CUTTING-EDGE APPROACHES FOR CNS PROTECTION AND REPAIR: FOCUS ON VASCULAR AND DEGENERATIVE DISORDERS

EDITED BY: Johannes Boltze, Marietta Zille, Stephan Schilling, Mathias Gelderblom, Gregory Jaye Bix, Piotr Walczak, Christoph Harms, Paulo Henrique Rosado-de-Castro and Emmanuel Pinteaux

PUBLISHED IN: Frontiers in Neuroscience, Frontiers in Neurology, Frontiers in Cellular Neuroscience and Frontiers in Aging Neuroscience

frontiers Research Topics

frontiers

Frontiers eBook Copyright Statement

The copyright in the text of individual articles in this eBook is the property of their respective authors or their respective institutions or funders. The copyright in graphics and images within each article may be subject to copyright of other parties. In both cases this is subject to a license granted to Frontiers.

The compilation of articles constituting this eBook is the property of Frontiers.

Each article within this eBook, and the eBook itself, are published under the most recent version of the Creative Commons CC-BY licence. The version current at the date of publication of this eBook is CC-BY 4.0. If the CC-BY licence is updated, the licence granted by Frontiers is automatically updated to the new version.

When exercising any right under the CC-BY licence, Frontiers must be attributed as the original publisher of the article or eBook, as applicable.

Authors have the responsibility of ensuring that any graphics or other materials which are the property of others may be included in the CC-BY licence, but this should be checked before relying on the CC-BY licence to reproduce those materials. Any copyright notices relating to those materials must be complied with.

Copyright and source acknowledgement notices may not be removed and must be displayed in any copy, derivative work or partial copy which includes the elements in question.

All copyright, and all rights therein, are protected by national and international copyright laws. The above represents a summary only. For further information please read Frontiers' Conditions for Website Use and Copyright Statement, and the applicable CC-BY licence.

ISSN 1664-8714
ISBN 978-2-88971-177-2
DOI 10.3389/978-2-88971-177-2

About Frontiers

Frontiers is more than just an open-access publisher of scholarly articles: it is a pioneering approach to the world of academia, radically improving the way scholarly research is managed. The grand vision of Frontiers is a world where all people have an equal opportunity to seek, share and generate knowledge. Frontiers provides immediate and permanent online open access to all its publications, but this alone is not enough to realize our grand goals.

Frontiers Journal Series

The Frontiers Journal Series is a multi-tier and interdisciplinary set of open-access, online journals, promising a paradigm shift from the current review, selection and dissemination processes in academic publishing. All Frontiers journals are driven by researchers for researchers; therefore, they constitute a service to the scholarly community. At the same time, the Frontiers Journal Series operates on a revolutionary invention, the tiered publishing system, initially addressing specific communities of scholars, and gradually climbing up to broader public understanding, thus serving the interests of the lay society, too.

Dedication to Quality

Each Frontiers article is a landmark of the highest quality, thanks to genuinely collaborative interactions between authors and review editors, who include some of the world's best academicians. Research must be certified by peers before entering a stream of knowledge that may eventually reach the public - and shape society; therefore, Frontiers only applies the most rigorous and unbiased reviews.
Frontiers revolutionizes research publishing by freely delivering the most outstanding research, evaluated with no bias from both the academic and social point of view. By applying the most advanced information technologies, Frontiers is catapulting scholarly publishing into a new generation.

What are Frontiers Research Topics?

Frontiers Research Topics are very popular trademarks of the Frontiers Journals Series: they are collections of at least ten articles, all centered on a particular subject. With their unique mix of varied contributions from Original Research to Review Articles, Frontiers Research Topics unify the most influential researchers, the latest key findings and historical advances in a hot research area! Find out more on how to host your own Frontiers Research Topic or contribute to one as an author by contacting the Frontiers Editorial Office: frontiersin.org/about/contact

CUTTING-EDGE APPROACHES FOR CNS PROTECTION AND REPAIR: FOCUS ON VASCULAR AND DEGENERATIVE DISORDERS

Topic Editors:
Johannes Boltze, University of Warwick, United Kingdom
Marietta Zille, University of Lübeck, Germany
Stephan Schilling, Fraunhofer Society (FHG), Germany
Mathias Gelderblom, University Medical Center Hamburg-Eppendorf, Germany
Gregory Jaye Bix, Tulane University, United States
Piotr Walczak, University of Maryland, Baltimore, United States
Christoph Harms, Charité – Universitätsmedizin Berlin, Germany
Paulo Henrique Rosado-de-Castro, D'Or Institute for Research and Education (IDOR), Brazil
Emmanuel Pinteaux, The University of Manchester, United Kingdom

Citation: Boltze, J., Zille, M., Schilling, S., Gelderblom, M., Bix, G. J., Walczak, P., Harms, C., Rosado-de-Castro, P. H., Pinteaux, E., eds. (2021). Cutting-Edge Approaches for CNS Protection and Repair: Focus on Vascular and Degenerative Disorders. Lausanne: Frontiers Media SA. doi: 10.3389/978-2-88971-177-2

Table of Contents

11 ***New Mechanistic Insights, Novel Treatment Paradigms, and Clinical Progress in Cerebrovascular Diseases***

Johannes Boltze, Jaroslaw A. Aronowski, Jerome Badaut, Marion S. Buckwalter, Mateo Caleo, Michael Chopp, Kunjan R. Dave, Nadine Didwischus, Rick M. Dijkhuizen, Thorsten R. Doeppner, Jens P. Dreier, Karim Fouad, Mathias Gelderblom, Karen Gertz, Dominika Golubczyk, Barbara A. Gregson, Edith Hamel, Daniel F. Hanley, Wolfgang Härtig, Friedhelm C. Hummel, Maulana Ikhsan, Miroslaw Janowski, Jukka Jolkkonen, Saravanan S. Karuppagounder, Richard F. Keep, Inga K. Koerte, Zaal Kokaia, Peiying Li, Fudong Liu, Ignacio Lizasoain, Peter Ludewig, Gerlinde A. S. Metz, Axel Montagne, Andre Obenaus, Alex Palumbo, Monica Pearl, Miguel Perez-Pinzon, Anna M. Planas, Nikolaus Plesnila, Ami P. Raval, Maria A. Rueger, Lauren H. Sansing, Farida Sohrabji, Charlotte J. Stagg, R. Anne Stetler, Ann M. Stowe, Dandan Sun, Akihiko Taguchi, Mickael Tanter, Sabine U. Vay, Raghu Vemuganti, Denis Vivien, Piotr Walczak, Jian Wang, Ye Xiong and Marietta Zille

26 ***Extracellular Vesicles Secreted in Response to Cytokine Exposure Increase Mitochondrial Oxygen Consumption in Recipient Cells***

Ashley E. Russell, Sujung Jun, Saumyendra Sarkar, Werner J. Geldenhuys, Sara E. Lewis, Stephanie L. Rellick and James W. Simpkins

38 ***Cell Type-Specific Human APP Transgene Expression by Hippocampal Interneurons in the Tg2576 Mouse Model of Alzheimer's Disease***

Corinna Höfling, Emira Shehabi, Peer-Hendrik Kuhn, Stefan F. Lichtenthaler, Maike Hartlage-Rübsamen and Steffen Roßner

50 ***Early Dyskinesias in Parkinson's Disease Patients With Parkin Mutation: A Primary Corticostriatal Synaptopathy?***

Jenny Sassone, Flavia Valtorta and Andrea Ciammola

57 ***Propensity Score-Matched Analysis of Lesion Patterns in Stroke Patients With Patent Foramen Ovale and Patients With Spontaneous Intracranial Artery Dissection***

Yangyang Huang, Yifan Cheng, Bei Shao, Xuanyou Zhou, Huazheng Liang, Jianhua Zhuang and Yong Bi

65 ***Correlates of Spreading Depolarization, Spreading Depression, and Negative Ultraslow Potential in Epidural Versus Subdural Electrocorticography***

Jens P. Dreier, Sebastian Major, Coline L. Lemale, Vasilis Kola, Clemens Reiffurth, Karl Schoknecht, Nils Hecht, Jed A. Hartings and Johannes Woitzik

85 ***Clinical Improvement Following Stroke Promptly Reverses Post-stroke Cellular Immune Alterations***

Antje Vogelgesang, Carl Witt, Christin Heuer, Juliane Schulze, Juliane Gellrich, Bettina von Sarnowski, Sönke Langner, Alexander Dressel and Johanna Ruhnau

94 ***Overexpression of CX3CR1 in Adipose-Derived Stem Cells Promotes Cell Migration and Functional Recovery After Experimental Intracerebral Hemorrhage***

Gaigai Li, Haihan Yu, Na Liu, Ping Zhang, Yingxin Tang, Yang Hu, Ye Zhang, Chao Pan, Hong Deng, Jiahui Wang, Qi Li and Zhouping Tang

106 ***Dipeptidyl Peptidase-4 Inhibitors for the Potential Treatment of Brain Disorders; A Mini-Review With Special Focus on Linagliptin and Stroke***

Vladimer Darsalia, Odd Erik Johansen, Grazyna Lietzau, Thomas Nyström, Thomas Klein and Cesare Patrone

115 ***Cross-Reactivity as a Mechanism Linking Infections to Stroke***

Guglielmo Lucchese, Agnes Flöel and Benjamin Stahl

123 ***MicroRNA-210-3p Targets RGMA to Enhance the Angiogenic Functions of Endothelial Progenitor Cells Under Hypoxic Conditions***

Wen-Jing Lu, Huai-Bin Liang, Yong-Fang Li, Xuan-Qiang Tu, Ji-Rong He, Kai-Qi Ding, Guo-Yuan Yang, Xiao-Yu Xin and Li-Li Zeng

134 ***Dysfunction of 67-kDa Laminin Receptor Disrupts BBB Integrity via Impaired Dystrophin/AQP4 Complex and p38 MAPK/VEGF Activation Following Status Epilepticus***

Hana Park, Seo-Hyeon Choi, Min-Jeong Kong and Tae-Cheon Kang

149 ***The Inflammatory Response After Ischemic Stroke: Targeting β_2 and β_1 Integrins***

Danielle N. Edwards and Gregory J. Bix

159 ***Fibrinogen Chains Intrinsic to the Brain***

Eugene V. Golanov, Martyn A. Sharpe, Angelique S. Regnier-Golanov, Gregory J. Del Zoppo, David S. Baskin and Gavin W. Britz

171 ***Generation of Oligodendrocyte Progenitor Cells From Mouse Bone Marrow Cells***

Yuan Zhang, Xin-Yu Lu, Giacomo Casella, Jing Tian, Ze-Qing Ye, Ting Yang, Juan-Juan Han, Ling-Yu Jia, Abdolmohamad Rostami and Xing Li

181 ***Canine Cognitive Dysfunction and Alzheimer's Disease – Two Facets of the Same Disease?***

Sonja Prpar Mihevc and Gregor Majdič

199 ***Telomere Length: A Potential Biomarker for the Risk and Prognosis of Stroke***

Yanjun Tian, Shuai Wang, Fengjuan Jiao, Qingsheng Kong, Chuanxin Liu and Yili Wu

207 ***Non-pulsed Sinusoidal Electromagnetic Field Rescues Animals From Severe Ischemic Stroke via NO Activation***

Lena P. Font, Miriam M. Cardonne, Hannelore Kemps, Raf Meesen, Oneida F. Salmon, Fidel G. González, Ivo Lambrichts, Jean-Michel Rigo, Bert Brône and Annelies Bronckaers

214 ***Proteostasis During Cerebral Ischemia***

Audrey M. Thiebaut, Elodie Hedou, Stefan J. Marciniak, Denis Vivien and Benoit D. Roussel

228 ***Old Dog New Tricks; Revisiting How Stroke Modulates the Systemic Immune Landscape***

Siddharth Krishnan and Catherine B. Lawrence

239 ***NK1-r Antagonist Treatment Comparable to Decompressive Craniectomy in Reducing Intracranial Pressure Following Stroke***
Annabel J. Sorby-Adams, Anna V. Leonard, Jan W. Hoving, Nawaf Yassi, Robert Vink, Adam J. Wells and Renée J. Turner

251 ***Determining the Temporal Profile of Intracranial Pressure Changes Following Transient Stroke in an Ovine Model***
Annabel J. Sorby-Adams, Anna V. Leonard, Levi E. Elms, Oana C. Marian, Jan W. Hoving, Nawaf Yassi, Robert Vink, Emma Thornton an Renée J. Turner

267 ***Intravenous Administration of Human Adipose Derived-Mesenchymal Stem Cells Is Not Efficient in Diabetic or Hypertensive Mice Subjected to Focal Cerebral Ischemia***
Gabrielle Mangin, Adrien Cogo, Anaïck Moisan, Philippe Bonnin, Benjamin Maïer and Nathalie Kubis on behalf of the RESSTORE Consortium

283 ***Delayed Effects of Acute Reperfusion on Vascular Remodeling and Late-Phase Functional Recovery After Stroke***
Violeta Durán-Laforet, David Fernández-López, Alicia García-Culebras, Juan González-Hijón, Ana Moraga, Sara Palma-Tortosa, Isaac García-Yébenes, Adrián Vega-Pérez, Ignacio Lizasoain and María Ángeles Moro

295 ***Re-thinking the Etiological Framework of Neurodegeneration***
Ximena Castillo, Susana Castro-Obregón, Benjamin Gutiérrez-Becker, Gabriel Gutiérrez-Ospina, Nikolaos Karalis, Ahmed A. Khalil, José Sócrates Lopez-Noguerola, Liliana Lozano Rodríguez, Eduardo Martínez-Martínez, Claudia Perez-Cruz, Judith Pérez-Velázquez, Ana Luisa Piña, Karla Rubio, Héctor Pedro Salazar García, Tauqeerunnisa Syeda, America Vanoye-Carlo, Arno Villringer, Katarzyna Winek and Marietta Zille

320 ***Dental Pulp Stem Cells: An Attractive Alternative for Cell Therapy in Ischemic Stroke***
Xiaoyan Lan, Zhengwu Sun, Chengyan Chu, Johannes Boltze and Shen Li

330 ***Therapeutic Potential of Neurotrophins for Repair After Brain Injury: A Helping Hand From Biomaterials***
Josh Houlton, Nashat Abumaria, Simon F. R. Hinkley and Andrew N. Clarkson

353 ***Pluripotent Stem Cells for Brain Repair: Protocols and Preclinical Applications in Cortical and Hippocampal Pathologies***
Claudia Alia, Marco Terrigno, Irene Busti, Federico Cremisi and Matteo Caleo

368 ***Acute Subcortical Infarcts Cause Secondary Degeneration in the Remote Non-involved Cortex and Connecting Fiber Tracts***
Xiao-Er Wei, Kai Shang, Jia Zhou, Ya-Jun Zhou and Yue-Hua Li

377 ***Topical Administration of a Soluble TNF Inhibitor Reduces Infarct Volume After Focal Cerebral Ischemia in Mice***
Minna Yli-Karjanmaa, Bettina Hjelm Clausen, Matilda Degn, Hans Gram Novrup, Ditte Gry Ellman, Peter Toft-Jensen, David E. Szymkowski, Allan Stensballe, Morten Meyer, Roberta Brambilla and Kate Lykke Lambertsen

395 ***Aging Neurovascular Unit and Potential Role of DNA Damage and Repair in Combating Vascular and Neurodegenerative Disorders***
Yan Li, Lv Xie, Tingting Huang, Yueman Zhang, Jie Zhou, Bo Qi, Xin Wang, Zengai Chen and Peiying Li

410 ***Potential Immunotherapeutic Targets on Myeloid Cells for Neurovascular Repair After Ischemic Stroke***
Ziyu Zhu, Li Zheng, Yan Li, Tingting Huang, Yu-Chieh Chao, Lijun Pan, Hui Zhu, Yanhua Zhao, Weifeng Yu and Peiying Li

425 ***Small Vessels are a Big Problem in Neurodegeneration and Neuroprotection***
Şefik Evren Erdener and Turgay Dalkara

445 ***Involvement of Epigenetic Mechanisms and Non-coding RNAs in Blood-Brain Barrier and Neurovascular Unit Injury and Recovery After Stroke***
Svetlana M. Stamatovic, Chelsea M. Phillips, Gabriela Martinez-Revollar, Richard F. Keep and Anuska V. Andjelkovic

460 ***Serial Metabolic Evaluation of Perihematomal Tissues in the Intracerebral Hemorrhage Pig Model***
Muhammad E. Haque, Refaat E. Gabr, Sarah D. George, Xiurong Zhao, Seth B. Boren, Xu Zhang, Shun-Ming Ting, Gunghua Sun, Khader M. Hasan, Sean Savitz and Jaroslaw Aronowski

468 ***The Potential of Biomaterial-Based Approaches as Therapies for Ischemic Stroke: A Systematic Review and Meta-Analysis of Pre-clinical Studies***
Faye Bolan, Irene Louca, Calvin Heal and Catriona J. Cunningham

480 ***New Perspective for Non-invasive Brain Stimulation Site Selection in Mild Cognitive Impairment: Based on Meta- and Functional Connectivity Analyses***
Jiao Liu, Binlong Zhang, Georgia Wilson, Jian Kong and the Alzheimer's Disease Neuroimaging Initiative

488 ***Stem Cell-Derived Exosomes Protect Astrocyte Cultures From* in vitro *Ischemia and Decrease Injury as Post-stroke Intravenous Therapy***
Xiaoyun Sun, Ji-Hye Jung, Oiva Arvola, Michelle R. Santoso, Rona G. Giffard, Phillip C. Yang and Creed M. Stary

497 ***Neurons Induced From Fibroblasts of c9ALS/FTD Patients Reproduce the Pathology Seen in the Central Nervous System***
Peter O. Bauer, Judith H. Dunmore, Hiroki Sasaguri and Vaclav Matoska

507 ***Small Vessel Disease***
Antoine M. Hakim

513 ***Enzymatic Digestion of Hyaluronan-Based Brain Extracellular Matrix* in vivo *Can Induce Seizures in Neonatal Mice***
Alena Balashova, Vladimir Pershin, Olga Zaborskaya, Natalia Tkachenko, Andrey Mironov, Evgeny Guryev, Leonid Kurbatov, Murat Gainullin and Irina Mukhina

525 ***Visualization and Quantification of Post-stroke Neural Connectivity and Neuroinflammation Using Serial Two-Photon Tomography in the Whole Mouse Brain***
Katherine Poinsatte, Dene Betz, Vanessa O. Torres, Apoorva D. Ajay, Shazia Mirza, Uma M. Selvaraj, Erik J. Plautz, Xiangmei Kong, Sankalp Gokhale, Julian P. Meeks, Denise M. O. Ramirez, Mark P. Goldberg and Ann M. Stowe

539 ***A Safe and Effective Magnetic Labeling Protocol for MRI-Based Tracking of Human Adult Neural Stem Cells***
Albrecht Stroh, Jenny Kressel, Roland Coras, Antje Y. Dreyer, Wenke Fröhlich, Annette Förschler, Donald Lobsien, Ingmar Blümcke, Saida Zoubaa, Jürgen Schlegel, Claus Zimmer and Johannes Boltze

549 ***Thyroid Hormones in the Brain and Their Impact in Recovery Mechanisms After Stroke***
Daniela Talhada, Cecília Reis Alves Santos, Isabel Gonçalves and Karsten Ruscher

565 ***Behcet's Disease With Cerebral Artery Infarction Caused by Cerebral Arteritis as an Early Symptom Only With Elevated Interleukin-8***
Hao Yin, Yun Song, Meimei Zheng, Ju Han and Jiyou Tang

572 ***Metabolic Changes in Focal Brain Ischemia in Rats Treated With Human Induced Pluripotent Stem Cell-Derived Neural Precursors Confirm the Beneficial Effect of Transplanted Cells***
Daniel Jirak, Natalia Ziolkowska, Karolina Turnovcova, Kristyna Karova, Eva Sykova, Pavla Jendelova and Nataliya Romanyuk

587 ***ApoA-I Mimetic Peptide Reduces Vascular and White Matter Damage After Stroke in Type-2 Diabetic Mice***
Xiaohui Wang, Rongwen Li, Alex Zacharek, Julie Landschoot-Ward, Michael Chopp, Jieli Chen and Xu Cui

600 ***Transcranial Current Stimulation Alters the Expression of Immune-Mediating Genes***
Monika Rabenstein, Marcus Unverricht-Yeboah, Meike Hedwig Keuters, Anton Pikhovych, Joerg Hucklenbroich, Sabine Ulrike Vay, Stefan Blaschke, Anne Ladwig, Helene Luise Walter, Magdalena Beiderbeck, Gereon Rudolf Fink, Michael Schroeter, Ralf Kriehuber and Maria Adele Rueger

608 ***The Delta-Subunit Selective $GABA_A$ Receptor Modulator, DS2, Improves Stroke Recovery via an Anti-inflammatory Mechanism***
Silke Neumann, Lily Boothman-Burrell, Emma K. Gowing, Thomas A. Jacobsen, Philip K. Ahring, Sarah L. Young, Karin Sandager-Nielsen and Andrew N. Clarkson

621 ***Opposite Effects of Neuroprotective Cannabinoids, Palmitoylethanolamide, and 2-Arachidonoylglycerol on Function and Morphology of Microglia***
Urszula Hohmann, Markus Pelzer, Joshua Kleine, Tim Hohmann, Chalid Ghadban and Faramarz Dehghani

636 ***Bioscaffold-Induced Brain Tissue Regeneration***
Michel Modo

662 ***Brain–Immune Interactions and Neuroinflammation After Traumatic Brain Injury***
Virginie Dinet, Klaus G. Petry and Jerome Badaut

674 ***Development of a Routinely Applicable Imaging Protocol for Fast and Precise Middle Cerebral Artery Occlusion Assessment and Perfusion Deficit Measure in an Ovine Stroke Model: A Case Study***
Andrea Maria Herrmann, Giorgio Franco Maria Cattaneo, Sebastian Alexander Eiden, Manuela Wieser, Elias Kellner, Christoph Maurer, Jörg Haberstroh, Christoph Mülling, Wolf-Dirk Niesen, Horst Urbach, Johannes Boltze, Stephan Meckel and Mukesch Johannes Shah

685 ***Proteostasis in Cerebral Small Vessel Disease***
Christof Haffner

695 ***Successes and Hurdles in Stem Cells Application and Production for Brain Transplantation***
Daniel Henriques, Ricardo Moreira, Jens Schwamborn, Luís Pereira de Almeida and Liliana S. Mendonça

710 ***Pericytes in Cerebrovascular Diseases: An Emerging Therapeutic Target***
Xiaojuan Su, Lingyi Huang, Yi Qu, Dongqiong Xiao and Dezhi Mu

722 ***A Pilot Study Investigating Changes in Capillary Hemodynamics and Its Modulation by Exercise in the APP-PS1 Alzheimer Mouse Model***
Xuecong Lu, Mohammad Moeini, Baoqiang Li, Yuankang Lu, Rafat Damseh, Philippe Pouliot, Éric Thorin and Frédéric Lesage

734 ***Viability and Contractility of Rat Brain Pericytes in Conditions That Mimic Stroke; an* in vitro *Study***
Mohammed Heyba, Lulwa Al-Abdullah, Andreas W. Henkel, Zeinab Sayed, Slava A. Malatiali and Zoran B. Redzic

744 ***Mean Platelet Volume-To-Lymphocyte Ratio Predicts Poor Functional Outcomes Among Ischemic Stroke Patients Treated With Intravenous Thrombolysis***
Si-Yan Chen, Yuan-Shao Lin, Yi-Fan Cheng, Hong Wang, Xiao-Ting Niu and Wan-Li Zhang

752 ***Effects of Transcranial Direct Current Stimulation (tDCS) and Exercises Treadmill on Autonomic Modulation of Hemiparetic Patients Due To Stroke—Clinic Test, Controlled, Randomized, Double-Blind***
Glauber Heinz, Katia De Angelis, Simone Dal Corso, Maria Helena Gomes De Sousa, Ariane Viana, Fernando Dos Santos, João Carlos Ferrari Corrêa and Fernanda Ishida Corrêa

764 ***Acute Treatment With Gleevec Does Not Promote Early Vascular Recovery Following Intracerebral Hemorrhage in Adult Male Rats***
Mohammed Abbas, Elizabeth Haddad, Mary Hamer, Derek Nowrangi, John Zhang, William J. Pearce, Jiping Tang and Andre Obenaus

781 ***Hierarchical Clustering Analyses of Plasma Proteins in Subjects With Cardiovascular Risk Factors Identify Informative Subsets Based on Differential Levels of Angiogenic and Inflammatory Biomarkers***
Zachary Winder, Tiffany L. Sudduth, David Fardo, Qiang Cheng, Larry B. Goldstein, Peter T. Nelson, Frederick A. Schmitt, Gregory A. Jicha and Donna M. Wilcock

791 ***Subarachnoid Hemorrhage Induces Dynamic Immune Cell Reactions in the Choroid Plexus***
Peter Solár, Ilona Klusáková, Radim Jančálek, Petr Dubový and Marek Joukal

804 ***Platelets in Amyloidogenic Mice are Activated and Invade the Brain***
Kathrin M. Kniewallner, Diana M. Bessa de Sousa, Michael S. Unger, Heike Mrowetz and Ludwig Aigner

818 ***Influence of Age-Related Complications on Clinical Outcome in Patients With Small Ruptured Cerebral Aneurysms***
Jianfeng Zheng, Xiaochuan Sun and Xiaodong Zhang

825 **In vivo *Two-Photon Imaging Reveals Acute Cerebral Vascular Spasm and Microthrombosis After Mild Traumatic Brain Injury in Mice***
Xinjia Han, Zhi Chai, Xingjie Ping, Li-Juan Song, Cungen Ma, Yiwen Ruan and Xiaoming Jin

837 ***Hypoxia-Inducible Factor 1α and 2α Have Beneficial Effects in Remote Ischemic Preconditioning Against Stroke by Modulating Inflammatory Responses in Aged Rats***
Xiangnan Du, Jian Yang, Cuiying Liu, Sainan Wang, Chencheng Zhang, Heng Zhao, Huishan Du and Xiaokun Geng

848 ***Gene Expression Dynamics at the Neurovascular Unit During Early Regeneration After Cerebral Ischemia/Reperfusion Injury in Mice***
Roxane-Isabelle Kestner, Franziska Mayser, Rajkumar Vutukuri, Lena Hansen, Stefan Günther, Robert Brunkhorst, Kavi Devraj and Waltraud Pfeilschifter

860 ***Isolation of Mouse Cerebral Microvasculature for Molecular and Single-Cell Analysis***
Hallel C. Paraiso, Xueqian Wang, Ping-Chang Kuo, Destin Furnas, Barbara A. Scofield, Fen-Lei Chang, Jui-Hung Yen and I-Chen Yu

873 ***Effects of Periprocedural Tirofiban vs. Oral Antiplatelet Drug Therapy on Posterior Circulation Infarction in Patients With Acute Intracranial Atherosclerosis-Related Vertebrobasilar Artery Occlusion***
Xuan Sun, Huijun Zhang, Xu Tong, Feng Gao, Gaoting Ma and Zhongrong Miao

880 ***Hypothesis and Theory: A Pathophysiological Concept of Stroke-Induced Acute Phase Response and Increased Intestinal Permeability Leading to Secondary Brain Damage***
Fabienne Ferrara, Vilia Zeisig, Sören Pietsch, Rita Rütten, Antje Y. Dreyer, Laura Pieper, Ann-Kathrin Schatzl, Damian D. McLeod, Henryk Barthel, Johannes Boltze, Wieland Schrödl and Björn Nitzsche

888 ***Reduced Post-ischemic Brain Injury in Transient Receptor* Potential Vanilloid 4 *Knockout Mice***
Koji Tanaka, Shoji Matsumoto, Takeshi Yamada, Ryo Yamasaki, Makoto Suzuki, Mizuho A. Kido and Jun-Ichi Kira

896 ***Serum-Based Proteomics Reveals Lipid Metabolic and Immunoregulatory Dysregulation in Cervical Artery Dissection With Stroke***
Yongtao Yang, Jing Peng, Suxia Wang, Jialu Huang, Hong Ran, Kangning Chen and Zhenhua Zhou

905 ***New PAR1 Agonist Peptide Demonstrates Protective Action in a Mouse Model of Photothrombosis-Induced Brain Ischemia***
Maksim Galkov, Ekaterina Kiseleva, Mikhail Gulyaev, Maria Sidorova and Liubov Gorbacheva

917 ***NEK7 Coordinates Rapid Neuroinflammation After Subarachnoid Hemorrhage in Mice***
Gen Li, Yushu Dong, Dongdong Liu, Zheng Zou, Guangzhi Hao, Xu Gao, Pengyu Pan and Guobiao Liang

931 ***A Semiquantitative Non-invasive Measurement of PcomA Patency in C57BL/6 Mice Explains Variance in Ischemic Brain Damage in Filament MCAo***
Samuel Knauss, Carolin Albrecht, Ulrich Dirnagl, Susanne Mueller, Christoph Harms, Christian Johannes Hoffmann, Stefan Paul Koch, Matthias Endres and Philipp Boehm-Sturm

942 ***Beta-Hydroxybutyrate Enhances BDNF Expression by Increasing H3K4me3 and Decreasing H2AK119ub in Hippocampal Neurons***
Erling Hu, Huan Du, Sen Shang, Yali Zhang and Xiaoyun Lu

955 ***Disrupted Regional Cerebral Blood Flow and Functional Connectivity in Pontine Infarction: A Longitudinal MRI Study***
Ying Wei, Luobing Wu, Yingying Wang, Jingchun Liu, Peifang Miao, Kaiyu Wang, Caihong Wang and Jingliang Cheng

968 ***LongShengZhi Capsule Attenuates Alzheimer-Like Pathology in APP/PS1 Double Transgenic Mice by Reducing Neuronal Oxidative Stress and Inflammation***
Zequn Yin, Xuerui Wang, Shihong Zheng, Peichang Cao, Yuanli Chen, Maoyun Yu, Chenzhong Liao, Zhongyuan Zhang, Jihong Han, Yajun Duan, Xiaoxiao Yang and Shuang Zhang

986 ***Hydrogen Sulfide Overproduction is Involved in Acute Ischemic Cerebral Injury Under Hyperhomocysteinemia***
Yan Ji, Yusheng Li, Zichen Zhao, Panxing Li and Yi Xie

1000 ***MiR-128-3p Alleviates Spinal Cord Ischemia/Reperfusion Injury Associated Neuroinflammation and Cellular Apoptosis via SP1 Suppression in Rat***
Dan Wang, Fengshou Chen, Bo Fang, Zaili Zhang, Yan Dong, Xiangyi Tong and Hong Ma

1015 ***Pathophysiological Changes and the Role of Notch-1 Activation After Decompression in a Compressive Spinal Cord Injury Rat Model***
Xing Cheng, Zhengran Yu, Jinghui Xu, Daping Quan and Houqing Long

1029 ***Improved Functional Outcome After Peripheral Nerve Stimulation of the Impaired Forelimb Post-stroke***
Shih-Yen Tsai, Jennifer A. Schreiber, Natalie S. Adamczyk, Joanna Y. Wu, Son T. Ton, Ryan C. Hofler, James S. Walter, Timothy E. O'Brien, Gwendolyn L. Kartje and Russ P. Nockels

frontiers in Aging Neuroscience

REVIEW
published: 28 January 2021
doi: 10.3389/fnagi.2021.623751

New Mechanistic Insights, Novel Treatment Paradigms, and Clinical Progress in Cerebrovascular Diseases

Johannes Boltze[1], Jaroslaw A. Aronowski[2], Jerome Badaut[3], Marion S. Buckwalter[4], Mateo Caleo[5,6], Michael Chopp[7,8], Kunjan R. Dave[9], Nadine Didwischus[1], Rick M. Dijkhuizen[10], Thorsten R. Doeppner[11], Jens P. Dreier[12,13,14,15], Karim Fouad[16], Mathias Gelderblom[17], Karen Gertz[12,18], Dominika Golubczyk[19], Barbara A. Gregson[20], Edith Hamel[21], Daniel F. Hanley[22], Wolfgang Härtig[23], Friedhelm C. Hummel[24,25], Maulana Ikhsan[26,27,28], Miroslaw Janowski[29], Jukka Jolkkonen[30], Saravanan S. Karuppagounder[31,32], Richard F. Keep[33], Inga K. Koerte[34,35], Zaal Kokaia[36], Peiying Li[37], Fudong Liu[38], Ignacio Lizasoain[39], Peter Ludewig[17], Gerlinde A. S. Metz[40], Axel Montagne[41], Andre Obenaus[42], Alex Palumbo[26,27,28], Monica Pearl[43], Miguel Perez-Pinzon[9], Anna M. Planas[44,45], Nikolaus Plesnila[46,47,48], Ami P. Raval[9], Maria A. Rueger[49], Lauren H. Sansing[50], Farida Sohrabji[51], Charlotte J. Stagg[52,53], R. Anne Stetler[54], Ann M. Stowe[55], Dandan Sun[56], Akihiko Taguchi[57], Mickael Tanter[58], Sabine U. Vay[49], Raghu Vemuganti[59], Denis Vivien[60,61], Piotr Walczak[29], Jian Wang[62], Ye Xiong[63] and Marietta Zille[26,27,28]*

[1]School of Life Sciences, University of Warwick, Warwick, United Kingdom, [2]Institute for Stroke and Cerebrovascular Diseases, McGovern Medical School, The University of Texas Health Science Center at Houston, Houston, TX, United States, [3]NRS UMR 5287, INCIA, Brain Molecular Imaging Team, University of Bordeaux, Bordeaux cedex, France, [4]Departments of Neurology and Neurological Sciences, and Neurosurgery, Wu Tsai Neurosciences Institute, Stanford School of Medicine, Stanford, CA, United States, [5]Neuroscience Institute, National Research Council, Pisa, Italy, [6]Department of Biomedical Sciences, University of Padua, Padua, Italy, [7]Department of Neurology, Henry Ford Hospital, Detroit, MI, United States, [8]Department of Physics, Oakland University, Rochester, MI, United States, [9]Peritz Scheinberg Cerebral Vascular Disease Research Laboratory, Department of Neurology, University of Miami Miller School of Medicine, Miami, FL, United States, [10]Biomedical MR Imaging and Spectroscopy Group, Center for Image Sciences, University Medical Center Utrecht and Utrecht University, Utrecht, Netherlands, [11]Department of Neurology, University Medical Center Göttingen, Göttingen, Germany, [12]Department of Neurology, Center for Stroke Research Berlin, Charité—Universitätsmedizin Berlin, Berlin, Germany, [13]Department of Experimental Neurology, Charité—Universitätsmedizin Berlin, Berlin, Germany, [14]Bernstein Center for Computational Neuroscience Berlin, Berlin, Germany, [15]Einstein Center for Neurosciences Berlin, Berlin, Germany, [16]Faculty of Rehabilitation Medicine and Institute for Neuroscience and Mental Health, University of Alberta, Edmonton, AB, Canada, [17]Department of Neurology, University Medical Center Hamburg-Eppendorf, Hamburg, Germany, [18]Berlin Institute of Health, Berlin, Germany, [19]Department of Neurosurgery, School of Medicine, University of Warmia and Mazury, Olsztyn, Poland, [20]Neurosurgical Trials Group, Institute of Neuroscience, The University of Newcastle upon Tyne, Newcastle upon Tyne, United Kingdom, [21]Laboratory of Cerebrovascular Research, Montreal Neurological Institute, McGill University, Montreal, QC, Canada, [22]Division of Brain Injury Outcomes, Johns Hopkins University, Baltimore, MD, United States, [23]Paul Flechsig Institute of Brain Research, University of Leipzig, Leipzig, Germany, [24]Clinical Neuroengineering, Center for Neuroprosthetics and Brain Mind Institute, Swiss Federal Institute of Technology Valais, Clinique Romande de Réadaptation, Sion, Switzerland, [25]Clinical Neuroscience, University of Geneva Medical School, Geneva, Switzerland, [26]Institute for Experimental and Clinical Pharmacology and Toxicology, University of Lübeck, Lübeck, Germany, [27]Fraunhofer Research Institution for Marine Biotechnology and Cell Technology, Lübeck, Germany, [28]Institute for Medical and Marine Biotechnology, University of Lübeck, Lübeck, Germany, [29]Department of Diagnostic Radiology and Nuclear Medicine, University of Maryland, Baltimore, MD, United States, [30]Department of Neurology, A.I. Virtanen Institute for Molecular Sciences, University of Eastern Finland, Kuopio, Finland, [31]Burke Neurological Institute, White Plains, NY, United States, [32]Feil Family Brain and Mind Research Institute, Weill Cornell Medicine, New York, NY, United States, [33]Department of Neurosurgery, University of Michigan, Ann Arbor, MI, United States, [34]Psychiatric Neuroimaging Laboratory, Brigham and Women's Hospital and Harvard Medical School, Boston, MA, United States, [35]Department of Child and Adolescent Psychiatry, Psychosomatic, and Psychotherapy, Ludwig Maximilians University, Munich, Germany, [36]Lund Stem Cell Center, Lund University, Lund, Sweden,

OPEN ACCESS

Edited by:
Eszter Farkas, University of Szeged, Hungary

Reviewed by:
Arthur Liesz, Ludwig Maximilian University of Munich, Germany
Anusha Mishra, Oregon Health and Science University, United States

***Correspondence:**
Johannes Boltze
johannes.boltze@warwick.ac.uk

Received: 30 October 2020
Accepted: 04 January 2021
Published: 28 January 2021

Citation:
Boltze J, Aronowski JA, Badaut J, Buckwalter MS, Caleo M, Chopp M, Dave KR, Didwischus N, Dijkhuizen RM, Doeppner TR, Dreier JP, Fouad K, Gelderblom M, Gertz K, Golubczyk D, Gregson BA, Hamel E, Hanley DF, Härtig W, Hummel FC, Ikhsan M, Janowski M, Jolkkonen J, Karuppagounder SS, Keep RF, Koerte IK, Kokaia Z, Li P, Liu F, Lizasoain I, Ludewig P, Metz GAS, Montagne A, Obenaus A, Palumbo A, Pearl M, Perez-Pinzon M, Planas AM, Plesnila N, Raval AP, Rueger MA, Sansing LH, Sohrabji F, Stagg CJ, Stetler RA, Stowe AM, Sun D, Taguchi A, Tanter M, Vay SU, Vemuganti R, Vivien D, Walczak P, Wang J, Xiong Y and Zille M (2021) New Mechanistic Insights, Novel Treatment Paradigms, and Clinical Progress in Cerebrovascular Diseases. Front. Aging Neurosci. 13:623751. doi: 10.3389/fnagi.2021.623751

[37]Department of Anesthesiology, Renji Hospital, School of Medicine, Shanghai Jiaotong University, Shanghai, China, [38]Department of Neurology, The University of Texas Health Science Center at Houston, McGovern Medical School, Houston, TX, United States, [39]Unidad de Investigación Neurovascular, Departamento Farmacología y Toxicología, Facultad de Medicina, Instituto Universitario de Investigación en Neuroquímica, Universidad Complutense de Madrid, Madrid, Spain, [40]Department of Neuroscience, Canadian Centre for Behavioural Neuroscience, University of Lethbridge, Lethbridge, AB, Canada, [41]Zilkha Neurogenetic Institute, Keck School of Medicine, University of Southern California, Los Angeles, CA, United States, [42]Department of Pediatrics, University of California, Irvine, Irvine, CA, United States, [43]The Russell H. Morgan Department of Radiology and Radiological Science, Johns Hopkins University School of Medicine, Baltimore, MD, United States, [44]Institut d'Investigacions Biomèdiques August Pi i Sunyer (IDIBAPS), Àrea de Neurociències, Barcelona, Spain, [45]Department d'Isquèmia Cerebral I Neurodegeneració, Institut d'Investigacions Biomèdiques de Barcelona (IIBB), Consejo Superior de Investigaciones Cientificas (CSIC), Barcelona, Spain, [46]Institute for Stroke and Dementia Research (ISD), Munich University Hospital, Munich, Germany, [47]Graduate School of Systemic Neurosciences (GSN), Munich University Hospital, Munich, Germany, [48]Munich Cluster of Systems Neurology (Synergy), Munich, Germany, [49]Faculty of Medicine and University Hospital, Department of Neurology, University of Cologne, Cologne, Germany, [50]Department of Neurology, Yale University School of Medicine, New Haven, CT, United States, [51]Women's Health in Neuroscience Program, Neuroscience and Experimental Therapeutics, Texas A&M College of Medicine, Bryan, TX, United States, [52]Nuffield Department of Clinical Neurosciences, Wellcome Centre for Integrative Neuroimaging, University of Oxford, Oxford, United Kingdom, [53]MRC Brain Network Dynamics Unit, University of Oxford, Oxford, United Kingdom, [54]Department of Neurology, Pittsburgh Institute of Brain Disorders and Recovery, University of Pittsburgh, Pittsburgh, PA, United States, [55]Department of Neurology and Neurotherapeutics, Peter O'Donnell Jr. Brain Institute, UT Southwestern Medical Center, Dallas, TX, United States, [56]Pittsburgh Institute for Neurodegenerative Disorders, University of Pittsburgh, PA, United States, [57]Department of Regenerative Medicine Research, Institute of Biomedical Research and Innovation, Kobe, Japan, [58]Institute of Physics for Medicine Paris, INSERM U1273, ESPCI Paris, CNRS FRE 2031, PSL University, Paris, France, [59]Department of Neurological Surgery, University of Wisconsin, Madison, WI, United States, [60]UNICAEN, INSERM, INSERM UMR-S U1237, Physiopathology and Imaging for Neurological Disorders (PhIND), Normandy University, Caen, France, [61]CHU Caen, Clinical Research Department, CHU de Caen Côte de Nacre, Caen, France, [62]Department of Human Anatomy, College of Medical Sciences, Zhengzhou University, Zhengzhou, China, [63]Department of Neurosurgery, Henry Ford Hospital, Detroit, MI, United States

The past decade has brought tremendous progress in diagnostic and therapeutic options for cerebrovascular diseases as exemplified by the advent of thrombectomy in ischemic stroke, benefitting a steeply increasing number of stroke patients and potentially paving the way for a renaissance of neuroprotectants. Progress in basic science has been equally impressive. Based on a deeper understanding of pathomechanisms underlying cerebrovascular diseases, new therapeutic targets have been identified and novel treatment strategies such as pre- and post-conditioning methods were developed. Moreover, translationally relevant aspects are increasingly recognized in basic science studies, which is believed to increase their predictive value and the relevance of obtained findings for clinical application.This review reports key results from some of the most remarkable and encouraging achievements in neurovascular research that have been reported at the 10th International Symposium on Neuroprotection and Neurorepair. Basic science topics discussed herein focus on aspects such as neuroinflammation, extracellular vesicles, and the role of sex and age on stroke recovery. Translational reports highlighted endovascular techniques and targeted delivery methods, neurorehabilitation, advanced functional testing approaches for experimental studies, pre-and post-conditioning approaches as well as novel imaging and treatment strategies. Beyond ischemic stroke, particular emphasis was given on activities in the fields of traumatic brain injury and cerebral hemorrhage in which promising preclinical and clinical results have been reported. Although the number of neutral outcomes in clinical trials is still remarkably high when targeting cerebrovascular diseases, we begin to evidence stepwise but continuous progress towards novel treatment options. Advances in preclinical and translational research as reported herein are believed to have formed a solid foundation for this progress.

Keywords: cell therapies, dementia, experimental therapy, hemorrhage, neuroprotection, neurorehabilitation, stroke, translational research

INTRODUCTION

Overcoming more than two decades of translational standstill and providing options to treat selected stroke patients in extended time windows, the advent of recanalization approaches has sparked a new dynamic in preclinical and clinical stroke research. With a catheter in place, i.e., in a reopened cerebral artery, we now have the opportunity to apply neuroprotective treatments exactly when and where they may exert their optimal benefit (Savitz et al., 2019). These new options have the potential to initiate a "renaissance of neuroprotectants." Neuroprotectants may also play an increasingly important role in the treatment of cerebral hemorrhages. Minimally invasive techniques for hematoma evacuation relying on specialized, catheter-based intervention strategies have been developed and were assessed in first clinical trials (Hanley et al., 2019). Neuroprotective agents may be delivered *via* those catheters once the hematoma was removed, and novel targets for neuroprotective interventions have been identified (Zille et al., 2017).

Nevertheless, the majority of patients still cannot benefit from the recent advances in acute interventions for cerebrovascular diseases. Among others, reasons comprise strict inclusion/exclusion and eligibility criteria, uncertainties regarding the optimal way to deliver such treatments as well as logistical challenges and limited availability of required infrastructure. Therefore, the need for new treatments being effective within therapeutic time windows beyond the range of hours as well as supporting long-term recovery and recuperation continues to exist. The development of these new treatments should take into account advances in basic science areas such as neuroimmunology, neurobiochemistry, and molecular biology, as well as cell-based approaches. Moreover, translational research shall reflect advances in imaging technologies and rehabilitation research and must consider aspects such as the influence of sex and age on therapeutic outcome.

The International Symposium on Neuroprotection and Neurorepair (ISN&N) discussed these aspects in the light of current therapeutic advances in cerebrovascular diseases. The ISN&N is a biennial meeting series on fundamental and translational neuroscience with a scope on cerebrovascular diseases and dementia (Boltze et al., 2011, 2012; Demuth et al., 2017). Attracting leading neuroscientists and clinicians from around the world, the meeting is characterized by intensive scientific exchange and discussions of new insights into neurovascular and neurodegenerative diseases. To share some of the most exciting reports with a wider academic community in a concise format, this review summarizes cross-selected, outstanding sessions from the 10th ISN&N that took place from October 9th to 11th 2018 in Radebeul near Dresden, Germany. It covers the main topics of the meeting, and puts a particular scope on translational and clinical aspects, as such providing a good overview of the field.

Conditioning Medicine: Basic Mechanisms and Clinical Potential

It is now well accepted that ischemic pre- and post-conditioning promotes ischemic neuroprotection in different modalities (e.g., pharmacological, remote, and ischemic) and in many different animal models (Wang et al., 2015). Novel mechanisms involved in conditioning were discussed and clinical views of how to apply conditioning strategies to thrombectomy were provided.

IL (Madrid, Spain) presented that toll-like receptor 4 (TLR4) has both protective (ischemic tolerance) and damaging (acute ischemia) roles in cerebral ischemia, including hemorrhagic transformation (Pradillo et al., 2009; Vartanian et al., 2011; García-Culebras et al., 2017). TLR4 deficiency increased the levels of alternative neutrophils (N2), which may be involved in the resolution of inflammation and in the neuroprotective effect observed after stroke (García-Culebras et al., 2019). New drugs blocking TLR4 (Fernández et al., 2018) may be useful for the treatment of patients with stroke.

RAS (Pittsburgh, PA, USA) demonstrated that ischemic neuroprotection can be achieved by dietary restriction, improving both gray and white matter outcomes and functional recovery (Zhang et al., 2018). Although the activation of sirtuins may be a potential contributor to ischemic neuroprotection (Haigis and Guarente, 2006; Guarente, 2008; Stetler et al., 2014), dietary restriction is also well known to affect the release of a variety of humoral factors, particularly from adipose tissue. Adiponectin release into the plasma occurs acutely after dietary restriction and increased levels in the serum. This was associated with beneficial outcomes, as global knockout of adiponectin negated the effects of dietary restriction on the subsequent ischemic injury. The effects may be due to penetration of adiponectin into the brain parenchyma and the subsequent binding to its receptors on neural cells in the context of the opening of the blood-brain barrier (BBB) after ischemic injury (Brochu-Gaudreau et al., 2010; Zhang et al., 2018). Whether this scenario or the alternative situation—wherein adiponectin acts directly on endothelial barrier function to exert protection—underlies the neuroprotective effects remains under investigation.

MP-P (Miami, FL, USA) reported a novel window for ischemic tolerance for preconditioning mimetics, which was previously limited to 48–72 h after cerebral ischemia (Narayanan et al., 2015). Resveratrol preconditioning yielded gene expression changes in 136 genes at 14 days after single administration: many of the 116 downregulated genes were related to transcription, synaptic signaling, and neurotransmission, resembling the metabolic depression observed in hibernating species. This downregulation of gene expression fits well with the hippocampal synaptic and electrophysiological depression observed with pre-conditioning mimetics (DeFazio et al., 2009; Neumann et al., 2015; Cohan et al., 2017). Also, glycolysis and mitochondrial respiration efficiency were increased upon resveratrol preconditioning (Koronowski et al., 2017; Khoury et al., 2019), indicating an increased reliance on energy-producing pathways.

PL (Shanghai, China) discussed anesthetic postconditioning as a valuable neuroprotection candidate (Cohan et al., 2017) as fast onset and short-acting anesthetics allow smooth anesthesia induction and faster anesthetic emergence to overcome the clinical limitation that neurological assessment during anesthesia or sedation is not possible. New technology-based anesthetic

drug delivery systems, such as target-controlled infusion, close loop infusion, and computer-assisted sedation systems allow better control of anesthesia (Struys et al., 2016; Zaouter et al., 2016). Dr. Li further reported about a planned clinical study in stroke patients undergoing endovascular thrombectomy to compare general anesthesia with and without anesthetic postconditioning for countering reperfusion injury after endovascular thrombectomy.

Overall, conditioning represents a clinically available therapeutic strategy for ischemic stroke, and the presented findings put forward our understanding of the underlying mechanisms and provided novel insights into its clinical application. However, to utilize its full potential, relevant aspects of heterogeneous patient populations such as age and sex have to be considered. Their relevance has already been shown in numerous studies.

Effect of Sex and Age on Post-ischemic Outcome and Therapy

Sex and age are known to affect stroke outcomes (Kim and Vemuganti, 2015). Their contribution concerning mechanisms of ionic imbalance, inflammation, microRNAs, and the interaction of long noncoding RNAs with epigenetics was discussed.

As the expression of the chloride influx transporter, Na-K-Cl cotransporter 1 (NKCC1) in male rodent brains starts earlier during development compared to female brains, targeting NKCC1 during post-injury in adulthood may be sex-dependent. Indeed, DS (Pittsburgh, PA, USA) showed that pharmacological blockade of NKCC1 protein has higher sensitivity in adult male mice than female mice for reducing post-ischemic brain injury (Huang et al., 2019).

FL (Houston, TX, USA) presented that post-stroke inflammation and microglial activation are sex- and age-dependent and that these differences exist throughout the lifespan (Zhao et al., 2017b; Ritzel et al., 2018). He also showed that sex-chromosomal effects in addition to sex hormones contribute to the differential outcomes between males and females after focal ischemia (McCullough et al., 2016).

AR (Miami, FL, USA) reported that the depletion of endogenous estrogen at reproductive senescence increases inflammasome proteins in the brain of females, but not in age-matched male rats (de Rivero Vaccari et al., 2016). In reproductively senescent females, extracellular vesicles (EVs) from reproductive organs carry inflammasome proteins to the brain leading to an exacerbated innate immune response that may be responsible for the increased severity of ischemic damage in senescent females (D'Adesky et al., 2018).

FS (Bryan, TX, USA) showed that stroke neuroprotectants may act in a sex-specific manner. Post-stroke administration of IGF-1 is neuroprotective after stroke. Preventing microRNA let-7f, thus upregulating IGF-1 which is reduced in aging animals and humans, is protective in young female rats. However, it is not neuroprotective in young males and even worsens outcomes in senescent females post-stroke (Selvamani et al., 2012; Sohrabji et al., 2019). Let7f also regulates caspase 3, and treatment with miR-363–3p mimic (repressing caspase-3) protects young and senescent females, but not males, after focal ischemia (Selvamani and Sohrabji, 2017). Thus, the neurotoxic effect seen in older females may be related to an increase in caspase-3 and its cell death pathways caused by the blocking of let7f (Sohrabji and Selvamani, 2019). These findings also illustrate the complexity of sex-specific neuroprotective actions that must be taken into consideration.

RV (Madison, WI, USA) presented that the long noncoding RNAs Fos downstream transcript (FosDT) is induced after stroke and that knockdown of FosDT with a siRNA cocktail protects the brain in both males and females and also aged animals (Mehta et al., 2015). The epigenetic modification hydroxymethylation that converts 5-methylcytosine to 5-hydroxymethylcytosine induced after stroke is neuroprotective in both sexes (Morris-Blanco et al., 2019).

In summary, the contribution of age and sex to the outcome of cerebrovascular diseases should be carefully considered in the development of novel therapeutic strategies.

Long-Term Neuroinflammation During Functional Recovery From Stroke

Inflammation has been regarded as a target to reduce brain damage in acute stroke. While dampening innate immune responses and addressing complement or danger signaling effectively reduces acute brain damage (Muhammad et al., 2008; Alawieh et al., 2018), certain inflammatory responses are necessary for repair as they induce cell migration, proliferation, matrix deposition, and tissue remodeling. This suggests that initial inflammatory reactions trigger a set of responses that may improve functional outcome in the long term.

AMP (Barcelona, Spain) reported that although monocytes and macrophages reach the brain within the first 4 days after stroke (Miró-Mur et al., 2016), macrophages persist for weeks in the damaged brain tissue (Wattananit et al., 2016; Mantovani, 2017). While they may have detrimental functions acutely, macrophages also play critical roles in long-term functional recovery (Wattananit et al., 2016). Besides, lymphocytes, which promote acute thromboinflammation through mechanisms that do not involve adaptive immune responses (Kleinschnitz et al., 2010), also infiltrate the brain in higher numbers during chronic phases, when adaptive immune responses may play a role in functional impairment (Selvaraj and Stowe, 2017).

AMS (Lexington, KY, USA) discussed that $CD8^+$ T cells (i.e., cytotoxic T cells) move into several regions interconnected to the infarct within 4 days after transient middle cerebral artery occlusion (tMCAO) in mice, where they remain and support recovery (Poinsatte et al., 2019). Antibody-mediated depletion of $CD8^+$ T cells improved motor recovery and reduced diapedesis of other leukocyte populations, including macrophages, neutrophils, and $CD4^+$ T cells (Selvaraj and Stowe, 2017).

MSB (Stanford, CA, USA) described that in a model of post-stroke cognitive impairment, mice have normal cognition and hippocampal long-term potentiation 1 week after a cortical stroke adjacent to the hippocampus, while within 7 weeks, cognitive impairment and progressive loss of long-term potentiation begin (Doyle et al., 2015). In parallel, antibody-producing B-lymphocytes accumulate in the infarct

core. Antibody levels increase in both the core and the surrounding brain parenchyma but the specificity of these antibodies could not (yet) be revealed. However, ablating B-lymphocytes prevents delayed cognitive impairment. Dr. Buckwalter further presented that B-lymphocytes are involved in this process in humans, suggesting that B cells may be critical targets for the development of post-stroke immunotherapies.

FS (Bryan, TX, USA) showed that anti-inflammatory miRNA therapy improves long-term affective dysfunction after ischemic stroke (Panta et al., 2019). Intravenous injection of mir363-3p mimics reduced infarct volume in the acute phase of stroke, ameliorated sensory-motor impairment, and attenuated transient increases of IL-6 and TNF-α. Depressive behaviors, assessed over 30–100 days after stroke, were also attenuated in mir363-3p treated animals (Panta et al., 2019). This indicates that a neuroprotectant that has anti-inflammatory properties may also improve affective dysfunction after stroke.

Taken together, these studies highlight the complex role of inflammation in the chronic phase after stroke and that modulating inflammation may require targeting a specific subset of inflammatory cells and proteins.

Targeting the Interplay Between Stem Cells and Neuroinflammation in Stroke Regeneration

Sustained neuroinflammation is also required to eliminate degenerating tissue, supplying a restorative milieu for stem cell-mediated repair. However, immune responses are often dysregulated and lead to detrimental effects on regeneration. Recent work aims to elucidate the complex and interwoven processes of neuroinflammation and stem cell-mediated regeneration after a stroke that may form the basis for novel therapeutic approaches to modulate these processes and their interactions.

SUV (Cologne, Germany) reported that differentially polarized microglia differ in their effects on the fate of neural stem cells (NSC) *in vitro* and *in vivo*, with pro-inflammatory microglia promoting the generation of astrocytes, while anti-inflammatory microglia support neurogenesis. Regardless of their polarization, the secretome of activated microglia inhibits NSC proliferation, increases NSC migration, and accelerates NSC differentiation (Vay et al., 2018). These combined effects suggest that activated microglia induce NSC to exit the cell cycle, to migrate towards a putative lesion site, and to attempt cell replacement by differentiation. Besides, NSC promotes functional restoration after stroke not only by cell replacement but also by modulating surrounding cells and inflammatory processes.

ZK (Lund, Sweden) discussed the significance of monocyte-derived macrophages (MDM) in supporting regenerative processes after ischemic stroke. MDM are recruited to the ischemic lesion site exhibiting a high degree of functional plasticity, changing from a pro- to an anti-inflammatory phenotype during the first weeks after stroke. Blockage of MDM recruitment worsens functional and structural outcomes after stroke (Wattananit et al., 2016; Kronenberg et al., 2018). Dr. Kokaia's work suggests that immune cells affect the regenerative capacity of the brain, most likely by modulating stem-cell-derived neuronal plasticity in the subventricular zone and the adjacent striatum (Laterza et al., 2017).

KG (Berlin, Germany) emphasized the beneficial role of anti-inflammatory MDM activated in the early phase after stroke. However, not only stroke-invading MDM but also brain-resident microglia are activated, and both MDM and microglia often display a mixture of phenotypic markers ("intermediate states") during the first weeks after stroke (Kronenberg et al., 2018).

Overall, the cross-talk between inflammatory cells acting as key regulators and endogenous or grafted neural stem cells acting as key effectors is highly relevant during post-stroke regeneration. Thus, therapeutic strategies based on modulating these cell entities and their interactions could be exploited to facilitate functional recovery after stroke.

Extracellular Vesicles: Therapy and Imaging

Although there is growing evidence that long-term benefits are produced by stem cells, particularly in sudden onset diseases, these cells are often short-lived after transplantation (Kim et al., 2012; Jablonska et al., 2016). Stem cells release EVs including exosomes that mediate therapeutic effects (Xin et al., 2012, 2013a; Zhang et al., 2015) and in certain conditions, they can achieve the same efficacy obtained by the administration of the stem cells themselves (Doeppner et al., 2015).

TD (Göttingen, Germany) explained the positive effects of mesenchymal stem cell-derived EVs (Doeppner et al., 2015). Interestingly, similar effects have recently been described for EVs derived from neural progenitor cells (Zheng et al., 2021). This suggests that EV-derived modes of action could be a general mechanism related to beneficial stem and progenitor cell effects. Apart from this, Dr. Doeppner also reported innovative therapeutic approaches such as the application of remote ischemic post-conditioning (for review and current clinical application please see Ji et al., 2019), defined as a transient and subcritical period of peripheral organ ischemia following cerebral ischemia, to exert beneficial but transient effects on recovery. Interestingly, post-conditioning also facilitated intracerebral transplantation of neural progenitor cells resulting in persistent protection and improved functional recovery (Doeppner et al., 2017).

YX (Detroit, MI, USA) discussed that exosomes elicit potent cellular responses *in vitro* and *in vivo* by delivering their cargos, including lipids, proteins, RNAs (miRNAs and mRNAs), and other macromolecules, to recipient cells (Xin et al., 2013a; Zhang et al., 2019). In turn, microRNAs regulate numerous genes that mediate beneficial therapeutic effects (Zhang et al., 2019) and exosomes with select miRNAs can be designed to provide further improved therapeutic efficacy (Xin et al., 2013b, 2017).

MJ (Baltimore, MD, USA) explained strategies for EV labeling and imaging to assess direct routes of EV delivery that are potentially more beneficial and to monitor EV biodistribution in the body. Iron oxide-based labeling is comparably easy as it is sufficient to apply a standard labeling protocol to

stem cells, from which EVs are subsequently derived (Busato et al., 2017; Dabrowska et al., 2018). While the signal is strong, its specificity is quite low due to other sources of hypointensities in tissues related to pathology. However, this approach may be particularly compelling to monitor EV delivery in real-time as the signal of the label can be subtracted from the background image obtained before the procedure (Walczak et al., 2017). Further labeling techniques based on radioisotopes are very attractive to assess EV biodistribution even in clinical settings, while other modalities such as fluorescence or bioluminescence labeling are limited to preclinical studies (Choi and Lee, 2016).

Summing up, cell-free exosome-based approaches may replace stem cells and become a major driving force for therapeutic interventions with the aid of engineering and imaging.

Traumatic Brain Injury Can Lead to Cerebrovascular Disease

A provocative question discussed was whether traumatic brain injury can serve as a model to study neurovascular unit dysfunction in cerebrovascular disease as their relationship has been proposed in recent studies (Pop and Badaut, 2011; Sandsmark et al., 2019).

NP (Munich, Germany) showed that controlled cortical impact in adult mice induces progressive cognitive decline (Mao et al., 2020). While motor function recovered partially after TBI, depression-like behavior and the loss of memory function were progressive. Increasing tissue loss in the corpus callosum, hippocampus, and hydrocephalus formation was also observed over time. Hence, experimental TBI in mice replicates the long-term sequelae post-trauma including dementia and depression that are observed in humans. It needs to be determined whether these changes are triggered by concomitant vascular injury or other, so far unknown mechanisms.

JB (Bordeaux, France) discussed the alteration of the NVU months after mild pediatric TBI in which changes of water channel expression on astrocytic endfeet adjacent to blood vessels have been observed (Fukuda et al., 2013). These changes are related to diffusion tensor imaging modifications in different brain structures at 12 months post-injury after a single impact.

Linked with NVU remodeling, AO (Irvine, CA, USA) presented the importance of the activation of the Wnt-Beta-catenin pathway in cerebral blood vessels after TBI (Salehi et al., 2018). After acute vascular loss post-TBI, new immature vessels occurred at the injury site 7 days after the injury. This coincided with decreased levels of β-catenin protein in the injury site but dramatically increased β-catenin protein expression in vessels. β-catenin and Wnt expression were particularly increased in perilesional vessels and are thought to promote new vessel formation into the injury site.

Overall, most of the pre-clinical models of TBI from mild to severe severities reproduce the long-term clinical changes described in the literature in terms of neuroimaging. IKK (Boston, MA, USA) reviewed noninvasive neuroimaging techniques that can help to bridge clinical and preclinical studies.

In summary, the presented data impressively showed that assessing long-term outcomes after TBI in preclinical models may be a suitable approach for a better understanding of the molecular and cellular processes in cerebrovascular diseases.

Targeting Acute Pathomechanisms Following Subarachnoid Hemorrhage

Subarachnoid hemorrhage (SAH) is a devastating type of stroke with a high mortality rate, especially during the acute phase after the ictus. Therefore, current strategies focus on minimizing early brain injury to reduce SAH-induced mortality and disability (Lantigua et al., 2015).

NP (Munich, Germany) reported that SAH causes acute and long-lasting constrictions of pial arterioles (microvascular spasm): the CO_2-reactivity is lost within the first 3 h, followed by an impairment of neurovascular coupling within 24 h after SAH. Within 1 month, CO_2-reactivity reestablishes, while neurovascular coupling does not recover (Balbi et al., 2017, 2020). Loss of neurovascular coupling may result in further brain damage after SAH due to an uncoupling of blood flow and metabolism, e.g., during cortical spreading depolarizations or even during normal brain activity.

SAH also induces acute spreading depolarizations as shown by JPD (Berlin, Germany) both in animal models and in patients (Dreier et al., 2018). These lead to severe hypoperfusion in tissue at risk for progressive injury, which may directly initiate infarction (Lückl et al., 2018).

RK (Ann Arbor, MI, USA) demonstrated that SAH induces BBB disruption (Egashira et al., 2016) and white matter injury acutely after the ictus (Guo et al., 2017). Dr. Keep further discussed the importance of clot-derived factors and the significance of hemorrhage extension into the ventricular system leading to injury and hydrocephalus. In particular, epiplexus cell activation was associated with hydrocephalus development and may occur in response to thrombin production after SAH (Wan et al., 2019).

BAG (Newcastle, Newcastle upon Tyne, UK) presented the ongoing Treatment of Poor-grade SubArachnoid Hemorrhage Trial 2 (TOPSAT2; ISRCTN15960635) that investigates whether early treatment compared to conventional treatment after neurological recovery improves functional outcome after 12 months in poor-grade aneurysmal SAH patients.

In summary, these reports demonstrated several acute pathomechanisms after SAH that present promising therapeutic targets that need to be further assessed in clinical trials of SAH.

Targeting the Hematoma and the Search for Protective Strategies in Intracerebral Hemorrhage

Another hemorrhagic subtype of stroke is intracerebral hemorrhage (ICH), which remains a major cause of mortality and permanent disability (Poon et al., 2014; van Asch et al., 2010). Recent studies targeting both primary and secondary injury components (Keep et al., 2012) were discussed in two mini-symposia of the 10th ISN&N.

As targeting primary injury by surgical evacuation using craniotomy does not improve functional outcome in large

surgical trials of ICH (STICH I and II; Potts and Riina, 2014), recent efforts focused on Minimally Invasive Surgery with Thrombolysis in ICH Evacuation (MISTIE). MISTIE featured the administration of alteplase (initially 1.0 mg in ml followed by up to nine 3 ml flushes every 8 h) *via* a soft catheter directly into a residual hematoma that was primarily addressed by clot aspiration (Hanley et al., 2019). DFH (Baltimore, MD, USA) reported no overall efficacy of the MISTIE procedure in phase III clinical trial. However, a subgroup analysis on the surgical performance showed that a hematoma reduction below 15 ml increases the chances of having a good outcome by 10% for each additional ml of hematoma removed (Awad et al., 2019). Furthermore, KRD (Miami, FL, USA) demonstrated that a novel hemostatic agent, red blood cell-derived microparticles (RMPs), which display negatively charged phosphatidylserines to induce coagulation, limited hematoma growth in a collagenase-induced model of ICH in rats. According to the pharmacokinetic and safety profile of RMPs, this agent is applicable in the clinics (Jy et al., 2018; Rehni et al., 2019). Since a complete evacuation of the hematoma is unlikely to be achieved in every patient, additional strategies targeting clot-derived factors are needed for ICH therapy.

Addressing neuroinflammation as a secondary injury component, LHS (Yale, New Haven, CT, USA) described the properties of leukocytes in the peripheral blood and hematoma evacuates from the MISTIE III clinical trial using RNA sequencing and provided evidence for the importance of efferocytosis in reducing inflammation in human macrophages (Chang et al., 2018). Furthermore, macrophages and microglia undergo acute activation during the first week after ICH, with microglia producing inflammatory cytokines and chemokines, and a decreasing expression of microglia-specific genes (Taylor et al., 2017). Other immune cells such as neutrophils are another source of damage and secondary injury as they infiltrate the brain in response to sterile inflammation triggered by ischemic stroke or ICH. JA (Houston, TX, USA) presented that neutrophils are plastic regarding their phenotype and the cytokine IL-27 can alter their gene expression during maturation in the bone marrow (Zhao et al., 2017a). After ICH, IL-27-modified neutrophils can deliver to the hematoma site more beneficial haptoglobin and lactoferrin to neutralize the toxicity of hemoglobin and iron and to limit the brain exposure to pro-oxidative and pro-inflammatory mediators normally transported by the infiltrating neutrophils.

As hemolysis leads to the release of blood breakdown products that induce cell death, targeting cell death is another strategy for secondary intervention. MZ (Lübeck, Germany) demonstrated that primary cortical neurons in culture die by a mixture of ferroptotic and necroptotic cell death when exposed to blood breakdown products (Zille et al., 2017). In contrast, cell death mechanisms underlying brain endothelial cell death after hemorrhagic stroke remain poorly understood (Zille et al., 2019). JW (Baltimore, MD, USA) demonstrated the co-existence of ultrastructural characteristics of ferroptosis, autophagy, and necroptosis after experimental ICH *in vivo* (Li et al., 2018). The inhibition of ferroptosis using the small molecule ferrostatin-1 improved neurological function and conferred protection after ICH (Li et al., 2017). Moreover, SSK (White Plains, NY, USA) showed that the ferroptosis inhibitor N-acetylcysteine improved functional recovery after ICH in mice by inhibiting toxic lipid products (Karuppagounder et al., 2018).

Taken together, the presented studies put forward the idea that targeting the hematoma is an important strategy in ICH therapy and that there should be a combinatorial approach consisting of primary intervention (to evacuate the hematoma) together with a secondary intervention (immunomodulatory and neuroprotective; **Figure 1**).

Next-Generation Functional Testing in Experimental Brain Research

The reliable assessment of functional improvement after cerebrovascular injury and potential treatment remains challenging. The recent development of new assessment strategies in experimental brain research considers several conceptual and methodological aspects.

GASM (Lethbridge, AB, Canada) showed that compensation after brain injury represents the primary process of functional improvement, i.e., the development of alternate behavioral strategies rather than the recovery of the original functions (Metz et al., 2005; Fouad et al., 2013). Compensatory behaviors are clearly recognizable and acquired through repetitive training in a task-specific manner (Girgis et al., 2007; Kirkland et al., 2012).

KF (Edmonton, AB, Canada) discussed recent advances that have exploited automated test apparatus solutions to enhance the efficacy of animal training and assessment (Fenrich et al., 2015; Bova et al., 2019) along with machine learning algorithms to identify discrete aspects of compensatory movement patterns (Ryait et al., 2019).

EH (Montreal, QC, Canada) showed that exercise-based rehabilitation and pharmacotherapy influence white matter inflammation and the degree of cognitive and cerebrovascular improvement, including neurovascular coupling, in a mouse model of vascular cognitive impairment and dementia (Trigiani and Hamel, 2017; Trigiani et al., 2019).

These observations open new avenues for the discovery of biomarkers that aid in the stratification of patients to personalized rehabilitation programs. The overarching goal of combined multi-level functional and molecular analysis is the improved translation of experimental innovations to clinical practice.

Cutting-Edge Brain Imaging in Disease and Regeneration

Magnetic resonance imaging (MRI) has been decisive in understanding cerebrovascular disease over the past decades. Besides MRI, functional ultrasound has recently evolved as an analog to functional MRI. Cutting-edge imaging-based findings were reported at the 10th ISN&N.

AM (Los Angeles, CA, USA) reported on brain imaging of vascular dysfunction to understand BBB breakdown and how this may contribute to cerebrovascular diseases, with a particular focus on dementia. Measuring BBB alterations *in vivo* can be challenging. Examples of how brain imaging (i.e., dynamic contrast-enhanced MRI) may contribute to a better

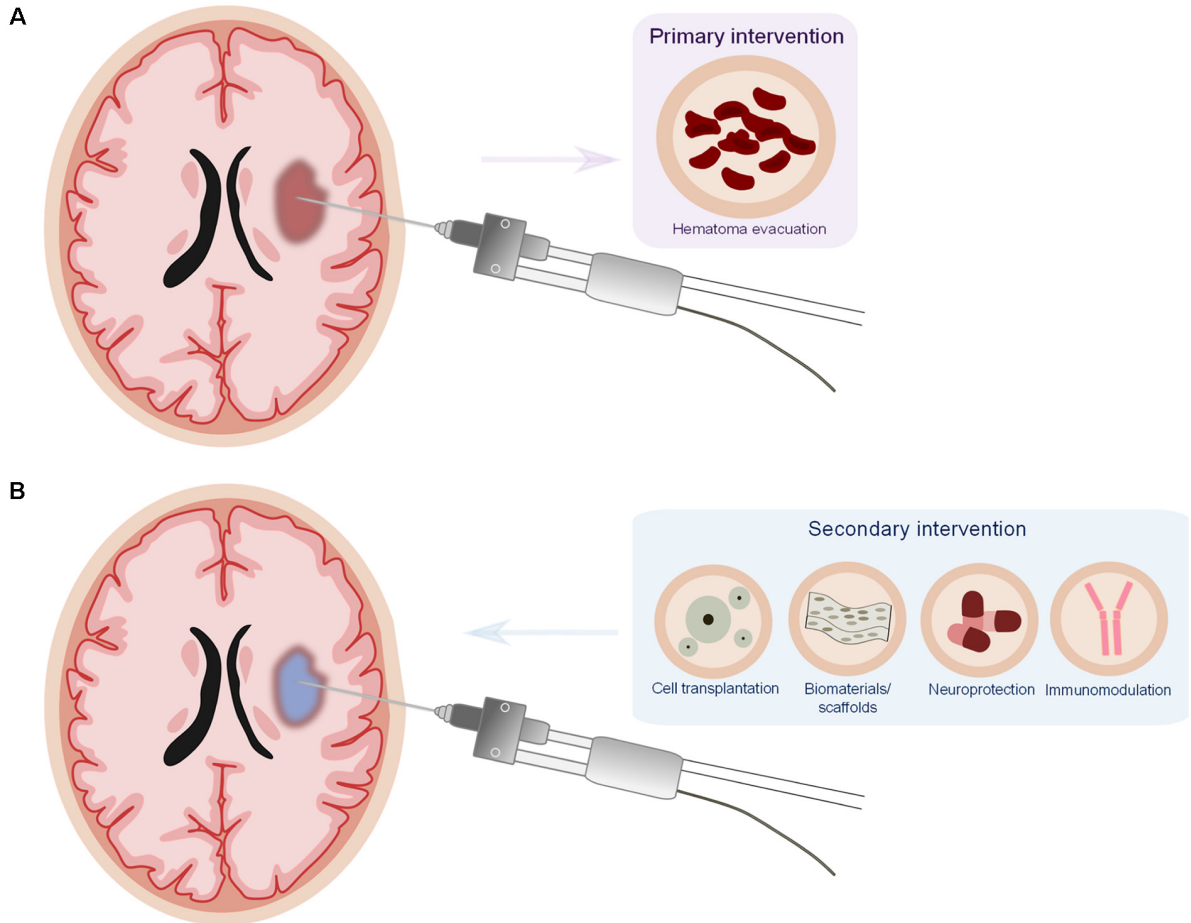

FIGURE 1 | Proposed model for a combinatorial therapy in intracerebral hemorrhage (ICH). **(A)** Minimally invasive surgery for the evacuation of the hematoma (primary intervention). **(B)** Minimally invasive surgery offers the particular opportunity to deliver potential therapeutics (cell transplantation, biomaterials/scaffolds, neuroprotective, and/or immunomodulatory drugs) as secondary intervention directly into the lesion site, reducing drug delivery issues and potential systemic side effects of the drugs.

diagnosis and prognosis of BBB alterations and how targeting the BBB can influence the course of neurological disorders have been discussed. Finally, an outlook on future approaches to better understand the cellular and molecular events underlying mechanisms between BBB breakdown and neurodegeneration was given (Montagne et al., 2017).

DV (Caen Cedex, France) focused on molecular MRI of neuroinflammation, including targeting vascular cell adhesion molecule 1 and P-selectin. The perspectives for the clinical application of this technology were discussed and he showed that molecular MRI of adhesion molecules, using micro-sized particles of iron oxide complexed with specific antibodies of adhesion molecules, may be useful for the diagnosis and prognosis of brain disorders (Gauberti et al., 2018).

RMD (Utrecht, The Netherlands) presented recent data that inform on correspondences between quantitative functional and structural connectivity measures in the mammalian brain from resting-state functional MRI, diffusion-weighted MRI, and neuronal tract tracing. Overall, despite methodological differences between studies, the current literature supports the hypothesis that structural connectivity provides the hardware from which functional connectivity emerges (Straathof et al., 2019). However, strong structural connections are not necessarily strong functional connections.

MT (Paris, France) spoke on recent progress in ultrafast ultrasound imaging. Neurologists and neuroradiologists warrant an imaging technique that can be performed at the bedside (as transcranial Doppler ultrasound), is repeatable (as arterial spin labeling MRI), provides quantitative measurement (as positron emission tomography), and measures multiple perfusion parameters (as perfusion computed tomography). The recent development of ultrafast ultrasound sequences and advances in high-frequency probes technologies combines all these criteria in a unique system. Specifically, it allows detecting subtle cerebral blood volume changes due to neurovascular coupling, which has led to the development of the ultrasound analog to functional MRI, functional ultrasound providing a high spatiotemporal resolution of cerebral blood flow and brain functioning in animals and humans (Rabut et al., 2019).

The presented imaging tools promise to further enhance our understanding of cerebrovascular disease in the future that will form the basis for the development of novel therapeutic strategies. Moreover, these new imaging techniques might develop into invaluable diagnostic tools augmenting current diagnostic procedures and leading to better clinical treatment by identifying patients with specific dysfunctions that would benefit from targeted interventions. They may also provide opportunities to use imaging biomarkers of vascular dysfunction in patients with TBI or cerebral small vessel disease.

Endovascular Approaches to Image and Treat Stroke: Beyond Thrombectomy

Modern mechanical thrombectomy techniques are highly efficient and have revolutionized the treatment of acute stroke patients with large vessel occlusion. However, the restoration of blood flow is insufficient to completely reverse the ischemic insult. The next phase of stroke intervention should therefore focus on reparative mechanisms that can be delivered with image-guidance (Chu et al., 2018) in the same setting after thrombectomy to further improve patient outcomes, as outlined by MP (Baltimore, MD, USA).

PW (Baltimore, MD, USA) stressed that the brain remains to be a challenging target for drug delivery with systemic injection frequently resulting in less than 1% of injected dose reaching the brain parenchyma. Due to compromised perfusion, drug accumulation in the stroke lesion is related to even higher uncertainty and unpredictability. Dr. Walczak presented approaches for spatially selective, intra-arterial drug and cell delivery guided with interventional MRI (**Figure 2**; **Supplementary Video 1**). High precision and reproducibility are achieved by visualization of trans-catheter pre-injections of a contrast agent using dynamic MRI. Imaging the trans-catheter perfusion territory facilitates optimization of that territory by modulating the infusion rate or the position of the catheter tip. Once the targeted volume is optimized, the drug (or any other therapeutic agent) is infused. This procedure improves the precision and efficiency of targeting (Walczak et al., 2017). In case BBB opening is desired or required, it can be implemented in the procedure by an additional step such as infusion of hyperosmotic mannitol (Chu et al., 2018).

As a new tomographic imaging method, PL (Hamburg, Germany) reported on magnetic particle imaging, which is a useful tool for the rapid assessment of the cerebral vasculature and perfusion in stroke due to its temporal resolution. Magnetic particle imaging provides great innovation potential to improve stroke imaging and treatment in the future (Ludewig et al., 2017).

DG (Olsztyn, Poland) presented a recently developed endovascular method for inducing ischemic stroke in swine (Golubczyk et al., 2020). To overcome the long-standing drawback due to the vascular rete preventing the navigation of endovascular catheters into the brain, her approach is to inject thrombin solution *via* the pharyngeal ascendant artery to occlude cerebral vessels. The entire procedure including the injection of a clot-forming solution, the blockage of vasculature and the evolution of stroke was visualized with MRI. This new model offers several important advantages including a minimally invasive approach in a species with large, gyrencephalic brain and overall high clinical relevance (Herrmann et al., 2019).

A potential treatment option, as outlined above, is targeting neuroinflammation. MG (Hamburg, Germany) reported on the influence of the post-ischemic inflammatory reaction on the fate of the ischemic brain (Gülke et al., 2018). He presented novel data on conserved proinflammatory pathways, which are crucial for the initiation of the damaging inflammatory reaction in the ischemic brain. Finally, he correlated the available experimental data with human clinical studies.

Taken together, the described tools and strategies are particularly relevant at the time of growing use of endovascular mechanical thrombectomy as the placement of intra-arterial catheters introduces the opportunity to implement intra-arterial adjuvant therapies.

Recent Advances in Neurorehabilitation Strategies in Stroke

As a result of improved acute stroke care, more and more patients survive, but many are left with permanent disabilities, making stroke a major cause of adult disability. Although neurorehabilitation is the only established stroke therapy being effective beyond acute stages of the disease, combinatorial approaches may strengthen the beneficial effects of neurorehabilitation strategies.

MC (Pisa, Italy) described rehabilitation of motor function in a mouse model of focal cortical stroke induced by photothrombosis. A robotic device (M-platform) was used for the daily training of the affected forelimb in combination with pharmacological contralesional silencing to dampen excessive transcallosal inhibition. Mice receiving this combined therapy displayed motor improvements that persisted beyond the treatment period and these were even generalized to non-trained tasks (Spalletti et al., 2017).

JJ (Kuopio, Finland) presented on combined cell therapy and rehabilitative training in experimental stroke. The transplantation of subventricular zone or human embryonic stem cells into the perilesional cortex was characterized by low cell survival (Hicks et al., 2009). Nonetheless, some improvement was observed in behavioral outcomes both when cells were transplanted alone or together with housing the experimental animals in an enriched environment i.e., mimicking rehabilitation. Likewise, the intravenous delivery of human adipose tissue-derived mesenchymal stem cells and exposure to the enriched environment improved forelimb function in the cylinder test and sticky label test (Mu et al., 2019).

CJS (Oxford, UK) discussed the role of non-invasive brain stimulation in recovery, which is a promising tool as it is relatively cheap, very well tolerated, and easy to use. However, the functional improvements demonstrated are highly variable across people. Various MRI approaches have been applied to predict the response to transcranial direct current stimulation in the motor system, indicating that a reduction of inhibition

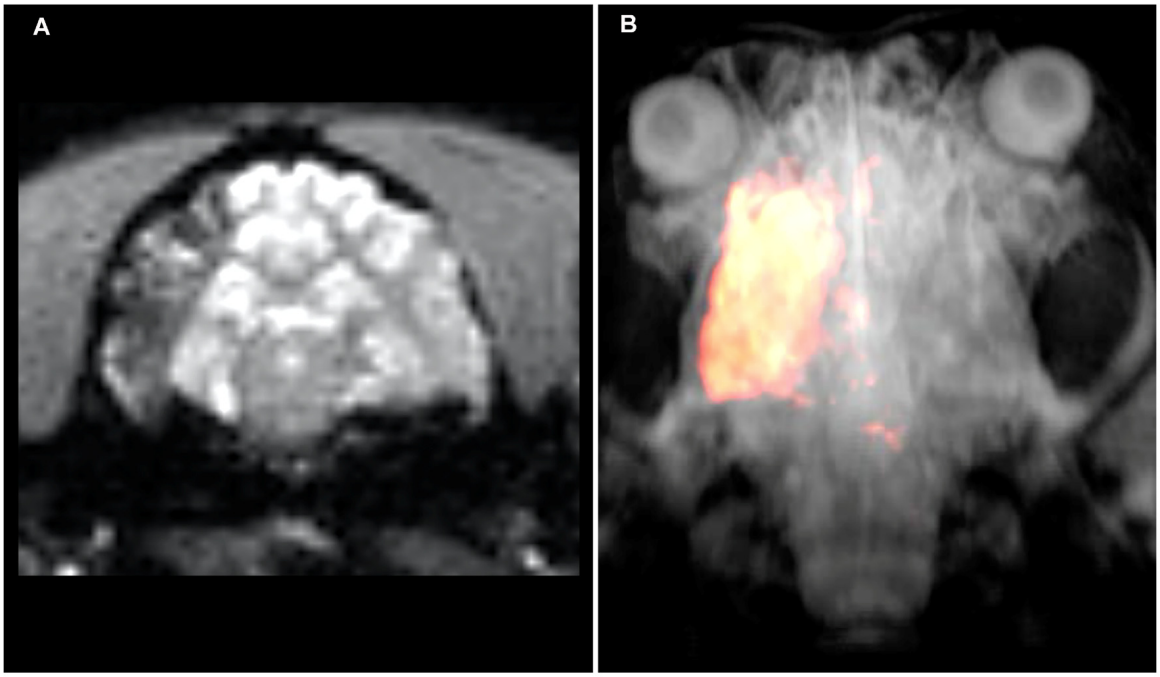

FIGURE 2 | Intraarterial magnetic resonance imaging (MRI)-guided injection of mesenchymal stem cells into the canine brain. **(A)** Raw T2*w MRI after intraarterial injection of superparamagnetic iron oxide particle-labeled mesenchymal stem cells showing cell accumulation throughout the ipsilateral middle cerebral artery territory. **(B)** Segmentation of hypo-intense pixels and 3D visualization of stem cell biodistribution. Please see the **Supplementary Video 1** for a dynamic visualization of stem cell injection.

in the primary motor cortex (M1) is a central mechanism for motor plasticity in humans, both in health and in recovery after stroke (Stagg et al., 2011; Blicher et al., 2015; Kolasinski et al., 2019). Indeed, GABA levels in the ipsilateral M1 cortex can predict the response to transcranial direct current stimulation (O'Shea et al., 2014).

FCH (Geneva, Switzerland) summarized the reasons for heterogeneous results of neurorehabilitative interventions, such as non-invasive brain stimulation, and discussed a paradigm shift from imprecision of "one treatment suits all" strategies towards personalized medicine approaches delivered in a manner tailored to the demands of the individual patient (Raffin and Hummel, 2018; Coscia et al., 2019). Structural MRI imaging and connectome analyses can be used to determine the functional outcome of patients to stratify patients towards specific brain stimulation protocols (Koch and Hummel, 2017; Schulz et al., 2017).

Taken together, these studies support the use of rehabilitation and neuromodulatory approaches for promoting post-stroke recovery. Although combination therapy and early delivery may be more effective, further studies with greater statistical power to cope with these complex experimental designs will be needed to determine the optimal treatment protocol, the effect of co-morbidities, and to explore underlying therapeutic mechanisms (Boltze et al., 2017). Moreover, novel imaging approaches as discussed in the section "Cutting-Edge Brain Imaging in Disease and Regeneration" (above) might be helpful to identify patients that may benefit from brain stimulation interventions.

OUTLOOK AND CONCLUSIONS

Based on the setbacks seen in the past decades of cerebrovascular disease research, the field has clearly consolidated and recognized the reasons for previous translational failure as exemplified in the field of cell therapies (Cui et al., 2019). Recent guidelines for translational research in that field stress, for instance, the importance of considering comorbidities, the use of highly predictive animal models and experimental settings as well as a closer interaction between preclinical and clinical research activities for more integrated study designs being able to inform each other (Boltze et al., 2019). Moreover, with the refinement of our research tools, some of which have been discussed herein, and increasing study quality (Ramirez et al., 2017), it seems that the translational roadblock is slowly overcome as new therapeutic concepts start to arise (Liebeskind et al., 2018). For instance, new combinations of recanalization and neuroprotecive approaches are believed to emerge for stroke (Savitz et al., 2019) and potentially ICH.

Encouraging progress is also witnessed in related fields such as vascular dementia or even Alzheimer's disease. For instance, significant progress has been made in understanding the vascular contribution to various form of dementia (Iadecola and Gottesman, 2018; Royea et al., 2020). While the role of

the frequent but treatable risk factors of dementia such as hypertension and hypercholesterinemia is better understood (Kaiser et al., 2014; Trigiani et al., 2019), new animal models of vascular cognitive impairment may facilitate translational research programs (Hainsworth et al., 2017). In parallel, new targets for pharmacological interventions have been identified (Loera-Valencia et al., 2019) and are expected to lead to future clinical trials (Howard et al., 2019). Although there will likely be setbacks on the way forward and we shall avoid premature enthusiasm as seen in the past, the "therapeutic nihilism" still observed in translational cerebrovascular research just 5 years ago has turned into new optimism.

The 11th ISN&N will continue to monitor the progress in the fields of basic translational and clinical cerebrovascular disease research. Moreover, it will extend its scope by partnering with the 18th International Conference on Brain Edema and Cellular Injury (BEM) for a single combined meeting in October 2022 in Berlin, Germany.

AUTHOR CONTRIBUTIONS

All authors listed have made a substantial, direct and intellectual contribution to the work, and approved it for publication.

FUNDING

We wish to express our gratitude to all institutions and people who supported the 10th ISN&N. First and foremost, we want to thank all meeting participants for their outstanding academic contributions. Moreover, we are particularly grateful to the Deutsche Forschungsgemeinschaft (grant number: BO 3518/2-1) and the International Society of Cerebral Blood Flow and Metabolism, both of which supported the meeting with generous grants. We further acknowledge all industrial sponsors and exhibitors for their academic and invaluable financial support.

ACKNOWLEDGMENTS

The Eventlab congress organizing team deserves special thanks for tireless and professional support that was not only crucial for carefully preparing the meeting, but also for running it successfully and smoothly.

SUPPLEMENTARY MATERIAL

The Supplementary Material for this article can be found online at: https://www.frontiersin.org/articles/10.3389/fnagi.2021.623751/full#supplementary-material.

REFERENCES

Alawieh, A., Langley, E. F., and Tomlinson, S. (2018). Targeted complement inhibition salvages stressed neurons and inhibits neuroinflammation after stroke in mice. *Sci. Transl. Med.* 10:eaao6459. doi: 10.1126/scitranslmed.aao6459

Awad, I. A., Polster, S. P., Carrión-Penagos, J., Thompson, R. E., Cao, Y., Stadnik, A., et al. (2019). Surgical performance determines functional outcome benefit in the minimally invasive surgery plus recombinant tissue plasminogen activator for intracerebral hemorrhage evacuation (MISTIE) procedure. *Neurosurgery* 84, 1157–1168. doi: 10.1093/neuros/nyz077

Balbi, M., Koide, M., Schwarzmaier, S. M., Wellman, G. C., and Plesnila, N. (2017). Acute changes in neurovascular reactivity after subarachnoid hemorrhage *in vivo*. *J. Cereb. Blood Flow Metab.* 37, 178–187. doi: 10.1177/0271678X15621253

Balbi, M., Vega, M. J., Lourbopoulos, A., Terpolilli, N. A., and Plesnila, N. (2020). Long-term impairment of neurovascular coupling following experimental subarachnoid hemorrhage. *J. Cereb. Blood Flow Metab.* 40, 1193–1202. doi: 10.1177/0271678X19863021

Blicher, J. U., Near, J., Næss-Schmidt, E., Stagg, C. J., Johansen-Berg, H., Nielsen, J. F., et al. (2015). GABA levels are decreased after stroke and GABA changes during rehabilitation correlate with motor improvement. *Neurorehabil. Neural Repair* 29, 278–286. doi: 10.1177/1545968314543652

Boltze, J., Kleinschnitz, C., Reymann, K. G., Reiser, G., Wagner, D. C., Kranz, A., et al. (2012). Neurovascular pathophysiology in cerebral ischemia, dementia and the ageing brain—current trends in basic, translational and clinical research. *Exp. Transl. Stroke Med.* 4:14. doi: 10.1186/2040-7378-4-14

Boltze, J., Kranz, A., Wagner, D. C., Reymann, K., Reiser, G., and Hess, D. C. (2011). Recent advances in basic and translational stroke research. *Expert Rev. Neurother.* 11, 199–202. doi: 10.1586/ern.10.202

Boltze, J., Modo, M. M., Mays, R. W., Taguchi, A., Jolkkonen, J., Savitz, S., et al. (2019). Stem cells as an emerging paradigm in stroke 4: advancing and accelerating preclinical research. *Stroke* 50, 3299–3306. doi: 10.1161/STROKEAHA.119.025436

Boltze, J., Nitzsche, F., Jolkkonen, J., Weise, G., Pösel, C., Nitzsche, B., et al. (2017). Concise review: increasing the validity of cerebrovascular disease models and experimental methods for translational stem cell research. *Stem Cells* 35, 1141–1153. doi: 10.1002/stem.2595

Bova, A., Kernodle, K., Mulligan, K., and Leventhal, D. (2019). Automated rat single-pellet reaching with 3-dimensional reconstruction of paw and digit trajectories. *J. Vis. Exp.* 149:e59979. doi: 10.3791/59979

Brochu-Gaudreau, K., Rehfeldt, C., Blouin, R., Bordignon, V., Murphy, B. D., and Palin, M. F. (2010). Adiponectin action from head to toe. *Endocrine* 37, 11–32. doi: 10.1007/s12020-009-9278-8

Busato, A., Bonafede, R., Bontempi, P., Scambi, I., Schiaffino, L., Benati, D., et al. (2017). Labeling and magnetic resonance imaging of exosomes isolated from adipose stem cells. *Curr. Protoc. Cell Biol.* 75, 3.44.1-3.44.15. doi: 10.1002/cpcb.23

Chang, C. F., Goods, B. A., Askenase, M. H., Hammond, M. D., Renfroe, S. C., Steinschneider, A. F., et al. (2018). Erythrocyte efferocytosis modulates macrophages towards recovery after intracerebral hemorrhage. *J. Clin. Invest.* 128, 607–624. doi: 10.1172/JCI95612

Choi, H., and Lee, D. S. (2016). Illuminating the physiology of extracellular vesicles. *Stem Cell Res. Ther.* 7:55. doi: 10.1186/s13287-016-0316-1

Chu, C., Liu, G., Janowski, M., Bulte, J. W. M., Li, S., Pearl, M., et al. (2018). Real-time MRI guidance for reproducible hyperosmolar opening of the blood-brain barrier in mice. *Front. Neurol.* 9:921. doi: 10.3389/fneur.2018.00921

Cohan, C. H., Stradecki-Cohan, H. M., Morris-Blanco, K. C., Khoury, N., Koronowski, K. B., Youbi, M., et al. (2017). Protein kinase C epsilon delays latency until anoxic depolarization through arc expression and GluR2 internalization. *J. Cereb. Blood Flow Metab.* 37, 3774–3788. doi: 10.1177/0271678X17712178

Coscia, M., Wessel, M. J., Chaudary, U., Millán, J. D. R., Micera, S., Guggisberg, A., et al. (2019). Neurotechnology-aided interventions for upper limb motor rehabilitation in severe chronic stroke. *Brain* 142, 2182–2197. doi: 10.1093/brain/awz181

Cui, L. L., Golubczyk, D., Tolppanen, A. M., Boltze, J., and Jolkkonen, J. (2019). Cell therapy for ischemic stroke: are differences in preclinical and clinical study

design responsible for the translational loss of efficacy? *Ann. Neurol.* 86, 5–16. doi: 10.1002/ana.25493

Dabrowska, S., Del Fattore, A., Karnas, E., Frontczak-Baniewicz, M., Kozlowska, H., Muraca, M., et al. (2018). Imaging of extracellular vesicles derived from human bone marrow mesenchymal stem cells using fluorescent and magnetic labels. *Int. J. Nanomedicine* 13, 1653–1664. doi: 10.2147/IJN.S159404

D'Adesky, N. D., de Rivero Vaccari, J. P., Bhattacharya, P., Schatz, M., Perez-Pinzon, M. A., Bramlett, H. M., et al. (2018). Nicotine alters estrogen receptor-β-regulated inflammasome activity and exacerbates ischemic brain damage in female rats. *Int. J. Mol. Sci.* 19:1330. doi: 10.3390/ijms19051330

DeFazio, R. A., Raval, A. P., Lin, H. W., Dave, K. R., Della-Morte, D., and Perez-Pinzon, M. A. (2009). GABA synapses mediate neuroprotection after ischemic and εPKC preconditioning in rat hippocampal slice cultures. *J. Cereb. Blood Flow Metab.* 29, 375–384. doi: 10.1038/jcbfm.2008.126

Demuth, H. U., Dijkhuizen, R. M., Farr, T. D., Gelderblom, M., Horsburgh, K., Iadecola, C., et al. (2017). Recent progress in translational research on neurovascular and neurodegenerative disorders. *Restor. Neurol. Neurosci.* 35, 87–103. doi: 10.3233/RNN-160690

de Rivero Vaccari, J. P., Patel, H. H., Brand, F. J. 3rd, Perez-Pinzon, M. A., Bramlett, H. M., and Raval, A. P. (2016). Estrogen receptor beta signaling alters cellular inflammasomes activity after global cerebral ischemia in reproductively senescence female rats. *J. Neurochem.* 136, 492–496. doi: 10.1111/jnc.13404

Doeppner, T. R., Doehring, M., Kaltwasser, B., Majid, A., Lin, F., Bähr, M., et al. (2017). Ischemic post-conditioning induces post-stroke neuroprotection *via* Hsp70-mediated proteasome inhibition and facilitates neural progenitor cell transplantation. *Mol. Neurobiol.* 54, 6061–6073. doi: 10.1007/s12035-016-0137-3

Doeppner, T. R., Herz, J., Görgens, A., Schlechter, J., Ludwig, A. K., Radtke, S., et al. (2015). Extracellular vesicles improve post-stroke neuroregeneration and prevent postischemic immunosuppression. *Stem Cells Transl. Med.* 4, 1131–1143. doi: 10.5966/sctm.2015-0078

Doyle, K. P., Quach, L. N., Solé, M., Axtell, R. C., Nguyen, T. V., Soler-Llavina, G. J., et al. (2015). B-lymphocyte-mediated delayed cognitive impairment following stroke. *J. Neurosci.* 35, 2133–2145. doi: 10.1523/JNEUROSCI.4098-14.2015

Dreier, J. P., Lemale, C. L., Kola, V., Friedman, A., and Schoknecht, K. (2018). Spreading depolarization is not an epiphenomenon but the principal mechanism of the cytotoxic edema in various gray matter structures of the brain during stroke. *Neuropharmacology* 134, 189–207. doi: 10.1016/j.neuropharm.2017.09.027

Egashira, Y., Hua, Y., Keep, R. F., Iwama, T., and Xi, G. (2016). Lipocalin 2 and blood-brain barrier disruption in white matter after experimental subarachnoid hemorrhage. *Acta Neurochir. Suppl.* 121, 131–134. doi: 10.1007/978-3-319-18497-5_23

Fenrich, K. K., May, Z., Hurd, C., Boychuk, C. E., Kowalczewski, J., Bennett, D. J., et al. (2015). Improved single pellet grasping using automated *ad libitum* full-time training robot. *Behav. Brain Res.* 281, 137–148. doi: 10.1016/j.bbr.2014.11.048

Fernández, G., Moraga, A., Cuartero, M. I., García-Culebras, A., Peña-Martínez, C., Pradillo, J. M., et al. (2018). TLR4-binding DNA aptamers show a protective effect against acute stroke in animal models. *Mol. Ther.* 26, 2047–2059. doi: 10.1016/j.ymthe.2018.05.019

Fouad, K., Hurd, C., and Magnuson, D. S. (2013). Functional testing in animal models of spinal cord injury: not as straight forward as one would think. *Front. Integr. Neurosci.* 7:85. doi: 10.3389/fnint.2013.00085

Fukuda, A. M., Adami, A., Pop, V., Bellone, J. A., Coats, J. S., Hartman, R. E., et al. (2013). Posttraumatic reduction of edema with aquaporin-4 RNA interference improves acute and chronic functional recovery. *J. Cereb. Blood Flow Metab.* 33, 1621–1632. doi: 10.1038/jcbfm.2013.118

García-Culebras, A., Durán-Laforet, V., Peña-Martínez, C., Moraga, A., Ballesteros, I., Cuartero, M. I., et al. (2019). Role of TLR4 (toll-like receptor 4) in N1/N2 neutrophil programming after stroke. *Stroke* 50, 2922–2932. doi: 10.1161/STROKEAHA.119.025085

García-Culebras, A., Palma-Tortosa, S., Moraga, A., García-Yébenes, I., Durán-Laforet, V., Cuartero, M. I., et al. (2017). Toll-like receptor 4 mediates hemorrhagic transformation after delayed tissue plasminogen activator administration in *in situ* thromboembolic stroke. *Stroke* 48, 1695–1699. doi: 10.1161/STROKEAHA.116.015956

Gauberti, M., Fournier, A. P., Docagne, F., Vivien, D., and Martinez de Lizarrondo, S. (2018). Molecular magnetic resonance imaging of endothelial activation in the central nervous system. *Theranostics* 8, 1195–1212. doi: 10.7150/thno.22662

Girgis, J., Merrett, D., Kirkland, S., Metz, G. A., Verge, V., and Fouad, K. (2007). Reaching training in rats with spinal cord injury promotes plasticity and task specific recovery. *Brain* 130, 2993–3003. doi: 10.1093/brain/awm245

Golubczyk, D., Kalkowski, L., Kwiatkowska, J., Zawadzki, M., Holak, P., Glodek, J., et al. (2020). Endovascular model of ischemic stroke in swine guided by real-time MRI. *Sci. Rep.* 10:17318. doi: 10.1038/s41598-020-74411-3

Guarente, L. (2008). Mitochondria—a nexus for aging, calorie restriction and sirtuins? *Cell* 132, 171–176. doi: 10.1016/j.cell.2008.01.007

Gülke, E., Gelderblom, M., and Magnus, T. (2018). Danger signals in stroke and their role on microglia activation after ischemia. *Ther. Adv. Neurol. Disord.* 11:1756286418774254. doi: 10.1177/1756286418774254

Guo, D., Wilkinson, D. A., Thompson, B. G., Pandey, A. S., Keep, R. F., Xi, G., et al. (2017). MRI characterization in the acute phase of experimental subarachnoid hemorrhage. *Transl. Stroke Res.* 8, 234–243. doi: 10.1007/s12975-016-0511-5

Haigis, M. C., and Guarente, L. P. (2006). Mammalian sirtuins—emerging roles in physiology, aging and calorie restriction. *Genes Dev.* 20, 2913–2921. doi: 10.1101/gad.1467506

Hainsworth, A. H., Allan, S. M., Boltze, J., Cunningham, C., Farris, C., Head, E., et al. (2017). Translational models for vascular cognitive impairment: a review including larger species. *BMC Med.* 15:16. doi: 10.1186/s12916-017-0793-9

Hanley, D. F., Thompson, R. E., Rosenblum, M., Yenokyan, G., Lane, K., McBee, N., et al. (2019). Efficacy and safety of minimally invasive surgery with thrombolysis in intracerebral haemorrhage evacuation (MISTIE III): a randomised, controlled, open-label, blinded endpoint phase 3 trial. *Lancet* 393, 1021–1032. doi: 10.1016/S0140-6736(19)30195-3

Herrmann, A. M., Meckel, S., Gounis, M. J., Kringe, L., Motschall, E., Mülling, C., et al. (2019). Large animals in neurointerventional research: a systematic review on models, techniques and their application in endovascular procedures for stroke, aneurysms and vascular malformations. *J. Cereb. Blood Flow Metab.* 39, 375–394. doi: 10.1177/0271678X19827446

Hicks, A. U., Lappalainen, R. S., Narkilahti, S., Suuronen, R., Corbett, D., Sivenius, J., et al. (2009). Transplantation of human embryonic stem cell-derived neural precursor cells and enriched environment after cortical stroke in rats: cell survival and functional recovery. *Eur. J. Neurosci.* 29, 562–574. doi: 10.1111/j.1460-9568.2008.06599.x

Howard, R., Zubko, O., Bradley, R., Harper, E., Pank, L., O'Brien, J., et al. (2019). Minocycline at 2 different dosages vs. placebo for patients with mild Alzheimer disease: a randomized clinical trial. *JAMA Neurol.* 77, 164–174. doi: 10.1001/jamaneurol.2019.3762

Huang, H., Bhuiyan, M. I. H., Jiang, T., Song, S., Shankar, S., Taheri, T., et al. (2019). A novel $Na^{+-}K^{+-}Cl^{-}$ cotransporter 1 inhibitor STS66* reduces brain damage in mice after ischemic stroke. *Stroke* 50, 1021–1025. doi: 10.1161/STROKEAHA.118.024287

Iadecola, C., and Gottesman, R. F. (2018). Cerebrovascular alterations in Alzheimer disease. *Circ. Res.* 123, 406–408. doi: 10.1161/CIRCRESAHA.118.313400

Jablonska, A., Drela, K., Wojcik-Stanaszek, L., Janowski, M., Zalewska, T., and Lukomska, B. (2016). Short-lived human umbilical cord-blood-derived neural stem cells influence the endogenous secretome and increase the number of endogenous neural progenitors in a rat model of lacunar stroke. *Mol. Neurobiol.* 53, 6413–6425. doi: 10.1007/s12035-015-9530-6

Ji, X., Zhao, W., Boltze, J., Li, S., Meng, R., Wang, Y., et al. (2019). Clinical practice guidelines of remote ischemic conditioning for the management of cerebrovascular diseases. *Cond. Med.* 2, 225–241.

Jy, W., Rehni, A. K., Bidot, C. Jr., Navarro-Quero, H., Haase, C. R., Koch, S., et al. (2018). Pharmacokinetics of human red blood cell microparticles prepared using high-pressure extrusion method. *Front. Pharmacol.* 9:599. doi: 10.3389/fphar.2018.00599

Kaiser, D., Weise, G., Möller, K., Scheibe, J., Pösel, C., Baasch, S., et al. (2014). Spontaneous white matter damage, cognitive decline and neuroinflammation in middle-aged hypertensive rats: an animal model of early-stage cerebral small vessel disease. *Acta Neuropathol. Commun.* 2:169. doi: 10.1186/s40478-014-0169-8

Karuppagounder, S. S., Alin, L., Chen, Y., Brand, D., Bourassa, M. W., Dietrich, K., et al. (2018). N-acetylcysteine targets 5 lipoxygenase-derived, toxic lipids and can synergize with prostaglandin E2 to inhibit ferroptosis and improve outcomes following hemorrhagic stroke in mice. *Ann. Neurol.* 84, 854–872. doi: 10.1002/ana.25356

Keep, R. F., Hua, Y., and Xi, G. (2012). Intracerebral haemorrhage: mechanisms of injury and therapeutic targets. *Lancet Neurol.* 11, 720–731. doi: 10.1016/S1474-4422(12)70104-7

Khoury, N., Xu, J., Stegelmann, S. D., Jackson, C. W., Koronowski, K. B., Dave, K. R., et al. (2019). Resveratrol preconditioning induces genomic and metabolic adaptations within the long-term window of cerebral ischemic tolerance leading to bioenergetic efficiency. *Mol. Neurobiol.* 56, 4549–4565. doi: 10.1007/s12035-018-1380-6

Kim, T. H., and Vemuganti, R. (2015). Effect of sex and age interactions on functional outcome after stroke. *CNS Neurosci. Ther.* 21, 327–336. doi: 10.1111/cns.12346

Kim, H., Walczak, P., Muja, N., Campanelli, J. T., and Bulte, J. W. (2012). ICV-transplanted human glial precursor cells are short-lived yet exert immunomodulatory effects in mice with EAE. *Glia* 60, 1117–1129. doi: 10.1002/glia.22339

Kirkland, S. W., Smith, L. K., and Metz, G. A. (2012). Task-specific compensation and recovery following focal motor cortex lesion in stressed rats. *J. Integr. Neurosci.* 11, 33–59. doi: 10.1142/S0219635212500033

Kleinschnitz, C., Schwab, N., Kraft, P., Hagedorn, I., Dreykluft, A., Schwarz, T., et al. (2010). Early detrimental T-cell effects in experimental cerebral ischemia are neither related to adaptive immunity nor thrombus formation. *Blood* 115, 3835–3842. doi: 10.1182/blood-2009-10-249078

Koch, P. J., and Hummel, F. C. (2017). Toward precision medicine: tailoring interventional strategies based on noninvasive brain stimulation for motor recovery after stroke. *Curr. Opin. Neurol.* 30, 388–397. doi: 10.1097/WCO.0000000000000462

Kolasinski, J., Hinson, E. L., Divanbeighi Zand, A. P., Rizov, A., Emir, U. E., and Stagg, C. J. (2019). The dynamics of cortical GABA in human motor learning. *J. Physiol.* 597, 271–282. doi: 10.1113/JP276626

Koronowski, K. B., Khoury, N., Saul, I., Loris, Z. B., Cohan, C. H., Stradecki-Cohan, H. M., et al. (2017). Neuronal SIRT1 (silent information regulator 2 homologue 1) regulates glycolysis and mediates resveratrol-induced ischemic tolerance. *Stroke* 48, 3117–3125. doi: 10.1161/STROKEAHA.117.018562

Kronenberg, G., Uhlemann, R., Richter, N., Klempin, F., Wegner, S., Staerck, L., et al. (2018). Distinguishing features of microglia- and monocyte-derived macrophages after stroke. *Acta Neuropathol.* 135, 551–568. doi: 10.1007/s00401-017-1795-6

Lantigua, H., Ortega-Gutierrez, S., Schmidt, J. M., Lee, K., Badjatia, N., Agarwal, S., et al. (2015). Subarachnoid hemorrhage: who dies and why? *Crit. Care* 19:309. doi: 10.1186/s13054-015-1036-0

Laterza, C., Wattananit, S., Uoshima, N., Ge, R., Pekny, R., Tornero, D., et al. (2017). Monocyte depletion early after stroke promotes neurogenesis from endogenous neural stem cells in adult brain. *Exp. Neurol.* 297, 129–137. doi: 10.1016/j.expneurol.2017.07.012

Li, Q., Han, X., Lan, X., Gao, Y., Wan, J., Durham, F., et al. (2017). Inhibition of neuronal ferroptosis protects hemorrhagic brain. *JCI Insight* 2:e90777. doi: 10.1172/jci.insight.90777

Li, Q., Weiland, A., Chen, X., Lan, X., Han, X., Durham, F., et al. (2018). Ultrastructural characteristics of neuronal death and white matter injury in mouse brain tissues after intracerebral hemorrhage: coexistence of ferroptosis, autophagy and necrosis. *Front. Neurol.* 9:581. doi: 10.3389/fneur.2018.00581

Liebeskind, D. S., Derdeyn, C. P., Wechsler, L. R., and STAIR X Consortium. (2018). STAIR X: emerging considerations in developing and evaluating new stroke therapies. *Stroke* 49, 2241–2247. doi: 10.1161/STROKEAHA.118.021424

Loera-Valencia, R., Cedazo-Minguez, A., Kenigsberg, P. A., Page, G., Duarte, A. I., Giusti, P., et al. (2019). Current and emerging avenues for Alzheimer's disease drug targets. *J. Intern. Med.* 286, 398–437. doi: 10.1111/joim.12959

Lückl, J., Lemale, C. L., Kola, V., Horst, V., Khojasteh, U., Oliveira-Ferreira, A. I., et al. (2018). The negative ultraslow potential, electrophysiological correlate of infarction in the human cortex. *Brain* 141, 1734–1752. doi: 10.1093/brain/awy102

Ludewig, P., Gdaniec, N., Sedlacik, J., Forkert, N. D., Szwargulski, P., Graeser, M., et al. (2017). Magnetic particle imaging for real-time perfusion imaging in acute stroke. *ACS Nano* 11, 10480–10488. doi: 10.1021/acsnano.7b05784

Mantovani, A. (2017). Wandering pathways in the regulation of innate immunity and inflammation. *J. Autoimmun.* 85, 1–5. doi: 10.1016/j.jaut.2017.10.007

Mao, X., Terpolilli, N. A., When, A., Cheng, S., Hellal, F., Liu, B., et al. (2020). Progressive histopathological damage occurring up to 1 year after experimental traumatic brain injury is associated with cognitive decline and depression-like behavior. *J. Neurotrauma* 37, 1331–1341. doi: 10.1089/neu.2019.6510

McCullough, L. D., Mirza, M. A., Xu, Y., Bentivegna, K., Steffens, E. B., Ritzel, R., et al. (2016). Stroke sensitivity in the aged: sex chromosome complement vs. gonadal hormones. *Aging* 8, 1432–1441. doi: 10.18632/aging.100997

Mehta, S. L., Kim, T., and Vemuganti, R. (2015). Long noncoding RNA FosDT promotes ischemic brain injury by interacting with REST-associated chromatin-modifying proteins. *J. Neurosci.* 35, 16443–16449. doi: 10.1523/JNEUROSCI.2943-15.2015

Metz, G. A., Antonow-Schlorke, I., and Witte, O. W. (2005). Motor improvements after focal cortical ischemia in adult rats are mediated by compensatory mechanisms. *Behav. Brain Res.* 162, 71–82. doi: 10.1016/j.bbr.2005.03.002

Miró-Mur, F., Pérez-de-Puig, I., Ferrer-Ferrer, M., Urra, X., Justicia, C., Chamorro, A., et al. (2016). Immature monocytes recruited to the ischemic mouse brain differentiate into macrophages with features of alternative activation. *Brain Behav. Immun.* 53, 18–33. doi: 10.1016/j.bbi.2015.08.010

Montagne, A., Zhao, Z., and Zlokovic, B. V. (2017). Alzheimer's disease: a matter of blood-brain barrier dysfunction? *J. Exp. Med.* 214, 3151–3169. doi: 10.1084/jem.20171406

Morris-Blanco, K. C., Kim, T., Lopez, M. S., Bertogliat, M. J., Chelluboina, B., and Vemuganti, R. (2019). Induction of DNA hydroxymethylation protects the brain after stroke. *Stroke* 50, 2513–2521. doi: 10.1161/STROKEAHA.119.025665

Mu, J., Bakreen, A., Juntunen, M., Korhonen, P., Oinonen, E., Cui, L., et al. (2019). Combined adipose tissue-derived mesenchymal stem cell therapy and rehabilitation in experimental stroke. *Front. Neurol.* 10:235. doi: 10.3389/fneur.2019.00235

Muhammad, S., Barakat, W., Stoyanov, S., Murikinati, S., Yang, H., Tracey, K. J., et al. (2008). The HMGB1 receptor RAGE mediates ischemic brain damage. *J. Neurosci.* 28, 12023–12031. doi: 10.1523/JNEUROSCI.2435-08.2008

Narayanan, S. V., Dave, K. R., Saul, I., and Perez-Pinzon, M. A. (2015). Resveratrol preconditioning protects against cerebral ischemic injury *via* nuclear erythroid 2-related factor 2. *Stroke* 46, 1626–1632. doi: 10.1161/STROKEAHA.115.008921

Neumann, J. T., Thompson, J. W., Raval, A. P., Cohan, C. H., Koronowski, K. B., and Perez-Pinzon, M. A. (2015). Increased BDNF protein expression after ischemic or PKC epsilon preconditioning promotes electrophysiologic changes that lead to neuroprotection. *J. Cereb. Blood Flow Metab.* 35, 121–130. doi: 10.1038/jcbfm.2014.185

O'Shea, J., Boudrias, M. H., Stagg, C. J., Bachtiar, V., Kischka, U., Blicher, J. U., et al. (2014). Predicting behavioural response to TDCS in chronic motor stroke. *Neuroimage* 85, 924–933. doi: 10.1016/j.neuroimage.2013.05.096

Panta, A., Pandey, S., Duncan, I. N., Duhamel, S., and Sohrabji, F. (2019). Mir363-3p attenuates post-stroke depressive-like behaviors in middle-aged female rats. *Brain Behav. Immun.* 78, 31–40. doi: 10.1016/j.bbi.2019.01.003

Poinsatte, K., Betz, D., Torres, V. O., Ajay, A. D., Mirza, S., Selvaraj, U. M., et al. (2019). Visualization and quantification of post-stroke neural connectivity and neuroinflammation using serial two-photon tomography in the whole mouse brain. *Front. Neurosci.* 13:1055. doi: 10.3389/fnins.2019.01055

Poon, M. T., Fonville, A. F., and Al-Shahi Salman, R. (2014). Long-term prognosis after intracerebral haemorrhage: systematic review and meta-analysis. *J. Neurol. Neurosurg. Psychiatry* 85, 660–667. doi: 10.1136/jnnp-2013-306476

Pop, V., and Badaut, J. (2011). A neurovascular perspective for long-term changes after brain trauma. *Transl. Stroke Res.* 2, 533–545. doi: 10.1007/s12975-011-0126-9

Potts, M. B., and Riina, H. A. (2014). Refining the role for evacuation of spontaneous intracerebral hematomas: results of STICH II. *World Neurosurg.* 82, 549–550. doi: 10.1016/j.wneu.2014.08.046

Pradillo, J. M., Fernández-López, D., García-Yébenes, I., Sobrado, M., Hurtado, O., Moro, M. A., et al. (2009). Toll-like receptor 4 is involved in neuroprotection afforded by ischemic preconditioning. *J. Neurochem.* 109, 287–294. doi: 10.1111/j.1471-4159.2009.05972.x

Rabut, C., Correia, M., Finel, V., Pezet, S., Pernot, M., Deffieux, T., et al. (2019). 4D functional ultrasound imaging of whole-brain activity in rodents. *Nat. Methods* 16, 994–997. doi: 10.1038/s41592-019-0572-y

Raffin, E., and Hummel, F. C. (2018). Restoring motor functions after stroke: multiple approaches and opportunities. *Neuroscientist* 24, 400–416. doi: 10.1177/1073858417737486

Ramirez, F. D., Motazedian, P., Jung, R. G., Di Santo, P., MacDonald, Z. D., Moreland, R., et al. (2017). Methodological rigor in preclinical cardiovascular studies: targets to enhance reproducibility and promote research translation. *Circ. Res.* 120, 1916–1926. doi: 10.1161/CIRCRESAHA.117.310628

Rehni, A. K., Shukla, V., Navarro Quero, H., Bidot, C. Jr., Haase, C. R., Crane, E. A. A., et al. (2019). Preclinical evaluation of safety and biodistribution of red cell microparticles: a novel hemostatic agent. *J. Cardiovasc. Pharmacol. Ther.* 24, 474–483. doi: 10.1177/1074248419838512

Ritzel, R. M., Lai, Y. J., Crapser, J. D., Patel, A. R., Schrecengost, A., Grenier, J. M., et al. (2018). Aging alters the immunological response to ischemic stroke. *Acta Neuropathol.* 136, 89–110. doi: 10.1007/s00401-018-1859-2

Royea, J., Martinot, P., and Hamel, E. (2020). Memory and cerebrovascular deficits recovered following angiotensin IV intervention in a mouse model of Alzheimer's disease. *Neurobiol. Dis.* 134:104644. doi: 10.1016/j.nbd.2019.104644

Ryait, H., Bermudez-Contreras, E., Harvey, M., Faraji, J., Mirza Agha, B., Gomez-Palacio Schjetnan, A., et al. (2019). Data-driven analyses of motor impairments in animal models of neurological disorders. *PLoS Biol.* 17:e3000516. doi: 10.1371/journal.pbio.3000516

Salehi, A., Jullienne, A., Baghchechi, M., Hamer, M., Walsworth, M., Donovan, V., et al. (2018). Up-regulation of Wnt/β-catenin expression is accompanied with vascular repair after traumatic brain injury. *J. Cereb. Blood Flow Metab.* 38, 274–289. doi: 10.1177/0271678X17744124

Sandsmark, D. K., Bashir, A., Wellington, C. L., and Diaz-Arrastia, R. (2019). Cerebral microvascular injury: a potentially treatable endophenotype of traumatic brain injury-induced neurodegeneration. *Neuron* 103, 367–379. doi: 10.1016/j.neuron.2019.06.002

Savitz, S. I., Baron, J. C., Fisher, M., and STAIR X Consortium. (2019). Stroke treatment academic industry roundtable X: brain cytoprotection therapies in the reperfusion era. *Stroke* 50, 1026–1031. doi: 10.1161/STROKEAHA.118.023927

Schulz, R., Park, E., Lee, J., Chang, W. H., Lee, A., Kim, Y. H., et al. (2017). Interactions between the corticospinal tract and premotor-motor pathways for residual motor output after stroke. *Stroke* 48, 2805–2811. doi: 10.1161/STROKEAHA.117.016834

Selvamani, A., Sathyan, P., Miranda, R. C., and Sohrabji, F. (2012). An antagomir to microRNA Let7f promotes neuroprotection in an ischemic stroke model. *PLoS One* 7:e32662. doi: 10.1371/journal.pone.0032662

Selvamani, A., and Sohrabji, F. (2017). Mir363-3p improves ischemic stroke outcomes in female but not male rats. *Neurochem. Int.* 107, 168–181. doi: 10.1016/j.neuint.2016.10.008

Selvaraj, U. M., and Stowe, A. M. (2017). Long-term T cell responses in the brain after an ischemic stroke. *Discov. Med.* 24, 323–333.

Sohrabji, F., Okoreeh, A., and Panta, A. (2019). Sex hormones and stroke: beyond estrogens. *Horm. Behav.* 111, 87–95. doi: 10.1016/j.yhbeh.2018.10.010

Sohrabji, F., and Selvamani, A. (2019). Sex differences in miRNA as therapies for ischemic stroke. *Neurochem. Int.* 127, 56–63. doi: 10.1016/j.neuint.2018.10.021

Spalletti, C., Alia, C., Lai, S., Panarese, A., Conti, S., Micera, S., et al. (2017). Combining robotic training and inactivation of the healthy hemisphere restores pre-stroke motor patterns in mice. *eLife* 6:e28662. doi: 10.7554/eLife.28662

Stagg, C. J., Bachtiar, V., and Johansen-Berg, H. (2011). The role of GABA in human motor learning. *Curr. Biol.* 21, 480–484. doi: 10.1016/j.cub.2011.01.069

Stetler, R. A., Leak, R. K., Gan, Y., Li, P., Zhang, F., Hu, X., et al. (2014). Preconditioning provides neuroprotection in models of CNS disease: paradigms and clinical significance. *Prog. Neurobiol.* 114, 58–83. doi: 10.1016/j.pneurobio.2013.11.005

Straathof, M., Sinke, M. R., Dijkhuizen, R. M., and Otte, W. M. (2019). A systematic review on the quantitative relationship between structural and functional network connectivity strength in mammalian brains. *J. Cereb. Blood Flow Metab.* 39, 189–209. doi: 10.1177/0271678X18809547

Struys, M. M., De Smet, T., Glen, J. I., Vereecke, H. E., Absalom, A. R., and Schnider, T. W. (2016). The history of target-controlled infusion. *Anesth. Analg.* 122, 56–69. doi: 10.1213/ANE.0000000000001008

Taylor, R. A., Chang, C. F., Goods, B. A., Hammond, M. D., Mac Grory, B., Ai, Y., et al. (2017). TGF-β1 modulates microglial phenotype and promotes recovery after intracerebral hemorrhage. *J. Clin. Invest.* 127, 280–292. doi: 10.1172/JCI88647

Trigiani, L. J., and Hamel, E. (2017). An endothelial link between the benefits of physical exercise in dementia. *J. Cereb. Blood Flow Metab.* 37, 2649–2664. doi: 10.1177/0271678X17714655

Trigiani, L. J., Royea, J., Tong, X. K., and Hamel, E. (2019). Comparative benefits of simvastatin and exercise in a mouse model of vascular cognitive impairment and dementia. *FASEB J.* 33, 13280–13293. doi: 10.1096/fj.201901002R

van Asch, C. J., Luitse, M. J., Rinkel, G. J., van der Tweel, I., Algra, A., and Klijn, C. J. (2010). Incidence, case fatality and functional outcome of intracerebral haemorrhage over time, according to age, sex and ethnic origin: a systematic review and meta-analysis. *Lancet Neurol.* 9, 167–176. doi: 10.1016/S1474-4422(09)70340-0

Vartanian, K. B., Stevens, S. L., Marsh, B. J., Williams-Karnesky, R., Lessov, N. S., and Stenzel-Poore, M. P. (2011). LPS preconditioning redirects TLR signaling following stroke: TRIF-IRF3 plays a seminal role in mediating tolerance to ischemic injury. *J. Neuroinflammation* 8:140. doi: 10.1186/1742-2094-8-140

Vay, S. U., Flitsch, L. J., Rabenstein, M., Rogall, R., Blaschke, S., Kleinhaus, J., et al. (2018). The plasticity of primary microglia and their multifaceted effects on endogenous neural stem cells *in vitro* and *in vivo*. *J. Neuroinflammation* 15:226. doi: 10.1186/s12974-018-1261-y

Walczak, P., Wojtkiewicz, J., Nowakowski, A., Habich, A., Holak, P., Xu, J., et al. (2017). Real-time MRI for precise and predictable intra-arterial stem cell delivery to the central nervous system. *J. Cereb. Blood Flow Metab.* 37, 2346–2358. doi: 10.1177/0271678X16665853

Wan, Y., Hua, Y., Garton, H. J. L., Novakovic, N., Keep, R. F., and Xi, G. (2019). Activation of epiplexus macrophages in hydrocephalus caused by subarachnoid hemorrhage and thrombin. *CNS Neurosci. Ther.* 25, 1134–1141. doi: 10.1111/cns.13203

Wang, Y., Reis, C., Applegate, R., Stier, G., Martin, R., and Zhang, J. H. (2015). Ischemic conditioning-induced endogenous brain protection: applications pre-, per- or post-stroke. *Exp. Neurol.* 272, 26–40. doi: 10.1016/j.expneurol.2015.04.009

Wattananit, S., Tornero, D., Graubardt, N., Memanishvili, T., Monni, E., Tatarishvili, J., et al. (2016). Monocyte-derived macrophages contribute to spontaneous long-term functional recovery after stroke in mice. *J. Neurosci.* 36, 4182–4195. doi: 10.1523/JNEUROSCI.4317-15.2016

Xin, H., Katakowski, M., Wang, F., Qian, J. Y., Liu, X. S., Ali, M. M., et al. (2017). MicroRNA cluster miR-17-92 cluster in exosomes enhance neuroplasticity and functional recovery after stroke in rats. *Stroke* 48, 747–753. doi: 10.1161/STROKEAHA.116.015204

Xin, H., Li, Y., Buller, B., Katakowski, M., Zhang, Y., Wang, X., et al. (2012). Exosome-mediated transfer of miR-133b from multipotent mesenchymal stromal cells to neural cells contributes to neurite outgrowth. *Stem Cells* 30, 1556–1564. doi: 10.1002/stem.1129

Xin, H., Li, Y., Cui, Y., Yang, J. J., Zhang, Z. G., and Chopp, M. (2013a). Systemic administration of exosomes released from mesenchymal stromal cells promote functional recovery and neurovascular plasticity after stroke in rats. *J. Cereb. Blood Flow Metab.* 33, 1711–1715. doi: 10.1038/jcbfm.2013.152

Xin, H., Li, Y., Liu, Z., Wang, X., Shang, X., Cui, Y., et al. (2013b). MiR-133b promotes neural plasticity and functional recovery after treatment of stroke with multipotent mesenchymal stromal cells in rats *via* transfer of exosome-

enriched extracellular particles. *Stem Cells* 31, 2737–2746. doi: 10.1002/stem.1409

Zaouter, C., Hemmerling, T. M., Lanchon, R., Valoti, E., Remy, A., Leuillet, S., et al. (2016). The feasibility of a completely automated total iv anesthesia drug delivery system for cardiac surgery. *Anesth. Analg.* 123, 885–893. doi: 10.1213/ANE.0000000000001152

Zhang, Z. G., Buller, B., and Chopp, M. (2019). Exosomes—beyond stem cells for restorative therapy in stroke and neurological injury. *Nat. Rev. Neurol.* 15, 193–203. doi: 10.1038/s41582-018-0126-4

Zhang, Y., Chopp, M., Meng, Y., Katakowski, M., Xin, H., Mahmood, A., et al. (2015). Effect of exosomes derived from multipluripotent mesenchymal stromal cells on functional recovery and neurovascular plasticity in rats after traumatic brain injury. *J. Neurosurg.* 122, 856–867. doi: 10.3171/2014.11.JNS14770

Zhang, J., Zhang, W., Gao, X., Zhao, Y., Chen, D., Xu, N., et al. (2018). Preconditioning with partial caloric restriction confers long-term protection against gray and white matter injury after transient focal ischemia. *J. Cereb. Blood Flow Metab.* 39, 1394–1409. doi: 10.1177/0271678X18785480

Zhao, X., Ting, S. M., Liu, C. H., Sun, G., Kruzel, M., Roy-O'Reilly, M., et al. (2017a). Neutrophil polarization by IL-27 as a therapeutic target for intracerebral hemorrhage. *Nat. Commun.* 8:602. doi: 10.1038/s41467-017-00770-7

Zhao, S. C., Wang, C., Xu, H., Wu, W. Q., Chu, Z. H., Ma, L. S., et al. (2017b). Age-related differences in interferon regulatory factor-4 and -5 signaling in ischemic brains of mice. *Acta Pharmacol. Sin.* 38, 1425–1434. doi: 10.1038/aps.2017.122

Zheng, X., Zhang, L., Kuang, Y., Venkataramani, V., Jin, F., Hein, K., et al. (2021). Extracellular vesicles derived from neural progenitor cells–a preclinical evaluation for stroke treatment in mice. *Transl. Stroke Res.* 12, 185–203. doi: 10.1007/s12975-020-00814-z

Zille, M., Ikhsan, M., Jiang, Y., Lampe, J., Wenzel, J., and Schwaninger, M. (2019). The Impact of endothelial cell death in the brain and its role after stroke: a systematic review. *Cell Stress* 3, 330–347. doi: 10.15698/cst2019.11.203

Zille, M., Karuppagounder, S. S., Chen, Y., Gough, P. J., Bertin, J., Finger, J., et al. (2017). Neuronal death after hemorrhagic stroke *in vitro* and *in vivo* shares features of ferroptosis and necroptosis. *Stroke* 48, 1033–1043. doi: 10.1161/STROKEAHA.116.015609

Conflict of Interest: The authors declare that the research was conducted in the absence of any commercial or financial relationships that could be construed as a potential conflict of interest.

The reviewer AL declared a shared affiliation, though no other collaboration, with several of the authors (IK, NP) to the handling Editor.

Copyright © 2021 Boltze, Aronowski, Badaut, Buckwalter, Caleo, Chopp, Dave, Didwischus, Dijkhuizen, Doeppner, Dreier, Fouad, Gelderblom, Gertz, Golubczyk, Gregson, Hamel, Hanley, Härtig, Hummel, Ikhsan, Janowski, Jolkkonen, Karuppagounder, Keep, Koerte, Kokaia, Li, Liu, Lizasoain, Ludewig, Metz, Montagne, Obenaus, Palumbo, Pearl, Perez-Pinzon, Planas, Plesnila, Raval, Rueger, Sansing, Sohrabji, Stagg, Stetler, Stowe, Sun, Taguchi, Tanter, Vay, Vemuganti, Vivien, Walczak, Wang, Xiong and Zille. This is an open-access article distributed under the terms of the Creative Commons Attribution License (CC BY). The use, distribution or reproduction in other forums is permitted, provided the original author(s) and the copyright owner(s) are credited and that the original publication in this journal is cited, in accordance with accepted academic practice. No use, distribution or reproduction is permitted which does not comply with these terms.

frontiers in Cellular Neuroscience

ORIGINAL RESEARCH
published: 14 February 2019
doi: 10.3389/fncel.2019.00051

Extracellular Vesicles Secreted in Response to Cytokine Exposure Increase Mitochondrial Oxygen Consumption in Recipient Cells

*Ashley E. Russell[1], Sujung Jun[2], Saumyendra Sarkar[2], Werner J. Geldenhuys[3], Sara E. Lewis[2], Stephanie L. Rellick[2] and James W. Simpkins[2]**

[1]*Department of Neuroscience, West Virginia University School of Medicine, Morgantown, WV, United States,* [2]*Department of Physiology and Pharmacology, West Virginia University School of Medicine, Morgantown, WV, United States,* [3]*Center for Basic and Translational Stroke Research, Department of Pharmaceutical Sciences, Rockefeller Neuroscience Institute, West Virginia University School of Pharmacy, Morgantown, WV, United States*

Extracellular vesicles (EVs) are small, membrane-bound nanoparticles released from most, if not all cells, and can carry functionally active cargo (proteins, nucleic acids) which can be taken up by neighboring cells and mediate physiologically relevant effects. In this capacity, EVs are being regarded as novel cell-to-cell communicators, which may play important roles in the progression of neurodegenerative diseases, like Alzheimer's disease (AD). Aside from the canonical physical hallmarks of this disease [amyloid β (Aβ) plaques, neurofibrillary tangles, and widespread cell death], AD is characterized by chronic neuroinflammation and mitochondrial dysfunction. In the current study, we sought to better understand the role of tumor necrosis factor-alpha (TNF-α), known to be involved in inflammation, in mediating alterations in mitochondrial function and EV secretion. Using an immortalized hippocampal cell line, we observed significant reductions in several parameters of mitochondrial oxygen consumption after a 24-h exposure period to TNF-α. In addition, after TNF-α exposure we also observed significant upregulation of two microRNAs (miRNAs; miR-34a and miR-146a) associated with mitochondrial dysfunction in secreted EVs. Despite this, when naïve cells are exposed to EVs isolated from TNF-α treated cells, mitochondrial respiration, proton leak, and reactive oxygen species (ROS) production are all significantly increased. Collectively these data indicate that a potent proinflammatory cytokine, TNF-α, induces significant mitochondrial dysfunction in a neuronal cell type, in part *via* the secretion of EVs, which significantly alter mitochondrial activity in recipient cells.

Keywords: neuroinflammation, microRNAs, mitochondria, extracellular vesicles, TNF-α

OPEN ACCESS

Edited by:
Gregory Jaye Bix,
University of Kentucky, United States

Reviewed by:
Zezong Gu,
University of Missouri, United States
Lezi E,
Duke University, United States
Heather Jane Mortiboys,
University of Sheffield, United Kingdom

****Correspondence:***
James W. Simpkins
jwsimpkins@hsc.wvu.edu

Received: *05 December 2018*
Accepted: *01 February 2019*
Published: *14 February 2019*

Citation:
Russell AE, Jun S, Sarkar S, Geldenhuys WJ, Lewis SE, Rellick SL and Simpkins JW (2019) Extracellular Vesicles Secreted in Response to Cytokine Exposure Increase Mitochondrial Oxygen Consumption in Recipient Cells. Front. Cell. Neurosci. 13:51. doi: 10.3389/fncel.2019.00051

Abbreviations: AD, Alzheimer's disease; TNF-α, tumor necrosis factor-α; Aβ, amyloid β; AMCs, age matched controls; ETC, electron transport chain; EVs, extracellular vesicles; miRNA, microRNA; ROS, reactive oxygen species; Ψm, mitochondrial membrane potential.

INTRODUCTION

Alzheimer's disease (AD) is a chronic neurodegenerative disease characterized by amyloid β (Aβ) plaques, neurofibrillary tangles, neuroinflammation, and mitochondrial dysfunction (Wyss-Coray and Rogers, 2012). Extracellular Aβ plaques activate microglia, prompting secretion of immunomodulatory molecules, including tumor necrosis factor-alpha (TNF-α; Hanisch, 2002). Elevated levels of this cytokine have been detected in the plasma (Fillit et al., 1991; Zuliani et al., 2007), cerebrospinal fluid (CSF; Tarkowski et al., 2003), and brains (Sharma et al., 2012) of AD patients when compared to healthy, age matched controls (AMCs). Further, several studies have implicated TNF-α as a key player in the formation of Aβ plaques (Blasko et al., 2000; Liao et al., 2004; Yamamoto et al., 2007), suggesting that this cytokine may participate in a vicious cycle of AD progression. TNF-α activates the transcription factor NF-κB (Schütze et al., 1995), which induces the transcription of many genes, including microRNAs (miRNAs); these small, non-coding RNAs function as gene repressors by base-pairing with complementary mRNAs and inhibiting protein translation, or accelerating the de-adenylation of the poly-A tail (Krek et al., 2005; Huntzinger and Izaurralde, 2011). Changes in expression of various miRNAs have been associated with inflammation and may influence AD progression.

Previous work from our laboratory assessed brain region-specific changes in miRNA expression, and observed significant upregulation of miR-34a and miR-146a in AD patients' temporal cortices, when compared to AMCs (Sarkar et al., 2016). Promotor analysis revealed that various components of the NF-κB family bind to the promotor region of both miR-34a (Sarkar et al., 2016) and miR-146a (Taganov et al., 2006), suggesting that the activation of pro-inflammatory pathways could lead to increased transcription of these miRNAs. Interestingly, these miRNAs target several mRNAs, which encode for proteins of the mitochondrial electron transport chain (ETC; Dasgupta et al., 2015; Sarkar et al., 2016). Indeed, overexpression of miR-146a in primary microglial cells (Jun et al., unpublished observation) or miR-34a in primary neurons (Sarkar et al., 2016) significantly reduced mitochondrial function, and repressed expression of all of the associated mitochondrial proteins that were assessed (Sarkar et al., 2016). Inflammation-induced upregulation of NF-κB may lead to aberrant expression of miR-34a and -146a and lead to translational repression of ETC proteins, thus contributing to the widespread reductions in glucose metabolism and dysregulated mitochondrial function observed in AD brains.

Intercellular communication allows for the transfer of information from one cell to another. The secretion of extracellular vesicles (EVs) affords the opportunity for cells to send important signaling molecules out into the extracellular environment to convey vital messages to neighboring cells (Harding et al., 1983; Pan et al., 1985; Valadi et al., 2007; Tkach and Théry, 2016). As EVs are encapsulated by a lipid bilayer, their contents (including proteins, DNA, and RNA) are protected from degrading enzymes, allowing for delivery of functional cargo. During periods of neuroinflammation, concentrations of circulating EVs have been shown to be significantly upregulated, and within the context of AD, EVs have been shown to confer noxious molecules, including Aβ (Rajendran et al., 2006; Sardar Sinha et al., 2018), to recipient cells and thereby participate in the spreading of AD pathology and neuroinflammation.

Inasmuch as neuroinflammation clearly occurs in affected individuals, and likely occurs years prior to onset of clinical symptoms, it is difficult to model *in vitro*, the effects of long-term inflammation. In the current study, we sought to characterize the role of acute TNF-α exposure on phenotypes seen in AD, including mitochondrial dysfunction, increased miRNA expression (e.g., miR-34a and miR-146a; Sarkar et al., 2016), and altered EV secretion in an immortalized hippocampal cell line (HT-22). Here we demonstrate that direct exposure to TNF-α for 24-h significantly reduces mitochondrial oxygen consumption, induces cellular death, and induces differential expression of miR-34a and miR-146a both within cells, and in secreted EVs. We also assessed the functional outcomes of exposing TNF-α naïve cells to TNF-α-induced EVs and found significant increases in mitochondrial oxygen consumption, proton leak, and reactive oxygen species (ROS) production.

MATERIALS AND METHODS

Cell Culture

The HT-22 immortalized mouse hippocampal cells were obtained from the Salk Institute for Biological Research (La Jolla, CA, USA). HT-22 cells were cultured in Hyclone Dulbecco's modified Eagle's medium (DMEM)/high glucose (Fisher Scientific, Waltham, MA, USA) with 10% fetal bovine serum (FBS; Atlanta Biologicals, Flowery Branch, GA, USA) and 1% penicillin/streptomycin (Fisher Scientific). When cells were at least 80% confluent, they were trypsinized and spun down at 325.5× *g* for 3 min. Cells were counted with a Nexcelom Bioscience Cellometer AutoT4 (Lawrence, MA, USA). Cell passages 5–18 were used for all experiments.

Cytokine Reconstitution and Exposure

Recombinant mouse TNF-α was purchased from R&D Systems (Minneapolis, MN, USA) and reconstituted at 100 μg/ml in phosphate-buffered saline (PBS) containing 0.1% bovine serum albumin. Dilutions were made in Hyclone DMEM/high glucose with 10% exosome-depleted FBS (Fisher Scientific), and 1% penicillin/streptomycin to obtain concentrations of 0.1, 1, and 10 ng/ml. The 24-h time point for TNF-α exposure was chosen as preliminary data suggested that shorter exposure period did not result in mitochondrial dysfunction (data not shown). Longer exposure periods were not tested due to the potential complication of TNF-α-induced neurotoxicity on cell number, which could affect readouts of all of the assessed parameters in this study.

EV Isolation From Cell Culture Media

Conditioned media was collected after a 24-h exposure to TNF-α and filtered through a Millex-AA Syringe Filter Unit, 0.80 μm (Millipore Sigma, Burlington, MA, USA) to remove cellular debris. EV isolation was performed as per the manufacturer's instructions using either the ExoRNeasy Serum Plasma Maxi Kit

(Qiagen, Germantown, MD, USA) utilized for RNA purification from EVs, or the ExoEasy Maxi Kit (Qiagen) for all other EV applications.

Briefly, 1 volume of filtered media was mixed with 1 volume of buffer XBP and then placed on a spin column and centrifuged at 500× *g* for 1 min. The flow-through was discarded and the column was washed with 10 ml buffer XWP and centrifuged at >3,000× *g* for 5 min. The column was then transferred to a new collection tube and the EVs were eluted with 700 μl QIAzol for downstream RNA purification, or 400 μl buffer XE for all other EV applications.

Particle Size Distributions and Concentrations

To determine if changes in EV concentrations after exposure to TNF-α could account for alterations in mitochondrial function, EVs were isolated from HT-22 cell conditioned media using the ExoEasy Maxi Kit (as described above) and profiled with the NanoSight NS300 (Malvern, Westborough MA, USA). In the final isolation step using the ExoEasy Maxi Kit, EVs were eluted from the spin column membrane in 400 μl XE Buffer. Suspended EVs were diluted 1:200 in sterile filtered PBS for injection into the NanoSignt NS300 unit. Capture and analysis settings were manually set according to the manufacturer's instructions. Particles were visualized using laser light scattering to quantify nanoparticles (10–1,000 nm) moving under Brownian motion as they pass through the flow chamber. The Nanoparticle Tracking Analysis (NTA) software generates particle size distributions and concentrations based on an analysis of both Brownian motion and light scattering observed from tracked particles.

EV Marker Dot Blot

The presence of several EV markers was assessed to ensure that isolated particles from control or TNF-α exposure groups were indeed EVs. Protein concentration was measured using a microBCA kit (Fisher). BSA standards were prepared in the same solution EVs were eluted in (XE Buffer). EVs were diluted in 2% sodium dodecyl sulfide (SDS) at a ratio of 1:10 to a final volume of 150 μl, and transferred to a 96 well clear bottom assay plate. The standard curve was prepared using 150 μl of each, in duplicate. Working reagent was prepared in a 25:24:1 ratio of reagents A, B, and C, respectfully. One-hundred and fifty microliter working reagent was added to each of the standards and diluted EV samples, and incubated at room temperature for 2 h on a shaker. The plate was read using a BioTek Synergy H1 Hybrid reader at 562 nm absorbance.

The Exo-Check Exosome Antibody Array (System Biosciences) was used to detect the presence of several EV markers as per the manufacturer's instructions. Briefly, from either control or TNF-α induced EVs, 200 μg protein was incubated with 600 μl Exosome Lysis buffer and vortexed. Next, the lysate mixture was combined with 9.4 mL Exosome Array Binding buffer and was then added to a pre-wet antibody array membrane and incubated overnight at 4°C on a shaker. The following day the membrane was washed and 10 mL Detection buffer was added to the membrane and incubated for 2 h on a shaker. Next, the membrane was washed 3× and 2 mL SuperSignal West Femto Chemi-luminescent Substrate (Fisher) developer solution was added and the membrane was imaged.

Mitochondrial Functional Assessment

HT-22 cells were seeded at 5 k per well in an XF^{e}96 cell culture microplate (Agilent, Santa Clara, CA, USA) for 24 h. Media was gently aspirated from the cells and replaced with 100 μl Hyclone DMEM/high glucose, supplemented with 10% exosome-depleted FBS and 1% penicillin/streptomycin, the various concentrations of TNF-α, or isolated TNF-α-induced EVs. For EV exposure, EVs were isolated from the media of HT-22 cells exposed to varying concentrations of TNF-α (0, 0.1, 1, and 10 ng/ml) for 24 h. As described above, EVs were isolated from 20 ml media of cytokine-exposed HT-22 cells and eluted from spin columns in 400 μl buffer XE. Assuming a high yield of recovery from a starting volume of 20 ml conditioned cell culture media, EVs eluted in 400 μl buffer XE would be concentrated 50×. To mimic *in vitro* EV concentrations from each cytokine exposure condition, EVs were diluted 50× in DMEM/high glucose, supplemented with 10% exosome-depleted FBS and 1% penicillin/streptomycin (i.e., 2 μl EVs suspended in buffer XE were diluted into 98 μl media per well). Various parameters of mitochondrial function were assessed using a Mito Stress kit, with the XF^{e}96 Analyzer. Using Wave 2.4.0 Desktop software, all mitochondrial assessments were calculated with the Agilent Seahorse XF Cell Mito Stress Test Report Generator. Non-mitochondrial oxygen consumption rate (OCR) was calculated as the minimum rate measurement after rotenone/antimycin A injection. Basal respiration was calculated by subtracting non-mitochondrial OCR from the last rate measurement before oligomycin injection. Maximal respiration was calculated by subtracting non-mitochondrial OCR from the maximum rate measurement after trifluorocarbonylcyanide phenylhydrazone (FCCP) injection. Proton leak was calculated by subtracting non-mitochondrial OCR from the minimum rate measurement after Oligomycin injection. ATP production was calculated by subtracting the minimum rate measurement after Oligomycin injection from the last rate measurement before Oligomycin injection. Lastly, spare respiratory capacity was calculating by subtracting basal respiration from maximal respiration. All measurements are displayed percent changes from control. All wells with a basal respiratory rate below 40 pmol/min were excluded from analysis.

While glycolysis was not directly measured, data on the extracellular acidification rate (ECAR) is an additional measurement collected while completing the Mito Stress test. From these measurements, basal levels of glycolytic activity can be determined. To determine basal glycolysis, the third measurement, prior to the injection of oligomycin, was used. For cells treated with TNF-α, the average ECAR reading was calculated, and was used to calculate percent of control for each of the TNF-α treatment groups (0, 0.1, 1, and 10 ng/ml). For cells treated with EVs derived from TNF-α exposed cells, the cells treated with the XE buffer served as the control, and percent of control was calculated in the same way in each of the treatment groups (0, 0.1, 1, and 10 ng/ml).

Lactate Dehydrogenase Assay

Cell death after cytokine or EV exposure was assessed using the Pierce™ lactate dehydrogenase (LDH) Cytotoxicity Assay (Fisher Scientific) kit. Reaction substrates were prepared as per the manufacturer's instructions. LDH assay was performed with the media from the XF^{e}96 cell culture microplate. Forty-five minutes prior to the end of the 24-h exposure period, 10 μl 10× lysis buffer was added to one control well, and the plate was placed back in the incubator. At the conclusion of the exposure period, 50 μl of media was carefully removed from each well and transferred to a new 96 well clear bottom assay plate. The well exposed to 10× lysis buffer was excluded from the mitochondrial functional assessment. Next, 50 μl of the LDH reaction mixture was added to each well, and the plate was incubated for 30 min at room temperature, protected from light. The reaction was stopped by adding 50 μl of LDH stop solution to each sample. The plate was read using the BioTek Synergy H1 Hybrid reader (BioTek, Winooski, VT, USA) at absorbance of 490 nm and 680 nm. Cell death was calculated as a percentage of total death, relative to maximal cell death induced by treatment with the 10× lysis buffer.

Intracellular and EV miRNA Analysis

Cells were seeded at 250 k per 10 cm cell culture dish and left to reach ∼80% confluency over the course of 48 h. Media was gently aspirated from cells, and replaced by 10 ml of Hyclone DMEM/high glucose, supplemented with 10% exosome-depleted FBS and 1% penicillin/streptomycin, or the various concentrations of TNF-α. After a 24-h exposure period the media was collected for EV isolation, and cell lysates were collected using a Cell Lifter (Corning, Corning, NY, USA), washed with PBS, and pelleted by centrifugation at 325.5× *g* for 3 min, followed by the addition of 700 μl QIAzol Lysis Reagent for RNA purification (Qiagen).

RNA was purified from EVs eluted in 700 μl QIAzol by using the exoRNeasy Serum Plasma Maxi Kit (Qiagen). For all EV samples, 3.5 μl miRNeasy Serum/Plasma Spike-In Control (*C. elegans* miR-39; at a concentration of 1.6 × 10^8 copies/μl) was added to each sample, followed by the addition of 90 μl chloroform and a 3 min incubation. Next the samples were centrifuged for 15 min at 12,000× *g* at 4°C. The upper aqueous phase (300 μl) was transferred to a new collection tube and mixed with 600 μl 100% ethanol. The solution was then placed on a RNeasy MinElute spin column and centrifuged at 12,000× *g* for 15 s. The flow through was discarded and 700 μl buffer RWT was added to the spin column and centrifuged at 12,000× *g* for 15 s. Two washes of 500 μl buffer RPE were then performed, the first lasting 15 s and the second lasting 2 min. The RNeasy MinElute spin column was then placed in a new collection tube and spun at 12,000× *g* for 5 min to dry the column membrane. Lastly, the column was placed in another collection tube and 28 μl RNase-free water was added to the center of the membrane and incubated for 1 min, and then centrifuged at 12,000× *g* for 1 min ending with the purified RNA eluted in the collection tube. Cellular RNA was purified using the miRNeasy Mini Kit (Qiagen) as per the manufacturer's instructions, similar to the purification process for EVs, as described above.

RNA concentrations for each sample were measured using Nano drop 2,000 spectrophotometer (Thermo Scientific). For cDNA synthesis, 0.75 μg total RNA containing miRNAs was reverse transcribed using the miScript II RT kit (Qiagen). A 10 μl total volume reaction mix was made using 2 μl 5× miScript HiSpec Buffer, 1 μl 10× miScript Nucleics Mix, 1 μl miScript Reverse Transcriptase Mix, and 6 μl Template RNA/nuclease-free water. Prior to use for quantitative real-time PCR (qRT-PCR), cDNA was diluted in nuclease-free water, at a ratio of 1:10.

Previous work from our laboratory indicates that of a panel of miRNAs assessed, only miR-34a and miR-146a showed disease-stage related increases in expression in both human AD and triple transgenic AD mouse (3xTgAD) brains. Therefore, expression of miR-34a and miR-146a were profiled for both EV and intracellular levels using target specific miScript primer assays and the miScript SYBR® Green PCR kit (Qiagen; 5 μl SYBR® Green; 1 μl Universal Primer; 1 μl Target Primer; 3 μl diluted cDNA). qRT-PCR reactions were performed in triplicate for each sample, using the CFX384 Touch™ RT PCR Detection System (Bio-Rad, Hercules, CA, USA) for 45 cycles as follows: 15 s at 94°C, 30 s at 55°C, 30 s at 70°C. Negative control reactions were included as wells containing only master mix and nuclease-free water (no template cDNA). All miRNA specific primers were miScript Primer Assays (Qiagen); Hs_RNU6-2_11 (MS00033740), Ce_miR-39_1 (219610), Hs_miR-34a (MS00003318), and Hs_miR-146a (MS00003535). The expression levels of target genes in EVs were standardized against those of the spike-in control, *C. elegans* miR-39 gene, detected in identical cDNA samples, while the expression levels of target genes in cell lysates was standardized against RNU6. Quantification of PCR amplified miRNA specific cDNA was done by comparative cycle threshold CT method ($2^{-\Delta\Delta CT}$).

EV Uptake *via* Naïve Cells

To determine if naïve HT-22 cells have the capacity to take up cytokine-induced EVs, cells were incubated with EVs labeled with Exo-Red Exosome RNA Fluorescent Label (System Biosciences, Palo Alto, CA, USA). EVs isolated from all TNF-α exposure groups were labeled as per the manufacturer's protocol. Briefly, ∼100 μg protein of isolated EVs were incubated with 50 μl Exo-Red for 10 min at 37°C. ExoQuick-TC reagent (100 μl) was then added to the labeled EV suspension and mixed by gentle inversion. This solution was incubated on ice for 30 min, followed by centrifugation at 14,000 rpm for 3 min. The supernatant was removed and the EV pellet was resuspended in 500 μl PBS. Next, 100 μl labeled EVs were added to naïve HT-22 cells in a 6-well dish (∼80% confluent), and imaged with the Nikon Swept Field Confocal microscope (Nikon, Melville, NY, USA) approximately 10 min after addition to naïve cells.

Mitochondrial Membrane Potential Assay

Mitochondrial membrane potential (Ψm) was measured using the tetramethylrhodamine, ethyl ester (TMRE; Abcam, Cambridge, United Kingdom) reagent. Cells were grown in a 96-well clear bottom black plate and exposed to TNF-α induced vesicles as described for the Seahorse assay. At the end of the

experiment, media was gently aspirated from the wells and replaced by 100 μl of 60 nM TMRE in cell culture media, and incubated at 37°C for 20 min, protected from light. Cells were gently washed three times with warmed HBSS and fluorescence was measured on a Synergy HT multimodal plate reader with excitation 549 nm and emission 575 nm.

Mitochondrial Superoxide Assay

The levels of mitochondrial superoxide in cells were determined using the MitoSOX^{TM} reagent (Fisher). Cells were grown in a 96-well clear bottom black plate and exposed to TNF-α induced vesicles as described for the Seahorse assay. At the end of the experiment, media was gently aspirated from the wells and replaced by 100 μl of 5 μm MitoSox in cell culture media and incubated for 10 min at 37°C, protected from light. Cells were gently washed three times with warmed HBSS and fluorescence was measured on a Synergy HT multimodal plate reader with excitation 510 nm and emission 580 nm.

Hydrogen Peroxide Assay

The hydrogen peroxide (H_2O_2) assay was performed using the Amplex Red Kit (Invitrogen). Cells were grown in a 96-well clear bottom black plate, and exposed to TNF-α induced vesicles as described for the Seahorse assay. At the end of the experiment, 50 μL of the Amplex Red reagent was added to the media in the plate without washing, and incubated for 30 min at room temperature. The fluorescence of the Amplex Red reagent was measured on a Synergy HT multimodal plate reader with excitation 530 nm and emission 590 nm.

Statistical Analyses

All biological experiments were repeated at least three times with $n = 3$–16 plates/wells per treatment. Results from the experiments are reported as means ± SEM. All quantitative data were assessed for significance using a one-way ANOVA with Dunnett's *post hoc* test. All results were analyzed by GraphPad Prism 8.0 software (GraphPad Software, La Jolla, CA, USA). A p value < 0.05 was used to establish significance; significance presented as $^{*}p < 0.05$, $^{**}p < 0.01$, $^{***}p < 0.001$, and $^{****}p < 0.0001$.

RESULTS

TNF-α Induces Mitochondrial Dysfunction and Cellular Death

A Seahorse mitochondrial stress test was conducted to assess mitochondrial function in HT-22 cells exposed to TNF-α for 24 h. Results indicate that TNF-α exposure reduced basal and maximal respiration, ATP production, and spare capacity in a dose-dependent manner, with significant reductions occurring at the two highest concentrations (1 and 10 ng/ml) compared to unexposed control cells (**Figures 1A–D**). These same concentrations of TNF-α induced significant proton leak (**Figure 1E**), which can reduce the Ψm, and uncouple oxidative phosphorylation (Terada, 1990; Jastroch et al., 2010). Significant, dose-dependent decreases in basal glycolysis were also detected as a result of TNF-α exposure (**Figure 1F**). Exposure to all concentrations of TNF-α lead to cell death as shown by significant increases in LDH present in the conditioned culture media (**Figure 1G**). In view of the apparent cell death induced by increasing doses of TNF-α (**Figure 1G**), the observed decline in oxidative phosphorylation (**Figures 1A–D**) and glycolysis (**Figure 1F**) may be caused by the loss of cells in the assay.

TNF-α Exposure Induces EV Secretion, but Not in a Dose-Dependent Fashion

We next assessed the ability of TNF-α exposure to induce EV secretion in this hippocampal cell line. Vesicles isolated from the conditioned media of TNF-α exposed cells were profiled using the NanoSight NS300. Interestingly, TNF-α exposure lead to increased EV particle number, however this effect does not appear to be dose-dependent (**Figures 2A,B**). Exposure to low (0.1 ng/ml) and high (10 ng/ml) concentrations of TNF-α significantly increased particle concentration, whereas exposure to 1 ng/ml TNF-α did not lead to particle concentrations above control. Additionally, TNF-α exposure did not alter vesicle size, as all EV size distributions were between ∼80 and 300 nm in diameter, consistent with what has been shown in the literature (van Niel et al., 2018).

As recommended by the International Society for EVs (Lötvall et al., 2014), we probed for the presence of several canonical EV markers, including ALIX, CD81, CD63, and TSG101. Vesicles isolated from both the control and TNF-α exposure groups expressed all of the expected markers (**Figure 2C**) indicating that EVs were indeed being isolated in the vesicle preparation.

TNF-α Alters miRNA Expression Intracellularly and in Secreted EVs

In order to determine the impact of acute TNF-α exposure on miRNA expression, we assayed miR-34a and miR-146a expression within cells and their secreted EVs 24-h after exposure. Interestingly, intracellular expression levels of miR-34a were not changed after exposure to TNF-α (**Figure 3A**), yet a dose-dependent significant upregulation of this miRNA was observed in the secreted EVs (**Figure 3B**). Intracellular miR-146a expression was significantly increased after TNF-α exposure with an apparent ceiling effect (**Figure 3C**), and was significantly increased in a dose-dependent fashion in secreted EVs (**Figure 3D**).

EVs Are Taken Up by, and Enhance Mitochondrial Function in Recipient Cells

Because the secreted EVs contained TNF-α dose-dependent increased expression of both miR-34a and miR-146a, we were interested in determining whether EV cargo could be delivered to TNF-α naïve recipient cells, and how this may affect their mitochondrial function. We exposed TNF-α naïve cells to EVs isolated from the media of TNF-α exposed cells whose RNA was fluorescently labeled; EVs delivered this RNA to naïve recipient cells (**Figure 4**). We then assessed mitochondrial function, using the XF^{e}96 Mito Stress kit, in EV-recipient cells at 24 h after exposure. To our surprise, we observed significant, dose-dependent increases in mitochondrial oxygen consumption after EV exposure (**Figures 5A–D**). Interestingly, we also observed significant increases in proton leak (**Figure 5E**)

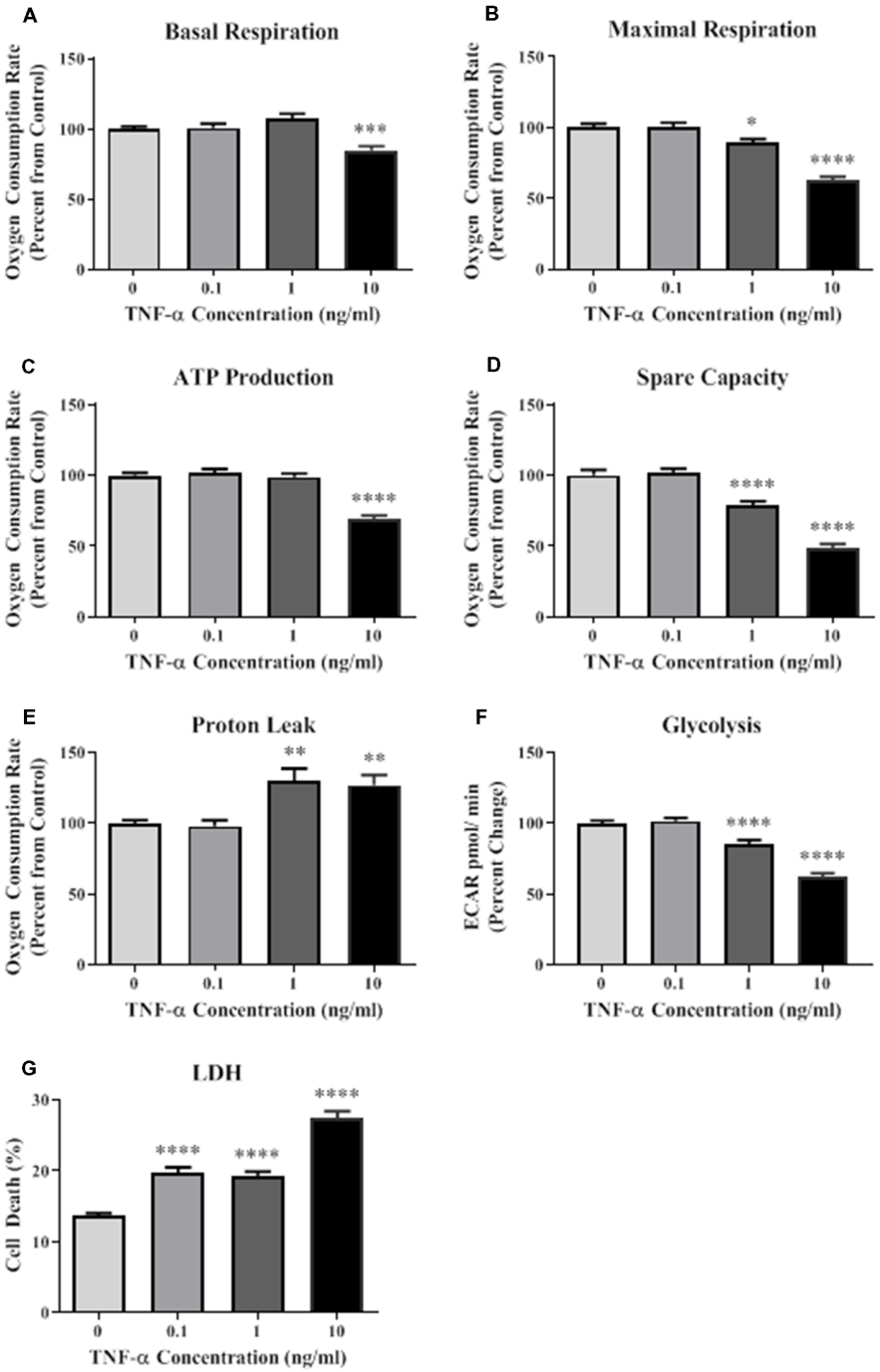

FIGURE 1 | Tumor necrosis factor-alpha (TNF-α) exposure significantly reduces cellular bioenergetic function and increases cell death. After 24 h exposure to TNF-α, basal respiration (**A**; $F_{(3,292)} = 11.90$, $p < 0.001$), maximal respiration (**B**; $F_{(3,292)} = 42.31$, $p < 0.0001$), ATP production (**C**; $F_{(3,292)} = 39.80$, $p < 0.0001$), and spare capacity (**D**; $F_{(3,292)} = 50.10$, $p < 0.0001$) were significantly reduced at the highest two concentrations. Proton leak (**E**; $F_{(3,202)} = 10.62$, $p < 0.0001$) was significantly increased. Glycolysis was also significantly reduced after TNF-α exposure (**F**; $F_{(3,164)} = 59.42$, $p < 0.0001$). Lactate dehydrogenase (LDH) data indicate that significant cell death occurred at all concentrations of TNF-α exposure (**G**; $F_{(3,223)} = 65.31$, $p < 0.0001$). $^{*}p < 0.05$, $^{**}p < 0.01$, $^{***}p < 0.001$, and $^{****}p < 0.0001$.

suggesting that although oxidative phosphorylation is increased, mitochondria are likely not functioning optimally, as protons are leaking across the membrane. We also observed a significant dose-dependent upregulation of basal glycolysis after exposure to EVs (**Figure 5F**). Unlike direct exposure to TNF-α, only EVs induced from the highest concentration of TNF-α (10 ng/ml) caused significant cell death in naïve cells (**Figure 5G**). The enhanced oxidative phosphorylation (**Figures 5A–D**) and

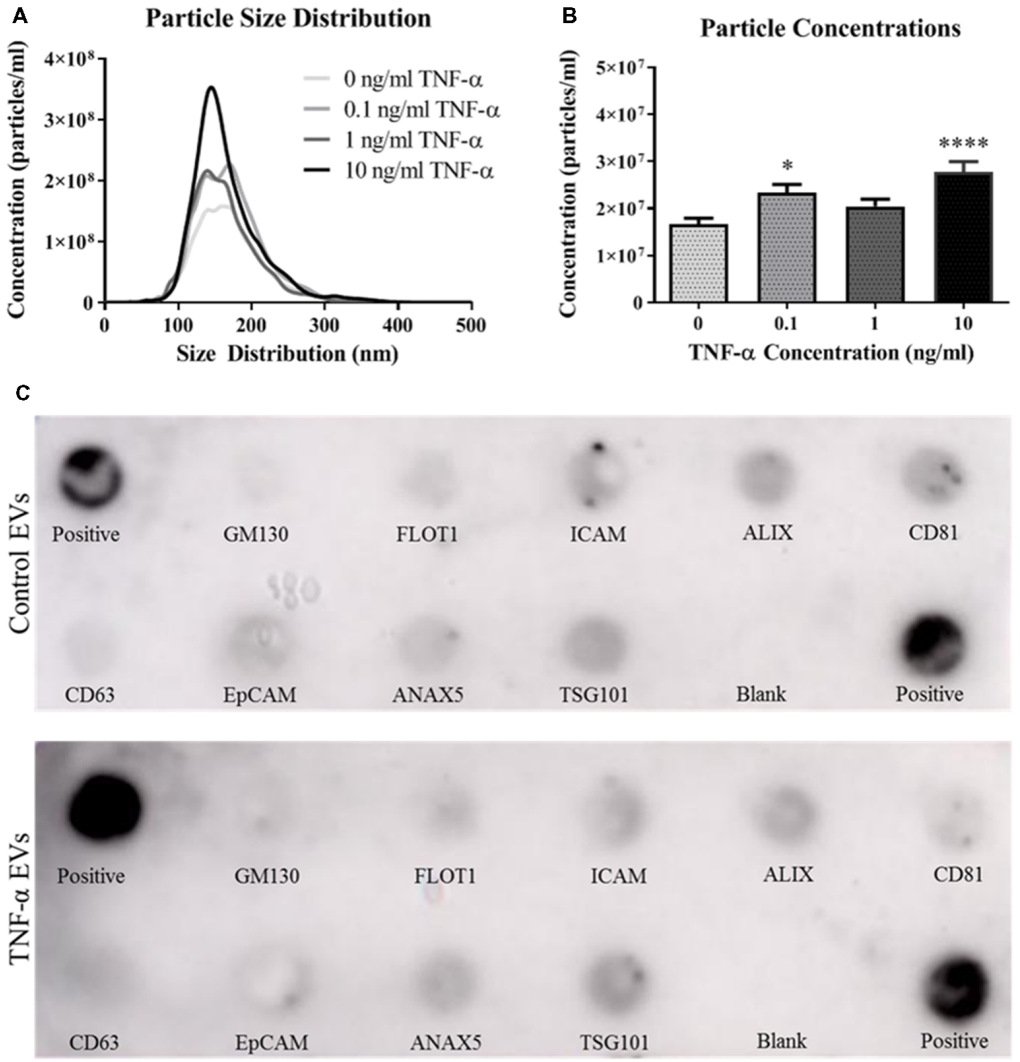

FIGURE 2 | TNF-α exposure induces secretion of extracellular vesicles (EVs). Particle size distributions calculated from the NanoSight NS300 show expected size ranges for EVs (**A**; $F_{(3,3,996)} = 7.06$, $p < 0.0001$). Overall particle concentrations for each TNF-α exposure group indicate that TNF-α exposure induces vesicle secretion **(B)**. TNF-α induces EVs expressing canonical markers and are appropriately sized. Canonical EV proteins and their locations on a dot blot are shown **(C)**. Presence of proteins expressed for control vesicles (**C**, top panel) and TNF-α (10 ng/ml) induced vesicles (**C**, bottom panel) are shown. $^{*}p < 0.05$, $^{****}p < 0.0001$.

glycolysis (**Figure 5F**) seen after exposure to TNF-α-induced EVs is likely an underestimate of the bioenergetic function of the cells exposed to 10 ng/ml TNF-α-induced EVs, as this group experienced significant cell death (**Figure 5G**).

EVs Increase ROS Production in Recipient Cells

Due to the increased proton leak observed in the Seahorse assay following EV exposure, we next assessed mitochondrial Ψm. We did not observe any significant changes in potential (**Figure 6A**) after a 24-h exposure period to TNF-α induced EVs.

We next assessed ROS production in cells exposed to TNF-α induced EVs. We observed a statistically significant increase in mitochondrial superoxide production when cells were incubated with EVs induced by 0, 0.1, and 1 ng/ml TNF-α, but not 10 ng/ml (**Figure 6B**); however, this result may be attributed to the significant amount of cell death observed in this group (**Figure 5G**). Additionally, we observed significant increases in H_2O_2 after exposure to EVs, with the highest amount generated in the 10 ng/ml TNF-α induced EV group (**Figure 6C**). As H_2O_2 has the capacity to induce neuronal cell death (Ricart and Fiszman, 2001), this may explain why we observed significant cellular death in this group (**Figure 5G**).

DISCUSSION

AD is characterized by neuroinflammation (Wyss-Coray and Rogers, 2012) and mitochondrial dysfunction (Swerdlow, 2018). In the present study, we observed that physiologically relevant levels of the proinflammatory cytokine TNF-α are capable of

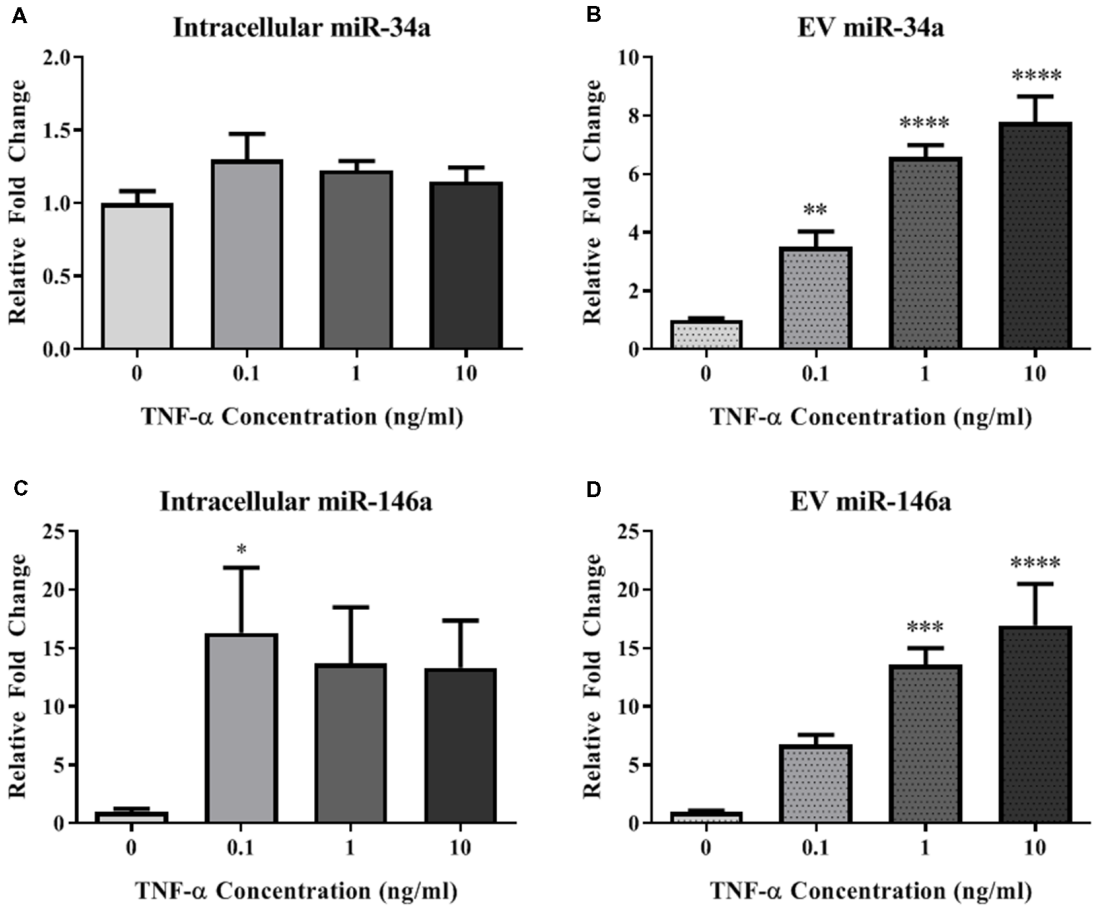

FIGURE 3 | TNF-α significantly alters microRNA (miRNA) expression profiles. TNF-α exposure did not significantly alter intracellular expression of miR-34a (**A**; $F_{(3,32)} = 1.29$, $p = 0.2951$), but did induce a dose-dependent increase in miR-34a expression within EVs (**B**; $F_{(3,31)} = 30.00$, $p < 0.0001$). Conversely, TNF-α exposure induced intracellular upregulation of miR-146a which trended towards significance (**C**; $F_{(3,32)} = 2.92$, $p = 0.0643$), as well as a significant, dose-dependent increases within EVs (**D**; $F_{(3,31)} = 13.15$, $p < 0.0001$). *$p < 0.05$, **$p < 0.01$, ***$p < 0.001$, and ****$p < 0.0001$.

causing significant cellular death and mitochondrial dysfunction in hippocampal neurons after a 24-h exposure period. We also demonstrate that TNF-α induced EVs are taken up by naïve cells, and significantly alter mitochondrial activity in recipient cells. Specifically, we observed increases in mitochondrial respiration, glycolysis, proton leak, and ROS production in recipient cells after 24 h of EV exposure. Together, these data suggest that direct exposure of TNF-α to a neuronal cell type is highly toxic, and the vesicles secreted in response to this exposure are capable of inducing a stress response in neighboring cells.

We observed significant downregulation of mitochondrial oxidative phosphorylation and glycolysis in HT-22 cells exposed to TNF-α for 24 h. Under some conditions, when oxidative phosphorylation is inhibited or reduced, neurons can increase glycolysis as a protective, compensatory mechanism (Bas-Orth et al., 2017). However, with the decline in oxidative phosphorylation observed in this study, there is no compensatory increase in glycolysis. We additionally assessed expression of several ETC proteins involved in oxidative phosphorylation (including NDUFC2 of complex I, SHDC of complex II, UQCRB of complex III, and Cytochrome C oxidase of complex IV) after TNF-α exposure, and observed no significant changes in expression (data not shown). High concentrations of LDH in the media, along with reductions in bioenergetic measurements indicate that these observations are likely a result of cell death due to exposure to the cytotoxic protein, TNF-α.

We have previously shown that overexpression of miR-34a significantly reduces mitochondrial function in neuronal cells (Sarkar et al., 2016). In view of our evidence that miR-146a, but not miR-34a, was increased intracellularly in HT-22 cells, miR-146a may be responsible for the TNF-α induced mitochondrial impairment observed in these cells. Indeed, overexpression of miR-146a significantly reduces cellular bioenergetics (Jun et al., unpublished observation). Additionally, TNF-α exposure caused a dose-dependent increase in both miR-34a and miR-146a in secreted EVs. In line with other reports, these results suggest differential packaging and secretion mechanisms which are dependent on specific miRNAs (Abels and Breakefield, 2016). The results from the current study support the concept that some miRNAs (e.g., miR-34a) may be

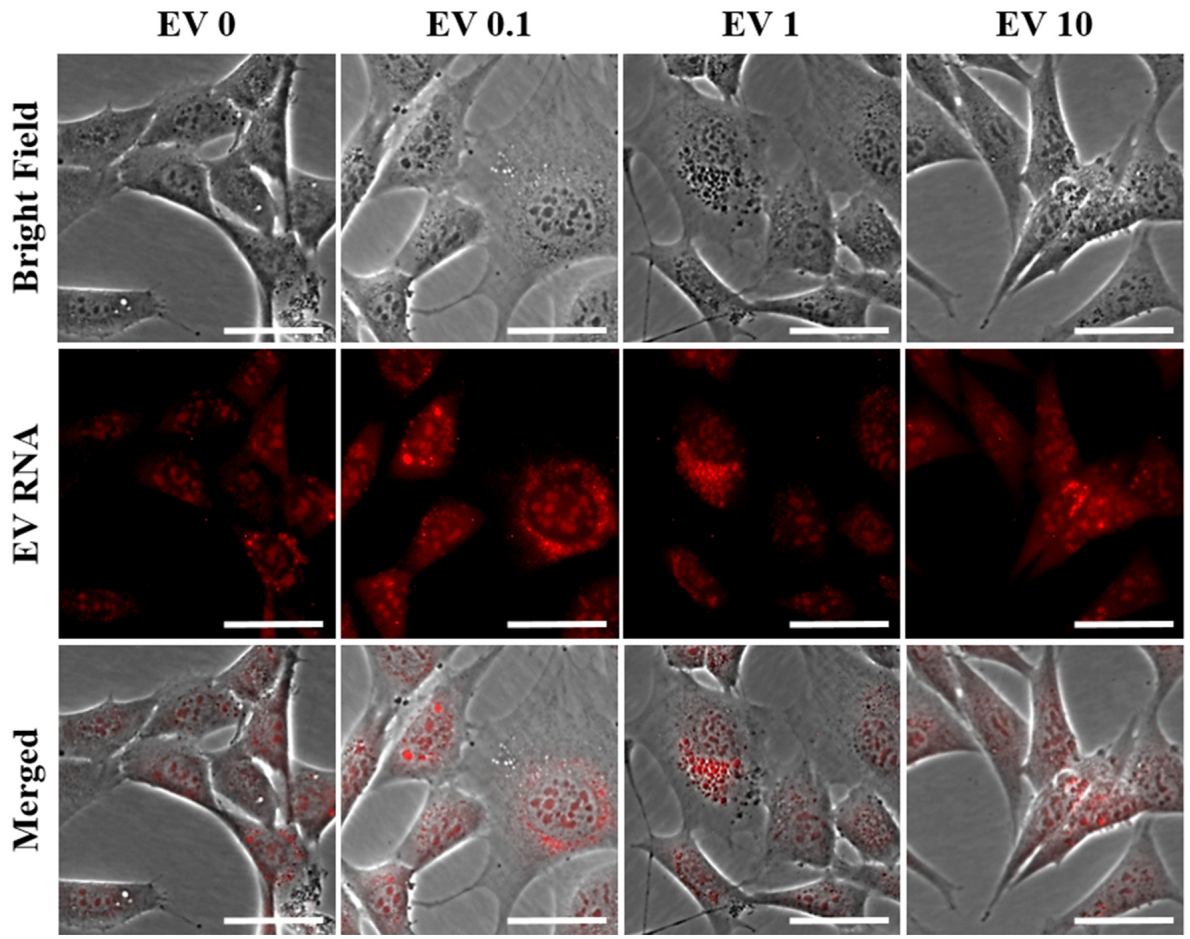

FIGURE 4 | Naïve cell EV uptake and functional consequences. EVs derived from control and all concentrations of TNF-α (0, 0.1, 1, and 10 ng/ml) are taken up by naïve cells as evidenced by punctate staining of red-labeled EV RNA present within naïve cells. Scale bar = 40 μm.

preferentially sorted out of cells (Jovicic and Gitler, 2017; Wei et al., 2017), however this interpretation is strictly speculative and requires further investigation.

As TNF-α exposure significantly elevated miR-34a and miR-146a expression within secreted EVs, we hypothesized that exposing naïve cells to TNF-α induced EVs would result in significant reduction of mitochondrial respiration due to miRNA-mediated repression of ETC protein translation. Interestingly, we observed significant increases in mitochondrial oxygen consumption in naïve cells exposed to these vesicles. In this study, only relative changes in miRNA expression were assessed, not definitive quantities. It has been postulated that there is fewer than one copy of an individual miRNA per EV (Chevillet et al., 2014; Wei et al., 2017), so it is likely that the absolute concentrations of miR-34a and miR-146a were not high enough to induce physiologically relevant repression of ETC proteins in recipient cells and cause reductions in oxygen consumption.

Several groups have also shown that exposure to EVs significantly increases mitochondrial respiration in recipient cells (Phinney et al., 2015; Sansone et al., 2017; Bland et al., 2018), and others have described that in response to stimulation, neurons are able to increase their rate of glycolysis (Yellen, 2018). This unexpected increase in mitochondrial activity may actually be a signal of mitochondrial stress, as we concomitantly observed dose-dependent increases in proton leak, suggesting that although oxidative phosphorylation is increased, the mitochondria are not actually functioning optimally. Indeed, a disproportionately large rate of mitochondrial oxygen consumption likely indicates an attempt to maintain Ψm as proton leak across occurs (Jastroch et al., 2010). Spare respiratory capacity is an indicator of mitochondria's ability to respond to stress (Hill et al., 2009). Here we observe significant elevation of spare capacity in cells exposed to EVs, which is likely the mechanism by which mitochondria were able to maintain Ψm, despite undergoing significant proton leak. As mitochondria are the main generators of ROS, it is likely that the increased oxygen consumption incurred by maintaining Ψm is responsible for significant ROS generation. Superoxide anions are quickly converted to less reactive H_2O_2 by superoxide dismutases (Lennicke et al., 2015), which may explain why we saw significantly more H_2O_2 than superoxide after EV exposure.

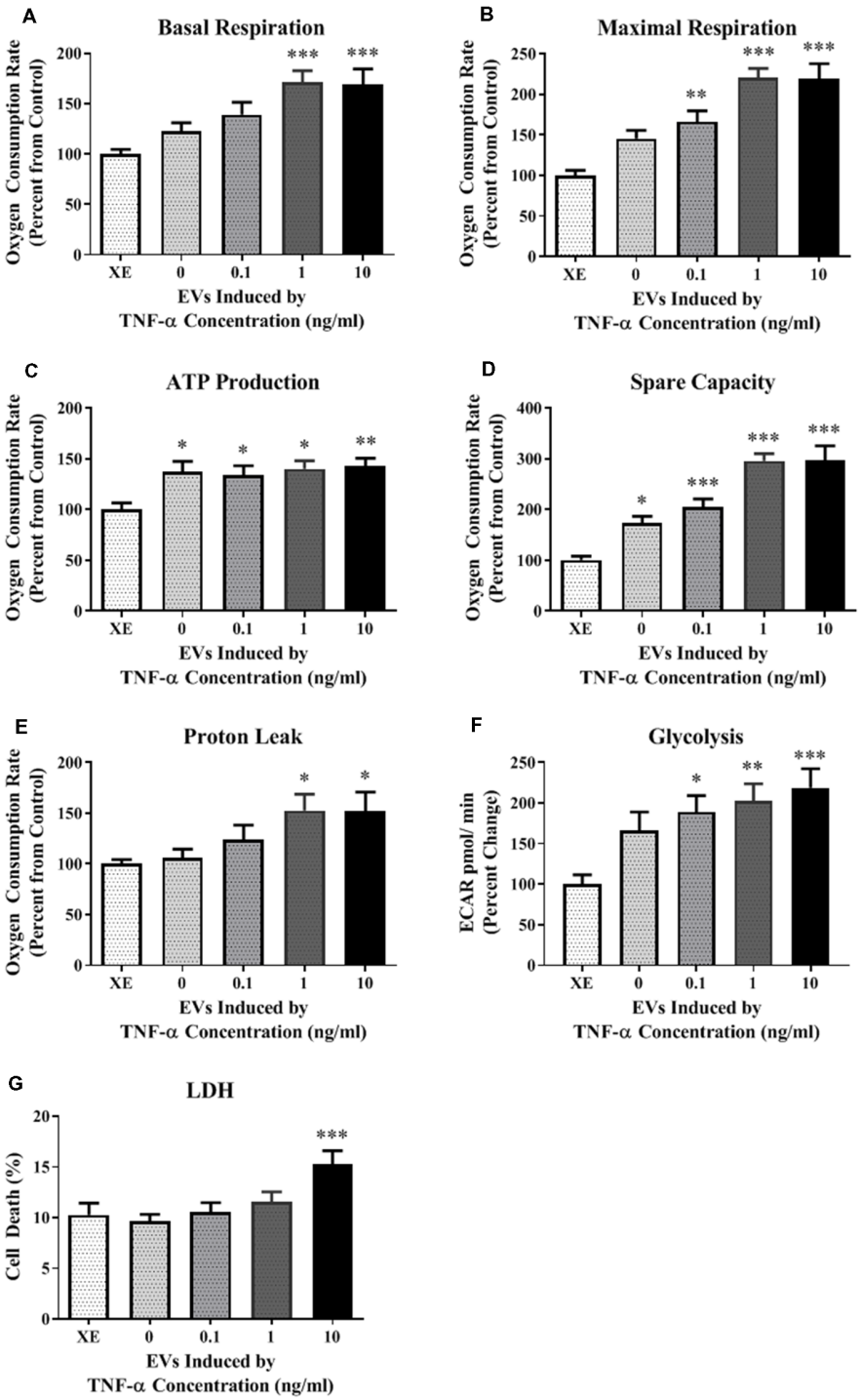

FIGURE 5 | TNF-α induced EVs significantly alter energy metabolism. Data are depicted as significant differences related to XE buffer as the control. TNF-α induced EVs significantly increased basal respiration (**A**; $F_{(4,67)} = 6.72$, $p = 0.0001$) and maximal respiration (**B**; $F_{(4,67)} = 15.05$, $p < 0.0001$), while exposure to all vesicles significantly increased ATP production (**C**; $F_{(4,67)} = 3.64$, $p = 0.0096$) and spare capacity (**D**; $F_{(4,67)} = 21.50$, $p < 0.0001$). Proton leak was also significantly increased at the highest TNF-α concentrations (**E**; $F_{(4,67)} = 3.07$, $p = 0.0221$). Exposure to these vesicles significantly increased glycolysis as well (**F**; $F_{(4,84)} = 5.024$, $p < 0.0011$). Significant cell death only occurred at the highest concentration (**G**; $F_{(4,44)} = 4.717$, $p = 0.003$). Additional analyses using 0 ng/ml TNF-α exposed EVs as control were also conducted. When 0 EVs were used as the control, the effects of TNF-α-induced EVs remained significant for basal respiration ($F_{(3,55)} = 3.614$, $p = 0.0187$), maximal respiration ($F_{(3,55)} = 7.607$, $p = 0.0002$), spare capacity ($F_{(3,55)} = 11.09$, $p < 0.0001$), and LDH ($F_{(3,35)} = 6.174$, $p = 0.0018$). There were no significant responses to TNF-α-induced EVs for ATP production ($F_{(3,55)} = 0.1857$, $p = 0.9057$), proton leak ($F_{(3,55)} = 2.266$, $p = 0.0909$), or glycolysis ($F_{(3,68)} = 1.039$, $p = 0.3809$). $^{*}p < 0.05$, $^{**}p < 0.01$, and $^{***}p < 0.001$.

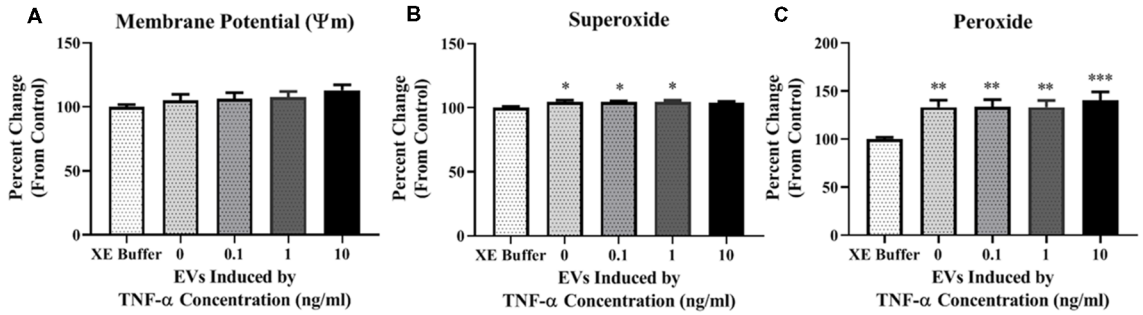

FIGURE 6 | TNF-α induced EVs alter reactive oxygen species (ROS) production in recipient cells. Data are depicted as significant differences related to XE buffer as the control. EVs do not have a significant impact on the inner mitochondrial membrane potential (Ψm; **A**; $F_{(4,115)} = 1.287$, $p = 0.2794$). Exposure of naïve cells to EVs significantly increases ROS production in the form of mitochondrial superoxide (**B**; $F_{(4,113)} = 2.787$, $p = 0.0298$), and hydrogen peroxide (H_2O_2; **C**; $F_{(4,85)} = 5.329$, $p = 0.0007$). Additional analyses using 0 ng/ml TNF-α exposed EVs as control were also conducted. There were no significant responses to TNF-α-induced EVs for membrane potential ($F_{(3,92)} = 0.5786$, $p = 0.6305$), mitochondrial superoxide ($F_{(3,90)} = 0.07873$, $p = 0.9714$), or H_2O_2 ($F_{(3,68)} = 0.2021$, $p = 0.8946$). $^*p < 0.5$, $^{**}p < 0.01$, and $^{***}p < 0.001$.

Our observation of altered mitochondrial function after a single exposure to TNF-α, or TNF-α induced EVs does not recapitulate the *in vivo* conditions of AD, as there is constant crosstalk between different cell types, and persistent, dynamic EV-cell interactions. However, the current findings suggest that neuronal, inflammation-derived EVs may acutely alter mitochondrial activity in recipient cells. The mitochondrial cascade hypothesis of AD posits that increased ROS induces mitochondrial DNA damage and reduces mitochondrial function; with time this initiates a "reset response" in which Aβ production is increased, leading to further generation of ROS in a vicious, positive feedback cycle (Swerdlow and Khan, 2004). While we have not identified the cargo within EVs that initiates this mitochondrial response, future studies will address this issue, as any component of EV-associated cargo may be responsible for these effects, e.g., direct transfer of specific proteins, mRNAs, or other miRNAs not assessed here.

Importantly, the current study provides novel insights on the role of inflammation-induced EVs in the inflamed and aging brain. The results underscore the importance of TNF-α, a canonical proinflammatory cytokine in the brain, as a regulator of mitochondrial function, miRNA expression, and EV secretion in neurons. Thus, TNF-α induced EVs may be drivers of the bioenergetic function and dysfunction throughout the brain in AD and other neuroinflammatory disorders.

DATA AVAILABILITY

The datasets generated for this study are available on request to the corresponding author.

AUTHOR CONTRIBUTIONS

AR, SJ, SS, WG, and JS designed studies. AR and WG performed research. AR, SJ, SL, and SR analyzed data. AR and JS wrote the article.

FUNDING

This work was supported by NIH Grants P20 GM109098, P01 AG027956, T32 AG052375 and U54 GM104942. Imaging experiments and image analysis were performed in the West Virginia University Imaging Facilities which have been supported by the WVU Cancer Institute and NIH grants P20RR016440 and P30RR032138/P30GM103488. Experiments were also performed in the West Virginia University Flow Cytometry and Single Cell Core Facility, which is supported by the following National Institutes of Health and the Institutional Development Awards (IDeA) grants U57GM104942 (WV CTSI), P30GM103488 (CoBRE), P20GM109098 (Stroke CoBRE) and P20GM103434 (INBRE).

REFERENCES

Abels, E. R., and Breakefield, X. O. (2016). Introduction to extracellular vesicles: biogenesis, RNA cargo selection, content, release, and uptake. *Cell. Mol. Neurobiol.* 36, 301–312. doi: 10.1007/s10571-016-0366-z

Bas-Orth, C., Tan, Y.-W., Lau, D., and Bading, H. (2017). Synaptic activity drives a genomic program that promotes a neuronal warburg effect. *J. Biol. Chem.* 292, 5183–5194. doi: 10.1074/jbc.m116.761106

Bland, C. L., Byrne-Hoffman, C. N., Fernandez, A., Rellick, S. L., Deng, W., and Klinke, D. J. (2018). Exosomes derived from B16F0 melanoma cells alter the transcriptome of cytotoxic T cells that impacts mitochondrial respiration. *FEBS J.* 285, 1033–1050. doi: 10.1111/febs.14396

Blasko, I., Veerhuis, R., Stampfer-Kountchev, M., Saurwein-Teissl, M., Eikelenboom, P., and Grubeck-Loebenstein, B. (2000). Costimulatory Effects of interferon-γ and Interleukin-1β or Tumor Necrosis Factor α on the Synthesis of Aβ1-40 and Aβ1-42 by Human Astrocytes. *Neurobiol. Dis.* 7, 682–689. doi: 10.1006/nbdi.2000.0321

Chevillet, J. R., Kang, Q., Ruf, I. K., Briggs, H. A., Vojtech, L. N., Hughes, S. M., et al. (2014). Quantitative and stoichiometric analysis of the microRNA content of exosomes. *Proc. Natl. Acad. Sci. U S A* 111, 14888–14893. doi: 10.1073/pnas.1408301111

Dasgupta, N., Peng, Y., Tan, Z., Ciraolo, G., Wang, D., and Li, R. (2015). miRNAs in mtDNA-less cell mitochondria. *Cell Death Discov.* 1:15004. doi: 10.1038/cddiscovery.2015.4

Fillit, H., Ding, W. H., Buee, L., Kalman, J., Altstiel, L., Lawlor, B., et al. (1991). Elevated circulating tumor necrosis factor levels in Alzheimer's disease. *Neurosci. Lett.* 129, 318–320. doi: 10.1016/0304-3940(91)90490-k

Hanisch, U.-K. (2002). Microglia as a source and target of cytokines. *Glia* 40, 140–155. doi: 10.1002/glia.10161

Harding, C., Heuser, J., and Stahl, P. (1983). Receptor-mediated endocytosis of transferrin and recycling of the transferrin receptor in rat reticulocytes. *J. Cell Biol.* 97, 329–339. doi: 10.1083/jcb.97.2.329

Hill, B. G., Dranka, B. P., Zou, L., Chatham, J. C., and Darley-Usmar, V. M. (2009). Importance of the bioenergetic reserve capacity in response to cardiomyocyte stress induced by 4-hydroxynonenal. *Biochem. J.* 424, 99–107. doi: 10.1042/bj20090934

Huntzinger, E., and Izaurralde, E. (2011). Gene silencing by microRNAs: contributions of translational repression and mRNA decay. *Nat. Rev. Genet.* 12, 99–110. doi: 10.1038/nrg2936

Jastroch, M., Divakaruni, A. S., Mookerjee, S., Treberg, J. R., and Brand, M. D. (2010). Mitochondrial proton and electron leaks. *Essays Biochem.* 47, 53–67. doi: 10.1042/bse0470053

Jovičic, A., and Gitler, A. D. (2017). Distinct repertoires of microRNAs present in mouse astrocytes compared to astrocyte-secreted exosomes. *PLoS One* 12:e0171418. doi: 10.1371/journal.pone.0171418

Krek, A., Grün, D., Poy, M. N., Wolf, R., Rosenberg, L., Epstein, E. J., et al. (2005). Combinatorial microRNA target predictions. *Nat. Genet.* 37, 495–500. doi: 10.1038/ng1536

Lennicke, C., Rahn, J., Lichtenfels, R., Wessjohann, L. A., and Seliger, B. (2015). Hydrogen peroxide—production, fate and role in redox signaling of tumor cells. *Cell Commun. Signal.* 13:39. doi: 10.1186/s12964-015-0118-6

Liao, Y.-F., Wang, B.-J., Cheng, H.-T., Kuo, L.-H., and Wolfe, M. S. (2004). Tumor Necrosis Factor-α, Interleukin-1β and Interferon-γ Stimulate γ-Secretase-mediated Cleavage of Amyloid Precursor Protein through a JNK-dependent MAPK Pathway. *J. Biol. Chem.* 279, 49523–49532. doi: 10.1074/jbc.M402034200

Lötvall, J., Hill, A. F., Hochberg, F., Buzás, E. I., Di Vizio, D., Gardiner, C., et al. (2014). Minimal experimental requirements for definition of extracellular vesicles and their functions: a position statement from the International Society for Extracellular Vesicles. *J. Extracell. Vesicles* 3:26913. doi: 10.3402/jev.v3.26913

Pan, B. T., Teng, K., Wu, C., Adam, M., and Johnstone, R. M. (1985). Electron microscopic evidence for externalization of the transferrin receptor in vesicular form in sheep reticulocytes. *J. Cell Biol.* 101, 942–948.

Phinney, D. G., Di Giuseppe, M., Njah, J., Sala, E., Shiva, S., St Croix, C. M., et al. (2015). Mesenchymal stem cells use extracellular vesicles to outsource mitophagy and shuttle microRNAs. *Nat. Commun.* 6:8472. doi: 10.1038/ncomms9472

Rajendran, L., Honsho, M., Zahn, T. R., Keller, P., Geiger, K. D., Verkade, P., et al. (2006). Alzheimer's disease beta-amyloid peptides are released in association with exosomes. *Proc. Natl. Acad. Sci. U S A* 103, 11172–11177. doi: 10.1073/pnas.0603838103

Ricart, K. C., and Fiszman, M. L. (2001). Hydrogen Peroxide-Induced Neurotoxicity in Cultured Cortical Cells Grown in Serum-Free and Serum-Containing Media. *Neurochem. Res.* 26, 801–808. doi: 10.1023/A:1011660001941

Sansone, P., Savini, C., Kurelac, I., Chang, Q., Amato, L. B., Strillacci, A., et al. (2017). Packaging and transfer of mitochondrial DNA *via* exosomes regulate escape from dormancy in hormonal therapy-resistant breast cancer. *Proc. Natl. Acad. Sci. U S A* 114, E9066–E9075. doi: 10.1073/pnas.1718630114

Sardar Sinha, M., Ansell-Schultz, A., Civitelli, L., Hildesjö, C., Larsson, M., Lannfelt, L., et al. (2018). Alzheimer's disease pathology propagation by exosomes containing toxic amyloid-beta oligomers. *Acta Neuropathol.* 136, 41–56. doi: 10.1007/s00401-018-1868-1

Sarkar, S., Jun, S., Rellick, S., Quintana, D. D., Cavendish, J. Z., and Simpkins, J. W. (2016). Expression of microRNA-34a in Alzheimer's disease brain targets genes linked to synaptic plasticity, energy metabolism, and resting state network activity. *Brain Res.* 1646, 139–151. doi: 10.1016/j.brainres.2016.05.026

Schütze, S., Wiegmann, K., Machleidt, T., and Krönke, M. (1995). TNF-induced activation of NF-κB. *Immunobiology* 193, 193–203.

Sharma, V., Thakur, V., Singh, S. N., and Guleria, R. (2012). Tumor necrosis factor and Alzheimer's disease: a cause and consequence relationship. *Klin. Psikofarmakol. Bülteni-Bulletin Clin. Psychopharmacol.* 22, 86–97. doi: 10.5455/bcp.20120112064639

Swerdlow, R. H. (2018). Mitochondria and mitochondrial cascades in Alzheimer's disease. *J. Alzheimers. Dis.* 62, 1403–1416. doi: 10.3233/JAD-170585

Swerdlow, R. H., and Khan, S. M. (2004). A "mitochondrial cascade hypothesis" for sporadic Alzheimer's disease. *Med. Hypotheses* 63, 8–20. doi: 10.1016/j.mehy.2003.12.045

Taganov, K. D., Boldin, M. P., Chang, K.-J., and Baltimore, D. (2006). NF-κB-dependent induction of microRNA miR-146, an inhibitor targeted to signaling proteins of innate immune responses. *Proc. Natl. Acad. Sci. U S A* 103, 12481–12486. doi: 10.1073/pnas.0605298103

Tarkowski, E., Andreasen, N., Tarkowski, A., and Blennow, K. (2003). Intrathecal inflammation precedes development of Alzheimer's disease. *J. Neurol. Neurosurg. Psychiatry* 74, 1200–1205. doi: 10.1136/jnnp.74.9.1200

Terada, H. (1990). Uncouplers of oxidative phosphorylation. *Environ. Health Perspect.* 87, 213–218. doi: 10.1289/ehp.9087213

Tkach, M., and Théry, C. (2016). Communication by extracellular vesicles: where we are and where we need to go. *Cell* 164, 1226–1232. doi: 10.1016/j.cell.2016.01.043

Valadi, H., Ekström, K., Bossios, A., Sjöstrand, M., Lee, J. J., and Lötvall, J. O. (2007). Exosome-mediated transfer of mRNAs and microRNAs is a novel mechanism of genetic exchange between cells. *Nat. Cell Biol.* 9, 654–659. doi: 10.1038/ncb1596

van Niel, G., D'Angelo, G., and Raposo, G. (2018). Shedding light on the cell biology of extracellular vesicles. *Nat. Rev. Mol. Cell Biol.* 19, 213–228. doi: 10.1038/nrm.2017.125

Wei, Z., Batagov, A. O., Schinelli, S., Wang, J., Wang, Y., El Fatimy, R., et al. (2017). Coding and noncoding landscape of extracellular RNA released by human glioma stem cells. *Nat. Commun.* 8:1145. doi: 10.1038/s41467-017-01196-x

Wyss-Coray, T., and Rogers, J. (2012). Inflammation in Alzheimer disease—a brief review of the basic science and clinical literature. *Cold Spring Harb. Perspect. Med.* 2:a006346. doi: 10.1101/cshperspect.a006346

Yamamoto, M., Kiyota, T., Horiba, M., Buescher, J. L., Walsh, S. M., Gendelman, H. E., et al. (2007). Interferon-γ and tumor necrosis factor-α regulate amyloid-β plaque deposition and β-secretase expression in swedish mutant APP transgenic mice. *Am. J. Pathol.* 170, 680–692. doi: 10.2353/ajpath.2007.060378

Yellen, G. (2018). Fueling thought: management of glycolysis and oxidative phosphorylation in neuronal metabolism. *J. Cell Biol.* 217, 2235–2246. doi: 10.1083/jcb.201803152

Zuliani, G., Ranzini, M., Guerra, G., Rossi, L., Munari, M. R., Zurlo, A., et al. (2007). Plasma cytokines profile in older subjects with late onset Alzheimer's disease or vascular dementia. *J. Psychiatr. Res.* 41, 686–693. doi: 10.1055/s-0039-1677803

Conflict of Interest Statement: The authors declare that the research was conducted in the absence of any commercial or financial relationships that could be construed as a potential conflict of interest.

Copyright © 2019 Russell, Jun, Sarkar, Geldenhuys, Lewis, Rellick and Simpkins. This is an open-access article distributed under the terms of the Creative Commons Attribution License (CC BY). The use, distribution or reproduction in other forums is permitted, provided the original author(s) and the copyright owner(s) are credited and that the original publication in this journal is cited, in accordance with accepted academic practice. No use, distribution or reproduction is permitted which does not comply with these terms.

frontiers in Neuroscience

ORIGINAL RESEARCH
published: 22 February 2019
doi: 10.3389/fnins.2019.00137

Cell Type-Specific Human APP Transgene Expression by Hippocampal Interneurons in the Tg2576 Mouse Model of Alzheimer's Disease

*Corinna Höfling[1], Emira Shehabi[1], Peer-Hendrik Kuhn[2], Stefan F. Lichtenthaler[3,4,5,6], Maike Hartlage-Rübsamen[1] and Steffen Roßner[1]**

[1] Paul-Flechsig-Institute for Brain Research, Leipzig University, Leipzig, Germany, [2] Institute of Pathology, Technical University of Munich, Munich, Germany, [3] Deutsches Zentrum für Neurodegenerative Erkrankungen, Munich, Germany, [4] Munich Cluster for Systems Neurology (SyNergy), Munich, Germany, [5] Neuroproteomics, School of Medicine, Klinikum Rechts der Isar, Technical University of Munich, Munich, Germany, [6] Institute for Advanced Study, Technical University of Munich, Garching, Germany

OPEN ACCESS

Edited by:
Johannes Boltze,
Fraunhofer-Institut für Zelltherapie und Immunologie (IZI), Germany

Reviewed by:
Dietmar R. Thal,
KU Leuven, Belgium
Serena Stanga,
University of Turin, Italy

***Correspondence:**
Steffen Roßner
steffen.rossner@medizin.uni-leipzig.de

Specialty section:
This article was submitted to Neurodegeneration, a section of the journal Frontiers in Neuroscience

Received: 11 December 2018
Accepted: 06 February 2019
Published: 22 February 2019

Citation:
Höfling C, Shehabi E, Kuhn P-H, Lichtenthaler SF, Hartlage-Rübsamen M and Roßner S (2019) Cell Type-Specific Human APP Transgene Expression by Hippocampal Interneurons in the Tg2576 Mouse Model of Alzheimer's Disease. Front. Neurosci. 13:137. doi: 10.3389/fnins.2019.00137

Amyloid precursor protein (APP) transgenic animal models of Alzheimer's disease have become versatile tools for basic and translational research. However, there is great heterogeneity of histological, biochemical, and functional data between transgenic mouse lines, which might be due to different transgene expression patterns. Here, the expression of human APP (hAPP) by GABAergic hippocampal interneurons immunoreactive for the calcium binding proteins parvalbumin, calbindin, calretinin, and for the peptide hormone somatostatin was analyzed in Tg2576 mice by double immunofluorescent microscopy. Overall, there was no GABAergic interneuron subpopulation that did not express the transgene. On the other hand, in no case all neurons of such a subpopulation expressed hAPP. In dentate gyrus molecular layer and in stratum lacunosum moleculare less than 10% of hAPP-positive interneurons co-express any of these interneuron markers, whereas in *stratum oriens* hAPP-expressing neurons frequently co-express these interneuron markers to different proportions. We conclude that these neurons differentially contribute to deficits in young Tg2576 mice before the onset of Abeta plaque pathology. The detailed analysis of distinct brain region and neuron type-specific APP transgene expression patterns is indispensable to understand particular pathological features and mouse line-specific differences in neuronal and systemic functions.

Keywords: Alzheimer's disease, animal model, amyloid precursor protein, hippocampus, interneuron, calcium-binding proteins

INTRODUCTION

Alzheimer's disease (AD) is histopathologically characterized by the formation of intracellular neurofibrillary tangles, principally made of tau protein and extracellular amyloid deposits composed of Abeta peptides that deposit in the parenchyma and in the vessel walls. These Abeta peptides are cleavage products generated by proteolytical processing of the amyloid precursor

protein (APP) by the β-secretase BACE1 (Lichtenthaler et al., 2011; Vassar et al., 2014) and the γ-secretase complex composed of presenilin-1 or -2, nicastrin, APH-1, and PEN-2 (Kimberly et al., 2003). Abeta plaques represent a final aggregation state of Abeta peptides and are used for *post mortem* AD diagnosis but can be also detected by positron emission tomography imaging in patients (Barthel and Sabri, 2017; Salloway et al., 2017).

A substantial gain of knowledge on mechanisms of amyloid pathology in AD was achieved by the analyses of transgenic mouse models overexpressing human APP (hAPP) with disease-promoting mutations that lead to early-onset AD in humans (Ameen-Ali et al., 2017; Sasaguri et al., 2017). However, these animal models differ significantly regarding the onset of pathology, spatial appearance of Abeta deposits, neuronal loss and deficits in learning and memory tasks as reviewed by Höfling et al. (2016) which hampers drawing general conclusions on defined pathogenic functions of Abeta peptides. Thus, a detailed analysis of the brain region and cell type-specific transgene expression patterns is indispensable to understand pathogenic mechanisms in each animal model. A very well characterized and frequently used transgenic model is the Tg2576 mouse established by Hsiao et al. (1996). These mice overexpress hAPP harboring the Swedish double mutation KM670/671NL and develop Abeta deposits starting in entorhinal cortex followed by hippocampus at around 11 months of age (Hsiao et al., 1996; Kawarabayashi et al., 2001; Hartlage-Rübsamen et al., 2011).

Interestingly, these mice display impaired hippocampus-dependent spatial learning, working memory, and contextual fear conditioning already at 6 months of age (King and Arendash, 2002), which is well before extracellular plaques appear in the brains of these mice. The deficiencies in spatial learning and memory consolidation are of particular interest since they resemble clinical aspects of AD patients such as disturbed spatial orientation (Kumar et al., 2015) and altered neuronal network activity (Allen et al., 2007; Brier et al., 2012; Sheline and Raichle, 2013). In that regard dendritic spine loss in the Tg2576 CA1 region (Lanz et al., 2003) and a decline in long-term potentiation (LTP) in dentate gyrus (DG) after performant path stimulation (Jacobsen et al., 2006) already detectable at 5 months of age point towards a pathogenic role of soluble, oligomeric Abeta prior to Abeta plaque formation. Additionally, using resting-state functional Magnetic Resonance Imaging (MRI), a hypersynchrony of functional connectivity in the hippocampus of 5-month-old Tg2576 mice was demonstrated (Shah et al., 2016) suggesting increased excitatory and/or reduced inhibitory neuronal activity. These pathogenic aspects have been frequently related to Abeta oligomer formation. However, a series of recent studies from different laboratories demonstrates that such disturbances may occur independently of Abeta formation. In particular, there appears to be a causal link between early pathogenic events including lysosomal autophagic pathology, hyperactivity in lateral entorhinal cortex, early brain network alterations in the CA1/subiculum and the generation of intracellular APP C-terminal fragments not cleaved by γ-secretase (Lauritzen et al., 2012, 2016; Xu et al., 2015; Mondragón-Rodríguez et al., 2018). In addition, the AD-related endosome dysfunction in Down syndrome was demonstrated to be independent of Abeta generation but to rely on the BACE1-catalyzed formation of the APP C-terminal fragment C99 (Jiang et al., 2010).

However, both the generation of soluble human Abeta and of C-terminal hAPP fragments require transgenic hAPP expression. In that regard, it is a still unaddressed question which specific neuronal populations are affected by hAPP overexpression in Tg2576 hippocampus. Theoretically, either neurons expressing the hAPP transgene or those exposed to extracellular Abeta assemblies might be specifically affected. Employing a novel, hAPP-specific rat monoclonal antibody we have recently demonstrated transgene expression by virtually all CA1 to CA3 pyramidal neurons and by scattered GABAergic interneurons throughout all hippocampal layers, but not by DG granule cells (Höfling et al., 2016). These interneurons represent a small proportion of hippocampal neurons but generate and control the rhythmic output of large populations of principal cells and modulate LTP (Chen et al., 2010; Huh et al., 2016), neurogenesis (Krezymon et al., 2013; Verdaguer et al., 2015), Abeta pathology (Ramos et al., 2006) as well as learning and memory (Perez-Cruz et al., 2011; Schmid et al., 2016). Thus, the observed early alterations in hippocampal network activity may be due to functional impairment of inhibitory GABAergic hippocampal interneurons expressing the hAPP transgene in Tg2576 mice. These GABAergic hippocampal interneurons can be subdivided based on shape, localization in defined hippocampal layers and the co-expression of specific calcium-binding proteins (CBPs) such as parvalbumin, calbindin, and calretinin as well as the peptide hormone somatostatin (Mátyás et al., 2004).

In order to identify hippocampal interneurons expressing the hAPP transgene in Tg2576 mice, double immunofluorescent labelings detecting hAPP and the CBPs and somatostatin were performed followed by quantitative stereological analyses. The data reported identify defined hippocampal populations of interneurons as cellular source for Abeta generation which may affect the neurons expressing the transgene themselves or anatomical target areas where Abeta peptides are released from these neurons.

MATERIALS AND METHODS

Animals

In order to identify GABAergic interneurons expressing the hAPP transgene we used 3-month-old female wild type ($N = 3$) and female Tg2576 mice ($N = 3$) on C57BL/6xSJL background in which transgene expression is driven by the hamster prion protein promoter (Hsiao et al., 1996). Female mice were chosen because they develop Abeta pathology earlier than males and display a higher amyloid load than males at the same age (Callahan et al., 2001) and are, therefore, used more often in experimental studies. Animals were housed at 23°C at 12 h day/12 h night cycles with food and water *ad libitum* in cages that contained red plastic houses (Tecniplast) and shredded paper flakes to allow nest building. All experimental protocols were approved by Landesdirektion Sachsen, license T28/16 and

all methods were carried out in accordance with the relevant guidelines and regulations.

Tissue Preparation

Mice were sacrificed by CO_2 inhalation and perfused transcardially with 50 ml 0.9% saline followed by perfusion with 80 ml 4% paraformaldehyde in PBS (0.1 M; pH 7.4). The brains were removed from the skull and postfixed by immersion in the same fixative overnight at 4°C. After cryoprotection in 30% sucrose in 0.1 M PBS for 3 days, coronal sections (30 μm) were cut at the level of Bregma −2.70 mm to Bregma −3.16 mm on a sliding microtome and collected in 0.1 M PBS.

Immunohistochemistry

In order to reveal the neuron type-specific labeling generated by the rat monoclonal anti-hAPP antibody 1D1 (15 μg/ml) in hippocampus of Tg2576 mice triple immunofluorescent labeling in combination with antibodies directed against the CBPs parvalbumin (rabbit anti-parvalbumin; Swant; 1:4,000), calbindin (rabbit anti-calbindin; Swant; 1:1,000), calretinin (rabbit anti-calretinin; Swant; 1:1,000) and against somatostatin (goat anti-somatostatin; Santa Cruz; 1:200) was performed. To allow normalization for total neuronal numbers a mixture of mouse anti-NeuN/anti-HuCD (1:1000 each; Invitrogen/Millipore) was added to the incubation cocktails. Brain sections were incubated with cocktails of primary antibodies overnight at 4°C. On the next day, sections were washed three times with TBS and were then incubated with cocktails of Cy3-conjugated donkey anti-rat (1:400; Dianova) and Cy2-conjugated donkey anti-rabbit or donkey anti-goat (1:400; Dianova) and Cy5-conjugated donkey anti-mouse (1:400; Dianova) for 60 min at room temperature. This procedure resulted in red labeling of hAPP-positive neurons, in green labeling of the respective interneuron types and in blue labeling of all neurons. After washing, sections were mounted onto glass slides and coverslipped.

Microscopy

Confocal laser scanning microscopy (LSM 510, Zeiss, Oberkochen, Germany) was performed to reveal co-localization of hAPP with parvalbumin, calbindin, calretinin, and somatostatin in hippocampus. For Cy2-labeled interneuron markers (green fluorescence), an argon laser with 488 nm excitation was used and emission from Cy2 was recorded at 510 nm applying a low-range band pass (505–550 nm). For Cy3-labeled hAPP (red fluorescence), a helium-neon-laser with 543 nm excitation was applied and emission from Cy3 at 570 nm was detected applying high-range band pass (560–615 nm). Photoshop CS2 (Adobe Systems, Mountain View, CA, United States) was used to process the images obtained by light and confocal laser scanning microscopy. Care was taken to keep the same brightness, sharpness, color saturation, and contrast in the various pictures.

Quantification of Neuronal Numbers

For quantification of neuronal numbers, images of immunohistochemical labelings were taken at a Keyence BZ-9000 microscope. The outline of hippocampal layers, the location of neurons inside these layers and quantitative analysis of the proportion of hAPP-immunoreactive interneuron populations were assessed by means of BZ-II Analyzer software (Keyence).

The expression of NeuN/HuCD, hAPP, parvalbumin, calbindin, calretinin, and somatostatin-positive neurons was investigated in both hippocampi of all animals. Each section was first viewed at low magnification (5×) for outlining the relevant hippocampal layers, and dissector frames were placed in a systematic consecutive fashion in the delineated regions of the sections. On average the post-processing shrinkage of the tissues resulted in a final section thickness of about 16 μm, which permitted a consistent sampling of 10 μm with the dissector and the use of guard zones of 2 μm on either sides of the section. All neurons that fell within the dissector frames were then counted at higher magnification (10×). In all sections analyzed, the total number of neurons in each hippocampal layer was set to 100%. The proportion of hAPP-immunoreactive neurons and neurons immunoreactive for interneuron markers was calculated and statistical differences were evaluated by unpaired *t* test.

RESULTS

The hAPP-specific 1D1 antibody used was shown by us to specifically detect the N-terminus of human, but not endogenous mouse APP in mouse brain sections (Höfling et al., 2016). In control experiments of the present study we included wild type mouse brain sections as negative control to validate specific hAPP transgene detection. In preceding experiments, we tested the 1D1 antibody at different concentrations on hAPP-transgenic Tg2576 and wild type mouse brain sections. With the highest 1D1 concentration not generating labeling in wild type mouse brain, we still observed the same pattern of labeling of hippocampal interneurons as reported below. The hippocampal formation can be subdivided into DG and hippocampus proper consisting of segments *cornu ammonis* (CA) 1, 2, 3, and 4. In addition, hippocampal layers with defined neuronal populations can be distinguished along these hippocampal subfields. In order to obtain highly detailed information on the specific distribution of hAPP expressing interneurons, our analyses were performed in hippocampal layers excluding pyramidal and granule cell layers. We observed hAPP expression in subsets of hippocampal interneurons ranging between 57 and 100% in hippocampal layers analyzed (**Table 1**). In contrast, endogenous mouse APP is ubiquitously expressed by virtually all neurons (Buxbaum et al., 1993; Neve et al., 1996) and critical for neuronal development and viability as well as for synapse formation and stabilization (Priller et al., 2006). Thus, endogenous mouse APP is expressed by almost all hippocampal neurons, whereas transgene expression of hAPP is limited to subsets of hippocampal neurons.

GABAergic Interneurons in Hippocampal Layers of Wild Type and Tg2576 Mice

First, we tested whether the numbers of CBP and somatostatin-expressing interneurons is similar in hippocampal layers of

TABLE 1 | Proportions of hAPP-positive neurons in hippocampal layers and proportions of hAPP-positive neurons expressing parvalbumin, calbindin, calretinin, and somatostatin.

	hilus	S. mol.	S. lac.	S. rad.	S. ori.
			% mean ± SEM		
hAPP/neurons	59.5 ± 15.0	100 ± 0	100 ± 0	63.6 ± 8.2	56.7 ± 3.4
parvalbumin/hAPP	3.7 ± 0.3	0.6 ± 0.2	0	4.0 ± 1.0	24.8 ± 3.6
calbindin/hAPP	1.2 ± 0.9	2.4 ± 0.2	4.9 ± 2.1	20.1 ± 9.6	41.3 ± 8.0
calretinin/hAPP	18.4 ± 6.4	3.3 ± 1.5	4.8 ± 1.5	4.3 ± 1.8	8.3 ± 2.1
somatostatin/hAPP	30.2 ± 4.6	0.1 ± 0.1	0.3 ± 0.3	10.7 ± 4.2	34.6 ± 2.5

S. mol., stratum moleculare; S. lac., stratum lacunosum moleculare; S. rad., stratum radiatum; S. ori., stratum oriens.

3-month-old wild type and hAPP-transgenic Tg2576 mice. Since the absolute number of neurons and the neuronal number per area differ strongly along the rostro-caudal extension of the hippocampal formation, the proportion of CBP- and somatostatin-containing neurons of all neurons was calculated in brain sections at a narrow brain cutting level of bregma −2.70 to Bregma −3.16 mm by immunofluorescent co-labeling of the CBP and somatostatin with a combination of the pan-neuronal markers NeuN/HuCD (**Figure 1**). Typical examples of these labelings of wild type and Tg2576 hippocampus are displayed in **Figure 1A**. Visual examination of the staining patterns indicated a similar appearance of all CBP analyzed as well as of somatostatin, while hAPP immunoreactivity was absent in wild type brain sections. Data of the quantitative analyses of these labelings are depicted in **Figures 1B–E**.

As to the expression of the different neuropeptides we detected striking differences in the hippocampus layer-specific abundance of CBP and somatostatin-positive neurons in wild type mice. For example, approximately 25% of neurons in *stratum oriens* were *parvalbumin*-immunoreactive, whereas only 5% in *stratum radiatum*, *stratum moleculare* and the hilus of DG displayed parvalbumin immunoreactivity and *stratum lacunosum moleculare* was completely devoid of parvalbumin neurons (**Figure 1B**). *Calbindin*-expressing neurons were highly abundant in *stratum oriens* and *stratum radiatum* (30% of all neurons) and to a lesser extent in neurons of *stratum moleculare* and *stratum lacunosum moleculare* (15% of all neurons), whereas in hilus of DG only 5% of all neurons expressed this protein (**Figure 1C**). An inverse pattern in the abundance across hippocampal layers was detected for *calretinin*-containing interneurons. Here, more than 30% of all neurons in the hilus of DG and in *stratum lacunosum moleculare* were calretinin-immunoreactive, whereas only 15% of neurons in *stratum radiatum* and *stratum oriens* and less than 10% of neurons in *stratum moleculare* were calretinin-immunoreactive (**Figure 1D**). Somatostatin-containing neurons were most abundant in *stratum oriens* and hilus of DG (30% of all neurons), followed by *stratum radiatum* (10% of all neurons) and were found to be absent in DG molecular layer and in *stratum lacunosum moleculare* (**Figure 1E**).

For most labelings, there were no statistically significant differences between wild type and Tg2576 mice in the abundance of parvalbumin-, calbindin-, calretinin-, or somatostatin-positive neurons in hippocampal layers analyzed (**Figures 1B–E**). The only exceptions are a lower proportion of parvalbumin-containing neurons in *stratum oriens* (**Figure 1B**) and a higher proportion of calretinin-immunoreactive neurons in *stratum moleculare* of Tg2576 mice (**Figure 1D**). Thus, in general, the appearance and distribution of GABAergic interneurons in hippocampus of young Tg2576 mice is preserved compared to the wild type.

Human APP Transgene Expression by Hippocampal GABAergic Interneurons

The transgenic hAPP was found to be expressed by interneurons across all hippocampal layers. We, therefore, wanted to analyze the hAPP transgene expression by hippocampal GABAergic interneurons in detail. In particular, the following questions were addressed. (i) Which proportion of hAPP-expressing hippocampal interneurons is immunoreactive for parvalbumin, calbindin, calretinin, and somatostatin in defined hippocampal layers? (ii) Which proportion of parvalbumin, calbindin, calretinin, and somatostatin-positive neurons expresses hAPP?

In general, there was no GABAergic interneuron subpopulation that did not express the hAPP transgene. On the other hand, in no case all neurons of such a subpopulation expressed hAPP (**Figures 2–5**). Typical examples of parvalbumin/hAPP double labelings in *stratum oriens* are shown in **Figure 2A**. Quantitative analysis revealed that of all hAPP transgene-expressing interneurons in *stratum oriens*, 25% were *parvalbumin*-immunoreactive, whereas in *stratum radiatum* and in hilus of DG only 5% and in *stratum moleculare* only 2% of hAPP-positive neurons displayed parvalbumin immunoreactivity. *Stratum lacunosum moleculare* did not have any neurons expressing both hAPP and parvalbumin (**Figure 2B**). On the other hand, of all parvalbumin-expressing neurons, 60 to 80% expressed the hAPP transgene in hilus of DG, *stratum moleculare*, *stratum radiatum*, and *stratum oriens*, respectively (**Figure 2C**).

Double immunofluorescent labelings for calbindin and hAPP in *stratum radiatum* are shown in **Figure 3A**. The proportion of hAPP expressing neurons positive for *calbindin* differed considerably between layers and in hippocampus proper amounted to 42% in *stratum oriens*, 20% in *stratum radiatum*, and 5% in *stratum lacunosum moleculare*, respectively, and in DG to 3% in *stratum moleculare* and 2% in the hilus (**Figure 3B**). Of all calbindin-expressing neurons, 70% expressed hAPP in *stratum*

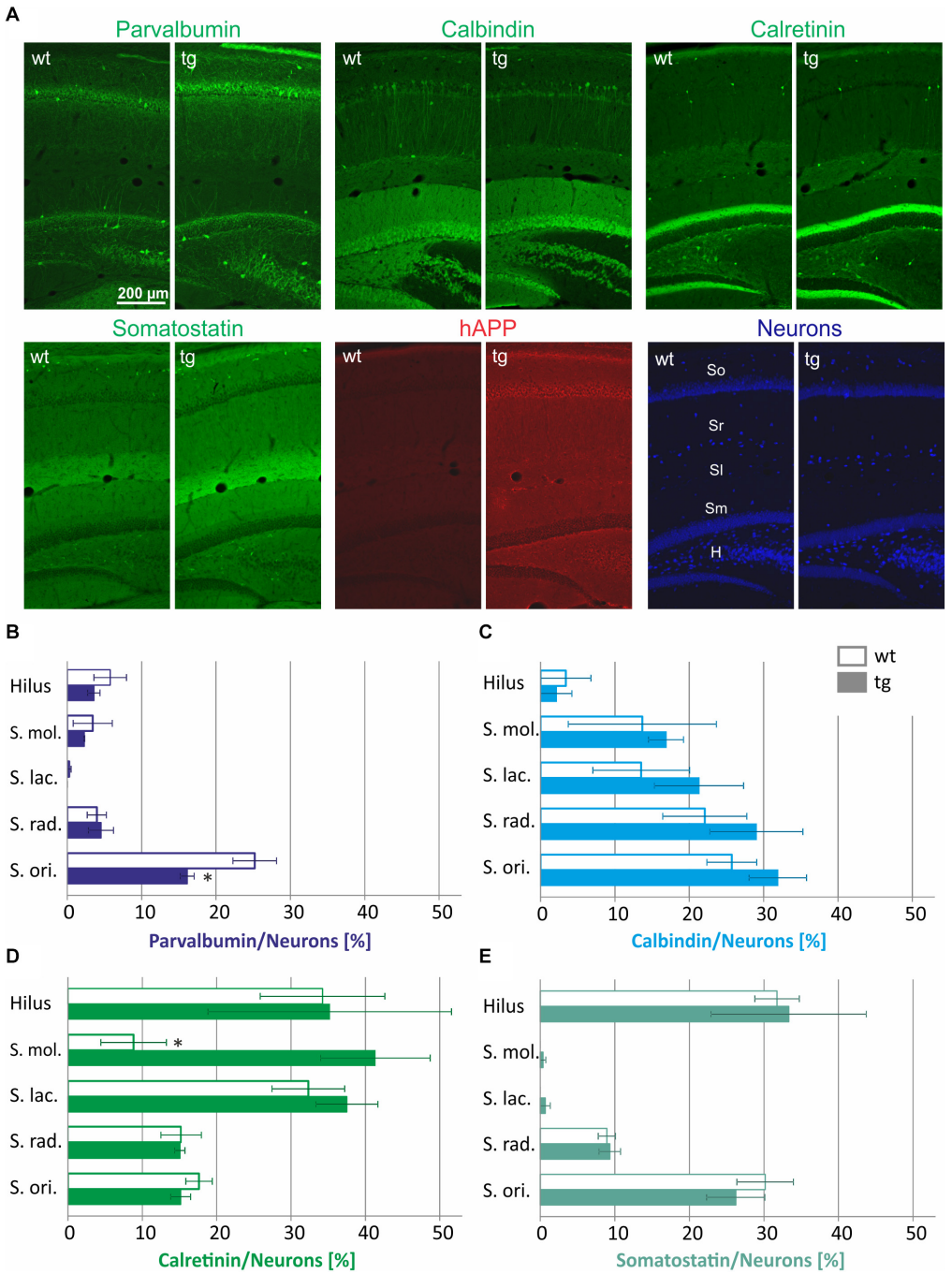

FIGURE 1 | Quantification of interneuron numbers in hippocampal layers of wild type (wt) and hAPP-transgenic Tg2576 mice (tg). In panel **(A)** typical staining patterns of parvalbumin-, calbindin-, calretinin-, somatostatin-, and hAPP-immunoreactive neurons are depicted in wt and tg mouse hippocampus. Note the similar labeling intensity in wt and tg brain sections for all antigens except hAPP. The hippocampal layers analyzed are indicated in the wt pan-neuronal labeling image (Neurons). In panels **B–E**, the proportions of parvalbumin-, calbindin-, calretinin-, and somatostatin-positive neurons in hippocampal layers of wt and tg mice are quantified. Total neuronal numbers in each layer (hilus 69.8 ± 2.8; S. mol 48.2 ± 6.7; S. lac. 68.5 ± 8.5; S. rad. 407.2 ± 49.0; S. ori. 269.5 ± 13.0) were set to 100%. Note the similar interneuron proportions in wt and tg hippocampus for most data analyzed. *significantly different from wild type ($p < 0.05$; unpaired t test).

oriens and approximately 40% in *stratum moleculare*, *stratum lacunosum moleculare*, and *stratum radiatum*, whereas less than 5% of calbindin-positive neurons in the hilus of DG expressed hAPP (**Figure 3C**).

The immunohistochemical co-localization of calretinin and hAPP in *stratum radiatum* is shown in **Figure 4A**. The highest proportion of hAPP expressing neurons that was positive for *calretinin* was detected in the hilus of DG (18%), followed

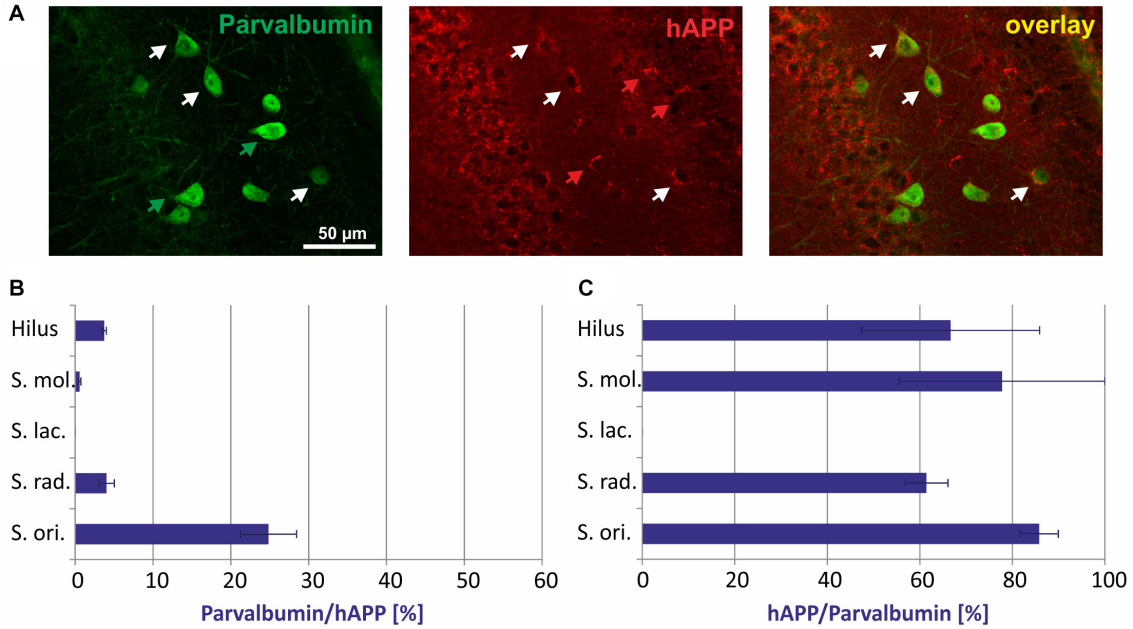

FIGURE 2 | Quantitative analyses of the co-localization between parvalbumin-immunoreactive neurons and hAPP-expressing interneurons in hippocampus of Tg2576 mice. Typical examples of double labelings in *stratum oriens* are shown in panel **(A)**. White arrows point to double-labeled neurons, green, and red arrows to neurons that are only labeled by green (parvalbumin) and red (hAPP) fluorescence, respectively. Quantitative analysis revealed that of all hAPP transgene-expressing interneurons 0% (in *stratum lacunosum moleculare*) to 25% (in *stratum oriens*) were parvalbumin-immunoreactive **(B)**. Of all parvalbumin-expressing neurons, 60 to 80% expressed the hAPP transgene in hilus of DG, *stratum moleculare*, *stratum radiatum*, and *stratum oriens* **(C)**.

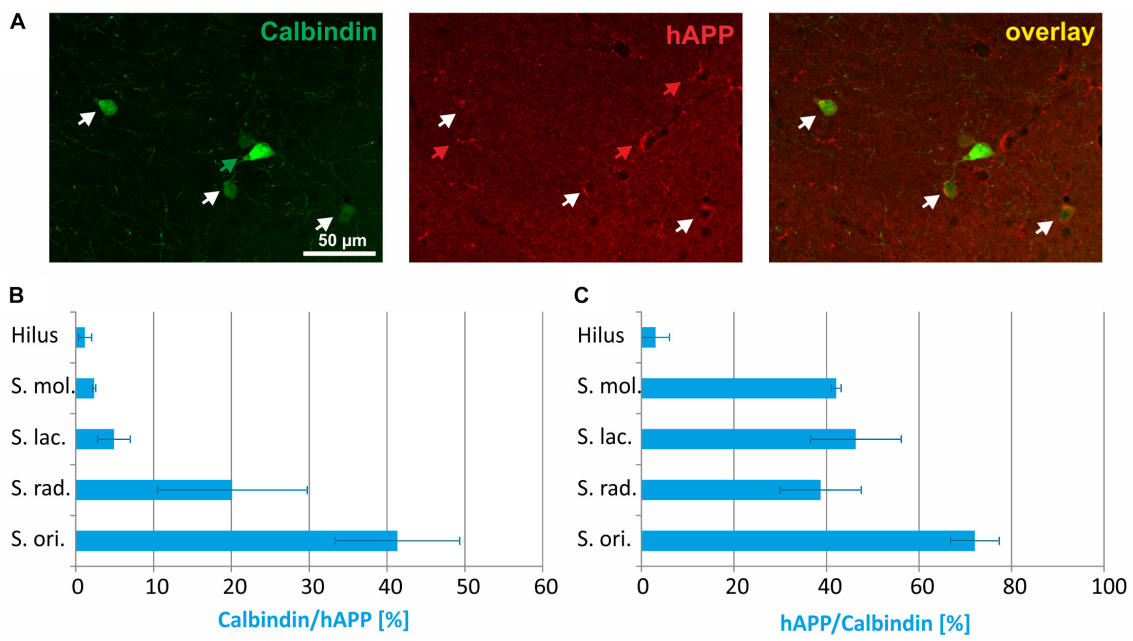

FIGURE 3 | Quantitative analyses of the co-localization between calbindin-immunoreactive neurons and hAPP-expressing interneurons in hippocampus of Tg2576 mice. Typical examples of double labelings in *stratum radiatum* are shown in panel **(A)**. White arrows point to double-labeled neurons, green, and red arrows to neurons that are only labeled by green (calbindin) and red (hAPP) fluorescence, respectively. Quantitative analysis revealed that of all hAPP transgene-expressing interneurons 2% (in DG hilus) to 42% (in *stratum oriens*) were calbindin-immunoreactive **(B)**. Of all calbindin-expressing neurons, 5 to 70% expressed the hAPP transgene **(C)**.

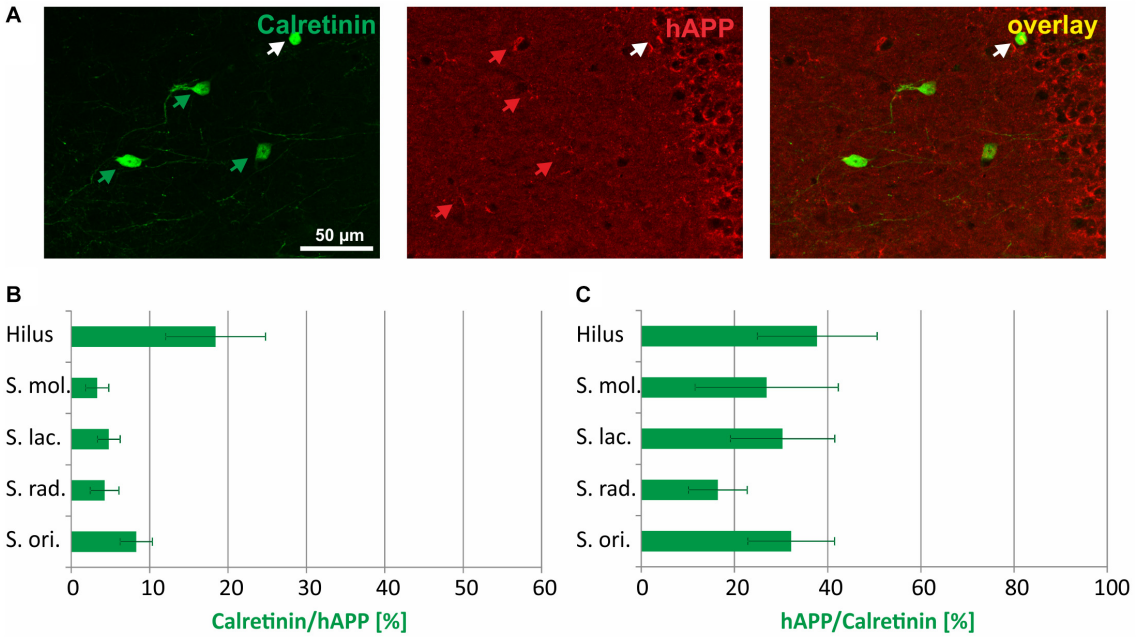

FIGURE 4 | Quantitative analyses of the co-localization between calretinin-immunoreactive neurons and hAPP-expressing interneurons in hippocampus of Tg2576 mice. Typical examples of double labelings in *stratum radiatum* are shown in panel **(A)**. White arrows point to double-labeled neurons, green, and red arrows to neurons that are only labeled by green (calretinin) and red (hAPP) fluorescence, respectively. Quantitative analysis revealed that of all hAPP transgene-expressing interneurons 4% (in *stratum moleculare*) to 18% (in DG hilus) were calretinin-immunoreactive **(B)**. Of all calretinin-expressing neurons, 18 to 38% expressed the hAPP transgene in defined hippocampal layers **(C)**.

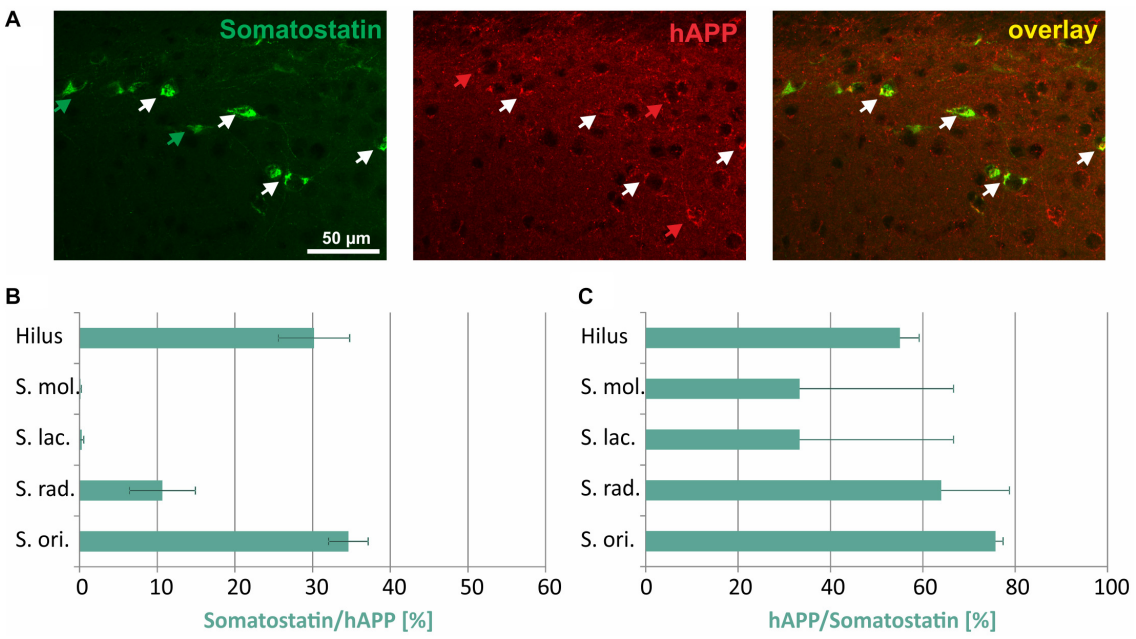

FIGURE 5 | Quantitative analyses of the co-localization between somatostatin-immunoreactive neurons and hAPP-expressing interneurons in hippocampus of Tg2576 mice. Typical examples of double labelings in *stratum oriens* are shown in panel **(A)**. White arrows point to double-labeled neurons, green, and red arrows to neurons that are only labeled by green (somatostatin) and red (hAPP) fluorescence, respectively. Quantitative analysis revealed that of all hAPP transgene-expressing interneurons 1 to 2% in *stratum moleculare* and *stratum lacunosum moleculare* to approximately 30% (in DG hilus and *stratum oriens*) were somatostatin-immunoreactive **(B)**. Of all somatostatin-expressing neurons, 30 to 76% expressed the hAPP transgene in all hippocampal layers **(C)**.

by *stratum oriens* (8%), *stratum lacunosum moleculare* (6%), *stratum radiatum* (5%), and *stratum moleculare* (4%) (**Figure 4B**). Across hippocampal layers, the proportion of calretinin-positive neurons expressing the hAPP transgene was rather homogenous, reaching 30 to 40% in hilus, and *stratum moleculare* of DG as well as *stratum lacunosum moleculare* and *stratum oriens* and 16% in *stratum radiatum* of hippocampus proper (**Figure 4C**).

In **Figure 5A**, typical examples of somatostatin/hAPP double immunofluorescent labelings in *stratum oriens* are displayed. Of all hAPP-positive neurons 30% in hilus of DG and 35% in *stratum oriens* were immunoreactive for *somatostatin*, whereas only 10% of hAPP-expressing neurons in *stratum radiatum* and 2% in *stratum moleculare* and in *stratum lacunosum moleculare* displayed somatostatin immunoreactivity (**Figure 5B**). In all hippocampal layers the proportion of somatostatin expressing neurons which was positive for the hAPP transgene was at least 25% (*stratum moleculare*, *stratum lacunosum moleculare*) and reached around 60% in hilus of DG and *stratum radiatum*, respectively, and 76% in *stratum oriens* (**Figure 5C**).

For a general overview, the proportions of hAPP-positive neurons expressing parvalbumin, calbindin, calretinin, and somatostatin across hippocampal layers are displayed in **Table 1** and the proportions of total parvalbumin-, calbindin-, calretinin-, and somatostatin-positive neurons expressing hAPP are given in **Table 2**.

When the proportion of hAPP-positive hippocampal interneurons co-expressing parvalbumin, calbindin, calretinin, and somatostatin is summed up in individual hippocampal layers, clear differences in hAPP transgene expression by these GABAergic interneurons can be established. In *stratum oriens*, the highest proportion of hAPP-expressing neurons was found to be immunoreactive for the interneuron markers tested (**Figure 6**). Among the hAPP-positive neurons in *stratum oriens*, most were immunoreactive for calbindin and somatostatin, respectively, followed by parvalbumin and calretinin (**Figure 6**). In contrast, in *stratum moleculare* and in *stratum lacunosum* moleculare less than 10% of hAPP-positive neurons expressed one of the markers investigated. Among those, most were immunoreactive for calbindin and calretinin but almost none for parvalbumin and somatostatin (**Figure 6**). In *stratum radiatum*, all four interneuron populations contributed to a total 40% of hAPP-expressing neurons, with calbindin and somatostatin-positive neurons having the biggest impact.

Thus, in defined hippocampal layers there are robust differences in CBP and somatostatin expression by hAPP-positive neurons ranging from 10% in *stratum moleculare* and *stratum lacunosum moleculare* to 100% in *stratum oriens*. Additionally, the proportion of specific GABAergic interneuron subtypes varies considerably in hippocampal layers with a large population of parvalbumin-positive hAPP neurons in *stratum oriens*, calbindin-positive hAPP neurons in *stratum oriens* and *stratum radiatum*, calretinin-positive hAPP neurons in hilus of DG and somatostatin-positive hAPP neurons in *stratum oriens* as well as in hilus of DG. It remains an open question why the promoter driving transgene expression is only active in a subset of the hippocampal interneuron populations investigated here. *Vice versa*, there is a high proportion of hAPP-positive neurons that does not express any of the interneuron markers studied; in particular in *stratum moleculare* and *stratum lacunosum moleculare*. These neurons apparently are subpopulations of hippocampal interneurons other than the ones depicted by CBP and somatostatin immunoreactivity. They might be distinguished based on different characteristics like morphology, wiring and neurochemical properties such as expression of neuropeptides, enzymes and receptors.

DISCUSSION

Many experimental studies using APP-transgenic AD animal models suffer from a lack of information on the distinct brain region and cell type-specific transgene expression patterns. These data are, however, the pre-requisite to understand pathogenic mechanisms on the subcellular, cellular, neuronal network and systemic level and to allow comparison of experimental outcome obtained from different transgenic mouse lines. Our data presented here indicate that defined interneuron populations in hippocampus expressing transgenic hAPP to different extents may selectively contribute to aspects of pathological disturbances and learning and memory deficits well before amyloid plaque pathology in Tg2576 mice. We decided to analyze young Tg2576 mice before the onset of amyloid pathology for hAPP expression because in older mice the affected neurons may have degenerated and thus escaped quantification.

Parvalbumin

In CA1 of hippocampal slices of 6- to 7-month-old Tg2576 mice LTP was found to be impaired, but restored in Tg2576 mice aged 14 to 19 months (Huh et al., 2016). The authors explained these findings with the selective loss of inhibitory

TABLE 2 | Proportions of parvalbumin-, calbindin-, calretinin-, and somatostatin-positive neurons expressing hAPP.

	Hilus	S. mol.	S. lac.	S. rad.	S. ori.
			% mean ± SEM		
hAPP/parvalbumin	66.7 ± 19.2	77.8 ± 22.2	0	61.5 ± 4.7	85.8 ± 4.1
hAPP/calbindin	3.0 ± 3.0	42.1 ± 1.1	46.3 ± 9.8	38.7 ± 8.8	72.1 ± 5.3
hAPP/calretinin	37.7 ± 12.9	26.9 ± 15.4	30.3 ± 11.2	16.4 ± 6.3	32.2 ± 9.3
hAPP/somatostatin	55.1 ± 4.2	33.3 ± 33.3	33.3 ± 33.3	64.0 ± 14.7	75.7 ± 1.6

S. mol., stratum moleculare; S. lac., stratum lacunosum moleculare; S. rad., stratum radiatum; S. ori., stratum oriens.

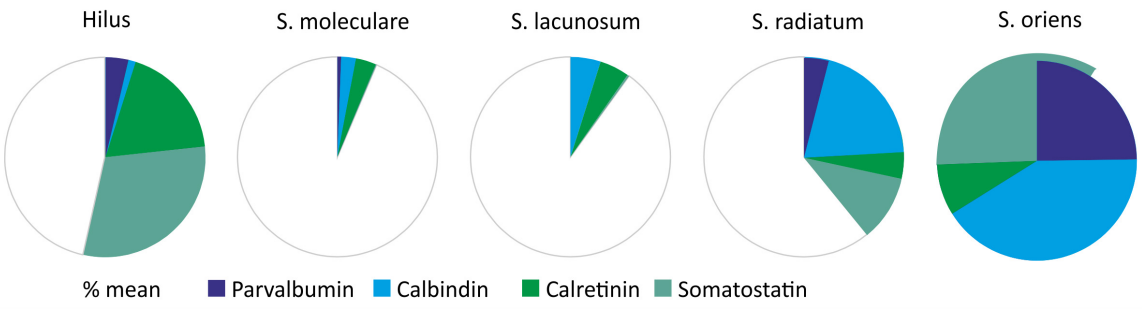

FIGURE 6 | In this Figure, the proportion of hAPP-positive hippocampal interneurons co-expressing parvalbumin, calbindin, calretinin, and somatostatin is summed up in individual hippocampal layers. In *stratum moleculare* and *stratum lacunosum moleculare* less than 10% of all hAPP-expressing neurons are immunoreactive for the four interneuron markers analyzed, whereas in *stratum radiatum* and DG hilus 40 to 50%, and in *stratum oriens* all hAPP-immunoreactive neurons are positive for these interneuron markers. Additionally, the contribution of individual interneuron types to the hAPP-expressing population varies considerably in hippocampal layers as indicated by the respective color.

parvalbumin-positive neurons in hippocampus during aging, which resulted in enhanced excitatory signaling (Huh et al., 2016). This notion is supported by findings on the critical role of parvalbumin interneurons for the down regulation of LTP at Schaffer collateral-CA1 synapses (Chen et al., 2010). Using resting-state functional MRI to assess brain functional connectivity in Tg2576 mice, network hypersynchrony was detected in hippocampus of 3- to 5-month-old Tg2576 mice but an age-dependent reduction in hippocampal functional connectivity was revealed in 8- and 18-month-old Tg2576 mice (Shah et al., 2016). Interestingly, in another hAPP-transgenic mouse model spontaneous epileptiform discharges induced by network hypersynchrony were attributed to impaired function of parvalbumin neurons (Verret et al., 2012). Our data suggest that hAPP transgene expression by parvalbumin-positive hippocampal GABAergic interneurons may contribute to the described impairments of neuronal network activity, LTP and, subsequently, hippocampus-dependent spatial learning. Moreover, Abeta deposits in old Tg2576 mice appear primarily in *strata oriens*, *lacunosum moleculare* and *moleculare* (Hartlage-Rübsamen et al., 2011), indicating a contribution of transgene expression by these neuronal populations to Abeta pathology. Similar conclusions have been drawn in a study using APP/PS1 mice, where reductions in parvalbumin, calbindin, and calretinin immunoreactivity in DG were more pronounced at Bregma levels with high Abeta plaque load than at Bregma levels with low plaque load (Popović et al., 2008).

Calbindin

The population of calbindin-immunoreactive neurons was demonstrated to be stable during aging in hippocampus of wild type mice between 3 and 18 months (Krezymon et al., 2013). In male Tg2576 mice, however, there was an age-dependent decline of calbindin immunoreactivity in the DG molecular layer resulting in significantly reduced calbindin immunoreactivity of 12- and 18-month-old Tg2576 mice compared to wild type mice. Preceding these changes in DG calbindin immunoreactivity, severe disturbances in hippocampal neurogenesis of Tg2576 mice were observed which compromised functional integration of new neurons into hippocampal circuits (Krezymon et al., 2013). Implications for a disturbed hippocampal neurogenesis were also obtained in the APPswe/PS1dE9 transgenic mouse model by reduced numbers of calretinin-positive and doublecortin-positive neurons in the subgranular zone of the DG hilus compared to wild type mice (Verdaguer et al., 2015). Moreover, in $hAPP_{FAD}$ mice, learning deficits correlated strongly with decreased levels of calbindin in the DG (Palop et al., 2003) and epigenetic suppression of hippocampal calbindin results in disturbance of spatial memory, whereas restoring calbindin expression in these mice improves performance in spatial memory (You et al., 2017).

Calretinin

In contrast to the high vulnerability of hippocampal calbindin-positive neurons in the human AD brain and its animal models, calretinin-positive fibers in proximity of Abeta plaques were shown to be less affected by dystrophic morphology than neurites containing neurofilament-triplet proteins in Tg2576 and APPswe/PS1dE9 mice and human AD affected brains (Mitew et al., 2013). However, the number of calretinin-positive interneurons is profoundly decreased in CA1 and CA2/3 hippocampal subfields of APP/PS1 mice at a very early stage of pathology, whereas hippocampal calretinin neurons belonging to the Caja-Retzius cells were not affected (Baglietto-Vargas et al., 2010). Interestingly, the early and selective calretinin cell loss preferentially occurred in parallel to the appearance of Abeta deposits in axonal terminal fields of these neurons (Baglietto-Vargas et al., 2010). Thus, the calretinin-positive population of hippocampal interneurons appears to be differentially affected by Abeta pathology.

Somatostatin

In addition to CBP-positive interneurons, a subpopulation of GABAergic hippocampal interneurons expressing the peptide hormone somatostatin has been demonstrated to be critically involved in learning and memory processes (Lovett-Barron et al., 2014), most likely by providing feedback inhibition to CA1

pyramidal neurons (Royer et al., 2012). In hippocampus of APP/PS1-transgenic mice, an early and substantial reduction of somatostatin-positive neurons, which correlated with Abeta pathology, was observed in hippocampal subfields CA1, CA2/3, and in DG (Ramos et al., 2006). The dysfunction of these neurons in APP/PS1 mice was shown to be associated with memory deficits (Schmid et al., 2016). Also in Tg2576 mice a significant reduction in the number of somatostatin-positive interneurons in *stratum oriens* of CA1 was reported and related to impairments of performance in contextual fear and spatial memory tasks (Perez-Cruz et al., 2011). Another line of evidence for the importance of somatostatin-positive hippocampal interneuron function for learning processes arises from pharmacological studies using somatostatin receptor 4 agonists (Sandoval et al., 2013). When Tg2576 mice were treated with the selective somatostatin receptor 4 agonist NNC 26-9100, learning improvements and reductions in oligomeric Abeta concentrations were observed (Sandoval et al., 2013).

Relation to AD

The presented data are relevant to the understanding of different aspects of synaptic, neuronal and network dysfunction in hippocampus of young and aged Tg2576 mice as well as systemic deficits in learning and memory and the contribution of defined hippocampal GABAergic subpopulations to these pathogenic processes. However, no direct conclusions can be drawn with regard to the involvement of these neuronal populations in AD pathogenesis because a higher, or lower, proportion of these neurons may express varying amounts of APP and produce pathogenic Abeta assemblies. Nevertheless, in the APP/PS1 model, the reduction of the number of parvalbumin expressing neurons in the CA1/2 hippocampal sublayer and of calretinin-immunoreactive neurons in DG is at the same order of magnitude as in *post mortem* hippocampal tissue from AD subjects (Takahashi et al., 2010). Reductions in the number of hippocampal parvalbumin-immunoreactive neurons in AD were already reported by Brady and Mufson (1997). They observed an up to 60% decrease in the number of parvalbumin-positive neurons in CA1/2/4 and DG, but not in CA3, subiculum, or presubiculum. They concluded, that the selective vulnerability of subsets of hippocampal parvalbumin neurons in AD may be related to differential connectivity. Accordingly, DG and CA1 parvalbumin-positive neurons connected to the cerebral cortex would be more vulnerable than neurons located in the subiculum or presubiculum, respectively, which are connectionally related to subcortical areas (Brady and Mufson, 1997). Hippocampal calbindin-immunoreactive neurons, on the other hand, were reported to be spared from neurofibrillary tangle formation and appeared to be unaffected by Abeta pathology at early stages of AD, whereas this resistance is lost at advanced disease stages (Iritani et al., 2001). Calbindin immunoreactive neurons in DG were also reported to be differentially affected in AD and other neurodegenerative disorders (Stefanits et al., 2014). The proportion of calbindin-negative DG granule neurons was found to increase with Braak stage of AD and was significantly higher than in Creutzfeldt-Jakob disease, argyrophilic grain disease, frontotemporal lobar degeneration-TDP types A and B, but not compared to frontotemporal lobar degeneration-Tau Pick's disease type (Stefanits et al., 2014). Also in entorhinal cortex, a major source of DG innervation, a differential impact of AD pathology on neurons expressing CBPs was reported (Mikkonen et al., 1999). Non-principal cells containing parvalbumin or calbindin were affected at early disease stages, whereas non-principal neurons containing calretinin were more viable, even in AD cases with severe entorhinal pathology (Mikkonen et al., 1999).

Non-neuronal hAPP Expression

In a recent study we demonstrated that hAPP expression is not neuron-specific but also detectable in subsets of resting astrocytes in neocortex and corpus callosum of Tg2576 mice before the onset of amyloid plaque formation (Heiland et al., 2019). In hippocampus, the majority of hAPP immunoreactivity arises from neurons, but there is also hAPP immunoreactivity present in glial cells of astrocytic morphology [see filmstrip links provided in Heiland et al. (2019)]. Although the proportion of astrocytic hAPP expression is low, we cannot rule out an astrocytic contribution to impairments in spatial navigation, learning, memory, hippocampal LTP formation, and neuronal network activity induced by Abeta or C-terminal APP fragments. Also in human brain, non-neuronal expression of APP mRNA has been demonstrated and related to pathology (Golde et al., 1990).

CONCLUSION

In this study, hAPP transgene expression by different populations of GABAergic interneurons in defined hippocampal layers of Tg2576 mice was investigated for the first time. Our results partly explain disturbed hippocampus-dependent processes and functions such as LTP, neuronal network activity, learning and spatial memory and neurogenesis. Thus, the detailed analysis of transgene expression patterns allows revealing pathological mechanisms and obtaining novel insights in hAPP-dependent disturbances in brain. Technical aspects of transgenic animal generation such as transgene isoform and promoter selection, the genomic integration of the transgene, co-pathologies and compensatory mechanisms result in strikingly different transgene expression patterns in different mouse lines (Höfling et al., 2016). We, therefore, strongly recommend carefully analyzing and comparing transgene expression patterns in different mouse lines used as animal models to mimic amyloid pathology of AD.

AUTHOR CONTRIBUTIONS

CH designed the study, carried out the experiments, analyzed the data, and drafted the manuscript. ES carried out the experiments and analyzed the data. P-HK and SL participated in designing the experiments and drafted the manuscript. MH-R designed the study, analyzed the data, and drafted the manuscript.

SR conceived, designed and coordinated the study and drafted the manuscript. All authors gave final approval for publication.

FUNDING

This work was supported by the German Federal Department of Education, Science and Technology, BMBF (grant #01ED1501B to SR) within the European Union Joint Program for Neurodegenerative Disease (JPND) Research, Project CrossSeeds, and by the Alzheimer Forschungsinitiative e.V. (AFI #16004) to SR as well as by the Centers of Excellence in Neurodegeneration program and the Helmholtz-Israel program to SL.

ACKNOWLEDGMENTS

We are grateful to Karen Hsiao-Ashe for providing Tg2576 mouse breeders. We acknowledge support from the German Research Foundation (DFG) and Leipzig University within the program of Open Access Publishing.

REFERENCES

Allen, G., Barnard, H., McColl, R., Hester, A. L., Fields, J. A., Weiner, M. F., et al. (2007). Reduced hippocampal functional connectivity in Alzheimer disease. *Arch. Neurol.* 64, 1482–1487. doi: 10.1001/archneur.64.10.1482

Ameen-Ali, K. E., Wharton, S. B., Simpson, J. E., Heath, P. R., Sharp, P., and Berwick, J. (2017). Review: neuropathology and behavioural features of transgenic murine models of Alzheimer's disease. *Neuropathol. Appl. Neurobiol.* 43, 553–570. doi: 10.1111/nan.12440

Baglietto-Vargas, D., Moreno-Gonzalez, I., Sanchez-Varo, R., Jimenez, S., Trujillo-Estrada, L., Sanchez-Mejias, E., et al. (2010). Calretinin interneurons are early targets of extracellular amyloid-beta pathology in PS1/AbetaPP Alzheimer mice hippocampus. *J. Alzheimers Dis.* 21, 119–132. doi: 10.3233/JAD-2010-100066

Barthel, H., and Sabri, O. (2017). Clinical use and utility of amyloid imaging. *J. Nucl. Med.* 58, 1711–1717. doi: 10.2967/jnumed.116.185017

Brady, D. R., and Mufson, E. J. (1997). Parvalbumin-immunoreactive neurons in the hippocampal formation of Alzheimer's diseased brain. *Neuroscience* 80, 1113–1125. doi: 10.1016/S0306-4522(97)00068-7

Brier, M., Thomas, J. B., Snyder, A. Z., Benzinger, T. L., Zhang, D., Raichle, M. E., et al. (2012). Loss of intranetwork and internetwork resting state functional connections with Alzheimer's disease progression. *J. Neurosci.* 32, 8890–8899. doi: 10.1523/JNEUROSCI.5698-11.2012

Buxbaum, J. D., Christensen, J. L., Ruefli, A. A., Greengard, P., and Loring, J. F. (1993). Expression of APP in brains of transgenic mice containing the entire human APP gene. *Biochem. Biophys. Res. Commn.* 197, 639–645. doi: 10.1006/bbrc.1993.2527

Callahan, M. J., Lipinski, W. J., Bian, F., Durham, R. A., Pack, A., and Walker, L. C. (2001). Augmented senile plaque load in aged female beta-amyloid precursor protein-transgenic mice. *Am. J. Pathol.* 158, 1173–1177. doi: 10.1016/S0002-9440(10)64064-3

Chen, Y. J., Zhang, M., Yin, D. M., Wen, L., Ting, A., Wang, P., et al. (2010). ErbB4 in parvalbumin-positive interneurons is critical for neuregulin 1 regulation of long-term potentiation. *Proc. Natl. Acad. Sci. U.S.A.* 107, 21818–21823. doi: 10.1073/pnas.1010669107

Golde, T. E., Estus, S., Usiak, M., Younkin, L. H., and Younkin, S. G. (1990). Expression of beta amyloid protein precursor mRNAs: recognition of a novel alternatively spliced form and quantitation in Alzheimer's disease using PCR. *Neuron* 4, 253–267. doi: 10.1016/0896-6273(90)90100-T

Hartlage-Rübsamen, M., Morawski, M., Waniek, A., Jäger, C., Zeitschel, U., Koch, B., et al. (2011). Glutaminyl cyclase contributes to the formation of focal and diffuse pyroglutamate (pGlu)-Aβ deposits in hippocampus via distinct cellular mechanisms. *Acta Neuropathol.* 121, 705–719. doi: 10.1007/s00401-011-0806-2

Heiland, T., Zeitschel, U., Puchades, M. A., Kuhn, P. H., Lichtenthaler, S. F., Bjaalie, J. G., et al. (2019). Defined astrocytic expression of human amyloid precursor protein in Tg2576 mouse brain. *Glia* 67, 393–403. doi: 10.1002/glia.23550

Höfling, C., Morawski, M., Zeitschel, U., Zanier, E. R., Moschke, K., Serdaroglu, A., et al. (2016). Differential transgene expression patterns in Alzheimer mouse models revealed by novel human amyloid precursor protein-specific antibodies. *Aging Cell* 15, 953–963. doi: 10.1111/acel.12508

Hsiao, K., Chapman, P., Nilsen, S., Eckman, C., Harigaya, Y., Younkin, S., et al. (1996). Correlative memory deficits, Abeta elevation, and amyloid plaques in transgenic mice. *Science* 274, 99–102. doi: 10.1126/science.274.5284.99

Huh, S., Baek, S. J., Lee, K. H., Whitcomb, D. J., Jo, J., Choi, S. M., et al. (2016). The reemergence of long-term potentiation in aged Alzheimer's disease mouse model. *Sci. Rep.* 6:29152. doi: 10.1038/srep29152

Iritani, S., Niizato, K., and Emson, P. C. (2001). Relationship of calbindin D28K-immunoreactive cells and neuropathological changes in the hippocampal formation of Alzheimer's disease. *Neuropathology* 21, 162–167. doi: 10.1046/j.1440-1789.2001.00393.x

Jacobsen, J. S., Wu, C. C., Redwine, J. M., Comery, T. A., Arias, R., Bowlby, M., et al. (2006). Early-onset behavioral and synaptic deficits in a mouse model of Alzheimer's disease. *Proc. Natl. Acad. Sci. U.S.A.* 103, 5161–5166. doi: 10.1073/pnas.0600948103

Jiang, Y., Mullaney, K. A., Peterhoff, C. M., Che, S., Schmidt, S. D., Boyer-Boiteau, A., et al. (2010). Alzheimer's-related endosome dysfunction in down syndrome is Abeta-independent but requires APP and is reversed by BACE-1 inhibition. *Proc. Natl. Acad. Sci. U.S.A.* 107, 1630–1635. doi: 10.1073/pnas.0908953107

Kawarabayashi, T., Younkin, L. H., Saido, T. C., Shoji, M., Ashe, K. H., and Younkin, S. G. (2001). Age-dependent changes in brain, CSF, and plasma amyloid (beta) protein in the Tg2576 transgenic mouse model of Alzheimer's disease. *J. Neurosci.* 21, 372–381. doi: 10.1523/JNEUROSCI.21-02-00372.2001

Kimberly, W. T., LaVoie, M. J., Ostaszewski, B. L., Ye, W., Wolfe, M. S., and Selkoe, D. J. (2003). Gamma-secretase is a membrane protein complex comprised of presenilin, nicastrin, Aph-1, and Pen-2. *Proc. Natl. Acad. Sci. U.S.A.* 100, 6382–6387. doi: 10.1073/pnas.1037392100

King, D. L., and Arendash, G. W. (2002). Behavioral characterization of the Tg2576 transgenic model of Alzheimer's disease through 19 months. *Physiol. Behav.* 75, 627–642. doi: 10.1016/S0031-9384(02)00639-X

Krezymon, A., Richetin, K., Halley, H., Roybon, L., Lassalle, J. M., Francès, B., et al. (2013). Modifications of hippocampal circuits and early disruption of adult neurogenesis in the tg2576 mouse model of Alzheimer's disease. *PLoS One* 8:e76497. doi: 10.1371/journal.pone.0076497

Kumar, A., Singh, A., and Ekavali (2015). A review on Alzheimer's disease pathophysiology and its management: an update. *Pharmacol. Rep.* 67, 195–203. doi: 10.1016/j.pharep.2014.09.004

Lanz, T. A., Carter, D. B., and Merchant, K. M. (2003). Dendritic spine loss in the hippocampus of young PDAPP and Tg2576 mice and its prevention by the ApoE2 genotype. *Neurobiol. Dis.* 13, 246–253. doi: 10.1016/S0969-9961(03)00079-2

Lauritzen, I., Pardossi-Piquard, R., Bauer, C., Brigham, E., Abraham, J. D., Ranaldi, S., et al. (2012). The β-secretase-derived C-terminal fragment of βAPP, C99, but not Aβ, is a key contributor to early intraneuronal lesions in triple-transgenic mouse hippocampus. *J. Neurosci.* 32, 16243a–16255a. doi: 10.1523/JNEUROSCI.2775-12.2012

Lauritzen, I., Pardossi-Piquard, R., Bourgeois, A., Pagnotta, S., Biferi, M. G., Barkats, M., et al. (2016). Intraneuronal aggregation of the β-CTF fragment of APP (C99) induces Aβ-independent lysosomal-autophagic pathology. *Acta Neuropathol.* 132, 257–276. doi: 10.1007/s00401-016-1577-6

Lichtenthaler, S. F., Haass, C., and Steiner, H. (2011). Regulated intramembrane proteolysis–lessons from amyloid precursor protein processing. *J. Neurochem.* 117, 779–796. doi: 10.1111/j.1471-4159.2011.07248.x

Lovett-Barron, M., Kaifosh, P., Kheirbek, M. A., Danielson, N., Zaremba, J. D., Reardon, T. R., et al. (2014). Dendritic inhibition in the hippocampus supports fear learning. *Science* 343, 857–863. doi: 10.1126/science.1247485

Mátyás, F., Freund, T. F., and Gulyás, A. I. (2004). Immunocytochemically defined interneuron populations in the hippocampus of mouse strains used in transgenic technology. *Hippocampus* 14, 460–481. doi: 10.1002/hipo.10191

Mikkonen, M., Alafuzoff, I., Tapiola, T., Soininen, H., and Miettinen, R. (1999). Subfield- and layer-specific changes in parvalbumin, calretinin and calbindin-D28K immunoreactivity in the entorhinal cortex in Alzheimer's disease. *Neuroscience* 92, 515–532. doi: 10.1016/S0306-4522(99)00047-0

Mitew, S., Kirkcaldie, M. T., Dickson, T. C., and Vickers, J. C. (2013). Neurites containing the neurofilament-triplet proteins are selectively vulnerable to cytoskeletal pathology in Alzheimer's disease and transgenic mouse models. *Front. Neuroanat.* 7:30. doi: 10.3389/fnana.2013.00030

Mondragón-Rodríguez, S., Gu, N., Manseau, F., and Williams, S. (2018). Alzheimer's transgenic model is characterized by very early brain network alterations and β-CTF fragment accumulation: reversal by β-Secretase inhibition. *Front. Cell. Neurosci.* 12:121. doi: 10.3389/fncel.2018.00121

Neve, R. L., Valletta, J. S., Li, Y., Ventosa-Michelman, M., Holtzman, D. M., and Mobley, W. C. (1996). A comprehensive study of the spatiotemporal pattern of b-amyloid precursor protein mRNA and protein in the rat brain: lack of modulation by exogenously applied nerve growth factor. *Mol. Brain Res.* 39, 185–197. doi: 10.1016/0169-328X(96)00007-1

Palop, J. J., Jones, B., Kekonius, L., Chin, J., Yu, G. Q., Raber, J., et al. (2003). Neuronal depletion of calcium-dependent proteins in the dentate gyrus is tightly linked to Alzheimer's disease-related cognitive deficits. *Proc. Natl. Acad. Sci. U.S.A.* 100, 9572–9577. doi: 10.1073/pnas.1133381100

Perez-Cruz, C., Nolte, M. W., van Gaalen, M. M., Rustay, N. R., Termont, A., Tanghe, A., et al. (2011). Reduced spine density in specific regions of CA1 pyramidal neurons in two transgenic mouse models of Alzheimer's disease. *J. Neurosci.* 31, 3926–3934. doi: 10.1523/JNEUROSCI.6142-10.2011

Popović, M., Caballero-Bleda, M., Kadish, I., and Van Groen, T. (2008). Subfield and layer-specific depletion in calbindin-D28K, calretinin and parvalbumin immunoreactivity in the dentate gyrus of amyloid precursor protein/presenilin 1 transgenic mice. *Neuroscience* 155, 182–191. doi: 10.1016/j.neuroscience.2008.05.023

Priller, C., Bauer, T., Mitteregger, G., Krebs, B., Kretzschmar, H. A., and Herms, J. (2006). Synapse formation and function is modulated by the amyloid precursor protein. *J. Neurosci.* 26, 7212–7221. doi: 10.1523/JNEUROSCI.1450-06.2006

Ramos, B., Baglietto-Vargas, D., del Rio, J. C., Moreno-Gonzalez, I., Santa-Maria, C., Jimenez, S., et al. (2006). Early neuropathology of somatostatin/NPY GABAergic cells in the hippocampus of a PS1xAPP transgenic model of Alzheimer's disease. *Neurobiol. Aging* 27, 1658–1672. doi: 10.1016/j.neurobiolaging.2005.09.022

Royer, S., Zemelman, B. V., Losonczy, A., Kim, J., Chance, F., Magee, J. C., et al. (2012). Control of timing, rate and bursts of hippocampal place cells by dendritic and somatic inhibition. *Nat. Neurosci.* 15, 769–775. doi: 10.1038/nn.3077

Salloway, S., Gamez, J. E., Singh, U., Sadowsky, C. H., Villena, T., Sabbagh, M. N., et al. (2017). Performance of [18F]flutemetamol amyloid imaging against the neuritic plaque component of CERAD and the current (2012) NIA-AA recommendations for the neuropathologic diagnosis of Alzheimer's disease. *Alzheimers Dement.* 9, 25–34.

Sandoval, K. E., Farr, S. A., Banks, W. A., Crider, A. M., Morley, J. E., and Witt, K. A. (2013). Somatostatin receptor subtype-4 agonist NNC 26-9100 mitigates the effect of soluble Aβ(42) oligomers via a metalloproteinase-dependent mechanism. *Brain Res.* 1520, 145–156. doi: 10.1016/j.brainres.2013.05.006

Sasaguri, H., Nilsson, P., Hashimoto, S., Nagata, K., Saito, T., De Strooper, B., et al. (2017). APP mouse models for Alzheimer's disease preclinical studies. *EMBO J.* 36, 2473–2487. doi: 10.15252/embj.201797397

Schmid, L. C., Mittag, M., Poll, S., Steffen, J., Wagner, J., Geis, H. R., et al. (2016). Dysfunction of somatostatin-positive interneurons associated with memory deficits in an Alzheimer's disease model. *Neuron* 92, 114–125. doi: 10.1016/j.neuron.2016.08.034

Shah, D., Praet, J., Latif Hernandez, A., Höfling, C., Anckaerts, C., Bard, F., et al. (2016). Early pathologic amyloid induces hypersynchrony of BOLD resting-state networks in transgenic mice and provides an early therapeutic window before amyloid plaque deposition. *Alzheimers Dement.* 12, 964–976. doi: 10.1016/j.jalz.2016.03.010

Sheline, Y. I., and Raichle, M. E. (2013). Resting state functional connectivity in preclinical Alzheimer's disease. *Biol. Psychiatry* 74, 340–347. doi: 10.1093/cercor/bhu259

Stefanits, H., Wesseling, C., and Kovacs, G. G. (2014). Loss of calbindin immunoreactivity in the dentate gyrus distinguishes Alzheimer's disease from other neurodegenerative dementias. *Neurosci. Lett.* 566, 137–141. doi: 10.1016/j.neulet.2014.02.026

Takahashi, H., Brasnjevic, I., Rutten, B. P., Van Der Kolk, N., Perl, D. P., Bouras, C., et al. (2010). Hippocampal interneuron loss in an APP/PS1 double mutant mouse and in Alzheimer's disease. *Brain Struct. Funct.* 214, 145–160. doi: 10.1007/s00429-010-0242-4

Vassar, R., Kuhn, P. H., Haass, C., Kennedy, M. E., Rajendran, L., Wong, P. C., et al. (2014). Function, therapeutic potential and cell biology of BACE proteases: current status and future prospects. *J. Neurochem.* 130, 4–28. doi: 10.1111/jnc.12715

Verdaguer, E., Brox, S., Petrov, D., Olloquequi, J., Romero, R., de Lemos, M. L., et al. (2015). Vulnerability of calbindin, calretinin and parvalbumin in a transgenic/knock-in APPswe/PS1dE9 mouse model of Alzheimer disease together with disruption of hippocampal neurogenesis. *Exp. Gerontol.* 69, 176–188. doi: 10.1016/j.exger.2015.06.013

Verret, L., Mann, E. O., Hang, G. B., Barth, A. M., Cobos, I., Ho, K., et al. (2012). Inhibitory interneuron deficit links altered network activity and cognitive dysfunction in Alzheimer model. *Cell* 149, 708–721. doi: 10.1016/j.cell.2012.02.046

Xu, W., Fitzgerald, S., Nixon, R. A., Levy, E., and Wilson, D. A. (2015). Early hyperactivity in lateral entorhinal cortex is associated with elevated levels of AβPP metabolites in the Tg2576 mouse model of Alzheimer's disease. *Exp. Neurol.* 264, 82–91. doi: 10.1016/j.expneurol.2014.12.008

You, J. C., Muralidharan, K., Park, J. W., Petrof, I., Pyfer, M. S., Corbett, B. F., et al. (2017). Epigenetic suppression of hippocampal calbindin-D28k by ΔFosB drives seizure-related cognitive deficits. *Nat. Med.* 23, 1377–1383. doi: 10.1038/nm.4413

Conflict of Interest Statement: The authors declare that the research was conducted in the absence of any commercial or financial relationships that could be construed as a potential conflict of interest.

Copyright © 2019 Höfling, Shehabi, Kuhn, Lichtenthaler, Hartlage-Rübsamen and Roßner. This is an open-access article distributed under the terms of the Creative Commons Attribution License (CC BY). The use, distribution or reproduction in other forums is permitted, provided the original author(s) and the copyright owner(s) are credited and that the original publication in this journal is cited, in accordance with accepted academic practice. No use, distribution or reproduction is permitted which does not comply with these terms.

frontiers in Neuroscience

MINI REVIEW
published: 26 March 2019
doi: 10.3389/fnins.2019.00273

Early Dyskinesias in Parkinson's Disease Patients With Parkin Mutation: A Primary Corticostriatal Synaptopathy?

Jenny Sassone[1,2]*, *Flavia Valtorta*[1,2] *and Andrea Ciammola*[3]

[1] Division of Neuroscience, IRCCS San Raffaele Scientific Institute, Milan, Italy, [2] Vita-Salute San Raffaele University, Milan, Italy, [3] Department of Neurology, IRCCS Istituto Auxologico Italiano, Milan, Italy

Mutations in the *PARKIN* gene cause early-onset Parkinson's disease (PD). Despite the high proportion of still missing phenotyping data in the literature devoted to early-onset PD, studies suggest that, as compared with late-onset PD, *PARKIN* patients show dystonia at onset and extremely dose-sensitive levodopa-induced dyskinesia (LID). What pathophysiological mechanisms underpin such early and atypical dyskinesia in patients with *PARKIN* mutations? Though the precise mechanisms underlying dystonia and LID are still unclear, evidence suggests that hyperkinetic disorders in PD are a behavioral expression of maladaptive functional and morphological changes at corticostriatal synapses induced by long-term dopamine (DA) depletion. However, since the dyskinesia in *PARKIN* patients can also be present at onset, other mechanisms beside the well-established DA depletion may play a role in the development of dyskinesia in these patients. Because cortical and striatal neurons express parkin protein, and parkin modulates the function of ionotropic glutamatergic receptors (iGluRs), an intriguing explanation may rest on the potential role of parkin in directly controlling the glutamatergic corticostriatal synapse transmission. We discuss the novel theory that loss of parkin function can dysregulate transmission at the corticostriatal synapses where they cause early maladaptive changes that co-occur with the changes stemming from DA loss. This hypothesis suggests an early striatal synaptopathy; it could lay the groundwork for pharmacological treatment of dyskinesias and LID in patients with *PARKIN* mutations.

Keywords: synaptopathy, glutamatergic transmission, parkin, dyskinesia, striatum

OPEN ACCESS

Edited by:
Gregory Jaye Bix,
University of Kentucky, United States

Reviewed by:
Mattia Volta,
EURAC Research, Italy
Sandeep Kumar Barodia,
The University of Alabama at Birmingham, United States

***Correspondence:**
Jenny Sassone
sassone.jenny@hsr.it

Specialty section:
This article was submitted to Neurodegeneration, a section of the journal Frontiers in Neuroscience

Received: *27 November 2018*
Accepted: *07 March 2019*
Published: *26 March 2019*

Citation:
Sassone J, Valtorta F and Ciammola A (2019) Early Dyskinesias in Parkinson's Disease Patients With Parkin Mutation: A Primary Corticostriatal Synaptopathy? Front. Neurosci. 13:273. doi: 10.3389/fnins.2019.00273

INTRODUCTION

Loss of function mutations in the *PARKIN* gene cause autosomal recessive juvenile parkinsonism (ARJP) (Kitada et al., 1998). Autopsy studies have shown that neuropathological changes in patients with *PARKIN* mutations differ from those observed in idiopathic Parkinson's disease (iPD). Unlike iPD, neuronal loss is greater in the substantia nigra pars compacta (SNpc) than in the locus coeruleus in most parkin cases. Also, Lewy bodies are not detected in the majority of parkin cases, suggesting a difference in the pathogenic processes between *PARKIN*-related disease and iPD

(Schneider and Alcalay, 2017). Also, *PARKIN*-associated, early-onset PD is phenotypically distinct from iPD. Recent reviews in the clinical literature on genetic PD have pointed to the lack of a detailed description of individual phenotypic features (Kasten et al., 2017, 2018). Evidence suggests, however, that unlike late-onset PD patients, parkin patients display dystonia at early disease stages and dyskinesia at exceedingly low dosages of levodopa (Wickremaratchi et al., 2011). Early dystonia and dyskinesia are also reported in other early-onset genetic forms of PD such as *PINK1* and *DJ1* (Lohmann et al., 2009). Since *PARKIN* mutations account for about three-quarters of PD cases with an age at onset of 30 years or younger, understanding the pathophysiological mechanisms that underlie early and atypical dystonia and dyskinesia in *PARKIN* patients is a key step toward achieving a more personalized treatment for this genetic condition and toward understanding the biological basis of this phenomena in other early-onset genetic forms of PD.

Here, we review the clinical evidence for early hyperkinetic symptoms in patients with *PARKIN* mutations and the recent evidence that parkin modulates glutamatergic neurotransmission. We discuss the hypothesis that early hyperkinetic symptoms of PD patients with *PARKIN* mutation may be considered manifestations of corticostriatal synaptopathy. These features can be linked to dopamine depletion, a well-recognized mechanism in the literature, but they also may be related to a potential direct effect of parkin on the corticostriatal synapse.

CLINICAL EVIDENCE FOR DYSTONIA AND DYSKINESIA IN PARKIN PATIENTS

Since the first description of juvenile parkinsonism caused by mutations of the *PARKIN* gene in two families (Kitada et al., 1998), dystonia has been proposed as a clinical hallmark of the disease (Schrag and Schott, 2006). Recent literature reviews have reported that an overall, clinically typical form of PD with early onset, slow progression, and excellent response to levodopa treatment is frequently associated with dystonia and dyskinesia in patients with *PARKIN* mutations (Grünewald et al., 2013; Kasten et al., 2018). Usually independent of levodopa intake, dystonia is described as the presenting symptom in a large percentage of *PARKIN* patients in whom it can be present in isolation for years before the appearance of parkinsonism (Khan et al., 2003). The reported phenotypic overlap between PD patients with *PARKIN* mutation and rare forms of dystonia-parkinsonism, such as levodopa-responsive dystonia (DRD), prompts screening for *PARKIN* mutations along with *GTP cyclohydrolase* 1 and *tyrosine hydroxylase* in clinically diagnosed DRD patients (Tassin et al., 2000; Wu et al., 2005, 2008; Schneider and Bhatia, 2010; Potulska-Chromik et al., 2017). To determine whether dystonia contributes to gait abnormalities in patients with *PARKIN* mutations, a recent study used a clinical computerized video motion analysis system to evaluate lower limb dystonia severity in 15 patients. Lower limb dystonia occurred in most *PARKIN* patients who displayed a specific, abnormal gait pattern that differed from the patterns observed in healthy controls independent of the OFF/ON state (Castagna et al., 2016).

In addition to dystonia, *PARKIN* patients show dyskinesia at exceedingly low dosages of levodopa as compared with late-onset PD patients. On average, the response to low doses of levodopa is reported as being excellent and sustained. However, the likelihood of developing LID is reportedly higher than in individuals with parkinsonism resulting from other aetiologies (Brüggemann and Klein, 1993; Paviour et al., 2004) and it is inducible by very-low-dose levodopa in some cases (Khan et al., 2003). While bradykinesia responds well even to low levodopa dosages in *PARKIN* patients, the same low doses seem to exacerbate dystonia already in very early stages of the disease. Although conflicting results have also been reported (Kasten et al., 2018), the present evidence suggests that the incidence of hyperkinetic disorders at earlier disease stages is higher in *PARKIN* patients than in those with iPD.

POTENTIAL MOLECULAR MECHANISMS UNDERLYING DYSTONIA AND DYSKINESIA

The precise mechanisms underlying dystonia and LID in PD are unknown. Studies on PD animal models, mainly dopamine-depleted animals, and PD patients strongly suggest that dyskinesia results from dysfunction of glutamatergic transmission from the cortex to the striatal medium spiny neurons (MSNs) (Picconi et al., 2017). MSNs are characterized by radially projecting dendrites densely studded with spines and receiving excitatory glutamatergic inputs from the cerebral cortex which form in the order of 5000 contacts per neuron (Graveland et al., 1985; David Smith and Paul Bolam, 1990; Yelnik et al., 1991). The dendritic spines bear the asymmetrical glutamatergic synapse on the head and the symmetric dopaminergic synapses on the neck (**Figure 1A**; David Smith and Paul Bolam, 1990). This characteristic synaptic triad boosted the widely accepted theory that dopamine (DA) physiologically modulates the strength of cortical inputs to the MSNs (Gerfen and Surmeier, 2011) and that long-term DA depletion occurring over the course of idiopathic PD triggers prominent secondary changes in the corticostriatal synapses (Picconi et al., 2017). Indeed, DA depletion leads to strong sensitization of post-synaptic D1 receptors, which is critical for the development of dyskinesia (Darmopil et al., 2009), and induces a variety of molecular changes in the downstream signaling pathways, including an increase in the state of phosphorylation of the DA- and cAMP-regulated phosphoprotein of 32 KDa (DARPP-32) (Santini et al., 2007; Heumann et al., 2014; Ruiz-Dediego et al., 2015; Solís et al., 2017). DARPP-32 phosphorylation promotes a cascade of intracellular events in MSNs: activation of extracellular signal-regulated kinase 1 and 2 (ERK1 and 2) and, as a consequence, activation of the ERK and the mammalian target of rapamycin complex 1 (mTORC1) signaling pathways (Santini et al., 2012; Heumann et al., 2014).

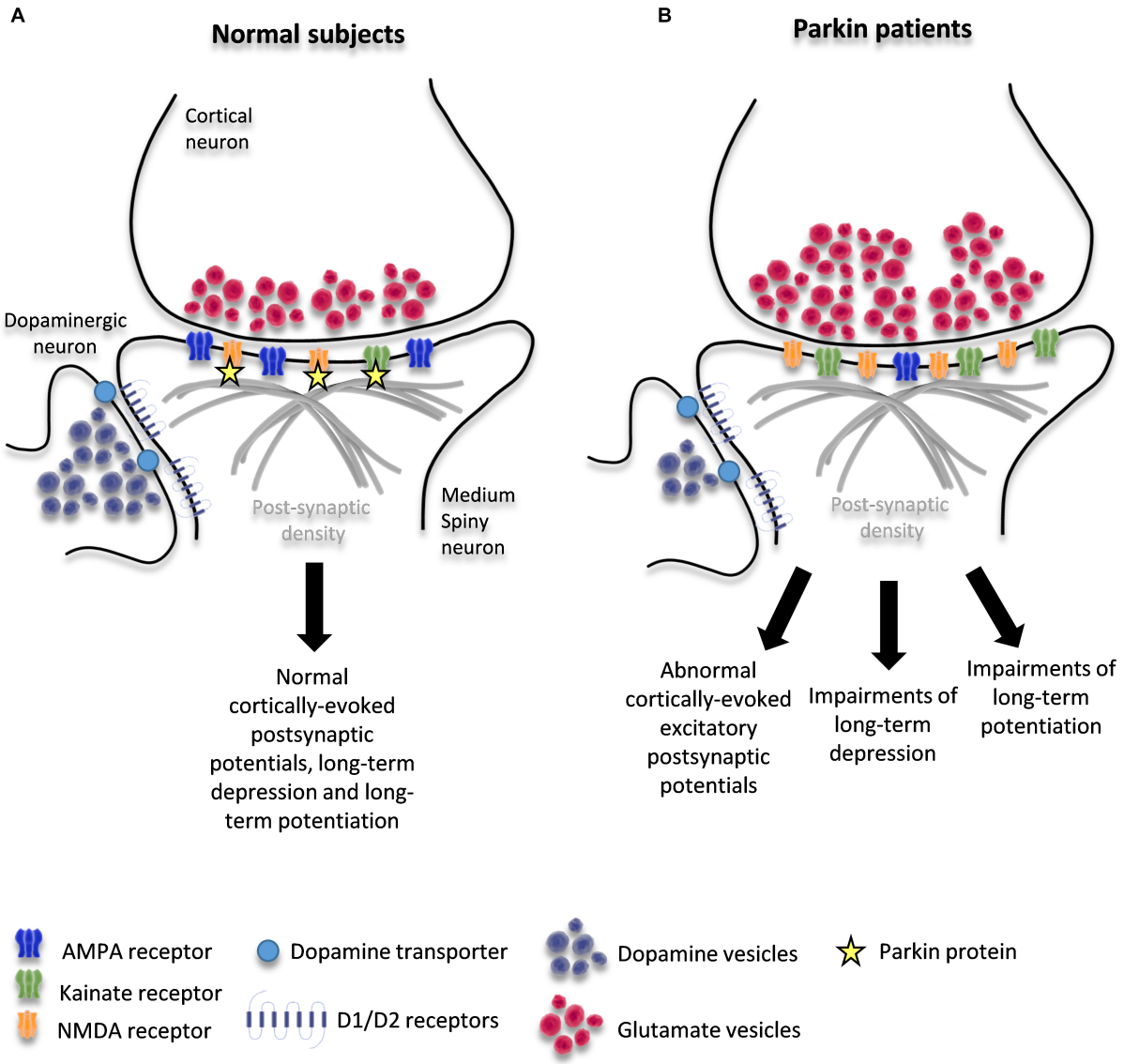

FIGURE 1 | Schematic diagram of corticostriatal synapse in healthy condition **(A)** and in patients with *PARKIN* mutations **(B)**. The figure shows the interaction of parkin with KAR and NMDAR and potential changes induced by loss of *PARKIN* function.

The molecular signatures that have recently emerged as key signals in LIDs are ERK1/2 phosphorylation (Pavón et al., 2006), abnormal activation of mitogen- and stress-activated protein kinase-1 (MSK-1), and phosphorylation of histone H3 (Santini et al., 2007; Heumann et al., 2014). The final result of this chain of events is a change in the molecular make-up of MSNs due to alterations in gene expression and protein synthesis that might account for maladaptive morphological plasticity at the corticostriatal synapse (Picconi et al., 2017). Morphological examination of MSNs in dopamine-depleted animals and in autopsy specimens from iPD patients has revealed dendrite atrophy, truncated dendrites, and decreased spine density (Stephens et al., 2005; Zaja-Milatovic et al., 2005; Suarez et al., 2016). These functional and morphological changes in the corticostriatal synapses are believed to result in dyskinesias (Picconi et al., 2017).

The question arises as to whether the same molecular mechanisms underlie the early and atypical dyskinesia displayed by *PARKIN* patients. Clinical studies with [18F] Dopa as a marker of the functional integrity of pre-synaptic dopamine nerve terminals have shown that *Parkin* mutated patients have widespread pre-synaptic dopaminergic deficits (Scherfler et al., 2004). So while the early hyperkinetic symptoms in patients with parkin mutations can be linked to DA depletion, the appearance of dyskinesia in early disease stages, before the onset of typical and cardinal signs of parkinsonism, suggests that additional mechanisms may be involved. In particular, dyskinesia-related molecular changes in patients with

PARKIN mutation may partially stem from dysfunctions of the corticostriatal synapses due to the loss of parkin function in these synapses.

THE POTENTIAL ROLE OF PARKIN AT THE CORTICOSTRIATAL SYNAPSE

In vitro studies have revealed that parkin can localize at the pre-synapse, where it associates with the cytoplasmic surface of synaptic vesicles (Kubo et al., 2001; Mouatt-Prigent et al., 2004) and binds to synaptotagmin-11, a pre-synaptic protein involved in synaptic vesicle formation, docking, and recycling (Huynh et al., 2003; Wang et al., 2018). The loss of parkin function may inhibit endocytosis and the processes of vesicle replenishment and recycling, leading to as yet undefined changes in neurotransmitter release. Interestingly, the pre-synaptic functions of parkin resemble the function of synuclein, another key protein involved in PD pathogenesis and a regulator of pre-synapse size and synaptic vesicle pool organization (Anwar et al., 2011; Vargas et al., 2017), additionally, the roles of other PD genes such as *DNAJC6*, *SYNJ1*, *SH3GL2, LRRK2*, and *VPS35* in the regulation of synaptic vesicle trafficking SVE are beginning to emerge (Nguyen et al., 2018).

In vitro studies on glutamatergic neurons showed that parkin can also localize at the post-synapse, where it directly modulates ionotropic glutamate receptor function. Parkin directly interacts with and ubiquitinates the GluK2 subunit of kainate receptor (KAR) and thus regulates its function: loss of parkin increases KAR levels in the human cortex and KAR function in glutamatergic hippocampal neurons *in vitro* (Maraschi et al., 2014). At the post-synapse, loss of parkin function probably leads to dysregulation of other neurotransmitter receptors as well: a study on brain tissues from parkin knockout mice showed up-regulation of KAR density, increased NMDA receptor density, and reduced AMPA receptor density throughout various brain regions (Cremer et al., 2015). The role of parkin in modulating AMPA receptors was further confirmed in an *in vitro* study showing that parkin-deficient hippocampal neurons exhibit significantly reduced AMPA receptor-mediated currents (Cortese et al., 2016). The suggested underlying mechanism is the decrease in the post-synaptic expression of the adaptor protein Homer1, which is necessary for coupling AMPAR endocytic zones with post-synaptic density. A more recent study evaluated the impact of four parkin point mutations on glutamatergic synaptic function in hippocampal neurons and found that these mutants alter NMDA and AMPA receptor-mediated currents and cell-surface levels and that they prevent the induction of long-term depression. The study demonstrated that parkin regulates NMDA receptor trafficking through ubiquitination of the subunit GluN1 and that the mutations impair ubiquitination activity (Zhu et al., 2018). Hence, the bulk of evidence strongly suggests that *PARKIN* mutations disturb glutamatergic synaptic transmission by directly changing NMDAR, AMPAR, and KAR receptor function. Since parkin is widely expressed in various brain regions and neuron types, including cortical neurons and MSNs, (Kitada et al., 1998; Stichel et al., 2000) it is conceivable that the loss of parkin directly induces pathological effects on these neurons and contributes to the pathophysiology of dyskinesia.

These studies on the localization of parkin and its capacity to directly regulate excitatory transmission constitute an important step toward understanding the functions of parkin at the synapses (Sassone et al., 2017). The complementary approach was to investigate the function of nigrostriatal and corticostriatal synapses in murine models knockout for *Parkin* gene. Unfortunately, studies on the nigrostriatal pathway revealed many discrepancies probably deriving from different experimental conditions and/or from *in vivo* age-dependent compensatory mechanisms. Increased spontaneous DA release from SNc DA neurons was found in *Parkin*-knockout mice aged 8 to 9 months (Goldberg et al., 2003). Decreased evoked DA release was found in 3-to-9-month-old *Parkin* knockout mice (Oyama et al., 2010). In the striatum of 22-month-old wild-type and *Parkin*-knockout mice, DA levels were reported to be indistinguishable (Perez and Palmiter, 2005). DA overflow in striatal slices from 6-to-8-week-old mice was found to be equal between wild-type and *Parkin*-knockout mice (Sanchez et al., 2014). Indeed, not all the evidence supports the idea that DA release is impaired in the nigrostriatal pathway of *Parkin*-knockout mice. Studies on corticostriatal synapses performed by intracellular recordings of MSNs revealed impairment in long-term depression and long-term potentiation in *Parkin*-knockout mice (Kitada et al., 2009). These results suggest that parkin is involved in the regulation of striatal synaptic plasticity. Unfortunately, however, *Parkin*-knockout mice do not show DA neuron loss, motor impairment, dystonic phenotype or hypersensitivity to levodopa (Perez and Palmiter, 2005). The authors suggest that this murine model may represent a tool to study the early stages of the disease (Dawson et al., 2010); nonetheless, its usefulness as a disease model is limited and complicates the interpretation of the results obtained on these mice. More promising results come from studies on dopaminergic neurons differentiated from induced human pluripotent stem cells. When glutamatergic transmission was studied in a mixed population of GABAergic, glutamatergic, and dopaminergic neurons differentiated from induced human pluripotent stem cells, *PARKIN* mutations were observed to potentiate glutamatergic transmission by modifying synaptic vesicle function at the pre-synaptic site of the corticostriatal synapse (Zhong et al., 2017). Moreover, the actions of dopamine on D1-class receptors were noted to be markedly altered in dopaminergic neurons differentiated from induced human pluripotent stem cells of PD patients with *PARKIN* mutations. In particular, as compared with control neurons, the parkin-deficient neurons had a stronger response to the activation of D1-class dopamine receptors (Zhong et al., 2017).

This raises the possibility that parkin could be involved in D1 receptor hypersensitization after dopaminergic denervation, an important mechanism underlying the dyskinesia in iPD (Heumann et al., 2014). Accordingly, a recent paper showed that parkin ubiquitinates and regulates the levels of STEP61, the striatal enriched protein tyrosine phosphatase, whereas clinically relevant parkin mutants fail to do so. Because STEP61 substrates include ERK1/2, it is conceivable that a parkin-induced

increase in STEP61 might influence D1 signaling in MSNs (Kurup et al., 2015).

Taken together, these findings suggest that parkin orchestrates a complex remodeling of corticostriatal synapses through multiple mechanisms. These mechanisms are likely to include changes due to DA depletion as well as those due to loss of parkin function at these synapses: alterations in the trafficking of glutamate vesicles at the glutamatergic pre-synapse and/or dysregulation of glutamate receptor levels on MSNs and/or dysregulation of D1-signaling. These mechanisms may be responsible for the precocious maladaptive plasticity of the corticostriatal synapses that leads to early dyskinesia (**Figure 1B**).

CONCLUSION

Since the parkin protein modulates glutamatergic receptor function and possibly glutamate release as well, it is conceivable that *PARKIN* mutation affects corticostriatal transmission, leading to early maladaptive changes in this glutamatergic synapse. This alteration could produce changes due to corticostriatal-induced depletion of DA at the synapses. What does this scenario imply for the development of specific and effective treatments? The only currently available drug for symptomatic treatment of dyskinesia is amantadine, an antiviral agent introduced in the early 1970s that also displays NMDA receptor antagonism (Hubsher et al., 2012). With a better understanding of the mechanisms by which parkin causes early dystonia and dyskinesia, researchers may be able to identify novel therapeutic targets and develop strategies that include drugs that act on the glutamatergic system. Such drugs are already under investigation for treating dyskinesias in iPD (Müller, 2017). Moreover, if our hypothesis proves true, the distinct molecular mechanisms underlying dyskinesia between *PARKIN* patients and late-onset PD patients could be relevant for devising precision medicine strategies for parkin patients. The recent discovery that LID is caused by a distinct and stable group of striatal neurons (Girasole et al., 2018) paves the way to further studies aimed at investigating the role of parkin in these neurons and at their corticostriatal synapse.

In conclusion, published data support the hypothesis of an early corticostriatal synaptopathy in parkin patients caused by parkin modulating the glutamatergic synapse. This hypothesis could provide a biological basis for studying the disease phenotype and lay the groundwork for the pharmacological treatment of PD patients with *PARKIN* mutation.

AUTHOR CONTRIBUTIONS

JS wrote first draft of the manuscript. FV and AC reviewed and critically revised the manuscript.

FUNDING

This work was supported by the Telethon Foundation (Grant GGP15167 to AC) and the Italian Ministry of Health (GR-2016-02361366 to JS).

ACKNOWLEDGMENTS

The authors wish to thank Floriano Girotti for critical revision and reading of the manuscript. The Michael J. Fox Foundation for Parkinson's Research (Grant MJFF14110 to JS).

REFERENCES

Anwar, S., Peters, O., Millership, S., Ninkina, N., Doig, N., Connor-Robson, N., et al. (2011). Functional alterations to the nigrostriatal system in mice lacking all three members of the synuclein family. *J. Neurosci.* 31, 7264–7274. doi: 10.1523/JNEUROSCI.6194-10.2011

Brüggemann, N., and Klein, C. (1993). "Parkin type of early-onset Parkinson disease," in *GeneReviews® [Internet]*, eds M. P. Adam, H. H. Ardinger, R. A. Pagon, S. E. Wallace, L. J. H. Bean, K. Stephens, et al. (Seattle, WA: University of Washington).

Castagna, A., Frittoli, S., Ferrarin, M., Del Sorbo, F., Romito, L. M., Elia, A. E., et al. (2016). Quantitative gait analysis in parkin disease: possible role of dystonia. *Mov. Disord.* 31, 1720–1728. doi: 10.1002/mds.26672

Cortese, G. P., Zhu, M., Williams, D., Heath, S., and Waites, C. L. (2016). Parkin deficiency reduces hippocampal glutamatergic neurotransmission by impairing AMPA receptor endocytosis. *J. Neurosci.* 36, 12243–12258. doi: 10.1523/JNEUROSCI.1473-16.2016

Cremer, J. N., Amunts, K., Schleicher, A., Palomero-Gallagher, N., Piel, M., Rösch, F., et al. (2015). Changes in the expression of neurotransmitter receptors in Parkin and DJ-1 knockout mice. quantitative multireceptor study. *Neuroscience* 311, 539–551. doi: 10.1016/j.neuroscience.2015.10.054

Darmopil, S., Martín, A. B., De Diego, I. R., Ares, S., and Moratalla, R. (2009). Genetic inactivation of dopamine D1 but Not D2 receptors inhibits L-DOPA-induced dyskinesia and histone activation. *Biol. Psychiatry* 66, 603–613. doi: 10.1016/j.biopsych.2009.04.025

David Smith, A., and Paul Bolam, J. (1990). The neural network of the basal ganglia as revealed by the study of synaptic connections of identified neurones. *Trends Neurosci.* 13, 259–265. doi: 10.1016/0166-2236(90)90106-K

Dawson, T. M., Ko, H. S., and Dawson, V. L. (2010). Genetic animal models of Parkinson's disease. *Neuron* 66, 646–661. doi: 10.1016/j.neuron.2010.04.034

Gerfen, C. R., and Surmeier, D. J. (2011). Modulation of striatal projection systems by dopamine. *Annu. Rev. Neurosci.* 34, 441–466. doi: 10.1146/annurev-neuro-061010-113641

Girasole, A. E., Lum, M. Y., Nathaniel, D., Bair-Marshall, C. J., Guenthner, C. J., Luo, L., et al. (2018). A subpopulation of striatal neurons mediates levodopa-induced dyskinesia. *Neuron* 97, 787–795. doi: 10.1016/j.neuron.2018.01.017

Goldberg, M. S., Fleming, S. M., Palacino, J. J., Cepeda, C., Lam, H. A., Bhatnagar, A., et al. (2003). Parkin-deficient mice exhibit nigrostriatal deficits but not loss of dopaminergic neurons. *J. Biol. Chem.* 278, 43628–43635. doi: 10.1074/jbc.M308947200

Graveland, G. A., Williams, R. S., and Difiglia, M. (1985). A golgi study of the human neostriatum: neurons and afferent fibers. *J. Comp. Neurol.* 234, 317–333. doi: 10.1002/cne.902340304

Grünewald, A., Kasten, M., Ziegler, A., and Klein, C. (2013). Next-generation phenotyping using the Parkin example: time to catch up with genetics. *JAMA Neurol.* 70, 1186–1191. doi: 10.1001/jamaneurol.2013.488

Heumann, R., Moratalla, R., Herrero, M. T., Chakrabarty, K., Drucker-Colín, R., Garcia-Montes, J. R., et al. (2014). Dyskinesia in Parkinson's disease: mechanisms and current non-pharmacological interventions. *J. Neurochem.* 130, 472–489. doi: 10.1111/jnc.12751

Hubsher, G., Haider, M., and Okun, M. S. (2012). Amantadine: the journey from fighting flu to treating Parkinson disease. *Neurology* 78, 1096–1099. doi: 10.1212/WNL.0b013e31824e8f0d

Huynh, D. P., Scoles, D. R., Nguyen, D., and Pulst, S. M. (2003). The autosomal recessive juvenile Parkinson disease gene product, parkin, interacts with and ubiquitinates synaptotagmin XI. *Hum. Mol. Genet.* 12, 2587–2597. doi: 10.1093/hmg/ddg269

Kasten, M., Hartmann, C., Hampf, J., Schaake, S., Westenberger, A., Vollstedt, E. J., et al. (2018). Genotype-phenotype relations for the Parkinson's disease genes Parkin, PINK1, DJ1: MDSGene systematic review. *Mov. Disord.* 33, 730–741. doi: 10.1002/mds.27352

Kasten, M., Marras, C., and Klein, C. (2017). Nonmotor signs in genetic forms of Parkinson's disease. *Int. Rev. Neurobiol.* 133, 129–178. doi: 10.1016/bs.irn.2017.05.030

Khan, N. L., Graham, E., Critchley, P., Schrag, A. E., Wood, N. W., Lees, A. J., et al. (2003). Parkin disease: a phenotypic study of a large case series. *Brain* 126, 1279–1292. doi: 10.1093/brain/awg142

Kitada, T., Asakawa, S., Hattori, N., Matsumine, H., Yamamura, Y., Minoshima, S., et al. (1998). Mutations in the parkin gene cause autosomal recessive juvenile parkinsonism. *Nature* 392, 605–608. doi: 10.1038/33416

Kitada, T., Pisani, A., Karouani, M., Haburcak, M., Martella, G., Tscherter, A., et al. (2009). Impaired dopamine release and synaptic plasticity in the striatum of Parkin-/- mice. *J. Neurochem.* 110, 613–621. doi: 10.1111/j.1471-4159.2009.06152.x

Kubo, S., Kitami, T., Noda, S., Shimura, H., Uchiyama, Y., Asakawa, S., et al. (2001). Parkin is associated with cellular vesicles. *J. Neurochem.* 78, 42–54. doi: 10.1046/j.1471-4159.2001.00364.x

Kurup, P. K., Xu, J., Videira, R. A., Ononenyi, C., Baltazar, G., Lombroso, P. J., et al. (2015). STEP 61 is a substrate of the E3 ligase parkin and is upregulated in Parkinson's disease. *Proc. Natl. Acad. Sci. U.S.A.* 112, 1202–1207. doi: 10.1073/pnas.1417423112

Lohmann, E., Thobois, S., Lesage, S., Broussolle, E., Du Montcel, S. T., Ribeiro, M. J., et al. (2009). A multidisciplinary study of patients with early-onset PD with and without parkin mutations. *Neurology* 72, 110–116. doi: 10.1212/01.wnl.0000327098.86861.d4

Maraschi, A. M., Ciammola, A., Folci, A., Sassone, F., Ronzitti, G., Cappelletti, G., et al. (2014). Parkin regulates kainate receptors by interacting with the GluK2 subunit. *Nat. Commun.* 5:5182. doi: 10.1038/ncomms6182

Mouatt-Prigent, A., Muriel, M. P., Gu, W. J., El Hachimi, K. H., Lücking, C. B., Brice, A., et al. (2004). Ultrastructural localization of parkin in the rat brainstem, thalamus and basal ganglia. *J. Neural Transm.* 111, 1209–1218. doi: 10.1007/s00702-004-0144-9

Müller, T. (2017). Current and investigational non-dopaminergic agents for management of motor symptoms (including motor complications) in Parkinson's disease. *Expert Opin. Pharmacother.* 18, 1457–1465. doi: 10.1080/14656566.2017.1373089

Nguyen, M., Wong, Y. C., Ysselstein, D., Severino, A., and Krainc, D. (2018). Synaptic, mitochondrial, and lysosomal dysfunction in parkinson's disease. *Trends Neurosci.* 42, 140–149. doi: 10.1016/j.tins.2018.11.001

Oyama, G., Yoshimi, K., Natori, S., Chikaoka, Y., Ren, Y. R., Funayama, M., et al. (2010). Impaired in vivo dopamine release in parkin knockout mice. *Brain Res.* 1352, 214–222. doi: 10.1016/j.brainres.2010.06.065

Paviour, D. C., Surtees, R. A. H., and Lees, A. J. (2004). Diagnostics considerations in juvenile parkinsonism. *Mov. Disord.* 19, 123–135. doi: 10.1002/mds.10644

Pavón, N., Martín, A. B., Mendialdua, A., and Moratalla, R. (2006). ERK phosphorylation and FosB expression are associated with L-DOPA-induced dyskinesia in hemiparkinsonian mice. *Biol. Psychiatry* 59, 64–74. doi: 10.1016/j.biopsych.2005.05.044

Perez, F. A., and Palmiter, R. D. (2005). Parkin-deficient mice are not a robust model of parkinsonism. *Proc. Natl. Acad. Sci. U.S.A.* 102, 2174–2179. doi: 10.1073/pnas.0409598102

Picconi, B., Hernández, L. F., Obeso, J. A., and Calabresi, P. (2017). Motor complications in Parkinson's disease: striatal molecular and electrophysiological mechanisms of dyskinesias. *Mov. Disord.* 33, 867–876. doi: 10.1002/mds.27261

Potulska-Chromik, A., Hoffman-Zacharska, D., Łukawska, M., and Kostera-Pruszczyk, A. (2017). Dopa-responsive dystonia or early-onset Parkinson disease – Genotype–phenotype correlation. *Neurol. Neurochir. Pol.* 51, 1–6. doi: 10.1016/j.pjnns.2016.07.013

Ruiz-Dediego, I., Mellstrom, B., Vallejo, M., Naranjo, J. R., and Moratalla, R. (2015). Activation of DREAM (Downstream Regulatory Element Antagonistic Modulator), a calcium-binding protein, reduces L-DOPA-induced dyskinesias in mice. *Biol. Psychiatry* 77, 95–105. doi: 10.1016/j.biopsych.2014.03.023

Sanchez, G., Varaschin, R. K., Büeler, H., Marcogliese, P. C., Park, D. S., and Trudeau, L. E. (2014). Unaltered striatal dopamine release levels in young Parkin knockout, Pink1 knockout, DJ-1 knockout and LRRK2 R1441G transgenic mice. *PLoS One* 9:e0094826. doi: 10.1371/journal.pone.0094826

Santini, E., Feyder, M., Gangarossa, G., Bateup, H. S., Greengard, P., and Fisone, G. (2012). Dopamine- and cAMP-regulated phosphoprotein of 32-kDa (DARPP-32)-dependent activation of extracellular signal-regulated kinase (ERK) and mammalian target of rapamycin complex 1 (mTORC1) signaling in experimental parkinsonism. *J. Biol. Chem.* 287, 27806–27812. doi: 10.1074/jbc.M112.388413

Santini, E., Valjent, E., Usiello, A., Carta, M., Borgkvist, A., Girault, J. A., et al. (2007). Critical involvement of cAMP/DARPP-32 and extracellular signal-regulated protein kinase signaling in L-DOPA-induced dyskinesia. *J. Neurosci.* 27, 6995–7005. doi: 10.1523/JNEUROSCI.0852-07.2007

Sassone, J., Serratto, G., Valtorta, F., Silani, V., Passafaro, M., and Ciammola, A. (2017). The synaptic function of parkin. *Brain* 140, 2265–2272. doi: 10.1093/brain/awx006

Scherfler, C., Khan, N. L., Pavese, N., Eunson, L., Graham, E., Lees, A. J., et al. (2004). Striatal and cortical pre- and postsynaptic dopaminergic dysfunction in sporadic parkin-linked parkinsonism. *Brain* 127, 1332–1342. doi: 10.1093/brain/awh150

Schneider, S. A., and Alcalay, R. N. (2017). Neuropathology of genetic synucleinopathies with parkinsonism: review of the literature. *Mov. Disord.* 32, 1504–1523. doi: 10.1002/mds.27193

Schneider, S. A., and Bhatia, K. P. (2010). Rare causes of dystonia parkinsonism. *Curr. Neurol. Neurosci. Rep.* 10, 431–439. doi: 10.1007/s11910-010-0136-0

Schrag, A., and Schott, J. M. (2006). Epidemiological, clinical, and genetic characteristics of early-onset parkinsonism. *Lancet Neurol.* 5, 355–363. doi: 10.1016/S1474-4422(06)70411-2

Solís, O., Garcia-Montes, J. R., González-Granillo, A., Xu, M., and Moratalla, R. (2017). Dopamine D3 receptor Modulates l-DOPA-Induced Dyskinesia by Targeting D1 Receptor-Mediated Striatal Signaling. *Cereb. Cortex* 27, 435–446. doi: 10.1093/cercor/bhv231

Stephens, B., Mueller, A. J., Shering, A. F., Hood, S. H., Taggart, P., Arbuthnott, G. W., et al. (2005). Evidence of a breakdown of corticostriatal connections in Parkinson's disease. *Neuroscience* 132, 741–754. doi: 10.1016/j.neuroscience.2005.01.007

Stichel, C. C., Augustin, M., Kühn, K., Zhu, X. R., Engels, P., Ullmer, C., et al. (2000). Parkin expression in the adult mouse brain. *Eur. J. Neurosci.* 12, 4181–4194.

Suarez, L. M., Solis, O., Aguado, C., Lujan, R., and Moratalla, R. (2016). L-DOPA oppositely regulates synaptic strength and spine morphology in D1 and D2 striatal projection neurons in dyskinesia. *Cereb. Cortex* 26, 4253–4264. doi: 10.1093/cercor/bhw263

Tassin, J., Dürr, A., Bonnet, A. M., Gil, R., Vidailhet, M., Lücking, C. B., et al. (2000). Levodopa-responsive dystonia. GTP cyclohydrolase I or parkin mutations? *Brain* 123, 1112–1121. doi: 10.1093/brain/123.6.1112

Vargas, K. J., Schrod, N., Davis, T., Fernandez-Busnadiego, R., Taguchi, Y. V., Laugks, U., et al. (2017). Synucleins Have Multiple Effects on Presynaptic Architecture. *Cell Rep.* 18, 161–173. doi: 10.1016/j.celrep.2016.12.023

Wang, C., Kang, X., Zhou, L., Chai, Z., Wu, Q., Huang, R., et al. (2018). Synaptotagmin-11 is a critical mediator of parkin-linked neurotoxicity and Parkinson's disease-like pathology. *Nat. Commun.* 9:81. doi: 10.1038/s41467-017-02593-y

Wickremaratchi, M. M., Knipe, M. D. W., Sastry, B. S. D., Morgan, E., Jones, A., Salmon, R., et al. (2011). The motor phenotype of Parkinson's disease in relation to age at onset. *Mov. Disord.* 26, 457–463. doi: 10.1002/mds.23469

Wu, R. M., Bounds, R., Lincoln, S., Hulihan, M., Lin, C. H., Hwu, W. L., et al. (2005). Parkin mutations and early-onset parkinsonism in a Taiwanese cohort. *Arch. Neurol.* 62, 82–87. doi: 10.1001/archneur.62.1.82

Wu, Z. Y., Lin, B., Chen, B., Zhao, G. X., Xie, H., Murong, S. X., et al. (2008). Molecular analyses of GCH-1, TH and parkin genes in Chinese dopa-responsive dystonia families. *Clin. Genet.* 74, 513–521. doi: 10.1111/j.1399-0004.2008.01039.x

Yelnik, J., Francis, C., Percheron, G., and Tandéa, D. (1991). Morphological taxonomy of the neurons of the primate striatum. *J. Comp. Neurol.* 313, 273–294. doi: 10.1002/cne.903130207

Zaja-Milatovic, S., Milatovic, D., Schantz, A. M., Zhang, J., Montine, K. S., Samii, A., et al. (2005). Dendritic degeneration in neostriatal medium spiny neurons in Parkinson disease. *Neurology* 64, 545–547. doi: 10.1212/01.WNL.0000150591.33787.A4

Zhong, P., Hu, Z., Jiang, H., Yan, Z., and Feng, J. (2017). Dopamine induces oscillatory activities in human midbrain neurons with parkin mutations. *Cell Rep.* 19, 1033–1044. doi: 10.1016/j.celrep.2017.04.023

Zhu, M., Cortese, G. P., and Waites, C. L. (2018). Parkinson's disease-linked Parkin mutations impair glutamatergic signaling in hippocampal neurons. *BMC Biol.* 16:100. doi: 10.1186/s12915-018-0567-7

Conflict of Interest Statement: The authors declare that the research was conducted in the absence of any commercial or financial relationships that could be construed as a potential conflict of interest.

Copyright © 2019 Sassone, Valtorta and Ciammola. This is an open-access article distributed under the terms of the Creative Commons Attribution License (CC BY). The use, distribution or reproduction in other forums is permitted, provided the original author(s) and the copyright owner(s) are credited and that the original publication in this journal is cited, in accordance with accepted academic practice. No use, distribution or reproduction is permitted which does not comply with these terms.

frontiers in Neurology

ORIGINAL RESEARCH
published: 24 April 2019
doi: 10.3389/fneur.2019.00418

Propensity Score-Matched Analysis of Lesion Patterns in Stroke Patients With Patent Foramen Ovale and Patients With Spontaneous Intracranial Artery Dissection

*Yangyang Huang[1,2], Yifan Cheng[2], Bei Shao[2], Xuanyou Zhou[3], Huazheng Liang[1], Jianhua Zhuang[4] and Yong Bi[1]**

[1] Department of Neurology, Shanghai Fourth People's Hospital, Tongji University, Shanghai, China, [2] Department of Neurology, The First Affiliated Hospital, Wenzhou Medical University, Wenzhou, China, [3] The First Clinical Medical Institute, The First Affiliated Hospital, Wenzhou Medical University, Wenzhou, China, [4] Department of Neurology, Changzheng Hospital, Second Military Medical University, Shanghai, China

OPEN ACCESS

Edited by:
Johannes Boltze, Fraunhofer-Institut für Zelltherapie und Immunologie (IZI), Germany

Reviewed by:
Bernhard Meier, Bern University Hospital, Switzerland
Gianfranco Butera, Policlinico San Donato (IRCCS), Italy

***Correspondence:**
Yong Bi
drbiyong@126.com

Specialty section:
This article was submitted to Stroke, a section of the journal Frontiers in Neurology

Received: *02 January 2019*
Accepted: *05 April 2019*
Published: *24 April 2019*

Citation:
Huang Y, Cheng Y, Shao B, Zhou X, Liang H, Zhuang J and Bi Y (2019) Propensity Score-Matched Analysis of Lesion Patterns in Stroke Patients With Patent Foramen Ovale and Patients With Spontaneous Intracranial Artery Dissection. Front. Neurol. 10:418. doi: 10.3389/fneur.2019.00418

Aims: To investigate the relationship between clinical and imaging features of stroke patients with patent foramen ovale (PFO) and those with spontaneous intracranial artery dissection (SIAD).

Materials and methods: We retrospectively examined both clinical and imaging results of 40 stroke patients with PFO and 29 with SIAD. To reduce selection bias, we conducted a propensity score-matching analysis. The patients' propensity scores were estimated using a logistic regression model based on the following variables: age, sex, hypertension, diabetes mellitus, hypercholesterolemia, cigarette smoking, stroke histories, and their NIHSS scores. We compared the pattern of cerebral DWI lesions between patients with PFO and those with SIAD.

Results: After propensity score matching, 21 pairs of patients were selected. Clinical characteristics of the 2 groups were well matched. The distribution of DWI lesion patterns differed between the 2 groups. Single lesions (cortical or subcortical) were more frequently observed in the PFO group than in the SIAD group ($P = 0.026$). Multiple lesions in one vascular territory occurred more frequently in the SIAD group than in the PFO group ($P = 0.035$).

Conclusion: The present study suggests that lesion patterns observed from DWI of patients with PFO and SIAD might provide clues to the etiology of infarcts. Single lesions (cortical or subcortical) might be a typical feature of PFO associated strokes, while multiple lesions in one vascular territory might be a specific feature of SIAD associated strokes.

Keywords: patent foramen ovale, spontaneous intracranial artery dissection, ischemic stroke, embolism, DWI

INTRODUCTION

Both patent foramen ovale (PFO) and spontaneous intracranial artery dissection (SIAD) are important stroke risk factors, especially in young and middle-aged adults (1–3). About 25% of patients with ischemic stroke are cryptogenic (4), and PFO is present in ∼54% of patients with cryptogenic stroke under 54 yeas (5). PFO and SIAD might result in strokes through different mechanisms. Promptly identifying the difference in the underlying mechanisms among young and middle-aged stroke patients will facilitate selection of the best therapy for the primary disease and prevention of recurrent strokes.

A prior study has assessed brain Magnetic resonance imaging (MRI) features of stroke patients due to PFO and SIAD and found that, a single non-territorial infarct seemed to favor strokes due to PFO, whereas territorial infarcts (with or without additional smaller lesions in the same territory) were more likely to occur in patients with arterial dissection (6). However, this study did not individually compare between patients with carotid dissection, vertebral dissection, and those with PFO, respectively, though the former two types of patients had different mechanisms of stroke pathogenesis. In SIAD, spontaneous cervical artery dissection showed different clinical and imaging features from spontaneous vertebral artery dissection (7, 8). Artery-to-artery embolism and reduced blood flow due to the primary lesion are the two basic mechanisms with which spontaneous cervical artery dissection led to strokes (9, 10), whereas artery-to-artery embolism is considered to be the primary mechanism with which spontaneous vertebral artery dissection led to strokes (11, 12). Therefore, it might be more reliable to individually analyze the imaging characters of carotid dissection and vertebral dissection patients. The other thing to note is that the baseline data of some studies are not consistent with each other, which leads to systemic bias in data analysis and subsequently the findings from these studies are not trustworthy.

In the present study, we aimed to analyze the difference in imaging findings between stroke patients with PFO and those with carotid dissection or vertebral dissection through propensity analysis. Results from this study will facilitate the diagnosis of these diseases in stroke patients and initiate appropriate therapies.

MATERIALS AND METHODS

Subjects

Stroke patients with PFO and SIAD, admitted to the Department of Neurology and Neurosurgery, the First Affiliated Hospital of Wenzhou Medical University between August 2010 and June 2018, were included in the present retrospective study. This study was approved by the Human Ethics Committee of the First Affiliated Hospital of Wenzhou Medical University.

Inclusion criteria for stroke patients due to SIAD were: (1) definite angiographic findings of dissection in intracranial arteries; (2) presence of ischemic stroke lesions on Diffusion-weighted imaging (DWI); (3) according to the TOAST criteria, no definite causes had been identified apart from dissection after a standardized workup; (4) PFO was excluded by transesophageal echocardiography (TEE) and transcranial Doppler (TCD); (5) Spontaneous cervical artery dissection was diagnosed based on ≥1 of the following 3 criteria: (1) intimal flap visible on carotid ultrasound; (2) mural hematoma visible on MRI or CT; (3) a non-atherosclerotic, tapered, flame-shaped ICA-occlusion or a string-like ICA-stenosis (7). A total of 31 patients were diagnosed with SIAD, one patient was excluded due to absence of lesions on DWI, and another patient excluded due to an extracranial artery dissection. As a result, 29 patients were included in the "SIAD group."

Inclusion criteria for stroke patients with PFO were: (1) presence of ischemic stroke lesions on DWI; (2) according to the TOAST criteria, no definite causes had been identified apart from PFO after a standardized etiological workup; (3) evaluated with a standard stroke protocol including DWI sequence; (4) The presence of PFO was confirmed by transesophageal echocardiography (TEE) and the presence of right-to-left shunt was tested by transcranial Doppler (TCD) (13, 14). Forty two patients with PFO and no other definite stroke causes were chosen, but 2 were excluded due to absence of lesions on DWI, the remaining 40 patients were included in the "PFO group." A flowchart of the selection process was shown in **Figure 1**.

We reviewed age, sex, medical histories, stroke histories, physical examination, laboratory test results, and stroke severity measured by the National Institute of Health Stroke Scale (NIHSS) score. Conventional vascular risk factors were identified and listed below: hypertension, diabetes mellitus, hypercholesterolemia, cigarette smoking.

All patients underwent brain Magnetic resonance imaging, transcranial doppler, carotid and vertebral artery ultrasound, magnetic resonance angiography/computer tomography angiography or digital subtraction angiography to exclude infarction due to extracranial or intracranial atherosclerosis. Chest x-ray, electrocardiogram, transthoracic echocardiography, and transesophageal echocardiography, 24 h electrocardiogram were applied to exclude infarction due to emboli from the heart. Laboratory tests for hypercoagulation states, vasculitis, or metabolic disorders were requested at the discretion of the treating physician.

Brain MR Imaging

MRI was performed using a 3.0-T MRI unit (Signa HDx; GE Medical Systems, Milwaukee, WI). Data were obtained from the DWI sequence. DWI was performed with a repetition time of 5,000 ms, echo time of 84 ms, field of view of 24 × 24 mm, matrix number of 128 × 128, and slice thickness of 5 mm.

The following 5 lesion patterns on DWI were shown in **Figures 2–5**, using a published classification system: (1) Pattern 1: single lesions (cortical, or subcortical); (2) Pattern 2: single lesions (corticosubcortical); (3) Pattern 3: multiple lesions in one vascular territory (anterior or posterior circulation); (4) Pattern 4: multiple lesions in multiple vascular territories (same side); (5) Pattern 5:multiple lesions in multiple vascular territories (different sides) (15, 16). Multiple lesions were defined as 2 or more isolated DWI-positive lesions within the same or multiple vascular territories (9). Multiple lesions were classified into unilateral anterior circulation, posterior circulation, bilateral anterior circulations, or anterior and posterior circulations. Based on the difference in supplying

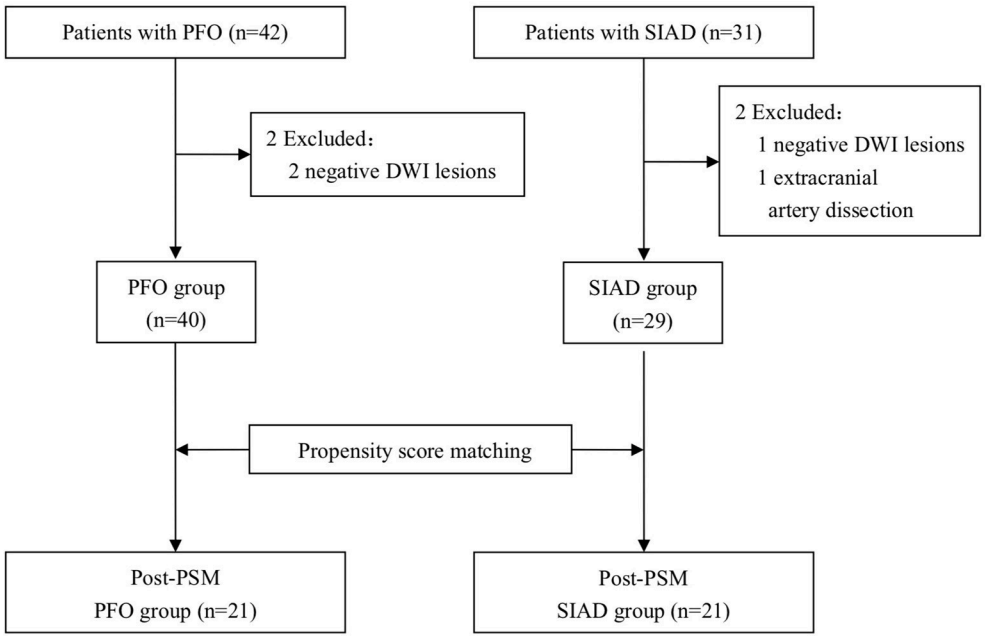

FIGURE 1 | Flowchart of the patient selection process.

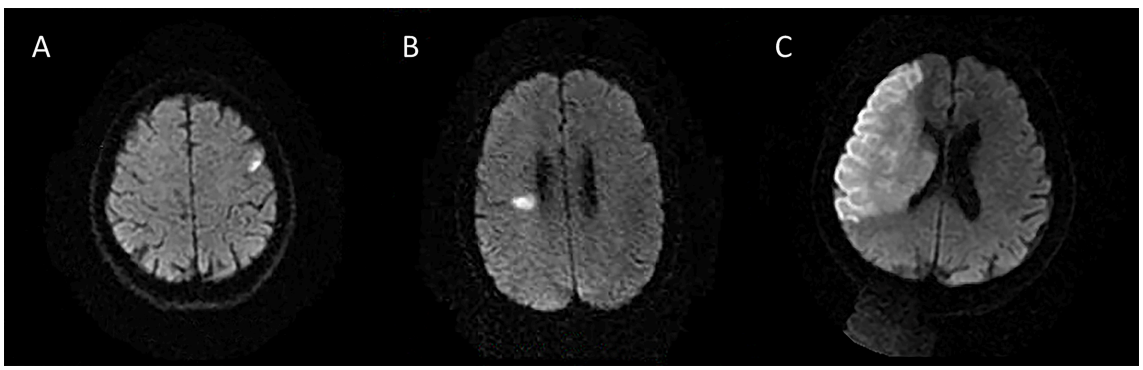

FIGURE 2 | Single lesions **(A)** (Pattern 1): single lesions (cortical). **(B)** (Pattern 1): single lesions (subcortical). **(C)** (Pattern 2): single lesions (corticosubcortical).

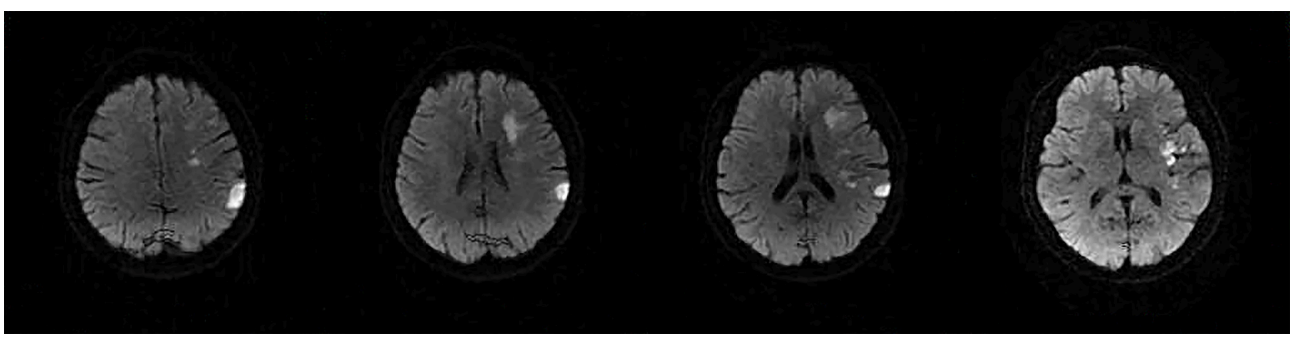

FIGURE 3 | (Pattern 3): multiple lesions in one vascular territory.

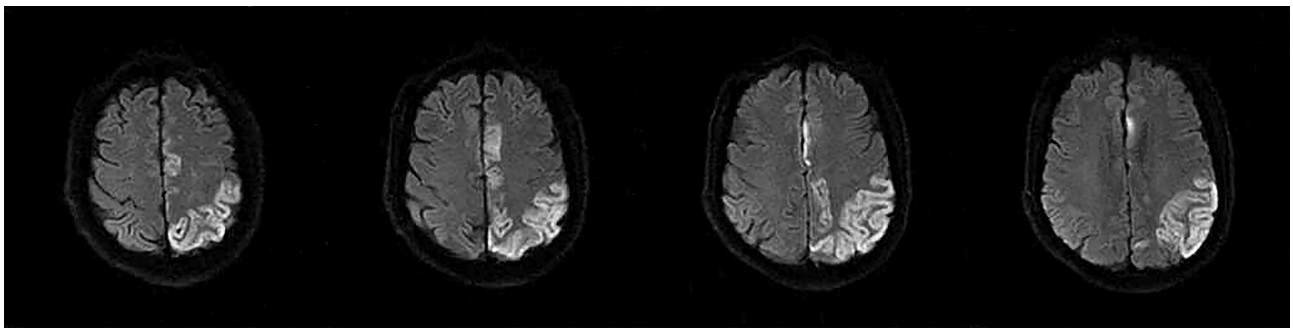

FIGURE 4 | (Pattern 4): multiple lesions in multiple vascular territories (same side).

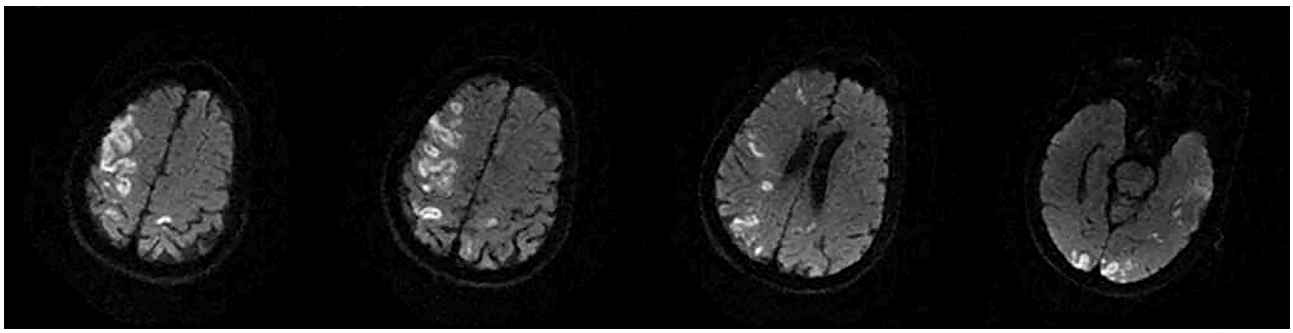

FIGURE 5 | (Pattern 5): multiple lesions in multiple vascular territories (different sides).

arteries, vascular territories were also divided into anterior circulation (carotid artery), posterior circulation (vertebral-basal artery), anterior and posterior circulations (carotid and vertebral-basal arteries).

Propensity Score Matching

We performed Propensity score matching (PSM) to reduce the possibility of selection bias and to adjust significant differences in baseline characteristics between the PFO and SIAD groups. The propensity score was estimated using a logistic regression model based on the following 8 variables: age, sex, hypertension, diabetes mellitus, hypercholesterolemia, cigarette smoking, stroke histories, and NIHSS scores. One-to-one pair matching was performed without replacement using a caliper of 0.20.

Statistical Analysis

Statistical analyses were performed using the statistical software package SPSS version 22.0. Continuous variables were presented as mean ± SD; categorical variables were expressed as frequencies. The statistical significance for inter-group differences was tested by the χ^2 test for categorical variables, the *t*-test for continuous variables, and the Mann–Whitney test for non-normal variables (e.g., NIHSS). The ROC curve was produced to predict the likelihood of right diagnosis of the underlying conditions based on findings from specific imaging results.

TABLE 1 | Comparison of the clinical characteristics of patients in the two groups.

Patient Characteristics	PFO, N, (%) ($n = 40$)	SIAD, N, (%) ($n = 29$)	*P*-Value
Age, y, mean ± *SD*[a]	46.85 ± 14.19	38.79 ± 9.10	0.006*
Male sex[b]	29 (73)	24 (83)	0.319
Vascular risk factors[b]			
Hypertension	15 (38)	4 (14)	0.057
Diabetes mellitus	3 (8)	2 (7)	1.000
Hypercholesterol	6 (15)	10 (34)	0.058
Cigarette smoking[b]	18 (45)	14 (48)	0.788
Stroke histories[b]	4 (10)	0	0.218
NIHSS score[c]	2.0 (1–6)	6.0 (1.5–9.5)	0.028*

PFO, patent foramen ovale; SIAD, spontaneous intracranial artery dissection; NIHSS, National Institutes of Health Stroke Scale.

**Statistically significant ($p \leq 0.05$).*

[a]Values expressed as mean ± standard deviation (SD).

[b]Values expressed as frequencies and percentages.

[c]Values expressed as median and interquartile range.

*P-values were determined with the use of independent **t**-test, the Pearson χ^2-test (or Fisher's exact test where appropriate) and Mann–Whitney test.*

RESULTS

Demographical Information of all Patients

Clinical characteristics of the PFO and SIAD groups were shown in **Table 1**. In the SIAD group, there were 17 (59%) patients

TABLE 2 | Comparison of the radiological data of patients in the two groups.

	PFO, N, (%) ($n = 40$)	SIAD, N, (%) ($n = 29$)	*P*-Value
DWI lesion patterns[a]			
Single lesions (Corticosubcortical)	3 (8)	7 (24)	0.112
Single lesions (Cortical or subcortical)	20 (50)	6 (21)	0.013*
Multiple lesions in one vascular territory	6 (15)	12 (41)	0.014*
Multiple lesions in several vascular territories (same side)	2 (5)	2 (7)	1.000
Multiple lesions in several vascular territories (different side)	9 (23)	2 (7)	0.157
Distribution of multiple lesions [a]	17 (43)	16 (55)	
Unilateral anterior circulation	8 (20)	12 (41)	0.053
Posterior circulation	7 (18)	6 (21)	0.738
Bilateral anterior circulation	4 (10)	0	0.218
Distribution of circulation [a]			
Anterior and posterior circulations	4 (10)	2 (7)	0.985
Anterior circulation	22 (55)	15 (52)	0.788
Posterior circulation	12 (30)	12 (41)	0.327
Anterior and posterior circulations	6 (15)	2 (7)	0.299

PFO, patent foramen ovale; SIAD, spontaneous intracranial artery dissection; DWI, diffusion-weighted imaging.
[a]Values expressed as frequencies and percentages.
P-values were determined with the use of Pearson χ^2-test (or Fisher's exact test where appropriate).

with vertebral artery dissection and 12 (41%) with cervical artery dissection. The mean age of patients in the PFO group (46.85 ± 14.19 years) was significantly older than that of the SIAD group (38.79 ± 9.10 years) ($p = 0.006$). The NIHSS score of the SIAD group was significantly higher than that of the PFO group ($P = 0.028$). The percentage of males was high in both groups (73 vs. 83%) and there was no significant difference between them ($P = 0.319$). No significant difference was observed in hypertension, diabetes mellitus, hypercholesterolemia, cigarette smoking, and stroke histories between the two groups.

Radiological data on DWI were presented in **Table 2**. The distribution of DWI lesion patterns differed between the 2 groups. Single lesions (cortical or subcortical, Pattern 1) was more frequent in the PFO group than in the SIAD group (50 vs. 21%; $P = 0.013$). Multiple lesions in one vascular territory (Pattern 3) were more frequently observed in the SIAD group than in the PFO group (41 vs. 15%; $P = 0.014$). Differences in the occurrence of other lesion patterns like single lesions (corticosubcortical, Pattern 2), multiple lesions in multiple vascular territories (same side and different sides, Pattern 4 and 5) did not reach statistical significance. Additionally, there was no difference in the distribution of multiple lesions between patients with PFO and those with SIAD. Six patients with PFO had both anterior and posterior circulations involved.

Propensity Score-Matched Cohort

Patients in the PFO and SIAD groups were matched 1 to 1 using PSM to minimize the effect of confounding factors. Twenty-one pairs of patients were selected and their clinical characteristics seemed to be well matched, and no significant differences were observed between the groups after PSM (**Table 3**).

TABLE 3 | Comparison of the clinical characteristics of patients in the two groups in the propensity score-matched cohort.

Patient Characteristics	PFO, N, (%) ($n = 21$)	SIAD, N, (%) ($n = 21$)	*P*-Value
Age, y, mean ± *SD*[a]	44.38 ± 16.624	37.86 ± 9.759	0.131
Male sex[b]	16 (76)	17 (81)	1.000
Vascular risk factors[b]			
Hypertension	3 (14)	2 (10)	1.000
Diabetes mellitus	1 (5)	2 (10)	1.000
Hypercholesterol	5 (24)	7 (33)	0.495
Cigarette smoking[b]	9 (43)	10 (48)	0.757
Stroke histories[b]	1 (5)	0	0.311
NIHSS score[C]	2.0 (1.0–6.0)	3 (1.0–7.5)	0.713

PFO, patent foramen ovale; SIAD, spontaneous intracranial artery dissection; NIHSS, National Institutes of Health Stroke Scale.
[a]Values expressed as mean ± standard deviation (SD).
[b]Values expressed as frequencies and percentages.
[c]Values expressed as median and interquartile range.
P-values were determined with the use of independent t-test, the Pearson χ^2-test (or Fisher's exact test where appropriate) and Mann–Whitney test.

Post-PSM comparison of radiological data were presented in **Table 4**. Single lesions (cortical or subcortical, Pattern 1) were still more frequently observed in the PFO group than in the SIAD group (57 vs. 19%; $P = 0.026$). Multiple lesions in one vascular territory were more frequently observed in the SIAD group than in the PFO group (43 vs. 10%; $P = 0.035$). Unlike the full cohort, single lesions (corticosubcortical, Pattern 2) were more frequently observed in the SIAD group than in the PFO group ($P = 0.048$). Differences in the percentage of other lesion patterns like multiple lesions in multiple vascular territories (same side and different sides) did not reach statistical significance. Distribution of multiple lesions in the PSM set did not reach significant difference. Lesions in the posterior circulation territory occurred more frequently in the SIAD group than in the PFO group (57 vs. 24%; $P = 0.028$). Five patients with PFO had both anterior and posterior circulations involved.

Receiver Operating Characteristic (ROC) Curve

ROC was produced to calculate the value of diagnosing PFO based on patterns of single cortical or subcortical infarcts. The area under ROC curve was 0.647 (**Figure 6**). Similarly, the area under ROC curve was 0.632 (**Figure 7**) for diagnosing SIAD based on the pattern of multiple infarcts in a single vascular territory.

DISCUSSION

The present study compared the imaging features between stroke patients with PFO and those with SIAD. In the full

TABLE 4 | Comparison of radiological data of patients in the two groups in the propensity score-matched cohort.

	PFO, N, (%) ($n = 21$)	SIAD, N, (%) ($n = 21$)	*P*-Value
DWI lesion patterns[a]			
Single lesions (Corticosubcortical)	0 (0)	5 (24)	0.048*
Single lesions (Cortical or subcortical)	12 (57)	4 (19)	0.026*
Multiple lesions in one vascular territory	2 (10)	9 (43)	0.035*
Multiple lesions in several vascular territories (same side)	2 (10)	1 (5)	1.000
Multiple lesions in several vascular territories (different side)	5 (24)	2 (10)	0.408
Distribution of multiple lesions [a]	10 (48)	12 (57)	0.537
Unilateral anterior circulation	2 (10)	5 (24)	0.408
Posterior circulation	2 (10)	6 (29)	0.116
Bilateral anterior circulation	1 (5)	0	1.000
Anterior and posterior circulations			
Distribution of circulation [a]	5 (24)	1 (5)	0.186
Anterior circulation	11 (52)	8 (38)	0.352
Posterior circulation	5 (24)	12 (57)	0.028*
Anterior and posterior circulations	5 (24)	1 (5)	0.186

PFO, patent foramen ovale; SIAD, spontaneous intracranial artery dissection; DWI, diffusion-weighted imaging.

**Statistically significance ($p \leq 0.05$).*

[a]Values expressed as frequencies and percentages.

P-values were determined with the use of Pearson χ^2-test (or Fisher's exact test where appropriate).

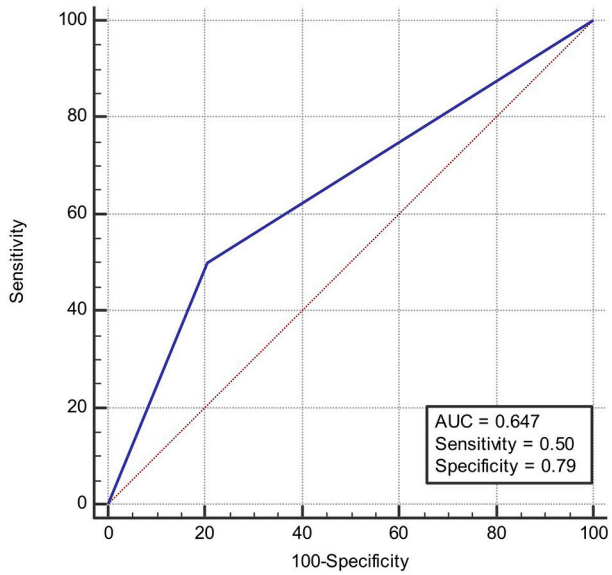

FIGURE 6 | Area under the ROC curve predicts the likelihood of PFO based on patterns of single cortical or subcortical infarcts.

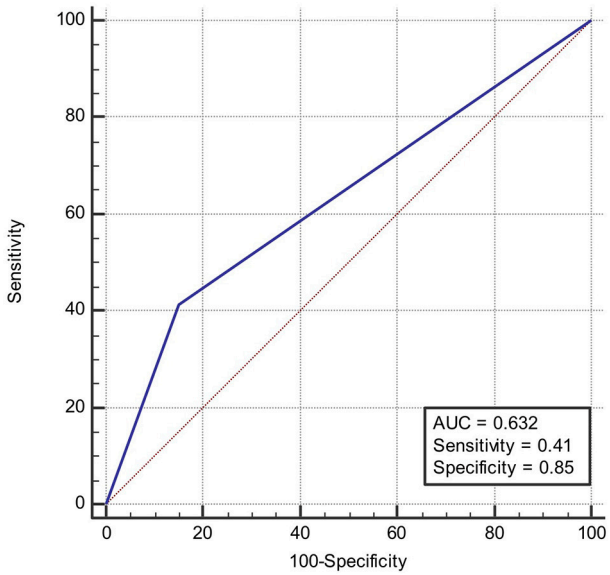

FIGURE 7 | Area under the ROC curve predicts the likelihood of SIAD based on patterns of multiple infarcts in a single vascular territory.

cohort, we found that patients with PFO were older and more likely to have hypertension than patients with SIAD, while the NIHSS score was higher in stroke patients with SIAD than in those with PFO. To minimize bias due to patient selection, we conducted PSM to match patients with PFO and those with SIAD. After PSM, significant difference was not observed in their clinical characteristics but their radiological findings. Single lesions (cortical or subcortical) were more frequently observed in patients with PFO than in those with SIAD, whereas multiple lesions in one vascular territory were more frequently observed in patients with SIAD than in those with PFO. Furthermore, single lesions (corticosubcortical), and posterior circulation involvement were more frequently observed in patients with SIAD than in those with PFO after PSM.

The finding that single lesions (cortical or subcortical) were more frequently observed in the PFO group than in the SIAD group, is consistent to some extent with findings of previous reports (6, 17, 18). Bonati et al. (6) found that among cerebral infarct patients with PFO, 42% (25/60) had single cortical or subcortical infarcts in areas not fulfilling the criteria for territorial infarct, whereas only 6% (2/33) of patients with SIAD had this type of cerebral infarct. This statistical difference is consistent with our findings. In another study (17), it was found that among 25 patients with PFO, 5 (20%) had single subcortical infarct with a diameter over 15 mm, which is significantly different from what was found in the non-PFO group (0%). In the non-PFO group, 8 out of 21 patients showed subcortical infarcts, but none of them showed single subcortical infarcts larger than 15 mm. Kim et al. (18) found that among 117 patients with PFO, 40 had a single subcortical infarct (34.2%), which is significantly different from what was found in patients with atrial fibrillation (11/358, 3.1%). In that study, 46.1% of patients showed large corticosubcortical infarcts, 19% showed confluent large infarcts with additional lesions, and 16.5% showed infarcts in multiple vascular territories. This indicates

that atrial fribrillation is more likely to result in infarcts in multiple vascular territories. However, the latter two studies have different baseline information of patients, which leads to bias in their conclusions. In the present study, 50% of patients with PFO had a single cortical or subcortical infarct, which was significantly higher than that of patients with SIAD (21%). The result remained significantly different after propensity analysis (57 vs. 21%). The advantage of the present study was that propensity analysis excluded the bias caused by confounding factors and that the result was more reliable. The underlying mechanism for this finding might be that the patent foramen ovale is relatively small in diameter, and only small thrombi from the periphery can pass it and flow to the carotid or vertebral artery. Therefore, the infarcts are relatively small and often localized to one vascular territory. The other major finding in our study was that multiple lesions in one vascular territory were observed more frequently in the SIAD group than in the PFO group, which was also in line with Bonati's study which showed that territorial infarcts (with or without additional smaller lesions in the same territory) were more likely to occur in patients with arterial dissection (61%, 20/33 vs. 27%,16/60). It is likely that carotid artery dissection or vertebral artery dissection often leads to artery to artery embolism, which subsequently results in multiple infarcts in one vascular territory. A large observational study showed that there was no association between PFO and multiple acute strokes in patients with PFO and cryptogenic strokes (19). Our results are consistent with their findings in that PFO predominantly leads to single infarcts. Calculating the area under ROC curve might be a good way in predicting the likelihood of suffering from PFO or SIAD. Based on the discussion above, we could conclude that single lesions (cortical or subcortical) could be a specific feature of stroke patients with PFO, and multiple lesions in one vascular territory a specific feature of stroke patients with dissection, which could provide further support for differentiating diagnosis of the two etiologies.

After dividing patients with SIAD into carotid dissection and vertebral dissection, it was found that infarcts were more frequently observed in the posterior circulation of SIAD patients than in PFO patients, which was consistent with previously published results (20). However, patients with PFO were more likely to have both anterior and posterior circulations involved than SIAD patients with only one patient in our SIAD group having both circulations involved. The possible reason for this was that PFO tends to result in paradoxical cardioembolic strokes. Emboli from the heart might block both anterior and posterior circulations simultaneously, while emboli from artery dissection only block anterior circulations or posterior circulation, although no statistical significance was observed in our study due to the size limit. Therefore, large-size studies are needed to show whether patients with PFO have more anterior circulation or posterior circulation involved than patients with SIAD.

The present study has several limitations. Firstly, it was a single-center study and the sample size was relatively small. After PSM, the number of patients was reduced to 21 in each group. Thus, a large-scale multi-center study is essential to confirm our conclusion. Secondly, a possible bias might arise from patient selection for TEE, because TEE was an invasive procedure, some suspicious mild PFO associated stroke might be excluded. Thirdly, the cost of MRI scan is high, as a result, some small hospitals cannot perform this test for patients. Fourthly, a study published by New England Journal of Medicine showed that 30 days ambulatory ECG monitoring improves the diagnosis of atrial fibrillation (21). The present study only monitored the patients for 24 h, and the positive diagnosis of atrial fibrillation is low, which might lead to bias in our analysis.

In conclusion, single lesions (cortical or subcortical) might be a typical feature of PFO associated strokes, while multiple lesions in one vascular territory might be a specific feature of arterial dissection associated strokes.

ETHICS STATEMENT

This study was carried out in accordance with the recommendations of the Ethics Committees of the First Affiliated Hospital of Wenzhou Medical University with written informed consent from all subjects. All subjects gave written informed consent in accordance with the Declaration of Helsinki. The protocol was approved by the Ethics Committees of the First Affiliated Hospital of Wenzhou Medical University.

AUTHOR CONTRIBUTIONS

YB designed the study. YH and XZ collected the data. JZ and BS analyzed the data. YH and YC drafted the manuscript. HL analyzed the data and edited the manuscript. YB and YH approved the final version of the manuscript. All authors have read and approved the final manuscript.

FUNDING

This work was funded by Shanghai Hongkou Municipal Commission of Health and Family Planning [grant number 1803-05].

REFERENCES

1. Miranda B, Fonseca AC, Ferro JM. Patent foramen ovale and stroke. *J Neurol*. (2018) 265:1943–9. doi: 10.1007/s00415-018-8865-0
2. Putaala J, Metso AJ, Metso TM, Konkola N, Kraemer Y, Haapaniemi E, et al. Analysis of 1008 consecutive patients aged 15 to 49 with first-ever ischemic stroke: the Helsinki young stroke registry. *Stroke*. (2009) 40:1195–203. doi: 10.1161/STROKEAHA.108.529883
3. Schievink WI. Spontaneous dissection of the carotid and vertebral arteries. *N Engl J Med*. (2001) 344:898–906. doi: 10.1056/NEJM200103223441206
4. Liberman AL, Prabhakaran S. Cryptogenic stroke: how to define it? How to treat it? *Curr Cardiol Rep*. (2013) 15:423. doi: 10.1007/s11886-013-0423-x

5. Leehat P, Mas JL, Lascault G, Loron P, Theard M, Klimczac M, et al. Prevalence of patent foramen ovale in patients with stroke. *N Engl J Med*. (1988) 318:1148–52. doi: 10.1056/NEJM198805053181802
6. Bonati LH, Wetzel SG, Kessel-Schaefer A, Lyrer PA, Engelter ST, Buser P. Diffusion-weighted imaging findings differ between stroke attributable to spontaneous cervical artery dissection and patent foramen ovale. *Eur J Neurol*. (2010) 17:307–13. doi: 10.1111/j.1468-1331.2009.02805.x
7. Morel A, Naggara O, Touze E, Raymond J, Mas JL, Meder JF, et al. Mechanism of ischemic infarct in spontaneous cervical artery dissection. *Stroke*. (2012) 43:1354–61. doi: 10.1161/STROKEAHA.111.643338
8. Bonati LH, Wetzel SG, Gandjour J, Baumgartner RW, Lyrer PA, Engelter ST, et al. Diffusion-weighted imaging in stroke attributable to internal carotid artery dissection: the significance of vessel patency. *Stroke*. (2008) 39:483–5. doi: 10.1161/STROKEAHA.107.496760
9. Koch S, Rabinstein AA, Romano JG, Forteza A. Diffusion-weighted magnetic resonance imaging in internal carotid artery dissection. *Arch Neurol*. (2004) 61:510–2. doi: 10.1001/archneur.61.4.510
10. Weiller C, Mullges W, Ringelstein EB, Buell U, Reiche W. Patterns of brain infarctions in internal carotid artery dissections. *Neurosurg Rev*. (1991) 14:111–3.
11. Lee JS, Yong SW, Bang OY, Shin YS, Kim BM, Kim SY. Comparison of spontaneous intracranial vertebral artery dissection with large artery disease. *Arch Neurol*. (2006) 63:1738–44. doi: 10.1001/archneur.63.12.1738
12. Koch S, Amir M, Rabinstein AA, Reyes-Iglesias Y, Romano JG, Forteza A. Diffusion-weighted magnetic resonance imaging in symptomatic vertebrobasilar atherosclerosis and dissection. *Arch Neurol*. (2005) 62:1228–31. doi: 10.1001/archneur.62.8.1228
13. Schuchlenz HW, Weihs W, Horner S, Quehenberger F. The association between the diameter of a patent foramen ovale and the risk of embolic cerebrovascular events. *Am J Med*. (2000) 109:456–62. doi: 10.1016/S0002-9343(00)00530-1
14. De Castro S, Cartoni D, Fiorelli M, Rasura M, Anzini A, Zanette EM, et al. Morphological and functional characteristics of patent foramen ovale and their embolic implications. *Stroke*. (2000) 31:2407–13. doi: 10.1161/01.STR.31.10.2407
15. Jauss M, Wessels T, Trittmacher S, Allendörfer J, Kaps M. Embolic lesion pattern in stroke patients with patent foramen ovale compared with patients lacking an embolic source. *Stroke*. (2006) 37:2159–61. doi: 10.1161/01.STR.0000231645.22128.ab
16. Kang DW, Chalela JA, Ezzeddine MA, , Warach S. Association of ischemic lesion patterns on early diffusion-weighted imaging with TOAST stroke subtypes. *Arch Neurol*. (2003) 60:1730–4. doi: 10.1001/archneur.60.12.1730
17. Boutet C, Rouffiange-Leclair L, Garnier P, , Quenet S, Delsart D, Varvat J, et al. Brain magnetic resonance imaging findings in cryptogenic stroke patients under 60 years with patent foramen ovale. *Eur J Radiol*. (2014) 83:824–8. doi: 10.1016/j.ejrad.2014.01.022
18. Kim BJ, Sohn H, Sun BJ, Song JK, Kang DW, Kim JS, et al. Imaging characteristics of ischemic strokes related to patent foramen ovale. *Stroke*. (2013) 44:3350–6. doi: 10.1161/STROKEAHA.113.002459
19. Thaler DE, Ruthazer R, Di Angelantonio E, , Di Tullio MR, Donovan JS, Elkind MS, et al. Neuroimaging findings in cryptogenic stroke patients with and without patent foramen ovale. *Stroke*. (2013) 44:675–80. doi: 10.1161/STROKEAHA.112.677039
20. Kwon JY, Kim NY, Suh DC, Kang DW, Kwon SU, Kim JS, et al. Intracranial and extracranial arterial dissection presenting with ischemic stroke: lesion location and stroke mechanism. *J Neurol Sci*. (2015) 358:371–6. doi: 10.1016/j.jns.2015.09.368
21. Gladstone DJ, Spring M, Dorian P, Thorpe KE, Hall J, Vaid H, et al. Atrial fibrillation in patients withcryptogenic stroke. *N Engl J Med*. (2014) 370:2467–77. doi: 10.1056/NEJMoa1311376

Conflict of Interest Statement: The authors declare that the research was conducted in the absence of any commercial or financial relationships that could be construed as a potential conflict of interest.

Copyright © 2019 Huang, Cheng, Shao, Zhou, Liang, Zhuang and Bi. This is an open-access article distributed under the terms of the Creative Commons Attribution License (CC BY). The use, distribution or reproduction in other forums is permitted, provided the original author(s) and the copyright owner(s) are credited and that the original publication in this journal is cited, in accordance with accepted academic practice. No use, distribution or reproduction is permitted which does not comply with these terms.

frontiers in Neuroscience

ORIGINAL RESEARCH
published: 24 April 2019
doi: 10.3389/fnins.2019.00373

Correlates of Spreading Depolarization, Spreading Depression, and Negative Ultraslow Potential in Epidural Versus Subdural Electrocorticography

Jens P. Dreier[1,2,3,4,5], Sebastian Major[1,2,3], Coline L. Lemale[1,3,6], Vasilis Kola[1], Clemens Reiffurth[1,3], Karl Schoknecht[1,2,3], Nils Hecht[1,6], Jed A. Hartings[7,8] and Johannes Woitzik[1,6]*

[1] Center for Stroke Research Berlin, Charité – Universitätsmedizin Berlin, Corporate Member of Freie Universität Berlin, Humboldt-Universität zu Berlin, and Berlin Institute of Health, Berlin, Germany, [2] Department of Neurology, Charité – Universitätsmedizin Berlin, Corporate Member of Freie Universität Berlin, Humboldt-Universität zu Berlin, and Berlin Institute of Health, Berlin, Germany, [3] Department of Experimental Neurology, Charité – Universitätsmedizin Berlin, Corporate Member of Freie Universität Berlin, Humboldt-Universität zu Berlin, and Berlin Institute of Health, Berlin, Germany, [4] Bernstein Center for Computational Neuroscience Berlin, Berlin, Germany, [5] Einstein Center for Neurosciences Berlin, Berlin, Germany, [6] Department of Neurosurgery, Charité – Universitätsmedizin Berlin, Corporate Member of Freie Universität Berlin, Humboldt-Universität zu Berlin, and Berlin Institute of Health, Berlin, Germany, [7] UC Gardner Neuroscience Institute, College of Medicine, University of Cincinnati, Cincinnati, OH, United States, [8] Department of Neurosurgery, College of Medicine, University of Cincinnati, Cincinnati, OH, United States

OPEN ACCESS

Edited by:
Gregory Jaye Bix, University of Kentucky, United States

Reviewed by:
Sergei Kirov, Augusta University, United States
Massimo Mantegazza, UMR7275 Institut de Pharmacologie Moléculaire et Cellulaire (IPMC), France

***Correspondence:**
Jens P. Dreier
jens.dreier@charite.de

Specialty section:
This article was submitted to Neurodegeneration, a section of the journal Frontiers in Neuroscience

Received: *02 February 2019*
Accepted: *01 April 2019*
Published: *24 April 2019*

Citation:
Dreier JP, Major S, Lemale CL, Kola V, Reiffurth C, Schoknecht K, Hecht N, Hartings JA and Woitzik J (2019) Correlates of Spreading Depolarization, Spreading Depression, and Negative Ultraslow Potential in Epidural Versus Subdural Electrocorticography. Front. Neurosci. 13:373. doi: 10.3389/fnins.2019.00373

Spreading depolarizations (SDs) are characterized by near-complete breakdown of the transmembrane ion gradients, neuronal oedema and activity loss (=depression). The SD extreme in ischemic tissue, termed 'terminal SD,' shows prolonged depolarization, in addition to a slow baseline variation called 'negative ultraslow potential' (NUP). The NUP is the largest bioelectrical signal ever recorded from the human brain and is thought to reflect the progressive recruitment of neurons into death in the wake of SD. However, it is unclear whether the NUP is a field potential or results from contaminating sensitivities of platinum electrodes. In contrast to Ag/AgCl-based electrodes in animals, platinum/iridium electrodes are the gold standard for intracranial direct current (DC) recordings in humans. Here, we investigated the full continuum including short-lasting SDs under normoxia, long-lasting SDs under systemic hypoxia, and terminal SD under severe global ischemia using platinum/iridium electrodes in rats to better understand their recording characteristics. Sensitivities for detecting SDs or NUPs were 100% for both electrode types. Nonetheless, the platinum/iridium-recorded NUP was 10 times smaller in rats than humans. The SD continuum was then further investigated by comparing subdural platinum/iridium and epidural titanium peg electrodes in patients. In seven patients with either aneurysmal subarachnoid hemorrhage or malignant hemispheric stroke, two epidural peg electrodes were placed 10 mm from a subdural strip. We found that 31/67 SDs (46%) on the subdural strip were also detected epidurally. SDs that had longer negative DC shifts and spread more widely across the subdural strip were more likely to be observed in epidural recordings. One patient displayed an SD-initiated NUP while undergoing brain death despite continued circulatory function. The NUP's amplitude was −150 mV subdurally and −67 mV

epidurally. This suggests that the human NUP is a bioelectrical field potential rather than an artifact of electrode sensitivity to other factors, since the dura separates the epidural from the subdural compartment and the epidural microenvironment was unlikely changed, given that ventilation, arterial pressure and peripheral oxygen saturation remained constant during the NUP. Our data provide further evidence for the clinical value of invasive electrocorticographic monitoring, highlighting important possibilities as well as limitations of less invasive recording techniques.

Keywords: cerebral ischemia, hypoxia, malignant hemispheric stroke, spreading depression, subarachnoid hemorrhage

INTRODUCTION

Spreading depolarization is the principal mechanism causing cytotoxic oedema and excitotoxicity in cerebral cortex and basal ganglia (Ochs and Van Harreveld, 1956; van Harreveld, 1959; Dreier et al., 2013, 2018a; Hinzman et al., 2015). Using ECoG, SD is observed as a large negative direct current (DC) shift (frequency band: <0.05 Hz). The SD continuum describes the spectrum from terminal SD in severely ischemic tissue to transient SDs with negative DC shifts of intermediate to short duration in tissue that is less ischemic or normal (Dreier and Reiffurth, 2015; Hartings et al., 2017b). Accordingly, SDs occur in human conditions ranging from CA, to stroke, to the harmless migraine aura (Dreier et al., 2006, 2018b; Dohmen et al., 2008; Lauritzen et al., 2011). This means that there are commonalities yet also considerable variations in SD properties along the continuum. Terminal SD, for example, is characterized by initiation of a NUP, which is similar to the negative DC shift of prolonged SD, but specifically refers to a negative potential component during progressive recruitment of neurons into cell death. The NUP has been recorded in patients dying in the wake of CA (Dreier et al., 2018b), in a patient with aSAH undergoing brain death despite continued circulatory function (Carlson et al., 2018), and in patients with ECI and DCI after aSAH (Oliveira-Ferreira et al., 2010; Dreier, 2011; Drenckhahn et al., 2012; Hartings et al., 2017c; Luckl et al., 2018).

The continuum is also manifested in the consequences of SD. In electrically active tissue, SD induces spreading depression of activity, which is measured in the AC-ECoG range (>0.5 Hz) (Dreier et al., 2017). The depression is short-lasting in normal tissue but progressively prolonged in metabolically impaired areas, such that SD can induce even persistent electrical inactivity (=isoelectricity) that develops in a spreading pattern (Oliveira-Ferreira et al., 2010). Thereafter, SDs cannot induce further spreading depression and are termed 'isoelectric SD' (Hartings et al., 2011). This state of electrical silence contrasts with 'non-spreading depression,' which is the electrical silence that develops in tissue simultaneously after the onset of severe ischemia, 1–5 min prior to terminal SD (Dreier, 2011; Dreier et al., 2018b). SD also induces tone alterations in resistance vessels, leading to either transient hyperemia (normal neurovascular response) in healthy tissue or severe hypoperfusion (inverse neurovascular response = spreading ischemia) in tissue at risk for progressive injury (Dreier et al., 1998; Shin et al., 2006). Experimentally, SI could be the sole cause of widespread cortical infarcts (Dreier et al., 2000). The continuum from SH to SI was recorded in patients with aSAH, TBI, and MHS (Dreier et al., 2009; Dreier, 2011; Woitzik et al., 2013; Hinzman et al., 2014).

Subdural recordings from platinum–iridium (Pt/Ir) electrodes have been the gold standard for intracranial monitoring of SDs in humans (Dreier et al., 2017; Eriksen et al., 2019). Despite the many translational successes achieved with these electrodes, Pt/Ir has some shortcomings as an electrode material for recording slow potentials, particularly in contrast to the Ag/AgCl-based electrodes used in animals (Masvidal-Codina et al., 2018). For instance, as a polarizable material, Pt/Ir has a capacitive nature that may result in filtering or distortion of slow potentials (Hartings et al., 2017a). Here, in an approach of reverse translation from bedside to bench (Fisher, 2013), we investigated how reliably Pt/Ir electrodes record negative DC shifts of varying duration, including the NUP, by studying the full SD continuum in rats under conditions of normoxia, hypoxia, and severe global ischemia. We then conducted a study of bench to bedside translation, based on the suggestion from animal experiments that epidural recordings are a possible semi-invasive alternative to subdural recordings (Iijima et al., 1992; Kang et al., 2013; Luckl et al., 2018). Epidural recordings are of interest as an intermediate step between invasive subdural and

Abbreviations: AC, alternating current; ACSF, artificial cerebrospinal fluid; Ag/AgCl, silver/silver chloride; ARRIVE, Animal Research: Reporting of *In Vivo* Experiments; aSAH, aneurysmal subarachnoid hemorrhage; ATP, adenosine triphosphate; BBB, blood–brain barrier; BMBF, Bundesministerium für Bildung und Forschung (Federal Ministry of Education and Research); CA, circulatory arrest; COSBID, Co-Operative Studies on Brain Injury Depolarizations; CT, computed tomography; CTA, computed tomography angiography; DC potential, direct current (steady) potential; DCD, organ donation after cardio-circulatory death; DCI, delayed cerebral ischemia; DFG, Deutsche Forschungsgemeinschaft; ECI, early cerebral ischemia; ECoG, electrocorticography; EEG, electroencephalography; EVD, extraventricular drainage; FiO_2, fraction of inspired oxygen; ICP, intracranial pressure; ICU, intensive care unit; IQR, interquartile range; $[K^+]_o$, extracellular potassium concentration; KCl, potassium chloride; LAGeSo, Landesamt für Gesundheit und Soziales Berlin; LDF, laser-doppler flowmetry; MAP, mean arterial pressure; MCA, middle cerebral artery; MHS, malignant hemispheric stroke; MRI, magnetic resonance imaging; NUP, negative ultraslow potential; p_aO_2, arterial pressure of oxygen; p_aCO_2, arterial pressure of carbon dioxide; PTDDD, peak total SD-induced depression duration of a recording day; $p_{ti}O_2$, tissue partial pressure of oxygen; Pt/Ir, platinum/iridium; rCBF, regional cerebral blood flow; SD, spreading depolarization; SH, spreading hyperemia; SI, spreading ischemia; STROBE, STrengthening the Reporting of OBservational studies in Epidemiology; TBI, traumatic brain injury; TDDD, total depression duration per recording day; WFNS, World Federation of Neurosurgical Societies.

non-invasive scalp EEG. Although correlates of SD were clearly identified in continuous scalp EEG recordings when performed simultaneously with subdural ECoG (Drenckhahn et al., 2012; Hartings et al., 2014), scalp EEG alone may not be sufficient to reliably diagnose SDs, particularly in patients with intact skulls (Hartings et al., 2018; Hofmeijer et al., 2018). Therefore, we investigated the performance of epidural titanium peg electrodes (Barnett et al., 1990) compared to subdural electrodes in detecting SDs in patients with either aSAH or MHS. In this series, we recorded a patient who displayed an SD-initiated NUP while undergoing brain death despite continued circulatory function, as in another case reported previously (Carlson et al., 2018). The NUP was recorded not only subdurally but also epidurally, providing further insight into the nature of this phenomenon.

MATERIALS AND METHODS

Animals

This study was carried out in accordance with the recommendations of the Landesamt für Gesundheit und Soziales Berlin (LAGeSo) (G0152/11). The protocol was approved by the LAGeSo (G0152/11). All experimental procedures were conducted in accordance with the Charité Animal Welfare Guidelines. The reporting of animal experiments complies with the ARRIVE Guidelines. Naïve, male, wild-type Wistar rats (n = 8; 250–400 g, ∼10–16 weeks old, supplied by Charles River, Germany) were anesthetized with 100 mg/kg body weight thiopental-sodium intraperitoneally (Trapanal, BYK Pharmaceuticals, Konstanz, Germany), tracheotomized, and artificially ventilated (Effenberger Rodent Respirator, Effenberger Med.-Techn. Gerätebau, Pfaffing/Attel, Germany). The left femoral artery and vein were cannulated. Body temperature was maintained at 38.0 ± 0.5°C using a heating pad. Systemic arterial pressure (Pressure Monitor BP-1, World Precision Instruments, Berlin, Germany) and expiratory pCO_2 (Heyer CO_2 Monitor EGM I, Bad Ems, Germany) were monitored. Arterial pO_2 (p_aO_2), pCO_2 (p_aCO_2) and pH were serially measured using a Compact 1 Blood Gas Analyzer (AVL Medizintechnik GmbH, Bad Homburg, Germany). Adequacy of the level of anesthesia was assessed with testing motor and blood pressure responses to tail pinch.

A parietal craniotomy was performed using a saline-cooled drill and the dura was removed. The composition of ACSF in mM was: NaCl 127.5; KCl 3.0; $CaCl_2$ 1.5; $MgSO_4$ 1.2; $NaHCO_3^-$ 24.5; glucose 3.7; urea 6.7 (Levasseur et al., 1975). The ACSF was equilibrated with a gas mixture containing 6.6% O_2, 5.9% CO_2, and 87.5% N_2. A pO_2 between 90 and 130 mmHg, a pCO_2 between 35 and 45 mmHg, and a pH between 7.35 and 7.45 were accepted as physiological. rCBF was continuously monitored using LDF (Periflux 4001, Perimed AB, Järfälla, Sweden). A double-barreled K^+-selective microelectrode was used to measure the intracortical DC/AC-ECoG and the extracellular K^+ concentration ($[K^+]_o$) in the open window (Petzold et al., 2005; Kang et al., 2013). The cortical measuring depth was 300 μm. In addition, two Pt/Ir plate electrodes (Ad-Tech Medical, Racine, WI, United States) were placed on the cortex as shown in **Figure 1A** (total diameter: 4 mm, contact surface: 2 mm, distance between electrode centers: 5 mm). An Ag/AgCl electrode was placed for a reference in the neck. Electrodes were connected to differential amplifiers (Jens Meyer, Munich, Germany). Analog-to-digital conversion was performed using a Power 1401 (Cambridge Electronic Design Limited, Cambridge, United Kingdom). Systemic arterial blood pressure as well as $[K^+]_o$, DC- and AC-ECoG, rCBF and expiratory pCO_2 were continuously recorded using a personal computer and Spike 2 software (version 6, Cambridge Electronic Design Limited).

Following surgical preparation, SDs were triggered first under normoxic conditions by applying a droplet of 2M KCl at a rostral burr hole. After cessation of SDs and recovery of baseline levels, hypoxia was then induced by gradually substituting N_2 for O_2 in the inspired air over ∼60 s. Thereafter, animals were monitored while hypoxia was maintained until animals died spontaneously. In some animals, additional SDs were provoked by KCl application during hypoxia.

Statistical Analysis in General

No prior information was available which would have enabled us to perform sample size estimations based on evidence. We thus chose a sample size of eight animals which is standard in the field. For the clinical pilot study, we had originally chosen a sample size of 20 patients, but peg electrodes were no longer available (see below). Therefore, only seven patients were included. All analyses were exploratory and are reported with the caveat that no formal power consideration was performed on them. All data in text and figures is given as median and IQR. We only used non-parametric tests because of the small sample sizes. The exact statistical tests are given in the text. $P \leq 0.05$ was accepted as significant.

Analysis of Animal Data

Animal data was prospectively collected and analyzed by comparing relative changes of rCBF and absolute changes of DC potential and $[K^+]_o$. rCBF changes were calculated in relation to baseline (=100%) using a zero level established after death. No animals were excluded from analysis. The data was analyzed in an un-blinded fashion with LabChart-8 software (ADInstruments, Bella Vista, NSW, Australia).

Patients

The study was carried out in accordance with the recommendations of the ethics committee of the Charité – Universitätsmedizin Berlin (EA4/175/17) with written informed consent from the patients or the patients' legally authorized representatives. All patients or patients' legally authorized representatives gave written informed consent in accordance with the Declaration of Helsinki. The protocol was approved by the ethics committee of the Charité – Universitätsmedizin Berlin. Results are reported in accordance with the STROBE guidelines[1]. Prospective inclusion and exclusion criteria for aSAH and MHS patients in the COSBID have been previously described (Woitzik et al., 2014; Winkler et al., 2017). Five patients with major aSAH and two patients with MHS were consecutively enrolled

[1]https://www.strobe-statement.org

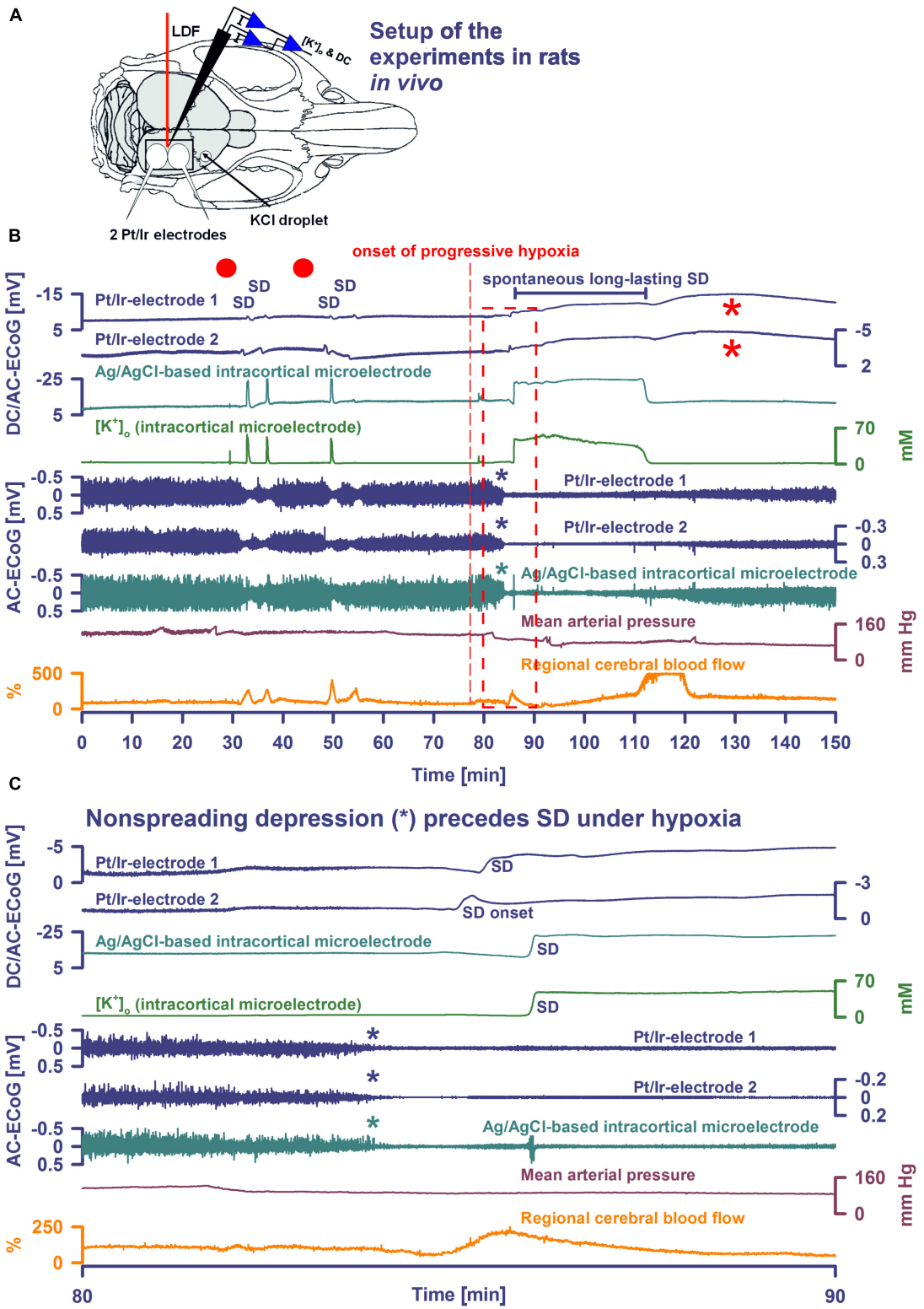

FIGURE 1 | Comparison of normoxic SD with hypoxic SD preceded by non-spreading depression of spontaneous activity. **(A)** Experimental setup in rats. LDF, laser-doppler flow probe; $[K^+]_o$ and DC, K^+-selective glass-microelectrode; Pt/Ir electrodes, platinum/iridium plate electrodes; KCl droplet, SD was triggered with a droplet containing KCl at 2M. Panel **(B)** shows the first half of an experiment with 4 KCl-induced SDs followed by the first spontaneous SD induced by hypoxia, and panel **(C)** shows the boxed portion of **(B)** with an expanded time scale. KCl application is marked with red dots.Traces 1–3: The full-band ECoG signal

(Continued)

FIGURE 1 | Continued
(DC/AC-ECoG) contains information on both the negative DC shift that identifies SD (Dreier, 2011) and the SD-induced depression of activity (negative is up for ECoG recordings shown in all figures). Note the differences in amplitude and shape of the DC shift between the gold standard recording technique in animals, the intracortical glass-microelectrode, and the Pt/Ir electrodes on the brain surface, gold standard in humans (cf. **Table 1**). For example, the amplitude ratio of the initial DC negativity divided by the subsequent DC positivity was significantly larger for the glass-microelectrode than for the Pt/Ir electrodes in normal tissue [Ag/AgCl: 9.1 (IQR = 8.0, 17.0); caudal Pt/Ir: 1.2 (IQR = 1.0, 1.7); rostral Pt/Ir: 1.0 (IQR = 0.7, 1.3), $P \leq 0.05$, $n = 7$, Kruskal–Wallis One-Way Analysis of Variance on Ranks with *post hoc* Dunn test]. Also note the spread of the SD in rostral (Pt/Ir-electrode 2)-caudal (Pt/Ir-electrode 1) direction. Trace 4: The hallmark of SD is the abrupt, near-complete breakdown of the transcellular ion concentration gradients. Here, the large SD-associated increase of $[K^+]_o$ is seen. Note the significant prolongation under hypoxia. Traces 5–7: The spontaneous activity is assessed in the higher frequency band between 0.5 and 45 Hz. Note that the SD under hypoxia is preceded by non-spreading depression of the spontaneous activity [blue and green asterisks in **(B,C)**]. Non-spreading depression precludes that the subsequent SD can induce spreading depression of the activity. Interestingly, the depression of activity was reversible after the SD despite continued hypoxia. Trace 8: MAP fell under hypoxia. Trace 9: SD-induced hyperemia under normoxia and hypoxia, respectively. Note the marked reactive hyperemia following the recovery from SD under hypoxia. Note also that the Pt/Ir electrodes in contrast to the glass microelectrode displayed a marked negative DC reverberation following the recovery from SD under hypoxia (red asterisks), which may hinder correct assessment of the duration of the negative DC shift of SD. The fourth SD under normoxia showed much smaller amplitude than the three previous SDs at both the Pt/Ir-electrode 2 and the Ag/AgCl-based intracortical microelectrode. Such amplitude reductions are sometimes observed in clusters of SDs and could, for example, result from a proportion of parenchymal cells that are still refractory after the previous SD.

at Campus Benjamin Franklin, Charité – Universitätsmedizin Berlin between June 2017 and January 2018 in this pilot study.

Neurosurgeons in charge recruited patients into invasive neuromonitoring when they assumed a potential benefit for the patient based on clinical presentation and preinterventional CT scan leading them to suspect an emerging serious risk of epileptic seizures or infarct progression. Patients at high risk often require ventilation and analgo-sedation. This limits neurological assessment. Therefore, diagnosis and treatment of secondary complications are often delayed. Invasive real-time neuromonitoring can help the neurointensivist to diagnose earlier and initiate treatment earlier (Dreier et al., 2017).

In patients with aSAH, a linear electrode strip (six Pt/Ir contacts spaced at 10 mm) (Wyler, Ad-Tech Medical, Racine, WI, United States) was placed on the cortical surface of the vascular territory of the aneurysm-carrying vessel following surgery to secure the aneurysm (Dreier et al., 2006, 2009). In two patients with MHS, the electrode strip was placed on perfused, non-infarcted periinfarct tissue after decompressive hemicraniectomy (Dohmen et al., 2008; Woitzik et al., 2013). In addition, two epidural titanium peg electrodes (Ad-Tech Medical) were implanted through two small burr holes separated by a distance of 10 mm from one another and at a distance of 10 mm to the subdural strip. Peg electrodes are conically shaped with a $\sim$10 mm^2 recording surface area in the epidural space. The tail of the electrodes was tunneled subcutaneously and exited 2–3 cm from the scalp incision. Technical aspects of implantation of subdural electrode strips have been described in detail elsewhere (Dreier et al., 2017).

Continuous ECoG and multimodal monitoring were performed following the COSBID recommendations while patients were in the ICU (Dreier et al., 2017). The near-DC/AC-ECoG (0.01–100 Hz) was recorded in five bipolar channels with a GT205 amplifier (ADInstruments). Data was sampled at 200 Hz and recorded and analyzed with a Powerlab 16/SP and LabChart-8 software. A subdermal Pt/Ir needle electrode on the frontal apex was used as reference. Additional monopolar, DC-coupled (0–100 Hz) recordings were performed with a BrainAmp amplifier (BrainProducts GmbH, Munich, Germany) and BrainVision Recorder software (BrainProducts GmbH). In one patient, the brain $p_{ti}O_2$ was measured using an intraparenchymal sensor (Licox CC1P1, Integra Lifesciences Corporation, Plainsboro, NJ, United States) (Dreier et al., 2009; Bosche et al., 2010; Hinzman et al., 2014; Winkler et al., 2017). ICP was monitored via ventricular drainage catheter (EVD) or ICP transducer (Codman or Camino Systems). The systemic arterial pressure was continuously recorded via radial artery catheter.

Analysis of Patient Data

No patients were excluded from analysis. The data was analyzed in an un-blinded fashion with LabChart-8 software. The first 24 h period after the initial insult was denoted as 'Day 0.' SDs were identified by the consecutive occurrence of slow potential changes ($<$0.05 Hz) of neighboring ECoG channels. The negative DC shift was measured from start to end, regardless of morphology or multi-phasic appearance. In electrically active tissue, SD typically causes spreading depression of spontaneous activity in the AC-ECoG range (0.5–45 Hz) (Dreier et al., 2006). The duration of the depression period was scored beginning at the initial decrease in the integral of power and ending at the start of the recovery phase. Depression durations were scored to measure the TDDD (Dreier et al., 2017). The peak TDDD (PTDDD) was defined as the maximal value among all recording days. SDs in electrically active tissue received the epithet 'spreading depression.' SDs measured in a zone of electrically inactive tissue were denoted with the adjective 'isoelectric.'

RESULTS

SD in Rats Under Normal Conditions

Figure 1A shows the experimental setup. During SD in normoxic rats, Pt/Ir electrodes recorded the negative DC shift of SD, albeit with early and late positivities not observed in micropipette recordings to such an extent. SD reached the rostral Pt/Ir electrode earlier than the caudal one [delay: median: 76 (IQR: 70–83) s] corresponding to a propagation velocity of 3.9 (IQR: 3.6–4.3) mm/min. SD caused a hyperemic response to 272 (IQR: 191–286) % of baseline [duration: 118 (IQR: 110–127) s]. In more detail, the recordings using the Ag/AgCl-based intracortical glass-microelectrode and the Pt/Ir electrodes are compared in **Figure 1B** and **Table 1**.

TABLE 1 | Characteristic changes along the SD continuum in rats *in vivo*.

Condition		Pre-SD DC positivity		SD DC negativity		Post-SD DC positivity		Negative DC reverberation post SD		Depression of activity	Increase of $[K^+]_o$ during SD	
		Amplitude (mV)	Duration (s)	Amplitude (mV)	Duration	Amplitude (mV)	Duration (s)	Amplitude (mV)	Duration (min)	Duration	Amplitude (mM)	Duration
Normoxia (*n* = 7)	Glass micro-electrode	Absent	Absent	−21.5 [(−19.4)–(−22.0)]	36 **s** (27–38)	1.8 (0.9–2.5)	92 (68–94)	Absent	Absent	x	From 3.0 (3.0–3.1) to 56.0 (46.0–61.5)	44 **s** (42–52)
	Rostral Pt/Ir electrode	Absent	Absent	−1.7 [(−1.4)–(−2.0)]	48 **s** (40–49)	1.4 (1.1–1.7)	99 (57–115)	−1.3 [(−0.8)–(−1.9)] (*n* = 4 out of 7)	11.0 (10.5–11.9) (*n* = 4 out of 7)	226 **s** (187–233)		
	Caudal Pt/Ir electrode	0.3 (0.2–0.9) (*n* = 3 out of 7)	35 (29–51)	−1.8 [(−1.4)–(−2.4)]	51 **s** (42–59)	1.9 (1.2–2.3)	89 (68–94)	−1.8 [(−1.5)–(−2.2)] (*n* = 4 out of 7)	16.7 (12.4–19.8) (*n* = 4 out of 7)	230 **s** (176–250)		
Hypoxia (*n* = 8)	Glass micro-electrode	1.8 (1.6–2.9) (*n* = 3 out of 8)	92 (80–136)	−17.4 [(−13.1)–(−18.3)]	*7.9 **min** (1.4–17.7) (***P* = 0.031**)	Absent	Absent	Absent	Absent		From 3.8 (3.6–5.0) to 51.5 (48.5–56.0)	*12.8 **min** (5.9–20.7) (*P* = 0.016)
	Rostral Pt/Ir electrode	0.1 (0.1–0.2) (*n* = 4 out of 8)	28 (25–33) (*n* = 4 out of 8)	*−3.9 [(−2.8)–(−5.9)] (***P* ≤ 0.05**)	*8.5 **min** (2.2–17.5) (***P* = 0.016**)	Absent	Absent	−1.9 [(−0.8)–(−7.2)] (*n* = 5 out of 8)	21.3 (12.7–22.1) (*n* = 5 out of 8)	**21.0 **min** (8.5–57.2) (*P* = 0.004)		
	Caudal Pt/Ir electrode	0.3 (0.2–0.4) (*n* = 4 out of 8)	28 (23–35) (*n* = 4 out of 8)	*−5.5 [(−2.9)–(−6.4)] (***P* ≤ 0.05**)	*9.3 **min** (2.2–18.4) (***P* = 0.016**)	Absent	Absent	−5.0 [(−3.5)–(−5.5)] (*n* = 5 out of 8)	*26.8 (19.1–27.4) (*n* = 5 out of 8) (***P* = 0.032**)	**21.7 **min** (10.3–54.0) (*P* = 0.004)		
During dying process (*n* = 8)	Glass micro-electrode	0.8 (0.6–1.0) (*n* = 4 out of 8)	47 (23–82) (*n* = 4 out of 8)	*−14.5 [(−12.2)–(−15.5)] (***P* ≤ 0.05**)	Terminal					Terminal	From *7.4 (6.0–8.0) (***P* = 0.05**) to 60.9 (57.2–68.5)	Terminal
	Rostral Pt/Ir electrode	1.2 (0.8–1.7) (*n* = 4 out of 8)	80 (44–115) (*n* = 4 out of 8)	−3.6 [(−0.2)–(−5.7)]	Terminal					Terminal	With delay gradual rise to 76.0 (73.0–78.0)	
	Caudal Pt/Ir electrode	1.2 (0.7–1.8) (*n* = 4 out of 8)	79 (47–125) (*n* = 4 out of 8)	*−4.9 [(−3.3)–(−7.3)] (***P* ≤ 0.05**)	Terminal					Terminal		

*Statistical comparisons were performed between SD under normoxia (control group), SD under hypoxia and the terminal SD using either Wilcoxon Signed Rank Test (two-group design) or Friedman Repeated Measures Analysis of Variance on Ranks with Dunn's post hoc test (three-group design versus control) (*P ≤ 0.05, **P ≤ 0.01). x: In recordings with microelectrodes, in contrast to Pt/Ir electrodes, the sharper negative DC shift of SD made it difficult to assess the depression periods using the integral of power. Data is given as median and IQR.*

Hypoxia-Induced SD in Rats

Partial replacement of O_2 with N_2 in the inspired air caused a decrease of arterial p_aO_2 from 102 (IQR: 95–120) to 36 (IQR: 33–39) mmHg, of hemoglobin saturation with O_2 from 98 (IQR: 97–98) to 51 (IQR: 43–52) %, of arterial pH from 7.37 (IQR: 7.36–7.39) to 6.99 (IQR: 6.88–7.22), of p_aCO_2 from 39 (IQR: 37–46) to 29 (IQR: 22–31) mmHg and of the base excess from −2.5 [IQR: (−1.4)–(−3.7)] to −23.7 [IQR: (−14.7)–(−27.3)] mM corresponding with hypoxia-induced metabolic acidosis (all $P \leq 0.05$, $n = 6$, Wilcoxon Signed Rank Tests). MAP significantly fell from 112 to 69 (IQR: 56–98) mmHg ($P = 0.016$, $n = 8$, Wilcoxon Signed Rank Test), although high doses of intravenous noradrenalin of up to 67 (IQR: 57–77) μg/kg/min were intravenously administered to maintain the systemic circulation. Although MAP decreased under hypoxia, rCBF significantly increased from 97 to 211 (IQR: 113–248) % ($P = 0.039$, $n = 8$, Wilcoxon Signed Rank Test).

Spreading depolarization developed spontaneously under hypoxia in four experiments (**Figures 1B,C**, **2A**) and was triggered by KCl application during hypoxia in the remaining ones (**Figure 3**). In all animals, initial SDs were transient with spontaneous recovery despite continued hypoxia. SDs induced spreading depression of activity under hypoxia in all animals except one in which non-spreading depression developed first (**Figure 1C**). Negative DC shifts, $[K^+]_o$ elevations, and depression periods were significantly prolonged under hypoxic compared to normoxic conditions (**Table 1**). Notably, Pt/Ir electrodes were able to record the SDs, but in contrast to Ag/AgCl microelectrodes, also displayed a negative DC reverberation in five of eight animals following the recovery from SD (**Figures 1B**, **2A** and **Table 1**). Similar to normoxia, SD occurred with a delay of 71 (IQR: 47–100) s between the two Pt/Ir electrodes. The rCBF response to SD was impaired under hypoxia and difficult to quantify due to heterogeneity. Often, no major change was seen during SD, but a delayed hyperemic response from 211 to 368 (IQR: 215–398) % followed recovery from long-lasting SDs (**Figures 1B**, **2A**). This was distinct from the hyperemia observed during SD in normoxic tissue. Thereafter, a relative oligemia to 135 (IQR: 76–182) % occurred (**Figure 2A**). The typical pattern of SI (Dreier et al., 1998; Dreier, 2011; Sugimoto et al., 2018) was not observed in any of the SDs under hypoxia that preceded the terminal one.

Terminal SD in Rats During the Dying Process

Seven animals died spontaneously from hypoxia and one from intravenous injection of an air embolus into the femoral vein. The phase transition from life to death was characterized by four events: loss of circulation, loss of respiration, loss of spontaneous brain activity and a terminal SD without repolarization. These changes occurred in all animals, but not necessarily in the same order. Four animals had CA before terminal SD and four after. Of animals dying spontaneously under hypoxia, MAP was 45 (IQR: 43–61) mmHg at the time the first of these events occurred. When CA occurred first, brain isoelectricity developed as non-spreading depression after 71 (IQR: 49–265) s, unless the tissue was already depressed, and terminal SD began 181 (IQR: 142–302) s ($n = 4$) after CA. When terminal SD occurred first, CA followed after a median delay of 878 s (range: 23–1740, $n = 4$). In all cases, the terminal SD appeared first at the rostral Pt/Ir electrode and spread either to the caudal Pt/Ir electrode with a median delay of 60 s (range: 11–195, $n = 7$) or to the glass microelectrode (delay: 12 s, $n = 1$). This is consistent with rodent imaging experiments, which showed that the persistent SD during global cerebral ischemia would usually spread from one point of origin in a rostral-caudal direction (Farkas et al., 2008, 2010; Bogdanov et al., 2016).

In four animals, isoelectricity developed in a non-spreading pattern and was followed by terminal SD. For instance, following the air embolus in one animal, MAP fell rapidly from 99 to 6 mmHg and respiratory fluctuations of expiratory pCO_2 ceased within 18 s; non-spreading depression caused isoelectricity within 26 s and terminal SD started after 98 s (**Figure 4**). In two other animals, progressive CA spontaneously developed with fluctuating drops in MAP and rCBF, and was followed by non-spreading depression and then terminal SD. In yet another case (**Figure 3**), non-spreading depression developed minutes after respiratory insufficiency and was then followed by terminal SD, which induced SI. Thereafter, CA developed.

The remaining animals showed diverse patterns in the development of isoelectric brain activity during the dying process. In one case, the terminal SD started when MAP was 44 mmHg, the respiratory rate was 71/min, and spontaneous brain activity was still present. The SD thus triggered a spreading depression that persisted through death (**Figure 2B**). 179 s after SD first appeared at the rostral Pt/Ir electrode, the LDF probe detected a marked SI with sharp drop of rCBF from 81 to 0%. Systemic CA and respiratory arrest started 23 and 42 s, respectively, after the onset of SI. In two other animals, terminal SDs started when the spontaneous activity was already depressed after previous SD-induced spreading depressions. These did not cause any obvious change in rCBF, which remained at 70 and 95%, respectively. Systemic circulatory and respiratory arrest, with simultaneous drop in rCBF, did not occur until 29 min later in one case, and 27 min in the other. The electrophysiological pattern was the same in the last animal, but terminal SD was preceded by progressive circulatory failure.

Epidural Recordings of SDs in Patients

Demographic details are given in **Table 2**. The total near-DC/AC-ECoG recording time from the cortical surface was 1117.5 h in the five patients with aSAH and 178.1 h in the two patients with MHS. Three patients had no SDs, but assessment was limited in one of these because recordings were artifact-laden. Three patients with aSAH had 98 SDs and one patient with MHS had 5 SDs. For further analysis, 808.0 h of simultaneous subdural DC/AC-ECoG and epidural DC/AC-ECoG recording time of sufficient quality was available during which 74 of the 103 SDs occurred. Ten of these occurred in patient 1, 16 in patient 4, 3 in patient 6, and 45 in patient 7. Seven of the 45 SDs in patient 7 occurred as part of the terminal cluster and are described further below.

The negative DC shift's peak-to-peak amplitude and duration of the remaining 67 SDs were 5.7 (IQR: 3.9–7.3) mV and

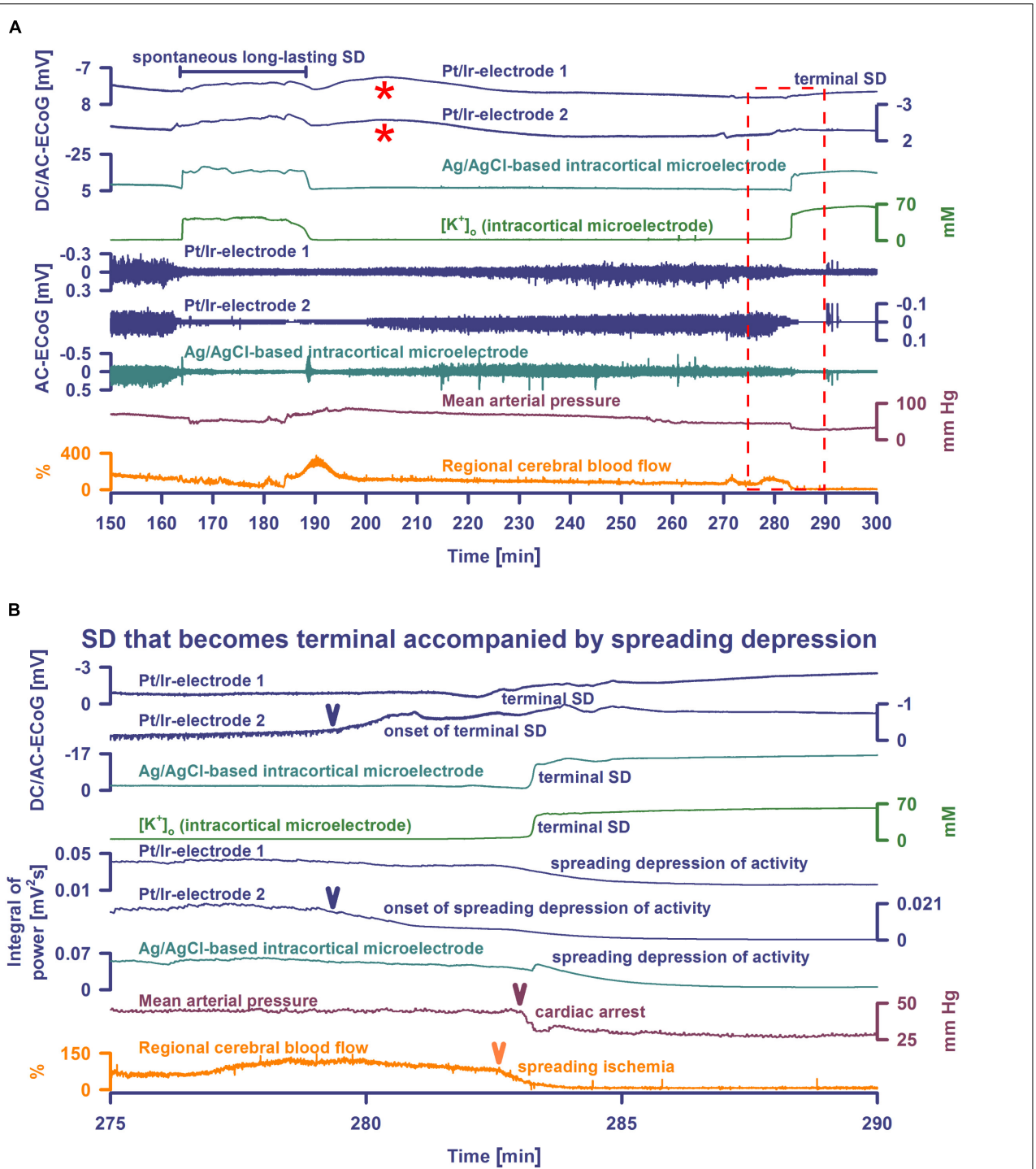

FIGURE 2 | Spontaneous SD during hypoxia compared with terminal SD in death. Traces are the same as in **Figure 1**. The Pt/Ir plate electrodes were compared with the K^+-selective glass microelectrode over the full SD continuum from SD in well-nourished tissue (0–80 min shown in **Figure 1**) to SD in hypoxic tissue to SD during global cerebral ischemia (terminal SD) (81–150 min shown in **Figure 1** and 150–300 min in **Figure 2**). Systemic hypoxia was induced by partial replacement of O_2 with N_2 in the inspired air. The negative DC shift is necessary and sufficient for identification of SD, and the duration of the negativity is a measure of the metabolic and excitotoxic burden imposed on tissue by SD (Dreier et al., 2017). Accordingly, it can be seen that both negative DC shift and increase of $[K^+]_o$ were markedly longer under hypoxia than under normoxia, and they were terminal after CA. Note that the Pt/Ir electrodes in contrast to the glass microelectrode displayed a marked negative DC reverberation following the recovery from SD under hypoxia (red asterisks), which may hinder correct assessment of the duration of the negative DC shift of SD. It is also interesting in this animal that terminal SD began spontaneously under hypoxia prior to the spontaneous CA and induced spreading depression of activity. Note the spread of the terminal SD in rostral (Pt/Ir-electrode 2)-caudal (Pt/Ir-electrode 1) direction. Panel **(B)** shows the same data from **(A)** on an expanded time scale (275–290 min). The terminal SD-induced spreading depression of the activity is shown in **(B)** using the integral of power of the spontaneous activity.

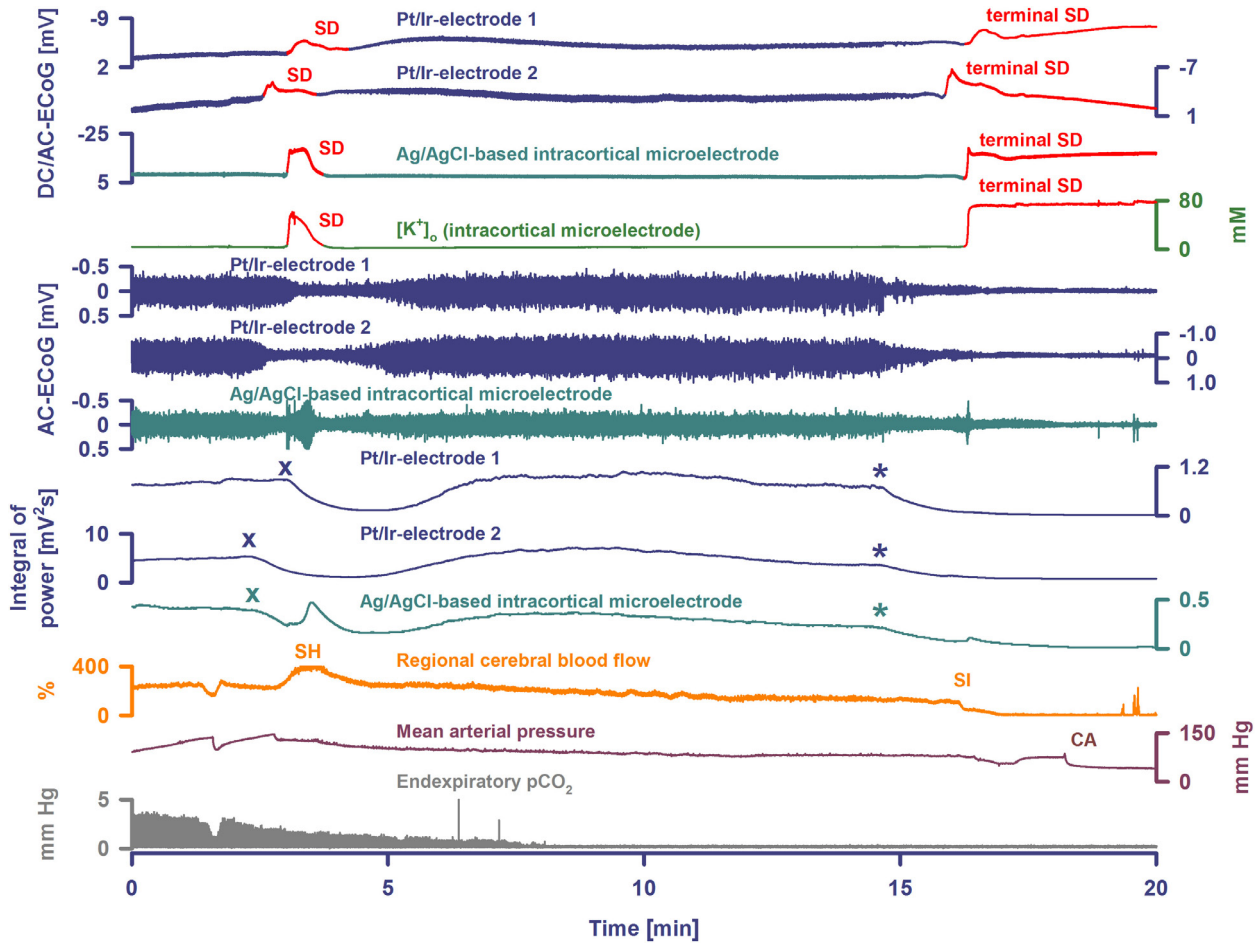

FIGURE 3 | Terminal SD during death in the rat brain. Traces are similar to **Figures 1**, **2**. A drop of KCl triggered the SD under hypoxia in this animal. Note that the hypoxic SD induced spreading depression of activity (cf. x) in contrast to the hypoxic SD in **Figure 1** which was preceded by non-spreading depression. Negative DC shift and $[K^+]_o$ were only mildly prolonged indicating that hypoxia was less severe during this experiment compared to the one displayed in **Figures 1**, **2**. Accordingly, SD induced a relatively normal spreading hyperemia (SH). Subsequently, the fraction of inspired oxygen (FiO_2) was further reduced, and a spontaneous, slowly progressive respiratory arrest (cf. end-expiratory pCO_2) eventually led to non-spreading depression of spontaneous activity (cf. asterisks). Thirty-five seconds after isoelectricity was established a spontaneous terminal SD occurred first at the rostral Pt/Ir electrode (rostral-caudal delay: 63 s) and triggered a marked spreading ischemia (SI) with rapid drop in rCBF from 112 to 1%. The SI was detected by the LDF probe 36 s after the SD had first appeared at the rostral Pt/Ir electrode. Circulatory arrest (CA) with a rapid drop in MAP occurred only 247 s after the onset of SI.

4.2 (IQR: 3.6–5.8) min. The AC-ECoG activity declined from 100 to 19 (IQR: 15–28) % during the SD-induced spreading depression. Median depression duration was 13.2 (IQR: 7.5–21.8) min. Median interval between SDs was 91 (IQR: 49–316) min.

With visual inspection of epidural DC-ECoG recordings alongside subdural recordings, negative DC shifts were identified for 31/67 (46%) SDs (**Figure 5C**). All 31 epidurally identified SDs occurred in patient 4 [14/16 SDs (88%)] and patient 7 [17/38 SDs (45%)] who had clustered SDs following COSBID's current working definition of a cluster that at least three SDs occurred within three or fewer consecutive recording hours (Dreier et al., 2017) (**Figure 6A**). When the 67 SDs were pooled, the 31 epidurally identified SDs involved significantly more subdural electrodes than the 36 SDs that could not be identified in epidural recordings (Mann–Whitney Rank Sum Test, $P \leq 0.001$, **Figures 5A,B**). Intervals between subsequent SDs were not significantly different between these two groups, but the subdural negative DC shift of epidurally identified SDs was significantly larger [5.4 (IQR: 3.9–7.8) mV versus 4.0 (IQR: 3.3–4.6) mV, Mann–Whitney Rank Sum Test, $P \leq 0.001$].

Subdural negative DC shifts were larger and shorter than epidural ones [6.1 (IQR: 5.3–7.5) versus 1.5 (IQR: 1.0–2.1) mV and 5.4 (IQR: 3.9–7.8) versus 7.2 (IQR: 4.6–13.5) min, $n = 31$, Wilcoxon Signed Rank Tests with $P \leq 0.001$]. Amplitudes and durations significantly correlated between subdural and epidural negative DC shifts (**Figure 6B**). Sometimes, a delay was noted between the onsets of the negative DC shift at the two epidural electrodes but this was difficult to quantify. SD-induced spreading depression of epidural AC-ECoG activity was only identified during 19 SDs (28%). In these, the decline in epidural AC-ECoG activity was slightly less pronounced than the subdural one [20 (IQR: 15–38) % versus 18 (IQR: 13–22) %]. Both activity

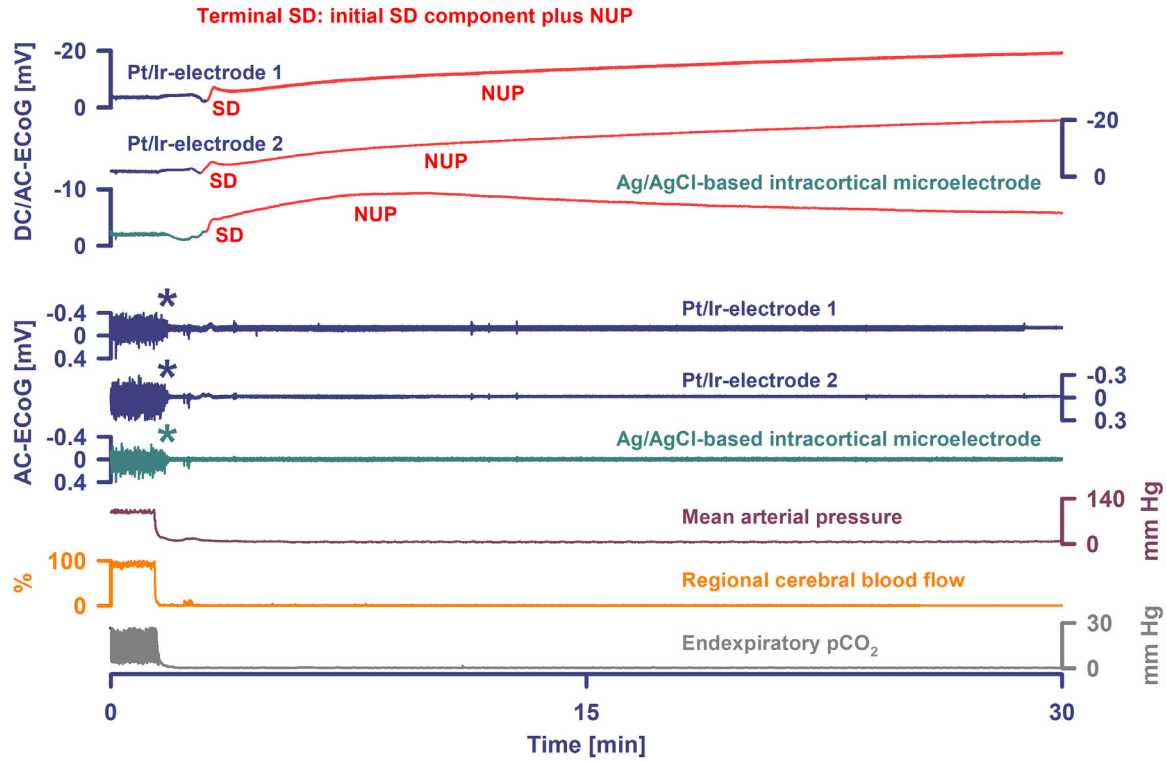

FIGURE 4 | Terminal SD in the wake of circulatory arrest. Sudden circulatory arrest was induced in this rat by injection of 10 ml of air into the heart via the femoral vein. MAP fell rapidly from 99 to 6 mmHg and respiratory fluctuations of expiratory pCO_2 ceased within 18 s; non-spreading depression caused isoelectricity within 26 s (asterisks) and terminal SD started after 98 s. Terminal SD showed an initial and a late negative DC component similar to human recordings (Dreier et al., 2018b). Whereas the initial one is the actual SD component, the late one is termed the NUP.

decline (Spearman Rank Order Correlation Coefficient: 0.599, $P = 0.00683$) and duration of spreading depression (Spearman Rank Order Correlation Coefficient: 0.898, $P = 0.0000002$) significantly correlated between epi- and subdural recordings.

A Case of Brain Death Recorded With Subdural and Epidural Electrodes

Patient 7 (cf. **Table 2**) was a 45-year-old woman with aSAH who presented with a WFNS score 4 on admission. The initial CT on Day 0 showed a grade 4 on the modified Fisher scale. CT angiography (CTA) revealed an aneurysm of the posterior communicating artery which was successfully treated with clip ligation on Day 0. After surgery, she was transferred to the ICU where prophylaxis of DCI with oral nimodipine commenced. The postoperative MRI scan on Day 1 showed widespread subarachnoid clots with oedema of the adjacent cortex. Laminar infarcts were seen at the frontal base, along the interhemispheric fissure and around a clot in the Sylvian fissure on the left side. No important parenchymal changes were noted on the CT scan on Day 3, but the CTA demonstrated signs of proximal vasospasm. Therefore, endovascular spasmolysis was performed. CT on Day 5 revealed progression of the cortical oedema. On Day 7, a wide and fixed left-sided pupil led to an emergency CT. This revealed a new infarct in the left MCA territory and a midline shift of 8 mm. Midazolam was added to the sedative regimen of propofol and sufentanil because of the increased ICP. On Day 9, another CT revealed progression of the infarct, 12 mm midline shift and beginning subfalcine herniation.

Occurrence of SDs, spreading depressions and isoelectric SDs during the clinical course are illustrated in **Figure 7B**. Clustered SDs on Day 8 after the initial hemorrhage are shown in the right panel of **Figure 6A**. Notably, when the last CT scan was performed on Day 9, the subdural electrode strip was still on viable cortex anterior to the infarct in the left MCA territory (**Figure 8**). Eleven hours thereafter, the last cluster of SDs started and led to a spreading depression with persistent loss of cortical activity through death as shown in **Figure 7A**. At all electrodes, SD then became terminal, since the negative potential shift, termed NUP, was persistent (20+ h). Additional SDs with reduced amplitude occurred superimposed on the NUP, similar to previous cases of focal or global brain death with maintained systemic circulation (Oliveira-Ferreira et al., 2010; Carlson et al., 2018; Luckl et al., 2018), but in contrast to cases when brain death followed systemic CA (Dreier et al., 2018b) (**Figure 8**). The NUP had an amplitude of −150 [IQR: (−136)–(−157)] mV at the subdural electrodes, and was also recorded at the two epidural electrodes (median amplitude: −67 mV).

At onset of the terminal cluster, MAP was at 120 mmHg, the heart rate was around 65 beats/min and the peripheral

TABLE 2 | Summary of demographic, treatment, and SD-related data of the patients.

aSAH (subdural electrode strip, bipolar near-DC/AC-ECoG recordings)												
No.	**Age range**	**Lesions**	**WFNS grade**	**Modified Fisher grade**	**Location of aneurysm**	**Intervention**	**Location of electrode**	**Total number of SDs**	**PTDDD (min)**	**Peak number of SDs/24 h**	**Peak number of iSDs/24 h**	**Recording time (h)**
1	80–85	Lesions remote from strip; early: ICH (P, l), PCA infarct (r); delayed infarcts: AchA (l), MCA (l), PCA (l); delayed lacunes: ACA (r), MCA (r), PICA (b), SCA (b)	5	4	MCA	Aneurysm clipping, EVD left frontal	F (l)	10	96.8	8.3	0.0	270.5
3	70–75	Lesions remote from strip; early: ICH (F, T, r)	5	3	MCA	Aneurysm clipping, EVD right frontal	F (r)	0	0.0	0.0	0.0	188.8
4	60–65	Delayed lesion close to strip; early: PCA infarct (l), lacunes: ACA (r), MCA (l), PCA (r); delayed infarcts: ACA (b)	5	4	ACoA	Aneurysm clipping, EVD left frontal	F (r)	16	259.8	6.3	3.0	191.1
5	60–65	Early lesion close to strip; early: ACA/MCA infarcts (l), ICH (T, l), SDH hem (l)	5	3	MCA	Aneurysm clipping	P (l)	Artifact-laden				278.4
7	40–45	Delayed lesion close to strip (**Figure 8**); early: ACA infarct (l), ICH (P, l); delayed infarct: MCA (l)	4	4	PCoA	Aneurysm clipping, EVD right frontal	F (l)	72	1440.0	23.9	12.5	188.6

MHS (subdural electrode strip, bipolar near-DC/AC-ECoG recordings)										
No.	**Age range**	**Lesions**	**Infarct etiology**	**Intervention**	**Location of electrode**	**Total number of SDs**	**PTDDD (min)**	**Peak number of SDs/24 h**	**Peak number of iSDs/24 h**	**Recording time (h)**
2	46–50	Territorial infarct MCA (r)	Suspicion of cardiac embolism due to NSTEMI	Decompressive hemicraniectomy	P, O (r)	0	0.0	0.0	0.0	78.6
6	70–75	Territorial infarct MCA/PCA (r)	Cardiac embolism due to atrial fibrillation	Decompressive hemicraniectomy	F (r)	3	37.9	3.4	0.0	99.5

iSD, isoelectric SD; PTDDD, peak total SD-induced depression duration of a recording day; WFNS, World Federation of Neurosurgical Societies; f, female; m, male; l, left; r, right; b, bilateral; hem, hemisphere; F, frontal; O, occipital; P, parietal; T, temporal; EVD, extraventricular drainage; ICH, intracerebral hemorrhage; NSTEMI, non-ST elevation myocardial infarction; SDH, subdural hematoma; ACA, anterior cerebral artery; AChA, anterior choroidal artery; ACoA, anterior communicating artery; PCoA, posterior communicating artery; MCA, middle cerebral artery; PCA, posterior cerebral artery; PICA, posterior inferior cerebellar artery; SCA, superior cerebellar artery.

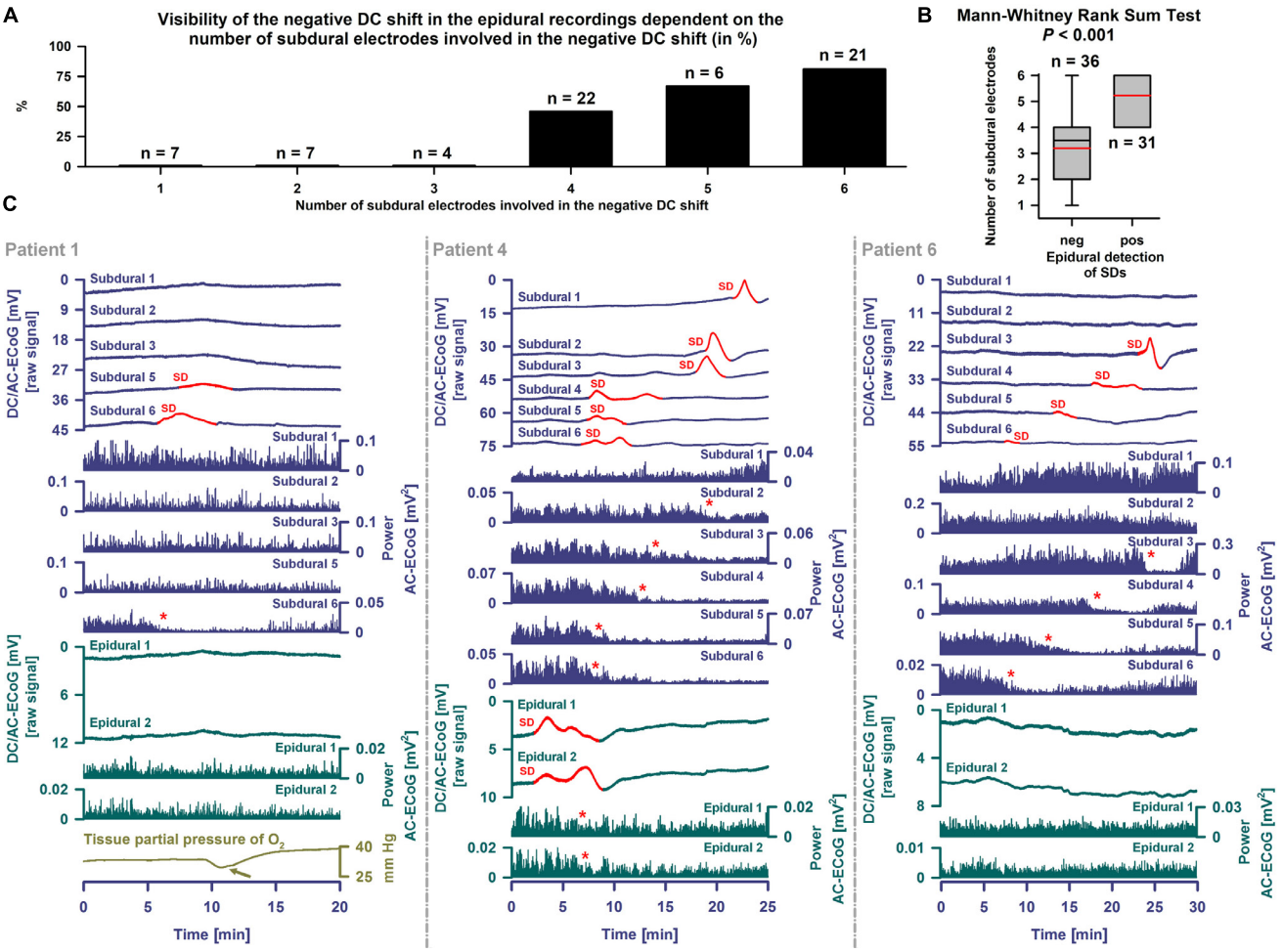

FIGURE 5 | Epidural and subdural recordings of single SDs. **(A)** The 31 epidurally identified SDs involved more subdural electrodes than the 36 SDs that could not be identified using epidural recordings. **(B)** When the SDs were pooled this was statistically significant (Mann–Whitney Rank Sum Test, $P \leq 0.001$). The whiskers (error bars) above and below the box indicate the 90th and 10th percentiles. The red reference line marks the mean. **(C)** SDs are observed as a negative DC shift propagating between neighboring electrodes (cf. top traces showing the DC/AC-ECoG (0–45 Hz) at the different electrodes, negative up). Red portions indicate potentials associated with SDs. SD-induced spreading depression is observed in the AC-ECoG recordings (0.5–45 Hz) as a rapidly developing reduction in the amplitudes of spontaneous activity that spreads together with SD between adjacent recording sites. The squared spontaneous activity is called AC-ECoG power (cf. Power AC-ECoG-traces from the different electrodes). In patient 1, 10 non-clustered SDs were recorded using subdural electrodes. Six SDs only occurred at electrode 6 and 4 also involved electrode 5. The left panel shows an example of one of these SDs. The red asterisk marks the SD-induced depression of activity at electrode 6. The light green arrow points at the SD-induced tissue hypoxia (Dreier et al., 2009; Bosche et al., 2010; Winkler et al., 2017). Different from the subdural recordings, the epidural ones did not allow clear identification of the SD, though there could be a correlate. By contrast, in patient 4 (middle panel), 14 of 16 SDs were not only seen subdurally but also epidurally. A non-clustered SD is displayed. The preceding SD occurred 12.5 h before and the subsequent one 25.1 h after this SD. Note that the SD involved all six subdural electrodes. At the epidural electrodes, not only the negative DC shift but also the SD-induced depression was visible. The red asterisks mark the SD-induced spreading depression of activity at subdural electrodes 2–5 and the two epidural electrodes. In patient 6 (right panel), the subdural DC/AC-ECoG of 3 SDs was available to the analysis. None of these showed an unambiguous correlate in the epidural DC/AC-ECoG. One of these is displayed here as an example.

O_2 saturation >98%. ICP was around 30 mmHg with a trend toward slow increase. The arterial blood gas analysis was normal, including serum lactate at 6 mg/dl, serum glucose at 155 mg/dl and normal serum electrolytes. However, shortly after onset of the terminal cluster, the patient was found to have an abrupt loss of brainstem reflexes with fixed dilated pupils. Serum lactate then increased to 12 mg/dl and serum glucose to 211 mg/dl; a sinus tachycardia up to 125/min developed. Following discussion with the family regarding the poor prognosis, the patient was terminally extubated 20 h later and expired shortly thereafter. Similar to the previous case of Carlson et al. (2018), the exact cause of death remained unclear given that there was no massive ICP increase suggestive of large stroke or oedema, and cardiac, pulmonary, and renal function were thought to be adequately supported. During CA at 20 h after brain death, a slow positive DC drift occurred which stabilized at 53 (IQR: 52–54) mV subdurally and 43 (IQR: 42–44) mV epidurally. No SDs were superimposed on this potential, consistent with the prior

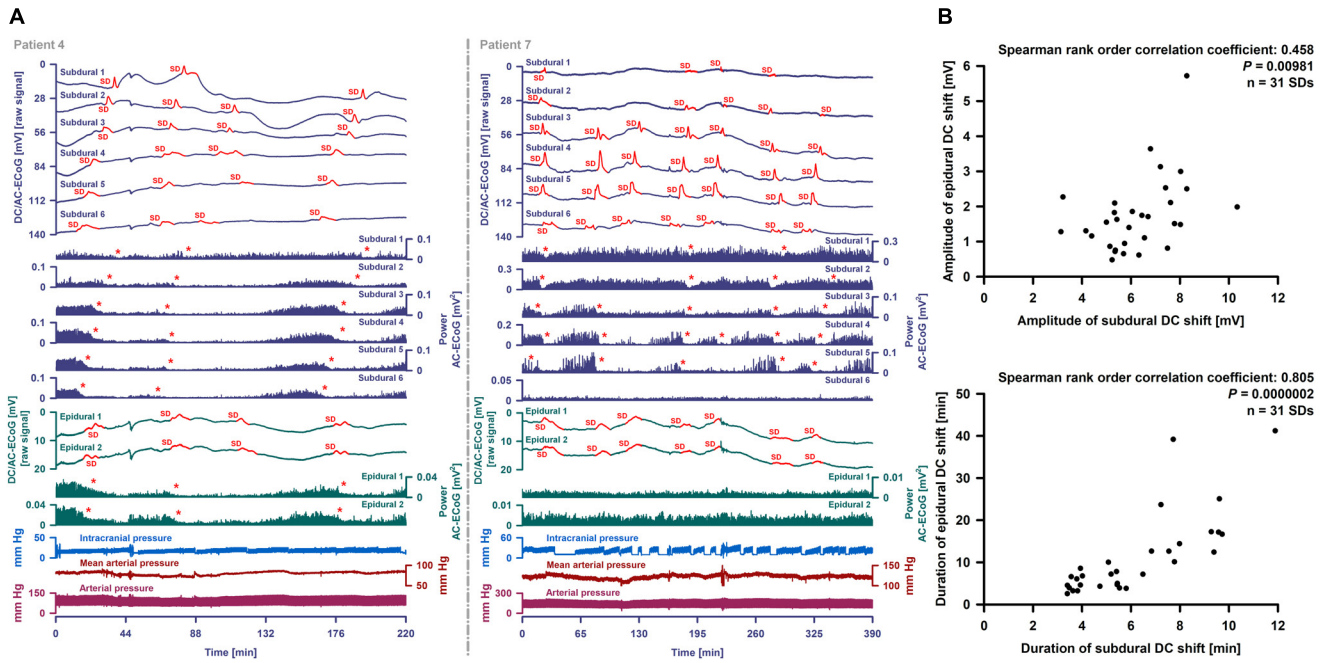

FIGURE 6 | Epidural and subdural recordings of clustered SDs. **(A)** Top six traces show the raw DC/AC-ECoG recordings from each subdural electrode (negative up). Red portions indicate potentials associated with SDs. SD-induced spreading depressions are assessed in the power of the AC-ECoG (traces 7–12). Below, the epidural recordings are shown. In the left panel, clustered SDs in patient 4 are displayed. Between an MRI on Day 2 and a CT on Day 9, the patient developed a new infarct in the vicinity of the recording strip. The SDs involved all subdural and epidural electrodes. The red asterisks mark the SD-induced spreading depressions. The third SD is an isoelectric one. In patient 7 (right panel), clustered SDs on Day 8 are shown. The electrodes were located close to a delayed cerebral infarct as shown in **Figure 8**. The SDs were observed both subdurally and epidurally in contrast to the SD-induced spreading depressions which were only seen at the subdural electrodes. **(B)** Amplitudes and durations significantly correlated between subdural and epidural negative DC shifts indicating SDs.

diagnosis of brain death and in contrast to cases where CA is the cause of subsequent brain death (Dreier et al., 2018b).

DISCUSSION

Terminal SD Under Progressive Hypoxia in Rats

The animal experiments confirmed the characteristic changes along the full SD continuum. Specifically, the duration of depolarization and near-complete breakdown of ion homeostasis, as indicated by the negative DC shift and increase of $[K^+]_o$, varied from short-lasting under normoxia to long-lasting under systemic hypoxia to persistent under severe global ischemia, since repolarization requires activation of energy-dependent membrane pumps such as Na, K-ATPases (LaManna and Rosenthal, 1975; Major et al., 2017). Short-lasting DC shifts thus indicate sufficient ATP at the recording site to fuel fast repolarization. This feature renders the negative DC shift duration a useful measure for (a) the tissue energy status and (b) the risk of injury (cytotoxic oedema and excitotoxicity) at the recording site as reviewed recently (Dreier et al., 2017; Hartings et al., 2017b).

A significant proportion of SD waves observed in patients have intermediate characteristics, as opposed to the two extremes of the SD wave in either severely ischemic or normal tissue (Dreier and Reiffurth, 2015; Dreier et al., 2017; Hartings et al., 2017b). In patients, SD waves of intermediate character might typically indicate moderate focal ischemia at the recording site. This interpretation is consistent with previous experimental observations in brain slices (Somjen, 2001) and also with the intermediate SDs recorded here in rats under systemic hypoxia. The uniformity of intermediate SDs, no matter whether they are recorded during focal ischemia or under systemic hypoxia, indicates that energy depletion is the decisive factor producing this pattern rather than, for example, diffusion of chemicals from the core of focal ischemia to the penumbra.

In contrast to the intermediate type, persistent SDs are those that are indefinitely prolonged at the recording location and will not repolarize unless oxygen and glucose availability improve. These typically occur following non-spreading depression of activity after onset of anoxia/severe ischemia, and thus historically are termed 'anoxic SD' (van Harreveld, 1946; Leão, 1947; Bures and Buresova, 1957; Marshall, 1959). However, SD can transform into intermediate and persistent types even in well-nourished tissue by the mechanism of SI, which reflects inverse neurovascular coupling (Dreier et al., 1998, 2001; Dreier, 2011; Sugimoto et al., 2018). Here, we observed SI in response to terminal SD in two out of four hypoxic animals in which the terminal SD preceded the CA. This corresponds well to previous observations under hypoxia (Sonn and Mayevsky, 2000; Sukhotinsky et al., 2008). Nonetheless, terminal SD did not cause

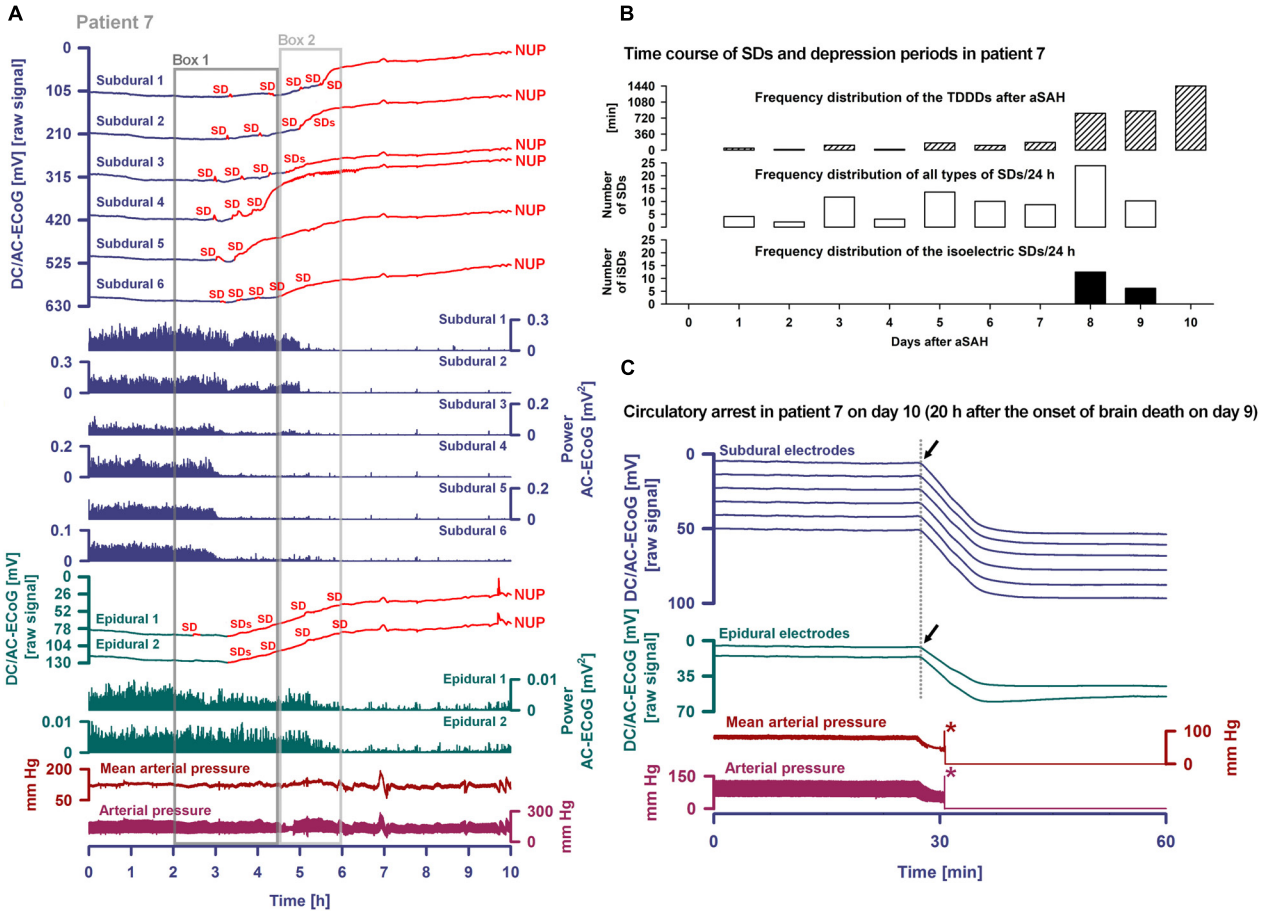

FIGURE 7 | Progress to brain death in patient 7. **(A)** The six top traces show a series of several transient SDs followed by terminal SD. The terminal SD consists of the initial SD component followed by the NUP (Dreier et al., 2018b). Traces 7–12 display the SD-induced spreading depression that persisted through death (observed as a reduction in the amplitudes of the AC-ECoG power propagating from electrode to electrode). SDs and NUP are smaller in the epidural than the subdural DC/AC-ECoG recordings. However, in particular the NUP is clearly visible also in the epidural recordings (traces 13 and 14). Also the terminal SD-induced depression of activity is seen at the epidural recordings (traces 15 and 16). Traces 17 and 18 display MAP and arterial pressure fluctuations. Regions of Box 1 outlined by the dark gray lines and of Box 2 outlined by the light gray lines are shown in detail in **Figure 8** which additionally gives the continuous ICP recordings. **(B)** The occurrence of SDs, SD-induced depression periods and isoelectric SDs in patient 7 over the whole clinical course. **(C)** When the patient underwent circulatory arrest 20 h after brain death the DC potential at all subdural and epidural electrodes showed a slow positive drift (positive down). The asterisks mark the moment when the arterial pressure monitoring was switched off.

any change in rCBF in the remaining two animals, and rCBF declined only when the systemic circulation ceased. These results evidence the continuum of hemodynamic responses to SD, which ranges from the normal hyperemic response to an increasingly inverse ischemic one (Dreier et al., 2009, 2018a).

Patterns in the development of electrocerebral silence during the dying process varied in the animals. The terminal SD could be preceded by non-spreading depression of activity, or it could trigger a spreading depression that persisted through death, or it could start when the spontaneous activity was already depressed after previous SD-induced spreading depressions. In rats, the pathophysiology of hypoxic-ischemic brain injury thus shows significant variations. In part, this may reflect whether the underlying condition is primarily hypoxic/anoxic versus abrupt circulatory collapse versus prolonged hypoperfusion. Nonetheless, the phase transition from life to death is always characterized by four events: loss of circulation, loss of respiration, loss of spontaneous brain activity and terminal SD. The latencies and even the order of the four events can vary dependent on the specific etiologies and circumstances of death.

The patterns observed in the present case and in 10 cases previously reported (Carlson et al., 2018; Dreier et al., 2018b) suggest that human death is characterized by similar variations. This is important not only for research on treatment strategies of cardiac arrest and stroke that may complement efforts to re-establish circulation, but also for the debate on organ donation after (a) either cardiocirculatory death (DCD), where death is declared between a few seconds and 10 min following the cessation of circulatory function (Boucek et al., 2008; Dhanani et al., 2012; Stiegler et al., 2012; van Veen et al., 2018), or (b) brain death.

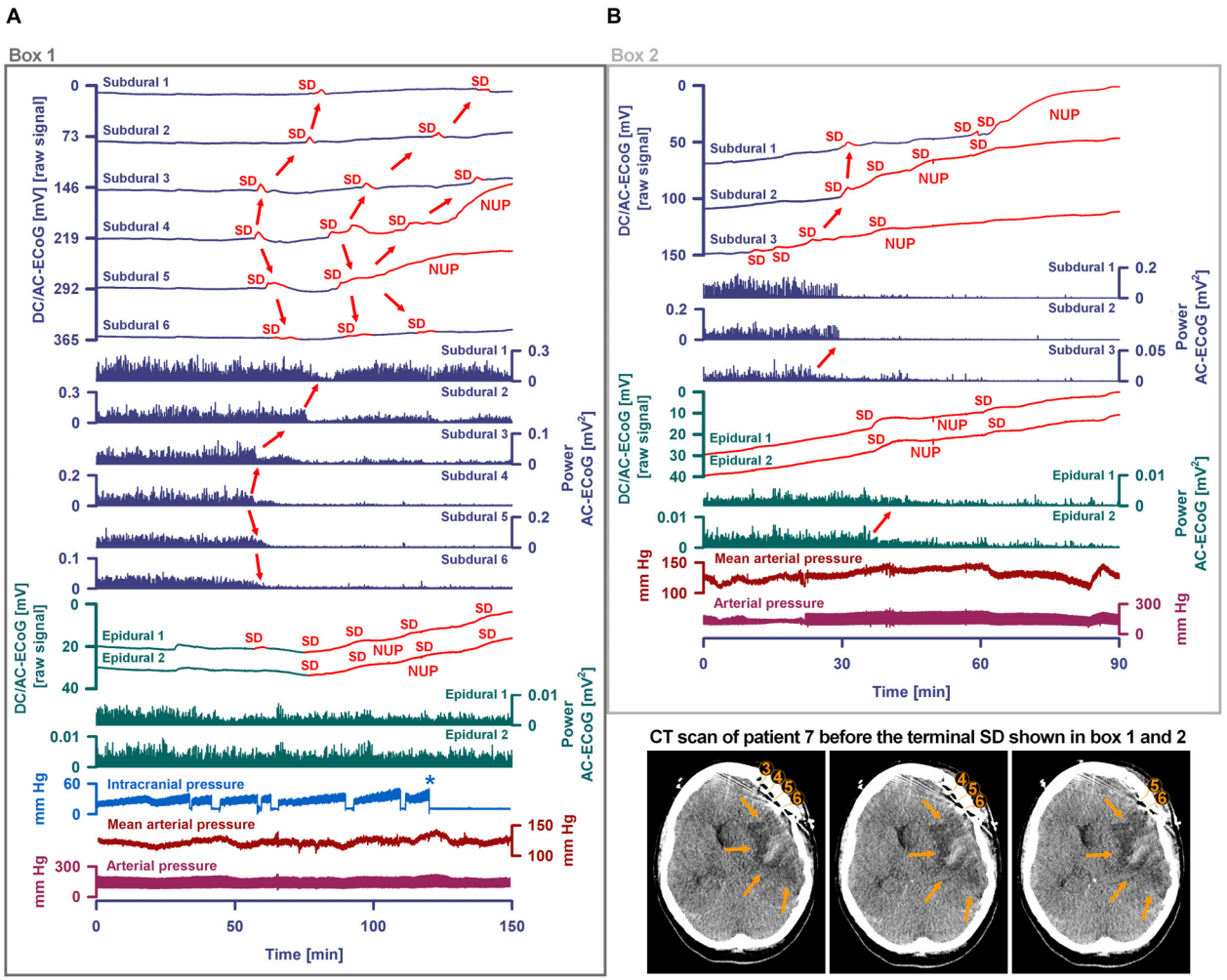

FIGURE 8 | Progress to brain death in patient 7. **(A)** A subset of the same traces in **Figure 7** is shown in greater detail. In addition, ICP is given. As outlined by Box 1 in **Figure 7**, the initial time period around the terminal SD is displayed. The SDs are marked in red. The second SD is a terminal one that starts at electrode 4 from where it spreads to electrode 5. The terminal nature of this event is indicated by the persistence of the negative DC shift. This negative potential develops further through time as a NUP, which is thought to reflect the progressive development of tissue necrosis. The red arrows mark the spreading depression of activity (middle traces). Whereas the spontaneous activity transiently recovered at subdural electrodes 1–3, the activity depression persisted through death at subdural electrodes 4–6 after the first SD. The continuous physiological variables in the bottom traces remained stable during the terminal SD. The asterisk marks the moment when the EVD was left open to counteract the ICP increase. **(B)** As outlined by Box 2 in **Figure 7**, the time period following the one in **(A)** is shown. The terminal SD spread further to subdural electrode 3 to 2 to 1. The activity depression at the subdural electrodes was eventually followed by activity depression at the epidural electrodes which persisted through death. Note that the NUP was superimposed by additional SDs of decreasing amplitude. In the right lower corner, three neighboring slices of the last CT scan are given, showing the subdural electrodes anterior to the delayed infarct in the MCA territory.

With regard to the terminal SD, it should be noted that propagation is not really the decisive property of SD and that depolarization of neurons can also take place in many other contexts. The main feature of SD is the abrupt, almost complete collapse of the small molecule gradients across cell membranes, which in the case of terminal SD is persistent and eventually leads to cell death under this condition.

Detection of SDs Using Subdural Electrodes

The animal experiments confirmed that subdural Pt/Ir electrodes reliably identify the full SD continuum. However, reliable measurement of negative DC shift durations may be complicated by multiple sensitivities of Pt/Ir electrodes, particularly in hypoxic conditions. Here, for instance we observed negative DC reverberations on Pt/Ir electrodes that were not present in Ag/AgCl electrodes. This pattern can also occur in human recordings (Drenckhahn et al., 2012). The underlying process is unclear, but may be related to the strong catalytic capacity of platinum in contrast to Ag/AgCl for many chemical reactions. To give but two examples: (a) platinum's catalytic effect on the redox reaction between hydrogen ions and molecular hydrogen renders the platinum-based hydrogen electrode method a standard among the various methods for measuring pH; (b) an additional

reaction catalyzed by platinum is the formation of water from molecular O_2 and hydrogen ions (Meunier and Popovic, 1988).

Detection of SDs Using Epidural Electrodes

A number of previous animal studies suggested that SD's negative DC shift can also be recorded using epidural electrodes (Iijima et al., 1992; Kang et al., 2013). Though subdural and intraparenchymal Pt/Ir electrodes show a good safety profile in humans (Stuart et al., 2010; Drenckhahn et al., 2016), at least theoretically, epidural electrodes pose a lower risk of bleeding and infection because they do not penetrate dura or brain (Beleza et al., 2010). However, here, only 46% of the subdurally recorded SDs could be identified using epidural electrodes. This relatively small yield may have resulted from the fact that only two epidural peg electrodes were used in each patient, in contrast to six electrodes on the subdural strip. This is supported by a previous analysis showing that a single recording location failed to detect 43% of all SDs that were identified based on consideration of a full six-electrode subdural strip (Hartings et al., 2017a). In addition, the ability to detect SDs using epidural electrodes depended on the features of a given SD. Thus, epidural electrodes were more likely to detect SDs when subdural negative DC shifts were longer and more subdural electrodes were involved in a given SD. Nonetheless, it is noteworthy that the DC shifts of SD were captured in titanium electrode recordings, since little is known about these electrodes in terms of interferences and DC recording properties. This deserves further study, not the least because titanium could also be used for intracranial recordings and is much less costly than Pt/Ir.

In a recent study, scalp EEG recordings in the rat failed to detect the negative DC shifts of SDs (Luckl et al., 2018). This supported the interpretation that DC-EEG shifts are only observable in human scalp recordings when there is an existing craniotomy (Drenckhahn et al., 2012; Hartings et al., 2014). For comparison, the median scalp DC-EEG amplitude was one twentieth of the subdural DC-ECoG amplitude (Drenckhahn et al., 2012), whereas the epidural amplitude in the present study was one quarter. The superiority of epidural peg electrodes over scalp EEG electrodes and their inferiority to subdural electrodes is congruent with findings from electrographic seizure detection (Beleza et al., 2010; Benovitski et al., 2017).

In epidural recordings, the SD-induced depression periods were even more difficult to detect than the negative DC shifts. The lower sensitivity of epidural than subdural electrodes to detect depression periods may be due to superposition of volume-conducted signals from more widespread cortical generators, due in particular to the spatial filtering of the dura. That is, epidural electrodes record from widespread sources including unaffected cortical regions that may mask and overwhelm smaller regions affected by spreading depression, making detection more difficult.

Limitations

The typical indication for the use of epidural peg electrodes in patients is the detection of epileptic foci. Unfortunately, the demand for epidural peg electrodes is low. For this reason, the manufacturer has recently discontinued their production. Therefore, we could not include more patients and the small size of the study is a limitation. However, our results provide guidance for planning future studies. For example, the next step could be to investigate whether depth electrodes placed epidurally instead of in the parenchyma are sufficient to detect SDs.

Terminal SDs Cause Electrocortical Silencing Prior to Clinical Brain Death

Similar to the previously reported case of Carlson et al. (2018), patient 7 progressed to brain death despite continued circulatory function. The neuromonitoring confirmed that (a) a series of SDs preceded the clinical signs of brain death, (b) SD-induced spreading depression initiated the final electrical silence recorded over the following 20 h, and (c) the terminal electrographic event was an SD, which initiated a NUP. The NUP is the largest bioelectrical signal ever recorded from the human brain and in the present case, similar to previous ones, had an amplitude of −150 mV (Carlson et al., 2018; Luckl et al., 2018). It is possible that the Pt/Ir-recorded NUP is not purely a biopotential, but results also in part from platinum sensitivities to diffusible chemicals. Nonetheless, the fact that the NUP was measured not only by the subdural but also the epidural electrodes affirms that the human NUP is a bioelectrical field potential. The epidural environment was likely unchanged with respect to signal-contaminating factors during the NUP, since systemic variables such as ventilation, MAP, and peripheral oxygen saturation stayed constant and the dura provides insulation from changes in the subdural compartment.

A clinical implication of this finding is that epidural electrodes may be sufficient to record the NUP. This could have relevance to patients who are at risk for secondary ischemia, but for whom placement of a subdural strip is not possible, due to lack of clinical indication for a craniotomy or a burr hole. Notably, the NUP occurs not only in brain death but also during ECI and DCI in aSAH patients (Oliveira-Ferreira et al., 2010; Dreier, 2011; Drenckhahn et al., 2012; Hartings et al., 2017c; Luckl et al., 2018). ECI and DCI predominantly affect the cerebral cortex (Birse and Tom, 1960; Stoltenburg-Didinger and Schwarz, 1987; Neil-Dwyer et al., 1994; Dreier et al., 2002; Rabinstein et al., 2005; Hartings et al., 2017c). A significant proportion of these ischemic events could thus be detectable by epidural recordings. A limitation might be that ECI- and DCI-associated NUPs are localized phenomena (Luckl et al., 2018) in contrast to the NUP during brain death (Carlson et al., 2018) or CA (Dreier et al., 2018b). Thus, recordings at multiple sites would be necessary because the exact location of future developing pathology is unknown when the neurosurgeon implants neuromonitoring devices.

When the patient underwent CA 20 h after brain death, a slow positive DC drift occurred. This was previously observed in cases of CA leading to brain death, where it occurred simultaneously with the parenchymal $p_{ti}O_2$ decline as measured by an O_2 sensor (Dreier et al., 2018b). The present findings suggest that this drift does not reflect a cerebral field potential of biological origin but

rather results from interferences, since neither brain parenchyma nor BBB should be able to generate field potentials 20 h after brain death. Consistent with this conclusion, no terminal SD was superimposed on the slow positive DC drift, in contrast to previous cases in which the brain was viable at the time of CA (Dreier et al., 2018b). The lack of terminal SD at this time, in addition to the clinical signs such as loss of brainstem reflexes and wide dilated pupils, further supports the conclusion that brain death occurred with the final cluster of SDs and associated NUP, 20 h earlier.

One remaining question is why the NUP can be at least 10 times larger in humans than in rats. The answer may relate to the different recording conditions of a closed subdural compartment in patients versus an open compartment in rats, since current leaks from the intended circuit may have occurred in the latter condition. Another possibility is that the NUP partially reflects the DC potential across the BBB and is caused by the profound interstitial and rCBF changes during the dying process. In this hypothesis, the zonal DC shift of SD, resulting from neurons and to a lesser extent from astrocytes (Makarova et al., 2008; Dreier et al., 2013), could be superimposed on a DC drift across the BBB. This hypothesis is indirectly supported by previous reports on profound differences in electrogenesis across the BBB between rats, rabbits, goats and dogs on the one hand and cats and non-human primates on the other (Tschirgi and Taylor, 1958; Held et al., 1964; Besson et al., 1970; Woody et al., 1970; Messeter and Siesjo, 1971; Kang et al., 2013). This notion may imply that future studies to uncover the generators of the NUP in humans should be performed in higher mammals rather than rodents. For example, swine share many features with humans in the pathogenesis of ischemic lesions after aSAH and would be interesting candidates for further study (Hartings et al., 2017c).

However, when considering various possible DC potential components that could contribute to the human NUP, it should not be forgotten that the NUP is experimentally defined not by simple quantifiable parameters such as its amplitude, but by three other more complex properties: (i) the beginning with SD, (ii) the fact that the ion shifts and cell oedema do not fully recover during this extremely long DC negativity, and (iii) the death of neurons (Dreier, 2011; Luckl et al., 2018). In this operational definition, however, it should be noted that the distinction of a NUP from a long-lasting SD, which has not exceeded the commitment point (Dreier and Reiffurth, 2015) and does not lead to cell damage, is currently not possible solely on the basis of electrophysiological criteria. In addition, the NUP may be experimentally of high amplitude, but may also be relatively shallow (Dreier et al., 2017). If the NUP is comparatively shallow, a cluster of SDs is typically superimposed on the NUP (Oliveira-Ferreira et al., 2010). This constellation indicates that only a fraction of the neurons in the tissue stays permanently depolarized, while the remaining fraction repolarizes after each SD. In contrast, the SD-initiated NUP in the wake of CA is typically of high amplitude and not associated with a cluster of superimposed SDs, as all neurons and astrocytes remain permanently depolarized and all cells will eventually die under this condition unless the tissue is reperfused in time.

CONCLUSION

The animal experiments indicated that Pt/Ir electrodes on the brain surface can record 100% of SDs, SD-induced spreading depressions, non-spreading depression and SD-initiated NUPs, but negative DC reverberations following the recovery from SD may complicate evaluation, especially evaluation of the NUP. To identify a very slow DC potential component as NUP, the context with other factors such as initiation by SD, possible superposition by SDs, persistent depression of neuronal activity, decrease of rCBF and $p_{ti}O_2$, occurrence of a new focal or global neurological deficit, a new ischemic lesion in sequential neuroimaging scans, or death should also be considered.

In theory, epidural electrodes are a semi-invasive alternative to subdural recordings and can be viewed as an intermediate step between invasive subdural and non-invasive scalp EEG. However, in our patients, only 46% of subdurally recorded SDs and 28% of subdurally recorded SD-induced spreading depressions were also detected epidurally. Using epidural electrodes, the NUP may be easier to detect than SDs or SD-induced spreading depressions, but measuring the initial SD component and the SD-induced persistent depression helps to distinguish the NUP from artifacts, so subdural electrodes also offer metrological advantages in the case of a NUP. Within the limits of a small study, all this indicates that the protocol investigated here with two epidural electrodes cannot replace subdural electrode strips in the clinic. The next step in the development could be to place depth electrodes with several contacts epidurally to improve the yield. In addition, such arrays could also be tested subdurally, as this could still be less invasive than the placement of a subdural electrode strip. The goal must be to find the least invasive method that still provides robust and reliable data of sufficient quality to make clinical decisions. At present, it is the subdural electrode strip that meets these criteria and whose properties need to be exceeded.

ETHICS STATEMENT

The animal study was carried out in accordance with the recommendations of the Landesamt für Arbeitsschutz, Gesundheitsschutz und technische Sicherheit Berlin (LAGetSi) (G0152/11). The protocol was approved by the Landesamt für Arbeitsschutz, Gesundheitsschutz und technische Sicherheit Berlin (LAGetSi) (G0152/11). All experimental procedures were conducted in accordance with the Charité Animal Welfare Guidelines. The reporting of animal experiments complies with the Animal Research: Reporting of *In Vivo* Experiments (ARRIVE) Guidelines. The clinical study was carried out in accordance with the recommendations of the ethics committee of the Charité – Universitätsmedizin Berlin (EA4/175/17) with written informed consent from the patients or the patients' legally authorized representatives. All patients or patients' legally authorized representatives gave written informed consent in accordance with the Declaration of Helsinki. The protocol was approved by the ethics committee of the Charité – Universitätsmedizin Berlin. Results are reported

in accordance with the STrengthening the Reporting of OBservational studies in Epidemiology (STROBE) guidelines (https://www.strobe-statement.org).

AUTHOR CONTRIBUTIONS

JD and JW contributed substantially to the conception and design of the work, and drafted and revised the manuscript for important intellectual content. SM, CL, VK, CR, KS, NH, and JH drafted corresponding sections of the manuscript. All authors have approved the final version to be published and agreed to be accountable for all aspects of the work.

FUNDING

This work was supported by grants of the Bundesministerium für Bildung und Forschung (BMBF) Center for Stroke Research Berlin 01 EO 0801 and Deutsche Forschungsgemeinschaft (DFG) DR 323/10-1 to JD, DFG DR 323/5-1 to JD and JW, DFG WO 1704/1-1 to JW, and the United States Army CDMRP PH/TBI Research Program (Contract No. W81XWH-08-2-0016) to JH.

ACKNOWLEDGMENTS

We acknowledge support from the DFG and the Open Access Publication Fund of Charité – Universitätsmedizin Berlin.

REFERENCES

Barnett, G. H., Burgess, R. C., Awad, I. A., Skipper, G. J., Edwards, C. R., and Luders, H. (1990). Epidural peg electrodes for the presurgical evaluation of intractable epilepsy. *Neurosurgery* 27, 113–115. doi: 10.1227/00006123-199007000-00016

Beleza, P., Remi, J., Feddersen, B., Peraud, A., and Noachtar, S. (2010). Epidural and foramen-ovale electrodes in the diagnostic evaluation of patients considered for epilepsy surgery. *Epileptic Disord.* 12, 48–53. doi: 10.1684/epd.2010.0297

Benovitski, Y. B., Lai, A., McGowan, C. C., Burns, O., Maxim, V., Nayagam, D. A. X., et al. (2017). Ring and peg electrodes for minimally-Invasive and long-term sub-scalp EEG recordings. *Epilepsy Res.* 135, 29–37. doi: 10.1016/j.eplepsyres.2017.06.003

Besson, J. M., Woody, C. D., Aleonard, P., Thompson, H. K., Albe-Fessard, D., and Marshall, W. H. (1970). Correlations of brain d-c shifts with changes in cerebral blood flow. *Am. J. Physiol.* 218, 284–291. doi: 10.1152/ajplegacy.1970.218.1.284

Birse, S. H., and Tom, M. I. (1960). Incidence of cerebral infarction associated with ruptured intracranial aneurysms. A study of 8 unoperated cases of anterior cerebral aneurysm. *Neurology* 10, 101–106. doi: 10.1212/WNL.10.2.101

Bogdanov, V. B., Middleton, N. A., Theriot, J. J., Parker, P. D., Abdullah, O. M., Ju, Y. S., et al. (2016). Susceptibility of primary sensory cortex to spreading depolarizations. *J. Neurosci.* 36, 4733–4743. doi: 10.1523/JNEUROSCI.3694-15.2016

Bosche, B., Graf, R., Ernestus, R. I., Dohmen, C., Reithmeier, T., Brinker, G., et al. (2010). Recurrent spreading depolarizations after subarachnoid hemorrhage decreases oxygen availability in human cerebral cortex. *Ann. Neurol.* 67, 607–617. doi: 10.1002/ana.21943

Boucek, M. M., Mashburn, C., Dunn, S. M., Frizell, R., Edwards, L., Pietra, B., et al. (2008). Pediatric heart transplantation after declaration of cardiocirculatory death. *N. Engl. J. Med.* 359, 709–714. doi: 10.1056/NEJMoa0800660

Bures, J., and Buresova, O. (1957). Die anoxische terminaldepolarisation als indikator der vulnerabilität der Großhirnrinde bei anoxie und ischämie. *Pflügers Arch.* 264, 325–334. doi: 10.1007/BF00364173

Carlson, A. P., Shuttleworth, C. W., Major, S., Lemale, C. L., Dreier, J. P., and Hartings, J. A. (2018). Terminal spreading depolarizations causing electrocortical silencing prior to clinical brain death: case report. *J. Neurosurg.* doi: 10.3171/2018.7.JNS181478 [Epub ahead of print].

Dhanani, S., Hornby, L., Ward, R., and Shemie, S. (2012). Variability in the determination of death after cardiac arrest: a review of guidelines and statements. *J. Intensive Care Med.* 27, 238–252. doi: 10.1177/0885066610396993

Dohmen, C., Sakowitz, O. W., Fabricius, M., Bosche, B., Reithmeier, T., Ernestus, R. I., et al. (2008). Spreading depolarizations occur in human ischemic stroke with high incidence. *Ann. Neurol.* 63, 720–728. doi: 10.1002/ana.21390

Dreier, J. P. (2011). The role of spreading depression, spreading depolarization and spreading ischemia in neurological disease. *Nat. Med.* 17, 439–447. doi: 10.1038/nm.2333

Dreier, J. P., Fabricius, M., Ayata, C., Sakowitz, O. W., William Shuttleworth, C., Dohmen, C., et al. (2017). Recording, analysis, and interpretation of spreading depolarizations in neurointensive care: review and recommendations of the COSBID research group. *J. Cereb. Blood Flow Metab.* 37, 1595–1625. doi: 10.1177/0271678X16654496

Dreier, J. P., Isele, T., Reiffurth, C., Offenhauser, N., Kirov, S. A., Dahlem, M. A., et al. (2013). Is spreading depolarization characterized by an abrupt, massive release of gibbs free energy from the human brain cortex? *Neuroscientist* 19, 25–42. doi: 10.1177/1073858412453340

Dreier, J. P., Major, S., Manning, A., Woitzik, J., Drenckhahn, C., Steinbrink, J., et al. (2009). Cortical spreading ischaemia is a novel process involved in ischaemic damage in patients with aneurysmal subarachnoid haemorrhage. *Brain* 132(Pt 7), 1866–1881. doi: 10.1093/brain/awp102

Dreier, J. P., Petzold, G., Tille, K., Lindauer, U., Arnold, G., Heinemann, U., et al. (2001). Ischaemia triggered by spreading neuronal activation is inhibited by vasodilators in rats. *J. Physiol.* 531(Pt 2), 515–526. doi: 10.1111/j.1469-7793.2001.0515i.x

Dreier, J. P., Sakowitz, O. W., Harder, A., Zimmer, C., Dirnagl, U., Valdueza, J. M., et al. (2002). Focal laminar cortical MR signal abnormalities after subarachnoid hemorrhage. *Ann. Neurol.* 52, 825–829. doi: 10.1002/ana.10383

Dreier, J. P., Woitzik, J., Fabricius, M., Bhatia, R., Major, S., Drenckhahn, C., et al. (2006). Delayed ischaemic neurological deficits after subarachnoid haemorrhage are associated with clusters of spreading depolarizations. *Brain* 129(Pt 12), 3224–3237. doi: 10.1093/brain/awl297

Dreier, J. P., Ebert, N., Priller, J., Megow, D., Lindauer, U., Klee, R., et al. (2000). Products of hemolysis in the subarachnoid space inducing spreading ischemia in the cortex and focal necrosis in rats: a model for delayed ischemic neurological deficits after subarachnoid hemorrhage? *J. Neurosurg.* 93, 658–666. doi: 10.3171/jns.2000.93.4.0658

Dreier, J. P., Korner, K., Ebert, N., Gorner, A., Rubin, I., Back, T., et al. (1998). Nitric oxide scavenging by hemoglobin or nitric oxide synthase inhibition by N-nitro-L-arginine induces cortical spreading ischemia when K+ is increased in the subarachnoid space. *J. Cereb. Blood Flow Metab.* 18, 978–990. doi: 10.1097/00004647-199809000-00007

Dreier, J. P., Lemale, C. L., Kola, V., Friedman, A., and Schoknecht, K. (2018a). Spreading depolarization is not an epiphenomenon but the principal mechanism of the cytotoxic edema in various gray matter structures of the brain during stroke. *Neuropharmacology* 134(Pt B), 189–207. doi: 10.1016/j.neuropharm.2017.09.027

Dreier, J. P., Major, S., Foreman, B., Winkler, M. K. L., Kang, E. J., Milakara, D., et al. (2018b). Terminal spreading depolarization and electrical silence in death of human cerebral cortex. *Ann. Neurol.* 83, 295–310. doi: 10.1002/ana.25147

Dreier, J. P., and Reiffurth, C. (2015). The stroke-migraine depolarization continuum. *Neuron* 86, 902–922. doi: 10.1016/j.neuron.2015.04.004

Drenckhahn, C., Windler, C., Major, S., Kang, E. J., Scheel, M., Vajkoczy, P., et al. (2016). Complications in aneurysmal subarachnoid hemorrhage patients with and without subdural electrode strip for electrocorticography. *J. Clin. Neurophysiol.* 33, 250–259. doi: 10.1097/WNP.0000000000000274

Drenckhahn, C., Winkler, M. K., Major, S., Scheel, M., Kang, E. J., Pinczolits, A., et al. (2012). Correlates of spreading depolarization in human scalp electroencephalography. *Brain* 135(Pt 3), 853–868. doi: 10.1093/brain/aws010

Eriksen, N., Rostrup, E., Fabricius, M., Scheel, M., Major, S., Winkler, M. K. L., et al. (2019). Early focal brain injury after subarachnoid hemorrhage correlates with spreading depolarizations. *Neurology* 92, e326–e341. doi: 10.1212/WNL.0000000000006814

Farkas, E., Bari, F., and Obrenovitch, T. P. (2010). Multi-modal imaging of anoxic depolarization and hemodynamic changes induced by cardiac arrest in the rat cerebral cortex. *Neuroimage* 51, 734–742. doi: 10.1016/j.neuroimage.2010.02.055

Farkas, E., Pratt, R., Sengpiel, F., and Obrenovitch, T. P. (2008). Direct, live imaging of cortical spreading depression and anoxic depolarisation using a fluorescent, voltage-sensitive dye. *J. Cereb. Blood Flow Metab.* 28, 251–62. doi: 10.1038/sj.jcbfm.9600569

Fisher, M. (2013). The spectrum of translational stroke research. *Neurol. Res.* 35, 443–447. doi: 10.1179/1743132813Y.0000000214

Hartings, J. A., Bullock, M. R., Okonkwo, D. O., Murray, L. S., Murray, G. D., Fabricius, M., et al. (2011). Spreading depolarisations and outcome after traumatic brain injury: a prospective observational study. *Lancet Neurol.* 10, 1058–1064. doi: 10.1016/S1474-4422(11)70243-5

Hartings, J. A., Li, C., Hinzman, J. M., Shuttleworth, C. W., Ernst, G. L., Dreier, J. P., et al. (2017a). Direct current electrocorticography for clinical neuromonitoring of spreading depolarizations. *J. Cereb. Blood Flow Metab.* 37, 1857–1870. doi: 10.1177/0271678X16653135

Hartings, J. A., Shuttleworth, C. W., Kirov, S. A., Ayata, C., Hinzman, J. M., Foreman, B., et al. (2017b). The continuum of spreading depolarizations in acute cortical lesion development: examining Leao's legacy. *J. Cereb. Blood Flow Metab.* 37, 1571–1594. doi: 10.1177/0271678X16654495

Hartings, J. A., York, J., Carroll, C. P., Hinzman, J. M., Mahoney, E., Krueger, B., et al. (2017c). Subarachnoid blood acutely induces spreading depolarizations and early cortical infarction. *Brain* 140, 2673–2690. doi: 10.1093/brain/awx214

Hartings, J. A., Ngwenya, L. B., Watanabe, T., and Foreman, B. (2018). Commentary: detecting cortical spreading depolarization with full band scalp electroencephalography: an illusion? *Front. Syst. Neurosci.* 12:19. doi: 10.3389/fnsys.2018.00019

Hartings, J. A., Wilson, J. A., Hinzman, J. M., Pollandt, S., Dreier, J. P., DiNapoli, V., et al. (2014). Spreading depression in continuous electroencephalography of brain trauma. *Ann. Neurol.* 76, 681–694. doi: 10.1002/ana.24256

Held, D., Fencl, V., and Pappenheimer, J. R. (1964). Electrical potential of cerebrospinal fluid. *J. Neurophysiol.* 27, 942–959. doi: 10.1152/jn.1964.27.5.942

Hinzman, J. M., DiNapoli, V. A., Mahoney, E. J., Gerhardt, G. A., and Hartings, J. A. (2015). Spreading depolarizations mediate excitotoxicity in the development of acute cortical lesions. *Exp. Neurol.* 267, 243–253. doi: 10.1016/j.expneurol.2015.03.014

Hinzman, J. M, Andaluz, N., Shutter, L. A., Okonkwo, D. O., Pahl, C., Strong, A. J., et al. (2014). Inverse neurovascular coupling to cortical spreading depolarizations in severe brain trauma. *Brain* 137, 2960–2972. doi: 10.1093/brain/awu241

Hofmeijer, J., van Kaam, C. R., van de Werff, B., Vermeer, S. E., Tjepkema-Cloostermans, M. C., and van Putten, M. (2018). Detecting cortical spreading depolarization with full band scalp electroencephalography: an illusion? *Front. Neurol.* 9:17. doi: 10.3389/fneur.2018.00017

Iijima, T., Mies, G., and Hossmann, K. A. (1992). Repeated negative DC deflections in rat cortex following middle cerebral artery occlusion are abolished by MK-801: effect on volume of ischemic injury. *J. Cereb. Blood Flow Metab.* 12, 727–733. doi: 10.1038/jcbfm.1992.103

Kang, E. J., Major, S., Jorks, D., Reiffurth, C., Offenhauser, N., Friedman, A., et al. (2013). Blood-brain barrier opening to large molecules does not imply blood-brain barrier opening to small ions. *Neurobiol. Dis.* 52, 204–218. doi: 10.1016/j.nbd.2012.12.007

LaManna, J. C., and Rosenthal, M. (1975). Effect of ouabain and phenobarbital on oxidative metabolic activity associated with spreading cortical depression in cats. *Brain Res.* 88, 145–149. doi: 10.1016/0006-8993(75)90963-4

Lauritzen, M., Dreier, J. P., Fabricius, M., Hartings, J. A., Graf, R., and Strong, A. J. (2011). Clinical relevance of cortical spreading depression in neurological disorders: migraine, malignant stroke, subarachnoid and intracranial hemorrhage, and traumatic brain injury. *J. Cereb. Blood Flow Metab.* 31, 17–35. doi: 10.1038/jcbfm.2010.191

Leão, A. A. P. (1947). Further observations on the spreading depression of activity in the cerebral cortex. *J. Neurophysiol.* 10, 409–414. doi: 10.1152/jn.1947.10.6.409

Levasseur, J. E., Wei, E. P., Raper, A. J., Kontos, A. A., and Patterson, J. L. (1975). Detailed description of a cranial window technique for acute and chronic experiments. *Stroke* 6, 308–317. doi: 10.1161/01.STR.6.3.308

Luckl, J., Lemale, C. L., Kola, V., Horst, V., Khojasteh, U., Oliveira-Ferreira, A. I., et al. (2018). The negative ultraslow potential, electrophysiological correlate of infarction in the human cortex. *Brain* 141, 1734–1752. doi: 10.1093/brain/awy102

Major, S., Petzold, G. C., Reiffurth, C., Windmuller, O., Foddis, M., Lindauer, U., et al. (2017). A role of the sodium pump in spreading ischemia in rats. *J. Cereb. Blood Flow Metab.* 37, 1687–1705. doi: 10.1177/0271678X16639059

Makarova, J., Gomez-Galan, M., and Herreras, O. (2008). Variations in tissue resistivity and in the extension of activated neuron domains shape the voltage signal during spreading depression in the CA1 in vivo. *Eur. J. Neurosci.* 27, 444–456. doi: 10.1111/j.1460-9568.2008.06022.x

Marshall, W. H. (1959). Spreading cortical depression of Leao. *Physiol. Rev.* 39, 239–279. doi: 10.1152/physrev.1959.39.2.239

Masvidal-Codina, E., Illa, X., Dasilva, M., Calia, A. B., Dragojevic, T., Vidal-Rosas, E. E., et al. (2018). High-resolution mapping of infraslow cortical brain activity enabled by graphene microtransistors. *Nat Mater.* 18, 280–288. doi: 10.1038/s41563-018-0249-4

Messeter, K., and Siesjo, B. K. (1971). The DC potential between CSF and plasma in respiratory acidosis. *Acta Physiol. Scand.* 83, 13–20. doi: 10.1111/j.1748-1716.1971.tb05046.x

Meunier, P. C., and Popovic, R. (1988). Optimization of the bare platinum electrode as an oxygen measurement system in photosynthesis. *Photosynth. Res.* 15, 271–279. doi: 10.1007/BF00047358

Neil-Dwyer, G., Lang, D. A., Doshi, B., Gerber, C. J., and Smith, P. W. (1994). Delayed cerebral ischaemia: the pathological substrate. *Acta Neurochir. (Wien)* 131, 137–145. doi: 10.1007/BF01401464

Ochs, S., and Van Harreveld, A. (1956). Cerebral impedance changes after circulatory arrest. *Am. J. Physiol.* 187, 180–192. doi: 10.1152/ajplegacy.1956.187.1.180

Oliveira-Ferreira, A. I., Milakara, D., Alam, M., Jorks, D., Major, S., Hartings, J. A., et al. (2010). Experimental and preliminary clinical evidence of an ischemic zone with prolonged negative DC shifts surrounded by a normally perfused tissue belt with persistent electrocorticographic depression. *J. Cereb. Blood Flow Metab.* 30, 1504–1519. doi: 10.1038/jcbfm.2010.40

Petzold, G. C., Windmuller, O., Haack, S., Major, S., Buchheim, K., Megow, D., et al. (2005). Increased extracellular K+ concentration reduces the efficacy of N-methyl-D-aspartate receptor antagonists to block spreading depression-like depolarizations and spreading ischemia. *Stroke* 36, 1270–1277. doi: 10.1161/01.STR.0000166023.51307.e0

Rabinstein, A. A., Weigand, S., Atkinson, J. L., and Wijdicks, E. F. (2005). Patterns of cerebral infarction in aneurysmal subarachnoid hemorrhage. *Stroke* 36, 992–997. doi: 10.1161/01.STR.0000163090.59350.5a

Shin, H. K., Dunn, A. K., Jones, P. B., Boas, D. A., Moskowitz, M. A., and Ayata, C. (2006). Vasoconstrictive neurovascular coupling during focal ischemic depolarizations. *J. Cereb. Blood Flow Metab.* 26, 1018–1030. doi: 10.1038/sj.jcbfm.9600252

Somjen, G. G. (2001). Mechanisms of spreading depression and hypoxic spreading depression-like depolarization. *Physiol. Rev.* 81, 1065–1096. doi: 10.1152/physrev.2001.81.3.1065

Sonn, J., and Mayevsky, A. (2000). Effects of brain oxygenation on metabolic, hemodynamic, ionic and electrical responses to spreading depression in the rat. *Brain Res.* 882, 212–216. doi: 10.1016/S0006-8993(00)02827-4

Stiegler, P., Sereinigg, M., Puntschart, A., Seifert-Held, T., Zmugg, G., Wiederstein-Grasser, I., et al. (2012). A 10min "no-touch" time – is it enough in DCD? A DCD animal study. *Transpl. Int.* 25, 481–492. doi: 10.1111/j.1432-2277.2012.01437.x

Stoltenburg-Didinger, G., and Schwarz, K. (1987). "Brain lesions secondary to subarachnoid hemorrhage due to ruptured aneurysms," in *Stroke and Microcirculation*, eds J. Cervós-Navarro and R. Ferszt (New York, NY: Raven Press), 471–480.

Stuart, R. M., Schmidt, M., Kurtz, P., Waziri, A., Helbok, R., Mayer, S. A., et al. (2010). Intracranial multimodal monitoring for acute brain injury: a single institution review of current practices. *Neurocrit. Care* 12, 188–198. doi: 10.1007/s12028-010-9330-9

Sugimoto, K., Nomura, S., Shirao, S., Inoue, T., Ishihara, H., Kawano, R., et al. (2018). Cilostazol decreases duration of spreading depolarization and spreading ischemia after aneurysmal subarachnoid hemorrhage. *Ann. Neurol.* 84, 873–885. doi: 10.1002/ana.25361

Sukhotinsky, I., Dilekoz, E., Moskowitz, M. A., and Ayata, C. (2008). Hypoxia and hypotension transform the blood flow response to cortical spreading depression from hyperemia into hypoperfusion in the rat. *J. Cereb. Blood Flow Metab.* 28, 1369–1376. doi: 10.1038/jcbfm.2008.35

Tschirgi, R. D., and Taylor, J. L. (1958). Slowly changing bioelectric potentials associated with the blood-brain barrier. *Am. J. Physiol.* 195, 7–22. doi: 10.1152/ajplegacy.1958.195.1.7

van Harreveld, A. (1946). Depolarisation in the spinal cord caused by asphyxiation. *Am. J. Physiol.* 147, 669–684. doi: 10.1152/ajplegacy.1946.147.4.669

van Harreveld, A. (1959). Compounds in brain extracts causing spreading depression of cerebral cortical activity and contraction of crustacean muscle. *J. Neurochem.* 3, 300–315. doi: 10.1111/j.1471-4159.1959.tb12636.x

van Veen, E., van der Jagt, M., Cnossen, M. C., Maas, A. I. R., de Beaufort, I. D., Menon, D. K., et al. (2018). Brain death and postmortem organ donation: report of a questionnaire from the CENTER-TBI study. *Crit. Care* 22:306. doi: 10.1186/s13054-018-2241-4

Winkler, M. K., Dengler, N., Hecht, N., Hartings, J. A., Kang, E. J., Major, S., et al. (2017). Oxygen availability and spreading depolarizations provide complementary prognostic information in neuromonitoring of aneurysmal subarachnoid hemorrhage patients. *J. Cereb. Blood Flow Metab.* 37, 1841–1856. doi: 10.1177/0271678X16641424

Woitzik, J., Hecht, N., Pinczolits, A., Sandow, N., Major, S., Winkler, M. K., et al. (2013). Propagation of cortical spreading depolarization in the human cortex after malignant stroke. *Neurology* 80, 1095–1102. doi: 10.1212/WNL.0b013e3182886932

Woitzik, J., Pinczolits, A., Hecht, N., Sandow, N., Scheel, M., Drenckhahn, C., et al. (2014). Excitotoxicity and metabolic changes in association with infarct progression. *Stroke* 45, 1183–1185. doi: 10.1161/STROKEAHA.113.004475

Woody, C. D., Marshall, W. H., Besson, J. M., Thompson, H. K., Aleonard, P., and Albe-Fessard, D. (1970). Brain potential shift with respiratory acidosis in the cat and monkey. *Am. J. Physiol.* 218, 275–283. doi: 10.1152/ajplegacy.1970.218.1.275

Conflict of Interest Statement: The authors declare that the research was conducted in the absence of any commercial or financial relationships that could be construed as a potential conflict of interest.

Copyright © 2019 Dreier, Major, Lemale, Kola, Reiffurth, Schoknecht, Hecht, Hartings and Woitzik. This is an open-access article distributed under the terms of the Creative Commons Attribution License (CC BY). The use, distribution or reproduction in other forums is permitted, provided the original author(s) and the copyright owner(s) are credited and that the original publication in this journal is cited, in accordance with accepted academic practice. No use, distribution or reproduction is permitted which does not comply with these terms.

frontiers in Neurology

ORIGINAL RESEARCH
published: 01 May 2019
doi: 10.3389/fneur.2019.00414

Clinical Improvement Following Stroke Promptly Reverses Post-stroke Cellular Immune Alterations

Antje Vogelgesang[1†], Carl Witt[1†], Christin Heuer[1], Juliane Schulze[1], Juliane Gellrich[1], Bettina von Sarnowski[1], Sönke Langner[2], Alexander Dressel[1,3] and Johanna Ruhnau[1]*

[1] Department of Neurology, University Medicine, Greifswald, Germany, [2] Department of Diagnostic Radiology and Neuroradiology, University Medicine, Greifswald, Germany, [3] Department of Neurology, Carl-Thiem-Klinikum, Cottbus, Germany

Background and Purpose: Stroke induces immediate profound alterations of the peripheral immune system rendering patients more susceptible to post-stroke infections. The precise mechanisms maintaining stroke-induced immune alterations (SIIA) remain unknown. High-Mobility-Group-Protein B1 (HMGB-1) is elevated for at least 7 days post-stroke and has been suggested to mediate SIIA. Patients with rapid clinical recovery of neurological deficits rarely develop severe infections. We therefore investigated whether rapid neurological recovery (either spontaneous or secondary to neurovascular recanalization therapy) alters the course of SIIA. National Institutes of Health Stroke Scale (NIHSS) served as surrogate marker for neurological improvement.

Methods: Fluorescence-activated cell sorting was used to define leukocyte subpopulations. C-reactive protein (CRP), procalcitonin (PCT), HMGB-1, GM-CSF; IFN-β, IFN-γ, IL-1β, IL-1RA, IL-2, IL-4, IL-5, IL-6, IL-10, IL-12, IL-17, IL-17F, IL-18, TNF-α, MIF, IL-8, MCP-1, MCP-4, MIP-3α, MIP-3β, Eotaxin, soluble IL-6 receptor, E-selectin, and P-selectin were analyzed by ELISA or Multiplex Assays. Serum miRNA expression changes were analyzed by qPCR.

Results: Cellular parameters were similar in the improved and non-improved cohort on admission. In patients with rapid clinical recovery absolute and relative leukocyte, neutrophil, and lymphocyte numbers normalized promptly overnight. In contrast, HMGB-1 serum levels did not differ between the two groups. Nine miRNA were found to be differentially expressed between improved and non-improved patients.

Conclusions: SIIA are detectable on admission of acute stroke patients. While it was assumed that post-stroke immunosuppression is rapidly reversed with improvement this is the first data set that shows that improvement actually is associated with a rapid reversal of SIIA demonstrating that SIIA require a constant signal to persist. The observation that HMGB-1 serum concentrations were similar in improved and non-improved cohorts argues against a role for this pro-inflammatory mediator in the maintenance of SIIA. Serum miRNA observed to be regulated in stroke in other publications was counter regulated with improvement in our cohort.

Keywords: stroke, immunosuppression, tissue plasminogen activator, HMGB-1, miRNA

OPEN ACCESS

Edited by:
Johannes Boltze, Fraunhofer-Institut für Zelltherapie und Immunologie (IZI), Germany

Reviewed by:
Anna M. Planas, Spanish National Research Council (CSIC), Spain
Muhib Khan, Michigan State University, United States

****Correspondence:***
Antje Vogelgesang
antje.vogelgesang@uni-greifswald.de

† These authors have contributed equally to this work

Specialty section:
This article was submitted to Stroke, a section of the journal Frontiers in Neurology

Received: *09 November 2018*
Accepted: *04 April 2019*
Published: *01 May 2019*

Citation:
Vogelgesang A, Witt C, Heuer C, Schulze J, Gellrich J, von Sarnowski B, Langner S, Dressel A and Ruhnau J (2019) Clinical Improvement Following Stroke Promptly Reverses Post-stroke Cellular Immune Alterations. Front. Neurol. 10:414. doi: 10.3389/fneur.2019.00414

INTRODUCTION

Post-stroke infections, predominantly pneumonia, are associated with increased mortality and impaired neurological outcome. In recent years, it has been clearly shown in both experimental stroke and stroke patients that these infections are closely related to stroke-induced immune alterations (SIIA) of the peripheral immune system (1, 2). SIIA develop within the first hours of ischemic stroke and persist at least for days up to weeks (3–5).

Stroke volume and stroke severity on admission as determined by NIHSS are associated with post-stroke infections (6) and patients with transitory ischemic attacks have significantly fewer infectious complications and show a milder immune response after stroke compared to patients with complete stroke (7) and it is likely that patients with initially severe ischemic stroke that improve after hyperacute treatment have a reduced risk of infections and will show milder immune alterations after stroke.

To date it is unknown how SIIA are maintained and how they are reversed. We have investigated whether SIIA are influenced by clinical improvement. We hypothesized that rapid clinical improvement is associated with a reversal of SIIA. If SIIA were self-maintained after the induction within the initial hours of stroke, the time course of cellular changes should be similar in patients with rapid neurological recovery compared to those with persistent neurological deficits. If SIIA required an ongoing signal from injured brain tissue to persist, it should be reversed rapidly in patients with neurological improvement. Therefore, we took advantage of the National Institutes of Health Stroke Scale (NIHSS) reduction from admission to day 1 as a marker for the neurological improvement. Experimental and human stroke studies delivered proof that the hypothalamic–pituitary–adrenal axis and the autonomic nervous system release catecholamines and glucocorticoids which results in stroke-induced immune suppression. These hormones and transmitters have a very short half-life and return to normal levels within 24 h after an initial increase induced by ischemic brain injury (6) while the functional deficits of the immune system persist (4).

In animal models High-Mobility-Group-Protein B1 (HMGB-1) has been suggested as an important mediator of SIIA (8, 9). Others and we have reported earlier that HMGB-1 is elevated post-stroke at least for 7 days while its decoy receptors sRAGE and esRAGE are not altered (5, 8). HMGB-1 binds DNA within the nucleus but can be passively released during brain cell death or actively secreted by immune cells as an alarmin. Post-stroke the amount of HMGB-1 correlates rather with the amount of leukocytes in the peripheral blood than with the brain lesion size (10). We quantified HMGB-1 in serum of the improved and non-improved stroke patient cohort on admission and on day 3 to determine its possible role for maintaining post-stroke immune suppression.

SIIA include quantitative and functional alterations of innate and adaptive immune cells. Granulocytes increase in number but lose their ability to fight bacterial infections through radical production and neutrophil extracellular trap release (3). Lymphocytes are lost from the peripheral blood of patients (4, 5). It is also known that IL-6 and CRP are significantly elevated in patients suffering from an ischemic stroke and that HLA-DR on monocytes is reduced (5, 11). We therefore quantified peripheral blood immune cells and a panel of cytokines, chemokines, and acute phase proteins within the serum of the improved and non-improved stroke patient cohort.

MiRNA are known to be important regulators of immune responses and several miRNA were found to be differentially expressed after stroke (12–14). We investigated fold changes of serum miRNA amounts on day 1 post-stroke between the improved and non-improved cohort.

MATERIALS

Patients and Controls

A *post hoc* analysis was performed on patients included in a prospective explorative study. This study recruited 40 ischemic stroke patients from the dedicated stroke unit of the University Medicine Greifswald from 2015 to 2016. Blood was sampled on admission within 24 h of stroke onset as well as on days 1, 2, 3, 4, 5, and 7 thereafter.

Patients aged $\geq$18 years suffering from ischemic middle cerebral artery (MCA) stroke were eligible for this study within 12 h after the onset of symptoms if their National Institutes of Health Stroke Scale (NIHSS) was $\geq$8 and if no signs of systemic infection were detected on admission (C-reactive protein (CRP) $\leq$50 mg/L and procalcitonin (PCT) $\leq$0.5 ng/mL). Patients receiving immunosuppressive drugs or diagnosed with a non-curatively treated malignoma were not recruited. Additional exclusion criteria were severe cerebral disorder in medical history (e.g., ischemic or haemorrhagic stroke, meningitis, encephalitis, severe cerebral trauma, or epilepsy), any contraindication for MRI (e.g., pace maker), clinically significant anemia (hemoglobin $<$ 3.7 mmol/l), immunosuppression and the lack of written informed consent by the patient himself or through a surrogate where appropriate (See **supplemental Table I**).

All patients received best medical care on a dedicated stroke unit according to local standards. Recanalization with recombinant tissue plasminogen activator (rtPA) and/or thrombectomy was carried out as clinically indicated. Age-matched control individuals were recruited from the ophthalmology clinics among patients scheduled to receive cataract surgery. Controls were neurologically and immunologically healthy. See the participants' characteristics in **Table 1**. The study was approved by the local ethics committee (No. BB 050/15).

METHODS

Blood Sampling

Blood was obtained immediately on admission (d0) and between 6:30 and 7:30 in the morning on days 1, 2, 3, 4, 5, and 7 in different quantities. Differential blood cell counts (XN9000, Sysmex, Norderstedt, Germany) and the values for PCT, IL-6 (Adivia Centaur XPT, Siemens Healthcare Diagnostics, Eschborn, Germany) and CRP (all measured with the Dimension Vista, Siemens Healthcare Diagnostics, Eschborn, Germany) were measured in the central laboratory facility of the University Medicine Greifswald.

TABLE 1 | Patients characteristics.

Variable	Patient group (*N* = 40)	Control group (*N* = 16)	Improved* (*N* = 13)	Non-improved (*N* = 27)
Age [Years, Mean ± Std.]	71 ± 14	71 ± 8	65 ± 16	73 ± 13
Sex [as % female]	55%	44%	69%	49%
BMI, Weight/Height^2 [Mean ± Std.]	28.45 ± 5.13	27.30 ± 3.42	30.43 ± 5.87	27.48 ± 4.53
CO-MORBIDITIES				
Hypertension [*n* (%)]	31 (77.5)	8 (50)	8 (61.5)	23 (85.2)
Diabetes mellitus [*n* (%)]	6 (15)	5 (31.9)	0 (0)	6 (22.2)
STROKE CHARACTERISTICA				
Etiology				
Large-artery artherosclerosis	10 (25)	NA$^{\#}$	4 (30.8)	6 (22.2)
Cardioembolism [*n* (%)]	19 (47.5)	NA$^{\#}$	6 (46.2)	13 (48.1)
Stroke of other determined Etiology [*n* (%)]	2 (5)	NA$^{\#}$	0	2 (7.4)
Stroke of undetermined Etiology [*n* (%)]	9 (22.5)	NA$^{\#}$	3 (27.1)	6 (22.2)
1. MRI Stroke Size [ml^3, Median (IQR)]	31.0 (11.9–78.8)	NA$^{\#}$	11.8 (4.5–23.8)$^{\$}$	61.5 (23.7–201.7)$^{\$}$
2. MRI Stroke Size [ml^3, Median (IQR)]	40.5 (9.4–80.1)	NA$^{\#}$	8 (5.9–13.1)$^{\$}$	63.0 (19.2–89.8)$^{\$}$
Initial NIHSS [Median (IQR)]	15 (11.25–21.00)	NA$^{\#}$	15 (11–19)	15 (12–21)
Infarct side [*n* (%) left-sided infarcts]	20 (50.0)	NA$^{\#}$	6 (46.2)	14 (51.9)
Treatment [*n* (%)]	30 (75.0)	NA$^{\#}$	13 (100.0)$^{\$}$	17 (63.0)$^{\$}$
Systemic Thrombolysis [*n* (%)]$^{\&}$	25 (62.5)	NA$^{\#}$	10 (76.9)	15 (55.6)
Mechanical Thrombectomy [*n* (%)]$^{\&}$	18 (45.0)	NA$^{\#}$	11 (84.6)$^{\$}$	7 (25.9)$^{\$}$
Combined Treatment [*n* (%)]	13 (32.5)	NA$^{\#}$	8 (30.8)$^{\$}$	5 (18.5)$^{\$}$

$^{\&}$*The numbers of systemic thrombolysis and mechanical thrombectomies are the total number of patients receiving the treatments and include patients receiving a combination of both.* NA$^{\#}$*, Not applicable.*

$^{\$}$*1. MRI Stroke: Mann Whitney test, p = 0.0170; 2. MRI Stroke: Mann Whitney test, p = 0.0120; Treatment: Fisher's exact test, p = 0.0164; Mechanical thrombectomy: Fisher's exact test, p = 0.007; Combined treatment: Fisher's exact test, p = 0.0114.*

**Clinical improvement was defined as a reduction of more than 25% of the NIHSS score from admission to day 1.*

Determination of Cell Subset

Fluorescence-activated cell sorting was used to measure cell counts for leukocytes, neutrophils, T cells, CD4+T cells, CD8+T cells, NK cells, and B cells (anti-CD45 FITC; anti-CD56 PE, anti-CD16 PE, anti-CD19 ECD, anti-CD3 PC5, IgG1 PC7, anti-CD4 PE, anti-CD8 PCD, anti-CD3 PC5 [Beckman Coulter]).

Determination of Inflammatory Mediators

All patients' sera were sampled on admission day (day 0), days 1, 3, and 5 and immediately frozen at −80°C for later analysis.

Biomarker determination was performed at the Multiplex Facility at University Leiden utilizing the multi-analyte profiling (xMAP) technology (Luminex, Austin, USA) for Cathepsin S, Eotaxin, E-selectin, GM-CSF; IFN-β, IFN-γ, IL-1β, IL-1RA, IL-2, IL-4, IL-5, IL-6, IL-8, IL-10, IL-12, IL-17, IL-17F, IL-18, MIF, MCP-1, MCP-4, MIP-3α, MIP-3β, P-selectin, MMP-3, soluble IL-6 receptor, TNF-α). To analyse stroke recovery effects and not inter-individual differences only those cytokines were included into the analysis where stroke patients with or without improvement had no differences on day of admission.

IL-6 was determined twice due to multiplex setup. We only show the results gained in the central laboratory facility of the University Medicine Greifswald which provide higher precision in terms of standard deviation and coefficient of variation.

HMGB-1 was determined by ELISA according to the manufacturer's instructions (IBL International, Hamburg, Germany) from serum samples gained and frozen at −80°C on admission and day 3. Haemolytic serum samples were excluded because they lead to false positive ELISA results. Some HMGB-1 levels exceeded the standard range and were set to the highest standard due to lack of sample for reanalysis.

Determination of Stroke Lesion Size

Diffusion weighted MRI images were used to calculate infarct sizes (3.0 Tesla). To analyse the location and stroke size images were analyzed using OSIRIX 5.6. To calculate the infarct size, the regions of interest were defined manually and the lesion volume was calculated semi-automatically. Initial MRI was performed between days 1 and 3; the second MRI was performed between days 5 and 7 post-stroke.

Statistical Analysis

Because this is a *post hoc* data analysis, group sizes were not calculated prior to analysis, but *post-hoc* power analysis suggests, that our group sizes are adequate to detect effect sizes from previous trials (4). All data sets were tested for adherence to the Gaussian distribution with the Kolmogorov-Smirnov test. Since some of the data failed the normality test we used non-parametric testing throughout. The Kruskal-Wallis test with Dunn's multiple comparison test as a post-test or the Mann-Whitney test were used as appropriate. For comparing dichotomous data fisher's exact test was used. Correlations were determined by Spearman analysis. GraphPad-PRISM 5.0 (GraphPad Software Inc., San Diego, CA, USA) was used for all analyses. A $p < 0.05$ was regarded as significant.

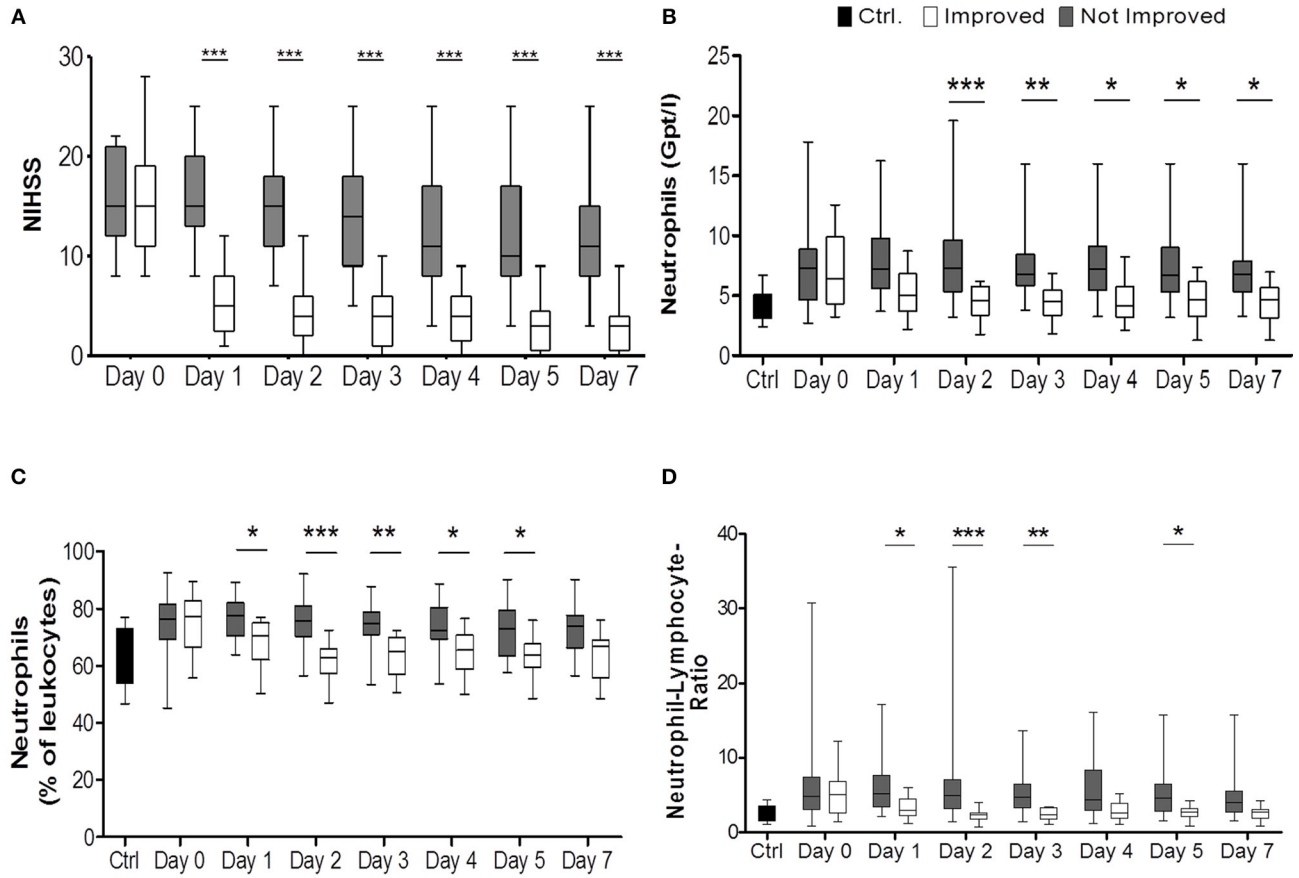

FIGURE 1 | Comparison of improved patients (white bars) vs. non-improved patients (gray bars) on the day of stroke unit admission (day 0), days 1, 2, 3, 4, 5, 7. National Institutes of Health Stroke Scale (NIHSS) served as surrogate marker for neurological improvement **(A)** ($n_{imp} = 13$, $n_{non-imp} = 27$). Healthy control patients are given in black bars. **(B)** illustrates the absolute numbers of neutrophils (Gpt/l) ($n_{imp} = 12$, $n_{non-imp} = 25$) while **(C)** shows relative numbers (%) ($n_{imp} = 12$, $n_{non-imp} = 25$). In **(D)** the lymphocyte-neutrophil ratio is shown ($n_{imp} = 12$, $n_{non-imp} = 25$). $^{*}p < 0.05$; $^{**}p < 0.01$; $^{***}p < 0.001$; Box and whiskers (Min–Max) are given.

MiRNA Groups were tested for differential expression by applying a *t*-test. None of the 9 herein found regulated miRNA passed a Benjamini-Hochberg correction to avoid false positive results at a significance level of 0.05. The results of the *t*-test reported in this manuscript are therefore explorative.

Definition of Clinical Improvement

To study the effect of rapid clinical improvement on SIIA we took advantage of the NIHSS score and defined a reduction of more than 25% from admission to day 1 as marker of rapid clinical improvement after stroke. Thirteen patients did profoundly improve by this definition while 27 patients did not (see **Table 1**; **Figure 1A**).

miRNA

We investigated fold changes of serum miRNA amounts on day 1 post-stroke between the improved and non-improved cohort. Serum miRNA was isolated from all patient samples and then analyzed by SYBR Green based miRCURY LNA PCR Human Panel I assay by Qiagen. The assay included 372 different miRNA. Samples were analyzed individually. Quality controls included melting curve analysis, calculation of amplification efficiency and comparison of Cq values to background level in the negative control sample. Spike-ins served as RNA isolation and cDNA synthesis control. To avoid data variation Quiagen controlled for hemolysis by the ratio between red blood cell miR-451 and miR-23a that is relatively stable in serum and plasma and not affected by hemolysis. Normalization was performed based on the average of the assays detected in all samples as this was shown to be the best normalization for qPCR studies involving numerous assays (15). For the present study, this included 43 assays.

RESULTS

Notably, all patients who improved rapidly after stroke according to our definition received some form of treatment, either mechanical thrombectomy or systemic thrombolysis with rtPA or both, while in the groups without rapid improvement only 63% of patients received some form of treatment. This difference was statistically significant ($p = 0.0164$). While both groups had nearly identical median NIHSS scores on admission

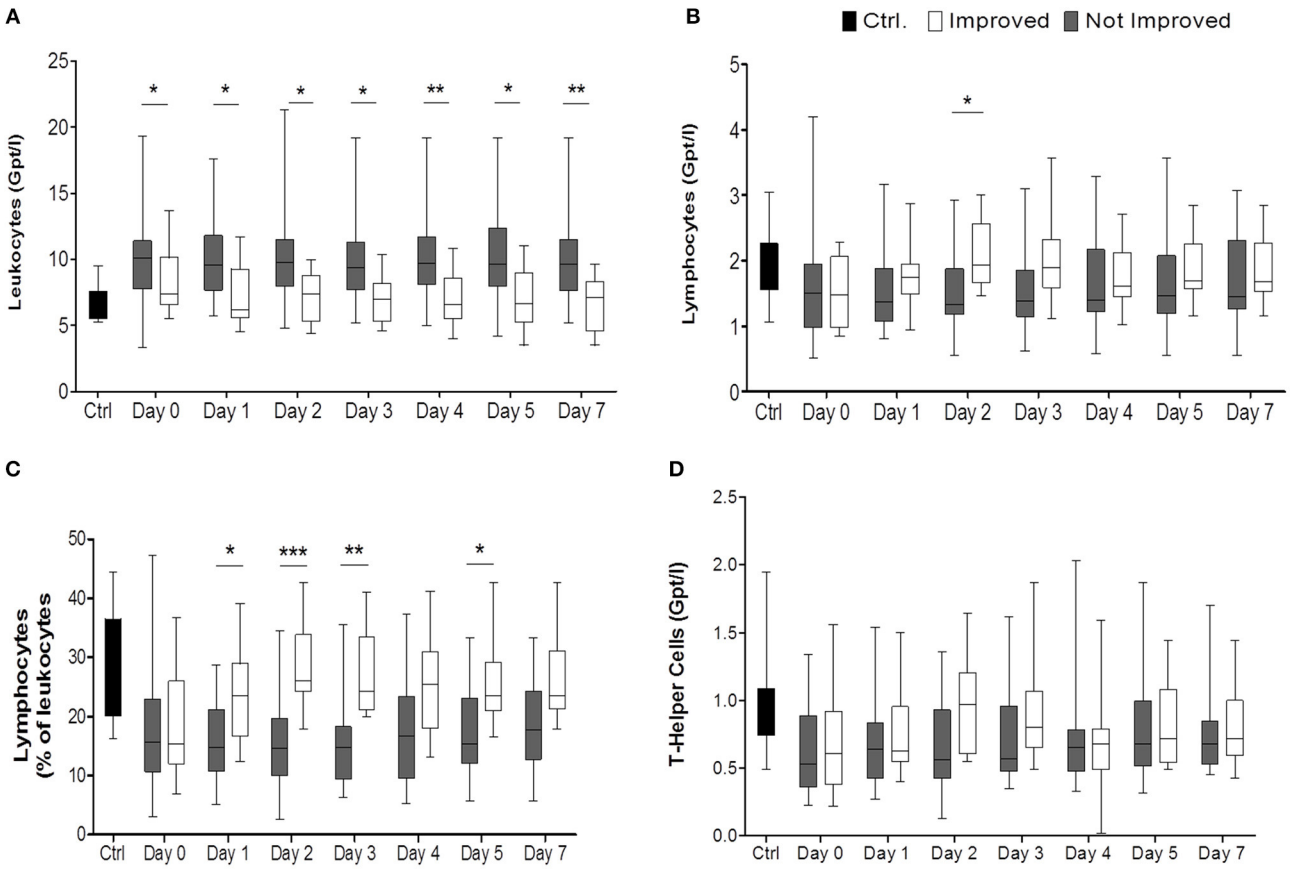

FIGURE 2 | Comparison of improved patients (white bars) vs. non-improved patients (gray bars) on the day of stroke unit admission (day 0), days 1, 2, 3, 4, 5, 7, while healthy control patients are given in black bars. In **(A)** the absolute numbers of leukocytes (Gpt/l) ($n_{imp} = 13$, $n_{non-imp} = 26$), in **(B)** absolute numbers of lymphocytes (Gpt/l) and in **(C)** relative numbers of lymphocytes (%) are shown. Absolute T helper cells (Gpt/l) are given in **(D)**. $^{*}p < 0.05$; $^{**}p < 0.01$; $^{***}p < 0.001$; Box and whiskers (Min–Max) are given ($n_{imp} = 12$, $n_{non-imp} = 25$).

[$NIHSS_{improved}$: 15 (IQR 11–19), $NIHSS_{non-improved}$: 15 (IQR 12-21)], median NIHSS scores were significantly different on all other days ($p < 0.0001$; **Figure 1A**). Stroke volumes measured by MRI after treatment and early improvement were markedly smaller for patients with clinical improvement compared to patients without clinical improvement (**Table 1**) between days 1 and 3 ($p = 0.001$) and days 5 and 7 ($p = 0.012$).

Cellular Parameters

Comparison of the total stroke cohort with controls revealed changes in agreement with previous reports: Total leukocyte numbers increased significantly on all days compared to controls (**Supplemental Figure IC**), and absolute and relative neutrophilia ($p_{absolute} = 0.0041$, **Figure 1C**; $p_{relative} = 0.0025$, **Supplemental Figures IA,B**) was observed. Also, the absolute number of CD4+ T cells was significantly reduced on admission and on day 1 ($p = 0.0345$, **Supplemental Figure IIA**). CD8+ T cells, NK cells, and B cells weren't altered in absolute numbers or percentage of parent leukocytes (**Supplemental Figures IIB–D**).

On admission, the immune alterations observed in patients with subsequent improvement and without improvement were remarkably similar, no significant differences were observed for the cell populations investigated.

Improved patients had lower neutrophil counts and frequency than non-improved patients from days 1 or 2 until day 7 after stroke ($p_{absolute} < 0.0001$; $p_{relative} < 0.0001$; *post-hoc*: days 1, 2, 3, 4, 5) (**Figures 1B,C**, **Supplemental Figures IIIB, IVA**). The lymphocyte-neutrophil ratio was significantly increased in patients without improvement on days 1, 2, 3, and 5 (**Figure 1D**, **Supplemental Figure IIID**).

From days 1 to 7 absolute leukocyte counts were significantly elevated in the non-improved group compared to the improved one ($p < 0.001$) (**Figure 2A**, **Supplemental Figure IIIA**). Non-improved patients had more pronounced absolute and relative lymphocytopenia during the observation period than patients with neurological improvement (for absolute numbers: $p < 0.0306$, *post-hoc*: day 2; for relative numbers: <0.0001, *post-hoc*: days 1, 2, 3, 5) (**Figures 2B,C**, **Supplemental Figures IIIC, IVB**). The absolute CD4+ T lymphocyte count tended to be higher in improved patients than in not improved patients especially on day 2 (**Figure 2D**). CD8+ T cells, NK cells, and B cell subpopulations did not differ between the two groups (data not shown).

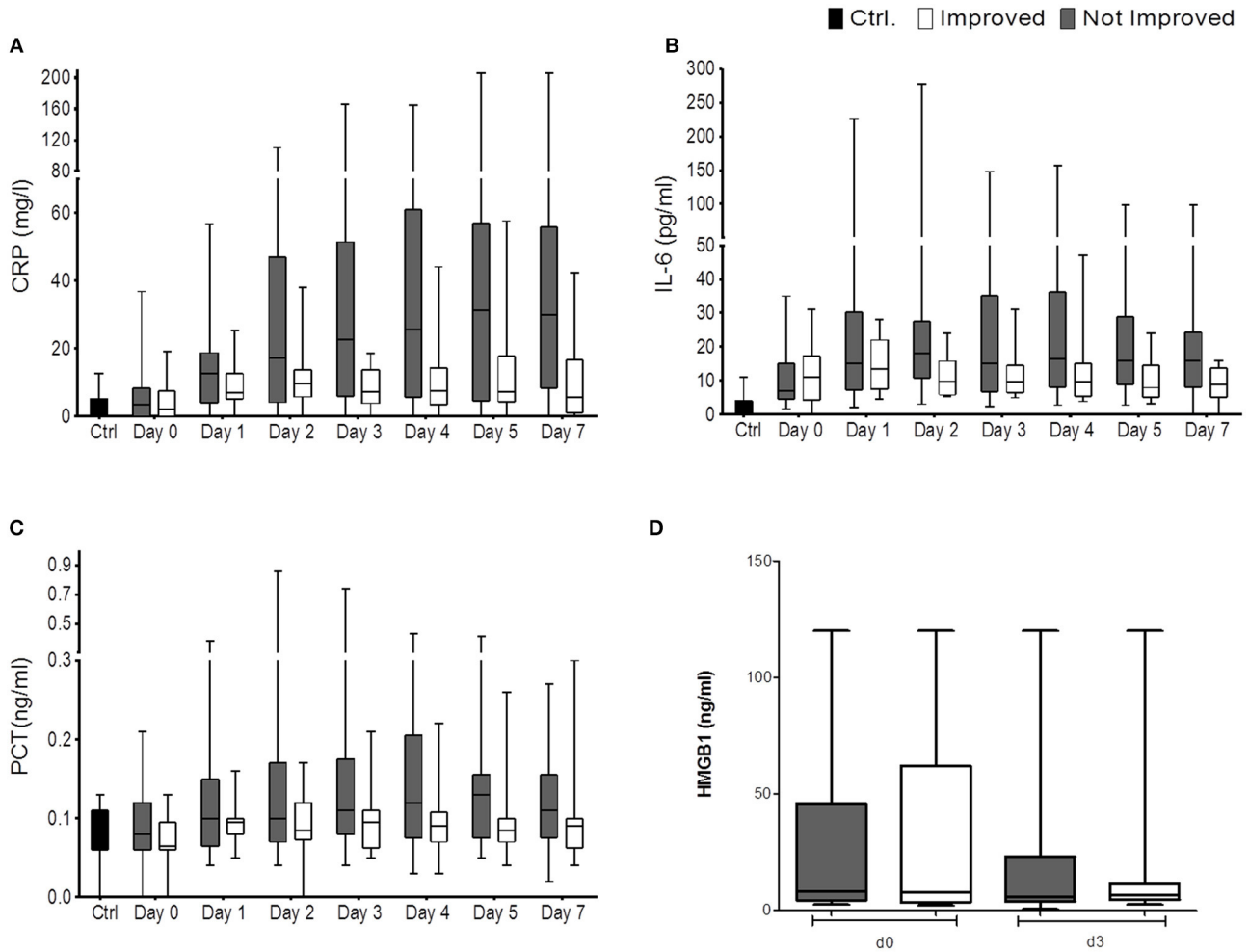

FIGURE 3 | CRP (mg/L) **(A)**, IL6 (pg/ml) **(B)**, PCT (ng/ml) **(C)**, and HMGB-1 **(D)** are shown for the comparison of improved patients (white bars) vs. non-improved patients (gray bars) on the day of stroke unit admission (day 0), days 1, 2, 3, 4, 5, 7 ($n_{imp} = 13$, $n_{non-imp} = 27$). HMGB-1 (in ng/ml) is shown for improved patients (white bars) and non-improved patients (gray bars) on the day of stroke unit admission (day 0) and day 3. Box and whiskers (Min–Max) are given ($n_{imp} = 11$, $n_{non-imp} = 16$).

Acute Phase Proteins

Despite an apparent trend toward higher CRP, PCT, and IL-6 in the non-improved cohort, statistical significance was not reached throughout the observation period (**Figures 3A–C**).

We found serum concentrations of HMGB-1 similar to our last study (5, 10). While the investigated immune alterations post-stroke had promptly reversed in the improved cohort, HMGB-1 concentrations were not differentially regulated between the improved and non-improved cohort at the investigated time points (**Figure 3D**).

Serum Pro- and Anti-inflammatory Cytokines, Chemokines, and Biomarkers

To analyse the effect of clinical improvement on soluble immune markers we measured cytokines (GM-CSF; IFN-β, IFN-γ, IL-1β, IL-1RA, IL-2, IL-4, IL-5, IL-6, IL-10, IL-12, IL-17, IL-17F, IL-18, TNF-α, MIF), chemokines (IL-8, MCP-1, MCP-4, MIP-3α, MIP-3β, Eotaxin), and biomarkers (Cathepsin S, MMP-3, soluble IL-6 receptor, E-selectin, P-selectin).

Cathepsin S was significantly elevated in the improved cohort on day 3 ($p = 0.0006$) (**Figure 4A**). MIP-3a and MMP-3 were significantly reduced from days 1 to 5 in the improved cohort and also displayed the same trend on admission (MIP-3a $p = 0.0001$; MMP-3 $p = 0.0003$) (**Figures 4B,C**). Other cytokines, chemokines, and biomarkers were not regulated or showed inter-individual differences on admission (data not shown).

Post-stroke Infections

We used a previously established definition of infections (4) to categorize patients. To fulfill these criteria patients had to show clinical signs of infection and have a serum CRP above 50 mg/L and PCT above 0.5 ng/mL. Only one patient in the non-improved cohort fulfilled all three criteria, suffering from pneumonia. Considering also patients fulfilling 1 or 2 criteria only (defined

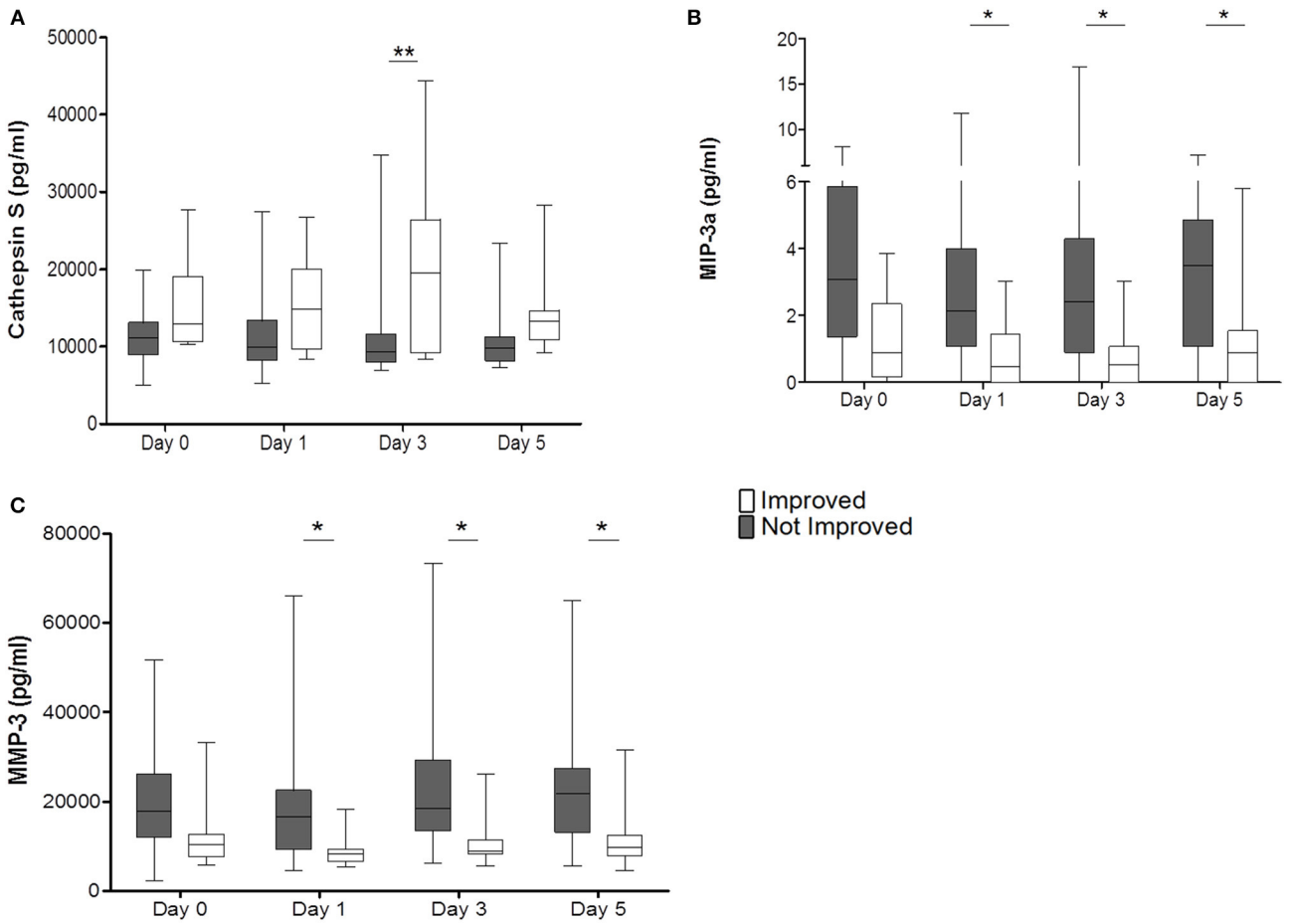

FIGURE 4 | Improved patients (white bars) and non-improved patients (gray bars) are given for Cathepsin S (pg/ml) **(A)**, MIP-3a (pg/ml) **(B)**, and MMP-3 (pg/ml) **(C)**. $^{*}p < 0.05$; $^{**}p < 0.01$; Box and whiskers (Min–Max) are given ($n_{imp} = 13$, $n_{non-imp} = 27$).

unclear infection status according to our criteria) 56% of the non-improved cohort had signs of infections, compared to 23% of the improved cohort.

miRNA

Forty three of the Three hundred and seventy two analyzed miRNA were detectable in all samples investigates. The average number of miRNA detected per sample was 112. Nine miRNA were differentially expressed between the improved and non-improved patient group (cut-off $p < 0.05$) (**Table 2**).

DISCUSSION

Post-stroke immune alterations are a well-described phenomenon. Its functional characteristics have been investigated in different immune cell populations and its clinical relevance is revealed by the fact that in human and experimental studies the extent of SIIA correlates with post-stroke infection (4, 7, 16, 17). While stroke severity and the extent of SIIA correlate (10), the relationship of early neurological recovery and SIIA has not been investigated. Here, we describe the novel observation that early clinical improvement is associated with a rapid reversal of SIIA in stroke patients within 24 h. At admission, patients with and without improvement had identical stroke severity, as measured with the NIHSS score [15 (IQR 11–19) vs. 15 (12–21)]. As a rough estimate the NIHSS on admission can be considered a surrogate marker for the tissue at risk. Therefore, the neurological improvement can be considered to correlate with rescued penumbra. While the MRI imaging would allow for a better assessment of tissue at risk and the volume of brain tissue rescued due to recanalization therapy this MRI data on admission were not available for this study. Although we only measured stroke lesion size between days 1 and 3 (MRI 1) and days 5 and 7 (MRI 2) after stroke the observation that the MRI lesions of patients with an improvement are markedly smaller than in patients without improvement supports the use of these surrogate markers. Among patients with rapid improvement, the treatment protected viable brain parenchyma in the penumbra and thereby not only reduced the neurological deficit (NIHSS) but also reverted parts of the SIIA.

While the initiation of SIIA has been in the focus of many studies, data on the mechanisms that maintain or reverse SIIA remain scarce. HMGB-1 has been suggested to play a

TABLE 2 | Top most differentially expressed miRNAs, showing the standard deviation (SD) across the groups, followed by average normalized Cq values for each group and fold change between the two groups.

miR name	SD1	SD0	Average dCq 1	Average dCq 0	Fold change	*p*-value	BH adj. *P*-value
hsa-let-7e-5p	0.77	0.92	−3.7	−4.4	1.6	0.020	0.83
hsa-miR-431-5p	0.30	0.28	−4.9	−5.7	1.7	0.022	0.83
hsa-miR-584-5p	0.83	0.67	−4.1	−3.5	−1.5	0.030	0.83
hsa-miR-145-5p	0.67	0.83	−1.9	−1.3	−1.5	0.033	0.83
hsa-miR-30c-5p	0.51	0.51	−2.0	−2.4	1.3	0.034	0.83
hsa-miR-181a-3p	0.69	0.75	−5.7	−6.9	2.3	0.036	0.83
hsa-miR-99a-5p	0.64	0.92	−3.6	−4.2	1.5	0.037	0.83
hsa-miR-505-3p	0.86	0.93	−3.8	−4.5	1.7	0.040	0.83
hsa-miR-148b-3p	0.57	1.0	−5.2	−5.8	1.5	0.049	0.91

The last two columns show the p-value from the t-test and the Benjamini-Hochberg adjusted p-value.

role in SIIA or influence the outcome of tested patients and animals in at least 6 studies (8–10, 18–20). With a given sample size that allows to detect large effect sizes only, we observed no difference in the regulation of HMGB-1 serum levels in patients with and without rapid clinical improvement. While our data do not support the hypothesis that HMGB-1 is involved in maintaining immunosuppression, additional studies are required to further define the role of HMGB-1 in stroke induced immunosuppression.

In our explorative analysis of miRNA expression we detected 9 miRNAs which were differentially regulated between improved and non-improved stroke patients. Five of these had been described as regulated in ischemic stroke compared to healthy controls. In agreement with our hypothesis, the miRNAs in the cohort of improved stroke patients appear to be regulated toward healthy controls. Of interest, miR99a which is enhanced in our improved cohort has been suggested to exert neuroprotective effects through inhibition of pro-caspase-3 and caspase-3 expression following cerebral ischemic stroke (21). Let-7e and miR-145 were reported to be upregulated by Sepramaniam et al. in acute stroke while miR-505 and miR-30c were reported to be downregulated (14). These miRNA were regulated in the opposite direction in our improved cohort accordingly.

MiRNA data regarding stroke are controversial discussed due to different methods, tissues, in man and animal studies (12–14, 21). Due to our small sample size our results are limited but proof the value of further investigations. Since miRNA seem to be differentially regulated between the improved and non-improved cohort they might emerge as possible targets for therapy to improve outcome especially in patients with an unsuccessful acute therapy.

Some limitations apply to our *post hoc* study. Due to the design of the original study the sample size is limited to 40 patients and no preceding sample size calculation was performed. As a consequence, resulting subgroups are small, limiting our power to the detection of large effects. Due to the exploratory nature of the study no adjustment for multiple testing was performed. Nevertheless, our findings are robust across the parameters investigated.

CONCLUSION

While the course of stroke induced immunosuppression and the gradual recovery of immune function after the first week from stroke onset is well-described the change of the patients' immune status in dependence on successful acute recovery due to recanalization strategies had not been investigated. Here we report the novel finding that successful recanalization therapies by rtPA and thrombectomy not only improve neurological function but also reverse SIIA promptly. The rapid recovery observed in the improved cohort therefore strongly supports the requirement of continuous signals to maintain stroke induced immune alterations as early as day 1 post-stroke to maintain SIIA. Future studies should therefore focus on brain injury-induced signal cascades to fight the detrimental effects of SIIA in severe ischemic stroke.

ETHICS STATEMENT

The study protocol was approved by the ethics committee of the Medical Faculty, University of Greifswald (No. BB 050/15). Controls gave direct informed and written consent to participate. Patients gave informed and written consent directly or through a surrogate.

AUTHOR CONTRIBUTIONS

AV, AD, and JR designed the study. CW, CH, and BvS recruited patients and controls. CW and CH evaluated the FACS and cytokine data. JG measured HMGB-1 and evaluated the data. SL evaluated stroke lesion size. JS, AV, AD, JR, and CW are responsible for data interpretation. AV, CW, JR, and AD wrote the manuscript.

FUNDING

AV received funding from the University of Greifswald—Käthe-Kluth-Research-Group. JR was funded by the Gerhard-Domagk-Program of the University Medicine

Greifswald. The funders had no role in the study design, data collection and analysis, decision to publish or preparation of the article.

ACKNOWLEDGMENTS

We thank the patients and their next of kin for participating in this study and stroke physicians for their support in the recruitment of patients. We thank Dr. Sabine Ameling for assistance in analyzing miRNA data. We thank Sonya Ceesay for supporting the study through control recruitment, blood sampling and data handling.

SUPPLEMENTARY MATERIAL

The Supplementary Material for this article can be found online at: https://www.frontiersin.org/articles/10.3389/fneur.2019.00414/full#supplementary-material

REFERENCES

1. Shi K, Wood K, Shi FD, Wang X, Liu Q. Stroke-induced immunosuppression and poststroke infection. *Stroke Vasc Neurol*. (2018) 3:34–41. doi: 10.1136/svn-2017-000123
2. Shim R, Wong CHY. Complex interplay of multiple biological systems that contribute to post-stroke infections. *Brain Behav Immun*. (2018) 70:10–20. doi: 10.1016/j.bbi.2018.03.019
3. Ruhnau J, Schulze K, Gaida B, Langner S, Kessler C, Broker B, et al. Stroke alters respiratory burst in neutrophils and monocytes. *Stroke*. (2014) 45:794–800. doi: 10.1161/STROKEAHA.113.003342
4. Vogelgesang A, Grunwald U, Langner S, Jack R, Broker BM, Kessler C, et al. Analysis of lymphocyte subsets in patients with stroke and their influence on infection after stroke. *Stroke*. (2008) 39:237–41. doi: 10.1161/STROKEAHA.107.493635
5. Vogelgesang A, May VE, Grunwald U, Bakkeboe M, Langner S, Wallaschofski H, et al. Functional status of peripheral blood t-cells in ischemic stroke patients. *PLoS ONE*. (2010) 5:e8718. doi: 10.1371/journal.pone.0008718
6. Chamorro A, Amaro S, Vargas M, Obach V, Cervera A, Gomez-Choco M, et al. Catecholamines, infection, and death in acute ischemic stroke. *J Neurol Sci*. (2007) 252:29–35. doi: 10.1016/j.jns.2006.10.001
7. Liesz A, Ruger H, Purrucker J, Zorn M, Dalpke A, Mohlenbruch M, et al. Stress mediators and immune dysfunction in patients with acute cerebrovascular diseases. *PLoS ONE*. (2013) 8:e74839. doi: 10.1371/journal.pone.0074839
8. Liesz A, Dalpke A, Mracsko E, Antoine DJ, Roth S, Zhou W, et al. Damp signaling is a key pathway inducing immune modulation after brain injury. *J Neurosci*. (2015) 35:583–98. doi: 10.1523/JNEUROSCI.2439-14.2015
9. Singh V, Roth S, Veltkamp R, Liesz A. Hmgb1 as a key mediator of immune mechanisms in ischemic stroke. *Antioxid Redox Signal*. (2016) 24:635–51. doi: 10.1089/ars.2015.6397
10. Schulze J, Zierath D, Tanzi P, Cain K, Shibata D, Dressel A, et al. Severe stroke induces long-lasting alterations of high-mobility group box 1. *Stroke*. (2013) 44:246–8. doi: 10.1161/STROKEAHA.112.676072
11. Harms H, Reimnitz P, Bohner G, Werich T, Klingebiel R, Meisel C, et al. Influence of stroke localization on autonomic activation, immunodepression, and post-stroke infection. *Cerebrovasc Dis*. (2011) 32:552–60. doi: 10.1159/000331922
12. Dharap A, Bowen K, Place R, Li LC, Vemuganti R. Transient focal ischemia induces extensive temporal changes in rat cerebral micrornaome. *J Cereb Blood Flow Metab*. (2009) 29:675–87. doi: 10.1038/jcbfm.2008.157
13. Ni J, Wang X, Chen S, Liu H, Wang Y, Xu X, et al. Microrna let-7c-5p protects against cerebral ischemia injury via mechanisms involving the inhibition of microglia activation. *Brain Behav Immun*. (2015) 49:75–85. doi: 10.1016/j.bbi.2015.04.014
14. Sepramaniam S, Tan JR, Tan KS, DeSilva DA, Tavintharan S, Woon FP, et al. Circulating micrornas as biomarkers of acute stroke. *Int J Mol Sci*. (2014) 15:1418–32. doi: 10.3390/ijms15011418
15. Mestdagh P, Van Vlierberghe P, De Weer A, Muth D, Westermann F, Speleman F, et al. A novel and universal method for microrna rt-qpcr data normalization. *Genome Biol*. (2009) 10:R64. doi: 10.1186/gb-2009-10-6-r64
16. Hug A, Dalpke A, Wieczorek N, Giese T, Lorenz A, Auffarth G, et al. Infarct volume is a major determiner of post-stroke immune cell function and susceptibility to infection. *Stroke*. (2009) 40:3226–32. doi: 10.1161/STROKEAHA.109.557967
17. Liesz A, Hagmann S, Zschoche C, Adamek J, Zhou W, Sun L, et al. The spectrum of systemic immune alterations after murine focal ischemia: immunodepression versus immunomodulation. *Stroke*. (2009) 40:2849–58. doi: 10.1161/STROKEAHA.109.549618
18. Goldstein RS, Gallowitsch-Puerta M, Yang L, Rosas-Ballina M, Huston JM, Czura CJ, et al. Elevated high-mobility group box 1 levels in patients with cerebral and myocardial ischemia. *Shock*. (2006) 25:571–4. doi: 10.1097/01.shk.0000209540.99176.72
19. Muhammad S, Barakat W, Stoyanov S, Murikinati S, Yang H, Tracey KJ, et al. The hmgb1 receptor rage mediates ischemic brain damage. *J Neurosci*. (2008) 28:12023–31. doi: 10.1523/JNEUROSCI.2435-08.2008
20. Yang Q-W, Wang J-Z, Li J-C, Zhou Y, Zhong Q, Lu F-L, et al. High-mobility group protein box-1 and its relevance to cerebral ischemia. *J Cereb Blood Flow Metab*. (2009) 30:243–54. doi: 10.1038/jcbfm.2009.202
21. Tao Z, Zhao H, Wang R, Liu P, Yan F, Zhang C, et al. Neuroprotective effect of microrna-99a against focal cerebral ischemia-reperfusion injury in mice. *J Neurol Sci*. (2015) 355:113–19. doi: 10.1016/j.jns.2015.05.036

Conflict of Interest Statement: The authors declare that the research was conducted in the absence of any commercial or financial relationships that could be construed as a potential conflict of interest.

Copyright © 2019 Vogelgesang, Witt, Heuer, Schulze, Gellrich, von Sarnowski, Langner, Dressel and Ruhnau. This is an open-access article distributed under the terms of the Creative Commons Attribution License (CC BY). The use, distribution or reproduction in other forums is permitted, provided the original author(s) and the copyright owner(s) are credited and that the original publication in this journal is cited, in accordance with accepted academic practice. No use, distribution or reproduction is permitted which does not comply with these terms.

frontiers in Neuroscience

ORIGINAL RESEARCH
published: 08 May 2019
doi: 10.3389/fnins.2019.00462

Overexpression of CX3CR1 in Adipose-Derived Stem Cells Promotes Cell Migration and Functional Recovery After Experimental Intracerebral Hemorrhage

Gaigai Li[1], Haihan Yu[1], Na Liu[1], Ping Zhang[1], Yingxin Tang[1], Yang Hu[1], Ye Zhang[1], Chao Pan[1], Hong Deng[1], Jiahui Wang[1], Qi Li[2] and Zhouping Tang[1]**

[1] Department of Neurology, Tongji Hospital, Tongji Medical College, Huazhong University of Science and Technology, Wuhan, China, [2] Department of Neurology, The First Affiliated Hospital of Chongqing Medical University, Chongqing, China

OPEN ACCESS

Edited by:
Gregory Jaye Bix,
University of Kentucky, United States

Reviewed by:
Qiang Liu,
Barrow Neurological Institute (BNI), United States
DaZhi Liu,
University of California, Davis, United States
Zahoor A. Shah,
The University of Toledo, United States

***Correspondence:**
Qi Li
qili_md@126.com
Zhouping Tang
ddjtzp@163.com

Specialty section:
This article was submitted to Neurodegeneration, a section of the journal Frontiers in Neuroscience

Received: 07 November 2018
Accepted: 24 April 2019
Published: 08 May 2019

Citation:
Li G, Yu H, Liu N, Zhang P, Tang Y, Hu Y, Zhang Y, Pan C, Deng H, Wang J, Li Q and Tang Z (2019) Overexpression of CX3CR1 in Adipose-Derived Stem Cells Promotes Cell Migration and Functional Recovery After Experimental Intracerebral Hemorrhage. Front. Neurosci. 13:462. doi: 10.3389/fnins.2019.00462

Stem cell therapy has emerged as a new promising therapeutic strategy for intracerebral hemorrhage (ICH). However, the efficiency of stem cell therapy is partially limited by low retention and engraftment of the delivered cells. Therefore, it's necessary to improve the migration ability of stem cells to the injured area in order to save the costs and duration of cell preparation. This study aimed to investigate whether overexpression of CX3CR1, the specific receptor of chemokine fractalkine (FKN), in adipose-derived stem cells (ADSCs) can stimulate the cell migration to the injured area in the brain, improve functional recovery and protect against cell death following experimental ICH. ADSCs were isolated from subcutaneous adipose tissues of rats. ICH was induced by means of an injection of collagenase type VII. ELISA showed that the expression levels of fractalkine/FKN were increased at early time points, with a peak at day 3 after ICH. And it was found that different passages of ADSCs could express the chemokine receptor CX3CR1. Besides, the chemotactic movements of ADSCs toward fractalkine have been verified by transwell migration assay. ADSCs overexpressing CX3CR1 were established through lentivirus transfection. We found that after overexpression of CX3CR1 receptor, the migration ability of ADSCs was increased both *in vitro* and *in vivo*. In addition, reduced cell death and improved sensory and motor functions were seen in the mice ICH model. Thus, ADSCs overexpression CX3CR1 might be taken as a promising therapeutic strategy for the treatment of ICH.

Keywords: intracerebral hemorrhage, adipose-derived stem cells, migration, fractalkine, FKN, CX3CR1

INTRODUCTION

Intracerebral hemorrhage (ICH) is a severe neurological disease with high morbidity and mortality (Balami and Buchan, 2012; Rabinstein, 2017). Current treatment options for ICH mainly include surgical evacuation of hematoma, reduction of intracranial pressure, prevention of cerebral edema, and general supportive measures (Mayer and Rincon, 2005; Rabinstein, 2017). In recent years,

stem cell therapy has emerged as a new promising therapeutic strategy for ICH (Sun et al., 2015; Hu et al., 2016; Bedini et al., 2018). It is reported that stem cells can promote functional recovery through the mechanisms of directly transdifferentiation, paracrine effects, and immune regulation (Bronckaers et al., 2014; Liu et al., 2014; Wei et al., 2017). Based on the results of these animal studies, clinical trials of stem cells for recent ICH and cerebral hemorrhage sequela are ongoing now (NCT03371329; NCT02283879). Adipose tissue is one of the most abundant and easily accessible sources for mesenchymal stem cell (MSCs), with the advantages of high yield, low immunogenicity and avoidance of ethical issues (Schäffler and Büchler, 2007; Forcales, 2015; Gutiérrez-Fernández et al., 2015). A large number of preclinical studies and several clinical trials have shown that adipose-derived stem cells (ADSCs) transplantation could reduce neuronal apoptosis, promote regeneration of neurons and vessels and improve functional recovery after brain injury (Gimble et al., 2012; Neirinckx et al., 2013; Gutiérrez-Fernández et al., 2015; Konala et al., 2016). It has been found in some studies that ADSCs can improve ICH-induced neurological deficits (Chen et al., 2012; Yang et al., 2012; Kuramoto et al., 2019).

It is generally believed that the efficiency of stem cell therapy to attenuate inflammation, or injuries after ischemia depends on the number of MSCs migrating and homing to the target tissues (Chavakis et al., 2008; Karp and Leng, 2009). Despite the tendency of MSCs migrating to the lesion site, however, only a small percentage of the infused MSCs reach the target tissue, due to the effects of entrapment in peripheral filter organs and the existence of blood-brain barrier (BBB) (Detante et al., 2009; Arbab et al., 2012; Liu et al., 2013; Tang et al., 2015). Furthermore, the exact mechanisms underlying the migration and homing of MSCs are not fully understood. It is proposed that like leukocyte homing, recruitment and incorporation of MSCs into injured tissues may also involve circulation, capture rolling, adhesion, crawling, transendothelial migration and interstitial migration (Chavakis et al., 2008; Emmanouil Chavakis, 2011; Nitzsche et al., 2017). Therefore, it is of great importance to enhance the migration ability of MSCs in order to improve cell engraftment and transplant efficiency. Up to now, studies about the migration and homing of exogenous MSCs for ICH treatment have been extremely rare.

Recently, it has been reported that the chemokines play pivotal roles in MSCs homing process, and MSCs exhibit chemotactic movement toward different chemokines (Stamatovic et al., 2003; Zhu et al., 2009; Guo et al., 2013; Li et al., 2015; Zhang et al., 2015; De Becker and Riet, 2016; Xiao et al., 2016; Xu et al., 2016). Fractalkine, or FKN for short, also known as CX3CL1, is one of the most abundant chemokines constitutively expressed on both neurons and astrocytes in the central nervous system (CNS) (Re and Przedborski, 2006; Miller et al., 2008). The specific receptor of Fractalkine /FKN, CX3CR1, is primarily expressed on microglial cells (Harrison et al., 1998). Meanwhile, an increased expression of fractalkine has been associated with development of ischemic stroke, brain and spinal cord injury and epilepsy (Xu et al., 2012; Poniatowski et al., 2017; Chen et al., 2018). Notably, elevated fractalkine levels at the lesion site can attract cells expressing CX3CR1, resulting in cell migration. Therefore, this study aimed to investigate whether overexpression of CX3CR1 in ADSCs can stimulate the cell migration to the injured brain, protect against neuronal apoptosis and improve functional recovery following experimental ICH.

MATERIALS AND METHODS

Animals

Adult male C57BL/6 mice (8–10 weeks, 20–25 g, n = 95) and female Sprague-Dawley rats (5 weeks, 100–120 g, n = 75) were obtained from the Animal Center of Tongji Hospital of Tongji Medical College of Huazhong University of Science and Technology (Wuhan, China). The experimental procedures were approved by the Experimental Animal Ethics Committee of Huazhong University of Science and Technology.

ICH Induction

Intracerebral hemorrhage was induced by a stereotactic intrastriatal injection of collagenase type VII (Sigma) as previously described (Pan et al., 2018). In brief, C57BL/6 male mice, 8–10 weeks old and weighing 20–25 g, were used in the experiments. Once anesthetized, the animals were fixed in a prone position in a stereotaxic frame, and a burr hole was drilled into the skull. Then, 0.1 U collagenase dissolved in 1 μl saline was stereotactically injected into the right basal ganglia (coordinates 0.2 mm anterior, 2.0 mm lateral, and 3.5 mm ventral to the bregma) at a rate of 0.2 μL/min. After injection, the syringe was left in place for 7 min and the needle was then withdrawn at a rate of 1 mm/min. After the suturing of wounds, all animals were monitored with free access to food and water.

Assessment of ICH Model

After 8 h of modeling, the neurologic function was evaluated with Zea Longa's five-grade scale (Longa et al., 1989). The five-point scoring criteria are as follows: a score of 0 indicated no neurologic deficit, a score of 1 (failure to extend left forepaw fully) indicated a mild focal neurologic deficit, a score of 2 (circling to the left) indicated a moderate focal neurologic deficit, and scores of 3 (falling to the left) and 4 (no spontaneous walk or a depressed level of consciousness) indicated severe focal deficits.

Isolation and Characterization of ADSCs

Adipose-derived stem cells were isolated from the subcutaneous inguinal adipose tissues of female Sprague-Dawley rats (weighing 100–120 g) as previously described (Zhang et al., 2014). Briefly, fatty plaques were cut into pieces (1 mm^3) and then digested with 0.1% collagenase Type I (Invitrogen) for 60 min at 37°C with gentle agitation. After centrifugation, the cell pellet was resuspended in the basal growth medium consisting of Dulbecco's modified Eagle medium/Ham's F12 (DMEM/F12; Hyclone) supplemented with 1% penicillin/streptomycin (Gibco), 1% L-glutamine (Gibco), and 10% fetal bovine serum (FBS; Sera Pro). Later, the suspension solution was filtered through a 40 μm cell strainer (BD Falcon) to remove debris. The remaining cells were seeded onto a 25 cm^2

tissue culture bottle (Eppendorf) and incubated at 37°C in a humidified atmosphere of 5% CO_2. After 1 h incubation, non-adherent cells were collected and transferred into a new culture bottle, in order to eliminate any impurities. The culture medium was changed in the following day and every 2–3 days thereafter. When reaching 80–90% confluency, the cells were detached by using a trypsin-EDTA solution (0.25% trypsin, 0.02% EDTA; Gibco) and were then passaged at a split ratio of 1:2. ADSCs between passages 2 and 5 were used for subsequent experiments.

Adipose-derived stem cells were analyzed for surface marker expression by flow cytometry. The isolated cells were incubated with fluorescein isothiocyanate (FITC)-conjugated antibodies against CD29, CD45 (eBioscience), phycoerythrin (PE)-conjugated antibodies against CD90, CD31 (BD Biosciences) and PBS (negative control) in a dark chamber at 4°C for 45 min. For each sample, at least 5×10^5 cells were acquired for detection and analysis.

Cell Transfection

The lentivirus for overexpressing CX3CR1 (LV-CX3CR1) and controls (Ubi-MCS-3FLAG-CBh-gcGFP-IRES-puromycin) were obtained commercially from GeneChem Corporation (Shanghai, China). When the ADSCs reached 30% confluency, lentiviral vectors were transferred to ADSC monolayer and incubated for 8 h [Multiplicity of Infection (MOI) = 40]. After lentivirus infection and transduction of ADSCs, CX3CR1-overexpressing cells (CX3CR1-GFP-ADSCs) and control cells (Ctr-GFP-ADSCs) were selected with 4 μg/ml puromycin. The effects of gene interference on CX3CR1 expression were verified using quantitative reverse transcription-polymerase chain reaction (qRT-PCR) and immunocytochemistry.

Enzyme-Linked Immune Sorbent Assay (ELISA)

Animals were terminally anesthetized at indicated time points after collagenase-induced ICH. The ipsilateral perihematomal brain tissues (bregma: −2 to 2 mm) were then removed and homogenized in PBS with protease inhibitors (900 μl of PBS were added to each 100 mg brain tissues). Quantitative analysis of mouse fractalkine/FKN was performed using a double-antibody sandwich ELISA Array Kit (Elabscience, China) according to manufacturer's instructions. In brief, tissue homogenates or standards were added to micro ELISA plate wells pre-coated with mouse fractalkine antibodies. Then, a biotinylated detection antibody specific for mouse fractalkine and avidin-horseradish peroxidase (HRP) conjugate was added into each micro plate well and incubated to wash away the free components. Afterward, the substrate solution was added into each well to yield a blue color, as a result of enzyme-substrate reaction. Immediately, sulfuric acid solution was added to terminate the reaction, which changed the color to yellow. The optical density (OD) was measured spectrophotometrically at a wavelength of 450 nm ± 2 nm. All determinations were performed in triple for each sample. Standard curve was generated to calculate the concentrations of fractalkine/FKN.

Transwell Migration Assay

The migration assay was performed by using transwell plates with pore size of 8 μm (Corning Costar). The upper chambers were loaded with $2.3 \sim 4 \times 10^4$ ADSCs in 200 μl of DMEM/F12, while the lower chambers were loaded with 600 μl of DMEM/F12 (negative control), DMEM/F12 containing 10% FBS (positive control), and different concentrations of recombined fractalkine/FKN dissolved in DMEM/F12 (Sigma). These chambers were incubated at 37°C with 5% CO_2. After 24 h of incubation, non-migrated cells on the upper surface of the filter were removed by gentle scraping and washed with PBS. Next, the adherent cells were fixed in 4% paraformaldehyde (PFA) for 20 min and then stained with 1% crystal violet for 30 min. The average number of migrated cells was determined by examining five random fields per well. All experiments were performed in triplicate for each group.

Cell Transplantation

Approximately $2 \sim 4 \times 10^5$ ADSCs in 2 μl PBS were transplanted into the right cerebral cortex (coordinates 0.1 mm posterior, 3.0 mm lateral, and 2.0 mm ventral to the bregma) of mice on the 3rd day after ICH. Mice were randomized allocated into three experimental groups: (1) PBS treatment; (2) Ctr-GFP-ADSC transplantation; and (3) CX3CR1-GFP-ADSC transplantation ($n = 7$ mice per group).

Adhesive Removal Test

The adhesive removal test is a sensitive method that assesses sensorimotor deficits in mice (Bouët et al., 2007). This test was carried out blind at days 1, 3, 7, 14, and 21 after cell transplantation. The mice were trained for 5 consecutive days before surgery, to obtain an optimal level of performance and to reduce the inter-individual variations. Before the experiment, each mouse was placed into a transparent perspex box (15 cm × 25 cm) for a habituation period of 60 s. Thereafter, two small pieces of adhesive surgical tape of equal size (0.3 cm × 0.4 cm) were placed with an equal pressure on each forepaw, covering their hairless parts (i.e., the three pads, thenar, and hypothenar). The order of placement (right or left) was alternated between each animal and session. The mice then transferred back to the perspex box, and the time for sensing and removing each adhesive tape were recorded with a maximum of 180 s.

Cylinder Test

The cylinder test was used to assess forelimb preference and asymmetry in each mouse on days 1, 3, 7, 14, and 21 after cell transplantation (Vahid-Ansari et al., 2016). Mice were placed in a transparent cylinder (diameter: 10 cm, height: 16.5 cm) for 10 min and the number of forepaw contacts to the cylinder wall was counted. The final score was calculated as: (Right forelimb movement – Left forelimb movement)/(Right forelimb movement + Left forelimb movement + both movement). The behavioral tests were performed by the two co-authors blind to the group of mice.

TTC Staining

Animals were sacrificed 3 days following transplantation of ADSCs. Hematoma volume was quantified using TTC staining method. Mice were perfused with normal saline solution, and then the brains were dissected and sectioned into 2 mm coronal sections from the frontal pole. The slices were incubated in a 2% solution of TTC at 37°C for 30 min. The sections were subsequently fixed with 4% paraformaldehyde solution. The volume of hematoma was calculated by summing the relative areas of hematoma from the individual sections and multiplying them by the distance between the sections.

Immunocytochemistry and Immunofluorescence Staining

Mice were transcardially perfused with saline and 4% PFA. The brains were dissected out and post-fixed in 4% PFA for 24 h, followed by dehydration with 25 and 30% sucrose. The brain tissues were cut into 30 μm thick sections (Leica CM1950, Germany) and picked up on a glass slide for staining. The tissue sections or adherent cells were then fixed in 4% PFA, washed three times with PBS, and incubated in 0.5% Triton X-100 for 30 min. After blocking with 5% Bovine Serum Albumin (BSA) for 1 h at room temperature, slices or cells were incubated with primary antibodies rabbit anti-CX3CL1 (1:500, Abcam, Cambridge), mouse anti-NeuN (1:500, Abcam, Cambridge), mouse anti-GFAP (1:500, Santa Cruz, CA, United States), rabbit anti-CX3CR1 (1:100, Abcam, Cambridge), goat anti-Iba-1 (1:100, Abcam, Cambridge), or chicken anti-GFP (1:1000, Abcam, Cambridge) at 4°C overnight. Secondary antibodies of FITC conjugated goat anti rabbit IgG (1:100, Boster Biological Technology Co., Ltd., United States), Cy3 conjugated goat anti mouse IgG (1:100, Boster Biological Technology Co., Ltd., United States), Cy3 conjugated donkey anti mouse IgG (1:200, Servicebio, China), Alexa Fluor® 594 donkey anti-goat IgG (1:400, life technologies, the United States) or Alexa Fluor® 488 conjugated Goat anti-chicken IgG (1:500, Abcam, Cambridge) were subsequently incubated for 1 h at 37°C. Counterstaining was performed with 4′,6-diamidino-2-phenylindole (DAPI; Beyotime, China).

Terminal Deoxynucleotidyltransferase-Mediated dUTP End Labeling (TUNEL) Staining

The paraffin-embedded tissue sections were prepared for TUNEL staining with the *in situ* Cell Death Detection Kit, POD (Roche, Switzerland). The numbers of TUNEL-positive cells were quantified with the use of Image-Pro Plus software. To determine the frequencies of apoptotic cells, five microscopic fields were examined for each sample. The apoptotic index was defined as the average proportion of TUNEL-positive cells in each area.

Western Blot

The total protein concentration in cells and tissues was determined using bicinchoninic acid assay (BCA) (Beyotime, China) according to manufacturer's instructions. After sodium dodecyl sulfate polyacrylamide gel electrophoresis (SDS-PAGE), the detected proteins were transferred onto nitrocellulose filter (NC) membranes. Subsequently, the membranes were blocked in 5% skim milk for 1 h at room temperature with gentle shaking. After that, the membranes were incubated with primary antibodies of rabbit anti-CX3CR1 (1:500, Abcam, Cambridge), mouse anti-bcl-2 (1:500, Santa Cruz, CA, United States), mouse anti-caspase-3 (1:500, Santa Cruz, CA, United States), and/or mouse anti-β-actin antibody (1:1000, Proteintech, China) at 4°C overnight, followed by 1 h incubation with anti-rabbit IgG (H+L) (DyLight 800 Conjugate; Cell Signaling Technology, United States) or anti-mouse IgG (H+L) (DyLight 800 Conjugate; Cell Signaling Technology, United States) secondary antibody at room temperature. The protein bands were visualized with Odyssey Infrared Imaging System (LI-COR Biosciences, Lincoln, NE, United States), and the intensity of each band was analyzed using Image J (National Institutes of Health, United States).

Statistical Analysis

All experimental data from three independent experiments were analyzed using SPSS software (version 20.0 for Windows, SPSS Inc., United States) and the results were expressed as mean ± standard deviation (SD). One-way analysis of variance (ANOVA) followed by Tukey's *post hoc* test was used for parametric data and multiple comparisons between groups. In **Figure 5D**, two-way ANOVA was used to assess the main effect of each independent variable and the latent interaction between them. *P*-values of less than 0.05 were considered statistically significant.

RESULTS

Increased Expression of Fractalkine/FKN After ICH

After the establishment of ICH model, the mice exhibited weakness of left limbs, uncoordinated movement and spontaneous rotation (**Figure 1A**). A proper size of hematoma could be induced with 0.1 U collagenase (**Figure 1B**). Mice scoring grades 1–3 of Zea Longa's scale were selected for further experiments. ELISA method was used to detect the dynamic changes of fractalkine in the brain tissue homogenates at 6 h, 12 h, and days 1, 2, 3, 5, and 7 after ICH. The results indicated that the expression levels of fractalkine were significantly increased at early time points, with a peak at day 3 after ICH (**Figure 1C**). Therefore, we transplanted ADSCs on the 3rd day after ICH in the following *in vivo* experiments. The immunofluorescence staining revealed that fractalkine was constitutively expressed in normal brain tissues by neurons and astrocytes, distributed mainly in the cortex, basal ganglia and other regions (**Figures 1D,E**).

Characterization of ADSCs

Primary ADSCs exhibited short bar shapes during the early stages, and maintained a spindle-shaped morphology thereafter

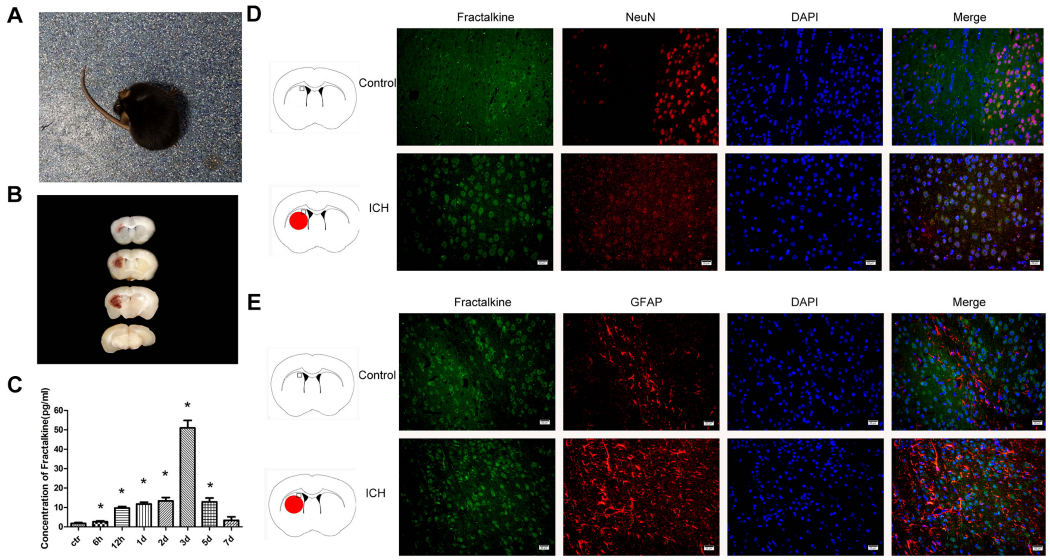

FIGURE 1 | Mice began to turn around spontaneously 8 h after ICH **(A)**, and hematoma was seen in the right basal ganglia at day 3 **(B)**. ELISA showed that the expression level of fractalkine could be increased at early time points, with a peak at day 3 after ICH **(C)** (n = 3 each group, $^*P < 0.001$, as compared to normal control group). Fractalkine, mainly produced by neurons and astrocytes, was constitutely expressed in basal ganglion of the brain tissue (**D,E**, scale bar = 20 μm; the square in the schema diagram showed the area where from the pictures were taken).

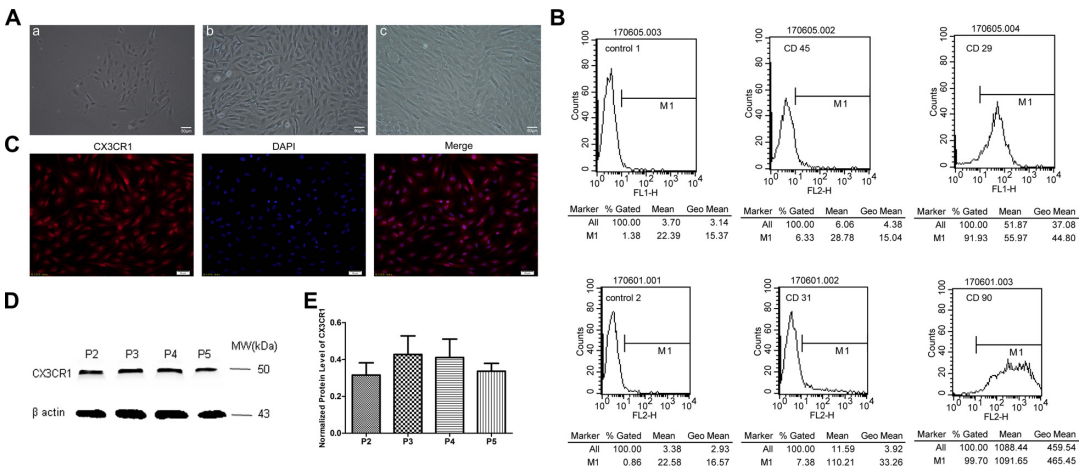

FIGURE 2 | Cellular morphology of ADSCs **(A)**. The primary ADSCs displayed short bar shapes initially (**a**, the 3rd day of cell culture), and maintained spindle-shaped morphology thereafter (**b**, the 7th day of cell culture) and could stable proliferate (**c**, passage 3 ADSCs) (scale bar = 50 μm). P2 ADSCs were positive for CD29 (91.93%) and CD90 (99.70%), and the expression level of CD45 (6.33%) and CD31 (7.38%) were very low **(B)**. P2-P5 ADSCs could stably expressed CX3CR1 in both membrane and cytoplasm detected by immunocytochemistry (**C**, scale bar = 50 μm) and western blot **(D,E)**.

(**Figure 2A**). Flow cytometry analysis showed that these cells were positive for MSC markers CD29 (91.93%) and CD90 (99.70%), while the expression of hematopoietic cell markers CD45 (6.33%) and CD31 (7.38%) were relatively low (**Figure 2B**).

CX3CR1 Protein Expression in ADSCs

The results of immunocytochemical staining revealed that ADSCs were found to express CX3CR1, which distributed mainly in the cell membrane and cytoplasm (**Figure 2C**). Western blot results demonstrated that the stable expression of CX3CR1 could be detected in ADSCs at passage 2–5 (**Figures 2D,E**).

Establishment of Stable CX3CR1 Overexpressing ADSCs

Following lentivirus transfection and puromycin screening, the transfection rate of ADSCs could remain up to 80–90% until day 11 of transfection (**Figure 3A**). The mRNA and protein expression levels of CX3CR1 were significantly higher ($P < 0.05$) in CX3CR1-GFP-ADSCs than normal ADSCs (**Figures 3B–D**).

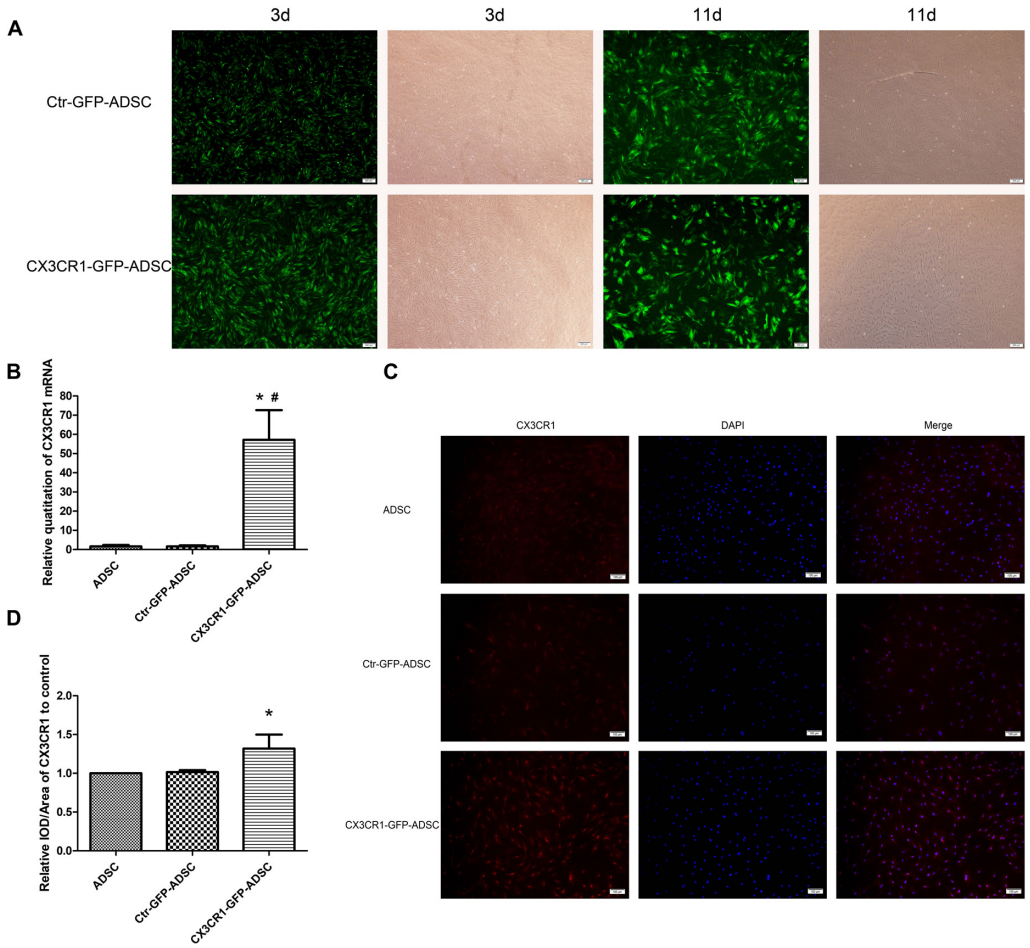

FIGURE 3 | After transfection with lentivirus and screen with puromycin, most ADSCs expressed the tag protein of GFP on the 3rd day, and the transfection rate could still remain at 80–90% till the 11th day (**A**, scale bar = 200 μm). qRT-PCR showed that mRNA expression levels of CX3CR1 in CX3CR1-GFP-ADSCs were significantly higher than the other two groups (**B**, $^{*}P < 0.01$, as compared with ADSC group; $^{\#}P < 0.01$, as compared with Ctr-GFP-ADSC group). IOD analysis of immunocytochemical images showed a higher CX3CR1 protein expression level in CX3CR1-GFP-ADSCs (**C,D**, scale bar = 100 μm; $^{*}P < 0.05$, as compared with ADSC group, IOD, integrated optical density).

Overexpression of CX3CR1 Augments ADSC Migration *in vitro*

Transwell migration assay was used to detect the chemotactic movements of ADSCs toward fractalkine/FKN. The results showed that the number of ADSCs migrated to the bottom of chamber was significantly increased with the elevated concentrations of fractalkine/FKN (**Figures 4A,B**). So FKN with the concentration of 200 ng/ml was loaded in the lower chamber in the following transwell migration assays to detect the migration ability of CX3CR1-GFP-ADSCs. The upper chamber was filled with (1) untransfected ADSCs, (2) Ctr-GFP-ADSCs, and (3) Ctr-GFP-ADSCs, and then the number of migrated cells toward FKN was compared. Finally, the augmented *in vitro* migration ability of CX3CR1-GFP-ADSCs was confirmed, as it migrated more efficiently toward FKN compared to untransfected ADSCs ($P < 0.05$). However, there were no statistically significant differences in the migration rate between Ctr-GFP-ADSCs and untransfected ADSCs (**Figures 4C,D**).

Overexpression of CX3CR1 Augments ADSCs Homing to the Hemorrhagic Brain

Most of the transplanted cells were distributed throughout the transplant area and survived on the 3rd day after transplantation (**Figure 5A**). Few ADSCs migrated to the lesion site over comparatively short distances. In contrast, more cells were seen to migrate to the target site in the CX3CR1-GFP-ADSC group as compared to the Ctr-GFP-ADSC group, and the distance of migration was comparatively longer (**Figures 5B,C**). We also detected the immunological response after transplantation. It was found that there was no obvious microglial activation against rat-derived ADSCs (**Supplementary Figure S1**).

ADSCs Overexpressing CX3CR1 Promote Functional Recovery After ICH

At day 21 after cell transplantation, the mice in both Ctr-GFP-ADSC and CX3CR1-GFP-ADSC groups had a tendency to sense

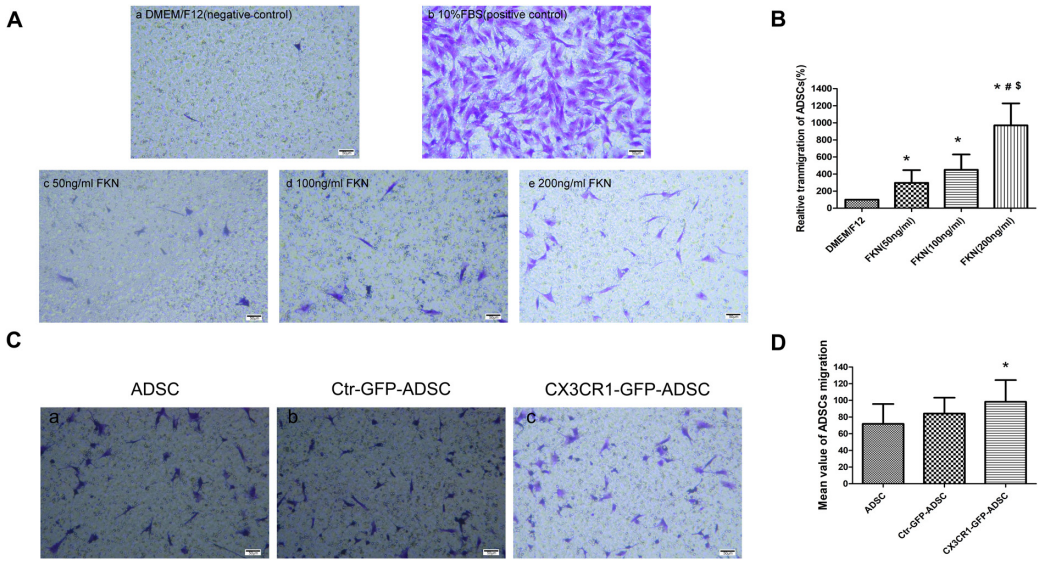

FIGURE 4 | *In vitro* transwell migration assay. Chemotactic movements of ADSCs toward fractalkine/FKN *in vitro* **(A)**. The lower compartment was filled with 600 μl DMEM/F12 (negative control) **(a)**, 10% FBS (positive control) **(b)**, 50 ng/ml FKN **(c)**, 100 ng/ml FKN **(d)**, and 200 ng/ml FKN **(e)** in DMEM/F12. The upper chamber were cell suspensions of ADSCs (2.3–2.4 × 10^4 cells/200 μl). It was found that the number of ADSCs directed migration to the bottom of chamber increased significantly with the increase of the concentration of fractalkine/FKN (**B**, relative transmigration of ADSCs = migration number of experimental group/migration number of negative control group,$^*P < 0.01$, as compared with DMEM/F12 group; $^{\#}P < 0.05$ as compared with FKN (50 ng/ml) group; $^{\$}P < 0.01$, as compared with FKN (100 ng/ml) group. *In vitro* migration ability of ADSCs after overexpressing CX3CR1 **(C)**. There were totally three groups: Ctr-GFP-ADSCs, CX3CR1-GFP-ADSCs, and untransfected ADSCs. The corresponding ADSCs (4 × 10^4 cells/200 μl) were placed in the upper chamber, and the lower chamber was loaded with 200 ng/ml FKN in the DMEM/F12 solution. The results showed that compared with untransfected ADSCs, CX3CR1 – GFP – ADSCs migrated more toward FKN (**D**, $^*P < 0.01$, as compared with ADSC group).

and remove stickers earlier and faster than those in the PBS group, as indicated by adhesive removal test (**Figures 5Da,b** and **Table 1**, $0.05 < P < 0.1$). In the cylinder test, scores were lower in CX3CR1-GFP-ADSC group than PBS group on days 7 post-transplantation, but no difference was observed between the Ctr-GFP-ADSC and PBS group (**Figure 5Dc** and **Table 1**, $P < 0.05$).

ADSCs Overexpressing CX3CR1 Reduce ICH-Induced Cell Death

The results of Western blot analysis revealed that anti-apoptotic protein bcl-2 expression level was significantly higher ($P < 0.05$) in the cell transplantation group (i.e., Ctr-GFP-ADSC and CX3CR1-GFP-ADSC groups) than that in the PBS group. However, no significant difference was observed between the two cell transplantation groups (**Figures 6A,B**). Meanwhile, the expression level of pro-apoptotic protein caspase-3 was significantly decreased ($P < 0.05$) in the CX3CR1-GFP-ADSC group compared to Ctr-GFP-ADSC and PBS groups (**Figures 6A,B**). TUNEL assay showed significantly reduced number of apoptotic cells in the cell transplantation groups compared to the PBS group ($P < 0.01$). Similarly, a significant difference ($P < 0.05$) was observed between Ctr-GFP-ADSC group and CX3CR1-GFP-ADSC group with respect to the apoptosis rate (**Figures 6C,D**). In addition, we also detected the hematoma volume in different groups. TTC staining showed that reduced volumes of hematoma were seen in both cell transplantation groups, but no difference was observed between the Ctr-GFP-ADSC and CX3CR1-GFP-ADSC group (**Supplementary Figure S2**).

DISCUSSION

Fractalkine/FKN, or CX3CL1, is the only member of CX3C subfamily of chemokines with two isoforms (Poniatowski et al., 2017). The membrane-bounded form of fractalkine is related to the adhesive effects, while the soluble form enhances the recruitment and activation of inflammatory cells (Réaux-Le Goazigo et al., 2013). Unlike most chemokine peptides, fractalkine can be expressed in non-hematopoietic tissues, including brain, kidney, lung, and heart. In particular, fractalkine is constitutively expressed in the CNS at relatively high levels, which produced mainly by neurons and astrocytes (Harrison et al., 1998; Re and Przedborski, 2006; Sciumè et al., 2010; Réaux-Le Goazigo et al., 2013). Meanwhile, its unique receptor CX3CR1, is primarily expressed on microglia (Donohue et al., 2012; Réaux-Le Goazigo et al., 2013). Previous studies reported that cerebrospinal fluid levels of soluble fractalkine are elevated in patients with traumatic brain injury and inflammatory brain diseases (Kastenbauer et al., 2003; Rancan et al., 2004). Similarly, increased serum levels of fractalkine have been reported in multiple sclerosis and systemic lupus erythematosus with neuropsychiatric involvement (Kastenbauer et al., 2003; Yajima et al., 2005). Here, we firstly detect the dynamic

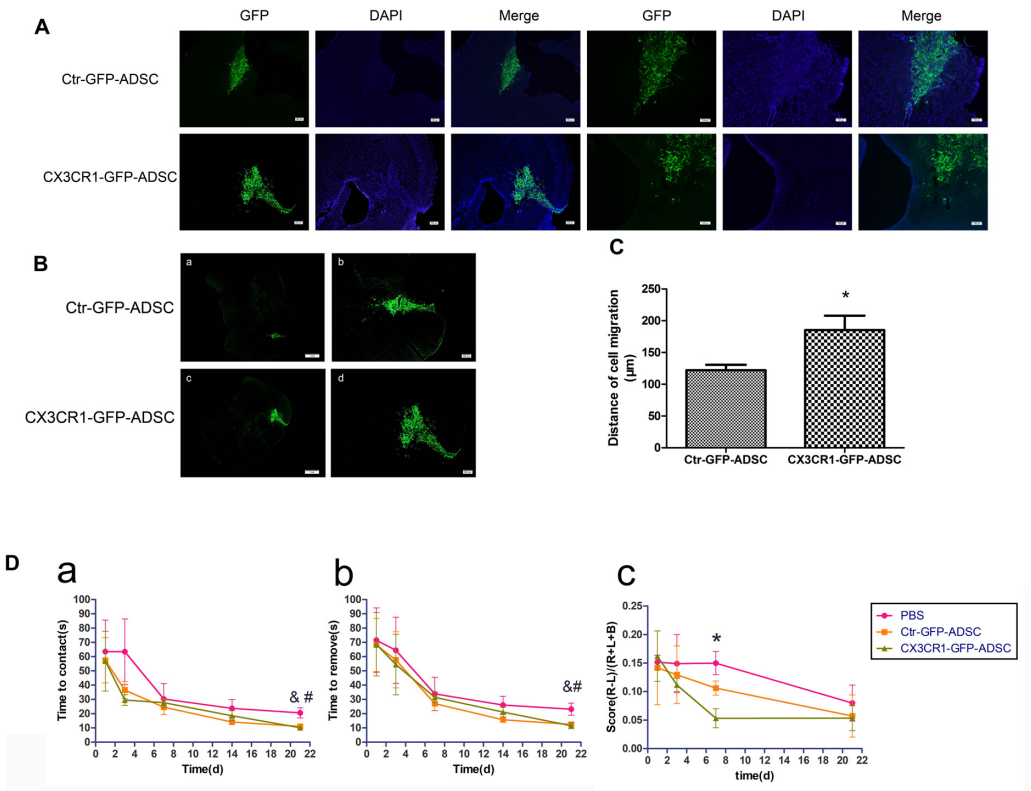

FIGURE 5 | Three days after transplantation, most of cells were distributed near the transplantation site (**A**, scale bar = 200 μm, 100 μm). Compared with Ctr-GFP-ADSC group, more CX3CR1 – GFP – ADSCs migrated toward the lesion loci (**B**, scale bar = 1 mm, 200 μm), and the distance of migration was comparatively longer (**C**, $^{*}P < 0.05$, as compared with Ctr-GFP-ADSC group). Adhesive removal test and cylinder test was use to assess functional recovery after cell transplantation in ICH **(D)**. Mice in both cell transplantation groups had a tendency to sense and remove stickers faster in the affected extremity on the 21st day after transplantation (**a**, time to contact the stickers in the left forepaw; **b**, time to remove the stickers in the left forepaw, $n = 7$ each group, $^{\&}P < 0.1$, Ctr-GFP-ADSC group vs. PBS group; $^{\#}P < 0.1$, CX3CR1-GFP-ADSC group vs. PBS group). In the cylinder test, scores were lower in CX3CR1-GFP-ADSC group than PBS group on days 7 post-transplantation, but no difference was observed between the Ctr-GFP-ADSC and PBS group (**c**, the final scores to assess forelimb preference and asymmetry, $n = 7$ each group, $^{*}P < 0.05$, CX3CR1-GFP-ADSC group vs. PBS group).

changes of fractalkine in brain tissue homogenates after ICH. We found that the levels of fractalkine can be increased at early time points, with a peak on the 3rd day after ICH. Despite controversies over the neuroprotective and neurotoxic roles of fractalkine (Donohue et al., 2012; Réaux-Le Goazigo et al., 2013), it is of great significance to study the dynamic changes of fractalkine expression after CNS diseases or injury. It's known that elevated fractalkine can attract endogenous or exogenous CX3CR1-expressing cells to migrate toward lesion loci. Consequently, studying the dynamic change of fractalkine can help to decide the time point of cell transplantation so that the grafting efficiency of stem cell therapy might be further improved through modifying infused cells or internal microenvironment. In addition, fractalkine expression has been considered as an essential biomarker in predicting the severity and prognosis of diseases (Kim et al., 2008; Donohue et al., 2012; Grosse et al., 2014).

Stem cell therapy is a promising therapeutic strategy for neurological diseases. It is generally believed that an adequate number of stem cells homing and migrating toward lesion site is important for efficient cell transplantation (Chavakis et al., 2008; Karp and Leng, 2009). Although infused cells tend to migrate to the lesion site, the decreased rate of cell homing, retention and survival can be the major limitations (Karp and Leng, 2009; Emmanouil Chavakis, 2011; Tang et al., 2015). MSC homing has been first defined by Karp and Leng (2009), as the arrest of MSCs within the vasculature of a tissue followed by transmigration across the endothelium. Recently, Nitzsche et al. (2017) expanded the definition of MSC homing to non-systemic and systemic homing according to MSC administration routes. However, the exact mechanisms underlying the homing and migration of MSCs are not fully understood. It is proposed that systemic homing require a coordinated multistep process involving ingress to the circulation, extravasation at the lesion vicinity, and interstitial migration toward the target site. For non-systemic homing, locally infused MSCs directly possess interstitial migration following activation and polarization (Chavakis et al., 2008; Emmanouil Chavakis, 2011; Nitzsche et al., 2017). Chemokines play an important role during the process of cell migration. In this study, we found that the expression level of fractalkine increased after ICH, and different passages of ADSCs express its receptor CX3CR1. Besides, the

TABLE 1 | The effects of ADSCs transplantation on functional recovery following intracerebral hemorrhage.

A. Adhesive removal test

Variants	Group	Days after transplantation				
		Day 1	Day 3	Day 7	Day 14	Day 21
Time to contact in the left(s)	PBS	63.57 ± 22.03	63.43 ± 23.06	30.29 ± 10.87	23.71 ± 6.19	20.57 ± 3.58
	Ctr-GFP-ADSC	57.43 ± 15.85	36.57 ± 6.08	24.57 ± 5.20	14.14 ± 1.44	11.00 ± 0.98*
	CX3CR1-GFP-ADSC	56.86 ± 20.95	29.57 ± 3.76	27.71 ± 3.15	18.57 ± 3.54	10.14 ± 1.86*
Time to remove in the left(s)	PBS	71.57 ± 22.60	64.43 ± 23.23	33.86 ± 11.66	26.00 ± 6.24	23.14 ± 4.20
	Ctr-GFP-ADSC	68.14 ± 18.54	57.71 ± 19.69	27.00 ± 5.00	15.71 ± 1.92	12.43 ± 1.11*
	CX3CR1-GFP-ADSC	68.71 ± 22.26	54.43 ± 21.22	31.43 ± 3.77	21.14 ± 3.41	11.57 ± 2.00*
Time to contact in the right(s)	PBS	20.86 ± 2.90	14.71 ± 3.08	11.57 ± 2.03	9.29 ± 0.64	6.29 ± 0.57
	Ctr-GFP-ADSC	19.14 ± 2.13	14.57 ± 3.30	11.86 ± 1.87	9.14 ± 1.99	7.29 ± 1.15
	CX3CR1-GFP-ADSC	19.00 ± 2.73	13.86 ± 2.51	11.14 ± 1.53	10.43 ± 2.18	7.29 ± 1.15
Time to remove in the right(s)	PBS	23.43 ± 3.21	20.43 ± 2.79	13.57 ± 2.17	11.14 ± 0.70	7.71 ± 0.97
	Ctr-GFP-ADSC	22.00 ± 2.73	18.43 ± 3.26	14.71 ± 2.99	10.71 ± 2.17	8.29 ± 1.34
	CX3CR1-GFP-ADSC	22.86 ± 4.75	18.00 ± 2.40	14.86 ± 3.38	12.14 ± 2.31	9.00 ± 1.62

B. Cylinder test

Variants	Group	Days after transplantation			
		Day 1	Day 3	Day 7	Day 21
Forelimb preference and asymmetry final scores	PBS	0.15 ± 0.01	0.15 ± 0.05	0.15 ± 0.02	0.08 ± 0.03
	Ctr-GFP-ADSC	0.14 ± 0.06	0.13 ± 0.05	0.11 ± 0.01	0.06 ± 0.04
	CX3CR1-GFP-ADSC	0.16 ± 0.04	0.11 ± 0.01	0.05 ± 0.02#	0.05 ± 0.02

*$P < 0.1$ compared to PBS group; #$P < 0.05$ compared to PBS group.

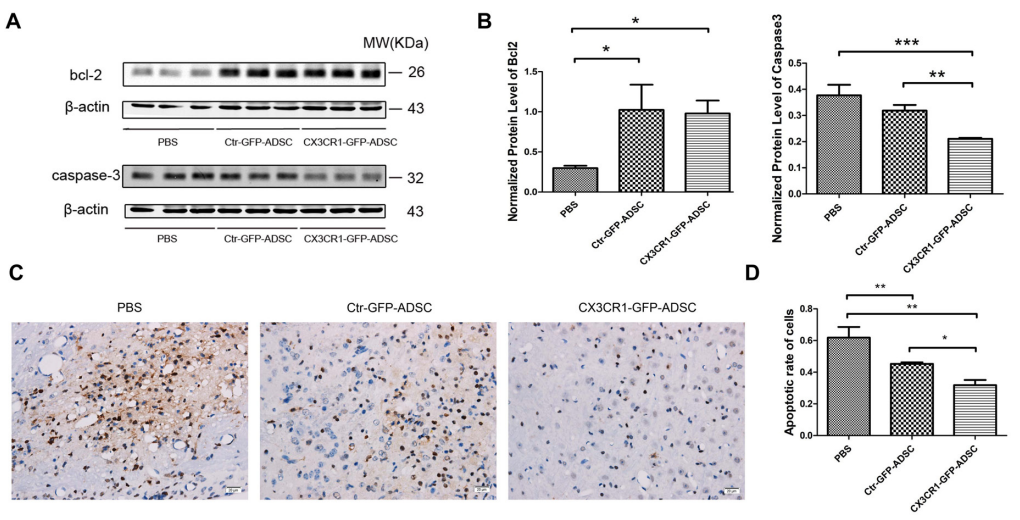

FIGURE 6 | Western blot showed that both cell transplantation group could reduce the expression of bcl-2, while the CX3CR1-GFP-ADSC group could more significantly lower the expression of caspase-3 compared to Ctr-GFP-ADSC and PBS group (**A,B**, *$P < 0.05$; **$P < 0.01$; ***$P < 0.001$). TUNEL staining showed that both cell transplantation groups could reduce the apoptosis rate of the foci (**C**, scale bar = 20 μm), and a lower apoptosis rate was found in the CX3CR1-GFP-ADSC group (**D**, *$P < 0.05$; **$P < 0.01$).

chemotactic movements of ADSCs toward fractalkine have been confirmed *in vitro*. So, we want to detect whether ADSCs overexpressing CX3CR1 could migrate more to the hemorrhagic site to achieve a higher therapeutic efficiency with the same former transplantation dosage.

Stem cell transplantation involves various delivery routes. Local infusion can be used to inject MSCs directly into the tissues of interest, but this strategy may not be clinically feasible due to its high invasiveness and diffusion limitations of nutrients and oxygen (Karp and Leng, 2009). Intravenous delivery has the

advantages of being more convenient, less invasive and much safer process than intrathecal or intracerebral administration (Lanza et al., 2009), but the MSCs homing is limited. It's reported that a high engraftment rate might be achieved by intra-arterial delivery, through the bypassing of filtration organs (Walczak et al., 2008). It still seems unclear whether systemically infused MSCs can actively migrate across BBB. MSCs were found to transmigrate across the brain microvascular endothelial cells monolayers *in vitro* through the transient intercellular gaps between them, but the endothelial cell monolayers do not fully recapitulate the *in vivo* BBB properties (Matsushita et al., 2011). In this study, we applied intracortical transplantation method to preliminarily investigate the short-term distribution and migration ability of CX3CR1 overexpressing ADSCs. Since the site of transplantation is relatively superficial, it is conducive to oxygen and nutrition diffusion. In addition, the short distance from the injection site to the injury center is favorable for observing the migration of cells.

The stable overexpression of CX3CR1 ADSCs (CX3CR1-GFP-ADSCs) were established with lentivirus transfection. Our findings demonstrated that the *in vitro* migration ability of ADSCs was increased after overexpressing CX3CR1. Additionally, the infused cells could survive until day 3 after transplantation, and a small part of ADSCs could migrate to the hemorrhagic brain site. In this study, CX3CR1-GFP-ADSC group showed better efficiency as compared to Ctr-GFP-ADSC group, with respect to the number of cells migrate toward the target region and their migration distances. There are various strategies to improve the migration ability of stem cells up to now (Li et al., 2017). And genetic manipulation remains one of the stable and efficient methods to improve their migration and mobility. However, the risk of malignant transformation and time-consuming should be noticed during the process (Liu et al., 2014). The ultimate aim of this study is to achieve increased homing and engraftment of MSCs by using lower or the same dosage of transplanted cells, in order to decrease the costs and duration of cell preparation (Maijenburg et al., 2012; Li et al., 2017). Interestingly, we observed the positive effects of ADSCs overexpressing CX3CR1 in reducing neuronal apoptosis and improving functional recovery after ICH. A tendency of improved sensory and motor functions and reduced expression of caspase-3 and increased expression of bcl-2 in CX3CR1-GFP-ADSC transplantation group were found in our research. Furthermore, a lower apoptosis rate around the foci was observed in CX3CR1-GFP-ADSC group as compared to Ctr-GFP-ADSC group. However, there are some limitations for our study. We transplanted rat ADSCs to the mice in this experiment, and human ADSCs will be used in our later studies, which is closer to the actual clinical situation. In addition, we should observe for a longer time to determine whether the transplanted ADSCs have teratogenic effects.

CONCLUSION

In summary, ADSCs overexpressing CX3CR1 demonstrated an increased migration ability both *in vitro* and *in vivo*, and may improve therapeutic efficiency in the ICH model.

ETHICS STATEMENT

The study was carried out in accordance with the recommendations in the Guide for the Care and Use of Laboratory Animals of the National Institutes of Health. The protocol was approved by competent ethics committees at Huazhong University of Science and Technology.

AUTHOR CONTRIBUTIONS

GL and HY were responsible for the cellular and animal experiments. GL performed the ELISA, immunohistochemical staining, qRT-PCR, and cell transplantation experiments. HY was responsible for the animal model and preparation of frozen sections of brain tissues. GL and HD performed the Western blot experiments. GL and JW performed the behavioral tests. NL, PZ, YT, YH, YZ, CP, QL, and ZT were responsible for the conception or design of the work. QL and ZT drafted the work or revisited it critically. All authors approved the final version of the manuscript.

FUNDING

This work was supported by grants from the National Natural Science Foundation of China (Nos. 81471201 and 81171089).

SUPPLEMENTARY MATERIAL

The Supplementary Material for this article can be found online at: https://www.frontiersin.org/articles/10.3389/fnins.2019.00462/full#supplementary-material

FIGURE S1 | Microglial activation against rat-derived ADSCs around the injection site 3 days after transplantation (scale bar = 50 μm).

FIGURE S2 | TTC staining showed that reduced volumes of hematoma were seen in both cell transplantation groups, but no difference was observed between the Ctr-GFP-ADSC and CX3CR1-GFP-ADSC group (**A,B**, $n = 3$ each group, $^*P < 0.0001$).

REFERENCES

Arbab, A. S., Thiffault, C., Navia, B., Victor, S. J., Hong, K., Zhang, L., et al. (2012). Tracking of In-111-labeled human umbilical tissue-derived cells (hUTC) in a rat model of cerebral ischemia using SPECT imaging. *BMC Med. Imaging* 12:33. doi: 10.1186/1471-2342-12-33

Balami, J. S., and Buchan, A. M. (2012). Complications of intracerebral haemorrhage. *Lancet Neurol.* 11, 101–118. doi: 10.1016/S1474-4422(11)70264-2

Bedini, G., Bersano, A., Zanier, E. R., Pischiutta, F., and Parati, E. A. (2018). Mesenchymal stem cell therapy in intracerebral haemorrhagic stroke. *Curr. Med. Chem.* 25, 2176–2197. doi: 10.2174/0929867325666180111101410

Bouët, V., Freret, T., Toutain, J., Divoux, D., Boulouard, M., and Schumann-Bard, P. (2007). Sensorimotor and cognitive deficits after transient middle cerebral artery occlusion in the mouse. *Exp. Neurol.* 203, 555–567. doi: 10.1016/j.expneurol.2006.09.006

Bronckaers, A., Hilkens, P., Martens, W., Gervois, P., Ratajczak, J., Struys, T., et al. (2014). Mesenchymal stem/stromal cells as a pharmacological and therapeutic approach to accelerate angiogenesis. *Pharmacol. Therapeut.* 143, 181–196. doi: 10.1016/j.pharmthera.2014.02.013

Chavakis, E., Urbich, C., and Dimmeler, S. (2008). Homing and engraftment of progenitor cells: a prerequisite for cell therapy. *J. Mol. Cell Cardiol.* 45, 514–522. doi: 10.1016/j.yjmcc.2008.01.004

Chen, C., Chu, S., Liu, D., Zhang, Z., Kong, L., Zhou, X., et al. (2018). Chemokines play complex roles in cerebral ischemia. *Neurochem. Int.* 112, 146–158. doi: 10.1016/j.neuint.2017.06.008

Chen, J., Tang, Y. X., Liu, Y. M., Chen, J., Hu, X. Q., Liu, N., et al. (2012). Transplantation of adipose-derived stem cells is associated with neural differentiation and functional improvement in a rat model of intracerebral hemorrhage. *CNS Neurosci. Ther.* 18, 847–854. doi: 10.1111/j.1755-5949.2012.00382.x

De Becker, A., and Riet, I. V. (2016). Homing and migration of mesenchymal stromal cells: how to improve the efficacy of cell therapy? *World J. Stem Cells* 8, 73–87. doi: 10.4252/wjsc.v8.i3.73

Detante, O., Moisan, A. C., Dimastromatteo, J., Richard, M., Riou, L., Grillon, E., et al. (2009). Intravenous administration of 99mTc-HMPAO-Labeled human mesenchymal stem cells after stroke: in vivo imaging and biodistribution. *Cell Transplant.* 18, 1369–1379. doi: 10.3727/096368909X474230

Donohue, M. M., Cain, K., Zierath, D., Shibata, D., Tanzi, P. M., and Becker, K. J. (2012). Higher plasma fractalkine is associated with better 6-month outcome from ischemic stroke. *Stroke* 43, 2300–2306. doi: 10.1161/STROKEAHA.112.657411

Emmanouil Chavakis, A. S. D. (2011). Homing of progenitor cells to ischemic tissues. *Antioxid. Redox Sign.* 15, 967–980. doi: 10.1089/ars.2010.3582

Forcales, S. (2015). Potential of adipose-derived stem cells in muscular regenerative therapies. *Front. Aging Neurosci.* 7:123. doi: 10.3389/fnagi.2015.00123

Gimble, J. M., Bunnell, B. A., and Guilak, F. (2012). Human adipose-derived cells: an update on the transition to clinical translation. *Regen. Med.* 7, 225–235. doi: 10.2217/rme.11.119

Grosse, G. M., Tryc, A. B., Dirks, M., Schuppner, R., Pflugrad, H., Lichtinghagen, R., et al. (2014). The temporal dynamics of plasma fractalkine levels in ischemic stroke: association with clinical severity and outcome. *J. Neuroinflamm.* 11:74. doi: 10.1186/1742-2094-11-74

Guo, J., Zhang, H., Xiao, J., Wu, J., Ye, Y., Li, Z., et al. (2013). Monocyte chemotactic protein-1 promotes the myocardial homing of mesenchymal stem cells in dilated cardiomyopathy. *Int. J. Mol. Sci.* 14, 8164–8178. doi: 10.3390/ijms14048164

Gutiérrez-Fernández, M., Otero-Ortega, L., Ramos-Cejudo, J., Rodríguez-Frutos, B., Fuentes, B., and Díez-Tejedor, E. (2015). Adipose tissue-derived mesenchymal stem cells as a strategy to improve recovery after stroke. *Expert Opin. Biol. Th.* 15, 873–881. doi: 10.1517/14712598.2015.1040386

Harrison, J. K., Jiang, Y., Chen, S., Xia, Y., Maciejewski, D., McNamara, R. K., et al. (1998). Role for neuronally derived fractalkine in mediating interactions between neurons and CX3CR1-expressing microglia. *Proc. Natl. Acad. Sci. U.S.A.* 95, 10896–10901. doi: 10.1073/pnas.95.18.10896

Hu, Y., Liu, N., Zhang, P., Pan, C., Zhang, Y., Tang, Y., et al. (2016). Preclinical studies of stem cell transplantation in intracerebral hemorrhage: a systemic review and meta-analysis. *Mol. Neurobiol.* 53, 5269–5277. doi: 10.1007/s12035-015-9441-6

Karp, J. M., and Leng, T. G. (2009). Mesenchymal stem cell homing: the devil is in the details. *Cell Stem Cell* 4, 206–216. doi: 10.1016/j.stem.2009.02.001

Kastenbauer, S., Koedel, U., Wick, M., Kieseier, B. C., Hartung, H. P., and Pfister, H. W. (2003). CSF and serum levels of soluble fractalkine (CX3CL1) in inflammatory diseases of the nervous system. *J. Neuroimmunol.* 137, 210–217. doi: 10.1016/s0165-5728(03)00085-7

Kim, T. S., Lim, H. K., Lee, J. Y., Kim, D. J., Park, S., Lee, C., et al. (2008). Changes in the levels of plasma soluble fractalkine in patients with mild cognitive impairment and Alzheimer's disease. *Neurosci. Lett.* 436, 196–200. doi: 10.1016/j.neulet.2008.03.019

Konala, V. B., Mamidi, M. K., Bhonde, R., Das, A. K., Pochampally, R., and Pal, R. (2016). The current landscape of the mesenchymal stromal cell secretome: a new paradigm for cell-free regeneration. *Cytotherapy* 18, 13–24. doi: 10.1016/j.jcyt.2015.10.008

Kuramoto, Y., Takagi, T., Tatebayashi, K., Beppu, M., Doe, N., Fujita, M., et al. (2019). Intravenous administration of human adipose-derived stem cells ameliorates motor and cognitive function for intracerebral hemorrhage mouse model. *Brain Res.* 1711, 58–67. doi: 10.1016/j.brainres.2018.12.042

Lanza, C., Morando, S., Voci, A., Canesi, L., Principato, M. C., Serpero, L. D., et al. (2009). Neuroprotective mesenchymal stem cells are endowed with a potent antioxidant effect in vivo. *J. Neurochem.* 110, 1674–1684. doi: 10.1111/j.1471-4159.2009.06268.x

Li, G., Hu, Y., Chen, Y., Tang, Z., Li, G., Hu, Y., et al. (2017). Strategies to improve the migration of mesenchymal stromal cells in cell therapy. *Transl. Neurosci. Clin.* 3, 159–175. doi: 10.18679/cn11-6030_r.2017.025

Li, J., Guo, W., Xiong, M., Han, H., Chen, J., Mao, D., et al. (2015). Effect of SDF-1/CXCR4 axis on the migration of transplanted bone mesenchymal stem cells mobilized by erythropoietin toward lesion sites following spinal cord injury. *Int. J. Mol. Med.* 36, 1205–1214. doi: 10.3892/ijmm.2015.2344

Liu, L., Eckert, M. A., Riazifar, H., Kang, D., Agalliu, D., and Zhao, W. (2013). From blood to the brain: can systemically transplanted mesenchymal stem cells cross the blood-brain barrier? *Stem Cells Int.* 2013, 1–7. doi: 10.1155/2013/435093

Liu, X., Ye, R., Yan, T., Yu, S. P., Wei, L., Xu, G., et al. (2014). Cell based therapies for ischemic stroke: from basic science to bedside. *Prog. Neurobiol.* 115, 92–115. doi: 10.1016/j.pneurobio.2013.11.007

Longa, E. Z., Weinstein, P. R., Carlson, S., and Cummins, R. (1989). Reversible middle cerebral artery occlusion without craniectomy in rats. *Stroke* 20, 84–91. doi: 10.1161/01.str.20.1.84

Maijenburg, M. W., van der Schoot, C. E., and Voermans, C. (2012). Mesenchymal stromal cell migration: possibilities to improve cellular therapy. *Stem Cells Dev.* 21, 19–29. doi: 10.1089/scd.2011.0270

Matsushita, T., Kibayashi, T., Katayama, T., Yamashita, Y., Suzuki, S., Kawamata, J., et al. (2011). Mesenchymal stem cells transmigrate across brain microvascular endothelial cell monolayers through transiently formed inter-endothelial gaps. *Neurosci. Lett.* 502, 41–45. doi: 10.1016/j.neulet.2011.07.021

Mayer, S. A., and Rincon, F. (2005). Treatment of intracerebral haemorrhage. *Lancet Neurol.* 4, 662–672.

Miller, R. J., Rostene, W., Apartis, E., Banisadr, G., Biber, K., Milligan, E. D., et al. (2008). Chemokine action in the nervous system. *J. Neurosci.* 28, 11792–11795.

Neirinckx, V., Coste, C., Rogister, B., and Wislet-Gendebien, S. (2013). Concise review: adult mesenchymal stem cells, adult neural crest stem cells, and therapy of neurological pathologies: a state of play. *Stem Cells Transl. Med.* 2, 284–296. doi: 10.5966/sctm.2012-0147

Nitzsche, F., Muller, C., Lukomska, B., Jolkkonen, J., Deten, A., and Boltze, J. (2017). Concise review: MSC adhesion cascade-insights into homing and transendothelial migration. *Stem Cells* 35, 1446–1460. doi: 10.1002/stem.2614

Pan, C., Liu, N., Zhang, P., Wu, Q., Deng, H., Xu, F., et al. (2018). EGb761 Ameliorates neuronal apoptosis and promotes angiogenesis in experimental intracerebral hemorrhage via RSK1/GSK3β pathway. *Mol. Neurobiol.* 55, 1556–1567. doi: 10.1007/s12035-016-0363-8

Poniatowski, A. A., Wojdasiewicz, P., Krawczyk, M., Szukiewicz, D., Gasik, R., Kubaszewski, A., et al. (2017). Analysis of the role of CX3CL1 (Fractalkine) and its receptor CX3CR1 in traumatic brain and spinal cord injury: insight into recent advances in actions of neurochemokine agents. *Mol. Neurobiol.* 54, 2167–2188. doi: 10.1007/s12035-016-9787-4

Rabinstein, A. A. (2017). Intracerebral haemorrhage: no good treatment but treatment helps. *Lancet* 389, 575–576. doi: 10.1016/s0140-6736(17)30002-8

Rancan, M., Bye, N., Otto, V. I., Trentz, O., Kossmann, T., Frentzel, S., et al. (2004). The chemokine fractalkine in patients with severe traumatic brain injury and a mouse model of closed head injury. *J. Cereb. Blood Flow Metab.* 24, 1110–1118. doi: 10.1097/01.wcb.0000133470.91843.72

Re, D. B., and Przedborski, S. (2006). Fractalkine: moving from chemotaxis to neuroprotection. *Nat. Neurosci.* 9, 859–861. doi: 10.1038/nn0706-859

Réaux-Le Goazigo, A., Van Steenwinckel, J., Rostène, W., and Mélik Parsadaniantz, S. (2013). Current status of chemokines in the adult CNS. *Prog. Neurobiol.* 104, 67–92. doi: 10.1016/j.pneurobio.2013.02.001

Schäffler, A., and Büchler, C. (2007). Concise review: adipose tissue-derived stromal cells-basic and clinical implications for novel cell-based therapies. *Stem Cells* 25, 818–827. doi: 10.1634/stemcells.2006-0589

Sciumè, G., Soriani, A., Piccoli, M., Frati, L., Santoni, A., and Bernardini, G. (2010). CX3CR1/CX3CL1 axis negatively controls glioma cell invasion and is modulated by transforming growth factor-beta1. *Neuro-Oncology* 12, 701–710. doi: 10.1093/neuonc/nop076

Stamatovic, S. M., Keep, R. F., Kunkel, S. L., and Andjelkovic, A. V. (2003). Potential role of MCP-1 in endothelial cell tight junction 'opening': signaling via Rho and Rho kinase. *J. Cell Sci.* 116, 4615–4628. doi: 10.1242/jcs.00755

Sun, J., Wei, Z. Z., Gu, X., Zhang, J. Y., Zhang, Y., Li, J., et al. (2015). Intranasal delivery of hypoxia-preconditioned bone marrow-derived mesenchymal stem cells enhanced regenerative effects after intracerebral hemorrhagic stroke in mice. *Exp. Neurol.* 272, 78–87. doi: 10.1016/j.expneurol.2015.03.011

Tang, Y., Zhang, C., Wang, J., Lin, X., Zhang, L., Yang, Y., et al. (2015). MRI/SPECT/fluorescent tri-modal probe for evaluating the homing and therapeutic efficacy of transplanted mesenchymal stem cells in a rat ischemic stroke model. *Adv. Funct. Mater.* 25, 1024–1034. doi: 10.1002/adfm.201402930

Vahid-Ansari, F., Lagace, D. C., and Albert, P. R. (2016). Persistent post-stroke depression in mice following unilateral medial prefrontal cortical stroke. *Transl. Psychiat.* 6, e863. doi: 10.1038/tp.2016.124

Walczak, P., Zhang, J., Gilad, A. A., Kedziorek, D. A., Ruiz-Cabello, J., Young, R. G., et al. (2008). Dual-modality monitoring of targeted intraarterial delivery of mesenchymal stem cells after transient ischemia. *Stroke* 39, 1569–1574. doi: 10.1161/STROKEAHA.107.502047

Wei, L., Wei, Z. Z., Jiang, M. Q., Mohamad, O., and Yu, S. P. (2017). Stem cell transplantation therapy for multifaceted therapeutic benefits after stroke. *Prog. Neurobiol.* 157, 49–78. doi: 10.1016/j.pneurobio.2017.03.003

Xiao, L. K., Peng, L., Jian, F. Z., Wei, C., Wei, Y. Y., Nan, S., et al. (2016). Stromal derived factor-1/CXCR4 axis involved in bone marrow mesenchymal stem cells recruitment to injured liver. *Stem Cells Int.* 2016:8906945. doi: 10.1155/2016/8906945

Xu, L., Zhao, Y., Wang, M., Song, W., Li, B., Liu, W., et al. (2016). Defocused low-energy shock wave activates adipose tissue-derived stem cells in vitro via multiple signaling pathways. *Cytotherapy* 18, 1503–1514. doi: 10.1016/j.jcyt.2016.08.009

Xu, Y., Zeng, K., Han, Y., Wang, L., Chen, D., Xi, Z., et al. (2012). Altered expression of CX3CL1 in patients with epilepsy and in a rat Model. *The American J. Pathol.* 180, 1950–1962. doi: 10.1016/j.ajpath.2012.01.024

Yajima, N., Kasama, T., Isozaki, T., Odai, T., Matsunawa, M., Negishi, M., et al. (2005). Elevated levels of soluble fractalkine in active systemic lupus erythematosus: potential involvement in neuropsychiatric manifestations. *Arthritis Rheum.* 52, 1670–1675. doi: 10.1002/art.21042

Yang, K. L., Lee, J. T., Pang, C. Y., Lee, T. Y., Chen, S. P., Liew, H. K., et al. (2012). Human adipose-derived stem cells for the treatment of intracerebral hemorrhage in rats via femoral intravenous injection. *Cell Mol. Biol. Lett.* 17, 376–392. doi: 10.2478/s11658-012-0016-5

Zhang, Y., Liu, N., Tang, Y., Yang, E., Dong, S., Huang, M., et al. (2014). Efficient generation of neural stem cell-like cells from rat adipose derived stem cells after lentiviral transduction with green fluorescent protein. *Mol. Neurobiol.* 50, 647–654. doi: 10.1007/s12035-014-8638-4

Zhang, Y., Zheng, J., Zhou, Z., Zhou, H., Wang, Y., Gong, Z., et al. (2015). Fractalkine promotes chemotaxis of bone marrow-derived mesenchymal stem cells towards ischemic brain lesions through Jak2 signaling and cytoskeletal reorganization. *FEBS J.* 282, 891–903. doi: 10.1111/febs.13187

Zhu, J., Zhou, Z., Liu, Y., and Zheng, J. (2009). Fractalkine and CX3CR1 are involved in the migration of intravenously grafted human bone marrow stromal cells toward ischemic brain lesion in rats. *Brain Res.* 1287, 173–183. doi: 10.1016/j.brainres.2009.06.068

Conflict of Interest Statement: The authors declare that the research was conducted in the absence of any commercial or financial relationships that could be construed as a potential conflict of interest.

Copyright © 2019 Li, Yu, Liu, Zhang, Tang, Hu, Zhang, Pan, Deng, Wang, Li and Tang. This is an open-access article distributed under the terms of the Creative Commons Attribution License (CC BY). The use, distribution or reproduction in other forums is permitted, provided the original author(s) and the copyright owner(s) are credited and that the original publication in this journal is cited, in accordance with accepted academic practice. No use, distribution or reproduction is permitted which does not comply with these terms.

frontiers in Neurology

MINI REVIEW
published: 08 May 2019
doi: 10.3389/fneur.2019.00493

Dipeptidyl Peptidase-4 Inhibitors for the Potential Treatment of Brain Disorders; A Mini-Review With Special Focus on Linagliptin and Stroke

Vladimer Darsalia[1], Odd Erik Johansen[2], Grazyna Lietzau[1], Thomas Nyström[1], Thomas Klein[3] and Cesare Patrone[1]**

[1] Department of Clinical Science and Education, Södersjukhuset, Internal Medicine, Karolinska Institutet, Stockholm, Sweden, [2] Boehringer Ingelheim, Asker, Norway, [3] Boehringer Ingelheim Pharma GmbH & Co. KG, Biberach, Germany

Cerebral stroke is a leading cause of death and persistent disability of elderly in the world. Although stroke prevention by targeting several risk factors such as diabetes and hypertension has decreased the stroke incidence, the total number of strokes is increasing due to the population aging and new preventive therapies are needed. Moreover, post-stroke acute pharmacological strategies aimed to reduce stroke-induced brain injury have failed in clinical trials despite being effective in animal models. Finally, approximately 30% of surviving stroke patients do not recover from stroke and remain permanently dependent on supportive care in activities of daily living. Therefore, strategies to improve stroke recovery in the post-acute phase are highly needed. Linagliptin is a dipeptidyl peptidase-4 inhibitor which is clinically approved to reduce hyperglycemia in type 2 diabetes. The regulation of glycemia by dipeptidyl peptidase-4 inhibition is mainly achieved by preventing endogenous glucagon-like peptide-1 (GLP-1) degradation. Interestingly, linagliptin has also shown glycaemia-independent beneficial effects in animal models of stroke, Parkinson's disease and Alzheimer's disease. In some case the preclinical data have been supported with some clinical data. Although potentially very interesting for the development of new strategies against stroke and neurodegenerative disorders, the mode of action of linagliptin in the brain is still largely unknown and seems to occur in a GLP-1R-independent manner. The purpose of this mini-review is to summarize and discuss the recent experimental and clinical work regarding the effects of linagliptin in the central nervous system, with special emphasis on acute neuroprotection, stroke prevention and post-stroke recovery. We also highlight the main questions in this research field that need to be addressed in clinical perspective.

Keywords: dipeptidyl peptidase-4 inhibitors, linagliptin, stroke, stroke recovery, neuroprotection

OPEN ACCESS

Edited by:
Gregory Jaye Bix,
University of Kentucky, United States

Reviewed by:
Richard F. Keep,
University of Michigan, United States
Guohua Xi,
University of Michigan Health System, United States

****Correspondence:***
Vladimer Darsalia
vladimer.darsalia@ki.se
orcid.org/0000-0002-6693-934X
Cesare Patrone
cesare.patrone@ki.se
orcid.org/0000-0003-0470-4606

Specialty section:
This article was submitted to Stroke, a section of the journal Frontiers in Neurology

Received: *12 March 2019*
Accepted: *23 April 2019*
Published: *08 May 2019*

Citation:
Darsalia V, Johansen OE, Lietzau G, Nyström T, Klein T and Patrone C (2019) Dipeptidyl Peptidase-4 Inhibitors for the Potential Treatment of Brain Disorders; A Mini-Review With Special Focus on Linagliptin and Stroke. Front. Neurol. 10:493. doi: 10.3389/fneur.2019.00493

INTRODUCTION

Stroke is a highly prevalent condition and a major cause of death and disabilities (1–5). Globally, 15 million people suffer a stroke every year with up to a 40% death rate (6). Of the surviving patients, up to 30% remain permanently disabled and require assistance in activities of daily living (5). In recent years, the incidence and mortality rates of stroke have significantly declined in high-income

countries (4, 7). The decrease in stroke incidence is probably due to targeted intervention programs against major stroke risk factors such as type 2 diabetes (T2D), obesity, smoking, sedentary lifestyle, hypertension, and alcohol abuse (8), while the decrease in mortality rate and disability could be attributed to faster intervention by thrombolytics and/or clot removal surgery resulting in blood flow restoration which minimize stroke damage (9). However, there is a significant geographic variations of stroke burden (10), and the total number of strokes and associated disability burden have substantially increased due to the increase of global population and life expectancy (4, 7). For instance, in Europe the number of elderly is projected to increase by 35% by 2050 (11). Thus, the total number of stroke cases is unlikely to decrease, unless more advanced preventive and/or curative strategies will be developed.

Potential future approaches to reduce acute stroke damage that have been investigated over the last decades are therapeutic hypothermia and pharmacological neuroprotection (12, 13). However, neither of these strategies have seen successful translation into clinical practice. The major obstacle for this type of strategies is the rapid tissue death in ischemic core and the limited effective intervention time-window in the ischemic *penumbra* (14–16).

Pharmacological interventions of stroke aimed toward recovery to combat chronic post-stroke disabilities is also promising based on animal studies, although full translation from bench-to-bed remains to be achieved (17–20).

Recent research suggests that stroke therapeutics could be developed from diabetes research. In fact, several studies have shown that anti-diabetic drugs targeting the glucagon-like protein 1 receptor [(GLP-1-receptor agonists and dipeptidyl peptidase-4 inhibitors (DPP-4i)] can mediate anti-stroke efficacy in animal models, and has been suggested to decrease the incidence of stroke in some clinical studies [reviewed in (21, 22)]. These drugs are in clinical use for T2D and their robust safety profile suggest high potential for the possible repositioning into stroke therapies.

The aim of this review was to summarize the recent experimental and clinical data regarding the effects of DPP-4i (also named gliptins) in the central nervous system, with special emphasis on linagliptin and stroke. Specifically, we focused our discussion about the effects of DPP-4i in relation to stroke prevention, acute neuroprotection, and post-stroke recovery. We also highlighted the main gaps of knowledge that will need to be addressed in clinical perspective.

METHODS

This review is based on a literature search in Pubmed, or at the scientific conference websites of major international cardiology (e.g., ESC, ESC HF, ACC, or AHA) or diabetes (i.e., EASD or ADA) societies until Jan 31st 2019. Pubmed was searched using free-text terms and medical subject heading. A uniform search strategy was applied to Pubmed to identify the reported studies. The primary MeSH terms and keywords used were as follows: dipeptidyl peptidase 4 inhibitor, DPP IV, gliptins, linagliptin, stroke, ischemia, neuroprotection, Parkinson's, Alzheimer's, dementia, neurogenesis, and neuroplasticity. Studies were screened by title, abstract and full text.

LINAGLIPTIN'S PHARMACOLOGY

Linagliptin is a once daily oral DPP-4i launched in 2011 for the treatment of T2D. The IC_{50} of linagliptin on its primary target, DPP-4, is 1 nM, which makes it one of the most potent inhibitors within the class (23). The other DPP-4 inhibitors possess lower potency in the range of IC_{50} 7–95 nM. Linagliptin shows high selectivity for DPP-4, over other dipeptidyl peptidases and related proteases (such as DPP-8 and 9) Chemically the drug is based on an optimized and unique xanthine scaffold (See **Figure 1**) possessing very slow dissociation from the human DPP-4 enzyme ($k_{off} < 0.00002\ s^{-1}$). This extremely slow off-rate is the main factor for the high affinity (K_D =6.6 pM) and results in a prolonged drug-target residence time over several hours (24).

Following absorption, linagliptin is distributed into tissues with high DPP-4 expression, e.g., the kidney and liver. At low concentrations (< 1 nM), 99% of linagliptin is bound to soluble and circulating DPP-4 and elimination is low. In higher concentrations (>100 nM) plasma DPP-4 is saturated and protein binding decreases to 70–80%. That is one of the reasons why in contrast to other DPP-4 inhibitors with linear pharmacokinetics, linagliptin is unique in having non-linear pharmacokinetics in the therapeutic dose (5 mg, human dose) range. The linagliptin's binding characteristics were shown to be absent in DPP-4 deficient animals (25). Moreover, renal excretion of linagliptin at its therapeutic dose is <7%, which is unique in the DPP-4 inhibitor class, that are primarily eliminated via the kidney (26). Linagliptin further shows low interaction with Cytochrom P450 and high stability in human cytosolic

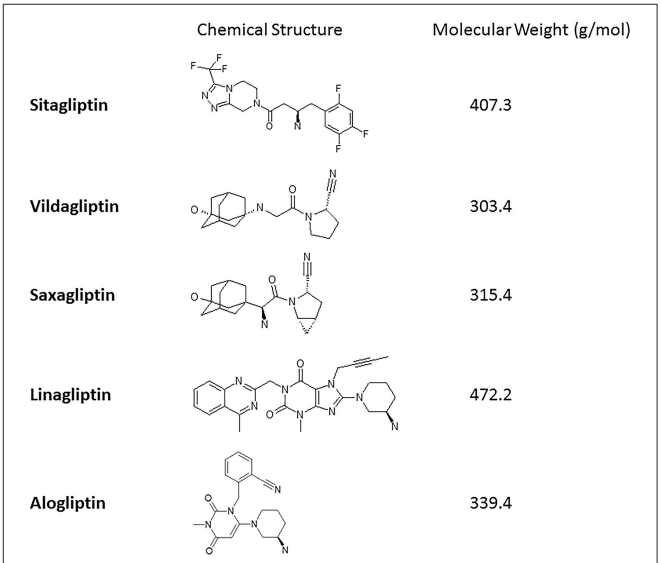

FIGURE 1 | The molecular structure and weight of selected DPP-4i.

and microsomal compartment, however linagliptin is a P-gp (P-glycoprotein) substrate (27) limiting penetration across the blood brain barrier (bbb) under normal conditions (28).

LINAGLIPTIN AND THE TREATMENT OF T2D

The concept behind DPP-4i for therapeutic use in T2D is based on the prolongation of the half-life of the incretins GLP-1 and glucose-dependent insulinotropic polypeptide (GIP), both secreted via specific endocrine gut cells following meal digestion. Incretins cause subsequently glucose-dependent insulin secretion for mainly postprandial glucose regulation. Further, DPP-4 inhibition suppresses glucagon secretion from α-cells. Numerous other substrates for DPP-4 have been described (29) such as SDF1α, GLP-2, NPY, substance P, which are activated or deactivated by the DPP-4 protease and play additional roles in inflammation, food intake, pain and vascular regulation, however less contribute to glucose control. Most clinically used DPP-4 inhibitors, like linagliptin, are once daily drugs because they show >80% inhibition of DPP-4 activity over 24 h. This is associated with the high increase of plasma GLP-1 and consistent reductions in elevated plasma glucose and HbA1c in various patient populations and across various background therapies (30). The recently completed cardiovascular outcome trial CARMELINA (CArdiovascular and Renal Microvascular outcomE study with LINAgliptin) confirmed the tolerability of linagliptin, and its cardiovascular (CV) safety, without any signal of heart failure (31). Due to an excretion primarily via the bile, linagliptin does not need dose adjustment, including in patients with T2D and impaired kidney function. CARMELINA proved safety in these renally impaired patients, and additionally showed a significant reduction in risk for progression albuminuria (32), which has not been assessed in a similar robust manner with the other members of the class of DPP-4 inhibitors.

LINAGLIPTIN MEDIATES BENEFICIAL EFFECTS IN EXPERIMENTAL MODELS OF BRAIN DISORDERS

Beside their glycemic properties, it has been recently reported that DPP-4 inhibitors can also affect the brain. For instance, studies have shown that DPP-4i exert neuroprotective actions in animal models of Parkinson's disease (PD) (33–35) and ongoing studies investigating the safety of intranasal delivery of the DPP-4i omarigliptin for the treatment of PD are ongoing (36). Moreover, D'Amico et al. (37) have shown that sitagliptin delayed AD-like pathology in a mouse model, and several studies confirmed these findings by using different DPP-4i inhibitors, including linagliptin [(38–41) and reviewed in (42)]. Other effects improving cognitive function, neuroplasticity and neurogenesis have been recently reported by employing vildagliptin (43), sitagliptin (44–48), and linagliptin (49). Furthermore, Hasegawa et al. (50) showed that linagliptin decreased hippocampal neuronal cell death and improved cognitive function in a model of aging. However, one study has also shown negative effects of sitagliptin in the brain, i.e., increased tau phosphorylation and insulin resistance (51). Finally, a recent study showed neuroprotection by sitagliptin in a model of brain trauma (52). In summary, although the passage of DPP-4i through the bbb in the damaged brain is undetermined and the mechanisms are unknown, the evidence of favorable effects of DPP-4i on brain complications is substantial.

LINAGLIPTIN PROVIDES ACUTE NEUROPROTECTION AFTER STROKE IN EXPERIMENTAL MODELS

It is difficult to study the potential efficacy of candidate drugs to reduce stroke risk using animal models. However, to determine the efficacy for acute neuroprotection, several animal models exist. A few studies have tested the potential efficacy of DPP-4i for acute neuroprotection and/or recovery after stroke. Moreover, acute ischemic stroke severity has been recently associated to changes in DPP-4 activity (53), suggesting that the regulation of this enzyme might have a therapeutic value.

Rohnert et al. (54) first showed that DPP-4 inhibition is neuroprotective in stroke via intracerebral administration of sitagliptin in the rat. We recently showed that 4 weeks per-oral pretreatment followed by 3 weeks post-stroke treatment with linagliptin reduced brain damage after stroke, in both normal and T2D/obese mice (55). Similar effects in non-diabetic rats were recently shown by Yang et al. (56) using alogliptin and by El-Sahar et al. (57) using vildagliptin. In the Yang et al. study, neuroprotection correlated to increased levels of brain BDNF. Moreover, DPP-4 inhibition by genistein resulted in similar findings (58). By using an experimental design consisting of chronic administration of linagliptin before and after stroke, Darsalia et al. (59) also showed that linagliptin-mediated neuroprotection against stroke occurred in correlation with increased neural stem cells proliferation (60) and, importantly, was not mediated by the GLP-1R.

A recent work by Ma et al. (61) has shown that the linagliptin treatment starting after stroke can decrease the stroke-induced brain damage in a rat model of transient cerebral ischemia induced by bilateral common carotid artery occlusion. Similar data using transient middle cerebral occlusion were reported by Chiazza et al. (62) who also showed that linagliptin improved functional recovery 3 days after stroke through the activation of the SDF-1α/CXCR4 pathway. Although one cannot rule out that the results of these two studies are due to the presence of linagliptin close to stroke time (suggesting acute neuroprotective effects), the data also suggest a pharmacological effect that goes beyond acute neuroprotection because the study design allowed extending the observation period from days to weeks after experimental stroke, thus evaluating the effects of linagliptin treatment in the post-stroke recovery phase. The likelihood of positive effects during the post-stroke recovery phase is also supported by the work of Darsalia et al. (59) showing that a single, acute *bolus* administration of linagliptin at stroke time was ineffective in reducing the brain damage. Furthermore, the potential role of DPP-4 inhibition in endogenous brain tissue

remodeling and repair processes after stroke has been recently suggested by Wesley et al. (63).

Whether DPP-4i leads to neuroprotection and promotes recovery after stroke by directly acting on neurons remains to be determined, although a recent *in vitro* study suggested direct neuroprotection in neural cells (64). However, additional cellular mechanisms may be involved. Indeed, Mi et al. (65) showed that linagliptin increases the *in vitro* proliferation of rat brain microvascular endothelial cells via the SIRT1/HIF-1α/VEGF pathway. Furthermore, recent works have shown that linagliptin improves cerebrovascular dysfunction and remodeling in a rat model of T2D, independent of glycemic control (66, 67).

Admission hyperglycemia is *per se* a negative prognostic marker for patients suffering acute ischemic stroke. Interestingly, hyperglycemia in patients without previously known diabetes is associated with a greater risk for poor outcome compared to patients with identified diabetes prior the stroke (68–70). Remarkably most of the effects reviewed here occurred independently from the regulation of glycemia in both normal and diabetic models, suggesting that the potential efficacy of DPP-4i to increase acute neuroprotection and/or recovery may be clinically relevant not only for the diabetic population under a DPP-4i-mediated therapy.

DPP-4 INHIBITORS AND STROKE PREVENTION WITH A FOCUS ON CARMELINA, A CARDIORENAL OUTCOME TRIAL WITH LINAGLIPTIN

The incidence of CV complications in T2D, including stroke, has declined substantially but it is still high (71). An increasing CV risk factor control attainment has probably contributed to this, and recently, it was demonstrated that maintaining control of glycated hemoglobin level, low-density lipoprotein cholesterol level, albuminuria, and blood pressure, as well as abstaining from smoking, was associated with no excess risk of CV death or stroke in T2D as compared to the general population (72). Interestingly, glycated hemoglobin was the strongest risk factor for stroke in this registry analysis.

Because, historically, there have been CV safety concerns regarding anti-diabetic drugs in the treatment of T2D, regulators in US and Europe focus specifically on this issue [(73) and http://www.ema.europa.eu/docs/en_GB/document_library/Scientific_guideline/2012/06/WC500129256.pdf], and as a response, fifteen CV outcome trials assessing 3 novel classes of antihyperglycemic therapies (i.e., DPP-4 inhibitors, GLP-1 receptor agonists, and SGLT-2 inhibitors) had been completed by end of 2018, of which none reported an increase in risk for major adverse CV events (MACE), whereas 6 agents have demonstrated CV benefits (74). Within the class of DPP-4i, four large CV outcome trials have been published till date for saxagliptin (75), sitagliptin (76), alogliptin (77), and linagliptin (32).

These trials have used the composite Major Adverse CV events (MACE); i.e., CV death, non-fatal myocardial infarction and stroke, with or without hospitalized unstable angina, as primary outcome. All trials have demonstrated CV safety, without incremental benefit for MACE, including no statistical significant difference in risk for non-fatal stroke. In the saxagliptin trial there was however a significantly higher numbers of patients hospitalized for heart failure (75), a signal also reported in the alogliptin trial (77). Due to this, the class has received a heart failure warning by the US Food and Drug Administration, especially if used in patients with high CV risk underlying heart and kidney disease (73). The linagliptin trial (CARMELINA®) (32) was designed to evaluate the CV safety and kidney outcomes of linagliptin in patients with T2D at high CV risk (75% of patients had prevalent kidney disease). Despite a frailer population, in comparison with the other DPP4i trials, linagliptin resulted in a non-inferior risk of MACE [compared to placebo added to standard care; hazard ratio 1.02 (95% CI: 0.89, 1.17)], including across a number of subgroups such as by sex and age, and did not affect the risk of heart failure [hazard ratio 0.90 (95% CI: 0.74, 1.08)] (31). Furthermore, the progression of albuminuria occurred less frequently in the linagliptin group [hazard ratio 0.86 (95% CI: 0.78, 0.95)] (32), but despite MACE safety, no significant protection for stroke [fatal/non-fatal stroke hazard ratio 0.91 (95% CI: 0.67, 1.23)] was observed. Nonetheless, their broad tolerability and the safety profile are today well-documented and a good choice for the pharmacology treatment of T2D. Importantly, it remains to be determined if these class of drugs can improve stroke outcome in the recovery phase (78) as it has been shown in several experimental studies. Interestingly, outcome trials with linagliptin (32, 79) will be exploring this question by determining the post-stroke functional outcome in a subgroup of patients hospitalized with stroke with T2D by using the modified rankin scale 3–6 months after stroke.

LINAGLIPTIN AND CLINICAL EFFECTS ON COGNITIVE OUTCOMES

Cognitive impairment, including mild cognitive impairment (MCI) and dementia, is increasingly recognized as an important T2D complication (80). High HbA1C concentration and glucose variability are negatively associated with subtle cognitive changes but the association is weak and more randomized controlled trials are needed (81). The underlying processes of cognitive dysfunction in T2D are largely unknown and till date, no pharmacological intervention has proven efficacious (82). Given that incretin therapies have emerged as a potential therapeutic lead for vascular brain injury, studying effects of these on cognitive outcomes are of interest. This is further supported by findings, in an observational study in elderly patients with T2D, that increased plasma DPP-4 activity is associated with elevated risk of MCI (83) and some small, and hypothesis generating, and underpowered, clinical observational studies, reporting some benefits of DPP-4i on clinical cognitive outcomes (84–86).

Both in CARMELINA, and in CAROLINA (a recently completed head-to-head study of linagliptin vs. the sulfonylurea glimepiride) cognitive studies with linagliptin have been completed, but none yet published. The CARMELINA-cognition and the CAROLINA-cognition sub-studies were integral parts of CARMELINA (32) and CAROLINA trials (87), respectively. Both cognition sub-studies aimed to test whether linagliptin prevents accelerated cognitive decline by applying the mini-mental state

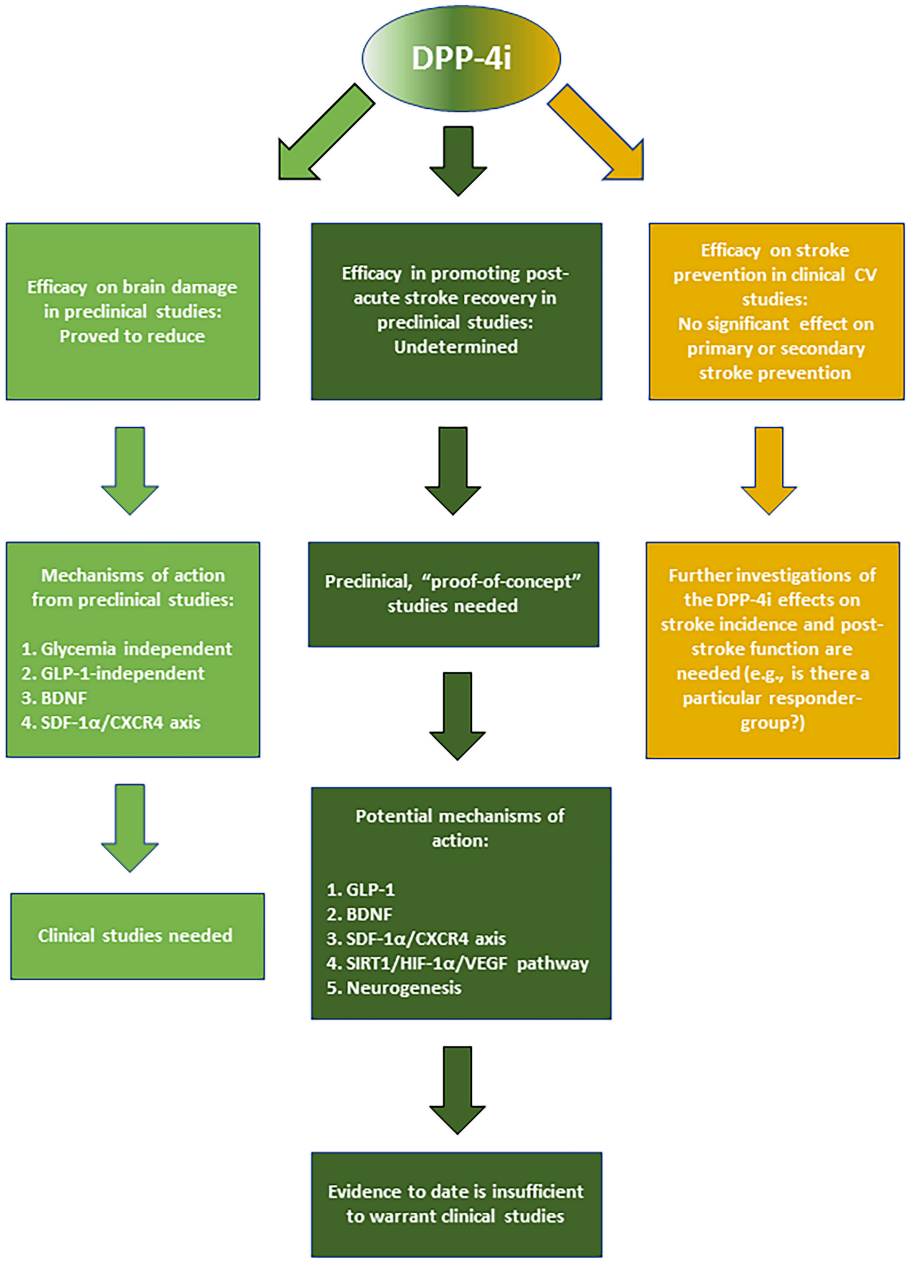

FIGURE 2 | Summary of the reported effects and mechanisms mediated by DPP-4i in stroke prevention, acute neuroprotection, and post-stroke recovery.

examination, as a measure of global cognitive function. In addition, more domain-sensitive composite measure of attention & executive functioning, using two additional tests: the Trail Making Test and the verbal fluency test, have been applied. The results of these sub-studies will be informative for refining the research area within this emerging and highly developing field.

FUTURE DIRECTIONS

Preclinical studies showing favorable effects of DPP-4i in several CNS disorders and stroke, encourage further research aiming to clinically reposition these diabetic drugs as active CNS-centric drugs. Clinical studies mainly investigating the safety of DPP4i have shown that these drugs are safe albeit no effect to decrease stroke incidence has been shown.

The clinical efficacy of acute neuroprotection after stroke is largely dependent on timely intervention within a very short therapeutic window (few hours from stroke onset), which is difficult to achieve. However, if the neuroprotective substance is systemically present at stroke time, the chances of minimizing stroke-induced tissue loss are significantly greater. The success of this strategy could be achieved in T2D patients (at high stroke

risk) who routinely take DPP-4i for the daily management of T2D. These patients could benefit from this treatment when suffering from stroke.

Another potential strategy to exploit the advantages of a DPP4i-based stroke therapy could be the promotion of stroke recovery and rehabilitation in the post-acute/chronic phase that could be theoretically applicable to all stroke patients. However, the potential of this approach has not yet been thoroughly investigated in animal studies and research in this field is highly needed, also in the clinical setting (78), including exploring whether there are differences in effects according to patient-characteristics; a field of emerging importance in the personalized medicine area. Indeed recent animal studies have shown pro-neurogenic (46), anti-inflammatory (54) and neuroplasticity (49) effects mediated by DPP-4i that could result beneficial in the post-stroke recovery phase and long-term clinical outcome.

Finally, studies are needed to understand the molecular mechanisms of DPP-4i in the brain, since the passage of DPP-4i through the bbb seems not to occur under normal conditions and after stroke is undetermined. Therefore, to study the mechanism of action of DPP4i in the brain substances with bbb permeability need to be synthesized in the future. Moreover, the systemic peripheral doses of GIP and GLP-1 after DPP-4i administration are low in comparison to GLP-1 agonists, e.g., in the pg range, and neuroprotection by linagliptin treatment has been shown to occur independently from GLP-1R (59). This suggest that alternative mechanisms are likely involved. Since the DPP-4 is an enzyme with over 40 known, biologically active substrates, many of which with proven CNS effects, the deeper understanding of how exactly DPP-4i regulate these substrates could lead to the identifications of new therapeutic targets in the CNS.

CONCLUSIONS

The demonstrated beneficial CNS effects in preclinical studies and the proven clinical safety of DPP-4i make them good candidates for their potential repositioning against stroke. While the data so far suggest that DPP-4i cannot reduce stroke risk, studies are needed to determine if T2D people who use them for daily T2D management could gain advantages in terms of reduced brain damage in the event of stroke. Both T2D and non-diabetic stroke patients could also benefit from the use of DPP-4i as post-stroke curative agents promoting recovery and rehabilitation in post-acute phase. However, more pre-clinical and clinical research is highly needed in this research field (See **Figure 2** for the summary of DPP-4i-mediated effects in stroke and potential mechanisms of action).

AUTHOR CONTRIBUTIONS

VD conceived and wrote the review. OJ wrote the Linagliptin and Clinical Effects on Cognitive Outcomes section and edited the manuscript. GL wrote the Introduction section. TN wrote and reviewed the DPP-4 Inhibitors and Stroke Prevention With a Focus on CARMELINA, a Cardiorenal Outcome Trial With Linagliptin section. TK conceived the review and wrote The Pharmacology of Linagliptin and Linagliptin and the Treatment of T2D sections. CP conceived, wrote, and coordinated the review.

FUNDING

Financial support in our laboratory is provided by the European Foundation for the Study of Diabetes (EFSD), the Swedish Research Council (2018-02483), the Swedish Heart-Lung Foundation (20160511), the Novo Nordisk foundation (NNF17OC0026924), Karolinska Institutet (Foundation for Geriatric Diseases), KI Stiftelser och Fonder, Stohnes Stiftelse, O. E. och Edla Johanssons Stiftelse, STROKE Riksförbundet, Gamla Tjänarinnor Stiftelse, and by the regional agreement on medical training and clinical research (ALF) between Stockholm County Council and the Karolinska Institutet. All foundations have provided funding that may also include publication costs.

REFERENCES

1. Thrift AG, Thayabaranathan T, Howard G, Howard VJ, Rothwell PM, Feigin VL, et al. Global stroke statistics. *Int J Stroke.* (2017) 12:13–32. doi: 10.1177/1747493016676285
2. Benjamin EJ, Muntner P, Alonso A, Bittencourt MS, Callaway CW, Carson AP, et al. Heart disease and stroke statistics−−2019 update: a report from the American Heart Association. *Circulation.* (2019) 139:e56–528. doi: 10.1161/CIR.0000000000000659
3. Bejot Y, Bailly H, Durier J, Giroud M. Epidemiology of stroke in Europe and trends for the 21st century. *Presse Med.* (2016) 45:e391–8. doi: 10.1016/j.lpm.2016.10.003
4. Feigin VL, Norrving B, Mensah GA. Global burden of stroke. *Circ Res.* (2017) 120:439–48. doi: 10.1161/CIRCRESAHA.116.308413
5. Ullberg T, Zia E, Petersson J, Norrving B. Changes in functional outcome over the first year after stroke: an observational study from the Swedish stroke register. *Stroke.* (2015) 46:389–94. doi: 10.1161/STROKEAHA.114.006538
6. WHO. *Global Atlas on Cardiovascular Disease Prevention and Control.* Geneva (2011). Available online at: https://www.who.int/cardiovascular_diseases/publications/atlas_cvd/en/ (accessed February, 2019).
7. Feigin VL, Forouzanfar MH, Krishnamurthi R, Mensah GA, Connor M, Bennett DA, et al. Global and regional burden of stroke during 1990–2010: findings from the Global Burden of Disease Study 2010. *Lancet.* (2014) 383:245–54. doi: 10.1016/S0140-6736(13)61953-4
8. Larsson SC, Akesson A, Wolk A. Primary prevention of stroke by a healthy lifestyle in a high-risk group. *Neurology.* (2015) 84:2224–8. doi: 10.1212/WNL.0000000000001637
9. Khandelwal P, Yavagal DR, Sacco RL. Acute ischemic stroke intervention. *J Am Coll Cardiol.* (2016) 67:2631–44. doi: 10.1016/j.jacc.2016.03.555
10. Kim AS, Johnston SC. Temporal and geographic trends in the global stroke epidemic. *Stroke.* (2013) 44:S123–5. doi: 10.1161/STROKEAHA.111.000067
11. United Nations DoEaSA. *Population Division, World Population Ageing—Highlights (ST/ESA/SER.A/397).* (2017). Available online at: http://www.un.org/en/development/desa/population/theme/ageing/WPA2017.shtml (accessed February, 2019).

12. Karnatovskaia LV, Wartenberg KE, Freeman WD. Therapeutic hypothermia for neuroprotection: history, mechanisms, risks, and clinical applications. *Neurohospitalist.* (2014) 4:153–63. doi: 10.1177/1941874413519802
13. Patel RAG, McMullen PW. Neuroprotection in the treatment of acute ischemic stroke. *Prog Cardiovasc Dis.* (2017) 59:542–8. doi: 10.1016/j.pcad.2017.04.005
14. Sena E, van der Worp HB, Howells D, Macleod M. How can we improve the pre-clinical development of drugs for stroke? *Trends Neurosci.* (2007) 30:433–9. doi: 10.1016/j.tins.2007.06.009
15. Cheng YD, Al-Khoury L, Zivin JA. Neuroprotection for ischemic stroke: two decades of success and failure. *NeuroRx.* (2004) 1:36–45. doi: 10.1602/neurorx.1.1.36
16. Minnerup J, Sutherland BA, Buchan AM, Kleinschnitz C. Neuroprotection for stroke: current status and future perspectives. *Int J f Mol Sci.* (2012) 13:11753–72. doi: 10.3390/ijms131011753
17. Roth S, Liesz A. Stroke research at the crossroads—where are we heading? *Swiss Med Wkly.* (2016) 146:w14329. doi: 10.4414/smw.2016.14329
18. Chollet F, Cramer SC, Stinear C, Kappelle LJ, Baron JC, Weiller C, et al. Pharmacological therapies in post stroke recovery: recommendations for future clinical trials. *J Neurol.* (2014) 261:1461–8. doi: 10.1007/s00415-013-7172-z
19. Viale L, Catoira NP, Di Girolamo G, Gonzalez CD. Pharmacotherapy and motor recovery after stroke. *Expert Rev Neurother.* (2018) 18:65–82. doi: 10.1080/14737175.2018.1400910
20. Yeo SH, Lim ZI, Mao J, Yau WP. Effects of central nervous system drugs on recovery after stroke: a systematic review and meta-analysis of randomized controlled trials. *Clin Drug Investig.* (2017) 37:901–28. doi: 10.1007/s40261-017-0558-4
21. Darsalia V, Klein T, Nystrom T, Patrone C. Glucagon-like receptor 1 agonists and DPP-4 inhibitors: anti-diabetic drugs with anti-stroke potential. *Neuropharmacology.* (2017) 136 (Pt B):280–6. doi: 10.1016/j.neuropharm.2017.08.022
22. Nauck MA, Meier JJ, Cavender MA, Abd El Aziz M, Drucker DJ. Cardiovascular actions and clinical outcomes with glucagon-like peptide-1 receptor agonists and dipeptidyl peptidase-4 inhibitors. *Circulation.* (2017) 136:849–70. doi: 10.1161/CIRCULATIONAHA.117.028136
23. Thomas L, Eckhardt M, Langkopf E, Tadayyon M, Himmelsbach F, Mark M. (R)-8-(3-amino-piperidin-1-yl)-7-but-2-ynyl-3-methyl-1-(4-methyl-quinazolin-2-ylm ethyl)-3,7-dihydro-purine-2,6-dione (BI 1356), a novel xanthine-based dipeptidyl peptidase 4 inhibitor, has a superior potency and longer duration of action compared with other dipeptidyl peptidase-4 inhibitors. *J Pharmacol Exp Ther.* (2008) 325:175–82. doi: 10.1124/jpet.107.135723
24. Schnapp G, Klein T, Hoevels Y, Bakker RA, Nar H. Comparative analysis of binding kinetics and thermodynamics of dipeptidyl peptidase-4 inhibitors and their relationship to structure. *J Med Chem.* (2016) 59:7466–77. doi: 10.1021/acs.jmedchem.6b00475
25. Retlich S, Withopf B, Greischel A, Staab A, Jaehde U, Fuchs H. Binding to dipeptidyl peptidase-4 determines the disposition of linagliptin (BI 1356)–investigations in DPP-4 deficient and wildtype rats. *Biopharm Drug Dispos.* (2009) 30:422–36. doi: 10.1002/bdd.676
26. Golightly LK, Drayna CC, McDermott MT. Comparative clinical pharmacokinetics of dipeptidyl peptidase-4 inhibitors. *Clin Pharmacokinet.* (2012) 51:501–14. doi: 10.1007/BF03261927
27. Ishiguro N, Shimizu H, Kishimoto W, Ebner T, Schaefer O. Evaluation and prediction of potential drug-drug interactions of linagliptin using *in vitro* cell culture methods. *Drug Metab Dispos.* (2013) 41:149–58. doi: 10.1124/dmd.112.048470
28. Fuchs H, Binder R, Greischel A. Tissue distribution of the novel DPP-4 inhibitor BI 1356 is dominated by saturable binding to its target in rats. *Biopharm Drug Dispos.* (2009) 30:229–40. doi: 10.1002/bdd.662
29. Gorrell MD. Dipeptidyl peptidase IV and related enzymes in cell biology and liver disorders. *Clin Sci.* (2005) 108:277–92. doi: 10.1042/CS20040302
30. Deeks ED. Linagliptin: a review of its use in the management of type 2 diabetes mellitus. *Drugs.* (2012) 72:1793–824. doi: 10.2165/11209570-000000000-00000
31. McGuire DK, Alexander JH, Johansen OE, Perkovic V, Rosenstock J, Cooper ME, et al. Linagliptin effects on heart failure and related outcomes in individuals with type 2 diabetes mellitus at high cardiovascular and renal risk in CARMELINA. *Circulation.* (2019) 139:351–61. doi: 10.1161/CIRCULATIONAHA.118.038352
32. Rosenstock J, Perkovic V, Johansen OE, Cooper ME, Kahn SE, Marx N, et al. Effect of linagliptin vs placebo on major cardiovascular events in adults with type 2 diabetes and high cardiovascular and renal risk: the CARMELINA randomized clinical trial. *JAMA.* (2018) 321:69–79. doi: 10.1001/jama.2018.18269
33. Badawi GA, Abd El Fattah MA, Zaki HF, El Sayed MI. Sitagliptin and liraglutide reversed nigrostriatal degeneration of rodent brain in rotenone-induced Parkinson's disease. *Inflammopharmacology.* (2017) 25:369–82. doi: 10.1007/s10787-017-0331-6
34. Abdelsalam RM, Safar MM. Neuroprotective effects of vildagliptin in rat rotenone Parkinson's disease model: role of RAGE-NFkappaB and Nrf2-antioxidant signaling pathways. *J Neurochem.* (2015) 133:700–7. doi: 10.1111/jnc.13087
35. Nassar NN, Al-Shorbagy MY, Arab HH, Abdallah DM. Saxagliptin: a novel antiparkinsonian approach. *Neuropharmacology.* (2015) 89:308–17. doi: 10.1016/j.neuropharm.2014.10.007
36. Ayoub BM, Mowaka S, Safar MM, Ashoush N, Arafa MG, Michel HE, et al. Repositioning of omarigliptin as a once-weekly intranasal anti-parkinsonian agent. *Sci Rep.* (2018) 8:8959. doi: 10.1038/s41598-018-27395-0
37. D'Amico M, Di Filippo C, Marfella R, Abbatecola AM, Ferraraccio F, Rossi F, et al. Long-term inhibition of dipeptidyl peptidase-4 in Alzheimer's prone mice. *Exp Gerontol.* (2010) 45:202–7. doi: 10.1016/j.exger.2009.12.004
38. Kosaraju J, Holsinger RM, Guo L, Tam KY. Linagliptin, a dipeptidyl peptidase-4 inhibitor, mitigates cognitive deficits and pathology in the 3xTg-AD mouse model of Alzheimer's disease. *Mol Neurobiol.* (2016) 54:6074–84. doi: 10.1007/s12035-016-0125-7
39. Kosaraju J, Murthy V, Khatwal RB, Dubala A, Chinni S, Muthureddy Nataraj SK, et al. Vildagliptin: an anti-diabetes agent ameliorates cognitive deficits and pathology observed in streptozotocin-induced Alzheimer's disease. *J Pharm Pharmacol.* (2013) 65:1773–84. doi: 10.1111/jphp.12148
40. Kosaraju J, Gali CC, Khatwal RB, Dubala A, Chinni S, Holsinger RM, et al. Saxagliptin: a dipeptidyl peptidase-4 inhibitor ameliorates streptozotocin induced Alzheimer's disease. *Neuropharmacology.* (2013) 72:291–300. doi: 10.1016/j.neuropharm.2013.04.008
41. Ma QH, Jiang LF, Mao JL, Xu WX, Huang M. Vildagliptin prevents cognitive deficits and neuronal apoptosis in a rat model of Alzheimer's disease. *Mol Med Rep.* (2018) 17:4113–9. doi: 10.3892/mmr.2017.8289
42. Angelopoulou E, Piperi C. DPP-4 inhibitors: a promising therapeutic approach against Alzheimer's disease. Ann Transl Med. (2018) 6:255. doi: 10.21037/atm.2018.04.41
43. Zhang DD, Shi N, Fang H, Ma L, Wu WP, Zhang YZ, et al. Vildagliptin, a DPP4 inhibitor, alleviates diabetes-associated cognitive deficits by decreasing the levels of apoptosis-related proteins in the rat hippocampus. *Exp Ther Med.* (2018) 15:5100–6. doi: 10.3892/etm.2018.6016
44. Dong Q, Teng SW, Wang Y, Qin F, Li Y, Ai LL, et al. Sitagliptin protects the cognition function of the Alzheimer's disease mice through activating glucagon-like peptide-1 and BDNF-TrkB signalings. *Neurosci Lett.* (2018) 696:184–90. doi: 10.1016/j.neulet.2018.12.041
45. Bachor TP, Marquioni-Ramella MD, Suburo AM. Sitagliptin protects proliferation of neural progenitor cells in diabetic mice. *Metab Brain Dis.* (2015) 30:885–93. doi: 10.1007/s11011-015-9656-2
46. Gault VA, Lennox R, Flatt PR. Sitagliptin, a dipeptidyl peptidase-4 inhibitor, improves recognition memory, oxidative stress and hippocampal

neurogenesis and upregulates key genes involved in cognitive decline. *Diab Obes Metab.* (2015) 17:403–13. doi: 10.1111/dom.12432
47. Tsai TH, Sun CK, Su CH, Sung PH, Chua S, Zhen YY, et al. Sitagliptin attenuated brain damage and cognitive impairment in mice with chronic cerebral hypo-perfusion through suppressing oxidative stress and inflammatory reaction. *J Hypertens.* (2015) 33:1001–13. doi: 10.1097/HJH.0000000000000529
48. Sakr HF. Effect of sitagliptin on the working memory and reference memory in type 2 diabetic Sprague-Dawley rats: possible role of adiponectin receptors 1. *J Physiol Pharmacol.* (2013) 64:613–23.
49. Lietzau G, Davidsson W, Ostenson CG, Chiazza F, Nathanson D, Pintana H, et al. Type 2 diabetes impairs odour detection, olfactory memory and olfactory neuroplasticity; effects partly reversed by the DPP-4 inhibitor Linagliptin. *Acta Neuropathol Commun.* (2018) 6:14. doi: 10.1186/s40478-018-0517-1
50. Hasegawa Y, Hayashi K, Takemoto Y, Cheng C, Takane K, Lin B, et al. DPP-4 inhibition with linagliptin ameliorates the progression of premature aging in klotho$^{-/-}$ mice. *Cardiovasc Diabetol.* (2017) 16:154. doi: 10.1186/s12933-017-0639-y
51. Kim DH, Huh JW, Jang M, Suh JH, Kim TW, Park JS, et al. Sitagliptin increases tau phosphorylation in the hippocampus of rats with type 2 diabetes and in primary neuron cultures. *Neurobiol Dis.* (2012) 46:52–8. doi: 10.1016/j.nbd.2011.12.043
52. DellaValle B, Brix GS, Brock B, Gejl M, Rungby J, Larsen A. Oral administration of sitagliptin activates CREB and is neuroprotective in murine model of brain trauma. *Front Pharmacol.* (2016) 7:450. doi: 10.3389/fphar.2016.00450
53. Baerts L, Brouns R, Kehoe K, Verkerk R, Engelborghs S, De Deyn PP, et al. Acute ischemic stroke severity, progression, and outcome relate to changes in dipeptidyl peptidase IV and fibroblast activation protein activity. *Transl Stroke Res.* (2017) 8:157–64. doi: 10.1007/s12975-016-0493-3
54. Rohnert P, Schmidt W, Emmerlich P, Goihl A, Wrenger S, Bank U, et al. Dipeptidyl peptidase IV, aminopeptidase N and DPIV/APN-like proteases in cerebral ischemia. *J Neuroinflamm.* (2012) 9:44. doi: 10.1186/1742-2094-9-44
55. Darsalia V, Ortsater H, Olverling A, Darlof E, Wolbert P, Nystrom T, et al. The DPP-4 inhibitor linagliptin counteracts stroke in the normal and diabetic mouse brain: a comparison with glimepiride. *Diabetes.* (2013) 62:1289–96. doi: 10.2337/db12-0988
56. Yang D, Nakajo Y, Iihara K, Kataoka H, Yanamoto H. Alogliptin, a dipeptidylpeptidase-4 inhibitor, for patients with diabetes mellitus type 2, induces tolerance to focal cerebral ischemia in non-diabetic, normal mice. *Brain Res.* (2013) 1517:104–13. doi: 10.1016/j.brainres.2013.04.015
57. El-Sahar AE, Safar MM, Zaki HF, Attia AS, Ain-Shoka AA. Sitagliptin attenuates transient cerebral ischemia/reperfusion injury in diabetic rats: implication of the oxidative-inflammatory-apoptotic pathway. *Life Sci.* (2015) 126:81–6. doi: 10.1016/j.lfs.2015.01.030
58. Rajput MS, Sarkar PD, Nirmal NP. Inhibition of DPP-4 activity and neuronal atrophy with genistein attenuates neurological deficits induced by transient global cerebral ischemia and reperfusion in streptozotocin-induced diabetic mice. *Inflammation.* (2017) 40:623–35. doi: 10.1007/s10753-017-0509-5
59. Darsalia V, Larsson M, Lietzau G, Nathanson D, Nystrom T, Klein T, et al. Gliptins-mediated neuroprotection against stroke requires chronic pre-treatment and is glucagon-like peptide-1 receptor independent. *Diab Obes Metab.* (2016) 18:537–41. doi: 10.1111/dom.12641
60. Darsalia V, Olverling A, Larsson M, Mansouri S, Nathanson D, Nystrom T, et al. Linagliptin enhances neural stem cell proliferation after stroke in type 2 diabetic mice. *Regul Pept.* (2014) 190–1:25–31. doi: 10.1016/j.regpep.2014.05.001
61. Ma M, Hasegawa Y, Koibuchi N, Toyama K, Uekawa K, Nakagawa T, et al. DPP-4 inhibition with linagliptin ameliorates cognitive impairment and brain atrophy induced by transient cerebral ischemia in type 2 diabetic mice. *Cardiovasc Diabetol.* (2015) 14:54. doi: 10.1186/s12933-015-0218-z
62. Chiazza F, Tammen H, Pintana H, Lietzau G, Collino M, Nystrom T, et al. The effect of DPP-4 inhibition to improve functional outcome after stroke is mediated by the SDF-1alpha/CXCR4 pathway. *Cardiovasc Diabetol.* (2018) 17:60. doi: 10.1186/s12933-018-0702-3
63. Wesley UV, Hatcher JF, Ayvaci ER, Klemp A, Dempsey RJ. Regulation of dipeptidyl peptidase IV in the post-stroke rat brain and *in vitro* ischemia: implications for chemokine-mediated neural progenitor cell migration and angiogenesis. *Mol Neurobiol.* (2017) 54:4973–85. doi: 10.1007/s12035-016-0039-4
64. Kornelius E, Lin CL, Chang HH, Li HH, Huang WN, Yang YS, et al. DPP-4 inhibitor linagliptin attenuates abeta-induced cytotoxicity through activation of AMPK in neuronal cells. *CNS Neurosci Ther.* (2015) 21:549–57. doi: 10.1111/cns.12404
65. Mi DH, Fang HJ, Zheng GH, Liang XH, Ding YR, Liu X, et al. DPP-4 inhibitors promote proliferation and migration of rat brain microvascular endothelial cells under hypoxic/high-glucose conditions, potentially through the SIRT1/HIF-1/VEGF pathway. *CNS Neurosci Ther.* (2018) 25:323–32. doi: 10.1111/cns.13042
66. Hardigan T, Yasir A, Abdelsaid M, Coucha M, El-Shaffey S, Li W, et al. Linagliptin treatment improves cerebrovascular function and remodeling and restores reduced cerebral perfusion in Type 2 diabetes. *Am J Physiol Regul Integr Comp Physiol.* (2016) 311:R466–77. doi: 10.1152/ajpregu.00057.2016
67. Yasir Y, Hardigan T, Ergul A. Diabetes-mediated middle cerebral artery remodeling is restored by linagliptin: interaction with the vascular smooth muscle cell endothelin system. *Life Sci.* (2016) 159:76–82. doi: 10.1016/j.lfs.2016.02.096
68. Lau LH, Lew J, Borschmann K, Thijs V, Ekinci EI. Prevalence of diabetes and its effects on stroke outcomes: a meta-analysis and literature review. *J Diab Investig.* (2018) 10:780–92. doi: 10.1111/jdi.12932
69. Capes SE, Hunt D, Malmberg K, Pathak P, Gerstein HC. Stress hyperglycemia and prognosis of stroke in nondiabetic and diabetic patients: a systematic overview. *Stroke.* (2001) 32:2426–32. doi: 10.1161/hs1001.096194
70. Weir CJ, Murray GD, Dyker AG, Lees KR. Is hyperglycaemia an independent predictor of poor outcome after acute stroke? Results of a long term follow up study. *BMJ.* (1997) 314:1303. doi: 10.1136/bmj.314.7090.1303
71. Rawshani A, Rawshani A, Franzen S, Eliasson B, Svensson AM, Miftaraj M, et al. Mortality and cardiovascular disease in type 1 and type 2 diabetes. *N Engl J Med.* (2017) 376:1407–18. doi: 10.1056/NEJMoa1608664
72. Rawshani A, Rawshani A, Franzen S, Sattar N, Eliasson B, Svensson AM, et al. Risk factors, mortality, and cardiovascular outcomes in patients with type 2 diabetes. *N Engl J Med.* (2018) 379:633–44. doi: 10.1056/NEJMoa1800256
73. Cefalu WT, Kaul S, Gerstein HC, Holman RR, Zinman B, Skyler JS, et al. Cardiovascular outcomes trials in type 2 diabetes: where do we go from here? Reflections from a diabetes care editors' expert forum. *Diab Care.* (2018) 41:14–31. doi: 10.2337/dci17-0057
74. McGuire DK, Marx N, Johansen OE, Inzucchi SE, Rosenstock J, George JT. FDA guidance on antihyperglycemic therapies for type 2 diabetes: one decade later. *Diab Obes Metab.* (2019) 21:1079–80. doi: 10.1111/dom.13645
75. Scirica BM, Bhatt DL, Braunwald E, Steg PG, Davidson J, Hirshberg B, et al. Saxagliptin and cardiovascular outcomes in patients with type 2 diabetes mellitus. *N Engl J Med.* (2013) 369:1317–26. doi: 10.1056/NEJMoa1307684
76. Green JB, Bethel MA, Armstrong PW, Buse JB, Engel SS, Garg J, et al. Effect of sitagliptin on cardiovascular outcomes in type 2 diabetes. *N Engl J Med.* (2015) 373:232–42. doi: 10.1056/NEJMoa1501352
77. White WB, Cannon CP, Heller SR, Nissen SE, Bergenstal RM, Bakris GL, et al. Alogliptin after acute coronary syndrome in patients with type 2 diabetes. *N Engl J Med.* (2013) 369:1327–35. doi: 10.1056/NEJMoa1305889
78. Darsalia V, Larsson M, Klein T, Patrone C. The high need for trials assessing functional outcome after stroke rather than stroke prevention with GLP-1 agonists and DPP-4 inhibitors. *Cardiovasc Diabetol.* (2018) 17:32. doi: 10.1186/s12933-018-0674-3

79. Marx N, Rosenstock J, Kahn SE, Zinman B, Kastelein JJ, Lachin JM, et al. Design and baseline characteristics of the CARdiovascular Outcome Trial of LINAgliptin Versus Glimepiride in Type 2 Diabetes (CAROLINA(R)). *Diab Vasc Dis Res.* (2015) 12:164–74. doi: 10.1177/1479164115570301
80. Biessels GJ, Despa F. Cognitive decline and dementia in diabetes mellitus: mechanisms and clinical implications. *Nat Rev Endocrinol.* (2018) 14:591–604. doi: 10.1038/s41574-018-0048-7
81. Geijselaers SLC, Sep SJS, Stehouwer CDA, Biessels GJ. Glucose regulation, cognition, and brain MRI in type 2 diabetes: a systematic review. *Lancet Diab Endocrinol.* (2015) 3:75–89. doi: 10.1016/S2213-8587(14)70148-2
82. Fink HA, Jutkowitz E, McCarten JR, Hemmy LS, Butler M, Davila H, et al. Pharmacologic interventions to prevent cognitive decline, mild cognitive impairment, and clinical alzheimer-type dementia: a systematic review. *Ann Intern Med.* (2018) 168:39–51. doi: 10.7326/M17-1529
83. Zheng T, Qin L, Chen B, Hu X, Zhang X, Liu Y, et al. Association of plasma DPP4 activity with mild cognitive impairment in elderly patients with type 2 diabetes: results from the GDMD study in China. *Diab Care.* (2016) 39:1594–601. doi: 10.2337/dc16-0316
84. Tasci I, Naharci MI, Bozoglu E, Safer U, Aydogdu A, Yilmaz BF, et al. Cognitive and functional influences of vildagliptin, a DPP-4 inhibitor, added to ongoing metformin therapy in elderly with type 2 diabetes. *Endocr Metab Immune Disord Drug Targets.* (2013) 13:256–63. doi: 10.2174/18715303113139990037
85. Kim YG, Jeon JY, Kim HJ, Kim DJ, Lee KW, Moon SY, et al. Risk of dementia in older patients with type 2 diabetes on dipeptidyl-peptidase IV inhibitors versus sulfonylureas: a real-world population-based cohort study. *J Clin Med.* (2018) 8:E28. doi: 10.3390/jcm8010028
86. Dumbrill JL, Moulton CD. Effects of incretin-based therapies on neurocognitive function in humans: a systematic review of the literature. *Prim Care Diab.* (2018) 12:51–8. doi: 10.1016/j.pcd.2017.06.009
87. Biessels GJ, Janssen J, van den Berg E, Zinman B, Espeland MA, Mattheus M, et al. Rationale and design of the CAROLINA(R)—cognition substudy: a randomised controlled trial on cognitive outcomes of linagliptin versus glimepiride in patients with type 2 diabetes mellitus. *BMC Neurol.* (2018) 18:7. doi: 10.1186/s12883-018-1014-7

Conflict of Interest Statement: Work in our laboratory is partly financed by Boehringer Ingelheim Pharma GmbH & Co. TK is employed at Boehringer Ingelheim Pharma GmbH & Co and Odd Erik Johansen by Boehringer Ingelheim Norway. TN has received unrestricted grants from AstraZenca and consultancy fees from Boehringer Ingelheim, Eli Lilly, Novo Nordisk, Merck, and Sanofi-Aventis.

The remaining authors declare that the research was conducted in the absence of any commercial or financial relationships that could be construed as a potential conflict of interest.

Copyright © 2019 Darsalia, Johansen, Lietzau, Nyström, Klein and Patrone. This is an open-access article distributed under the terms of the Creative Commons Attribution License (CC BY). The use, distribution or reproduction in other forums is permitted, provided the original author(s) and the copyright owner(s) are credited and that the original publication in this journal is cited, in accordance with accepted academic practice. No use, distribution or reproduction is permitted which does not comply with these terms.

frontiers in Neurology

HYPOTHESIS AND THEORY
published: 14 May 2019
doi: 10.3389/fneur.2019.00469

Cross-Reactivity as a Mechanism Linking Infections to Stroke

Guglielmo Lucchese[1,2]*, *Agnes Flöel*[1] and *Benjamin Stahl*[1,3,4,5]

[1] Department of Neurology, University of Greifswald, Greifswald, Germany, [2] Department of Computing, Goldsmiths, University of London, London, United Kingdom, [3] Department of Neurology, Charité Universitätsmedizin Berlin, Berlin, Germany, [4] Department of Neurophysics, Max Planck Institute for Human Cognitive and Brain Sciences, Leipzig, Germany, [5] Psychologische Hochschule Berlin, Berlin, Germany

The relevance of infections as risk factor for cerebrovascular disease is being increasingly recognized. Nonetheless, the pathogenic link between the two entities remains poorly understood. Consistent with recent advances in medicine, the present work addresses the hypothesis that infection-induced immune responses may affect human proteins associated with stroke. Applying established procedures in bioinformatics, the pathogen antigens and the human proteins were searched for common sequences using pentapeptides as probes. The resulting data demonstrate massive peptide sharing between infectious pathogens—such as *Chlamydia pneumoniae*, *Streptococcus pneumoniae*, *Tannerella forsythia, Haemophilus influenzae*, Influenza A virus, and Cytomegalovirus—and human proteins related to risk of ischemic and hemorrhagic stroke. Moreover, the shared peptides are also evident in a number of epitopes experimentally proven immunopositive in the human host. The present findings suggest cross-reactivity as a potential mechanistic link between infections and stroke.

Keywords: stroke, infections, cross-reactivity, peptides, inflammation

OPEN ACCESS

Edited by:
Gregory Jaye Bix,
University of Kentucky, United States

Reviewed by:
Adam Denes,
Institute of Experimental Medicine (MTA), Hungary
Pietro Enea Lazzerini,
University of Siena, Italy

***Correspondence:**
Guglielmo Lucchese
guglielmo.lucchese@uni-greifswald.de

Specialty section:
This article was submitted to Stroke, a section of the journal Frontiers in Neurology

Received: *27 January 2019*
Accepted: *17 April 2019*
Published: *14 May 2019*

Citation:
Lucchese G, Flöel A and Stahl B (2019) Cross-Reactivity as a Mechanism Linking Infections to Stroke. Front. Neurol. 10:469. doi: 10.3389/fneur.2019.00469

INTRODUCTION

When considered separately from other cardiovascular diseases, stroke ranks fifth among all causes of death (1) and, critically, its incidence is on the rise (2).

The etiology of stroke is multifactorial with various environmental and genetic risk factors. Hypertension, diabetes and insulin resistance, smoking, dyslipidemia, obesity, heavy alcohol consumption, atrial fibrillation, and carotid stenosis are all established and well-investigated modifiable risk factors of stroke (3–5).

Additionally, there is evidence that environmental factors may also increase risk of stroke, including viral and bacterial infections, such as periodontitis (6) and respiratory infections (7), and infection with *Chlamydia pneumoniae* (8) or Cytomegalovirus (9). However, relatively little is known so far about the role of different pathogens as well as the molecular basis and the mechanisms that potentially link infections to stroke.

Here we set out to investigate whether or not infections can induce immune responses capable of cross-reacting with human proteins that, when altered, have been associated with stroke. Our hypothesis was that immune responses induced by infectious agents might cross-react with crucial stroke-related proteins, thus contributing to the multifactorial pathogenesis of cerebrovascular disease.

To address this hypothesis, we analyzed pathogens, as well as proteins that are known to be associated with increased risk of ischemic and hemorrhagic stroke by searching for common peptides that might underlie cross-reactions.

Specifically, we analyzed antigens from the following pathogens that have been reported to have a possible influence on stroke: the periodontal bacterium *Tannerella forsythia* (10), *Haemophilus influenza* (11), *Streptococcus pneumoniae* (7), *Chlamydia pneumoniae* (8), Influenza A viruses (12, 13), and Human Cytomegalovirus (9).

METHODS

We analyzed the amino acid (aa) primary sequence of pathogen antigens (with short name and UniProt ID in parentheses):

- Surface antigen repeat/outer membrane protein (OMP; UniProtKB: A0A0F7WYE8_CHLPN) from *Chlamydia pneumoniae*;
- Pneumococcal vaccine antigen A (PVAA;UniProtKB: PVAA_STRR6) from *Streptococcus pneumoniae*;
- Surface antigen BspA (BspA; UniProtKB: O68831_TANFO) from *Tannerella forsythia*;
- Outer membrane antigenic lipoprotein B (LPPB; UniProtKB: LPPB_HAEIN) from *Haemophilus influenzae* (strain ATCC 51907);
- Hemagglutinin (HA H1N1; UniProtKB: HEMA_I34A1) from Influenza A virus (strain A/Puerto Rico/8/1934 H1N1);
- Hemagglutinin (HA H5N1; UniProtKB: HEMA_I96A0) from Influenza A virus (strain A/Goose/Guangdong/1/1996 H5N1);
- Hemagglutinin (HA H3N2; UniProtKB: HEMA_I68A6) from Influenza A virus (strain A/Northern Territory/60/1968 H3N2); and
- 65 kDa phosphoprotein (pp65; UniProtKB: PP65_HCMVM) from Human Cytomegalovirus (HCMV; strain Merlin).

The primary sequence of pathogen antigens was dissected into partially overlapping pentapeptides with a one-residue-offset: i.e., MFKRI, FKRIR, KRIRR, and so on. Then, each pentapeptide was analyzed for occurrences within a library consisting of primary sequences of human proteins involved in stroke. The human protein library was *a priori* chosen from the UniProtKB Database (https://www.uniprot.org) (14) using the keyword "stroke." We obtained an unbiased list of 74 human proteins (in)directly associated with stroke (**Table S1**). Stroke-related proteins are indicated as UniProtKB entry names throughout the present article, except when discussed in detail. The pathogen antigens and the human proteins were searched for common sequences using the pentapeptide as a probe unit because a pentapeptide is an immunobiological determinant sufficient for epitope-paratope interaction and for inducing specific immune responses (15–18).

The immunologic potential of the shared peptides was analyzed using the Immune Epitope Database (IEDB; www.iedb.org) (19). All evaluations were based only on epitopic sequences that had been experimentally validated as immunopositive in the human host.

This linear peptide similarity analysis procedure has been used and described before (20, 21).

RESULTS

In a detailed overview, **Table 1** shows that 49 out of the 74 human stroke-related proteins share peptide sequences with antigens from pathogens that proved to be (in)directly involved in stroke (6–10). It can be seen that

- The pathogen vs. human peptide overlap is unexpectedly high when considering that the probability for two proteins to share a pentapeptide is 1 out of 20^{-5}, that is, 0.0000003125 or close to zero.
- The peptide overlap varies widely, with *T. forsythia* BspA and Influenza A HA H3N2 being the pathogen more and less involved in the peptide sharing, respectively.
- The high number of stroke-related proteins involved in the viral peptide overlap precludes a detailed protein-by-protein analysis. However, an example worth noting is the human ATP-binding cassette sub-family C member nine (ABCC9 or SUR2) that shares peptide sequences with all of the pathogen antigens analyzed, with the exception of the Influenza A HA H3N2 virus. ABCC9 is a subunit of ATP-sensitive potassium channels (K_{ATP}) that can form cardiac and smooth muscle-type KATP channels with KCNJ11 and mediates neuroprotection (22).

In summary, **Table 1** describes a peptide platform that connects the infectious agents under analysis human proteins related to stroke.

Subsequently, in order to define the immunologic potential of the shared peptides, we conducted analyses throughout the peptide immunome cataloged in the Immune Epitope Database (IEDB; www.iedb.org) (19). The search was finalized to identify epitopic sequences corresponding to (or containing) the peptide sequences shared between stroke-related infectious agents and stroke-related human proteins. It was found that a great number of the shared peptides listed in **Table 1** are also distributed through hundreds of epitopic sequences with an immunological potential. A list of such epitopic sequences is reported in **Table 2.**

CONCLUSION

Stroke risk appears to be the result of a complex combination of multiple genetic non-modifiable and environmental modifiable factors that can be further classified as either "traditional" or new, "emerging" ones (23). As highlighted by Grau et al. (24, 25), the occurrence of stroke is only partially explained by traditional modifiable cardiovascular

TABLE 1 | Peptide sharing between pathogen antigens and human proteins that have been associated with stroke[1].

Shared peptides[a,b]	Human protein involved in the peptide [Sharing b,c]
***C. pneumoniae* OMP:**	
ITNYL	**ABCC9**. ATP-binding cassette sub-family C member 9
RKFLL	CCM2. Cerebral cavernous malformations 2 protein
RKFLL; **KGFVS**	CCM2L. Cerebral cavernous malformations 2 protein-like
ASSVD; LEHNQ	CSF1R. Macrophage colony-stimulating factor 1 receptor
IALHL	**DAPK1**. Death-associated protein kinase 1
SEGKT	FA5. Coagulation factor V
PTTGI	GNAQ. Guanine nucleotide-binding protein G(q) subunit alpha
EGPCG	HTRA1. Serine protease HTRA1
NTTAE	KCNE2. Potassium voltage-gated channel subfamily E member 2
GFRCL; LRSSA	NOTC3. Neurogenic locus notch homolog protein 3
VSAAG	**NU155**. Nuclear pore complex protein Nup155
SGLGG	PAWR. PRKC apoptosis WT1 regulator protein
SGNQV	PDE4D. cAMP-specific 3′,5′-cyclic phosphodiesterase 4D
GYFAS	**RN213**. E3 ubiquitin-protein ligase RNF213
DSPRT; SPRTP	SAMH1. Deoxynucleoside triphosphate triphosphohydrolase SAMHD1
***S. pneumoniae* PVAA:**	
LAMIY	**ABCC9**. ATP-binding cassette sub-family C member 9
TVAPL; VAPLL	KCNA5. Potassium voltage-gated channel subfamily A member 5
AQNGK	KLOT. Klotho
SASGS	LMNA. Prelamin-A/C
LVLAV	NMDE2. Glutamate receptor ionotropic, NMDA 2B
IQTLT	NU5M. NADH-ubiquinone oxidoreductase chain 5
***T. forsythia* BspA:**	
AWTAR; SGTKT	A4. Amyloid-beta A4 protein
GLTTI; LTITN	**ABCC9**. ATP-binding cassette sub-family C member 9
TLSAL	BI1. Bax inhibitor 1
APGRA	CO4A2. Collagen alpha-2(IV) chain
GKKAV	COQ8A. Atypical kinase COQ8A, mitochondrial
IIFVS	CXA5. Gap junction alpha-5 protein
NCGAL	GATA5. Transcription factor GATA-5
HSLQS	GATA6. Transcription factor GATA-6
LGATA; GATAQ	IL4. Interleukin-4
DALTT	ITIH4. Inter-alpha-trypsin inhibitor heavy chain H4
AGGAL; VTTIG	KCNQ1. Potassium voltage-gated channel subfamily KQT member 1
TAPDA	KRIT1. Krev interaction trapped protein 1
EGFAL	LYAM3. P-selectin
VTQNP	NMDE2. Glutamate receptor ionotropic, NMDA 2B
DGVNT; SGTTG	NOTC3. Neurogenic locus notch homolog protein 3
GLFLL	SCN4B. Sodium channel subunit beta-4
TLPNS	SCN5A. Sodium channel protein type 5 subunit alpha
TLPDG; VTLPN	SYLM. Probable leucine—tRNA ligase, mitochondrial
LPDAL; LTLSA; SGLTS; TLPDA	**ZFHX3**. Zinc finger homeobox protein 3
***H. influenzae* LPPB:**	
TSNFP; GIDIS	ABCC9. ATP-binding cassette sub-family C member 9
LLLPL	ACE. Angiotensin-converting enzyme
SFLLL; TTTVS	ANF. Natriuretic peptides A
AQPAF	CSF1R. Macrophage colony-stimulating factor 1 receptor
ILVAD	ENPP4. Bis(5′-adenosyl)-triphosphatase ENPP4
VTSSV	GATA6. Transcription factor GATA-6

(Continued)

TABLE 1 | Continued

Shared peptides[a,b]	Human protein involved in the peptide [Sharing b,c]
GNLII	ITIH4. Inter-alpha-trypsin inhibitor heavy chain H4
PGANG; SGSRG	KCNA5. Potassium voltage-gated channel subfamily A member 5
APDYS; PDYSK; DYSKI; TYTPG	KRIT1. Krev interaction trapped protein 1
SNVGG; SPSVP	NU155. Nuclear pore complex protein Nup155
AYLAG	PDE3A. cGMP-inhibited 3′,5′-cyclic phosphodiesterase A
LLPLS;**AYLAG**; **VTSSV**; QEVKA	RN213. E3 ubiquitin-protein ligase RNF213
GPIKS	SCN5A. Sodium channel protein type 5 subunit alpha
KKSFL	SYLM. Probable leucine–tRNA ligase, mitochondrial
Influenza A HA H1N1:	
DGVKL	ADA2. Adenosine deaminase 2
LLVSL	ATP6. ATP synthase subunit a
ENAYV	**ABCC9**. ATP-binding cassette sub-family C member 9
ASSLV	PDE3A. cGMP-inhibited 3′,5′-cyclic phosphodiesterase A
AELLV; **ELLVL**; LLVLL; LVLLV	**DAPK1**. Death-associated protein kinase 1
TVLEK; YVSVV; QTPLG; FLDIW	**RN213**. E3 ubiquitin-protein ligase RNF213
TSNAS	NMDE2. Glutamate receptor ionotropic, NMDA 2B
CALAA	GAS6. Growth arrest-specific protein 6
LLVLL;YAADQ; KVDGV	KLOT. Klotho
EELRE	LMNA. Prelamin-A/C
YSEES	**ZFHX3**. Zinc finger homeobox protein 3
Influenza A HA H5N1:	
LLAIV	AL5AP. Arachidonate 5-lipoxygenase-activating protein
LLLAI	**ABCC9**. ATP-binding cassette sub-family C member 9
AQDIL; ISGVK	PDE4D. cAMP-specific 3′,5′-cyclic phosphodiesterase 4D
LLLAI	CYTC. Cystatin-C
QRLVP; **AELLV**; **ELLVL**	**DAPK1**. Death-associated protein kinase 1
ILEKT; LKHLL; **VSSAC**	**RN213**. E3 ubiquitin-protein ligase RNF213
EGGWQ	KLOT. Klotho
SLALA	NU5M. NADH-ubiquinone oxidoreductase chain 5
KIVLL; LVLAT	**NU155**. Nuclear pore complex protein Nup155
ARLNR; SIYST	KCNQ1. Potassium voltage-gated channel subfamily KQT member 1
VSSAC	SCN1B. Sodium channel subunit beta-1
VPEWS	TBX5. T-box transcription factor TBX5
SVAGW	S19A2. Thiamine transporter 1
SLALA	GATA5. Transcription factor GATA-5
Influenza A HA H3N2:	
GGSNA; **AELLV**	**DAPK1**. Death-associated protein kinase 1
INSNG	SAMH1. Deoxynucleoside triphosphate triphosphohydrolase SAMHD1
KITYG	MYL4. Myosin light chain 4
LLGDP	KCNA5. Potassium voltage-gated channel subfamily A member 5
ISFAI	HTRA1. Serine protease HTRA1
VLNVT	SCN3B. Sodium channel subunit beta-3

[1] *References in **Table S1** (Supplementary Material).*
[a] *Viral/bacterial antigens are described under Methods. Further details at https://www.uniprot.org (14).*
[b] *Multiple occurrences in bold.*
[c] *Human proteins given as UniProt entry and name. Further details at https://www.uniprot.org (14).*

risk factors, such as increasing blood pressure, cigarette smoking, and diabetes mellitus. Most importantly, infectious diseases appear to play a key role in contributing to the risk of stroke and are to be counted among "emerging" modifiable risk factors that receive increasing scientific interest (6–10, 23, 26, 27).

Searching for possible immunopathogenic links between infection and risk of stroke, the present study aimed to analyze

TABLE 2 | Epitopes immunopositive in the human host and containing peptide sequences common to antigens from stroke-related pathogens and human proteins associated with stroke.

1	2	1	2	1	2	1	2
58129	SGLTSlf	459109	sLLPLShlv	554097	lvesyTLPDGrii	634993	mplhVAPLLaa
66225	tSGLTSl	466105	gtdpLVLAV	554098	lvesyTLPDGriikv	637221	slsdLLVSL
66817	ttSGLTS	467909	LLLPLnlev	554195	mfehllNSNGikpv	638032	tpLLLPLaa
69631	vLLVSLgai	471133	SPRTPppltv	555093	qgDGVKLhlkakaev	638320	vhEGPCGisy
79809	ELLVLLenertld	471667	tlAELLVLL	555672	rlsrlqekEELRE	642301	eqklnrypASSLVvvr
113324	dgFLDlWtynAELLV	475091	aekeNTTAEl	557456	vlvesyTLPDGrii	642391	etpvyLGATAgmrll
113533	idlwsynAELLVal	476155	ASSLVdtpk	559587	gnENAYVkngklhls	644577	iekdliilLGATAvedrl
143137	tSASGSgedaidesg	476488	avdDGVNTf	563134	evAELLVkh	644669	iifgASSVDf
150977	eeaklnreeiDGVKL	478710	GLTTllknv	570114	AELLVshga	645002	inhvvSVAGWgisd
151075	ynAELLVLLenertl	482488	nelLVADty	571918	EELRElaesw	645986	kpTLSALpsplvtsg
151076	ypgdfidyEELREql	482780	nrypASSLV	573110	haCALAAslw	648442	qgkdlqqYVSVVvld
163409	setdaLRSSA	482921	pkyvksnrLVLATg	574223	kpagpLGATA	649953	sldrSLALAaeep
164690	fLLVLLdyqgmlp	483957	reSNVGGiqql	575691	nrypASSLVvv	691126	klnrypASSLVvvr
164772	gvdtGlDlShsdf	485150	rySGNQVlf	577376	rVLNVTnlef	691145	kpTLSALpsplvts
178609	avvvlkrLPDALadg	485418	sedpsGKKAVl	577393	rvqGYFASf	691655	neqklnrypASSLVv
182409	stvASSLVLLVSLga	487836	TVLEKfrylpk	578014	SPRTPnrsv	692295	skpTLSALpsplvtsg
182414	yqilaiystvASSLV	488193	vifftSGTTGfpk	578015	SPRTPsntp	694354	eskrKKSFLlcig
184585	lrTTTVSgkl	488539	vVAPLLrkv	578016	SPRTPsntpsa	695746	pltspttsqLRSSAp
190442	hELLVLvkkaq	488926	ypASSLVvv	578044	SPSVPktsa	695843	pSASGSsgntptppn
194133	llaAWTARa	489284	LLLPLpvpa	579718	vyLKHLLpk	695894	pttsqLRSSApshaq
196781	slLEKTsay	490154	araLLLPLl	581635	aeLLLPLkvl	696039	qLRSSApshaqtpwp
213534	kssSGTKTtk	492412	irfgLLPLSm	581817	anatLLPLSl	699244	aqhSGLGGvshy
223189	ldLLLPLnl	492430	irfSGTTGqm	582446	eeLLLPLly	699571	asiVAPLLl
223510	pelLLLPL	492987	lepcsrlLLLPLl	583971	iamhaaLLLAl	699594	aslVAPLLi
223880	seeLLLPLl	493322	mpepasrclLLLPL	584143	ildksVAPLL	699595	aslVAPLLl
226701	yvftLLVSL	493610	plLLVSLw	584764	kgVSAAGilek	700497	deVTLPNvv
240338	sASSLVnldslv	493947	qrqqLLVSL	584945	klrEELREk	700729	difqQTPLGr
243935	FLDlWtyna	495137	srlLLLPLl	587249	prclLLVLL	700885	dpSGTKTcidtkeg
419699	gpprlLLLPL	495478	traLLLPLl	587956	raqggLLVLL	702273	EELREkyrry
423950	alLKHLLsy	496437	eirTVLEKl	589061	rrgELLVLr	702274	EELRElanky
424543	fLLPLSlif	497010	tpvyLGATAgmrll	590120	srsKlVLLv	703553	erySGNQVl
426499	nfkAWTARy	504703	clyvLLLAl	590169	stsSPSVPk	704661	evvtSEGKTk
430136	fspdLLGDPdny	505049	elitlLEKT	590856	vpglcllvll	705071	fAQPAFml
430260	fTVLEKfry	505187	fasVAPLLef	590986	vsgTLPDGhmp	706516	fsLLPLShl
435575	rrlLLLPLl	505268	flaptfSGLTSi	592071	dttyinhvvSVAGWg	710491	ielLEKTttiy
435576	rrlLLLPLll	507273	mpllLLLPL	594553	atiEELRErvw	711114	ipingSPRTPr
436423	apfGPlKSidm	507346	mtlLLLPL	595684	gLLAlVkv	711645	itnvAELLV
437494	gAGGALfvhrd	507484	palSPSVPl	600696	qttTVLEKy	712552	kfpeiVAPLL
437792	gSGLGGltdk	510341	ypASSLVv	601366	rTLPDGthel	713254	klkikelre
440682	SPRTPvspvkf	511858	ardSLALArpkssdvy	601983	sryLLPLSalgtvag	713313	kLLLAlktk
441210	TVLEKvyel	518869	inhvvSVAGWgisdg	602564	tiEELRErvw	716976	ltneKlVLL
442404	apaAPGRAl	519272	itlLEKTvspdrle	610338	QEVKAitkl	720288	qhyelcSGNQV
443560	erySGNQVlf	520276	kqqeLLVSL	611939	rrvkAELLV	721762	rgaLLPLSi
444320	glsLLPLSek	521984	lrqaAGGALqvvhsr	614291	asfaplSFAlk	722338	rlLLLPLl
445722	kpkhPTTGl	523925	qaAGGALqvvhsrql	615815	evAELLVrh	722416	rlprLLVLL
448068	rvrvPTTGl	532960	mPTTGlney	616957	glvnSGLTSv	723746	rvpaLLVLL
448661	SPRTPpqrf	535612	ELLVLrqkhsepsrf	620774	kvleAELLVLr	723778	rvpsLLVLL
448662	SPRTPtpfkhal	537116	nkvleAELLVLrqkh	623038	qrAGGALsi	724649	SEGKTfqly
448918	sryLLPLSa	541075	allpAGGALqh	627837	vPTTGliey	724650	SEGKTkpli
449866	VSAAGlvqgl	541668	eEELREkqay	628836	AELLVkgyei	725019	sgdGPlKSv
453784	flpllLLVLL	541699	EELREkqay	628959	ailhLLVSL	725662	slVAPLLi
456288	LLLAliphv	544699	rggaAGGALp	630008	dvAGGALthsll	727559	TAPDAaltl
456316	LLLPLplll	545442	srvpLLLPL	632600	iLLLPLhtg	728413	TLPDGthel
457304	ntlLLVSL	548131	hLLGDPmanv	633968	lLLLPLpvpa	728445	TLSALyarr
457363	pekTLSALl	551494	esyTLPDGrii	634370	lprLLVLLa	729508	tvpdLLLPL
458091	rlAELLVsv	553367	kpvlqkyAELLV	634991	mplhVAPLL	732341	yAPDYSsrl

Column 1: Epitopes listed according to the IEDB-ID number. Epitope details and references at www.immuneepitope.org (19). Column 2: Sequences common to pathogen antigens and human proteins related to stroke are indicated in capital letters.

the potential immunologic relationship between pathogens and human proteins that, when altered, have been associated with risk of stroke. In line with our hypothesis, we found that immune cross-reactions between infectious pathogens and human stroke-related proteins might occur, thus increasing the risk of stroke (see **Tables 1**, **2**).

The immunologically relevant peptide sharing reported in the present study depicts a complex scenario. Some potential molecular targets of cross-reactions are proteins belonging to the cardiovascular system, thus possibly directly accounting for cerebrovascular damage. Other possible targets are proteins of the immune system, thus suggesting mechanisms resulting in immune dysregulation which could lead to cerebrovascular damage.

An example of the first type of potential targets are ion-channels, particularly potassium (K^+) and sodium (Na^+) channels (ABCC9, KCNE2, KCNA5, KCNQ1, SCN4B, SCN5A, SCN1B, SCN3B, see **Table 1**). Accordingly, a growing body of evidence points to the involvement of cardiac K^+ and Na^+ channel dysfunction (cardiac channelopathies as a result of genetic mutations and/or inflammatory mechanisms) in the pathogenesis of atrial fibrillation (AF), an established risk factor for stroke (28, 29). Moreover, autoantibodies targeting ion-channels may be involved in cardiac arrhythmias (30). In light of the potential cross-reactivity suggested by the observed peptide sharing, AF and subsequent stroke could result from antibodies primarily targeting epitopes of infective agents but also cross-reacting with cardiac ion channels. For instance, activating antibodies could lead to a gain-of-function of K^+-channels and inhibiting antibodies to a loss-of-function of of Na^+-channels. This could promote re-entry or increase susceptibility to early and/or delayed afterdepolarizations, two mechanisms that can generate AF (31, 32).

The second class of potential targets includes proteins that actively modulate the inflammatory response, such as cytokines and colony-stimulating factor receptors (IL-4, macrophage colony-stimulating factor 1 receptor, see **Table 1**) (33, 34). IL-4, for example, is a well-investigated tolerogenic cytokine that is able to suppress inflammatory responses and organ-specific autoimmunity in both animal models and humans (35, 36). It is then conceivable that autoantibodies downregulating the function of these proteins can promote inflammatory responses, thus increasing the risk of cerebrovascular damage and stroke. Indeed, inflammatory responses appear to be crucial in the pathogenesis of stroke by inducing atherosclerosis progression, pro-thrombotic activation, and AF—among other mechanisms (37). Inflammation can therefore be considered as one key factor underpinning the relationship between classical stroke risk factors and comorbidities. It appears that not just single infections, but overall infectious burden from multiple agents predicts stroke incidence. Moreover, poor outcome may be proportional to systemic inflammatory burden both in patients and experimental models. For instance, Influenza and Streptococcus infection seem to contribute to stroke incidence and outcome, and evidence from experimental models indicate that blocking inflammatory processes might be an effective prevention strategy (38, 39).

The increasingly recognized relevance of inflammation in stroke is consistent with a possible role of peptide sharing-based cross-reactivity as contributing factors to cerebrovascular damage. In fact, the past two decades of immunologic research have radically changed the way we think of inflammation and innate immunity. It is now known that innate immune responses can "specifically" drive the following adaptive responses through recognition of pathogen-associated molecular patterns (PAMPs) (40, 41). That is to say that peptide epitopes, cell-wall components, and other PAMPs activate immune cells already from the very first stages of immune reactions and drive inflammation. Indeed, there are examples of cross-reactivity between host and pathogen-associated molecular patterns: identical inflammasomes and toll-like receptors (TLRs) recognizing molecular fingerprints of both pathogens (the PAMPs) and injured host cells (so-called danger-associated molecular patterns; DAMPs). For instance, both bacteria LPS and HMGB1 from injured host cells activate TLR4, with consequent inflammation in various tissues including the brain (41, 42). TLR- and inflammasome-dependent pathways seem to be important drivers of inflammation, vascular disease, and reportedly contribute to stroke outcome (43, 44).

Our preliminary results underline the importance of further experimental efforts to define the molecular basis through which microbial infections might contribute to an increased risk of stroke (45–50). Future studies should evaluate immunoreactivity against the peptides shared by infectious pathogens and human stroke-related proteins in sera from stroke patients. Possibly, such serological analyses could also help identify specific markers predicting a higher risk of stroke and might therefore be useful to design preventive strategies following an infection. The ultimate translational relevance of our finding lies in the possibility of adopting effective individualized primary and secondary preventive strategies in patients at risk for stroke after infections. Generic hygienic measure, as well as antibiotic prophylaxis and vaccination campaigns have already been proposed and tested with contrasting results (37). Identifying and stratifying patients according to individual biomarker profiles would allow to personalize treatment for each patient, thus possibly increasing overall efficacy.

Until now, stroke is a leading cause of preventable death and adult disability (1–5, 47–52), but preventive strategies mostly concentrate on traditional cardiovascular risk factors (53–56). Moreover, "cryptogenic" stroke (i.e., ischemic stroke with no obvious cause) poses a challenge in terms of primary and secondary prevention (57, 58).

Given the burden of cerebrovascular disease, and the potential to identify immunological markers that may then serve as prognostic indicators of risk of cerebrovascular damage after an infection, our results justify further intensive research on the cross-reactive link between infections and risk of stroke.

AUTHOR CONTRIBUTIONS

GL formulated the hypothesis, analyzed the data and wrote the manuscript. GL, AF, and BS interpreted the data, revised and finalized the manuscript.

FUNDING

We acknowledge support for the Article Processing Charge from the DFG (German Research Foundation, 393148499) and the Open Access Publication Fund of the University of Greifswald and from the Deutsche Forschungsgemeinschaft to AF (SFB1315 TP B03).

SUPPLEMENTARY MATERIAL

The Supplementary Material for this article can be found online at: https://www.frontiersin.org/articles/10.3389/fneur.2019.00469/full#supplementary-material

REFERENCES

1. Benjamin EJ, Virani SS, Callaway CW, Chamberlain AM, Chang AR, Cheng S, et al. Heart disease and stroke statistics-2018 update: a report from the American Heart Association. *Circulation.* (2018) 137:e67–e492. doi: 10.1161/CIR.0000000000000573
2. Cabral NL, Freire AT, Conforto AB, Dos Santos N, Reis FI, Nagel V, et al. Increase of stroke incidence in young adults in a middle-income country: a 10-year population-based study. *Stroke.* (2017) 48:2925–30. doi: 10.1161/STROKEAHA.117.018531
3. Kirshner HS. Differentiating ischemic stroke subtypes: risk factors and secondary prevention. *J Neurol Sci.* (2009) 279:1–8. doi: 10.1016/j.jns.2008.12.012
4. Tonk M, Haan J. A review of genetic causes of ischemic and hemorrhagic stroke. *J Neurol Sci.* (2007) 257:273–9. doi: 10.1016/j.jns.2007.01.037
5. Hankey GJ. Stroke. *Lancet.* (2017) 389:641–54. doi: 10.1016/S0140-6736(16)30962-X
6. Leira Y, Seoane J, Blanco M, Rodríguez-Yáñez M, Takkouche B, Blanco J, et al. Association between periodontitis and ischemic stroke: a systematic review and meta-analysis. *Eur J Epidemiol.* (2017) 32:43–53. doi: 10.1007/s10654-016-0170-6
7. Blackburn R, Zhao H, Pebody R, Hayward A, Warren-Gash C. Laboratory-confirmed respiratory infections as predictors of hospital admission for myocardial infarction and stroke: time-series analysis of english data for 2004-2015. *Clin Infect Dis.* (2018) 67:8–17. doi: 10.1093/cid/cix1144
8. Wimmer ML, Sandmann-Strupp R, Saikku P, Haberl RL. Association of chlamydial infection with cerebrovascular disease. *Stroke.* (1996) 27:2207–10. doi: 10.1161/01.STR.27.12.2207
9. Wang H, Peng G, Bai J, He B, Huang K, Hu X, et al. Cytomegalovirus infection and relative risk of cardiovascular disease (ischemic heart disease, stroke, and cardiovascular death): a meta-analysis of prospective studies up to 2016. *J Am Heart Assoc.* (2017) 6:e005025. doi: 10.1161/JAHA.116.005025
10. Chukkapalli SS, Rivera-Kweh MF, Velsko IM, Chen H, Zheng D, Bhattacharyya I, et al. Chronic oral infection with major periodontal bacteria *Tannerella forsythia* modulates systemic atherosclerosis risk factors and inflammatory markers. *Pathog Dis.* (2015) 73:ftv009. doi: 10.1093/femspd/ftv009
11. Takeoka M, Takahashi T. Infectious and inflammatory disorders of the circulatory system and stroke in childhood. *Curr Opin Neurol.* (2002) 15:159–64. doi: 10.1097/00019052-200204000-00006
12. Ekstrand JJ. Neurologic complications of influenza. *Semin Pediatr Neurol.* (2012) 19:96–100. doi: 10.1016/j.spen.2012.02.004
13. Urbanek C, Palm F, Grau AJ. Influenza and stroke risk: a key target not to be missed? *Infect Disord Drug Targets.* (2010) 10:122–31. doi: 10.2174/187152610790963474
14. UniProt Consortium T. UniProt: the universal protein knowledgebase. *Nucleic Acids Res.* (2018) 46:2699. doi: 10.1093/nar/gky092
15. Reddehase MJ, Rothbard JB, Koszinowski UH. A pentapeptide as minimal antigenic determinant for MHC class I-restricted T lymphocytes. *Nature.* (1989) 337:651–3. doi: 10.1038/337651a0
16. Frank SA. *Immunology and Evolution of Infectious Disease.* Princeton, NJ: Princeton University Press (2002).
17. Kanduc D. Pentapeptides as minimal functional units in cell biology and immunology. *Curr Protein Pept Sci.* (2013) 14:111–20. doi: 10.2174/1389203711314020003
18. Kanduc D. Homology, similarity, and identity in peptide epitope immunodefinition. *J Pept Sci.* (2012) 18:487–94. doi: 10.1002/psc.2419
19. Vita R, Overton JA, Greenbaum JA, Ponomarenko J, Clark JD, Cantrell JR, et al. The immune epitope database (IEDB) 3.0. *Nucleic Acids Res.* (2015) 43 (Database issue): D405–12. doi: 10.1093/nar/gku938
20. Lucchese G, Capone G, Kanduc D. Peptide sharing between influenza A H1N1 hemagglutinin and human axon guidance proteins. *Schizophr Bull.* (2014) 40:362–75. doi: 10.1093/schbul/sbs197
21. Lucchese G, Stahl B. Peptide sharing between viruses and DLX Proteins: a potential cross-reactivity pathway to neuropsychiatric disorders. *Front Neurosci.* (2018) 12:150. doi: 10.3389/fnins.2018.00150
22. Liu R, Wang H, Xu B, Chen W, Turlova E, Dong N, et al. Cerebrovascular safety of sulfonylureas: the role of KATP channels in neuroprotection and the risk of stroke in patients with type 2 diabetes. *Diabetes.* (2016) 65:2795–809. doi: 10.2337/db15-1737
23. Boehme AK, Esenwa C, Elkind MS. Stroke risk factors, genetics, and prevention. *Circ Res.* (2017) 120:472–95. doi: 10.1161/CIRCRESAHA.116.308398
24. Grau AJ, Brandt T. Do multiple chronic infections increase the risk of stroke? the infectious burden concept. *Arch Neurol.* (2010) 67:16–17. doi: 10.1001/archneurol.2009.301
25. Grau AJ, Urbanek C, Palm F. Common infections and the risk of stroke. *Nat Rev Neurol.* (2010) 6:681–94. doi: 10.1038/nrneurol.2010.163
26. Manousakis G, Jensen MB, Chacon MR, Sattin JA, Levine RL. The interface between stroke and infectious disease: infectious diseases leading to stroke and infections complicating stroke. *Curr Neurol Neurosci Rep.* (2009) 9:28–34. doi: 10.1007/s11910-009-0005-x
27. Elkind MS, Ramakrishnan P, Moon YP, Boden-Albala B, Liu KM, Spitalnik SL, et al. Infectious burden and risk of stroke: the northern Manhattan study. *Arch Neurol.* (2010) 67:33–8. doi: 10.1001/archneurol.2009.271
28. Hucker WJ, Saini H, Lubitz SA, Ellinor PT. Atrial fibrillation genetics: is there a practical clinical value now or in the future? *Can J Cardiol.* (2016) 32, 1300–5. doi: 10.1016/j.cjca.2016.02.032
29. Lazzerini PE, Capecchi PL, El-Sherif N, Laghi-Pasini F, Boutjdir M. Emerging arrhythmic risk of autoimmune and inflammatory cardiac channelopathies. *J Am Heart Assoc.* (2018) 7:e010595. doi: 10.1161/JAHA.118.010595
30. Lazzerini PE, Capecchi PL, Laghi-Pasini F, Boutjdir M. Autoimmune channelopathies as a novel mechanism in cardiac arrhythmias. *Nat Rev Cardiol.* (2017) 14:521–35. doi: 10.1038/nrcardio.2017.61
31. Nattel S, Burstein B, Dobrev D. Atrial remodeling and atrial fibrillation: mechanisms and implications. *Circ Arrhythm Electrophysiol.* (2008) 1:62–73. doi: 10.1161/CIRCEP.107.754564
32. Nattel S, Dobrev D. Electrophysiological and molecular mechanisms of paroxysmal atrial fibrillation. *Nat Rev Cardiol.* (2016) 13:575–90. doi: 10.1038/nrcardio.2016.118
33. Sredni-Kenigsbuch D. TH1/TH2 cytokines in the central nervous system. *Int J Neurosci.* (2002) 112:665–703. doi: 10.1080/00207450290025725

34. Hamilton JA, Achuthan A. Colony stimulating factors and myeloid cell biology in health and disease. *Trends Immunol.* (2013) 34:81–9. doi: 10.1016/j.it.2012.08.006
35. Yang WC, Hwang YS, Chen YY, Liu CL, Shen CN, Hong WH, et al. Interleukin-4 supports the suppressive immune responses elicited by regulatory T cells. *Front Immunol.* (2017) 8:1508. doi: 10.3389/fimmu.2017.01508
36. Guenova E, Skabytska Y, Hoetzenecker W, Weindl G, Sauer K, Tham M, et al. IL-4 abrogates TH17 cell-mediated inflammation by selective silencing of IL-23 in antigen-presenting cells. *Proc Natl Acad Sci USA.* (2015) 112:2163–8. doi: 10.1073/pnas.1416922112
37. Esenwa CC, Elkind MS. Inflammatory risk factors, biomarkers and associated therapy in ischaemic stroke. *Nat Rev Neurol.* (2016) 12:594–604. doi: 10.1038/nrneurol.2016.125
38. Muhammad S, Haasbach E, Kotchourko M, Strigli A, Krenz A, Ridder DA, et al. Influenza virus infection aggravates stroke outcome. *Stroke.* (2011) 42:783–91. doi: 10.1161/STROKEAHA.110.596783
39. Dénes Á, Pradillo JM, Drake C, Sharp A, Warn P, Murray KN, et al. *Streptococcus pneumoniae* worsens cerebral ischemia via interleukin 1 and platelet glycoprotein Ibα. *Ann Neurol.* (2014) 75:670–83. doi: 10.1002/ana.24146
40. Root-Bernstein R, Fairweather D. Complexities in the relationship between infection and autoimmunity. *Curr Allergy Asthma Rep.* (2014) 14:407. doi: 10.1007/s11882-013-0407-3
41. Mills K. H. TLR-dependent T cell activation in autoimmunity. *Nat Rev Immunol.* (2011) 11:807–22. doi: 10.1038/nri3095
42. Aucott H, Lundberg J, Salo H, Klevenvall L, Damberg P, Ottosson L, et al. Neuroinflammation in response to intracerebral injections of different HMGB1 redox isoforms. *J Innate Immun.* (2018) 10:215–27. doi: 10.1159/000487056
43. Kim ID, Lee H, Kim SW, Lee HK, Choi J, Han PL, et al. Alarmin HMGB1 induces systemic and brain inflammatory exacerbation in post-stroke infection rat model. *Cell Death Dis.* (2018) 9:426. doi: 10.1038/s41419-018-0438-8
44. Vogelgesang A, May VE, Grunwald U, Bakkeboe M, Langner S, Wallaschofski H, et al. Functional status of peripheral blood T-cells in ischemic stroke patients. *PLoS ONE.* (2010) 5:e8718. doi: 10.1371/journal.pone.0008718
45. Emsley HC, Hopkins SJ. Acute ischaemic stroke and infection: recent and emerging concepts. *Lancet Neurol.* (2008) 7:341–53. doi: 10.1016/S1474-4422(08)70061-9
46. Lindsberg PJ, Grau AJ. Inflammation and infections as risk factors for ischemic stroke. *Stroke.* (2003) 34:2518–32. doi: 10.1161/01.STR.0000089015.51603.CC
47. Kuklina EV, Tong X, George MG, Bansil P. Epidemiology and prevention of stroke: a worldwide perspective. *Expert Rev Neurother.* (2012) 12:199–208. doi: 10.1586/ern.11.99
48. Kim AS, Johnston SC. Temporal and geographic trends in the global stroke epidemic. *Stroke.* (2013) 44 (6 Suppl. 1):S123–5. doi: 10.1161/STROKEAHA.111.000067
49. Tan RY, Markus HS. Monogenic causes of stroke: now and the future. *J Neurol.* (2015) 262:2601–16. doi: 10.1007/s00415-015-7794-4
50. Kim YD, Cha MJ, Kim J, Lee DH, Lee HS, Nam CM, et al. Long-term mortality in patients with coexisting potential causes of ischemic stroke. *Int J Stroke.* (2015) 10:541–6. doi: 10.1111/ijs.12013
51. Carrera E, Maeder-Ingvar M, Rossetti AO, Devuyst G, Bogousslavsky J, . Trends in risk factors, patterns and causes in hospitalized strokes over 25 years: the Lausanne Stroke Registry. *Cerebrovasc Dis.* (2007) 24:97–103. doi: 10.1159/000103123
52. Inzitari D, Eliasziw M, Gates P, Sharpe BL, Chan RK, Meldrum HE, et al. The causes and risk of stroke in patients with asymptomatic internal-carotid-artery stenosis. North American Symptomatic Carotid Endarterectomy Trial Collaborators. *N Engl J Med.* (2000) 342:1693–700. doi: 10.1056/NEJM200006083422302
53. Rothstein L, Jickling GC. Ischemic stroke biomarkers in blood. *Biomark Med.* (2013) 7:37–47. doi: 10.2217/bmm.12.104
54. Simats A, García-Berrocoso T, Montaner J. Neuroinflammatory biomarkers: from stroke diagnosis and prognosis to therapy. *Biochim Biophys Acta.* (2016) 1862:411–24. doi: 10.1016/j.bbadis.2015.10.025
55. Pullagurla SR, Baird AE, Adamski MG, Soper SA. Current and future bioanalytical approaches for stroke assessment. *Bioanalysis.* (2015) 7:1017–35. doi: 10.4155/bio.15.40
56. Salat D, Penalba A, García-Berrocoso T, Campos-Martorell M, Flores A, Pagola J, et al. Immunological biomarkers improve the accuracy of clinical risk models of infection in the acute phase of ischemic stroke. *Cerebrovasc Dis.* (2013) 35:220–7. doi: 10.1159/000346591
57. Fonseca AC, Ferro JM. Cryptogenic stroke. *Eur J Neurol.* (2015) 22:618–23. doi: 10.1111/ene.12673
58. Saver JL. Clinical practice. Cryptogenic stroke. *N Engl J Med.* (2016) 374:2065–74. doi: 10.1056/NEJMcp1503946

Conflict of Interest Statement: AF received consulting fees from Bayer and Novartis and honoraria for oral presentations from Novartis, Böhringer-Ingelheim, Lilly, and Biogen Idec (unrelated to current research).

The remaining authors declare that the research was conducted in the absence of any commercial or financial relationships that could be construed as a potential conflict of interest.

Copyright © 2019 Lucchese, Flöel and Stahl. This is an open-access article distributed under the terms of the Creative Commons Attribution License (CC BY). The use, distribution or reproduction in other forums is permitted, provided the original author(s) and the copyright owner(s) are credited and that the original publication in this journal is cited, in accordance with accepted academic practice. No use, distribution or reproduction is permitted which does not comply with these terms.

frontiers in Cellular Neuroscience

ORIGINAL RESEARCH
published: 21 May 2019
doi: 10.3389/fncel.2019.00223

MicroRNA-210-3p Targets RGMA to Enhance the Angiogenic Functions of Endothelial Progenitor Cells Under Hypoxic Conditions

Wen-Jing Lu[1,2†], Huai-Bin Liang[1†], Yong-Fang Li[1], Xuan-Qiang Tu[1], Ji-Rong He[1], Kai-Qi Ding[1], Guo-Yuan Yang[1], Xiao-Yu Xin[1] and Li-Li Zeng[1]**

[1] Department of Neurology, Ruijin Hospital, School of Medicine, Shanghai Jiao Tong University, Shanghai, China,
[2] Department of Rehabilitation Medicine, Huashan Hospital, Fudan University, Shanghai, China

OPEN ACCESS

Edited by:
Gregory Jaye Bix,
University of Kentucky, United States

Reviewed by:
Hermona Soreq,
The Hebrew University of Jerusalem, Israel
Simona Candiani,
University of Genoa, Italy

***Correspondence:**
Xiao-Yu Xin
xiaoyu2004@163.com
Li-Li Zeng
llzeng@126.com

[†] These authors have contributed equally to this work

Specialty section:
This article was submitted to Cellular Neuropathology, a section of the journal Frontiers in Cellular Neuroscience

Received: 07 January 2019
Accepted: 02 May 2019
Published: 21 May 2019

Citation:
Lu W-J, Liang H-B, Li Y-F, Tu X-Q, He J-R, Ding K-Q, Yang G-Y, Xin X-Y and Zeng L-L (2019) MicroRNA-210-3p Targets RGMA to Enhance the Angiogenic Functions of Endothelial Progenitor Cells Under Hypoxic Conditions. Front. Cell. Neurosci. 13:223. doi: 10.3389/fncel.2019.00223

Endothelial progenitor cells (EPCs) are multipotential stem cells considered to have immense clinical value for revascularization. However, the clinical application of EPCs has been hampered by their clinical potency in ischemic anoxic environments. This study aimed to explore the effect of microRNA-210 (miR-210) on EPCs under oxygen-glucose deprivation (OGD) conditions. We generated a model of EPCs cultured under OGD conditions to simulate ischemia and explore the expression of miR-210 *in vitro*. With longer exposure to hypoxia, we found that miR-210-3p expression was highly upregulated in OGD groups compared to that in controls from 4 to 24 h, but not miR-210-5p. We then transfected a miR-210-3p mimic and inhibitor into EPCs, and after 24 h, we exposed them to OGD conditions for 4 h to simulate ischemia. We detected miR-210 by real-time polymerase chain reaction (RT-PCR) and tested the proliferation, migration, and tube formation of normal EPCs and OGD-treated EPCs by CCK-8, transwell chamber, and Matrigel assays, respectively. The direct targets of miR-210-3p were predicted using miRWalk. Compared to that in normal EPCs, higher miR-210-3p expression was found in OGD-treated EPCs ($p < 0.05$). Moreover, upregulation of miR-210-3p was found to promote proliferation, migration, and tube formation in EPCs under normal and OGD conditions ($p < 0.05$), whereas down-regulation inhibited these abilities in OGD-treated EPCs ($p < 0.05$). Repulsive guidance molecule A (RGMA), a negative regulator of angiogenesis, was predicted to be a target of miR-210-3p. Accordingly, upregulation of miR-210-3p was found to inhibit its expression at the protein level in OGD-treated EPCs, whereas downregulation of miR-210-3p inhibited its expression ($p < 0.05$). A dual-luciferase reporter system confirmed that RGMA is a direct target of miR-210-3p. MicroRNA-210-3p overexpression enhances the angiogenic properties of OGD-treated EPCs by inhibiting RGMA.

Keywords: angiogenesis, endothelial progenitor cells, oxygen-glucose deprivation injury, microRNA-210-3p, repulsive guidance molecule A

INTRODUCTION

Characterized by high mortality, morbidity, and disability, ischemic stroke causes immense health and economic burdens to families and society (Benjamin et al., 2017). However, the pathogenesis of stroke remains unclear and there are currently no effective treatments.

Endothelial progenitor cells (EPCs) are multipotential stem cells considered to have immense clinical value for revascularization. Previous research has demonstrated that EPCs can differentiate into mature endothelial cells (ECs) to take part in angiogenesis and vasculogenesis after cerebral ischemic injury (Chong et al., 2016). They have also been shown to participate in the repair of dysfunctional endothelia and to suppress endothelial injury through their direct incorporation into newly forming vessels or the secretion of pro-angiogenic growth factors or cytokines (Asahara et al., 2011). However, the clinical application of EPCs has been hampered by the limited numbers of surviving cells and their clinical potency in ischemic anoxic environments, in addition to the controversies surrounding their identities and functions (Zhao et al., 2013). Our study began with the key point of improving the ability of EPCs to resist hypoxia and ischemia.

As a class of conserved, single-stranded, endogenous, non-coding RNA, microRNAs (miRNAs) exert physiological effects mainly by negatively regulating gene expression at the post-transcriptional level. Further, they have been widely researched in both experimental and clinical settings. Usually, one miRNA can target more than one mRNA and one mRNA is targeted by more than one miRNA (Lim et al., 2005). This phenomenon results in the formation of an intricate regulatory network that plays important roles in biological processes such as cell proliferation, differentiation, apoptosis, early development, immunity, hematopoiesis and longevity, and angiogenesis, among others (Xu et al., 2003; Calin et al., 2004; Chen, 2004; Wang et al., 2009; de Rie et al., 2017). MicroRNA-210 (miR-210), the key hypoxia-related miRNA, was found to be upregulated in many different types of cells under hypoxic conditions. Studies revealed that this miRNA is involved in angiogenesis, regulating the cell cycle, differentiation, deoxyribonucleic acid repair, and apoptosis by targeting Ephrin-A3, E2F3, NPTX1, RAD52, ACVR1B, MNT, and CASP8AP2, among others (Chan and Loscalzo, 2010). Moreover, miR-210 improves cardiac function in a murine model of myocardial infarction by inhibiting apoptosis and enhancing angiogenesis (Hu et al., 2010). We have previously performed the peripheral blood miRNAs expression profiling in patients with acute cerebral ischemia (Zeng et al., 2016), and miR-210 is one of 10 significant differentially expressed miRNAs. Our previous studies also demonstrated that it is upregulated during the acute stage following cerebral ischemia in transient middle cerebral occlusion (tMCAO) mice (Zeng et al., 2016). Further, its overexpression was found to promote angiogenesis and neurogenesis and improve the prognosis of mice with cerebral ischemia by upregulating vascular endothelial growth factor (VEGF) and brain-derived neurotrophic factor (BDNF) levels (Zeng et al., 2014). MiR-210 has robust anti-hypoxia ability (Chan and Loscalzo, 2010), and it has been reported that miR-210 could enhance the hypoxia tolerance of bone marrow mesenchymal stem cells (MSCs) (Chang et al., 2013). Recent research has shown loading miR-210 in EPCs derived exosomes could boost the beneficial effects on hypoxia/reoxygenation injured human ECs (Ma et al., 2018). However, the function of miR-210 on EPCs was not previously known. Therefore, we hypothesized that the function of EPCs under ischemic conditions might be improved by miR-210 overexpression. We considered that the combination of miR-210 and EPCs could be a more effective therapy for treating stroke.

In this study, we used an *in vitro* cell model with oxygen-glucose deprivation (OGD) injury to simulate an ischemic environment. We investigated the possible functions of miR-210 in EPC under the hypoxic condition and further explored the potential underlying molecular mechanism in controlling cellular behavior.

MATERIALS AND METHODS

Cell Culture and OGD Treatment

Endothelial progenitor cells were extracted from the umbilical cord blood of the healthy parturient women. Umbilical cord blood was provided by the International Peace Maternity and Child Health Hospital, School of Medicine, Shanghai Jiao Tong University, Shanghai, China. And all participants were informed about the study protocol and given written informed consent according to the Declaration of Helsinki principles. The study protocol was approved by the Ethics Committee of Ruijin Hospital, Shanghai Jiao Tong University School of Medicine. Cells were cultured in Endothelial Growth Medium-2 (EGM-2) (Lonza, United States) at 37 ± 1°C with 5% CO_2, 90 ± 2% humidity in 10-cm^2 culture dishes. To mimic ischemia conditions *in vitro*, the culture medium was replaced and washed with phosphate buffered saline (PBS) (HyClone, United States), and cells were placed in an airtight experimental hypoxia chamber containing a gas mixture comprising 95% N_2 and 5% CO_2 for 4, 12, or 24 h. EPCs cultured with normal oxygen levels served as controls. All cells were collected for total RNA extraction using TRIzol (Invitrogen, United States). EPCs used in all experiments were fourth to the sixth generation.

Immunocytochemistry

Endothelial progenitor cells were washed with PBS (HyClone, United States), and then fixed in 4% paraformaldehyde (PFA) for 10 min. EPCs were then washed with PBS three times after PFA was discarded. Cells were permeabilized with 0.3% Triton-100 (Sigma-Aldrich, United States) for 10 min and blocked with 10% bovine serum albumin (BSA) (Sigma-Aldrich, United States) for 1 h. EPCs were incubated for 20 h at 4°C with primary antibodies in PBS as follows: polyclonal sheep anti-CD31 (1:200; R&D, United States), polyclonal sheep anti-CD34 (1:200; R&D, United States), polyclonal rabbit anti-Von Willebrand Factor (vWF) (1:200; Abcam, United Kingdom), polyclonal goat anti-KDR (1:200; R&D, United States), polyclonal rabbit anti- repulsive guidance molecule A (RGMA) (1:300; Abcam, United Kingdom). The

secondary antibodies were Alexa 488/594-conjugated donkey anti-sheep/rabbit/goat (1:1000; Invitrogen, United States) and the nuclei were stained by adding DAPI (1:1000; Invitrogen, United States). All samples were observed with a confocal laser scanning microscope (Leica, Germany).

Flow Cytometry

Endothelial progenitor cells were digested and centrifugalized when the cell density was 80–90%. Cells were then resuspended in PBS at a concentration of 1×10^7/ml. We used 1×10^6 cells in a 100-μl sample (test). EPCs were incubated with fluorescent antibodies including CD34-PE (1:5; BD Biosciences, United States), CD31-PE (1:5; BD Biosciences, United States), KDR-APC (1:5; BD Biosciences, United States), CD105-APC (1:20; BD Biosciences, United States), and CD133-PE (1:10; Miltenyi Biotec, Germany) in the dark for 30 min on the ice. Without washing, samples were analyzed by flow cytometry.

Cell Transfection

For miR-210-3p overexpression and suppression, a miR-210-3p mimic (5′-CUGUGCGUGUGACAGCGGCUGA-3′), miR-210-3p inhibitor (5′-UCAGCCGCUGUCACACGCACAG-3′), mimic control (5′-GCGCUCGUGGAGUGCGUGUCAA-3′) and inhibitor control (5′-GCCAGAGCCUGACCGCUACCUA-3′) were purchased from TuoRan (Shanghai, China). According to the manufacturer's protocol, we transfected mimic or mimic control at a concentration of 50 nM and inhibitor or inhibitor control at a concentration of 200 nM using Lipofectamine 2000 (Invitrogen, United States) in accordance with the manufacturer's instructions. All related experiments were performed within 24 h after transfection.

RNA Extraction, Reverse Transcription, and Real-Time PCR

Using the protocol for TRIzol (Invitrogen, United States), RNA extraction was performed. RNA concentration and purity were detected using the NanoDrop1000 spectrophotometer (Thermo Fisher Scientific, United States). Samples with an absorbance ratio at 260–280 nm between 1.8 and 2.0 were adopted. The Starter Kit (EXIQON, Denmark) was used for reverse transcription and real-time quantitative polymerase chain reaction (qPCR) according to the manufacturer's protocol in the measurement of miR-210. A fast real-time PCR system (7900 HT, ABI) was used for this amplification. The relative expression of miR-210 was normalized to the expression of the internal reference U6 and calculated by the $2^{-\Delta\Delta Ct}$ relative quantification method. As for RGMA (forward primer 5′-TCACCGACCGCTTCCAGACC-3′; reverse primers 3′-CTCCTTCACCAGTTACGACACCTC-5′), the PrimeScript^{TM} RT reagent Kit (Takara, Japan) was used for reverse transcription and real-time qPCR according to the manufacturer's protocol in the measurement of RGMA. The relative expression of RGMA was normalized to the expression of the internal reference GAPDH (forward primer 5′-GATGGTGAAGGTCGGTGTGA-3′; reverse primers 3′-TGAACTTGCCGTGGGTAGAG-5′) and calculated by the $2^{-\Delta\Delta Ct}$ relative quantification method.

Proliferation Assay

We used the cell counting kit-8 (CCK-8) (Dojindo, Japan) to examine EPC proliferation. For this, 1×10^4 cells with 100 μl of EGM-2 were inoculated into each well of a 96-well plate and incubated for 24 h. Then, a new medium containing CCK-8 reagent (10:1 v/v) was added to each well. Cells were further incubated at 37°C for 2 h. The absorption at 450 nm was examined using a microplate reader.

Migration Assay

As a classical *in vitro* model of angiogenesis, migration was assessed in 24-well plates with 8.0-mm pore polycarbonate membranes inserted (Corning, United States). In brief, we added 800 μl of EGM-2 into each well of the 24-well plate, which was followed by inserting chambers with polycarbonate membranes. Then, 2×10^4 cells with 200 μl of EBM-2 were added into each chamber in triplicate. After further incubation for 20 h, cells were fixed with PFA and stained with crystal violet for 10 min. The images of cells that migrated across the membrane were captured using a microscope (Leica, Germany). The tinctorial cells under the membranes were then counted and analyzed.

Tube Formation Assay

As another classical *in vitro* model of angiogenesis, tube formation assays were carried out in 96-well plates. Approximately 40 μl of Matrigel (BD, United States) was added into each well of a 96-well plate and incubated at 37°C for 30 min for solidification. Then, 1.5×10^4 cells were inoculated into the coated plate in triplicate. After culturing for 8 h at 37°C. After having obtained a series of three-dimensional focal stack images of the microvascular structure via a bright field microscope, we imported the stack images into Intensify3D to enhance and optimize the cell signal (Yayon et al., 2018). Then we used the AngioTool to calculate the tube length as previously reported (Zudaire et al., 2011).

Western Blotting

Endothelial progenitor cells were lysed and proteins were extracted separately from cells with radioimmunoprecipitation assay buffer (10 mM Tris/HCl, pH 8.0, 150 mM NaCl, 1 mM EDTA, 1% sodium deoxycholate, 1% Triton X-100, 0.1% SDS, and protease inhibitor cocktails) at 4°C and centrifuged at 12000 × *g* for 25 min to remove cell debris. The supernatant was transferred to a new tube and mixed with 5× loading buffer. For the detection of RGMA, samples were electrophoresed with a 10% polyacrylamide gel, and the proteins were electrophoretically transferred to polyvinylidene difluoride membranes. The membranes were blocked with Block Ace (Sangon, China) and incubated with a polyclonal rabbit anti-RGMA antibody (1:1000; Abcam, United Kingdom) and a monoclonal mouse anti-GAPDH antibody (1:1000; Invitrogen, United States) in TBST for 16 h at 4 °C. Antibodies were detected by incubating the samples with an HRP-conjugated secondary antibody (1:5000; Invitrogen, United States) for 1 h at room temperature. The blots were detected using Super Signal West Femto Substrate (Thermo Fisher Scientific, United States) and a

LAS-4000 imaging system. For densitometric quantification, the band density of RGMA relative to that of β-actin was quantified by NIH ImageJ software.

Luciferase Reporter Assays

In this study, the full length of the 3′UTR sequence was cloned (base from 1636 to 3227) to construct the luciferase reporter vectors. The full 3′UTR fragments from *RGMA* containing the predicted miR-210-3p-binding sites were amplified by PCR and subcloned downstream of the luciferase gene in the luciferase vector. The 3′UTR of *RGMA* with or without the mutant sequence was then amplified. For luciferase assays, EPCs were cultured in 24-well plates and co-transfected with 200 ng of firefly luciferase constructs, 4 ng of *Renilla* luciferase plasmid, and 50 nmol/L miR-210-3p mimic using Lipofectamine 2000. *Renilla* luciferase activity was measured using a dual-luciferase reporter assay 48 h after transfection. The results were expressed as relative luciferase activity (firefly luciferase/*Renilla* luciferase).

Data Analysis and Statistics

All statistical tests were performed using GraphPad Prism7. Data are presented as the mean ± SEM. Three or more replicates were always performed for each experiment in all assays. Statistical analyses were performed by one-way ANOVA followed by Student-Newman-Keuls tests. A probability value of $p < 0.05$ was considered statistically significant.

RESULTS

Culture and Identification of EPCs

We extracted mononuclear cells from the umbilical cord blood of healthy parturient women using lymphocyte separation liquid. The medium was changed twice per week until primary EPCs were passaged. Primary EPCs grew out at approximately the third week. We could see small, cobblestone-shaped cell clusters and growth and proliferation were highly apparent (**Figure 1A**). We subjected the fourth generation of EPCs to direct staining (**Figure 1B**) and under the microscope, we could see that nearly half of EPCs were stained for CD34 (green) and CD31 (green), whereas most of the EPCs were stained for KDR (red) and vWF (red). Flow cytometric analysis (**Figure 1C**) was used to identify the proportion of EPCs that were stained with endothelial surface antigens (CD105, 88.5%; CD31, 94.8%; KDR, 45.78∼63.85%) and stem cell surface markers (CD34, 59.54%; CD133, 2.12%). Our results thus showed that cultured cells derived from human cord blood were EPCs.

Upregulation of MiR-210-3p in EPCs Under OGD Conditions

We next generated a model of EPCs cultured under OGD conditions to simulate ischemia and explore the expression of miR-210 *in vitro*. Although the majority of EPCs survived when deprived of oxygen and glucose for 4 h, cell debris could still be observed under the microscope. With longer exposure to hypoxia, EPCs became deformed and disaggregated and died progressively from 4 to 24 h (**Figure 2A**). Correspondingly, miR-210-3p expression was highly upregulated in OGD groups compared to that in controls, whereas miR-210-5p expression was upregulated in OGD groups compared to expression in controls but did not rise markedly; in addition, there were no differences in expression among groups subjected to OGD for 4, 12, and 24 h (**Figure 2B**).

Upregulated MiR-210-3p Enhances the Angiogenic Ability of EPCs Under Normal Oxygen Conditions

To elucidate the involvement of miR-210-3p in the functional behaviors of EPCs, we transfected a miR-210-3p mimic, mimic control, miR-210-3p inhibitor, and inhibitor control into EPCs and subjected them to normal oxygen conditions. MiR-210-3p was upregulated in the mimic group but was not downregulated by the inhibitor (**Figure 3A**). We chose CCK-8, transwell, and Matrigel assays to test the proliferation (**Figure 3B**), migration (**Figure 3C**), and tube formation (**Figure 3D**) abilities, respectively, of these cells. Results showed that the EPC-miR-210-3p mimic group exhibited enhanced proliferative and migration abilities compared to EPCs alone. A similar outcome was observed for tube formation assays. Further, the EPC-miR-210-3p mimic group displayed the best tube formation ability among all groups. Other experimental conditions had no effect on EPCs. These data suggested that upregulated miR-210-3p expression enhances the angiogenic ability of EPCs under normal oxygen conditions.

Upregulated MiR-210-3p Enhances the Angiogenic Ability of EPCs Under OGD Conditions

To further elucidate the involvement of miR-210-3p in the functional behaviors of EPCs, we transfected a miR-210-3p mimic, mimic control, miR-210-3p inhibitor, and inhibitor control into EPCs under OGD conditions and performed the same experiments. MiR-210-3p was upregulated in the mimic group and downregulated in the inhibitor group (**Figure 4A**). We found that the EPC-miR-210-3p mimic group still exhibited enhanced proliferation, migration, and tube formation compared to those in EPCs alone under OGD conditions. However, the EPC-miR-210-3p inhibitor group showed the opposite result. Specifically, miR-210-3p inhibitor treatment resulted in reduced proliferation, subdued migration, and diminished tube formation (**Figures 4B–D**). These data suggested that upregulated miR-210-3p enhances the angiogenic ability of EPCs under OGD conditions, and in contrast, that downregulation of miR-210-3p inhibits these processes.

MiR-210-3p Targets RGMA

We next investigated the involvement of upregulated miR-210-3p, induced by OGD, in regulating RGMA expression in EPCs. First, the nucleotide coding region of *RGMA* mRNA was analyzed. A screen utilizing the online miRWalk software revealed putative binding between miR-210-3p and the *RGMA* 3′UTR. Further, *RGMA* mRNA expression was increased in EPCs

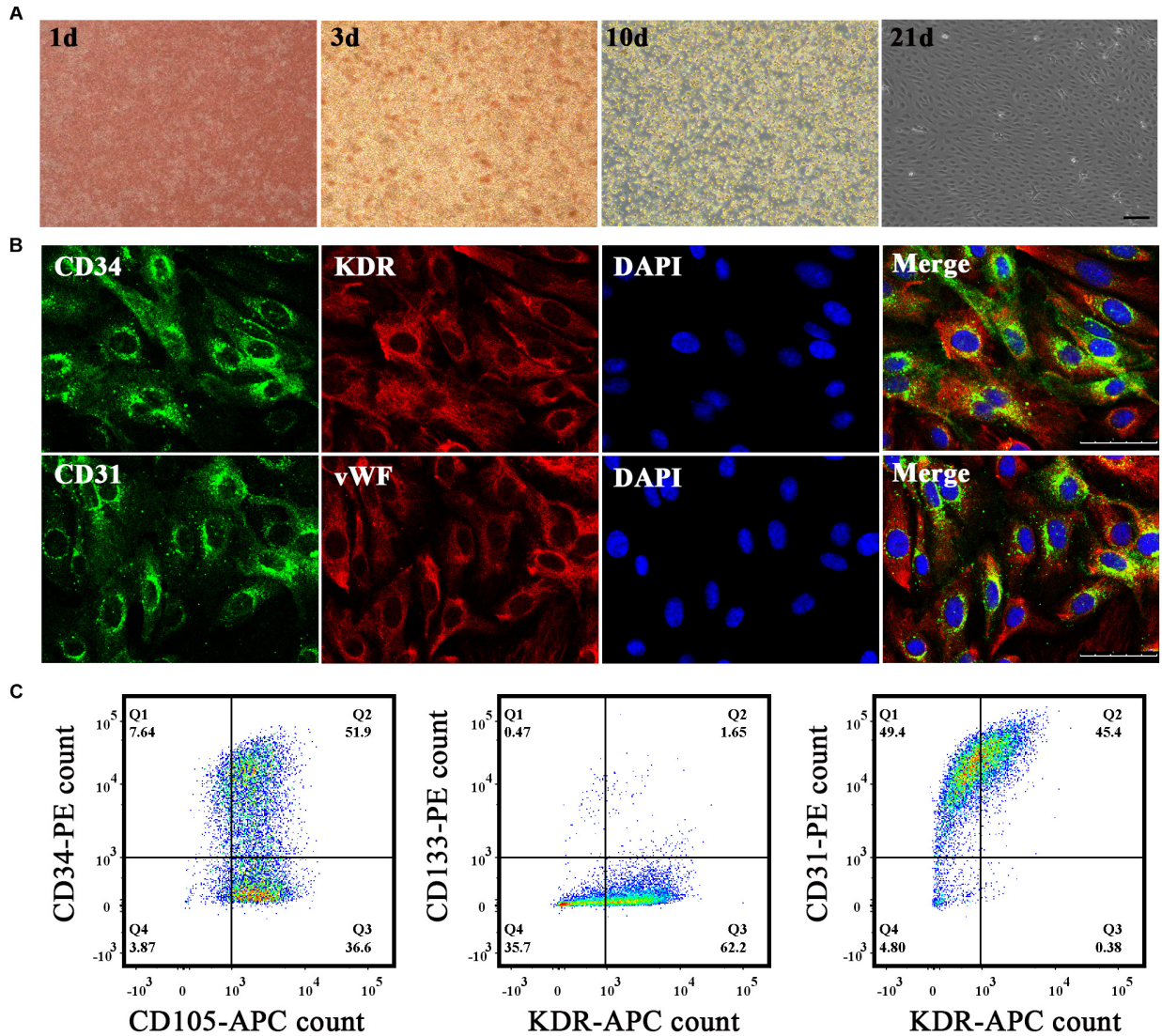

FIGURE 1 | Cultivation and identification of endothelial progenitor cells (EPCs). **(A)** EPCs were extracted from umbilical cord blood and morphological changes in primary EPCs were observed *in vitro* on the first, third, tenth, and twenty-first days successively under a microscope. Bar = 100 μm. **(B)** Immunohistochemistry staining results to identify EPCs. Biomarkers adopted were CD34, CD31, KDR, and vWF. Bar = 50 μm. **(C)** Flow cytometry results to identify EPCs. Biomarkers adopted were CD34, CD105, CD133, KDR, and CD31.

alone under OGD conditions (**Figure 5A**) but there was no difference among groups after mimic or inhibitor of miR-210-3p was transfected into EPCs under OGD conditions (**Figure 5B**). Subsequent experiments showed that the protein expression of RGMA was significantly suppressed in the miR-210-3p mimic group of EPCs but increased in the miR-210-3p inhibitor group (**Figures 5C,D** and **Supplementary Figure S1**). In addition, when performing reported assays, co-transfection of RGMA-WT and the miR-210-3p mimic resulted in the significant downregulation of luciferase activity compared to that with transfection of RGMA-WT alone or with co-transfection of RGMA-MT and the miR-210-3p mimic. In addition, upon comparing RGMA-WT alone and RGMA-MT and miR-210-3p mimic co-transfection groups, no significant difference was noted, supporting the contention that the miR-210 mimic can directly bind the *RGMA* 3′UTR (**Figure 5E**). Hence, *RGMA* is a target of miR-210-3p.

DISCUSSION

The results presented in our study are the first to reveal that miR-210-3p is overexpressed in OGD-treated EPCs. Further, miR-210-3p overexpression might enhance the angiogenic ability of EPCs under hypoxia conditions via the suppression of RGMA expression at the protein level. This study could provide a theoretical basis to uncover the molecular mechanisms underlying recovery after stroke and suggest a new treatment approach for this event.

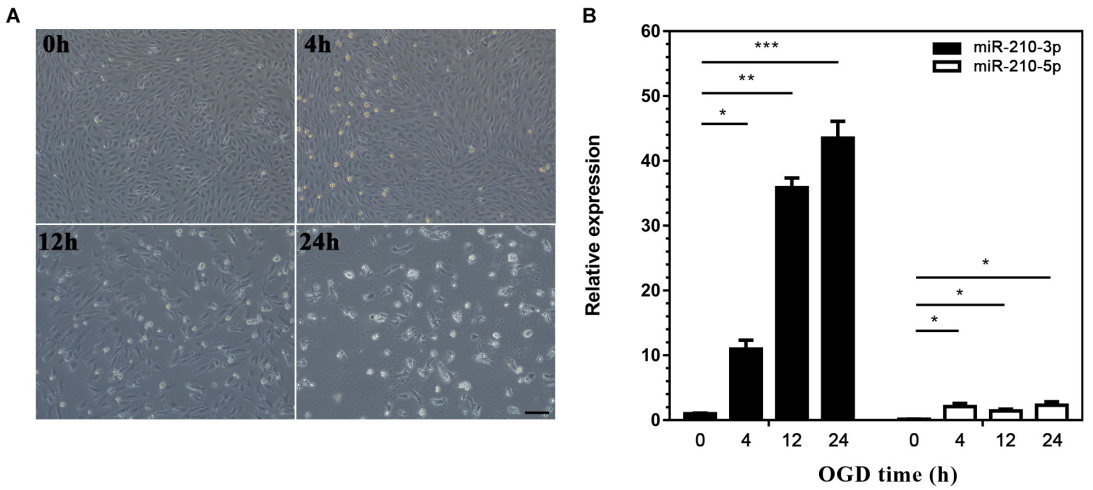

FIGURE 2 | Construction of oxygen and glucose deprivation (OGD) model and expression of microRNA (miR)-210. **(A)** Endothelial progenitor cells (EPCs) were exposed to OGD conditions for 0, 4, 12, and 24 h to simulate ischemia. Bar = 100 μm. **(B)** Real-time PCR was used to detected miR-210 expression in OGD-treated EPCs; $n = 3$ per group. Data are presented as the mean ± SEM, $^{*}p < 0.05$, $^{**}p < 0.01$, and $^{***}p < 0.001$.

Previously, only the 3-arm of precursor microRNA (designated as the guide strand) was thought to mature and become functional, whereas the complementary 5′-arm (referred to as microRNA* or the passenger strand) was considered destined for degradation. However, research results in recent years have discovered that both arms of the pre-microRNA might be expressed differently and modulate various aspects of biological processes (Essandoh et al., 2016). To avoid confusion, miRNA/miRNA* nomenclature is now replaced by miRNA-3p and miRNA-5p, respectively. To this end, we explored the expression of both arms of miR-210, namely miR-210-3p and miR210-5p, in OGD-treated EPCs. MiR-210-3p is the guide-strand that integrates into the RNA-induced silencing complex, whereas miR-210-5p is the passenger-strand that is inactivated through degradation (Bartel, 2004). In this study, we examined the expression of miR-210-3p and miR-210-5p on EPC cells after OGD in the meantime. The results showed that the expression of miR-210-3p was significantly increased after hypoxia, which was several tens of times higher than the baseline level. And the expression of miR-210-3p was positively correlated with OGD time. However, Although 5p increased after ischemia, the expression of miR-210-5p was very low, only 3–5 times higher than baseline, and there was no noticeable correlation with time increase. Based on the above facts, we speculate that during the formation process of mature miRNAs (miR-210-3p and -5p) from precursor miR-210, miR-210-3p plays the major biological function. So for subsequent experiments on EPC function under hypoxic conditions, we focused on miR-210-3p to explore the underlying molecular mechanism.

With a functional hypoxia-responsive element in its promoter region (Huang et al., 2009), miR-210 has been found to be expressed at high levels in many cell types such as cardiomyocytes (Martinez et al., 2017), adipose-derived stem cells (Kim et al., 2013), and tumor cells (Ying et al., 2011; McCormick et al., 2013) upon exposure to hypoxia. Moreover, miR-210 has been shown to be related to the development of different diseases including immunological diseases (Wang et al., 2014), cancers (Ying et al., 2011; McCormick et al., 2013), and cardiovascular and cerebrovascular diseases (Zeng et al., 2016; Martinez et al., 2017). Accumulating evidence has shown the diverse functions of miR-210 in multiple critical biological processes concerned with hypoxia such as cell cycle, proliferation, angiogenesis, apoptosis, DNA damage repair, mitochondrial metabolism, differentiation, and tumor growth. Hypoxia decreases cell viability, migration and invasion while increasing apoptosis. Previous studies demonstrated that miR-210 is upregulated in the serum of patients with acute cerebral infarction and that it might be involved in the pathogenesis of this disease by regulating the proliferation and apoptosis of endothelial cells (Wang et al., 2018). Similar to these results, our study demonstrated that the overexpression of miR-210, and specifically miR-210-3p, is precise and protects EPCs against OGD injury, in addition to enhancing angiogenesis in OGD-treated EPCs. We also showed that a miR-210-3p mimic could ameliorate hypoxia-induced injury in EPCs, whereas a miR-210-3p inhibitor had the opposite effects. In addition, among all data, statistics showed that the expression of miR-210-3p could not be suppressed under normal oxygen conditions to affect cell function. We suggested that this might due to its low original expression such that the inhibitors could not function efficiently. However, inhibitors worked well and restrained the angiogenic ability of EPCs under OGD conditions, which confirmed our hypothesis. Based on these data, miR-210-3p might have a possible proangiogenic effect on EPCs.

Research indicates that EPCs can contribute to the growth of new blood vessels, potentially restoring the health of ischemic tissue (Tongers et al., 2010; Fadini et al., 2012). Upon searching ClinicalTrials.gov, many trials involving EPCs for the treatment of ischemia have used systemic infusion directly as the delivery method. However, most results showed poor efficacy due to high cell death and a lack of control with respect to cell targeting.

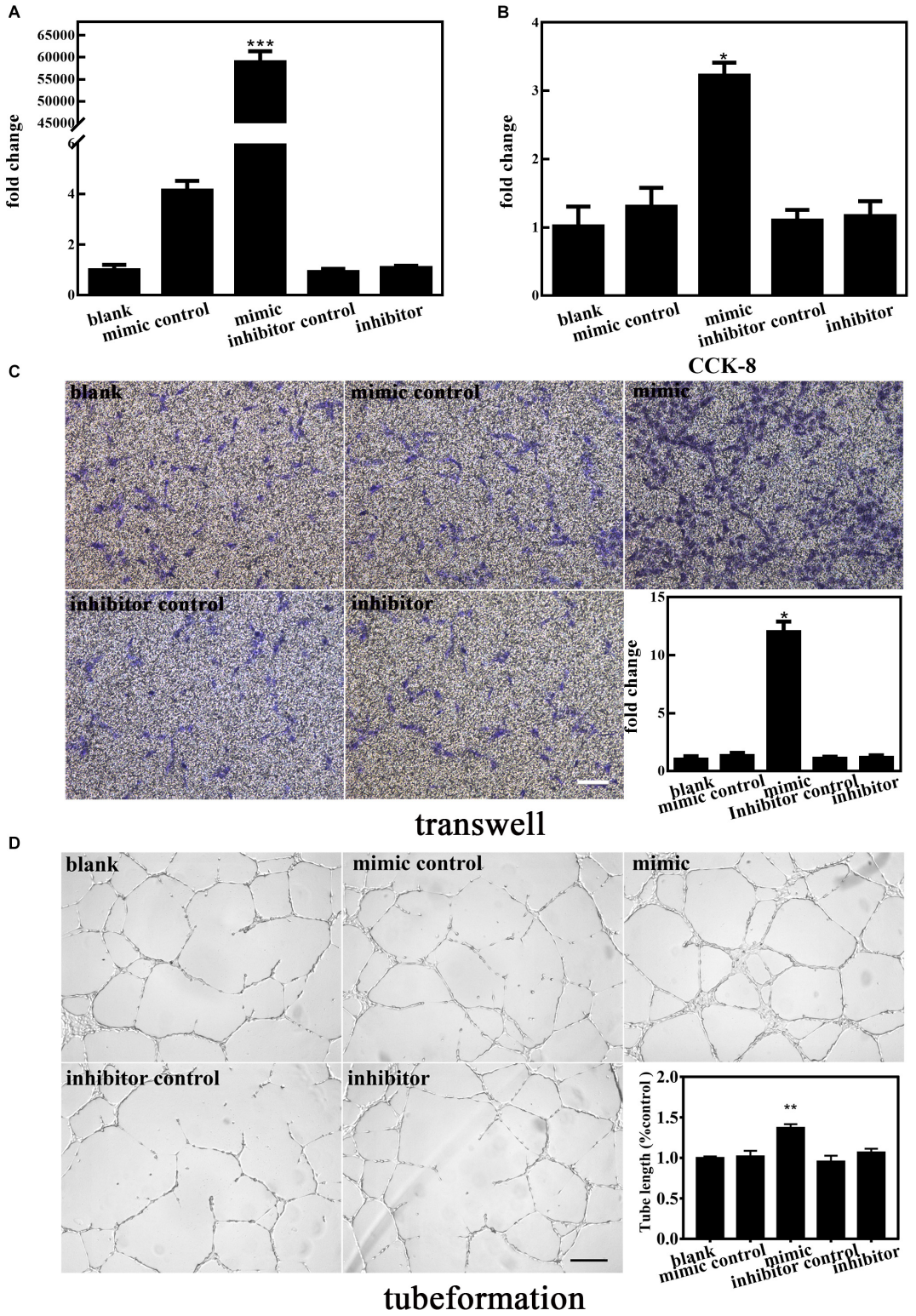

FIGURE 3 | Effect of altered miR-210-3p expression on normal endothelial progenitor cell (EPC) angiogenesis. **(A)** Expression of miR-210-3p increased obviously in the mimic group. **(B)** Graph of CCK-8 results showed that the proliferation rate in the mimic group was improved compared to that in the other four groups. **(C)** Representative images showing EPC migration. Bar graph indicates that overexpression of miR-210-3p in EPCs resulted in enhanced migration ability. Bar = 100 μm. **(D)** Representative images showing EPC tube formation ability. Bar graph indicates that overexpression of miR-210-3p in EPCs resulted in larger tube length. Bar = 250 μm; $n = 3$ per group. Data are presented as the mean ± SEM, $^{*}p < 0.05$, $^{**}p < 0.01$, and $^{***}p < 0.001$.

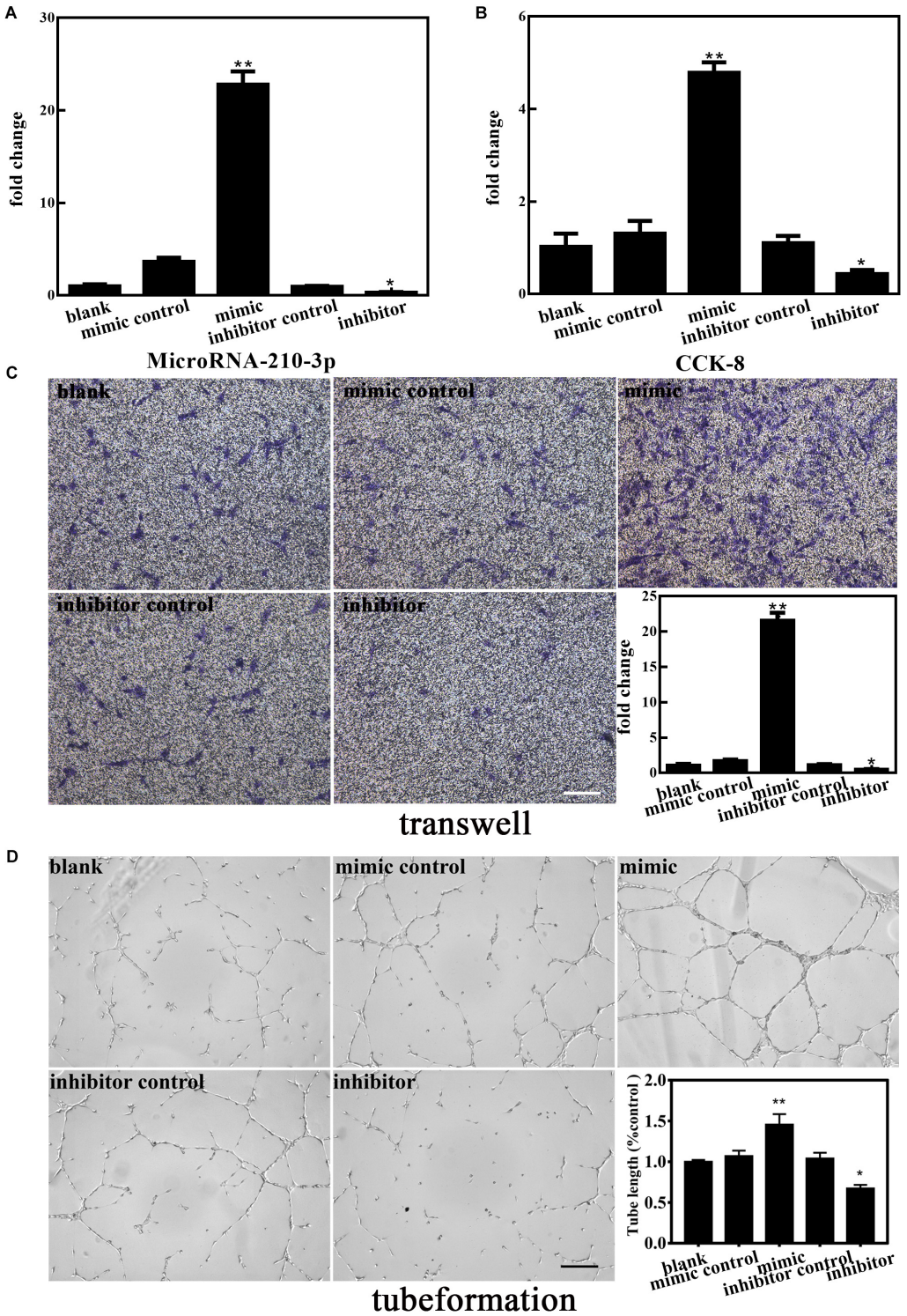

FIGURE 4 | Effect of altered miR-210-3p expression on angiogenesis of endothelial progenitor cells (EPCs) under oxygen and glucose deprivation (OGD). **(A)** The expression of miR-210-3p increased in the mimic group but the opposite results were observed in the inhibitor group. **(B)** Graph of CCK-8 results showing that the proliferation rate in the mimic group was improved compared to that in the blank group, with opposite results in the inhibitor group. **(C)** Representative images showing the effects of 4 h of OGD on EPC migration. Bar graph indicating that the overexpression of miR-210-3p under OGD conditions for 4 h resulted in higher migration ability, with opposite results observed in the inhibitor group. Bar = 100 μm. **(D)** Representative images showing tube formation under the condition of OGD for 4 h in EPCs. Bar graph indicating that the overexpression of miR-210-3p resulted in EPCs resulted in larger tube length under the OGD condition, with opposite results observed in the inhibitor group. Bar = 100 μm; $n = 3$ per group. Data are presented as the mean ± SEM, $^{*}p < 0.05$ and $^{**}p < 0.01$.

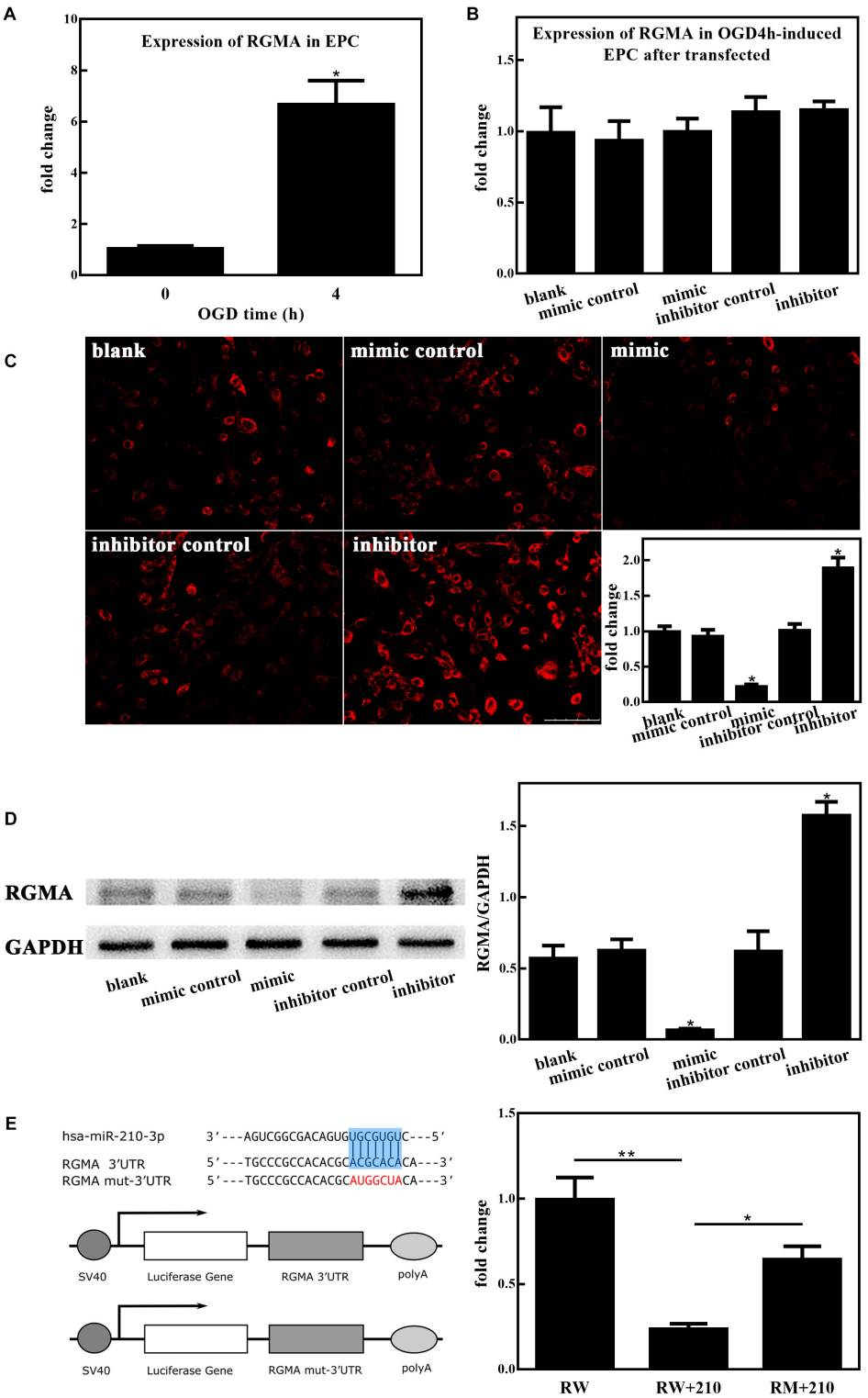

FIGURE 5 | MiR-210-3p overexpression enhances angiogenesis by inhibiting RGMA. **(A)** Bar graph indicating that the expression of *RGMA* mRNA increased in endothelial progenitor cells (EPCs) upon culture under oxygen and glucose deprivation (OGD) conditions for 4 h. **(B)** There were no statistically significant differences among groups in terms of the expression of *RGMA* mRNA. **(C,D)** Immunohistochemistry staining and western blot results of EPCs cultured under conditions of OGD for 4 h after transfection; the expression of RGMA protein were reduced in the mimic group, and opposite results were observed in the inhibitor group. Bar = 100 μm. **(E)** Luciferase reporter assay showing that miR-210-3p can directly bind *RGMA*; $n = 3$ per group. Data are presented as the mean ± SEM, $^{*}p < 0.05$ and $^{**}p < 0.01$.

EPCs are thus limited in their applications. One strategy to improve therapeutic outcomes is to combine such approaches with molecular therapy, thereby improving the survival rates and increasing the probability that cells will contribute to new blood vessel growth. We suggest that miR-210-3p overexpression could help to solve the existing problems and contribute to the application of EPCs to clinical treatment.

To shed light on the molecular mechanisms underlying the miR-210-3p-mediated control of cellular behavior, we used a bioinformatics method to virtually screen possible targets of miR-210-3p. Based on this, we focused on the interaction between miR-210-3p and *RGMA*, as results indicated that RGMA could be negatively regulated by miR-210-3p. Additional luciferase reporter assays further established that the *RGMA* 3′UTR was recognized by miR-210-3p. In previous studies, RGMA was shown to limit axonal regeneration after CNS injury (Hata et al., 2006) and to modulate T cell responses involved in autoimmune encephalomyelitis (Muramatsu et al., 2011). In summary, early research on RGMA was mainly focused on inflammation and autoimmune diseases. Recently, studies on the correlation between RGMA and ischemic disease have increased gradually. Zhang et al. found that RGMA suppresses the proliferation, tube formation, and migration of ECs by downregulating VEGF and p-FAK (Tyr397) via neogenin and Unc5b *in vitro* (Zhang et al., 2017). Wang et al. reported that RGMA might suppress angiogenesis via VEGF, Ang2, Ang1, and BDNF after cerebral ischemia/reperfusion injury through neogenin, thereby inhibiting neovascularization (Wang et al., 2018). Results of our study found that miR-210-3p overexpression has positive effects on cell proliferation, tube formation, and migration, suggesting that miR-210-3p might function through the negative regulation of RGMA. In addition, there was no difference in *RGMA* mRNA expression among groups, whereas the protein expression was significantly suppressed by a miR-210-3p mimic, suggesting that this miRNA primarily acts on gene translation and post-translational modification instead of transcription. Our study is the first to report that RGMA is a target of miR-210-3p in EPCs under hypoxia, and is consistent with previous reports (Wang et al., 2018) on the function of RGMA in ECs.

CONCLUSION

In conclusion, we report that miR-210-3p protects EPCs against OGD injury and enhances angiogenesis in OGD-treated EPCs. The suppression of RGMA, directly regulated by miR-210-3p overexpression, might partially contribute to the protection against hypoxic injury in EPCs and enhanced angiogenesis. Considering the potential application of these results, there are still many unknowns that require further exploration. For example, it will be more stringent to perform an unbiased screen by mass proteomics to identify the preferred targets of this miR. Secondly, downstream signaling pathways, in addition to the interaction between miR-210-3p and RGMA, in OGD-treated EPCs need to be studied. Moreover, we also need to further design related experiments *in vivo* to investigate Whether miR-210-3p overexpression could enhance the angiogenic function of EPCs on an MCAO mice model and the post-stroke long-term functional recovery.

AUTHOR CONTRIBUTIONS

L-LZ involved in all aspects of the study, supervised the tissue assay analysis, and participated in the study design, data analysis, and revision of the manuscript. X-YX participated in the revision of the manuscript and data analysis. W-JL drafted the enclosed manuscript and collected the human donor cells. H-BL performed the data analysis. Y-FL, X-QT, and K-QD revised the manuscript. J-RH and G-YY participated in the design of the present study and revision of the manuscript.

FUNDING

This work was supported by the National Natural Science Foundation of China (NSFC) (81471246 to L-LZ).

ACKNOWLEDGMENTS

We are sincerely grateful to all study participants. We would like to thank Editage for English language editing.

SUPPLEMENTARY MATERIAL

The Supplementary Material for this article can be found online at: https://www.frontiersin.org/articles/10.3389/fncel.2019.00223/full#supplementary-material

REFERENCES

Asahara, T., Kawamoto, A., and Masuda, H. (2011). Concise review: circulating endothelial progenitor cells for vascular medicine. *Stem Cells* 29, 1650–1655. doi: 10.1002/stem.745

Bartel, D. P. (2004). MicroRNAs: genomics, biogenesis, mechanism, and function. *Cell* 116, 281–297.

Benjamin, E. J., Blaha, M. J., Chiuve, S. E., Cushman, M., Das, S. R., Deo, R., et al. (2017). Heart disease and stroke statistics—2017 update: a report from the american heart association. *Circulation* 135, e146–e603.

Calin, G. A., Liu, C.-G., Sevignani, C., Ferracin, M., Felli, N., Dumitru, C. D., et al. (2004). MicroRNA profiling reveals distinct signatures in B cell chronic lymphocytic leukemias. *Proc. Natl. Acad. Sci. U.S.A.* 101, 11755–11760. doi: 10.1073/pnas.0404432101

Chan, S. Y., and Loscalzo, J. (2010). MicroRNA-210 a unique and pleiotropic hypoxamir. *Cell Cycle* 9, 1072–1083. doi: 10.4161/cc.9.6.11006

Chang, W., Lee, C. Y., Park, J.-H., Park, M.-S., Maeng, L.-S., Yoon, C. S., et al. (2013). Survival of hypoxic human mesenchymal stem cells is enhanced by a positive feedback loop involving miR-210 and hypoxia-inducible factor 1. *J. Vet. Sci.* 14, 69–76.

Chen, C.-Z. (2004). MicroRNAs modulate hematopoietic lineage differentiation. *Science* 303, 83–86. doi: 10.1126/science.1091903

Chong, M. S. K., Ng, W. K., and Chan, J. K. Y. (2016). Concise review: endothelial progenitor cells in regenerative medicine: applications and

challenges: endothelial progenitors in regenerative medicine. *Stem Cells Transl. Med.* 5, 530–538. doi: 10.5966/sctm.2015-0227

de Rie, D., Abugessaisa, I., Alam, T., Arner, E., Arner, P., Ashoor, H., et al. (2017). An integrated expression atlas of miRNAs and their promoters in human and mouse. *Nat. Biotechnol.* 35, 872–878. doi: 10.1038/nbt.3947

Essandoh, K., Li, Y., Huo, J., and Fan, G.-C. (2016). MiRNA-mediated macrophage polarization and its potential role in the regulation of inflammatory response. *Shock* 46, 122–131. doi: 10.1097/SHK.0000000000000604

Fadini, G. P., Losordo, D., and Dimmeler, S. (2012). Critical reevaluation of endothelial progenitor cell phenotypes for therapeutic and diagnostic use. *Circ. Res.* 110, 624–637. doi: 10.1161/CIRCRESAHA.111.243386

Hata, K., Fujitani, M., Yasuda, Y., Doya, H., Saito, T., Yamagishi, S., et al. (2006). RGMa inhibition promotes axonal growth and recovery after spinal cord injury. *J. Cell Biol.* 173, 47–58. doi: 10.1083/jcb.200508143

Hu, S., Huang, M., Li, Z., Jia, F., Ghosh, Z., Lijkwan, M. A., et al. (2010). MicroRNA-210 as a novel therapy for treatment of ischemic heart disease. *Circulation* 122, S124–S131. doi: 10.1161/CIRCULATIONAHA.109.928424

Huang, X., Ding, L., Bennewith, K. L., Tong, R. T., Welford, S. M., Ang, K. K., et al. (2009). Hypoxia-inducible mir-210 regulates normoxic gene expression involved in tumor initiation. *Mol. Cell* 35, 856–867. doi: 10.1016/j.molcel.2009.09.006

Kim, J. H., Park, S. G., Song, S.-Y., Kim, J. K., and Sung, J.-H. (2013). Reactive oxygen species-responsive miR-210 regulates proliferation and migration of adipose-derived stem cells via PTPN2. *Cell Death Dis.* 4:e588. doi: 10.1038/cddis.2013.117

Lim, L. P., Lau, N. C., Garrett-Engele, P., Grimson, A., Schelter, J. M., Castle, J., et al. (2005). Microarray analysis shows that some microRNAs downregulate large numbers of target mRNAs. *Nature* 433, 769–773.

Ma, X., Wang, J., Li, J., Ma, C., Chen, S., Lei, W., et al. (2018). Loading MiR-210 in endothelial progenitor cells derived exosomes boosts their beneficial effects on hypoxia/reoxygeneation-injured human endothelial cells via protecting mitochondrial function. *Cell. Physiol. Biochem.* 46, 664–675. doi: 10.1159/000488635

Martinez, S. R., Ma, Q., Dasgupta, C., Meng, X., and Zhang, L. (2017). MicroRNA-210 suppresses glucocorticoid receptor expression in response to hypoxia in fetal rat cardiomyocytes. *Oncotarget* 8, 80249–80264. doi: 10.18632/oncotarget.17801

McCormick, R. I., Blick, C., Ragoussis, J., Schoedel, J., Mole, D. R., Young, A. C., et al. (2013). miR-210 is a target of hypoxia-inducible factors 1 and 2 in renal cancer, regulates ISCU and correlates with good prognosis. *Br. J. Cancer* 108, 1133–1142. doi: 10.1038/bjc.2013.56

Muramatsu, R., Kubo, T., Mori, M., Nakamura, Y., Fujita, Y., Akutsu, T., et al. (2011). RGMa modulates T cell responses and is involved in autoimmune encephalomyelitis. *Nat. Med.* 17, 488–494. doi: 10.1038/nm.2321

Tongers, J., Roncalli, J. G., and Losordo, D. W. (2010). Role of endothelial progenitor cells during ischemia-induced vasculogenesis and collateral formation. *Microvasc. Res.* 79, 200–206. doi: 10.1016/j.mvr.2010.01.012

Wang, H., Flach, H., Onizawa, M., Wei, L., McManus, M. T., and Weiss, A. (2014). Negative regulation of Hif1a expression and TH17 differentiation by the hypoxia-regulated microRNA miR-210. *Nat. Immunol.* 15, 393–401. doi: 10.1038/ni.2846

Wang, Y., Keys, D. N., Au-Young, J. K., and Chen, C. (2009). MicroRNAs in embryonic stem cells. *J. Cell. Physiol.* 218, 251–255. doi: 10.1002/jcp.21607

Wang, Y., Zhang, R., Xing, X., Guo, J., Xie, F., Zhang, G., et al. (2018). Repulsive guidance molecule a suppresses angiogenesis after ischemia/reperfusion injury of middle cerebral artery occlusion in rats. *Neurosci. Lett.* 662, 318–323. doi: 10.1016/j.neulet.2017.10.036

Xu, P., Vernooy, S. Y., Guo, M., and Hay, B. A. (2003). The Drosophila microRNA Mir-14 suppresses cell death and is required for normal fat metabolism. *Curr. Biol.* 13, 790–795. doi: 10.1016/s0960-9822(03)00250-1

Yayon, N., Dudai, A., Vrieler, N., Amsalem, O., London, M., and Soreq, H. (2018). Intensify3d: normalizing signal intensity in large heterogenic image stacks. *Sci. Rep.* 8:4311. doi: 10.1038/s41598-018-22489-1

Ying, Q., Liang, L., Guo, W., Zha, R., Tian, Q., Huang, S., et al. (2011). Hypoxia-inducible MicroRNA-210 augments the metastatic potential of tumor cells by targeting vacuole membrane protein 1 in hepatocellular carcinoma. *Hepatology* 54, 2064–2075. doi: 10.1002/hep.24614

Zeng, L.-L., He, X.-S., Liu, J.-R., Zheng, C.-B., Wang, Y.-T., and Yang, G.-Y. (2016). Lentivirus-mediated overexpression of microRNA-210 improves long-term outcomes after focal cerebral ischemia in mice. *CNS Neurosci. Ther.* 22, 961–969. doi: 10.1111/cns.12589

Zeng, L., He, X., Wang, Y., Tang, Y., Zheng, C., Cai, H., et al. (2014). MicroRNA-210 overexpression induces angiogenesis and neurogenesis in the normal adult mouse brain. *Gene Ther.* 21, 37–43. doi: 10.1038/gt.2013.55

Zhang, G., Wang, R., Cheng, K., Li, Q., Wang, Y., Zhang, R., et al. (2017). Repulsive guidance molecule a inhibits angiogenesis by downregulating VEGF and phosphorylated focal adhesion kinase in vitro. *Front. Neurol.* 8:504. doi: 10.3389/fneur.2017.00504

Zhao, Y.-H., Yuan, B., Chen, J., Feng, D.-H., Zhao, B., Qin, C., et al. (2013). Endothelial progenitor cells: therapeutic perspective for ischemic stroke. *CNS Neurosci. Ther.* 19, 67–75. doi: 10.1111/cns.12040

Zudaire, E., Gambardella, L., Kurcz, C., and Vermeren, S. (2011). A computational tool for quantitative analysis of vascular networks. *PLoS One* 6:e27385. doi: 10.1371/journal.pone.0027385

Conflict of Interest Statement: The authors declare that the research was conducted in the absence of any commercial or financial relationships that could be construed as a potential conflict of interest.

Copyright © 2019 Lu, Liang, Li, Tu, He, Ding, Yang, Xin and Zeng. This is an open-access article distributed under the terms of the Creative Commons Attribution License (CC BY). The use, distribution or reproduction in other forums is permitted, provided the original author(s) and the copyright owner(s) are credited and that the original publication in this journal is cited, in accordance with accepted academic practice. No use, distribution or reproduction is permitted which does not comply with these terms.

frontiers in Cellular Neuroscience

ORIGINAL RESEARCH
published: 24 May 2019
doi: 10.3389/fncel.2019.00236

Dysfunction of 67-kDa Laminin Receptor Disrupts BBB Integrity via Impaired Dystrophin/AQP4 Complex and p38 MAPK/VEGF Activation Following Status Epilepticus

*Hana Park[1,2], Seo-Hyeon Choi[1,2], Min-Jeong Kong[1,2] and Tae-Cheon Kang[1,2]**

[1] Department of Anatomy and Neurobiology, College of Medicine, Hallym University, Chuncheon, South Korea, [2] Institute of Epilepsy Research, College of Medicine, Hallym University, Chuncheon, South Korea

Status epilepticus (SE, a prolonged seizure activity) impairs brain-blood barrier (BBB) integrity, which results in secondary complications following SE. The non-integrin 67-kDa laminin receptor (67-kDa LR) plays a role in cell adherence to laminin (a major glycoprotein component in basement membrane), and participates laminin-mediated signaling pathways including p38 mitogen-activated protein kinase (p38 MAPK). Thus, we investigated the role of 67-kDa LR in SE-induced vasogenic edema formation in the rat piriform cortex (PC). SE diminished 67-kDa LR expression, but increased laminin expression, in endothelial cells accompanied by the reduced SMI-71 (a rat BBB barrier marker) expression. Astroglial 67-kDa LR expression was also reduced in the PC due to massive astroglial loss. 67-kDa LR neutralization led to serum extravasation in the PC concomitant with the reduced SMI-71 expression. 67-kDa LR neutralization also decreased expressions of dystrophin and aquaporin-4 (AQP4). In addition, it increased p38 MAPK phosphorylation and expressions of vascular endothelial growth factor (VEGF), laminin and endothelial nitric oxide synthase (eNOS), which were abrogated by SB202190, a p38 MAPK inhibitor. Therefore, our findings indicate that 67-kDa LR dysfunction may disrupt dystrophin-AQP4 complex, which would evoke vasogenic edema formation and subsequent laminin over-expression via activating p38 MAPK/VEGF axis.

Keywords: SMI-71, eNOS, SB202190, laminin, vasogenic edema

OPEN ACCESS

Edited by:
Gregory Jaye Bix,
University of Kentucky, United States

Reviewed by:
Hermona Soreq,
Hebrew University of Jerusalem, Israel
Yu-Feng Wang,
Harbin Medical University, China

***Correspondence:**
Tae-Cheon Kang
tckang@hallym.ac.kr

Specialty section:
This article was submitted to Cellular Neurophysiology, a section of the journal Frontiers in Cellular Neuroscience

Received: *16 March 2019*
Accepted: *09 May 2019*
Published: *24 May 2019*

Citation:
Park H, Choi S-H, Kong M-J and Kang T-C (2019) Dysfunction of 67-kDa Laminin Receptor Disrupts BBB Integrity via Impaired Dystrophin/AQP4 Complex and p38 MAPK/VEGF Activation Following Status Epilepticus. Front. Cell. Neurosci. 13:236. doi: 10.3389/fncel.2019.00236

INTRODUCTION

Vasogenic edema is the most common type of brain edema and a result from increased capillary permeability due to breakdown in intact brain-blood barrier (BBB) that is important for the maintenance of brain homeostasis. Vasogenic edema results in an abrupt increase in intracranial pressure and abnormal blood-brain transports of serum-derived molecules, which affect neuronal excitability, properties of regenerating (recovering) vessels, white matter injury and reactive gliosis in brain tumor, exposure of insecticides, traumatic brain injury (TBI), ischemia and brain inflammation (Papadopoulos et al., 2004; Song et al., 2004; Bloch et al., 2005; Kim et al., 2010b;

Li and Ehrich, 2013; Kim Y.J. et al., 2015; Ko and Kang, 2015; Bennett et al., 2016; Zhao et al., 2018; Sun et al., 2019). Therefore, the prevention or attenuation of vasogenic edema formation is one of the major therapeutic strategies, which help to alleviate undesirable secondary complications in various neurological diseases.

Status epilepticus (SE) is a medical emergency condition with significant mortality showing continuous seizure activity. SE is considered as one of the precipitating factors for temporal lobe epilepsy (TLE) that is observed in one-third of all cases of epilepsy. Human TLE patients present neuronal loss and reactive astrogliosis in various brain regions including the hippocampus, which are influenced by SE (Fountain, 2000; Koh et al., 2005; Téllez-Zenteno and Hernández-Ronquillo, 2012; Sørensen and Kokaia, 2013). Similar to human patients, SE-induced epilepsy animal models show massive neuronal loss and astroglial dysfunctions in the various brain regions. Furthermore, vasogenic edema is one of the early post-SE events in the hippocampus and extrahippocampal limbic systems including the piriform cortex (PC). Since serum extravasation during vasogenic edema formation leads to spreading depolarizations and epileptiform discharges due to neuronal hyperexcitability, dysfunction of astrocytes and potassium buffering (Sisodiya et al., 2002; Löscher and Potschka, 2005; Kim Y.J. et al., 2015; Lippmann et al., 2017), it is likely that vasogenic edema may be one of the risk factors inducing pharmacoresistant epilepsy and life-threatening complications following SE.

The BBB consists of endothelial cells, astroglial endfeet, pericytes and basement membrane (BM; Banerjee and Bhat, 2007). The BM is vital for endothelial cell adhesion, migration and stabilization under physiological conditions. The BM is a structural and specialized complex of extracellular matrix protein including laminin, fibronectin, vitronectin, collagen, and heparin sulfate proteoglycans (Tilling et al., 2002; Yurchenco and Patton, 2009). Among them, laminin is a major glycoprotein component of BMs in vessels, and is involved in cellular adhesion and migratory processes (Miner, 2008). Thus, laminin is essential for vascular development, vessel dilation and physical integrity (Thyboll et al., 2002). Interestingly, laminin expression is remarkably upregulated in the BM of vessels following SE (Biagini et al., 2008; Gualtieri et al., 2012). Indeed, we have reported that laminin over-expression is closely relevant to the repair of BBB disruption accompanied by the reconstruction of endothelial barrier following SE (Kim et al., 2014). However, the underlying mechanism of up-regulation of laminin expression in vasogenic edema formation has not been fully elucidated.

The laminin functions are mediated by cell-surface receptors of two main classes: the integrins and the non-integrin 67-kDa laminin receptor (67-kDa LR; Lesot et al., 1983; Malinoff and Wicha, 1983; Rao et al., 1983). 67-kDa LR is composed of a 32 ∼ 33 kDa precursor (approximately 37 kDa in sodium dodecyl sulfate polyacrylamide gel electrophoresis). 67-kDa LR plays a role in cell adherence to laminin and stabilizes or modulates the binding of laminin to other receptors (Pellegrini et al., 1994; Ardini et al., 1998). In addition, 67-kDa LR is involved in laminin-mediated extracellular signal-regulated kinase 1/2 (ERK1/2), c-Jun N-terminal kinase (JNK) and p38 mitogen-activated protein kinase (p38 MAPK) signaling pathways (Givant-Horwitz et al., 2004). It also binds to several exogenous agents (including prion proteins, viruses and bacteria) and regulates cellular migration, viability and cytoskeleton reorganization (Wewer et al., 1986; Rao et al., 1989; Huang and Jong, 2009; Vana et al., 2009; Kielian et al., 2010). Furthermore, 67-kDa LR is expressed in the adult rat brain (Baloui et al., 2004). With respect to these profiles of 67-kDa LR, elucidating the correlation between 67-kDa LR expression and vasogenic edema formation may be noteworthy to understand the mechanisms of BBB disruption and laminin over-expression in response to SE. Therefore, during the course of this study, we investigated the alteration in 67-kDa LR expression induced by SE, and the effect of blockade of 67-kDa LR by neutralization on laminin expression or BBB integrity in efforts to understand the role of vascular dysfunction in epileptogenic insult.

MATERIALS AND METHODS

Experimental Animals and Chemicals

Male Sprague-Dawley (SD) rats (7 weeks old) were used in the present study. Animals were housed in a controlled temperature (22 ± 2°C), humidity (55 ± 5%) and a light-dark cycle (12:12). Food and tap water were provided *ad libitum* throughout the experiments. All experimental protocols described below were approved by the Institutional Animal Care and Use Committee of Hallym University (Chuncheon, South Korea). Every effort was made to reduce the number of animals employed and to minimize animal's discomfort. All reagents were obtained from Sigma-Aldrich (St. Louis, MO, United States), except as noted.

SE Induction

Rats were pretreated with an intraperitoneal injection of LiCl (127 mg/kg i.p) 24 h before the pilocarpine (PILO) treatment. Animals were intraperitoneally (i.p) treated with PILO (30 mg/kg) 20 min after atropine methylbromide (5 mg/kg i.p.). PILO injection resulted in stereotypical behavioral responses, which included the following: akinesia, staring, salivation, facial automatisms, slight tremors and head bobbing. These behavior responses built up progressively into motor limbic seizures that recurred repeatedly and rapidly developed into SE characterized by forelimb clonus and tonic-clonic seizures with loss of righting reflexes. SE was defined by continuous or intermittent seizures without full recovery between seizures. Control animals received an equal volume of normal saline instead of PILO after the pretreatment with atropine methylbromide. Diazepam (Valium; Hoffman la Roche; 10 mg/kg, i.p.) was administered 2 h after onset of SE and repeated, as needed. Three days after SE, animals were used for Western blot and immunohistochemistry.

Surgery

Under Isoflurane anesthesia (3% induction, 1.5–2% for surgery and 1.5% maintenance in a 65:35 mixture of N_2O:O_2), animals were infused each chemical into the right lateral ventricle (1 mm posterior; 1.5 mm lateral; −3.5 mm depth to the bregma) with a brain infusion kit 1 and an Alzet 1003D osmotic pump (Alzet,

United States) for 3 days. Osmotic pump contained (1) control IgG (Abcam, #ab37425, United Kingdom, 50 ug/ml) + vehicle, (2) control IgG + SB202190 (a p38 MAPK inhibitor, 0.3 mg/ml), (3) anti-67-kDa LR IgG (Abcam, #133645, United Kingdom, 50 ug/ml) + vehicle and (4) anti-67-kDa LR IgG (Abcam, #133645, United Kingdom, 50 ug/ml) + SB202190 (0.3 mg/ml). In pilot study and our previous studies (Kim et al., 2016; Ko and Kang, 2017), each compound treatment did not show behavioral and neurological defects and could not change the seizure susceptibility and seizure severity in response to PILO in normal animals. Three days after surgery (infusion), animals were used for Western blot and immunohistochemistry.

Western Blot

After animals were sacrificed via decapitation, the PC was obtained. The PC tissues were homogenized, and determined protein concentration using a Micro BCA Protein Assay Kit (Pierce Chemical, United States). Western blot was performed by the standard protocol. Membranes were incubated with primary antibody against 67-kDa LR (Abcam, #133645, United Kingdom, diluted 1:1,000), aquaporin-4 (AQP4, Alomone labs, #AQP-004, Israel, 1:5,000), dystrophin (Abcam, #ab15277, United Kingdom, diluted 1:5,000), endothelial nitric oxide synthase (eNOS, Abcam, #ab66127, United Kingdom, diluted 1:1,000), laminin (Abcam, #ab11575, United Kingdom, diluted 1:1,000), p38 MAPK (Cell signaling, #9212, United States, diluted 1:1000) or p-p38 MAPK (Abbiotec, #251246, United States, diluted 1:200), rat IgG (Vector, #PI9400, United States, diluted 1:200) or VEGF (Abcam, #ab46154, United Kingdom, diluted 1:1000) and visualized by an ECL Kit (Amersham, United States). The bands were detected and quantified on ImageQuant LAS4000 system (GE Healthcare, United States). As an internal reference, rabbit anti-β-actin primary antibody (#A5316, 1:5000) was used. The values of each sample were normalized with the corresponding amount of β-actin. The ratio of phosphoprotein to total protein was described as phosphorylation ratio.

Immunohistochemistry

Rats were anesthetized with urethane anesthesia (1.5 g/kg, i.p.) and intracardially perfused with 4% paraformaldehyde in 0.1 M phosphate buffer (PB, pH 7.4). Subsequently, brains were post-fixed in the same fixative overnight, followed by cryoprotection with 30% sucrose/0.1 M PBS, and sectioned at 30 μm with a cryo-microtome. Standard procedures for immunohistochemistry were used to detect vasogenic edema formation. Briefly, free-floating sections were washed three times in PBS (0.1 M, pH 7.3). Next, to inactivate the endogenous peroxidase, slides were incubated in 3% H_2O_2 and 10% methanol in PBS (0.1 M) for 20 min at room temperature. Later, sections were incubated in biotinylated rat IgG (Vector, #BA9400, United States, diluted 1:200) and ABC complex (Vector, #PK-6100, United States, diluted 1:200). Tissue sections were developed in 3,3′-diaminobenzidine in 0.1 M Tris buffer and mounted on gelatin-coated slides. The volume of vasogenic edema lesion in the PC was measured by AxioVision Rel. 4.8 software and estimated by the modified Cavalieri method: $V = \Sigma area \times$ section thickness (30 μm) $\times$ 1/the fraction of the sections (1/6). The volumes are reported in mm^3 (Kim et al., 2016).

Some sections were incubated with a cocktail solution containing the primary antibodies against 67-kDa LR (Abcam, #ab133775, United Kingdom, diluted 1:500), AQP4 (Alomone labs, #AQP-004, Israel, diluted 1:500), dystrophin (Abcam, #ab15277, United Kingdom, diluted 1:500), eNOS (Abcam, #ab66127, United Kingdom, diluted 1:500), glial fibrillary acidic protein (GFAP, Millipore, #MAB3402, United States, diluted 1:5,000), laminin (Abcam, #ab11575, United Kingdom, diluted 1:200) and SMI-71 (Covance, #SMI-71R, United States, diluted 1:1000) in PBS containing 0.3% Triton X-100 overnight at room temperature. Thereafter, sections were visualized with appropriate Cy2- and Cy3-conjugated secondary antibodies. Immunoreaction was observed using an Axio Scope microscope (Carl Zeiss Inc., Germany). To establish the specificity of the immunostaining, a negative control test was carried out with preimmune serum instead of the primary antibody. No immunoreactivity was observed for the negative control in any structures (data not shown). All experimental procedures in this study were performed under the same conditions and in parallel. To quantify relative fluorescence intensity, sections (10 sections per each animal) were captured using an AxioImage M2 microscope. A 300-μm^2 box was then randomly placed within the region of interest. Thereafter, mean fluorescence intensity of each section was measured by using AxioVision Rel. 4.8 software. Fluorescence intensity measurements were represented as the number of a 256 gray scale. Fluorescence intensity values were corrected by subtracting the average values of background noise (mean background intensity) obtained from five image inputs. Fluorescent intensity of each section was standardized by setting the threshold level (mean background intensity obtained from five image inputs). Manipulation of the images was restricted to threshold and brightness adjustments to the whole image (Kim et al., 2013, 2014; Kim and Kang, 2017).

Statistical Analysis

Quantitative data are expressed as mean ± standard error of the mean. Data are analyzed by Student *t*-test or one-way ANOVA followed by Newman–Keuls *post hoc* test. A $p < 0.05$ is considered to be statistically different.

RESULTS

SE-Induced Reduction in 67-kDa LR Expression in Vasogenic Edema Lesion

Consistent with our previous studies (Sheen et al., 2011; Kim et al., 2012, 2013, 2014), **Figure 1** shows that SE led to serum extravasation in the PC ($p < 0.05$ vs. control animals, Student *t*-test, $n = 7$, respectively). In addition, SE increased laminin expression to 3.2-fold of control level in the PC ($p < 0.05$ vs. control animals, Student *t*-test, $n = 7$, respectively; **Figures 1A,B** and **Supplementary Figure S1**). However, 67-kDa LR expression level was diminished to ∼ 0.68-fold of control level in this region ($p < 0.05$ vs. control animals, Student

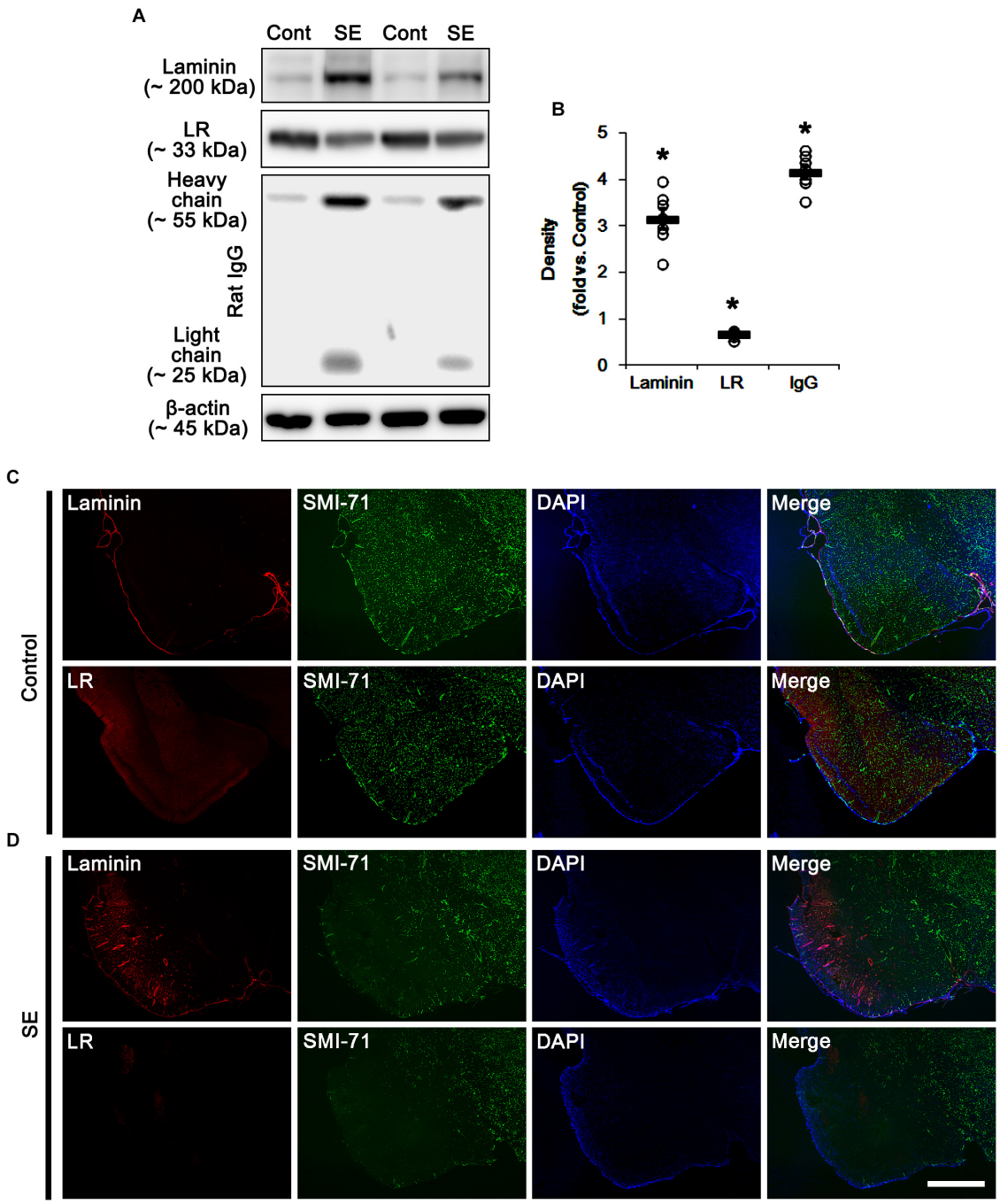

FIGURE 1 | Alterations in laminin and 67-kDa LR (LR) expression in the PC following SE. **(A)** Western blot image for expression levels of laminin and 67-kDa LR, and serum extravasation following SE. SE increases laminin expression and serum extravasation, but reduces 67-kDa LR expression. **(B)** Quantitative values (mean ± S.E.M) of the Western blot data concerning expression levels of laminin and 67-kDa LR, serum extravasation induced by SE (n = 7, respectively). Open circles indicate each individual value. Horizontal bars indicate mean value. Significant differences are $^*p < 0.05$ vs. control animals (Student t-test). **(C,D)** Representative photographs of expression levels of laminin and 67-kDa LR in vasogenic edema (SMI-71-deleted) lesion in the PC in control **(C)**- and post-SE condition **(D)**. In SMI-71-deleted area, laminin expression is enhanced, while 67-kDa LR expression is decreased. Bar = 400 μm.

t-test, n = 7, respectively; **Figures 1A,B** and **Supplementary Figure S1**). Furthermore, SE reduced SMI-71 (a rat BBB barrier antibody) expression in the PC (**Figures 1C,D**), which is an indicative of vasogenic edema formation (Sheen et al., 2011; Kim et al., 2012, 2013, 2014). However, laminin expression was increased in SMI-71-deleted areas in the PC (**Figures 1C,D**). Although laminin over-expression would predict astroglial loss following SE (Gualtieri et al., 2012; Willis et al., 2013), our

previous study has revealed that laminin over-expression is not relevant to astroglial death induced by SE. This is because laminin expression is unaltered in the frontoparietal cortex where vasogenic edema is not detected following SE. Furthermore, laminin over-expression is ameliorated by inhibition of vasogenic edema formation and during recovery of vasogenic edema (Kim et al., 2014). Thus, the present data revel that SE-induced BBB disruption may be a cause of laminin over-expression, and that the subsequent laminin over-expression may be one of compensatory responses for recovery of BBB integrity. In contrast to laminin expression, 67-kDa LR expression was decreased in SMI-71-deleted areas in the PC (**Figures 1C,D**), indicating 67-kDa LR expression may be relevant to BBB integrity.

Decreased 67-kDa LR Expression in Astrocytes Following SE

Next, we investigated the cellular localizations of laminin and 67-kDa LR in the PC. In control animals, laminin expression was detected in endothelial cells, and 67-kDa LR expression was weakly observed in endothelial cells and astrocytes within the PC (**Figure 2A**). Following SE, laminin expression was increased in vasogenic edema lesion within the PC where astroglial loss was observed ($p < 0.05$ vs. control animals, Student *t*-test, $n = 7$, respectively; **Figures 2B,C**). In contrast to laminin, 67-kDa LR expression was diminished in endothelial cells accompanied by loss of SMI-71 expression. Astroglial 67-kDa LR expression was also reduced in the PC due to massive astroglial loss. In addition, the remaining astrocytes in this region showed the decrease in 67-kDa LR expression ($p < 0.05$ vs. control animals, Student *t*-test, $n = 7$, respectively; **Figures 2B,C**). These findings indicate that SE-induced down-regulation of 67-kDa LR expression may be relevant to vasogenic edema formation.

Laminin Over-Expression and BBB Disruption Induced by 67-kDa LR Neutralization

In our previous study, we have reported that control IgG and interleukin-18 antibody infusions differently affects SE-induced vasogenic formation in the PC (Jung et al., 2012). To directly confirm the role of 67-kDa LR in vasogenic edema formation, thus, we applied 67-kDa LR antibody infusion (neutralization) to control animals and explored its effect on BBB integrity. As compared to control IgG, 67-kDa LR neutralization led to serum extravasation in the PC without changing 67-kDa LR expression level ($p < 0.05$ vs. control IgG, Student *t*-test, $n = 7$, respectively; **Figures 3A,B** and **Supplementary Figure S1**). 67-kDa LR antiserum increased laminin expression to 2.26-fold of control IgG level in the PC ($p < 0.05$ vs. control IgG, Student *t*-test, $n = 7$, respectively; **Figures 3A,B** and **Supplementary Figure S1**). It also up-regulated laminin and eNOS expressions in endothelial cells, accompanied by the reduced SMI-71 expression in this region ($p < 0.05$ vs. control IgG, Student *t*-test, $n = 7$, respectively; **Figures 3A–F**). Together with the data obtained from SE induction, our findings indicate that the blockade of 67-kDa LR functionality may lead to vasogenic edema formation by BBB breakdowns, and that 67-kDa LR may negatively regulate laminin expression in BM of brain capillary.

67-kDa LR Neutralization-Induced Reductions in Dystrophin and AQP4 Expression in Astrocytes and Endothelial Cells

In the present study, we found that SE and 67-kDa LR neutralization induced laminin over-expression, which is closely relevant to the repair of BBB disruption accompanied by the reconstruction of endothelial barrier (Kim et al., 2014). Interestingly, laminin interacts with dystrophin-glycoprotein complex that maintains the anchoring astroglial endfeet to BM, the polarized expression of AQP4 water channel and the BBB integrity (Neely et al., 2001; Nico et al., 2003; Wolburg et al., 2009), which are down-regulated by SE (Kim et al., 2010b; Sheen et al., 2011). With respect to these previous reports, it is likely that 67-kDa LR-mediated regulation of dystrophin expression would maintain AQP4 expression and BBB integrity under physiological condition. Consistent with our previous studies (Kim et al., 2010b; Sheen et al., 2011), the expression of dystrophin and AQP4 were observed in astrocytes and brain capillaries in control IgG-infused animals. 67-kDa LR neutralization decreased dystrophin and AQP4 expressions without astroglial loss in the PC ($p < 0.05$ vs. control IgG, Student *t*-test, $n = 7$, respectively; **Figures 4A–E** and **Supplementary Figure S2**). Therefore, our findings indicate that 67-kDa LR may play a role in maintenance of dystrophin-AQP4 complex in astrocytes and brain capillaries.

Elevated p38 MAPK Phosphorylation Induced by 67-kDa LR Neutralization

The remaining question is what underlying signaling pathway is involved in vasogenic edema formation induced by 67-kDa LR neutralization. Recently, we have reported that p38 MAPK-mediated VEGF over-expression leads to BBB breakdown following SE (Kim et al., 2016; Kim and Kang, 2017). Interestingly, reduced 67-kDa LR expression increased p38 MAPK phosphorylation (activation), regardless of the exposure to exogenous laminin (Givant-Horwitz et al., 2004). Furthermore, mice lacking dystrophin show but a high endogenous p38 MAPK phosphorylation, as compared to wild-type animals (Smythe and Forwood, 2012; Wissing et al., 2014). Therefore, it is likely that 67-kDa LR-mediated regulation of dystrophin expression may be one of the up-stream signals to regulate BBB integrity via p38 MAPK/VEGF axis.

In the present study, 67-kDa LR neutralization led to up-regulation of p38 MAPK phosphorylation and VEGF expression in the PC, as compared to control IgG ($p < 0.05$ vs. control IgG, one-way ANOVA, $n = 7$, respectively; **Figures 5A,B,E** and **Supplementary Figure S2**). SB202190 (a p38 MAPK inhibitor) co-treatment did not affect 67-kDa LR expression levels in both control IgG- and 67-kDa LR IgG-infused animals (**Figures 5A,C** and **Supplementary Figure S2**). However,

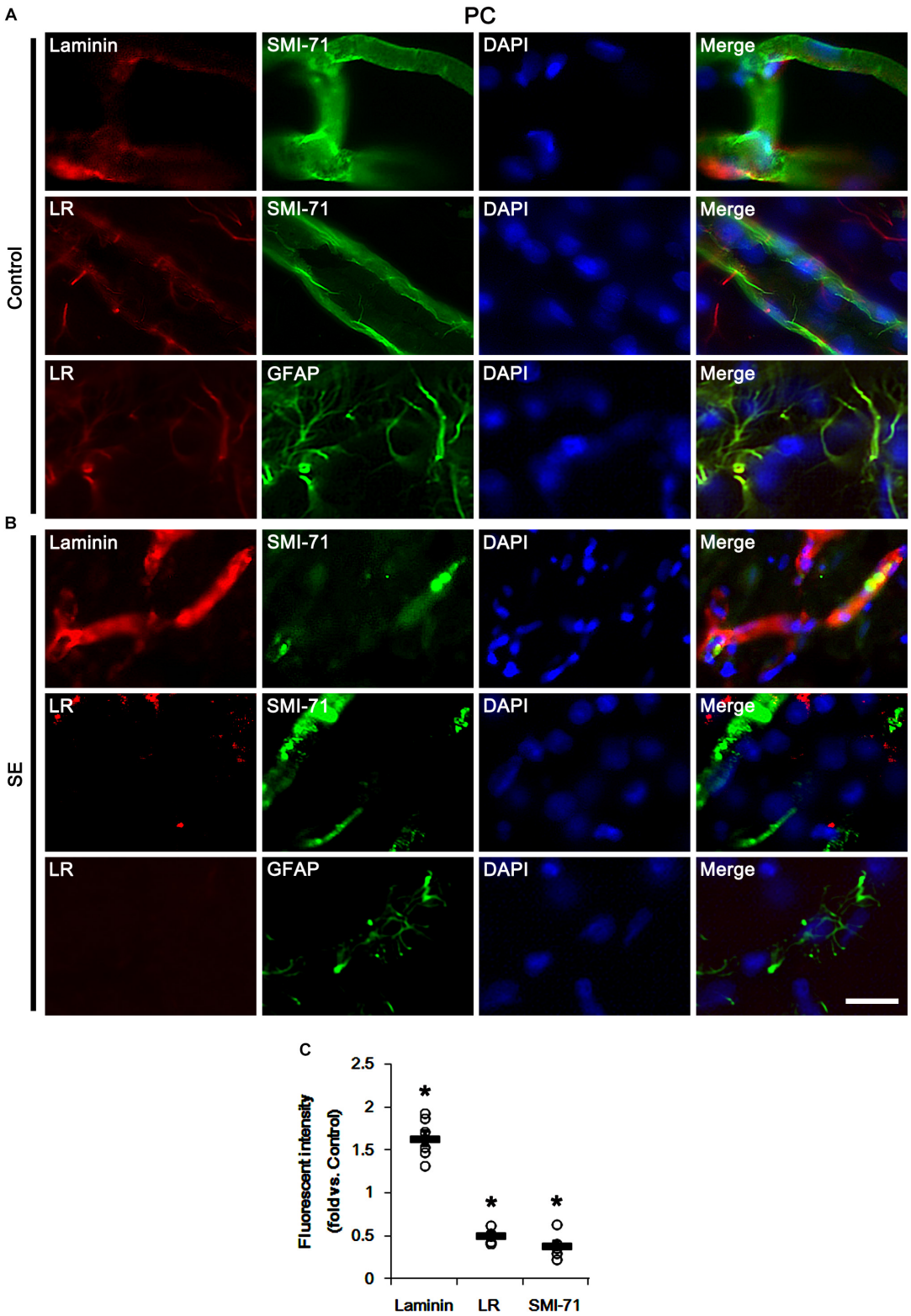

FIGURE 2 | Alterations in laminin and 67-kDa LR (LR) expression in capillaries and astrocytes within the PC following SE. **(A,B)** Representative photographs of SMI-71, laminin and 67-kDa LR expression in control **(A)**- and post-SE animals **(B)**. SE increases laminin expression, but reduces 67-kDa LR expression, accompanied by BBB disruptions (SMI-71 degradation) in capillaries. SE also diminished astroglial 67-kDa LR expression. Bar = 12.5 μm. **(C)** Quantitative values (mean ± S.E.M) of the fluorescent intensities of laminin, 67-kDa LR and SMI-71 (n = 7, respectively). Open circles indicate each individual value. Horizontal bars indicate mean value. Significant differences are *$p < 0.05$ vs. control animals (Student t-test).

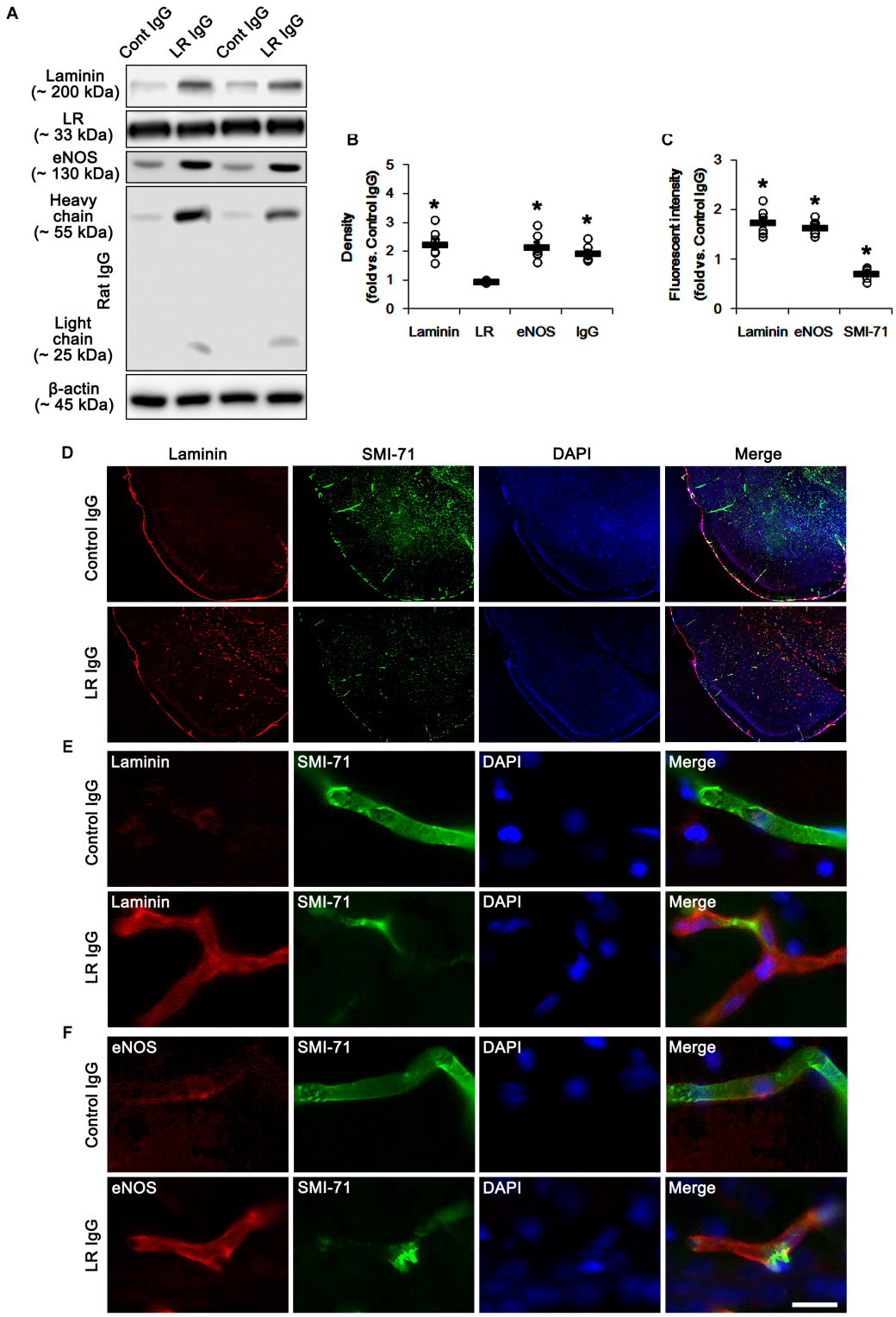

FIGURE 3 | 67-kDa LR (LR) neutralization-induced serum extravasation in normal animals. **(A)** Western blot image for expression levels of laminin, 67-kDa LR and eNOS, and serum extravasation induced by 67-kDa LR neutralization. 67-kDa LR IgG infusion increases expression levels of laminin and eNOS and serum extravasation, without changing 67-kDa LR expression. **(B)** Quantitative values (mean ± S.E.M) of the Western blot data concerning expression levels of laminin, 67-kDa LR and eNOS, and serum extravasation induced by 67-kDa LR neutralization ($n = 7$, respectively). Open circles indicate each individual value. Horizontal bars indicate mean value. Significant differences are $^*p < 0.05$ vs. control IgG (Student t-test). **(C)** Quantitative values (mean ± S.E.M) of the fluorescent intensities of SMI-71, eNOS and laminin ($n = 7$, respectively). Significant differences are $^*p < 0.05$ vs. control IgG (Student t-test). **(D–F)** Representative photographs of expression levels of laminin, eNOS, and SMI-71 in the PC. Bar = 400 μm **(D)** and 12.5 μm **(E,F)**.

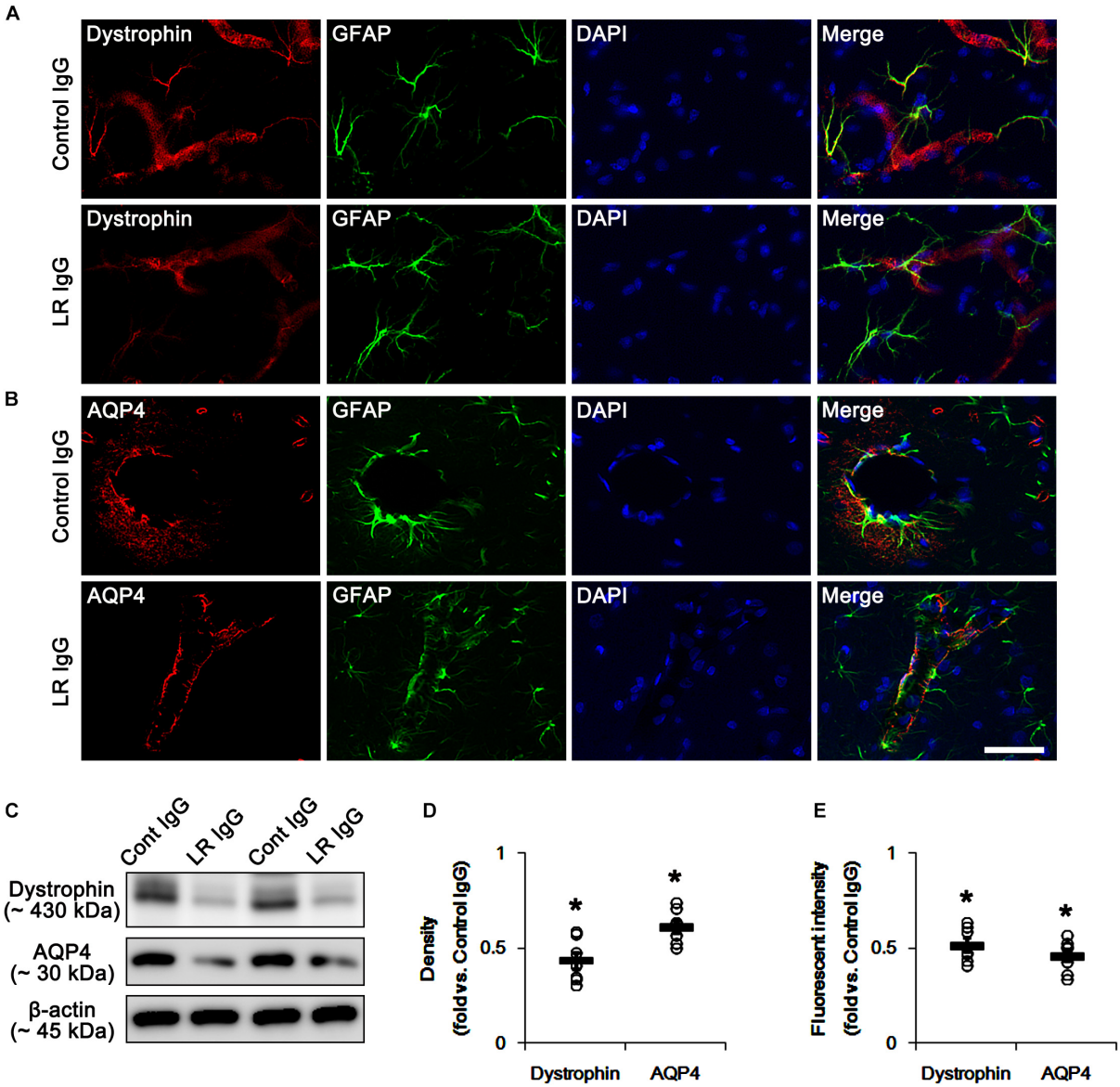

FIGURE 4 | Effect of 67-kDa LR (LR) neutralization on dystrophin and AQP4 expression in the PC of normal animals. **(A,B)** Representative photographs of dystrophin **(A)** and AQP4 **(B)** expressions in the PC. As compare to vehicle, 67-kDa LR neutralization leads to the reduction in dystrophin and AQP4 expressions in the PC. Bar = 12.5 μm. **(C)** Western blot image for expression levels of dystrophin and AQP4. **(D,E)** Quantitative values (mean ± S.E.M) of the Western blot data **(D)** and the fluorescent intensities concerning expression levels of dystrophin and AQP4 induced by 67-kDa LR neutralization (n = 7, respectively). Open circles indicate each individual value. Horizontal bars indicate mean value. Significant differences are *$p < 0.05$ vs. control IgG (Student t-test).

SB202190 co-treatment abrogated p38 MAPK activation, eNOS induction, VEGF induction and laminin over-expression induced by 67-kDa LR neutralization, although it could not abolish reductions in dystrophin and AQP4 expressions ($p < 0.05$ vs. vehicle, one-way ANOVA, $n = 7$, respectively; **Figures 5A–H** and **Supplementary Figure S2**). Furthermore, SB202190 inhibited serum extravasation in the PC induced by 67-kDa LR IgG ($p < 0.05$ vs. vehicle, one-way ANOVA, $n = 7$, respectively; **Figures 5I,J**). Thus, our findings indicate that the disruption of dystrophin-AQP4 complex by 67-kDa LR dysfunctions may trigger vasogenic edema formation and laminin over-expression by activating p38 MAPK-mediated VEGF expression.

DISCUSSION

Recently, we have reported that p38 MAPK-mediated VEGF over-expression leads to phosphatidylinositol-3-kinase (PI3K)/AKT-mediated eNOS activation during SE-induced vasogenic edema formation, which is also regulated by tumor necrosis factor-α (TNF-α)/nuclear factor-κB (NF-κB)/endothelin

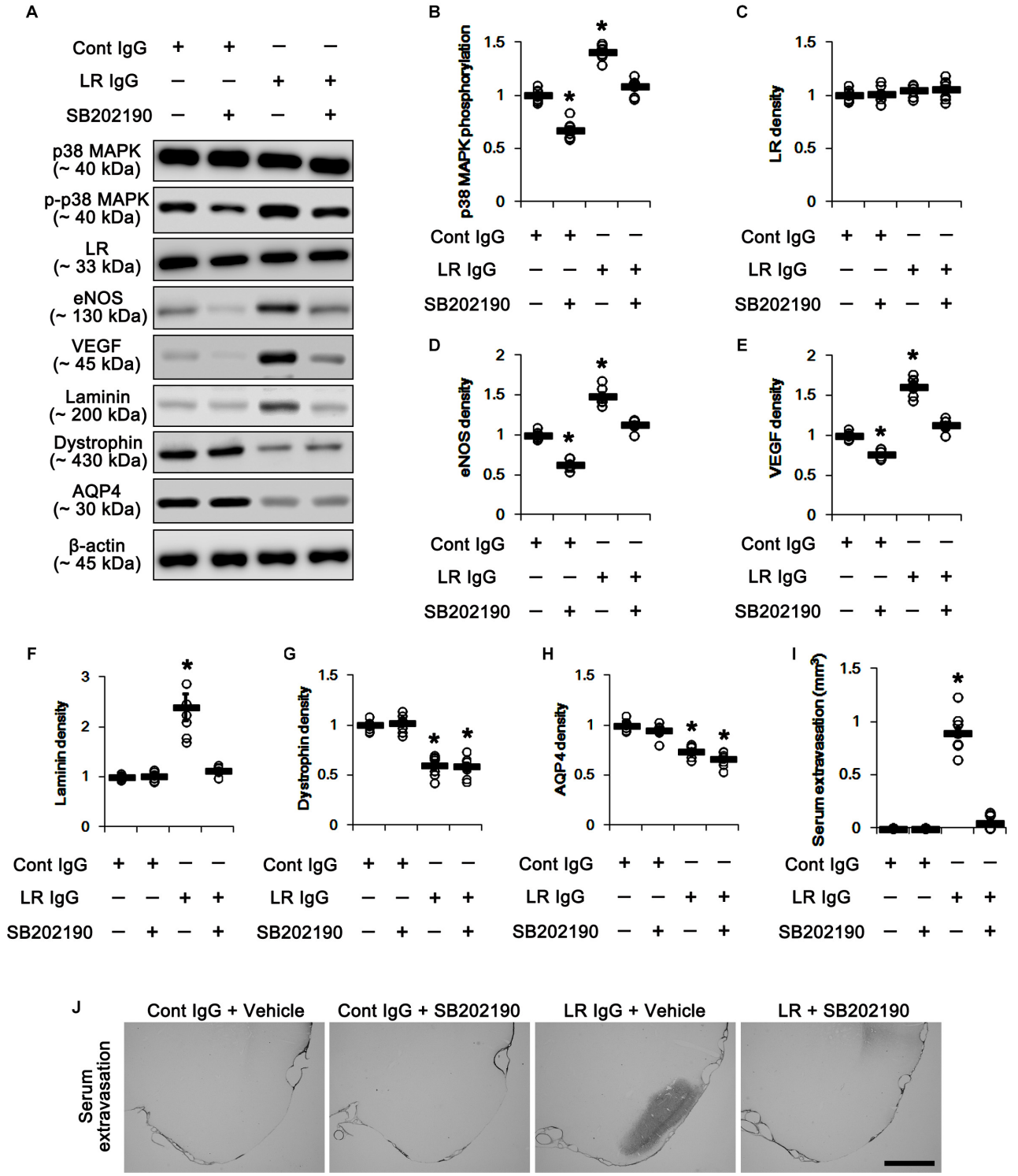

FIGURE 5 | Effect of 67-kDa LR (LR) neutralization and SB202190 co-treatment on serum extravasation in the PC of normal animals. **(A)** Western blot image for expression levels of p38 MAPK, phospho (p)-p38 MAPK, 67-kDa LR, eNOS, VEGF, laminin, dystrophin, and AQP4. **(B–H)** Quantitative values (mean ± S.E.M) of the Western blot data concerning expression levels of phospho (p)-p38 MAPK, 67-kDa LR, eNOS, VEGF, laminin, dystrophin, and AQP4 (n = 7, respectively). Open circles indicate each individual value. Horizontal bars indicate mean value. Significant differences are *$p < 0.05$ vs. control IgG (one-way ANOVA). **(I,J)** Quantitative values (mean ± S.E.M) of areas (n = 7, respectively; **(I)** and representative photographs **(J)** of serum extravasation in the PC. *$p < 0.05$ vs. control IgG (one-way ANOVA). Bar = 400 μm.

B (ET_B) receptor-mediated signaling pathway (Kim et al., 2016; Min and Kang, 2016; Kim and Kang, 2017). However, we could not elucidate the up-stream effectors/signaling pathways concerning p38 MAPK/VEGF-mediated vasogenic edema formation. In the present study, we found that 67-kDa LR might inhibit this signaling pathway by maintaining the integrity of dystrophin-AQP4 complex (**Figure 6**).

Consistent with previous studies (Castronovo et al., 1991; Guo et al., 1992), the present study shows that 67-kDa LR is identified in astrocytes and vascular endothelial cells. Furthermore, SE diminished its expression level in the PC. The present data also reveal that 67-kDa LR neutralization evoked the up-regulations of p38 MAPK phosphorylation, VEGF induction and eNOS expression in the normal animals, accompanied by serum extravasation and the reduced dystrophin expression, which were abrogated by SB202190. VEGF is a chemokine inducing impairment of BBB integrity, which potentially causes vasogenic edema (Pavlicek et al., 2000; Walter et al., 2001; Argaw et al., 2009; Bates, 2010; Kim et al., 2016; Kim and Kang, 2017). Aforementioned, 67-kDa LR and dystrophin expression levels regulate p38 MAPK activity (Givant-Horwitz et al., 2004; Smythe and Forwood, 2012; Wissing et al., 2014), and activation of p38 MAPK-VEGF axis participates in SE-induced vasogenic edema via the increased PI3K/AKT-mediated eNOS expression (Kim et al., 2016; Kim and Kang, 2017). Thus, our findings indicate that the reduced 67-kDa LR expression may be one of the up-stream molecules to regulate this signaling pathway during vasogenic edema formation. On the other hand, it is plausible that 67-kDa LR neutralization-induced up-regulations of p38 MAPK phosphorylation, VEGF induction, laminin and eNOS expression would be an adaptive reaction to rescue the BBB breakdown rather than a part of further detrimental mechanisms. If this hypothesis were true, the blockade of p38 MAPK signaling pathway would deteriorate vasogenic edema formation induced by 67-kDa LR neutralization. However, the present study reveals that SB202190 co-treatment mitigated serum extravasation induced by 67-kDa LR IgG infusion. Therefore, our findings suggest that 67-kDa LR may negatively regulate p38 MAPK/VEGF axis, which evokes BBB disruption.

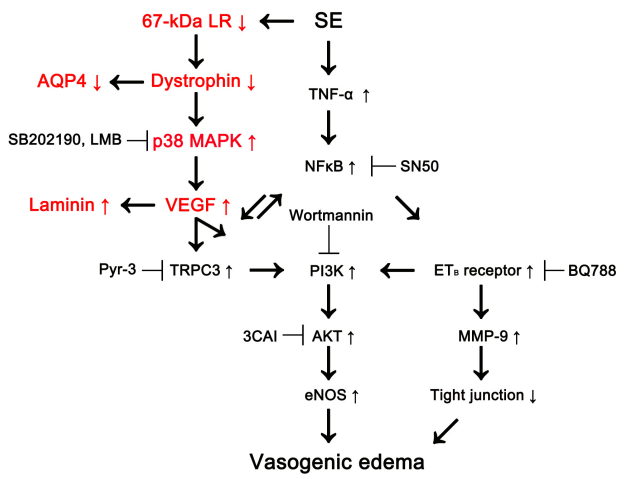

FIGURE 6 | Scheme of role of 67-kDa LR in vasogenic edema formation induced by SE based on the present data and previous reports (Kim et al., 2013, 2016; Kim J.Y. et al., 2015; Min and Kang, 2016). SE reduces 67-kDa LR and dystrophin expressions in astrocytes and endothelial cells, which activates p38 MAPK/VEGF axis. Subsequently, VEGF increases eNOS activity via transient receptor potential canonical channel-3 (TRPC3)/PI3K/AKT signaling pathway, which evokes vasogenic edema formation, along with ET_B receptor activation. Down-regulation of dystrophin also decreases AQP4 expression leading to exacerbation of vasogenic edema. In addition, VEGF induces laminin over-expression for recovery of damaged brain capillaries.

In addition to VEGF, p38 MAPK activates cytosolic phospholipase A2 (cPLA2) that mediates arachidonic acid metabolism causing BBB dysfunction and edema. Indeed, p38 MAPK/cPLA2 pathway promotes BBB disruption with secondary vasogenic edema after ischemia-reperfusion injury (Nito et al., 2008). Furthermore, p38 MAPK activates Src family kinase regulates BBB permeability in response to VEGF. p38MAPK/VEGF/Src kinase pathway is also involved in BBB disruption and vasogenic edema formation via inflammation-associated BBB dysfunction in subarchnoid hemorrhage (Han et al., 2018), ischemic stroke (Liang et al., 2009) and cold-induced brain injury, but not experimental pneumococcal meningitis (Paul et al., 2007). Therefore, it is not excluded the possibilities that p38 MAPK-VEGF axis would lead to SE-induced vasogenic edema formation activating the cPLA2 and Src pathways.

Brain-blood barrier breakdown induces the leakage of albumin from blood into brain tissue. Albumin activates microglia and affects its cytokine releases and synthesis of inducible nitric oxide synthase (iNOS) via p38 MAPK pathway (Ralay Ranaivo and Wainwright, 2010; Yang et al., 2016). In addition, albumin results in the productions of inflammatory mediators, matrix metalloproteinase-9 (MMP-9) and myosin light chain kinase (MLCK) in astrocytes through p38 MAPK activation, which lead to disruption of vascular barrier integrity by the reorganization of the cytoskeleton and the dissociation of laminin as well as tight junctions (Rossi et al., 2011; Ralay Ranaivo et al., 2012; Kim Y.J. et al., 2015; Amtul et al., 2018). With respect to these previous reports, it is likely that extravasation of albumin may also reinforce p38 MAPK/VEGF signal pathway, accompanied by down-regulation of 67-kDa LR expression, following vasogenic edema formation.

The interaction between laminin and dystrophin plays an important role in the BBB integrity and AQP4 polarization in brain capillaries and astrocytes (Neely et al., 2001; Nico et al., 2003; Wolburg et al., 2009; Kim et al., 2010b; Sheen et al., 2011). Absence of dystrophin or deletion of base pairs in the dystrophin gene is a cause of Duchenne and Becker muscular dystrophy, which are allelic X-linked disorders with a progressive muscle weakness, a static cognitive impairment, autism and problems of behavior and attention (Young et al., 2008; de Brouwer et al., 2014). In mice models, deletion of dystrophin increases blood-retinal barrier (BRB) permeability by VEGF over-expression, and AQP4 delocalization/down-regulation (El Mathari et al., 2015; Vacca et al., 2016). In the brain, dystrophin deletion also reduces AQP4 expression over perivascular astroglial endfoot membranes (Enger et al., 2012). However, the regulatory signaling pathways for AQP4

expression have been still controversial. For example, p38 MAPK and JNK inhibitors decrease AQP4 protein levels in cultured human primary cortical astrocytes (Salman et al., 2017). In contrast, temozolomide (an effective drug for malignant glioma) decreases AQP4 expression level with increasing p38 MAPK phosphorylation, which is blocked by p38 MAPK inhibitor (Chen et al., 2017). Similarly, ERK1/2 pathway down-regulates AQP4 expression in scratch-injured astrocytes (Shi et al., 2015), while ERK1/2 activation up-regulates AQP4 expression in oxygen-glucose deprivation-recovery-induced injury (Qi et al., 2011). In the present study, 67-kDa LR neutralization diminished expression levels of dystrophin and AQP4 in the PC. These findings indicate that 67-kDa LR-mediated regulation of dystrophin expression may maintain AQP4 expression and BBB integrity under physiological condition. The present study also demonstrates that SB201290 did not affect expression levels of dystrophin and AQP4 in control IgG-infused animals. Furthermore, SB202190 co-treatment could not affect decreases in dystrophin and AQP4 expressions, although it abolished serum extravasation induced by 67-kDa LR neutralization. These findings indicate that impairment of dystrophin-AQP4 complex without activation of p38 MAPK/VEGF signaling pathway may not trigger BBB disruption in the PC, and that p38 MAPK activity may not influence expressions of dystrophin and AQP4. Indeed, AQP4 deletion does not affect the brain morphology and baseline intracranial pressure under physiological condition, while it worsens vasogenic edema in a freeze-injury model and a brain tumor edema model (Papadopoulos et al., 2004). Furthermore, acetazolamide (an AQP4 inhibitor) exacerbates vasogenic edema and astroglial loss in the PC following SE, although it did not induce vasogenic edema under physiological conditions (Kim et al., 2010b). Therefore, our findings suggest that the disruption of dystrophin may trigger BBB breakdown by activating p38 MAPK-mediated VEGF expression, and subsequently may aggravate vasogenic edema due to diminishing AQP4−dependent vasogenic water elimination.

Laminin is a key component of vascular BMs and contributes to vascular permeability by generating the physical barrier of the gliovascular BM and BBB maturation (Menezes et al., 2014). Laminin is also involved in the communication among the cellular components forming the gliovascular units via the integrins and non-integrin receptors (Lesot et al., 1983; Malinoff and Wicha, 1983; Rao et al., 1983; Menezes et al., 2014). In the present study, SE resulted in the down-regulated 67-kDa LR expression accompanied by laminin over-expression. Furthermore, 67-kDa LR neutralization evoked the similar effects in normal animals. Considering the essential roles of laminin in brain vascular development and vessel integrity (Thyboll et al., 2002) and its proteolytic cleavage by 67-kDa LR (Ardini et al., 2002), it is likely that the SE-induced reduction in 67-kDa LR expression and 67-kDa LR neutralization may up-regulate laminin expression to inhibit or recover vasogenic edema formation. Furthermore, SB202190 co-treatment abrogated laminin expression and serum extravasation induced by 67-kDa LR neutralization. Therefore, our findings indicate that 67-kDa LR dysfunction may up-regulate laminin expression via p38 MAPK/VEGF signaling pathway, and that laminin over-expression may be a secondary adaptive response to serum extravasation.

Similar to 67-kDa LR neutralization, recombinant tissue plasminogen activator (r-tPA) induces BBB disruption, and subsequently results in vasogenic edema (Copin et al., 2011), which is mitigated by p38 MAPK inhibitor (Garraud et al., 2016). Rosuvastatin (a lipid-lowering agent) also ameliorates r-tPA-induced BBB damage by reducing the activities of JNK and p38 MAPK (Lu et al., 2018). Indeed, tPA activates ERK1/2, JNK, AKT and p38 MAPK signaling pathways (Pineda et al., 2012). Thus, it is plausible that 67-kDa LR neutralization may lead to vasogenic edema through tPA activation and various signaling pathways as well as p38 MAPK. Further studies are needed to validate the relationship between 67-kDa LR and tPA and the related signaling pathways.

Pilocarpine is a cholinergic agent, which activates muscarinic M1 receptors (Hamilton et al., 1997; Kim and Kang, 2011). Acetylcholine induces vasodilation by eNOS activation (Gericke et al., 2013) and cholinesterase inhibitors such as chlorpyrifos and paraoxon (organophosphorus insecticides) evoke vasogenic edema (Song et al., 2004; Li and Ehrich, 2013). Thus, it is presumable that the direct PILO-mediated eNOS activation would affect seizure activity and vasogenic edema formation, although we blocked its peripheral cholinergic effects by atropine methylbromide in the present study. Recently, our laboratory reveals that *N*-nitro-L-arginine methyl ester (L-NAME, a non-selective NOS inhibitor) abrogates NO synthesis without altering seizure activity in response to PILO by the real-time simultaneous monitoring of NO and EEG. Thus, we have speculated that NO synthesis may be a consequent response to seizure activity, and that NO itself may not be directly involved in ictogenesis (Lee and Kim, 2018; Jeon and Kim, 2018). Furthermore, ET_B receptor antagonist attenuated vasogenic edema formation via reducing eNOS expression without altering PILO-induced seizure activity (Kim J.Y. et al., 2015). Therefore, it is unlikely that the direct cholinergic effect of PILO on eNOS activity may not influence seizure activity and vasogenic edema formation, at least in our model.

Various brain insults induce an osmotic potential across central necrotic tissue, inflammatory reaction, tight junction degradation and protein extravasation, which are regulated by inflammatory cytokines, MMP, VEGF and leukocyte/neutrophil infiltration (for review; Jha et al., 2019). Similar to other disease models, SE-induced vasogenic edema formation is relevant to neuroinflammation, MMP-9 activation and neutrophil infiltration (Kim et al., 2010a, 2012; Jung et al., 2012; Kim J.Y. et al., 2015). Thus, it is likely that the fundamental mechanisms of vasogenic edema formation induced by SE may be similar to those under various pathophysiological conditions. However, there are many underlying factors including age, sex and genetics to contribute vasogenic edema formation in animal model and human patients. For example, the major population of patients of posterior reversible encephalopathy syndrome (PRES), which is a neurotoxic encephalopathic state showing seizures and SE with white matter vasogenic edema in occipital and parietal lobes, is woman (Kamiya-Matsuoka and Tummala, 2017). Therefore, it seems that vasogenic edema would show

gender-dependent characteristics. Indeed, sex steroids influences vascular reactivity in the brain via various signaling molecules including eNOS (Krause et al., 2006; Parikh et al., 2017). However, AQP4 expression is down-regulated in glioma patients without gender−dependent difference in AQP4 expression, although sex hormones such as estrogen, progesterone and testosterone modulate AQP4 expression in astrocytes (Warth et al., 2007). Ischemic stroke also shows the relative protection from brain injury in the female as compared with male, which is conferred by endogenous sex steroids. However, AQP4 is not involved in gender-specific differences in stroke volume and finally, the perivascular pool of AQP4 does not alter after ischemic stroke (Liu et al., 2008). Furthermore, age and genetic polymorphisms (e.g., cytokines, apolipoprotien E, Tau, and mitochondrial genes) affect BBB integrity (Song et al., 2004; Bennett et al., 2016). Therefore, studies concerning gender-, age-, and genetic-based difference in vasogenic edema formation in animal models and human patients are needed to elucidate the underlying mechanisms, the prediction of outcome and clinical management in various neurological diseases relevant to vasogenic edema.

CONCLUSION

In conclusion, to the best of our knowledge, the present data show novel evidence that 67-kDa LR may be one of the up-stream regulators of dystrophin/p38 MAPK/VEGF/eNOS axis, which plays an important role in the maintenance of BBB integrity (**Figure 6**). Thus, our findings suggest that 67-kDa LR-mediated astroglio-vascular interface may be a therapeutic target for treatment of vasogenic edema.

DATA AVAILABILITY

All datasets generated for this study are included in the manuscript and/or the **Supplementary Files**.

ETHICS STATEMENT

All experimental protocols described below were approved by the Institutional Animal Care and Use Committee of Hallym University (Chuncheon, South Korea). Every effort was made to reduce the number of animals employed and to minimize animal's discomfort.

AUTHOR CONTRIBUTIONS

T-CK designed and supervised the project, analyzed the data, and wrote the manuscript. All authors performed the experiments described in the manuscript.

FUNDING

This work was supported by Hallym University (HRF-201903-011).

SUPPLEMENTARY MATERIAL

The Supplementary Material for this article can be found online at: https://www.frontiersin.org/articles/10.3389/fncel.2019.00236/full#supplementary-material

REFERENCES

Amtul, Z., Yang, J., Nikolova, S., Lee, T. Y., Bartha, R., and Cechetto, D. F. (2018). The dynamics of impaired blood-brain barrier restoration in a rat model of co-morbid Injury. *Mol. Neurobiol.* 55, 8071–8083. doi: 10.1007/s12035-018-0904-4

Ardini, E., Pesole, G., Tagliabue, E., Magnifico, A., Castronovo, V., Sobel, M. E., et al. (1998). The 67-kDa laminin receptor originated from a ribosomal protein that acquired a dual function during evolution. *Mol. Biol. Evol.* 15, 1017–1025. doi: 10.1093/oxfordjournals.molbev.a026000

Ardini, E., Sporchia, B., Pollegioni, L., Modugno, M., Ghirelli, C., Castiglioni, F., et al. (2002). Identification of a novel function for 67-kDa laminin receptor: increase in laminin degradation rate and release of motility fragments. *Cancer Res.* 62, 1321–1325.

Argaw, A. T., Gurfein, B. T., Zhang, Y., Zameer, A., and John, G. R. (2009). VEGF-mediated disruption of endothelial CLN-5 promotes blood-brain barrier breakdown. *Proc. Natl. Acad. Sci. U.S.A.* 106, 1977–1982. doi: 10.1073/pnas.0808698106

Baloui, H., von Boxberg, Y., Vinh, J., Weiss, S., Rossier, J., Nothias, F., et al. (2004). Cellular prion protein/laminin receptor: distribution in adult central nervous system and characterization of an isoform associated with a subtype of cortical neurons. *Eur. J. Neurosci.* 20, 2605–2616. doi: 10.1111/j.1460-9568.2004.03728.x

Banerjee, S., and Bhat, M. A. (2007). Neuron-glial interactions in blood-brain barrier formation. *Annu. Rev. Neurosci.* 30, 235–258. doi: 10.1146/annurev.neuro.30.051606.094345

Bates, D. O. (2010). Vascular endothelial growth factors and vascular permeability. *Cardiovasc. Res.* 87, 262–271. doi: 10.1093/cvr/cvq105

Bennett, E. R., Reuter-Rice, K., and Laskowitz, D. T. (2016). "Genetic influences in traumatic brain injury," in *Translational Research in Traumatic Brain Injury*, eds D. Laskowitz and G. Grant (Boca Raton, FL: CRC Press).

Biagini, G., Baldelli, E., Longo, D., Contri, M. B., Guerrini, U., Sironi, L., et al. (2008). Proepileptic influence of a focal vascular lesion affecting entorhinal cortex-CA3 connections after status epilepticus. *J. Neuropathol. Exp. Neurol.* 67, 687–701. doi: 10.1097/NEN.0b013e318181b8ae

Bloch, O., Papadopoulos, M. C., Manley, G. T., and Verkman, A. S. (2005). Aquaporin-4 gene deletion in mice increases focal edema associated with staphylococcal brain abscess. *J. Neurochem.* 95, 254–262. doi: 10.1111/j.1471-4159.2005.03362.x

Castronovo, V., Claysmith, A. P., Barker, K. T., Cioce, V., Krutzsch, H. C., and Sobel, M. E. (1991). Biosynthesis of the 67 kDa high affinity laminin receptor. *Biochem. Biophys. Res. Commun.* 177, 177–183. doi: 10.1016/0006-291x(91)91965-f

Chen, Y., Gao, F., Jiang, R., Liu, H., Hou, J., Yi, Y., et al. (2017). Down-regulation of AQP4 expression via p38 MAPK signaling in temozolomide-induced glioma cells growth inhibition and invasion impairment. *J. Cell. Biochem.* 118, 4905–4913. doi: 10.1002/jcb.26176

Copin, J. C., Bengualid, D. J., Da Silva, R. F., Kargiotis, O., Schaller, K., and Gasche, Y. (2011). Recombinant tissue plasminogen activator induces blood-brain barrier breakdown by a matrix metalloproteinase-9-independent pathway after transient focal cerebral ischemia in mouse. *Eur. J. Neurosci.* 34, 1085–1092. doi: 10.1111/j.1460-9568.2011.07843.x

de Brouwer, A. P., Nabuurs, S. B., Verhaart, I. E., Oudakker, A. R., Hordijk, R., Yntema, H. G., et al. (2014). A 3-base pair deletion, c.9711_9713del, in DMD results in intellectual disability without muscular dystrophy. *Eur. J. Hum. Genet.* 22, 480–485. doi: 10.1038/ejhg.2013.169

El Mathari, B., Sene, A., Charles-Messance, H., Vacca, O., Guillonneau, X., Grepin, C., et al. (2015). Dystrophin Dp71 gene deletion induces retinal vascular inflammation and capillary degeneration. *Hum. Mol. Genet.* 24, 3939–3947. doi: 10.1093/hmg/ddv132

Enger, R., Gundersen, G. A., Haj-Yasein, N. N., Eilert-Olsen, M., Thoren, A. E., Vindedal, G. F., et al. (2012). Molecular scaffolds underpinning macroglial polarization: an analysis of retinal Müller cells and brain astrocytes in mouse. *Glia* 60, 2018–2026. doi: 10.1002/glia.22416

Fountain, N. B. (2000). Status epilepticus: risk factors and complications. *Epilepsia* 41, S23–S30.

Garraud, M., Khacef, K., Vion, A. C., Leconte, C., Yin, M., Renard, J. M., et al. (2016). Recombinant tissue plasminogen activator enhances microparticle release from mouse brain-derived endothelial cells through plasmin. *J. Neurol. Sci.* 370, 187–195. doi: 10.1016/j.jns.2016.09.026

Gericke, A., Goloborodko, E., Sniatecki, J. J., Steege, A., Wojnowski, L., and Pfeiffer, N. (2013). Contribution of nitric oxide synthase isoforms to cholinergic vasodilation in murine retinal arterioles. *Exp. Eye Res.* 109, 60–66. doi: 10.1016/j.exer.2013.01.012

Givant-Horwitz, V., Davidson, B., and Reich, R. (2004). Laminin-induced signaling in tumor cells: the role of the M(r) 67,000 laminin receptor. *Cancer Res.* 64, 3572–3579. doi: 10.1158/0008-5472.can-03-3424

Gualtieri, F., Curia, G., Marinelli, C., and Biagini, G. (2012). Increased perivascular laminin predicts damage to astrocytes in CA3 and piriform cortex following chemoconvulsive treatments. *Neuroscience* 218, 278–294. doi: 10.1016/j.neuroscience.2012.05.018

Guo, N. H., Krutzsch, H. C., Vogel, T., and Roberts, D. D. (1992). Interactions of a laminin-binding peptide from a 33-kDa protein related to the 67-kDa laminin receptor with laminin and melanoma cells are heparin-dependent. *J. Biol. Chem.* 267, 17743–17747.

Hamilton, S. E., Loose, M. D., Qi, M., Levey, A. I., Hille, B., McKnight, G. S., et al. (1997). Disruption of the m1 receptor gene ablates muscarinic receptor-dependent M current regulation and seizure activity in mice. *Proc. Natl. Acad. Sci. U.S.A.* 94, 13311–13316. doi: 10.1073/pnas.94.24.13311

Han, Y. W., Liu, X. J., Zhao, Y., and Li, X. M. (2018). Role of Oleanolic acid in maintaining BBB integrity by targeting p38MAPK/VEGF/Src signaling pathway in rat model of subarachnoid hemorrhage. *Eur. J. Pharmacol.* 839, 12–20. doi: 10.1016/j.ejphar.2018.09.018

Huang, S. H., and Jong, A. (2009). Evolving role of laminin receptors in microbial pathogenesis and therapeutics of CNS infection. *Future Microbiol.* 4, 959–962. doi: 10.2217/fmb.09.67

Jeon, A. R., and Kim, J. E. (2018). PDI knockdown inhibits seizure activity in acute seizure and chronic epilepsy rat models via S-nitrosylation-independent thiolation on NMDA receptor. *Front. Cell. Neurosci.* 12:438. doi: 10.3389/fncel.2018.00438

Jha, R. M., Kochanek, P. M., and Simard, J. M. (2019). Pathophysiology and treatment of cerebral edema in traumatic brain injury. *Neuropharmacology* 145, 230–246. doi: 10.1016/j.neuropharm.2018.08.004

Jung, H. K., Ryu, H. J., Kim, M. J., Kim, W. I., Choi, H. K., Choi, H. C., et al. (2012). Interleukin-18 attenuates disruption of brain-blood barrier induced by status epilepticus within the rat piriform cortex in interferon-γ independent pathway. *Brain Res.* 1447, 126–134. doi: 10.1016/j.brainres.2012.01.057

Kamiya-Matsuoka, C., and Tummala, S. (2017). Electrographic patterns in patients with posterior reversible encephalopathy syndrome and seizures. *J. Neurol. Sci.* 375, 294–298. doi: 10.1016/j.jns.2017.02.017

Kielian, M., Chanel-Vos, C., and Liao, M. (2010). Alphavirus entry and membrane fusion. *Viruses* 2, 796–825. doi: 10.3390/v2040796

Kim, D. S., Min, S. J., Kim, M. J., Kim, J. E., and Kang, T. C. (2016). Leptomycin B ameliorates vasogenic edema formation induced by status epilepticus via inhibiting p38 MAPK/VEGF pathway. *Brain Res.* 1651, 27–35. doi: 10.1016/j.brainres.2016.09.023

Kim, J. E., and Kang, T. C. (2011). The P2X7 receptor-pannexin-1 complex decreases muscarinic acetylcholine receptor-mediated seizure susceptibility in mice. *J. Clin. Invest.* 121, 2037–2047. doi: 10.1172/JCI44818

Kim, J. E., and Kang, T. C. (2017). TRPC3- and ET(B) receptor-mediated PI3K/AKT activation induces vasogenic edema formation following status epilepticus. *Brain Res.* 1672, 58–64. doi: 10.1016/j.brainres.2017.07.020

Kim, J. E., Ryu, H. J., Choi, S. Y., and Kang, T. C. (2012). Tumor necrosis factor-α-mediated threonine 435 phosphorylation of p65 nuclear factor-κB subunit in endothelial cells induces vasogenic edema and neutrophil infiltration in the rat piriform cortex following status epilepticus. *J. Neuroinflamm.* 9:6. doi: 10.1186/1742-2094-9-6

Kim, J. E., Ryu, H. J., and Kang, T. C. (2013). Status epilepticus induces vasogenic edema via tumor necrosis factor-α/endothelin-1-mediated two different pathways. *PLoS One* 8:e74458. doi: 10.1371/journal.pone.0074458

Kim, J. E., Ryu, H. J., Yeo, S. I., and Kang, T. C. (2010a). P2X7 receptor regulates leukocyte infiltrations in rat frontoparietal cortex following status epilepticus. *J. Neuroinflamm.* 7:65. doi: 10.1186/1742-2094-7-65

Kim, J. E., Yeo, S. I, Ryu, H. J., Kim, M. J., Kim, D. S., Jo, S. M., et al. (2010b). Astroglial loss and edema formation in the rat piriform cortex and hippocampus following pilocarpine-induced status epilepticus. *J. Comp. Neurol.* 518, 4612–4628. doi: 10.1002/cne.22482

Kim, J. Y., Ko, A. R., Hyun, H. W., and Kang, T. C. (2015). ETB receptor-mediated MMP-9 activation induces vasogenic edema via ZO-1 protein degradation following status epilepticus. *Neuroscience* 304, 355–367. doi: 10.1016/j.neuroscience.2015.07.065

Kim, Y. J., Kim, J. E., Choi, H. C., Song, H. K., and Kang, T. C. (2015). Cellular and regional specific changes in multidrug efflux transporter expression during recovery of vasogenic edema in the rat hippocampus and piriform cortex. *BMB Rep.* 48, 348–353. doi: 10.5483/bmbrep.2015.48.6.237

Kim, Y. J., Kim, J. Y., Ko, A. R., and Kang, T. C. (2014). Over-expression of laminin correlates to recovery of vasogenic edema following status epilepticus. *Neuroscience* 275, 146–161. doi: 10.1016/j.neuroscience.2014.06.005

Ko, A. R., and Kang, T. C. (2015). Mannitol induces selective astroglial death in the CA1 region of the rat hippocampus following status epilepticus. *BMB Rep.* 48, 507–512. doi: 10.5483/bmbrep.2015.48.9.013

Ko, A. R., and Kang, T. C. (2017). TRPC6-mediated ERK1/2 phosphorylation prevents dentate granule cell degeneration via inhibiting mitochondrial elongation. *Neuropharmacology* 121, 120–129. doi: 10.1016/j.neuropharm.2017.05.004

Koh, S., Mathern, G. W., Glasser, G., Wu, J. Y., Shields, W. D., Jonas, R., et al. (2005). Status epilepticus and frequent seizures: incidence and clinical characteristics in pediatric epilepsy surgery patients. *Epilepsia* 46, 1950–1954. doi: 10.1111/j.1528-1167.2005.00340.x

Krause, D. N., Duckles, S. P., and Pelligrino, D. A. (2006). Influence of sex steroid hormones on cerebrovascular function. *J. Appl. Physiol.* 101, 1252–1261. doi: 10.1152/japplphysiol.01095.2005

Lee, D. S., and Kim, J. E. (2018). PDI-mediated S-nitrosylation of DRP1 facilitates DRP1-S616 phosphorylation and mitochondrial fission in CA1 neurons. *Cell Death Dis.* 9:869. doi: 10.1038/s41419-018-0910-5

Lesot, H., Kuhl, U., and Mark, K. (1983). Isolation of a laminin-binding protein from muscle cell membranes. *EMBO J.* 2, 861–865. doi: 10.1002/j.1460-2075.1983.tb01514.x

Li, W., and Ehrich, M. (2013). Transient alterations of the blood-brain barrier tight junction and receptor potential channel gene expression by chlorpyrifos. *J. Appl. Toxicol.* 33, 1187–1191. doi: 10.1002/jat.2762

Liang, S., Pong, K., Gonzales, C., Chen, Y., Ling, H. P., Mark, R. J., et al. (2009). Neuroprotective profile of novel SRC kinase inhibitors in rodent models of cerebral ischemia. *J. Pharmacol. Exp. Ther.* 331, 827–835. doi: 10.1124/jpet.109.156562

Lippmann, K., Kamintsky, L., Kim, S. Y., Lublinsky, S., Prager, O., Nichtweiss, J. F., et al. (2017). Epileptiform activity and spreading depolarization in the blood-brain barrier-disrupted peri-infarct hippocampus are associated with impaired GABAergic inhibition and synaptic plasticity. *J. Cereb. Blood Flow Metab.* 37, 1803–1819. doi: 10.1177/0271678X16652631

Liu, X., Zhang, W., Alkayed, N. J., Froehner, S. C., Adams, M. E., Amiry-Moghaddam, M., et al. (2008). Lack of sex-linked differences in cerebral edema and aquaporin-4 expression after experimental stroke. *J. Cereb. Blood Flow Metab.* 28, 1898–1906. doi: 10.1038/jcbfm.2008.83

Löscher, W., and Potschka, H. (2005). Blood-brain barrier active efflux transporters: ATP-binding cassette gene family. *NeuroRx* 2, 86–89.

Lu, D., Mai, H. C., Liang, Y. B., Xu, B. D., Xu, A. D., and Zhang, Y. S. (2018). Beneficial role of rosuvastatin in blood-brain barrier damage following experimental ischemic stroke. *Front. Pharmacol.* 9:926. doi: 10.3389/fphar.2018.00926

Malinoff, H. L., and Wicha, M. S. (1983). Isolation of a cell surface receptor protein for laminin from murine fibrosarcoma cells. *J. Cell Biol.* 96, 1475–1479. doi: 10.1083/jcb.96.5.1475

Menezes, M. J., McClenahan, F. K., Leiton, C. V., Aranmolate, A., Shan, X., and Colognato, H. (2014). The extracellular matrix protein laminin α2 regulates the maturation and function of the blood-brain barrier. *J. Neurosci.* 34, 15260–15280. doi: 10.1523/JNEUROSCI.3678-13.2014

Min, S. J., and Kang, T. C. (2016). Positive feedback role of TRPC3 in TNF-α-mediated vasogenic edema formation induced by status epilepticus independent of ET(B) receptor activation. *Neuroscience* 337, 37–47. doi: 10.1016/j.neuroscience.2016.09.005

Miner, J. H. (2008). Laminins and their roles in mammals. *Microsc. Res. Tech.* 71, 349–356. doi: 10.1002/jemt.20563

Neely, J. D., Amiry-Moghaddam, M., Ottersen, O. P., Froehner, S. C., Agre, P., and Adams, M. E. (2001). Syntrophin-dependent expression and localization of aquaporin-4 water channel protein. *Proc. Natl. Acad. Sci. U.S.A.* 98, 14108–14113. doi: 10.1073/pnas.241508198

Nico, B., Frigeri, A., Nicchia, G. P., Corsi, P., Ribatti, D., Quondamatteo, F., et al. (2003). Severe alterations of endothelial and glial cells in the blood-brain barrier of dystrophic mdx mice. *Glia* 42, 235–251. doi: 10.1002/glia.10216

Nito, C., Kamada, H., Endo, H., Niizuma, K., Myer, D. J., and Chan, P. H. (2008). Role of the p38 mitogen-activated protein kinase/cytosolic phospholipase A2 signaling pathway in blood-brain barrier disruption after focal cerebral ischemia and reperfusion. *J. Cereb. Blood Flow Metab.* 28, 1686–1696. doi: 10.1038/jcbfm.2008.60

Papadopoulos, M. C., Manley, G. T., Krishna, S., and Verkman, A. S. (2004). Aquaporin-4 facilitates reabsorption of excess fluid in vasogenic brain edema. *FASEB J.* 18, 1291–1293. doi: 10.1096/fj.04-1723fje

Parikh, N. S., Schweitzer, A. D., Young, R. J., Giambrone, A. E., Lyo, J., Karimi, S., et al. (2017). Corticosteroid therapy and severity of vasogenic edema in posterior reversible encephalopathy syndrome. *J. Neurol. Sci.* 380, 11–15. doi: 10.1016/j.jns.2017.06.044

Paul, R., Angele, B., Popp, B., Klein, M., Riedel, E., Pfister, H. W., et al. (2007). Differential regulation of blood-brain barrier permeability in brain trauma and pneumococcal meningitis-role of Src kinases. *Exp. Neurol.* 203, 158–167. doi: 10.1016/j.expneurol.2006.08.003

Pavlicek, V., Marti, H. H., Grad, S., Gibbs, J. S., Kol, C., Wenger, R. H., et al. (2000). Effects of hypobaric hypoxia on vascular endothelial growth factor and the acute phase response in subjects who are susceptible to high-altitude pulmonary oedema. *Eur. J. Appl. Physiol.* 81, 497–503. doi: 10.1007/s004210050074

Pellegrini, R., Martignone, S., Menard, S., and Colnaghi, M. I. (1994). Laminin receptor expression and function in small-cell lung carcinoma. *Int. J. Cancer* 8, 116–120. doi: 10.1002/ijc.2910570725

Pineda, D., Ampurdanés, C., Medina, M. G., Serratosa, J., Tusell, J. M., and Saura, J. (2012). Tissue plasminogen activator induces microglial inflammation via a noncatalytic molecular mechanism involving activation of mitogen-activated protein kinases and Akt signaling pathways and annexinA2 and galectin-1 receptors. *Glia* 60, 526–540. doi: 10.1002/glia.22284

Qi, L. L., Fang, S. H., Shi, W. Z., Huang, X. Q., Zhang, X. Y., Lu, Y. B., et al. (2011). CysLT2 receptor-mediated AQP4 up-regulation is involved in ischemic-like injury through activation of ERK and p38 MAPK in rat astrocytes. *Life Sci.* 88, 50–56. doi: 10.1016/j.lfs.2010.10.025

Ralay Ranaivo, H., Hodge, J. N., Choi, N., and Wainwright, M. S. (2012). Albumin induces upregulation of matrix metalloproteinase-9 in astrocytes via MAPK and reactive oxygen species-dependent pathways. *J. Neuroinflamm.* 9:68. doi: 10.1186/1742-2094-9-68

Ralay Ranaivo, H., and Wainwright, M. S. (2010). Albumin activates astrocytes and microglia through mitogen-activated protein kinase pathways. *Brain Res.* 1313, 222–231. doi: 10.1016/j.brainres.2009.11.063

Rao, C. N., Castronovo, V., Schmitt, M. C., Wewer, U. M., Claysmith, A. P., Liotta, L. A., et al. (1989). Evidence for a precursor of the high-affinity metastasis-associated murine laminin receptor. *Biochemistry* 28, 7476–7486. doi: 10.1021/bi00444a047

Rao, N. C., Barsky, S. H., Terranova, V. P., and Liotta, L. A. (1983). Isolation of a tumor cell laminin receptor. *Biochem. Biophys. Res. Commun.* 111, 804–808. doi: 10.1016/0006-291x(83)91370-0

Rossi, J. L., Ralay Ranaivo, H., Patel, F., Chrzaszcz, M., Venkatesan, C., and Wainwright, M. S. (2011). Albumin causes increased myosin light chain kinase expression in astrocytes via p38 mitogen-activated protein kinase. *J. Neurosci. Res.* 89, 852–861. doi: 10.1002/jnr.22600

Salman, M. M., Sheilabi, M. A., Bhattacharyya, D., Kitchen, P., Conner, A. C., Bill, R. M., et al. (2017). Transcriptome analysis suggests a role for the differential expression of cerebral aquaporins and the MAPK signalling pathway in human temporal lobe epilepsy. *Eur. J. Neurosci.* 46, 2121–2132. doi: 10.1111/ejn.13652

Sheen, S. H., Kim, J. E., Ryu, H. J., Yang, Y., Choi, K. C., and Kang, T. C. (2011). Decrease in dystrophin expression prior to disruption of brain-blood barrier within the rat piriform cortex following status epilepticus. *Brain Res.* 1369, 173–183. doi: 10.1016/j.brainres.2010.10.080

Shi, Z. F., Zhao, W. J., Xu, L. X., Dong, L. P., Yang, S. H., and Yuan, F. (2015). Downregulation of aquaporin 4 expression through extracellular signal-regulated kinases1/2 activation in cultured astrocytes following scratch-injury. *Biomed. Environ. Sci.* 28, 199–205. doi: 10.3967/bes2015.026

Sisodiya, S. M., Lin, W. R., Harding, B. N., Squier, M. V., and Thom, M. (2002). Drug resistance in epilepsy: expression of drug resistance proteins in common causes of refractory epilepsy. *Brain* 125, 22–31. doi: 10.1093/brain/awf002

Smythe, G. M., and Forwood, J. K. (2012). Altered mitogen-activated protein kinase signaling in dystrophic (mdx) muscle. *Muscle Nerve* 46, 374–383. doi: 10.1002/mus.23312

Song, X., Pope, C., Murthy, R., Shaikh, J., Lal, B., and Bressler, J. P. (2004). Interactive effects of paraoxon and pyridostigmine on blood-brain barrier integrity and cholinergic toxicity. *Toxicol. Sci.* 78, 241–247. doi: 10.1093/toxsci/kfh076

Sørensen, A. T., and Kokaia, M. (2013). Novel approaches to epilepsy treatment. *Epilepsia* 54, 1–10. doi: 10.1111/epi.12000

Sun, M., Shinoda, Y., and Fukunaga, K. (2019). KY-226 protects blood-brain barrier function through the Akt/FoxO1 signaling pathway in brain ischemia. *Neuroscience* 399, 89–102. doi: 10.1016/j.neuroscience.2018.12.024

Téllez-Zenteno, J. F., and Hernández-Ronquillo, L. (2012). A review of the epidemiology of temporal lobe epilepsy. *Epilepsy Res. Treat.* 2012:630853. doi: 10.1155/2012/630853

Thyboll, J., Kortesmaa, J., Cao, R., Soininen, R., Wang, L., Iivanainen, A., et al. (2002). Deletion of the laminin alpha4 chain leads to impaired microvessel maturation. *Mol. Cell. Biol.* 22, 1194–1202. doi: 10.1128/mcb.22.4.1194-1202.2002

Tilling, T., Engelbertz, C., Decker, S., Korte, D., Hüwel, S., and Galla, H. J. (2002). Expression and adhesive properties of basement membrane proteins in cerebral capillary endothelial cell cultures. *Cell Tissue Res.* 310, 19–29. doi: 10.1007/s00441-002-0604-1

Vacca, O., Charles-Messance, H., El Mathari, B., Sene, A., Barbe, P., Fouquet, S., et al. (2016). AAV-mediated gene therapy in Dystrophin-Dp71 deficient mouse leads to blood-retinal barrier restoration and oedema reabsorption. *Hum. Mol. Genet.* 25, 3070–3079.

Vana, K., Zuber, C., Pflanz, H., Kolodziejczak, D., Zemora, G., Bergmann, A. K., et al. (2009). LRP/LR as an alternative promising target in therapy of prion diseases, Alzheimer's disease and cancer. *Infect. Disord. Drug Targets* 9, 69–80. doi: 10.2174/187152651090900069

Walter, R., Maggiorini, M., Scherrer, U., Contesse, J., and Reinhart, W. H. (2001). Effects of high-altitude exposure on vascular endothelial growth factor levels in man. *Eur. J. Appl. Physiol.* 85, 113–117. doi: 10.1007/s004210100419

Warth, A., Simon, P., Capper, D., Goeppert, B., Tabatabai, G., Herzog, H., et al. (2007). Expression pattern of the water channel aquaporin-4 in human gliomas is associated with blood-brain barrier disturbance but not with patient survival. *J. Neurosci. Res.* 85, 1336–1346. doi: 10.1002/jnr.21224

Wewer, U. M., Liotta, L. A., Jaye, M., Ricca, G. A., Drohan, W. N., Claysmith, A. P., et al. (1986). Altered levels of laminin receptor mRNA in various human

carcinoma cells that have different abilities to bind laminin. *Proc. Natl. Acad. Sci. U.S.A.* 83, 7137–7141. doi: 10.1073/pnas.83.19.7137

Willis, C. L., Camire, R. B., Brule, S. A., and Ray, D. E. (2013). Partial recovery of the damaged rat blood-brain barrier is mediated by adherens junction complexes, extracellular matrix remodeling and macrophage infiltration following focal astrocyte loss. *Neuroscience* 250, 773–785. doi: 10.1016/j.neuroscience.2013.06.061

Wissing, E. R., Boyer, J. G., Kwong, J. Q., Sargent, M. A., Karch, J., McNally, E. M., et al. (2014). P38α MAPK underlies muscular dystrophy and myofiber death through a Bax-dependent mechanism. *Hum. Mol. Genet.* 23, 5452–5463. doi: 10.1093/hmg/ddu270

Wolburg, H., Noell, S., Mack, A., Wolburg-Buchholz, K., and Fallier-Becker, P. (2009). Brain endothelial cells and the glio-vascular complex. *Cell Tissue Res.* 335, 75–96. doi: 10.1007/s00441-008-0658-9

Yang, L. L., Zhou, Y., Tian, W. D., Li, H. J., Kang-Chu-Li, Miao, X., et al. (2016). Electromagnetic pulse activated brain microglia via the p38 MAPK pathway. *Neurotoxicology* 52, 144–149. doi: 10.1016/j.neuro.2015.12.008

Young, H. K., Barton, B. A., Waisbren, S., Portales Dale, L., Ryan, M. M., Webster, R. I., et al. (2008). Cognitive and psychological profile of males with Becker muscular dystrophy. *J. Child Neurol.* 23, 155–162. doi: 10.1177/0883073807307975

Yurchenco, P. D., and Patton, B. L. (2009). Developmental and pathogenic mechanisms of basement membrane assembly. *Curr. Pharm. Des.* 15, 1277–1294. doi: 10.2174/138161209787846766

Zhao, F., Deng, J., Xu, X., Cao, F., Lu, K., Li, D., et al. (2018). Aquaporin-4 deletion ameliorates hypoglycemia-induced BBB permeability by inhibiting inflammatory responses. *J. Neuroinflamm.* 15:157. doi: 10.1186/s12974-018-1203-8

Conflict of Interest Statement: The authors declare that the research was conducted in the absence of any commercial or financial relationships that could be construed as a potential conflict of interest.

Copyright © 2019 Park, Choi, Kong and Kang. This is an open-access article distributed under the terms of the Creative Commons Attribution License (CC BY). The use, distribution or reproduction in other forums is permitted, provided the original author(s) and the copyright owner(s) are credited and that the original publication in this journal is cited, in accordance with accepted academic practice. No use, distribution or reproduction is permitted which does not comply with these terms.

frontiers in Neuroscience

REVIEW
published: 28 May 2019
doi: 10.3389/fnins.2019.00540

The Inflammatory Response After Ischemic Stroke: Targeting β_2 and β_1 Integrins

Danielle N. Edwards[1,2] *and Gregory J. Bix*[3,4]*

[1] Sanders–Brown Center on Aging, University of Kentucky, Lexington, KY, United States, [2] Department of Neuroscience, University of Kentucky, Lexington, KY, United States, [3] Department of Neurology, University of Kentucky, Lexington, KY, United States, [4] Department of Neurosurgery, University of Kentucky, Lexington, KY, United States

Ischemic stroke is a leading cause of death and disability with limited therapeutic options. Resulting inflammatory mechanisms after reperfusion (removal of the thrombus) result in cytokine activation, calcium influx, and leukocytic infiltration to the area of ischemia. In particular, leukocytes migrate toward areas of inflammation by use of integrins, particularly integrins β_1 and β_2. Integrins have been shown to be necessary for leukocyte adhesion and migration, and thus are of immediate interest in many inflammatory diseases, including ischemic stroke. In this review, we identify the main integrins involved in leukocytic migration following stroke ($\alpha_L\beta_2$, $\alpha_D\beta_2$, $\alpha_4\beta_1$, and $\alpha_5\beta_1$) and targeted clinical therapeutic interventions.

Keywords: ischemic stroke, integrins, inflammation, leukocytes, clinical trial results

OPEN ACCESS

Edited by:
Xin Qi,
Case Western Reserve University, United States

Reviewed by:
Jan Rossaint,
University of Münster, Germany
Shan Huang,
University of California, Los Angeles, United States

****Correspondence:***
Gregory J. Bix
gregorybix@uky.edu

Specialty section:
This article was submitted to Neurodegeneration, a section of the journal Frontiers in Neuroscience

Received: *07 March 2019*
Accepted: *09 May 2019*
Published: *28 May 2019*

Citation:
Edwards DN and Bix GJ (2019) The Inflammatory Response After Ischemic Stroke: Targeting β_2 and β_1 Integrins. Front. Neurosci. 13:540. doi: 10.3389/fnins.2019.00540

INTRODUCTION

Ischemic stroke is a leading cause of death and disability in the United States with limited therapeutic interventions available, including tissue plasminogen activator (t-PA) and endovascular mechanical thrombectomy (Rao et al., 2014; Benjamin et al., 2017; Rai et al., 2017). These interventions are focused on the removal of the thrombus, restoring blood flow, oxygen and glucose to hypoperfused areas, but are unable to affect the inflammatory, necrotic, and blood-brain barrier (BBB) mechanism that follow. In particular, the initial inflammatory cascade is initiated by the decrease in ATP production, release of cytokines, influx of intracellular calcium, reactive oxygen species, etc., that develops during occlusion and continues for days afterward (Sandoval and Witt, 2008). Using shear forces from cerebral blood flow, marrow-derived leukocytes (including polymorphonuclear leukocytes (PMNs), neutrophils, lymphocytes and monocytes) are recruited to the site of injury (Dereski et al., 1993; del Zoppo, 1994; Stefanidakis and Koivunen, 2006).

For the purpose of this review, we will focus on the recruitment and rolling of leukocytes under the direction of integrins, as well as some of their ligands following reperfusion after ischemic stroke. We will then introduce recent β_2 and β_1 integrin-specific stroke clinical trials, and, finally, discuss potential future directions for the field.

LEUKOCYTIC INFILTRATION FOLLOWING ISCHEMIC STROKE

Leukocyte Recruitment

The initial endothelial response upregulates endothelial selectins, particularly P-selectin and E-selectin, translocating them from an intracellular, inactive state, to the available extracellular matrix for leukocytic binding, while the upregulation of L-selectin on the leukocyte is essential for recruitment to the site of injury (Bargatze et al., 1994). Both are acutely regulated, P-selectin at

15 min and E-selectin at 2 h post ischemia. These extracellularly located selectins then facilitate the recruitment and activation of leukocytes to the area of ischemia (Zhang et al., 1998). Leukocytes then undergo a conformational change, facilitating polarization and the development of certain cellular characteristics: a leading edge, main body, and rear-uropod protrusion. The uropod, or posterior protrusion, in fast moving leukocytes promotes mobility, while the leading protrusions (lamellipodia and filopodia, small leg-like projections) are less likely to be used due to the rate limiting interaction with actin filaments (Ridley et al., 2003) (summarized in **Figure 1**). Though this mechanism is less obvious in the highly mobile leukocytes. Once leukocytes are bound to selectins, additional binding to integrins and adhesion molecules (intracellular adhesion molecule (ICAMs and vascular adhesion molecule-1 (VCAM) occurs, permitting leukocytic rolling (del Pozo et al., 1995; Lorant et al., 1995; Kindzelskii et al., 1996; Becker, 2002). Additional damage can occur once at the site of ischemia, as infiltration into the brain parenchyma across the BBB destroys surrounding vasculature (Clark et al., 1993; Chou et al., 2004), and leukocytes continually release additional factors (reactive oxygen species, cytokines, and proteases) that enhance leukocytic recruitment (Wang et al., 2008).

Leukocyte Infiltration

At the site of injury, leukocytes continue to increase binding on cerebrovasculature up to 48 h following ischemic stroke, and use transendothelial migration as a method for infiltration from the cerebrovasculature into the surrounding brain parenchyma. Early adhesion, prior to 24 h following reperfusion, is attributed to neutrophils. Within 30 min to a few hours following reperfusion, neutrophils arrive at the site of injury, peaking at maximum expression around 1–3 days, though expression can still be detected 7–15 days later in preclinical stroke models (Weston et al., 2007). This upregulation is also seen in ischemic stroke patients, where neutrophils have been detected beginning at 6 h, with radiolabeled imaging, and continue to be detected up to 72 h (Aspey et al., 1989). The early recruitment and infiltration of neutrophils across the BBB appears to be highly significant in stroke, as high neutrophilic infiltration is associated with damaged cerebrovasculature (Enzmann et al., 2013), while depletion reduces infarct volume and dysfunction in stroke models (Chou et al., 2004).

As reperfusion injury continues, the circulating leukocytes switch from neutrophils to mononucleuar leukocytes (monocytes/lymphocytes) which dominate the adherent culture from 24 h to 7 days post reperfusion (Schroeter et al., 1994; Stevens et al., 2002; Ishikawa et al., 2005). Of the two types of lymphocytes, B- and T-, T cells have emerged as the dominant, damage-inducing lymphocyte in ischemic stroke (Brait et al., 2011). Preclinical studies have shown that the inhibition of all lymphocytes results in smaller infarct and improved neurological outcomes, but only the reintroduction of T-lymphocytes to mice reversed any benefits (Yilmaz et al., 2006; Kleinschnitz et al., 2010). Activated T-lymphocytes, not B-, have been detected in patients up to 60 days post-stroke, and are correlated with an increased risk of stroke reoccurrence and death (Tarkowski et al., 1995; Nadareishvili et al., 2004).

Clinical Importance of Leukocytes

Multiple studies have established the importance of leukocytic adherence and infiltration into the brain parenchyma following ischemic stroke, but targeting the leukocytes has a high degree of risk. This is evident as inhibition of leukocytic cells increase the occurrence of bacterial infection and mortality as evident by Leukocytic Adhesion Deficiency (LAD-1) (Stefanidakis and Koivunen, 2006). Because these cells are necessary for bacterial resistance, systemic inhibition following ischemic stroke is exceptionally risky. However, studies in stroke patients show a strong correlation between increased levels of peripheral leukocytes and neutrophils, and increased infarct volume (Price et al., 2004; Buck et al., 2008). Thus, some current therapeutic strategies have focused on the inflammatory cascade have focused on blocking the adhesion and infiltration of cells at the site of injury, primarily endothelial expressed ICAMs and VCAM. This method has shown success in preclinical studies, but has failed to translate to the clinic. Thus, the focus has switched to directly targeting the integrins, a primary mediator of leukocyte adhesion, rather than their ligands, as discussed above. This review is focused on integrins β_2 and β_1 that have shown promise in therapeutically targeting the ischemic stroke inflammatory cascade.

ROLE OF INTEGRINS POST-STROKE: AN OVERVIEW

Integrins are a diverse group of heterodimers composed of 18 different α and β subunits, creating 24 unique combinations. Integrins exist on every cell type, while exhibiting a high diversity of ligands and grouped into four different receptor groups: RGD (Arg-Gly-Asp), laminin receptors, collagen receptors, and leukocyte-specific receptors. Within these groups, integrins can have a variety of ligands and roles following ischemic stroke (reviewed in Edwards and Bix, 2019). Under normal cerebrovascular conditions, integrins are in a highly inactive state, typically in a bent conformation (Takagi et al., 2002; Nishida et al., 2006). Following ischemic stroke, activation signals are sent. Chemokines are translocated to the lumen, on the apical side of endothelial cells, to induce "inside-out" signaling (Chavakis, 2012). Integrins then undergo a conformational change to increase integrin affinity for potential ligands while enhancing detection by localizing to the leading or rear-facing edge of the leukocyte's cell wall for ligand detection (Ridley et al., 2003; Hyun et al., 2009). Activated integrins then bind to available ligands, permitting leukocytic rolling and intracellular signaling. This is termed "outside-in" signaling (Hato et al., 1998; Tominaga et al., 1998; Ley et al., 2007). Leukocytes continue movement to the site of injury, looking for areas to cross the endothelial cell barrier, and eventually coming to a halt. Aggregation/clustering of integrins increases binding avidity (strength of binding), preventing flow conditions from detaching leukocytes from the endothelial cells (Ley et al., 2007). Using transmigration, leukocytes will infiltrate into the cerebral parenchyma using these integrin-ligand connections.

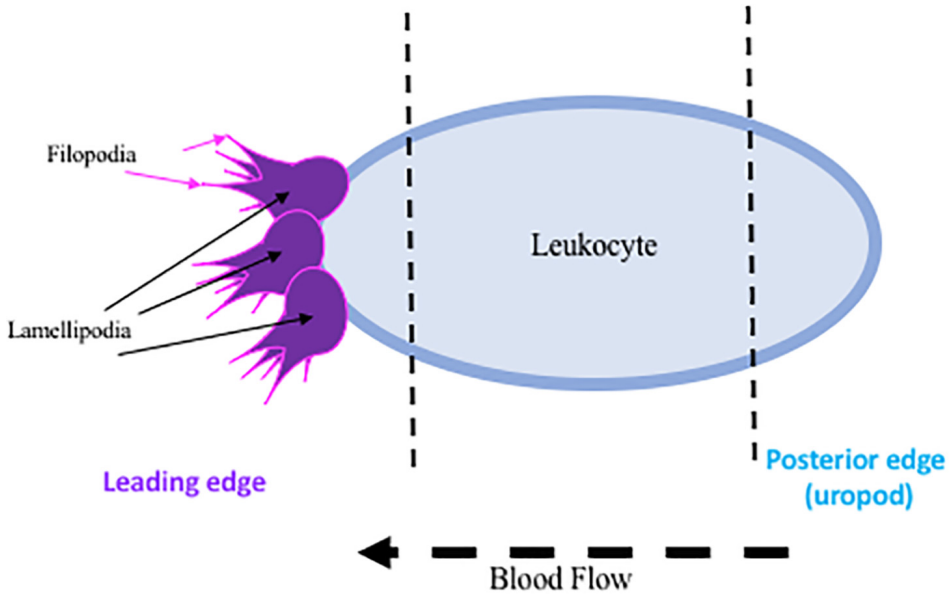

FIGURE 1 | Representative diagram of regions of interest on activated leukocytes.

β_2 Integrins

β_2 integrins are the only group of integrins exclusively expressed on leukocytes (derived from hematopoietic cells) (Schenkel et al., 2004), and like most integrins, are highly conserved across species (Schittenhelm et al., 2017). They are also the most highly expressed integrin on circulating blood leukocytes, tending to cluster at the retraction area of the cell (the rear), in both an active and inactive state, compared to other β_1, β_4, β_3, and β_7 integrins found on circulating leukocytes (Pierini et al., 2000; Lindbom and Werr, 2002). Genetic leukocyte adhesion changes (LAD-1, as discussed above) has been attributed to mutations in the β_2 subunit, reducing β_2 expression. Thus, leukocytic movement is reduced on the cell surface with less movement toward the site of inflammation (Arnaout, 1990; Scharffetter-Kochanek et al., 1998). Importantly, in β_2 inhibited mice, there is not total arrest of leukocytic recruitment or infiltration (Pierini et al., 2000), suggesting that other factors likely play a role. There are 4 identified heterodimers of β_2 integrins, and of these, the most highly studied are $\alpha_L\beta_2$ and $\alpha_M\beta_2$ in ischemic stroke, and will be reviewed in more detail below. The other β_2 integrins, $\alpha_X\beta_2$ and $\alpha_D\beta_2$, have not been individually studied in the context of stroke as have $\alpha_L\beta_2$ and $\alpha_M\beta_2$ integrins, though CD18 (β_2) inhibition in addition to t-PA has been shown to increase the time window of t-PA administration without an increase in hemorrhagic transformation in a rat embolic stroke model (Zhang et al., 1999). Furthermore, **Figure 2** summarizes the results in this section.

$\alpha_L\beta_2$ Integrin

Integrin $\alpha_L\beta_2$ is also referred to as CD11a/CD18 and LFA-1 (lymphocyte functional-associating antigen-1). $\alpha_L\beta2$ integrin acutely increases in ischemic stroke patients, with detectable amounts through 72 h associated around the area of ischemia (Gerhard et al., 2000; Zhao et al., 2002). This suggests a correlation between $\alpha_L\beta_2$ integrin expression and inflammatory damage following ischemia. $\alpha_L\beta_2$ is expressed on all leukocytes (Soriano et al., 1999), though at particularly high levels on T-lymphocytes (Hammond et al., 2014; Walling and Kim, 2018). In healthy individuals, extracted blood analysis revealed that $\alpha_L\beta_2$ activation requires leukocytic rolling on P- or E-selectins, inducing an active conformational change (Kuwano et al., 2010), but it is the binding of chemokines g-protein coupled receptors (GPCR) and Rap-1 activation that induces the high-affinity conformational state of $\alpha_L\beta_2$ (Steffen et al., 1994; Greenwood et al., 1995; Ghandour et al., 2007). In this state, $\alpha_L\beta_2$ has many possible ligands, ICAM-1, ICAM-2, ICAM-3, ICAM-4, ICAM-5, and junctional adhesion molecule-1 (JAM-1) (Marlin and Springer, 1987; de Fougerolles et al., 1991, 1994; Tian et al., 2000), though ICAM-1 is preferentially bound (Walling and Kim, 2018). The high avidity $\alpha_L\beta_2$-ICAM-1 complex, once formed, allows t-lymphocytes to move against circulatory flow and the shear forces, resulting in the high-speed movement of leukocytes (Katakai et al., 2013; Dominguez et al., 2015).

In an intraluminal model of experimental ischemic stroke, $\alpha_L\beta_2$ inhibition with the use of transgenic mice results in reduced infarct volume, edema volume and mortality. However, this phenomenon is evident in transient, but not permanent middle cerebral artery occlusion (Arumugam et al., 2004). This may be due to the previously mentioned high avidity of $\alpha_L\beta_2$-ICAM-1 bonds, and is evident in an *in vitro* study using $\alpha_L\beta_2$ (LFA-1) knock-in mice that experience high avidity through binding of lymphocytes mediated through ICAM-1 binding, but are unable to continue movement due to a non-polarized uropod (Park et al., 2010). An explanation for this phenomenon may be that the recycling process within the leukocyte is overwhelmed (Shaw et al., 2004). By enhancing $\alpha_L\beta_2$ expression, recycling may not be able to allow for dislocation of $\alpha_L\beta_2$-ICAM-1

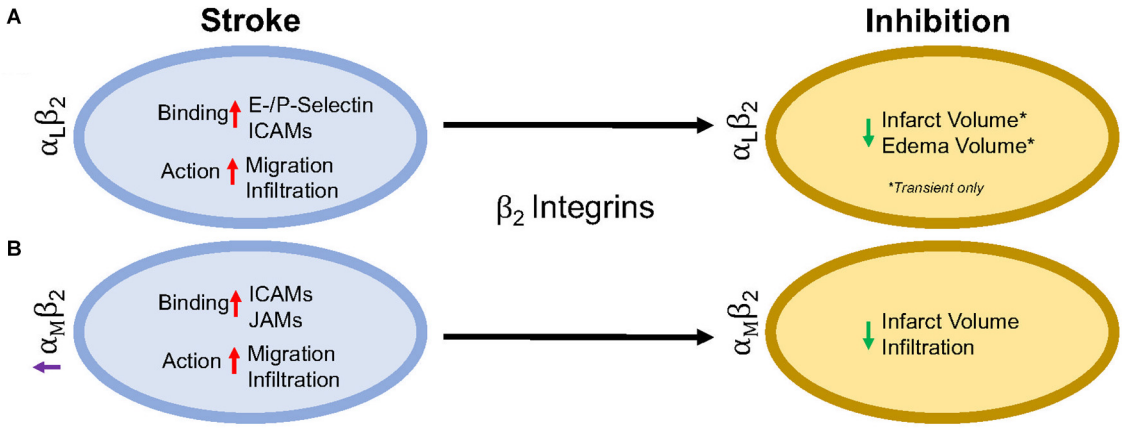

FIGURE 2 | Representative image of the β_2 integrin response following experimental stroke and inhibitory antibody treatment in preclinical trials. Inhibition of **(A)** $\alpha_L\beta_2$ and **(B)** $\alpha_M\beta_2$ integrins post-stroke responses and effects.

complexes, preventing movement from the loss of high adhesion bonds. Enhanced $\alpha_L\beta_2$ expression could be a potential new avenue for therapy, especially if no enhanced mortality, infection, etc., are observed.

Independently, ICAMs play a significant role in inflammation following ischemic stroke. ICAM-1, in particular, is acutely increased in both cultured human endothelial cells undergoing hypoxia and following intraluminal suture middle cerebral artery occlusion, while expression remains sustained for up to a week post-injury (Hess et al., 1994a,b; Zhang et al., 1995). ICAM-2, another possible ligand, does not change in expression following cytokine stimulation (de Fougerolles et al., 1991; Nortamo et al., 1991a,b). Furthermore, serum of ischemic stroke patients contains soluble ICAM-1, but not ICAM-2 in addition to being a risk factor (Kaplanski et al., 1994; Shyu et al., 1997). Antibodies targeting ICAM-1 in rodents and humans have shown contradictory results. An intraluminal suture middle cerebral artery occlusion model in mice and rats showed a decrease in leukocyte infiltration and infarct volume (Connolly et al., 1996; Kitagawa et al., 1998; Vemuganti et al., 2004), while one study reported opposing effects (Furuya et al., 2001). ICAM-1 inhibition was translated to the clinic through testing of the murine ICAM-1 antibody, Enlimomab in ischemic stroke. Unfortunately, the study was halted early due to increased rate of infection, infarct volumes, neurological scores and mortality for patients (Furuya et al., 2001).

$\alpha_M\beta_2$ Integrin

Integrin $\alpha_M\beta_2$, also known as CD11b/CD18 and Mac-1 (macrophage-1 antigen), exhibits many similarities to $\alpha_L\beta_2$ through its expression on all leukocytes (Springer et al., 1979), and common ligand binding partners such as the family of ICAMs and JAMs (von Andrian et al., 1991). Additional ligands are fibrinogen, heparin (von Andrian et al., 1991), elastase (Cai and Wright, 1996), complement C3 fragment (C3bi) (Micklem and Sim, 1985), kinogen components, and urokinase and its receptor (Chavakis et al., 1999). Just as $\alpha_L\beta_2$, hypoxia induced factors (cytokines, chemokines, etc.) induce conformational change of $\alpha_M\beta_2$ to a high affinity ligand-binding state (Stanimirovic et al., 1997). Binding assays with ICAM-1 as a ligand and both $\alpha_L\beta_2$ and $\alpha_M\beta_2$ as receptors show $\alpha_L\beta_2$ integrin is preferably bound (Lub et al., 1996). This suggests that the binding sites on both $\alpha_L\beta_2$ and $\alpha_M\beta_2$ compete for ICAM-1 binding.

Following experimental ischemic stroke in rats, integrin $\alpha_M\beta_2$ is upregulated (Campanella et al., 2002), and has shown benefit when inhibited. Antibodies against both CD11b/CD18 reduce infarct volume and reestablish cerebral blood flow as a result of decreased neutrophil infiltration following intraluminal stroke surgery (Chen et al., 1994; Bowes et al., 1995; Zhang et al., 1995). In a different approach, the addition of recombinant neutrophil inhibitory factor (rNIF) inhibits a binding domain on Mac-1 and yields similar results in the same intraluminal occlusion model (Jiang et al., 1998). Furthermore, and similarly to $\alpha_L\beta_2$ integrin inhibition, inhibition of $\alpha_M\beta_2$ is also effective in transient, but not permanent experimental ischemic stroke in an embolic occlusion model (Zhang et al., 2003).

β_1 Integrins

β_1 integrins are a diverse set of integrins, with laminin-binding, collagen-binding, RGD-binding and leukocyte heterodimers. β_1 integrins are not as highly expressed on leukocytes as β_2 integrins, but they do play a major role in leukocyte adhesion and migration following ischemic stroke. The activity of β_1 integrins is similar to β_2 integrins. They undergo a conformational change to induce "inside-out" and "outside-in" cellular signaling (Campanero et al., 1994). As the cells migrate, the β_1 integrins are most commonly clustered around the uropod, but will be located in any area of the leukocyte that is in contact with the endothelial cell or extracellular matrix (Campanero et al., 1994; Caimi et al., 2001). Inhibition of the β_1 integrin, just as with β_2 integrin inhibition, does not fully stop leukocyte rolling. However, when both β_1 and β_2 integrins are inhibited, complete leukocyte arrest occurs (Lobb and Hemler, 1994; Pierini et al., 2000). This suggests that both β_1 and β_2 integrins are necessary for leukocyte migration, regardless of expression load. Of all the β_1 integrins, both $\alpha_4\beta_1$ and $\alpha_5\beta_1$

appear to be the most highly expressed and the most studied in post-stroke inflammation. The other β_1 integrin expressed on leukocytes, $\alpha_9\beta_1$, has not been studied in the context of stroke as its expression and role has not yet been fully elucidated in the brain. **Figure 3** summarizes the results discussed in this section.

$\alpha_4\beta_1$ Integrin

$\alpha_4\beta_1$, also known as CD49d/CD29 VLA-4 (very late antigen-4), is localized primarily to leukocytes (neutrophils, monocytes, lymphocytes, macrophages, etc.) and microglia as a leukocyte-specific receptor. Additionally, α_4 will also dimerize with β_4, which is found in gut endothelium (Hammond et al., 2014). Activation of $\alpha_4\beta_1$ integrin results from the binding of upregulated chemokines to GPCRs in the same manner as $\alpha_L\beta_2$ as discussed above (Vajkoczy et al., 2001). This stimulates binding to $\alpha_4\beta_1$'s preferred ligand, VCAM-1, but experiments have shown some preference for paxillin ICAM-1 (Steffen et al., 1994; Ghandour et al., 2007), and fibronectin (Hart and Greaves, 2010) as well. Interestingly, instead of using the β_1 submit of the heterodimer for binding, integrin $\alpha_4\beta_1$ uses its α subunit of $\alpha_4\beta_1$ to mediate binding to VCAM-1 (Luo et al., 2007).

Preclinical ischemic stroke studies targeting $\alpha_4\beta_1$ have shown increasingly varied results. Most researchers reported a decrease in VCAM-1 expression, cytokine production, and infiltrating leukocytes (Liesz et al., 2011; Langhauser et al., 2014; Llovera et al., 2015), but this reduction in inflammation did not result in reduced infarct volumes or functional deficit following analysis of a randomized preclinical trial involving six different centers (Llovera et al., 2015). Langhauser et al went one step further and found that no treatment paradigm (prophylactic or therapeutic) and no model (transient or permanent) showed efficacy (Langhauser et al., 2014). On the other hand, both Becker, 2002 and Relton et al., 2000 found that inhibition of α_4 improved both infarct volumes and functional deficits. When a preclinical randomized control trial was implemented at multiple centers, researchers found efficacy only in patients with small infarct volumes (Llovera et al., 2015). Collectively, these contradictory results may be caused by a couple of scenarios, 1) the varying expression of integrin $\alpha_4\beta_1$ expression following ischemic stroke resulting in continued leukocyte infiltration, or 2) integrin $\alpha_4\beta_1$ is not a primary driver of post-stroke pathophysiology, but other factors, including other integrins, promote leukocyte migration (Hammond et al., 2014).

$\alpha_5\beta_1$ Integrin

$\alpha_5\beta_1$, also known as CD49e/CD29 and VLA-5, plays an as yet largely undetermined role in inflammation, with studies primarily limited to cell culture. What is known is that leukocytes express different β_1 integrins with $\alpha_5\beta_1$ composing around 50% of all β_1 –integrins expressed on neutrophils (Pierini et al., 2000) and monocytes (Pacifici et al., 1994). Additionally, $\alpha_5\beta_1$ is necessary for leukocyte adhesion. Only inhibition of both $\alpha_5\beta_1$ and β_2 integrins completely blocks adhesion *in vitro* (Pierini et al., 2000), while inhibition of $\alpha_5\beta_1$ alone prevents transmigration across the BBB (Labus et al., 2018) *in vitro*. As an RGD receptor, fibronectin has been shown to be the primary and preferred [over other potential ligands such as fibrinogen (Suehiro et al., 1997)] ligand for $\alpha_5\beta_1$ on endothelial cells and leukocytes (Schaffner et al., 2013; Bharadwaj et al., 2017). Importantly, in the presence of activated $\alpha_L\beta_2$, leukocyte $\alpha_5\beta_1$ binding to fibronectin is enhanced (Bohnsack, 1992; Loike et al., 1999; Gronholm et al., 2016). $\alpha_5\beta_1$ integrin expression is induced by cytokines, particularly TNFα (Li et al., 2011) toward the leading edge of the cell in contrast with other integrins at the uropod (Pierini et al., 2000). Furthermore, $\alpha_5\beta_1$ integrin appears to be highly sensitive to calcium (Pierini et al., 2000), an ion that is increased rapidly following reperfusion (Sandoval and Witt, 2008). Upon calcium buffering, $\alpha_5\beta_1$ expression moves from the front of the cell to the uropod and the leukocyte becomes elongated. The change in expression localization and morphology is attributed to non-movement as the leukocyte cannot detach $\alpha_5\beta_1$ from the vascular wall (Pierini et al., 2000). Recently, Edwards et al. (2019) found that inhibition of $\alpha_5\beta_1$ integrin by the small peptide ATN-161 prevented CD45+ leukocytes from infiltrating the brain

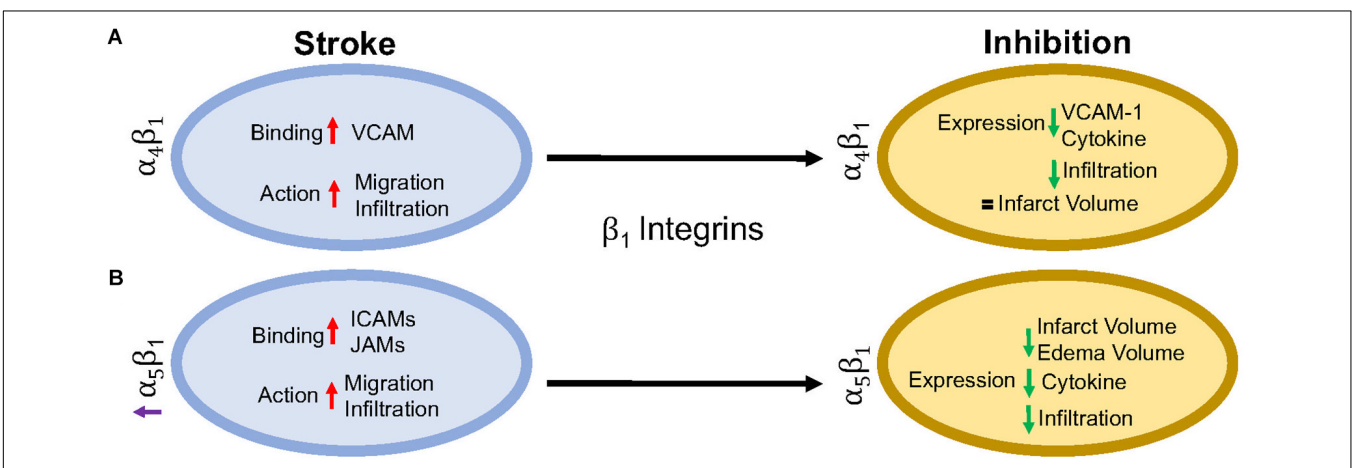

FIGURE 3 | Representative image of the β_1 integrin response following experimental stroke and inhibitory antibody treatment in preclinical trials. Inhibition of **(A)** $\alpha_4\beta_1$ and **(B)** $\alpha_5\beta_1$ integrins post-stroke responses and effects.

parenchyma following the tandem/transient common carotid artery/middle cerebral artery occlusion model. Additionally, mice were observed to have reduced BBB permeability, functional deficits, edema, and infarct volume following middle cerebral artery occlusion (Roberts et al., 2015; Edwards et al., 2019). Thus, targeting $\alpha_5\beta_1$ after ischemic stroke could be a new avenue for reduction of inflammation following ischemic stroke.

CLINICAL IMPLICATIONS

The preclinical studies discussed here point towards the potential of targeting β_2 and β_1 integrins in the treatment of post-stroke inflammation. Though their potential has not fully been elucidated, many clinical trials, not just limited to stroke, have been approved in the last 10 years targeting these integrins.

The most common target for post-stroke inflammation are the β_2 integrins. Though some efficacy has been reported, no clinical stroke trials to date have targeted the α_L subunit in stroke patients. However, one clinical trial with the monoclonal antibody, Efalizumab, has shown promise in decreasing T-lymphocyte rolling in patients with moderate-severe plaque psoriasis (Lebwhohl et al., 2003).

In preclinical studies targeting $\alpha_M\beta_2$, a hookworm isolated recombinant glycoprotein targeting rNIF (UK279276) (Zhang et al., 2003) and humanized Hu23F2G (Leukarrest) (Yenari et al., 1998), were both shown to decrease infarct volume and increase functional recovery following reperfusion. Both therapies had negligible side effects in Phase 1 studies and thus were continued to a Phase II study, respectively, before the trials were halted due to no observed efficacy (Becker, 2002; Krams et al., 2003). The failure to target $\alpha_M\beta_2$ integrin may be due to the observation that human ischemic stroke patients do not experience the increase in $\alpha_M\beta_2$ expression as seen in rodent stroke models (Caimi et al., 2001). Interestingly, when given in conjunction with United Kingdom279276, patients experienced a slight improvement (Krams et al., 2003), but no follow-up has been conducted. This interesting effect may be worth additional investigation in future clinical trials.

Clinical inhibition of β_1 integrins, on the other hand, is small and varied. Of the current clinical trials, one trial has emerged targeting $\alpha_4\beta_1$ in the context of ischemic stroke. The monoclonal antibody targeting the α_4 subunit (Natalizumab) has been successful in protecting patients from relapses in multiple sclerosis (Polman et al., 2006) and Crohn's disease (Sandborn et al., 2015). However, in a Phase II ischemic stroke study, patients receiving Natalizumab showed no improvement in infarct growth or neurological scores over 30 days. Furthermore, two patients (out of 79) died from serious infections attributed to Natalizumab treatment (Elkins et al., 2017). At this time, there are no further clinical trials planned.

FUTURE CONSIDERATIONS

As discussed in this review, targeting leukocytic integrins has had limited to no efficacy in clinical trials. Importantly, these studies have collectively employed only three different therapeutics and two targets; there are still significant areas that can be investigated. Though not discussed here, most preclinical investigations have focused on the ligands themselves rather than the integrin as the therapeutic target, highlighting the continued importance of integrins in stroke.

It is also important to note that preclinical studies carried out in rodents inadequately model the post-stroke pathophysiology that patients experience. Preclinical stroke research is also typically limited, focusing on one species, sex, and age that do not necessarily match the demographic of stroke patients (see Kahle and Bix, 2012 for a review of this topic). Furthermore, as the changes following stroke and/or reperfusion are inadequately understood, identifying appropriate therapeutic targets that translate from the lab to clinical trials, has been particularly challenging.

However, this does not suggest abandoning therapeutic trials for ischemic stroke. As mentioned above, stroke is a leading cause of death and disability, separate from cardiovascular disease. This will not improve without intervention with our aging and obese population. Fortunately, with the advent of stroke mortality-altering therapies, i.e., t-PA and endovascular mechanical thrombectomy, our financial burden has shifted to aftercare. When we review the amount of trials performed for thrombolytic agents (Multicentre Acute Stroke Trial–Italy (MAST-I) Group, 1995; National Institute of Neurological Disorders and Stroke rt-Pa Stroke Study Group, 1995; The Multicenter Acute Stroke Trial–Europe Study Group, 1996) and endovascular thrombectomy [MR CLEAN (Berkhemer et al., 2015), ESCAPE (Goyal et al., 2015), EXTEND IA (Campbell et al., 2015), SWIFT PRIME (Saver et al., 2015), and REVASCAT (Jovin et al., 2015)] as potential treatments of ischemic stroke, it is obvious that the complexities of stroke affect the outcome of the clinical trial. This includes, but is not limited to, the time a patient takes to arrive at an ER, time to treatment, location of the stroke, amount of surrounding collaterals, current medications and co-morbidities (diabetes, cancer, etc.), and if the patient has experienced multiple strokes.

Based on current advances, as well as previous failures, a focus on integrins as a therapeutic target for stroke is emerging. A significant reason for this focus may be the complex, multi-dimensional role that integrins appear to play in brain pathophysiology. Integrins are diverse, existing on all cell types with varying roles depending upon expression and activation. This complexity can represent a significant challenge to integrin-targeted therapies inasmuch as such therapies could have diverse, even unintended off-target effects. However, we believe that this can be overcome by a better understanding of how integrin function and expression is altered after stroke, with the potential to exploit stroke-dependent integrin changes to therapeutic effect. For example, identifying a specific integrin to be upregulated in select cells in the post-stroke brain or brain-targeting cells, but not in other organs, could render it a viable therapeutic target. This emphasizes the need and importance of preclinical stroke research to discover and unravel the complexities of integrin biology. We are confident that such studies will result in viable new stroke therapies.

CONCLUSION

In this review, we have implicated integrins as an area of research for limiting inflammation following ischemic stroke. To date, therapeutic inhibition of $\alpha_L\beta_2$, $\alpha_M\beta_2$, and $\alpha_4\beta_1$ has shown promising results in preclinical studies, but translation to the clinic has been disappointing. Going forward, more targeted antibodies to all reactive β_1 and β_2 integrins after ischemic stroke may prove more beneficial, but more research needs to be done to completely understand the human inflammatory response and how that relates to changes in preclinical models.

AUTHOR CONTRIBUTIONS

DE wrote the manuscript. DE and GB edited the manuscript.

REFERENCES

Arnaout, M. A. (1990). Leukocyte adhesion molecules deficiency: its structural basis, pathophysiology and implications for modulating the inflammatory response. *Immunol. Rev.* 114, 145–180. doi: 10.1111/j.1600-065x.1990.tb00564.x

Arumugam, T. V., Salter, J. W., Chidlow, J. H., Ballantyne, C. M., Kevil, C. G., and Granger, D. N. (2004). Contributions of LFA-1 and Mac-1 to brain injury and microvascular dysfunction induced by transient middle cerebral artery occlusion. *Am. J. Physiol. Heart Circ. Physiol.* 287, H2555–H2560. doi: 10.1152/ajpheart.00588.2004

Aspey, B., Jessimer, C., Pereira, S., and Harrison, M. (1989). Do leukocytes have a role in the cerebral no-reflow phenomenon? *J. Neurol. Neurosurg. Psychiatry* 52, 526–528. doi: 10.1136/jnnp.52.4.526

Bargatze, R., Kurk, S., Butcher, E., and Jutila, M. (1994). Neutrophils roll on adherent neutrophils bound to cytokine-induced endothelial cells via L-selectin on the rolling cells. *J. Exp. Med.* 180, 1785–1792. doi: 10.1084/jem.180.5.1785

Becker, K. (2002). Anti-leukocyte antibodies: leukarrest (Hu23F2G) and enlimomab (R6.5) in acute stroke. *Curr. Med. Res. Opin.* 18(Suppl. 2), 18–22.

Benjamin, E. J., Blaha, M. J., Chiuve, S. E., Cushman, M., Das, S. R., Deo, R., et al. (2017). Heart disease and stroke statistics—2017 update: a report from the american heart association. *Stroke* 137, 1–459.

Berkhemer, O. A., Fransen, P. S., Beumer, D., van den Berg, L. A., Lingsma, H. F., Yoo, A. J., et al. (2015). A randomized trial of intraarterial treatment for acute ischemic stroke. *N. Engl. J. Med.* 372, 11–20. doi: 10.1056/NEJMoa1411587

Bharadwaj, M., Strohmeyer, N., Colo, G. P., Helenius, J., Beerenwinkel, N., Schiller, H. B., et al. (2017). alphaV-class integrins exert dual roles on alpha5beta1 integrins to strengthen adhesion to fibronectin. *Nat. Commun.* 8:14348. doi: 10.1038/ncomms14348

Bohnsack, J. (1992). CD18-independent neutrophil adherence to laminin is mediated by the integrin VLA-6. *Blood* 79, 1545–1552.

Bowes, M., Rothlein, R., Fagan, S., and Zivin, J. (1995). Monoclonal antibodies preventing leukocyte activation reduce experimental neurologic injury and enhance efficacy of thrombolytic therapy. *Neurology* 45, 815–819. doi: 10.1212/WNL.45.4.815

Brait, V. H., Rivera, J., Broughton, B. R., Lee, S., Drummond, G. R., and Sobey, C. G. (2011). Chemokine-related gene expression in the brain following ischemic stroke: no role for CXCR2 in outcome. *Brain Res.* 1372, 169–179. doi: 10.1016/j.brainres.2010.11.087

Buck, B. H., Liebeskind, D. S., Saver, J. L., Bang, O. Y., Yun, S. W., Starkman, S., et al. (2008). Early neutrophilia is associated with volume of ischemic tissue in acute stroke. *Stroke* 39, 355–360. doi: 10.1161/STROKEAHA.107.490128

Cai, T., and Wright, S. (1996). Human leukocyte elastase is an endogenous ligand for the integrin CR3 (CDllb/CD18, Mac-l, alphaM beta2) and modulates polymorphonuclear leukocyte adhesion. *J. Exp. Med.* 184, 1213–1223. doi: 10.1084/jem.184.4.1213

Caimi, G., Canino, B., Ferrara, F., Montana, M., Musso, M., Porretto, F., et al. (2001). Granulocyte integrins before and after activation in acute ischaemic stroke. *J. Neurol. Sci.* 186, 23–26. doi: 10.1016/s0022-510x(01)00495-6

Campanella, M., Sciorati, C., Tarozzo, G., and Beltramo, M. (2002). Flow cytometric analysis of inflammatory cells in ischemic rat brain. *Stroke* 33, 586–592. doi: 10.1161/hs0202.103399

Campanero, M., Sanchez-Mateos, P., del Pozo, M., and Sanchez-Madrid, F. (1994). ICAM-3 regulates lymphocyte morphology and integrin-mediated T cell interaction with endothelial cell and extracellular matrix ligands. *J. Cell Biol.* 127, 867–878. doi: 10.1083/jcb.127.3.867

Campbell, B. C., Mitchell, P. J., Kleinig, T. J., Dewey, H. M., Churilov, L., Yassi, N., et al. (2015). Endovascular therapy for ischemic stroke with perfusion-imaging selection. *N. Engl. J. Med.* 372, 1009–1018. doi: 10.1056/NEJMoa1414792

Chavakis, T. (2012). Leucocyte recruitment in inflammation and novel endogenous negative regulators thereof. *Eur. J. Clin. Invest.* 42, 686–691. doi: 10.1111/j.1365-2362.2012.02677

Chavakis, T., May, A., Preissner, K., and Kanse, S. (1999). Molecular mechanisms of zinc-dependent leukocyte adhesion involving the urokinase receptor and B2-integrins. *Blood* 93, 2976–2983.

Chen, H., Chopp, M., Zhang, R., Bodzin, G., Chen, Q., Rusche, J., et al. (1994). Anti-CD11b monoclonal antibody reduces ischemic cell damage after transient focal cerebral ischemia in rat. *Ann. Neurol.* 35, 458–463. doi: 10.1002/ana.410350414

Chou, W., Choi, D., Zhang, H., Mu, D., McMahon, T., Kharazia, V., et al. (2004). Neutrophil protein kinase Cδ as a mediator of stroke-reperfusion injury. *J. Clin. Invest.* 114, 49–56. doi: 10.1172/JCI200421655

Clark, R., Lee, E., Fish, C., White, R., Price, W. J., Jonak, Z., et al. (1993). Development of tissue damage, inflammation, and resolution following stroke: an immunohistochemical and quantitative planimetric study. *Brain Res. Bull.* 31, 565–572. doi: 10.1016/0361-9230(93)90124-t

Connolly, E., Winfree, C., Springer, T. A., Naka, Y., Liao, H., Yan, S., et al. (1996). Cerebral protection in homozygous null ICAM-1 mice after middle cerebral artery occlusion. *J. Clin. Invest.* 97, 209–216. doi: 10.1172/jci118392

de Fougerolles, A., Qin, X., and Springer, T. (1994). Characterization of the function of intercellular adhesion molecule (ICAM)-3 and comparison with ICAM-1 and ICAM-2 in immune responses. *J. Exp. Med.* 179, 619–629. doi: 10.1084/jem.179.2.619

de Fougerolles, A., Stacker, S., Schwarting, R., and Springer, T. (1991). Characterization of ICAM-2 and evidence for a third counter-receptor for LFA-1. *J. Exp. Med.* 174, 253–267. doi: 10.1084/jem.174.1.253

del Pozo, M. A., Sánchez-Mateos, P., Nieto, M., and Sánchez-Madrid, F. (1995). Chemokines regulate cellular polarization and adhesion receptor redistribution during lymphocyte interaction with endothelium and extracellular matrix. Involvement of cAMP signaling pathway. *J. Cell Biol.* 131, 495–508. doi: 10.1083/jcb.131.2.495

del Zoppo, G. (1994). Microvascular changes during cerebral ischemia and reperfusion. *Cerebrovasc. Brain Metab. Rev.* 6, 47–96.

Dereski, M., Chopp, M., Knight, R., Rodolosi, L., and Garcia, J. (1993). The heterogeneous temporal evolution of focal ischemic neuronal damage in the rat. *Acta Neuropathol.* 85, 327–333.

Dominguez, G. A., Anderson, N. R., and Hammer, D. A. (2015). The direction of migration of T-lymphocytes under flow depends upon which adhesion receptors are engaged. *Integr. Biol.* 7, 345–355. doi: 10.1039/c4ib00201f

Edwards, D., and Bix, G. (2019). Roles of integrins and extracellular matrix proteins after ischemic stroke. *Am. J. Physiol. Cell Physiol.* 316, C252–C263. doi: 10.1152/ajpcell.00151.2018

Edwards, D. N., Salmeron, K., Lukins, D., Trout, A., Fraser, J. F., and Bix, G. J. (2019). "Integrin a5b1 inhibition by ATN-161 reduces blood-brain barrier permeability, neuroinflammation, and is neuroprotective," in *Proceedings of the Abstract, International Stroke Conference 2019*, Honolulu.

Elkins, J., Vetkamp, R., Montaner, J., Johnston, S., Singhal, A., Becker, K., et al. (2017). Safety and efficacy of natalizumab in patients with acute ischemic stroke (ACTION): a randomized, placebo-controlled, double-blind phase 2 trial. *Lancet Neurol.* 16, 217–226. doi: 10.1016/S1474-4422(16)30357-X

Enzmann, G., Mysiorek, C., Gorina, R., Cheng, Y. J., Ghavampour, S., Hannocks, M. J., et al. (2013). The neurovascular unit as a selective barrier to polymorphonuclear granulocyte (PMN) infiltration into the brain after ischemic injury. *Acta Neuropathol.* 125, 395–412. doi: 10.1007/s00401-012-1076-3

Furuya, K., Takeda, H., Azhar, S., McCarron, R., Chen, Y., Ruetzler, C., et al. (2001). Examination of several potential mechanisms for the negative outcome in a clinical stroke trial of enlimomab, a murine anti-human intercellular adhesion molecule-1 antibody: a bedside-to-bench study. *Stroke* 32, 2665–2674. doi: 10.1161/hs3211.098535

Gerhard, A., Neumaier, B., Elitok, E., Glatting, G., Tomczak, R., Ludolph, A., et al. (2000). In vivo imaging of activated microglia using [11C]PK11195 and positron emission tomography in patients after ischemic stroke. *Neuroreport* 11, 2957–2960. doi: 10.1097/00001756-200009110-00025

Ghandour, H., Cultere, X., Alvarez, A., Luscinskas, F., and Mayadas, T. (2007). Essential role for Rap1 GTPase and its guanine exchange factor CalDAG-GEFI in LFA-1 but not VLA-4 integrin mediated human T-cell adhesion. *Blood* 110, 3682–3690. doi: 10.1182/blood-2007-

Goyal, M., Demchuk, A. M., Menon, B. K., Eesa, M., Rempel, J. L., Thornton, J., et al. (2015). Randomized assessment of rapid endovascular treatment of ischemic stroke. *N. Engl. J. Med.* 372, 1019–1030. doi: 10.1056/NEJMoa1414905

Greenwood, J., Wang, Y., and Calder, V. (1995). Lymphocyte adhesion and transendothelial migration in the central nervous system: the role of LFA-1, ICAM-1, VLA-4 and VCAM-1. off. *Immunology* 86, 408–415.

Gronholm, M., Jahan, F., Bryushkova, E. A., Madhavan, S., Aglialoro, F., Soto Hinojosa, L., et al. (2016). LFA-1 integrin antibodies inhibit leukocyte alpha4beta1-mediated adhesion by intracellular signaling. *Blood* 128, 1270–1281. doi: 10.1182/blood-2016-03-705160

Hammond, M. D., Ambler, W. G., Ai, Y., and Sansing, L. H. (2014). alpha4 integrin is a regulator of leukocyte recruitment after experimental intracerebral hemorrhage. *Stroke* 45, 2485–2487. doi: 10.1161/STROKEAHA.114.005551

Hart, R., and Greaves, D. (2010). Chemerin contributes to inflammation by promoting macrophage adhesion to VCAM-1 and fibronectin through clustering of VLA-1 and VLA-5. *J. Immunol.* 185, 3728–3739. doi: 10.4049/jimmunol.0902154

Hato, T., Pampori, N., and Shattil, S. J. (1998). Complementary roles for receptor clustering and conformational change in the adhesive and signaling functions of integrin aIIb b3. *J. Cell Biol.* 141, 1685–1695. doi: 10.1083/jcb.141.7.1685

Hess, D., Bhutwala, T., Sheppard, J., Zhao, W., and Smith, J. (1994a). ICAM-1 expression on human brain microvascular endothelial cells. *Neurosci. Lett.* 168, 201–204. doi: 10.1016/0304-3940(94)90450-2

Hess, D., Zhao, W., Carroll, J., McEachin, M., and Buchanan, K. (1994b). Increased expression of ICAM-1 during reoxygenation in brain endothelial cells. *Stroke* 25, 1463–1468.

Hyun, Y., Lefort, C., and Kim, M. (2009). Leukocyte integrins and their ligand interactions. *Immunol. Res.* 45, 195–208. doi: 10.1007/s12026-009-8101-1

Ishikawa, M., Vowinkel, T., Stokes, K. Y., Arumugam, T. V., Yilmaz, G., Nanda, A., et al. (2005). CD40/CD40 ligand signaling in mouse cerebral microvasculature after focal ischemia/reperfusion. *Circulation* 111, 1690–1696. doi: 10.1161/01.CIR.0000160349.42665.0C

Jiang, N., Chopp, M., and Chahwala, S. (1998). Neutrophil inhibitory factor treatment of focal cerebral ischemia in the rat. *Brain Res.* 788, 25–34. doi: 10.1016/s0006-8993(97)01503-5

Jovin, T. G., Chamorro, A., Cobo, E., de Miquel, M. A., Molina, C. A., Rovira, A., et al. (2015). Thrombectomy within 8 hours after symptom onset in ischemic stroke. *N. Engl. J. Med.* 372, 2296–2306. doi: 10.1056/NEJMoa1503780

Kahle, M. P., and Bix, G. J. (2012). Successfully climbing the "STAIRs": surmounting failed translation of experimental ischemic stroke treatments. *Stroke Res. Treat.* 2012, 1–8. doi: 10.1155/2012/374098

Kaplanski, G., Farnaier, C., Benoliel, A. M., Foa, C., Kaplanski, S., and Bongrand, P. (1994). A novel role for E- and P-selectins: shape control of endothelial cell monolayers. *J. Cell Sci.* 107, 2449–2457.

Katakai, T., Habiro, K., and Kinashi, T. (2013). Dendritic cells regulate high-speed interstitial T cell migration in the lymph node via LFA-1/ICAM-1. *J. Immunol.* 191, 1188–1199. doi: 10.4049/jimmunol.1300739

Kitagawa, K., Matsumoto, M., Mabuchi, T., Yagita, Y., O'htsuki, T., Hori, M., et al. (1998). Deficiency of intercellular adhesion molecule 1 attenuates microcirculatory disturbance and infarction size in focal cerebral ischemia. *JCBFM* 18, 1336–1345. doi: 10.1097/00004647-199812000-00008

Kindzelskii, A. L., Laska, Z. O., Todd, R. F., and Petyy, H. R. (1996). Urokinase-type plasminogen activator receptor reversibly dissociates from complement receptor type 3 (alpha M beta 2' CD11b/CD18) during neutrophil polarization. *J. Immunol.* 156, 297–309.

Kleinschnitz, C., Schwab, N., Kraft, P., Hagedorn, I., Dreykluft, A., Schwarz, T., et al. (2010). Early detrimental T-cell effects in experimental cerebral ischemia are neither related to adaptive immunity nor thrombus formation. *Blood* 115, 3835–3842. doi: 10.1182/blood-2009-10-249078

Krams, M., Lees, K. R., Hacke, W., Grieve, A. P., Orgogozo, J. M., Ford, G. A., et al. (2003). Acute stroke therapy by inhibition of neutrophils (ASTIN): an adaptive dose-response study of UK-279,276 in acute ischemic stroke. *Stroke* 34, 2543–2548. doi: 10.1161/01.STR

Kuwano, Y., Spelten, O., Zhang, H., Ley, K., and Zarbock, A. (2010). Rolling on E- or P-selectin induces the extended but not high-affinity conformation of LFA-1 in neutrophils. *Blood* 116, 617–624. doi: 10.1182/blood-2010-01-266122

Labus, J., Woltje, K., Stolte, K. N., Hackel, S., Kim, K. S., Hildmann, A., et al. (2018). IL-1beta promotes transendothelial migration of PBMCs by upregulation of the FN/alpha5beta1 signaling pathway in immortalized human brain microvascular endothelial cells. *Exp. Cell Res.* 373, 99–111. doi: 10.1016/j.yexcr.2018.10.002

Langhauser, F., Kraft, P., Gob, E., Leinweber, J., Schuhmann, M. K., Lorenz, K., et al. (2014). Blocking of alpha4 integrin does not protect from acute ischemic stroke in mice. *Stroke* 45, 1799–1806. doi: 10.1161/STROKEAHA.114.005000

Lebwhohl, M., Tyring, S., Hamilton, T., Toth, D., Glazer, S., Tawflk, N., et al. (2003). A novel targeted T-cell modulator, efalizumab, for plaque psoriasis. *N. Eng. J. Med.* 349, 2004–2013. doi: 10.1056/NEJMoa030002

Ley, K., Laudanna, C., Cybulsky, M. I., and Nourshargh, S. (2007). Getting to the site of inflammation: the leukocyte adhesion cascade updated. *Nat. Rev. Immunol.* 7, 678–689. doi: 10.1038/nri2156

Li, B., Pozzi, A., and Young, P. P. (2011). TNFalpha accelerates monocyte to endothelial transdifferentiation in tumors by the induction of integrin alpha5 expression and adhesion to fibronectin. *Mol. Cancer Res.* 9, 702–711. doi: 10.1158/1541-7786.MCR-10-0484

Liesz, A., Zhou, W., Mracsko, E., Karcher, S., Bauer, H., Schwarting, S., et al. (2011). Inhibition of lymphocyte trafficking shields the brain against deleterious neuroinflammation after stroke. *Brain* 134(Pt 3), 704–720. doi: 10.1093/brain/awr008

Lindbom, L., and Werr, J. (2002). Integrin-dependent neutrophil migration in extravascular tissue. *Semin. Immunol.* 14, 115–121. doi: 10.1006/smim.2001.0348

Llovera, G., Hofmann, K., Roth, S., Salas-Perdomo, A., Ferrer-Ferrer, M., Perego, C., et al. (2015). Results of a preclinical randomized controlled multicenter trial (pRCT): anti-CD49d treatment for acute brain ischemia. *Sci. Transl. Med.* 7:299ra121. doi: 10.1126/scitranslmed.aaa9853

Lobb, R. R., and Hemler, M. E. (1994). The pathophysiologic role of alpha 4 integrins in vivo. *J. Clin. Invest.* 94, 1722–1728. doi: 10.1172/JCI117519

Loike, J., Cao, L., Budhu, S., Maracantonio, E., Khoury, J., Hoffman, S., et al. (1999). Differential regulation of b1 integrins by chemoattractants regulates neutrophil migration through fibrin. *J. Cell Biol.* 144, 1047–1056. doi: 10.1083/jcb.144.5.1047

Lorant, D., McEver, R., McIntyre, T. M., Moore, K., Prescott, S. M., and Zimmerman, G. A. (1995). Activation of polymorphonuclear leukocytes reduces their adhesion to P-selectin and causes redistribution of ligands for P-selectin on their surfaces. *J. Clin. Invest.* 96, 171–182. doi: 10.1172/jci118018

Lub, M., van Koyk, Y., and Figdor, C. (1996). Competition between lymphocyte function-associated antigen 1 (CD11a/CD18) and Mac-1 (CD11b/CD18) for binding to intercellular adhesion molecule-1 (CD54). *J. Leukoc. Biol.* 59, 648–655. doi: 10.1002/jlb.59.5.648

Luo, B. H., Carman, C. V., and Springer, T. A. (2007). Structural basis of integrin regulation and signaling. *Annu. Rev. Immunol.* 25, 619–647. doi: 10.1146/annurev.immunol.25.022106.141618

Marlin, S., and Springer, T. (1987). Purified intercellular adhesion molecule-1 (ICAM-1) is a ligand for lymphocyte function-associated antigen 1 (LFA-1). *Cell* 51, 813–819. doi: 10.1016/0092-8674(87)90104-8

Micklem, K., and Sim, R. (1985). Isolation of complement-fragment-iC3b-binding proteins by affinity chromatography. *Biochemistry* 231, 233–236. doi: 10.1042/bj2310233

Multicenter Acute Stroke Trial–Europe Study Group (1996). Thrombolytic therapy with streptokinase in acute ischemic stroke. *N. Engl. J. Med.* 335, 145–150. doi: 10.1056/nejm199607183350301

Multicentre Acute Stroke Trial–Italy (Mast-. (I)) Group (1995). Randomised controlled trial of streptokinase, aspirin, and combination of both in treatment of acute ischaemic stroke. *Lancet* 346, 1509–1514. doi: 10.1016/s0140-6736(95)92049-8

Nadareishvili, Z., Li, H., Wright, V., Maric, D., Warach, S., Hallenbeck, J., et al. (2004). Elevated pro-inflammatory CD4+CD28+ lymphocytes and stroke recurrence and death. *Neurology* 63, 1446–1451. doi: 10.1212/01.wnl.0000142260.61443.7c

National Institute of Neurological Disorders and Stroke rt-Pa Stroke Study Group (1995). Tissue plasminogen activator for acute ischemic stroke. *N. Engl. J. Med.* 333, 1581–1587.

Nishida, N., Xie, C., Shimaoka, M., Cheng, Y., Walz, T., and Springer, T. A. (2006). Activation of leukocyte beta2 integrins by conversion from bent to extended conformations. *Immunity* 25, 583–594. doi: 10.1016/j.immuni.2006.07.016

Nortamo, P., Li, R., Renkonen, R., Timonen, T., Prieto, J., Patarroyo, M., et al. (1991a). The expression of human intercellular adhesion molecule-2 is refractory to inflammatory cytokines. *Eur. J. Immunol.* 21, 2629–2632. doi: 10.1002/eji.1830211049

Nortamo, P., Salcedo, R., Timonen, T., Patarroyo, M., and Gahmber, C. (1991b). A monoclonal antibody to the human leukocyte adhesion molecule intercellular adhesion molecule-2. Cellular distribution and molecular characterization of the antigen. *J. Immunol.* 146, 2530–2535.

Pacifici, R., Roman, J., Kimble, R., Civitelli, R., Brownfield, C., and Bizzarri, C. (1994). Ligand binding to monocyte alpha 5 beta 1 integrin activates the alpha 2 beta 1 receptor via the alpha 5 subunit cytoplasmic domain and protein kinase C. *J. Immunol.* 153, 2222–2233.

Park, E. J., Peixoto, A., Imai, Y., Goodarzi, A., Cheng, G., Carman, C. V., et al. (2010). Distinct roles for LFA-1 affinity regulation during T-cell, diapedesis, and interstitial migration in lymph nodes. *Immunology* 115, 1572–1581. doi: 10.1182/blood-2009-08-237917

Pierini, L. M., Lawson, M. A., Eddy, R. J., Hendey, B., and Maxfield, F. R. (2000). Oriented endocytic recycling of a5b1 in motile neutrophils. *Blood* 95, 2471–2480.

Polman, C., O"Conner, P., Havrdova, E., Hutchinson, M., Kappos, L., Miller, D., et al. (2006). A randomized, placebo-controlled trial of natalizumab for relapsing multiple sclerosis. *N. Eng. J. Med.* 354, 899–910. doi: 10.1056/NEJMoa044397

Price, C. J., Menon, D. K., Peters, A. M., Ballinger, J. R., Barber, R. W., Balan, K. K., et al. (2004). Cerebral neutrophil recruitment, histology, and outcome in acute ischemic stroke: an imaging-based study. *Stroke* 35, 1659–1664. doi: 10.1161/01.STR.0000130592.71028.92

Rai, A. T., Seldon, A. E., Boo, S., Link, P. S., Domico, J. R., Tarabishy, A. R., et al. (2017). A population-based incidence of acute large vessel occlusions and thrombectomy eligible patients indicates significant potential for growth of endovascular stroke therapy in the USA. *J. Neurointerv. Surg.* 9, 722–726. doi: 10.1136/neurintsurg-2016-012515

Rao, N. M., Levine, S. R., Gornbein, J. A., and Saver, J. L. (2014). Defining clinically relevant cerebral hemorrhage after thrombolytic therapy for stroke: analysis of the National Institute of Neurological Disorders and Stroke tissue-type plasminogen activator trials. *Stroke* 45, 2728–2733. doi: 10.1161/STROKEAHA.114.005135

Relton, J., Sloan, K., Frew, E., Whalley, E., Adams, S., and Lobb, R. (2000). Inhibition of alpha4 integrins protects against transient focal cerebral ischemia in normotensive and hypertensive rats. *Stroke* 32, 199–205. doi: 10.1161/01.str.32.1.199

Ridley, A., Schwartz, M., Burridge, K., Firtel, R., Ginsberg, M., Borisy, G., et al. (2003). Cell migration: integrating signals from front to back. *Science* 302, 1704–1709. doi: 10.1126/science.1092053

Roberts, J., de Hoog, L., and Bix, G. J. (2015). Mice deficient in endothelial alpha5 integrin are profoundly resistant to experimental ischemic stroke. *J. Cereb. Blood Flow Metab.* 37, 85–96. doi: 10.1177/0271678X15616979

Sandborn, W., Colombel, J., Enns, R., Feagen, B., Hanauer, S., Lawrence, I., et al. (2015). Natalizumab induction and maintenance therapy for crohn's disease. *N. Eng. J. Med.* 372:2074. doi: 10.1056/NEJMx140055

Sandoval, K. E., and Witt, K. A. (2008). Blood-brain barrier tight junction permeability and ischemic stroke. *Neurobiol. Dis.* 32, 200–219. doi: 10.1016/j.nbd.2008.08.005

Saver, J. L., Goyal, M., Bonafe, A., Diener, H. C., Levy, E. I., Pereira, V. M., et al. (2015). Stent-retriever thrombectomy after intravenous t-PA vs. t-PA alone in stroke. *N. Engl. J. Med.* 372, 2285–2295. doi: 10.1056/NEJMoa1415061

Schaffner, F., Ray, A. M., and Dontenwill, M. (2013). Integrin alpha5beta1, the fibronectin receptor, as a pertinent therapeutic target in solid tumors. *Cancers* 5, 27–47. doi: 10.3390/cancers5010027

Scharffetter-Kochanek, K., Lu, H., Norman, K., van Nood, N., Munoz, F., Grabbe, S., et al. (1998). Spontaneous skin ulceration and defective T cell function in CD18 null mice. *J. Exp. Med.* 188, 119–131. doi: 10.1084/jem.188.1.119

Schenkel, A. R., Mamdouh, Z., and Muller, W. A. (2004). Locomotion of monocytes on endothelium is a critical step during extravasation. *Nat. Immunol.* 5, 393–400. doi: 10.1038/ni1051

Schittenhelm, L., Hilkens, C. M., and Morrison, V. L. (2017). beta2 integrins as regulators of dendritic cell, monocyte, and macrophage function. *Front. Immunol.* 8:1866. doi: 10.3389/fimmu.2017.01866

Schroeter, M., Jander, S., Witte, O., and Stoll, G. (1994). Local immune responses in the rat cerebral cortex after middle cerebral artery occlusion. *J. Neuroimmunol.* 55, 195–203. doi: 10.1016/0165-5728(94)90010-8

Shaw, S. K., Ma, S., Kim, M. B., Rao, R. M., Hartman, C. U., Froio, R. M., et al. (2004). Coordinated redistribution of leukocyte LFA-1 and endothelial cell ICAM-1 accompany neutrophil transmigration. *J. Exp. Med.* 200, 1571–1580. doi: 10.1084/jem.20040965

Shyu, K., Chang, H., and Lin, C. (1997). Serum levels of intercellular adhesion molecule-1 and E-selectin in patients with acute ischaemic stroke. *J. Neurosci.* 244, 90–93. doi: 10.1007/s004150050055

Soriano, S., Coxon, A., Wang, Y., Frosch, M., Lipton, S., Hickey, P., et al. (1999). Mice deficient in Mac-1 (CD11b/CD18) are less susceptible to cerebral ischemia/reperfusion injury. *Stroke* 30, 134–139. doi: 10.1161/01.str.30.1.134

Springer, T. A., Galfre, G., Secher, D., and Milstein, C. (1979). Mac-1: a macrophage differentiation antigen identified by monoclonal antibody. *Eur. J. Immunol.* 9, 301–306. doi: 10.1002/eji.1830090410

Stanimirovic, D., Wong, J., Shapiro, A., and Durkin, J. (1997). Increase in surface expression of ICAM-1, VCAM-1 and E-selectin in human cerebromicrovascular endothelial cells subjected to ischemia-like insults. *Acta Neurochir. Suppl.* 70, 12–16. doi: 10.1007/978-3-7091-6837-0_4

Stefanidakis, M., and Koivunen, E. (2006). Cell-surface association between matrix metalloproteinases and integrins: role of the complexes in leukocyte migration and cancer progression. *Blood* 108, 1441–1450. doi: 10.1182/blood-2006-02-005363

Steffen, B., Butcher, E., and Engelhardt, B. (1994). Evidence for involvement of ICAM-1 and VCAM-1 in lymphocyte interaction with endothelium in experimental autoimmune encephalomyelitis in the central nervous system in the SJL/J mouse. *Am. J. Pathol.* 145, 189–201.

Stevens, S., Bao, J., Hollis, J., Lessov, N., Clark, W., and Stenzel-Poore, M. (2002). The use of flow cytometry to evaluate temporal changes in inflammatory cells following focal cerebral ischemia in mice. *Brain Res.* 932, 110–119. doi: 10.1016/s0006-8993(02)02292-8

Suehiro, K., Gailit, J., and Plow, E. F. (1997). Fibrinogen is a ligand for integrin alpha5beta1 on endothelial cells. *J. Biol. Chem.* 272, 5360–5366. doi: 10.1074/jbc.272.8.5360

Takagi, J., Petre, B., Walz, T., and Springer, T. A. (2002). Global conformational rearrangements in integrin extracellular domains in outside-in and inside-out signaling. *Cell* 110, 599–611. doi: 10.1016/s0092-8674(02)00935-2

Tarkowski, E., Naver, H., Walling, B., Blomstrand, C., and Tarkowski, A. (1995). Lateralization of T-lymphocyte responses in patients with stroke. Effect of sympathetic dysfunction? *Stroke* 26, 57–62. doi: 10.1161/01.str.26.1.57

Tian, L., Kilgannon, P., Yoshihara, Y., Mori, K., Gallatin, W., Carpen, O., et al. (2000). Binding of T lymphocytes to hippocampal neurons through ICAM-5 (telencephalin) and characterization of its interaction with the leukocyte integrin CD11a/CD18. *Eur. J. Immunol.* 30, 810–818. doi: 10.1002/1521-4141(200003)30:3<810::aid-immu810>3.3.co;2-o

Tominaga, Y., Kita, T., Satoh, A., Asai, S., Kato, K., Ishikawa, K., et al. (1998). Affinity and kintetic analysis of the molecular interaction of ICAM-1 and leukocyte function-associated antigen-1. *J. Immunol.* 161, 4016–4022.

Vajkoczy, P., Laschinger, M., and Engelhardt, B. (2001). α4-integrin-VCAM-1 binding mediates G protein–independent capture of encephalitogenic T cell blasts to CNS white matter microvessels. *J. Clin. Invest.* 108, 557–565. doi: 10.1172/JCI200112440

Vemuganti, R., Dempsey, R. J., and Bowen, K. K. (2004). Inhibition of intercellular adhesion molecule-1 protein expression by antisense oligonucleotides is neuroprotective after transient middle cerebral artery occlusion in rat. *Stroke* 35, 179–184. doi: 10.1161/01.STR

von Andrian, U., Chambers, J., McEvoy, L., Bargatze, R., Arfors, K., and Butcher, E. (1991). Two-step model of leukocyte-endothelial cell interaction in inflammation: distinct roles for LECAM-1 and the leukocyte beta2 integrins in vivo. *Proc. Natl. Acad. Sci. U.S.A.* 88, 7538–7542. doi: 10.1073/pnas.88.17.7538

Walling, B. L., and Kim, M. (2018). LFA-1 in T cell migration and differentiation. *Front. Immunol.* 9:952. doi: 10.3389/fimmu.2018.00952

Wang, W. Z., Fang, X. H., Stephenson, L. L., Khiabani, K. T., and Zamboni, W. A. (2008). Ischemia/reperfusion-induced necrosis and apoptosis in the cells isolated from rat skeletal muscle. *J. Orthop. Res.* 26, 351–356. doi: 10.1002/jor.20493

Weston, R. M., Jones, N. M., Jarrott, B., and Callaway, J. K. (2007). Inflammatory cell infiltration after endothelin-1-induced cerebral ischemia: histochemical and myeloperoxidase correlation with temporal changes in brain injury. *JCBFM* 27, 100–114. doi: 10.1038/sj.jcbfm.9600324

Yenari, M. A., Kunis, D., Sun, G., Onley, D., Watson, L., Turner, S., et al. (1998). Hu23F2G, an antibody recognizing the leukocyte CD11/CD18 integrin, reduces injury in a rabbit model of transient focal cerebral ischemia. *Exp. Neurol.* 153, 223–233. doi: 10.1006/exnr.1998.6876

Yilmaz, G., Arumugam, T. V., Stokes, K. Y., and Granger, D. N. (2006). Role of T lymphocytes and interferon-gamma in ischemic stroke. *Circulation* 113, 2105–2112. doi: 10.1161/CIRCULATIONAHA.105.593046

Zhang, L., Zhang, Z. G., Zhang, R. L., Lu, M., Krams, M., and Chopp, M. (2003). Effects of a selective CD11b/CD18 antagonist and recombinant human tissue plasminogen activator treatment alone and in combination in a rat embolic model of stroke. *Stroke* 34, 1790–1795. doi: 10.1161/01.STR.0000077016.55891.2E

Zhang, R., Chopp, M., Zhang, Z., Jiang, N., and Powers, C. (1998). The expression of P- and E-selectins in three models of middle cerebral artery occlusion. *Brain Res.* 785, 207–214. doi: 10.1016/s0006-8993(97)01343-7

Zhang, R., Zhang, Z., and Chopp, M. (1999). Increased therapeutic efficacy with rt-PA and anti-CD18 antibody treatment of stroke in the rat. *Neurology* 52, 273–279.

Zhang, Z., Chopp, M., Tang, W., Jiang, N., and Zhang, R. (1995). Postischemic treatment (2-4 h) with anti-CDllb and anti-CD18 monoclonal antibodies are neuroprotective after transient (2 h) focal cerebral ischemia in the rat. *Brain Res.* 698, 79–85. doi: 10.1016/0006-8993(95)00830-j

Zhao, H., Dong, X., Wang, X., Li, X., Zhuang, F., Stoltz, J. F., et al. (2002). Studies on single-cell adhesion probability between lymphocytes and endothelial cells with micropipette technique. *Microvasc. Res.* 63, 218–226. doi: 10.1006/mvre.2001.2390

Conflict of Interest Statement: The authors declare that the research was conducted in the absence of any commercial or financial relationships that could be construed as a potential conflict of interest.

Copyright © 2019 Edwards and Bix. This is an open-access article distributed under the terms of the Creative Commons Attribution License (CC BY). The use, distribution or reproduction in other forums is permitted, provided the original author(s) and the copyright owner(s) are credited and that the original publication in this journal is cited, in accordance with accepted academic practice. No use, distribution or reproduction is permitted which does not comply with these terms.

frontiers in Neuroscience

ORIGINAL RESEARCH
published: 29 May 2019
doi: 10.3389/fnins.2019.00541

Fibrinogen Chains Intrinsic to the Brain

Eugene V. Golanov[1], Martyn A. Sharpe[1], Angelique S. Regnier-Golanov[1], Gregory J. Del Zoppo[2], David S. Baskin[1] and Gavin W. Britz[1]*

[1] Department of Neurosurgery, Houston Methodist Hospital, Houston, TX, United States, [2] Division of Hematology, University of Washington School of Medicine, Seattle, WA, United States

We observed fine fibrin deposition along the paravascular spaces in naive animals, which increased dramatically following subarachnoid hemorrhage (SAH). Following SAH, fibrin deposits in the areas remote from the hemorrhage. Traditionally it is thought that fibrinogen enters subarachnoid space through damaged blood brain barrier. However, deposition of fibrin remotely from hemorrhage suggests that fibrinogen chains Aα, Bβ, and γ can originate in the brain. Here we demonstrate *in vivo* and *in vitro* that astroglia and neurons are capable of expression of fibrinogen chains. SAH in mice was induced by the filament perforation of the circle of Willis. Four days after SAH animals were anesthetized, transcardially perfused and fixed. Whole brain was processed for immunofluorescent (IF) analysis of fibrin deposition on the brain surface or in brains slices processed for fibrinogen chains Aα, Bβ, γ immunohistochemical detection. Normal human astrocytes were grown media to confluency and stimulated with NOC-18 (100 μM), TNF-α (100 nM), ATP-γ-S (100 μM) for 24 h. Culture was fixed and washed/permeabilized with 0.1% Triton and processed for IF. Four days following SAH fibrinogen chains Aα IF associated with glia limitans and superficial brain layers increased 3.2 and 2.5 times ($p < 0.05$ and $p < 0.01$) on the ventral and dorsal brain surfaces respectively; fibrinogen chains Bβ increased by 3 times ($p < 0.01$) on the dorsal surface and fibrinogen chain γ increased by 3 times ($p < 0.01$) on the ventral surface compared to sham animals. Human cultured astrocytes and neurons constitutively expressed all three fibrinogen chains. Their expression changed differentially when exposed for 24 h to biologically significant stimuli: TNFα, NO or ATP. Western blot and RT-qPCR confirmed presence of the products of the appropriate molecular weight and respective mRNA. We demonstrate for the first time that mouse and human astrocytes and neurons express fibrinogen chains suggesting potential presence of endogenous to the brain fibrinogen chains differentially changing to biologically significant stimuli. SAH is followed by increased expression of fibrinogen chains associated with glia limitans remote from the hemorrhage. We conclude that brain astrocytes and neurons are capable of production of fibrinogen chains, which may be involved in various normal and pathological processes.

Keywords: fibrinogen, brain, astrocytes, neurons, subarachnoid hemorrhage, intrinsic, fibrinogen chain, fibrin

OPEN ACCESS

Edited by:
Johannes Boltze, Fraunhofer-Institut für Zelltherapie und Immunologie (IZI), Germany

Reviewed by:
Richard F. Keep, University of Michigan, United States
Anatol Manaenko, University Hospital Erlangen, Germany

****Correspondence:***
Eugene V. Golanov
evgolanov@houstonmethodist.org; egolanov@gmail.com

Specialty section:
This article was submitted to Neurodegeneration, a section of the journal Frontiers in Neuroscience

Received: *01 April 2019*
Accepted: *09 May 2019*
Published: *29 May 2019*

Citation:
Golanov EV, Sharpe MA, Regnier-Golanov AS, Del Zoppo GJ, Baskin DS and Britz GW (2019) Fibrinogen Chains Intrinsic to the Brain. Front. Neurosci. 13:541. doi: 10.3389/fnins.2019.00541

INTRODUCTION

Arrest of cerebrospinal fluid (CSF) flow can be triggered by subarachnoid hemorrhage (SAH). Following SAH, fibrin is deposited in the paravascular space hindering CSF flow (Gaberel et al., 2014; Siler et al., 2014; Golanov et al., 2017). The blockage of CSF flow can be partially reversed by rt-PA or anti-tissue factor (TF, FIII) antibodies, suggesting that fibrin deposition in subarachnoid space (SS) may play an important role in CSF arrest (Gaberel et al., 2014; Siler et al., 2014; Golanov et al., 2017).

Astrocyte endfeet form the glia limitans on the brain surface placing astrocytes, a primary source of TF in the brain (Eddleston et al., 1993), in direct contact with blood following SAH. Activation of factor VII to factor VIIa in the blood and its interaction with TF (to form the TF: VIIa complex), initiate the extrinsic pathway of coagulation that ultimately convert prothrormbin to thrombin and hence promote fibrin formation.

Fibrinogen is not considered to be present in the brain, unless there is breach of the cerebral vasculature blood-brain or permeability barrier (BBB) and leakage of plasma/blood into the neuropil or fluid spaces (Akassoglou and Strickland, 2002; Adams et al., 2004; Petersen et al., 2018). Levels of fibrinogen in the CSF are very low, ∼0.65 μg/ml (Thompson, 2005), especially compared to the blood levels of fibrinogen (2–3 mg/ml) (Redman and Xia, 2001; Colman and Budzynski, 2011).

Blood coagulation is considered to participate in certain intravascular immunity responses targeted toward immobilization of the foreign agent (Doolittle, 2011, 2016; Gaertner and Massberg, 2016), and thus is a part of acute phase response (Gruys et al., 2005; Cray et al., 2009). Fibrinogen and prothrombin are necessary components of both intrinsic and extrinsic coagulation pathways. Fibrinogen is a 340 kDa glycoprotein consisting of three dimers. Each dimer is formed by identical polypeptides formed by fibrinogen chains Aα, Bβ, and γ, respectively. Fibrinogen is assembled in the endoplasmic reticulum of hepatocytes with the help of chaperon proteins, contains 29 disulfide bonds, and after glycosylation is released into the circulation (Redman and Xia, 2001; Mosesson, 2005; Weisel, 2005). Each of the three polypeptide chains forming fibrinogen is encoded by the respective genes, FGA, FGB, and FGG. It is thought that these genes are paralogs and are common for extant vertebrates (Doolittle et al., 1997). Thrombin, serine protease, which is present in brain (Deschepper et al., 1991; Dihanich et al., 1991) cleaves fibrinogen releasing fibrinopeptide A and B and initiating of fibrin polymerization and fibrin gel formation (Weisel, 2005).

Earlier observations and our recent experiments (Golanov et al., 2017) suggest that fibrin in the subarachnoid/paravascular space present in naïve animals and is being deposited in the areas remote from the hemorrhage following the SAH (Suzuki et al., 1977). Fibrin(ogen) was observed intracellularly (Marik et al., 2007; Yates et al., 2017) under pathological conditions such as multiple sclerosis. It is generally accepted that BBB insufficiency leads to blood-born fibrinogen penetration into the brain and consequent formation of fibrin depositions accompanying neurological disorders (Petersen et al., 2018).

The majority of circulating fibrinogen is being synthesis in liver (Tennent et al., 2007). However, fibrinogen can also be synthesized in extrahepatic sites such as bone marrow, lungs, intestine epithelial cells (see Weisel, 2005). We hypothesize that non-vascular brain cells, including astroglia and, probably, neurons, are capable of expressing fibrinogen chains Aα, Bβ, and γ, which, in turn, may exert multiple effects in the brain in normal and pathological conditions. Here we provide *in vivo* and *in vitro* data that support this hypothesis.

MATERIALS AND METHODS

All animal procedures were conducted in accord with the U.S. National Institutes of Health "Guide for the care and use of laboratory animals" and approved by the Institutional Animal Care and Use Committee of Houston Methodist Research Institute, Houston, TX, United States. Animals were housed in the institutional animal facilities on 12 h day/night cycle with *ad libitum* access to food and water. Studies were performed in sixteen 10–14 weeks old male C56BL/6J mice (Jackson Labs).

General Procedures

Anesthesia was induced by placing animals in a closed chamber flushed with 3% isoflurane in air; after reaching sufficient depth of anesthesia the animals were maintained at depth by 1.5–1.75% isoflurane in 80%/20% N2/O2 mixture delivered by facemask. Core body temperature was maintained at 37°C using a thermoblanket with the feedback from the rectal probe.

SAH in Mice

Subarachnoid hemorrhage was triggered by monofilament perforation of the Circle of Willis as previously described (Bederson et al., 1995; Parra et al., 2002; Feiler et al., 2010). Briefly, animals were anesthetized and placed in the supine position. The left common, external and internal carotid arteries were exposed through the midline incision. All three arteries were mobilized using silk sutures (7-0). The stump was formed from the external carotid artery by cutting it between two ligatures. A proline monofilament (6-0) was advanced into the internal carotid artery the stump until slight resistance was felt. The filament was advanced further forward for ∼1 mm and withdrawn. The stump was ligated, the wound was closed, and the animal was allowed to recover. In the sham group, the filament was advanced to the resistance point and withdrawn without perforation. After surgery, the animals were allowed to recovery and then returned to the home cage.

Immunohistochemistry

Four days after SAH (or sham operation) the mice were deeply anesthetized and sacrificed by transcardiac perfusion with saline followed by 4% paraformaldehyde in PBS. Brains were removed, post-fixed for 24 h, and cryoprotected in 30% sucrose in PBS until complete submersion. The brains were quick frozen on dry ice, embedded in mounting media (NEG50, Richard-Allan Scientific, Thermo Scientific), and stored at −80°C until further processed. Ten micrometer thick coronal sections were prepared using a

cryotome (Microm HM550, Thermo Scientific) and collected on glass slides. The glass slides with samples were washed in PBS-0.3% Triton X-100 for 30 min at room temperature, rinsed in distilled water, and air dried. A paraffin pen was used to contour the brain slices on the glass slides (ImmEdge Pen, Vector Laboratories). After the slides were rinsed in PBS to re-wet tissue, the sections were blocked with 2% normal donkey serum (Jackson ImmunoResearch) in PBS-0.3% Triton X-100 for 2 h. After blocking, the slides were incubated overnight (12–14 h) with the primary specific antibodies against fibrinogen-α, -β and -γ chains (1:200; rabbit polyclonal; Proteintech). The slides were washed three times for 15 min in PBS-0.3% Triton X-100, and then incubated with secondary antibodies for 3 h (donkey anti-rabbit-Alexa Fluor® 488 and Alexa Fluor® 594; 1:1000; Life Technologies, Thermo Fisher Scientific). The slides were rinsed in PBS and distilled water, covered with protective Fluorescent Mounting Medium with DAPI (GBI Labs), glass covered, and sealed with nail polish. In control slides, primary antibodies were omitted.

Cell Cultures

Normal human astrocytes (NHA) were obtained from Lonza (Walkersville, MD, United States) and human cortical neurons (HCN) from the American Type Culture Collection (ATCC, Manassas, VA, United States) and grown subject to vendor recommendations. NHA were grown in Astrocyte Basal Medium supplemented with 3% FBS, glutamine, insulin, fhEGF, GA-1000, and ascorbic acid. HCN were prepared using ATCC-formulated Dulbecco's modified Eagle's medium (cat# 30-2002) and supplemented with 10% FBS. HCN and NHA were grown to confluence in the appropriate media on Costar 96-well growth plates (Corning, NYC, NY, United States), and were grown for 24 h in the presence/absence of all effectors, in a total volume of 250 μL. The cells were fixed in ice-cold 4% PFA, were washed/permeabilized with 0.1% Triton X-100 in PBS, and then treated with Dako protein blocking solution. The cells were then incubated in 0.1% avidin (Sigma) for 30 min, washed and then incubated 10 μM biotin for 15 min, and washed in PBS.

The following primary antibodies were used: rabbit polyclonal fibrinogen chain Aα antibody ([H-300] (Santa Cruz Biotechnology, Santa Cruz, CA, United States), fibrinogen chain Bβ antibody ([H-270] Santa Cruz), fibrinogen chain γ antibody ([H-194] Santa Cruz) and mouse monoclonal antibodies to GFAP ([2A5] Santa Cruz). The following secondary antibodies were used: Donkey Anti-Mouse IgG H&L (Alexa Fluor® 488) (ab150105) and (Alexa Fluor® 594) (ab150108), Donkey Anti-Rabbit IgG H&L (Alexa Fluor® 488) (ab150073) and (Alexa Fluor® 594) (ab150076), all from Abcam (Abcam, Cambridge, MA, United States). All antibodies were diluted using Dako antibody diluent (S3022) at 1:100 for the primary antibodies and 1:250 for the secondary antibodies. Cell nuclei were labeled using DAPI.

Culture Stimulation

Normal human astrocytes and neurons grown to confluence were stimulated with the nitric oxide donor, NOC-18 (100 μM; Santa Cruz, CA, United States), tumor necrosis factor alpha, TNF-α (100 nM; Life Technologies, Carlsbad, CA, United States), or the stable ATP analog, ATP-γ-S (100 μM, Sigma, MS) for 24 h. The cultures were fixed and washed/permeabilized with 0.1% Triton and processed for quantitative immunofluorescence.

Fluorescent Imaging

Fluorescent images were captured using a Nikon Eclipse TE2000-E at 4×, 20×, or 30× magnification using a CoolSnap ES digital camera system (Roper Scientific) containing a CCD-1300-Y/HS 1392-1040 imaging array that is cooled by Peltier. Images were recorded and analyzed using Nikon NIS-Elements software (Elements 3.22.11). All images were saved as JPEG2000 files using Nikon NIS-Elements. In culture, cell numbers in the field of view in one well were counted manually, using DAPI nuclei fluorescence, and after background removal, fluorophore levels were calculated as signal/cell. Statistical analysis consisted of ANOVA followed by t-test using Bonferroni multiple-comparison correction.

To evaluate the intensity of fluorescence in the brain tissue, the fluorescent images of the ventral and dorsal regions of interest (ROI) were taken at 20x using standard exposure time by blinded to the experiment observer and processed simultaneously. Using ImageJ software color channels were split and equally thresholded after subtraction of the background and converted into binary images (Iliff et al., 2012). Five ROI were measured in each animal and fluorophore levels were calculated followed by statistical analysis using ANOVA followed by Bonferroni multiple comparison. All data expressed as mean ± SEM.

Human Brain Tissue Sections

Human brain tissue samples were procured, after obtaining signed informed consent and institutional review, from patients undergoing surgically indicated resection of malignant gliomas at the Houston Methodist Hospital. Tissue was collected directly from the operating room, given an identifying code to ensure patient confidentiality, and fixed in ice-cold 4% paraformaldehyde (PFA) within 15 min of removal. For details see Sharpe and Baskin (2016).

The tissue microarray block was sliced into 5-μm sections that were affixed to slides and dried. Slides were dewaxed four times in xylene, twice in isopropanol, and rehydrated using graded ethanol. The slides were washed and permeabilized using PBS (Fisher Scientific, Waltham, MA, United States) containing 0.1% Triton X-100. Epitope retrieval was done by heating the slides in Na-citrate buffer (100 mM, pH 6.0) at $< 100°C$ for 30 min, followed by cooling slowly to bench temperature. After washing in PBS, endogenous peroxidase activity was eliminated using mild conditions: 1.8% H2O2 for 5 min, 1% Periodate for 5 min, 0.02% NaBH4 for 2 min. The slides were blocked using Serum-Free Protein Block (Dako North America, Inc., Carpinteria, CA, United States) and incubated with primary antibodies (same that were used for mouse tissue processing) overnight at room temperature, at 1:100 dilution. After washing in PBS, the HiDefTM HRP-polymer system (Cell Marque, Rocklin, CA, United States) was used to functionalize with peroxidase, and visualization was performed using the Dako DAB chromogen kit according to manufacturer's guidelines. Additional slides

were also incubated with either hematoxylin/100 mM LiOH to render the nuclei blue for visualization of cells using transmission microscopy or 0.1% cresyl violet solution for 3 min, followed by washing (Nissl Staining).

Western Blot

Normal human astrocytes cell cultures were collected at confluence and processed for protein extraction. Cell pellets were lysed with RIPA buffer (Thermo Fisher Scientific) by pipetting them up and down and then placed for 30 min on an orbital shaker at 4°C. Proteins were quantified by Pierce BCA Protein Assay Kit (Thermo Fisher Scientific) and resolved by 4–15% SDS-PAGE Gel (Bio-Rad) according to the manufacturer's instruction.

Antibodies used were: rabbit anti-fibrinogen-Aα, anti-fibrinogen-Bβ and γ (1:1000, respectively H-300, H-270 and C-20; Santa Cruz Biotechnologies, Santa Cruz, CA, United States); anti-goat-HRP (1:2000; 81-1620; Thermo Fisher Scientific) and anti-rabbit-HRP (1:2000, 1706515; Bio-Rad).

RNA Extraction and RT-qPCR

Total RNA was extracted from NHA cell cultures (n = 3) using Aurum Total RNA mini kit (Bio-Rad). RNA concentration was determined using a NanoDrop ND-1000 spectrophotometer (NanoDrop, Rockland, DE, United States). Quantitative RT–PCR was run with 20ng of RNA using the 1-step Rt-qPCR mix from Bio-Rad according to the supplier's protocol. Amplification was done using SYBR green chemistry on CFX96 Real-Time PCR System (Bio-Rad). Each sample was run in duplicate. PCR primers were designed with primer designing tool from NCBI and manufactured by Sigma. Hprt was used as the reference gene. The following primers' sequences were used: FibA-α, 5′-AGA CAT CAA TCT GCC TGC AAA-3′ and 5′-AGT GGT CAA CGA ATG AGA ATC C-3′; FibB-β, 5′-GTC CCA AGG TGT CAA CGA CAA-3′ and 5′-CTC TCT TCT TGT CAA GGG GTC G-3′; Fib-γ 5′-TTA TTG TCC AAC TAC CTG TGG C-3′ and 5′-GAC TTC AAA GTA GCA GCG TCT AT-3′; HPRT, 5′-CCT GGC GTC GTG ATT AGT GAT-3′ and 5′-GGG CTA CAA TGT GAT GGC CT-3′.

Down-Regulation of the FibA-α, FibB-β, and Fib-γ in NHA Cells by siRNA

FGA siRNA (assay# s5115), FGB siRNA (s5119) FGG siRNAs (s5179) and negative control #1 (#4390843) were obtained from Thermo Fisher Scientific. Each siRNA concentration was titrated in 96-well tissue culture plate, in triplicates, with final concentrations ranging from 0 nm to 49 nM, in 7 nm increment. Briefly, each siRNA was dissolved in 200 μl of OPTI-MEM I Reduced Serum Medium (Gibco) mixed in equal volume of Lipofectamine RNAiMAx (Invitrogen, Carlsbad, CA, United States) with a final amount of 0.64 μl/well. siRNA and Lipofectamine were left for 5 min at room temperature for complexes to form, according to manufacturer's instructions, and then were added to each well, mixed gently and incubated at 37°C for 48 h. At 48 h, cells were fixed in ice-cold 4% PFA. Rabbit polyclonal antibodies against human fibrinogen chain Aα antibody (20645-1-AP), fibrinogen chain Bβ antibody (16747-1-AP), and fibrinogen chain γ antibody (15841-1-AP) from Proteintech (Rosemont, IL, United States), were used. Donkey anti-Rabbit IgG H&L (Alexa Fluor®594) (A21207, Invitrogen, Carlsbad, CA, United States) were used as a secondary antibody. Immunofluorescence was processed as described above.

RESULTS

Changes in Fibrinogen Chains Immunofluorescence Following SAH

In the first series of experiments we explored changes in the fibrinogen chains by immunofluorescence (IF) in the superficial layers of the parietal cortex and ventral surface of the mouse brain. We avoided areas on the ventral surface (especially) of the brain with visible signs of blood. Two groups of animals were compared: animals, in which the Circle of Willis was perforated 4 days before euthanasia and sham-operated animals in which no perforation was performed. Four days following SAH fibrinogen chains Aα IF associated with glia limitans and superficial layers of the ventral and dorsal superficial brain parenchyma increased 3.2 and 2.5 times ($p < 0.05$ and $p < 0.01$), respectively; fibrinogen chain Bβ increased by 3 times ($p < 0.01$) on the dorsal surface and fibrinogen chain γ increased by 3 times ($p < 0.01$) on the ventral surface compared to sham animals (**Figures 1A–C**). Importantly the changes in all three fibrinogen chains were un-coordinated suggesting differential distribution of fibrinogen chains in the dorsal and ventral superficial layers of the brain parenchyma.

Besides the increase in the presence of fibrinogen chains in the glia limitans and brain parenchyma, astrocytes and other cells also demonstrated the presence of fibrinogen chains immunoreactivity. Specifically, immunofluorescence of the cell-associated fibrinogen chains changed in the hippocampal dentate gyrus 4 days following the SAH (**Figure 2**).

Human Normal Astrocytes

Next, we explored whether NHA alone are capable of expressing fibrinogen chains. Indeed, immunochemical staining revealed that isolated astrocytes express immunoreactivity of all three fibrinogen chains (**Figure 3**). To determine whether the immunofluorescence was associated with the proteins we performed western blot analysis of the cell, and observed three bands with the molecular weights close to those reported for all three fibrinogen chains (McDonagh et al., 1972) (**Figure 4**).

Effect of siRNA on the Expression of Fibrinogen Chains in Normal Human Astrocytes

Following exploration of the fibrinogen chains proteins immunoreactivity levels in NHA we investigated silencing of the respective genes FGA, FGB and FGG using siRNA will suppress fibrinogen chains proteins immunofluorescence. Lipofection of the NHA with the specific siRNA, known to silence fibrinogen chains genes (Takezawa et al., 2013) we observed significant decrease of fibrinogen chains immunoreactivity in NHA. Specific

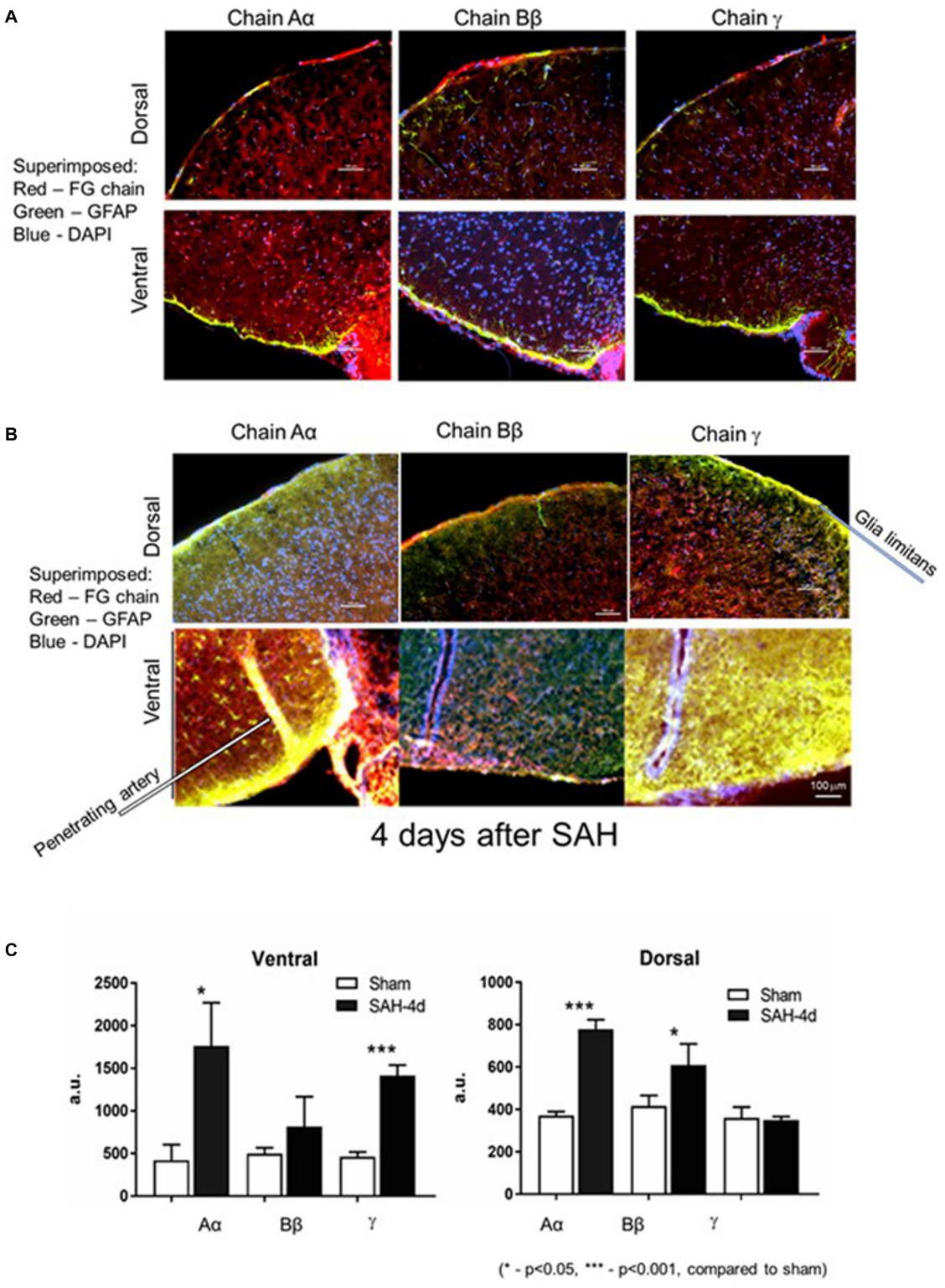

FIGURE 1 | Distribution of fibrinogen chains (FG) Aα, Bβ, and γ in *glia limitans* and superficial layers of the brain dorsal and ventral surfaces **(A)** 4 days after surgery in sham hemorrhage animals and **(B)** 4 days after subarachnoid hemorrhage. **(C)** Changes in immunofluorescent intensity of the respective fibrinogen chains 4 days following the subarachnoid hemorrhage. Dorsal, dorsal surface of the brain; Ventral, ventral surface of the brain of the same animal. Red, fibrinogen chain; green, GFAP; blue, DAPI. a.u., arbitrary units. Bar – 100 μm. (3 animals/group; 5 ROI/animal, $^*p < 0.05$).

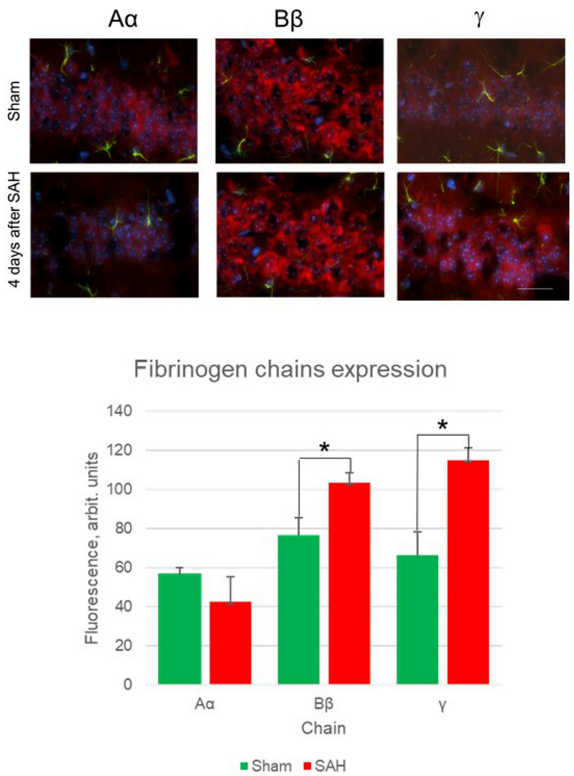

FIGURE 2 | Fibrinogen chains expression changes 4 days after sham surgery and 4 days after SAH (upper panels) and quantification of immunofluorescence between sham animals and 4 days after SAH in hippocampal dentate gyrus. (5 animals/group, $*p < 0.05$, bar 100 μm).

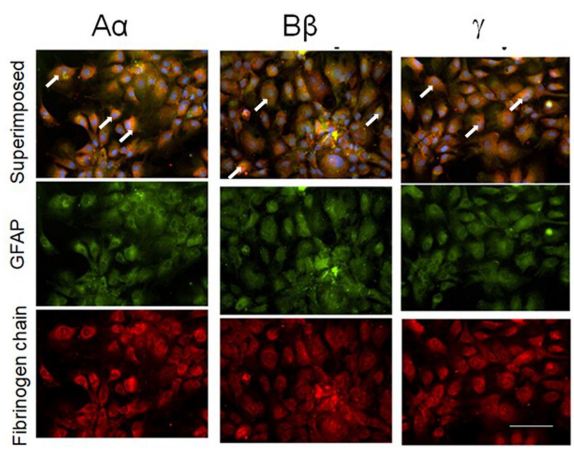

FIGURE 3 | Normal human cultured astrocytes constitutively express all three fibrinogen chains immunofluorescence. Note co-localization (white arrows) of fibrinogen chains immunofluorescence and immunofluorescence of astrocytes labeled with GFAP antibodies. (bar – 100 μm).

siRNA decreased expression immunoreactive of fibrinogen chain Aα by 76%, fibrinogen Bβ by 80% and fibrinogen chain γ by 78%, respectively, at the concentration of siRNA of 49 nM (**Figure 5**).

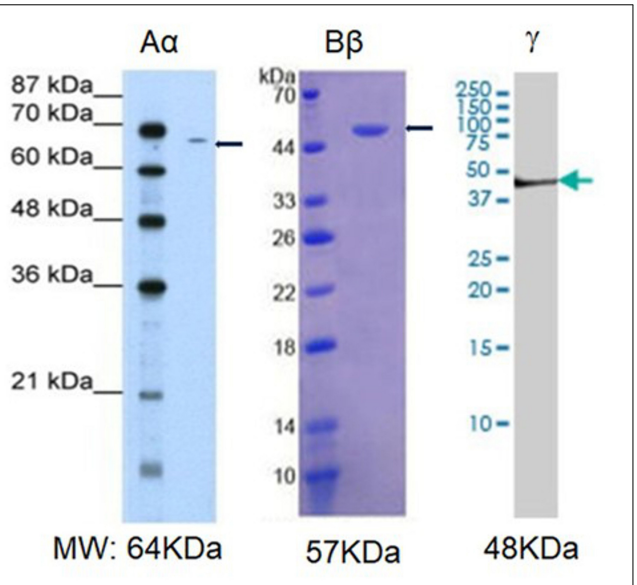

FIGURE 4 | Western blot analysis of the fibrinogen immunopositive chains in normal human astrocytic culture. MW, established molecular weight of fibrinogen chains (Sharpe and Baskin, 2016).

Decrease of the levels of fibrinogen chains after silencing of respective genes strongly suggest that that fibrinogen chains observed in NHA culture are of NHA origin and not resulting from external contamination, e.g., by bovine calf serum.

Reaction to Biologically Significant Stimuli

In the following experiments, we explored whether expression of the fibrinogen chains can be modified by biologically important signals including (i) TNF-α, the cytokine associated with the acute phase reaction of inflammation, (ii) the slow releasing NO donor diethylenetriamine (NOC-18), which is known to participate in various processes, including the inflammatory response, and (iii) stable ATP analog, which is a danger-associated molecule, which initiates protective responses, including the inflammatory response. Expression of the fibrinogen chains differentially changed when exposed for 24 h to these biological stimuli (**Table 1**). Importantly, levels of immunoreactivity of each chain did not correlate. While fibrinogen chain Aα levels, determined by changes in

TABLE 1 | Changes in specific fibrinogen chains (FC) IF (arbitrary units/cell) in cultured human astrocytes in response to exposure to TNFα, NO-donor (NOC-18) and stable ATP analog (ATP-γ-S) (triplicates, 3 fields of view/well, m ± SEM).

	FC Aα	FC Bβ	FC γ
Control	1.00 ± 0.07	1.00 ± 0.12	1.00 ± 0.13
TNFα	1.48 ± 0.21*	0.92 ± 0.14	0.79 ± 0.04
NOC-18	1.41 ± 0.18*	1.14 ± 0.20	0.89 ± 0.08
ATP-γS	0.82 ± 0.12	0.58 ± 0.11*	0.66 ± 0.07*

*$p < 0.01$.

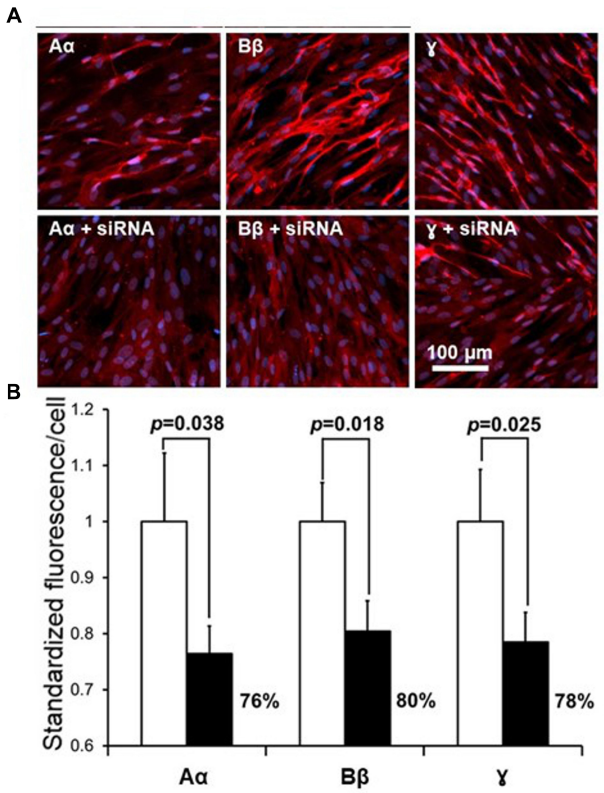

FIGURE 5 | Effect of suppression of fibrinogen chains genes by siRNA in the culture of normal human astrocytes. **(A)** Representative fluorescent fields of view in control cultures (upper row) and in culture transfected with respective siRNA. Red fluorescence, fibrinogen chains; blue, DAPIB. Quantification of the suppression of fibrinogen chains expression by normal human astrocytic culture by siRNA. (**B**, Fluorescence was normalized by the determining the calculation of fluorescence/single cell, see Materials and Methods, all measurements were done in triplicate and three fields of view were taken in each well).

immunofluorescence, increased by ∼50% ($p < 0.01$), fibrinogen chain Bβ levels decreased by almost 50% and did not change significantly to other stimuli. Fibrinogen chain γ also decreased in response to ATP administration. These experiments strongly indicate that fibrinogen chains differentially regulated by biologically significant stimuli (**Figure 6A** and **Table 1**).

RT-qPCR in Astrocytes

The presence of the specific proteins suggested by immunohistochemistry would imply the presence of the specific mRNA if these proteins are being constitutively produced by cultured cells. To establish the presence of the transcription signal we performed RT-qPCR analysis of the presence of specific fibrinogen chain mRNA. Our results demonstrated the presence of the specific mRNA for each chain in the cultured astrocytes suggesting local transcription of the fibrinogen chains. Importantly, the levels of all three fibrinogens chains mRNA not only differed but were modulated differently by different biologically significant stimuli. These experiments strongly suggested that human astrocytes are capable of synthesizing fibrinogen chains, expression of which depends on the specific context (**Figure 6B**).

Human Cortical Neurons

Similarly, we explored constitutive expression and changes in fibrinogen chain immunoreactivities in the culture of human neurons. Human cortical neurons also demonstrated background expression of the fibrinogen chains. Exposure of cortical neurons to pro-inflammatory stimuli (TNF-α and ATP) changed the expression of fibrinogen chains as evaluated by immunofluorescence (**Figure 7A**). These changes were also differential and dependent on the type of stimulus. However, the pattern of the responses to similar stimuli differed from those observed in human astrocyte culture. Fibrinogen chain Bβ level increased by 85%, at the same time fibrinogen chain γ increased by over 100% in response to administration of ATP in neurons, while it decreased in response to ATP in astrocytes (**Figure 7B** and **Table 2**).

Human Tissue

After establishing that cultured human neurons and astrocytes are capable of expressing the three fibrinogen chains and that increases in fibrinogen chain-associated immunofluorescence in the mouse brain, including their intracellular localization, we analyzed whether fibrinogen chains are present in human brain tissue. We analyzed brain parenchyma samples obtained from different human brain structures (amygdala, hypothalamus) and observed that single cell-associated fibrinogen chain–associated immunofluorescence can be observed in human brain cells that displayed neuronal or astrocyte morphology, while there was no fibrinogen chain-related immunoreactivity in the extracellular space (**Figure 8**).

DISCUSSION

We demonstrate, for the first time, that astrocytes and neurons express fibrinogen chains suggesting potential presence of endogenous to the brain fibrinogen chains. Along with others we observed fibrin deposition in the areas remote to hemorrhage following the SAH (Suzuki et al., 1977; Golanov et al., 2017). It is conceivable that in spite of the remote location of the fibrin deposition in the subarachnoid space following the SAH fibrinogen and associated coagulation factors of the extrinsic pathway diffuse there along with CSF and polymerize through the

TABLE 2 | Changes in specific fibrinogen chains (FC) IF (arbitrary units/cell) in cultured human cortical neurons in response to exposure to TNFα, and stable ATP analog (ATP-γ-S) (triplicates, 3 fields of view/well, m ± SEM).

	FC Aα	FC Bβ	FC γ
Control	1.00 ± 0.38	1.00 ± 0.32	1.00 ± 0.13
TNFα	1.76 ± 0.39	1.59 ± 0.56	2.43 ± 1.03
ATP-γS	1.19 ± 0.12	1.85 ± 0.54*	2.28 ± 0.72*

*$p < 0.01$.

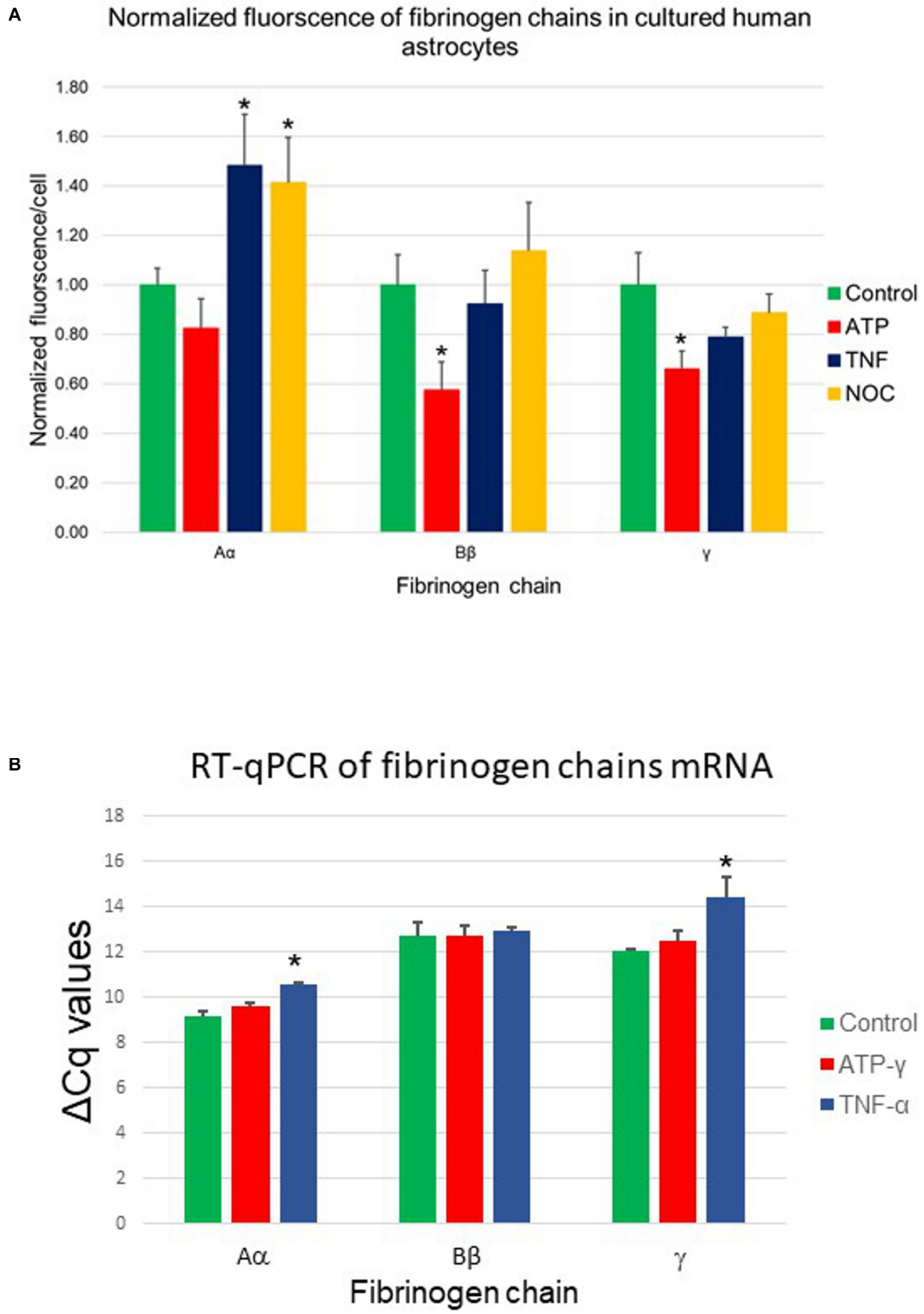

FIGURE 6 | (A) Changes in fibrinogen chains immunofluorescence in normal human astrocytes differentially affected by 24-h exposure to pro-inflammatory stimuli. Aα, fibrinogen chain Aα; Bβ, fibrinogen chain Bβ; γ, fibrinogen chain γ; TNFα, tumor necrosis factor α; NOC, NO-donor and ATP-γ, stable ATP analog (three plates, each stimulus in triplicates, three fields of view). **(B)** Changes in fibrinogen chains mRNA (RT-qPCR) in normal human astrocytic culture in response to biologically significant stimuli. TNFα, tumor necrosis factor α; ATP-γ, stable ATP analog, $^*p < 0.05$). (Three plates, each stimulus in triplicates).

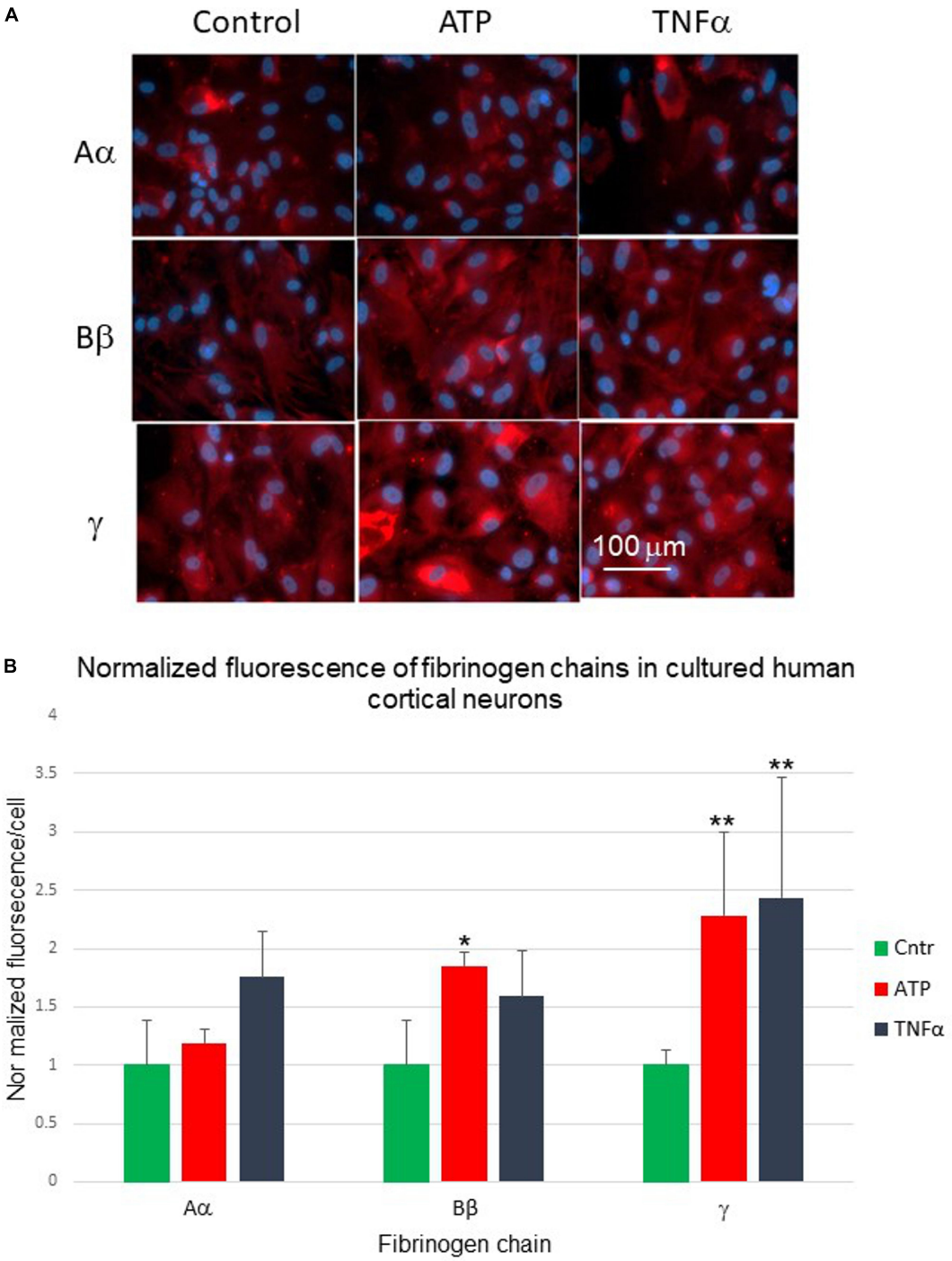

FIGURE 7 | (A) Changes in fibrinogen chains immunofluorescence in normal human cortical neurons differentially affected by 24-h exposure to pro-inflammatory stimuli. Aα, fibrinogen chain Aα; Bβ, fibrinogen chain Bβ; γ, fibrinogen chain γ, **(B)** Normalized quantification of the changes of the fibrinogen chains fluorescence in normal human cortical neurons culture in response to biologically significant stimuli. (ATP, stable ATP-γ; TNFα, tumor necrosis factor α; $*p < 0.05$; $**p < 0.01$). (Three plates, each stimulus in triplicates).

extrinsic pathway as it is known that the bounding glia limitans contains high levels of TF that can initiate fibrinogen conversion to fibrin (Golanov et al., 2017). In our described experiments cells of the glia limitans also demonstrated high levels of fibrinogen chains, which conceivably could be endocytosed from the CSF. Similarly, increased levels of fibrinogen chains in the parenchyma following the SAH could be due to changes in the permeability barrier of cerebral microvessels following the SAH

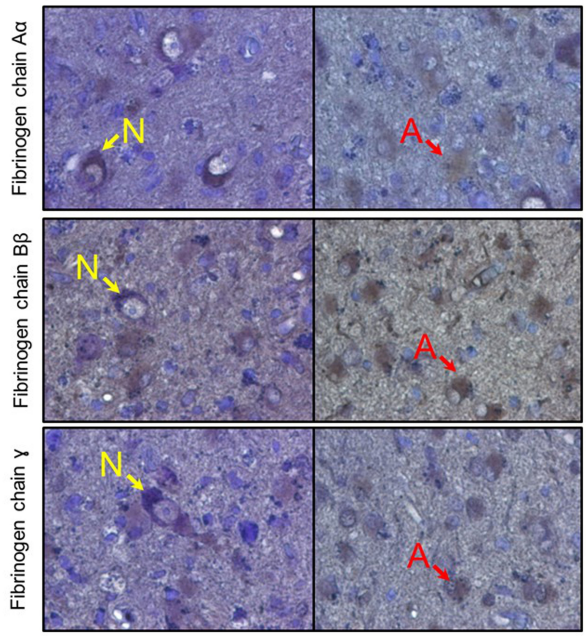

FIGURE 8 | Immunoreactive detection (DAB + hematoxylin) of fibrinogen chains in human brain samples (amygdala). Rows represent respective fibrinogen chains. N, indicate neurons, A, indicate astrocytes.

even in the remote sites, where no blood elements were observed (Davalos and Akassoglou, 2012; Petersen et al., 2018). However, in our experiments changes in the levels of fibrinogen chains were not correlated. Moreover, the fibrinogen chains were also accumulated in the intraparenchymal cells. These observations suggest that fibrinogen chains at least partially can be of local origin, i.e., generated by the glia limitans and other non-vascular brain cells. Furthermore, fibrinogen chain immunoreactivities were also detectable in the hippocampal dentate gyrus, where no blood was observed.

We also explored NHA and cortical human neuron cultures for the presence of the three fibrinogen chains. Immunohistochemistry revealed the intracellular presence of all three fibrinogen chains in human astrocytes and neurons. It can be argued that cultured cells endocytosed fibrinogen from the FBS-containing culture media. Western blot revealed presence of the specific fibrinogen chain proteins with the appropriate molecular weight. Low levels of fibrinogen in calf fetal serum and washing the cells before fixation (Ayache et al., 2006) decrease probability of cell "contamination" with the exogenous fibrinogen chains. However, this does not completely exclude origination of intracellular fibrin chains from the serum fibrinogen. Corroborating are our findings that the astrocyte cultures express the specific mRNAs for each chain, the observation which supports the hypothesis of an intracellular origin of the fibrinogen chains.

Allen atlas also demonstrates possible wide spread expression of fibrinogen chain Aα[1], presence of expression, though much more limited, of fibrinogen chains Bβ[2] and γ[3] (Morris et al., 2010). Expression of fibrinogen γ in the brain was demonstrated earlier (Haidaris and Courtney, 1990). These data provide additional support for the possible fibrinogen chains expression by the mouse brains.

Moreover, immunohistochemically determined levels of fibrinogen chains varied differentially in response to exposure to biologically significant signals. Importantly, responses, for example, of fibrinogen chain γ differed in neurons and astrocytes to the same signal, ATP-γS. These data suggest that the expression of the fibrinogen chains in cultured human neurons and astrocytes is intrinsic and regulated independently of each other.

Taken together these data strongly suggest the possibility that all three fibrinogen chains can be expressed in the brain, by neurons and astrocytes.

Fibrinogen chains appears in numerous brain pathologies: multiple sclerosis, Alzheimer's disease, EAE, posttraumatic demyelination as well as possible involvement in depression (Davalos and Akassoglou, 2012; Chiam et al., 2015; Petersen et al., 2018). In all cases it was suggested that the cause of appearance of fibrinogen in the brain is a "leaky" BBB. Indeed, in most cases the cerebral microvessel permeability barrier is abnormal and allows fibrinogen to enter the brain (Davalos and Akassoglou, 2012; Petersen et al., 2018). Because of fibrin deposits appear in Alzheimer's disease often localized near vessels a role for an altered blood-brain barrier has been suggested (Ryu and McLarnon, 2009; Sagare et al., 2013). However, there are also fibrin deposits in the neuropil without clear BBB disruption (Bien-Ly et al., 2015), which might occur due to the local production of fibrinogen.

Notably, fibrinogen chains as independent units are capable of interacting with various molecules (Weisel, 2005). Fibrinogen chains Aα and γ are capable of interaction with the various integrins such as αMβ2, αIIIβV mostly through their fibrinogen-related domain Arg–Gly–Asp (RGD) (Smith et al., 1990; Suehiro et al., 2000; Lishko et al., 2002; Yakubenko et al., 2002; Podolnikova et al., 2003; Ugarova et al., 2003; Lilja and Ivaska, 2018). The important role of integrins in the regulation of extracellular matrix and synaptic activity is well-established (Wu and Reddy, 2012; Park and Goda, 2016; Lilja and Ivaska, 2018). It is conceivable that fibrinogen chains Aα and γ can play modulatory roles through their interaction with various integrins in neuronal activity and other processes. Longer fibrinogen-related domain (Doolittle et al., 2012) of fibrinogen chain Bβ and fibrinogen chain γ also interacts with TLR-4 (Zuliani-Alvarez et al., 2017) potentially playing important roles in innate immunity and inflammation (Trotta et al., 2014). Fibrinogen chain Aα also interacts with fibronectin and TGF-β playing roles in the neuroinflammation (Engvall et al., 1978; Schachtrup et al., 2010; Webster et al., 2017). Fibrinogen chain Bβ can interact with VE-cadherin and β-amyloid (Yakovlev and Medved, 2009; Ahn et al., 2010). Fibrinogen chain γ is capable of interaction with ICAM-1 (Altieri et al., 1995). As our experiments demonstrated, fibrinogen chains differentially respond to biologically significant

[1]http://mouse.brain-map.org/experiment/show/68442907

[2]http://mouse.brain-map.org/experiment/show/68638095

[3]http://mouse.brain-map.org/gene/show/63741

and pro-inflammatory signals. It is conceivable that intrinsic fibrinogens chains play roles in the brain pathology and brain responses to various stimuli. Fibrin(ogen) itself is known to exert damaging effects on brain tissue (Ryu et al., 2009). However, the origin of separate fibrinogen chains could be different, extrinsic and intrinsic. It is conceivable that intrinsic fibrinogen chains can exert pleiotropic effects modulating various processes in norm and pathology.

CONCLUSION

Our data strongly suggest that neurons and astrocytes are capable of production of fibrinogen chains, which may be involved in various normal processes and brain pathology. Additional experiments are necessary to establish (a). whether cell/structure-specific fibrinogen chain genes knock-outs/knock-ins would have specific phenotype; (b) what physiological/behavioral effects fibrinogen chains alone would exercise being introduced directly into the brain; (c) to what extent they are capable to modify synaptic functions; (d) whether they play specific roles in various brain pathologies. The possibility that fibrinogen chains may have intrinsic to the brain origin open new intriguing venues for our understanding of established brain pathologies, including SAH.

CONTRIBUTION TO THE FIELD STATEMENT

Discovery of the expression of all fibrinogen chains by astrocytes and neurons in the brain *in vivo* and *vitro* suggests that fibrinogen observed in various neuropathological conditions can be of endogenous to the brain origin. Demonstration that the fibrinogen chains are differentially regulated by pro-inflammatory stimuli suggests that fibrinogen chains may play different role in brain functioning and brain response to the neuroinflammatory processes occurring during various neurological diseases. Traditionally it is thought that fibrinogen enters brain/subarachnoid space through damaged blood brain barrier. We demonstrate for the first time that mouse and human astrocytes and neurons express fibrinogen chains suggesting potential presence of endogenous to the brain fibrinogen chains differentially changing to biologically significant stimuli. SAH is followed by increased expression of fibrinogen chains associated with glia limitans remote from the hemorrhage. We conclude that brain astrocytes and neurons are capable of production of fibrinogen chains, which may be involved in various normal and pathological processes in the brain.

DATA AVAILABILITY

The datasets generated for this study are available on request to the corresponding author.

AUTHOR CONTRIBUTIONS

EG, MS, and AR-G conceived, planned, and carried out the experiments, processed the data, and wrote the manuscript. GDZ conceived and planned the experiments, analyzed the data, and edited the manuscript. DB and GB planned the experiments, interpreted the data, and edited the manuscript.

REFERENCES

Adams, R. A., Passino, M., Sachs, B. D., Nuriel, T., and Akassoglou, K. (2004). Fibrin mechanisms and functions in nervous system pathology. *Mol. Interv.* 4, 163–176.

Ahn, H. J., Zamolodchikov, D., Cortes-Canteli, M., Norris, E. H., Glickman, J. F., and Strickland, S. (2010). Alzheimer's disease peptide beta-amyloid interacts with fibrinogen and induces its oligomerization. *Proc. Natl. Acad. Sci. U.S.A.* 107, 21812–21817. doi: 10.1073/pnas.1010373107

Akassoglou, K., and Strickland, S. (2002). Nervous system pathology: the fibrin perspective. *Biol. Chem.* 383, 37–45.

Altieri, D. C., Duperray, A., Plescia, J., Thornton, G. B., and Languino, L. R. (1995). Structural recognition of a novel fibrinogen gamma chain sequence (117-133) by intercellular adhesion molecule-1 mediates leukocyte-endothelium interaction. *J. Biol. Chem.* 270, 696–699.

Ayache, S., Panelli, M. C., Byrne, K. M., Slezak, S., Leitman, S. F., Marincola, F. M., et al. (2006). Comparison of proteomic profiles of serum, plasma, and modified media supplements used for cell culture and expansion. *J. Transl. Med.* 4:40.

Bederson, J. B., Germano, I. M., and Guarino, L. (1995). Cortical blood flow and cerebral perfusion pressure in a new noncraniotomy model of subarachnoid hemorrhage in the rat. *Stroke* 26, 1086–1091.

Bien-Ly, N., Boswell, C. A., Jeet, S., Beach, T. G., Hoyte, K., Luk, W., et al. (2015). Lack of widespread BBB disruption in alzheimer's disease models: focus on therapeutic antibodies. *Neuron* 88, 289–297. doi: 10.1016/j.neuron.2015.09.036

Chiam, J. T., Dobson, R. J., Kiddle, S. J., and Sattlecker, M. (2015). Are blood-based protein biomarkers for Alzheimer's disease also involved in other brain disorders? a systematic review. *J. Alzheimers Dis.* 43, 303–314. doi: 10.3233/JAD-140816

Colman, R. W., and Budzynski, A. Z. (2011). *Blood Coagulation and Fibrinolysis. Comprehensive Physiology*. Hoboken, NJ: John Wiley & Sons, Inc.

Cray, C., Zaias, J., and Altman, N. H. (2009). Acute phase response in animals: a review. *Comp. Med.* 59, 517–526.

Davalos, D., and Akassoglou, K. (2012). Fibrinogen as a key regulator of inflammation in disease. *Semin. Immunopathol.* 34, 43–62. doi: 10.1007/s00281-011-0290-8

Deschepper, C. F., Bigornia, V., Berens, M. E., and Lapointe, M. C. (1991). Production of thrombin and antithrombin III by brain and astroglial cell cultures. *Brain Res. Mol. Brain Res.* 11, 355–358.

Dihanich, M., Kaser, M., Reinhard, E., Cunningham, D., and Monard, D. (1991). Prothrombin mRNA is expressed by cells of the nervous system. *Neuron* 6, 575–581.

Doolittle, R. F. (2011). Coagulation in vertebrates with a focus on evolution and inflammation. *J. Innate. Immun.* 3, 9–16. doi: 10.1159/000321005

Doolittle, R. F. (2016). The conversion of fibrinogen to fibrin: a brief history of some key events. *Matrix Biol.* 60–61, 5–7. doi: 10.1016/j.matbio.2016.08.002

Doolittle, R. F., McNamara, K., and Lin, K. (2012). Correlating structure and function during the evolution of fibrinogen-related domains. *Protein Sci.* 21, 1808–1823. doi: 10.1002/pro.2177

Doolittle, R. F., Spraggon, G., and Everse, S. J. (1997). Evolution of vertebrate fibrin formation and the process of its dissolution. *Ciba Found. Symp.* 212, 4–17; discussion 17–23.

Eddleston, M., de la Torre, J. C., Oldstone, M. B., Loskutoff, D. J., Edgington, T. S., and Mackman, N. (1993). Astrocytes are the primary source of tissue factor in the murine central nervous system. a role for astrocytes in cerebral hemostasis. *J. Clin. Invest.* 92, 349–358.

Engvall, E., Ruoslahti, E., and Miller, E. J. (1978). Affinity of fibronectin to collagens of different genetic types and to fibrinogen. *J. Exp. Med.* 147, 1584–1595.

Feiler, S., Friedrich, B., Scholler, K., Thal, S. C., and Plesnila, N. (2010). Standardized induction of subarachnoid hemorrhage in mice by intracranial pressure monitoring. *J. Neurosci. Methods* 190, 164–170. doi: 10.1016/j.jneumeth.2010.05.005

Gaberel, T., Gakuba, C., Goulay, R., Martinez De Lizarrondo, S., Hanouz, J. L., Emery, E., et al. (2014). Impaired glymphatic perfusion after strokes revealed by contrast-enhanced mri: a new target for fibrinolysis? *Stroke* 45, 3092–3096. doi: 10.1161/STROKEAHA.114.006617

Gaertner, F., and Massberg, S. (2016). Blood coagulation in immunothrombosis-At the frontline of intravascular immunity. *Semin. Immunol.* 28, 561–569. doi: 10.1016/j.smim.2016.10.010

Golanov, E. V., Bovshik, E. I., Wong, K. K., Pautler, R. G., Foster, C. H., Federley, R. G., et al. (2017). Subarachnoid hemorrhage - induced block of cerebrospinal fluid flow: role of brain coagulation factor III (tissue factor). *J. Cereb. Blood Flow Metab.* 38, 793–808. doi: 10.1177/0271678X17701157

Gruys, E., Toussaint, M. J., Niewold, T. A., and Koopmans, S. J. (2005). Acute phase reaction and acute phase proteins. *J. Zhejiang Univ. Sci. B* 6, 1045–1056.

Haidaris, P. J., and Courtney, M. A. (1990). Tissue-specific and ubiquitous expression of fibrinogen gamma-chain mRNA. *Blood Coagul. Fibrinolysis.* 1, 433–437.

Iliff, J. J., Wang, M., Liao, Y., Plogg, B. A., Peng, W., Gundersen, G. A., et al. (2012). A paravascular pathway facilitates CSF flow through the brain parenchyma and the clearance of interstitial solutes, including amyloid beta. *Sci. Transl. Med.* 4:147ra11. doi: 10.1126/scitranslmed.3003748

Lilja, J., and Ivaska, J. (2018). Integrin activity in neuronal connectivity. *J. Cell Sci.* 131:jcs212803. doi: 10.1242/jcs.212803

Lishko, V. K., Kudryk, B., Yakubenko, V. P., Yee, V. C., and Ugarova, T. P. (2002). Regulated unmasking of the cryptic binding site for integrin alpha M beta 2 in the gamma C-domain of fibrinogen. *Biochemistry* 41, 12942–12951.

Marik, C., Felts, P. A., Bauer, J., Lassmann, H., and Smith, K. J. (2007). Lesion genesis in a subset of patients with multiple sclerosis: a role for innate immunity? *Brain* 130(Pt 11), 2800–2815.

McDonagh, J., Messel, H., McDonagh, R. P. Jr., Murano, G., and Blomback, B. (1972). Molecular weight analysis of fibrinogen and fibrin chains by an improved sodium dodecyl sulfate gel electrophoresis method. *Biochim. Biophys. Acta* 257, 135–142.

Morris, J. A., Royall, J. J., Bertagnolli, D., Boe, A. F., Burnell, J. J., Byrnes, E. J., et al. (2010). Divergent and nonuniform gene expression patterns in mouse brain. *Proc. Natl. Acad. Sci. U.S.A.* 107, 19049–19054. doi: 10.1073/pnas.1003732107

Mosesson, M. W. (2005). Fibrinogen and fibrin structure and functions. *J. Thromb. Haemost.* 3, 1894–1904.

Park, Y. K., and Goda, Y. (2016). Integrins in synapse regulation. *Nat. Rev. Neurosci.* 17, 745–756. doi: 10.1038/nrn.2016.138

Parra, A., McGirt, M. J., Sheng, H., Laskowitz, D. T., Pearlstein, R. D., and Warner, D. S. (2002). Mouse model of subarachnoid hemorrhage associated cerebral vasospasm: methodological analysis. *Neurol. Res.* 24, 510–516.

Petersen, M. A., Ryu, J. K., and Akassoglou, K. (2018). Fibrinogen in neurological diseases: mechanisms, imaging and therapeutics. *Nat. Rev. Neurosci.* 19, 283–301. doi: 10.1038/nrn.2018.13

Podolnikova, N. P., Yakubenko, V. P., Volkov, G. L., Plow, E. F., and Ugarova, T. P. (2003). Identification of a novel binding site for platelet integrins alpha IIb beta 3 (GPIIbIIIa) and alpha 5 beta 1 in the gamma C-domain of fibrinogen. *J. Biol. Chem.* 278, 32251–32258.

Redman, C. M., and Xia, H. (2001). Fibrinogen biosynthesis. assembly, intracellular degradation, and association with lipid synthesis and secretion. *Ann. N.Y. Acad. Sci.* 936, 480–495.

Ryu, J. K., Davalos, D., and Akassoglou, K. (2009). Fibrinogen signal transduction in the nervous system. *J. Thromb. Haemost.* 7(Suppl. 1), 151–154.

Ryu, J. K., and McLarnon, J. G. (2009). A leaky blood-brain barrier, fibrinogen infiltration and microglial reactivity in inflamed Alzheimer's disease brain. *J. Cell Mol. Med.* 13, 2911–2925. doi: 10.1111/j.1582-4934.2008.00434.x

Sagare, A. P., Bell, R. D., and Zlokovic, B. V. (2013). Neurovascular defects and faulty amyloid-beta vascular clearance in Alzheimer's disease. *J. Alzheimers Dis.* 33(Suppl. 1), S87–S100.

Schachtrup, C., Ryu, J. K., Helmrick, M. J., Vagena, E., Galanakis, D. K., Degen, J. L., et al. (2010). Fibrinogen triggers astrocyte scar formation by promoting the availability of active TGF-beta after vascular damage. *J. Neurosci.* 30, 5843–5854. doi: 10.1523/JNEUROSCI.0137-10.2010

Sharpe, M. A., and Baskin, D. S. (2016). Monoamine oxidase B levels are highly expressed in human gliomas and are correlated with the expression of HiF-1alpha and with transcription factors Sp1 and Sp3. *Oncotarget* 7, 3379–3393. doi: 10.18632/oncotarget.6582

Siler, D. A., Gonzalez, J. A., Wang, R. K., Cetas, J. S., and Alkayed, N. J. (2014). Intracisternal administration of tissue plasminogen activator improves cerebrospinal fluid flow and cortical perfusion after subarachnoid hemorrhage in mice. *Transl. Stroke Res.* 5, 227–237. doi: 10.1007/s12975-014-0329-y

Smith, J. W., Ruggeri, Z. M., Kunicki, T. J., and Cheresh, D. A. (1990). Interaction of integrins alpha v beta 3 and glycoprotein IIb-IIIa with fibrinogen. differential peptide recognition accounts for distinct binding sites. *J. Biol. Chem.* 265, 12267–12271.

Suehiro, K., Mizuguchi, J., Nishiyama, K., Iwanaga, S., Farrell, D. H., and Ohtaki, S. (2000). Fibrinogen binds to integrin alpha(5)beta(1) via the carboxyl-terminal RGD site of the Aalpha-chain. *J. Biochem.* 128, 705–710.

Suzuki, S., Ishii, M., Ottomo, M., and Iwabuchi, T. (1977). Changes in the subarachnoid space after experimental subarachnoid haemorrhage in the dog: scanning electron microscopic observation. *Acta Neurochirurg.* 39, 1–14.

Takezawa, Y., Matsuda, K., Terasawa, F., Sugano, M., Honda, T., and Okumura, N. (2013). siRNA down-regulation of FGA mRNA in HepG2 cells demonstrated that heterozygous abnormality of the Aalpha-chain gene does not affect the plasma fibrinogen level. *Thromb. Res.* 131, 342–348. doi: 10.1016/j.thromres.2013.01.010

Tennent, G. A., Brennan, S. O., Stangou, A. J., O'Grady, J., Hawkins, P. N., and Pepys, M. B. (2007). Human plasma fibrinogen is synthesized in the liver. *Blood* 109, 1971–1974.

Thompson, E. J. (2005). *Proteins of Cerebrospinal Fluid,* 2nd ed. San Diego, CA: Elsevier Academic Press, 325.

Trotta, T., Porro, C., Calvello, R., and Panaro, M. A. (2014). Biological role of Toll-like receptor-4 in the brain. *J. Neuroimmunol.* 268, 1–12. doi: 10.1016/j.jneuroim.2014.01.014

Ugarova, T. P., Lishko, V. K., Podolnikova, N. P., Okumura, N., Merkulov, S. M., Yakubenko, V. P., et al. (2003). Sequence gamma 377-395(P2), but not gamma 190-202(P1), is the binding site for the alpha MI-domain of integrin alpha M beta 2 in the gamma C-domain of fibrinogen. *Biochemistry* 42, 9365–9373.

Webster, K. M., Sun, M., Crack, P., O'Brien, T. J., Shultz, S. R., and Semple, B. D. (2017). Inflammation in epileptogenesis after traumatic brain injury. *J. Neuroinflam.* 14:10. doi: 10.1186/s12974-016-0786-1

Weisel, J. W. (2005). Fibrinogen and fibrin. *Adv. Protein Chem.* 70, 247–299.

Wu, X., and Reddy, D. S. (2012). Integrins as receptor targets for neurological disorders. *Pharmacol. Ther.* 134, 68–81. doi: 10.1016/j.pharmthera.2011.12.008

Yakovlev, S., and Medved, L. (2009). Interaction of fibrin(ogen) with the endothelial cell receptor VE-cadherin: localization of the fibrin-binding site within the third extracellular VE-cadherin domain. *Biochemistry* 48, 5171–5179. doi: 10.1021/bi900487d

Yakubenko, V. P., Lishko, V. K., Lam, S. C., and Ugarova, T. P. (2002). A molecular basis for integrin alphaMbeta 2 ligand binding promiscuity. *J. Biol. Chem.* 277, 48635–48642.

Yates, R. L., Esiri, M. M., Palace, J., Jacobs, B., Perera, R., and DeLuca, G. C. (2017). Fibrin(ogen) and neurodegeneration in the progressive multiple sclerosis cortex. *Ann. Neurol.* 82, 259–270. doi: 10.1002/ana.24997

Zuliani-Alvarez, L., Marzeda, A. M., Deligne, C., Schwenzer, A., McCann, F. E., Marsden, B. D., et al. (2017). Mapping tenascin-C interaction with toll-like receptor 4 reveals a new subset of endogenous inflammatory triggers. *Nat. Commun.* 8:1595. doi: 10.1038/s41467-017-01718-7

Conflict of Interest Statement: The authors declare that the research was conducted in the absence of any commercial or financial relationships that could be construed as a potential conflict of interest.

Copyright © 2019 Golanov, Sharpe, Regnier-Golanov, Del Zoppo, Baskin and Britz. This is an open-access article distributed under the terms of the Creative Commons Attribution License (CC BY). The use, distribution or reproduction in other forums is permitted, provided the original author(s) and the copyright owner(s) are credited and that the original publication in this journal is cited, in accordance with accepted academic practice. No use, distribution or reproduction is permitted which does not comply with these terms.

frontiers in Cellular Neuroscience

METHODS
published: 05 June 2019
doi: 10.3389/fncel.2019.00247

Generation of Oligodendrocyte Progenitor Cells From Mouse Bone Marrow Cells

*Yuan Zhang[1†], Xin-Yu Lu[1†], Giacomo Casella[2†], Jing Tian[1†], Ze-Qing Ye[1], Ting Yang[1], Juan-Juan Han[1], Ling-Yu Jia[1], Abdolmohamad Rostami[2] and Xing Li[1]**

[1] The Key Laboratory of Medicinal Resources and Natural Pharmaceutical Chemistry, National Engineering Laboratory for Resource Development of Endangered Crude Drugs in Northwest China, The Ministry of Education, College of Life Sciences, Shaanxi Normal University, Xi'an, China, [2] Department of Neurology, Thomas Jefferson University, Philadelphia, PA, United States

Oligodendrocyte progenitor cells (OPCs) are a subtype of glial cells responsible for myelin regeneration. Oligodendrocytes (OLGs) originate from OPCs and are the myelinating cells in the central nervous system (CNS). OLGs play an important role in the context of lesions in which myelin loss occurs. Even though many protocols for isolating OPCs have been published, their cellular yield remains a limit for clinical application. The protocol proposed here is novel and has practical value; in fact, OPCs can be generated from a source of autologous cells without gene manipulation. Our method represents a rapid, and high-efficiency differentiation protocol for generating mouse OLGs from bone marrow-derived cells using growth-factor defined media. With this protocol, it is possible to obtain mature OLGs in 7–8 weeks. Within 2–3 weeks from bone marrow (BM) isolation, after neurospheres formed, the cells differentiate into Nestin$^+$ Sox2$^+$ neural stem cells (NSCs), around 30 days. OPCs specific markers start to be expressed around day 38, followed by RIP$^+$O4$^+$ around day 42. CNPase$^+$ mature OLGs are finally obtained around 7–8 weeks. Further, bone marrow-derived OPCs exhibited therapeutic effect in shiverer (Shi) mice, promoting myelin regeneration and reducing the tremor. Here, we propose a method by which OLGs can be generated starting from BM cells and have similar abilities to subventricular zone (SVZ)-derived cells. This protocol significantly decreases the timing and costs of the OLGs differentiation within 2 months of culture.

Keywords: oligodendrocyte progenitor cells, oligodendrocytes, neurospheres, bone marrow, autologous cells

OPEN ACCESS

Edited by:
Paulo Henrique Rosado-de-Castro, D'Or Institute for Research and Education (IDOR), Brazil

Reviewed by:
Jorge Matias-Guiu, Complutense University of Madrid, Spain
Enrica Boda, University of Turin, Italy

****Correspondence:***
Xing Li
xingli_xian@126.com

[†] These authors have contributed equally to this work

Specialty section:
This article was submitted to Non-Neuronal Cells, a section of the journal Frontiers in Cellular Neuroscience

Received: *14 December 2018*
Accepted: *17 May 2019*
Published: *05 June 2019*

Citation:
Zhang Y, Lu X-Y, Casella G, Tian J, Ye Z-Q, Yang T, Han J-J, Jia L-Y, Rostami A and Li X (2019) Generation of Oligodendrocyte Progenitor Cells From Mouse Bone Marrow Cells. Front. Cell. Neurosci. 13:247. doi: 10.3389/fncel.2019.00247

INTRODUCTION

Oligodendrocyte progenitor cells (OPCs) are present in both the white and gray matter of the adult central nervous system (CNS); upon oligodendrocytes (OLGs) injury, OPCs contribute to OLGs regeneration and remyelination (Duncan et al., 2018). OPCs are characterized by expression of platelet-derived growth factor receptor alpha (PDGFRα), neural/glial antigen 2 (NG2), and A2B5 (Dietrich et al., 2002; Zhu et al., 2008; Sim et al., 2011); they represent a high proliferative cell population resident in the CNS of adult mammals and humans (Mekhail et al., 2012; Clemente et al., 2013). OLGs derived from OPCs and are the myelinating cells of the CNS. Once OPCs differentiate into mature OLGs, they extend multiple processes that individually ensheath axons and then proceed to generate the concentric layers of the

modified cell membrane that compose myelin (Goldman and Kuypers, 2015). Thanks to their remyelinating ability, several groups used OPCs transplantation as a therapeutic strategy for CNS diseases (Kim et al., 2012; Najm et al., 2013; Yang et al., 2013). Indeed, OPCs can be used as a safe treatment for spinal cord injury (Nori et al., 2018), stroke (Wang et al., 2018), Parkinson's disease (Ahmed et al., 2013), and cerebral palsy (Rumajogee et al., 2018).

The transplantation of exogenous OPCs can represent a suitable treatment for chronic demyelinating disorders (Czepiel et al., 2015). The most common methods for obtaining functional OPCs, use mouse embryonic stem cell (ESCs) or pluripotent stem cells (Li et al., 2013; Wang et al., 2013; Kuai et al., 2015; Manley et al., 2017), or reprogrammed fibroblasts expressing a defined set of transcription factors (TFs) (Najm et al., 2013; Yang et al., 2013; Yamashita et al., 2017). Even if, OPCs transplantation has shown promising result in rodents (Goldman and Kuypers, 2015), its application remains far from the clinic. Several barriers should be overcome such as, whether OPCs can successfully migrate to the lesion (Foster et al., 1995), or their reprogramming can induce aberrant phenotype with consequent side-effects, as reported in some study in which next-generation sequencing was used (Liu et al., 2019). Other well-reported approaches used SVZ, from rodent CNS, as a source for isolating functional OPCs (Dincman et al., 2012; Zhu et al., 2014; Lu et al., 2015); however, due to the low cellular yield these methods have not guaranteed any feasibility for clinical application (Yang et al., 2010). Recently, it has been demonstrated that OPCs can be generated from bone marrow (BM) (Cristofanilli et al., 2011). These bone marrow-derived OPCs, induced with specific growth factor media, have shown similar morphology and cellular markers to canonical OPCs (Nazm Bojnordi et al., 2015).

We describe here a detailed protocol for generating OPCs and mature OLGs from autologous mouse bone marrow-derived neural stem cells (NSCs). Our method consists of two main steps. The first step provides the differentiation and generation of neurospheres from bone marrow-derived NSCs; the second one consists of neurospheres-derived OPCs differentiation within 1 week, using specific media. Respect to a previous report (Douvaras and Fossati, 2015), our protocol enables to produce autologous OLGs in 52 days.

Obtaining a high number of autologous OLGs is relevant to the clinic. For addressing this aspect, we tested the myelination ability of our bone marrow-derived OPCs, in a genetic model of congenital dysmyelination, shiverer (Shi) mice. Bone marrow-derived OPCs induced remyelination and significantly reduced tremor in treated mice. According to our data, this protocol is suitable for producing in large scale autologous OPCs, research aimed at understanding oligodendrocyte biology, and finally, it may represent a screening platform for myelinating compounds.

MATERIALS AND METHODS

Animals

C57BL/6 (The Fourth Military Medical University), SJL, and C3H mouse strains (The Jackson laboratory) are all appropriate for this protocol. Mice were kept in clean cages with a maximum of 5 mice per cage, in a controlled environment with 12/12 h of light/dark cycles and food *ad libitum* throughout the experimental procedures. All experimental procedures and protocols are approved by the Animal Management and Committee of Shaanxi Normal University. At the same time, by the approved institutional guidelines and regulations.

BM-NSCs were given by injection of single cells suspension (2×10^5 cells in 20 μl PBS/each mouse) by intracerebroventricular (i.c.v.) injection, into 1 week-old Shi mice. PBS-treated age-sex- and strain-matched mice were used as controls. All groups of animals were observed for 35 days.

Preparation of Neural Stem Cell Proliferation Media (NSC-PM)

A total of 200 ml of NSC-PM media is prepared mixing 150 ml of DMEM/F12 with 4 ml of B27, 2 ml of Penicillin-streptomycin (50 U/ml), 2 ml of Non-essential amino acid solution (0.1 mM), 2 ml HEPES (10 mM), 2 ml of sodium pyruvate (1 mM; all purchased from Thermo Fisher Scientific), 40 μl of epidermal growth factor (EGF, 20 ng/ml, stock concentration: 100 μg/ml; PeproTech), and 40 μl of basic fibroblast growth factor (bFGF, 10 ng/ml, stock concentration: 50 μg/ml; PeproTech). DMEM/F12 is added to a final volume of 200 ml, filter with a bottle-top filter (0.22 μm) and store at 4°C. We suggest to use complete media within 2 weeks.

Preparation of OPC Proliferation Media (OPC-PM)

A total of 50 ml of OPC-PM is prepared mixing 30 ml of DMEM/F12 with 1 ml of B27, 0.5 ml of N2, 0.5 ml of GlutaMax (2 mM), 0.5 ml of Penicillin-streptomycin (50 U/ml), 0.5 ml of Non-essential amino acid solution (0.1 mM), 0.5 ml of sodium pyruvate (1 mM; all purchased from Thermo Fisher Scientific), 10 μl of platelet-derived growth factor-AA (PDGF-AA, 20 ng/ml, stock concentration: 100 μg/ml; PeproTech), and 20 μl of bFGF (20 ng/ml, stock concentration: 50 μg/ml; PeproTech). DMEM/F12 is added to a final volume of 50 ml, filter with a bottle-top filter (0.22 μm) and store at 4°C. We suggest to use complete media within 2 weeks.

Preparation of Early OLGs Differentiation Media (EOLG-DM)

A total of 25 ml of EOLG-DM is prepared mixing 15 ml of DMEM/F12 with 0.5 ml of B27, 0.25 ml of N2, 0.25 ml of GlutaMax (2 mM), 0.25 ml of Penicillin-streptomycin (50 U/ml), 0.25 ml of Non-essential amino acid solution (0.1 mM), 0.25 ml of sodium pyruvate (1 mM; all purchased from Thermo Fisher Scientific), 50 μl of triiodo-l-thyronine (T3, 40 ng/ml, stock concentration: 20 μg/ml; Sigma-Aldrich), 20 μl of sonic hedgehog (Shh) (40 ng/ml stock, concentration: 50 μg/ml), 20 μl of Noggin (40 ng/ml, stock concentration: 50 μg/ml), 5 μl of insulin-like growth factor (IGF, 100 ng/ml, stock concentration: 500 μg/ml; all purchased from PeproTech), and 25 μl of neurotrophin 3 (NT-3, 10 ng/ml; Sigma-Aldrich). DMEM/F12 is added to a final volume of 25 ml, filter with a bottle-top

filter (0.22 μm) and store at 4°C. We suggest to use complete media within 1 week.

Preparation of Late OLGs Differentiation Media (LOLG-DM)

A total of 10 ml of LOLG-DM is prepared mixing 10 ml of EOLG-DM with 5 μl of 3′,5′-cyclic adenosine monophosphate (cAMP, 50 μM, stock concentration: 50 μg/ml; Sigma-Aldrich). The fresh media should be using within 1 week. For preparing Poly-D-lysine coating solution, stock at 0.1 % (wt/vol) 50 mL of sterile tissue culture grade water to 5 mg of poly-D-lysine (Sigma-Aldrich). Poly-D-lysine solution can be stored at 4°C for 3 months. Coating culture plates with the poly-D-lysine coating solution (0.5 ml per well for 24 well plate) and keep them for 2 h in 37°C incubator or overnight at 4°C. Remove coating solution and wash three times with sterile ddH_2O. After poly-D-lysine coated, add 1 μg/ml laminin (Sigma-Aldrich) solution for 2 h in 37°C incubator or overnight at 4°C. Laminin should be slowly thawed at 2–8°C for avoiding any solidification process. Dilute in a balanced salt solution and coat culture surface with a minimal volume. Remove coating solution, wash three times with sterile ddH_2O and dry completely in a tissue culture hood. Allow to air dry at least 5 min before introducing cells and media. Poly-D-lysine and laminin-coated coverslips: Place sterilized coverslips into the wells of a 24 well plate. The procedure followed the Poly-D-lysine coating and Laminin coating. The coverslips will float on the surface of the solution. Make sure the coverslips are completely immersed in the coating buffer to ensure the coverslips are well coated.

Isolation and Culture of NSCs From Murine SVZ and Bone Marrow

SVZ-derived NSCs were isolated from adult C57BL/6 mice as described previously with minor modification (Yang et al., 2009). Briefly, C57BL/6 mice 8 weeks old were euthanized and the SVZ region was harvested under sterile conditions and placed in DMEM media. After a brief washing with DMEM media, tissues were cut into 1 mm^3 pieces and digested by neural tissue dissociation kits (Miltenyi Biotec). The cells were suspended in serum-free DMEM/F12 (Invitrogen) supplied with 2% B27 supplements (Invitrogen), 20 ng/ml EGF (Peprotech) and 10 ng/ml bFGF (Peprotech), along with 100 IU/ml penicillin and 100 μg/ml Streptomycin (Sigma).

Bone marrow cells were isolated according to a previously described protocol (Swamydas and Lionakis, 2013). Finally, the cells were suspended in NSC-PM media at 10^6 cells/ml, and plated on poly-D-lysine, and laminin coated 24 well plate for 4 days. We suggest to replace half of the media with fresh NSC-PM media every 4 days. The media should be changed softly and slowly to avoid lifting the adhered NSCs (This is the critical step).

The formation of cellular clusters that resemble neurospheres becomes evident after 10–14 days. For cell detachment, aspirate the media, add 500 μl accutase (Thermo Fisher Scientific), and incubate at room temperature (22–25°C) for 2 min. Use 200 μl pipette to carefully suspend the adhered cell and transfer to a 15 ml conical tube. Shake the tube 10 times/min for total 3 min and add 4.5 ml DPBS for centrifuge (300 × *g*, 10 min). Next, suspend the cell pellet in NSC-PM media at 1×10^5 cells/ml, and plate the cell in non-coated 6 cm plate. After 4 days, the neurospheres can observe under the microscope. Collect suspended neurospheres from culture dish and transfer to a 15 ml conical tube. Centrifuge the cell at 100 × *g* for 1 min. Gently aspirate media leaving the neurospheres at the bottom of tube. Resuspend neurospheres in 5 ml DPBS and centrifuge the cell at 100 × g for 1 min to remove the media residues. Gently aspirate media leaving the neurospheres at the bottom of tube and add 1 ml of accutase to the cell culture and incubate 5 min at room temperature. Mildly shake the tube 10 times/min. If any neurosphere remains visible, after 4 min accutase incubation, we suggest to pipette gentle up and down until all the visible neurospheres are in a single cell suspension. The accutase media will change the color from carnation to oyster white. Then, add 4 ml of fresh media to the tube and centrifuge the cells at 200 × *g* for 4 min. Gently aspirate the supernatant and resuspend cells in fresh media. Transfer the cell 1×10^5 cells/ml to a new culture dish and incubate at 37°C for NSCs expanded. Cells can be frozen at this step. For visualization of results, seed the cell at 1×10^5 cells/ml in a poly-D-lysine and laminin coated 24 well plate with coverslips. Cells were fixed using 4% paraformaldehyde for immunocytochemical staining.

Bone Marrow-Derived NSCs Differentiation and Proliferation

To test the proliferation capacity of bone marrow-derived NSCs, growth curve of bone marrow-derived NSCs was determined followed previous method (Yang et al., 2010). Briefly, the newly formed neurospheres were digested to the single cells and plated at a density of 1.0×10^5 cell/ml and cultured in NSC-PM. At days 6, 11, 16 and 21, neurospheres in each well were digested into single cells; cell numbers were counted by hemocytometer. SVZ derived NSCs were used in the parallel experiment to compare the proliferate ratio.

To evaluate the differentiation ability of bone marrow-derived NSCs, single cells were plated on poly-D-lysine/laminin coated coverslip at a density of 1.0×10^4 cells/ml and cultured in specific NSCs differentiation media (Li et al., 2016). In brief, for neuron differentiation, Neurobasal media was supplemented with 2% B27, 2 mM GlutaMax-I and 0.5 mM cAMP. For astrocyte differentiation, DMEM was supplemented with 1% N2, 2 mM GlutaMax-I and 1% FBS. The oligodendrocyte differentiation media requires Neurobasal media supplemented with 2% B27, 2 mM GlutaMax-I and 20 ng/ml T3. Over 2 weeks, NSCs in differentiation media changed morphology and developed markers of neurons, astrocytes, and OLGs as determined by immunocytochemistry staining. To determine the number of cells expressing a specific antigen, five areas of each coverslip were examined, and the percentage of positive cells labeled for a specific neural marker in the total number of $DAPI^+$ cells was expressed as the mean value of specific neural differentiation.

OPCs Differentiation

Once neurospheres reach 100–250 μm of diameter, dissociate the neurospheres with accutase. Start by stepping suspend the cell pellet in NSC-PM media at 1×10^5 cells/ml until transfer the cell 1×10^5 cells/ml to a new culture dish and incubate at 37°C for NSCs expanded to the end. Finally, The cells are seeded on the poly-D-lysine, and laminin coated plate at 5×10^3 cells/ml in the NSC-PM media. After 1–2 days, over 90% cells will be adhered to the bottom, change the media to OPC-PM. Incubate the plate in a 37°C, 5% CO_2 incubator and perform media changes every 2 days for 8 days. Cells can be frozen at this step.

OLGs Maturation

At day 9, aspirate the OPC-PM media, gently rinse with DPBS to remove the growth factor (i.e., PDGF-AA and bFGF), and add fresh EOLG-DM (500 μl/well/24 well plate) for inducing differentiation of OLGs. OPCs will proliferate few times. If the cells reach 90% confluency, it might be necessary to split the cells at a 1:4–6 ratio. After 4 days, the media is changed to LOLG-DM. Adding cAMP will accelerate the branch outgrowth for OLGs differentiation. Repeat these steps for 3 times, after 2 weeks.

Immunofluorescence Staining

For immunocytochemistry, cells were fixed in 4% paraformaldehyde at room temperature for 30 min. Then, incubate with 0.3% TritonX-100 (in PBS) for 15 min at room temperature and wash with PBS. The primary antibody is diluted to a suitable concentration with a blocking solution (10% horse serum in PBS). The following primary antibodies were used: anti-A2B5 (MA1-90445, Thermo Fisher Scientific), anti-CNPase (ab44289, Abcam), anti-Ki67 (ab15580, Abcam), anti-Nestin (MAB353, Milipore), anti-NG2 (MAB5384, Milipore), anti-O4 (NL1326V, R&D), anti-RIP (ab72139, Abcam), and anti-SOX2 (ab97959, Abcam). Primary antibodies were washed out with PBS three times after overnight incubation at 4°C. The corresponding Alexa Fluor 488/594 conjugated secondary antibodies (both from Jackson ImmunoResearch Laboratories) were used for 2 h at room temperature. After wash, the ProLong™ Gold Antifade Mountant with DAPI buffer (P36931, Thermo Fisher Scientific) were used for mounting slides. Results were visualized by fluorescent microscopy (Nikon Eclipse E600; Nikon, Melville, NY, United States). Quantitative image analysis was performed using ImagePro (Media Cybernetics).

Bone Marrow NSC-Derived OPCs Transplantation Into Shi Mice

Newborn double-homozygous Shi (Mbp^{Shi}/Mbp^{Shi}) mice (The Jackson Laboratory, Bar Harbor, ME, United States) were injected with dissociated single OPCs. The protocol followed previous work with minor modifications (Zhang et al., 2019). Briefly, to generate the lentivirus expression of mCherry protein, the backbone of pCDH-CMV-MCS-EF1-copGFP (System Biosciences) was used. Subsequently, the copGFP was replaced by mCherry and puromycin was inserted into the multiple clone sites. The positive plasmid was confirmed by sequencing and using for lentivirus packaging. OPCs were transfected with lentiviral expressed mcherry, and positive cells were selected by puromycin. Then, mcherry $OPCs^+$ were transplanted bilaterally in the corpus callosum of 1 week-old Shi mice (2.0×10^5 cell/mice). PBS-treated age-sex-, strain-matched mice, and sham control mice were used. After 5 weeks from the treatment, mice were anesthetized, and brains were isolated and fixed with 4% paraformaldehyde and cryoprotected using 30% sucrose. CNS coronal sections were stained with myelin basic protein (MBP) antibody (ab40390, Abcam) for evaluating the differentiation process of mcherry $OPCs^+$. Tremor (Trembling time/total time) was analyzed for evaluating disease development. Kaplan-Meier analysis was used to assess the survival rate as described (Shinkai et al., 1992).

Statistical Analysis

Statistical analyses were performed using GraphPad Prism software (GraphPad, La Jolla, CA, United States). Data are presented as mean ± SD. Experiments with 2 groups were tested for statistical significance using unpaired, 2-tailed Student's *t*-tests. When comparing two groups at different time points, data were analyzed by two-way analysis of variance (ANOVA) with Tukey's multiple comparisons test. Comparisons between two groups were carried out with Student's *t*-test. Values of $p < 0.05$ were considered significant.

RESULTS

Timeline of Bone Marrow-Derived Mature Oligodendrocyte Differentiation

The timeline of our protocol is shown in **Figure 1**. In the first step, NSCs are differentiated from BM cells. After BM isolation, the cells are seeded at high density (5×10^5 cell per cm^2) on poly-D-lysine/laminin coated 24-well plate. *In vitro*, the presence EGF and fibroblast growth factor-2 (FGF2) mimic the NSCs culture environment, inducing NSCs proliferation. In the second stage, NSCs are induced to become OPCs. Here, the adherent cultures are dissociated to form spheres in suspension. Although $Sox2^+Nestin^+$ cells can also form spheres, the presence of recombinant protein PDGFα will gradually enrich the $NG2^+A2B5^+$ cell population (Neri et al., 2010). The final stage is the transition from OPCs to mature OLGs, by exposing the cells to T3, NT-3, Noggin, Shh, and IGF (Najm et al., 2013; Douvaras and Fossati, 2015).

Neurosphere Differentiation Step

For NSCs generation, BM from autologous adult mice can efficiency generate neurospheres. During neurosphere differentiation step, we are usually able to observe three stages (**Figure 2A**). (1) After 1 week in culture, individual cells exhibit high proliferative ability. (2) Two weeks later cells form neurospheres. (3) At 3–4 weeks, the neurospheres increased in size and gradually detached from the bottom of the culture plate. To characterize the bone marrow-derived NSCs, we compared the proliferative capacity with the SVZ-derived NSCs. We collected the neurosphere, dissociated, and re-plated at

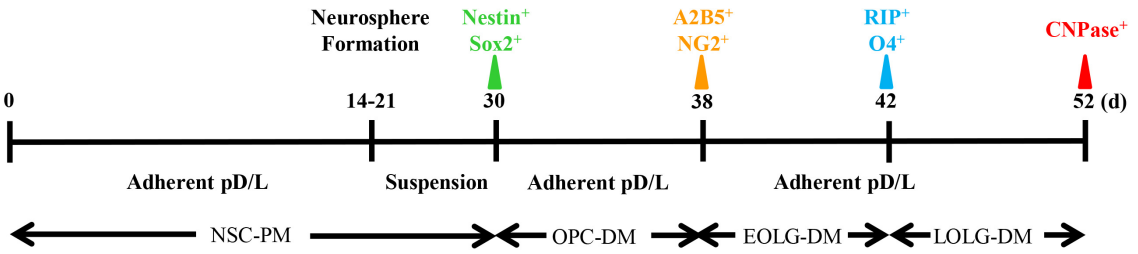

FIGURE 1 | Timeline of oligodendrocyte differentiation. Multicolor triangles represent recommended time points for evaluating the expression of stage-specific markers through immunofluorescence.

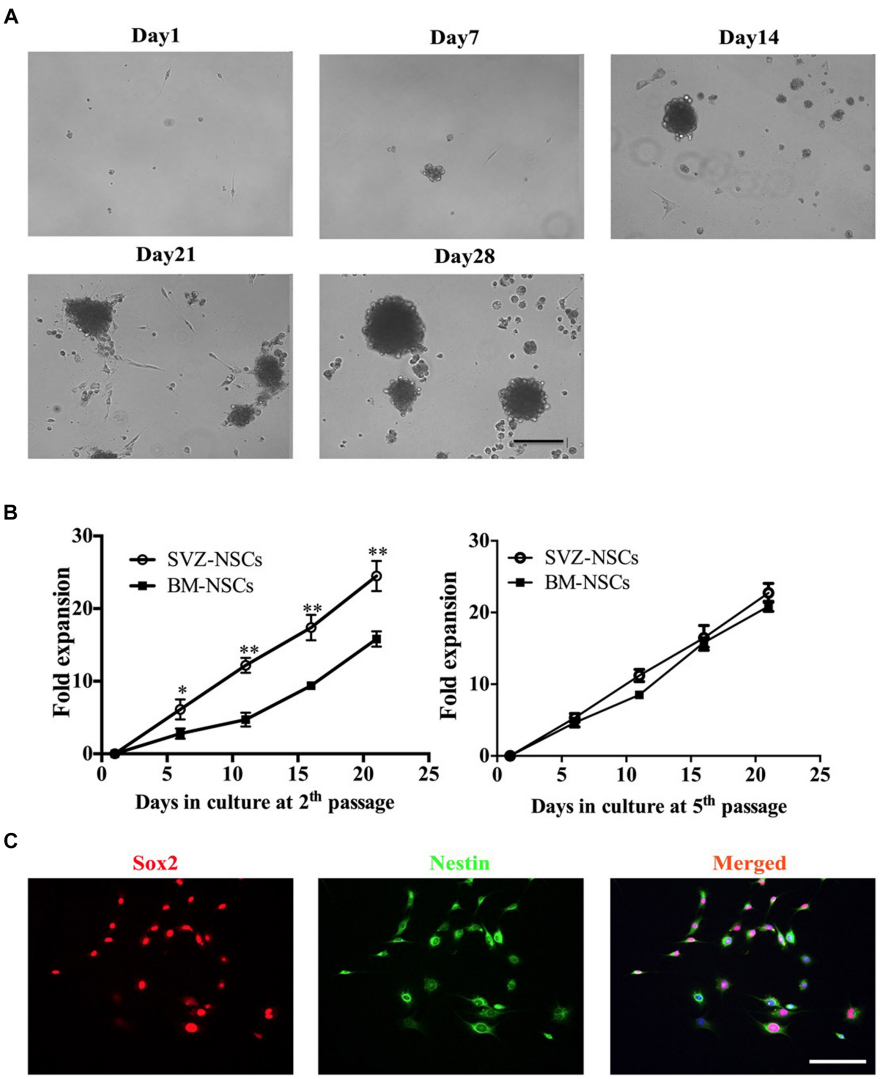

FIGURE 2 | Generation of bone marrow-derived NSCs *in vitro*. BM-NSCs were isolated and expanded from bone marrow of adult C57BL/6 mice and cultured in DMEM/F12 containing 20 ng/ml EGF, 20 ng/ml Bfgf, and 2% B27 supplements. **(A)** Single cells were seeded in poly-D-lysine- and laminin-coated plates. After 7 days, the cells showed obvious proliferation. After 14 days, the NSCs gradually formed neurospheres. After 21–28 days, neurospheres increased size, and detached from the bottom of the culture plate. **(B)** Growth curves of BM-NSCs and SVZ-NSCs. Single cells at the second and fifth passages were seeded at a density of 1.0×10^5 cells/ml and cultured in proliferation media. At days 6, 11, 16 and 21, neurospheres in each well were digested into single cells; cell numbers were counted by hemocytometer. At least 5 wells were evaluated at each time point. Data represent the mean ± SD from three repeated experiments from separately generated cultures, $^*p < 0.05$, $^{**}p < 0.01$, as determined by two-way ANOVA with Tukey's multiple comparison test. **(C)** Neurospheres dissociated with accutase and plated in the coated coverslips were immunostained for NSC markers Sox2 and Nestin. Scale bar = 50 μm.

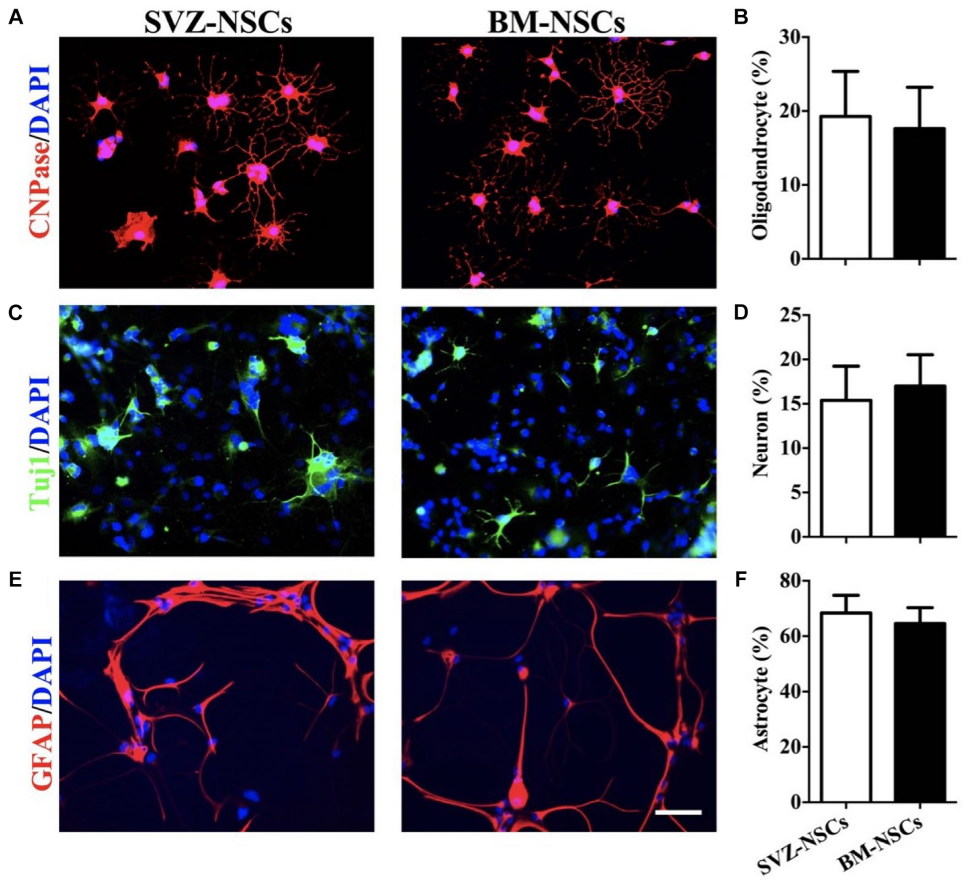

FIGURE 3 | BM-NSCs differentiation *in vitro*. Examples of NSCs that differentiated into **(A)** OLGs (CNPase$^+$), **(C)** neuron (Tuj1$^+$), and **(E)** astrocytes (GFAP$^+$), after 1 week with specific differentiation media. Scale bar = 50 μm. **(B,D,F)** Quantitative analysis of differentiated cells. Data are shown as mean values ± SD (n = 5 each group) and are representative of three experiments. Significance difference was analyzed by Student's t-test.

1.0×10^5 cell/ml for a next round cell expansion. We next compared the proliferation capacity of bone marrow- and SVZ-NSCs. BM and SVZ-NSCs from passages 2 and 5 were seeded and cultured in NSC-PM. At day 6, 11, 16, and 21, the neurospheres formed and re-dissociated to single cells, and the cell number were counted by hemocytometer. The proliferation rate of BM-NSCs was significantly slower than SVZ-NSC at the early stage, whereas there was no obviously difference in proliferation capacity at passage 5 (**Figure 2B**). To identify the BM-NSCs, single cells were transferred onto poly-D-lysine and laminin pre-coated coverslips and used for immunostaining with Sox2 and Nestin. We can observe over 95% cells are Sox2 and Nestin-positive cells at passage 5 (**Figure 2C**).

Differentiation Potential of BM-NSCs

To test the differentiation potential of BM-NSCs *in vitro*, neurospheres were used and cultured in specific neuron/astrocyte/oligodendrocyte differentiation media. After 2 weeks, BM-NSCs, plated in presence of differentiation media, changed morphology and developed markers of neuron, astrocytes, and OLGs, as shown by immunocytochemistry staining. We compared the differentiation capacity of BM-NSCs and SVZ-NSCs. There are no significant difference about the percentage of CNPase$^+$, Tuj1$^+$, and GFAP$^+$ cells between BM-NSCs and SVZ-NSCs. These results indicated that BM-NSCs can differentiate into neural cell lineages (**Figure 3**).

OPCs Differentiation and Oligodendrocyte Maturation Process

To assess whether the enrichment of OPCs obtained by differentiation media could be exploited for increasing the yield of mature OLGs, OPCs grown in EOLG-DM media for 4 days were shift to LOLG-DM media for additional 10 days. Cells grown for 14 days in OPC-PM media were used as control. Cells were then analyzed for the presence of A2B5$^+$, NG2$^+$, RIP$^+$, O4$^+$, and CNPase$^+$ cells. For OPCs differentiation, single NSCs were seed on poly-D-lysine, and laminin coated plates or coverslips in the OPCs differentiation media. Cells exhibited strong proliferation ability and grew faster under the proliferation condition (**Figure 4A**). These OPCs expressed A2B5 and NG2, as shown by immunostaining (**Figures 4B,C**). Moreover, OPC-spheres can be cultured with OPCs media without differentiation.

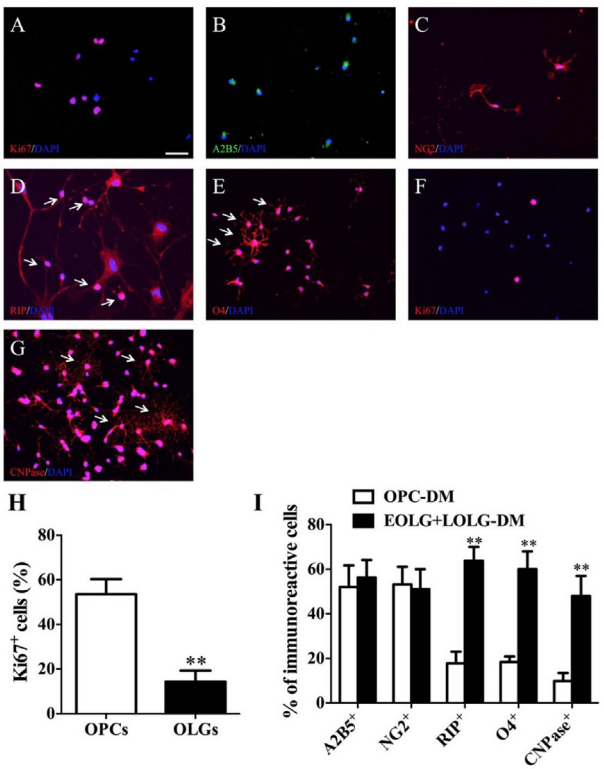

FIGURE 4 | Fundamental steps of BM-NSCs OLGs differentiation. **(A)** Expression of Ki-67 at day 38, as shown by immunofluorescence analysis. **(B,C)** Immunofluorescence staining of progenitor cells at day 38, expressing A2B5, and NG2. **(D,E)** RIP and O4 staining show cells ramified morphology. **(F)** Expression of Ki-67 which in late stage of OLGs differentiation (day 52). **(G)** At the end of differentiation stage, CNPase$^+$ OLGs show typical ramified morphology. **(H)** OPCs and OLGs proliferation **(A,F)** was quantified as percentage of Ki67-positive cells. Scale bar = 50 μm. **(I)** The percentages of A2B5$^+$, NG2$^+$, RIP$^+$, O4$^+$, and CNPase$^+$ cells are present in EOLG+LOLG-DM cultures as compared to OPC-PM cultures. Data are expressed as the mean ± SD, three independent experiments, $^{**}p < 0.01$, Student's *t*-test.

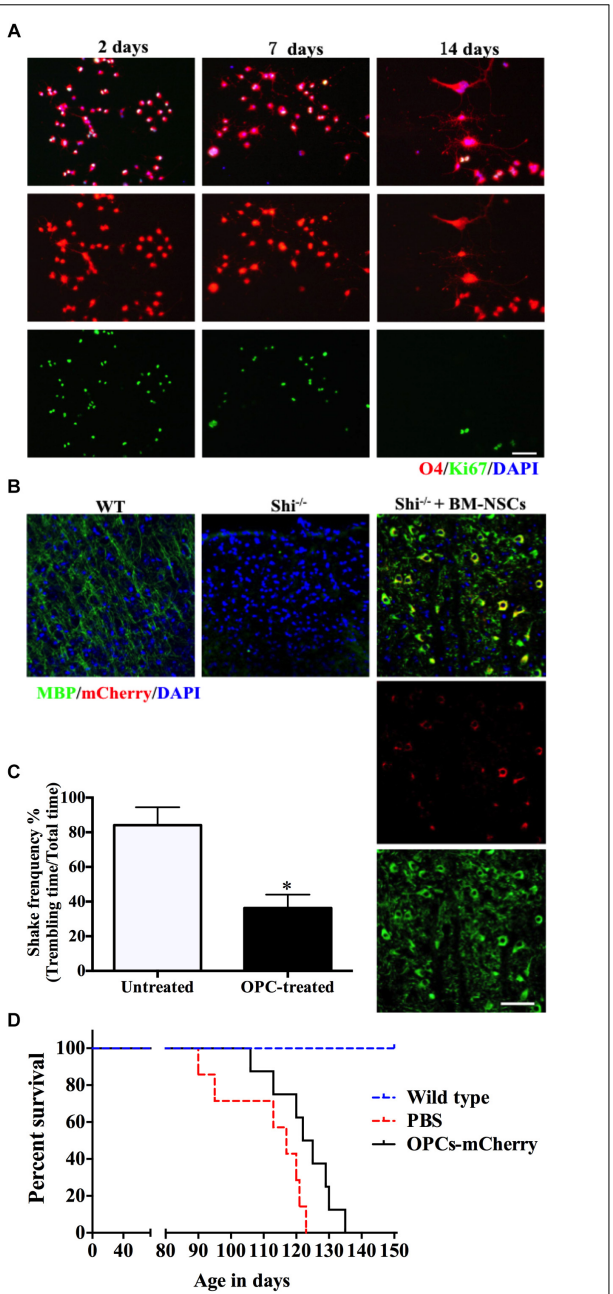

FIGURE 5 | BM-NSCs OLGs differentiation *in vitro* and transplantation in Shi mice. **(A)** BM-NSCs were cultured in oligodendrocyte differentiation media for 48 h, 1 week, and 2 weeks for O4 (differentiation marker) and Ki-67 (proliferation marker) staining. **(B)** Fluorescence staining of BM-NSCs (mCherry$^+$ cells), after 35 days post injection, show myelination (MBP$^+$) in the contralateral striatum. Scale bar = 50 μm. **(C)** Quantification of tremor of Shi mice treated with OPCs. **(D)** Transplanted OPCs prolong the survival of Shi mice compared with PBS-treated ($n = 9$). Symbols represent mean ± SD. $^*p < 0.05$, Student's *t*-test.

They can further form immature OLGs (e.g., RIP$^+$ and O4$^+$) when are grown in OLGs differentiation media for 1 week (**Figures 4D,E**).

For OLGs maturation, OPCs were grown in presence of oligodendrocyte differentiation media. Cells gradually stopped to proliferate (Ki67$^+$) (**Figures 4F,H**) and started to differentiate into mature OLGs (CNPase$^+$). About 50 % of the CNPase$^+$ OLGs exhibited complex membrane morphology indicating OPCs differentiation into mature OLGs successfully (**Figures 4G,I**).

OPCs and Mature OLGs Generation From Autologous Mouse Bone Marrow-Derived NSCs

Our method allows to isolate OPCs, using a selective detachment procedure, generate mature OLGs *in vitro* (**Figure 5A**), and induce remyelination after transplantation into the dysmyelinated Shi mice (**Figure 5B**). Although immunofluorescence analysis showed abundant MBP$^+$mCherry$^+$ cells, the transplanted cells were more like "non-completedly myelinating" cells. We hypothesized that these cells would become mature at later time points and

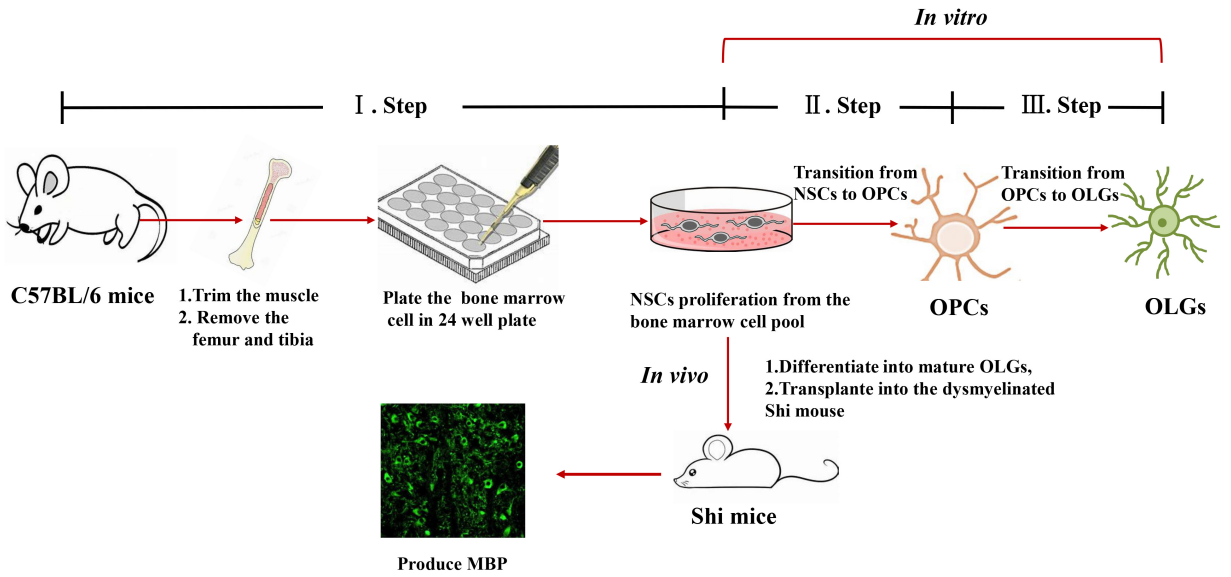

FIGURE 6 | Representative scheme of the protocol for generating OPCs and OLGs from autologous mouse bone marrow-derived NSCs.

express more MBP$^+$ myelin internodes. To define whether our BM-NSCs had the potential to form functional OLGs *in vivo*, the tremor and survival rate were test in the subsequent experiment. After OPCs transplantation, the tremor was significantly decreased compared the untreated Shi mice (**Figure 5C** and **Supplementary Videos 1, 2**). As shown in **Figure 5D**, the survival rate of mice transplanted with OPCs was increased, with a range of 106–135 days. All PBS-treated Shi mice died, over a range of 90–125 days postnatally. These results indicated that BM-OPCs could successfully differentiate into functionally OLGs, induce remyelination, and increase survival rate in Shi mice. The experimental design overview for this protocol is shown in **Figure 6**.

DISCUSSION

Oligodendrocyte progenitor cells can be isolated from the SVZ of adult mammalian and expanded *in vitro* for producing mature OLGs (Chen et al., 2007). However, with this method, a little number of mature OLGs can be obtained. Recent studies showed that it is possible to differentiate OPCs from BM cells (Yang et al., 2010; Nazm Bojnordi et al., 2015). Indeed, bone marrow-derived OPCs showed distinct neural cell markers and morphology (Abbaszadeh et al., 2013). The possibility to get a high number of mature OLGs, starting from bone marrow, represents an accessible, and alternative manner respect to canonical methods in which OPCs are generated from SVZ-derived cells. OPCs transplantation either intravenous (i.v.) or i.c.v. has shown to promote remyelination *in vivo* (Sher et al., 2012; Wu et al., 2012); thus its therapeutic potential is relevant for demyelination disorders.

Currently, there are several methods for obtaining functional OLGs (Garcia-Leon and Verfaillie, 2016). Nazm Bojnordi et al. (2015) used BM stromal cells for producing functional Olig2 and O4$^+$ cells. These OPCs successfully promoted the remyelination, in LPS-induced demyelination model; however, the efficiency was unclear. Further, OPCs isolation from ESCs or induced pluripotent stem cells (iPSCs), is an effective way for repairing and preventing the progression of demyelinating lesions (Douvaras et al., 2014; Thiruvalluvan et al., 2016). However, ESCs-derived OPCs may lack of stability and safety. It has been shown that NSCs possess less risk of potential tumorigenicity than ESCs or iPSCs (Zhao et al., 2015). The generation of OPCs from BM is consistent with what demonstrated so far (Yang et al., 2010; Hojjat-Allah et al., 2013; Nazm Bojnordi et al., 2015). Our method mainly consists of three steps, bone marrow-derived NSCs generation, NSCs-OPCs differentiation, and OLGs maturation. These data also focused on the derivation of OLGs from OPCs using assorted agents. In all of these steps, we use conditioned-media containing essential growth factors such as T3, Shh, IGF, and NT-3. We, also, use Noggin for negatively regulating bone morphogenetic protein (BMP) pathway, which blocked oligodendrocyte maturation (Najm et al., 2013). Although this protocol does not significantly improve the differentiation efficiency, compared with previous work, the timing is shorter (from 75 to 95 and 52 days) (Chen et al., 2007; Douvaras and Fossati, 2015). Our findings provide an alternative, fast strategy for obtaining functional OLGs from BM cells after just 40–50 days of differentiation. Here, we use the congenital dysmyelination model of Shi mice to show that BM-OPCs improved the mice survival. Our protocol can generate OPCs from BM-NSCs providing sufficient cell sources from autologous and inducing remyelination.

One generally OPCs generating strategies is that the cell need transduction of several TFs by lentiviral (Han et al., 2012; Najm et al., 2013). Virus-mediated gene delivery required higher biosafety levels and still need to be considered for

clinical application (Capetian et al., 2016). In our protocol, we choose a well-established, and effective custom differentiation media system (Najm et al., 2013; Baskin et al., 2016). These differentiation media contain several growth factors (EGF, FGF, PDGF, Shh, Noggin, IGF, and NT-3) which used in different proliferation or differentiation stage were sufficient for inducing cell differentiation into mature OLGs. The manner of using growth factor is safer than viral or small molecules to treat cell or neurodegeneration disease (Tuszynski et al., 2015; De et al., 2017). The specificity of growth factors to recognize its target is better than small molecules especially in high dose (such as concentration > 10 μM) (Weiss et al., 2007). Also, when withdrawing the growth factors such as FGF, EGF et al., cell will cease to proliferate and avoid the risk of formation tumor cell. In a previous report, T3 was used as an inducer to differentiate into oligodendrocyte-like cells using autologous BM stromal cells (Kaka et al., 2012; Hojjat-Allah et al., 2013). Compared with their researches, we have demonstrated that mouse OLGs can be produced from bone marrow-derived cells *in vitro*, indicating that our method is more reliable. Together, this protocol indicates that our bone marrow-derived OPCs represent a simple, safe, valuable and promising cell-based therapy strategy for myelin repair and neurodegeneration disease.

ETHICS STATEMENT

All experimental procedures and protocols are approved by the Animal Management and Committee of Shaanxi Normal University. At the same time, in accordance with the approved institutional guidelines and regulations.

AUTHOR CONTRIBUTIONS

YZ and XL conceived and designed the experiments. YZ, X-YL, JT, J-JH, and Z-QY carried out the experiments. TY, L-YJ, and XL analyzed the data. YZ, X-YL, GC, JT, and XL wrote the manuscript. AR and XL supervised the study and revised the manuscript. All authors read and approved the final manuscript.

FUNDING

This study was supported by the Chinese National Natural Science Foundation (Grant Nos. 81771345 and 81501062), the Natural Science Foundation of Shaanxi Province, China (Grant Nos. 2018JZ3001, 2018JQ8033, and 2017043) and the Fundamental Research Funds for the Central Universities (Grant Nos. GK201903062, GK20182010, GK201701009, 2018CSLZ018, 2018CSLZ019, and 2018CSLZ020).

SUPPLEMENTARY MATERIAL

The Supplementary Material for this article can be found online at: https://www.frontiersin.org/articles/10.3389/fncel.2019.00247/full#supplementary-material

REFERENCES

Abbaszadeh, H. A., Tiraihi, T., Delshad, A. R., Saghedi Zadeh, M., and Taheri, T. (2013). Bone marrow stromal cell transdifferentiation into oligodendrocyte-like cells using triiodothyronine as a inducer with expression of platelet-derived growth factor alpha as a maturity marker. *Iran. Biomed. J.* 17, 62–70.

Ahmed, Z., Asi, Y. T., Lees, A. J., Revesz, T., and Holton, J. L. (2013). Identification and quantification of oligodendrocyte precursor cells in multiple system atrophy, progressive supranuclear palsy and Parkinson's disease. *Brain Pathol.* 23, 263–273. doi: 10.1111/j.1750-3639.2012.00637.x

Baskin, J. M., Wu, X., Christiano, R., Oh, M. S., Schauder, C. M., Gazzerro, E., et al. (2016). The leukodystrophy protein FAM126A (hyccin) regulates PtdIns(4)P synthesis at the plasma membrane. *Nat. Cell Biol.* 18, 132–138. doi: 10.1038/ncb3271

Capetian, P., Azmitia, L., Pauly, M. G., Krajka, V., Stengel, F., Bernhardi, E. M., et al. (2016). Plasmid-based generation of induced neural stem cells from adult human fibroblasts. *Front. Cell Neurosci.* 10:245. doi: 10.3389/fncel.2016.00245

Chen, Y., Balasubramaniyan, V., Peng, J., Hurlock, E. C., Tallquist, M., Li, J., et al. (2007). Isolation and culture of rat and mouse oligodendrocyte precursor cells. *Nat. Protoc.* 2, 1044–1051. doi: 10.1038/nprot.2007.149

Clemente, D., Ortega, M. C., Melero-Jerez, C., and de Castro, F. (2013). The effect of glia-glia interactions on oligodendrocyte precursor cell biology during development and in demyelinating diseases. *Front. Cell Neurosci.* 7:268. doi: 10.3389/fncel.2013.00268

Cristofanilli, M., Harris, V. K., Zigelbaum, A., Goossens, A. M., Lu, A., Rosenthal, H., et al. (2011). Mesenchymal stem cells enhance the engraftment and myelinating ability of allogeneic oligodendrocyte progenitors in dysmyelinated mice. *Stem Cells Dev.* 20, 2065–2076. doi: 10.1089/scd.2010.0547

Czepiel, M., Boddeke, E., and Copray, S. (2015). Human oligodendrocytes in remyelination research. *Glia* 63, 513–530. doi: 10.1002/glia.22769

De, D., Halder, D., Shin, I., and Kim, K. K. (2017). Small molecule-induced cellular conversion. *Chem. Soc. Rev.* 46, 6241–6254. doi: 10.1039/c7cs00330g

Dietrich, J., Noble, M., and Mayer-Proschel, M. (2002). Characterization of A2B5+ glial precursor cells from cryopreserved human fetal brain progenitor cells. *Glia* 40, 65–77. doi: 10.1002/glia.10116

Dincman, T. A., Beare, J. E., Ohri, S. S., and Whittemore, S. R. (2012). Isolation of cortical mouse oligodendrocyte precursor cells. *J. Neurosci. Methods* 209, 219–226. doi: 10.1016/j.jneumeth.2012.06.017

Douvaras, P., and Fossati, V. (2015). Generation and isolation of oligodendrocyte progenitor cells from human pluripotent stem cells. *Nat. Protoc.* 10, 1143–1154. doi: 10.1038/nprot.2015.075

Douvaras, P., Wang, J., Zimmer, M., Hanchuk, S., O'Bara, M. A., Sadiq, S., et al. (2014). Efficient generation of myelinating oligodendrocytes from primary progressive multiple sclerosis patients by induced pluripotent stem cells. *Stem Cell Rep.* 3, 250–259. doi: 10.1016/j.stemcr.2014.06.012

Duncan, I. D., Radcliff, A. B., Heidari, M., Kidd, G., August, B. K., and Wierenga, L. A. (2018). The adult oligodendrocyte can participate in remyelination. *Proc. Natl. Acad. Sci. U.S.A.* 115, E11807–E11816. doi: 10.1073/pnas.1808064115

Foster, L. M., Landry, C., Phan, T., and Campagnoni, A. T. (1995). Conditionally immortalized oligodendrocyte cell lines migrate to different brain regions and elaborate 'myelin-like' membranes after transplantation into neonatal shiverer mouse brains. *Dev. Neurosci.* 17, 160–170. doi: 10.1159/000111284

Garcia-Leon, J. A., and Verfaillie, C. M. (2016). Stem cell-derived oligodendroglial cells for therapy in neurological diseases. *Curr. Stem Cell Res. Ther.* 11, 569–577. doi: 10.2174/1574888x10666150902095312

Goldman, S. A., and Kuypers, N. J. (2015). How to make an oligodendrocyte. *Development* 142, 3983–3995. doi: 10.1242/dev.126409

Han, D. W., Tapia, N., Hermann, A., Hemmer, K., Hoing, S., Arauzo-Bravo, M. J., et al. (2012). Direct reprogramming of fibroblasts into neural stem cells by defined factors. *Cell Stem Cell* 10, 465–472. doi: 10.1016/j.stem.2012.02.021

Hojjat-Allah, A., Ali Reza, D., Majid Saghedi, Z., and Taher, T. (2013). Bone marrow stromal cell transdifferentiation into oligodendrocyte-like cells using triiodothyronine as a inducer with expression of platelet-derived growth factor α as a maturity marker. *Iran. Biomed. J.* 17, 62–70. doi: 10.6091/ibj.11162.2013

Kaka, G. R., Tiraihi, T., Delshad, A., Arabkheradmand, J., and Kazemi, H. (2012). In vitro differentiation of bone marrow stromal cells into oligodendrocyte-like cells using triiodothyronine as inducer. *Int. J. Neurosci.* 122, 237–247. doi: 10.3109/00207454.2011.642037

Kim, H., Walczak, P., Kerr, C., Galpoththawela, C., Gilad, A. A., Muja, N., et al. (2012). Immunomodulation by transplanted human embryonic stem cell-derived oligodendroglial progenitors in experimental autoimmune encephalomyelitis. *Stem Cells* 30, 2820–2829. doi: 10.1002/stem.1218

Kuai, X. L., Ni, R. Z., Zhou, G. X., Mao, Z. B., Zhang, J. F., Yi, N., et al. (2015). Transplantation of mouse embryonic stem cell-derived oligodendrocytes in the murine model of globoid cell leukodystrophy. *Stem Cell Res. Ther.* 6:30. doi: 10.1186/s13287-015-0024-2

Li, X., Zhang, Y., Yan, Y., Ciric, B., Ma, C. G., Gran, B., et al. (2016). Neural stem cells engineered to express three therapeutic factors mediate recovery from chronic stage CNS autoimmunity. *Mol. Ther.* 24, 1456–1469. doi: 10.1038/mt.2016.104

Li, Y., Gautam, A., Yang, J., Qiu, L., Melkoumian, Z., Weber, J., et al. (2013). Differentiation of oligodendrocyte progenitor cells from human embryonic stem cells on vitronectin-derived synthetic peptide acrylate surface. *Stem Cells Dev.* 22, 1497–1505. doi: 10.1089/scd.2012.0508

Liu, C., Hu, X., Li, Y., Lu, W., Li, W., Cao, N., et al. (2019). Conversion of mouse fibroblasts into oligodendrocyte progenitor-like cells through a chemical approach. *J. Mol. Cell Biol.* doi: 10.1093/jmcb/mjy088 [Epub ahead of print].

Lu, Y., Yang, Y., Wang, Z., Wang, C., Du, Q., Wang, Q., et al. (2015). Isolation and culture of human oligodendrocyte precursor cells from neurospheres. *Brain Res. Bull.* 118, 17–24. doi: 10.1016/j.brainresbull.2015.08.008

Manley, N. C., Priest, C. A., Denham, J., Wirth, E. D. III, and Lebkowski, J. S. (2017). Human embryonic stem cell-derived oligodendrocyte progenitor cells: preclinical efficacy and safety in cervical spinal cord injury. *Stem Cells Transl. Med.* 6, 1917–1929. doi: 10.1002/sctm.17-0065

Mekhail, M., Almazan, G., and Tabrizian, M. (2012). Oligodendrocyte-protection and remyelination post-spinal cord injuries: a review. *Prog. Neurobiol.* 96, 322–339. doi: 10.1016/j.pneurobio.2012.01.008

Najm, F. J., Lager, A. M., Zaremba, A., Wyatt, K., Caprariello, A. V., Factor, D. C., et al. (2013). Transcription factor-mediated reprogramming of fibroblasts to expandable, myelinogenic oligodendrocyte progenitor cells. *Nat. Biotechnol.* 31, 426–433. doi: 10.1038/nbt.2561

Nazm Bojnordi, M., Ghasemi, H. H., and Akbari, E. (2015). Remyelination after lysophosphatidyl choline-induced demyelination is stimulated by bone marrow stromal cell-derived oligoprogenitor cell transplantation. *Cell. Tissues Org.* 200, 300–306. doi: 10.1159/000437350

Neri, M., Maderna, C., Ferrari, D., Cavazzin, C., Vescovi, A. L., and Gritti, A. (2010). Robust generation of oligodendrocyte progenitors from human neural stem cells and engraftment in experimental demyelination models in mice. *PLoS One* 5:e10145. doi: 10.1371/journal.pone.0010145

Nori, S., Khazaei, M., Ahuja, C. S., Yokota, K., Ahlfors, J. E., Liu, Y., et al. (2018). Human oligodendrogenic neural progenitor cells delivered with chondroitinase abc facilitate functional repair of chronic spinal cord injury. *Stem Cell Rep.* 11, 1433–1448. doi: 10.1016/j.stemcr.2018.10.017

Rumajogee, P., Altamentova, S., and Li, L. (2018). Exogenous neural precursor cell transplantation results in structural and functional recovery in a hypoxic-ischemic hemiplegic mouse model. *eNeuro* 5:ENEURO.369–ENEURO.318. doi: 10.1523/eneuro.0369-18.2018

Sher, F., Amor, S., Gerritsen, W., Baker, D., Jackson, S. L., Boddeke, E., et al. (2012). Intraventricularly injected Olig2-NSCs attenuate established relapsing-remitting EAE in mice. *Cell Trans.* 21, 1883–1897. doi: 10.3727/096368911x637443

Shinkai, Y., Rathbun, G., Lam, K. P., Oltz, E. M., Stewart, V., Mendelsohn, M., et al. (1992). RAG-2-deficient mice lack mature lymphocytes owing to inability to initiate V(D)J rearrangement. *Cell* 68, 855–867. doi: 10.1016/0092-8674(92)90029-c

Sim, F. J., McClain, C. R., Schanz, S. J., Protack, T. L., Windrem, M. S., and Goldman, S. A. (2011). CD140a identifies a population of highly myelinogenic, migration-competent and efficiently engrafting human oligodendrocyte progenitor cells. *Nat. Biotechnol.* 29, 934–941. doi: 10.1038/nbt.1972

Swamydas, M., and Lionakis, M. S. (2013). Isolation, purification and labeling of mouse bone marrow neutrophils for functional studies and adoptive transfer experiments. *J. Vis. Exp.* 10:e50586. doi: 10.3791/50586

Thiruvalluvan, A., Czepiel, M., Kap, Y. A., Mantingh-Otter, I., Vainchtein, I., Kuipers, J., et al. (2016). Survival and Functionality of Human Induced Pluripotent Stem Cell-Derived Oligodendrocytes in a Nonhuman Primate Model for Multiple Sclerosis. *Stem Cells Transl. Med.* 5, 1550–1561. doi: 10.5966/sctm.2016-0024

Tuszynski, M. H., Yang, J. H., Barba, D., Hs, U., Bakay, R. A., Pay, M. M., et al. (2015). Nerve growth factor gene therapy: activation of neuronal responses in alzheimer disease. *JAMA Neurol.* 72, 1139–1147. doi: 10.1001/jamaneurol.2015.1807

Wang, S., Bates, J., Li, X., Schanz, S., Chandler-Militello, D., Levine, C., et al. (2013). Human iPSC-derived oligodendrocyte progenitor cells can myelinate and rescue a mouse model of congenital hypomyelination. *Cell Stem Cell* 12, 252–264. doi: 10.1016/j.stem.2012.12.002

Wang, X., Li, R., Zacharek, A., Landschoot-Ward, J., Wang, F., Wu, K. H., et al. (2018). Administration of downstream ApoE attenuates the adverse effect of brain ABCA1 deficiency on stroke. *Int. J. Mol. Sci.* 19:3368. doi: 10.3390/ijms19113368

Weiss, W. A., Taylor, S. S., and Shokat, K. M. (2007). Recognizing and exploiting differences between RNAi and small-molecule inhibitors. *Nat. Chem. Biol.* 3, 739–744. doi: 10.1038/nchembio1207-739

Wu, B., Sun, L., Li, P., Tian, M., Luo, Y., and Ren, X. (2012). Transplantation of oligodendrocyte precursor cells improves myelination and promotes functional recovery after spinal cord injury. *Injury* 43, 794–801. doi: 10.1016/j.injury.2011.09.013

Yamashita, T., Miyamoto, Y., Bando, Y., Ono, T., Kobayashi, S., Doi, A., et al. (2017). Differentiation of oligodendrocyte progenitor cells from dissociated monolayer and feeder-free cultured pluripotent stem cells. *PLoS One* 12:e0171947. doi: 10.1371/journal.pone.0171947

Yang, J., Jiang, Z., Fitzgerald, D. C., Ma, C., Yu, S., Li, H., et al. (2009). Adult neural stem cells expressing IL-10 confer potent immunomodulation and remyelination in experimental autoimmune encephalitis. *J. Clin. Invest.* 119, 3678–3691. doi: 10.1172/jci37914

Yang, J., Yan, Y., Ciric, B., Yu, S., Guan, Y., Xu, H., et al. (2010). Evaluation of bone marrow- and brain-derived neural stem cells in therapy of central nervous system autoimmunity. *Am. J. Pathol.* 177, 1989–2001. doi: 10.2353/ajpath.2010.091203

Yang, N., Zuchero, J. B., Ahlenius, H., Marro, S., Ng, Y. H., Vierbuchen, T., et al. (2013). Generation of oligodendroglial cells by direct lineage conversion. *Nat. Biotechnol.* 31, 434–439. doi: 10.1038/nbt.2564

Zhang, Y., Lu, X. Y., Ye, Z. Q., Ciric, B., Ma, C. G., Rostami, A., et al. (2019). Combination therapy with fingolimod and neural stem cells promotes functional myelination in vivo through a non-immunomodulatory mechanism. *Front. Cell Neurosci.* 13:14. doi: 10.3389/fncel.2019.00014

Zhao, Y., Zhao, T., Guan, J., Zhang, X., Fu, Y., Ye, J., et al. (2015). A XEN-like state bridges somatic cells to pluripotency during chemical reprogramming. *Cell* 163, 1678–1691. doi: 10.1016/j.cell.2015.11.017

Zhu, B., Zhao, C., Young, F. I., Franklin, R. J., and Song, B. (2014). Isolation and long-term expansion of functional, myelinating oligodendrocyte progenitor cells from neonatal rat brain. *Curr. Protoc. Stem Cell Biol.* 31, 1–15. doi: 10.1002/9780470151808.sc02d17s31

Zhu, X., Bergles, D. E., and Nishiyama, A. (2008). NG2 cells generate both oligodendrocytes and gray matter astrocytes. *Development* 135, 145–157. doi: 10.1242/dev.004895

Conflict of Interest Statement: The authors declare that the research was conducted in the absence of any commercial or financial relationships that could be construed as a potential conflict of interest.

Copyright © 2019 Zhang, Lu, Casella, Tian, Ye, Yang, Han, Jia, Rostami and Li. This is an open-access article distributed under the terms of the Creative Commons Attribution License (CC BY). The use, distribution or reproduction in other forums is permitted, provided the original author(s) and the copyright owner(s) are credited and that the original publication in this journal is cited, in accordance with accepted academic practice. No use, distribution or reproduction is permitted which does not comply with these terms.

frontiers in Neuroscience

REVIEW
published: 12 June 2019
doi: 10.3389/fnins.2019.00604

Canine Cognitive Dysfunction and Alzheimer's Disease – Two Facets of the Same Disease?

Sonja Prpar Mihevc[1] *and Gregor Majdič*[1,2]*

[1] Veterinary Faculty, Institute for Preclinical Sciences, University of Ljubljana, Ljubljana, Slovenia, [2] Medical Faculty, Institute for Physiology, University of Maribor, Maribor, Slovenia

Neurodegenerative diseases present a major and increasing burden in the societies worldwide. With aging populations, the prevalence of neurodegenerative diseases is increasing, yet there are no effective cures and very few treatment options are available. Alzheimer's disease is one of the most prevalent neurodegenerative conditions and although the pathology is well studied, the pathogenesis of this debilitating illness is still poorly understood. This is, among other reasons, also due to the lack of good animal models as laboratory rodents do not develop spontaneous neurodegenerative diseases and human Alzheimer's disease is only partially mimicked by transgenic rodent models. On the other hand, older dogs commonly develop canine cognitive dysfunction, a disease that is similar to Alzheimer's disease in many aspects. Dogs show cognitive deficits that could be paralleled to human symptoms such as disorientation, memory loss, changes in behavior, and in their brains, beta amyloid plaques are commonly detected both in extracellular space as senile plaques and around the blood vessels. Dogs could be therefore potentially a very good model for studying pathological process and novel treatment options for Alzheimer's disease. In the present article, we will review the current knowledge about the pathogenesis of canine cognitive dysfunction, its similarities and dissimilarities with Alzheimer's disease, and developments of novel treatments for these two diseases with a focus on canine cognitive dysfunction.

Keywords: brain, neurodegeneration, canine cognitive dysfunction, Alzheimer's disease, amyloid beta, TAU, animal model, treatment

OPEN ACCESS

Edited by:
Marietta Zille,
Universität zu Lübeck, Germany

Reviewed by:
Ling Li,
University of Minnesota Twin Cities, United States
Wolfgang Härtig,
Leipzig University, Germany
Björn Nitzsche,
Leipzig University, Germany

***Correspondence:**
Gregor Majdič
gregor.majdic@vf.uni-lj.si

Specialty section:
This article was submitted to Neurodegeneration, a section of the journal Frontiers in Neuroscience

Received: *24 March 2019*
Accepted: *27 May 2019*
Published: *12 June 2019*

Citation:
Prpar Mihevc S and Majdič G (2019) Canine Cognitive Dysfunction and Alzheimer's Disease – Two Facets of the Same Disease? Front. Neurosci. 13:604. doi: 10.3389/fnins.2019.00604

INTRODUCTION

Neurodegenerative diseases such as Alzheimer's disease (AD), Parkinson's disease, Huntington's disease, frontotemporal dementia, amyotrophic lateral sclerosis, and others are a major growing public health problem associated with aging, as aging is the greatest risk factor for neurodegeneration. The global number of people living with dementia more than doubled from 1990 to 2016 (GBD 2016 Dementia Collaborators, 2019). These diseases now affect nearly 50 million individuals, and the incidence is projected to triple by 2050. AD and other dementias are associated with alterations in cell type-specific function, including gliosis, neuronal dysfunction and cell death. The pathognomic cause is the condensation of certain proteins into insoluble aggregates and this aggregates damage vulnerable neurons and glial cells. These inclusions of misfolded proteins build up in the brain during normal aging and during the progression of adult-onset dementias.

Neurodegenerative diseases do not occur spontaneously in laboratory mice and rats, but do occur in several other mammalian species. Studies of neurodegenerative diseases in animals

have shown strong similarities between cognitive dysfunction in dogs and human AD and between AD in humans and most other primates (Cummings et al., 1993; Cummings and Cotman, 1995; Dodart et al., 2002; Chambers et al., 2011; Braidy et al., 2015; Schütt et al., 2016). Canine cognitive dysfunction (CCD), also known as canine cognitive dysfunction syndrome (CDS) or canine dementia affects up to 60% of older dogs, mostly dogs older than 11 years (Fast et al., 2013b). The prevalence of CCD does not differ between breeds (Salvin et al., 2010) and there are no breed specific differences in clinical signs or pathology of the disease. However, as larger dog breeds have shorter life span than the smaller ones (Greer et al., 2007), clinical signs of CCD are more often observed and reported in smaller dogs (Vite and Head, 2014; Schmidt et al., 2015). Due to its similarity with AD, CCD is extremely interesting as a model for human disease. CCD is also a major problem for health of older dogs, and is thus also interesting from the point of view of the development of new veterinary diagnostic procedures/markers and medicines for treating this disease in dogs.

In dogs and humans, dementia often affects cerebral gyri (cerebral atrophy) and shows as widening of sulci together with ventricular enlargement (Borràs et al., 1999; Toepper, 2017). Neuronal loss and cortical atrophy has been described in several brain regions including cortex, hippocampus and parts of the limbic system in cognitively impaired dogs (Tapp et al., 2004; Siwak-Tapp et al., 2008), similarly to human brain affected by AD (West et al., 2000). In human patients, AD has a preclinical stage with the clinical symptoms not yet evident but with pathological changes in the brain already present, which is followed by mild cognitive impairment stage which gradually culminates in dementia due to AD, with severe cognitive and functional decline (Bature et al., 2017). The onset of AD, detected clinically at the mild cognitive impairment stage, is characterized by a subtle decline in memory functions, followed by changes in personality, deterioration of language functions and eventually motor dysfunction (Braak and Braak, 1997). These deficits in cognition and behavior are mirrored in the AD-related regional brain destruction. Similarly to these signs in humans, the most obvious signs of CCD, deduced by standard cognition tests, are loss of memory, poor or completely lost sense of orientation, changes in behavior and confusion (Bain et al., 2001). Most common symptoms include disorientation, anxiousness, dogs get easily scared, do not recognize their owner, become aggressive or apathetic, have difficulty controlling the secretion of body fluids, change circadian rhythms and others.

NEUROPATHOLOGICAL FEATURES OF NEURODEGENERATIVE DISEASES

Role of Protein Aggregates in Neurodegenerative Diseases

Protein aggregation is an established pathogenic mechanism in AD, although little is known about the initiation of this process *in vivo*. As human brain research largely depends on the results of postmortem studies, an insight into the early stages of the disease, when protein aggregates are most likely to occur, is difficult. Novel and better animal models would therefore be very helpful to study the progress of AD in humans. The clinical course of the disease in humans could be monitored by brain imaging (CT, MRI). The exact connection between protein aggregates, such as extracellular amyloid-β (Aβ) plaques and intracellular neurofibrillary tangles (NFTs), the latter composed of hyperphosphorylated microtubule associated protein (TAU), in the brains of patients with AD, and neurodegeneration is therefore still unknown. It does seem that the AD is caused by the accumulation of amyloid plaques and neurofibrillary fibers, although this is not absolutely confirmed and generally accepted (Medeiros et al., 2011). Stronger evidence that aggregates do trigger neurodegeneration (the so-called amyloid hypothesis) and are not just a consequence of the neurodegeneration, is provided by mutations in the gene for the amyloid beta precursor protein (APP) present in some human patients with AD (Selkoe, 1991; Hardy and Higgins, 1992; Hardy and Selkoe, 2002; Lansbury and Lashuel, 2006). Similarly, amyloid plaques are present in different brain regions in dogs with CCD clinical symptoms, and they can be present even before clinical signs of this disease become obvious.

In general, age-related neurodegenerative disorders are complex and multifaceted pathologies, wherein the formation of large aggregates and/or high concentrations of toxic proteins prevent the proper function of neuronal cells, leading to ischemia and eventually tissue removal. The spread of AD pathology follows a characteristic topographic pattern, different for the two proteins involved in the pathology, Aβ and TAU (Brettschneider et al., 2015). TAU aggregates first develop in the locus coeruleus, then in entorhinal cortex followed by hippocampus and neocortex. Aβ plaques firstly appear in the neocortex, and later in allocortical, diencephalic and basal ganglia structures and in the brainstem (Brettschneider et al., 2015; Jucker and Walker, 2018). These aggregates spread in a prion-like manner, forming intracellular and extracellular deposits. TAU, Aβ, and also Parkinson disease associated α-synuclein, exist in different conformational variants ('strains') that show seeding properties and exert different levels of neurotoxicity, which could be the source of heterogeneity of neurodegenerative diseases (Aguzzi, 2014). The seeding potential of these aggregates was recently substantiated by demonstrating propagation of structural variants of Aβ in their distinct conformations through template-directed folding of naïve Aβ peptides (Condello and Stöehr, 2018). Prion-like transmission and seeding has been also observed for TAU (DeVos et al., 2018). Similar mechanism may be involved in young, pre-depositing APP transgenic mice which developed cerebral β-amyloidosis and associated pathology after being intracerebrally injected with Aβ-containing brain extracts from human patients with AD (Meyer-Luehmann et al., 2006; Langer et al., 2011). Interestingly, even intraperitoneal inoculation with Aβ extracts induced β-amyloidosis in the brains of APP transgenic mice after prolonged incubation times (Eisele et al., 2010). Likewise, soluble oligomers from blood and

cerebrospinal fluid (CSF) of an aged dog with CCD were neurotoxic to human neuroblastoma cell line, and canine CSF derived Aβ induced the *in vitro* aggregation of synthetic human Aβ peptides (Rusbridge et al., 2018). Spreading of misfolded Aβ oligomers in a prion-like mechanism might also exploit exosomes, which can seed Aβ not only as vehicles for the neuron-to-neuron transfer (Zheng et al., 2017; Sardar Sinha et al., 2018) but also between distant brain regions (i.e., from the dentate gyrus to other regions of hippocampus and to the cortex) (Zheng et al., 2017).

The Neuropathology in the Brain Parenchyma

The most prominent neuropathological signs of AD are accumulation of Aβ in a form of extracellular plaques in the brain parenchyma and also in the walls of blood vessels (cerebral amyloid angiopathy, CAA), and abnormally phosphorylated protein TAU that accumulates in NFTs (Braak and Braak, 1991; Nelson et al., 2012). These pathological features are believed to cause cognitive and behavioral changes. The amino acid sequence of APP and of the enzymes involved in the processing of Aβ peptides from APP, are highly homologous between humans and dogs (Johnstone et al., 1991; Sarasa and Pesini, 2009; Sarasa et al., 2010). Major canine APP isoforms are APP-770, APP-751, APP-714, and APP-695 (Sarasa et al., 2010). The alignment of the longest canine amyloid-beta precursor protein isoform (APP-770) sequence with protein sequence of human amyloid-beta precursor protein show 96.9% amino acid identity and 98.3% similarity (**Figure 1A**), making them almost identical. The expression patterns of canine APP isoforms are almost similar to the patterns previously detected for human APP isoforms (Yasojima et al., 2001; Sarasa et al., 2010). APP is a single-pass transmembrane protein with a large extracellular domain and a short cytoplasmic tail. The domain structure of APP-770 is shown in **Figure 1B**, the neuronal isoform APP-695 lacks the KPI domain (Müller et al., 2017). In contrary to APP, there is a difference in the TAU protein sequence between dogs and humans. **Figure 1C** shows the longest TAU isoform alignment between dog and human protein sequences with 84% similarity. Interestingly, the four microtubule-binding regions (4R) and the C-terminal regions (**Figures 1C,D**) are identical.

Amyloid-β was found to be present in the form of insoluble plaques in the area of the cerebral cortex in humans and dogs, and cognitive impairment in elderly dogs was in some studies strongly associated with the accumulation of Aβ in the brain (Cummings et al., 1993; Cummings and Cotman, 1995; Pugliese et al., 2006; Rofina et al., 2006; Barnes et al., 2016). However, in two other studies there was no significant correlation between the amount of Aβ brain load and CCD symptoms (Chambers et al., 2011; Ozawa et al., 2016) so the clear connection between Aβ load in the brain and clinical signs of CCD has not been firmly established yet. Although Aβ plaques are generally detected as extracellular deposits of diffuse and neuritic plaques in humans and dogs, some studies also reported the presence of Aβ deposits inside individual neurons in the canine brain (Cummings et al., 1993; Yu et al., 2011). Similarly, intraneuronal Aβ accumulation in human AD brains has been reported by many groups (reviewed in detail by Gouras et al., 2010).

In dogs, formation and maturation of Aβ deposits was observed by immunostaining throughout the canine cortical gray matter layers in a four-stage distribution, which is also characteristic for human AD, and this, according to some studies, correlates with the severity of cognitive deficit in the dog (Bosch et al., 2012) and varies as a function of age and size (weight) in companion dogs (Rofina et al., 2006; Schmidt et al., 2015). The Aβ load was higher in small and medium size dogs, which can be explained by the longer life span of smaller dogs and thus longer time necessary to accumulate these deposits (Schmidt et al., 2015). Most of the studies, on CCD brains, were made on geriatric dogs of different breeds and sizes, hence in this review the pathology is mainly described without further specifications of individual dogs characteristics. The canine prefrontal cortex is normally the site of disease onset (**Figure 2**), which spreads progressively to the parietal, entorhinal and occipital cortices, and lesions in certain brain regions correlate with certain behavioral deficits, as shown in **Table 1**. In separate studies amyloid plaques of mainly diffuse type were detected in several regions of canine brain, in the frontal and temporal cortex (Ishihara et al., 1991; Colle et al., 2000; Pugliese et al., 2006; Schmidt et al., 2015; Ozawa et al., 2016; Schütt et al., 2016; Smolek et al., 2016), in entorhinal cortex and hippocampus (Cummings et al., 1993; Colle et al., 2000; Yu et al., 2011; Schmidt et al., 2015; Borghys et al., 2017) and parietal cortex (Yu et al., 2011). Hippocampal deposits of a subspecies of pyroglutamyl Aβ, the highly neurotoxic pE3AA, were also detected in demented dogs (Schmidt et al., 2015). These plaques were more abundant in small and medium dogs (Schmidt et al., 2015). Studies further suggest that earlier assembly states of Aβ, such as oligomers and protofibrils, may be neurotoxic in the dog's brain (Head et al., 2010). The levels of Aβ soluble oligomers in the CSF correlated inversely with Aβ load in the CCD affected beagle brains (Head et al., 2010). Precipitates from the CSF of demented Samoyed dog with CCD acted highly neurotoxic in *in vitro* tests and were more neurotoxic than the synthetic oligomeric and fibrillary forms of Aβ (Rusbridge et al., 2018).

Besides Aβ plaques, recruitment and activation of astrocytes and microglial cells has been noticed in dogs with CCD (astrocytosis, microgliosis) (Smolek et al., 2016; Rusbridge et al., 2018) along with astrocyte hypertrophy (Borràs et al., 1999). Furthermore, the levels of pathological Aβ in the canine prefrontal cortex were positively correlated with age but neither with the severity of cognitive deficits (Gómez-Pinedo et al., 2016) nor the neuronal cell loss (Cummings et al., 1993). Neprilysin (NEP) mRNA, coding for a pivotal Aβ-degrading protein, was poorly expressed in the prefrontal cortex of aged dogs with CCD (Canudas et al., 2014), similar to human AD brain, where areas with higher Aβ aggregation express lower levels of NEP (Reilly, 2001).

Aged dogs with cognitive impairment exhibit degeneration of noradrenergic neurons, which correlates with higher levels of Aβ deposits in the prefrontal cortex (Insua et al., 2010). Likewise, in human AD, locus coeruleus degeneration and loss of cortical noradrenergic neurons occurs already at early stage (Kelly et al., 2017). The activity of the canine cholinergic system

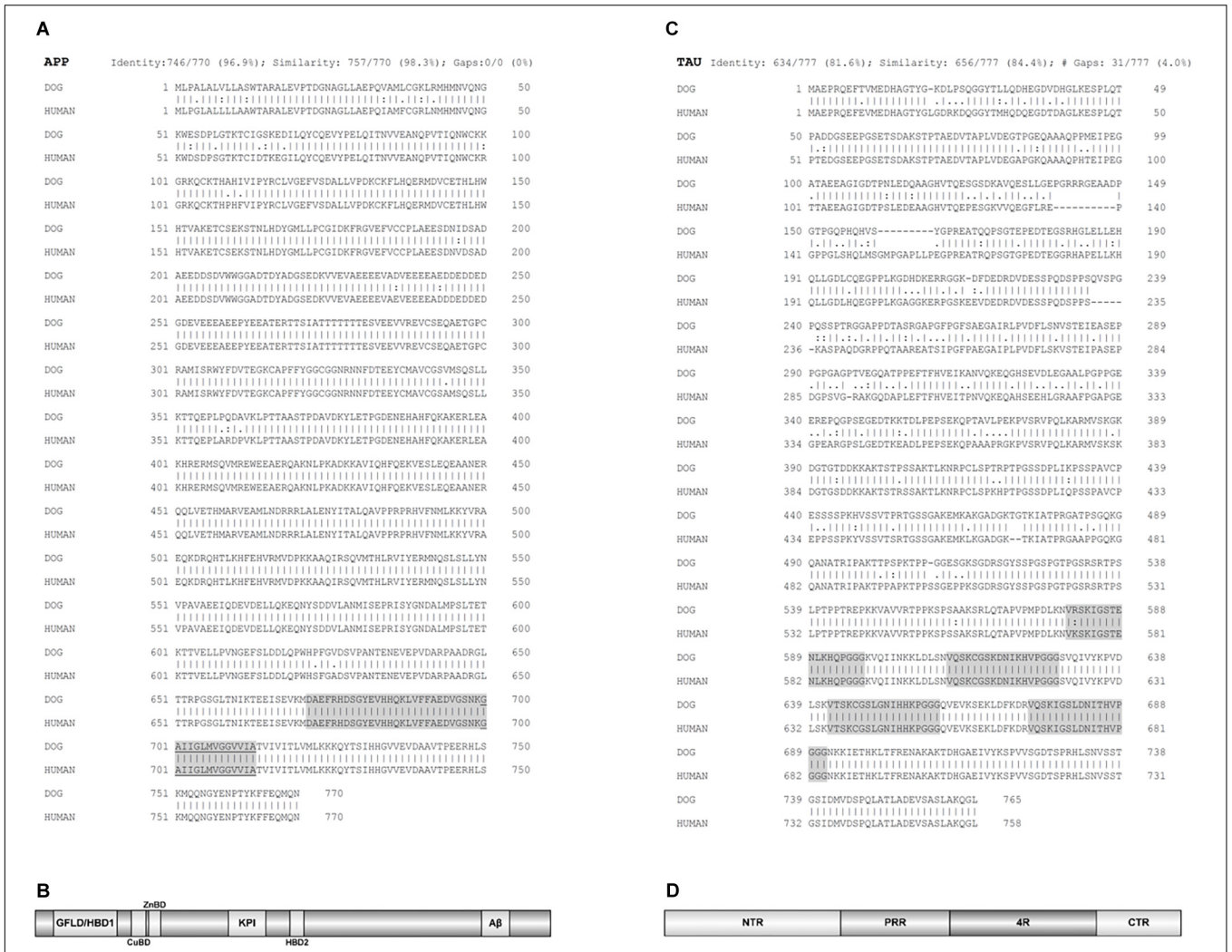

FIGURE 1 | Protein sequences alignments between dog and human amyloid-beta precursor protein (APP) and TAU. **(A)** The alignment of the longest canine APP isoform (APP-770) sequence with protein sequence of human APP. Aligned sequences share 96.9% amino acid identity and 98.3% similarity. Of note, the sequence identity of canine APP-695 isoform, the predominant APP isoform in the canine brain, and human APP is 87.5%. Highlighted is Aβ domain and underlined the membrane bound part of this domain. **(B)** Domain structure of APP. Isoform APP-770 is depicted. HBD1/GFLD, heparin binding domain 1/growth factor like domain; CuBD, copper binding domain; ZnBD, zinc binding domain; KPI, Kunitz-type protease inhibitor domain (not present in APP-695); Aβ, amyloid beta domain, the latter anchors APP in the cell membrane. The α-, β-, and γ-secretase cleavage sites are directly adjacent or inside the Aβ domain region, which is also most mutation prone, thus enabling alternative cleavage of APP and its divergent aggregation propensities. **(C)** Alignment of the longest TAU protein isoform, out of six existing, of dog and human TAU. Aligned TAU sequences share 81.6% amino acid identity and 84.4% similarity. Highlighted are four microtubule-binding regions (4R). **(D)** Domain structure of TAU. The basic organization is shown. NTR, N-terminal region; PRR, proline-rich region; 4R, four microtubule-binding regions (some isoforms have three); CTR, C-terminal region. The PRR and 4R domains are subject of most posttranslational modifications, while the CTR enables interactions with microtubules and plasma membrane. EMBOSS Needle pairwise sequence alignment (Madeira et al., 2019) was performed. A line (|) indicates positions which have a single, fully conserved residue. A colon (:) indicates conservation between groups of strongly similar properties and a dot (.) indicates conservation between groups of weakly similar properties. The domain organization was depicted by software illustrator of biological sequences (IBS) (Liu et al., 2015). Figure made by the authors.

also declines with age (Araujo et al., 2005b). Number of basal forebrain cholinergic neurons was significantly reduced in aged cognitively impaired dogs in comparison to aged cognitive unimpaired and young dogs, but unlike for noradrenergic neurons, this reduction of cholinergic neurons did not correlate with the extent of Aβ cortical load (Insua et al., 2012). As in CCD, cholinergic neurons located in the basal forebrain, including the neurons that form the nucleus basalis of Meynert, are usually lost in AD (Whitehouse et al., 1981). In human patients, the cholinergic neurons appear most vulnerable to Aβ pathology, followed by glutamatergic and GABAergic neurons (Bell et al., 2006). The synaptic loss correlates with the disease progression and destruction of cholinergic neurons contributes to memory and attention deficits in AD (Terry et al., 1991). These alterations in neurotransmitter systems, with reduced neuronal and synaptic function have also been observed in dogs (Landsberg et al., 2012) and result in clinical symptoms of CCD. The employment of the canine

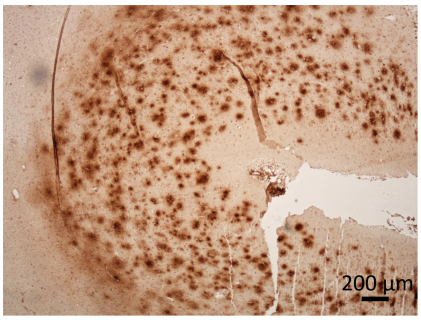

FIGURE 2 | Presence of Aβ in the cerebral cortex of a dog with CCD. The dense plaques detected in superficial cortical layers and diffuse plaques in deeper layers of prefrontal cortex. The dog was 17-years-old of a mixed breed. Immunoperoxidase staining with antibodies against Aβ (purified anti-β-Amyloid, 17-24 Antibody, BioLegend, #800701) with diaminobenzidine (DAB) as chromogen (brown), counter stained with hematoxylin. Original microphotograph made by the authors.

model to examine the effect of the cholinesterase inhibitors in treatment of CCD is described in details under "Treatment and drug development".

TAU protein, another important factor in neurodegenerative diseases, is encoded by *MAPT* (microtubule associated protein tau) gene. Mutations in this gene have not been linked to AD, but cause a familial form of frontotemporal dementia (Olszewska et al., 2016). However, in human AD, intraneuronal NFTs composed of hyperphosphorylated TAU and misfolded insoluble TAU protein aggregates and extracellular Aβ inclusions are both present and necessary for the diagnosis of the disease. In AD NFTs form initially in the locus coeruleus, then entorhinal cortex and further progress to the hippocampus, anterior cingulate cortex, visual association area and finally to the primary visual cortex in the occipital lobe (Ossenkoppele et al., 2016; Hoenig et al., 2018). Interestingly, TAU neurofibrillary inclusions were only rarely identified in canine brain, for instance only in one dog in one study (Smolek et al., 2016) and in three dogs in another study (Schmidt et al., 2015). Increased phosphorylation of TAU was observed at some amino acid sites in canine brain, although no study so far confirmed the presence of vast mature NFTs deposits as are typically observed in human AD. In one study, cytoplasmic deposits of phosphorylated TAU (pTAUThr181) were detected in the prefrontal cortex, but no NFTs were observed (Pugliese et al., 2006). Smolek et al. (2016) detected increased presence of phosphorylated TAU protein (pTAU) in synaptosomes of demented dogs. This could suggest that dementia in dogs might be partially caused by the weakening of the synaptic function, caused by pTAU, and not by the toxic effects of NFTs. This is further supported by the increase in TAU hyperphosphorylation in individual cortical neurons and by pTAU subcellular distribution shift from perinuclear to granular cytoplasmic and nuclear, which correlates with dog's age (Pugliese et al., 2006). Expression of pTAUSer396 and accumulation of ubiquitin were also significantly increased in the parietal cortex and dorsal part of the hippocampus in old dogs when compared to expression in humans (Pugliese et al., 2006; Yu et al., 2011). Specifically, pTAUSer396 expressing astrocytes and neurons with co-localization of pTAUSer396 and ubiquitin were also observed in the parietal cortices and hippocampi of dogs with CCD (Yu et al., 2011). However, cytoplasmic aggregates of normally predominately nuclear proteins, TAR DNA-binding protein (TDP-43) and fused in sarcoma (FUS), which are strongly associated with frontotemporal dementia and amyotrophic lateral sclerosis in human patients, were not detected in the canine brain with CCD (Smolek et al., 2016).

Neurodegenerative diseases occur spontaneously in other domestic animals, especially in cats (Chambers et al., 2015), although brain pathology in these other species is much less studied. In the hippocampi of naturally aged domestic cats, Aβ accumulation, NFTs formation and neuronal loss were observed (Chambers et al., 2015) and this might contribute to cognitive decline in this species, although this has not yet been firmly established. Cognitive deficit may occur in the horse, as clinical signs similar to cognitive impairment have been observed, but no detailed studies focusing on age-related neurologic aberrances have been conducted so far. In one study, TAU protein was shown to be present in equine hippocampal neurons, but no NFTs were detected (Capucchio et al., 2010). Some horses develop equine motor neuron disease, but none have been associated with pathological accumulation of dementia related proteins (El-Assaad et al., 2012; Youssef et al., 2016). Interestingly, a recent study negated the belief that abnormally behaving stereotypic horses (*Equus caballus*) are cognitively impaired (Briefer Freymond et al., 2018).

Neurodegenerative diseases most likely occur in many other mammalian species, but there are very limited reports about these. The reports are focusing on the presence of Aβ deposits and phosphorylated TAU and/or NFTs, which are detected post mortem, not describing the cognitive deficit, this is of course more difficult to observe in wild life animals or in this aspect less characterized species. Diffuse deposits of Aβ were observed in the parietal cortex of dolphins and more compact senile plaques in their cerebellum (Di Guardo, 2018). Sheep and goats (Braak et al., 1994; Nelson et al., 1994; Nelson and Saper, 1995), cheetah (Serizawa et al., 2012), bison (Härtig et al., 2000, 2001), bears (Cork et al., 1988) and most species of nonhuman primates (Schultz et al., 2000a,b; Rosen et al., 2008; Oikawa et al., 2010; Perez et al., 2013, 2016; Rodriguez-Callejas et al., 2016; Reid et al., 2017) also develop amyloid plaques and/or harbor phosphorylated TAU laden neurons, but most of them do not have NFTs present in their central nervous systems (as reviewed in Youssef et al., 2016). However, AT8-immunostained pTAUSer202 and pTAUThr205 were found in the brains of brown lemur, rhesus monkey, baboons, rabbit, guanaco, and bison (Härtig et al., 2000). Furthermore, NFTs were revealed by Gallyas staining in aged bison (Härtig et al., 2001).

There have been speculations on the reasons for the lack of NFTs in the canine brain and in the brains of other animals (Kuroki et al., 1997; Youssef et al., 2016). First possibility

TABLE 1 | Affected brain regions and underlying cognitive deficits in dogs.

Brain region	Pathology	Cognitive decline	References
Prefrontal cortex	Aβ	Executive function, behavioral changes [cognitive performance, loss of previously learned behaviors (e.g., house soiling)], motor skills, attention, emotions and impulse control (fearfulness, aggression, stereotypic pacing or circling)	Bosch et al., 2012
Frontal cortex	Aβ	Changes in executive functions (inhibitory control and complex working memory)	Ishihara et al., 1991; Schmidt et al., 2015; Smolek et al., 2016
Parietal cortex	Aβ	Sensory association, learning and memory	Yu et al., 2011; Nešić et al., 2017
Entorhinal cortex	Aβ, NFTs*	Visual learning, memory	Schmidt et al., 2015; Smolek et al., 2016
Occipital cortex	Aβ	Learning and memory (visual association area, visual cortex)	Martin et al., 2011
Temporal cortex	Aβ, NFTs*	Visual memory (facial recognition), emotions	Smolek et al., 2016
Hippocampus	Aβ, NFTs*	Changes in sleep–wake cycles, appetite control, complex working memory	Colle et al., 2000; Pugliese et al., 2006; Yu et al., 2011; Schmidt et al., 2015; Smolek et al., 2016
Cerebral cortex (not further specified)	Aβ	Disorientation, decrease in social interactions, changes in sleep–wake cycles, loss of prior housetraining, increased anxiety, changes in level of activity	Colle et al., 2000; Pugliese et al., 2006; Yu et al., 2011
Cerebral capillaries and arteries	Aβ - CAA	Lower perceptual speed and episodic memory	Ishihara et al., 1991; Colle et al., 2000; Yu et al., 2011
Meningeal blood vessels	Aβ - CAA		Ishihara et al., 1991; Borràs et al., 1999; Colle et al., 2000; Yu et al., 2011; Nešić et al., 2017

**NTFs are rarely detected in CCD.*

is the dissimilarity between canine TAU protein sequence in comparison to human's. Secondly, the lifespan of dogs might be too short to develop NFTs, as Aβ deposition precedes NTFs formation. Thirdly, although the amyloid protein sequence is highly conserved between species, its N-terminal part is not, which might influence TAU phosphorylation and its subsequent aggregation into NFTs. Therefore, it seems that only humans develop the full blown AD pathology with amyloid plaques, NFTs and dementia. There have been few reports of possible AD in aged great apes (Rosen et al., 2008; Perez et al., 2013, 2016), although also in these the TAU pathology was very limited. Several reasons for this exceptional vulnerability of humans to develop AD have been proposed (Arendt et al., 2017; Walker and Jucker, 2017). Predisposition to develop AD might arise as early as during embryonic development over the period of neurogenesis, this was inferred from the modular deposition of AD related cerebral deposits which mirrors the formation and migration of neurons and on a larger scale development of brain regions (Arendt et al., 2017). In humans, the relative brain size is much larger than in any other animal and this expansion is due to longer duration of brain development as well as higher number of neuronal progenitor cell division cycles, the latter giving rise to genomic aberrations, which in turn can be the origin of AD (Arendt et al., 2017). Furthermore, the neurons display genomic mosaicism, which was detected in neurons of approximately 10% of normally aged people. These neurons were shown to preferentially undergo apoptosis in AD (Arendt et al., 2010). The extent of neuronal genomic mosaicism is brain region specific and correlates with differential vulnerability to neurofibrillary pathology (Arendt et al., 2015). Moreover, the pathological TAU conversion might commence as early as in children (Braak and Del Tredici, 2012), although it has not been firmly established if these processes are transient in nature. The canine model would therefore serve as an accessible and suitable model to further delineate why, except for humans, are other species less susceptible to develop tauopathies.

The Neuropathology of Cerebral Blood Vessels

In patients with AD, accumulation of Aβ is often observed in the walls of blood vessels in the brain. This is called CAA and is caused by pathological deposits of Aβ and other proteins in the cerebral arterioles and capillaries of the leptomeninges and cortex. It is considered as an early and integral part of AD pathogenesis and the prevalence of CAA in AD is over 70% (Attems, 2005). CAA is a risk factor for hemorrhagic stroke and contributes to AD dementia. Atherosclerosis may also cause cerebrovascular dysfunction that may lead to cognitive decline as well as stroke (Shabir et al., 2018). The accumulation of amyloid in the walls of blood vessels is common in elderly people, patients with CAA and in almost all patients with AD (Kumar-Singh, 2008). The most CAA affected brain regions are the leptomeninges and frontal and temporal cortices (Borràs et al., 1999) with Aβ deposits in arteries, arterioles, capillaries, venules, and veins. The CAA disease progresses from mild, to moderate to severe stage, this is from almost intact blood vessels with minor Aβ deposits to extensive vascular Aβ load, which disrupts vessel architecture and exacerbates microangiopathies, microaneurysmal dilatation, and fibrinoid necrosis (Revesz et al., 2002).

In aged dogs Aβ deposits are detected both in the brain parenchyma and in the walls of cerebral blood vessels (Ishihara et al., 1991; Uchida et al., 1992; Borràs et al., 1999;

Colle et al., 2000; Brettschneider et al., 2015; Schmidt et al., 2015; Ozawa et al., 2016; Nešić et al., 2017; Rusbridge et al., 2018), further suggesting similarities between AD in humans and CCD in dogs (**Figures 2**, **3**). The amyloidotic blood vessels in the brains of dogs were observed by Congo red stainings as well as by antibodies directed against Aβ. Vascular Aβ deposition mainly consists of $A\beta_{40}$ in humans, but both $A\beta_{40}$ and $A\beta_{42}$ were detected in dogs (Kumar-Singh, 2008; Chambers et al., 2012). In canine CAA, the most affected region is the frontal cortex, where Aβ is often present in microvascular parenchymal lesions in elderly dogs. In dogs with CCD an overlap between the density and anatomical distribution of CAA and parenchymal plaques was observed (Nešić et al., 2017). The CAA consistently increased with age, but did not correlate with the CCD score (Ozawa et al., 2016). Intracerebral hemorrhages have also been described in association with CAA in dogs (Uchida et al., 1990). A recent case reported multiple infarcts and brain hemorrhages in a dog with CAA and CCD, with cerebral and vascular Aβ deposits (Rodrigues et al., 2018). Pathological hallmarks of CCD and AD are summarized in **Table 2**.

TABLE 2 | Pathological hallmarks of CCD and/or AD.

Abnormality	CCD	AD
Cognitive decline	+	+
Brain atrophy	+	+
Neuronal damage and death	+	+
Aβ accumulation in brain parenchyma	+	+
Diffuse Aβ plaques	+	+
Dense-core Aβ plaques	–	+
Aβ accumulation in blood vessel walls (CAA)	+	+
Neurofibrillary tangles (NTFs) formation	–	+
Microglial dysfunction	+	+
Astrocyte dysfunction	+	+
Astroglial hypertrophy and hyperplasia	+	+
Oxidative brain damage	+	+
Mitochondrial dysfunction	+	+
Cholinergic dysfunction	+	+
Impaired neuronal glucose metabolism	+	+

GENETICS

The incidence of human neurodegeneration and associated dementias is sporadic and is only rarely due to hereditary changes that are linked with genetic mutations. The majority of AD cases are sporadic late-onset (LOAD) with an unknown etiology (Cacace et al., 2016). The other rare AD form is genetically determined familial AD. Known specific gene mutations are the root cause for the development of familial form of AD (Selkoe, 1997). Most of the patients with early onset, familial form of AD have mutations in one of the two presenilin proteins (PSEN1 and PSEN2) (Bekris et al., 2010), which are proteins with a role in Aβ generation. Mutations also occur in *APP* gene (Selkoe, 1997). Polymorphism in APOEε4 allele of apolipoprotein E gene (*APOE*) is the major genetic risk factor for LOAD along with polymorphism in *TREM2* gene, which has a role in maintaining normal immune functions in the brain (reviewed in detail in Wolfe et al., 2018). In population studies, several genetic loci have been identified as risk factors for AD (e.g., *CLU, CR1, APP, PICALM, BIN1, ABCA7, MS4A, MEF2C CD33, EPHA1, CD2AP, APOE, TRIP4, TREM2, SORL1*), although the connection between genes in these loci and pathogenesis of AD has not been established (Ashford, 2004; Karch et al., 2012; Mäkelä et al., 2018). Interestingly, the *APOE4* polymorphism is unique to humans and its evolvement from the presumably ancestral primate form might have been instrumental for the AD pathogenesis (Mahley and Rall, 1999; Walker and Jucker, 2017).

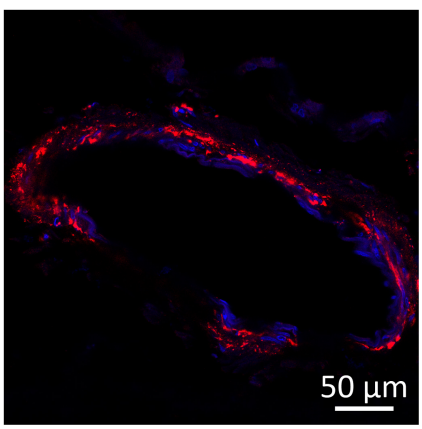

FIGURE 3 | Amyloid beta (red) detected by immunofluorescence staining in the wall of a leptomeningeal blood vessel in the frontal cortex from a 15-years-old Pit Bull Terrier. Nuclei were counterstained with DAPI (blue). The antibody employed is the same as in **Figure 2**. Original microphotograph made by the authors.

Some presenilin mutations and mutations in *APP* have been connected to CAA (Hendriks et al., 1992; Grabowski et al., 2001; Rossi et al., 2004; Bugiani et al., 2010; Sellal et al., 2017) and also a polymorphism in the neprilysin gene was associated with CAA (Kumar-Singh, 2008), although the exact connections between these mutations and AD/CAA symptoms and progression are not yet understood. Furthermore, APOEε4 was shown to be a risk factor for CAA and both APOEε2 and ε4 alleles are associated with more severe forms of CAA (Nelson et al., 2013; Yu et al., 2015).

No mutations in specific genes have been reported in dogs with CCD so far. The only neurodegenerative disease in dogs that has been linked to specific mutation is degenerative myelopathy (DM), a condition caused by both demyelination and axonal loss in the canine spinal cord. In dogs with this disease, mutations have been found in a gene SOD1, coding for superoxide dismutase enzyme (Nakamae et al., 2015; Kobatake et al., 2016). Interestingly, this gene is in human patients associated with some forms of familial amyotrophic lateral sclerosis (Rosen et al., 1993). Beside mutations in SOD1 gene, risk for developing DM in dogs, as well as onset of disease, seem to be partially modulated by gene encoding SP110 nuclear body protein (SP110) at least in Pembroke Welsh Corgis (Ivansson et al., 2016). No other

mutations or disease modifying loci related to neurodegeneration have been detected in dogs so far and thus, little is known about the potential genetic risks or genetic predisposition for CCD and CAA.

BIOMARKERS

Neurodegenerative diseases are particularly challenging diseases, as they are difficult to diagnose in the initial stages. Although many years of research have been devoted to the identification of suitable biomarkers, preferably in blood, that would allow early diagnosis or even prediction of AD in humans, such markers remain elusive. Numerous candidates have been identified in both blood and CSF, but none of the markers identified so far have been used routinely in the clinics. CSF levels of Aβ, total TAU and hyperphosphorylated TAU are the most often monitored variables, along with PET molecular imaging of amyloid and TAU deposition, in diagnosis of early stages of AD (McKhann et al., 2011).

In dogs there are no biological markers that would allow accurate and early diagnosis of CCD. In most cases assessment of cognitive functions through several neuropsychological tests and excluding other conditions with overlapping symptoms is sufficient to confirm diagnosis when the disease has progressed, but markers for detecting disease in early stages would be very useful in veterinary medicine.

In dogs with CCD, plasma $A\beta_{42}$, a longer Aβ isoform which is more fibrillogenic and associated with disease, was monitored as a biomarker potentially linked to CCD (González-Martínez et al., 2011; Schütt et al., 2015). One study showed highest $A\beta_{42}$ plasma levels in younger healthy dogs, and significantly higher $A\beta_{42}$ plasma levels in mildly cognitively impaired dogs in comparison to severely impaired dogs (González-Martínez et al., 2011). However, another study reported the opposite with highest $A\beta_{42}$ plasma levels in CCD dogs (Schütt et al., 2015). Plasma ratio of $A\beta_{40}$ and $A\beta_{42}$, was shown to be similar in human AD and CCD as in healthy individuals (Mayeux et al., 2003; Lopez et al., 2008; González-Martínez et al., 2011) although in some studies decreases in plasma $A\beta_{42}$ were an indicator of faster progression of CCD and AD (Pesini et al., 2009; González-Martínez et al., 2011). This points to a possible disease mechanism wherein aggregation and accumulation of Aβ in the brain results in lower levels of Aβ in plasma and CSF. A more recent human study showed decrease in plasma Aβ during the dementia stage of AD and increased levels of Aβ in plasma during vascular disease (Janelidze et al., 2016).

In healthy aged dogs with age related Aβ deposits, a decrease in levels of $A\beta_{42}$, but not $A\beta_{40}$ was detected in CSF (Head et al., 2010). Similarly, in elderly people $A\beta_{42}$ has been monitored in CSF and the decrease in $A\beta_{42}$ is suggested as biomarker for Aβ deposition in the brain and has been observed alongside brain atrophy (Fagan et al., 2009; Racine et al., 2016). Although CSF Aβ content decreased in the aging dog (Head et al., 2010), high levels of Aβ in the CSF of young and middle-aged dogs also correlated with impaired learning (Borghys et al., 2017). This infers high CSF Aβ levels in younger dogs, which are not likely to harbor depositions of amyloid in their brains yet, as an early biomarker for the development of cognitive impairment. One study also reported an increase of lactate, pyruvate and potassium concentrations in CSF of dogs correlating with severe cognitive impairment (Pugliese et al., 2005), but this has not been firmly established or confirmed. Therefore, there are no biomarkers available to monitor and predict CCD progress in dogs. Future studies aiming to develop such biomarkers would be needed, hoping to provide biomarkers for early detection of this disease.

DIAGNOSIS OF CCD

Although CCD is highly prevalent the disease is severely under-diagnosed, affecting a growing population of aged dogs. The diagnosis of CCD is a diagnosis of elimination. The illness exacerbating symptoms, commonly also observed in CCD, must be excluded, such as brain tumors, hypertension, other neurological conditions, metabolic and hormonal imbalances, etc. Screening and diagnosis of CCD is primarily based on observation of clinical signs which are summarized by the acronym DISHAA [Disorientation, altered social Interactions, altered Sleep–wake cycles, House soiling and loss of other learned behaviors, altered Activity levels and increasing Anxiety (Ruehl et al., 1995; Neilson et al., 2001; Azkona et al., 2009; Rosado et al., 2012; Fast et al., 2013b; Madari et al., 2015)]. Sleeping during the day and restless at night, decreased interaction, disorientation at home and anxiety are common symptoms (Fast et al., 2013b).

The diagnosis depends largely on the owners and the veterinarians to observe and diagnose the disease, which is in most cases overlooked and symptoms attributed to the aging of dogs. To facilitate the detection of CCD, veterinarians can use a screening questionnaire that includes a list of possible signs. Several questionnaires are available and based on the scores the stage of dog's cognitive decline can be identified (Colle et al., 2000; Neilson et al., 2001; Osella et al., 2007; Azkona et al., 2009; Golini et al., 2009; Salvin et al., 2011; Landsberg et al., 2012; Rosado et al., 2012; Fast et al., 2013b; Madari et al., 2015). Madari et al. (2015) have proposed criteria for discrimination of three stages of the disease, these are mild cognitive impairment, moderate cognitive impairment, and severe cognitive impairment. The severity and progression of CCD disease is identified by Canine Dementia Scale (CADES), which contains 17 items distributed into four domains related to changes in dogs' behavior (spatial orientation, social interactions, sleep–wake cycles, and house soiling) (Madari et al., 2015). The Canine Cognitive Dysfunction Rating Scale (CCDR) is another questionnaire (Salvin et al., 2011), which is comprised of 13 behavioral items distributed into four domains, namely orientation, memory, apathy, impaired olfaction, and locomotion (Salvin et al., 2011). The cognitive deficits in dogs with CCD with regards to affected brain regions are summarized in **Table 1**. Cognitive impairment parallels the symptomology of AD. Performance on tasks involving complex learning and working memory are impaired first, along with executive function, visuospatial ability and complex learning deficits, with disease progression impairments in discrimination learning and behavioral

changes are common (Neilson et al., 2001; Tapp et al., 2003; Studzinski et al., 2006; Madari et al., 2015).

MRI diagnosis is only rarely performed in dogs, due to possible complications during anesthesia and cost restraints. In dogs with CCD, as in humans with AD, MRI shows brain atrophy and include ventricular enlargement as well as widened and well-demarcated cerebral sulci. Measuring the thickness of the interthalamic adhesion in CCD was employed as a parameter for quantifying canine brain atrophy (Hasegawa et al., 2005; Noh et al., 2017). In demented canine brain MRI can be a useful tool to detect other abnormalities of the brain, possibly causing dementia such as leukoaraiosis (periventricular white matter hyperintensities) and brain microhemorrhages (Dewey et al., 2019). In human brain imaging a variant of amyloid-binding histological dye Thioflavin T, [^{11}C]PiB, has been used as a tracer to detect Aβ using PET (positron-emission tomography) scans. In dogs this compound failed to detect the full amyloid load in the brain, established by *ex vivo* histopathological investigation (Fast et al., 2013a).

In general, the diagnosis of human AD is set similarly. First by ruling out other possible causes for symptoms and then by detection of CSF and plasma biomarker levels, tests of memory, problem solving, attention, counting, and language, which can be followed by MRI and PET scans (Hane et al., 2017). As in dogs, the cause of dementia can only be confirmed with certainty postmortem.

TREATMENT AND DRUG DEVELOPMENT

Current treatment approaches for AD in humans are focused on helping people maintain mental function, manage behavioral symptoms, and slow or delay the symptoms of the disease. Unfortunately, there is no effective treatment for AD. Drugs that are used today in the management of AD can only alleviate the symptoms, and even that only temporarily. Cholinesterase inhibitors (donepezil, rivastigmine, and galantamine) have been approved for the management of AD in humans. Drugs acting as acetylcholinesterase inhibitors reduce the activity of the acetylcholine esterase which degrades acetylcholine, thus increasing the amount of acetylcholine available in the brain and therefore stimulate brain cells which receive more synaptic inputs (reviewed in Winblad et al., 2016). This very unspecific treatment can slow the disease progression for 6–12 months, and even achieve temporary improvement as shown for donepezil (Birks and Harvey, 2018), but does not cure the disease which will eventually progress. Another drug used for the treatment of AD is memantine that acts on the glutamatergic system by blocking NMDA (*N*-methyl-D-aspartate) receptors. A recent random-effects network meta-analysis of 41 randomized controlled trials reveled the most suitable dosages of cholinesterase inhibitors and memantine to treat patients with mild, moderate and severe AD (Dou et al., 2018). Although these pharmacological interventions have beneficial effects on cognition, function and global clinical impression, these treatments do not alleviate the neuropsychiatric symptoms (Dou et al., 2018). Unfortunately, there have been numerous clinical trials with many candidate drugs, but most of these had negative outcomes (Cummings et al., 2018).

Treatment of Canine Dementia

Current treatment options for CCD target prevention, slowing and/or improving the cognitive decline in dogs. Some drugs or food supplements are available for senior dogs and might act neuroprotective. Some enhance the blood flow into the brain, others work as antioxidants and more effort is now directed to slowing the progression of the disease instead of providing only symptomatic treatment. One commonly prescribed drug for cognitive impaired dogs is selegiline, which acts as an inhibitor of monoamine oxidase B (MAOB), thus reducing degradation of several neurotransmitters in the brain, and may have neuroprotective effects on dopaminergic, noradrenergic and cholinergic neurons (Landsberg, 2005; Magyar, 2011). Another drug that is occasionally used is nicergoline, which increases the blood flow through the brain. It may enhance neuronal transmission and act neuroprotective, increase dopamine and noradrenaline turnover and inhibit platelet aggregation (Landsberg, 2005). Propentofylline also has a neuroprotective role as it inhibits the production of free radicals and reduces the activation of microglial cell, thus acting anti-inflammatory (Frampton et al., 2003). Antidepressants such as selective serotonin reuptake inhibitors fluoxetine and sertraline, amitriptyline, paroxetine and anxiolytics benzodiazepines, gabapentin, valproic acid and buspirone can also be used to treat the anxiety and aggression which may accompany CCD. Clomipramin is an antidepressant commonly prescribed for dogs with anxiety (Landsberg, 2005), but these are all symptomatic treatments and do not treat the disease itself. *S*-adenosylmethionine tosylate supplementation was reported to be safe and effective in improving signs of age-related mental decline in dogs (Rème et al., 2008).

There are also some nutraceutical preparations available for dogs, which are based on natural products and/or supplement formulations. Behavioral enrichment alongside with antioxidant-rich diet and exercise is an approach for maintaining cognitive function and slowing the progression of CCD in senior pets. As means of preventative intervention, aging beagles were fed a diet rich in antioxidant, which improved cognition, maintained cognition and reduced oxidative damage and Aβ pathology in treated dogs (Milgram et al., 2004; Dowling and Head, 2012). Another longitudinal survey in beagles looked at the proteomic changes following administration of antioxidant-rich diet in combination with behavioral enrichment (Opii et al., 2008). Following treatment, the levels of oxidative stress biomarkers decreased and the increased expression levels of Cu/Zn superoxide dismutase, fructose-bisphosphate aldolase C, creatine kinase, glutamate dehydrogenase and glyceraldehyde-3-phosphate dehydrogenase correlated with improved cognition (Opii et al., 2008). In addition, some other studies implicated the nutrition as cognition modifying factor in dogs (Araujo et al., 2005a; Siwak et al., 2005; Osella et al., 2007; Christie et al., 2009; Head et al., 2009; Snigdha et al., 2011, 2012; Katina et al., 2016;

Chapagain et al., 2018), highlighting combination of nutraceutical supplements directed at several mechanisms of pathological aging, in combination with behavioral enrichment, as more effective (Araujo et al., 2005a, 2008). Dogs receiving both an antioxidant-rich diet and environmental enrichment showed increased levels of brain-derived neurotrophic factor (BDNF) mRNA when compared to untreated aged dogs. As a result of increase in BDNF mRNA, the cognitive performance improved and the amount of cortical Aβ deposits decreased (Fahnestock et al., 2012). Interesting is the finding that neuronal loss in the hippocampus, occurring in the aged dogs, could be partially reversed by more engagement with the dog, i.e., with stimulation of brain function (Siwak et al., 2000).

Animal Models for Developing Novel Treatments

In comparison to transgenic mouse models, natural animal models better represent the pathophysiology of AD. Models of "physiologically" aged rats, degus and dogs are useful for studying mechanistic aspects of AD, which are also very valuable in the development of therapeutics that would alleviate age-related declines in cognitive function. Mouse models for AD research carry mutations, found in familial AD, and are artificially accumulating Aβ plaques and NFTs. Whether mice are good models have been thoroughly discussed elsewhere (Götz et al., 2018). Several drugs have cleared the amyloid load in mice but failed to do so in people with AD. Recently the genetic background and environmental factors have been demonstrated as the variability in AD development, which was partially recognized by incorporating genetic diversity into mouse models of AD (Neuner et al., 2018). Transgenic minipigs expressing *APP695* or *PSEN1* have also been developed but have not shown the histopathological nor the cognitive impairment signs (Holm et al., 2016). Therefore, natural animal models of species with spontaneously occurring neurodegeneration are potentially more useful in developing and testing novel treatments for such diseases.

To date, most of the drugs in development for AD treatment have been directed toward the removal of amyloid plaques or NFTs, not taking into the account the multifactorial causation of the disease. Several experimental drugs that have successfully removed plaques from mouse brains have not lessened the symptoms of AD in people. For instance, drugs acting as BACE1 (beta-site amyloid precursor protein cleaving enzyme-1) inhibitors had failed in Phase II/III clinical trials (Hawkes, 2017; Dobrowolska Zakaria and Vassar, 2018; Egan et al., 2018). A BACE1 inhibitor verubecestat successfully blocked the accumulation of amyloid protein in mice (Villarreal et al., 2017), rats and monkeys (Kennedy et al., 2016), but did not reduce cognitive or functional decline in patients with mild to moderate AD (Egan et al., 2018). Although decrease in Aβ biomarkers in CSF and brain has been noticed after treatment with BACE1 inhibitors, the failure to prevent cognitive decline might have been due to irreversible neurotoxic accumulation of Aβ that occurred prior to the start of the treatment. For this reason, focus is on the development of therapies that commence at presymptomatic stage (preclinical stage and the stage of mild cognitive impairment) although for this, development of novel, useful biomarkers, is also crucial.

As canine cognitive decline and human Alzheimer's disease show neuropathological, cognitive and behavioral parallels, the testing of products for the treatment of AD in canine model could be useful to determine the efficacy of these compounds in humans, and also to develop novel therapeutic agents for the treatment of senior dogs. Several drugs have been tested in elderly dogs and their suitability and effectiveness correlated with results obtained in human trials, when available. Drugs tested in dogs are listed in **Table 3**.

BACE1 is a protease that controls the formation of Aβ and most likely plays an important role in the development of pathogenesis in AD. The usefulness of BACE1 small-molecule inhibitor LY2886721 has been tested in a dog model and in humans in the first clinical phase (May et al., 2015). It significantly reduced plasma and CSF Aβ levels both in dogs and healthy volunteers (May et al., 2015). After administration of two BACE1 inhibitors (cyclic sulfoxide hydroxyethylamine NB-B4 and oxazine derivative NB-C8) a unique pattern of secreted Aβ peptides was observed in canine CSF (Mattsson et al., 2012). Besides the expected reduced levels of $A\beta_{40}$ and $A\beta_{42}$, reduced levels of $A\beta_{1-34}$ and increased levels of $A\beta_{5-40}$ were detected, which were proposed as prognostic markers of BACE1 inhibition therapies (Mattsson et al., 2012). A recent survey, using BACE1 inhibitor CNP520, demonstrated reduced brain and CSF Aβ in rats, dogs, and reduced CSF Aβ in humans and was assessed to be well tolerated in healthy adults and further clinical trials are ongoing (Neumann et al., 2018). A cardiovascular disease drug, atorvastatin, has been investigated in a canine model of dementia whether it could reduce Aβ plaques, BACE1 protein levels and oxidative stress (Barone et al., 2012). It does offer some neuroprotective role through the up-regulation of enzyme biliverdin reductase-A (Barone et al., 2012). Selegiline (L-deprenyl), a type B monoamine oxidase inhibitor, has been reported to prolong the survival of aged dogs (Ruehl et al., 1997) and in some cases improve visuospatial working memory (Head et al., 1996). However, in subsequent studies only a small subset of dogs seemed to show improvement, pointing to a minor clinical relevance of selegiline administration (Campbell et al., 2001). Furthermore, several human AD trials provided no evidence of clinically meaningful benefits of selegiline administration for people with AD (Birks and Flicker, 2003). Interestingly, although selegiline was shown to be fairly ineffective in the treatment of CCD, it is still the only FDA-approved treatment for CCD.

Testing the same compounds in dogs and humans provided similar findings also in other studies. CP-118,954, an acetylcholinesterase inhibitor, showed minimal cognitive enhancing effects in dogs and human clinical trials were discontinued (Studzinski et al., 2005). Donepezil administration enhanced memory in dogs (Araujo et al., 2011a). Phenserine, an acetylcholinesterase inhibitor which also inhibits synthesis of Aβ and acts as a cognitive enhancing therapeutic, improved learning and working memory in geriatric dogs (Studzinski et al., 2005; Araujo et al., 2011a). Its administration showed

TABLE 3 | Pharmacological interventions tested in dogs with cognitive decline.

Name/type	Mode of action	Testing in dog	Results/outcomes	References
LY2886721	BACE1 inhibitor	Pharmacology study in dogs and clinical trial in healthy volunteers	Aβ lowering in plasma and CSF	May et al., 2015
Selegiline (L-deprenyl)	MAOB inhibitor	Longitudinal study	Higher life expectancy (cognitive status not monitored)	Ruehl et al., 1997
Selegiline (L-deprenyl)	MAOB inhibitor	Performance studies	Improved visuospatial working memory (in only a subset of dogs)	Head et al., 1996; Campbell et al., 2001; Studzinski et al., 2005
Atorvastatin	Reduction of Aβ and BACE1	Longitudinal study	Neuroprotective	Barone et al., 2012
Adrafinil	A wakefulness-promoting agent (eugeroic) with nootropic effects	Longitudinal study; pharmacological study	A significant increase in locomotion; improved learning; impaired working memory	Siwak et al., 2000; Studzinski et al., 2005
Ampakine	Positive modulator of AMPA receptors (enhance excitatory glutamatergic neurotransmission)	Pharmacological study	Decrease of performance accuracy; may have memory impairing effects	Studzinski et al., 2005
CP-118,954	Acetylcholinesterase inhibitor	Pharmacological study	Minimal cognitive enhancing effects	Studzinski et al., 2005
Phenserine	Acetylcholinesterase inhibitor	Pharmacological study; performance study	Enhancing effects on memory and learning; improved performance (only in a subset of dogs treated)	Studzinski et al., 2005; Araujo et al., 2011a
Donepezil	Acetylcholinesterase inhibitor	Performance study	memory enhancement	Araujo et al., 2011a
CNP520	BACE1 inhibitor	Dogs, human	Safe to use in dogs; tolerated in healthy humans; ongoing clinical trials	Neumann et al., 2018
Antioxidant-rich diet with cognitive enrichment	/	Dogs	Improved cognition	Opii et al., 2008; Dowling and Head, 2012
Anti-Aβ immunotherapy	Passive vaccination with injections of antibodies against $A\beta_{42}$	Dogs	Reduced amyloid plaques and reduced astrogliosis	Head et al., 2008; Neus Bosch et al., 2015; Davis et al., 2017

similar results in Phase II human clinical trials, suggesting its effectiveness in improving memory in AD patients, but in Phase III human clinical trial, with patients with mild to moderate AD, no significant differences between the phenserine treated and placebo groups were noticed and the trial was discontinued (Thatte, 2005). There has been further discussions if this trial, and several other AD trials, failed due to procedural errors rather than due to a lack of drug efficacy (Winblad et al., 2010). In more recent studies patients with mild AD showed improvement in cognition following phenserine treatments, this was mirrored also by an increase in CSF $A\beta_{40}$ (Kadir et al., 2008; Nordberg et al., 2015). There is another mode of action of phenserine in AD, namely inhibition of neuronal self-induced preprogrammed cell death, which further clinical trials might pursue (Becker et al., 2018). Ampakine (drug that alters the glutaminergic system) also failed in human AD trials and in dogs with age-associated memory disorder and dementia showed insignificant memory-enhancing effects after treatment with ampakine (Studzinski et al., 2005). Dogs, treated with adrafinil, a mild central nervous system stimulant used to relieve excessive sleepiness and inattention in elderly patients, were more attentive (Siwak et al., 2000). Cholinergic hypofunction might play a role in age-dependent cognitive decline in dogs (Araujo et al., 2011b), this was determined by administration of muscarinic cholinergic receptor antagonist scopolamine, which induces transient memory impairment. Similar findings were presented for aged and demented humans (Schliebs and Arendt, 2011). All these suggest that dogs might be a very good preclinical model for developing and testing new drugs for AD in humans.

Besides BACE1 and cholinesterase inhibitors several attempts have been made to develop immunotherapy treatments directed against Aβ or TAU (Bittar et al., 2018). A range of TAU-targeted immunotherapies have entered clinical development (recently reviewed in Novak et al., 2018). Clinical trials in patients with AD, which were administered Aβ peptide with conjugate to stimulate the immune response (i.e., active immunization) or anti-Aβ antibodies (i.e., passive immunization) have shown modest results and also serious side effects (reviewed in detail in Wisniewski and Drummond, 2016).

In dogs, Aβ immunotherapy could reduce the presence of amyloid plaques and astroglial reaction in aged individuals (Neus Bosch et al., 2015). A vaccine directed against fibrillary Aβ (anti-$A\beta_{42}$) reduced the presence of Aβ plaques in canine prefrontal cortex and improved the function of the frontal cortex, thus resulting in cognitive benefits (Head et al., 2008). Anti-$A\beta_{42}$ vaccination of dogs with CCD, in combination with behavioral enrichment, resulted in reduced presence of Aβ plaques in the brain, a significant maintenance of learning abilities over time

and cognitive maintenance with no improvement in cognition (Davis et al., 2017). This anti-Aβ vaccine, however, also increased the frequency of brain microhemorrhages (Davis et al., 2017) which is commonly observed in the development of these immunotherapies also in human trials and could be very serious side effect. Similarly to pharmacological compounds, immunotherapies in both dogs and humans have provided modest improvements at most, yet similarities between human and canine patients again highlight the parallels between diseases and usefulness of dogs as a preclinical model for AD.

CONCLUSION

Risks for age-related AD and CCD are a complicated interplay between aging, genetic risk factors and environmental influences. CCD in dogs is similar to human AD with respect to APP processing, amyloid plaque deposition and cognitive dysfunction. As dogs age, they have been shown to accumulate amyloid plaques, but, dissimilar to human AD patients, dog brain rarely contains NFTs. Aβ peptide accumulates in the canine brain extracellular space in the form of soluble oligomers, fibrils and Aβ plaques. Its toxic accumulation is believed to be responsible for the neuronal dysfunction and degeneration although the severity of the disease does not always correlate with amyloid burden, but might correlate with toxic fibril polymorphs.

Dogs over 7–8 years seem to be interesting, naturally occurring model organism for aging/dementia that fairly faithfully recapitulate human disease. They are potentially much more useful as rodent models as in laboratory rodents neurodegenerative diseases do not occur spontaneously. Furthermore, genetically modified mice used in research often show very different neurodegeneration courses, as seen in humans. Dogs also spontaneously develop vasculopathies, such as CAA, and perhaps vascular dementia although this has not yet been truly studied, and are therefore also valuable as models to decipher the age and/or dementia related cerebrovascular changes that often accompany or even precede neurodegeneration in human patients.

There are no effective treatments for neurodegenerative disorders, practically all currently available treatments are symptomatic. This is partially related to the poor understanding of the pathogenesis of these diseases, and partly due to the lack of good animal models. Cholinesterase or secretase inhibitor therapy or immunotherapy has been attempted in dogs with CDD, with overlapping results to human AD trials. The neuroprotective effects of cognitive enrichment, alongside with antioxidant-rich diet, show benefits in managing the disease progression and severity in both humans and dogs. Similar results with various drugs do suggest that dogs are useful model to study both pathogenesis and novel treatments for AD in the future.

Taken together, animal studies are important to dissect the molecular and cellular processes specific to AD pathology. Dogs with CCD not only develop isomorphic changes in human cognition and brain pathology, but also accurately predicted the efficacy of known AD treatments and would be therefore good models for testing new substances that affect the lowering of Aβ levels or the reduction or degradation of aggregates associated with AD. This would benefit human patients, but could also help dog patients as any successful treatments could be also introduced into clinical veterinary medicine with the aim to successfully treat this debilitating disease in canine patients.

AUTHOR CONTRIBUTIONS

Both authors have made a substantial contribution to this work.

FUNDING

This work was supported by European Social Fund and Slovenian Research Agency (ARRS) Research Program P4-0053.

REFERENCES

Aguzzi, A. (2014). Neurodegeneration: Alzheimer's disease under strain. *Nature* 512, 32–34. doi: 10.1038/512032a

Araujo, J. A., Greig, N. H., Ingram, D. K., Sandin, J., de Rivera, C., and Milgram, N. W. (2011a). Cholinesterase inhibitors improve both memory and complex learning in aged beagle dogs. *J. Alzheimers Dis.* 26, 143–155. doi: 10.3233/JAD-2011-110005

Araujo, J. A., Landsberg, G. M., Milgram, N. W., and Miolo, A. (2008). Improvement of short-term memory performance in aged beagles by a nutraceutical supplement containing phosphatidylserine, Ginkgo biloba, vitamin E, and pyridoxine. *Can. Vet. J.* 49, 379–385.

Araujo, J. A., Nobrega, J. N., Raymond, R., and Milgram, N. W. (2011b). Aged dogs demonstrate both increased sensitivity to scopolamine impairment and decreased muscarinic receptor density. *Pharmacol. Biochem. Behav.* 98, 203–209. doi: 10.1016/j.pbb.2011.01.005

Araujo, J. A., Studzinski, C. M., Head, E., Cotman, C. W., and Milgram, N. W. (2005a). Assessment of nutritional interventions for modification of age-associated cognitive decline using a canine model of human aging. *Age* 27, 27–37. doi: 10.1007/s11357-005-4001-z

Araujo, J. A., Studzinski, C. M., and Milgram, N. W. (2005b). Further evidence for the cholinergic hypothesis of aging and dementia from the canine model of aging. *Prog. Neuropsychopharmacol. Biol. Psychiatry* 29, 411–422. doi: 10.1016/j.pnpbp.2004.12.008

Arendt, T., Brückner, M. K., and Lösche, A. (2015). Regional mosaic genomic heterogeneity in the elderly and in Alzheimer's disease as a correlate of neuronal vulnerability. *Acta Neuropathol.* 130, 501–510. doi: 10.1007/s00401-015-1465-5

Arendt, T., Brückner, M. K., Mosch, B., and Lösche, A. (2010). Selective cell death of hyperploid neurons in Alzheimer's disease. *Am. J. Pathol.* 177, 15–20. doi: 10.2353/ajpath.2010.090955

Arendt, T., Stieler, J., and Ueberham, U. (2017). Is sporadic Alzheimer's disease a developmental disorder? *J. Neurochem.* 143, 396–408. doi: 10.1111/jnc.14036

Ashford, J. W. (2004). APOE genotype effects on Alzheimer's disease onset and epidemiology. *J. Mol. Neurosci.* 23, 157–165.

Attems, J. (2005). Sporadic cerebral amyloid angiopathy: pathology, clinical implications, and possible pathomechanisms. *Acta Neuropathol.* 110, 345–359. doi: 10.1007/s00401-005-1074-9

Azkona, G., García-Belenguer, S., Chacón, G., Rosado, B., León, M., and Palacio, J. (2009). Prevalence and risk factors of behavioural changes associated with age-related cognitive impairment in geriatric dogs. *J. Small Anim. Pract.* 50, 87–91. doi: 10.1111/j.1748-5827.2008.00718.x

Bain, M. J., Hart, B. L., Cliff, K. D., and Ruehl, W. W. (2001). Predicting behavioral changes associated with age-related cognitive impairment in dogs. *J. Am. Vet. Med. Assoc.* 218, 1792–1795. doi: 10.2460/javma.2001.218.1792

Barnes, J., Cotton, P., Robinson, S., and Jacobsen, M. (2016). Spontaneous pathology and routine clinical pathology parameters in aging beagle dogs: a comparison with adolescent and young adults. *Vet. Pathol.* 53, 447–455. doi: 10.1177/0300985815610390

Barone, E., Mancuso, C., Di Domenico, F., Sultana, R., Murphy, M. P., Head, E., et al. (2012). Biliverdin reductase-A: a novel drug target for atorvastatin in a dog pre-clinical model of Alzheimer disease. *J. Neurochem.* 120, 135–146. doi: 10.1111/j.1471-4159.2011.07538.x

Bature, F., Guinn, B.-A., Pang, D., and Pappas, Y. (2017). Signs and symptoms preceding the diagnosis of Alzheimer's disease: a systematic scoping review of literature from 1937 to 2016. *BMJ Open* 7:e015746. doi: 10.1136/bmjopen-2016-015746

Becker, R. E., Greig, N. H., Schneider, L. S., Ballard, C., Aarsland, D., Lahiri, D. K., et al. (2018). (-)-Phenserine and inhibiting apoptosis: in pursuit of a novel intervention for Alzheimer's disease. *Curr. Alzheimer Res.* 15, 883–891. doi: 10.2174/1567205015666180110120026

Bekris, L. M., Yu, C.-E., Bird, T. D., and Tsuang, D. W. (2010). Genetics of Alzheimer Disease. *J. Geriatr. Psychiatry Neurol.* 23, 213–227. doi: 10.1177/0891988710383571

Bell, K. F. S., Ducatenzeiler, A., Ribeiro-da-Silva, A., Duff, K., Bennett, D. A., and Cuello, A. C. (2006). The amyloid pathology progresses in a neurotransmitter-specific manner. *Neurobiol. Aging* 27, 1644–1657. doi: 10.1016/j.neurobiolaging.2005.09.034

Birks, J., and Flicker, L. (2003). Selegiline for Alzheimer's disease. *Cochrane Database Syst. Rev.* 1:CD000442. doi: 10.1002/14651858.CD000442

Birks, J. S., and Harvey, R. J. (2018). Donepezil for dementia due to Alzheimer's disease. *Cochrane Database Syst. Rev.* 6:CD001190. doi: 10.1002/14651858.CD001190.pub3

Bittar, A., Sengupta, U., and Kayed, R. (2018). Prospects for strain-specific immunotherapy in Alzheimer's disease and tauopathies. *NPJ Vaccines* 3:9. doi: 10.1038/s41541-018-0046-8

Borghys, H., Van Broeck, B., Dhuyvetter, D., Jacobs, T., de Waepenaert, K., Erkens, T., et al. (2017). Young to middle-aged dogs with high amyloid-β levels in cerebrospinal fluid are impaired on learning in standard cognition tests. *J. Alzheimers Dis.* 56, 763–774. doi: 10.3233/JAD-160434

Borràs, D., Ferrer, I., and Pumarola, M. (1999). Age-related changes in the brain of the dog. *Vet. Pathol.* 36, 202–211. doi: 10.1354/vp.36-3-202

Bosch, M. N., Pugliese, M., Gimeno-Bayón, J., Rodríguez, M. J., and Mahy, N. (2012). Dogs with cognitive dysfunction syndrome: a natural model of Alzheimer's disease. *Curr. Alzheimer Res.* 9, 298–314. doi: 10.2174/156720512800107546

Braak, H., and Braak, E. (1991). Neuropathological stageing of Alzheimer-related changes. *Acta Neuropathol.* 82, 239–259. doi: 10.1007/bf00308809

Braak, H., and Braak, E. (1997). Frequency of stages of alzheimer-related lesions in different age categories. *Neurobiol. Aging* 18, 351–357. doi: 10.1016/S0197-4580(97)00056-0

Braak, H., Braak, E., and Strothjohann, M. (1994). Abnormally phosphorylated tau protein related to the formation of neurofibrillary tangles and neuropil threads in the cerebral cortex of sheep and goat. *Neurosci. Lett.* 171, 1–4. doi: 10.1016/0304-3940(94)90589-4

Braak, H., and Del Tredici, K. (2012). Where, when, and in what form does sporadic Alzheimer's disease begin? *Curr. Opin. Neurol.* 25, 708–714. doi: 10.1097/WCO.0b013e32835a3432

Braidy, N., Poljak, A., Jayasena, T., Mansour, H., Inestrosa, N. C., and Sachdev, P. S. (2015). Accelerating Alzheimer's research through "natural" animal models. *Curr. Opin. Psychiatry* 28, 155–164. doi: 10.1097/YCO.0000000000000137

Brettschneider, J., Del Tredici, K., Lee, V. M.-Y., and Trojanowski, J. Q. (2015). Spreading of pathology in neurodegenerative diseases: a focus on human studies. *Nat. Rev. Neurosci.* 16, 109–120. doi: 10.1038/nrn3887

Briefer Freymond, S., Ruet, A., Grivaz, M., Fuentes, C., Zuberbühler, K., Bachmann, I., et al. (2018). Stereotypic horses (Equus caballus) are not cognitively impaired. *Anim. Cogn.* 22, 17–33. doi: 10.1007/s10071-018-1217-8

Bugiani, O., Giaccone, G., Rossi, G., Mangieri, M., Capobianco, R., Morbin, M., et al. (2010). Hereditary cerebral hemorrhage with amyloidosis associated with the E693K mutation of APP. *Arch. Neurol.* 67, 987–995. doi: 10.1001/archneurol.2010.178

Cacace, R., Sleegers, K., and Van Broeckhoven, C. (2016). Molecular genetics of early-onset Alzheimer's disease revisited. *Alzheimers Dement.* 12, 733–748. doi: 10.1016/j.jalz.2016.01.012

Campbell, S., Trettien, A., and Kozan, B. (2001). A noncomparative open-label study evaluating the effect of selegiline hydrochloride in a clinical setting. *Vet. Ther.* 2, 24–39.

Canudas, J., Insua, D., Sarasa, L., González-Martínez, A., Suárez, M. L., Santamarina, G., et al. (2014). Neprilysin is poorly expressed in the prefrontal cortex of aged dogs with cognitive dysfunction syndrome. *Int. J. Alzheimers Dis.* 2014:483281. doi: 10.1155/2014/483281

Capucchio, M. T., Márquez, M., Pregel, P., Foradada, L., Bravo, M., Mattutino, G., et al. (2010). Parenchymal and vascular lesions in ageing equine brains: histological and immunohistochemical studies. *J. Comp. Pathol.* 142, 61–73. doi: 10.1016/j.jcpa.2009.07.007

Chambers, J. K., Mutsuga, M., Uchida, K., and Nakayama, H. (2011). Characterization of AβpN3 deposition in the brains of dogs of various ages and other animal species. *Amyloid* 18, 63–71. doi: 10.3109/13506129.2011.570385

Chambers, J. K., Tokuda, T., Uchida, K., Ishii, R., Tatebe, H., Takahashi, E., et al. (2015). The domestic cat as a natural animal model of Alzheimer's disease. *Acta Neuropathol. Commun.* 3:78. doi: 10.1186/s40478-015-0258-3

Chambers, J. K., Uchida, K., and Nakayama, H. (2012). White matter myelin loss in the brains of aged dogs. *Exp. Gerontol.* 47, 263–269. doi: 10.1016/j.exger.2011.12.003

Chapagain, D., Virányi, Z., Huber, L., Serra, J., Schoesswender, J., and Range, F. (2018). Effect of age and dietary intervention on discrimination learning in pet dogs. *Front. Psychol.* 9:2217. doi: 10.3389/fpsyg.2018.02217

Christie, L.-A., Opii, W. O., and Head, E. (2009). Strategies for improving cognition with aging: insights from a longitudinal study of antioxidant and behavioral enrichment in canines. *Age* 31, 211–220. doi: 10.1007/s11357-008-9063-2

Colle, M.-A., Hauw, J.-J., Crespeau, F., Uchihara, T., Akiyama, H., Checler, F., et al. (2000). Vascular and parenchymal Abeta deposition in the aging dog: correlation with behavior. *Neurobiol. Aging* 21, 695–704. doi: 10.1016/s0197-4580(00)00113-5

Condello, C., and Stöehr, J. (2018). Aβ propagation and strains: Implications for the phenotypic diversity in Alzheimer's disease. *Neurobiol. Dis.* 109, 191–200. doi: 10.1016/j.nbd.2017.03.014

Cork, L. C., Powers, R. E., Selkoe, D. J., Davies, P., Geyer, J. J., and Price, D. L. (1988). Neurofibrillary Tangles and Senile Plaques in Aged Bears. *J. Neuropathol. Exp. Neurol.* 47, 629–641. doi: 10.1097/00005072-198811000-00006

Cummings, B. J., and Cotman, C. W. (1995). Image analysis of beta-amyloid load in Alzheimer's disease and relation to dementia severity. *Lancet* 346, 1524–1528. doi: 10.1016/s0140-6736(95)92053-6

Cummings, B. J., Su, J. H., Cotman, C. W., White, R., and Russell, M. J. (1993). Beta-amyloid accumulation in aged canine brain: a model of early plaque formation in Alzheimer's disease. *Neurobiol. Aging* 14, 547–560. doi: 10.1016/0197-4580(93)90038-d

Cummings, J., Ritter, A., and Zhong, K. (2018). Clinical trials for disease-modifying therapies in Alzheimer's disease: a primer, lessons learned, and a blueprint for the future. *J. Alzheimers Dis.* 64, S3–S22. doi: 10.3233/JAD-179901

Davis, P. R., Giannini, G., Rudolph, K., Calloway, N., Royer, C. M., Beckett, T. L., et al. (2017). Aβ vaccination in combination with behavioral enrichment in aged beagles: effects on cognition, Aβ, and microhemorrhages. *Neurobiol. Aging* 49, 86–99. doi: 10.1016/j.neurobiolaging.2016.09.007

DeVos, S. L., Corjuc, B. T., Oakley, D. H., Nobuhara, C. K., Bannon, R. N., Chase, A., et al. (2018). Synaptic Tau seeding precedes Tau pathology in human Alzheimer's disease brain. *Front. Neurosci.* 12:267. doi: 10.3389/fnins.2018.00267

Dewey, C. W., Davies, E. S., Xie, H., and Wakshlag, J. J. (2019). Canine cognitive dysfunction: pathophysiology, diagnosis, and treatment. *Vet. Clin. North Am. Small Anim. Pract.* 49, 477–499. doi: 10.1016/j.cvsm.2019.01.013

Di Guardo, G. (2018). Alzheimer's disease, cellular prion protein, and dolphins. *Alzheimers Dement.* 14, 259–260. doi: 10.1016/j.jalz.2017.12.002

Dobrowolska Zakaria, J. A., and Vassar, R. J. (2018). A promising, novel, and unique BACE1 inhibitor emerges in the quest to prevent Alzheimer's disease. *EMBO Mol. Med.* 10:e9717. doi: 10.15252/emmm.201809717

Dodart, J. C., Mathis, C., Bales, K. R., and Paul, S. M. (2002). Does my mouse have Alzheimer's disease? *Genes Brain Behav.* 1, 142–155. doi: 10.1034/j.1601-183x.2002.10302.x

Dou, K.-X., Tan, M.-S., Tan, C.-C., Cao, X.-P., Hou, X.-H., Guo, Q.-H., et al. (2018). Comparative safety and effectiveness of cholinesterase inhibitors and memantine for Alzheimer's disease: a network meta-analysis of 41 randomized controlled trials. *Alzheimers Res. Ther.* 10:126. doi: 10.1186/s13195-018-0457-9

Dowling, A. L. S., and Head, E. (2012). Antioxidants in the canine model of human aging. *Biochim. Biophys. Acta* 1822, 685–689. doi: 10.1016/j.bbadis.2011.09.020

Egan, M. F., Kost, J., Tariot, P. N., Aisen, P. S., Cummings, J. L., Vellas, B., et al. (2018). Randomized Trial of Verubecestat for Mild-to-Moderate Alzheimer's Disease. *N. Engl. J. Med.* 378, 1691–1703. doi: 10.1056/NEJMoa1706441

Eisele, Y. S., Obermüller, U., Heilbronner, G., Baumann, F., Kaeser, S. A., Wolburg, H., et al. (2010). Peripherally applied Abeta-containing inoculates induce cerebral beta-amyloidosis. *Science* 330, 980–982. doi: 10.1126/science.1194516

El-Assaad, I., Di Bari, J. A., Yasuda, K., Divers, T. J., Summers, B. A., de Lahunta, A., et al. (2012). Differential expression of TAR DNA-binding protein (TDP-43) in the central nervous system of horses afflicted with equine motor neuron disease (EMND): a preliminary study of a potential pathologic marker. *Vet. Res. Commun.* 36, 221–226. doi: 10.1007/s11259-012-9533-y

Fagan, A. M., Head, D., Shah, A. R., Marcus, D., Mintun, M., Morris, J. C., et al. (2009). Decreased cerebrospinal fluid Abeta(42) correlates with brain atrophy in cognitively normal elderly. *Ann. Neurol.* 65, 176–183. doi: 10.1002/ana.21559

Fahnestock, M., Marchese, M., Head, E., Pop, V., Michalski, B., Milgram, W. N., et al. (2012). BDNF increases with behavioral enrichment and an antioxidant diet in the aged dog. *Neurobiol. Aging* 33, 546–554. doi: 10.1016/j.neurobiolaging.2010.03.019

Fast, R., Rodell, A., Gjedde, A., Mouridsen, K., Alstrup, A. K., Bjarkam, C. R., et al. (2013a). PiB fails to map amyloid deposits in cerebral cortex of aged dogs with canine cognitive dysfunction. *Front. Aging Neurosci.* 5:99. doi: 10.3389/fnagi.2013.00099

Fast, R., Schütt, T., Toft, N., Møller, A., and Berendt, M. (2013b). An observational study with long-term follow-up of canine cognitive dysfunction: clinical characteristics, survival, and risk factors. *J. Vet. Intern. Med.* 27, 822–829. doi: 10.1111/jvim.12109

Frampton, M., Harvey, R. J., and Kirchner, V. (2003). Propentofylline for dementia. *Cochrane Database Syst. Rev.* 2:CD002853. doi: 10.1002/14651858.CD002853

GBD 2016 Dementia Collaborators (2019). Global, regional, and national burden of Alzheimer's disease and other dementias, 1990-2016: a systematic analysis for the Global Burden of Disease Study 2016. *Lancet Neurol.* 18, 88–106. doi: 10.1016/S1474-4422(18)30403-4

Golini, L., Colangeli, R., Tranquillo, V., and Mariscoli, M. (2009). Association between neurologic and cognitive dysfunction signs in a sample of aging dogs. *J. Vet. Behav.* 4, 25–30. doi: 10.1016/j.jveb.2008.09.033

Gómez-Pinedo, U., Villar-Quiles, R. N., Galán, L., Matías-Guiu, J. A., Benito-Martin, M. S., Guerrero-Sola, A., et al. (2016). Immununochemical markers of the amyloid cascade in the hippocampus in motor neuron diseases. *Front. Neurol.* 7:195. doi: 10.3389/fneur.2016.00195

González-Martínez, Á., Rosado, B., Pesini, P., Suárez, M.-L., Santamarina, G., García-Belenguer, S., et al. (2011). Plasma β-amyloid peptides in canine aging and cognitive dysfunction as a model of Alzheimer's disease. *Exp. Gerontol.* 46, 590–596. doi: 10.1016/j.exger.2011.02.013

Götz, J., Bodea, L.-G., and Goedert, M. (2018). Rodent models for Alzheimer disease. *Nat. Rev. Neurosci.* 19, 583–598. doi: 10.1038/s41583-018-0054-8

Gouras, G. K., Tampellini, D., Takahashi, R. H., and Capetillo-Zarate, E. (2010). Intraneuronal β-amyloid accumulation and synapse pathology in Alzheimer's disease. *Acta Neuropathol.* 119, 523–541. doi: 10.1007/s00401-010-0679-9

Grabowski, T. J., Cho, H. S., Vonsattel, J. P., Rebeck, G. W., and Greenberg, S. M. (2001). Novel amyloid precursor protein mutation in an Iowa family with dementia and severe cerebral amyloid angiopathy. *Ann. Neurol.* 49, 697–705. doi: 10.1002/ana.1009

Greer, K. A., Canterberry, S. C., and Murphy, K. E. (2007). Statistical analysis regarding the effects of height and weight on life span of the domestic dog. *Res. Vet. Sci.* 82, 208–214. doi: 10.1016/j.rvsc.2006.06.005

Hane, F. T., Robinson, M., Lee, B. Y., Bai, O., Leonenko, Z., and Albert, M. S. (2017). Recent progress in Alzheimer's disease research, part 3: diagnosis and treatment. *J. Alzheimers Dis.* 57, 645–665. doi: 10.3233/JAD-160907

Hardy, J., and Selkoe, D. J. (2002). The amyloid hypothesis of Alzheimer's disease: progress and problems on the road to therapeutics. *Science* 297, 353–356. doi: 10.1126/science.1072994

Hardy, J. A., and Higgins, G. A. (1992). Alzheimer's disease: the amyloid cascade hypothesis. *Science* 256, 184–185.

Härtig, W., Klein, C., Brauer, K., Schüppel, K.-F., Arendt, T., Bigl, V., et al. (2001). Hyperphosphorylated protein tau is restricted to neurons devoid of perineuronal nets in the cortex of aged bison. *Neurobiol. Aging* 22, 25–33. doi: 10.1016/S0197-4580(00)00179-2

Härtig, W., Klein, C., Brauer, K., Schüppel, K. F., Arendt, T., Brückner, G., et al. (2000). Abnormally phosphorylated protein tau in the cortex of aged individuals of various mammalian orders. *Acta Neuropathol.* 100, 305–312. doi: 10.1007/s004010000183

Hasegawa, D., Yayoshi, N., Fujita, Y., Fujita, M., and Orima, H. (2005). Measurement of interthalamic adhesion thickness as a criteria for brain atrophy in dogs with and without cognitive dysfunction (dementia). *Vet. Radiol. Ultrasound* 46, 452–457. doi: 10.1111/j.1740-8261.2005.00083.x

Hawkes, N. (2017). Merck ends trial of potential Alzheimer's drug verubecestat. *BMJ* 356:j845. doi: 10.1136/bmj.j845

Head, E., Hartley, J., Kameka, A. M., Mehta, R., Ivy, G. O., Ruehl, W. W., et al. (1996). The effects of L-deprenyl on spatial short term memory in young and aged dogs. *Prog. Neuropsychopharmacol. Biol. Psychiatry* 20, 515–530. doi: 10.1016/0278-5846(96)00014-0

Head, E., Nukala, V. N., Fenoglio, K. A., Muggenburg, B. A., Cotman, C. W., and Sullivan, P. G. (2009). Effects of age, dietary, and behavioral enrichment on brain mitochondria in a canine model of human aging. *Exp. Neurol.* 220, 171–176. doi: 10.1016/j.expneurol.2009.08.014

Head, E., Pop, V., Sarsoza, F., Kayed, R., Beckett, T. L., Studzinski, C. M., et al. (2010). Amyloid-beta peptide and oligomers in the brain and cerebrospinal fluid of aged canines. *J. Alzheimers Dis.* 20, 637–646. doi: 10.3233/JAD-2010-1397

Head, E., Pop, V., Vasilevko, V., Hill, M., Saing, T., Sarsoza, F., et al. (2008). A two-year study with fibrillar beta-amyloid (Abeta) immunization in aged canines: effects on cognitive function and brain Abeta. *J. Neurosci.* 28, 3555–3566. doi: 10.1523/JNEUROSCI.0208-08.2008

Hendriks, L., van Duijn, C. M., Cras, P., Cruts, M., Van Hul, W., van Harskamp, F., et al. (1992). Presenile dementia and cerebral haemorrhage linked to a mutation at codon 692 of the beta-amyloid precursor protein gene. *Nat. Genet.* 1, 218–221. doi: 10.1038/ng0692-218

Hoenig, M. C., Bischof, G. N., Seemiller, J., Hammes, J., Kukolja, J., Onur, Ö. A., et al. (2018). Networks of tau distribution in Alzheimer's disease. *Brain* 141, 568–581. doi: 10.1093/brain/awx353

Holm, I. E., Alstrup, A. K. O., and Luo, Y. (2016). Genetically modified pig models for neurodegenerative disorders. *J. Pathol.* 238, 267–287. doi: 10.1002/path.4654

Insua, D., Corredoira, A., González-Martínez, A., Suárez, M.-L., Santamarina, G., Sarasa, M., et al. (2012). Expression of p75(NTR), a marker for basal forebrain cholinergic neurons, in young and aged dogs with or without cognitive dysfunction syndrome. *J. Alzheimers Dis.* 28, 291–296. doi: 10.3233/JAD-2011-110905

Insua, D., Suárez, M.-L., Santamarina, G., Sarasa, M., and Pesini, P. (2010). Dogs with canine counterpart of Alzheimer's disease lose noradrenergic neurons. *Neurobiol. Aging* 31, 625–635. doi: 10.1016/j.neurobiolaging.2008.05.014

Ishihara, T., Gondo, T., Takahashi, M., Uchino, F., Ikeda, S., Allsop, D., et al. (1991). Immunohistochemical and immunoelectron microscopical characterization of cerebrovascular and senile plaque amyloid in aged dogs' brains. *Brain Res.* 548, 196–205. doi: 10.1016/0006-8993(91)91122-h

Ivansson, E. L., Megquier, K., Kozyrev, S. V., Murén, E., Körberg, I. B., Swofford, R., et al. (2016). Variants within the SP110 nuclear body protein modify risk of canine degenerative myelopathy. *Proc. Natl. Acad. Sci. U.S.A.* 113, E3091–E3100. doi: 10.1073/pnas.1600084113

Janelidze, S., Stomrud, E., Palmqvist, S., Zetterberg, H., van Westen, D., Jeromin, A., et al. (2016). Plasma β-amyloid in Alzheimer's disease and vascular disease. *Sci. Rep.* 6:26801. doi: 10.1038/srep26801

Johnstone, E. M., Chaney, M. O., Norris, F. H., Pascual, R., and Little, S. P. (1991). Conservation of the sequence of the Alzheimer's disease amyloid peptide in dog, polar bear and five other mammals by cross-species polymerase chain reaction analysis. *Brain Res. Mol. Brain Res.* 10, 299–305. doi: 10.1016/0169-328x(91)90088-f

Jucker, M., and Walker, L. C. (2018). Propagation and spread of pathogenic protein assemblies in neurodegenerative diseases. *Nat. Neurosci.* 21, 1341–1349. doi: 10.1038/s41593-018-0238-6

Kadir, A., Andreasen, N., Almkvist, O., Wall, A., Forsberg, A., Engler, H., et al. (2008). Effect of phenserine treatment on brain functional activity and amyloid in Alzheimer's disease. *Ann. Neurol.* 63, 621–631. doi: 10.1002/ana.21345

Karch, C. M., Jeng, A. T., Nowotny, P., Cady, J., Cruchaga, C., and Goate, A. M. (2012). Expression of novel Alzheimer's disease risk genes in control and Alzheimer's disease brains. *PLoS One* 7:e50976. doi: 10.1371/journal.pone.0050976

Katina, S., Farbakova, J., Madari, A., Novak, M., and Zilka, N. (2016). Risk factors for canine cognitive dysfunction syndrome in Slovakia. *Acta Vet. Scand.* 58:17. doi: 10.1186/s13028-016-0196-5

Kelly, S. C., He, B., Perez, S. E., Ginsberg, S. D., Mufson, E. J., and Counts, S. E. (2017). Locus coeruleus cellular and molecular pathology during the progression of Alzheimer's disease. *Acta Neuropathol. Commun.* 5:8. doi: 10.1186/s40478-017-0411-2

Kennedy, M. E., Stamford, A. W., Chen, X., Cox, K., Cumming, J. N., Dockendorf, M. F., et al. (2016). The BACE1 inhibitor verubecestat MK-8931 reduces CNS β-amyloid in animal models and in Alzheimer's disease patients. *Sci. Transl. Med.* 8:363ra150. doi: 10.1126/scitranslmed.aad9704

Kobatake, Y., Sakai, H., Tsukui, T., Yamato, O., Kohyama, M., Sasaki, J., et al. (2016). Localization of a mutant SOD1 protein in E40K-heterozygous dogs: implications for non-cell-autonomous pathogenesis of degenerative myelopathy. *J. Neurol. Sci.* 372, 369–378. doi: 10.1016/j.jns.2016.10.034

Kumar-Singh, S. (2008). Cerebral amyloid angiopathy: pathogenetic mechanisms and link to dense amyloid plaques. *Genes Brain Behav.* 7(Suppl. 1), 67–82. doi: 10.1111/j.1601-183X.2007.00380.x

Kuroki, K., Uchida, K., Kiatipattanasakul, W., Nakamura, S., Yamaguchi, R., Nakayama, H., et al. (1997). Immunohistochemical detection of tau protein in various non-human animal brains. *Neuropathology* 17, 174–180. doi: 10.1111/j.1440-1789.1997.tb00034.x

Landsberg, G. (2005). Therapeutic agents for the treatment of cognitive dysfunction syndrome in senior dogs. *Prog. Neuropsychopharmacol. Biol. Psychiatry* 29, 471–479. doi: 10.1016/j.pnpbp.2004.12.012

Landsberg, G. M., Nichol, J., and Araujo, J. A. (2012). Cognitive dysfunction syndrome: a disease of canine and feline brain aging. *Vet. Clin. North Am. Small Anim. Pract.* 42, 749–768, vii. doi: 10.1016/j.cvsm.2012.04.003

Langer, F., Eisele, Y. S., Fritschi, S. K., Staufenbiel, M., Walker, L. C., and Jucker, M. (2011). Soluble Aβ seeds are potent inducers of cerebral β-amyloid deposition. *J. Neurosci.* 31, 14488–14495. doi: 10.1523/JNEUROSCI.3088-11.2011

Lansbury, P. T., and Lashuel, H. A. (2006). A century-old debate on protein aggregation and neurodegeneration enters the clinic. *Nature* 443, 774–779. doi: 10.1038/nature05290

Liu, W., Xie, Y., Ma, J., Luo, X., Nie, P., Zuo, Z., et al. (2015). IBS: an illustrator for the presentation and visualization of biological sequences. *Bioinformatics* 31, 3359–3361. doi: 10.1093/bioinformatics/btv362

Lopez, O. L., Kuller, L. H., Mehta, P. D., Becker, J. T., Gach, H. M., Sweet, R. A., et al. (2008). Plasma amyloid levels and the risk of AD in normal subjects in the Cardiovascular Health Study. *Neurology* 70, 1664–1671. doi: 10.1212/01.wnl.0000306696.82017.66

Madari, A., Farbakova, J., Katina, S., Smolek, T., Novak, P., Weissova, T., et al. (2015). Assessment of severity and progression of canine cognitive dysfunction syndrome using the CAnine DEmentia Scale (CADES). *Appl Anim. Behav. Sci.* 171, 138–145. doi: 10.1016/j.applanim.2015.08.034

Madeira, F., Park, Y. M., Lee, J., Buso, N., Gur, T., Madhusoodanan, N., et al. (2019). The EMBL-EBI search and sequence analysis tools APIs in 2019. *Nucleic Acids Res.* [Epub ahead of print].

Magyar, K. (2011). The pharmacology of selegiline. *Int. Rev. Neurobiol.* 100, 65–84. doi: 10.1016/B978-0-12-386467-3.00004-2

Mahley, R. W., and Rall, S. C. (1999). Is epsilon4 the ancestral human apoE allele? *Neurobiol. Aging* 20, 429–430. doi: 10.1016/s0197-4580(99)00081-0

Mäkelä, M., Kaivola, K., Valori, M., Paetau, A., Polvikoski, T., Singleton, A. B., et al. (2018). Alzheimer risk loci and associated neuropathology in a population-based study (Vantaa 85+). *Neurol. Genet.* 4:e211. doi: 10.1212/NXG.0000000000000211

Martin, S. B., Dowling, A. L. S., and Head, E. (2011). Therapeutic interventions targeting Beta amyloid pathogenesis in an aging dog model. *Curr. Neuropharmacol.* 9, 651–661. doi: 10.2174/157015911798376217

Mattsson, N., Rajendran, L., Zetterberg, H., Gustavsson, M., Andreasson, U., Olsson, M., et al. (2012). BACE1 inhibition induces a specific cerebrospinal fluid β-amyloid pattern that identifies drug effects in the central nervous system. *PLoS One* 7:e31084. doi: 10.1371/journal.pone.0031084

May, P. C., Willis, B. A., Lowe, S. L., Dean, R. A., Monk, S. A., Cocke, P. J., et al. (2015). The potent BACE1 inhibitor LY2886721 elicits robust central Aβ pharmacodynamic responses in mice, dogs, and humans. *J. Neurosci.* 35, 1199–1210. doi: 10.1523/JNEUROSCI.4129-14.2015

Mayeux, R., Honig, L. S., Tang, M.-X., Manly, J., Stern, Y., Schupf, N., et al. (2003). Plasma A[beta]40 and A[beta]42 and Alzheimer's disease: relation to age, mortality, and risk. *Neurology* 61, 1185–1190.

McKhann, G. M., Knopman, D. S., Chertkow, H., Hyman, B. T., Jack, C. R., Kawas, C. H., et al. (2011). The diagnosis of dementia due to Alzheimer's disease: recommendations from the National Institute on Aging-Alzheimer's Association workgroups on diagnostic guidelines for Alzheimer's disease. *Alzheimers Dement.* 7, 263–269. doi: 10.1016/j.jalz.2011.03.005

Medeiros, R., Baglietto-Vargas, D., and LaFerla, F. M. (2011). The role of tau in Alzheimer's disease and related disorders. *CNS Neurosci. Ther.* 17, 514–524. doi: 10.1111/j.1755-5949.2010.00177.x

Meyer-Luehmann, M., Coomaraswamy, J., Bolmont, T., Kaeser, S., Schaefer, C., Kilger, E., et al. (2006). Exogenous induction of cerebral beta-amyloidogenesis is governed by agent and host. *Science* 313, 1781–1784. doi: 10.1126/science.1131864

Milgram, N. W., Head, E., Zicker, S. C., Ikeda-Douglas, C., Murphey, H., Muggenberg, B. A., et al. (2004). Long-term treatment with antioxidants and a program of behavioral enrichment reduces age-dependent impairment in discrimination and reversal learning in beagle dogs. *Exp. Gerontol.* 39, 753–765. doi: 10.1016/j.exger.2004.01.007

Müller, U. C., Deller, T., and Korte, M. (2017). Not just amyloid: physiological functions of the amyloid precursor protein family. *Nat. Rev. Neurosci.* 18, 281–298. doi: 10.1038/nrn.2017.29

Nakamae, S., Kobatake, Y., Suzuki, R., Tsukui, T., Kato, S., Yamato, O., et al. (2015). Accumulation and aggregate formation of mutant superoxide dismutase 1 in canine degenerative myelopathy. *Neuroscience* 303, 229–240. doi: 10.1016/j.neuroscience.2015.06.066

Neilson, J. C., Hart, B. L., Cliff, K. D., and Ruehl, W. W. (2001). Prevalence of behavioral changes associated with age-related cognitive impairment in dogs. *J. Am. Vet. Med. Assoc.* 218, 1787–1791. doi: 10.2460/javma.2001.218.1787

Nelson, P. T., Alafuzoff, I., Bigio, E. H., Bouras, C., Braak, H., Cairns, N. J., et al. (2012). Correlation of Alzheimer disease neuropathologic changes with cognitive status: a review of the literature. *J. Neuropathol. Exp. Neurol.* 71, 362–381. doi: 10.1097/NEN.0b013e31825018f7

Nelson, P. T., Greenberg, S. G., and Saper, C. B. (1994). Neurofibrillary tangles in the cerebral cortex of sheep. *Neurosci. Lett.* 170, 187–190. doi: 10.1016/0304-3940(94)90270-4

Nelson, P. T., Pious, N. M., Jicha, G. A., Wilcock, D. M., Fardo, D. A., Estus, S., et al. (2013). APOE-ε2 and APOE-ε4 Correlate with Increased Amyloid Accumulation in Cerebral Vasculature. *J. Neuropathol. Exp. Neurol.* 72, 708–715. doi: 10.1097/NEN.0b013e31829a25b9

Nelson, P. T., and Saper, C. B. (1995). Ultrastructure of neurofibrillary tangles in the cerebral cortex of sheep. *Neurobiol. Aging* 16, 315–323. doi: 10.1016/0197-4580(94)00175-z

Nešić, S., Kukolj, V., Marinkoviæ, D., Vuèiæeviæ, I., and Jovanoviæ, M. (2017). Histological and immunohistochemical characteristics of cerebral amyloid angiopathy in elderly dogs. *Vet. Q.* 37, 1–7. doi: 10.1080/01652176.2016.1235301

Neumann, U., Ufer, M., Jacobson, L. H., Rouzade-Dominguez, M.-L., Huledal, G., Kolly, C., et al. (2018). The BACE-1 inhibitor CNP520 for prevention trials in Alzheimer's disease. *EMBO Mol. Med.* 10:e9316. doi: 10.15252/emmm.201809316

Neuner, S. M., Heuer, S. E., Huentelman, M. J., O'Connell, K. M. S., and Kaczorowski, C. C. (2018). Harnessing genetic complexity to enhance translatability of Alzheimer's disease mouse models: a path toward precision medicine. *Neuron* 101, 399–411.e5. doi: 10.1016/j.neuron.2018.11.040

Neus Bosch, M., Pugliese, M., Andrade, C., Gimeno-Bayón, J., Mahy, N., and Rodriguez, M. J. (2015). Amyloid-β immunotherapy reduces amyloid plaques and astroglial reaction in aged domestic dogs. *Neurodegener. Dis.* 15, 24–37. doi: 10.1159/000368672

Noh, D., Choi, S., Choi, H., Lee, Y., and Lee, K. (2017). Evaluation of interthalamic adhesion size as an indicator of brain atrophy in dogs with and without cognitive dysfunction. *Vet. Radiol. Ultrasound* 58, 581–587. doi: 10.1111/vru.12528

Nordberg, A., Kadir, A., Andreasen, N., Almkvist, O., Wall, A., Långström, B., et al. (2015). Correlations between Alzheimer's Disease Cerebrospinal Fluid Biomarkers and Cerebral Glucose Metabolism after 12 Months of Phenserine Treatment. *J. Alzheimers Dis.* 47, 691–704. doi: 10.3233/JAD-132474

Novak, P., Kontsekova, E., Zilka, N., and Novak, M. (2018). Ten Years of Tau-Targeted Immunotherapy: The Path Walked and the Roads Ahead. *Front. Neurosci.* 12:798. doi: 10.3389/fnins.2018.00798

Oikawa, N., Kimura, N., and Yanagisawa, K. (2010). Alzheimer-type tau pathology in advanced aged nonhuman primate brains harboring substantial amyloid deposition. *Brain Res.* 1315, 137–149. doi: 10.1016/j.brainres.2009.12.005

Olszewska, D. A., Lonergan, R., Fallon, E. M., and Lynch, T. (2016). Genetics of Frontotemporal Dementia. *Curr. Neurol. Neurosci. Rep.* 16:107. doi: 10.1007/s11910-016-0707-9

Opii, W. O., Joshi, G., Head, E., Milgram, N. W., Muggenburg, B. A., Klein, J. B., et al. (2008). Proteomic identification of brain proteins in the canine model of human aging following a long-term treatment with antioxidants and a program of behavioral enrichment: relevance to Alzheimer's disease. *Neurobiol. Aging* 29, 51–70. doi: 10.1016/j.neurobiolaging.2006.09.012

Osella, M. C., Re, G., Odore, R., Girardi, C., Badino, P., Barbero, R., et al. (2007). Canine cognitive dysfunction syndrome: prevalence, clinical signs and treatment with a neuroprotective nutraceutical. *Appl. Anim. Behav. Sci.* 105, 297–310. doi: 10.1016/j.applanim.2006.11.007

Ossenkoppele, R., Schonhaut, D. R., Schöll, M., Lockhart, S. N., Ayakta, N., Baker, S. L., et al. (2016). Tau PET patterns mirror clinical and neuroanatomical variability in Alzheimer's disease. *Brain* 139, 1551–1567. doi: 10.1093/brain/aww027

Ozawa, M., Chambers, J. K., Uchida, K., and Nakayama, H. (2016). The Relation between canine cognitive dysfunction and age-related brain lesions. *J. Vet. Med. Sci.* 78, 997–1006. doi: 10.1292/jvms.15-0624

Perez, S. E., Raghanti, M. A., Hof, P. R., Kramer, L., Ikonomovic, M. D., Lacor, P. N., et al. (2013). Alzheimer's disease pathology in the neocortex and hippocampus of the western lowland gorilla (*Gorilla gorilla* gorilla). *J. Comp. Neurol.* 521, 4318–4338. doi: 10.1002/cne.23428

Perez, S. E., Sherwood, C. C., Cranfield, M. R., Erwin, J. M., Mudakikwa, A., Hof, P. R., et al. (2016). Early Alzheimer's disease-type pathology in the frontal cortex of wild mountain gorillas (*Gorilla beringei beringei*). *Neurobiol. Aging* 39, 195–201. doi: 10.1016/j.neurobiolaging.2015.12.017

Pesini, P., Boada, M., Martínez-Lage, P., Tárraga, L., Monleón, I., Pérez-Grijalva, V., et al. (2009). Differences in beta amyloid pool in blood discriminate between amnesic mild cognitive impairment patients and healthy controls. *J. Nutr. Health Aging* 13:850.

Pugliese, M., Carrasco, J. L., Andrade, C., Mas, E., Mascort, J., and Mahy, N. (2005). Severe cognitive impairment correlates with higher cerebrospinal fluid levels of lactate and pyruvate in a canine model of senile dementia. *Prog. Neuropsychopharmacol. Biol. Psychiatry* 29, 603–610. doi: 10.1016/j.pnpbp.2005.01.017

Pugliese, M., Mascort, J., Mahy, N., and Ferrer, I. (2006). Diffuse beta-amyloid plaques and hyperphosphorylated tau are unrelated processes in aged dogs with behavioral deficits. *Acta Neuropathol.* 112, 175–183. doi: 10.1007/s00401-006-0087-3

Racine, A. M., Koscik, R. L., Nicholas, C. R., Clark, L. R., Okonkwo, O. C., Oh, J. M., et al. (2016). Cerebrospinal fluid ratios with Aβ42 predict preclinical brain β-amyloid accumulation. *Alzheimers Dement.* 2, 27–38. doi: 10.1016/j.dadm.2015.11.006

Reid, S. J., Mckean, N. E., Henty, K., Portelius, E., Blennow, K., Rudiger, S. R., et al. (2017). Alzheimer's disease markers in the aged sheep (*Ovis aries*). *Neurobiol. Aging* 58, 112–119. doi: 10.1016/j.neurobiolaging.2017.06.020

Reilly, C. E. (2001). Neprilysin content is reduced in Alzheimer brain areas. *J. Neurol.* 248, 159–160. doi: 10.1007/s004150170259

Rème, C. A., Dramard, V., Kern, L., Hofmans, J., Halsberghe, C., and Mombiela, D. V. (2008). Effect of S-adenosylmethionine tablets on the reduction of age-related mental decline in dogs: a double-blinded, placebo-controlled trial. *Vet. Ther.* 9, 69–82.

Revesz, T., Holton, J. L., Lashley, T., Plant, G., Rostagno, A., Ghiso, J., et al. (2002). Sporadic and familial cerebral amyloid angiopathies. *Brain Pathol.* 12, 343–357. doi: 10.1111/j.1750-3639.2002.tb00449.x

Rodrigues, L. L., Mesquita, L. P., Costa, R. C., Gomes, R. G., Biihrer, D. A., and Maiorka, P. C. (2018). Multiple infarcts and hemorrhages in the central nervous system of a dog with cerebral amyloid angiopathy: a case report. *BMC Vet. Res.* 14:370. doi: 10.1186/s12917-018-1700-0

Rodriguez-Callejas, J. D., Fuchs, E., and Perez-Cruz, C. (2016). Evidence of Tau Hyperphosphorylation and Dystrophic Microglia in the Common Marmoset. *Front. Aging Neurosci.* 8:315. doi: 10.3389/fnagi.2016.00315

Rofina, J. E., van Ederen, A. M., Toussaint, M. J. M., Secrève, M., van der Spek, A., van der Meer, I., et al. (2006). Cognitive disturbances in old dogs suffering from the canine counterpart of Alzheimer's disease. *Brain Res.* 1069, 216–226. doi: 10.1016/j.brainres.2005.11.021

Rosado, B., González-Martínez, A., Pesini, P., García-Belenguer, S., Palacio, J., Villegas, A., et al. (2012). Effect of age and severity of cognitive dysfunction on spontaneous activity in pet dogs - part 1: locomotor and exploratory behaviour. *Vet. J.* 194, 189–195. doi: 10.1016/j.tvjl.2012.03.025

Rosen, D. R., Siddique, T., Patterson, D., Figlewicz, D. A., Sapp, P., Hentati, A., et al. (1993). Mutations in Cu/Zn superoxide dismutase gene are associated with familial amyotrophic lateral sclerosis. *Nature* 362, 59–62. doi: 10.1038/362059a0

Rosen, R. F., Farberg, A. S., Gearing, M., Dooyema, J., Long, P. M., Anderson, D. C., et al. (2008). Tauopathy with paired helical filaments in an aged chimpanzee. *J. Comp. Neurol.* 509, 259–270. doi: 10.1002/cne.21744

Rossi, G., Giaccone, G., Maletta, R., Morbin, M., Capobianco, R., Mangieri, M., et al. (2004). A family with Alzheimer disease and strokes associated with A713T mutation of the APP gene. *Neurology* 63, 910–912. doi: 10.1212/01.wnl.0000137048.80666.86

Ruehl, W. W., Bruyette, D. S., DePaoli, A., Cotman, C. W., Head, E., Milgram, N. W., et al. (1995). Canine cognitive dysfunction as a model for human age-related cognitive decline, dementia and Alzheimer's disease: clinical presentation, cognitive testing, pathology and response to 1-deprenyl therapy. *Prog. Brain Res.* 106, 217–225. doi: 10.1016/s0079-6123(08)61218-2

Ruehl, W. W., Entriken, T. L., Muggenburg, B. A., Bruyette, D. S., Griffith, W. C., and Hahn, F. F. (1997). Treatment with L-deprenyl prolongs life in elderly dogs. *Life Sci.* 61, 1037–1044. doi: 10.1016/s0024-3205(97)00611-5

Rusbridge, C., Salguero, F. J., David, M. A., Faller, K. M. E., Bras, J. T., Guerreiro, R. J., et al. (2018). An aged Canid with behavioral deficits exhibits blood and cerebrospinal fluid amyloid beta oligomers. *Front. Aging Neurosci.* 10:7. doi: 10.3389/fnagi.2018.00007

Salvin, H. E., McGreevy, P. D., Sachdev, P. S., and Valenzuela, M. J. (2011). The canine cognitive dysfunction rating scale (CCDR): a data-driven and ecologically relevant assessment tool. *Vet. J.* 188, 331–336. doi: 10.1016/j.tvjl.2010.05.014

Salvin, H. E., McGreevy, P. D., Sachdev, P. S., and Valenzuela, M. J. (2010). Under diagnosis of canine cognitive dysfunction: a cross-sectional survey of older companion dogs. *Vet. J.* 184, 277–281. doi: 10.1016/j.tvjl.2009.11.007

Sarasa, L., Gallego, C., Monleón, I., Olvera, A., Canudas, J., Montañés, M., et al. (2010). Cloning, sequencing and expression in the dog of the main amyloid precursor protein isoforms and some of the enzymes related with their processing. *Neuroscience* 171, 1091–1101. doi: 10.1016/j.neuroscience.2010.09.042

Sarasa, M., and Pesini, P. (2009). Natural non-trasgenic animal models for research in Alzheimer's disease. *Curr. Alzheimer Res.* 6, 171–178. doi: 10.2174/156720509787602834

Sardar Sinha, M., Ansell-Schultz, A., Civitelli, L., Hildesjö, C., Larsson, M., Lannfelt, L., et al. (2018). Alzheimer's disease pathology propagation by exosomes containing toxic amyloid-beta oligomers. *Acta Neuropathol.* 136, 41–56. doi: 10.1007/s00401-018-1868-1

Schliebs, R., and Arendt, T. (2011). The cholinergic system in aging and neuronal degeneration. *Behav. Brain Res.* 221, 555–563. doi: 10.1016/j.bbr.2010.11.058

Schmidt, F., Boltze, J., Jäger, C., Hofmann, S., Willems, N., Seeger, J., et al. (2015). Detection and Quantification of β-Amyloid, Pyroglutamyl Aβ, and Tau in Aged Canines. *J. Neuropathol. Exp. Neurol.* 74, 912–923. doi: 10.1097/NEN.0000000000000230

Schultz, C., Dehghani, F., Hubbard, G. B., Thal, D. R., Struckhoff, G., Braak, E., et al. (2000a). Filamentous tau pathology in nerve cells, astrocytes, and oligodendrocytes of aged baboons. *J. Neuropathol. Exp. Neurol.* 59, 39–52. doi: 10.1093/jnen/59.1.39

Schultz, C., Hubbard, G. B., Rüb, U., Braak, E., and Braak, H. (2000b). Age-related progression of tau pathology in brains of baboons. *Neurobiol. Aging* 21, 905–912. doi: 10.1016/s0197-4580(00)00176-7

Schütt, T., Helboe, L., Pedersen, L. Ø., Waldemar, G., Berendt, M., and Pedersen, J. T. (2016). Dogs with cognitive dysfunction as a spontaneous model for early Alzheimer's disease: a translational study of neuropathological and inflammatory markers. *J. Alzheimers Dis.* 52, 433–449. doi: 10.3233/JAD-151085

Schütt, T., Toft, N., and Berendt, M. (2015). Cognitive Function, Progression of Age-related Behavioral Changes, Biomarkers, and Survival in Dogs More Than 8 Years Old. *J. Vet. Intern. Med.* 29, 1569–1577. doi: 10.1111/jvim.13633

Selkoe, D. J. (1991). The molecular pathology of Alzheimer's disease. *Neuron* 6, 487–498.

Selkoe, D. J. (1997). Alzheimer's disease: genotypes, phenotypes, and treatments. *Science* 275, 630–631. doi: 10.1126/science.275.5300.630

Sellal, F., Wallon, D., Martinez-Almoyna, L., Marelli, C., Dhar, A., Oesterlé, H., et al. (2017). APP Mutations in Cerebral Amyloid Angiopathy with or without Cortical Calcifications: Report of Three Families and a Literature Review. *J. Alzheimers Dis.* 56, 37–46. doi: 10.3233/JAD-160709

Serizawa, S., Chambers, J. K., and Une, Y. (2012). Beta amyloid deposition and neurofibrillary tangles spontaneously occur in the brains of captive cheetahs (*Acinonyx jubatus*). *Vet. Pathol.* 49, 304–312. doi: 10.1177/0300985811410719

Shabir, O., Berwick, J., and Francis, S. E. (2018). Neurovascular dysfunction in vascular dementia, Alzheimer's and atherosclerosis. *BMC Neurosci.* 19:62. doi: 10.1186/s12868-018-0465-5

Siwak, C. T., Gruet, P., Woehrlé, F., Muggenburg, B. A., Murphey, H. L., and Milgram, N. W. (2000). Comparison of the effects of adrafinil, propentofylline, and nicergoline on behavior in aged dogs. *Am. J. Vet. Res.* 61, 1410–1414. doi: 10.2460/ajvr.2000.61.1410

Siwak, C. T., Tapp, P. D., Head, E., Zicker, S. C., Murphey, H. L., Muggenburg, B. A., et al. (2005). Chronic antioxidant and mitochondrial cofactor administration improves discrimination learning in aged but not young dogs. *Prog. Neuropsychopharmacol. Biol. Psychiatry* 29, 461–469. doi: 10.1016/j.pnpbp.2004.12.011

Siwak-Tapp, C. T., Head, E., Muggenburg, B. A., Milgram, N. W., and Cotman, C. W. (2008). Region specific neuron loss in the aged canine hippocampus is reduced by enrichment. *Neurobiol. Aging* 29, 39–50. doi: 10.1016/j.neurobiolaging.2006.09.018

Smolek, T., Madari, A., Farbakova, J., Kandrac, O., Jadhav, S., Cente, M., et al. (2016). Tau hyperphosphorylation in synaptosomes and neuroinflammation are associated with canine cognitive impairment. *J. Comp. Neurol.* 524, 874–895. doi: 10.1002/cne.23877

Snigdha, S., Astarita, G., Piomelli, D., and Cotman, C. W. (2012). Effects of diet and behavioral enrichment on free fatty acids in the aged canine brain. *Neuroscience* 202, 326–333. doi: 10.1016/j.neuroscience.2011.12.002

Snigdha, S., Berchtold, N., Astarita, G., Saing, T., Piomelli, D., and Cotman, C. W. (2011). Dietary and behavioral interventions protect against age related activation of caspase cascades in the canine brain. *PLoS One* 6:e24652. doi: 10.1371/journal.pone.0024652

Studzinski, C. M., Araujo, J. A., and Milgram, N. W. (2005). The canine model of human cognitive aging and dementia: pharmacological validity of the model for assessment of human cognitive-enhancing drugs. *Prog. Neuropsychopharmacol. Biol. Psychiatry* 29, 489–498. doi: 10.1016/j.pnpbp.2004.12.014

Studzinski, C. M., Christie, L.-A., Araujo, J. A., Burnham, W. M., Head, E., Cotman, C. W., et al. (2006). Visuospatial function in the beagle dog: an early marker of cognitive decline in a model of human aging and dementia. *Neurobiol. Learn. Mem.* 86, 197–204. doi: 10.1016/j.nlm.2006.02.005

Tapp, P. D., Siwak, C. T., Estrada, J., Head, E., Muggenburg, B. A., Cotman, C. W., et al. (2003). Size and reversal learning in the beagle dog as a measure of executive function and inhibitory control in aging. *Learn. Mem.* 10, 64–73. doi: 10.1101/lm.54403

Tapp, P. D., Siwak, C. T., Gao, F. Q., Chiou, J.-Y., Black, S. E., Head, E., et al. (2004). Frontal lobe volume, function, and beta-amyloid pathology in a canine model of aging. *J. Neurosci.* 24, 8205–8213. doi: 10.1523/JNEUROSCI.1339-04.2004

Terry, R. D., Masliah, E., Salmon, D. P., Butters, N., DeTeresa, R., Hill, R., et al. (1991). Physical basis of cognitive alterations in Alzheimer's disease: synapse loss is the major correlate of cognitive impairment. *Ann. Neurol.* 30, 572–580. doi: 10.1002/ana.410300410

Thatte, U. (2005). Phenserine Axonyx. *Curr. Opin. Investig. Drugs* 6, 729–739.

Toepper, M. (2017). Dissociating Normal Aging from Alzheimer's Disease: A View from Cognitive Neuroscience. *J. Alzheimers Dis.* 57, 331–352. doi: 10.3233/JAD-161099

Uchida, K., Miyauchi, Y., Nakayama, H., and Goto, N. (1990). Amyloid angiopathy with cerebral hemorrhage and senile plaque in aged dogs. *Nippon Juigaku Zasshi* 52, 605–611. doi: 10.1292/jvms1939.52.605

Uchida, K., Nakayama, H., Tateyama, S., and Goto, N. (1992). Immunohistochemical analysis of constituents of senile plaques and cerebro-vascular amyloid in aged dogs. *J. Vet. Med. Sci.* 54, 1023–1029. doi: 10.1292/jvms.54.1023

Villarreal, S., Zhao, F., Hyde, L. A., Holder, D., Forest, T., Sondey, M., et al. (2017). Chronic Verubecestat Treatment Suppresses Amyloid Accumulation in Advanced Aged Tg2576-AβPPswe Mice Without Inducing Microhemorrhage. *J. Alzheimers Dis.* 59, 1393–1413. doi: 10.3233/JAD-170056

Vite, C. H., and Head, E. (2014). Aging in the canine and feline brain. *Vet. Clin. North Am. Small Anim. Pract.* 44, 1113–1129. doi: 10.1016/j.cvsm.2014.07.008

Walker, L. C., and Jucker, M. (2017). The Exceptional Vulnerability of Humans to Alzheimer's Disease. *Trends Mol. Med.* 23, 534–545. doi: 10.1016/j.molmed.2017.04.001

West, M. J., Kawas, C. H., Martin, L. J., and Troncoso, J. C. (2000). The CA1 region of the human hippocampus is a hot spot in Alzheimer's disease. *Ann. N. Y. Acad. Sci.* 908, 255–259. doi: 10.1111/j.1749-6632.2000.tb06652.x

Whitehouse, P. J., Price, D. L., Clark, A. W., Coyle, J. T., and DeLong, M. R. (1981). Alzheimer disease: evidence for selective loss of cholinergic neurons in the nucleus basalis. *Ann. Neurol.* 10, 122–126. doi: 10.1002/ana.410100203

Winblad, B., Amouyel, P., Andrieu, S., Ballard, C., Brayne, C., Brodaty, H., et al. (2016). Defeating Alzheimer's disease and other dementias: a priority for European science and society. *Lancet Neurol.* 15, 455–532. doi: 10.1016/S1474-4422(16)00062-4

Winblad, B., Giacobini, E., Frölich, L., Friedhoff, L. T., Bruinsma, G., Becker, R. E., et al. (2010). Phenserine Efficacy in Alzheimer's disease. *J. Alzheimers Dis.* 22, 1201–1208. doi: 10.3233/JAD-2010-101311

Wisniewski, T., and Drummond, E. (2016). Developing therapeutic vaccines against Alzheimer's disease. *Expert Rev. Vaccines* 15, 401–415. doi: 10.1586/14760584.2016.1121815

Wolfe, C. M., Fitz, N. F., Nam, K. N., Lefterov, I., and Koldamova, R. (2018). The Role of APOE and TREM2 in Alzheimer's Disease-Current Understanding and Perspectives. *Int. J. Mol. Sci.* 20:E81. doi: 10.3390/ijms20010081

Yasojima, K., McGeer, E. G., and McGeer, P. L. (2001). Relationship between beta amyloid peptide generating molecules and neprilysin in Alzheimer disease and normal brain. *Brain Res.* 919, 115–121. doi: 10.1016/s0006-8993(01)03008-6

Youssef, S. A., Capucchio, M. T., Rofina, J. E., Chambers, J. K., Uchida, K., Nakayama, H., et al. (2016). Pathology of the aging brain in domestic and laboratory animals, and animal models of human neurodegenerative diseases. *Vet. Pathol.* 53, 327–348. doi: 10.1177/0300985815623997

Yu, C.-H., Song, G.-S., Yhee, J.-Y., Kim, J.-H., Im, K.-S., Nho, W.-G., et al. (2011). Histopathological and immunohistochemical comparison of the brain

of human patients with Alzheimer's disease and the brain of aged dogs with cognitive dysfunction. *J. Comp. Pathol.* 145, 45–58. doi: 10.1016/j.jcpa.2010.11.004

Yu, L., Boyle, P. A., Nag, S., Leurgans, S., Buchman, A. S., Wilson, R. S., et al. (2015). APOE and cerebral amyloid angiopathy in community dwelling older persons. *Neurobiol. Aging* 36, 2946–2953. doi: 10.1016/j.neurobiolaging.2015.08.008

Zheng, T., Pu, J., Chen, Y., Mao, Y., Guo, Z., Pan, H., et al. (2017). Plasma exosomes spread and cluster around β-amyloid plaques in an animal model of Alzheimer's disease. *Front. Aging Neurosci.* 9:12. doi: 10.3389/fnagi.2017.00012

Conflict of Interest Statement: The authors declare that the research was conducted in the absence of any commercial or financial relationships that could be construed as a potential conflict of interest.

Copyright © 2019 Prpar Mihevc and Majdič. This is an open-access article distributed under the terms of the Creative Commons Attribution License (CC BY). The use, distribution or reproduction in other forums is permitted, provided the original author(s) and the copyright owner(s) are credited and that the original publication in this journal is cited, in accordance with accepted academic practice. No use, distribution or reproduction is permitted which does not comply with these terms.

frontiers in Neurology

MINI REVIEW
published: 13 June 2019
doi: 10.3389/fneur.2019.00624

Telomere Length: A Potential Biomarker for the Risk and Prognosis of Stroke

Yanjun Tian[1†], *Shuai Wang*[2,3†], *Fengjuan Jiao*[2,3†], *Qingsheng Kong*[1], *Chuanxin Liu*[1] and *Yili Wu*[1,2,3*]

[1] Collaborative Innovation Center for Birth Defect Research and Transformation of Shandong Province, Jining Medical University, Jining, China, [2] Shandong Collaborative Innovation Center for Diagnosis, Treatment and Behavioral Interventions of Mental Disorders, Institute of Mental Health, Jining Medical University, Jining, China, [3] Shandong Key Laboratory of Behavioral Medicine, School of Mental Health, Jining Medical University, Jining, China

Stroke is one of the leading causes of death and disability worldwide. Age is associated with increased risk of stroke, while telomere length shortening plays a pivotal role in the process of aging. Moreover, telomere length shortening is associated with many risk factors of stroke in addition to age. Accumulated evidence shows that short leukocyte telomere length is not only associated with stroke occurrence but also associated with post-stroke recovery in the elderly population. In this review, we aimed to summarize the association between leukocyte telomere length and stroke, and discuss that telomere length might serve as a potential biomarker to predict the risk and prognosis of stroke.

Keywords: telomere, telomerase, telomere length, risk of stroke, prognosis of stroke

OPEN ACCESS

Edited by:
Gregory Jaye Bix,
University of Kentucky, United States

Reviewed by:
Marc De Buyzere,
Ghent University, Belgium
Robert Y. Zee,
Tufts Medical Center, United States

***Correspondence:**
Yili Wu
yili_wu2004@yahoo.ca;
wuyili@mail.jnmc.edu.cn

[†] *These authors have contributed equally to this work*

Specialty section:
This article was submitted to Stroke, a section of the journal Frontiers in Neurology

Received: *14 December 2018*
Accepted: *28 May 2019*
Published: *13 June 2019*

Citation:
Tian Y, Wang S, Jiao F, Kong Q, Liu C and Wu Y (2019) Telomere Length: A Potential Biomarker for the Risk and Prognosis of Stroke. Front. Neurol. 10:624. doi: 10.3389/fneur.2019.00624

INTRODUCTION

Stroke is an acute cerebrovascular disease caused by the disruption of blood supply. As the second leading cause of death and the third leading cause of disability worldwide (1), stroke brings heavy burden to both family and health care system. The incidence of stroke is increased with age and ∼65% of stroke cases occur in individuals older than 65 years. In addition to age *per se*, various risk factors of stroke are age-related, including hypertension, atherosclerosis, atrial fibrillation, high cholesterol, and diabetes. Telomere length (TL) shortening is associated with age and many other risk factors of stroke. Consistently, a number of studies indicated that stroke occurrence is associated with short leukocyte telomere length (LTL) (2–4). Moreover, accumulated evidence indicates that short LTL is also associated with the post-stroke recovery. Therefore, we aimed to summarize the association between LTL and stroke, and discuss the potential of TL as a biomarker to predict the risk and prognosis of stroke.

TL MAINTENANCE

Telomeres

Human telomeres are specialized structure of DNA-protein complex, capping the end of linear chromosomes. Human telomeric DNA consists of a variable number of tandem repeats of double-stranded TTAGGG and a 3′ G-rich single-stranded overhang, known as the G-tail (5). The length of double-stranded repeats ranges from 2 to 30 kb, while the length of 3′ overhang is around 150 nt. The invasion of 3′ G-tail into the double-stranded region forms a high order structure and a triple-stranded structure, called T-(telomere) loop and D-(displacement) loop, respectively

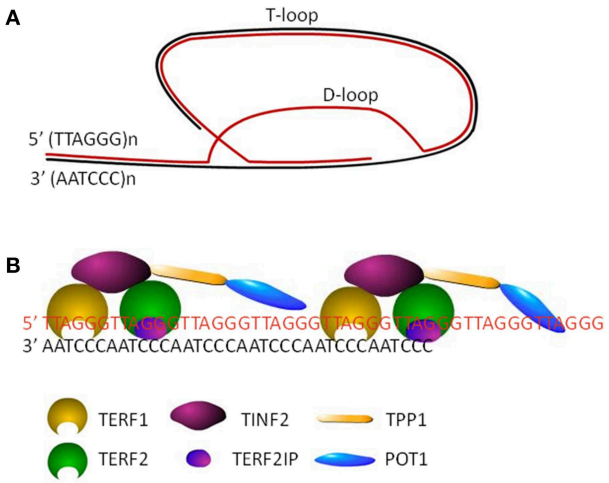

FIGURE 1 | The structure of telomeres. **(A)** Cap structure of telomeres consists of a T-loop and a D-loop. **(B)** The shelterin complex, including TERF1, TERF2, TINF2, TERF2IP, TPP1, and POT1, maintains the stability of loop structures by binding to the telomeric DNA.

(6) (**Figure 1A**). Shelterin complex, the protein components of telomere, includes six subunits, telomeric repeat binding factor 1 (TERF1), telomeric repeat binding factor 2 (TERF2), TERF2 interacting protein (TERF2IP), TERF1-interacting nuclear factor 2 (TINF2), tripeptidyl peptidase I (TPP1), and protection of telomeres 1 (POT1) (**Figure 1B**). TERF1/TERF2 and POT1 bind directly to double-stranded and single-stranded telomeric DNA, respectively (**Figure 1B**). TERF2IP, the partner of TERF2, interacts solely with TERF2, while TINF2 connects TERF1, and TERF2. POT1 is tethered to TERF1 and TERF2 via an interaction between TPP1 and TINF2 (7). Telomeric DNA along with the shelterin protein complex maintains the specialized telomere structure and protects the ends of chromosomes from degradation, fusion, and recombination for maintaining genomic integrity (8). Moreover, mammalian CTC1-STN1-TEN1 (CST) complex does localize to telomeres, which resembles the Cdc13-Stn1-Ten1 complex from *Saccharomyces cerevisiae* in that the STN1 and TEN1 subunits are conserved. CST complex binds to single strand DNA in a non-sequence specific manner and plays a key role in telomere replication (9–11). In addition, various DNA repair proteins contribute to telomere maintenance including TL maintenance via interacting with telomere proteins or modifying telomere proteins, including Polβ, FEN1, APE1, XPF-ERCC1 complex, and MRN complex which are involved in base excision repair pathway, nucleotide excision repair pathway and double strand break repair pathway, respectively (12–15).

Telomerase

Inability of DNA polymerase complex to replicate the 3′-end of the lagging strand in linear chromosomes leads to telomere shortening by each cycle of DNA replication during cell division, so-called end replication problem. As the number of cell division increases, TL is gradually shortened. When TL is reduced to the critical length, cells stop dividing and may enter cellular senescence or apoptosis (16). To counter this issue, human telomerase is responsible for synthesizing telomeric DNA to compensate the erosion of TL during DNA replication. Telomerase is a unique ribonucleoprotein enzymatic complex consisting of a RNA component and a protein component, telomerase RNA component (TERC), and telomerase reverse transcriptase (TERT). TERC is a non-coding RNA which is essential for telomere synthesis by serving as a template for the elongation of telomere 3′ overhang of the telomeric G-rich strand, while TERT catalyzes the process by its reverse transcriptase activity (17). In mammalian, telomerase is active only in germ cells, some types of stem cells and cancer cells, while most human somatic cells lack telomerase activity. Moreover, the activity of telomerase is regulated by the shelterin complex, CST complex, and telomeric repeat containing RNA (TERRA) which is transcribed from telomeric DNA. For example, shelterin complex control telomerase-dependent telomere elongation through a TERF1-mediated negative regulatory pathway, i.e., the more TERF1 is binding to telomeres, the less telomerase accesses to the ends of telomeres leading to less telomere elongation (13, 18, 19). In addition, the phosphoryaltion and PARylation of TERF1 promotes the release of TERF1 from telomeres contributing to telomere lengthening (13, 20, 21). Recently, the structure of telomerase with telomeric DNA has been resolved, which will promote the understanding the function of telomerase (22).

TL AND STROKE

TL maintenance is critical for human health as telomere shortening is associated with aging and various age-related diseases. Leukocyte telomere length (LTL) is served as a marker in a number of association studies of aging and age-related diseases (3, 23–26). The alteration of LTL has been observed in patients with stroke, which is one of the most common age-related diseases leading to death and disability. The positive association between short LTL and the risk of stroke was reported in the case-control studies from China, while the short LTL was also associated with post-stroke death (2, 25, 27, 28). In a 10-year prospective study from the United States, the positive association between short LTL and increased risk of stroke was only existed in the population ranging from 65 to 73 years old, but not in the population beyond 73 years old (29). A study from Europe showed that short LTL was associated with cerebrovascular accidents in the hypertensive patients with left ventricular hypertrophy aged 55–80 years (30). Moreover, short LTL was associated with higher mortality rate in patients with cardiovascular diseases aged 60 years or older (31). However, two nested case-control studies from the United States have not found the positive association between LTL and stroke (32, 33). In addition, no association between short LTL and stroke was found in a 29-year cohort study from Denmark (34). It has to be noted that the participants aged 30–55, 40–84, and 30–60 years, respectively, in the three studies when the blood samples were collected. It highly suggested that the positive

association between short LTL and the risk of stroke or post-stroke death might only exist in the aged population although further validation is necessary. Recently, two meta-analysis have been performed to investigate the association between TL and stroke. First, a meta-analysis including 11 studies showed that shortened TL is significantly associated with stroke, even though subgroup analysis showed equivocal results for both prospective ($n = 7$, $p = 0.051$) and retrospective ($n = 4$, $p = 0.067$) studies (35). The high heterogeneity, particularly age difference, and reduced sample size might contribute the equivocal results of the subgroup analysis. Another meta-analysis based on causal inference approaches using TL-related SNPs as instrumental variables did not support the causal effect of shorter TL on ischemic stroke (36). It has to be noted that age, one of the most important covariates, was not considered in this study. As previous studies do indicate that the positive association between short LTL and the risk of stroke or post-stroke death might only exist in the aged population, the effect of age might need to be taken into consideration in future studies. Currently, although mechanisms of the positive association between short LTL and stroke in the elderly remain elusive, multiple signaling pathways may contribute the positive association, e.g., apelin-apelin receptor mediated signaling pathway, histone deacetylases mediated epigenetic regulation (37, 38).

RISK FACTORS OF STROKE AND TL

Age

Age is one of the major risk factors of stroke (39). The incidence of stroke is increased with age, and the mean age at first-ever stroke was more than 68 years (40). TL is considered as a marker of the biological aging process because it shortens with each cell division. The estimated shortening rate is about 25–27 base pairs per year with individual difference (23, 41, 42). However, the actual LTL shortening rate is about 31–72 base pairs per year (23, 43). It suggests that many factors may contribute to LTL shortening in addition to end replication problem. For example, oxidative stress-induced oxidative DNA damage could lead to telomere uncapping and subsequent telomere shortening, while telomere shortening further enhances oxidative stress forming a vicious cycle (44–47). Age-related increase of oxidative damage is observed in human (48, 49). Moreover, increased evidence suggests that reduction of mitochondria function contributes to the aging process (50). Dysfunction of mitochondria contributes to age-related increase of oxidative stress, which in turn leads to TL shortening (51). Furthermore, multiple molecules (e.g., apelin, HDAC4, RCAN1, α-synuclein), altered in stroke are implicated in aging process, premature disorders (e.g., Down syndrome, Werner syndrome) and age-related disorders (e.g., Alzheimer's disease, Parkinson's disease, Huntington's disease) (37, 38, 52–66). Thus, age-related physiological or pathological alterations may also contribute to TL shortening.

Genetic Factors

Growing evidence indicates that genetic factors play a major role in stroke and family history of stroke is associated with increased stroke risk (67–69). Genomewide association study (GWAS) showed that the heritability for all ischemic stroke was 37.9%, while the heritability varied markedly in different subtypes of stroke, 32.6% for cardioembolic stroke, 40.3% for large-vessel stroke and 16.1% for small-vessel stroke (70). It was also reported that genetic factors appeared to be more important in large-vessel and small-vessel strokes than in cardioembolic stroke (71). Moreover, various genetic variants associated with short telomeres also contribute to the risk of stroke. For example, genetic variants of *ACYP2* and *TSPYL6* were associated with shorter telomere, which did contribute to the increased risk of stroke (72, 73).

Obesity

Obesity is associated with elevated risk of stroke. A number of studies showed that obesity is consistently associated with increased inflammation and oxidative stress, which promotes telomere shortening (74–80). Valdes et al. found that LTL of obese women was 240 bp shorter than that of age-matched lean women (41). A couple of cross-sectional studies showed a negative correlation between LTL and obesity (81, 82), whereas others did not show significant associations between LTL and obesity (83, 84). A recent meta-analysis showed there is a tendency toward demonstrating negative correlation between obesity and TL. Although 39 of 63 studies showed either weak or moderate correlation between obesity and TL, heterogeneity among the selected studies made the relationship of obesity and TL still open (85).

Smoking and Alcohol Intake

Smoking is a well-established risk factor for all forms of stroke (86–88). Even passive smoking significantly increases the risk of stroke (89–91). Meta-analysis including 30 studies showed that shorter LTL was among ever smokers compared to never smokers, while the dosage of smoking was negatively associated with LTL (92). Moreover, Valdes et al. showed that each pack-year smoked caused an additional loss of 5 base pairs of LTL per year (41). Babizhayev et al. reported that telomere attrition can serve as a biomarker of the oxidative stress and inflammation induced by tobacco smoking (93). In addition, heavy alcohol consumption was strongly associated with a reduced LTL in participants aged ≥65 years (94).

Psychological Stress and Depression

Numerous studies demonstrated that psychological stress caused by negative life event, work stress, illness etc. has significant effect on the risk of stroke (95–98). Accelerated LTL shortening was associated with psychological stress, which might be caused by psychological stress-induced higher oxidative stress and lower telomerase activity (99, 100). In addition, depression is a strong risk factor for stroke, while long-term stress could lead to depression (101, 102). Although the association between LTL and depression was inconsistent, two meta-analyses showed that short LTL was associated with depression (103, 104).

Age-Related Diseases

Hypertension

Hypertension is one of the most important modifiable risk factors for stroke. The strong, direct, linear, and continuous association between increased blood pressure and stroke risk was observed, while intensive blood pressure lowering appears to be beneficial for the reduction of stroke incidence (105–109). Two studies showed that LTL was negatively associated with pulse pressure and hypertension (110, 111). Importantly, meta-analyses from 3,097 participants showed that LTL of hypertensive patients was significantly shorter than that of controls (112).

Diabetes

Diabetes is an independent risk factor for stroke with a 2-fold increased risk in stroke for diabetic patients (113). Compared with control individuals, TL is significantly shorter in patients with type 1 diabetes or type 2 diabetes (114–121). For example, LTL was significantly shorter in type 2 diabetes cases compared with controls over a wide age range in a retrospective case-control study comprising 4,016 subjects (121). Moreover, the escalated telomere attrition was associated with insulin resistance in young adults aged from 21.0 to 43.5 years, which might be caused by increased oxidative stress, metabolic and inflammatory factors (122). In addition, the inverse association between LTL and body mass index (BMI)was observed (120).

Cardiovascular Diseases

Short LTL are associated with various cardiovascular diseases (CVD) including atherosclerosis, myocardial infarction, coronary artery disease (CAD) and atrial fibrillation (AF) (123–129). For example, short TL was associated with severe CAD adjusting for age and sex (123). A recent systematic review and meta-analysis from 43,725 participants and 8,400 patients suggested that LTL was inversely associated with the risk of coronary heart disease independent of conventional vascular risk factors (26). LTL was shorter in patients with myocardial infarction than that in age-matched control individuals (124). In a prospective study, Chen et al. examined LTL at baseline to predict the incidence and progression of carotid atherosclerosis (130). Compared to participants in the highest LTL tertile, those in the lowest tertile had significantly elevated risk for both incident plaque and plaque progression (130). A recent study indicated that telomere shortening may constitute a novel factor for cardioembolic stroke in patients with AF (129).

Although the underlying mechanism of the relationship between short LTL and CVD remains elusive, booming studies have provided a number of hypotheses (131–133). First, genomic evidence showed that inheritance of shorter telomere might act as a cause of CVD. Genome-wide association studies (GWAS) identified a small set of loci, including SNPs within *TERT* and *TERC*, but all with very small R^2 values (<0.5%) (72, 134). Moreover, it has been reported that cardiovascular risk-related systemic oxidative stress and inflammation might accelerate telomere attrition (135). In addition, the attrition-rate hypothesis implies that variation in adult telomere attrition rates might be more important than TL inheritance (136), indicating that telomere attrition rate could serve as a clinical atherosclerosis CVD biomarker. However, a smaller longitudinal study did not show and so on an association between leukocyte telomere attrition rate and atherosclerosis (137).

CONCLUSIONS

Short LTL is positively associated with stroke in the elderly population. In addition, multiple risk factors of stroke are associated with shortened LTL, e.g., age, smoking, alcohol intake, psychological stress, while the possibility of short LTL as an independent risk indicator of stroke still remains. It indicates that LTL might serve as a potential biomarker to evaluate the risk of stroke in the elderly. Moreover, short LTL was also positively associated with the mortality of stroke and cardiovascular diseases, indicating that LTL might be a potential biomarker to predict the prognosis of stroke.

AUTHOR CONTRIBUTIONS

YT, SW, FJ, QK, and CL wrote the manuscript. YW formulated and revised the manuscript.

FUNDING

This work was supported by grants from National Natural Science Foundation of China (81771147), Natural Science Foundation of Shandong Province of China (ZR2016HM30, ZR2016HM55), Medical and Health Science and Technology Planning Project of Shandong Province of China (2018WS463), Supporting Fund for Teachers' Research of Jining Medical University (JY2017KJ039, JY2017JS006, JY2017JS003), the Startup Fund from Jining Medical University (to FJ).

REFERENCES

1. Donnan GA. International journal of stroke. Editorial. *Int J Stroke.* (2008) 3:157. doi: 10.1111/j.1747-4949.2008.00208.x
2. Ding H, Chen C, Shaffer JR, Liu L, Xu Y, Wang X, et al. Telomere length and risk of stroke in Chinese. *Stroke.* (2012) 43:658–63. doi: 10.1161/STROKEAHA.111.637207
3. D'mello MJ, Ross SA, Briel M, Anand SS, Gerstein H, Pare G. Association between shortened leukocyte telomere length and cardiometabolic outcomes: systematic review and meta-analysis. *Circ Cardiovasc Genet.* (2015) 8:82–90. doi: 10.1161/CIRCGENETICS.113.000485
4. Hamad R, Walter S, Rehkopf DH. Telomere length and health outcomes: a two-sample genetic instrumental variables analysis. *Exp Gerontol.* (2016) 82:88–94. doi: 10.1016/j.exger.2016.06.005
5. Blackburn EH, Epel ES, Lin J. Human telomere biology: a contributory and interactive factor in aging, disease risks, and protection. *Science.* (2015) 350:1193–8. doi: 10.1126/science.aab3389

6. Griffith JD, Comeau L, Rosenfield S, Stansel RM, Bianchi A, Moss H, et al. Mammalian telomeres end in a large duplex loop. *Cell.* (1999) 97:503–14. doi: 10.1016/S0092-8674(00)80760-6
7. Schmutz I, De Lange T. Shelterin. *Curr Biol.* (2016) 26:R397–9. doi: 10.1016/j.cub.2016.01.056
8. Lu W, Zhang Y, Liu D, Songyang Z, Wan M. Telomeres-structure, function, and regulation. *Exp Cell Res.* (2013) 319:133–41. doi: 10.1016/j.yexcr.2012.09.005
9. Miyake Y, Nakamura M, Nabetani A, Shimamura S, Tamura M, Yonehara S, et al. RPA-like mammalian Ctc1-Stn1-Ten1 complex binds to single-stranded DNA and protects telomeres independently of the Pot1 pathway. *Mol Cell.* (2009) 36:193–206. doi: 10.1016/j.molcel.2009.08.009
10. Surovtseva YV, Churikov D, Boltz KA, Song X, Lamb JC, Warrington R, et al. Conserved telomere maintenance component 1 interacts with STN1 and maintains chromosome ends in higher eukaryotes. *Mol Cell.* (2009) 36:207–18. doi: 10.1016/j.molcel.2009.09.017
11. Stewart JA, Wang F, Chaiken MF, Kasbek C, Chastain PD, Wright WE, et al. Human CST promotes telomere duplex replication and general replication restart after fork stalling. *EMBO J.* (2012) 31:3537–49. doi: 10.1038/emboj.2012.215
12. Muftuoglu M, Wong HK, Imam SZ, Wilson DM III, Bohr VA, Opresko PL. Telomere repeat binding factor 2 interacts with base excision repair proteins and stimulates DNA synthesis by DNA polymerase beta. *Cancer Res.* (2006) 66:113–24. doi: 10.1158/0008-5472.CAN-05-2742
13. Wu Y, Xiao S, Zhu XD. MRE11-RAD50-NBS1 and ATM function as co-mediators of TRF1 in telomere length control. *Nat Struct Mol Biol.* (2007) 14:832–40. doi: 10.1038/nsmb1286
14. Wu Y, Mitchell TR, Zhu XD. Human XPF controls TRF2 and telomere length maintenance through distinctive mechanisms. *Mech Ageing Dev.* (2008) 129:602–10. doi: 10.1016/j.mad.2008.08.004
15. Miller AS, Balakrishnan L, Buncher NA, Opresko PL, Bambara RA. Telomere proteins POT1, TRF1 and TRF2 augment long-patch base excision repair *in vitro*. *Cell Cycle.* (2012) 11:998–1007. doi: 10.4161/cc.11.5.19483
16. Collado M, Blasco MA, Serrano M. *Cell*ular senescence in cancer and aging. *Cell.* (2007) 130:223–33. doi: 10.1016/j.cell.2007.07.003
17. Greider CW, Blackburn EH. A telomeric sequence in the RNA of Tetrahymena telomerase required for telomere repeat synthesis. *Nature.* (1989) 337:331–7. doi: 10.1038/337331a0
18. Van Steensel B, De Lange T. Control of telomere length by the human telomeric protein TRF1. *Nature.* (1997) 385:740–3. doi: 10.1038/385740a0
19. Ancelin K, Brunori M, Bauwens S, Koering CE, Brun C, Ricoul M, et al. Targeting assay to study the cis functions of human telomeric proteins: evidence for inhibition of telomerase by TRF1 and for activation of telomere degradation by TRF2. *Mol Cell Biol.* (2002) 22:3474–87. doi: 10.1128/MCB.22.10.3474-3487.2002
20. Ye JZ, De Lange T. TIN2 is a tankyrase 1 PARP modulator in the TRF1 telomere length control complex. *Nat Genet.* (2004) 36:618–23. doi: 10.1038/ng1360
21. Li B, Qiao R, Wang Z, Zhou W, Li X, Xu W, et al. Crystal structure of a tankyrase 1-telomere repeat factor 1 complex. *Acta Crystallogr F Struct Biol Commun.* (2016) 72:320–7. doi: 10.1107/S2053230X16004131
22. Jiang J, Wang Y, Susac L, Chan H, Basu R, Zhou ZH, et al. Structure of Telomerase with Telomeric DNA. *Cell.* (2018) 173:1179–90 e1113. doi: 10.1016/j.cell.2018.04.038
23. Muezzinler A, Zaineddin AK, Brenner H. A systematic review of leukocyte telomere length and age in adults. *Ageing Res Rev.* (2013) 12:509–19. doi: 10.1016/j.arr.2013.01.003
24. Sanders JL, Newman AB. Telomere length in epidemiology: a biomarker of aging, age-related disease, both, or neither? *Epidemiol Rev.* (2013) 35:112–31. doi: 10.1093/epirev/mxs008
25. Zhang W, Chen Y, Wang Y, Liu P, Zhang M, Zhang C, et al. Short telomere length in blood leucocytes contributes to the presence of atherothrombotic stroke and haemorrhagic stroke and risk of post-stroke death. *Clin Sci.* (2013) 125:27–36. doi: 10.1042/CS20120691
26. Haycock PC, Heydon EE, Kaptoge S, Butterworth AS, Thompson A, Willeit P. Leucocyte telomere length and risk of cardiovascular disease: systematic review and meta-analysis. *BMJ.* (2014) 349:g4227. doi: 10.1136/bmj.g4227
27. Jiang X, Dong M, Cheng J, Huang S, He Y, Ma K, et al. Decreased leukocyte telomere length (LTL) is associated with stroke but unlikely to be causative. *PLoS ONE.* (2013) 8:e68254. doi: 10.1371/journal.pone.0068254
28. Li J, Feng C, Li L, Yang S, Chen Y, Hui R, et al. The association of telomere attrition with first-onset stroke in Southern Chinese: a case-control study and meta-analysis. *Sci Rep.* (2018) 8:2290. doi: 10.1038/s41598-018-20434-w
29. Fitzpatrick AL, Kronmal RA, Gardner JP, Psaty BM, Jenny NS, Tracy RP, et al. Leukocyte telomere length and cardiovascular disease in the cardiovascular health study. *Am J Epidemiol.* (2007) 165:14–21. doi: 10.1093/aje/kwj346
30. Fyhrquist F, Silventoinen K, Saijonmaa O, Kontula K, Devereux RB, De Faire U, et al. Telomere length and cardiovascular risk in hypertensive patients with left ventricular hypertrophy: the LIFE study. *J Hum Hypertens.* (2011) 25:711–8. doi: 10.1038/jhh.2011.57
31. Cawthon RM, Smith KR, O'brien E, Sivatchenko A, Kerber RA. Association between telomere length in blood and mortality in people aged 60 years or older. *Lancet.* (2003) 361:393–5. doi: 10.1016/S0140-6736(03)12384-7
32. Zee RY, Castonguay AJ, Barton NS, Ridker PM. Relative leukocyte telomere length and risk of incident ischemic stroke in men: a prospective, nested case-control approach. *Rejuvenation Res.* (2010b) 13:411–4. doi: 10.1089/rej.2009.0975
33. Schurks M, Prescott J, Dushkes R, De Vivo I, Rexrode KM. Telomere length and ischaemic stroke in women: a nested case-control study. *Eur J Neurol.* (2013) 20:1068–74. doi: 10.1111/ene.12135
34. Ellehoj H, Bendix L, Osler M. Leucocyte telomere length and risk of cardiovascular disease in a cohort of 1,397 danish men and women. *Cardiology.* (2016) 133:173–7. doi: 10.1159/000441819
35. Jin X, Pan B, Dang X, Wu H, Xu D. Relationship between short telomere length and stroke: a meta-analysis. *Medicine.* (2018) 97:e12489. doi: 10.1097/MD.0000000000012489
36. Cao W, Li X, Zhang X, Zhang J, Sun Q, Xu X, et al. No causal effect of telomere length on ischemic stroke and its subtypes: a mendelian randomization study. *Cells.* (2019) 8:159. doi: 10.3390/cells8020159
37. Wu Y, Wang X, Zhou X, Cheng B, Li G, Bai B. Temporal expression of apelin/apelin receptor in ischemic stroke and its therapeutic potential. *Front Mol Neurosci/.* (2017) 10:1. doi: 10.3389/fnmol.2017.00001
38. Kong Q, Hao Y, Li X, Wang X, Ji B, Wu Y. HDAC4 in ischemic stroke: mechanisms and therapeutic potential. *Clin Epigenet.* (2018) 10:117. doi: 10.1186/s13148-018-0549-1
39. Benjamin EJ, Virani SS, Callaway CW, Chamberlain AM, Chang AR, Cheng S, et al. Heart disease and stroke statistics-2018 update: a report from the american heart association. *Circulation.* (2018) 137, e67–e492. doi: 10.1161/CIR.0000000000000558
40. Appelros P, Stegmayr B, Terent A. Sex differences in stroke epidemiology: a systematic review. *Stroke.* (2009) 40:1082–90. doi: 10.1161/STROKEAHA.108.540781
41. Valdes AM, Andrew T, Gardner JP, Kimura M, Oelsner E, Cherkas LF, et al. Obesity, cigarette smoking, and telomere length in women. *Lancet.* (2005) 366:662–4. doi: 10.1016/S0140-6736(05)66630-5
42. Zhu H, Belcher M, Van Der Harst P. Healthy aging and disease: role for telomere biology? *Clin Sci.* (2011) 120:427–40. doi: 10.1042/CS20100385
43. Vera E, Bernardes De Jesus B, Foronda M, Flores JM, Blasco MA. The rate of increase of short telomeres predicts longevity in mammals. *Cell Rep.* (2012) 2:732–7. doi: 10.1016/j.celrep.2012.08.023
44. Demissie S, Levy D, Benjamin EJ, Cupples LA, Gardner JP, Herbert A, et al. Insulin resistance, oxidative stress, hypertension, and leukocyte telomere length in men from the Framingham Heart Study. *Aging Cell.* (2006) 5:325–30. doi: 10.1111/j.1474-9726.2006.00224.x
45. Sampson MJ, Winterbone MS, Hughes JC, Dozio N, Hughes DA. Monocyte telomere shortening and oxidative DNA damage in type 2 diabetes. *Diabetes Care.* (2006) 29:283–9. doi: 10.2337/diacare.29.02.06.dc05-1715
46. Mourkioti F, Kustan J, Kraft P, Day JW, Zhao MM, Kost-Alimova M, et al. Role of telomere dysfunction in cardiac failure in Duchenne muscular dystrophy. *Nat Cell Biol.* (2013) 15:895–904. doi: 10.1038/ncb2790
47. Sharifi-Sanjani M, Oyster NM, Tichy ED, Bedi KCR, Harel O, Margulies KB, et al. Cardiomyocyte-specific telomere shortening is a distinct

signature of heart failure in humans. *J Am Heart Assoc.* (2017) 6:e005086. doi: 10.1161/JAHA.116.005086
48. Smith CD, Carney JM, Starke-Reed PE, Oliver CN, Stadtman ER, Floyd RA, et al. Excess brain protein oxidation and enzyme dysfunction in normal aging and in Alzheimer disease. *Proc Natl Acad Sci USA.* (1991) 88:10540–3. doi: 10.1073/pnas.88.23.10540
49. Abdul HM, Sultana R, St. Clair DK, Markesbery WR, Butterfield DA. Oxidative damage in brain from human mutant APP/PS-1 double knock-in mice as a function of age. *Free Radic Biol Med.* (2008) 45:1420–5. doi: 10.1016/j.freeradbiomed.2008.08.012
50. Wei YH, Wu SB, Ma YS, Lee HC. Respiratory function decline and DNA mutation in mitochondria, oxidative stress and altered gene expression during aging. *Chang Gung Med J.* (2009) 32:113–32.
51. Dzitoyeva S, Chen H, Manev H. Effect of aging on 5-hydroxymethylcytosine in brain mitochondria. *Neurobiol Aging.* (2012) 33:2881–91. doi: 10.1016/j.neurobiolaging.2012.02.006
52. Chang KT, Min KT. Drosophila melanogaster homolog of Down syndrome critical region 1 is critical for mitochondrial function. *Nat Neurosci.* (2005) 8:1577–85. doi: 10.1038/nn1564
53. Cho KO, Kim YS, Cho YJ, Kim SY. Upregulation of DSCR1 (RCAN1 or Adapt78) in the peri-infarct cortex after experimental stroke. *Exp Neurol.* (2008) 212:85–92. doi: 10.1016/j.expneurol.2008.03.017
54. Sun X, Wu Y, Chen B, Zhang Z, Zhou W, Tong Y, et al. Regulator of calcineurin 1 (RCAN1) facilitates neuronal apoptosis through caspase-3 activation. *J Biol Chem.* (2011) 286:9049–62. doi: 10.1074/jbc.M110.177519
55. Sobrado M, Ramirez BG, Neria F, Lizasoain I, Arbones ML, Minami T, et al. Regulator of calcineurin 1 (Rcan1) has a protective role in brain ischemia/reperfusion injury. *J Neuroinflamm.* (2012) 9:48. doi: 10.1186/1742-2094-9-48
56. Wu Y, Song W. Regulation of RCAN1 translation and its role in oxidative stress-induced apoptosis. *FASEB J.* (2013) 27:208–21. doi: 10.1096/fj.12-213124
57. Sun X, Wu Y, Herculano B, Song W. RCAN1 overexpression exacerbates calcium overloading-induced neuronal apoptosis. *PLoS ONE.* (2014) 9:e95471. doi: 10.1371/journal.pone.0095471
58. Wu Y, Ly PT, Song W. Aberrant expression of RCAN1 in Alzheimer's pathogenesis: a new molecular mechanism and a novel drug target. *Mol Neurobiol.* (2014) 50:1085–97. doi: 10.1007/s12035-014-8704-y
59. Wu Y, Deng Y, Zhang S, Luo Y, Cai F, Zhang Z, et al. Amyloid-beta precursor protein facilitates the regulator of calcineurin 1-mediated apoptosis by downregulating proteasome subunit alpha type-5 and proteasome subunit beta type-7. *Neurobiol Aging.* (2015) 36:169–77. doi: 10.1016/j.neurobiolaging.2014.07.029
60. Wu Y, Hou F, Wang X, Kong Q, Han X, Bai B. Aberrant expression of histone deacetylases 4 in cognitive disorders: molecular mechanisms and a potential target. *Front Mol Neurosci.* (2016) 9:114. doi: 10.3389/fnmol.2016.00114
61. Christoffersen M, Frikke-Schmidt R, Nordestgaard BG, Tybjaerg-Hansen A. Genetic variation in WRN and ischemic stroke: general population studies and meta-analyses. *Exp Gerontol.* (2017) 89:69–77. doi: 10.1016/j.exger.2017.01.005
62. Marto JP, Dias M, Alves JN, Montes V, Beato-Coelho J, Marques-Matos C, et al. Stroke in adults with Down syndrome. *J Neurol Sci.* (2017) 375:279–80. doi: 10.1016/j.jns.2017.02.014
63. Qiu J, Wang X, Wu F, Wan L, Cheng B, Wu Y, et al. Low dose of apelin-36 attenuates ER stress-associated apoptosis in rats with ischemic stroke. *Front Neurol.* (2017) 8:556. doi: 10.3389/fneur.2017.00556
64. Fu Q, Wu Y. RCAN1 in the inverse association between Alzheimer's disease and cancer. *Oncotarget.* (2018) 9:54–66. doi: 10.18632/oncotarget.23094
65. Wu F, Qiu J, Fan Y, Zhang Q, Cheng B, Wu Y, et al. Apelin-13 attenuates ER stress-mediated neuronal apoptosis by activating Galphai/Galphaq-CK2 signaling in ischemic stroke. *Exp Neurol.* (2018) 302:136–44. doi: 10.1016/j.expneurol.2018.01.006
66. Zhang S, Cai F, Wu Y, Bozorgmehr T, Wang Z, Huang D, et al. A presenilin-1 mutation causes Alzheimer disease without affecting Notch signaling. *Mol Psychiatry*. (2018) doi: 10.1038/s41380-018-0101-x. [Epub ahead of print].
67. Flossmann E, Schulz UG, Rothwell PM. Systematic review of methods and results of studies of the genetic epidemiology of ischemic stroke. *Stroke.* (2004) 35:212–27. doi: 10.1161/01.STR.0000107187.84390.AA
68. Kumar P, Misra S, Kumar A, Faruq M, Shakya S, Vardhan G, et al. Transforming growth factor-beta1 (C509T, G800A, and T869C) gene polymorphisms and risk of ischemic stroke in North Indian population: a hospital-based case-control study. *Ann Indian Acad Neurol.* (2017) 20:5–12. doi: 10.4103/0972-2327.199910
69. Tian T, Jin G, Yu C, Lv J, Guo Y, Bian Z, et al. Family history and stroke risk in china: evidence from a large cohort study. *J Stroke.* (2017) 19:188–95. doi: 10.5853/jos.2016.01270
70. Bevan S, Traylor M, Adib-Samii P, Malik R, Paul NL, Jackson C, et al. Genetic heritability of ischemic stroke and the contribution of previously reported candidate gene and genomewide associations. *Stroke.* (2012) 43:3161–7. doi: 10.1161/STROKEAHA.112.665760
71. Schulz UG, Flossmann E, Rothwell PM. Heritability of ischemic stroke in relation to age, vascular risk factors, and subtypes of incident stroke in population-based studies. *Stroke.* (2004) 35:819–24. doi: 10.1161/01.STR.0000121646.23955.0f
72. Codd V, Nelson CP, Albrecht E, Mangino M, Deelen J, Buxton JL, et al. Identification of seven loci affecting mean telomere length and their association with disease. *Nat Genet.* (2013) 45:422–427; 427e421–422. doi: 10.1038/ng.2528
73. Liang Y, Zhang R, Zhang S, Ji G, Shi P, Yang T, et al. Association of ACYP2 and TSPYL6 genetic polymorphisms with risk of ischemic stroke in han chinese population. *Mol Neurobiol.* (2017) 54:5988–95. doi: 10.1007/s12035-016-0086-x
74. Von Zglinicki T, Saretzki G, Docke W, Lotze C. Mild hyperoxia shortens telomeres and inhibits proliferation of fibroblasts: a model for senescence? *Exp Cell Res.* (1995) 220:186–93. doi: 10.1006/excr.1995.1305
75. Halvorsen TL, Beattie GM, Lopez AD, Hayek A, Levine F. Accelerated telomere shortening and senescence in human pancreatic islet cells stimulated to divide *in vitro*. *J Endocrinol.* (2000) 166:103–9. doi: 10.1677/joe.0.1660103
76. Suzuki K, Ito Y, Ochiai J, Kusuhara Y, Hashimoto S, Tokudome S, et al. Relationship between obesity and serum markers of oxidative stress and inflammation in Japanese. *Asian Pac J Cancer Prev.* (2003) 4:259–66.
77. Kurz DJ, Decary S, Hong Y, Trivier E, Akhmedov A, Erusalimsky JD. Chronic oxidative stress compromises telomere integrity and accelerates the onset of senescence in human endothelial cells. *J Cell Sci.* (2004) 117:2417–26. doi: 10.1242/jcs.01097
78. Rankin JW, Andreae MC, Oliver Chen CY, O'keefe SF. Effect of raisin consumption on oxidative stress and inflammation in obesity. *Diabetes Obes Metab.* (2008) 10:1086–96. doi: 10.1111/j.1463-1326.2008.00867.x
79. Sohet FM, Neyrinck AM, Pachikian BD, De Backer FC, Bindels LB, Niklowitz P, et al. Coenzyme Q10 supplementation lowers hepatic oxidative stress and inflammation associated with diet-induced obesity in mice. *Biochem Pharmacol.* (2009) 78:1391–400. doi: 10.1016/j.bcp.2009.07.008
80. Njajou OT, Cawthon RM, Blackburn EH, Harris TB, Li R, Sanders JL, et al. Shorter telomeres are associated with obesity and weight gain in the elderly. *Int J Obes.* (2012) 36:1176–9. doi: 10.1038/ijo.2011.196
81. Zannolli R, Mohn A, Buoni S, Pietrobelli A, Messina M, Chiarelli F, et al. Telomere length and obesity. *Acta Paediatr.* (2008) 97:952–4. doi: 10.1111/j.1651-2227.2008.00783.x
82. Al-Attas OS, Al-Daghri NM, Alokail MS, Alfadda A, Bamakhramah A, Sabico S, et al. Adiposity and insulin resistance correlate with telomere length in middle-aged Arabs: the influence of circulating adiponectin. *Eur J Endocrinol.* (2010) 163:601–7. doi: 10.1530/EJE-10-0241
83. Diaz VA, Mainous AG, Player MS, Everett CJ. Telomere length and adiposity in a racially diverse sample. *Int J Obes.* (2010) 34:261–5. doi: 10.1038/ijo.2009.198
84. Maceneaney OJ, Kushner EJ, Westby CM, Cech JN, Greiner JJ, Stauffer BL, et al. Endothelial progenitor cell function, apoptosis, and telomere length in overweight/obese humans. *Obesity.* (2010) 18:1677–82. doi: 10.1038/oby.2009.494
85. Mundstock E, Sarria EE, Zatti H, Mattos Louzada F, Kich Grun L, Herbert Jones M, et al. Effect of obesity on telomere length: systematic review and meta-analysis. *Obesity.* (2015) 23:2165–74. doi: 10.1002/oby.21183

86. Shah RS, Cole JW. Smoking and stroke: the more you smoke the more you stroke. *Expert Rev Cardiovasc Ther.* (2010) 8:917–32. doi: 10.1586/erc.10.56
87. Goldstein LB, Bushnell CD, Adams RJ, Appel LJ, Braun LT, Chaturvedi S, et al. Guidelines for the primary prevention of stroke: a guideline for healthcare professionals from the American Heart Association/American Stroke Association. *Stroke.* (2011) 42:517–84. doi: 10.1161/STR.0b013e3181fcb238
88. Meschia JF, Bushnell C, Boden-Albala B, Braun LT, Bravata DM, Chaturvedi S, et al. Guidelines for the primary prevention of stroke: a statement for healthcare professionals from the American Heart Association/American Stroke Association. *Stroke.* (2014) 45:3754–832. doi: 10.1161/STR.0000000000000046
89. Oono IP, Mackay DF, Pell JP. Meta-analysis of the association between secondhand smoke exposure and stroke. *J Public Health.* (2011) 33:496–502. doi: 10.1093/pubmed/fdr025
90. Malek AM, Cushman M, Lackland DT, Howard G, Mcclure LA. Secondhand smoke exposure and stroke: the reasons for geographic and racial differences in stroke (REGARDS) study. *Am J Prev Med.* (2015) 49:e89–97. doi: 10.1016/j.amepre.2015.04.014
91. Lin MP, Ovbiagele B, Markovic D, Towfighi A. Association of secondhand smoke with stroke outcomes. *Stroke.* (2016a) 47:2828–35. doi: 10.1161/STROKEAHA.116.014099
92. Astuti Y, Wardhana A, Watkins J, Wulaningsih W, Network PR. Cigarette smoking and telomere length: a systematic review of 84 studies and meta-analysis. *Environ Res.* (2017) 158:480–9. doi: 10.1016/j.envres.2017.06.038
93. Babizhayev MA, Savel'yeva EL, Moskvina SN, Yegorov YE. Telomere length is a biomarker of cumulative oxidative stress, biologic age, and an independent predictor of survival and therapeutic treatment requirement associated with smoking behavior. *Am J Ther.* (2011) 18:e209–26. doi: 10.1097/MJT.0b013e3181cf8ebb
94. Wang H, Kim H, Baik I. Associations of alcohol consumption and alcohol flush reaction with leukocyte telomere length in Korean adults. *Nutr Res Pract.* (2017) 11:334–9. doi: 10.4162/nrp.2017.11.4.334
95. O'donnell MJ, Xavier D, Liu L, Zhang H, Chin SL, Rao-Melacini P, et al. Risk factors for ischaemic and intracerebral haemorrhagic stroke in 22 countries (the INTERSTROKE study): a case-control study. *Lancet.* (2010) 376:112–23. doi: 10.1016/S0140-6736(10)60834-3
96. Henderson KM, Clark CJ, Lewis TT, Aggarwal NT, Beck T, Guo H, et al. Psychosocial distress and stroke risk in older adults. *Stroke.* (2013) 44:367–72. doi: 10.1161/STROKEAHA.112.679159
97. Booth J, Connelly L, Lawrence M, Chalmers C, Joice S, Becker C, et al. Evidence of perceived psychosocial stress as a risk factor for stroke in adults: a meta-analysis. *BMC Neurol.* (2015) 15:233. doi: 10.1186/s12883-015-0456-4
98. Ramirez-Moreno JM, Munoz Vega P, Espada S, Bartolome Alberca S, Aguirre J, Peral D. Association between self-perceived psychological stress and transitory ischaemic attack and minor stroke: a case-control study. *Neurologia.* (2017). doi: 10.1016/j.nrl.2017.09.012. [Epub ahead of print].
99. Epel ES, Blackburn EH, Lin J, Dhabhar FS, Adler NE, Morrow JD, et al. Accelerated telomere shortening in response to life stress. *Proc Natl Acad Sci USA.* (2004) 101:17312–5. doi: 10.1073/pnas.0407162101
100. Wolkowitz OM, Mellon SH, Epel ES, Lin J, Dhabhar FS, Su Y, et al. Leukocyte telomere length in major depression: correlations with chronicity, inflammation and oxidative stress–preliminary findings. *PLoS ONE.* (2011) 6:e17837. doi: 10.1371/journal.pone.0017837
101. Dong JY, Zhang YH, Tong J, Qin LQ. Depression and risk of stroke: a meta-analysis of prospective studies. *Stroke.* (2012) 43:32–7. doi: 10.1161/STROKEAHA.111.630871
102. Jackson CA, Mishra GD. Depression and risk of stroke in midaged women: a prospective longitudinal study. *Stroke.* (2013) 44:1555–60. doi: 10.1161/STROKEAHA.113.001147
103. Lin PY, Huang YC, Hung CF. Shortened telomere length in patients with depression: a meta-analytic study. *J Psychiatr Res.* (2016b) 76:84–93. doi: 10.1016/j.jpsychires.2016.01.015
104. Ridout KK, Ridout SJ, Price LH, Sen S, Tyrka AR. Depression and telomere length: a meta-analysis. *J Affect Disord.* (2016) 191:237–47. doi: 10.1016/j.jad.2015.11.052
105. Lewington S, Clarke R, Qizilbash N, Peto R, Collins R, Prospective Studies C. Age-specific relevance of usual blood pressure to vascular mortality: a meta-analysis of individual data for one million adults in 61 prospective studies. *Lancet.* (2002) 360:1903–13. doi: 10.1016/S0140-6736(02)11911-8
106. Chobanian AV, Bakris GL, Black HR, Cushman WC, Green LA, Izzo JL, et al. The seventh report of the joint national committee on prevention, detection, evaluation, and treatment of high blood pressure: the JNC 7 report. *JAMA.* (2003) 289:2560–72. doi: 10.1001/jama.289.19.2560
107. Ettehad D, Emdin CA, Kiran A, Anderson SG, Callender T, Emberson J, et al. Blood pressure lowering for prevention of cardiovascular disease and death: a systematic review and meta-analysis. *Lancet.* (2016) 387:957–67. doi: 10.1016/S0140-6736(15)01225-8
108. Thomopoulos C, Parati G, Zanchetti A. Effects of blood pressure lowering on outcome incidence in hypertension: 7. Effects of more vs less intensive blood pressure lowering and different achieved blood pressure levels - updated overview and meta-analyses of randomized trials. *J Hypertens.* (2016) 34:613–22. doi: 10.1097/HJH.0000000000000881
109. Xie X, Atkins E, Lv J, Bennett A, Neal B, Ninomiya T, et al. Effects of intensive blood pressure lowering on cardiovascular and renal outcomes: updated systematic review and meta-analysis. *Lancet.* (2016) 387:435–43. doi: 10.1016/S0140-6736(15)00805-3
110. Jeanclos E, Schork NJ, Kyvik KO, Kimura M, Skurnick JH, Aviv A. Telomere length inversely correlates with pulse pressure and is highly familial. *Hypertension.* (2000) 36:195–200. doi: 10.1161/01.HYP.36.2.195
111. Benetos A, Okuda K, Lajemi M, Kimura M, Thomas F, Skurnick J, et al. Telomere length as an indicator of biological aging: the gender effect and relation with pulse pressure and pulse wave velocity. *Hypertension.* (2001) 37:381–85. doi: 10.1161/01.HYP.37.2.381
112. Tellechea ML, Pirola CJ. The impact of hypertension on leukocyte telomere length: a systematic review and meta-analysis of human studies. *J Hum Hypertens.* (2017) 31:99–105. doi: 10.1038/jhh.2016.45
113. Boehme AK, Esenwa C, Elkind MS. Stroke risk factors, genetics, and prevention. *Circ Res.* (2017) 120:472–95. doi: 10.1161/CIRCRESAHA.116.308398
114. Jeanclos E, Krolewski A, Skurnick J, Kimura M, Aviv H, Warram JH, et al. Shortened telomere length in white blood cells of patients with IDDM. *Diabetes.* (1998) 47:482–6. doi: 10.2337/diabetes.47.3.482
115. Adaikalakoteswari A, Balasubramanyam M, Mohan V. Telomere shortening occurs in Asian Indian Type 2 diabetic patients. *Diabet Med.* (2005) 22:1151–6. doi: 10.1111/j.1464-5491.2005.01574.x
116. Adaikalakoteswari A, Balasubramanyam M, Ravikumar R, Deepa R, Mohan V. Association of telomere shortening with impaired glucose tolerance and diabetic macroangiopathy. *Atherosclerosis.* (2007) 195:83–9. doi: 10.1016/j.atherosclerosis.2006.12.003
117. Uziel O, Singer JA, Danicek V, Sahar G, Berkov E, Luchansky M, et al. Telomere dynamics in arteries and mononuclear cells of diabetic patients: effect of diabetes and of glycemic control. *Exp Gerontol.* (2007) 42:971–8. doi: 10.1016/j.exger.2007.07.005
118. Olivieri F, Lorenzi M, Antonicelli R, Testa R, Sirolla C, Cardelli M, et al. Leukocyte telomere shortening in elderly Type2DM patients with previous myocardial infarction. *Atherosclerosis.* (2009) 206:588–93. doi: 10.1016/j.atherosclerosis.2009.03.034
119. Salpea KD, Talmud PJ, Cooper JA, Maubaret CG, Stephens JW, Abelak K, et al. Association of telomere length with type 2 diabetes, oxidative stress and UCP2 gene variation. *Atherosclerosis.* (2010) 209:42–50. doi: 10.1016/j.atherosclerosis.2009.09.070
120. Zee RY, Castonguay AJ, Barton NS, Germer S, Martin M. Mean leukocyte telomere length shortening and type 2 diabetes mellitus: a case-control study. *Transl Res.* (2010a) 155:166–9. doi: 10.1016/j.trsl.2009.09.012
121. Shen Q, Zhao X, Yu L, Zhang Z, Zhou D, Kan M, et al. Association of leukocyte telomere length with type 2 diabetes in mainland Chinese populations. *J Clin Endocrinol Metab.* (2012) 97:1371–4. doi: 10.1210/jc.2011-1562
122. Gardner JP, Li S, Srinivasan SR, Chen W, Kimura M, Lu X, et al. Rise in insulin resistance is associated with escalated telomere attrition. *Circulation.* (2005) 111:2171–7. doi: 10.1161/01.CIR.0000163550.70487.0B

123. Samani NJ, Boultby R, Butler R, Thompson JR, Goodall AH. Telomere shortening in atherosclerosis. *Lancet.* (2001) 358:472–3. doi: 10.1016/S0140-6736(01)05633-1
124. Brouilette S, Singh RK, Thompson JR, Goodall AH, Samani NJ. White cell telomere length and risk of premature myocardial infarction. *Arterioscler Thromb Vasc Biol.* (2003) 23:842–6. doi: 10.1161/01.ATV.0000067426.96344.32
125. Benetos A, Gardner JP, Zureik M, Labat C, Xiaobin L, Adamopoulos C, et al. Short telomeres are associated with increased carotid atherosclerosis in hypertensive subjects. *Hypertension.* (2004) 43:182–5. doi: 10.1161/01.HYP.0000113081.42868.f4
126. Farzaneh-Far R, Cawthon RM, Na B, Browner WS, Schiller NB, Whooley MA. Prognostic value of leukocyte telomere length in patients with stable coronary artery disease: data from the Heart and Soul Study. *Arterioscler Thromb Vasc Biol.* (2008) 28:1379–84. doi: 10.1161/ATVBAHA.108.167049
127. Huzen J, Van Veldhuisen DJ, Van Gilst WH, Van Der Harst P. Telomeres and biological ageing in cardiovascular disease. *Ned Tijdschr Geneeskd.* (2008) 152:1265–70.
128. O'donnell CJ, Demissie S, Kimura M, Levy D, Gardner JP, White C, et al. Leukocyte telomere length and carotid artery intimal medial thickness: the Framingham Heart Study. *Arterioscler Thromb Vasc Biol.* 28:1165–71. doi: 10.1161/ATVBAHA.107.154849
129. Allende M, Molina E, Gonzalez-Porras JR, Toledo E, Lecumberri R, Hermida J. Short leukocyte telomere length is associated with cardioembolic *stroke* risk in patients with atrial fibrillation. *Stroke.* (2016) 47:863–5. doi: 10.1161/STROKEAHA.115.011837
130. Chen S, Lin J, Matsuguchi T, Blackburn E, Yeh F, Best LG, et al. Short leukocyte telomere length predicts incidence and progression of carotid atherosclerosis in American Indians: the Strong Heart Family Study. *Aging.* (2014) 6:414–27. doi: 10.18632/aging.100671
131. Rietzschel ER, Bekaert S, De Meyer T. Telomeres and atherosclerosis: the attrition of an attractive hypothesis. *J Am Coll Cardiol.* (2016) 67:2477–9. doi: 10.1016/j.jacc.2016.03.541
132. De Meyer T, De Buyzere ML. Telomeres and atherosclerosis: the intricate pursuit of mechanistic insight through epidemiology. *Hypertension.* (2017) 70:243–4. doi: 10.1161/HYPERTENSIONAHA.117.09454
133. De Meyer T, Nawrot T, Bekaert S, De Buyzere ML, Rietzschel ER, Andres V. Telomere length as cardiovascular aging biomarker: JACC review topic of the week. *J Am Coll Cardiol.* (2018) 72:805–13. doi: 10.1016/j.jacc.2018.06.014
134. Scheller Madrid A, Rode L, Nordestgaard BG, Bojesen SE. Short telomere length and ischemic heart disease: observational and genetic studies in 290 022 individuals. *Clin Chem.* (2016) 62:1140–9. doi: 10.1373/clinchem.2016.258566
135. Bekaert S, De MT, Rietzschel ER, De Buyzere ML, De BD, Langlois M, et al. Telomere length and cardiovascular risk factors in a middle-aged population free of overt cardiovascular disease. *Aging Cell.* (2007) 6:639–47. doi: 10.1111/j.1474-9726.2007.00321.x
136. De Meyer T, Rietzschel ER, De Buyzere ML, Langlois MR, De Bacquer D, Segers P, et al. Systemic telomere length and preclinical atherosclerosis: the Asklepios Study. *Eur Heart J.* (2009) 30:3074–81. doi: 10.1093/eurheartj/ehp324
137. Toupance S, Labat C, Temmar M, Rossignol P, Kimura M, Aviv A, et al. Short telomeres, but not telomere attrition rates, are associated with carotid atherosclerosis. *Hypertension.* (2017) 70:420–5. doi: 10.1161/HYPERTENSIONAHA.117.09354

Conflict of Interest Statement: The authors declare that the research was conducted in the absence of any commercial or financial relationships that could be construed as a potential conflict of interest.

Copyright © 2019 Tian, Wang, Jiao, Kong, Liu and Wu. This is an open-access article distributed under the terms of the Creative Commons Attribution License (CC BY). The use, distribution or reproduction in other forums is permitted, provided the original author(s) and the copyright owner(s) are credited and that the original publication in this journal is cited, in accordance with accepted academic practice. No use, distribution or reproduction is permitted which does not comply with these terms.

frontiers in Neuroscience

BRIEF RESEARCH REPORT
published: 19 June 2019
doi: 10.3389/fnins.2019.00561

Non-pulsed Sinusoidal Electromagnetic Field Rescues Animals From Severe Ischemic Stroke via NO Activation

Lena P. Font[1,2], Miriam M. Cardonne[2], Hannelore Kemps[1], Raf Meesen[1], Oneida F. Salmon[2], Fidel G. González[2], Ivo Lambrichts[1], Jean-Michel Rigo[1], Bert Brône[1†] and Annelies Bronckaers[1*†]*

[1] Faculty of Medicine and Life Sciences, BIOMED, UHasselt – Hasselt University, Diepenbeek, Belgium, [2] Centro Nacional de Electromagnetismo Aplicado, Universidad de Oriente, Santiago de Cuba, Cuba

OPEN ACCESS

Edited by:
Johannes Boltze,
Fraunhofer-Institut für Zelltherapie und Immunologie (IZI), Germany

Reviewed by:
Maria Domercq,
University of the Basque Country, Spain
Zemin Wang,
Harvard Medical School, United States

***Correspondence:**
Bert Brône
bert.brone@uhasselt.be
Annelies Bronckaers
annelies.bronckaers@uhasselt.be

[†] These authors have contributed equally to this work

Specialty section:
This article was submitted to Neurodegeneration, a section of the journal Frontiers in Neuroscience

Received: 18 February 2019
Accepted: 15 May 2019
Published: 19 June 2019

Citation:
Font LP, Cardonne MM, Kemps H, Meesen R, Salmon OF, González FG, Lambrichts I, Rigo J-M, Brône B and Bronckaers A (2019) Non-pulsed Sinusoidal Electromagnetic Field Rescues Animals From Severe Ischemic Stroke via NO Activation. Front. Neurosci. 13:561. doi: 10.3389/fnins.2019.00561

Despite the high prevalence and devastating outcome, only a few treatment options for cerebral ischemic stroke exist. Based on the nitric oxide (NO)-stimulating capacity of Non-pulsed Sinusoidal Electromagnetic Field (NP-SEMF) and the possible neuroprotective role of NO in ischemic stroke, we hypothesized that NP-SEMF is able to enhance survival and neurological outcome in a rat model of cerebral ischemia. The animals, in which ischemic injury was induced by occlusion of both common carotid arteries, received 20 min of NP-SEMF of either 10 or 60 Hz daily for 4 days. NP-SEMF dramatically increased survival, reduced the size of the infarcted brain area and significantly improved the neurological score of the surviving rats. Corresponding to previous reports, NP-SEMF was able to induce NO production *in vitro*. The importance of NO as a key signaling molecule was highlighted by inhibition of the NP-SEMF beneficial effects in the rat stroke model after blocking NO synthase (NOS). Our results indicate for the first time that NP-SEMF exposure (13.5 mT at 60 and 10 Hz) improves the survival and neurological outcome of rats subjected to cerebral ischemia and that this effect is mediated by NO, underlining the great therapeutic potential of NP-SEMF as a therapy for ischemic stroke.

Keywords: cerebral ischemia, nitric oxide, electromagnetic field, endothelial cell, neuroprotection

INTRODUCTION

Cerebral ischemic stroke is caused by the occlusion of a major artery in the brain, which results in extensive brain tissue loss. Cerebral ischemic stroke is a major cause of mortality and disability worldwide (Kissela et al., 2009; Feigin et al., 2014). Currently, the only available treatment options are tissue plasminogen activator and thrombectomy, which have significant effectivity after stroke. However, these therapies can only be used in a small subset of cases, indicating the clear need for new interventions (Zhang et al., 2013).

Nitric oxide (NO) is an important signaling molecule that is synthesized from its precursor L-arginine by nitric oxide synthase (NOS). Following stroke, NO produced by the neuronal and

inducible isoforms of NOS exerts neurotoxic effects, while NO supplied by endothelial NOS (eNOS) is beneficial by stimulating several mechanisms such as vasodilation, angiogenesis, and neurogenesis. As a consequence of these later positive effects, NO donors display therapeutic effects in animal stroke models (Terpolilli et al., 2012; Garry et al., 2015). Extremely low frequency electromagnetic field (ELF-MF) has been shown to induce NO production (Jelenkovic et al., 2006; Bragin et al., 2015). ELF-MF is defined by a magnetic flux below 20 mT with a frequency range of 1 to 300 Hz and is applied in a pulsed or non-pulsed fashion. Pulsed ELF-MF is intensively investigated and used in the clinic to treat delayed union bone fractures and wounds (Pesce et al., 2013). Furthermore, pulsed ELF-MF is beneficial in preclinical models of hind limb ischemia (Li et al., 2015), myocardial infarction (Yuan et al., 2010; Hao et al., 2014) and traumatic brain injury (Rasouli et al., 2012). In contrast, NP-SEMF is less studied but shows clinical promise in a rat model of Huntington's disease (Tasset et al., 2012). Although the precise cellular mechanism activated by ELF-MF is poorly characterized, NO is induced by both pulsed ELF-MF and NP-SEMF in the brains of healthy rats (Jelenkovic et al., 2006; Bragin et al., 2015).

Because of the promising preclinical data of NO donors as a stroke therapy and the ability of NP-SEMF to induce NO production, we investigated the effect of NP-SEMF in a rat model of cerebral ischemia. We also studied the influence of NOS inhibition on NP-SEMF-induced neuroprotective effects. To our knowledge, this study is the first to show the therapeutic effect of NP-SEMF in brain ischemia and its NO-dependence.

MATERIALS AND METHODS

Generation of NP-SEMF

Based on our previous results using NP-SEMF for pain relief (Niubó Elías et al., 2010), we used an electromagnetic field strength of 13.5 mT and a non-pulsed sinusoidal frequency of 10 and 60 Hz during a short application of 20 min. NP–SEMF was generated using a coil (ferromagnetic core radius 16 mm; wire diameter 0.20 mm; 950 turns) connected to a Magnetic Stimulator NaK-02. The NaK-02 function generator was coupled to a power amplifier (high fidelity amplifier; bandwidth 10 Hz–20 kHz; output 60 W) to generate a continuous sinusoidal current source (for detailed specifications see **Supplementary Data S1**). The resulting magnetic field showed a sinusoidal distribution in function of time as exemplified in **Figure 1A**. During the exposure time, a continuous sinusoidal current was applied without intervals, which is in contrast to pulsed ELF-MF.

Permanent Bilateral Common Carotid Arteries Occlusion (2CCAO Model) in Rats

Cerebral ischemia was induced in Wistar rats (6–8 weeks old), in which both common carotid arteries were permanently occluded with 5-0 silk suture (Yamaguchi et al., 2005). Animals that died immediately after the procedure or demonstrated bleeding during surgery were excluded. Treated groups (10 and 60 Hz both 13.5 mT) were repeatedly exposed to NP-SEMF during 20 min on 4 subsequent days, with first exposure 3 h after injury (experimental setup, see **Figure 1B**). A group of sham operated animals, which were subjected to the same surgical intervention but without vessel occlusion, was also included. Survival was evaluated daily for 7 days. The open field test was performed to assess general locomotor activity (measuring the number crossing the fourth quadrant) and spontaneous exploratory activity (measuring the number of rears, thus the frequency at which the rodent stands on its hind legs). This was done before surgery (baseline level) and 7 days after surgery. Neurological outcome was scored double blindly 24 h and 7 days after surgery (**Supplementary Table S1**) (Menzies et al., 1992). Experimental procedures were approved by the "Scientific and Ethic Council of the CNEA." All conducted experiments were performed according the standard biosecurity and UHasselt (BIOMED), and CNEA safety procedures.

Staining of Brain Sections With 2,3,5-Triphenyltetrazolium Chloride (TTC)

Seven days after surgery, animals were sacrificed. Brain slices of 1 mm were made and stained for 30 min in a 2% TTC solution (Sigma, St. Louis, MO, United States). TTC stains non-damaged tissue in red, while death tissue remains white. Infarct quantification was performed on digital photographs using ImageJ (NIH, Bethesda, MD, United States).

NO Production by HMEC-1 Cells After NP-SEMF

Human immortalized microvascular endothelial cells (HMEC-1) were seeded in 24 well plates (40,000 cells/well). 24 h later, the medium was replaced and cells were treated with NP-SEMF (13.5 mT, 20 min. 10 or 60 Hz) with or without the NOS inhibitor L-NMMA at different concentrations (1.5 mM, 150 μM, 15 μM and 1.5 μM). L-NMMA was added 15 min before NP-SEMF (A scheme of the experimental setup is provided in **Supplementary Figure S2**). 1 h or 24 h later, medium was collected and the amount of nitrite (a non-volatile breakdown product of NO) was measured using Griess assay (Promega, Leiden, Netherlands).

In vivo Inhibition of NO After NP-SEMF Treatment

Cerebral ischemia was induced in male Wistar rats by 2CCAO. The NOS inhibitor (L-NAME) was injected intraperitoneally (20 mg/kg) (Delwing et al., 2005) once 15 min before surgery and daily 15 min before NP-SEMF treatment. Untreated animals received an intraperitoneal saline injection. Survival was monitored daily. At day 7, the rats were sacrificed and TTC staining was performed.

Statistical Analysis

Statistical analysis was done with Graphpad Prism software (Graphpad, San Diego, CA, United States). Statistical significance was set at $p < 0.05$.

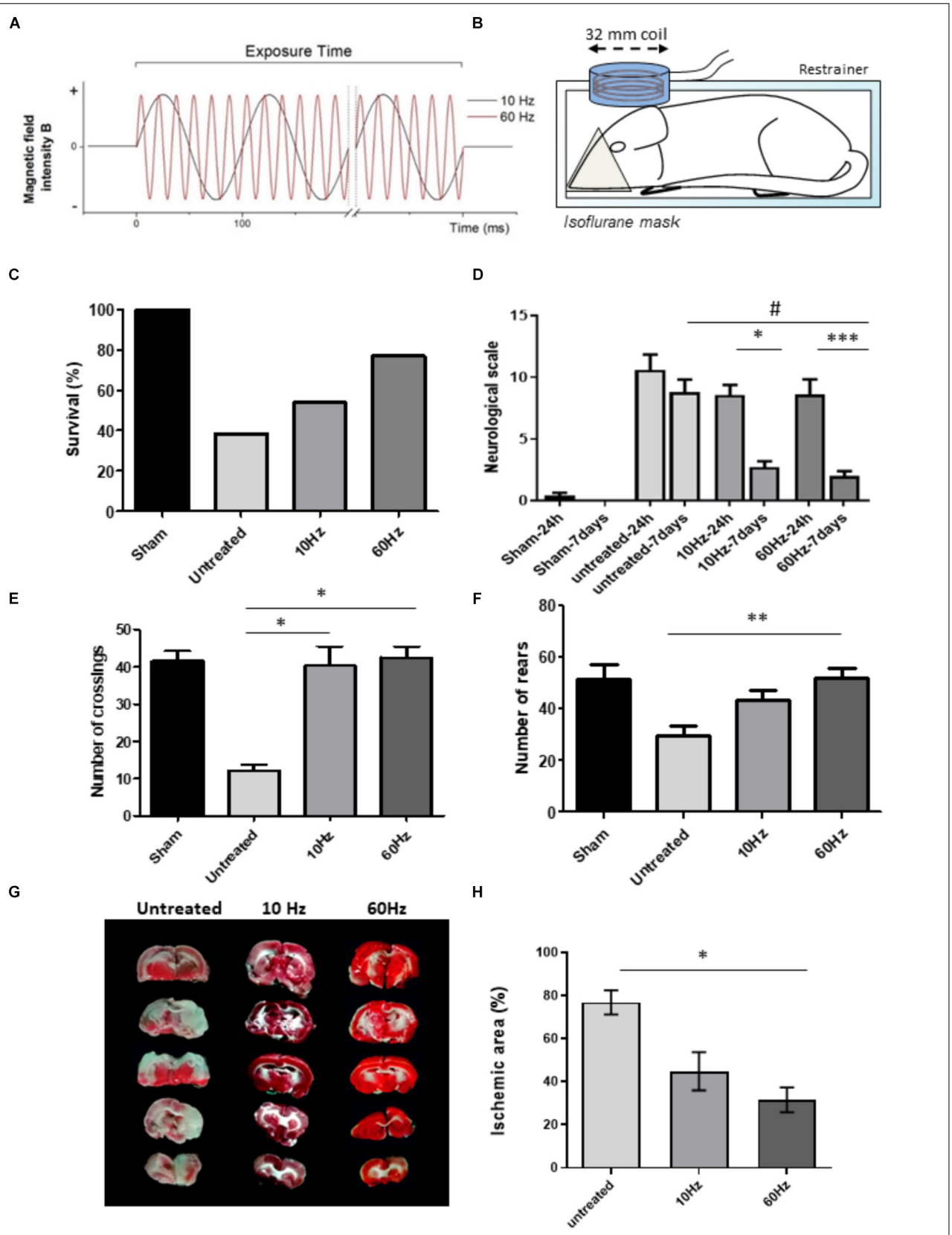

FIGURE 1 | Continued

FIGURE 1 | Beneficial effects of NP-SEMF in a rat model of ischemic stroke. Cerebral ischemia was induced by using the standard two-vessel occlusion (2CCAO) protocol in Wistar rats. Treated groups (10 and 60 Hz both 13.5 mT; n = 13/group) were repeatedly exposed to non-pulsed sinusoidal electromagnetic field (NP-SEMF) during 20 min on 4 subsequent days. The first exposure was performed 3 h after injury. **(A)** Graph showing the properties of the applied NP-SEMF. Sinusoidal magnetic waves were generated at either 10 or 60 Hz in a continuous fashion during the exposure time. **(B)** Scheme of the experimental set-up for the rat study. Rats were restricted in a plastic restrainer while receiving the anesthetic isoflurane during the NP-SEMF treatment. The plastic enclosed coil which has a diameter of 32 mm generates the NP-SEMF and is placed on top of the skull. **(C)** Survival was evaluated 7 days following stroke induction. Only 38% of the untreated animals survived 7 days after surgery while survival rates were substantially higher after NP-SEMF treatment (54% for 10 Hz and 77% for 60 Hz). **(D)** Neurological score was determined 24 h and 7 days after injury on the surviving animals. A higher score represents a higher number of deficits. n = 5/sham group and n = 13/untreated and treated groups. $^{*}p \leq 0.05$ and $^{***}p \leq 0.001$ 24 h vs. 7 days; $^{\#}p \leq 0.001$ 60 Hz NP-SEMF 7 days vs. untreated 7 days post-surgery. All calculated with a Kruskall–Wallis test and Dunnett's *post hoc* test. **(E)** Open field test was assessed before surgery (baseline) and 7 days after surgery. The frequency to cross the fourth quadrant was measured to assess the effect on locomotion. $^{*}p \leq 0.05$ vs. untreated, as analyzed with a Kruskal–Wallis test with a Dunnett's *post hoc* test. **(F)** In the open field tests, the number of rears (i.e., animal raises his forepaws) was measured as an indication of spontaneous exploratory behavior. $^{**}p \leq 0.01$ as analyzed with a Kruskal–Wallis test with a Dunnett's *post hoc* test. **(G)** Brain slices were stained with TTC to determine infarct size in 2CCAO animals. **(H)** The damaged area as well as the whole brain area was quantified using ImageJ. For every animal, the area of affected brain tissue was quantified and calculated as % of total brain area. Next, the averages of all animals of the same experimental group were made (5 sections/brain, n = 8/group, data represent average ± standard deviation). TTC was performed 7 days after surgery, on animals without treatment and animals which received 10 Hz or 60 Hz NP-SEMF. $^{*}p \leq 0.05$, $^{***}p \leq 0.001$ vs. control, as analyzed with a Kruskal–Wallis test with a Dunnett's *post hoc* test.

RESULTS

NP-SEMF Has Beneficial Effects in a Rat Model of Stroke

Cerebral ischemia was induced in rats by permanent occlusion of the two common carotid vessels. Animals where either untreated or received NP-SEMF treatment (10 or 60 Hz both 13.5 mT; n = 13/group) for 20 min during 4 subsequent days. Without treatment, the surgery causes death of 62% of the animals after 7 days (**Figure 1C**). NP-SEMF considerably improved the survival rates by 1.4-fold for 10 Hz and by 2.0-fold for 60 Hz. The neurological scale was assessed after 24 h and 7 days post-surgery (**Figure 1D**). For the untreated group, no statistical differences were found between 24 h and 7 days. In contrast, in both NP-SEMF groups, a significant improvement was evident after 7 days (from 8.6 ± 1.2 to 2.7 ± 0.5 for 10 Hz, and from 8.6 ± 0.8 to 2.0 ± 1.1 for 60 Hz). Functional outcome was measured with the open field test (**Figures 1E,F**). NP-SEMF treatment induced a significant improvement of locomotion as shown by a rescued frequency of crossing the fourth quadrant: from 12.2 ± 1.5 (untreated) to 40.2 ± 5.2 (10 Hz) and 42.5 ± 3.0 (60 Hz). The number of rears was significantly increased for the 60 Hz treated group (29.6 ± 3.8 in untreated animals versus 51.7 ± 4.1 in 60 Hz).

During NP-SEMF, animals are anesthetized with isoflurane and placed in a restrainer. To rule out any effect of this procedure, we studied animals (with 2CCAO) placed in the restrainer but without switching on the magnetic flux (= sham exposed animals) (**Supplementary Figure S1**). No amelioration in survival nor neurological outcome were observed.

NP-SEMF reduced the severity of the ischemic brain damage (**Figures 1G,H**). TTC staining 7 days after injury revealed that untreated animals displayed large white infarcted areas in both the cortex and the striatum as quantified with ImageJ. The infarcted brain area was reduced by more than 50% after 60 Hz NP-SEMF treatment and the remaining lesions were mainly located in the striatum. The percentage of ischemic brain area in control animals was significantly reduced from 76.9 ± 5.6% toward 31.5 ± 5.8% in animals treated with 60 Hz. 10 Hz application did lead to a slight reduction in lesion size, although this difference was not statistically significant.

Inhibition of NOS Decreased NP-SEMF-Induced NO Production *in vitro*

To verify that NP-SEMF acts via NO, the NO production was indirectly measured with the Griess assay in HMEC-1 cells (**Figure 2A**). Nitrite concentration (and thus NO) was significantly increased 24 h after 60 Hz NP-SEMF (3.9 ± 1.3 μM in 60 Hz vs. control). The involvement of NOS was studied using the general NOS inhibitor L-NMMA, which was able to dose-dependently inhibit the NP-SEMF-triggered NO production (**Figures 2B,C**). The IC_{50} for 10 Hz was estimated 59.88 μM after 1 h and 85.53 μM after 24 h; The IC_{50} for 60 Hz was 7.3 μM after 1 h and 2.7 μM after 24 h.

NOS-Derived NO Was Essential for NP-SEMF-Effectivity *in vivo*

To prove the involvement of NO in the neuroprotective action of NP-SEMF after ischemic stroke, the general NOS blocker L-NAME was injected in 2CCAO rats to inhibit NO formation. The beneficial effect of NP-SEMF at 60 Hz on survival 7 days after ischemic stroke disappeared when NO-synthesis was blocked (**Figure 2D**). Inhibition of NOS with L-NAME inhibited the protective effect of NP-SEMF on tissue damage as the lesion size (in % of total area) was significantly increased (NP-SEMF+L-NAME 69.1 ± 3.4 vs. NP-SEMF alone 34.5 ± 6.2). The tissue damage in animals treated with both NP-SEMF and L-NAME were similar in size compared to the untreated group (**Figure 2E**). These results indicate that NO is a key signaling molecule by which NP-SEMF protects the brain from tissue damage after ischemic stroke.

DISCUSSION

As several studies have demonstrated the ability of ELF-MF to alter NO production and since NO has been suggested to be beneficial in stroke, we explored the use of NP-SEMF in a rat

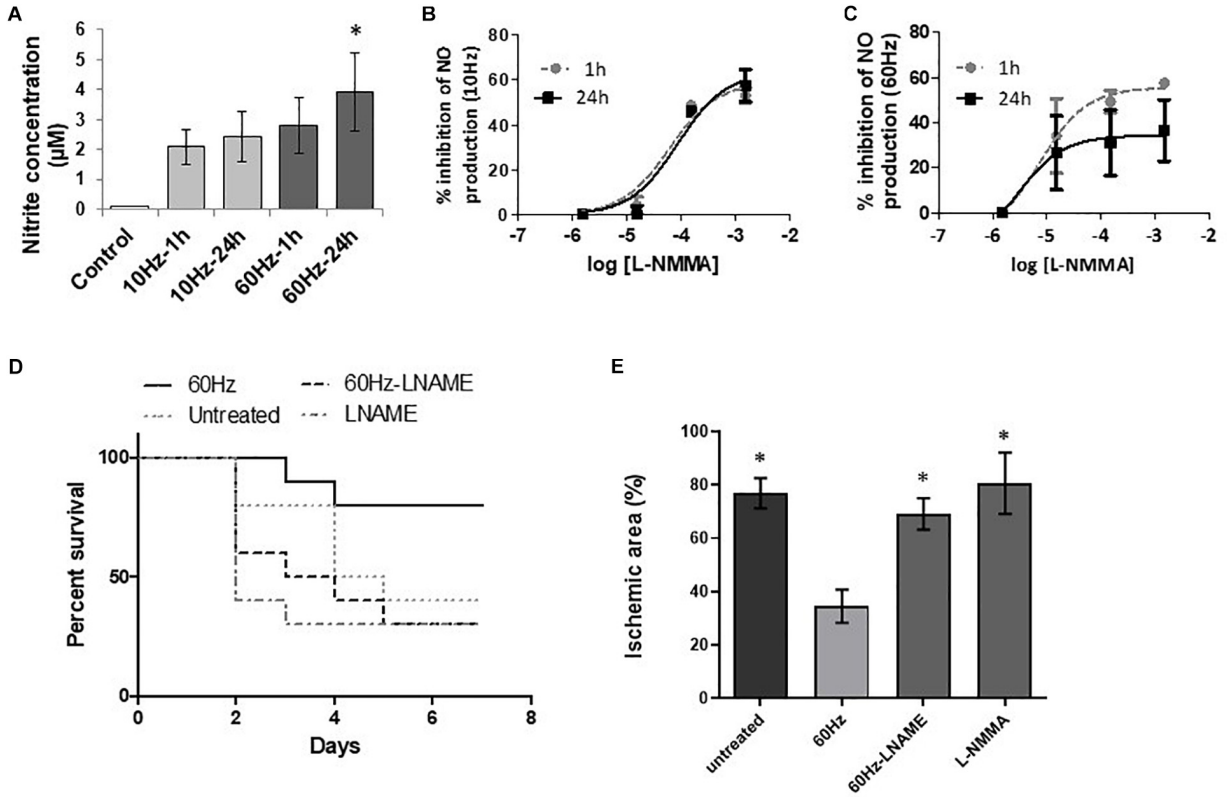

FIGURE 2 | Involvement of NO as key mediator of the beneficial effects of NP-SEMF. **(A)** Nitrite concentration (as an indirect measure for the NO concentration) induced by NP-SEMF was measured by Griess reaction, 1 h or 24 h after treatment of NP-SEMF for 20 min (13.5 mT at 10 or 60 Hz). Values are expressed as mean ± SD, $n = 4$, $^*p \leq 0.05$, as calculated with Kruskal-Wallis ANOVA test with a Dunnett's *post hoc* test. **(B)** Inhibitor effect of L-NMMA (1.5 mM, 150 μM, 15 μM, 1.5 μM) on NO production by HMEC-1 subjected to 10 Hz NP-SEMF for 20 min, $n = 4$. NO production was measured 1 h or 24 h after treatment. **(C)** Inhibitor effect of L-NMMA on NO release by HMEC-1 subjected to 60 Hz NP-SEMF. NO production was measured 1 h or 24 h after treatment, $n = 4$. **(D)** Rats were subjected to 2CCAO and received either no treatment, L-NAME injections, 60 Hz NP-SEMF or combination of L-NAME and NP-SEMF. L-NAME was injected at a dose of 20 mg/kg, 15 min before surgery and before each NP-SEMF treatment (13.5 mT for 20 min at 10 or 60 Hz). Kaplan-Meier graph shows the survival rates of these four groups during 7 days after surgery ($n = 10$/group). The percentage of surviving animals was higher after NP-SEMF treatment. L-NAME injection inhibited the beneficial effect of NP-SEMF on survival. **(E)** The ischemic area in the brain of the surviving rats was measured by TTC staining 7 days after surgery and calculated as ischemic area (in % of total area). Treatment of L-NAME obliterates the neuroprotective effect of NP-SEMF. $n = 4$/group, $^*p \leq 0.05$ vs. 60 Hz, according to a Kruskal–Wallis ANOVA test with a Dunnett's *post hoc* test.

model of severe cerebral ischemic stroke. Daily applications of 20 min of NP-SEMF (10 and 60 Hz) significantly improved survival, locomotion, and neurological outcome. The lesion size was dramatically reduced in rats treated with 60 Hz NP-SEMF. Our study confirmed that NO is the key player in this beneficial effect of NP-SEMF. NP-SEMF increased NO production in HMEC-1 cells, which was inhibited by the NOS-inhibitor L-NMMA. Moreover, the NOS blocker L-NAME reversed the beneficial effects of NP-SEMF in rats subjected to 2CCAO. This is in line with previous findings which showed that L-NAME prevents blood flow induction by pulsed ELF-MF in healthy rat brains (Bragin et al., 2015). Accordingly, L-NAME also reduced the angiogenic effects of endothelial cells induced by pulsed ELF-MF (Li et al., 2015).

We postulate that NP-SEMF is effective by inducing NO. In the acute phases of stroke, relative NO depletion occurs, leading to a reduction of cerebral blood flow (CBF) and the development of secondary damage. Therefore, increasing post-ischemic NO content to augment CBF toward the lesion is considered to be a promising treatment strategy for ischemic stroke. Indeed, numerous animal studies demonstrate the efficacy of NO donors or inhaled gaseous NO as an ischemic stroke therapy (Garry et al., 2015). Nevertheless, in the clinic, application of the NO precursor L-arginine or the NO donor glyceryl trinitrate has no beneficial effects in ischemic stroke (Bath et al., 2000), while other strategies based on NO (such as NO inhalation) are still in the experimental stage (Terpolilli et al., 2016). It is highly likely that NP-SEMF has a similar effect as NO donors or gaseous NO. An additional advantage of NP-SEMF is that it locally induces NO production in regions with interrupted blood flow, whereas gaseous NO or NO donors are administered systemically so might not reach the damaged regions and may provoke unwanted side effects (Garry et al., 2015). Possibly, NP-SEMF also activates other pathways independent of NO.

The mechanism by which NP-SEMF stimulates NO production remains to be investigated in detail. Previous studies

on healthy brains show enhanced NO levels in the brain but the underlying mechanism could not be revealed. NP-SEMF induces eNOS and iNOS expression in human keratinocytes (Patruno et al., 2010), while pulsed ELF-MF enhances phosphorylation of eNOS in a mouse hindlimb ischemia model (Li et al., 2015).

Taken together, our data clearly show the high potential of NP-SEMF to improve neurological outcome, lesion size and survival in a rat model of stroke. The fact that an electromagnetic field of low frequency during short time frames causes such a tremendous improvement sparks hope to translate this new "electroceutical" into the clinic.

DATA AVAILABILITY

The datasets generated for this study are available on request to the corresponding authors.

ETHICS STATEMENT

This study was carried out in accordance with the regulations of Scientific and Ethic Council of the CNEA (Centro Nacional de Electromagnetismo Aplicado), Santiago de Cuba, Cuba. The protocol was approved by the "Scientific and Ethic Council of the CNEA" (Centro Nacional de Electromagnetismo Aplicado), Santiago de Cuba, Cuba.

AUTHOR CONTRIBUTIONS

LF carried out the *in vivo* experiments and wrote the first draft of the manuscript. LF, HK, and AB carried out the *in vitro* experiments, histology, and prepared the figures. LF, MC, AB, and BB were involved in data interpretation. MC designed the NP-SEMF equipment. FG was responsible for device calibration. LF, AB, BB, HK, MC, RM, FG, OS, IL, and J-MR contributed to the project design and reviewed the manuscript. All authors who contributed to manuscript revision, read, and approved the submitted version.

FUNDING

This work was supported by the Belgian Development Cooperation through VLIR-UOS (Flemish Interuniversity Council-University Cooperation for Development) in the context of the Institutional University Cooperation Program with Universidad de Oriente and the Institutional Research Founds of the Centro Nacional de Electromagnetismo Aplicado, Cuba, and through BOF-BILA, doctoral grants in the framework of the bilateral cooperation, University Hasselt. AB benefits from a research grant of the FWO (Research Foundation – Flanders-Grant Nos. 1266015N and 1522518N).

ACKNOWLEDGMENTS

We would like to acknowledge Petra Bex and Neldris Zamora Suárez for their excellent technical assistance. HMEC-1 were a kind gift of the Centers for Disease Control and Prevention (Atlanta, GA, United States).

SUPPLEMENTARY MATERIAL

The Supplementary Material for this article can be found online at: https://www.frontiersin.org/articles/10.3389/fnins.2019.00561/full#supplementary-material

REFERENCES

Bath, F. J., Butterworth, R. J., and Bath, P. M. (2000). Nitric oxide donors (nitrates), L-arginine, or nitric oxide synthase inhibitors for acute ischaemic stroke. *Cochrane Database Syst. Rev.* 4:CD000398. doi: 10.1002/14651858.CD000398

Bragin, D. E., Statom, G. L., Hagberg, S., and Nemoto, E. M. (2015). Increases in microvascular perfusion and tissue oxygenation via pulsed electromagnetic fields in the healthy rat brain. *J. Neurosurg.* 122, 1239–1247. doi: 10.3171/2014.8.JNS132083

Delwing, D., Goncalves, M. C., Sarkis, J. J., and Wyse, A. T. (2005). L-NAME administration prevents the inhibition of nucleotide hydrolysis by rat blood serum subjected to hyperargininemia. *Amino Acids* 29, 267–272. doi: 10.1007/s00726-005-0216-7

Feigin, V. L., Forouzanfar, M. H., Krishnamurthi, R., Mensah, G. A., Connor, M., Bennett, D. A., et al. (2014). Global and regional burden of stroke during 1990-2010: findings from the global burden of disease study 2010. *Lancet* 383, 245–254. doi: 10.1007/s00726-005-0216-7

Garry, P. S., Ezra, M., Rowland, M. J., Westbrook, J., and Pattinson, K. T. (2015). The role of the nitric oxide pathway in brain injury and its treatment–from bench to bedside. *Exp. Neurol.* 263, 235–243. doi: 10.1016/j.expneurol.2014.10.017

Hao, C. N., Huang, J. J., Shi, Y. Q., Cheng, X. W., Li, H. Y., Zhou, L., et al. (2014). Pulsed electromagnetic field improves cardiac function in response to myocardial infarction. *Am. J. Transl. Res.* 6, 281–290. doi: 10.1016/j.expneurol.2014.10.017

Jelenkovic, A., Janac, B., Pesic, V., Jovanovic, D. M., Vasiljevic, I., and Prolic, Z. (2006). Effects of extremely low-frequency magnetic field in the brain of rats. *Brain Res. Bull.* 68, 355–360. doi: 10.1016/j.brainresbull.2005.09.011

Kissela, B., Lindsell, C. J., Kleindorfer, D., Alwell, K., Moomaw, C. J., Woo, D., et al. (2009). Clinical prediction of functional outcome after ischemic stroke: the surprising importance of periventricular white matter disease and race. *Stroke* 40, 530–536. doi: 10.1161/STROKEAHA.108.521906

Li, R. L., Huang, J. J., Shi, Y. Q., Hu, A., Lu, Z. Y., Weng, L., et al. (2015). Pulsed electromagnetic field improves postnatal neovascularization in response to hindlimb ischemia. *Am. J. Transl. Res.* 7, 430–444. doi: 10.1161/strokeaha.108.521906

Menzies, S. A., Hoff, J. T., and Betz, A. L. (1992). Middle cerebral artery occlusion in rats: a neurological and pathological evaluation of a reproducible model. *Neurosurgery* 31, 100–106; discussion106–107.

Niubó Elías, M. M., Lahera Cabrales, R., Rodríguez Arias, O. D., and Marañón Cardonne, M. (2010). Magnetoterapia para alivio del dolor por artrosis cervical. *Medisan* 14:161.

Patruno, A., Amerio, P., Pesce, M., Vianale, G., Di Luzio, S., Tulli, A., et al. (2010). Extremely low frequency electromagnetic fields modulate expression of inducible nitric oxide synthase, endothelial nitric oxide synthase and cyclooxygenase-2 in the human keratinocyte cell line hacat: potential therapeutic effects in wound healing. *Br. J. Dermatol.* 162, 258–266. doi: 10.1111/j.1365-2133.2009.09527.x

Pesce, M., Patruno, A., Speranza, L., and Reale, M. (2013). Extremely low frequency electromagnetic field and wound healing: implication of cytokines as biological mediators. *Eur. Cytokine Netw.* 24, 1–10. doi: 10.1684/ecn.2013.0332

Rasouli, J., Lekhraj, R., White, N. M., Flamm, E. S., Pilla, A. A., Strauch, B., et al. (2012). Attenuation of interleukin-1beta by pulsed electromagnetic fields after traumatic brain injury. *Neurosci. Lett.* 519, 4–8. doi: 10.1016/j.neulet.2012.03.089

Tasset, I., Medina, F. J., Jimena, I., Aguera, E., Gascon, F., Feijoo, M., et al. (2012). Neuroprotective effects of extremely low-frequency electromagnetic fields on a huntington's disease rat model: effects on neurotrophic factors and neuronal density. *Neuroscience* 209, 54–63. doi: 10.1016/j.neuroscience.2012.02.034

Terpolilli, N. A., Feiler, S., Dienel, A., Muller, F., Heumos, N., Friedrich, B., et al. (2016). Nitric oxide inhalation reduces brain damage, prevents mortality, and improves neurological outcome after subarachnoid hemorrhage by resolving early pial microvasospasms. *J. Cereb. Blood Flow Metab.* 36, 2096–2107. doi: 10.1177/0271678X15605848

Terpolilli, N. A., Moskowitz, M. A., and Plesnila, N. (2012). Nitric oxide: considerations for the treatment of ischemic stroke. *J. Cereb. Blood Flow Metab.* 32, 1332–1346. doi: 10.1038/jcbfm.2012.12

Yamaguchi, M., Calvert, J. W., Kusaka, G., and Zhang, J. H. (2005). One-stage anterior approach for four-vessel occlusion in rat. *Stroke* 36, 2212–2214. doi: 10.1161/01.STR.0000182238.08510.c5

Yuan, Y., Wei, L., Li, F., Guo, W., Li, W., Luan, R., et al. (2010). Pulsed magnetic field induces angiogenesis and improves cardiac function of surgically induced infarcted myocardium in sprague-dawley rats. *Cardiology* 117, 57–63. doi: 10.1159/000321459

Zhang, R. L., Zhang, Z. G., and Chopp, M. (2013). Targeting nitric oxide in the subacute restorative treatment of ischemic stroke. *Expert Opin. Investig. Drugs* 22, 843–851. doi: 10.1517/13543784.2013.793672

Conflict of Interest Statement: The authors declare that the research was conducted in the absence of any commercial or financial relationships that could be construed as a potential conflict of interest.

Copyright © 2019 Font, Cardonne, Kemps, Meesen, Salmon, González, Lambrichts, Rigo, Brône and Bronckaers. This is an open-access article distributed under the terms of the Creative Commons Attribution License (CC BY). The use, distribution or reproduction in other forums is permitted, provided the original author(s) and the copyright owner(s) are credited and that the original publication in this journal is cited, in accordance with accepted academic practice. No use, distribution or reproduction is permitted which does not comply with these terms.

frontiers in Neuroscience

REVIEW
published: 19 June 2019
doi: 10.3389/fnins.2019.00637

Proteostasis During Cerebral Ischemia

Audrey M. Thiebaut[1†], Elodie Hedou[1†], Stefan J. Marciniak[2,3], Denis Vivien[1,4] and Benoit D. Roussel[1]*

[1] INSERM, INSERM UMR-S U1237, Physiopathology and Imaging of Neurological Disorders, University of Caen Normandy, Caen, France, [2] Cambridge Institute for Medical Research, University of Cambridge, Cambridge, United Kingdom, [3] Department of Medicine, Addenbrooke's Hospital, University of Cambridge, Cambridge, United Kingdom, [4] Department of Clinical Research, University of Caen Normandy, Caen, France

Cerebral ischemia is a complex pathology involving a cascade of cellular mechanisms, which deregulate proteostasis and lead to neuronal death. Proteostasis refers to the equilibrium between protein synthesis, folding, transport, and protein degradation. Within the brain proteostasis plays key roles in learning and memory by controlling protein synthesis and degradation. Two important pathways are implicated in the regulation of proteostasis: the unfolded protein response (UPR) and macroautophagy (called hereafter autophagy). Both are necessary for cell survival, however, their over-activation in duration or intensity can lead to cell death. Moreover, UPR and autophagy can activate and potentiate each other to worsen the issue of cerebral ischemia. A better understanding of autophagy and ER stress will allow the development of therapeutic strategies for stroke, both at the acute phase and during recovery. This review summarizes the latest therapeutic advances implicating ER stress or autophagy in cerebral ischemia. We argue that the processes governing proteostasis should be considered together in stroke, rather than focusing either on ER stress or autophagy in isolation.

Keywords: stroke, autophagy, ER stress, proteostasis, mTOR

OPEN ACCESS

Edited by:
Mathias Gelderblom, University Medical Center Hamburg-Eppendorf, Germany

Reviewed by:
Pedro Domingos, Institute of Chemical and Biological Technology, New University of Lisbon, Portugal
Maria Xilouri, Biomedical Research Foundation of the Academy of Athens, Greece

***Correspondence:**
Benoit D. Roussel
broussel@cyceron.fr

[†]These authors have contributed equally to this work

Specialty section:
This article was submitted to Neurodegeneration, a section of the journal Frontiers in Neuroscience

Received: *26 March 2019*
Accepted: *03 June 2019*
Published: *19 June 2019*

Citation:
Thiebaut AM, Hedou E, Marciniak SJ, Vivien D and Roussel BD (2019) Proteostasis During Cerebral Ischemia. Front. Neurosci. 13:637. doi: 10.3389/fnins.2019.00637

Abbreviations: 3-MA, 3-methyladenine; AMP, adenosine monophosphate; AMPAR, α-amino-3-hydroxy-5-methyl-4-isoxazolepropionic acid receptor; AMPK, AMP-activated protein kinase; ATF4, activating transcription factor 4; ATF6, activating transcription factor 6; Atg, autophagy-regulated; Atg16L1, Atg16-like 1; ATP, adenosine triphosphate; Baf, bafilomycin; BBB, blood-brain barrier; BCAo, Bilateral cerebral artery occlusion; Bcl-2, B cell lymphoma 2; BiP, binding immunoglobulin protein; BMVECs, brain microvascular endothelial cells; CA, cornu ammonis; CHOP, CCAT/enhancer homologous protein; CICR, calcium-induced calcium release; CMA, chaperone-mediated autophagy; CREB, cAMP response element binding protein; CSF, cerebrospinal fluid; DAPK1, death-associated protein kinase 1; eIF2α, eukaryotic translation initiation factor 2α; ER, endoplasmic reticulum; ERAD, ER-associated protein degradation; FIP200, focal adhesion kinase family interacting protein of 200 kDa; FOXO1, forkhead box O1; GABARAP, ϒ-aminobutyric acid receptor-associated protein; GADD34, growth arrest and DNA damage inducible 34; GATE-16, Golgi-associated ATPase enhancer of 16 kDa; GFAP, glial fibrillary acidic protein; GFP, green fluorescence protein; Grp78, Glucose regulated protein 78; HI, hypoxia-ischemia; HIF-1α, hypoxia-inducible factor-1α; hsc70, heat-shock cognate protein of 70 kDa; IP3R, inositol trisphosphate receptor; IPC, ischemic preconditioning; IRE1, inositol-requiring enzyme 1; JNK1, Jun N-terminal kinase 1; LAMP2A, lysosomal-associated membrane protein 2A; LC3, light chain 3; miR-9a-5p, micro-RNA-9a-5p; mTOR, mammalian target of rapamycin; mTORC1, mammalian target of rapamycin complex 1; NF-κB, Nuclear factor-κB; NMDA, N-methyl-D-aspartate; OGD, oxygen and glucose deprivation; P70S6K, P70 ribosomal protein S6 kinase; PE, phosphatidylethanolamine; PERK, protein kinase R-like endoplasmic reticulum kinase; PI3K, phosphatidylinositol 3-kinase; PI3P, phosphatidylinositol 3-phosphate; pMCAO, permanent model of middle cerebral artery occlusion; Rheb, Ras homolog enriched in brain; RIP1K, receptor-interacting protein 1 kinase; SERCA, sarcoendoplasmic reticular calcium-ATPase; SGK, serum and glucocorticoid kinase; siRNA, small interfering RNA; SNAP29, synaptosomal-associated protein 29; SNARE, soluble N-ethylmaleimide-sensitive-factor attachment protein receptor; SQSTM1, sequestosome 1; STX17, syntaxin 17; tMCAo, transient MCAo; tPA, tissue-type plasminogen activator; TSC1/2, tuberous sclerosis complex 1 and 2; TSC2, tuberous sclerosis complex 2; ULK1, Unc-51-like kinase; UPR, unfolded protein response; VAMP8, vesicle-associated membrane protein 8; VPS15, vacuolar protein sorting 15; VPS34, vacuolar protein sorting 34; XBP1, X-box bonding protein 1.

INTRODUCTION

Cerebral ischemia is a major cause of adult mortality and disability in developed countries. It is characterized by a reduction of cerebral blood flow, leading to a dramatic drop of energetic supply, altered cellular homeostasis and finally cell death (Doyle et al., 2008; Yepes et al., 2009). Several pathways leading to neuronal death are activated during ischemic events. Historically, glutamate receptor-mediated excitotoxicity, apoptosis and inflammation have been shown to be important parts of ischemia-mediated neuronal death (Dirnagl et al., 1999). More recently, ER stress via the UPR (Roussel et al., 2013) and autophagy (Liu et al., 2010) pathways, either at the acute phase or during recovery, has received much attention in the stroke research field.

To date, only two therapeutic approaches are available to promote reperfusion during ischemic stroke: the recent mechanical clot removal (endovascular thrombectomy), and thrombolysis by tPA (Thiebaut et al., 2018). Of note, tPA administration is often combined with endovascular thrombectomy, especially in patients with large vessel occlusion (Berkhemer et al., 2015). However, both treatments have their own limits: tPA has a narrow therapeutic window (4.5 h after stroke onset) (Hacke et al., 2008), presents a risk of hemorrhagic transformation and has a low recanalisation rate (National Institute of Neurological Disorders and Stroke rt-Pa Stroke Study Group, 1995; Thiebaut et al., 2018); while endovascular thrombectomy is restricted to large vessel occlusions (Berkhemer et al., 2015). Several strategies of neuroprotection have been tested in stroke, but no clinical trials have demonstrated any beneficial effect in patients (Young et al., 2007). To overcome this challenge, better stroke models and trial designs are required, and integration of multiple complex signaling pathways will be necessary to provide a complete understanding of stroke (Karsy et al., 2017).

Among such pathways, those maintaining proteostasis appear especially relevant as they encompass many responses, from changes in protein synthesis and folding to secretion and degradation. Moreover, altered proteostasis is implicated in both the acute and recovery phases of stroke (Wang and Yang, 2018). The UPR, which is the proteostasis control system affecting the ER, maintains the balance between protein synthesis, folding and degradation within the organelle (Roussel et al., 2013). On the other hand, protein or organelle degradation during stroke is mainly driven by autophagy (with ubiquitination and SUMOylation), and more particularly, macroautophagy (called hereafter autophagy) (Liu et al., 2010).

AUTOPHAGY AND CEREBRAL ISCHEMIA

Autophagy is a protein degradation system highly conserved in all eukaryotes. Its name comes from Greek roots: "auto" which means "self" and "phagy" which means "eating." This self-protecting catabolic process is required for restoring cellular homeostasis under nutrient starvation or metabolic stress by degrading or recycling long-lived or misfolded proteins and damaged organelles (Klionsky et al., 2016). Depending on the mode of cargo delivery, three types of autophagy have been described: microautophagy, CMA and macroautophagy.

Microautophagy is a non-selective lysosomal degradative process referring to as the direct engulfment of cytoplasmic materials by the lysosome. In microautophagy, the lysosomal membrane is randomly invaginated to trap portions of the cytosol (**Figure 1A**). Microautophagy is known to play several roles, such as the regulation of the ratio of lipid to protein at the lysosomal surface, the maintenance of organelle size, the membrane composition and lipid metabolism. It can occur simultaneously with macroautophagy or simply be a constitutive method to degrade long-lived proteins and membrane proteins (Iwata et al., 2005; Krick et al., 2009).

Chaperone-mediated autophagy is a selective lysosomal degradative process requiring the presence within the substrate protein of a specific amino acid motif recognized by the chaperone hsc70. All cargo recognized by hsc70 are delivered to lysosomes where they bind to the LAMP2A (Bandyopadhyay et al., 2008; **Figure 1B**). Then, they are translocated one-by-one into lysosomes assisted by a chaperone located in the lysosomal lumen. CMA contributes to protein quality control through selective removal of altered or damaged proteins (Zhang and Cuervo, 2008).

In contrast to microautophagy and CMA, macroautophagy involves sequestration of the cargo away from the lysosome. Macroautophagy requires the synthesis of an autophagosome, a double-layered membrane structure, to transport cellular cargo targeted for degradation. Autophagosomes then fuse with lysosomes to form autophagolysosomes resulting in the degradation of their contents (**Figure 1C**). Because macroautophagy is the most abundant and characterized form of autophagy, our review will primarily focus on its mechanisms and effects in cerebral ischemia.

Autophagy occurs at a basal level in all mammalian cells and is regulated by conditions such as starvation, oxidative stress or hypoxia, and can also be triggered by obesity, diabetes, inflammation and cancer. The induction of autophagy appears as a promising therapeutic strategy for neurodegenerative diseases with protein misfolding and aggregation (Alzheimer's diseases, Parkinson's disease, Tauopathies, Huntington's disease, and various spinocerebellar ataxias) (Rubinsztein et al., 2012).

Autophagy Mechanisms in Physiopathological Conditions

Autophagy Processes and Signaling Pathway

The most common experimental approaches to induce autophagy are either nutrient starvation and or the use of rapamycin to inhibit the mTOR. Autophagy activates the ULK1 complex (ULK1, also known as Atg1 for intervention of autophagy-regulated 1), Atg13, and FIP200 (Noda and Ohsumi, 1998). The ULK1 complex also regulates the activation of a class III PI3K complex formed by Beclin-1, VPS34, and VPS15. When phosphorylated by ULK1, Beclin-1 promotes the generation of PI3P by VPS34, which upgrades autophagosomal

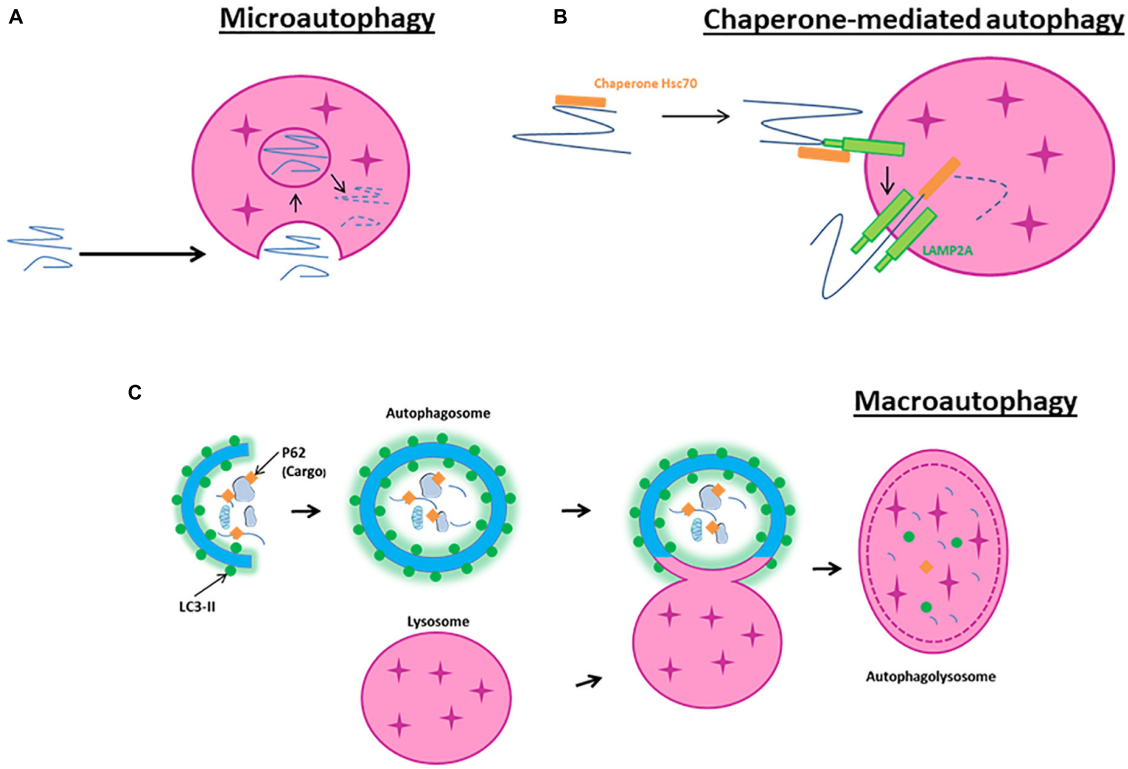

FIGURE 1 | Schematic model of autophagy. **(A)** Macroautophagy is the result of the fusion of an autophagosome, a double membrane vacuole transporting cellular cargo that has been targeted for degradation, with a lysosome. **(B)** Microautophagy is a non-selective lysosomal degradative process that involves direct engulfment of cytoplasmic materials by the invagination of the lysosome. **(C)** Chaperone-mediated autophagy involves the direct translocation, through LAMP2A, of specific proteins containing a motif recognized by a chaperone named hsc70 (heat-shock cognate protein of 70 kDa).

membrane nucleation (Russell et al., 2013; **Figure 2A**). On the other hand, Beclin-1 can bind to the anti-apoptotic protein Bcl-2 leading to the inhibition of autophagy (Pattingre et al., 2005). In response to starvation, JNK1 phosphorylates Bcl-2 allowing its release from Beclin-1 and the induction of autophagy (Pattingre et al., 2009; **Figure 2B**).

In addition to these two complexes, other Atg proteins are hierarchically required for the biogenesis of autophagosomes. Atg5 and Atg12, co-operate with Atg7, to promote the formation of an Atg5-Atg12- Atg16L1 complex, and thus facilitate the cargo recruitment and autophagosomes membrane elongation. The microtubule-associated protein light chain 3 (LC3, also named Atg8) is cleaved by Atg4 to yield LC3-I, then, LC3-I is conjugated to PE by Atg7 and Atg3 to become LC3-II (Mizushima et al., 2011). p62, also called SQSTM1, binds to ubiquitinated proteins, targeting them for degradation into autolysosomes through its binding to LC3-II in the autophagosome (Myeku and Figueiredo-Pereira, 2011). LC3-II is essential for phagophore formation, with the participation of GABARAP/GATE-16 subfamily members in later stages of autophagosome formation, in particular for phagophore elongation, closure and fusion (Weidberg et al., 2010). Autophagosome can acquire membranes from multiple sources including the ER, the Golgi apparatus, the plasma membrane and the mitochondrial outer membrane. This process requires the involvement of the only transmembrane Atg protein, Atg9, which is present in single-membrane vesicles providing membranes for early autophagosome formation (Yamamoto et al., 2012). The fusion between the autophagosome and the lysosome requires the recruitment from the ER and mitochondria of the SNARE protein STX17. STX17 interacts with SNAP29 and VAMP8 to form a *trans*-SNARE complex and mediates autophagosome-lysosomes fusion (Itakura et al., 2012).

Autophagy Activation in Brain Ischemia

Nitatori et al. (1995) were the first to demonstrate, by electron microscopy, an increase in cathepsin B-immunopositive lysosomes, in the CA1 pyramidal neurons 3 days after an ischemic insult. Since then, the evidence for activation of autophagy has continued to accumulate. For example, beclin 1 is activated and associated to a LC3-II increase following neonatal hypoxia-ischemia (HI) (Carloni et al., 2008) and focal cerebral ischemia (Rami et al., 2008). In neonatal cerebral HI, in addition to the increase in autophagosomal formation (characterized by an increase of LC3-II), there is also an increase of lysosomal activity in damaged cortical and CA3 neurons, suggesting an increase in the autophagic flux (Ginet et al., 2009). These results are confirmed in a pMCAO. Moreover, immunofluorescence shows strong co-localisation of autophagosomal puncta (LC3-II) and lysosomes (cathepsin D and LAMP1) (Puyal et al., 2009).

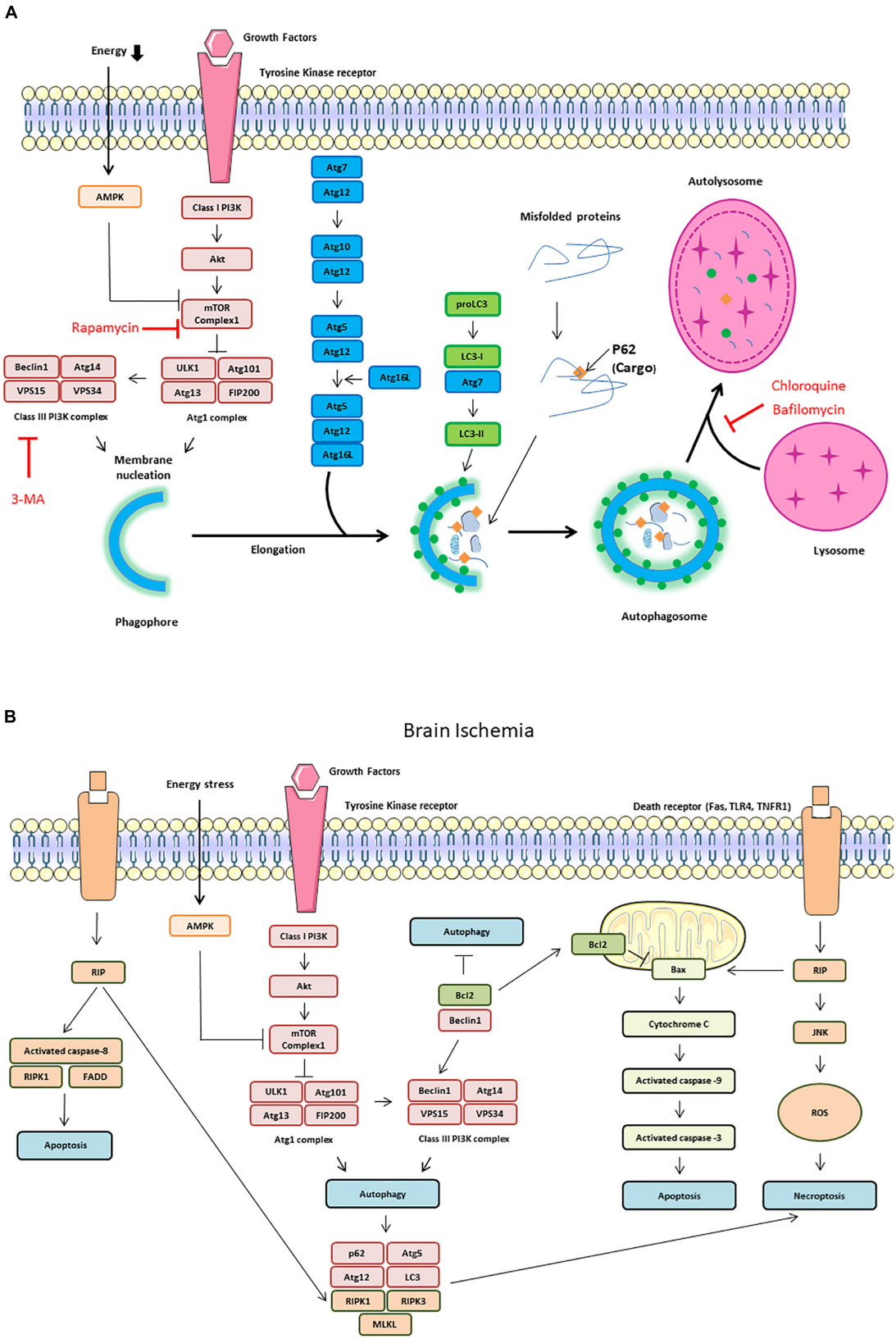

FIGURE 2 | Continued

FIGURE 2 | Autophagy signaling pathway. Autophagy is induced by an energetic stress, leading to AMPK activation; or by growth factors starvation, leading to the inhibition of the class I phosphatidylinositol 3-kinase (PI3K)/Akt/mammalian target of rapamycin (mTOR) pathway. Two complexes can be involved in autophagy induction: ULK1 complex composed of autophagy-regulated 101 (Agt1), Atg101, FIP200, and ULK1 and class III PI3K complex form by Beclin-1, vacuolar protein sorting 34 (VPS34) and vacuolar protein sorting 15 (VPS15). **(A)** Schematic illustration of autophagy initiation and autophagosome formation. Different Atg proteins including Atg5-Atg12-Atg16L and the microtubule-associated protein LC3-II are involved in double membrane elongation and in autophagosome-lysosome fusion. P62 binds to ubiquitinated proteins targeting them for degradation in the autolysosomes. Rapamycin can activate autophagy by inhibiting mTOR Complex 1. Both 3-MA (3-methyladenine), chloroquine and Bafilomycin are autophagy inhibitors by, respectively, inhibiting Class III PI3K complex and autophagosome/lysosome fusion. **(B)** Schematic illustration of cross talk and interaction among autophagy, apoptosis and necroptosis during brain ischemia. The dissociation of Beclin1 and Bcl-2 is also responsible of autophagy increase. The receptor interacting protein (RIP) Kinase 1 activation by death receptors, such as Fas, TLR4 and TNFR1, is responsible of Jun N-terminal kinase 1 (JNK1) pathway activation, ROS (reactive oxygen species) release and necroptosis. RIP1 interacts with FADD (Fas-Associated protein with Death Domain) and TRADD (Tumor necrosis factor receptor type 1-associated DEATH domain protein) to induce extrinsic apoptosis. RIP1 is also involved in intrinsic (mitochondrial) apoptosis through cytochrome C release which activates caspase-9 and capase-3.

Furthermore, a study with 37 acute ischemic stroke patients revealed that CSF and serum levels of both Beclin-1 and LC3 are increased compared to control patients (Li et al., 2015), suggesting that autophagic cells die and release these markers in the circulation. Levels of Beclin1 and LC3 in CSF are positively correlated with infarct volumes and the severity of neurological deficits (NIHSS and Modified Rankin Scale) (Li et al., 2015). In addition, the expression of autophagic and apoptotic genes is increased in blood samples of ischemic stroke patients (Guo et al., 2017). However, Liu et al. (2010) reported that autophagy pathway is up-regulated after cerebral ischemia/reperfusion, but fails to operate correctly. They propose the idea that at least a part of the accumulation of protein aggregate-associated organelles seen following ischemia is due to the failure of autophagosomes to fuse with lysosomes (Liu et al., 2010).

After brain ischemia, autophagy-related signaling pathways are dramatically activated. In neonatal HI, Akt and CREB are activated in neurons and both phospho-Akt and phospho-CREB colocalized with Beclin-1. In this model, it has been shown that activation of autophagy activated by rapamycin was neuroprotective, and this was associated with the activation of Akt/CREB signaling (Carloni et al., 2010). During ischemia, a decrease in ATP concentration increases the AMP/ATP ratio and activates AMPK. Active AMPK leads to phosphorylation of TSC1/2 (tuberous sclerosis proteins 1 and 2) and inhibition of mTORC1 activity through Rheb. Several groups have reported the involvement of AMPK signaling pathway in the mediation of autophagy-related neuroprotection in brain ischemia (Wang et al., 2012; Gabryel et al., 2014; Jiang et al., 2014; Dai et al., 2017). Conversely, a study has shown that inhibition of AMPK activity inhibits autophagy and alleviates focal cerebral ischemia injury in mice by restoring mTORC1 activity (Fu et al., 2016). Autophagy may also be increased by the HIF-1α, a key transcription factor activated by the low oxygen conditions observed during cerebral ischemia (Xin et al., 2011; Yang et al., 2014; Zhang et al., 2018).

Role of Autophagy in Cerebral Ischemia

While brain ischemia is known to induce autophagy, its protective or deleterious role remains unclear. Indeed, *in vitro* and *in vivo* studies report contradictory effects of autophagy induction during ischemia.

Neuronal Autophagy in the Ischemia Brain

Neuronal autophagy occurs early during cerebral ischemia, with autophagosomes and autolysosomes detectable just 1 h after pMCAo, and increasing up to 12 h thereafter (Wen et al., 2008). In line with this, Tian et al. (2010) showed, using GFP-LC3 transgenic mice, increased levels of autophagosomes in the ipsilateral hemisphere at 1, 3, and 6 days following tMCAo, with a peak at 1 day. The cells containing GFP-LC3-punctae were mostly neurons (Tian et al., 2010). Indeed, during cerebral ischemia, autophagy is predominantly a neuronal phenomenon (Carloni et al., 2008; Rami et al., 2008; Ginet et al., 2009; Puyal et al., 2009).

Autophagy and Neuronal Death in Brain Ischemia

After cerebral ischemia, the number of GFP-LC3-punctae/TUNEL (terminal deoxynucleotidyl transferase-mediated dUTP-digoxigenin nick end labeling) double-positive cells increases in both the core and the peri-ischemic area (Tian et al., 2010). In addition, dying neurons displaying intense vacuolisation and numerous autophagosomes are detected 6 h after HI in neonatal rats, with a peak at 24 h. These dying neurons display some features of apoptosis such as chromatin condensation, cytoplasmic shrinkage, and relatively well-preserved organelles, suggesting that autophagy could precede apoptosis (Ginet et al., 2009). Uchiyama (2001) have shown that inhibiting autophagy protects neuron-like differentiated PC12 cells from apoptosis following serum deprivation, suggesting that autophagy is involved in neuronal cell death *in vitro*. This association between neuronal death and autophagy has led to the term "autophagic death" (**Figure 2B**). Beclin 1 has been reported to be involved in autophagic death. RNAi against Beclin-1 reduces neuronal autophagy and apoptosis in tMCAo model (Zheng et al., 2009). In addition, Beclin 1 knockdown inhibits autophagosomal formation and alleviates apoptotic neurodegeneration in the ipsilateral thalamus following focal ischemia (Xing et al., 2012).

Apoptosis is not the only mechanism involved in ischemia-induced cell death. In 2005, a study shown that an intracerebroventricular injection of necrostatin-1, an inhibitor of necroptosis (programmed necrosis), decreases the infarct volume in a mouse MCAo model (Degterev et al., 2005). A recent work demonstrates in a pMCAo model, that the RIP1K-regulated necroptosis contribute to ischemia-mediated neuronal and astrocytic cell death through the activation of autophagic pathways (Ni et al., 2018). Furthermore, necrostatin-1 decreases LC3-II level and autophagy (Ni et al., 2018). On the other hand, pre-treatment with 3-MA, an inhibitor of autophagy and PI3K,

prevents neuronal necroptosis at 7 days of reperfusion in a severe model of global cerebral ischemia (Wang et al., 2011).

Despite controversial findings suggesting that ischemia induces autophagy only in the hippocampal CA1 region (Gao et al., 2015), it has been suggested that hippocampal CA1 and CA3 regions present a differential response to ischemia-induced autophagy, with CA1 neurons mostly undergoing apoptosis without autophagy, while CA3 neurons mostly undergo autophagic death (Ginet et al., 2009; Papadakis et al., 2013). The reasons for these subpopulation differences remain to be established.

Deleterious Autophagy in Brain Ischemia

In both primary cultures of neurons and SH-SY5Y cells subjected to OGD, autophagic cell death occurs and can be reversed by 3-MA, a PI3Ks inhibitor (Shi et al., 2012). Bao et al. (2017) suggest that this effect is dependent of autophagy-induced AMPAR subunits GluR1, GluR2, and GluR3 upregulation during OGD, leading to an increase of cytoplasmic Ca^{2+} levels. In rats subjected to transient focal cerebral ischemia, intraventricular injection of 3-MA dramatically reduces the lesion volume (by 46%) whereas an inhibitor of apoptosis does not provide protection (Puyal et al., 2009). Several inhibitors of autophagy (3-MA, bafilomycin, and the cathepsin B inhibitor Z-FA-fmk) significantly reduce the increase of autophagosome and autolysosome, the downregulation of Bcl2, infarct volume, brain oedema and motor deficits in a rat model of pMCAO (Wen et al., 2008). Thus, it seems that decreasing autophagy both *in vitro* and *in vivo* during cerebral ischemia is beneficial (Cui et al., 2013; Jiang et al., 2017; Ryan et al., 2018).

Knocking down Beclin1 and Atg7 with siRNA reduce autophagy and excitotoxic cell death induced by both kainate and hypoxia in primary neurons (Ginet et al., 2014). Atg7 deficient mice show nearly complete protection from HI-induced caspase-3 activation and hippocampal pyramidal neuronal death (Koike et al., 2008). Furthermore selective neuronal deletion of Atg7 reduces autophagy and infarct volume by 42% in neonatal mice subjected to HI (Xie et al., 2016). Overexpression of microRNA-9a-5p (miR-9a-5p) decreases Atg5 protein level, leading to a decrease of infarct volume and neurological deficit in a rat model of MCAo (Wang et al., 2018).

Protective Autophagy in Brain Ischemia

In Wang et al. (2012) have shown that 3-MA pre-treatment is deleterious in a rat model of MCAo. The inhibition of autophagy by 3-MA or wortmannin, both PI3Ks inhibitor, accelerates the progression toward necrotic cell death in neonatal HI model. Conversely, rapamycin, increases Beclin 1 expression and reduces necrotic cell death and brain damage (Carloni et al., 2008). Both ischemic preconditioning (IPC) and permanent focal ischemia induce autophagy activation by up-regulating LC3-II and Beclin-1. IPC treatment significantly reduces infarct volume, brain oedema and motor deficits, whereas 3-MA and bafilomycin suppress IPC-induced neuroprotection (Sheng et al., 2010). The neuroprotective action of rapamycin has been confirmed in several models of MCAo (Chauhan et al., 2011; Buckley et al., 2014). Finally, neuronal autophagy upon brain ischemia seems to be a part of pro-survival signaling pathway, that involves PI3K/Akt/TSC2 /mTOR/P70S6K signaling pathway (Wang et al., 2012; Papadakis et al., 2013) and Akt/CREB pathway (Carloni et al., 2010). IPC-induced autophagy is also neuroprotective and this effect has been suggested to be dependent of the amelioration of ER stress (Sheng et al., 2012). Inhibition of autophagy with Atg7 knock down increase ischemia-induced neuronal apoptosis in OGD and MCAo model. Mitochondrial clearance is reversed by 3-MA and Atg7 silencing, suggesting that mitophagy underlies the neuroprotection by autophagy (Zhang et al., 2013). Moreover, Atg7 silencing reverses the neuroprotection induced by an ER stress activator (Zhang et al., 2014). In fact both tunicamycin and thapsigargin protect against ischemic brain injury by activating mitochondrial autophagy during reperfusion. Interestingly, this effect is reversed by the inhibition of autophagy (Zhang et al., 2014). Knocking out arrestin-β1, which is upregulated after cerebral ischemia, protects neurons from OGD by impairing the interaction between Beclin-1 and PIK3 catalytic subunit type 3, thus decreasing autophagy (Wang et al., 2014). Beclin-1 seems central, as caveolin1, an integral membrane protein, is able to activate autophagy through its binding to Beclin-1/VPS34 complex: in Caveolin1 knock out mice, autophagy is impaired, leading to greater tMCAo-induced cerebral infarct (Nah et al., 2017).

Endothelial Autophagy in Brain Ischemia

In Engelhardt et al. (2015) have published a comparative study to characterize BBB-associated cells responses to HI. BMVECs exhibit greater responsiveness and sensitivity to OGD than astrocytes and pericytes. This is associated with the stabilization of HIF-1α, early disruption of cellular cytoskeleton and metabolism impairment, but unlike perivascular cells, BMVECs appear unable to induce autophagy. BMVECs are specialized endothelial cells, connected by tight junction and display intimate contact with supporting pericytes, astrocytes, microglia, and neurons in order to maintain the structural and functional integrity of the BBB. Brain ischemia and thrombolysis therapy with tPA induce BBB disruption, brain oedema and neuronal injury (Thiebaut et al., 2018). Several groups support the idea that autophagy induces endothelial cell injury and BBB disruption. Indeed focal ischemia, in NF-κB p50 knockout mice, induces autophagy like-injury in BMVECs together with a disruption of BBB integrity (Li et al., 2013). It appears that autophagy is beneficial for BMVECs and BBB integrity. In Li et al. (2014) shown that enhancing autophagy by rapamycin and lithium reverses OGD-induced collapsing of tight junction and decreases tMCAo-induced BBB leakage and brain oedema; while 3-MA intensifies BMVECs apoptosis. Supporting these results, the knockdown of Beclin-1 attenuates autophagy processes and reduces the viability of endothelial cells subjected to OGD, while treatment with rapamycin increases cell viability (Urbanek et al., 2014). Similarly, chloroquine-induced autophagy inhibition enhances BBB permeability during pMCAo in diabetic rats. By opposition to the results of Engelhart and collaborators, this group observed autophagy activation in BMVECs after ischemia (Fang et al., 2015).

Astrocytic Autophagy in Brain Ischemia

During brain ischemia, glial cells, especially astrocytes, play a crucial role. They are involved in water transport, ion homeostasis, glutamate uptake, cerebral blood flow regulation, cerebral inflammation, maintenance of the BBB integrity, modulation of neuroplasticity and the secretion of neurotrophic and neuroprotective factors (Nedergaard et al., 2003).

In Tian et al. (2010) have shown, in a mouse model of MCAo, that GFP-LC3-punctae positive cells were mostly neurons rather than astrocytes or microglial cells in the peri-ischemic area, suggesting that glial cells may be more resistant to brain ischemia-induced autophagy than neurons. Nonetheless, a few groups report that ischemia induces an increase of astrocytic autophagy (Qin et al., 2010; Zhang et al., 2010; Engelhardt et al., 2015). Autophagosomes start to appear in the cytoplasm of astrocytes within the ischemic cortex 1 h after pMCAo and in the cytoplasm of primary astrocytes 1 h after OGD, with a peak at 3 h (Qin et al., 2010). The number of lysosomes significantly increases 6 h after pMCAo and OGD. In addition, they observe an increase of LC3-II, Beclin-1, LAMP2 and lysosomal cathepsin B expression. 3-MA and bafilomycin decrease ischemia-induced autophagy, apoptosis and necrosis, suggesting that autophagic/lysosomal activation may contribute to ischemic injury of astrocytes (Qin et al., 2010). This is partially confirmed by the fact that RIP1K knockdown decreases autophagy, increases GFAP levels, and attenuates astrocytic necrotic cell death in the ischemic cortex (Ni et al., 2018). RIP1K-mediated necroptosis may play important roles in ischemia-induced neuronal and astrocytic cell death through the activation of autophagic-lysosomal pathway (Ni et al., 2018). In the same line, breviscapine provides neuroprotection in the penumbra by decreasing both astrocytic and neuronal autophagy induced by tMCAo (Pengyue et al., 2017).

In contrast, inhibition of AMPK, by siRNA targeting AMPKα1 or by a pharmacological inhibitor, attenuates autophagy and astrocyte viability following OGD. This work supports the idea that during ischemia AMPK is involved in the induction of protective autophagy in astrocytes (Gabryel et al., 2014). Furthermore, when the astrocytic autophagy is specifically enhanced, by using AAV-GFAP-ATG7, it leads to neuroprotection in astrocytes/neurons co-cultures exposed to OGD and improves neurological outcome following tMCAo (Liu et al., 2018).

It is important to mention that many inhibitors used in the autophagy field are not always selective. For example, 3-MA and wortmannin inhibit both class I and class III PI3K, and each class of PI3K has its own, and sometimes opposite, effect on autophagy (Petiot et al., 2000). Furthermore, the use of rapamycin to inhibit mTORC1 does not only affect autophagy, as mTORC1 is involved in cell growth, cell survival protein synthesis and ribosomes biogenesis (Boutouja et al., 2019). Rapamycin can also inhibit mTOR complex 2, a complex known to have pro-survival and pro-proliferation effect by increasing Akt and SGK (Boutouja et al., 2019). The use of these poorly selective autophagy inhibitors could explain some of the discrepancies observed in the literature.

ER STRESS AND CEREBRAL ISCHEMIA

Another important consequence of cerebral ischemia is ER stress. The ER is an important organelle for the folding of all secreted and membrane proteins. In stress conditions, such as ischemia, the ER cannot assume correctly its functions and triggers an adaptive program called the UPR, leading to two distinct actions: (i) an early inhibition of protein synthesis; (ii) a delayed upregulation of genes that promote protein folding and degradation (Marciniak and Ron, 2006).

In Def Webster and Ames (1965), it was first noted that neurons of the rabbit retinas show swelling of their ER when subjected to OGD. Although initially reversible, this change becomes irreversible when OGD lasts more than 30 min. Similar distension of the ER was subsequently reported in neurons in a rat model of MCAo reperfusion injury (Dietrich et al., 1989), implicating ER dysfunction in the complex process of ischemic neuronal damage.

The threat of ER is detected in cells by three sensors that are present at the ER membrane, PERK, IRE1, and ATF, each mediating a separate branch of the UPR (**Figure 3**).

The PERK branch: the inhibition of protein synthesis is an early response to ER stress mediated by PERK (PKR-like endoplasmic reticulum eIF2α kinase) (Harding et al., 1999). Under physiological conditions, PERK is held inactive by its binding to the chaperone BiP (binding immunoglobulin protein, also known as Grp78). Upon stress, the kinase is activated by the release of BiP and phosphorylates its sole cytoplasmic target, eIF2α (Marciniak et al., 2006). This is a regulator of the initiation of protein synthesis. In teleological terms, a "goal" of the PERK branch activation is to prevent the further accumulation of misfolded proteins (Roussel et al., 2013). However, despite a global shutdown of protein translation due to the phosphorylation of eIF2α, some mRNAs are translated more efficiently (Harding et al., 2003). This is the case of ATF4, leading to a transcriptional program of stress-responsive genes including CHOP (C/EBP homologous protein) (Harding et al., 2003). The observation that Chop−/− animals and cells are resistant to ER stress, led some to suggest CHOP functions to promote ER stress-induced cell death. This is not fully supported, however, by analysis of the genes regulated by CHOP (Marciniak et al., 2004). Instead, CHOP appears to regulate a program that promotes the recovery of protein synthesis and secretion following the recovery of ER stress. For example, CHOP induces expression of GADD34 (protein phosphatase 1 regulatory subunit 15A), which is responsible for the dephosphorylation of eIF2α and thus the recovery of normal protein translation (Roussel et al., 2013). In this light, the ATF4-CHOP-GADD34 axis can be viewed as a negative feedback loop opposing the effects of PERK. It is therefore likely that the apparent "pro-death" role that has been attributed to CHOP is too simplistic. The recovery of translation is essential for normal functioning of

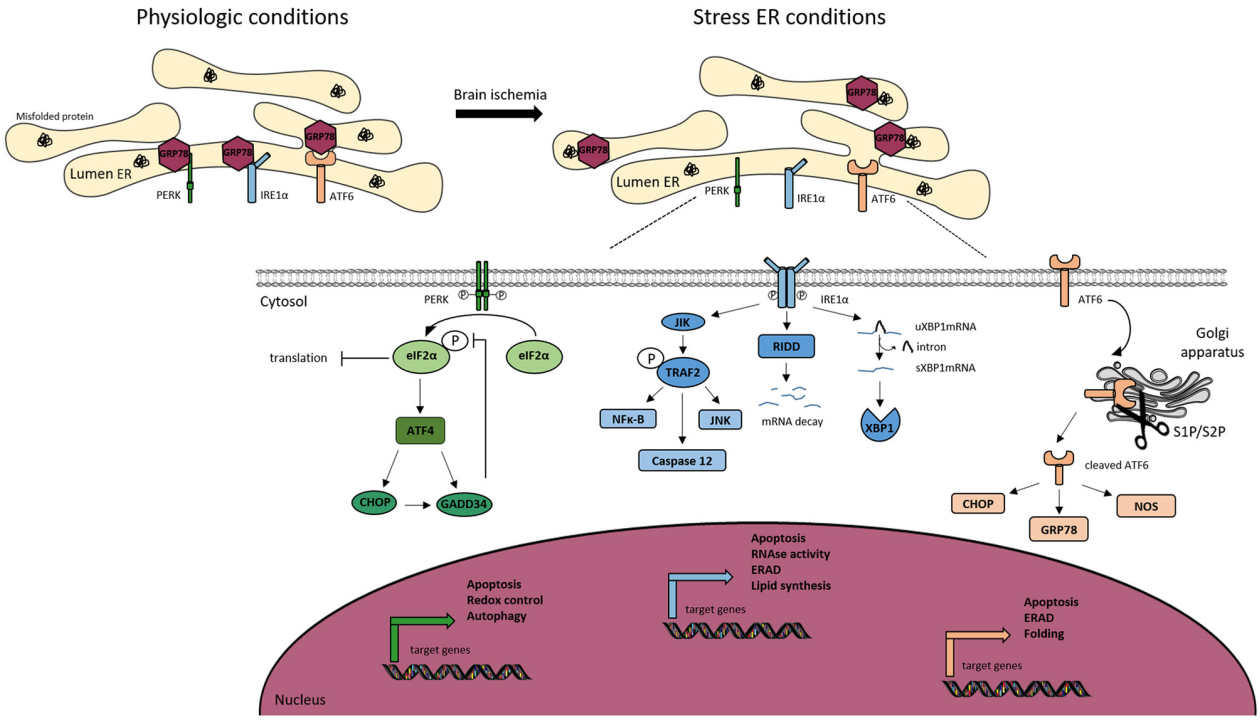

FIGURE 3 | Endoplasmic reticulum (ER) stress signaling. Under physiological conditions, the Glucose Related Protein 78 (GRP78) binds to the three ER transmembrane sensors; protein kinase RNA-like ER kinase (PERK), inositol-requiring kinase 1α (IRE1α) and activating transcription factor 6 (ATF6), and maintains them inactive. Ischemic stroke induces ER stress, leading to the activation of the UPR. Under stress conditions, GRP78 dissociates from the ER sensors to bind to misfolded proteins, allowing the *trans*-autophosphorylation of PERK. P-PERK phosphorylates the eukaryotic translation initiation factor 2α (eIF2α), which decreases the global protein translation. Paradoxically, P-eIF2α allows the transcription of activating transcription factor 4 (ATF4), CCAT/enhancer binding protein homologous protein (CHOP). Both P-eIF2α and CHOP can activate the translation of growth arrest and DNA damage inducible gene/protein 34 (GADD34). The latter creates a feedback mechanism by dephosphorylating eiF2α. PERK is associated to apoptosis, autophagy and redox control. IRE1α dimerizes and *trans*-autophosphorylates, to splice the unspliced mRNA XBP1 (uXBP1) into spliced XBP1 (sXBP1). IRE1α activates c-jun-N-terminal-inhibiting kinase (JIK) and allows the recruitment of TNF receptor-associated factor 2 (TRAF2), leading to the activation of nuclear factor κ-B (NFκ-B), caspase 12 and c-jun-N-terminal kinase (JNK) pathway. IRE1α activates Regulated IRE1-Dependent Decay (RIDD) leading to the degradation of selected mRNAs. IRE1α is also involved in apoptosis, ER-associated degradation (ERAD) and lipid synthesis. The activation of ATF6 is dependent of its cleavage by S1P and S2P endopeptidases in the Golgi apparatus. Cleaved ATF6 induces the transcription of GRP78, nitric oxide synthase (NOS) and CHOP. Moreover, cleaved ATF6 controls ERAD, apoptosis and protein folding.

the cell following mild ER stress, but perhaps in pathology, for example cerebral ischemia, there are benefits from disabling the normal rapid recovery of protein synthesis. This clearly has exciting therapeutic implications and many groups are currently developing approaches to antagonize the ATF4-CHOP-GADD34 axis for therapeutic benefit.

The ATF6 branch: like PERK, ATF6 is held inactive by the binding to BiP. Under stressed conditions, ATF6 is free to traffic to the Golgi apparatus where it is cleaved to release a soluble transcription factor for protein folding and degradation genes (Hillary and Fitzgerald, 2018).

The IRE1 branch: the activation of IRE1 is similar to that of ATF6 and PERK, but IRE1 is an endoribonuclease that triggers the splicing of the mRNA XBP1 (Calfon et al., 2002). The splicing induces a frameshift, allowing the active form of the protein. Proteins that fail to fold in the ER are eventually returned to the cytoplasm and targeted for degradation by the proteasome in process called ERAD. Many proteins of the ERAD machinery are induced by XBP1 (Yoshida et al., 2003). During intense ER stress, IRE1 also degrades many mRNAs located at the ER membrane through a mechanism called regulated IRE1-dependent decay (RIDD) (Hollien and Weissman, 2006). This helps further to reduce the load of new proteins entering the ER to be folded.

UPR in Cerebral Ischemia

The ER is the main storage site for intracellular calcium, a central second messenger mediating diverse physiological processes in neurons, including secretion, synaptic plasticity and cell death (Zundorf and Reiser, 2011). Molecular chaperones that reside within the ER require high calcium concentrations to function efficiently (Michalak et al., 2002). This high calcium environment is maintained by the constant pumping of calcium from the cytosol into the ER by the SERCA (Doutheil et al., 1999b). Release of calcium back into the cytosol happens through the IP3R channel, which can be triggered by extracellular signals, or by the ryanodine receptor, activated by cytosolic calcium itself during CICR. Both lead to signaling but, if sustained, they deplete ER calcium stores and can induce chaperone dysfunction (Szydlowska and Tymianski, 2010). During cerebral ischemia, the

influx of extracellular calcium via the NMDA receptor mediates glutamate-dependent neurotoxicity (Lopez-Atalaya et al., 2008). The rise in intracellular calcium triggers the release of ER calcium from ryanodine-sensitive stores, which is known to exacerbate CA1 hippocampal neuronal damage during global cerebral ischemia-reperfusion (Xing et al., 2004; Bull et al., 2008). Accordingly, inhibition of calcium release with the ryanodine receptor antagonist dantrolene decreases brain injury in animal models of both neonatal and adult HI (Wei and Perry, 1996; Gwak et al., 2008). While commonly attributed to the effects of cytosolic calcium, it is likely that effects on ER protein folding will also be important in these pathological conditions. Moreover, during cerebral ischemia, lack of ATP affects protein maturation (Kumar et al., 2003), and at the same time energy depletion leads to failure of the SERCA pumps (Doutheil et al., 1999b), contributing to the global ER calcium depletion and causing chaperone failure. Thus, the redistribution of calcium from ER to cytosol delivers a double blow to neurons, which exacerbates neurotoxicity (Paschen and Doutheil, 1999; Parsons et al., 1999).

The deregulation of ER-calcium homeostasis causing chaperone failure and activation of the UPR is readily apparent in many animal models of cerebral ischemia, including mice with BCAo (Kumar et al., 2001) or MCAo (Mengesdorf et al., 2002), rats with middle carotid artery occlusion with (Nakka et al., 2010) or without (Rissanen et al., 2006) reperfusion, cardiac arrest with reperfusion (Kumar et al., 2003) and a model of cortical spreading depression in rats (Schneeloch et al., 2004). This induction of ER stress during cerebral ischemia is responsible for the shutdown of protein translation seen during stroke (Burda et al., 1994; DeGracia et al., 1996; Hayashi et al., 2003; Kumar et al., 2003). It involves the activation of the stress-sensing PERK (Kumar et al., 2001; Li et al., 2005; Rissanen et al., 2006) that phosphorylates the translation initiation factor eIF2α, leading to the attenuation of new protein synthesis and disaggregation of polyribosomes (Althausen et al., 2001; Nakka et al., 2010).

Also, CHOP expression is elevated in several animal models of cerebral ischemia, including MCAo (Qi et al., 2004) and BCAo in mice (Tajiri et al., 2004; Osada et al., 2009), as well as MCAo and global ischemia in rats (Hayashi et al., 2005). Chop knockout (−/−) mice are more resistant to a BCAo type of ischemia than their wild-type littermates (Tajiri et al., 2004), and depletion of CHOP using RNA-interference in primary cultures of astrocytes partially prevents cell death in response to OGD (Benavides et al., 2005), suggesting that CHOP regulates a genetic program that is toxic in the context of cerebral ischemia. It has been shown that GADD34 is a target gene of CHOP responsible for some of the tissue damage seen in animal models of ER stress (Marciniak et al., 2004). This phosphatase is induced under conditions of cerebral ischemia (Doutheil et al., 1999a; Paschen et al., 2004; Li et al., 2005; Owen et al., 2005) and is detectable by immunostaining in the peri-infarct penumbra up to 24 h following the induction of stroke in rats (Imai et al., 2002; McCaig et al., 2005). As discussed already, it is therefore plausible that the toxicity attributed to CHOP is in fact the result of re-established protein translation mediated by GADD34 (Marciniak et al., 2004): it might be a mechanism implicated in reperfusion-mediated damage in cerebral ischemia. If this is the case, attenuation of protein translation should protect neurons from accumulating misfolded proteins. Consistent with this theory, salubrinal, a putative GADD34 inhibitor, has been shown to decrease ER stress and kainate-induced neurotoxicity *in vitro* (Sokka et al., 2007). However, the specificity of salubrinal has been questioned many times, since it was first demonstrated to work only *in vivo* (Boyce et al., 2005), and more recently its inhibitory effect has been shown to be really limited (Crespillo-Casado et al., 2017). IRE1, which splices the mRNA encoding the transcription factor XBP1, also shows activation during cerebral ischemia, for example in the cortex of mice after MCAo (Paschen et al., 2003; Morimoto et al., 2007) and BCAo (Tajiri et al., 2004). By contrast, ATF6 signaling remains a subject of debate: ATF6 expression was increased following MCAO in rats (Rissanen et al., 2006), but activation could not be demonstrated in an ischemia-reperfusion model by cardiac arrest in rats (Kumar et al., 2003).

CROSSTALK BETWEEN AUTOPHAGY AND ER STRESS

Autophagy and ER stress are important signaling pathways, but when dysregulated can lead to cell death, such like during cerebral ischemia. A well-balanced activation of these processes allow the maintenance or the recovery of proteostasis. However, their over-activation, by duration or intensity, tips the scale from a protective to a deleterious role (Roussel et al., 2013; Chen et al., 2014).

Although, as mentioned in the introduction, several interactions exist between ER stress and autophagy, in particular when misfolded proteins accumulate within the ER and activate PERK to induce autophagy (Kouroku et al., 2007). Moreover, downstream targets of PERK, like ATF4 and CHOP, induce the transcription of genes related to autophagy in response to both ER stress and amino acid starvation (B'Chir et al., 2013). During hypoxia, ATF4 facilitates autophagosome expansion through a binding to a cAMP response element-binding site within the *LC3b* promoter (Rzymski et al., 2010). Other sensors are also involved in autophagy induction, such as IRE1 by dissociating Beclin1 from its binding with Bcl2 (Wei et al., 2008). In addition, IRE1 also induces autophagy by activating AMPK in response to nitric oxide (Meares et al., 2011). XBP1, the mRNA processed by IRE1, is important for the negative feedback of ER stress-mediated autophagy, especially via its interaction with FOXO1 (Zhou et al., 2011). Interestingly, a genetic screen in *Drosophila* shows that both XBP1 loss of function and spliced-XBP1 overexpression lead to the induction of autophagy (Arsham and Neufeld, 2009). Finally, ATF6 has also been implicated in ER stress-mediated autophagy. By increasing the expression of DAPK1 (Gade et al., 2014), ATF6 promotes the dissociation of Beclin1 from Bcl2, leading to autophagy activation (Zalckvar et al., 2009).

In a mouse model of tMCAo, both ER stress and autophagy markers increase, suggesting a dual activation of ER stress and autophagy (Feng et al., 2017). It seems then important when

studying proteostasis in cerebral ischemia, to pay attention to both phenomena and not only ER stress or autophagy.

Some studies also demonstrate an action of autophagy on ER stress. Indeed, the use of 3MA in a rat model of MCAo alters the ER stress response and leads to the stimulation of apoptosis and the enlargement of the cerebral infarct (Zhang et al., 2018). Similarly, Carloni et al. (2014) show a reduced ER stress activation and a better protection after neonatal HI when they increase autophagy with rapamycin. A possible explanation might be that CHOP induces death by inhibiting autophagy (Lei et al., 2017). This has been demonstrated in hepatocellular carcinoma cells, where ER stress inducer increases apoptosis and autophagy, while autophagy inhibitor promotes apoptosis and autophagy activator decreases ER stress-induced apoptosis (Lei et al., 2017). However, this hypothesis needs to be confirmed in neurons under ischemic/hypoxic challenge.

Finally, ER stress has been reported to cause the translocation of ER chaperones to the cell surface. BiP is the best described chaperone at the cell surface, and can act as a general co-receptor (Gonzalez-Gronow et al., 2009), with roles in autophagy, cancer and neuroprotection (Casas, 2017). Interestingly, cell-surface BiP can regulate autophagy by at least two mechanisms: by activating the PI3K/AKT pathway (Liu et al., 2013); and by associating to α2-macroglobulin receptor to activate mTOR signaling (Misra and Pizzo, 2012). Under OGD conditions, BiP is also at the neuronal surface (Louessard et al., 2017), and its binding to tPA results in a decrease in ER stress activation and neuroprotection (Louessard et al., 2017). In another model of hypoxia-induced apoptosis, the activation of neuronal-surface BiP by a synthetic peptide is also protective (Goldenberg-Cohen et al., 2012), reinforcing its role in neuroprotection during cerebral ischemia.

CONCLUSION

Many neurological diseases, including cerebral ischemia, are associated with complete or partial activation of the UPR, perturbations in calcium homeostasis, autophagy dysfunctions, and finally cell death. Both an appreciation of the crucial role for ER homeostasis, the multiple forms that ER dysfunction can take, the regulation and the consequences of autophagy are now providing novel therapeutic strategies.

We propose a model in which proteostasis dysfunction spans a continuous spectrum from the UPR to autophagy, with probably a direct regulation of autophagy by the UPR as mentioned above. In cerebral ischemia, both pathways will be triggered to a greater or lesser degree, depending of stroke intensity, itself depending of the occlusion type and localisation. In each case, the relative contribution of each response and their interactions would need to be determined if rational approaches to therapy are to be developed.

Also, special attention should be given to studies using pharmacological approaches. As scientists, we all know that pharmacological treatments are really convenient, but we have to keep in mind that a "specific" drug has a lot of off targets actions. For example, it has been recently shown that GSK2606414, a PERK inhibitor, and KIRA6, an IRE1 inhibitor, are not only UPR specific (Mahameed et al., 2019). In fact they also inhibit KIT (also called CD117), a receptor tyrosine kinase involved in signal transduction pathways such as ERK and PI3K/AKT, upstream of mTOR and autophagy. In fact, many pharmacological activators and inhibitors are not as specific as they are supposed to be, and thus participate to discrepancies.

AUTHOR CONTRIBUTIONS

AT and EH did the research and wrote the autophagy and the ER stress part, respectively, and made the figures. SM has actively participated to the writing of the ER stress section and made useful comments on the whole manuscript. DV made corrections and comments on the manuscript. BR organized the review, wrote the introduction and the last section on the interactions between the autophagy and the ER stress, and made final corrections.

REFERENCES

Althausen, S., Mengesdorf, T., Mies, G., Olah, L., Nairn, A. C., Proud, C. G., et al. (2001). Changes in the phosphorylation of initiation factor eIF-2alpha, elongation factor eEF-2 and p70 S6 kinase after transient focal cerebral ischaemia in mice. *J. Neurochem.* 78, 779–787. doi: 10.1046/j.1471-4159.2001.00462.x

Arsham, A. M., and Neufeld, T. P. (2009). A genetic screen in *Drosophila* reveals novel cytoprotective functions of the autophagy-lysosome pathway. *PLoS One* 29:e6068. doi: 10.1371/journal.pone.0006068

Bandyopadhyay, U., Kaushik, S., Varticovski, L., and Cuervo, A. M. (2008). The chaperone-mediated autophagy receptor organizes in dynamic protein complexes at the lysosomal membrane. *Mol. Cell. Biol.* 28, 5747–5763. doi: 10.1128/MCB.02070-07

Bao, L., Li, R. H., Li, M., Jin, M. F., Li, G., Han, X., et al. (2017). Autophagy-regulated AMPAR subunit upregulation in in vitro oxygen glucose deprivation/reoxygenation-induced hippocampal injury. *Brain Res.* 1, 65–71. doi: 10.1016/j.brainres.2017.05.019

B'Chir, W., Maurin, A. C., Carraro, V., Averous, J., Jousse, C., Muranishi, Y., et al. (2013). The eIF2alpha/ATF4 pathway is essential for stress-induced autophagy gene expression. *Nucleic Acids Res.* 41, 7683–7699. doi: 10.1093/nar/gkt563

Benavides, A., Pastor, D., Santos, P., Tranque, P., and Calvo, S. (2005). CHOP plays a pivotal role in the astrocyte death induced by oxygen and glucose deprivation. *Glia* 52, 261–275. doi: 10.1002/glia.20242

Berkhemer, O. A., Fransen, P. S., Beumer, D., van den Berg, L. A., Lingsma, H. F., Yoo, A. J., et al. (2015). A randomized trial of intraarterial treatment for acute ischemic stroke. *N. Engl. J. Med.* 1, 11–20.

Boutouja, F., Stiehm, C. M., and Platta, H. W. (2019). mTOR: a cellular regulator interface in health and disease. *Cells* 2:8. doi: 10.3390/cells8010018

Boyce, M., Bryant, K. F., Jousse, C., Long, K., Harding, H. P., Scheuner, D., et al. (2005). A selective inhibitor of eIF2alpha dephosphorylation protects cells from ER stress. *Science* 11, 935–939. doi: 10.1126/science.1101902

Buckley, K. M., Hess, D. L., Sazonova, I. Y., Periyasamy-Thandavan, S., Barrett, J. R., Kirks, R., et al. (2014). Rapamycin up-regulation of autophagy reduces infarct size and improves outcomes in both permanent MCAL, and embolic MCAO, murine models of stroke. *Exp.Transl. Stroke Med.* 6:8. doi: 10.1186/2040-7378-6-8

Bull, R., Finkelstein, J. P., Galvez, J., Sanchez, G., Donoso, P., Behrens, M. I., et al. (2008). Ischemia enhances activation by Ca2+ and redox modification of ryanodine receptor channels from rat brain cortex. *J. Neurosci.* 17, 9463–9472. doi: 10.1523/JNEUROSCI.2286-08.2008

Burda, J., Martin, M. E., Garcia, A., Alcazar, A., Fando, J. L., and Salinas, M. (1994). Phosphorylation of the alpha subunit of initiation factor 2 correlates with the inhibition of translation following transient cerebral ischaemia in the rat. *Biochem J.* 302(Pt 2), 335–338. doi: 10.1042/bj3020335

Calfon, M., Zeng, H., Urano, F., Till, J. H., Hubbard, S. R., Harding, H. P., et al. (2002). IRE1 couples endoplasmic reticulum load to secretory capacity by processing the XBP-1 mRNA. *Nature* 3, 92–96. doi: 10.1038/415092a

Carloni, S., Albertini, M. C., Galluzzi, L., Buonocore, G., Proietti, F., and Balduini, W. (2014). Increased autophagy reduces endoplasmic reticulum stress after neonatal hypoxia-ischemia: role of protein synthesis and autophagic pathways. *Exp. Neurol.* 255, 103–112. doi: 10.1016/j.expneurol.2014.03.002

Carloni, S., Buonocore, G., and Balduini, W. (2008). Protective role of autophagy in neonatal hypoxia-ischemia induced brain injury. *Neurobiol. Dis.* 32, 329–339. doi: 10.1016/j.nbd.2008.07.022

Carloni, S., Girelli, S., Scopa, C., Buonocore, G., Longini, M., and Balduini, W. (2010). Activation of autophagy and Akt/CREB signaling play an equivalent role in the neuroprotective effect of rapamycin in neonatal hypoxia-ischemia. *Autophagy* 6, 366–377. doi: 10.4161/auto.6.3.11261

Casas, C. (2017). GRP78 at the Centre of the Stage in Cancer and Neuroprotection. *Front. Neurosci.* 11:177. doi: 10.3389/fnins.2017.00177

Chauhan, A., Sharma, U., Jagannathan, N. R., Reeta, K. H., and Gupta, Y. K. (2011). Rapamycin protects against middle cerebral artery occlusion induced focal cerebral ischemia in rats. *Behav. Brain Res.* 1, 603–609. doi: 10.1016/j.bbr.2011.08.035

Chen, W., Sun, Y., Liu, K., and Sun, X. (2014). Autophagy: a double-edged sword for neuronal survival after cerebral ischemia. *Neural Regener. Res.* 15, 1210–1216. doi: 10.4103/1673-5374.135329

Crespillo-Casado, A., Chambers, J. E., Fischer, P. M., Marciniak, S. J., and Ron, D. (2017). PPP1R15A-mediated dephosphorylation of eIF2alpha is unaffected by Sephin1 or Guanabenz. *eLife* 27:26109. doi: 10.7554/eLife.26109

Cui, D. R., Wang, L., Jiang, W., Qi, A. H., Zhou, Q. H., and Zhang, X. L. (2013). Propofol prevents cerebral ischemia-triggered autophagy activation and cell death in the rat hippocampus through the NF-kappaB/p53 signaling pathway. *Neuroscience* 29, 117–132. doi: 10.1016/j.neuroscience.2013.04.054

Dai, S. H., Chen, T., Li, X., Yue, K. Y., Luo, P., Yang, L. K., et al. (2017). Sirt3 confers protection against neuronal ischemia by inducing autophagy: involvement of the AMPK-mTOR pathway. *Free Radical Biol. Med.* 108, 345–353. doi: 10.1016/j.freeradbiomed.2017.04.005

Def Webster, H., and Ames, A. (1965). Reversible and irreversible changes in the fine structure of nervous tissue during oxygen and glucose deprivation. *J. Cell Biol.* 1, 885–909. doi: 10.1083/jcb.26.3.885

DeGracia, D. J., Neumar, R. W., White, B. C., and Krause, G. S. (1996). Global brain ischemia and reperfusion: modifications in eukaryotic initiation factors associated with inhibition of translation initiation. *J. Neurochem.* 67, 2005–2012. doi: 10.1046/j.1471-4159.1996.67052005.x

Degterev, A., Huang, Z., Boyce, M., Li, Y., Jagtap, P., Mizushima, N., et al. (2005). Chemical inhibitor of nonapoptotic cell death with therapeutic potential for ischemic brain injury. *Nat. Chem. Biol.* 1, 112–119. doi: 10.1038/nchembio711

Dietrich, W. D., Nakayama, H., Watson, B. D., and Kanemitsu, H. (1989). Morphological consequences of early reperfusion following thrombotic or mechanical occlusion of the rat middle cerebral artery. *Acta Neuropathol.* 78, 605–614. doi: 10.1007/bf00691287

Dirnagl, U., Iaola, C., and Moskowitz, M. A. (1999). Pathobiology of ischaemic stroke: an integrated view. *Trends Neurosci.* 22, 391–397. doi: 10.1016/s0166-2236(99)01401-0

Doutheil, J., Althausen, S., Gissel, C., and Paschen, W. (1999a). Activation of MYD116 (gadd34) expression following transient forebrain ischemia of rat: implications for a role of disturbances of endoplasmic reticulum calcium homeostasis. *Brain Res. Mol. Brain Res.* 8, 225–232. doi: 10.1016/s0169-328x(98)00276-9

Doutheil, J., Treiman, M., Oschlies, U., and Paschen, W. (1999b). Recovery of neuronal protein synthesis after irreversible inhibition of the endoplasmic reticulum calcium pump. *Cell Calcium* 25, 419–428. doi: 10.1054/ceca.1999.0042

Doyle, K. P., Simon, R. P., and Stenzel-Poore, M. P. (2008). Mechanisms of ischemic brain damage. *Neuropharmacology* 55, 310–318. doi: 10.1016/j.neuropharm.2008.01.005

Engelhardt, S., Huang, S. F., Patkar, S., Gassmann, M., and Ogunshola, O. O. (2015). Differential responses of blood-brain barrier associated cells to hypoxia and ischemia: a comparative study. *Fluids Barriers CNS* 17:4. doi: 10.1186/2045-8118-12-4

Fang, L., Li, X., Zhong, Y., Yu, J., Yu, L., Dai, H., et al. (2015). Autophagy protects human brain microvascular endothelial cells against methylglyoxal-induced injuries, reproducible in a cerebral ischemic model in diabetic rats. *J. Neurochem.* 135, 431–440. doi: 10.1111/jnc.13277

Feng, D., Wang, B., Wang, L., Abraham, N., Tao, K., Huang, L., et al. (2017). Pre-ischemia melatonin treatment alleviated acute neuronal injury after ischemic stroke by inhibiting endoplasmic reticulum stress-dependent autophagy via PERK and IRE1 signalings. *J. Pineal Res.* 62:e12395. doi: 10.1111/jpi.12395

Fu, L., Huang, L., Cao, C., Yin, Q., and Liu, J. (2016). Inhibition of AMP-activated protein kinase alleviates focal cerebral ischemia injury in mice: interference with mTOR and autophagy. *Brain Res.* 1, 103–111. doi: 10.1016/j.brainres.2016.08.035

Gabryel, B., Kost, A., Kasprowska, D., Liber, S., Machnik, G., Wiaderkiewicz, R., et al. (2014). AMP-activated protein kinase is involved in induction of protective autophagy in astrocytes exposed to oxygen-glucose deprivation. *Cell Biol. Int.* 38, 1086–1097. doi: 10.1002/cbin.10299

Gade, P., Manjegowda, S. B., Nallar, S. C., Maachani, U. B., Cross, A. S., and Kalvakolanu, D. V. (2014). Regulation of the death-associated protein kinase 1 expression and autophagy via ATF6 requires apoptosis signal-regulating kinase 1. *Mol. Cell. Biol.* 34, 4033–4048. doi: 10.1128/MCB.00397-14

Gao, C., Cai, Y., Zhang, X., Huang, H., Wang, J., Wang, Y., et al. (2015). Ischemic Preconditioning Mediates Neuroprotection against Ischemia in Mouse Hippocampal CA1 Neurons by Inducing Autophagy. *PLoS One* 10:e0137146. doi: 10.1371/journal.pone.0137146

Ginet, V., Puyal, J., Clarke, P. G., and Truttmann, A. C. (2009). Enhancement of autophagic flux after neonatal cerebral hypoxia-ischemia and its region-specific relationship to apoptotic mechanisms. *Am. J. Pathol.* 175, 1962–1974. doi: 10.2353/ajpath.2009.090463

Ginet, V., Spiehlmann, A., Rummel, C., Rudinskiy, N., Grishchuk, Y., Luthi-Carter, R., et al. (2014). Involvement of autophagy in hypoxic-excitotoxic neuronal death. *Autophagy* 10, 846–860. doi: 10.4161/auto.28264

Goldenberg-Cohen, N., Raiter, A., Gaydar, V., Dratviman-Storobinsky, O., Goldstein, T., Weizman, A., et al. (2012). Peptide-binding GRP78 protects neurons from hypoxia-induced apoptosis. *Apoptosis* 17, 278–288. doi: 10.1007/s10495-011-0678-x

Gonzalez-Gronow, M., Selim, M. A., Papalas, J., and Pizzo, S. V. (2009). GRP78: a multifunctional receptor on the cell surface. *Antioxid. Redox Signal.* 11, 2299–2306. doi: 10.1089/ARS.2009.2568

Guo, Y., Ma, Y., Zhang, Y., Zhou, L., Huang, S., Wen, Y., et al. (2017). Autophagy-related gene microarray and bioinformatics analysis for ischemic stroke detection. *Biochem. Biophys. Res. Commun.* 15, 48–55. doi: 10.1016/j.bbrc.2017.05.099

Gwak, M., Park, P., Kim, K., Lim, K., Jeong, S., Baek, C., et al. (2008). The effects of dantrolene on hypoxic-ischemic injury in the neonatal rat brain. *Anesth. Analog.* 106, 227–233. doi: 10.1213/01.ane.0000287663.81050.38

Hacke, W., Kaste, M., Bluhmki, E., Brozman, M., Davalos, A., Guidetti, D., et al. (2008). Thrombolysis with alteplase 3 to 4.5 hours after acute ischemic stroke. *N. Engl. J. Med.* 25, 1317–1329.

Harding, H. P., Zhang, Y., and Ron, D. (1999). Protein translation and folding are coupled by an endoplasmic-reticulum-resident kinase. *Nature* 21, 271–274. doi: 10.1038/16729

Harding, H. P., Zhang, Y., Zeng, H., Novoa, I., Lu, P. D., Calfon, M., et al. (2003). An integrated stress response regulates amino acid metabolism and resistance to oxidative stress. *Mol. Cell* 11, 619–633. doi: 10.1016/s1097-2765(03)00105-9

Hayashi, T., Saito, A., Okuno, S., Ferrand-Drake, M., and Chan, P. H. (2003). Induction of GRP78 by ischemic preconditioning reduces endoplasmic reticulum stress and prevents delayed neuronal cell death. *J. Cereb. Blood Flow Metab.* 23, 949–961. doi: 10.1097/01.wcb.0000077641.41248.ea

Hayashi, T., Saito, A., Okuno, S., Ferrand-Drake, M., Dodd, R. L., and Chan, P. H. (2005). Damage to the endoplasmic reticulum and activation of apoptotic

machinery by oxidative stress in ischemic neurons. *J. Cereb. Blood Flow Metab.* 25, 41–53. doi: 10.1038/sj.jcbfm.9600005

Hillary, R. F., and Fitzgerald, U. (2018). A lifetime of stress: ATF6 in development and homeostasis. *J. Biomed. Sci.* 25:48. doi: 10.1186/s12929-018-0453-1

Hollien, J., and Weissman, J. S. (2006). ay of endoplasmic reticulum-localized mRNAs during the unfolded protein response. *Science* 7, 104–107. doi: 10.1126/science.1129631

Imai, H., Harland, J., McCulloch, J., Graham, D. I., Brown, S. M., and Macrae, I. M. (2002). Specific expression of the cell cycle regulation proteins, GADD34 and PCNA, in the peri-infarct zone after focal cerebral ischaemia in the rat. *Eur. J. Neurosci.* 15, 1929–1936. doi: 10.1046/j.1460-9568.2002.02025.x

Itakura, E., Kishi-Itakura, C., and Mizushima, N. (2012). The hairpin-type tail-anchored SNARE syntaxin 17 targets to autophagosomes for fusion with endosomes/lysosomes. *Cell* 7, 1256–1269. doi: 10.1016/j.cell.2012.11.001

Iwata, A., Christianson, J. C., Bucci, M., Ellerby, L. M., Nukina, N., Forno, L. S., et al. (2005). Increased susceptibility of cytoplasmic over nuclear polyglutamine aggregates to autophagic degradation. *Proc. Natl. Acad. Sci. U.S.A.* 13, 13135–13140. doi: 10.1073/pnas.0505801102

Jiang, T., Yu, J. T., Zhu, X. C., Wang, H. F., Tan, M. S., Cao, L., et al. (2014). Acute metformin preconditioning confers neuroprotection against focal cerebral ischaemia by pre-activation of AMPK-dependent autophagy. *Br. J. Pharmacol.* 171, 3146–3157. doi: 10.1111/bph.12655

Jiang, W. W., Huang, B. S., Han, Y., Deng, L. H., and Wu, L. X. (2017). Sodium hydrosulfide attenuates cerebral ischemia/reperfusion injury by suppressing overactivated autophagy in rats. *FEBS Open Biol.* 7, 1686–1695. doi: 10.1002/2211-5463.12301

Karsy, M., Brock, A., Guan, J., Taussky, P., Kalani, M. Y., and Park, M. S. (2017). Neuroprotective strategies and the underlying molecular basis of cerebrovascular stroke. *Neurosurg. Focus* 42:E3. doi: 10.3171/2017.1.FOCUS16522

Klionsky, D. J., Abdelmohsen, K., Abe, A., Abedin, M. J., Abeliovich, H., Acevedo Arozena, A., et al. (2016). Guidelines for the use and interpretation of assays for monitoring autophagy (3rd edition). *Autophagy* 12, 1–222.

Koike, M., Shibata, M., Tadakoshi, M., Gotoh, K., Komatsu, M., Waguri, S., et al. (2008). Inhibition of autophagy prevents hippocampal pyramidal neuron death after hypoxic-ischemic injury. *Am. J. Pathol.* 172, 454–469. doi: 10.2353/ajpath.2008.070876

Kouroku, Y., Fujita, E., Tanida, I., Ueno, T., Isoai, A., Kumagai, H., et al. (2007). ER stress (PERK/eIF2alpha phosphorylation) mediates the polyglutamine-induced LC3 conversion, an essential step for autophagy formation. *Cell Death Differ.* 14, 230–239. doi: 10.1038/sj.cdd.4401984

Krick, R., Muhe, Y., Prick, T., Bredschneider, M., Bremer, S., Wenzel, D., et al. (2009). Piecemeal microautophagy of the nucleus: genetic and morphological traits. *Autophagy* 5, 270–272. doi: 10.4161/auto.5.2.7639

Kumar, R., Azam, S., Sullivan, J. M., Owen, C., Cavener, D. R., Zhang, P., et al. (2001). Brain ischemia and reperfusion activates the eukaryotic initiation factor 2alpha kinase. *PERK. J. Neurochem.* 77, 1418–1421. doi: 10.1046/j.1471-4159.2001.00387.x

Kumar, R., Krause, G. S., Yoshida, H., Mori, K., and DeGracia, D. J. (2003). Dysfunction of the unfolded protein response during global brain ischemia and reperfusion. *J. Cereb. Blood Flow Metab.* 23, 462–471. doi: 10.1097/01.wcb.0000056064.25434.ca

Lei, Y., Wang, S., Ren, B., Wang, J., Chen, J., Lu, J., et al. (2017). CHOP favors endoplasmic reticulum stress-induced apoptosis in hepatocellular carcinoma cells via inhibition of autophagy. *PLoS One* 12:e0183680. doi: 10.1371/journal.pone.0183680

Li, F., Hayashi, T., Jin, G., Deguchi, K., Nagotani, S., Nagano, I., et al. (2005). The protective effect of dantrolene on ischemic neuronal cell death is associated with reduced expression of endoplasmic reticulum stress markers. *Brain Res.* 28, 59–68. doi: 10.1016/j.brainres.2005.04.058

Li, H., Gao, A., Feng, D., Wang, Y., Zhang, L., Cui, Y., et al. (2014). Evaluation of the protective potential of brain microvascular endothelial cell autophagy on blood-brain barrier integrity during experimental cerebral ischemia-reperfusion injury. *Transl. Stroke Res.* 5, 618–626. doi: 10.1007/s12975-014-0354-x

Li, H., Qiu, S., Li, X., Li, M., and Peng, Y. (2015). Autophagy biomarkers in CSF correlates with infarct size, clinical severity and neurological outcome in AIS patients. *J. Transl. Med.* 14:359. doi: 10.1186/s12967-015-0726-3

Li, W. L., Yu, S. P., Chen, D., Yu, S. S., Jiang, Y. J., Genetta, T., et al. (2013). The regulatory role of NF-kappaB in autophagy-like cell death after focal cerebral ischemia in mice. *Neuroscience* 6, 16–30. doi: 10.1016/j.neuroscience.2013.03.045

Liu, C., Gao, Y., Barrett, J., and Hu, B. (2010). Autophagy and protein aggregation after brain ischemia. *J. Neurochem.* 115, 68–78. doi: 10.1111/j.1471-4159.2010.06905.x

Liu, R., Li, X., Gao, W., Zhou, Y., Wey, S., Mitra, S. K., et al. (2013). Monoclonal antibody against cell surface GRP78 as a novel agent in suppressing PI3K/AKT signaling, tumor growth, and metastasis. *Clin. Cancer Res.* 15, 6802–6811. doi: 10.1158/1078-0432.CCR-13-1106

Liu, X., Tian, F., Wang, S., Wang, F., and Xiong, L. (2018). Astrocyte autophagy flux protects neurons against oxygen-glucose deprivation and ischemic/reperfusion injury. *Rejuvenation Res.* 21, 405–415. doi: 10.1089/rej.2017.1999

Lopez-Atalaya, J. P., Roussel, B. D., Levrat, D., Parcq, J., Nicole, O., Hommet, Y., et al. (2008). Toward safer thrombolytic agents in stroke: molecular requirements for NMDA receptor-mediated neurotoxicity. *J. Cereb. Blood Flow Metab.* 28, 1212–1221. doi: 10.1038/jcbfm.2008.14

Louessard, M., Bardou, I., Lemarchand, E., Thiebaut, A. M., Parcq, J., Leprince, J., et al. (2017). Activation of cell surface GRP78 reases endoplasmic reticulum stress and neuronal death. *Cell Death Differ.* 24, 1518–1529. doi: 10.1038/cdd.2017.35

Mahameed, M., Wilhelm, T., Darawshi, O., Obiedat, A., Tommy, W. S., Chintha, C., et al. (2019). The unfolded protein response modulators GSK2606414 and KIRA6 are potent KIT inhibitors. *Cell Death Dis.* 1:300. doi: 10.1038/s41419-019-1523-3

Marciniak, S. J., Garcia-Bonilla, L., Hu, J., Harding, H. P., and Ron, D. (2006). Activation-dependent substrate recruitment by the eukaryotic translation initiation factor 2 kinase PERK. *J. Cell Biol.* 16, 201–209. doi: 10.1083/jcb.200508099

Marciniak, S. J., and Ron, D. (2006). Endoplasmic reticulum stress signaling in disease. *Physiol. Rev.* 86, 1133–1149. doi: 10.1152/physrev.00015.2006

Marciniak, S. J., Yun, C. Y., Oyadomari, S., Novoa, I., Zhang, Y., Greis, R., et al. (2004). CHOP induces death by promoting protein synthesis and oxidation in the stressed endoplasmic reticulum. *Genes Dev.* 15, 3066–3077. doi: 10.1101/gad.1250704

McCaig, D., Imai, H., Gallagher, L., Graham, D. I., Harland, J., Moira Brown, S., et al. (2005). Evolution of GADD34 expression after focal cerebral ischaemia. *Brain Res.* 9, 51–61. doi: 10.1016/j.brainres.2004.11.058

Meares, G. P., Hughes, K. J., Naatz, A., Papa, F. R., Urano, F., Hansen, P. A., et al. (2011). IRE1-dependent activation of AMPK in response to nitric oxide. *Mol. Cell. Biol.* 31, 4286–4297. doi: 10.1128/MCB.05668-11

Mengesdorf, T., Proud, C. G., Mies, G., and Paschen, W. (2002). Mechanisms underlying suppression of protein synthesis induced by transient focal cerebral ischemia in mouse brain. *Exp. Neurol.* 177, 538–546. doi: 10.1006/exnr.2002.8002

Michalak, M., Robert Parker, J. M., and Opas, M. (2002). Ca2+ signaling and calcium binding chaperones of the endoplasmic reticulum. *Cell Calcium* 32, 269–278. doi: 10.1016/s0143416002001884

Misra, U. K., and Pizzo, S. V. (2012). Receptor-recognized alpha(2)-macroglobulin binds to cell surface-associated GRP78 and activates mTORC1 and mTORC2 signaling in prostate cancer cells. *PLoS One* 7:e51735. doi: 10.1371/journal.pone.0051735

Mizushima, N., Yoshimori, T., and Ohsumi, Y. (2011). The role of Atg proteins in autophagosome formation. *Annu. Rev. Cell Dev. Biol.* 27, 107–132. doi: 10.1146/annurev-cellbio-092910-154005

Morimoto, N., Oida, Y., Shimazawa, M., Miura, M., Kudo, T., Imaizumi, K., et al. (2007). Involvement of endoplasmic reticulum stress after middle cerebral artery occlusion in mice. *Neuroscience* 29, 957–967. doi: 10.1016/j.neuroscience.2007.04.017

Myeku, N., and Figueiredo-Pereira, M. E. (2011). Dynamics of the degradation of ubiquitinated proteins by proteasomes and autophagy: association with sequestosome 1/p62. *J. Biol. Chem.* 24, 22426–22440. doi: 10.1074/jbc.M110.149252

Nah, J., Yoo, S. M., Jung, S., Jeong, E. I., Park, M., Kaang, B. K., et al. (2017). Phosphorylated CAV1 activates autophagy through an interaction with

BECN1 under oxidative stress. *Cell Death Dis.* 25:e2822. doi: 10.1038/cddis.2017.71

Nakka, V. P., Gusain, A., and Raghubir, R. (2010). Endoplasmic reticulum stress plays critical role in brain damage after cerebral ischemia/reperfusion in rats. *Neurotox Res.* 17, 189–202. doi: 10.1007/s12640-009-9110-5

National Institute of Neurological Disorders and Stroke rt-Pa Stroke Study Group (1995). Tissue plasminogen activator for acute ischemic stroke. *N. Engl. J. Med.* 14, 1581–1587.

Nedergaard, M., Ransom, B., and Goldman, S. A. (2003). New roles for astrocytes: redefining the functional architecture of the brain. *Trends Neurosci.* 26, 523–530. doi: 10.1016/j.tins.2003.08.008

Ni, Y., Gu, W. W., Liu, Z. H., Zhu, Y. M., Rong, J. G., Kent, T. A., et al. (2018). RIP1K Contributes to Neuronal and Astrocytic Cell Death in Ischemic Stroke via Activating Autophagic-lysosomal Pathway. *Neuroscience* 10, 60–74. doi: 10.1016/j.neuroscience.2017.10.038

Nitatori, T., Sato, N., Waguri, S., Karasawa, Y., Araki, H., Shibanai, K., et al. (1995). Delayed neuronal death in the CA1 pyramidal cell layer of the gerbil hippocampus following transient ischemia is apoptosis. *J. Neurosci.* 15, 1001–1011. doi: 10.1523/jneurosci.15-02-01001.1995

Noda, T., and Ohsumi, Y. (1998). Tor, a phosphatidylinositol kinase homologue, controls autophagy in yeast. *J. Biol. Chem.* 13, 3963–3966. doi: 10.1074/jbc.273.7.3963

Osada, N., Kosuge, Y., Kihara, T., Ishige, K., and Ito, Y. (2009). Apolipoprotein E-deficient mice are more vulnerable to ER stress after transient forebrain ischemia. *Neurochem. Int.* 54, 403–409. doi: 10.1016/j.neuint.2009.01.010

Owen, C. R., Kumar, R., Zhang, P., McGrath, B. C., Cavener, D. R., and Krause, G. S. (2005). PERK is responsible for the increased phosphorylation of eIF2alpha and the severe inhibition of protein synthesis after transient global brain ischemia. *J. Neurochem.* 94, 1235–1242. doi: 10.1111/j.1471-4159.2005.03276.x

Papadakis, M., Hadley, G., Xilouri, M., Hoyte, L. C., Nagel, S., McMenamin, M. M., et al. (2013). Tsc1 (hamartin) confers neuroprotection against ischemia by inducing autophagy. *Nat. Med.* 19, 351–357. doi: 10.1038/nm.3097

Parsons, J. T., Churn, S. B., and DeLorenzo, R. J. (1999). Global ischemia-induced inhibition of the coupling ratio of calcium uptake and ATP hydrolysis by rat whole brain microsomal Mg(2+)/Ca(2+) ATPase. *Brain Res.* 10, 32–41. doi: 10.1016/s0006-8993(99)01504-8

Paschen, W., Aufenberg, C., Hotop, S., and Mengesdorf, T. (2003). Transient cerebral ischemia activates processing of xbp1 messenger RNA indicative of endoplasmic reticulum stress. *J. Cereb. Blood Flow Metab.* 23, 449–461. doi: 10.1097/00004647-200304000-00009

Paschen, W., and Doutheil, J. (1999). Disturbances of the functioning of endoplasmic reticulum: a key mechanism underlying neuronal cell injury? *J. Cereb. Blood Flow Metab.* 19, 1–18. doi: 10.1097/00004647-199901000-00001

Paschen, W., Hayashi, T., Saito, A., and Chan, P. H. (2004). GADD34 protein levels increase after transient ischemia in the cortex but not in the CA1 subfield: implications for post-ischemic recovery of protein synthesis in ischemia-resistant cells. *J. Neurochem.* 90, 694–701. doi: 10.1111/j.1471-4159.2004.02555.x

Pattingre, S., Bauvy, C., Carpentier, S., Levade, T., Levine, B., and Codogno, P. (2009). Role of JNK1-dependent Bcl-2 phosphorylation in ceramide-induced macroautophagy. *J. Biol. Chem.* 30, 2719–2728. doi: 10.1074/jbc.M805920200

Pattingre, S., Tassa, A., Qu, X., Garuti, R., Liang, X. H., Mizushima, N., et al. (2005). Bcl-2 antiapoptotic proteins inhibit Beclin 1-dependent autophagy. *Cell* 23, 927–939. doi: 10.1016/j.cell.2005.07.002

Pengyue, Z., Tao, G., Hongyun, H., Liqiang, Y., and Yihao, D. (2017). Breviscapine confers a neuroprotective efficacy against transient focal cerebral ischemia by attenuating neuronal and astrocytic autophagy in the penumbra. *Biomed. Pharmacother.* 90, 69–76. doi: 10.1016/j.biopha.2017.03.039

Petiot, A., Ogier-Denis, E., Blommaart, E. F., Meijer, A. J., and Codogno, P. (2000). Distinct classes of phosphatidylinositol 3'-kinases are involved in signaling pathways that control macroautophagy in HT-29 cells. *J. Biol. Chem.* 14, 992–998. doi: 10.1074/jbc.275.2.992

Puyal, J., Vaslin, A., Mottier, V., and Clarke, P. G. (2009). Postischemic treatment of neonatal cerebral ischemia should target autophagy. *Ann. Neurol.* 66, 378–389. doi: 10.1002/ana.21714

Qi, X., Okuma, Y., Hosoi, T., and Nomura, Y. (2004). Edaravone protects against hypoxia/ischemia-induced endoplasmic reticulum dysfunction. *J. Pharmacol. Exp. Ther.* 311, 388–393. doi: 10.1124/jpet.104.069088

Qin, A. P., Liu, C. F., Qin, Y. Y., Hong, L. Z., Xu, M., Yang, L., et al. (2010). Autophagy was activated in injured astrocytes and mildly reased cell survival following glucose and oxygen deprivation and focal cerebral ischemia. *Autophagy* 6, 738–753. doi: 10.4161/auto.6.6.12573

Rami, A., Langhagen, A., and Steiger, S. (2008). Focal cerebral ischemia induces upregulation of Beclin 1 and autophagy-like cell death. *Neurobiol. Dis.* 29, 132–141. doi: 10.1016/j.nbd.2007.08.005

Rissanen, A., Sivenius, J., and Jolkkonen, J. (2006). Prolonged bihemispheric alterations in unfolded protein response related gene expression after experimental stroke. *Brain Res.* 4, 60–66. doi: 10.1016/j.brainres.2006.02.095

Roussel, B. D., Kruppa, A. J., Miranda, E., Crowther, D. C., Lomas, D. A., and Marciniak, S. J. (2013). Endoplasmic reticulum dysfunction in neurological disease. *Lancet Neurol.* 12, 105–118. doi: 10.1016/s1474-4422(12)70238-7

Rubinsztein, D. C., Codogno, P., and Levine, B. (2012). Autophagy modulation as a potential therapeutic target for diverse diseases. *Nat. Rev. Drug Discov.* 11, 709–730. doi: 10.1038/nrd3802

Russell, R. C., Tian, Y., Yuan, H., Park, H. W., Chang, Y. Y., Kim, J., et al. (2013). ULK1 induces autophagy by phosphorylating Beclin-1 and activating VPS34 lipid kinase. *Nat. Cell Biol.* 15, 741–750. doi: 10.1038/ncb2757

Ryan, F., Khodagholi, F., Dargahi, L., Minai-Tehrani, D., and Ahmadiani, A. (2018). Temporal pattern and crosstalk of necroptosis markers with autophagy and apoptosis associated proteins in ischemic hippocampus. *Neurotox Res.* 34, 79–92. doi: 10.1007/s12640-017-9861-3

Rzymski, T., Milani, M., Pike, L., Buffa, F., Mellor, H. R., Winchester, L., et al. (2010). Regulation of autophagy by ATF4 in response to severe hypoxia. *Oncogene* 5, 4424–4435. doi: 10.1038/onc.2010.191

Schneeloch, E., Wenkel, S., Mies, G., and Paschen, W. (2004). Spreading depression activates unfolded protein response. *Neurosci. Lett.* 16, 37–40. doi: 10.1016/j.neulet.2004.06.061

Sheng, R., Liu, X. Q., Zhang, L. S., Gao, B., Han, R., Wu, Y. Q., et al. (2012). Autophagy regulates endoplasmic reticulum stress in ischemic preconditioning. *Autophagy* 8, 310–325. doi: 10.4161/auto.18673

Sheng, R., Zhang, L. S., Han, R., Liu, X. Q., Gao, B., and Qin, Z. H. (2010). Autophagy activation is associated with neuroprotection in a rat model of focal cerebral ischemic preconditioning. *Autophagy* 6, 482–494. doi: 10.4161/auto.6.4.11737

Shi, R., Weng, J., Zhao, L., Li, X. M., Gao, T. M., and Kong, J. (2012). Excessive autophagy contributes to neuron death in cerebral ischemia. *CNS Neurosci. Thera.* 18, 250–260. doi: 10.1111/j.1755-5949.2012.00295.x

Sokka, A. L., Putkonen, N., Mudo, G., Pryazhnikov, E., Reijonen, S., Khiroug, L., et al. (2007). Endoplasmic reticulum stress inhibition protects against excitotoxic neuronal injury in the rat brain. *J. Neurosci.* 24, 901–908. doi: 10.1523/jneurosci.4289-06.2007

Szydlowska, K., and Tymianski, M. (2010). Calcium, ischemia and excitotoxicity. *Cell Calcium* 47, 122–129. doi: 10.1016/j.ceca.2010.01.003

Tajiri, S., Oyadomari, S., Yano, S., Morioka, M., Gotoh, T., Hamada, J. I., et al. (2004). Ischemia-induced neuronal cell death is mediated by the endoplasmic reticulum stress pathway involving CHOP. *Cell Death Differ.* 11, 403–415. doi: 10.1038/sj.cdd.4401365

Thiebaut, A. M., Gauberti, M., Ali, C., Martinez De Lizarrondo, S., Vivien, D., Yepes, M., et al. (2018). The role of plasminogen activators in stroke treatment: fibrinolysis and beyond. *Lancet Neurol.* 17, 1121–1132. doi: 10.1016/S1474-4422(18)30323-5

Tian, F., Deguchi, K., Yamashita, T., Ohta, Y., Morimoto, N., Shang, J., et al. (2010). In vivo imaging of autophagy in a mouse stroke model. *Autophagy* 6, 1107–1114. doi: 10.4161/auto.6.8.13427

Uchiyama, Y. (2001). Autophagic cell death and its execution by lysosomal cathepsins. *Arch. Histol. Cytol.* 64, 233–246. doi: 10.1679/aohc.64.233

Urbanek, T., Kuczmik, W., Basta-Kaim, A., and Gabryel, B. (2014). Rapamycin induces of protective autophagy in vascular endothelial cells exposed to oxygen-glucose deprivation. *Brain Res.* 17, 1–11. doi: 10.1016/j.brainres.2014.01.017

Wang, J. Y., Xia, Q., Chu, K. T., Pan, J., Sun, L. N., Zeng, B., et al. (2011). Severe global cerebral ischemia-induced programmed necrosis of hippocampal CA1 neurons in rat is prevented by 3-methyladenine: a widely used inhibitor

of autophagy. *J. Neuropathol. Exp. Neurol.* 70, 314–322. doi: 10.1097/NEN.0b013e31821352bd

Wang, N., Yang, L., Zhang, H., Lu, X., Wang, J., Cao, Y., et al. (2018). MicroRNA-9a-5p alleviates ischemia injury after focal cerebral ischemia of the rat by targeting ATG5-mediated autophagy. *Cell. Physiol. Biochem.* 45, 78–87. doi: 10.1159/000486224

Wang, P., Guan, Y. F., Du, H., Zhai, Q. W., Su, D. F., and Miao, C. Y. (2012). Induction of autophagy contributes to the neuroprotection of nicotinamide phosphoribosyltransferase in cerebral ischemia. *Autophagy* 8, 77–87. doi: 10.4161/auto.8.1.18274

Wang, P., Xu, T. Y., Wei, K., Guan, Y. F., Wang, X., Xu, H., et al. (2014). ARRB1/beta-arrestin-1 mediates neuroprotection through coordination of BECN1-dependent autophagy in cerebral ischemia. *Autophagy* 10, 1535–1548. doi: 10.4161/auto.29203

Wang, Z., and Yang, W. (2018). Impaired capacity to restore proteostasis in the aged brain after ischemia: implications for translational brain ischemia research. *Neurochem. Int.* doi: 10.1016/j.neuint.2018.12.018 [Epub ahead of print].

Wei, H., and Perry, D. C. (1996). Dantrolene is cytoprotective in two models of neuronal cell death. *J. Neurochem.* 67, 2390–2398. doi: 10.1046/j.1471-4159.1996.67062390.x

Wei, Y., Pattingre, S., Sinha, S., Bassik, M., and Levine, B. (2008). JNK1-mediated phosphorylation of Bcl-2 regulates starvation-induced autophagy. *Mol. Cell* 20, 678–688. doi: 10.1016/j.molcel.2008.06.001

Weidberg, H., Shvets, E., Shpilka, T., Shimron, F., Shinder, V., and Elazar, Z. (2010). LC3 and GATE-16/GABARAP subfamilies are both essential yet act differently in autophagosome biogenesis. *EMBO J.* 2, 1792–1802. doi: 10.1038/emboj.2010.74

Wen, Y. D., Sheng, R., Zhang, L. S., Han, R., Zhang, X., Zhang, X. D., et al. (2008). Neuronal injury in rat model of permanent focal cerebral ischemia is associated with activation of autophagic and lysosomal pathways. *Autophagy* 4, 762–769. doi: 10.4161/auto.6412

Xie, C., Ginet, V., Sun, Y., Koike, M., Zhou, K., Li, T., et al. (2016). Neuroprotection by selective neuronal deletion of Atg7 in neonatal brain injury. *Autophagy* 12, 410–423. doi: 10.1080/15548627.2015.1132134

Xin, X. Y., Pan, J., Wang, X. Q., Ma, J. F., Ding, J. Q., Yang, G. Y., et al. (2011). 2-methoxyestradiol attenuates autophagy activation after global ischemia. *Can. J. Neurol. Sci.* 38, 631–638. doi: 10.1017/s031716710001218x

Xing, H., Azimi-Zonooz, A., Shuttleworth, C. W., and Connor, J. A. (2004). Caffeine releasable stores of Ca2+ show depletion prior to the final steps in delayed CA1 neuronal death. *J. Neurophysiol.* 92, 2960–2967. doi: 10.1152/jn.00015.2004

Xing, S., Zhang, Y., Li, J., Zhang, J., Li, Y., Dang, C., et al. (2012). Beclin 1 knockdown inhibits autophagic activation and prevents the secondary neurodegenerative damage in the ipsilateral thalamus following focal cerebral infarction. *Autophagy* 8, 63–76. doi: 10.4161/auto.8.1.18217

Yamamoto, H., Kakuta, S., Watanabe, T. M., Kitamura, A., Sekito, T., Kondo-Kakuta, C., et al. (2012). Atg9 vesicles are an important membrane source during early steps of autophagosome formation. *J. Cell Biol.* 23, 219–233. doi: 10.1083/jcb.201202061

Yang, Z., Zhao, T. Z., Zou, Y. J., Zhang, J. H., and Feng, H. (2014). Hypoxia Induces autophagic cell death through hypoxia-inducible factor 1alpha in microglia. *PLoS One* 9:e96509. doi: 10.1371/journal.pone.0096509

Yepes, M., Roussel, B. D., Ali, C., and Vivien, D. (2009). Tissue-type plasminogen activator in the ischemic brain: more than a thrombolytic. *Trends Neurosci.* 32, 48–55. doi: 10.1016/j.tins.2008.09.006

Yoshida, H., Matsui, T., Hosokawa, N., Kaufman, R. J., Nagata, K., and Mori, K. (2003). A time-dependent phase shift in the mammalian unfolded protein response. *Dev. Cell* 4, 265–271. doi: 10.1016/s1534-5807(03)00022-4

Young, A. R., Ali, C., Duretete, A., and Vivien, D. (2007). Neuroprotection and stroke: time for a compromise. *J. Neurochem.* 103, 1302–1309. doi: 10.1111/j.1471-4159.2007.04866.x

Zalckvar, E., Berissi, H., Mizrachy, L., Idelchuk, Y., Koren, I., Eisenstein, M., et al. (2009). DAP-kinase-mediated phosphorylation on the BH3 domain of beclin 1 promotes dissociation of beclin 1 from Bcl-XL and induction of autophagy. *EMBO Rep.* 10, 285–292. doi: 10.1038/embor.2008.246

Zhang, C., and Cuervo, A. M. (2008). Restoration of chaperone-mediated autophagy in aging liver improves cellular maintenance and hepatic function. *Nat. Med.* 14, 959–965. doi: 10.1038/nm.1851

Zhang, T., Liu, X., Li, Q., Wang, J., Jia, W., and Sun, X. (2010). Exacerbation of ischemia-induced amyloid-beta generation by diabetes is associated with autophagy activation in mice brain. *Neurosci. Lett.* 2, 215–220. doi: 10.1016/j.neulet.2010.05.064

Zhang, T., Lu, D., Yang, W., Shi, C., Zang, J., Shen, L., et al. (2018). HMG-CoA Reductase Inhibitors Relieve Endoplasmic Reticulum Stress by Autophagy Inhibition in Rats With Permanent Brain Ischemia. *Front. Neurosci.* 12:405. doi: 10.3389/fnins.2018.00405

Zhang, X., Yan, H., Yuan, Y., Gao, J., Shen, Z., Cheng, Y., et al. (2013). Cerebral ischemia-reperfusion-induced autophagy protects against neuronal injury by mitochondrial clearance. *Autophagy* 9, 1321–1333. doi: 10.4161/auto.25132

Zhang, X., Yuan, Y., Jiang, L., Zhang, J., Gao, J., Shen, Z., et al. (2014). Endoplasmic reticulum stress induced by tunicamycin and thapsigargin protects against transient ischemic brain injury: involvement of PARK2-dependent mitophagy. *Autophagy* 1, 1801–1813. doi: 10.4161/auto.32136

Zheng, Y. Q., Liu, J. X., Li, X. Z., Xu, L., and Xu, Y. G. (2009). RNA interference-mediated downregulation of Beclin1 attenuates cerebral ischemic injury in rats. *Acta Pharmacol. Sin.* 30, 919–927. doi: 10.1038/aps.2009.79

Zhou, Y., Lee, J., Reno, C. M., Sun, C., Park, S. W., Chung, J., et al. (2011). Regulation of glucose homeostasis through a XBP-1-FoxO1 interaction. *Nat. Med.* 17, 356–365. doi: 10.1038/nm.2293

Zundorf, G., and Reiser, G. (2011). Calcium dysregulation and homeostasis of neural calcium in the molecular mechanisms of neurodegenerative diseases provide multiple targets for neuroprotection. *Antioxid. Redox Signal.* 1, 1275–1288. doi: 10.1089/ars.2010.3359

Conflict of Interest Statement: The authors declare that the research was conducted in the absence of any commercial or financial relationships that could be construed as a potential conflict of interest.

Copyright © 2019 Thiebaut, Hedou, Marciniak, Vivien and Roussel. This is an open-access article distributed under the terms of the Creative Commons Attribution License (CC BY). The use, distribution or reproduction in other forums is permitted, provided the original author(s) and the copyright owner(s) are credited and that the original publication in this journal is cited, in accordance with accepted academic practice. No use, distribution or reproduction is permitted which does not comply with these terms.

frontiers in Neurology

MINI REVIEW
published: 02 July 2019
doi: 10.3389/fneur.2019.00718

Old Dog New Tricks; Revisiting How Stroke Modulates the Systemic Immune Landscape

Siddharth Krishnan [1,2,3*] *and Catherine B. Lawrence* [1,4]

[1] *Faculty of Biology, Medicine and Health, Manchester Academic Health Science Centre, Lydia Becker Institute of Immunology and Inflammation, University of Manchester, Manchester, United Kingdom,* [2] *Manchester Collaborative Centre for Inflammation Research, University of Manchester, Manchester, United Kingdom,* [3] *Division of Infection, Immunity and Respiratory Medicine, Faculty of Biology, Medicine and Health, Manchester Academic Health Science Centre, University of Manchester, Manchester, United Kingdom,* [4] *Division of Neuroscience and Experimental Psychology, Faculty of Biology, Medicine and Health, Manchester Academic Health Science Centre, University of Manchester, Manchester, United Kingdom*

Infections in the post-acute phase of cerebral ischaemia impede optimal recovery by exacerbating morbidity and mortality. Our review aims to reconcile the increased infection susceptibility of patients post-stroke by consolidating our understanding of compartmentalised alterations to systemic immunity. Mounting evidence has catalogued alterations to numerous immune cell populations but an understanding of the mechanisms of long-range communication between the immune system, nervous system and other organs beyond the involvement of autonomic signalling is lacking. By taking our cues from established and emerging concepts of neuro-immune interactions, immune-mediated inter-organ cross-talk, innate immune training and the role of microbiota-derived signals in central nervous system (CNS) function we will explore mechanisms of how cerebral ischaemia could shape systemic immune function. In this context, we will also discuss a key question: how are immune requirements critical for mediating repair of the ischaemic insult balanced by the need for anti-microbial immunity post-stroke, given that they are mediated by mutually exclusive immune networks? Our reformed understanding of the immune landscape post-stroke and novel mechanisms at play could guide targeted therapeutic interventions and initiate a step-change in the clinical management of these infectious complications post-stroke.

Keywords: cerebral ischaemia, post-stroke infection, systemic immunity, innate immune training, neuroimmunology

OPEN ACCESS

Edited by:
Johannes Boltze,
University of Warwick,
United Kingdom

Reviewed by:
Adam Denes,
Institute of Experimental Medicine (MTA), Hungary
Brad A. Sutherland,
University of Tasmania, Australia
Renée Jade Turner,
University of Adelaide, Australia

***Correspondence:**
Siddharth Krishnan
siddharth.krishnan@manchester.ac.uk

Specialty section:
This article was submitted to Stroke, a section of the journal Frontiers in Neurology

Received: *29 March 2019*
Accepted: *18 June 2019*
Published: *02 July 2019*

Citation:
Krishnan S and Lawrence CB (2019) Old Dog New Tricks; Revisiting How Stroke Modulates the Systemic Immune Landscape. Front. Neurol. 10:718. doi: 10.3389/fneur.2019.00718

Ischaemic stroke imposes a significant burden on health-care systems and societies across the globe as a consequence of the morbidity and mortality associated with the condition (1, 2). In addition to neurological deficits, infectious complications such as pneumonia and urinary tract infections post-stroke also pose a hurdle to optimal recovery, affecting a significant proportion of patients and exacerbating mortality risk (3–7). Despite significant leaps in our understanding of key players in the immune response post-stroke (8–19) and biomarkers of infection (4, 20, 21), therapy using statins (for immunomodulation), prophylactic beta-blockers (to target sympathetic activation), and antibiotics (to control infection) have proved ineffective in treating infection (22–26). Equally, attempts to improve stroke outcome using neuroprotective therapies to harness the immune system such as dexamethasone, erythropoietin, and many others have been met with limited success in the clinic; in part, due to undesirable effects on systemic immunity. Yet, the

question of whether drugs that possess immunomodulatory properties can be purposed for stroke patients remains to be resolved (27). What is clear, however, is the onset of a plethora of immunological alterations involving diverse immune cells and tissues that is essential for both neurological recovery as well as the occurrence of systemic infections through impairments in anti-microbial immunity (13). In this review, we collate previously described alterations to systemic immunity, and delineate how long-range communication between the CNS and the periphery shapes immune control by taking our cues from data that does not examine stroke. We will finally examine whether the cost of tissue repair (of the ischaemic damage) is impairment in anti-microbial immunity and consequently, increased infection susceptibility.

THE SYSTEMIC IMMUNE LANDSCAPE OF STROKE

To date, there is a wealth of information surrounding the spectrum of immune alterations that ensue following a stroke in both patients as well as models of experimental stroke. The onset of immunological alterations in the central nervous system (CNS) is sequential; neutrophils are recruited hours after stroke by activated microglia and endothelial cells, followed by monocytes a few days following the insult, whilst T and B cells infiltrate the ischaemic tissue in the succeeding weeks (28–32). This contrasts immune alterations in peripheral tissues where stroke drives alterations to the hepatic cytokine networks as early as 6 h post-stroke whilst other systemic immune effects present 24 h post-stroke, affecting both myeloid and lymphoid populations (12, 14, 17, 33–35). However, the mechanisms by which these rapidly-elicited immune changes morph into immune suppression remain poorly defined.

As well as directly altering immune networks, stroke-driven systemic cytokine signals have also emerged as key players that have been implicated to have divergent effects on outcome following stroke (16, 36, 37). Importantly, hepatic interleukin (IL)-6 and chemokine (C-X-C motif) ligand 1 (CXCL1) drive a rapid and transient inflammatory response (35, 38) whilst primed splenocytes secrete tumour necrosis factor (TNF)-α, interferon (IFN)-γ, chemokine (C-C motif) ligand 2 (CCL2) and IL-2 (39); and granulocyte colony stimulating factor (G-CSF) mobilises monocytes and neutrophils from the bone marrow following experimental stroke (40, 41). Moreover, stroke has also been shown to compromise humoral responses through the induction of hypogammaglobulinaemia via the excretional loss of immunoglobulin (Ig) G and impairments in innate-like B cell responses facilitating IgM loss (12, 42).

Many groups have implicated the loss of lymphocytes (T and natural killer (NK) cells), termed lymphopenia, in circulation as a central feature of stroke-induced immune suppression in patients (43–45), a hallmark also replicated in experimental stroke (14, 45, 46). It is thought that the remaining T lymphocytes are also fundamentally altered, being primed to mount a type-1 response through increased IFN-γ and IL-2 production even years after the ischaemic insult (47). In fact, experimental models of stroke have also demonstrated that $CD4^+$ T cells in Peyer's patches (lymphoid tissue in the small intestine) of mice are primed to secrete increased levels of IL-17 and IFN-γ (15). Similarly, there is also an activation of innate lymphocytes such as invariant natural killer T cells (iNKT) cells in the liver in tandem with a cessation of their patrolling behaviour in the sinusoids (48). Additionally, stroke also leads to the apoptotic loss of splenic marginal zone B cells (12) whilst their loss in the blood and bone marrow is predominantly driven by alterations in lymphopoiesis (49).

As such, even innate immune responses are compromised in stroke patients with impairments in the oxidative burst of neutrophils (34) as well as shifts in the proportions and properties of monocyte populations (9, 17, 50, 51). Specifically, as classical and intermediate monocytes expand within the circulating monocyte pool (50, 51) they accrue deficiencies in their anti-microbial immunity as evidenced by their shedding of CD163, tolerance to endotoxin and their inability to secrete key cytokines such as TNF-α, IL-6, and CCL2. These monocytes, also through their increased secretion of IL-10 and downregulation of human leukocyte antigen-DR isotype (HLA-DR) thus acquire an immune suppressed state (16, 17, 33, 46, 52–54). That said, CD74, the invariant polypeptide chain associated with the HLA complex is upregulated in the peripheral blood mononuclear cells of patients (55). Despite being capable of processing and transporting antigens, monocytes, nevertheless, are not professional antigen-presenting cells (56, 57). Consequently, it remains to be determined if the loss of HLA-DR functionally impacts these monocytes in their ability to prime T cell responses post-stroke. Indeed, murine models of experimental stroke have also implicated impairments in monocyte function with an increase in splenic monocytes; both macrophages and monocytes in the spleen downregulate their expression of major histocompatibility complex II (MHCII) (58, 59). By contrast, the role of non-classical monocytes following stroke is less clear in both patients and experimental models of stroke (60, 61).

THE DYNAMIC INTERACTIONS BETWEEN THE CNS AND SYSTEMIC IMMUNITY IN STROKE

Thus far, we have discussed compartmentalised alterations to systemic immunity post-stroke. In this section, we shall highlight how recruited immune cells interface with locally resident cells and the milieu of cytokines following ischaemic injury in stroke. The identification of meningeal lymphatics in the dural sinuses of the CNS (62, 63) as well as previously undescribed subsets of CNS-resident immune cells such as type 2 innate lymphoid cells (ILC2) (64) has reformed our understanding of immunity in the CNS and its frontiers. It is particularly salient to probe the role of these ILC2s post-stroke given their established function in mediating type 2 immunity (65–69) and the critical role of type 2 immunity in mediating tissue repair (70–73). Essentially, type 2 immunity is an ancient arm of the immune system that is mobilised during infection by multicellular metazoan parasites such as helminths that can drive tissue injury as they develop in the host (70, 74, 75). Characterised by the cytokines IL-3,

IL-4, IL-5, IL-9, IL-10, and IL-13, it can be orchestrated by a large repertoire of cells including expanded populations of macrophages, T cell, ILCs, and other sentinels of tissue injury to mediate tissue repair in parallel with parasite expulsion (73, 76, 77). As a result, it becomes important to appreciate the reciprocal regulation that exists between the CNS and systemic immunity in homeostasis (78–80) and how injury to the brain modulates this cross-talk during stroke.

Local cytokine cues facilitate neutrophil recruitment to the ischaemic hemisphere as early as 6 h post-stroke in an intercellular adhesion molecule-1-dependent manner (28, 81). Neutrophils are thought to exacerbate the initial injury through the release of proteases and neutrophil extracellular traps (NETs) that exert neurotoxic effects (82, 83). In particular, the release of matrix metalloproteinase-9, a gelatinase, is thought to compromise the integrity of the blood-brain barrier (BBB) (84, 85) and promote the development of oedema (86). Despite being short-lived, it is thought that neutrophils can take on polarisation states through the acquisition of Ym1 and CD206 expression which has been suggested to be important for their clearance and the resolution of inflammation post-stroke (87).

The role of microglia through their interaction with peripherally-derived leukocytes adds an extra layer of complexity as they are double-edged swords with the capacity to propagate and curtail inflammation, and support neurogenesis (88, 89). Through the acquisition of a classically activated state as a result of astrocytic signals and/or microglial CD8 signalling, they secrete pro-inflammatory cytokines including TNF-α, IL-1α that induce neurotoxic astrocytes (90) and disrupt the integrity of the BBB post-stroke (91). By contrast, they are also capable of limiting neuroinflammation by restraining neutrophil recruitment through the effects of transforming growth factor (TGF)-β on astrocyte-derived CXCL1 (92), limiting neuronal excitotoxicity (93) as well as myelin auto-reactivity (94).

Being one of the first responders to injury or infection (95–97), it comes as no surprise that monocytes are rapidly recruited from the periphery to the ischaemic brain post-stroke (9, 19, 31, 79). Whilst they can infiltrate the brain parenchyma through a breached BBB (98), studies have also demonstrated that the choroid plexus is another means of access to the CNS (95, 99). By employing the CD73 enzyme for extravasation and transmigration, monocytes are thought to infiltrate the CNS via the choroid plexus through interactions between the vascular cell adhesion molecule 1 (VCAM-1) and very late antigen-4 (VLA-4). In the CNS, monocytes are an acute source of pro-inflammatory cytokines that drive neuroinflammation following which the milieu of cytokines directs their differentiation into macrophages with features of alternative activation such as arginase-1 and Ym1 expression to mediate tissue repair (61, 100–103). Nevertheless, the interactions between microglia and monocyte-derived macrophages are indispensable for restraining and resolution of long-term microglial inflammation (61, 104) and promoting neurological recovery in diverse settings of CNS injury (95, 99). Despite their ability to engraft in this niche and mediate repair in contexts of inflammation, studies have shown that these monocyte-derived macrophages maintain a distinct transcriptional identity and cannot replenish microglia (105–107). Although this has been ascribed to the embryonic origins of microglia that are seeded from the yolk sac (108–110), the dynamics of this niche remain unclear in stroke.

Amongst leukocytes recruited to the infarcted brain, T cells are one of the last responders and their dynamics are equally complex with studies suggesting that their functions *in situ* are influenced by not just the subset but also the route of entry into the CNS (8, 111, 112). It is thought that γδ T cells gain access to the injured brain through the leptomeninges in a C-C chemokine receptor (CCR) type 6-dependent manner (8, 113, 114) meanwhile other T cells can access the CNS through the choroid plexus (112) in addition to migrating across a breached BBB (111). Consequently, γδ T cells exacerbate ischaemic damage through their production of IL-17 (8, 113, 114) whilst $CD4^+$ T cells can take on a type 2 activation state and mediate tissue repair through the production of IL-4 in synergy with macrophages (72, 73, 111).

In conjunction with the previously described alterations to systemic immunity it can thus be observed that stroke initiates a complex cycle of events in the ischaemic brain that shapes immunity and inflammation at distal sites. The notion that inflammation at one site can affect other sites is not a new concept as studies have demonstrated that infection-driven inflammation or antigenic challenges in the lungs are capable of promoting the homing of $CD4^+$ T cells to the gastrointestinal tract where they can drive pathology or protective immunity (115, 116). In this paradigm, it is worth noting that γδ T cells are recruited from the intestinal tract (8) where stroke also modulates inflammation in the Peyer's patches whilst driving shifts in microbial communities (15). It can therefore be observed that by fuelling neuroinflammation, ischaemic damage concurrently shapes immune networks in peripheral tissues such as the blood, bone marrow, and spleen that in turn amplify neuroinflammation and inter-organ cross-talk.

THE REACHES OF STROKE: MEANS OF IMMUNE CONTROL

Given the diverse range of immune alterations elicited by stroke, it is conceivable that long-range communication mechanisms between the CNS and the peripheral immune system is a prerequisite to mediating these effects. By employing established and emerging immunological data that does not investigate stroke, we will outline plausible mechanisms of how inflammation and injury in the brain in the context of stroke can shape immune networks at distal sites. Thus, we will highlight possible mechanisms that cerebral ischaemia could utilise to effect compartmentalised changes to systemic immunity and add to the concepts of autonomic dysfunction by suggesting avenues of research (**Figure 1**).

Autonomic Signalling

Mounting evidence has ascribed the alterations in systemic immunity to be consequence of increased autonomic signalling, particularly an over activation of the sympathetic nervous system (SNS) through the excessive release of catecholamines, in both

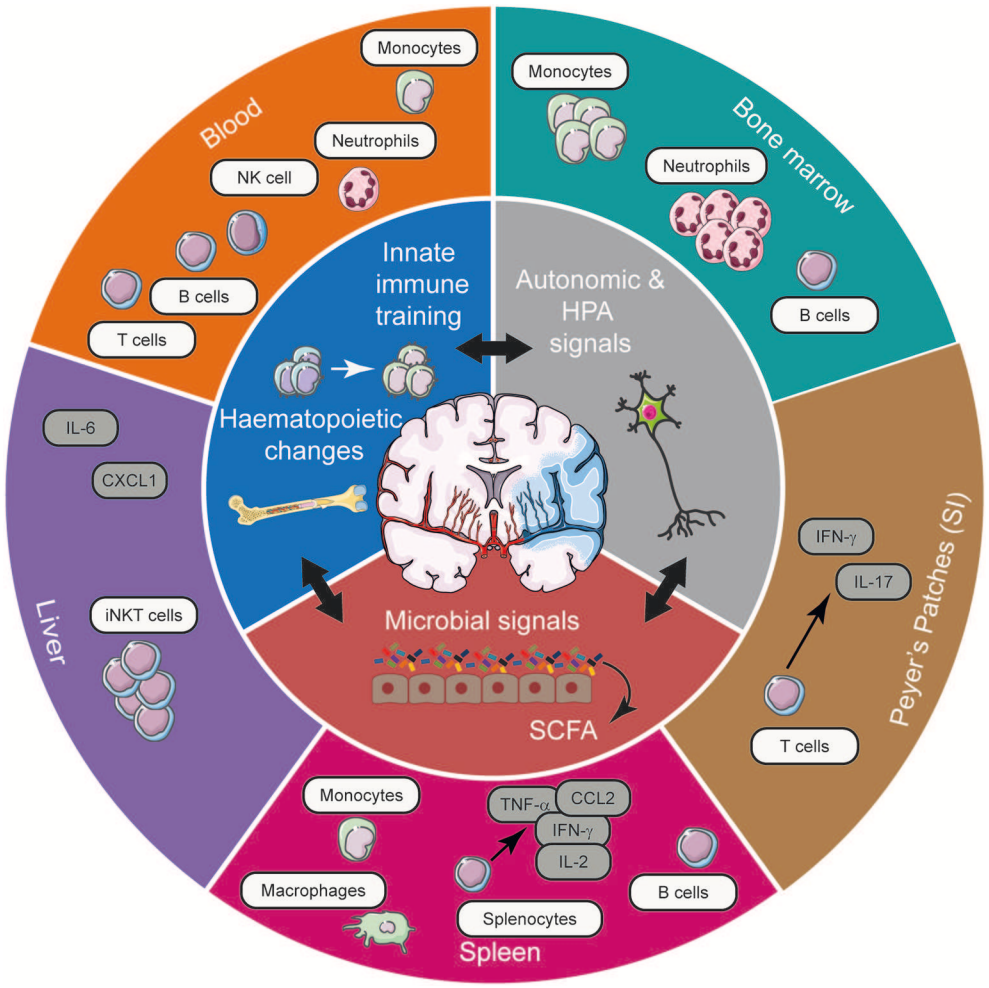

FIGURE 1 | The spectrum of systemic immune alterations post-stroke and the potential mechanisms exploited by stroke to mediate these long-range effects. Stroke, through its effects on autonomic and HPA axis activation, innate immune training, and microbial communities in the gut can gain access to various tissues to shape the systemic immune landscape, affecting cellular, and cytokine networks. Acting in synergy, these means of long-range communication modulate the frequency and functional responsiveness of a plethora of immune cells, tuning the quality of the immune response elicited in various tissues in response to CNS injury. CCL2, chemokine (C-C motif) ligand 2; CXCL1, chemokine (C-X-C motif) ligand 1; IFN-γ, interferon- γ; HPA, hypothalamic-pituitary-adrenal; IL, interleukin; iNKT cell, invariant natural killer T cell; NK cell, natural killer cell; SCFA, short chain fatty acids; SI, small intestine; TNF-α, tumour necrosis factor-α.

patients (43, 117, 118) and experimental stroke (12, 14, 48). Studies have also implicated aberrant cholinergic input (45, 119, 120) and glucocorticoid signalling via the hypothalamic-pituitary-adrenal (HPA) axis (14, 49, 121) in mediating systemic immune dysfunction; again through the excessive release of stress mediators such as cortisol and glucocorticoids into the circulation. In addition to being shaped by circulating catecholamines, many tissues that exhibit altered immune profiles post-stroke such as the gut, lung, spleen, and bone marrow are in fact hard-wired to the SNS (39, 122–125). Mechanistically, it has been posited that neurogenic input from autonomic signals as well as the HPA axis could calibrate systemic immunity by the direct effects of stress mediators on immune cells through adrenergic (126, 127), cholinergic (128, 129) and glucocorticoid receptor signalling (130, 131). Intriguingly, the phenomenon of immunosuppression driven by autonomic and HPA axis-derived signals is not restricted to stroke but is also observed in the broader context of CNS injury such as traumatic brain and spinal cord injury (132–134). Hence, a broader understanding of fundamental neuronal pathways linking the CNS and immune system could guide therapeutic interventions to alleviate infectious complications driven by CNS injury.

Innate Immune Training

Emerging evidence has highlighted the training of innate immune responses by diverse stimuli such as pathogen-associated molecular patterns or cytokines and consequently, the development of immunological memory, a concept traditionally confined to the realms of adaptive immunity (135–144). Given the transient existence of innate cells such as monocytes and neutrophils, it is thought that trained innate immunity is a means to elicit a targeted and enhanced immune reaction

to suit host requirements. This has been shown to drive immunometabolic reprogramming via epigenetic rewiring (139, 141) or the replacement of these cells *en masse* through the generation of functionally poised ones via alterations in haematopoietic output (135, 144). To put this in the context of stroke, recent work has demonstrated that microglial training resulting from repeated administration of bacterial endotoxin is capable of curtailing IL-1β secretion as well as microglial activation (and hence neuroinflammation) following cerebral ischaemia (136). Equally, it is plausible that stroke itself could elicit the training of immune cells in the periphery through its effects on the bone marrow. For example, it has been shown that stroke increases the generation of classical monocytes as a consequence of altered myelopoietic output post-stroke (40). As the bone marrow receives rich sympathetic innervation, it can be envisaged that stroke-driven autonomic signals could tune myelopoiesis to facilitate tissue repair by transducing signals through distinct adrenergic receptor subtypes (125, 145–148). Therefore, the predisposition to repair and replace the entire pool of monocytes and the duration of these changes could impact infection susceptibility as well as the response to a subsequent stroke.

Microbiota-Derived Signals

The interaction of stroke with the commensal microbiota in the gastrointestinal tract is extremely nuanced. Not only does the commensal microbiome play a role in shaping stroke outcome (despite the precise effect being unclear) (8, 15, 18, 149–152) but stroke also mediates shifts in key microbial communities like Firmicutes and Bacteroidetes (153). In homeostasis, the microbiome itself calibrates immunity within the gut microenvironment as well as distal sites through the symbiotic relationship of diverse microbial communities with immune networks by means of microbial metabolites (154–157). In light of data suggesting a detrimental effect of the gut microbiota on stroke outcome (assessed by infarct volume) as well as their role in seeding bacteria that drive pneumonia (8, 149), it therefore becomes difficult to reconcile how commensal bacteria mediate such effects given their indispensable roles in calibrating immunity in homeostasis and injury (158–163). Nevertheless, it is conceivable that the leakiness of the gut barrier induced by stroke (15) could promote the systemic dissemination of pathobionts such as *Enterococcus* spp., *Escherichia coli,* and *Morganella morganii* (149) or result in shifts in key microbial communities that could directly impact systemic immune networks and consequently, stroke outcome (153). Equally, microbial metabolites such as short-chain fatty acids for example, butyrate and propionate are capable of modulating myelopoietic output (increasing the generation of functionally poised monocytes, macrophages and dendritic cells), indicating their ability to train innate immune responses as well (156, 157). In light of these data, it is reasonable to hypothesise that stroke, by shaping gut microbial communities, could also train myeloid responses through the generation of primed progenitors, simultaneously influencing immune networks, shaping both infarct repair and infection susceptibility in distal tissues such as the lungs and bone marrow. However, the precise contributions of stroke in driving shifts in microbial communities and innate immune training remain to be elucidated.

A BALANCING ACT: ISCHAEMIC INJURY REPAIR VS. ANTI-MICROBIAL IMMUNITY

Thus far, we have summarised the plethora of effects that stroke has on systemic immunity as well as the means it employs to shape immune function, taking our cues from established and emerging immunological evidence. Taken together, the net effect of the immune alterations elicited by stroke appear to facilitate the repair of the ischaemic insult given that both mononuclear phagocytes as well as T cells appear to adopt an alternatively activated state (14, 31, 61). This is unsurprising as a large body of evidence has identified critical roles for type 2 immunity in mediating tissue repair, a response conserved across vertebrates (74, 75, 164–166). Studies have shown that type 2 cytokines such as IL-4 and IL-13 promote the alternative activation of macrophages via the expression of molecules such as arginase and Ym1 and facilitate collagen fibril assembly (70, 72, 73, 167). However, mononuclear phagocytes with the predisposition to take on an alternatively activated fate remain in circulation and police the immune responses in various tissues but their plasticity, and hence ability, to classically activate and then mediate antimicrobial immunity is questionable. This is due to the fact that the transcriptional and epigenetic landscapes that drive classical and alternative activation, at least in macrophages, are mutually opposing (168). Although tissue-resident macrophages can reversibly polarise in a GATA6-dependent manner (169), whether these principles apply to monocytes and in the context of stroke requires further investigation.

Viewing the paradigm from the vantage point of an immunologist raises some pertinent questions. Is the cost of repairing the ischaemic damage an impairment of antimicrobial defences? Are the various effects on systemic immunity a means to dampen immune responses to antigens that are now exposed to the immune system through a breached BBB following a stroke? Intriguingly, studies have identified that some contexts of stroke (170–174) and other settings of spinal cord (132) and traumatic brain injury (175–177) could also initiate auto-immunity through antibodies to myelin-derived proteins. As a result, immunosuppression post-stroke could be construed as a means to dampen debilitating auto-immunity post-stroke by skewing immunity towards a type 2 phenotype and limiting the splenic B cell pool to constrain humoral and T cell-mediated immunity towards exposed brain antigens. The simultaneous autonomic activation could educate monocytes to take on features of alternative activation in order to augment repair of the injured brain tissue prior to entry though alterations in haematopoiesis in the bone marrow. An inadvertent consequence of this cascade could be increased infection susceptibility due to inadequate plasticity in the polarisation fate acquired during generation. Thus, the systemic availability of poised mononuclear phagocytes could underpin impaired antimicrobial defences in the lungs but it remains to be determined if this is indeed the case.

CONCLUDING REMARKS

Data from clinical and pre-clinical paradigms of stroke highlight a diverse range of effects on systemic immunity that can be mediated directly and indirectly by the ischaemic damage. An appreciation of not just the changes themselves but the means employed to elicit them could inform the choice of viable therapies to mitigate infections post-stroke by digressing from traditional choices of antibiotics and beta-blockers. It is therefore imperative we re-examine data from clinical trials of immunotherapy in settings of auto-immunity and cancer to appreciate the remit of immunotherapy. By taking cues from these studies, the clinical trials of immunomodulatory therapies in stroke could provide insight into the fundamental mechanisms at play and more importantly, the suitability of immunotherapies for bolstering neuroprotection and antimicrobial immunity in stroke. This in turn could guide approaches for targeted therapies in the clinical management of neuroprotection and infection to improve outcome following stroke.

AUTHOR CONTRIBUTIONS

SK conceived the idea for the manuscript. SK and CL wrote and edited the manuscript together.

ACKNOWLEDGMENTS

We would like to acknowledge the BBSRC grant BB/M025977/1 awarded to Dr. Joanne E. Konkel which supports SK. We would also like to thank Dr. Catriona Cunningham and Flora McClure for critical review of this manuscript and acknowledge Servier Medical Art for templates used in the figure.

REFERENCES

1. O'Donnell MJ, Chin SL, Rangarajan S, Xavier D, Liu L, Zhang H, et al. Global and regional effects of potentially modifiable risk factors associated with acute stroke in 32 countries (INTERSTROKE): a case-control study. *Lancet*. (2016) 388:761–75. doi: 10.1016/S0140-6736(16)30506-2
2. Di Carlo A. Human and economic burden of stroke. *Age Ageing*. (2009) 38:4–5. doi: 10.1093/ageing/afn282
3. Armstrong JR, Mosher BD. Aspiration pneumonia after stroke: intervention and prevention. *Neurohospitalist*. (2011) 1:85–93. doi: 10.1177/1941875210395775
4. Hoffmann S, Harms H, Ulm L, Nabavi DG, Mackert BM, Schmehl I, et al. Stroke-induced immunodepression and dysphagia independently predict stroke-associated pneumonia - the PREDICT study. *J Cereb Blood Flow Metab*. (2017) 37:3671–82. doi: 10.1177/0271678X16671964
5. Ovbiagele B, Hills NK, Saver JL, Johnston SC, California Acute Stroke Prototype Registry Investigators. Frequency and determinants of pneumonia and urinary tract infection during stroke hospitalization. *J Stroke Cerebrovasc Dis*. (2006) 15:209–13. doi: 10.1016/j.jstrokecerebrovasdis.2006.05.004
6. Vermeij FH, Scholte op Reimer WJ, de Man P, van Oostenbrugge RJ, Franke CL, de Jong G, et al. Stroke-associated infection is an independent risk factor for poor outcome after acute ischemic stroke: data from the Netherlands Stroke Survey. *Cerebrovasc Dis*. (2009) 27:465–71. doi: 10.1159/000210093
7. Westendorp WF, Nederkoorn PJ, Vermeij JD, Dijkgraaf MG, van de Beek D. Post-stroke infection: a systematic review and meta-analysis. *BMC Neurol*. (2011) 11:110. doi: 10.1186/1471-2377-11-110
8. Benakis C, Brea D, Caballero S, Faraco G, Moore J, Murphy M, et al. Commensal microbiota affects ischemic stroke outcome by regulating intestinal gammadelta T cells. *Nat Med*. (2016) 22:516–23. doi: 10.1038/nm.4068
9. Chamorro Á, Meisel A, Planas AM, Urra X, van de Beek D, Veltkamp R. The immunology of acute stroke. *Nat Rev Neurol*. (2012) 8:401–10. doi: 10.1038/nrneurol.2012.98
10. Gelderblom M, Gallizioli M, Ludewig P, Thom V, Arunachalam P, Rissiek B, et al. IL-23 (Interleukin-23)-producing conventional dendritic cells control the detrimental IL-17 (Interleukin-17) response in stroke. *Stroke*. (2018) 49:155–64. doi: 10.1161/STROKEAHA.117.019101
11. Liesz A, Hagmann S, Zschoche C, Adamek J, Zhou W, Sun L, et al. The spectrum of systemic immune alterations after murine focal ischemia: immunodepression versus immunomodulation. *Stroke*. (2009) 40:2849–58. doi: 10.1161/STROKEAHA.109.549618
12. McCulloch L, Smith CJ, McColl BW. Adrenergic-mediated loss of splenic marginal zone B cells contributes to infection susceptibility after stroke. *Nat Commun*. (2017) 8:15051. doi: 10.1038/ncomms16151
13. Meisel C, Schwab JM, Prass K, Meisel A, Dirnagl U. Central nervous system injury-induced immune deficiency syndrome. *Nat Rev Neurosci*. (2005) 6:775–86. doi: 10.1038/nrn1765
14. Prass K, Meisel C, Höflich C, Braun J, Halle E, Wolf T, et al. Stroke-induced immunodeficiency promotes spontaneous bacterial infections and is mediated by sympathetic activation reversal by poststroke T helper cell type 1-like immunostimulation. *J Exp Med*. (2003) 198:725–36. doi: 10.1084/jem.20021098
15. Singh V, Roth S, Llovera G, Sadler R, Garzetti D, Stecher B, et al. Microbiota dysbiosis controls the neuroinflammatory response after stroke. *J Neurosci*. (2016) 36:7428–40. doi: 10.1523/JNEUROSCI.1114-16.2016
16. Smith CJ, Emsley HC, Udeh CT, Vail A, Hoadley ME, Rothwell NJ, et al. Interleukin-1 receptor antagonist reverses stroke-associated peripheral immune suppression. *Cytokine*. (2012) 58:384–9. doi: 10.1016/j.cyto.2012.02.016
17. Urra X, Cervera A, Obach V, Climent N, Planas AM, Chamorro A. Monocytes are major players in the prognosis and risk of infection after acute stroke. *Stroke*. (2009) 40:1262–8. doi: 10.1161/STROKEAHA.108.532085
18. Winek K, Meisel A, Dirnagl U. Gut microbiota impact on stroke outcome: fad or fact? *J Cereb Blood Flow Metab*. (2016) 36:891–8. doi: 10.1177/0271678X16636890
19. Iadecola C, Anrather J. The immunology of stroke: from mechanisms to translation. *Nat Med*. (2011) 17:796–808. doi: 10.1038/nm.2399
20. Hochmeister S, Engel O, Adzemovic MZ, Pekar T, Kendlbacher P, Zeitelhofer M, et al. Lipocalin-2 as an infection-related biomarker to predict clinical outcome in ischemic stroke. *PLoS ONE*. (2016) 11:e0154797. doi: 10.1371/journal.pone.0154797
21. Warusevitane A, Karunatilake D, Sim J, Smith C, Roffe C. Early diagnosis of pneumonia in severe stroke: clinical features and the diagnostic role of C-reactive protein. *PLoS ONE*. (2016) 11:e0150269. doi: 10.1371/journal.pone.0150269
22. Lin SP, Long YM, Chen XH. The effects of statins on infections after stroke or transient ischemic attack: a meta-analysis. *PLoS ONE*. (2015) 10:e0130071. doi: 10.1371/journal.pone.0130071
23. Maier IL, Karch A, Mikolajczyk R, Bähr M, Liman J. Effect of beta-blocker therapy on the risk of infections and death after acute stroke–a historical cohort study. *PLoS ONE*. (2015) 10:e0116836. doi: 10.1371/journal.pone.0116836
24. Westendorp WF, Vermeij JD, Brouwer MC, Roos YB, Nederkoorn PJ, van de Beek D, et al. Pre-stroke use of beta-blockers does not lower post-stroke infection rate: an exploratory analysis of the preventive antibiotics in stroke study. *Cerebrovasc Dis*. (2016) 42:506–11. doi: 10.1159/000450926
25. Xi YG, Tian X, Chen WQ, Zhang S, Zhang S, Ren WD, et al. Antibiotic prophylaxis for infections in patients with acute stroke: a systematic

review and meta-analysis of randomized controlled trials. *Oncotarget*. (2017) 8:81075–87. doi: 10.18632/oncotarget.19039
26. Kalra L, Irshad S, Hodsoll J, Simpson M, Gulliford M, Smithard D, et al. Prophylactic antibiotics after acute stroke for reducing pneumonia in patients with dysphagia (STROKE-INF): a prospective, cluster-randomised, open-label, masked endpoint, controlled clinical trial. *Lancet*. (2015) 386:1835–44. doi: 10.1016/S0140-6736(15)00126-9
27. Smith CJ, Denes A, Tyrrell PJ, Di Napoli M. Phase II anti-inflammatory and immune-modulating drugs for acute ischaemic stroke. *Expert Opin Investig Drugs*. (2015) 24:623–43. doi: 10.1517/13543784.2015.1020110
28. Perez-de-Puig I, Miró-Mur F, Ferrer-Ferrer M, Gelpi E, Pedragosa J, Justicia C, et al. Neutrophil recruitment to the brain in mouse and human ischemic stroke. *Acta Neuropathol.* (2015) 129:239–57. doi: 10.1007/s00401-014-1381-0
29. Doyle KP, Quach LN, Solé M, Axtell RC, Nguyen TV, Soler-Llavina GJ, et al. B-lymphocyte-mediated delayed cognitive impairment following stroke. *J Neurosci.* (2015) 35:2133–45. doi: 10.1523/JNEUROSCI.4098-14.2015
30. Liesz A, Zhou W, Mracskó É, Karcher S, Bauer H, Schwarting S, et al. Inhibition of lymphocyte trafficking shields the brain against deleterious neuroinflammation after stroke. *Brain.* (2011) 134(Pt 3):704–20. doi: 10.1093/brain/awr008
31. Miró-Mur F, Pérez-de-Puig I, Ferrer-Ferrer M, Urra X, Justicia C, Chamorro A, et al. Immature monocytes recruited to the ischemic mouse brain differentiate into macrophages with features of alternative activation. *Brain Behav Immun.* (2016) 53:18–33. doi: 10.1016/j.bbi.2015.08.010
32. Jin R, Yang G, Li G. Inflammatory mechanisms in ischemic stroke: role of inflammatory cells. *J Leukoc Biol.* (2010) 87:779–89. doi: 10.1189/jlb.1109766
33. Chamorro A, Amaro S, Vargas M, Obach V, Cervera A, Torres F, et al. Interleukin 10, monocytes and increased risk of early infection in ischaemic stroke. *J Neurol Neurosurg Psychiatry*. (2006) 77:1279–81. doi: 10.1136/jnnp.2006.100800
34. Ruhnau J, Schulze K, Gaida B, Langner S, Kessler C, Bröker B, et al. Stroke alters respiratory burst in neutrophils and monocytes. *Stroke*. (2014) 45:794–800. doi: 10.1161/STROKEAHA.113.003342
35. Chapman KZ, Dale VQ, Dénes A, Bennett G, Rothwell NJ, Allan SM, et al. A rapid and transient peripheral inflammatory response precedes brain inflammation after experimental stroke. *J Cereb Blood Flow Metab.* (2009) 29:1764–8. doi: 10.1038/jcbfm.2009.113
36. Emsley HC, Smith CJ, Georgiou RF, Vail A, Hopkins SJ, Rothwell NJ, et al. A randomised phase II study of interleukin-1 receptor antagonist in acute stroke patients. *J Neurol Neurosurg Psychiatry*. (2005) 76:1366–72. doi: 10.1136/jnnp.2004.054882
37. Smith CJ, Hulme S, Vail A, Heal C, Parry-Jones AR, Scarth S, et al. SCIL-STROKE (Subcutaneous Interleukin-1 Receptor Antagonist in Ischemic Stroke): a randomized controlled phase 2 trial. *Stroke*. (2018) 49:1210–6. doi: 10.1161/STROKEAHA.118.020750
38. Campbell SJ, Perry VH, Pitossi FJ, Butchart AG, Chertoff M, Waters S, et al. Central nervous system injury triggers hepatic CC and CXC chemokine expression that is associated with leukocyte mobilization and recruitment to both the central nervous system and the liver. *Am J Pathol.* (2005) 166:1487–97. doi: 10.1016/S0002-9440(10)62365-6
39. Offner H, Subramanian S, Parker SM, Afentoulis ME, Vandenbark AA, Hurn PD. Experimental stroke induces massive, rapid activation of the peripheral immune system. *J Cereb Blood Flow Metab.* (2006) 26:654–65. doi: 10.1038/sj.jcbfm.9600217
40. Courties G, Herisson F, Sager HB, Heidt T, Ye Y, Wei Y, et al. Ischemic stroke activates hematopoietic bone marrow stem cells. *Circ Res.* (2015) 116:407–17. doi: 10.1161/CIRCRESAHA.116.305207
41. Denes A, McColl BW, Leow-Dyke SF, Chapman KZ, Humphreys NE, Grencis RK, et al. Experimental stroke-induced changes in the bone marrow reveal complex regulation of leukocyte responses. *J Cereb Blood Flow Metab.* (2011) 31:1036–50. doi: 10.1038/jcbfm.2010.198
42. Liesz A, Roth S, Zorn M, Sun L, Hofmann K, Veltkamp R. Acquired immunoglobulin G deficiency in stroke patients and experimental brain ischemia. *Exp Neurol.* (2015) 271:46–52. doi: 10.1016/j.expneurol.2015.04.021
43. Harms H, Reimnitz P, Bohner G, Werich T, Klingebiel R, Meisel C, et al. Influence of stroke localization on autonomic activation, immunodepression, and post-stroke infection. *Cerebrovasc Dis.* (2011) 32:552–60. doi: 10.1159/000331922
44. Hug A, Dalpke A, Wieczorek N, Giese T, Lorenz A, Auffarth G, et al. Infarct volume is a major determiner of post-stroke immune cell function and susceptibility to infection. *Stroke.* (2009) 40:3226–32. doi: 10.1161/STROKEAHA.109.557967
45. Liu Q, Jin WN, Liu Y, Shi K, Sun H, Zhang F, et al. Brain ischemia suppresses immunity in the periphery and brain via different neurogenic innervations. *Immunity*. (2017) 46:474–87. doi: 10.1016/j.immuni.2017.02.015
46. Vogelgesang A, Grunwald U, Langner S, Jack R, Bröker BM, Kessler C, et al. Analysis of lymphocyte subsets in patients with stroke and their influence on infection after stroke. *Stroke*. (2008) 39:237–41. doi: 10.1161/STROKEAHA.107.493635
47. Theodorou GL, Marousi S, Ellul J, Mougiou A, Theodori E, Mouzaki A, et al. T helper 1 (Th1)/Th2 cytokine expression shift of peripheral blood CD4+ and CD8+ T cells in patients at the post-acute phase of stroke. *Clin Exp Immunol.* (2008) 152:456–63. doi: 10.1111/j.1365-2249.2008.03650.x
48. Wong CH, Jenne CN, Lee WY, Léger C, Kubes P. Functional innervation of hepatic iNKT cells is immunosuppressive following stroke. *Science*. (2011) 334:101–5. doi: 10.1126/science.1210301
49. Courties G, Frodermann V, Honold L, Zheng Y, Herisson F, Schloss MJ, et al. Glucocorticoids regulate bone marrow B lymphopoiesis after stroke. *Circ Res*. (2019) 124:1372–85. doi: 10.1161/CIRCRESAHA.118.314518
50. Kaito M, Araya S, Gondo Y, Fujita M, Minato N, Nakanishi M, et al. Relevance of distinct monocyte subsets to clinical course of ischemic stroke patients. *PLoS ONE*. (2013) 8:e69409. doi: 10.1371/journal.pone.0069409
51. Grosse GM, Schulz-Schaeffer WJ, Teebken OE, Schuppner R, Dirks M, Worthmann H, et al. Monocyte subsets and related chemokines in carotid artery stenosis and ischemic stroke. *Int J Mol Sci*. (2016) 17:433. doi: 10.3390/ijms17040433
52. Haeusler KG, Schmidt WU, Föhring F, Meisel C, Helms T, Jungehulsing GJ, et al. Cellular immunodepression preceding infectious complications after acute ischemic stroke in humans. *Cerebrovasc Dis*. (2008) 25:50–8. doi: 10.1159/000111499
53. Hernández-Jiménez E, Gutierrez-Fernández M, Cubillos-Zapata C, Otero-Ortega L, Rodríguez-Frutos B, Toledano V, et al. Circulating monocytes exhibit an endotoxin tolerance status after acute ischemic stroke: mitochondrial DNA as a putative explanation for poststroke infections. *J Immunol.* (2017) 198:2038–46. doi: 10.4049/jimmunol.1601594
54. Zhang DP, Yan FL, Xu HQ, Zhu YX, Yin Y, Lu HQ. A decrease of human leucocyte antigen-DR expression on monocytes in peripheral blood predicts stroke-associated infection in critically-ill patients with acute stroke. *Eur J Neurol.* (2009) 16:498–505. doi: 10.1111/j.1468-1331.2008.02512.x
55. Yang L, Kong Y, Ren H, Li M, Wei CJ, Shi E, et al. Upregulation of CD74 and its potential association with disease severity in subjects with ischemic stroke. *Neurochem Int*. (2017) 107:148–55. doi: 10.1016/j.neuint.2016.11.007
56. Jakubzick C, Gautier EL, Gibbings SL, Sojka DK, Schlitzer A, Johnson TE, et al. Minimal differentiation of classical monocytes as they survey steady-state tissues and transport antigen to lymph nodes. *Immunity*. (2013) 39:599–610. doi: 10.1016/j.immuni.2013.08.007
57. Jakubzick CV, Randolph GJ, Henson PM. Monocyte differentiation and antigen-presenting functions. *Nat Rev Immunol.* (2017) 17:349–62. doi: 10.1038/nri.2017.28
58. McCulloch L, Alfieri A, McColl BW. Experimental stroke differentially affects discrete subpopulations of splenic macrophages. *Front Immunol.* (2018) 9:1108. doi: 10.3389/fimmu.2018.01108
59. Liesz A, Dalpke A, Mracsko E, Antoine DJ, Roth S, Zhou W, et al. DAMP signaling is a key pathway inducing immune modulation after brain injury. *J Neurosci.* (2015) 35:583–98. doi: 10.1523/JNEUROSCI.2439-14.2015
60. Michaud JP, Pimentel-Coelho PM, Tremblay Y, Rivest S. The impact of Ly6Clow monocytes after cerebral hypoxia-ischemia in adult mice. *J Cereb Blood Flow Metab.* (2014) 34:e1–9. doi: 10.1038/jcbfm.2014.80
61. Wattananit S, Tornero D, Graubardt N, Memanishvili T, Monni E, Tatarishvili J, et al. Monocyte-derived macrophages contribute to spontaneous long-term functional recovery after stroke in mice. *J Neurosci.* (2016) 36:4182–95. doi: 10.1523/JNEUROSCI.4317-15.2016

62. Absinta M, Ha SK, Nair G, Sati P, Luciano NJ, Palisoc M, et al. Human and nonhuman primate meninges harbor lymphatic vessels that can be visualized noninvasively by MRI. *Elife*. (2017) 6:e29738. doi: 10.7554/eLife.29738
63. Louveau A, Smirnov I, Keyes TJ, Eccles JD, Rouhani SJ, Peske JD, et al. Structural and functional features of central nervous system lymphatic vessels. *Nature*. (2015) 523:337–41. doi: 10.1038/nature14432
64. Gadani SP, Smirnov I, Smith AT, Overall CC, Kipnis J. Characterization of meningeal type 2 innate lymphocytes and their response to CNS injury. *J Exp Med.* (2017) 214:285–96. doi: 10.1084/jem.20161982
65. Spencer SP, Wilhelm C, Yang Q, Hall JA, Bouladoux N, Boyd A, et al. Adaptation of innate lymphoid cells to a micronutrient deficiency promotes type 2 barrier immunity. *Science.* (2014) 343:432–7. doi: 10.1126/science.1247606
66. Brestoff JR, Kim BS, Saenz SA, Stine RR, Monticelli LA, Sonnenberg GF, et al. Group 2 innate lymphoid cells promote beiging of white adipose tissue and limit obesity. *Nature*. (2015) 519:242–6. doi: 10.1038/nature14115
67. Monticelli LA, Buck MD, Flamar AL, Saenz SA, Tait Wojno ED, Yudanin NA, et al. Arginase 1 is an innate lymphoid-cell-intrinsic metabolic checkpoint controlling type 2 inflammation. *Nat Immunol.* (2016) 17:656–65. doi: 10.1038/ni.3421
68. Wallrapp A, Riesenfeld SJ, Burkett PR, Abdulnour RE, Nyman J, Dionne D, et al. The neuropeptide NMU amplifies ILC2-driven allergic lung inflammation. *Nature.* (2017) 549:351–6. doi: 10.1038/nature24029
69. Klose CSN, Mahlakõiv T, Moeller JB, Rankin LC, Flamar AL, Kabata H, et al. The neuropeptide neuromedin U stimulates innate lymphoid cells and type 2 inflammation. *Nature*. (2017) 549:282–6. doi: 10.1038/nature23676
70. Allen JE, Sutherland TE. Host protective roles of type 2 immunity: parasite killing and tissue repair, flip sides of the same coin. *Semin Immunol.* (2014) 26:329–40. doi: 10.1016/j.smim.2014.06.003
71. Minutti CM, Modak RV, Macdonald F, Li F, Smyth DJ, Dorward DA, et al. A macrophage-pericyte axis directs tissue restoration via amphiregulin-induced transforming growth factor beta activation. *Immunity*. (2019) 50:645–654.e6. doi: 10.1016/j.immuni.2019.01.008
72. Minutti CM, Knipper JA, Allen JE, Zaiss DM. Tissue-specific contribution of macrophages to wound healing. *Semin Cell Dev Biol.* (2017) 61:3–11. doi: 10.1016/j.semcdb.2016.08.006
73. Minutti CM, Jackson-Jones LH, García-Fojeda B, Knipper JA, Sutherland TE, Logan N, et al. Local amplifiers of IL-4Ralpha-mediated macrophage activation promote repair in lung and liver. *Science*. (2017) 356:1076–80. doi: 10.1126/science.aaj2067
74. Allen JE, Wynn TA. Evolution of Th2 immunity: a rapid repair response to tissue destructive pathogens. *PLoS Pathog.* (2011) 7:e1002003. doi: 10.1371/journal.ppat.1002003
75. Skugor S, Glover KA, Nilsen F, Krasnov A. Local and systemic gene expression responses of Atlantic salmon (*Salmo salar* L.) to infection with the salmon louse (*Lepeophtheirus salmonis*). *BMC Genomics*. (2008) 9:498. doi: 10.1186/1471-2164-9-498
76. Jenkins SJ, Ruckerl D, Thomas GD, Hewitson JP, Duncan S, Brombacher F, et al. IL-4 directly signals tissue-resident macrophages to proliferate beyond homeostatic levels controlled by CSF-1. *J Exp Med.* (2013) 210:2477–91. doi: 10.1084/jem.20121999
77. Allen JE, Maizels RM. Diversity and dialogue in immunity to helminths. *Nat Rev Immunol*. (2011) 11:375–88. doi: 10.1038/nri2992
78. Kipnis J, Multifaceted interactions between adaptive immunity and the central nervous system. *Science*. (2016) 353:766–71. doi: 10.1126/science.aag2638
79. Prinz M, Priller J. The role of peripheral immune cells in the CNS in steady state and disease. *Nat Neurosci.* (2017) 20:136–44. doi: 10.1038/nn.4475
80. Engelhardt B, Vajkoczy P, Weller RO. The movers and shapers in immune privilege of the CNS. *Nat Immunol.* (2017) 18:123–31. doi: 10.1038/ni.3666
81. Connolly ES Jr, Winfree CJ, Springer TA, Naka Y, Liao H, Yan SD, et al. Cerebral protection in homozygous null ICAM-1 mice after middle cerebral artery occlusion. Role of neutrophil adhesion in the pathogenesis of stroke. *J Clin Invest*. (1996) 97:209–16. doi: 10.1172/JCI118392
82. Allen C, Thornton P, Denes A, McColl BW, Pierozynski A, Monestier M, et al. Neutrophil cerebrovascular transmigration triggers rapid neurotoxicity through release of proteases associated with decondensed DNA. *J Immunol*. (2012) 189:381–92. doi: 10.4049/jimmunol.1200409
83. Stowe AM, Adair-Kirk TL, Gonzales ER, Perez RS, Shah AR, Park TS, et al. Neutrophil elastase and neurovascular injury following focal stroke and reperfusion. *Neurobiol Dis.* (2009) 35:82–90. doi: 10.1016/j.nbd.2009.04.006
84. McColl BW, Rothwell NJ, Allan SM. Systemic inflammation alters the kinetics of cerebrovascular tight junction disruption after experimental stroke in mice. *J Neurosci.* (2008) 28:9451–62. doi: 10.1523/JNEUROSCI.2674-08.2008
85. Justicia C, Panés J, Solé S, Cervera A, Deulofeu R, Chamorro A, et al. Neutrophil infiltration increases matrix metalloproteinase-9 in the ischemic brain after occlusion/reperfusion of the middle cerebral artery in rats. *J Cereb Blood Flow Metab.* (2003) 23:1430–40. doi: 10.1097/01.WCB.0000090680.07515.C8
86. García-Culebras A, Durán-Laforet V, Peña-Martínez C, Ballesteros I, Pradillo JM, Díaz-Guzmán J, et al. Myeloid cells as therapeutic targets in neuroinflammation after stroke: specific roles of neutrophils and neutrophil-platelet interactions. *J Cereb Blood Flow Metab.* (2018) 38:2150–64. doi: 10.1177/0271678X18795789
87. Cuartero MI, Ballesteros I, Moraga A, Nombela F, Vivancos J, Hamilton JA, et al. N2 neutrophils, novel players in brain inflammation after stroke: modulation by the PPARgamma agonist rosiglitazone. *Stroke*. (2013) 44:3498–508. doi: 10.1161/STROKEAHA.113.002470
88. Thored P, Heldmann U, Gomes-Leal W, Gisler R, Darsalia V, Taneera J, et al. Long-term accumulation of microglia with proneurogenic phenotype concomitant with persistent neurogenesis in adult subventricular zone after stroke. *Glia*. (2009) 57:835–49. doi: 10.1002/glia.20810
89. Neumann J, Gunzer M, Gutzeit HO, Ullrich O, Reymann KG, Dinkel K. Microglia provide neuroprotection after ischemia. *FASEB J.* (2006) 20:714–6. doi: 10.1096/fj.05-4882fje
90. Liddelow SA, Guttenplan KA, Clarke LE, Bennett FC, Bohlen CJ, Schirmer L, et al. Neurotoxic reactive astrocytes are induced by activated microglia. *Nature*. (2017) 541:481–7. doi: 10.1038/nature21029
91. Pradillo JM, Denes A, Greenhalgh AD, Boutin H, Drake C, McColl BW, et al. Delayed administration of interleukin-1 receptor antagonist reduces ischemic brain damage and inflammation in comorbid rats. *J Cereb Blood Flow Metab*. (2012) 32:1810–9. doi: 10.1038/jcbfm.2012.101
92. Li D, Lang W, Zhou C, Wu C, Zhang F, Liu Q, et al. Upregulation of microglial ZEB1 ameliorates brain damage after acute ischemic stroke. *Cell Rep*. (2018) 22:3574–86. doi: 10.1016/j.celrep.2018.03.011
93. Szalay G, Martinecz B, Lénárt N, Környei Z, Orsolits B, Judák L, et al. Microglia protect against brain injury and their selective elimination dysregulates neuronal network activity after stroke. *Nat Commun.* (2016) 7:11499. doi: 10.1038/ncomms11499
94. Römer C, Engel O, Winek K, Hochmeister S, Zhang T, Royl G, et al. Blocking stroke-induced immunodeficiency increases CNS antigen-specific autoreactivity but does not worsen functional outcome after experimental stroke. *J Neurosci*. (2015) 35:7777–94. doi: 10.1523/JNEUROSCI.1532-14.2015
95. Ge R, Tornero D, Hirota M, Monni E, Laterza C, Lindvall O, et al. Choroid plexus-cerebrospinal fluid route for monocyte-derived macrophages after stroke. *J Neuroinflammation.* (2017) 14:153. doi: 10.1186/s12974-017-0909-3
96. Leuschner F, Rauch PJ, Ueno T, Gorbatov R, Marinelli B, Lee WW, et al. Rapid monocyte kinetics in acute myocardial infarction are sustained by extramedullary monocytopoiesis. *J Exp Med*. (2012) 209:123–37. doi: 10.1084/jem.20111009
97. Strauss-Ayali D, Conrad SM, Mosser DM.Monocyte subpopulations and their differentiation patterns during infection. *J Leukoc Biol.* (2007) 82:244–52. doi: 10.1189/jlb.0307191
98. McColl BW, Rothwell NJ, Allan SM. Systemic inflammatory stimulus potentiates the acute phase and CXC chemokine responses to experimental stroke and exacerbates brain damage via interleukin-1- and neutrophil-dependent mechanisms. *J Neurosci.* (2007) 27:4403–12. doi: 10.1523/JNEUROSCI.5376-06.2007

99. Shechter R, Miller O, Yovel G, Rosenzweig N, London A, Ruckh J, et al. Recruitment of beneficial M2 macrophages to injured spinal cord is orchestrated by remote brain choroid plexus. *Immunity*. (2013) 38:555–69. doi: 10.1016/j.immuni.2013.02.012
100. Gliem M, Schwaninger M, Jander S. Protective features of peripheral monocytes/macrophages in stroke. *Biochim Biophys Acta*. (2016) 1862:329–38. doi: 10.1016/j.bbadis.2015.11.004
101. Garcia-Bonilla L, Faraco G, Moore J, Murphy M, Racchumi G, Srinivasan J, et al. Spatio-temporal profile, phenotypic diversity, and fate of recruited monocytes into the post-ischemic brain. *J Neuroinflammation*. (2016) 13:285. doi: 10.1186/s12974-016-0750-0
102. Ritzel RM, Patel AR, Grenier JM, Crapser J, Verma R, Jellison ER, et al. Functional differences between microglia and monocytes after ischemic stroke. *J Neuroinflammation*. (2015) 12:106. doi: 10.1186/s12974-015-0329-1
103. Chu HX, Broughton BR, Kim HA, Lee S, Drummond GR, Sobey CG. Evidence that Ly6C(hi) monocytes are protective in acute ischemic stroke by promoting M2 macrophage polarization. *Stroke*. (2015) 46:1929–37. doi: 10.1161/STROKEAHA.115.009426
104. Greenhalgh AD, Zarruk JG, Healy LM, Baskar Jesudasan SJ, Jhelum P, Salmon CK, et al. Peripherally derived macrophages modulate microglial function to reduce inflammation after CNS injury. *PLoS Biol*. (2018) 16:e2005264. doi: 10.1371/journal.pbio.2005264
105. Cronk JC, Filiano AJ, Louveau A, Marin I, Marsh R, Ji E, et al. Peripherally derived macrophages can engraft the brain independent of irradiation and maintain an identity distinct from microglia. *J Exp Med*. (2018) 215:1627–47. doi: 10.1084/jem.20180247
106. Shemer A, Grozovski J, Tay TL, Tao J, Volaski A, Süß P, et al. Engrafted parenchymal brain macrophages differ from microglia in transcriptome, chromatin landscape and response to challenge. *Nat Commun*. (2018) 9:5206. doi: 10.1038/s41467-018-07548-5
107. Huang Y, Xu Z, Xiong S, Sun F, Qin G, Hu G, et al. Repopulated microglia are solely derived from the proliferation of residual microglia after acute depletion. *Nat Neurosci*. (2018) 21:530–40. doi: 10.1038/s41593-018-0090-8
108. Prinz M, Priller J. Microglia and brain macrophages in the molecular age: from origin to neuropsychiatric disease. *Nat Rev Neurosci*. (2014) 15:300–12. doi: 10.1038/nrn3722
109. Prinz M, Erny D, Hagemeyer N. Ontogeny and homeostasis of CNS myeloid cells. *Nat Immunol*. (2017) 18:385–92. doi: 10.1038/ni.3703
110. Goldmann T, Wieghofer P, Jordão MJ, Prutek F, Hagemeyer N, Frenzel K, et al. Origin, fate and dynamics of macrophages at central nervous system interfaces. *Nat Immunol*. (2016) 17:797–805. doi: 10.1038/ni.3423
111. Brait VH, Arumugam TV, Drummond GR, Sobey CG. Importance of T lymphocytes in brain injury, immunodeficiency, and recovery after cerebral ischemia. *J Cereb Blood Flow Metab*. (2012) 32:598–611. doi: 10.1038/jcbfm.2012.6
112. Llovera G, Benakis C, Enzmann G, Cai R, Arzberger T, Ghasemigharagoz A, et al. The choroid plexus is a key cerebral invasion route for T cells after stroke. *Acta Neuropathol*. (2017) 134:851–68. doi: 10.1007/s00401-017-1758-y
113. Arunachalam P, Ludewig P, Melich P, Arumugam TV, Gerloff C, Prinz I, et al. CCR6 (CC Chemokine Receptor 6) is essential for the migration of detrimental natural interleukin-17-producing gammadelta T cells in stroke. *Stroke*. (2017) 48:1957–65. doi: 10.1161/STROKEAHA.117.016753
114. Shichita T, Sugiyama Y, Ooboshi H, Sugimori H, Nakagawa R, Takada I, et al. Pivotal role of cerebral interleukin-17-producing gammadeltaT cells in the delayed phase of ischemic brain injury. *Nat Med*. (2009) 15:946–50. doi: 10.1038/nm.1999
115. Wang J, Li F, Wei H, Lian ZX, Sun R, Tian Z. Respiratory influenza virus infection induces intestinal immune injury via microbiota-mediated Th17 cell-dependent inflammation. *J Exp Med*. (2014) 211:2397–410. doi: 10.1084/jem.20140625
116. Ruane D, Brane L, Reis BS, Cheong C, Poles J, Do Y, et al. Lung dendritic cells induce migration of protective T cells to the gastrointestinal tract. *J Exp Med*. (2013) 210:1871–88. doi: 10.1084/jem.20122762
117. Liesz A, Rüger H, Purrucker J, Zorn M, Dalpke A, Möhlenbruch M, et al. Stress mediators and immune dysfunction in patients with acute cerebrovascular diseases. *PLoS ONE*. (2013) 8:e74839. doi: 10.1371/journal.pone.0074839
118. Chamorro A, Amaro S, Vargas M, Obach V, Cervera A, Gómez-Choco M, et al. Catecholamines, infection, and death in acute ischemic stroke. *J Neurol Sci*. (2007) 252:29–35. doi: 10.1016/j.jns.2006.10.001
119. Lafargue M, Xu L, Carlès M, Serve E, Anjum N, Iles KE, et al. Stroke-induced activation of the alpha7 nicotinic receptor increases *Pseudomonas aeruginosa* lung injury. *FASEB J*. (2012) 26:2919–29. doi: 10.1096/fj.11-197384
120. Engel O, Akyüz L, da Costa Goncalves AC, Winek K, Dames C, Thielke M, et al. Cholinergic pathway suppresses pulmonary innate immunity facilitating pneumonia after stroke. *Stroke*. (2015) 46:3232–40. doi: 10.1161/STROKEAHA.115.008989
121. Mracsko E, Liesz A, Karcher S, Zorn M, Bari F, Veltkamp R. Differential effects of sympathetic nervous system and hypothalamic-pituitary-adrenal axis on systemic immune cells after severe experimental stroke. *Brain Behav Immun*. (2014) 41:200–9. doi: 10.1016/j.bbi.2014.05.015
122. Veiga-Fernandes H, Mucida D. Neuro-immune interactions at barrier surfaces. *Cell*. (2016) 165:801–11. doi: 10.1016/j.cell.2016.04.041
123. Matteoli G, Boeckxstaens GE. The vagal innervation of the gut and immune homeostasis. *Gut*. (2013) 62:1214–22. doi: 10.1136/gutjnl-2012-302550
124. Chamorro A, Urra X, Planas AM. Infection after acute ischemic stroke: a manifestation of brain-induced immunodepression. *Stroke*. (2007) 38:1097–103. doi: 10.1161/01.STR.0000258346.68966.9d
125. Katayama Y, Battista M, Kao WM, Hidalgo A, Peired AJ, Thomas SA, et al. Signals from the sympathetic nervous system regulate hematopoietic stem cell egress from bone marrow. *Cell*. (2006) 124:407–21. doi: 10.1016/j.cell.2005.10.041
126. Pirzgalska RM, Seixas E, Seidman JS, Link VM, Sánchez NM, Mahú I, et al. Sympathetic neuron-associated macrophages contribute to obesity by importing and metabolizing norepinephrine. *Nat Med*. (2017) 23:1309–18. doi: 10.1038/nm.4422
127. Shaked I, Hanna RN, Shaked H, Chodaczek G, Nowyhed HN, Tweet G, et al. Transcription factor Nr4a1 couples sympathetic and inflammatory cues in CNS-recruited macrophages to limit neuroinflammation. *Nat Immunol*. (2015) 16:1228–34. doi: 10.1038/ni.3321
128. Pavlov VA, Parrish WR, Rosas-Ballina M, Ochani M, Puerta M, Ochani K, et al. Brain acetylcholinesterase activity controls systemic cytokine levels through the cholinergic anti-inflammatory pathway. *Brain Behav Immun*. (2009) 23:41–5. doi: 10.1016/j.bbi.2008.06.011
129. Borovikova LV, Ivanova S, Zhang M, Yang H, Botchkina GI, Watkins LR, et al. Vagus nerve stimulation attenuates the systemic inflammatory response to endotoxin. *Nature*. (2000) 405:458–62. doi: 10.1038/35013070
130. Varga G, Ehrchen J, Tsianakas A, Tenbrock K, Rattenholl A, Seeliger S, et al. Glucocorticoids induce an activated, anti-inflammatory monocyte subset in mice that resembles myeloid-derived suppressor cells. *J Leukoc Biol*. (2008) 84:644–50. doi: 10.1189/jlb.1107768
131. van de Garde MD, Martinez FO, Melgert BN, Hylkema MN, Jonkers RE, Hamann J. Chronic exposure to glucocorticoids shapes gene expression and modulates innate and adaptive activation pathways in macrophages with distinct changes in leukocyte attraction. *J Immunol*. (2014) 192:1196–208. doi: 10.4049/jimmunol.1302138
132. Held KS, Lane TE. Spinal cord injury, immunodepression, and antigenic challenge. *Semin Immunol*. (2014) 26:415–20. doi: 10.1016/j.smim.2014.03.003
133. Kraft P, Drechsler C, Schuhmann MK, Gunreben I, Kleinschnitz C. Characterization of peripheral immune cell subsets in patients with acute and chronic cerebrovascular disease: a case-control study. *Int J Mol Sci*. (2015) 16:25433–49. doi: 10.3390/ijms161025433
134. Schwulst SJ, Trahanas DM, Saber R, Perlman H. Traumatic brain injury-induced alterations in peripheral immunity. *J Trauma Acute Care Surg*. (2013) 75:780–8. doi: 10.1097/TA.0b013e318299616a

135. Askenase MH, Han SJ, Byrd AL, Morais da Fonseca D, Bouladoux N, Wilhelm C, et al. Bone-marrow-resident NK cells prime monocytes for regulatory function during infection. *Immunity*. (2015) 42:1130–42. doi: 10.1016/j.immuni.2015.05.011
136. Wendeln AC, Degenhardt K, Kaurani L, Gertig M, Ulas T, Jain G, et al. Innate immune memory in the brain shapes neurological disease hallmarks. *Nature*. (2018) 556:332–8. doi: 10.1038/s41586-018-0023-4
137. Bekkering S, Arts RJW, Novakovic B, Kourtzelis I, van der Heijden CDCC, Li Y, et al. Metabolic induction of trained immunity through the mevalonate pathway. *Cell*. (2018) 172:135–146.e9. doi: 10.1016/j.cell.2017.11.025
138. van der Meer JW, Joosten LA, Riksen N, Netea MG. Trained immunity: a smart way to enhance innate immune defence. *Mol Immunol*. (2015) 68:40–4. doi: 10.1016/j.molimm.2015.06.019
139. Christ A, Günther P, Lauterbach MAR, Duewell P, Biswas D, Pelka K, et al. Western diet triggers NLRP3-dependent innate immune reprogramming. *Cell*. (2018) 172:162–175.e14. doi: 10.1016/j.cell.2017.12.013
140. Netea MG, Joosten LA, Latz E, Mills KH, Natoli G, Stunnenberg HG, et al. Trained immunity: a program of innate immune memory in health and disease. *Science*. (2016) 352:aaf1098. doi: 10.1126/science.aaf1098
141. Quintin J, Saeed S, Martens JHA, Giamarellos-Bourboulis EJ, Ifrim DC, Logie C, et al. Candida albicans infection affords protection against reinfection via functional reprogramming of monocytes. *Cell Host Microbe*. (2012) 12:223–32. doi: 10.1016/j.chom.2012.06.006
142. Netea MG, van Crevel R. BCG-induced protection: effects on innate immune memory. *Semin Immunol*. (2014) 26:512–7. doi: 10.1016/j.smim.2014.09.006
143. Netea MG, van der Meer JW. Trained immunity: an ancient way of remembering. *Cell Host Microbe*. (2017) 21:297–300. doi: 10.1016/j.chom.2017.02.003
144. Mitroulis I, Ruppova K, Wang B, Chen LS, Grzybek M, Grinenko T, et al. Modulation of myelopoiesis progenitors is an integral component of trained immunity. *Cell*. (2018) 172:147–161.e12. doi: 10.1016/j.cell.2017.11.034
145. Dénes A, Boldogkoi Z, Uhereczky G, Hornyák A, Rusvai M, Palkovits M, et al. Central autonomic control of the bone marrow: multisynaptic tract tracing by recombinant pseudorabies virus. *Neuroscience*. (2005) 134:947–63. doi: 10.1016/j.neuroscience.2005.03.060
146. Méndez-Ferrer S, Lucas D, Battista M, Frenette PS. Haematopoietic stem cell release is regulated by circadian oscillations. *Nature*. (2008) 452:442–7. doi: 10.1038/nature06685
147. Vasamsetti SB, Florentin J, Coppin E, Stiekema LCA, Zheng KH, Nisar MU, et al. Sympathetic neuronal activation triggers myeloid progenitor proliferation and differentiation. *Immunity*. (2018) 49:93–106.e7. doi: 10.1016/j.immuni.2018.05.004
148. Maryanovich M, Zahalka AH, Pierce H, Pinho S, Nakahara F, Asada N, et al. Adrenergic nerve degeneration in bone marrow drives aging of the hematopoietic stem cell niche. *Nat Med*. (2018) 24:782–91. doi: 10.1038/s41591-018-0030-x
149. Stanley D, Mason LJ, Mackin KE, Srikhanta YN, Lyras D, Prakash MD, et al. Translocation and dissemination of commensal bacteria in post-stroke infection. *Nat Med*. (2016) 22:1277–84. doi: 10.1038/nm.4194
150. Wen SW, Wong CHY. An unexplored brain-gut microbiota axis in stroke. *Gut Microbes*. (2017) 8:601–6. doi: 10.1080/19490976.2017.1344809
151. Winek K, Dirnagl U, Meisel A. The gut microbiome as therapeutic target in central nervous system diseases: implications for stroke. *Neurotherapeutics*. (2016) 13:762–74. doi: 10.1007/s13311-016-0475-x
152. Winek K, Engel O, Koduah P, Heimesaat MM, Fischer A, Bereswill S, et al. Depletion of cultivatable gut microbiota by broad-spectrum antibiotic pretreatment worsens outcome after murine stroke. *Stroke*. (2016) 47:1354–63. doi: 10.1161/STROKEAHA.115.011800
153. Spychala MS, Venna VR, Jandzinski M, Doran SJ, Durgan DJ, Ganesh BP, et al. Age-related changes in the gut microbiota influence systemic inflammation and stroke outcome. *Ann Neurol*. (2018) 84:23–36. doi: 10.1002/ana.25250
154. Thion MS, Low D, Silvin A, Chen J, Grisel P, Schulte-Schrepping J, et al. Microbiome influences prenatal and adult microglia in a sex-specific manner. *Cell*. (2018) 172:500–516.e16. doi: 10.1016/j.cell.2017.11.042
155. Belkaid Y, Hand TW. Role of the microbiota in immunity and inflammation. *Cell*. (2014) 157:121–41. doi: 10.1016/j.cell.2014.03.011
156. Trompette A, Gollwitzer ES, Pattaroni C, Lopez-Mejia IC, Riva E, Pernot J, et al. Dietary fiber confers protection against flu by shaping Ly6c(-) patrolling monocyte hematopoiesis and CD8(+) T cell metabolism. *Immunity*. (2018) 48:992–1005.e8. doi: 10.1016/j.immuni.2018.04.022
157. Trompette A, Gollwitzer ES, Yadava K, Sichelstiel AK, Sprenger N, Ngom-Bru C, et al. Gut microbiota metabolism of dietary fiber influences allergic airway disease and hematopoiesis. *Nat Med*. (2014) 20:159–66. doi: 10.1038/nm.3444
158. Mortha A, Chudnovskiy A, Hashimoto D, Bogunovic M, Spencer SP, Belkaid Y, et al. Microbiota-dependent crosstalk between macrophages and ILC3 promotes intestinal homeostasis. *Science*. (2014) 343:1249288. doi: 10.1126/science.1249288
159. Naik S, Bouladoux N, Linehan JL, Han SJ, Harrison OJ, Wilhelm C, et al. Commensal-dendritic-cell interaction specifies a unique protective skin immune signature. *Nature*. (2015) 520:104–8. doi: 10.1038/nature14052
160. Harrison OJ, Linehan JL, Shih HY, Bouladoux N, Han SJ, Smelkinson M, et al. Commensal-specific T cell plasticity promotes rapid tissue adaptation to injury. *Science*. (2019) 363:eaat6280. doi: 10.1126/science.aat6280
161. Belkaid Y, Bouladoux N, Hand TW. Effector and memory T cell responses to commensal bacteria. *Trends Immunol*. (2013) 34:299–306. doi: 10.1016/j.it.2013.03.003
162. Belkaid Y, Naik S. Compartmentalized and systemic control of tissue immunity by commensals. *Nat Immunol*. (2013) 14:646–53. doi: 10.1038/ni.2604
163. Hepworth MR, Monticelli LA, Fung TC, Ziegler CG, Grunberg S, Sinha R, et al. Innate lymphoid cells regulate CD4+ T-cell responses to intestinal commensal bacteria. *Nature*. (2013) 498:113–7. doi: 10.1038/nature12240
164. Tapia VS, Herrera-Rojas M, Larrain J. JAK-STAT pathway activation in response to spinal cord injury in regenerative and non-regenerative stages of *Xenopus laevis*. *Regeneration*. (2017) 4:21–35. doi: 10.1002/ireg2.74
165. Secombes CJ, Zou J. Evolution of interferons and interferon receptors. *Front Immunol*. (2017) 8:209. doi: 10.3389/fimmu.2017.00209
166. Gause WC, Wynn TA, Allen JE. Type 2 immunity and wound healing: evolutionary refinement of adaptive immunity by helminths. *Nat Rev Immunol*. (2013) 13:607–14. doi: 10.1038/nri3476
167. Knipper JA, Willenborg S, Brinckmann J, Bloch W, Maaß T, Wagener R, et al. Interleukin-4 receptor alpha signaling in myeloid cells controls collagen fibril assembly in skin repair. *Immunity*. (2015) 43:803–16. doi: 10.1016/j.immuni.2015.09.005
168. Piccolo V, Curina A, Genua M, Ghisletti S, Simonatto M, Sabò A, et al. Opposing macrophage polarization programs show extensive epigenomic and transcriptional cross-talk. *Nat Immunol*. (2017) 18:530–40. doi: 10.1038/ni.3710
169. Okabe Y, Medzhitov R. Tissue-specific signals control reversible program of localization and functional polarization of macrophages. *Cell*. (2014) 157:832–44. doi: 10.1016/j.cell.2014.04.016
170. Jin WN, Gonzales R, Feng Y, Wood K, Chai Z, Dong JF, et al. Brain ischemia induces diversified neuroantigen-specific T-cell responses that exacerbate brain injury. *Stroke*. (2018) 49:1471–8. doi: 10.1161/STROKEAHA.118.020203
171. Becker KJ, Tanzi P, Zierath D, Buckwalter MS. Antibodies to myelin basic protein are associated with cognitive decline after stroke. *J Neuroimmunol*. (2016) 295–296:9–11. doi: 10.1016/j.jneuroim.2016.04.001
172. Doyle KP, Buckwalter MS. Does B lymphocyte-mediated autoimmunity contribute to post-stroke dementia? *Brain Behav Immun*. (2017) 64:1–8. doi: 10.1016/j.bbi.2016.08.009

173. Gee JM, Kalil A, Thullbery M, Becker KJ. Induction of immunologic tolerance to myelin basic protein prevents central nervous system autoimmunity and improves outcome after stroke. *Stroke*. (2008) 39:1575–82. doi: 10.1161/STROKEAHA.107.501486
174. Urra X, Miró F, Chamorro A, Planas AM. Antigen-specific immune reactions to ischemic stroke. *Front Cell Neurosci*. (2014) 8:278. doi: 10.3389/fncel.2014.00278
175. Zhang Z, Zoltewicz JS, Mondello S, Newsom KJ, Yang Z, Yang B, et al. Human traumatic brain injury induces autoantibody response against glial fibrillary acidic protein and its breakdown products. *PLoS ONE*. (2014) 9:e92698. doi: 10.1371/journal.pone.0092698
176. Javidi E, Magnus T. Autoimmunity after ischemic stroke and brain injury. *Front Immunol*. (2019) 10:686. doi: 10.3389/fimmu.2019.00686
177. Guaraldi F, Grottoli S, Arvat E, Ghigo E. Hypothalamic-pituitary autoimmunity and traumatic brain injury. *J Clin Med*. (2015) 4:1025–35. doi: 10.3390/jcm4051025

Conflict of Interest Statement: The authors declare that the research was conducted in the absence of any commercial or financial relationships that could be construed as a potential conflict of interest.

Copyright © 2019 Krishnan and Lawrence. This is an open-access article distributed under the terms of the Creative Commons Attribution License (CC BY). The use, distribution or reproduction in other forums is permitted, provided the original author(s) and the copyright owner(s) are credited and that the original publication in this journal is cited, in accordance with accepted academic practice. No use, distribution or reproduction is permitted which does not comply with these terms.

frontiers in Neuroscience

ORIGINAL RESEARCH
published: 05 July 2019
doi: 10.3389/fnins.2019.00681

NK1-r Antagonist Treatment Comparable to Decompressive Craniectomy in Reducing Intracranial Pressure Following Stroke

Annabel J. Sorby-Adams[1]†, Anna V. Leonard[1†], Jan W. Hoving[2,3], Nawaf Yassi[4], Robert Vink[5], Adam J. Wells[6] and Renée J. Turner[1]*

[1] Adelaide Medical School and Adelaide Centre for Neuroscience Research, The University of Adelaide, Adelaide, SA, Australia, [2] Department of Medicine and Neurology, Melbourne Brain Centre at the Royal Melbourne Hospital, The University of Melbourne, Parkville, VIC, Australia, [3] Department of Radiology, Amsterdam UMC, University of Amsterdam, Amsterdam, Netherlands, [4] Florey Institute of Neuroscience and Mental Health, Parkville, VIC, Australia, [5] Division of Health Sciences, University of South Australia, Adelaide, SA, Australia, [6] Department of Neurosurgery, Royal Adelaide Hospital, Adelaide, SA, Australia

OPEN ACCESS

Edited by:
Christoph Harms,
Charité – University Medicine Berlin, Germany

Reviewed by:
Sandeep Kumar Barodia,
The University of Alabama at Birmingham, United States
Zareen Amtul,
Independent Researcher, London, Canada

***Correspondence:**
Annabel J. Sorby-Adams
annabel.sorby-adams@adelaide.edu.au

[†]These authors have contributed equally to this work

Specialty section:
This article was submitted to Neurodegeneration, a section of the journal Frontiers in Neuroscience

Received: 07 March 2019
Accepted: 13 June 2019
Published: 05 July 2019

Citation:
Sorby-Adams AJ, Leonard AV, Hoving JW, Yassi N, Vink R, Wells AJ and Turner RJ (2019) NK1-r Antagonist Treatment Comparable to Decompressive Craniectomy in Reducing Intracranial Pressure Following Stroke. Front. Neurosci. 13:681. doi: 10.3389/fnins.2019.00681

Background and Purpose: The morbidity and early mortality associated with stroke is largely attributable to cerebral edema and elevated intracranial pressure (ICP). Existing pharmacotherapies do not target the underlying pathophysiology and are often ineffective in sustainably lowering ICP, whilst decompressive craniectomy (DC) surgery is life-saving yet with surgical/peri-operative risk and increased morbidity in the elderly. Accordingly, there is an urgent need for therapies that directly target the mechanisms of edema genesis. Neurogenic inflammation, mediated by substance P (SP) binding to the tachykinin NK1 receptor (NK1-r), is associated with blood-brain barrier (BBB) disruption, cerebral edema and poor outcome post-stroke. NK1-r antagonist treatment ameliorates BBB dysfunction and cerebral edema in rodent stroke models. However, treatment has not been investigated in a large animal model, an important step toward clinical translation. Consequently, the current study compared the efficacy of NK1-r antagonist treatment to DC surgery in reducing ICP post-stroke in a clinically relevant ovine model.

Methods: Anesthetized female Merino sheep (65 ± 6 kg, 18–24 months) underwent sham surgery (n = 4) or permanent middle cerebral artery occlusion (n = 22). Stroke animals were randomized into one of 5 treatments: 1×NK1 bolus (4 h), 2×NK1 bolus (4 h;9 h), 3×NK1 bolus (4 h;9 h;14 h), DC surgery (performed at 4 h) or saline vehicle. ICP, blood pressure and blood gasses were monitored for 24 h post-stroke. At 24 h post-stroke anesthetized animals underwent MRI followed by perfusion and brains removed and processed for histological assessment.

Results: 2×NK1, 3×NK1 administration or DC surgery significantly ($p < 0.05$) reduced ICP compared to vehicle. 1×NK1 was ineffective in sustainably lowering ICP. On MRI,

midline shift and cerebral edema were more marked in vehicles compared to NK1-r treatment groups.

Conclusion: Two or three boluses of NK1-r antagonist treatment reduced ICP comparable to DC surgery, suggesting it may provide a novel alternative to invasive surgery for the management of elevated ICP.

Keywords: intracranial pressure, cerebral edema, substance P, decompressive craniectomy, blood-brain barrier, stroke

INTRODUCTION

Elevated intracranial pressure (ICP) arising as a result of malignant cerebral edema is the leading cause of death in the first week following stroke (Hacke et al., 1996). Despite the devastating impact of elevated ICP on patient outcome, clinical management remains sub-optimal. Pharmacological interventions for ICP management are limited, and while osmotic therapies (including mannitol and hypertonic saline) are used in some centers (Zhang et al., 2018), there is no evidence that these therapies are independently effective in improving outcome. Furthermore, the efficacy of other pharmacotherapies including corticosteroids and barbiturates remains ambiguous for the treatment of post-stroke cerebral edema (Brogan and Manno, 2015). In selected patients with malignant middle cerebral artery (MCA) territory infarction, surgical intervention with decompressive craniectomy (DC) may be required. This procedure rapidly alleviates pressure by removing a large portion of the skull and opening the dura overlying the brain, thereby providing space for the edematous brain to swell freely until cerebral edema resolves, typically beyond the first week following stroke (Xiao-feng et al., 2005). However, although this procedure reduces compression on cerebral structures and the risk of life-threatening tonsillar herniation, it is also associated with increased morbidity in those aged greater than 60 years, the patient population in which stroke is most prevalent (Jüttler et al., 2007; Das et al., 2019). It is clear that current pharmacological and surgical interventions are inadequate as they target the symptoms, rather than the underlying cause of cerebral edema and concomitant rise in ICP (Bardutzky and Schwab, 2007; Simard et al., 2007). An enhanced understanding of the mechanisms that underlie the genesis of cerebral edema and raised ICP is critical for the development of more targeted and effective treatments.

Although factors associated with the pathogenesis of cerebral edema are not completely understood, neurogenic inflammation has been identified as a potential therapeutic target (Stumm et al., 2001; Turner et al., 2006; Corrigan et al., 2016a). Neurogenic inflammation is a neurally mediated process involving the release of neuropeptides, including substance P (SP) and calcitonin gene-related peptide, which initiate vasodilation, increased microvascular permeability and edema (Hokfelt et al., 2000). Although well established as a precipitant of edema development within peripheral tissues such as the skin and lungs (Alves et al., 1999), neurogenic inflammation remained largely unexplored as a potential mechanism of cerebral edema development (Lewis et al., 2013; Sorby-Adams et al., 2017). This was until studies depleting neuropeptides or blocking the action of SP at the tachykinin NK1 receptor (NK1-r), to which SP binds preferentially, showed a ubiquitous role for this process in the genesis of cerebral edema following stroke and traumatic brain injury (TBI) (Vink et al., 2003; Nimmo et al., 2004; Turner et al., 2006, 2011; Donkin et al., 2009; Turner and Vink, 2012, 2014; Corrigan et al., 2016a). Specifically, increased SP immunoreactivity within the penumbral perivascular tissue is associated with profound BBB disruption and cerebral edema at 24 h post-stroke and poor functional outcomes up to 7 days following middle cerebral artery occlusion (MCAO) in rats, with NK1-r blockade ameliorating these effects (Turner et al., 2011; Turner and Vink, 2012, 2014; Corrigan et al., 2016a). Increased plasma SP levels have also been reported clinically following severe acute ischemic stroke, elevated levels of which were associated with increased mortality (Lorente et al., 2016). Comparable alterations in SP levels have also been observed in clinical TBI correlating with injury severity and mortality (Lorente et al., 2015).

The cumulative evidence from these studies suggests an important role for SP in the development of cerebral edema and poor outcome following acute CNS injury. However, pre-clinical stroke evaluation of the NK1-r antagonist has been limited to small animal stroke models, with the most extensive screening to date performed in small and large animal models of TBI. Whilst rodent species are essential for establishing basic biological processes, it is often difficult to obtain clinically relevant outcome measures, thereby limiting clinical translation. Given the extremely poor translation of stroke neuroprotection from the laboratory to the clinic (Xu and Pan, 2013), evaluation of promising therapies in a large, intermediate species is essential. Species such as sheep are an ideal candidate for such studies due to the ability to utilize clinically relevant outcome measures in addition to similarities in neuroanatomical structure, including gyrencephalic cerebral organization and significant portion of white matter (Sorby-Adams et al., 2018). Of particular relevance when investigating elevated ICP, however, is the strong tentorium cerebelli of the sheep, separating supra- and infratentorial compartments, bearing structural similarity to that of the human (Dostovic et al., 2016). In the setting of clinical malignant cerebral edema, this leads to compartmentalization of pressure within the supratentorial space, tonsillar herniation, and ultimately often fatal compression of the brain stem as the brain attempts to alleviate dangerously elevated ICP. Indeed, ovine stroke models replicate key clinical hallmarks following

stroke including elevated ICP, cerebral edema, midline shift and tonsillar herniation (Wells et al., 2012; Wells et al., 2015; Sorby-Adams et al., 2018).

As such, the aim of the present study was to determine the effect of inhibition of SP with an NK1-r antagonist, compared to DC surgery, on ICP following permanent ischemic stroke in an ovine model.

MATERIALS AND METHODS

Animals and Experimental Design

Female Merino sheep ($n = 26$) aged 18–24 months old (65 ± 6 kg) were allocated to the study. Animals were randomized into either sham surgery or permanent MCA occlusion (MCAO). Following induction of stroke animals were then randomized into one of the following groups: (1) saline vehicle treatment at 4 h post-stroke ($n = 6$); (2) 1× bolus NK1 antagonist at 4 h post-stroke ($n = 3$); (3) 2× boluses of NK1 antagonist at 4 h and 9 h post-stroke ($n = 3$); (4) 3× boluses of NK1 antagonist at 4, 9 and 14 h post-stroke ($n = 6$); or (5) decompressive craniectomy ($n = 5$) at 4 h post-stroke. Note that the dose for the NK1-r antagonist treatment was the same across all the NK1-r treatment groups, the only difference was the number of boluses that each group received, either one (1×NK1), two (2×NK1), or three (3×NK1) boluses. The NK1-r antagonist used in the study was a test compound supplied by PresSuraNeuro prepared at a concentration of 1 mg/ml in warmed saline (37°C) and administered at a dose of 1 ml/kg via an indwelling jugular venous catheter, as per previous studies in our laboratory (Vink et al., 2017).

Anesthesia and Physiological Monitoring

Anesthesia was induced with intravenous thiopentone (1000 mg in 20 mL, Jurox Pty Ltd., Australia) and maintained with 1.5% inhalational isoflurane (Veterinary Companies of Australia Pty Ltd., Australia) in a mixture of oxygen and room air (500:5000 ml/min), plus intravenous ketamine (Parnell Australia Pty Ltd., Australia) infusion at 4 mg/kg/hr via a femoral venous line. These two anesthetic agents were used in combination to avoid the intrinsic neuroprotective properties of either above certain doses, and to maintain a twilight general anesthesia (Hudetz and Pagel, 2010; Schifilliti et al., 2010). With the animal supine, an arterial catheter was placed in the right femoral artery for continuous blood pressure monitoring and periodic arterial blood gas sampling, and a venous catheter inserted for anesthetic and fluid administration. The animal was then placed prone in the sphinx position, a burr hole drilled in the right parietal bone posterior to the coronal suture and approximately 20 mm from the sagittal suture, dura perforated, and skull bolts secured. A Codman microsensor ICP probe (Codman & Shurtleff Inc., MA, United States) was introduced into the bolt, calibrated and inserted intraparenchymally to measure ICP within the supratentorial compartment. Using LabChart Reader (v 8.1.1), mean arterial blood pressure (MABP) and ICP were continuously recorded through the 24 h monitoring period. Arterial blood gas sampling was conducted prior to MCAO or sham surgery and at hourly intervals throughout the monitoring period until the completion of the experiment to maintain physiological pO_2, pCO_2, and pH.

Surgical Approach to MCAO

We have previously described the surgical approach to proximal MCAO in detail (Wells et al., 2012, 2015). Briefly, a 50 mm vertical incision was made posterior to the right eye, terminating at the zygomatic arch. The underlying muscle was retracted, coronoid process removed, and the skull revealed. A small craniotomy was performed at the junction of the parietal and squamous temporal bones with a high-speed pneumatic drill using a 5 mm cutting burr (Midas Rex, Medtronic, MN, United States). All intra-dural work was carried out with loupe magnification and a head mounted light source (Surgical Acuity, WI, United States). A horse-shoe shaped durotomy was performed with an inferiorly based flap allowing for gentle upward retraction of the anterior temporal lobe to achieve visualization of the proximal MCA. Animals then either underwent sham surgery in which the proximal MCA was dissected but not occluded, or permanent MCA in which the proximal MCA was occluded via Malis bipolar diathermy forceps (Valleylab Inc., CO, United States). The exposed brain was irrigated with saline during surgery to prevent dehydration of the cerebral cortex. After completion of sham or MCAO surgery the dura was approximated and synthetic dura (Durepair, Medtronic) interleaved under the existing dura (in the case of dural retraction following incision) and closed watertight with ethyl cyanoacrylate (Bostik, Australia). Once dural closure was confirmed and no leakage of CSF observed, the craniotomy site was reinforced with dental acrylic cement (Lang Dental, IL, United States) that was manipulated into the edge of the craniotomy and the wound closed in layers, maintaining the shape of the cranial cavity and importantly, the homeostasis of ICP dynamics. For animals allocated to the DC group, at 4h following stroke the wound was opened, dental acrylic removed, and the craniotomy site widened (3 cm × 6 cm) to allow for decompression. A dural pouch was created using Durepair to expand the intracranial cavity, after which the bone was left off and the overlying skin sutured closed, simulating clinical DC and expansile duraplasty. For all groups, the head was then returned to a neutral position for monitoring under general anesthesia.

Magnetic Resonance Imaging

At 24 h following stroke or sham surgery onset animals were placed under general anesthesia (3% isoflurane) in a 1.5 Tesla Siemens Sonata (Siemens AG, Munich, Germany) magnetic resonance imaging (MRI) scanner. The scanning sequence included time-of-flight magnetic resonance angiography (TOF MRA; TR 26.0 ms, TE 3.69 ms, slice thickness 0.50 mm, slices per slab 48), diffusion weighted imaging (DWI; TR 5600.0 ms, TE 80 ms, slice thickness 3.0 mm, slices per slab 25), fluid attenuated inversion recovery (FLAIR; TR 5000.0 ms, TE 386 ms, slice thickness 0.9 mm, slices per slab 96), T1 (TR 2300.0 ms, TE 2.58 ms, slice thickness 0.9 mm, slices per slab 96) and T2 (TR 3200 ms, TE 410 ms, slice thickness 0.9 mm, slices per slab 96) weighted images.

The degree of midline shift on MRI was used as a marker of the amount of expansion of the infarcted hemisphere, indicative of cerebral edema. Extent of shift from the midline was assessed using axial T2-weighted scans and measured in mm from the septum pellucidum at the level of the foramen of Monro (Horos DICOM image viewer v3.1.1). To calculate cerebral edema, coronal FLAIR images were analyzed using Horos (v3.1.1). After optimal adjustment of brightness and contrast, edema volume was determined from sequences using computer-aided manual tracing of the hyperintense lesion by a blinded assessor. The areas were then summed and multiplied by the slice thickness to give a total volume in cm^3.

To calculate infarct volume, segmentation tools in ITK-SNAP (v 3.7) were used to perform semi-automated segmentation of the MRI diffusion lesions using diffusion-weighted images (Yushkevich et al., 2006). A combination of "three-dimensional active contour segmentation" and subsequent manual post-processing of the segmentation while adjusting image thresholds was performed to maximize reproducibility whilst excluding artifacts. The "three-dimensional active contour segmentation" consisted of multiple steps: First, in the pre-segmentation phase, independent component analysis automatically segmented parts of the DWI image and these were manually identified as foreground or background. To obtain an optimal distinction between foreground and background, thresholds of the image windows were adjusted. After thresholding, a "speed image" with a separate foreground and background was created. Next, in the active contour phase, seed regions were manually placed within the region of interest (ROI). These seeds were then automatically grown within the ROIs to form the temporary segmentation. Subsequently, areas that were not automatically included in the "active contour segmentation," were manually included in the follow-up infarct segmentation. The total volume of the segmentation was exported and reported in cm^3 for analysis.

Histological Examination

Following MRI, intravenous heparin (5000I.U./5 ml; Pfizer, NY, United States) was administered and animals euthanized via common carotid perfusion fixation with cold Tris–buffered saline under Isoflurane anesthesia. The brains were subsequently removed and sliced into 10 mm coronal slices using a custom-made matrix. Sections were then immersion fixed in 10% neutral-buffered formalin for a minimum of 14 days prior to being processed, embedded in paraffin wax and sectioned coronally at 5 micron intervals for histological examination by hematoxylin and eosin (H&E), albumin (1:2000, Dako Pty Ltd., A0001), SP (1:5000 citrate retrieval, Abcam Pty Ltd., ab14184), NKI-r (1:1000 citrate retrieval, Advanced Targeting Systems Pty Ltd., AB-N-33AP) and caveolin-1 (cav-1; 1:1000 EDTA retrieval, Cell Signaling Technologies Pty Ltd., 3238) immunohistochemistry.

Statistical Analysis

All data are expressed as mean ± SD. Physiological data (arterial blood pressure, pH, pO_2, pCO_2) were analyzed using one-way analysis of variance (ANOVA) followed by Tukey's *post hoc* tests (Prism v.8.0.1, Graphpad, CA, United States). Values were averaged for each treatment group across all time points and reported as a single value. Raw ICP and MABP data underwent a logarithmic exponential transformation as previously described and were expressed as geometric mean ± SD (Matthews et al., 1990; Wells et al., 2015). ICP was analyzed by two-way ANOVA and lesion volume, cerebral edema and midline shift data were analyzed by one-way ANOVA, all followed by Tukey's *post hoc* tests. A p-value of < 0.05 was considered significant. Correlations were performed between cerebral edema and midline shift and ICP and cerebral edema to determine the relationship between these variables.

RESULTS

Surgery, Mortality and Physiological Parameters

All experimental procedures were carried out without complication and there was no premature mortality or unexpected events in any of the groups. Basic physiological parameters are expressed in **Table 1**. For all groups, there was no statistically significant difference in pO_2, pCO_2, or pH at any of the time-points following stroke. However, there was a statistically significant difference in MABP between sham, 1×NK1 (p = 0.02) DC (p = 0.02) and 3×NK1 (p = 0.006) treatment groups.

Intracranial Pressure

Intracranial pressure remained physiologically stable across all time points in sham animals (9 ± 3 mmHg). At both 4 and 9 h post-stroke, there was no significant difference in ICP between sham or any of the stroke groups. By 14 h following injury, ICP in vehicle animals was significantly elevated (24 ± 11 mmHg) compared to shams (10 ± 3 mmHg) (p = 0.019). However, no difference in ICP was seen between vehicle or any of the treatment groups at this time-point (**Figure 1**).

Intracranial pressure in vehicle animals continued to rise and by 19 h post-stroke measured 32 ± 11 mmHg, which was significantly elevated (p = 0.0002) compared to shams recording an ICP of 13 ± 6 mmHg. By 19 h there was a significant reduction in ICP seen in 2×NK1 (18 ± 4 mmHg; p = 0.013), 3×NK1 (17 ± 7 mmHg; p = 0.015), and DC (19 ± 11 mmHg; p = 0.042) treated animals compared to vehicle. Conversely, there was no reduction ($p > 0.05$) in ICP seen following 1×NK1 treatment

TABLE 1 | Basic physiological parameters.

Group	pCO_2 (mmHg) ± SD	pO_2 (mmHg) ± SD	MABP (mmHg) ± SD	pH (−log $[H^+]$) ± SD
Sham	43 ± 8.41	113 ± 14.09	79 ± 8.78	7.48 ± 0.039
Vehicle	40 ± 6.09	127 ± 31.28	104 ± 10.17	7.46 ± 0.062
1×NK1	36 ± 2.55	138 ± 25.06	112 ± 10.18	7.51 ± 0.033
2×NK1	43 ± 6.56	149 ± 33.99	98 ± 5.81	7.45 ± 0.031
3×NK1	37 ± 2.34	135 ± 20.53	111 ± 15.66	7.52 ± 0.018
DC	42 ± 3.78	150 ± 17.22	108 ± 10.65	7.45 ± 0.082

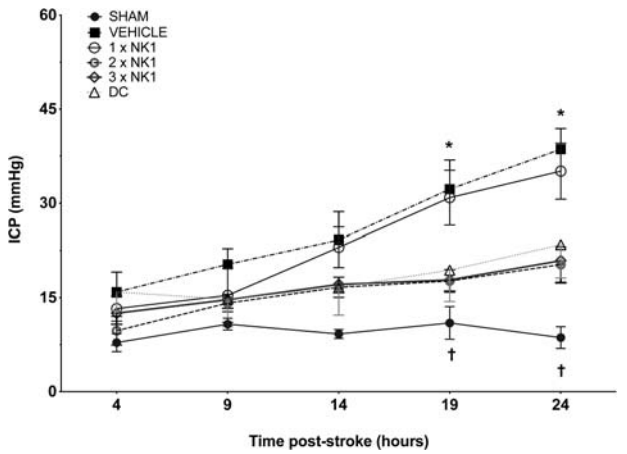

FIGURE 1 | 24 h ICP following MCAO. There was no significant difference in sham ICP across any of the time points. At 14 h post-stoke ICP was elevated in vehicle animals compared to sham ($p < 0.05$) and by 19 h post-stroke, ICP was significantly elevated in vehicle ($p < 0.001$) and 1×NK1 ($p < 0.01$) treated animals when compared to 2×NK1 ($p < 0.05$), 3×NK1 ($p < 0.05$) and DC treatment groups ($p < 0.05$). By 24 h, ICP remained significantly elevated in vehicle animals compared to sham ($p < 0.0001$), 2×NK1 ($p < 0.01$), 3×NK1 ($p < 0.01$) and DC ($p < 0.05$) treatment groups. ICP also remained elevated at 24 h post-stroke in 1×NK1 treatment groups compared to sham ($p < 0.001$) and 2×NK1 ($p < 0.05$). Data presented as mean ± SD. *$p < 0.05$ compared to sham; †$p < 0.05$ compared to vehicle.

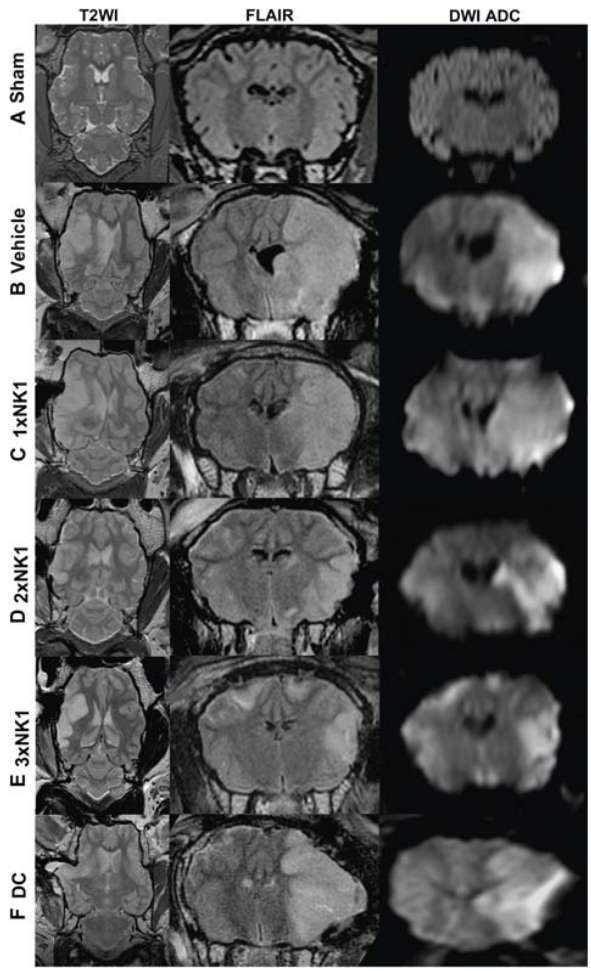

FIGURE 2 | MRI findings 24 h post-MCAO. There was no evidence of hyperintensity or tissue deformation seen in sham animals **(A)**. Midline shift was evident in all stroke animals as seen on axial T2-weighted images **(B–D)**. Cerebral edema as shown in coronal FLAIR MRI images was greater in vehicle **(B)**, DC **(F)** and 1×NK1 **(C)** groups compared with 2×NK1 **(D)** and 3×NK1 **(E)** groups. This was associated with a smaller diffusion lesion volume as shown in DWI ADC images in the coronal plane. Note the transcalvarial herniation through the craniotomy site in DC treated animals **(F)**.

(31 ± 9 mmHg) compared to vehicle, with ICP remaining significantly elevated compared to sham ($p = 0.002$).

By 24 h post-stroke, ICP in vehicle animals had continued to rise (39 ± 7 mmHg) and remained significantly elevated compared to shams (12 ± 8 mmHg; $p < 0.001$), DC (23 ± 12 mmHg; $p = 0.013$), 2×NK1 (20 ± 6 mmHg; $p < 0.001$), and 3×NK1 (19 ± 7 mmHg; $p < 0.005$) treated animals. ICP continued to rise in the 1×NK1 treatment group (35 ± 9 mmHg) and remained significantly elevated compared to both shams ($p < 0.001$) and 2×NK1 ($p = 0.029$) treatment groups. ICP in 2×NK1 and 3×NK1 treatment groups was comparable ($p > 0.05$) to DC across all time points following stroke. No rebound increases in ICP were observed following 2×NK1 or 3×NK1 treatment at any time-point post-stroke.

MRI

Magnetic resonance imaging was unremarkable in sham animals ($n = 4$) with no evidence of cerebral edema, midline shift or infarction (**Figure 2A**). All stroke animals showed evidence of hyperintensity on T2-weighted and FLAIR images in the territory MCA, indicative of the infarct core and surrounding vasogenic edema (**Figure 2**). In addition, DC treated animals showed evidence of transcalvarial herniation through the craniectomy site (**Figure 2D**). No animals showed evidence of tonsillar herniation or brain stem compression on MRI (data not shown).

Cerebral edema calculated on FLAIR MRI (**Figure 3** and **Table 2**) was reduced in DC ($p = 0.012$) and 1×NK1 treatment groups ($p = 0.042$) when compared to vehicle (**Figure 3A**). However, treatment with 2×NK1 ($p = 0.001$) and 3×NK1 ($p = 0.001$) was associated with a more significant reduction in cerebral edema volume compared to vehicle (**Figure 3A**). Midline shift was evident in all stroke animals (**Table 2**) with no statistical significance seen between groups ($p = 0.2$; **Figure 3B**). Nevertheless, there was a moderate positive relationship between the volume of cerebral edema and the degree of midline shift ($r = 0.46$; **Figure 3C**). No significant differences ($p = 0.17$) were observed in infarct volume across any of the treatment groups following stroke, as measured on DWI MRI (**Figure 3D**).

Histological Analysis

H&E

There was no evidence of tissue injury or infarction in sham tissue (**Figure 4A**). Following stroke (**Figure 4B**) there was marked tissue pallor and loss of gray-white matter differentiation,

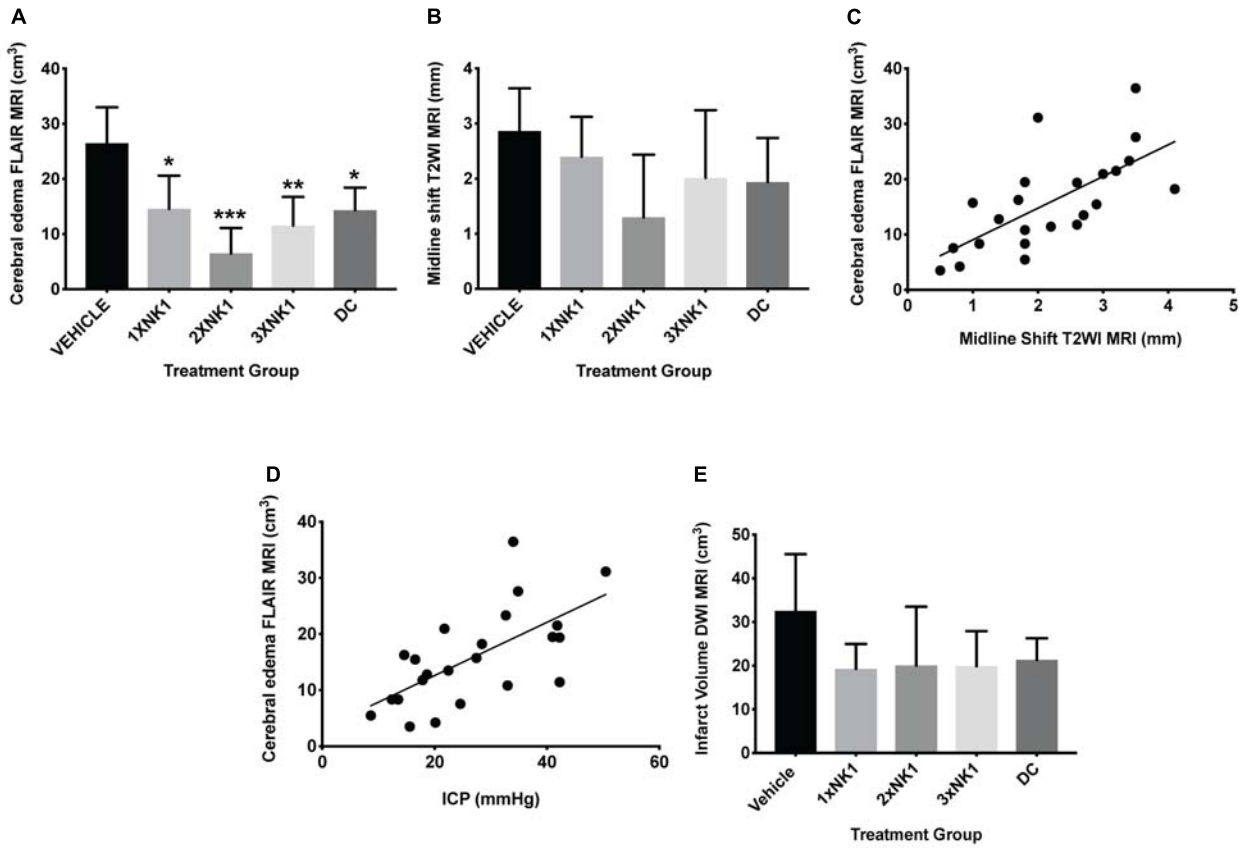

FIGURE 3 | Cerebral edema and infarct volume findings at 24 h post-MCAO. Cerebral edema volume, as measured on FLAIR MRI **(A)**, was decreased in 1×NK1 ($p < 0.05$), 2×NK1 ($p < 0.001$), 3×NK1 ($p < 0.01$), and DC ($p < 0.05$) treatment groups when compared to vehicle. There was no difference in midline shift in any of the vehicle or treatment groups post-stroke **(B)**. Despite this, there was a relative moderate positive correlation between cerebral edema and midline shift **(C)**. There was also a moderate positive correlation between cerebral edema and ICP measured at 24 h post-stroke **(D)**. There was no significant difference in infarct volume **(E)** as measured on DWI MRI between any treatment groups. *$p < 0.05$, **$p < 0.01$ and ***$p < 0.001$ compared to vehicle.

indicative of infarction within the MCA territory of the right hemisphere. 1×NK1 (**Figure 4C**) treatment tissue was comparable to vehicles, however, there was an increased preservation of tissue, in particular the sub-cortical white matter, in the 2×NK1 (**Figure 4D**), 3×NK1 (**Figure 4E**) and DC (**Figure 4F**) treated groups.

Albumin

There was minimal evidence of albumin extravasation in sham tissue (**Figure 4A**). Following stroke, marked albumin extravasation, indicative of BBB breakdown and subsequent vasogenic cerebral edema formation, was observed both macroscopically within the infarcted territory and microscopically in the perivascular tissue of the infarct in vehicles (**Figure 4B**), 1×NK1 (**Figure 4C**) and DC (**Figure 4F**), when compared to shams (**Figure 4A**), 2×NK1 (**Figure 4D**) and 3×NK1 (**Figure 4E**) treatment groups.

SP

There was low to no observable immunoreactivity of SP in sham tissue (**Figure 5A**). Furthermore, similarly low levels of SP immunoreactivity were observed in the infarcted hemisphere of vehicle and each of the treatment groups following stroke.

NK1-r

Low levels of perivascular NK1-r immunoreactivity were observed in sham tissue (**Figure 5B**). Following stroke, an increase in perivascular NK1-r immunoreactivity was observed in vehicle and DC treated groups, which was not observed in any of the NK1 treatment groups.

Cav-1

Little to no perivascular cav-1 immunoreactivity was observed in sham tissue (**Figure 5C**). Following stroke, a marked increase in perivascular cav-1 immunoreactivity was observed in vehicles (E), 1×NK1 (F) and DC (L) tissue when compared to sham (D), 2×NK1 (J) and 3×NK1(K) tissue.

DISCUSSION

In this study we have demonstrated that administration of two or three boluses of an NK1-r antagonist is effective

TABLE 2 | MRI characteristics post-MCAO.

Treatment	Edema FLAIR MRI (cm^3)	Midline Shift T2 (mm)	Infarct DWI MRI (cm^3)
Vehicle			
86	19.48	1.8	33.9
87	36.45	3.5	24.5
60	20.96	3	25.9
66	31.14	2	34.4
57	27.61	3.5	20.1
59	23.32	3.4	56.5
Mean ± SD	25.56 ± 6.10	2.87 ± 0.71	32.55 ± 11.85
1×NK1			
69	10.84	1.8	22.1
75	21.51	3.2	23
88	11.44	2.2	12.7
Mean ± SD	14.60 ± 6.0	2.40 ± 0.72	19.27 ± 5.70
2×NK1			
70	4.230	0.8	8.3
72	3.520	0.5	17.2
91	11.789	2.6	34.7
Mean ± SD	6.51 ± 4.58	1.30 ± 1.14	20.07 ± 13.43
3×NK1			
71	5.49	1.8	11.6
73	13.50	2.7	20.7
74	7.56	0.7	10.6
76	8.33	1.1	20.8
89	18.23	4.1	32.1
90	16.27	1.7	23.7
Mean ± SD	11.56 ± 5.17	2.02 ± 1.23	19.92 ± 8.0
DC			
101	19.38	2.6	26.8
102	15.46	2.9	23.7
105	15.74	1	16.6
106	12.80	1.4	15.6
107	8.36	1.8	24
Mean ± SD	14.35 ± 4.08	1.94 ± 0.78	21.34 ± 4.95

in reducing ICP following stroke in a clinically relevant ovine model. This reduction in ICP following treatment was associated with improved BBB integrity, as shown by albumin immunohistochemistry, and a trend toward reduction in the volume of cerebral edema in the infarcted hemisphere. These findings corroborate previous experimental (Vink et al., 2003; Nimmo et al., 2004; Turner et al., 2006, 2011; Donkin et al., 2009; Corrigan et al., 2012, 2016b; Turner and Vink, 2012, 2014) and clinical (Lorente et al., 2015, 2016) studies to further support the role of SP in the pathogenesis of elevated ICP, cerebral edema and increased permeability of the BBB following acute CNS injury. Indeed, the reduction in ICP following treatment observed in this study is consistent with findings in an ovine model of TBI (Vink et al., 2017). Taken together, we have now successfully demonstrated the efficacy of NK1-r antagonist treatment for the reduction of cerebral edema and its consequences in both rodent and sheep models of stroke (Turner et al., 2006, 2011; Turner and Vink, 2012, 2014) and TBI (Donkin et al., 2009; Corrigan et al., 2012, 2016b; Vink et al., 2017). Taken together these findings clearly demonstrate that SP release is a ubiquitous feature of acute CNS injury and that blockade of this pathway is able to preserve BBB integrity and halt the development of cerebral edema and subsequent rise in ICP.

Despite the clear treatment effect of blocking the NK1-r to reduce ICP in this study, we did not observe a significant increase in perivascular SP immunoreactivity within the infarcted territory in any of the treatment groups following stroke. This is in keeping with our previous findings in a rodent model of MCAO (Turner, 2007), where minimal SP immunoreactivity was observed following permanent MCAO, yet profound perivascular staining was identified following transient MCAO with reperfusion. These observations are most likely due to the fact that in the setting of permanent MCAO, the release and peak in SP occurs acutely due to the severity of the ischemic insult. As such, SP has likely been degraded by the time of tissue harvest at 24 h post-stroke. In comparison, in previous rodent transient MCAO studies, perivascular SP immunoreactivity was observed primarily in the penumbral tissue. The relative proportion of penumbra to ischemic core is likely to be much less following permanent compared to transient MCAO due to the extensive collateral failure with longer durations of ischemia. Not surprisingly, this suggests that the magnitude and timing of SP release in the neurogenic inflammatory response is dependent upon the duration and severity of the ischemic insult (Corrigan et al., 2016b). Indeed, following vascular occlusion, temporary changes in transient receptor potential channels of c-fibers as a result of alterations in temperature, pH and ligand binding instigates release of SP (Hokfelt et al., 1975). When there is no reperfusion, compromised cells undergo ischemic necrosis quickly with associated acute changes in cellular function, leading to a rapid return of receptor channel potential and decrease in SP release. Comparatively, in the setting of transient MCAO, compromised cells in the penumbra experience long durations of electrical silence and alterations in neuronal function, leading to sustained activation of c-fibers and persistent SP release (Astrup et al., 1981; Turner, 2007; Hofmeijer and Van Putten, 2012). Taken together, these findings may provide an explanation as to why SP was not observed on IHC in this study.

We did not observe any effect on infarct volume following NK1-r antagonist treatment, irrespective of the number of boluses administered. This is not surprising considering that we used a permanent stroke model and given that the NK1-r antagonist is targeting BBB disruption and not other pathways in the ischemic injury cascade. Indeed, a transient stroke model with reperfusion followed by delivery of an NK1-r antagonist may yield different results on infarct volume. Nevertheless, we also did not observe an effect on infarct volume at 24 hrs following 2 h MCAO thread occlusion in our rodent studies (Turner et al., 2011). In these previous rat studies, however, we did demonstrate that increased perivascular SP immunoreactivity was associated with increased BBB permeability, profound cerebral edema and persistent functional deficits (Turner et al., 2006, 2011; Turner and Vink, 2012, 2014).

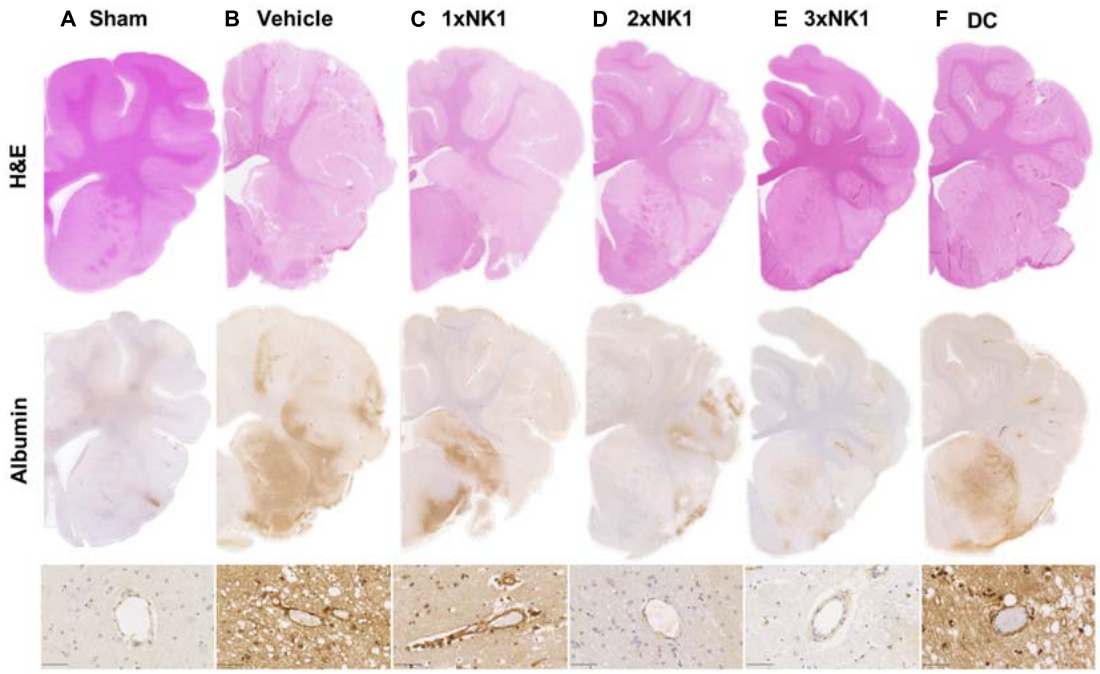

FIGURE 4 | Hematoxylin and Eosin staining and albumin immunoreactivity in **(A)** sham, **(B)** vehicle, **(C)** 1×NK1, **(D)** 2×NK1, **(E)** 3×NK1, and **(F)** DC animals. H&E staining shows evidence of pallor and reduced gray white matter differentiation, which is especially prominent in vehicles and 1×NK1 treated animals. Enhanced albumin extravasation was seen macroscopically in vehicle, 1×NK1 and DC treated animals compared to sham, 2×NK1 and 3×NK1 treatment groups. This pattern of albumin staining is consistent with the perivascular staining seen in microscopic images. Scale bar 50 μm, 40× magnification.

In this study we have identified that increased BBB permeability was sustained to 24 h post-stroke in vehicle-treated animals, as identified by the increased albumin extravasation. Furthermore, the corresponding increase in perivascular caveolin-1 immunoreactivity in the vehicle group may provide an explanation for persistent changes barrier permeability seen. Caveolae are invaginations of the plasma membrane present in endothelial cells, including those that comprise the BBB, with a key role in regulating transcytosis of large molecules, including albumin, across the barrier (Abbott et al., 2006). Cav-1 is an integral protein for caveolae formation, with upregulation associated with enhanced albumin extravasation and the development of vasogenic cerebral edema (Nag et al., 2007). Furthermore, cav-1 is shown to be upregulated following rodent cortical-cold injury and feline TBI, despite maintenance of tight junction (TJ) integrity (Povlishock et al., 1978; Nag et al., 2007), suggesting that physical breakdown of the barrier through loss of TJ is not necessary for the development of cerebral edema. The NK1-r is located within caveolae, suggesting that its activation may play a role in regulating transcytosis (Monastyrskaya et al., 2005; Kubale et al., 2007). Indeed, this is consistent with the observation of reduced barrier permeability following NK1-r antagonist administration (Donkin et al., 2007; Turner et al., 2011; Turner and Vink, 2012, 2014; Corrigan et al., 2016a; Vink et al., 2017). It is proposed that SP release following acute CNS injury leads to NK1-r activation, including those located within the caveolae of endothelial cells. This precipitates enhanced transcytosis of albumin across the barrier, altering the osmotic gradient leading to the development of vasogenic edema. Inhibition of transcytosis-mediated albumin extravasation through administration of the NK1-r antagonist attenuates unfavorable alterations in osmotic gradient across the barrier, thus preventing the abnormal accumulation of water in the parenchyma and subsequent development of edema and rise in ICP.

As previously mentioned, in this study we were able to reliability measure changes in ICP throughout the 24 h monitoring period. Clinical studies investigating fluctuations in ICP following malignant MCA stroke have recorded pressures as high as 43 mmHg in patients that died, compared with 28 mmHg in survivors (Hacke et al., 1996). In the present study pressures as high as 50 mmHg were recorded in vehicle animals, however, two or three boluses of the NK1-r antagonist were sufficient to sustainably reduce ICP to less than 30 mmHg. Furthermore, 2×NK1 treated animals recorded pressures of less than 20 mmHg throughout the 24 h monitoring period, with the exception of one animal, and 3 boluses of the antagonist was sufficient to maintain pressures below 25 mmHg, again with the exception of one animal who recorded a maximum pressure of 28 mmHg. One dose of the NK1-r antagonist, however, was insufficient to produce a treatment effect with pressures averaging 35 mmHg. These findings suggest that multiple boluses of the NK1-r antagonist is a potentially viable therapeutic strategy to reduce elevated ICP following stroke, with the ability to bring about a clinically meaningful and sustainable reduction

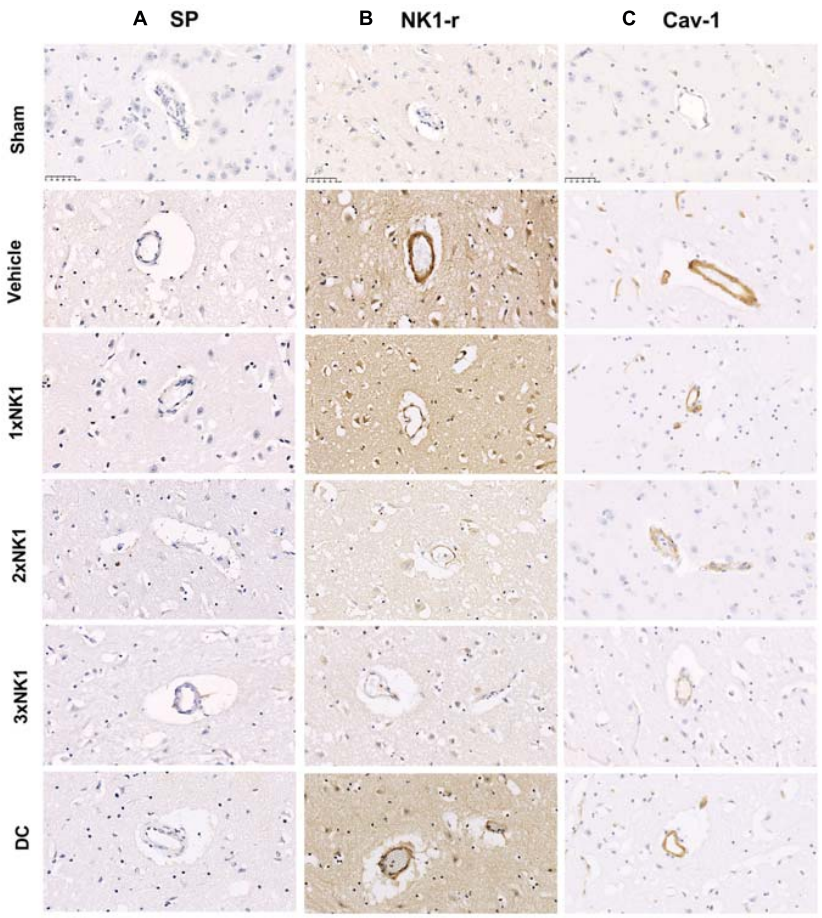

FIGURE 5 | SP, NK1-r and caveolin-1 immunoreactivity. There was no identifiable increase in SP, NK1-r or cav-1 immunoreactivity in sham animals. Low levels of SP immunoreactivity were seen perivascularly in vehicle, 1×NK1, 2×NK1, 3×NK1 and DC groups **(A)**. This was concordant with an increase in NK1-r immunoreactivity, which was most prominent in vehicle, 1×NK1 and DC animals **(B)**. Cav-1 immunoreactivity was significantly enhanced in 1×NK1, 2×NK1 and DC treatment groups when compared to vehicle and 1×NK1 **(C)**. Scale bar: 50 μm, 40× magnification.

in pressure comparable to that observed in surviving patients (Hacke et al., 1996).

Furthermore, the reduction in ICP we observed with repeated NK1-r boluses was comparable to surgical decompression, which is encouraging given the limitations of current available pharmacotherapies used for ICP management, often necessitating early DC. Indeed, DC performed before clinical signs of herniation is shown to improve functional outcomes however surgery performed after onset of clinical deterioration may be too late to yield beneficial outcomes (Shah et al., 2019). Furthermore, although DC is the most powerful tool currently available to combat elevated ICP, the procedure is highly invasive, benefits remain controversial and the long-term implications of the procedure on ICP dynamics are not well understood (Funchal et al., 2018; Lilja-Cyron et al., 2019; Shah et al., 2019). A pooled analysis of the randomized control trials DECIMAL, HAMLET, and DESTINY, compared early DC with best available conventional medical management in patients with evidence of MCA territory hypersensitivity and a National Institute of Health Stroke Scale (NIHSS) > 15/20 (Jüttler et al., 2007; Vahedi et al., 2007a,b; Hofmeijer et al., 2009; Geurts et al., 2013). These studies found that that DC significantly reduced fatality rates and improved functional outcome compared with conventional pharmacotherapy alone. However, whilst some studies report reduced mortality and improved survival, it is at the cost of a higher number of individuals that are moderately severely disabled following the procedure (Vahedi et al., 2007a; Kurland et al., 2015). This becomes an issue of increasing concern given that DC is associated with higher mortality rates in those aged greater than 60 years of age, the most prevalent stroke patient population (Hofmeijer et al., 2009; Benjamin et al., 2018). The correlation between age and functional outcome remains an extremely important pre-treatment prognostic factor in deciding if patients should undergo DC (Chen et al., 2007), further highlighting the need for development of new therapies that can be administered to a wider patient population in a safe and timely manner, eliminating the need for surgical decompression and risk of associated morbidity. In this study we have demonstrated that repeated dosing of NK1-r antagonist treatment was able

to reduce ICP comparable to DC surgery, thus providing an alternate treatment strategy, circumventing the need for invasive surgery.

Limitations

Although we have established that the NK1-r antagonist is an effective strategy to lower ICP and we have previously determined that the ovine model is viable candidate for the screening of promising novel therapeutics, we must acknowledge the limitations of the study.

Due to the invasive nature of the surgery and significant deficits that ensued following permanent MCAO, animals were required to be maintained under anesthesia for the duration of the experiment. We recognize that human patients are rarely under the influence of anesthesia on stroke onset, and that the use of anesthetic agents may affect outcome measures. Despite this, the agents used for induction and maintenance were chosen to reduce any potential neuroprotective or damaging effects, as previously described in detail (Wells et al., 2015). Indeed, as ketamine is known for its neuroprotective properties, and inhalation isoflurane for its sub-neuroprotection and association with reduced blood pressure, the combination was used to bring about a countering effect. The synergistic use of these agents permitted adequate anesthesia with controlled MABP whilst preventing inadvertent neuroprotection as a confounding factor, an important consideration when modeling acute ischemic stroke. It must be acknowledged, however, that we did observe significant differences in MABP across several of the groups. Nevertheless, these alterations in MABP did not follow the same pattern as the alterations in ICP so it is therefore unlikely that they significantly contributed to the observed treatment effects. The differences in MABP observed between groups most likely reflects both the within group and between group heterogeneity in the amount of isoflurane required to maintain twilight anesthesia during surgery whilst balancing with ketamine to maintain adequate blood pressure.

Furthermore, only female animals were used in the present study due to the inherent need for catheterization of animals during long-duration anesthesia. Females were selected preferentially over males upon veterinary advice given the difficulty in catheterizing the highly convoluted male urethra.

Though we were able to establish a significant increase in ICP following ovine stroke, MRI findings were not strongly correlated with ICP. Although the relationship between ICP and cerebral edema well established and promising in this study, we acknowledge that the small sample sizes in this study may have led to a low statistical power. Furthermore, it must be noted that this is frequently seen in clinical stroke cases, where MRI and computed tomography (CT) findings are not always a good predictor of ICP. Due to facility access, MRI was not possible in the entire cohort, leading to uneven group sizes. Despite a larger cohort available for ICP in both treatment and vehicle groups, only animals with matching ICP/MRI data were included, leading to variations in group sizes. Furthermore, the reliable measurement of cerebral edema on MRI at a single time-point is somewhat contentious, as the hyperintensity of vasogenic edema is difficult to distinguish from the lesion itself. The measurement of the entire FLAIR lesion volume therefore includes areas of infarction as well as edema, and is thus an indirect measure of edema volume. A more robust approach to measuring edema evolution would be to perform sequential MRI's and evaluate the change in diffusion lesion volume between 2 times points following reperfusion, which was not possible in this study due to cost. It should also be acknowledged that whilst MRI findings did not correlate with ICP, we were able to observe MRI features similar to that seen clinically, including transcalvarial herniation in DC treated animals and reduced midline shift. Finally, testing of multiple NK1-r antagonists was not feasible in this study given the time and cost involved in conducting sheep experiments. However, in our rodent studies of TBI we have previously tested 2 different NK1-r antagonists and recorded comparable results (Donkin, 2006) which provided the basis for the use of the agent in the present study.

For future studies we will work alongside the animal ethics committee of the South Australian Health and Medical Research Institute (SAHMRI) to develop a survival model of transient MCAO which obviates the need for long duration anesthesia, allowing for the study of conscious animals following induction of stroke and assessment of long-term functional changes.

CONCLUSION

Multiple boluses of an NK1-r antagonist is effective in lowering ICP following ovine stroke, producing a reduction in ICP that is comparable to decompressive surgery. We propose that the mechanism by which the NK1-r antagonist is exerting its effect is largely via caveolae mediated albumin transcytosis. Administration of the NK1-r is thus preventing abnormal albumin extravasation from the vasculature to the brain parenchyma and ameliorating the subsequent development of vasogenic edema and rise in ICP. These findings suggest that NK1-r antagonist treatment may represent a novel intervention for the management of elevated ICP following stroke.

DATA AVAILABILITY

All datasets generated for this study are included in the manuscript and/or the supplementary files.

ETHICS STATEMENT

All experimental procedures were approved by the Animal Ethics Committees of the University of Adelaide (M-2011-240) and the South Australian Health and Medical Research Institute (SAHMRI; SAM104/11) and conducted according to guidelines established for the use of animals in experimental research as outlined by the Australian National Health and Medical Research Council code of practice for the care and use of animals for scientific purposes (8th edition, 2013).

AUTHOR CONTRIBUTIONS

AW, RV, RT, and AL conceived and designed the experiments. AW, RT, and AL carried out the experiments. AS-A, NY, JH, and RT analyzed the data. AS-A, RT, and AL wrote the manuscript.

FUNDING

This work was supported by the National Health and Medical Research Council (NHMRC; Project grant GNT1082556) and by the Neurosurgical Research Foundation (Adelaide, SA, Australia). RT was supported by the NHMRC Post-Doctoral Training Fellowship. AW was supported by the NHMRC Post-Graduate Fellowship.

ACKNOWLEDGMENTS

We would like to thank Sunthara Rajan Perumal for the acquisition of the MRI and Shenyi Peng, Tony Nguyen, and Martina Kontos for their contribution to the MRI analysis. We would also like to acknowledge the facilities and scientific and technical assistance of the National Imaging Facility, a National Collaborative Research Infrastructure Strategy (NCRIS) capability, at LARIF and SAHMRI.

REFERENCES

Abbott, N. J., Ronnback, L., and Hansson, E. (2006). Astrocyte-endothelial interactions at the blood-brain barrier. *Nat. Rev. Neurosci.* 7, 41–53. doi: 10.1038/nrn1824

Alves, R. V., Campos, M. M., Santos, A. R., and Calixto, J. B. (1999). Receptor subtypes involved in tachykinin-mediated edema formation. *Peptides* 20, 921–927. doi: 10.1016/s0196-9781(99)00082-0

Astrup, J., Siesjo, B. K., and Symon, L. (1981). Thresholds in cerebral ischemia - the ischemic penumbra. *Stroke* 12, 723–725. doi: 10.1161/01.str.12.6.723

Bardutzky, J., and Schwab, S. (2007). Antiedema therapy in ischemic stroke. *Stroke* 38, 3084–3094. doi: 10.1161/strokeaha.107.490193

Benjamin, E. J., Virani, S. S., Callaway, C. W., Chamberlain, A. M., Chang, A. R., and Cheng, S. (2018). Heart disease and stroke statistics-2018 update: a report From the American heart association. *Circulation* 137, e67-e492.

Brogan, M., and Manno, E. (2015). Treatment of malignant brain edema and increased intracranial pressure after stroke. *Cur. Treat. Options Neurol.* 17, 1–11.

Chen, C.-C., Cho, D.-Y., and Tsai, S.-C. (2007). Outcome of and prognostic factors for decompressive hemicraniectomy in malignant middle cerebral artery infarction. *J. Clin. Neurosci.* 14, 317–321. doi: 10.1016/j.jocn.2005.05.024

Corrigan, F., Leonard, A., Ghabriel, M., Van Den Heuvel, C., and Vink, R. (2012). A substance P antagonist improves outcome in female sprague dawley rats following diffuse traumatic brain injury. *CNS Neurosci. Ther.* 18, 513–515. doi: 10.1111/j.1755-5949.2012.00332.x

Corrigan, F., Mander, K. A., Leonard, A. V., and Vink, R. (2016a). Neurogenic inflammation after traumatic brain injury and its potentiation of classical inflammation. *J. Neuroinflammation* 13:264.

Corrigan, F., Vink, R., and Turner, R. J. (2016b). Inflammation in acute CNS injury: a focus on the role of substance P. *Br. J. Pharmacol.* 173, 703–715. doi: 10.1111/bph.13155

Das, S., Mitchell, P., Ross, N., and Whitfield, P. C. (2019). Decompressive hemicraniectomy in the treatment of malignant middle cerebral artery infarction: a meta-analysis. *World Neurosurgery* 123, 8–16. doi: 10.1016/j.wneu.2018.11.176

Donkin, J. D. (2006). *The effects of the neuropeptide substance P on outcome following experimental traumatic brain injury in rats*. Adelaide: University of Adelaide.

Donkin, J. J., Nimmo, A. J., Cernak, I., Blumbergs, P. C., and Vink, R. (2009). Substance P is associated with the development of brain edema and functional deficits after traumatic brain injury. *J. Cereb. Blood Flow Metab.* 29, 1388–1398. doi: 10.1038/jcbfm.2009.63

Donkin, J. J., Turner, R. J., Hassan, I., and Vink, R. (2007). Substance P in traumatic brain injury. *Prog. Brain Res.* 161, 97–109.

Dostovic, Z., Dostovic, E., Smajlovic, D., Ibrahimagic, O. C., and Avdic, L. (2016). Brain edema after ischaemic stroke. *Med. Arch.* 70, 339–341.

Funchal, B. F., Alves, M. M., Suriano, I. C., Chaddad-Neto, F. E., Ferraz, M., and Silva, G. S. (2018). Intracranial pressure following decompressive hemicraniectomy for malignant cerebral infarction: clinical and treatment correlations. *Arq Neuropsiquiatr.* 76, 812–815. doi: 10.1590/0004-282X20180132

Geurts, M., Van Der Worp, H. B., Kappelle, L. J., Amelink, G. J., Algra, A., and Hofmeijer, J. (2013). Surgical decompression for space-occupying cerebral infarction: outcomes at 3 years in the randomized HAMLET trial. *Stroke* 44, 2506–2508. doi: 10.1161/STROKEAHA.113.002014

Hacke, W., Schwab, S., Horn, M., Spranger, M., De Georgia, M., and Von Kummer, R. (1996). 'Malignant' middle cerebral artery territory infarction: clinical course and prognostic signs. *Arch. Neurol.* 53, 309–315.

Hofmeijer, J., Kappelle, L. J., Algra, A., Amelink, G. J., Van Gijn, J., and Van Der Worp, H. B. (2009). Surgical decompression for space-occupying cerebral infarction (the hemicraniectomy after middle cerebral artery infarction with life-threatening edema trial [HAMLET]): a multicentre, open, randomised trial. *Lancet. Neurol.* 8, 326–333. doi: 10.1016/S1474-4422(09)70047-X

Hofmeijer, J., and Van Putten, M. J. (2012). Ischemic cerebral damage: an appraisal of synaptic failure. *Stroke* 43, 607–615. doi: 10.1161/STROKEAHA.111.632943

Hokfelt, T., Broberger, C., Xu, Z. Q., Sergeyev, V., Ubink, R., and Diez, M. (2000). Neuropeptides–an overview. *Neuropharmacology* 39, 1337–1356. doi: 10.1016/s0028-3908(00)00010-1

Hokfelt, T., Kellerth, J. O., Nilsson, G., and Pernow, B. (1975). Substance P: localisation in the central nervous system and in some primary sensory neurones. *Science* 190, 889–890. doi: 10.1126/science.242075

Hudetz, J. A., and Pagel, P. S. (2010). Neuroprotection by ketamine: a review of the experimental and clinical evidence. *J. Cardiothorac. Vasc. Anesth.* 24, 131–142. doi: 10.1053/j.jvca.2009.05.008

Jüttler, E., Schwab, S., Schmiedek, P., Unterberg, A., Hennerici, M., Woitzik, J., et al. (2007). Decompressive surgery for the treatment of malignant infarction of the middle cerebral artery (DESTINY): a randomized, controlled trial. *Stroke* 38, 2518–2525. doi: 10.1161/strokeaha.107.485649

Kubale, V., Abramovic, Z., Pogacnik, A., Heding, A., Sentjurc, M., and Vrecl, M. (2007). Evidence for a role of caveolin-1 in neurokinin-1 receptor plasma-membrane localization, efficient signaling, and interaction with beta-arrestin 2. *Cell Tissue Res.* 330, 231–245. doi: 10.1007/s00441-007-0462-y

Kurland, D. B., Khaladj-Ghom, A., Stokum, J. A., Carusillo, B., Karimy, J. K., Gerzanich, V., et al. (2015). Complications associated with decompressive craniectomy: a systematic review. *Neurocrit. care* 23, 292–304. doi: 10.1007/s12028-015-0144-7

Lewis, K. M., Turner, R. J., and Vink, R. (2013). Blocking neurogenic inflammation for the treatment of acute disorders of the central nervous system. *Int. J. Inflam.* 2013:578480.

Lilja-Cyron, A., Andresen, M., Kelsen, J., Andreasen, T. H., Fugleholm, K., and Juhler, M. (2019). Long-term effect of decompressive craniectomy on intracranial pressure and possible implications for intracranial fluid movements. *Neurosurgery* doi: 10.1093/neuros/nyz049 [Epub ahead of print].

Lorente, L., Martín, M. M., Almeida, T., Hernández, M., Ramos, L., Argueso, M., et al. (2015). Serum substance p levels are associated with severity and mortality in patients with severe traumatic brain injury. *Crit. Care* 19:192. doi: 10.1186/s13054-015-0911-z

Lorente, L., Martín, M. M., Almeida, T., Pérez-Cejas, A., Ramos, L., Argueso, M., et al. (2016). Serum Levels of Substance P and Mortality in Patients with a Severe Acute Ischemic Stroke. *Int.J. Mol. Sci.* 17:991. doi: 10.3390/ijms17060991

Matthews, J. N., Altman, D. G., Campbell, M. J., and Royston, P. (1990). Analysis of serial measurements in medical research. *BMJ* 300, 230–235. doi: 10.1136/bmj.300.6719.230

Monastyrskaya, K., Hostettler, A., Buergi, S., and Draeger, A. (2005). The NK1 receptor localizes to the plasma membrane microdomains, and its activation is dependent on lipid raft integrity. *J. Biol. Chem.* 280, 7135–7146. doi: 10.1074/jbc.m405806200

Nag, S., Venugopalan, R., and Stewart, D. J. (2007). Increased caveolin-1 expression precedes decreased expression of occludin and claudin-5 during blood-brain barrier breakdown. *Acta Neuropathol.* 114, 459–469. doi: 10.1007/s00401-007-0274-x

Nimmo, A. J., Cernak, I., Heath, D. L., Hu, X., Bennett, C. J., and Vink, R. (2004). Neurogenic inflammation is associated with development of edema and functional deficits following traumatic brain injury in rats. *Neuropeptides* 38, 40–47. doi: 10.1016/j.npep.2003.12.003

Povlishock, J. T., Becker, D. P., Sullivan, H. G., and Miller, J. D. (1978). Vascular permeability alterations to horseradish peroxidase in experimental brain injury. *Brain Res.* 153, 223–239. doi: 10.1016/0006-8993(78)90404-3

Schifilliti, D., Grasso, G., Conti, A., and Fodale, V. (2010). Anaesthetic-related neuroprotection intravenous or inhalational agents? *CNS Drugs* 24, 893–907. doi: 10.2165/11584760-000000000-00000

Shah, A., Almenawer, S., and Hawryluk, G. (2019). Timing of decompressive craniectomy for ischemic stroke and traumatic brain injury: a review. *Front. Neurol.* 10:11. doi: 10.3389/fneur.2019.00011

Simard, J. M., Kent, T. A., Chen, M., Tarasov, K. V., and Gerzanich, V. (2007). Brain oedema in focal ischaemia: molecular pathophysiology and theoretical implications. *Lancet. Neurol.* 6, 258–268. doi: 10.1016/s1474-4422(07)70055-8

Sorby-Adams, A. J., Marcoionni, A. M., Dempsey, E. R., Woenig, J. A., and Turner, R. J. (2017). The role of neurogenic inflammation in blood-brain barrier disruption and development of cerebral oedema following acute central nervous system (cns) injury. *Int. J. Mol. Sci.* 18:E1788.

Sorby-Adams, A. J., Vink, R., and Turner, R. J. (2018). Large animal models of stroke and traumatic brain injury as translational tools. *Am. J. physiol. Regul. Integr. comp. physiol.* 315, R165–R190. doi: 10.1152/ajpregu.00163.2017

Stumm, R., Culmsee, C., Schafer, M. K., Krieglstein, J., and Weihe, E. (2001). Adaptive plasticity in tachykinin and tachykinin receptor expression after focal cerebral ischemia is differentially linked to gabaergic and glutamatergic cerebrocortical circuits and cerebrovenular endothelium. *J. Neurosci.* 21, 798–811. doi: 10.1523/jneurosci.21-03-00798.2001

Turner, R. E. J. (2007). *Characterising the role of substance P in acute ischaemic stroke*. Thesis. University of Adelaide. Adelaide.

Turner, R. J., Blumbergs, P. C., Sims, N. R., Helps, S. C., Rodgers, K. M., and Vink, R. (2006). Increased substance P immunoreactivity and edema formation following reversible ischemic stroke. *Acta Neurochir Suppl.* 96, 263–266. doi: 10.1007/3-211-30714-1_56

Turner, R. J., Helps, S. C., Thornton, E., and Vink, R. (2011). A substance P antagonist improves outcome when administered 4 h after onset of ischemic stroke. *Brain Res.* 1393, 84–90. doi: 10.1016/j.brainres.2011.03.066

Turner, R. J., and Vink, R. (2012). Combined tissue plasminogen activator and an NK1 tachykinin receptor antagonist: an effective treatment for reperfusion injury following acute ischemic stroke in rats. *Neuroscience* 220, 1–10. doi: 10.1016/j.neuroscience.2012.06.047

Turner, R. J., and Vink, R. (2014). NK1 tachykinin receptor treatment is superior to capsaicin pre-treatment in improving functional outcome following acute ischemic stroke. *Neuropeptides* 48, 267–272. doi: 10.1016/j.npep.2014.07.002

Vahedi, K., Hofmeijer, J., Juettler, E., Vicaut, E., George, B., Algra, A., et al. (2007a). Early decompressive surgery in malignant infarction of the middle cerebral artery: a pooled analysis of three randomised controlled trials. *Lancet. Neurol.* 6, 215–222. doi: 10.1016/s1474-4422(07)70036-4

Vahedi, K., Vicaut, E., Mateo, J., Kurtz, A., Orabi, M., Guichard, J.-P., et al. (2007b). Sequential-design, multicenter, randomized, controlled trial of early decompressive craniectomy in malignant middle cerebral artery infarction (DECIMAL Trial). *Stroke* 38, 2506–2517. doi: 10.1161/strokeaha.107.485235

Vink, R., Gabrielian, L., and Thornton, E. (2017). The Role of Substance P in Secondary Pathophysiology after Traumatic Brain Injury. *Front. Neurol.* 8:304. doi: 10.3389/fneur.2017.00304

Vink, R., Young, A., Bennett, C. J., Hu, X., Connor, C. O., Cernak, I., et al. (2003). Neuropeptide release influences brain edema formation after diffuse traumatic brain injury. *Acta Neurochir. Suppl.* 86, 257–260. doi: 10.1007/978-3-7091-0651-8_55

Wells, A. J., Vink, R., Blumbergs, P. C., Brophy, B. P., Helps, S. C., Knox, S. J., et al. (2012). A surgical model of permanent and transient middle cerebral artery stroke in the sheep. *PLoS One* 7:e42157. doi: 10.1371/journal.pone.0042157

Wells, A. J., Vink, R., Helps, S., Knox, S. J., Blumbergs, P. C., and Turner, R. J. (2015). Elevated intracranial pressure and cerebral edema following permanent mca occlusion in an ovine model. *PLoS One* 10:e0130512. doi: 10.1371/journal.pone.0130512

Xiao-feng, Y., Yu, Y., Wei-Wei, H., Gu, L., Jin-Fang, X., Xue-Qun, Z., et al. (2005). Is decompressive craniectomy for malignant middle cerebral artery infarction of any worth? *J. Zhejiang Univ. Sci. B* 6, 644–649. doi: 10.1631/jzus.2005.b0644

Xu, S. Y., and Pan, S. Y. (2013). The failure of animal models of neuroprotection in acute ischemic stroke to translate to clinical efficacy. *Med. sci. Monit. Basic Res.* 19, 37–45.

Yushkevich, P. A., Piven, J., Hazlett, H. C., Smith, R. G., Ho, S., Gee, J. C., et al. (2006). User-guided 3D active contour segmentation of anatomical structures: significantly improved efficiency and reliability. *Neuroimage* 31, 1116–1128. doi: 10.1016/j.neuroimage.2006.01.015

Zhang, W., Neal, J., Lin, L., Dai, F., Hersey, D. P., Mcdonagh, D. L., et al. (2018). Mannitol in critical care and surgery over 50+ years: a systematic review of randomized controlled trials and complications with meta-analysis. *J. Neurosurg. Anesthesiol.* 31, 273–284. doi: 10.1097/ANA.0000000000000520

Conflict of Interest Statement: The authors declare that the research was conducted in the absence of any commercial or financial relationships that could be construed as a potential conflict of interest.

Copyright © 2019 Sorby-Adams, Leonard, Hoving, Yassi, Vink, Wells and Turner. This is an open-access article distributed under the terms of the Creative Commons Attribution License (CC BY). The use, distribution or reproduction in other forums is permitted, provided the original author(s) and the copyright owner(s) are credited and that the original publication in this journal is cited, in accordance with accepted academic practice. No use, distribution or reproduction is permitted which does not comply with these terms.

frontiers in Neuroscience

ORIGINAL RESEARCH
published: 09 July 2019
doi: 10.3389/fnins.2019.00587

Determining the Temporal Profile of Intracranial Pressure Changes Following Transient Stroke in an Ovine Model

Annabel J. Sorby-Adams[1], Anna V. Leonard[1], Levi E. Elms[1], Oana C. Marian[1], Jan W. Hoving[2,3], Nawaf Yassi[2,4], Robert Vink[5], Emma Thornton[1] and Renée J. Turner[1]*

[1] Adelaide Medical School, Adelaide Centre for Neuroscience Research, The University of Adelaide, Adelaide, SA, Australia, [2] Department of Medicine and Neurology, Melbourne Brain Centre at the Royal Melbourne Hospital, University of Melbourne, Melbourne, VIC, Australia, [3] Department of Radiology, Amsterdam UMC, University of Amsterdam, Amsterdam, Netherlands, [4] Florey Institute of Neuroscience and Mental Health, Melbourne, VIC, Australia, [5] Division of Health Sciences, University of South Australia, Adelaide, SA, Australia

OPEN ACCESS

Edited by:
Johannes Boltze, University of Warwick, United Kingdom

Reviewed by:
Lucy Anne Murtha, The University of Newcastle, Australia
Bruno Meloni, The University of Western Australia, Australia
Donald Stein, Emory University, United States

***Correspondence:**
Annabel J. Sorby-Adams annabel.sorby-adams@adelaide.edu.au

Specialty section:
This article was submitted to Neurodegeneration, a section of the journal Frontiers in Neuroscience

Received: *31 March 2019*
Accepted: *23 May 2019*
Published: *09 July 2019*

Citation:
Sorby-Adams AJ, Leonard AV, Elms LE, Marian OC, Hoving JW, Yassi N, Vink R, Thornton E and Turner RJ (2019) Determining the Temporal Profile of Intracranial Pressure Changes Following Transient Stroke in an Ovine Model. Front. Neurosci. 13:587. doi: 10.3389/fnins.2019.00587

Background and Purpose: Cerebral edema and elevated intracranial pressure (ICP) are the leading cause of death in the first week following stroke. Despite this, current treatments are limited and fail to address the underlying mechanisms of swelling, highlighting the need for targeted treatments. When screening promising novel agents, it is essential to use clinically relevant large animal models to increase the likelihood of successful clinical translation. As such, we sought to develop a survival model of transient middle cerebral artery occlusion (tMCAO) in the sheep and subsequently characterize the temporal profile of cerebral edema and elevated ICP following stroke in this novel, clinically relevant model.

Methods: Merino-sheep (27M;31F) were anesthetized and subject to 2 h tMCAO with reperfusion or sham surgery. Following surgery, animals were allowed to recover and returned to their home pens. At preselected times points ranging from 1 to 7 days post-stroke, animals were re-anesthetized, ICP measured for 4 h, followed by imaging with MRI to determine cerebral edema, midline shift and infarct volume (FLAIR, T2 and DWI). Animals were subsequently euthanized and their brain removed for immunohistochemical analysis. Serum and cerebrospinal fluid samples were also collected and analyzed for substance P (SP) using ELISA.

Results: Intracranial pressure and MRI scans were normal in sham animals. Following stroke, ICP rose gradually over time and by 5 days was significantly ($p < 0.0001$) elevated above sham levels. Profound cerebral edema was observed as early as 2 days post-stroke and continued to evolve out to 6 days, resulting in significant midline shift which was most prominent at 5 days post-stroke ($p < 0.01$), in keeping with increasing ICP. Serum SP levels were significantly elevated ($p < 0.01$) by 7 days post-tMCAO.

Conclusion: We have successfully developed a survival model of ovine tMCAO and characterized the temporal profile of ICP. Peak ICP elevation, cerebral edema and

midline shift occurred at days 5–6 following stroke, accompanied by an elevation in serum SP. Our findings suggest that novel therapeutic agents screened in this model targeting cerebral edema and elevated ICP would most likely be effective when administered prior to 5 days, or as early as possible following stroke onset.

Keywords: intracranial pressure, cerebral edema, stroke, large animal model, blood-brain barrier

INTRODUCTION

Worldwide, over 15 million people suffer a stroke each year, of which one third will die and one third will remain permanently disabled as a result (Feigin et al., 2017). Cerebral ischemia initiates a cascade of interrelated events precipitating brain tissue injury and cell death (Ayata and Ropper, 2002). Of these secondary injury processes, increased microvascular permeability and loss of structural integrity of the blood-brain barrier (BBB) are key to the development of cerebral edema, a pathological state in which fluid abnormally accumulates in the extracellular space of the cerebral parenchyma, resulting in an overall increase in brain volume. This leads to a subsequent rise in intracranial pressure (ICP), which has devastating consequences including infarct expansion, displacement of brain tissue, tonsillar herniation, and death (Steiner et al., 2001; Raslan and Bhardwaj, 2007; Battey et al., 2014; Kim et al., 2015).

Stroke patients often exhibit a progressive and slow evolution of brain injury, with cerebral edema and elevated ICP presenting some days following initial insult to tissue, most commonly around 3–5 days following onset (Hewitt and Ellory, 2012). Despite the devastating impact of cerebral edema and elevated ICP, however, existing treatments fail to address the underlying pathophysiology, thereby limiting their efficacy (Battey et al., 2014). Novel therapies that target the underlying cause of swelling and prevent the evolution of cerebral edema and elevated ICP are urgently required to improve post-stroke outcomes. To this end, our laboratory has identified that the tachykinin neuropeptide substance P (SP) is a key mediator in BBB dysfunction and development of cerebral edema following stroke (Turner et al., 2006, 2011; Turner and Vink, 2012) and traumatic brain injury (TBI) (Vink et al., 2003; Nimmo et al., 2004; Donkin et al., 2009; Corrigan et al., 2012). Specifically, SP release leads to neurogenic inflammation, manifesting following acute central nervous system (CNS) injury as increased BBB permeability and the development of cerebral edema. Furthermore, we have established that blockade of the receptor for SP, the tachykinin NK1 receptor (NK1-r), reduces both BBB permeability and cerebral edema in rodent models of stroke (Turner et al., 2011; Turner and Vink, 2012, 2014) and TBI (Donkin et al., 2009; Corrigan et al., 2012, 2016), suggesting that this is a common feature of acute brain injury.

An enhanced understanding of the underlying pathophysiology of cerebral edema and elevated ICP following stroke is essential in guiding the development of more effective therapies, and pre-clinical stroke studies are an essential step in this process. However, the poor clinical translation of stroke therapies from the laboratory to the clinic to date has emphasized the importance of appropriate species and model selection (Casals et al., 2011). The use of large intermediate species for these studies is paramount in the pre-clinical phase to improve translation to the clinic due to similarities in neuroanatomical structure, such as a large gyrencephalic brain that is closer in similarity to that of the human compared with many widely adopted small animal models. In light of this, a number of large animal species are used as pre-clinical stroke models, including sheep (Boltze et al., 2008; Wells et al., 2012, 2015), dogs (Qureshi et al., 2004; Cameron et al., 2008; Boulos et al., 2011; Christoforidis et al., 2011), pigs (Sakoh et al., 2000; Watanabe et al., 2007; Platt et al., 2014), and non-human primates (Nehls et al., 1986; Tagaya et al., 1997; Yuji et al., 2001; D'Ambrosio et al., 2004; Furuichi et al., 2007), each with their own inherent advantages and disadvantages (Sorby-Adams et al., 2018). Although gyrencephalic non-human primates are of great value in modeling the human condition, the cost, housing requirements and ethical considerations may preclude their use in large scale studies. Pigs are a widely used experimental species in models of cardiovascular (Suzuki et al., 2011; Kamoi et al., 2014) and TBI studies worldwide (Lighthall, 1988; Pfenninger et al., 1989; Ross et al., 1994; Duhaime et al., 2000; Manley et al., 2006), however, the Yucatan mini-pig is not available in Australia, and the rapidly increasing bodyweight of other strains can make long-term studies difficult. Sheep are an accessible experimental species and have been used extensively to model a number of neurological conditions, including non-accidental head injury (Sandoz et al., 2012; Anderson et al., 2014), TBI (Vink et al., 2008; Vink et al., 2017), and Huntington's Disease (Reid et al., 2013; Morton et al., 2014). Although sheep have earned a reputation as unintelligent animals, the evidence is quite to the contrary, as sheep demonstrate excellent facial recognition, executive decision making and emotional processing, often comparable to humans on equivalent tasks (Tate et al., 2006; Keith et al., 2007; Morton and Avanzo, 2011). Specifically, the high proportion of white to gray matter in the sheep brain is of particular benefit when studying the pathophysiology of edema and ICP, given that edematous fluid accumulates in the white matter following ischaemic stroke (Jha, 2003; Mahajan and Bhagat, 2016). The strong fibrous tentorium cerebelli of the sheep, comparable with that of the human, also prevents the brain from moving downward to accommodate increased volume of the edematous brain, resulting in persistent elevations in ICP, midline shift and tonsillar herniation all of which are seen clinically. Additional advantages of large animal models, is the ability to take multiple serum and cerebrospinal fluid (CSF) samples from an individual animal over time which is not possible in rodents, as well as using clinical physiological monitoring equipment and magnetic resonance imaging (MRI). As such, large animal stroke models, including the sheep, are

an excellent additional screening tool following evaluation in rodents prior to progression to clinical trials.

There are two models of ovine middle cerebral artery occlusion (MCAO) currently in use (Boltze et al., 2008; Wells et al., 2012) both of which involve permanent occlusion of the MCA. In the Boltze model (Boltze et al., 2008) the craniotomy is left open so that animals are effectively given decompression at the time of stroke, allowing for the investigation of long-term time-points without premature mortality, although intracranial pressure dynamics cannot be investigated. Conversely, in the Wells model (Wells et al., 2012, 2015) the craniotomy is closed following MCAO so that the evolution of ICP can be accurately studied. However, survival time-points beyond 24 h are not possible in this model due to the resulting malignant MCA infarction and ethical requirement to maintain animals under anesthesia for the duration of the experiment. As such, there is a clear requirement for an ovine MCAO stroke model where the MCA is temporarily occluded to study the effects of reperfusion injury and longer time-points following stroke onset. Furthermore, there is an increasing incidence of patients who successfully recanalize following stroke onset. This is largely due to the increased use of endovascular clot retrieval for reperfusion of large strokes, such as occlusion of the internal carotid artery (ICA) or M1 segment of the MCA (Goyal et al., 2016). The mechanical recanalization of the MCA able to be produced in a transient MCAO model closely aligns with the vascular reperfusion achieved with endovascular thrombectomy, and thus may be more representative of the human condition.

Accordingly, the aims of the present study were to: (1) develop a survival model of ovine MCAO stroke with reperfusion; (2) characterize the temporal profile of intracranial pressure changes following stroke; and (3) determine the contribution of SP to BBB permeability and cerebral edema that develops in this model. By determining the clinical course of ICP in this model, an optimal time window for administration of novel therapeutic agents targeting elevated ICP due to cerebral edema can be established.

MATERIALS AND METHODS

Experimental Design

A total of 58 (n = 27M;31F) merino sheep (weight range 65 ± 7 kg; age 18–36 months) were used in this study. Animals (3M and 3F/time point) were pre-operatively randomized to daily post-stroke survival time points ranging from 1–7 days. Animals allocated to the post-stroke time-points underwent two surgeries: tMCAO surgery with recovery, and ICP monitoring on the designated day post-stroke. An additional group of animals underwent the surgical procedure without MCAO and acted as sham controls (n = 4F). These animals had ICP continuously recorded for 4 h immediately following the sham surgical procedure. Finally, an additional follow up cohort of 12 animals (n = 6F;6M) underwent stroke surgery and were included to obtain serum and CSF samples over the 7-day post-stroke time-course. This was not possible in the main stroke cohort due to the risk that repeat CSF sampling might potentiate changes in intracranial dynamics leading to inaccurate measurements of ICP. All animals were group housed in conventional sheep paddocks for a minimum of 2 weeks prior to surgery to allow for acclimatization. Animals were then moved to individual indoor pens 48 h prior to surgery and fasted over night for a minimum of 12 h prior to the procedure.

Experimental Procedure

Animal Preparation and Anesthesia

Anesthesia was induced with a combination of intravenous ketamine (0.05 ml/kg, 100 mg/kg Injection, CEVA, Australia) and diazepam (0.08 ml/kg, 5 mg/ml Injection, Pamlin, CEVA, Australia). Following induction, animals were intubated via endotracheal tube insertion to ensure airway patency for ventilation. Animals were then positioned on the operating table on their left side, with hind limbs exposed for arterial access. An arterial catheter was inserted in the left hind leg for blood gas sampling and a cannula inserted into the external jugular vein for fluid and drug administration. Intraoperative anesthesia was maintained via a combination of inhalational isoflurane (Henry Shein, Australia; 1.5–2.0%) in 100% oxygen and intravenous (jugular) ketamine at an infusion rate of 4 mg/kg/h. Crystalloid fluids were administered throughout surgery via continuous intravenous infusion with compound sodium lactate (Baxter Health, Australia) to assist hydration and ionic balance. In addition, intraarterial sodium chloride (Baxter Health, Australia) was infused at a rate sufficient to ensure arterial catheter patency. Following surgery, animals were recovered and treated with subcutaneous antibiotic Rilexine (1 ml/10 kg every 12 h, 15 g/100 ml Cephalexin, VIBRAC, Australia), NSAID Carprieve (0.7 mg/kg, 50 mg/ml every 12 h, Carprofen, Norbrook, Australia) and opioid Temgesic (1.0 ml, 324 ug/ml Buprenorphine hydrochloride, one dose post-operatively, Reckin Benckiser, Australia) for pain relief. Antibiotic and NSAID treatment was continued for a minimum of 3 days following surgery, with additional opioid and/or NSAID administered as required thereafter for pain management.

Surgical Approach

A model of ovine stroke was modified from previously published works (Wells et al., 2012, 2015) in order to achieve tMCAO with reperfusion (**Figure 1**). This modification enabled the recovery of animals from surgery and the study of longer time-points (beyond 24 h) following stroke. In this particular approach, it was necessary to keep the coronoid process of the mandible intact and preserve the surrounding temporalis muscle to ensure animals were able to masticate following surgery. To achieve this, a 50 mm curved horizontal incision was made posterior to the orbital rim of the right eye and terminating anterior to the ear. Upon incision, the temporalis muscle was retracted and the coronoid process elevated to expose the underlying skull. Cervical retractors (Codman) were inserted and blades adjusted to provide space for a small craniotomy to be drilled at the junction of the parietal and squamous temporal bones with a high-speed pneumatic drill using a 5 mm cutting burr (Midas Rex, Medtronic, MN, United States). Following craniotomy, a horse shoe durotomy was performed, the brain exposed and the anterior temporal lobe gently retracted to expose the right

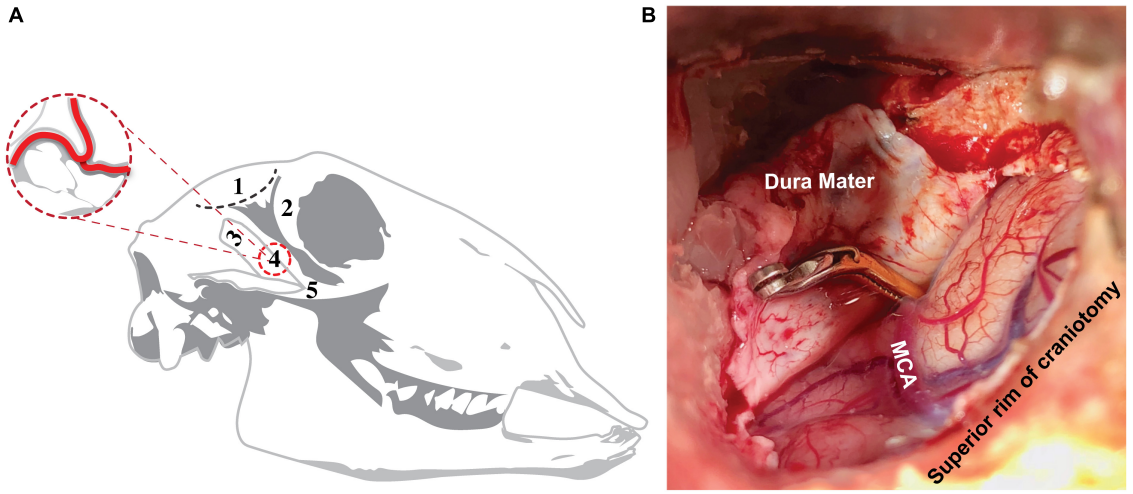

FIGURE 1 | Surgical approach to ovine transient MCAO. Surgical approach **(A)**, showing site of incision (1; black dashed line) posterior to the orbital rim (2) and superior to the coronoid process (3). This approach enabled the skull base to be accessed without disrupting the coronoid process or zygomatic arch (5), allowing for craniotomy (4) and direct access to the MCA, whilst ensuring post-operative recovery of the animal and the ability to masticate following the procedure. Superior view of craniotomy site **(B)** showing the aneurysm clip applied to the proximal MCA.

proximal MCA. A small amount of CSF was aspirated to ensure sufficient visualization of the proximal MCA, however, this was kept to a minimum to reduce the impact on intracranial volume. Gentle dissection of the MCA from the arachnoid mater was performed to allow for a temporary aneurysm clip (Aesculap) to be applied proximal to the MCA bifurcation using a clip applicator (YASARGIL Aneurysm clip system, Aesculap). Successful clipping of the MCA resulted in an immediate decrease in vessel caliber, confirming reduced blood flow. The dura was then gently re-opposed onto the brain and the craniotomy site filled with sterile saline to prevent dehydration of the underlying cortical tissue and the surgical site draped. The clip was left *in situ* for 2 h and subsequently removed with clip applicators to achieve reperfusion. Visual confirmation of reperfusion was noted when the caliber of the vessel increased and blood returned to the distal MCA. Successful reperfusion also was confirmed on magnetic resonance angiography (MRA) MRI performed at the pre-selected timepoints.

Following reperfusion, the dura was approximated and interleaved with synthetic dura (Durepair, Medtronic, Australia) to cover the exposed brain. Dural closure was then achieved with ethyl cyanoacrylate (Bostik, Australia), and the bone previously removed reinserted into the craniotomy site and reinforced with dental acrylic cement (Sledgehammer, Keystone, Germany) to create a watertight seal, thus restoring intracranial dynamics. The surgical site was then treated with 1.0 ml 0.5% local anesthetic Marcain (bupivacaine hydrochloride 5 mg/ml, AstraZeneca, Australia) and closed using a 0.1 Vicryl braided polyglactin Suture (ETHICON, Australia) using the horizontal mattress suture technique of wound closure to minimize risk of infection. The animal was removed from anesthesia, extubated and pain relief administered prior to transfer into a post-operative recovery pen. Mean arterial blood pressure (MABP) was monitored at 5-min intervals throughout surgery via application of a pediatric blood pressure cuff (Delfi Medical, Canada) on the upper left front limb. Blood gas samples (Machine AVL Scientific Corporation United States, Manufactured by Hersteller, OPTI Critical Care Analyzer–Model OPTI3, Serial No. OP3-2759) were acquired hourly via arterial catheter sampling to determine pO_2, pCO_2, hematocrit, hemoglobin, pH, Na^+ and K^+ levels. End tidal CO_2 was also recorded at regular intervals. Animals were maintained on a heating pad throughout all surgical procedures and rectal temperature checked hourly to ensure maintenance of body temperature within normal ovine limits (37.5–39.0°C).

ICP Measurement

At 4 h prior to the pre-determined post-stroke time-point, or immediately following surgery in shams, anesthetized (using aforesaid isoflurane and ketamine maintenance protocols) animals were placed prone in the sphinx position on the operating table. Bilateral burr holes were drilled into the left and right parietal bones, posterior to the coronal suture and approximately 20 mm from the sagittal suture. The dura was perforated and skull bolts secured, following which Codman microsensor ICP probes (Codman Neuro, DePuy Synthes, Australia) were inserted to an approximate depth of 15 mm into the brain parenchyma and ICP recorded continuously for a period of 4 h post-MCAO induction or sham surgery (LabChart Reader, ADInstruments, v. 8.1.1). Two-point calibration (0 and 100 mmHg) was performed prior to insertion of probes and at the end of the recording period to confirm measurement accuracy. ICP readings selected for final analysis (left or right) were based on calibration data, with readings preferentially selected from the right hemisphere probe. Raw ICP data underwent a logarithmic exponential transformation as previously described and was expressed as geometric mean ± SEM (Matthews et al., 1990; Wells et al., 2015).

MRI

Following the 4-h ICP monitoring period, animals were moved to a 1.5T Siemens Syngo2004A (Siemens AG, Munich, Germany) MRI scanner, during which they were maintained under general anesthesia (3% isoflurane). Sequences were acquired including time-of-flight MRA (TOF MRA; TR 26 ms, TE 3.69 ms, slice thickness 0.50 mm), diffusion weighted imaging (DWI; TR 5600 ms, TE 80 ms, slice thickness 3.0 mm), fluid attenuated inversion recovery (FLAIR; TR 5000 ms, TE 386 ms, slice thickness 0.9 mm), T1-weighted imaging (TR 2300 ms, TE 2.58ms, slice thickness 0.9 mm) and T2-weighted imaging (TR 3200 ms, TE 410 ms, slice thickness 0.9 mm). T1-weighted post-contrast images were also acquired following intravenous administration of 1 mL/kg gadolinium-diethylene-triamine-pentaacetic acid (GAD) (Magnevist, Bayer HealthCare, Germany) to determine the extent of BBB breakdown on MRI.

The degree of midline shift was used as a surrogate marker for the anatomical sequalae of cerebral edema. Shift from the midline was assessed using axial T2-weighted scans and measured in mm from the septum pellucidum at the level of the foramen of Monro (Horos DICOM image viewer v3.1.1). To calculate cerebral edema, coronal FLAIR images were analyzed using Horos DICOM image viewer (v3.1.1). After optimal adjustment of brightness and contrast, edema volume was determined from sequences using computer-aided manual tracing of the hyperintense lesion by a blinded assessor. The areas were then summed and multiplied by the slice thickness to give a total volume in cm^3.

To calculate infarct volume, segmentation tools in ITK-SNAP (v3.7) were used to perform semi-automated segmentation of the MRI diffusion lesions using diffusion-weighted images (Yushkevich et al., 2006). A combination of "three-dimensional active contour segmentation" and subsequent manual post-processing of the segmentation while adjusting image thresholds was performed to maximize reproducibility whilst excluding artifacts. The "three-dimensional active contour segmentation" consisted of multiple steps: First, in the pre-segmentation phase, independent component analysis automatically segmented parts of the DWI image and these were manually identified as foreground or background. To obtain an optimal distinction between foreground and background, thresholds of the image windows were adjusted. After thresholding, a "speed image" with a separate foreground and background was created. Next, in the active contour phase, seed regions were manually placed within the region of interest (ROI). These seeds were then automatically grown within the ROIs to form the temporary segmentation. Subsequently, areas that were not automatically included in the "active contour segmentation," were manually included in the follow-up infarct segmentation. The total volume of the segmentation was exported and reported in cm^3 for analysis.

Perfusion and Histological Examination

Following MRI, intravenous heparin (5000 I.U./5 ml; Pfizer, NY, United States) was administered and animals humanely euthanized via common carotid perfusion fixation with cold TRIS-buffered saline under isoflurane anesthesia. The brains were subsequently removed and sliced into 10 mm coronal slices using a custom-made sheep brain matrix. Sections were then immersion fixed in 10% neutral-buffered formalin for a minimum of 14 days prior to being processed, embedded in paraffin wax and sectioned coronally at 5-micron intervals to identify albumin, SP, and caveolin-1 via immunohistochemistry (**Table 1**).

Serum and CSF Collection

Blood samples were collected (BD-Vacutainer®-SST™-II-Advance-Tube) from animals (n = 12, 6M;6F) pre-injury and at 4, 8, 12, and 16 h post-stroke and on days 1, 3, 5, and 7 via jugular venipuncture. Following collection, samples were centrifuged (10 min at 2000g) and serum extracted into 10 × 500 µl aliquots and stored at −80°C. CSF was collected via lumbosacral tap prior to induction of stroke and on days 1, 3, and 6 thereafter. Note that this was performed in the follow up cohort, and these animals did not undergo ICP monitoring so there were no concerns regarding multiple CSF draws and the associated effects on ICP measurement accuracy. Prior to collection, animals were induced with combination diazepam and ketamine as previously described. The animals were then placed in the prone position on a surgical table and the sagittal plane of the animals vertebrae manipulated so that it was perpendicular with the horizontal plane of the bench. The animal was shaved to allow for clear access to the lumbosacral joint and appropriate visualization for landmarks. Palpation of the hips was performed to determine the correct sagittal plane orientation of the spine and the optimal site for CSF collection was determined via identification of the midline depression between the last lumbar and first sacral vertebrae. The area was cleaned using a 4% chlorhexidine preoperative surgical scrub brush (BD E-Z Scrub™), povidone-iodine applied and site surgically prepared. A steriseal spinal needle with stylet (Becton Dickinson Medical Technology) was inserted perpendicular to the skin and the needle advanced slowly through the subcutaneous tissue and interarcuate ligament until a sudden drop in resistance was felt indicating the advancement through the dural membrane and entry into the subarachnoid space. The stylet was then removed and 2 ml of CSF aspirated via a syringe and deposited into a 3 ml container; sample placed immediately on ice for 20 min, centrifuged (15 min at 3000g), extracted into 3 × 500 µl aliquots and stored at −80°C.

Analysis of Serum and CSF

Serum and CSF samples were used to quantify expression of SP using enzyme-linked immunosorbent assay (ELISA)

TABLE 1 | Immunohistochemistry protocols.

Antibody	Dilution	Retrieval	Brand	Catalog no.
Albumin	1:2000	No retrieval	Dako	A0001
SP	1:5000	Citrate	Abcam	ab14184
Caveolin-1	1:500	EDTA	Cell Signaling Technologies	3238

according to the manufacturer's instructions (Abcam; KIT-ab133029). All samples were diluted 1:4 in assay buffer for appropriate compliance with each individual plate standard curve. Standards, serum and CSF test samples were run and the plate immediately analyzed following addition of the stop solution using a spectrophotometric microplate reader (Synergy HTX, multi-mode reader). At optical density of 405 nm light absorbance was calculated to give an inverse reading of SP proportional to its captured measure on the plate.

Statistical Analysis

All data are expressed as mean ± SEM. Physiological data (MABP, pH, pO_2, and pCO_2) were analyzed using one-way analysis of variance (ANOVA) followed by Tukey's *post hoc* tests (Prism v.8.0.1, Graphpad, CA, United States). ICP, infarct volume, cerebral edema and midline shift data were analyzed by one-way ANOVA with multiple comparisons followed by Tukey's *post hoc* tests. ELISA evaluation was performed for each plate using individually generated standard curves and an R-value of 0.9709 was accepted to improve the efficacy of inter-plate accuracy. ELISA values were then analyzed via one-way ANOVA with Tukey's *post hoc*. Pearson's correlations were run between midline shift and cerebral edema, cerebral edema and ICP and midline shift and ICP to determine the relationship between variables. A two-way ANOVA with Sidak's multiple comparison test was run to determine gender differences in physiological variables during both surgery and ICP monitoring. Gender discrepancies were also established for infarct volume, cerebral oedema, midline shift and ICP in addition to CSF and serum SP via two-way ANOVA with Sidak's *post hoc*. A p-value < 0.05 and R-value > 0.04 was considered significant.

RESULTS

Surgery, Mortality, and Post-operative Course

There was no premature mortality of animals in the present study. One animal was excluded due to insufficient reperfusion following MCAO as seen on MRA, resulting in a permanent rather than a transient occlusion (**Figure 2**). In all other temporary occlusions of the MCA reperfusion was successfuly achieved and confirmed on MRA. A further four animals were excluded due to significant anesthetic difficulties which confounded the experimental course (n = 2 in 2 days group; n = 2 in 3 days group). Specifically, the excluded animals were unstable throughout the induction of stroke surgery, necessitating repeat boluses of ketamine and diazepam and an increased rate of isoflurane to maintain surgical levels of anesthesia, which resulted in significantly lowered MABP, decreased cerebral perfusion pressure and ultimately profound infarct expansion.

All animals were able to use their jaw and masticate to eat following surgery. A comprehensive behavioral analysis was beyond the scope of this study, however, all animals in the ICP cohort were observed for jaw alignment and eating behavior, the presence/absence of fetlock weakness and demeanor throughout the post-stroke period. A total of 9/42 animals demonstrated evidence of jaw misalignment following stroke surgery, which persisted to the end of the experiment in 3/9 animals. Although 25/42 animals showed reduced food intake post-stroke when compared to their pre-stroke daily intake, body weight remained within acceptable limits (< 15% reduction from pre-stroke weight). A total of 14/42 animals showed fetlock weakness following stroke, manifesting as knuckling of the distal forelimb which was most commonly observed on day 1 and typically resolved by day 4 post-stroke.

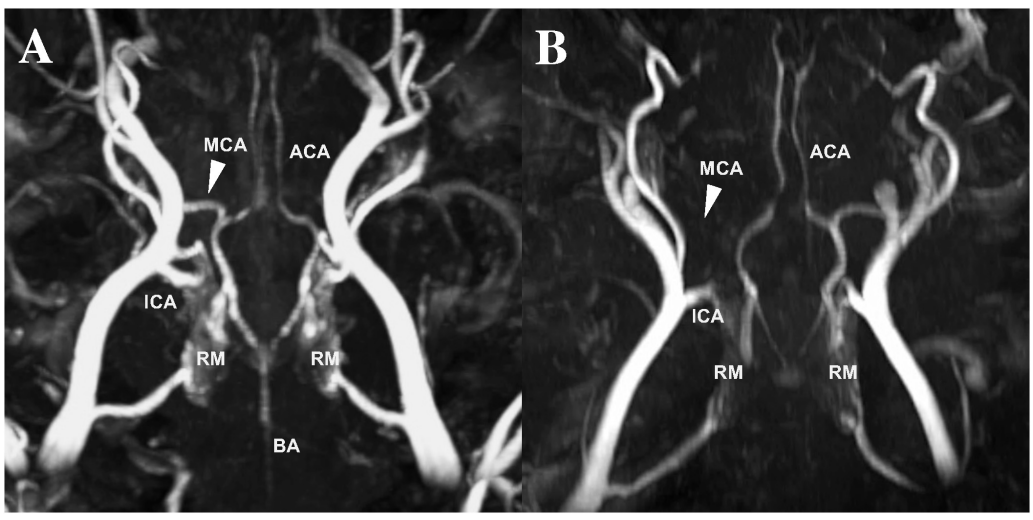

FIGURE 2 | MCA reperfusion following transient MCAO **(A)** compared to permanent MCAO **(B)** on time-of-flight MRA. Evidence of vessel patency, indicated by the white arrow, following clip removal in transient MCAO animals compared to permanent MCAO animals, where the vessel cannot be visualized MRA (data not reported). MCA, middle cerebral artery; ACA, anterior cerebral artery; ICA, internal carotid artery; BA, basilar artery; RM, rete mirabile.

A decline in demeanor, as demonstrated by a lowered head position and droopy ears, was observed in 26/42 animals and was most prevalent at days 5–7 post-stroke, coinciding with elevated ICP.

Physiological Parameters

Physiological variables for pCO_2, MABP, and pH were within normal limits for all groups throughout the duration of the experiment (**Table 2**). As animals were maintained on 100% oxygen (oxygen 6.0 L/min) through the course of surgery and ICP monitoring this resulted in pO_2 values that were significantly above the normal clinical range of 90–100 mmHg. These observations, however, were observed across all experimental groups. No significant difference ($p > 0.05$; **Table 1**) in pO_2, pCO_2, or pH were observed amongst groups during stroke surgery or the 4-h period of ICP monitoring. There was however a statistically significant decrease in MABP during the ICP monitoring period seen at 1-day post-stroke compared with 4 ($p = 0.04$) and 7 ($p = 0.01$) days.

Intracranial Pressure

Intracranial pressure remained within normal limits for the duration of the 4-h monitoring period in sham animals (8 ± 2 mmHg). From 1 to 4 days following tMCAO, ICP levels were comparable to sham ($p > 0.05$; **Figure 3**). However, by 5 days post-stroke, ICP was significantly elevated (28 ± 10 mmHg; $p < 0.0001$) from sham levels and post-stroke days 1–4 ($p < 0.0001$). ICP remained significantly elevated out to 6 days post-stroke when compared to shams (25 ± 5 mmHg; $p = 0.0001$) and 1 ($p = 0.0001$), 2 ($p = 0.0003$), 3 ($p = 0.03$) and 4 day ($p = 0.0007$) post-stroke time points. By 7 days, ICP began to decline (18 ± 2 mmHg; $p = 0.02$ when compared to 5 days), but remained significantly elevated compared to sham ($p = 0.04$), although not significantly different ($p > 0.05$) from recordings on days 1, 2, 3, 4, and 6 post-stroke.

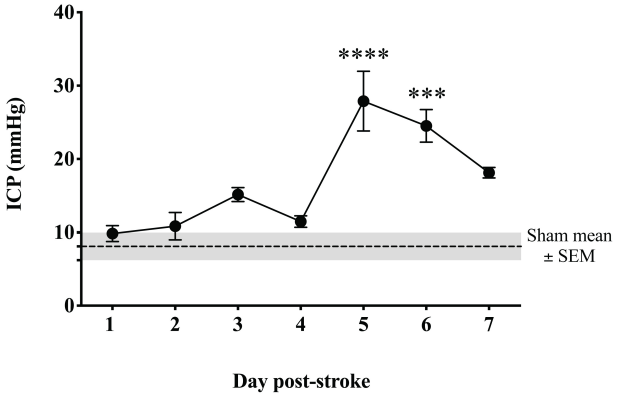

FIGURE 3 | Temporal profile of ICP following transient MCAO. ICP was significantly elevated at 5 days ($p < 0.001$) and 6 days ($p < 0.05$) post-stroke when compared to sham. By 7 days, ICP began to resolve though remained elevated compared to sham ($p < 0.05$). ****$p < 0.0001$; and ***$p < 0.001$ compared to sham. $n = 6$/time-point, $n = 4$ sham.

MRI

Magnetic resonance imaging was normal in sham animals, with no evidence of infarction, cerebral edema or midline shift (data not shown). At each time-point following stroke there was evidence of MCA recanalization following clip removal as seen on MRA, with the aforementioned exception of one animal that was excluded due to persistent MCAO (**Figure 3**). All stroke animals showed evidence of hyperintensity on T2-weighted and FLAIR images in the territory MCA, indicative of the infarct core and surrounding extracellular edema (**Figure 4**). There was no significant difference in infarct volume at any of the time points post-stroke as measured on DWI MRI (**Figure 5A**).

Cerebral edema evolved over time from 1 to 6 days post-tMCAO, with the largest volume of cerebral edema seen at 5 (8.86 ± 2.03 cm^3) and 6 days (7.01 ± 0.9 cm^3). This increase in the volume of edema was accompanied by increased extravasation of GAD across the barrier, as seen in T1 post-contrast sequences, indicative of BBB breakdown (**Figure 4**). However, although a qualitative evolution of cerebral edema post-stroke was apparent (**Figure 4**), accompanied by increased GAD contrast, there was no statistically significant difference between time-points (**Figure 5B**; $p > 0.05$). Midline shift was evident in all stroke animals, the degree of which evolved over time following stroke (**Figure 5C**) and was most prominent at 5 days post-stroke (3.92 ± 0.59 mm) when compared to 1 ($p = 0.002$) and 7 days ($p = 0.04$), in keeping with ICP findings. No animals showed evidence of tonsillar herniation or brain stem compression on MRI (data not shown).

Despite the fact that cerebral edema findings were not significantly different between time points, there was a moderate positive correlation seen between midline shift and cerebral edema calculations ($r = 0.49$; **Figure 6A**). However, there was no positive correlation seen between ICP and cerebral edema ($r = 0.23$; **Figure 6B**) or ICP and midline shift ($r = 0.20$; **Figure 6C**).

SP ELISA

A reduction in serum SP was observed between 4 and 16 h following transient MCAO, however, changes were not significant ($p > 0.05$; **Figure 7**). At 7-days post-stroke, SP levels were significantly elevated compared to 16 h ($p = 0.002$) and days 1 ($p = 0.04$), 4 ($p = 0.04$), 8 ($p = 0.008$) and 12 ($p = 0.003$) following occlusion. Despite a qualitative increase, the concentration of serum SP at day 7 was not significantly elevated ($p > 0.05$) when compared to pre-stroke measurements. Furthermore, despite a relative increase in SP seen in the serum post-stroke, no significant changes ($p > 0.05$) in SP levels in the CSF (**Figure 7**) were observed at any time-point following MCAO.

Gender Comparisons

No differences in pCO_2, pO_2, MABP or pH were seen between sexes during either stroke surgery or ICP monitoring ($p > 0.05$; **Table 2**). There was no significant difference in ICP between male and female animals at any of the post-stroke time-points ($p = 0.93$; **Figure 8A**). Furthermore, there was no significant difference in infarct volume ($p = 0.79$; **Figure 8B**), cerebral edema ($p = 0.41$; **Figure 8C**) or midline shift ($p = 0.39$; **Figure 8D**)

TABLE 2 | Surgical and intracranial pressure monitoring physiological parameters.

Group	Surgery day			ICP monitoring			Surgery day			ICP Monitoring		
	Male	**Female**	**All animals**	**Male**	**Female**	**All animals**	**Male**	**Female**	**All animals**	**Male**	**Female**	**All animals**
	PCO_2 (mmHg) ± SEM						**PO_2 (mmHg) ± SEM**					
Sham		43.19 ± 3.43						112.77 ± 5.75				
1 Day	41.19 ± 3.39	39.83 ± 2.07	40.51 ± 1.80	36.08 ± 1.61	37.42 ± 2.32	36.75 ± 1.30	213.94 ± 50.81	213.08 ± 66.77	213.51 ± 37.52	294.36 ± 64.89	191.64 ± 38.27	243 ± 40.78
2 Day	43.83 ± 2.05	45.25 ± 2.84	44.54 ± 1.60	38.33 ± 1.02	41.42 ± 2.14	39.88 ± 1.27	200.17 ± 37.13	83.67 ± 10.83	141.92 ± 31.27	166.67 ± 14.21	250.92 ± 62.62	208.79 ± 34.34
3 Day	46.58 ± 1.72	46.25 ± 1.50	46.42 ± 1.02	47.28 ± 2.98	40.25 ± 1.75	44.47 ± 2.43	289.50 ± 96.27	187.0 ± 38.56	238.25 ± 51.73	241.81 ± 126.13	237.38 ± 72.13	240.03 ± 72.76
4 Day	46.81 ± 3.13	43.0 ± 3.47	44.90 ± 2.26	42.89 ± 0.45	38.17 ± 4.19	40.53 ± 2.16	193.00 ± 73.93	113.50 ± 8.75	153.25 ± 37.74	304.67 ± 47.92	163.0 ± 17.10	233.83 ± 39.00
5 Day	50.08 ± 3.17	44.33 ± 2.51	47.21 ± 2.22	41.58 ± 0.79	39.58 ± 2.19	40.58 ± 1.13	193.83 ± 30.12	188.47 ± 57.77	191.15 ± 29.16	228.17 ± 70.65	251.33 ± 29.37	239.75 ± 34.61
6 Day	45.42 ± 2.38	41.33 ± 1.62	43.38 ± 1.58	47.75 ± 1.75	42.83 ± 1.96	45.29 ± 1.61	342.33 ± 101.85	217.58 ± 76.33	279.96 ± 63.39	319.56 ± 122.91	422.67 ± 57.68	371.11 ± 64.95
7 Day	47.67 ± 1.88	44.08 ± 2.24	45.80 ± 3.76	42.75 ± 2.89	46.25 ± 0.88	44.50 ± 1.56	172.08 ± 79.94	116.50 ± 8.62	144.29 ± 38.04	313.03 ± 83.77	280.83 ± 48.43	296.93 ± 43.87
	MABP (mmHg) ± SEM						**pH ± SEM**					
Sham		79.35 ± 6.27						7.46 ± 0.02				
1 Day	84.61 ± 12.54	86.17 ± 8.80	85.39 ± 6.86	97.25 ± 8.76	77.64 ± 8.54	87.44 ± 7.01	7.43 ± 0.03	7.44 ± 0.01	7.43 ± 0.01	7.42 ± 0.01	7.42 ± 0.03	7.42 ± 0.01
2 Day	74.17 ± 0.87	92.92 ± 4.01	106.98 ± 25.30	88.50 ± 11.35	107.39 ± 17.88	96.44 ± 10.66	7.43 ± 0.02	7.45 ± 0.04	7.44 ± 0.02	7.43 ± 0.03	7.48 ± 0.03	7.45 ± 0.02
3 Day	75.42 ± 5.47	91.42 ± 4.03	83.42 ± 4.69	93.75 ± 14.42	99.88 ± 12.63	96.20 ± 8.97	7.41 ± 0.04	7.41 ± 0.01	7.41 ± 0.02	7.39 ± 0.04	7.41 ± 0.03	7.40 ± 0.02
4 Day	92.75 ± 3.82	84.17 ± 3.99	88.46 ± 3.13	116.33 ± 10.19	127.50 ± 6.91	121.92 ± 6.05*	7.41 ± 0.02	7.44 ± 0.02	7.42 ± 0.02	7.35 ± 0.05	7.48 ± 0.02	7.41 ± 0.04
5 Day	96.75 ± 1.32	80.97 ± 13.45	88.86 ± 7.00	117.92 ± 7.58	104.75 ± 1.98	111.33 ± 4.58	7.38 ± 0.02	7.43 ± 0.07	7.40 ± 0.02	7.47 ± 0.02	7.43 ± 0.07	7.45 ± 0.03
6 Day	78.67 ± 9.04	91.17 ± 2.98	119.56 ± 6.87	122.67 ± 2.85	108.42 ± 5.21	115.54 ± 4.15	7.39 ± 0.03	7.45 ± 0.01	7.42 ± 0.02	7.40 ± 0.02	7.44 ± 0.03	7.42 ± 0.02
7 Day	114.17 ± 11.28	84.25 ± 10.31	99.21 ± 9.56	137.42 ± 17.12	116.75 ± 10.33	127.08 ± 10.07*	7.40 ± 0.02	7.42 ± 0.02	7.41 ± 0.01	7.48 ± 0.02	7.44 ± 0.03	7.46 ± 0.02

*$p < 0.05$ compared to day 1.

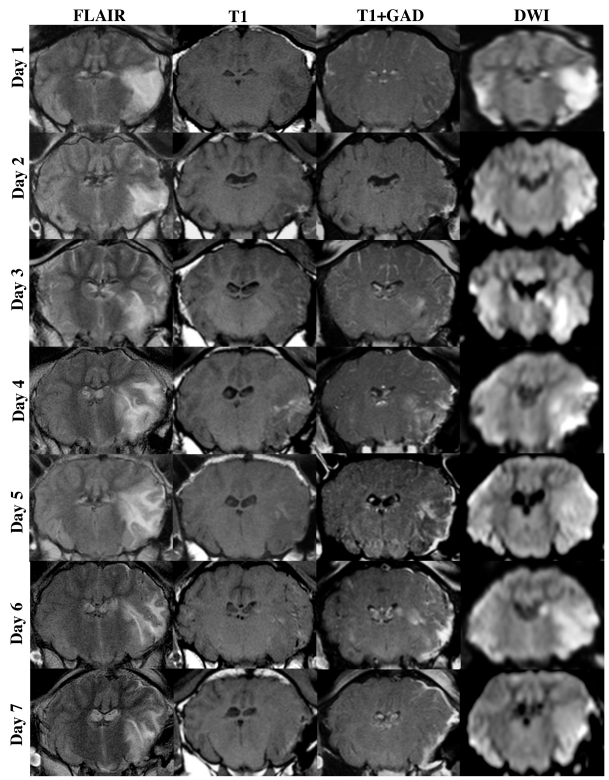

FIGURE 4 | MRI findings following transient MCAO. Cerebral edema, as shown in coronal FLAIR MRI images, evolved from 1–6 days following stroke, beginning to resolve by 7 days. This evolution in cerebral edema was associated with enhanced extravasation of GAD across the BBB as seen on T1 weighted post-contrast series (T1+GAD) when compared to pre-contrast T1 series. Lesion volume, as shown in DWI MRI images, was comparable across time-points following stroke.

seen between sexes following stroke. SP levels in the serum were not significantly different between males and females ($p = 0.41$; **Figure 8E**). However, there was a significant increase in SP seen in the CSF (**Figure 8F**) of females when compared to males pre-stroke ($p = 0.002$), and at 1 ($p < 0.0001$), 3 ($p < 0.0001$) and 6 ($p = 0.002$) days post-stroke although there were no significant within group differences observed in the females at any time-point pre- or post-stroke ($p = 0.18$).

Immunohistochemistry

Albumin

There was minimal evidence of albumin extravasation in sham tissue (**Figure 9**). Following stroke, marked albumin extravasation, indicative of BBB breakdown and subsequent vasogenic cerebral edema formation, was observed both macroscopically within the infarcted territory and microscopically in the perivascular tissue of the infarct, most prominent of which was at 5 and 6 days post-stroke.

SP

Little to no perivascular SP immunoreactivity was observed in sham tissue (**Figure 10**, Substance P, S). Following stroke, a marked increase in perivascular SP immunoreactivity was observed in tissue at 5 and 6 days, which was still evident at 7 days, although less pronounced.

Cav-1

Low levels of caveolin-1 immunoreactivity were observed in sham tissue (**Figure 10**, Caveolin-1, S). Following stroke, an increase in perivascular caveolin-1 immunoreactivity was identifiable which was particularly evident at 5 and 6 days post-stroke.

DISCUSSION

This study is the first to describe a surgical approach to ovine tMCAO with reperfusion. Through this study we have successfully developed a model that conserves tissue and permits post-operative recuperation, allowing for investigation into the pathophysiology of ischemic stroke, in particular post-stroke complications such as BBB disruption, development of cerebral edema and elevated ICP. This method of transient stroke induction provides a clinically relevant model in which promising novel treatments targeting stroke and its complications can be screened.

Although a number of studies have reported raised ICP following stroke in small animal models (Beard et al., 2015; Murtha et al., 2015) and large animal species at early time-points (Wells et al., 2015) this study is the first in which ICP was recorded out to 7 days post-stoke in a large gyrencephalic species. Using this model we have successfully characterized the temporal profile and established that ICP peaks at 5–6 days following ovine transient MCAO. These findings are comparable to the human patients, where ICP is shown to peak 3–5 days post-stroke, indicating that our model reliably replicates the clinical situation (Battey et al., 2014). The modest difference in the time course between the ovine model and humans may reflect the additional time taken to restore intracranial dynamics following surgery due to CSF aspiration required for optimal visualization of the proximal MCA. Indeed, a closed skull approach to MCAO where ICP dynamics are maintained through the induction of stroke may yield a timeline of ICP changes that directly align with clinical pathogenesis, however, this was not possible due to the complex ovine extracranial cerebrovasculature, in particular the rete mirabile, which precludes vascular access via the ICA for insertion of a balloon catheter, autologous clot or other occlusive agent.

Regardless, at 5–6 days post-stroke we consistently observed elevated ICP readings above 20 mmHg. In the clinic, ICP readings of ≥20 mmHg warrant investigation for possible treatment and intervention (Lavinio and Menon, 2011; Battey et al., 2014), as persistently elevated ICP is associated with poor outcome following ischemic stroke, widely accepted as being attributable to the development of edema in the cerebral parenchyma (Ayata and Ropper, 2002). Despite this, conflicting studies have reported an elevation of ICP in the absence of cerebral edema following small ischemic stroke in rats (Beard et al., 2015;

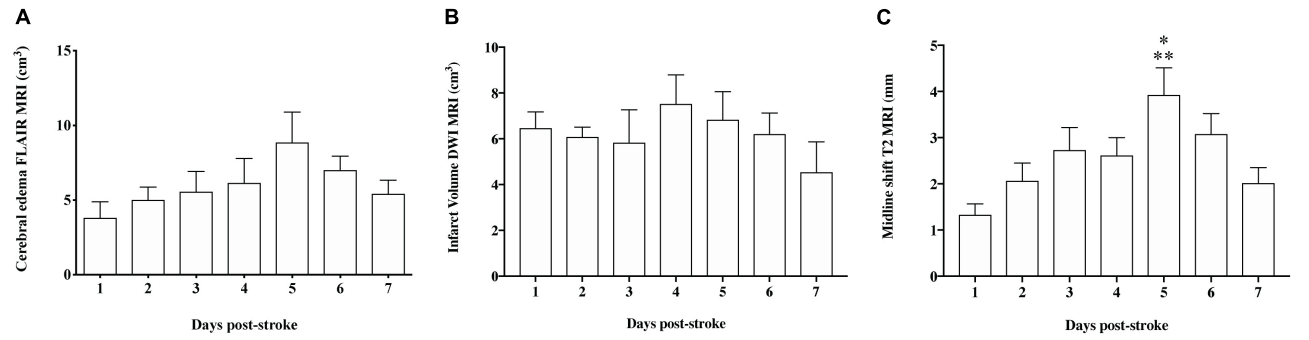

FIGURE 5 | Quantification of infarct volume, cerebral edema, and midline shift on MRI. **(A)** There was no significant difference ($p > 0.05$) in infarct volume at any of the time-points following stroke. **(B)** The evolution of cerebral edema showed a similar pattern to ICP, however, changes were not significant ($p > 0.05$). **(C)** Midline shift was significantly greater at 5 days when compared to 1 (<0.01) and 7 ($p < 0.05$) days post-stroke. Data shown as mean ± SEM. *$p < 0.05$ compared to 7 days, **$p < 0.01$ compared to 1 day. n = 6/time-point.

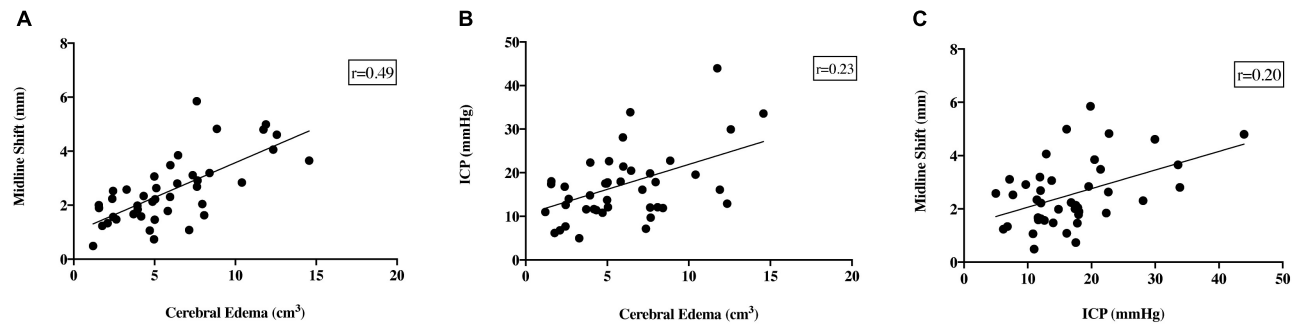

FIGURE 6 | Relationship between ICP, cerebral edema, midline shift and infarct volume. There was a moderate positive correlation seen between cerebral edema and midline shift (r = 0.49, **A**). Despite this, there was no correlation seen between ICP and cerebral edema (r = 0.23, **B**), or ICP and midline shift (r = 0.20, **C**). NB data from all time points was used for comparison between variables.

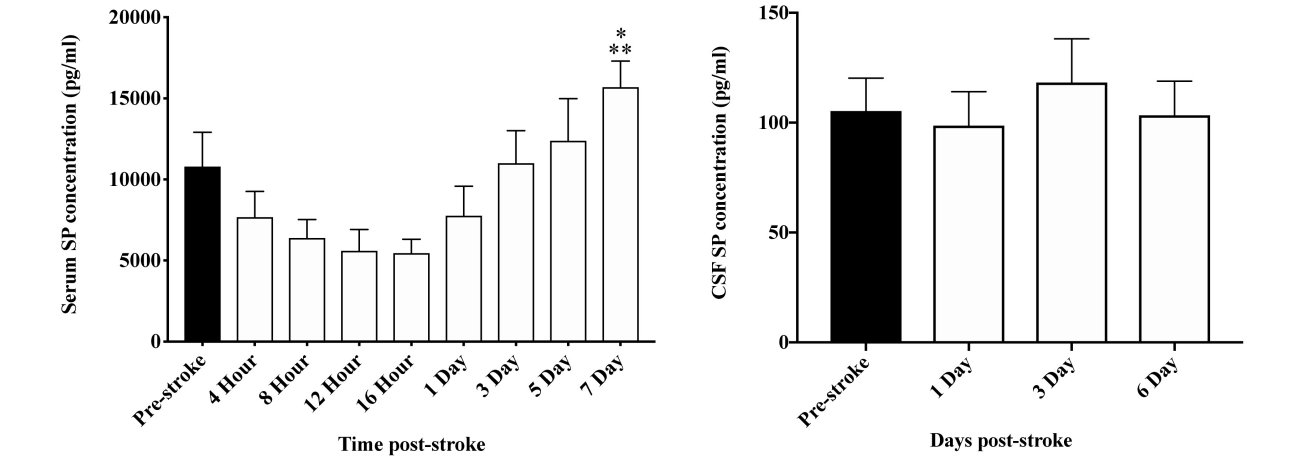

FIGURE 7 | Temporal profile of serum and CSF SP levels following stroke. At 7 days post-stroke, SP in the serum was significantly elevated compared with levels seen at 4 h ($p < 0.05$), 8, 12, and 16 h ($p < 0.01$), and 1 day ($p < 0.05$) following stroke. Furthermore, despite a qualitative increase, SP concentration pre-stroke was comparable to day 7 post-stroke. In the CSF, there was no significant difference seen in SP levels at days 1, 3, and 6 post-stroke ($p > 0.05$). Data shown as mean ± SEM. *$p < 0.05$ compared to 4 h and 1 day; **$p < 0.01$ compared to 8, 12, and 16 h. n = 12/time-point serum; n = 8/time-point CSF.

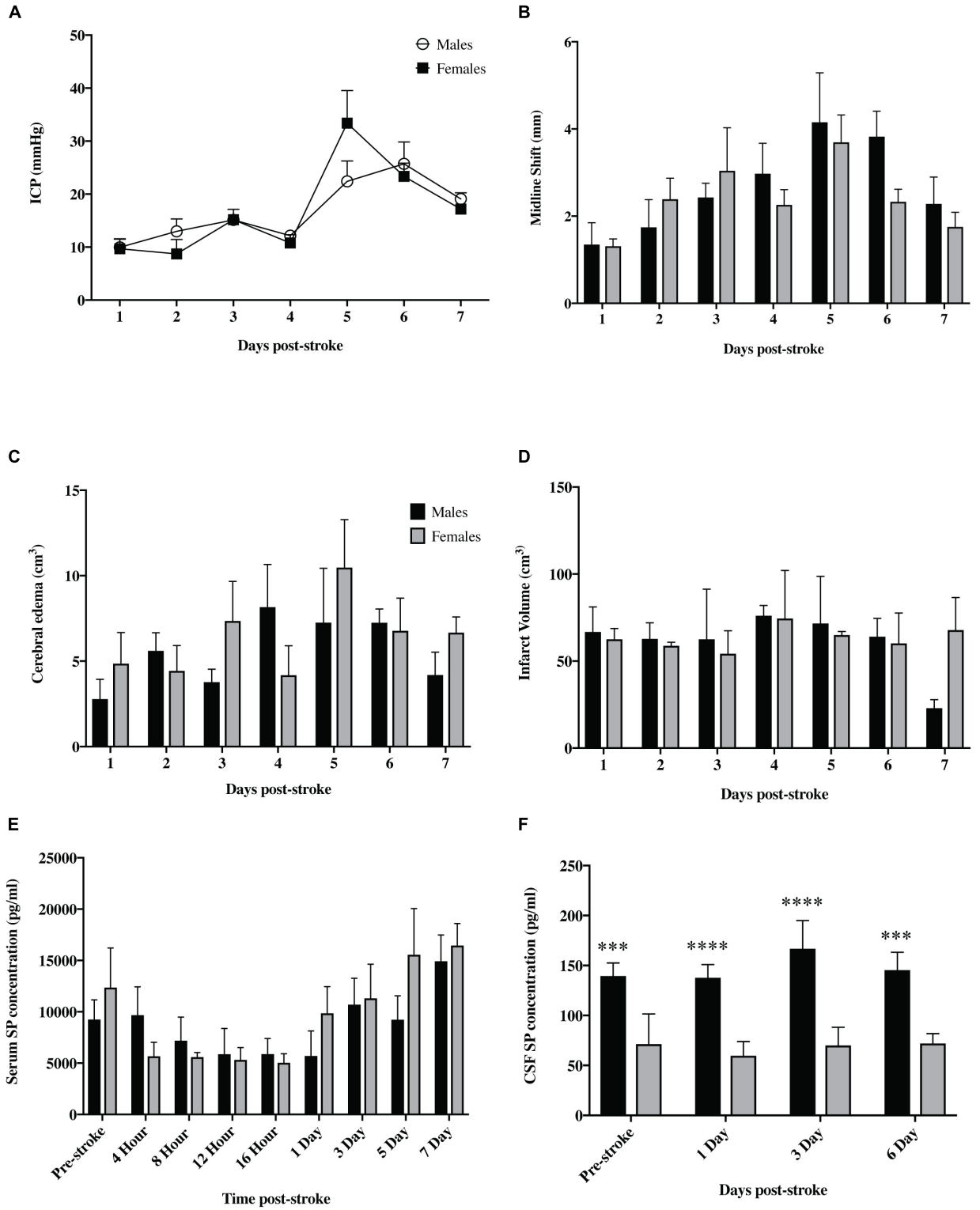

FIGURE 8 | Sex differences following tMCAO. There was no significant difference in ICP **(A)** seen between sexes at any of the post-stroke time points ($p > 0.05$). Furthermore, there was no significant difference seen between males and females in infarct volume **(B)**, cerebral edema **(C)**, or midline shift **(D)** ($p > 0.05$). SP levels in the serum **(E)** were not significantly different between sexes ($p > 0.05$) but were significantly elevated in the CSF **(F)** of female animals compared to males at both pre and post-stroke time points ($p < 0.01$). Data shown as mean ± SEM. ***$p < 0.01$ and ****$p < 0.0001$ females compared to males. n = 3/time-point ICP infarct volume, midline shift and edema; n = 6/time-point for serum; n = 4/time-point CSF.

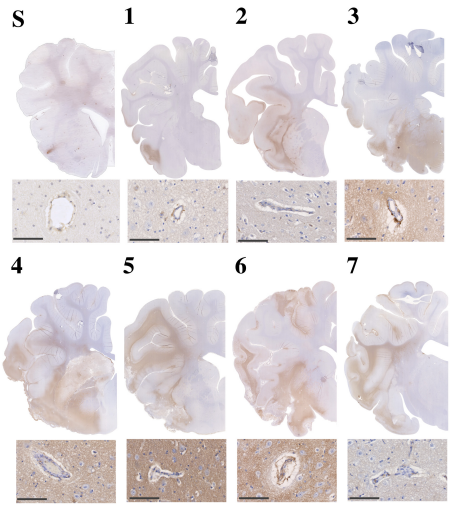

FIGURE 9 | Albumin immunoreactivity in sham (S) and post-stroke animals at 1 (1), 2 (2), 3 (3), 4 (4), 5 (5), 6 (6) and 7 days (7) post-stoke. Enhanced albumin extravasation evolved over time following stroke and was most prominent at 4–6 days following tMCAO. This pattern of albumin staining was consistent with perivascular staining seen microscopically. Microscopic images scale bar 100 μm, 40× magnification.

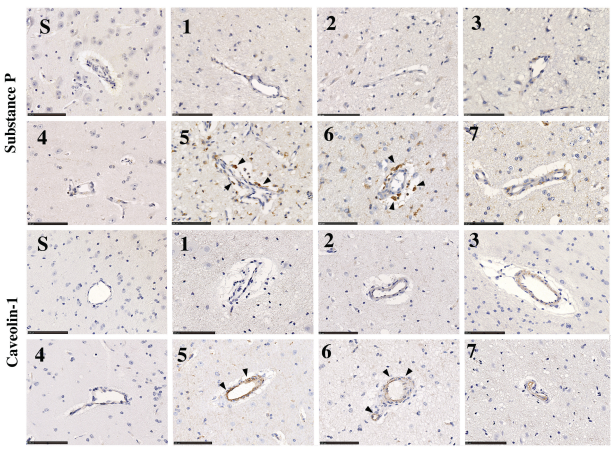

FIGURE 10 | SP and caveolin-1 immunoreactivity in sham (S) and post-stroke animals at 1 (1), 2 (2), 3 (3), 4 (4), 5 (5), 6 (6), and 7 days (7) post-stoke. There was no identifiable immunoreactivity of SP or caveolin-1 in sham animals (S). Low levels of SP immunoreactivity were seen perivascularly at 1–4 days post-stroke. At 5 and 6 days following transient MCAO, there was an increase in SP seen in the perivascular tissue of the ischemic penumbra in the affected hemisphere. This increase in SP was concordant with an increase in caveolin-1 immunoreactivity perivascularly, which was most evident at 5–6 days. Arrows indicate increased immunoreactivity of SP and cav-1 seen surrounding vessels. Scale bar 100 μm, 40× magnification.

Murtha et al., 2015). However, the underlying pathophysiology of increased ICP was not reported and requires further investigation. Furthermore, in the case of larger hemispheric strokes seen clinically, such as that of proximal MCAO or ICA occlusion, there is a positive correlation between cerebral edema and elevated ICP (Engelhorn et al., 2002). However, we did not observe such a relationship in this study, which may reflect the within group variability and different cohorts that were required to populate the time course. Furthermore, when measuring elevated ICP following stroke, the influence of autoregulation must also be taken into consideration. The ability to maintain cerebral homeostasis plays an important role in moderating the pathogenesis of elevated ICP. A loss of autoregulation has been shown to enhance the progression of ischemia and development of cerebral edema, and thus plays an important role during MCA reperfusion (Dohmen et al., 2007). It is proposed that autoregulation may be enhanced quite early following stroke, and become dampened at 6 days post-stroke (Reinhard et al., 2012), in keeping with our observations of significantly elevated ICP at 6 days post-stroke. Furthermore, elevated ICP is associated with a decreased ability to autoregulate following head injury, indicating a strong positive correlation between the two (Reinhard et al., 2012).

We observed an evolution of cerebral edema over time following stroke, although changes were not significant between time-points. Nevertheless, it is widely accepted that the increased volume of the brain as a result of cerebral edema positively correlates with subsequent elevations in ICP (Battey et al., 2014; Beard et al., 2015; Brogan and Manno, 2015). The development of vasogenic cerebral edema in particular occurs following loss of integrity of the BBB, permitting the abnormal extravasation of proteins across the damaged barrier. This creates an osmotic drive pulling water from the vasculature into the extracellular cerebral parenchyma, leading to an overall increase in brain volume and concomitant rise in ICP (Battey et al., 2014). Our study was able to confirm that there was disruption to BBB via visualization of the GAD contrast medium within the brain parenchyma, suggesting that the cerebral edema seen was vasogenic in nature. This finding was substantiated by the increased extravasation of albumin following tMCAO, which was most prominent at 5–6 days post-stroke. Albumin is unable to cross the intact barrier under physiological conditions due to its large size and structure (Quinlan et al., 2005). Previous studies have established that albumin crosses the barrier via the transcellular pathway, facilitated by caveolae (Abbott et al., 2006), of which caveolin-1 (cav-1) is an integral component (Nag et al., 2007). Indeed, increased barrier permeability in association with caveolin-1 upregulation was observed in the absence of tight junction breakdown, confirming the integral role of caveolae in the maintenance of barrier integrity (Povlishock et al., 1978; Nag et al., 2007). Our IHC findings of increased cav-1 immunoreactivity at 5–6 days post-stroke corroborate this, providing a potential mechanism driving sustained barrier permeability and the evolution of cerebral edema. Furthermore, the volumetric enlargement of the brain as a result of vasogenic edema leads to displacement of cerebral tissue and subsequent shift of the midline, a critical state in which compression of adjacent brain structures precedes potentially fatal tonsillar herniation (Huttner and Schwab, 2009). We observed significant midline shift at 5 days following stroke in keeping with elevated ICP. As such, our findings of enhanced GAD, albumin and cav-1 immunoreactivity at 5–6 days post-stroke suggest a loss of barrier integrity at this time-point, precipitating the development

of vasogenic cerebral edema, extensive midline shift and the subsequent rise in ICP seen in this model.

We also demonstrated that serum SP levels were increased at 7 days following stroke when compared to pre-stroke values. This followed a non-significant decline in serum SP at 4 h which continued to decline out to 16 h following injury. This suggests a peak increase in the levels of serum SP may occur ahead of the 4 h-post-stroke sampling time-point. Indeed, rodent TBI studies have reported an early peak in plasma SP levels at 30 min post-injury but a decline by 5 h post-injury (Donkin and Vink, 2010) Similarly, SP levels were increased in serum samples obtained within 12 h following the onset of both clinical stroke (Bruno et al., 2003; Lorente et al., 2016) and TBI (Lorente et al., 2015), with higher levels associated with early mortality. Although some discrepancy between experimental and clinical time-points exists, it is important to acknowledge that it is difficult to draw firm comparisons given the complications in obtaining clinical samples at acute time-points. We also examined SP levels in the CSF following stroke, though observed no differences at 1, 3, or 6 day time-points. Although females consistently had higher CSF SP levels compared to males at all post-stroke time-points, there was no significant change in these levels post-stroke. This suggests that females have higher baseline levels of SP. Indeed, gender differences in the SP response have previously been observed (Pittenger et al., 2016; Simões et al., 2018). A comprehensive sampling regime, including sampling at 4 and 6 days post-stroke for serum and 4 and 5 days post-stroke for CSF, would be required to populate a detailed time-course of changes in SP in the serum and CSF in the setting of ischemic stroke, and may reveal changes beyond those observed in the current cohort. Nevertheless, the increase in serum SP levels we observed, in conjunction with the increased barrier permeability and vasogenic edema seen with albumin IHC and MRI, support a potential role for SP in the genesis of cerebral edema and development of elevated ICP in this model. Indeed, our rodent stroke studies support this (Turner et al., 2006, 2011; Corrigan et al., 2012, 2016; Turner and Vink, 2012, 2014) and corroborates our recent work demonstrating the efficacy of NK1-r antagonist treatment in reducing ICP in an ovine model of permanent MCAO (Sorby-Adams et al., 2019). Taken together, these findings suggest that neurogenic inflammation occurs following ischemic stroke and may contribute to the increased BBB permeability and elevated ICP observed, suggesting that blocking the action of SP with a tachykinin NK1-r antagonist may be an effective strategy to mitigate these post-stroke complications and thus improve outcome.

LIMITATIONS AND FUTURE DIRECTIONS

Although the findings of this study demonstrate successful model development and clearly show the evolution of ICP following stroke, limitations must be acknowledged. It must firstly be recognized that human patients are rarely under anesthesia when suffering a stroke. This is of particular importance due to the implied effects of anesthesia, both protective and deleterious. Ketamine has been shown to have neuroprotective effects (Hudetz and Pagel, 2010), whilst isoflurane is associated with respiratory depression, decreased MABP and thus diminished oxygen supply to neuronal cells (Murr et al., 1993), exacerbating cerebral ischemia. These limitations have been discussed in detail in our previous studies (Wells et al., 2012, 2015), however, due to the nature of the surgical procedure, anesthesia is unavoidable (Lin et al., 1997). The decision to maintain animals on a combination of ketamine and isoflurane was made on the basis of prolonged duration (4–5 h) of surgical procedures. The anesthetic combination produces a countering effect, eliminating the neuroprotective effect of pure ketamine and the respiratory distress associated with pure isoflurane, thus reducing confounding factors of anesthetic agents administered alone (Schifilliti et al., 2010).

There was a large within group variability, particularly for the MRI parameters, seen at each of the time-points following stroke. This may reflect differences in collateral flow or autoregulation capacity within the individual animals. Indeed, there is a considerable degree of variation in the severity and timing of cerebral edema in human patients following stroke. Furthermore, there may be some variability due to the severity of stroke in addition to the relative age of the sheep compared with the greater stroke population. In this study we used sheep aged 18–24 months, which are the equivalent to mid-adulthood in humans, whereas clinical stroke most commonly occurs in those over 60 years of age. Furthermore, the exclusion of experimental animals due to anesthetic complications or lack of reperfusion decreased the total sample size. This could be addressed by increasing the overall sample size for each group to increase statistical power. It must also be acknowledged that we used different cohorts of animals to generate the stroke ICP data, sham ICP data and serum/CSF for the ELISAs. This led to an inability to run true correlations between groups, for example between the SP and ICP datasets, limiting the conclusions we can draw regarding the potential relationship between serum/CSF SP and ICP. Furthermore, there was some discrepancy seen between elevated ICP and edema at 5–6 days in the first cohort and elevated serum SP seen at 7 days in the second cohort. Our findings suggest that SP is involved in the evolution of edema, however, given that different cohorts used in this study it was difficult to establish a definitive relationship between the two. As such, the differences in the time course of SP elevations and increased ICP are most likely attributable to the different cohorts used for each of these outcome measures.

In order to reduce the number of animals required we utilized a cohort of sham animals that underwent sham surgery immediately followed by ICP monitoring. We acknowledge that we would have preferentially used the same regime as the stroke cohort but it was not possible to generate an additional sham control cohort for this study alone. When measuring ICP, values would ideally be obtained from the same animal from 1–7 days post-stroke to look at the evolution of pressure individual

to that animal. This could be addressed through the use of a telemetric system to remotely and non-invasively measure ICP. As sheep are quadrupeds however, some question remains regarding the impact of head position, in particular when feeding, on ICP measurements obtained using this method. Furthermore, the use of individual cohorts of animals benefited this study by allowing us to harvest the brain at specific time-points following stroke and perform IHC accordingly, an important aspect to understanding the evolution of the injury. The reliable measurement of cerebral edema on MRI at a single time-point is somewhat contentious, as the hyperintensity of vasogenic edema is difficult to distinguish from the lesion itself. The measurement of the entire FLAIR lesion volume therefore includes areas of infarction as well as edema and is therefore an indirect measure of edema volume. A more robust approach to measuring edema would be to undergo sequential MRI's and evaluate the change in diffusion lesion volume between 2 time points following reperfusion, which was not feasible in this study due to cost. Furthermore, although GAD was utilized, T1 weighted MRI images were only taken at a single time-point following administration. As such, it is difficult to obtain a quantitative measure of GAD extravasation across the barrier. A more robust approach to this would be to obtain dynamic contrast enhanced (DCE) and dynamic susceptibility contrast (DSC) sequences to generate clinically relevant measurements of barrier permeability. Finally, although gender differences were examined in this study the hormonal status of the female animals at the time of stroke and monitoring period was not known.

CONCLUSION

In this study, we have successfully developed a surgical approach to tMCAO with reperfusion in the sheep that permits recovery and the examination of long-term time-points following stroke. In this novel model we have determined the temporal profile of ICP, showing that ICP peaks at 5–6 days following stroke, in conjunction with midline shift, an evolution of cerebral edema, increased serum SP levels, enhanced SP immunoreactivity and increased albumin extravasation. These results suggest a role of SP in BBB disruption and the subsequent genesis of cerebral edema and associated rise in ICP following stroke. As such, agents targeting elevated ICP and cerebral edema would be most effective when administered prior to 6 days post-stroke, or as early as possible following stroke-onset. We conclude that this ovine model provides a promising platform to screen novel treatments targeting post-stroke complications and verify treatment efficacy prior to clinical assessment.

DATA AVAILABILITY

All datasets generated for this study are included in the manuscript and/or the supplementary files.

ETHICS STATEMENT

All experimental procedures were approved by the Animal Ethics Committees of The University of Adelaide (M-2014-015) and South Australian Health and Medical Research Institute (SAHMRI SAM 3; SAM 141). Experiments were conducted in accordance with the Australian National Health and Medical Research Council code of practice for the care and use of animals for scientific purposes (8th edition, 2013).

AUTHOR CONTRIBUTIONS

AS-A, RV, RT, and AL conceived and designed the experiments. AS-A, RT, ET, OM, and LE performed the experiments. AS-A, LE, JH, and NY analyzed the data. AS-A and RT wrote the manuscript.

FUNDING

This study was supported by funding from the National Health and Medical Research Council (NHMRC; Project Grant 1082556) and the NeuroSurgical Research Foundation (Australia).

ACKNOWLEDGMENTS

We would like to thank Sunthara Rajan Perumal for the acquisition of the MRI. We would also like to acknowledge the facilities and technical assistance of the National Imaging Facility, a National Collaborative Research Infrastructure Strategy (NCRIS) capability, at LARIF, SAHMRI.

REFERENCES

Abbott, N. J., Ronnback, L., and Hansson, E. (2006). Astrocyte-endothelial interactions at the blood-brain barrier. *Nat. Rev. Neurosci.* 7, 41–53. doi: 10.1038/nrn1824

Anderson, R. W., Sandoz, B., Dutschke, J. K., Finnie, J. W., Turner, R. J., Blumbergs, P. C., et al. (2014). Biomechanical studies in an ovine model of non-accidental head injury. *J. Biomech.* 47, 2578–2583. doi: 10.1016/j.jbiomech.2014.06.002

Ayata, C., and Ropper, A. H. (2002). Ischaemic brain oedema. *J. Clin. Neurosci.* 9, 113–124. doi: 10.1054/jocn.2001.1031

Battey, T. W. K., Karki, M., Singhal, A. B., Wu, O., Sadaghiani, S., Campbell, B. C. V., et al. (2014). Brain edema predicts outcome after nonlacunar ischemic stroke. *Stroke* 45:3643. doi: 10.1161/STROKEAHA.114.006884

Beard, D. J., Mcleod, D. D., Logan, C. L., Murtha, L. A., Imtiaz, M. S., Van Helden, D. F., et al. (2015). Intracranial pressure elevation reduces flow through collateral vessels and the penetrating arterioles they supply. a possible explanation for 'collateral failure' and infarct expansion after ischemic stroke. *J. Cereb. Blood Flow Metab.* 35, 861–872. doi: 10.1038/jcbfm.2015.2

Boltze, J., Förschler, A., Nitzsche, B., Waldmin, D., Hoffmann, A., Boltze, C. M., et al. (2008). Permanent middle cerebral artery occlusion in sheep: a novel large animal model of focal cerebral ischemia. *J. Cereb. Blood Flow Metab.* 28, 1951–1964. doi: 10.1038/jcbfm.2008.89

Boulos, A. S., Deshaies, E. M., Dalfino, J. C., Feustel, P. J., Popp, A. J., and Drazin, D. (2011). Tamoxifen as an effective neuroprotectant in an endovascular canine model of stroke. *J. Neurosur.* 114:1117. doi: 10.3171/2010.8.JNS09352

Brogan, M., and Manno, E. (2015). Treatment of malignant brain edema and increased intracranial pressure after stroke. *Curr. Treat. Options Neurol.* 17, 1–11.

Bruno, G., Tega, F., Bruno, A., Graf, U., Corelli, F., Molfetta, R., et al. (2003). The role of substance P in cerebral ischemia. *Int. J. Immunopathol. Pharmacol.* 16, 67–72.

Cameron, R., Greg, C., Amir, A., Marinos, K., Valerie, B., Sashwati, R., et al. (2008). Minimally invasive neuroradiologic model of preclinical transient middle cerebral artery occlusion in canines. *Proc. Natl. Acad. Sci. U.S.A.* 105:14100. doi: 10.1073/pnas.0806678105

Casals, J. B., Pieri, N. C. G., Feitosa, M. L. T., Ercolin, A. C. M., Roballo, K. C. S., Barreto, R. S. N., et al. (2011). Use of animal models for stroke research: a review. *Comp. Med.* 61, 305–313.

Christoforidis, G. A., Rink, C., Kontzialis, M. S., Mohammad, Y., Koch, R. M., Abduljalil, A. M., et al. (2011). An endovascular canine middle cerebral artery occlusion model for the study of leptomeningeal collateral recruitment. *Invest. Radiol.* 46, 34–40. doi: 10.1097/RLI.0b013e3181f0cbc7

Corrigan, F., Leonard, A., Ghabriel, M., Van Den Heuvel, C., and Vink, R. (2012). A substance P antagonist improves outcome in female sprague dawley rats following diffuse traumatic brain injury. *CNS Neurosci. Ther.* 18, 513–515. doi: 10.1111/j.1755-5949.2012.00332.x

Corrigan, F., Mander, K. A., Leonard, A. V., and Vink, R. (2016). Neurogenic inflammation after traumatic brain injury and its potentiation of classical inflammation. *J Neuroinflammation* 13:264.

D'Ambrosio, A. L., Sughrue, M. E., Mocco, J., Mack, W. J., King, R. G., Agarwal, S., et al. (2004). A modified transorbital baboon model of reperfused stroke. *Methods Enzymol.* 386:60. doi: 10.1016/s0076-6879(04)86002-6

Dohmen, C., Bosche, B., Graf, R., Reithmeier, T., Ernestus, R.-I., Brinker, G., et al. (2007). Identification and clinical impact of impaired cerebrovascular autoregulation in patients with malignant middle cerebral artery infarction. *Stroke* 38:56. doi: 10.1161/01.str.0000251642.18522.b6

Donkin, J. J., Nimmo, A. J., Cernak, I., Blumbergs, P. C., and Vink, R. (2009). Substance P is associated with the development of brain edema and functional deficits after traumatic brain injury. *J. Cereb. Blood Flow Metab.* 29, 1388–1398. doi: 10.1038/jcbfm.2009.63

Donkin, J. J., and Vink, R. (2010). Mechanisms of cerebral edema in traumatic brain injury: therapeutic developments. *Curr. Opin. Neurol.* 23, 293–299. doi: 10.1097/WCO.0b013e328337f451

Duhaime, A. C., Margulies, S. S., Durham, S. R., O'rourke, M. M., Golden, J. A., Marwaha, S., et al. (2000). Maturation-dependent response of the piglet brain to scaled cortical impact. *J. Neurosurg.* 93, 455–462. doi: 10.3171/jns.2000.93.3.0455

Engelhorn, T., Von Kummer, R., Reith, W., Forsting, M., and Doerfler, A. (2002). What is effective in malignant middle cerebral artery infarction: reperfusion, craniectomy, or both? An experimental study in rats. *Stroke* 33, 617–622. doi: 10.1161/hs0202.102374

Feigin, V. L., Norrving, B., and Mensah, G. A. (2017). Global Burden of Stroke. *Circ. Res.* 120:439. doi: 10.1161/CIRCRESAHA.116.308413

Furuichi, Y., Maeda, M., Matsuoka, N., Mutoh, S., and Yanagihara, T. (2007). Therapeutic time window of tacrolimus (FK506) in a nonhuman primate stroke model: comparison with tissue plasminogen activator. *Exp. Neurol.* 204, 138–146. doi: 10.1016/j.expneurol.2006.10.003

Goyal, M., Menon, B. K., Van Zwam, W. H., Dippel, D. W. J., Mitchell, P. J., Demchuk, A. M., et al. (2016). Endovascular thrombectomy after large-vessel ischaemic stroke: a meta-analysis of individual patient data from five randomised trials. *Lancet* 387, 1723–1731. doi: 10.1016/S0140-6736(16)00163-X

Hewitt, A., and Ellory, C. (2012). Brain oedema, intracranial pressure and cerebral blood flow. *Surgery* 30, 102–106. doi: 10.1016/j.mpsur.2011.12.004

Hudetz, J. A., and Pagel, P. S. (2010). Neuroprotection by Ketamine: a review of the experimental and clinical evidence. *J. Cardio. Vasc. Anesth.* 24, 131–142. doi: 10.1053/j.jvca.2009.05.008

Huttner, H. B., and Schwab, S. (2009). Malignant middle cerebral artery infarction: clinical characteristics, treatment strategies, and future perspectives. *Lancet Neurol.* 8, 949–958. doi: 10.1016/S1474-4422(09)70224-8

Jha, S. (2003). Cerebral edema and its management. *Med. J. Arm. Forces India* 59, 326–331. doi: 10.1016/s0377-1237(03)80147-8

Kamoi, S., Pretty, C., Docherty, P., Squire, D., Revie, J., Chiew, Y. S., et al. (2014). Continuous stroke volume estimation from aortic pressure using zero dimensional cardiovascular model: proof of concept study from porcine experiments. *PLoS One* 9:e102476. doi: 10.1371/journal.pone.0102476

Keith, M. K., Ana, P. D. C., Andrea, E. L., Michael, R. H., and Jon, W. P. (2007). Sheep don't forget a face. *Nature* 447:346. doi: 10.1038/nature05882

Kim, H., Jin, S. T., Kim, Y. W., Kim, S. R., Park, I. S., and Jo, K. W. (2015). Predictors of malignant brain edema in middle cerebral artery infarction observed on CT angiography. *J. Clin. Neurosci.* 22, 554–560. doi: 10.1016/j.jocn.2014.08.021

Lavinio, A., and Menon, D. K. (2011). Intracranial pressure: why we monitor it, how to monitor it, what to do with the number and what's the future? *Curr. Opin. Anaesthesiol.* 24, 117–123. doi: 10.1097/ACO.0b013e32834458c5

Lighthall, J. W. (1988). Controlled cortical impact: a new experimental brain injury model. *J. Neurotrauma* 5, 1–15. doi: 10.1089/neu.1988.5.1

Lin, H. C., Purohit, R. C., and Powe, T. A. (1997). Anesthesia in sheep with propofol or with xylazine-ketamine followed by halothane. *Vet. Surg.* 26, 247–252. doi: 10.1111/j.1532-950x.1997.tb01494.x

Lorente, L., Martin, M. M., Almeida, T., Hernandez, M., Ramos, L., Argueso, M., et al. (2015). Serum substance P levels are associated with severity and mortality in patients with severe traumatic brain injury. *Crit. Care* 19:192. doi: 10.1186/s13054-015-0911-z

Lorente, L., Martín, M. M., Almeida, T., Pérez-Cejas, A., Ramos, L., Argueso, M., et al. (2016). Serum levels of substance P and mortality in patients with a severe acute ischemic stroke. *Int. J. Mol. Sci.* 17:991. doi: 10.3390/ijms17060991

Mahajan, S., and Bhagat, H. (2016). Cerebral oedema: pathophysiological mechanisms and experimental therapies. *J. Neuroanaesthesiol. Crit. Care* 3, 22-28.

Manley, G. T., Rosenthal, G., Lam, M., Morabito, D., Yan, D., Derugin, N., et al. (2006). Controlled cortical impact in swine: pathophysiology and biomechanics. *J. Neurotrauma* 23, 128–139. doi: 10.1089/neu.2006.23.128

Matthews, J. N., Altman, D. G., Campbell, M. J., and Royston, P. (1990). Analysis of serial measurements in medical research. *BMJ* 300:230. doi: 10.1136/bmj.300.6719.230

Morton, A. J., and Avanzo, L. (2011). Executive decision-making in the domestic sheep. *PLoS One* 6:e15752. doi: 10.1371/journal.pone.0015752

Morton, A. J., Rudiger, S. R., Wood, N. I., Sawiak, S. J., Brown, G. C., Mclaughlan, C. J., et al. (2014). Early and progressive circadian abnormalities in Huntington's disease sheep are unmasked by social environment. *Hum. Mol. Genet.* 23, 3375–3383. doi: 10.1093/hmg/ddu047

Murr, R., Schurer, L., Berger, S., Enzenbach, R., Peter, K., and Baethmann, A. (1993). Effects of isoflurane, fentanyl, or thiopental anesthesia on regional cerebral blood flow and brain surface PO2 in the presence of a focal lesion in rabbits. *Anesth. Analg.* 77, 898–907.

Murtha, L. A., Mcleod, D. D., Pepperall, D., Mccann, S. K., Beard, D. J., Tomkins, A. J., et al. (2015). Intracranial pressure elevation after ischemic stroke in rats: cerebral edema is not the only cause, and short-duration mild hypothermia is a highly effective preventive therapy. *J. Cereb. Blood Flow Metab.* 35, 2109–2109. doi: 10.1038/jcbfm.2015.209

Nag, S., Venugopalan, R., and Stewart, D. J. (2007). Increased caveolin-1 expression precedes decreased expression of occludin and claudin-5 during blood-brain barrier breakdown. *Acta Neuropathol.* 114, 459–469. doi: 10.1007/s00401-007-0274-x

Nehls, D. G., Cartwright, M., and Spetzler, R. F. (1986). Experimental primate stroke model. *Neurosurgery* 18:388.

Nimmo, A. J., Cernak, I., Heath, D. L., Hu, X., Bennett, C. J., and Vink, R. (2004). Neurogenic inflammation is associated with development of edema and functional deficits following traumatic brain injury in rats. *Neuropeptides* 38, 40–47. doi: 10.1016/j.npep.2003.12.003

Pfenninger, E. G., Reith, A., Breitig, D., Grunert, A., and Ahnefeld, F. W. (1989). Early changes of intracranial pressure, perfusion pressure, and blood flow after acute head injury. Part 1: an experimental study of the underlying pathophysiology. *J. Neurosurg.* 70, 774–779. doi: 10.3171/jns.1989.70.5.0774

Pittenger, S. T., Swalve, N., Chou, S., Smith, M. D., Hoonakker, A. J., Pudiak, C. M., et al. (2016). Sex differences in neurotensin and substance P following nicotine self-administration in rats. *Synapse* 70, 336–346. doi: 10.1002/syn.21907

Platt, S. R., Holmes, S. P., Howerth, E. W., Duberstein, K. J. J., Dove, C. R., Kinder, H. A., et al. (2014). Development and characterization of a Yucatan miniature

biomedical pig permanent middle cerebral artery occlusion stroke model. *Exp. Trans. Stroke Med.* 6:5. doi: 10.1186/2040-7378-6-5

Povlishock, J. T., Becker, D. P., Sullivan, H. G., and Miller, J. D. (1978). Vascular permeability alterations to horseradish peroxidase in experimental brain injury. *Brain Res.* 153, 223–239. doi: 10.1016/0006-8993(78)90404-3

Quinlan, G. J., Martin, G. S., and Evans, T. W. (2005). Albumin: biochemical properties and therapeutic potential. *Hepatology* 41, 1211–1219. doi: 10.1002/hep.20720

Qureshi, A., Boulos, A., Hanel, R., Suri, M., Yahia, A., Alberico, R., et al. (2004). Randomized comparison of intra-arterial and intravenous thrombolysis in a canine model of acute basilar artery thrombosis. *J Devoted Neuro. Int. Neuroradiol.* 46, 988–995. doi: 10.1007/s00234-004-1180-8

Raslan, A., and Bhardwaj, A. (2007). Medical management of cerebral edema. *Neurosurg. Focus* 22:E12.

Reid, S. J., Patassini, S., Handley, R. R., Rudiger, S. R., Mclaughlan, C. J., Osmand, A., et al. (2013). Further molecular characterisation of the OVT73 transgenic sheep model of Huntington's disease identifies cortical aggregates. *J. Huntington's Dis.* 2:279. doi: 10.3233/JHD-130067

Reinhard, M., Rutsch, S., and Hetzel, A. (2012). Cerebral autoregulation in acute ischemic stroke. *Perspect. Med.* 1:194. doi: 10.1016/j.permed.2012.02.028

Ross, D. T., Meaney, D. F., Sabol, M. K., Smith, D. H., and Gennarelli, T. A. (1994). Distribution of forebrain diffuse axonal injury following inertial closed head injury in miniature swine. *Exp. Neurol.* 126, 291–299.

Sakoh, M., Røhl, L., Gyldensted, C., Gjedde, A., and Ostergaard, L. (2000). Cerebral blood flow and blood volume measured by magnetic resonance imaging bolus tracking after acute stroke in pigs: comparison with (15)OH(2)O positron emission tomography. *Stroke* 31:1958. doi: 10.1161/01.str.31.8.1958

Sandoz, B., Dutshke, J., Liu, Q., Manavis, J., Finnie, J. W., Vink, R., et al. (2012). In vivo biomechanical response of ovine heads to shaken baby syndrome events. *Comput. Methods Biomech. Biomed. Eng.* 15(Suppl. 1), 293–294. doi: 10.1080/10255842.2012.713640

Schifilliti, D., Grasso, G., Conti, A., and Fodale, V. (2010). Anaesthetic-Related Neuroprotection Intravenous or Inhalational Agents? *CNS Drugs* 24, 893–907. doi: 10.2165/11584760-000000000-00000

Simões, A. L. B., Silva, G. A. R., Giorgetto, C., De Cassia Do Carmo-Campos, E., Dias, F. J., and Fazan, V. P. S. (2018). Substance P in dorsal root ganglion neurons in young and adult rats, after nociceptive stimulation during the neonatal period. *Anatom. Record* 301, 849–861. doi: 10.1002/ar.23755

Sorby-Adams, A. J., Leonard, A. V., Hoving, J. W., Yassi, N., Vink, R., Wells, A. J., et al. (2019). NK1-r antagonist treatment comparable to decompressive craniectomy in reducing intracranial pressure following stroke. *Front. Neurosci.* doi: 10.3389/fnins.2019.00681

Sorby-Adams, A. J., Vink, R., and Turner, R. J. (2018). Large animal models of stroke and traumatic brain injury as translational tools. *Am. J. Physiol. Regul. Integr. Comp. Physiol.* 315:R165. doi: 10.1152/ajpregu.00163.2017

Steiner, T., Weber, R., and Krieger, D. (2001). Increased intracerebral pressure following stroke. *Curr. Treat. Options Neurol.* 3, 441–450. doi: 10.1007/s11940-001-0032-7

Suzuki, Y., Yeung, A. C., and Ikeno, F. (2011). The representative porcine model for human cardiovascular disease. *J. Biomed. Biotechnol.* 2011:195483.

Tagaya, M., Liu, K. F., Copeland, B., Seiffert, D., Engler, R., Garcia, J. H., et al. (1997). DNA scission after focal brain ischemia temporal differences in two species. *Stroke* 28:1245. doi: 10.1161/01.str.28.6.1245

Tate, A. J., Fischer, H., Leigh, A. E., and Kendrick, K. M. (2006). Behavioural and neurophysiological evidence for face identity and face emotion processing in animals. *Philos. Trans. Biol. Sci.* 361, 2155–2172. doi: 10.1098/rstb.2006.1937

Turner, R. J., Blumbergs, P. C., Sims, N. R., Helps, S. C., Rodgers, K. M., and Vink, R. (2006). Increased substance P immunoreactivity and edema formation following reversible ischemic stroke. *Acta Neurochir. Suppl.* 96, 263–266. doi: 10.1007/3-211-30714-1_56

Turner, R. J., Helps, S. C., Thornton, E., and Vink, R. (2011). A substance P antagonist improves outcome when administered 4 h after onset of ischemic stroke. *Brain Res.* 1393, 84–90. doi: 10.1016/j.brainres.2011.03.066

Turner, R. J., and Vink, R. (2012). Combined tissue plasminogen activator and an NK1 tachykinin receptor antagonist: an effective treatment for reperfusion injury following acute ischemic stroke in rats. *Neuroscience* 220, 1–10. doi: 10.1016/j.neuroscience.2012.06.047

Turner, R. J., and Vink, R. (2014). NK1 tachykinin receptor treatment is superior to capsaicin pre-treatment in improving functional outcome following acute ischemic stroke. *Neuropeptides* 48, 267–272. doi: 10.1016/j.npep.2014.07.002

Vink, R., Bhatia, K. D., and Reilly, P. L. (2008). The relationship between intracranial pressure and brain oxygenation following traumatic brain injury in sheep. *Acta Neurochir. Suppl.* 102, 189–192. doi: 10.1007/978-3-211-85578-2_37

Vink, R., Gabrielian, L., and Thornton, E. (2017). The role of substance P in secondary pathophysiology after traumatic brain injury. *Front. Neurol.* 8:304. doi: 10.3389/fneur.2017.00304

Vink, R., Young, A., Bennett, C. J., Hu, X., Connor, C. O., Cernak, I., et al. (2003). Neuropeptide release influences brain edema formation after diffuse traumatic brain injury. *Acta Neurochir. Suppl.* 86, 257–260. doi: 10.1007/978-3-7091-0651-8_55

Watanabe, H., Sakoh, M., Andersen, F., Rodell, A., Sørensen, J. C., Østergaard, L., et al. (2007). Statistical mapping of effects of middle cerebral artery occlusion (MCAO) on blood flow and oxygen consumption in porcine brain. *J. Neurosci. Methods* 160, 109–115. doi: 10.1016/j.jneumeth.2006.08.016

Wells, A. J., Vink, R., Blumbergs, P. C., Brophy, B. P., Helps, S. C., Knox, S. J., et al. (2012). A surgical model of permanent and transient middle cerebral artery stroke in the sheep. *PLoS One* 7:e42157. doi: 10.1371/journal.pone.0042157

Wells, A. J., Vink, R., Helps, S., Knox, S. J., Blumbergs, P. C., and Turner, R. J. (2015). Elevated intracranial pressure and cerebral edema following permanent MCA occlusion in an ovine model. *PLoS One* 10:e0130512. doi: 10.1371/journal.pone.0130512

Yuji, K., Chiaki, Y., Masafumi, T., Yasuhiro, H., Akira, N., Go, K., et al. (2001). Serial changes in cerebral blood flow and flow–metabolism uncoupling in primates with acute thromboembolic stroke. *J. Cereb. Blood Flow Metab.* 21:202. doi: 10.1097/00004647-200103000-00003

Yushkevich, P. A., Piven, J., Hazlett, H. C., Smith, R. G., Ho, S., Gee, J. C., et al. (2006). User-guided 3D active contour segmentation of anatomical structures: significantly improved efficiency and reliability. *Neuroimage* 31, 1116–1128. doi: 10.1016/j.neuroimage.2006.01.015

Conflict of Interest Statement: The authors declare that the research was conducted in the absence of any commercial or financial relationships that could be construed as a potential conflict of interest.

Copyright © 2019 Sorby-Adams, Leonard, Elms, Marian, Hoving, Yassi, Vink, Thornton and Turner. This is an open-access article distributed under the terms of the Creative Commons Attribution License (CC BY). The use, distribution or reproduction in other forums is permitted, provided the original author(s) and the copyright owner(s) are credited and that the original publication in this journal is cited, in accordance with accepted academic practice. No use, distribution or reproduction is permitted which does not comply with these terms.

frontiers in Neuroscience

ORIGINAL RESEARCH
published: 16 July 2019
doi: 10.3389/fnins.2019.00718

Intravenous Administration of Human Adipose Derived-Mesenchymal Stem Cells Is Not Efficient in Diabetic or Hypertensive Mice Subjected to Focal Cerebral Ischemia

Gabrielle Mangin[1], Adrien Cogo[1,2], Anaïck Moisan[3], Philippe Bonnin[1,2,4], Benjamin Maïer[1] and Nathalie Kubis[1,2,4] on behalf of the RESSTORE Consortium*

[1] INSERM, U965, CART, Paris, France, [2] INSERM, U1148, Laboratory for Vascular and Translational Science, Universite de Paris, Paris, France, [3] Unité de Thérapie et d'Ingénierie Cellulaire, EFS Auvergne Rhône Alpes, Saint-Ismier, France, [4] Service de Physiologie Clinique-Explorations Fonctionnelles, AP-HP, Hôpital Lariboisière, Paris, France

OPEN ACCESS

Edited by:
Johannes Boltze, University of Warwick, United Kingdom

Reviewed by:
Andrew N. Clarkson, University of Otago, New Zealand
Jan-Kolja Strecker, University of Münster, Germany
Alison Willing, University of South Florida, United States

***Correspondence:**
Nathalie Kubis
nathalie.kubis@aphp.fr

Specialty section:
This article was submitted to Neurodegeneration, a section of the journal Frontiers in Neuroscience

Received: *06 April 2019*
Accepted: *26 June 2019*
Published: *16 July 2019*

Citation:
Mangin G, Cogo A, Moisan A, Bonnin P, Maïer B and Kubis N (2019) Intravenous Administration of Human Adipose Derived-Mesenchymal Stem Cells Is Not Efficient in Diabetic or Hypertensive Mice Subjected to Focal Cerebral Ischemia. Front. Neurosci. 13:718. doi: 10.3389/fnins.2019.00718

As the second cause of death and cognitive decline in industrialized countries, stroke is a major burden for society. Vascular risks factors such as hypertension and diabetes are involved in most stroke patients, aggravate stroke severity, but are still poorly taken into account in preclinical studies. Microangiopathy and sustained inflammation are exacerbated, likely explaining the severity of stroke in those patients. We sought to demonstrate that intravenous administration of human adipose derived-mesenchymal stem cells (hADMSC) that have immunomodulatory properties, could accelerate sensorimotor recovery, prevent long-term spatial memory impairment and promote neurogenesis, in diabetic or hypertensive mice, subjected to permanent middle cerebral artery occlusion (pMCAo). Diabetic (streptozotocin IP) or hypertensive (L-NAME in drinking water) male C57Bl6 mice subjected to pMCAo, were treated by hADMSC (500,000 cells IV) 2 days after cerebral ischemia induction. Infarct volume, neurogenesis, microglial/macrophage density, T-lymphocytes density, astrocytes density, and vessel density were monitored 7 days after cells injection and at 6 weeks. Neurological sensorimotor deficit and spatial memory were assessed until 6 weeks post-stroke. Whatever the vascular risk factor, hADMSC showed no effect on functional sensorimotor recovery or cognitive decline prevention at short or long-term assessment, nor significantly modified neurogenesis, microglial/macrophage, T-lymphocytes, astrocytes, and vessel density. This work is part of a European program (H2020, RESSTORE). We discuss the discrepancy of our results with those obtained in rats and the optimal cell injection time frame, source and type of cells according to the species stroke model. A comprehensive understanding of the mechanisms preventing recovery should help for successful clinical translation, but first could allow identifying good and bad responders to cell therapy in stroke.

Keywords: stroke, cell therapy, adipose tissue, cognitive decline, inflammation, behavior

INTRODUCTION

Stroke is currently the second cause of death and cognitive decline worldwide (Snyder et al., 2015; World Health Organization [WHO], 2018). Recanalization treatments, either by rtPA (recombinant tissue plasminogen activator) or thrombectomy, can only be used at the acute phase, with less than 10% of patients being concerned (Bhaskar et al., 2018). In that context, cell therapy, using stem cells/progenitors or differentiated cells, was developed in order to potentially repair tissue damage and improve neurological outcome taking advantage of a wider therapeutic window (Mangin and Kubis, 2018).

Among them, mesenchymal stem cells (MSCs) are particularly attractive. They are multipotent cells capable of differentiating into at least one differentiated cell type depending on environmental conditions (Chamberlain et al., 2007). These cells improve neurological deficit after stroke in both mice (Chen et al., 2003) and rats (Li et al., 1999; Cho et al., 2012) but their mechanism of action is still poorly understood, although neurogenesis, angiogenesis and immunomodulation, all contributing to new neuronal networks formation, have been associated to improved neurological recovery (Chen et al., 2014).

Mesenchymal cells derive from multiple sources such as bone marrow, cord blood, or adipose tissue, this last one offering numerous advantages. A large number of cells can be easily collected by liposuccion. Expansion of cells is easier than when MSC are derived from bone marrow (BM-MSC), the other largest source of MSC and they could be more effective than BM-MSC (Mangin et al., 2019). Indeed, they proliferate better *in vitro* and further reduce the cerebral ischemic-related damage in a mouse model of transient middle cerebral artery occlusion (tMCAo) compared to cells isolated from bone marrow (Ikegame et al., 2011). In addition, they showed an excellent safety profile in 8 clinical trials representing 321 patients (Lalu et al., 2012) and their low immunogenicity after allogeneic administration (Pers and Jorgensen, 2013) make them a likely "ready-to-use" therapeutic product.

Up to date, few studies have considered the impact of vascular risk factors on stroke outcome. This is quite surprising since hypertension, the first leading vascular risk factor for stroke, is still dramatically underdiagnosed, with only 32.5% of hypertensive patients being pharmacologically treated and controlled (Chow et al., 2013). Diabetes is another independent risk factor for stroke, tripling its incidence (Mankovsky and Ziegler, 2004). These data are particularly alarming since the diabetic population will double by 2030 (Shaw et al., 2010). These two vascular risk factors are associated with increased disability, death (Knopman et al., 2001; Ettehad et al., 2016) and post-stroke cognitive decline (Gorelick et al., 2011). As hypertensive and diabetic patients are at higher risk of stroke and therefore potential candidates for cell therapy, understanding how vascular risk factors influence donors' cells properties and efficiency is therefore mandatory (Mangin and Kubis, 2018).

This work if part of a H2020 program (RESSTORE) that includes clinical and preclinical work-packages, and whose aim is to assess the efficiency of cell therapy in stroke taken into account vascular risk factors. Preclinical evaluation complied with the STAIRS (Liu et al., 2009) and STEPS II (Savitz et al., 2011) recommendations. Mesenchymal stem cells derived from human adipose tissue (hADMSC) obtained from healthy donor, were injected intravenously 2 days after induction of a focal cerebral ischemia in mice in which hypertension or diabetes had been previously induced. The primary objective of our work was to evaluate the short (1 week) and long-term (6 weeks) consequences on neurological sensorimotor and cognitive decline and on stroke volume. Neurogenesis, inflammation, and angiogenesis were secondarily evaluated.

MATERIALS AND METHODS

All experiments and surgical procedures were performed according to the European Community Directive (2010/63/EU), the ARRIVE (Animal Research Reporting In Vivo Experiments) guidelines, and the French national guidelines for the care and use of laboratory animals. The study was specifically approved by our local institutional ethics committee (CE121#/17581v6) and by the French ministry of Higher Education for Research and Innovation (APAFIS#5431-2016031912549126 v2).

Experimental Design

The experimental design is summarized in **Figure 1**. Experiments were performed on male adult C57/BL6 mice (Janvier Labs, Le Genest-Saint-Isle, France) housed in a 12 h/light/dark cycle with food and water *ad libitum*. Prior to stroke, either hypertension or diabetes was induced. The duration of sustained hyperglycemia and elevated blood pressure were determined to be the minimal duration to induce an increased sensorimotor deficit compared to age-matched mice without vascular risk factors. Because timing differed between diabetic (2 months) and hypertensive mice (4 months), control groups were matched with age. At day 0 (D0), permanent occlusion of middle cerebral artery was performed. At day 1 (D1), mice undergone cerebral MRI to be randomized in treated or untreated groups, according to the infarct volume and IV hADMSC or PBS were intravenously (IV) delivered the day after (D2). Sensorimotor evaluation was conducted from D-1 until D14, open field at D28 and cognitive assessment between D30 and D38. Stroke volume measured after Cresyl violet staining was assessed at day 9 (7 days after hADMSC delivery) and neuroblasts density, microglia/macrophages cells density, T-Lymphocytes density, astrocytes density, and vessels density assessment were performed 1-week post-hADMSC delivery (9 days post-stroke, D9) or 40 days post-stroke (D40), i.e., at the end of the cognitive assessment period, to evaluate the histological consequences of hADMSC injection. Thus, a subset of mice was sacrificed at D9 and another at D40 for histological and immunohistochemical analyses.

The following groups were evaluated: untreated non-diabetic (ND-PBS) and diabetic (D-PBS) mice and treated non-diabetic (ND-hADMSC) and diabetic (D-hADMSC) mice; untreated non-hypertensive (NHT-PBS) and hypertensive (HT-PBS) mice and treated non-hypertensive mice (NHT-hADMSC) and hypertensive mice (HT-hADMSC).

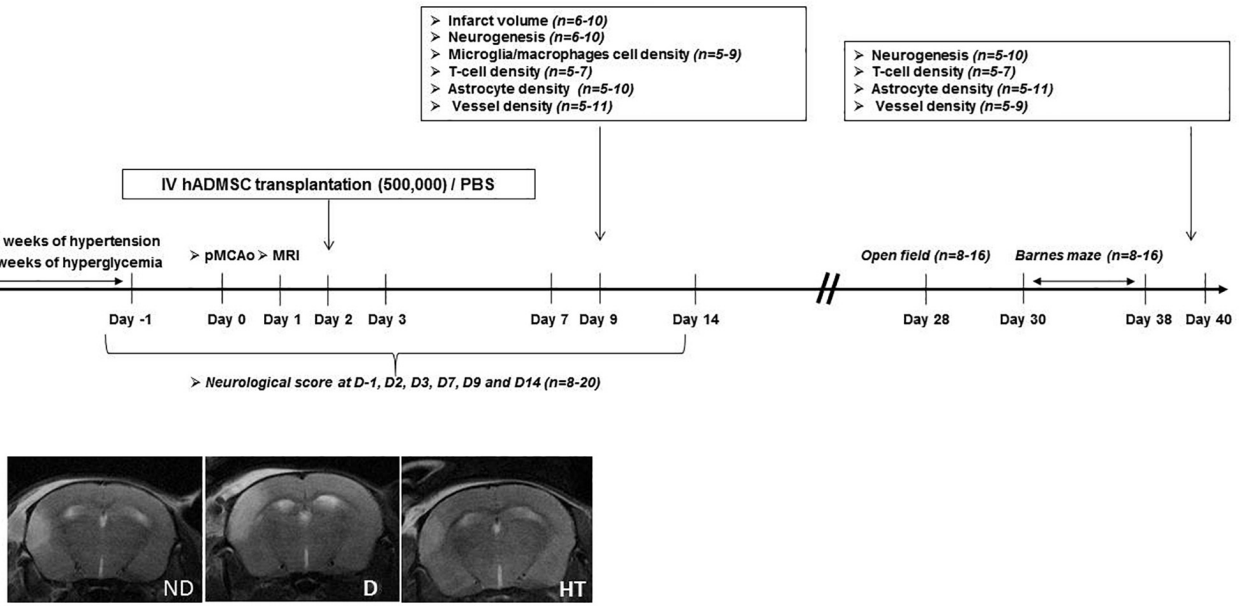

FIGURE 1 | Experimental protocol and time schedule for hypertensive and diabetic mice. hADMSC, human adipose derived mesenchymal stem cells; pMCAo, permanent, middle cerebral artery occlusion; n, number of mice.

In a separate set of diabetic and hypertensive mice, vasoreactivity was assessed after 8 weeks of diabetes and hypertension induction, by measuring with Doppler ultrasound the variations of mean blood flow velocity at the basilar trunk after CO_2 inhalation.

All experiments were conducted by investigators blinded to the status (diabetic and non-diabetic, hypertensive, and non-hypertensive) and the treatment (hADMSC or PBS).

Diabetes Induction

At 6 weeks of age, C57Bl6/J mice were randomized to receive for five consecutive days intraperitoneal (IP) injections of STZ (60 mg/kg in 100 μL of citrate buffer) to induce diabetes or 100 μL of citrate buffer for non-diabetic mice. To ensure that mice became diabetic, blood glucose levels were monitored once a week by collecting blood through a skin incision at the tail. Only mice with sustained hyperglycemia above 300 mg/dL were considered as diabetic (90% of treated mice).

Hypertension Induction

At 6 weeks of age, C57Bl6/J mice were randomized to receive during 16 weeks L-NAME [*N*(G)-nitro-L-arginine methyl ester, 60 mg/kg/day] in drinking water to induce hypertension, or without L-NAME for the non-hypertensive mice. Systolic and diastolic blood pressure and heart rate were measured after 2 weeks of habituation once a week until sacrifice, using a tail-cuff plethysmograph connected to a computerized system (BP-2000 computerized system, Visitech Systems, Apex, NC, United States). Measurements were performed in vigil mice, placed on a heating blanket. All mice became hypertensive.

Doppler Imaging of Cerebral Vasoreactivity to Inhaled CO_2

Cerebral vasoreactivity was assessed in all groups after 8 weeks of hyperglycemia and hypertension induction as previously described (Poittevin et al., 2015). This time point was previously determined in preliminary studies to be the shortest time to impair vasoreactivity. Ultrasound measurements were performed under 0.5% isoflurane anesthesia, using an echocardiograph (Acuson S3000, Siemens, Erlangen, Germany), equipped with a 14-MHz probe (14L5 SP). As previously described, time-averaged mean blood flow velocities were measured at the basilar trunk under air and after 5 min of breathing a gas mixture of 16% O_2, 5% CO_2, and 70% N_2.

Permanent Middle Cerebral Artery (pMCAo) Induction

This procedure has already been fully described (Poittevin et al., 2013). Briefly, at D0, mice were anesthetized by isoflurane (initially 2%, followed by 1.5 to 1.8% in O_2) and body temperature was continuously maintained at 37 ± 0.5°C during the whole procedure using a heating blanket (Homeothermic Blanket Control Unit; Harvard Apparatus Limited, United Kingdom). The permanent focal cerebral ischemia was induced by electrocoagulation of the left middle cerebral artery. The whole procedure did not exceed 10 min.

Cerebral MRI

MR examinations were performed at D1 at the FRIM plateform using a 7.0 Tesla MR unit (PharmaScan, Bruker Biospin, Ettlingen, Germany) equipped with a surface coil with an internal diameter of 10 mm, in thermoregulated and anesthetized

(2% isoflurane in O_2) mice. T2-weighted imaging [Rapid Imaging with Refocused Echoies (RARE) sequence was used with the following parameters: effective TE: 33 ms, TR: 2742 ms, NEX: 1, Flip angle: 180°] was performed in order to measure infarct volume (Medical Image Processing, Analysis and Visualization or MIPAV software, NIH, Bethesda, MD, United States) and T2*-weighted imaging [a Fast Low Angle Shot (FLASH) sequence was used with the following parameters: 15 axial slices 1 mm thick, TE: 8 ms, TR: 600 ms, NEX: 2, Flip angle: 30°, FOV: 2 cm × 2 cm, MTX: 256 × 256] to verify that there was no hemorrhage in any of these mice.

hADMSC Collection

Adipose tissue was harvested from the subcutaneous abdominal adipose tissue by lipo-aspiration from one young healthy female then transferred to the cell therapy unit for digestion. Negativity of the donor for HIV1/2, HBV, HCV, HTLV1/2, HSV1/2, Syphilis, CMV, and EBV serology was verified in order to be compliant with the Directive 2006/17/EC. At the end of the aspiration procedure, adipose tissue was transferred to the Etablissement Français du Sang (EFS) cell therapy unit for digestion according to an internal procedure. The adipose tissue stem cell line RESSTORE01 (Master Cell Bank/Stock no. 1—Donor RESSSTORE01, Batch no. 591133643763) was cultured in the growth medium Alpha MEM (Macopharma) supplemented with 5% human platelet lysate (Stemulate, Cook Medical, United States). The medium was changed twice each week and cells were passaged when they reached (85%) confluence. The cells were detached with TrypLE Select (Life Technologies) for 7–10 min. The RESSTORE01 cell phenotype was analyzed with flow cytometry (FACS Canto II, BD Biosciences) at passage P1. The BD Stemflow hMSC Analysis kit (ref: 562245, Becton Dickinson) was used to phenotype the ADSC that were characterized by the expression of the surface markers CD73, CD44, CD105, and CD90. In addition, in order to identify non-mesenchymal cell contamination, specific markers of monocytes/macrophages (CD11b), lymphocytes (CD19), pan-leucocytes (CD45), hematopoietic stem cells (CD34), and HLA-DR were performed. The expression of these positive markers should be ≥90% and ≤5% for the negative markers. These specifications have been established based on the recommendations of the International Society for Cellular Therapy. These hADMSC were harvested after expansion in MEMα medium (Thermofisher) and human platelet lysate 5% (Cook Regentec). At D2 post-stroke 500,000 cells in 0.2 mL PBS were administered through the retroorbital vein.

Sensorimotor Deficit Assessment

Mice underwent a neurological evaluation consisting of five tests: neurological score, grip and string test, beam walking test and pole test, currently used in our laboratory (Poittevin et al., 2013, 2015; Hilal et al., 2018) and that have been fully described elsewhere (Frechou et al., 2019). The maximum global score was 19, with the lower neurologic score corresponding to a more severe deficit. The assessment was performed at D-1 (habituation stage, the mouse being its own control), D2 (just before cell infusion), D3, D7, D9, and D14 in all groups.

Cognitive Assessment

Before testing spatial memory (Barnes maze), we evaluated the sensorimotor deficit as well as spontaneous locomotor activity (open field) at D28, since residual neurological sensorimotor deficit or anxiety could otherwise introduce a bias in the interpretation of the Barnes maze. Cognitive assessment was performed in a dedicated room where mice were placed 2 weeks before in order to acclimate to the room where they were subjected to a 12 h night-day cycle with food and water provided *ad libitum*.

Open Field

Residual sensorimotor deficit and potential anxiety likely to cause the mice to "freeze," could interfere with the Barnes maze evaluation thus skewing the results. We used the open-field as previously described (Cifuentes et al., 2015). Spontaneous activity (distance traveled in cm and mean velocity in cm/s) was measured automatically for 30 min by an EthoVision XT system and analyzed by EthoVision XT 11.5 tracking software (Noldus, Wageningen, Netherlands). Open field activity was assessed at D28 in all groups that were then tested on the Barnes Maze platform.

Barnes Maze

The Barnes maze is an open space 1 m in diameter, consisting of 20 holes spaced equidistantly around the circumference; one escape box is placed under one of the holes that the mouse will learn to find using visual cues placed in the behavior room. Mice are trained three times a day with a 15-min rest between each trial and recorded with a camera.

As previously described (Cifuentes et al., 2017), at D30, the mouse has to learn the location of the escape box on four consecutive days, named the training phase (1st day to 4th day of evaluation). After 2 days of resting (7th day of evaluation), mice are tested on their ability to recall the place of the escape box, named the retention phase. The next day (8th day), the escape is box is changed from its original location and mice have to adapt, learn and memorize the new location during 2 days (8th day and 9th day). During this last phase or reversal phase, brain plasticity is evaluated. During each phase, the latency to escape (seconds) is measured.

Assessment of Infarct Volume

At D9, 1 week after hADMSC IV administration, mice were transcardiacally perfused with heparinized saline, followed by 4% paraformaldehyde (PFA). Brain was removed, post-fixed overnight in PFA and cryoprotected in 20% sucrose. Coronal 30 μm-thick sections were cut frozen using a cryostat CM 1950 (Leica Biosystems, Nußloch, Germany). Every eight 30 μm-thick floating section was stained with Cresyl violet. Using ImageJ software (National Institutes of Health, Bethesda, MD, United States), the cortical infarct area was measured to calculate the stroke volume (mm^3) by integrating measured areas and distances between sections. Measured infarct volume was corrected for edema with the following formula: corrected infarct volume = measured infarct volume × (contralateral

hemisphere volume/ipsilateral hemisphere volume) as already described (Poittevin et al., 2013).

Assessment of Histological Response to hADMSC

Thirty μm-thick coronal floating sections were incubated with primary antibody overnight at 4°C to detect neuroblasts using anti-doublecortin (DCX) (1:4000, Abcam, Cambridge, United Kingdom); microglial cells using anti-Iba1 (1:200, Wako, Japan), T-lymphocytes using anti-CD3 (1/200, Dako, Santa Clara, United States), astrocytes using anti-GFAP (1:200, Millipore, Burlington, MA, United States) and vessels using the anti-glucose transporter-1 (Glut-1) (1:500, Millipore, Burlington, MA, United States). Appropriate fluorescent-labeled secondary alexa fluor 594 or 488 antibodies (Molecular Probes, Eugene, OR, United States 1:400) were applied for 1 h at room temperature. Specificity was checked by omitting the primary antibody. As doublecortin is expressed in newborn and migrating neurons, we assumed that DCX+ cells reflect neurogenesis (Brown et al., 2003; Jin et al., 2010).

Morphological Analysis

Cells density assessments were conducted blindly (vascular risk factor and treatment) at D9 and D40 and performed on three coronal brain sections at +0.80, −0.80, and −1.20 mm relative to bregma, that consistently contained the infarct area.

Neuroblasts density was assessed by calculating the DCX-positive area (X10) using NIH ImageJ software, in the whole ipsilateral hemisphere to stroke, actually only found in the subventricular zone and along the corpus callosum along which they migrate toward the lesion.

Microglial/macrophage density was assessed by calculating the Iba1-positive area (X5) using NIH ImageJ software in the peri-infarct area.

T-cell density was manually assessed by counting CD3+ cells in each section, actually only present in the infarct area, and expressed as the number of CD3+ cells per section.

Astrocytes density was assessed by calculating the GFAP-positive area in 2 R.O.I (X40) using NIH ImageJ software in the peri-infarct area.

Vessel density was assessed by calculating the GLUT-1-positive area (X20) using NIH ImageJ software in the peri-infarct area.

All calculated areas were expressed as arbitrary units.

Statistical Analysis

Statistical analyses were performed using Prism 7.02 software (GraphPad, San Diego, CA, United States). The data are expressed in mean ± SD. The Shapiro–Wilk normality test was used to assess whether the data corresponded to a Gaussian distribution. Comparisons between the four groups of diabetic mice or of hypertensive mice were analyzed using either ANOVA or a Kruskal–Wallis test. Two-way ANOVA for repeated measures was used to analyze data of the training (1^{st} to 4^{th} days) and reversal (8^{th} to 9^{th} days) phases in the Barnes maze. *Post hoc* analyses were performed using Bonferroni's multiple comparison tests. A value of $p < 0.05$ was considered statistically significant.

RESULTS

Mean glycemia was not significantly different at D-1 between D-PBS (451.7 ± 59.7 mg/dl) and D-hADMSC mice (431.8 ± 50.1 mg/dl). No mice died whatever the group during surgery and during follow-up. hADMSC did not significantly modify glycemia in diabetic mice during follow-up until D40 (460.3 ± 56.6 mg/dl) compared to untreated D-PBS mice (493.3 ± 70.9 mg/dl) (n = 13–14).

Before stroke, systolic and diastolic blood pressure were significantly higher in HT mice (134.9 ± 5.9/89.0 ± 7.2 mmHg) compared to NHT mice (114.0 ± 7.0/78.6 ± 6.2 mmHg) ($p < 0.0001$). After stroke and during follow-up, hADMSC did not significantly modify systolic blood pressure (NHT-PBS: 104.9 ± 14.1 mmHg vs. NHT-hADMSC 111.7 ± 6.3 mmHg; HT-PBS: 138.3 ± 7.2 mmHg vs. HT-hADMSC: 136.2 ± 11.2 mmHg), or diastolic blood pressure (NHT-PBS: 82.1 ± 9.5 mmHg vs. NHT-hADMSC: 80.9 ± 6.5 mmHg; HT-PBS: 86.3 ± 7.3 mmHg vs. HT-hADMSC: 90.1 ± 6.6 mmHg). Heart rate (beats per min) did not differ significantly between groups (NHT-PBS: 536 ± 10 vs. NHT-hADMSC: 522 ± 17 vs. HT-PBS: 518 ± 36 vs. HT-hADMSC 507 ± 35) (n = 18–20). No mice died whatever the group during surgery and during follow-up.

Doppler Imaging of Cerebral Vasoreactivity to Inhaled CO_2

Cerebral vasoreactivity was assessed 8 weeks after the induction of chronic hyperglycemia or chronic hypertension, before cerebral ischemic induction. Mean blood flow velocities at the basilar trunk were not significantly modified after CO_2 inhalation in diabetic mice (air: 12.0 ± 1.7 versus CO_2: 11.0 ± 1.4 cm/s) (n = 7) and in hypertensive mice (air: 15.7 ± 2.2 versus CO_2: 15.8 ± 2.6 cm/s) (n = 14), whereas they were significantly increased when compared to the same control mice (non-diabetic and non-hypertensive mice) (air: 15.4 ± 2.4 versus CO_2: 17.7 ± 2.2 cm/s, p = 0.0001) (n = 9), indicating that in this last group only, CO_2 induced arteriolar vasodilation.

Sensorimotor Deficit

At D2, compared to D-1, we observed a significant reduction in the neurological score in diabetic and hypertensive mice compared to control non-diabetic and non-hypertensive mice, indicating that both diabetes and hypertension induced a more severe sensorimotor deficit compared to mice that were subjected to the same pMCAo stroke model but without vascular risk factor. From D2 to D9, this deficit significantly persisted over time until complete recovery by D14, except in D-PBS that had nevertheless completely recovered by D28. However, whatever the time of evaluation, there was no significant difference in the neurological score between untreated and treated mice whatever the risk factor, indicating that hADMSC had no effect on sensorimotor recovery (**Figures 2A,B** and **Tables 1**, **2**).

Open Field

The ability of mice to spontaneously walk the equivalent distance with similar velocity was verified in the open field,

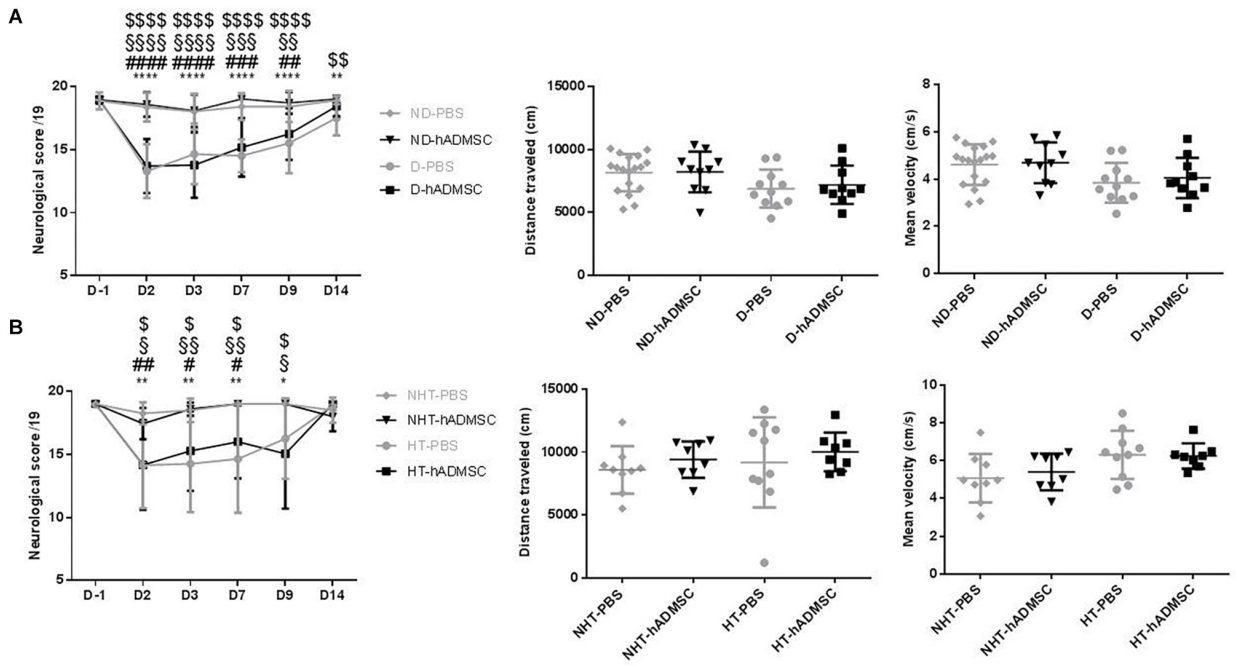

FIGURE 2 | Assessment of sensorimotor deficit between D-1 and D14 and of spontaneous locomotor activity measured at D28 in ND-PBS, untreated non-diabetic mice; ND-hADMSC, treated non-diabetic mice; D-PBS, untreated diabetic mice and D-hADMSC, treated diabetic mice (n = 13–20) **(A)** and NHT-PBS, untreated non-hypertensive mice; NHT-hADMSC, treated non-hypertensive mice; HT-PBS, untreated hypertensive mice and HT-hADMSC, treated hypertensive mice (n = 8–20) **(B)**. Diabetic and hypertensive mice showed a more severe sensorimotor deficit than control mice during the whole evaluation until they fully recovered at D14 except D-PBS mice ($p < 0.01$ versus ND-PBS and $p < 0.01$ versus ND-hADMSC). No differences were evidenced between untreated and treated mice. At D28, no differences were evidenced between mice in the total distance traveled or mean velocity at open field; $^{*}p < 0.05$, $^{**}p < 0.01$, $^{****}p < 0.0001$ between ND-PBS versus D-PBS mice and NHT-PBS versus HT-PBS mice; $^{\#}p < 0.05$, $^{\#\#}p < 0.01$, $^{\#\#\#}p < 0.001$, $^{\#\#\#\#}p < 0.0001$ between ND-PBS versus D-hADMSC and between NHT-PBS versus HT-hADMSC; $^{\S}p < 0.05$, $^{\S\S}p < 0.01$, $^{\S\S\S}p < 0.001$, $^{\S\S\S\S}p < 0.0001$ between ND-hADMSC versus D-PBS and between NHT-hADMSC versus HT-PBS; $^{\$}p < 0.05$, $^{\$\$}p < 0.01$, $^{\$\$\$\$}p < 0.0001$ between ND-hADMSC versus D-hADMSC and NHT-hADMSC versus HT-hADMSC.

before the Barnes Maze evaluation. Indeed, any residual motor impairment could skew the interpretation of spatial long-term memory. No differences were observed between mice in the distance traveled or mean velocity in the diabetic groups or in the hypertensive groups, whether the mice were treated or untreated (**Figures 2A,B**).

Barnes Maze

In the training phase, D-hADMSC had an impaired learning ability at the 2nd and 3rd day compared to ND-PBS ($p < 0.01$ and $p < 0.001$, respectively). At the 3rd day, D-PBS also presented an impairment compared to ND-PBS ($p < 0.05$) and D-hADMSC compared to ND-hADMSC ($p < 0.01$). However, all mice learned the same on the 4th day. In the retention phase, only diabetic mice without treatment showed a delayed latency to escape reflecting an impaired long-term memory ability (ND-PBS versus D-PBS, $p < 0.001$). D-hADMSC did not show differences compared to non-diabetic mice, nor with D-PBS mice. On the reversal phase, all diabetic mice had an impaired cerebral plasticity compared to non-diabetic mice (ND-PBS versus D-PBS, $p < 0.01$; ND-PBS

TABLE 1 | Sensorimotor assessment in diabetic mice.

Day	ND-PBS (n = 20)	ND-hADMSC (n = 16)	D-PBS (n = 14)	D-hADMSC (n = 13)
D-1	18.85 ± 0.67	18.94 ± 0.25	19.00 ± 0.00	18.92 ± 0.28
D2	18.35 ± 1.14	18.56 ± 0.96	13.29 ± 2.13	13.69 ± 2.14
D3	18.00 ± 1.41	18.06 ± 1.29	14.64 ± 2.41	13.77 ± 2.59
D7	18.40 ± 1.08	19.00 ± 0.00	14.50 ± 1.31	15.17 ± 2.38
D9	18.40 ± 1.23	18.69 ± 0.87	15.50 ± 2.38	16.23 ± 2.048
D14	18.90 ± 0.32	19.00 ± 0.00	17.50 ± 1.38	18.43 ± 0.79

Control diabetic (D-PBS) and non-diabetic (ND-PBS) mice, treated diabetic (D-hADMSC), and non-diabetic mice (ND-hADMSC).

TABLE 2 | Sensorimotor assessment in hypertensive mice.

Days	NHT-PBS (n = 8)	NHT-hADMSC (n = 10)	HT-PBS (n = 20)	HT-hADMSC (n = 18)
D-1	19.00 ± 0,00	18.89 ± 0.33	19.00 ± 0.00	19.00 ± 0.00
D2	18.25 ± 0.89	17.44 ± 1.24	14.15 ± 3.41	14.17 ± 3.55
D3	18.50 ± 0.93	18.60 ± 0.52	14.25 ± 3,82	15.28 ± 3.16
D7	19.00 ± 0.00	19.00 ± 0.00	14.65 ± 4.27	16.00 ± 2.89
D9	19.00 ± 0.00	19.00 ± 0.00	16.25 ± 3.19	15.50 ± 4.32

Control hypertensive (HT-PBS) and non-hypertensive mice (NHT-PBS) and treated hypertensive (HT-hADMSC) and non-hypertensive mice (NHT-hADMSC).

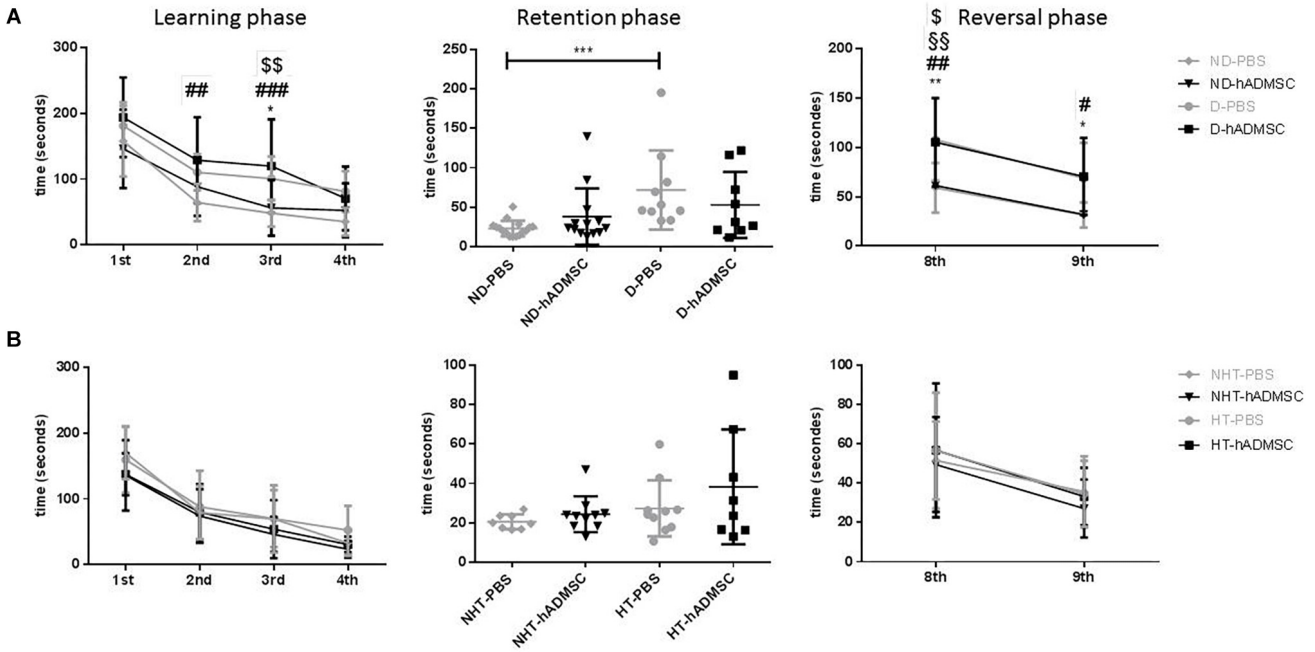

FIGURE 3 | Assessment of long-term spatial memory between D30 and D38 in ND-PBS, untreated non-diabetic mice; ND-hADMSC, treated non-diabetic mice; D-PBS, untreated diabetic mice and D-hADMSC, treated diabetic mice (n = 9–16) **(A)** and NHT-PBS, untreated non-hypertensive mice; NHT-hADMSC, treated non-hypertensive mice; HT-PBS, untreated hypertensive mice and HT-hADMSC, treated hypertensive mice (n = 8–10) **(B)**. hADMSC did not significantly modify the latency to escape of pMCAo mice whatever the risk factor; $^{*}p < 0.05$, $^{**}p < 0.01$, $^{***}p < 0.001$, ND-PBS versus D-PBS; $^{\#}p < 0.05$, $^{\#\#}p < 0.01$, $^{\#\#\#}p < 0.001$, $^{\#\#\#\#}p < 0.0001$ ND-PBS versus D-hADMSC; $^{\S}p < 0.05$, $^{\S\S}p < 0.01$, $^{\S\S\S}p < 0.001$, $^{\S\S\S\S}p < 0.0001$ ND-hADMSC versus D-PBS; $^{\$}p < 0.05$, $^{\$\$}p < 0.01$, $^{\$\$\$}p < 0.001$, $^{\$\$\$\$}p < 0.0001$ ND-hADMSC versus D-hADMSC.

versus D-hADMSC, $p < 0.01$; ND-hADMSC versus D-PBS, $p < 0.01$; ND-hADMSC versus D-hADMSC, $p < 0.05$). This impairment was also present on the 9th day for D-PBS mice and D-hADMSC compared to ND-PBS mice ($p < 0.05$) (**Figure 3A** and **Table 3**).

To summarize, hADMSC injected intravenously 2 days after a focal cerebral ischemia failed to protect from post-stroke cognitive impairment in diabetic mice.

In hypertensive mice, we evidenced no differences in the training phase, the retention phase or the reversal phase between the four groups, indicating that 16 weeks of hypertension did not induce a worse post-stroke cognitive impairment compared to non-hypertensive mice subjected to a focal cerebral ischemia. As we have previously shown (Mangin et al., 2019) that pMCAo mice, without vascular risk factor, does not have significantly modified scores at Barnes Maze, our results would indicate that our model did not produce cognitive impairment in hypertensive mice. The effect of hADSMC could therefore not be evaluated (**Figure 3B** and **Table 4**).

Infarct Volume

Infarct volume was not significantly modified at day 9 in the diabetic groups or in the hypertensive groups, whether the mice were treated or untreated (**Figure 4**).

TABLE 3 | Barnes maze in diabetic mice.

Days	ND-PBS (n = 16)	ND-hADMSC (n = 13)	D-PBS (n = 10)	D-hADMSC (n = 9)
1st	157.80 ± 53.71	146.00 ± 59.73	181.20 ± 35.50	194.00 ± 60.40
2nd	64.60 ± 28.10	88.63 ± 44.34	110.50 ± 27.29	128.90 ± 65.16
3rd	48.35 ± 20.47	56.46 ± 42.37	101.00 ± 33.31	119.90 ± 70.87
4th	35.26 ± 20.97	52.70 ± 40.81	81.38 ± 30.90	70.76 ± 48.27
7th	23.23 ± 9.85	38.29 ± 35.77	71.80 ± 50.08	53.02 ± 41.96
8th	59.09 ± 25.23	61.35 ± 30.93	107.90 ± 41.58	105.30 ± 44.89
9th	31.53 ± 12.80	32.13 ± 17.95	72.71 ± 32.68	57.20 ± 43.07

Control diabetic (D-PBS) and non-diabetic (ND-PBS) mice, treated diabetic (D-hADMSC), and non-diabetic mice (ND-hADMSC).

TABLE 4 | Barnes maze in hypertensive mice.

Days	NHT-PBS (n = 9)	NHT-hADMSC (n = 10)	HT-PBS (n = 10)	HT-hADMSC (n = 8)
1st	170.20 ± 40.06	135.80 ± 53.44	159.60 ± 50.13	137.40 ± 31.63
2nd	79.38 ± 40.17	74.10 ± 40.59	88.22 ± 54.67	80.18 ± 42.32
3rd	69.61 ± 51.14	46.22 ± 26.37	70.14 ± 43.29	54.19 ± 44.01
4th	33.09 ± 19.45	23.67 ± 12.43	52.63 ± 37.05	30.92 ± 12.06
7th	20.60 ± 3.76	24.46 ± 9.08	27.13 ± 14.28	38.32 ± 29.13
8th	51.53 ± 19.76	49.45 ± 24.09	56.59 ± 29.37	56.67 ± 34.05
9th	35.75 ± 17.88	27.12 ± 14.78	33.20 ± 14.60	34.47 ± 16.90

Control hypertensive (HT-PBS) and non-hypertensive mice (NHT-PBS) and treated hypertensive (HT-hADMSC), and non-hypertensive mice (NHT-hADMSC).

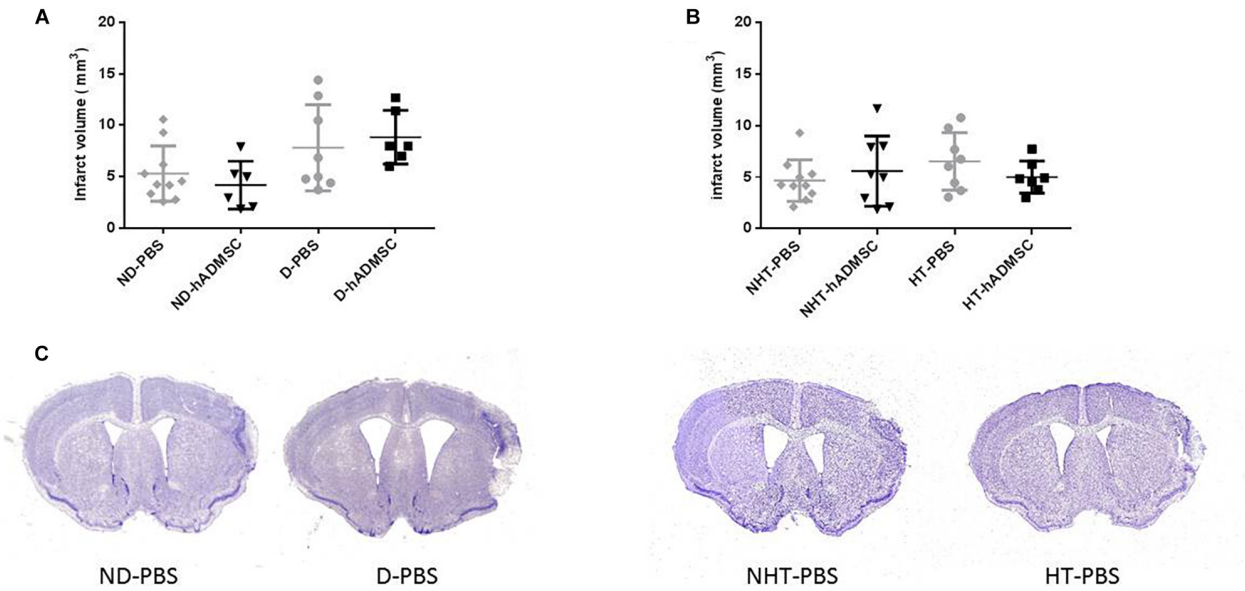

FIGURE 4 | Assessment of infarct volume at D9 in ND-PBS, untreated non-diabetic mice; ND-hADMSC, treated non-diabetic mice; D-PBS, untreated diabetic mice and D-hADMSC, treated diabetic mice (n = 6–10) **(A)** and NHT-PBS, untreated non-hypertensive mice; NHT-hADMSC, treated non-hypertensive mice; HT-PBS, untreated hypertensive mice and HT-hADMSC, treated hypertensive mice (n = 7–10) **(B)**. hADMSC did not significantly reduce infarct volume whatever the risk factor. Representative crésyl violet sections of infarct areas for non-diabetic, diabetic, non-hypertensive, and hypertensive mice **(C)**.

Neurogenesis, Microglial/Macrophages, T Lymphocytes, Astrocytes, and Vessel Density and Were Not Significantly Modified by hADMSC in Diabetic and Hypertensive Mice

Neurogenesis

Comparison of the DCX-positive area was performed in order to assess neurogenesis between groups. At D9, no differences were evidenced between untreated and treated non-diabetic and diabetic mice and between untreated and treated non-hypertensive and hypertensive mice.

At D40, there was an overall ANOVA significance between untreated and treated non-diabetic and diabetic mice ($p < 0.01$). The DCX-positive area was significantly increased in D-hADMSC mice (1.6 ± 0.28 mm^3) compared to ND-PBS mice (0.42 ± 0.40 mm^3) ($p < 0.001$), whereas there was no significant difference with the other groups (1.01 ± 0.51 mm^3, ND-hADMSC mice; 1.14 ± 0.57 mm^3, D-PBS mice). No differences were evidenced between untreated and treated non-hypertensive and hypertensive mice.

Between D9 and D40, there was a significant reduction in neuroblasts density in ND-PBS ($p < 0.001$), ND-hADMSC ($p < 0.05$), D-PBS ($p < 0.05$) and D-hADMSC mice ($p < 0.05$), and in NHT-PBS ($p < 0.05$) and NHT-hADMSC mice ($p < 0.01$); no differences were observed in HT-PBS and HT-hADMSC mice over time (**Figure 5**).

Microglial/Macrophages Density

Comparison of the Iba1-positive area was performed in order to assess microglial/macrophages density between groups. Microglia/macrophage cells (Iba1+) adopted a round amoeboid shape in the peri-infarct area, indicating a change in the state of activation. At D9, no differences were evidenced between untreated and treated non-diabetic and diabetic mice or between untreated and treated non-hypertensive and hypertensive mice (**Figure 6**).

At D40, rare microglial/macrophages were evidenced on sections, and therefore no quantification was performed.

T Lymphocytes Density

Comparison of CD3+ cells density was performed in order to assess T lymphocytes density between groups. At D9, no differences were evidenced between untreated and treated non-diabetic and diabetic mice or between untreated or treated non-hypertensive or hypertensive mice.

At D40, no differences were evidenced between untreated and treated non-diabetic and diabetic mice or between untreated or treated non-hypertensive or hypertensive mice.

Between D40 and D9, there was a significant increase in CD3+ cells density in D-PBS mice (84.3 ± 58/section versus 40.6 ± 15.0/section) ($p < 0.05$) only, whereas there were no significant differences in the CD3+ cells density between treated diabetic mice and untreated or treated non-diabetic mice. No differences were observed between untreated or treated non-hypertensive or hypertensive mice overtime (**Figure 7**).

Astrocytes Density

Comparison of the GFAP-positive area was performed in order to assess astrocytes density between groups. Activated astrocytes only were considered, when they adopted a narrow cell body and thickened their branches. At D9, no differences were

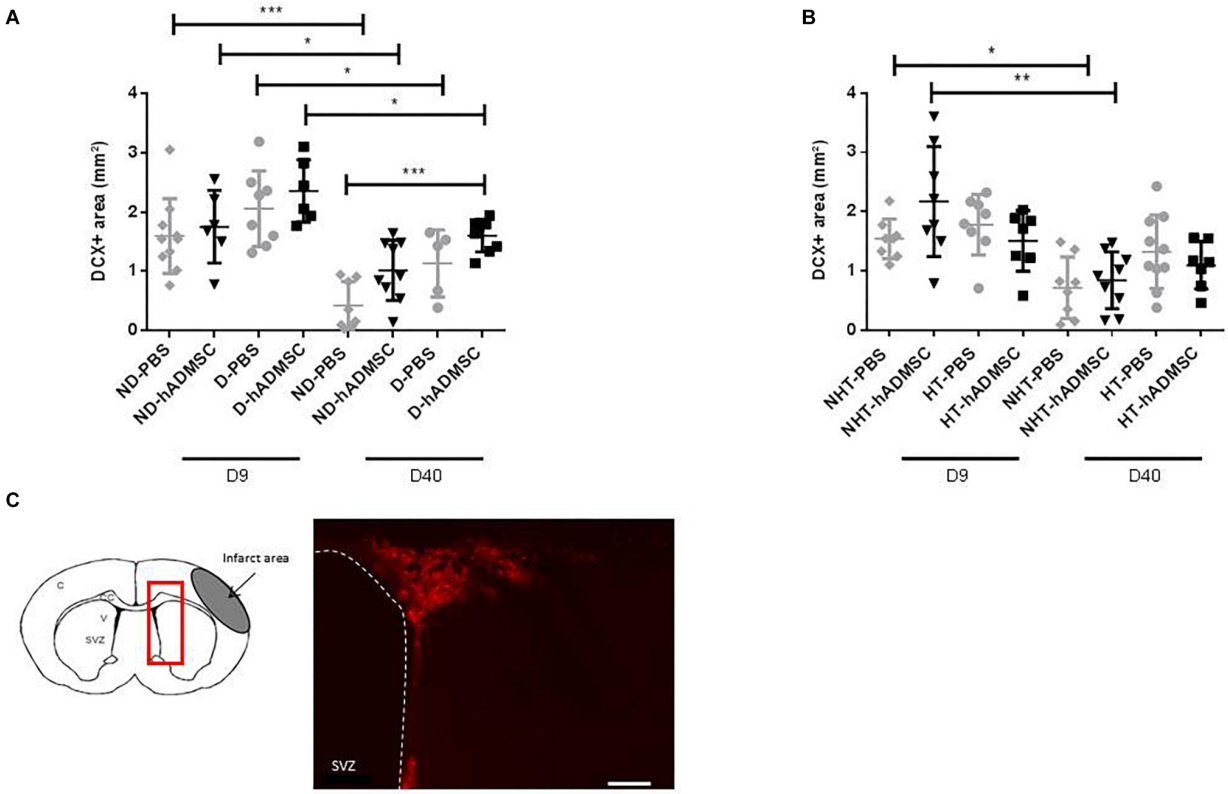

FIGURE 5 | Assessment of neuroblasts density at D9 and D40 in ND-PBS, untreated non-diabetic mice; ND-hADMSC, treated non-diabetic mice; D-PBS, untreated diabetic mice and D-hADMSC, treated diabetic mice (D9: n = 6–10, D40: n = 5–9) **(A)** and NHT-PBS, untreated non-hypertensive mice; NHT-hADMSC, treated non-hypertensive mice; HT-PBS, untreated hypertensive mice and HT-hADMSC, treated hypertensive mice (D9: n = 7–8, D40: n = 7–10) **(B)**. hADMSC did not significantly increase neuroblasts density except at D40 in D-hADMSC mice compared to ND-PBS mice. Between D9 and D40, a significant decrease in neuroblasts density was evidenced in ND-PBS, $p < 0.001$; ND-hADMSC, $p < 0.05$; D-PBS, $p < 0.05$; D-hADMSC, $p < 0.05$) and in NHT-PBS ($p < 0.05$) and NHT-hADMSC ($p < 0.01$). *$p < 0.05$, **$p < 0.01$, ***$p < 0.001$. DCX immunostaining in the SVZ of untreated diabetic mice, at D9 and at D40, scale bar: 50 μm; C, cortex; V, ventricle; SVZ, subventricular zone; red square, region of interest **(C)**.

evidenced between untreated and treated non-diabetic and diabetic mice. There was an overall significant difference between untreated or treated non-hypertensive or hypertensive mice ($p = 0.02$) and the GFAP-positive area was significantly decreased in HT-PBS (2.59 ± 0.35 A.U.) compared to NHT-PBS mice (8.06 ± 4.58 A.U.) ($p < 0.05$). No differences were evidenced with the other groups.

At D40, no differences were evidenced between untreated and treated non-diabetic and diabetic mice. There was an overall significant difference between untreated or treated non-hypertensive or hypertensive mice ($p = 0.015$) and the GFAP-positive area was significantly increased in HT-hADMSC mice (12.07 ± 2.43 A.U.) versus NHT-PBS mice (5.22 ± 4.52 A.U.) ($p < 0.05$), whereas no differences were evidenced with the other groups.

Between D40 and D9, the GFAP-positive area was significantly reduced in ND-PBS (2.04 ± 0.94 A.U. versus 10.90 ± 4.01 A.U.) ($p < 0.0001$), ND-hADMSC (2.79 ± 1.85 A.U. versus 9.72 ± 5.95 A.U.) ($p < 0.05$), D-PBS (2.34 ± 1.56 A.U. versus 10.49 ± 2.87 A.U.) ($p < 0.01$), and D-hADMSC (4.26 ± 1.74 A.U. versus 8.15 ± 0.80 A.U.) ($p < 0.01$) mice. By contrast, the GFAP-positive area was significantly increased in HT-PBS mice (13.47 ± 4.34 A.U. versus 2.59 ± 0.35 A.U.) ($p < 0.01$) and HT-hADMSC mice (12.07 ± 2.43 A.U. versus 5.49 ± 2.31 A.U.) ($p < 0.001$) (**Figure 8**).

Vessel Density

Comparison of the GLUT-1-positive area was performed in order to assess vessel density between groups. At D9 or at D40, no differences were evidenced between untreated and treated non-diabetic and diabetic mice or between untreated or treated non-hypertensive or hypertensive mice.

Between D9 and D40, no differences in the GLUT-1-positive area were evidenced between untreated and treated non-diabetic and diabetic mice or between untreated or treated non-hypertensive or hypertensive mice (**Figure 9**).

DISCUSSION

We showed that IV administration of hADMSC 2 days after focal cerebral ischemia induction did not significantly modify infarct

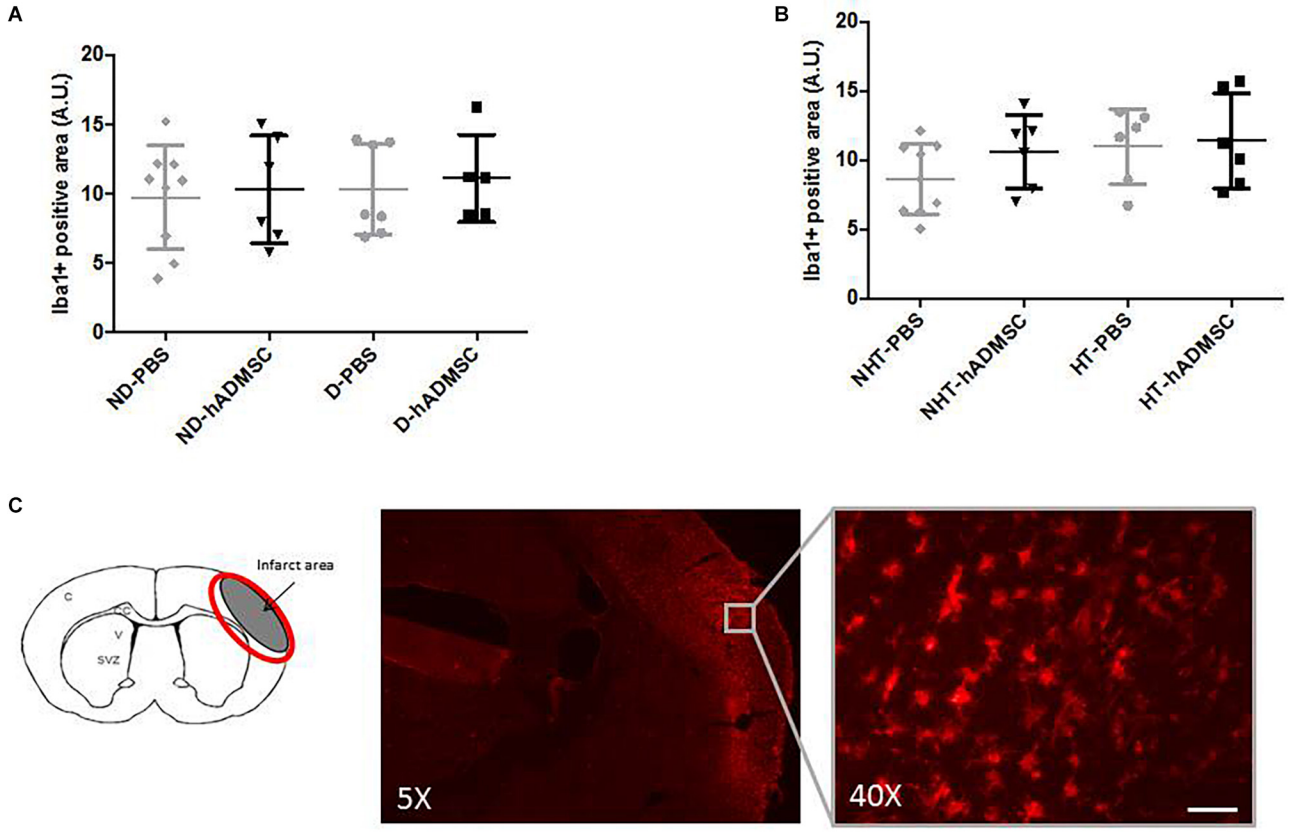

FIGURE 6 | Assessment of Iba1+ cell density at D9 in ND-PBS, untreated non-diabetic mice; ND-hADMSC, treated non-diabetic mice; D-PBS, untreated diabetic mice and D-hADMSC, treated diabetic mice (n = 5–9) **(A)** and NHT-PBS, untreated non-hypertensive mice; NHT-hADMSC, treated non-hypertensive mice; HT-PBS, untreated hypertensive mice and HT-hADMSC, treated hypertensive mice (n = 6–9) **(B)**. No significant reduction in microglia/macrophages density by hADMSC was evidenced whatever the risk factor. Iba1 immunostaining in D-PBS mice with magnification showing amoeboid cells, scale bar: 50 μm; C, cortex; V, ventricle; SVZ, subventricular zone; red circle: region of interest **(C)**.

volume, short and long-term functional outcome in diabetic or hypertensive mice neither was associated with significant modification of neurogenesis, inflammatory cells density or angiogenesis, whatever the analysis time frame.

Most of preclinical studies investigating the beneficial effect of cell therapy have been performed in healthy young male rodents, even when vascular risk factors are known to worsen the infarct lesion, functional outcome and mortality, and therefore question the efficiency of cell therapy. We have used a diabetic stroke model that we previously characterized (Poittevin et al., 2015). Streptozotocin induced chronic hyperglycemia was associated after 8 weeks to impaired vasoreactivity and decreased brain eNOS and nNOS expression. After stroke induction, diabetic mice had an increased sensori-motor disability (Poittevin et al., 2015) and presented cognitive impairment at D30 compared to non-diabetic mice (Mangin et al., 2019). For the hypertensive model, we used L-NAME in daily drinking water that induced chronic mild hypertension, rather than chronic infusion of angiotensin 2 that is responsible for a more severe hypertension and requires additional surgery for angiotensin 2 pump implantation (Cifuentes et al., 2015, 2017). This model was also associated with impaired vasoreactivity after 8 weeks, but to achieve a sensori-motor impairment in our experimental conditions, we had to administer L-NAME during 16 weeks.

Cell therapy in post-stroke diabetic rodents has already been investigated using various cell types, sources and administration pathways. Allogenic bone-marrow derived MSC (BM-MSC) from healthy rats have been intravenously injected 1 day after stroke in type 1 diabetic rats, and 3 days after stroke in type 2 diabetic rats subjected to tMCAo. In the first case, blood-brain-barrier permeability and mortality were increased with an opposite outcome in the second case (Chen et al., 2011; Ding et al., 2016). In type 2 diabetic rats, xenogenic human BM-MSC that were IV delivered 3 days after a tMCAo, significantly improved neurological function without affecting infarct volume. Endothelial progenitor cells (EPCs) isolated from human umbilical cord blood and IV delivered immediately after reperfusion in type 1 diabetic mice subjected to a tMCAo, reduced blood-brain barrier leakage, reduced infarct volume and attenuated neurological impairment (Geng et al., 2017). By contrast, intraarterial delivery of allogenic BM-EPC in type 2 diabetic mice, 24 h after induction of a photothrombotic stroke, failed to significantly improve behavioral scores and infarct volume (Bai et al., 2015). Diabetes models, stroke models, species,

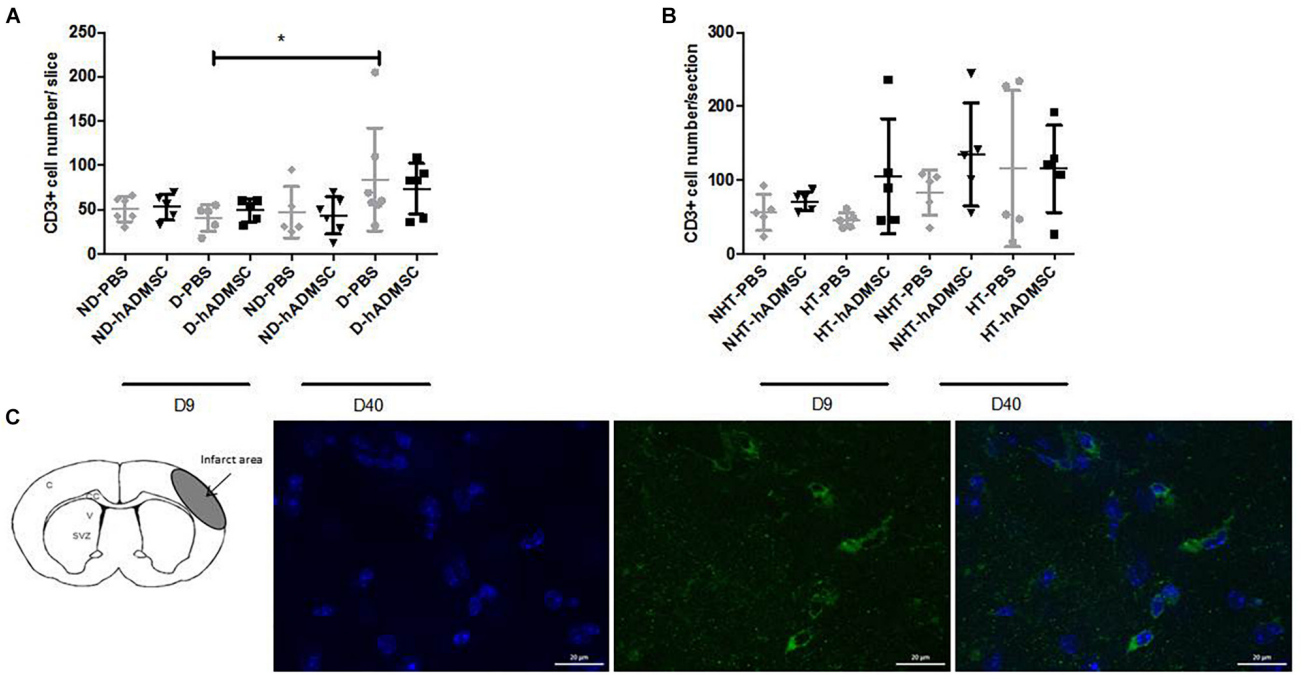

FIGURE 7 | Assessment of CD3+ cells density at D9 and D40 in ND-PBS, untreated non-diabetic mice; ND-hADMSC, treated non-diabetic mice; D-PBS, untreated diabetic mice and D-hADMSC, treated diabetic mice (D9: $n = 5–6$, D40: $n = 5–7$) **(A)** and NHT-PBS, untreated non-hypertensive mice; NHT-hADMSC, treated non-hypertensive mice; HT-PBS, untreated hypertensive mice and HT-hADMSC, treated hypertensive mice (D9: $n = 5–7$, D40: $n = 5$) **(B)**. hADMSC did not significantly modify the T-lymphocytes density whatever the risk factor. Between D9 and D40, there was a significant increase in T-lymphocytes density in D-PBS mice ($^*p < 0.05$). From left to right, DAPI, CD3 and merge immunostaining, scale bar: 20 μm; C, cortex; V, ventricle; SVZ, subventricular zone **(C).**

delay of injection after stroke and allograft versus xenograft differed between studies and with ours, precluding direct comparison. Interestingly, xenograft or delayed injection of BM-MSC, up to 3 days, in diabetic animals, was not an impediment to improved outcome. Cell therapy in hypertensive rodents have only been investigated in spontaneously hypertensive rats. BM-derived mononuclear cells did not succeed in demonstrating sensori-motor improvement when IV transplanted 1 h after induction of a photothrombotic stroke (Diederich et al., 2014) or IV transplanted 3 h after reperfusion in a tMCAo stroke model (Minnerup et al., 2014), nor did umbilical cord blood mononuclear cells (Weise et al., 2014). Only maternal placenta derived MSC that were intravenously administered, led to an improvement of functional outcome (Kranz et al., 2010). These mitigate results underline the necessity to integrate co-morbidity factors into stroke models.

The source of MSC may matter. Adipose tissue is an interesting alternative donor tissue to bone marrow. Lipoaspiration allows easy collection of great quantities of cells (Mangin and Kubis, 2018). In addition, and in a translational point of view, ADMSC have a low immunogenicity profile enabling allogeneic administration with good tolerance. When transplanted in a tMCAo model, allogenic ADMSC IV delivered soon after reperfusion, showed a remarkable attenuation of ischemic damage compared to BM-MSC treated mice (Ikegame et al., 2011). In rats, a beneficial effect of ADMSC was observed whatever the IV (Gutierrez-Fernandez et al., 2015) or IA (Huang et al., 2017) administration, in a pMCAo and tMCAo model, respectively. Interestingly, xenogeneic ADMSC or allogeneic ADMSC showed equal efficacy in terms of functional recovery and decreased ischemic brain damage when IV delivered 30 min after pMCAo (Gutierrez-Fernandez et al., 2015). To summarize, ADMSC seem to be more promising than BM-MSC, the xenograft and allograft are of equal efficacy, they have been constantly reported to improve functional outcome in rats and mice, the tMCAo stroke model being the most widely used. However, none of these animals had associated vascular risk factors and cells were constantly administered, within 24 h after cerebral ischemia induction, both conditions that might explain our negative results.

Our model is not questioned since, using the same pMCAo model in diabetic mice, we previously showed a dramatic functional improvement and a reduced infarct volume following treatment with the immunomodulatory drug glatiramer acetate (Mangin et al., 2019), with peripheral blood mononuclear cells pretreated with ephrin-B2 in diabetic (personal unpublished data) but also in non-diabetic mice (Hilal et al., 2018). In literature, cell therapy is mainly reported in tMCAo stroke models. However, the pMCAo model offers many advantages. The tMCAO stroke model in diabetic mice is associated with a high mortality after 7 days which prevents any further follow-up (Poittevin et al., 2015). We had previously shown that diabetic mice developed post-stroke dementia after pMCAo (Mangin et al., 2019), which was one of the functional outcomes we

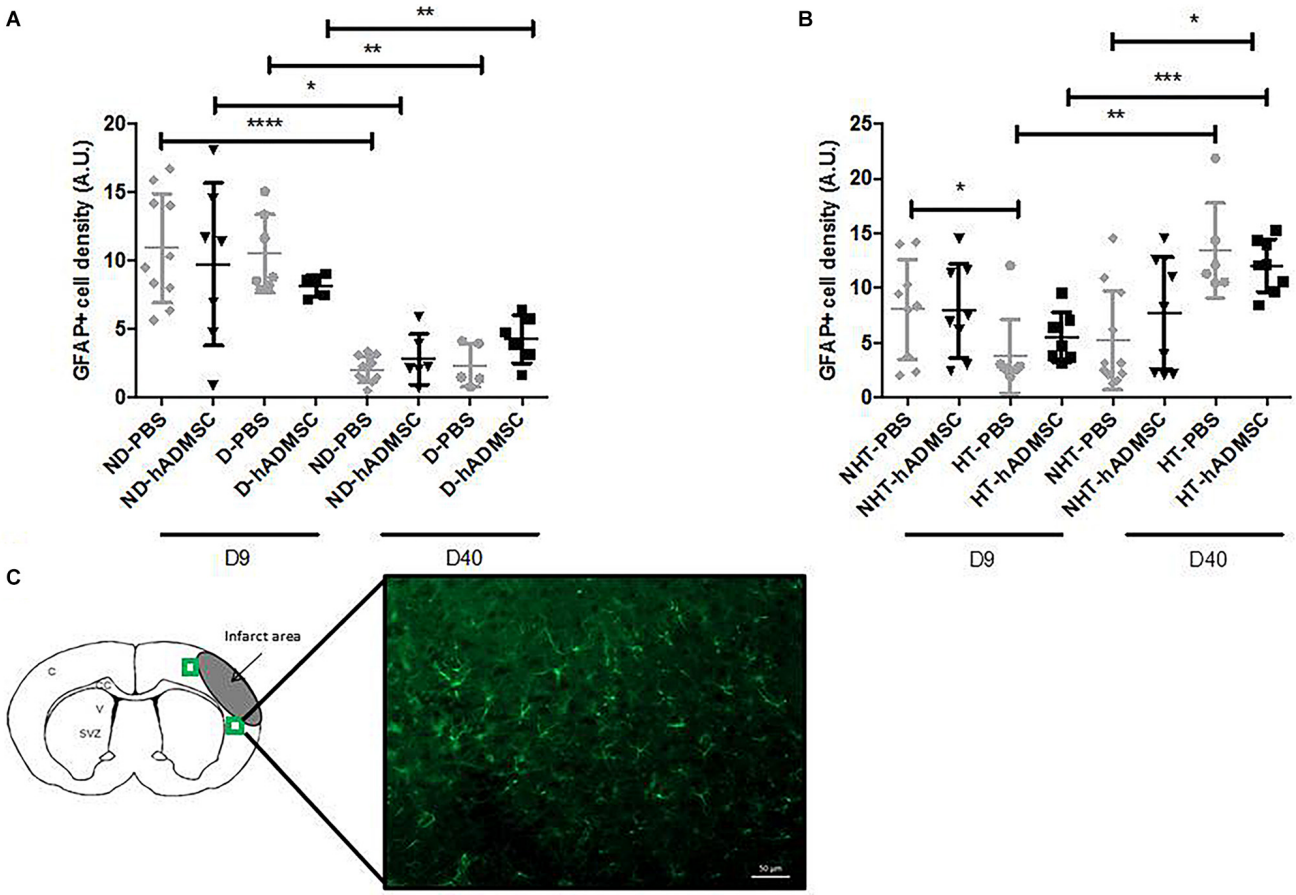

FIGURE 8 | Assessment of GFAP+ cells density at D9 and D40 in ND-PBS, untreated non-diabetic mice; ND-hADMSC, treated non-diabetic mice; D-PBS, untreated diabetic mice and D-hADMSC, treated diabetic mice (D9: n = 5–10, D40: n = 5–11) **(A)** and NHT-PBS, untreated non-hypertensive mice; NHT-hADMSC, treated non-hypertensive mice; HT-PBS, untreated hypertensive mice and HT-hADMSC, treated hypertensive mice (D9: n = 7–9, D40: n = 6–11) **(B)**. hADMSC did not significantly modify the astrocytes density whatever the risk factor. Between D9 and D40, there was a significant reduction in activated astrocytes in ND-PBS, ND-hADMSC, D-PBS, and D-hADMSC mice and a significant increase in activated astrocytes in HT-PBS and HT-hADMSC mice; $^{*}p < 0.05$, $^{**}p < 0.01$, $^{***}p < 0.001$, $^{****}p < 0.0001$. GFAP immunostaining, scale bar: 50 µm; C, cortex; V, ventricle; SVZ, subventricular zone; green squares: regions of interest **(C).**

wanted to explore. The smaller infarct, restricted to the cortex was crucial in our model, because we did want to spare the hippocampus from the neuronal damage. Moreover, it was recently reported that even a minor stroke increases the incidence of post-stroke dementia and that diabetes is the only vascular risk factor identified (Pendlebury et al., 2019). Although the infarct is smaller in this pMCAo stroke model compared to the tMCAo model in mice, brain inflammation is exacerbated (Zhou et al., 2013) and even more in diabetic mice (Mangin et al., 2019) and in hypertensive rats (Moller et al., 2015). This is important to consider since the efficiency of hADMSC is related to their "immunomodulatory properties" (Leu et al., 2010; Melief et al., 2013). At last, "healthy" non-diabetic and non-hypertensive mice subjected to a pMCAo presented little sensorimotor deficit that recovered completely very quickly and prevented us to evaluate any effect of cells in those mice, but this was not the primary endpoint of our study.

We cannot rule out that a different culture procedure might have led to different results. The fact that hADMSC were collected from only one donor might question the efficiency of these cells. However, using the cells of the same donor, Mu et al. (2019) succeeded in demonstrating functional improvement in treated non-diabetic adult male Sprague Dawley rats, subjected to focal cerebral ischemia, and using the sticky label test. However, this does not exclude that there might be variability in the response that should be tested by comparing the efficiency of these cells between various donors. Also, the delay of injection might have been too late. In our previous cell therapy studies in pMCAO mice, we constantly IV transplanted the cells within the first 24 h after stroke induction (Nih et al., 2012; Hilal et al., 2018) and a beneficial effect was observed when ADMSC were IV (Gutierrez-Fernandez et al., 2015) or IA administered (Huang et al., 2017), 30 min and 24 h respectively after the cerebral ischemia induction. The 48 h delay was chosen in that particular study to get along with the parallel clinical trial that aimed to widen the therapeutic window and because mice were randomized according to the infarct volume determined at cerebral MRI the day before.

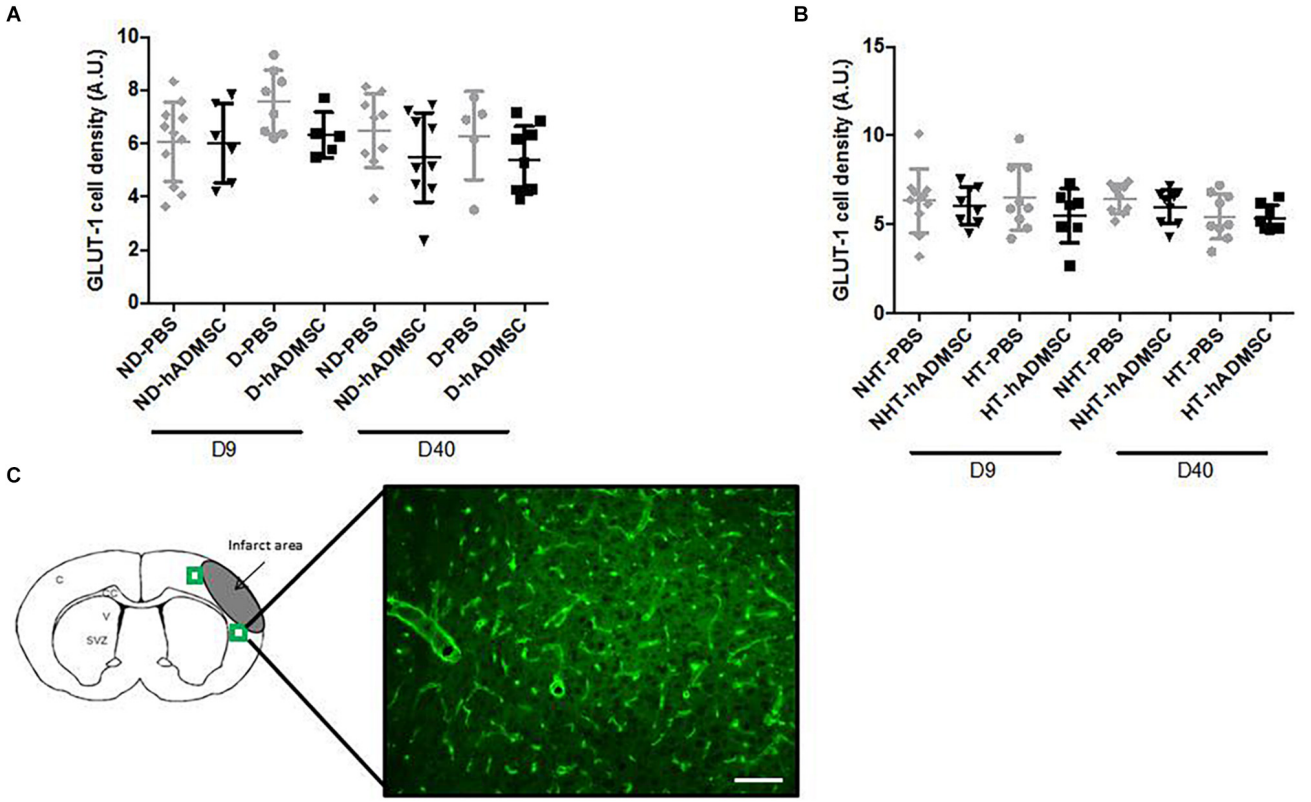

FIGURE 9 | Assessment of GLUT-1+ cells area at D9 and D40 in ND-PBS, untreated non-diabetic mice; ND-hADMSC, treated non-diabetic mice; D-PBS, untreated diabetic mice; and D-hADMSC, treated diabetic mice (D9: n = 5–11, D40: n = 5–9) **(A)** and NHT-PBS, untreated non-hypertensive mice; NHT-hADMSC, treated non-hypertensive mice; HT-PBS, untreated hypertensive mice and HT-hADMSC, treated hypertensive mice (D9: n = 7–10, D40: n = 8–9) **(B)**. Vessel density was not significantly modified over time and hADMSC did not significantly modify the vessels density whatever the risk factor. GLUT-1 immunostaining, scale bar: 100 μm; C, cortex; V, ventricle; SVZ, subventricular zone; green squares: regions of interest **(C)**.

The discrepancies of our results between mice and those obtained in rats by the other teams of the RESSTORE project (Mu et al., 2019), could be related to species differences in the immune system. In an *in vitro* model of oxygen-glucose deprivation on primary cultures of neurons, astrocytes, microglia in rats, mice or humans, the cytokines levels were differently expressed between all three species (Du et al., 2017), or even may be present in one species and not in the other (Mestas and Hughes, 2004). MSC have been shown to secrete cytokines and growth factors that inhibit T cells proliferation, decrease TNFα secreted by dendritic cells (Uccelli et al., 2008) and at the same time polarize lymphocytes and microglial cells to an "anti-inflammatory" and beneficial phenotype (Ankrum et al., 2014). Although hADMSC have been reported to have a higher immunomodulatory capacity than BM-derived counterparts, including increase of IL-6 and TGF-β1 (Melief et al., 2013) and decrease of IL-18 (Leu et al., 2010), we did not evidence any modification of microglial/macrophages, T lymphocytes, or astrocytes densities between treated and untreated mice, when adding co-morbidity, but we did not measure brain cytokines levels. We cannot exclude either a participation of peripheral immune organs and modification of blood immune cells and cytokines release to stroke response and to comorbid factors. Indeed, spleen and systemic immune response have shown contribution to the pathophysiology of stroke (Offner et al., 2006; Vendrame et al., 2006), diabetes (Tong et al., 2017), and hypertension (McMaster et al., 2015) that could impede neurorepair.

Untreated hypertensive mice presented a reduced astrocytes density in the peri-infarct area compared to non-hypertensive mice at D9 and, on the contrary, increased astrocytes density in treated hypertensive mice compared to untreated mice at D40. Moreover, untreated and treated hypertensive mice had increased astrocytes density between D9 and D40. Given the complex role of astrocytes following stroke, this increased glial scar at D40 is difficult to interpret as being a simple epiphenomenon or as a key event resulting in the absence of neurorepair (Morrison and Filosa, 2019).

Post-stroke dementia will eventually affect 25% of patients (Iadecola, 2013). This is a particular important heath issue since it is the second cause of cognitive decline after Alzheimer's disease and that there is no current treatment to prevent or cure the disease. Still too few studies evaluate this aspect because of the need for models that must be maintained over time, complying with the increased early mortality when adding comorbidity (Poittevin et al., 2015). We found that diabetic mice with

pMCAo presented altered spatial memory at Barnes maze but not non-diabetic pMCAO mice (Mangin et al., 2019). Structural alterations in the hippocampus, which is involved in information processing related to spatial memory, have already been observed after focal brain ischemia, with neurodegeneration in the CA1 zone in particular (Wang et al., 2004). Diabetes by itself can also decrease neuronal density (Artola et al., 2005; Amin et al., 2013) and impair long-term potentiation in rats (Artola et al., 2005). In our model, both conditions (pMCAo + diabetes) were necessary to alter the Barnes Maze, that also evaluates brain plasticity (Martin et al., 2000), but again hADMSC did not prevent spatial memory impairment in those mice. MSC beneficial effects rely partly on the promulgation of neurogenesis (Leu et al., 2010; Bao et al., 2011), limitation of neuronal death (Gutiérrez-Fernández et al., 2013), and angiogenesis promotion (Wang et al., 2008) none of which having been observed in treated mice. We failed to show spatial memory impairment in our hypertensive mice after 16 weeks of mild elevated blood pressure, although impaired vasoreactivity after 8 weeks was evidenced just as for diabetic mice. If the duration of the hypertension was appropriate to induce a sensorimotor deficit, we cannot exclude that both the duration of hypertension and/or the time points chosen to assess the Barnes maze test were inadequate and that a later evaluation would have been more contributive.

CONCLUSION

These negative results are of utmost importance, given the importance of vascular risk factors in stroke patients. Comorbid animals should be part of all preclinical stroke studies and could avoid considerable unnecessary costs in clinical studies. The next preclinical study will focus on time administration and other models of vascular risk factors. If hADMSC prove then to be efficient, we will have the opportunity, by comparing the molecular pathways, to explore the in depths-mechanisms involved by these human ADMSC.

MEMBERS OF RESSTORE STEERING COMMITTEE

O. Detante, Coordinator/Principal Investigator, Université Grenoble Alpes, Centre Hospitalier Universitaire Grenoble Alpes, Grenoble, France; E. Diez Tejedor (Principal Investigator, Servicio Madrileno de Salud, La Paz University Hospital, IdiPAZ Research Institute, Autonoma University of Madrid, Madrid, Spain; B. Fuentes, Servicio Madrileno de Salud, La Paz University Hospital, IdiPAZ Research Institute, Autonoma University of Madrid, Madrid, Spain, Madrid, Spain; M. Hommel, Université Grenoble Alpes Grenoble, France; A. Jaillard, Université Grenoble Alpes, Centre Hospitalier Universitaire Grenoble Alpes, Grenoble, France; J. Jolkkonen, University of Eastern Finland, Kuopio, Finland; R. Mikulik, St Anne's University Hospital, Brno, Czechia; A. Moisan, Etablissement Français du sang, Saint-Ismier, France; F. Moniche, Neurology Department, Hospital Universitario Virgen del Rocio, Seville, Spain; J. Montaner, Vall d'Hebron Research Institute, Barcelona, Spain; A. Bustamante, Vall d'Hebron Research Institute, Barcelona, Spain; K. Muir, University of Glasgow, Glasgow, United Kingdom; H. Numminen, Pirkanmaa Hospital District, Finland; S. Miettinen, University of Tampere, Tampere, Finland; D. Koubi, Finovatis CEO, Lyon, France; C. Bollart, sponsor, Centre Hospitalier Universitaire Grenoble Alpes Grenoble, France. T. Keinonen, MEDFILES Oy CEO, Kuopio, Finland.

DATA AVAILABILITY

The raw data supporting the conclusions of this manuscript will be made available by the authors, without undue reservation, to any qualified researcher.

ETHICS STATEMENT

All experiments and surgical procedures were performed according to the European Community Directive (2010/63/EU), the ARRIVE (Animal Research Reporting In Vivo Experiments) guidelines, and the French national guidelines for the care and use of laboratory animals. The study was approved by the French ministry of Higher Education for Research and Innovation (APAFIS#5431-2016031912549126 v2).

AUTHOR CONTRIBUTIONS

GM performed the mice experiments including the acquisition and interpretation of data and drafted the manuscript. AC performed the analysis and interpretation of the data. AM provided the hADMSC. PB performed the Doppler experiments and analyses. BM performed experiments including the acquisition and interpretation of data. NK conceived and designed the study, and drafted and edited the manuscript. All authors read and approved the final manuscript.

FUNDING

The RESSTORE project received funding from the European Union's Horizon 2020 Research and Innovation Programme under the Grant Agreement No. 681044 RESSTORE project (www.resstore.eu) and GM was directly funded by the RESSTORE project.

ACKNOWLEDGMENTS

The authors thank the FRIM platform (UMS34), University of Paris Diderot, member of France Life Imaging (grant ANR-11-INBS-0006) and IDEX Imagerie Du Vivant networks, and in collaboration with the IAME group (UMR1137), the Institut des Vaisseaux et du Sang (Hospital Lariboisière, Paris).

REFERENCES

Amin, S. N., Younan, S. M., Youssef, M. F., Rashed, L. A., and Mohamady, I. (2013). A histological and functional study on hippocampal formation of normal and diabetic rats. *F1000Research* 2:151. doi: 10.12688/f1000research.2-151.v1

Ankrum, J. A., Ong, J. F., and Karp, J. M. (2014). Mesenchymal stem cells: immune evasive, not immune privileged. *Nat. Biotechnol.* 32, 252–260. doi: 10.1038/nbt.2816

Artola, A., Kamal, A., Ramakers, G. M., Biessels, G. J., and Gispen, W. H. (2005). Diabetes mellitus concomitantly facilitates the induction of long-term depression and inhibits that of long-term potentiation in hippocampus. *Eur. J. Neurosci.* 22, 169–178. doi: 10.1111/j.1460-9568.2005.04205.x

Bai, Y. Y., Wang, L., Chang, D., Zhao, Z., Lu, C. Q., Wang, G., et al. (2015). Synergistic effects of transplanted endothelial progenitor cells and rwj 67657 in diabetic ischemic stroke models. *Stroke* 46, 1938–1946. doi: 10.1161/STROKEAHA.114.008495

Bao, X., Wei, J., Feng, M., Lu, S., Li, G., Dou, W., et al. (2011). Transplantation of human bone marrow-derived mesenchymal stem cells promotes behavioral recovery and endogenous neurogenesis after cerebral ischemia in rats. *Brain Res.* 1367, 103–113. doi: 10.1016/j.brainres.2010.10.063

Bhaskar, S., Stanwell, P., Cordato, D., Attia, J., and Levi, C. (2018). Reperfusion therapy in acute ischemic stroke: dawn of a new era? *BMC Neurol.* 18:8. doi: 10.1186/s12883-017-1007-y

Brown, J. P., Couillard-Despres, S., Cooper-Kuhn, C. M., Winkler, J., Aigner, L., and Kuhn, H. G. (2003). Transient expression of doublecortin during adult neurogenesis. *J. Comp. Neurol.* 467, 1–10. doi: 10.1002/cne.10874

Chamberlain, G., Fox, J., Ashton, B., and Middleton, J. (2007). Concise review: mesenchymal stem cells: their phenotype, differentiation capacity, immunological features, and potential for homing. *Stem Cells* 25, 2739–2749. doi: 10.1634/stemcells.2007-0197

Chen, J., Li, Y., Katakowski, M., Chen, X., Wang, L., Lu, D., et al. (2003). Intravenous bone marrow stromal cell therapy reduces apoptosis and promotes endogenous cell proliferation after stroke in female rat. *J. Neurosci. Res.* 73, 778–786. doi: 10.1002/jnr.10691

Chen, J., Venkat, P., Zacharek, A., and Chopp, M. (2014). Neurorestorative therapy for stroke. *Front. Hum. Neurosci.* 8:382. doi: 10.3389/fnhum.2014.00382

Chen, J., Ye, X., Yan, T., Zhang, C., Yang, X.-P., Cui, X., et al. (2011). Adverse effects of bone marrow stromal cell treatment of stroke in diabetic rats. *Stroke* 42, 3551–3558. doi: 10.1161/STROKEAHA.111.627174

Cho, Y. J., Song, H. S., Bhang, S., Lee, S., Kang, B. G., Lee, J. C., et al. (2012). Therapeutic effects of human adipose stem cell-conditioned medium on stroke. *J. Neurosci. Res.* 90, 1794–1802. doi: 10.1002/jnr.23063

Chow, C. K., Teo, K. K., Rangarajan, S., Islam, S., Gupta, R., Avezum, A., et al. (2013). Prevalence, awareness, treatment, and control of hypertension in rural and urban communities in high-, middle-, and low-income countries. *JAMA* 310, 959–968. doi: 10.1001/jama.2013.184182

Cifuentes, D., Poittevin, M., Bonnin, P., Ngkelo, A., Kubis, N., Merkulova-Rainon, T., et al. (2017). Inactivation of nitric oxide synthesis exacerbates the development of alzheimer disease pathology in apppss1 mice (amyloid precursor protein/presenilin-1). *Hypertension* 70, 613–623. doi: 10.1161/HYPERTENSIONAHA.117.09742

Cifuentes, D., Poittevin, M., Dere, E., Broqueres-You, D., Bonnin, P., Benessiano, J., et al. (2015). Hypertension accelerates the progression of Alzheimer-like pathology in a mouse model of the disease. *Hypertension* 65, 218–224. doi: 10.1161/HYPERTENSIONAHA.114.04139

Diederich, K., Schmidt, A., Beuker, C., Strecker, J. K., Wagner, D. C., Boltze, J., et al. (2014). Granulocyte colony-stimulating factor (G-CSF) treatment in combination with transplantation of bone marrow cells is not superior to G-CSF treatment alone after cortical stroke in spontaneously hypertensive rats. *Front. Cell. Neurosci.* 8:411. doi: 10.3389/fncel.2014.00411

Ding, G., Chen, J., Chopp, M., Li, L., Yan, T., Li, Q., et al. (2016). Cell treatment for stroke in type two diabetic rats improves vascular permeability measured by MRI. *PLoS One* 11:e0149147. doi: 10.1371/journal.pone.0149147

Du, Y., Deng, W., Wang, Z., Ning, M., Zhang, W., Zhou, Y., et al. (2017). Differential subnetwork of chemokines/cytokines in human, mouse, and rat brain cells after oxygen-glucose deprivation. *J. Cereb. Blood Flow Metab.* 37, 1425–1434. doi: 10.1177/0271678X16656199

Ettehad, D., Emdin, C. A., Kiran, A., Anderson, S. G., Callender, T., Emberson, J., et al. (2016). Blood pressure lowering for prevention of cardiovascular disease and death: a systematic review and meta-analysis. *Lancet* 387, 957–967. doi: 10.1016/S0140-6736(15)01225-8

Frechou, M., Margaill, I., Marchand-Leroux, C., and Beray-Berthat, V. (2019). Behavioral tests that reveal long-term deficits after permanent focal cerebral ischemia in mouse. *Behav. Brain Res.* 360, 69–80. doi: 10.1016/j.bbr.2018.11.040

Geng, J., Wang, L., Qu, M., Song, Y., Lin, X., Chen, Y., et al. (2017). Endothelial progenitor cells transplantation attenuated blood-brain barrier damage after ischemia in diabetic mice via HIF-1alpha. *Stem Cell Res. Ther.* 8:163. doi: 10.1186/s13287-017-0605-3

Gorelick, P. B., Scuteri, A., Black, S. E., Decarli, C., Greenberg, S. M., Iadecola, C., et al. (2011). Vascular contributions to cognitive impairment and dementia: a statement for healthcare professionals from the american heart association/american stroke association. *Stroke* 42, 2672–2713. doi: 10.1161/str.0b013e3182299496

Gutierrez-Fernandez, M., Rodriguez-Frutos, B., Ramos-Cejudo, J., Otero-Ortega, L., Fuentes, B., Vallejo-Cremades, M. T., et al. (2015). Comparison between xenogeneic and allogeneic adipose mesenchymal stem cells in the treatment of acute cerebral infarct: proof of concept in rats. *J. Trans. Med.* 13:46. doi: 10.1186/s12967-015-0406-3

Gutiérrez-Fernández, M., Rodríguez-Frutos, B., Ramos-Cejudo, J., Teresa Vallejo-Cremades, M., Fuentes, B., Cerdán, S., et al. (2013). Effects of intravenous administration of allogenic bone marrow- and adipose tissue-derived mesenchymal stem cells on functional recovery and brain repair markers in experimental ischemic stroke. *Stem Cell Res. Ther.* 4:11. doi: 10.1186/scrt159

Hilal, R., Poittevin, M., Pasteur-Rousseau, A., Cogo, A., Mangin, G., Chevauche, M., et al. (2018). Diabetic ephrin-B2-stimulated peripheral blood mononuclear cells enhance poststroke recovery in mice. *Stem Cells Int.* 2018:2431567. doi: 10.1155/2018/2431567

Huang, H., Lin, F., Jiang, J., Chen, Y., Mei, A., and Zhu, P. (2017). Effects of intra-arterial transplantation of adipose-derived stem cells on the expression of netrin-1 and its receptor DCC in the peri-infarct cortex after experimental stroke. *Stem Cell Res. Ther.* 8:223. doi: 10.1186/s13287-017-0671-6

Iadecola, C. (2013). The pathobiology of vascular dementia. *Neuron* 80, 844–866. doi: 10.1016/j.neuron.2013.10.008

Ikegame, Y., Yamashita, K., Hayashi, S.-I., Mizuno, H., Tawada, M., You, F., et al. (2011). Comparison of mesenchymal stem cells from adipose tissue and bone marrow for ischemic stroke therapy. *Cytotherapy* 13, 675–685. doi: 10.3109/14653249.2010.549122

Jin, K., Wang, X., Xie, L., Mao, X. O., and Greenberg, D. A. (2010). Transgenic ablation of doublecortin-expressing cells suppresses adult neurogenesis and worsens stroke outcome in mice. *Proc. Natl. Acad. Sci. U.S.A.* 107, 7993–7998. doi: 10.1073/pnas.1000154107

Knopman, D., Boland, L. L., Mosley, T., Howard, G., Liao, D., Szklo, M., et al. (2001). Cardiovascular risk factors and cognitive decline in middle-aged adults. *Neurology* 56, 42–48. doi: 10.1212/wnl.56.1.42

Kranz, A., Wagner, D. C., Kamprad, M., Scholz, M., Schmidt, U. R., Nitzsche, F., et al. (2010). Transplantation of placenta-derived mesenchymal stromal cells upon experimental stroke in rats. *Brain Res.* 1315, 128–136. doi: 10.1016/j.brainres.2009.12.001

Lalu, M. M., McIntyre, L., Pugliese, C., Fergusson, D., Winston, B. W., Marshall, J. C., et al. (2012). Safety of cell therapy with mesenchymal stromal cells (SafeCell): a systematic review and meta-analysis of clinical trials. *PLoS One* 7:e47559. doi: 10.1371/journal.pone.0047559

Leu, S., Lin, Y. C., Yuen, C. M., Yen, C. H., Kao, Y. H., Sun, C. K., et al. (2010). Adipose-derived mesenchymal stem cells markedly attenuate brain infarct size and improve neurological function in rats. *J. Trans. Med.* 8:63. doi: 10.1186/1479-5876-8-63

Li, F., Han, S. S., Tatlisumak, T., Liu, K. F., Garcia, J. H., Sotak, C. H., et al. (1999). Reversal of acute apparent diffusion coefficient abnormalities and delayed neuronal death following transient focal cerebral ischemia in rats. *Ann. Neurol.* 46, 333–342. doi: 10.1002/1531-8249(199909)46:3<333::aid-ana9>3.0.co;2-x

Liu, S., Zhen, G., Meloni, B. P., Campbell, K., and Winn, H. R. (2009). Rodent stroke model guidelines for preclinical stroke trials. *J. Exp. Stroke Trans. Med.* 2, 2–27.

Mangin, G., and Kubis, N. (2018). Cell therapy for ischemic stroke: how to turn a promising preclinical research into a successful clinical story. *Stem Cell Rev.* 15, 176–193. doi: 10.1007/s12015-018-9864-3

Mangin, G., Poittevin, M., Charriaut-Marlangue, C., Giannesini, C., Merkoulova-Rainon, T., and Kubis, N. (2019). Glatiramer acetate reduces infarct volume in diabetic mice with cerebral ischemia and prevents long-term memory loss. *Brain Behav. Immun.* [Epub ahead of print],

Mankovsky, B. N., and Ziegler, D. (2004). Stroke in patients with diabetes mellitus. *Diab. Metab. Res. Rev.* 20, 268–287.

Martin, S. J., Grimwood, P. D., and Morris, R. G. (2000). Synaptic plasticity and memory: an evaluation of the hypothesis. *Annu. Rev. Neurosci.* 23, 649–711. doi: 10.1146/annurev.neuro.23.1.649

McMaster, W. G., Kirabo, A., Madhur, M. S., and Harrison, D. G. (2015). Inflammation, immunity, and hypertensive end-organ damage. *Circ. Res.* 116, 1022–1033. doi: 10.1161/CIRCRESAHA.116.303697

Melief, S. M., Zwaginga, J. J., Fibbe, W. E., and Roelofs, H. (2013). Adipose tissue-derived multipotent stromal cells have a higher immunomodulatory capacity than their bone marrow-derived counterparts. *Stem Cells Trans. Med.* 2, 455–463. doi: 10.5966/sctm.2012-0184

Mestas, J., and Hughes, C. C. (2004). Of mice and not men: differences between mouse and human immunology. *J. Immunol.* 172, 2731–2738. doi: 10.4049/jimmunol.172.5.2731

Minnerup, J., Wagner, D. C., Strecker, J. K., Posel, C., Sevimli-Abdis, S., Schmidt, A., et al. (2014). Bone marrow-derived mononuclear cells do not exert acute neuroprotection after stroke in spontaneously hypertensive rats. *Front. Cell. Neurosci.* 7:288. doi: 10.3389/fncel.2013.00288

Moller, K., Posel, C., Kranz, A., Schulz, I., Scheibe, J., Didwischus, N., et al. (2015). Arterial hypertension aggravates innate immune responses after experimental stroke. *Front. Cell. Neurosci.* 9:461. doi: 10.3389/fncel.2015.00461

Morrison, H. W., and Filosa, J. A. (2019). Stroke and the neurovascular unit: glial cells, sex differences, and hypertension. *Am. J. Physiol. Cell Physiol.* 316, C325–C339. doi: 10.1152/ajpcell.00333.2018

Mu, J., Bakreen, A., Juntunen, M., Korhonen, P., Oinonen, E., Cui, L., et al. (2019). Combined adipose tissue-derived mesenchymal stem cell therapy and rehabilitation in experimental stroke. *Front. Neurol.* 10:235. doi: 10.3389/fneur.2019.00235

Nih, L. R., Deroide, N., Leré-Déan, C., Lerouet, D., Soustrat, M., Levy, B. I., et al. (2012). Neuroblast survival depends on mature vascular network formation after mouse stroke: role of endothelial and smooth muscle progenitor cell co-administration. *Eur. J. Neurosci.* 35, 1208–1217. doi: 10.1111/j.1460-9568.2012.08041.x

Offner, H., Subramanian, S., Parker, S. M., Wang, C., Afentoulis, M. E., Lewis, A., et al. (2006). Splenic atrophy in experimental stroke is accompanied by increased regulatory T cells and circulating macrophages. *J. Immunol.* 176, 6523–6531. doi: 10.4049/jimmunol.176.11.6523

Pendlebury, S. T., Rothwell, P. M., and Oxford Vascular, S. (2019). Incidence and prevalence of dementia associated with transient ischaemic attack and stroke: analysis of the population-based oxford vascular study. *Lancet Neurol.* 18, 248–258. doi: 10.1016/s1474-4422(18)30442-3

Pers, Y.-M., and Jorgensen, C. (2013). Cellules souches mésenchymateuses: actualités et perspectives thérapeutiques dans les maladies auto-immunes. *Médecine Thérapeutique* 19, 207–214.

Poittevin, M., Bonnin, P., Pimpie, C., Riviere, L., Sebrie, C., Dohan, A., et al. (2015). Diabetic microangiopathy: impact of impaired cerebral vasoreactivity and delayed angiogenesis after permanent middle cerebral artery occlusion on stroke damage and cerebral repair in mice. *Diab. Metab. Res. Rev.* 64, 999–1010. doi: 10.2337/db14-0759

Poittevin, M., Deroide, N., Azibani, F., Delcayre, C., Giannesini, C., Levy, B. I., et al. (2013). Glatiramer acetate administration does not reduce damage after cerebral ischemia in mice. *J. Neuroimmunol.* 254, 55–62. doi: 10.1016/j.jneuroim.2012.09.009

Savitz, S. I., Chopp, M., Deans, R., Carmichael, T., Phinney, D., Wechsler, L., et al. (2011). Stem cell therapy as an emerging paradigm for stroke (STEPS) II. *Stroke* 42, 825–829. doi: 10.1161/STROKEAHA.110.601914

Shaw, J. E., Sicree, R. A., and Zimmet, P. Z. (2010). Global estimates of the prevalence of diabetes for 2010 and 2030. *Diab. Res. Clin. Pract.* 87, 4–14. doi: 10.1016/j.diabres.2009.10.007

Snyder, H. M., Corriveau, R. A., Craft, S., Faber, J. E., Greenberg, S. M., Knopman, D., et al. (2015). Vascular contributions to cognitive impairment and dementia including Alzheimer's disease. *Alzheimer's Dementia* 11, 710–717.

Tong, H. V., Luu, N. K., Son, H. A., Hoan, N. V., Hung, T. T., Velavan, T. P., et al. (2017). Adiponectin and pro-inflammatory cytokines are modulated in vietnamese patients with type 2 diabetes mellitus. *J. Diab. Invest.* 8, 295–305. doi: 10.1111/jdi.12579

Uccelli, A., Moretta, L., and Pistoia, V. (2008). Mesenchymal stem cells in health and disease. *Nat. Rev. Immunol.* 8, 726–736. doi: 10.1038/nri2395

Vendrame, M., Gemma, C., Pennypacker, K. R., Bickford, P. C., Davis Sanberg, C., Sanberg, P. R., et al. (2006). Cord blood rescues stroke-induced changes in splenocyte phenotype and function. *Exp. Neurol.* 199, 191–200. doi: 10.1016/j.expneurol.2006.03.017

Wang, J. H., Liu, N., Du, H. W., Weng, J. S., Chen, R. H., Xiao, Y. C., et al. (2008). [Effects of adipose-derived stem cell transplantation on the angiogenesis and the expression of bFGF and VEGF in the brain post focal cerebral ischemia in rats]. *Chinese J. Cell. Mol. Immunol.* 24, 958–961.

Wang, W., Redecker, C., Bidmon, H. J., and Witte, O. W. (2004). Delayed neuronal death and damage of GDNF family receptors in CA1 following focal cerebral ischemia. *Brain Res.* 1023, 92–101. doi: 10.1016/j.brainres.2004.07.034

Weise, G., Lorenz, M., Posel, C., Maria Riegelsberger, U., Storbeck, V., Kamprad, M., et al. (2014). Transplantation of cryopreserved human umbilical cord blood mononuclear cells does not induce sustained recovery after experimental stroke in spontaneously hypertensive rats. *J. Cereb. Blood Flow Metab.* 34, e1–e9. doi: 10.1038/jcbfm.2013.185

World Health Organization [WHO] (2018). The top 10 causes of death. Available at: http://www.who.int/news-room/fact-sheets/detail/the-top-10-causes-of-death (accessed May 24, 2018).

Zhou, W., Liesz, A., Bauer, H., Sommer, C., Lahrmann, B., Valous, N., et al. (2013). Postischemic brain infiltration of leukocyte subpopulations differs among murine permanent and transient focal cerebral ischemia models. *Brain Pathol.* 23, 34–44. doi: 10.1111/j.1750-3639.2012.00614.x

Conflict of Interest Statement: The authors declare that the research was conducted in the absence of any commercial or financial relationships that could be construed as a potential conflict of interest.

Copyright © 2019 Mangin, Cogo, Moisan, Bonnin, Maïer and Kubis. This is an open-access article distributed under the terms of the Creative Commons Attribution License (CC BY). The use, distribution or reproduction in other forums is permitted, provided the original author(s) and the copyright owner(s) are credited and that the original publication in this journal is cited, in accordance with accepted academic practice. No use, distribution or reproduction is permitted which does not comply with these terms.

frontiers in Neuroscience

ORIGINAL RESEARCH
published: 23 July 2019
doi: 10.3389/fnins.2019.00767

Delayed Effects of Acute Reperfusion on Vascular Remodeling and Late-Phase Functional Recovery After Stroke

*Violeta Durán-Laforet†, David Fernández-López†, Alicia García-Culebras, Juan González-Hijón, Ana Moraga, Sara Palma-Tortosa, Isaac García-Yébenes, Adrián Vega-Pérez, Ignacio Lizasoain and María Ángeles Moro**

Unidad de Investigación Neurovascular, Departamento de Farmacología y Toxicología, Facultad de Medicina, Instituto Universitario de Investigación en Neuroquímica, Universidad Complutense de Madrid, Instituto de Investigación Hospital 12 de Octubre (i+12), Madrid, Spain

OPEN ACCESS

Edited by:
Emmanuel Pinteaux, The University of Manchester, United Kingdom

Reviewed by:
Zhongwu Liu, Henry Ford Hospital, United States
Yongting Wang, Shanghai Jiao Tong University, China

***Correspondence:**
María Ángeles Moro
neurona@ucm.es

†Co-first authors

Specialty section:
This article was submitted to Neurodegeneration, a section of the journal Frontiers in Neuroscience

Received: *30 March 2019*
Accepted: *09 July 2019*
Published: *23 July 2019*

Citation:
Durán-Laforet V, Fernández-López D, García-Culebras A, González-Hijón J, Moraga A, Palma-Tortosa S, García-Yébenes I, Vega-Pérez A, Lizasoain I and Moro MÁ (2019) Delayed Effects of Acute Reperfusion on Vascular Remodeling and Late-Phase Functional Recovery After Stroke. Front. Neurosci. 13:767. doi: 10.3389/fnins.2019.00767

Tissue perfusion is a necessary condition for vessel survival that can be compromised under ischemic conditions. Following stroke, delayed effects of early brain reperfusion on the vascular substrate necessary for remodeling, perfusion and maintenance of proper peri-lesional hemodynamics are unknown. Such aspects of ischemic injury progression may be critical for neurological recovery in stroke patients. This study aims to describe the impact of early, non-thrombolytic reperfusion on the vascular brain component and its potential contribution to tissue remodeling and long-term functional recovery beyond the acute phase after stroke in 3-month-old male C57bl/6 mice. Permanent (pMCAO) and transient (60 min, tMCAO) brain ischemia mouse models were used for characterizing the effect of early, non-thrombolytic reperfusion on the brain vasculature. Analysis of different vascular parameters (vessel density, proliferation, degeneration and perfusion) revealed that, while early middle cerebral artery recanalization was not sufficient to prevent sub-acute vascular degeneration within the ischemic brain regions, brain reperfusion promoted a secondary wave of vascular remodeling in the peri-lesional regions, which led to improved perfusion of the ischemic boundaries and late-phase neurological recovery. This study concluded that acute, non-thrombolytic artery recanalization following stroke favors late-phase vascular remodeling and improves peri-lesional perfusion, contributing to secondary functional recovery.

Keywords: brain, recanalization, perfusion, blood-brain barrier, angiogenesis, stroke

INTRODUCTION

Long-term, stroke-induced vascular remodeling is a key process governing neural tissue reorganization in response to injury (Navarro-Sobrino et al., 2011; Chen et al., 2014). Local tissue perfusion, hemodynamics and proper neurovascular coupling in the peri-lesional regions contribute to support the metabolic demands necessary for neuronal plasticity and for the survival and differentiation of migrating neural progenitors (Thored et al., 2007; Snapyan et al., 2009), two processes that may underlie long-term functional recovery. Indeed, a functional correlation exists

between delayed blood flow restoration and neurological recovery in stroke patients (Krupinski et al., 1993; Chopp et al., 2007; Arkuszewski et al., 2009; Navarro-Sobrino et al., 2011). Additionally, in the context of vascular remodeling upon damage, vascular perfusion is necessary for vessel survival, stimulates vessel outgrowth and precludes endothelial degeneration (Dimmeler et al., 1996; Haga et al., 2003; Yamamoto et al., 2003). Thus, acute artery recanalization may condition the long-term survival of a vascular substrate for remodeling and vascularization of the ischemic and peri-ischemic brain regions during the chronic neural repair phase after stroke. Several studies have explored vascular remodeling after stroke (Marti et al., 2000; Wei et al., 2001; Zhang et al., 2002; Hayashi et al., 2003; Schaffer et al., 2006; Mostany et al., 2010; Hayakawa et al., 2012; Mao et al., 2014; Marks et al., 2014). In the present report, we intend to go further and elucidate the implication of vessel reperfusion after brain ischemia and also to compare it with a non-reperfusion scenario.

Early restoration of brain tissue perfusion is the main strategy currently pursued in the acute management of stroke patients. However, between 17 and 24% of ischemic stroke patients experience spontaneous arterial recanalization within the first 24 h after stroke onset in the absence of induced thrombolysis (Kassem-Moussa and Graffagnino, 2002; Rha and Saver, 2007). Adding to this, the number of patients undergoing recanalization induced by mechanical thrombectomy or thrombus removal in the absence of thrombolysis is increasing (Smith et al., 2017). In spite of its relative frequency, clinical studies describing the impact of non-thrombolytic reperfusion on the long-term progression of the brain vascular component are scarce. In this study, we have characterized for the first time the effect of arterial recanalization on key components of sub-acute (24h-5d) vascular responses and long-term (7d-14d) vascular remodeling both in the ischemic and the peri-lesional brain regions, focusing on critical aspects for late-phase recovery such as local tissue perfusion, blood-brain barrier functionality and permissiveness of the glial scar for remodeling of the brain vascular network in C57bl/6 mice.

RESULTS

Early Reperfusion Is Not Sufficient to Prevent Sub-Acute Vessel Degeneration After Stroke

The presence of perfused vessels in the sub-acute phase was measured within the infarction at 72 h and 5 days after stroke by quantification of intravascular FITC-lectin intensity. Symmetric fields of view in the contralateral cortex were used as internal controls. The tMCAO procedure led to increased sub-acute perfused vessels irrigating the infarction at 72 h ($p < 0.05$, **Figures 1B,D**) and 5 days ($p = 0.07$, **Figures 1C,D**) as compared to pMCAO. The impact of early reperfusion on the vascular niche was characterized within the infarction by two different approaches: 1) quantification of vascular cell proliferation as a measure of stroke-induced angiogenesis and 2) quantification of vessel density as end-point parameter for vascular remodeling. Vascular cell proliferation was analyzed cumulatively by combining several protocols of BrdU administration (**Supplementary Figure 2A**). Following permanent artery occlusion (pMCAO group), vascular proliferation labeled from 24h after stroke was evident from 48h up to the latest time studied, 5 days after stroke (**Figures 2A,A′** arrowheads, **B**). When measured at 72 h, early reperfusion led to increased cumulative vascular cell proliferation (**Figures 2B,B′** arrowheads, **B**), suggesting an enhancement of the proliferative vascular response to stroke in presence of reperfusion. However, cumulative proliferating cell numbers were similar between pMCAO and tMCAO groups at 5 days ($p > 0.05$, **Figures 2A,B**). Additionally, vessel density decreased after both pMCAO and tMCAO at 48 h up to 5 days after stroke and was not affected by differences in vascular cell proliferation (**Figures 2A,C**), suggesting that proliferation could be counteracted by vascular degeneration, regardless of the presence of reperfusion. This was supported by the occasional presence of vessels with recognizable tip cells showing a crown of extended filopodia, a characteristic feature of angiogenesis (**Figure 2D**, arrowheads) next to interrupted vessels with narrowed lumen, a typical feature of vascular degeneration (**Figure 2D**, arrows). Vessel degeneration was further revealed by identification of endothelial cells undergoing active apoptosis after both pMCAO and tMCAO (**Figure 2A**, Isolectin-B4$^+$/caspase-3$^+$). Together, these observations indicate that improved local measurement of perfused vessels and increased vascular cell proliferation achieved by early reperfusion are not sufficient to prevent sub-acute vessel degeneration within the infarction.

Acute Reperfusion Favors Peri-Lesional Vascular Remodeling Two Weeks After Stroke

The effect of acute reperfusion on long-term vascular remodeling was studied within the infarcted and peri-lesional regions 2 weeks after stroke (regions of interest and BrdU administration protocol are shown in **Supplementary Figures 2B,C**, respectively). Reperfusion achieved by tMCAO led to increased vascular cell proliferation within the infarction between post-stroke days 7 and 10 ($p < 0.05$, **Figures 3A,B**), corresponding with the days of BrdU administration (**Supplementary Figure 2B**). Increased proliferation was reflected in higher vessel density quantified at post-stroke day 14, as compared to pMCAO ($p < 0.05$, **Figures 3A,B**). Additionally, protein expression of the pro-angiogenic factor VEGF-A was better preserved within the infarction after tMCAO ($p < 0.05$, **Figure 3C**). In peri-lesional regions, active vascular cell proliferation was observed to a similar extent after pMCAO and tMCAO ($p > 0.05$, **Figure 3B**). Also, no differences on vessel density were detected within this region ($p > 0.05$, **Figure 3B**).

In order to further characterize the functionality of the remodeling vessels at 14 days after injury, structural and functional blood-brain barrier parameters were analyzed. No permeability of the BBB was detected on the Evans Blue *in vivo* permeability assay (representative brain in **Figure 3D**) regardless

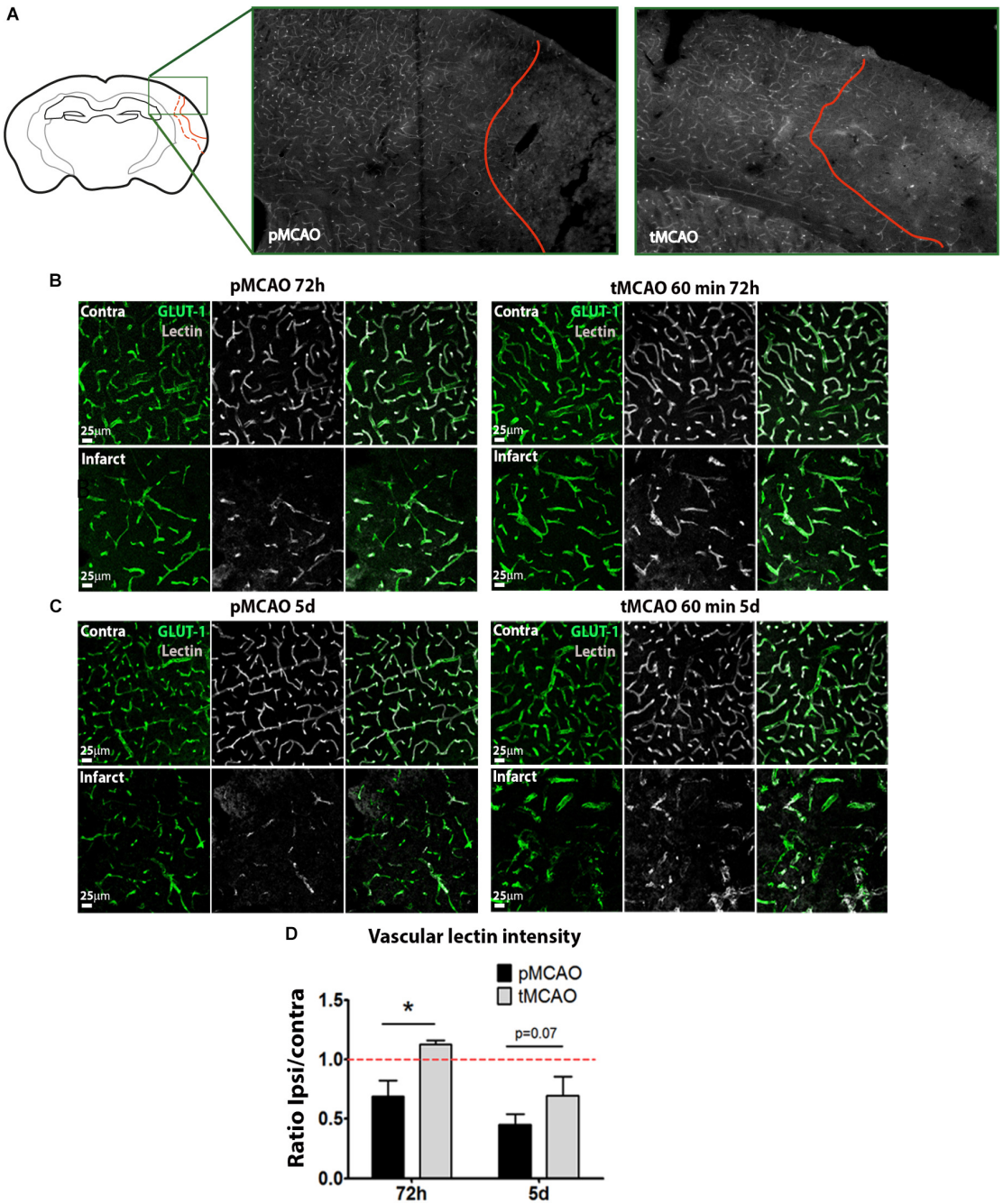

FIGURE 1 | (A) Representative images of the whole area of study comprising the healthy tissue, the peri-infarct and the infarct. **(B,C)** Representative confocal fluorescence micrographs (20x) showing perfusion intensity in ischemic and contralateral regions at 72 h **(B)** and 5 days **(C)** after pMCAO or 60-min tMCAO. Intravascular perfusion (lectin, gray) was analyzed in Glut-1^{+} vessels (green). **(D)** Quantification of average lectin intensity in vessels expressed as ratio of ischemic/contralateral (internal control) sub-acutely (n = 6–7). * Student's t-test $p < 0.05$ vs. pMCAO.

of the presence of early reperfusion. Tight junction protein expression (Claudin-5 and ZO-1) was generally preserved within infarcted and peri-lesional regions, also regardless of the presence of early reperfusion (western blots in **Figure 3D**).

While fluorescent background precluded the quantification of lectin perfusion within the infarction, analysis of vascular lectin intensity within the peri-lesional regions showed that acute recanalization led to a sustained presence of perfused vessels, indicative of local perfusion, in the regions surrounding the injured tissue ($p < 0.05$, **Figures 4A,B**). Improved peri-lesional perfusion was also reflected in the protein levels of hypoxia-inducible factor-1α (HIF-1α) at 14 days after injury within

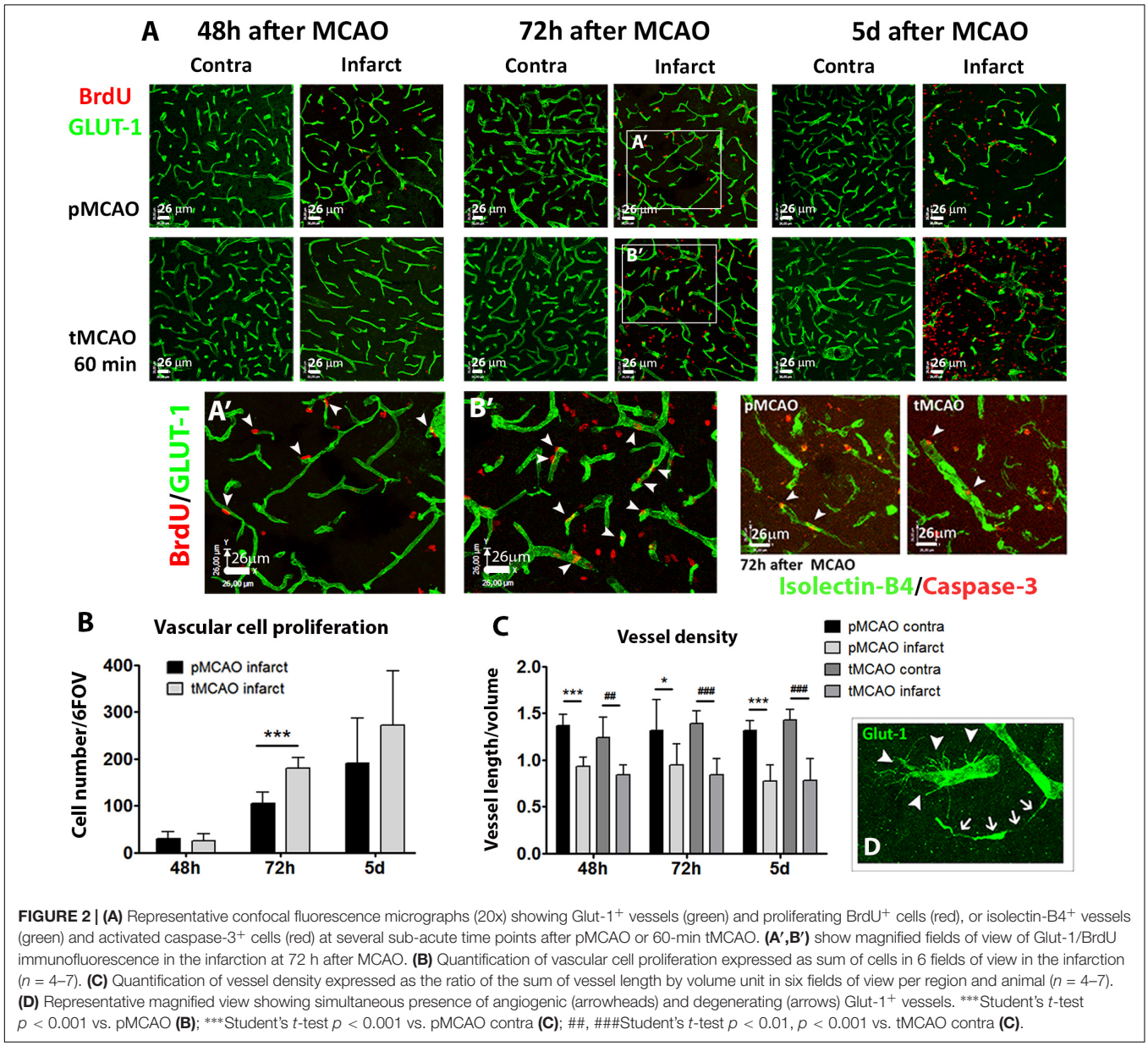

FIGURE 2 | (A) Representative confocal fluorescence micrographs (20x) showing Glut-1$^+$ vessels (green) and proliferating BrdU$^+$ cells (red), or isolectin-B4$^+$ vessels (green) and activated caspase-3$^+$ cells (red) at several sub-acute time points after pMCAO or 60-min tMCAO. **(A′,B′)** show magnified fields of view of Glut-1/BrdU immunofluorescence in the infarction at 72 h after MCAO. **(B)** Quantification of vascular cell proliferation expressed as sum of cells in 6 fields of view in the infarction (n = 4–7). **(C)** Quantification of vessel density expressed as the ratio of the sum of vessel length by volume unit in six fields of view per region and animal (n = 4–7). **(D)** Representative magnified view showing simultaneous presence of angiogenic (arrowheads) and degenerating (arrows) Glut-1$^+$ vessels. ***Student's t-test $p < 0.001$ vs. pMCAO **(B)**; ***Student's t-test $p < 0.001$ vs. pMCAO contra **(C)**; ##, ###Student's t-test $p < 0.01$, $p < 0.001$ vs. tMCAO contra **(C)**.

the infarction, that were significantly lower in animals with acute reperfusion compared to those that underwent permanent ischemia ($p < 0.05$, **Figure 4C**).

Together, our data indicate that early reperfusion favors long-term peri-lesional perfusion and vascular remodeling within the infarction, while preserving BBB integrity.

Glial Scar Shows Features of Higher Permissiveness for Brain Tissue Remodeling After Acute Reperfusion

The glial scar formed in response to CNS injury may preclude tissue repair. Expression of protein markers of two cell populations typically present in the glial scar (GFAP for reactive astrocytes and PDGFR-β for stromal cells of pericytic origin) was quantified at post-stroke day 14 in the infarcted and peri-lesional regions. GFAP expression was expressed to similar extent in both regions after pMCAO and tMCAO ($p > 0.05$, **Figures 5A,B**). PDGFR-β was also expressed to a similar extent in both stroke models ($p > 0.05$, **Figures 5A,B**). In contrast, expression of collagen type-IV, a matrix protein abundantly expressed in the scar, as well as of one of its main degrading proteases, MMP-9, were substantially reduced in animals that underwent acute reperfusion as compared to animals with pMCAO ($p < 0.01$, **Figures 5A–C**). Both intact collagen type-IV (∼230 kDa) and the two main degradation fragments (∼82 kDa and ∼42 kDa) were decreased (**Figure 5C**), suggesting that decreased levels of intact proteins are not a result of increased degradation and that alteration of matrix composition in the glial scar is a long-term effect of acute reperfusion.

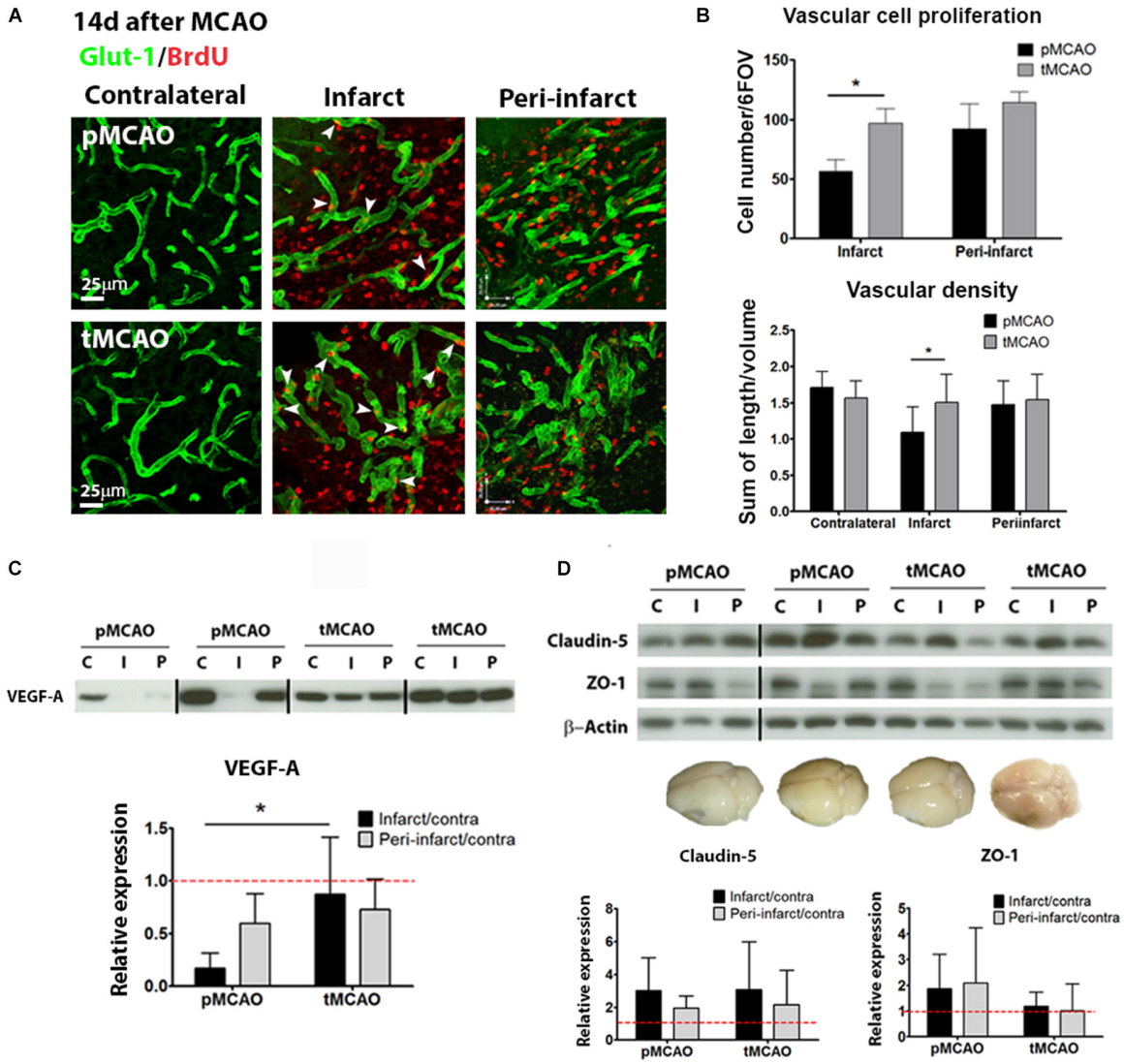

FIGURE 3 | (A) Representative confocal fluorescence micrographs (40x) showing Glut-1$^+$ vessels (green) and proliferating BrdU$^+$ cells (red) at post-stroke day 14. **(B)** Quantification of vascular cell proliferation (n = 6–8) and vascular density (n = 7–9) at post-stroke day 14. **(C)** Cropped blots from a representative VEGF-A western blot and quantification in contralateral (C), infarcted (I) and peri-lesional (P) tissue at post-stroke day 14. Complete gels are shown in **Supplementary Figure 3** (n = 5–6). **(D)** Cropped blots from representative ZO-1 (n = 5–6) and claudin-5 (n = 4–6) western blots and quantifications, and brain photographs showing absence of *in vivo* BBB permeability at post-stroke day 14. Complete gels are shown in **Supplementary Figure 3**. * Student's t-test $p < 0.05$ vs. pMCAO.

Acute Reperfusion Favors Late-Phase Functional Recovery

A final question that remained open in the study was if delayed affectation of peri-lesional remodeling mediated by acute reperfusion is associated to on an improvement on long-term injury progression and functional recovery. To address this question, late-phase functional recovery (beyond 48 h after stroke) was characterized in mice after pMCAO and tMCAO.

Lesion size at 24 h was similar in mice subjected to pMCAO and 60-min tMCAO (**Figures 6A,B**). Neurological deficits at 48 h were also comparable between both groups (not shown). In contrast, late-phase recovery from acute deficits (expressed as percentage of recovery versus the deficits observed at 48 h) was significantly higher in mice that underwent early artery recanalization at 7 and 14 days ($p < 0.05$, **Figure 6C**). However, injury progression (up to 14 days) was similar after pMCAO and tMCAO ($p > 0.05$, **Figure 6D**), indicating that recovery is not related to a reduction of injury size and could be related to the observed enhancement of vascular function in the peri-lesional regions.

DISCUSSION

An adequate restoration of tissue perfusion during the first hours after stroke is the main strategic pursued to reduce brain injury. This approach is especially effective when salvageable tissue

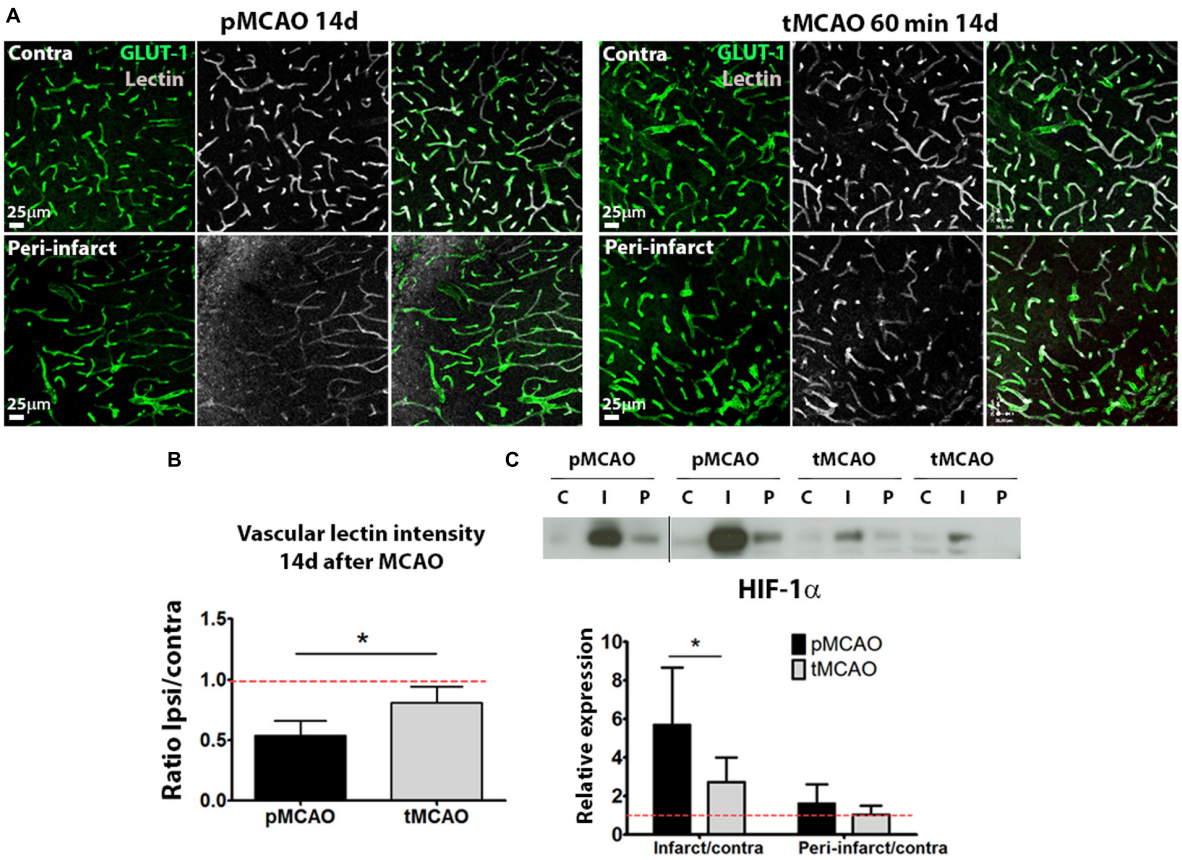

FIGURE 4 | (A) Representative confocal fluorescence micrographs (20x) showing perfusion intensity in ischemic and contralateral regions at post-stroke day 14. **(B)** Quantification of average lectin intensity in vessels expressed as ratio of ischemic/contralateral (internal control) sub-acutely. **(C)** Cropped blots from a representative HIF-1α western blot and quantification at post-stroke day 14, expressed as ratio ischemic/contralateral. Complete gels are shown in **Supplementary Figure 3** (n = 5–6). *Student's t-test $p < 0.05$ vs. pMCAO.

remains within the ischemic territory. However, it is assumed that stroke-induced injury is permanently established within the first 48 h after stroke regardless of the initial presence of salvageable penumbral tissue (Heiss et al., 1992; Darby et al., 1999; Markus et al., 2004). One of the most interesting findings in this study is that, beyond the known acute effects on brain injury, reperfusion also impacts vascular remodeling and peri-lesional hemodynamics in the long-term. More importantly, delayed effects of acute reperfusion may underlie late-phase functional recovery occurring after injury consolidation. This conclusion extends the clinical importance of achieving early reperfusion for the chronic recovery phase after stroke.

Importantly, as soon as 24 h after stroke there was a significant decrease in vascular coverage within the injured tissue regardless of the presence of tissue reperfusion, despite the fact that vascular degeneration occurred faster after pMCAO than after tMCAO. However, even though reperfusion prolonged vessel survival in the core, eventually restoration of brain perfusion was insufficient to rescue endothelial cells from death caused by ischemia-reperfusion injury. Notably, our data provide new knowledge on the vascular dynamics at the infarct core, an area that remains so far quite understudied.

Relating to this, recent studies have shown that reperfusion is not always complete at the capillary level, since no-reflow phenomenon has been observed in approximately 32% of capillaries within the injured tissue due to sustained constriction of contractile vascular cells, which can in turn trigger capillary degeneration (Yemisci et al., 2009; Hill et al., 2015). Adding to this, reperfusion itself exacerbates endogenous damaging mechanisms that can affect the survival of brain vessels such as oxidative stress and neuroinflammation (Eltzschig and Eckle, 2011; Iadecola and Anrather, 2011), thus increasing blood-brain barrier leakage and vasogenic oedema (Barber et al., 2005; Krueger et al., 2015) and ultimately compromising vessel survival.

The loss of capillary coverage within the infarcted tissue could potentially be compensated by vascular cell proliferation. Consistent with previous reports (Seevinck et al., 2010; Hossmann, 2012), we have observed a peak in vascular cell proliferation between 48 and 72 h after stroke. Interestingly, this peak of proliferation was increased by reperfusion, but was not reflected in higher vascular coverage later on. The simultaneous presence of apoptotic (activated caspase-3^{+}) vascular cells observed is in agreement with a prior study (Hayashi et al., 2003), and confirms the co-existence of vascular proliferation

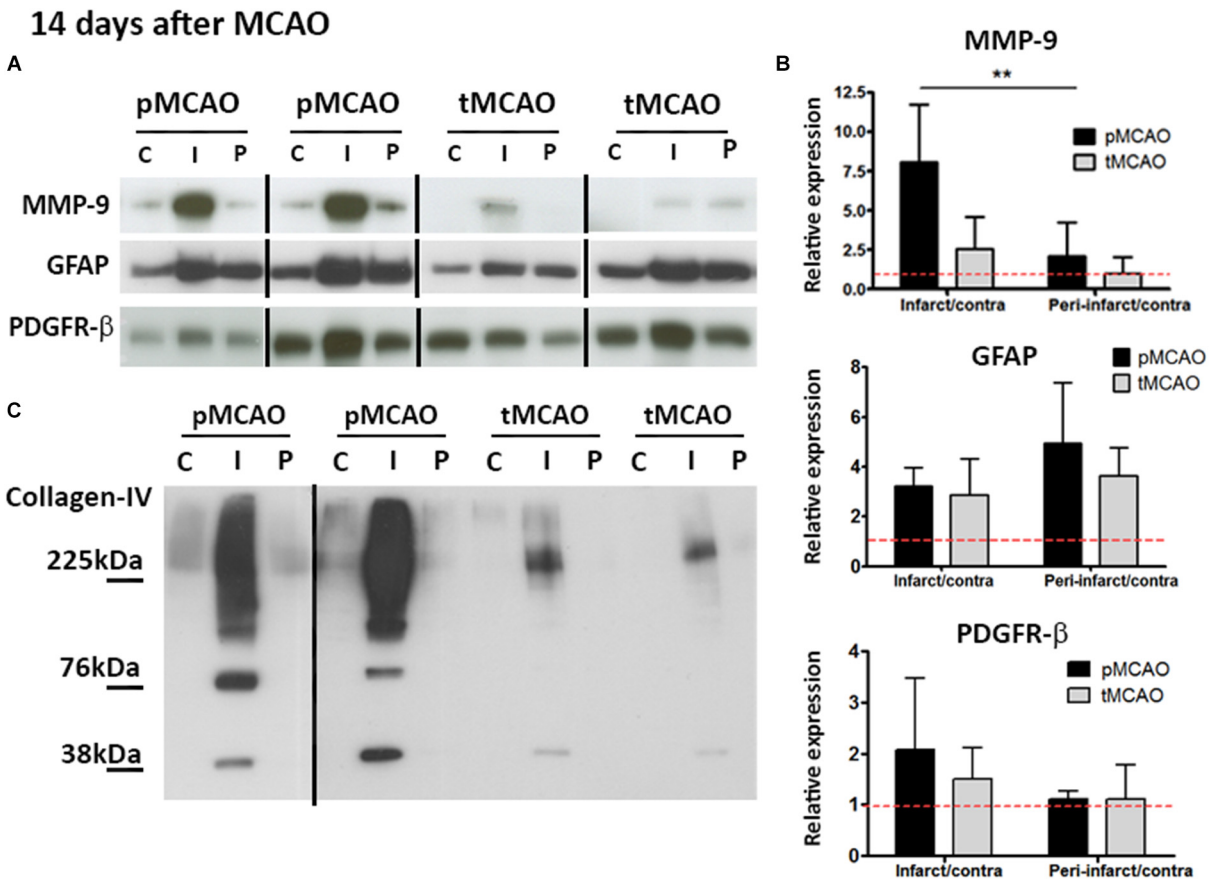

FIGURE 5 | (A,B) Cropped blots from representative MMP-9 (n = 5–6), GFAP (n = 4–5), and PDGFR-β (n = 5–6) western blots **(A)** and quantifications **(B)** in contralateral **(C)**, infarcted (I) and peri-lesional (P) regions at post-stroke day 14. **Student's t-test $p < 0.01$ vs. infarct/contra. Complete gels are shown in **Supplementary Figure 3**. **(C)** Representative collagen-IV cropped western blots showing expression of non-degraded protein (225 kDa) and degradation fragments (76 and 38 kDa) at post-stroke day 14. Complete gels are shown in **Supplementary Figure 3**.

and degeneration. Of note, absence of increased vessel density in response to proliferation conflicts with previous reports (Marti et al., 2000; Hayashi et al., 2003), but is a clear observation in our study. Interestingly, our observations at later time points reveal a secondary wave (between post-stroke days 7 and 10) of vascular proliferation within the ischemic and peri-lesional tissue, also described in previous studies (Wei et al., 2001; Zhang et al., 2002). Once more, in spite of the active proliferation and vascular remodeling observed in the peri-lesional regions, vascular coverage remained unchanged regardless of the presence of acute recanalization, in agreement with a previous long-term longitudinal study using intravital microscopy (Mostany et al., 2010). The same study concludes that absence of local angiogenesis does not preclude restoration of cerebral blood flow in the peri-lesional regions. Similarly, improved peri-lesional perfusion that we observed after acute tissue reperfusion can occur in the absence of angiogenesis.

We acknowledge that our study has certain limitations. For instance, transient mechanical vascular occlusion has been suggested not to be a fully adequate model of naturally occurring stroke (Hossmann, 2012) although, in our study, it was deemed appropriate in order to investigate the effect of reperfusion versus the permanent occlusion. In our work, comparisons are established between ipsi- and contralesional sides, thus assuming that the contralesional one does not show any major changes as previously described (Seevinck et al., 2010). However, we cannot discard that minor variations in the contralesional vasculature might take place. In addition, the differential contribution of local (angiogenesis) and/or peripheral (vasculogenesis) endothelial cells/progenitors to vascular outgrowth and remodeling as well as the contribution of recruited collaterals to the improvement of peri-lesional perfusion observed after acute recanalization have not been specifically addressed. It is known that vasculogenesis plays a role in post-stroke vascular remodeling (Hayakawa et al., 2012; Mao et al., 2014), but no correlation with restoration of local cerebral blood flow has been found so far. Regarding collateral circulation, the fact that injury size at 72 h after stroke was similar after pMCAO and tMCAO suggests that compensatory collateral perfusion may occur in the absence of reperfusion, as previously reported (Wei et al., 2001; Schaffer et al., 2006). A clinical study has shown that reperfusion following artery recanalization is a better prognostic marker of good outcome than of good collateral

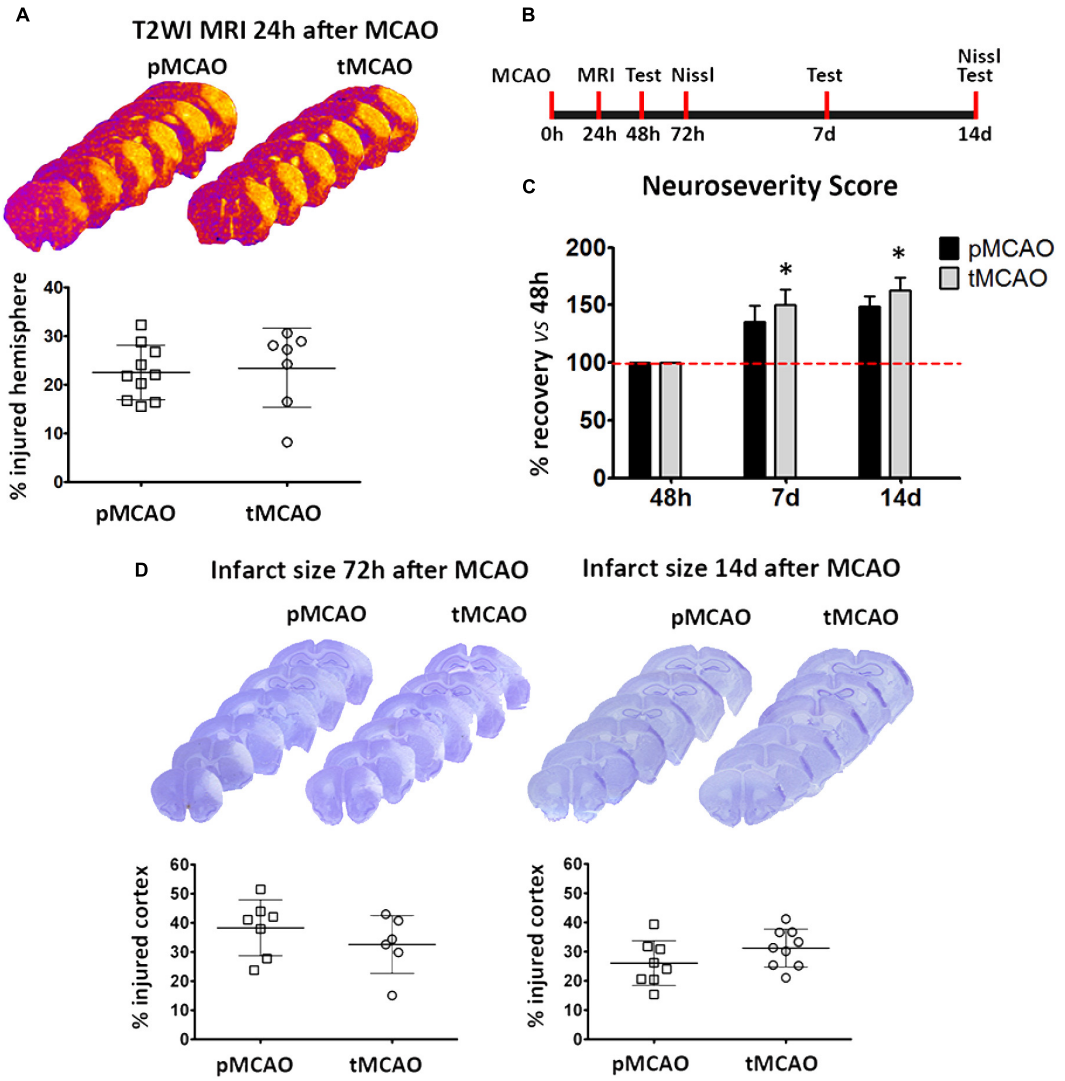

FIGURE 6 | (A) Representative series of T2WI-MRI planes and volumetric quantification showing infarct volumes at 24 h after pMCAO or tMCAO. **(B)** Schematic representation of the experimental design for the measurement of infarct volume and functional deficits after MCAO. **(C)** Data from functional assessment performed at 48 h (basal), 7 and 14 days after pMCAO or tMCAO (n = 7). **(D)** Representative series of Nissl-stained brain sections and corresponding graphs showing the extent of ischemic injury at 72 h and 14 days after permanent (pMCAO) or transient (60 min) middle cerebral artery occlusion (tMCAO). *Two-way ANOVA $p < 0.05$ vs. pMCAO.

circulation (Marks et al., 2014). Collaterals contribute to improve reperfusion following recanalization (Heiss et al., 1992; Darby et al., 1999; Kassem-Moussa and Graffagnino, 2002; Markus et al., 2004; Barber et al., 2005; Rha and Saver, 2007; Yemisci et al., 2009; Seevinck et al., 2010; Bang et al., 2011; Eltzschig and Eckle, 2011; Iadecola and Anrather, 2011; Hossmann, 2012; Liebeskind et al., 2014; Marks et al., 2014; Hill et al., 2015; Krueger et al., 2015; Smith et al., 2017), but to our knowledge a reverse effect of recanalization on collateral circulation has not been yet described. However, we acknowledge the possibility that leptomeningeal collateral remodeling induced by reperfusion may have contributed to the outcomes described here. As far as functional recovery is concerned, our study explores up to 14 days after MCAO; further studies are required to ascertain whether this effect remains at later time points. Finally, reperfusion in the tMCAO was assessed visually. Although this is a quite straightforward procedure when a craniectomy has been performed, as in our case, we acknowledge that this method lacks the resolution of laser Doppler flowmetry.

Our exploration of the injury scar has revealed interesting effects of acute recanalization, especially in what refers to the extracellular matrix composition and turnover. We focused on characterizing expression of the reactive astrocytes marker GFAP and the pericyte marker PDGFR-β, since recent studies have described that a specific subpopulation of pericytes characterized by the expression of this marker are the main source of stromal

cells forming the scar as a result of spinal cord injury (Göritz et al., 2011; Soderblom et al., 2013). While recanalization affected neither GFAP nor PDGR-β protein expression, collagen type-IV was much more abundant in the absence of acute reperfusion, as it was the expression of its degrading protease MMP-9 and its degradation fragments. Increased MMP-9 expression could be a response to higher accumulation of collagen-IV within the injury scar, which ultimately would interfere with tissue remodeling processes in spite of a higher local MMP-9 activity. While collagen type-IV is not a growth inhibitory molecule *per se* (Tonge et al., 1997; Joosten et al., 2000), collagen meshworks in the scar can allocate other inhibitory factors that preclude vascular and neural growth signaling (Hermanns et al., 2006; Klapka and Müller, 2006), effects that may have important consequences on the endogenous mechanisms of repair. In agreement with this hypothesis, an important observation of our study is that functional outcome in the long term (7–14 days) was improved in animals that underwent early recanalization. Since the size of the lesion was though not affected, our findings strongly support that recanalization-induced enhanced vascular function in the peri-lesional regions of these animals accounts for the long-term recovery observed. These observations open the path to a more complete characterization of the effect of acute reperfusion on injury scar formation and composition, with the functional relevance that these processes may have for tissue repair and functional recovery during the chronic phase after stroke.

MATERIALS AND METHODS

All data generated or analyzed during this study are included in this published article (and its **Supplementary Information Files**).

Animals

All experiments were performed in 3-month-old male C57bl/6 mice obtained from Jackson Laboratories. Mice were kept in a ventilated room with controlled temperature and with a 12-h dark/light cycle and were fed *ad libitum* with standard food and water. All experimental protocols had been approved by the Animal Welfare Committee of the Complutense University of Madrid and were in accordance to the guidelines of the Madrid Autonomous Community Government (RD 53/2013) following the European directives 86/609/CEE and 2003/65/CE. Results are reported according to ARRIVE guidelines. Details on the experimental design and number of animals used in each study are provided in **Supplementary Figure 1**.

Induction of Focal Brain Ischemia

Mice were anesthetized and maintained during surgery at 1–2% isoflurane in a 30%/70% mixture of O_2/N_2O and body temperature was maintained at physiological levels with a heating blanket during the surgery and anesthesia recovery. Mice were exposed to focal brain ischemia by distal occlusion of the middle cerebral artery (MCAO). To study the effect of acute reperfusion, two modes of occlusion were used after randomization: permanent middle cerebral artery occlusion (pMCAO, with no reperfusion) and transient MCAO (60 min occlusion followed by reperfusion, tMCAO). MCAO was achieved through ligation of the artery with a 9-0 suture just before its bifurcation into the frontal and parietal branches (Hernández-Jiménez et al., 2013). For tMCAO, the ligation was removed after 60 min and recanalization of the artery was visually assessed. The ipsilateral common carotid artery was also occluded permanently (pMCAO) or transiently (tMCAO) prior to ligation of the MCA. Researchers were blind to the experimental groups thereafter. After surgery mice were returned to their cages with *ad libitum* access to food and water. Mice were observed until anesthesia recovery and once a day until euthanasia. When appropriate, mice were euthanized with a lethal dose of pentobarbital or an overdose of isoflurane.

Experimental Groups

Mice were allocated in experimental groups by randomization by coin toss. A complete chart describing experimental groups, number of animals per group, dead animals (2 mice, 2%) and procedures can be found in **Supplementary Figures 1**, **2**.

Determination of Brain Infarct Size

Infarct size was determined at 24h by T2WI Magnetic Resonance. From 72h to 14d the injured tissue was measured by histological quantification on Nissl-stained serial sections.

T2WI Magnetic Resonance

MRI was performed on a 1 T benchtop MRI scanner [Icon (1T-MRI); Bruker BioSpin GmbH, Ettlingen, Germany]. The system consists of a 1 T permanent magnet (without extra cooling required for the magnet). Its gradient coil provides 450 mT/m. MRI experiments consisted of a series three dimensional T2 weighted images (T2WI) used to evaluate the vascular oedema. Three-dimensional T2WI were acquired using a rapid acquisition with relaxation enhancement (RARE) technique, with a repetition time (TR) = 2350 s, RARE factor = 16, and interecho interval = 15.83 ms, resulting in an effective echo time (TE) = 95 ms, number of average = 1, the field of view (FOV) = 16 × 16 × 8 mm. The acquired matrix size was 96 × 96 × 16 and the resolution 0.167 × 0.167 × 0.500 mm. Infarcts were visualized with the Image J software. The areas of infarcted tissue, the whole ipsilateral hemisphere, and the whole contralateral hemisphere were delineated in all consecutive sections. Data were corrected for edema and expressed as % of injured hemisphere by applying the formula $[(Vol_{Contra}\text{-}Vol_{UninjuredIpsi})/Vol_{Contra}] \times 100$.

Histology

Cryoprotected brains were sliced using a freezing microtome (Leica) and 30 μm serial sections covering the brain were obtained. Serial sections were stained with cresyl violet and infarct volume was measured stereologically (using the software StereoInvestigator, MicroBrightField) or by ImageJ analysis at 72 h and 14 days after MCAO. The contralateral cortex and the uninjured ipsilateral cortex were traced on 10 serial

sections (spaced 300 μm, covering approximately from bregma 1.3 to −2.3 mm) and volumes were calculated using the Cavalieri estimation obtaining a coefficient of error Gundersen ($m = 1$) < 0.05 in all cases. Infarct size was obtained by applying the formula for oedema correction [(Vol_{Contra}-$Vol_{UninjuredIpsi}$)/Vol_{Contra}] × 100 and was expressed as percentage of injured ipsilateral cortex.

Assessment of Neurological Deficits

Neuroseverity Score (James et al., 2009; Hernández-Jiménez et al., 2017) was used to measure functional deficits induced by MCAO in the mice. Motor activity score (Krupinski et al., 1993; Dimmeler et al., 1996; Kassem-Moussa and Graffagnino, 2002; Haga et al., 2003; Yamamoto et al., 2003; Chopp et al., 2007; Arkuszewski et al., 2009; Snapyan et al., 2009; Smith et al., 2017) is based on spontaneous activity, symmetry in the use of the limbs, equilibrium and coordination and sensory score (Krupinski et al., 1993; Dimmeler et al., 1996; Haga et al., 2003; Chopp et al., 2007; Thored et al., 2007; Arkuszewski et al., 2009; Snapyan et al., 2009) is based on tactile, vibrissae, visual and proprioceptive responses, that were measured in the contralateral side of the animalś; body. A minimum score of 7 reflects most severe neurological deficit and a maximum score of 21 reflects absence of deficits. The 48h measurement was taken as the basal value as we consider this time as the starting point of the angiogenesis process.

In vivo Blood-Brain Barrier Permeability Assay

Mice were injected intravenously with 2% Evans Blue (2 mg/kg, Sigma) 30 min before termination at 14 days after MCAO and perfused transcardiacally with saline solution until blood was removed from the system. Contralateral and ipsilateral cortices were collected, weighted and immediately flash-frozen. Cortices were then homogenized in 250 μl 1:2 saline/50% TCA solution and homogenates were centrifuged at 10000 g for 15 min. Supernatants were collected and loaded 1:4 in 95% ethanol on a 96-well plated. Fluorescence (620 nm excitation/680 nm emission) was measured using a fluorimeter. Lowest detection level limited by the current state of the technique was 0.1 μg/ml.

Immunofluorescence

Thirty micrometer-thickness brain serial sections were stained by free-floating immunofluorescence. Sections were incubated with primary antibodies (see **Table 1** for a list of antibodies, dilutions and conditions) in blocking solution (5% Normal Serum) overnight at 4°C and then incubated with secondary antibodies conjugated to the corresponding fluorophores. For proliferation analysis, BrdU (50 mg/kg) was injected intraperitoneally once daily following the experimental designs shown in **Supplementary Figure 2**. For BrdU staining sections were incubated with 2N HCl at 37°C for 30 min prior to incubation with the primary antibodies. For vessel perfusion analysis, *Lycopersicon esculentum* lectin was injected intravenously 20 min prior to animal sacrifice and observed by direct FITC fluorescence under the microscope.

TABLE 1 | Antibodies, vendors and concentrations used in immunofluorescence and western blot assays.

Antibody/marker	*RRID*	*Dilution*
Immunofluorescence		
Rabbit anti-Glut-1	Millipore Cat# 07-1401, RRID:AB_1587074	1:500
Rat anti-BrdU	Bio-Rad Cat# MCA2060T, RRID:AB_10015293	1:100
Rabbit anti-cleaved caspase-3	Cell Signaling Technology Cat# 9661, RRID:AB_2341188	1:500
FITC-lectin	Vector Laboratories Cat# FL-1171, RRID:AB_2307440	−−
Isolectin B4-Alexa647		1:100
Western blotting		
Rabbit anti-VEGF	Santa Cruz Biotechnology Cat# sc-152, RRID:AB_2212984	1:1000
Mouse anti-Claudin-5	Thermo Fisher Scientific Cat# 35-2500, RRID:AB_2533200	1:1000
Rabbit anti-ZO-1	Innovative Research Cat# 61-7300, RRID:AB_138452	1:1000
Mouse anti-HIF-1α	Millipore Cat# MAB5382, RRID:AB_177967	1:500
Mouse anti-GFAP	Millipore Cat# IF03L, RRID:AB_2294571	1:1000
Goat anti-PDGFR-β	R and D Systems Cat# AF1042, RRID:AB_2162633	1:500
Goat anti-MMP-9	R and D Systems Cat# AF909, RRID:AB_355706	1:500
Rabbit anti-Collagen type IV	Abcam Cat# ab6586, RRID:AB_305584	1:1000

Image Acquisition and Quantification

Regions of interest were defined as follows: infarcted cortex -where infarct rim was clearly visible in MRI images, and in Nissl (as shown in **Figure 1A**, by an abundant nuclei area) and immunofluorescence stainings (increased fluorescence background)- and mirroring region in the contralateral cortex (48 h, 72 h and 5 days), peri-lesional cortex (1 field immediately adjacent to the infarct rim, clearly visible by the presence of the glial scar) and the mirroring contralateral cortex (14 days). Representative images of the area comprising the infarct, the peri-infarct and the healthy tissue were taken with a 5× lens. Z-stacks used for perfusion quantification were captured using a 20x lens and analyzed volumetrically using Volocity software (Improvision). Close-up images were captured with a 40× oil-immersion lens. Vascular coverage was expressed as the sum of length of vessels (Glut-1^+ objects) per unit of volume. Vascular tortuosity was calculated separately for each object by the ratio length/longest axis, and average vascular diameter was obtained for each vessel and expressed as a diameter size distribution for the vessel population. Cell proliferation associated to vessels was calculated by the quantification of $BrdU^+$ cells with whole nuclear staining in contact with Glut-1^+ vessels. Quantification of variations in local perfusion was performed by the analysis of the fluorescence intensity of FITC-lectin in Glut-1^+ vessels following subtraction of background intensity. Images were captured under same exact conditions in the infarcted and contralateral cortex at sub-acute time points (72 h and 5 days)

and in the ischemic boundaries and the contralateral cortex at 14 days. Data are expressed as sum of values obtained from 6 different fields of view per region of interest in each animal.

Western Blot

Whole brain lysates were prepared from flash frozen samples by homogenization in 1x Lysis Buffer (Cell Signaling) containing protease inhibitors (Roche). Western blot membranes were obtained after PAGE-SDS and protein transfer to PVDF membranes. Membranes were incubated with primary antibodies (see **Table 1** for list of antibodies, dilutions and conditions) in 5% non-fat milk in 0.2% Tween-20 TBS and HRP-conjugated secondary antibodies. Band intensity was measured by ImageJ, and data are expressed by normalization to values in the uninjured contralateral tissue due to the high variability between individuals. For that reason, the contralateral tissue was used as internal control in **Figures 3C**, **4C**, **5A**. In **Figure 3D** data are expressed by normalization with actin.

Statistical Analysis

Data were expressed as mean ± SD. Data sets were tested for normality (Kolmogorov-Smirnoff test). Student's *t*-test was used for comparison of two datasets and one- or two-way ANOVA was used for comparison of multiple datasets and variables. For comparisons against a defined value (eg.- ratio/ipsi contra = 1) a one-sample *t*-test was used. A p-value < 0.05 was considered statistically significant.

DATA AVAILABILITY

No datasets were generated or analyzed for this study.

ETHICS STATEMENT

All experimental protocols had been approved by the Animal Welfare Committee of the Complutense University of Madrid, and were in accordance to the guidelines of the Madrid Autonomous Community Government (RD 53/2013) following the European directives 86/609/CEE and 2003/65/CE. Results are reported according to ARRIVE guidelines.

AUTHOR CONTRIBUTIONS

DF-L, VD-L, MÁM, and IL designed the research. VD-L, DF-L, JG-H, AM, AG-C, SP-T, IG-Y, and AV-P performed the research. VD-L, DF-L, IG-Y, and AV-P analyzed the data. DF-L, MÁM, and IL wrote the manuscript. All authors reviewed the manuscript.

FUNDING

This work was supported by grants from the Spanish Ministry of Economy and Competitiveness SAF2015-68632-R (MÁM) and CSD2010-00045 (MÁM), from the Instituto de Salud Carlos III (ISCIII) and co-financed by the Fondo Europeo de Desarrollo Regional (FEDER) "A way to achieve Europe" FIS PI17/01601 (IL) and RETICS RD16/0019/0009 (IL), and from Regional Madrid Government B2017/BMD-3688 (IL).

SUPPLEMENTARY MATERIAL

The Supplementary Material for this article can be found online at: https://www.frontiersin.org/articles/10.3389/fnins.2019.00767/full#supplementary-material

REFERENCES

Arkuszewski, M., Swiat, M., and Opala, G. (2009). Perfusion computed tomography in prediction of functional outcome in patients with acute ischaemic stroke. *Nucl. Med. Rev. Cent. East. Eur.* 12, 89–94.

Bang, O. Y., Saver, J. L., Kim, S. J., Kim, G. M., Chung, C. S., Ovbiagele, B., et al. (2011). Collateral flow predicts response to endovascular therapy for acute ischemic stroke. *Stroke* 42, 693–699. doi: 10.1161/STROKEAHA.110.595256

Barber, P. A., Hoyte, L., Kirk, D., Foniok, T., Buchan, A., and Tuor, U. (2005). Early T1- and T2-weighted MRI signatures of transient and permanent middle cerebral artery occlusion in a murine stroke model studied at 9.4*T*. *Neurosci. Lett.* 388, 54–59. doi: 10.1016/j.neulet.2005.06.067

Chen, J., Venkat, P., Zacharek, A., and Chopp, M. (2014). Neurorestorative therapy for stroke. *Front. Hum. Neurosci.* 8:382. doi: 10.3389/fnhum.2014.00382

Chopp, M., Zhang, Z. G., and Jiang, Q. (2007). Neurogenesis, angiogenesis, and MRI indices of functional recovery from stroke. *Stroke* 38, 827–831. doi: 10.1161/01.str.0000250235.80253.e9

Darby, D. G., Barber, P. A., Gerraty, R. P., Desmond, P. M., Yang, Q., Parsons, M., et al. (1999). Pathophysiological topography of acute ischemia by combined diffusion-weighted and perfusion MRI. *Stroke* 30, 2043–2052. doi: 10.1161/01.str.30.10.2043

Dimmeler, S., Haendeler, J., Rippmann, V., Nehls, M., and Zeiher, A. M. (1996). Shear stress inhibits apoptosis of human endothelial cells. *FEBS Lett.* 399, 71–74. doi: 10.1016/s0014-5793(96)01289-6

Eltzschig, H. K., and Eckle, T. (2011). Ischemia and reperfusion–from mechanism to translation. *Nat. Med.* 17, 1391–1401. doi: 10.1038/nm.2507

Göritz, C., Dias, D. O., Tomilin, N., Barbacid, M., Shupliakov, O., and Frisén, J. (2011). A pericyte origin of spinal cord scar tissue. *Science* 333, 238–242. doi: 10.1126/science.1203165

Haga, M., Chen, A., Gortler, D., Dardik, A., and Sumpio, B. E. (2003). Shear stress and cyclic strain may suppress apoptosis in endothelial cells by different pathways. *Endothelium* 10, 149–157. doi: 10.1080/10623320390233463

Hayakawa, K., Pham, L.-D. D., Katusic, Z. S., Arai, K., and Lo, E. H. (2012). Astrocytic high-mobility group box 1 promotes endothelial progenitor cell-mediated neurovascular remodeling during stroke recovery. *Proc. Natl. Acad. Sci. U.S.A.* 109, 7505–7510. doi: 10.1073/pnas.1121146109

Hayashi, T., Noshita, N., Sugawara, T., and Chan, P. H. (2003). Temporal profile of angiogenesis and expression of related genes in the brain after ischemia. *J. Cereb. Blood Flow Metab.* 23, 166–180. doi: 10.1097/01.wcb.0000041283.53351.cb

Heiss, W. D., Huber, M., Fink, G. R., Herholz, K., Pietrzyk, U., Wagner, R., et al. (1992). Progressive derangement of periinfarct viable tissue in ischemic stroke. *J. Cereb. Blood Flow Metab.* 12, 193–203. doi: 10.1038/jcbfm.1992.29

Hermanns, S., Klapka, N., Gasis, M., and Müller, H. W. (2006). The collagenous wound healing scar in the injured central nervous system inhibits axonal regeneration. *Adv. Exp. Med. Biol.* 557, 177–190. doi: 10.1007/0-387-30128-3_11

Hernández-Jiménez, M., Hurtado, O., Cuartero, M. I., Ballesteros, I., Moraga, A., Pradillo, J. M., et al. (2013). Silent information regulator 1 protects the brain against cerebral ischemic damage. *Stroke* 44, 2333–2337. doi: 10.1161/STROKEAHA.113.001715

Hernández-Jiménez, M., Peña-Martínez, C., Godino, M. D. C., Díaz-Guzmán, J., Moro, M. Á, and Lizasoain, I. (2017). Test repositioning for functional assessment of neurological outcome after experimental stroke in mice. *PLoS One* 12:e0176770. doi: 10.1371/journal.pone.0176770

Hill, R. A., Tong, L., Yuan, P., Murikinati, S., Gupta, S., Grutzendler, J., et al. (2015). Regional Blood Flow in the Normal and Ischemic Brain Is Controlled by Arteriolar Smooth Muscle Cell Contractility and Not by Capillary Pericytes. *Neuron* 87, 95–110. doi: 10.1016/j.neuron.2015.06.001

Hossmann, K.-A. (2012). The two pathophysiologies of focal brain ischemia: implications for translational stroke research. *J. Cereb. Blood Flow Metab.* 32, 1310–1316. doi: 10.1038/jcbfm.2011.186

Iadecola, C., and Anrather, J. (2011). The immunology of stroke: from mechanisms to translation. *Nat. Med.* 17, 796–808. doi: 10.1038/nm.2399

James, M. L., Sullivan, P. M., Lascola, C. D., Vitek, M. P., and Laskowitz, D. T. (2009). Pharmacogenomic effects of apolipoprotein e on intracerebral hemorrhage. *Stroke* 40, 632–639. doi: 10.1161/STROKEAHA.108.530402

Joosten, E. A. J., Dijkstra, S., Brook, G. A., Veldman, H., and Bär, P. R. (2000). Collagen IV deposits do not prevent regrowing axons from penetrating the lesion site in spinal cord injury. *J. Neurosci. Res.* 62, 686–691. doi: 10.1002/1097-4547(20001201)62:5<686::aid-jnr7>3.0.co;2-l

Kassem-Moussa, H., and Graffagnino, C. (2002). Nonocclusion and spontaneous recanalization rates in acute ischemic stroke: a review of cerebral angiography studies. *Arch. Neurol.* 59, 1870–1873.

Klapka, N., and Müller, H. W. (2006). Collagen matrix in spinal cord injury. *J. Neurotrauma* 23, 422–435.

Krueger, M., Bechmann, I., Immig, K., Reichenbach, A., Härtig, W., and Michalski, D. (2015). Blood-brain barrier breakdown involves four distinct stages of vascular damage in various models of experimental focal cerebral ischemia. *J. Cereb. Blood Flow Metab.* 35, 292–303. doi: 10.1038/jcbfm.2014.199

Krupinski, J., Kaluza, J., Kumar, P., Wang, M., and Kumar, S. (1993). Prognostic value of blood vessel density in ischaemic stroke. *Lancet* 342, 742. doi: 10.1016/0140-6736(93)91734-4

Liebeskind, D. S., Tomsick, T. A., Foster, L. D., Yeatts, S. D., Carrozzella, J., Demchuk, A. M., et al. (2014). Collaterals at Angiography and Outcomes in the Interventional Management of Stroke (IMS) III Trial. *Stroke* 45, 759–764. doi: 10.1161/STROKEAHA.113.004072

Mao, L., Huang, M., Chen, S. C., Li, Y. N., Xia, Y. P., He, Q. W., et al. (2014). Endogenous endothelial progenitor cells participate in neovascularization via CXCR4/SDF-1 axis and improve outcome after stroke. *CNS Neurosci. Ther.* 20, 460–468. doi: 10.1111/cns.12238

Marks, M. P., Lansberg, M. G., Mlynash, M., Olivot, J. M., Straka, M., Kemp, S., et al. (2014). Effect of Collateral Blood Flow on Patients Undergoing Endovascular Therapy for Acute Ischemic Stroke. *Stroke* 45, 1035–1039. doi: 10.1161/strokeaha.113.004085

Markus, R., Reutens, D. C., Kazui, S., Read, S., Wright, P., Pearce, D. C., et al. (2004). Hypoxic tissue in ischaemic stroke: persistence and clinical consequences of spontaneous survival. *Brain* 127, 1427–1436. doi: 10.1093/brain/awh162

Marti, H. J., Bernaudin, M., Bellail, A., Schoch, H., Euler, M., Petit, E., et al. (2000). Hypoxia-induced vascular endothelial growth factor expression precedes neovascularization after cerebral ischemia. *Am. J. Pathol.* 156, 965–976. doi: 10.1016/s0002-9440(10)64964-4

Mostany, R., Chowdhury, T. G., Johnston, D. G., Portonovo, S. A., Carmichael, S. T., Portera-Cailliau, C., et al. (2010). Local hemodynamics dictate long-term dendritic plasticity in peri-infarct cortex. *J. Neurosci.* 30, 14116–14126. doi: 10.1523/JNEUROSCI.3908-10.2010

Navarro-Sobrino, M., Rosell, A., Hernández-Guillamon, M., Penalba, A., Boada, C., Domingues-Montanari, S., et al. (2011). A large screening of angiogenesis biomarkers and their association with neurological outcome after ischemic stroke. *Atherosclerosis* 216, 205–211. doi: 10.1016/j.atherosclerosis.2011.01.030

Rha, J.-H., and Saver, J. L. (2007). The Impact of Recanalization on Ischemic Stroke Outcome: A Meta-Analysis. *Stroke* 38, 967–973. doi: 10.1161/01.str.0000258112.14918.24

Schaffer, C. B., Friedman, B., Nishimura, N., Schroeder, L. F., Tsai, P. S., Ebner, F. F., et al. (2006). Two-photon imaging of cortical surface microvessels reveals a robust redistribution in blood flow after vascular occlusion. *PLoS Biol.* 4:e22. doi: 10.1371/journal.pbio.0040022

Seevinck, P. R., Deddens, L. H., and Dijkhuizen, R. M. (2010). Magnetic resonance imaging of brain angiogenesis after stroke. *Angiogenesis* 13, 101–111. doi: 10.1007/s10456-010-9174-0

Smith, E. E., Saver, J. L., Cox, M., Liang, L., Matsouaka, R., Xian, Y., et al. (2017). *Rapid increase in endovascular thrombectomy for acute ischemic stroke in the United States: Data from get with the guidelines-stroke*. Available at: http://www.abstractsonline.com/pp8/#!/4172/presentation/12316

Snapyan, M., Lemasson, M., Brill, M. S., Blais, M., Massouh, M., Ninkovic, J., et al. (2009). Vasculature guides migrating neuronal precursors in the adult mammalian forebrain via brain-derived neurotrophic factor signaling. *J. Neurosci.* 29, 4172–4188. doi: 10.1523/JNEUROSCI.4956-08.2009

Soderblom, C., Luo, X., Blumenthal, E., Bray, E., Lyapichev, K., Ramos, J., et al. (2013). Perivascular fibroblasts form the fibrotic scar after contusive spinal cord injury. *J. Neurosci.* 33, 13882–13887. doi: 10.1523/JNEUROSCI.2524-13.2013

Thored, P., Wood, J., Arvidsson, A., Cammenga, J., Kokaia, Z., and Lindvall, O. (2007). Long-term neuroblast migration along blood vessels in an area with transient angiogenesis and increased vascularization after stroke. *Stroke* 38, 3032–3039. doi: 10.1161/strokeaha.107.488445

Tonge, D. A., Golding, J. P., Edbladh, M., Kroon, M., Ekström, P. E., and Edström, A. (1997). Effects of extracellular matrix components on axonal outgrowth from peripheral nerves of adult animals in vitro. *Exp. Neurol.* 146, 81–90. doi: 10.1006/exnr.1997.6498

Wei, L., Erinjeri, J. P., Rovainen, C. M., and Woolsey, T. A. (2001). Collateral growth and angiogenesis around cortical stroke. *Stroke* 32, 2179–2184. doi: 10.1161/hs0901.094282

Yamamoto, K., Takahashi, T., Asahara, T., Ohura, N., Sokabe, T., Kamiya, A., et al. (2003). Proliferation, differentiation, and tube formation by endothelial progenitor cells in response to shear stress. *J. Appl. Physiol.* 95, 2081–2088. doi: 10.1152/japplphysiol.00232.2003

Yemisci, M., Gursoy-Ozdemir, Y., Vural, A., Can, A., Topalkara, K., and Dalkara, T. (2009). Pericyte contraction induced by oxidative-nitrative stress impairs capillary reflow despite successful opening of an occluded cerebral artery. *Nat. Med.* 15, 1031–1037. doi: 10.1038/nm.2022

Zhang, Z. G., Zhang, L., Tsang, W., Soltanian-Zadeh, H., Morris, D., Zhang, R., et al. (2002). Correlation of VEGF and angiopoietin expression with disruption of blood-brain barrier and angiogenesis after focal cerebral ischemia. *J. Cereb. Blood Flow Metab.* 22, 379–392. doi: 10.1097/00004647-200204000-00002

Conflict of Interest Statement: The authors declare that the research was conducted in the absence of any commercial or financial relationships that could be construed as a potential conflict of interest.

Copyright © 2019 Durán-Laforet, Fernández-López, García-Culebras, González-Hijón, Moraga, Palma-Tortosa, García-Yébenes, Vega-Pérez, Lizasoain and Moro. This is an open-access article distributed under the terms of the Creative Commons Attribution License (CC BY). The use, distribution or reproduction in other forums is permitted, provided the original author(s) and the copyright owner(s) are credited and that the original publication in this journal is cited, in accordance with accepted academic practice. No use, distribution or reproduction is permitted which does not comply with these terms.

frontiers in Neuroscience

REVIEW
published: 24 July 2019
doi: 10.3389/fnins.2019.00728

Re-thinking the Etiological Framework of Neurodegeneration

*Ximena Castillo[1,2], Susana Castro-Obregón[3], Benjamin Gutiérrez-Becker[4], Gabriel Gutiérrez-Ospina[5], Nikolaos Karalis[6], Ahmed A. Khalil[7,8,9], José Sócrates Lopez-Noguerola[10], Liliana Lozano Rodríguez[11], Eduardo Martínez-Martínez[12], Claudia Perez-Cruz[13], Judith Pérez-Velázquez[14,15], Ana Luisa Piña[16], Karla Rubio[17], Héctor Pedro Salazar García[18], Tauqeerunnisa Syeda[13], America Vanoye-Carlo[19], Arno Villringer[7,8,9], Katarzyna Winek[20,21] and Marietta Zille[22,23,24]**

[1] Instituto de Neurobiología, Universidad Nacional Autónoma de México, Mexico City, Mexico, [2] Institute of Neurobiology, University of Puerto Rico, San Juan, PR, United States, [3] Instituto de Fisiología Celular, Universidad Nacional Autónoma de México, Mexico City, Mexico, [4] Artificial Intelligence in Medical Imaging KJP, Ludwig Maximilian University of Munich, Munich, Germany, [5] Laboratorio de Biología de Sistemas, Departamento de Biología Celular y Fisiología, Instituto de Investigaciones Biomédicas y Coordinación de Psicobiología y Neurociencias, Facultad de Psicología, Universidad Nacional Autónoma de México, Mexico City, Mexico, [6] Friedrich Miescher Institute for Biomedical Research, Basel, Switzerland, [7] Center for Stroke Research Berlin, Charité-Universitätsmedizin Berlin, Berlin, Germany, [8] Berlin School of Mind and Brain, Humboldt-Universität zu Berlin, Berlin, Germany, [9] Department of Neurology, Max Planck Institute for Human Cognitive and Brain Sciences, Leipzig, Germany, [10] School of Health Sciences, Department of Gerontology, Autonomous University of Hidalgo State, Pachuca, Mexico, [11] Departamento de Bioquímica, Facultad de Medicina, Universidad Nacional Autónoma de México, Mexico City, Mexico, [12] Cell Communication & Extracellular Vesicles Laboratory, Instituto Nacional de Medicina Genómica, Mexico City, Mexico, [13] National Polytechnic Institute, Center of Research in Advanced Studies, Mexico City, Mexico, [14] Departamento de Matemáticas y Mecánica, Instituto de Investigaciones en Matemáticas Aplicadas y Sistemas, Universidad Nacional Autónoma de México, Mexico City, Mexico, [15] Mathematische Modellierung Biologischer Systeme, Fakultät für Mathematik, Technische Universität München, Munich, Germany, [16] Department of Neurosurgery, Charité-Universitätsmedizin Berlin, Berlin, Germany, [17] Lung Cancer Epigenetics, Max Planck Institute for Heart and Lung Research, Bad Nauheim, Germany, [18] Leibniz-Forschungsinstitut für Molekulare Pharmakologie, Berlin, Germany, [19] Laboratorio de Neurociencias, Instituto Nacional de Pediatría, Secretaría de Salud, Mexico City, Mexico, [20] The Shimon Peres Postdoctoral Fellow at the Edmond and Lily Safra Center for Brain Sciences, The Hebrew University of Jerusalem, Jerusalem, Israel, [21] Department of Experimental Neurology, Charité-Universitätsmedizin Berlin, Berlin, Germany, [22] Institute for Experimental and Clinical Pharmacology and Toxicology, University of Lübeck, Lübeck, Germany, [23] Institute for Medical and Marine Biotechnology, University of Lübeck, Lübeck, Germany, [24] Fraunhofer Research Institution for Marine Biotechnology and Cell Technology, Lübeck, Germany*

OPEN ACCESS

Edited by:
Aurel Popa-Wagner, University Hospital Essen, Germany

Reviewed by:
Daniela Galimberti, University of Milan, Italy
Jukka Jolkkonen, University of Eastern Finland, Finland

***Correspondence:**
Marietta Zille
marietta.zille@pharma.uni-luebeck.de

Specialty section:
This article was submitted to Neurodegeneration, a section of the journal Frontiers in Neuroscience

Received: *31 March 2019*
Accepted: *28 June 2019*
Published: *24 July 2019*

Citation:
Castillo X, Castro-Obregón S, Gutiérrez-Becker B, Gutiérrez-Ospina G, Karalis N, Khalil AA, Lopez-Noguerola JS, Rodríguez LL, Martínez-Martínez E, Perez-Cruz C, Pérez-Velázquez J, Piña AL, Rubio K, García HPS, Syeda T, Vanoye-Carlo A, Villringer A, Winek K and Zille M (2019) Re-thinking the Etiological Framework of Neurodegeneration. Front. Neurosci. 13:728. doi: 10.3389/fnins.2019.00728

Neurodegenerative diseases are among the leading causes of disability and death worldwide. The disease-related socioeconomic burden is expected to increase with the steadily increasing life expectancy. In spite of decades of clinical and basic research, most strategies designed to manage degenerative brain diseases are palliative. This is not surprising as neurodegeneration progresses "silently" for decades before symptoms are noticed. Importantly, conceptual models with heuristic value used to study neurodegeneration have been constructed retrospectively, based on signs and symptoms already present in affected patients; a circumstance that may confound causes and consequences. Hence, innovative, paradigm-shifting views of the etiology of these diseases are necessary to enable their timely prevention and treatment. Here, we outline four alternative views, not mutually exclusive, on different etiological paths toward neurodegeneration. First, we propose neurodegeneration as being a secondary outcome of a primary cardiovascular cause with vascular pathology disrupting the vital homeostatic interactions between the vasculature and the brain, resulting in

cognitive impairment, dementia, and cerebrovascular events such as stroke. Second, we suggest that the persistence of senescent cells in neuronal circuits may favor, together with systemic metabolic diseases, neurodegeneration to occur. Third, we argue that neurodegeneration may start in response to altered body and brain trophic interactions established via the hardwire that connects peripheral targets with central neuronal structures or by means of extracellular vesicle (EV)-mediated communication. Lastly, we elaborate on how lifespan body dysbiosis may be linked to the origin of neurodegeneration. We highlight the existence of bacterial products that modulate the gut-brain axis causing neuroinflammation and neuronal dysfunction. As a concluding section, we end by recommending research avenues to investigate these etiological paths in the future. We think that this requires an integrated, interdisciplinary conceptual research approach based on the investigation of the multimodal aspects of physiology and pathophysiology. It involves utilizing proper conceptual models, experimental animal units, and identifying currently unused opportunities derived from human data. Overall, the proposed etiological paths and experimental recommendations will be important guidelines for future cross-discipline research to overcome the translational roadblock and to develop causative treatments for neurodegenerative diseases.

Keywords: lifespan, vascular pathology, senescence, body–brain trophism, dysbiosis

INTRODUCTION

Neurological disorders are the leading cause of disability-adjusted life-years and the second-leading cause of deaths worldwide. This burden has increased substantially over the past 25 years because of expanding population numbers and aging (GBD 2015 Neurological Disorders Collaborator Group, 2017) and will continue to grow in the coming decades due to the further increase in life expectancy.

At intermediate and advanced stages, frequently by the time a diagnosis is made, neurodegeneration has affected higher brain areas that control cognitive, sensory, and motor functions. Because the majority of cases are seen by the age of 50 or older in both men and women, many scientists think of neurodegenerative diseases as processes that reflect abnormal aging. Likewise, since neurodegeneration involves the loss of neuronal populations brain-wide, many researchers believe that neuronal death results from altered processes intrinsic to the nervous system, such as neuroinflammation, abnormal accumulation or deteriorated clearance of toxic proteins, and reduced anti-oxidative defenses.

Hence, current explicative models of neurodegenerative diseases account for signs and symptoms already seen in affected patients. In fact, the majority of these causative models have been formulated in retrospect, based on what is already present in the patient's brain. Given the nature of these models, it is difficult to identify real causes from mere consequences and epiphenomena. This is even more puzzling given that neurodegenerative diseases are life-spanning processes that start silently at least 20 to 30 years before the pathological signs and symptoms are recognized by patients and diagnosed by physicians. In addition, accumulating information suggests an extraneural origin of neurodegeneration.

Clearly, the essential premises guiding research on neurodegenerative diseases seem at least partly incorrect and somewhat misleading. This may explain why, despite researchers' best efforts, neurodegeneration is still a growing health concern and the reason why therapeutic measures are currently palliative, while preventive approaches are often ineffective (Crous-Bou et al., 2017; Hsu and Marshall, 2017; Klein and Tyrlikova, 2017).

Here, we outline four different paths as the basis for a paradigm shift toward an etiologic view on neurodegeneration: (1) the vascular origin of neurodegeneration, (2) cellular senescence as the origin of neurodegeneration, (3) body–brain trophic interactions as the origin of neurodegeneration, and (4) lifespan gut dysbiosis as the origin of neurodegeneration. We did not cover here genetic components as risk factors for neurodegeneration, a comprehensive analysis of which can be found elsewhere (Brainstorm et al., 2018). We provide concrete recommendations on how to investigate the discussed etiological paths experimentally in future studies. This work is the result of the discussions that took place during the German-Mexican Roundtable Exploring New Etiological Paths Towards Neurodegeneration in October 2018.

THE VASCULAR ORIGIN OF NEURODEGENERATION

Neurons depend on blood vessels to deliver oxygen and nutrients, for the removal of carbon dioxide and other by-products of metabolism from the brain's interstitial space, which helps to maintain the homeostasis of the cerebral microenvironment. Therefore, to function properly, it is thought that the cerebral circulation has developed adaptive mechanisms to provide the

trophic molecules and energy substrates needed for neuronal cells at different times and regions, depending on neural activity (Girouard and Iadecola, 2006).

The recognition of these mechanisms led to the concept of neurovascular coupling (Roy and Sherrington, 1890), which refers to the dynamic functional change in cerebral blood flow that occurs in response to local neuronal activity (Dirnagl, 1997; Kisler et al., 2017; Villringer, 1997). This response increases cerebral blood flow within the activated brain regions to fulfill energy demands in a process known as functional hyperemia.

The main players of these dynamic adjustments in the cerebral blood flow are neurons, glia, and vascular cells. All of them come together in a functional morphological entity termed the "neurovascular unit". This view explains why cerebrovascular diseases linked to neurodegeneration are considered as stand-alone etiopathological states (Przedborski et al., 2003; Brown et al., 2005). Vascular diseases, however, may be the forerunners of neurodegeneration. In support of this, it has been shown that shifts in blood pressure lead neurons to adjust the excitability thresholds according to brain perfusion levels, safeguarding their homeostasis. Hence, vascular diseases may occur first and then later neurodegeneration may follow, if the process of neurovascular coupling proceeds ineffectively (Moore and Cao, 2008; Kim et al., 2016).

Cerebral blood vessels originate from large cerebral arteries arising from the circle of Willis. As they find the way through the brain, large cerebral arteries divide into pial arteries and arterioles, which grow gradually deeper and form the penetrating arteries and arterioles that become progressively smaller until they turn into cerebral capillaries (Wittko-Schneider et al., 2014). The development of nerves and astrocytes originating from central and peripheral sources is closely associated with cerebral arteries, arterioles, and capillaries as demonstrated by the observation that the inhibition of angiogenesis during development is accompanied by severe developmental defects in specific regions of the central nervous system (CNS) (Hallene et al., 2006). This highlights the importance of blood vessels during brain formation.

There are different steps and mediators underlying neurovascular coupling. Briefly, neurons and interneurons are responsible for the initiation and modulation of the vascular response by the activation of NMDA and AMPA receptors, which leads to an increase of intracellular Ca^{2+} and calcium-dependent enzymes that exert effects on the endothelium, astrocytes, and pericytes. Because of their close association with synapses and microvessels, astrocytes are in charge of the neurovascular transmission of signals to the capillaries and arterioles while endothelial cells exert a retrograde propagation of vasomotor responses to regulate cerebral blood flow (Iadecola, 2017). The endothelium also regulates the vascular tone by releasing potent relaxing and contracting factors that readjust the vascular musculature and maintain a healthy homeostasis of the vascular wall.

Nitric oxide (NO), prostacyclins, endothelial-derived hyperpolarizing factor (EDHF), and endothelin have been proposed as the main vasoactive factors related to the endothelial response to neural activity. NO promotes the vasodilation of cerebral blood vessels by stimulating soluble guanylate cyclase in the vascular muscle, leading to an intracellular increase of cGMP and relaxation (Schmidt and Walter, 1994). NO is generated by three different isoforms of the enzyme NO synthase (NOS): neuronal (nNOS), inducible (iNOS), and endothelial NOS (eNOS).

In the CNS, nNOS is mainly located in neurons, astrocytes, and neuronal stem cells and has been implicated in synaptic plasticity and in the central control of blood pressure. Abnormal NO signaling is likely to contribute to a variety of neurodegenerative pathologies such as excitotoxicity following stroke, multiple sclerosis (MS), Alzheimer's disease (AD), and Parkinson's disease (PD) (Calabrese et al., 2007).

iNOS expression had initially been shown for macrophages, but it is now clear that it can be induced by cytokines in a variety of cell types in the context of inflammation (Li et al., 1991). During episodes of acute inflammation, the role of NO appears to be protective, while chronic iNOS expression is detrimental. The high levels of NO produced by activated macrophages and other cells may not only be toxic to microbes, parasites, or tumor cells, but may also harm healthy cells (Wong and Billiar, 1995).

Endothelial NOS is mostly expressed in endothelial cells, although the isozyme has been detected in certain neurons of the brain (Caviedes et al., 2017). eNOS-derived NO is a well-known physiological vasodilator and an inhibitor of platelet aggregation and adhesion, but it also inhibits leukocyte adhesion and vascular inflammation, controls vascular smooth muscle proliferation, stimulates angiogenesis, and activates endothelial progenitor cells (Forstermann and Sessa, 2012).

In addition to the production and release of NO, cyclooxygenase produces prostacyclin, which induces the relaxation of cerebral vessels by the activation of adenylate cyclase with the accumulation of cAMP and the activation of potassium channels. Similarly, in large cerebral arteries, the production of EDHF by the cytochrome P-450 monooxygenase metabolism of arachidonic acid causes relaxation by hyperpolarizing the underlying vascular muscle through the activation of potassium channels. The contribution of EDHF increases as the vessel size decreases, with a predominance of EDHF activity in resistance vessels and a compensatory upregulation of hyperpolarization in states characterized by reduced NO availability (Ozkor and Quyyumi, 2011).

Besides vasodilatory factors, under certain conditions, the cerebral endothelium produces vasoconstrictive substances such as endothelins leading to a potent and long-lasting contraction of cerebral vessels dependent on extracellular calcium and the activation of protein kinase C (Faraci and Heistad, 1998).

The alterations of any of the cellular players involved in the neurovascular unit may impair its coupling and functional hyperemia, resulting in an alteration of homeostasis leading to brain dysfunction (Iadecola, 2004).

Heart and Vascular Diseases and the Origin of Neurodegeneration

According to the World Health Organization, cardiovascular diseases (CVDs) lead to one-third of all annual deaths globally,

which is about 17.9 million total deaths (Lim et al., 2012). CVDs are disorders of the heart and blood vessels and include among others coronary heart disease, cerebrovascular disease, and rheumatic heart disease. A large number of studies have reported a strong relationship between indices of vascular pathology (such as carotid intima-media thickness, arterial stiffness, and small-artery remodeling) and cognitive impairment and neurodegeneration (Gorelick et al., 2011).

Because the factors contributing to vascular pathology are often preventable or treatable, targeting them may prove useful for preventing or delaying the onset of neurodegenerative diseases. Epidemiological studies show that treating hypertension and hyperlipidemia reduces the incidence of neurodegenerative diseases (Larsson and Markus, 2018) and slows down the rate of cognitive impairment (Deschaintre et al., 2009). Here, we will focus on the main CVDs known to promote changes in the cerebral microvasculature that lead to neurodegeneration in the long run.

Hypertension

Hypertension – or blood pressure at or beyond 130 mmHg/80 mmHg (systolic/diastolic blood pressure) according to the 2017 American College of Cardiology/American Heart Association guidelines (Whelton et al., 2018) – affects one billion people worldwide and leads to nine million deaths every year (Lim et al., 2012). In normotensive individuals, cerebrovascular autoregulation counteracts the cerebrovascular effects of the fluctuations in arterial pressure that occur during normal activities. Cerebral arteries relax when arterial pressure decreases and constrict when arterial pressure rises. The role of this vascular adjustment is the maintenance of a stable cerebral perfusion despite changes in systemic arterial pressure.

Hypertension alters cerebrovascular autoregulation (Sadoshima et al., 1983) by impairing endothelium-dependent relaxation (Faraci and Heistad, 1998). Hypertension promotes vascular hypertrophy, remodeling, and atherosclerosis in large cerebral arteries and lipohyalinosis in penetrating arterioles. These changes are damaging because they reduce the lumen of the vessel and increase vascular resistance (Dickinson, 2001). In humans, longstanding hypertension induces the deposition of collagen and fibronectin as well as elastin fragmentation, leading to an increased stiffness of the wall of large arteries (Henskens et al., 2008). Hypertension also affects neurovascular coupling as shown by a reduction in the normal increase in cerebral blood flow elicited in the posterior parietal and thalamic areas during cognitive tasks in patients with chronic untreated hypertension relative to normotensive individuals (Jennings et al., 2005).

The disruption of the adjustment mechanisms by a sustained increase in the blood pressure has been linked to different neurodegenerative diseases such as stroke (MacMahon et al., 1990). Hypertension is also considered an important modifiable risk factor for late-life cognitive decline and non-amnestic mild cognitive impairment in the mid-aged population (Knopman et al., 2001; Reitz et al., 2007). The Honolulu Asia aging study demonstrated an association between elevated levels of blood pressure in middle age and vascular dementia (Launer et al., 2000).

Atherosclerosis

Atherosclerosis, a progressive disease, characterized by the accumulation of lipids and fibrous elements in the large arteries, is a major cause of heart disease and stroke (Banerjee and Chimowitz, 2017).

The damage leading to atherosclerosis is elicited over years and is highly influenced by lifestyle. The pathogenic sequence starts with the recruitment of circulating monocytes into the intima, where they differentiate into macrophages and internalize modified lipoproteins to become foam cells (fat-laden M2 macrophages). Then, chemokines and growth factors induce the proliferation of neighboring smooth muscle cells and the synthesis of extracellular matrix components within the intimal compartment, generating a fibromuscular plaque that undergoes progressive structural remodeling resulting in the formation of a fibrous cap, overlying a lipid-rich, necrotic core accompanied by varying degrees of matrix remodeling and calcification (Lusis, 2000). If a rupture of the plaque occurs, the highly thrombogenic contents of the necrotic core are released to the lumen of the vessel, promoting atherothrombotic occlusion.

Epidemiological and post-mortem studies have shown that the atherosclerosis of the arteries that supply the brain is associated with a two- to threefold increased odds of dementia (Hofman et al., 1997; van Oijen et al., 2007; Wendell et al., 2012; Dearborn et al., 2017). Interestingly, this association is independent of the effects of cerebral infarction (Dolan et al., 2010), which can result from the atherosclerosis-induced occlusion of vessels.

Cerebral Small-Vessel Disease

Cerebral small-vessel disease comprises white matter lesions (WMLs), lacunar infarcts, and cerebral microbleeds and is a frequent neuroimaging finding (best seen on magnetic resonance images) in elderly people (de Leeuw et al., 2001).

Factors such as arterial stiffness, also related to aging and hypertension, are considered to expose the small vessels in the brain to highly pulsatile pressure and flow (Poels et al., 2012). This causes thickening of the arterial media of these vessels, which gradually narrows the lumen. In addition, atherosclerotic plaques in large arteries can encroach on the origins of smaller arteries, blocking the blood flow to areas supplied by these arteries. Subcortical white matter is particularly susceptible to such changes, as its blood supply depends on small arteries that get progressively smaller as they descend from the cortex to the deeper parts of the brain. Hypoxia ensues, causing edema, demyelination, and infarction of the white matter.

Cerebral small-vessel disease is associated with an increased risk of cognitive decline, dementia, stroke, balance disturbances, and parkinsonism (Bohnen and Albin, 2011). Individuals with an identical WML pattern present clinically heterogeneous complaints in cognitive and motor performance, ranging from no complaints to dementia and parkinsonism, which means other factors determine the cognitive or motor outcome (de Leeuw et al., 2001). Possible explanations for this heterogeneity are the lack of sensitivity of conventional magnetic resonance imaging to the early loss of microstructural integrity in the normal-appearing white matter (Scheltens et al., 1995), the disagreement on how lesions underlying small-vessel disease

are classified (Wardlaw et al., 2013), and the efficiency of compensation mechanisms that prevent further cognitive and motor deterioration (Mondadori et al., 2006).

Atrial Fibrillation

Atrial fibrillation (AF) is the most common arrhythmia affecting 1 to 2% of the general population (Andrade et al., 2014). AF is characterized by disturbances that promote ectopic firing and reentrant mechanisms that lead to impaired atrial function [for a review on the pathophysiology of AF, refer to (Andrade et al., 2014)].

AF can lead to reduced cardiac output, intermittent cerebral hypoperfusion, and transient hypertension in the cerebral capillaries (Anselmino et al., 2016). Such changes have been suggested as possible mediators of AF-related brain damage. On the other hand, AF may be a manifestation of a broader systemic illness that involves widespread inflammation and platelet activation, which can also lead to impaired cerebrovascular function (Dietzel et al., 2018).

AF is associated with increased morbidity and mortality and has long been known as one of the main risk factors for embolic stroke (Kamel et al., 2016). It is now also considered a risk factor for dementia. de Bruijn et al. (2015) analyzed the association of prevalent and incident AF with incident dementia in 6514 dementia-free patients, revealing not only a positive association between AF and the development of dementia but also that the association was strongest for younger participants with the longest duration of AF. These findings have been replicated by several studies (Nishtala et al., 2018), some of which have shown that the association between AF and dementia is independent of the occurrence of embolic stroke (Ryden et al., 2019) and the use of anticoagulants (Graves et al., 2017). Future investigation will determine if optimal treatment of AF can prevent or postpone cognitive decline and dementia.

Vascular Pathology in Neurodegenerative Diseases

The link between vascular risk factors and neurodegenerative disease is strengthened by the evidence showing that vascular and neurodegenerative pathophysiological changes often co-exist in patients with a diverse spectrum of neurodegenerative diseases. Several lines of evidence even suggest that vascular mechanisms are *directly* involved in the pathophysiology of neurodegenerative diseases.

The event that triggers the onset of a stroke, such as the rupture of an atherosclerotic plaque, the embolization of a blood clot, or the damage to a vessel and subsequent bleeding, is often preceded by vascular pathophysiological changes that accumulate over time. One of the earliest changes is endothelial dysfunction induced by oxidative stress (Roquer et al., 2009), which occurs as a result of the aforementioned cerebrovascular risk factors. Immediately after the onset of stroke, a series of overlapping pathophysiological changes occur leading to neuronal death within and beyond the initial area of damage. These include critically low blood flow, the accumulation of free oxygen radicals, the sustained or spreading depolarization of neurons, acidosis, tissue inflammation, damage to the blood–brain barrier (BBB), and regulated cell death (Mergenthaler et al., 2004).

The same vascular mechanisms that lead to acute stroke can also lead to cognitive impairment (Popa-Wagner et al., 2010). In the condition known as vascular dementia (or vascular cognitive impairment), the consequences of these pathophysiological changes are the primary cause of neurodegeneration. They include the development of multiple or strategically located infarcts, damage to the myelin sheath and axons, small cerebral hemorrhages, chronic cerebral hypoperfusion, and brain atrophy (Iadecola, 2013). Each of these represents damaged tissue, and the accumulation of damage eventually manifests as cognitive impairment (Gorelick et al., 2011).

Vascular pathology leading to white matter damage, manifesting as WML, seems to play a particularly important role in the pathogenesis of vascular dementia (Iadecola, 2013). Very often, however, both vascular and neurodegenerative changes contribute to the development of dementia, resulting in a condition known as "mixed" dementia.

The link between vascular pathology and neurodegeneration has also been thoroughly studied in AD. Vascular damage, initiated by vascular and genetic predisposing factors, precedes the accumulation of beta-amyloid (Aβ), which eventually leads to neurodegeneration in AD (Nelson et al., 2016). Neuroimaging studies support this theory, showing that reduced CBF and abnormal neurovascular coupling occurs in elderly people at the risk of AD before they show the hallmarks of the disease such as brain atrophy, cognitive impairment, or accumulation of Aβ (Smith et al., 1999; Bookheimer et al., 2000; Ruitenberg et al., 2005).

Vascular damage may facilitate neurodegeneration by altering a major route through which substances are cleared from the interstitial space of the brain parenchyma. This route is known as the glymphatic system, which facilitates the movement of fluid from perivascular (Virchow-Robin) spaces surrounding pial arterioles to the interstitium into spaces surrounding the brain's deep veins and then to the cervical lymph nodes (Jessen et al., 2015).

Vascular risk factors cause blockages in and around small arteries, which can manifest as an enlargement of the perivascular spaces (Gouw et al., 2011) that are visible on structural magnetic resonance images (Wardlaw et al., 2013). These enlarged spaces are a sign of impeded interstitial fluid flow and hence impaired clearance of substances from the brain parenchyma, and have been linked to an increased risk of dementia (Buerge et al., 2011; Ramirez et al., 2015) and stroke (Mills et al., 2007; Selvarajah et al., 2009).

Interestingly, the spatial distribution of these enlarged perivascular spaces has been linked to different underlying pathologies. A predominant distribution in the basal ganglia indicates vascular disease caused by hypertension (Selvarajah et al., 2009; Charidimou et al., 2013), while a white matter distribution is related to cerebral amyloid angiopathy (Martinez-Ramirez et al., 2013; Charidimou et al., 2014), caused by the accumulation of Aβ protein in the walls of the cerebral and meningeal vessels.

Cerebral amyloid angiopathy, which leads to intracerebral hemorrhage that aggravates the cognitive impairment (Cordonnier, 2011), is found in more than 80% of AD patients (Jellinger, 2010). Aβ itself is a potent vasoconstrictor (Thomas et al., 1996), worsening the hypoperfusion, which, if severe enough, directly injures neurons. However, even milder hypoperfusion alters protein synthesis and plays a role in neurodegeneration (Iadecola, 2004). The critical role of hypoperfusion is supported by the evidence that the induction of chronic global hypoperfusion in animal models causes memory impairment, the accumulation of Aβ, and synaptic dysfunction (Walsh et al., 2002; Koike et al., 2010; Wang et al., 2010).

Blood–brain barrier dysfunction, which involves damage to pericytes and endothelial tight junction molecules, has been observed in several neurodegenerative diseases, including AD, PD, amyotrophic lateral sclerosis (ALS), and Huntington's disease (Zlokovic, 2008; Chao et al., 2009; Duran-Vilaregut et al., 2009; Henkel et al., 2009; Kalaria, 2010; Alvarez et al., 2011). Vascular damage worsens the situation, both by leading to further BBB dysfunction and because low blood flow traps potentially neurotoxic proteins such as Aβ that pass through the leaky barrier. These proteins, which include immunoglobulins, plasmin, thrombin, and albumin, further reduce blood flow and cause vasogenic brain edema, oxidative stress, and axonal demyelination (Chen and Strickland, 1997; Mhatre et al., 2004; Farrall and Wardlaw, 2009; Chen et al., 2010). In patients, this BBB dysfunction is detectable using neuroimaging and the analysis of the biomarkers of neurodegenerative diseases in the cerebrospinal fluid (Olsson et al., 2016; Sweeney et al., 2018).

The presence and severity of vascular damage occurring at the cellular and molecular level, affect the clinical course of neurodegenerative diseases. Large neuropathological studies show the post-mortem presence of infarcts, lacunes, leukoencephalopathy, atherosclerosis, or hemorrhages in 80% of AD patients compared to 67% of similarly aged people without cognitive impairment (Toledo et al., 2013).

Interestingly, the effects of vascular pathology and neurodegeneration on cognitive decline seem to be synergistic, particularly in patients with moderate AD pathology (Zekry et al., 2002; Choi et al., 2011; Lee et al., 2014). Studies show that the worse the vascular pathology in patients with AD, the worse the cognitive impairment (Snowdon et al., 1997; Song et al., 2007; White, 2009). AD patients with infarcts or microangiopathic white matter disease also experience faster cognitive decline (Silvestrini et al., 2006; Helzner et al., 2009).

CELLULAR SENESCENCE AS THE ORIGIN OF NEURODEGENERATION

Since a main feature of aging is the accumulation of senescent cells in various tissues (van Deursen, 2014; Calcinotto et al., 2019), cellular senescence has emerged as a key potential contributor to neurodegenerative and cerebrovascular diseases (Baker and Petersen, 2018; Kritsilis et al., 2018).

Cellular senescence is a phenotype characterized by a durable cell cycle withdrawal (i.e., cells do not respond to mitogens), associated with the expression of tumor suppressors $p21^{CIP1/WAF1}$ (encoded by *Cdkn1a*) and/or $p16^{INK4A}$ (encoded by *Cdkn2a*), as well as by apoptosis resistance (**Figure 1**). Senescent cells display a flattened and vacuolated morphology with abundant stress granules and accumulate lipofuscin. There is a persistent DNA damage response commonly detected by the presence of γH2AX foci, while the most common feature is an increase in the lysosomal activity of the enzyme senescence-associated beta galactosidase isoform (SA-B-Gal), which has been widely used for their detection. Some senescent cells exhibit a formation of senescence-associated heterochromatin

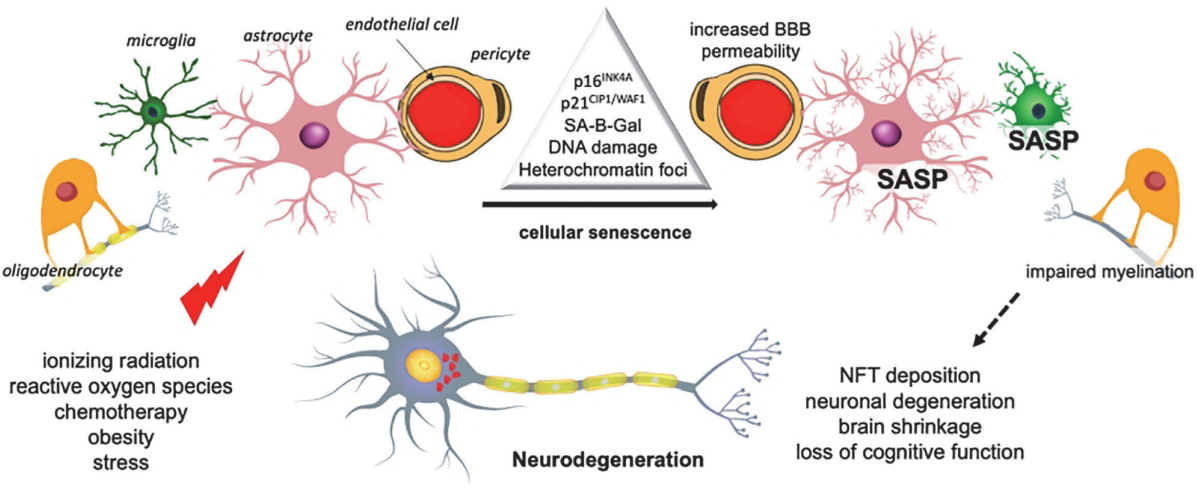

FIGURE 1 | Senescence-mediated neurodegeneration. Cellular senescence can be induced by several stimuli in the different brain cells. Senescence of microglia and astrocytes results in inflammation and the loss of trophic support. Oligodendrocyte senescence reduces myelin, which affects transmission and the BBB may be compromised by endothelial cells senescence. These changes have an impact on the integrity and viability of neurons and ultimately brain function [based on Chinta et al. (2015)]. SASP, senescence-associated secretory phenotype.

foci (SAHF), which are domains enriched in the transcription-silencing histone H2A variant, macroH2A.

However, the most important feature of senescent cells is the secretion of pro-inflammatory cytokines, growth factors, extracellular enzymes, and metalloproteases, collectively known as senescence-associated secretory phenotype (SASP) (Chow and Herrup, 2015; Ask et al., 2018). In early stages, the secretion of cytokines by senescent cells promotes the migration and infiltration of effector immune cells and the secretion of growth factors and proteases, which facilitate tissue repair and remodeling (Munoz-Espin and Serrano, 2014; Davaapil et al., 2017).

Yet, persisting cytokine signaling, as occurs in aging, contributes among other processes to chronic inflammation (*inflammaging*), a major contributor to age-related dysfunctions. SASP molecules also have an autocrine role, fostering the senescent phenotype, and a paracrine role inducing senescence in surrounding cells (Coppe et al., 2010). Notably, during aging, senescent cells accumulate and persist in different organs, including the brain, and are associated with the onset of several diseases (Munoz-Espin and Serrano, 2014).

To avoid confusion, it is however important to differentiate between aging, often termed "senescence" and cellular senescence. Aging is featured by an accumulation of senescent cells, but not all aged cells have the unique cellular senescence phenotype. Further investigations are needed to understand why senescent cells accumulate with aging, perhaps involving a combination of immune system malfunction failing to eliminate them, with changes in senescent cells themselves so that they become less efficiently recognized.

Senescence in Neurodegenerative Diseases

More recent *in vitro* and *in vivo* evidence strengthens the hypothesis of cellular senescence as causative of neurodegeneration. Dysfunctional astrocytes with senescent hallmarks have been detected in post-mortem human brain tissue from patients with ALS, PD, and AD (Bhat et al., 2012; Chinta et al., 2015, 2018; Turnquist et al., 2016). Mouse models and *in vitro* studies provide further evidence of senescence in microglia (Bussian et al., 2018), endothelial cells (Broadwell, 1989), neural stem cells and possibly oligodendrocytes (Kritsilis et al., 2018), which may contribute to neurodegenerative disorders.

Moreover, several senescent features have recently been described in studies of both physiological aging and neurodegenerative diseases using different models, including AD, PD, MS, and stroke (Kritsilis et al., 2018; Walton and Andersen, 2019), supporting the idea that cellular senescence may contribute to neurodegeneration and cerebrovascular disease in a far-reaching way (reviewed by Baker and Petersen, 2018; Walton and Andersen, 2019).

In a recent publication, using weighted gene co-expression analysis, Mukherjee et al. (2019) found a microglial signature of 17 genes that are strongly related with both aging and neurodegenerative diseases, not only in human brains but also in neurodegenerative murine models. An early study from Bhat et al. (2012) suggested that $p16^{INK4A}$-positive astrocytes may increase the risk for sporadic AD, since the prefrontal cortex of AD patients harbors a significant increase of senescent astrocytes expressing $p16^{INK4a}$ and matrix metalloproteinase-1 (MMP-1).

Also, the *in vitro* exposure of astrocytes to $A\beta_{1-42}$ triggers senescence, leading to the secretion of pro-inflammatory cytokines, including interleukin 6 (Bhat et al., 2012). Chinta and colleagues also demonstrated an increase of senescent astrocytes in brain tissue from PD patients, and found that cultured murine and human astrocytes exposed to paraquat (an herbicide associated with sporadic PD) become senescent. Interestingly, the depletion of senescent cells diminished neurodegeneration (Chinta et al., 2018), suggesting that senescence may be the cause, not the consequence of neurodegeneration.

Cellular senescence has also been considered as a therapeutic target in MS (Oost et al., 2018). Although MS is regarded as a classical autoimmune disease, it has been hypothesized that the driver of the autoreactive immune response in MS is actually a primary neurodegenerative process (Trapp and Nave, 2008). The senescence of microglia, T-cells, astrocytes, endothelial cells, and oligodendrocytes, among other cell types, is implicated in MS pathophysiology (Oost et al., 2018). Even though no study has been conducted for senescent cell detection on post-mortem tissue of MS patients, there is initial evidence in animal models about the role of cellular senescence on MS progression (Oost et al., 2018).

Senescence and Synaptic Plasticity

Another common hallmark of neurodegenerative pathologies is the alteration in synaptic structure and function during the early stages of the disease, which is related to subcellular reorganization preceding cell loss. The mechanisms underlying these pathologies are not fully understood. In fact, a decline in synaptic plasticity may be linked to the phenomenon of senescence. Unfortunately, there are only a few studies that have investigated the effect of senescence on the synaptic machinery. However, there is growing evidence of the changes in neuroplasticity caused by inflammation, oxidative stress, and protein misfolding, that may be linked to SASP action as well as the influence of senescence in glial cells, which are associated with an impairment in the neuroplasticity machinery (Gan et al., 2018).

The hippocampus has been pointed out as a brain structure with high plasticity and prone to neurodegeneration with age (Kreutzmann et al., 2015). The neurogenic capacity of the hippocampal dentate gyrus is reduced during aging. This reduction correlates with an impairment in memory formation and is accompanied by other changes, such as an increase of pro-inflammatory cytokines as well as a reduction of neurotrophic and vascular factors (Seib and Martin-Villalba, 2015; Fan et al., 2017).

Aging is also associated with changes in the hippocampal perforant pathway and its synapses, with the dentate gyrus being particularly affected (Wenk and Barnes, 2000). A decrease of synapses and changes in the morphology of dendrites and their spines have been linked to atrophy and a dysfunction of the aged hippocampus (Rogers et al., 1984). A synapto-proteome

study in old animals revealed a general decrease in the expression of neurotransmission regulation proteins, such as post-synaptic density 95, synaptosomal nerve-associated protein 25, shiga toxin 1, synapsin 1 and 2, synaptophysin, and vesicle-associated membrane protein (Wang et al., 2007; VanGuilder et al., 2010; Orock et al., 2019).

Moreover, a recent breakthrough paper, using a classical model of neurodegeneration, shows the accumulation of senescent astrocytes and microglia, but not neurons, in the brains of mice overexpressing human TauP301S. The genetic clearance of senescent glial cells prevented neurofibrillary tangle (NFT) deposition, the degeneration of hippocampal neurons, brain shrinkage, and the thinning of the dentate gyrus, thus preserving cognitive function. The transgenic mice that did not undergo a senescent transformation of microglia cells maintained their cognitive functions (Bussian et al., 2018).

Interestingly, neurogenesis and learning and memory can be impaired when blood and plasma from aged animals are transfused to young animals, showing that systemic factors can affect brain integrity. This phenomenon may be related to chemokine levels, especially the C–C Motif Chemokine Ligand 2 (CCL2), an important SASP component (Villeda et al., 2011). It is possible that when senescent astrocytes accumulate, they release SASP factors that lead to NFT deposition and other neurodegenerative hallmarks in surrounding neurons, oligodendrocytes, microglia, and endothelial cells (**Figure 1**). Investigating senescent cell accumulation in the periphery and in the nervous system should help to understand the process of aging of the brain and, more importantly, neurodegeneration in an integrative way.

Cellular Senescence in Stroke

Cellular senescence accompanying neurological conditions involves many cell types of the CNS (Walton and Andersen, 2019), which may also be of great importance in the case of brain injury following stroke (Buga et al., 2013). Most studies in this field, however, focused on the effects of aging rather than on cellular senescence. The timing of the cellular and genetic response to brain tissue injury is dysregulated in aged animal models due to a premature accumulation of BrdU-positive microglia and astrocytes, activated oligodendrocytes, and degenerated neurons (Popa-Wagner et al., 2007).

There is no consensus whether and to what extent age influences infarct size: several studies reported larger (Popa-Wagner et al., 2011) or smaller ischemic lesions in aged animals when compared to young rodents (Manwani et al., 2013; Ritzel et al., 2018). However, irrespective of the infarct size, aged animals have worse functional when compared to young ones (Popa-Wagner et al., 2011; Ritzel et al., 2018). The slow tissue recovery and rapid development of damage after injuries like stroke in aged animals may be linked to several factors such as a reduced expression of genes linked to neuroprotective pathways, high and accelerated cell death, high oxidative stress by mitochondrial dysfunction, increased permeability of the BBB, high phagocytic activity of brain macrophages, autophagic dysfunction, as well as an imbalanced inflammatory state (Popa-Wagner et al., 2007, 2011; Petcu et al., 2008).

Furthermore, the immune response to ischemic brain injury differs between aged and young mice. In a recent report, older mice displayed an increased number of brain-infiltrating and peripheral neutrophils with decreased phagocytic potential, increased levels of reactive oxygen species and extracellular matrix-degrading enzymes (Ritzel et al., 2018). Rawji and colleagues reported that aging also affects brain-resident immune cells. Aged microglia express excessive amounts of pro-inflammatory cytokines and proliferate at increased rates, but simultaneously display defective phagocytosis and decreased motility. Interestingly, aged peripheral monocytes seem to share the features of impaired phagocytosis and reduced motility, but are less prone to activation and proliferation (Rawji et al., 2016).

Since aging has been linked to the accumulation of senescent cells (van Deursen, 2014; Calcinotto et al., 2019), we speculate that cellular senescence may contribute to the outcome after stroke. However, there is a need for more studies, exploring specifically the impact of cellular senescence rather than the global effects of aging. *In vitro* and *in vivo* experiments show that aging influences the state of endothelial cells, pericytes, and tight junctions, in turn resulting in a compromised function of the BBB (Yamazaki et al., 2016). Acute stroke leads to increased permeability and BBB breakdown, associated with worse outcome in stroke patients (Brouns et al., 2011).

Astrocytes in aged brains display the features of cellular senescence and SASP (Salminen et al., 2011), possibly impacting surrounding cells also in the case of acute brain damage. In the context of senescence hallmarks, human astrocytes are highly sensitive to oxidative stress and trigger a senescence program when faced with multiple types of stressors (Crowe et al., 2016; Liddell, 2017).

Chronic low-grade inflammation contributes to the increased risk of cerebrovascular disease (Lucas et al., 2006) and was shown to be a feature of the aging (Buga et al., 2013). The SASP in many cell types, including peripheral immune cells, astrocytes and microglia may influence a chronic inflammatory state observed in aging (Buga et al., 2013).

Taking into consideration the pathogenesis of cerebrovascular diseases, it is important to mention that cellular senescence may play a role in comorbidities and conditions known as risk factors for stroke (Buga et al., 2013). Cellular senescence impacts the formation and state of atherosclerotic plaques (Ritzel et al., 2018) and endothelial cells showing the hallmarks of senescence triggered by stressors like changes in glucose levels, homocysteine or elevated blood pressure (Tian and Li, 2014) may play a role in age-related vascular diseases. Since cellular stress induces senescence, it remains to be experimentally tested whether stroke itself triggers senescence in brain cells, which may influence the CNS microenvironment, have long-term consequences and an impact on the outcome after cerebral insults.

Systemic Metabolic Disease, Cellular Senescence, and Neurodegeneration

Risk factors in many neurodegenerative disorders include systemic metabolic diseases (see section "Impact of Peripheral Metabolic Disorders on Neurodegeneration"), which, in fact, favor the accumulation of senescent cells by facilitating the

functional changes of cellular distribution and regulation of adipose tissue. As mentioned before, cellular senescence in aging may contribute to a chronic inflammatory state in the brain and peripheral tissues (Buga et al., 2013).

Interestingly, obesity generates an accelerated state of aging, pro-oxidant factors as well as glucotoxicity (Hardie et al., 2006; Eberle and Ament, 2012). It is also associated with an increased senescent cell burden and a wide range of neurodegenerative and neuropsychiatric diseases (Gariepy et al., 2011; Hryhorczuk et al., 2013; Morsi et al., 2018). Ogrodnik and colleagues demonstrated that, in obese mice, glial cells show increased markers of cellular senescence in the periventricular region of the lateral ventricle, a region in close proximity to the neurogenic niche (Ogrodnik et al., 2019).

Furthermore, the affected glial cells in obese mice display excessive fat accumulation, which is in agreement with the role of glial cells on the senescence-mediated induction of neurodegeneration. Since SASP contributes to inflammation, metabolic dysregulation, progeria, pulmonary fibrosis, geriatric syndromes, and the loss of resilience, the clearance of senescent cells may delay or even alleviate multiple age-related diseases (Kirkland and Tchkonia, 2017).

Taking into consideration the increasing body of evidence on the role of cellular senescence in neurodegenerative, cerebrovascular, and metabolic disorders, we propose to investigate senescent cell accumulation in the periphery and in the nervous system as well as the influence of SASP on processes in the CNS, such as neuroplasticity, specific cellular populations, and on the brain–body signaling. This will help to understand the normal process of aging and senescence in an integrative way.

BODY–BRAIN TROPHIC INTERACTIONS AS THE ORIGIN OF NEURODEGENERATION

The disruption of the bidirectional interaction between neurons and the cells they innervate has not been considered as a putative etiologic mechanism of neurodegeneration. According to the trophic theory of neural connections, the body is represented several times within the nervous system along the sensory and motor pathways (Purves, 1988). Thus, changes in size and function of the body must be accompanied by changes in their neural representation at a central level, which may include neurite remodeling and functional adaptations.

Furthermore, novel requirements of the body affect the peripheral and central connections of peripheral neurons. In early phases of metabolic disorders, adipocytes and immune cells are related to peripheral nerve remodeling of both sympathetic and sensory fibers (Pellegrinelli et al., 2018; Yamazaki et al., 2018). In addition, the alteration of the enteric nervous system (ENS) may be a conduit to induce changes in the CNS. Future studies oriented to understand the interactions between neurons and the cells they innervate would help to discover biomarkers for early diagnosis and to monitor disease progression. Here, we present a brief summary of the experimental evidence related to the early events of neurodegeneration in the body and discuss possible mechanisms of intercellular communication that may be operating (**Figure 2**).

Pathological Events in the Peripheral Nervous System

Various neurodegenerative diseases share common molecular and cellular mechanisms including the misfolding of proteins that undergo conformational changes leading to tissue deposition and the formation of inclusion bodies. Increasing evidence suggests that these neurodegenerative proteinopathies may originate in the peripheral nervous system (Wakabayashi et al., 2010) or even across the body.

In PD and dementia with Lewy bodies (DLBs), the histopathological hallmark is the occurrence of neuronal α-synuclein aggregates, also known as Lewy bodies. Lewy bodies are typically found in the substantia nigra in PD. However, LBs can also be present in peripheral organs, neural or not, including the sympathetic ganglia, ENS, cardiac and pelvic plexuses, submandibular gland, adrenal medulla, and the skin (Beach et al., 2010; Wakabayashi et al., 2010). Moreover, in the early pathological stages of PD, α-synuclein pathology is present first in the dorsal motor nucleus of the glossopharyngeal and vagal nerves as well as the anterior olfactory nucleus (Braak et al., 2003a).

In AD, NFTs are observed in the spinal and sympathetic ganglia. However, it seems that they develop independently of the cerebral AD pathology (Shankle et al., 1993). In ALS, TDP-43 is a major component of the ubiquitinated inclusions and also occurs in the neurons of the spinal ganglia (Nishihira et al., 2008).

Sensory abnormalities have been described in neurodegenerative diseases including PD and AD. In this regard, the loss of olfaction represents an important early clinical symptom frequently preceding motor and cognitive impairments typically observed in these neurodegenerative diseases (Driver-Dunckley et al., 2014; Doty, 2017; Marin et al., 2018; Rey et al., 2018). The olfactory system may be particularly affected in neurodegenerative diseases as seen by the accumulation of pathological protein aggregates in olfactory structures including the anterior olfactory nucleus, the olfactory bulb, and the olfactory epithelium (OE) (Doty, 2017; Marin et al., 2018; Rey et al., 2018).

Given that the OE is directly accessible to external factors, it is vulnerable to environmental insults. Thus, external agents (toxins, bacteria, viruses, air pollutants) may trigger neurodegeneration through the OE (Rey et al., 2018). Once these agents enter the brain via the OE, they may cause protein misfolding and the spreading of protein aggregates in a prion-like manner throughout the olfactory pathway to other anatomically connected brain regions (Doty, 2017).

Moreover, xenobiotics and particles in contact with the OE can also induce the production of reactive oxygen species triggering a local inflammatory reaction in a similar way to that induced by misfolded proteins (Lema Tome et al., 2013). Alternatively, the enhanced expression of misfolding-prone proteins in olfactory structures may make those regions prone to develop certain diseases (Duda et al., 1999; Taguchi et al., 2016; Kim et al., 2018).

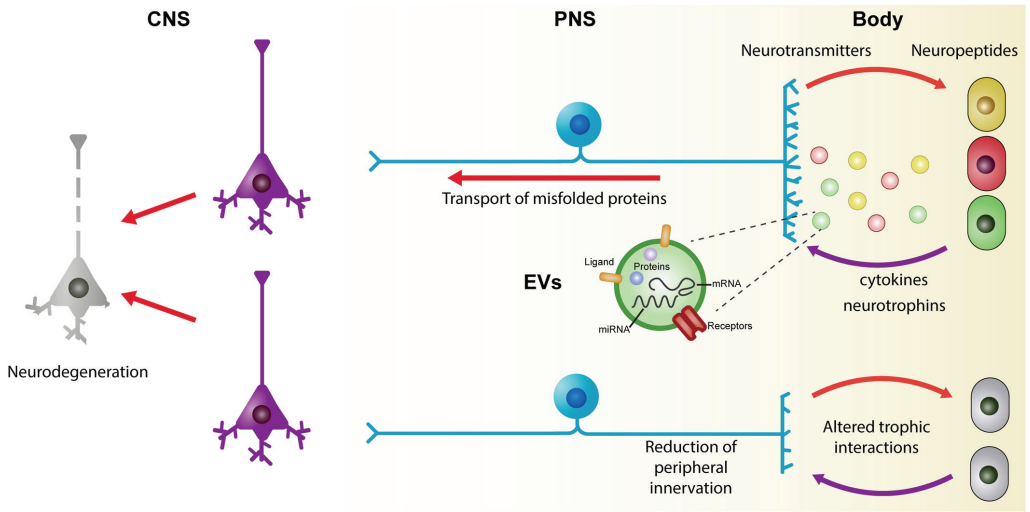

FIGURE 2 | The role of trophic interactions between the brain and the body in the development of neurodegenerative diseases. Under physiologic conditions, there is a continuous exchange of information between neurons and their targets. Neurons control several aspects of the cells they innervate by the release of neuropeptides and neurotransmitters. Reciprocally, peripheral cells modulate neuronal physiology by the release of several molecules including neurotrophins and cytokines. Recently, extracellular vesicles (EVs) have been considered as key players in the development and progression of chronic and degenerative diseases. An alteration of the homeostatic state of peripheral cells is reflected on the molecular cargo of EVs which, in turn, can affect the functioning of the neurons. Common to several chronic and neurodegenerative diseases, there is a reduction of peripheral innervation which leads to a disturbance of the trophic relation between the body and the central nervous system. A continuous alteration of these interactions during maturity of individuals may underlie some of the early events that reflect on neuronal death during aging. CNS, central nervous system; EVs, extracellular vesicles; PNS, peripheral nervous system.

Pain abnormalities are part of the clinical features in patients with PD and the impaired nociceptive processing depends on nociceptor degeneration (Nolano et al., 2008; Reichling and Levine, 2011; Conte et al., 2013). Skin biopsies of PD patients reveal a decrease in cutaneous autonomic innervation, free epidermal nerve endings, and encapsulated sensory endings (Dabby et al., 2006; Nolano et al., 2008). The severity of PD correlates with the loss of Meissner corpuscles and epidermal nerve fibers, accompanied by a reduction in cold and pain perception (Nolano et al., 2008).

The accumulation of misfolded proteins such as α-synuclein and parkin due to a dysfunction of the ubiquitin-proteasome system may partially explain the painful nociceptor dysfunction (Saha et al., 2000). In AD, pain perception seems not to be reduced. However, more studies are necessary to document whether sensory innervation is modified in AD and other neurodegenerative diseases (Cole et al., 2006). Of note, it is important to mention that different mechanisms involving both peripheral and central pain pathways may play a role in sensory dysfunction.

Autonomic dysfunction is present in several neurodegenerative diseases including PD, multiple system atrophy, AD, and other types of dementia such as DLB, PD with dementia, and frontotemporal lobar degeneration (Idiaquez and Roman, 2011; Coon et al., 2018). Orthostatic hypotension has been widely reported in patients with PD and DLBs as seen by the decreased cardiac uptake of the noradrenaline analog meta-iodobenzylguanidine (Orimo et al., 2005).

The presence of orthostatic hypertension may be due to the depletion of cardiac vagal sympathetic nerves as well as the α-synuclein pathology in sympathetic ganglia and adrenal gland that have been reported in Lewy body diseases, which includes PD, PD with dementia, and DLB (Wakabayashi et al., 2010). Interestingly, sympathetic denervation precedes neuronal loss in the sympathetic ganglia (Orimo et al., 2005). Autonomic dysfunction in AD may also be affected by neuropathological changes in central autonomic networks (Collins et al., 2012). Future studies should focus on the temporality of autonomic alterations in neurodegenerative diseases.

Gastrointestinal dysfunction is closely linked to the dysfunction of the ENS. Enteric dysfunction has been reported in PD, AD, ALS, and frontotemporal dementia (Rao and Gershon, 2016). Biopsies of PD patients have demonstrated the presence of Lewy-type pathology in enteric neurons suggesting a role of the ENS in the onset of the disease (Kupsky et al., 1987; Wakabayashi et al., 1988, 1990). The unmyelinated axons of enteric neurons may increase their susceptibility to PD and due to their multiple synaptic terminals may promote the propagation of α-synuclein aggregates via connected ganglia (Chalazonitis and Rao, 2018).

Likewise, in AD patients, Aβ immunoreactivity is found in the submucosa of the intestine (Joachim et al., 1989). In addition, amyloid precursor protein expression is present in the enteric neurons of AD patients (Arai et al., 1991). However, in contrast to PD, data from human samples in AD are still sparse. Other autonomic dysfunctions reported include urinary symptoms, sexual and thermoregulatory, dysfunction, and sleep disturbances (Postuma et al., 2015; Racosta et al., 2015; Pfeiffer, 2016). A better characterization of peripheral damage is required

in those cases where there is evidence of alteration in the peripheral innervation.

Impact of Peripheral Metabolic Disorders on Neurodegeneration

An increasing body of evidence suggests that metabolic disturbances may contribute to neurodegenerative processes in the CNS. We discuss here briefly the impact of diabetes mellitus (DM) and obesity on neurodegeneration.

Diabetes mellitus is one of the most common metabolic diseases and a major disorder of insulin regulation with increasing incidence (Duarte et al., 2012). Especially type 2 diabetes (T2D) is a highly complex, multifactorial metabolic disease, characterized by a progressive pancreatic β-cell failure (relative insulin deficiency), decreased insulin action and peripheral insulin resistance (Campbell, 2011; Carvalho et al., 2012).

T2D develops under a cluster of risk factors that includes high blood glucose, obesity, increased blood triacylglycerols and insulin resistance, which individually or collectively, also increase the risk for neurodegeneration/neuronal death, functional and structural brain changes, culminating in cognitive dysfunction that underlies dementia-type disorders (e.g., AD), which may arise from a complex interplay between T2D and brain aging. Additionally, decreased brain insulin levels/signaling and glucose metabolism in both pathologies further suggests that an effective treatment strategy for one disorder maybe also beneficial in the other (Duarte et al., 2013).

Obesity is clinically identified based on measurements of body mass index, but can be generally defined as the condition in which excess body fat has accumulated to an extent that can negatively affect health. This definition is based on the dramatically enhanced risk for a myriad of disorders, including T2D, CVD, gastrointestinal and respiratory disorders, and several types of cancer (for review, see Haslam and James, 2005). Furthermore, abdominal obesity is a component of the metabolic syndrome, which additionally combines insulin resistance or glucose intolerance, atherogenic dyslipidemia, elevated blood pressure, and increased expression of prothrombotic and proinflammatory markers (for review, see Olufadi and Byrne, 2008) and is an important risk factor for T2D, CVD, and stroke.

While the consequences of obesity on metabolic and cardiovascular pathophysiology are well-studied, epidemiological and experimental data are beginning to reveal that the CNS may also be detrimentally affected by obesity and obesity-induced metabolic dysfunction. In particular, data show that obesity is associated with cognitive decline and enhanced vulnerability to brain injury, while experimental studies in animal models confirm a profile of increased susceptibility to brain damage and decreased cognitive function (Bruce-Keller et al., 2009).

Recent data suggest that both AD and PD can manifest systemic alterations in energy metabolism (e.g., increased insulin resistance and dysregulation of glucose metabolism). Moreover emerging evidence that dietary restriction can forestall the development of AD and PD is consistent with a major "metabolic" component to these diseases, and provides optimism that these devastating brain disorders of aging may be largely preventable (Blum-Degen et al., 1995; Mattson et al., 1999).

Advanced glycation end products generated by chronic hyperglycemia and their receptor RAGE provide critical links between diabetes and AD (Vicente Miranda et al., 2016; Fleitas et al., 2018). Obesity, diabetes, and metabolic syndrome increase the risk of cognitive decline and dementia, including not only vascular dementia, but also AD and PD (Roriz-Filho et al., 2009).

However, due to increased incidence, especially in the aging population, the impact of metabolic disease on neurodegenerative processes will increase tremendously in the upcoming decades. We believe therefore that potential therapeutic approaches aiming at preventing/treating neurodegenerative diseases should include metabolic disorders.

Altered Body–Brain Trophic Communication

Accumulating evidence suggests that patients with neurodegenerative diseases commonly develop sensory and autonomic dysfunctions during maturity. This raises the possibility that the peripheral nervous system may be the gateway to alter brain physiology. The trophic theory of neural connections states that there is a mutual dependence between neurons and their targets (Purves, 1988; Qureshi and Mehler, 2013; Holm et al., 2018). Olfactory or gastrointestinal alterations may reflect a distortion of the communication between a variety of cell types and peripheral neurons. The repercussion of these altered interactions on the development of neurodegenerative diseases are still underexplored. Moreover, the mechanisms of cellular communication between peripheral cells and the nervous system are not fully characterized.

Recently, a novel system of intercellular communication has been proposed to modulate changes in neuronal physiology and to participate in the propagation of misfolded proteins (Fevrier et al., 2004; Asai et al., 2015; Grey et al., 2015; Polanco et al., 2016). This system is mediated by membranous organelles denominated as EVs, which can travel from the periphery to the brain and vice versa (Li et al., 2018).

Apparently, all the cell types of the body can release EVs to transmit information in the form of proteins, RNAs, and lipids. EVs are classified according to their subcellular origin in exosomes when originating from multivesicular bodies and in ectosomes (or microvesicles) when formed from the plasma membrane (Thery et al., 2018). Despite the technical challenges to study the functional role of different EVs subpopulations, their participation in both the maintenance of tissue homeostasis and the progression of chronic degenerative diseases is becoming clearer.

Extracellular vesicles are involved in several processes of brain development and normal functioning, including synapse formation, synaptic plasticity, and communication between glia and neurons. The signaling proteins of hydrophobic nature, such as the Wnt family members and other regulatory proteins, are loaded into EVs (Korkut et al., 2009; Coulter et al., 2018; Lee et al., 2018). During mammalian brain development, the vesicular secretion of the

growth factor sonic hedgehog promotes the proliferation of neural progenitors.

Interestingly, the loss of function of the complex charged multivesicular body proteins 1A reduces the number of intraluminal vesicles and the secretion of a specific subtype of EVs whose functions can be directly related to sonic hedgehog signaling (Coulter et al., 2018). At the *Drosophila* neuromuscular junction, EVs containing the Wnt-binding protein Evennes Interrupt and the Wnt 1 homolog Wingless promote synaptic growth when released from the presynaptic terminal (Korkut et al., 2009; Koles et al., 2012).

There is a constant reciprocal exchange of information through EVs between the pre- and post-synapse to modulate fine aspects of synaptic maturation and remodeling. In rat hippocampal neurons, excitatory synapses can be eliminated by a mechanism dependent on the delivery of Proline-Rich 7 by exosomes to induce the degradation of the post-synaptic density protein-95 (Lee et al., 2018).

Extracellular vesicles contents also influence long-term memory and synaptic plasticity. In neuronal cultures from mouse hippocampus and in neuromuscular junction preparations from *Drosophila*, oligomers of the activity-regulated cytoskeleton-associated protein and its own mRNA are transported through exosomes to the post-synapse (Ashley et al., 2018; Pastuzyn et al., 2018). The translation of the exosomal activity-regulated cytoskeleton-associated protein mRNA increases by the activation of the group 1 metabotropic glutamate receptors (Pastuzyn et al., 2018). The notion that neurons constantly use EV-mediated communication is reinforced by the fact that the release of EVs is activity-dependent and that the delivery of the cargo from presynaptic cells enables retrograde signaling from the post-synaptic cells (Lachenal et al., 2011; Korkut et al., 2013; Lee et al., 2018).

The general hypothesis on the role of EVs related to the development of neurodegenerative diseases relies on their potential to transport protein aggregates, which has been reviewed elsewhere (Howitt and Hill, 2016). Here, we would like to center the discussion on the possibility that a bidirectional exchange of information through EVs between peripheral cells and neurons may have a long-term impact on the brain physiology.

Emerging evidence suggests that both central and peripheral neurons can uptake EVs from a variety of cell types. Thus, under certain circumstances, EVs derived from peripheral cells contain proteins or RNAs that can be deleterious for neuronal functioning. In agreement with this notion, exosomes derived from hyperglycemic Schwann cells contain microRNAs that suppress axonal growth *in vitro* (Jia et al., 2018). Moreover, hyperglycemic Schwann cell-derived exosomes contribute to the development of diabetic peripheral neuropathy when injected into a diabetic mouse (Jia et al., 2018).

Similarly, the CNS can also be affected by the information transported by systemic exosomes. An increase of inflammatory cytokines in the brain and microglial and astrocytic activation is observed after the intravenous injection of serum-derived exosomes from lipopolysaccharide (LPS)-challenged mice (Balusu et al., 2016; Li et al., 2018). Dorsal root ganglion neurons modulate immune cells in the periphery by the release of neuropeptides.

Recent findings also indicate that EV-mediated communication can be an additional mechanism operating during trauma. After nerve injury, dorsal root ganglia neuron-derived exosomes loaded with microRNA-21 increase the infiltration of inflammatory macrophages, which contributes to neuronal sensitization (Simeoli et al., 2017). Further work is required to obtain insights whether EVs from peripheral cells modulate cellular processes in the brain under physiological conditions and which factors can alter the messages coming from the periphery (Ridder et al., 2014).

Despite the few studies focusing on the influence of peripherally derived EVs on peripheral neurons, it is likely that peripheral terminals establish a bidirectional interaction with the cellular elements surrounding them. Both sensory and autonomic axon terminals usually end as free nerve endings in the extracellular matrix intercalated between different cell types. Peripheral neurons are responsive to EVs derived from mesenchymal stem cells and Schwann cells (Lopez-Verrilli et al., 2013, 2016; Ching et al., 2018; Sun et al., 2018; Shiue et al., 2019). The general observation of these studies, performed in conditions of neuronal damage, is that EVs reduce the inflammatory state and have a beneficial role in axonal growth both *in vivo* and *in vitro*.

Taken together, these findings indicate that neurons are susceptible to modify their functioning or gene expression profile as a result of incorporating EVs from neighboring cells. A challenge for future studies is to determine if EVs from any cell source can modify neuronal functioning and how these events are associated with physiological alterations that precede neurodegeneration in the brain.

GUT DYSBIOSIS AS THE ORIGIN OF NEURODEGENERATION

Microbiota is defined as a community of all microorganisms living in our body. Microbiota therefore includes all taxonomic domains such as fungi, protozoa, viruses, and bacteria. Bacterial microbiota living in the gut (further referred as GM) represent about 90% of all microbiota in the body (Thursby and Juge, 2017), with an estimated ratio of human:bacterial cells close to 1:1 (Sender et al., 2016). This large number of bacteria offers different benefits to the host, confers protection against pathogens (Baumler and Sperandio, 2016), regulates host immunity (Gensollen et al., 2016), and products originating from bacterial fermentation can be used as a source of energy for colonocytes (den Besten et al., 2013).

A delicate balance exists between the GM composition and its interaction with the host, while an imbalance in this composition is commonly known as dysbiosis. Gut dysbiosis has been implicated in the development of chronic diseases, such as irritable bowel syndrome (Raskov et al., 2016), coeliac disease (Verdu et al., 2015) as well as metabolic disorders, including obesity, metabolic syndrome, and T2D (Holmes et al., 2011;

TABLE 1 | Alterations in gut microbiota at PHYLUM level in AD patients and AD transgenic mice.

Model	Bacterial phylum INCREASED	Bacterial phylum DECREASED	References
AD patients	Actinobacteria	Bacteroidetes	Zhuang et al., 2018
AD patients	Bacteroidetes	Firmicutes	Vogt et al., 2017
3×TG-AD mice 8 months old	Firmicutes	–	Sanguinetti et al., 2018
3×Tg-AD mice 24 months old	–	Tenericutes Cyanobacteria	Bonfili et al., 2017
APP/PS1 mice 8 months old	Firmicutes	Bacteroidetes Proteobacteria	Park et al., 2017
APP/PS1 mice 1 month old	Firmicutes	Bacteroidetes	Harach et al., 2017
APP/PS1 mice 8 months old	Bacteroidetes Tenericutes	Firmicutes Verrucomicrobia Proteobacteria Actinobacteria	Harach et al., 2017
5×FAD mice 9 weeks old	Firmicutes	Bacteroidetes	Brandscheid et al., 2017

Carding et al., 2015; Zhang et al., 2015; Baothman et al., 2016; Org et al., 2017).

Notably, those metabolic diseases, when developed during adulthood, are considered important risk factors for AD (Alzheimer's Association, 2016; Livingston et al., 2017). Furthermore, metabolic alterations are known to induce peripheral low-grade chronic inflammation, associated with higher incidence of neurodegenerative diseases. In AD, systemic inflammation during prodromal stages shortens disease onset (Tao et al., 2018), whereas dysregulation of the gastrointestinal function and colonic inflammation diminished immune competence and preceded motor symptoms in PD patients (Dobbs et al., 1999; Braak et al., 2003b; Lebouvier et al., 2009; Villaran et al., 2010; Forsyth et al., 2011).

During aging, there is an increased permeability of the gut epithelium (Tran and Greenwood-Van Meerveld, 2013). This condition allows bacteria and bacterial products to translocate through the disrupted gut barrier reaching peripheral organs (Zevin et al., 2016). Newest reports suggest that translocated bacteria may even reach the brain (Roberts et al., 2018), where an exacerbated immune reaction can lead to neurodegeneration. These observations remain however to be investigated in detail.

Gut Microbiota Alterations in Neurodegenerative Diseases

Recent reports concomitantly demonstrate a gut dysbiosis in PD (Minato et al., 2017; Wu et al., 2017), ALS, and AD patients (Cattaneo et al., 2017; Vogt et al., 2017).

Understanding how GM may be implicated in brain pathologies requires a clear comparison among the data reported from different research groups. The GM is mainly dominated by four phyla: Firmicutes, Bacteroidetes, Actinobacteria, and Proteobacteria (Szablewski, 2018). The first studies described GM alterations only at the phylum level. However, recent advances in sequencing techniques allow distinction at the species level, which is advantageous since the different species of bacteria belonging to the same genus affect host physiology in a different manner. We compared previously published GM data obtained from AD patients and AD mice models. We noted a strong variation between studies: at phylum level, most transgenic models coincide with an increased abundance of Firmicutes but a decreased abundance of Bacteriodetes (**Table 1**). Whereas at the family and upper taxonomical levels (i.e., genus/species), there is no more consistency (**Table 2**).

Importantly, variations in the experimental design or the type of samples can be observed. Moreover, differences in the animal model, chronological stage of the pathology (age), handling and diet significantly impact GM (Mueller et al., 2006; Hufeldt et al., 2010; Sanchez-Tapia et al., 2017). Thus, experimental variations among published studies may explain discrepancies in the GM composition in AD.

Despite this strong variation, we can observe a general increased abundance of pro-inflammatory bacteria in AD mice and AD patients (Kountouras et al., 2009; Zhan et al., 2016; Cattaneo et al., 2017; Shen et al., 2017; Vogt et al., 2017; Zhang et al., 2017; Syeda et al., 2018) compared to controls. Furthermore, in AD transgenic mice, longitudinal studies clearly indicate an age-associated gut dysbiosis, culminating in a strong pro-inflammatory environment along the development of brain pathological hallmarks (Shen et al., 2017; Zhang et al., 2017; Syeda et al., 2018).

How Can the GM Affect Brain Function or Even Cause Neurodegeneration?

A bidirectional communication between the gastrointestinal system and the brain has been described and has led to the concept of gut-brain axis (Collins and Bercik, 2013). Recent studies illustrated the role of GM in brain Aβ aggregation, as GM absence in germ-free condition (Harach et al., 2017) or GM partial depletion by antibiotic treatment (Minter et al., 2016) reduced the amyloid burden and microglia activation in AD transgenic mice. However, it is still unclear which factors may be associated with the above described gut-brain axis in brain pathologies.

Several groups have implicated the neurotoxin LPS present in the outer membrane of gram-negative bacteria. LPS plays key roles in the host-pathogen interactions of the innate immune system (Hill and Lukiw, 2015; Maldonado et al., 2016). Alterations in the GM composition/abundance are associated with enhanced plasma levels of LPS (Avila-Nava et al., 2017;

TABLE 2 | Alterations in gut microbiota in AD patients and AD mice at FAMILY, GENUS, and SPECIES levels.

Model	Bacterial family (f.)/genus (g.)/ species (g. s.) INCREASED	Bacterial family (f.)/genus (g.)/ species (g. s.) DECREASED	References
AD patients	*g. Escherichia/Shigella*	*g.s. Eubacterium rectale*	Cattaneo et al., 2017
AD patients	*f. Bacteroidaceae* *f. Rikenellaceae* *f. Gemellaceae* *g. Bilophila* *g. Phascolarctobacterium* *g. Gemella* *g. Bacteroides* *g. Alistipes*	*f. Ruminococcaceae* *f. Turicibacteraceae* *f. Peptostreptococcaceae* *f. Clostridiaceae* *f. Mogibacteriaceae* *f. Bifidobacteriaceae* *g. SMB53* *g. Dialister* *g. Clostridium* *g. Turicibacter* *g. cc115*	Vogt et al., 2017
AD patients	*f. Ruminococcaceae* *f. Enterococcaceae* *f. Lactobacillaceae*	*f. Lanchnospiraceae* *f. Bacteroidaceae* *f. Veillonellaceae*	Zhuang et al., 2018
3XTG-AD mice 24 months old	*g. Prevotellaceae* *g. Enterococcus* *g. Streptococcus* *g. Turicibacter* *g. Ruminococcus* *g. Desulfovibrionaceae* *g. Flexispira*	*g. Turicibacter* *g. Prevotella* *g. Ruminococcus* *g. Flexispira*	Bonfili et al., 2017
APP/PS1 mice 8 months old	*f. Rikenellaceae* *f. S24-7*	*g. Allobaculum* *g. Akkermansia*	Harach et al., 2017
APP/PS1 mice 8 months old	*f. Aerococcaceae* *f. Leuconostocaceae* *f. Lactobacillaceae* *f. Pseudomonadaceae* *f. Caulobacteraceae* *f. Cytophagaceae* *f. Sphingobacteriaceae* *f. Corynebacteriaceae*	*f. Sphingomonadaceae* *f. Comamonadaceae* *f. Rhodocyclaceae* *f. Flavobacteriaceae*	Park et al., 2017
3XTG-AD mice 8 months old	*f. Enterococcaceae* *f. Turicibacteraceae*	*f. S24-7* *f. Bifidobacteriaceae*	Sanguinetti et al., 2018
3XTG-AD mice 9 months old	*g.s. Prevotella copri* *g.s. Lactobacillus ruminis* *g.s. Streptococcus anginosus* *g.s. Actinobacillus parahaemolyticus* *g.s. Haemophilus parainfluenzae*	*g.s. Bacteroides fragilis* *g.s. Faecalibacterium prausnitzii* *g.s. Akkermansia muciniphila*	Syeda et al., 2018

Sanchez-Tapia et al., 2017), which may result in an exacerbated metabolic endotoxemia (Cani et al., 2012), a condition characterized by inflammation and the increased release of pro-inflammatory cytokines.

Systemic infections have been related to a higher possibility to develop AD (Holmes et al., 2009) as well as early motor dysfunction in PD patients (Dobbs et al., 1999). Therefore, long-term gut microbiota alterations and gut dysbiosis resulting in a pro-inflammatory environment and inflammation may be linked to brain dysfunction in aging.

As a proof of concept, LPS is detected in the parenchyma and blood vessels of both, non-demented aged and AD brain samples, but at a higher level in diseased tissues (Zhao et al., 2015, 2017; Zhan et al., 2016). LPS also increases in the plasma of AD transgenic mice compared to wild type controls (Syeda et al., 2018). In PD patients, higher plasma LPS correlates with α-synuclein aggregation (Forsyth et al., 2011). Furthermore, LPS is a well-known neuroinflammatory agent driving the generation of $A\beta_{1-42}$ (Lee et al., 2008; Asti and Gioglio, 2014; Hill and Lukiw, 2015; Zhao et al., 2015). LPS administration to mice results in memory impairment, Aβ aggregation, and astrocyte activation (Lee et al., 2008). Therefore, gut dysbiosis may enhance LPS to the blood circulation and even to the brain, producing glia activation and protein aggregation, both important features of neurodegenerative diseases.

Another bacterial product related to the development of neurodegenerative diseases are short-chain fatty acids (SCFAs). SCFAs are produced by the GM after the degradation of non-digestible polysaccharides, with butyrate, acetate, and propionate being the more abundant fermentation products (Wong et al., 2006). About 95% of the SCFAs produced in the gut are absorbed within the colon (Hoyles et al., 2018), while butyrate is used by the colonocytes as an energy source. In order to maintain an optimal equilibrium between intestinal SCFAs and the concentration in the body, the gut intestinal barrier increases its mucus production

(Rios-Covian et al., 2016), while the liver clears the majority of propionate and butyrate from the portal circulation (Bloemen et al., 2010). However, SCFAs can be transported through the bloodstream to reach the brain.

Some alterations in fecal SCFAs concentration have been described in AD transgenic mice compared to controls (Bonfili et al., 2017; Zhang et al., 2017). Butyrate, a well-known neuroprotective agent (Minamiyama et al., 2004; Govindarajan et al., 2011; Liu et al., 2015), is reduced in the fecal samples of AD mice (Zhang et al., 2017). Other reports show increased propionate levels in brain tissue of AD transgenic mice compared to wild type controls, an event associated with GM dysbiosis (Syeda et al., 2018). Although, propionate has some beneficial effects [e.g., on the BBB (Hoyles et al., 2018)], excessive propionate alters dopamine, serotonin, and glutamate systems in a manner similar to that observed in autism spectrum disorders (El-Ansary et al., 2012; Li et al., 2017).

Fecal samples of children with autism spectrum disorder present an increased level of propionate (Wang et al., 2012). In addition, genetic diseases that affect the function of the enzyme propionyl-CoA carboxylase (such as propionic acidemia) are characterized by high levels of propionate and high incidence of dementia (Grunert et al., 2013), while in AD patients, increased levels of acetate and propionate have been found in saliva samples compared to healthy controls (Figueira et al., 2016; Yilmaz et al., 2017). Although, the effects of butyrate and propionate are still controversially discussed, several data support a role of the imbalance between butyrate and propionate in the pathogenesis of AD (Syeda et al., 2018).

Another important pathway connecting the brain and the GM is the involvement of the immune system (Fung et al., 2017) studied, e.g., in stroke. According to recent reports, in the experimental rodent models, stroke leads to dysbiosis (Benakis et al., 2016; Houlden et al., 2016; Singh et al., 2016; Stanley et al., 2018) and dysbiosis may have an effect on the course of the disease (Benakis et al., 2016; Singh et al., 2016; Stanley et al., 2016). This may be linked to GM-related fine-tuning of the balance between pro-inflammatory/anti-inflammatory immune responses primarily in the gut, followed by an infiltration of immune cells to the CNS after injury. Interestingly, pro-inflammatory T-helper cell 17 and γδ T cells found in the ischemic CNS originate from the intestine and the infiltration of these subpopulations has been linked with unfavorable outcome (Benakis et al., 2016; Singh et al., 2016).

However, the optimal (in terms of prognosis after stroke) composition of the GM has not been identified yet and is possibly difficult to pinpoint. Some findings indicate that the complete absence (in germ-free mice) or deep antibiotic depletion of GM can be detrimental, leading to increased infarct volumes (Singh et al., 2018) or increased mortality not related to lesion size (Winek et al., 2016). Alterations in GM have also been identified in stroke patients (Yin et al., 2015; Stanley et al., 2016). Due to its metabolic capacities, GM can also contribute to the pathogenesis of the diseases considered as the risk factors of stroke, like obesity (for review Torres-Fuentes et al., 2017) and atherosclerosis (Karlsson et al., 2012; Tang et al., 2013) (for review, see Li and Tang, 2017).

We can conclude that a predominantly pro-inflammatory GM and the release of neurotoxic substances may negatively affect brain functions, causing systemic and central inflammation over decades. This is in support of the recent hypothesis of an infectious etiology for neurodegenerative diseases, such as AD (Bhattacharjee and Lukiw, 2013; Little et al., 2014; Maheshwari and Eslick, 2015; Itzhaki et al., 2016). The substances released from the GM (i.e., LPS and SCFAs) may be implicated in the pathogenesis of several neurodegenerative diseases; however, more data are still needed to clearly understand this gut-brain-immune interaction.

FROM CONSEQUENCES TO CAUSES: ACADEMIC AND PRECLINICAL CONSIDERATIONS

As we have described above, the neurocentric view entertained as the predominant focus of our effort in treating neurodegeneration is likely insufficient to ensure successful therapeutic intervention.

The Lack of Adequate Experimental Models to Study the Etiology

Investigating the pathophysiological processes behind neurodegeneration in detail requires the use of animal models. A plethora of animal models of neurodegeneration exists, and the nuances of these models are beyond the scope of this manuscript (for recent reviews, see Gitler et al., 2017; Dawson et al., 2018; Ransohoff, 2018).

However, two general problems with current models seem to be particularly widespread and contribute to our limited success in extrapolating findings from preclinical research to patients. Firstly, they often fail to fully integrate our understanding of the etiology of the diseases they are meant to represent, often being restricted to inducing the disease in a single way, despite multiple inducing factors being responsible for the human disease. Secondly, animals used as the model organism of specific diseases often do not exhibit similar comorbidities and demographic characteristics (such as age or gender) seen in human patients. Examples of such problems are the rodent models of stroke, particularly ones that involve surgical ligation or occlusion of blood vessels in otherwise healthy, young animals (van der Worp et al., 2010; Mergenthaler and Meisel, 2012).

Another important issue is the way these models are characterized. For animal models to be used to study neurodegeneration, two essential steps must be taken. First, the validity of the model for the question at hand should be thoroughly and systematically investigated. This is preferably done in a multi-centric and multi-disciplinary way to ensure the generalizability and robustness of the results. Second, the external (face, construct, and predictive) validity of the model (Willner, 1984) should be empirically and thoroughly tested, as well as the inter-rater agreement on, and replicability of, the model's characteristics (McKinney and Bunney, 1969). Such studies aimed at characterizing the model should be very clearly

and unequivocally separated from experiments using the model to test hypotheses, such as the effect of an intervention on the course of the model's progression.

For these strategies to be successful, research into and using these models must be conducted in the setting of appropriate, rigorous, and transparent experimental design and reporting (Kilkenny et al., 2010; Holman et al., 2016; Percie du Sert et al., 2017). Beyond that, we should make an active effort to think of the drawbacks of the models and methods we have used and how this may restrict or bias the knowledge we gain from such studies (Garner et al., 2017). Finally, we need a framework for integrating the knowledge gained from individual studies using different models and methods to address similar research questions. Systematic reviews and quantitative meta-analyses, widely used for knowledge synthesis in clinical research, may be helpful tools to help us achieve this.

Studying Human Disease in Human Systems

Although animal models are a powerful tool toward understanding the etiology of neurodegenerative diseases, they still present considerable limitations (Jucker, 2010). As a consequence, there has been little success translating the knowledge obtained from model organisms to therapeutically valuable outcomes. This constraint can only be addressed by studying neurodegenerative diseases directly on humans.

The recent increase in the generation of digital data including imaging, genotypic, and phenotypic information coupled with a fast development of computational methods allows us to obtain new insights from this massive amount of data. Major efforts from consortiums such as the Alzheimer's Disease Initiative (ADNI), the Australian Imaging, Biomarkers & Lifestyle Study of Ageing (AIBL), the Parkinson's Progression Markers Initiative (PPMI) or more recently the United Kingdom Biobank have made available an unprecedented amount of data, which can be exploited through the use of big data algorithms.

Having large amounts of information coming from heterogeneous populations and acquisition systems increases the power of statistic approaches and reduces the risk of bias. Big data approaches are inherently limited since in general they cannot be used to perform causal inference, but rather to find correlations or associations between variables. However, these correlations have proven to be an invaluable tool for hypothesis generation, drug and safety surveillance, disease and treatment heterogeneity among many other applications (Lee and Yoon, 2017).

Such computational models have been used for example to build a model of senescence signaling via DNA damage, insulin-TOR, FoxO3a transcription factors, oxidative stress response, mitochondrial regulation, and mitophagy using a systems biology approach (Dalle Pezze et al., 2014). A recent review of mathematical models in neurodegenerative diseases reports several mathematical models involving some of the processes we addressed above, such as energy metabolism and synaptic plasticity (Lloret-Villas et al., 2017). A multivariate Bayesian model of biomarker measurements was used to estimate AD dementia onset age (Bilgel and Jedynak, 2019). Similarly, multivariate models have been used to relate image based morphological features to the risk of dementia (Gutierrez Becker et al., 2018; Cole et al., 2019).

Recent trends in stem cell methods have also opened new possibilities for human brain cell cultures, which can in turn be used to model neurodegeneration. Induced pluripotent stem cells and neural stem cell cultures can now be used to generate human neurons from human and sometimes patient cells (Abud et al., 2017; Korhonen et al., 2018). This has been reviewed extensively elsewhere (Xie and Tang, 2016; Robbins and Price, 2017).

CONCLUSION

Disease is typically defined in juxtaposition to the state of health, which has been even more generally defined as "a state of complete physical, mental, and social well-being" (International Health Conference, 2002). However, in order to characterize a bodily or mental state as diseased, we need a more practical, operational definition of the healthy state, characterized in terms of physiological parameters and defined by the description of the steady state functioning of the body and its subsystems.

Typically, pathophysiological events of neurodegeneration are detected through behavioral observations and self-reporting and subsequently confirmed and classified using neurological examination and diagnostic imaging. The result of this diagnostic approach usually reveals typical defining features for each neurological disease (such as hemorrhage, tumor, or deformations), that allows the classification of the disorder. However, these defining characteristics are not necessarily the root causes of the disease but rather elements of the disease manifestation or even merely epiphenomena. In addition to the complex and usually obscure causal relationships giving rise to brain disorders, a parameter that further complicates the identification of causation is the widespread and intricate comorbidities between presumably distinct and unrelated disorders.

Together, these facts limit the therapeutic potential to treat the symptoms rather than the causes. The complex causality chain hinders the early detection and treatment of the root causes of brain disorders overall and neurodegeneration more specifically. These limitations highlight the critical need for a drastic shift of perspective and the improvement of the models used to investigate and understand neurodegenerative diseases.

Given the complexity of the brain and its disorders, researchers and clinicians have retreated to a highly segregated approach, focusing on describing subsets of the symptoms of each disease and trying to identify mechanistic explanations and treatments for those symptoms. However, the lack of a holistic perspective, taking into account the deviations from the default homeostatic state at an organismal level, renders this endeavor nearly impossible and doomed to fail.

Importantly, characterizing the expected, default healthy brain, is a necessary precondition to being able to identify and meaningfully interpret the deviations from it. Thus, characterizing and understanding the brain function in health is of paramount importance in the attempt to understand and treat the diseased brain.

In summary, there is an identifiable need for an interdisciplinary approach to explore the brain function at multiple levels, from molecular to systems, while maintaining a holistic perspective that treats the brain as an element of a complex system, rather than a separate entity. Using this approach, fundamental research can proceed hand-in-hand and maintain a constant dialogue with clinical research, to propose, improve, and revise current models of health and disease.

We hope that our work inspires the opening of new research avenues among those interested in understanding and pursuing the complexities of the "neuro-degenerating" brain focusing on lifespan processes. Therefore, the proposed etiological paths and suggestions will be important guidelines for future cross-discipline research to overcome the translational roadblock and to develop causative treatments for neurological disorders.

AUTHOR CONTRIBUTIONS

AP, GG-O, and MZ applied for funding and organized the workshop. AK, AP, AV, BG-B, MZ, NK, and XC were participants of the subgroup "The Vascular Origin of Neurodegeneration." AV-C, JP-V, KR, KW, LR, and SC-O of the subgroup "Cellular Senescence as the Origin of Neurodegeneration." CP-C, EM-M, GG-O, HG, and JL-N of the subgroup "Body–Brain Trophic Interactions as the Origin of Neurodegeneration." Accordingly, the authors wrote the respective sections of this manuscript, except CP-C who together with TS wrote the section "Gut Dysbiosis as the Origin of Neurodegeneration" with contributions from KW. AP contributed to the section "Body–Brain Trophic Interactions as the Origin of Neurodegeneration." BG-B wrote the section on "Studying Human Disease in Human Systems." AK on "The Lack of Adequate Experimental Models to Study the Etiology." NK wrote the conclusion. MZ wrote the remaining sections of the manuscript. AV commented on the manuscript. All authors discussed and commented on the final version of the manuscript.

FUNDING

This work was supported by a grant from the German Federal Ministry of Education and Research (BMBF grant number 01DN18054) to MZ, AP, and GG-O.

ACKNOWLEDGMENTS

This is a spin-off article from the workshop "German-Mexican Roundtable Exploring New Etiological Paths Towards Neurodegeneration," which took place at the Instituto de Investigaciones Biomédicas at the National Autonomous University of México, Mexico City, on October 15–17th, 2018. Miguel Morales Pacheco helped in the design of **Figure 1**.

REFERENCES

Abud, E. M., Ramirez, R. N., Martinez, E. S., Healy, L. M., Nguyen, C. H. H., Newman, S. A., et al. (2017). iPSC-derived human microglia-like cells to study neurological diseases. *Neuron* 94, 278–293.e9.

Alvarez, J. I., Cayrol, R., and Prat, A. (2011). Disruption of central nervous system barriers in multiple sclerosis. *Biochim. Biophys. Acta* 1812, 252–264. doi: 10.1016/j.bbadis.2010.06.017

Alzheimer's Association (2016). 2016 Alzheimer's disease facts and figures. *Alzheimers Dement* 12, 459–509. doi: 10.1016/j.jalz.2016.03.001

Andrade, J., Khairy, P., Dobrev, D., and Nattel, S. (2014). The clinical profile and pathophysiology of atrial fibrillation: relationships among clinical features, epidemiology, and mechanisms. *Circ. Res.* 114, 1453–1468. doi: 10.1161/circresaha.114.303211

Anselmino, M., Scarsoglio, S., Saglietto, A., Gaita, F., and Ridolfi, L. (2016). Transient cerebral hypoperfusion and hypertensive events during atrial fibrillation: a plausible mechanism for cognitive impairment. *Sci. Rep.* 6: 28635.

Arai, H., Lee, V. M., Messinger, M. L., Greenberg, B. D., Lowery, D. E., and Trojanowski, J. Q. (1991). Expression patterns of beta-amyloid precursor protein (beta-APP) in neural and nonneural human tissues from Alzheimer's disease and control subjects. *Ann. Neurol.* 30, 686–693. doi: 10.1002/ana.410300509

Asai, H., Ikezu, S., Tsunoda, S., Medalla, M., Luebke, J., Haydar, T., et al. (2015). Depletion of microglia and inhibition of exosome synthesis halt tau propagation. *Nat. Neurosci.* 18, 1584–1593. doi: 10.1038/nn.4132

Ashley, J., Cordy, B., Lucia, D., Fradkin, L. G., Budnik, V., and Thomson, T. (2018). Retrovirus-like gag protein arc1 binds RNA and traffics across synaptic boutons. *Cell* 172, 262–274.e11. doi: 10.1016/j.cell.2017.12.022

Ask, T. F., Lugo, R. G., and Sutterlin, S. (2018). The neuro-immuno-senescence integrative model (NISIM) on the negative association between parasympathetic activity and cellular senescence. *Front. Neurosci.* 12:726. doi: 10.3389/fnins.2018.00726

Asti, A., and Gioglio, L. (2014). Can a bacterial endotoxin be a key factor in the kinetics of amyloid fibril formation? *J. Alzheimers Dis.* 39, 169–179. doi: 10.3233/jad-131394

Avila-Nava, A., Noriega, L. G., Tovar, A. R., Granados, O., Perez-Cruz, C., Pedraza-Chaverri, J., et al. (2017). Food combination based on a pre-hispanic Mexican diet decreases metabolic and cognitive abnormalities and gut microbiota dysbiosis caused by a sucrose-enriched high-fat diet in rats. *Mol. Nutr. Food Res.* 61:1501023. doi: 10.1002/mntr.201501023

Baker, D. J., and Petersen, R. C. (2018). Cellular senescence in brain aging and neurodegenerative diseases: evidence and perspectives. *J. Clin. Invest.* 128, 1208–1216. doi: 10.1172/jci95145

Balusu, S., Van Wonterghem, E., De Rycke, R., Raemdonck, K., Stremersch, S., Gevaert, K., et al. (2016). Identification of a novel mechanism of blood-brain communication during peripheral inflammation via choroid plexus-derived extracellular vesicles. *EMBO Mol. Med.* 8, 1162–1183. doi: 10.15252/emmm.201606271

Banerjee, C., and Chimowitz, M. I. (2017). Stroke caused by atherosclerosis of the major intracranial arteries. *Circ. Res.* 120, 502–513. doi: 10.1161/circresaha.116.308441

Baothman, O. A., Zamzami, M. A., Taher, I., Abubaker, J., and Abu-Farha, M. (2016). The role of gut microbiota in the development of obesity and diabetes. *Lipids Health Dis.* 15, 108.

Baumler, A. J., and Sperandio, V. (2016). Interactions between the microbiota and pathogenic bacteria in the gut. *Nature* 535, 85–93. doi: 10.1038/nature18849

Beach, T. G., Adler, C. H., Sue, L. I., Vedders, L., Lue, L., White Iii, C. L., et al. (2010). Multi-organ distribution of phosphorylated alpha-synuclein histopathology in subjects with Lewy body disorders. *Acta Neuropathol.* 119, 689–702. doi: 10.1007/s00401-010-0664-3

Benakis, C., Brea, D., Caballero, S., Faraco, G., Moore, J., Murphy, M., et al. (2016). Commensal microbiota affects ischemic stroke outcome by regulating intestinal gammadelta T cells. *Nat. Med.* 22, 516–523. doi: 10.1038/nm.4068

Bhat, R., Crowe, E. P., Bitto, A., Moh, M., Katsetos, C. D., Garcia, F. U., et al. (2012). Astrocyte senescence as a component of Alzheimer's disease. *PLoS One* 7:e45069. doi: 10.1371/journal.pone.0045069

Bhattacharjee, S., and Lukiw, W. J. (2013). Alzheimer's disease and the microbiome. *Front. Cell Neurosci.* 7:153. doi: 10.3389/fncel.2013.00153

Bilgel, M., and Jedynak, B. M. (2019). Predicting time to dementia using a quantitative template of disease progression. *Alzheimers Dement* 11, 205–215. doi: 10.1016/j.dadm.2019.01.005

Bloemen, J. G., Olde Damink, S. W., Venema, K., Buurman, W. A., Jalan, R., and Dejong, C. H. (2010). Short chain fatty acids exchange: is the cirrhotic, dysfunctional liver still able to clear them? *Clin. Nutr.* 29, 365–369. doi: 10.1016/j.clnu.2009.10.002

Blum-Degen, D., Frolich, L., Hoyer, S., and Riederer, P. (1995). Altered regulation of brain glucose metabolism as a cause of neurodegenerative disorders? *J. Neural Transm. Suppl.* 46, 139–147.

Bohnen, N. I., and Albin, R. L. (2011). White matter lesions in Parkinson disease. *Nat Rev Neurol* 7, 229–236. doi: 10.1038/nrneurol.2011.21

Bonfili, L., Cecarini, V., Berardi, S., Scarpona, S., Suchodolski, J. S., Nasuti, C., et al. (2017). Microbiota modulation counteracts Alzheimer's disease progression influencing neuronal proteolysis and gut hormones plasma levels. *Sci. Rep.* 7:2426.

Bookheimer, S. Y., Strojwas, M. H., Cohen, M. S., Saunders, A. M., Pericak-Vance, M. A., Mazziotta, J. C., et al. (2000). Patterns of brain activation in people at risk for Alzheimer's disease. *N. Engl. J. Med.* 343, 450–456.

Braak, H., Del Tredici, K., Rub, U., De Vos, R. A., Jansen Steur, E. N., and Braak, E. (2003a). Staging of brain pathology related to sporadic Parkinson's disease. *Neurobiol. Aging* 24, 197–211. doi: 10.1016/s0197-4580(02)00065-9

Braak, H., Rub, U., Gai, W. P., and Del Tredici, K. (2003b). Idiopathic Parkinson's disease: possible routes by which vulnerable neuronal types may be subject to neuroinvasion by an unknown pathogen. *J. Neural Transm.* 110, 517–536. doi: 10.1007/s00702-002-0808-2

Brainstorm, C., Anttila, V., Bulik-Sullivan, B., Finucane, H. K., Walters, R. K., Bras, J., et al. (2018). Analysis of shared heritability in common disorders of the brain. *Science* 360:eaap8757.

Brandscheid, C., Schuck, F., Reinhardt, S., Schafer, K. H., Pietrzik, C. U., Grimm, M., et al. (2017). Altered gut microbiome composition and tryptic activity of the 5xFAD Alzheimer's mouse model. *J. Alzheimers Dis.* 56, 775–788. doi: 10.3233/jad-160926

Broadwell, R. D. (1989). Transcytosis of macromolecules through the blood-brain barrier: a cell biological perspective and critical appraisal. *Acta Neuropathol.* 79, 117–128. doi: 10.1007/bf00294368

Brouns, R., Wauters, A., De Surgeloose, D., Marien, P., and De Deyn, P. P. (2011). Biochemical markers for blood-brain barrier dysfunction in acute ischemic stroke correlate with evolution and outcome. *Eur. Neurol.* 65, 23–31. doi: 10.1159/000321965

Brown, R. C., Lockwood, A. H., and Sonawane, B. R. (2005). Neurodegenerative diseases: an overview of environmental risk factors. *Environ. Health Perspect.* 113, 1250–1256. doi: 10.1289/ehp.7567

Bruce-Keller, A. J., Keller, J. N., and Morrison, C. D. (2009). Obesity and vulnerability of the CNS. *Biochim. Biophys. Acta* 1792, 395–400.

Buerge, C., Steiger, G., Kneifel, S., Wetzel, S., Wollmer, M. A., Probst, A., et al. (2011). Lobar dementia due to extreme widening of virchow-robin spaces in one hemisphere. *Case Rep. Neurol.* 3, 136–140. doi: 10.1159/000329267

Buga, A. M., Di Napoli, M., and Popa-Wagner, A. (2013). Preclinical models of stroke in aged animals with or without comorbidities: role of neuroinflammation. *Biogerontology* 14, 651–662. doi: 10.1007/s10522-013-9465-0

Bussian, T. J., Aziz, A., Meyer, C. F., Swenson, B. L., Van Deursen, J. M., and Baker, D. J. (2018). Clearance of senescent glial cells prevents tau-dependent pathology and cognitive decline. *Nature* 562, 578–582. doi: 10.1038/s41586-018-0543-y

Calabrese, V., Mancuso, C., Calvani, M., Rizzarelli, E., Butterfield, D. A., and Stella, A. M. (2007). Nitric oxide in the central nervous system: neuroprotection versus neurotoxicity. *Nat. Rev. Neurosci.* 8, 766–775. doi: 10.1038/nrn2214

Calcinotto, A., Kohli, J., Zagato, E., Pellegrini, L., Demaria, M., and Alimonti, A. (2019). Cellular senescence: aging, cancer, and injury. *Physiol. Rev.* 99, 1047–1078. doi: 10.1152/physrev.00020.2018

Campbell, R. K. (2011). Clarifying the role of incretin-based therapies in the treatment of type 2 diabetes mellitus. *Clin. Ther.* 33, 511–527. doi: 10.1016/j.clinthera.2011.04.015

Cani, P. D., Osto, M., Geurts, L., and Everard, A. (2012). Involvement of gut microbiota in the development of low-grade inflammation and type 2 diabetes associated with obesity. *Gut Microbes* 3, 279–288. doi: 10.4161/gmic.19625

Carding, S., Verbeke, K., Vipond, D. T., Corfe, B. M., and Owen, L. J. (2015). Dysbiosis of the gut microbiota in disease. *Microb Ecol. Health Dis.* 26:26191.

Carvalho, C., Cardoso, S., Correia, S. C., Santos, R. X., Santos, M. S., Baldeiras, I., et al. (2012). Metabolic alterations induced by sucrose intake and Alzheimer's disease promote similar brain mitochondrial abnormalities. *Diabetes Metab. Res. Rev.* 61, 1234–1242. doi: 10.2337/db11-1186

Cattaneo, A., Cattane, N., Galluzzi, S., Provasi, S., Lopizzo, N., Festari, C., et al. (2017). Association of brain amyloidosis with pro-inflammatory gut bacterial taxa and peripheral inflammation markers in cognitively impaired elderly. *Neurobiol. Aging* 49, 60–68. doi: 10.1016/j.neurobiolaging.2016.08.019

Caviedes, A., Varas-Godoy, M., Lafourcade, C., Sandoval, S., Bravo-Alegria, J., Kaehne, T., et al. (2017). Endothelial nitric oxide synthase is present in dendritic spines of neurons in primary cultures. *Front. Cell Neurosci.* 11:180. doi: 10.3389/fncel.2017.00180

Chalazonitis, A., and Rao, M. (2018). Enteric nervous system manifestations of neurodegenerative disease. *Brain Res.* 1693, 207–213. doi: 10.1016/j.brainres.2018.01.011

Chao, Y. X., He, B. P., and Tay, S. S. (2009). Mesenchymal stem cell transplantation attenuates blood brain barrier damage and neuroinflammation and protects dopaminergic neurons against MPTP toxicity in the substantia nigra in a model of Parkinson's disease. *J. Neuroimmunol.* 216, 39–50. doi: 10.1016/j.jneuroim.2009.09.003

Charidimou, A., Jaunmuktane, Z., Baron, J. C., Burnell, M., Varlet, P., Peeters, A., et al. (2014). White matter perivascular spaces: an MRI marker in pathology-proven cerebral amyloid angiopathy? *Neurology* 82, 57–62. doi: 10.1212/01.wnl.0000438225.02729.04

Charidimou, A., Meegahage, R., Fox, Z., Peeters, A., Vandermeeren, Y., Laloux, P., et al. (2013). Enlarged perivascular spaces as a marker of underlying arteriopathy in intracerebral haemorrhage: a multicentre MRI cohort study. *J. Neurol. Neurosurg. Psychiatry* 84, 624–629. doi: 10.1136/jnnp-2012-304434

Chen, B., Cheng, Q., Yang, K., and Lyden, P. D. (2010). Thrombin mediates severe neurovascular injury during ischemia. *Stroke* 41, 2348–2352. doi: 10.1161/strokeaha.110.584920

Chen, Z. L., and Strickland, S. (1997). Neuronal death in the hippocampus is promoted by plasmin-catalyzed degradation of laminin. *Cell* 91, 917–925. doi: 10.1016/s0092-8674(00)80483-3

Ching, R. C., Wiberg, M., and Kingham, P. J. (2018). Schwann cell-like differentiated adipose stem cells promote neurite outgrowth via secreted exosomes and RNA transfer. *Stem Cell Res. Ther.* 9:266.

Chinta, S. J., Woods, G., Demaria, M., Rane, A., Zou, Y., Mcquade, A., et al. (2018). Cellular senescence is induced by the environmental neurotoxin paraquat and contributes to neuropathology linked to Parkinson's Disease. *Cell Rep.* 22, 930–940. doi: 10.1016/j.celrep.2017.12.092

Chinta, S. J., Woods, G., Rane, A., Demaria, M., Campisi, J., and Andersen, J. K. (2015). Cellular senescence and the aging brain. *Exp. Gerontol.* 68, 3–7.

Choi, B. R., Lee, S. R., Han, J. S., Woo, S. K., Kim, K. M., Choi, D. H., et al. (2011). Synergistic memory impairment through the interaction of chronic cerebral hypoperfusion and amlyloid toxicity in a rat model. *Stroke* 42, 2595–2604. doi: 10.1161/strokeaha.111.620179

Chow, H. M., and Herrup, K. (2015). Genomic integrity and the ageing brain. *Nat. Rev. Neurosci.* 16, 672–684. doi: 10.1038/nrn4020

Cole, J. H., Marioni, R. E., Harris, S. E., and Deary, I. J. (2019). Brain age and other bodily 'ages': implications for neuropsychiatry. *Mol. Psychiatry* 24, 266–281. doi: 10.1038/s41380-018-0098-1

Cole, L. J., Farrell, M. J., Duff, E. P., Barber, J. B., Egan, G. F., and Gibson, S. J. (2006). Pain sensitivity and fMRI pain-related brain activity in Alzheimer's disease. *Brain* 129, 2957–2965. doi: 10.1093/brain/awl228

Collins, O., Dillon, S., Finucane, C., Lawlor, B., and Kenny, R. A. (2012). Parasympathetic autonomic dysfunction is common in mild cognitive impairment. *Neurobiol. Aging* 33, 2324–2333. doi: 10.1016/j.neurobiolaging.2011.11.017

Collins, S. M., and Bercik, P. (2013). Gut microbiota: intestinal bacteria influence brain activity in healthy humans. *Nat. Rev. Gastroenterol. Hepatol.* 10, 326–327. doi: 10.1038/nrgastro.2013.76

Conte, A., Khan, N., Defazio, G., Rothwell, J. C., and Berardelli, A. (2013). Pathophysiology of somatosensory abnormalities in Parkinson disease. *Nat. Rev. Neurol.* 9, 687–697. doi: 10.1038/nrneurol.2013.224

Coon, E. A., Cutsforth-Gregory, J. K., and Benarroch, E. E. (2018). Neuropathology of autonomic dysfunction in synucleinopathies. *Mov. Disord.* 33, 349–358. doi: 10.1002/mds.27186

Coppe, J. P., Desprez, P. Y., Krtolica, A., and Campisi, J. (2010). The senescence-associated secretory phenotype: the dark side of tumor suppression. *Annu. Rev. Pathol.* 5, 99–118. doi: 10.1146/annurev-pathol-121808-102144

Cordonnier, C. (2011). Brain microbleeds: more evidence, but still a clinical dilemma. *Curr. Opin. Neurol.* 24, 69–74. doi: 10.1097/wco.0b013e328341f8c0

Coulter, M. E., Dorobantu, C. M., Lodewijk, G. A., Delalande, F., Cianferani, S., Ganesh, V. S., et al. (2018). The ESCRT-III protein CHMP1A mediates secretion of sonic hedgehog on a distinctive subtype of extracellular vesicles. *Cell Rep.* 24, 973–986.e8. doi: 10.1016/j.celrep.2018.06.100

Crous-Bou, M., Minguillon, C., Gramunt, N., and Molinuevo, J. L. (2017). Alzheimer's disease prevention: from risk factors to early intervention. *Alzheimers Res. Ther.* 9:71.

Crowe, E. P., Tuzer, F., Gregory, B. D., Donahue, G., Gosai, S. J., Cohen, J., et al. (2016). Changes in the transcriptome of human astrocytes accompanying oxidative stress-induced senescence. *Front. Aging Neurosci.* 8:208. doi: 10.3389/fnagi.2016.00208

Dabby, R., Djaldetti, R., Shahmurov, M., Treves, T. A., Gabai, B., Melamed, E., et al. (2006). Skin biopsy for assessment of autonomic denervation in Parkinson's disease. *J. Neural Transm.* 113, 1169–1176. doi: 10.1007/s00702-005-0431-0

Dalle Pezze, P., Nelson, G., Otten, E. G., Korolchuk, V. I., Kirkwood, T. B., Von Zglinicki, T., et al. (2014). Dynamic modelling of pathways to cellular senescence reveals strategies for targeted interventions. *PLoS Comput. Biol.* 10:e1003728. doi: 10.1371/journal.pcbi.1003728

Davaapil, H., Brockes, J. P., and Yun, M. H. (2017). Conserved and novel functions of programmed cellular senescence during vertebrate development. *Development* 144, 106–114. doi: 10.1242/dev.138222

Dawson, T. M., Golde, T. E., and Lagier-Tourenne, C. (2018). Animal models of neurodegenerative diseases. *Nat. Neurosci.* 21, 1370–1379.

de Bruijn, R. F., Heeringa, J., Wolters, F. J., Franco, O. H., Stricker, B. H., Hofman, A., et al. (2015). Association between atrial fibrillation and dementia in the general population. *JAMA Neurol.* 72, 1288–1294.

de Leeuw, F. E., De Groot, J. C., Achten, E., Oudkerk, M., Ramos, L. M., Heijboer, R., et al. (2001). Prevalence of cerebral white matter lesions in elderly people: a population based magnetic resonance imaging study. The rotterdam scan study. *J. Neurol. Neurosurg. Psychiatry* 70, 9–14. doi: 10.1136/jnnp.70.1.9

Dearborn, J. L., Zhang, Y., Qiao, Y., Suri, M. F. K., Liu, L., Gottesman, R. F., et al. (2017). Intracranial atherosclerosis and dementia: the atherosclerosis risk in communities (ARIC) study. *Neurology* 88, 1556–1563. doi: 10.1212/wnl.0000000000003837

den Besten, G., Van Eunen, K., Groen, A. K., Venema, K., Reijngoud, D. J., and Bakker, B. M. (2013). The role of short-chain fatty acids in the interplay between diet, gut microbiota, and host energy metabolism. *J. Lipid Res.* 54, 2325–2340. doi: 10.1194/jlr.r036012

Deschaintre, Y., Richard, F., Leys, D., and Pasquier, F. (2009). Treatment of vascular risk factors is associated with slower decline in Alzheimer disease. *Neurology* 73, 674–680. doi: 10.1212/wnl.0b013e3181b59bf3

Dickinson, C. J. (2001). Why are strokes related to hypertension? Classic studies and hypotheses revisited. *J. Hypertens.* 19, 1515–1521. doi: 10.1097/00004872-200109000-00001

Dietzel, J., Haeusler, K. G., and Endres, M. (2018). Does atrial fibrillation cause cognitive decline and dementia? *Europace* 20, 408–419. doi: 10.1093/europace/eux031

Dirnagl, U. (1997). Metabolic aspects of neurovascular coupling. *Adv. Exp. Med. Biol.* 413, 155–159. doi: 10.1007/978-1-4899-0056-2_17

Dobbs, R. J., Charlett, A., Purkiss, A. G., Dobbs, S. M., Weller, C., and Peterson, D. W. (1999). Association of circulating TNF-alpha and IL-6 with ageing and parkinsonism. *Acta Neurol. Scand.* 100, 34–41. doi: 10.1111/j.1600-0404.1999.tb00721.x

Dolan, H., Crain, B., Troncoso, J., Resnick, S. M., Zonderman, A. B., and Obrien, R. J. (2010). Atherosclerosis, dementia, and Alzheimer disease in the baltimore longitudinal study of aging cohort. *Ann. Neurol.* 68, 231–240.

Doty, R. L. (2017). Olfactory dysfunction in neurodegenerative diseases: is there a common pathological substrate? *Lancet Neurol.* 16, 478–488. doi: 10.1016/s1474-4422(17)30123-0

Driver-Dunckley, E., Adler, C. H., Hentz, J. G., Dugger, B. N., Shill, H. A., Caviness, J. N., et al. (2014). Olfactory dysfunction in incidental Lewy body disease and Parkinson's disease. *Parkinsonism Relat. Disord.* 20, 1260–1262. doi: 10.1016/j.parkreldis.2014.08.006

Duarte, A. I., Candeias, E., Correia, S. C., Santos, R. X., Carvalho, C., Cardoso, S., et al. (2013). Crosstalk between diabetes and brain: glucagon-like peptide-1 mimetics as a promising therapy against neurodegeneration. *Biochim. Biophys. Acta* 1832, 527–541. doi: 10.1016/j.bbadis.2013.01.008

Duarte, A. I., Moreira, P. I., and Oliveira, C. R. (2012). Insulin in central nervous system: more than just a peripheral hormone. *J. Aging Res.* 2012:384017.

Duda, J. E., Shah, U., Arnold, S. E., Lee, V. M., and Trojanowski, J. Q. (1999). The expression of alpha-, beta-, and gamma-synucleins in olfactory mucosa from patients with and without neurodegenerative diseases. *Exp. Neurol.* 160, 515–522. doi: 10.1006/exnr.1999.7228

Duran-Vilaregut, J., Del Valle, J., Camins, A., Pallas, M., Pelegri, C., and Vilaplana, J. (2009). Blood-brain barrier disruption in the striatum of rats treated with 3-nitropropionic acid. *Neurotoxicology* 30, 136–143. doi: 10.1016/j.neuro.2008.10.007

Eberle, C., and Ament, C. (2012). Diabetic and metabolic programming: mechanisms altering the intrauterine milieu. *ISRN Pediatr.* 2012:975685.

El-Ansary, A. K., Ben Bacha, A., and Kotb, M. (2012). Etiology of autistic features: the persisting neurotoxic effects of propionic acid. *J. Neuroinflammation* 9:74.

Fan, X., Wheatley, E. G., and Villeda, S. A. (2017). Mechanisms of hippocampal aging and the potential for rejuvenation. *Annu. Rev. Neurosci.* 40, 251–272. doi: 10.1146/annurev-neuro-072116-031357

Faraci, F. M., and Heistad, D. D. (1998). Regulation of the cerebral circulation: role of endothelium and potassium channels. *Physiol. Rev.* 78, 53–97. doi: 10.1152/physrev.1998.78.1.53

Farrall, A. J., and Wardlaw, J. M. (2009). Blood-brain barrier: ageing and microvascular disease–systematic review and meta-analysis. *Neurobiol. Aging* 30, 337–352. doi: 10.1016/j.neurobiolaging.2007.07.015

Fevrier, B., Vilette, D., Archer, F., Loew, D., Faigle, W., Vidal, M., et al. (2004). Cells release prions in association with exosomes. *Proc. Natl. Acad. Sci. U.S.A.* 101, 9683–9688. doi: 10.1073/pnas.0308413101

Figueira, J., Jonsson, P., Nordin Adolfsson, A., Adolfsson, R., Nyberg, L., and Ohman, A. (2016). NMR analysis of the human saliva metabolome distinguishes dementia patients from matched controls. *Mol. Biosyst.* 12, 2562–2571. doi: 10.1039/c6mb00233a

Fleitas, C., Pinol-Ripoll, G., Marfull, P., Rocandio, D., Ferrer, I., Rampon, C., et al. (2018). proBDNF is modified by advanced glycation end products in Alzheimer's disease and causes neuronal apoptosis by inducing p75 neurotrophin receptor processing. *Mol. Brain* 11:68.

Forstermann, U., and Sessa, W. C. (2012). Nitric oxide synthases: regulation and function. *Eur. Heart J.* 33, 829–837 doi: 10.1093/eurheartj/ehr304

Forsyth, C. B., Shannon, K. M., Kordower, J. H., Voigt, R. M., Shaikh, M., Jaglin, J. A., et al. (2011). Increased intestinal permeability correlates with sigmoid mucosa alpha-synuclein staining and endotoxin exposure markers in early Parkinson's disease. *PLoS One* 6:e28032. doi: 10.1371/journal.pone.0028032

Fung, T. C., Olson, C. A., and Hsiao, E. Y. (2017). Interactions between the microbiota, immune and nervous systems in health and disease. *Nat. Neurosci.* 20, 145–155. doi: 10.1038/nn.4476

Gan, L., Cookson, M. R., Petrucelli, L., and La Spada, A. R. (2018). Converging pathways in neurodegeneration, from genetics to mechanisms. *Nat. Neurosci.* 21, 1300–1309. doi: 10.1038/s41593-018-0237-7

Gariepy, G., Wang, J., Lesage, A., and Schmitz, N. (2011). Obesity and the risk of disability in a 12-year cohort study: the role of psychological distress. *Soc. Psychiatry Psychiatr. Epidemiol.* 46, 1173–1179. doi: 10.1007/s00127-010-0284-1

Garner, J. P., Gaskill, B. N., Weber, E. M., Ahloy-Dallaire, J., and Pritchett-Corning, K. R. (2017). Introducing therioepistemology: the study of how knowledge is gained from animal research. *Lab Anim.* 46, 103–113. doi: 10.1038/laban.1224

GBD 2015 Neurological Disorders Collaborator Group (2017). Global, regional, and national burden of neurological disorders during 1990-2015: a systematic analysis for the global burden of disease study 2015. *Lancet Neurol.* 16, 877–897.

Gensollen, T., Iyer, S. S., Kasper, D. L., and Blumberg, R. S. (2016). How colonization by microbiota in early life shapes the immune system. *Science* 352, 539–544. doi: 10.1126/science.aad9378

Girouard, H., and Iadecola, C. (2006). Neurovascular coupling in the normal brain and in hypertension, stroke, and Alzheimer disease. *J. Appl. Physiol.* 100, 328–335. doi: 10.1152/japplphysiol.00966.2005

Gitler, A. D., Dhillon, P., and Shorter, J. (2017). Neurodegenerative disease: models, mechanisms, and a new hope. *Dis. Model Mech.* 10, 499–502. doi: 10.1242/dmm.030205

Gorelick, P. B., Scuteri, A., Black, S. E., Decarli, C., Greenberg, S. M., Iadecola, C., et al. (2011). Vascular contributions to cognitive impairment and dementia: a statement for healthcare professionals from the american heart association/american stroke association. *Stroke* 42, 2672–2713. doi: 10.1161/str.0b013e3182299496

Gouw, A. A., Seewann, A., Van Der Flier, W. M., Barkhof, F., Rozemuller, A. M., Scheltens, P., et al. (2011). Heterogeneity of small vessel disease: a systematic review of MRI and histopathology correlations. *J. Neurol. Neurosurg. Psychiatry* 82, 126–135. doi: 10.1136/jnnp.2009.204685

Govindarajan, N., Agis-Balboa, R. C., Walter, J., Sananbenesi, F., and Fischer, A. (2011). Sodium butyrate improves memory function in an Alzheimer's disease mouse model when administered at an advanced stage of disease progression. *J. Alzheimers Dis.* 26, 187–197. doi: 10.3233/jad-2011-110080

Graves, K. G., May, H. T., Jacobs, V., Bair, T. L., Stevens, S. M., Woller, S. C., et al. (2017). Atrial fibrillation incrementally increases dementia risk across all CHADS2 and CHA2DS2VASc strata in patients receiving long-term warfarin. *Am. Heart J.* 188, 93–98. doi: 10.1016/j.ahj.2017.02.026

Grey, M., Dunning, C. J., Gaspar, R., Grey, C., Brundin, P., Sparr, E., et al. (2015). Acceleration of alpha-synuclein aggregation by exosomes. *J. Biol. Chem.* 290, 2969–2982. doi: 10.1074/jbc.m114.585703

Grunert, S. C., Mullerleile, S., De Silva, L., Barth, M., Walter, M., Walter, K., et al. (2013). Propionic acidemia: clinical course and outcome in 55 pediatric and adolescent patients. *Orphanet J. Rare Dis.* 8:6. doi: 10.1186/1750-1172-8-6

Gutierrez Becker, B., Klein, T., Wachinger, C., Alzheimer's Disease Neuroimaging Initiative., The Australian Imaging Biomarkers, and Lifestyle flagship study of ageing (2018). Gaussian process uncertainty in age estimation as a measure of brain abnormality. *Neuroimage* 175, 246–258. doi: 10.1016/j.neuroimage.2018.03.075

Hallene, K. L., Oby, E., Lee, B. J., Santaguida, S., Bassanini, S., Cipolla, M., et al. (2006). Prenatal exposure to thalidomide, altered vasculogenesis, and CNS malformations. *Neuroscience* 142, 267–283. doi: 10.1016/j.neuroscience.2006.06.017

Harach, T., Marungruang, N., Duthilleul, N., Cheatham, V., Mc Coy, K. D., Frisoni, G., et al. (2017). Reduction of abeta amyloid pathology in appps1 transgenic mice in the absence of gut microbiota. *Sci. Rep.* 7:41802.

Hardie, D. G., Hawley, S. A., and Scott, J. W. (2006). AMP-activated protein kinase–development of the energy sensor concept. *J. Physiol.* 574, 7–15. doi: 10.1113/jphysiol.2006.108944

Haslam, D. W., and James, W. P. (2005). Obesity. *Lancet* 366, 1197–1209.

Helzner, E. P., Luchsinger, J. A., Scarmeas, N., Cosentino, S., Brickman, A. M., Glymour, M. M., et al. (2009). Contribution of vascular risk factors to the progression in Alzheimer disease. *Arch. Neurol.* 66, 343–348.

Henkel, J. S., Beers, D. R., Wen, S., Bowser, R., and Appel, S. H. (2009). Decreased mRNA expression of tight junction proteins in lumbar spinal cords of patients with ALS. *Neurology* 72, 1614–1616. doi: 10.1212/wnl.0b013e3181a41228

Henskens, L. H., Kroon, A. A., Van Oostenbrugge, R. J., Gronenschild, E. H., Fuss-Lejeune, M. M., Hofman, P. A., et al. (2008). Increased aortic pulse wave velocity is associated with silent cerebral small-vessel disease in hypertensive patients. *Hypertension* 52, 1120–1126. doi: 10.1161/hypertensionaha.108.119024

Hill, J. M., and Lukiw, W. J. (2015). Microbial-generated amyloids and Alzheimer's disease (AD). *Front. Aging Neurosci.* 7:9. doi: 10.3389/fnagi.2015.00009

Hofman, A., Ott, A., Breteler, M. M., Bots, M. L., Slooter, A. J., Van Harskamp, F., et al. (1997). Atherosclerosis, apolipoprotein E, and prevalence of dementia and Alzheimer's disease in the rotterdam Study. *Lancet* 349, 151–154. doi: 10.1016/s0140-6736(96)09328-2

Holm, M. M., Kaiser, J., and Schwab, M. E. (2018). Extracellular vesicles: multimodal envoys in neural maintenance and repair. *Trends Neurosci.* 41, 360–372. doi: 10.1016/j.tins.2018.03.006

Holman, C., Piper, S. K., Grittner, U., Diamantaras, A. A., Kimmelman, J., Siegerink, B., et al. (2016). Where have all the rodents gone? the effects of attrition in experimental research on cancer and stroke. *PLoS Biol.* 14:e1002331. doi: 10.1371/journal.pbio.1002331

Holmes, C., Cunningham, C., Zotova, E., Woolford, J., Dean, C., Kerr, S., et al. (2009). Systemic inflammation and disease progression in Alzheimer disease. *Neurology* 73, 768–774. doi: 10.1212/wnl.0b013e3181b6bb95

Holmes, E., Li, J. V., Athanasiou, T., Ashrafian, H., and Nicholson, J. K. (2011). Understanding the role of gut microbiome-host metabolic signal disruption in health and disease. *Trends Microbiol.* 19, 349–359. doi: 10.1016/j.tim.2011.05.006

Houlden, A., Goldrick, M., Brough, D., Vizi, E. S., Lenart, N., Martinecz, B., et al. (2016). Brain injury induces specific changes in the caecal microbiota of mice via altered autonomic activity and mucoprotein production. *Brain Behav. Immun.* 57, 10–20. doi: 10.1016/j.bbi.2016.04.003

Howitt, J., and Hill, A. F. (2016). Exosomes in the pathology of neurodegenerative diseases. *J. Biol. Chem.* 291, 26589–26597. doi: 10.1074/jbc.r116.757955

Hoyles, L., Snelling, T., Umlai, U. K., Nicholson, J. K., Carding, S. R., Glen, R. C., et al. (2018). Microbiome-host systems interactions: protective effects of propionate upon the blood-brain barrier. *Microbiome* 6:55.

Hryhorczuk, C., Sharma, S., and Fulton, S. E. (2013). Metabolic disturbances connecting obesity and depression. *Front. Neurosci.* 7:177. doi: 10.3389/fnins.2013.00177

Hsu, D., and Marshall, G. A. (2017). Primary and secondary prevention trials in Alzheimer disease: looking back, Moving Forward. *Curr. Alzheimer Res.* 14, 426–440.

Hufeldt, M. R., Nielsen, D. S., Vogensen, F. K., Midtvedt, T., and Hansen, A. K. (2010). Variation in the gut microbiota of laboratory mice is related to both genetic and environmental factors. *Comp. Med.* 60, 336–347.

Iadecola, C. (2004). Neurovascular regulation in the normal brain and in Alzheimer's disease. *Nat. Rev. Neurosci.* 5, 347–360. doi: 10.1038/nrn1387

Iadecola, C. (2013). The pathobiology of vascular dementia. *Neuron* 80, 844–866. doi: 10.1016/j.neuron.2013.10.008

Iadecola, C. (2017). The neurovascular unit coming of age: a journey through neurovascular coupling in health and disease. *Neuron* 96, 17–42. doi: 10.1016/j.neuron.2017.07.030

Idiaquez, J., and Roman, G. C. (2011). Autonomic dysfunction in neurodegenerative dementias. *J. Neurol. Sci.* 305, 22–27. doi: 10.1016/j.jns.2011.02.033

International Health Conference (2002). Constitution of the World Health Organization. 1946. *Bull. World Health Organ.* 80, 983–984.

Itzhaki, R. F., Lathe, R., Balin, B. J., Ball, M. J., Bearer, E. L., Braak, H., et al. (2016). Microbes and Alzheimer's disease. *J. Alzheimers Dis.* 51, 979–984.

Jellinger, K. A. (2010). Prevalence and impact of cerebrovascular lesions in Alzheimer and lewy body diseases. *Neurodegener. Dis.* 7, 112–115. doi: 10.1159/000285518

Jennings, J. R., Muldoon, M. F., Ryan, C., Price, J. C., Greer, P., Sutton-Tyrrell, K., et al. (2005). Reduced cerebral blood flow response and compensation among patients with untreated hypertension. *Neurology* 64, 1358–1365. doi: 10.1212/01.wnl.0000158283.28251.3c

Jessen, N. A., Munk, A. S., Lundgaard, I., and Nedergaard, M. (2015). The glymphatic system: a beginner's guide. *Neurochem. Res.* 40, 2583–2599.

Jia, L., Chopp, M., Wang, L., Lu, X., Szalad, A., and Zhang, Z. G. (2018). Exosomes derived from high-glucose-stimulated schwann cells promote development of diabetic peripheral neuropathy. *FASEB J.* doi: 10.1096/fj.201800597R. [Epub ahead of print].

Joachim, C. L., Mori, H., and Selkoe, D. J. (1989). Amyloid beta-protein deposition in tissues other than brain in Alzheimer's disease. *Nature* 341, 226–230. doi: 10.1038/341226a0

Jucker, M. (2010). The benefits and limitations of animal models for translational research in neurodegenerative diseases. *Nat. Med.* 16, 1210–1214. doi: 10.1038/nm.2224

Kalaria, R. N. (2010). Vascular basis for brain degeneration: faltering controls and risk factors for dementia. *Nutr. Rev.* 68(Suppl 2), S74–87.

Kamel, H., Okin, P. M., Elkind, M. S., and Iadecola, C. (2016). Atrial fibrillation and mechanisms of stroke: time for a new model. *Stroke* 47, 895–900. doi: 10.1161/strokeaha.115.012004

Karlsson, F. H., Fak, F., Nookaew, I., Tremaroli, V., Fagerberg, B., Petranovic, D., et al. (2012). Symptomatic atherosclerosis is associated with an altered gut metagenome. *Nat. Commun.* 3:1245.

Kilkenny, C., Browne, W. J., Cuthill, I. C., Emerson, M., and Altman, D. G. (2010). Improving bioscience research reporting: the arrive guidelines for reporting animal research. *PLoS Biol.* 8:e1000412. doi: 10.1371/journal.pbio.1000412

Kim, J. Y., Rasheed, A., Yoo, S. J., Kim, S. Y., Cho, B., Son, G., et al. (2018). Distinct amyloid precursor protein processing machineries of the olfactory system. *Biochem. Biophys. Res. Commun.* 495, 533–538. doi: 10.1016/j.bbrc.2017.10.153

Kim, K. J., Ramiro Diaz, J., Iddings, J. A., and Filosa, J. A. (2016). Vasculo-neuronal coupling: retrograde vascular communication to brain neurons. *J. Neurosci.* 36, 12624–12639. doi: 10.1523/jneurosci.1300-16.2016

Kirkland, J. L., and Tchkonia, T. (2017). Cellular senescence: a translational perspective. *EBioMedicine* 21, 21–28. doi: 10.1016/j.ebiom.2017.04.013

Kisler, K., Nelson, A. R., Montagne, A., and Zlokovic, B. V. (2017). Cerebral blood flow regulation and neurovascular dysfunction in Alzheimer disease. *Nat. Rev. Neurosci.* 18, 419–434. doi: 10.1038/nrn.2017.48

Klein, P., and Tyrlikova, I. (2017). Prevention of epilepsy: should we be avoiding clinical trials? *Epilepsy Behav.* 72, 188–194. doi: 10.1016/j.yebeh.2017.05.024

Knopman, D., Boland, L. L., Mosley, T., Howard, G., Liao, D., Szklo, M., et al. (2001). Cardiovascular risk factors and cognitive decline in middle-aged adults. *Neurology* 56, 42–48. doi: 10.1212/wnl.56.1.42

Koike, M. A., Green, K. N., Blurton-Jones, M., and Laferla, F. M. (2010). Oligemic hypoperfusion differentially affects tau and amyloid-{beta}. *Am. J. Pathol.* 177, 300–310. doi: 10.2353/ajpath.2010.090750

Koles, K., Nunnari, J., Korkut, C., Barria, R., Brewer, C., Li, Y., et al. (2012). Mechanism of evenness interrupted (Evi)-exosome release at synaptic boutons. *J. Biol. Chem.* 287, 16820–16834. doi: 10.1074/jbc.m112.342667

Korhonen, P., Malm, T., and White, A. R. (2018). 3D human brain cell models: new frontiers in disease understanding and drug discovery for neurodegenerative diseases. *Neurochem. Int.* 120, 191–199. doi: 10.1016/j.neuint.2018.08.012

Korkut, C., Ataman, B., Ramachandran, P., Ashley, J., Barria, R., Gherbesi, N., et al. (2009). Trans-synaptic transmission of vesicular Wnt signals through Evi/Wntless. *Cell* 139, 393–404. doi: 10.1016/j.cell.2009.07.051

Korkut, C., Li, Y., Koles, K., Brewer, C., Ashley, J., Yoshihara, M., et al. (2013). Regulation of postsynaptic retrograde signaling by presynaptic exosome release. *Neuron* 77, 1039–1046. doi: 10.1016/j.neuron.2013.01.013

Kountouras, J., Boziki, M., Gavalas, E., Zavos, C., Grigoriadis, N., Deretzi, G., et al. (2009). Eradication of *helicobacter* pylori may be beneficial in the management of Alzheimer's disease. *J. Neurol.* 256, 758–767.

Kreutzmann, J. C., Havekes, R., Abel, T., and Meerlo, P. (2015). Sleep deprivation and hippocampal vulnerability: changes in neuronal plasticity, neurogenesis and cognitive function. *Neuroscience* 309, 173–190. doi: 10.1016/j.neuroscience.2015.04.053

Kritsilis, M., Sophia, V. R., Koutsoudaki, P. N., Evangelou, K., Gorgoulis, V. G., and Papadopoulos, D. (2018). Ageing, cellular senescence and neurodegenerative disease. *Int. J. Mol. Sci.* 19:E2937.

Kupsky, W. J., Grimes, M. M., Sweeting, J., Bertsch, R., and Cote, L. J. (1987). Parkinson's disease and megacolon: concentric hyaline inclusions (Lewy bodies) in enteric ganglion cells. *Neurology* 37, 1253–1255.

Lachenal, G., Pernet-Gallay, K., Chivet, M., Hemming, F. J., Belly, A., Bodon, G., et al. (2011). Release of exosomes from differentiated neurons and its regulation by synaptic glutamatergic activity. *Mol. Cell. Neurosci.* 46, 409–418. doi: 10.1016/j.mcn.2010.11.004

Larsson, S. C., and Markus, H. S. (2018). Does treating vascular risk factors prevent dementia and Alzheimer's disease? a systematic review and meta-analysis. *J. Alzheimers Dis.* 64, 657–668. doi: 10.3233/jad-180288

Launer, L. J., Ross, G. W., Petrovitch, H., Masaki, K., Foley, D., White, L. R., et al. (2000). Midlife blood pressure and dementia: the honolulu-asia aging study. *Neurobiol. Aging* 21, 49–55. doi: 10.1016/s0197-4580(00)00096-8

Lebouvier, T., Chaumette, T., Paillusson, S., Duyckaerts, C., Bruley Des Varannes, S., Neunlist, M., et al. (2009). The second brain and Parkinson's disease. *Eur. J. Neurosci.* 30, 735–741.

Lee, C. H., and Yoon, H. J. (2017). Medical big data: promise and challenges. *Kidney Res. Clin. Pract.* 36, 3–11. doi: 10.23876/j.krcp.2017.36.1.3

Lee, J. W., Lee, Y. K., Yuk, D. Y., Choi, D. Y., Ban, S. B., Oh, K. W., et al. (2008). Neuro-inflammation induced by lipopolysaccharide causes cognitive impairment through enhancement of beta-amyloid generation. *J. Neuroinflammation* 5:37. doi: 10.1186/1742-2094-5-37

Lee, M. J., Seo, S. W., Na, D. L., Kim, C., Park, J. H., Kim, G. H., et al. (2014). Synergistic effects of ischemia and beta-amyloid burden on cognitive decline in patients with subcortical vascular mild cognitive impairment. *JAMA Psychiatry* 71, 412–422.

Lee, S. H., Shin, S. M., Zhong, P., Kim, H. T., Kim, D. I., Kim, J. M., et al. (2018). Reciprocal control of excitatory synapse numbers by Wnt and Wnt inhibitor PRR7 secreted on exosomes. *Nat. Commun.* 9:3434.

Lema Tome, C. M., Tyson, T., Rey, N. L., Grathwohl, S., Britschgi, M., and Brundin, P. (2013). Inflammation and alpha-synuclein's prion-like behavior in Parkinson's disease–is there a link? *Mol. Neurobiol.* 47, 561–574.

Li, D. Y., and Tang, W. H. W. (2017). Gut microbiota and atherosclerosis. *Curr. Atheroscler. Rep.* 19:39.

Li, J. J., Wang, B., Kodali, M. C., Chen, C., Kim, E., Patters, B. J., et al. (2018). In vivo evidence for the contribution of peripheral circulating inflammatory exosomes to neuroinflammation. *J. Neuroinflammation* 15:8.

Li, L. M., Kilbourn, R. G., Adams, J., and Fidler, I. J. (1991). Role of nitric oxide in lysis of tumor cells by cytokine-activated endothelial cells. *Cancer Res.* 51, 2531–2535.

Li, Q., Han, Y., Dy, A. B. C., and Hagerman, R. J. (2017). The gut microbiota and autism spectrum disorders. *Front. Cell. Neurosci.* 11:120. doi: 10.3389/fncel.2017.00120

Liddell, J. R. (2017). Are astrocytes the predominant cell type for activation of nrf2 in aging and neurodegeneration? *Antioxidants* 6:E65

Lim, S. S., Vos, T., Flaxman, A. D., Danaei, G., Shibuya, K., Adair-Rohani, H., et al. (2012). A comparative risk assessment of burden of disease and injury attributable to 67 risk factors and risk factor clusters in 21 regions, 1990-2010: a systematic analysis for the global burden of disease study 2010. *Lancet* 380, 2224–2260.

Little, C. S., Joyce, T. A., Hammond, C. J., Matta, H., Cahn, D., Appelt, D. M., et al. (2014). Detection of bacterial antigens and Alzheimer's disease-like pathology in the central nervous system of BALB/c mice following intranasal infection with a laboratory isolate of *Chlamydia pneumoniae*. *Front. Aging Neurosci.* 6:304. doi: 10.3389/fnagi.2014.00304

Liu, J., Sun, J., Wang, F., Yu, X., Ling, Z., Li, H., et al. (2015). Neuroprotective effects of clostridium butyricum against vascular dementia in mice via metabolic butyrate. *Biomed Res. Int.* 2015:412946.

Livingston, G., Sommerlad, A., Orgeta, V., Costafreda, S. G., Huntley, J., Ames, D., et al. (2017). Dementia prevention, intervention, and care. *Lancet* 390, 2673–2734.

Lloret-Villas, A., Varusai, T. M., Juty, N., Laibe, C., Le Novere, N., Hermjakob, H., et al. (2017). The impact of mathematical modeling in understanding the mechanisms underlying neurodegeneration: evolving dimensions and future directions. *CPT Pharmacometrics Syst. Pharmacol.* 6, 73–86. doi: 10.1002/psp4.12155

Lopez-Verrilli, M. A., Caviedes, A., Cabrera, A., Sandoval, S., Wyneken, U., and Khoury, M. (2016). Mesenchymal stem cell-derived exosomes from different sources selectively promote neuritic outgrowth. *Neuroscience* 320, 129–139. doi: 10.1016/j.neuroscience.2016.01.061

Lopez-Verrilli, M. A., Picou, F., and Court, F. A. (2013). Schwann cell-derived exosomes enhance axonal regeneration in the peripheral nervous system. *Glia* 61, 1795–1806. doi: 10.1002/glia.22558

Lucas, S. M., Rothwell, N. J., and Gibson, R. M. (2006). The role of inflammation in CNS injury and disease. *Br. J. Pharmacol.* 147 Suppl 1, S232-S240.

Lusis, A. J. (2000). Atherosclerosis. *Nature* 407, 233–241.

MacMahon, S., Peto, R., Cutler, J., Collins, R., Sorlie, P., Neaton, J., et al. (1990). Blood pressure, stroke, and coronary heart disease. Part 1, prolonged differences in blood pressure: prospective observational studies corrected for the regression dilution bias. Lancet 335, 765–774. doi: 10.1016/0140-6736(90)90878-9

Maheshwari, P., and Eslick, G. D. (2015). Bacterial infection and Alzheimer's disease: a meta-analysis. *J. Alzheimers. Dis.* 43, 957–966. doi: 10.3233/jad-140621

Maldonado, R. F., Sa-Correia, I., and Valvano, M. A. (2016). Lipopolysaccharide modification in Gram-negative bacteria during chronic infection. *FEMS Microbiol. Rev.* 40, 480–493. doi: 10.1093/femsre/fuw007

Manwani, B., Liu, F., Scranton, V., Hammond, M. D., Sansing, L. H., and Mccullough, L. D. (2013). Differential effects of aging and sex on stroke induced

inflammation across the lifespan. *Exp. Neurol.* 249, 120–131. doi: 10.1016/j.expneurol.2013.08.011

Marin, C., Vilas, D., Langdon, C., Alobid, I., Lopez-Chacon, M., Haehner, A., et al. (2018). Olfactory dysfunction in neurodegenerative diseases. *Curr. Allergy Asthma Rep.* 18:42.

Martinez-Ramirez, S., Pontes-Neto, O. M., Dumas, A. P., Auriel, E., Halpin, A., Quimby, M., et al. (2013). Topography of dilated perivascular spaces in subjects from a memory clinic cohort. *Neurology* 80, 1551–1556. doi: 10.1212/wnl.0b013e31828f1876

Mattson, M. P., Pedersen, W. A., Duan, W., Culmsee, C., and Camandola, S. (1999). Cellular and molecular mechanisms underlying perturbed energy metabolism and neuronal degeneration in Alzheimer's and Parkinson's diseases. *Ann. N. Y. Acad. Sci.* 893, 154–175. doi: 10.1111/j.1749-6632.1999.tb07824.x

McKinney, W. T. Jr., and Bunney, W. E. Jr. (1969). Animal model of depression. I. Review of evidence: implications for research. *Arch. Gen. Psychiatry* 21, 240–248.

Mergenthaler, P., Dirnagl, U., and Meisel, A. (2004). Pathophysiology of stroke: lessons from animal models. *Metab. Brain Dis.* 19, 151–167. doi: 10.1023/b:mebr.0000043966.46964.e6

Mergenthaler, P., and Meisel, A. (2012). Do stroke models model stroke? Dis Model Mech 5, 718–725. doi: 10.1242/dmm.010033

Mhatre, M., Nguyen, A., Kashani, S., Pham, T., Adesina, A., and Grammas, P. (2004). Thrombin, a mediator of neurotoxicity and memory impairment. *Neurobiol. Aging* 25, 783–793. doi: 10.1016/s0197-4580(03)00192-1

Mills, S., Cain, J., Purandare, N., and Jackson, A. (2007). Biomarkers of cerebrovascular disease in dementia. *Br. J. Radiol.* 80 Spec No 2, S128-S145.

Minamiyama, M., Katsuno, M., Adachi, H., Waza, M., Sang, C., Kobayashi, Y., et al. (2004). Sodium butyrate ameliorates phenotypic expression in a transgenic mouse model of spinal and bulbar muscular atrophy. *Hum. Mol. Genet.* 13, 1183–1192. doi: 10.1093/hmg/ddh131

Minato, T., Maeda, T., Fujisawa, Y., Tsuji, H., Nomoto, K., Ohno, K., et al. (2017). Progression of Parkinson's disease is associated with gut dysbiosis: two-year follow-up study. *PLoS One* 12:e0187307. doi: 10.1371/journal.pone.0187307

Minter, M. R., Zhang, C., Leone, V., Ringus, D. L., Zhang, X., Oyler-Castrillo, P., et al. (2016). Antibiotic-induced perturbations in gut microbial diversity influences neuro-inflammation and amyloidosis in a murine model of Alzheimer's disease. *Sci. Rep.* 6:30028.

Mondadori, C. R., Buchmann, A., Mustovic, H., Schmidt, C. F., Boesiger, P., Nitsch, R. M., et al. (2006). Enhanced brain activity may precede the diagnosis of Alzheimer's disease by 30 years. *Brain* 129, 2908–2922. doi: 10.1093/brain/awl266

Moore, C. I., and Cao, R. (2008). The hemo-neural hypothesis: on the role of blood flow in information processing. *J. Neurophysiol.* 99, 2035–2047. doi: 10.1152/jn.01366.2006

Morsi, M., Maher, A., Aboelmagd, O., Johar, D., and Bernstein, L. (2018). A shared comparison of diabetes mellitus and neurodegenerative disorders. *J. Cell Biochem.* 119, 1249–1256. doi: 10.1002/jcb.26261

Mueller, S., Saunier, K., Hanisch, C., Norin, E., Alm, L., Midtvedt, T., et al. (2006). Differences in fecal microbiota in different European study populations in relation to age, gender, and country: a cross-sectional study. *Appl. Environ. Microbiol.* 72, 1027–1033. doi: 10.1128/aem.72.2.1027-1033.2006

Mukherjee, S., Klaus, C., Pricop-Jeckstadt, M., Miller, J. A., and Struebing, F. L. (2019). A microglial signature directing human aging and neurodegeneration-related gene networks. *Front. Neurosci.* 13:2. doi: 10.3389/fnins.2019.00002

Munoz-Espin, D., and Serrano, M. (2014). Cellular senescence: from physiology to pathology. *Nat. Rev. Mol. Cell Biol.* 15, 482–496. doi: 10.1038/nrm3823

Nelson, A. R., Sweeney, M. D., Sagare, A. P., and Zlokovic, B. V. (2016). Neurovascular dysfunction and neurodegeneration in dementia and Alzheimer's disease. *Biochim. Biophys. Acta* 1862, 887–900. doi: 10.1016/j.bbadis.2015.12.016

Nishihira, Y., Tan, C. F., Onodera, O., Toyoshima, Y., Yamada, M., Morita, T., et al. (2008). Sporadic amyotrophic lateral sclerosis: two pathological patterns shown by analysis of distribution of TDP-43-immunoreactive neuronal and glial cytoplasmic inclusions. *Acta Neuropathol.* 116, 169–182. doi: 10.1007/s00401-008-0385-z

Nishtala, A., Piers, R. J., Himali, J. J., Beiser, A. S., Davis-Plourde, K. L., Saczynski, J. S., et al. (2018). Atrial fibrillation and cognitive decline in the framingham heart study. *Heart Rhythm* 15, 166–172. doi: 10.1016/j.hrthm.2017.09.036

Nolano, M., Provitera, V., Estraneo, A., Selim, M. M., Caporaso, G., Stancanelli, A., et al. (2008). Sensory deficit in Parkinson's disease: evidence of a cutaneous denervation. *Brain* 131, 1903–1911. doi: 10.1093/brain/awn102

Ogrodnik, M., Zhu, Y., Langhi, L. G. P., Tchkonia, T., Kruger, P., Fielder, E., et al. (2019). Obesity-induced cellular senescence drives anxiety and impairs neurogenesis. Cell Metab. 29(5), 1061-1077.e8

Olsson, B., Lautner, R., Andreasson, U., Ohrfelt, A., Portelius, E., Bjerke, M., et al. (2016). CSF and blood biomarkers for the diagnosis of Alzheimer's disease: a systematic review and meta-analysis. *Lancet Neurol.* 15, 673–684. doi: 10.1016/s1474-4422(16)00070-3

Olufadi, R., and Byrne, C. D. (2008). Clinical and laboratory diagnosis of the metabolic syndrome. *J. Clin. Pathol.* 61, 697–706. doi: 10.1136/jcp.2007.048363

Oost, W., Talma, N., Meilof, J. F., and Laman, J. D. (2018). Targeting senescence to delay progression of multiple sclerosis. *J. Mol. Med.* 96, 1153–1166. doi: 10.1007/s00109-018-1686-x

Org, E., Blum, Y., Kasela, S., Mehrabian, M., Kuusisto, J., Kangas, A. J., et al. (2017). Relationships between gut microbiota, plasma metabolites, and metabolic syndrome traits in the METSIM cohort. *Genome Biol.* 18:70.

Orimo, S., Amino, T., Yokochi, M., Kojo, T., Uchihara, T., Takahashi, A., et al. (2005). Preserved cardiac sympathetic nerve accounts for normal cardiac uptake of MIBG in PARK2. *Mov. Disord.* 20, 1350–1353. doi: 10.1002/mds.20594

Orock, A., Logan, S., and Deak, F. (2019). Age-related cognitive impairment: role of reduced synaptobrevin-2 levels in memory and synaptic plasticity deficits. *J. Gerontol. A Biol. Sci. Med. Sci.* doi: 10.1093/gerona/glz013 [Epub ahead of print].

Ozkor, M. A., and Quyyumi, A. A. (2011). Endothelium-derived hyperpolarizing factor and vascular function. *Cardiol. Res. Pract.* 2011:156146.

Park, J. Y., Choi, J., Lee, Y., Lee, J. E., Lee, E. H., Kwon, H. J., et al. (2017). Metagenome analysis of bodily microbiota in a mouse model of Alzheimer disease using bacteria-derived membrane vesicles in blood. *Exp. Neurobiol.* 26, 369–379.

Pastuzyn, E. D., Day, C. E., Kearns, R. B., Kyrke-Smith, M., Taibi, A. V., Mccormick, J., et al. (2018). The neuronal gene arc encodes a repurposed retrotransposon gag protein that mediates intercellular RNA transfer. *Cell* 172, 275-288.e18.

Pellegrinelli, V., Peirce, V. J., Howard, L., Virtue, S., Turei, D., Senzacqua, M., et al. (2018). Adipocyte-secreted BMP8b mediates adrenergic-induced remodeling of the neuro-vascular network in adipose tissue. *Nat. Commun.* 9:4974.

Percie du Sert, N., Alfieri, A., Allan, S. M., Carswell, H. V., Deuchar, G. A., Farr, T. D., et al. (2017). The improve guidelines (Ischaemia models: procedural refinements of in vivo experiments). *J. Cereb. Blood Flow Metab.* 37, 3488–3517. doi: 10.1177/0271678x17709185

Petcu, E. B., Sfredel, V., Platt, D., Herndon, J. G., Kessler, C., and Popa-Wagner, A. (2008). Cellular and molecular events underlying the dysregulated response of the aged brain to stroke: a mini-review. *Gerontology* 54, 6–17. doi: 10.1159/000112845

Pfeiffer, R. F. (2016). Non-motor symptoms in Parkinson's disease. *Parkinsonism Relat. Disord.* 22(Suppl 1), S119-S122.

Poels, M. M. F., Zaccai, K., Verwoert, G. C., Vernooij, M. W., Hofman, A., van der Lugt, A., et al. (2012). Arterial stiffness and cerebral small vessel disease: the rotterdam scan study. *Stroke* 43, 2637–2642. doi: 10.1161/strokeaha.111.642264

Polanco, J. C., Scicluna, B. J., Hill, A. F., and Gotz, J. (2016). Extracellular vesicles isolated from the brains of rTg4510 mice seed tau protein aggregation in a threshold-dependent manner. *J. Biol. Chem.* 291, 12445–12466. doi: 10.1074/jbc.m115.709485

Popa-Wagner, A., Buga, A. M., and Kokaia, Z. (2011). Perturbed cellular response to brain injury during aging. *Ageing Res. Rev.* 10, 71–79. doi: 10.1016/j.arr.2009.10.008

Popa-Wagner, A., Carmichael, S. T., Kokaia, Z., Kessler, C., and Walker, L. C. (2007). The response of the aged brain to stroke: too much, too soon? *Curr. Neurovasc. Res.* 4, 216–227. doi: 10.2174/156720207781387213

Popa-Wagner, A., Pirici, D., Petcu, E. B., Mogoanta, L., Buga, A. M., Rosen, C. L., et al. (2010). Pathophysiology of the vascular wall and its relevance for cerebrovascular disorders in aged rodents. *Curr. Neurovasc. Res.* 7, 251–267. doi: 10.2174/156720210792231813

Postuma, R. B., Adler, C. H., Dugger, B. N., Hentz, J. G., Shill, H. A., Driver-Dunckley, E., et al. (2015). REM sleep behavior disorder and neuropathology in Parkinson's disease. *Mov. Disord.* 30, 1413–1417.

Przedborski, S., Vila, M., and Jackson-Lewis, V. (2003). Neurodegeneration: what is it and where are we? *J. Clin. Invest.* 111, 3–10.

Purves, D. (1988). *Body and Brain: A Trophic Theory of Neural Connections*. Cambridge, MA: Harvard University Press.

Qureshi, I. A., and Mehler, M. F. (2013). Towards a 'systems'-level understanding of the nervous system and its disorders. *Trends Neurosci.* 36, 674–684. doi: 10.1016/j.tins.2013.07.003

Racosta, J. M., Kimpinski, K., Morrow, S. A., and Kremenchutzky, M. (2015). Autonomic dysfunction in multiple sclerosis. *Auton. Neurosci.* 193, 1–6. doi: 10.1016/j.autneu.2015.06.001

Ramirez, J., Berezuk, C., Mcneely, A. A., Scott, C. J., Gao, F., and Black, S. E. (2015). Visible virchow-robin spaces on magnetic resonance imaging of Alzheimer's disease patients and normal elderly from the sunnybrook dementia study. *J. Alzheimers. Dis.* 43, 415–424. doi: 10.3233/jad-132528

Ransohoff, R. M. (2018). All (animal) models (of neurodegeneration) are wrong. Are they also useful? *J. Exp. Med.* 215, 2955–2958. doi: 10.1084/jem.20182042

Rao, M., and Gershon, M. D. (2016). The bowel and beyond: the enteric nervous system in neurological disorders. *Nat. Rev. Gastroenterol. Hepatol.* 13, 517–528. doi: 10.1038/nrgastro.2016.107

Raskov, H., Burcharth, J., Pommergaard, H. C., and Rosenberg, J. (2016). Irritable bowel syndrome, the microbiota and the gut-brain axis. *Gut Microbes* 7, 365–383. doi: 10.1080/19490976.2016.1218585

Rawji, K. S., Mishra, M. K., Michaels, N. J., Rivest, S., Stys, P. K., and Yong, V. W. (2016). Immunosenescence of microglia and macrophages: impact on the ageing central nervous system. *Brain* 139, 653–661. doi: 10.1093/brain/awv395

Reichling, D. B., and Levine, J. D. (2011). Pain and death: neurodegenerative disease mechanisms in the nociceptor. *Ann. Neurol.* 69, 13–21. doi: 10.1002/ana.22351

Reitz, C., Tang, M. X., Manly, J., Mayeux, R., and Luchsinger, J. A. (2007). Hypertension and the risk of mild cognitive impairment. *Arch. Neurol.* 64, 1734–1740.

Rey, N. L., Wesson, D. W., and Brundin, P. (2018). The olfactory bulb as the entry site for prion-like propagation in neurodegenerative diseases. *Neurobiol. Dis.* 109, 226–248. doi: 10.1016/j.nbd.2016.12.013

Ridder, K., Keller, S., Dams, M., Rupp, A. K., Schlaudraff, J., Del Turco, D., et al. (2014). Extracellular vesicle-mediated transfer of genetic information between the hematopoietic system and the brain in response to inflammation. *PLoS Biol.* 12:e1001874. doi: 10.1371/journal.pbio.1001874

Rios-Covian, D., Ruas-Madiedo, P., Margolles, A., Gueimonde, M., De Los Reyes-Gavilan, C. G., and Salazar, N. (2016). Intestinal short chain fatty acids and their link with diet and human health. *Front. Microbiol.* 7:185. doi: 10.3389/fmicb.2016.00185

Ritzel, R. M., Lai, Y. J., Crapser, J. D., Patel, A. R., Schrecengost, A., Grenier, J. M., et al. (2018). Aging alters the immunological response to ischemic stroke. *Acta Neuropathol.* 136, 89–110. doi: 10.1007/s00401-018-1859-2

Robbins, J. P., and Price, J. (2017). Human induced pluripotent stem cells as a research tool in Alzheimer's disease. *Psychol. Med.* 47, 2587–2592. doi: 10.1017/s0033291717002124

Roberts, R. C., Farmer, C. B., and Walker, C. K. (2018). "The human brain microbiome; there are bacteria in our brains!," *Conference Report at the Society for Neuroscience Meeting*, San Diego, CA.

Rogers, J., Zornetzer, S. F., Bloom, F. E., and Mervis, R. E. (1984). Senescent microstructural changes in rat cerebellum. *Brain Res.* 292, 23–32. doi: 10.1016/0006-8993(84)90886-2

Roquer, J., Segura, T., Serena, J., and Castillo, J. (2009). Endothelial dysfunction, vascular disease and stroke: the ARTICO study. *Cerebrovasc. Dis.* 27 (Suppl 1), 25–37. doi: 10.1159/000200439

Roriz-Filho, J. S., Sa-Roriz, T. M., Rosset, I., Camozzato, A. L., Santos, A. C., Chaves, M. L., et al. (2009). (Pre)diabetes, brain aging, and cognition. *Biochim. Biophys. Acta* 1792, 432–443.

Roy, C. S., and Sherrington, C. S. (1890). On the regulation of the blood-supply of the brain. *J. Physiol.* 11, 85-158.17.

Ruitenberg, A., Den Heijer, T., Bakker, S. L., Van Swieten, J. C., Koudstaal, P. J., Hofman, A., et al. (2005). Cerebral hypoperfusion and clinical onset of dementia: the rotterdam study. *Ann. Neurol.* 57, 789–794. doi: 10.1002/ana.20493

Ryden, L., Zettergren, A., Seidu, N. M., Guo, X., Kern, S., Blennow, K., et al. (2019). Atrial fibrillation increases the risk of dementia amongst older adults even in the absence of stroke. *J. Intern. Med.* 286, 101–110

Sadoshima, S., Busija, D. W., and Heistad, D. D. (1983). Mechanisms of protection against stroke in stroke-prone spontaneously hypertensive rats. *Am. J. Physiol.* 244, H406–412.

Saha, A. R., Ninkina, N. N., Hanger, D. P., Anderton, B. H., Davies, A. M., and Buchman, V. L. (2000). Induction of neuronal death by alpha-synuclein. *Eur. J. Neurosci.* 12, 3073–3077. doi: 10.1046/j.1460-9568.2000.00210.x

Salminen, A., Ojala, J., Kaarniranta, K., Haapasalo, A., Hiltunen, M., and Soininen, H. (2011). Astrocytes in the aging brain express characteristics of senescence-associated secretory phenotype. *Eur. J. Neurosci.* 34, 3–11. doi: 10.1111/j.1460-9568.2011.07738.x

Sanchez-Tapia, M., Aguilar-Lopez, M., Perez-Cruz, C., Pichardo-Ontiveros, E., Wang, M., Donovan, S. M., et al. (2017). Nopal (*Opuntia ficus indica*) protects from metabolic endotoxemia by modifying gut microbiota in obese rats fed high fat/sucrose diet. *Sci. Rep.* 7:4716.

Sanguinetti, E., Collado, M. C., Marrachelli, V. G., Monleon, D., Selma-Royo, M., Pardo-Tendero, M. M., et al. (2018). Microbiome-metabolome signatures in mice genetically prone to develop dementia, fed a normal or fatty diet. *Sci. Rep.* 8:4907.

Scheltens, P., Barkhof, F., Leys, D., Wolters, E. C., Ravid, R., and Kamphorst, W. (1995). Histopathologic correlates of white matter changes on MRI in alzheimer's disease and normal aging. *Neurology* 45, 883–888. doi: 10.1212/wnl.45.5.883

Schmidt, H. H., and Walter, U. (1994). NO at work. *Cell* 78, 919–925.

Seib, D. R., and Martin-Villalba, A. (2015). Neurogenesis in the normal ageing hippocampus: a mini-review. *Gerontology* 61, 327–335. doi: 10.1159/000368575

Selvarajah, J., Scott, M., Stivaros, S., Hulme, S., Georgiou, R., Rothwell, N., et al. (2009). Potential surrogate markers of cerebral microvascular angiopathy in asymptomatic subjects at risk of stroke. *Eur. Radiol.* 19, 1011–1018. doi: 10.1007/s00330-008-1202-8

Sender, R., Fuchs, S., and Milo, R. (2016). Revised estimates for the number of human and bacteria cells in the body. *PLoS Biol.* 14:e1002533. doi: 10.1371/journal.pbio.1002533

Shankle, W. R., Landing, B. H., Ang, S. M., Chui, H., Villarreal-Engelhardt, G., and Zarow, C. (1993). Studies of the enteric nervous system in Alzheimer disease and other dementias of the elderly: enteric neurons in Alzheimer disease. *Mod. Pathol.* 6, 10–14.

Shen, L., Liu, L., and Ji, H. F. (2017). Alzheimer's disease histological and behavioral manifestations in transgenic mice correlate with specific gut microbiome state. *J. Alzheimers. Dis.* 56, 385–390. doi: 10.3233/jad-160884

Shiue, S. J., Rau, R. H., Shiue, H. S., Hung, Y. W., Li, Z. X., Yang, K. D., et al. (2019). Mesenchymal stem cell exosomes as a cell-free therapy for nerve injury-induced pain in rats. *Pain* 160, 210–223. doi: 10.1097/j.pain.0000000000001395

Silvestrini, M., Pasqualetti, P., Baruffaldi, R., Bartolini, M., Handouk, Y., Matteis, M., et al. (2006). Cerebrovascular reactivity and cognitive decline in patients with Alzheimer disease. *Stroke* 37, 1010–1015. doi: 10.1161/01.str.0000206439.62025.97

Simeoli, R., Montague, K., Jones, H. R., Castaldi, L., Chambers, D., Kelleher, J. H., et al. (2017). Exosomal cargo including microRNA regulates sensory neuron to macrophage communication after nerve trauma. *Nat. Commun.* 8:1778.

Singh, V., Roth, S., Llovera, G., Sadler, R., Garzetti, D., Stecher, B., et al. (2016). Microbiota dysbiosis controls the neuroinflammatory response after stroke. *J. Neurosci.* 36, 7428–7440. doi: 10.1523/jneurosci.1114-16.2016

Singh, V., Sadler, R., Heindl, S., Llovera, G., Roth, S., Benakis, C., et al. (2018). The gut microbiome primes a cerebroprotective immune response after stroke. *J. Cereb. Blood Flow Metab.* 38, 1293–1298. doi: 10.1177/0271678x18780130

Smith, C. D., Andersen, A. H., Kryscio, R. J., Schmitt, F. A., Kindy, M. S., Blonder, L. X., et al. (1999). Altered brain activation in cognitively intact individuals at high risk for Alzheimer's disease. *Neurology* 53, 1391–1396.

Snowdon, D. A., Greiner, L. H., Mortimer, J. A., Riley, K. P., Greiner, P. A., and Markesbery, W. R. (1997). Brain infarction and the clinical expression of Alzheimer disease. The nun study. *JAMA* 277, 813–817. doi: 10.1001/jama.277.10.813

Song, I. U., Kim, J. S., Kim, Y. I., Eah, K. Y., and Lee, K. S. (2007). Clinical significance of silent cerebral infarctions in patients with Alzheimer disease. *Cogn. Behav. Neurol.* 20, 93–98. doi: 10.1097/wnn.0b013e31805d859e

Stanley, D., Mason, L. J., Mackin, K. E., Srikhanta, Y. N., Lyras, D., Prakash, M. D., et al. (2016). Translocation and dissemination of commensal bacteria in post-stroke infection. *Nat. Med.* 22, 1277–1284. doi: 10.1038/nm.4194

Stanley, D., Moore, R. J., and Wong, C. H. Y. (2018). An insight into intestinal mucosal microbiota disruption after stroke. *Sci. Rep.* 8:568.

Sun, G., Li, G., Li, D., Huang, W., Zhang, R., Zhang, H., et al. (2018). HucMSC derived exosomes promote functional recovery in spinal cord injury mice via attenuating inflammation. *Mater. Sci. Eng. C Mater. Biol. Appl.* 89, 194–204. doi: 10.1016/j.msec.2018.04.006

Sweeney, M. D., Sagare, A. P., and Zlokovic, B. V. (2018). Blood-brain barrier breakdown in Alzheimer disease and other neurodegenerative disorders. *Nat. Rev. Neurol.* 14, 133–150. doi: 10.1038/nrneurol.2017.188

Syeda, T., Sanchez-Tapia, M., Pinedo-Vargas, L., Granados, O., Cuervo-Zanatta, D., Rojas-Santiago, E., et al. (2018). Bioactive food abates metabolic and synaptic alterations by modulation of gut microbiota in a mouse model of Alzheimer's disease. *J. Alzheimers. Dis.* 66, 1657–1682. doi: 10.3233/jad-180556

Szablewski, L. (2018). Human gut microbiota in health and Alzheimer's disease. *J. Alzheimers. Dis.* 62, 549–560. doi: 10.3233/jad-170908

Taguchi, K., Watanabe, Y., Tsujimura, A., and Tanaka, M. (2016). Brain region-dependent differential expression of alpha-synuclein. *J. Comp. Neurol.* 524, 1236–1258. doi: 10.1002/cne.23901

Tang, W. H., Wang, Z., Levison, B. S., Koeth, R. A., Britt, E. B., Fu, X., et al. (2013). Intestinal microbial metabolism of phosphatidylcholine and cardiovascular risk. *N. Engl. J. Med.* 368, 1575–1584. doi: 10.1056/nejmoa1109400

Tao, Q., Ang, T. F. A., Decarli, C., Auerbach, S. H., Devine, S., Stein, T. D., et al. (2018). Association of chronic low-grade inflammation with risk of Alzheimer disease in ApoE4 carriers. *JAMA Netw. Open* 1, e183597. doi: 10.1001/jamanetworkopen.2018.3597

Thery, C., Witwer, K. W., Aikawa, E., Alcaraz, M. J., Anderson, J. D., Andriantsitohaina, R., et al. (2018). Minimal information for studies of extracellular vesicles 2018 (MISEV2018): a position statement of the international society for extracellular vesicles and update of the MISEV2014 guidelines. *J. Extracell. Vesicles* 7:1535750.

Thomas, T., Thomas, G., Mclendon, C., Sutton, T., and Mullan, M. (1996). beta-Amyloid-mediated vasoactivity and vascular endothelial damage. *Nature* 380, 168–171. doi: 10.1038/380168a0

Thursby, E., and Juge, N. (2017). Introduction to the human gut microbiota. *Biochem. J.* 474, 1823–1836. doi: 10.1042/bcj20160510

Tian, X. L., and Li, Y. (2014). Endothelial cell senescence and age-related vascular diseases. *J. Genet. Genom.* 41, 485–495. doi: 10.1016/j.jgg.2014.08.001

Toledo, J. B., Arnold, S. E., Raible, K., Brettschneider, J., Xie, S. X., Grossman, M., et al. (2013). Contribution of cerebrovascular disease in autopsy confirmed neurodegenerative disease cases in the national Alzheimer's coordinating centre. *Brain* 136, 2697–2706. doi: 10.1093/brain/awt188

Torres-Fuentes, C., Schellekens, H., Dinan, T. G., and Cryan, J. F. (2017). The microbiota-gut-brain axis in obesity. *Lancet Gastroenterol. Hepatol.* 2, 747–756.

Tran, L., and Greenwood-Van Meerveld, B. (2013). Age-associated remodeling of the intestinal epithelial barrier. *J. Gerontol. A Biol. Sci. Med. Sci.* 68, 1045–1056. doi: 10.1093/gerona/glt106

Trapp, B. D., and Nave, K. A. (2008). Multiple sclerosis: an immune or neurodegenerative disorder? *Annu. Rev. Neurosci.* 31, 247–269. doi: 10.1146/annurev.neuro.30.051606.094313

Turnquist, C., Horikawa, I., Foran, E., Major, E. O., Vojtesek, B., Lane, D. P., et al. (2016). p53 isoforms regulate astrocyte-mediated neuroprotection and neurodegeneration. *Cell Death. Differ.* 23, 1515–1528. doi: 10.1038/cdd.2016.37

van der Worp, H. B., Howells, D. W., Sena, E. S., Porritt, M. J., Rewell, S., O'collins, V., et al. (2010). Can animal models of disease reliably inform human studies? *PLoS Med.* 7:e1000245. doi: 10.1371/journal.pmed.1000245

van Deursen, J. M. (2014). The role of senescent cells in ageing. *Nature* 509, 439–446. doi: 10.1038/nature13193

van Oijen, M., De Jong, F. J., Witteman, J. C., Hofman, A., Koudstaal, P. J., and Breteler, M. M. (2007). Atherosclerosis and risk for dementia. *Ann. Neurol.* 61, 403–410.

VanGuilder, H. D., Yan, H., Farley, J. A., Sonntag, W. E., and Freeman, W. M. (2010). Aging alters the expression of neurotransmission-regulating proteins in the hippocampal synaptoproteome. *J. Neurochem.* 113, 1577–1588.

Verdu, E. F., Galipeau, H. J., and Jabri, B. (2015). Novel players in coeliac disease pathogenesis: role of the gut microbiota. *Nat. Rev. Gastroenterol. Hepatol.* 12, 497–506. doi: 10.1038/nrgastro.2015.90

Vicente Miranda, H., El-Agnaf, O. M., and Outeiro, T. F. (2016). Glycation in Parkinson's disease and Alzheimer's disease. *Mov. Disord.* 31, 782–790.

Villaran, R. F., Espinosa-Oliva, A. M., Sarmiento, M., De Pablos, R. M., Arguelles, S., Delgado-Cortes, M. J., et al. (2010). Ulcerative colitis exacerbates lipopolysaccharide-induced damage to the nigral dopaminergic system: potential risk factor in Parkinson's disease. *J. Neurochem.* 114, 1687–1700. doi: 10.1111/j.1471-4159.2010.06879.x

Villeda, S. A., Luo, J., Mosher, K. I., Zou, B., Britschgi, M., Bieri, G., et al. (2011). The ageing systemic milieu negatively regulates neurogenesis and cognitive function. *Nature* 477, 90–94. doi: 10.1038/nature10357

Villringer, A. (1997). Understanding functional neuroimaging methods based on neurovascular coupling. *Adv. Exp. Med. Biol.* 413, 177–193. doi: 10.1007/978-1-4899-0056-2_20

Vogt, N. M., Kerby, R. L., Dill-Mcfarland, K. A., Harding, S. J., Merluzzi, A. P., Johnson, S. C., et al. (2017). Gut microbiome alterations in Alzheimer's disease. *Sci. Rep.* 7:13537.

Wakabayashi, K., Mori, F., Tanji, K., Orimo, S., and Takahashi, H. (2010). Involvement of the peripheral nervous system in synucleinopathies, tauopathies and other neurodegenerative proteinopathies of the brain. *Acta Neuropathol.* 120, 1–12. doi: 10.1007/s00401-010-0706-x

Wakabayashi, K., Takahashi, H., Ohama, E., and Ikuta, F. (1990). Parkinson's disease: an immunohistochemical study of Lewy body-containing neurons in the enteric nervous system. *Acta Neuropathol.* 79, 581–583. doi: 10.1007/bf00294234

Wakabayashi, K., Takahashi, H., Takeda, S., Ohama, E., and Ikuta, F. (1988). Parkinson's disease: the presence of Lewy bodies in Auerbach's and *Meissner's plexuses*. *Acta Neuropathol.* 76, 217–221. doi: 10.1007/bf00687767

Walsh, D. M., Klyubin, I., Fadeeva, J. V., Cullen, W. K., Anwyl, R., Wolfe, M. S., et al. (2002). Naturally secreted oligomers of amyloid beta protein potently inhibit hippocampal long-term potentiation in vivo. *Nature* 416, 535–539. doi: 10.1038/416535a

Walton, C. C., and Andersen, J. K. (2019). Unknown fates of (brain) oxidation or UFO: close encounters with neuronal senescence. *Free Radic Biol. Med.* 134, 695–701 doi: 10.1016/j.freeradbiomed.2019.01.012

Wang, L., Christophersen, C. T., Sorich, M. J., Gerber, J. P., Angley, M. T., and Conlon, M. A. (2012). Elevated fecal short chain fatty acid and ammonia concentrations in children with autism spectrum disorder. *Dig. Dis. Sci.* 57, 2096–2102. doi: 10.1007/s10620-012-2167-7

Wang, R., Tang, Y., Feng, B., Ye, C., Fang, L., Zhang, L., et al. (2007). Changes in hippocampal synapses and learning-memory abilities in age-increasing rats and effects of tetrahydroxystilbene glucoside in aged rats. *Neuroscience* 149, 739–746. doi: 10.1016/j.neuroscience.2007.07.065

Wang, X., Xing, A., Xu, C., Cai, Q., Liu, H., and Li, L. (2010). Cerebrovascular hypoperfusion induces spatial memory impairment, synaptic changes, and amyloid-beta oligomerization in rats. *J. Alzheimers Dis.* 21, 813–822. doi: 10.3233/jad-2010-100216

Wardlaw, J. M., Smith, E. E., Biessels, G. J., Cordonnier, C., Fazekas, F., Frayne, R., et al. (2013). Neuroimaging standards for research into small vessel disease and its contribution to ageing and neurodegeneration. *Lancet Neurol.* 12, 822–838.

Wendell, C. R., Waldstein, S. R., Ferrucci, L., O'brien, R. J., Strait, J. B., and Zonderman, A. B. (2012). Carotid atherosclerosis and prospective risk of dementia. *Stroke* 43, 3319–3324. doi: 10.1161/strokeaha.112.672527

Wenk, G. L., and Barnes, C. A. (2000). Regional changes in the hippocampal density of AMPA and NMDA receptors across the lifespan of the rat. *Brain Res.* 885, 1–5. doi: 10.1016/s0006-8993(00)02792-x

Whelton, P. K., Carey, R. M., Aronow, W. S., Casey, D. E. Jr., Collins, K. J., Dennison Himmelfarb, C., et al. (2018). 2017 ACC/AHA/AAPA/ABC/ACPM/AGS/APhA/ASH/ASPC/NMA/PCNA guideline for the prevention, detection, evaluation, and management of high blood pressure in adults: a report of the american college of cardiology/american heart association task force on clinical practice guidelines. *Hypertension* 71, e13-e115.

White, L. (2009). Brain lesions at autopsy in older Japanese-American men as related to cognitive impairment and dementia in the final years of life: a summary report from the Honolulu-Asia aging study. *J. Alzheimers. Dis.* 18, 713–725. doi: 10.3233/jad-2009-1178

Willner, P. (1984). The validity of animal models of depression. *Psychopharmacology* 83, 1–16. doi: 10.1007/bf00427414

Winek, K., Engel, O., Koduah, P., Heimesaat, M. M., Fischer, A., Bereswill, S., et al. (2016). Depletion of cultivatable gut microbiota by broad-spectrum antibiotic pretreatment worsens outcome after murine stroke. *Stroke* 47, 1354–1363. doi: 10.1161/strokeaha.115.011800

Wittko-Schneider, I. M., Schneider, F. T., and Plate, K. H. (2014). Cerebral angiogenesis during development: who is conducting the orchestra? *Methods Mol. Biol.* 1135, 3–20. doi: 10.1007/978-1-4939-0320-7_1

Wong, J. M., and Billiar, T. R. (1995). Regulation and function of inducible nitric oxide synthase during sepsis and acute inflammation. *Adv. Pharmacol.* 34, 155–170. doi: 10.1016/s1054-3589(08)61084-4

Wong, J. M., De Souza, R., Kendall, C. W., Emam, A., and Jenkins, D. J. (2006). Colonic health: fermentation and short chain fatty acids. *J. Clin. Gastroenterol.* 40, 235–243.

Wu, S. C., Cao, Z. S., Chang, K. M., and Juang, J. L. (2017). Intestinal microbial dysbiosis aggravates the progression of Alzheimer's disease in drosophila. *Nat. Commun.* 8:24.

Xie, N., and Tang, B. (2016). The application of human iPSCs in neurological diseases: from bench to bedside. *Stem Cells Int.* 2016:6484713.

Yamazaki, T., Li, W., Yang, L., Li, P., Cao, H., Motegi, S. I., et al. (2018). Whole mount adult ear skin imaging reveals defective neuro-vascular branching morphogenesis in obese and type 2 diabetic mouse models. *Sci. Rep.* 8:430.

Yamazaki, Y., Baker, D. J., Tachibana, M., Liu, C. C., Van Deursen, J. M., Brott, T. G., et al. (2016). Vascular cell senescence contributes to blood-brain barrier breakdown. *Stroke* 47, 1068–1077. doi: 10.1161/strokeaha.115.010835

Yilmaz, A., Geddes, T., Han, B., Bahado-Singh, R. O., Wilson, G. D., Imam, K., et al. (2017). Diagnostic biomarkers of Alzheimer's disease as identified in Saliva using 1H NMR-based metabolomics. *J. Alzheimers. Dis.* 58, 355–359. doi: 10.3233/jad-161226

Yin, J., Liao, S. X., He, Y., Wang, S., Xia, G. H., Liu, F. T., et al. (2015). Dysbiosis of gut microbiota with reduced trimethylamine-N-Oxide level in patients with large-artery atherosclerotic stroke or transient ischemic attack. *J. Am. Heart Assoc.* 4:e002699.

Zekry, D., Duyckaerts, C., Moulias, R., Belmin, J., Geoffre, C., Herrmann, F., et al. (2002). Degenerative and vascular lesions of the brain have synergistic effects in dementia of the elderly. *Acta Neuropathol.* 103, 481–487. doi: 10.1007/s00401-001-0493-5

Zevin, A. S., Mckinnon, L., Burgener, A., and Klatt, N. R. (2016). Microbial translocation and microbiome dysbiosis in HIV-associated immune activation. *Curr. Opin. HIV AIDS* 11, 182–190. doi: 10.1097/coh.0000000000000234

Zhan, X., Stamova, B., Jin, L. W., Decarli, C., Phinney, B., and Sharp, F. R. (2016). Gram-negative bacterial molecules associate with Alzheimer disease pathology. *Neurology* 87, 2324–2332. doi: 10.1212/wnl.0000000000003391

Zhang, C., Yin, A., Li, H., Wang, R., Wu, G., Shen, J., et al. (2015). Dietary modulation of gut microbiota contributes to alleviation of both genetic and simple obesity in children. *EBioMed.* 2, 968–984. doi: 10.1016/j.ebiom.2015.07.007

Zhang, L., Wang, Y., Xiayu, X., Shi, C., Chen, W., Song, N., et al. (2017). Altered gut microbiota in a mouse model of Alzheimer's disease. *J. Alzheimers Dis.* 60, 1241–1257. doi: 10.3233/jad-170020

Zhao, Y., Cong, L., and Lukiw, W. J. (2017). Lipopolysaccharide (LPS) accumulates in neocortical neurons of Alzheimer's disease (AD) brain and impairs transcription in human neuronal-glial primary co-cultures. *Front. Aging. Neurosci.* 9:407. doi: 10.3389/fnagi.2017.00407

Zhao, Y., Dua, P., and Lukiw, W. J. (2015). Microbial sources of amyloid and relevance to amyloidogenesis and alzheimer's disease (AD). *J. Alzheimers. Dis. Parkinsonism* 5:177.

Zhuang, Z. Q., Shen, L. L., Li, W. W., Fu, X., Zeng, F., Gui, L., et al. (2018). Gut microbiota is altered in patients with Alzheimer's disease. *J. Alzheimers. Dis.* 63, 1337–1346.

Zlokovic, B. V. (2008). The blood-brain barrier in health and chronic neurodegenerative disorders. *Neuron* 57, 178–201. doi: 10.1016/j.neuron.2008.01.003

Conflict of Interest Statement: The authors declare that the research was conducted in the absence of any commercial or financial relationships that could be construed as a potential conflict of interest.

Copyright © 2019 Castillo, Castro-Obregón, Gutiérrez-Becker, Gutiérrez-Ospina, Karalis, Khalil, Lopez-Noguerola, Rodríguez, Martínez-Martínez, Perez-Cruz, Pérez-Velázquez, Piña, Rubio, García, Syeda, Vanoye-Carlo, Villringer, Winek and Zille. This is an open-access article distributed under the terms of the Creative Commons Attribution License (CC BY). The use, distribution or reproduction in other forums is permitted, provided the original author(s) and the copyright owner(s) are credited and that the original publication in this journal is cited, in accordance with accepted academic practice. No use, distribution or reproduction is permitted which does not comply with these terms.

frontiers in Neurology

MINI REVIEW
published: 02 August 2019
doi: 10.3389/fneur.2019.00824

Dental Pulp Stem Cells: An Attractive Alternative for Cell Therapy in Ischemic Stroke

Xiaoyan Lan[1], *Zhengwu Sun*[2], *Chengyan Chu*[1], *Johannes Boltze*[3†] *and Shen Li*[1*†]

[1] *Department of Neurology, Dalian Municipal Central Hospital Affiliated to Dalian Medical University, Dalian, China,* [2] *Department of Pharmacy, Dalian Municipal Central Hospital Affiliated to Dalian Medical University, Dalian, China,* [3] *School of Life Sciences, University of Warwick, Coventry, United Kingdom*

Ischemic stroke is a major cause of disability and mortality worldwide, but effective restorative treatments are very limited at present. Regenerative medicine research revealed that stem cells are promising therapeutic options. Dental pulp stem cells (DPSCs) are autologously applicable cells that origin from the neural crest and exhibit neuro-ectodermal features next to multilineage differentiation potentials. DPSCs are of increasing interest since they are relatively easy to obtain, exhibit a strong proliferation ability, and can be cryopreserved for a long time without losing their multi-directional differentiation capacity. Besides, use of DPSCs can avoid fundamental problems such as immune rejection, ethical controversy, and teratogenicity. Therefore, DPSCs provide a tempting prospect for stroke treatment.

Keywords: stem cells, dental pulp stem cells, stroke, brain ischemia, cell therapy

OPEN ACCESS

Edited by:
Jean-Marc Olivot,
Centre Hospitalier Universitaire de Toulouse, France

Reviewed by:
Yi-Je Chen,
University of California, Davis, United States
Jukka Jolkkonen,
University of Eastern Finland, Finland

***Correspondence:**
Shen Li
listenlishen@hotmail.com

†These authors have contributed equally to this work

Specialty section:
This article was submitted to Stroke, a section of the journal Frontiers in Neurology

Received: *15 March 2019*
Accepted: *17 July 2019*
Published: *02 August 2019*

Citation:
Lan X, Sun Z, Chu C, Boltze J and Li S (2019) Dental Pulp Stem Cells: An Attractive Alternative for Cell Therapy in Ischemic Stroke. Front. Neurol. 10:824. doi: 10.3389/fneur.2019.00824

The past decade has witnessed intense advancement and tremendous therapeutic achievements in the ability to diagnose and treat stroke, a cerebrovascular disease of which 87% is ischemic in nature. Nevertheless, stroke remains a major cause of disability, morbidity, and mortality worldwide, and constitutes a major socioeconomic problem (1, 2). Ischemic stroke, due to partially or completely blocked blood flow in a cerebral artery, causes ischemic necrosis of brain tissue seriously impairing the health of affected individuals. The main therapeutic strategy for ischemic stroke is timely recanalization. This can either be achieved by tissue-type plasminogen activator application or mechanical thrombectomy. Particularly the latter can be applied up to 24 h after stroke in patients exhibiting a penumbra, and has revolutionized acute stroke treatment. However, the absolute number of patients qualifying for recanalization remains very low (3, 4). Hence, additional treatment approaches being effective beyond the first hours after stroke onset are urgently required.

Stem cell transplantation is a promising strategy to restore neurological function after stroke (5). Experimental stem cell transplantation in animals showed that numerous cell populations can improve functional recovery by a broad spectrum of mechanisms (6–8). Several kinds of stem cells are currently considered for therapy. These include embryonic stem cells (ESCs), fetal stem/progenitor cells, induced pluripotent stem cells (iPSCs), and adult stem cells. While embryonic or induced pluripotent stem cells exhibit a tremendous differentiation potential, they may also inherit a risk for tumor formation (9). The use of embryonic stem cells or fetal stem/progenitor cells raises ethical concerns. Adult stem cells show a limited proliferation and differentiation potential, but can still be beneficial after stroke due numerous mechanisms beyond tissue restoration. They are further believed to be safer in clinical application and their use is ethically less challenging (9–13).

Recent systematic reviews and meta-analyses on the most prominent adult stem cell therapy candidates, mesenchymal stem cells (MSCs), presented evidence that MSCs improve the outcome

after stroke in animals (14) and patients, and confirmed the safety and feasibility of the approach (15). Nevertheless, there is still a lack of adult (stem) cells that can be derived from an autologous source, and may exhibit therapeutic abilities beyond those of MSCs.

DENTAL PULP STEM CELLS (DPSCs): A NEW SOURCE OF ADULT STEM CELLS

The dental pulp is a soft tissue located in the center of teeth. It comprises blood vessels, neural fibers, and connective tissue. The dental pulp contains both mesenchymal and ectodermal tissue as well as neural crest cells (16). Limited dentinal repair in the postnatal organism relies on specialized precursor cell populations residing in the dental pulp tissue. Gronthos et al. first reported the isolation and characterization of stem cells from dental pulp tissue of the third molar in 2000 (17). DPSCs are ectoderm-derived stem cells, originating from migrating neural crest cells (**Figure 1**). They are a subpopulation among dental pulp cells (DPCs) which possess MSC properties, such as a fibroblast-like morphology, adherence to a plastic surface, as well as surface marker expression, proliferation and colony forming behavior similar to that of MSCs (18, 19). It is not clear whether or not DPSCs are a kind of MSC population. Given their differentiation abilities as reviewed below, it might be assumed that DPSCs are a more naïve stem cell population that also, but not exclusively, exhibits MSC properties. A major benefit of DPSCs is that they can be isolated during routine dental procedures such as the eruption of deciduous teeth or extraction of impacted wisdom teeth (20) in simple and autologous fashion without ethical concerns. Another primary advantage of DPSCs is their potential for cell banking. Several studies have demonstrated that DPSCs retain their stem cell properties after long cryopreservation (21, 22). This is essential as cryopreservation can impact therapeutic capacities of other adult stem cell-containing populations in stroke (23). In addition, DPSC cultures can be established from extracted human molars with high efficiency, even after the whole tooth has been cryopreserved for up to 1 month (24). DPSCs also exhibit a multilineage differentiation potential into chondrocytes, adipocytes, odontoblasts, and potentially even neural-like cells (25–28).

Currently, there are no specific markers that uniquely define DPSCs. In general, DPSCs, as a heterogeneous population, express a variety of markers similar to MSCs (**Table 1**) (**Figure 1**), and do not express hematopoietic markers such as CD14, CD19, CD34, and CD45 (18, 26, 29–32). DPSCs isolated by their high proliferative potential tend to include a large population of cells expressing $CD44^+$, $CD90^+$, and $CD166^+$. However, DPSCs also express stemness-related markers similar to ESCs such as Oct-3/4, Nanog, and Sox-2, as well as the cytoskeleton-related markers nestin and vimentin (**Figure 1**) (33–35). They further express insulin-like growth factor 1 receptor (IGF1R) which is regarded as a pluripotency marker in ESCs. DPSC-secreted IGF1 interacts with IGF1R through an autocrine signaling pathway to maintain self-renewal and proliferation potential (36).

In addition, DPSCs (as neural crest-derived stem cells) not only express a number of neural stem cell (NSC) associated markers including nestin (26, 37) and Sox2 (38) (**Figure 1**), but also express low basal levels of markers associated with mature central nervous system cell types, including the neuronal markers βIII-tubulin, microtubule-associated protein 2 (MAP2), neurofilaments (NF) (33, 39), NeuN (40), the astrocytic marker glial fibrillary acidic protein (GFAP) (26, 33), and oligodendrocyte-associated CNPase (33). Taken together, this suggests that DPSCs can indeed differentiate into neuron-like cells under appropriate conditions, and differentiated cells even exhibit typical electrophysiological properties after neuronal differentiation (41, 42).

DPSCs AS A POTENTIAL CANDIDATE FOR THERAPY OF NEUROLOGICAL DISEASES

Brain-derived NSCs are considered a promising population for stroke treatment due to their ability to self-renew and to differentiate into neural cells types (neurons, astrocytes, oligodendrocytes) (43). However, autologous harvest of adult human NSCs requires neurosurgical procedures due to their brain parenchymal residence (44), while allogeneic or even xenogenic NSCs grafting imposes the risk of graft rejection and additional immunological damage. Only a limited number of clinical trials currently explore the potential of NSCs for stroke treatment because of these limitations.

Adult stem cells or stem cell-containing populations are more frequently applied in translational research. As stated above, DPSCs share many biological characteristics with MSCs including bone marrow MSCs (BM-MSCs), adipose tissue-derived stem cells (ADSCs) and umbilical cord MSCs (UC-MSCs) but there are some variations in their proliferation potential (17, 27, 45), differentiation potential (17, 27, 46), immunomodulatory activity (27), secretome characteristics, and secretory capacity (47–49). Specifically, DPSCs have a higher proliferation rate and a greater clonogenic potential than MSCs (17, 45). Next to DPSCs, the DPC population also contains a higher number of stem/progenitor cells as compared to bone marrow (50). This may be attributed to the developmental state of the respective tissues. All teeth, even the permanent molars, are generated early in individual development and rest in the jar until they erupt. Abilities and capacities of stem cells may be much better preserved in tissue with a slow turnover such as the dental pulp when compared to BM, which exhibits a tremendous turnover throughout life apart from some niches. DPSCs maintain their high rate of proliferation even after extensive subculturing.

Like MSCs, DPSCs can differentiate into cells of mesenchymal and non-mesenchymal tissues *in vitro* and *in vivo*. However, DPSCs exhibit stronger odontogenesis and neurogenesis capabilities, in turn being not as potent to produce adipogeneic, osteogeneic and chondrogeneic tissue than BM-MSCs (51) and ADSCs (46). Besides, DPSCs also have immunomodulatory capacities exceeding those of BM-MSCs, for example a higher suppression rate of T lymphocyte growth (17, 27).

DPSCs exhibit superior neuroprotective and neuro-supportive properties in neurological injuries and pathologies as

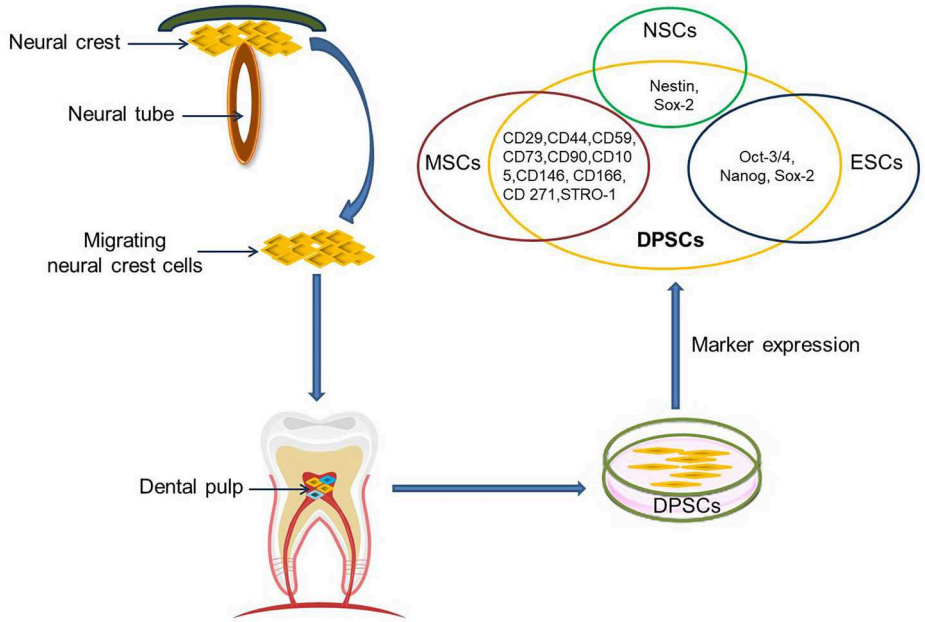

FIGURE 1 | DPSCs origin, isolation, and marker expression. DPSCs originate from migrating neural crest cells, coming to rest in dental pulp, and express markers overlapping with MSCs, ESCs, and NCSs.

TABLE 1 | Characteristics of DPSCs.

	Marker expression overlapping with			*In vitro* multipotency	Secretomes
MSCs	**ESCs**	**NSCs**	**Mature cells**		
CD29, CD44, CD59, CD73, CD90, CD105, CD146, CD166, CD 271, STRO-1	Oct-3/4, Nanog, Sox-2	Nestin,Sox-2	MAP2, NF, βIII-tubulin, NeuN (neurons), GFAP, S100 (astrocytes), CNPase (oligodendrocytes)	Adipo, chondro, myo, osteo, neuro, odonto	Neuroprotective effect: BDNF, GDNF, VEGF, NGF, IGF-1, PDGF, CNTF, RANTES, GM-CSF; Anti-apoptotic effect: MCP-1, FRACTALKINE; Immunomodulation effect: FLT-3, TGF-β, IL-6

MAP2, microtubule associated protein 2; NF, Neurofilament; GFAP, glial fibrillary acidic protein; adipo, adipocyte; chondro, chondrocyte; myo, myoblast; neuro, neuronal cell; odonto, odontoblast; osteo, osteoblast. BDNF, brain-derived neurotrophic factor; GDNF, glial cell-derived neurotrophic factor; VEGF, vascular endothelial growth factor; NGF, nerve growth factor; PDGF, platelet derived growth factor; CNTF, ciliary neurotrophic factor, FLT-3, fms-related tyrosine kinase 3; GM-CSF, granulocyte-macrophage colony-stimulating factor; MCP-1, monocyte chemotactic protein 1; TGF-β, transforming growth factor-β; IL-6, interleukin-6.

compared with BM-MSCs and ADSCs (52). This might be related to a higher expression of trophic factors including brain derived neurotrophic factor (BDNF), glial cell-derived neurotrophic factor (GDNF), nerve growth factor (NGF), vascular endothelial growth factor (VEGF), and platelet derived growth factor (PDGF) in DPSCs as compared to BM-MSCs (47, 48), although the spectrum of growth and trophic factors secretion is similar (53). DPSCs also express higher quantities of CXCL14 and monocyte chemoattractant protein 1 (MCP-1) than ADSCs (49). Besides, the DPSC secretome contains higher concentrations of RANTES, FRACTALKINE, fms-related tyrosine kinase 3 (FLT-3), granulocyte-macrophage colony-stimulating factor (GM-CSF), and MCP-1 than the BM-MSCs secretome (54). DPSCs show higher angiogenic and neurogenic potentials in ectopic transplantation models compared to BM-MSCs and ADSCs, and exhibit the highest migration capacity. Transplantation of DPSCs in a mouse hindlimb ischemia model produced higher blood flow and capillary density than transplantation of BM-MSCs and ADSCs, which being associated with superior recovery of limb movement abilities and reduction of ischemic hindlimb damage (55). DPSCs also mediate stronger anti-apoptotic effects in a microenvironment challenged by oxidative and serum deprivation than BM-MSCs, ADSCs and UC-MSCs (45).

Cell size and diameter are important for safety after intravascular delivery as they are the major, but not the only, determinants of vascular obstruction and complications (56) (**Table 2**). Previously reported studies showed that the cell diameter of human DPSCs is around 15–16 μm (59), which is comparable to NSCs (57, 58) but slightly smaller than for most MSC populations (57, 60) including human BM-MSCs (61). Still this means that one has to expect a considerable pulmonary passage filtering effect after intravenous delivery, as well as a risk for microembolism after intraarterial administration (62).

TABLE 2 | Overview of cell size of cell populations.

Cell population	Cell diameter	Cell source
NSCs (57, 58)	16 μm	Human fetal brain
DPSCs (59)	15–16 μm	Human dental pulp
MSCs (57, 60)	17–18 μm	Bone marrow; adipose tissue; human umbilical cord blood
Hematopoietic stem/progenitor cells (57)	6–10 μm	Bone marrow; peripheral blood; cord blood
Mononuclear cells (57, 60)	7 μm	Bone marrow; peripheral blood; cord blood

Hence, thorough investigations identifying the optimal route of DPSC administration by considering safety and efficacy aspects are recommended in DPSC translational research.

DPSCs FOR ISCHEMIC NEURONAL DAMAGE: *IN VITRO* EFFECTS

Treatment with immunosorted IGF1R$^+$ DPSCs significantly modulates neurite regeneration and anti-inflammation in primary cortical cultures subject to oxygen/glucose deprivation (OGD) (36). DPSCs cultivated on adult mouse hippocampal slices were able to stimulate neurogenesis in both the CA1 zone and at the edges of the hippocampal slices through neurotrophic support *in vitro* (41). Besides, DPSCs can protect primary hippocampal, mesencephalic (63) and dopaminergic neurons (64) from β-amyloid peptide and 6-OHDA induced toxicity, respectively. Furthermore, DPSCs and conditioned medium from DPSCs show superior protective, migratory, and angiogenic effects in OGD-injured astrocytes as compared to BM-MSCs (52, 65). Reducing reactive gliosis, reactive oxygen species production and inflammatory mediators might contribute to this protective effect (52).

DPSCs EFFECTS AFTER ISCHEMIC STROKE *IN VIVO*

Human DPSCs can differentiate toward functionally active neurons under appropriate culture conditions (66–68). This comes on top of their bystander effects, indicating that DPSCs might provide enhanced therapeutic capacities in neurological diseases including stroke, Parkinson's disease, Alzheimer's disease, and spinal cord injury (52, 63, 69). To date, there are several preclinical studies demonstrating that DPSCs exert neuroprotective effect resulting in improved functional outcome and reduced infract volumes in rodent stroke models (**Table 3**) (52, 66, 68, 70–76). No obvious deleterious effects were observed in these studies (66, 68, 71–73, 75), but have not been always explicitly looked for.

A number of remarkable improvements were seen in behavioral tests (**Table 3**), underpinning the considerable effect DPSCs may exert after ischemic stroke. However, many of the behavioral tests used are known for a tendency to overestimate true functional recovery in standard rodent models so future research may also include the use of highly specific behavioral readout systems (77).

During ischemia, neurons are unable to maintain normal transmembrane ion gradient and balance, resulting in cell death by apoptosis, excitatory toxicity, and oxidative stress. Inflammatory reactions contribute to cell death in subacute and even chronic stages what can be exacerbated in the presence of important stroke risk factors (78, 79). These pathophysiological processes are interrelated and can trigger each other, forming a vicious cycle (80, 81). Indeed, neuroinflammation and immune response after stroke have been recognized as key factors contributing to overall brain damage and the extent of neurological deficit (82). The administration of DPSCs during the acute phase of stroke dampens inflammation *in vivo*, and can promote recovery from in post-ischemia/reperfusion brain injury (70). Moreover, intracerebral transplantation of DPSCs or immunosorted IGF1R$^+$ DPSCs into the ischemically injured neonatal murine brain significantly increases immunomodulation, enhances poststroke recovery, and promotes neuroplasticity (36, 67). Further, intravenous transplantation of DPSCs or DPSC-derived neurosphere cells significantly ameliorates the impact of global cerebral ischemia, decreases neuronal cell death in the hippocampal CA1 region, improves neuromotor and cognitive function as well as overall survival rates in stroke animals (73). Moreover, intracerebral transplantation of DPSCs also enhanced poststroke functional recovery after brain injury through increasing expression of the anti-apoptotic protein Bcl-2 (67).

Transplanted DPSCs can migrate into the boundary of ischemic areas, and express neural cell and NSC markers such as βIII tubulin, doublecortin (DCX), nestin, and NF (72). The cells' beneficial effects may even be exerted after xenogeneic transplantation as evidenced by a study showing that porcine DPSCs (CD31$^-$/CD146$^-$ side population cells) injection promotes recovery form motor impairment and reduced infarct volume, promoted migration and differentiation of endogenous NSCs, and finally induced vasculogenesis after stroke in rats (66).

DPSC EXOSOMES—GREAT OPPORTUNITIES FOR CELL THERAPY WITHOUT CELLS

The limited survival, differentiation and integration of DPSC-derived cells into the ischemically lesioned brain implies that the functional improvement is more likely mediated through bystander effects rather than cell replacement and differentiation (33). It has been well-documented that the MSC secretome contains a variety of cytokines, chemokines, and growth factors, along with extracellular vesicles (EVs). The most important EVs in MSC-conditioned medium are exosomes, which are of "nano" size (30–100 nm in diameter) (83, 84). EVs play an important role in intercellular communication because they can transfer RNA, micro-RNA, proteins, membrane receptors and even organelles (mitochondria) between cells (85, 86). MSC-derived EVs are of increasing interest since they may have

TABLE 3 | Overview of DPSCs therapy for ischemic stroke animal models.

Cell type and dose	Delivery method	Delivery time	Animal model	Transplantation paradigm	Function and mechanisms	Primary endpoint and effect sizes
Human DPSCs; 6 × 10^5 in 4 μl (68)	Intracerebral (striatum and cortex)	24 h after MCAO	Rat MCAO (2 h)	Xenogeneic	Improved functional recovery; Differentiation into astrocytes; Paracrine effects.	Neuroscore: 35% improve ($p < 0.05$)*
Human DPSCs; 4 × 10^6 in 500 μl (52)	Intravenous (tail vein)	24 h after MCAO	Rat MCAO (2 h)	Xenogeneic	Improved functional recovery and reduced infarct volume; Differentiated into astrocytes and neuron-like cells; Promoted angiogenesis and inhibited astrogliosis.	Infract volume: 44% decrease, ($p < 0.05$); mNSS: 38% improve ($p < 0.05$)*
Human DPSCs; 1 × 10^6 in 1 ml (70)	Intravenous (tail vein)	immediately after MCAO	Rat MCAO (90 min)	Xenogeneic	Reduced the infarct volume and improved the neurological recovery; Inflammation modulation; BBB permeability modulation; Promoted angiogenesis.	Infract volume: 23% decrease ($p < 0.01$); Rotarod test: 108% improve ($p < 0.01$) *; Forelimb grip strength: 54% improve ($p < 0.05$)*
Rat DPSCs; 3 × 10^6 in 300 μl (71)	Intravenous (tail vein)	24 h after MCAO	Rat MCAO (2 h)	Allogeneic Homologous	Enhanced sensorimotor functional recovery; Differentiation into neuronal progenitor cells and neuron-like cells, and triggered neurogenesis.	mNSS: 52% improve ($p < 0.05$)*; Adhesive-removal test: 38% improve ($p < 0.05$)*
Rat DPSCs; 1 × 10^6 in 500 μl (72)	Intravenous (tail vein)	24 h after MCAO	Rat MCAO (2 h)	Allogeneic Homologous	Reduced infarct volume and cerebral edema; Differentiated into neuron-like cells	Infract volume: 31% decrease ($p < 0.05$)
Rat DPSCs and dental pulp-derived neurospheres; 1×10^6 in 1 ml (73)	Intravenous (tail vein)	3 h after brain ischemia	Rat severe forebrain ischemia model (11 min)	Allogeneic Homologous	Improved survival rate and cognitive function; Reduced the dead neurons of hippocampus CA1.	Survival rate: 36% improve ($p < 0.05$); Water-maze test: 62% improve ($p < 0.05$)*
Human DPSCs; 1 × 10^6 in 1 ml (74)	Intravenous (tail vein)	immediately and 3 h after MCAO	Rat MCAO (90 min)	Xenogeneic	Reduced ischemic damage and improved functional recovery; Inflammation modulation	Infract volume: 30% decrease ($p < 0.05$); Rotarod test: 97% improve ($p < 0.01$)*; Forelimb grip strength: 40% improve ($p < 0.01$)*

**Compare with vehicle-treated stroke animals.*

a comparable therapeutic potential to MSCs themselves, but are relatively safer in application, and can pass through the BBB far more easily than cells (87). Studies demonstrated that administration of BM-MSC or ESC-derived exosomes could significantly increases neurogenesis and vasculogenesis, and promotes functional recovery in stroke animal (88, 89).

Likewise, accumulating evidence demonstrated the potent neuroprotective properties of DPSC-derived EVs. An *in vitro* study showed that DPSC-EVs which were grown on laminin-coated microcarriers display neuroprotective properties in 6-OHDA-exposed human dopaminergic neurons (90). DPSC-EVs also reduce cytotoxicity through anti-apoptotic mechanism by upregulating endogenous Bcl-2, and decrease the expression of the pro-apoptotic regulator Bax in Aβ peptide-exposed human neuroblastoma (SH-SY5Y) cells (54). An *in vivo* study showed that exosomes derived from DPSCs have beneficial effects after focal cerebral ischemia in the rat by stimulating angiogenesis and neurogenesis (91). In addition, the therapeutic potential of DPSC-derived conditioned medium (CM) was found to be similar to that of the injection of living cells in animal model of stroke, leading to motor function improvement and infarct volume reduction (76). Moreover, CM from human DPSCs also induced significant neuroprotection, enhanced neuronal sprouting, and reduced neuroinflammation in a mouse model of Alzheimer disease (92). DPSC-derived exosomes were further shown to exert strong anti-inflammatory effects at levels comparable to those of glucocorticoids. They also suppress cathepsin B and matrix metalloproteinase (MMP) activities at the site of inflammation in mice, likely mediated by the transport of annexin A1, phospholipases, and lipid mediators to the site of inflammation (93). Taken as a whole, these studies showed the potential of DPSC-derived exosomes for the treatment of central nervous system disorders.

Investigation of molecules within EVs provides new insight to EV-mediated beneficial mechanism, although determining the exact composition and content of the exosomal content (cargo) produced by different cell types is hard to establish due to inevitable differences regarding the conditions in which the cells are prepared and processed (83). High-throughput mass spectrometry-based analysis of proteins revealed some surface receptors (CD105, CD73, CD29, CD81, and CD44), signaling molecules (many of which are involved in controlling of TGF-β, BMP, MAPK, and PPAR recipient cell signaling pathways), adhesion molecules and MSC-associated markers which may account for the therapeutic potential of MSC-derived EVs (94, 95). Baglio et al. (96) reported a substantial similarity between the most represented miRNAs in ADSC and BM-MSC exosomes, but their relative proportions are different. The top 5 most abundant miRNAs (accounted for 50 % of the total miRNA reads) in ADSC exosomes were miR-486-5p, miR-10a-5p, miR-10b-5p, miR-191-5p, and miR-222-3p, while miR-143-3p, miR-10b-5p, miR-486-5p, miR-22-3p, and miR-21-5p were among the most abundant for BM-MSC exosomes. Besides, exosome libraries were highly enriched in the class of tRNAs, which represented >50 % of total small RNAs in ADSC exosomes and 23–35% in BM-MSC exosomes. However, since the studies of DPSC exosomes are just at the initial stage, there is no exactly content of these exosomes reported.

POSSIBLE MECHANISMS OF DPSC THERAPY FOR ISCHEMIC STROKE

Previous studies suggested that human DPSCs potentially differentiate into functional neural progenitors or neurons which may integrate into the brain (64, 97, 98). Similarly, studies showed that grafted DPSCs survive, migrated to infarct boundary zones, and differentiate into neurons and astrocytes in the rat. The cells also express neuron-specific markers including βIII tubulin and NF (52, 72). However, only a very small part of transplanted DPSCs (2.3 ± 0.7%) survived in the post-stroke brain, migrated to the peri-infarction areas, and differentiated into astrocytes (51.0 ± 8.6% $GFAP^+$) in preference to neurons (8.7 ± 6.1% $NeuN^+$) (68). Hence, the therapeutic potential of DPSCs is believed to be mainly exerted by their bystander effects (**Figure 2**) (76).

DPSCs have the potential to improve the microenvironment and enhancing neurogenesis (47, 64, 99, 100). DPSCs also have been shown to exert potent immune-modulatory properties *via* inhibition of activated T cell responses (27) and peripheral blood mononuclear cell proliferation (101), regulating the expression of inflammatory factors such as TGF-β and interleukin (IL)-6 (102), and the induction of Fas ligand-mediated T cell apoptosis (103). Although the suppression of T cell proliferation seen in *in vitro* studies is now established, this property of DPSCs may not be the sole mechanism of action *in vivo*, particularly since blood circulation increases the number of T cells perpetually. More studies are therefore warranted to further understand the interaction between DPSCs and the immune system because this cross talk has important therapeutic implications.

LIMITATIONS OF DPSCs AND CHALLENGES RELATED TO THEIR USE

Though DPSCs have a higher proliferation rate than MSCs, it still needs at least 1 to 2 months to acquire enough cells for therapy from primary isolation (104) (**Table 4**), which may limit their use at the acute stage of acute onset diseases. The long-term side effects associated with the use of DPSCs also have not been sufficiently studied so far. Further studies are warranted to clarify possible long-term risks associated with the use of these cells, as well as optimal cell preparation, storage and application procedures including routes and time points of application. Tailored potency assays for clinical trials are also lacking, and the optimal route of delivery awaits detailed investigation. Moreover, clinical investigation of the cells has just started (105) so appropriate double-blinded, randomized clinical trials have not yet been reported, currently preventing any conclusion on a potential clinical efficacy of these cells. In addition, further studies thoroughly assessing efficacy, safety and also the content of DPSC-derived EVs are required since EVs are highly promising therapeutic tools for regenerative medicine, but a thorough proof of concept is still missing. Additional research is also needed to capitalize on the DPSC differentiation potential. This might require specialized stroke models, for instance mimicking lacunar stroke, that may be more permissible

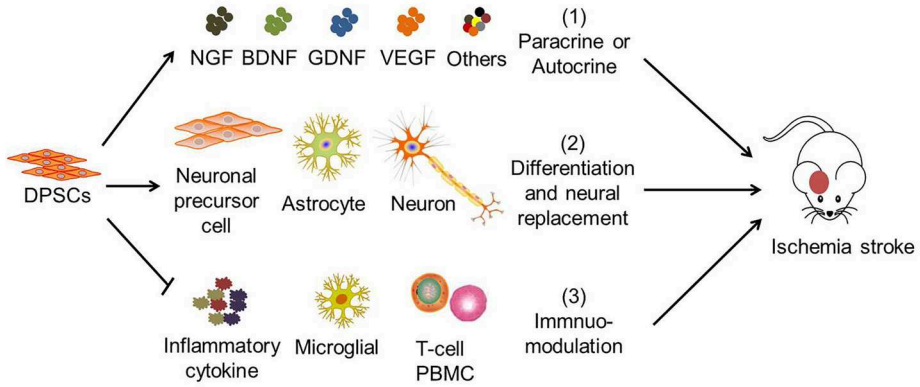

FIGURE 2 | The mechanisms of DPSC therapy for ischemic stroke. The therapeutic effects of DPSCs in stroke are attributed to (1) paracrine or autocrine production of cytokines and growth factors, (2) neural replacement through differentiation into neuronal progenitor cells, astrocytes and neuron-like cells, (3) immuno-modulation with mitigation of pro-inflammatory cytokine expression, of microglial activation, inhibition of activated T-cell response, and peripheral blood mononuclear cell (PBMC) proliferation. (1) and (3) are believed to be the main therapeutic effects of DPSCs.

TABLE 4 | The comparison of DPSCs with other stem cells.

	DPSCs	ESCs	NSCs	MSCs		
				BM-MSCs	ADSCs	UC-MSCs
Basic abilities						
Proliferation potential	++	++	+/–	+	+	++
Neurogenic differentiation	+	++	++	+/–	+/–	+/–
Migration abilities	++	++	+	+	+	+
Autologous application abilities	++	––	–	++	++	–
Required cultivation time to achieve sufficient cell numbers	1–2 months	1–2 months	>2 months	1–2 months	1–2 months	1–2 months
Cryopreservation abilities	+	+	+/–	+	+	+
Cell banking opportunities for adults	+	+/–	–	+/–	+/–	+/–
General amount of information available about cell properties	–	+	+	++	+	+

(++) very high, (+) high, (+/–) average, (–) low, (––) very low.

for tissue restoration, and/or the use of biomaterials to support cell engraftment and survival (106).

CONCLUSIONS

This review summarizes the main DPSC characteristics including surface marker expression, proliferation and differentiation potential, cytokine and trophic factor secretion ability, as well as therapeutic effects in *in vitro* and *in vivo* stroke models. It also elucidates important underlying therapeutic mechanisms. DPSCs express a variety of markers that are found on MSCs, ESCs, and NSCs. Although they can differentiate into different types of neuronal cells, bystander effects are believed to be their predominant therapeutic mechanism. DPSCs are widely available, easily accessible, and can support well-established stroke therapies, thereby potentially extending the therapeutic time window and/or augmenting the therapeutic impact. DPSCs differ from the other adult stem cell populations due to their embryonic origin from the neural crest and are of special interest because of their neurotropic character, which makes DPSCs and their exosomes particularly attractive as a new therapeutic tool for the alleviation of symptoms of stroke and, potentially, other neurodegenerative diseases. Besides, DPSCs exhibit a higher proliferation rate, higher expression of trophic factors, stronger neuroprotective effects and neuro-supportive properties *in vitro* and *in vivo* than MSC populations (**Table 4**), which provide a tempting prospect for stroke treatment.

AUTHOR CONTRIBUTIONS

XL, ZS, and CC wrote the manuscript. JB and SL designed the literature assessment strategy and edited the manuscript.

FUNDING

The work was fund by the National Natural Science Foundation of China (81300985), Natural Science Foundation of Liaoning Province (2015020549), LiaoNing Revitalization Talents Program (XLYC1807124) and Dalian Municipal Health and Family Planning Project (1711014, 1811014).

REFERENCES

1. Rothwell PM. The high cost of not funding stroke research: a comparison with heart disease and cancer. *Lancet.* (2001) 357:1612–6. doi: 10.1016/s0140-6736(00)04730-9
2. Zhang Y, Zhang P, Shen X, Tian S, Wu Y, Zhu Y, et al. Early exercise protects the blood-brain barrier from ischemic brain injury via the regulation of MMP-9 and occludin in rats. *Int J Mol Sci.* (2013) 14:11096–112. doi: 10.3390/ijms140611096
3. Brandt T, von Kummer R, Muller-Kuppers M, Hacke W. Thrombolytic therapy of acute basilar artery occlusion. Variables affecting recanalization and outcome. *Stroke.* (1996) 27:875–81.
4. Goyal M, Demchuk AM, Menon BK, Eesa M, Rempel JL, Thornton J, et al. Randomized assessment of rapid endovascular treatment of ischemic stroke. *N Engl J Med.* (2015) 372:1019–30. doi: 10.56/NEJMoa1414905
5. Janowski M, Wagner DC, Boltze J. Stem cell-based tissue replacement after stroke: factual necessity or notorious fiction? *Stroke.* (2015) 46:2354–63. doi: 10.1161/STROKEAHA.114.007803
6. Scheibe F, Ladhoff J, Huck J, Grohmann M, Blazej K, Oersal A, et al. Immune effects of mesenchymal stromal cells in experimental stroke. *J Cereb Blood Flow Metab.* (2012) 32:1578–88. doi: 10.038/jcbfm.2012.55
7. Trounson A, McDonald C. Stem cell therapies in clinical trials: progress and challenges. *Cell Stem Cell.* (2015) 17:11–22. doi: 10.1016/j.stem.2015.06.007
8. Boese AC, Le QE, Pham D, Hamblin MH, Lee JP. Neural stem cell therapy for subacute and chronic ischemic stroke. *Stem Cell Res Ther.* (2018) 9:154. doi: 10.1186/s13287-018-0913-2
9. Leong WK, Lewis MD, Koblar SA. Concise review: preclinical studies on human cell-based therapy in rodent ischemic stroke models: where are we now after a decade? *Stem Cells.* (2013) 31:1040–3. doi: 10.02/stem.348
10. Prockop DJ, Brenner M, Fibbe WE, Horwitz E, Le Blanc K, Phinney DG, et al. Defining the risks of mesenchymal stromal cell therapy. *Cytotherapy.* (2010) 12:576–8. doi: 10.3109/14653249.2010.507330
11. Lees JS, Sena ES, Egan KJ, Antonic A, Koblar SA, Howells DW, et al. Stem cell-based therapy for experimental stroke: a systematic review and meta-analysis. *Int J Stroke.* (2012) 7:582–8. doi: 10.1111/j.747-4949.2012.00797.x
12. Savitz SI. Developing cellular therapies for stroke. *Stroke.* (2015) 46:2026–31. doi: 10.1161/STROKEAHA.115.007149
13. Kalladka D, Muir KW. Brain repair: cell therapy in stroke. *Stem Cells Cloning.* (2014) 7:31–44. doi: 10.2147/SCCAA.S38003
14. Sarmah D, Agrawal V, Rane P, Bhute S, Watanabe M, Kalia K, et al. Mesenchymal stem cell therapy in ischemic stroke: a meta-analysis of preclinical studies. *Clin Pharmacol Ther.* (2018) 103:990–8. doi: 10.1002/cpt.927
15. Nagpal A, Choy FC, Howell S, Hillier S, Chan F, Hamilton-Bruce MA, et al. Safety and effectiveness of stem cell therapies in early-phase clinical trials in stroke: a systematic review and meta-analysis. *Stem Cell Res Ther.* (2017) 8:191. doi: 10.1186/s13287-017-0643-x
16. Kerkis I, Kerkis A, Dozortsev D, Stukart-Parsons GC, Gomes Massironi SM, Pereira LV, et al. Isolation and characterization of a population of immature dental pulp stem cells expressing OCT-4 and other embryonic stem cell markers. *Cells Tissues Organs.* (2006) 184:105–16. doi: 10.1159/000099617
17. Gronthos S, Mankani M, Brahim J, Robey PG, Shi S. Postnatal human dental pulp stem cells (DPSCs) *in vitro* and *in vivo*. *Proc Natl Acad Sci USA.* (2000) 97:13625–30. doi: 10.1073/pnas.240309797
18. Martens W, Bronckaers A, Politis C, Jacobs R, Lambrichts I. Dental stem cells and their promising role in neural regeneration: an update. *Clin Oral Investig.* (2013) 17:1969–83. doi: 10.007/s00784-013-1030-3
19. Dominici M, Le Blanc K, Mueller I, Slaper-Cortenbach I, Marini F, Krause D, et al. Minimal criteria for defining multipotent mesenchymal stromal cells. The international society for cellular therapy position statement. *Cytotherapy.* (2006) 8:315–7. doi: 10.1080/14653240600855905
20. Egusa H, Sonoyama W, Nishimura M, Atsuta I, Akiyama K. Stem cells in dentistry–part I: stem cell sources. *J Prosthodont Res.* (2012) 56:151–65. doi: 10.1016/j.jpor.2012.06.001
21. Zhang W, Walboomers XF, Shi S, Fan M, Jansen JA. Multilineage differentiation potential of stem cells derived from human dental pulp after cryopreservation. *Tissue Eng.* (2006) 12:2813–23. doi: 10.1089/ten.2006.12.813
22. Papaccio G, Graziano A, d'Aquino R, Graziano MF, Pirozzi G, Menditti D, et al. Long-term cryopreservation of dental pulp stem cells (SBP-DPSCs) and their differentiated osteoblasts: a cell source for tissue repair. *J Cell Physiol.* (2006) 208:319–25. doi: 10.1002/jcp.20667
23. Weise G, Lorenz M, Posel C, Maria Riegelsberger U, Storbeck V, Kamprad M, et al. Transplantation of cryopreserved human umbilical cord blood mononuclear cells does not induce sustained recovery after experimental stroke in spontaneously hypertensive rats. *J Cereb Blood Flow Metab.* (2014) 34:e1–9. doi: 10.1038/jcbfm.2013.185
24. Perry BC, Zhou D, Wu X, Yang FC, Byers MA, Chu TM, et al. Collection, cryopreservation, and characterization of human dental pulp-derived mesenchymal stem cells for banking and clinical use. *Tissue Eng Part C Methods.* (2008) 14:149–56. doi: 10.1089/ten.tec.2008.0031
25. Fawzy El-Sayed KM, Dorfer C, Fandrich F, Gieseler F, Moustafa MH, Ungefroren H. Adult mesenchymal stem cells explored in the dental field. *Adv Biochem Eng Biotechnol.* (2013) 130:89–103. doi: 10.1007/10_2012_151
26. Gronthos S, Brahim J, Li W, Fisher LW, Cherman N, Boyde A, et al. Stem cell properties of human dental pulp stem cells. *J Dent Res.* (2002) 81:531–5. doi: 10.1177/154405910208100806
27. Pierdomenico L, Bonsi L, Calvitti M, Rondelli D, Arpinati M, Chirumbolo G, et al. Multipotent mesenchymal stem cells with immunosuppressive activity can be easily isolated from dental pulp. *Transplantation.* (2005) 80:836–42. doi: 10.1097/01.tp.0000173794.72151.88
28. Balic A, Aguila HL, Caimano MJ, Francone VP, Mina M. Characterization of stem and progenitor cells in the dental pulp of erupted and unerupted murine molars. *Bone.* (2010) 46:1639–51. doi: 10.016/j.bone.2010.02.019
29. Kawashima N. Characterisation of dental pulp stem cells: a new horizon for tissue regeneration? *Arch Oral Biol.* (2012) 57:1439–58. doi: 10.016/j.archoralbio.2012.08.010
30. Palmieri A, Pezzetti F, Graziano A, Riccardo D, Zollino I, Brunelli G, et al. Comparison between osteoblasts derived from human dental pulp stem cells and osteosarcoma cell lines. *Cell Biol Int.* (2008) 32:733–8. doi: 10.1016/j.cellbi.2008.02.003
31. Foudah D, Redondo J, Caldara C, Carini F, Tredici G, Miloso M. Human mesenchymal stem cells express neuronal markers after osteogenic and adipogenic differentiation. *Cell Mol Biol Lett.* (2013) 18:163–86. doi: 10.2478/s11658-013-0083-2
32. Blondheim NR, Levy YS, Ben-Zur T, Burshtein A, Cherlow T, Kan I, et al. Human mesenchymal stem cells express neural genes, suggesting a neural predisposition. *Stem Cells Dev.* (2006) 15:141–64. doi: 10.1089/scd.2006.15.141
33. Sakai K, Yamamoto A, Matsubara K, Nakamura S, Naruse M, Yamagata M, et al. Human dental pulp-derived stem cells promote locomotor recovery after complete transection of the rat spinal cord by multiple neuro-regenerative mechanisms. *J Clin Invest.* (2012) 122:80–90. doi: 10.1172/JCI59251
34. Cheng PH, Snyder B, Fillos D, Ibegbu CC, Huang AH, Chan AW. Postnatal stem/progenitor cells derived from the dental pulp of adult chimpanzee. *BMC Cell Biol.* (2008) 9:20. doi: 10.1186/471-2121-9-20
35. Kiraly M, Porcsalmy B, Pataki A, Kadar K, Jelitai M, Molnar B, et al. Simultaneous PKC and cAMP activation induces differentiation of human dental pulp stem cells into functionally active neurons. *Neurochem Int.* (2009) 55:323–32. doi: 10.1016/j.neuint.2009.03.017
36. Chiu HY, Lin CH, Hsu CY, Yu J, Hsieh CH, Shyu WC. IGF1R(+) dental pulp stem cells enhanced neuroplasticity in hypoxia-ischemia model. *Mol Neurobiol.* (2017) 54:8225–41. doi: 10.1007/s12035-016-0210-y
37. Patel M, Smith AJ, Sloan AJ, Smith G, Cooper PR. Phenotype and behaviour of dental pulp cells during expansion culture. *Arch Oral Biol.* (2009) 54:898–908. doi: 10.1016/j.archoralbio.2009.06.008
38. Karbanova J, Soukup T, Suchanek J, Pytlik R, Corbeil D, Mokry J. Characterization of dental pulp stem cells from impacted third molars cultured in low serum-containing medium. *Cells Tissues Organs.* (2011) 193:344–65. doi: 10.1159/000321160
39. Osathanon T, Nowwarote N, Pavasant P. Basic fibroblast growth factor inhibits mineralization but induces neuronal differentiation by human dental pulp stem cells through a FGFR and PLCgamma signaling pathway. *J Cell Biochem.* (2011) 112:1807–16. doi: 10.002/jcb.23097

40. Foudah D, Monfrini M, Donzelli E, Niada S, Brini AT, Orciani M, et al. Expression of neural markers by undifferentiated mesenchymal-like stem cells from different sources. *J Immunol Res.* (2014) 2014:987678. doi: 10.1155/2014/987678
41. Xiao L, Ide R, Saiki C, Kumazawa Y, Okamura H. Human dental pulp cells differentiate toward neuronal cells and promote neuroregeneration in adult organotypic hippocampal slices *in vitro*. *Int J Mol Sci.* (2017) 18:E1745. doi: 10.3390/ijms18081745
42. Li D, Zou XY, El-Ayachi I, Romero LO, Yu Z, Iglesias-Linares A, et al. Human dental pulp stem cells and gingival mesenchymal stem cells display action potential capacity *in vitro* after neuronogenic differentiation. *Stem Cell Rev.* (2018) 15:67–81. doi: 10.1007/s12015-018-9854-5
43. Ross JJ, Verfaillie CM. Evaluation of neural plasticity in adult stem cells. *Philos Trans R Soc Lond B Biol Sci.* (2008) 363:199–205. doi: 10.1098/rstb.2006.21
44. Palmer TD, Schwartz PH, Taupin P, Kaspar B, Stein SA, Gage FH. Cell culture. Progenitor cells from human brain after death. *Nature.* (2001) 411:42–3. doi: 10.1038/35075141
45. Zhang Y, Xing Y, Jia L, Ji Y, Zhao B, Wen Y, et al. An *in vitro* comparative study of multisource derived human mesenchymal stem cells for bone tissue engineering. *Stem Cells Dev.* (2018) 27:1634–45. doi: 10.089/scd.2018.0119
46. Jin Q, Yuan K, Lin W, Niu C, Ma R, Huang Z. Comparative characterization of mesenchymal stem cells from human dental pulp and adipose tissue for bone regeneration potential. *Artif Cells Nanomed Biotechnol.* (2019) 47:1577–84. doi: 10.080/21691401.2019.1594861
47. Mead B, Logan A, Berry M, Leadbeater W, Scheven BA. Paracrine-mediated neuroprotection and neuritogenesis of axotomised retinal ganglion cells by human dental pulp stem cells: comparison with human bone marrow and adipose-derived mesenchymal stem cells. *PLoS ONE.* (2014) 9:e109305. doi: 10.1371/journal.pone.0109305
48. Caseiro AR, Pereira T, Ivanova G, Luis AL, Mauricio AC. Neuromuscular regeneration: perspective on the application of mesenchymal stem cells and their secretion products. *Stem Cells Int.* (2016) 2016:9756973. doi: 10.1155/2016/9756973
49. Hayashi Y, Murakami M, Kawamura R, Ishizaka R, Fukuta O, Nakashima M. CXCL14 and MCP1 are potent trophic factors associated with cell migration and angiogenesis leading to higher regenerative potential of dental pulp side population cells. *Stem Cell Res Ther.* (2015) 6:111. doi: 10.1186/s13287-015-0088-z
50. Alge DL, Zhou D, Adams LL, Wyss BK, Shadday MD, Woods EJ, et al. Donor-matched comparison of dental pulp stem cells and bone marrow-derived mesenchymal stem cells in a rat model. *J Tissue Eng Regen Med.* (2010) 4:73–81. doi: 10.1002/term.220
51. Mayo V, Sawatari Y, Huang CY, Garcia-Godoy F. Neural crest-derived dental stem cells–where we are and where we are going. *J Dent.* (2014) 42:1043–51. doi: 10.16/j.jdent.2014.04.007
52. Song M, Lee JH, Bae J, Bu Y, Kim EC. Human dental pulp stem cells are more effective than human bone marrow-derived mesenchymal stem cells in cerebral ischemic injury. *Cell Trans.* (2017) 26:1001–16. doi: 10.3727/096368916X694391
53. Ye X, Hu J, Cui G. therapy effects of bone marrow stromal cells on ischemic stroke. *Oxid Med Cell Longev.* (2016) 2016:7682960. doi: 10.1155/2016/7682960
54. Ahmed Nel M, Murakami M, Hirose Y, Nakashima M. Therapeutic potential of dental pulp stem cell secretome for Alzheimer's disease treatment: an *in vitro* study. *Stem Cells Int.* (2016) 2016:8102478. doi: 10.1155/2016/8102478
55. Ishizaka R, Hayashi Y, Iohara K, Sugiyama M, Murakami M, Yamamoto T, et al. Stimulation of angiogenesis, neurogenesis and regeneration by side population cells from dental pulp. *Biomaterials.* (2013) 34:1888–97. doi: 10.016/j.biomaterials.2012.10.045
56. Ge J, Guo L, Wang S, Zhang Y, Cai T, Zhao RC, et al. The size of mesenchymal stem cells is a significant cause of vascular obstructions and stroke. *Stem Cell Rev.* (2014) 10:295–303. doi: 10.1007/s12015-013-9492-x
57. Boltze J, Arnold A, Walczak P, Jolkkonen J, Cui L, Wagner DC. The dark side of the force–constraints and complications of cell therapies for stroke. *Front Neurol.* (2015) 6:155. doi: 10.3389/fneur.2015.00155
58. Li T, Li C, Zhang CY, Zhao J. Effect of accutase or trypsin dissociation on the apoptosis of human striatum-derived neural stem cells. *Zhongguo Yi Xue Ke Xue Yuan Xue Bao.* (2015) 37:185–94. doi: 10.3881/j.issn.1000-503X.2015.02.009
59. Suchanek J, Soukup T, Visek B, Ivancakova R, Kucerova L, Mokry J. Dental pulp stem cells and their characterization. *Biomed Pap Med Fac Univ Palacky Olomouc Czech Repub.* (2009) 153:31–5. doi: 10.5507/bp.2009.005
60. Fischer UM, Harting MT, Jimenez F, Monzon-Posadas WO, Xue H, Savitz SI, et al. Pulmonary passage is a major obstacle for intravenous stem cell delivery: the pulmonary first-pass effect. *Stem Cells Dev.* (2009) 18:683–92. doi: 10.1089/scd.2008.0253
61. Nishimura M, Nguyen L, Watanabe N, Fujita Y, Sawamoto O, Matsumoto S. Development and characterization of novel clinical grade neonatal porcine bone marrow-derived mesenchymal stem cells. *Xenotransplantation.* (2019) 15:12501. doi: 10.1111/xen.12501
62. Cui LL, Kerkela E, Bakreen A, Nitzsche F, Andrzejewska A, Nowakowski A, et al. The cerebral embolism evoked by intra-arterial delivery of allogeneic bone marrow mesenchymal stem cells in rats is related to cell dose and infusion velocity. *Stem Cell Res Ther.* (2015) 6:11. doi: 10.1186/scrt544
63. Apel C, Forlenza OV, de Paula VJ, Talib LL, Denecke B, Eduardo CP, et al. The neuroprotective effect of dental pulp cells in models of Alzheimer's and Parkinson's disease. *J Neural Transm (Vienna).* (2009) 116:71–8. doi: 10.1007/s00702-008-0135-3
64. Nosrat IV, Smith CA, Mullally P, Olson L, Nosrat CA. Dental pulp cells provide neurotrophic support for dopaminergic neurons and differentiate into neurons *in vitro*; implications for tissue engineering and repair in the nervous system. *Eur J Neurosci.* (2004) 19:2388–98. doi: 10.1111/j.0953-816X.2004.03314.x
65. Song M, Jue SS, Cho YA, Kim EC. Comparison of the effects of human dental pulp stem cells and human bone marrow-derived mesenchymal stem cells on ischemic human astrocytes *in vitro*. *J Neurosci Res.* (2015) 93:973–83. doi: 10.1002/jnr.23569
66. Sugiyama M, Iohara K, Wakita H, Hattori H, Ueda M, Matsushita K, et al. Dental pulp-derived CD31(-)/CD146(-) side population stem/progenitor cells enhance recovery of focal cerebral ischemia in rats. *Tissue Eng Part A.* (2011) 17:1303–11. doi: 10.089/ten.TEA.2010.0306
67. Yamagata M, Yamamoto A, Kako E, Kaneko N, Matsubara K, Sakai K, et al. Human dental pulp-derived stem cells protect against hypoxic-ischemic brain injury in neonatal mice. *Stroke.* (2013) 44:551–4. doi: 10.1161/STROKEAHA.112.676759
68. Leong WK, Henshall TL, Arthur A, Kremer KL, Lewis MD, Helps SC, et al. Human adult dental pulp stem cells enhance poststroke functional recovery through non-neural replacement mechanisms. *Stem Cells Transl Med.* (2012) 1:177–87. doi: 10.5966/sctm.2011-0039
69. Yang C, Li X, Sun L, Guo W, Tian W. Potential of human dental stem cells in repairing the complete transection of rat spinal cord. *J Neural Eng.* (2017) 14:026005. doi: 10.1088/1741-2552/aa596b
70. Sowa K, Nito C, Nakajima M, Suda S, Nishiyama Y, Sakamoto Y, et al. Impact of dental pulp stem cells overexpressing hepatocyte growth factor after cerebral ischemia/reperfusion in rats. *Mol Ther Methods Clin Dev.* (2018) 10:281–90. doi: 10.1016/j.omtm.2018.07.009
71. Zhang X, Zhou Y, Li H, Wang R, Yang D, Li B, et al. Intravenous administration of DPSCs and BDNF improves neurological performance in rats with focal cerebral ischemia. *Int J Mol Med.* (2018) 41:3185–94. doi: 10.892/ijmm.2018.3517
72. Zhang X, Zhou Y, Li H, Wang R, Yang D, Li B, et al. Transplanted dental pulp stem cells migrate to injured area and express neural markers in a rat model of cerebral ischemia. *Cell Physiol Biochem.* (2018) 45:258–66. doi: 10.1159/000486772
73. Kumasaka A, Kanazawa K, Ohke H, Miura I, Miura Y. Post-ischemic intravenous administration of allogeneic dental pulp-derived neurosphere cells ameliorated outcomes of severe forebrain ischemia in rats. *Neurocrit Care.* (2017) 26:133–42. doi: 10.1007/s12028-016-0304-4
74. Nito C, Sowa K, Nakajima M, Sakamoto Y, Suda S, Nishiyama Y, et al. Transplantation of human dental pulp stem cells ameliorates brain damage following acute cerebral ischemia. *Biomed Pharmacother.* (2018) 108:1005–14. doi: 10.1016/j.biopha.2018.09.084

75. Yang KL, Chen MF, Liao CH, Pang CY, Lin PY. A simple and efficient method for generating Nurr1-positive neuronal stem cells from human wisdom teeth (tNSC) and the potential of tNSC for stroke therapy. *Cytotherapy.* (2009) 11:606–17. doi: 10.1080/14653240902806994
76. Inoue T, Sugiyama M, Hattori H, Wakita H, Wakabayashi T, Ueda M. Stem cells from human exfoliated deciduous tooth-derived conditioned medium enhance recovery of focal cerebral ischemia in rats. *Tissue Eng Part A.* (2013) 19:24–9. doi: 10.1089/ten.TEA.2011.0385
77. Boltze J, Lukomska B, Jolkkonen J. Mesenchymal stromal cells in stroke: improvement of motor recovery or functional compensation? *J Cereb Blood Flow Metab.* (2014) 34:1420–1. doi: 10.038/jcbfm.2014.94
78. Moller K, Boltze J, Posel C, Seeger J, Stahl T, Wagner DC. Sterile inflammation after permanent distal MCA occlusion in hypertensive rats. *J Cereb Blood Flow Metab.* (2014) 34:307–15. doi: 10.1038/jcbfm.2013.199
79. Moller K, Posel C, Kranz A, Schulz I, Scheibe J, Didwischus N, et al. Arterial hypertension aggravates innate immune responses after experimental stroke. *Front Cell Neurosci.* (2015) 9:461. doi: 10.3389/fncel.2015.00461
80. Siesjo BK. Pathophysiology and treatment of focal cerebral ischemia. Part II: mechanisms of damage and treatment. *J Neurosurg.* (1992) 77:337–54. doi: 10.3171/jns.1992.77.3.0337
81. Titomanlio L, Fernandez-Lopez D, Manganozzi L, Moretti R, Vexler ZS, Gressens P. Pathophysiology and neuroprotection of global and focal perinatal brain injury: lessons from animal models. *Pediatr Neurol.* (2015) 52:566–84. doi: 10.1016/j.pediatrneurol.2015.01.016
82. Offner H, Vandenbark AA, Hurn PD. Effect of experimental stroke on peripheral immunity: CNS ischemia induces profound immunosuppression. *Neuroscience.* (2009) 158:1098–111. doi: 10.16/j.neuroscience.2008.05.033
83. Raposo G, Stoorvogel W. Extracellular vesicles: exosomes, microvesicles, and friends. *J Cell Biol.* (2013) 200:373–83. doi: 10.1083/jcb.201211138
84. van der Pol E, Boing AN, Harrison P, Sturk A, Nieuwland R. Classification, functions, and clinical relevance of extracellular vesicles. *Pharmacol Rev.* (2012) 64:676–705. doi: 10.1124/pr.112.005983
85. Ratajczak J, Miekus K, Kucia M, Zhang J, Reca R, Dvorak P, et al. Embryonic stem cell-derived microvesicles reprogram hematopoietic progenitors: evidence for horizontal transfer of mRNA and protein delivery. *Leukemia.* (2006) 20:847–56. doi: 10.1038/sj.leu.2404132
86. Yu B, Zhang X, Li X. Exosomes derived from mesenchymal stem cells. *Int J Mol Sci.* (2014) 15:4142–57. doi: 10.3390/ijms15034142
87. Alvarez-Erviti L, Seow Y, Yin H, Betts C, Lakhal S, Wood MJ. Delivery of siRNA to the mouse brain by systemic injection of targeted exosomes. *Nat Biotechnol.* (2011) 29:341–5. doi: 10.1038/nbt.807
88. Xin H, Li Y, Cui Y, Yang JJ, Zhang ZG, Chopp M. Systemic administration of exosomes released from mesenchymal stromal cells promote functional recovery and neurovascular plasticity after stroke in rats. *J Cereb Blood Flow Metab.* (2013) 33:1711–5. doi: 10.038/jcbfm.2013.152
89. Kalani A, Chaturvedi P, Kamat PK, Maldonado C, Bauer P, Joshua IG, et al. Curcumin-loaded embryonic stem cell exosomes restored neurovascular unit following ischemia-reperfusion injury. *Int J Biochem Cell Biol.* (2016) 79:360–9. doi: 10.1016/j.biocel.2016.09.002
90. Jarmalaviciute A, Tunaitis V, Pivoraite U, Venalis A, Pivoriunas A. Exosomes from dental pulp stem cells rescue human dopaminergic neurons from 6-hydroxy-dopamine-induced apoptosis. *Cytotherapy.* (2015) 17:932–9. doi: 10.1016/j.jcyt.2014.07.013
91. Stanko P, Altanerova U, Jakubechova J, Repiska V, Altaner C. Dental mesenchymal stem/stromal cells and their exosomes. *Stem Cells Int.* (2018) 2018:8973613. doi: 10.1155/2018/8973613
92. Mita T, Furukawa-Hibi Y, Takeuchi H, Hattori H, Yamada K, Hibi H, et al. Conditioned medium from the stem cells of human dental pulp improves cognitive function in a mouse model of Alzheimer's disease. *Behav Brain Res.* (2015) 293:189–97. doi: 10.1016/j.bbr.2015.07.043
93. Pivoraite U, Jarmalaviciute A, Tunaitis V, Ramanauskaite G, Vaitkuviene A, Kaseta V, et al. Exosomes from human dental pulp stem cells suppress carrageenan-induced acute inflammation in mice. *Inflammation.* (2015) 38:1933–41. doi: 10.007/s10753-015-0173-6
94. Kim HS, Choi DY, Yun SJ, Choi SM, Kang JW, Jung JW, et al. Proteomic analysis of microvesicles derived from human mesenchymal stem cells. *J Proteome Res.* (2012) 11:839–49. doi: 10.1021/pr200682z
95. Vallabhaneni KC, Penfornis P, Dhule S, Guillonneau F, Adams KV, Mo YY, et al. Extracellular vesicles from bone marrow mesenchymal stem/stromal cells transport tumor regulatory microRNA, proteins, and metabolites. *Oncotarget.* (2015) 6:4953–67. doi: 10.18632/oncotarget.3211
96. Baglio SR, Rooijers K, Koppers-Lalic D, Verweij FJ, Perez Lanzon M, Zini N, et al. Human bone marrow- and adipose-mesenchymal stem cells secrete exosomes enriched in distinctive miRNA and tRNA species. *Stem Cell Res Ther.* (2015) 6:127. doi: 10.1186/s13287-015-0116-z
97. Kiraly M, Kadar K, Horvathy DB, Nardai P, Racz GZ, Lacza Z, et al. Integration of neuronally predifferentiated human dental pulp stem cells into rat brain *in vivo*. *Neurochem Int.* (2011) 59:371–81. doi: 10.1016/j.neuint.2011.01.006
98. Fang CZ, Yang YJ, Wang QH, Yao Y, Zhang XY, He XH. Intraventricular injection of human dental pulp stem cells improves hypoxic-ischemic brain damage in neonatal rats. *PLoS ONE.* (2013) 8:e66748. doi: 10.1371/journal.pone.0066748
99. Nosrat IV, Widenfalk J, Olson L, Nosrat CA. Dental pulp cells produce neurotrophic factors, interact with trigeminal neurons *in vitro*, and rescue motoneurons after spinal cord injury. *Dev Biol.* (2001) 238:120–32. doi: 10.1006/dbio.2001.0400
100. Matsushita K, Motani R, Sakuta T, Yamaguchi N, Koga T, Matsuo K, et al. The role of vascular endothelial growth factor in human dental pulp cells: induction of chemotaxis, proliferation, and differentiation and activation of the AP-1-dependent signaling pathway. *J Dent Res.* (2000) 79:1596–603. doi: 10.177/00220345000790081201
101. Wada N, Menicanin D, Shi S, Bartold PM, Gronthos S. Immunomodulatory properties of human periodontal ligament stem cells. *J Cell Physiol.* (2009) 219:667–76. doi: 10.1002/jcp.21710
102. Tomic S, Djokic J, Vasilijic S, Vucevic D, Todorovic V, Supic G, et al. Immunomodulatory properties of mesenchymal stem cells derived from dental pulp and dental follicle are susceptible to activation by toll-like receptor agonists. *Stem Cells Dev.* (2011) 20:695–708. doi: 10.1089/scd.2010.0145
103. Zhao Y, Wang L, Jin Y, Shi S. Fas ligand regulates the immunomodulatory properties of dental pulp stem cells. *J Dent Res.* (2012) 91:948–54. doi: 10.1177/0022034512458690
104. Dong Q, Wang Y, Mohabatpour F, Zheng L, Papagerakis S, Chen D, et al. Dental pulp stem cells: isolation, characterization, expansion, and odontoblast differentiation for tissue engineering. *Methods Mol Biol.* (2019) 1922:91–101. doi: 10.1007/978-1-4939-9012-2_9
105. Nagpal A, Kremer KL, Hamilton-Bruce MA, Kaidonis X, Milton AG, Levi C, et al. TOOTH (The Open study Of dental pulp stem cell Therapy in Humans): study protocol for evaluating safety and feasibility of autologous human adult dental pulp stem cell therapy in patients with chronic disability after stroke. *Int J Stroke.* (2016) 11:575–85. doi: 10.1177/1747493016641111
106. Modo MM, Jolkkonen J, Zille M, Boltze J. Future of animal modeling for poststroke tissue repair. *Stroke.* (2018) 49:1099–106. doi: 10.161/STROKEAHA.117.018293

Conflict of Interest Statement: The authors declare that the research was conducted in the absence of any commercial or financial relationships that could be construed as a potential conflict of interest.

Copyright © 2019 Lan, Sun, Chu, Boltze and Li. This is an open-access article distributed under the terms of the Creative Commons Attribution License (CC BY). The use, distribution or reproduction in other forums is permitted, provided the original author(s) and the copyright owner(s) are credited and that the original publication in this journal is cited, in accordance with accepted academic practice. No use, distribution or reproduction is permitted which does not comply with these terms.

frontiers in Neuroscience

REVIEW
published: 02 August 2019
doi: 10.3389/fnins.2019.00790

Therapeutic Potential of Neurotrophins for Repair After Brain Injury: A Helping Hand From Biomaterials

*Josh Houlton[1], Nashat Abumaria[2,3], Simon F. R. Hinkley[4] and Andrew N. Clarkson[1]**

[1] Brain Health Research Centre, Department of Anatomy, University of Otago, Dunedin, New Zealand, [2] State Key Laboratory of Medical Neurobiology, MOE Frontiers Center for Brain Science, Institute of Brain Science, Fudan University, Shanghai, China, [3] Department of Laboratory Animal Science, Shanghai Medical College, Fudan University, Shanghai, China, [4] The Ferrier Research Institute, Victoria University of Wellington, Petone, New Zealand

OPEN ACCESS

Edited by:
Piotr Walczak,
Johns Hopkins Medicine,
United States

Reviewed by:
Huib Versnel,
University Medical Center Utrecht,
Netherlands
Petr A. Slominsky,
Institute of Molecular Genetics (RAS),
Russia

***Correspondence:**
Andrew N. Clarkson
andrew.clarkson@otago.ac.nz

Specialty section:
This article was submitted to Neurodegeneration, a section of the journal Frontiers in Neuroscience

Received: 14 March 2019
Accepted: 15 July 2019
Published: 02 August 2019

Citation:
Houlton J, Abumaria N, Hinkley SFR and Clarkson AN (2019) Therapeutic Potential of Neurotrophins for Repair After Brain Injury: A Helping Hand From Biomaterials. Front. Neurosci. 13:790. doi: 10.3389/fnins.2019.00790

Stroke remains the leading cause of long-term disability with limited options available to aid in recovery. Significant effort has been made to try and minimize neuronal damage following stroke with use of neuroprotective agents, however, these treatments have yet to show clinical efficacy. Regenerative interventions have since become of huge interest as they provide the potential to restore damaged neural tissue without being limited by a narrow therapeutic window. Neurotrophins, such as brain-derived neurotrophic factor (BDNF), and their high affinity receptors are actively produced throughout the brain and are involved in regulating neuronal activity and normal day-to-day function. Furthermore, neurotrophins are known to play a significant role in both protection and recovery of function following neurodegenerative diseases such as stroke and traumatic brain injury (TBI). Unfortunately, exogenous administration of these neurotrophins is limited by a lack of blood-brain-barrier (BBB) permeability, poor half-life, and rapid degradation. Therefore, we have focused this review on approaches that provide a direct and sustained neurotrophic support using pharmacological therapies and mimetics, physical activity, and potential drug delivery systems, including discussion around advantages and limitations for use of each of these systems. Finally, we discuss future directions of biomaterial drug-delivery systems, including the incorporation of heparan sulfate (HS) in conjunction with neurotrophin-based interventions.

Keywords: neurotrophins, BDNF, Trk receptor, p75 neurotrophic receptor, hydrogel, microsphere encapsulation, electrospun fibers, HSPG

INTRODUCTION

Stroke consistently remains a leading cause of death and disability worldwide (Mozaffarian et al., 2015). While stroke preferentially affects older people, stroke can affect anyone of any age, race, or gender (Feigin et al., 2014). In addition, ethnic disparities are known to exist, for instance, New Zealand Māori, and Pacific Island populations experience a stroke at a much younger age than Europeans (Feigin et al., 2006). With the global population continuing to age, the number of people suffering from a stroke and subsequently living with a lasting disability is also expected to rise. As a result, there is an urgent and unmet need to find treatment options to aid in improving recovery of lost functions.

The central nervous system CNS has a limited capacity to regenerate, which is one of the main causes for why stroke patients recover poorly. In addition, there is a lack of spontaneous recovery seen after stroke, leading to a large personal, and societal burden (Mozaffarian et al., 2015). This burden has led research into investigating neural mechanisms of regeneration and repair, in the hope to restore and improve lost functions following stroke. Depending on the neuronal area affected by the stroke (i.e., motor, speech, or language centers), rehabilitation, mental practice, and music therapies have all been shown to increase the capacity to recover after a stroke (Johansson, 2011). However, in patients who have had a large stroke, rehabilitation is less effective in facilitating an improvement in functional recovery (Johansson, 2011).

Significant work has shown that exogenous administration of GFs can help facilitate the repair of injured CNS tissue via their ability to regulate neuronal growth and survival (Connor and Dragunow, 1998; Sofroniew et al., 2001; Berretta et al., 2014). In particular, BDNF has been highlighted as being a key regulator of rehabilitation-induced recovery after stroke (Ploughman et al., 2007, 2009). Moreover, activity-driven increases in BDNF have also been shown to promote motor recovery after stroke (Fritsch et al., 2010; Clarkson et al., 2011).

The regenerative capabilities of neurotrophin-mediated interventions have already been observed in preclinical models of neurodegenerative diseases. Specifically, systemic administration of BDNF, NGF, and NT-3 have been reported to enhance neurite outgrowth, neurogenesis, and functional recovery in rodent models of stroke (Grill et al., 1997; Jakeman et al., 1998; Ramer et al., 2000; Winkler et al., 2000; Schäbitz et al., 2004, 2007). However, the translation of such treatments into a clinical setting has been challenged by poor BBB permeability, off-target effects on the PNS, and short half-life (Chan et al., 2017). Approximately 98 percent of all compounds targeting the CNS have failed to cross the BBB (Pardridge, 2005), creating a need for alternative approaches. As a novel solution to this issue, various biomaterials have been engineered to provide an effective, and sustained drug-delivery system to the injured brain. These systems allow stem cells and/or small drug molecules including neurotrophins to bypass the BBB (Aizawa et al., 2008) and be delivered directly to the site of injury.

Heparan sulfate, as the GAG cleaved from its protein backbone, is thought to provide a novel approach for the delivery of neurotrophins to the injured CNS. HS plays a critical role in coordinating GFs and mediating their biological potential (Xu and Esko, 2014). This highly sulfated biopolymer is ideally suited as a component of a biomaterial therapeutic for brain injury. It is chemically stable, physiologically tolerated, has a demonstrated long-term benefit to wound repair by tunable protein-interactions and has been demonstrated to tolerate the level of γ-irradiation treatment required to sterilize sufficiently medical-device-like materials (Smith et al., 2018). In addition, HS has demonstrated a remarkable propensity to stabilize short-lived GF's in what appears to be a selective fashion (Wang et al., 2014; Wijesinghe et al., 2017).

The effects of BDNF and other GFs have previously been investigated in various stroke models and have shown strong regenerative potential (Berretta et al., 2014). In general, BDNF is believed to have a beneficial effect on stroke recovery via several mechanisms: protection against acute ischemic injury (Schäbitz et al., 2007), increased angiogenesis (Kermani and Hempstead, 2007), neurogenesis (Schäbitz et al., 2007), and neural repair (Mamounas et al., 2000) as well as enhanced synaptic plasticity (Waterhouse and Xu, 2009; Clarkson et al., 2011). Whilst the use of BDNF and other GFs to promote neuroprotection and minimize the spread of damage during the acute phase of injury has been extensively studied (Pardridge, 2005; Wu, 2005; Cai et al., 2014), this work will not be reviewed here. This review instead summarizes past experimental evidence that highlights how neurotrophins have shown potential as a delayed treatment option for aiding in repair and regeneration of neural tissue for stroke and other neurodegenerative diseases. In addition, we discuss novel biomaterial delivery systems that have been utilized to enhance the delivery of neurotrophins to the CNS, as utilizing such delivery systems have resulted in a further improvement in

Abbreviations: AAV, adeno-associated viral vector; ALS, amyotrophic lateral sclerosis; AMPA, α-amino-3-hydroxy-5-methyl-4-isoxazolepropionic acid; Ang1, angiopoietin-1; BBB, blood-brain-barrier; BDNF, brain-derived neurotrophic factor; BMA, basilar membrane area; BMP, bone morphogenic protein; BSA, bovine serum albumin; CMT1A, Charcot-Marie-Tooth type 1A; CNS, central nervous system; CREB, cAMP-response element-binding protein; CST, corticospinal tract; DAG, diacylglycerol; DRG, dorsal root ganglion; ECM, extracellular matrix; ERK, extracellular signal-regulated kinase; FGF, fibroblast growth factor; GABA, gamma-Aminobutyric acid; GAG, glycosaminoglycan; GAP43, growth associated protein 43; GFs, growth factors; GFAP, glial fibrillary acidic protein; GSK-3, glycogen synthase kinase 3; HS, heparan sulfate; HSPG, HS containing proteoglycan; IP3, inositol triphosphate; JNK, c-Jun N-terminal kinase; LTP, long-term potentiation; MAP-2, microtubule-associated protein-2; MAPK, mitogen-activated protein kinase; MSC, mesenchymal stem cells; MCAo, middle cerebral artery occlusion; NADE, $p75^{NTR}$-associated cell death executor; NF-kB, nuclear factor kappa-light-chain-enhancer of activated B cells; NGF, nerve growth factor; NIS, Neuropathy Impairment Score; NPC, neural progenitor cell; NRIF, neurotrophin-interacting factor; NT-3, neurotrophin-3; NSC, neural stem cells; NSPC, neural stem progenitor cell; p75NTR, p75 neurotrophin receptor; PI3K, phosphatidylinositol-3 kinase; PAGE, polyacrylamide gel electrophoresis; PCL, poly(ε-caprolactone); PEG, polyethylene glycol; PG, proteoglycan; PGA, poly y-glutamic acid; PKC, protein kinase C; PLA, poly(lactic acid); PLLA, poly-L-lactide; PLC-γ1, phospholipase C-γ1; PLGA, poly(lactide-co-glycolide); PNI, peripheral nerve injury; PNS, peripheral nervous system; PPE, poly(phosphoester); RhoA, ras homolog gene family member A; SC, spinal cord; SC-1, Schwann-Cell 1; SCI, spinal cord injury; SVZ, subventricular zone; SGZ, sub granular zone; SNP, single nucleotide polymorphism; TBI, traumatic brain injury; TFs, transcription factors; Trk, tropomyosin receptor kinase; VEGF, vascular endothelial growth factor.

functional recovery when treatment is delayed by days to weeks post injury.

Stroke Pathophysiology and Mechanisms of Endogenous Repair

Stroke occurs when blood flow to the brain is either obstructed by an occlusion (ischemic) or following rupturing (hemorrhagic) of a cerebral blood vessel. Lack of oxygen and glucose, and a build-up of toxic by-products, cause the areas of the brain deprived of blood flow to undergo a chain of pathological events (ischemic cascade), ultimately leading to cell death, and loss of function associated with that region of the brain (Dirnagl et al., 1999). As time passes, a lack of reperfusion to the penumbra (regions surrounding the core infarct) results in further expansion until the stroke is fully formed. Whilst neuroprotective agents have shown preclinical success at restoring reperfusion and minimizing cellular damage, they are only effective when administered within the first few hours following stroke onset and have failed to translate into clinical use, with the exception of thrombolytic compounds (Moretti et al., 2015). As a result, much needed stroke research unraveling the mechanisms associated with neuroregeneration and repair in the days to weeks following a stroke have highlighted a number of targetable treatment options, some of which have already resulted in the establishment of clinical trials.

Whilst the CNS shows limited capacity for regeneration and repair, under pathological conditions such as stroke, axonal sprouting, endogenous neurogenesis, and spontaneous functional recovery appear to be enhanced (Carmichael et al., 2001; Benowitz and Carmichael, 2010). In addition, Stroemer et al. (1995) reported that both GAP-43 and synaptophysin, two proteins involved with neurite growth and synaptogenesis; are upregulated throughout the neocortex 2 weeks following a focal infarct in rats. Further, these researchers show a positive correlation between improved locomotor function and stroke-induced elevations in GAP-43 and synaptophysin. It has since been established that enhancing neuronal connections throughout the ischemic brain via pharmacological interventions correlates with an improvement in functional motor recovery after stroke (Lee et al., 2004; Overman et al., 2012; Clarkson et al., 2013; Cook et al., 2017).

Neurogenesis occurs continuously in two areas of the healthy adult CNS: the SVZ of the lateral ventricle, and the subgranular zone (SGZ) of the hippocampal dentate gyrus. In these areas, self-renewing multipotent cells known as NSPCs differentiate into both neuronal, and glial cells (Taupin, 2006). Under physiological conditions these NSPCs migrate to the dentate gyrus or olfactory bulb to replenish the continuously dying granule cells or olfactory neurons, respectively. Following acute injury to the CNS, these resident neural progenitors may also be induced in an attempt to replace damaged neurons (Zhang et al., 2005; Greenberg, 2007). Supporting this notion, many animal models of stroke have reported the upregulation of SVZ and SGZ neurogenesis, peaking around 7–10 days post-stroke (Iwai et al., 2002, 2003; Parent et al., 2002; Carmichael et al., 2005). Furthermore, stroke-induced local changes to the microvasculature has been found to attract neuroblasts generated within the SVZ and facilitate their migration to the ischemic boundary zone (peri-infarct), an area lying lateral to the stroke (Carmichael et al., 2005; Yamashita et al., 2006; Thored et al., 2007).

Interestingly, preclinical research indicates NSPCs offer the majority of their regenerative potential through bystander effects, specifically by providing a rich source of GFs to the injured tissue rather than contributing to structural reconstruction (Chen et al., 2000). Supporting this, preclinical work has shown that MSCs facilitate an improvement in functional recovery, even though they fail to differentiate into mature neurons or glia when grafted into the ischemic boundary zone of rats exposed to a MCAo (Chen et al., 2000). Moreover, at least a portion of the therapeutic potential of MSCs has been ascribed to their ability to enhance endogenous neurogenesis and protect newborn cells from deleterious environments (Yoo et al., 2008), both of which are mechanisms mediated by neurotrophin signaling pathways. Although explicit evidence directly linking enhanced neurogenesis and functional recovery is sparse, a direct causal relationship seems probable with almost all neuroregenerative agents that improve neurological function following stroke also potentiating neurogenesis (Zhang et al., 2001; Wang et al., 2004; Schäbitz et al., 2007; Cook et al., 2017). Of note, HS has also been demonstrated to support the proliferation (without differentiation) of stem cells *ex vivo* (Dombrowski et al., 2009; Wijesinghe et al., 2017).

In addition to changes in neurogenesis, angiogenesis and axonal sprouting, work over the past few years has highlighted a chronic imbalance in brain excitability following stroke (Clarkson, 2012). Specifically, stroke has been reported to weaken transcallosal inhibition from the ipsilesional hemisphere onto the intact, contralesional hemisphere (Murase et al., 2004; Duque et al., 2005). This further exacerbates an increase in tonic GABAergic inhibition onto the stroked hemisphere, limiting its potential for cortical plasticity, and spontaneous recovery after stroke (Clarkson et al., 2010). Indeed, restoring neuronal excitability in the ipsilesional stroke hemisphere via increasing AMPA activity, and/or dampening tonic GABAergic inhibition has shown great promise to enhance recovery of lost function (Clarkson et al., 2010, 2015; Orfila et al., 2017). Whilst the above evidence collectively supports an intrinsic capability of the ischemic brain to regenerate and repair itself, it must be reiterated that these mechanisms alone are most often insufficient to cause a complete reversal of the functional impairment (Yamashita and Abe, 2012). Furthermore, age-related decreases in neurogenesis (Cooper-Kuhn et al., 2004; Kernie and Parent, 2010) and angiogenesis (Sonntag et al., 1997) have been reported, making it even harder for endogenous repair mechanisms to overcome damage and promote recovery. Accordingly, regenerative interventions have begun to target the potentiation of these endogenous mechanisms to try and maximize functional recovery in animal models of stroke and other neurodegenerative conditions such as SCI and Alzheimer's disease (Wang et al., 2004; Piantino et al., 2006; Schäbitz et al., 2007; Weishaupt et al., 2014; Choi et al., 2018). This has been demonstrated in the case of the endogenous stimulation of key

GF's by addition of HS on a biomaterial support to the wound site (Murali et al., 2013).

Neurotrophins for Repair and Regeneration

Neurotrophins are the predominant mediators of neuronal survival and regeneration throughout the CNS, making them of particular interest in neuroregenerative research. The neurotrophin family consists of several main GFs, including NGF, BDNF, and NT-3. All neurotrophins are initially synthesized as precursor proteins, known as pro-neurotrophins. These pro-neurotrophins can then be cleaved intracellularly by furin or proconvertases, or extracellularly by metalloproteases and plasmin, to form stable mature neurotrophins. Whilst mature neurotrophins selectively bind to their respective Trk to exert neurotrophic effects, pro-neurotrophins have been found to conduct somewhat opposing, pro-apoptotic effects through the $p75^{NTR}$/sortilin receptor (see **Figure 1**: further information on neurotrophin signaling pathways can be found below; (Nykjaer et al., 2004; Teng et al., 2005). This finding has left the scientific world moving away from the passive function of these pro-domains, and has brought a new level of complexity to the role and function of neurotrophin signaling in the CNS (Zanin et al., 2017).

The expression of both neurotrophins and their respective receptors typically decrease with age, indicating neurons and glia yield a limited trophic ability to combat natural, and pathological neurodegeneration (Webster et al., 2002; Lommatzsch et al., 2005). In support of this, reduced BDNF expression in the hippocampus has been shown to correlate with impairments in both spatial and working memory in gerbils and rats (Schaaf et al., 2001; Hwang et al., 2006). Furthermore, excitotoxic lesions to the nigrostriatal pathway increases BDNF expression in the striatum of young, but not aged rats (Yurek and Fletcher-Turner, 2000, 2001). Similarly, lesions to the medial septum significantly elevates hippocampal levels of NGF in young rats only (Scott et al., 1994). Interestingly, further assessment of these young rats revealed an enhancement in neurite outgrowth compared to their aged counterparts (Scott et al., 1994; Kaseloo et al., 1996).

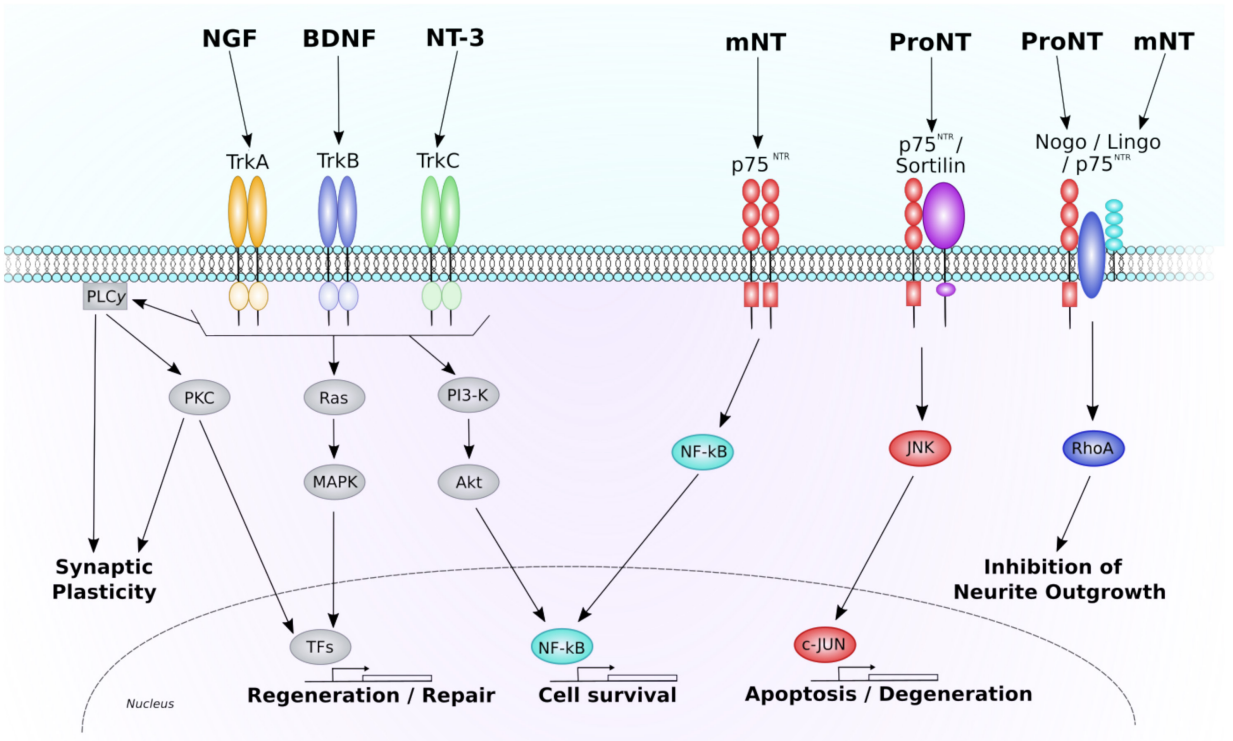

FIGURE 1 | Neurotrophin signaling through the $p75^{NTR}$ and Trk receptors. This diagram depicts the major intracellular signaling pathways associated through each neurotrophin receptor. Each Trk receptor isoform binds mature neurotrophins and acts through three predominant pathways. Activation of PLC-γ1 results in PKC-mediated promotion of synaptic plasticity. Activation of Ras initiates MAPK-mediated promotion of neuronal regeneration and growth. Activation of PI3-K results in activation of Akt and promotion of NF-κB-mediated cell survival. Each of these pathways are also known to regulate genetic transcription, further promoting pro-survival, and regenerative gene expression. The $p75^{NTR}$ receptor also regulates three main pathways. When a mature neurotrophin binds to an isolated $p75^{NTR}$ NF-κB-mediated cell survival is promoted. If the $p75^{NTR}$ is co-expressed with the sortilin receptor, pro-neurotrophins can bind, and cause activation of JNK-c-Jun mediated cell death and degeneration. A receptor complex consisting of Nogo, $p75^{NTR}$, and Lingo1 can bind both pro- and mature-neurotrophins to alter neurite outgrowth in a RhoA-dependent manner. NGF, nerve growth factor; BDNF, brain-derived neurotrophic factor; NT-3, neurotrophin-3; Trk, tropomyosin receptor kinase; mNT, mature neurotrophin; ProNT, proneurotrophin; $p75^{NTR}$, pan neurotrophin receptor 75; PLC*γ1*, phospholipase C gamma one; PKC, protein kinase C; MAPK, mitogen-activated protein kinase; TFs, transcription factors; PI3-K, phosphoinositide 3-kinase; NF-kB, nuclear factor kappa-light-chain-enhancer of activated B cells; JNK, c-Jun N-terminal kinase.

Evidence from preclinical animal models also supports an age-related difference in expression of BDNF, with stroke inducing a lessened elevation of BDNF in aged mice compared to young stroke controls (Clarkson et al., 2015). In summary, aging exacerbates the degree of functional impairment as a consequence of damage to the brain, relative to young animals. This is thought to be in part, due to the differing recovery trajectories observed in aged and young animals, including differences in spontaneous recovery, neurogenic activity, and the neuronal sprouting transcriptome (Li S. et al., 2010; Hermann and Chopp, 2012). Therefore, it has been postulated that age-specific interventions may be required to maximize the effectiveness of regenerative interventions. Specifically, aged animals may require a combinatorial intervention to gain functional recovery to the same extent as young mice. Supporting this, systemic administration of the high impact AMPAKine (positive allosteric modulator of AMPA receptors), CX1837, has been reported to stimulate an increase in BDNF expression and promote functional recovery in aged mice following photothrombotic strokes (Clarkson et al., 2015). Interestingly, the use of low impact AMPAkines (positive allosteric modulator of AMPA receptors) have failed to elicit functional recovery in the same animal model (Clarkson et al., 2011). Although neurotrophins mediate intrinsic repair mechanisms, the above collectively supports that their intrinsic regeneration abilities decline during aging.

Neurotrophin Signaling Pathways

The neurotrophin family shares two common classes of transmembrane receptors; the Trk receptors that bind the mature neurotrophins, and the $p75^{NTR}$, a receptor from the tumor necrosis factor (TNF) receptor superfamily that preferentially binds the pro-neurotrophins. Whilst the low-affinity $p75^{NTR}$ binds to all members of the neurotrophin family with similar nanomolar affinities (Bothwell, 1995), each neurotrophin shows preference for different Trk receptor isoforms; specifically, NGF binds to the TrkA, BDNF to TrkB, and NT-3 to TrkC. Once a mature neurotrophin has bound to its respective Trk receptor, the Trk receptor dimerizes and undergoes transphosphorylation to specific intracellular tyrosine kinase residues. These phosphorylated tyrosine-kinase residues act as docking sites for adaptor proteins that allow additional kinases to be recruited for activation of intracellular signaling pathways (see **Figure 1**).

Activation of the Trk receptor is known to phosphorylate and activate PLC-γ1 and its associated second messenger signaling pathway. PLCγ activity generally generates two distinct second messenger systems: IP3 and DAG, both of which increase intracellular release of calcium (Ca^{2+}) and stimulate PKC-mediated signaling, resulting in enhanced neuronal and synaptic plasticity (Chao, 2003; Yoshii and Constantine-Paton, 2010). Trk receptors have also been found to activate Ras, a small GTP-binding protein that further activates the MAPK signaling pathway to generate ERK. ERK then phosphorylates and activates a range of TFs including CREB, causing downstream transcriptional changes to genes that control neuronal differentiation and neurite outgrowth (Kaplan and Miller, 2000). Another major pathway activated by Trk receptors is the PI3-K pathway, which leads to downstream activation of the serine/theronine kinase, AKT to promote NF-kB-mediated neuronal survival (Reichardt, 2006). The PI3K/AKT signaling pathway plays a central role in regulating cell growth, proliferation, and survival under physiological and pathological conditions (Cantley, 2002). In addition, PI3K/AKT signaling has been revealed to contribute to axonal sprouting in cultured hippocampal neurons (Atwal et al., 2000; Sanchez et al., 2001; Jaworski et al., 2005), which is an important mechanism underlying post-stroke functional recovery (Li S. et al., 2010; Overman et al., 2012; Clarkson et al., 2013). For instance, in a recent paper by Clarkson et al. (2015), experimenters combined systemic administration of a high impact AMPAKine, CX1837, and local hydrogel delivery of BDNF, resulting in a synergistic increase in phosphorylation of AKT, MEK, and CREB in aged (22–24 months old) mice. This upregulation was observed in parallel to increased functional recovery of motor function. In addition, recent work has also shown that modulation of GSK-3 after stroke can enhance axonal outgrowth (Ueno et al., 2012). Activation of the AKT/GSK-3/CREB pathway has also been observed in other age-related neurological disorders such as Alzheimer's disease, with activation of this pathway leading to an improvement in cognitive function (Tang et al., 2014). To this end the full complement of Trk-mediated signaling pathways that play a role in post-stroke recovery, or their involvement in mechanisms associated with recovery, still remain to be full elucidated.

Whilst neurotrophins signal via two different receptor pathways, most of the attention has been focused on the activation of Trk receptors and their subsequent biological effects (see **Figure 1**). However, over the past couple of decades research has also begun to investigate the surprisingly diverse functions of $p75^{NTR}$, including a somewhat paradoxical involvement in pro-apoptotic signaling (Reichardt, 2006). Most neuronal populations that respond to neurotrophins co-express both $p75^{NTR}$ and Trk receptors. Whilst the exact mechanism remains elusive, the interaction between these two receptors is known to positively modulate Trk function following binding of a mature neurotrophin (Reichardt, 2006). Contrastingly, in the absence of Trk, $p75^{NTR}$ can also promote apoptotic signaling when a complex is formed with sortilin, a Vps10-domain containing protein that acts as a co-receptor for pro-neurotrophin binding (Nykjaer et al., 2004; Teng et al., 2005). In this scenario the activated pro-neurotrophin-receptor complex activates Rac, a GTP-binding protein that promotes the JNK cascade (Harrington et al., 2002), leading to activation of pro-apoptotic genes and apoptotic cell death (Reichardt, 2006).

The $p75^{NTR}$ itself lacks any catalytic intracellular domains, however, it is able to signal via several adaptor proteins. Specifically, $p75^{NTR}$-mediated recruitment of NRIF1/NRIF2, NADE and SC-1 can activate several apoptotic signals including Rac, JNK and NF-kB (Mukai et al., 2000; Dechant and Barde, 2002; Yeiser et al., 2004). The $p75^{NTR}$ is also known to form a signaling complex with the transmembrane proteins Lingo-1 and Nogo-66 (NgR1) receptor, a receptor previously reported to inhibit axonal sprouting and neural plasticity (Schwab, 2010).

Although it is not fully understood how, this receptor complex is known to activate the small GTPase protein, RhoA, leading to inhibition of oligodendrocyte differentiation and myelination, and inhibition of axonal growth in the CNS (Tan et al., 2011). Both pro-neurotrophins and mature neurotrophins have been reported to bind to the $p75^{NTR}$/NgR1/Lingo1 receptor complex, with opposing effects on neurite growth being observed (Lehmann et al., 1999; Deinhardt et al., 2011; Sun et al., 2012). Specifically, introduction of proBDNF or proNGF to neuronal cultures induces growth cone collapse (i.e., the developing or regenerating tip of a neurite) and inhibition of further neurite extension (Lehmann et al., 1999; Deinhardt et al., 2011; Sun et al., 2012). Contrastingly, binding of mature forms of BDNF and NGF to this receptor complex appears to inhibit RhoA activity leading to subsequent disinhibition of neurite outgrowth (Yamashita et al., 1999). Collectively, these findings indicate bidirectional effects of $p75^{NTR}$ depending on both the ligands and receptors present in a particular neuronal microenvironment. It must be reiterated, however, that the mature neurotrophins' enhanced affinity for the Trk receptor counteracts the proapoptotic action of $p75^{NTR}$ activity, resulting in the predominant function of neurotrophin being trophic.

Nerve Growth Factor (NGF)

In the early 1950's Levi-Montalcini (1987) first discovered NGF, demonstrating its' ability to regulate the survival and maturation of developing PNS neurons. NGF has since become one of the best characterized members of the neurotrophin family, acting on many neuronal and glial cell populations throughout the nervous system to promote axonal sprouting, dendritic arborization, and cell body growth (Cuello, 1996; Debeir et al., 1999; Sofroniew et al., 2001). Moreover, recent work has highlighted an interaction between NGF and cells from the immune-hematopoietic linage, including mast cells (Skaper, 2017). Specifically, mast cells have been found to synthesize and release NGF, with NGF also acting back on mast cells to promote survival (Skaper, 2017). Further, NGF concentrations are elevated in various inflammatory and autoimmune states in humans, such as multiple sclerosis and chronic arthritis (Aloe et al., 1992; Laudiero et al., 1992). Whilst this area of research is in its infancy, these findings suggest that under certain conditions, NGF may be able to promote inflammatory cascades, and have deleterious effects on surrounding tissues, arguing a more complicated role of this neurotrophin than previously thought.

Various CNS injuries such as ischemia, seizure-activity and trauma induce a rapid upregulation in the expression of NGF and the TrkA receptor (Lindvall et al., 1994; Goss et al., 1998; Gottlieb and Matute, 1999; Dmitrieva et al., 2016). Although the exact function of this injury-induced upregulation is not fully understood, several lines of evidence suggest enhanced NGF signaling may facilitate the repair of damaged nervous tissue. For example, implantation of fibroblasts, genetically modified to secrete NGF reduce cholinergic cell death and promote axonal sprouting in the aged rats and non-human primates undergoing lesion-induced degeneration (Kawaja and Gage, 1991; Kordower et al., 1994). Moreover, exogenous NGF has also been reported to have a similar effect on transected SC axons, promoting regeneration of damaged axons and restoration of stimulus-driven electrophysiological activity (Ramer et al., 2000). However, it must be noted that the ability of NGF to promote functional recovery in animal models of neurodegenerative diseases remains largely understudied with somewhat opposing findings. For example, enhanced NGF-induced sprouting following SCI is known to be a primary cause of autonomic dysreflexia, a condition in which potentially life threatening episodic hypertension is triggered by stimulation of sensory nerves in the body below the site of injury (Krenz et al., 1999; Weaver et al., 2006). In these situations, enhanced NGF signaling stimulates sprouting of small-diameter primary afferent fibers, thereby amplifying SC reflexes, and promoting dysreflexia. For a more detailed discussion of NGF treatment's mixed success for treating SCI see a recent review by Keefe et al. (2017).

The systemic administration of NGF in clinical trials has also revealed a variety of adverse side effects including marked reductions in body weight, and myalgia to the muscles of the trunk and back (Petty et al., 1994; Eriksdotter Jönhagen et al., 1998). Despite this, the topical administration of recombinant human NGF to the eyes of patients with ophthalmological diseases such as neurotrophic keratitis and dry eye disease has shown promise in relieving symptoms and promoting healing of the damage eye (Bonini et al., 2018; Rocco et al., 2018; Sacchetti et al., 2019).

Brain-Derived Neurotrophic Factor (BDNF)

Brain-derived neurotrophic factor is the most abundant neurotrophin in the CNS (Andero et al., 2014). BDNF-TrkB signaling is well documented to regulate a wide range of neuronal functions including cell survival, neuronal differentiation and migration, neurite outgrowth, and facilitation of LTP and plasticity (Encinas et al., 1999; Boyd and Gordon, 2003b; Pang and Lu, 2004). Both BDNF and its high affinity receptor, TrkB, are widely produced throughout the CNS with high expression being observed in areas such as the neocortex, hypothalamus, and amygdala (Connor and Dragunow, 1998; Binder and Scharfman, 2004).

Studies using *in situ* hybridization have revealed a stroke-induced upregulation of BDNF mRNA expression in both the ipsilateral cortex and hippocampus in rat models of forebrain ischemia (Comelli et al., 1993; Kokaia et al., 1995; Dmitrieva et al., 2016). This upregulation appears to peak within the first 12 h after stroke and remains elevated as late as 1 week later (Béjot et al., 2011; Clarkson et al., 2011). Indeed, stroke-induced changes in BDNF protein have also been observed, with microsphere embolism-induced MCAo causing elevated BDNF expression over a similar time course (Miyake et al., 2002). However, these changes appear to vary across brain regions, with a suppression in BDNF protein expression being observed in the parietal cortex 24-h after MCAo in rats (Kokaia et al., 1995). The expression of BDNF and TrkB levels are also modulated in animal models of SCI (Ikeda et al., 2001) and traumatic brain injury (TBI), which occurs following blunt or penetrating forces

to the skull causing damage to white matter tracts, intracranial hemorrhaging, and ischemia (Rostami et al., 2014).

It must be noted, however, that stroke-induced increases in endogenous BDNF are insufficient to reverse functional impairments (Li B. et al., 2010). Supplementing the ischemic brain with exogenous BDNF has thus been investigated over the past few decades, with research supporting BDNF-enhanced axonal sprouting (Mansour-Robaey et al., 1994; Batchelor et al., 2000, 2002; Mamounas et al., 2000), angiogenesis (Kermani and Hempstead, 2007), neurogenesis (Schäbitz et al., 2007), neuronal plasticity (Yacoubian and Lo, 2000; Zakharenko et al., 2003), and behavioral recovery (Schäbitz et al., 2004; Guan et al., 2012). Importantly, several studies have also reported that a critical threshold in BDNF activity is required in order to achieve an improvement in functional recovery in the weeks following stroke (Ploughman et al., 2009; Clarkson et al., 2011; MacLellan et al., 2011). This was first shown following enriched rehabilitation has been found to only improve motor recovery in rats with elevated BDNF levels post-MCAo (MacLellan et al., 2011). Furthermore, suppressing endogenous BDNF translation with antisense oligonucleotides prevents such improvements (Ploughman et al., 2009). Clarkson et al. (2011) further demonstrated functional motor recovery in mice following administration of a BDNF-inducing AMPAkine following photothrombotic stroke. This effect was not observed when a non-BDNF inducing AMPAkine was applied, or when BDNF function was inhibited with the BDNF ligand decoy, TrkB-Fc (Clarkson et al., 2011). Interestingly, BDNF and the TrkB receptor is abundantly expressed throughout the sensory neurons in the inner ear, leading many researchers to investigate the potential of BDNF in treating deafness (Ramekers et al., 2012). For example, Shibata et al. (2010) treated neomycin-deafened rats with transgenic vectors overexpressing the gene for BDNF within the BMA of the inner ear. Results showed that treatment with the BDNF vectors could promote regrowth of damaged nerve fibers into the cochlear epithelium and enhance survival of spinal ganglion neurons.

Given neurotrophic effects of BDNF it is reasonable to presume that the injury-induced upregulation of BDNF and is receptor acts to restrict pro-apoptotic signaling following injury. Further support for this notion lies in clinical studies investigating a common SNP of the BDNF gene, where valine is substituted for methionine at codon 66 (BDNF val*66*met, otherwise known as rs6265). A resulting 19–30% reduction in activity-dependent secretion of BDNF protein has been reported in humans carrying this SNP (Shimizu et al., 2004), with worse functional outcomes being reported in these individuals following a stroke (Siironen et al., 2007; Mirowska-Guzel et al., 2012). Be that as it may, the val*66*met allele has also been reported to promote recovery of executive function in individuals with TBI (Krueger et al., 2011). Moreover, knock-in-mice homozygous for the Met allele have been reported to display enhanced functional recovery following chronic stroke (Qin et al., 2014). These findings argue a more complicated role of this SNP that requires future investigation to clarify its role following CNS injury.

To date, only a few studies have conducted clinical trials investigating BDNF as a therapeutic intervention. Both intrathecal and subcutaneous administrations of BDNF have been found to be well tolerated in ALS patients (Beck et al., 1994; Bradley, 1999; Ochs et al., 2000). The neurorehabilitative potential of BDNF, however, was not observed due small cohort size and limited half-life. Other proposed factors limiting BDNF's success in human trials includes the difficulty of producing sufficient amounts of BDNF for use in human interventions, and the lack of studies investigating higher doses of BDNF in animal models (Nagahara and Tuszynski, 2011). However, the use of biomaterial drug-delivery systems holds promise in circumventing these issues, as lower concentrations of BDNF can be administered directly to the brain without worrying about BBB passage as discussed below.

Neurotrophin-3 (NT-3)

Neurotrophin-3 is another member of the neurotrophic family, sharing 55 percent amino acid homology with BDNF, and NGF (Maness et al., 1994). Contrasting to other members of the neurotrophin family, NT-3 expression within the CNS appears to peak at the time of fetal development, during which time NT-3 plays a strong role in neuronal survival, and differentiation (Ernfors et al., 1990; Maisonpierre et al., 1990; Ghosh and Greenberg, 1995). NT-3 conducts most of its trophic effects through a high affinity interaction with the TrkC receptor (Lamballe et al., 1991). However, at high concentrations NT-3 is also known to interact with other Trk isoforms at a much lower affinity compared to that of NGF and BDNF (Clary and Reichardt, 1994; Strohmaier et al., 1996).

Maisonpierre et al. (1990) first reported in 1990 that induction of the NT-3 gene facilitated neurite outgrowth in DRG explants. NT-3 has since been reported to mediate aspects of neurogenesis, with NT-3 neutralizing antibodies, and conditional NT-3 knockouts both causing significant reductions in NSPC differentiation and survival (Ghosh and Greenberg, 1995; Barnabé-Heider and Miller, 2003; Shimazu et al., 2006).

Contrasting with the other members of the neurotrophin family, NT-3 mRNA expression is significantly reduced in the first 12–24 h following injury to the CNS (Kokaia et al., 1995; Boris-Möller et al., 1998; Boyd and Gordon, 2003a). This is likely an intrinsic mechanism to help minimize damage, as conditional NT-3 knockout animals and animals administered NT-3 neutralizing antibodies have smaller infarct volumes following MCAo stroke and enhanced survival of axotomized corticospinal neurons, respectively, indicating a detrimental role of NT-3 in the acute phase of injury (Giehl and Tetzlaff, 1996; Bates et al., 2002). However, contrasting reports show intrathecal and intraventricular administration of NT-3 promote neurite extension, axonal sprouting, and neuronal survival when administered immediately after trauma to the SC (Schnell et al., 1994; Bradbury et al., 1999). Based on these findings, it is possible that NT-3 has differing rolls in both the CNS and PNS after injury, however, further work is required to confirm this hypothesis.

Contrary to findings showing early administration of NT-3 to the CNS being damaging, delayed administration of NT-3 (>3 days) after stroke appear to promote protection and repair (Zhang et al., 1999). NSCs engineered to overexpress NT-3 have been found to enhance neuronal differentiation in the

penumbra and infarct cavity when administered to mice 3 days after hypoxic-ischemic injury (Park et al., 2006). Furthermore, Duricki et al. (2015, 2018) showed that intramuscular injections or prolonged subcutaneous infusion of human recombinant NT-3, given 24 h after endothelin-1 and MCAO-induced stroke, can enhance sensorimotor recovery in elderly rats. Interestingly, anterograde tracing revealed NT-3-enhanced neuroplasticity in the CST, with increased numbers of fibers extending from the intact to affected side. This change in plasticity has also been reported by Weishaupt et al. (2014) in a rat model of SCI, with enhanced axonal sprouting being observed from injured CST axons following intrathecal injections of a NT-3 expressing AAV.

To the best of our knowledge, the therapeutic potential of NT-3 has not been investigated in clinical trials for neurodegenerative CNS diseases (Bezdjian et al., 2016). However, phase I and II clinical trials in neurologically healthy adults have confirmed that NT-3 administration is safe and well tolerated (Chaudhry et al., 2000; Parkman et al., 2003). Furthermore, a pilot clinical study showed potential for the subcutaneous administration of NT-3 in patients with CMT1A, a PNS neuropathy resulting from a mutation to a gene for peripheral myelin protein in Schwann cells (Sahenk et al., 2005). Results revealed that patients treated with NT-3 showed significant improvement in the Mayo Clinic NIS and sensory modality function, compared to those treated with a placebo. It is hypothesized that these behavioral changes occur as a result of NT-3-mediated regeneration of sensory nerves. Whilst these findings do support the potential of NT-3 use clinically, larger cohort studies are required.

Biomaterial-Based Delivery of Neurotrophins

It is already well established that neurotrophins play a major role in regulating neuroregenerative processes and facilitating an improvement in functional recovery in various animal models of neurodegenerative diseases. However, the translation of growth factor-based treatments into the clinic has been challenged by extremely poor BBB permeability, short therapeutic half-life and undesirable PNS side-effects, such as bone pains and increased hematocrit (Zhang et al., 2001; Ren and Finklestein, 2005; Lanfranconi et al., 2011; Chan et al., 2017). In 2006, an international panel of 44 experts conducted a forefront study identifying the top ten most promising applications of regenerative medicine for improving health in developing countries (Greenwood et al., 2006). Applications were evaluated for disease burden, therapeutic impact, feasibility, affordability, acceptability, and indirect benefits. The use of growth factor-seeded scaffolds for directing and enhancing SC and PNI was named in the top ten. Since then, it has become evident that this technology can be effectively applied into rehabilitative and regenerative approaches in other CNS injuries and diseases, in the hope to overcome the barriers faced by systemic administration.

The term biomaterial refers to a material that has been engineered to interact with a biological system, being tuned to hold various biodegradable, biocompatible, cytocompatible, physical, and topographical properties. The effect of altering these properties will not be included within the scope of this review, but the authors direct readers to the following review for their own reading (Führmann et al., 2017). Biomaterial scaffolds used in medical and scientific research are generally synthesized from biodegradable, aliphatic poly(esters) such as PLGA, PGA, PCL, PLA, PLLA, and poly(phosphoesters) (PPEs). These poly(esters) are preferentially used due to their excellent biocompatibility and biodegradability and their current FDA approval for use as a drug delivery system (Lewis, 1990). Proteinaceous scaffolds utilizing materials such as foamed-collagen (e.g., freeze-dried) also fulfill the requirements for biomedical implants that can exhibit controlled biodegradation.

When engineered specifically for stroke, biomaterials are typically designed to degrade in synchrony with the hosts healing process whilst supporting the efficacy of NSPCs grafts, and/or to amplify endogenous repair mechanisms with a sustained release of therapeutic agents (Bhatia, 2010; Wang L. et al., 2012). Although hundreds of biomaterials have been generated and investigated in the past decade, they can be generally categorized into the following categories, which will be discussed in relation to neurotrophin-based interventions below: microspheres, electrospun nanofibers and hydrogels (see **Figure 2**). The following studies are summarized in **Tables 1**, **2** to highlight past use of neurotrophins for regenerative interventions without (see **Table 1**) or with (see **Table 2**) biomaterial drug-delivery systems, respectively.

Microsphere-Based Delivery Systems

Microspheres, also known as microparticles, are polymeric spheres with a diameter between one and 1000 μm. Historically, microsphere technology has been utilized for a diverse range of applications including cosmetics, electronics, and material engineering. In medical and scientific fields, microspheres are used to encapsulate drugs, and mediate their release to an injury site.

There are many techniques employed for microencapsulation of drugs including phase separation/precipitation, emulsion-solvent evaporation/extraction, spray drying and *in situ* polymerization (Jain, 2000). Each method has its own advantages and disadvantages, leaving the synthesis process to be chosen based on the application involved (i.e., polymer attributes, site of drug action, and therapy duration). The most common method of encapsulation is the emulsion-solvent extraction/evaporation method, which results in lyophilized ready to inject drug-loaded microspheres. In contrast to systemic methods of neurotrophin administration, microsphere-based drug delivery systems can be surgically injected straight into the injury site, avoiding issues with BBB passage. Microspheres also offer the advantage of being highly tunable with choice of polymer, particle size, and method of erosion all altering the rate of drug delivery from microspheres (Xu et al., 2002). Drug-loaded microspheres can also be injected into the peripheral circulation as they can cross the BBB. Furthermore, as loaded neurotrophins are encapsulated they are not enzymatically degraded until the microsphere degrades, thereby increasing the therapeutic half-life.

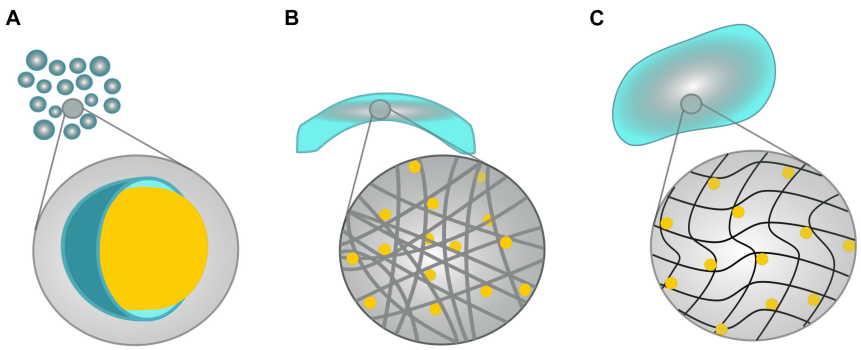

FIGURE 2 | Schematic of possible biomaterial scaffolds. Although hundreds of biomaterials have been generated, they fall neatly into four main categories: **(A)** Microspheres are small, polymeric spheres (shown in blue) that encapsulate a target drug or molecule (as depicted by the yellow sphere). **(B)** Electrospun fibers consist of long, usually cylindrical, and fibers that are commonly crafted into tubes or conduits. Target drugs can either be bound to the fibers themselves, or left to freely diffuse from the fiber network. **(C)** Hydrogels consist of hydrophilic, polymeric networks that swell to conform to cavities formed by neurodegenerative diseases/injuries, and facilitate the passive release of target molecules.

Santos et al. (2016) have illustrated the neurotrophic potential of PLGA microspheres loaded with NGF or BDNF. When applied to organotypic cultures derived from the SC and DRG, both of the loaded-microspheres enhanced neurite outgrowth when assessed 1 week after application. In contrast, free BDNF or NGF alone failed to show neurotrophic effects at this time, supporting the augmentation of neurotrophic effects as a direct result of microsphere encapsulation (Santos et al., 2016). In this same study, Santos et al. (2016) further confirmed a neurotrophic effect in a rat model of PNI. Briefly, neurotrophin encapsulated microspheres were loaded into a silicon tube filled with collagen gel before being injected into transected sciatic nerves. The use of retrograde tracers confirmed silicon tubes loaded with either NGF- or BDNF-loaded microspheres significantly increased the number of regenerated motor neuron axons in the SC, compared to control tubes loaded with free-floating neurotrophins. Furthermore, tubes loaded with encapsulated-NT-3 significantly increased the number of sensory axons in the DRG compared to free-floating controls (Santos et al., 2016). Similarly, sustained release of NGF from PLGA microspheres has also been reported by De Boer et al. (2010, 2011) with increased neurite outgrowth being observed as late as 35 days following subcutaneous implantation of the PLGA microspheres in rats. However, it should be noted that the long-term functional recovery observed in rats receiving the NGF-loaded microspheres was no greater than that of rats receiving autologous grafts (De Boer et al., 2011). The authors suggested that this may due to a "catch-up" or "blow through" effect, where intrinsic regeneration of the rat sciatic nerve is thought to be so effective that minor or early intervention-induced differences go unnoticed when long term regeneration is accessed (Young et al., 2001; De Boer et al., 2011). It is also possible that NGF exposure from the microspheres had stopped before a lasting NGF-mediated trophic effect could have been induced, resulting in a rebound effect.

The application of microsphere technology to stroke remains sparse due to several reasons. Whilst microspheres do support the sustained release of neurotrophins, the use of microspheres alone lack the mechanical support that benefits injuries with large lesion sites (i.e., stroke, SCI) (Sharp et al., 2012). Another major issue lies in the difficulty of sustaining the release of GFs in order to maintain levels within a given concentration range, an issue hampered by the challenge to create microspheres of a consistent diameter (Mohtaram et al., 2013). Further, it is known that there is a higher, initial burst of compound release from microspheres that restricts the overall duration and concentration of release (Binan et al., 2014). In attempts to overcome this, Bertram et al. (2010) have produced a PLGA-PLLA-PEG based microsphere delivery system that yields a consistent release of NGF without an initial burst, and with delivery lasting as long as 65 days. Nevertheless, the application of polymeric microspheres for therapeutic interventions has been found to be safe and well tolerated in human trials of brain tumors (Brem and Gabikian, 2001). Additionally, treatments utilizing neurotrophin-loaded microspheres in conjunction with other biomaterial scaffolds are emerging and showing promise (Xu et al., 2003; Lampe et al., 2011; Ju et al., 2014). For instance, Ju et al. (2014) investigated the therapeutic potential of loading PLGA microspheres with VEGF and Ang1, two factors that stimulate angiogenesis. The loaded microspheres were then embedded within a hyaluronic acid-derived hydrogel (containing anti-Nogo receptors) and injected into the stroke cavity of mice. Animals treated with the composite system showed enhanced angiogenesis around ischemic regions and facilitated recovery of locomotor function 6 weeks post-stroke. It is worth highlighting that to the best of our knowledge, no one has compared these hybrid delivery systems to systems containing the single biomaterial type, leaving the exact benefit of these hybrid models requiring future investigation.

Electrospun Nanofibers and Conduits

Another fabrication technique that has proven useful in generating tunable, three-dimensional scaffolds consisting of micro-, and nano-sized fibers is electrospinning. Electrospinning was initially designed to generate textiles and filters before being proposed to produce wound dressing material (Doshi and Reneker, 1995). Nowadays, electrospun nanofibers are commonly used as neural scaffolds due to their ability to mimic

TABLE 1 | Evidence supporting the neuroregenerative properties of classical neuroptrophin use in the context of treatments for CNS disease/injury.

Neurotrophin	Species	Disease model/Injury	Intervention/Treatment	Neuroregenerative effect	References
NGF	Rat	Unilateral lesion to nucleus basalis	Implantation of NGF-secreting fibroblasts	Enhanced NGF-induced axonal growth	Kawaja and Gage, 1991
	Rhesus Monkeys	Unilateral transection of the fornix	Implantation of NGF-secreting fibroblasts	Enhanced sprouting of cholinergic fibers	Kordower et al., 1994
	Rat	Complete crush injuries to the cervical DRG	Intrathecal NGF via osmotic minipumps	Regrowth of unmyelinated DRG fibers, restoration of behavioral sensitivity and stimulus-driven postsynaptic activity	Ramer et al., 2000
	Rat	Immunotoxic lesions to the CBF	Intracerebroventricular NGF via osmotic minipumps	Hypertrophy and enhanced axonal growth in CBF neurons, improved spatial orientation in a water maze	Winkler et al., 2000
BDNF	Rat	Optic nerve transection	Intravitreal BDNF injections	Enhanced local regrowth of RGC axons near the optic disc	Mansour-Robaey et al., 1994
	Mice	Striatal lesion	Intrastriatal infusion of BDNF antisense oligonucleotides via minipumps	Suppressed peri-wound dopaminergic sprouting	Batchelor et al., 2000
	Rat	PCA-induced lesions (forebrain or hippocampus)	BDNF infusions to lesion site via osmotic minipumps	Enhanced sprouting of 5-HT axons at the lesion site (both the forebrain and hippocampus)	Mamounas et al., 2000
	Rat	Complete transection of the thoracic spinal cord	Intrathecal BDNF via osmotic minipumps	Enhanced functional recovery of the hindlimb, modest sprouting of cholinergic fibers within injury cavity	Jakeman et al., 1998
	Rat	Photothrombotic stroke to the parietal cortex	Intravenous BDNF injections	Enhanced functional recovery of motor function, promoted widespread neuronal remodeling	Schäbitz et al., 2004
	Rat	Photothrombotic stroke to the parietal cortex	Intravenous BDNF injections	Enhanced functional recovery of sensorimotor function, neurogenesis (DG) and SVZ progenitor cell migration	Schäbitz et al., 2007
	Rat	MCAO via permanent intraluminal vascular occlusion	Intraventricular injections of CBD-bound BDNF	Enhanced SVZ progenitor cell proliferation, enhanced angiogenesis and improved neurological performance	Guan et al., 2012
	Rat	Endothelin-1-induced MCAO	Intraventricular infusion of BDNF antisense oligonucleotides via minipumps	Attenuated rehabilitation-mediated functional recovery of motor skills	Ploughman et al., 2009
	Mice	Photothrombotic stroke to the motor cortex	TrkB-Fc-embedded hydrogel into stroke cavity	Occluded AMPAkine-mediated and spontaneous functional recovery	Clarkson et al., 2011
NT-3	Mice	N/A	Conditional NT-3 knockout	Impaired NPC differentiation and LTP, deficits in spatial memory	Shimazu et al., 2006
	Rat	Partial bilateral transection of the thoracic spinal cord	Intrathecal NT-3 injection	Enhanced axonal sprouting of transected corticospinal tract	Schnell et al., 1994
	Rat	Partial bilateral crushing of the thoracic spinal cord	Intrathecal NT-3 via osmotic minipumps	Enhanced axonal growth within and outside the lesion site	Bradbury et al., 1999
		Focal hypoxic-ischemic brain injury	Implantation of NT-3-overexpressing NSCs	Promoted NSC differentiation into neurons, dampened glial scarring	Park et al., 2006
	Rat	Partial bilateral transection of the thoracic spinal cord	Implantation of NT-3-secreting fibroblasts	Enhanced axonal growth around and distal to lesion site, partial recovery of motor function	Grill et al., 1997

DRG, dorsal root ganglion; CBF, cholinergic basal forebrain; RGC, retinal ganglion cells; PCA, p-chloroamphetamine; DG, dentate gyrus; SVZ, subventricular zone; MCAO, middle cerebral artery occlusion; CBD, collagen binding domain; TrkB-Fc, tropomyosin receptor kinase B-Fc; NPC, neural progenitor cell; LTP, long term potentiation; NSC, neural stem cells.

TABLE 2 | Examples of biomaterial-based neurotrophin treatments for regeneration and repair following CNS disease/injury *in vivo*.

Neurotrophin	Species	Disease model/Injury	Biomaterial/Treatment	Effect of treatment	References
NGF	Rat	Sciatic nerve transection	Nerve conduits loaded with NGF-embedded PLGA microspheres	Enhanced regeneration of motor and sensory axons	Santos et al., 2016
	Rat	Sciatic nerve transection	NGF-loaded PCL nerve conduit	Significantly enhanced mean axon diameter and myelin thickness, increased total number of regenerated fibers, enhanced recovery of electromyographic function	Liu et al., 2011
	Rat	Sciatic nerve transection	NGF-loaded chitosan conduit	Facilitated axonal regeneration, enhanced target muscle innervation and motor recovery	Wang H. et al., 2012
BDNF	Rat	Sciatic nerve transection	Nerve conduits loaded with NGF-embedded PLGA microspheres	Enhanced regeneration of sensory axons	Santos et al., 2016
	Mouse	Photothrombotic stroke to the motor cortex	Hyaluronan-based hydrogels loaded with BDNF	Improved recovery of motor function	Clarkson et al., 2015
	Mouse	Photothrombotic stroke to the motor cortex/L-NIO induced stroke	Hyaluronan-based hydrogels loaded with BDNF	Enhanced axonal sprouting, enhanced migration of neuroblasts to the peri-infarct cortex, enhanced recovery of forelimb function	Cook et al., 2017
	Rat	Acute brain injury via needle insertion	Electrospun PCL sacffolds embedded with a BDNF-mimetic	Redirected endogenous neuroblasts toward the scaffold, enhanced neuroblasts integration and promoted local neurite sprouting	Fon et al., 2014
NT-3	Rat	Complete transection of the thoracic spinal cord	Multichannel PLGA conduits loaded with rhNT-3	Enhanced axonal regrowth between spinal cord stumps, partial recovery of hindlimb locomotor function	Fan et al., 2011
	Rat	Partial bilateral transection of the dorsal spinal cord	Collagen-derived hydrogel loaded with NT-3	Enhanced regrowth of CST axons, mild improvements in motor function	Houweling et al., 1998
	Rat	Partial bilateral transection of the dorsal spinal cord	Acrylate-based hydrogel loaded with NT-3	Enhanced axonal outgrowth in the CST and raphespinal tract, recovery of locomotor function	Piantino et al., 2006

rhNT-3, recombinant human neurotrophin-3; L-NIO, N5-(1-iminoethyl)-L-ornithine; CST, corticospinal tract.

the structure and surface-to-volume ratio of the ECM (Chew et al., 2005; Alhosseini et al., 2012; Jiang et al., 2012). Compared to other biomaterials, electrospun nanofibers offer the advantage of an easily adaptable shape and structure, reduced initial drug release and enhanced cell or drug attachment (Han et al., 2011). Conversely, electrospinning has proven difficult to maintain consistency in fiber sizes, with concerns also being placed on the use of toxic solvents involved in the synthesis of polymer-drug emulsions (Li et al., 2002).

Many groups have encapsulated neurotrophic factors within electrospun nanofibers and shown retention of neurotrophic factor bioactivity. For instance, Chew et al. (2005) showed the sustained release of NGF from *E*-caprolactone and ethyl ethylene phosphate (PCLEEP) electrospun copolymers. Three months after loading, NGF was still being released and capable of causing mild differentiative effects upon PC12 cells. PCL nanofibers have also been reported to release a NGF-BSA mixture for as long as 28 days, with significantly enhanced neurite outgrowth still being observed in PC12 cells (Valmikinathan et al., 2009). Similarly, electrospun PLC nanofibers that have been tethered to BDNF have been found to promote neurite extension and NSPC proliferation and differentiation into neurons and oligodendrocytes (Horne et al., 2009).

Electrospun scaffolds and conduits have been extensively studied as an intervention for SCI and peripheral nerve regeneration. In these injuries, axonal repair requires fine, ordered control to ensure functional recovery. Electrospun nanofiber scaffolds alone have already demonstrated the ability to promote stem cell proliferation and differentiation, and more importantly, enhance the outgrowth of new connections from neurons in the direction of aligned nanofibers (Yang et al., 2005; Corey et al., 2007; Xie et al., 2009). Fan et al. (2011) further illustrated the regenerative potential of a multichannel PLGA conduit loaded with recombinant human NT-3. Following complete transection of the thoracic SC in rats, use of retrograde tracing confirmed axonal regrowth between caudal and rostral SC stumps, with partial locomotor recovery also being observed 150 days post-injury. The use of NGF-loaded electrospun conduits has also been investigated in order to aid the regeneration of the PNS (Liu et al., 2011). Supporting this, chitosan-based conduits preloaded with NGF have been shown to facilitate the re-establishment of nerve function following injury to the sciatic nerves, with improved muscle innervation and functional recovery of motor function being observed 24 weeks after treatment (Wang H. et al., 2012). Furthermore, Liu et al. (2011) showed that PCL electrospun fibers containing NGF could promote nerve regeneration and improve electromyographic function in a rodent model of PNI. Amazingly, this electrospun treatment was found to provide the same degree of recovery as autografts, which is the current "gold standard" of nerve regeneration (Liu et al., 2011).

The use of neurotrophin-embedded electrospun fibers in the injured brain has been questioned due to the haphazard arrangement of the cerebrum and the invasive nature of electrospun conduit application. However, Fon et al. (2014) conducted a study to investigate the use of electrospun PCL scaffolds embedded with a small molecule BDNF-mimetic following acute injury to the brain. The PCL scaffolds were implanted toward the SVZ, with the needle tract resulting from implantation acting as the acute injury. Eight days after injury, authors found scaffold implantation with and without the BDNF mimetic, facilitated a significant increase in neuroblast migration from the rostral migratory stream (RMS) to the injury site. In contrast, at 21 days post-injury, a significant increase in neuroblast migration was only observed in animals treated with scaffolds containing the BDNF-mimetic (Fon et al., 2014). These findings suggest that electrospun fibers may be able to direct neurogenic processes to the injured brain, including influencing neuroblast infiltration into 3D biomaterial scaffolds. In further support of this notion, Rivet et al. (2015) investigated the use of a hybrid biomaterial system that utilized hydrogels loaded with PLLA-fibronectin electrospun fiber fragments. Sixty days after implantation into the striatum of rats, immunohistology revealed enhanced astrocyte and macrophage/microglia infiltration into the scaffolds. Whilst these findings support that resident cells of the brain were able to locate and utilize cues from the electrospun fibers, further works is needed to confirm the regenerative potential of these systems.

Hydrogel-Based Neurotrophin Delivery Systems

First introduced as a novel material to construct soft contact lenses, Wichterle and Lim (1960) displayed the plausibility of using a porous material with low immunoreactivity in a living organism. Hydrogels have since become of immense interest as a vehicle for drug administration throughout the biomedical and pharmaceutical worlds. Hydrogels refer to three-dimensional, hydrophilic, polymeric networks that are capable of absorbing large amounts of water, or biological fluids (Peppas et al., 2000). Opposed to the fixed encapsulation of GFs, hydrogels allow neurotrophins to be blended into a polymer scaffold, resulting in a steady release of the neurotrophins from within the implantation site as the gel slowly biodegrades.

Compared to the other biomaterials, hydrogels offer many advantages for application in stroke treatments. Hydrogels typically express low toxicity, have a minimally invasive administration procedure, and have a relatively soft consistency that resembles neural tissue (Ratner and Hoffman, 1976). Additionally, *in situ* hydrogels show the unique ability to swell and fill the irregular conformations of stroke-induced lesions. This is hugely advantageous as it provides maximal mechanical and sustained pharmaceutical support directly to the damaged tissue. Specifically, drugs embedded into hydrogels have a sustained, consistent release into surrounding tissue lasting around 2–3 weeks (Tae et al., 2006; Overman et al., 2012; Clarkson et al., 2015; Cook et al., 2017). This overcomes various difficulties encountered by other delivery systems including increased adverse side effects resulting from higher doses and injuries acquired during repetitive drug administrations.

Hydrogels are known to yield anti-inflammatory and regenerative properties when used as a vehicle for NSPCs *in vivo*. For instance, a hyaluronan-heparin-collagen based hydrogel was able to promote survival of NSPCs and reduce infiltration of

inflammatory cells following photothrombotic stroke in mice (Zhong et al., 2010). Similarly, Park et al. (2002) demonstrated the ability of a PGA-derived hydrogel to enhance neuronal differentiation and neurite elongation, reduce monocyte infiltration, and minimize glial scarring when used as a scaffold for NSPC application in a mouse model of hypoxic-induced ischemia. Further, the anti-inflammatory properties of hydrogels themselves have also been observed in rat models of SC injury (Woerly et al., 1998). These intrinsic properties of hydrogels make them ideal candidates as a drug-delivery system for neurotrophin-based treatments, in the hope to further maximize repair, and functional recovery.

The use of BDNF-embedded hydrogels has shown huge promise in repairing the ischemic brain and promoting functional recovery (Clarkson et al., 2015; Cook et al., 2017). A promising study from the Carmichael lab investigated the use of a BDNF-loaded hyaluronan-based hydrogel that was cross-linked with PEG, in two mouse models of stroke (Cook et al., 2017). In both models, treatment beginning at 1-week post-stroke was sufficient to induce significant axonal sprouting throughout cortical and cortico-striatal regions. These animals further displayed enhanced migration of neuroblasts to the peri-infarct cortex and improved functional recovery of forelimb activity. Worth noting, the regenerative potential of BDNF-loaded hydrogels has also been confirmed in aged mice receiving photothrombotic strokes, however, the magnitude of recovery was less than that of young mice (Clarkson et al., 2015). Hydrogels embedded with NT-3 have also displayed neuroregenerative properties when applied as a therapeutic intervention for SCI (Houweling et al., 1998; Piantino et al., 2006). Early work with a NT-3 embedded collagen-derived hydrogel revealed significant regrowth of CST axons following bilateral transection of the dorsal SC in rats (Houweling et al., 1998). In the same animal model, an acrylate-based hydrogel loaded with NT-3 was found to facilitate motor performance on the horizontal ladder walking task and the Basso-Beattie-Bresnahan locomotor score (Piantino et al., 2006). Collectively, the above highlights the benefits of hydrogel-derived delivery systems, providing sustained support to the injured brain and facilitating repair of nervous tissue.

Heparan Sulfate Proteoglycans (HSPGs): A Promising Future Delivery System

The neuronal ECM is a complex and dynamic environment composed of a wide variety of glycoproteins and PGs. PGs are a group of proteins that consist of long, unbranched GAGs side chains covalently linked to a core protein. Interestingly, many GFs are known to require the presence of these extracellular GAGs in order to exert their biological function (Taipale and Keski-Oja, 1997; Whitelock and Iozzo, 2005).

Heparan sulfates are a subset of the class of linear GAG polysaccharide sugars. HS, as extracted from tissue sources and cleaved from its protein component, presents as a ∼15 kDa polymeric mixture. Constructed from a repeating disaccharide comprised of a glucosamine α – linked (1–4) to an uronic acid [glucuronic (*D*-GlcA) or the C-5 epimer iduronic (*L*-IdoA)]. Varying degrees and combinations of acetylation, sulfation or no-substitution at the amine moiety, as well as O-sulfation at the 2-position of the uronic acid and/or 6-position of the glucosamine gives rise to a considerable number of disaccharide permutations (Carnachan et al., 2016). These in turn can be combined into a vastly complex linear array. Enzymatic depolymerization generally reveals eight main disaccharide components (Carnachan et al., 2016), with the most abundant constituent being non-sulfated and comprising ∼30% of the population (as described in **Figure 3**).

Heparan sulfates are particularly evident during times of tissue growth and repair (Gallagher, 1989; Bernfield et al., 1999). Over the past decade the involvement of HS and/or HSPGs in cellular signaling mechanisms has become more and more evident. Many HSPGs are known to be involved in both synaptic and structural neuroplasticity, regulating synaptogenesis, LTP, and dendritic spine maturation (Ksiazek et al., 2007; Allen et al., 2012; Senkov, 2014). Several studies have also discovered HSPG-mediated potentiation of neurite outgrowth and cell migration *in vitro* (Walz et al., 1997; Hu, 2001; Jung Kim et al., 2003).

Many of the regenerative and reparative properties of HS are thought to be mediated through GAGs ability to act as a medium-affinity co-receptor for binding GF's to their receptors (Bespalov et al., 2011; Chen et al., 2012). This GF-GAG interaction further enhances protein stability and bioavailability of GFs and their receptors (Chen et al., 2012; Chan et al., 2017). HSPGs are also highly sulfated giving the sugar a unique ability to create large binding pockets that can be utilized to house an abundance of GFs. Supporting this notion, early work from Kanato et al. (2009) used horizontal native- PAGE and gel chromatography analysis to confirm a direct molecular interaction between HS and the neurotrophins NT-3 and BDNF. The resulting complex was found to bind to both $p75^{NTR}$ and TrkB, respectively, in a manner similar to polysialic acid, a protein that has been proposed to house and mediate BDNF concentrations and function (Kanato et al., 2008). Whilst this interaction remains to be identified both *in vitro* and *in vivo*, the above findings do support the idea that GAGs may regulate local GF concentrations, which could further serve to provide a reservoir of neurotrophins on cell surfaces or around the ECM. However, is should also be acknowledged that the exact role of HS with respect to its interaction with GFs, still requires future investigation (Lander, 2007).

The therapeutic use of HS remains sparsely investigated due to the low yield experienced when fractionating heparanoid raw materials (sourced as byproduct from Heparin manufacture). This is further complicated by limited supply and quality control of HS (Mulloy et al., 2016). The preparation of individual oligosaccharides remains highly costly, time consuming and difficult (DeAngelis et al., 2013), but recent advancements in technology have led to innovative synthetic or chemoenzymatic approaches allowing access to significantly longer purified HS structures (Kuberan et al., 2003; Liu et al., 2010; Tyler et al., 2015). However, the heterogeneity of native HS means synthesis of even a small portion of the structural diversity that is found in nature, even if limited in size to as small as an octasaccharide, is a daunting challenge.

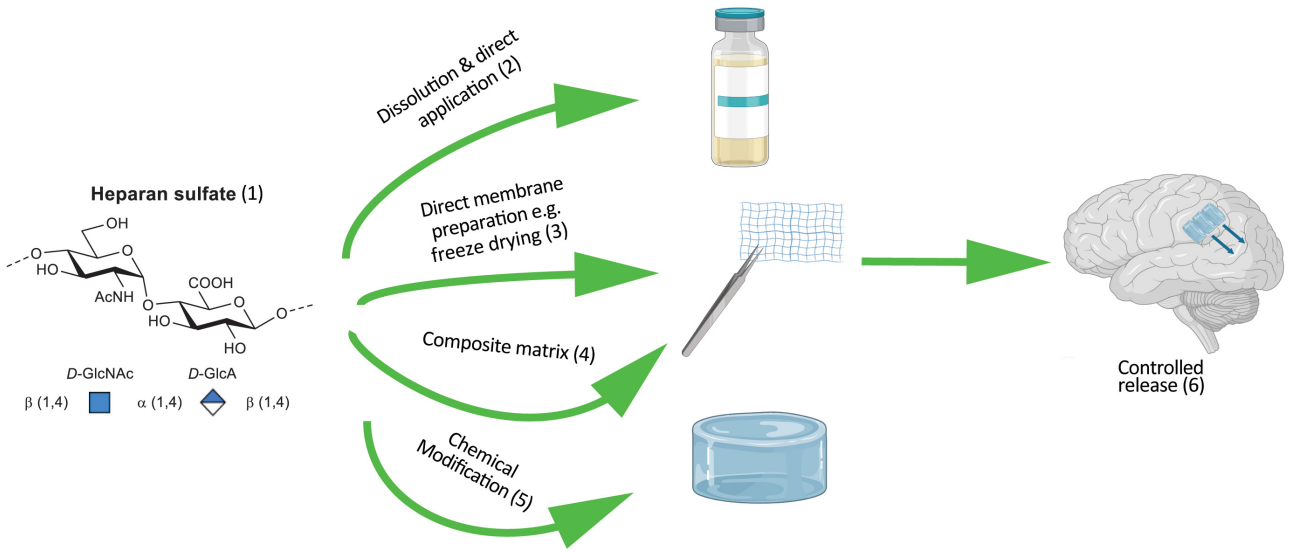

FIGURE 3 | Schematic of incorporating HS into therapeutic devices. (1) Synthetic HS that approximates the degree of sulfation and acetylation of naturally occurring HS can be derived from heparin through chemical modifications. Example modifications of HS and composition of device. (2) HS adsorbed onto a collagen membrane. (3) Solid form of HS as a carbohydrate foam. (4) Electrostatically bound HS (net –ve charge) protein substrate (net +ve charge). (5) Pegylated, alkylated or alternative chemical modification of HS to control hydrophobicity and release for direct coating onto a device. (6) Device characteristics tuned to release HS into the extracellular matrix facilitating tissue regeneration.

Whilst literature investigating the ability of HS and heparin to cross the BBB is sparse, several studies suggest that these molecules may in fact cross the BBB. Early *in vitro* work has indicated Heparin of 3000 Da and smaller fragments (i.e., di, tetra, and hexasaccharides) can all cross a BBB barrier in a model system, without any obvious correlation with size to transport efficiency (Leveugle et al., 1998). Ma et al. (2002) have since reported BBB passage of small fragments of C3, a low molecular weight (2000 ± 200 Da) heparin-derived oligosaccharide designed for treatment of vascular dementia and Alzheimer's disease. Specifically, C3 was able to penetrate the BBB and retain its' inhibitory effect on factor Xa after systemic administration to non-human primates (Ma et al., 2002). Further supporting evidence has come from a recent study by Hippensteel et al. (2019) who found fluorescein-labeled HS fragments penetrated the BBB during sepsis and inhibited BDNF-mediated hippocampal memory. In addition, they further show that the binding affinity of HS fragments to BDNF increased with sulfation at the 2-O-position of iduronic acid and N-position of glucosamine (Hippensteel et al., 2019). These findings support that sulfation at these sites is critical for memory impairments, although it has not been shown if this is the case for all cognitive domains. Whilst, the involvement of these sulfation sites in post-stroke motor and sensory impairments is yet to be investigated. Given that poor BBB passage is thought to be an underlying cause for a lack of clinical translation of compounds targeting the CNS (Pardridge, 2005), HS may prove extremely useful as a backbone for therapeutic interventions targeting the injured brain.

Although HS application into CNS disease is extremely limited so far, a recent study by Hill et al. (2012) illustrated the neuroregenerative potential of the HSPG glypican, in the MCAo model of stroke. Intracerebral glypican was administered through micro-osmotic pumps for a week following stroke, which resulted in a significant decrease in GFAP and increased MAP2 expression in the peri-infarct region. These findings support a glypican-mediated reduction in astrocyte activation and enhanced neuronal survival, respectively. Furthermore, when put through various sensorimotor tasks glypican-treated animals performed significantly better when assessed 10- and 14-days after stroke, compared to control animals (Hill et al., 2012). Another HSPG, Perlecan domain V, has also been shown to afford neuroprotection in both young and aged mice (Bix et al., 2013). Perlecan domain V has also been shown to regulate both VEGF and BDNF levels (Lee et al., 2011; Bix et al., 2013). Whilst the regenerative potential of Perlecan domain V when administrated via a hydrogel or other biomaterial has yet to be studied, it is likely that similar if not better effects would be observed compared to when Perlecan domain V is given systemically.

A key component of biomaterial design lies in the topography and three-dimensional structure of its' scaffold (Führmann et al., 2017). Given the physiological role of HS chains in supporting the ECM of the CNS, the incorporation of HS chains into biomaterial scaffolds has been of interest in the field of regeneration and repair. Fibrin glue loaded with a HS scaffold has been shown to increase mineralized bone deposition and osteogenic marker expression, reflecting enhanced bone repair (Woodruff et al., 2007). Microcomputed tomography further revealed almost complete closure of chronic cranial defects sites in rats 3 months after treatment with the fibrin-HS glue, compared

to minimal healing seen in fibrin glue without HS chains (Woodruff et al., 2007).

Heparan sulfates, as the sodium salt, demonstrates very good water solubility and only when solutions get above 10% w/w does any increase in viscosity become apparent. In an anhydrous form it will reach an equilibrium water-content of 13% at room temperature, which must be accommodated for (or freshly freeze-dried material must be used) or else dose control in constructs becomes erroneous (Murali et al., 2013). Other salt-forms are generally more problematic in terms of physical handling; the pyridinium salt, for example, being very hygroscopic. This solubility means a preformed porous substrate can be dosed with a solution (**Figure 3**, direct application) prior to wound inclusion (Murali et al., 2013). Alternatively, solid support foams can readily be prepared through freeze drying a solution of neat HS, or by combining HS with other materials in solution to form a stable solid matrix (**Figure 3**, composite matrix and or membrane preparation). Pre-formed microspheres or membranes generated through electrospinning as depicted in **Figure 2** may have the HS included during preparation and/or adsorbed into the construct or coated onto the material surface.

Collagenous matrices with covalently attached HS chains have also been found to promote matrix integrity, facilitate angiogenesis and reduce foreign body reactions when implanted subcutaneously into rats (Pieper et al., 2000). Early *in vitro* work has also confirmed a trophic effect of HS-incorporation on cells of the CNS. Guan et al. (2013) discovered that a chitosan-gelatin scaffold containing GAGs, HA, and HS, promoted NSC/NPC adhesion, survival and long-term growth. A similar finding was observed by Uygun et al. (2009) who recorded increased MSC density, migration, and proliferation of MSCs cultured on chitosan membranes modified with HS chains. The trophic potential of HS-embedded biomaterial scaffolds has also been acknowledged by Mammadov et al. (2012), who illustrated that combining a heparan-sulfate-mimicking peptide nanofibers with a laminin-derived nanofiber scaffold significantly enhances neurite outgrowth of PC-12 neurons. The above literature supports the use of HS-seeded biomaterials for neurotrophin-mediated regeneration, leaving the translational potential of such treatments to future research. It is also worth noting that in the body, HS chains are manufactured as a PG, which are present in the ECM at relatively high concentrations compared to free HS fragments (i.e., mg/mL. PPM) (Lander and Selleck, 2000). Certainly, it is recognized that the shedding of HS chains from HSPGs can release sequestered GFs to stimulate GF activity (Yu et al., 2017). However, it remains a matter of debate as to whether or not all GF-GAG interactions are mediated by HS chains or the full HSPG (i.e., HS chains and protein core). For example, the HSPG, glypican, requires the presence of its HS chains in order to facilitate FGF-2 (Song et al., 1997; Lander and Selleck, 2000) but not BMP signaling (Kirkpatrick et al., 2006). Furthermore, the protein core of glypican has been found to bind and promote Hedgehog (Hh) signaling without the involvement of HS chains (Capurro et al., 2008). Future work elucidating the exact molecular mechanism associated with this GF-HS interaction will help guide the development of HS-embedded biomaterials for therapeutic application.

CONCLUDING REMARKS

Neurodegenerative diseases, such as stroke, remain the leading cause of adult death and disability worldwide. With the aging population on the rise, and these diseases preferentially affecting the elderly, there is a growing interest in the development of interventions that can fight against neurological decline and enhance functional recovery. Protective therapies for stroke are massively limited due to the narrow window of opportunity that is required for success. Consequently, the generation of regenerative interventions have become of utmost importance to help treat stroke at a clinically relevant time point, and to successfully translate findings from bench to bedside.

After decades of preclinical studies and still no successful treatments for stroke recovery in humans, researchers have agreed that future work investigating the neurobiology, and progression of post-stroke recovery (both spontaneous and treatment-induced) will be crucial on the journey toward the identification of key molecular targets and an optimal time of intervention (Bernhardt et al., 2017; Corbett et al., 2017). Armed with this knowledge, the scientific and medical worlds will have the greatest chance of providing maximal recovery from stroke in multidisciplinary phase II clinical trials.

Neurotrophins have shown great promise in modulating the injured brain and promoting functional recovery in preclinical models of neurodegenerative disease. However, the clinical success of these treatments is yet to be observed due to poor BBB passage, short half-life and lack of sufficient quantities for clinical use. The use of biomaterials creates a unique delivery system that alters the pharmacokinetic profile of neurotrophins and offers a mechanism to penetrate the BBB and treat the injured brain with concentrations that are only a fraction of those used during systemic administration. Recent animal-based experimental research has shown great promise using biomaterial-delivery systems to deliver neurotrophins to enhance functional recovery, with each biomaterial type yielding distinct properties that suit different biomedical applications. For example, the linear nature of electrospun conduits has shown the most success in promoting controlled nerve regeneration in animal models of SCI (Fan et al., 2011; Wang H. et al., 2012). Alternatively, the ability of hydrogels to expand and fill irregular injury sites in conditions such as stroke has proven extremely useful for providing additional mechanical stability that other biomaterial systems lack.

Heparan sulfates offers a new therapeutic potential in promoting rapid tissue regeneration. It has shown significant benefit in repair of large defects in controlled wound sites (Murali et al., 2013; Wang et al., 2014) yet its full therapeutic benefit is unexplored, in no small way due to availability and reliability of supply (Mulloy et al., 2016). The versatility of this biopolymer, intrinsic to cellular regulation, is well suited to biomaterial applications *in vivo*: it is extremely well tolerated, readily decomposed by native enzymatic processes, is compatible with accepted medical device materials (e.g., collagen sponge or

hydrogels) and can be included into device technologies through a variety of mechanisms.

Of note, an exciting biomaterial approach that is emerging involves not just one, but many biomaterial types combined into a hybrid delivery system. Early work with this technology has shown the fine-tuned release of multiple GFs over different release profiles (Burdick et al., 2006). Specifically, the sequential release of glial cell-derived neurotrophic factor (GDNF)- and BDNF-loaded PLGA microspheres was achieved by loading neurotrophins to opposite ends of a PEG-based hydrogel implant (Lampe et al., 2011). Healthy rats given the combinational treatment, with the implant being applied to target the striatum (BDNF) and sustantia nigra (GDNF) with the hope of assisting transplant survival and long-term axon extension, respectively, in future work with animal models of Parkinson's disease. Results showed that GDNF was released within 28 days of implantation, whereas BDNF release was observed as late as 56 days. Due to the recency of the development of these sequential drug-delivery systems, they have sparsely been investigated in animal models of CNS injury or disease. Nonetheless, given the complex spatiotemporal, pathological events that occur in the days to weeks to months following neurodegenerative diseases, these delivery systems will yield great promise with delivery of multiple GFs to appropriate regions of the brain at relevant therapeutic time points to maximize recovery.

To ensure such treatment options translate into the clinic, much needed follow-up studies are required and clinical validation studies to be undertaken. Given the knowledge we have already gained around neurotrophic signaling especially with respect to BDNF-mediated improvements in functional recovery and the advances made in the biomaterial-delivery field, there is an exciting prospect of being able to deliver a potential treatment to contribute toward recovery from stroke and other neurological disorders.

AUTHOR CONTRIBUTIONS

JH, NA, SH, and AC wrote and edited the final version of the manuscript. JH prepared the figures. AC conceived the idea for the review of the manuscript.

FUNDING

This work was supported by a Ministry of Business, Innovation and Employment grant (No. CONT-46417-CRFSI-UOO) to AC.

REFERENCES

Aizawa, Y., Leipzig, N., Zahir, T., and Shoichet, M. (2008). The effect of immobilized platelet derived growth factor AA on neural stem/progenitor cell differentiation on cell-adhesive hydrogels. *Biomaterials* 29, 4676–4683. doi: 10.1016/j.biomaterials.2008.08.018

Alhosseini, S. N., Moztarzadeh, F., Mozafari, M., Asgari, S., Dodel, M., Samadikuchaksaraei, A., et al. (2012). Synthesis and characterization of electrospun polyvinyl alcohol nanofibrous scaffolds modified by blending with chitosan for neural tissue engineering. *Int. J. Nanomedicine* 7, 25–34. doi: 10.2147/IJN.S25376

Allen, N. J., Bennett, M. L., Foo, L. C., Wang, G. X., Chakraborty, C., Smith, S. J., et al. (2012). Astrocyte glypicans 4 and 6 promote formation of excitatory synapses via GluA1 AMPA receptors. *Nature* 486, 410–414. doi: 10.1038/nature11059

Aloe, L., Tuveri, M. A., Carcassi, U., and Levi-Montalcini, R. (1992). Nerve growth factor in the synovial fluid of patients with chronic arthritis. *Arthritis Rheum.* 35, 351–355. doi: 10.1002/art.1780350315

Andero, R., Choi, D. C., and Ressler, K. J. (2014). BDNF-TrkB receptor regulation of distributed adult neural plasticity, memory formation, and psychiatric disorders. *Prog. Mol. Biol. Transl. Sci.* 122, 169–192. doi: 10.1016/B978-0-12-420170-5.00006-4

Atwal, J. K., Massie, B., Miller, F. D., and Kaplan, D. R. (2000). The TrkB-Shc site signals neuronal survival and local axon growth via MEK and PI3-kinase. *Neuron* 27, 265–277. doi: 10.1016/s0896-6273(00)00035-0

Barnabé-Heider, F., and Miller, F. D. (2003). Endogenously produced neurotrophins regulate survival and differentiation of cortical progenitors via distinct signaling pathways. *J. Neurosci.* 23, 5149–5160. doi: 10.1523/jneurosci.23-12-05149.2003

Batchelor, P. E., Liberatore, G., Porritt, M. J., Donnan, G. A., and Howells, D. W. (2000). Inhibition of brain-derived neurotrophic factor and glial cell line-derived neurotrophic factor expression reduces dopaminergic sprouting in the injured striatum. *Eur. J. Neurosci.*, 3462–3468. doi: 10.1046/j.1460-9568.2000.00239.x

Batchelor, P. E., Porritt, M. J., Martinello, P., Parish, C., Liberatore, G., Donnan, G. A., et al. (2002). Macrophages and microglia produce local trophic gradients that stimulate axonal sprouting toward but not beyond the wound edge. *Mol. Cell. Neurosci.* 21, 436–453. doi: 10.1006/mcne.2002.1185

Bates, B., Hirt, L., Thomas, S. S., Akbarian, S., Le, D., Amin-Hanjani, S., et al. (2002). Neurotrophin-3 promotes cell death induced in cerebral ischemia, oxygen-glucose deprivation, and oxidative stress: possible involvement of oxygen free radicals. *Neurobiol. Dis.* 9, 24–37. doi: 10.1006/nbdi.2001.0458

Beck, T., Lindholm, D., Castren, E., and Wree, A. (1994). Brain-derived neurotrophic factor protects against ischemic cell damage in rat hippocampus. *J. Cereb. Blood Flow Metab.* 14, 689–692. doi: 10.1038/jcbfm.1994.86

Béjot, Y., Prigent-Tessier, A., Cachia, C., Giroud, M., Mossiat, C., Bertrand, N., et al. (2011). Time-dependent contribution of non neuronal cells to BDNF production after ischemic stroke in rats. *Neurochem. Int.* 58, 102–111. doi: 10.1016/j.neuint.2010.10.019

Benowitz, L. I., and Carmichael, S. T. (2010). Promoting axonal rewiring to improve outcome after stroke. *Neurobiol. Dis.* 37, 259–266. doi: 10.1016/j.nbd.2009.11.009

Bernfield, M., Götte, M., Park, P. W., Reizes, O., Fitzgerald, M. L., Lincecum, J., et al. (1999). Functions of cell surface heparan sulfate proteoglycans. *Ann. Rev. Biochem.* 68, 729–777. doi: 10.1146/annurev.biochem.68.1.729

Bernhardt, J., Hayward, K. S., Kwakkel, G., Ward, N. S., Wolf, S. L., Borschmann, K., et al. (2017). Agreed definitions and a shared vision for new standards in stroke recovery research: the stroke recovery and rehabilitation roundtable taskforce. *Int. J. Stroke* 12, 444–450. doi: 10.1177/1747493017711816

Berretta, A., Tzeng, Y. C., and Clarkson, A. N. (2014). Post-stroke recovery: the role of activity-dependent release of brain-derived neurotrophic factor. *Expert Rev. Neurother.* 14, 1335–1344. doi: 10.1586/14737175.2014.969242

Bertram, J. P., Rauch, M. F., Chang, K., and Lavik, E. B. (2010). Using polymer chemistry to modulate the delivery of neurotrophic factors from degradable microspheres: delivery of BDNF. *Pharm. Res.* 27, 82–91. doi: 10.1007/s11095-009-0009-x

Bespalov, M. M., Sidorova, Y. A., Tumova, S., Ahonen-Bishopp, A., Magalhães, A. C., Kulesskiy, E., et al. (2011). Heparan sulfate proteoglycan syndecan-3 is a novel receptor for GDNF, neurturin, and artemin. *J. Cell Biol.* 192, 153–169. doi: 10.1083/jcb.201009136

Bezdjian, A., Kraaijenga, V., Ramekers, D., Versnel, H., Thomeer, H., Klis, S., et al. (2016). Towards clinical application of neurotrophic factors to the auditory

nerve; assessment of safety and efficacy by a systematic review of neurotrophic treatments in humans. *Int. J. Mol. Sci.* 17:1981. doi: 10.3390/ijms17121981

Bhatia, S. K. (2010). Tissue engineering for clinical applications. *Biotechnol. J.* 5, 1309–1323. doi: 10.1002/biot.201000230

Binan, L., Ajji, A., De Crescenzo, G., and Jolicoeur, M. (2014). Approaches for neural tissue regeneration. *Stem Cell Rev. Rep.* 10, 44–59.

Binder, D. K., and Scharfman, H. E. (2004). Brain-derived neurotrophic factor. *Growth factors* 22, 123–131.

Bix, G. J., Gowing, E. K., and Clarkson, A. N. (2013). Perlecan domain V is neuroprotective and affords functional improvement in a photothrombotic stroke model in young and aged mice. *Transl. Stroke Res.* 4, 515–523. doi: 10.1007/s12975-013-0266-1

Bonini, S., Lambiase, A., Rama, P., Sinigaglia, F., Allegretti, M., Chao, W., et al. (2018). Phase II randomized, double-masked, vehicle-controlled trial of recombinant human nerve growth factor for neurotrophic keratitis. *Ophthalmology* 125, 1332–1343. doi: 10.1016/j.ophtha.2018.02.022

Boris-Möller, F., Kamme, F., and Wieloch, T. (1998). The effect of hypothermia on the expression of neurotrophin mRNA in the hippocampus following transient cerebral ischemia in the rat. *Mol. Brain Res.* 63, 163–173. doi: 10.1016/s0169-328x(98)00286-1

Bothwell, M. (1995). Functional interactions of neurotrophins and neurotrophin receptors. *Annu. Rev. Neurosci.* 18, 223–253. doi: 10.1146/annurev.neuro.18.1.223

Boyd, J. G., and Gordon, T. (2003a). Glial cell line-derived neurotrophic factor and brain-derived neurotrophic factor sustain the axonal regeneration of chronically axotomized motoneurons in vivo. *Exp. Neurol.* 183, 610–619. doi: 10.1016/s0014-4886(03)00183-3

Boyd, J. G., and Gordon, T. (2003b). Neurotrophic factors and their receptors in axonal regeneration and functional recovery after peripheral nerve injury. *Mol. Neurobiol.* 27, 277–323.

Bradbury, E. J., Khemani, S., Von, R., Priestley, J. V., and Mcmahon, S. B. (1999). NT-3 promotes growth of lesioned adult rat sensory axons ascending in the dorsal columns of the spinal cord. *Eur. J. Neurosci.* 11, 3873–3883. doi: 10.1046/j.1460-9568.1999.00809.x

Bradley, W. G. (1999). A controlled trial of recombinant methionyl human BDNF in ALS. *Neurology* 52, 1427–1433.

Brem, H., and Gabikian, P. (2001). Biodegradable polymer implants to treat brain tumors. *J. Controll. release* 74, 63–67. doi: 10.1016/s0168-3659(01)00311-x

Burdick, J. A., Ward, M., Liang, E., Young, M. J., and Langer, R. (2006). Stimulation of neurite outgrowth by neurotrophins delivered from degradable hydrogels. *Biomaterials* 27, 452–459. doi: 10.1016/j.biomaterials.2005.06.034

Cai, J., Hua, F., Yuan, L., Tang, W., Lu, J., Yu, S., et al. (2014). Potential therapeutic effects of neurotrophins for acute and chronic neurological diseases. *BioMed Res. Int.* 2014:601084.

Cantley, L. C. (2002). The phosphoinositide 3-kinase pathway. *Science* 296, 1655–1657. doi: 10.1126/science.296.5573.1655

Capurro, M. I., Xu, P., Shi, W., Li, F., Jia, A., and Filmus, J. (2008). Glypican-3 inhibits Hedgehog signaling during development by competing with patched for Hedgehog binding. *Dev. Cell* 14, 700–711. doi: 10.1016/j.devcel.2008.03.006

Carmichael, S. T., Ohab, J., and Nguyen, J. (2005). Post-stroke neurogenesis and the neurovascular niche: newly born neuroblasts localize to peri-infarct cortex in close association with the vascular endothelium. *J. Cereb. Blood Flow Metab.* 25, S214–S214.

Carmichael, S. T., Wei, L., Rovainen, C. M., and Woolsey, T. A. (2001). New patterns of intracortical projections after focal cortical stroke. *Neurobiol. Dis.* 8, 910–922. doi: 10.1006/nbdi.2001.0425

Carnachan, S. M., Bell, T. J., Sims, I. M., Smith, R. A. A., Nurcombe, V., Cool, S. M., et al. (2016). Determining the extent of heparan sulfate depolymerisation following heparin lyase treatment. *Carbohydr. Polym.* 152, 592–597. doi: 10.1016/j.carbpol.2016.07.024

Chan, S. J., Love, C., Spector, M., Cool, S. M., Nurcombe, V., and Lo, E. H. (2017). Endogenous regeneration: engineering growth factors for stroke. *Neurochem. Int.* 107, 57–65. doi: 10.1016/j.neuint.2017.03.024

Chao, M. V. (2003). Neurotrophins and their receptors: a convergence point for many signalling pathways. *Nat. Rev. Neurosci.* 4, 299–309. doi: 10.1038/nrn1078

Chaudhry, V., Giuliani, M., Petty, B., Lee, D., Seyedsadr, M., Hilt, D., et al. (2000). Tolerability of recombinant-methionyl human neurotrophin-3 (r-metHuNT3) in healthy subjects. *Muscle Nerve* 23, 189–192. doi: 10.1002/(sici)1097-4598(200002)23:2<189::aid-mus7>3.0.co;2-8

Chen, G., Gulbranson, D. R., Yu, P., Hou, Z., and Thomson, J. A. (2012). Thermal stability of fibroblast growth factor protein is a determinant factor in regulating self-renewal, differentiation, and reprogramming in human pluripotent stem cells. *Stem Cells* 30, 623–630. doi: 10.1002/stem.1021

Chen, J., Li, Y., and Chopp, M. (2000). Intracerebral transplantation of bone marrow with BDNF after MCAo in rat. *Neuropharmacology* 39, 711–716. doi: 10.1016/s0028-3908(00)00006-x

Chew, S. Y., Wen, J., Yim, E. K., and Leong, K. W. (2005). Sustained release of proteins from electrospun biodegradable fibers. *Biomacromolecules* 6, 2017–2024. doi: 10.1021/bm0501149

Choi, S. H., Bylykbashi, E., Chatila, Z. K., Lee, S. W., Pulli, B., Clemenson, G. D., et al. (2018). Combined adult neurogenesis and BDNF mimic exercise effects on cognition in an Alzheimer's mouse model. *Science* 361:eaan8821. doi: 10.1126/science.aan8821

Clarkson, A. N. (2012). Perisynaptic GABA receptors: the overzealous protector. *Adv. Pharm. Sci.* 2012:708428. doi: 10.1155/2012/708428

Clarkson, A. N., Huang, B. S., Macisaac, S. E., Mody, I., and Carmichael, S. T. (2010). Reducing excessive GABA-mediated tonic inhibition promotes functional recovery after stroke. *Nature* 468, 305–309. doi: 10.1038/nature09511

Clarkson, A. N., Lopez-Valdes, H. E., Overman, J. J., Charles, A. C., Brennan, K. C., and Thomas Carmichael, S. (2013). Multimodal examination of structural and functional remapping in the mouse photothrombotic stroke model. *J. Cereb. Blood Flow Metab.* 33, 716–723. doi: 10.1038/jcbfm.2013.7

Clarkson, A. N., Overman, J. J., Zhong, S., Mueller, R., Lynch, G., and Carmichael, S. T. (2011). AMPA receptor-induced local brain-derived neurotrophic factor signaling mediates motor recovery after stroke. *J. Neurosci.* 31, 3766–3775. doi: 10.1523/JNEUROSCI.5780-10.2011

Clarkson, A. N., Parker, K., Nilsson, M., Walker, F. R., and Gowing, E. K. (2015). Combined ampakine and BDNF treatments enhance poststroke functional recovery in aged mice via AKT-CREB signaling. *J. Cereb. Blood Flow Metab.* 35, 1272–1279. doi: 10.1038/jcbfm.2015.33

Clary, D. O., and Reichardt, L. F. (1994). An alternatively spliced form of the nerve growth factor receptor TrkA confers an enhanced response to neurotrophin 3. *Proc. Natl. Acad. Sci. U.S.A.* 91, 11133–11137. doi: 10.1073/pnas.91.23.11133

Comelli, M., Guidolin, D., Seren, M., Zanoni, R., Canella, R., Rubini, R., et al. (1993). Time course, localization and pharmacological modulation of immediate early inducible genes, brain-derived neurotrophic factor and trkB messenger RNAs in the rat brain following photochemical stroke. *Neuroscience* 55, 473–490. doi: 10.1016/0306-4522(93)90517-j

Connor, B., and Dragunow, M. (1998). The role of neuronal growth factors in neurodegenerative disorders of the human brain. *Brain Res. Brain Res. Rev.* 27, 1–39. doi: 10.1016/s0165-0173(98)00004-6

Cook, D. J., Nguyen, C., Chun, H. N., Llorente, L. L., Chiu, A. S., Machnicki, M., et al. (2017). Hydrogel-delivered brain-derived neurotrophic factor promotes tissue repair and recovery after stroke. *J. Cereb. Blood Flow Metab.* 37, 1030–1045. doi: 10.1177/0271678X16649964

Cooper-Kuhn, C. M., Winkler, J., and Kuhn, H. G. (2004). Decreased neurogenesis after cholinergic forebrain lesion in the adult rat. *J. Neurosci. Res.* 77, 155–165. doi: 10.1002/jnr.20116

Corbett, D., Carmichael, S. T., Murphy, T. H., Jones, T. A., Schwab, M. E., Jolkkonen, J., et al. (2017). Enhancing the alignment of the preclinical and clinical stroke recovery research pipeline: consensus-based core recommendations from the stroke recovery and rehabilitation roundtable translational working group. *Int. J. Stroke* 12, 462–471. doi: 10.1177/1747493017711814

Corey, J. M., Lin, D. Y., Mycek, K. B., Chen, Q., Samuel, S., Feldman, E. L., et al. (2007). Aligned electrospun nanofibers specify the direction of dorsal root ganglia neurite growth. *J. Biomed. Mater. Res. Part A* 83, 636–645. doi: 10.1002/jbm.a.31285

Cuello, A. C. (1996). Effects of trophic factors on the CNS cholinergic phenotype. *Prog. Brain Res.* 109, 347–358. doi: 10.1016/s0079-6123(08)62117-2

De Boer, R., Knight, A. M., Borntraeger, A., Hébert-Blouin, M. N., Spinner, R. J., Malessy, M. J., et al. (2011). Rat sciatic nerve repair with a poly-lactic-co-glycolic

acid scaffold and nerve growth factor releasing microspheres. *Microsurgery* 31, 293–302. doi: 10.1002/micr.20869

De Boer, R., Knight, A. M., Spinner, R. J., Malessy, M. J., Yaszemski, M. J., and Windebank, A. J. (2010). In vitro and in vivo release of nerve growth factor from biodegradable poly-lactic-co-glycolic-acid microspheres. *J. Biomed. Mater. Res. Part A* 95, 1067–1073. doi: 10.1002/jbm.a.32900

DeAngelis, P. L., Liu, J., and Linhardt, R. J. (2013). Chemoenzymatic synthesis of glycosaminoglycans: re-creating, re-modeling and re-designing nature's longest or most complex carbohydrate chains. *Glycobiology* 23, 764–777. doi: 10.1093/glycob/cwt016

Debeir, T., Saragovi, H. U., and Cuello, A. C. (1999). A nerve growth factor mimetic TrkA antagonist causes withdrawal of cortical cholinergic boutons in the adult rat. *Proc. Natl. Acad. Sci. U.S.A.* 96, 4067–4072. doi: 10.1073/pnas.96.7.4067

Dechant, G., and Barde, Y.-A. (2002). The neurotrophin receptor p75NTR: novel functions and implications for diseases of the nervous system. *Nat. Neurosci.* 5, 1131–1136. doi: 10.1038/nn1102-1131

Deinhardt, K., Kim, T., Spellman, D. S., Mains, R. E., Eipper, B. A., Neubert, T. A., et al. (2011). Neuronal growth cone retraction relies upon proneurotrophin receptor signaling through Rac. *Sci. Signal.* 4:ra82. doi: 10.1126/scisignal.2002060

Dirnagl, U., Iadecola, C., and Moskowitz, M. A. (1999). Pathobiology of ischaemic stroke: an integrated view. *Trends Neurosci.* 22, 391–397. doi: 10.1016/s0166-2236(99)01401-0

Dmitrieva, V., Stavchansky, V., Povarova, O., Skvortsova, V., Limborska, S., and Dergunova, L. (2016). Effects of ischemia on the expression of neurotrophins and their receptors in rat brain structures outside the lesion site, including on the opposite hemisphere. *Mol. Biol.* 50, 684–692. doi: 10.1134/s0026893316030067

Dombrowski, C., Song, S. J., Chuan, P., Lim, X., Susanto, E., Sawyer, A. A., et al. (2009). Heparan sulfate mediates the proliferation and differentiation of rat mesenchymal stem cells. *Stem Cells Dev.* 18, 661–670. doi: 10.1089/scd.2008.0157

Doshi, J., and Reneker, D. H. (1995). Electrospinning process and applications of electrospun fibers. *J. Electrost.* 35, 151–160. doi: 10.1016/0304-3886(95)00041-8

Duque, J., Hummel, F., Celnik, P., Murase, N., Mazzocchio, R., and Cohen, L. G. (2005). Transcallosal inhibition in chronic subcortical stroke. *Neuroimage* 28, 940–946. doi: 10.1016/j.neuroimage.2005.06.033

Duricki, D., Kakanos, S., Haenzi, B., Wayman, C., Cash, D., and Moon, L. (2018). Subcutaneous neurotrophin-3 infusion induces corticospinal neuroplasticity and improvements in dexterity and walking in elderly rats after large cortical stroke. *bioRxiv* [Preprint]. doi: 10.1101/427864

Duricki, D. A., Hutson, T. H., Kathe, C., Soleman, S., Gonzalez-Carter, D., Petruska, J. C., et al. (2015). Delayed intramuscular human neurotrophin-3 improves recovery in adult and elderly rats after stroke. *Brain* 139, 259–275. doi: 10.1093/brain/awv341

Encinas, M., Iglesias, M., Llecha, N., and Comella, J. (1999). Extracellular-regulated kinases and phosphatidylinositol 3-kinase are involved in brain-derived neurotrophic factor-mediated survival and neuritogenesis of the neuroblastoma cell line SH-SY5Y. *J. Neurochem.* 73, 1409–1421. doi: 10.1046/j.1471-4159.1999.0731409.x

Eriksdotter Jönhagen, M., Nordberg, A., Amberla, K., Bäckman, L., Ebendal, T., Meyerson, B., et al. (1998). Intracerebroventricular infusion of nerve growth factor in three patients with Alzheimer's disease. *Dement. Geriatr. Cogn. Disord.* 9, 246–257. doi: 10.1159/000017069

Ernfors, P., Ibanez, C. F., Ebendal, T., Olson, L., and Persson, H. (1990). Molecular cloning and neurotrophic activities of a protein with structural similarities to nerve growth factor: developmental and topographical expression in the brain. *Proc. Natl. Acad. Sci. U.S.A.* 87, 5454–5458. doi: 10.1073/pnas.87.14.5454

Fan, J., Zhang, H., He, J., Xiao, Z., Chen, B., Xiaodan, J., et al. (2011). Neural regrowth induced by PLGA nerve conduits and neurotrophin-3 in rats with complete spinal cord transection. *J. Biomed. Mater. Res. Part B* 97, 271–277. doi: 10.1002/jbm.b.31810

Feigin, V., Carter, K., Hackett, M., Barber, P. A., Mcnaughton, H., Dyall, L., et al. (2006). Ethnic disparities in incidence of stroke subtypes: auckland regional community stroke study, 2002–2003. *Lancet Neurol.* 5, 130–139. doi: 10.1016/s1474-4422(05)70325-2

Feigin, V. L., Forouzanfar, M. H., Krishnamurthi, R., Mensah, G. A., Connor, M., Bennett, D. A., et al. (2014). Global and regional burden of stroke during 1990–2010: findings from the global burden of disease study 2010. *Lancet* 383, 245–255. doi: 10.1016/s0140-6736(13)61953-4

Fon, D., Al-Abboodi, A., Chan, P. P., Zhou, K., Crack, P., Finkelstein, D. I., et al. (2014). Effects of GDNF-loaded injectable gelatin-based hydrogels on endogenous neural progenitor cell migration. *Adv. Healthc. Mater.* 3, 761–774. doi: 10.1002/adhm.201300287

Fritsch, B., Reis, J., Martinowich, K., Schambra, H. M., Ji, Y., Cohen, L. G., et al. (2010). Direct current stimulation promotes BDNF-dependent synaptic plasticity: potential implications for motor learning. *Neuron* 66, 198–204. doi: 10.1016/j.neuron.2010.03.035

Führmann, T., Anandakumaran, P. N., and Shoichet, M. S. (2017). Combinatorial therapies after spinal cord injury: how can biomaterials help? *Adv. Healthc. Mater.* 6:1601130. doi: 10.1002/adhm.201601130

Gallagher, J. T. (1989). The extended family of proteoglycans: social residents of the pericellular zone. *Curr. Opin. Cell Biol.* 1, 1201–1218. doi: 10.1016/s0955-0674(89)80072-9

Ghosh, A., and Greenberg, M. E. (1995). Distinct roles for bFGF and NT-3 in the regulation of cortical neurogenesis. *Neuron* 15, 89–103. doi: 10.1016/0896-6273(95)90067-5

Giehl, K. M., and Tetzlaff, W. (1996). BDNF and NT-3, but not NGF, prevent axotomy-induced death of rat corticospinal neurons in vivo. *Eur. J. Neurosci.* 8, 1167–1175. doi: 10.1111/j.1460-9568.1996.tb01284.x

Goss, J. R., O'malley, M. E., Zou, L., Styren, S. D., Kochanek, P. M., and Dekosky, S. T. (1998). Astrocytes are the major source of nerve growth factor upregulation following traumatic brain injury in the rat. *Exp. Neurol.* 149, 301–309. doi: 10.1006/exnr.1997.6712

Gottlieb, M., and Matute, C. (1999). Expression of nerve growth factor in astrocytes of the hippocampal CA1 area following transient forebrain ischemia. *Neuroscience* 91, 1027–1034. doi: 10.1016/s0306-4522(98)00612-5

Greenberg, D. A. (2007). Neurogenesis and stroke. *CNS Neurol. Disord. Drug Targets* 6, 321–325.

Greenwood, H. L., Singer, P. A., Downey, G. P., Martin, D. K., Thorsteinsdottir, H., and Daar, A. S. (2006). Regenerative medicine and the developing world. *PLoS Med* 3:e381. doi: 10.1371/journal.pmed.0030381

Grill, R., Murai, K., Blesch, A., Gage, F., and Tuszynski, M. (1997). Cellular delivery of neurotrophin-3 promotes corticospinal axonal growth and partial functional recovery after spinal cord injury. *J. Neurosci.* 17, 5560–5572. doi: 10.1523/jneurosci.17-14-05560.1997

Guan, J., Tong, W., Ding, W., Du, S., Xiao, Z., Han, Q., et al. (2012). Neuronal regeneration and protection by collagen-binding BDNF in the rat middle cerebral artery occlusion model. *Biomaterials* 33, 1386–1395. doi: 10.1016/j.biomaterials.2011.10.073

Guan, S., Zhang, X.-L., Lin, X.-M., Liu, T.-Q., Ma, X.-H., and Cui, Z.-F. (2013). Chitosan/gelatin porous scaffolds containing hyaluronic acid and heparan sulfate for neural tissue engineering. *J. Biomater. Sci. Polym. Ed.* 24, 999–1014. doi: 10.1080/09205063.2012.731374

Han, N., Rao, S. S., Johnson, J., Parikh, K. S., Bradley, P. A., Lannutti, J. J., et al. (2011). Hydrogel–electrospun fiber mat composite coatings for neural prostheses. *Front. Neuroeng.* 4:2. doi: 10.3389/fneng.2011.00002

Harrington, A. W., Kim, J. Y., and Yoon, S. O. (2002). Activation of Rac GTPase by p75 is necessary for c-jun N-terminal kinase-mediated apoptosis. *J. Neurosci.* 22, 156–166. doi: 10.1523/jneurosci.22-01-00156.2002

Hermann, D. M., and Chopp, M. (2012). Promoting brain remodelling and plasticity for stroke recovery: therapeutic promise and potential pitfalls of clinical translation. *Lancet Neurol.* 11, 369–380. doi: 10.1016/S1474-4422(12)70039-X

Hill, J. J., Jin, K., Mao, X. O., Xie, L., and Greenberg, D. A. (2012). Intracerebral chondroitinase ABC and heparan sulfate proteoglycan glypican improve outcome from chronic stroke in rats. *Proc. Natl. Acad. Sci.* 109, 9155–9160. doi: 10.1073/pnas.1205697109

Hippensteel, J. A., Anderson, B. J., Orfila, J. E., Mcmurtry, S. A., Dietz, R. M., Su, G., et al. (2019). Circulating heparan sulfate fragments mediate septic cognitive dysfunction. *J. Clin. Invest.* 129, 1779–1784. doi: 10.1172/JCI124485

Horne, M. K., Nisbet, D. R., Forsythe, J. S., and Parish, C. L. (2009). Three-dimensional nanofibrous scaffolds incorporating immobilized BDNF promote

proliferation and differentiation of cortical neural stem cells. *Stem Cells Dev.* 19, 843–852. doi: 10.1089/scd.2009.0158

Houweling, D., Lankhorst, A., Gispen, W., Bär, P., and Joosten, E. (1998). Collagen containing neurotrophin-3 (NT-3) attracts regrowing injured corticospinal axons in the adult rat spinal cord and promotes partial functional recovery. *Exp. Neurol.* 153, 49–59. doi: 10.1006/exnr.1998.6867

Hu, H. (2001). Cell-surface heparan sulfate is involved in the repulsive guidance activities of Slit2 protein. *Nat. Neurosci.* 4, 695–702.

Hwang, I. K., Yoo, K.-Y., Jung, B.-K., Cho, J. H., Kim, D.-H., Kang, T.-C., et al. (2006). Correlations between neuronal loss, decrease of memory, and decrease expression of brain-derived neurotrophic factor in the gerbil hippocampus during normal aging. *Exp. Neurol.* 201, 75–83. doi: 10.1016/j.expneurol.2006.02.129

Ikeda, O., Murakami, M., Ino, H., Yamazaki, M., Nemoto, T., Koda, M., et al. (2001). Acute up-regulation of brain-derived neurotrophic factor expression resulting from experimentally induced injury in the rat spinal cord. *Acta Neuropathol.* 102, 239–245.

Iwai, M., Sato, K., Kamada, H., Omori, N., Nagano, I., Shoji, M., et al. (2003). Temporal profile of stem cell division, migration, and differentiation from subventricular zone to olfactory bulb after transient forebrain ischemia in gerbils. *J. Cereb. Blood Flow Metab.* 23, 331–341. doi: 10.1097/01.wcb.0000050060.57184.e7

Iwai, M., Sato, K., Omori, N., Nagano, I., Manabe, Y., Shoji, M., et al. (2002). Three steps of neural stem cells development in gerbil dentate gyrus after transient ischemia. *J. Cereb. Blood Flow Metab.* 22, 411–419. doi: 10.1097/00004647-200204000-00005

Jain, R. A. (2000). The manufacturing techniques of various drug loaded biodegradable poly (lactide-co-glycolide)(PLGA) devices. *Biomaterials* 21, 2475–2490. doi: 10.1016/s0142-9612(00)00115-0

Jakeman, L. B., Wei, P., Guan, Z., and Stokes, B. T. (1998). Brain-derived neurotrophic factor stimulates hindlimb stepping and sprouting of cholinergic fibers after spinal cord injury. *Exp. Neurol.* 154, 170–184. doi: 10.1006/exnr.1998.6924

Jaworski, J., Spangler, S., Seeburg, D. P., Hoogenraad, C. C., and Sheng, M. (2005). Control of dendritic arborization by the phosphoinositide-3'-kinase-Akt-mammalian target of rapamycin pathway. *J. Neurosci.* 25, 11300–11312. doi: 10.1523/jneurosci.2270-05.2005

Jiang, X., Cao, H. Q., Shi, L. Y., Ng, S. Y., Stanton, L. W., and Chew, S. Y. (2012). Nanofiber topography and sustained biochemical signaling enhance human mesenchymal stem cell neural commitment. *Acta Biomater.* 8, 1290–1302. doi: 10.1016/j.actbio.2011.11.019

Johansson, B. (2011). Current trends in stroke rehabilitation. A review with focus on brain plasticity. *Acta Neurol. Scand.* 123, 147–159. doi: 10.1111/j.1600-0404.2010.01417.x

Ju, R., Wen, Y., Gou, R., Wang, Y., and Xu, Q. (2014). The experimental therapy on brain ischemia by improvement of local angiogenesis with tissue engineering in the mouse. *Cell Transplant.* 23, S83–S95. doi: 10.3727/096368914X684998

Jung Kim, M., Cotman, S. L., Halfter, W., and Cole, G. J. (2003). The heparan sulfate proteoglycan agrin modulates neurite outgrowth mediated by FGF-2. *Dev. Neurobiol.* 55, 261–277. doi: 10.1002/neu.10213

Kanato, Y., Kitajima, K., and Sato, C. (2008). Direct binding of polysialic acid to a brain-derived neurotrophic factor depends on the degree of polymerization. *Glycobiology* 18, 1044–1053. doi: 10.1093/glycob/cwn084

Kanato, Y., Ono, S., Kitajima, K., and Sato, C. (2009). Complex formation of a brain-derived neurotrophic factor and glycosaminoglycans. *Biosci. Biotechnol. Biochem.* 73, 2735–2741. doi: 10.1271/bbb.90637

Kaplan, D. R., and Miller, F. D. (2000). Neurotrophin signal transduction in the nervous system. *Curr. Opin. Neurobiol.* 10, 381–391. doi: 10.1016/s0959-4388(00)00092-1

Kaseloo, P. A., Lis, A., Asada, H., Barone, T. A., and Plunkett, R. J. (1996). In vitro assessment of neurotrophic activity from the striatum of aging rats. *Neurosci. Lett.* 218, 157–160. doi: 10.1016/s0304-3940(96)13146-3

Kawaja, M. D., and Gage, F. H. (1991). Reactive astrocytes are substrates for the growth of adult CNS axons in the presence of elevated levels of nerve growth factor. *Neuron* 7, 1019–1030. doi: 10.1016/0896-6273(91)90346-2

Keefe, K., Sheikh, I., and Smith, G. (2017). Targeting neurotrophins to specific populations of neurons: NGF, BDNF, and NT-3 and their relevance for treatment of spinal cord injury. *Int. J. Mol. Sci.* 18:548. doi: 10.3390/ijms18030548

Kermani, P., and Hempstead, B. (2007). Brain-derived neurotrophic factor: a newly described mediator of angiogenesis. *Trends Cardiovasc. Med.* 17, 140–143. doi: 10.1016/j.tcm.2007.03.002

Kernie, S. G., and Parent, J. M. (2010). Forebrain neurogenesis after focal Ischemic and traumatic brain injury. *Neurobiol. Dis.* 37, 267–274. doi: 10.1016/j.nbd.2009.11.002

Kirkpatrick, C. A., Knox, S. M., Staatz, W. D., Fox, B., Lercher, D. M., and Selleck, S. B. (2006). The function of a Drosophila glypican does not depend entirely on heparan sulfate modification. *Dev. Biol.* 300, 570–582. doi: 10.1016/j.ydbio.2006.09.011

Kokaia, Z., Zhao, Q., Kokaia, M., Elmér, E., Metsis, M., Smith, M.-L., et al. (1995). Regulation of brain-derived neurotrophic factor gene expression after transient middle cerebral artery occlusion with and without brain damage. *Exp. Neurol.* 136, 73–88. doi: 10.1006/exnr.1995.1085

Kordower, J. H., Winn, S. R., Liu, Y.-T., Mufson, E. J., Sladek, J. R., Hammang, J. P., et al. (1994). The aged monkey basal forebrain: rescue and sprouting of axotomized basal forebrain neurons after grafts of encapsulated cells secreting human nerve growth factor. *Proc. Natl. Acad. Sci. U.S.A.* 91, 10898–10902. doi: 10.1073/pnas.91.23.10898

Krenz, N. R., Meakin, S. O., Krassioukov, A. V., and Weaver, L. C. (1999). Neutralizing intraspinal nerve growth factor blocks autonomic dysreflexia caused by spinal cord injury. *J. Neurosci.* 19, 7405–7414. doi: 10.1523/jneurosci.19-17-07405.1999

Krueger, F., Pardini, M., Huey, E. D., Raymont, V., Solomon, J., Lipsky, R. H., et al. (2011). The role of the Met66 brain-derived neurotrophic factor allele in the recovery of executive functioning after combat-related traumatic brain injury. *J. Neurosci.* 31, 598–606. doi: 10.1523/JNEUROSCI.1399-10.2011

Ksiazek, I., Burkhardt, C., Lin, S., Seddik, R., Maj, M., Bezakova, G., et al. (2007). Synapse loss in cortex of agrin-deficient mice after genetic rescue of perinatal death. *J. Neurosci.* 27, 7183–7195. doi: 10.1523/jneurosci.1609-07.2007

Kuberan, B., Lech, M. Z., Beeler, D. L., Wu, Z. L., and Rosenberg, R. D. (2003). Enzymatic synthesis of antithrombin III–binding heparan sulfate pentasaccharide. *Nat. Biotechnol.* 21, 1343–1346. doi: 10.1038/nbt885

Lamballe, F., Klein, R., and Barbacid, M. (1991). trkC, a new member of the trk family of tyrosine protein kinases, is a receptor for neurotrophin-3. *Cell* 66, 967–979. doi: 10.1016/0092-8674(91)90442-2

Lampe, K. J., Kern, D. S., Mahoney, M. J., and Bjugstad, K. B. (2011). The administration of BDNF and GDNF to the brain via PLGA microparticles patterned within a degradable PEG-based hydrogel: protein distribution and the glial response. *J. Biomed. Mater. Res. Part A* 96, 595–607. doi: 10.1002/jbm.a.33011

Lander, A. D. (2007). Morpheus unbound: reimagining the morphogen gradient. *Cell* 128, 245–256. doi: 10.1016/j.cell.2007.01.004

Lander, A. D., and Selleck, S. B. (2000). The elusive functions of proteoglycans: in vivo veritas. *J. Cell Biol.* 148, 227–232. doi: 10.1083/jcb.148.2.227

Lanfranconi, S., Locatelli, F., Corti, S., Candelise, L., Comi, G., Baron, P., et al. (2011). Growth factors in ischemic stroke. *J. Cell. Mol. Med.* 15, 1645–1687. doi: 10.1111/j.1582-4934.2009.00987.x

Laudiero, L. B., Aloe, L., Levi-Montalcini, R., Buttinelli, C., Schilter, D., Gillessen, S., et al. (1992). Multiple sclerosis patients express increased levels of β-nerve growth factor in cerebrospinal fluid. *Neurosci. Lett.* 147, 9–12. doi: 10.1016/0304-3940(92)90762-v

Lee, B., Clarke, D., Al Ahmad, A., Kahle, M., Parham, C., Auckland, L., et al. (2011). Perlecan domain V is neuroprotective and proangiogenic following ischemic stroke in rodents. *J. Clin. Invest.* 121, 3005–3023. doi: 10.1172/JCI46358

Lee, J.-K., Kim, J.-E., Sivula, M., and Strittmatter, S. M. (2004). Nogo receptor antagonism promotes stroke recovery by enhancing axonal plasticity. *J. Neurosci.* 24, 6209–6217. doi: 10.1523/jneurosci.1643-04.2004

Lehmann, M., Fournier, A., Selles-Navarro, I., Dergham, P., Sebok, A., Leclerc, N., et al. (1999). Inactivation of Rho signaling pathway promotes CNS axon regeneration. *J. Neurosci.* 19, 7537–7547. doi: 10.1523/jneurosci.19-17-07537.1999

Leveugle, B., Ding, W., Laurence, F., Dehouck, M. P., Scanameo, A., Cecchelli, R., et al. (1998). Heparin oligosaccharides that pass the blood-brain barrier inhibit beta-amyloid precursor protein secretion and heparin binding to beta-amyloid peptide. *J. Neurochem.* 70, 736–744. doi: 10.1046/j.1471-4159.1998.70020736.x

Levi-Montalcini, R. (1987). The nerve growth factor 35 years later. *Science* 237, 1154–1162. doi: 10.1126/science.3306916

Lewis, D. H. (1990). Controlled release of bioactive agents from lactide/glycolide polymers. *Drugs Pharm. Sci.* 45, 1–41.

Li, B., Piao, C.-S., Liu, X.-Y., Guo, W.-P., Xue, Y.-Q., Duan, W.-M., et al. (2010). Brain self-protection: the role of endogenous neural progenitor cells in adult brain after cerebral cortical ischemia. *Brain Res.* 1327, 91–102. doi: 10.1016/j.brainres.2010.02.030

Li, S., Overman, J. J., Katsman, D., Kozlov, S. V., Donnelly, C. J., Twiss, J. L., et al. (2010). An age-related sprouting transcriptome provides molecular control of axonal sprouting after stroke. *Nat. Neurosci.* 13, 1496–1504. doi: 10.1038/nn.2674

Li, W. J., Laurencin, C. T., Caterson, E. J., Tuan, R. S., and Ko, F. K. (2002). Electrospun nanofibrous structure: a novel scaffold for tissue engineering. *J. Biomed. Mater. Res. Part A* 60, 613–621.

Lindvall, O., Kokaia, Z., Bengzon, J., Elmer, E., and Kokaia, M. (1994). Neurotrophins and brain insults. *Trends Neurosci.* 17, 490–496. doi: 10.1016/0166-2236(94)90139-2

Liu, J. J., Wang, C. Y., Wang, J. G., Ruan, H. J., and Fan, C. Y. (2011). Peripheral nerve regeneration using composite poly (lactic acid-caprolactone)/nerve growth factor conduits prepared by coaxial electrospinning. *J. Biomed. Mater. Res. Part A* 96, 13–20. doi: 10.1002/jbm.a.32946

Liu, R., Xu, Y., Chen, M., Weïwer, M., Zhou, X., Bridges, A. S., et al. (2010). Chemoenzymatic design of heparan sulfate oligosaccharides. *J. Biol. Chem.* 285, 34240–34249. doi: 10.1074/jbc.m110.159152

Lommatzsch, M., Zingler, D., Schuhbaeck, K., Schloetcke, K., Zingler, C., Schuff-Werner, P., et al. (2005). The impact of age, weight and gender on BDNF levels in human platelets and plasma. *Neurobiol. Aging* 26, 115–123. doi: 10.1016/j.neurobiolaging.2004.03.002

Ma, Q., Dudas, B., Hejna, M., Cornelli, U., Lee, J. M., Lorens, S., et al. (2002). The blood-brain barrier accessibility of a heparin-derived oligosaccharides C3. *Thromb. Res.* 105, 447–453. doi: 10.1016/s0049-3848(02)00050-6

MacLellan, C. L., Keough, M. B., Granter-Button, S., Chernenko, G. A., Butt, S., and Corbett, D. (2011). A critical threshold of rehabilitation involving brain-derived neurotrophic factor is required for poststroke recovery. *Neurorehabil. Neural Repair* 25, 740–748. doi: 10.1177/1545968311407517

Maisonpierre, P. C., Belluscio, L., Squinto, S., Ip, N. Y., Furth, M. E., Lindsay, R. M., et al. (1990). Neurotrophin-3: a neurotrophic factor related to NGF and BDNF. *Science* 247, 1446–1452.

Mammadov, B., Mammadov, R., Guler, M. O., and Tekinay, A. B. (2012). Cooperative effect of heparan sulfate and laminin mimetic peptide nanofibers on the promotion of neurite outgrowth. *Acta Biomater.* 8, 2077–2086. doi: 10.1016/j.actbio.2012.02.006

Mamounas, L. A., Altar, C. A., Blue, M. E., Kaplan, D. R., Tessarollo, L., and Lyons, W. E. (2000). BDNF promotes the regenerative sprouting, but not survival, of injured serotonergic axons in the adult rat brain. *J. Neurosci.* 20, 771–782. doi: 10.1523/jneurosci.20-02-00771.2000

Maness, L. M., Kastin, A. J., Weber, J. T., Banks, W. A., Beckman, B. S., and Zadina, J. E. (1994). The neurotrophins and their receptors: structure, function, and neuropathology. *Neurosci. Biobehav. Rev.* 18, 143–159. doi: 10.1016/0149-7634(94)90043-4

Mansour-Robaey, S., Clarke, D., Wang, Y., Bray, G., and Aguayo, A. (1994). Effects of ocular injury and administration of brain-derived neurotrophic factor on survival and regrowth of axotomized retinal ganglion cells. *Proc. Natl. Acad. Sci. U.S.A.* 91, 1632–1636. doi: 10.1073/pnas.91.5.1632

Mirowska-Guzel, D., Gromadzka, G., Czlonkowski, A., and Czlonkowska, A. (2012). BDNF- 270 C> T polymorphisms might be associated with stroke type and BDNF- 196 G> A corresponds to early neurological deficit in hemorrhagic stroke. *J. Neuroimmunol.* 249, 71–75. doi: 10.1016/j.jneuroim.2012.04.011

Miyake, K., Yamamoto, W., Tadokoro, M., Takagi, N., Sasakawa, K., Nitta, A., et al. (2002). Alterations in hippocampal GAP-43, BDNF, and L1 following sustained cerebral ischemia. *Brain Res.* 935, 24–31. doi: 10.1016/s0006-8993(02)02420-4

Mohtaram, N. K., Montgomery, A., and Willerth, S. M. (2013). Biomaterial-based drug delivery systems for the controlled release of neurotrophic factors. *Biomed. Mater.* 8:022001. doi: 10.1088/1748-6041/8/2/022001

Moretti, A., Ferrari, F., and Villa, R. F. (2015). Neuroprotection for ischaemic stroke: current status and challenges. *Pharm. Therap.* 146, 23–34. doi: 10.1016/j.pharmthera.2014.09.003

Mozaffarian, D., Benjamin, E. J., Go, A. S., Arnett, D. K., Blaha, M. J., Cushman, M., et al. (2015). Executive summary: heart disease and stroke statistics—2015 update. *Circulation* 131, 434–441.

Mukai, J., Hachiya, T., Shoji-Hoshino, S., Kimura, M. T., Nadano, D., Suvanto, P., et al. (2000). NADE, a p75NTR-associated cell death executor, is involved in signal transduction mediated by the common neurotrophin receptor p75NTR. *J. Biol. Chem.* 275, 17566–17570. doi: 10.1074/jbc.c000140200

Mulloy, B., Wu, N., Gyapon-Quast, F., Lin, L., Zhang, F., Pickering, M. C., et al. (2016). Abnormally high content of free glucosamine residues identified in a preparation of commercially available porcine intestinal heparan sulfate. *Anal. Chem.* 88, 6648–6652. doi: 10.1021/acs.analchem.6b01662

Murali, S., Rai, B., Dombrowski, C., Lee, J. L., Lim, Z. X., Bramono, D. S., et al. (2013). Affinity-selected heparan sulfate for bone repair. *Biomaterials* 34, 5594–5605. doi: 10.1016/j.biomaterials.2013.04.017

Murase, N., Duque, J., Mazzocchio, R., and Cohen, L. G. (2004). Influence of interhemispheric interactions on motor function in chronic stroke. *Ann. Neurol.* 55, 400–409. doi: 10.1002/ana.10848

Nagahara, A. H., and Tuszynski, M. H. (2011). Potential therapeutic uses of BDNF in neurological and psychiatric disorders. *Nat. Rev. Drug Discov.* 10, 209–219. doi: 10.1038/nrd3366

Nykjaer, A., Lee, R., Teng, K. K., Jansen, P., Madsen, P., Nielsen, M. S., et al. (2004). Sortilin is essential for proNGF-induced neuronal cell death. *Nature* 427, 843–848. doi: 10.1038/nature02319

Ochs, G., Penn, R. D., York, M., Giess, R., Beck, M., Tonn, J., et al. (2000). A phase I/II trial of recombinant methionyl human brain derived neurotrophic factor administered by intrathecal infusion to patients with amyotrophic lateral sclerosis. *Amyotroph. Lateral Scler. Other Motor Neuron Disord.* 1, 201–206. doi: 10.1080/14660820050515197

Orfila, J. E., Grewal, H., Dietz, R. M., Strnad, F., Shimizu, T., Moreno, M., et al. (2017). Delayed inhibition of tonic inhibition enhances functional recovery following experimental ischemic stroke. *J. Cereb. Blood Flow Metab.* 39, 1005–1014. doi: 10.1177/0271678X17750761

Overman, J. J., Clarkson, A. N., Wanner, I. B., Overman, W. T., Eckstein, I., Maguire, J. L., et al. (2012). A role for ephrin-A5 in axonal sprouting, recovery, and activity-dependent plasticity after stroke. *Proc. Natl. Acad. Sci.* 109, E2230–E2239. doi: 10.1073/pnas.1204386109

Pang, P. T., and Lu, B. (2004). Regulation of late-phase LTP and long-term memory in normal and aging hippocampus: role of secreted proteins tPA and BDNF. *Ageing Res. Rev.* 3, 407–430. doi: 10.1016/j.arr.2004.07.002

Pardridge, W. M. (2005). The blood-brain barrier: bottleneck in brain drug development. *NeuroRx* 2, 3–14. doi: 10.1602/neurorx.2.1.3

Parent, J. M., Vexler, Z. S., Gong, C., Derugin, N., and Ferriero, D. M. (2002). Rat forebrain neurogenesis and striatal neuron replacement after focal stroke. *Ann. Neurol.* 52, 802–813. doi: 10.1002/ana.10393

Park, K. I., Himes, B. T., Stieg, P. E., Tessler, A., Fischer, I., and Snyder, E. Y. (2006). Neural stem cells may be uniquely suited for combined gene therapy and cell replacement: evidence from engraftment of neurotrophin-3-expressing stem cells in hypoxic–ischemic brain injury. *Exp. Neurol.* 199, 179–190. doi: 10.1016/j.expneurol.2006.03.016

Park, K. I., Teng, Y. D., and Snyder, E. Y. (2002). The injured brain interacts reciprocally with neural stem cells supported by scaffolds to reconstitute lost tissue. *Nat. Biotechnol.* 20, 1111–1117. doi: 10.1038/nbt751

Parkman, H. P., Rao, S. S., Reynolds, J. C., Schiller, L. R., Wald, A., Miner, P. B., et al. (2003). Neurotrophin-3 improves functional constipation. *Am. J. Gastroenterol.* 98, 1338–1347. doi: 10.1016/s0002-9270(03)00252-1

Peppas, N. A., Bures, P., Leobandung, W., and Ichikawa, H. (2000). Hydrogels in pharmaceutical formulations. *Eur. J. Pharm. Biopharm.* 50, 27–46. doi: 10.1016/s0939-6411(00)00090-4

Petty, B. G., Cornblath, D. R., Adornato, B. T., Chaudhry, V., Flexner, C., Wachsman, M., et al. (1994). The effect of systemically administered recombinant human nerve growth factor in healthy human subjects. *Ann. Neurol.* 36, 244–246. doi: 10.1002/ana.410360221

Piantino, J., Burdick, J., Goldberg, D., Langer, R., and Benowitz, L. (2006). An injectable, biodegradable hydrogel for trophic factor delivery enhances axonal rewiring and improves performance after spinal cord injury. *Exp. Neurol.* 201, 359–367. doi: 10.1016/j.expneurol.2006.04.020

Pieper, J., Van Wachem, P., Van Luyn, M., Brouwer, L., Hafmans, T., Veerkamp, J., et al. (2000). Attachment of glycosaminoglycans to collagenous matrices

modulates the tissue response in rats. *Biomaterials* 21, 1689–1699. doi: 10.1016/s0142-9612(00)00052-1

Ploughman, M., Attwood, Z., White, N., Doré, J. J., and Corbett, D. (2007). Endurance exercise facilitates relearning of forelimb motor skill after focal ischemia. *Eur. J. Neurosci.* 25, 3453–3460. doi: 10.1111/j.1460-9568.2007.05591.x

Ploughman, M., Windle, V., Maclellan, C. L., White, N., Dore, J. J., and Corbett, D. (2009). Brain-derived neurotrophic factor contributes to recovery of skilled reaching after focal ischemia in rats. *Stroke* 40, 1490–1495. doi: 10.1161/STROKEAHA.108.531806

Qin, L., Jing, D., Parauda, S., Carmel, J., Ratan, R. R., Lee, F. S., et al. (2014). An adaptive role for BDNF Val66Met polymorphism in motor recovery in chronic stroke. *J. Neurosci.* 34, 2493–2502. doi: 10.1523/JNEUROSCI.4140-13.2014

Ramekers, D., Versnel, H., Grolman, W., and Klis, S. F. (2012). Neurotrophins and their role in the cochlea. *Hear. Res.* 288, 19–33. doi: 10.1016/j.heares.2012.03.002

Ramer, M. S., Priestley, J. V., and Mcmahon, S. B. (2000). Functional regeneration of sensory axons into the adult spinal cord. *Nature* 403, 312–316. doi: 10.1038/35002084

Ratner, B. D., and Hoffman, A. S. (1976). *Synthetic Hydrogels for Biomedical Applications*. Washington, DC: ACS Publications.

Reichardt, L. F. (2006). Neurotrophin-regulated signalling pathways. *Philos. Trans. R. Soc. Lond. B* 361, 1545–1564. doi: 10.1098/rstb.2006.1894

Ren, J. M., and Finklestein, S. P. (2005). Growth factor treatment of stroke. *Curr. Drug Targets CNS Neurol. Disord.* 4, 121–125. doi: 10.2174/1568007053544101

Rivet, C. J., Zhou, K., Gilbert, R. J., Finkelstein, D. I., and Forsythe, J. S. (2015). Cell infiltration into a 3D electrospun fiber and hydrogel hybrid scaffold implanted in the brain. *Biomatter* 5:e1005527. doi: 10.1080/21592535.2015.1005527

Rocco, M. L., Soligo, M., Manni, L., and Aloe, L. (2018). Nerve growth factor: early studies and recent clinical trials. *Curr. Neuropharm.* 16, 1455–1465. doi: 10.2174/1570159X16666180412092859

Rostami, E., Krueger, F., Plantman, S., Davidsson, J., Agoston, D., Grafman, J., et al. (2014). Alteration in BDNF and its receptors, full-length and truncated TrkB and p75NTR following penetrating traumatic brain injury. *Brain Res.* 1542, 195–205. doi: 10.1016/j.brainres.2013.10.047

Sacchetti, M., Lambiase, A., Schmidl, D., Schmetterer, L., Ferrari, M., Mantelli, F., et al. (2019). Effect of recombinant human nerve growth factor eye drops in patients with dry eye: a phase IIa, open label, multiple-dose study. *Br. J. Ophthalmol.* doi: 10.1136/bjophthalmol-2018-312470 [Epub ahead of print].

Sahenk, Z., Nagaraja, H., Mccracken, B., King, W., Freimer, M., Cedarbaum, J., et al. (2005). NT-3 promotes nerve regeneration and sensory improvement in CMT1A mouse models and in patients. *Neurology* 65, 681–689. doi: 10.1212/01.wnl.0000171978.70849.c5

Sanchez, S., Sayas, C. L., Lim, F., Diaz-Nido, J., Avila, J., and Wandosell, F. (2001). The inhibition of phosphatidylinositol-3-kinase induces neurite retraction and activates GSK3. *J. Neurochem.* 78, 468–481. doi: 10.1046/j.1471-4159.2001.00453.x

Santos, D., Giudetti, G., Micera, S., Navarro, X., and Del Valle, J. (2016). Focal release of neurotrophic factors by biodegradable microspheres enhance motor and sensory axonal regeneration in vitro and in vivo. *Brain Res.* 1636, 93–106. doi: 10.1016/j.brainres.2016.01.051

Schaaf, M. J., Workel, J. O., Lesscher, H. M., Vreugdenhil, E., Oitzl, M. S., and De Kloet, E. R. (2001). Correlation between hippocampal BDNF mRNA expression and memory performance in senescent rats. *Brain Res.* 915, 227–233. doi: 10.1016/s0006-8993(01)02855-4

Schäbitz, W.-R., Berger, C., Kollmar, R., Seitz, M., Tanay, E., Kiessling, M., et al. (2004). Effect of brain-derived neurotrophic factor treatment and forced arm use on functional motor recovery after small cortical ischemia. *Stroke* 35, 992–997. doi: 10.1161/01.str.0000119754.85848.0d

Schäbitz, W.-R., Steigleder, T., Cooper-Kuhn, C. M., Schwab, S., Sommer, C., Schneider, A., et al. (2007). Intravenous brain-derived neurotrophic factor enhances poststroke sensorimotor recovery and stimulates neurogenesis. *Stroke* 38, 2165–2172. doi: 10.1161/strokeaha.106.477331

Schnell, L., Schneider, R., Kolbeck, R., Barde, Y.-A., and Schwab, M. E. (1994). Neurotrophin-3 enhances sprouting of corticospinal tract during development and after adult spinal cord lesion. *Nature* 367, 170–173. doi: 10.1038/367170a0

Schwab, M. E. (2010). Functions of Nogo proteins and their receptors in the nervous system. *Nat. Rev. Neurosci.* 11, 799–811. doi: 10.1038/nrn2936

Scott, S. A., Liang, S., Weingartner, J. A., and Crutcher, K. A. (1994). Increased NGF-like activity in young but not aged rat hippocampus after septal lesions. *Neurobiol. Aging* 15, 337–346. doi: 10.1016/0197-4580(94)90029-9

Senkov, O. (2014). The role of highly sulfated heparan sulfates in LTP, theta and gamma oscillations and contextual discrimination in fear conditioning paradigm. *Biology* 44, 591–595.

Sharp, K. G., Dickson, A. R., Marchenko, S. A., Yee, K. M., Emery, P. N., Laidmåe, I., et al. (2012). Salmon fibrin treatment of spinal cord injury promotes functional recovery and density of serotonergic innervation. *Exp. Neurol.* 235, 345–356. doi: 10.1016/j.expneurol.2012.02.016

Shibata, S. B., Cortez, S. R., Beyer, L. A., Wiler, J. A., Di Polo, A., Pfingst, B. E., et al. (2010). Transgenic BDNF induces nerve fiber regrowth into the auditory epithelium in deaf cochleae. *Exp. Neurol.* 223, 464–472. doi: 10.1016/j.expneurol.2010.01.011

Shimazu, K., Zhao, M., Sakata, K., Akbarian, S., Bates, B., Jaenisch, R., et al. (2006). NT-3 facilitates hippocampal plasticity and learning and memory by regulating neurogenesis. *Learn. Mem.* 13, 307–315. doi: 10.1101/lm.76006

Shimizu, E., Hashimoto, K., and Iyo, M. (2004). Ethnic difference of the BDNF 196G/A (val66met) polymorphism frequencies: the possibility to explain ethnic mental traits. *Am. J. Med. Gen. Part B* 126, 122–123. doi: 10.1002/ajmg.b.20118

Siironen, J., Juvela, S., Kanarek, K., Vilkki, J., Hernesniemi, J., and Lappalainen, J. (2007). The Met allele of the BDNF Val66Met polymorphism predicts poor outcome among survivors of aneurysmal subarachnoid hemorrhage. *Stroke* 38, 2858–2860. doi: 10.1161/strokeaha.107.485441

Skaper, S. D. (2017). Nerve growth factor: a neuroimmune crosstalk mediator for all seasons. *Immunology* 151, 1–15. doi: 10.1111/imm.12717

Smith, R. A. A., Chua, R. J. E., Carnachan, S. M., Tan, C. L. L., Sims, I. M., Hinkley, S. F. R., et al. (2018). Retention of the Structure and Function of Heparan Sulfate Biomaterials After Gamma Irradiation. *Tissue Eng. Part A* 24, 729–739. doi: 10.1089/ten.TEA.2017.0263

Sofroniew, M. V., Howe, C. L., and Mobley, W. C. (2001). Nerve growth factor signaling, neuroprotection, and neural repair. *Annu. Rev. Neurosci.* 24, 1217–1281. doi: 10.1146/annurev.neuro.24.1.1217

Song, H. H., Shi, W., and Filmus, J. (1997). OCI-5/rat glypican-3 binds to fibroblast growth factor-2 but not to insulin-like growth factor-2. *J. Biol. Chem.* 272, 7574–7577. doi: 10.1074/jbc.272.12.7574

Sonntag, W. E., Lynch, C. D., Cooney, P. T., and Hutchins, P. M. (1997). Decreases in cerebral microvasculature with age are associated with the decline in growth hormone and insulin-like growth factor 1. *Endocrinology* 138, 3515–3520. doi: 10.1210/en.138.8.3515

Stroemer, R. P., Kent, T. A., and Hulsebosch, C. E. (1995). Neocortical neural sprouting, synaptogenesis, and behavioral recovery after neocortical infarction in rats. *Stroke* 26, 2135–2144. doi: 10.1161/01.str.26.11.2135

Strohmaier, C., Carter, B., Urfer, R., Barde, Y., and Dechant, G. (1996). A splice variant of the neurotrophin receptor trkB with increased specificity for brain-derived neurotrophic factor. *EMBO J.* 15, 3332–3337. doi: 10.1002/j.1460-2075.1996.tb00698.x

Sun, Y., Lim, Y., Li, F., Liu, S., Lu, J.-J., Haberberger, R., et al. (2012). ProBDNF collapses neurite outgrowth of primary neurons by activating RhoA. *PLoS One* 7:e35883. doi: 10.1371/journal.pone.0035883

Tae, G., Scatena, M., Stayton, P. S., and Hoffman, A. S. (2006). PEG-cross-linked heparin is an affinity hydrogel for sustained release of vascular endothelial growth factor. *J. Biomater. Sci. Polym. Ed.* 17, 187–197. doi: 10.1163/156856206774879090

Taipale, J., and Keski-Oja, J. (1997). Growth factors in the extracellular matrix. *FASEB J.* 11, 51–59.

Tan, H.-B., Zhong, Y.-S., Cheng, Y., and Shen, X. (2011). Rho/ROCK pathway and neural regeneration: a potential therapeutic target for central nervous system and optic nerve damage. *Int. J. Ophthalm.* 4, 652–657. doi: 10.3980/j.issn.2222-3959.2011.06.16

Tang, M., Shi, S., Guo, Y., Xu, W., Wang, L., Chen, Y., et al. (2014). GSK-3/CREB pathway involved in the gx-50's effect on Alzheimer's disease. *Neuropharmacology* 81, 256–266. doi: 10.1016/j.neuropharm.2014.02.008

Taupin, P. (2006). Therapeutic potential of adult neural stem cells. *Recent Pat. CNS Drug Discov.* 1, 299–303. doi: 10.2174/157488906778773670

Teng, H. K., Teng, K. K., Lee, R., Wright, S., Tevar, S., Almeida, R. D., et al. (2005). ProBDNF induces neuronal apoptosis via activation of a receptor complex of

p75NTR and sortilin. *J. Neurosci.* 25, 5455–5463. doi: 10.1523/jneurosci.5123-04.2005

Thored, P., Wood, J., Arvidsson, A., Cammenga, J., Kokaia, Z., and Lindvall, O. (2007). Long-term neuroblast migration along blood vessels in an area with transient angiogenesis and increased vascularization after stroke. *Stroke* 38, 3032–3039. doi: 10.1161/strokeaha.107.488445

Tyler, P. C., Guimond, S. E., Turnbull, J. E., and Zubkova, O. V. (2015). Single-entity heparan sulfate glycomimetic clusters for therapeutic applications. *Angew. Chem. Int. Ed. Engl.* 54, 2718–2723. doi: 10.1002/anie.201410251

Ueno, Y., Chopp, M., Zhang, L., Buller, B., Liu, Z., Lehman, N. L., et al. (2012). Axonal outgrowth and dendritic plasticity in the cortical peri-infarct area after experimental stroke. *Stroke* 43, 2221–2228. doi: 10.1161/STROKEAHA.111.646224

Uygun, B. E., Stojsih, S. E., and Matthew, H. W. (2009). Effects of immobilized glycosaminoglycans on the proliferation and differentiation of mesenchymal stem cells. *Tissue Eng. Part A* 15, 3499–3512. doi: 10.1089/ten.tea.2008.0405

Valmikinathan, C. M., Defroda, S., and Yu, X. (2009). Polycaprolactone and bovine serum albumin based nanofibers for controlled release of nerve growth factor. *Biomacromolecules* 10, 1084–1089. doi: 10.1021/bm8012499

Walz, A., Mcfarlane, S., Brickman, Y. G., Nurcombe, V., Bartlett, P. F., and Holt, C. E. (1997). Essential role of heparan sulfates in axon navigation and targeting in the developing visual system. *Development* 124, 2421–2430.

Wang, C., Poon, S., Murali, S., Koo, C. Y., Bell, T. J., Hinkley, S. F., et al. (2014). Engineering a vascular endothelial growth factor 165-binding heparan sulfate for vascular therapy. *Biomaterials* 35, 6776–6786. doi: 10.1016/j.biomaterials.2014.04.084

Wang, H., Zhao, Q., Zhao, W., Liu, Q., Gu, X., and Yang, Y. (2012). Repairing rat sciatic nerve injury by a nerve-growth-factor-loaded, chitosan-based nerve conduit. *Biotechnol. Appl. Biochem.* 59, 388–394. doi: 10.1002/bab.1031

Wang, L., Shansky, J., Borselli, C., Mooney, D., and Vandenburgh, H. (2012). Design and fabrication of a biodegradable, covalently crosslinked shape-memory alginate scaffold for cell and growth factor delivery. *Tissue Eng. Part A* 18, 2000–2007. doi: 10.1089/ten.TEA.2011.0663

Wang, L., Zhang, Z., Wang, Y., Zhang, R., and Chopp, M. (2004). Treatment of stroke with erythropoietin enhances neurogenesis and angiogenesis and improves neurological function in rats. *Stroke* 35, 1732–1737. doi: 10.1161/01.str.0000132196.49028.a4

Waterhouse, E. G., and Xu, B. (2009). New insights into the role of brain-derived neurotrophic factor in synaptic plasticity. *Mol. Cell. Neurosci.* 42, 81–89. doi: 10.1016/j.mcn.2009.06.009

Weaver, L. C., Marsh, D. R., Gris, D., Brown, A., and Dekaban, G. A. (2006). Autonomic dysreflexia after spinal cord injury: central mechanisms and strategies for prevention. *Prog. Brain Res.* 152, 245–263. doi: 10.1016/s0079-6123(05)52016-8

Webster, M. J., Weickert, C. S., Herman, M. M., and Kleinman, J. E. (2002). BDNF mRNA expression during postnatal development, maturation and aging of the human prefrontal cortex. *Dev. Brain Res.* 139, 139–150. doi: 10.1016/s0165-3806(02)00540-0

Weishaupt, N., Mason, A., Hurd, C., May, Z., Zmyslowski, D., Galleguillos, D., et al. (2014). Vector-induced NT-3 expression in rats promotes collateral growth of injured corticospinal tract axons far rostral to a spinal cord injury. *Neuroscience* 272, 65–75. doi: 10.1016/j.neuroscience.2014.04.041

Whitelock, J. M., and Iozzo, R. V. (2005). Heparan sulfate: a complex polymer charged with biological activity. *Chem. Rev.* 105, 2745–2764. doi: 10.1021/cr010213m

Wichterle, O., and Lim, D. (1960). Hydrophilic gels for biological use. *Nature* 185, 117–118. doi: 10.1038/185117a0

Wijesinghe, S. J., Ling, L., Murali, S., Qing, Y. H., Hinkley, S. F., Carnachan, S. M., et al. (2017). Affinity selection of FGF2-binding heparan sulfates for ex vivo expansion of human mesenchymal stem cells. *J. Cell Physiol.* 232, 566–575. doi: 10.1002/jcp.25454

Winkler, J., Ramirez, G. A., Thal, L. J., and Waite, J. J. (2000). Nerve growth factor (NGF) augments cortical and hippocampal cholinergic functioning after p75NGF receptor-mediated deafferentation but impairs inhibitory avoidance and induces fear-related behaviors. *J. Neurosci.* 20, 834–844. doi: 10.1523/jneurosci.20-02-00834.2000

Woerly, S., Pinet, E., De Robertis, L., Bousmina, M., Laroche, G., Roitback, T., et al. (1998). Heterogeneous PHPMA hydrogels for tissue repair and axonal regeneration in the injured spinal cord. *J. Biomater. Sci. Polym. Ed.* 9, 681–711. doi: 10.1163/156856298x00091

Woodruff, M. A., Rath, S. N., Susanto, E., Haupt, L. M., Hutmacher, D. W., Nurcombe, V., et al. (2007). Sustained release and osteogenic potential of heparan sulfate-doped fibrin glue scaffolds within a rat cranial model. *J. Mol. Histol.* 38, 425–433. doi: 10.1007/s10735-007-9137-y

Wu, D. (2005). Neuroprotection in experimental stroke with targeted neurotrophins. *NeuroRx* 2, 120–128. doi: 10.1602/neurorx.2.1.120

Xie, J., Willerth, S. M., Li, X., Macewan, M. R., Rader, A., Sakiyama-Elbert, S. E., et al. (2009). The differentiation of embryonic stem cells seeded on electrospun nanofibers into neural lineages. *Biomaterials* 30, 354–362. doi: 10.1016/j.biomaterials.2008.09.046

Xu, D., and Esko, J. D. (2014). Demystifying heparan sulfate-protein interactions. *Annu. Rev. Biochem.* 83, 129–157. doi: 10.1146/annurev-biochem-060713-035314

Xu, X., Yee, W.-C., Hwang, P. Y., Yu, H., Wan, A. C., Gao, S., et al. (2003). Peripheral nerve regeneration with sustained release of poly (phosphoester) microencapsulated nerve growth factor within nerve guide conduits. *Biomaterials* 24, 2405–2412. doi: 10.1016/s0142-9612(03)00109-1

Xu, X., Yu, H., Gao, S., Mao, H.-Q., Leong, K. W., and Wang, S. (2002). Polyphosphoester microspheres for sustained release of biologically active nerve growth factor. *Biomaterials* 23, 3765–3772. doi: 10.1016/s0142-9612(02)00116-3

Yacoubian, T. A., and Lo, D. C. (2000). Truncated and full-length TrkB receptors regulate distinct modes of dendritic growth. *Nat. Neurosci.* 3, 342–349. doi: 10.1038/73911

Yamashita, T., and Abe, K. (2012). Potential treatment strategies for enhancing neuroplasticity and regeneration after ischemic stroke. *Future Neurol.* 7, 279–285. doi: 10.2217/fnl.12.12

Yamashita, T., Ninomiya, M., Acosta, P. H., García-Verdugo, J. M., Sunabori, T., Sakaguchi, M., et al. (2006). Subventricular zone-derived neuroblasts migrate and differentiate into mature neurons in the post-stroke adult striatum. *J. Neurosci.* 26, 6627–6636. doi: 10.1523/jneurosci.0149-06.2006

Yamashita, T., Tucker, K. L., and Barde, Y.-A. (1999). Neurotrophin binding to the p75 receptor modulates Rho activity and axonal outgrowth. *Neuron* 24, 585–593. doi: 10.1016/s0896-6273(00)81114-9

Yang, F., Murugan, R., Wang, S., and Ramakrishna, S. (2005). Electrospinning of nano/micro scale poly (L-lactic acid) aligned fibers and their potential in neural tissue engineering. *Biomaterials* 26, 2603–2610. doi: 10.1016/j.biomaterials.2004.06.051

Yeiser, E. C., Rutkoski, N. J., Naito, A., Inoue, J.-I., and Carter, B. D. (2004). Neurotrophin signaling through the p75 receptor is deficient in traf6-/-mice. *J. Neurosci.* 24, 10521–10529. doi: 10.1523/jneurosci.1390-04.2004

Yoo, S.-W., Kim, S.-S., Lee, S.-Y., Lee, H.-S., Kim, H.-S., Lee, Y.-D., et al. (2008). Mesenchymal stem cells promote proliferation of endogenous neural stem cells and survival of newborn cells in a rat stroke model. *Exp. Mol. Med.* 40, 387. doi: 10.3858/emm.2008.40.4.387

Yoshii, A., and Constantine-Paton, M. (2010). Postsynaptic BDNF-TrkB signaling in synapse maturation, plasticity, and disease. *Dev. Neurobiol.* 70, 304–322. doi: 10.1002/dneu.20765

Young, C., Miller, E., Nicklous, D. M., and Hoffman, J. R. (2001). Nerve growth factor and neurotrophin-3 affect functional recovery following peripheral nerve injury differently. *Restor. Neurol. Neurosci.* 18, 167–175.

Yu, S., Lv, H., Zhang, H., Jiang, Y., Hong, Y., Xia, R., et al. (2017). Heparanase-1-induced shedding of heparan sulfate from syndecan-1 in hepatocarcinoma cell facilitates lymphatic endothelial cell proliferation via VEGF-C/ERK pathway. *Biochem. Biophys. Res. Commun.* 485, 432–439. doi: 10.1016/j.bbrc.2017.02.060

Yurek, D. M., and Fletcher-Turner, A. (2000). Lesion-induced increase of BDNF is greater in the striatum of young versus old rat brain. *Exp. Neurol.* 161, 392–396. doi: 10.1006/exnr.1999.7274

Yurek, D. M., and Fletcher-Turner, A. (2001). Differential expression of GDNF, BDNF, and NT-3 in the aging nigrostriatal system following a neurotoxic lesion. *Brain Res.* 891, 228–235. doi: 10.1016/s0006-8993(00)03217-0

Zakharenko, S. S., Patterson, S. L., Dragatsis, I., Zeitlin, S. O., Siegelbaum, S. A., Kandel, E. R., et al. (2003). Presynaptic BDNF required for a presynaptic but not postsynaptic component of LTP at hippocampal CA1-CA3 synapses. *Neuron* 39, 975–990. doi: 10.1016/s0896-6273(03)00543-9

Zanin, J. P., Unsain, N., and Anastasia, A. (2017). Growth factors and hormones pro-peptides: the unexpected adventures of the BDNF prodomain. *J. Neurochem.* 141, 330–340. doi: 10.1111/jnc.13993

Zhang, R., Zhang, L., Zhang, Z., Wang, Y., Lu, M., Lapointe, M., et al. (2001). A nitric oxide donor induces neurogenesis and reduces functional deficits after stroke in rats. *Ann. Neurol.* 50, 602–611. doi: 10.1002/ana.1249

Zhang, R. L., Zhang, Z. G., and Chopp, M. (2005). Neurogenesis in the adult ischemic brain: generation, migration, survival, and restorative therapy. *Neuroscientist* 11, 408–416. doi: 10.1177/1073858405278865

Zhang, W., Kitagawa, H., Hayashi, T., Sasaki, C., Sakai, K., Warita, H., et al. (1999). Topical application of neurotrophin-3 attenuates ischemic brain injury after transient middle cerebral artery occlusion in rats. *Brain Res.* 842, 211–214. doi: 10.1016/s0006-8993(99)01818-1

Zhong, J., Chan, A., Morad, L., Kornblum, H. I., Fan, G., and Carmichael, S. T. (2010). Hydrogel matrix to support stem cell survival after brain transplantation in stroke. *Neurorehabil. Neural Repair* 24, 636–644. doi: 10.1177/1545968310361958

Conflict of Interest Statement: The authors declare that the research was conducted in the absence of any commercial or financial relationships that could be construed as a potential conflict of interest.

Copyright © 2019 Houlton, Abumaria, Hinkley and Clarkson. This is an open-access article distributed under the terms of the Creative Commons Attribution License (CC BY). The use, distribution or reproduction in other forums is permitted, provided the original author(s) and the copyright owner(s) are credited and that the original publication in this journal is cited, in accordance with accepted academic practice. No use, distribution or reproduction is permitted which does not comply with these terms.

frontiers in Neuroscience

REVIEW
published: 06 August 2019
doi: 10.3389/fnins.2019.00684

Pluripotent Stem Cells for Brain Repair: Protocols and Preclinical Applications in Cortical and Hippocampal Pathologies

Claudia Alia[1†], Marco Terrigno[2†], Irene Busti[1,3], Federico Cremisi[2,4] and Matteo Caleo[1,5,6]*

[1] CNR Neuroscience Institute, National Research Council (CNR), Pisa, Italy, [2] Laboratory of Biology, Scuola Normale Superiore, Pisa, Italy, [3] Department of Neuroscience, Psychology, Drugs and Child Health Area, School of Psychology, University of Florence, Florence, Italy, [4] Biophysics Institute (IBF), National Research Council (CNR), Pisa, Italy, [5] Department of Biomedical Sciences, University of Padua, Padua, Italy, [6] Padua Neuroscience Center, University of Padua, Padua, Italy

OPEN ACCESS

Edited by:
Johannes Boltze, University of Warwick, United Kingdom

Reviewed by:
Tristan Bouschet, INSERM U1191 Institut de Génomique Fonctionnelle (IGF), France
Zaal Kokaia, Lund Stem Cell Center, Sweden
Daniel Tornero, University of Barcelona, Spain

****Correspondence:***
Claudia Alia
alia@in.cnr.it

† These authors have contributed equally to this work as first authors

Specialty section:
This article was submitted to Neurodegeneration, a section of the journal Frontiers in Neuroscience

Received: *15 May 2019*
Accepted: *14 June 2019*
Published: *06 August 2019*

Citation:
Alia C, Terrigno M, Busti I, Cremisi F and Caleo M (2019) Pluripotent Stem Cells for Brain Repair: Protocols and Preclinical Applications in Cortical and Hippocampal Pathologies. Front. Neurosci. 13:684. doi: 10.3389/fnins.2019.00684

Brain injuries causing chronic sensory or motor deficit, such as stroke, are among the leading causes of disability worldwide, according to the World Health Organization; furthermore, they carry heavy social and economic burdens due to decreased quality of life and need of assistance. Given the limited effectiveness of rehabilitation, novel therapeutic strategies are required to enhance functional recovery. Since cell-based approaches have emerged as an intriguing and promising strategy to promote brain repair, many efforts have been made to study the functional integration of neurons derived from pluripotent stem cells (PSCs), or fetal neurons, after grafting into the damaged host tissue. PSCs hold great promises for their clinical applications, such as cellular replacement of damaged neural tissues with autologous neurons. They also offer the possibility to create *in vitro* models to assess the efficacy of drugs and therapies. Notwithstanding these potential applications, PSC-derived transplanted neurons have to match the precise sub-type, positional and functional identity of the lesioned neural tissue. Thus, the requirement of highly specific and efficient differentiation protocols of PSCs in neurons with appropriate neural identity constitutes the main challenge limiting the clinical use of stem cells in the near future. In this Review, we discuss the recent advances in the derivation of telencephalic (cortical and hippocampal) neurons from PSCs, assessing specificity and efficiency of the differentiation protocols, with particular emphasis on the genetic and molecular characterization of PSC-derived neurons. Second, we address the remaining challenges for cellular replacement therapies in cortical brain injuries, focusing on electrophysiological properties, functional integration and therapeutic effects of the transplanted neurons.

Keywords: pluripotent stem cells, stroke, cortex, hippocampus, brain injuries, brain repair, cell-based therapy, differentiation protocols

INTRODUCTION

Brain injuries represent a large variety of disabling pathologies. They may originate from different causes and affect distinct brain locations, leading to an enormous multiplicity of various symptoms ranging from cognitive deficits to sensorimotor disabilities. They can also result in secondary disturbances, such as epileptic foci, which occur within the lesioned and perilesional tissues

(Herman, 2002). Indeed, frequently a secondary functional damage can take place in a region distant from the first insult (e.g., the hippocampus after traumatic brain injury), providing an explanation for cognitive and memory deficits arising after a brain lesion (Girgis et al., 2016). Brain injuries can have traumatic or non-traumatic etiologies, including focal brain lesions, anoxia, tumors, aneurysms, vascular malformations, encephalitis, meningitis and stroke (Teasell et al., 2007). In particular, stroke covers a vast majority of acquired brain lesions. *Stroke* is usually referred to as a sudden cerebrovascular dysfunction leading to focal deficits and/or impairment of global brain functions and lasting more than 24 h (Mackay and Mensah, 2004). Since brain function is strictly dependent on a constant supply of oxygen and glucose, normally assured by blood circulation, a sudden block of blood supply determines suppression of neural function in less than 1 min, primarily due to interference with synaptic functions (Hofmeijer and Van Putten, 2012). Brief blood deprivations may cause only a reversible damage, which becomes permanent only if the circulation is not promptly restored (Krnjević, 2008; Vrselja et al., 2019). The neocortex represents the highest level of cognitive and sensorimotor integration, and it is therefore not surprising that, independently of different etiologies, lesions occurring in the cerebral cortex are particularly impacting on the clinical phenotype (Delavaran et al., 2013). For example, an insult occurring in the motor cortex results in functional impairment of one or more body parts contralateral to the infarct. The degree of the motor impairment depends on many factors, such as the extent of the lesion, the identity of the damaged region and the effectiveness of the initial neuroprotective interventions.

Following stroke, there is a window of neuroplasticity during which the greatest gains in recovery occur (Zeiler and Krakauer, 2013). Indeed, in the first weeks after stroke a limited spontaneous restoration of function may be observed, and about 30% of stroke survivors are able to carry on everyday activities (Activity of Daily Living or ADLs, i.e., eating, drinking, walking, etc.) without any help (Mozaffarian et al., 2014). However, other patients do not recover at all (Winters et al., 2018). In particular, impairments of upper and lower limbs make very hard to retain a sufficient degree of independence in ADLs. These impairments can be ameliorated with a variable degree of success, through rehabilitation of the affected body parts, including several physical activities improving strength and coordination of the affected muscles and promoting recover of motility. Furthermore, combining rehabilitation with treatments that enhance neuroplasticity has been demonstrated to boost recovery (Alia et al., 2017; Spalletti et al., 2017) but further steps forward in the field are necessary for clinical translation.

Besides physical rehabilitation and plasticizing treatments, another therapeutic approach is cell-based therapy, which has been pioneered in the therapy of Parkinson Disease (PD). Indeed, initial studies showed that fetal dopaminergic neurons grafted in the striatum ameliorated PD symptoms, both in animal models (Herman and Abrous, 1994) and in patients (Lindvall et al., 1990; Kordower et al., 1998). Since fetal transplantation poises both ethical issues and technical challenges (Robertson, 2001), other non-neural cells, such as mesenchymal stem cells (MSCs), may represent a more accessible alternative. In fact, MSCs can be readily derived from various sources, show a low immunogenic effect and proved to be beneficial in stroke treatment (Eckert et al., 2013; Zhang and Chopp, 2013). Notably, MSCs-conditioned medium alone is sufficient for a similar therapeutic effect, suggesting that the beneficial effect is likely due to a bystander effect and trophic support, rather than actual cell replacement (Eckert et al., 2013). Recent clinical trials proved the safety of immortalized neural cells when stereotaxically injected in the brain of patients with stable paresis of the arm following an ischemic stroke (Kalladka et al., 2016). Finally, induced pluripotent stem cells (iPSCs) are easily accessible, since they can be reprogrammed starting from somatic cells, can be *in vitro* differentiated in the desired type of neurons and, being autologously derived and carry low risk of immune rejection (Jung et al., 2012; Trounson and DeWitt, 2016).

Due to the high clinical relevance of cerebral lesions, protocols to differentiate neural stem cells in telencephalic neurons are highly valuable. These protocols are frequently inspired by findings in neural development.

DEVELOPMENTALLY INSPIRED STEM CELLS DIFFERENTIATION PARADIGMS

Attempts to generate identity-specific cortical neurons require exploitation of the right embryonic developmental signals in a culture dish. The six layers of the mammalian neocortex originate from inside-out in a timely regulated manner during embryonic development and are characterized by a specific pattern of gene expression and connectivity (reviewed in: Rubenstein, 2011; Bronner and Hatten, 2013; Greig et al., 2013; Lodato and Arlotta, 2015). Both intrinsic and environmental factors control the progressive restriction of competence of cortical progenitors resulting in the sequential generation of the different cortical neurons, with deeper layer cortical neurons generated earlier than upper layer neurons (Gorski et al., 2002; Kriegstein and Noctor, 2004; Molyneaux et al., 2007).

The hippocampus arises from the invagination of the dorsal midline of the telencephalon, adjacent to the cortical hem. The boundaries between choroid plexus, cortical hem and hippocampus are defined early in development by the non-overlapping expression of molecular markers signatures. In particular, BMP4/7 are strongly expressed by the choroid plexus (Grove et al., 1998; Bulchand et al., 2001), while the cortical hem expresses high level of WNT3a, WNT2, and WNT5, whose signaling is essential for the correct development of the hippocampus (Grove et al., 1998) (**Figure 1A**). Consistently, experiments in which the cortical hem is ablated, or hem-dependent WNT expression is abrogated or compromised, showed the crucial role of the cortical hem in the hippocampal development (Grove et al., 1998; Grove and Tole, 1999; Lee et al., 2000). The Dentate Gyrus (DG), the CA1 and CA3 layers are the different fields forming the hippocampal formation; each one has its own cellular composition, morphology, connectivity and expresses specific molecular markers. In particular, KA1, a glutamate receptor subunit, is detectable in the CA3, while SCIP, a POU-domain transcription factor, is expressed in the CA1. The

pyramidal neurons of the CA1-3 originate in the more dorsal ventricular zone of the hippocampus and then migrate toward the pial surface on a glial scaffold (Nadarajah et al., 2001), while the DG cells arise from a smaller and specialized medial region close to the fimbria, the dentate neuroepithelium (Danglot et al., 2006). Furthermore, new neurons are generated in the hippocampus of rodents throughout life, while cortical neurogenesis rapidly subsides after birth (Eriksson et al., 1998; van Praag et al., 2002). This makes hippocampus the region of choice to assay the ability of *in vitro* produced PSC-derived hippocampal-like neural cells to make projections and to send them to appropriate targets.

Pluripotent stem cells cultured in low-density, serum-free and feeder-free conditions, in absence of any exogenous growth factor, readily differentiate into neural progenitor cells (Tropepe et al., 2001; Ying et al., 2003). This process faithfully reproduces *in vivo* neurogenesis (reviewed in: van den Ameele et al., 2014; Brown et al., 2018; Varrault et al., 2019), following the same timely regulated sequential neurogenic waves observed in vivo (Eiraku et al., 2008; Gaspard et al., 2008; Bertacchi et al., 2013; Molyneaux et al., 2015), which is therefore conserved *in vitro* (Shen et al., 2006). In fact, differentiating PSCs give rise to neural rosettes expressing the early neural markers Sox1, Pax6 and Nestin and closely resembling the early embryonic neural tube (Perrier et al., 2004). When dissociated and replated, PSC-derived neural rosettes give rise to neural progenitor cells (NPCs) which subsequently differentiate into a heterogeneous mixture of different subtypes of neurons (GABAergic, dopaminergic, serotonergic, and cholinergic), astrocytes and oligodendrocytes (Zhang et al., 2001; Barberi et al., 2003). Furthermore, PSCs cultured in this conditions spontaneously acquire an anterior dorsal neural identity (Watanabe et al., 2005; Pankratz et al., 2007), while the addition of growth factors to the medium can steer the differentiation of PSCs toward midbrain/hindbrain (Kawasaki et al., 2000; Perrier et al., 2004) or spinal cord (Wichterle et al., 2002; Li et al., 2009) fates. Thus, PSCs are first committed toward an anterior neural fate and successively patterned by caudalizing factors to acquire a more posterior neural identity, supporting a mammalian model of default neural induction (Muñoz-Sanjuán and Brivanlou, 2002; Smukler et al., 2006; Stern, 2006; Levine and Brivanlou, 2007; Gaulden and Reiter, 2008). Finally, recent evidence suggest that the regionalization of the presumptive neural ectoderm precedes neural commitment; indeed these results further support the notion that FGF, WNT and RA signaling are required for the acquisition of posterior neural identity by PSCs differentiating *in vitro* (Metzis et al., 2018).

The positional identity of neural cells obtained by pluripotent cell during *in vitro* differentiation is often established by the simple study of their neurotransmitter phenotype (Eiraku and Sasai, 2011; Shi et al., 2012; Yu et al., 2014; Shiraishi et al., 2017), or by deeper investigation of their molecular nature through methods of global gene expression analysis (Bertacchi et al., 2013, 2014; Espuny-Camacho et al., 2013; Leemput et al., 2014; Edri et al., 2015; Yao et al., 2017; Terrigno et al., 2018a). However, specific neural subtypes present in different areas of the adult brain show, in addition to distinct gene expression profiles, also defined connectivity patterns, electrophysiological proprieties and morphologies (Cadwell et al., 2015; Fuzik et al., 2015; Tiklová et al., 2019). Whereas the molecular signature of neurons can be established prior their transplantation, the evaluation of all the other parameters require *in vivo* analysis. Understanding how to obtain a precise subtype of neuron, patterned with the proper temporal and positional identity, is pivotal and might have considerable repercussion on possible clinical applications.

In this review, we have considered available protocols to differentiate murine and human pluripotent stem cells into cortical- or hippocampal-like stem cells (**Figures 2**, **3**) expressing at least a forebrain marker (FOXG1 or EMX1/2) and an early cortical or hippocampal marker (TBR1/2, BCL11B or PROX1).

Derivation of Cortical-Like Neurons From Pluripotent Stem Cells

The derivation of cortical-like neurons from PSCs was first reported a decade ago by the laboratories of Pierre Vanderhaeghen (Gaspard et al., 2008) and Yoshiki Sasai (Eiraku et al., 2008). Interestingly, Sasai's protocol is also the first report on 3D cortical organoid from both murine and human PSCs obtained by inhibiting both the endogenous WNT and TGFβ signaling. On the contrary, in Vanderhaeghen's protocol PSCs are cultured as low density adherent monolayer in a minimal, chemically defined medium supplied with a SHH inhibitor, Cyclopamine. Indeed, these authors pioneered the generation of cortical-like cells from PSCs, paving the road for the subsequent studies on human PSCs and induced PSCs (**Figures 2**, **3**). Notably, cortical-like cultures, expressing anterior neural markers (FOXG1 and EMX1/2) and enriched in several cortical cell types (BCL11B, TBR1/2, SATB2, BRN2, and CUX1), can be obtained by simply differentiating PSCs, cultured in suspension as embryoid bodies (Ebs), or as attached monolayer, in a chemically defined minimum medium, devoid of any grow factors (Gaspard et al., 2008; Li et al., 2009; Zeng et al., 2010; Lancaster et al., 2013). However, most authors block endogenous posteriorizing or ventralizing factors (**Figure 1**) to promote the commitment toward an anterior dorsal fate and enrich the culture in cortical cell types (Eiraku et al., 2008; Gaspard et al., 2008; Mariani et al., 2012; Shi et al., 2012; Bertacchi et al., 2013, 2014; Espuny-Camacho et al., 2013, 2018; Kadoshima et al., 2013; Renner et al., 2013; Yu et al., 2014; Paşca et al., 2015; Sakaguchi et al., 2015; Motono, 2016; Gunhanlar et al., 2017; Sarkar et al., 2018; Terrigno et al., 2018a), including BMP inhibitors (Noggin, BMPR1A-Fc, LDN193189, or Dorsomorphin), WNT inhibitors (Dkk1, IWR-1-endo, 53AH, or WNTC59) and TGFβ inhibitors (Lefty, SB431542). In addition, the default fate of PSC-derived neural progenitors appears to be dorsal, thus fewer protocols include the inhibition of SHH signaling (Gaspard et al., 2008; Yu et al., 2014; Sarkar et al., 2018).

Interestingly, by default PSC-derived cortical neurons appear to acquire mainly limbic and occipital cortical identities (Gaspard et al., 2008; Bertacchi et al., 2013; Terrigno et al., 2018b). In fact, cortical-like cultures show high levels of posterior cortical markers, namely COUP-TF1 (Gaspard et al., 2008; Bertacchi et al., 2013; Terrigno et al., 2018b), an orphan nuclear receptor that is expressed in a high posterior-lateral to low anterior-medial expression gradient by both progenitors and cortical neurons, and is required to balance the antero-posterior patterning of the

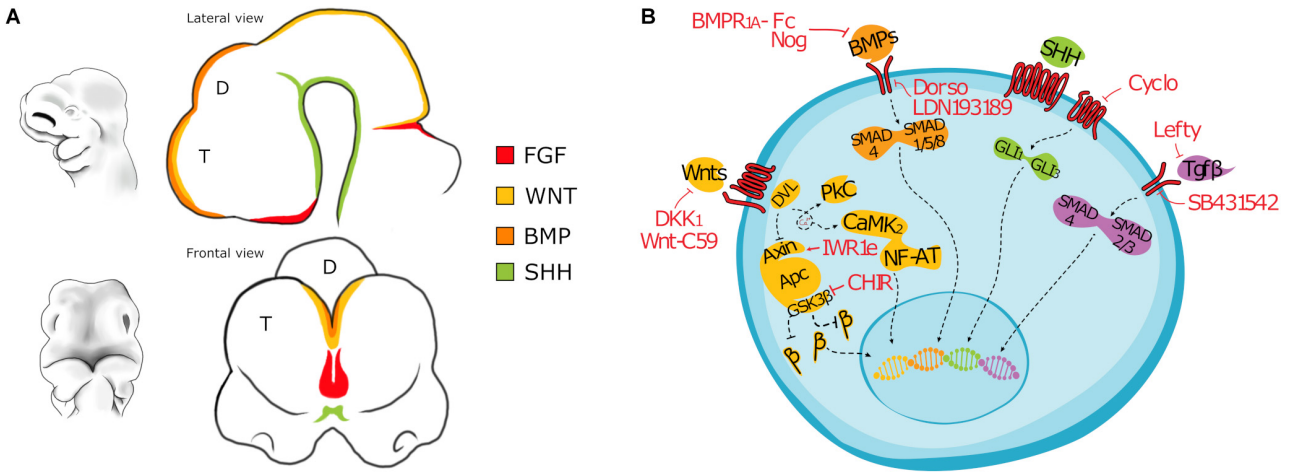

FIGURE 1 | (A) Drawing depicting the main morphogens involved in the patterning of the forebrain of a mouse embryo (E10). T, Telencephalon; D, Diencephalon. **(B)** Cartoon showing main signaling pathways active in differentiating PSC and the inhibitors most commonly used. BMP signaling: Noggin, Bone Morphogenetic Protein Receptor 1A Fc chimera (BMPR1A-Fc), LDN193189, or Dorsomorphin; WNT signaling: CHIR99021, Dickkopf-related protein 1 (Dkk1), IWR-1-endo, 53AH or WNT-C59; TGFβ signaling: Lefty, SB431542; SHH signaling: Cyclopamine. β: β-catenin (CTNNB1).

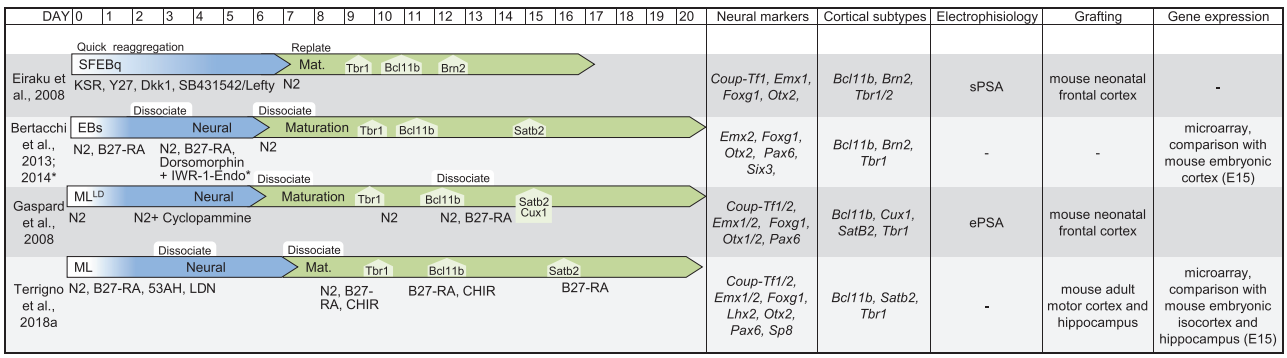

FIGURE 2 | Table showing original reports of differentiation protocols of murine PSCs in cortical and hippocampal neurons. For each entry we indicated (from left to right): reference, schematic layout of the protocol, neural markers, cell-type markers, electrophysiological proprieties, target of transplantation assay to assess integration, global gene expression analysis to identify cell positional identity. If the information was available, we indicated the time of emergence of main cortical cell types (TBR1, BCL11B, BRN2, SATB2, and CUX1). Due to the sheer number of studies on this topic, derivative reports of minor modifications to previously published protocols are not included in this table. SFEBq, serum-free culture of embryoid body-like aggregates; EB, embryoid body; ML, monolayer; LD, low-density; sPSA, spontaneous post-synaptic activity; ePSA, evoked post-synaptic activity.

neocortex (Armentano et al., 2007; Liu et al., 2010). In addition, heterotopic transplantation experiments into the adult murine cortex showed patterns of projection strikingly similar to grafted embryonic visual cortical cells (Michelsen et al., 2015; Espuny-Camacho et al., 2018), supporting the hypothesis of a default occipital fate for PSC-derived neurons. Indeed, treatment with the morphogen FGF8 can induce frontal motor cortical fates in PSC-derived cultures (Eiraku et al., 2008; Kadoshima et al., 2013; Imaizumi et al., 2018; Terrigno et al., 2018b). Intriguingly, Motono et al. reported the generation of PSC-derived anterior cortical neurons (low COUP-TF1 / high SP8 expression) by blocking both the canonical and non-canonical WNT signaling with an inhibitor of Porcupine (PORCN), a membrane-bound O-acyltransferase involved in the palmitoylation, and subsequent secretion, of WNT proteins (Motono et al., 2016). Although these results remain to be confirmed by whole genome expression profiling of the cells and a more extensive analysis of their morphology and connectivity following homotopic and heterotopic transplantation, they are yet another example of how culture conditions profoundly influence the positional identity of PSC-derived cortical neurons. Finally, since different protocol to obtain cells with anterior cortical identity are now available (Eiraku et al., 2008; Kadoshima et al., 2013; Motono, 2016; Imaizumi et al., 2018; Terrigno et al., 2018b), further studies should focus on PSC-derived neurons with motor cortical identity transplanted in the damaged motor cortex.

Besides positional identity, the cellular composition of the cell culture has great clinical implications, since the projection pattern of transplanted PSC-derived neurons varies according to their cellular identity. That is, TBR1- and BCL11B-positive

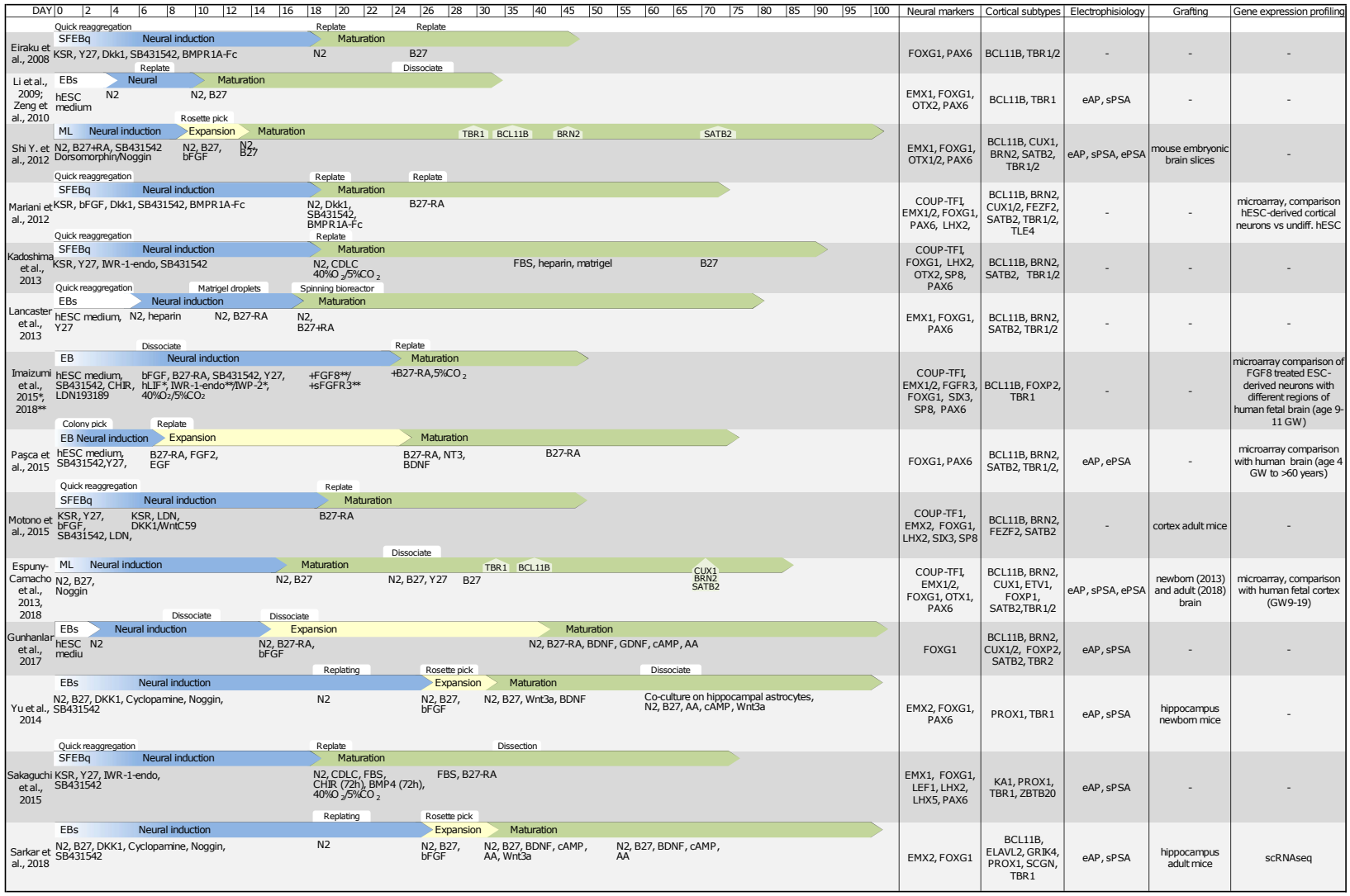

FIGURE 3 | Table showing original reports of differentiation protocols of human PSCs in cortical and hippocampal neurons. With same criteria as those indicated in **Figure 2** SFEBq, serum-free culture of embryoid body-like aggregates; EB, embryoid body; ML, monolayer; scRNAseq, single cell RNA sequencing; eAP, evoked action potential; sPSA, spontaneous post-synaptic activity; ePSA, evoked post-synaptic activity.

PSC-derived neurons transplanted in the adult brain generate, respectively, cortico-thalamic and corticofugal projections (Espuny-Camacho et al., 2013; Michelsen et al., 2015), consistently with the connectivity of normal TBR1- and BCL11B-positive cells. In fact, differentiating PSCs can generate all the cell-types of the six cortical layers (van den Ameele et al., 2014), although culture conditions strongly influence their ratio. Indeed, the production of cortical pyramidal neurons by PSCs cultured in minimal medium as monolayer cultures is strongly skewed toward lower layer identity (Gaspard et al., 2008; Espuny-Camacho et al., 2013). However, the proportion of upper cortical neurons can be increased by supplying retinoids during dual SMAD inhibition (Shi et al., 2012), by transplantation in host brain (Espuny-Camacho et al., 2013) or by culturing PSCs as aggregates (Eiraku et al., 2008; Mariani et al., 2012; Lancaster et al., 2013). Organoid cortical cultures more faithfully reproduce several features of *in vivo* corticogenesis (reviewed in Lancaster and Knoblich, 2014; Di Lullo and Kriegstein, 2017; Giandomenico and Lancaster, 2017), such as migration of newborn neurons on radial glia processes (Bamba et al., 2017), interkinetic nuclear migration (Paşca et al., 2015), and interactions and connections between different regions of the neuroepithelium, such as the interneuron migration and cortical invasion in 3D co-cultures of dorsalized and ventralized PSC-derived neurons (Birey et al., 2017). Finally, although these methods do not allow the identification of the signals responsible for PSC specification, aggregate cultures display higher axonal outgrowth (Chandrasekaran et al., 2017) and cell survival (Daviaud et al., 2018) following cortical transplantation, holding great promises for *in vitro* modeling of neurodegenerative diseases (Quadrato et al., 2016).

During telencephalic development, GABAergic interneurons are generated in the subpallial caudal and medial ganglionic eminence (CGE and MGE) and migrate tangentially to the cortex and hippocampus (Marín and Rubenstein, 2001; Xu et al., 2004; Hansen et al., 2013; Ma et al., 2013). Several neurological disorders are caused by dysfunctions of the GABAergic system and in the last decades GABAergic cell-based therapies have emerged as a promising treatment in restoring the lost balance between inhibitory and excitatory circuits (Danjo et al., 2011; reviewed in Alvarez Dolado and Broccoli, 2011; Hunt et al., 2013; Shetty and Upadhya, 2016). Furthermore, several groups were able to efficiently generate forebrain GABAergic interneurons from PSCs (Gaspard et al., 2008; Li et al., 2009; Zeng et al., 2010; Falk et al., 2012; Germain et al., 2013; Liu et al., 2013; Maroof et al., 2013; Nicholas et al., 2013; Tornero et al., 2013; Yuan et al., 2015; Liao et al., 2016; Sun et al., 2016; Xu et al., 2016). However, due to the ventral origin of the forebrain interneurons, PSCs committed in culture to dorsal telencephalic fates, such as cortex and hippocampus, generate mainly glutamatergic neurons (Zhang et al., 2001; Bibel et al., 2004; Eiraku et al., 2008; Gaspard et al., 2008, 2009; Bertacchi et al., 2013, 2014; Espuny-Camacho et al., 2013; Yu et al., 2014; Michelsen et al., 2015; Livesey et al., 2016; Motono, 2016; Sarkar et al., 2018; Terrigno et al., 2018a). Since GABA-ergic inhibition is essential for maintaining the balanced activity of cortical neural circuits and for the development of neural network activity (Ben-Ari et al., 2007), grafting of PSC-derived cortical or hippocampal cultures enriched with interneurons could have significant clinical repercussions and should be further investigated.

Derivation of Hippocampal-Like Neurons From Pluripotent Stem Cells

The first report of PSC-derived neural progenitors committed to a medial pallial identity was by Sasai and colleagues (Eiraku et al., 2008). Since then, several authors described methods to commit PSC to either choroid plexus or hippocampus (**Figures 1**, **2**; Yu et al., 2014; Sakaguchi et al., 2015; Sarkar et al., 2018; Terrigno et al., 2018a). Most of these protocols share an initial phase of WNT, BMP and TGFβ inhibition, followed by activation of BMP and WNT signaling, by either suppling WNT3a or a small-molecule inhibitor of GSK3 (CHIR). In particular, Sakaguchi et al. showed that a short-term activation of WNT and BMP signaling in anteriorized neural progenitors specifies a hippocampal primordium-like tissue *in vitro*, expressing the hippocampal markers ZBTB20, KA1 and PROX1; while a prolonged treatment results in increased expression of LMX1A and TTR, markers of choroid plexus (Sakaguchi et al., 2015). Consistently, other authors showed that double inhibition of WNT and BMP endogenous signaling in differentiating PSC followed by timely activation of WNT signaling results in hippocampal specification (Yu et al., 2014; Sarkar et al., 2018; Terrigno et al., 2018a). In particular, the laboratory of Fred Gage showed that a prolonged treatment with WNT3a results in the commitment of PSC to DG fate, while a shorter treatment and with a lower concentration of WNT3a specifies CA3 identity (Yu et al., 2014; Sarkar et al., 2018). Notably, PSC-derived hippocampal-like neurons, but not cortical-like cells, transplanted into adult hippocampus were capable of long-term survival, contacted relevant targets of the hippocampal formation and formed functional synaptic contacts with the host network, further confirming the importance of the identity match between transplanted cells and surrounding environment (Terrigno et al., 2018a).

IN VIVO INTEGRATION AND THERAPEUTIC EFFECT OF GRAFTED EXOGENOUS NEURAL CELLS IN THE BRAIN

Once obtained the cell type(s) of interest, the next step is to evaluate if these cells can properly integrate in the host tissue, sending short and long projections to their natural targets and rebuilding damaged circuitry. Neurons suitable for transplantation must be able to integrate into the host context, produce the appropriate type of neurotransmitter and neurotransmitter receptors and develop synapses with functionally relevant targets and electrophysiological properties of mature neurons.

Anatomical Characterization of Grafted Neurons in the Host Circuits

Initial reports showed that the outgrowth from grafts of fetal neurons in adult host brain was limited and dependent on the site of injection (Gonzalez et al., 1988; Isacson et al., 1988; Fricker et al., 1999). The first consistent observation of long-distance axons and extensive innervation of the host brain by fetal transplants following experimental deletion of cortical projection neurons was reported by Hernit-Grant and Macklis (1996) and Fricker-Gates et al. (2002). However, in these studies the specificity of efferent projections from the grafted cells toward appropriate host target sites was not assessed. Subsequently, Gaillard et al., 2007 described the reconstruction of damaged cortical circuitry in adult mice and the formation of long-range projections targeting the appropriate host regions, notably the pyramidal tract and the spinal cord. 2 months after the transplantation of fetal cortical tissue in the damaged motor cortex, they observed outgoing projections toward most of the cortical and subcortical targets of the cortical motor neurons, comparable to those established by neurons of the contralesional motor cortex. Furthermore, they verified that most of the grafted neurons sent projections along motor pathways, by injecting the retrograde tracer cholera toxin in the brain regions where fibers were found (i.e., thalamus and dorsolateral caudate putamen). Interestingly, the fact that in the same study visual grafts were not competent to replace degenerating motor pathways suggests that transplanted cells retain positional identity and functional capability of the donor. Altogether, these initial reports showed that transplanted embryonic neurons are able to extend long-range projections to distant targets with great specificity, suggesting that guidance cues persist in the adult brain or are re-expressed after injury, although no electrophysiological and/or behavioral evidence was provided to corroborate the anatomical observations (Gaillard et al., 2007).

More recently, Falkner et al. (2016) performed *in vivo* 2-photon imaging of embryonic cortical neurons transplanted 7 days after ablation of layer II-III callosal projecting neurons in the monocular visual cortex, evaluating longitudinal structural maturation, morphology, dendrite elongation and spine refinement of grafted neurons. Notably, already at 3–4 days post-transplantation, grafted neurons extended branched neurites, with identifiable growth cone and boutons, followed by the formation of apical dendrites which reached complete development within 4 weeks post-transplantation (wpt). Spine and bouton density greatly increased up to 4 wpt and then reached a plateau, while turnover rates increased at 5 wpt and subsequently stabilized after 8 wpt. Interestingly, as soon as 5 wpt, grafted cells displayed appropriate identity of pyramidal neurons and projected to the natural targets of V1 neurons, including ipsilateral visual areas, retrosplenial and entorhinal cortices and the corpus callosum. Furthermore, grafted cells received topographically correct synaptic inputs from appropriate cortical and subcortical regions, as assessed by performing monosynaptic rabies virus tracing. Overall, the authors showed that fetal neurons integrate adequately into the adult cerebral cortex, mature over time and re-establish a normal pattern of projection according to their original positional identity.

As previously discussed, in the last decade several groups worked to overcome the ethical and technical challenges of using fetal tissue, developing protocols to differentiate both mouse and human embryonic stem cells into neurons with appropriate cellular identity and area specification (**Figures 1**, **2**).

Among the first, Pierre Vanderhaeghen and collaborators showed that murine PSC-derived pyramidal neurons grafted into the frontal cortex of neonatal mice and analyzed after 1 month displayed specific patterns of axonal projections corresponding to visual and limbic occipital cortex, despite the frontal site of transplantation (Gaspard et al., 2008). Furthermore, cultures transplanted at later stages of differentiation were enriched in later-born, superficial layer cell types. A similar pattern of projections was found 2 months after transplantation of human PSC-derived cortical neurons in frontal cortex of mouse pups, although 6 months post-transplantation the selectivity of these cells to contact the appropriate targets seems to decrease, with axonal projections reaching a wider range of regions, including motor and somatosensory areas (Espuny-Camacho et al., 2013). Noteworthy, Ideguchi and colleagues found no intrinsic regional identity in their PSC-derived pyramidal neurons, showing instead projection patterns coherent with the site of transplantation (Ideguchi et al., 2010). Thus, there may be a variability (likely depending on the protocol used for the differentiation) in the ability of the transplanted cells to retain the identity acquired *in vitro*.

In subsequent studies by Vanderhaeghen and collaborators, murine and human PSC-derived neurons were transplanted in a model of visual cortex lesion in adult mice and the re-establishment of the damaged pathways was assessed from 4 to 90 days after grafting (Michelsen et al., 2015). Grafted cells successfully differentiated, mainly in glutamatergic neurons, and showed reciprocal long-range axonal projections with targets of the damaged cortex such as the ipsilateral and contralateral cortex (layers II/III/IV), striatum (V), thalamus (VI) and midbrain/hindbrain nuclei (layer V). This study further confirmed that transplanted neurons display layer-specific patterns of projection in accordance with their molecular identity and consistent with the pattern of projection of native neurons of the visual cortex. Interestingly, these results were only obtained following homotopic transplantation in visual and not in motor cortex, as also confirmed by transplantation of fetal visual and motor cortical neural precursors. Human PSC-derived neurons maintained positional identity after transplantation and displayed the same projection properties of corresponding mouse cells, but required a longer time of maturation (Espuny-Camacho et al., 2018). Taken together, these results suggest that the success of transplantation in adult cortex is highly dependent on a strict match between the areal identity of the lesioned cortex and the positional identity of transplanted cells (Gaspard et al., 2008; Espuny-Camacho et al., 2013, 2018; Michelsen et al., 2015).

Among the first reports of mouse PSC used as cell therapy in animal models of stroke, Bühnemann et al. (2006) found that PSC-derived neural precursors transplanted into an Endothelin-1 (ET-1)-induced corticostriatal ischemic lesion,

or in the perilesional striatum in rats, survived for up to 12 weeks and differentiated into distinct neuronal subtypes without expressing a specific cortical area-specific identity. However, the size of the surviving graft decreased from 4 to 12 weeks, probably due to graft rejection despite cyclosporine treatment, while paucity of fibers and high neuron mortality rate did not allow a proper analysis of the projection pattern.

Tornero et al., 2013 transplanted human IPSCs-derived, cortically committed or non-committed neural precursors, in the perilesional somatosensory cortex of a rat stroke model obtained by middle cerebral artery occlusion (MCAO). After 2 months they found that non-fated neural precursors cells (NPCs) proliferate more than their cortical counterpart. Both cell types migrated toward the ischemic lesion, but cortically fated cells differentiated more efficiently into TBR1- and SATB2-positive cortical neurons with a pyramidal morphology (Tornero et al., 2013). The same authors reported that grafted iPSC-derived cortical NPCs received synaptic inputs from the same areas as endogenous neurons (e.g., perilesional and contralateral cortex, ipsilateral and contralateral claustrum, specific thalamic nuclei, globus pallidus, etc.) as shown by the injection of a modified rabies virus that labeled monosynaptic afferents to grafted neurons. Finally, 6 months post-transplantation, immunoelectron microscopy confirmed that grafted neurons exhibited the ultrastructural features of mature neurons and formed synaptic contacts with host axon terminals, showing all of the ultrastructural criteria for synapses (Tornero et al., 2017).

Our group recently developed a protocol to produce either hippocampal or isocortical neurons that were then co-transplanted in healthy and lesioned brain regions. The analysis of *in vivo* projection pattern revealed that the different molecular identity acquired *in vitro* profoundly affect the different ability of these cells to extend axonal projections. In fact, we found that, accordingly to their molecular identity, isocortical neural precursors were not able to project once transplanted in the dentate gyrus (DG) of the hippocampus, contrary to PSC-derived hippocampal cells that properly elongated fibers to CA3 following endogenous hippocampal pathways. Instead, when grafted in their proper healthy cortical region, isocortical neurons sent projections toward the motor cortex and other cortical and subcortical targets. Interestingly, consistently with previous findings (de la Rosa-Prieto et al., 2017), fiber quantification revealed that the presence of an ischemic cortical lesion had an impressive impact in increasing the number of projections from isocortical cells, possibly through the same cellular mechanisms that spontaneously trigger and enhance post-stroke endogenous neural regeneration (Lindvall and Kokaia, 2015). Following stroke, the cortical cells elongated far reaching process that successfully integrated in motor pathways channeling in corticospinal tract segments, as the internal capsule (Terrigno et al., 2018b). However, PSC-derived isocortical cells transplanted into either intact or photothrombotic motor cortex failed in sending projections to thalamic nuclei and midbrain, in keeping with previous observations (Michelsen et al., 2015). This finding suggests that they might simply have maintained a general isocortical identity and that a further motor specification step may be required to generate also thalamic and midbrain projections.

Due to the clinical relevance and incidence of cortico-striatal lesions in humans, transplantation studies using neural precursors to rebuild lost circuitry focus mostly on sensory and motor cortices and striatum. However, since 1995 Fred Gage's laboratory explored the possibility of transplanting cells in the hippocampus, publishing evidence that hippocampal neural stem cells long expanded *in vitro*, can integrate in the dentate gyrus and differentiate into mature neurons (Gage et al., 1995, 1998). Subsequently, it has been shown that pyramidal neurons obtained *in vitro*, integrate in the hippocampus, spreading throughout the CA3 region and the hilus, and elongate long projections to the contralateral hippocampus (Englund et al., 2002).

Electrophysiological Properties of Grafted Neurons

Studying electrophysiological properties of grafted neurons is an unavoidable step to demonstrate the effective integration in the pre-existing circuitry and the formation of active synapses with the host tissue.

Different strategies can be adopted to study functional properties of grafted neurons, each one with its own limitations. Whole cell patch clamp in an *ex vivo* preparation permits the visualization of fluorescent grafted cells with the certainty to record from a single grafted neuron, allowing the experimenter to precisely study the input/output connectivity of the transplanted cells with surrounding neurons. However, with this *ex vivo* technique it is not possible to test the response of grafted neurons to more physiological environmental events, such as somatic or visual stimuli. On the other hand, during *in vivo* electrophysiological recordings it is challenging to unambiguously identify grafted cells within the cortex, posing uncertainty on the source of the recorded activity. However, appropriate strategies have been developed to overcome these limitations.

Several studies showed that neurons transplanted in the cortex differentiate and mature in functional neurons, which are characterized by appropriate electrophysiological properties of resting membrane potential, spontaneous and induced action potentials (APs) and spontaneous post-synaptic activity in voltage or current clamp configuration (Bühnemann et al., 2006; Daadi et al., 2009; Oki et al., 2012; Espuny-Camacho et al., 2013, 2018; Tornero et al., 2013; Michelsen et al., 2015). In one of the first reports, Bühnemann et al. (2006) studied the electrophysiological proprieties of murine neural progenitors transplanted in a stroke model. The authors showed appropriate voltage-gated sodium and potassium currents with reversal potential similar to control neurons and blocked them using specific drugs (TTX and TEA, respectively). In addition, they recorded APs and spontaneous excitatory post-synaptic currents in graft-derived cells indicating synaptic input. Moreover, spontaneous APs decreased their duration over time (3 to 6 weeks after transplantation) suggesting that maturation processes could take place in this window (Bühnemann et al., 2006).

Action potentials of murine and human grafted neurons, transplanted both in naïve and pathological conditions, have been recorded in spontaneous conditions or in voltage clamp configuration, using a depolarizing current (Daadi et al., 2009; Oki et al., 2012; Espuny-Camacho et al., 2013, 2018; Tornero et al., 2013; Michelsen et al., 2015). Interestingly, many of these studies reported both excitatory and inhibitory spontaneous post-synaptic activity of transplanted cells. This activity was totally blocked using AMPA, NMDA or GABA antagonists (CNQX, AP-V and Gabazine, respectively), indicating that transplanted cells successfully received inputs from resident neurons. Specific inputs from host neurons have been detected by electrically stimulating a cortical site far away from the transplant (e.g., the contralateral cortex) and visualizing post-synaptic activity (PSP or PSC) in some of the grafted cells, although action potentials were not reported, suggesting mature and functional host-to-neurons synapses but with a low density distribution (Oki et al., 2012; Espuny-Camacho et al., 2013, 2018; Tornero et al., 2013). In addition to electrical stimulation, optogenetic tools have been exploited to study afferent connectivity to grafted neurons. In fact, Tornero et al. (2013) reported host thalamic inputs to transplanted iPSC-derived cells that differentiated into pyramidal neurons and fast spiking interneurons. After light stimulation of the host neurons expressing Channelrhodopsin-2 in the ventral thalamic nuclei, EPSP and EPSC were detected in grafted neurons 3 months after transplantation in the ipsilesional somatosensory cortex (Tornero et al., 2017).

In another recent study, Wuttke et al. (2018) tested the callosal host inputs on grafted PSC-derived neurons, using a remarkably clean optogenetic approach. TdTomato-conjugated Channelrhodopsin-2 was *in utero* electroporated in correspondence to the layer II-III neuron production peak during corticogenesis (E14.5). At birth, they transplanted PSC-derived neurons in the contralateral homotopic region to the electroporaton site. Starting from P21, in acute slice, they patched grafted neurons (GFP+) surrounded by TdTomato fibers arising from contralateral callosal projecting neurons. In voltage-clamp configurations, grafted neurons showed spontaneous excitatory and inhibitory post-synaptic activity (EPSC and IPSC). After light stimulation of the contralateral ChR2-electroporeted neurons, authors found post-synaptic currents in grafted neurons, although no action potentials occurred (Wuttke et al., 2018). Notably, based on the latencies between the onsets of the light pulses and the light-evoked postsynaptic currents, the authors were able to distinguish between excitatory, monosynaptic transcallosal connections and polysynaptic, inhibitory inputs mediated by local interneurons. Finally, the authors assessed whether the grafted cells established functional contacts with the host neurons. Thus, after grafting ChR2-TdTomato cells in the neonatal cortex, they patched host neurons and optogenetically stimulated transplanted cells. They found that stimulation of grafted neurons induced EPSC in endogenous cells with a greater efficiency in ipsilateral compared to contralateral host neurons (Wuttke et al., 2018).

The main challenge of cell therapy in adult disease models is to obtain neurons behaving as the endogenous counterparts and properly responsive to environmental stimuli. In this regard, Pierre Vanderhaeghen and colleagues (Michelsen et al., 2015) tested the responsiveness to a visual stimulus of *in vitro* differentiated murine pyramidal visual cortex neurons, after their transplantation in the visual cortex of adult mice that was previously lesioned by ibotenic acid injection. The authors performed extracellular recordings in anesthetized animals 3–9 months after the transplant, placing the electrode in the center of the transplant and performing juxtacellular neurobiotin injection after the recordings. Grafted neurons showed spontaneous action potential firing with frequencies similar to control neurons. Then, they tested whether a physiological stimulus (1-s flash) was able to evoke spike activity in grafted neurons and found that half of recorded neurons increased their firing rate after flash presentation, with latencies and frequencies similar to naïve control neurons (Michelsen et al., 2015).

Falkner et al. (2016) reported functional maturation of murine grafted neurons in visual cortex after a selective degeneration of callosal projecting neurons in adult mice. The authors transplanted E14.5–E15.5 fetal cortical cells previously transduced with a calcium indicator. From 4 to 15 weeks post-transplantation they performed 2-photon imaging sessions, presenting gratings to the contralateral eye and reported a refinement over time of the orientation preference with sharp tuning properties in the later sessions (Falkner et al., 2016). These data are remarkable as the transplanted neurons appear to assume tuning properties indistinguishable from endogenous pyramidal cells.

Tornero et al. (2013) grafted human iPSCs-derived cortical neural precursor cells in the somatosensory cortex, 1 week after MCAO. Animals were subjected to extracellular recordings 3 months after transplantation, during tactile stimulation of different parts of the body. In these experiments the electrode was placed in the core of the transplant at least 70 μm far away from the border. Spike sorting allowed the identification of single unit responses. Authors reported an increased firing rate of some grafted neurons after stimulation of nose, forelimbs or hindlimbs, with latencies ranging from 9 to 32 ms. Moreover, spontaneous activity in some of the recorded neurons was inhibited by tactile stimulation but with a longer latency (46 to 85 ms) indicating a fine integration of these neurons in the cortical network, responding with an opposite directionality to stimuli from different parts of the body. In addition to single unit recordings, Local Field Potentials (LFPs) were also analyzed in this paper. Authors demonstrated that the evoked potential after nose stimulation was affected in untreated MCAO rats, showing a longer latency with respect to healthy animals. Grafting IPSC-derived cortical neurons rescued this deficit, shortening the latencies and making them similar to those of naïve rats (Tornero et al., 2017). Indeed, this is one of the few studies in which functional recovery after stroke was corroborated by electrophysiological evidences, suggesting that the therapeutic effect of the grafted neurons may be, at least in part, mediated by actual cellular replacement.

In animal models of epilepsy, several studies reported reduction of electrographic seizure activity mediated by neural

transplantation (Hattiangady et al., 2008; Baraban et al., 2009; Maisano et al., 2012; Hunt et al., 2013; Southwell et al., 2014). In particular, it has been showed that grafting fetal interneurons, derived from human PSCs, in the hippocampus of a pilocarpine-induced temporal lobe epilepsy murine model, rescued the epileptic phenotype, with a very significant decrease in the number of seizures and amelioration of cognitive deficits and hyperactivity (Cunningham et al., 2014). 4 months post-transplantation, grafted interneurons were integrated in the hippocampus and showed spontaneous post-synaptic currents and regular membrane potential properties. In addition, efferent graft-to-host connections were tested using whole-cell patch clamp of endogenous neurons during optogenetic stimulation of Chr2-expressing cells. Post-synaptic activity induced by blue light stimulation in host neighboring neurons was totally abolished by the GABA antagonist bicuculline, thus demonstrating correct and mutual integration (Cunningham et al., 2014).

Overall, these results suggest that exogenous neurons can successfully integrate in a pre-existing neural network, developing mature synaptic contacts with resident neurons. In selected cases, transplanted neurons appear to contribute to rescue functional deficits. To determine the extent of integration within the host circuitry, it is now of paramount importance to assess how the grafted cells respond in awake animals during physiologically relevant behaviors. So far, only sensory stimuli have been used to drive grafted neurons. Thus, it would be of great interest to evaluate the responsiveness of transplanted cells during motor tasks. Hopefully, further research will shed light on these important questions.

Therapeutic Effectiveness of Cell Replacement Therapies

The final goal of cell-based therapies is to improve recovery from functional deficits. In this context, beneficial effects of grafted cells can be ascribed to two, not mutually exclusive, mechanisms: (i) grafted cells could enhance functional recovery by secreting trophic factors and molecules with a neuroprotective/neuroplastic effect (also known as bystander effect); (ii) transplanted neurons could properly rebuild damaged circuitry, reestablishing lost sensorimotor synaptic connections. Consistently, cell-based therapy efforts are either directed toward grafting cells to produce and release trophic factors on site, or toward obtaining neurons with a specific identity in order to promote actual cell-replacement. Indeed, the fact that in several reports grafted cells were not detected in transplanted animals, despite an apparent functional improvement, indicates that: (i) the beneficial effect of the grafting was not related to long-term cell integration in the host neuronal circuitry and was exerted in the initial phase before the cells degenerated and (ii) the effect might be due to secretion of beneficial molecules released from grafted cells, or from resident cells stimulated by the grafting, in early post-implantation phase (Ramos-Cabrer et al., 2010; Oki et al., 2012; Hermanto, 2017).

Vascular endothelial growth factor (VEGF) has been implicated in mediating cell-induced functional recovery (Lee et al., 2007). In fact, neurons derived from human neural stem cells and overexpressing VEGF improved animal performance in the rotarod and limb placement tests when transplanted in the perilesional tissue after a hemorrhagic lesion, with early effects (8 days post-transplantation). Cells overexpressing VEGF also increased microvessels proliferation and diminished apoptotic cell death (Lee et al., 2007). Subsequently, Horie et al. (2011) confirmed that VEGF was responsible for the therapeutic effect of grafted neurons. They transplanted neurospheres in the peri-ischaemic cortex and observed an amelioration in the vibrissa-evoked forelimb placing test. Intriguingly, the recovery was totally abolished when VEGF was sequestered by a specific monoclonal antibody. In addition, histological investigations also reported a better blood brain barrier integrity, increased neovascularization and reduced inflammation (Horie et al., 2011). Moreover, the same authors showed that VEGF-mediated beneficial effects positively modulate axonal transport of host neurons, and stimulated axonal sprouting and dendritic plasticity (Andres et al., 2011).

It is generally accepted that grafted neurons could improve recovery by modulating neural plasticity. Indeed, transplanted interneurons induce plasticity in the host brain as reported by Southwell and colleagues, who demonstrated that grafting inhibitory interneurons in the adult visual cortex could re-open the critical period for ocular dominance plasticity (Southwell et al., 2010). In line with these results, hippocampal neural stem cells co-transplanted with astrocytes and microvascular endothelial cells in the hippocampus improved memory deficit after experimental stroke (Cai et al., 2015). Moreover, motor improvements have been reported following grafting of human derived neural precursors in rats with stroke (Daadi et al., 2008; Tornero et al., 2013; Tatarishvili et al., 2014), and after combination of grafting and exposure to enriched environment (Hicks et al., 2009). Recent findings confirmed the synergistic effect of coupling transplantation of murine E14.5 cortical NPCs with physical exercise, resulting in an increased and targeted fiber extension and a better motor improvement after aspiration of motor cortex in rats (Shimogawa et al., 2019).

CONCLUSION

The final goal of neuroscientists working in cell therapy for brain diseases is to restore injured neural circuits, thus rescuing physiological impairments. Among the challenges faced by the clinical application of cell-based therapies is the choice of the cell source (fetal cells, embryonic PSCs or iPSCs). Indeed, both embryonic PSCs and fetal transplantations raise ethical issues, since fetuses are hardly a reliable and scalable source of material. Thus, iPSCs represent a good choice from a translational point of view, showing low immunogenicity and posing no ethical concerns. Human Leukocyte Antigen (HLA)-matched banking of iPSCs would reduce both the time and the cost associated with the derivation of clinically compliant induced pluripotent stem cell lines (reviewed in: Solomon et al., 2015) and several

groups are making continuing efforts to improve the immune compatibility of PSCs, reducing the risk of immune rejection caused by HLA mismatching (Rong et al., 2014; Gornalusse et al., 2017; Xu et al., 2019). In addition, of great importance is the development of footprint-free reprogramming tools, to induce pluripotency while preserving the genetic stability of the reprogrammed cells and reducing the risk of tumorigenesis after transplantation, together with optimized protocols, allowing a more efficient cell replacement of the different damaged brain regions (reviewed in Martin, 2017). Finally, further preclinical studies should involve chemogenetic and optogenetic tools for stimulating activity of transplanted neurons and endogenous cells, during specific tasks in which these cells are involved. This would facilitate the strengthening of correct and effective synaptic contacts among grafted and naïve neurons, via mechanisms of Hebbian plasticity. Indeed, the establishment of new neuronal circuitry required for functional recovery after brain injuries likely depends on the same mechanisms of synaptic plasticity that drive experience-dependent refinement of connections during brain development.

AUTHOR CONTRIBUTIONS

All authors revised, wrote, and discussed the manuscript.

FUNDING

CA was supported by a fellowship from the Accademia Nazionale dei Lincei. This work was supported by the H2020 EXCELLENT SCIENCE – European Research Council (ERC) under grant agreement ID no. 692943 (BrainBIT).

REFERENCES

Alia, C., Spalletti, C., Lai, S., Panarese, A., Lamola, G., Bertolucci, F., et al. (2017). Neuroplastic changes following brain ischemia and their contribution to stroke recovery: novel approaches in neurorehabilitation. *Front. Cell Neurosci.* 11:76. doi: 10.3389/fncel.2017.00076

Alvarez Dolado, M., and Broccoli, V. (2011). GABAergic neuronal precursor grafting: implications in brain regeneration and plasticity. *Neural Plast.* 2011:384216. doi: 10.1155/2011/384216

Andres, R. H., Horie, N., Slikker, W., Keren-Gill, H., Zhan, K., Sun, G., et al. (2011). Human neural stem cells enhance structural plasticity and axonal transport in the ischaemic brain. *Brain* 134, 1777–1789. doi: 10.1093/brain/awr094

Armentano, M., Chou, S. J., Srubek Tomassy, G., Leingärtner, A., O'Leary, D. D. M. M., and Studer, M. (2007). COUP-TFI regulates the balance of cortical patterning between frontal/motor and sensory areas. *Nat. Neurosci.* 10, 1277–1286. doi: 10.1038/nn1958

Bamba, Y., Kanemura, Y., Okano, H., and Yamasaki, M. (2017). Visualization of migration of human cortical neurons generated from induced pluripotent stem cells. *J. Neurosci. Methods* 289, 57–63. doi: 10.1016/j.jneumeth.2017.07.004

Baraban, S. C., Southwell, D. G., Estrada, R. C., Jones, D. L., Sebe, J. Y., Alfaro-Cervello, C., et al. (2009). Reduction of seizures by transplantation of cortical GABAergic interneuron precursors into Kv1.1 mutant mice. *Proc. Natl. Acad. Sci. U.S.A.* 106, 15472–15477. doi: 10.1073/pnas.0900141106

Barberi, T., Klivenyi, P., Calingasan, N. Y., Lee, H., Kawamata, H., Loonam, K., et al. (2003). Neural subtype specification of fertilization and nuclear transfer embryonic stem cells and application in parkinsonian mice. *Nat. Biotechnol.* 21, 1200–1207. doi: 10.1038/nbt870

Ben-Ari, Y., Gaiarsa, J.-L., Tyzio, R., and Khazipov, R. (2007). GABA: a pioneer transmitter that excites immature neurons and generates primitive oscillations. *Physiol. Rev.* 87, 1215–1284. doi: 10.1152/physrev.00017.2006

Bertacchi, M., Pandolfini, L., D'Onofrio, M., Brandi, R., and Cremisi, F. (2014). The double inhibition of endogenously produced BMP and Wnt factors synergistically triggers dorsal telencephalic differentiation of mouse ES cells. *Dev. Neurobiol.* 75, 66–79. doi: 10.1002/dneu.22209

Bertacchi, M., Pandolfini, L., Murenu, E., Viegi, A., Capsoni, S., Cellerino, A., et al. (2013). The positional identity of mouse ES cell-generated neurons is affected by BMP signaling. *Cell Mol. Life. Sci.* 70, 1095–1111. doi: 10.1007/s00018-012-1182-3

Bibel, M., Richter, J., Schrenk, K., Tucker, K. L., Staiger, V., Korte, M., et al. (2004). Differentiation of mouse embryonic stem cells into a defined neuronal lineage. *Nat. Neurosci.* 7, 1003–1009.

Birey, F., Andersen, J., Makinson, C. D., Islam, S., Wei, W., Huber, N., et al. (2017). Assembly of functionally integrated human forebrain spheroids. *Nature* 545:54. doi: 10.1038/nature22330

Bronner, M., and Hatten, M. E. (2013). "Neurogenesis and Migration," in *Fundamental Neuroscience*, 4th Edn, eds L. R. Squire, D. Berg, F. Bloom, S. Lac, A. Ghosh and N. C. Spitzer (Waltham, MA: Elsevier), 339–361. doi: 10.1016/b978-0-12-385870-2.00015-9

Brown, J., Quadrato, G., and Arlotta, P. (2018). "Chapter four - studying the brain in a dish: 3d cell culture models of human brain development and disease," in *Human Embryonic Stem Cells in Development*, ed. A. H. Brivanlou (Cambridge: Academic Press), 99–122. doi: 10.1016/bs.ctdb.2018.03.002

Bühnemann, C., Scholz, A., Bernreuther, C., Malik, C. Y., Braun, H., Schachner, M., et al. (2006). Neuronal differentiation of transplanted embryonic stem cell-derived precursors in stroke lesions of adult rats. *Brain* 129, 3238–3248. doi: 10.1093/brain/awl261

Bulchand, S., Grove, E. A., Porter, F. D., and Tole, S. (2001). LIM-homeodomain gene Lhx2 regulates the formation of the cortical hem. *Mech. Dev.* 100, 165–175. doi: 10.1016/s0925-4773(00)00515-3

Cadwell, C. R., Palasantza, A., Jiang, X., Berens, P., Deng, Q., Yilmaz, M., et al. (2015). Electrophysiological, transcriptomic and morphologic profiling of single neurons using Patch-seq. *Nat. Biotechnol.* 34:199. doi: 10.1038/nbt.3445

Cai, Q., Chen, Z., Song, P., Wu, L., Wang, L., Deng, G., et al. (2015). Co-transplantation of hippocampal neural stem cells and astrocytes and microvascular endothelial cells improve the memory in ischemic stroke rat. *Int. J. Clin. Exp. Med.* 8, 13109–13117.

Chandrasekaran, A., Avci, H. X., Ochalek, A., Rösingh, L. N., Molnár, K., László, L., et al. (2017). Comparison of 2D and 3D neural induction methods for the generation of neural progenitor cells from human induced pluripotent stem cells. *Stem Cell Res.* 25, 139–151. doi: 10.1016/j.scr.2017.10.010

Cunningham, M., Cho, J.-H., Leung, A., Savvidis, G., Ahn, S., Moon, M., et al. (2014). hPSC-derived maturing GABAergic interneurons ameliorate seizures and abnormal behavior in epileptic mice. *Cell Stem Cell* 15, 559–573. doi: 10.1016/j.stem.2014.10.006

Daadi, M. M., Li, Z., Arac, A., Grueter, B. A., Sofilos, M., Malenka, R. C., et al. (2009). Molecular and magnetic resonance imaging of human embryonic stem cell-derived neural stem cell grafts in ischemic rat brain. *Mol. Ther.* 17, 1282–1291. doi: 10.1038/mt.2009.104

Daadi, M. M., Maag, A.-L., and Steinberg, G. K. (2008). Adherent self-renewable human embryonic stem cell-derived neural stem cell line: functional engraftment in experimental stroke model Chan-Ling T, ed. *PLoS One* 3:e1644. doi: 10.1371/journal.pone.0001644

Danglot, L., Triller, A., and Marty, S. (2006). The development of hippocampal interneurons in rodents. *Hippocampus* 16, 1032–1060. doi: 10.1002/hipo.20225

Danjo, T., Eiraku, M., Muguruma, K., Watanabe, K., Kawada, M., Yanagawa, Y., et al. (2011). Subregional specification of embryonic stem cell-derived ventral telencephalic tissues by timed and combinatory treatment with extrinsic signals. *J. Neurosci.* 31, 1919–1933. doi: 10.1523/JNEUROSCI.5128-10.2011

Daviaud, N., Friedel, R. H., and Zou, H. (2018). Vascularization and engraftment of transplanted human cerebral organoids in mouse cortex. *eNeuro* 5, ENEURO.219–ENEURO.218. doi: 10.1523/ENEURO.0219-18.2018

de la Rosa-Prieto, C., Laterza, C., Gonzalez-Ramos, A., Wattananit, S., Ge, R., Lindvall, O., et al. (2017). Stroke alters behavior of human skin-derived neural progenitors after transplantation adjacent to neurogenic area in rat brain. *Stem Cell Res. Ther.* 8:59. doi: 10.1186/s13287-017-0513-6

Delavaran, H., Sjunnesson, H., Arvidsson, A., Lindvall, O., Norrving, B., van Westen, D., et al. (2013). Proximity of brain infarcts to regions of endogenous neurogenesis and involvement of striatum in ischaemic stroke. *Eur. J. Neurol.* 20, 473–479. doi: 10.1111/j.1468-1331.2012.03877.x

Di Lullo, E., and Kriegstein, A. R. (2017). The use of brain organoids to investigate neural development and disease. *Nat. Rev. Neurosci.* 18, 573–584. doi: 10.1038/nrn.2017.107

Eckert, M. A., Vu, Q., Xie, K., Yu, J., Liao, W., Cramer, S. C., et al. (2013). Evidence for high translational potential of mesenchymal stromal cell therapy to improve recovery from ischemic stroke. *J. Cereb. Blood Flow Metab.* 33, 1322–1334. doi: 10.1038/jcbfm.2013.91

Edri, R., Yaffe, Y., Ziller, M. J., Mutukula, N., Volkman, R., David, E., et al. (2015). Analysing human neural stem cell ontogeny by consecutive isolation of Notch active neural progenitors. *Nat. Commun.* 6:6500. doi: 10.1038/ncomms7500

Eiraku, M., and Sasai, Y. (2011). Mouse embryonic stem cell culture for generation of three-dimensional retinal and cortical tissues. *Nat. Protoc.* 7, 69–79. doi: 10.1038/nprot.2011.429

Eiraku, M., Watanabe, K., Matsuo-Takasaki, M., Kawada, M., Yonemura, S., Matsumura, M., et al. (2008). Self-organized formation of polarized cortical tissues from escs and its active manipulation by extrinsic signals. *Cell Stem Cell* 3, 519–532. doi: 10.1016/j.stem.2008.09.002

Englund, U., Bjorklund, A., Wictorin, K., Lindvall, O., and Kokaia, M. (2002). Grafted neural stem cells develop into functional pyramidal neurons and integrate into host cortical circuitry. *Proc. Natl. Acad. Sci. U.S.A.* 99, 17089–17094. doi: 10.1073/pnas.252589099

Eriksson, P. S., Perfilieva, E., Bjork-Eriksson, T., Alborn, A. M., Nordborg, C., Peterson, D. A., et al. (1998). Neurogenesis in the adult human hippocampus. *Nat. Med.* 4, 1313–1317.

Espuny-Camacho, I., Michelsen, K. A., Linaro, D., Bilheu, A., Acosta-Verdugo, S., Herpoel, A., et al. (2018). Human pluripotent stem-cell-derived cortical neurons integrate functionally into the lesioned adult murine visual cortex in an area-specific way. *Cell Rep.* 23, 2732–2743. doi: 10.1016/j.celrep.2018.04.094

Espuny-Camacho, I., Michelsen, K a, Gall, D., Linaro, D., Hasche, A., Bonnefont, J., et al. (2013). Pyramidal neurons derived from human pluripotent stem cells integrate efficiently into mouse brain circuits in vivo. *Neuron* 77, 440–456. doi: 10.1016/j.neuron.2012.12.011

Falk, A., Koch, P., Kesavan, J., Takashima, Y., Ladewig, J., Alexander, M., et al. (2012). Capture of neuroepithelial-like stem cells from pluripotent stem cells provides a versatile system for in vitro production of human neurons. *PLoS One* 7:e29597. doi: 10.1371/journal.pone.0029597

Falkner, S., Grade, S., Dimou, L., Conzelmann, K.-K., Bonhoeffer, T., Götz, M., et al. (2016). Transplanted embryonic neurons integrate into adult neocortical circuits. *Nature* 539, 248–253. doi: 10.1038/nature20113

Fricker, R. A., Carpenter, M. K., Winkler, C., Greco, C., Gates, M. A., and Björklund, A. (1999). Site-specific migration and neuronal differentiation of human neural progenitor cells after transplantation in the adult rat brain. *J. Neurosci.* 19, 5990–6005. doi: 10.1523/jneurosci.19-14-05990.1999

Fricker-Gates, R. A., Shin, J. J., Tai, C. C., Catapano, L. A., and Macklis, J. D. (2002). Late-stage immature neocortical neurons reconstruct interhemispheric connections and form synaptic contacts with increased efficiency in adult mouse cortex undergoing targeted neurodegeneration. *J. Neurosci.* 22, 4045–4056. doi: 10.1523/jneurosci.22-10-04045.2002

Fuzik, J., Zeisel, A., Máté, Z., Calvigioni, D., Yanagawa, Y., Szabó, G., et al. (2015). Integration of electrophysiological recordings with single-cell RNA-seq data identifies neuronal subtypes. *Nat. Biotechnol.* 34:175. doi: 10.1038/nbt.3443

Gage, F. H., Coates, P. W., Palmer, T. D., Kuhn, H. G., Fisher, L. J., Suhonen, J. O., et al. (1995). Survival and differentiation of adult neuronal progenitor cells transplanted to the adult brain. *Proc. Natl. Acad. Sci. U.S.A.* 92, 11879–11883. doi: 10.1073/pnas.92.25.11879

Gage, F. H., Kempermann, G., Palmer, T. D., Peterson, D. A., and Ray, J. (1998). Multipotent progenitor cells in the adult dentate gyrus. *J. Neurobiol.* 36, 249–266. doi: 10.1002/(sici)1097-4695(199808)36:2<249::aid-neu11>3.0.co;2-9

Gaillard, A., Prestoz, L., Dumartin, B., Cantereau, A., Morel, F., Roger, M., et al. (2007). Reestablishment of damaged adult motor pathways by grafted embryonic cortical neurons. *Nat. Neurosci.* 10, 1294–1299. doi: 10.1038/nn1970

Gaspard, N., Bouschet, T., Herpoel, A., Naeije, G., van den Ameele, J., and Vanderhaeghen, P. (2009). Generation of cortical neurons from mouse embryonic stem cells. *Nat. Protoc.* 4, 1454–1463. doi: 10.1038/nprot.2009.157

Gaspard, N., Bouschet, T., Hourez, R., Dimidschstein, J., Naeije, G., van den Ameele, J., et al. (2008). An intrinsic mechanism of corticogenesis from embryonic stem cells. *Nature* 455, 351–357. doi: 10.1038/nature07287

Gaulden, J., and Reiter, J. F. (2008). Neur-ons and neur-offs: Regulators of neural induction in vertebrate embryos and embryonic stem cells. *Hum. Mol. Genet.* 17, R60–R66. doi: 10.1093/hmg/ddn119

Germain, N. D., Banda, E. C., Becker, S., Naegele, J. R., and Grabel, L. B. (2013). Derivation and isolation of NKX2.1-positive basal forebrain progenitors from human embryonic stem cells. *Stem Cells Dev.* 22, 1477–1489. doi: 10.1089/scd.2012.0264

Giandomenico, S. L., and Lancaster, M. A. (2017). Probing human brain evolution and development in organoids. *Curr. Opin. Cell Biol.* 44, 36–43. doi: 10.1016/j.ceb.2017.01.001

Girgis, F., Pace, J., Sweet, J., and Miller, J. P. (2016). Hippocampal neurophysiologic changes after mild traumatic brain injury and potential neuromodulation treatment approaches. *Front. Syst. Neurosci.* 10:8. doi: 10.3389/fnsys.2016.00008

Gonzalez, M. F., Sharp, F. R., and Loken, J. E. (1988). Fetal frontal cortex transplanted to injured motor/sensory cortex of adult rats: reciprocal connections with host thalamus demonstrated with WGA-HRP. *Exp. Neurol.* 99, 154–165. doi: 10.1016/0014-4886(88)90135-5

Gornalusse, G. G., Hirata, R. K., Funk, S. E., Riolobos, L., Lopes, V. S., Manske, G., et al. (2017). HLA-E-expressing pluripotent stem cells escape allogeneic responses and lysis by NK cells. *Nat. Biotechnol.* 35, 765–772. doi: 10.1038/nbt.3860

Gorski, J. A., Talley, T., Qiu, M., Puelles, L., Rubenstein, J. L. R., and Jones, K. R. (2002). Cortical excitatory neurons and glia, but not GABAergic neurons, are produced in the Emx1-expressing lineage. *J. Neurosci.* 22, 6309–6314. doi: 10.1523/jneurosci.22-15-06309.2002

Greig, L. C., Woodworth, M. B., Galazo, M. J., Padmanabhan, H., and Macklis, J. D. (2013). Molecular logic of neocortical projection neuron specification, development and diversity. *Nat. Rev. Neurosci.* 14, 755–769. doi: 10.1038/nrn3586

Grove, E. A., and Tole, S. (1999). Patterning events and specification signals in the developing hippocampus. *Cereb. Cortex* 9, 551–561. doi: 10.1093/cercor/9.6.551

Grove, E. A., Tole, S., Limon, J., Yip, L., and Ragsdale, C. W. (1998). The hem of the embryonic cerebral cortex is defined by the expression of multiple Wnt genes and is compromised in Gli3-deficient mice. *Development* 125, 2315–2325.

Gunhanlar, N., Shpak, G., van der Kroeg, M., Gouty-Colomer, L. A., Munshi, S. T., Lendemeijer, B., et al. (2017). A simplified protocol for differentiation of electrophysiologically mature neuronal networks from human induced pluripotent stem cells. *Mol. Psychiatry* 23, 1336–1344. doi: 10.1038/mp.2017.56

Hansen, D. V., Lui, J. H., Flandin, P., Yoshikawa, K., Rubenstein, J. L., Alvarez-Buylla, A., et al. (2013). Non-epithelial stem cells and cortical interneuron production in the human ganglionic eminences. *Nat. Neurosci.* 16:1576. doi: 10.1038/nn.3541

Hattiangady, B., Rao, M. S., and Shetty, A. K. (2008). Grafting of striatal precursor cells into hippocampus shortly after status epilepticus restrains chronic temporal lobe epilepsy. *Exp. Neurol.* 212, 468–481. doi: 10.1016/j.expneurol.2008.04.040

Herman, J.-P., and Abrous, N. D. (1994). Dopaminergic neural grafts after fifteen years: results and perspectives. *Prog. Neurobiol.* 44, 1–35. doi: 10.1016/0301-0082(94)90055-8

Herman, S. T. (2002). Epilepsy after brain insult: targeting epileptogenesis. *Neurology* 59, S21–S26.

Hermanto, Y. (2017). Transplantation of feeder-free human induced pluripotent stem cell – derived cortical neuron progenitors in adult male Wistar rats with focal brain ischemia. *J. Neurosci. Res.* 96, 863–874. doi: 10.1002/jnr.24197

Hernit-Grant, C. S., and Macklis, J. D. (1996). Embryonic neurons transplanted to regions of targeted photolytic cell death in adult mouse somatosensory cortex re-form specific callosal projections. *Exp. Neurol.* 139, 131–142. doi: 10.1006/exnr.1996.0088

Hicks, A. U., Lappalainen, R. S., Narkilahti, S., Suuronen, R., Corbett, D., Sivenius, J., et al. (2009). Transplantation of human embryonic stem cell-derived neural precursor cells and enriched environment after cortical stroke in rats: cell survival and functional recovery. *Eur. J. Neurosci.* 29, 562–574. doi: 10.1111/j.1460-9568.2008.06599.x

Hofmeijer, J., and Van Putten, M. J. A. M. (2012). Ischemic cerebral damage: An appraisal of synaptic failure. *Stroke* 43, 607–615. doi: 10.1161/STROKEAHA.111.632943

Horie, N., Pereira, M. P., Niizuma, K., Sun, G., Keren-Gill, H., Encarnacion, A., et al. (2011). Transplanted stem cell-secreted vascular endothelial growth factor effects poststroke recovery. *Inflam. Vasc. Repair. Stem Cells* 29, 274–285. doi: 10.1002/stem.584

Hunt, R. F., Girskis, K. M., Rubenstein, J. L., Alvarez-Buylla, A., and Baraban, S. C. (2013). GABA progenitors grafted into the adult epileptic brain control seizures and abnormal behavior. *Nat. Neurosci.* 16:692. doi: 10.1038/nn.3392

Ideguchi, M., Palmer, T. D., Recht, L. D., and Weimann, J. M. (2010). Murine embryonic stem cell-derived pyramidal neurons integrate into the cerebral cortex and appropriately project axons to subcortical targets. *J. Neurosci.* 30, 894–904. doi: 10.1523/JNEUROSCI.4318-09.2010

Imaizumi, K., Fujimori, K., Ishii, S., Otomo, A., Hosoi, Y., Miyajima, H., et al. (2018). Rostrocaudal areal patterning of human PSC-derived cortical neurons by FGF8 signaling. *eneuro* 5, ENEURO.368–ENEURO.317. doi: 10.1523/ENEURO.0368-17.2018

Isacson, O., Wictorin, K., Fischer, W., Sofroniew, M. V., and Björklund, A. (1988). Fetal cortical cell suspension grafts to the excitotoxically lesioned neocortex: anatomical and neurochemical studies of trophic interactions. *Prog. Brain Res.* 78, 13–26. doi: 10.1016/s0079-6123(08)60261-7

Jung, Y., Bauer, G., and Nolta, J. A. (2012). Concise review: induced pluripotent stem cell-derived mesenchymal stem cells: progress toward safe clinical products. *Stem Cells* 30, 42–47. doi: 10.1002/stem.727

Kadoshima, T., Sakaguchi, H., Nakano, T., Soen, M., Ando, S., Eiraku, M., et al. (2013). Self-organization of axial polarity, inside-out layer pattern, and species-specific progenitor dynamics in human ES cell-derived neocortex. *Proc. Natl. Acad. Sci. U.S.A.* 110, 20284–20289. doi: 10.1073/pnas.1315710110

Kalladka, D., Sinden, J., Pollock, K., Haig, C., McLean, J., Smith, W., et al. (2016). Human neural stem cells in patients with chronic ischaemic stroke (PISCES): a phase 1, first-in-man study. *Lancet* 388, 787–796. doi: 10.1016/S0140-6736(16)30513-X

Kawasaki, H., Mizuseki, K., Nishikawa, S., Kaneko, S., Kuwana, Y., Nakanishi, S., et al. (2000). Induction of midbrain dopaminergic neurons from ES cells by stromal cell-derived inducing activity. *Neuron* 28, 31–40. doi: 10.1016/s0896-6273(00)00083-0

Kordower, J. H., Freeman, T. B., Chen, E. Y., Mufson, E. J., Sanberg, P. R., Hauser, R. A., et al. (1998). Fetal nigral grafts survive and mediate clinical benefit in a patient with Parkinson's disease. *Mov. Disord.* 13, 383–393. doi: 10.1002/mds.870130303

Kriegstein, A. R., and Noctor, S. C. (2004). Patterns of neuronal migration in the embryonic cortex. *Trends Neurosci.* 27, 392–399. doi: 10.1016/j.tins.2004.05.001

Krnjević, K. (2008). Electrophysiology of cerebral ischemia. *Neuropharmacology* 55, 319–333. doi: 10.1016/j.neuropharm.2008.01.002

Lancaster, M. A., and Knoblich, J. A. (2014). Generation of cerebral organoids from human pluripotent stem cells. *Nat. Protoc.* 9, 2329–2340. doi: 10.1038/nprot.2014.158

Lancaster, M. A., Renner, M., Martin, C., Wenzel, D., Bicknell, S., Hurles, M. E., et al. (2013). Europe PMC funders group cerebral organoids model human brain development and microcephaly. *Nature* 501, 373–379.

Lee, H. J., Kim, K. S., Park, I. H., and Kim, S. U. (2007). Human neural stem cells over-expressing VEGF provide neuroprotection, angiogenesis and functional recovery in mouse stroke model lohuizen M van, ed. *PLoS One* 2:e156. doi: 10.1371/journal.pone.0000156

Lee, S. M., Tole, S., Grove, E., and McMahon, A. P. (2000). A local Wnt-3a signal is required for development of the mammalian hippocampus. *Development* 127, 457–467.

Leemput, J., Van De Boles, N. C., Kiehl, T. R., Corneo, B., Lederman, P., Menon, V., et al. (2014). NeuroResource CORTECON?: a temporal transcriptome analysis of in vitro human cerebral cortex development from human embryonic stem cells. *Neuron* 83, 51–68. doi: 10.1016/j.neuron.2014.05.013

Levine, A. J., and Brivanlou, A. H. (2007). Proposal of a model of mammalian neural induction. *Dev. Biol.* 308, 247–256. doi: 10.1016/j.ydbio.2007.05.036

Li, X.-J., Zhang, X., Johnson, M. A., Wang, Z.-B., LaVaute, T., and Zhang, S.-C. (2009). Coordination of sonic hedgehog and Wnt signaling determines ventral and dorsal telencephalic neuron types from human embryonic stem cells. *Development* 136, 4055–4063. doi: 10.1242/dev.036624

Liao, M.-C., Muratore, C. R., Gierahn, T. M., Sullivan, S. E., Srikanth, P., De Jager, P. L., et al. (2016). Single-cell detection of secreted aβ and sappα from human ipsc-derived neurons and astrocytes. *J. Neurosci.* 36, 1730–1746. doi: 10.1523/JNEUROSCI.2735-15.2016

Lindvall, O., and Kokaia, Z. (2015). Neurogenesis following stroke affecting the adult brain. *Cold Spring Harb. Perspect. Biol.* 7:a019034. doi: 10.1101/cshperspect.a019034

Lindvall, O., Rehncrona, S., Brundin, P., Gustavii, B., Astedt, B., Widner, H., et al. (1990). Neural transplantation in Parkinson's disease: the Swedish experience. *Prog. Brain Res.* 82, 729–734.

Liu, Q., Dwyer, N. D., and O'Leary, D. D. (2010). Differential expression of COUP-TFI, CHL1, and two novel genes in developing neocortex identified by differential display PCR. *J. Neurosci.* 20, 7682–7690. doi: 10.1523/jneurosci.20-20-07682.2000

Liu, Y., Weick, J. P., Liu, H., Krencik, R., Zhang, X., Ma, L., et al. (2013). Medial ganglionic eminence-like cells derived from human embryonic stem cells correct learning and memory deficits. *Nat. Biotechnol.* 31, 440–447. doi: 10.1038/nbt.2565

Livesey, M. R., Magnani, D., Hardingham, G. E., Chandran, S., and Wyllie, D. J. A. (2016). Functional properties of in vitro excitatory cortical neurons derived from human pluripotent stem cells. *J. Physiol.* 594, 6573–6582. doi: 10.1113/JP270660

Lodato, S., and Arlotta, P. (2015). Generating neuronal diversity in the mammalian cerebral cortex. *Annu. Rev. Cell Dev. Biol.* 31, 699–720. doi: 10.1146/annurev-cellbio-100814-125353

Ma, T., Wang, C., Wang, L., Zhou, X., Tian, M., Zhang, Q., et al. (2013). Subcortical origins of human and monkey neocortical interneurons. *Nat. Neurosci.* 16:1588. doi: 10.1038/nn.3536

Mackay, J., and Mensah, G. A. (2004). The atlas of heart disease and stroke. *J. Hum. Hyper.* 19:505. doi: 10.1038/sj.jhh.1001852

Maisano, X., Litvina, E., Tagliatela, S., Aaron, G. B., Grabel, L. B., and Naegele, J. R. (2012). Differentiation and functional incorporation of embryonic stem cell-derived GABAergic interneurons in the dentate gyrus of mice with temporal lobe epilepsy. *J. Neurosci.* 32, 46–61. doi: 10.1523/JNEUROSCI.2683-11.2012

Mariani, J., Simonini, M. V., Palejev, D., Tomasini, L., Coppola, G., Szekely, A. M., et al. (2012). Modeling human cortical development in vitro using induced pluripotent stem cells. *Proc. Natl. Acad. Sci. U.S.A.* 109, 12770–12775. doi: 10.1073/pnas.1202944109

Marín, O., and Rubenstein, J. L. R. (2001). A long, remarkable journey: Tangential migration in the telencephalon. *Nat. Rev. Neurosci.* 2, 780–790. doi: 10.1038/35097509

Maroof, A. M., Keros, S., Tyson, J. A., Ying, S. W., Ganat, Y. M., Merkle, F. T., et al. (2013). Directed differentiation and functional maturation of cortical interneurons from human embryonic stem cells. *Cell Stem Cell* 12, 559–572. doi: 10.1016/j.stem.2013.04.008

Martin, U. (2017). Therapeutic application of pluripotent stem cells: challenges and risks. *Front. Med.* 4:229. doi: 10.3389/fmed.2017.00229

Metzis, V., Steinhauser, S., Pakanavicius, E., Gouti, M., Stamataki, D., Ivanovitch, K., et al. (2018). Nervous system regionalization entails axial allocation before neural differentiation. *Cell* 175, 1105.e–1118.e. doi: 10.1016/j.cell.2018.09.040

Michelsen, K. A., Acosta-Verdugo, S., Benoit-Marand, M., Espuny-Camacho, I., Gaspard, N., Saha, B., et al. (2015). Area-specific reestablishment of damaged circuits in the adult cerebral cortex by cortical neurons derived from mouse embryonic stem cells. *Neuron* 85, 982–997. doi: 10.1016/j.neuron.2015.02.001

Molyneaux, B. J., Arlotta, P., Menezes, J. R. L., and Macklis, J. D. (2007). Neuronal subtype specification in the cerebral cortex. *Nat. Rev. Neurosci.* 8, 427–437. doi: 10.1038/nrn2151

Molyneaux, B. J., Goff, L. A., Brettler, A. C., Chen, H. H., Brown, J. R., Hrvatin, S., et al. (2015). DeCoN: Genome-wide analysis of invivo transcriptional dynamics during pyramidal neuron fate selection in neocortex. *Neuron* 85, 275–288. doi: 10.1016/j.neuron.2014.12.024

Motono, M. (2016). Tissue engineering and regenerative medicine wnt-c59, a small-molecule WNT inhibitor, efficiently neurons from human pluripotent stem cells. *Stem Cell Transl. Med.* 5, 552–560. doi: 10.5966/sctm.2015-0261

Motono, M., Ioroi, Y., Ogura, T., and Takahashi, J. (2016). Tissue engineering and regenerative medicine WNT-C59, a small-molecule WNT inhibitor, efficiently neurons from human pluripotent stem cells. *Stem Cell Transl Med* 5, 552–560. doi: 10.5966/sctm.2015-0261

Mozaffarian, D., Benjamin, E. J., Go, A. S., Arnett, D. K., Blaha, M. J., Cushman, M., et al. (2014) Heart disease and stroke statistics–2015 update: a report from the American Heart Association. *Circulation* 131:e29-322. doi: 0.161/CIR.0000000000000152

Muñoz-Sanjuán, I., and Brivanlou, A. H. (2002). Neural induction, the default model and embryonic stem cells. *Nat. Rev. Neurosci.* 3, 271–280. doi: 10.1038/nrn786

Nadarajah, B., Brunstrom, J. E., Grutzendler, J., Wong, R. O. L., and Pearlman, A. L. (2001). Two modes of radial migration in early development of the cerebral cortex. *Nat. Neurosci.* 4, 143–150. doi: 10.1038/83967

Nicholas, C. R., Chen, J., Tang, Y., Southwell, D. G., Chalmers, N., Vogt, D., et al. (2013). Functional maturation of hPSC-derived forebrain interneurons requires an extended timeline and mimics human neural development. *Cell Stem Cell* 12, 573–586. doi: 10.1016/j.stem.2013.04.005

Oki, K., Tatarishvili, J., Wood, J., Koch, P., Wattananit, S., Mine, Y., et al. (2012). Human-induced pluripotent stem cells form functional neurons and improve recovery after grafting in stroke-damaged brain. *Stem Cells* 30, 1120–1133. doi: 10.1002/stem.1104

Pankratz, M. T., Li, X.-J., Lavaute, T. M., Lyons, E. A., Chen, X., and Zhang, S.-C. (2007). Directed neural differentiation of human embryonic stem cells via an obligated primitive anterior stage. *Stem Cells* 25, 1511–1520. doi: 10.1634/stemcells.2006-0707

Paşca, A. M., Sloan, S. A., Clarke, L. E., Tian, Y., Makinson, C. D., Huber, N., et al. (2015). Functional cortical neurons and astrocytes from human pluripotent stem cells in 3D culture. *Nat. Methods* 12, 671–678. doi: 10.1038/nmeth.3415

Perrier, A. L., Tabar, V., Barberi, T., Rubio, M. E., Bruses, J., Topf, N., et al. (2004). Derivation of midbrain dopamine neurons from human embryonic stem cells. *Proc. Natl. Acad. Sci. U.S.A* 101, 12543–12548. doi: 10.1073/pnas.0404700101

Quadrato, G., Brown, J., and Arlotta, P. (2016). The promises and challenges of human brain organoids as models of neuropsychiatric disease. *Nat. Med.* 22:1220. doi: 10.1038/nm.4214

Ramos-Cabrer, P., Justicia, C., Wiedermann, D., and Hoehn, M. (2010). Stem cell mediation of functional recovery after stroke in the Rat Kleinschnitz C, ed. *PLoS One* 5:e12779. doi: 10.1371/journal.pone.0012779

Renner, M., Knoblich, J. A., Wenzel, D., Lancaster, M. A., Hurles, M. E., Homfray, T., et al. (2013). Cerebral organoids model human brain development and microcephaly. *Nature* 501, 373–379. doi: 10.1038/nature12517

Robertson, J. A. (2001). Human embryonic stem cell research: ethical and legal issues. *Nat. Rev. Genet.* 2, 74–78. doi: 10.1038/35047594

Rong, Z., Wang, M., Hu, Z., Stradner, M., Zhu, S., Kong, H., et al. (2014). An effective approach to prevent immune rejection of human ESC-derived allografts. *Cell Stem Cell* 14, 121–130. doi: 10.1016/j.stem.2013.11.014

Rubenstein, J. L. R. (2011). Annual research review: development of the cerebral cortex: implications for neurodevelopmental disorders. *J. Child Psychol. Psychiatry* 52, 339–355. doi: 10.1111/j.1469-7610.2010.02307.x

Sakaguchi, H., Kadoshima, T., Soen, M., Narii, N., Ishida, Y., Ohgushi, M., et al. (2015). Generation of functional hippocampal neurons from self-organizing human embryonic stem cell-derived dorsomedial telencephalic tissue. *Nat. Commun.* 6:8896. doi: 10.1038/ncomms9896

Sarkar, A., Mei, A., Paquola, A. C. M., Stern, S., Bardy, C., Klug, J. R., et al. (2018). Efficient generation of CA3 neurons from human pluripotent stem cells enables modeling of hippocampal connectivity in vitro. *Cell Stem Cell* 22, 684.e–697.e. doi: 10.1016/j.stem.2018.04.009

Shen, Q., Wang, Y., Dimos, J. T., Fasano, C. A., Phoenix, T. N., Lemischka, I. R., et al. (2006). The timing of cortical neurogenesis is encoded within lineages of individual progenitor cells. *Nat. Neurosci.* 9, 743–751. doi: 10.1038/nn1694

Shetty, A. K., and Upadhya, D. (2016). GABA-ergic cell therapy for epilepsy: advances, limitations and challenges. *Neurosci. Biobehav. Rev.* 62, 35–47. doi: 10.1016/j.neubiorev.2015.12.014

Shi, Y., Kirwan, P., Smith, J., Robinson, H. P. C., and Livesey, F. J. (2012). Human cerebral cortex development from pluripotent stem cells to functional excitatory synapses. *Nat. Neurosci.* 15, 477–486. doi: 10.1038/nn.3041

Shimogawa, T., Sakaguchi, H., Kikuchi, T., Tsuchimochi, R., Sano, N., Torikoshi, S., et al. (2019). Therapeutic effects of combined cell transplantation and locomotor training in rats with brain injury. *Npj Regen. Med.* 4:13. doi: 10.1523/JNEUROSCI.5359-13.2014

Shiraishi, A., Muguruma, K., and Sasai, Y. (2017). Generation of thalamic neurons from mouse embryonic stem cells. *Development* 144, 1211–1220. doi: 10.1242/dev.144071

Smukler, S. R., Runciman, S. B., Xu, S., and van der Kooy, D. (2006). Embryonic stem cells assume a primitive neural stem cell fate in the absence of extrinsic influences. *J. Cell Biol.* 172, 79–90. doi: 10.1083/jcb.200508085

Solomon, S., Pitossi, F., and Rao, M. S. (2015). Banking on iPSC- Is it Doable and is it Worthwhile. *Stem Cell Rev. Rep.* 11, 1–10. doi: 10.1007/s12015-014-9574-4

Southwell, D. G., Froemke, R. C., Alvarez-Buylla, A., Stryker, M. P., and Gandhi, S. P. (2010). Cortical plasticity induced by inhibitory neuron transplantation. *Science* 327, 1145–1148. doi: 10.1126/science.1183962

Southwell, D. G., Nicholas, C. R., Basbaum, A. I., Stryker, M. P., Kriegstein, A. R., Rubenstein, J. L., et al. (2014). Interneurons from embryonic development to cell-based therapy. *Science* 344:1240622. doi: 10.1126/science.1240622

Spalletti, C., Alia, C., Lai, S., Panarese, A., Conti, S., Micera, S., et al. (2017). Combining robotic training and inactivation of the healthy hemisphere restores pre-stroke motor patterns in mice. *Elife* 6:e28662. doi: 10.7554/eLife.28662

Stern, C. D. (2006). Neural induction: 10 years on since the "default model". *Curr. Opin. Cell Biol.* 18, 692–697. doi: 10.1016/j.ceb.2006.09.002

Sun, A. X., Yuan, Q., Tan, S., Xiao, Y., Wang, D., Khoo, A. T. T., et al. (2016). Direct induction and functional maturation of forebrain gabaergic neurons from human pluripotent stem cells. *Cell Rep.* 16, 1929–1941. doi: 10.1016/j.celrep.2016.07.035

Tatarishvili, J., Oki, K., Monni, E., Koch, P., Memanishvili, T., Buga, A.-M., et al. (2014). Human induced pluripotent stem cells improve recovery in stroke-injured aged rats. *Restor. Neurol. Neurosci.* 32, 547–558. doi: 10.3233/RNN-140404

Teasell, R., Bayona, N., Marshall, S., Cullen, N., Bayley, M., Chundamala, J., et al. (2007). A systematic review of the rehabilitation of moderate to severe acquired brain injuries. *Brain Inj.* 21, 107–112.

Terrigno, M., Bertacchi, M., Pandolfini, L., Baumgart, M., Calvello, M., Cellerino, A., et al. (2018a). The microRNA miR-21 is a mediator of FGF8 action on cortical COUP-TFI translation. *Stem Cell Rep.* 11, 756–769. doi: 10.1016/j.stemcr.2018.08.002

Terrigno, M., Busti, I., Alia, C., Pietrasanta, M., Arisi, I., D'Onofrio, M., et al. (2018b). Neurons generated by mouse ESCs with hippocampal or cortical identity display distinct projection patterns when co-transplanted in the adult brain. *Stem Cell Rep.* 10, 1016–1029. doi: 10.1016/j.stemcr.2018.01.010

Tiklová, K., Björklund, ÅK., Lahti, L., Fiorenzano, A., Nolbrant, S., Gillberg, L., et al. (2019). Single-cell RNA sequencing reveals midbrain dopamine neuron diversity emerging during mouse brain development. *Nat. Commun.* 10:581. doi: 10.1038/s41467-019-08453-1

Tornero, D., Tsupykov, O., Granmo, M., Rodriguez, C., Grønning-Hansen, M., Thelin, J., et al. (2017). Synaptic inputs from stroke-injured brain to grafted human stem cell-derived neurons activated by sensory stimuli. *Brain* 140, 692–706. doi: 10.1093/brain/aww347

Tornero, D., Wattananit, S., Madsen, M. G., Koch, P., Wood, J., Tatarishvili, J., et al. (2013). Human induced pluripotent stem cell-derived cortical neurons integrate in stroke-injured cortex and improve functional recovery. *Brain* 136, 3561–3577. doi: 10.1093/brain/awt278

Tropepe, V., Hitoshi, S., Sirard, C., Mak, T. W., Rossant, J., and van der Kooy, D. (2001). Direct neural fate specification from embryonic stem cells: a primitive mammalian neural stem cell stage acquired through a default mechanism. *Neuron* 30, 65–78. doi: 10.1016/s0896-6273(01)00263-x

Trounson, A., and DeWitt, N. D. (2016). Pluripotent stem cells progressing to the clinic. *Nat. Rev. Mol. Cell Biol.* 17, 194–200. doi: 10.1038/nrm.2016.10

van den Ameele, J., Tiberi, L., Vanderhaeghen, P., and Espuny-Camacho, I. (2014). Thinking out of the dish: what to learn about cortical development using pluripotent stem cells. *Trends Neurosci.* 37, 334–342. doi: 10.1016/j.tins.2014.03.005

van Praag, H., Schinder, A. F., Christie, B. R., Toni, N., Palmer, T. D., and Gage, F. H. (2002). Functional neurogenesis in the adult hippocampus. *Nature* 415, 1030–1034.

Varrault, A., Journot, L., and Bouschet, T. (2019). Cerebral cortex generated from pluripotent stem cells to model corticogenesis and rebuild cortical circuits: in vitro veritas? *Stem Cells Dev.* 33:scd.2018.0233. doi: 10.1089/scd.2018.0233

Vrselja, Z., Daniele, S. G., Silbereis, J., Talpo, F., Morozov, Y. M., Sousa, A. M. M., et al. (2019). Restoration of brain circulation and cellular functions hours post-mortem. *Nature* 568, 336–343. doi: 10.1038/s41586-019-1099-1

Watanabe, K., Kamiya, D., Nishiyama, A., Katayama, T., Nozaki, S., Kawasaki, H., et al. (2005). Directed differentiation of telencephalic precursors from embryonic stem cells. *Nat. Neurosci.* 8, 288–296.

Wichterle, H., Lieberam, I., Porter, J. A., and Jessell, T. M. (2002). Directed differentiation of embryonic stem cells into motor neurons. *Cell* 110, 385–397.

Winters, C., Kwakkel, G., van Wegen, E. E. H., Nijland, R. H. M., Veerbeek, J. M., and Meskers, C. G. M. (2018). Moving stroke rehabilitation forward: the need to change research Harvey RL, ed. *NeuroRehabilitation* 43, 19–30. doi: 10.3233/nre-172393

Wuttke, T. V., Markopoulos, F., Padmanabhan, H., Wheeler, A. P., Murthy, V. N., and Macklis, J. D. (2018). Developmentally primed cortical neurons maintain fidelity of differentiation and establish appropriate functional connectivity after transplantation. *Nat. Neurosci.* 21, 517–529. doi: 10.1038/s41593-018-0098-0

Xu, H., Wang, B., Ono, M., Kagita, A., Fujii, K., Sasakawa, N., et al. (2019). Targeted disruption of HLA genes via CRISPR-Cas9 generates iPSCs with enhanced immune compatibility. *Cell Stem Cell* 24, 566.e–578.e. doi: 10.1016/j.stem.2019.02.005

Xu, J. C., Fan, J., Wang, X., Eacker, S. M., Kam, T. I., Chen, L., et al. (2016). Cultured networks of excitatory projection neurons and inhibitory interneurons for studying human cortical neurotoxicity. *Sci. Transl. Med.* 8:333ra48. doi: 10.1126/scitranslmed.aad0623

Xu, Q., Cobos, I., De La Cruz, E., Rubenstein, J. L., and Anderson, S. A. (2004). Origins of cortical interneuron subtypes. *J. Neurosci.* 24:2612. doi: 10.1523/jneurosci.5667-03.2004

Yao, Z., Mich, J. K., Ku, S., Menon, V., Krostag, A. R., Martinez, R. A., et al. (2017). A single-cell roadmap of lineage bifurcation in human esc models of embryonic brain development. *Cell Stem Cell* 20, 120–134. doi: 10.1016/j.stem.2016.09.011

Ying, Q.-L., Stavridis, M., Griffiths, D., Li, M., and Smith, A. (2003). Conversion of embryonic stem cells into neuroectodermal precursors in adherent monoculture. *Nat. Biotechnol.* 21, 183–186. doi: 10.1038/nbt780

Yu, D. X., Di Giorgio, F. P., Yao, J., Marchetto, M. C., Brennand, K., Wright, R., et al. (2014). Modeling hippocampal neurogenesis using human pluripotent stem cells. *Stem Cell Rep.* 2, 295–310. doi: 10.1016/j.stemcr.2014.01.009

Yuan, F., Fang, K. H., Cao, S. Y., Qu, Z. Y., Li, Q., Krencik, R., et al. (2015). Efficient generation of region-specific forebrain neurons from human pluripotent stem cells under highly defined condition. *Sci. Rep.* 5, 1–11. doi: 10.1038/srep18550

Zeiler, S. R., and Krakauer, J. W. (2013). The interaction between training and plasticity in the poststroke brain. *Curr. Opin. Neurol.* 26, 609–616. doi: 10.1097/WCO.0000000000000025

Zeng, H., Guo, M., Martins-Taylor, K., Wang, X., Zhang, Z., Park, J. W., et al. (2010). Specification of region-specific neurons including forebrain glutamatergic neurons from human induced pluripotent stem cells. *PLoS One* 5:e11853. doi: 10.1371/journal.pone.0011853

Zhang, J., and Chopp, M. (2013). Cell-based therapy for ischemic stroke. *Expert Opin. Biol. Ther.* 13, 1229–1240. doi: 10.1517/14712598.2013.804507

Zhang, S. C., Wernig, M., Duncan, I. D., Brüstle, O., and Thomson, J. A. (2001). In vitro differentiation of transplantable neural precursors from human embryonic stem cells. *Nat. Biotechnol.* 19, 1129–1133. doi: 10.1038/nbt1201-1129

Conflict of Interest Statement: The authors declare that the research was conducted in the absence of any commercial or financial relationships that could be construed as a potential conflict of interest.

Copyright © 2019 Alia, Terrigno, Busti, Cremisi and Caleo. This is an open-access article distributed under the terms of the Creative Commons Attribution License (CC BY). The use, distribution or reproduction in other forums is permitted, provided the original author(s) and the copyright owner(s) are credited and that the original publication in this journal is cited, in accordance with accepted academic practice. No use, distribution or reproduction is permitted which does not comply with these terms.

frontiers in Neurology

ORIGINAL RESEARCH
published: 07 August 2019
doi: 10.3389/fneur.2019.00860

Acute Subcortical Infarcts Cause Secondary Degeneration in the Remote Non-involved Cortex and Connecting Fiber Tracts

Xiao-Er Wei[1†], *Kai Shang*[1†], *Jia Zhou*[1], *Ya-Jun Zhou*[2] *and Yue-Hua Li*[1*]

[1] *Institute of Diagnostic and Interventional Radiology, Shanghai Jiao Tong University Affiliated Sixth People's Hospital, Shanghai, China,* [2] *Department of Neurology, Shanghai Jiao Tong University Affiliated Sixth People's Hospital, Shanghai, China*

Background and Purpose: Remote white matter and cortex reorganization may contribute to functional reorganization and clinical outcome after acute infarcts. To determine the microstructural changes in the remote intact corticospinal tract (CST) and precentral gyrus cortex connected to the acute infarct after subcortical stroke involving the CST over 6 months.

Methods: Twenty-two patients with subcortical stroke involving the CST underwent magnetic resonance imaging (MRI) and clinical assessment in the acute phase (baseline) and 6 months (follow–up) after the stroke. The MRI sequences included T1-weighted imaging, T2–weighted imaging, fluid-attenuated inversion recovery, diffusion tensor imaging (DTI), and diffusion kurtosis imaging. Fractional anisotropy (FA) and track–density imaging (TDI) values were generated using DTI data for the centrum semiovale, corona radiata, posterior limb of internal capsule, and cerebral peduncle. The mean kurtosis (MK) value of the precentral gyrus cortex was calculated. Changes in the FA, TDI, and MK values between the baseline and follow-up and the relationship between these changes were analyzed.

Results: The TDI and FA values of all parts of the ipsilesional (IL) CST, including the noninvolved upper and lower parts, decreased at the 6-month follow-up ($P < 0.001$). The MK values of the stroke lesion ($P < 0.001$) and IL precentral gyrus cortex ($P = 0.002$) were lower at follow-up than at the baseline. The ΔTDI ($r = 0.689$, $P < 0.001$) and Δ FA values ($r = 0.463$, $P = 0.03$) of the noninvolved upper part of the IL CST were positively correlated with the ΔMK value of the IL precentral gyrus cortex.

Conclusion: Secondary degeneration occurred in the remote part of the CST and the remote IL precentral gyrus cortex after subcortical stroke involving the CST. The secondary degeneration in the upper part of the CST was correlated with that in the IL precentral gyrus cortex.

Keywords: stroke, diffusion tensor imaging (DTI), corticospinal tract (CST), diffusion kurtosis imaging (DKI), track-density imaging, precentral gyrus

OPEN ACCESS

Edited by:
Johannes Boltze, University of Warwick, United Kingdom

Reviewed by:
Masaaki Hori, Toho University, Japan
Dong-Hoon Lee, University of Sydney, Australia

***Correspondence:**
Yue-Hua Li
liyuehua312@163.com

[†]*These authors have contributed equally to this work*

Specialty section:
This article was submitted to Stroke, a section of the journal Frontiers in Neurology

Received: *19 June 2019*
Accepted: *25 July 2019*
Published: *07 August 2019*

Citation:
Wei X-E, Shang K, Zhou J, Zhou Y-J and Li Y-H (2019) Acute Subcortical Infarcts Cause Secondary Degeneration in the Remote Non-involved Cortex and Connecting Fiber Tracts. Front. Neurol. 10:860. doi: 10.3389/fneur.2019.00860

INTRODUCTION

Ischemic stroke is a leading cause of death and long-term disability. Motor disability is one of the most common sequelae of stroke. In stroke survivors who do not receive timely and effective arterial thrombolysis or thrombectomy in the hyperacute phase to salvage the ischemic brain tissue, movement function can still be recovered to a certain extent mainly through the structural reorganization of the central nervous system after brain damage (1, 2). Cortical regions that are distant from the acute ischemic infarct are considered to play an important role in this reorganization (3–5). Secondary damage and degeneration of the remote white-matter tracts connected to the acute ischemic infarct as well as focal cortical thinning in remote cortical regions related to the infarct lesion have been reported after subcortical stroke (6, 7). A magnetic resonance spectroscopy (MRS) study showed that the *N*-acetylacetate (NAA) value of the intact primary motor cortex (M1) decreased after subcortical stroke, indicating neuronal depression, and dysfunction in the M1 area due to ischemia and/or diaschisis of the remote white-matter tracts connected to the acute ischemic infarcts (8). However, other studies have shown that the volume of the remote intact cortex may increase or remain unchanged during the post-stroke rehabilitation period (9, 10). Therefore, there is some controversy about the changes in the volume of the distal intact cortex after subcortical stroke. Possible reasons for this controversy may include differences in follow-up duration, and extent and location of the stroke lesions. Nevertheless, the above studies do suggest that the microstructure of the intact cortex connected to the area of subcortical stroke may change over time.

Diffusion tensor imaging (DTI) and fractional anisotropy (FA), a measurement typically associated with tract integrity, have been used to evaluate cerebral reorganization after ischemic stroke (11, 12). However, DTI cannot precisely evaluate fiber orientation in voxels containing more than one principal fiber direction, for example, in the case of crossing or branching fiber tracks. Another limitation of DTI is partial volume effects due to the coexistence of different types of tissue architecture in the same voxel (13). Recently, track-density imaging (TDI), a new technique with sub-millimeter resolution, was developed using a new algorithm based on whole-brain fiber-tracking. The intensity of TDI maps is proportional to the number of streamlines traversing each voxel. Although whole-brain TDI maps are generated using diffusion-weighted imaging (DWI) data, they provide higher spatial resolution than that of the acquired diffusion MRI data (e.g., FA maps) (14, 15). In addition, diffusion kurtosis imaging (DKI), which is based on non-Gaussian water distribution, can more sensitively detect changes in the tissue microstructure than conventional DWI (16, 17). Therefore, DKI may have certain advantages in evaluating cortical structural remodeling after cerebral infarction.

The aim of this study was to use TDI and DTI combined with DKI to explore the microstructural changes in the corticospinal tract (CST) involved by the stroke lesion as well as the remote intact CST and precentral gyrus cortex connected to the acute infarct during a 6-month follow-up period. In this way, we hoped to provide quantitative information about structural remodeling after subcortical stroke.

MATERIALS AND METHODS

Patients

The study was approved by the institutional review board of our hospital. Written informed consent was obtained from all patients or their legal representatives. We enrolled patients with subcortical ischemic stroke who were treated in our center between September 2016 and June 2018. The inclusion criteria were as follows: (a) subcortical ischemic stroke involving the CST, (b) first-ever stroke occurred within 2 weeks of onset, and (c) ischemic stroke involving only one hemisphere, as confirmed by magnetic resonance imaging (MRI). The exclusion criteria were as follows: (a) any cortical ischemic lesion, (b) previous infarct lesion involving the CST on the initial MRI scan, (c) intracranial hemorrhage, (d) recurrent stroke, or other neurological disorders that may affect limb motor function, and (e) death during the 6-month follow-up period. A total of 22 patients were enrolled in this study. The average age of the patients was 63.0 ± 10.47 years, and the ratio of male-to-female patients was 12:10. No new cerebral ischemic stroke occurred in any of the patients during the 6-month follow-up. The mean time of the first MRI examination was 4.59 ± 1.44 days after onset, and the mean follow-up duration was 187.95 ± 5.52 days. Neurological function recovered to a certain extent during the follow-up. The clinical characteristics and demographics are shown in **Table 1**.

Clinical Assessment

The severity of neurological symptoms was evaluated using the National Institutes of Health Stroke Scale (NIHSS), the Fugl-Meyer Upper Extremity (FM-UE) scale, and the modified Rankin Scale (mRS) in the acute phase and at 6 months after the stroke.

MRI Protocol

MRI was performed in the acute phase (baseline) and at 6 months (follow-up) after the stroke by using a clinical 3.0-T MR scanner (Magnetom Verio, Siemens Healthcare, Erlangen, Germany) with an eight-channel head coil. The MRI sequences were as follows: axial fast spin echo T1-weighted (repetition time [TR]/echo time [TE] = 2,000/9 ms, inversion time [TI] = 860 ms, 24 slices with slice thickness = 5 mm, field of view [FOV] = 220 × 220 mm, matrix = 204 × 320); T2-weighted imaging (TR/TE = 6,000/95 ms, FOV = 220 × 220 mm, matrix = 244 × 384, 24 slices with slice thickness = 5 mm); fluid-attenuated inversion recovery (TR/TE = 8,500/94 ms, TI = 2438.9 ms, 24 slices with slice thickness = 5 mm, FOV = 220 × 220 mm, matrix = 324 × 512); and spin echo echoplanar conventional DWI (FOV = 220 × 220 mm, TR/TE = 5,000 ms/60 ms, resolution = 162 × 162, b = 0 and 1,000 s/mm^2, 28 slices with slice thickness = 4 mm). Both DTI and DKI were carried out using a spin echo echoplanar imaging diffusion sequence (for DTI, FOV = 220 × 220 mm, TR/TE = 8,831 ms/95 ms, resolution = ×, 54 slices with slice

TABLE 1 | Clinical characteristics and demographics.

Demographics and Characteristics ($n = 22$)	
Male, *n* (%)	12 (60)
Age (years, mean ± SD)	63.0 ± 10.47
Location of infarction, *n* (%)	
Left posterior limb of the internal capsule	6 (27.3)
Right posterior limb of the internal capsule	4 (18.2)
Left corona radiata	6 (27.3)
Left centrum semiovale	2 (9.1)
Right centrum semiovale	2 (9.1)
Vascular risk factors, *n* (%)	
Hypertension	15 (68.2)
Diabetes mellitus	10 (45.5)
Hypercholesterolemia	14 (63.6)
Clinical assessment (mean ± SD)	
Time from symptom onset to first (baseline) MRI (days)	4.59 ± 1.44
Time from symptom onset to follow-up MRI (days)	187.95 ± 5.52
NIHSS score at baseline	10.45 ± 2.36
NIHSS score at follow-up*	4.73 ± 1.49
FM-UE scale score at baseline	19.64 ± 5.34
FM-UE scale score at follow-up*	40.68 ± 6.54
mRS score at baseline	2.41 ± 0.80
mRS at follow-up*	1.41 ± 0.50

*$P < 0.05$ as compared to the baseline.
MRI, magnetic resonance imaging; NIHSS, National Institutes of Health Stroke Scale; FM-UE, Fugl-Meyer Upper-Extremity; mRS, Modified Rankin Scale.

thickness = 2 mm); for DKI, FOV = 220 × 220 mm, TR/TE = 6,100 ms/109 ms, resolution = ×, 54 slices with slice thickness = 2 mm) with 30 different diffusion encoding directions. For each direction, DTI with two b values (b = 0 and 1,000 s/mm^2) and DKI with six b values (b = 0, 500, 1,000, 1,500, 2,000, and 2,500 s/mm^2) were acquired. The total scan time of all sequences was about 25 min.

Data Processing

Whole-brain fiber-tracking maps and super-resolution TDI maps were generated using the MRtrix package (http://www.mrtrix.org/). First, the high-angular resolution diffusion imaging data were corrected for eddy-current distortion. The T2W images were used as the reference data for motion correction. The Brain Extraction Tool (BET2version2.1) from the FMRIB software library (http://www.fmrib.ox.ac.uk/fsl) was used to calculate the margins of the brain and skull and to remove the skull and scalp tissues. Then, constrained spherical deconvolution (CSD) was used to obtain multiple fiber orientations, and second-order integration was used to generate probabilistic tractography. Track lengths <0.5 mm were discarded, and the tractography termination criteria were as follows: exit the brain (or the numerical phantom) or when the CSD bra orientation distribution amplitude was <0.1. The resulting streamlines were then used to generate maps of track density at 0.25 mm isotropic spatial resolution in the DICOM format for side-by-side comparisons. FA maps were created using FMRIB's Diffusion Toolbox (FSL, Oxford, UK).

DKI post-processing was performed using the Diffusional Kurtosis Estimator (http://www.nitrc.org/projects/dke), where the diffusivity and kurtosis maps were generated using all DKI images. Before the calculation, motion correction through a 6-parameter rigid-body transformation was applied to all DKI images. After the calculation, the mean kurtosis (MK) map was generated.

According to the location of the stroke lesion, the CST was divided into the ipsilesional (IL) CST and contralesional (CL) CST. Regions of interest (ROIs) of FA and TDI were manually drawn along the CST on FA pseudo-color maps at the baseline. First, the whole-brain fiber-tracking map and TDI map were used as a reference, and ROIs were manually drawn at the level of the centrum semiovale, corona radiata, posterior limb of the internal capsule, and cerebral peduncle of the CST. If the above sites of the CST were involved by the stroke lesion, the involved part of the CST was also included in the ROI. The ROIs of the CL CST corresponded to those of the IL CST. We analyzed the impact of the stroke lesion on the remote intact CST based on the level of the CST involved by the stroke lesion. The mean value of the ROIs above the level at which the CST was involved by the stroke lesion was considered to be the value of the remote intact upper part of the CST. Similarly, the mean value of the ROIs below the level of involvement was considered to be the value of the remote intact lower part of the CST. For example, when the posterior limb of the internal capsule was involved by the stroke lesion, the mean value of the area between the corona radiata and the centrum semiovale was considered the value of the remote intact upper part of the CST, and the value of the cerebral peduncle was considered the value of the remote intact lower part of the CST. If the centrum semiovale was involved by the stroke lesion, an extra ROI was manually drawn on the IL CST between the involved centrum semiovale and the precentral gyrus cortex to evaluate the change in the remote intact upper part of the CST. The difference value of TDI and FA (ΔTDI and ΔFA) between follow-up and baseline in the remote intact upper part and lower part of the CST was calculated. The ROI on the CL CST corresponded to this manually drawn ROI (**Figure 1**). To determine the mean kurtosis (MK) value, we manually drew an ROI on the stroke lesion based on the hyperintensity on DWI. Another ROI was manually drawn on the corresponding CL area. According to the location of the stroke lesion, the precentral gyrus was also divided into an IL and CL part. Six ROIs were manually drawn on the precentral gyrus cortex, and the mean value of these six ROIs was considered to be the MK value of the precentral gyrus (**Figure 2**). The difference value of MK (ΔMK) between follow-up and baseline in the precentral gyrus cortex was also calculated.

Statistical Analysis

SPSS v16.0 (IBM, Armonk, NY, USA) was used for statistical analyses. Differences in clinical outcomes (FM-UE scale, NIHSS, and mRS scores) between the baseline and follow-up were analyzed using the Wilcoxon signed-rank tests. Differences in quantitative MRI measurements (TDI, FA, and MK) between the baseline and follow-up were analyzed using the paired *t*-test. The correlations (r) between ΔTDI and ΔFA in the IL

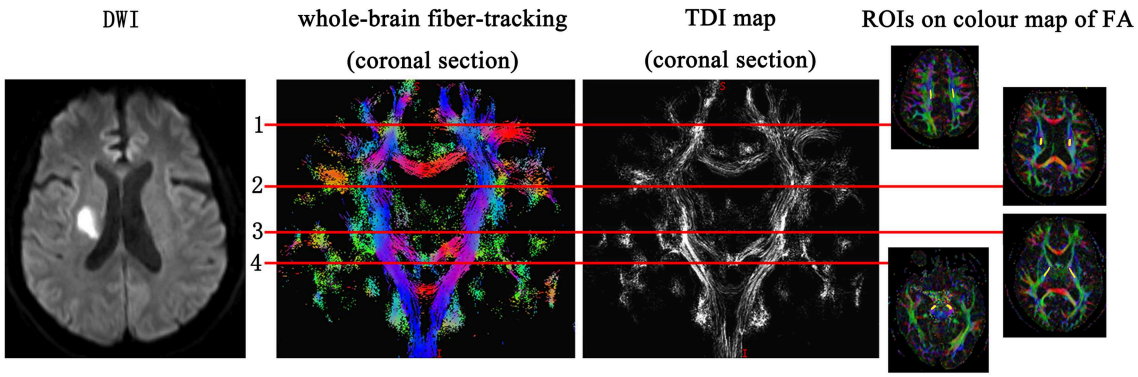

FIGURE 1 | Regions of interest (ROIs) on the corticospinal tract (CST) were manually drawn at the level of the centrum semiovale, corona radiata, posterior limb of the internal capsule, and cerebral peduncle. If any of the above parts of CST were involved by the stroke lesion, the involved part of the CST was also included in the ROI.

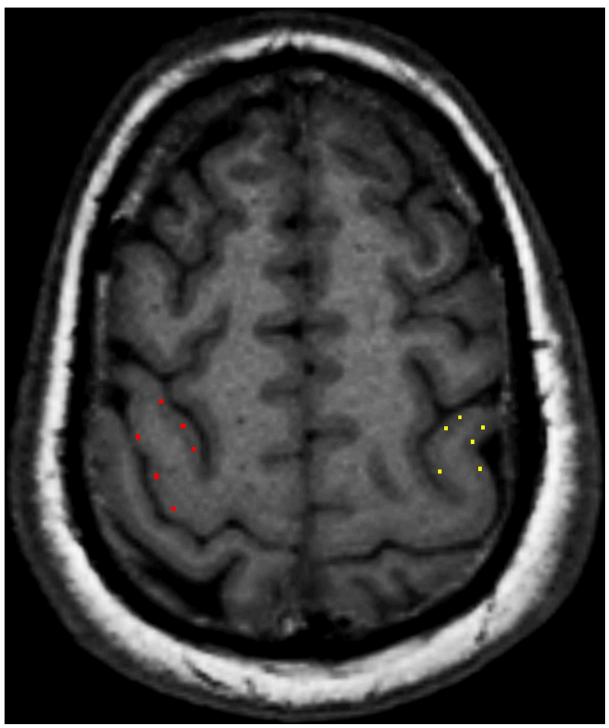

FIGURE 2 | Six regions of interest (ROIs) were manually drawn on the precentral gyrus cortex, and the mean value of these six ROIs was considered to be the mean kurtosis (MK) value of the precentral gyrus cortex.

CST and ΔMK in the IL precentral gyrus cortex were calculated using the Pearson correlation test. $P < 0.05$ was considered statistically significant.

RESULTS

Changes in the TDI and FA Values of the CST

In the case of the IL CST, the TDI and FA values of all levels were lower at the 6-month follow-up than at the baseline (all $P < 0.001$). In the case of the CL CST, however, no differences were found in the TDI and FA values at any level between the baseline and follow-up (**Tables 2**, **3**).

The TDI values of the non-involved upper (ΔTDI, 0.406) and lower parts (ΔTDI, 0.512) of the IL CST were lower at the 6-month follow-up than at the baseline ($P < 0.001$). Similarly, the FA values of the non-involved upper (ΔFA, 0.131) and lower parts (ΔFA, 0.173) of the IL CST were lower at follow-up than at the baseline ($P < 0.001$). In the case of the CL CST, the TDI and FA values of the parts corresponding to the non-involved upper ($P = 0.93$ and $P = 0.935$, respectively) and lower parts ($P = 0.995$ and $P = 0.38$, respectively) of the IL CST showed no significant difference between the follow-up and baseline (**Figures 3**, **4**).

Changes in the MK Values of the Stroke Lesion and Precentral Gyrus Cortex

The MK value of the stroke lesion was significantly lower at follow-up than at the baseline ($P < 0.001$); however, the corresponding CL ROI showed no significant change in MK value ($P = 0.368$). The MK value of the IL precentral gyrus cortex was lower (ΔMK, 0.052) at follow-up than at the baseline ($P = 0.002$), while the value of the CL precentral gyrus cortex showed no significant change ($P = 0.472$; **Table 4**, **Figure 3**).

Relationship Between the ΔTDI and ΔFA Values of the IL CST and the ΔMK Value of the IL Precentral Gyrus

The ΔTDI ($r = 0.689$, $P < 0.001$) and ΔFA values ($r = 0.463$, $P = 0.03$) of the non-involved upper part of the IL CST were positively correlated with the ΔMK value of the IL precentral gyrus (**Figure 5**). In contrast, the ΔTDI ($r = -0.062$, $P = 0.783$) and ΔFA values ($r = 0.31$, $P = 0.16$) of the non-involved lower part of the IL CST did not correlate with the ΔMK value of the IL precentral gyrus cortex.

DISCUSSION

In this study, we used DTI, TDI, and DKI to examine patients with subcortical infarction involving the CST in the acute phase

TABLE 2 | Changes in TDI value of the CST at the baseline and at follow-up.

ROIs of CST	Ipsilesional			Contralesional		
	Baseline	Follow-up	*P*	Baseline	Follow-up	*P*
Centrum semiovale	2.627 ± 0.655	2.082 ± 0.947	<0.001	2.895 ± 0.160	2.875 ± 0.128	0.136
Corona radiata	1.826 ± 0.382	1.096 ± 0.714	<0.001	2.092 ± 0.121	2.078 ± 0.123	0.287
Posterior limb of internal capsule	1.765 ± 0.535	1.069 ± 0.634	<0.001	2.198 ± 0.182	2.204 ± 0.192	0.728
Cerebral peduncle	1.879 ± 0.111	1.384 ± 0.188	<0.001	1.867 ± 0.103	1.872 ± 0.114	0.678

TDI, track-density imaging; CST, corticospinal tract; ROI, region of interest.

TABLE 3 | Changes in FA value of CST at baseline and follow-up.

ROIs of CST	Ipsilesional			Contralesional		
	Baseline	Follow-up	*P*	Baseline	Follow-up	*P*
Centrum semiovale	0.523 ± 0.118	0.374 ± 0.18	<0.001	0.582 ± 0.028	0.585 ± 0.030	0.351
Corona radiata	0.509 ± 0.160	0.320 ± 0.196	<0.001	0.615 ± 0.018	0.616 ± 0.024	0.794
Posterior limb of internal capsule	0.513 ± 0.136	0.289 ± 0.208	<0.001	0.626 ± 0.017	0.624 ± 0.020	0.553
Cerebral peduncle	0.569 ± 0.026	0.394 ± 0.042	<0.001	0.572 ± 0.026	0.568 ± 0.028	0.393

FA, fractional anisotropy; CST, corticospinal tract; ROI, region of interest.

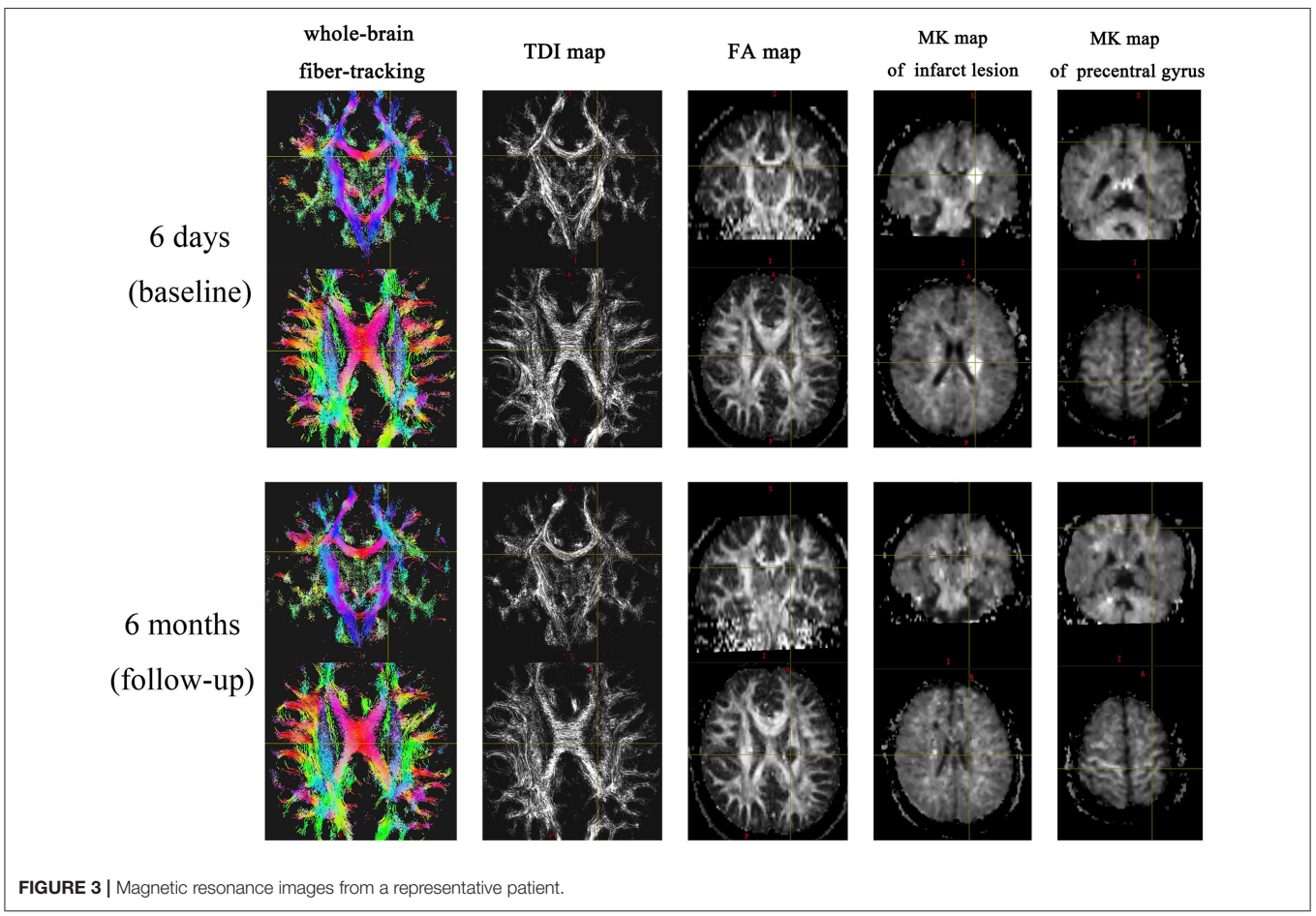

FIGURE 3 | Magnetic resonance images from a representative patient.

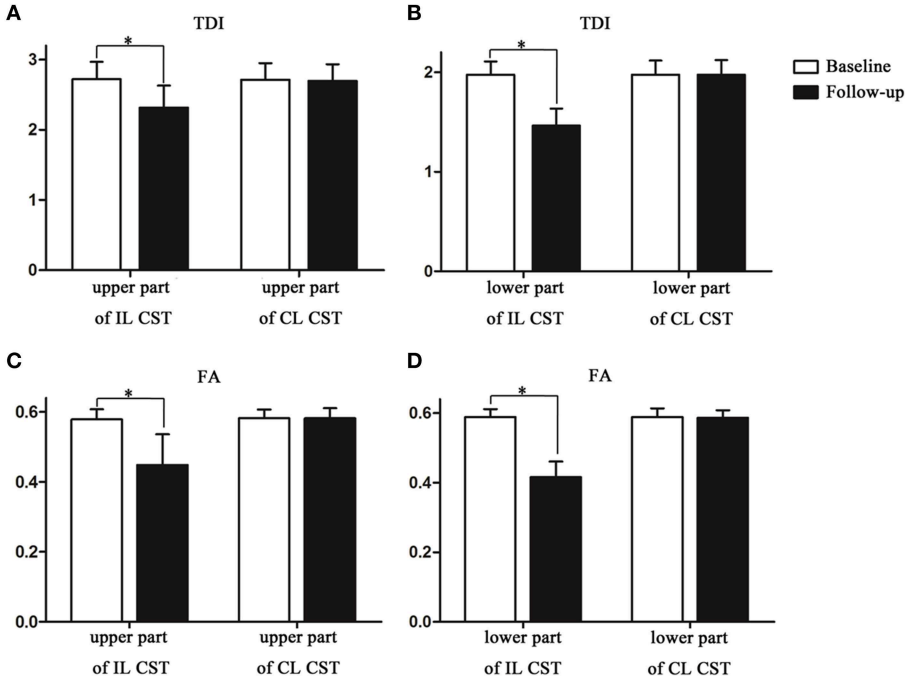

FIGURE 4 | The track-density imaging (TDI) and fractional anisotropy (FA) values of the non-involved lower and upper parts of the corticospinal tract (CST) at the baseline and at follow-up. **(A)** The comparison of TDI values in the non-involved upper part of the IL CST and the CL CST between baseline and follow-up. **(B)** The comparison of TDI values in the non-involved lower part of the IL CST and the CL CST between baseline and follow-up. **(C)** The comparison of FA values in the non-involved upper part of the IL CST and the CL CST between baseline and follow-up. **(D)** The comparison of FA values in the non-involved lower part of the IL CST and the CL CST between baseline and follow-up. *$P < 0.05$.

TABLE 4 | Changes in MK value of stroke lesion and precentral gyrus cortex at baseline and follow-up.

	Ipsilesional			Contralesional		
	Baseline	**Follow-up**	***P***	**Baseline**	**Follow-up**	***P***
Stroke lesion	2.759 ± 0.241	0.343 ± 0.132	<0.001	1.738 ± 0.116	1.745 ± 0.121	0.368
Precentral gyrus cortex	0.99 ± 0.128	0.938 ± 0.131	0.002	0.974 ± 0.117	0.963 ± 0.110	0.472

MK, mean kurtosis value.

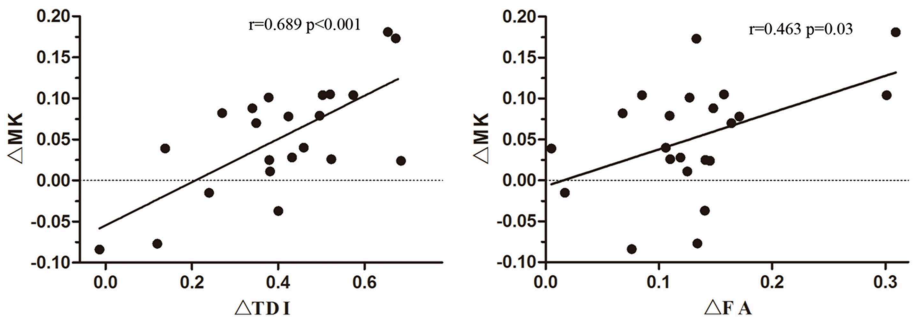

FIGURE 5 | Correlation of the ΔMK value of the ipsilesional (IL) precentral gyrus cortex with the ΔTDI and ΔFA values of the non-involved upper part of the corticospinal tract (CST).

and 6 months after onset. The results showed that (a) the TDI and FA values were reduced in both the involved part and the remote intact part of the IL CST, (b) the MK value decreased in the infarct lesion as well as in the IL precentral gyrus, and

(c) the ΔTDI and ΔFA values of the non-involved upper part of the IL CST were correlated with the ΔMK value of the IL precentral gyrus.

In this study, the neurological function of ischemic stroke patients recovered to a certain extent during the 6-month follow-up. A previous study has shown that during the post-stroke rehabilitation process, both the white matter and cortex may undergo a certain degree of structural remodeling to compensate for impaired neurological function (18). After ischemic stroke, nerve fibers disintegrate due to ischemia, hypoxia, and necrosis of the local tissue. In addition, axonal injury and demyelination occur in the remote intact tissue due to Wallerian degeneration (19, 20). Therefore, the integrity and number of nerve fibers decrease. We used TDI combined with FA to monitor changes in the CST after subcortical infarction involving the CST. TDI accurately reflects the number of white matter fibers passing through a voxel (14), while FA values reflect the integrity of white-matter fibers (11). Thus, both these parameters could reflect the severity of damage to the local white-matter fibers. Our results showed that during follow-up, the TDI and FA values decreased in the centrum semiovale, corona radiata, posterior limb of the internal capsule, and cerebral peduncle of the IL CST compared to the baseline, indicating that the number and integrity of white-matter fibers in the IL CST reduced during the 6-month follow-up. Among our patients, most ischemic stroke lesions were located in the posterior limb of the internal capsule and corona radiata. Only four stoke lesions were located in the centrum semiovale, while the cerebral peduncle was not involved at all by the stroke. Nevertheless, the TDI and FA values of the cerebral peduncle and the non-involved upper part of the IL CST reduced during the follow-up, confirming that the integrity and number of remote non-involved nerve fibers reduced after stroke.

To understand the changes in the remote non-involved nerve fibers of the IL CST, we divided the CST into a lower and an upper part according to the location of the infarct. Consistent with previous studies (21, 22), our results showed that the TDI and FA values reduced in both the non-involved lower and upper parts of the IL CST during follow-up, indicating that the integrity and number of fibers reduced in both the proximal and distal parts of the remote non-involved IL CST. In addition to the changes in the infarct itself, the infarct lesion will cut off the nutritional supply and synaptic connection between the inferior nerve fibers and the upper cortex, leading to Wallerian degeneration of the inferior nerve fibers, which causes axonal and myelin sheath disintegration and nerve fiber atrophy (19, 20). These changes lead to a reduction in the TDI and FA values. We also found a similar reduction in the non-involved upper part of the IL CST. Although Wallerian degeneration mainly occurred in the descending nerve fibers, one study has shown that Wallerian degeneration can occur in a retrograde fashion and affect the upper nerve fibers (23). However, the mechanism underlying the decrease in the number and integrity of fibers in the non-involved upper part of the IL CST is unknown (24)—some studies have shown that the secondary degeneration of nerve fibers may be bi-directional (25, 26). In addition, the downward transmission of excitatory stimulation of the remote intact cortical neurons may be not smooth due to the involvement of the CST by the infarct, leading to loss of local synaptic inputs and atrophy of the non-involved upper part of the IL CST (6). This may be one of the reasons for the decrease in the TDI and FA values of the non-involved upper part of the IL CST.

Besides the nerve fibers, the cortex also plays an important role in the structural reorganization after cerebral infarction (27). Although the IL cortex was not involved by the subcortical infarction, the activation areas induced by impaired limb movement switched to the corresponding CL motor cortex or other distal cortical areas (3, 5). Other studies have found that the thickness and NAA value of the cortex connected with the nerve fibers involved by the subcortical infarction changed during follow-up (6, 8). In this study, DKI was used to analyze the changes in the infarct lesion and the IL precentral gyrus cortex; the results showed that besides the changes in the infarct, the MK value of the IL precentral gyrus cortex decreased during the follow-up, indicating that the complexity of the internal structure of the precentral gyrus cortex decreased. The connected cortex may be transsynaptic affected by the secondary degeneration of the non-involved upper part of the IL CST. Loss of synaptic input due to the infarct could induce compromised metabolism. The secondary degeneration and compromised metabolism could induce changes such as neuronal apoptosis and atrophy in the cortex connected with the involved nerve fibers after subcortical stroke (28). In addition, loss of synaptic input may lead to the shrinkage of dendrites and cell bodies (6). These pathological changes may reduce the complexity of the focal microenvironment to a certain extent, thereby reducing the MK value.

The above findings raise the question of whether there is any correlation between the structural remodeling in the remote non-involved CST and the connected cortex after subcortical stroke. Our results showed that the ΔTDI and ΔFA values of the non-involved upper part of the IL CST were positively correlated with the ΔMK value of the IL precentral gyrus cortex, while no correlation was found between the ΔTDI and ΔFA values of the lower part of the IL CST and the ΔMK value of the IL precentral gyrus cortex. Both the upper fibers and the remote cortex were located above the level of the infarct and were directly connected. The loss of synaptic input to the cortex could cause degeneration and atrophy of the connected nerve fibers, which in turn may cause atrophy of the neuronal bodies and dendrites (6). Therefore, it is unsurprising that there would be a correlation between the upper fibers and the remote cortex. The connection between the non-involved lower part of the IL CST and the remote IL precentral gyrus cortex was cut off by the infarct lesion, so there was no linear correlation between the ΔTDI and ΔFA values of the non-involved lower part of the IL CST and the ΔMK value of the remote IL precentral gyrus cortex. We also found that the degree of correlation was higher for ΔTDI than for ΔFA. Although DTI can evaluate the integrity of white-matter fibers, it has some limitations in evaluating complex fibers, such as cross fibers (13). TDI, which is an ultra-high resolution technology, may more accurately evaluate changes in cross fibers than FA (14, 15). In this study, lesions were mainly located in the centrum semiovale, corona radiata, and posterior limb of the internal capsule, so the ROIs of the non-involved upper part of the IL CST

were located in the centrum semiovale and corona radiata, which have many bundles of cross fibers. Therefore, TDI might be more sensitive than FA to reflect changes in the CST.

Studies have shown that both the CL CST and cortex may undergo structural remodeling and functional reorganization to a certain extent after cerebral infarction (3, 5). However, the TDI and FA values of the CL CST and the MK values of the CL precentral gyrus cortex did not change during the 6-month follow-up. This may be because the compensatory function switched to the IL hemisphere with the partial recovery of motor function. In addition, differences in infarction site and follow-up duration may be possible reasons.

There are some limitations to this study. First, the small sample size may have introduced some bias. Second, this study focused on the cortex of the IL precentral gyrus connected with the IL CST; other cortical regions were not analyzed. We evaluated the IL precentral gyrus cortex because it is directly connected to the CST, thus it may reflect more intuitively the impact of subcortical stroke involving the CST. Third, only two time points were used in this study, and these could not reflect dynamic changes in the CST and cortex of the precentral gyrus. Finally, we did not analyze the relationship of the changes in the CST and precentral gyrus with neurological function. The main purpose of this study was to determine the microstructural changes in the IL CST and IL precentral gyrus cortex, and other cortical regions were not analyzed. Therefore, simply evaluating the relationship of the changes in the IL CST and IL precentral gyrus cortex with neurological function may have some deficiencies.

In conclusion, our results showed that subcortical infarction involving the CST not only reduced the number and integrity of the remote IL CST but also caused changes in the remote IL precentral gyrus cortex. The changes in the number and integrity of the nerve fibers in the non-involved upper part of the IL CST were correlated with microstructural changes in the IL precentral gyrus cortex. In addition, TDI was more sensitive than FA to detect pathological changes in the CST after subcortical stroke, and may be used as a tool to evaluate pathological changes in white-matter fibers.

DATA AVAILABILITY

All datasets generated for this study are included in the manuscript/supplementary files.

AUTHOR CONTRIBUTIONS

X-EW and Y-HL conceived and designed of the study. X-EW and KS organized the database. X-EW, KS, JZ, and Y-JZ performed the follow-up and MRI scan. The processing of MRI was performed by X-EW, KS, and JZ. X-EW wrote the first draft of the manuscript. Y-HL and Y-JZ wrote sections of the manuscript. All authors read and approved the submitted version.

FUNDING

This study was supported by Shanghai Health and Family Planning Commission research projects (No. 20164Y0065), the Medical-Engineering Cross Project of Shanghai Jiaotong University (Grant No. YG2015MS19), Shanghai Municipal Education Commission-Gaofeng Clinical Medicine Grant Support (No. 2016427), the National Natural Scientific Fund of China (Nos. 81471656, 81671673, 81871329, and 81301213), Youth Medical Talents-Medical Imaging Practitioner Program, and Shanghai key discipline of medical imaging (No. 2017ZZ02005).

REFERENCES

1. Havsteen I, Madsen KH, Christensen H, Christensen A, Siebner HR. Diagnostic approach to functional recovery: functional magnetic resonance imaging after stroke. *Front Neurol Neurosci*. (2013) 32:9–25. doi: 10.1159/000346408
2. Jiang Q, Zhang ZG, Chopp M. MRI evaluation of white matter recovery after brain injury. *Stroke*. (2010) 41(Suppl 10):S112–3. doi: 10.1161/STROKEAHA.110.595629
3. Cai J, Ji Q, Xin R, Zhang D, Na X, Peng R, et al. Contralesional cortical structural reorganization contributes to motor recovery after sub-cortical stroke: longitudinal voxel-based morphometry study. *Front Hum Neurosci*. (2016) 10:393. doi: 10.3389/fnhum.2016.00393
4. Dodd KC, Nair VA, Prabhakaran V. Role of the contralesional vs. Ipsilesional hemisphere in stroke recovery. *Front Hum Neurosci*. (2017) 21:469. doi: 10.3389/fnhum.2017.00469
5. Sinke MR, Otte WM, van Meer MP, van der Toorn A, Dijkhuizen RM. Modified structural network backbone in the contralesional hemisphere chronically after stroke in rat brain. *J Cereb Blood Flow Metab*. (2018) 38:1642–53. doi: 10.1177/0271678X17713901
6. Duering M, Righart R, Wollenweber FA, Zietemann V, Gesierich B, Dichgans M. Acute infarcts cause focal thinning in remote cortex via degeneration of connecting fiber tracts. *Neurology*. (2015) 84:1685–92. doi: 10.1212/WNL.0000000000001502
7. Lukic S, Barbieri E, Wang X, Caplan D, Kiran S, Rapp B, et al. Right hemisphere grey matter volume and language functions in stroke Aphasia. *Neural Plast*. (2017) 2017:5601509. doi: 10.1155/2017/5601509
8. Cirstea CM, Savage CR, Nudo RJ, Cohen LG, Yeh HW, Choi IY, et al. Handgrip-related activation in the primary motor cortex relates to underlying neuronal metabolism after stroke. *Neurorehabil Neural Repair*. (2014) 28:433–42. doi: 10.1177/1545968313516868
9. Schaechter JD, Moore CI, Connell BD, Rosen BR, Dijkhuizen RM. Structural and functional plasticity in the somatosensory cortex of chronic stroke patients. *Brain*. (2006) 129(Pt 10):2722–33. doi: 10.1093/brain/awl214
10. Brodtmann A, Pardoe H, Li Q, Lichter R, Ostergaard L, Cumming T. Changes in regional brain volume three months after stroke. *J Neurol Sci*. (2012) 322:122–8. doi: 10.1016/j.jns.2012.07.019
11. Owen M, Ingo C, Dewald JPA. Upper extremity motor impairments and microstructural changes in bulbospinal pathways in chronic hemiparetic stroke. *Front Neurol*. (2017) 8:257. doi: 10.3389/fneur.2017.00257
12. Jung WB, Han YH, Chung JJ, Chae SY, Lee SH, Im GH, et al. Spatiotemporal microstructural white matter changes in diffusion tensor imaging after transientfocal ischemic stroke in rats. *NMR Biomed*. (2017) 30:e3704. doi: 10.1002/nbm.3704
13. Po C, Kalthoff D, Kim YB, Nelles M, Hoehn M. White matter reorganization and functional response after focal cerebral ischemia in the rat. *PLoS ONE*. (2012) 7:e45629. doi: 10.1371/journal.pone.0045629

14. Calamante F, Tournier JD, Smith RE, Connelly A. A generalized framework for super-resolution track-weighted imaging. *Neuroimage*. (2012) 59:2494–503. doi: 10.1016/j.neuroimage.2011.08.099
15. Calamante F, Tournier JD, Jackson GD, Connelly A. Track-density imaging (TDI): super-resolution white matter imaging using whole-brain track-density mapping. *Neuroimage*. (2010) 53:1233–43. doi: 10.1016/j.neuroimage.2010.07.024
16. Yin J, Sun H, Wang Z, Ni H, Shen W, Sun PZ. Diffusion kurtosis imaging of acute infarction: comparison with routine diffusion and follow-up MR imaging. *Radiology*. (2018) 287:651–7. doi: 10.1148/radiol.2017170553
17. Wu Y, Kim J, Chan ST, Zhou IY, Guo Y, Igarashi T, et al. Comparison of image sensitivity between conventional tensor-based and fast diffusion kurtosis imaging protocols in a rodent model of acute ischemic stroke. *NMR Biomed*. (2016) 29:625–30. doi: 10.1002/nbm.3506
18. Zhang J, Zhang Y, Wang L, Sang L, Yang J, Yan R, et al. Disrupted structural and functional connectivity networks in ischemic stroke patients. *Neuroscience*. (2017) 364:212–25. doi: 10.1016/j.neuroscience.2017.09.009
19. Guo AH, Hao FL, Liu LF, Wang BJ, Jiang XF. An assessment of the correlation between early postinfarction pyramidal tract Wallerian degeneration and nerve function recovery using diffusion tensor imaging. *Genet Mol Res*. (2017) 16:gmr16019035. doi: 10.4238/gmr16019035
20. Ma C, Liu A, Li Z, Zhou X, Zhou S. Longitudinal study of diffusion tensor imaging properties of affected cortical spinal tracts in acute and chronic hemorrhagic stroke. *J Clin Neurosci*. (2014) 21:1388–92. doi: 10.1016/j.jocn.2013.11.032
21. Kim B, Fisher BE, Schweighofer N, Leahy RM, Haldar JP, Choi S, et al. A comparison of seven different DTI-derived estimates of corticospinal tract structural characteristics in chronic stroke survivors. *J Neurosci Methods*. (2018) 304:66–75. doi: 10.1016/j.jneumeth.2018.04.010
22. Schaechter JD, Fricker ZP, Perdue KL, Helmer KG, Vangel MG, Greve DN, et al. Microstructural status of ipsilesional and contralesional corticospinal tract correlates with motorskill in chronic stroke patients. *Hum Brain Mapp*. (2009) 30:3461–74. doi: 10.1002/hbm.20770
23. Liang Z, Zeng J, Zhang C, Liu S, Ling X, Xu A, et al. Longitudinal investigations on the anterograde and retrograde degeneration in the pyramidaltract following pontine infarction with diffusion tensor imaging. *Cerebrovasc Dis*. (2008) 25:209–16. doi: 10.1159/000113858
24. Takenobu Y, Hayashi T, Moriwaki H, Nagatsuka K, Naritomi H, Fukuyama H. Motor recovery and microstructural change in rubro-spinal tract in subcortical stroke. *Neuroimage Clin*. (2013) 4:201–8. doi: 10.1016/j.nicl.2013.12.003
25. Kanamori A, Catrinescu MM, Belisle JM, Costantino S, Levin LA. Retrograde and Wallerian axonal degeneration occur synchronously after retinal ganglion cell axotomy. *Am J Pathol*. (2012) 181:62–73. doi: 10.1016/j.ajpath.2012.03.030
26. Liang Z, Zeng J, Liu S, Ling X, Xu A, Yu J, et al. A prospective study of secondary degeneration following subcortical infarction using diffusiontensor imaging. *J Neurol Neurosurg Psychiatry*. (2007) 78:581–6. doi: 10.1136/jnnp.2006.099077
27. Larsen LH, Zibrandtsen IC, Wienecke T, Kjaer TW, Langberg H, Nielsen JB, et al. Modulation of task-related cortical connectivity in the acute and subacute phase after stroke. *Eur J Neurosci*. (2018) 47:1024–32. doi: 10.1111/ejn.13874
28. Fan F, Zhu C, Chen H, Qin W, Ji X, Wang L, et al. Dynamic brain structural changes after left hemisphere subcortical stroke. *Hum Brain Mapp*. (2013) 34:1872–81. doi: 10.1002/hbm.22034

Conflict of Interest Statement: The authors declare that the research was conducted in the absence of any commercial or financial relationships that could be construed as a potential conflict of interest.

Copyright © 2019 Wei, Shang, Zhou, Zhou and Li. This is an open-access article distributed under the terms of the Creative Commons Attribution License (CC BY). The use, distribution or reproduction in other forums is permitted, provided the original author(s) and the copyright owner(s) are credited and that the original publication in this journal is cited, in accordance with accepted academic practice. No use, distribution or reproduction is permitted which does not comply with these terms.

frontiers in Neuroscience

ORIGINAL RESEARCH
published: 07 August 2019
doi: 10.3389/fnins.2019.00781

Topical Administration of a Soluble TNF Inhibitor Reduces Infarct Volume After Focal Cerebral Ischemia in Mice

*Minna Yli-Karjanmaa[1†], Bettina Hjelm Clausen[1,2†], Matilda Degn[3], Hans Gram Novrup[1], Ditte Gry Ellman[1], Peter Toft-Jensen[1], David E. Szymkowski[4], Allan Stensballe[5], Morten Meyer[1,2], Roberta Brambilla[1,2,6] and Kate Lykke Lambertsen[1,2,7]**

[1] Department of Neurobiology Research, Institute of Molecular Medicine, University of Southern Denmark, Odense, Denmark, [2] BRIDGE – Brain Research Inter-Disciplinary Guided Excellence, Department of Clinical Research, University of Southern Denmark, Odense, Denmark, [3] Pediatric Oncology Laboratory, Department of Pediatrics and Adolescent Medicine, University Hospital Rigshospitalet, Copenhagen, Denmark, [4] Xencor Inc., Monrovia, CA, United States, [5] Department of Health Science and Technology, University of Aalborg, Aalborg, Denmark, [6] The Miami Project to Cure Paralysis, University of Miami Miller School of Medicine, Miami, FL, United States, [7] Department of Neurology, Odense University Hospital, Odense, Denmark

OPEN ACCESS

Edited by:
Mathias Gelderblom, University Medical Center Hamburg-Eppendorf, Germany

Reviewed by:
Qiang Liu, Barrow Neurological Institute (BNI), United States
Mikhail Yu. Stepanichev, Institute of Higher Nervous Activity and Neurophysiology (RAS), Russia

***Correspondence:**
Kate Lykke Lambertsen
klambertsen@health.sdu.dk

† These authors have contributed equally to this work

Specialty section:
This article was submitted to Neurodegeneration, a section of the journal Frontiers in Neuroscience

Received: *28 March 2019*
Accepted: *11 July 2019*
Published: *07 August 2019*

Citation:
Yli-Karjanmaa M, Clausen BH, Degn M, Novrup HG, Ellman DG, Toft-Jensen P, Szymkowski DE, Stensballe A, Meyer M, Brambilla R and Lambertsen KL (2019) Topical Administration of a Soluble TNF Inhibitor Reduces Infarct Volume After Focal Cerebral Ischemia in Mice. Front. Neurosci. 13:781. doi: 10.3389/fnins.2019.00781

Background: Tumor necrosis factor, which exists both as a soluble (solTNF) and a transmembrane (tmTNF) protein, plays an important role in post-stroke inflammation. The objective of the present study was to test the effect of topical versus intracerebroventricular administration of XPro1595 (a solTNF inhibitor) and etanercept (a solTNF and tmTNF inhibitor) compared to saline on output measures such as infarct volume and post-stroke inflammation in mice.

Methods: Adult male C57BL/6 mice were treated topically (2.5 mg/ml/1μl/h for 3 consecutive days) or intracerebroventricularly (1.25 mg/kg/0.5 ml, once) with saline, XPro1595, or etanercept immediately after permanent middle cerebral artery occlusion (pMCAO). Mice were allowed to survive 1 or 3 days. Infarct volume, microglial and leukocyte profiles, and inflammatory markers were evaluated.

Results: We found that topical, and not intracerebroventricular, administration of XPro1595 reduced infarct volume at both 1 and 3 days after pMCAO. Etanercept showed no effect. We observed no changes in microglial or leukocyte populations. XPro1595 increased gene expression of *P2ry12* at 1 day and *Trem2* at 1 and 3 days, while decreasing *Cx3cr1* expression at 1 and 3 days after pMCAO, suggesting a change in microglial activation toward a phagocytic phenotype.

Conclusion: Our data demonstrate that topical administration of XPro1595 for 3 consecutive days decreases infarct volumes after ischemic stroke, while modifying microglial activation and the inflammatory response post-stroke. This suggests that inhibitors of solTNF hold great promise for future neuroprotective treatment in ischemic stroke.

Keywords: ischemic stroke, behavior, cytokines, microglial activation, neuroprotection

INTRODUCTION

Inflammatory events after ischemic stroke contribute to secondary injury mechanisms that can expand tissue injury and are thus targets of new treatment options (Lambertsen et al., 2018). Tumor necrosis factor (TNF) is a multifunctional, proinflammatory cytokine that participates in all phases of ischemic stroke, from development to repair and long-term inflammatory effects (reviewed in Hallenbeck, 2002). It exists both as a transmembrane (tmTNF) and a soluble (solTNF) protein, the latter released via proteolytic cleavage by TNFα converting enzyme (TACE, also called ADAM17) (Black et al., 1997). TNF mediates its effects via TNF receptor 1 (TNFR1, p55TNFR) and 2 (TNFR2, p75TNFR); solTNF primarily mediates acute and chronic inflammation, while tmTNF has been shown to support innate immune function and promote neuronal survival and axonal remyelination, synaptic function, and neurotransmission (Ruuls et al., 2001; Alexopoulou et al., 2006; Brambilla et al., 2011; Barnum et al., 2014; Cavanagh et al., 2016). In ischemic stroke, TNF plays an important role in infarct development (Lambertsen et al., 2018). In support of this, conventional (Lambertsen et al., 2009) and conditional myeloid (Clausen et al., 2016a) deletion of TNF resulted in increased infarct volumes in mice subjected to permanent middle cerebral artery occlusion (pMCAO). Interestingly, genetic ablation of solTNF using tmTNF$^{\Delta/\Delta}$ mice resulted in decreased infarct volumes after pMCAO (Madsen et al., 2016), suggesting that inhibition of solTNF, but preservation of tmTNF, is required for neuroprotection in ischemic stroke.

Current FDA- and EMA-approved TNF inhibitors are used for treating chronic autoimmune inflammatory diseases such as rheumatoid arthritis, inflammatory bowel disease, and psoriasis (Lis et al., 2014), where they also relieve potential symptoms of depression (Tyring et al., 2006). The dimeric Fc-fusion protein etanercept targets both tmTNF and solTNF. Being a large (150 kDa) protein, it is not able to cross the blood-brain barrier. When administered perispinally, however, etanercept improved neurological outcome in patients with chronic stroke, traumatic brain injury and Alzheimer's disease (Griffin, 2008; Tobinick, 2011; Tobinick et al., 2012; and reviewed in Lambertsen et al., 2018). The downside of drugs like etanercept is that inhibition of both solTNF and tmTNF can provoke demyelination and induce neuropathies, infections, sepsis, congestive heart failure and lupus, emphasizing the importance of leaving tmTNF available to preserve adequate function of the innate immune system (Scheinfeld, 2004). XPro1595 is a dominant-negative inhibitor of solTNF (Steed et al., 2003). In animal models of multiple sclerosis, XPro1595 promotes axonal preservation and remyelination (Brambilla et al., 2011); in Parkinson's disease XPro1595 reduces neuronal loss (McCoy et al., 2006; Barnum et al., 2014); in Alzheimer's disease it decreases beta-amyloid plaques and promotes synaptic function (Cavanagh et al., 2016; MacPherson et al., 2017); and in spinal cord injury it decreases lesion volume (Novrup et al., 2014). We have previously shown that using etanercept and XPro1595 for systemic inhibition of TNF improved functional outcome and affected the inflammatory response after pMCAO in mice, but with no effect on infarct volume (Clausen et al., 2014). The altered inflammatory response after systemic administration of TNF inhibitors was likely a result of peripheral immunomodulation that decreased the granulocyte infiltration to the ischemic lesion, which was earlier shown to be neuroprotective (Soriano et al., 1999; Clausen et al., 2014). Peripheral treatment likely also changed microglial activation (Clausen et al., 2014). In light of these studies and our earlier studies demonstrating that topical (and not systemic) administration of XPro1595 decreased lesion size following moderate spinal cord injury (Novrup et al., 2014), we hypothesized that topical and/or intracerebroventricular (i.c.v.) delivery of XPro1595 would reduce lesion size, ameliorate brain inflammation, and improve functional outcome after focal cerebral ischemia in mice.

Abbreviations: 3-MPST, 3-mercaptopyruvate sulfurtransferase; Arg1, arginase 1; CCL2, C-C motif chemokine ligand 2; CV, coefficient of variation; CXCL1, C-X-C motif chemokine ligand 1; CXCL10, C-X-C motif chemokine ligand 10; Cx3cr1, C-X3-C motif chemokine receptor 1; FBS, fetal bovine serum; FDR, false discovery rate; FMO, fluorescence minus one; HBSS, Hanks' Balanced Salt Solution; HGTD-P, human growth and transformation-dependent protein; HPGDS, hematopoetic prostaglandin D synthase; HPRT1, hypoxanthine phosphoribosyltransferase 1; i.c.v., intracerebroventricular; IL-1β, interleukin-1β, INOS, inducible nitric oxide synthase; LPS, lipopolysaccharide; MCA, middle cerebral artery; MECP, methyl-CgP-binding protein 2; MFI, mean fluorescent intensity; MPO, myeloperoxidase; PBS, phosphate buffered saline; pMCAO, permanent middle cerebral artery occlusion; P2ry12, P2Y purinoceptor 12; PYCARD, apoptosis-associated speck-like protein containing CARD; RIN, RNA integrity factor; RT-PCR, reverse transcriptase-polymerase chain reaction; s.c., subcutaneously; solTNF, soluble tumor necrosis factor; SSC, side scatter; TACE, tumor necrosis factor alpha converting enzyme; tmTNF, transmembrane tumor necrosis factor; TNF, tumor necrosis factor; TNFR1, tumor necrosis factor 1; TNFR2, tumor necrosis factor 2; Trem2, triggering receptor expressed on myeloid cells-2; UPLC-MS/MS, ultra-performance liquid chromatography-tandem mass spectrometry.

MATERIALS AND METHODS

Animals

Adult male C57BL/6 mice (aged 7–8 weeks) were purchased from Taconic Ltd. (Ry, Denmark) and transferred to the Biomedical Laboratory at the University of Southern Denmark, Odense, Denmark. tmTNF$^{\Delta/\Delta}$ (Ruuls et al., 2001) breeding couples were kindly donated by Dr. Tacchini-Cottier, University of Lausanne, Switzerland and a breeding colony was established at the Biomedical Laboratory at the University of Southern Denmark. Animals were housed under diurnal lighting conditions, and food and water were available *ad libitum*. Mice were allowed to acclimatize for at least 1 week before behavioral testing. All animal experiments were approved by the Danish Animal Inspectorate under the Ministry of Food and Agriculture (J. No. 2013-15-2934-00924).

Permanent Middle Cerebral Artery Occlusion

Permanent occlusion of the distal part of the middle cerebral artery was performed by electrocoagulation under Hypnorm-Dormicum anesthesia (fentanyl citrate (0.315 mg/ml, Jansen-Cilag), fluanisone (10 mg/ml, Jansen-Cilag, Birkerød, Denmark), and midazolam (5 mg/ml, Hoffmann-La Roche, Hvidovre, Denmark) as routinely done in our laboratory (Lambertsen et al.,

2001, 2009; Clausen et al., 2014, 2016b). Post-operatively, mice were injected with 0.9% physiological saline subcutaneously (s.c.) and placed in a 28°C heating cabinet for 24 h. Mice with 3 days survival were returned to the conventional animal facility after 24 h. Buprenorphine hydrochloride (0.001 mg/20 g Temgesic, Schering-Plough, Ballerup, Denmark) was administered three times at 8 h intervals starting immediately prior to surgery. Sham mice were subjected to similar surgery but without electrocoagulation of the middle cerebral artery (MCA).

Pharmacological Treatment

Saline, XPro1595 (Xencor Inc., Monrovia, CA, United States), or etanercept (Enbrel, Amgen-Wyeth, Thousand Oak, CA, United States) was administered topically using mini-osmotic pumps (Alzet, 1003D, Durect Corporation, Cupertino, CA, United States) implanted 30 min after pMCAO. XPro1595 and etanercept were diluted in saline for the final concentration. The pumps were placed in such a way that the delivering end of the catheter was on top of the infarct core. The catheter was sutured to the musculature, and the suture and placement of it were secured using Vetbond (3M Animal Care Products, St. Paul, MN, United States). The pumps were set to deliver either saline (0.9% physiological NaCl) with a flow of 1 μl/h, XPro1595 or etanercept with a flow of 2.5 mg/ml/1μl/h for 3 consecutive days, as previously described (Novrup et al., 2014).

In addition, intracerebroventricular (i.c.v.) injection of saline, XPro1595, or etanercept was performed 30 min after pMCAO. For i.c.v. delivery, animals were fixed in a stereotactic frame (David Kopf Instruments, United States) immediately after pMCAO, and anesthesia was maintained with isoflurane (2% isoflurane in O_2). One single i.c.v. injection (0.5 μl) of either saline, XPro1595 (1.25 mg/kg), or etanercept (1.25 mg/kg) was administered using a 2 μl Hamilton micro-syringe. The injection was made in the left lateral ventricle using the following coordinates with reference to bregma: anterior -0.2 mm; lateral 0.9 mm; ventral 2.5 mm; tooth-bar -1.0 mm. After injection, the syringe was left in place for a further 5 min before being slowly retracted.

Group Size and Study Design

Groups of mice for infarct volumetric, functional, and inflammatory analyses consisted of mice treated topically for 1 day (n = 7–11/group) or for 3 days (n = 20/group) or mice treated i.c.v. for 1 day (n = 6–7/group) or for 3 days (n = 20/group) after pMCAO. Animals were excluded from the study if the infarct volume was less than 3 mm^3 due to lack of successful occlusion of the MCA. Animals with MCA bleedings were excluded due to hematoma formation. A total of 29 mice subjected to pMCAO were excluded due to lack of infarct or bleedings.

To evaluate microglial and leukocyte profiles, a group of sham-treated mice were allowed to survive 3 days (n = 5/group). Mice allowed to survive for 1 day (n = 5–6/group) or 3 days (n = 5/group) after pMCAO were included for flow cytometric studies.

Mortality was 9% and independent of treatment. In total, in the day one groups, 2 mice treated topically with saline, 1 mouse treated topically with XPro1595, 1 mouse treated i.c.v. with XPro1595, and 1 mouse treated i.c.v. with etanercept died. In the day 3 groups, 1 mouse with 3 days survival treated topically with saline, 2 mice treated topically with XPro1595, and 1 mouse treated topically with etanercept, 2 mice treated i.c.v. with saline, 1 mouse treated i.c.v. with XPro1595, and 3 mice treated i.c.v. with etanercept died.

Behavioral Tests

Functional outcome was evaluated using the Hargreaves test (2 days after surgery) and a grip strength test (3 days after surgery). Prior to behavioral testing, mice were allowed to acclimatize in the behavior room. Neuromuscular testing of mice with mini-osmotic pumps was not possible as the pumps were placed in subcutaneous pockets on the lateral back of the mice and affected the animals' balance. Behavioral testing was therefore only performed with i.c.v. treated mice.

Thermal Nociception Assay

Thermal hyperalgesia was evaluated using the Hargreaves nociception assay (Hargreaves et al., 1988). The plantar test (37370, Ugo Basile, Comerio VA, Italy) was used to measure the withdrawal latencies after predisposing the hind paws to heat (Clausen et al., 2016b). Five measurements were registered for each hind paw prior to and 2 days after pMCAO; the lowest and highest values were excluded, and the mean was calculated. Data are presented as symmetry between contra- and ipsilateral hind paws prior to and after surgery. The mice were allowed to recover for 15 min between trials. Mice were excluded if they did not complete all the trials. In total, four animals were excluded.

Grip Strength

Grip strength was measured 1 day prior to and 3 days after surgery using a grip strength meter (BIO-GT-3, BIOSEB, Vitrolles, France). We measured the peak force generated when the mouse loosened its grip when being gently pulled horizontally backwards. We tested both the front right (R) and the front left (L) paw as well as the total grip strength. The peak force (g) of five trials was recorded, and the highest score was registered. Results are presented as delta (Δ) grip strength in grams (g), representing the difference in grip strength prior to and after pMCAO (Lambertsen et al., 2009; Clausen et al., 2014). Mice were excluded if they could not complete the trials with both paws separately and together. A total of four mice were excluded.

Tissue Processing

Fresh Frozen Tissue

Animals were sacrificed by cervical dislocation 1 or 3 days after induction of ischemia. Brains were dissected, frozen in CO_2 snow, and stored at −80°C until further processing. Brains were cut into six parallel series of 30 μm thick sections as previously described (Clausen et al., 2014).

Flow Cytometric Tissue

Mice treated topically with saline, XPro1595, or etanercept were sacrificed 1 or 3 days after pMCAO or 3 days after sham surgery. All mice were given an overdose of pentobarbital

(200 mg/ml) containing lidocaine hydrochloride (20 mg/ml) (Glostrup Apotek, Glostrup, Denmark) and perfused through the left ventricle with phosphate buffered saline (PBS, pH 7.4). Ipsilateral and contralateral cortices were dissected and placed in Hanks' balanced salt solution (HBSS) containing 10% fetal bovine serum (FBS). Lymph nodes were collected for positive detection of T cells. A pool of cells collected from ipsilateral cortices was used for fluorescence minus one (FMO), and isotype controls and a contralateral pool with cells from lymph nodes for compensation. Live/dead cell staining was performed using eBioscience Fixable Viability Dye eFluor 506 (Thermo Fisher Scientific, Roskilde, Denmark).

The tissue was mechanically dissociated using 70 μm cell strainers (BD Biosciences) as previously described (Madsen et al., 2016). Samples were washed with FACS buffer containing HBSS, 2% FBS, and 0.1% sodium azide, fixed with BD Cytofix/Cytoperm (BD Biosciences) and blocked for non-specific binding using 50 μg/ml Syrian Hamster Gamma Globulin (Trichem) and Mouse BD Fc Block (BD Biosciences) diluted in FACS buffer. For detection of microglia and leukocytes, cells were incubated with CD45-PerCP-Cy5.5 (clone 30-F11) and CD11b-PE (clone M7/70).

For separation of macrophages and granulocytes, the following antibodies were used: Ly6C-PE-Cy7 (clone AL21) and Ly6G-BV421 (clone 1A8). T cells were detected with CD3-APC (clone 145-2C11). Respective isotype controls were: IgG2b-PerCP-Cy5.5 (clone A95-1), IgG2b-PE (clone A95-1), IgM-PE-Cy7 (clone R4-22), IgG2a-BV421 (clone R35-95), and IgG1κ-APC (clone A19-3). All antibodies were from BD Biosciences. Flow cytometry was performed as previously described using FACSVerse (BD Biosciences) and analyzed by FACSuite software (Clausen et al., 2014). Positive staining for $CD45^{dim}CD11b^{+}$ microglia, $CD45^{high}CD11b^{+}LY6C^{+}Ly6G^{-}$ macrophages, $CD45^{+}CD3^{+}$ T cells, and $CD45^{high}CD11b^{+}Ly6C^{+}Ly6G^{+}$ granulocytes was determined based on FMO controls and intensity of the respective isotype control as previously described (Clausen et al., 2016a; Madsen et al., 2016). A total of 1,000,000 events were collected using side scatter (SSC). The mean fluorescence intensity (MFI) was calculated as the geometric mean of each population.

Infarct Volumetric and Rostrocaudal Distribution Analysis

Every sixth section was stained with Toluidine blue, and infarct volume was estimated based on Cavalieri's principle for volume estimation as previously described (Gregersen et al., 2000; Lambertsen et al., 2009). The rostrocaudal distribution of the infarct was estimated 3,600 μm anterior of the anterior commissure to 3,600 μm posterior of the anterior commissure as previously described (Clausen et al., 2016a; Madsen et al., 2016).

Real-Time Polymerase Chain Reaction (RT-PCR)

One series of brain tissue was used for RT-PCR. The RNA was extracted using the TRIzol (Invitrogen) method as previously described (Meldgaard et al., 2006). Purity of RNA was controlled spectrophotometrically with 260/280 and 230/260 values using NanoDrop (Thermo Fisher Scientific). Degradation of RNA was measured by RNA integrity factor (RIN) using Agilent 2100 Bioanalyzer (Agilent Genomics). Samples were used for PCR if they had a RIN factor of 7.6 or above. RNA was reverse transcribed into complementary DNA (cDNA) according to the High-Capacity cDNA Reverse Transcription kit protocol (Applied Biosystems). PCR was performed according to the Maxima SYBR Green/ROX qPCR Master Mix (2X) (Thermo Fisher Scientific) protocol. Primer sequences used for RT-PCR (**Table 1**) were designed to target exon-exon junctions whenever possible. Primers were ordered from TAG Copenhagen. Values were normalized to hypoxanthine phosphoribosyltransferase 1 (HPRT1) mRNA, and relative values were calculated relative to a calibrator pool of unmanipulated mice as previously described (Meldgaard et al., 2006).

Cytokine and Receptor Protein Expression and Drug Concentration Analysis

One series of brain tissue was lysed in Complete Mesoscale buffer according to the manufacturer's protocol (Mesoscale Discovery, Rockville, MD, United States). Protein concentrations were determined according to the protocol from Micro BCA protein

TABLE 1 | Primer sequences for RT-PCR.

Gene	Primer sequence	Product length
CD11b	F: 5′ cggaaagtagtgagagaactgtttc 3′	114 bp
	R: 5′ cttataatccaagggatcaccgaattt 3′	
CX3CR1	F: 5′ cctgcctctgagaaatggag 3′	332 bp
	R: 5′ atctctccagcccctgaaat 3′	
	F: 5′ cagcatcgaccggtacctt 3′	65 bp
	R: 5′ gctgcactgtccggttgtt 3′	
Arg1	Mm00475988_m1 from Life technologies	65 bp
CCL2	F: 5′ ccccactcacctgctgctac 3′	86 bp
	R: 5′ cctgctgctggtgattctctt 3′	
CXCL10	F: 5′ gccgtcatttttctgcctcatcct 3′	113 bp
	R: 5′ ctcattctcactggcccgtcatc 3′	
CXCL1	F: 5′ catggctgggattcacctcaag 3′	113 bp
	R: 5′ ggcaagcctcgcgaccattct 3′	
TREM2	F: 5′ cagccctgtcccaagccctcaac 3′	134 bp
	R: 5′ ctcctcacccagctgccgacacc 3′	
P2RY12	F: 5′ tctttgctgggctcatcacgaa 3′	167 bp
	R: 5′ aggcccggctcccagtttag 3′	
iNOS	F: 5′ ggacagcacagaatgttccagaa 3′	104 bp
	R: 5′ caaaatctctccactgccccag 3′	
IL-1β	F: 5′ tgtaatgaaagacggcacac 3′	68 bp
	R: 5′ tcttctttgggtattgcttgg 3′	
TNFR1	F: 5′ gcccgaagtctactccatcatttg 3′	91 bp
	R: 5′ ggctggggaggggctggagttag 3′	
TNFR2	F: 5′ gcccagccaaactccaagcatc 3′	133 bp
	R: 5′ tcctaacatcagcagacccagtg 3′	
HPRT1	F′: 5′-aagcagtacagccccaaaatg-3′	
	R′: 5′-aaatccaacaaagtctggcctgta-3′	

F, forward; R, reverse.

assay kit (Thermo Fischer Scientific). Cytokine and chemokine concentrations were estimated using an MSD Mouse Pro-Inflammatory V-Plex Plus Kit (Mesoscale Discovery) and TNF receptor concentrations using the Mouse TNF-RI and TNFR-II Ultra-Sensitive Kits (Mesoscale Discovery). XPro1595 levels were measured in ischemic brain tissue lysates using a human TNF V-Plex immunoassay (Mesoscale Discovery) as previously described (Karamita et al., 2017). The standard in the kit was replaced with XPro1595, which was diluted in the kit diluent number 2. Etanercept levels were measured using a human TNFRII Ultra-Sensitive immunoassay (Mesoscale Discovery) (Karamita et al., 2017). The standard in the kit was replaced with etanercept diluted in the kit diluent number 2. All kits were read on a SECTOR Imager 6000 plate reader (Mesoscale Discovery) according to the manufacturer's instructions. All samples were run in duplex, and coefficient of variation (CV) values below 25% were accepted.

Characterization of Cells From Mice With Genetic Ablation of SolTNF

Cell Purification for Proteomics

Microglia and neurons were purified from cortices from adult (8 weeks) tmTNF$^{\Delta/\Delta}$ and tmTNF$^{wt/wt}$ mice by MACS affinity-based cell sorting (Miltenyi Biotech, Bergisch-Gladbach, Germany) as previously described (Clausen et al., 2016b). Mice were sacrificed by cervical dislocation, cortices dissociated with Neuronal dissociation papain kit (P) (Miltenyi Biotech) and microglia and neurons purified according to the manufacturer's protocol. The cell suspensions were incubated with monoclonal CD11b beads (Miltenyi Biotech) and applied to LS magnetic separation columns (Miltenyi Biotech) attached to a magnetic field for positive selection of microglia. The flow through was further incubated with Neuron Isolation Kit (Miltenyi Biotech) and applied to LD magnetic separation columns (Miltenyi Biotech) for negative selection of neurons. The cell pellets were stored at −80°C until preparation for mass spectrometry.

Sample Preparation/Digestion for Mass Spectrometry

Microglia and neurons were prepared using a filter-aided sample preparation protein digestion protocol essentially according to Kruse Meyer et al. (2015). Briefly, samples were lysed in cold lysis buffer (5% sodium deoxycholate, 50 mM triethylammonium bicarbonate, pH 8.5) and homogenized by bead beating (Bullet Blender Gold (NextAdvance, United States); 0.9–2.0 mm steel bead blend; Setting 10; 2 × 5 min; +4°C) and heat-denaturized at 95°C for 5 min. Protein concentrations were estimated using a NanoDrop 1000 UV-Vis spectrophotometer (Thermo Fisher Scientific) using bovine serum albumin as reference standard. Protein lysate was transferred to a 10 kDa molecular weight cutoff spin-filter (Millipore, Billerica, MA, United States) and protein disulfide bonds were reduced with 10 mM tris(2-carboxyethyl)phosphine (Thermo Fisher Scientific) for 30 min. Afterward, cysteine residues were blocked with 50 mM chloroacetamide (Sigma-Aldrich, St. Louis, MO, United States) for 30 min in the dark. Protein digestion was performed with sequencing grade modified trypsin (Promega, Madison, WI, United States) at an enzyme to substrate ratio of 1:50 (w/w) for 16 h at 37°C. The peptide material was eluted from the spin-filter, acidified with trifluoroacetic acid to a final concentration of 1% and purified by phase inversions with ethyl acetate 1:2 (v/v). The peptide rich aqueous phase was dried down in a vacuum centrifuge.

UPLC-MS/MS Sample Analysis

Ultra-performance liquid chromatography-tandem mass spectrometry (UPLC-MS/MS) analysis was performed using an UltiMate 3000 UPLC system (Thermo Fisher Scientific) coupled online to a Q Exactive HF mass spectrometer (Thermo Fisher Scientific). Peptide material was separated on a 75 cm C18 Acclaim PepMap100 analytical column (Thermo Fisher Scientific) with 96% solvent A (0.1% FA) and 4% solvent B (0.1% FA in acetonitrile), which was increased to 30% solvent B on a 60 min ramp gradient at a constant flow rate of 250 nL/min. Eluting peptides were introduced directly into the mass spectrometer by a picotip emitter for electrospray ionization (New Objective, Woburn, MA, United States).

The mass spectrometer was operated in positive mode using a data-dependent TOP12 acquisition method with the following settings: mass range m/z 400–1200; isolation window m/z 1.6; NCE 27; charge state exclusion: unassigned, 1, >6; peptide match preferred; dynamic exclusion 30 s.

Protein Quantification and Filtering

The .RAW files were investigated by Progenesis QI for Proteomics to access the chromatographic quality. The raw data were searched with two complementary label free quantitative approaches: MaxQuant (v1.5.6.0) against the UniProt Mouse reference proteome database with isoforms (UP000000589, November 2016). Standard settings were employed in MaxQuant, including max two tryptic missed cleavages, and a first search with 20 ppm mass tolerance followed by data calibration and a main search with 4.5 ppm mass tolerance. The match between runs feature was enabled to allow the transfer of identified precursors between different runs, based on accurate mass and retention time. The following peptide modifications were found to be abundant with the applied protocol and were included in the search: carbamidomethylated cysteine residues (fixed), acetylation of the N-terminal of proteins (variable), oxidation of methionine (variable). Identified proteins and peptide spectral matches were filtered to <1% false discovery rate (FDR) using a forward/reverse database search strategy in MaxQuant, and proteins tagged as common contaminants were removed. Relative protein quantities were calculated by summing the unique peptide peak areas of each protein in MaxQuant using the LFQ (label-free quantitation) feature. Additional filtering steps were employed in Perseus (v1.5.6.0): (1) The quantitation of any protein was required to be based on at least two unique peptides. (2) Unique peptides were required to be quantifiable in at least three of the tmTNF$^{wt/wt}$ or tmTNF$^{\Delta/\Delta}$ samples. (3) Pearson's correlation coefficients (R) between the technical repeats should be greater than 0.95, based on log2 transformed protein LFQ values.

Data Processing

All abundances were log2-transformed and proteins with less than two unique peptides and (>50% missing values) filtered out. Proteins with a statistically significant mean abundance difference between the $tmTNF^{wt/wt}$ and $tmTNF^{\Delta/\Delta}$ samples were identified by independent two-sample t-tests in Perseus, with permutation-based truncation using standard parameters (s0 = 0.1, 250 randomizations) to correct for multiple hypothesis testing. In this way, the p-value requirement was adjusted to expect <5% false positives among the statistically significant findings.

The MS data has been deposited to the ProteomeXchange Consortium[1] via the PRIDE partner repository with dataset identifiers PXD014440. Protein-protein interaction analysis was performed by STRING[2].

Phagocytosis Assay

In order to test phagocytic activity of primary microglia derived from $tmTNF^{wt/wt}$ and $tmTNF^{\Delta/\Delta}$ mice, the microglia were plated, activated and incubated with fluorescent beads. As a measure of phagocytic activity, the number of engulfed beads was counted and morphological changes estimated as previously described (Al-Ali et al., 2017; Gao et al., 2017). Microglial cultures were prepared using brain tissue from $tmTNF^{\Delta/\Delta}$ (n = 3) and $tmTNF^{wt/wt}$ (n = 6) pups at post-natal age 5–7. The meninges and blood vessels were removed, and brains collected in ice-cold HBSS without Ca^{2+} and Mg^{2+} (Thermo Fisher Scientific) under sterile conditions. Cortices were processed using Neural Tissue Dissociation Kit (P) (Miltenyi Biotech) according to the manufacturer's protocol. Cell suspensions were filtered through 70 μm cell strainers (BD Biosciences, San Jose, CA, United States) and washed with HBSS with Ca^{2+} and Mg^{2+} (Thermo Fisher Scientific). Cell suspensions were centrifuged, and the pellet used for MACS sorting. Microglia were purified by MACS sorting using magnetic $CD11b^{+}$ beads on LS columns (Miltenyi Biotech) and cultured in culture medium A (76 % Dulbecco's modified Eagle's medium (DMEM) (Thermo Fisher Scientific), 20% FBS (Thermo Fisher Scientific), 1% minimum essential media (MEM) (Thermo Fisher Scientific), 1% penicillin streptomycin (Thermo Fisher Scientific), 1% Glutamax™ (Gibco, Thermo Fisher Scientific), 1% pyruvate (Thermo Fisher Scientific)) on poly-L-ornithine-coated plates in a humified CO_2 incubator at 37°C. After 3 days half of the media was changed to culture medium B (86% DMEM, 10% FBS, 1% MEM, 1% penicillin streptomycin, 1% Glutamax™, 1% pyruvate). Four days after the media change microglia were activated by adding 100 ng/mL LPS (Invitrogen, Thermo Fisher Scientific) for 24 h. After activation, FluoSpheres™ Carboxylate-Modified Microspheres (1.0 μm, 505/515, yellow-green fluorescent) (Thermo Fisher Scientific) were added onto the cultured cells. After 2 h phagocytosis was terminated by adding cold culture medium B. Cells were fixed with 4% paraformaldehyde, blocked in 5% normal goat serum in tris-buffered saline and incubated overnight in anti-Iba1 antibody (1:500, Fujifilm Wako Pure Chemical Corporation, Japan). The next day, cells were stained using alexa 594-conjugated anti-rabbit antibody (1:750, Alexa594 Molecular Probes) (Thermo Fisher Scientific) and 4′,6-diamidino-2-phenylindol (DAPI) (Thermo Fisher Scientific). Pictures were taken using a FV1000 (Olympus) confocal microscope from nine randomly chosen positions per coverslip. Analysis of phagocytosis measured as engulfed beads/cell and cell morphology measured as cell area, membrane irregularity and perimeter length was done by automated counting software Puntomorph[3] (Al-Ali et al., 2017).

Statistical Analysis

Data are presented as mean ± SEM. Statistical comparison between the three groups (saline, Xpro1595, and etanercept) was assessed by one-way ANOVA followed by Tukey's *post hoc* test (GraphPad Prism Software Inc., San Diego, CA, United States). Comparison of the rostrocaudal distribution of the infarct and comparison of phagocytosis in $tmTNF^{\Delta/\Delta}$ and $tmTNF^{wt/wt}$ microglia were tested by two-way ANOVA followed by Tukey's *post hoc* test. Statistical significance of the asymmetry of the paws in the grip strength test and the Hargreaves nociception test was tested by Student's paired *t*-test. Normal distribution of variables was tested using both Brown-Forsythe and Bartlett's tests. Significance was set at $p \leq 0.05$.

RESULTS

Topical Delivery of XPro1595 Decreases Infarct Volume 1 and 3 Days After pMCAO

Infarct volumes were estimated in Toluidine blue-stained brain sections from mice treated topically or i.c.v. with saline, XPro1595, or etanercept and allowed to survive 1 or 3 days after pMCAO (**Figure 1** and **Supplementary Figure 1A**). At day 1, infarct volumes were significantly reduced in mice treated topically with XPro1595 compared to mice treated topically with saline (**Figure 1B**). Etanercept treatment showed no effect. The rostrocaudal distribution of the infarcts was comparable between groups (**Figure 1C**). At day 3, infarct volumes were also significantly reduced in mice treated topically with XPro1595 (**Figure 1E**). Again, the rostrocaudal distribution of the infarct was comparable between groups (**Figure 1F**).

Intracerebroventricular administration of XPro1595 or etanercept was not effective in decreasing infarct size (**Supplementary Figure 1A**). In support of this, we observed no difference in functional outcomes as assessed by the Hargreaves thermal hyperalgesia (**Supplementary Figure 1B**) or grip strength tests (**Supplementary Figures 1C,D**), except for a total

[1]http://proteomecentral.proteomexchange.org

[2]http://string-db.org

[3]https://github.com/HA-Lab/PuntoMorph

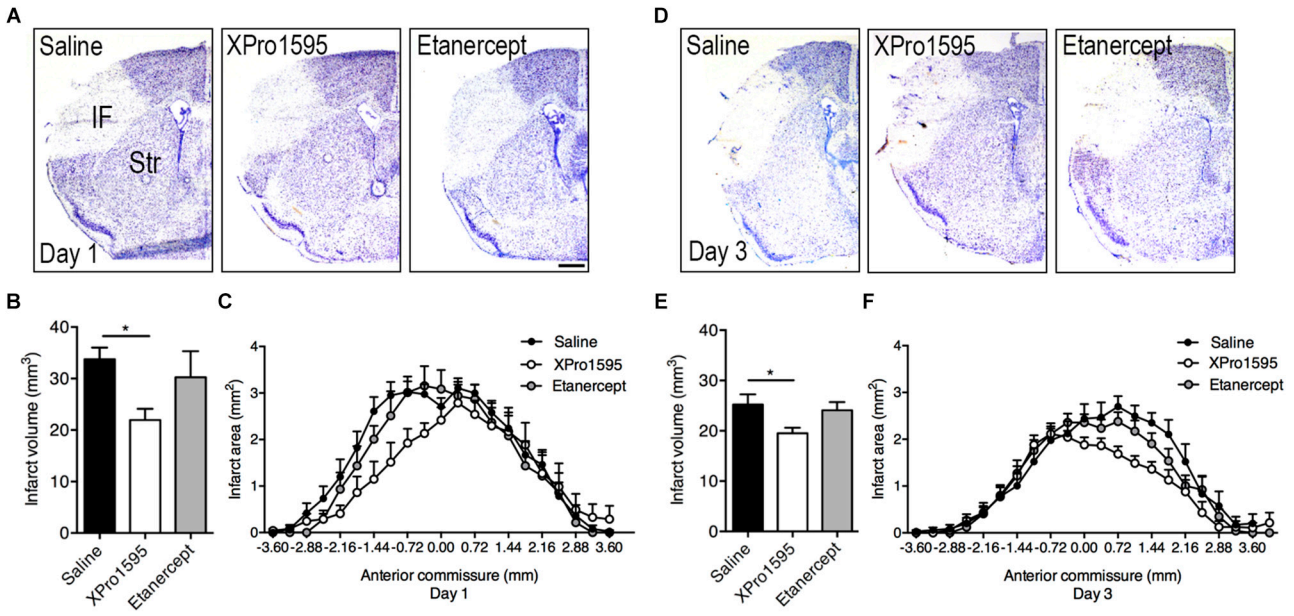

FIGURE 1 | Infarct volume and rostrocaudal distribution after topical administration of TNF inhibitors. **(A)** Toluidine blue-stained brain sections of mice treated topically with saline, XPro1595, or etanercept and allowed to survive 1 day after pMCAO. Scalebar 500 μm. **(B)** Infarct volume estimation 1 day after pMCAO. N(saline) = 11; n(XPro1595) = 6; n(etanercept) = 4. **(C)** Rostrocaudal distribution of the infarct 1 day after pMCAO. **(D)** Toluidine blue-stained brain sections of mice treated topically with saline, XPro1595, or etanercept and allowed to survive 3 days after pMCAO. **(E)** Infarct volume estimation 3 days after pMCAO. N(saline) = 12; n(XPro1595) = 15; n(etanercept) = 17. **(F)** Rostrocaudal distribution of the infarct 3 days after pMCAO. *$p \leq 0.05$, one-way ANOVA followed by Tukey's *post hoc* test.

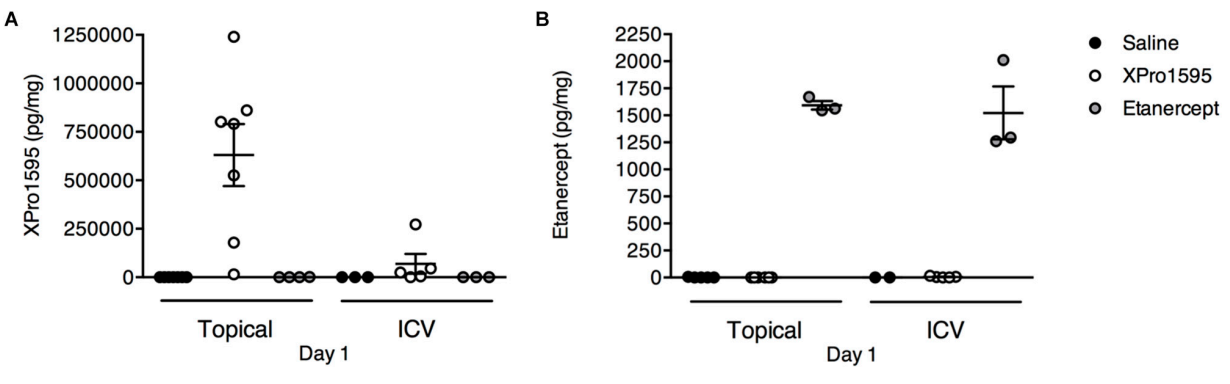

FIGURE 2 | Detection of TNF inhibitors in ischemic brain tissue 24 h after pMCAO. **(A)** Concentration of XPro1595 in brain tissue after topical and i.c.v. administration. *N* = 4–7/group (excluded due to too high CV values: saline pump, *n* = 4; saline i.c.v., *n* = 2). **(B)** Concentration of etanercept in brain tissue after topical and i.c.v. administration. *N* = 2–6/group (excluded due to too high CV values: saline i.c.v., *n* = 2; XPro1595 i.c.v., *n* = 1).

weaker grip strength on day 3 compared to baseline in mice treated with etanercept (**Supplementary Figure 1D**).

XPro1595 and Etanercept Can Be Detected in Brain Ischemic Tissue

To validate the presence of XPro1595 and etanercept and estimate their concentrations in the ischemic brain following topical and i.c.v. delivery, we measured the concentration of XPro1595 and etanercept 1 day after pMCAO (**Figures 2A,B**). We found topical administration to be an efficient method to deliver a high concentration of XPro1595 to neural tissue (**Figure 2A**). After topical administration, the concentration of XPro1595 in brain tissue 1 day after pMCAO was 630,300 ± 160,000 pg/mg. The concentration of XPro1595 was lower after i.c.v. administration, with a mean of 69,400 ± 51,300 pg/mg (**Figure 2A**). This concentration in the neural tissue is, however, sufficient to neutralize solTNF and to promote neuroprotection, based on previous publications in an animal model of Alzheimer's disease (MacPherson et al., 2017).

Etanercept was detected in the brain tissue after both delivery routes (**Figure 2B**). The concentration of etanercept in brain tissue 1 day after pMCAO was 1,600 pg/mg after topical administration and 1,500 ± 200 pg/mg after i.c.v.

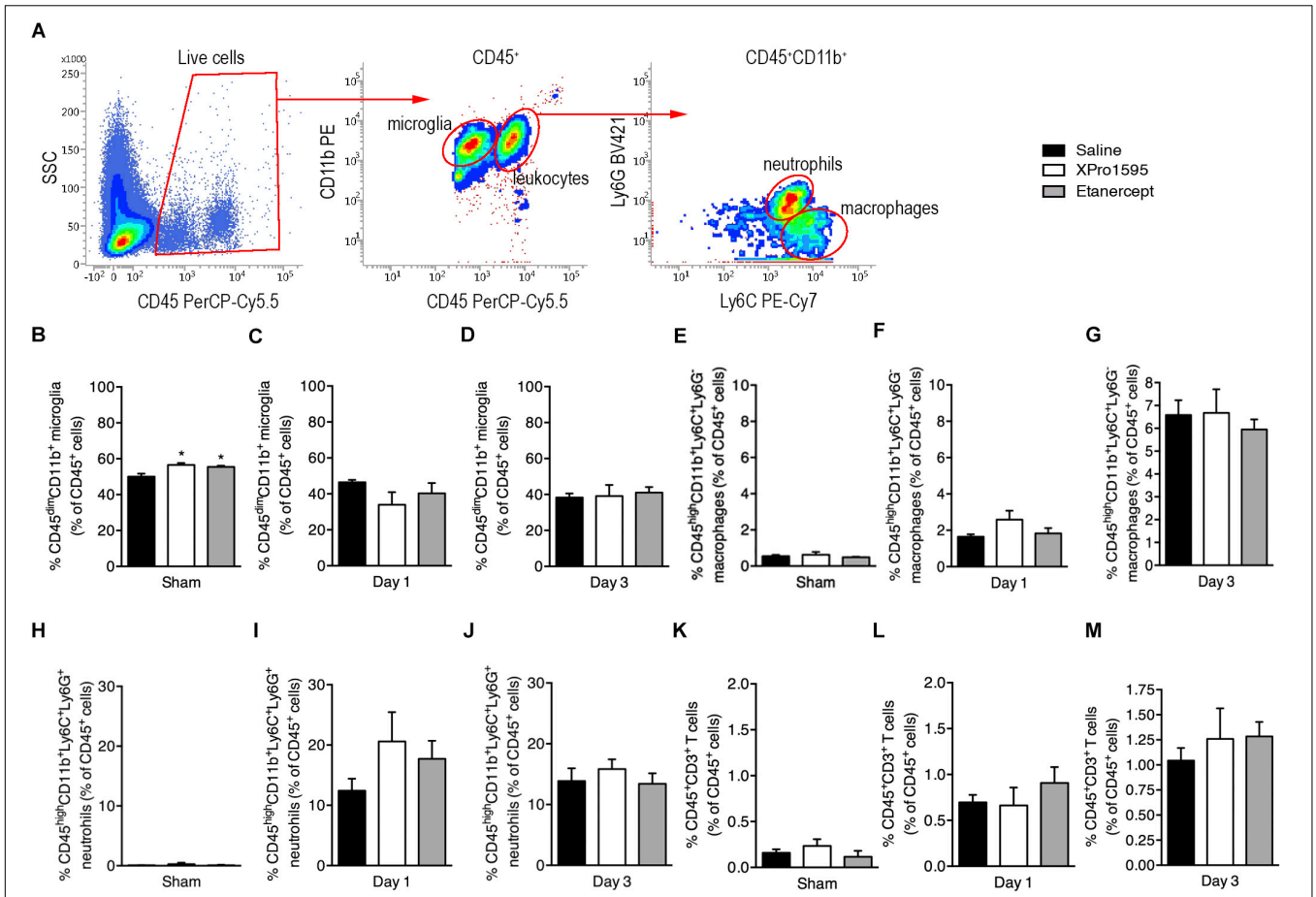

FIGURE 3 | Flow cytometric analysis of ipsilateral hemispheres in sham and pMCAO mice after topical saline, XPro1595, or etanercept treatment**. (A)** Gating strategy for CD45$^+$ cells, CD45^{dim}CD11b$^+$ microglia, CD45^{high}CD11b$^+$ leukocytes, CD45^{high}CD11b$^+$Ly6C$^+$Ly6G$^-$ macrophages, and CD45^{high}CD11b$^+$Ly6C$^+$Ly6G$^+$ granulocytes. **(B–D)** Changes in CD45^{dim}CD11b$^+$ microglia presented as % of CD45$^+$ cells 3 days after sham surgery or 1 or 3 days after pMCAO. **(E–G)** Changes in CD45^{high}CD11b$^+$Ly6C$^+$Ly6G$^-$ macrophages presented as % of CD45$^+$ cells after sham surgery or 1 or 3 days after pMCAO. **(H–J)** Changes in CD45^{high}CD11b$^+$Ly6C$^+$Ly6G$^+$ granulocytes presented as % of CD45$^+$ cells after sham surgery or 1 or 3 days after pMCAO. **(K–M)** Changes in CD3$^+$ T cells presented as % of CD45$^+$ cells after sham surgery or 1 or 3 days after pMCAO. N(sham) = 3–5/group; n(day 1) = 4–5/group; n(day 3) = 5/group; *$p \leq 0.05$; one-way ANOVA followed by Tukey's *post hoc* test.

administration. This demonstrated that both XPro1595 and etanercept successfully accessed the ischemic brain tissue.

Topical Treatment With XPro1595 Does Not Affect Microglial and Leukocyte Cell Populations After pMCAO

To investigate potential changes in microglial and leukocyte populations in mice subjected to pMCAO and treated topically with saline, XPro1595 or etanercept, we performed flow cytometry and gated for CD45^{dim}CD11b$^+$ microglia, CD45^{dim}CD11b$^+$Ly6C$^+$Ly6G$^-$ macrophages, CD45^{dim}CD11b$^+$Ly6C$^+$Ly6G$^+$ granulocytes (**Figure 3A**), and CD45$^+$CD3$^+$ T cells.

We found that compared to saline, both Xpro1595 and etanercept treatment increased the percentage of microglia in the ipsilateral cortex 3 days after sham surgery (**Figure 3B**), whereas no difference was observed between groups at day 1 (**Figure 3C**) or day 3 (**Figure 3D**) after pMCAO. In all groups of mice 3 days after pMCAO, the microglial population constituted ∼80% of all live CD45$^+$ cells in the contralateral cortex, with only ∼60% in sham. By 1 day after pMCAO the microglial population constituted ∼60% of all live CD45$^+$ cells (**Supplementary Figures 2A–C**). The percentage of infiltrating macrophages (**Figures 3E–G**), granulocytes (**Figures 3H–J**), and T cells (**Figures 3K–M**) did not differ between groups at any time point investigated, although the percentages of cells increased over time in the ipsilateral cortex (**Figures 3E–M**) and remained relatively constant in the contralateral cortex (**Supplementary Figures 2D–L**).

Since microglia and macrophages upregulate their expression of CD11b and CD45 after ischemia (Ito et al., 2001; Ponomarev et al., 2005; Clausen et al., 2008; Morrison and Filosa, 2013), their activation status was evaluated based on the MFI of these cell surface markers. MFIs of CD11b and CD45 were comparable between treatment groups 3 days after sham surgery

and 1 and 3 days after pMCAO (**Supplementary Figures 3A–L**). However, both microglia and leukocytes seemed to downregulate their expression of CD11b and upregulate their expression of CD45 3 days after pMCAO, which was not the case in sham mice and 1 day after pMCAO (**Supplementary Figures 3A–L**, please compare C to A and B; I to G and H; F to D and E; and L to J and K).

XPro1595 Affects Microglial Activation

We next investigated changes in mRNA expression of selected microglial/macrophage and inflammatory markers in brain tissue derived from mice subjected to pMCAO and treated topically (**Figure 4**) or i.c.v. (**Supplementary Figure 4**) with saline, XPro1595, or etanercept and allowed to survive 1 or 3 days after pMCAO.

We found *Tnf* mRNA expression to be significantly upregulated 1 and 3 days after pMCAO in mice treated topically with XPro1595 when compared to saline- and etanercept-treated mice (**Figure 4A**). *Tnfrsf1a* (TNFR1, **Figure 4B**) and *Tnfrsf1b* (TNFR2, **Figure 4C**) mRNA expression was comparable between treatment groups at both days 1 and 3 after pMCAO. At 3 days, *Il-1beta* mRNA levels were significantly upregulated in mice treated topically with XPro1595 compared to saline- and etanercept-treated mice (**Figure 4D**), whereas no significant changes in *Nos2* (iNOS) mRNA expression was observed between groups, although XPro1595 tended to downregulate the expression at 3 days ($p = 0.08$; **Figure 4E**).

To study whether TNF inhibition using XPro1595 or etanercept affects chemokine gene expression, we measured the mRNA levels of *Cxcl1*, *Cxcl10,* and *Ccl2* at 1 and 3 days after pMCAO. Topical etanercept treatment significantly increased *Cxcl1* mRNA compared to saline and XPro1595 at day 1 and compared to XPro1595 at day 3 after pMCAO (**Figure 4F**). In contrast, *Cxcl10* mRNA levels decreased at day 3 in mice treated topically with etanercept compared to saline (**Figure 4G**), and *Ccl2* mRNA levels significantly increased at day 3 in XPro1595-treated mice compared to both saline- and etanercept-treated mice (**Figure 4H**).

We further measured mRNA expression levels of microglial/macrophage markers *Cx3cr1*, *P2ry12*, *Trem2*, *Cd11b,* and *Arg1*. We found that at days 1 and 3 after pMCAO, topical XPro1595 treatment decreased *Cx3cr1* mRNA expression compared to saline-treated mice (**Figure 4I**). In contrast, *P2ry12* mRNA expression was significantly increased at 1 day after pMCAO in topically XPro1595-treated mice compared to saline-treated mice (**Figure 4J**), as well as *Trem2* mRNA expression at 1 and 3 days after pMCAO (**Figure 4K**). *Cd11b* and *Arg1* mRNA levels were comparable between groups except for a significant decrease in *Arg1* mRNA levels in XPro1595-treated mice at day 3 (**Figures 4L,M**).

Even though i.c.v. administration of TNF inhibitors had no effect on infarct volume or functional outcome, we also investigated potential changes in mRNA expression after i.c.v. injection of XPro1595 or etanercept (**Supplementary Figure 4**). We observed no change in *Tnf*, *Tnfrsf1a*, *Tnfrsf1b*, *Il-1beta*, *Nos2*, *Cxcl1*, *Cx3cr1*, or *CD11b* mRNA expression between groups. Etanercept significantly increased *Cxcl10* mRNA levels compared to saline at day 1 and compared to both XPro1595 and saline 3 days after pMCAO (**Supplementary Figure 4**). Also, *P2ry12* mRNA levels increased significantly at day 1 in etanercept-treated mice compared to saline- and Xpro1595-treated mice, and *Ccl2* and *Trem2* mRNA levels increased significantly at day 3, while *Arg1* decreased significantly.

Cytokine, Chemokine, and TNF Receptor Expression in Brain Tissue 1 and 3 Days After TNF Inhibitor Treatment

To study whether topical (**Figure 5**) or i.c.v. (**Supplementary Figure 5**) XPro1595 and etanercept treatment after pMCAO affected cytokines, TNF receptor and/or chemokine protein levels, we measured TNF, TNFR1, TNFR2, IL-1β, CXCL1, IL-6, IL-10, IL-4, IL-5, and IL-12p70 levels in brain tissue 1 day after pMCAO, when neuroinflammation is maximal (Lambertsen et al., 2012), in addition to 3 days after pMCAO using multiplex ELISA.

We found that despite increased *Tnf* mRNA expression after topical XPro1595 treatment, the protein expression tended to be downregulated in XPro1595-treated mice ($p = 0.06$, **Figure 5A**), whereas TNF levels in etanercept-treated mice were comparable to saline-treated mice 1 day after pMCAO. At 3 days, TNF levels had increased significantly in etanercept-treated mice compared to saline-treated mice. Compared to topical saline treatment, etanercept treatment downregulated TNFR1 levels at day 1, which also showed tendency to be downregulated after XPro1595 treatment ($p = 0.08$), whereas TNFR1 levels were comparable at 3 days (**Figure 5B**). Topical treatment had no effect on expression of TNFR2, IL-1β, Cxcl1, IL-6, IL-10, IL-4, IL-5, or IL-12p70 (**Figures 5C–J**).

Intracerebroventricular administration of TNF inhibitors showed no effect on the TNF or TNFR1 protein expression (**Supplementary Figures 5A,B**) although TNFR2 was downregulated after etanercept-treatment compared to saline treatment 1 day after pMCAO (**Supplementary Figure 5C**). Treatment with XPro1595 showed a tendency toward reducing TNFR2 levels at day 1 after pMCAO ($p = 0.07$) (**Supplementary Figure 5C**). At 1 day after pMCAO, etanercept treatment significantly increased IL-1β levels compared to saline (**Supplementary Figure 5D**), but no effect was observed on CXCL1, IL-6, IL-10, IL-4, IL-5, or IL-12p70 levels (**Supplementary Figures 5E–J**).

tmTNF Microglia Have an Upregulated Expression of Phagocytosis-Related Proteins

In order to investigate the hypothesis that ablation of solTNF improves microglial phagocytosis, we investigated differentially expressed proteins in microglia derived from $tmTNF^{\Delta/\Delta}$ and $tmTNF^{wt/wt}$ mice using mass spectrometry. In total, 1,564 proteins with two or more unique peptides were quantified by label free quantification in microglia cells (**Supplementary Table 1**). Of these, 87 proteins were differentially regulated between $tmTNF^{wt/wt}$ and $tmTNF^{\Delta/\Delta}$ mice (**Figure 6A**). Several of the upregulated proteins, 3-mercaptopyruvate

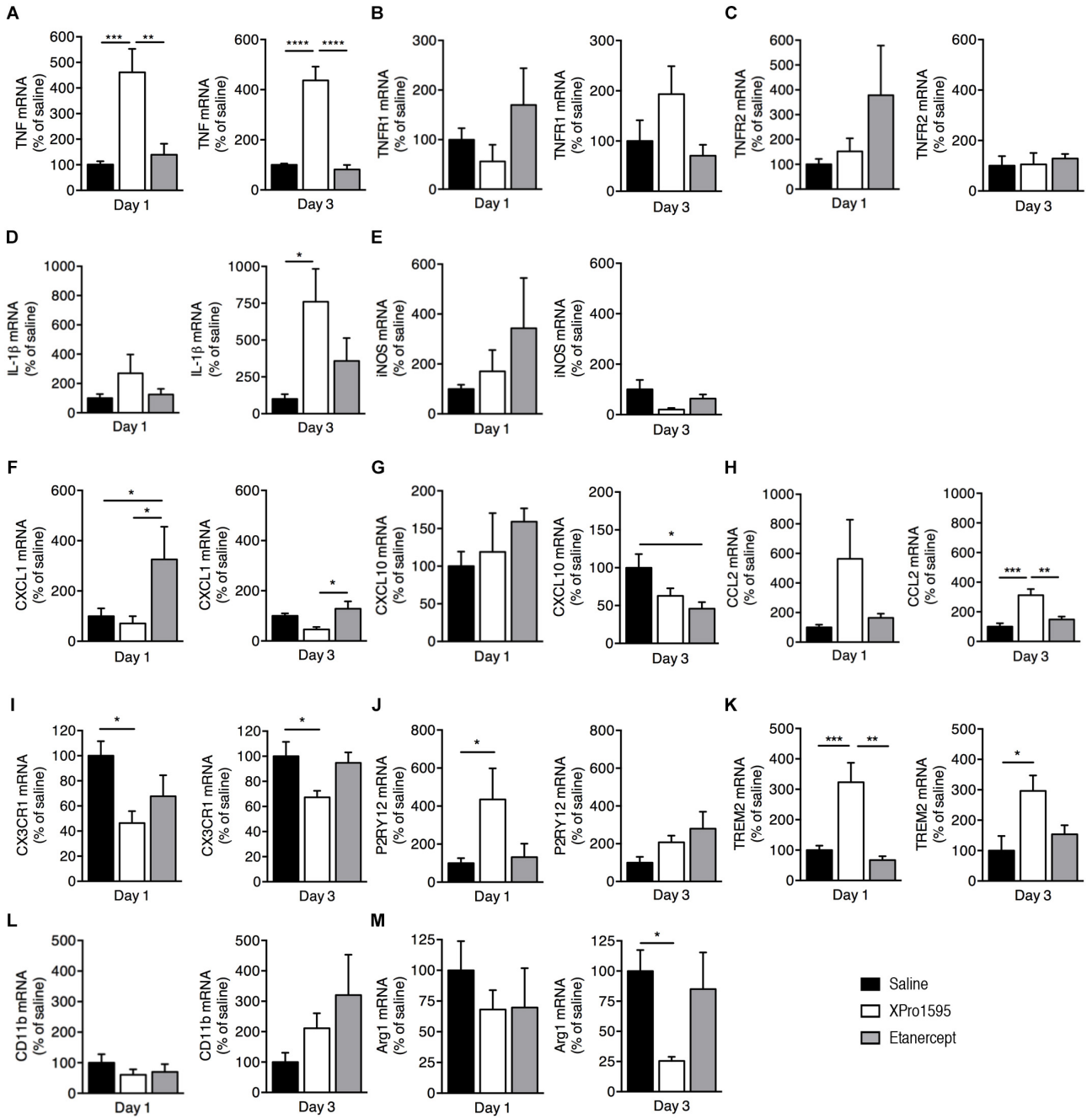

FIGURE 4 | Inflammatory gene profile 1 and 3 days after pMCAO in mice treated topically with saline, XPro1595, or etanercept. mRNA expression of cytokines, pro-inflammatory molecules, chemokines, and microglial markers presented as % of gene expression in saline-treated animals **(A–M). (A)** Expression of *Tnf* mRNA. **(B)** Expression of *Tnfrsf1a* (TNFR1) mRNA. **(C)** Expression of *Tnfrsf1b* (TNFR2) mRNA. **(D)** Expression of *Il1*β mRNA. **(E)** Expression of *Nos2* (iNOS) mRNA. **(F)** Expression of *Cxcl1* mRNA. **(G)** Expression of *Cxcl10* mRNA. **(H)** Expression of *Ccl2* mRNA. **(I)** Expression of *Cx3cr1* mRNA. **(J)** Expression of *P2ry12* mRNA. **(K)** Expression of *Trem2* mRNA. **(L)** Expression of *CD11b* mRNA. **(M)** Expression of *Arg1* mRNA. N(day 1) = 4–11/group, n(day 3) = 5–6/group; $*p \leq 0.05$, $**p \leq 0.01$, $***p \leq 0.001$, $****p \leq 0.0001$; one-way ANOVA followed by Tukey's *post hoc* test.

sulfurtransferase (3-MPST), hematopoietic prostaglandin D synthase (HPGDS) and apoptosis-associated speck-like protein containing a CARD (PYCARD/ASC) are neuroprotective (Liu et al., 2009; Chen et al., 2015; Kimura et al., 2017; Shan et al., 2017) or related to regulation of phagocytosis (Rajakariar et al., 2007; Ippagunta et al., 2011). 3-MPST has previously been shown to be upregulated in activated microglia treated with a neuroprotective compound (Cobourne-Duval et al., 2018). tmTNF expressing microglia had an increased expression of HPGDS, which is known to be expressed in

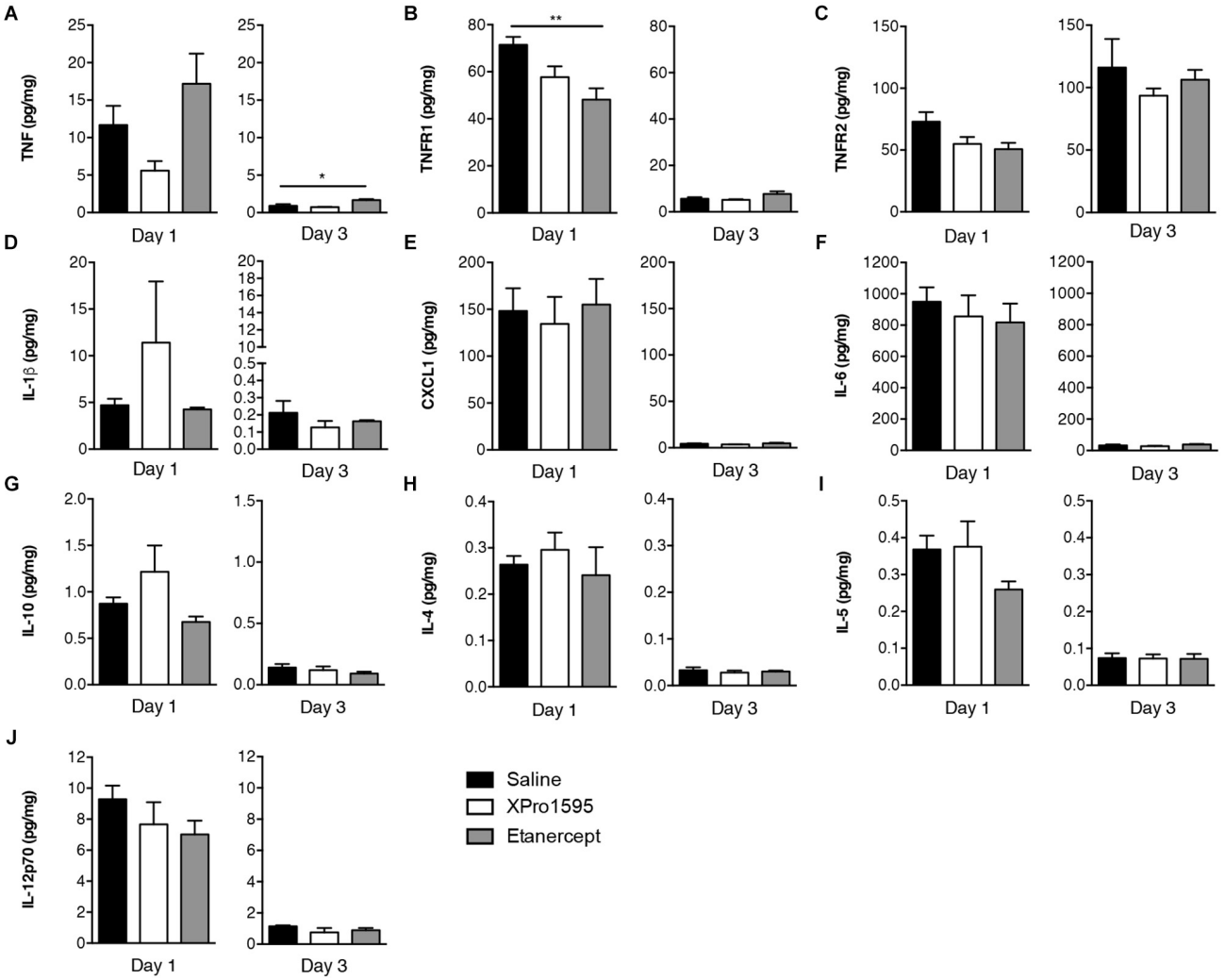

FIGURE 5 | Cytokine and TNF receptor protein expression in brain tissue 1 and 3 days after pMCAO in mice treated topically with saline, XPro1595, or etanercept. **(A)** Expression of TNF (n = 4–11/group). **(B)** Expression of TNFR1 (n = 4–11/group). **(C)** Expression of TNFR2 (n = 4–10/group). **(D)** Expression of IL-1β (n = 3–11/group). **(E)** Expression of CXCL1 (n = 3–11/group). **(F)** Expression of IL-6 (n = 3–9/group). **(G)** Expression of IL-10 (n = 3–10/group). **(H)** Expression of IL-4 (n = 2–11/group). **(I)** Expression of IL-5 (n = 4–10/group). **(J)** Expression of IL-12p70 (n = 4–11/group). $^{**}p \leq 0.01$; one-way ANOVA with Tukey's *post hoc* test.

activated microglia in the core of the infarct after ischemic stroke and to enhance their differentiation into a phagocytic phenotype (Mohri et al., 2003; Liu et al., 2007). PYCARD/ASC supports the function of a normal immune system (Ippagunta et al., 2011). Among the downregulated proteins was MPO. Interestingly, upregulation of myeloperoxidase (MPO) expression is linked to pathological phagocytosis of myelin leading to demyelination in patients with multiple sclerosis (Minohara et al., 2006; Gray et al., 2008). Moreover, the expression of Methyl-CpG-binding protein 2 (MECP2) (Cronk et al., 2015) was downregulated in tmTNF expressing microglia. The absence of microglial MECP2 has shown to increase *Tnf* mRNA expression (Cronk et al., 2015). Interestingly, tmTNF expressing microglia had downregulated expression of Histone H1.5, which promotes microglial proinflammatory functions (Gilthorpe et al., 2013), Heat shock protein 27, which is neuroprotective in ischemic brain (Stetler et al., 2012) and Heat shock 70 kDa protein 1, which functions as a chaperone (Stetler et al., 2010) supporting earlier studies showing solTNF to be needed for optimal control of inflammatory response (Ruuls et al., 2001; Musicki et al., 2006; Dambuza et al., 2011; DeBerge et al., 2014). Downregulation of Human growth and transformation-dependent protein (HGTD-P), a protein which is proapoptotic in ischemia (Qu et al., 2009), and downregulation of Vimentin, which has been shown to mediate microglial activation (Jiang et al., 2012), supports the beneficial function of tmTNF. Two other histones, Histone H4 and Core histone macro-H2A.1 were downregulated in tmTNF expressing microglia. String analysis of the differentially regulated proteins in microglia showed clustering of the aforementioned immune system-related proteins Histone H1.5, Heat shock protein 27,

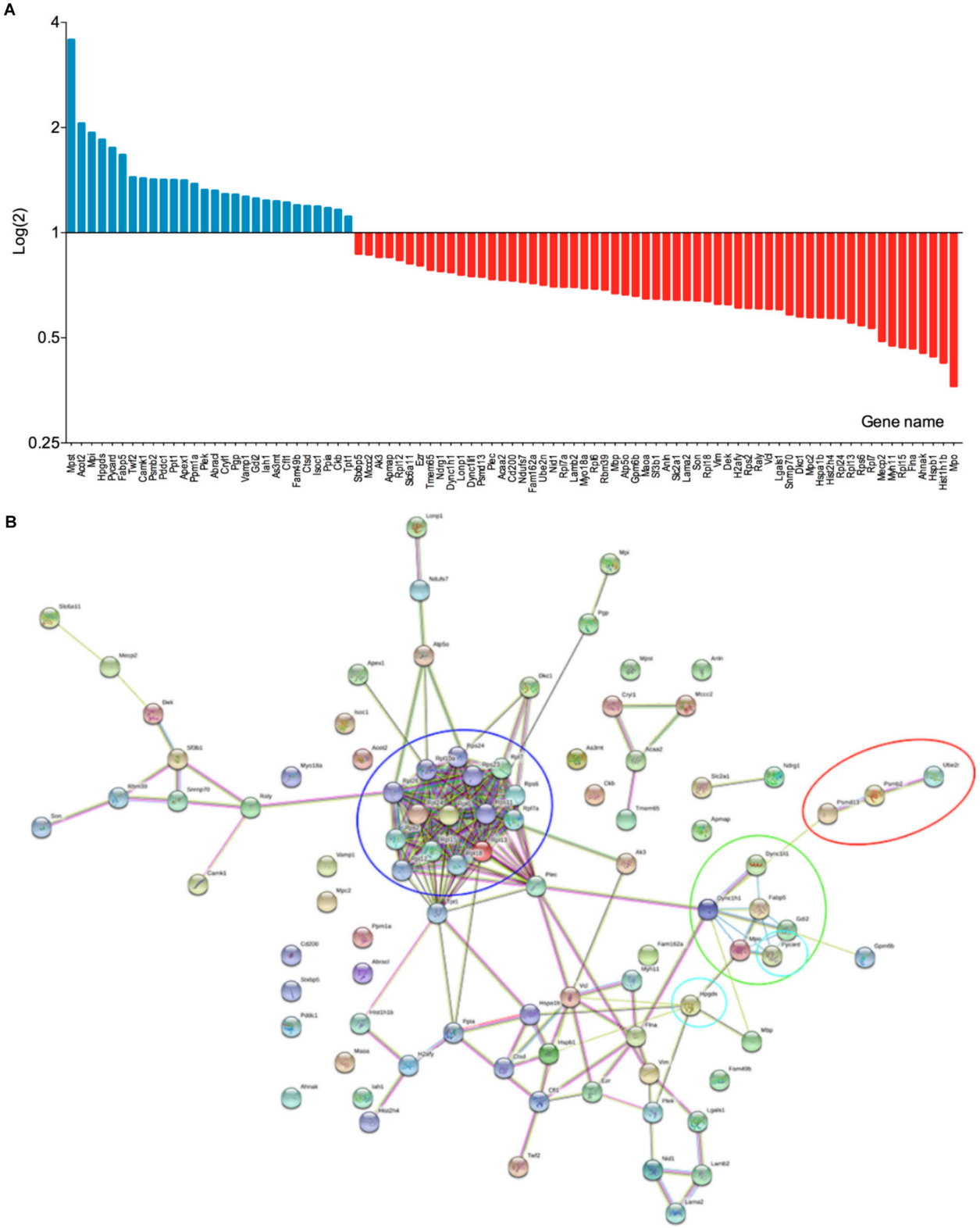

FIGURE 6 | Proteome analysis of primary microglia from tmTNF$^{wt/wt}$ and tmTNF$^{\Delta/\Delta}$ mice. **(A)** Differentially expressed proteins in tmTNF$^{wt/wt}$ and tmTNF$^{\Delta/\Delta}$ microglia (n = 4/group). **(B)** String analysis of differentially expressed proteins in tmTNF$^{wt/wt}$ and tmTNF$^{\Delta/\Delta}$ microglia. Red circle, FCERI-mediated NF-kappa B activation; blue circle, ribosomal proteins; green circle, neutrophil degranulation; turquoise circles, proteins related to phagocytosis.

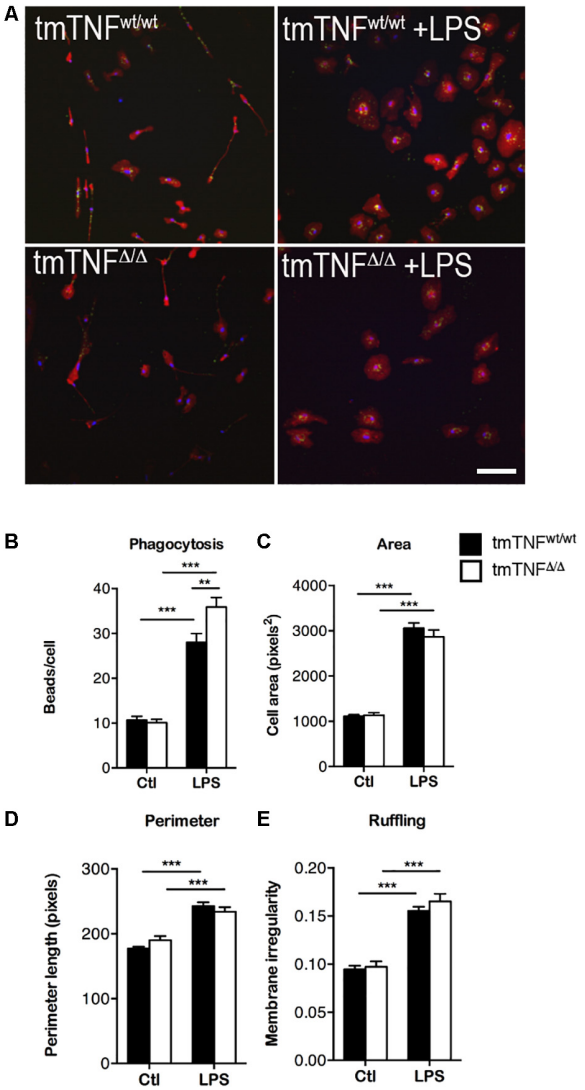

FIGURE 7 | Microglia from tmTNF$^{\Delta/\Delta}$ mice have increased phagocytic activity after LPS activation. **(A)** Primary microglia cultures stained for Iba1 (red) and DAPI (blue) demonstrating phagocytosis of FluoSpheres Carboxylate-Modified Microspheres (green). Staining of tmTNF$^{wt/wt}$ microglia (upper left), tmTNF$^{wt/wt}$ + LPS (upper right), tmTNF$^{\Delta/\Delta}$ (lower left), tmTNF$^{\Delta/\Delta}$ + LPS (lower right). Scalebar = 100μm. **(B)** Engulfed beads/cell in tmTNF$^{wt/wt}$ and tmTNF$^{\Delta/\Delta}$ microglia. N(tmTNF$^{wt/wt}$) = 426 cells/25 FOV, n(tmTNF$^{wt/wt}$ + LPS) = 282 cells/17 FOV, n(tmTNF$^{\Delta/\Delta}$) = 169 cells/20 FOV, n(tmTNF$^{\Delta/\Delta}$ + LPS) = 137 cells/20 FOV. [Two-way ANOVA: treatment $^{***}p < 0.001$, $F_{(1, 78)} = 6.03$; genotype $^{*}p < 0.05$, $F_{(1, 78)} = 210.1$; interaction $^{**}p < 0.01$ $F_{(1, 78)} = 8.05$]. **(C–E)** Morphological features of microglia before and after LPS activation. **(C)** Area. [Two-way ANOVA: treatment $^{***}p < 0.001$, $F_{(1, 78)} = 373.3$]. **(D)** Perimeter. [Two-way ANOVA: treatment $^{***}p < 0.001$, $F_{(1, 78)} = 96.08$]. **(E)** Ruffling. [Two-way ANOVA: treatment $^{***}p < 0.001$, $F_{(1, 78)} = 132.5$]. For C-E, N(tmTNF$^{wt/wt}$) = 426 cells/25 FOV, n(tmTNF$^{wt/wt}$ + LPS) = 282 cells/17 FOV, n(tmTNF$^{\Delta/\Delta}$) = 169 cells/20 FOV, n(tmTNF$^{\Delta/\Delta}$ + LPS) = 137 cells/20 FOV. LPS, lipopolysaccharide; FOV, field of view.

Methyl-CpG-binding protein 2, Heat shock 70 kDa protein, Core histone macro-H2A.1, Vimentin, HPGDS, and Histone H4 (**Figure 6B**).

Microglia Expressing Only tmTNF Display Improved Phagocytic Properties

Due to the upregulated expression of phagocytosis-related proteins in microglia expressing only tmTNF, we next investigated the phagocytic properties and morphological changes 1 day after LPS stimulation in primary microglia derived from 5 to 7 days old tmTNF$^{\Delta/\Delta}$ and tmTNF$^{wt/wt}$ pups (**Figure 7A**). Phagocytosing microglia have a neuroprotective role in clearing apoptotic cells and debris after stroke (Neumann et al., 2009; Sierra et al., 2013). At 1 day after LPS stimulation, the phagocytic activity of microglia derived from tmTNF$^{\Delta/\Delta}$ pups was significantly increased compared to microglia derived from tmTNF$^{wt/wt}$ pups, measured as engulfed beads per cell (**Figure 7B**). Cell area (**Figure 7C**), perimeter length (**Figure 7D**), and membrane irregularity (**Figure 7E**) increased significantly after LPS activation in both tmTNF$^{wt/wt}$ and tmTNF$^{\Delta/\Delta}$ microglia indicating both tmTNF$^{wt/wt}$ and tmTNF$^{\Delta/\Delta}$ microglia to take an amoeboid form after LPS activation. Cell morphology was, however, comparable between tmTNF$^{wt/wt}$ and tmTNF$^{\Delta/\Delta}$ microglia after LPS activation (**Figures 7A,C–E**).

Proteomic Characterization of Neurons Derived From tmTNF$^{\Delta/\Delta}$ and tmTNF$^{wt/wt}$ Mice

In total, 763 proteins with two or more unique peptides were quantified by label free quantification in neurons. Of them, 11 proteins were differentially expressed between tmTNF$^{\Delta/\Delta}$ and tmTNF$^{wt/wt}$ mice (**Supplementary Figure 6**). Calcium-activated potassium channel subunit alpha-1 ($K_{Ca}1.1$) was upregulated in tmTNF$^{\Delta/\Delta}$ mice. HGTD-P that promotes apoptosis in ischemia (Qu et al., 2009) was downregulated in neurons derived from tmTNF$^{\Delta/\Delta}$ mice suggesting improved neuroprotection.

DISCUSSION

In the present study, we found that topical administration of the selective solTNF inhibitor XPro1595 decreased infarct volumes 1 and 3 days after pMCAO. Inhibition of TNF by the non-selective solTNF and tmTNF inhibitor etanercept showed no effect. Furthermore, there was no reduction in infarct volume or improvement in functional outcome when TNF inhibitors were delivered by i.c.v. administration, even though the concentrations of the inhibitors in brain tissue were sufficient to neutralize TNF and potentially promote neuroprotection as demonstrated in previous studies using animal models of Alzheimer's disease (MacPherson et al., 2017).

We have previously shown that topical, but not systemic, administration of XPro1595 decreased lesion volume and improved functional outcome after moderate spinal cord injury (Novrup et al., 2014). Systemic administration of XPro1595 and etanercept had no effect on the infarct volume after pMCAO (Clausen et al., 2014), and systemic etanercept administration had no effect after transient focal cerebral ischemia (Sumbria et al., 2012), indicating that TNF inhibitors have to be administered directly to infarcted brain tissue and not by

intracerebroventricular or peripheral routes. The length of treatment may also play a role in suppressing the infarct formation in the acute phase of ischemic stroke. It is known that the infarct volume correlates with functional outcome (Saver et al., 1999; Yoo et al., 2012), and since TNF inhibitors are known to improve functional outcome even without reduction in infarct volume when administered systemically (Clausen et al., 2014), assessment of the functional outcome would have been ideal to evaluate the neuroprotective effects of topical XPro1595 administration. Evaluation of the functional outcome was impossible, however, due to the placement of the mini-osmotic pumps in topically treated animals.

The expression of *Tnf* mRNA in central nervous system has been shown to peak 12 h after pMCAO in mice (Lambertsen et al., 2005, 2009), and TNF protein expression 24 h after pMCAO (Lambertsen et al., 2005, 2009; Clausen et al., 2008). Expression of *Tnf* mRNA in the contralateral hemisphere has been shown to remain at baseline levels after pMCAO (Lambertsen et al., 2009). In permanent focal cerebral ischemia, TNF is believed to exert its neuroprotective effects through TNFR1 (Taoufik et al., 2007; Lambertsen et al., 2009). *Tnfr1* mRNA expression peaks 1–2 days after pMCAO (Lambertsen et al., 2007, 2009), while the protein expression can be detected from 4 to 6 h until 5 days (Botchkina et al., 1997; Lambertsen et al., 2007). The expression of *Tnfr2* increases 1–10 days after pMCAO and reaches its peak 5 days after occlusion (Lambertsen et al., 2007). The protein expression of TNFR2 can be detected 24 h after pMCAO (Botchkina et al., 1997). In our study, topical administration of XPro1595 tended to suppress the expression of TNF protein 1 day after pMCAO, while gene expression was significantly upregulated due to the feedback mechanism by which TNF induces its own gene expression when the amount of available protein is repressed. In addition, inhibition of both solTNF and tmTNF with etanercept downregulated TNFR1 protein levels at day 1. Together with earlier findings that TNFR1 knock-out mice develop larger infarct volumes (Bruce et al., 1996; Gary et al., 1998) and neuroprotection in ischemic stroke is mediated through the TNFR1-NFκB-FLIP(L)-ERK1/2 pathway (Taoufik et al., 2007; Lambertsen et al., 2009; Marques-Fernandez et al., 2013), downregulation of TNFR1 is likely to contribute to the lack of neuroprotection after TNF inhibition with etanercept (Gary et al., 1998; Lambertsen et al., 2009). Given the neuroprotective effect of TNFR2 signaling in our spinal cord injury model (Novrup et al., 2014) and the protective effect of this receptor in chronic, inflammatory conditions such as multiple sclerosis (Brambilla et al., 2011; Gao et al., 2017), we cannot exclude that TNFR2 signaling on microglia may have contributed to the protective effects observed after topical XPro1595 treatment.

TNF is primarily secreted by activated resident microglia and at later time points by infiltrating macrophages after pMCAO (Clausen et al., 2008; Lambertsen et al., 2009). In contrast to earlier studies showing that systemic inhibition of solTNF increased the number of microglia 6 and 24 h after pMCAO (Clausen et al., 2014), flow cytometric analysis of the percentage of microglia and infiltrating macrophages or their CD11b and CD45 MFI values showed no difference between treatment groups. Interestingly, the number of $CD45^{dim}CD11b^{+}$ microglia was higher in sham mice treated with either TNF inhibitor when compared to saline-treated mice. In contrast to earlier studies where XPro1595 decreased glial activation in an animal model of Parkinson's disease (Barnum et al., 2014), it is possible that topical administration of XPro1595 shifted the microglial phenotype without influencing the activation status of the cells. In support of this, *Cx3cr1* mRNA levels were significantly downregulated after 1 and 3 days of topical administration of XPro1595. Also, CX3CR1 deficiency has been shown to be neuroprotective in the early phase after ischemia by promoting microglial polarization to an M2-like phenotype and to decrease microglial activation and neurotoxicity by decreasing the expression of M1-like microglial phenotype that is associated with proinflammatory molecules; all of which lead to smaller infarct volumes (Fumagalli et al., 2013; Tang et al., 2014). XPro1595 also increased the expression of *P2ry12*, a protein related to resting state microglia (Haynes et al., 2006), 1 day after pMCAO when administered topically, suggesting that XPro1595 decreases microglial activation as earlier reported (Barnum et al., 2014; Hsiao et al., 2014; Novrup et al., 2014; MacPherson et al., 2017). Furthermore, the expression of *Trem2* was upregulated 1 and 3 days after pMCAO in mice treated topically with XPro1595. Trem2-knock out mice have altered microglial phagocytosis and larger infarct volumes after cerebral ischemia (Takahashi et al., 2005; Kawabori et al., 2015), supporting earlier studies where XPro1595 was found to promote neuroprotection by improving phagocytosis of dying neurons and cell debris in demyelinated lesions in an animal model of multiple sclerosis (Karamita et al., 2017). Chemokine expression was also altered after treatment with TNF inhibitors.

In the present study, topical administration of XPro1595 increased the relative expression of *Ccl2* mRNA 3 days after pMCAO. CCL2 is necessary for hypoxia-required ischemic tolerance, and upregulation after XPro1595 treatment supports the neuroprotective properties of the selective solTNF inhibitor (Stowe et al., 2012; Wacker et al., 2012). *Cxcl1* mRNA, a proinflammatory granulocyte attracting chemokine expressed by monocytes and granulocytes, was upregulated in etanercept-treated but not XPro1595-treated mice 1 and 3 days after pMCAO. However, there was no difference in the CXCL1 protein levels or in granulocyte infiltration between the treatment groups, contradicting earlier findings where systemic treatment with TNF inhibitors decreased the number of infiltrating granulocytes (Clausen et al., 2014) and TNF deficiency increased the number of infiltrating leukocytes 24 h after pMCAO (Lambertsen et al., 2009).

Intracerebroventricular administration of XPro1595 or etanercept had no effect on the infarct volume nor any beneficial effect on functional outcome despite both drugs being shown to access neural tissue in therapeutically relevant concentrations. In both experimental conditions (i.c.v. versus topical administration), XPro1595 and etanercept were present in more than 1000-fold excess of TNF in the ischemic brain tissue. However, it is possible that despite the penetration of XPro1595 and etanercept, the drugs did not reach their site of action, the penumbra, within the therapeutic window, which in our pMCAO model has been shown to be 6 h (Clausen et al., 2006).

Proteomic characterization of microglia derived from tmTNF$^{\Delta/\Delta}$ mice revealed that several phagocytosis-related proteins were significantly upregulated compared to proteins from microglia derived from tmTNF$^{wt/wt}$ mice. Microglia derived from tmTNF$^{\Delta/\Delta}$ mice showed an upregulated expression of 3-MPST, an enzyme protecting cells from oxidative stress by producing redox regulators (Kimura et al., 2017). In addition, 3-MPST regulates hydrogen sulfide production, which has been shown to promote phagocytosis (Dufton et al., 2012), functions as a vasodilator supporting blood flow (Zhao et al., 2001), and promotes angiogenesis (Papapetropoulos et al., 2009). Among the upregulated proteins was HPGDS, which is upregulated in microglia and macrophages after ischemic stroke and is likely to promote microglia/macrophage differentiation to the phagocytic phenotype (Mohri et al., 2003, 2006; Liu et al., 2007). In addition, HPGDS inhibits production of reactive oxygen species and downregulates the expression of the pro-inflammatory cytokine IL-1β through the formation of prostaglandins (Gomez-Abellan et al., 2015). Microglia derived from tmTNF$^{\Delta/\Delta}$ mice also had an upregulated expression of PYCARD/ASC. PYCARD/ASC deficient mice have impaired lymphocyte migration and are deficient in the number of lymphocytes and dendritic cells in secondary lymphoid organs compromising the normal immune system function (Ippagunta et al., 2011). Upregulation of the microglial PYCARD/ASC could contribute to the maintenance of the innate immune system and the secondary lymphoid organs where tmTNF has shown to be crucial (Ruuls et al., 2001; Alexopoulou et al., 2006). Among the downregulated proteins in tmTNF expressing microglia was MPO, a reactive oxygen species generating enzyme known to be expressed by leukocytes and to increase in cerebral ischemia (Lau and Baldus, 2006; Breckwoldt et al., 2008). Inhibition of MPO increases the proliferation and survival of neurons in animal models of ischemic stroke (Kim et al., 2016). In addition, HGTD-P, that mediates apoptosis in the ischemic brain when activated by hypoxia-inducible factor-1 (Qu et al., 2009), was downregulated in tmTNF expressing microglia.

In order to study whether the up- and downregulation of the phagocytosis-related proteins would affect microglial phagocytosis *in vitro*, we tested phagocytic capacity after 1 day of LPS stimulation. Primary microglia derived from tmTNF$^{\Delta/\Delta}$ mice showed increased phagocytic activity that most likely can lead to increased clearing of debris thereby promoting neuronal survival in the ischemic area when solTNF is ablated. Earlier studies have demonstrated increased phagocytosis after inhibition of solTNF (Karakantza et al., 2003) and impaired phagocytic ability of TNFR2 deficient microglia (Gao et al., 2017). Since tmTNF preferentially binds to TNFR2, it is likely that phagocytosis is regulated through the tmTNF-TNFR2 pathway. In the present study, we also show that inhibition of solTNF by XPro1595 increased the gene expression of *Trem2*, a receptor that is known to be involved in promoting microglial phagocytosis (Takahashi et al., 2005), an upregulation that was likely to increase microglial phagocytosis in mice treated topically with XPro1595.

This study demonstrates that selective inhibition of solTNF is neuroprotective after pMCAO when administered topically for 1 and 3 consecutive days. Furthermore, topical administration of XPro1595 promotes a phagocytic, microglial phenotype possibly supporting a neurotrophic environment in the ischemic lesion. We suggest that topical administration of XPro1595 has potential to be clinically beneficial in treating patients with ischemic stroke.

DATA AVAILABILITY

The datasets generated for this study are available on request to the corresponding author.

ETHICS STATEMENT

The Danish Animal Inspectorate under the Ministry of Food and Agriculture (J. No. 2013-15-2934-00924).

AUTHOR CONTRIBUTIONS

MY-K, BC, HN, DE, MM, and KL conducted animal surgeries. MD assisted with flow cytometric analyses and helped analyze and interpret data. AS and PT-J performed proteomics. RB performed experiments and helped draft the manuscript. DS provided the XPro1595 and gave useful input to the drafting of the manuscript. MY-K, BC, and KL performed experiments, interpreted results, performed statistical analyses, and wrote the manuscript. KL conceived the study. All authors read and approved the final manuscript.

FUNDING

This work was supported by research grants from Rector's Funds (KL), the Danish Council for Independent Research (KL, DFF–4183-00033), the Lundbeck Foundation (KL, R173-2014-955), the Carlsberg Foundation (KL, 2007_01_0176), Fonden til Laegevidenskabens Fremme (MY-K), Overlaegeraadets Legatudvalg (MY-K), NIH-NINDS (RB, 1R01NS094522-01), the Italian Multiple Sclerosis Foundation (RB, FISM 2015/R/7), the US National Multiple Sclerosis Society (RB, NMSS PP-1804-30716), and The Miami Project To Cure Paralysis. The mass spectrometry proteomics data have been deposited to the ProteomeXchange Consortium via the PRIDE [1] partner repository with the dataset identifier PXD014440.

ACKNOWLEDGMENTS

We acknowledge skilled technical help from technicians Ulla Damgaard Munk and Charlotte Skouboe. RIO, University of Southern Denmark, is acknowledged for support and guidance throughout this study. Claire Gudex is acknowledged for proof-reading the manuscript.

SUPPLEMENTARY MATERIAL

The Supplementary Material for this article can be found online at: https://www.frontiersin.org/articles/10.3389/fnins.2019.00781/full#supplementary-material

REFERENCES

Al-Ali, H., Gao, H., Dalby-Hansen, C., Peters, V. A., Shi, Y., and Brambilla, R. (2017). High content analysis of phagocytic activity and cell morphology with PuntoMorph. *J. Neurosci. Methods* 291, 43–50. doi: 10.1016/j.jneumeth.2017.08.004

Alexopoulou, L., Kranidioti, K., Xanthoulea, S., Denis, M., Kotanidou, A., Douni, E., et al. (2006). Transmembrane TNF protects mutant mice against intracellular bacterial infections, chronic inflammation and autoimmunity. *Eur. J. Immunol.* 36, 2768–2780. doi: 10.1002/eji.200635921

Barnum, C. J., Chen, X., Chung, J., Chang, J., Williams, M., Grigoryan, N., et al. (2014). Peripheral Administration of the Selective Inhibitor of Soluble Tumor Necrosis Factor (TNF) XPro(R)1595 Attenuates Nigral Cell Loss and Glial Activation in 6-OHDA Hemiparkinsonian Rats. *J. Parkinsons Dis.* 4, 349–360. doi: 10.3233/JPD-140410

Black, R. A., Rauch, C. T., Kozlosky, C. J., Peschon, J. J., Slack, J. L., Wolfson, M. F., et al. (1997). A metalloproteinase disintegrin that releases tumour-necrosis factor-alpha from cells. *Nature* 385, 729–733. doi: 10.1038/385729a0

Botchkina, G. I., Meistrell, M. E. III, Botchkina, I. L., and Tracey, K. J. (1997). Expression of TNF and TNF receptors (p55 and p75) in the rat brain after focal cerebral ischemia. *Mol. Med.* 3, 765–781. doi: 10.1007/bf03401714

Brambilla, R., Ashbaugh, J. J., Magliozzi, R., Dellarole, A., Karmally, S., Szymkowski, D. E., et al. (2011). Inhibition of soluble tumour necrosis factor is therapeutic in experimental autoimmune encephalomyelitis and promotes axon preservation and remyelination. *Brain* 134(Pt 9), 2736–2754. doi: 10.1093/brain/awr199

Breckwoldt, M. O., Chen, J. W., Stangenberg, L., Aikawa, E., Rodriguez, E., Qiu, S., et al. (2008). Tracking the inflammatory response in stroke in vivo by sensing the enzyme myeloperoxidase. *Proc. Natl. Acad. Sci. U.S.A.* 105, 18584–18589. doi: 10.1073/pnas.0803945105

Bruce, A. J., Boling, W., Kindy, M. S., Peschon, J., Kraemer, P. J., Carpenter, M. K., et al. (1996). Altered neuronal and microglial responses to excitotoxic and ischemic brain injury in mice lacking TNF receptors. *Nat. Med.* 2, 788–794. doi: 10.1038/nm0796-788

Cavanagh, C., Tse, Y. C., Nguyen, H. B., Krantic, S., Breitner, J. C., Quirion, R., et al. (2016). Inhibiting tumor necrosis factor-alpha before amyloidosis prevents synaptic deficits in an Alzheimer's disease model. *Neurobiol. Aging* 47, 41–49. doi: 10.1016/j.neurobiolaging.2016.07.009

Chen, W. L., Niu, Y. Y., Jiang, W. Z., Tang, H. L., Zhang, C., Xia, Q. M., et al. (2015). Neuroprotective effects of hydrogen sulfide and the underlying signaling pathways. *Rev. Neurosci.* 26, 129–142. doi: 10.1515/revneuro-2014-0051

Clausen, B., Degn, M., Martin, N., Couch, Y., Karimi, L., Ormhoj, M., et al. (2014). Systemically administered anti-TNF therapy ameliorates functional outcomes after focal cerebral ischemia. *J. Neuroinflammation* 11:203. doi: 10.1186/PREACCEPT-2982253041347736

Clausen, B. H., Degn, M., Sivasaravanaparan, M., Fogtmann, T., Andersen, M. G., Trojanowsky, M. D., et al. (2016a). Conditional ablation of myeloid TNF increases lesion volume after experimental stroke in mice, possibly via altered ERK1/2 signaling. *Sci. Rep.* 6:29291. doi: 10.1038/srep29291

Clausen, B. H., Lambertsen, K. L., Dagnaes-Hansen, F., Babcock, A. A., von Linstow, C. U., Meldgaard, M., et al. (2016b). Cell therapy centered on IL-1Ra is neuroprotective in experimental stroke. *Acta Neuropathol.* 131, 775–791. doi: 10.1007/s00401-016-1541-5

Clausen, B. H., Lambertsen, K. L., Babcock, A. A., Holm, T. H., Dagnaes-Hansen, F., and Finsen, B. (2008). Interleukin-1beta and tumor necrosis factor-alpha are expressed by different subsets of microglia and macrophages after ischemic stroke in mice. *J. Neuroinflammation* 5:46. doi: 10.1186/1742-2094-5-46

Clausen, B. H., Lambertsen, K. L., and Finsen, B. (2006). Glyceraldehyde-3-phosphate dehydrogenase versus toluidine blue as a marker for infarct volume estimation following permanent middle cerebral artery occlusion in mice. *Exp. Brain Res.* 175, 60–67. doi: 10.1007/s00221-006-0526-3

Cobourne-Duval, M. K., Taka, E., Mendonca, P., and Soliman, K. F. A. (2018). Thymoquinone increases the expression of neuroprotective proteins while decreasing the expression of pro-inflammatory cytokines and the gene expression NFkappaB pathway signaling targets in LPS/IFNgamma -activated BV-2 microglia cells. *J. Neuroimmunol.* 320, 87–97. doi: 10.1016/j.jneuroim.2018.04.018

Cronk, J. C., Derecki, N. C., Ji, E., Xu, Y., Lampano, A. E., Smirnov, I., et al. (2015). Methyl-CpG binding protein 2 regulates microglia and macrophage gene expression in response to inflammatory stimuli. *Immunity* 42, 679–691. doi: 10.1016/j.immuni.2015.03.013

Dambuza, I., Keeton, R., Allie, N., Hsu, N. J., Randall, P., Sebesho, B., et al. (2011). Reactivation of M. tuberculosis infection in trans-membrane tumour necrosis factor mice. *PLoS One* 6:e25121. doi: 10.1371/journal.pone.0025121

DeBerge, M. P., Ely, K. H., and Enelow, R. I. (2014). Soluble, but not transmembrane, TNF-alpha is required during influenza infection to limit the magnitude of immune responses and the extent of immunopathology. *J. Immunol.* 192, 5839–5851. doi: 10.4049/jimmunol.1302729

Dufton, N., Natividad, J., Verdu, E. F., and Wallace, J. L. (2012). Hydrogen sulfide and resolution of acute inflammation: a comparative study utilizing a novel fluorescent probe. *Sci. Rep.* 2:499. doi: 10.1038/srep00499

Fumagalli, S., Perego, C., Ortolano, F., and De Simoni, M. G. (2013). CX3CR1 deficiency induces an early protective inflammatory environment in ischemic mice. *Glia* 61, 827–842. doi: 10.1002/glia.22474

Gao, H., Danzi, M. C., Choi, C. S., Taherian, M., Dalby-Hansen, C., Ellman, D. G., et al. (2017). Opposing functions of microglial and macrophagic tnfr2 in the pathogenesis of experimental autoimmune encephalomyelitis. *Cell Rep.* 18, 198–212. doi: 10.1016/j.celrep.2016.11.083

Gary, D. S., Bruce-Keller, A. J., Kindy, M. S., and Mattson, M. P. (1998). Ischemic and excitotoxic brain injury is enhanced in mice lacking the p55 tumor necrosis factor receptor. *J. Cereb. Blood Flow Metab.* 18, 1283–1287. doi: 10.1097/00004647-199812000-00001

Gilthorpe, J. D., Oozeer, F., Nash, J., Calvo, M., Bennett, D. L., Lumsden, A., et al. (2013). Extracellular histone H1 is neurotoxic and drives a pro-inflammatory response in microglia. *F1000Res* 2:148. doi: 10.12688/f1000research.2-148.v1

Gomez-Abellan, V., Montero, J., Lopez-Munoz, A., Figueras, A., Arizcun, M., Mulero, V., et al. (2015). Professional phagocytic granulocyte-derived PGD2 regulates the resolution of inflammation in fish. *Dev. Comp. Immunol.* 52, 182–191. doi: 10.1016/j.dci.2015.04.017

Gray, E., Thomas, T. L., Betmouni, S., Scolding, N., and Love, S. (2008). Elevated activity and microglial expression of myeloperoxidase in demyelinated cerebral cortex in multiple sclerosis. *Brain Pathol.* 18, 86–95. doi: 10.1111/j.1750-3639.2007.00110.x

Gregersen, R., Lambertsen, K., and Finsen, B. (2000). Microglia and macrophages are the major source of tumor necrosis factor in permanent middle cerebral artery occlusion in mice. *J. Cereb. Blood Flow Metab.* 20, 53–65. doi: 10.1097/00004647-200001000-00009

Griffin, W. S. (2008). Perispinal etanercept: potential as an Alzheimer therapeutic. *J. Neuroinflammation* 5:3. doi: 10.1186/1742-2094-5-3

Hallenbeck, J. M. (2002). The many faces of tumor necrosis factor in stroke. *Nat. Med.* 8, 1363–1368. doi: 10.1038/nm1202-1363

Hargreaves, K., Dubner, R., Brown, F., Flores, C., and Joris, J. (1988). A new and sensitive method for measuring thermal nociception in cutaneous hyperalgesia. *Pain* 32, 77–88. doi: 10.1016/0304-3959(88)90026-7

Haynes, S. E., Hollopeter, G., Yang, G., Kurpius, D., Dailey, M. E., Gan, W. B., et al. (2006). The P2Y12 receptor regulates microglial activation by extracellular nucleotides. *Nat. Neurosci.* 9, 1512–1519. doi: 10.1038/nn1805

Hsiao, H. Y., Chiu, F. L., Chen, C. M., Wu, Y. R., Chen, H. M., Chen, Y. C., et al. (2014). Inhibition of soluble tumor necrosis factor is therapeutic in Huntington's disease. *Hum. Mol. Genet.* 23, 4328–4344. doi: 10.1093/hmg/ddu151

Ippagunta, S. K., Malireddi, R. K., Shaw, P. J., Neale, G. A., Vande Walle, L., Green, D. R., et al. (2011). The inflammasome adaptor ASC regulates the function of adaptive immune cells by controlling Dock2-mediated Rac activation and actin polymerization. *Nat. Immunol.* 12, 1010–1016. doi: 10.1038/ni.2095

Ito, D., Tanaka, K., Suzuki, S., Dembo, T., and Fukuuchi, Y. (2001). Enhanced expression of Iba1, ionized calcium-binding adapter molecule 1, after transient focal cerebral ischemia in rat brain. *Stroke* 32, 1208–1215. doi: 10.1161/01.str.32.5.1208

Jiang, S. X., Slinn, J., Aylsworth, A., and Hou, S. T. (2012). Vimentin participates in microglia activation and neurotoxicity in cerebral ischemia. *J. Neurochem.* 122, 764–774. doi: 10.1111/j.1471-4159.2012.07823.x

Karakantza, M., Maniatis, A., Metallinos, C. I., Papapetropoulos, T., and Paschalis, C. (2003). In vivo platelet activation in ischemic stroke patients. *Stroke* 34, e174–e175. doi: 10.1161/01.STR.0000092400.93742.81

Karamita, M., Barnum, C., Mobius, W., Tansey, M. G., Szymkowski, D. E., Lassmann, H., et al. (2017). Therapeutic inhibition of soluble brain TNF promotes remyelination by increasing myelin phagocytosis by microglia. *JCI Insight* 2:87455. doi: 10.1172/jci.insight.87455

Kawabori, M., Kacimi, R., Kauppinen, T., Calosing, C., Kim, J. Y., Hsieh, C. L., et al. (2015). Triggering receptor expressed on myeloid cells 2 (TREM2) deficiency attenuates phagocytic activities of microglia and exacerbates ischemic damage in experimental stroke. *J. Neurosci.* 35, 3384–3396. doi: 10.1523/JNEUROSCI.2620-14.2015

Kim, H., Wei, Y., Lee, J. Y., Wu, Y., Zheng, Y., Moskowitz, M. A., et al. (2016). myeloperoxidase inhibition increases neurogenesis after ischemic stroke. *J. Pharmacol. Exp. Ther.* 359, 262–272. doi: 10.1124/jpet.116.235127

Kimura, Y., Koike, S., Shibuya, N., Lefer, D., Ogasawara, Y., and Kimura, H. (2017). 3-Mercaptopyruvate sulfurtransferase produces potential redox regulators cysteine- and glutathione-persulfide (Cys-SSH and GSSH) together with signaling molecules H2S2, H2S3 and H2S. *Sci. Rep.* 7:10459. doi: 10.1038/s41598-017-11004-7

Kruse Meyer, M., Andersen, M., Bennike, T. B., Birkelund, S., Andersen, G. N., and Stensballe, A. (2015). Effect of IL-6R inhibition with tocilizumab on the proteome of peripheral blood mononuclear cells from a rheumatoid arthritis patient. *J. Proteomics Bioinform.* 8:12. doi: 10.4172/jpb.1000380

Lambertsen, K. L., Biber, K., and Finsen, B. (2012). Inflammatory cytokines in experimental and human stroke. *J. Cereb. Blood Flow Metab.* 32, 1677–1698. doi: 10.1038/jcbfm.2012.88

Lambertsen, K. L., Clausen, B. H., Babcock, A. A., Gregersen, R., Fenger, C., Nielsen, H. H., et al. (2009). Microglia protect neurons against ischemia by synthesis of tumor necrosis factor. *J. Neurosci.* 29, 1319–1330. doi: 10.1523/JNEUROSCI.5505-08.2009

Lambertsen, K. L., Clausen, B. H., Fenger, C., Wulf, H., Owens, T., Dagnaes-Hansen, F., et al. (2007). Microglia and macrophages express tumor necrosis factor receptor p75 following middle cerebral artery occlusion in mice. *Neuroscience* 144, 934–949. doi: 10.1016/j.neuroscience.2006.10.046

Lambertsen, K. L., Finsen, B., and Clausen, B. H. (2018). Post-stroke inflammation-target or tool for therapy? *Acta Neuropathol.* 137, 693–714. doi: 10.1007/s00401-018-1930-z

Lambertsen, K. L., Gregersen, R., Drojdahl, N., Owens, T., and Finsen, B. (2001). A specific and sensitive method for visualization of tumor necrosis factor in the murine central nervous system. *Brain Res. Brain Res. Protoc.* 7, 175–191. doi: 10.1016/s1385-299x(01)00062-9

Lambertsen, K. L., Meldgaard, M., Ladeby, R., and Finsen, B. (2005). A quantitative study of microglial-macrophage synthesis of tumor necrosis factor during acute and late focal cerebral ischemia in mice. *J. Cereb. Blood Flow Metab.* 25, 119–135. doi: 10.1038/sj.jcbfm.9600014

Lau, D., and Baldus, S. (2006). Myeloperoxidase and its contributory role in inflammatory vascular disease. *Pharmacol. Ther.* 111, 16–26. doi: 10.1016/j.pharmthera.2005.06.023

Lis, K., Kuzawinska, O., and Balkowiec-Iskra, E. (2014). Tumor necrosis factor inhibitors - state of knowledge. *Arch. Med. Sci.* 10, 1175–1185. doi: 10.5114/aoms.2014.47827

Liu, M., Eguchi, N., Yamasaki, Y., Urade, Y., Hattori, N., and Urabe, T. (2007). Focal cerebral ischemia/reperfusion injury in mice induces hematopoietic prostaglandin D synthase in microglia and macrophages. *Neuroscience* 145, 520–529. doi: 10.1016/j.neuroscience.2006.12.018

Liu, M., Eguchi, N., Yamasaki, Y., Urade, Y., Hattori, N., and Urabe, T. (2009). Protective role of hematopoietic prostaglandin D synthase in transient focal cerebral ischemia in mice. *Neuroscience* 163, 296–307. doi: 10.1016/j.neuroscience.2009.06.027

MacPherson, K. P., Sompol, P., Kannarkat, G. T., Chang, J., Sniffen, L., Wildner, M. E., et al. (2017). Peripheral administration of the soluble TNF inhibitor XPro1595 modifies brain immune cell profiles, decreases beta-amyloid plaque load, and rescues impaired long-term potentiation in 5xFAD mice. *Neurobiol. Dis.* 102, 81–95. doi: 10.1016/j.nbd.2017.02.010

Madsen, P. M., Clausen, B. H., Degn, M., Thyssen, S., Kristensen, L. K., Svensson, M., et al. (2016). Genetic ablation of soluble tumor necrosis factor with preservation of membrane tumor necrosis factor is associated with neuroprotection after focal cerebral ischemia. *J. Cereb. Blood Flow. Metab* 36, 1553–1569. doi: 10.1177/0271678X15610339

Marques-Fernandez, F., Planells-Ferrer, L., Gozzelino, R., Galenkamp, K. M., Reix, S., Llecha-Cano, N., et al. (2013). TNFalpha induces survival through the FLIP-L-dependent activation of the MAPK/ERK pathway. *Cell Death Dis.* 4:e493. doi: 10.1038/cddis.2013.25

McCoy, M. K., Martinez, T. N., Ruhn, K. A., Szymkowski, D. E., Smith, C. G., Botterman, B. R., et al. (2006). Blocking soluble tumor necrosis factor signaling with dominant-negative tumor necrosis factor inhibitor attenuates loss of dopaminergic neurons in models of Parkinson's disease. *J. Neurosci.* 26, 9365–9375. doi: 10.1523/JNEUROSCI.1504-06.2006

Meldgaard, M., Fenger, C., Lambertsen, K. L., Pedersen, M. D., Ladeby, R., and Finsen, B. (2006). Validation of two reference genes for mRNA level studies of murine disease models in neurobiology. *J. Neurosci. Methods* 156, 101–110. doi: 10.1016/j.jneumeth.2006.02.008

Minohara, M., Matsuoka, T., Li, W., Osoegawa, M., Ishizu, T., Ohyagi, Y., et al. (2006). Upregulation of myeloperoxidase in patients with opticospinal multiple sclerosis: positive correlation with disease severity. *J. Neuroimmunol.* 178, 156–160. doi: 10.1016/j.jneuroim.2006.05.026

Mohri, I., Eguchi, N., Suzuki, K., Urade, Y., and Taniike, M. (2003). Hematopoietic prostaglandin D synthase is expressed in microglia in the developing postnatal mouse brain. *Glia* 42, 263–274. doi: 10.1002/glia.10183

Mohri, I., Taniike, M., Taniguchi, H., Kanekiyo, T., Aritake, K., Inui, T., et al. (2006). Prostaglandin D2-mediated microglia/astrocyte interaction enhances astrogliosis and demyelination in twitcher. *J. Neurosci.* 26, 4383–4393. doi: 10.1523/JNEUROSCI.4531-05.2006

Morrison, H. W., and Filosa, J. A. (2013). A quantitative spatiotemporal analysis of microglia morphology during ischemic stroke and reperfusion. *J. Neuroinflammation* 10:4. doi: 10.1186/1742-2094-10-4

Musicki, K., Briscoe, H., Tran, S., Britton, W. J., and Saunders, B. M. (2006). Differential requirements for soluble and transmembrane tumor necrosis factor in the immunological control of primary and secondary Listeria monocytogenes infection. *Infect. Immun.* 74, 3180–3189. doi: 10.1128/IAI.02004-05

Neumann, H., Kotter, M. R., and Franklin, R. J. (2009). Debris clearance by microglia: an essential link between degeneration and regeneration. *Brain* 132(Pt 2), 288–295. doi: 10.1093/brain/awn109

Novrup, H. G., Bracchi-Ricard, V., Ellman, D. G., Ricard, J., Jain, A., Runko, E., et al. (2014). Central but not systemic administration of XPro1595 is therapeutic following moderate spinal cord injury in mice. *J. Neuroinflammation* 11:159. doi: 10.1186/s12974-014-0159-6

Papapetropoulos, A., Pyriochou, A., Altaany, Z., Yang, G., Marazioti, A., Zhou, Z., et al. (2009). Hydrogen sulfide is an endogenous stimulator of angiogenesis. *Proc. Natl. Acad. Sci. U.S.A.* 106, 21972–21977. doi: 10.1073/pnas.0908047106

Ponomarev, E. D., Shriver, L. P., Maresz, K., and Dittel, B. N. (2005). Microglial cell activation and proliferation precedes the onset of CNS autoimmunity. *J. Neurosci. Res.* 81, 374–389. doi: 10.1002/jnr.20488

Qu, Y., Mao, M., Zhao, F., Zhang, L., and Mu, D. (2009). Proapoptotic role of human growth and transformation-dependent protein in the developing rat brain after hypoxia-ischemia. *Stroke* 40, 2843–2848. doi: 10.1161/STROKEAHA.109.553644

Rajakariar, R., Hilliard, M., Lawrence, T., Trivedi, S., Colville-Nash, P., Bellingan, G., et al. (2007). Hematopoietic prostaglandin D2 synthase controls the onset and resolution of acute inflammation through PGD2 and 15-deoxyDelta12 14 PGJ2. *Proc. Natl. Acad. Sci. U.S.A.* 104, 20979–20984. doi: 10.1073/pnas.0707394104

Ruuls, S. R., Hoek, R. M., Ngo, V. N., McNeil, T., Lucian, L. A., Janatpour, M. J., et al. (2001). Membrane-bound TNF supports secondary lymphoid organ structure but is subservient to secreted TNF in driving autoimmune inflammation. *Immunity* 15, 533–543. doi: 10.1016/s1074-7613(01)00215-1

Saver, J. L., Johnston, K. C., Homer, D., Wityk, R., Koroshetz, W., Truskowski, L. L., et al. (1999). Infarct volume as a surrogate or auxiliary outcome measure in ischemic stroke clinical trials. The RANTTAS Investigators. *Stroke* 30, 293–298. doi: 10.1161/01.str.30.2.293

Scheinfeld, N. (2004). A comprehensive review and evaluation of the side effects of the tumor necrosis factor alpha blockers etanercept, infliximab and adalimumab. *J. Dermatolog. Treat* 15, 280–294. doi: 10.1080/09546630410017275A6NLET3WGCNW1D14

Shan, H., Chu, Y., Chang, P., Yang, L., Wang, Y., Zhu, S., et al. (2017). Neuroprotective effects of hydrogen sulfide on sodium azideinduced autophagic cell death in PC12 cells. *Mol. Med. Rep.* 16, 5938–5946. doi: 10.3892/mmr.2017.7363

Sierra, A., Abiega, O., Shahraz, A., and Neumann, H. (2013). Janus-faced microglia: beneficial and detrimental consequences of microglial phagocytosis. *Front. Cell Neurosci.* 7:6. doi: 10.3389/fncel.2013.00006

Soriano, S. G., Coxon, A., Wang, Y. F., Frosch, M. P., Lipton, S. A., Hickey, P. R., et al. (1999). Mice deficient in Mac-1 (CD11b/CD18) are less susceptible to cerebral ischemia/reperfusion injury. *Stroke* 30, 134–139. doi: 10.1161/01.str.30.1.134

Steed, P. M., Tansey, M. G., Zalevsky, J., Zhukovsky, E. A., Desjarlais, J. R., Szymkowski, D. E., et al. (2003). Inactivation of TNF signaling by rationally designed dominant-negative TNF variants. *Science* 301, 1895–1898. doi: 10.1126/science.1081297

Stetler, R. A., Gan, Y., Zhang, W., Liou, A. K., Gao, Y., Cao, G., et al. (2010). Heat shock proteins: cellular and molecular mechanisms in the central nervous system. *Prog. Neurobiol.* 92, 184–211. doi: 10.1016/j.pneurobio.2010.05.002

Stetler, R. A., Gao, Y., Zhang, L., Weng, Z., Zhang, F., Hu, X., et al. (2012). Phosphorylation of HSP27 by protein kinase D is essential for mediating neuroprotection against ischemic neuronal injury. *J. Neurosci.* 32, 2667–2682. doi: 10.1523/JNEUROSCI.5169-11.2012

Stowe, A. M., Wacker, B. K., Cravens, P. D., Perfater, J. L., Li, M. K., Hu, R., et al. (2012). CCL2 upregulation triggers hypoxic preconditioning-induced protection from stroke. *J. Neuroinflammation* 9:33. doi: 10.1186/1742-2094-9-33

Sumbria, R. K., Boado, R. J., and Pardridge, W. M. (2012). Brain protection from stroke with intravenous TNFalpha decoy receptor-Trojan horse fusion protein. *J. Cereb. Blood Flow Metab.* 32, 1933–1938. doi: 10.1038/jcbfm.2012.97

Takahashi, K., Rochford, C. D., and Neumann, H. (2005). Clearance of apoptotic neurons without inflammation by microglial triggering receptor expressed on myeloid cells-2. *J. Exp. Med.* 201, 647–657. doi: 10.1084/jem.20041611

Tang, Z., Gan, Y., Liu, Q., Yin, J. X., Liu, Q., Shi, J., et al. (2014). CX3CR1 deficiency suppresses activation and neurotoxicity of microglia/macrophage in experimental ischemic stroke. *J. Neuroinflammation* 11:26. doi: 10.1186/1742-2094-11-26

Taoufik, E., Valable, S., Muller, G. J., Roberts, M. L., Divoux, D., Tinel, A., et al. (2007). FLIP(L) protects neurons against in vivo ischemia and in vitro glucose deprivation-induced cell death. *J. Neurosci.* 27, 6633–6646. doi: 10.1523/jneurosci.1091-07.2007

Tobinick, E. (2011). Rapid improvement of chronic stroke deficits after perispinal etanercept: three consecutive cases. *CNS Drugs* 25, 145–155. doi: 10.2165/11588400-000000000-00000

Tobinick, E., Kim, N. M., Reyzin, G., Rodriguez-Romanacce, H., and DePuy, V. (2012). Selective TNF inhibition for chronic stroke and traumatic brain injury: an observational study involving 629 consecutive patients treated with perispinal etanercept. *CNS Drugs* 26, 1051–1070. doi: 10.1007/s40263-012-0013-2

Tyring, S., Gottlieb, A., Papp, K., Gordon, K., Leonardi, C., Wang, A., et al. (2006). Etanercept and clinical outcomes, fatigue, and depression in psoriasis: double-blind placebo-controlled randomised phase III trial. *Lancet* 367, 29–35. doi: 10.1016/S0140-6736(05)67763-X

Wacker, B. K., Perfater, J. L., and Gidday, J. M. (2012). Hypoxic preconditioning induces stroke tolerance in mice via a cascading HIF, sphingosine kinase, and CCL2 signaling pathway. *J. Neurochem.* 123, 954–962. doi: 10.1111/jnc.12047

Yoo, A. J., Chaudhry, Z. A., Nogueira, R. G., Lev, M. H., Schaefer, P. W., Schwamm, L. H., et al. (2012). Infarct volume is a pivotal biomarker after intra-arterial stroke therapy. *Stroke* 43, 1323–1330. doi: 10.1161/STROKEAHA.111.639401

Zhao, W., Zhang, J., Lu, Y., and Wang, R. (2001). The vasorelaxant effect of H(2)S as a novel endogenous gaseous K(ATP) channel opener. *EMBO J.* 20, 6008–6016. doi: 10.1093/emboj/20.21.6008

Conflict of Interest Statement: DS was an employee of Xencor and holds stock and stock options in the company.

The remaining authors declare that the research was conducted in the absence of any commercial or financial relationships that could be construed as a potential conflict of interest.

Copyright © 2019 Yli-Karjanmaa, Clausen, Degn, Novrup, Ellman, Toft-Jensen, Szymkowski, Stensballe, Meyer, Brambilla and Lambertsen. This is an open-access article distributed under the terms of the Creative Commons Attribution License (CC BY). The use, distribution or reproduction in other forums is permitted, provided the original author(s) and the copyright owner(s) are credited and that the original publication in this journal is cited, in accordance with accepted academic practice. No use, distribution or reproduction is permitted which does not comply with these terms.

frontiers in Neuroscience

REVIEW
published: 08 August 2019
doi: 10.3389/fnins.2019.00778

Aging Neurovascular Unit and Potential Role of DNA Damage and Repair in Combating Vascular and Neurodegenerative Disorders

Yan Li[1†], Lv Xie[1†], Tingting Huang[1], Yueman Zhang[1], Jie Zhou[1], Bo Qi[1], Xin Wang[1], Zengai Chen[2] and Peiying Li[1]*

[1] Department of Anesthesiology, Renji Hospital, School of Medicine, Shanghai Jiao Tong University, Shanghai, China, [2] Department of Radiology, Renji Hospital, School of Medicine, Shanghai Jiao Tong University, Shanghai, China

OPEN ACCESS

Edited by:
Gregory Jaye Bix, University of Kentucky, United States

Reviewed by:
Ana Margarida Ledo, University of Coimbra, Portugal
Kazuhide Hayakawa, Massachusetts General Hospital, United States
Ken Arai, Massachusetts General Hospital – Harvard Medical School, United States
Josephine Lok, Massachusetts General Hospital – Harvard Medical School, United States

***Correspondence:**
Peiying Li
peiyingli.md@gmail.com

† These authors have contributed equally to this work

Specialty section:
This article was submitted to Neurodegeneration, a section of the journal Frontiers in Neuroscience

Received: *30 March 2019*
Accepted: *11 July 2019*
Published: *08 August 2019*

Citation:
Li Y, Xie L, Huang T, Zhang Y, Zhou J, Qi B, Wang X, Chen Z and Li P (2019) Aging Neurovascular Unit and Potential Role of DNA Damage and Repair in Combating Vascular and Neurodegenerative Disorders. Front. Neurosci. 13:778. doi: 10.3389/fnins.2019.00778

Progressive neurological deterioration poses enormous burden on the aging population with ischemic stroke and neurodegenerative disease patients, such as Alzheimers' disease and Parkinson's disease. The past two decades have witnessed remarkable advances in the research of neurovascular unit dysfunction, which is emerging as an important pathological feature that underlies these neurological disorders. Dysfunction of the unit allows penetration of blood-derived toxic proteins or leukocytes into the brain and contributes to white matter injury, disturbed neurovascular coupling and neuroinflammation, which all eventually lead to cognitive dysfunction. Recent evidences suggest that aging-related oxidative stress, accumulated DNA damage and impaired DNA repair capacities compromises the genome integrity not only in neurons, but also in other cell types of the neurovascular unit, such as endothelial cells, astrocytes and pericytes. Combating DNA damage or enhancing DNA repair capacities in the neurovascular unit represents a promising therapeutic strategy for vascular and neurodegenerative disorders. In this review, we focus on aging related mechanisms that underlie DNA damage and repair in the neurovascular unit and introduce several novel strategies that target the genome integrity in the neurovascular unit to combat the vascular and neurodegenerative disorders in the aging brain.

Keywords: aging, neurovascular unit, cerebral ischemia, DNA damage, DNA repair, blood brain barrier

INTRODUCTION

Aging populations are forcing nations and societies to confront the problem of an increasing prevalence of ischemic stroke and neurodegenerative diseases, including Parkinson's disease (PD) and Alzheimer's disease (AD). Specifically, approximately 4.7 million Americans were living with the most common neurodegenerative disease AD in 2010; by 2050 this number reaches 16 million (Hebert et al., 2013). Of note, the epidemiological trends of dementia are expected to cause an immense burden on health-care expenditure (Yang et al., 2013). Meanwhile, our understanding of these neurological disorders is still rudimentary, effective disease-modifying drugs are warranted to treat these disorders.

The neurovascular unit (NVU) is a functional unit with multiple components in the central nervous system (CNS), including vascular cells [pericytes, vascular smooth muscle cells (VSMCs), endothelial cells], glial cells (astrocytes, microglia, oligodendrocytes) and neurons (Banks et al., 2018). These cells together, ultimately determine the function of NVU and their responses in health and disease (Mazeika and Doraiswamy, 2002; Lo and Rosenberg, 2009; Cai et al., 2017). Aging related NVU dysfunction falls into two categories, NVU dysfunction resulting from normal aging or cell senescence and pathological NVU dysfunction under aging-related diseases, such as cerebral ischemic stroke, PD and AD (Cai et al., 2017). The pathological NVU dysfunction has emerged as an important element in the neuronal injury of ischemic stroke and neurodegenerative diseases, in which neuronal cell death, glial cell activation, blood-brain barrier (BBB) disruption, and penetration of peripheral immune cells may ensue with the diseases progress (Mazeika and Doraiswamy, 2002; Lo and Rosenberg, 2009; Cai et al., 2017; Baker and Petersen, 2018). Maintenance of genome integrity is a prerequisite for the maintenance of the normal function of the brain. However, aging not only results in accumulated DNA damages in neurons, the center of the NVU, including DNA breaks, cross-links, and bases mismatch (McKinnon, 2013; Lodato et al., 2018), but also impairs multiple DNA repair mechanisms (Santos et al., 2013; Chow and Herrup, 2015; Zhao et al., 2017). In this review, we provide new insights into DNA damage and repair in neurons and also discuss the potential role of DNA damage and repair in the other cell types of the aging NVU. Novel therapeutic strategies targeting DNA damage and repair that may have the potential to combat the neuronal injury after ischemic stroke and neurodegenerative disorders such as PD and AD will also be introduced.

VULNERABILITY OF THE NVU IN THE AGING BRAIN

Changes of the Aging NVU

Living cells gradually exhibit features of senescence, which are characterized by sustained cell cycle arrest and release of senescence-associated secretory phenotype (SASP) throughout the body, including the brain (Mazeika and Doraiswamy, 2002; Lo and Rosenberg, 2009; Cai et al., 2017). Compelling evidence indicates that senescence cells in the brain are associated with multiple neurodegenerative diseases (Baker and Petersen, 2018). Meanwhile, dysfunction of NVU in the aging brain plays fundamental role in the pathology of ischemic stroke and also in the progressive neurological deterioration of neurodegenerative diseases (Cai et al., 2017). Since it was first proposed in 2001, the concept of NVU is attracting increasing research attention (Lo and Rosenberg, 2009). With aging, substantial changes occur in all components of the NVU, including neurons, glial cells, vascular cells as well as the basal lamina matrix within the brain vasculature (Mazeika and Doraiswamy, 2002; Lo and Rosenberg, 2009; Cai et al., 2017; **Figure 1**).

Aging related changes in the NVU usually result in the impaired BBB integrity and penetration of blood derived proteins, such as fibrinogen and plasminogen, which has recently been suggested to clot and form insoluble pro-inflammatory fibrin deposit in the brain (Cortes-Canteli et al., 2015; D'Angelo et al., 2018; Maugeri et al., 2018). Fibrin deposits are associated with amyloid plaques, pericyte loss, dystrophic neurites, and activated microglia in AD, demyelinated multiple sclerosis and stroke (Petersen et al., 2017; Ryu et al., 2018; Brait et al., 2019; Freeze et al., 2019). Fibrin deposits can damage the brain function via a variety of mechanisms: (1) it binds to the CD11b-CD18 integrin receptor and promotes cognitive deficits in a mouse model of AD (Merlini et al., 2019); (2) it can induce reactive oxygen species (ROS) production and the activation of nicotinamide adenine dinucleotide phosphate (NADPH) oxidase, which increases the expression of proinflammatory genes (Ryu et al., 2018; Merlini et al., 2019); (3) it induces adaptive immune responses in the brain and inhibits oligodendrocyte precursor cells (OPCs) and suppresses remyelination (Ryu et al., 2015; Petersen et al., 2017; Lai et al., 2018); (4) it binds Aβ thus forming the Aβ-fibrinogen complex which blocks fibrin degradation and induces neurodegeneration by sustaining fibrin deposition and enhancing chronic CD11b-mediated microglia activation in the CNS (Cortes-Canteli et al., 2010; Zhao et al., 2010; Lai et al., 2018); (5) fibrinogen leads to axonal retraction (Schachtrup et al., 2007) and BBB damage, thus promoting neuroinflammation (Paul et al., 2007). Likewise, plasminogen, the blood protein synthesized in the liver is recently suggested as a regulator of brain inflammatory action and AD pathology (Baker et al., 2018). Depletion of plasminogen/plasmin in peripheral blood, but not in the brain, is highly protective from Aβ deposition and a neuroinflammatory response in a 5XFAD (Tg6799) AD mouse model (Baker et al., 2018; **Figure 2**).

Aging, with a plethora of mechanisms, affects all the components of the NVU. Aging may also impact the cell-cell interaction within the NVU and ultimately lead to NVU dysfunction and compromised BBB.

Aging Neurons in the NVU

In the NVU, neurons are the most susceptible cell type due to their high metabolic rate and are the most vulnerable to aging associated cell injuries (Cai et al., 2017). During aging, their capacity for ROS clearance reduces, making them more vulnerable to oxidative stress (Nicholls and Budd, 2000; Mattson and Magnus, 2006). Meanwhile, calcium dysregulation and decreased expression of calcium binding proteins further increase ROS production, exacerbating neuronal apoptosis and NVU injury in the aging brain (He et al., 1997). On the other hand, the regenerative capacities of neurons decline in an age-dependent manner, including neurogenesis (Smith et al., 2015), synaptic remodeling, synaptogenesis, axonal sprouting and dendritic remodeling (Skaper et al., 2017).

In addition to neuron itself, the interaction between neuron and glia cells may change with aging. There are a variety of neurotrophic factors that have been shown to play important roles in the neuron-glial interaction (Poyhonen et al., 2019). On one hand, the trophic factors produced from neurons, such as brain-derived neurotrophic factor (BDNF) and nerve growth factor (NGF), support the normal

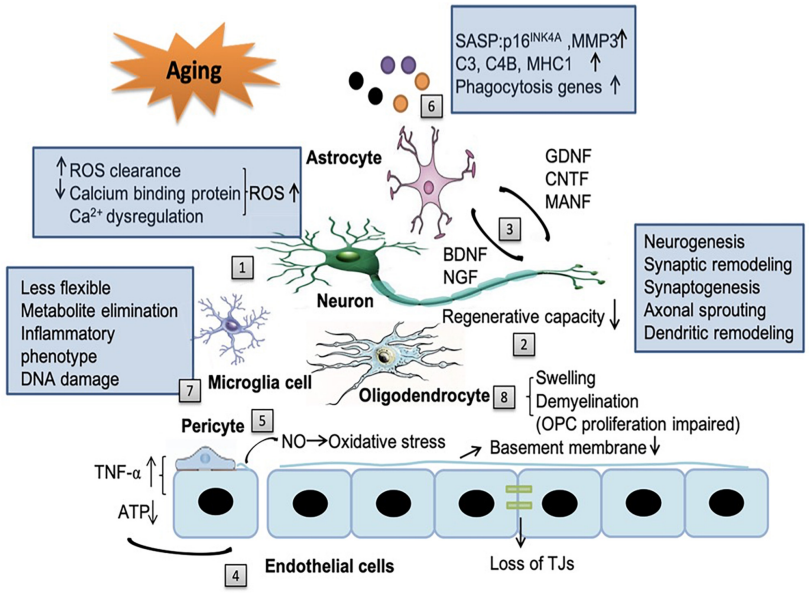

FIGURE 1 | The impact of aging on the neurovascular unit (NVU) components. Aging affects all the components of NVU. [1] In neurons, the capacity for reduced ROS clearance capacity, decreased expression of calcium binding proteins and Ca^{2+} dysregulation induced reactive oxygen species (ROS) production all contribute to the exacerbated neuronal injury. [2] The regenerative capacities of neurons decline in an age-dependent manner, including neurogenesis, synaptic remodeling, synaptogenesis, axonal sprouting and dendritic remodeling. [3] Aging reduces the release of neurotrophic factors from neurons, such as brain-derived neurotrophic factor (BDNF) and nerve growth factor (NGF) and also factors from astrocytes, such as glial cell-line derived neurotrophic factor (GDNF), ciliary neurotrophic factor (CNTF) and mesencephalic astrocyte-derived neurotrophic factor (MANF). The alteration of these factors in aging brain contribute to cognitive decline. [4] With aging, endothelial cells can secrete some noxious factors, such as tumor necrosis factor-α (TNF-α), consume increased amount of ATP, decrease the thickness of basement membrane and disrupt tight junction. In addition, the cross-talk among endothelial cells, astrocytes, and pericytes can modify the secretion of TNF-α. [5] Senile pericytes generate more nitric oxide (NO) and further increase the oxidative stress in the NVU. [6] Senescent astrocytes express senescence-associated secretory phenotype (SASP), such as $p16^{INK4A}$, matrix metallopeptidase 3 (MMP3), complement system genes (C3 and C4B), major histocompatibility complex 1 (MHC1) and upregulate phagocytosis genes, which enhance neuroinflammation and contribute to cognitive decline. [7] With aging, microglia become more rigid and less flexible in mobility. Their capacity to eliminate endogenous metabolites decreases. Aged microglia develop a more inflammatory phenotype and accumulates more DNA damages. [8] Senile oligodendrocytes have swelling morphology and lead to broad and irreversible demyelination which impair the ability of the proliferation of OPCs.

function of NVU (Budni et al., 2015). On the other hand, the factors produced from the glial cells, such as glial cell-line derived neurotrophic factor (GDNF), ciliary neurotrophic factor (CNTF), mesencephalic astrocyte-derived neurotrophic factor (MANF) and et al promote synaptic and neuronal growth, pruning, myelination and neuronal cell survival (Poyhonen et al., 2019). However, with aging, the alterations in their expression may contribute to cognitive decline in aging related neurodegenerative diseases (Budni et al., 2015). Astrocytes in the aging brain can also express characteristic SASP proteins, which may turn them into proinflammatory phenotypes and disrupt the functional neuron-glial interaction, thus progressively impair the neuronal functions (Salminen et al., 2011; Chinta et al., 2015).

Aging Brain Vasculature

Endothelial cells, one of the key components of the blood brain barrier and the NVU, maintain the integrity of the BBB and the hemostasis of the brain along with the tight junctions between endothelial cells, basement membrane, pericytes and astrocyte endfeet (Lo and Rosenberg, 2009). The cross-talk among endothelial cells, astrocytes, and pericytes of NVU may modify the cytokine secretion patterns of endothelial cells, such as tumor necrosis factor-α (TNF-α) (Banks et al., 2018). With aging, oxidative stress occurs in human endothelial cells and the permeability of BBB increases (Donato et al., 2007; Bake et al., 2009; Lee et al., 2012; Cai et al., 2017). Increased endothelial concentration of TNF-α, decreased thickness of basement membrane, loss of tight junctions (TJs), such as occludin and zonula occludens-1 (ZO-1), reduced secretion of trophic factors from brain pericytes have all been suggested as potential mechanisms underlying the aging associated injury of the NVU (Emerich et al., 2005; Bell et al., 2010; Elahy et al., 2015).

Central nervous system pericytes are embedded in the basement membrane. They generate diverse functional responses with neighboring cells, such as regulating BBB permeability, clearance of toxic metabolites, capillary hemodynamic responses, angiogenesis and neuroinflammation (Sweeney et al., 2016; Villasenor et al., 2017; Khennouf et al., 2018). During aging, the number of pericytes decreases in the brain and the loss of $NG2^{+}$ pericytes is associated with Aβ1-40 in AD patients (Bell et al., 2010). Mechanistically, fibril-enriched preparations (fibril-EP) Aβ1-40 exposure can reduce the cell viability of pericytes and it also increases caspase 3/7 activity, which may induce pericyte apoptosis (Schultz et al., 2018). The PDGF-BB/PDGFRβ (platelet-derived growth factor-BB/platelet-derived growth factor

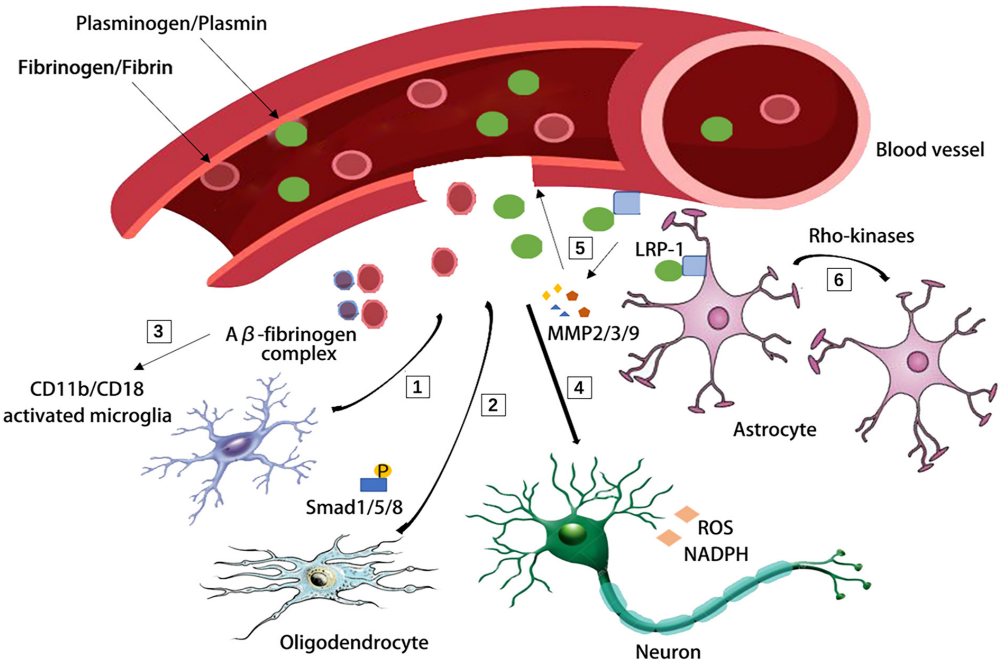

FIGURE 2 | Blood-derived fibrinogen and plasminogen mediated brain pathology through several different mechanisms. [1] Fibrin deposit causes CD11b-CD18 microglia activation in the 5XFAD mouse model of AD. [2] Fibrinogen causes phosphorylation of Smad 1/5/8 and inhibits oligodendrocyte progenitor cells. [3] Aβ-fibrinogen complex enhances chronic CD11b-mediated microglia activation. [4] Fibrin deposit induces reactive oxygen species (ROS) production and triphosphopyridine nucleotide (NADPH) oxidase activation and leads to axonal retraction. [5] The activation of low density lipoprotein receptor-related protein 1 (LRP-1) on endothelial cells was suggested to induce the degradation of tight junctions and base membrane by matrix metallopeptidase-9, matrix metallopeptidase-2, matrix metallopeptidase-3 (MMP-9, MMP-2, and MMP-3). [6] The LRP-1 on astrocytes activates the Rho kinases and mediates the retraction of astrocytic endfeet from vessel walls.

receptor β) signaling plays a pivotal role in the age-dependent pericyte regulation of the BBB integrity. Partially disrupted or deficient of the PDGF-BB/PDGFRβ signaling results in BBB breakdown in an age-dependent manner, which allows accumulation of neurotoxic blood-derived proteins in the brain (Armulik et al., 2010; Sweeney et al., 2016). Senile pericytes contain high smooth muscle actin and the smooth muscle cells generate more nitric oxide (NO), which can react with O^2-anions, causing severe oxidative stress (Hughes et al., 2006; Cai et al., 2017). Dysfunction of pericytes may ultimately result in comprised blood supply of the NVU due to contractile rigor (Sweeney et al., 2016).

The Impact of Aging on Brain Glial Cells

As the most numerous glial cells in the CNS, astrocytes not only provide structural and nutritional supports for neurons, but also participate in the composition of the NVU (Helms et al., 2017; Banks et al., 2018). In senile astrocytes, increased oxidative metabolism and disturbed glutamate regulation can impair their energy support capacity to neurons and cause neuronal excitotoxicity (Maragakis and Rothstein, 2006; Simpson et al., 2010; Cai et al., 2017). Senile astrocytes in the brain also express senescence-associated secretory phenotype (SASP), such as $p16^{INK4A}$ and matrix metalloproteinase 3 (MMP3), which enhances age-related neuroinflammation and exacerbates the functional decline of the aging brain (Salminen et al., 2011; Baker and Petersen, 2018). Recently, the accumulation of senile astrocytes were causally linked to neuronal cell loss and subsequent cognitive impairment (Bussian et al., 2018). Clearance of p16Ink4a-positive senescent astrocytes and microglia using INK-ATTAC transgenic mice prevents gliosis and deposition of neurofibrillary tangle in the cortex and hippocampus (Bussian et al., 2018). On the other hand, aging astrocytes activate the immune system and contribute to cognitive decline. It was recently demonstrated that the complement system genes in astrocytes, such as C3 and C4B were upregulated in the aging brain (Boisvert et al., 2018; Clarke et al., 2018). There's also an upregulation in antigen presenting genes such as major histocompatibility complex I (MHC I), and phagocytosis genes, such as *Pros1, Mfge8, Megf10, and Lrp1*, thus contributing to the low level inflammatory state characteristic of aging (Mangold et al., 2017; Clarke et al., 2018). However, the MHC I and the phagocytosis gene expression may not be detrimental all the time, they may also promote the clearance of the myelin debris and preserve the cognitive function during aging (Nag and Wadhwa, 2012; Lazarczyk et al., 2016).

Microglia has long been recognized as the main executor of inflammation after acute and chronic brain injuries (Perry and Holmes, 2014; Jin et al., 2017; Kluge et al., 2018). It has been recently shown that neocortical resident microglia are long-lived, with a median lifetime of well over 15 months. About half of the microglia can survive the entire lifespan in

mouse (Fuger et al., 2017). With aging, microglia become less flexible in mobility, which makes them become more rigid and less efficient during their daily patrol in the brain (Norden and Godbout, 2013; Perry and Holmes, 2014; Babcock et al., 2015). Their capacity to eliminate endogenous metabolites (e.g. amyloid-beta peptides) also decreases with aging (Norden and Godbout, 2013; Perry and Holmes, 2014; Babcock et al., 2015). Aged microglia develop a more inflammatory phenotype, which is primed, reactive or sensitized, and the activation is amplified and prolonged and more difficult to resolve compared to non-aged microglia (Norden and Godbout, 2013; Perry and Holmes, 2014). In addition, mutations and DNA damages accumulate in microglia with aging (Mrak and Griffin, 2005). Therefore, it's well recognized that microglial senescence may contribute to age-related neurodegenerative diseases. Although it does not directly participate in the composition of NVU, its interaction with the BBB after central nervous system disorders is getting increasing attention in the field.

Oligodendrocytes are one of the glial cells providing support and insulation to axons in the brain. Senile oligodendrocytes have swelling morphology which includes degenerated myelin sheaths in the cytoplasm (Peters, 2009). With aging, the injuries to myelin and the oligodendrocytes increase while the ability of the brain to repair and renew in response to these injuries declines, leading to broad and irreversible demyelination in various age-related CNS insults (Cai et al., 2017; Petersen et al., 2017). Demyelination results in exposure of unwrapped axons, which in turn stimulates the proliferation of OPCs and remyelination (Petersen et al., 2017). However, the remyelination efficiency is significantly impaired in the aged brain, causing a significantly lower axonal conduction velocity, which may also contribute to the progressive neurological deterioration in those aged individuals with neurodegenerative disorders (Peters and Sethares, 2002; Peters, 2009).

Collectively, the aging related changes in the NVU are illustrated in **Figure 1**.

Senile NVU and Cerebral Ischemic Stroke

As the fourth leading cause of death and the primary cause of disability worldwide, stroke poses enormous burden to the family and society (Donahue and Hendrikse, 2018). More than 80% of strokes occur in patients aged 65 or more (Ritzel et al., 2018). Aging is not only a risk factor of cerebral ischemic stroke, but also an indicator of poorer outcome (Cai et al., 2017; Yang and Paschen, 2017). Compared to younger patients, the elderly has higher rates of mortality and disability (Ritzel et al., 2018).

Aging can affect the NVU in a variety of ways (Salinet et al., 2018). Apart from the above mentioned direct impacts of aging on the NVU components, aging can also impair the systemic milieu and alter the immunological response and lead to further exacerbated brain injury after stroke (Pan et al., 2017; Ritzel et al., 2018; Wang et al., 2018). Reduced expression of sirtuin-1 in brain microvessels may also contribute to the increased brain permeability in aged mice after stroke (Stamatovic et al., 2018). However, the capacity of the aged NVU to recover from ischemic stroke is impaired (Jiang et al., 2018). Of note, with aging, BBB breakdown may occur before marked cognitive dysfunction occurs, which may predispose aged patient to post-stroke dementia (Nation et al., 2019). However, the causal link between aging-related NVU dysfunction and post-stroke dementia has not been well-established yet.

Intimate Association Between AD and NVU Dysfunction

Alzheimer's disease is a chronic neurodegenerative disease that constitutes 60–70% of dementia cases (Herholz et al., 2018). Emerging evidence suggests BBB disruption may serve as a critical pathway that initiates the onset of AD (Arvanitakis et al., 2016; Sweeney et al., 2018b). Using an advanced dynamic contrast-enhanced magnetic resonance imaging (DCE-MRI) protocol, it's demonstrated that compromise of the BBB is an early event in the hippocampus during aging and it may contribute to the progressive impairment of cognitive function. Thus, BBB breakdown can also serve as an early biomarker of human cognitive dysfunction (Montagne et al., 2015; Barry Erhardt et al., 2018; Nation et al., 2019).

Multiple lines of evidence suggest that there are pronounced NVU dysfunction in AD brains (Miners et al., 2018). BBB disruption has been found in the postmortem brain of AD patients, such as substantially reduced TJs proteins, occludin, claudin-5, and ZO-1 in capillaries, leading to increased fibrinogen leakages in the brain parenchyma (Carrano et al., 2011, 2012; Zlokovic, 2011). Aβ42 is likely to disrupt the organization of TJs and adherent junction between endothelial cells, thereby disturbing their barrier function (Carrano et al., 2011, 2012; Zlokovic, 2011). The receptor for advanced glycation end-products (RAGE)-mediated Aβ cytotoxicity is involved in damaging the BBB integrity (Kook et al., 2012; Wan et al., 2015). High degree of Aβ burden is associated with redistribution and even loss of aquaporin 4 (AQP4) on astrocytic end-foot membranes (Yang et al., 2011; Zeppenfeld et al., 2017). Retraction and swelling in astrocytic end-feet is involved in the Aβ mediated impairment of cerebral vascular function and cerebral metabolism (Merlini et al., 2011). Coverages of microvessels by pericytes are significantly reduced in AD brains and it inversely correlated with the extravasation of the blood-drived proteins including immunoglobulin G and fibrin (Sengillo et al., 2013; Winkler et al., 2014). Furthermore, reduced pericyte coverage in AD may further exacerbate cerebral hypoperfusion and Aβ clearance impairment (Dalkara et al., 2011). Deficiency of pericytes causes accelerated brain Aβ deposition and cerebral amyloid angiopathy formation in the brain of a mouse AD model (Sagare et al., 2013). With compelling evidence suggesting an intimate association of NVU dysfunction and AD, it's reasonable to envision that protecting the aging NVU may be a promising strategy to treat AD **(Figure 3)**.

Aging NVU and PD

Parkinson's disease is a progressive long-term neurodegenerative disorder in the aged population. It is characterized by degeneration of dopaminergic neurons in the substantia nigra

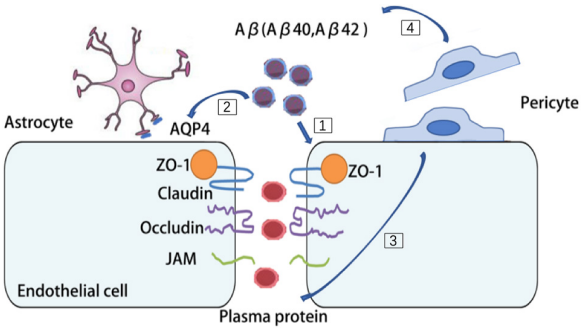

FIGURE 3 | Aβ burden contribute to multiple cell types dysfunction in AD brains. [1] Aβ42 disrupt the organization of tight junctions (TJs) and adherent junction in endothelial cells. [2] Aβ burden redistribute aquaporin 4 (AQP4) on astrocytes and cause retraction and swelling of astrocytic end-feet. [3] In AD brains, pericytes detach from microvessels and cause leakage of plasma protein. [4] Deficiency of pericytes cause accelerated brain Aβ deposition.

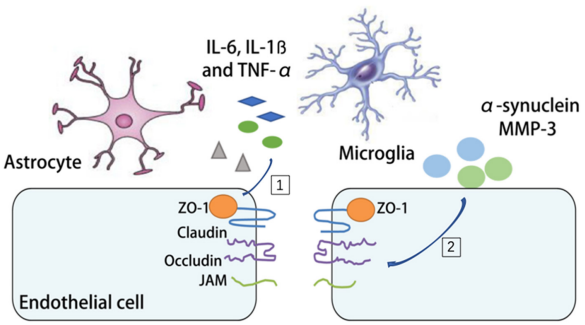

FIGURE 4 | The mechanism of BBB disruption in PD. [1] The release of interleukin 6 (IL-6), interleukin-1ß (IL-1ß) and tumor necrosis factor-α (TNF-α) by microglia and astrocytes during PD is associated with the rearrangement of tight junctions (TJs). [2] The deposition of α-synuclein and matrix metallopeptidase 3 (MMP3) increases BBB permeability and neuroinflammation in PD.

with accumulated α-synuclein. The relationship between the aging NVU and PD resides in two aspects. On one hand, increased oxidative stress, disturbed mitophagy, reduced energy support and impaired mitochondria repair with aging can all lead to dopaminergic neuronal cell injury and cell loss (Gredilla et al., 2010; Fivenson et al., 2017). On the other hand, the pathological changes of the PD brain, such as α-synuclein deposition and increased MMP-3 alter BBB permeability and neuroinflammation in PD (Chung et al., 2013; Jangula and Murphy, 2013). There is clinical evidence of BBB disruption during PD development (Ohlin et al., 2011; Lee and Pienaar, 2014). By measuring the albumin ratio, it's demonstrated that PD patients exhibit significant differences in albumin ratio, which indicates BBB dysfunction (Jangula and Murphy, 2013). Several mechanisms have been proposed to explain the BBB disruption in PD. Astrocytes have intimate contact with dopaminergic neurons, especially those with unmyelinated axons (Rodriguez et al., 2014). In the aging brain, instead of providing protection and support, the senile astrocytes along with microglia produce cytokines, chemokines (interleukin 6 (IL-6), interleukin-1ß (IL-1ß) and TNF-α) and ROS, which disrupt the integrity of the NVU, rearrange TJs ZO-1 and occludin and propel disease progression (Gredilla et al., 2010; Collins et al., 2012; Rodriguez et al., 2015; Fivenson et al., 2017). In addition, increased oxidative stress, neuroinflammatory processes and infiltration of peripheral immune cells have all been linked to BBB disruption in PD, although still controversial (Block et al., 2007; Appel, 2009; Chung et al., 2016). So far it still remains unknown whether NVU targeted therapy could be protective against PD (**Figure 4**).

ACCUMULATED DNA DAMAGE IN MULTIPLE CELL TYPES IN THE AGING NVU

Progressive DNA damage accumulation is linked to cellular senescence and organismal aging. Most DNA damage is referred to oxidative DNA damage, an endonuclease-independent process resulting from ROS attacks, posing a major threat for the genome stability in the aging brain (McKinnon, 2013). There are several types of DNA damage, such as DNA breaks, cross-links, and bases mismatch (e.g., oxidative lesions) (Hayflick, 2007), among which DNA strand breaks are the most frequently encountered and detrimental. When classified depending on their mechanisms of action, DNA damage can be divided into two distinctive types: active DNA damage and passive DNA damage. It's emerging that DNA damage accumulation underlies age-related neurodegenerative diseases, such as stroke, AD and PD [88]. Among the NVU cells, neurons are the most widely studied cell type in terms of DNA damage and repair. However, DNA damage in endothelial cells and glial cells are also getting increasing attention due to their fundamental role in the NVU. We summarize different types of DNA damages in different neuronal cells in the NVU following ischemic stroke, AD and PD in **Supplementary Table 1**.

Accumulated DNA Damage in the NVU and the Relationship With Neurodegenerative Diseases

Neurons are highly vulnerable to oxidative stress induced DNA damage due to its high metabolic and mitochondrial activity, oxygen consumption, as well as high rates of transcription and translation (Lu et al., 2014; D'apolito et al., 2018). This condition, together with the impaired DNA repair capacity, can lead to a high accumulation of DNA damage which ultimately result in neurodegenerative processes (Choi et al., 2012; Suberbielle et al., 2015; Hou et al., 2018). Persistent accumulation of DNA damages, including oxidative DNA damages, single-strand breaks (SSBs), and double-strand breaks (DSBs), have been found in neurons of both AD and PD patients and experimental animal models (Adamec et al., 1999; Abolhassani et al., 2017). Cortical neurons prepared from 8-oxodeoxyguanine/8-oxoguanine glycosylase (8-oxo-dG/OGG1) double deficient adult mouse brains exhibit increased 8-oxoguanine (8-oxoG) accumulation in mitochondrial DNA and significantly poor

neuritogenesis *in vitro* in the absence of antioxidants in AD (Abolhassani et al., 2017). In PD patients, a significant increase in 8-hydroxy-2'-deoxyguanosine (8-OHdG) levels was shown in mtDNA in nigrostriatal dopaminergic neurons [69]. After ischemic stroke, there are also pronounced formation of apurinic/apyrimidinic (AP) sites base modifications (e.g., 8-oxodG, 8-OHdG, and 8-oxoG), SSBs and DSBs in ischemic neurons (D'apolito et al., 2018). The DNA damages in neurons of different neurodegenerative diseases are summarized in **Supplementary Table 1**.

DNA damages also surface in brain vascular endothelial cells and lead to endothelial apoptosis and cell loss, which contributes to cognitive decline in AD and ischemic stroke via a number of mechanisms (Chen et al., 1997; Ou and Schumacher, 2018): (1) increased apoptosis in endothelial cells results in reduced cerebral blood flow due to stiffened vasculature; (2) compromised BBB integrity can cause unregulated passage of blood-derived protein into the brain and increased infiltration of peripheral immune cells; (3) generalized NVU dysfunction, which will impact both astrocytes and neurons, leads to reduced function of the NVU and a pro-inflammatory environment in the brain (Jadavji et al., 2015). Detailed DNA damage types identified in endothelial cells are also summarized in **Supplementary Table 1**.

Astrocytes play critical roles in the maintenance and protection of neurons especially acute or chronic injury encountered, they are also vulnerable to oxidative DNA damage (Fluteau et al., 2015). Astrocyte oxidative DNA damage and their response to oxidative DNA damage are related to the progression of cognitive impairment (Waller et al., 2018) and cerebral ischemic injuries (Chen et al., 1997; Matsuda et al., 2009). In addition, the activation of astrocytes has a profound impact on the glial scar formation and NVU remodeling after stroke (Nahirney et al., 2016; Yanev et al., 2017; Blochet et al., 2018). However, evidence of DNA damages in astrocytes in AD or PD is relatively limited. There is even conflicting data showing reduced DNA-dependent protein kinase expression and DNA-damage associated molecules H2A histone family member X (H2AX) in Alzheimer's disease (Simpson et al., 2010). Therefore, the role of astrocytic DNA damage in the development of neurodegenerative diseases remains obscure and warrants further investigation.

Pericytes are adjacent to capillaries and essential to the regulation and limitation of the transport of various substances, thereby play important roles in the regulation of the BBB permeability and NVU functions (Bell et al., 2010; Fernandez-Klett et al., 2013; Montagne et al., 2018; Sweeney et al., 2018a). The oxidative DNA damage and repair in pericytes are poorly understood comparing to neuronal cells and endothelia cells. However, pericyte loss has been evidenced as an important contributor for BBB disruption and NVU dysfunction in AD, white matter dysfunction and ischemic stroke (Bell et al., 2010; Fernandez-Klett et al., 2013; Montagne et al., 2018; Sweeney et al., 2018a). Pericytes incubated with Aβ express high levels of cyclin D1 and integrin alpha 5 (ITGa5), which represents disturbed cell cycle and increased cell apoptosis (Davis et al., 1999; Miao et al., 2005). Thymosin β10 (Thyβ10) is supposed to mediate the Aβ induced compromise of the actin network and increased expression of cyclin D1 and Thyβ10 in AD brain, may eventually lead to apoptosis in cerebrovascular cells (Gugliandolo et al., 2018; Knopman, 2019). However, whether different types of DNA damages participate in the pericyte loss during neurodegenerative diseases remains to be explored.

Collectively, there are compelling evidence showing that a variety of DNA damage molecules in neurons contribute to ischemic stroke, AD and PD, such as 8-OHdG, 8-oxodG, γ-H2AX and et al. as listed in **Supplementary Table 1**. While oxidative DNA damage and repair in other cell types of the NVU remains poorly understood and warrants further investigation.

Impaired DNA Damage Responses in the NVU in the Aging Brain

Once DNA damage occurs, it can be sensed by DNA damage responses (DDR), several signaling pathways can be triggered to initiate cell injury (Lee and Paull, 2005; Ciccia and Elledge, 2010; Shiloh, 2014; Lavin et al., 2015). Phosphoinositide 3-kinase (PI3K)-related kinases (PIKKs) can phosphorylate downstream proteins to activate DNA damage responses. There are three types of PIKKs DNA-dependent protein kinase that can be recruited to DNA damage sites, DNA-dependent protein kinase catalytic subunit (DNA-PKcs), Ataxia-telangiectasia mutated (ATM), and taxia-telangiectasia and Rad-3-related (ATR) (Blackford and Jackson, 2017). DNA-PKcs is required to form an active DNA-PK complex with Ku70/80 for DNA repair of double strand breaks, which is accompanied by non-homologous end-jointing (NHEJ), which will be discussed later. ATR is activated by single strand break and stalled DNA replication forks while ATM can be activated directly by oxidative stress and DNA damage, mainly double strand DNA damage (Li et al., 2011; Blackford and Jackson, 2017; D'apolito et al., 2018). Once ATM is activated, it phosphorylates a multitude of substrates, including nuclear respiratory factor 1 (NRF1), p53-binding protein 1 (53BP1), mediator of DNA damage checkpoint protein 1 (MDC1), breast cancer type 1 susceptibility protein (BRCA1) MRE11/RAD50/NBS1(MRN) and H2AX to activate cell cycle checkpoints and initiate DNA repair. When ATM phosphonates NRF1, it leads to enhanced electron transport chain and mitochondrial function (Chow et al., 2019). If the damage is too severe to be repaired, ATM can direct the cell to apoptosis (Lee and Paull, 2005; Ciccia and Elledge, 2010; Shiloh, 2014; Lavin et al., 2015).

Among the three PIKKs, both ATM and DNA-PKcs have been implicated to play fundamental roles in aging and neurodegenerative diseases (Chung, 2018; Gal et al., 2018). DNA-PKcs has been found in the amygdala of cognitively impaired patients (Gal et al., 2018). Both Aβ (1-42) oligomers and aggregated Aβ (25-35) have been shown to inhibit DNA-PK kinase activity, compromising double strand break repair (NHEJ) and sensitizing cells to non-lethal oxidative injury (Cardinale et al., 2012). ATM-centered DNA damage response has been shown to progressively decline with aging, but significantly increased phospho-ATM immunoreactivity has been found in dopaminergic neurons in PD mouse model (Cornelis et al., 2018; Milanese et al., 2018; Qian et al., 2018). Excessive ROS stimulates ATM-dependent phosphorylation of drebrin, a

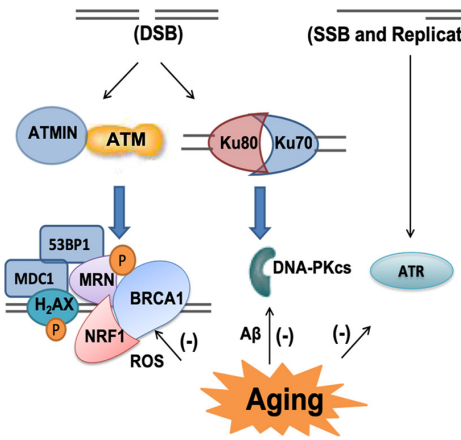

FIGURE 5 | PIKKs-related signaling pathway in the aging brain. There are three types of phosphoinositide 3-kinase (PI3K)-related kinases (PIKKs) DNA-dependent protein kinase including ataxia-telangiectasia mutated (ATM), DNA protein kinase catalytic subunit (DNA-PKcs) and taxia-telangiectasia and Rad-3-related (ATR). ATM can be activated by double-strand breaks (DSB) and it phosphorylates a multitude of substrates, including nuclear respiratory factor 1 (NRF1), H2A histone family member X (H2AX), mediator of DNA damage checkpoint protein 1 (MDC1), p53-binding protein 1 (53BP1), breast cancer type 1 susceptibility protein (BRCA1) and MRE11/RAD50/NBS1 (MRN). As an interactor of ATM, ATMIN plays important role in its response to oxidative stress and aging related DNA damage. DNA-PKcs is required to form an active DNA-PK complex with Ku70/80. ATR is activated by single-strand breaks (SSB) and replication arrest. In aging and AD brain, all these DNA damage response pathways have been shown to progressively decline.

regulator of cytoskeletal functions during neuronal development. The phosphorylation of drebrin improves structural and functional changes in the aging and AD synapse by enhancing the protein stability (Kreis et al., 2019). Depletion of ATM interactor (ATMIN), an interactor of ATM in the murine nervous system resulted in reduced numbers in dopaminergic neurons and increased mortality of aging mutant mice (Kanu and Behrens, 2008; Kanu et al., 2010; **Figure 5**).

Poly (ADP-ribose; PAR) polymerase-1 (PARP-1) is another enzyme that can be activated by oxidative stress and DNA damages, including single and double strand breaks. It belongs to NAD^+-dependent enzymes in eukaryotes. Cellular DNA damages, especially SSB, trigger overactivation of PARP-1, followed by NAD^+ depletion and lead to depletion of energy supply and mitochondrial impairment (Vosler et al., 2009; Fang et al., 2014). PARP-1 activation helps translocation of apoptosis-inducing factor (AIF) from the mitochondrion to the nucleus and also for the macrophage inhibitory factor (MIF) to translocate from the cytoplasm to the nucleus, where both of them can induce pro-death processes (Wang et al., 2016; D'apolito et al., 2018). Importantly, PARP-1 is not always detrimental, although overactivation of PARP-1 usually leads to pro-death cellular signals, its recognition of DNA damage is also important in initiating DNA repair (Vida et al., 2016). Of note, significant changes in the activity of PARPs have been detected in ischemic stroke (Andrabi et al., 2011; Nakajima et al., 2015), AD (Martire et al., 2016) and PD (Kam et al., 2018; Olsen and Feany, 2019; **Figure 6**).

As described above, mounting evidence suggests that aging not only results in accumulated DNA damages in the NVU comprising cells, but also affects the DNA damage response pathways, which contribute to the evolution of neuronal injuries in ischemic stroke and also neurodegenerative diseases. On the other hand, cells are equipped with delicate mechanisms to repair the DNA damages. However, with aging, the DNA repair capacities are impaired, which are associated with exacerbated ischemic brain injury and the progression of neurodegenerative diseases as we will discuss in the following part.

Impaired DNA Repair Capacities in Aging Brain

Although DNA damage is inevitable during aging, the cells have endogenous mechanism to repair these damages. The main DNA repair pathways include base excision repair (BER), nucleotide excision repair (NER), homologous recombination (HR), NHEJ and DNA mismatch repair (MMR) (Wyman and Kanaar, 2006; Iyama and Wilson, 2013; **Figure 7**).

Base excision repair is the primary nuclear and mitochondrial repair pattern for oxidative DNA damage, recognizing and replacing DNA modifications characterized by small base modifications (Li et al., 2011, D'apolito et al., 2018). BER is initiated by various DNA glycosylases, such as OGG1, endonuclease III-like 1 (NTH1), endonuclease VIII-like 1 (NEIL1) and endonuclease VIII-like 3 (NEIL3). These glycosylases excise the damaged bases and generate an AP site in DNA. The resulting AP site is then recognized by AP endonuclease 1 (APE1), which cleaves the phosphodiester backbone 5' to the AP site, leaving a nick with a 3'-OH group and a 5'-deoxyribose phosphate (dRP) residue. Next, the dRP is removed and filled in by "short-patch" repair or "long-patch" repair (D'apolito et al., 2018). Short patch repair involves sequential single-nucleotide gap-filling in which DNA polymerase beta (Polβ) synthesizes a single nucleotide to fill the gap and DNA ligase III-XRCC1 complex seals the nick between the newly synthesized nucleotide and the DNA template. Long patch repair is initiated by flap endonuclease-1 (FEN1) and usually produces a repair tract of at least two, most frequently four nucleotides (D'apolito et al., 2018).

With aging, the BER process becomes less effective (Niedernhofer et al., 2018), leading to accumulated DNA damage lesions that contribute to age-related degenerative diseases (Santos et al., 2013; Chow and Herrup, 2015). Firstly, the reduction in DNA damage recognition by reduced expression of DNA-PK and H2AX leads to impaired DNA damage recognition, which is associated with neuronal cell loss and glial responses in AD (Myung et al., 2008; Simpson et al., 2010). Secondly, the declined glycosylase activity and reduced DNA polymerase activity have been linked to aging related reduction of BER (Best, 2009). In the aged cerebellum, uracil DNA glycosylase (UDG) declined nearly 50% and OGG1 declined 90% (Best, 2009). In human studies, impaired BER function and the decreased BER capacity could be related to a reduction of Polβ activity and

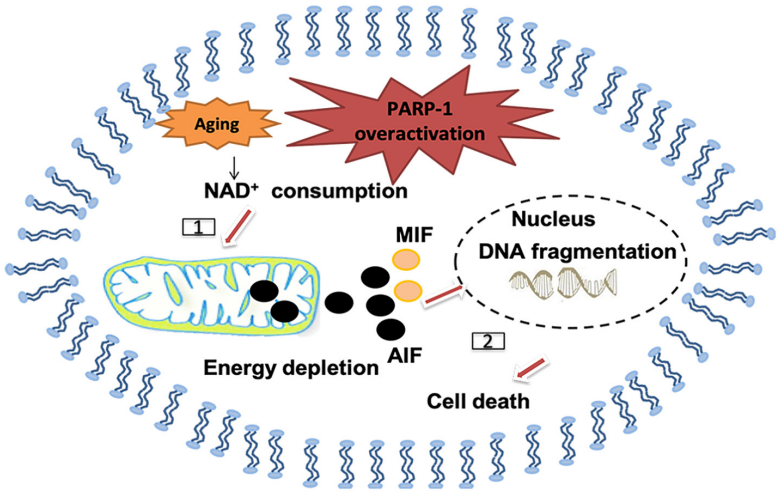

FIGURE 6 | Polymerase-1 over-activation causes cell death in the senile brain. [1] NAD^+ as the substrate for poly ADP-ribose polymerase (PARP) may be depleted and causes energy depletion in mitochondrial, especially in the senile brain. [2] PAR may directly cause the release of apoptosis inducing factor (AIF) from mitochondrial and transport into the nucleus, thus promoting macrophage migration inhibitory factor (MIF) to translocate from the cytoplasm to the nucleus and cause DNA fragmentation.

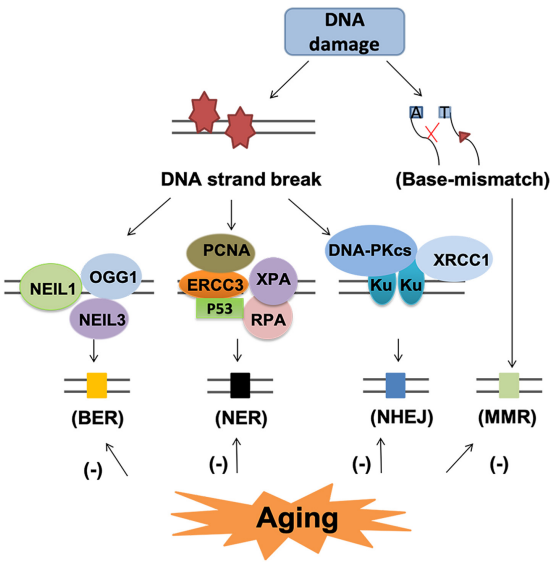

FIGURE 7 | DNA repair pathway and subsequent events in the aging brain. DNA repair pathway include base excision repair (BER), nucleotide excision repair (NER), non-homologous end-joining (NHEJ) and mismatch repair (MMR). Each pathway involved several various molecules. BER and NER are basic nuclear and mitochondrial DNA repair pathway for DNA strand break. NHEJ and MMR are two different pathways for the repair of base-mismatch. All the repair mechanisms become less effective with age, thus, may lead to accumulated DNA lesions and increase the risk of neurodegenerative diseases.

decreased glycosylase UDG in aging related neurodegenerative diseases (Sykora et al., 2013; Leandro et al., 2015). Recently, epigenetic events such as DNA methylation have also been identified to contribute to aging process and defective BER repair system (Dor and Cedar, 2018). Hypermethylation of the BER-related genes results in decreased expression these genes, especially OGG1, which is associated with reduced BER-related incision activity in AD and PD (Blanch et al., 2016).

The NER pathway is a versatile and complex system able to repair different types of DNA helix distorting lesions. In the aged humans, there are reduced expression of NER proteins, such as complementation group 3 (ERCC3), proliferating cell nuclear antigen (PCNA), replication protein A (RPA), xeroderma pigmentosum A (XPA) and tumor protein p53 (p53) (Gorbunova et al., 2007). However, the mechanism underlying this decline remains obscure. Treatment with short oligonucleotides that mimics DNA damage upregulated the levels of NER proteins in aged cells, suggesting decreased NER enzymes or altered induction of DNA damage response may underlie the decline of NER activity (Goukassian et al., 2002). The expression of NER proteins, such as ERCC1, is suggested to be associated with AD and PD (Sepe et al., 2016; Jensen et al., 2018).

Non-homologous end-jointing is a process to restore double stranded breaks of DNA. DNA-dependent protein kinase (DNA-PK) and its activator Ku play important roles initiating the NHEJ process upon binding to the DNA ends of DSBs (Kanungo, 2016). Reduced NHEJ activity as well as DNA-PKcs and Ku protein levels have been shown in aging and AD brains (Vyjayanti and Rao, 2006; Sharma, 2007; Kanungo, 2016). The level of Ku may be one of the mechanisms underlying the age-related decline of NHEJ (Rulten and Caldecott, 2013). Deficiency of Ku80 can induce Aβ generation, which in turn potentiates the degradation of DNA-PKcs and consequently reduced activity of NHEJ (Rulten and Caldecott, 2013).

Mismatch repair system provides two main genetic stabilization functions: correction of errors generated during replication and ensuring the fidelity of recombination. Mutations in MMR genes increase with aging but the function of MMR

declines (Bak et al., 2014). The mutagenic MMR has detrimental effects in neurodegenerative diseases for repeat expansions promotion (Bak et al., 2014). For AD patients, elevated DSB accumulation, reduction of DSB repair proteins such as DNA-PKcs and MRN complex proteins, and impaired BER activity all contribute to cell apoptosis or permanent cell-cycle arrest (Andreassi, 2008; Madabhushi et al., 2014).

Therefore, both increased DNA damage accumulation and defected DNA repair mechanisms have been identified in ischemic stroke, AD and PD. However, most of the above-mentioned studies focus the changes in neurons, but not other cell types of the NVU. Thus, it still remains unknown whether the above changes are directly associated with the NVU dysfunction in the aged brain. But, we envision that DNA damage and repair targeted therapy may help to preserve the NVU function and thus improve the outcome of these diseases. In the following part, we will introduce some potential therapeutic strategies that target DNA damage and repair in the treatment of ischemic stroke and neurodegenerative disorders.

POTENTIAL THERAPEUTIC STRATEGIES TARGETING DNA DAMAGE AND REPAIR IN AGE-RELATED VASCULAR AND NEURODEGENERATIVE DISORDERS

Several strategies have been proposed to combat the DNA damage in neurodegenerative diseases, such as prophylactically or therapeutically using antioxidants. Glutathione (GSH), vitamin E, selenium and superoxide dismutase have all been suggested to protect against oxidation and reduce DNA damage directly or stimulate the activity of DNA repair enzymes (Tomasetti et al., 2001; Mangialasche et al., 2010; Persson et al., 2014; Poprac et al., 2017).

Stimulating nuclear factors or increasing the activity of DNA repair enzymes can be another potential strategy to reduce the DNA damage and combat the neurodegenerative diseases. Forkhead box O3 (FOXO3a), the main isoform of FOXO transcription factors, has been shown to regulate the DNA repair genes. Inhibition of FOXO3a is associated with suppressed DNA damage response and attenuated Alzheimer-type pathology (Fluteau et al., 2015; Shi et al., 2016). In addition, there are a variety of DNA repair enzymes and proteins that can be targeted to combat the neuronal injuries, such as Apurinic/apyrimidinic endonuclease 1 (APE1), ATMIN, endonuclease VIII-like1 (NEIL1) DNA glycosylase, Polβ and DNA polymerase gamma (Polγ). APE1 is a critical BER enzyme that repairs AP sites. It has been shown to enhance neuronal survival after oxidative stress, provide neuroprotection against ischemic brain injury (Stetler et al., 2010; Leak et al., 2015) and also protect against Aβ25-35-induced neurotoxicity (Kaur et al., 2015). Administration of an endogenous small neuropeptide, pituitary adenylate cyclase-activating polypeptide (PACAP), is shown to induce APE1 expression and thus reduces oxidative DNA stress and reduce neuronal cell death after cerebral ischemia (Stetler et al., 2010). In addition, direct NAD repletion could markedly restore the DNA repair activity and reduce the accumulation of DNA damage (Wang et al., 2008). ATMIN is an essential component of the ATM signaling pathway (Kanu et al., 2010). ATMIN has same function in DNA repair system and deficiency of ATMIN will cause neurological disorders (Kanu and Behrens, 2008). Endonuclease VIII-like1 (NEIL1) DNA glycosylase is one of eleven mammalian DNA glycosylases that take part in the first step of the BER pathway (Prakash et al., 2016). Early research showed that NEIL1 function is important in brain-related diseases, such as AD (Canugovi et al., 2014). Polβ renders neurons vulnerable to reductions in cellular energy levels, sustain or elevate Polβ or DNA repair levels may protect neurons against dysfunction and degeneration in aging and AD (Sykora et al., 2015). Suitable supplement of Polγ may relieve PD syndrome (Gaweda-Walerych and Zekanowski, 2013). Collectively, these prophylactic or therapeutic DNA damage and repair targeting treatments appear to be a promising strategy to combat the DNA damage in neurodegenerative diseases **Supplementary Table 2**.

CONCLUSION

Aging related accumulation of DNA damage is emerging as important mechanism that underlies the neuronal injuries after ischemic stroke and neurodegenerative diseases like AD and PD. On the other hand, recent studies have highlighted the important role of NVU dysfunction and subsequent BBB damage and penetration of blood-derived substances, such as fibrinogen and plasminogen in the development of these diseases. In addition, aging related changes in the DNA damage responses and DNA repair signaling are also intimately associated with the progression of different types of age-related neurodegenerative diseases. Therefore, we envision that targeting DNA damage and DNA repair may serve as a promising strategy to combat the NVU dysfunction after ischemic stroke and neurodegenerative diseases. Although a variety of DNA damage and repair targeted treatments have been proposed to treat these neurological disorders, it still remains unknown whether these treatments can effectively improve the NVU function in these neurological disorders. Further investigations are warranted for a better understanding of DNA damage and repair related NVU dysfunction to explore new treatment ideas for multiple neurodegenerative disorders.

AUTHOR CONTRIBUTIONS

All authors listed have made a substantial, direct and intellectual contribution to the work, and approved it for publication.

FUNDING

PL is supported by the National Natural Science Foundation of China (NSFC) grant 81722017, the Rising Star Program of the Shanghai Science and Technology Committee (16QA1402600),

and the Shanghai Municipal Education Commission—Gaofeng Clinical Medicine Grant Support (20181805). ZC is supported by Shanghai Municipal Natural Science Foundation (16ZR1420700) and the Medical Guidance Project (19411971200) from Shanghai Science and Technology Committee.

SUPPLEMENTARY MATERIAL

The Supplementary Material for this article can be found online at: https://www.frontiersin.org/articles/10.3389/fnins.2019.00778/full#supplementary-material

REFERENCES

Abolhassani, N., Leon, J., Sheng, Z., Oka, S., Hamasaki, H., Iwaki, T., et al. (2017). Molecular pathophysiology of impaired glucose metabolism, mitochondrial dysfunction, and oxidative DNA damage in Alzheimer's disease brain. *Mech. Ageing Dev.* 161, 95–104. doi: 10.1016/j.mad.2016.05.005

Adamec, E., Vonsattel, J. P., and Nixon, R. A. (1999). DNA strand breaks in Alzheimer's disease. *Brain Res.* 849, 67–77.

Andrabi, S. A., Kang, H. C., Haince, J. F., Lee, Y. I., Zhang, J., Chi, Z., et al. (2011). Iduna protects the brain from glutamate excitotoxicity and stroke by interfering with poly(ADP-ribose) polymer-induced cell death. *Nat. Med.* 17, 692–699. doi: 10.1038/nm.2387

Andreassi, M. G. (2008). DNA damage, vascular senescence and atherosclerosis. *J. Mol. Med.* 86, 1033–1043. doi: 10.1007/s00109-008-0358-7

Appel, S. H. (2009). CD4+ T cells mediate cytotoxicity in neurodegenerative diseases. *J. Clin. Invest.* 119, 13–15. doi: 10.1172/JCI38096

Armulik, A., Genove, G., Mae, M., Nisancioglu, M. H., Wallgard, E., Niaudet, C., et al. (2010). Pericytes regulate the blood-brain barrier. *Nature* 468, 557–561.

Arvanitakis, Z., Capuano, A. W., Leurgans, S. E., Bennett, D. A., and Schneider, J. A. (2016). Relation of cerebral vessel disease to Alzheimer's disease dementia and cognitive function in elderly people: a cross-sectional study. *Lancet Neurol.* 15, 934–943. doi: 10.1016/S1474-4422(16)30029-1

Babcock, A. A., Ilkjaer, L., Clausen, B. H., Villadsen, B., Dissing-Olesen, L., Bendixen, A. T., et al. (2015). Cytokine-producing microglia have an altered beta-amyloid load in aged APP/PS1 Tg mice. *Brain Behav. Immun.* 48, 86–101. doi: 10.1016/j.bbi.2015.03.006

Bak, S. T., Sakellariou, D., and Pena-Diaz, J. (2014). The dual nature of mismatch repair as antimutator and mutator: for better or for worse. *Front. Genet.* 5:287. doi: 10.3389/fgene.2014.00287

Bake, S., Friedman, J. A., and Sohrabji, F. (2009). Reproductive age-related changes in the blood brain barrier: expression of IgG and tight junction proteins. *Microvasc. Res.* 78, 413–424. doi: 10.1016/j.mvr.2009.06.009

Baker, D. J., and Petersen, R. C. (2018). Cellular senescence in brain aging and neurodegenerative diseases: evidence and perspectives. *J. Clin. Invest.* 128, 1208–1216. doi: 10.1172/JCI95145

Baker, S. K., Chen, Z. L., Norris, E. H., Revenko, A. S., Macleod, A. R., and Strickland, S. (2018). Blood-derived plasminogen drives brain inflammation and plaque deposition in a mouse model of Alzheimer's disease. *Proc. Natl. Acad. Sci. U.S.A.* 115, E9687–E9696. doi: 10.1073/pnas.1811172115

Banks, W. A., Kovac, A., and Morofuji, Y. (2018). Neurovascular unit crosstalk: Pericytes and astrocytes modify cytokine secretion patterns of brain endothelial cells. *J. Cereb. Blood Flow Metab.* 38, 1104–1118. doi: 10.1177/0271678X17740793

Barry Erhardt, E., Pesko, J. C., Prestopnik, J., Thompson, J., Caprihan, A., and Rosenberg, G. A. (2018). Biomarkers identify the Binswanger type of vascular cognitive impairment. *J. Cereb. Blood Flow Metab.* doi: 10.1177/0271678X18762655 [Epub ahead of print].

Bell, R. D., Winkler, E. A., Sagare, A. P., Singh, I., Larue, B., Deane, R., et al. (2010). Pericytes control key neurovascular functions and neuronal phenotype in the adult brain and during brain aging. *Neuron* 68, 409–427. doi: 10.1016/j.neuron.2010.09.043

Best, B. P. (2009). Nuclear DNA damage as a direct cause of aging. *Rejuvenation Res.* 12, 199–208. doi: 10.1089/rej.2009.0847

Blackford, A. N., and Jackson, S. P. (2017). ATM, ATR, and DNA-PK: the trinity at the heart of the DNA damage response. *Mol. Cell* 66, 801–817. doi: 10.1016/j.molcel.2017.05.015

Blanch, M., Mosquera, J. L., Ansoleaga, B., Ferrer, I., and Barrachina, M. (2016). Altered mitochondrial DNA methylation pattern in alzheimer disease-related pathology and in parkinson disease. *Am. J. Pathol.* 186, 385–397. doi: 10.1016/j.ajpath.2015.10.004

Blochet, C., Buscemi, L., Clement, T., Gehri, S., Badaut, J., and Hirt, L. (2018). Involvement of caveolin-1 in neurovascular unit remodeling after stroke: effects on neovascularization and astrogliosis. *J. Cereb. Blood Flow Metab.* doi: 10.1177/0271678X18806893 [Epub ahead of print].

Block, M. L., Zecca, L., and Hong, J. S. (2007). Microglia-mediated neurotoxicity: uncovering the molecular mechanisms. *Nat. Rev. Neurosci.* 8, 57–69. doi: 10.1038/nrn2038

Boisvert, M. M., Erikson, G. A., Shokhirev, M. N., and Allen, N. J. (2018). The aging astrocyte transcriptome from multiple regions of the mouse brain. *Cell Rep.* 22, 269–285. doi: 10.1016/j.celrep.2017.12.039

Brait, V. H., Miro-Mur, F., Perez-De-Puig, I., Notario, L., Hurtado, B., Pedragosa, J., et al. (2019). CD69 plays a beneficial role in ischemic stroke by dampening endothelial activation. *Circ. Res.* 124, 279–291. doi: 10.1161/CIRCRESAHA.118.313818

Budni, J., Bellettini-Santos, T., Mina, F., Garcez, M. L., and Zugno, A. I. (2015). The involvement of BDNF, NGF and GDNF in aging and Alzheimer's disease. *Aging Dis.* 6, 331–341. doi: 10.14336/AD.2015.0825

Bussian, T. J., Aziz, A., Meyer, C. F., Swenson, B. L., Van Deursen, J. M., and Baker, D. J. (2018). Clearance of senescent glial cells prevents tau-dependent pathology and cognitive decline. *Nature* 562, 578–582. doi: 10.1038/s41586-018-0543-y

Cai, W., Zhang, K., Li, P., Zhu, L., Xu, J., Yang, B., et al. (2017). Dysfunction of the neurovascular unit in ischemic stroke and neurodegenerative diseases: an aging effect. *Ageing Res. Rev.* 34, 77–87. doi: 10.1016/j.arr.2016.09.006

Canugovi, C., Shamanna, R. A., Croteau, D. L., and Bohr, V. A. (2014). Base excision DNA repair levels in mitochondrial lysates of Alzheimer's disease. *Neurobiol. Aging* 35, 1293–1300. doi: 10.1016/j.neurobiolaging.2014.01.004

Cardinale, A., Racaniello, M., Saladini, S., De Chiara, G., Mollinari, C., De Stefano, M. C., et al. (2012). Sublethal doses of beta-amyloid peptide abrogate DNA-dependent protein kinase activity. *J. Biol. Chem.* 287, 2618–2631. doi: 10.1074/jbc.M111.276550

Carrano, A., Hoozemans, J. J., Van Der Vies, S. M., Rozemuller, A. J., Van Horssen, J., and De Vries, H. E. (2011). Amyloid Beta induces oxidative stress-mediated blood-brain barrier changes in capillary amyloid angiopathy. *Antioxid. Redox Signal.* 15, 1167–1178. doi: 10.1089/ars.2011.3895

Carrano, A., Hoozemans, J. J., Van Der Vies, S. M., Van Horssen, J., De Vries, H. E., and Rozemuller, A. J. (2012). Neuroinflammation and blood-brain barrier changes in capillary amyloid angiopathy. *Neurodegener Dis.* 10, 329–331. doi: 10.1159/000334916

Chen, J., Jin, K., Chen, M., Pei, W., Kawaguchi, K., Greenberg, D. A., et al. (1997). Early detection of DNA strand breaks in the brain after transient focal ischemia: implications for the role of DNA damage in apoptosis and neuronal cell death. *J. Neurochem.* 69, 232–245. doi: 10.1046/j.1471-4159.1997.69010232.x

Chinta, S. J., Woods, G., Rane, A., Demaria, M., Campisi, J., and Andersen, J. K. (2015). Cellular senescence and the aging brain. *Exp. Gerontol.* 68, 3–7.

Choi, D. H., Cristovao, A. C., Guhathakurta, S., Lee, J., Joh, T. H., Beal, M. F., et al. (2012). NADPH oxidase 1-mediated oxidative stress leads to dopamine neuron death in Parkinson's disease. *Antioxid. Redox Signal.* 16, 1033–1045. doi: 10.1089/ars.2011.3960

Chow, H. M., Cheng, A., Song, X., Swerdel, M. R., Hart, R. P., and Herrup, K. (2019). ATM is activated by ATP depletion and modulates mitochondrial function through NRF1. *J. Cell Biol.* 218, 909–928. doi: 10.1083/jcb.201806197

Chow, H.-M., and Herrup, K. (2015). Genomic integrity and the ageing brain. *Nat. Rev. Neurosci.* 16, 672–684. doi: 10.1038/nrn4020

Chung, J. H. (2018). The role of DNA-PK in aging and energy metabolism. *FEBS J.* 285, 1959–1972. doi: 10.1111/febs.14410

Chung, Y. C., Kim, Y. S., Bok, E., Yune, T. Y., Maeng, S., and Jin, B. K. (2013). MMP-3 contributes to nigrostriatal dopaminergic neuronal loss, BBB damage, and neuroinflammation in an MPTP mouse model of Parkinson's disease. *Mediators Inflamm.* 2013:370526. doi: 10.1155/2013/370526

Chung, Y. C., Shin, W. H., Baek, J. Y., Cho, E. J., Baik, H. H., Kim, S. R., et al. (2016). CB2 receptor activation prevents glial-derived neurotoxic mediator production, BBB leakage and peripheral immune cell infiltration and rescues dopamine neurons in the MPTP model of Parkinson's disease. *Exp. Mol. Med.* 48:e205. doi: 10.1038/emm.2015.100

Ciccia, A., and Elledge, S. J. (2010). The DNA damage response: making it safe to play with knives. *Mol. Cell* 40, 179–204. doi: 10.1016/j.molcel.2010.09.019

Clarke, L. E., Liddelow, S. A., Chakraborty, C., Munch, A. E., Heiman, M., and Barres, B. A. (2018). Normal aging induces A1-like astrocyte reactivity. *Proc. Natl. Acad. Sci. U.S.A.* 115, E1896-E1905. doi: 10.1073/pnas.1800165115

Collins, L. M., Toulouse, A., Connor, T. J., and Nolan, Y. M. (2012). Contributions of central and systemic inflammation to the pathophysiology of Parkinson's disease. *Neuropharmacology* 62, 2154–2168. doi: 10.1016/j.neuropharm.2012.01.028

Cornelis, F. M. F., Monteagudo, S., Guns, L. K. A., Den Hollander, W., Nelissen, R., Storms, L., et al. (2018). ANP32A regulates ATM expression and prevents oxidative stress in cartilage, brain, and bone. *Sci. Transl. Med.* 10:eaar8426. doi: 10.1126/scitranslmed.aar8426

Cortes-Canteli, M., Mattei, L., Richards, A. T., Norris, E. H., and Strickland, S. (2015). Fibrin deposited in the Alzheimer's disease brain promotes neuronal degeneration. *Neurobiol. Aging* 36, 608–617. doi: 10.1016/j.neurobiolaging.2014.10.030

D'apolito, M., Colia, A. L., Manca, E., Pettoello-Mantovani, M., Sacco, M., Maffione, A. B., et al. (2018). Urea memory: transient cell exposure to urea causes persistent mitochondrial ros production and endothelial dysfunction. *Toxins* 10:410.

Cortes-Canteli, M., Paul, J., Norris, E. H., Bronstein, R., Ahn, H. J., Zamolodchikov, D., et al. (2010). Fibrinogen and beta-amyloid association alters thrombosis and fibrinolysis: a possible contributing factor to Alzheimer's disease. *Neuron* 66, 695–709. doi: 10.1016/j.neuron.2010.05.014

Dalkara, T., Gursoy-Ozdemir, Y., and Yemisci, M. (2011). Brain microvascular pericytes in health and disease. *Acta Neuropathol.* 122, 1–9. doi: 10.1007/s00401-011-0847-6

D'Angelo, G., Impellizzeri, P., Marseglia, L., Montalto, A. S., Russo, T., Salamone, I., et al. (2018). Current status of laboratory and imaging diagnosis of neonatal necrotizing enterocolitis. *Ital. J. Pediatr.* 44:84. doi: 10.1186/s13052-018-0528-3

Davis, J., Cribbs, D. H., Cotman, C. W., and Van Nostrand, W. E. (1999). Pathogenic amyloid beta-protein induces apoptosis in cultured human cerebrovascular smooth muscle cells. *Amyloid* 6, 157–164. doi: 10.3109/13506129909007321

Donahue, M. J., and Hendrikse, J. (2018). Improved detection of cerebrovascular disease processes: introduction to the journal of cerebral blood flow and metabolism special issue on cerebrovascular disease. *J. Cereb. Blood Flow Metab.* 38, 1387–1390. doi: 10.1177/0271678X17739802

Donato, A. J., Eskurza, I., Silver, A. E., Levy, A. S., Pierce, G. L., Gates, P. E., et al. (2007). Direct evidence of endothelial oxidative stress with aging in humans: relation to impaired endothelium-dependent dilation and upregulation of nuclear factor-kappaB. *Circ. Res.* 100, 1659–1666. doi: 10.1161/01.res.0000269183.13937.e8

Dor, Y., and Cedar, H. (2018). Principles of DNA methylation and their implications for biology and medicine. *Lancet* 392, 777–786. doi: 10.1016/S0140-6736(18)31268-6

Elahy, M., Jackaman, C., Mamo, J. C., Lam, V., Dhaliwal, S. S., Giles, C., et al. (2015). Blood-brain barrier dysfunction developed during normal aging is associated with inflammation and loss of tight junctions but not with leukocyte recruitment. *Immun. Ageing* 12:2. doi: 10.1186/s12979-015-0029-9

Emerich, D. F., Skinner, S. J. M., Borlongan, C. V., Vasconcellos, A. V., and Thanos, C. G. (2005). The choroid plexus in the rise, fall and repair of the brain. *Bioessays* 27, 262–274. doi: 10.1002/bies.20193

Fang, E. F., Scheibye-Knudsen, M., Brace, L. E., Kassahun, H., Sengupta, T., Nilsen, H., et al. (2014). Defective mitophagy in XPA via PARP-1 hyperactivation and NAD(+)/SIRT1 reduction. *Cell* 157, 882–896. doi: 10.1016/j.cell.2014.03.026

Fernandez-Klett, F., Potas, J. R., Hilpert, D., Blazej, K., Radke, J., Huck, J., et al. (2013). Early loss of pericytes and perivascular stromal cell-induced scar formation after stroke. *J. Cereb. Blood Flow Metab.* 33, 428–439. doi: 10.1038/jcbfm.2012.187

Fivenson, E. M., Lautrup, S., Sun, N., Scheibye-Knudsen, M., Stevnsner, T., Nilsen, H., et al. (2017). Mitophagy in neurodegeneration and aging. *Neurochem. Int.* 109, 202–209. doi: 10.1016/j.neuint.2017.02.007

Fluteau, A., Ince, P. G., Minett, T., Matthews, F. E., Brayne, C., Garwood, C. J., et al. (2015). The nuclear retention of transcription factor FOXO3a correlates with a DNA damage response and increased glutamine synthetase expression by astrocytes suggesting a neuroprotective role in the ageing brain. *Neurosci. Lett.* 609, 11–17. doi: 10.1016/j.neulet.2015.10.001

Freeze, W. M., Bacskai, B. J., Frosch, M. P., Jacobs, H. I. L., Backes, W. H., Greenberg, S. M., et al. (2019). Blood-brain barrier leakage and microvascular lesions in cerebral amyloid angiopathy. *Stroke* 50, 328–335. doi: 10.1161/STROKEAHA.118.023788

Fuger, P., Hefendehl, J. K., Veeraraghavalu, K., Wendeln, A. C., Schlosser, C., Obermuller, U., et al. (2017). Microglia turnover with aging and in an Alzheimer's model via long-term in vivo single-cell imaging. *Nat. Neurosci.* 20, 1371–1376. doi: 10.1038/nn.4631

Gal, J., Chen, J., Katsumata, Y., Fardo, D. W., Wang, W. X., Artiushin, S., et al. (2018). Detergent insoluble proteins and inclusion body-like structures immunoreactive for PRKDC/DNA-PK/DNA-PKcs, FTL, NNT, and AIFM1 in the amygdala of cognitively impaired elderly persons. *J. Neuropathol. Exp. Neurol.* 77, 21–39. doi: 10.1093/jnen/nlx097

Gaweda-Walerych, K., and Zekanowski, C. (2013). The impact of mitochondrial DNA and nuclear genes related to mitochondrial functioning on the risk of Parkinson's disease. *Curr. Genomics* 14, 543–559. doi: 10.2174/1389202914666131210211033

Gorbunova, V., Seluanov, A., Mao, Z., and Hine, C. (2007). Changes in DNA repair during aging. *Nucleic Acids Res.* 35, 7466–7474. doi: 10.1093/nar/gkm756

Goukassian, D. A., Bagheri, S., El-Keeb, L., Eller, M. S., and Gilchrest, B. A. (2002). DNA oligonucleotide treatment corrects the age-associated decline in DNA repair capacity. *FASEB J.* 16, 754–756. doi: 10.1096/fj.01-0829fje

Gredilla, R., Bohr, V. A., and Stevnsner, T. (2010). Mitochondrial DNA repair and association with aging–an update. *Exp. Gerontol.* 45, 478–488. doi: 10.1016/j.exger.2010.01.017

Gugliandolo, E., D'amico, R., Cordaro, M., Fusco, R., Siracusa, R., Crupi, R., et al. (2018). Neuroprotective effect of artesunate in experimental model of traumatic brain injury. *Front. Neurol.* 9:590. doi: 10.3389/fneur.2018.00590

Hayflick, L. (2007). Biological aging is no longer an unsolved problem. *Ann. N. Y. Acad. Sci.* 1100, 1–13. doi: 10.1196/annals.1395.001

He, H., Lam, M., Mccormick, T. S., and Distelhorst, C. W. (1997). Maintenance of calcium homeostasis in the endoplasmic reticulum by Bcl-2. *J. Cell Biol.* 138, 1219–1228. doi: 10.1083/jcb.138.6.1219

Hebert, L. E., Weuve, J., Scherr, P. A., and Evans, D. A. (2013). Alzheimer disease in the United States (2010–2050) estimated using the 2010 census. *Neurology* 80, 1778–1783. doi: 10.1212/WNL.0b013e31828726f5

Helms, H. C., Aldana, B. I., Groth, S., Jensen, M. M., Waagepetersen, H. S., Nielsen, C. U., et al. (2017). Characterization of the L-glutamate clearance pathways across the blood-brain barrier and the effect of astrocytes in an in vitro blood-brain barrier model. *J. Cereb. Blood Flow Metab.* 37, 3744–3758. doi: 10.1177/0271678X17690760

Herholz, K., Haense, C., Gerhard, A., Jones, M., Anton-Rodriguez, J., Segobin, S., et al. (2018). Metabolic regional and network changes in Alzheimer's disease subtypes. *J. Cereb. Blood Flow Metab.* 38, 1796–1806. doi: 10.1177/0271678X17718436

Hou, Y., Lautrup, S., Cordonnier, S., Wang, Y., Croteau, D. L., Zavala, E., et al. (2018). NAD(+) supplementation normalizes key Alzheimer's features and DNA damage responses in a new AD mouse model with introduced DNA repair deficiency. *Proc. Natl. Acad. Sci. U.S.A.* 115, E1876–E1885. doi: 10.1073/pnas.1718819115

Hughes, S., Gardiner, T., Hu, P., Baxter, L., Rosinova, E., and Chan-Ling, T. (2006). Altered pericyte-endothelial relations in the rat retina during aging: implications for vessel stability. *Neurobiol. Aging* 27, 1838–1847. doi: 10.1016/j.neurobiolaging.2005.10.021

Iyama, T., and Wilson, D. M., III. (2013). DNA repair mechanisms in dividing and non-dividing cells. *DNA Repair* 12, 620–636. doi: 10.1016/j.dnarep.2013.04.015

Jadavji, N. M., Farr, T. D., Lips, J., Khalil, A. A., Boehm-Sturm, P., Foddis, M., et al. (2015). Elevated levels of plasma homocysteine, deficiencies in dietary folic acid and uracil-DNA glycosylase impair learning in a mouse model of vascular

cognitive impairment. *Behav. Brain Res.* 283, 215–226. doi: 10.1016/j.bbr.2015.01.040

Jangula, A., and Murphy, E. J. (2013). Lipopolysaccharide-induced blood brain barrier permeability is enhanced by alpha-synuclein expression. *Neurosci. Lett.* 551, 23–27. doi: 10.1016/j.neulet.2013.06.058

Jensen, H. L. B., Lillenes, M. S., Rabano, A., Gunther, C. C., Riaz, T., Kalayou, S. T., et al. (2018). Expression of nucleotide excision repair in Alzheimer's disease is higher in brain tissue than in blood. *Neurosci. Lett.* 672, 53–58. doi: 10.1016/j.neulet.2018.02.043

Jiang, X., Suenaga, J., Pu, H., Wei, Z., Smith, A. D., Hu, X., et al. (2018). Post-stroke administration of omega-3 polyunsaturated fatty acids promotes neurovascular restoration after ischemic stroke in mice: efficacy declines with aging. *Neurobiol. Dis.* 126, 62–75. doi: 10.1016/j.nbd.2018.09.012

Jin, W. N., Shi, S. X., Li, Z., Li, M., Wood, K., Gonzales, R. J., et al. (2017). Depletion of microglia exacerbates postischemic inflammation and brain injury. *J. Cereb. Blood Flow Metab.* 37, 2224–2236.

Kam, T. I., Mao, X., Park, H., Chou, S. C., Karuppagounder, S. S., Umanah, G. E., et al. (2018). Poly(ADP-ribose) drives pathologic alpha-synuclein neurodegeneration in Parkinson's disease. *Science* 362:eaat8407. doi: 10.1126/science.aat8407

Kanu, N., and Behrens, A. (2008). ATMINistrating ATM signalling: regulation of ATM by ATMIN. *Cell Cycle* 7, 3483–3486. doi: 10.4161/cc.7.22.7044

Kanu, N., Penicud, K., Hristova, M., Wong, B., Irvine, E., Plattner, F., et al. (2010). The ATM cofactor ATMIN protects against oxidative stress and accumulation of DNA damage in the aging brain. *J. Biol. Chem.* 285, 38534–38542. doi: 10.1074/jbc.M110.145896

Kanungo, J. (2016). DNA-PK Deficiency in Alzheimer's disease. *J. Neurol. Neuromedicine* 1, 17–22. doi: 10.29245/2572.942x/2016/3.1016

Kaur, N., Dhiman, M., Perez-Polo, J. R., and Mantha, A. K. (2015). Ginkgolide B revamps neuroprotective role of apurinic/apyrimidinic endonuclease 1 and mitochondrial oxidative phosphorylation against Abeta25-35 -induced neurotoxicity in human neuroblastoma cells. *J. Neurosci. Res.* 93, 938–947. doi: 10.1002/jnr.23565

Khennouf, L., Gesslein, B., Brazhe, A., Octeau, J. C., Kutuzov, N., Khakh, B. S., et al. (2018). Active role of capillary pericytes during stimulation-induced activity and spreading depolarization. *Brain* 141, 2032–2046. doi: 10.1093/brain/awy143

Kluge, M. G., Abdolhoseini, M., Zalewska, K., Ong, L. K., Johnson, S. J., Nilsson, M., et al. (2018). Spatiotemporal analysis of impaired microglia process movement at sites of secondary neurodegeneration post-stroke. *J. Cereb. Blood Flow Metab.* doi: 10.1177/0271678X18797346 [Epub ahead of print].

Knopman, D. S. (2019). Bad news and good news in AD, and how to reconcile them. *Nat. Rev. Neurol.* 15, 61–62. doi: 10.1038/s41582-018-0131-7

Kook, S. Y., Hong, H. S., Moon, M., Ha, C. M., Chang, S., and Mook-Jung, I. (2012). Abeta(1)(-)(4)(2)-RAGE interaction disrupts tight junctions of the blood-brain barrier via Ca(2)(+)-calcineurin signaling. *J. Neurosci.* 32, 8845–8854. doi: 10.1523/JNEUROSCI.6102-11.2012

Kreis, P., Gallrein, C., Rojas-Puente, E., Mack, T. G. A., Kroon, C., Dinkel, V., et al. (2019). ATM phosphorylation of the actin-binding protein drebrin controls oxidation stress-resistance in mammalian neurons and C. *elegans*. *Nat. Commun.* 10:486. doi: 10.1038/s41467-019-08420-w

Lai, S., Mastroluca, D., Letizia, C., Petramala, L., Perrotta, A. M., Digaeta, A., et al. (2018). Magnetic resonance imaging 3T and total fibrotic volume in autosomal dominant polycystic kidney disease. *Intern. Med. J.* 48, 1505–1513. doi: 10.1111/imj.14039

Lavin, M. F., Kozlov, S., Gatei, M., and Kijas, A. W. (2015). ATM-dependent phosphorylation of all three members of the MRN complex: from sensor to adaptor. *Biomolecules* 5, 2877–2902. doi: 10.3390/biom5042877

Lazarczyk, M. J., Kemmler, J. E., Eyford, B. A., Short, J. A., Varghese, M., Sowa, A., et al. (2016). Major Histocompatibility Complex class I proteins are critical for maintaining neuronal structural complexity in the aging brain. *Sci. Rep.* 6:26199. doi: 10.1038/srep26199

Leak, R. K., Li, P., Zhang, F., Sulaiman, H. H., Weng, Z., Wang, G., et al. (2015). Apurinic/apyrimidinic endonuclease 1 upregulation reduces oxidative DNA damage and protects hippocampal neurons from ischemic injury. *Antioxid. Redox Signal.* 22, 135–148. doi: 10.1089/ars.2013.5511

Leandro, G. S., Sykora, P., and Bohr, V. A. (2015). The impact of base excision DNA repair in age-related neurodegenerative diseases. *Mutat. Res.* 776, 31–39. doi: 10.1016/j.mrfmmm.2014.12.011

Lee, H., and Pienaar, I. S. (2014). Disruption of the blood-brain barrier in Parkinson's disease: curse or route to a cure? *Front. Biosci.* 19, 272–280. doi: 10.2741/4206

Lee, J. H., and Paull, T. T. (2005). ATM activation by DNA double-strand breaks through the Mre11-Rad50-Nbs1 complex. *Science* 308, 551–554. doi: 10.1126/science.1108297

Lee, P., Kim, J., Williams, R., Sandhir, R., Gregory, E., Brooks, W. M., et al. (2012). Effects of aging on blood brain barrier and matrix metalloproteases following controlled cortical impact in mice. *Exp. Neurol.* 234, 50–61. doi: 10.1016/j.expneurol.2011.12.016

Li, P., Hu, X., Gan, Y., Gao, Y., Liang, W., and Chen, J. (2011). Mechanistic insight into DNA damage and repair in ischemic stroke: exploiting the base excision repair pathway as a model of neuroprotection. *Antioxid. Redox Signal.* 14, 1905–1918. doi: 10.1089/ars.2010.3451

Lo, E. H., and Rosenberg, G. A. (2009). The neurovascular unit in health and disease: introduction. *Stroke* 40, S2–S3.

Lodato, M. A., Rodin, R. E., Bohrson, C. L., Coulter, M. E., Barton, A. R., Kwon, M., et al. (2018). Aging and neurodegeneration are associated with increased mutations in single human neurons. *Science* 359, 555–559. doi: 10.1126/science.aao4426

Lu, T., Aron, L., Zullo, J., Pan, Y., Kim, H., Chen, Y., et al. (2014). REST and stress resistance in ageing and Alzheimer's disease. *Nature* 507, 448–454. doi: 10.1038/nature13163

Madabhushi, R., Pan, L., and Tsai, L. H. (2014). DNA damage and its links to neurodegeneration. *Neuron* 83, 266–282. doi: 10.1016/j.neuron.2014.06.034

Mangialasche, F., Kivipelto, M., Mecocci, P., Rizzuto, D., Palmer, K., Winblad, B., et al. (2010). High plasma levels of vitamin E forms and reduced Alzheimer's disease risk in advanced age. *J. Alzheimers Dis.* 20, 1029–1037. doi: 10.3233/JAD-2010-091450

Mangold, C. A., Masser, D. R., Stanford, D. R., Bixler, G. V., Pisupati, A., Giles, C. B., et al. (2017). CNS-wide sexually dimorphic induction of the major histocompatibility complex 1 pathway with aging. *J. Gerontol. A Biol. Sci. Med. Sci.* 72, 16–29. doi: 10.1093/gerona/glv232

Maragakis, N. J., and Rothstein, J. D. (2006). Mechanisms of disease: astrocytes in neurodegenerative disease. *Nat. Clin. Pract. Neurol.* 2, 679–689. doi: 10.1038/ncpneuro0355

Martire, S., Fuso, A., Mosca, L., Forte, E., Correani, V., Fontana, M., et al. (2016). Bioenergetic impairment in animal and cellular models of Alzheimer's disease: PARP-1 inhibition rescues metabolic dysfunctions. *J. Alzheimers Dis.* 54, 307–324. doi: 10.3233/JAD-151040

Matsuda, S., Umeda, M., Kato, H., and Araki, T. (2009). Glial damage after transient focal cerebral ischemia in rats. *J. Mol. Neurosci.* 38, 220–226. doi: 10.1007/s12031-008-9165-4

Mattson, M. P., and Magnus, T. (2006). Ageing and neuronal vulnerability. *Nat. Rev. Neurosci.* 7, 278–294. doi: 10.1038/nrn1886

Maugeri, N., Capobianco, A., Rovere-Querini, P., Ramirez, G.A ., Tombetti, E., Valle, P. D., et al. (2018). Platelet microparticles sustain autophagy-associated activation of neutrophils in systemic sclerosis. *Sci. Transl. Med.* 10:eaao3089. doi: 10.1126/scitranslmed.aao3089

Mazeika, G., and Doraiswamy, P. M. (2002). "Structural Changes in the Aging Brain," in *Principles and Practice of Geriatric Psychiatry*. eds Anand Kumar, C. L. E. Katona (Hoboken, NJ: John Wiley & Sons, Ltd), 23-24.

McKinnon, P. J. (2013). Maintaining genome stability in the nervous system. *Nat. Neurosci.* 16, 1523–1529. doi: 10.1038/nn.3537

Merlini, M., Meyer, E. P., Ulmann-Schuler, A., and Nitsch, R. M. (2011). Vascular beta-amyloid and early astrocyte alterations impair cerebrovascular function and cerebral metabolism in transgenic arcAbeta mice. *Acta Neuropathol.* 122, 293–311. doi: 10.1007/s00401-011-0834-y

Merlini, M., Rafalski, V. A., Rios Coronado, P. E., Gill, T. M., Ellisman, M., Muthukumar, G., et al. (2019). Fibrinogen induces microglia-mediated spine elimination and cognitive impairment in an Alzheimer's disease model. *Neuron* 101, 1099.e6–1108.e6. doi: 10.1016/j.neuron.2019.01.014

Miao, J., Xu, F., Davis, J., Otte-Holler, I., Verbeek, M. M., and Van Nostrand, W. E. (2005). Cerebral microvascular amyloid beta protein deposition induces

vascular degeneration and neuroinflammation in transgenic mice expressing human vasculotropic mutant amyloid beta precursor protein. *Am. J. Pathol.* 167, 505–515. doi: 10.1016/s0002-9440(10)62993-8

Milanese, C., Cerri, S., Ulusoy, A., Gornati, S.V., Plat, A., Gabriels, S., et al. (2018). Activation of the DNA damage response in vivo in synucleinopathy models of Parkinson's disease. *Cell. Death Dis.* 9:818. doi: 10.1038/s41419-018-0848-7

Miners, J. S., Schulz, I., and Love, S. (2018). Differing associations between Abeta accumulation, hypoperfusion, blood-brain barrier dysfunction and loss of PDGFRB pericyte marker in the precuneus and parietal white matter in Alzheimer's disease. *J. Cereb. Blood Flow Metab.* 38, 103–115. doi: 10.1177/0271678X17690761

Montagne, A., Barnes, S. R., Sweeney, M. D., Halliday, M. R., Sagare, A. P., Zhao, Z., et al. (2015). Blood-brain barrier breakdown in the aging human hippocampus. *Neuron* 85, 296–302. doi: 10.1016/j.neuron.2014.12.032

Montagne A., Nikolakopoulou A. M., Zhao Z. Sagare A. P., Si G., Lazic D. et al. (2018). Pericyte degeneration causes white matter dysfunction in the mouse central nervous system. *Nature Medicine* 24, 326–337. doi: 10.1038/nm.4482

Mrak, R. E., and Griffin, W. S. (2005). Glia and their cytokines in progression of neurodegeneration. *Neurobiol. Aging* 26, 349–354. doi: 10.1016/j.neurobiolaging.2004.05.010

Myung, N. H., Zhu, X., Kruman, I. I., Castellani, R. J., Petersen, R. B., Siedlak, S. L., Perry, G., et al. (2008). Evidence of DNA damage in Alzheimer disease: phosphorylation of histone H2AX in astrocytes. *Age* 30, 209–215. doi: 10.1007/s11357-008-9050-7

Nag, T.C., and Wadhwa, S. (2012). Accumulation of lipid inclusions in astrocytes of aging human optic nerve. *Acta Biol. Hung.* 63(Suppl. 1) 54–64. doi: 10.1556/ABiol.63.2012.Suppl.1.6

Nahirney, P. C., Reeson, P., and Brown, C. E. (2016). Ultrastructural analysis of blood-brain barrier breakdown in the peri-infarct zone in young adult and aged mice. *J. Cereb. Blood Flow Metab.* 36, 413–425. doi: 10.1177/0271678X15608396

Nakajima, H., Kubo, T., Ihara, H., Hikida, T., Danjo, T., Nakatsuji, M., et al. (2015). Nuclear-translocated Glyceraldehyde-3-phosphate dehydrogenase promotes poly(ADP-ribose) Polymerase-1 activation during oxidative/nitrosative stress in stroke. *J. Biol. Chem.* 290, 14493–14503. doi: 10.1074/jbc.M114.635607

Nation, D. A., Sweeney, M. D., Montagne, A., Sagare, A. P., D'orazio, L. M., Pachicano, M., et al. (2019). Blood-brain barrier breakdown is an early biomarker of human cognitive dysfunction. *Nat. Med.* 25, 270–276. doi: 10.1038/s41591-018-0297-y

Nicholls, D. G., and Budd, S. L. (2000). Mitochondria and neuronal survival. *Physiol. Rev.* 80, 315–360. doi: 10.1152/physrev.2000.80.1.315

Niedernhofer, L. J., Gurkar, A. U., Wang, Y., Vijg, J., Hoeijmakers, J. H. J., and Robbins, P. D. (2018). Nuclear genomic instability and aging. *Annu. Rev. Biochem.* 87, 295–322.

Norden, D. M., and Godbout, J. P. (2013). Review: microglia of the aged brain: primed to be activated and resistant to regulation. *Neuropathol. Appl. Neurobiol.* 39, 19–34. doi: 10.1111/j.1365-2990.2012.01306.x

Ohlin, K. E., Francardo, V., Lindgren, H. S., Sillivan, S. E., O'sullivan, S. S., Luksik, A. S., et al. (2011). Vascular endothelial growth factor is upregulated by L-dopa in the parkinsonian brain: implications for the development of dyskinesia. *Brain* 134, 2339–2357. doi: 10.1093/brain/awr165

Olsen, A. L., and Feany, M. B. (2019). PARP inhibitors and Parkinson's disease. *N Engl. J. Med.* 380, 492–494.

Ou, H. L., and Schumacher, B. (2018). DNA damage responses and p53 in the aging process. *Blood* 131, 488–495. doi: 10.1182/blood-2017-07-746396

Pan, M., Wang, P., Zheng, C., Zhang, H., Lin, S., Shao, B., et al. (2017). Aging systemic milieu impairs outcome after ischemic stroke in rats. *Aging Dis.* 8, 519–530. doi: 10.14336/AD.2017.0710

Paul, J., Strickland, S., and Melchor, J. P. (2007). Fibrin deposition accelerates neurovascular damage and neuroinflammation in mouse models of Alzheimer's disease. *J. Exp. Med.* 204, 1999–2008. doi: 10.1084/jem.20070304

Perry, V.H., and Holmes, C. (2014). Microglial priming in neurodegenerative disease. *Nat. Rev. Neurol.* 10, 217–224. doi: 10.1038/nrneurol.2014.38

Persson, T., Popescu, B. O., and Cedazo-Minguez, A. (2014). Oxidative stress in Alzheimer's disease: why did antioxidant therapy fail? *Oxid. Med. Cell Longev.* 2014:427318. doi: 10.1155/2014/427318

Peters, A. (2009). The effects of normal aging on myelinated nerve fibers in monkey central nervous system. *Front. Neuroanat.* 3:11. doi: 10.3389/neuro.05.011

Peters, A., and Sethares, C. (2002). Aging and the myelinated fibers in prefrontal cortex and corpus callosum of the monkey. *J. Comp. Neurol.* 442, 277–291. doi: 10.1002/cne.10099

Petersen M. A., Ryu J. K., Chang K. J., Etxeberria A., Bardehle S., Mendiola A. S., Kamau-Devers W. (2017). Fibrinogen activates bmp signaling in oligodendrocyte progenitor cells and inhibits remyelination after vascular damage. *Neuron* 96, 1003.e7–1012.e7. doi: 10.1016/j.neuron.2017.10.008

Poprac, P., Jomova, K., Simunkova, M., Kollar, V., Rhodes, C. J., and Valko, M. (2017). Targeting free radicals in oxidative stress-related human diseases. *Trends Pharmacol. Sci.* 38, 592–607. doi: 10.1016/j.tips.2017.04.005

Poyhonen, S., Er, S., Domanskyi, A., and Airavaara, M. (2019). Effects of neurotrophic factors in glial cells in the central nervous system: expression and properties in neurodegeneration and injury. *Front. Physiol.* 10:486. doi: 10.3389/fphys.2019.00486

Prakash, A., Cao, V. B., and Doublie, S. (2016). Phosphorylation sites identified in the NEIL1 DNA glycosylase are potential targets for the JNK1 kinase. *PLoS One* 11:e0157860. doi: 10.1371/journal.pone.0157860

Qian, M., Liu, Z., Peng, L., Tang, X., Meng, F., Ao, Y., et al. (2018). Boosting ATM activity alleviates aging and extends lifespan in a mouse model of progeria. *eLife* 7:e34836. doi: 10.7554/eLife.34836

Ritzel, R. M., Lai, Y. J., Crapser, J. D., Patel, A. R., Schrecengost, A., Grenier, J. M., et al. (2018). Aging alters the immunological response to ischemic stroke. *Acta Neuropathol.* 136, 89–110. doi: 10.1007/s00401-018-1859-2

Rodriguez, M., Morales, I., Rodriguez-Sabate, C., Sanchez, A., Castro, R., Brito, J. M., et al. (2014). The degeneration and replacement of dopamine cells in Parkinson's disease: the role of aging. *Front. Neuroanat.* 8:80. doi: 10.3389/fnana.2014.00080

Rodriguez, M., Rodriguez-Sabate, C., Morales, I., Sanchez, A., and Sabate, M. (2015). Parkinson's disease as a result of aging. *Aging Cell* 14, 293–308.

Rulten, S. L., and Caldecott, K. W. (2013). DNA strand break repair and neurodegeneration. *DNA Repair* 12, 558–567. doi: 10.1016/j.dnarep.2013.04.008

Ryu, J. K., Rafalski, V. A., Meyer-Franke, A., Adams, R. A., Poda, S. B., Rios Coronado, P. E., et al. (2018). Fibrin-targeting immunotherapy protects against neuroinflammation and neurodegeneration. *Nat. Immunol.* 19, 1212–1223. doi: 10.1038/s41590-018-0232-x

Ryu J. K., Petersen M. A., Murray S. G., Baeten K. M., Meyer-Franke A., Chan J. P. et al. (2015). Blood coagulation protein fibrinogen promotes autoimmunity and demyelination via chemokine release and antigen presentation. *Nat. commun.* 6:8164. doi: 10.1038/ncomms9164

Sagare, A. P., Bell, R. D., Zhao, Z., Ma, Q., Winkler, E. A., Ramanathan, A., et al. (2013). Pericyte loss influences Alzheimer-like neurodegeneration in mice. *Nat. Commun.* 4:2932. doi: 10.1038/ncomms3932

Salinet, A. S., Silva, N. C., Caldas, J., De Azevedo, D. S., De-Lima-Oliveira, M., Nogueira, R. C., et al. (2018). Impaired cerebral autoregulation and neurovascular coupling in middle cerebral artery stroke: influence of severity? *J. Cereb. Blood Flow Metab.* doi: 10.1177/0271678X18794835 [Epub ahead of print].

Salminen, A., Ojala, J., Kaarniranta, K., Haapasalo, A., Hiltunen, M., and Soininen, H. (2011). Astrocytes in the aging brain express characteristics of senescence-associated secretory phenotype. *Eur. J. Neurosci.* 34, 3–11. doi: 10.1111/j.1460-9568.2011.07738.x

Santos, R. X., Correia, S. C., Zhu, X., Smith, M. A., Moreira, P. I., Castellani, R. J., et al. (2013). Mitochondrial DNA oxidative damage and repair in aging and Alzheimer's disease. *Antioxid. Redox Signal.* 18, 2444–2457. doi: 10.1089/ars.2012.5039

Schachtrup, C., Lu, P., Jones, L. L., Lee, J. K., Lu, J., Sachs, B. D., et al. (2007). Fibrinogen inhibits neurite outgrowth via beta 3 integrin-mediated phosphorylation of the EGF receptor. *Proc. Natl. Acad. Sci. U.S.A.* 104, 11814–11819. doi: 10.1073/pnas.0704045104

Schultz, N., Brannstrom, K., Byman, E., Moussaud, S., Nielsen, H. M., Olofsson, A., et al. (2018). Amyloid-beta 1-40 is associated with alterations in NG2+ pericyte population ex vivo and in vitro. *Aging Cell* 17:e12728. doi: 10.1111/acel.12728

Sengillo, J. D., Winkler, E. A., Walker, C. T., Sullivan, J. S., Johnson, M., and Zlokovic, B. V. (2013). Deficiency in mural vascular cells coincides with blood-brain barrier disruption in Alzheimer's disease. *Brain Pathol.* 23, 303–310. doi: 10.1111/bpa.12004

Sepe, S., Milanese, C., Gabriels, S., Derks, K. W., Payan-Gomez, C., Van, I. W. F., et al. (2016). Inefficient DNA repair is an aging-related modifier of parkinson's disease. *Cell Rep.* 15, 1866–1875. doi: 10.1016/j.celrep.2016.04.071

Sharma, S. (2007). Age-related nonhomologous end joining activity in rat neurons. *Brain Res. Bull.* 73, 48–54. doi: 10.1016/j.brainresbull.2007.02.001

Shi, C., Zhu, J., Leng, S., Long, D., and Luo, X. (2016). Mitochondrial FOXO3a is involved in amyloid beta peptide-induced mitochondrial dysfunction. *J. Bioenerg. Biomembr.* 48, 189–196. doi: 10.1007/s10863-016-9645-0

Shiloh, Y. (2014). ATM: expanding roles as a chief guardian of genome stability. *Exp. Cell Res.* 329, 154–161. doi: 10.1016/j.yexcr.2014.09.002

Simpson, J. E., Ince, P. G., Haynes, L. J., Theaker, R., Gelsthorpe, C., Baxter, L., et al. (2010). Population variation in oxidative stress and astrocyte DNA damage in relation to Alzheimer-type pathology in the ageing brain. *Neuropathol. Appl. Neurobiol.* 36, 25–40. doi: 10.1111/j.1365-2990.2009.01030.x

Skaper, S. D., Facci, L., Zusso, M., and Giusti, P. (2017). Synaptic plasticity, dementia and Alzheimer disease. *CNS Neurol. Disord. Drug Targets* 16, 220–233. doi: 10.2174/1871527316666170113120853

Smith, L. K., He, Y., Park, J. S., Bieri, G., Snethlage, C. E., Lin, K., et al. (2015). beta2-microglobulin is a systemic pro-aging factor that impairs cognitive function and neurogenesis. *Nat Med.* 21, 932–937. doi: 10.1038/nm.3898

Stamatovic, S. M., Martinez-Revollar, G., Hu, A., Choi, J., Keep, R. F., and Andjelkovic, A. V. (2018). Decline in Sirtuin-1 expression and activity plays a critical role in blood-brain barrier permeability in aging. *Neurobiol. Dis.* 126, 105–116. doi: 10.1016/j.nbd.2018.09.006

Stetler, R. A., Gao, Y., Zukin, R. S., Vosler, P. S., Zhang, L., Zhang, F., et al. (2010). Apurinic/apyrimidinic endonuclease APE1 is required for PACAP-induced neuroprotection against global cerebral ischemia. *Proc. Natl. Acad. Sci. U.S.A.* 107, 3204–3209. doi: 10.1073/pnas.1000030107

Suberbielle, E., Djukic, B., Evans, M., Kim, D. H., Taneja, P., Wang, X., et al. (2015). DNA repair factor BRCA1 depletion occurs in Alzheimer brains and impairs cognitive function in mice. *Nat. Commun.* 6:8897. doi: 10.1038/ncomms9897

Sweeney, M. D., Ayyadurai, S., and Zlokovic, B. V. (2016). Pericytes of the neurovascular unit: key functions and signaling pathways. *Nat. Neurosci.* 19, 771–783. doi: 10.1038/nn.4288

Sweeney, M. D., Kisler, K., Montagne, A., Toga, A. W., and Zlokovic, B. V. (2018a). The role of brain vasculature in neurodegenerative disorders. *Nat. Neurosci.* 21, 1318–1331. doi: 10.1038/s41593-018-0234-x

Sweeney, M. D., Sagare, A. P., and Zlokovic, B. V. (2018b). Blood-brain barrier breakdown in Alzheimer disease and other neurodegenerative disorders. *Nat. Rev. Neurol.* 14, 133–150. doi: 10.1038/nrneurol.2017.188

Sykora, P., Misiak, M., Wang, Y., Ghosh, S., Leandro, G. S., Liu, D., et al. (2015). DNA polymerase beta deficiency leads to neurodegeneration and exacerbates Alzheimer disease phenotypes. *Nucleic Acids Res.* 43, 943–959. doi: 10.1093/nar/gku1356

Sykora, P., Yang, J. L., Ferrarelli, L. K., Tian, J., Tadokoro, T., Kulkarni, A., et al. (2013). Modulation of DNA base excision repair during neuronal differentiation. *Neurobiol. Aging* 34, 1717–1727. doi: 10.1016/j.neurobiolaging.2012.12.016

Tomasetti, M., Alleva, R., Borghi, B., and Collins, A.R. (2001). In vivo supplementation with coenzyme Q10 enhances the recovery of human lymphocytes from oxidative DNA damage. *FASEB J* 15, 1425–1427. doi: 10.1096/fj.00-0694fje

Vida, A., Abdul-Rahman, O., Miko, E., Brunyanszki, A., and Bai, P. (2016). Poly(ADP-Ribose) polymerases in aging - friend or foe? *Curr. Protein Pept. Sci.* 17, 705–712. doi: 10.2174/1389203717666160419144959

Villasenor, R., Kuennecke, B., Ozmen, L., Ammann, M., Kugler, C., Gruninger, F., et al. (2017). Region-specific permeability of the blood-brain barrier upon pericyte loss. *J. Cereb. Blood Flow Metab.* 37, 3683–3694. doi: 10.1177/0271678X17697340

Vosler, P. S., Sun, D., Wang, S., Gao, Y., Kintner, D. B., Signore, A. P., et al. (2009). Calcium dysregulation induces apoptosis-inducing factor release: cross-talk between PARP-1- and calpain-signaling pathways. *Exp. Neurol.* 218, 213–220. doi: 10.1016/j.expneurol.2009.04.032

Vyjayanti, V. N., and Rao, K. S. (2006). DNA double strand break repair in brain: reduced NHEJ activity in aging rat neurons. *Neurosci. Lett.* 393, 18–22. doi: 10.1016/j.neulet.2005.09.053

Waller, R., Murphy, M., Garwood, C. J., Jennings, L., Heath, P. R., Chambers, A., et al. (2018). Metallothionein-I/II expression associates with the astrocyte DNA damage response and not Alzheimer-type pathology in the aging brain. *Glia* 66, 2316–2323. doi: 10.1002/glia.23465

Wan, W., Cao, L., Liu, L., Zhang, C., Kalionis, B., Tai, X., et al. (2015). Abeta(1-42) oligomer-induced leakage in an in vitro blood-brain barrier model is associated with up-regulation of RAGE and metalloproteinases, and down-regulation of tight junction scaffold proteins. *J. Neurochem.* 134, 382–393. doi: 10.1111/jnc.13122

Wang, L., Zhou, Y., Yin, J., Gan, Y., Wang, X., Wen, D., et al. (2018). Cancer exacerbates ischemic brain injury via Nrp1 (Neuropilin 1)-mediated accumulation of regulatory T cells within the tumor. *Stroke* 49, 2733–2742. doi: 10.1161/STROKEAHA.118.021948

Wang, S., Xing, Z., Vosler, P.S., Yin, H., Li, W., Zhang, F., et al. (2008). Cellular NAD replenishment confers marked neuroprotection against ischemic cell death: role of enhanced DNA repair. *Stroke* 39, 2587–2595. doi: 10.1161/STROKEAHA.107.509158

Wang, Y., An, R., Umanah, G. K., Park, H., Nambiar, K., Eacker, S. M., et al. (2016). A nuclease that mediates cell death induced by DNA damage and poly(ADP-ribose) polymerase-1. *Science* 354:aad6872.

Winkler, E. A., Sagare, A.P., and Zlokovic, B. V. (2014). The pericyte: a forgotten cell type with important implications for Alzheimer's disease? *Brain Pathol.* 24, 371–386. doi: 10.1111/bpa.12152

Wyman, C., and Kanaar, R. (2006). DNA double-strand break repair: all's well that ends well. *Annu. Rev. Genet.* 40, 363–383. doi: 10.1146/annurev.genet.40.110405.090451

Yanev, P., Seevinck, P. R., Rudrapatna, U. S., Bouts, M. J., Van Der Toorn, A., Gertz, K., et al. (2017). Magnetic resonance imaging of local and remote vascular remodelling after experimental stroke. *J. Cereb. Blood Flow Metab.* 37, 2768–2779. doi: 10.1177/0271678X16674737

Yang, J., Lunde, L. K., Nuntagij, P., Oguchi, T., Camassa, L. M., Nilsson, L. N., et al. (2011). Loss of astrocyte polarization in the tg-ArcSwe mouse model of Alzheimer's disease. *J. Alzheimers Dis.* 27, 711–722. doi: 10.3233/JAD-2011-110725

Yang, W., and Paschen, W. (2017). Is age a key factor contributing to the disparity between success of neuroprotective strategies in young animals and limited success in elderly stroke patients? Focus on protein homeostasis. *J. Cereb. Blood Flow Metab.* 37, 3318–3324. doi: 10.1177/0271678X17723783

Yang, Z., Lin, P. J., and Levey, A. (2013). Monetary costs of dementia in the United States. *N. Engl. J. Med.* 369, 489–490. doi: 10.1056/nejmc1305541

Zeppenfeld, D. M., Simon, M., Haswell, J. D., D'abreo, D., Murchison, C., Quinn, J. F., et al. (2017). Association of perivascular localization of Aquaporin-4 with cognition and Alzheimer disease in aging brains. *JAMA Neurol.* 74, 91–99. doi: 10.1001/jamaneurol.2016.4370

Zhao, X., Krishnamurthy, N., Burrows, C. J., and David, S. S. (2010). Mutation versus repair: NEIL1 removal of hydantoin lesions in single-stranded, bulge, bubble, and duplex DNA contexts. *Biochemistry* 49, 1658–1666. doi: 10.1021/bi901852q

Zhao, Z., Ong, L. K., Johnson, S., Nilsson, M., and Walker, F. R. (2017). Chronic stress induced disruption of the peri-infarct neurovascular unit following experimentally induced photothrombotic stroke. *J. Cereb. Blood Flow Metab.* 37, 3709–3724.

Zlokovic, B. V. (2011). Neurovascular pathways to neurodegeneration in Alzheimer's disease and other disorders. *Nat. Rev. Neurosci.* 12, 723–738. doi: 10.1038/nrn3114

Conflict of Interest Statement: The authors declare that the research was conducted in the absence of any commercial or financial relationships that could be construed as a potential conflict of interest.

Copyright © 2019 Li, Xie, Huang, Zhang, Zhou, Qi, Wang, Chen and Li. This is an open-access article distributed under the terms of the Creative Commons Attribution License (CC BY). The use, distribution or reproduction in other forums is permitted, provided the original author(s) and the copyright owner(s) are credited and that the original publication in this journal is cited, in accordance with accepted academic practice. No use, distribution or reproduction is permitted which does not comply with these terms.

frontiers in Neuroscience

REVIEW
published: 09 August 2019
doi: 10.3389/fnins.2019.00758

Potential Immunotherapeutic Targets on Myeloid Cells for Neurovascular Repair After Ischemic Stroke

Ziyu Zhu[1†], Li Zheng[1†], Yan Li[1], Tingting Huang[1], Yu-Chieh Chao[1], Lijun Pan[2], Hui Zhu[1], Yanhua Zhao[1], Weifeng Yu[1] and Peiying Li[1*]*

[1] Department of Anesthesiology, Renji Hospital, School of Medicine, Shanghai Jiaotong University, Shanghai, China,
[2] Department of Radiology, Renji Hospital, School of Medicine, Shanghai Jiaotong University, Shanghai, China

OPEN ACCESS

Edited by:
Johannes Boltze,
University of Warwick,
United Kingdom

Reviewed by:
Lidia Garcia-Bonilla,
Cornell University, United States
Thomas Blank,
University of Freiburg, Germany
Luke Michael Healy,
McGill University, Canada
Ken Arai,
Massachusetts General Hospital and Harvard Medical School, United States

***Correspondence:**
Weifeng Yu
ywf808@yeah.net
Peiying Li
peiyingli.md@gmail.com

[†] These authors have contributed equally to this work

Specialty section:
This article was submitted to Neurodegeneration, a section of the journal Frontiers in Neuroscience

Received: 01 April 2019
Accepted: 08 July 2019
Published: 09 August 2019

Citation:
Zhu Z, Zheng L, Li Y, Huang T, Chao Y-C, Pan L, Zhu H, Zhao Y, Yu W and Li P (2019) Potential Immunotherapeutic Targets on Myeloid Cells for Neurovascular Repair After Ischemic Stroke. Front. Neurosci. 13:758. doi: 10.3389/fnins.2019.00758

Neurological deficits and cognitive dysfunctions caused by acute ischemic stroke pose enormous burden to the stroke families and the communities. Restoration of the normal function of the neurovascular unit following ischemic stroke is critical for improving neurological recovery and cognitive functions after stroke. Recent evidence suggests that the myeloid cells including both the resident microglia and infiltrating monocytes/macrophages and neutrophils are highly plastic in response to the environmental cues. They intimately interact with multiple components of the neurovascular unit in response to the alarmins, danger associated pattern molecules (DAMPs) and other signals released from the ischemic brain. The aim of this review is to discuss the reciprocal interactions between the myeloid cells and the ischemic neurovascular unit during the late repair phase of cerebral ischemic stroke. We also summarize potential immunotherapeutic targets on myeloid cells and new therapeutic approaches targeting myeloid cells, such as cell transplantation, mitochondrial dynamic and extracellular vesicles-based therapy et al to enhance neurovascular repair for better stroke recovery.

Keywords: stroke, neurovascular unit, brain repair, myeloid cell, microglia, macrophage, neutrophil

INTRODUCTION

The neurovascular unit (NVU) is composed by neurons, endothelial cells, pericytes, smooth muscle cells, astrocytes, microglia and extracellular matrix components. It maintains brain homeostasis of the brain (Banks et al., 2018; Morrison and Filosa, 2019). All the components of NVU interact with each other to maintain the neuronal milieu that is required for proper neuronal functioning by balancing energy, preserving the integrity of the blood brain barrier (BBB), releasing neurotrophic factors, uptake and recycling of neurotransmitters and et al. (Halassa et al., 2007; Charveriat et al., 2017). In response to cerebral ischemic stroke, the integrity of the BBB compromises leading to leakage of harmful blood components into the CNS, immune cell infiltration, and aberrant transport and clearance of molecules. All these changes contribute to the dysfunction of the NVU which is associated with long term neurological impairments (Fisher and Saver, 2015; Villaseñor et al., 2017). The reconstruction of NVU and the remodeling of neuronal circuitry turns out as an essential player in long-term neurological recovery after stroke (Gurer et al., 2009; Lake et al., 2017). However, the repair of NVU is a complex

process involving clearing of neuronal debris, neurogenesis, angiogenesis, establishing the new neuronal circuitry, controlling neuroinflammation and et al. (Lake et al., 2017; Zhao Z. et al., 2017), thus it remains as a big challenge to promote the NVU repair after ischemic brain injury.

After ischemic stroke, both glial cells and peripheral immune cells can be activated by a variety of mechanisms, including neuronal "help me" signals, like lipocalin-2 (Xing et al., 2014; Blochet et al., 2018), interleukin 4 (IL-4) (Zhao et al., 2015), and a complex mixture of extracellular proteins functioning as damage associated molecular patterns (DAMPs), such as high-mobility group box 1 (HMGB1), hypoxia-inducible factor 1α (HIF-1α), S100B and et al. (Chamorro et al., 2012; Fu et al., 2015; Li et al., 2018b). Notably, myeloid immune cells are gaining increasing attention due to their unique function in anti-inflammation, clearing cellular debris and promoting neuronal plasticity (Iadecola and Anrather, 2011; Shichita et al., 2014; Fu et al., 2015; Zhao S. C. et al., 2017; Wang X. et al., 2018).

Myeloid cells are blood cells that arise from a large heterogeneous multipotent stem cell population, the hematopoietic stem cells (HSC) lineage (Kondo et al., 1997; Akashi et al., 2000) which resides in the bone marrow and possess the ability to give rise to diverse cell types in the immune system and the blood, including granulocytes, monocytes, erythrocytes and platelets (Paul et al., 2015). Some myeloid populations can develop directly from yolk sac progenitors without apparent bone marrow intermediates, such as tissue resident macrophages (Kondo et al., 1997; Akashi et al., 2000; Shibata and Suzuki, 2017). Although peripheral monocyte-derived macrophages and microglia can both be developed from the same yolk sac progenitors, they should not be considered as one cellular population in the injured brain (Greenhalgh et al., 2018). After injury, monocyte-derived macrophages can enter the brain and directly communicate with microglia and suppress the microglia-mediated phagocytosis and inflammation after spinal cord injury (Greenhalgh et al., 2018). In the central nervous system (CNS), the main tissue resident macrophages including perivascular macrophages (PVM), meningeal macrophages (MM), and choroid plexus macrophages (CPM) (Henning et al., 2009) and microglia migrate into the CNS during early neural development depending on transcription factor Pu.1 and Irf8 (Hanisch and Kettenmann, 2007; Kierdorf et al., 2013).

In the recent decades, microglia and monocytes/macrophages are intensively studied in the context of cerebral ischemic brain injury (Hu et al., 2012; Garcia-Culebras et al., 2018), with compelling evidence emerging, thus we mainly focused on these cells in this review. After cerebral ischemia, both residential microglia and macrophages can be activated within 24 h and the infiltration of monocyte-derived macrophages and activation of microglia peaks within 3–4 days after stroke onset (Lalancette-Hebert et al., 2007; Gelderblom et al., 2009; Wattananit et al., 2016). Polymorphonuclear neutrophil granulocytes (PMNs) are another myeloid cell population that can infiltrate into the ischemic brain and affect ischemic brain injury (Frijns and Kappelle, 2002). These innate immune cells play important roles in determining the ischemic infarcts. For example, PMNs release matrix metallopeptidase 9 (MMP-9) which degrades the BBB and exacerbates ischemic brain injury (Li et al., 2013a) and tissue-plasminogen activator related hemorrhagic transformation (Mao et al., 2017). Selective microglia elimination disturbed neuronal calcium responses, increased calcium overload and increased the incidence of spreading depolarization, thus significantly increased the infarct size by 60% (Szalay et al., 2016). Depletion of monocyte/macrophages in cerebral ischemic stroke reduced hemorrhagic infarct transformation or reduced brain injury in monocyte/macrophage depleted stroke mice (Gliem et al., 2012; Ma et al., 2016). However, there's also a recent study showed no impact on stroke outcome with monocyte/macrophages depleted (Schmidt et al., 2017).

Recent researches have highlighted that the impact of these myeloid cells on the ischemic brain injury largely depend on different phenotypes at different stages of stroke (Kurisu et al., 2018). As it's well-known that microglia and macrophages can be divided into different phenotypes depending on their functions on the inflammatory responses (Mantovani et al., 2013; Guruswamy and ElAli, 2017). Classically-activated (M1) microglia/macrophages usually secret pro-inflammatory cytokines, such as inducible nitric oxide synthase (iNOS), tumor necrosis factor α (TNFα), interleukin 23 (IL-23), interleukin 1β (IL-1β), interleukin 12 (IL-12) and et al. (Mills et al., 2000; Guruswamy and ElAli, 2017; Li et al., 2017), while alternatively activated (M2) microglia/macrophages are characterized by their production of anti-inflammatory cytokines, such as interleukin 10 (IL-10) and transforming growth factor β (TGF-β) (Gordon and Taylor, 2005; Guruswamy and ElAli, 2017) and they can be polarized with IL-4 via a signal transducer and activator of transcription 6 (STAT6)-dependent pathway (Stein et al., 1992; Gao et al., 2015). Recent studies further identified more specific subpopulation of M2 microglia/macrophages, such as M2a, M2b, M2c, and Mox (Hu et al., 2015). Importantly, the phenotypes and functions of these cells are highly dynamic after ischemic injury (Tsuyama et al., 2018). Likewise, PMNs may also have different phenotypes in different stages after ischemic stroke, a pro-inflammatory so called N1 and an anti-inflammatory N2 phenotype (Fridlender et al., 2009).

However, the terminology of microglial/macrophage polarization was questioned and believed to hinder research progress (Ransohoff, 2016). There are far more phenotypes of microglia/macrophages than M1/M2, such as amyotrophic lateral sclerosis specific microglia (Chiu et al., 2013), phagocytic monocyte-derived macrophages (Yamasaki et al., 2014), immunosuppressive $CD11c^{+}$ microglia and et al. (Kan et al., 2015). There are also cases that microglia/macrophage may concurrently display both pro- and anti-inflammatory phenotypes (Morganti et al., 2016). In addition, transcriptomics and genomic studies reveal that the function of microglia are versatile beyond immune responses, such as synaptic modulation and neurotrophic support (Wes et al., 2016). Single-cell RNA-sequencing gene profiling showed that macrophages in traumatic brain injury are not comprised of distinctly polarized cell subsets, instead, these macrophages are uniquely and broadly activated (Kim et al., 2016). Therefore, it is not rigorous to classify microglia/macrophages imprudently into M1/M2 classifications (Ransohoff, 2016).

Recently, compelling evidence is suggesting the role of the distinct "healing" myeloid cells during the restoration of NVU after stroke, including phagocytosis of damaged neuronal debris, promoting neurogenesis and angiogenesis, re-establishment of the neuronal circuitry, improving white matter repair and et al. during different phases after stroke (**Figure 1**).

In this review, we will summarize the distinct functions of different subsets of myeloid cells during the "repair" of NVU discuss the identified mechanisms underlying their restoration of the NVU after stroke.

DIVERGENT FUNCTIONS OF THE "HEALING" MYELOID CELLS DURING NVU REPAIR AFTER ISCHEMIC STROKE

Phagocytosis of Damaged Tissue Debris After Stroke

By removing necrotic tissues, myeloid cells may accelerate brain repair by enhanced phagocytosis after intracerebral hemorrhage (ICH) (Wan et al., 2016; Fumagalli et al., 2019). Using structured illumination microscopy, a super-resolution technique which helps study phagocytosis, it was shown that myeloid cells were encompassed with potent phagocytic abilities once they infiltrated into the ischemic brain (Fumagalli et al., 2019). There are several different receptors expressed on microglia/macrophages that mediate the phagocytosis of these cells, including class A, class B scavenger receptors, the surface receptor triggering receptor expressed on myeloid cells-2 (TREM2), complement receptors (CRs) (Dustin, 2016), mannose receptors (Galea et al., 2005) and the mer receptor tyrosine kinase (MerTK) (Healy et al., 2016, 2017). In addition, purinergic receptors, such as P2Y12 receptors as key regulators of microglia process extension, also contribute to their responses to brain injury (Kluge et al., 2017; Fukumoto et al., 2018). We will briefly summarize the phagocytic aspects of some recently studied receptors after stroke (**Figure 2**).

The Class A Scavenger Receptors

The class A scavenger receptor includes macrophage scavenger receptor 1(Msr1) and macrophage receptor with collagenous structure (Marco). Msr1 is also known as CD204. Both of these receptors are important for the clearance of DAMPs, including peroxiredoxins, high mobility group box 1 protein and S100 calcium-binding protein A8/9 from the ischemic brain (Milne et al., 2005; Shichita et al., 2017). Msr1 is up-regulated in infiltrating mononuclear phagocytes from day 1 to day 3 after stroke onset and is dependent on the transcription factor Mafb, which plays an important role in the regulation of lineage-specific hematopoiesis (Shichita et al., 2017). Combined Msr1 and Marco deficiency results in sustained inflammation, leading to impaired clearance of DAMPs and ultimately an enlarged infarct volume and exacerbated neurological deficits (Shichita et al., 2017). The expression level of Msr1 helps to distinguish the repairing macrophages from inflammatory ones, since $Msr1^{hi}$ macrophages express less inflammatory cytokines (TNF-α, IL-lβ, and IL- 23) and are instead the major sources of insulin-like growth factor-1(IGF-1), a neurotrophic factor (Shichita et al., 2017).

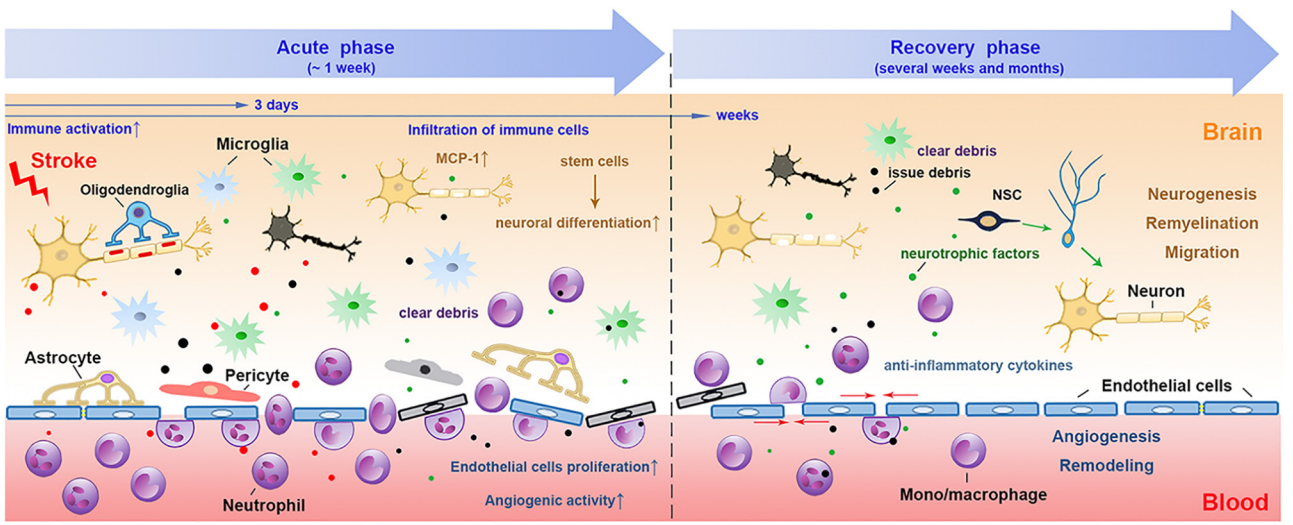

FIGURE 1 | The involvement of myeloid immune cells during the NVU repair after cerebral ischemic stroke. In the acute phase of ischemic stroke, the damaged associated signals from the ischemic brain activate resident and peripheral myeloid immune cells, such as microglia, peripheral mono/macrophages and neutrophils. These cells penetrate into the CNS through the disrupted BBB from 1 day after stroke, peaking at 2–3 days and may last for several weeks. The phagocytic function of myeloid cells enables them to remove tissue debris in both acute and repair stages. During the recovery phase after stroke, myeloid cells with strong plasticity could differentiate into different phenotypes and release several neurovascular nutritional factors, which may enhance neurovascular regeneration and remodeling up to weeks and months after stroke. NVU, neurovascular unit; CNS, central nervous system; BBB, blood brain barrier; NSC, neural stem cells.

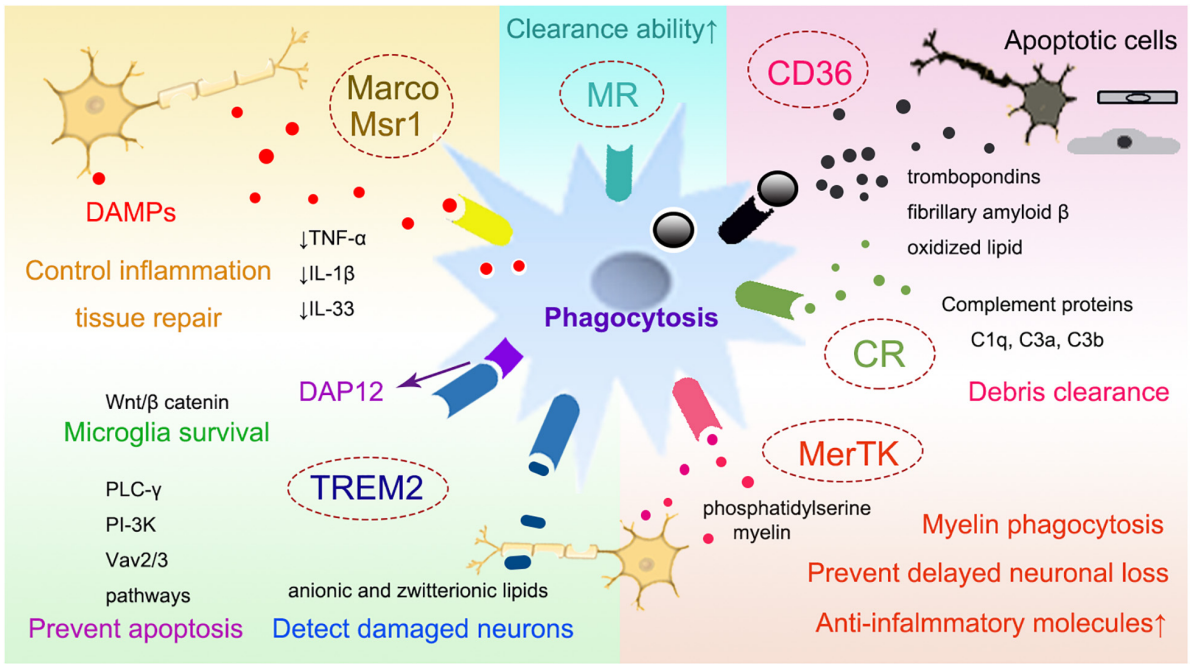

FIGURE 2 | The receptors that mediate phagocytosis of myeloid immune cells. Several receptors have been suggested to mediate the phagocytosis of myeloid cells, such as the class A scavenger receptor Marco and Msr1, the class B scavenger receptor CD36, TREM2, CRs, MRs, and MerTK. Myeloid cells can phagocytose the DAMPs released from damaged neurons with the receptors such as Msr1 and Marco, which subsequently downregulate the neurovascular inflammation and enhance brain repair. Through CD36, myeloid cells can also clear tissue debris from apoptotic cells, thrombospondins, oxidized lipid, et al. TREM2 is important for preventing microglia apoptosis, it also promotes the survival of microglia via the Wnt/β catenin pathway. Complement receptor, such as CR1 and CR3, may bind to apoptotic neuronal cells and contribute to clearing debris and limiting neuroinflammation. MerTK is associated with the myeloid phagocytosis of myelin, neurons and eryptotic erythrocytes, leading to prevent delayed neuronal loss after stroke. CD36, cluster of differentiation 36; TREM2, triggering receptor expressed on myeloid cells 2; CRs, complement receptors; MRs, mannose receptors; MerTK, the mer receptor tyrosine kinase; DAMP, danger associated molecular pattern; Msr1, macrophage scavenger receptor 1; Marco, macrophage receptor with collagenous structure.

The Class B Scavenger Receptor Cluster of Differentiation 36 (CD36)

The class B scavenger receptor CD36, is a highly glycosylated integral membrane protein expressed in microglia and monocytes/macrophages (Cho et al., 2005; Woo et al., 2016). With high affinity toward apoptotic cells and many ligands such as thrombospondins (TSPs), fibrillary amyloid β and oxidized lipids, CD36 has been suggested to play a pivotal role in the clearance of cell debris during the recovery phase in post-stroke brains (Cho et al., 2005; Woo et al., 2016; Stamova et al., 2018). Stroke induces increased mRNA expression of CD36 and TSP-1/2 mRNA levels in the ipsilateral hemisphere both during the acute and recovery phases (Woo et al., 2016). Deletion of CD36 results in poorer outcome due to lack of attenuation of nuclear factor-κB (NF-κB) mediated inflammation and diminished removal of apoptotic neuronal debris (Woo et al., 2012). CD36 deficiency or SS-31, a cell permeable tetra-peptide known to down-regulate CD36 pathway, significantly attenuated monocyte chemoattractant protein 1 (MCP-1), C-C chemokine receptor type 2 (CCR2) mRNA up-regulation and injury size in the transient ischemic stroke (Kim et al., 2015). Increased expression of CD36 expression in monocyte/macrophages has been associated with higher phagocytic indices in the brain immune cells after ischemic stroke (Woo et al., 2016).

The Surface Receptor TREM2

The surface receptor TREM2 is expressed exclusively on myeloid cells, including brain microglia (Hakola, 1972; Nasu et al., 1973). It was first identified as a genetic cause of neurodegenerative disease called Nasu-Hakola disease [or polycystic lipomembranous osteodysplasia with sclerosing leukoencephalopathy (PLOSL)] (Hakola, 1972; Nasu et al., 1973). It is characterized as axonal degeneration and white matter loss, as well as cortical atrophy in clinical patients (Sasaki et al., 2015). TREM2 binds anionic carbohydrates, anionic bacterial products and various phospholipids (Daws et al., 2003; Cannon et al., 2012). It transmits intracellular signals through the associated transmembrane adapter DNAX activation protein of 12 kDa (DAP12), an immune-receptor tyrosine-based activation motif (ITAM)-bearing adapter molecule that transduces activating signals in natural killer (NK) and myeloid cells (Peng et al., 2010). DAP 12 can recruit the protein tyrosine kinase Syk, which phosphorates phosphoinositide phospholipase C-γ (PLC-γ), phosphoinositide 3-kinases (PI3Ks) and Vav2/3 to induce the mobilization of intracellular calcium and the reorganization of actin and prevent apoptosis (Peng et al., 2010). TREM2 also stabilizes β-catenin by inhibiting its degradation via the Akt/GSK3β signaling pathway, thus promotes microglial survival (Zheng et al., 2017). TREM2 expression has been associated

with phagocytic activities of microglia in cerebral ischemia and Alzheimer's disease (AD) (Kawabori et al., 2015; Wu et al., 2017; Kurisu et al., 2018; Wei et al., 2019). Loss of TREM2 results in reduced phagocytosis of a variety of substrates, including apoptotic neurons (Hsieh et al., 2009), amyloid plaques and anionic and zwitterionic lipids on damaged neurons (Wang et al., 2015; Yuan et al., 2016). Using bone marrow chimeric mice, it has been shown that TREM2 on the brain microglia is more essential to post-stroke recovery compared to those on circulating macrophages (Kurisu et al., 2018).

CRs in Myeloid Cells

The complement system is emerging as an important player of cerebral ischemic brain injury. A variety of complement proteins have been shown to be induced after cerebral ischemic stroke, such as C1q, C3a and C3b (Fumagalli et al., 2019). It has been shown that C1q can bind to apoptotic neuronal cells and produce opsonizing C3b and C4b fragments, which are responsible for phagocytosis of apoptotic cells. Furthermore, C1q also binds to IgM, pentraxin-3 and serum amyloid P component during the C1q-mediated removal of apoptotic cells. $C1q^{-/-}$ mice exhibited impaired elimination of immune complexes and were more susceptible to neuroinflammation (Orsini et al., 2014). There are several CRs that have been linked to the phagocytic function of myeloid cells, such as CR1 and CR3 (Dustin, 2016). CR1 is a membrane-bound glycoprotein and is a receptor for C3b and C4b. It has been shown that the expression of CR1 on microglia was increased after lipopolysaccharide (LPS) induction and played a detrimental role in neuronal death after LPS stimulation or in the pathology of AD. However, the role of CR1 in the context of ischemic stroke remains unknown. CR3, also known as CD11b/CD18 or Mac-1(Ma et al., 2019) is a member of the integrin β2 subfamily. It is deeply involved in the innate immune responses and also the induction of phagocytosis by interacting with its ligand iC3b. The phagocytosis mediated by C3b is usually beneficial for clearing debris, apoptotic or necrotic neurons and limiting neuroinflammation after brain injury (Rotshenker, 2003; Fourgeaud and Boulanger, 2007).

Mannose Receptors (MRs)

The MRs, also known as cluster of differentiation 206, CD206, are C-type lectin which can express on microglia/macrophages, dendritic cells and et al. The extracellular region of MRs include an N-terminal cysteine-rich domain that is able to bind sugars with high affinity, such as mannose and fructose, thus scavenging unwanted high mannose N-linked glycoproteins from the circulation (Lee et al., 2002). The expression of MRs has been shown to increase after cerebral ischemic stroke in the phagocytic microglia/macrophages within the ischemic boundary (Giraldi-Guimaraes et al., 2012). Induction of increased MRs expression is believed to enhance the clearance ability of microglia/macrophages and thus provide neuroprotection against ischemic stroke (Giraldi-Guimaraes et al., 2012).

Tyrosine Kinase Receptor, MerTK

MerTK is a member of tyrosine kinase receptor family that plays important role in mediating phagocytosis by myeloid cells. The expression of MerTK is correlated with the myelin phagocytosis of myeloid cells not only in multiple sclerosis (Healy et al., 2016, 2017), but also the phagocytosis of ischemic neurons after cerebral ischemia (Neher et al., 2013). After ischemic stroke, the expression MerTK was transiently upregulated. Inhibition of MerTK may prevent delayed neuronal loss after stroke (Neher et al., 2013). In the model of ICH, loss of MerTK reduced hematoma clearance and exacerbated iron deposition, thus worsened neurological recovery (Chang et al., 2018). Therefore, MerTK is a receptor that is associated the phagocytosis of a variety targets, such as myelin, neurons and erythrocytes.

Collectively, there are multiple phagocytic receptors expressed on myeloid cells that are promising in clearing the debris and promoting brain repair after stroke. However, the roles and the underlying mechanisms of some phagocytic receptors remain largely unknown in the context of cerebral ischemia and thus warrant further investigation.

Anti-inflammatory Effect of Myeloid Cells and Brain Repair After Stroke

Mounting studies have suggested that the alternatively activated or anti-inflammatory phenotype of microglia/macrophages are characterized in their anti-inflammatory effects, with the signature proteins expressed, such as arginase-1, CD206 or macrophage MR, Ym1 and TGF β and IL-10 (Gordon and Taylor, 2005; Hu et al., 2015; Miro-Mur et al., 2016; Ge et al., 2017; Gaceb et al., 2018). Several mechanisms have been suggested to induce the anti-inflammatory effect of microglia and macrophages, such as the activation of chemokine (C-X3-C motif) ligand 1-CX3C chemokine receptor 1 (CX3CL1-CX3CR1) signaling, IL-33/ST2 signaling and IL-4/peroxisome proliferator-activated receptor γ (PPARγ) signaling (Mizuno et al., 2003; Lyons et al., 2009; Liu X. et al., 2016; Yang et al., 2017). High expression of endogenous CX3CL1 in neurons acts as an "on" signal to stop the quiescent state of microglia and leads to a tonic activation of CX3CR1 on microglia and acts as a neuronal "off" signal maintaining microglia in a quiescent state (Biber et al., 2007; Eyo and Wu, 2013). $CX3CR1^{+}Ly6C^{low}$ "patrolling" monocytes may play a role in repair processes in the ischemic brain (Garcia-Bonilla et al., 2016). However, there are also studies showing that $Ly6C^{hi}$ monocytes are protective in acute ischemic stroke by promoting macrophage polarization (Chu et al., 2015). IL-4 was able to induce peroxisome proliferator-activated receptor γ (PPARγ) activation thereby enhanced long-term functional recovery of cerebral ischemic stroke (Zhao et al., 2015). ST2, a member of the IL-1 receptor family, and its ligand interleukin-33(IL-33) play critical roles in immune regulation and inflammatory responses. ST2 deficiency aggravates neurological deficits up to 7 d after transient middle cerebral artery occlusion (Yang et al., 2017). The IL-33/ST2 signaling potentiates the expression of IL-10 and other anti-inflammatory genes in primary microglia and stimulates the production of IL-10 from microglia, which, in turn, enhances neuronal survival after ischemic insult (Yang et al., 2017).

Recent evidence suggests that similar to the concept of classically activated and alternatively activated macrophages, neutrophils also have pro-inflammatory and anti-inflammatory phenotypes, called N1 and N2 phenotypes

(Fridlender et al., 2009; Cuartero et al., 2013). Modulation of PPARγ with rosiglitazone results PMN to shift toward a more pronounced N2-phenotype after stroke (Cuartero et al., 2013). Notably, the anti-inflammatory N2 neutrophils were found to limit excessive immune response, promoting neuronal survival and successful brain remodeling after ischemic stroke and ICH (Hermann et al., 2018). Interleukin-27/lactoferrin is suggested to modulate neutrophil functions toward a "beneficial" phenotype in the treatment of ICH (Zhao X. et al., 2017).

Given the compelling evidence suggesting the association of anti-inflammatory phenotype of these myeloid cells with brain repair after stroke and ICH, the roles and mechanisms of the myeloid cell associated NVU repair remain to be further explored. Furthermore, it was recently demonstrated that lack of myeloid lineage cell autophagy could aggravate the inflammation after cerebral ischemic stroke, suggesting a conflicting role of myeloid cells in the neuroinflammation after stroke (Kotoda et al., 2018). In general, neuroinflammation is a complex and constantly evolving cellular process. However, we need to be cognizant of the fact that we still do not know which aspects of neuroinflammation are beneficial and which are detrimental. It is not by chance that there are no successful anti-inflammatory therapies to treat stroke patients, not least due to the risks surrounding immunosuppression (Smith et al., 2015; Siniscalchi et al., 2016), bringing other side effects like depression (Wium-Andersen et al., 2017).

Promoting Neurogenesis and Angiogenesis

Neurogenesis

Neurogenesis is a key step toward recovery from cerebral ischemic stroke (Sun et al., 2018). It is a natural process that occurs in the adult hippocampus everyday as was shown by a previous study measuring the concentration of nuclear-bomb-test-derived ^{14}C in genomic DNA (Spalding et al., 2013). After stroke, neurogenesis can be induced in the ipsilateral subventricular zone (SVZ) 1 to 2 weeks after the ischemic insult and cell proliferation returns to baseline 6 weeks later (Thored et al., 2006). In addition, stroke also induces neuroblasts to differentiate into neurons (Arvidsson et al., 2002) or to elicit a neurogenic program in striatal astrocytes in mice (Magnusson et al., 2014).

Microglia possess the ability to support neurogenesis after ischemic stroke through pleiotropic mechanisms (Ziv et al., 2006; Kettenmann et al., 2011). During 2, 6 and 16 weeks after middle cerebral artery occlusion, there are more activated microglia migrating from the ipsilateral SVZ to the striatum together with neuroblasts in rats (Thored et al., 2009). These microglia exhibit pro-neurogenic phenotypes with increased expression of IGF-1, which can promote proliferation and differentiation of neural stem cells (NSCs) (Thored et al., 2009) and contribute to neural repair and survival after ischemic injury (Zhu et al., 2009). Removal of proliferating microglia by ganciclovir treatment decreases the level of neurotrophic IGF1, leading to the exacerbation of ischemic neuronal damage and deteriorated stroke outcomes (Lalancette-Hebert et al., 2007). Therefore, microglia are believed to have a predominantly repairing function in promoting the survival of neurons in the resolution phase of ischemic brain injury (Szalay et al., 2016).

Brain-derived neurotrophic factor (BDNF) is another important neurotropic protein that can be produced by microglia after stroke (Cook et al., 2017; Verma et al., 2017). It has been shown to regulate synaptic function and promote multiple learning tasks performance (Coull et al., 2005; Parkhurst et al., 2013). The micro-environment of microglia/macrophage is critical for their pro-neurogenic properties. Microglia activated by IL-4 and interferon γ (IFNγ) promote neurogenesis, while LPS activated microglia block neurogenesis in hippocampal slice cultures (Butovsky et al., 2005; Liu et al., 2013). Modulation the polarization of microglia/macrophages with chronic metformin treatment is associated with enhanced angiogenesis and neurogenesis after cerebral ischemic stroke (Jin et al., 2014). Meningeal macrophage polarization induced by BCG vaccination is helpful for the neurogenesis and spatial cognition (Qi et al., 2017). In the neuron-macrophage co-culture, it has been shown that molecular factors secreted by macrophages can promote neurite outgrowth (Yun et al., 2018).

Angiogenesis and Vascular Remodeling

Remodeling of the cerebral vasculature after cerebral ischemic stroke involves angiogenesis and also the growth of new blood vessels from pre-existing vascular tree, both of which ultimately promotes the re-establishment of the microcirculation and the blood supply to the damaged brain tissue (Lapi and Colantuoni, 2015). Vascular remodeling can last for more than 3 weeks after cerebral ischemia. It has been associated with improved neurological outcome after stroke (Lapi and Colantuoni, 2015). Vascular endothelial growth factor (VEGF) and endothelium-released nitric oxide are important factors in the generation of new vessels and formation of new vasculature during microvascular remodeling (Lapi and Colantuoni, 2015). Monocytes/macrophages can express interleukin-8 (IL-8), VEGF, TGF-β, prostaglandin, and MMP-9, all of which can enhance the angiogenic process after stroke (Sanberg et al., 2010). In addition to secreting angiogenic factors, macrophages can also repair the ruptured vascular mechanically (Liu C. et al., 2016). Using i*n vivo* time-lapse imaging in zebrafish, it has been shown that macrophage arrive at the cerebral vascular rupture lesion and extend their filopodia or lamellipodia to physically adhere to both endothelial ends (Liu C. et al., 2016). Furthermore, these macrophages can promote the ligation and the repair of the rupture by generating mechanical traction forces to pull the endothelial ends (Liu C. et al., 2016; **Figure 3**).

Re-establishment of the Neuronal Circuit by Enhancing Axonal Sprouting and Synaptic Plasticity

To achieve functional recovery after stroke, the newly generated or differentiated neurons need reorganization and rewiring in the ischemic lesion. These remodeling processes are often

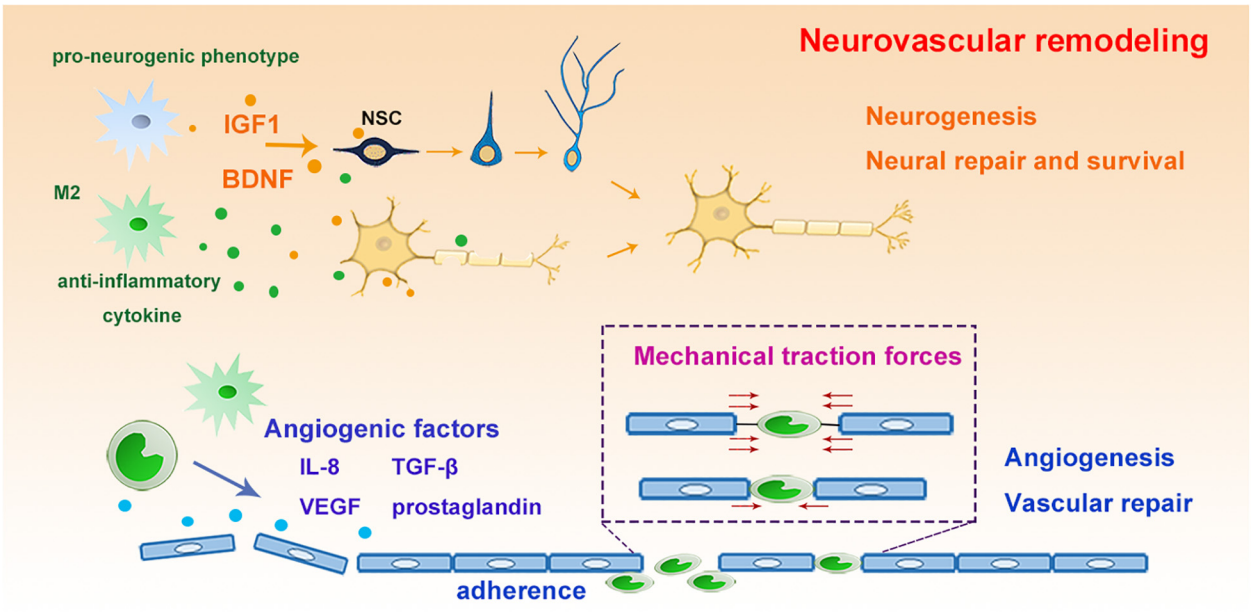

FIGURE 3 | The roles of myeloid cells for neurovascular remodeling. Microglia switch into pro-neurogenic phenotype and anti-inflammatory phenotype with increased release of IGF-1, BDNF and anti-inflammatory cytokines, which promote the proliferation and differentiation of NSCs, leading to enhanced neurogenesis, neural repair and NSC survival and differentiation. Furthermore, myeloid cells express angiogenic factors as IL-8, VEGF et al to promote vascular repair. Moreover, they could generate mechanical traction forces to pull the injured endothelial ends, rebuilding the ligation to enhance repair. IGF, insulin-like growth factor; BDNF, brain derived neurotrophic factor; NSC, neural stem cells; IL-8, interleukin 8; VEGF, vascular endothelial growth factor.

associated with the sprouting of spared axons and modifying the synaptic networks to establish new circuits (Chu et al., 2015). Interestingly, emerging evidence is suggesting that microglia can rapidly modify neuronal activity, modulate synaptic function and promote the integration of NPCs from endogenous neurogenic niches into functional networks after brain injury (Wake et al., 2013; Sandvig et al., 2018). In addition, recent evidence suggests that microglia/macrophages play an important role in the remyelination through protecting oligodendrocytes, augmenting oligodendrogenesis and promoting oligodendrocyte progenitor cell (OPC) differentiation both in stroke and other neurodegenerative diseases (Miron et al., 2013; Moore et al., 2015; Hagemeyer et al., 2017). By regulating the phenotypic switch of microglia with IL-4 or inducing iron-releasing phenotype with noggin, a bone morphogenetic protein (BMP) antagonist, the "healing" capacity toward remyelination of microglia can be significantly enhanced (Shin et al., 2018). Administration of iron-sulfur glutaredoxin 2, the oxidoreductase, inhibits peroxynitrite formation thus reduces the nitric oxide release from activated microglia and protects oligodendrocytes from myelin damage in experimental autoimmune encephalomyelitis (Lepka et al., 2017). Activation of microglia with IL-13 or IL-10 not only induces generation of OPCs from the SVZ after focal demyelination in the corpus callosum (Naruse et al., 2018), but also enhances the survival and differentiation of these cells during CNS remyelination (Miron et al., 2013; **Figure 4**).

POTENTIAL THERAPEUTIC STRATEGIES TARGETING MYELOID CELLS IN THE TREATMENT OF ISCHEMIC STROKE

Bone Marrow Derived Stem Mononuclear Cells Transplantation

Bone-marrow derived mononuclear cells (MNCs) based therapy is gaining increasing attention because of the pleotropic effects in improving neurological recovery after stroke (Brenneman et al., 2010; Vahidy et al., 2016; Yang et al., 2016). Interestingly, with increased expression of IL-10, IL-6, MCP-1, VEGF, and TNF-α, post-stroke MNCs treatment leads to a better recovery on neurological testing and reduces lesion size as compared to pre-stroke MNCs (Yang et al., 2012). In 2016, thirty-nine patients with subacute ischemic cerebral infarct due to large artery occlusion in the middle cerebral artery (MCA) territory were recruited to receive bone marrow mononuclear (BMMN) stem cell transplantation. The study suggests that it is safe to transplant autologous BMMN stem cell intra-arterially in subacute MCA ischemic stroke patients, but unfortunately, no significant improvement of motor, language disturbance, or infarction volume was detected in the stem cell-treated group as compared to the non-treated group within an observation period of 12 months (Deierborg et al., 2010).

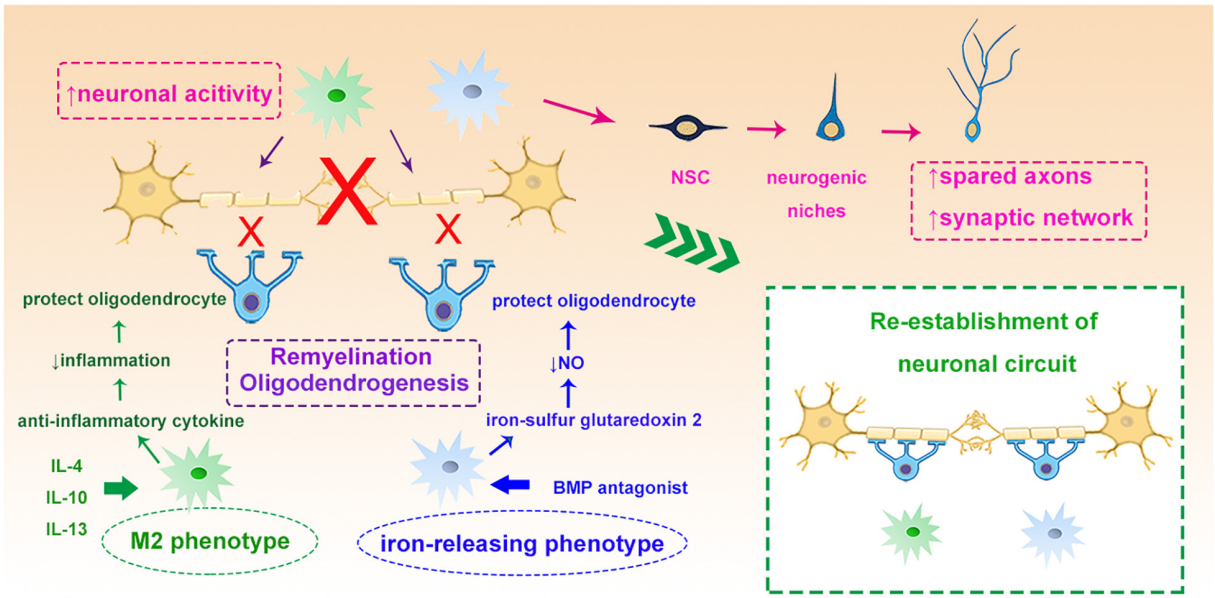

FIGURE 4 | Myeloid cells and neuronal circuit re-establishment. Myeloid cells such as microglia can modify neuronal activity and stimulate the NSCs to sprout axons and rebuild synaptic networks. IL-4 induced M2 myeloid cells and BMP antagonist induced iron-releasing microglia protect oligodendrocytes through different mechanisms, such as enhancing remyelination and oligodendrogenesis, which all contribute to the re-establishment of the neuronal circuit. NSC, neural stem cells; IL-4, interleukin 4; BMP, bone morphogenetic protein.

Adoptive Transfer of Monocytes/Macrophages

It's recently proposed that preconditioned monocytes/macrophages may play an endogenous protective role after ischemic brain injury (Garcia-Bonilla et al., 2018). Depletion of circulating monocytes/macrophages or selective targeting of CCR2 in bone marrow-derived cells exacerbated the BBB disruption and thus caused delayed clinical deterioration and hemorrhagic conversion of the infarctions after stroke (Gliem et al., 2012). On the other hand, transfer of splenic monocytes isolated from preconditioned mice into naive mice 7 h after transient MCAO reduced ischemic brain injury (Garcia-Bonilla et al., 2018). Mechanistically, gene expression and functional studies showed that IL-10, inducible nitric oxide synthase, and CCR2 in monocytes are essential for the neuroprotection (Garcia-Bonilla et al., 2018). Interestingly, a clinical study with 13 stroke patients and 13 case-control stroke patients showed that intrathecal injection of autologous M2 macrophages in stroke patients is safe and may lead to improved neurological recovery (Chernykh et al., 2016). Although the study is still preliminary with a small sample size, it opens up a new direction toward myeloid-cell based stroke therapy to protect the ischemic brain.

Nevertheless, when it comes to immune-cell based therapy, it's always important to consider the condition of the recipients. For example, in our previous study, we found adoptive transfer of regulatory T cells or *in vivo* expansion of regulatory T cells could protect against cerebral ischemic injury (Li et al., 2013b; Zhang et al., 2018) and meanwhile preserve the immune homeostasis after stroke (Li et al., 2013b). However, the immune suppressive regulatory T cells may be attracted to the tumor via the VEGF-neuropilin 1 signaling when the stroke recipient is complicated by cancer (Wang L. et al., 2018). Other critical issues related to immune cell-based therapy include availability or preparation of immune cells, major histocompatibility complex molecules which may initiate immune responses, preservation of purified immune cells and et al., all of which hinder the clinical translation of immune cell-based therapies.

Mitochondrial Dynamic of Myeloid Cells as Therapeutic Target

Mitochondria, a highly dynamic cellular organelle that plays pivotal role in metabolism and apoptosis is also deeply involved in the interplay between cellular metabolism and both innate and adaptive immune responses (Tur et al., 2017). They govern the dependence of cellular metabolism and the coordination of the tricarboxylic acid (TCA) cycle to modulate oxidative phosphorylation rates and adenosine triphosphate (ATP) production, as well as the important intermediates to support other metabolic processes (Tur et al., 2017). Therapeutically restoring mitochondrial function can reprogram inflammatory macrophages into anti-inflammatory cells by regulating cellular metabolic pathways (Van den Bossche et al., 2016). Alternatively activated or naive macrophages predominantly use oxidative phosphorylation for their energy support, whereas the aerobic glycolysis and pentose phosphate pathway can be robustly enhanced in classically activated macrophages (Liu and Ho, 2018), with significantly increased

glucose uptake. Whereas the fatty acids uptake is enhanced to support anti-inflammatory microglia/macrophage polarization and functions (Van den Bossche et al., 2016). As the central regulator of cellular metabolism, mitochondria are emerging as a pivotal therapeutic target to regulate the phenotype polarization of microglia/macrophages (Mehta et al., 2017). After cerebral ischemic stroke, enhanced glycolysis and fatty acid synthesis have been found in peripheral T cells, with increased expression of acetyl-coenzyme A (Wang et al., 2019). Hyper-glycolysis can induce the key glycolytic enzyme hexokinase 2 (HK2), which further results in accumulated acetyl-coenzyme A and subsequent histone acetylation and transcriptional activation of interleukin (IL)-1β and over-activation of the microglia-mediated neuroinflammation after cerebral ischemic stroke (Li et al., 2018a). However, it still should be kept in mind that the phenotypes of microglia/macrophages are far more complicated than pro-inflammatory or anti-inflammatory as we mentioned above. How does the mitochondria function and the metabolic process affect other phenotypes still remains largely unknown.

Immunological Effects of Extracellular Vesicles (EVs) on Ischemic Stroke

Extracellular vesicles (EVs) which can be released by almost all cell types can appear in all body fluids as membrane-surrounded vesicles. There are two distinct types of EV according to their origin: shedding microvesicles apoptotic bodies and exosomes. Because exosomes are able to cross the BBB and the blood-cerebrospinal fluid barrier, it allows crosstalk between the periphery and the brain. On one hand, damaged endothelium releases pro-inflammatory factors and EVs that pass through the compromised BBB after stroke. These EVs can activate microglia and astrocytes to release pro-inflammatory cytokines (TNFα, IL1β) (Zagrean et al., 2018). On the other hand, exosomes are emerging as a powerful diagnostic tool and a promising therapeutic shuttle of natural nanoparticles (Zagrean et al., 2018). It has been suggested that microglia-derived exosomes may contain microRNAs (miR-124-3p) that can inhibit neuronal inflammation and promote neurite outgrowth by transferring into neurons after traumatic brain injury (Ponomarev et al., 2013; Huang et al., 2018).

TABLE 1 | Potential immunotherapeutic targets on myeloid cells for NVU repair after stroke.

Cellular targets	Functions and underlying mechanisms	References
Msr1	Clearance of DAMPs; reduce the expression of inflammatory cytokines	Shichita et al., 2017
CD36	Clearance of cell debris; attenuation of nuclear factor-κB mediated inflammation;	Cho et al., 2005; Woo et al., 2012
TREM2	Promotes microglial survival by inhibiting β-catenin degradation *via* the Akt/GSK3β signaling pathway; phagocytosis apoptotic neurons, amyloid plaques and anionic and zwitterionic lipids on damaged neurons	Hsieh et al., 2009; Wang et al., 2015; Yuan et al., 2016; Zheng et al., 2017
CR1	Induction of phagocytosis by interacting with its ligands; clearing debris, apoptotic or necrotic neurons and limiting neuroinflammation	Rotshenker, 2003; Fourgeaud and Boulanger, 2007
MRs	Enhance the clearance ability of microglia/macrophages	Giraldi-Guimaraes et al., 2012
MerTK	Phagocytosis of ischemic neurons; clearance of hetatoma and reduce iron deposition	Neher et al., 2013; Chang et al., 2018
arginase-1, CD206, Ym1 and TGF β and IL-10	Induce the anti-inflammatory effect of microglia and macrophages by activating CX3CL1-CX3CR1 signaling, IL-33/ST2 signaling and neuronal IL-4, PPARγ	Mizuno et al., 2003; Lyons et al., 2009; Zhao et al., 2015; Liu X. et al., 2016; Yang et al., 2017
PPARγ in N2 neutrophils	Limit excessive immune response, promoting neuronal survival and successful brain remodeling after ischemic stroke and ICH	Hermann et al., 2018
lactoferrin	Iron-scavenging and clearance of hetatoma	Zhao X. et al., 2017
IGF-1	Promote proliferation and differentiation of NSCs	Thored et al., 2009
BDNF	Regulate synaptic function and promote multiple learning tasks performance	Coull et al., 2005
IL-8, VEGF, TGF-β, prostaglandin, MMP-9	Enhance the angiogenic process	Sanberg et al., 2010
Filopodia or lamellipodia	Physically adhere to both endothelial ends at the cerebral vascular rupture lesion	Liu C. et al., 2016
iron-releasing phenotype of microglia	Promoting oligodendrocyte progenitor cell differentiation	Shin et al., 2018
EVs, exosomes, miRNA124-3p	Inhibit neuronal inflammation and promote neurite outgrowth	Ponomarev et al., 2013; Huang et al., 2018

NVU, neurovascular unit; Msr1, macrophage scavenger receptor 1; DAMP, damage associated molecular patterns; CD36, cluster of differentiation 36; TREM2, triggering receptor expressed on myeloid cells-2; CR, complement receptor; MR, mannose receptor; MerTK, mer receptor tyrosine kinase; PPARγ, peroxisome proliferator-activated receptor γ; CX3CL1-CX3CR1, chemokine (C-X3-C motif) ligand 1-CX3C chemokine receptor 1; IL-33, interleukin 33; IL-4, interleukin 4; ICH, intracerebral hemorrhage; IGF-1, insulin-like growth factor-1; NSC, neural stem cell; BDNF, brain-derived neurotrophic factor; IL-8, interleukin 8; VEGF, vascular endothelial growth factor; TGF-β, transforming growth factor β; MMP-9, matrix metallopeptidase 9; EVs, extracellular vesicles.

In addition, intravenous administration of macrophage exosomes can cross the BBB which serve as natural nanocarriers to deliver a cargo protein, the brain derived neurotrophic factor to the injured brain (Yuan et al., 2017). Treatment with exosomes secreted from LPS-stimulated macrophage or MNCs has been shown to reduce brain infarct volume and improve neurological function after focal cerebral ischemic stroke (Altmann et al., 2014; Zheng et al., 2019). In addition, exosomes derived from several different cell types, such as mesenchymal stromal cells, adipose-derived stem cells (ADSCs), embryonic stem cells (ESCs) and neural stem cells (NSCs) (Rufino-Ramos et al., 2017; Cunningham et al., 2018; Webb et al., 2018), and exosomes from these cells have been shown to reduce ischemic volume, promote white matter repair and help neurovascular restoration following ischemia-reperfusion injury (Xin et al., 2013; Otero-Ortega et al., 2017; Jiang et al., 2018; Venkat et al., 2018; Webb et al., 2018). Therefore, it's reasonable to envision that the exosome from the "healing" type of myeloid cells holds the promise to serve as an intriguing therapeutic strategy for future stroke therapy.

CONCLUDING REMARKS AND FUTURE PERSPECTIVES

As highlighted in this review, myeloid cells play an important role in tissue remodeling during the late stage of stroke via pleiotropic mechanisms, such as inhibiting immune inflammation, devouring harmful factors, removing tissue fragments, secreting neurotrophic substances, et al. Scavenger receptors such as Msf1, CD36, TREM2, CRs, MRs and MerTK all contribute to the clearing of necrotic debris and set the stage for NVU remodeling in the repair phase. Several mechanisms are involved in their anti- inflammatory functions to turn into potential protective phenotype through secreting anti-inflammatory cytokines such as IL-10 and TGF-β. With their "healing" effects during neurovascular renewal, myeloid cells are promising to provide novel therapeutic targets (**Table 1**). Meanwhile, myeloid cell-based therapy, such as bone marrow derived myeloid stem cell perfusion, mitochondrial therapy and EVs-based therapy are also gaining increasing attention for the stroke treatment. However, there are myriad unknown areas that warrant further investigation to foster novel therapeutic strategies, such as the complex mix of "help me" signals that initiate the activation and functional switching of myeloid cells, the interactions between the NVU repair processes and myeloid cells and the underlying mechanisms. As our understanding of the role of myeloid cells in the post-stroke NVU repair grows, we may have the potential to design better myeloid cell targeted treatments to improve the neurological outcome of stroke patients.

AUTHOR CONTRIBUTIONS

All authors listed have made a substantial, direct and intellectual contribution to the work, and approved it for publication.

FUNDING

PL is supported by the National Natural Science Foundation of China (NSFC) grant 81722017 and the Shanghai Municipal Education Commission—Gaofeng Clinical Medicine Grant Support (20181805). WY is supported by the National Natual Science Foundation of China (81571048). YC is supported by the National Natural Science Foundation of China (NSFC) grant 81801095.

REFERENCES

Akashi, K., Traver, D., Miyamoto, T., and Weissman, I. L. (2000). A clonogenic common myeloid progenitor that gives rise to all myeloid lineages. *Nature* 404, 193–197. doi: 10.1038/35004599

Altmann, P., Mildner, M., Haider, T., Traxler, D., Beer, L., Ristl, R., et al. (2014). Secretomes of apoptotic mononuclear cells ameliorate neurological damage in rats with focal ischemia. *F1000Res* 3:131. doi: 10.12688/f1000research.4219.2

Arvidsson, A., Collin, T., Kirik, D., Kokaia, Z., and Lindvall, O. (2002). Neuronal replacement from endogenous precursors in the adult brain after stroke. *Nat. Med.* 8, 963–970. doi: 10.1038/nm747

Banks, W. A., Kovac, A., and Morofuji, Y. (2018). Neurovascular unit crosstalk: pericytes and astrocytes modify cytokine secretion patterns of brain endothelial cells. *J. Cereb. Blood Flow Metab.* 38, 1104–1118. doi: 10.1177/0271678X17740793

Biber, K., Neumann, H., Inoue, K., and Boddeke, H. W. (2007). Neuronal 'On' and 'Off' signals control microglia. *Trends Neurosci.* 30, 596–602. doi: 10.1016/j.tins.2007.08.007

Blochet, C., Buscemi, L., Clément, T., Gehri, S., Badaut, J., and Hirt, L. (2018). Involvement of caveolin-1 in neurovascular unit remodeling after stroke: effects on neovascularization and astrogliosis. *J. Cereb. Blood Flow Metab.* doi: 10.1177/0271678X18806893 [Epub ahead of print].

Brenneman, M., Sharma, S., Harting, M., Strong, R., Cox, C. S. Jr., Aronowski, J., et al. (2010). Autologous bone marrow mononuclear cells enhance recovery after acute ischemic stroke in young and middle-aged rats. *J. Cereb. Blood Flow Metab.* 30, 140–149. doi: 10.1038/jcbfm.2009.198

Butovsky, O., Talpalar, A. E., Ben-Yaakov, K., and Schwartz, M. (2005). Activation of microglia by aggregated beta-amyloid or lipopolysaccharide impairs MHC-II expression and renders them cytotoxic whereas IFN-gamma and IL-4 render them protective. *Mol. Cell. Neurosci.* 29, 381–393. doi: 10.1016/j.mcn.2005.03.005

Cannon, J. P., O'driscoll, M., and Litman, G. W. (2012). Specific lipid recognition is a general feature of CD300 and TREM molecules. *Immunogenetics* 64, 39–47. doi: 10.1007/s00251-011-0562-4

Chamorro, A., Meisel, A., Planas, A. M., Urra, X., Van De Beek, D., and Veltkamp, R. (2012). The immunology of acute stroke. *Nat. Rev. Neurol.* 8, 401–410. doi: 10.1038/nrneurol.2012.98

Chang, C. F., Goods, B. A., Askenase, M. H., Hammond, M. D., Renfroe, S. C., Steinschneider, A. F., et al. (2018). Erythrocyte efferocytosis modulates macrophages towards recovery after intracerebral hemorrhage. *J. Clin. Invest.* 128, 607–624. doi: 10.1172/JCI95612

Charveriat, M., Naus, C. C., Leybaert, L., Saez, J. C., and Giaume, C. (2017). Connexin-dependent neuroglial networking as a new therapeutic target. *Front. Cell. Neurosci.* 11:174. doi: 10.3389/fncel.2017.00174

Chernykh, E. R., Shevela, E. Y., Starostina, N. M., Morozov, S. A., Davydova, M. N., Menyaeva, E. V., et al. (2016). Safety and therapeutic potential of M2 macrophages in stroke treatment. *Cell Transplant.* 25, 1461–1471. doi: 10.3727/096368915X690279

Chiu, I. M., Morimoto, E. T., Goodarzi, H., Liao, J. T., O'keeffe, S., Phatnani, H. P., et al. (2013). A neurodegeneration-specific gene-expression signature of acutely isolated microglia from an amyotrophic lateral sclerosis mouse model. *Cell Rep.* 4, 385–401. doi: 10.1016/j.celrep.2013.06.018

Cho, S., Park, E. M., Febbraio, M., Anrather, J., Park, L., Racchumi, G., et al. (2005). The class B scavenger receptor CD36 mediates free radical production and tissue injury in cerebral ischemia. *J. Neurosci.* 25, 2504–2512. doi: 10.1523/jneurosci.0035-05.2005

Chu, H. X., Broughton, B. R., Kim, H. A., Lee, S., Drummond, G. R., and Sobey, C. G. (2015). Evidence that Ly6C(hi) monocytes are protective in acute ischemic stroke by promoting M2 macrophage polarization. *Stroke* 46, 1929–1937. doi: 10.1161/STROKEAHA.115.009426

Cook, D. J., Nguyen, C., Chun, H. N., Llorente, I. L., Chiu, A. S., Machnicki, M., et al. (2017). Hydrogel-delivered brain-derived neurotrophic factor promotes tissue repair and recovery after stroke. *J. Cereb. Blood Flow Metab.* 37, 1030–1045. doi: 10.1177/0271678X16649964

Coull, J. A., Beggs, S., Boudreau, D., Boivin, D., Tsuda, M., Inoue, K., et al. (2005). BDNF from microglia causes the shift in neuronal anion gradient underlying neuropathic pain. *Nature* 438, 1017–1021. doi: 10.1038/nature04223

Cuartero, M. I., Ballesteros, I., Moraga, A., Nombela, F., Vivancos, J., Hamilton, J. A., et al. (2013). N2 neutrophils, novel players in brain inflammation after stroke: modulation by the PPARgamma agonist rosiglitazone. *Stroke* 44, 3498–3508. doi: 10.1161/STROKEAHA.113.002470

Cunningham, C. J., Redondo-Castro, E., and Allan, S. M. (2018). The therapeutic potential of the mesenchymal stem cell secretome in ischaemic stroke. *J. Cereb. Blood Flow Metab.* 38, 1276–1292. doi: 10.1177/0271678X18776802

Daws, M. R., Sullam, P. M., Niemi, E. C., Chen, T. T., Tchao, N. K., and Seaman, W. E. (2003). Pattern recognition by TREM-2: binding of anionic ligands. *J. Immunol.* 171, 594–599. doi: 10.4049/jimmunol.171.2.594

Deierborg, T., Roybon, L., Inacio, A. R., Pesic, J., and Brundin, P. (2010). Brain injury activates microglia that induce neural stem cell proliferation ex vivo and promote differentiation of neurosphere-derived cells into neurons and oligodendrocytes. *Neuroscience* 171, 1386–1396. doi: 10.1016/j.neuroscience.2010.09.045

Dustin, M. L. (2016). Complement receptors in myeloid cell adhesion and phagocytosis. *Microbiol. Spectr.* 4, doi: 10.1128/microbiolspec.MCHD-0034-2016

Eyo, U. B., and Wu, L. J. (2013). Bidirectional microglia-neuron communication in the healthy brain. *Neural Plast.* 2013:456857.

Fisher, M., and Saver, J. L. (2015). Future directions of acute ischaemic stroke therapy. *Lancet Neurol.* 14, 758–767. doi: 10.1016/S1474-4422(15)00054-X

Fourgeaud, L., and Boulanger, L. M. (2007). Synapse remodeling, compliments of the complement system. *Cell* 131, 1034–1036. doi: 10.1016/j.cell.2007.11.031

Fridlender, Z. G., Sun, J., Kim, S., Kapoor, V., Cheng, G., Ling, L., et al. (2009). Polarization of tumor-associated neutrophil phenotype by TGF-beta: "N1" versus "N2". *TAN. Cancer Cell* 16, 183–194. doi: 10.1016/j.ccr.2009.06.017

Frijns, C. J., and Kappelle, L. J. (2002). Inflammatory cell adhesion molecules in ischemic cerebrovascular disease. *Stroke* 33, 2115–2122. doi: 10.1161/01.str.0000021902.33129.69

Fu, Y., Liu, Q., Anrather, J., and Shi, F. D. (2015). Immune interventions in stroke. *Nat. Rev. Neurol.* 11, 524–535.

Fukumoto, Y., Tanaka, K. F., Parajuli, B., Shibata, K., Yoshioka, H., Kanemaru, K., et al. (2018). Neuroprotective effects of microglial $P2Y_1$ receptors against ischemic neuronal injury. *J. Cereb. Blood Flow Metab.* doi: 10.1177/0271678X18805317 [Epub ahead of print].

Fumagalli, S., Fiordaliso, F., Perego, C., Corbelli, A., Mariani, A., De Paola, M., et al. (2019). The phagocytic state of brain myeloid cells after ischemia revealed by superresolution structured illumination microscopy. *J. Neuroinflammation* 16:9. doi: 10.1186/s12974-019-1401-z

Gaceb, A., Özen, I., Padel, T., Barbariga, M., and Paul, G. (2018). Pericytes secrete pro-regenerative molecules in response to platelet-derived growth factor-BB. *J. Cereb. Blood Flow Metab.* 38, 45–57. doi: 10.1177/0271678X17719645

Galea, I., Palin, K., Newman, T. A., Van Rooijen, N., Perry, V. H., and Boche, D. (2005). Mannose receptor expression specifically reveals perivascular macrophages in normal, injured, and diseased mouse brain. *Glia* 49, 375–384. doi: 10.1002/glia.20124

Gao, S., Zhou, J., Liu, N., Wang, L., Gao, Q., Wu, Y., et al. (2015). Curcumin induces M2 macrophage polarization by secretion IL-4 and/or IL-13. *J. Mol. Cell. Cardiol.* 85, 131–139. doi: 10.1016/j.yjmcc.2015.04.025

Garcia-Bonilla, L., Brea, D., Benakis, C., Lane, D. A., Murphy, M., Moore, J., et al. (2018). Endogenous protection from ischemic brain injury by preconditioned monocytes. *J. Neurosci.* 38, 6722–6736. doi: 10.1523/JNEUROSCI.0324-18.2018

Garcia-Bonilla, L., Faraco, G., Moore, J., Murphy, M., Racchumi, G., Srinivasan, J., et al. (2016). Spatio-temporal profile, phenotypic diversity, and fate of recruited monocytes into the post-ischemic brain. *J. Neuroinflammation* 13:285.

Garcia-Culebras, A., Duran-Laforet, V., Pena-Martinez, C., Ballesteros, I., Pradillo, J. M., Diaz-Guzman, J., et al. (2018). Myeloid cells as therapeutic targets in neuroinflammation after stroke: specific roles of neutrophils and neutrophil-platelet interactions. *J. Cereb. Blood Flow Metab.* 38, 2150–2164. doi: 10.1177/0271678X18795789

Ge, R., Tornero, D., Hirota, M., Monni, E., Laterza, C., Lindvall, O., et al. (2017). Choroid plexus-cerebrospinal fluid route for monocyte-derived macrophages after stroke. *J. Neuroinflammation* 14:153. doi: 10.1186/s12974-017-0909-3

Gelderblom, M., Leypoldt, F., Steinbach, K., Behrens, D., Choe, C. U., Siler, D. A., et al. (2009). Temporal and spatial dynamics of cerebral immune cell accumulation in stroke. *Stroke* 40, 1849–1857. doi: 10.1161/STROKEAHA.108.534503

Giraldi-Guimaraes, A., De Freitas, H. T., Coelho Bde, P., Macedo-Ramos, H., Mendez-Otero, R., Cavalcante, L. A., et al. (2012). Bone marrow mononuclear cells and mannose receptor expression in focal cortical ischemia. *Brain Res.* 1452, 173–184. doi: 10.1016/j.brainres.2012.03.002

Gliem, M., Mausberg, A. K., Lee, J. I., Simiantonakis, I., Van Rooijen, N., Hartung, H. P., et al. (2012). Macrophages prevent hemorrhagic infarct transformation in murine stroke models. *Ann. Neurol.* 71, 743–752. doi: 10.1002/ana.23529

Gordon, S., and Taylor, P. R. (2005). Monocyte and macrophage heterogeneity. *Nat. Rev. Immunol.* 5, 953–964. doi: 10.1038/nri1733

Greenhalgh, A. D., Zarruk, J. G., Healy, L. M., Baskar Jesudasan, S. J., Jhelum, P., Salmon, C. K., et al. (2018). Peripherally derived macrophages modulate microglial function to reduce inflammation after CNS injury. *PLoS Biol.* 16:e2005264. doi: 10.1371/journal.pbio.2005264

Gurer, G., Gursoy-Ozdemir, Y., Erdemli, E., Can, A., and Dalkara, T. (2009). Astrocytes are more resistant to focal cerebral ischemia than neurons and die by a delayed necrosis. *Brain Pathol.* 19, 630–641. doi: 10.1111/j.1750-3639.2008.00226.x

Guruswamy, R., and ElAli, A. (2017). Complex roles of microglial cells in ischemic stroke pathobiology: new insights and future directions. *Int. J. Mol. Sci.* 18:496. doi: 10.3390/ijms18030496

Hagemeyer, N., Hanft, K. M., Akriditou, M. A., Unger, N., Park, E. S., Stanley, E. R., et al. (2017). Microglia contribute to normal myelinogenesis and to oligodendrocyte progenitor maintenance during adulthood. *Acta Neuropathol.* 134, 441–458. doi: 10.1007/s00401-017-1747-1

Hakola, H. P. (1972). Neuropsychiatric and genetic aspects of a new hereditary disease characterized by progressive dementia and lipomembranous polycystic osteodysplasia. *Acta Psychiatr. Scand. Suppl.* 232, 1–173.

Halassa, M. M., Fellin, T., Takano, H., Dong, J. H., and Haydon, P. G. (2007). Synaptic islands defined by the territory of a single astrocyte. *J. Neurosci.* 27, 6473–6477. doi: 10.1523/jneurosci.1419-07.2007

Hanisch, U. K., and Kettenmann, H. (2007). Microglia: active sensor and versatile effector cells in the normal and pathologic brain. *Nat. Neurosci.* 10, 1387–1394. doi: 10.1038/nn1997

Healy, L. M., Jang, J. H., Won, S. Y., Lin, Y. H., Touil, H., Aljarallah, S., et al. (2017). MerTK-mediated regulation of myelin phagocytosis by macrophages generated from patients with MS. *Neurol. Neuroimmunol. Neuroinflamm.* 4:e402. doi: 10.1212/NXI.0000000000000402

Healy, L. M., Perron, G., Won, S. Y., Michell-Robinson, M. A., Rezk, A., Ludwin, S. K., et al. (2016). MerTK is a functional regulator of myelin phagocytosis by human myeloid cells. *J. Immunol.* 196, 3375–3384. doi: 10.4049/jimmunol.1502562

Henning, E. C., Ruetzler, C. A., Gaudinski, M. R., Hu, T. C., Latour, L. L., Hallenbeck, J. M., et al. (2009). Feridex preloading permits tracking of CNS-resident macrophages after transient middle cerebral artery occlusion. *J. Cereb. Blood Flow Metab.* 29, 1229–1239. doi: 10.1038/jcbfm.2009.48

Hermann, D. M., Kleinschnitz, C., and Gunzer, M. (2018). Implications of polymorphonuclear neutrophils for ischemic stroke and intracerebral

hemorrhage: predictive value, pathophysiological consequences and utility as therapeutic target. *J. Neuroimmunol.* 321, 138–143. doi: 10.1016/j.jneuroim.2018.04.015

Hsieh, C. L., Koike, M., Spusta, S. C., Niemi, E. C., Yenari, M., Nakamura, M. C., et al. (2009). A role for TREM2 ligands in the phagocytosis of apoptotic neuronal cells by microglia. *J. Neurochem.* 109, 1144–1156. doi: 10.1111/j.1471-4159.2009.06042.x

Hu, X., Leak, R. K., Shi, Y., Suenaga, J., Gao, Y., Zheng, P., et al. (2015). Microglial and macrophage polarization-new prospects for brain repair. *Nat. Rev. Neurol.* 11, 56–64. doi: 10.1038/nrneurol.2014.207

Hu, X., Li, P., Guo, Y., Wang, H., Leak, R. K., Chen, S., et al. (2012). Microglia/macrophage polarization dynamics reveal novel mechanism of injury expansion after focal cerebral ischemia. *Stroke* 43, 3063–3070. doi: 10.1161/STROKEAHA.112.659656

Huang, S., Ge, X., Yu, J., Han, Z., Yin, Z., Li, Y., et al. (2018). Increased miR-124-3p in microglial exosomes following traumatic brain injury inhibits neuronal inflammation and contributes to neurite outgrowth via their transfer into neurons. *FASEB J.* 32, 512–528. doi: 10.1096/fj.201700673R

Iadecola, C., and Anrather, J. (2011). The immunology of stroke: from mechanisms to translation. *Nat. Med.* 17, 796–808. doi: 10.1038/nm.2399

Jiang, M., Wang, H., Jin, M., Yang, X., Ji, H., Jiang, Y., et al. (2018). Exosomes from MiR-30d-5p-ADSCs reverse acute ischemic stroke-induced, autophagy-mediated brain injury by promoting M2 microglial/macrophage polarization. *Cell. Physiol. Biochem.* 47, 864–878. doi: 10.1159/000490078

Jin, Q., Cheng, J., Liu, Y., Wu, J., Wang, X., Wei, S., et al. (2014). Improvement of functional recovery by chronic metformin treatment is associated with enhanced alternative activation of microglia/macrophages and increased angiogenesis and neurogenesis following experimental stroke. *Brain Behav. Immun.* 40, 131–142. doi: 10.1016/j.bbi.2014.03.003

Kan, M. J., Lee, J. E., Wilson, J. G., Everhart, A. L., Brown, C. M., Hoofnagle, A. N., et al. (2015). Arginine deprivation and immune suppression in a mouse model of Alzheimer's disease. *J. Neurosci.* 35, 5969–5982. doi: 10.1523/JNEUROSCI.4668-14.2015

Kawabori, M., Kacimi, R., Kauppinen, T., Calosing, C., Kim, J. Y., Hsieh, C. L., et al. (2015). Triggering receptor expressed on myeloid cells 2 (TREM2) deficiency attenuates phagocytic activities of microglia and exacerbates ischemic damage in experimental stroke. *J. Neurosci.* 35, 3384–3396. doi: 10.1523/JNEUROSCI.2620-14.2015

Kettenmann, H., Hanisch, U. K., Noda, M., and Verkhratsky, A. (2011). Physiology of microglia. *Physiol. Rev.* 91, 461–553. doi: 10.1152/physrev.00011.2010

Kierdorf, K., Erny, D., Goldmann, T., Sander, V., Schulz, C., Perdiguero, E. G., et al. (2013). Microglia emerge from erythromyeloid precursors via Pu.1- *and Irf*8-dependent pathways. *Nat. Neurosci.* 16, 273–280. doi: 10.1038/nn.3318

Kim, C. C., Nakamura, M. C., and Hsieh, C. L. (2016). Brain trauma elicits non-canonical macrophage activation states. *J Neuroinflammation* 13:117. doi: 10.1186/s12974-016-0581-z

Kim, E. H., Tolhurst, A. T., Szeto, H. H., and Cho, S. H. (2015). Targeting CD36-mediated inflammation reduces acute brain injury in transient, but not permanent, ischemic stroke. *CNS Neurosci. Ther.* 21, 385–391. doi: 10.1111/cns.12326

Kluge, M. G., Kracht, L., Abdolhoseini, M., Ong, L. K., Johnson, S. J., Nilsson, M., et al. (2017). Impaired microglia process dynamics post-stroke are specific to sites of secondary neurodegeneration. *Glia* 65, 1885–1899. doi: 10.1002/glia.23201

Kondo, M., Weissman, I. L., and Akashi, K. (1997). Identification of clonogenic common lymphoid progenitors in mouse bone marrow. *Cell* 91, 661–672. doi: 10.1016/s0092-8674(00)80453-5

Kotoda, M., Furukawa, H., Miyamoto, T., Korai, M., Shikata, F., Kuwabara, A., et al. (2018). Role of myeloid lineage cell autophagy in ischemic brain injury. *Stroke* 49, 1488–1495. doi: 10.1161/STROKEAHA.117.018637

Kurisu, K., Zheng, Z., Kim, J. Y., Shi, J., Kanoke, A., Liu, J., et al. (2018). Triggering receptor expressed on myeloid cells-2 expression in the brain is required for maximal phagocytic activity and improved neurological outcomes following experimental stroke. *J. Cereb. Blood Flow Metab.* doi: 10.1177/0271678X18817282 [Epub ahead of print].

Lake, E. M. R., Bazzigaluppi, P., Mester, J., Thomason, L. A. M., Janik, R., Brown, M., et al. (2017). Neurovascular unit remodelling in the subacute stage of stroke recovery. *Neuroimage* 146, 869–882. doi: 10.1016/j.neuroimage.2016.09.016

Lalancette-Hebert, M., Gowing, G., Simard, A., Weng, Y. C., and Kriz, J. (2007). Selective ablation of proliferating microglial cells exacerbates ischemic injury in the brain. *J. Neurosci.* 27, 2596–2605. doi: 10.1523/jneurosci.5360-06.2007

Lapi, D., and Colantuoni, A. (2015). Remodeling of cerebral microcirculation after ischemia-reperfusion. *J. Vasc. Res.* 52, 22–31. doi: 10.1159/000381096

Lee, S. J., Evers, S., Roeder, D., Parlow, A. F., Risteli, J., Risteli, L., et al. (2002). Mannose receptor-mediated regulation of serum glycoprotein homeostasis. *Science* 295, 1898–1901. doi: 10.1126/science.1069540

Lepka, K., Volbracht, K., Bill, E., Schneider, R., Rios, N., Hildebrandt, T., et al. (2017). Iron-sulfur glutaredoxin 2 protects oligodendrocytes against damage induced by nitric oxide release from activated microglia. *Glia* 65, 1521–1534. doi: 10.1002/glia.23178

Li, M., Li, Z., Ren, H., Jin, W. N., Wood, K., Liu, Q., et al. (2017). Colony stimulating factor 1 receptor inhibition eliminates microglia and attenuates brain injury after intracerebral hemorrhage. *J. Cereb. Blood Flow Metab.* 37, 2383–2395. doi: 10.1177/0271678X16666551

Li, P., Gan, Y., Sun, B. L., Zhang, F., Lu, B., Gao, Y., et al. (2013a). Adoptive regulatory T-cell therapy protects against cerebral ischemia. *Ann. Neurol.* 74, 458–471. doi: 10.1002/ana.23815

Li, P., Mao, L., Zhou, G., Leak, R. K., Sun, B. L., Chen, J., et al. (2013b). Adoptive regulatory T-cell therapy preserves systemic immune homeostasis after cerebral ischemia. *Stroke* 44, 3509–3515. doi: 10.1161/STROKEAHA.113.002637

Li, Y., Lu, B., Sheng, L., Zhu, Z., Sun, H., Zhou, Y., et al. (2018a). Hexokinase 2-dependent hyperglycolysis driving microglial activation contributes to ischemic brain injury. *J. Neurochem.* 144, 186–200. doi: 10.1111/jnc.14267

Li, Y., Zhu, Z. Y., Huang, T. T., Zhou, Y. X., Wang, X., Yang, L. Q., et al. (2018b). The peripheral immune response after stroke-A double edge sword for blood-brain barrier integrity. *CNS Neurosci. Ther.* 24, 1115–1128. doi: 10.1111/cns.13081

Liu, C., Wu, C., Yang, Q., Gao, J., Li, L., Yang, D., et al. (2016). Macrophages mediate the repair of brain vascular rupture through direct physical adhesion and mechanical traction. *Immunity* 44, 1162–1176. doi: 10.1016/j.immuni.2016.03.008

Liu, J., Hjorth, E., Zhu, M., Calzarossa, C., Samuelsson, E. B., Schultzberg, M., et al. (2013). Interplay between human microglia and neural stem/progenitor cells in an allogeneic co-culture model. *J. Cell. Mol. Med.* 17, 1434–1443. doi: 10.1111/jcmm.12123

Liu, P. S., and Ho, P. C. (2018). Mitochondria: a master regulator in macrophage and T cell immunity. *Mitochondrion* 41, 45–50. doi: 10.1016/j.mito.2017.11.002

Liu, X., Liu, J., Zhao, S., Zhang, H., Cai, W., Cai, M., et al. (2016). Interleukin-4 is essential for microglia/macrophage m2 polarization and long-term recovery after cerebral ischemia. *Stroke* 47, 498–504. doi: 10.1161/STROKEAHA.115.012079

Lyons, A., Lynch, A. M., Downer, E. J., Hanley, R., O'sullivan, J. B., Smith, A., et al. (2009). Fractalkine-induced activation of the phosphatidylinositol-3 kinase pathway attentuates microglial activation in vivo and in vitro. *J. Neurochem.* 110, 1547–1556. doi: 10.1111/j.1471-4159.2009.06253.x

Ma, Y., Li, Y., Jiang, L., Wang, L., Jiang, Z., Wang, Y., et al. (2016). Macrophage depletion reduced brain injury following middle cerebral artery occlusion in mice. *J. Neuroinflammation* 13:38. doi: 10.1186/s12974-016-0504-z

Ma, Y., Liu, Y., Zhang, Z., and Yang, G. Y. (2019). Significance of complement system in ischemic stroke: a comprehensive review. *Aging Dis.* 10, 429–462. doi: 10.14336/AD.2019.0119

Magnusson, J. P., Goritz, C., Tatarishvili, J., Dias, D. O., Smith, E. M., Lindvall, O., et al. (2014). A latent neurogenic program in astrocytes regulated by Notch signaling in the mouse. *Science* 346, 237–241. doi: 10.1126/science.346.6206.237

Mantovani, A., Biswas, S. K., Galdiero, M. R., Sica, A., and Locati, M. (2013). Macrophage plasticity and polarization in tissue repair and remodelling. *J. Pathol.* 229, 176–185. doi: 10.1002/path.4133

Mao, L., Li, P., Zhu, W., Cai, W., Liu, Z., Wang, Y., et al. (2017). Regulatory T cells ameliorate tissue plasminogen activator-induced brain haemorrhage after stroke. *Brain* 140, 1914–1931. doi: 10.1093/brain/awx111

Mehta, M. M., Weinberg, S. E., and Chandel, N. S. (2017). Mitochondrial control of immunity: beyond ATP. *Nat. Rev. Immunol.* 17, 608–620. doi: 10.1038/nri.2017.66

Mills, C. D., Kincaid, K., Alt, J. M., Heilman, M. J., and Hill, A. M. (2000). M-1/M-2 macrophages and the Th1/Th2 paradigm. *J. Immunol.* 164, 6166–6173. doi: 10.4049/jimmunol.164.12.6166

Milne, S. A., Mcgregor, A. L., Mcculloch, J., and Sharkey, J. (2005). Increased expression of macrophage receptor with collagenous structure (MARCO) in mouse cortex following middle cerebral artery occlusion. *Neurosci. Lett.* 383, 58–62. doi: 10.1016/j.neulet.2005.03.065

Miro-Mur, F., Perez-De-Puig, I., Ferrer-Ferrer, M., Urra, X., Justicia, C., Chamorro, A., et al. (2016). Immature monocytes recruited to the ischemic mouse brain differentiate into macrophages with features of alternative activation. *Brain Behav. Immun.* 53, 18–33. doi: 10.1016/j.bbi.2015.08.010

Miron, V. E., Boyd, A., Zhao, J. W., Yuen, T. J., Ruckh, J. M., Shadrach, J. L., et al. (2013). M2 microglia and macrophages drive oligodendrocyte differentiation during CNS remyelination. *Nat. Neurosci.* 16, 1211–1218. doi: 10.1038/nn.3469

Mizuno, T., Kawanokuchi, J., Numata, K., and Suzumura, A. (2003). Production and neuroprotective functions of fractalkine in the central nervous system. *Brain Res.* 979, 65–70. doi: 10.1016/s0006-8993(03)02867-1

Moore, C. S., Cui, Q. L., Warsi, N. M., Durafourt, B. A., Zorko, N., Owen, D. R., et al. (2015). Direct and indirect effects of immune and central nervous system-resident cells on human oligodendrocyte progenitor cell differentiation. *J. Immunol.* 194, 761–772. doi: 10.4049/jimmunol.1401156

Morganti, J. M., Riparip, L. K., and Rosi, S. (2016). Call Off the Dog(ma): M1/M2 polarization is concurrent following traumatic brain injury. *PLoS One* 11:e0148001. doi: 10.1371/journal.pone.0148001

Morrison, H. W., and Filosa, J. A. (2019). Stroke and the neurovascular unit: glial cells, sex differences, and hypertension. *Am. J. Physiol. Cell Physiol.* 316, C325–C339. doi: 10.1152/ajpcell.00333.2018

Naruse, M., Shibasaki, K., Shimauchi-Ohtaki, H., and Ishizaki, Y. (2018). Microglial activation induces generation of oligodendrocyte progenitor cells from the subventricular zone after focal demyelination in the corpus callosum. *Dev. Neurosci.* 40, 54–63. doi: 10.1159/000486332

Nasu, T., Tsukahara, Y., and Terayama, K. (1973). A lipid metabolic disease-"membranous lipodystrophy"-an autopsy case demonstrating numerous peculiar membrane-structures composed of compound lipid in bone and bone marrow and various adipose tissues. *Acta Pathol. Jpn.* 23, 539–558. doi: 10.1111/j.1440-1827.1973.tb01223.x

Neher, J. J., Emmrich, J. V., Fricker, M., Mander, P. K., Thery, C., and Brown, G. C. (2013). Phagocytosis executes delayed neuronal death after focal brain ischemia. *Proc. Natl. Acad. Sci. U.S.A.* 110, E4098–E4107. doi: 10.1073/pnas.1308679110

Orsini, F., De Blasio, D., Zangari, R., Zanier, E. R., and De Simoni, M. G. (2014). Versatility of the complement system in neuroinflammation, neurodegeneration and brain homeostasis. *Front. Cell Neurosci.* 8:380. doi: 10.3389/fncel.2014.00380

Otero-Ortega, L., Laso-Garcia, F., Gomez-De Frutos, M. D., Rodriguez-Frutos, B., Pascual-Guerra, J., Fuentes, B., et al. (2017). White matter repair after extracellular vesicles administration in an experimental animal model of subcortical stroke. *Sci. Rep.* 7:44433. doi: 10.1038/srep44433

Parkhurst, C. N., Yang, G., Ninan, I., Savas, J. N., Yates, J. R. III, Lafaille, J. J., et al. (2013). Microglia promote learning-dependent synapse formation through brain-derived neurotrophic factor. *Cell* 155, 1596–1609. doi: 10.1016/j.cell.2013.11.030

Paul, F., Arkin, Y., Giladi, A., Jaitin, D. A., Kenigsberg, E., Keren-Shaul, H., et al. (2015). Transcriptional heterogeneity and lineage commitment in myeloid progenitors. *Cell* 163, 1663–1677. doi: 10.1016/j.cell.2015.11.013

Peng, Q., Malhotra, S., Torchia, J. A., Kerr, W. G., Coggeshall, K. M., and Humphrey, M. B. (2010). TREM2- and DAP12-dependent activation of PI3K requires DAP10 and is inhibited by SHIP1. *Sci. Signal.* 3:ra38. doi: 10.1126/scisignal.2000500

Ponomarev, E. D., Veremeyko, T., and Weiner, H. L. (2013). MicroRNAs are universal regulators of differentiation, activation, and polarization of microglia and macrophages in normal and diseased CNS. *Glia* 61, 91–103. doi: 10.1002/glia.22363

Qi, F., Zuo, Z., Yang, J., Hu, S., Yang, Y., Yuan, Q., et al. (2017). Combined effect of BCG vaccination and enriched environment promote neurogenesis and spatial cognition via a shift in meningeal macrophage M2 polarization. *J. Neuroinflammation* 14:32. doi: 10.1186/s12974-017-0808-7

Ransohoff, R. M. (2016). A polarizing question: do M1 and M2 microglia exist? *Nat. Neurosci.* 19, 987–991. doi: 10.1038/nn.4338

Rotshenker, S. (2003). Microglia and macrophage activation and the regulation of complement-receptor-3 (CR3/MAC-1)-mediated myelin phagocytosis in injury and disease. *J. Mol. Neurosci.* 21, 65–72. doi: 10.1385/jmn:21:1:65

Rufino-Ramos, D., Albuquerque, P. R., Carmona, V., Perfeito, R., Nobre, R. J., and Pereira De Almeida, L. (2017). Extracellular vesicles: novel promising delivery systems for therapy of brain diseases. *J. Control Release* 262, 247–258. doi: 10.1016/j.jconrel.2017.07.001

Sanberg, P. R., Park, D. H., Kuzmin-Nichols, N., Cruz, E., Hossne, N. A. Jr., Buffolo, E., et al. (2010). Monocyte transplantation for neural and cardiovascular ischemia repair. *J. Cell. Mol. Med.* 14, 553–563. doi: 10.1111/j.1582-4934.2009.00903.x

Sandvig, I., Augestad, I. L., Haberg, A. K., and Sandvig, A. (2018). Neuroplasticity in stroke recovery. The role of microglia in engaging and modifying synapses and networks. *Eur. J. Neurosci.* 47, 1414–1428. doi: 10.1111/ejn.13959

Sasaki, A., Kakita, A., Yoshida, K., Konno, T., Ikeuchi, T., Hayashi, S., et al. (2015). Variable expression of microglial DAP12 and TREM2 genes in Nasu-Hakola disease. *Neurogenetics* 16, 265–276. doi: 10.1007/s10048-015-0451-3

Schmidt, A., Strecker, J. K., Hucke, S., Bruckmann, N. M., Herold, M., Mack, M., et al. (2017). Targeting different monocyte/macrophage subsets has no impact on outcome in experimental stroke. *Stroke* 48, 1061–1069. doi: 10.1161/STROKEAHA.116.015577

Shibata, M., and Suzuki, N. (2017). Exploring the role of microglia in cortical spreading depression in neurological disease. *J. Cereb. Blood Flow Metab.* 37, 1182–1191. doi: 10.1177/0271678X17690537

Shichita, T., Ito, M., Morita, R., Komai, K., Noguchi, Y., Ooboshi, H., et al. (2017). MAFB prevents excess inflammation after ischemic stroke by accelerating clearance of damage signals through MSR1. *Nat. Med.* 23, 723–732. doi: 10.1038/nm.4312

Shichita, T., Ito, M., and Yoshimura, A. (2014). Post-ischemic inflammation regulates neural damage and protection. *Front. Cell Neurosci.* 8:319. doi: 10.3389/fncel.2014.00319

Shin, J. A., Kim, Y. A., Kim, H. W., Kim, H. S., Lee, K. E., Kang, J. L., et al. (2018). Iron released from reactive microglia by noggin improves myelin repair in the ischemic brain. *Neuropharmacology* 133, 202–215. doi: 10.1016/j.neuropharm.2018.01.038

Siniscalchi, A., Iannacchero, R., Anticoli, S., Pezzella, F. R., De Sarro, G., and Gallelli, L. (2016). Anti-inflammatory strategies in stroke: a potential therapeutic target. *Curr. Vasc. Pharmacol.* 14, 98–105. doi: 10.2174/1570161113666150923111329

Smith, C. J., Denes, A., Tyrrell, P. J., and Di Napoli, M. (2015). Phase II anti-inflammatory and immune-modulating drugs for acute ischaemic stroke. *Expert Opin. Investig. Drugs* 24, 623–643. doi: 10.1517/13543784.2015.1020110

Spalding, K. L., Bergmann, O., Alkass, K., Bernard, S., Salehpour, M., Huttner, H. B., et al. (2013). Dynamics of hippocampal neurogenesis in adult humans. *Cell* 153, 1219–1227. doi: 10.1016/j.cell.2013.05.002

Stamova, B., Ander, B. P., Jickling, G., Hamade, F., Durocher, M., Zhan, X., et al. (2018). The intracerebral hemorrhage blood transcriptome in humans differs from the ischemic stroke and vascular risk factor control blood transcriptomes. *J. Cereb. Blood Flow Metab.* doi: 10.1177/0271678X18769513 [Epub ahead of print].

Stein, M., Keshav, S., Harris, N., and Gordon, S. (1992). Interleukin 4 potently enhances murine macrophage mannose receptor activity: a marker of alternative immunologic macrophage activation. *J. Exp. Med.* 176, 287–292. doi: 10.1084/jem.176.1.287

Sun, P., Liu, D. Z., Jickling, G. C., Sharp, F. R., and Yin, K. J. (2018). MicroRNA-based therapeutics in central nervous system injuries. *J. Cereb. Blood Flow Metab.* 38, 1125–1148. doi: 10.1177/0271678X18773871

Szalay, G., Martinecz, B., Lenart, N., Kornyei, Z., Orsolits, B., Judak, L., et al. (2016). Microglia protect against brain injury and their selective elimination dysregulates neuronal network activity after stroke. *Nat. Commun.* 7:11499. doi: 10.1038/ncomms11499

Thored, P., Arvidsson, A., Cacci, E., Ahlenius, H., Kallur, T., Darsalia, V., et al. (2006). Persistent production of neurons from adult brain stem cells during recovery after stroke. *Stem Cells* 24, 739–747. doi: 10.1634/stemcells.2005-0281

Thored, P., Heldmann, U., Gomes-Leal, W., Gisler, R., Darsalia, V., Taneera, J., et al. (2009). Long-term accumulation of microglia with proneurogenic phenotype concomitant with persistent neurogenesis in adult subventricular zone after stroke. *Glia* 57, 835–849. doi: 10.1002/glia.20810

Tsuyama, J., Nakamura, A., Ooboshi, H., Yoshimura, A., and Shichita, T. (2018). Pivotal role of innate myeloid cells in cerebral post-ischemic sterile inflammation. *Semin Immunopathol.* 40, 523–538. doi: 10.1007/s00281-018-0707-8

Tur, J., Vico, T., Lloberas, J., Zorzano, A., and Celada, A. (2017). Macrophages and mitochondria: a critical interplay between metabolism, signaling, and the functional activity. *Adv. Immunol.* 133, 1–36. doi: 10.1016/bs.ai.2016.12.001

Vahidy, F. S., Rahbar, M. H., Zhu, H., Rowan, P. J., Bambhroliya, A. B., and Savitz, S. I. (2016). systematic review and meta-analysis of bone marrow-derived mononuclear cells in animal models of ischemic stroke. *Stroke* 47, 1632–1639. doi: 10.1161/STROKEAHA.116.012701

Van den Bossche, J., Baardman, J., Otto, N. A., Van Der Velden, S., Neele, A. E., Van Den Berg, S. M., et al. (2016). Mitochondrial dysfunction prevents repolarization of inflammatory macrophages. *Cell Rep.* 17, 684–696. doi: 10.1016/j.celrep.2016.09.008

Venkat, P., Chen, J., and Chopp, M. (2018). Exosome-mediated amplification of endogenous brain repair mechanisms and brain and systemic organ interaction in modulating neurological outcome after stroke. *J. Cereb. Blood Flow Metab.* 38, 2165–2178. doi: 10.1177/0271678X18782789

Verma, R., Cronin, C. G., Hudobenko, J., Venna, V. R., Mccullough, L. D., and Liang, B. T. (2017). Deletion of the P2X4 receptor is neuroprotective acutely, but induces a depressive phenotype during recovery from ischemic stroke. *Brain Behav. Immun.* 66, 302–312. doi: 10.1016/j.bbi.2017.07.155

Villaseñor, R., Kuennecke, B., Ozmen, L., Ammann, M., Kugler, C., Gruninger, F., et al. (2017). Region-specific permeability of the blood-brain barrier upon pericyte loss. *J. Cereb. Blood Flow Metab.* 37, 3683–3694. doi: 10.1177/0271678X17697340

Wake, H., Moorhouse, A. J., Miyamoto, A., and Nabekura, J. (2013). Microglia: actively surveying and shaping neuronal circuit structure and function. *Trends Neurosci.* 36, 209–217. doi: 10.1016/j.tins.2012.11.007

Wan, S., Cheng, Y., Jin, H., Guo, D., Hua, Y., Keep, R. F., et al. (2016). microglia activation and polarization after intracerebral hemorrhage in mice: the role of protease-activated receptor-1. *Transl Stroke Res.* 7, 478–487. doi: 10.1007/s12975-016-0472-8

Wang, L., Zhou, Y., Yin, J., Gan, Y., Wang, X., Wen, D., et al. (2018). Cancer exacerbates ischemic brain injury via Nrp1 (Neuropilin 1)-mediated accumulation of regulatory T cells within the tumor. *Stroke* 49, 2733–2742. doi: 10.1161/STROKEAHA.118.021948

Wang, X., Xuan, W., Zhu, Z. Y., Li, Y., Zhu, H., Zhu, L., et al. (2018). The evolving role of neuro-immune interaction in brain repair after cerebral ischemic stroke. *CNS Neurosci. Ther.* 24, 1100–1114. doi: 10.1111/cns.13077

Wang, X., Zhou, Y., Tang, D., Zhu, Z., Li, Y., Huang, T., et al. (2019). ACC1 (Acetyl Coenzyme A Carboxylase 1) is a potential immune modulatory target of cerebral ischemic stroke. *Stroke* 50, 1869–1878. doi: 10.1161/STROKEAHA.119.024564

Wang, Y., Cella, M., Mallinson, K., Ulrich, J. D., Young, K. L., Robinette, M. L., et al. (2015). TREM2 lipid sensing sustains the microglial response in an Alzheimer's disease model. *Cell* 160, 1061–1071. doi: 10.1016/j.cell.2015.01.049

Wattananit, S., Tornero, D., Graubardt, N., Memanishvili, T., Monni, E., Tatarishvili, J., et al. (2016). Monocyte-derived macrophages contribute to spontaneous long-term functional recovery after stroke in mice. *J. Neurosci.* 36, 4182–4195. doi: 10.1523/JNEUROSCI.4317-15.2016

Webb, R. L., Kaiser, E. E., Scoville, S. L., Thompson, T. A., Fatima, S., Pandya, C., et al. (2018). Human neural stem cell extracellular vesicles improve tissue and functional recovery in the murine thromboembolic stroke model. *Transl Stroke Res.* 9, 530–539. doi: 10.1007/s12975-017-0599-2

Wei, C. J., Cui, P., Li, H., Lang, W. J., Liu, G. Y., and Ma, X. F. (2019). Shared genes between Alzheimer's disease and ischemic stroke. *CNS Neurosci Ther.* doi: 10.1111/cns.13117 [Epub ahead of print].

Wes, P. D., Holtman, I. R., Boddeke, E. W., Moller, T., and Eggen, B. J. (2016). Next generation transcriptomics and genomics elucidate biological complexity of microglia in health and disease. *Glia* 64, 197–213. doi: 10.1002/glia.22866

Wium-Andersen, I. K., Wium-Andersen, M. K., Jorgensen, M. B., and Osler, M. (2017). Anti-inflammatory treatment and risk for depression after first-time stroke in a cohort of 147 487 Danish patients. *J. Psychiatry Neurosci.* 42, 320–330.

Woo, M. S., Wang, X., Faustino, J. V., Derugin, N., Wendland, M. F., Zhou, P., et al. (2012). Genetic deletion of CD36 enhances injury after acute neonatal stroke. *Ann. Neurol.* 72, 961–970. doi: 10.1002/ana.23727

Woo, M. S., Yang, J., Beltran, C., and Cho, S. (2016). Cell surface CD36 protein in monocyte/macrophage contributes to phagocytosis during the resolution phase of ischemic stroke in mice. *J. Biol. Chem.* 291, 23654–23661. doi: 10.1074/jbc.m116.750018

Wu, R., Li, X., Xu, P., Huang, L., Cheng, J., Huang, X., et al. (2017). TREM2 protects against cerebral ischemia/reperfusion injury. *Mol. Brain* 10:20. doi: 10.1186/s13041-017-0296-9

Xin, H., Li, Y., Cui, Y., Yang, J. J., Zhang, Z. G., and Chopp, M. (2013). Systemic administration of exosomes released from mesenchymal stromal cells promote functional recovery and neurovascular plasticity after stroke in rats. *J. Cereb. Blood Flow Metab.* 33, 1711–1715. doi: 10.1038/jcbfm.2013.152

Xing, C., Wang, X., Cheng, C., Montaner, J., Mandeville, E., Leung, W., et al. (2014). Neuronal production of lipocalin-2 as a help-me signal for glial activation. *Stroke* 45, 2085–2092. doi: 10.1161/STROKEAHA.114.005733

Yamasaki, R., Lu, H., Butovsky, O., Ohno, N., Rietsch, A. M., Cialic, R., et al. (2014). Differential roles of microglia and monocytes in the inflamed central nervous system. *J. Exp. Med.* 211, 1533–1549. doi: 10.1084/jem.20132477

Yang, B., Parsha, K., Schaar, K., Xi, X., Aronowski, J., and Savitz, S. I. (2016). Various cell populations within the mononuclear fraction of bone marrow contribute to the beneficial effects of autologous bone marrow cell therapy in a rodent stroke model. *Transl. Stroke Res.* 7, 322–330. doi: 10.1007/s12975-016-0462-x

Yang, B., Xi, X., Aronowski, J., and Savitz, S. I. (2012). Ischemic stroke may activate bone marrow mononuclear cells to enhance recovery after stroke. *Stem Cells Dev* 21, 3332–3340. doi: 10.1089/scd.2012.0037

Yang, Y., Liu, H., Zhang, H., Ye, Q., Wang, J., Yang, B., et al. (2017). ST2/IL-33-Dependent Microglial Response Limits Acute Ischemic Brain Injury. *J Neurosci* 37, 4692–4704. doi: 10.1523/JNEUROSCI.3233-16.2017

Yuan, D., Zhao, Y., Banks, W. A., Bullock, K. M., Haney, M., Batrakova, E., et al. (2017). Macrophage exosomes as natural nanocarriers for protein delivery to inflamed brain. *Biomaterials* 142, 1–12. doi: 10.1016/j.biomaterials.2017.07.011

Yuan, P., Condello, C., Keene, C. D., Wang, Y., Bird, T. D., Paul, S. M., et al. (2016). TREM2 haplodeficiency in mice and humans impairs the microglia barrier function leading to decreased amyloid compaction and severe axonal dystrophy. *Neuron* 92, 252–264. doi: 10.1016/j.neuron.2016.09.016

Yun, H. J., Kim, E. H., and Kim, B. G. (2018). Neuron-macrophage co-cultures to activate macrophages secreting molecular factors with neurite outgrowth activity. *J. Vis. Exp.* 30:e56920. doi: 10.3791/56920

Zagrean, A. M., Hermann, D. M., Opris, I., Zagrean, L., and Popa-Wagner, A. (2018). Multicellular crosstalk between exosomes and the neurovascular unit after cerebral ischemia. Therapeutic implications. *Front. Neurosci.* 12:811. doi: 10.3389/fnins.2018.00811

Zhang, H., Xia, Y., Ye, Q., Yu, F., Zhu, W., Li, P., et al. (2018). In vivo expansion of regulatory T cells with IL-2/IL-2 antibody complex protects against transient ischemic stroke. *J. Neurosci.* 38, 10168–10179. doi: 10.1523/JNEUROSCI.3411-17.2018

Zhao, S. C., Ma, L. S., Chu, Z. H., Xu, H., Wu, W. Q., and Liu, F. (2017). Regulation of microglial activation in stroke. *Acta Pharmacol. Sin* 38, 445–458. doi: 10.1038/aps.2016.162

Zhao, X., Ting, S. M., Liu, C. H., Sun, G., Kruzel, M., Roy-O'reilly, M., et al. (2017). Neutrophil polarization by IL-27 as a therapeutic target for intracerebral hemorrhage. *Nat. Commun.* 8:602. doi: 10.1038/s41467-017-00770-7

Zhao, X., Wang, H., Sun, G., Zhang, J., Edwards, N. J., and Aronowski, J. (2015). Neuronal interleukin-4 as a modulator of microglial pathways and ischemic brain damage. *J. Neurosci.* 35, 11281–11291. doi: 10.1523/JNEUROSCI.1685-15.2015

Zhao, Z., Ong, L. K., Johnson, S., Nilsson, M., and Walker, F. R. (2017). Chronic stress induced disruption of the peri-infarct neurovascular unit following

experimentally induced photothrombotic stroke. *J. Cereb. Blood Flow Metab.* 37, 3709–3724. doi: 10.1177/0271678X17696100

Zheng, H., Jia, L., Liu, C. C., Rong, Z., Zhong, L., Yang, L., et al. (2017). TREM2 promotes microglial survival by activating Wnt/beta-Catenin pathway. *J. Neurosci.* 37, 1772–1784. doi: 10.1523/JNEUROSCI.2459-16.2017

Zheng, Y., He, R., Wang, P., Shi, Y., Zhao, L., and Liang, J. (2019). Exosomes from LPS-stimulated macrophages induce neuroprotection and functional improvement after ischemic stroke by modulating microglial polarization. *Biomater Sci.* 7, 2037–2049. doi: 10.1039/c8bm01449c

Zhu, W., Fan, Y., Hao, Q., Shen, F., Hashimoto, T., Yang, G. Y., et al. (2009). Postischemic IGF-1 gene transfer promotes neurovascular regeneration after experimental stroke. *J. Cereb. Blood Flow Metab.* 29, 1528–1537. doi: 10.1038/jcbfm.2009.75

Ziv, Y., Ron, N., Butovsky, O., Landa, G., Sudai, E., Greenberg, N., et al. (2006). Immune cells contribute to the maintenance of neurogenesis and spatial learning abilities in adulthood. *Nat. Neurosci.* 9, 268–275. doi: 10.1038/nn1629

Conflict of Interest Statement: The authors declare that the research was conducted in the absence of any commercial or financial relationships that could be construed as a potential conflict of interest.

Copyright © 2019 Zhu, Zheng, Li, Huang, Chao, Pan, Zhu, Zhao, Yu and Li. This is an open-access article distributed under the terms of the Creative Commons Attribution License (CC BY). The use, distribution or reproduction in other forums is permitted, provided the original author(s) and the copyright owner(s) are credited and that the original publication in this journal is cited, in accordance with accepted academic practice. No use, distribution or reproduction is permitted which does not comply with these terms.

frontiers in Neurology

REVIEW
published: 16 August 2019
doi: 10.3389/fneur.2019.00889

Small Vessels Are a Big Problem in Neurodegeneration and Neuroprotection

Şefik Evren Erdener[1] *and Turgay Dalkara*[1,2]*

[1] *Institute of Neurological Sciences and Psychiatry, Hacettepe University, Ankara, Turkey,* [2] *Department of Neurology, Faculty of Medicine, Hacettepe University, Ankara, Turkey*

The cerebral microcirculation holds a critical position to match the high metabolic demand by neuronal activity. Functionally, microcirculation is virtually inseparable from other nervous system cells under both physiological and pathological conditions. For successful bench-to-bedside translation of neuroprotection research, the role of microcirculation in acute and chronic neurodegenerative disorders appears to be under-recognized, which may have contributed to clinical trial failures with some neuroprotectants. Increasing data over the last decade suggest that microcirculatory impairments such as endothelial or pericyte dysfunction, morphological irregularities in capillaries or frequent dynamic stalls in blood cell flux resulting in excessive heterogeneity in capillary transit may significantly compromise tissue oxygen availability. We now know that ischemia-induced persistent abnormalities in capillary flow negatively impact restoration of reperfusion after recanalization of occluded cerebral arteries. Similarly, microcirculatory impairments can accompany or even precede neural loss in animal models of several neurodegenerative disorders including Alzheimer's disease. Macrovessels are relatively easy to evaluate with radiological or experimental imaging methods but they cannot faithfully reflect the downstream microcirculatory disturbances, which may be quite heterogeneous across the tissue at microscopic scale and/or happen fast and transiently. The complexity and size of the elements of microcirculation, therefore, require utilization of cutting-edge imaging techniques with high spatiotemporal resolution as well as multidisciplinary team effort to disclose microvascular-neurodegenerative connection and to test treatment approaches to advance the field. Developments in two photon microscopy, ultrafast ultrasound, and optical coherence tomography provide valuable experimental tools to reveal those microscopic events with high resolution. Here, we review the up-to-date advances in understanding of the primary microcirculatory abnormalities that can result in neurodegenerative processes and the combined neurovascular protection approaches that can prevent acute as well as chronic neurodegeneration.

Keywords: capillary, microcirculation, pericytes, oxygen extraction, flow heterogeneity, neuroprotection, neurodegeneration

OPEN ACCESS

Edited by:
Johannes Boltze, University of Warwick, United Kingdom

Reviewed by:
Brad A. Sutherland, University of Tasmania, Australia
Leif Østergaard, Center of Functionally Integrative Neuroscience and MINDLab, Denmark

***Correspondence:**
Turgay Dalkara
tdalkara@hacettepe.edu.tr

Specialty section:
This article was submitted to Neurodegeneration, a section of the journal Frontiers in Neurology

Received: *12 May 2019*
Accepted: *01 August 2019*
Published: *16 August 2019*

Citation:
Erdener ŞE and Dalkara T (2019) Small Vessels Are a Big Problem in Neurodegeneration and Neuroprotection. Front. Neurol. 10:889. doi: 10.3389/fneur.2019.00889

INTRODUCTION

Cerebral microcirculation is a fundamental element for proper cerebral functioning since it is the main transport and distribution system for oxygen and nutrients that fuel the high and continuously changing metabolic demand of the brain tissue. The anatomical and physiological features of small vessels, which mainly consist of vasculature $<100\,\mu m$ in diameter (1), where most of the metabolic exchange takes place, are considerably different from large vessels and these differences make them difficult to study experimentally and virtually inaccessible in human beings. Over the last years, advances in imaging technologies and modeling made such investigations possible and increased the recognition of microcirculatory pathologies in acute and chronic neurodegenerative conditions, revealing novel mechanisms and potential therapeutic strategies. In this review, the structural and functional principles of cerebral microcirculation and its pathophysiological relevance will be discussed.

CAPILLARY DYSFUNCTION

The Complexity of Microcirculation

The brain is a vascular organ as much as it is neuronal. The anatomy of cerebral vasculature is unique and optimized to provide continuous blood supply to the brain. Extensive anastomoses between pial vessels on the surface ensure that extra blood can be shuffled to the activated brain area demanding more energy. As illustrated in **Figure 1**, progressive branching of penetrating arteries into a high-density meshwork of capillaries allows for adequate delivery of nutrients, such that there is a capillary within 10–20 μm of every neuron (4, 5). The density of capillary mesh correlates with neuronal density and differs between cortical layers or brain regions. Unlike simplified illustrations, capillary networks have a complex structure, branching in various directions, forming loops, and curls to optimally match the tissue demand.

Tissue blood flow is provided by the pressure gradient across the microcirculatory bed vascular resistance, which is largely determined by the vascular diameter and blood viscosity (6). The focal brain activity is highly variable; hence, regional metabolic requirements change fast and continuously. This requires a precise spatial and temporal control of the local blood flow. Consequently, flow changes are tightly coupled to neuronal activity through a set of mechanisms integrated within the *neurovascular unit* (7, 8). This *neurovascular coupling* can be mediated by both feed-forward (neuronal activity itself directly regulates blood flow) or feed-back (the metabolic consequences of increased activity regulates blood flow) mechanisms (8, 9).

Studying microcirculation is challenging in animals as well as humans because of the structural and functional complexity of the system. This has caused a delay in understanding role of microcirculatory dysfunction in neurological disorders, which is more relevant than previously thought. The microcirculatory dynamics are fast and heterogeneous, so we need tools that can acquire data with high spatial (in microns) and temporal (in milliseconds) resolution. Most of the available information on capillary flow and oxygenation is based on magnetic resonance imaging (MRI) as well as direct *in vivo* microscopic imaging that can be performed only in animals. Two-photon microscopy (TPM) through a cranial window in rodents provides high resolution angiogram of the capillary network and, red blood cell (RBC) flux and speed estimation within individual capillaries (12–14). Phosphorescence lifetime microscopy (PLIM) adds assessment of the oxygen with subcapillary resolution both in microvasculature and cerebral tissue (2, 15–22). Optical coherence tomography (OCT), which is sensitive to motion of scattering particles enable visualizing RBC flow label-free. Unlike TPM that images a limited area, OCT-angiography allows visualizing hundreds of capillaries simultaneously through the cortical mantle (10, 23–26). In MRI, a voxel of 1 mm^3 reflects merely an average of many capillaries but MRI has the advantage of imaging whole brain non-invasively (27).

Studies with these instruments have revealed that the increase in capillary blood flow occurs slightly before or in synchrony with upstream vessels, suggesting a direct role to the microcirculation to coordinate functional hyperemia response (29–32). Under resting state, most of the oxygen release into the tissue occurs at the precapillary arteriole level, while distal capillaries become an additional a site of oxygen extraction during functional hyperemia (2). Especially during baseline conditions, the capillary pO_2 distribution is highly heterogeneous, some capillaries have very low oxygen, while not necessarily making the tissue around them critically hypoxic but particularly vulnerable to fluctuations in blood flow and/or increase in metabolic demand (2, 16).

Microcirculation Plays an Active Role in Neurovascular Coupling

Models for blood flow simulation and oxygen transport / extraction (34–38) suggest that capillary flow patterns are important to determine tissue oxygen availability (37–39). While cerebral capillaries are normally almost always perfused with plasma during rest and activated conditions, the flow speeds of RBCs, like spatial oxygen distribution, are heterogeneous at baseline. This is caused by variability in capillary diameters, pressure gradients, and non-Newtonian fluid characteristics of blood, resulting in different RBC and plasma fractions in different capillaries that can affect the flow patterns (40) (**Figure 2C**). In a recent study, monitoring of capillaries frame-by-frame by OCT angiography revealed frequent temporary stalls that lasted for few seconds-minutes in individual capillaries (10) (**Figure 2A**). These temporal flow fluctuations can be caused by RBCs or white blood cells (WBCs) getting stuck or slowed down inside capillaries (10, 11, 41) because of their relatively large size compared to the capillary lumen (**Figure 2B**). They are more prevalent in capillaries closer to the distal end of the microcirculation, where pressure gradients are lower and RBCs are slower, and also where endothelial adhesion molecules like intercellular cell adhesion molecule-1 (ICAM-1) have higher expression (42). During functional activation, RBC flow speeds increase to make flow distribution in capillary bed more homogeneous and the dynamic stalls diminish (10) (**Figures 2D,E**). This homogeneous

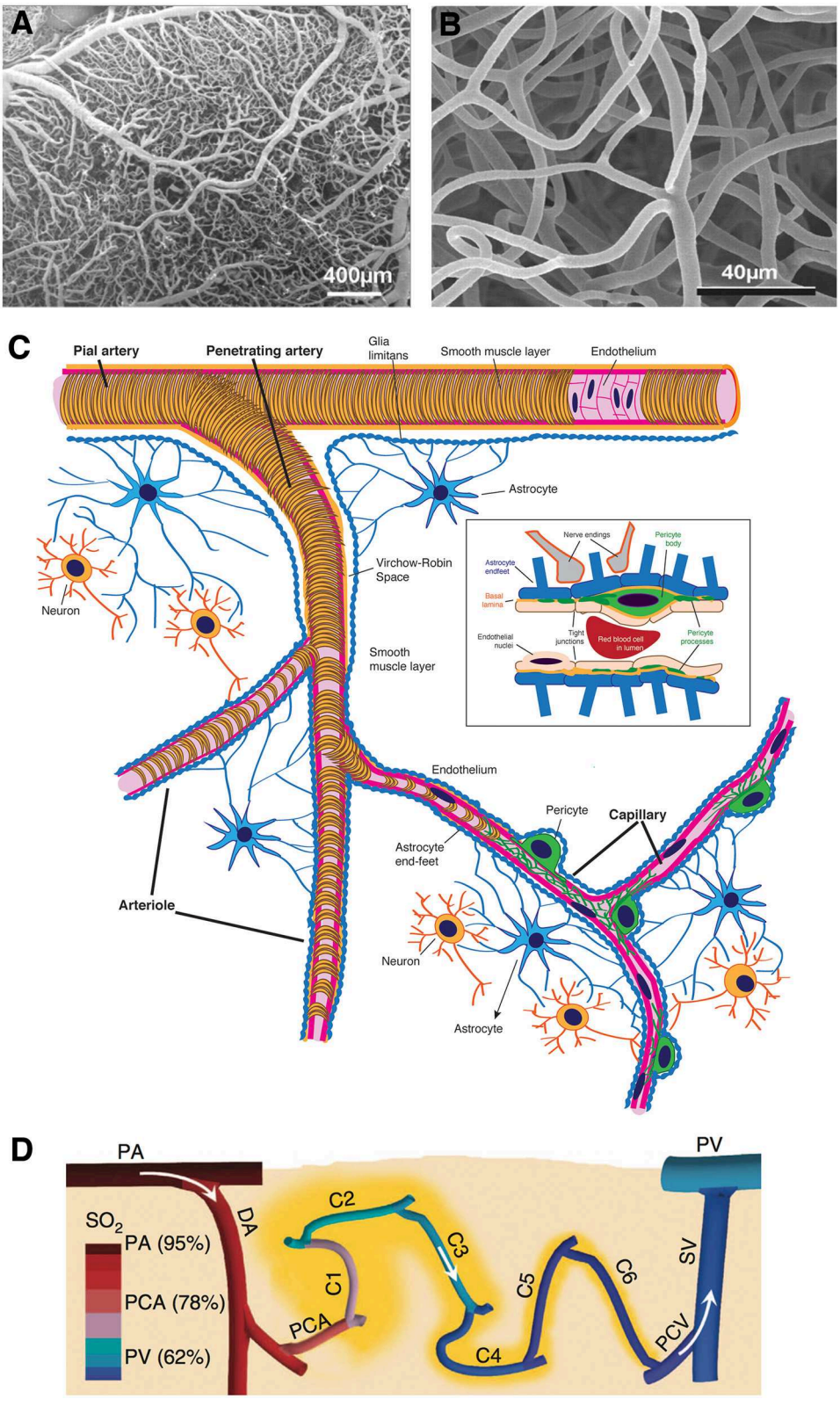

FIGURE 1 | Morphological features of cerebral microcirculation. **(A,B)** Dense external coverage of the surface by pial arteries and veins which are interconnected via anastomoses and collateral vessels then gives rise to a complex meshwork of capillaries, composed of segments about 60–70 μm in length. **(C)** Penetrating arteries

(Continued)

FIGURE 1 | originating from pial vasculature dive into the cortical tissue without forming any further anastomoses. Immediately surrounded by the cerebrospinal fluid-filled spaces called *perivascular spaces* or *Virchow-Robin spaces* along their course, penetrating arteries then give rise an extensive tree of small vessels as they branch into arterioles (30–100 μm diameter), precapillary arterioles (10–30 μm), and capillaries (<10 μm), respectively. As arterioles turn into capillaries, the perivascular space disappears, making the capillary wall adjacent to the parenchyma. **(D)** Capillaries branch out for 5–6 times on average (2) as they release oxygen into the tissue, until they converge on postcapillary venules that drain into ascending veins. (**A,B** reproduced by permission from: PNAS, Meyer et al. (3) ©2008 National Academy of Sciences. **(D)** reprinted by permission from: Nature Communications, Sakadžić et al. (2) ©2014 Springer Nature).

transformation in oxygenation and flow speeds is essential for optimum oxygen extraction. Because, in case of heterogeneous flows, some capillaries have higher flow velocity compared to the neighboring vessels and they act as thoroughfare channels, shunting highly-oxygenated RBCs through the microcirculation to leave little time for oxygen release (37). This is important because it has been shown that increasing overall arterial blood flow to a capillary bed with heterogeneous flow distribution can paradoxically worsen oxygen availability to the tissue (38, 43, 44). For this reason, functional blood flow responses in the brain need to be actively regulated at the capillary level and not solely by dilating arterioles. This function is realized by structural and metabolic collaboration between neurons, endothelia, astrocytes and pericytes, the building blocks of the neurovascular unit.

Endothelium is the common inner lining of all types of vasculature, including capillaries. In the central nervous system (CNS) tight junctions between endothelial cells form the critical layer of the blood brain barrier (BBB) that controls material passage into the parenchyma. In the healthy setting, endothelium prevents paracellular plasma leakage by tight junctions and there is a low level of transcytotic vesicle trafficking through endothelial cells (45, 46). Oxygen and carbon dioxide, on the other hand, can freely diffuse across the capillary wall bidirectionally (46–48), allowing rapid gas exchange. The endothelium, basal membrane, and astrocyte end feet together form the capillary wall and the BBB (49). Degradation of BBB either due to basal lamina changes, endothelial or astrocyte damage is a common feature of many neurodegenerative disorders which have microcirculatory pathologies. While there is no smooth muscle layer in the capillary wall, there is another contractile cell, the pericyte located at the periphery of microvessel wall and embedded into the basal membrane layers (50). Pericytes have a contractile apparatus, which is similar to that of smooth muscle cells. Pericyte processes concentrically surround the capillaries, enabling them to regulate the capillary diameter (51, 52). Pericytes have also been shown to contribute to BBB formation and maintenance, to immunological modulation, angiogenesis, and capillary reorganization (53–55). Pericytes therefore are attractive candidates for capillary-level control of neurovascular coupling. Indeed, pericyte relaxation during functional activation has been shown to precede or being closely coincident with functional hyperemia (30, 51). The strong interactions between pericytes and endothelial cells and astrocytes further underline their strategic role in microcirculation (56, 57).

Astrocyte end-feet around microvessels are critical elements for neuron-microvessel communication. Nearby neuronal activity is sensed by astrocyte processes as extracellular adenosine triphosphate (ATP) and glutamate increase around synapses. Calcium signals triggered in astrocytes lead to cyclooxygenase activation and release of vasodilatory prostaglandins from end-feet surrounding the capillaries (58, 59). This is one of the basic mechanisms for translation of neuronal activity to vasoactive regulation. Other mechanisms involving metabolic and paracrine interactions within elements of the tightly integrated neurovascular unit are also present and contribution of each varies between brain regions. For example, astrocyte processes are also metabolically coupled to excitatory synapses; they rapidly breakdown glycogen to release lactate as an energy supply to neurons (60). An intriguing feature of the astrocyte network is the gap junctions between end-feet integrated to the capillary wall. Activity-induced calcium signaling can rapidly propagate around microvasculature to provide a coordinated response in a given area (59, 61–63). Capillary pericytes readily respond to the local release of vasodilatory prostaglandins (30). Endothelial cells, which are electrically coupled to other endothelial cells and to smooth muscle cells via gap junctions (64–67), have also been shown to propagate membrane depolarizations and calcium waves along the vasculature, releasing nitric oxide (NO) in consequence (68), adding to the coordinated microvascular regulation. Interneurons are also directly involved in vasoactive regulation. For example, stimulation of GABAergic interneurons has been shown to produce a biphasic blood flow response, hyperemia, followed by vasoconstriction, similar to the somatosensory activation response, by releasing NO and neuropeptide Y, respectively (69–72). Interestingly, red blood cells within the capillary lumen themselves can also take active role in capillary flow regulation by releasing ATP in response to focal acidosis, hypoxia, shear stress, or mechanical stimuli (73–76). The ATP release can be initiated by opening of pannexin channels or voltage-dependent anion channels in erythrocytes (75, 77). ATP, by binding to purinergic receptors can trigger NO or prostaglandin release from the endothelium (73) generating a local vasodilatory response to match the oxygen demand in the stagnated microenvironment (73).

The mechanisms of neurovascular regulation should be recognized in the setting of an integrated vascular network, where different levels of microcirculation may work in concert in addition to a tight compartmentalization. For example, arterioles appear to favor the vasoactive signals coming from interneurons coding the activity in a larger cohort of neurons in contrast to capillary regulation responding to very focal demand translated by adjacent astrocytes (69, 78). Arterioles also respond to signals coming up through the endothelia to accommodate the blood volume demand by the downstream microcirculatory bed (58, 59, 61–63).

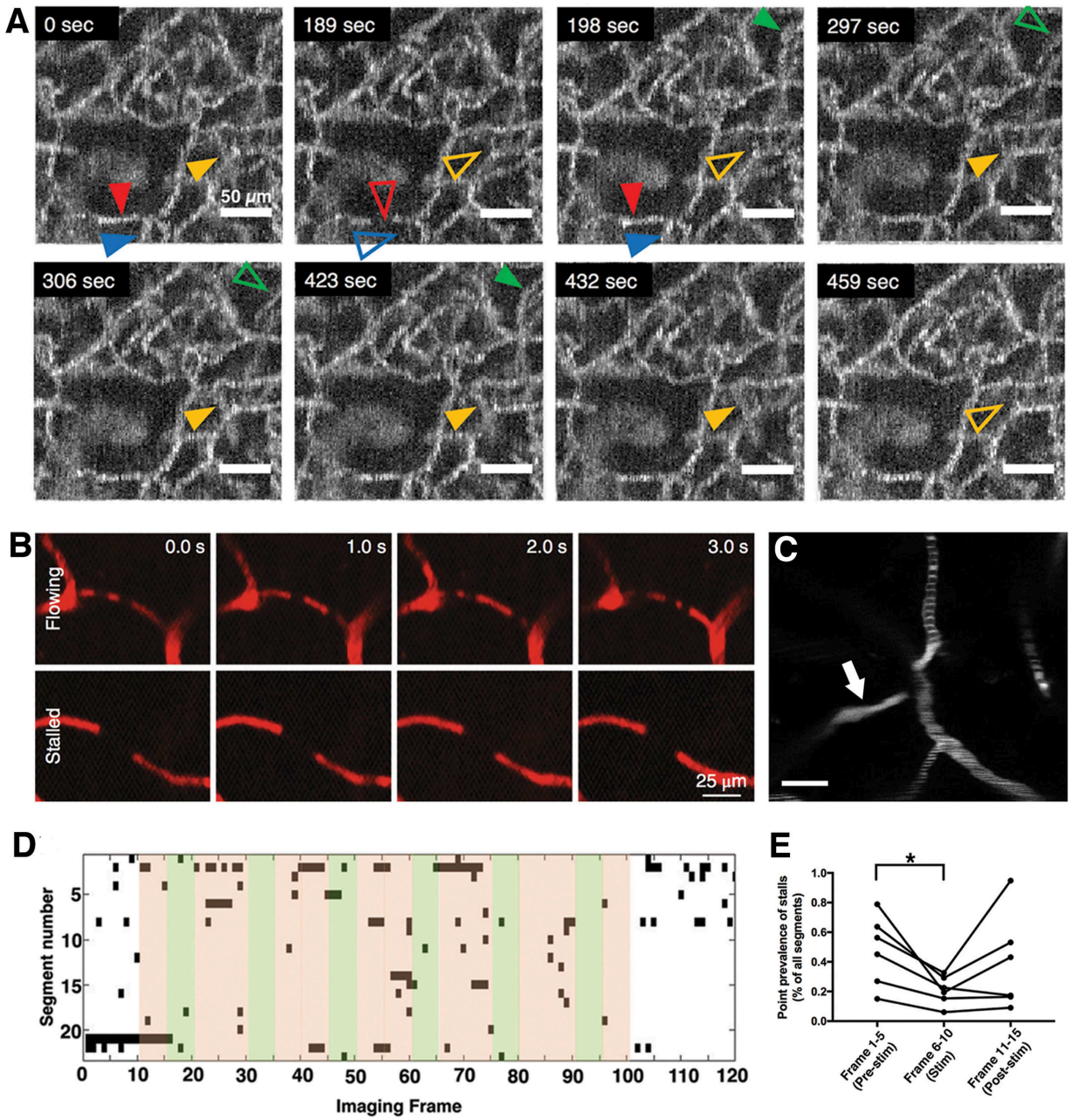

FIGURE 2 | Irregularity and heterogeneity in capillary flow **(A)** OCT angiogram time-series identify capillary segments with stalling red blood cells. Individual segments (arrowheads) with temporary interruptions of RBC flux simply lose OCT angiogram signal. Hollow arrowheads indicate a stalled capillary segment (10). **(B)** Two photon microscopy time series with fluorescent labeled plasma can identify flowing and stalled capillaries based on the motion of unlabeled cells as seen in black (11). **(C)** A single time-point two-photon angiogram of a set of capillary branches at ∼100 μm below cortical surface shows heterogeneous distribution of RBC flux. Segments with higher flow have thinner and denser RBC-bands whereas slower flow is indicated by thicker and more scarce bands. One segment (arrow) has no RBCs flowing but is still filled with fluorescent labeled plasma. Scalebar: 20 μm) **(D)** Matrix plot of individual stall events in a region of interest, acquired during a functional stimulation experiment, with a frame period of 9 s. Every black points denotes a stall in a particular capillary. Green shades indicate whisker stimulation. **(E)** The frequency of capillary stalls is dynamically modulated during functional stimulation; stall prevalence was significantly lower during functional hyperemia. *Statistical significance ($p < 0.05$). (**A,D,E** reproduced by permission from: JCBFM, Erdener et al. (10); **(B)** reprinted by permission from: Nature Neuroscience, Cruz Hernandez et al. (11), ©2019 Springer Nature).

Microcirculatory Failure

Since oxygen availability in the tissue relies on the distribution of capillary flow patterns and their heterogeneity, the absolute quantitative level of cerebral blood flow (CBF) may not always reflect accurate supply-demand match at microscopic level. In routine clinical practice of cerebrovascular medicine, main focus

is on the evaluation of adequate arterial flow and luminal patency, as they can be easily imaged by widely available radiological techniques. In the setting of a CBF drop, particularly to ischemic levels (below ∼20 ml/100 g/min in humans) (79), there is a prominent decrease in tissue oxygen tension paralleled by a relative increase in oxygen extraction. However, experimental and computer simulation data indicate that the tissue oxygen availability may be compromised even in the absence of a flow-limiting condition (37, 38). This arises from "capillary dysfunction," causing excessive flow heterogeneity in the capillary bed and failing to homogenize in response to increasing functional demand. This heterogeneity causes certain capillary segments to transit oxygenated RBCs too fast for enough oxygen to be released to tissue (36, 44). A classic example of this phenomenon is the hyperperfusion syndrome (38, 80, 81), a temporary excessive hyperemia after recanalization of an occluded cerebral artery, which paradoxically results in low tissue oxygenation (38). Very slow flux rates in some capillaries may also lead to a reduced oxygen delivery due to insufficient number of RBCs transiting. Any factor introducing irregularity to the capillary flow, results in a higher standard deviation in distribution of RBC velocities and/or transit times across the microvascular bed, i.e., the capillary transit time heterogeneity (CTH). However, it should be noted that increased CTH may passively increase with high mean transit time (MTT), the average time that contrast bolus traverse between arterial and venous ends (43). Importantly, the relative transit time heterogeneity (CTH/MTT), i.e., the coefficient of variation of transit times, can distinguish between true microcirculatory heterogeneity and a passive increase in CTH with low CBF and elevated MTT. The relationship between CBF, CTH, oxygen extraction fraction (OEF), and tissue oxygen can be evaluated with computational models (36, 82, 83). These models show that, CTH is, counter intuitively; homogenized with very low flow rates to maximize O_2 extraction in poorly perfused tissue (37, 82). The detailed evaluation of mathematical models is beyond the scope of this review and the reader is referred to excellent papers on this subject (84, 85). MRI data can be used to prepare MTT, CTH, and OEF maps with use of appropriate mathematical models (27). These tools have been useful for evaluation of capillary dysfunction in acute ischemic stroke and Alzheimer's disease patients (36, 38, 43, 82, 86).

The capillary dysfunction can arise from almost any element within the neurovascular unit. A thin (0.5 μm) glycoprotein coating in the luminal side of the endothelium, called glycocalyx, facilitates passage of blood cells (87–89). Glycocalyx can degrade very fast with excessive inflammatory stimuli like lipopolysaccharides, hyperglycemia, ischemia, and oxidative stress (90). A degraded glycocalyx exposes underlying endothelium to physical interaction with blood cells. This usually results in a higher degree of cellular adhesion. Each cellular plug, whether permanent or transient, can then increase resistance in that particular segment, change pressure gradient, flux, and hematocrit distribution in nearby capillary bed and cause irregular hemodynamics. A relative increase in hematocrit in other capillaries within the same network may increase the tendency for plugging.

Endothelial cell dysfunction can significantly contribute to dysregulated capillary flow. This dysfunction includes a reduction in endothelium-derived nitric oxide availability. Moreover, gap-junction uncoupling between endothelial cells increases functional shunting by introducing irregularities to the microvascular cross-sectional profiles, caused by desynchronized regulation of smooth muscle or pericyte tone (91, 92). A dysfunctional endothelium is also more prone to leukocyte adhesion, as nitric oxide is a well-recognized modulator of leukocyte adhesion (92–94). Leukocyte plugs and resultant flow stalls in capillaries can unfavorably affect flow patterns and, the release of leukocyte-derived oxygen radicals or cytokines can damage the endothelium and overlying glycocalyx. BBB breakdown may accompany a damaged and dysfunctional endothelium. Endothelium, besides these barrier-forming and material exchange functions, is also involved in immunological regulation, leukocyte adhesion and regulation of thrombosis as well as vascular tone (95).

Pericytes maintain the BBB, interact with immune cells (96) and, since they are contractile, regulate capillary flow distribution within the microvascular network. Both constriction or dilation of capillaries mediated by pericytes can result in stalls in cellular flow or functional shunts (32). Pericytes contract or constrict with changes in oxygen tension, with exposure to reactive oxygen radicals, noradrenaline, ATP and endothelin (28, 30, 53, 97), while glutamate, adenosine, lactate, nitric oxide, and C-type natriuretic peptide cause relaxation (30, 97–99). Besides active contractile changes, loss of pericytes themselves can cause capillary dysfunction (100). Amyloid-beta has been shown to cause pericyte degeneration (101, 102), which may be a possible link between neurodegenerative disorders and microcirculatory dysfunction. Hyperglycemia directly causes pericyte death or migration, hence, leaky newly-formed microvessels are typical features of diabetic retinopathy (99, 103). Pericytes have been shown to migrate along or away from vasculature following traumatic injury (104, 105). With pathological stimuli, pericyte process coverage over capillary wall can decrease, further disrupting microvascular physiology (106, 107).

Finally, the physicochemical properties of plasma or blood cells themselves can introduce microcirculatory heterogeneity. As noted above, RBCs and WBCs have large diameters compared to capillaries therefore they need to squeeze through the narrow capillary lumen, significantly making passage challenging and vulnerable to disturbances (108). Even subtle capillary constrictions can therefore dramatically affect RBC perfusion distribution in a capillary network (36, 82). Changes in cell count, size, stiffness, flexibility, and adhesion can affect the capillary transit (8). In experimental models of polycythemia vera and essential thrombocythemia, it has been shown that individual capillaries are clogged by RBCs, and then platelets, affecting the CBF (41). Rheological properties, like deformability of RBCs can affect microcirculatory efficiency as seen in diabetes (109). Blockade of capillaries by activated neutrophils are also observed in cerebral ischemia (110–113). Dehydration and elevated homocysteine can increase plasma viscosity and/or hematocrit, causing formation of RBC aggregates, and capillary plugs (38, 114). It should be noted that plasma may continue to

flow though even when there is no cellular flow in a capillary, unfavorably affecting tissue survival as plasma provides glucose to the hypo-oxygenized tissue, promoting lactate production and tissue acidosis (28, 115–117).

The tissue can tolerate a certain degree of capillary dysfunction by regulating upstream arteriolar flow (either increasing or decreasing) to optimize oxygen extraction (37, 44, 118–120). A reduction in resting CBF and suppression of functional hemodynamic responses can be a part of this compensation (37, 121). But after a certain degree of CTH, usually accompanied by a higher level of capillary diameter irregularities, glycocalyx damage, elevated blood viscosity, leukocyte adhesion, and excessive red blood cell stalls, the supplied oxygen cannot sustain neuronal homeostasis any more (36). At this level of severe capillary dysfunction, where CBF is close to the ischemic threshold, slight changes in metabolic needs, systemic blood pressure, leukocyte count, or blood viscosity may cause appearance of hypoxic/ischemic neurological symptoms (36, 37). These events can also cause irreversible morphological changes in microcirculation, like capillary pruning, or appearance of string capillaries with no functional lumen (122–124). It should be noted that all these pathological events described above could occur in the absence of a flow-limiting condition, like arterial occlusion, or stenosis.

MICROCIRCULATORY DYSFUNCTION IN NEURODEGENERATION

Small Vessel Disease

Small vessel disease is a clinical and imaging phenomenon caused by different etiologies and characterized by pathological changes in vasculature with a diameter $<100\,\mu m$, including, arterioles, venules, and capillaries (1, 125). It is a common cause of cognitive impairment, gait problems and disability in the elderly (125). Uncontrolled hypertension or diabetes are among the leading risk factors for this chronic vasculopathy characterized with concentric smooth muscle thickening, especially in penetrating vessels as well as pericyte degeneration, basal membrane thickening, endothelial, and astrocyte end-feet swelling in capillaries (38, 126–129). Pro-inflammatory conditions in the endothelium increases tendency to leukocyte adhesion and activation in this pathologic setting (130–134). The slowly progressive worsening of microcirculatory structure and function may result in neuronal loss, brain atrophy, and the white matter changes detected as leukoaraiosis or diffuse white matter hyperintensities with MRI (135, 136). While capillary-level damage may insidiously progress over time, acute vascular events, like spontaneous rupture, or thrombosis of already damaged arteriolar branches (137–141), leading to stepwise clinical deterioration (1). It is not surprising that either the chronic progressive vasculopathy or acute ischemic events superimposed on this is a primary cause of microcirculatory dysfunction, the details of which are outlined in the next section.

Ischemic Stroke

Currently, the only approved treatment of an acute ischemic stroke is prompt recanalization within few hours either by mechanical thrombectomy or thrombolysis with intravenous or intra-arterial tissue plasminogen activator. At the present, this treatment approach only takes large vessel recanalization into account. However, tissue reperfusion is usually incomplete, hence oxygen extraction is not optimal even after complete recanalization (38). In the ischemic brain, pericytes contract in response to hypoxia and reactive oxygen species (28). This luminal narrowing and irregularities can easily block cellular passage, while plasma may continue to flow. Recanalization of the artery does not resolve this microvascular dysfunction as the capillary constrictions are sustained, leading to the no-reflow phenomenon (142, 143) (**Figures 3A–E**). The quality of capillary perfusion after recanalization is indeed a better indicator of functional outcome than recanalization itself (144, 145). If the capillary flow patterns are extremely dysfunctional and heterogeneous, the recanalization may in fact introduce more functional shunting, paradoxically reducing the oxygen availability (36, 38, 146).

In the ischemic brain, activated neutrophils can also temporarily plug capillaries with their large size and stiff cytoplasm, and can disturb the RBC transit (108). As a clinical evidence, leukocytosis and a high neutrophil fraction are bad prognostic factors in ischemic stroke (147–150). Stroke incidence as well as stroke-related mortality is higher during acute infections (36, 151). The dynamic microcirculatory dysfunction may continue after stroke onset, potentially contributing to infarct expansion over the subsequent days despite recanalization (152–155). One essential way to prevent infarct growth appears to reverse any capillary flow disturbance in addition to large artery recanalization. It is also becoming clear that the definition of ischemic tissue based solely on the level of CBF decrease is insufficient and the capillary flow patterns must also be taken into account (36).

The ischemia-induced microvascular dysfunction progresses in a graded fashion. With a temporary decrease in perfusion pressure in a normal and compliant microvasculature, the cells transiting the microvasculature slow down, since there is less driving force due to lower pressure gradient. Accordingly, MTT values increase. The CTH calculated based on the standard deviation of transit times in multiple pathways across the capillary bed proportionally increases as well. Thereby, the relative transit heterogeneity (RTH=CTH/MTT) remains unchanged and oxygen delivery to the tissue can still be sufficient to match the demand. However, with ongoing ischemia, structural irregularities, like constrictions, and glycocalyx damage in capillaries emerge, making cellular passage complicated (**Figures 3F–L**). This time, the increase in CTH will be higher than what can be mathematically expected from prolongation of MTTs. The disproportional increase in CTH will yield to higher RTH values, pointing to a specific dysfunction in microcirculation that can result in suboptimal oxygen extraction for the ischemic tissue. The above simplified progressive microcirculatory deterioration is the most likely scenario taking place in the ischemic penumbra, corresponding to a potentially salvageable tissue with timely and efficient recanalization, whereas it can also undergo permanent damage with increasing microvascular damage and oxygenation failure

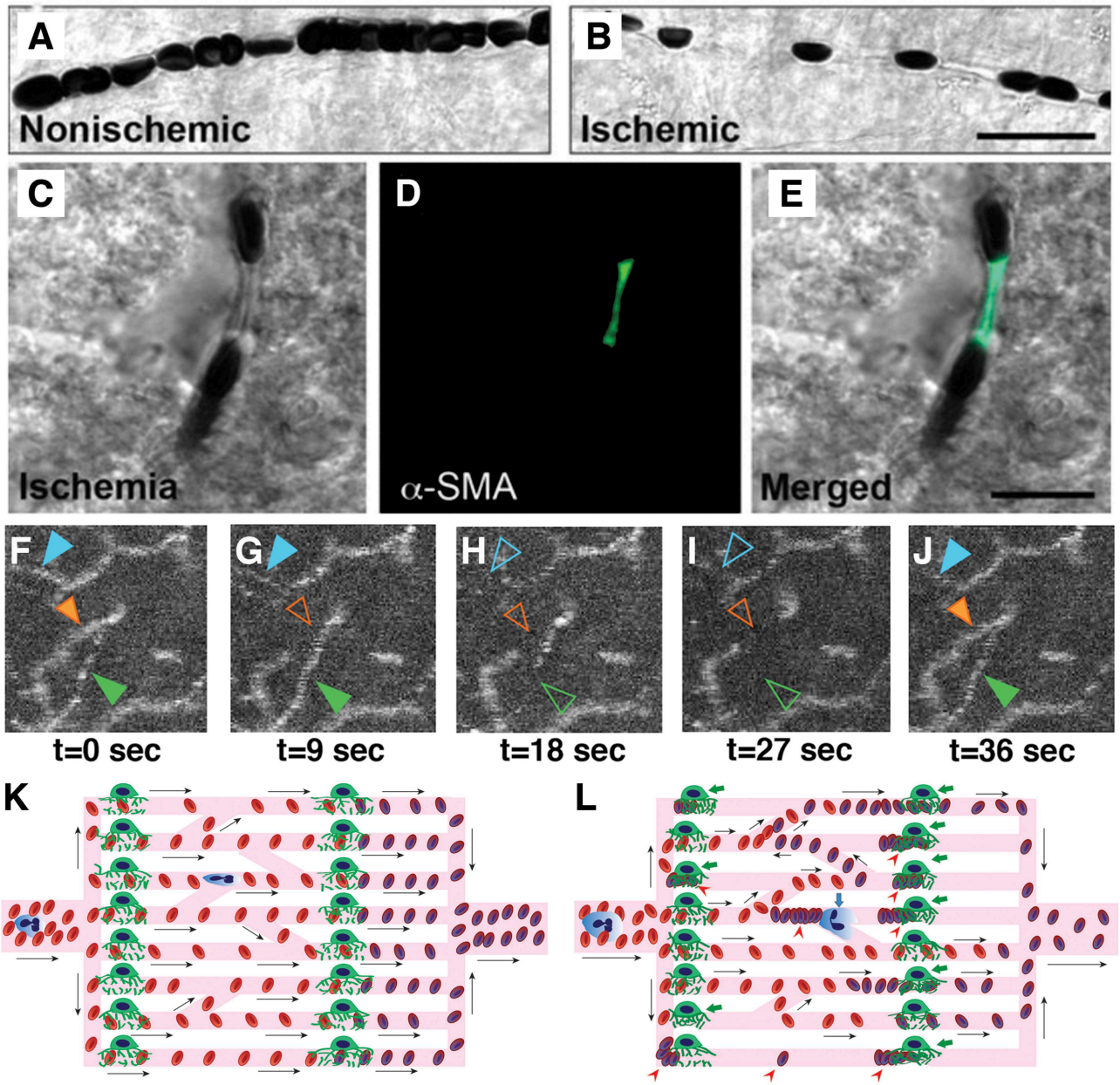

FIGURE 3 | Capillary dysfunction in ischemic stroke and flow-limiting conditions. **(A,B)** Differential interference contrast (DIC) microscopy images illustrate frequent interruptions in the erythrocyte column in an ischemic capillary contrary to a continuous row of erythrocytes flowing through a non-ischemic capillary. Scale bar: 20 μm. **(C–E)** The constricted segments colocalized with α-smooth muscle actin (α-SMA) immunoreactive pericytes. Scale bar: 10 μm. **(F–J)** Very high frequency of dynamic RBC flow stalls in ischemic penumbra shown with OCT angiogram time-series (Manuscript* in preparation). **(K)** Ideally, capillary flow should be homogeneous across a capillary bed to optimize oxygen extraction. Arrows indicate direction of cell motion. **(L)** Pericyte contractions, and increased plugging of leukocytes and red blood cells as a result of ischemia-induced capillary dysfunction, introduce severe heterogeneity into the microcirculation, resulting in redistributions of flow, and pathological shunting. This can profoundly reduce the oxygen delivery into the tissue, even if the total plasma-perfused capillary count and absolute arterial input is the same. Green arrows indicate constricted pericytes, red arrowheads indicate stagnant red blood cells, blue arrow indicates a plugged leukocyte. Deoxygenated RBCs are darker and bluish in color. [**A–E** reproduced by permission from: Nature Medicine, Yemisci et al. (28)]. (*Manuscript by authors: Erdener SE, Tang J, Kilic K, Postnov D, Giblin JT, Kura S, Chen A, Vayisoglu T, Sakadzic S, Schaffer CB and Boas DA).

(82). In the most severe form of ischemia, complete capillary occlusions that do not allow even passage of plasma emerge. This end-stage level of capillary dysfunction, paradoxically leads to homogenization of capillary transit times measured from remaining patent ones in the severely ischemic tissue that is destined to infarct regardless of recanalization (82). This low CTH probably reflects flow in maximally dilated flowing capillaries and does not take into account the occluded ones.

The phrasing may at first sound at odds with the capillary flow homogenization during normal functional hyperemia that provides optimal oxygen extraction (37). Although it may be a similar neurovascular coupling effort for the tissue to optimize blood flow using the capillaries left available (82), the absolute amount of blood passing through the tissue this time is simply very low, decreasing cerebral blood volume below the viability threshold (156).

Chronic cerebral hypoperfusion, even if it doesn't cause full-blown ischemia, can have long-term effects on microcirculatory structure. Experimental OCT data in mice with carotid artery occlusion show a local micro-heterogeneity of capillary flow and oxygen supply even at non-ischemic global blood flow levels (49). The functional changes are accompanied by histological signs of microglia and astrocyte activation along with capillary dilatation, remodeling, increased tortuosity, and even amyloid-beta accumulation (157–159). These structural pathologies can further contribute to the progression of capillary dysfunction. Recently, severity of carotid stenosis have been associated with accumulation of cortical cerebral microinfarcts and poor cognitive performance, even in patients who did not experience acute ischemic stroke (160). Preoperative capillary transit time heterogeneity measured by MRI, an indicator for capillary dysfunction, predicts the functional independency (i.e., Modified Rankin Scale) following endovascular treatment in patients with symptomatic bilateral high-grade carotid stenosis (161).

Subarachnoid Hemorrhage

Subarachnoid hemorrhage shares many common pathophysiological features with cerebral ischemia, because the blood products in cerebrospinal fluid (CSF) can trigger arteriolar and microvascular vasospasms (162). Hemoglobin breakdown products and concomitant formation of reactive oxygen species by iron released from hemoglobin (163) as well as release of vasoconstrictive mediators like endothelin-1 and thromboxane into the CSF may play roles in vasospasm (39, 164). Vasospasms emerge usually a few days after the initial hemorrhage. Like in cerebral ischemia, there is profound increase in capillary transit time heterogeneity after subarachnoid hemorrhage, caused by microarteriolar constrictions (165), reactive oxygen radicals, astrocyte end-feet swelling, leukocyte increase, and activation (39). There are numerous capillaries either without RBCs but with plasma, or with stationary RBCs in them (166). Capillaries with smaller diameters have been shown to have less probability to be perfused with RBCs (167). Because of these disturbances in microcirculation, attempts to relax the vasospasm in large arteries are not very effective. The microcirculatory pathology may begin even before gross vasospasm settles in. Within a few minutes after experimental subarachnoid hemorrhage, there is a heterogeneous slowing down of capillary flow with prominent irregularities, even though there is some dilation in penetrating vessels and precapillary arterioles (168, 169). Dilatory response to CO_2 is lost and an inverse neurovascular coupling response, i.e., constriction instead of expected hyperemia with sensory stimulation is observed 24 h after experimental subarachnoid hemorrhage (170). Whether this flow suppression is an outcome of pathologically high capillary heterogeneity or is a compensatory CBF decrease to optimize oxygen extraction is currently unknown (39).

Traumatic Brain Injury/Chronic Traumatic Encephalopathy

Ischemic injury is a well-known histological hallmark of traumatic contusion injuries (171). A reduction in global CBF almost always accompanies a contusion or traumatic hematoma. If the injury is severe, vasospasms in large vessels can emerge similar to subarachnoid hemorrhage, causing multifocal infarcts. Elevated intracranial pressure due to traumatic injury in animal models caused severely disturbed capillary flow and limited oxygen and solute extraction due to heterogeneity and shunts in the capillary bed (37, 172). This can be partly explained by a direct negative effect of increased intracranial pressure on cerebral perfusion pressure. The decrease in CBF can last for 12 h and functional blood flow responses are usually suppressed during this period (173, 174). Histologically, there is evidence of astrocyte end-feet swelling, pericyte contraction, and increased expression of smooth muscle actin (174). Also, pericytes have been shown to detach from the vessel wall early after the traumatic insult (105), which might contribute to blood-brain dysfunction in capillary bed (175). Capillaries have been shown to be the major site of vascular leakage in animal models after cortical trauma (176). Increased inflammatory protein expression and activation of leukocytes promote cellular adhesion, therefore limiting RBC passage and causing functional capillary stalls and shunts (108, 174). Leukocytosis, like in ischemic stroke, is associated with poor outcome following traumatic brain injury (172).

Interestingly, a gross contusion, hematoma, or intracranial pressure increase is not necessary for microcirculatory abnormalities to develop. A single mild concussion in mice can also decrease CBF 30–40% up to 24 h, as measured with diffuse correlation spectroscopy (177). With repetitive injuries, the oligemic response can extend to 72 h (177). The microcirculatory disturbances induced by mild injuries are independent of increases in intracranial pressure (178). Instead, cortical spreading depolarizations (CSD) multifocally triggered after such insults correlate with neuronal injury and cerebral microbleeds (172). CSDs are self-propagating waves of intense neuroglial depolarization, followed by prolonged suppression of neural activity. Whereas, CSDs associated with migraine aura are benign, repetitive CSDs can cause tissue injury in the setting of subarachnoid hemorrhage or cause infarct expansion during cerebral ischemia, in the form of peri-infarct spreading depolarizations (179–184). In a healthy brain, CSDs can initiate a hyperemic response followed by a long-term oligemia but, in an already ischemic brain, the hyperemia is reversed to oligemia during the depolarization phase (185). CSD waves cause sustained disturbances in capillary flow, causing massive, and heterogeneous changes in erythrocyte velocities (186). Pericytes contract during CSD in response to an increase in cytoplasmic calcium (187). Neurovascular coupling can disappear for hours, causing a supply-demand mismatch, contributing to tissue injury (186, 187). The reduced (inverse)

CBF response to increased metabolic load during massive depolarization could help increase O_2 extraction by slowing flux rates (186).

Repetitive concussions are associated with chronic traumatic encephalopathy (CTE), a cause of early onset dementia and psychiatric disorders especially in boxers or American football players and also in military veterans exposed to blast injuries (188). Autopsy brain samples from CTE patients and also rodent models have evidence of microcirculatory pathology, characterized with swollen astrocytic end-feet and processes forming tangles around capillaries, blood-brain barrier breakdown, and perivascular deposition of hyperphosphorylated tau especially in deep cortical regions (189–192). Even a single blast exposure or concussive cortical impact in mice has been shown to trigger a progressive tauopathy with evidence of microvascular injury and neurodegeneration, which started in the area of exposure first but spread distally over months (193–195).

Alzheimer's Disease

A reduction in CBF is observed early in Alzheimer's disease (AD) patients and this has been proposed as a predictor of progression to overt AD from mild cognitive impairment (196–198). Many vascular risk factors like coronary heart disease, dyslipidemia, hypertension are associated with AD (199). The underlying mechanisms and possible impact of the reduction in CBF and microcirculatory abnormalities in the pathogenesis of neurodegeneration are under investigation to better characterize the cause-effect relationship. In mouse models, impaired cerebral perfusion has been shown to stimulate amyloid-beta deposition. Tau protein can also be hyperphosphorylated under hypoxic conditions, even after brief and temporary episodes (200). After global brain ischemia, expression of tau protein increases in CA1 area of hippocampus in mice, one of the most severely affected areas in AD related to memory functions (201). Interestingly, perivascular zones around penetrating arterioles, the bottlenecks of the cerebral blood supply, are one of the initial areas showing tau and amyloid beta deposition (202).

Electron microscopy has identified capillary wall damage, basal membrane thickening and pericyte degeneration in autopsy brains from AD patients (203). In MRI studies, cognitive performance and level of cortical atrophy were found to be associated with low CBF, high CTH, and low oxygen extraction (86, 204). Similar dynamic abnormalities have also been found in transgenic AD mice, with insufficient flow homogenization, lower resting CBF, and reduced cortical oxygen availability (205).

A recent study using *in vivo* two photon microscopy in transgenic mice with excessive amyloid deposition demonstrated that an increased number of cortical capillaries had stalled blood flow due to neutrophils adhered to vessel wall (11) (**Figures 4A–C**). These stalls have also been found to correlate with amyloid deposition and, targeting neutrophil adhesion improved blood flow and cognitive performance (11). Another longitudinal study tracked obstructed capillaries and identified a VEGF-dependent pruning mechanism with regression of endothelial cells, causing uncompensated capillary loss (206). Perivascular macrophages, in response to amyloid-beta, can release reactive oxygen species that can aggravate microcirculatory dysfunction (207). Mouse models of increased hyperphosphorylated tau expression revealed capillary constrictions surrounded by swollen astrocyte processes (208), formation of abnormal spiraling capillary morphologies with impaired blood cell flux (33) (**Figures 4D,E**).

Transgenic mice with pericyte deficiency have been shown to have impaired capillary perfusion and neurovascular coupling, reduced oxygen supply, blood-brain barrier disruption, white matter degeneration and, importantly, progressive AD-like pathology (including progressive tauopathy and neuronal loss), resulting in accelerated cognitive decline (31, 100, 209–211). A recent study in AD patients showed reduced levels of platelet-derived growth factor-B, a pericyte marker, in precuneus, a cortical area affected in AD (101). We do not know exactly how pericytes degenerate progressively in those conditions, but there are some clues. For example, external introduction or overexpression of amyloid-β can damage pericytes directly (209, 212, 213) and conversely, pericytes can themselves be a zone of production of amyloid-β-associated proteins (214). Hypertension, dyslipidemia, and ApoE4 isoforms, all independent risk factors for AD, can also impair pericyte structure and function, that can potentially initiate a neurodegenerative phenotype (215–220). Pathogenic hyperphosphorylated tau, on the other hand, promotes BBB injury directly (221); the possibility that this injury may be related to pericyte damage, however, remains to be investigated.

Other Chronic Neurodegenerative Diseases

Accumulating evidence suggests that several other progressive neurodegenerative conditions may also involve primary microcirculatory pathologies, Like AD and CTE as discussed above, other tauopathies such as corticobasal degeneration (CBD), progressive supranuclear palsy (PSP) and amyotrophic lateral sclerosis (ALS) exhibit possible microvascular involvement (222).

In Parkinson's disease, both experimental and clinical data suggest microvascular involvement. Capillary loss and abnormal fragmented capillaries or endothelial clusters can be detected in substantia nigra, cerebral cortex and brain stem in pathological brain samples (223). There are also compensatory new vessel formations, which are possibly immature and leaky. In animal models produced by MPTP treatment, decreased capillary density or formation of abnormal endothelial clusters have been reported as observed in autopsy brains (224).

CBD and PSP are two atypical and rapidly progressive forms of parkinsonism. In postmortem brains of CBD and PSP patients, prominent accumulation of hyperphosphorylated tau in close proximity to vasculature, astrocytic proliferation, and hypertrophy as well as reduced capillary diameter have been detected (225, 226). These findings are difficult to test experimentally since there are no established animal models of these conditions. There are transgenic mouse models, however, available for another tauopathy, ALS, with mutations in superoxide-dismutase (SOD1) (227), tar DNA binding protein

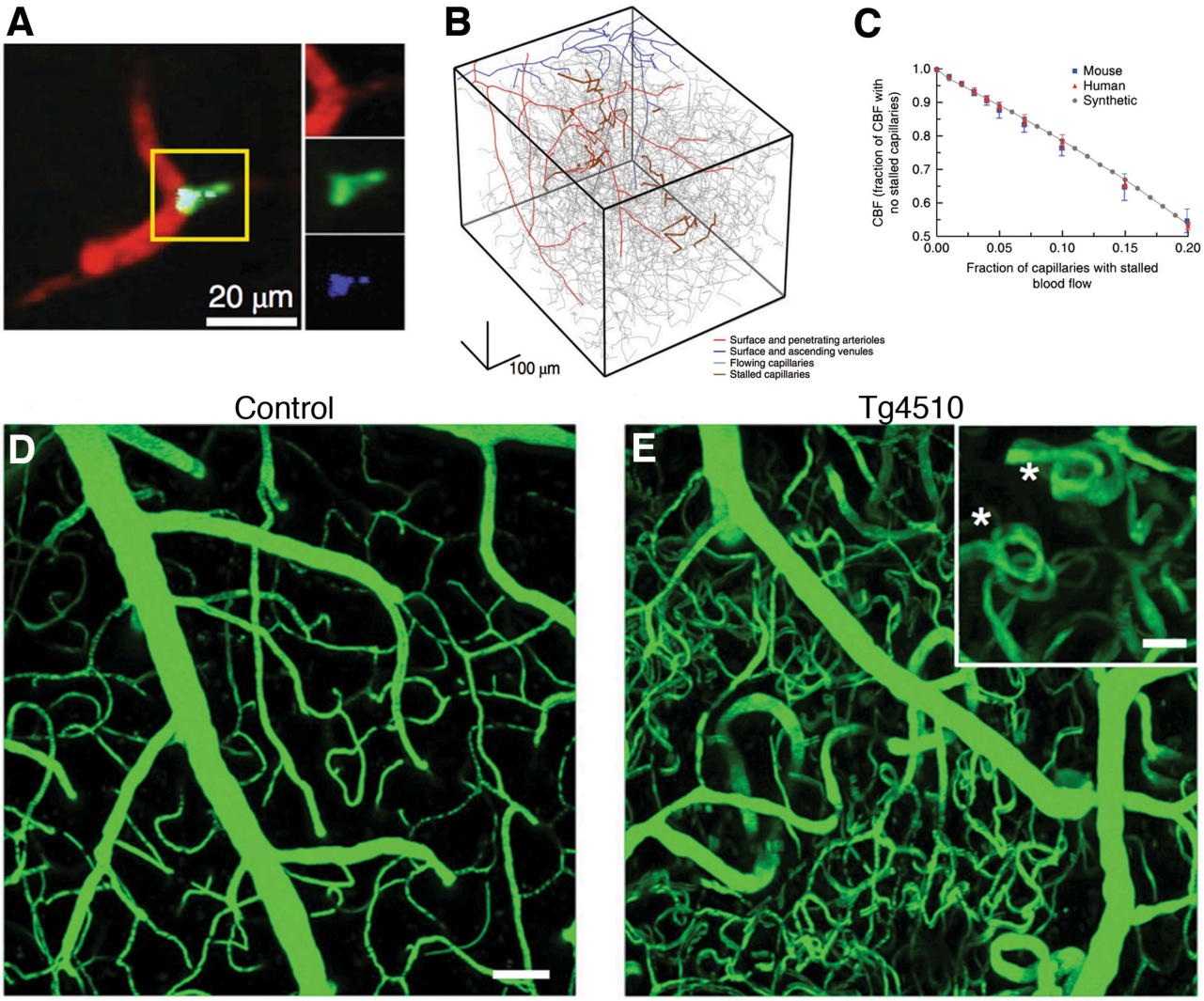

FIGURE 4 | Microcirculatory changes in experimental models of Alzheimer's disease. **(A)** There is increased fraction of stalled capillaries in double-transgenic mice overexpressing amyloid-beta (APP/SW1) due to increased plugging by leukocytes (Green: rhodamine-G labeled leukocyte, red: Texas-red labeled plasma). **(B)** Vascular network tracings show distribution of stalled capillaries. **(C)** Although the fraction of stalled capillaries may seem small, computer simulations on capillary networks show a prominent decrease in overall cerebral blood flow with gradual introduction of stalls. **(D,E)** In another model, 15 month-old mice overexpressing pathological form of hyperphosphorylated tau (Tg4510) show abnormal capillary morphology, number and density (spiral shapes as shown with asterisks(*)). Scale bar 50 μm (inset: 20 μm) There is increased number of stagnant of leukocytes also in these capillaries (not shown here). (**A–C** reprinted by permission from: Nature Neuroscience, Cruz Hernandez (11) © 2019 Springer Nature; **(D,E)** reproduced from Bennett et al. (33), by rights granted under a Creative Commons BY-NC-ND license).

(TARDBP/TDP43) (228), fused in sarcoma (FUS) (229), or C9orf72 (230) genes. SOD1 mouse model exhibits progressive decrease in the anterior gray matter of the spinal cord, beginning from the presymptomatic stage before neuronal degeneration, and is accompanied by a reduction in capillary diameter and density as well as slowing down of RBC flow (231). The flow-metabolism coupling is also disrupted as glucose utilization in contrast to the oxygen availability is increased especially in early stages. These findings become more profound as the disease progresses (232). At present, there is no reported data on microvascular features of mice with other ALS-related mutations, however, future studies might provide deeper insight. In ALS patients, the cerebral blood flow is decreased especially in the prefrontal cortex (233, 234) and a clinical picture of frontotemporal dementia can accompany ALS (235). In ALS patients, the blood-spinal cord barrier is also damaged and extravasated hemoglobin and hemosiderin deposits can be detected in perivascular areas (236). In ALS transgenic mice, there is data showing capillary pericyte degeneration and blood-spinal cord barrier leakage, which can precede motor neuron degeneration (231, 237).

Finally in epilepsy, a group of disorders characterized with chronic repetitive seizures, progressive neurodegeneration can occur over time and also a single prolonged seizure can

initiate such degeneration (238, 239). This has previously been attributed to glutamate-induced excitotoxicity (240). Since there is usually increased blood flow in seizure foci (241–243), one would not readily suspect from impaired oxygenation as a possible cause of neuronal loss. But as discussed above, capillary dysfunction may occur in the setting of increased cerebral blood flow (38). An elegant study with *in vivo* two-photon microscopy, however, identified individual capillaries with pericyte contractions and accompanying stalls in blood flow in hippocampus of epileptic mice during seizures and those abnormal capillary vasodynamics created an environment with irregular capillary flow and possibly microscopic hypoxia, which was associated with neurodegeneration in close proximity of constricted capillaries (244).

POSSIBLE THERAPEUTIC APPROACHES TO IMPROVE CAPILLARY FLOW AND OXYGENATION

The above-discussed findings strongly suggest that, to slow down or to reverse the acute and chronic neurodegeneration, the microcirculatory structures and dynamics must also be taken into account. Interventions to improve the microcirculation need to have specific targets to homogenize capillary flow and optimize oxygen and glucose extraction that would meet the metabolic needs at all times. These approaches should complement interventions for the macrovessels. Any attempt to increase the cerebral blood flow without correcting microcirculatory disturbances may aggravate heterogeneous shunting and paradoxically worsen oxygen extraction (38).

Reactive Oxygen Species and Pericyte Contraction

Various scavengers can target reactive oxygen species that are responsible for vasospasms as well as capillary pericyte contraction and endothelial dysfunction. One of these, N-tert-Butyl-α-phenylnitrone (PBN), has been shown to improve microcirculation in a mouse model of cerebral ischemia, improving tissue injury and functional outcome (245). Since NO depletion may be contributory to capillary constriction, nitric oxide inhalation as well as nitrite infusion have been suggested to improve microcirculation and tissue oxygenation in various models of neurovascular disorders (246–252). Like nitric oxide, adenosine is involved in active physiological regulation of microvascular diameter and perfusion (58, 253). Adenosine is endogenously released as a metabolic end product of cerebral activity and external adenosine administration increases capillary diameter by relaxing pericytes in both myocardial and cerebral microcirculation, under ischemic conditions (99, 254–256). A major problem with nitric oxide donors and adenosine-based therapies is their systemic side effects, including systemic cardiovascular and respiratory changes (257–260). Novel strategies that allow targeted cerebral delivery of such potent drugs, like squalenoyl adenosine nanoassemblies (99), or nanoparticulated nitric oxide donors (261), and also inhaled nitric oxide that does not have systemic cardiovascular side effects, can be highly useful to promote clinical translation of this pharmacologic potential.

Capillary pericytes constrict in response to adrenergic receptor activation and with endothelin, therefore their antagonists could be considered as potential therapeutic targets (51, 262). Pericyte constriction is calcium-dependent as it involves actin machinery (30). Voltage-gated calcium channel blockers have been shown to decrease pericyte constrictions and also pericyte death, improving capillary transit time homogenization (262, 263). Ca^{+2}-activated chloride channels can also potentiate pericyte depolarization and constriction and can be another target (262, 264). Rho-kinase pathway inhibition can reverse abnormal pericyte contractions (265, 266) and this approach has been found to be neuroprotective in mouse models of cerebral ischemia (267–269).

Glycocalyx Integrity

Shedding of glycocalyx can impair homogeneities in RBC flux and increase endothelial-leukocyte adhesion. Glycocalyx has been protected by anti-thrombin administration in a rat sepsis model and this treatment decreased leukocyte adhesion, improving microcirculatory blood flow in mesentery (270, 271). Avoiding hyperglycemia is also beneficial for glycocalyx integrity (271). Similarly, a hydroxyethyl starch improved lung microcirculation by preventing experimental glycocalyx degradation by heparinase (90). Therefore, restoring glycocalyx integrity can be another potential treatment approach.

Blood Viscosity and Hematology

Since increased leukocyte count, activation, and increase in hematocrit (either due to higher RBC number or dehydration) increase capillary clogging, stalls and heterogeneity, blood viscosity, and endothelial adhesion could be one of the possible targets. Phosphodiesterase inhibitors like pentoxifylline increase RBC flexibility and decrease blood viscosity (272, 273) and they can indeed improve microcirculatory profile while their direct effects on augmenting NO activity might be another contributor to this (274). Prevention of dehydration and concomitant infections could also be beneficial for a regular and optimal capillary flow (38). These two factors are among the most common triggers of delirium and cognitive fluctuations in elderly patients with dementia (275).

Decreasing leukocyte count has been reported to provide a beneficial outcome in animal models of cerebral ischemia (276). A monoclonal antibody against Ly6G surface proteins on neutrophils has improved microcirculation by reversing neutrophil-mediated capillary stalls in mice, increased blood flow and behavioral scores acutely in mice, an effect attributed to modulation of neutrophil adhesion in capillaries (11). The same antibody has been found to be beneficial in mice with subarachnoid hemorrhage (277) and after stroke in hyperlipidemic mice (278). The exact physiological role and endogenous receptor of Ly6G is currently unknown (279) but these experimental data require further investigations.

Other innovative approaches to modulate rheological parameters of blood cells are continuously being developed.

Drag-reducing polymers improved flexibility of RBCs, decreasing cell stasis in capillaries, and plasma separation in capillary branching points, improving capillary flow heterogeneity in cerebral and myocardial ischemia models (280–282). Uptake of plasma-derived extracellular vesicles by RBCs have recently been shown to increase their deformability (283, 284).

CONCLUSION

Our review can help the recognition that many microvascular pathogenetic mechanisms are shared across a variety of acute and chronic neurological conditions and these mechanisms are not simply by-standers but are actually role-players, emerging in very early phases of neurodegenerative conditions. With advancement of optical microscopy, MRI-based imaging tools having higher spatiotemporal resolution as well as computer models, the physiology and vulnerabilities of the microcirculation will be better elucidated. Investigators in the field should not be surprised to see the introduction of previously unknown details, which will eventually lead to much better neuroprotectants for many neurological disorders within the next decades.

AUTHOR CONTRIBUTIONS

ŞE drafted the manuscript and prepared the figures. TD drafted and critically revised the manuscript.

FUNDING

TD work is supported by Turkish Academy of Sciences. ŞE work is supported by Turkish Neurological Society and The Science Academy, Turkey.

ACKNOWLEDGMENTS

The authors would like to thank Dr. David A. Boas (Boston University) and Dr. Sava Sakadzic (Massachusetts General Hospital) for their supervision of ŞE postdoctoral studies and helpful discussions.

REFERENCES

1. Bosetti F, Galis ZS, Bynoe MS, Charette M, Cipolla MJ, Del Zoppo GJ, et al. "Small blood vessels: big health problems?": scientific recommendations of the national institutes of health workshop. *J Am Heart Assoc.* (2016) 5:e004389. doi: 10.1161/JAHA.116.004389
2. Sakadžić S, Mandeville ET, Gagnon L, Musacchia JJ, Yaseen MA, Yucel MA, et al. Large arteriolar component of oxygen delivery implies a safe margin of oxygen supply to cerebral tissue. *Nat Commun.* (2014) 5:5734. doi: 10.1038/ncomms6734
3. Meyer EP, Ulmann-Schuler A, Staufenbiel M, Krucker T. Altered morphology and 3D architecture of brain vasculature in a mouse model for Alzheimer's disease. *Proc Natl Acad Sci USA*. (2008) 105:3587–92. doi: 10.1073/pnas.0709788105
4. Mabuchi T, Lucero J, Feng A, Koziol JA, del Zoppo GJ. Focal cerebral ischemia preferentially affects neurons distant from their neighboring microvessels. *J Cereb Blood Flow Metab.* (2005) 25:257–66. doi: 10.1038/sj.jcbfm.9600027
5. Lovick TA, Brown LA, Key BJ. Neurovascular relationships in hippocampal slices: physiological and anatomical studies of mechanisms underlying flow-metabolism coupling in intraparenchymal microvessels. *Neuroscience.* (1999) 92:47–60. doi: 10.1016/S0306-4522(98)00737-4
6. Kanno I, Masamoto K. Bridging macroscopic and microscopic methods for the measurements of cerebral blood flow: toward finding the determinants in maintaining the CBF homeostasis. In: *New Horizons in Neurovascular Coupling: A Bridge Between Brain Circulation and Neural Plasticity*. Vol. 255. 1st ed. (Amsterdam: Elsevier B.V.) (2016).
7. Raichle ME, Mintun MA. Brain Work and Brain Imaging. *Annu Rev Neurosci.* (2006) 29:449–76. doi: 10.1146/annurev.neuro.29.051605.112819
8. Østergaard L, Jørgensen MB, Knudsen GM. Low on energy? An energy supply-demand perspective on stress and depression. *Neurosci Biobehav Rev.* (2018) 94:248–70. doi: 10.1016/j.neubiorev.2018.08.007
9. Iadecola C, Nedergaard M. Glial regulation of the cerebral microvasculature. *Nat Neurosci.* (2007) 10:1369–76. doi: 10.1038/nn2003
10. Erdener SE, Tang J, Sajjadi A, Kiliç K, Kura S, Schaffer CB, et al. Spatio-temporal dynamics of cerebral capillary segments with stalling red blood cells. *J Cereb Blood Flow Metab.* (2019) 39:886–900. doi: 10.1177/0271678X17743877
11. Cruz Hernández JC, Bracko O, Kersbergen CJ, Muse V, Haft-Javaherian M, Berg M, et al. Neutrophil adhesion in brain capillaries reduces cortical blood flow and impairs memory function in Alzheimer's disease mouse models. *Nat Neurosci.* (2019) 22:413–20. doi: 10.1038/s41593-018-0329-4
12. Shih AY, Driscoll JD, Drew PJ, Nishimura N, Schaffer CB, Kleinfeld D. Two-photon microscopy as a tool to study blood flow and neurovascular coupling in the rodent brain. *J Cereb Blood Flow Metab.* (2012) 32:1277–309. doi: 10.1038/jcbfm.2011.196
13. Kisler K, Lazic D, Sweeney MD, Plunkett S, El Khatib M, Vinogradov SA, et al. *In vivo* imaging and analysis of cerebrovascular hemodynamic responses and tissue oxygenation in the mouse brain. *Nat Protoc.* (2018) 13:1377–402. doi: 10.1038/nprot.2018.034
14. Kleinfeld D, Mitra PP, Helmchen F, Denk W. Fluctuations and stimulus-induced changes in blood flow observed in individual capillaries in layers 2 through 4 of rat neocortex. *Proc Natl Acad Sci USA.* (1998) 95:15741–6. doi: 10.1073/pnas.95.26.15741
15. Yaseen MA, Srinivasan VJ, SakadŽić S, Radhakrishnan H, Gorczynska I, Wu W, et al. Microvascular oxygen tension and flow measurements in rodent cerebral cortex during baseline conditions and functional activation. *J Cereb Blood Flow Metab.* (2011) 31:1051–63. doi: 10.1038/jcbfm.2010.227
16. Devor A, Sakadzic S, Saisan PA, Yaseen MA, Roussakis E, Srinivasan VJ, et al. "Overshoot" of O2 is required to maintain baseline tissue oxygenation at locations distal to blood vessels. *J Neurosci.* (2011) 31:13676–81. doi: 10.1523/JNEUROSCI.1968-11.2011
17. SakadŽic S, Yaseen MA, Jaswal R, Roussakis E, Dale AM, Buxton RB, et al. Two-photon microscopy measurement of cerebral metabolic rate of oxygen using periarteriolar oxygen concentration gradients. *Neurophotonics.* (2016) 3:045005. doi: 10.1117/1.NPh.3.4.045005
18. Sakadzić S, Yuan S, Dilekoz E, Ruvinskaya S, Vinogradov SA, Ayata C, et al. Simultaneous imaging of cerebral partial pressure of oxygen and blood flow during functional activation and cortical spreading depression. *Appl Opt.* (2009) 48:D169–77. doi: 10.1364/AO.48.00D169
19. Sinks LE, Robbins GP, Roussakis E, Troxler T, Hammer DA, Vinogradov SA. Two-photon microscopy of oxygen: polymersomes as probe carrier vehicles. *J Phys Chem B.* (2010) 114:14373–82. doi: 10.1021/jp100353v
20. Lecoq J, Parpaleix A, Roussakis E, Ducros M, Houssen YG, Vinogradov SA, et al. Simultaneous two-photon imaging of oxygen and blood flow in deep cerebral vessels. *Nat Med.* (2011) 17:893–8. doi: 10.1038/nm.2394
21. Esipova TV, Barrett MJP, Erlebach E, Masunov AE, Weber B, Vinogradov SA. Oxyphor 2P: a high-performance probe for deep-tissue longitudinal oxygen imaging. *Cell Metab.* (2019) 29:736–44. doi: 10.1016/j.cmet.2018.12.022
22. Devor A, SakadŽić S, Srinivasan VJ, Yaseen MA, Nizar K, Saisan PA, Tian P, et al. Frontiers in optical imaging of cerebral blood flow and metabolism. *J Cereb Blood Flow Metab.* (2012) 32:1259–76. doi: 10.1038/jcbfm.2011.195

23. Srinivasan VJ, SakadŽić S, Gorczynska I, Ruvinskaya S, Wu W, Fujimoto JG, et al. Quantitative cerebral blood flow with optical coherence tomography. *Opt Express.* (2010) 18:2477. doi: 10.1364/OE.18.002477
24. Tang J, Erdener SE, Fu B, Boas DA. Capillary red blood cell velocimetry by phase-resolved optical coherence tomography. *Opt Lett.* (2017) 42:3976. doi: 10.1364/OL.42.003976
25. Lee J, Wu W, Jiang JY, Zhu B, Boas DA. Dynamic light scattering optical coherence tomography. *Opt Express.* (2012) 20:22262–77. doi: 10.1364/OE.20.022262
26. Tang J, Erdener SE, Li B, Fu B, Sakadzic S, Carp SA, et al. Shear-induced diffusion of red blood cells measured with dynamic light scattering-optical coherence tomography. *J Biophotonics.* (2018) 11:1–10. doi: 10.1002/jbio.201700070
27. Mouridsen K, Hansen MB, Østergaard L, Jespersen SN. Reliable estimation of capillary transit time distributions using DSC-MRI. *J Cereb Blood Flow Metab.* (2014) 34:1511–21. doi: 10.1038/jcbfm.2014.111
28. Yemisci M, Gursoy-Ozdemir Y, Vural A, Can A, Topalkara K, Dalkara T. Pericyte contraction induced by oxidative-nitrative stress impairs capillary reflow despite successful opening of an occluded cerebral artery. *Nat Med.* (2009) 15:1031–7. doi: 10.1038/nm.2022
29. Iadecola C. The neurovascular unit coming of age: a journey through neurovascular coupling in health and disease. *Neuron.* (2017) 96:17–42. doi: 10.1016/j.neuron.2017.07.030
30. Hall CN, Reynell C, Gesslein B, Hamilton NB, Mishra A, Sutherland BA, et al. Capillary pericytes regulate cerebral blood flow in health and disease. *Nature.* (2014) 508:55–60. doi: 10.1038/nature13165
31. Kisler K, Nelson AR, Rege SV, Ramanathan A, Wang Y, Ahuja A, et al. Pericyte degeneration leads to neurovascular uncoupling and limits oxygen supply to brain. *Nat Neurosci.* (2017) 20:406–16. doi: 10.1038/nn.4489
32. Lee J, Wu W, Boas DA. Early capillary flux homogenization in response to neural activation. *J Cereb Blood Flow Metab.* (2016) 36:375–80. doi: 10.1177/0271678X15605851
33. Bennett RE, Robbins AB, Hu M, Cao X, Betensky RA, Clark T, et al. Tau induces blood vessel abnormalities and angiogenesis-related gene expression in P301L transgenic mice and human Alzheimer's disease. *Proc Natl Acad Sci USA*. (2018) 115:E1289–98. doi: 10.1073/pnas.1710329115
34. Gagnon L, SakadŽić S, Lesage F, Pouliot P, Dale AM, Devor A, et al. Validation and optimization of hypercapnic-calibrated fMRI from oxygen-sensitive two-photon microscopy. *Philos Trans R Soc B Biol Sci.* (2016) 371:20150359. doi: 10.1098/rstb.2015.0359
35. Cheng X, Berman AJL, Polimeni JR, Buxton RB, Gagnon L, Devor A, et al. Dependence of the MR signal on the magnetic susceptibility of blood studied with models based on real microvascular networks. *Magn Reson Med.* (2019) 81:3865–74. doi: 10.1002/mrm.27660
36. Østergaard L, Jespersen SN, Mouridsen K, Mikkelsen IK, Jonsdottír KÝ, Tietze A, et al. The role of the cerebral capillaries in acute ischemic stroke: the extended penumbra model. *J Cereb Blood Flow Metab.* (2013) 33:635–48. doi: 10.1038/jcbfm.2013.18
37. Jespersen SN, Østergaard L. The roles of cerebral blood flow, capillary transit time heterogeneity, and oxygen tension in brain oxygenation and metabolism. *J Cereb Blood Flow Metab.* (2012) 32:264–77. doi: 10.1038/jcbfm.2011.153
38. Østergaard L, Engedal TS, Moreton F, Hansen MB, Wardlaw JM, Dalkara T, et al. Cerebral small vessel disease: capillary pathways to stroke and cognitive decline. *J Cereb Blood Flow Metab.* (2016) 36:302–25. doi: 10.1177/0271678X15606723
39. Østergaard L, Aamand R, Karabegovic S, Tietze A, Blicher JU, Mikkelsen IK, et al. The role of the microcirculation in delayed cerebral ischemia and chronic degenerative changes after subarachnoid hemorrhage. *J Cereb Blood Flow Metab.* (2013) 33:1825–37. doi: 10.1038/jcbfm.2013.173
40. Balogh P, Bagchi P. Analysis of red blood cell partitioning at bifurcations in simulated microvascular networks. *Phys Fluids.* (2018) 30:051902. doi: 10.1063/1.5024783
41. Santisakultarm TP, Paduano CQ, Stokol T, Southard TL, Nishimura N, Skoda RC, et al. Stalled cerebral capillary blood flow in mouse models of essential thrombocythemia and polycythemia vera revealed by *in vivo* two-photon imaging. *J Thromb Haemost.* (2014) 12:2120–30. doi: 10.1111/jth.12738
42. Kataoka H, Kim SW, Plesnila N. Leukocyte-endothelium interactions during permanent focal cerebral ischemia in mice. *J Cereb Blood Flow Metab.* (2004) 24:668–76. doi: 10.1097/01.WCB.0000117812.35136.5B
43. Østergaard L, Jespersen SN, Engedahl T, Jiménez EG, Ashkanian M, Hansen MB, et al. Capillary dysfunction: its detection and causative role in dementias and stroke. *Curr Neurol Neurosci Rep.* (2015) 15:557. doi: 10.1007/s11910-015-0557-x
44. Angleys H, Østergaard L, Jespersen SN. The effects of capillary transit time heterogeneity (CTH) on brain oxygenation. *J Cereb Blood Flow Metab.* (2015) 35:806–17. doi: 10.1038/jcbfm.2014.254
45. Daneman R, Prat A. The blood–brain barrier. *Cold Spring Harb Perspect Biol.* (2015) 7:a020412. doi: 10.1101/cshperspect.a020412
46. Gu Y, Zheng G, Xu M, Li Y, Chen X, Zhu W, et al. Caveolin-1 regulates nitric oxide-mediated matrix metalloproteinases activity and blood-brain barrier permeability in focal cerebral ischemia and reperfusion injury. *J Neurochem.* (2012) 120:147–56. doi: 10.1111/j.1471-4159.2011.07542.x
47. Oldendorf WH, Cornford ME, Brown WJ. The large apparent work capability of the blood-brain barrier: a study of the mitochondrial content of capillary endothelial cells in brain and other tissues of the rat. *Ann Neurol.* (1977) 1:409–17. doi: 10.1002/ana.410010502
48. Friis ML, Paulson OB, Hertz MM. Carbon dioxide permeability of the blood-brain barrier in man: The effect of acetazolamide. *Microvasc Res.* (1980) 20:71–80. doi: 10.1016/0026-2862(80)90020-5
49. Srinivasan VJ, Yu E, Radhakrishnan H, Can A, Climov M, Leahy C, et al. Micro-heterogeneity of flow in a mouse model of chronic cerebral hypoperfusion revealed by longitudinal doppler optical coherence tomography and angiography. *J Cereb Blood Flow Metab.* (2015) 35:1552–60. doi: 10.1038/jcbfm.2015.175
50. Armulik A, Abramsson A, Betsholtz C. Endothelial/pericyte interactions. *Circ Res.* (2005) 97:512–23. doi: 10.1161/01.RES.0000182903.16652.d7
51. Peppiatt CM, Howarth C, Mobbs P, Attwell D. Bidirectional control of CNS capillary diameter by pericytes. *Nature.* (2006) 443:700–4. doi: 10.1038/nature05193
52. Risau W, Wolburg H. Development of the blood-brain barrier. *Trends Neurosci.* (1990) 13:174–8. doi: 10.1016/0166-2236(90)90043-A
53. Dore-Duffy P, LaManna JC. Physiologic angiodynamics in the brain. *Antioxid Redox Signal.* (2007) 9:1363–71. doi: 10.1089/ars.2007.1713
54. Thomas WE. Brain macrophages: on the role of pericytes and perivascular cells. *Brain Res Brain Res Rev.* (1999) 31:42–57. doi: 10.1016/S0165-0173(99)00024-7
55. Armulik A, Genové G, Mäe M, Nisancioglu MH, Wallgard E, Niaudet C, et al. Pericytes regulate the blood-brain barrier. *Nature.* (2010) 468:557–61. doi: 10.1038/nature09522
56. ElAli A, Thériault P, Rivest S. The role of pericytes in neurovascular unit remodeling in brain disorders. *Int J Mol Sci.* (2014) 15:6453–74. doi: 10.3390/ijms15046453
57. Yang S, Jin H, Zhu Y, Wan Y, Opoku EN, Zhu L, et al. Diverse functions and mechanisms of pericytes in ischemic stroke. *Curr Neuropharmacol.* (2017) 15:892–905. doi: 10.2174/1570159X15666170112170226
58. Attwell D, Buchan AM, Charpak S, Lauritzen M, MacVicar BA, Newman EA. Glial and neuronal control of brain blood flow. *Nature.* (2010) 468:232–43. doi: 10.1038/nature09613
59. Jakovcevic D, Harder DR. Role of astrocytes in matching blood flow to neuronal activity. In: Schatten GP, editor. *Current Topics in Developmental Biology*. Vol. 79. (San Diego, CA: Academic Press) (2007). p. 75–97. doi: 10.1016/S0070-2153(06)79004-4
60. Magistretti PJ, Allaman I. Lactate in the brain: from metabolic end-product to signalling molecule. *Nat Rev Neurosci.* (2018) 19:235–49. doi: 10.1038/nrn.2018.19
61. Bennett MVL, Contreras JE, Bukauskas FF, Sáez JC. New roles for astrocytes: gap junction hemichannels have something to communicate. *Trends Neurosci.* (2003) 26:610–7. doi: 10.1016/j.tins.2003.09.008
62. Parys B, Côté A, Gallo V, De Koninck P, Sík A. Intercellular calcium signaling between astrocytes and oligodendrocytes via gap junctions in culture. *Neuroscience.* (2010) 167:1032–43. doi: 10.1016/j.neuroscience.2010.03.004
63. Gu X, Chen W, Volkow ND, Koretsky AP, Du C, Pan Y. Synchronized astrocytic Ca2+responses in neurovascular coupling during somatosensory

stimulation and for the resting state. *Cell Rep.* (2018) 23:3878–90. doi: 10.1016/j.celrep.2018.05.091
64. Segal SS, Duling BR. Flow control among microvessels coordinated by intercellular conduction. *Science.* (1986) 234:868–70. doi: 10.1126/science.3775368
65. Isakson BE, Damon DN, Day KH, Liao Y, Duling BR. Connexin40 and connexin43 in mouse aortic endothelium: evidence for coordinated regulation. *Am J Physiol Heart Circ Physiol.* (2006) 290:H1199–205. doi: 10.1152/ajpheart.00945.2005
66. Little TL, Beyer EC, Duling BR. Connexin 43 and connexin 40 gap junctional proteins are present in arteriolar smooth muscle and endothelium *in vivo*. *Am J Physiol Circ Physiol.* (1995) 268:H729–39. doi: 10.1152/ajpheart.1995.268.2.H729
67. Pries AR, Höpfner M, le Noble F, Dewhirst MW, Secomb TW. The shunt problem: control of functional shunting in normal and tumour vasculature. *Nat Rev Cancer.* (2010) 10:587–93. doi: 10.1038/nrc2895
68. Isakson BE, Kronke G, Kadl A, Leitinger N, Duling BR. Oxidized phospholipids alter vascular connexin expression, phosphorylation, and heterocellular communication. *Arterioscler Thromb Vasc Biol.* (2006) 26:2216–21. doi: 10.1161/01.ATV.0000237608.19055.53
69. Uhlirova H, Kiliç K, Tian P, Thunemann M, Desjardins M, Saisan PA, et al. Cell type specificity of neurovascular coupling in cerebral cortex. *Elife.* (2016) 5:14315. doi: 10.7554/eLife.14315
70. Anenberg E, Chan AW, Xie Y, LeDue JM, Murphy TH. Optogenetic stimulation of GABA neurons can decrease local neuronal activity while increasing cortical blood flow. *J Cereb Blood Flow Metab.* (2015) 35:1579–86. doi: 10.1038/jcbfm.2015.140
71. Cauli B, Tong X-K, Rancillac A, Serluca N, Lambolez B, Rossier J, et al. Cortical GABA interneurons in neurovascular coupling: relays for subcortical vasoactive pathways. *J Neurosci.* (2004) 24:8940–9. doi: 10.1523/JNEUROSCI.3065-04.2004
72. Du W, Stern JE, Filosa JA. Neuronal-derived nitric oxide and somatodendritically released vasopressin regulate neurovascular coupling in the rat hypothalamic supraoptic nucleus. *J Neurosci.* (2015) 35:5330–41. doi: 10.1523/JNEUROSCI.3674-14.2015
73. Sprague RS, Stephenson AH, Ellsworth ML. Red not dead: signaling in and from erythrocytes. *Trends Endocrinol Metab.* (2007) 18:350–5. doi: 10.1016/j.tem.2007.08.008
74. Zhang H, Shen Z, Hogan B, Barakat AI, Misbah C. ATP release by red blood cells under flow: model and simulations. *Biophys J.* (2018) 115:2218–29. doi: 10.1016/j.bpj.2018.09.033
75. Marginedas-Freixa I, Alvarez CL, Moras M, Leal Denis MF, Hattab C, et al. Human erythrocytes release ATP by a novel pathway involving VDAC oligomerization independent of pannexin-1. *Sci Rep.* (2018) 8:11384. doi: 10.1038/s41598-018-29885-7
76. Belcik JT, Davidson BP, Xie A, Wu MD, Yadava M, Qi Y, et al. Augmentation of muscle blood flow by ultrasound cavitation is mediated by ATP and purinergic signaling. *Circulation.* (2017) 135:1240–52. doi: 10.1161/CIRCULATIONAHA.116.024826
77. Sridharan M, Adderley SP, Bowles EA, Egan TM, Stephenson AH, Ellsworth ML, Sprague RS. Pannexin 1 is the conduit for low oxygen tension-induced ATP release from human erythrocytes. *Am J Physiol Heart Circ Physiol.* (2010) 299:H1146–52. doi: 10.1152/ajpheart.00301.2010
78. Takano T, Tian G-F, Peng W, Lou N, Libionka W, Han X, et al. Astrocyte-mediated control of cerebral blood flow. *Nat Neurosci.* (2006) 9:260–7. doi: 10.1038/nn1623
79. Astrup J, Siesjö BK, Symon L. Thresholds in cerebral ischemia - the ischemic penumbra. *Stroke.* (1981) 12:723–5. doi: 10.1161/01.STR.12.6.723
80. Iihara K, Okawa M, Hishikawa T, Yamada N, Fukushima K, Iida H, et al. Slowly progressive neuronal death associated with postischemic hyperperfusion in cortical laminar necrosis after high-flow bypass for a carotid intracavernous aneurysm. *J Neurosurg.* (2010) 112:1254–9. doi: 10.3171/2009.9.JNS09345
81. Wegener S, Artmann J, Luft AR, Buxton RB, Weller M, Wong EC. The time of maximum post-ischemic hyperperfusion indicates infarct growth following transient experimental ischemia. *PLoS ONE.* (2013) 8:e65322. doi: 10.1371/journal.pone.0065322
82. Engedal TS, Hjort N, Hougaard KD, Simonsen CZ, Andersen G, Mikkelsen IK, et al. Transit time homogenization in ischemic stroke – A novel biomarker of penumbral microvascular failure? *J Cereb Blood Flow Metab.* (2018) 38:2006–20. doi: 10.1177/0271678X17721666
83. Park CS, Payne SJ. Modelling the effects of cerebral microvasculature morphology on oxygen transport. *Med Eng Phys.* (2016) 38:41–7. doi: 10.1016/j.medengphy.2015.09.004
84. Gagnon L, Smith AF, Boas DA, Devor A, Secomb TW, SakadŽić S. Modeling of cerebral oxygen transport based on *in vivo* microscopic imaging of microvascular network structure, blood flow, and oxygenation. *Front Comput Neurosci.* (2016) 10:1–20. doi: 10.3389/fncom.2016.00082
85. Lücker A, Secomb TW, Barrett MJP, Weber B, Jenny P. The relation between capillary transit times and hemoglobin saturation heterogeneity. part 2: capillary networks. *Front Physiol.* (2018) 9:1296. doi: 10.3389/fphys.2018.01296
86. Eskildsen SF, Gyldensted L, Nagenthiraja K, Nielsen RB, Hansen MB, Dalby RB, et al. Increased cortical capillary transit time heterogeneity in Alzheimer's disease: a DSC-MRI perfusion study. *Neurobiol Aging.* (2017) 50:107–18. doi: 10.1016/j.neurobiolaging.2016.11.004
87. Secomb TW, Hsu R, Pries AR. A model for red blood cell motion in glycocalyx-lined capillaries. *Am J Physiol.* (1998) 274:H1016–22. doi: 10.1152/ajpheart.1998.274.3.H1016
88. Vink H, Duling BR. Identification of distinct luminal domains for macromolecules, erythrocytes, and leukocytes within mammalian capillaries. *Circ Res.* (1996) 79:581–9. doi: 10.1161/01.RES.79.3.581
89. McClatchey PM, Schafer M, Hunter KS, Reusch JEB. The endothelial glycocalyx promotes homogenous blood flow distribution within the microvasculature. *Am J Physiol Heart Circ Physiol.* (2016) 311:H168–76. doi: 10.1152/ajpheart.00132.2016
90. Strunden MS, Bornscheuer A, Schuster A, Kiefmann R, Goetz AE, Heckel K. Glycocalyx degradation causes microvascular perfusion failure in the *ex vivo* perfused mouse lung. *Shock.* (2012) 38:559–66. doi: 10.1097/SHK.0b013e31826f2583
91. Mas M. A close look at the endothelium: its role in the regulation of vasomotor tone. *Eur Urol Suppl.* (2009) 8:48–57. doi: 10.1016/j.eursup.2008.10.011
92. Favero G, Paganelli C, Buffoli B, Rodella LF, Rezzani R. Endothelium and its alterations in cardiovascular diseases: life style intervention. *Biomed Res Int.* (2014) 2014:801896. doi: 10.1155/2014/801896
93. Lefer AM. Nitric oxide: nature's naturally occurring leukocyte inhibitor. *Circulation.* (1997) 95:553–4. doi: 10.1161/01.CIR.95.3.553
94. Kubes P, Suzuki M, Granger DN. Nitric oxide: an endogenous modulator of leukocyte adhesion. *Proc Natl Acad Sci USA.* (1991) 88:4651–5. doi: 10.1073/pnas.88.11.4651
95. Cines DB, Pollak ES, Buck CA, Loscalzo J, Zimmerman GA, McEver RP, et al. Endothelial cells in physiology and in the pathophysiology of vascular disorders. *Blood.* (1998) 91:3527–61.
96. Wang S, Cao C, Chen Z, Bankaitis V, Tzima E, Sheibani N, et al. Pericytes regulate vascular basement membrane remodeling and govern neutrophil extravasation during inflammation. *PLoS ONE.* (2012) 7:e45499. doi: 10.1371/journal.pone.0045499
97. Schmid F, Reichold J, Weber B, Jenny P. The impact of capillary dilation on the distribution of red blood cells in artificial networks. *Am J Physiol Heart Circ Physiol.* (2015) 308:H733–42. doi: 10.1152/ajpheart.00335.2014
98. Špiranec K, Chen W, Werner F, Nikolaev VO, Naruke T, Koch F, et al. Endothelial C-type natriuretic peptide acts on pericytes to regulate microcirculatory flow and blood pressure. *Circulation.* (2018) 138:494–508. doi: 10.1161/CIRCULATIONAHA.117.033383
99. Gaudin A, Yemisci M, Eroglu H, Lepetre-Mouelhi S, Turkoglu OF, Dönmez-Demir B, et al. Squalenoyl adenosine nanoparticles provide neuroprotection after stroke and spinal cord injury. *Nat Nanotechnol.* (2014) 9:1054–62. doi: 10.1038/nnano.2014.274
100. Bell RD, Winkler EA, Sagare AP, Singh I, LaRue B, Deane R, et al. Pericytes control key neurovascular functions and neuronal phenotype in the adult brain and during brain aging. *Neuron.* (2010) 68:409–27. doi: 10.1016/j.neuron.2010.09.043

101. Miners JS, Schulz I, Love S. Differing associations between Aβ accumulation, hypoperfusion, blood–brain barrier dysfunction and loss of PDGFRB pericyte marker in the precuneus and parietal white matter in Alzheimer's disease. *J Cereb Blood Flow Metab.* (2018) 38:103–15. doi: 10.1177/0271678X17690761
102. Schultz N, Brännström K, Byman E, Moussaud S, Nielsen HM, Olofsson A, et al. Amyloid-beta 1-40 is associated with alterations in NG2+ pericyte population *ex vivo* and *in vitro*. *Aging Cell.* (2018) 17:e12728. doi: 10.1111/acel.12728
103. Lin W, Ma X, Hao M, Zhou H, Yu X, Shao N, et al. Liraglutide attenuates the migration of retinal pericytes induced by advanced glycation end products. *Peptides.* (2018) 105:7–13. doi: 10.1016/j.peptides.2018.05.003
104. Reeves C, Jardim AP, Sisodiya SM, Thom M, Liu JYW. Spatiotemporal dynamics of PDGFRβ expression in pericytes and glial scar formation in penetrating brain injuries in adults. *Neuropathol Appl Neurobiol.* (2019). doi: 10.1111/nan.12539. [Epub ahead of print].
105. Dore-Duffy P, Owen C, Balabanov R, Murphy S, Beaumont T, Rafols JA. Pericyte migration from the vascular wall in response to traumatic brain injury. *Microvasc Res.* (2000) 60:55–69. doi: 10.1006/mvre.2000.2244
106. Berthiaume AA, Grant RI, McDowell KP, Underly RG, Hartmann DA, Levy M, et al. Dynamic remodeling of pericytes *in vivo* maintains capillary coverage in the adult mouse brain. *Cell Rep.* (2018) 22:8–16. doi: 10.1016/j.celrep.2017.12.016
107. Berthiaume AA, Hartmann DA, Majesky MW, Bhat NR, Shih AY. Pericyte structural remodeling in cerebrovascular health and homeostasis. *Front Aging Neurosci.* (2018) 10:210. doi: 10.3389/fnagi.2018.00210
108. Mazzoni MC, Schmid-Schonbein GW. Mechanisms and consequences of cell activation in the microcirculation. *Cardiovasc Res.* (1996) 32:709–19. doi: 10.1016/S0008-6363(96)00146-0
109. Barnes AJ, Locke P, Scudder PR, Dormandy TL, Dormandy JA, Slack J. Is hyperviscosity a treatable component of diabetic microcirculatory disease? *Lancet.* (1977) 2:789–91. doi: 10.1016/S0140-6736(77)90724-3
110. Mori E, del Zoppo GJ, Chambers JD, Copeland BR, Arfors KE. Inhibition of polymorphonuclear leukocyte adherence suppresses no-reflow after focal cerebral ischemia in baboons. *Stroke.* (1992) 23:712–8. doi: 10.1161/01.STR.23.5.712
111. del Zoppo GJ, Schmid-Schönbein GW, Mori E, Copeland BR, Chang CM. Polymorphonuclear leukocytes occlude capillaries following middle cerebral artery occlusion and reperfusion in baboons. *Stroke.* (1991) 22:1276–83. doi: 10.1161/01.STR.22.10.1276
112. Ritter LS, Orozco JA, Coull BM, McDonagh PF, Rosenblum WI. Leukocyte accumulation and hemodynamic changes in the cerebral microcirculation during early reperfusion after stroke editorial comment. *Stroke.* (2000) 31:1153–61. doi: 10.1161/01.STR.31.5.1153
113. Clark WM, Coull BM, Briley DP, Mainolfi E, Rothlein R. Circulating intercellular adhesion molecule-1 levels and neutrophil adhesion in stroke. *J Neuroimmunol.* (1993) 44:123–5. doi: 10.1016/0165-5728(93)90275-4
114. Harris AG, Skalak TC. Effects of leukocyte capillary plugging in skeletal muscle ischemia-reperfusion injury. *Am J Physiol.* (1996) 271:H2653–60. doi: 10.1152/ajpheart.1996.271.6.H2653
115. Theilen H, Schröck H, Kuschinsky W. Gross persistence of capillary plasma perfusion after middle cerebral artery occlusion in the rat brain. *J Cereb Blood Flow Metab.* (1994) 14:1055–61. doi: 10.1038/jcbfm.1994.138
116. Villringer A, Them A, Lindauer U, Einhäupl K, Dirnagl U. Capillary perfusion of the rat brain cortex. An *in vivo* confocal microscopy study. *Circ Res.* (1994) 75:55–62. doi: 10.1161/01.RES.75.1.55
117. Abounader R, Vogel J, Kuschinsky W. Patterns of capillary plasma perfusion in brains of conscious rats during normocapnia and hypercapnia. *Circ Res.* (1995) 76:120–6. doi: 10.1161/01.RES.76.1.120
118. Bookheimer SY, Strojwas MH, Cohen MS, Saunders AM, Pericak-Vance MA, Mazziotta JC, et al. Patterns of brain activation in people at risk for Alzheimer's disease. *N Engl J Med.* (2000) 343:450–6. doi: 10.1056/NEJM200008173430701
119. Scarmeas N, Habeck CG, Stern Y, Anderson KE. APOE genotype and cerebral blood flow in healthy young individuals. *JAMA.* (2003) 290:1581–2. doi: 10.1001/jama.290.12.1581
120. Kim T, Richard Jennings J, Kim SG. Regional cerebral blood flow and arterial blood volume and their reactivity to hypercapnia in hypertensive and normotensive rats. *J Cereb Blood Flow Metab.* (2014) 34:408–14. doi: 10.1038/jcbfm.2013.197
121. Angleys H, Jespersen SN, Østergaard L. The effects of capillary transit time heterogeneity on the BOLD signal. *Hum Brain Mapp.* (2018) 39:2329–52. doi: 10.1002/hbm.23991
122. Brown WR. A review of string vessels or collapsed, empty basement membrane tubes. *J Alzheimer Dis.* (2010) 21:725–39. doi: 10.3233/JAD-2010-100219
123. Hunter JM, Kwan J, Malek-Ahmadi M, Maarouf CL, Kokjohn TA, Belden C, et al. Morphological and pathological evolution of the brain microcirculation in aging and alzheimer's disease. *PLoS ONE.* (2012) 7:e36893. doi: 10.1371/journal.pone.0036893
124. Tong X-K, Hamel E. Simvastatin restored vascular reactivity, endothelial function and reduced string vessel pathology in a mouse model of cerebrovascular disease. *J Cereb Blood Flow Metab.* (2015) 35:512–20. doi: 10.1038/jcbfm.2014.226
125. Pantoni L. Cerebral small vessel disease: from pathogenesis and clinical characteristics to therapeutic challenges. *Lancet Neurol.* (2010) 9:689–701. doi: 10.1016/S1474-4422(10)70104-6
126. Price TO, Eranki V, Banks WA, Ercal N, Shah GN. Topiramate treatment protects blood-brain barrier pericytes from hyperglycemia-induced oxidative damage in diabetic mice. *Endocrinology.* (2012) 153:362–72. doi: 10.1210/en.2011-1638
127. McCuskey PA, McCuskey RS. *In vivo* and electron microscopic study of the development of cerebral diabetic microangiography. *Microcirc Endothelium Lymphatics.* (1984) 1:221–44.
128. Tagami M, Nara Y, Kubota A, Fujino H, Yamori Y. Ultrastructural changes in cerebral pericytes and astrocytes of stroke-prone spontaneously hypertensive rats. *Stroke.* (1990) 21:1064–71. doi: 10.1161/01.STR.21.7.1064
129. Junker U, Jaggi C, Bestetti G, Rossi GL. Basement membrane of hypothalamus and cortex capillaries from normotensive and spontaneously hypertensive rats with streptozotocin-induced diabetes. *Acta Neuropathol.* (1985) 65:202–8. doi: 10.1007/BF00686999
130. Wood KC, Hebbel RP, Granger DN. Endothelial cell NADPH oxidase mediates the cerebral microvascular dysfunction in sickle cell transgenic mice. *FASEB J.* (2005) 19:989–91. doi: 10.1096/fj.04-3218fje
131. Gidday JM, Park TS, Shah AR, Gonzales ER. Modulation of basal and postischemic leukocyte-endothelial adherence by nitric oxide. *Stroke.* (1998) 29:1423–30. doi: 10.1161/01.STR.29.7.1423
132. Fraticelli A, Serrano CV, Bochner BS, Capogrossi MC, Zweier JL. Hydrogen peroxide and superoxide modulate leukocyte adhesion molecule expression and leukocyte endothelial adhesion. *Biochim Biophys Acta.* (1996) 1310:251–9. doi: 10.1016/0167-4889(95)00169-7
133. Vink H, Constantinescu AA, Spaan JA. Oxidized lipoproteins degrade the endothelial surface layer : implications for platelet-endothelial cell adhesion. *Circulation.* (2000) 101:1500–2. doi: 10.1161/01.CIR.101.13.1500
134. Czarnowska E, Karwatowska-Prokopczuk E. Ultrastructural demonstration of endothelial glycocalyx disruption in the reperfused rat heart. Involvement of oxygen free radicals. *Basic Res Cardiol.* (1995) 90:357–64. doi: 10.1007/BF00788496
135. Pantoni L, Garcia JH. Pathogenesis of leukoaraiosis. *Stroke.* (1997) 28:652–59. doi: 10.1161/01.STR.28.3.652
136. Salat DH. Imaging small vessel-associated white matter changes in aging. *Neuroscience.* (2014) 276:174–86. doi: 10.1016/j.neuroscience.2013.11.041
137. Pires PW, Dams Ramos CM, Matin N, Dorrance AM. The effects of hypertension on the cerebral circulation. *Am J Physiol Heart Circ Physiol.* (2013) 304:H1598–614. doi: 10.1152/ajpheart.00490.2012
138. Shi Y, Wardlaw JM. Update on cerebral small vessel disease: a dynamic whole-brain disease. *Stroke Vasc Neurol.* (2016) 1:83–92. doi: 10.1136/svn-2016-000035
139. Martinez-Quinones P, McCarthy CG, Watts SW, Klee NS, Komic A, Calmasini FB, Priviero F, et al. Hypertension induced morphological and physiological changes in cells of the arterial wall. *Am J Hypertens.* (2018) 31:1067–78. doi: 10.1093/ajh/hpy083
140. Umemura T, Kawamura T, Hotta N. Pathogenesis and neuroimaging of cerebral large and small vessel disease in type 2 diabetes: a possible link

between cerebral and retinal microvascular abnormalities. *J Diabetes Investig.* (2017) 8:134–48. doi: 10.1111/jdi.12545
141. Caplan LR. Diabetes and brain ischemia. *Diabetes.* (1996) 45(Suppl 3):S95–7. doi: 10.2337/diab.45.3.S95
142. Gursoy-Ozdemir Y, Yemisci M, Dalkara T. Microvascular protection is essential for successful neuroprotection in stroke. *J Neurochem.* (2012) 123:2–11. doi: 10.1111/j.1471-4159.2012.07938.x
143. Dalkara T, Arsava EM. Can restoring incomplete microcirculatory reperfusion improve stroke outcome after thrombolysis? *J Cereb Blood Flow Metab.* (2012) 32:2091–9. doi: 10.1038/jcbfm.2012.139
144. De Silva DA, Fink JN, Christensen S, Ebinger M, Bladin C, Levi CR, et al. Assessing reperfusion and recanalization as markers of clinical outcomes after intravenous thrombolysis in the echoplanar imaging thrombolytic evaluation trial (EPITHET). *Stroke.* (2009) 40:2872–4. doi: 10.1161/STROKEAHA.108.543595
145. Soares BP, Tong E, Hom J, Cheng SC, Bredno J, Boussel L, et al. Reperfusion is a more accurate predictor of follow-up infarct volume than recanalization: a proof of concept using CT in acute ischemic stroke patients. *Stroke.* (2010) 41:e34–40. doi: 10.1161/STROKEAHA.109.568766
146. Liu S, Shi H, Liu W, Furuichi T, Timmins GS, Liu KJ. Interstitial pO2 in ischemic penumbra and core are differentially affected following transient focal cerebral ischemia in rats. *J Cereb Blood Flow Metab.* (2004) 24:343–9. doi: 10.1097/01.WCB.0000110047.43905.01
147. Maestrini I, Strbian D, Gautier S, Haapaniemi E, Moulin S, Sairanen T, et al. Higher neutrophil counts before thrombolysis for cerebral ischemia predict worse outcomes. *Neurology.* (2015) 85:1408–16. doi: 10.1212/WNL.0000000000002029
148. Zhang J, Ren Q, Song Y, He M, Zeng Y, Liu Z, Xu J. Prognostic role of neutrophil–lymphocyte ratio in patients with acute ischemic stroke. *Medicine.* (2017) 96:e8624. doi: 10.1097/MD.0000000000008624
149. Fang YN, Tong MS, Sung PH, Chen YL, Chen CH, Tsai NW, et al. Higher neutrophil counts and neutrophil-to-lymphocyte ratio predict prognostic outcomes in patients after non-atrial fibrillation-caused ischemic stroke. *Biomed J.* (2017) 40:154–62. doi: 10.1016/j.bj.2017.03.002
150. Wang H, Zhang M, Hao Y, Zi W, Yang D, Zhou Z, et al. Early prediction of poor outcome despite successful recanalization after endovascular treatment for anterior large vessel occlusion stroke. *World Neurosurg.* (2018) 115:e312–21. doi: 10.1016/j.wneu.2018.04.042
151. Elkind MS. Why now? Moving from stroke risk factors to stroke triggers. *Curr Opin Neurol.* (2007) 20:51–7. doi: 10.1097/WCO.0b013e328012da75
152. Davis S, Donnan GA. Time is Penumbra: imaging, selection and outcome. The Johann jacob wepfer award 2014. *Cerebrovasc Dis.* (2014) 38:59–72. doi: 10.1159/000365503
153. Guadagno JV, Jones PS, Aigbirhio FI, Wang D, Fryer TD, Day DJ, et al. Selective neuronal loss in rescued penumbra relates to initial hypoperfusion. *Brain.* (2008) 131:2666–78. doi: 10.1093/brain/awn175
154. Baron JC, Yamauchi H, Fujioka M, Endres M. Selective neuronal loss in ischemic stroke and cerebrovascular disease. *J Cereb Blood Flow Metab.* (2014) 34:2–18. doi: 10.1038/jcbfm.2013.188
155. Phan TG, Wright PM, Markus R, Howells DW, Davis SM, Donnan GA. Salvaging the ischaemic penumbra: more than just reperfusion? *Clin Exp Pharmacol Physiol.* (2002) 29:1–10. doi: 10.1046/j.1440-1681.2002.03609.x
156. Murphy BD, Fox AJ, Lee DH, Sahlas DJ, Black SE, Hogan MJ, et al. Identification of penumbra and infarct in acute ischemic stroke using computed tomography perfusion-derived blood flow and blood volume measurements. *Stroke.* (2006) 37:1771–7. doi: 10.1161/01.STR.0000227243.96808.53
157. Bordeleau M, ElAli A, Rivest S. Severe chronic cerebral hypoperfusion induces microglial dysfunction leading to memory loss in APPswe/PS1 mice. *Oncotarget.* (2016) 7:11864–80. doi: 10.18632/oncotarget.7689
158. ElAli A, Thériault P, Préfontaine P, Rivest S. Mild chronic cerebral hypoperfusion induces neurovascular dysfunction, triggering peripheral beta-amyloid brain entry and aggregation. *Acta Neuropathol Commun.* (2013) 1:75. doi: 10.1186/2051-5960-1-75
159. Song J, Nan D, He Q, Yang L, Guo H. Astrocyte activation and capillary remodeling in modified bilateral common carotid artery occlusion mice. *Microcirculation.* (2017) 24:e12366. doi: 10.1111/micc.12366
160. Takasugi J, Miwa K, Watanabe Y, Okazaki S, Todo K, Sasaki T, et al. Cortical cerebral microinfarcts on 3T magnetic resonance imaging in patients with carotid artery stenosis. *Stroke.* (2019) 50:639–44. doi: 10.1161/STROKEAHA.118.023781
161. Mundiyanapurath S, Ringleb PA, Diatschuk S, Hansen MB, Mouridsen K, Østergaard L, et al. Capillary transit time heterogeneity is associated with modified rankin scale score at discharge in patients with bilateral high grade internal carotid artery stenosis. *PLoS ONE.* (2016) 11:e0158148. doi: 10.1371/journal.pone.0158148
162. Crowley RW, Medel R, Dumont AS, Ilodigwe D, Kassell NF, Mayer SA, et al. Angiographic vasospasm is strongly correlated with cerebral infarction after subarachnoid hemorrhage. *Stroke.* (2011) 42:919–23. doi: 10.1161/STROKEAHA.110.597005
163. Macdonald RL, Weir BK. A review of hemoglobin and the pathogenesis of cerebral vasospasm. *Stroke.* (1991) 22:971–82. doi: 10.1161/01.STR.22.8.971
164. Takeuchi K, Miyata N, Renic M, Harder DR, Roman RJ. Hemoglobin NO, and 20-HETE interactions in mediating cerebral vasoconstriction following SAH. *Am J Physiol Regul Integr Comp Physiol.* (2006) 290:R84–9. doi: 10.1152/ajpregu.00445.2005
165. Friedrich B, Müller F, Feiler S, Schöller K, Plesnila N. Experimental subarachnoid hemorrhage causes early and long-lasting microarterial constriction and microthrombosis: an *in-vivo* microscopy study. *J Cereb Blood Flow Metab.* (2012) 32:447–55. doi: 10.1038/jcbfm.2011.154
166. Anzabi M, Angleys H, Aamand R, Ardalan M, Mouridsen K, Rasmussen PM, et al. Capillary flow disturbances after experimental subarachnoid hemorrhage: a contributor to delayed cerebral ischemia? *Microcirculation.* (2018) 26:e12516. doi: 10.1111/micc.12516
167. McConnell ED, Wei HS, Reitz KM, Kang H, Takano T, Vates GE, et al. Cerebral microcirculatory failure after subarachnoid hemorrhage is reversed by hyaluronidase. *J Cereb Blood Flow Metab.* (2016) 36:1537–52. doi: 10.1177/0271678X15608389
168. Ishikawa M, Kajimura M, Morikawa T, Tsukada K, Tsuji T, Kusaka G, et al. Cortical microcirculatory disturbance in the super acute phase of subarachnoid hemorrhage - *In vivo* analysis using two-photon laser scanning microscopy. *J Neurol Sci.* (2016) 368:326–33. doi: 10.1016/j.jns.2016.06.067
169. Wang KC, Tang SC, Lee JE, Tsai JC, Lai DM, Lin WC, et al. Impaired microcirculation after subarachnoid hemorrhage in an *in vivo* animal model. *Sci Rep.* (2018) 8:1–15. doi: 10.1038/s41598-018-31709-7
170. Balbi M, Koide M, Wellman GC, Plesnila N. Inversion of neurovascular coupling after subarachnoid hemorrhage *in vivo*. *J Cereb Blood Flow Metab.* (2017) 37:3625–34. doi: 10.1177/0271678X16686595
171. Graham DI, Adams JH. Ischaemic brain damage in fatal head injuries. *Lancet.* (1971) 1:265–6. doi: 10.1016/S0140-6736(71)91003-8
172. Bragin DE, Bush RC, Nemoto EM. Effect of cerebral perfusion pressure on cerebral cortical microvascular shunting at high intracranial pressure in rats. *Stroke.* (2013) 44:177–81. doi: 10.1161/STROKEAHA.112.668293
173. Martin NA, Patwardhan R V, Alexander MJ, Africk CZ, Lee JH, Shalmon E, et al. Characterization of cerebral hemodynamic phases following severe head trauma: hypoperfusion, hyperemia, and vasospasm. *J Neurosurg.* (1997) 87:9–19. doi: 10.3171/jns.1997.87.1.0009
174. Østergaard L, Engedal TS, Aamand R, Mikkelsen R, Iversen NK, Anzabi M, et al. Capillary transit time heterogeneity and flow-metabolism coupling after traumatic brain injury. *J Cereb Blood Flow Metab.* (2014) 34:1585–98. doi: 10.1038/jcbfm.2014.131
175. Villaseñor R, Kuennecke B, Ozmen L, Ammann M, Kugler C, Grüninger F, et al. Region-specific permeability of the blood–brain barrier upon pericyte loss. *J Cereb Blood Flow Metab.* (2017) 37:3683–94. doi: 10.1177/0271678X17697340
176. Schwarzmaier SM, Gallozzi M, Plesnila N. Identification of the vascular source of vasogenic brain edema following traumatic brain injury using *in vivo* 2-photon microscopy in mice. *J Neurotr.* (2015) 32:990–1000. doi: 10.1089/neu.2014.3775
177. Buckley EM, Miller BF, Golinski JM, Sadeghian H, McAllister LM, Vangel M, et al. Decreased microvascular cerebral blood flow assessed by diffuse correlation spectroscopy after repetitive concussions in mice. *J Cereb Blood Flow Metab.* (2015) 35:1995–2000. doi: 10.1038/jcbfm.2015.161

178. Bellapart J, Abi-Fares C, Cuthbertson K, Dunster K, Diab S, Platts DG, et al. Cerebral microcirculation during mild head injury after a contusion and acceleration experimental model in sheep. *Brain Inj.* (2016) 30:1542–51. doi: 10.1080/02699052.2016.1199894
179. Hartings JA, York J, Carroll CP, Hinzman JM, Mahoney E, Krueger B, et al. Subarachnoid blood acutely induces spreading depolarizations and early cortical infarction. *Brain.* (2017) 140:2673–90. doi: 10.1093/brain/awx214
180. Eriksen N, Rostrup E, Fabricius M, Scheel M, Major S, Winkler MKL, et al. Early focal brain injury after subarachnoid hemorrhage correlates with spreading depolarizations. *Neurology.* (2019) 92:e326–41. doi: 10.1212/WNL.0000000000006814
181. Strong AJ, Anderson PJ, Watts HR, Virley DJ, Lloyd A, Irving EA, et al. Peri-infarct depolarizations lead to loss of perfusion in ischaemic gyrencephalic cerebral cortex. *Brain.* (2006) 130:995–1008. doi: 10.1093/brain/awl392
182. Woitzik J, Hecht N, Pinczolits A, Sandow N, Major S, Winkler MKL, et al. Propagation of cortical spreading depolarization in the human cortex after malignant stroke. *Neurology.* (2013) 80:1095–102. doi: 10.1212/WNL.0b013e3182886932
183. Eikermann-Haerter K, Hyun Lee J, Yuzawa I, Liu CH, Zhou Z, Kyoung Shin H, et al. Migraine mutations increase stroke vulnerability by facilitating ischemic depolarizations. *Circulation.* (2012) 125:335–45. doi: 10.1161/CIRCULATIONAHA.111.045096
184. Kumagai T, Walberer M, Nakamura H, Endepols H, Sué M, Vollmar S, et al. Distinct spatiotemporal patterns of spreading depolarizations during early infarct evolution: evidence from real-time imaging. *J Cereb Blood Flow Metab.* (2011) 31:580–92. doi: 10.1038/jcbfm.2010.128
185. Ayata C, Lauritzen M. Spreading depression, spreading depolarizations, and the cerebral vasculature. *Physiol Rev.* (2015) 95:953–93. doi: 10.1152/physrev.00027.2014
186. Østergaard L, Dreier JP, Hadjikhani N, Jespersen SN, Dirnagl U, Dalkara T. Neurovascular coupling during cortical spreading depolarization and -depression. *Stroke.* (2015) 46:1392–401. doi: 10.1161/STROKEAHA.114.008077
187. Khennouf L, Gesslein B, Brazhe A, Octeau JC, Kutuzov N, Khakh BS, et al. Active role of capillary pericytes during stimulation-induced activity and spreading depolarization. *Brain.* (2018) 141:2032–46. doi: 10.1093/brain/awy143
188. Shahim P, Tegner Y, Gustafsson B, Gren M, Ärlig J, Olsson M, et al. Neurochemical aftermath of repetitive mild traumatic brain injury. *JAMA Neurol.* (2016) 73:1308–15. doi: 10.1001/jamaneurol.2016.2038
189. Aldag M, Armstrong RC, Bandak F, Bellgowan PSF, Bentley T, Biggerstaff S, et al. The biological basis of chronic traumatic encephalopathy following blast injury: a literature review. *J Neurotr.* (2017) 34:S-26-S-43. doi: 10.1089/neu.2017.5218
190. McKee AC, Cantu RC, Nowinski CJ, Hedley-Whyte ET, Gavett BE, Budson AE, et al. Chronic traumatic encephalopathy in athletes: progressive tauopathy after repetitive head injury. *J Neuropathol Exp Neurol.* (2009) 68:709–35. doi: 10.1097/NEN.0b013e3181a9d503
191. McKee AC, Stein TD, Kiernan PT, Alvarez VE. The neuropathology of chronic traumatic encephalopathy. *Brain Pathol.* (2015) 25:350–64. doi: 10.1111/bpa.12248
192. Sahyouni R, Gutierrez P, Gold E, Robertson RT, Cummings BJ. Effects of concussion on the blood-brain barrier in humans and rodents. *J Concussion.* (2017). doi: 10.1177/2059700216684518. [Epub ahead of print].
193. Tagge CA, Fisher AM, Minaeva OV, Gaudreau-Balderrama A, Moncaster JA, Zhang XL, et al. Concussion, microvascular injury, and early tauopathy in young athletes after impact head injury and an impact concussion mouse model. *Brain.* (2018) 141:422–58. doi: 10.1093/brain/awx350
194. Goldstein LE, Fisher AM, Tagge CA, Zhang XL, Velisek L, Sullivan JA, et al. Chronic traumatic encephalopathy in blast-exposed military veterans and a blast neurotrauma mouse model. *Sci Transl Med.* (2012) 4:134ra60. doi: 10.1016/j.jalz.2012.05.592
195. Zanier ER, Bertani I, Sammali E, Pischiutta F, Chiaravalloti MA, Vegliante G, et al. Induction of a transmissible tau pathology by traumatic brain injury. *Brain.* (2018) 141:2685–99. doi: 10.1093/brain/awy193
196. Wolters FJ, Zonneveld HI, Hofman A, van der Lugt A, Koudstaal PJ, Vernooij MW, et al. Heart-brain connection collaborative research group. cerebral perfusion and the risk of dementia. *Circulation.* (2017) 136:719–28. doi: 10.1161/CIRCULATIONAHA.117.027448
197. Dai W, Lopez OL, Carmichael OT, Becker JT, Kuller LH, Gach HM. Mild cognitive impairment and alzheimer disease: patterns of altered cerebral blood flow at MR imaging. *Radiology.* (2009) 250:856–66. doi: 10.1148/radiol.2503080751
198. Iturria-Medina Y, Sotero RC, Toussaint PJ, Mateos-Pérez JM, Evans AC, Alzheimer's disease neuroimaging initiative. Early role of vascular dysregulation on late-onset Alzheimer's disease based on multifactorial data-driven analysis. *Nat Commun.* (2016) 7:11934. doi: 10.1038/ncomms11934
199. Santos CY, Snyder PJ, Wu WC, Zhang M, Echeverria A, Alber J. Pathophysiologic relationship between Alzheimer's disease, cerebrovascular disease, and cardiovascular risk: a review and synthesis. *Alzheimer's Dement.* (2017) 7:69–87. doi: 10.1016/j.dadm.2017.01.005
200. Qiu L, Ng G, Tan EK, Liao P, Kandiah N, Zeng L. Chronic cerebral hypoperfusion enhances Tau hyperphosphorylation and reduces autophagy in Alzheimers disease mice. *Sci Rep.* (2016) 6:23964. doi: 10.1038/srep23964
201. Pluta R, Bogucka-Kocka A, Ułamek-Kozioł M, Bogucki J, Januszewski S, Kocki J, et al. Ischemic tau protein gene induction as an additional key factor driving development of Alzheimer's phenotype changes in CA1 area of hippocampus in an ischemic model of Alzheimer's disease. *Pharmacol Rep.* (2018) 70:881–84. doi: 10.1016/j.pharep.2018.03.004
202. Kuroiwa T. Experimental cerebral ischemia: the contribution of the Bethesda Group. *Acta Neurochir Suppl.* (2010) 106:17–9. doi: 10.1007/978-3-211-98811-4_2
203. Farkas E, De Jong GI, De Vos RAI, Jansen Steur ENH, Luiten PGM. Pathological features of cerebral cortical capillaries are doubled in Alzheimer's disease and Parkinson's disease. *Acta Neuropathol.* (2000) 100:395–402. doi: 10.1007/s004010000195
204. Nielsen RB, Egefjord L, Angleys H, Mouridsen K, Gejl M, Møller A, et al. Capillary dysfunction is associated with symptom severity and neurodegeneration in Alzheimer's disease. *Alzheimer Dement.* (2017) 13:1143–53. doi: 10.1016/j.jalz.2017.02.007
205. Gutiérrez-Jiménez E, Angleys H, Rasmussen PM, West MJ, Catalini L, Iversen NK, et al. Disturbances in the control of capillary flow in an aged APPswe/PS1ΔE9 model of Alzheimer's disease. *Neurobiol Aging.* (2018) 62:82–94. doi: 10.1016/j.neurobiolaging.2017.10.006
206. Reeson P, Choi K, Brown CE. VEGF signaling regulates the fate of obstructed capillaries in mouse cortex. *Elife.* (2018) 7:e33670. doi: 10.7554/eLife.33670
207. Park L, Uekawa K, Garcia-Bonilla L, Koizumi K, Murphy M, Pistik R, et al. Brain perivascular macrophages initiate the neurovascular dysfunction of alzheimer Aβ peptides. *Circ Res.* (2017) 121:258–69. doi: 10.1161/CIRCRESAHA.117.311054
208. Jaworski T, Lechat B, Demedts D, Gielis L, Devijver H, Borghgraef P, et al. Dendritic degeneration, neurovascular defects, and inflammation precede neuronal loss in a mouse model for tau-mediated neurodegeneration. *Am J Pathol.* (2011) 179:2001–15. doi: 10.1016/j.ajpath.2011.06.025
209. Sagare AP, Bell RD, Zhao Z, Ma Q, Winkler EA, Ramanathan A, et al. Pericyte loss influences Alzheimer-like neurodegeneration in mice. *Nat Commun.* (2013) 4:1–14. doi: 10.1038/ncomms3932
210. Sengillo JD, Winkler EA, Walker CT, Sullivan JS, Johnson M, Zlokovic B V. Deficiency in mural vascular cells coincides with blood-brain barrier disruption in Alzheimer's disease. *Brain Pathol.* (2013) 23:303–10. doi: 10.1111/bpa.12004
211. Montagne A, Nikolakopoulou AM, Zhao Z, Sagare AP, Si G, Lazic D, et al. Pericyte degeneration causes white matter dysfunction in the mouse central nervous system. *Nat Med.* (2018) 24:326–37. doi: 10.1038/nm.4482
212. Wilhelmus MMM, Otte-Höller I, van Triel JJJ, Veerhuis R, Maat-Schieman MLC, Bu G, et al. Lipoprotein receptor-related protein-1 mediates amyloid-beta-mediated cell death of cerebrovascular cells. *Am J Pathol.* (2007) 171:1989–99. doi: 10.2353/ajpath.2007.070050
213. Rensink AAM, Verbeek MM, Otte-Höller I, ten Donkelaar HT, de Waal RMW, Kremer B. Inhibition of amyloid-beta-induced cell death in human brain pericytes *in vitro*. *Brain Res.* (2002) 952:111–21. doi: 10.1016/S0006-8993(02)03218-3

214. Verbeek MM, Otte-Höller I, Ruiter DJ, de Waal RM. Human brain pericytes as a model system to study the pathogenesis of cerebrovascular amyloidosis in Alzheimer's disease. *Cell Mol Biol.* (1999) 45:37–46.
215. Toth P, Tucsek Z, Sosnowska D, Gautam T, Mitschelen M, Tarantini S, et al. Age-related autoregulatory dysfunction and cerebromicrovascular injury in mice with angiotensin II-induced hypertension. *J Cereb Blood Flow Metab.* (2013) 33:1732–42. doi: 10.1038/jcbfm.2013.143
216. Kruyer A, Soplop N, Strickland S, Norris EH. Chronic hypertension leads to neurodegeneration in the TgSwDI mouse model of alzheimer's disease. *Hypertens.* (2015) 66:175–82. doi: 10.1161/HYPERTENSIONAHA.115.05524
217. Thériault P, ElAli A, Rivest S. High fat diet exacerbates Alzheimer's disease-related pathology in APPswe/PS1 mice. *Oncotarget.* (2016) 7:67808–27. doi: 10.18632/oncotarget.12179
218. Casey CS, Atagi Y, Yamazaki Y, Shinohara M, Tachibana M, Fu Y, et al. Apolipoprotein E inhibits cerebrovascular pericyte mobility through a RhoA protein-mediated pathway. *J Biol Chem.* (2015) 290:14208–17. doi: 10.1074/jbc.M114.625251
219. Halliday MR, Rege SV, Ma Q, Zhao Z, Miller CA, Winkler EA, et al. Accelerated pericyte degeneration and blood-brain barrier breakdown in apolipoprotein E4 carriers with Alzheimer's disease. *J Cereb Blood Flow Metab.* (2016) 36:216–27. doi: 10.1038/jcbfm.2015.44
220. Zlokovic BV. Cerebrovascular effects of apolipoprotein E: implications for Alzheimer disease. *JAMA Neurol.* (2013) 70:440–4. doi: 10.1001/jamaneurol.2013.2152
221. Vidal R, Calero M, Piccardo P, Farlow MR, Unverzagt FW, Méndez E, et al. Senile dementia associated with amyloid beta protein angiopathy and tau perivascular pathology but not neuritic plaques in patients homozygous for the APOE-epsilon4 allele. *Acta Neuropathol.* (2000) 100:1–12. doi: 10.1007/s004010051186
222. Kolinko Y, Krakorova K, Cendelin J, Tonar Z, Kralickova M. Microcirculation of the brain: morphological assessment in degenerative diseases and restoration processes. *Rev Neurosci.* (2014) 26:75–93. doi: 10.1515/revneuro-2014-0049
223. Guan J, Pavlovic D, Dalkie N, Waldvogel HJ, O'Carroll SJ, Green CR, et al. Vascular degeneration in parkinsons disease. *Brain Pathol.* (2013) 23:154–64. doi: 10.1111/j.1750-3639.2012.00628.x
224. Sarkar S, Raymick J, Mann D, Bowyer J, Hanig J, Schmued L, et al. Neurovascular changes in acute, sub-acute and chronic mouse models of parkinson's disease. *Curr Neurovasc Res.* (2014) 11:48–61. doi: 10.2174/1567202610666131124234506
225. Shibuya K, Yagishita S, Nakamura A, Uchihara T. Perivascular orientation of astrocytic plaques and tuft-shaped astrocytes. *Brain Res.* (2011) 1404:50–4. doi: 10.1016/j.brainres.2011.06.014
226. Desai Bradaric B, Patel A, Schneider JA, Carvey PM, Hendey B. Evidence for angiogenesis in Parkinson's disease, incidental Lewy body disease, and progressive supranuclear palsy. *J Neural Transm.* (2012) 119:59–71. doi: 10.1007/s00702-011-0684-8
227. Wong PC, Pardo CA, Borchelt DR, Lee MK, Copeland NG, Jenkins NA, et al. An adverse property of a familial ALS-linked SOD1 mutation causes motor neuron disease characterized by vacuolar degeneration of mitochondria. *Neuron.* (1995) 14:1105–16. doi: 10.1016/0896-6273(95)90259-7
228. Caccamo A, Majumder S, Oddo S. Cognitive decline typical of frontotemporal lobar degeneration in transgenic mice expressing the 25-kDa C-terminal fragment of TDP-43. *Am J Pathol.* (2012) 180:293–302. doi: 10.1016/j.ajpath.2011.09.022
229. Qiu H, Lee S, Shang Y, Wang WY, Au KF, Kamiya S, et al. ALS-associated mutation FUS-R521C causes DNA damage and RNA splicing defects. *J Clin Invest.* (2014) 124:981–99. doi: 10.1172/JCI72723
230. O'Rourke JG, Bogdanik L, Muhammad AKMG, Gendron TF, Kim KJ, Austin A, et al. C9orf72 BAC transgenic mice display typical pathologic features of ALS/FTD. *Neuron.* (2015) 88:892–901. doi: 10.1016/j.neuron.2015.10.027
231. Miyazaki K, Ohta Y, Nagai M, Morimoto N, Kurata T, Takehisa Y, et al. Disruption of neurovascular unit prior to motor neuron degeneration in amyotrophic lateral sclerosis. *J Neurosci Res.* (2011) 89:718–28. doi: 10.1002/jnr.22594
232. Miyazaki K, Masamoto K, Morimoto N, Kurata T, Mimoto T, Obata T, et al. Early and progressive impairment of spinal blood flow-glucose metabolism coupling in motor neuron degeneration of ALS model mice. *J Cereb Blood Flow Metab.* (2012) 32:456–67. doi: 10.1038/jcbfm.2011.155
233. Abrahams S, Goldstein LH, Kew JJ, Brooks DJ, Lloyd CM, Frith CD, et al. Frontal lobe dysfunction in amyotrophic lateral sclerosis. A PET study. *Brain.* (1996) 119(Pt 6):2105–20. doi: 10.1093/brain/119.6.2105
234. Ishikawa T, Morita M, Nakano I. Constant blood flow reduction in premotor frontal lobe regions in ALS with dementia – a SPECT study with 3D-SSP. *Acta Neurol Scand.* (2007) 116:340–4. doi: 10.1111/j.1600-0404.2007.00876.x
235. van Es MA, Hardiman O, Chio A, Al-Chalabi A, Pasterkamp RJ, Veldink JH, et al. Amyotrophic lateral sclerosis. *Lancet.* (2017) 390:2084–98. doi: 10.1016/S0140-6736(17)31287-4
236. Winkler EA, Sengillo JD, Sullivan JS, Henkel JS, Appel SH, Zlokovic BV. Blood-spinal cord barrier breakdown and pericyte reductions in amyotrophic lateral sclerosis. *Acta Neuropathol.* (2013) 125:111–20. doi: 10.1007/s00401-012-1039-8
237. Zhong Z, Deane R, Ali Z, Parisi M, Shapovalov Y, O'Banion MK, et al. ALS-causing SOD1 mutants generate vascular changes prior to motor neuron degeneration. *Nat Neurosci.* (2008) 11:420–2. doi: 10.1038/nn2073
238. Meldrum BS. Concept of activity-induced cell death in epilepsy: historical and contemporary perspectives. *Prog Brain Res.* (2002) 135:3–11. doi: 10.1016/S0079-6123(02)35003-9
239. Farrell JS, Wolff MD, Teskey GC. Neurodegeneration and Pathology in Epilepsy: Clinical and Basic Perspectives. In: *Advances in Neurobiology*. (2017). p. 317–34. doi: 10.1007/978-3-319-57193-5_12
240. Mehta A, Prabhakar M, Kumar P, Deshmukh R, Sharma PL. Excitotoxicity: bridge to various triggers in neurodegenerative disorders. *Eur J Pharmacol.* (2013) 698:6–18. doi: 10.1016/j.ejphar.2012.10.032
241. Ko SB, Ortega-Gutierrez S, Choi HA, Claassen J, Presciutti M, Schmidt JM, et al. Status epilepticus–induced hyperemia and brain tissue hypoxia after cardiac arrest. *Arch Neurol.* (2011) 68:1323–6. doi: 10.1001/archneurol.2011.240
242. Johnson AC, Cipolla MJ. Altered hippocampal arteriole structure and function in a rat model of preeclampsia: potential role in impaired seizure-induced hyperemia. *J Cereb Blood Flow Metab.* (2017) 37:2857–69. doi: 10.1177/0271678X16676287
243. Wichert-Ana L, de Azevedo-Marques PM, Oliveira LF, Terra-Bustamante VC, Fernandes RMF, Santos AC, et al. Interictal hyperemia correlates with epileptogenicity in polymicrogyric cortex. *Epilepsy Res.* (2008) 79:39–48. doi: 10.1016/j.eplepsyres.2007.12.018
244. Leal-Campanario R, Alarcon-Martinez L, Rieiro H, Martinez-Conde S, Alarcon-Martinez T, Zhao X, et al. Abnormal capillary vasodynamics contribute to ictal neurodegeneration in epilepsy. *Sci Rep.* (2017) 7:43276. doi: 10.1038/srep43276
245. Taskiran-Sag A, Yemisci M, Gursoy-Ozdemir Y, Erdener SE, Karatas H, Yuce D, et al. Improving microcirculatory reperfusion reduces parenchymal oxygen radical formation and provides neuroprotection. *Stroke.* (2018) 49:1267–75. doi: 10.1161/STROKEAHA.118.020711
246. Jung KH, Chu K, Ko SY, Lee ST, Sinn DI, Park DK, et al. Early intravenous infusion of sodium nitrite protects brain against *in vivo* ischemia-reperfusion injury. *Stroke.* (2006) 37:2744–50. doi: 10.1161/01.STR.0000245116.40163.1c
247. Fathi AR, Pluta RM, Bakhtian KD, Qi M, Lonser RR. Reversal of cerebral vasospasm via intravenous sodium nitrite after subarachnoid hemorrhage in primates. *J Neurosurg.* (2011) 115:1213–20. doi: 10.3171/2011.7.JNS11390
248. Cantow K, Flemming B, Ladwig-Wiegard M, Persson PB, Seeliger E. Low dose nitrite improves reoxygenation following renal ischemia in rats. *Sci Rep.* (2017) 7:14597. doi: 10.1038/s41598-017-15058-5
249. Terpolilli NA, Kim SW, Thal SC, Kataoka H, Zeisig V, Nitzsche B, et al. Inhalation of nitric oxide prevents ischemic brain damage in experimental stroke by selective dilatation of collateral arterioles. *Circ Res.* (2012) 110:727–38. doi: 10.1161/CIRCRESAHA.111.253419
250. Terpolilli NA, Kim SW, Thal SC, Kuebler WM, Plesnila N. Inhaled nitric oxide reduces secondary brain damage after traumatic brain injury in mice. *J Cereb Blood Flow Metab.* (2013) 33:311–8. doi: 10.1038/jcbfm.2012.176

251. Garry PS, Ezra M, Rowland MJ, Westbrook J, Pattinson KTS. The role of the nitric oxide pathway in brain injury and its treatment–from bench to bedside. *Exp Neurol.* (2015) 263:235–43. doi: 10.1016/j.expneurol.2014.10.017
252. Terpolilli NA, Feiler S, Dienel A, Müller F, Heumos N, Friedrich B, et al. Nitric oxide inhalation reduces brain damage, prevents mortality, and improves neurological outcome after subarachnoid hemorrhage by resolving early pial microvasospasms. *J Cereb Blood Flow Metab.* (2016) 36:2096–107. doi: 10.1177/0271678X15605848
253. Li J, Iadecola C. Nitric oxide and adenosine mediate vasodilation during functional activation in cerebellar cortex. *Neuropharmacology.* (1994) 33:1453–61. doi: 10.1016/0028-3908(94)90049-3
254. O'Farrell FM, Mastitskaya S, Hammond-Haley M, Freitas F, Wah WR, Attwell D. Capillary pericytes mediate coronary no-reflow after myocardial ischaemia. *Elife.* (2017) 6:e29280. doi: 10.7554/eLife.29280
255. Costa MA, Paiva AE, Andreotti JP, Cardoso MV, Cardoso CD, Mintz A, et al. Pericytes constrict blood vessels after myocardial ischemia. *J Mol Cell Cardiol.* (2018) 116:1–4. doi: 10.1016/j.yjmcc.2018.01.014
256. Dalkara T, Alarcon-Martinez L. Cerebral microvascular pericytes and neurogliovascular signaling in health and disease. *Brain Res.* (2015) 1623:3–17. doi: 10.1016/j.brainres.2015.03.047
257. Biaggioni I, Olafsson B, Robertson RM, Hollister AS, Robertson D. Cardiovascular and respiratory effects of adenosine in conscious man. Evidence for chemoreceptor activation. *Circ Res.* (1987) 61:779–86. doi: 10.1161/01.RES.61.6.779
258. Abreu A, Mahmarian JJ, Nishimura S, Boyce TM, Verani MS. Tolerance and safety of pharmacologic coronary vasodilation with adenosine in association with thallium-201 scintigraphy in patients with suspected coronary artery disease. *J Am Coll Cardiol.* (1991) 18:730–5. doi: 10.1016/0735-1097(91)90796-C
259. Gaston B. Summary: systemic effects of inhaled nitric oxide. *Proc Am Thorac Soc.* (2006) 3:170–2. doi: 10.1513/pats.200506-049BG
260. den Uil CA, Brugts JJ. Impact of intravenous nitroglycerin in the management of acute decompensated heart failure. *Curr Heart Fail Rep.* (2015) 12:87–93. doi: 10.1007/s11897-014-0230-8
261. Seabra AB, Duran N. Nanoparticulated nitric oxide donors and their biomedical applications. *Mini Rev Med Chem.* (2017) 17:216–23. doi: 10.2174/1389557516666160808124624
262. Cheng J, Korte N, Nortley R, Sethi H, Tang Y, Attwell D. Targeting pericytes for therapeutic approaches to neurological disorders. *Acta Neuropathol.* (2018) 136:507–23. doi: 10.1007/s00401-018-1893-0
263. Sugiyama T, Kawamura H, Yamanishi S, Kobayashi M, Katsumura K, Puro DG. Regulation of P2X $_7$ -induced pore formation and cell death in pericyte-containing retinal microvessels. *Am J Physiol.* (2005) 288:C568–76. doi: 10.1152/ajpcell.00380.2004
264. Wu DM, Kawamura H, Sakagami K, Kobayashi M, Puro DG. Cholinergic regulation of pericyte-containing retinal microvessels. *Am J Physiol Circ Physiol.* (2003) 284:H2083–90. doi: 10.1152/ajpheart.01007.2002
265. Kutcher ME, Herman IM. The pericyte: cellular regulator of microvascular blood flow. *Microvasc Res.* (2009) 77:235–46. doi: 10.1016/j.mvr.2009.01.007
266. Niego B, Lee N, Larsson P, De Silva TM, Au AE-L, McCutcheon F, et al. Selective inhibition of brain endothelial Rho-kinase-2 provides optimal protection of an *in vitro* blood-brain barrier from tissue-type plasminogen activator and plasmin. *PLoS ONE.* (2017) 12:e0177332. doi: 10.1371/journal.pone.0177332
267. Shin HK, Salomone S, Potts EM, Lee SW, Millican E, Noma K, et al. Rho-kinase inhibition acutely augments blood flow in focal cerebral ischemia via endothelial mechanisms. *J Cereb Blood Flow Metab.* (2007) 27:998–1009. doi: 10.1038/sj.jcbfm.9600406
268. Hyun Lee J, Zheng Y, von Bornstadt D, Wei Y, Balcioglu A, Daneshmand A, et al. Selective ROCK2 inhibition in focal cerebral ischemia. *Ann Clin Transl Neurol.* (2014) 1:2–14. doi: 10.1002/acn3.19
269. Shin HK, Huang PL, Ayata C. Rho-Kinase inhibition improves ischemic perfusion deficit in hyperlipidemic mice. *J Cereb Blood Flow Metab.* (2014) 34:284–87. doi: 10.1038/jcbfm.2013.195
270. Iba T, Levy JH, Hirota T, Hiki M, Sato K, Murakami T, et al. Protection of the endothelial glycocalyx by antithrombin in an endotoxin-induced rat model of sepsis. *Thromb Res.* (2018) 171:1–6. doi: 10.1016/j.thromres.2018.09.042
271. Iba T, Levy JH. Derangement of the endothelial glycocalyx in sepsis. *J Thromb Haemost.* (2019) 17:283–94. doi: 10.1111/jth.14371
272. Gresele P, Momi S, Falcinelli E. Anti-platelet therapy: phosphodiesterase inhibitors. *Br J Clin Pharmacol.* (2011) 72:634–46. doi: 10.1111/j.1365-2125.2011.04034.x
273. Muravyov AV, Yakusevich VV, Chuchkanov FA, Maimistova AA, Bulaeva SV, Zaitsev LG. Hemorheological efficiency of drugs, targeting on intracellular phosphodiesterase activity: *in vitro* study. *Clin Hemorheol Microcirc.* (2007) 36:327–34.
274. Zhang Q, Wang G, Yuan W, Wu J, Wang M, Li C. The effects of phosphodiesterase-5 inhibitor sildenafil against post-resuscitation myocardial and intestinal microcirculatory dysfunction by attenuating apoptosis and regulating microRNAs expression: essential role of nitric oxide syntheses signaling. *J Transl Med.* (2015) 13:177. doi: 10.1186/s12967-015-0550-9
275. Magny E, Le Petitcorps H, Pociumban M, Bouksani-Kacher Z, Pautas É, Belmin J, et al. Predisposing and precipitating factors for delirium in community-dwelling older adults admitted to hospital with this condition: a prospective case series. *PLoS ONE.* (2018) 13:e0193034. doi: 10.1371/journal.pone.0193034
276. Jickling GC, Liu D, Ander BP, Stamova B, Zhan X, Sharp FR. Targeting neutrophils in ischemic stroke: translational insights from experimental studies. *J Cereb Blood Flow Metab.* (2015) 35:888–901. doi: 10.1038/jcbfm.2015.45
277. Provencio JJ, Altay T, Smithason S, Moore SK, Ransohoff RM. Depletion of Ly6G/C(+) cells ameliorates delayed cerebral vasospasm in subarachnoid hemorrhage. *J Neuroimmunol.* (2011) 232:94–100. doi: 10.1016/j.jneuroim.2010.10.016
278. Herz J, Sabellek P, Lane TE, Gunzer M, Hermann DM, Doeppner TR. Role of neutrophils in exacerbation of brain injury after focal cerebral ischemia in hyperlipidemic mice. *Stroke.* (2015) 46:2916–25. doi: 10.1161/STROKEAHA.115.010620
279. Lee PY, Wang JX, Parisini E, Dascher CC, Nigrovic PA. Ly6 family proteins in neutrophil biology. *J Leukoc Biol.* (2013) 94:585–94. doi: 10.1189/jlb.0113014
280. Hu F, Wang Y, Gong K, Ge G, Cao M, Zhao P, et al. Protective effects of drag-reducing polymers on ischemic reperfusion injury of isolated rat heart. *Clin Hemorheol Microcirc.* (2016) 62:1–11. doi: 10.3233/CH-151925
281. Bragin DE, Peng Z, Bragina OA, Statom GL, Kameneva MV, Nemoto EM. Improvement of impaired cerebral microcirculation using rheological modulation by drag-reducing polymers. *Adv Exp Med Biol.* (2016) 923:239–44. doi: 10.1007/978-3-319-38810-6_32
282. Bragin DE, Kameneva MV, Bragina OA, Thomson S, Statom GL, Lara DA, et al. Rheological effects of drag-reducing polymers improve cerebral blood flow and oxygenation after traumatic brain injury in rats. *J Cereb Blood Flow Metab.* (2017) 37:762–75. doi: 10.1177/0271678X16684153
283. Subramani K, Raju SP, Chu X, Warren M, Pandya CD, Hoda N, et al. Effect of plasma-derived extracellular vesicles on erythrocyte deformability in polymicrobial sepsis. *Int Immunopharmacol.* (2018) 65:244–47. doi: 10.1016/j.intimp.2018.10.011
284. Sorkin R, Bergamaschi G, Kamsma D, Brand G, Dekel E, Ofir-Birin Y, et al. Probing cellular mechanics with acoustic force spectroscopy. *Mol Biol Cell.* (2018) 29:2005–11. doi: 10.1091/mbc.E18-03-0154

Conflict of Interest Statement: The authors declare that the research was conducted in the absence of any commercial or financial relationships that could be construed as a potential conflict of interest.

Copyright © 2019 Erdener and Dalkara. This is an open-access article distributed under the terms of the Creative Commons Attribution License (CC BY). The use, distribution or reproduction in other forums is permitted, provided the original author(s) and the copyright owner(s) are credited and that the original publication in this journal is cited, in accordance with accepted academic practice. No use, distribution or reproduction is permitted which does not comply with these terms.

frontiers in Neuroscience

REVIEW
published: 20 August 2019
doi: 10.3389/fnins.2019.00864

Involvement of Epigenetic Mechanisms and Non-coding RNAs in Blood-Brain Barrier and Neurovascular Unit Injury and Recovery After Stroke

*Svetlana M. Stamatovic[1], Chelsea M. Phillips[2], Gabriela Martinez-Revollar[1], Richard F. Keep[3,4] and Anuska V. Andjelkovic[1,3]**

[1] Department of Pathology, University of Michigan Medical School, Ann Arbor, MI, United States, [2] Neuroscience Graduate Program, University of Michigan Medical School, Ann Arbor, MI, United States, [3] Department of Neurosurgery, University of Michigan Medical School, Ann Arbor, MI, United States, [4] Department of Molecular Integrative Physiology, University of Michigan Medical School, Ann Arbor, MI, United States

OPEN ACCESS

Edited by:
Marietta Zille, Universität zu Lübeck, Germany

Reviewed by:
Yun Jiang, University of Lübeck, Germany
Megan Bourassa, New York Academy of Sciences, United States

***Correspondence:**
Anuska V. Andjelkovic
anuskaa@med.umich.edu

Specialty section:
This article was submitted to Neurodegeneration, a section of the journal Frontiers in Neuroscience

Received: *14 May 2019*
Accepted: *31 July 2019*
Published: *20 August 2019*

Citation:
Stamatovic SM, Phillips CM, Martinez-Revollar G, Keep RF and Andjelkovic AV (2019) Involvement of Epigenetic Mechanisms and Non-coding RNAs in Blood-Brain Barrier and Neurovascular Unit Injury and Recovery After Stroke. Front. Neurosci. 13:864. doi: 10.3389/fnins.2019.00864

Cessation of blood flow leads to a complex cascade of pathophysiological events at the blood-vascular-parenchymal interface which evolves over time and space, and results in damage to neural cells and edema formation. Cerebral ischemic injury evokes a profound and deleterious upregulation in inflammation and triggers multiple cell death pathways, but it also induces a series of the events associated with regenerative responses, including vascular remodeling, angiogenesis, and neurogenesis. Emerging evidence suggests that epigenetic reprograming could play a pivotal role in ongoing post-stroke neurovascular unit (NVU) changes and recovery. This review summarizes current knowledge about post-stroke recovery processes at the NVU, as well as epigenetic mechanisms and modifiers (e.g., DNA methylation, histone modifying enzymes and microRNAs) associated with stroke injury, and NVU repair. It also discusses novel drug targets and therapeutic strategies for enhancing post-stroke recovery.

Keywords: blood brain barrier, neurovascular unit, stroke injury, inflammation, DNA methylation, histone deacetylases, microRNA, non-coding RNA

INTRODUCTION

Stroke is defined as an abrupt onset of focal or global neurological symptoms caused by a blockage of cerebral vessels (ischemic stroke), rupture of blood vessels (hemorrhage), or transient occlusion of small blood vessels (transient ischemic attack). It is particularly prevalent in the aging population, with people over 65 years old accounting for ∼75% of all registered cases (Hollander et al., 2003). Ischemic stroke is further subdivided based on the caliber of occluded vessels into macro- and microvascular (i.e., lacuna stroke), and based on the origin of clot-causing blockage into (a) thrombotic stroke where clot form inside brain blood vessels, and (b) thromboembolic/embolic stroke where clots form elsewhere in the body and travel toward and lodge in brain blood vessels (Reed et al., 2014; Topcuoglu et al., 2018; Tsai et al., 2018).

Pathophysiologically, cessation of blood flow leads to a complex cascade of events at the blood-vascular-parenchymal interface which evolves over time and space, and results in damage to neural

cells and edema formation (Dirnagl et al., 1999; Allen et al., 2012). The central events in the hyperacute phase (within minutes and up to 6 h) include compromised mitochondrial function, anaerobic glycolysis, decreased pH (acid condition), impaired ATP production and reduced ion pump activity. As a consequence, cells swell and die, predominantly due to accumulation of lactic acid, ions (Ca^{2+} and Na^{+}) and increased water influx (Dirnagl et al., 1999; Ginsberg, 2008; Nagy and Nardai, 2017).

There follows a cascade of events in the acute and subacute phase (hours to 7 days), including blood-brain barrier (BBB), and neurovascular unit (NVU) damage characterized by mitochondrial failure, robust production of reactive oxygen species (ROS) (superoxide O_2, hydrogen peroxide, and peroxynitrite), excitotoxicity (release of glutamate from dying neurons), activation of matrix metalloproteinases (MMP2, astrocytes; MMP3, MMP9 endothelial cells and neutrophils), BBB damage triggering inflammation and blood cell infiltration (neutrophils, monocytes) that can lead to further cell death, and cellular and vasogenic edema (Enzmann et al., 2013; Posada-Duque et al., 2014; Sifat et al., 2017). The secondary damage mostly takes place in the penumbra surrounding the core infarct and its progression can extend into the chronic phase after stroke.

Paralleling these injury processes, there is activation of endogenous protective and repair mechanisms that include vascular remodeling, angiogenesis, and neurogenesis (Chopp et al., 2007; Venna et al., 2014). The degree of these ongoing repair processes on one side and persistent inflammation/damaging processes on the other determines stroke recovery and the potential risk of another stroke.

There is mounting evidence on the importance of epigenetic factors in stroke. The purpose of this review is to examine how such factors impact the cerebrovasculature in stroke injury and recovery, focusing on effects at the BBB, and NVU. There is debate over whether non-coding RNAs should be included as an epigenetic mechanism and this review will cover their effects as well as other epigenetic mechanisms.

THE BLOOD-BRAIN BARRIER AND NEUROVASCULAR UNIT IN STROKE

The blood-brain barrier is a highly complex and dynamic barrier, formed by an interdependent network of brain capillary endothelial cells, endowed with barrier properties. The BBB strictly regulates paracellular permeability due to the presence of tight junctions (TJs) between endothelial cells. Those TJs are built by intricate interactions between transmembrane proteins (claudins -5, -3, -1, -12, occludin, and JAM-A), important for paracellular space occlusion, scaffolding proteins (ZO-1, -2), and the actin cytoskeleton vital for physical support and TJ function (Daneman et al., 2010; Stamatovic et al., 2016). The transcellular interactions of claudin-5 play the major role in occluding the paracellular space (Nitta et al., 2003; Ohtsuki et al., 2007). Any loosening of its adhesive interactions directly affects BBB integrity and increases paracellular permeability. The BBB role of other claudins with lower expression is still uncertain and under investigation (Tietz and Engelhardt, 2015; Sladojevic et al., 2019). BBB function is also dependent on the perivascular microenvironment, which contains cells (e.g., pericytes, astrocytes, and perivascular macrophages), neuronal endings and tissue unique extracellular matrix (Mae et al., 2011; Muoio et al., 2014). Because of this functional integration, nearly two decades ago, the concept of a BBB was broadened to a new structure, the NVU.

The neurovascular unit is composed of BBB-endowed endothelial cells and a perivascular milieu composed from cells including pericytes, smooth muscle cells, astrocytes, perivascular macrophages/microglia, neurons/neuronal endings, and extracellular matrix. The NVU mediates neurovascular coupling, modulating vessel tone (Mae et al., 2011; Muoio et al., 2014). These intimately and reciprocally linked cells and matrix generate a complex structure that regulates exchange between blood and brain, oxygen and nutrient delivery, and regional cerebral blood flow. It is essential for maintaining circulatory and brain homeostasis.

In stroke, blood-brain barrier, and neurovascular unit dysfunction actively contributes to injury pathogenesis, being a "solid substrate" for ongoing injuring processes (oxidative stress, inflammation, and cytotoxicity), contributing to ischemic core (infarct) formation in the acute phase of stroke, and facilitating the progression of injury in the subacute and chronic phases. For example, in the early (acute) phase of stroke, NVU dysfunction is characterized by disruption of BBB integrity/BBB breakdown (disassembly of TJ complex, decreases in the TJ proteins claudin-5, occludin, and ZO-1) that leads to vasogenic brain edema, a life-threatening acute stroke complication (Bauer et al., 2010; Zehendner et al., 2011; Sladojevic et al., 2014). The cell components of the NVU undergo a series of transformations during injury. Brain endothelial cells, for example, are affected very early by cytotoxic effects with dysfunction of ion channels and transporters (e.g., Na^{+}-K^{+}-Cl^{-} cotransporter, and Na^{+}/H^{+} exchanger), release of extracellular vesicles and conversion of brain endothelial cells toward a proinflammatory and prothrombotic phenotype due to upregulation of protease-activated receptor 1 (PAR-1), tissue factor, and matrix metalloproteinases (MMPs) (Zhu et al., 2008; Bauer et al., 2010; Yamashita and Abe, 2011; Chen et al., 2015). The proinflammatory phenotype of brain endothelial cells involves an upregulation of endothelial adhesive molecules (ICAM-1, VCAM-1, P-, and E- selectins) that guide leukocyte infiltration in the acute inflammatory phase response and T and B cells infiltration in the late phase (Kleinschnitz et al., 2013; Zhou et al., 2013; Sladojevic et al., 2014). Overall, inflammation is thought to worsen acute ischemic injury, contributing to chronic focal inflammation and restricting functional recovery. However, inflammation is also involved in tissue repair.

In the hyperacute phase after stroke, pericytes may be involved in vasoconstriction, causing capillary occlusion (no-reflow phenomenon), while later, by switching to pro-inflammatory phenotype, they may enhance BBB permeability, and brain edema formation (Hall et al., 2014; Underly et al., 2017). Ischemia triggers a series of damaging reactions in astrocytes including mitochondrial dysfunction, energy depletion, ion

disequilibrium, increased glutamate and Ca^{2+}, aquaporin 4 (AQP4) channel activation, increased water permeability, and cell swelling (Friedman et al., 2009; Ito et al., 2009; Hertz et al., 2014; Mogoanta et al., 2014). It results in the release of oxidative stress products and inflammatory cytokines/chemokines (IL1, IL6, IL15, CCL2, CXCL1, CXCL10, CXCL12, and IP-10), proinflammatory associated small molecules [S100 Ca^{2+}-binding protein B (S100B) and nitric oxide (NO)] that enhance the inflammatory post-stroke response (Yamashita et al., 2000; Hill et al., 2004; Mori et al., 2008; Shin et al., 2014; Liu H. et al., 2015; Chen et al., 2018).

Perivascular macrophages and microglia play an important role in the stroke-induced inflammatory response via production of proinflammatory cytokines (IL1|*upbeta* TNFα IL6, IL12) and ROS (Drake et al., 2011; Liu H. et al., 2015; Wu et al., 2016; He et al., 2019). They trigger the first line of inflammation at the NVU in the acute phase of stroke. Notable changes also occur in the extracellular matrix. At early time points (within hours), there is MMP-related basement membrane degradation with reductions in agrin, SPARC, perlecan, laminin, and fibronectin (Sole et al., 2004; Castellanos et al., 2007; Lee et al., 2011; Ji and Tsirka, 2012; Lloyd-Burton et al., 2013). This ultimately leads to increased BBB disruption, accumulation of new extracellular matrix proteins (i.e., chondroitin sulfate proteoglycan neurocan and osteopontin) and leakage of plasma proteins, such as fibrinogen, into the CNS. This mediates inflammation, edema, and potentially hemorrhagic transformation (**Figure 1**).

THE BLOOD-BRAIN BARRIER AND NEUROVASCULAR UNIT IN STROKE RECOVERY

In post-stroke conditions, the NVU has the ability and capacity for remodeling, and this is becoming a very important therapeutic target for enhancing stroke recovery. Remodeling involves complex and tightly tuned interactions between neurons, glial and brain endothelial cells, recruitment of endothelial and neural progenitor cells, and inflammatory blood cells (monocytes, T and B lymphocytes), governing new blood vessel formation, glial cell remodeling of extracellular matrix, for augmented improvement of the NVU, and neurological recovery.

Blood-brain barrier recovery involves *de novo* synthesis of junctional proteins and reestablishing barrier integrity to reduce further brain damage. It is important to highlight that BBB recovery is limited and complete pre-stroke impermeability is difficult to achieve. Ongoing angiogenic processes, as well as defects in the structural repair (e.g., imbalance in the synthesis of claudins essential for TJ function) play a role in the prolonged BBB leakiness days after stroke (Yang Y. et al., 2015; Xu H. et al., 2017; Sladojevic et al., 2019). Whether there are benefits of BBB post-stroke leakage is still a controversial issue. From the perspective of stroke treatment, it may facilitate brain drug delivery. However, it may allow uncontrolled entry of blood components into brain fueling inflammation.

In neurovascular unit remodeling after stroke, cellular elements have important roles in recovery. Pericytes are a

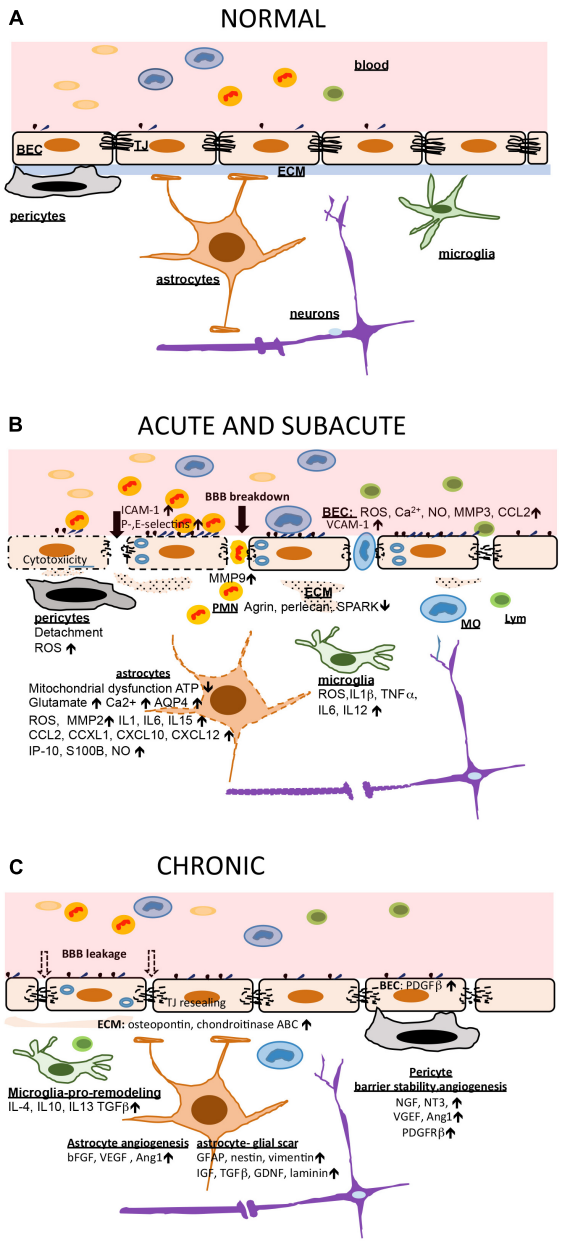

FIGURE 1 | Blood brain barrier (BBB) and neurovascular unit (NVU) in ischemic injury and post-stroke recovery. **(A)** In healthy conditions, the BBB is intact and other NVU components, including the extracellular matrix (ECM), support and preserve brain homeostasis. **(B)** Cessation of blood flow triggers a chain reaction at the BBB and NVU. The early events are mostly characterized by cytotoxicity, mitochondrial dysfunction and accumulation of ROS which further cause BBB breakdown (tight junction, TJ, disruption), neuronal injury guided by astrocytes, and triggering an acute inflammatory response. Brain endothelial cells (BEC) increase adhesion receptor expression allowing leukocyte (predominantly polymorphonuclear neutrophils; PMNs) entry which adds to BBB injury. Microglia and astrocytes produced large amount of proinflammatory cytokines and chemokines amplifying inflammation. Early pericyte detachment support BBB instability and breakdown. This support vasogenic brain edema formation. **(C)** The subacute and chronic phase of stroke is characterized by increased second wave of inflammation with monocyte (MO) and lymphocyte (Lym) entry but also

(Continued)

FIGURE 1 | Continued
ongoing repair processes (BBB recovery and angiogenesis). Microglia become source of anti-inflammatory cytokines and have a role in phagocytosing dead cells. Astrocytes are a source of growth factors supporting angiogenesis, and also source of extracellular matrix building a gliotic scar. Pericytes establish interactions with BEC, supporting barrier stabilization and new vessel formation. The BBB, with new TJ protein synthesis, undergo partial sealing.

source of neurotrophins and have a role in stabilizing the BBB and protecting brain parenchyma from leukocyte infiltration (Shimizu et al., 2012; Yang et al., 2017). They also promote angiogenesis and neurogenesis. Astrocytes undergo structural and functional transformation (reactive gliosis), manifested as increased expression of the intermediate filament protein glial fibrillary acidic protein (GFAP), cell proliferation, and synthesis of extracellular matrix to form the glial scar and demarcate the infarct necrotic core. Higher production of GFAP, nestin and vimentin in NVU negatively affect cell-cell communication at NVU during the subacute and chronic phase of stroke, while production of insulin-like growth factor, transforming growth factor β (TGFβ), and other growth factors as well as laminin by astrocytes enhance NVU recovery processes (Cekanaviciute et al., 2014; Yao et al., 2014; Okoreeh et al., 2017). During post-stroke NVU recovery, microglia transform to a M2 pro-remodeling phenotype, releasing anti-inflammatory cytokines (e.g., IL10) and growth factors. They switch astrocytes to anti-inflammatory phenotype, supporting clean-up phagocytosis, diminishing leukocyte-endothelial cells interaction, decreasing expression and activation of cytokine receptors, promoting NO-induced vasodilatation, and reducing ROS production and oxidative stress by inhibiting NADPH oxidase (Weston et al., 2013; Brifault et al., 2015; Yang Y. et al., 2015).

The extracellular matrix also plays an important role in NVU remodeling and stroke recovery. Interaction between the matrix and its receptors on NVU cells regulate cell survival, migration and focal bioavailability of growth factors essential for repair processes, including angiogenesis and neurogenesis. For example, while osteopontin is normally produced in development, its activity post-stroke, via αvβ3 receptors on astrocytes, promotes astrocyte migration and glial scar formation (Ellison et al., 1999; Suzuki et al., 2010). On the other hand, fibrinogen shifts its mechanism of action from the αvβ3 receptor to regulating transforming growth factor -β on astrocytes promoting reactive astrocytosis (Schachtrup et al., 2010; Beck and Schachtrup, 2012). Synthesis and upregulation of new extracellular matrix components like chondroitinase ABC may rescue the "injury type" of extracellular matrix by degrading proteoglycans (neurocan) that affect neuronal growth to further enhance the recovery processes (Hill et al., 2012; Chen et al., 2014; **Figure 1**).

Overall, targeting the NVU in stroke may have long lasting effects by preventing tissue damage in the early hours after stroke and enhancing ongoing recovery processes chronically after stroke. It is, however, very important to highlight that the functional response of NVU cells to stroke as well as the degree of recovery post-stroke will depend on the functional status of the NVU before the stroke which is affected by many co-morbidities (e.g., age, diabetes and hypertension).

EPIGENETIC REGULATION OF BBB AND NVU RECOVERY AFTER STROKE

An overview of decades of stroke research and a variety of identified targets, has unfortunately highlighted that current therapeutic approaches to limit ischemic brain injury have almost all failed, the exception being reperfusion. In recent years, approaches have started to shift toward preventing injury progression and enhancing repair and regeneration after stroke. Targets include inflammation and injury progression, neuronal repair to prevent ischemic cell-death and cerebrovascular remodeling that may prevent further injury progression. The NVU has a focal position in these new approaches to treat stroke.

How to approach treatment of stroke recovery when many conventional approaches (e.g., anti-oxidative, anti-inflammatory) have failed? It has to be taken into consideration that the recovery process is complex and tightly regulated. Many genes are involved in the temporal and spatial regulation of restoration of function with a high degree of individual variation that may depend upon multiple factors. An emerging field, epigenetics, holds promise for a better understanding of what regulates recovery after stroke and the potential success of modulating that process.

Epigenetics is defined as the interaction between environmental factors and the genome that may be heritable and modified gene expression or phenotype without changes in DNA sequences (Hendrich and Willard, 1995). Epigenetic mechanisms (e.g., DNA methylation, post-translational modification of histones) provide an additional level of tight control at the transcriptional level that differentially modifies gene expression and protein activity. In addition, cells possess a powerful machinery in non-coding RNAs, particularly microRNAs (miRs), that regulates gene expression at the post-transcriptional level. Coordinate and cooperative activity of epigenetics factors and miRs form circuits that regulate gene expression profiles and support cell function. Considering the far-reaching effects of epigenetics and miRs on gene regulation, these factors may have a key role in regulating plasticity during repair after stroke and be a key target for enhancing NVU recovery. In this review, we highlight some of the mechanisms that take place at the NVU and are involved in epigenetic and miRs remodeling of the NVU in stroke.

DNA METHYLATION

DNA methylation is an epigenetic mechanism characterized by covalent addition of methyl (CH_3) group to DNA that modifies gene function and expression. The best characterized methylation process occurs on the 5-carbon of the cytosine ring resulting in 5-methylcytosine (5-mC). 5-mC is found exclusively as paired

symmetrical methylation of a CpG site where cytosine nucleotide is located next to a guanidine nucleotide (Zeng and Chen, 2019). In genomic DNA, most CpG sites are methylated while CpG islands (clusters) located in proximity to promoter regions endure unmethylated allowing the regulation of gene expression, transcriptional repression (Bird, 1986). DNA methylation occurs via a family of enzymes, the DNA methyltransferases (DNMTs). Five types of DNA methyltransferases have been described: DNMT1- maintains existing methylation patterns following DNA replication, DNMT2 -which can act as a nuclear as well tRNA methytransferase, DNMT3a and DNMT3b responsible for establishing *de novo* methylation patterns and DNMT3L which does not mediate methylation but interacts with histone deacetylase 1 (HDAC1) (Hsieh, 1999; Aapola et al., 2002; Goll and Bestor, 2005; Goll et al., 2006; Ren et al., 2018). It is also important to highlight that DNMT may regulate the expression of certain miRs by direct methylation of miR promoter regions, adding additional layer of DNMT activity at the post-transcriptional level via miRs (Dakhlallah et al., 2013; Nicholson et al., 2017).

Early research investigating epigenetic changes following middle cerebral artery occlusion (MCAO) in mice demonstrated upregulated global DNA methylation within the brain, and genetic or pharmacologic DNMT inhibition decreased stroke severity (Endres et al., 2000). Within the NVU, altered DNA methylation is associated with both BBB injury and recovery, suggesting a biphasic pattern of post-stroke DNA methylation. Mouse MCAO leads to hypermethylation of the tissue inhibitor of metalloproteinase 2 (TIMP2) promoter. The resulting decrease in TIMP2 expression is associated with increased matrix metalloproteinase 9 (MMP9) activity and BBB hyperpermeability, with DNMT inhibition rescuing BBB permeability (Mondal et al., 2019). However, increased DNMT activity post-stroke is also implicated in angiogenesis. Oxygen-glucose deprivation (OGD) in cerebral endothelial cells promotes hypermethylation of the thrombospondin-1 promoter. As thrombospondin-1 inhibits angiogenesis, such promoter hypermethylation suggests DNMT activity promotes post-stroke angiogenesis (Hu et al., 2006). While research investigating post-stroke DNMT activity within the NVU is limited, current studies suggest a dual role of DNMTs within the NVU. An intriguing recent clinical study by Baccarelli et al. (2010) found that blood DNA hypomethylation was associated with a high risk stroke occurrence and total mortality, suggesting that DNMT activity could be a potential biomarker in post-stroke recovery.

To fully delineate the effects of post-stroke DNMT activity, future research must investigate: (1) specific genes with altered methylation patterns, and (2) the pattern of DNA methylation over time. As post-stroke DNMT activity is implicated in both BBB injury and recovery, investigating post-stroke methylation temporal patterns will begin to elucidate the complex roles of DNMTs in ischemic stroke.

HISTONE MODIFICATIONS

DNA wraps around histones forming nucleosomes and creating organized chromatin. Histones are octameric proteins containing modifiable N-terminal residues and post-translational histone modifications alter chromatin accessibility, leading to either transcriptional activation or repression. One well-characterized histone modification is the addition or removal of an acetyl group to lysine residues. Generally, histone acetyltransferases (HATs) add acetyl groups to lysine residues allowing transcription, as the acetyl group disrupts the interaction between the histone residue and DNA. Histone deacetylases (HDACs) remove acetyl groups, leading to transcriptional repression. Ultimately, a balance between HAT and HDAC activity regulates histone acetylation (Narlikar et al., 2002; Li et al., 2007; Kassis et al., 2017). Another form of histone modification is methylation. Methyl group are added on histone N terminal tails at either lysine or arginine residues (Klose and Zhang, 2007). The combination of methylation/demethylation pattern and interplay between lysine or arginine methylases and demethytransferases governs the transcriptional activation/repression of certain genes (Klose and Zhang, 2007; Migliori et al., 2010).

The HDAC superfamily consists of 18 different subtypes in four different classes. Expression of different HDACs within the brain varies by cell type, and mouse MCAO alters HDAC expression in a cell-specific manner (Baltan et al., 2011). Within the NVU, ischemic stroke upregulates astrocytic expression of HDAC2 and HDAC8 (Baltan et al., 2011; Demyanenko et al., 2018). Interestingly, ischemic stroke prominently upregulates HDAC2 in astrocytic processes and end-feet, suggesting HDAC2 affects the NVU post-stroke (Baltan et al., 2011). Current research has demonstrated that increased HDAC expression leads to BBB injury, as HDAC inhibition rescues BBB permeability observed in rodent models of ischemic stroke, including those with increased stroke severity (Park and Sohrabji, 2016; Shi et al., 2016). OGD upregulates endothelial HDAC9 expression and is associated with decreased expression of TJ proteins, such as ZO-1, claudin-5, and occludin. Genetically targeting HDAC9 pre-OGD rescues altered TJ protein expression in endothelial cells (Shi et al., 2016). Other studies indicate post-stroke HDAC expression induces inflammation and oxidative injury. Although contextualized within post-stroke neuroprotection, these studies potentially indicate a mechanism through which altered HDAC expression contributes to barrier injury as well (Wang et al., 2012; Patnala et al., 2017). HDAC inhibitors show a variety of effects after stroke. Valproic acid and sodium butyrate (class I, IIa and III inhibitor) repressed the nuclear translocation of NFκB subunit p65, mitigate MMP9 activity and restore the BBB integrity after stroke by regulating the expression of tight junction proteins, claudin-5, and ZO-1 (Wang et al., 2011; Park and Sohrabji, 2016). Non-specific HDAC inhibition also switches the pro-inflammatory microglial response to anti-inflammatory (Patnala et al., 2017). Likewise, pre-OGD HDAC inhibition promotes anti-oxidative enzyme expression in macrophages in a histone-independent manner (Wang et al., 2012).

While most studies focus on enzyme-mediated changes in histone acetylation, another mechanism through which histone acetylation may be altered in ischemic stroke is through histone eviction. Exposing endothelial cells to hypoxic conditions results in histone eviction from specific promoter regions, such as the eNOS promoter, and replacement with hypoacetylated histones

(Fish et al., 2010). Overall, studies investigating the role of histone acetylation in post-stroke recovery indicate that increased HDAC expression and histone hypoacetylation promotes BBB injury.

The specific pattern of histone methylation, and activity of histone lysine methylases and demethylases are important for stroke occurrence and regulation of stroke injury and recovery (Chisholm et al., 2015; Miao et al., 2015; Chakravarty et al., 2017). For example, the pattern of histone 3 methylation of lysine 4 or 9 residues in astrocytes, regulates different gene expression and may regulate the severity of stroke in rodents (Chisholm et al., 2015). The activity of histone lysine methylases (G9a lysine methylases) and demethylases (KDM4B lysine demethylases) was linked to inflammation by regulating TNFa mediated ICAM-1 and VCAM-1 expression in cerebral blood vessels and neutrophil infiltration (Choi et al., 2017). In addition, TNFa serum levels were closely correlated with H3K9Ac and H3K4me3 activity, suggesting an effect on stroke outcomes (Gomez-Uriz et al., 2014). Histone arginine methylation also plays a role in the inflammatory response after stroke. Hypomethylation of histone arginine residues and low asymmetric dimethylarginine (ADMA) levels are associated with increased inflammation and stroke risk in a hyperhomocysteinemia rodent model (Esse et al., 2013). Furthermore, ADMA and symmetric dimethylarginine (SDMA) expression levels were reported to be linked with inflammatory mediator expression (CCL2, IL6, S100B, MMP9, and tissue inhibitor of matrix metalloproteinase-1) and the expression of these mediators and inflammation closely correlated with histone arginine methylation (Chen et al., 2012). ADMA levels are potential biomarkers for stroke injury.

Multiple HDAC inhibitors have already undergone clinical testing for a variety of diseases, with vorinostat approved for treating T cell lymphoma and panobinostat for multiple myeloma (McClure et al., 2018). A non-specific HDAC inhibitor, valproic acid, has been used for many years in the treatment of epilepsy, although there are questions over whether those effects are mediated by HDAC inhibition. The knowledge from those clinical trials may help facilitate translation of HDAC inhibitors to the clinic, as may the generation of new inhibitors of specific HDAC subtypes that might lessen drug side effects (Cao et al., 2018).

Intriguing candidates for regulating BBB and NVU recovery after stroke are the sirtuins. Sirtuins are nicotinamide adenine dinucleotide (NAD^+) dependent class III histone deacetylases, first discovered in *Saccharomyces cerevisiae* as silent information regulator 2 (Sir2). There are seven mammalian sirtuins homologs (Sirt1-7) localized in nucleus (Sirt1, Sirt6, and Sirt7), mitochondria (Sirt3, Sirt4, and Sirt5), and cytoplasm (Sirt2). Generally, they are implicated in regulating aging, metabolism and cell cycle (Inoue et al., 2007). Besides targeting histones, sirtuins (i.e., Sirt1) can interact with specific DNA binding transcription factors and coregulators (i.e., FOXO, hypoxia inducible factor 1a, PGC1a) and deacetylation of these non-histone targets are responsible for transcriptional regulation and both negative and positive regulation of target gene expression (Andreou et al., 2012; Shukla et al., 2016; Chen et al., 2019).

Epigenetic roles of sirtuins, predominantly Sirt1 and 3, are described in stroke injury via acetylation/deacetylation of targets. Limited data highlight the role of Sirt1 in neuroprotection in the settings of stroke by deacetylation and subsequent inhibition of p53- and NFkB-induced inflammatory and apoptotic pathways, regulation of microglia activity via CX3CR1, brain endothelial cell protection by inhibiting nitric oxide synthesis, and balancing Sirt3 (mitochondrial Sirt) activation after stroke injury (Yang F. et al., 2015; Sellner et al., 2016; Chen T. et al., 2018). Resveratrol, a potent activator of Sirt1, has neuroprotective effects after stroke (enhancing neurite outgrowth and synaptogenesis) and vascular protective effects, reducing the chance of recurrent stroke (Tang et al., 2017). In addition, Sirt1 regulates BBB integrity in aging and CNS infection (Castro et al., 2016; Stamatovic et al., 2019). Although the role of sirtuins in NVU and BBB recovery after stroke is still largely unexplored, emerging data on sirtuin effects on the BBB, endothelial cells, and stroke, put these molecules, and particularly Sirt1, as important targets for epigenetic modification of NVU and BBB in stroke recovery (**Table 1**).

To determine the mechanisms leading to BBB injury in ischemic stroke, future research should determine which genes have altered expression due to aberrant HDAC activity. Because both HDAC and HAT activity determine histone acetylation patterns, post-stroke HAT activity within the NVU also needs to be determined.

NON-CODING RNAs (ncRNAs)

Non-coding RNAs represent a group of untranslated regulatory RNA molecules able to modify one or more genes/protein function affecting multiple cellular pathways in biological processes. Non-coding RNAs include ribosomal RNA (rRNA), transfer RNA (tRNA), small (<200 nucleotides), and long (>200 nucleotides) RNAs. Small ncRNA include large group of miRs, piwi-interacting RNAs (piRNA), small nuclear RNAs (snRNA), small nucleolar RNAs (snoRNA), and promoter associated small RNAs. Long ncRNAs are divided into long intergenic ncRNAs, long iontronic ncRNAs, telomeric ncRNAs, pseudogene transcripts, enhancer RNAs and promoter associated long RNAs. Small and long ncRNAs differ in origin, processing and mechanisms of action (Wei et al., 2017).

MICRORNAS

MicroRNAs are a class of short (∼20–25 nucleotides) non-coding RNAs capable of regulating gene/protein expression by inhibiting translation. Located in cytoplasm, miRs build RNA-induced silencing complexes (RISCs) by binding with Argonaute (Ago) proteins. Direct binding of miR-RISCs to complementary and unique 3′ UTR (untranslated) sequence motifs on target mRNAs, leads to sequestration or degradation of the target mRNA and translational silencing. miRs have multivalent properties, targeting multiple genes, and regulating protein expression in several key cellular processes (cell differentiation, cell cycle progression and apoptosis) (Ambros, 2001; Vishnoi and Rani, 2017). miR expression and function is closely associated with and dependent on interaction with epigenetic factors

TABLE 1 | NVU HDAC cell expression profile and effect in post-stroke recovery.

	NVU cells	Target	Effect	References
	HDAC class I			
HDAC1	Neurons	?	Neurotoxic	Formisano et al., 2015; Demyanenko et al., 2018
HDAC2	Neurons Astrocytes	?PSD-95, synapsin	Regulate neuroplasticity	Formisano et al., 2015; Tang et al., 2017
HDAC3	Neurons	?	Neurotoxic	Chen et al., 2012
HDAC8	Microglia	?MMP9, Cox2/iNOS	Microglia	Demyanenko et al., 2018
	HDAC class II (a and b)			
HDAC4 (a)	Neurons BEC	HMBG1 HIF- a, VEGF CREB Nox4, MMP9	Neuronal death Angiogenesis Neurogenesis Tight junctions	He et al., 2013; Kassis et al., 2015; Zhang Q.-Y. et al., 2017
HDAC5 (a)	Neurons	Neurotoxic (HMBG1)		He et al., 2013
HDAC7 (a)	Undefined			
HDAC9 (a)	BEC	Tight junction proteins Cox2/iNOS, NFkB	BBB integrity Inflammation	Shi et al., 2016; Lu et al., 2018
HDAC6 (b)	Neurons	Nrf2	Oxidative stress	Gaisina et al., 2018
HDAC10 (b)	Undefined			
	HDAC class III			
SIRT1	BEC, astrocytes		BBB integrity angiogenesis	Zheng et al., 2018; Sun et al., 2019; Xu et al., 2019
SIRT2	Neurons	FOXO3a	Apoptosis	She et al., 2018
SIRT3	BEC, astrocytes, microglial	p53, NFkB	Oxidative stress	Chen T. et al., 2018; Yang et al., 2018
SIRT4	Neurons	FOXO	Neurotoxic	Sangaletti et al., 2017
SIRT5	BEC		Diminish BBB integrity	Diaz-Cañestro et al., 2018
SIRT6	Neurons	Nrf2		Zhang W. et al., 2017
SIRT7	Undefined	?	Post-stroke biomarker	Wong et al., 2015
	HDAC class IV			
HDAC11	Undefined	?	Neurotoxic ?	Chen et al., 2012

BEC, brain endothelial cells; NVU, neurovascular unit; HDAC, histone deacetylase; Sirt, sirtuin; PSD-95, postsynaptic density protein 95; HMBG1, high-mobility group protein 1; FOXO, forkhead box protein; HIF-a, hypoxia inducible factor-a; CREB, cAMP response element binding protein.

(DMNT and HDAC) (Dakhlallah et al., 2013; Lee et al., 2017; Nicholson et al., 2017). Together they form complex circuits for transcriptional and post-transcriptional regulation of genes. To date, ∼2000 miR family members have been identified in human, and it is assumed that miRs could regulate ∼60% of all mammalian mRNAs. The family classification is based on a common miR ancestor (Vishnoi and Rani, 2017). Family members share similar physiological function but not always primary sequence or secondary structure. miRs are linked to many disease conditions and represent both potential therapeutic targets but also biomarkers.

MicroRNA are highly differentially expressed in brain tissue and they play key roles in development, physiology, and disease. Cerebral ischemia triggers selective and temporally regulated miR expression that regulate stress responses (e.g., excitotoxicity, oxidative stress, and apoptosis) as well as a spectrum of other processes (e.g., transcription, inflammation, and angiogenesis) (Mirzaei et al., 2018). Intriguingly, miR expression in brain is mirrored by differential expression of miRs implicated in endothelial cell and vascular function, erythropoiesis, angiogenesis, neural function, and hypoxia, even several months after the onset of stroke. This suggests that miRs play role in the response to cerebral ischemia and can serve as clinical biomarkers of stroke and post-stroke injury/recovery. In stroke and post-stroke remodeling of the BBB and NVU, a spectrum of miRs are involved varying with time, cell-specific target and recovery process. Importantly, due to the ability of miRs to target multiple molecules, often one miR is found to be on the interface of ongoing angiogenesis, inflammation, and/or oxidative stress.

Several miRs play a critical role in regulating post-stroke inflammation at the NVU. miR126 is highly expressed and considered as endothelial specific. It is one of the most heavily studied miRs and it is a potent regulator of vascular inflammation. miR126 modulates/downregulates expression of an adhesion molecule, VCAM, and controls leukocyte extravasation into brain (Yuan et al., 2016). Similarly, miR31 and miR17-3p regulate/antagonize the expression of E-selectins and ICAM-1 reducing neutrophil adhesion and post-stroke leukocyte infiltration (Staszel et al., 2011). miR98 and let-7g decrease leukocyte adhesion to and migration across the BBB (Rom et al., 2015). Two other miRs, miR155 and let-7, also have anti-inflammatory effects. They regulate expression of molecules important in stroke recovery including IL4, IL10, and BDNF in microglia and down-regulate iNOS and IL6 (Rom et al., 2015; Xiang et al., 2017; Greco et al., 2018; Lu et al., 2018). Intriguingly, miR155 has proinflammatory effects in the brain after stroke. It regulates macrophage signaling, differentiation and proinflammatory phenotype by diminishing the balance between suppressor of cytokine signaling 1 (SOCS-1) protein,

and upregulating of inflammatory molecules such as iNOS (Lopez-Ramirez et al., 2014; Liu Y. et al., 2015; Cerutti et al., 2016). miR155 also stimulates expression of TNFα and IL1β via NFκB and toll-like receptor 4 (TLR4), and downregulation of myeloid differentiation primary response gene (MyD88) (Tarassishin et al., 2011). Furthermore, administration of miR155 antagomir decreased post-stroke inflammation, reduced neuronal apoptosis and improved neurological deficits (Pena-Philippides et al., 2016). Similar to the effect of miR155, an antagomir for miR210 decreased expression of proinflammatory cytokines IL6, TNFα, IL1β, CCL2, and CCL3 reducing the neurological impairment, putting miR210 as potent regulator of inflammation during stroke recovery (Huang et al., 2018).

Intriguingly, miRs are also associated with inflammasome activity. The inflammasome is a cytosolic complex that plays a role in ischemic stroke by promoting inflammatory and cell death mechanisms. miR223 has a role in suppressing the NLRP3 inflammasome by binding to its 3′ UTR sites and consequent inhibition of IL1β and caspase-1 activity, reducing brain edema and improving neurological score (Maitrias et al., 2017). The miRs, miR124, miR132a and 149-5a also have anti-inflammatory effects after stroke by inhibiting CCAAT/enhanced-binding protein (C/EBP-alpha) and downstream factor PU.1, promoting microglia quiescence, and suppressing activation of microglia and consequently reducing the expression of proinflammatory cytokines and suppressing proinflammatory mediators like NFκB, TNFα, and IL6 (Wanet et al., 2012; Yu et al., 2017; Wan et al., 2018).

Nuclear factor erythroid 2-related factor 2 (Nrf2) is a master regulator of anti-oxidant defense mechanisms that plays a critical role in limiting ischemia-induced brain injury, including BBB disruption (Alfieri et al., 2013). Papp et al. (2012) examined the Nrf2 interactome and identified 85 miRs involved in post-transcriptional regulation of Nrf2 (Wang et al., 2016). After transient MCAO in mice, Wang et al. (2016) found a marked increase in miR93 and that a miR93 antagomir reduced brain injury. The antagomir markedly increased brain Nrf2 levels as well as hemeoxygenase-1, a protein regulated by Nrf2; i.e., miR93 acts as a repressor of Nrf2, and antagonizing its actions may be a therapeutic approach for stroke (Wang et al., 2016).

Another miR, miR1 is indicated to have an important role in regulating neurotropic factors, apoptosis, neurogenesis and the generation of synapses (Talebi et al., 2019). Indicated as being an important target in treating neurodegenerative diseases as well myocardial infraction, miR1 suppression has a protective effect in stroke by reducing BBB permeability and brain edema and improving neurological deficits (Talebi et al., 2019). Similarly, miR15a is considered as a master regulator of cerebral vascular dysfunction after ischemic stroke. Intriguingly, after ischemic episodes, PPARγ and PPARd modulate miR15a expression at the cerebrovasculature, reducing injury and enhancing vascular recovery (Yin et al., 2010, 2013). Therefore, targeting miR15a is a promising strategy for protecting the BBB and the NVU after stroke.

Other processes regulated by miRs in post-stroke recovery include angiogenesis and BBB stability. In post-stroke associated angiogenesis, the miR expression profile is associated with the degree of post-stroke angiogenisis. Some miRs regulating angiogenic processes include miR225, miR335, miR139-5p, miR203, miR708, miR193 and miR494, which are predominantly downregulated, as well as miR224, miR210, miR204, miR322, miR100, miR450a, miR322, miR331 and miR101a which are upregulated in post-stroke angiogenesis (Lou et al., 2012; Yin et al., 2015). These miRs regulate expression of fibroblast growth factor (bFGF) and vascular endothelial growth factor (VEGF) in endothelial cells (miR15a and miR126), tube formation (miR139, miR335, and miR107), cell migration (miR210), targeting Dicer-1 and consequently VEGF (miR107) (Tome et al., 2011; Ye et al., 2014; Li et al., 2015; Zhu et al., 2017). One recent study indicated that functional polymorphism in the 3′ UTR site of angiopoietin-1 gene affects the binding sites of miR211, and can reduce the risk of stroke occurrence, while miR129-5p ameliorates inflammation and promotes revascularization after stroke (Chen et al., 2010; Li X.Q. et al., 2017).

Evidence indicates that several miRs are critical in regulating BBB integrity after stroke. A miR491-5p decrease leads to increased risk of cerebral ischemia and worsening stroke-induced BBB disruption by directly regulating expression of MMP9 (Yan et al., 2011). Suppression of miR155 2 days after ischemia in an experimental mouse stroke model decreased vascular leakage and promoted revascularization through stabilization of TJs and preservation of the BBB (Greco et al., 2018). Two recent studies showed that inhibiting miR130a in cerebral ischemia reduced BBB permeability, brain edema and enhanced neurological function by targeting Homeobox1 (Chen et al., 2010; Saito et al., 2011). A recent study by Yao et al. (2018) showed that miR21 suppresses MAP2K3 expression in brain endothelial cells regulating barrier permeability and exacerbation of brain edema and ischemic injury. miR149-5p also regulates BBB stability and NVU remodeling after cerebral ischemia. In addition, a miR149 polymorphism was reported to be associated with ischemic stroke pathogenesis (Jeon et al., 2013). A recent study by Wan et al. (2018) reported that miR149-5p targets the sphingosine phosphate receptor 2 (S1PR2) and regulates pericyte migration and N-cadherin expression. Thus, treatment with an agomir of miR149-5p attenuated BBB permeability and improved outcomes after transient MCAO.

A number of miRs are considered as cell specific. In the line with that, miRs mostly involved in regulating endothelial cell function include miR126, miR17-92, miR23-27-24, miR222-22, miR99, miR20b, miR101, and Let-7b (Mishra and Singh, 2013). Astrocytes at the NVU are regulated by miR29b, that regulates AQP4 expression, as well as by miR130a, and miR320a (Sepramaniam et al., 2012; Song et al., 2015; Wang et al., 2015). miR130a is expressed in brain endothelial cells and pericytes. It regulates occludin expression via HoxA5 as well MMP2 and -9 (Wang et al., 2018). Intriguingly, miR130a is downregulated after ischemic conditioning in astrocytes and pericytes which may indirectly affect TJ complex structure and brain endothelial barrier permeability. A summary of miR activities at the BBB and post-stroke NVU recovery is presented in **Figure 2**.

An important aspect of miRs in stroke and post-stroke recovery is whether changes in their circulating levels reflect the degree/type of injury and potential recovery. For example,

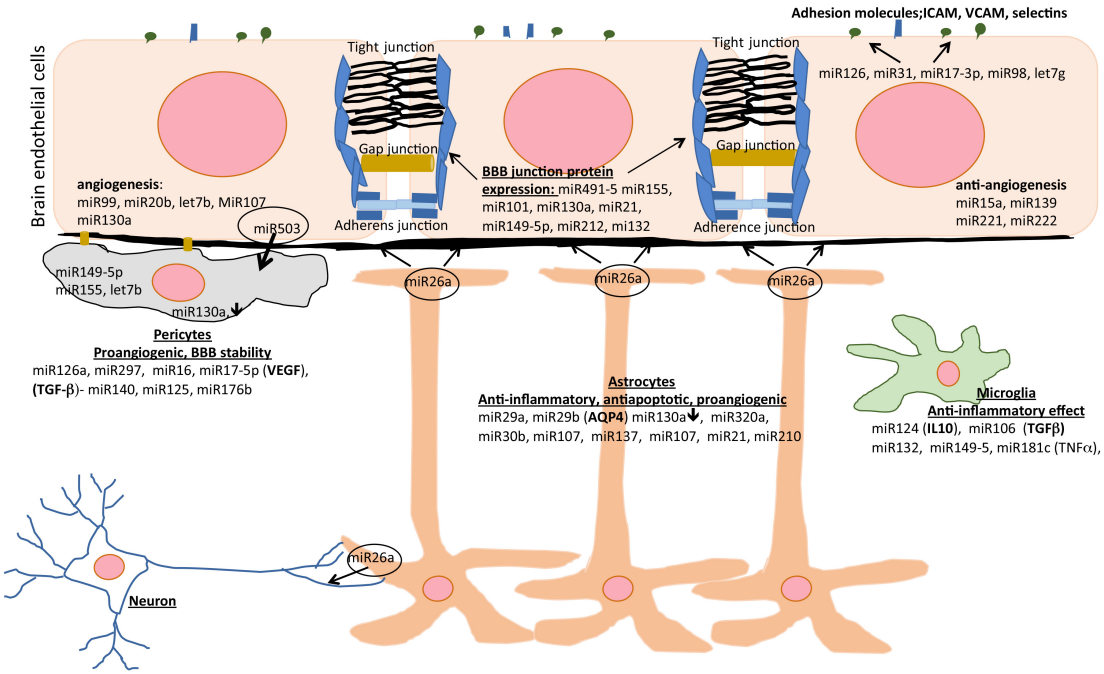

FIGURE 2 | The effects of miRs on different cell types of the NVU during post-stroke recovery. Different miRs modulate inflammation, angiogenesis, apoptosis, and blood-brain barrier (BBB) integrity and represent therapeutic area to enhance post-stroke recovery. AQP4, aquaporin-4; ICAM, intercellular adhesion molecule; IL-10, interleukin-10; TGF-β, transforming growth factor beta; VCAM, vascular cell adhesion molecule; VEGF, vascular endothelial growth factor.

blood levels of miR30a and miR126 in patients with ischemic stroke are reduced for 24 weeks (Long et al., 2013). Another example is a differential pattern of expression across different stroke subtypes for a miR, let-7b. Let-7b was lower in stroke patients of a large atherosclerosis subtype compared to non-stroke patients, whereas in other ischemic stroke subtypes, let-7b was higher than in healthy individuals (Long et al., 2013). Thus, screening of different types of miRs may serve as a useful tool to assess the risks and prognosis of specific stroke subtypes and stroke recovery.

It should be noted that while miRs have actions in the cells where they are produced, they can also have effects on other distant cells. One mechanism is via the cellular release and uptake of exosomes. That type of extracellular vesicle contains a wide range of molecules, including miRs. Exosomes are being examined both as biomarkers for stroke and as a therapeutic modality (Hong et al., 2018). Exosomes are produced and taken up by all cells of the NVU, having an important role in cellular crosstalk, including in stroke (Zagrean et al., 2018), potentially via the effects of miRs. Thus, Xu et al. recently found that exosomes released by neurons regulate BBB permeability in zebrafish (Xu B. et al., 2017; Zagrean et al., 2018). Those exosomes contained miR132 and delivery of that miR regulated adherens junction function in the cerebral endothelium (Xu B. et al., 2017).

Apart from the role of endogenous exosomes, there is interest in using exogenous exosomes as a delivery platform, including loading such exosomes with select miRs (Beuzelin and Kaeffer, 2018). Thus, bacterial-based mini-cells have been loaded with a miR16-based mimic and given to patients with malignant pleural mesothelioma (van Zandwijk et al., 2017). Such approaches might be used to limit stroke-induced NBVU/BBB injury or enhance recovery.

The above description suggests that miR agonists (agomirs) and antagonists (antagomirs) may be attractive targets for reducing ischemia-induced BBB and NVU dysfunction and improving post-stroke recovery, particularly as each miR many affect multiple processes. There are, however, hurdles that will need to be overcome. The ability of miRs to affect multiple pathways suggests that special attention may be required for potential side-effects of treatment. There is also the question of delivery of the therapeutic to the appropriate target. Targeting the cerebral endothelium may be easier than targeting other cells of the NVU where the miR, agomir or antagomir would have to cross the BBB. Progress has been made in adeno-associated viruses that will cross the BBB that might serve as a route for delivery.

OTHER NON-CODING RNAs

Currently, most studies have focused on the role of small ncRNA in regulating the BBB and NVU function in stroke. However, several recent studies have identified stroke-responsive piRNAs and lncRNAs (Alishahi et al., 2019). LncRNAs are not junk RNA but act as functional regulator elements in epigenetic regulation. They regulate gene function at different levels including but not limited to chromatin modification, and transcriptional and post-transcriptional mechanisms.

LncRNAs are longer than 200 nucleotides and have less sequence conservation than short ncRNA. Similar to short ncRNAs (miRs), lncRNAs regulate many important physiological processes including apoptosis, autophagy, immune response, and angiogenesis. LncRNAs may act as competitors to endogenous RNAs, acting as miR sponges or antagomirs (Alishahi et al., 2019). Recently, lncRNAs have been identified as being involved in human diseases. One lncRNA, Malat1 is involved in protecting against cerebrovascular ischemic injury. It is upregulated in brain endothelial cells by ischemia-like conditions and reduces injury. Malat1 acts by being a sponge for miR26b, regulating brain endothelial cell autophagy and survival under ischemic conditions (Li Z. et al., 2017).

CONCLUSION

The epigenetic mechanisms and the non-coding RNAs involved in BBB and NVU changes in stroke and stroke recovery are slowly emerging. That information holds great promise for better understanding of stroke pathology but also for developing new strategies for successful stroke recovery. In the future, both epigenetic factors and non-coding RNAs may have dual roles, as therapeutic targets and as biomarkers mirroring NVU injury and recovery processes. Epigenetic mechanisms are attractive targets as they affect multiple pathways. Histone deacetylase inhibitors are already used clinically for some disease states and more HDAC subtype-specific inhibitors are being developed. While the importance of miRs in a wide variety of disease states is recognized, there are still hurdles to cross in translating that to the clinic, particularly for neurological conditions such as stroke. However, the pleiotropic effects of epigenetic mechanisms and non-coding RNAs make them attractive and exciting therapeutic targets for limiting post-stroke NVU injury and enhancing recovery.

AUTHOR CONTRIBUTIONS

All authors contributed to the writing, illustration, and reviewing of the manuscript.

FUNDING

This work was supported by the Public Health Service grants: RFA057928 from the National Institute of Aging (AA) and 1-16-IBS-008 from the American Diabetes Association (AA) and NIH T-32-NS07640 (CP).

REFERENCES

Aapola, U., Liiv, I., and Peterson, P. (2002). Imprinting regulator DNMT3L is a transcriptional repressor associated with histone deacetylase activity. *Nucleic Acids Res.* 30, 3602–3608. doi: 10.1093/nar/gkf474

Alfieri, A., Srivastava, S., Siow, R. C. M., Cash, D., Modo, M., Duchen, M. R., et al. (2013). Sulforaphane preconditioning of the Nrf2/HO-1 defense pathway protects the cerebral vasculature against blood-brain barrier disruption and neurological deficits in stroke. *Free Radic. Biol. Med.* 65, 1012–1022. doi: 10.1016/j.freeradbiomed.2013.08.190

Alishahi, M., Ghaedrahmati, F., Kolagar, T. A., Winlow, W., Nikkar, N., Farzaneh, M., et al. (2019). Long non-coding RNAs and cell death following ischemic stroke. *Metab. Brain Dis.* doi: 10.1007/s11011-019-00423-2 [Epub ahead of print].

Allen, L. M., Hasso, A. N., Handwerker, J., and Farid, H. (2012). Sequence-specific MR imaging findings that are useful in dating ischemic stroke. *Radiographics* 32, 1285–1297; discussion 1297–1289.

Ambros, V. (2001). microRNAs: tiny regulators with great potential. *Cell* 107, 823–826.

Andreou, K., Rajendran, R., Krstic-Demonacos, M., and Demonacos, C. (2012). Regulation of CXCR4 gene expression in breast cancer cells under diverse stress conditions. *Int. J. Oncol.* 41, 2253–2259. doi: 10.3892/ijo.2012.1643

Baccarelli, A., Wright, R., Bollati, V., Litonjua, A., Zanobetti, A., Tarantini, L., et al. (2010). Ischemic heart disease and stroke in relation to blood DNA methylation. *Epidemiology* 21, 819–828. doi: 10.1097/ede.0b013e3181f20457

Baltan, S., Bachleda, A., Morrison, R. S., and Murphy, S. P. (2011). Expression of histone deacetylases in cellular compartments of the mouse brain and the effects of ischemia. *Transl Stroke Res.* 2, 411–423. doi: 10.1007/s12975-011-0087-z

Bauer, A. T., Burgers, H. F., Rabie, T., and Marti, H. H. (2010). Matrix metalloproteinase-9 mediates hypoxia-induced vascular leakage in the brain via tight junction rearrangement. *J. Cereb. Blood Flow Metab.* 30, 837–848. doi: 10.1038/jcbfm.2009.248

Beck, K., and Schachtrup, C. (2012). Vascular damage in the central nervous system: a multifaceted role for vascular-derived TGF-beta. *Cell Tissue Res.* 347, 187–201. doi: 10.1007/s00441-011-1228-0

Beuzelin, D., and Kaeffer, B. (2018). Exosomes and miRNA-Loaded Biomimetic Nanovehicles, a Focus on Their Potentials Preventing Type-2 Diabetes Linked to Metabolic Syndrome. *Front. Immunol.* 9:2711. doi: 10.3389/fimmu.2018.02711

Bird, A. P. (1986). CpG-rich islands and the function of DNA methylation. *Nature* 321, 209–213. doi: 10.1038/321209a0

Brifault, C., Gras, M., Liot, D., May, V., Vaudry, D., and Wurtz, O. (2015). Delayed pituitary adenylate cyclase-activating polypeptide delivery after brain stroke improves functional recovery by inducing m2 microglia/macrophage polarization. *Stroke* 46, 520–528. doi: 10.1161/strokeaha.114.006864

Cao, F., Zwinderman, M. R. H., and Dekker, F. J. (2018). The process and strategy for developing selective histone deacetylase 3 inhibitors. *Molecules* 23:E551.

Castellanos, M., Sobrino, T., Millan, M., Garcia, M., Arenillas, J., Nombela, F., et al. (2007). Serum cellular fibronectin and matrix metalloproteinase-9 as screening biomarkers for the prediction of parenchymal hematoma after thrombolytic therapy in acute ischemic stroke: a multicenter confirmatory study. *Stroke* 38, 1855–1859. doi: 10.1161/strokeaha.106.481556

Castro, V., Bertrand, L., Luethen, M., Dabrowski, S., Lombardi, J., Morgan, L., et al. (2016). Occludin controls HIV transcription in brain pericytes via regulation of SIRT-1 activation. *FASEB J.* 30, 1234–1246. doi: 10.1096/fj.15-277673

Cekanaviciute, E., Fathali, N., Doyle, K. P., Williams, A. M., Han, J., and Buckwalter, M. S. (2014). Astrocytic transforming growth factor-beta signaling reduces subacute neuroinflammation after stroke in mice. *Glia* 62, 1227–1240. doi: 10.1002/glia.22675

Cerutti, C., Soblechero-Martin, P., Wu, D., Lopez-Ramirez, M. A., De Vries, H., Sharrack, B., et al. (2016). MicroRNA-155 contributes to shear-resistant leukocyte adhesion to human brain endothelium in vitro. *Fluids Barriers CNS* 13:8.

Chakravarty, S., Jhelum, P., Bhat, U. A., Rajan, W. D., Maitra, S., Pathak, S. S., et al. (2017). Insights into the epigenetic mechanisms involving histone lysine methylation and demethylation in ischemia induced damage and repair has therapeutic implication. *Biochim. Biophys. Acta Mol. Basis Dis.* 1863, 152–164. doi: 10.1016/j.bbadis.2016.09.014

Chen, J., Yang, T., Yu, H., Sun, K., Shi, Y., Song, W., et al. (2010). A functional variant in the 3'-UTR of angiopoietin-1 might reduce stroke risk by interfering with the binding efficiency of microRNA 211. *Hum. Mol. Genet.* 19, 2524–2533. doi: 10.1093/hmg/ddq131

Chen, S., Martens-Lobenhoffer, J., Weissenborn, K., Kielstein, J. T., Lichtinghagen, R., Deb, M., et al. (2012). Association of dimethylarginines and mediators of inflammation after acute ischemic stroke. *J. Neuroinflammation.* 9:251.

Chen, T., Dai, S. H., Li, X., Luo, P., Zhu, J., Wang, Y. H., et al. (2018). Sirt1-Sirt3 axis regulates human blood-brain barrier permeability in response to ischemia. *Redox Biol.* 14, 229–236. doi: 10.1016/j.redox.2017.09.016

Chen, X. R., Liao, S. J., Ye, L. X., Gong, Q., Ding, Q., Zeng, J. S., et al. (2014). Neuroprotective effect of chondroitinase ABC on primary and secondary brain injury after stroke in hypertensive rats. *Brain Res.* 1543, 324–333. doi: 10.1016/j.brainres.2013.12.002

Chen, Y., Wang, L., Zhang, L., Chen, B., Yang, L., Li, X., et al. (2018). Inhibition of connexin 43 hemichannels alleviates cerebral ischemia/reperfusion injury via the TLR4 signaling pathway. *Front. Cell Neurosci.* 12:372. doi: 10.3389/fncel.2018.00372

Chen, Y. J., Wallace, B. K., Yuen, N., Jenkins, D. P., Wulff, H., and O'donnell, M. E. (2015). Blood-brain barrier KCa3.1 channels: evidence for a role in brain Na uptake and edema in ischemic stroke. *Stroke* 46, 237–244. doi: 10.1161/strokeaha.114.007445

Chen, Y. S., Liu, H. M., and Lee, T. Y. (2019). Ursodeoxycholic acid regulates hepatic energy homeostasis and white adipose tissue macrophages polarization in leptin-deficiency obese mice. *Cells* 8:253 doi: 10.3390/cells8030253

Chisholm, N. C., Henderson, M. L., Selvamani, A., Park, M. J., Dindot, S., Miranda, R. C., et al. (2015). Histone methylation patterns in astrocytes are influenced by age following ischemia. *Epigenetics* 10, 142–152. doi: 10.1080/15592294.2014.1001219

Choi, J. Y., Yoon, S. S., Kim, S. E., and Ahn, Jo, S. (2017). KDM4B histone demethylase and G9a regulate expression of vascular adhesion proteins in cerebral microvessels. *Sci. Rep.* 7:45005.

Chopp, M., Zhang, Z. G., and Jiang, Q. (2007). Neurogenesis, angiogenesis, and MRI indices of functional recovery from stroke. *Stroke* 38, 827–831. doi: 10.1161/01.str.0000250235.80253.e9

Dakhlallah, D., Batte, K., Wang, Y., Cantemir-Stone, C. Z., Yan, P., Nuovo, G., et al. (2013). Epigenetic regulation of miR-17˜92 contributes to the pathogenesis of pulmonary fibrosis. *Am. J. Respir. Crit. Care Med.* 187, 397–405.

Daneman, R., Zhou, L., Agalliu, D., Cahoy, J. D., Kaushal, A., and Barres, B. A. (2010). The mouse blood-brain barrier transcriptome: a new resource for understanding the development and function of brain endothelial cells. *PLoS One* 5:e13741. doi: 10.1371/journal.pone.0013741

Demyanenko, S., Neginskaya, M., and Berezhnaya, E. (2018). Expression of class i histone deacetylases in ipsilateral and contralateral hemispheres after the focal photothrombotic infarction in the mouse brain. *Transl Stroke Res.* 9, 471–483. doi: 10.1007/s12975-017-0595-6

Diaz-Cañestro, C., Merlini, M., Bonetti, N. R., Liberale, L., Wüst, P., Briand-Schumacher, S., et al. (2018). Sirtuin 5 as a novel target to blunt blood-brain barrier damage induced by cerebral ischemia/reperfusion injury. *Int. J. Cardiol.* 260, 148–155. doi: 10.1016/j.ijcard.2017.12.060

Dirnagl, U., Iadecola, C., and Moskowitz, M. A. (1999). Pathobiology of ischaemic stroke: an integrated view. *Trends Neurosci.* 22, 391–397. doi: 10.1016/s0166-2236(99)01401-0

Drake, C., Boutin, H., Jones, M. S., Denes, A., Mccoll, B. W., Selvarajah, J. R., et al. (2011). Brain inflammation is induced by co-morbidities and risk factors for stroke. *Brain Behav. Immun.* 25, 1113–1122. doi: 10.1016/j.bbi.2011.02.008

Ellison, J. A., Barone, F. C., and Feuerstein, G. Z. (1999). Matrix remodeling after stroke. De novo expression of matrix proteins and integrin receptors. *Ann. N. Y. Acad. Sci.* 890, 204–222. doi: 10.1111/j.1749-6632.1999.tb07996.x

Endres, M., Meisel, A., Biniszkiewicz, D., Namura, S., Prass, K., Ruscher, K., et al. (2000). DNA methyltransferase contributes to delayed ischemic brain injury. *J. Neurosci.* 20, 3175–3181. doi: 10.1523/jneurosci.20-09-03175.2000

Enzmann, G., Mysiorek, C., Gorina, R., Cheng, Y. J., Ghavampour, S., Hannocks, M. J., et al. (2013). The neurovascular unit as a selective barrier to polymorphonuclear granulocyte (PMN) infiltration into the brain after ischemic injury. *Acta Neuropathol.* 125, 395–412. doi: 10.1007/s00401-012-1076-3

Esse, R., Florindo, C., Imbard, A., Rocha, M. S., De Vriese, A. S., Smulders, Y. M., et al. (2013). Global protein and histone arginine methylation are affected in a tissue-specific manner in a rat model of diet-induced hyperhomocysteinemia. *Biochim. Biophys. Acta* 1832, 1708–1714. doi: 10.1016/j.bbadis.2013.05.013

Fish, J. E., Yan, M. S., Matouk, C. C., St Bernard, R., Ho, J. J., Gavryushova, A., et al. (2010). Hypoxic repression of endothelial nitric-oxide synthase transcription is coupled with eviction of promoter histones. *J. Biol. Chem.* 285, 810–826. doi: 10.1074/jbc.m109.067868

Formisano, L., Guida, N., Valsecchi, V., Cantile, M., Cuomo, O., Vinciguerra, A., et al. (2015). Sp3/REST/HDAC1/HDAC2 complex represses and Sp1/HIF-1/p300 complex activates ncx1 gene transcription, in brain ischemia and in ischemic brain preconditioning, by epigenetic mechanism. *J. Neurosci.* 35, 7332–7348. doi: 10.1523/JNEUROSCI.2174-14.2015

Friedman, B., Schachtrup, C., Tsai, P. S., Shih, A. Y., Akassoglou, K., Kleinfeld, D., et al. (2009). Acute vascular disruption and aquaporin 4 loss after stroke. *Stroke* 40, 2182–2190. doi: 10.1161/strokeaha.108.523720

Gaisina, I. N., Lee, S. H., Kaidery, N. A., Aissa, M. B., Ahuja, M., Smirnova, N. N., et al. (2018). Activation of Nrf2 and hypoxic adaptive response contribute to neuroprotection elicited by phenylhydroxamic acid selective HDAC6 inhibitors. *ACS Chem. Neurosci.* 9, 894–900. doi: 10.1021/acschemneuro.7b00435

Ginsberg, M. D. (2008). Neuroprotection for ischemic stroke: past, present and future. *Neuropharmacology* 55, 363–389. doi: 10.1016/j.neuropharm.2007.12.007

Goll, M. G., and Bestor, T. H. (2005). Eukaryotic cytosine methyltransferases. *Annu. Rev. Biochem.* 74, 481–514. doi: 10.1146/annurev.biochem.74.010904.153721

Goll, M. G., Kirpekar, F., Maggert, K. A., Yoder, J. A., Hsieh, C. L., Zhang, X., et al. (2006). Methylation of tRNAAsp by the DNA methyltransferase homolog Dnmt2. *Science* 311, 395–398. doi: 10.1126/science.1120976

Gomez-Uriz, A. M., Goyenechea, E., Campion, J., De Arce, A., Martinez, M. T., Puchau, B., et al. (2014). Epigenetic patterns of two gene promoters (TNF-alpha and PON) in stroke considering obesity condition and dietary intake. *J. Physiol. Biochem.* 70, 603–614. doi: 10.1007/s13105-014-0316-5

Greco, R., Demartini, C., Zanaboni, A. M., Blandini, F., Amantea, D., and Tassorelli, C. (2018). Endothelial nitric oxide synthase inhibition triggers inflammatory responses in the brain of male rats exposed to ischemia-reperfusion injury. *J. Neurosci. Res.* 96, 151–159. doi: 10.1002/jnr.24101

Hall, C. N., Reynell, C., Gesslein, B., Hamilton, N. B., Mishra, A., Sutherland, B. A., et al. (2014). Capillary pericytes regulate cerebral blood flow in health and disease. *Nature* 508, 55–60. doi: 10.1038/nature13165

He, M., Zhang, B., Wei, X., Wang, Z., Fan, B., Du, P., et al. (2013). HDAC4/5-HMGB1 signalling mediated by NADPH oxidase activity contributes to cerebral ischaemia/reperfusion injury. *J. Cell. Mol. Med.* 17, 531–542. doi: 10.1111/jcmm.12040

He, S., Liu, R., Li, B., Huang, L., Fan, W., Tembachako, C. R., et al. (2019). Propagermanium, a CCR2 inhibitor, attenuates cerebral ischemia/reperfusion injury through inhibiting inflammatory response induced by microglia. *Neurochem. Int.* 125, 99–110. doi: 10.1016/j.neuint.2019.02.010

Hendrich, B. D., and Willard, H. F. (1995). Epigenetic regulation of gene expression: the effect of altered chromatin structure from yeast to mammals. *Hum. Mol. Genet.* 4, 1765–1777. doi: 10.1093/hmg/4.suppl_1.1765

Hertz, L., Xu, J., Chen, Y., Gibbs, M. E., Du, T., Hertz, L., et al. (2014). Antagonists of the vasopressin V1receptor and of the beta(1)-adrenoceptor inhibit cytotoxic brain edema in stroke by effects on astrocytes Ű but the mechanisms differ. *Curr. Neuropharmacol.* 12, 308–323. doi: 10.2174/1570159X12666140828222723

Hill, J. J., Jin, K., Mao, X. O., Xie, L., and Greenberg, D. A. (2012). Intracerebral chondroitinase ABC and heparan sulfate proteoglycan glypican improve outcome from chronic stroke in rats. *Proc. Natl. Acad. Sci. U. S. A.* 109, 9155–9160. doi: 10.1073/pnas.1205697109

Hill, W. D., Hess, D. C., Martin-Studdard, A., Carothers, J. J., Zheng, J., Hale, D., et al. (2004). SDF-1 (CXCL12) is upregulated in the ischemic penumbra following stroke: association with bone marrow cell homing to injury. *J. Neuropathol. Exp. Neurol.* 63, 84–96. doi: 10.1093/jnen/63.1.84

Hollander, M., Koudstaal, P. J., Bots, M. L., Grobbee, D. E., Hofman, A., and Breteler, M. M. (2003). Incidence, risk, and case fatality of first ever stroke in

the elderly population. The Rotterdam Study. *J. Neurol. Neurosurg. Psychiatry* 74, 317–321. doi: 10.1136/jnnp.74.3.317

Hong, S. B., Yang, H., Manaenko, A., Lu, J., Mei, Q., and Hu, Q. (2018). Potential of exosomes for the treatment of stroke. *Cell Transplant.* doi: 10.1177/0963689718816990 [Epub ahead of print].

Hsieh, C.L. (1999). In vivo activity of murine de novo methyltransferases, Dnmt3a and Dnmt3b. *Mol. Cell Biol.* 19, 8211-8218.

Hu, C. J., Chen, S. D., Yang, D. I., Lin, T. N., Chen, C. M., Huang, T. H., et al. (2006). Promoter region methylation and reduced expression of thrombospondin-1 after oxygen-glucose deprivation in murine cerebral endothelial cells. *J. Cereb. Blood Flow Metab.* 26, 1519–1526. doi: 10.1038/sj.jcbfm.9600304

Huang, L., Ma, Q., Li, Y., Li, B., and Zhang, L. (2018). Inhibition of microRNA-210 suppresses pro-inflammatory response and reduces acute brain injury of ischemic stroke in mice. *Exp. Neurol.* 300, 41–50. doi: 10.1016/j.expneurol.2017.10.024

Inoue, T., Hiratsuka, M., Osaki, M., and Oshimura, M. (2007). The molecular biology of mammalian SIRT proteins: SIRT2 in cell cycle regulation. *Cell Cycle* 6, 1011–1018. doi: 10.4161/cc.6.9.4219

Ito, U., Hakamata, Y., Kawakami, E., and Oyanagi, K. (2009). Degeneration of astrocytic processes and their mitochondria in cerebral cortical regions peripheral to the cortical infarction: heterogeneity of their disintegration is closely associated with disseminated selective neuronal necrosis and maturation of injury. *Stroke* 40, 2173–2181. doi: 10.1161/strokeaha.108.534990

Jeon, Y. J., Kim, O. J., Kim, S. Y., Oh, S. H., Oh, D., Kim, O. J., et al. (2013). Association of the miR-146a, miR-149, miR-196a2, and miR-499 polymorphisms with ischemic stroke and silent brain infarction risk. *Arterioscler Thromb Vasc Biol.* 33, 420–430. doi: 10.1161/atvbaha.112.300251

Ji, K., and Tsirka, S. E. (2012). Inflammation modulates expression of laminin in the central nervous system following ischemic injury. *J. Neuroinflammation* 9:159.

Kassis, H., Shehadah, A., Chopp, M., Roberts, C., and Zhang, Z. G. (2015). Stroke induces nuclear shuttling of histone deacetylase 4. *Stroke* 46, 1909–1915. doi: 10.1161/STROKEAHA.115.009046

Kassis, H., Shehadah, A., Chopp, M., and Zhang, Z. G. (2017). Epigenetics in stroke recovery. *Genes* 8:89 doi: 10.3390/genes8030089

Kleinschnitz, C., Kraft, P., Dreykluft, A., Hagedorn, I., Gobel, K., Schuhmann, M. K., et al. (2013). Regulatory T cells are strong promoters of acute ischemic stroke in mice by inducing dysfunction of the cerebral microvasculature. *Blood* 121, 679–691. doi: 10.1182/blood-2012-04-426734

Klose, R. J., and Zhang, Y. (2007). Regulation of histone methylation by demethylimination and demethylation. *Nat. Rev. Mol. Cell Biol.* 8, 307–318. doi: 10.1038/nrm2143

Lee, B., Clarke, D., Al Ahmad, A., Kahle, M., Parham, C., Auckland, L., et al. (2011). Perlecan domain V is neuroprotective and proangiogenic following ischemic stroke in rodents. *J. Clin. Invest.* 121, 3005–3023. doi: 10.1172/jci46358

Lee, D. Y., Lin, T. E., Lee, C. I., Zhou, J., Huang, Y. H., Lee, P. L., et al. (2017). MicroRNA-10a is crucial for endothelial response to different flow patterns via interaction of retinoid acid receptors and histone deacetylases. *Proc. Natl. Acad. Sci. U. S. A.* 114, 2072–2077. doi: 10.1073/pnas.1621425114

Li, B., Gogol, M., Carey, M., Lee, D., Seidel, C., and Workman, J. L. (2007). Combined action of PHD and chromo domains directs the Rpd3S HDAC to transcribed chromatin. *Science* 316, 1050–1054. doi: 10.1126/science.1139004

Li, X. Q., Chen, F. S., Tan, W. F., Fang, B., Zhang, Z. L., and Ma, H. (2017). Elevated microRNA-129-5p level ameliorates neuroinflammation and blood-spinal cord barrier damage after ischemia-reperfusion by inhibiting HMGB1 and the TLR3-cytokine pathway. *J. Neuroinflammation* 14:205.

Li, Y., Mao, L., Gao, Y., Baral, S., Zhou, Y., and Hu, B. (2015). MicroRNA-107 contributes to post-stroke angiogenesis by targeting Dicer-1. *Sci. Rep.* 5:13316.

Li, Z., Li, J., and Tang, N. (2017). Long noncoding RNA Malat1 is a potent autophagy inducer protecting brain microvascular endothelial cells against oxygen-glucose deprivation/reoxygenation-induced injury by sponging miR-26b and upregulating ULK2 expression. *Neuroscience* 354, 1–10. doi: 10.1016/j.neuroscience.2017.04.017

Liu, H., Wei, X., Kong, L., Liu, X., Cheng, L., Yan, S., et al. (2015). NOD2 is involved in the inflammatory response after cerebral ischemia-reperfusion injury and triggers NADPH oxidase 2-derived reactive oxygen species. *Int. J. Biol. Sci.* 11, 525–535. doi: 10.7150/ijbs.10927

Liu, Y., Pan, Q., Zhao, Y., He, C., Bi, K., Chen, Y., et al. (2015). MicroRNA-155 regulates ROS production, NO generation, apoptosis and multiple functions of human brain microvessel endothelial cells under physiological and pathological conditions. *J. Cell. Biochem.* 116, 2870–2881. doi: 10.1002/jcb.25234

Lloyd-Burton, S. M., York, E. M., Anwar, M. A., Vincent, A. J., and Roskams, A. J. (2013). SPARC regulates microgliosis and functional recovery following cortical ischemia. *J. Neurosci.* 33, 4468–4481. doi: 10.1523/jneurosci.3585-12.2013

Long, G., Wang, F., Li, H., Yin, Z., Sandip, C., Lou, Y., et al. (2013). Circulating miR-30a, miR-126 and let-7b as biomarker for ischemic stroke in humans. *BMC Neurol.* 13:178. doi: 10.1186/1471-2377-13-178

Lopez-Ramirez, M. A., Wu, D., Pryce, G., Simpson, J. E., Reijerkerk, A., King-Robson, J., et al. (2014). MicroRNA-155 negatively affects blood-brain barrier function during neuroinflammation. *FASEB J.* 28, 2551–2565. doi: 10.1096/fj.13-248880

Lou, Y. L., Guo, F., Liu, F., Gao, F. L., Zhang, P. Q., Niu, X., et al. (2012). miR-210 activates notch signaling pathway in angiogenesis induced by cerebral ischemia. *Mol. Cell Biochem.* 370, 45–51. doi: 10.1007/s11010-012-1396-6

Lu, Y., Huang, Z., Hua, Y., and Xiao, G. (2018). Minocycline promotes BDNF expression of N2a cells via Inhibition of miR-155-mediated repression after oxygen-glucose deprivation and reoxygenation. *Cell Mol. Neurobiol.* 38, 1305–1313. doi: 10.1007/s10571-018-0599-0

Mae, M., Armulik, A., and Betsholtz, C. (2011). Getting to know the cast - cellular interactions and signaling at the neurovascular unit. *Curr. Pharm Des.* 17, 2750–2754. doi: 10.2174/138161211797440113

Maitrias, P., Metzinger-Le Meuth, V., Nader, J., Reix, T., Caus, T., and Metzinger, L. (2017). The involvement of miRNA in carotid-related stroke. *Arterioscler Thromb Vasc Biol.* 37, 1608–1617. doi: 10.1161/atvbaha.117.309233

McClure, J. J., Li, X., and Chou, C. J. (2018). Advances and challenges of HDAC inhibitors in cancer therapeutics. *Adv. Cancer Res.* 138, 183–211. doi: 10.1016/bs.acr.2018.02.006

Miao, Z., He, Y., Xin, N., Sun, M., Chen, L., Lin, L., et al. (2015). Altering 5-hydroxymethylcytosine modification impacts ischemic brain injury. *Hum. Mol. Genet.* 24, 5855–5866. doi: 10.1093/hmg/ddv307

Migliori, V., Phalke, S., Bezzi, M., and Guccione, E. (2010). Arginine/lysine-methyl/methyl switches: biochemical role of histone arginine methylation in transcriptional regulation. *Epigenomics* 2, 119–137. doi: 10.2217/epi.09.39

Mirzaei, H., Momeni, F., Saadatpour, L., Sahebkar, A., Goodarzi, M., Masoudifar, A., et al. (2018). MicroRNA: relevance to stroke diagnosis, prognosis, and therapy. *J. Cell Physiol.* 233, 856–865. doi: 10.1002/jcp.25787

Mishra, R., and Singh, S. K. (2013). HIV-1 Tat C modulates expression of miRNA-101 to suppress VE-cadherin in human brain microvascular endothelial cells. *J. Neurosci.* 33, 5992–6000. doi: 10.1523/jneurosci.4796-12.2013

Mogoanta, L., Ciurea, M., Pirici, I., Margaritescu, C., Simionescu, C., Ion, D. A., et al. (2014). Different dynamics of aquaporin 4 and glutamate transporter-1 distribution in the perineuronal and perivascular compartments during ischemic stroke. *Brain Pathol.* 24, 475–493. doi: 10.1111/bpa.12134

Mondal, N. K., Behera, J., Kelly, K. E., George, A. K., Tyagi, P. K., and Tyagi, N. (2019). Tetrahydrocurcumin epigenetically mitigates mitochondrial dysfunction in brain vasculature during ischemic stroke. *Neurochem. Int.* 122, 120–138. doi: 10.1016/j.neuint.2018.11.015

Mori, T., Tan, J., Arendash, G. W., Koyama, N., Nojima, Y., and Town, T. (2008). Overexpression of human S100B exacerbates brain damage and periinfarct gliosis after permanent focal ischemia. *Stroke* 39, 2114–2121. doi: 10.1161/strokeaha.107.503821

Muoio, V., Persson, P. B., and Sendeski, M. M. (2014). The neurovascular unit - concept review. *Acta Physiol.* 210, 790–798. doi: 10.1111/apha.12250

Nagy, Z., and Nardai, S. (2017). Cerebral ischemia/repefusion injury: from bench space to bedside. *Brain Res. Bull.* 134, 30–37. doi: 10.1016/j.brainresbull.2017.06.011

Narlikar, G. J., Fan, H. Y., and Kingston, R. E. (2002). Cooperation between complexes that regulate chromatin structure and transcription. *Cell* 108, 475–487. doi: 10.1016/s0092-8674(02)00654-2

Nicholson, C. J., Seta, F., Lee, S., and Morgan, K. G. (2017). MicroRNA-203 mimics age-related aortic smooth muscle dysfunction of cytoskeletal pathways. *J. Cell Mol. Med.* 21, 81–95. doi: 10.1111/jcmm.12940

Nitta, T., Hata, M., Gotoh, S., Seo, Y., Sasaki, H., Hashimoto, N., et al. (2003). Size-selective loosening of the blood-brain barrier in claudin-5-deficient mice. *J. Cell Biol.* 161, 653–660. doi: 10.1083/jcb.200302070

Ohtsuki, S., Sato, S., Yamaguchi, H., Kamoi, M., Asashima, T., and Terasaki, T. (2007). Exogenous expression of claudin-5 induces barrier properties in

cultured rat brain capillary endothelial cells. *J. Cell Physiol.* 210, 81–86. doi: 10.1002/jcp.20823

Okoreeh, A. K., Bake, S., and Sohrabji, F. (2017). Astrocyte-specific insulin-like growth factor-1 gene transfer in aging female rats improves stroke outcomes. *Glia* 65, 1043–1058. doi: 10.1002/glia.23142

Papp, D., Lenti, K., Modos, D., Fazekas, D., Dul, Z., Turei, D., et al. (2012). The NRF2-related interactome and regulome contain multifunctional proteins and fine-tuned autoregulatory loops. *FEBS Lett.* 586, 1795–1802. doi: 10.1016/j.febslet.2012.05.016

Park, M. J., and Sohrabji, F. (2016). The histone deacetylase inhibitor, sodium butyrate, exhibits neuroprotective effects for ischemic stroke in middle-aged female rats. *J. Neuroinflammation* 13:300.

Patnala, R., Arumugam, T. V., Gupta, N., and Dheen, S. T. (2017). HDAC inhibitor sodium butyrate-mediated epigenetic regulation enhances neuroprotective function of microglia during ischemic stroke. *Mol. Neurobiol.* 54, 6391–6411. doi: 10.1007/s12035-016-0149-z

Pena-Philippides, J.C., Caballero-Garrido, E., Lordkipanidze, T., and Roitbak, T. (2016). In vivo inhibition of miR-155 significantly alters post-stroke inflammatory response. *J. Neuroinflammation* 13:287.

Posada-Duque, R. A., Barreto, G. E., and Cardona-Gomez, G. P. (2014). Protection after stroke: cellular effectors of neurovascular unit integrity. *Front. Cell. Neurosci.* 8:231. doi: 10.3389/fncel.2014.00231

Reed, G. L., Houng, A. K., and Wang, D. (2014). Microvascular thrombosis, fibrinolysis, ischemic injury, and death after cerebral thromboembolism are affected by levels of circulating alpha2-antiplasmin. *Arterioscler Thromb Vasc Biol.* 34, 2586–2593. doi: 10.1161/atvbaha.114.304530

Ren, W., Gao, L., and Song, J. (2018). Structural Basis of DNMT1 and DNMT3A-Mediated DNA Methylation. *Genes* 9:E620.

Rom, S., Dykstra, H., Zuluaga-Ramirez, V., Reichenbach, N. L., and Persidsky, Y. (2015). miR-98 and let-7g* protect the blood-brain barrier under neuroinflammatory conditions. *J. Cereb. Blood Flow Metab.* 35, 1957–1965. doi: 10.1038/jcbfm.2015.154

Saito, K., Kondo, E., and Matsushita, M. (2011). MicroRNA 130 family regulates the hypoxia response signal through the P-body protein DDX6. *Nucleic Acids Res.* 39, 6086–6099. doi: 10.1093/nar/gkr194

Sangaletti, R., D'Amico, M., Grant, J., Della-Morte, D., and Bianchi, L. (2017). Knock-out of a mitochondrial sirtuin protects neurons from degeneration in *Caenorhabditis elegans*. *PLoS Genet.* 13:e1006965. doi: 10.1371/journal.pgen.1006965

Schachtrup, C., Ryu, J. K., Helmrick, M. J., Vagena, E., Galanakis, D. K., Degen, J. L., et al. (2010). Fibrinogen triggers astrocyte scar formation by promoting the availability of active TGF-beta after vascular damage. *J. Neurosci.* 30, 5843–5854. doi: 10.1523/jneurosci.0137-10.2010

Sellner, S., Paricio-Montesinos, R., Spiess, A., Masuch, A., Erny, D., Harsan, L. A., et al. (2016). Microglial CX3CR1 promotes adult neurogenesis by inhibiting Sirt 1/p65 signaling independent of CX3CL1. *Acta Neuropathol. Commun.* 4, 102.

Sepramaniam, S., Ying, L. K., Armugam, A., Wintour, E. M., and Jeyaseelan, K. (2012). MicroRNA-130a represses transcriptional activity of aquaporin 4 M1 promoter. *J. Biol. Chem.* 287, 12006–12015. doi: 10.1074/jbc.m111.280701

She, D. T., Wong, L. J., Baik, S.-H., and Arumugam, T. V. (2018). SIRT2 inhibition confers neuroprotection by downregulation of FOXO3a and MAPK signaling pathways in ischemic stroke. *Mol. Neurobiol.* 55, 9188–9203. doi: 10.1007/s12035-018-1058-0

Shi, W., Wei, X., Wang, Z., Han, H., Fu, Y., Liu, J., et al. (2016). HDAC9 exacerbates endothelial injury in cerebral ischaemia/reperfusion injury. *J. Cell Mol. Med.* 20, 1139–1149. doi: 10.1111/jcmm.12803

Shimizu, F., Sano, Y., Saito, K., Abe, M. A., Maeda, T., Haruki, H., et al. (2012). Pericyte-derived glial cell line-derived neurotrophic factor increase the expression of claudin-5 in the blood-brain barrier and the blood-nerve barrier. *Neurochem. Res.* 37, 401–409. doi: 10.1007/s11064-011-0626-8

Shin, J. H., Park, Y. M., Kim, D. H., Moon, G. J., Bang, O. Y., Ohn, T., et al. (2014). Ischemic brain extract increases SDF-1 expression in astrocytes through the CXCR2/miR-223/miR-27b pathway. *Biochim. Biophys. Acta* 1839, 826–836. doi: 10.1016/j.bbagrm.2014.06.019

Shukla, S., Sharma, A., Pandey, V. K., Raisuddin, S., and Kakkar, P. (2016). Concurrent acetylation of FoxO1/3a and p53 due to sirtuins inhibition elicit Bim/PUMA mediated mitochondrial dysfunction and apoptosis in berberine-treated HepG2 cells. *Toxicol. Appl. Pharmacol.* 291, 70–83. doi: 10.1016/j.taap.2015.12.006

Sifat, A. E., Vaidya, B., and Abbruscato, T. J. (2017). Blood-brain barrier protection as a therapeutic strategy for acute ischemic stroke. *AAPS J.* 19, 957–972. doi: 10.1208/s12248-017-0091-7

Sladojevic, N., Stamatovic, S. M., Johnson, A. M., Choi, J., Hu, A., Dithmer, S., et al. (2019). Claudin-1-dependent destabilization of the blood-brain barrier in chronic stroke. *J. Neurosci.* 39, 743–757. doi: 10.1523/jneurosci.1432-18.2018

Sladojevic, N., Stamatovic, S. M., Keep, R. F., Grailer, J. J., Sarma, J. V., Ward, P. A., et al. (2014). Inhibition of junctional adhesion molecule-A/LFA interaction attenuates leukocyte trafficking and inflammation in brain ischemia/reperfusion injury. *Neurobiol. Dis.* 67, 57–70. doi: 10.1016/j.nbd.2014.03.010

Sole, S., Petegnief, V., Gorina, R., Chamorro, A., and Planas, A. M. (2004). Activation of matrix metalloproteinase-3 and agrin cleavage in cerebral ischemia/reperfusion. *J. Neuropathol. Exp. Neurol.* 63, 338–349. doi: 10.1093/jnen/63.4.338

Song, Y. C., Li, W. J., and Li, L. Z. (2015). Regulatory effect of miRNA 320a on expression of aquaporin 4 in brain tissue of epileptic rats. *Asian Pac. J. Trop Med.* 8, 807–812. doi: 10.1016/j.apjtm.2015.09.006

Stamatovic, S. M., Johnson, A. M., Keep, R. F., and Andjelkovic, A. V. (2016). Junctional proteins of the blood-brain barrier: new insights into function and dysfunction. *Tissue Barriers* 4:e1154641. doi: 10.1080/21688370.2016.1154641

Stamatovic, S. M., Martinez-Revollar, G., Hu, A., Choi, J., Keep, R. F., and Andjelkovic, A. V. (2019). Decline in sirtuin-1 expression and activity plays a critical role in blood-brain barrier permeability in aging. *Neurobiol. Dis.* 126, 105–116. doi: 10.1016/j.nbd.2018.09.006

Staszel, T., Zapala, B., Polus, A., Sadakierska-Chudy, A., Kiec-Wilk, B., Stepien, E., et al. (2011). Role of microRNAs in endothelial cell pathophysiology. *Pol. Arch. Med. Wewn.* 121, 361–366.

Sun, P., Bu, F., Min, J.-W., Munshi, Y., Howe, M. D., Liu, L., et al. (2019). Inhibition of calcium/calmodulin-dependent protein kinase kinase (CaMKK) exacerbates impairment of endothelial cell and blood-brain barrier after stroke. *Eur. J. Neurosci.* 49, 27–39. doi: 10.1111/ejn.14223

Suzuki, H., Hasegawa, Y., Kanamaru, K., and Zhang, J. H. (2010). Mechanisms of osteopontin-induced stabilization of blood-brain barrier disruption after subarachnoid hemorrhage in rats. *Stroke* 41, 1783–1790. doi: 10.1161/strokeaha.110.586537

Talebi, A., Rahnema, M., and Bigdeli, M. R. (2019). Effect of intravenous injection of antagomiR-1 on brain ischemia. *Mol. Biol. Rep.* 46, 1149–1155. doi: 10.1007/s11033-018-04580-y

Tang, F., Guo, S., Liao, H., Yu, P., Wang, L., Song, X., et al. (2017). Resveratrol enhances neurite outgrowth and synaptogenesis via sonic hedgehog signaling following oxygen-glucose deprivation/reoxygenation injury. *Cell Physiol. Biochem.* 43, 852–869. doi: 10.1159/000481611

Tarassishin, L., Loudig, O., Bauman, A., Shafit-Zagardo, B., Suh, H. S., and Lee, S. C. (2011). Interferon regulatory factor 3 inhibits astrocyte inflammatory gene expression through suppression of the proinflammatory miR-155 and miR-155. *Glia* 59, 1911–1922. doi: 10.1002/glia.21233

Tietz, S., and Engelhardt, B. (2015). Brain barriers: crosstalk between complex tight junctions and adherens junctions. *J. Cell. Biol.* 209, 493–506. doi: 10.1083/jcb.201412147

Tome, M., Lopez-Romero, P., Albo, C., Sepulveda, J. C., Fernandez-Gutierrez, B., Dopazo, A., et al. (2011). miR-335 orchestrates cell proliferation, migration and differentiation in human mesenchymal stem cells. *Cell. Death Differ.* 18, 985–995. doi: 10.1038/cdd.2010.167

Topcuoglu, M. A., Liu, L., Kim, D. E., and Gurol, M. E. (2018). Updates on prevention of cardioembolic strokes. *J. Stroke* 20, 180–196. doi: 10.5853/jos.2018.00780

Tsai, H. H., Kim, J. S., Jouvent, E., and Gurol, M. E. (2018). Updates on prevention of hemorrhagic and lacunar strokes. *J. Stroke* 20, 167–179. doi: 10.5853/jos.2018.00787

Underly, R. G., Levy, M., Hartmann, D. A., Grant, R. I., Watson, A. N., and Shih, A. Y. (2017). Pericytes as Inducers of Rapid, Matrix Metalloproteinase-9-Dependent Capillary Damage during Ischemia. *J. Neurosci.* 37, 129–140. doi: 10.1523/jneurosci.2891-16.2017

van Zandwijk, N., Pavlakis, N., Kao, S. C., Linton, A., Boyer, M. J., Clarke, S., et al. (2017). Safety and activity of microRNA-loaded minicells in patients with recurrent malignant pleural mesothelioma: a first-in-man, phase 1, open-label, dose-escalation study. *Lancet Oncol.* 18, 1386–1396. doi: 10.1016/s1470-2045(17)30621-6

Venna, V. R., Li, J., Hammond, M. D., Mancini, N. S., and Mccullough, L. D. (2014). Chronic metformin treatment improves post-stroke angiogenesis and recovery after experimental stroke. *Eur. J. Neurosci.* 39, 2129–2138. doi: 10.1111/ejn.12556

Vishnoi, A., and Rani, S. (2017). MiRNA biogenesis and regulation of diseases: an overview. *Methods Mol. Biol.* 1509, 1–10. doi: 10.1007/978-1-4939-6524-3_1

Wan, Y., Jin, H. J., Zhu, Y. Y., Fang, Z., Mao, L., He, Q., et al. (2018). MicroRNA-149-5p regulates blood-brain barrier permeability after transient middle cerebral artery occlusion in rats by targeting S1PR2 of pericytes. *FASEB J.* 32, 3133–3148. doi: 10.1096/fj.201701121r

Wanet, A., Tacheny, A., Arnould, T., and Renard, P. (2012). miR-212/132 expression and functions: within and beyond the neuronal compartment. *Nucleic Acids Res.* 40, 4742–4753. doi: 10.1093/nar/gks151

Wang, B., Zhu, X., Kim, Y., Li, J., Huang, S., Saleem, S., et al. (2012). Histone deacetylase inhibition activates transcription factor Nrf2 and protects against cerebral ischemic damage. *Free Radic. Biol. Med.* 52, 928–936. doi: 10.1016/j.freeradbiomed.2011.12.006

Wang, P., Liang, X., Lu, Y., Zhao, X., and Liang, J. (2016). MicroRNA-93 downregulation ameliorates cerebral ischemic injury through the Nrf2/HO-1 defense pathway. *Neurochem. Res.* 41, 2627–2635. doi: 10.1007/s11064-016-1975-0

Wang, Y., Huang, J., Ma, Y., Tang, G., Liu, Y., Chen, X., et al. (2015). MicroRNA-29b is a therapeutic target in cerebral ischemia associated with aquaporin 4. *J. Cereb. Blood Flow Metab.* 35, 1977–1984. doi: 10.1038/jcbfm.2015.156

Wang, Y., Wang, M. D., Xia, Y. P., Gao, Y., Zhu, Y. Y., Chen, S. C., et al. (2018). MicroRNA-130a regulates cerebral ischemia-induced blood-brain barrier permeability by targeting Homeobox A5. *FASEB J.* 32, 935–944. doi: 10.1096/fj.201700139rrr

Wang, Z., Leng, Y., Tsai, L. K., Leeds, P., and Chuang, D. M. (2011). Valproic acid attenuates blood-brain barrier disruption in a rat model of transient focal cerebral ischemia: the roles of HDAC and MMP-9 inhibition. *J. Cereb. Blood Flow Metab.* 31, 52–57. doi: 10.1038/jcbfm.2010.195

Wei, J. W., Huang, K., Yang, C., and Kang, C. S. (2017). Non-coding RNAs as regulators in epigenetics (Review). *Oncol. Rep.* 37, 3–9.

Weston, R. M., Lin, B., Dusting, G. J., and Roulston, C. L. (2013). Targeting oxidative stress injury after ischemic stroke in conscious rats: limited benefits with apocynin highlight the need to incorporate long term recovery. *Stroke Res. Treat.* 2013:648061.

Wong, Y.-H., Wu, C.-C., Lai, H.-Y., Jheng, B.-R., Weng, H.-Y., Chang, T.-H., et al. (2015). Identification of network-based biomarkers of cardioembolic stroke using a systems biology approach with time series data. *BMC Syst. Biol.* 9(Suppl 6):S4. doi: 10.1186/1752-0509-9-S6-S4

Wu, M. H., Huang, C. C., Chio, C. C., Tsai, K. J., Chang, C. P., Lin, N. K., et al. (2016). Inhibition of peripheral TNF-alpha and downregulation of microglial activation by alpha-lipoic acid and etanercept protect rat brain against ischemic stroke. *Mol. Neurobiol.* 53, 4961–4971. doi: 10.1007/s12035-015-9418-5

Xiang, W., Tian, C., Peng, S., Zhou, L., Pan, S., and Deng, Z. (2017). Let-7i attenuates human brain microvascular endothelial cell damage in oxygen glucose deprivation model by decreasing toll-like receptor 4 expression. *Biochem. Biophys. Res. Commun.* 493, 788–793. doi: 10.1016/j.bbrc.2017.08.093

Xu, B., He, X., Sui, Y., Wang, X., Wang, X., Ren, L., et al. (2019). Ginkgetin aglycone attenuates neuroinflammation and neuronal injury in the rats with ischemic stroke by modulating STAT3/JAK2/SIRT1. *Folia Neuropathol.* 57, 16–23. doi: 10.5114/fn.2019.83827

Xu, B., Zhang, Y., Du, X. F., Li, J., Zi, H. X., Bu, J. W., et al. (2017). Neurons secrete miR-132-containing exosomes to regulate brain vascular integrity. *Cell Res.* 27, 882–897. doi: 10.1038/cr.2017.62

Xu, H., Cao, Y., Yang, X., Cai, P., Kang, L., Zhu, X., et al. (2017). ADAMTS13 controls vascular remodeling by modifying VWF reactivity during stroke recovery. *Blood* 130, 11–22. doi: 10.1182/blood-2016-10-747089

Yamashita, K., Kataoka, Y., Sakurai-Yamashita, Y., Shigematsu, K., Himeno, A., Niwa, M., et al. (2000). Involvement of glial endothelin/nitric oxide in delayed neuronal death of rat hippocampus after transient forebrain ischemia. *Cell Mol. Neurobiol.* 20, 541–551.

Yamashita, T., and Abe, K. (2011). Therapeutic approaches to vascular protection in ischemic stroke. *Acta Med. Okayama.* 65, 219–223.

Yan, W., Zhang, W., Sun, L., Liu, Y., You, G., Wang, Y., et al. (2011). Identification of MMP-9 specific microRNA expression profile as potential targets of anti-invasion therapy in glioblastoma multiforme. *Brain Res.* 1411, 108–115. doi: 10.1016/j.brainres.2011.07.002

Yang, F., Zhou, L., Wang, D., Wang, Z., and Huang, Q. Y. (2015). Minocycline ameliorates hypoxia-induced blood-brain barrier damage by inhibition of HIF-1alpha through SIRT-3/PHD-2 degradation pathway. *Neuroscience* 304, 250–259. doi: 10.1016/j.neuroscience.2015.07.051

Yang, X., Geng, K.-Y., Zhang, Y.-S., Zhang, J.-F., Yang, K., Shao, J.-X., et al. (2018). Sirt3 deficiency impairs neurovascular recovery in ischemic stroke. *CNS Neurosci. Ther.* 24, 775–783. doi: 10.1111/cns.12853

Yang, S., Jin, H., Zhu, Y., Wan, Y., Opoku, E. N., Zhu, L., et al. (2017). Diverse functions and mechanisms of pericytes in ischemic stroke. *Curr. Neuropharmacol.* 15, 892–905.

Yang, Y., Salayandia, V. M., Thompson, J. F., Yang, L. Y., Estrada, E. Y., and Yang, Y. (2015). Attenuation of acute stroke injury in rat brain by minocycline promotes blood-brain barrier remodeling and alternative microglia/macrophage activation during recovery. *J. Neuroinflammation* 12:26. doi: 10.1186/s12974-015-0245-4

Yao, X., Wang, Y., and Zhang, D. (2018). microRNA-21 confers neuroprotection against cerebral ischemia-reperfusion injury and alleviates blood-brain barrier disruption in rats via the MAPK signaling pathway. *J. Mol. Neurosci.* 65, 43–53. doi: 10.1007/s12031-018-1067-5

Yao, Y., Chen, Z. L., Norris, E. H., and Strickland, S. (2014). Astrocytic laminin regulates pericyte differentiation and maintains blood brain barrier integrity. *Nat. Commun.* 5:3413.

Ye, P., Liu, J., He, F., Xu, W., and Yao, K. (2014). Hypoxia-induced deregulation of miR-126 and its regulative effect on VEGF and MMP-9 expression. *Int. J. Med. Sci.* 11, 17–23. doi: 10.7150/ijms.7329

Yin, K. J., Deng, Z., Hamblin, M., Xiang, Y., Huang, H., Zhang, J., et al. (2010). Peroxisome proliferator-activated receptor delta regulation of miR-15a in ischemia-induced cerebral vascular endothelial injury. *J. Neurosci.* 30, 6398–6408. doi: 10.1523/jneurosci.0780-10.2010

Yin, K. J., Fan, Y., Hamblin, M., Zhang, J., Zhu, T., Li, S., et al. (2013). KLF11 mediates PPARgamma cerebrovascular protection in ischaemic stroke. *Brain* 136, 1274–1287. doi: 10.1093/brain/awt002

Yin, K. J., Hamblin, M., and Chen, Y. E. (2015). Angiogenesis-regulating microRNAs and Ischemic Stroke. *Curr. Vasc. Pharmacol.* 13, 352–365. doi: 10.2174/1570161113119990016

Yu, A., Zhang, T., Duan, H., Pan, Y., Zhang, X., Yang, G., et al. (2017). MiR-124 contributes to M2 polarization of microglia and confers brain inflammatory protection via the C/EBP-alpha pathway in intracerebral hemorrhage. *Immunol. Lett.* 182, 1–11. doi: 10.1016/j.imlet.2016.12.003

Yuan, X., Chen, J., and Dai, M. (2016). Paeonol promotes microRNA-126 expression to inhibit monocyte adhesion to ox-LDL-injured vascular endothelial cells and block the activation of the PI3K/Akt/NF-kappaB pathway. *Int. J. Mol. Med.* 38, 1871–1878. doi: 10.3892/ijmm.2016.2778

Zagrean, A. M., Hermann, D. M., Opris, I., Zagrean, L., and Popa-Wagner, A. (2018). Multicellular crosstalk between exosomes and the neurovascular unit after cerebral ischemia. Therapeutic Implications. *Front. Neurosci.* 12:811. doi: 10.3389/fnins.2018.00811

Zehendner, C. M., Librizzi, L., De Curtis, M., Kuhlmann, C. R., and Luhmann, H. J. (2011). Caspase-3 contributes to ZO-1 and Cl-5 tight-junction disruption in rapid anoxic neurovascular unit damage. *PLoS One* 6:e16760. doi: 10.1371/journal.pone.0016760

Zeng, Y., and Chen, T. (2019). DNA methylation reprogramming during mammalian development. *Genes* 10:257 doi: 10.3390/genes10040257

Zhang, Q.-Y., Wang, Z.-J., Sun, D.-M., Wang, Y., Xu, P., Wu, W.-J., et al. (2017). Novel therapeutic effects of leonurine on ischemic stroke: new mechanisms of BBB integrity. *Oxid Med. Cell Longev.* 2017:7150376. doi: 10.1155/2017/7150376

Zhang, W., Wei, R., Zhang, L., Tan, Y., and Qian, C. (2017). Sirtuin 6 protects the brain from cerebral ischemia/reperfusion injury through NRF2 activation. *Neuroscience* 366, 95–104. doi: 10.1016/j.neuroscience.2017.09.035

Zheng, X.-W., Shan, C.-S., Xu, Q.-Q., Wang, Y., Shi, Y.-H., Wang, Y., et al. (2018). Buyang huanwu decoction targets SIRT1/VEGF pathway to promote angiogenesis after cerebral ischemia/reperfusion injury. *Front. Neurosci.* 12:911. doi: 10.3389/fnins.2018.00911

Zhou, W., Liesz, A., Bauer, H., Sommer, C., Lahrmann, B., Valous, N., et al. (2013). Postischemic brain infiltration of leukocyte subpopulations differs among murine permanent and transient focal cerebral ischemia models. *Brain Pathol.* 23, 34–44. doi: 10.1111/j.1750-3639.2012.00614.x

Zhu, H. L., Luo, W. Q., and Wang, H. (2008). Iptakalim protects against hypoxic brain injury through multiple pathways associated with ATP-sensitive potassium channels. *Neuroscience* 157, 884–894. doi: 10.1016/j.neuroscience.2008.09.033

Zhu, Z., Gan, X., and Yu, H. (2017). NFkappaBmiR15abFGF/VEGFA axis contributes to the impaired angiogenic capacity of BMMSCs in high fat dietfed mice. *Mol. Med. Rep.* 16, 7609–7616. doi: 10.3892/mmr.2017.7498

Conflict of Interest Statement: The authors declare that the research was conducted in the absence of any commercial or financial relationships that could be construed as a potential conflict of interest.

Copyright © 2019 Stamatovic, Phillips, Martinez-Revollar, Keep and Andjelkovic. This is an open-access article distributed under the terms of the Creative Commons Attribution License (CC BY). The use, distribution or reproduction in other forums is permitted, provided the original author(s) and the copyright owner(s) are credited and that the original publication in this journal is cited, in accordance with accepted academic practice. No use, distribution or reproduction is permitted which does not comply with these terms.

frontiers in Neuroscience

ORIGINAL RESEARCH
published: 21 August 2019
doi: 10.3389/fnins.2019.00888

Serial Metabolic Evaluation of Perihematomal Tissues in the Intracerebral Hemorrhage Pig Model

Muhammad E. Haque[1], Refaat E. Gabr[2], Sarah D. George[1], Xiurong Zhao[1], Seth B. Boren[1], Xu Zhang[3], Shun-Ming Ting[1], Gunghua Sun[1], Khader M. Hasan[2], Sean Savitz[1] and Jaroslaw Aronowski[1]*

[1] *Institute for Stroke and Cerebrovascular Diseases, McGovern Medical School, The University of Texas Health Science Center at Houston, Houston, TX, United States,* [2] *Diagnostic and Interventional Imaging, McGovern Medical School, The University of Texas Health Science Center at Houston, Houston, TX, United States,* [3] *Biostatistics, Epidemiology, and Research Design Component, Center for Clinical and Translational Sciences, McGovern Medical School, The University of Texas Health Science Center at Houston, Houston, TX, United States*

Purpose: Perihematomal edema (PHE) occurs in patients with intracerebral hemorrhage (ICH) and is often used as surrogate of secondary brain injury. PHE resolves over time, but little is known about the functional integrity of the tissues that recover from edema. In a pig ICH model, we aimed to assess metabolic integrity of perihematoma tissues by using non-invasive magnetic resonance spectroscopy (MRS).

Materials and Methods: Fourteen male Yorkshire pigs with an average age of 8 weeks were intracerebrally injected with autologous blood to produce ICH. Proton MRS data were obtained at 1, 7, and 14 days after ICH using a whole-body 3.0T MRI system. Point-resolved spectroscopy (PRESS)-localized 2D chemical shift imaging (CSI) was acquired. The concentration of *N*-Acetylaspartate (NAA), Choline (Cho), and Creatine (Cr) were measured within the area of PHE, tissues adjacent to the injury with no or negligible edema (ATNE), and contralesional brain tissue. A linear mixed model was used to analyze the evolution of metabolites in perihematomal tissues, with p-value < 0.05 indicating statistical significance.

Results: The perihematoma volume gradually decreased from 2.38 ± 1.23 ml to 0.41 ± 0.780 ml ($p < 0.001$) over 2 weeks. Significant ($p < 0.001$) reductions in NAA, Cr, and Cho concentrations were found in the PHE and ATNE regions compared to the contralesional hemisphere at day 1 and 7 after ICH. All three metabolites were significantly ($p < 0.001$) restored in the PHE tissue on day 14, but remained persistently low in the ATNE area, and unaltered in the contralesional voxel.

Conclusion: This study highlights the potential of MRS to probe salvageable tissues within the perihematoma in the sub-acute phase of ICH. Altered metabolites within the PHE and ATNE regions in addition to edema and hematoma volumes were explored as possible markers for tissue recovery. Perihematomal tissue with PHE demonstrated a more reversible injury compared to the tissue adjacent to the injury without edema, suggesting a potentially beneficial role of edema.

Keywords: intracerebral hemorrhage, pig ICH model, perihematomal edema, magnetic resonance spectroscopy, serial neuroimaging study

OPEN ACCESS

Edited by:
Aurel Popa-Wagner,
University Hospital Essen, Germany

Reviewed by:
Dazhi Liu,
University of California, Davis, United States
Guodong Cao,
University of Pittsburgh, United States

****Correspondence:***
Muhammad E. Haque
Muhammad.E.Haque@uth.tmc.edu

Specialty section:
This article was submitted to Neurodegeneration, a section of the journal Frontiers in Neuroscience

Received: *09 May 2019*
Accepted: *07 August 2019*
Published: *21 August 2019*

Citation:
Haque ME, Gabr RE, George SD, Zhao X, Boren SB, Zhang X, Ting S-M, Sun G, Hasan KM, Savitz S and Aronowski J (2019) Serial Metabolic Evaluation of Perihematomal Tissues in the Intracerebral Hemorrhage Pig Model. Front. Neurosci. 13:888. doi: 10.3389/fnins.2019.00888

INTRODUCTION

Intracerebral hemorrhage (ICH) often results in hemiparesis or hemiplegia. ICH accounts for about 10–15% of all strokes, and is associated with a high mortality and long-term disability rate (Feigin et al., 2009). ICH-induced deaths may occur within hours to days of the ictus (Feigin et al., 2009; Hemphill et al., 2015). The sequelae of ICH pathogenesis consist of primary injury with the rupture of blood vessels, physical compression, and disruption of brain tissues by the expanding blood mass. The secondary injury is associated with hematoma toxicity, oxidative stress, neuroinflammation, blood-brain barrier disruption, and consequent robust edema Perihematomal edema (PHE) (Wagner et al., 2003; Cherubini et al., 2005; Babu et al., 2012; Selim and Sheth, 2015; Lim-Hing and Rincon, 2017; Bernstein et al., 2018).

Initial cytotoxic edema progresses into mainly vasogenic edema, which is coupled with extravasation of blood fluid that contains plasma proteins, and has been proposed to contribute to additional injury (Xi et al., 2001; Keep et al., 2012a; Selim and Norton, 2018). One study reported a significant proportion of swollen cells in the inner and outer rims of the perihematoma with a small proportion of shrunken dark cells within 24 h after onset (Qureshi et al., 2001). ICH-induced neuroinflammation has been characterized by the presence of neutrophils, microglia, and macrophage/monocyte around the hemorrhagic foci (Castejon et al., 2005; Bakhshayesh et al., 2014; Zhao et al., 2007, 2017; Zhang et al., 2017). The location, expansion and retraction of hematoma and PHE volumes are used as a prognostic tool in humans and rodents (Aronowski and Hall, 2005; Falcone et al., 2013; Grunwald et al., 2017; Al-Shahi Salman et al., 2018; Klahr et al., 2018; Volbers et al., 2018). Because of the clinical importance of PHE, there is great interest to understand the pathophysiology and develop therapeutic agents targeting PHE. Serial and cross-sectional neuroimaging studies have reported a reduction of edema over time (Murthy et al., 2016; Ozdinc et al., 2016; Rodriguez-Luna et al., 2016; Liu et al., 2019), however, there is little known about the functional and structural restoration of those tissues after edema resolution.

N-acetylaspartate (NAA), choline (Cho), and creatine (Cr) are three major brain metabolites, seen on proton magnetic resonance spectroscopy (MRS) (^{1}H-MRS), which are often used as surrogate markers of neuronal health, cell proliferation, and cellular energy, respectively (Prado et al., 2002; Madhavarao and Namboodiri, 2006; Rigotti et al., 2007; Rackayova et al., 2017). Alterations in these metabolites were documented in patients with ischemic stroke, providing useful markers of tissue health (Fenstermacher and Narayana, 1990; Felber et al., 1992; Kang et al., 2000; Bivard et al., 2014). However, only a limited number of reports characterized these changes in patients with ICH (Kobayashi et al., 2001). Wagner reported a significant reduction in NAA in patients with a subarachnoid hemorrhage and Kobayashi reported a reduction in the ipsilesional NAA/Cr ratio in the motor cortex in patients with poor outcomes (Kobayashi et al., 2001; Wagner et al., 2013). Another study also demonstrated a significant reduction in NAA/Cr ratio in the primary motor cortices remote from the locus of injury (Yang et al., 2017). However, only few neuroimaging studies investigated metabolic changes in the PHE. Two studies by Carhuapoma et al. (2000, 2005) reported the presence of lactate and increased apparent diffusion coefficient in the PHE regions in ICH patients. In an animal study, Yin et al. (2006) showed significant apoptosis and reduction in NAA/Cr ratio in the PHE within 24 h of ICH onset. However, to the best of our knowledge, no study used spectroscopy to probe metabolic activities of the perihematoma region during post-ICH recovery, especially to understand the fate of peri-hematomal tissue regarding its functional recovery vs. irreversible damage.

The primary objective of this study was to assess the metabolic integrity of the perihematoma region over 2 weeks after injury using the ICH pig model. We used non-invasive MRS to probe neuronal viability/functionality in the perihematoma and the tissue adjacent to the injury with no apparent edema.

MATERIALS AND METHODS

Animal studies were approved by our institution's Animal Welfare Committee. The studies followed the guidelines outlined in the *Guide for the Care and Use of Laboratory Animals* from the National Institutes of Health.

Induction of ICH

Fourteen male Yorkshire pigs were studied with average age/weight of 8 ± 2 weeks/13.4 ± 2.4 kg. Procedural details were described elsewhere (Haque et al., 2018). Briefly, animals were sedated with ketamine (25 mg/kg, IM) and maintained under isoflurane throughout surgery. During the surgery, animals were wrapped in a blanket (to maintain body temperature), intubated, and catheterized to monitor physiological variables. To produce lobar ICH, a cranial burr hole was drilled 11 mm to the right of the sagittal and 11 mm anterior to the coronal suture. Hemorrhage was induced by pressure controlled infusion of autologous blood into the right frontal hemisphere, first 1.0 mL infused over 10 min followed by additional 1.5 ml after a 5 min interval.

Image Acquisition

Pigs were serially imaged on 1, 7, and 14 days after the surgery. During imaging, animals were ventilated with an average of 18 breaths-per-minute with maximum airway pressure of 20 cm-H_2O, oxygen saturation level (SpO_2) of 97%, typical end-tidal CO_2 of 47 mmHg, heart rate 120 beats-per-minute, and body temperature 98.6°C. Anesthesia was maintained with 2% isoflurane mixed with oxygen.

Animals were positioned prone in 3.0 Tesla Philips Ingenia MRI system (Philips, Best, Netherlands) and imaged using an eight-channel head coil. Anatomical imaging included: 3D T_1-weighted (TR/TE = 10/4.8 ms), 3D coronal T_2-weighted (TR/TE = 3500/267 ms), and 3D fluid attenuated inversion recovery (FLAIR, TR/TI/TE = 4800/1650/129 ms) with a field-of-view of 200 × 200 × 86 mm^3. Multivoxel spectral data were obtained using point resolved spectroscopy (PRESS)-localized two-dimensional chemical shift imaging (CSI) with

TR/TE = 2000/144 ms, matrix size = 9 × 9, bandwidth = 2000 Hz, and voxel size = 15 × 15 × 15 mm^3.

Spectral Analysis and Metabolite Quantification

All spectral integration and phase correction were performed manually using in-house software in Matlab (The Mathworks, Natick, MA, United States). The metabolite peaks at 2.01, 3.03, 3.19 ppm were referenced to NAA, Cr, and Cho, respectively, with respect to the unsuppressed water signal at 4.7 ppm. The absolute concentration of the metabolites was quantified using the unsuppressed water peak as an internal reference (Ernst et al., 1993; Kreis et al., 1993) with T_1 and T_2 correction for metabolite and water using the following equation:

$$C_m = \frac{A_m N_w (1-e^{-TR/T_{1w}}) e^{-TE/T_{2w}}}{A_w N_m (1-e^{-TR/T_{1m}}) e^{-TE/T_{2m}}} C_w \quad (1)$$

where C_m is metabolite concentration, A_m (A_w) is the area under the metabolite (water) peak, T_{1m} (T_{1w}) is the longitudinal relaxation time of metabolite (water), T_{2m} (T_{2w}) is the transverse relaxation time of metabolite (water), N_m (N_w) is the number of hydrogen atoms in the metabolite (water) molecule, TR is the repetition time, TE is echo time, and C_w is the reference water concentration in tissue. Previously reported T_{1m}, T_{1w}, T_{2m}, T_{2w}, and C_w at 3T systems were used in the calculation (Reyngoudt et al., 2010). Concentration is reported in milli-mole (mM) units.

To characterize biochemical events in brain tissue directly affected by ICH, we identified one voxel within the PHE, ATNE, and contralesional hemisphere and measured its absolute metabolite concentrations.

Lesion Volume Measurements

A semi-automated seed growing algorithm in Analyze 12.0 (Analyze Direct, Inc., KS, United States) was used to measure edema and hematoma volume on FLAIR images by a single rater. The rater selected two seed points within the hyperintense edema and hypointense hematoma and a region-growing algorithm automatically expanded the seed points within the 3D space of the image. Manual editing of the lesion volume was done when necessary.

Statistical Analysis

Cerebral metabolite concentrations were analyzed by the mixed model (Littell et al., 1998). The fixed effects in the model included brain regions (PHE, PHNE and contralesional), polychotomous time (1, 7, and 14 days), and interaction between hemisphere and polychotomous time. The random effects in the model included animal and interaction between animal and brain regions. These random effects led to a nested covariance matrix accounting for correlation of measurements due to the same animal and a different level of correlation for measurements due to the same hemisphere of the brain. The edema and hematoma volume were analyzed by the mixed models including polychotomous time as a fixed effect and animal as a random effect. Two-sided p-values of less than 0.05 were considered statistically significant. All statistical analyses were performed using the SAS software (version 9.4, the SAS Institute, Cary, NC, United States).

RESULTS

Twelve pigs completed all three imaging time points. One pig died during imaging on day 1 and was excluded from the analysis. Another pig died one day prior to the last imaging on day 14.

Representative MRI images demonstrating changes in the PHE region and hematoma volumes at three time points in a representative pig are shown in **Figure 1**. The computer calculated region of interest (ROIs) showing the boundaries were used to calculate the intracranial (ICV), hematoma, and edema volumes. There was no statistically significant change in ICV between day 1 (70.3 ± 6.5 ml), day 7 (72.9 ± 7.6 ml), and day 14 (74.2 ± 7.6 ml). ICH resulted in a 2.38 ± 1.23 ml PHE on day 1 that progressively resolved over the course of 2 weeks, reducing by 23.1% on day 7 and by 82.7% on day 14 ($p < 0.001$) (**Figure 1D**). Our model of ICH generated a hematoma volume of 1.00 ± 0.79 ml on day 1 after the surgery. The hematoma underwent progressive clearance and was reduced by 15.7% on day 7 and by 38.3% on day 14 ($p < 0.001$), as compared to day 1 (**Figure 1E**), indicating effective hematoma clearance.

Representative anatomical locations of MRS data collection are illustrated in **Figures 2A–C**. The locations were similarly applied across all 13 analyzed pigs and were selected on day 1 to signify presence of PHE, adjacent non-edematous tissues (ATNE), and the contralesional brain tissue. Our analyses demonstrate a clear pattern of metabolite loss around the hematoma at day 1 after ICH with strong restoration of NAA and Cho concentrations in the PHE, and unexpectedly poor restoration of all the metabolites in ATNE tissue, as assessed on day 7 and day 14 (**Figures 2D–L**). Specifically, the NAA concentration in both PHE and ATNE regions was reduced ($p < 0.001$) in response to ICH, as compared to contralesional tissue on day 1 and day 7 (**Figure 3A**), suggesting that ICH imposes dysfunction that affects neurons in the perilesional brain. The loss in NAA was transient in the PHE regions, as NAA was largely restored by day 14. Unexpectedly, NAA in the ATNE was still reduced 2 weeks after ICH, suggesting the more permanent nature of injury/dysfunction in the region containing no edema than in the regions spared by edema. The NAA concentration in PHE recovered from 9.70 ± 2.7 mM at day 1 to 14.79 ± 2.5 mM ($p < 0.001$) at day 14, values equivalent to NAA levels in the contralesional region. However, there was virtually no recovery in NAA content in the ATNE between day 1 and 14 (9.45 ± 3.1 vs. 9.99 ± 2.1 mM, $p = 0.51$). There was no change in NAA content in contralesional regions (13.7 ± 2.1 vs. 14.5 ± 2.0, $p = 0.36$) between the first and last time points.

As compared to the contralesional tissue, the Cr concentration in response to ICH was reduced ($p < 0.001$) within both the PHE and ATNE regions and remained reduced for 14 days, through the end of the experiment (**Figure 3B**). Unlike in the case of NAA, which was fully restored, Cr levels both in PHE and ATNE were only partially restored (3.62 ± 1.7 mM to 6.23 ± 2.9 mM; $p = 0.001$ for PHE and 3.46 ± 1.2 vs. 5.15 ± 2.4 mM, $p = 0.023$

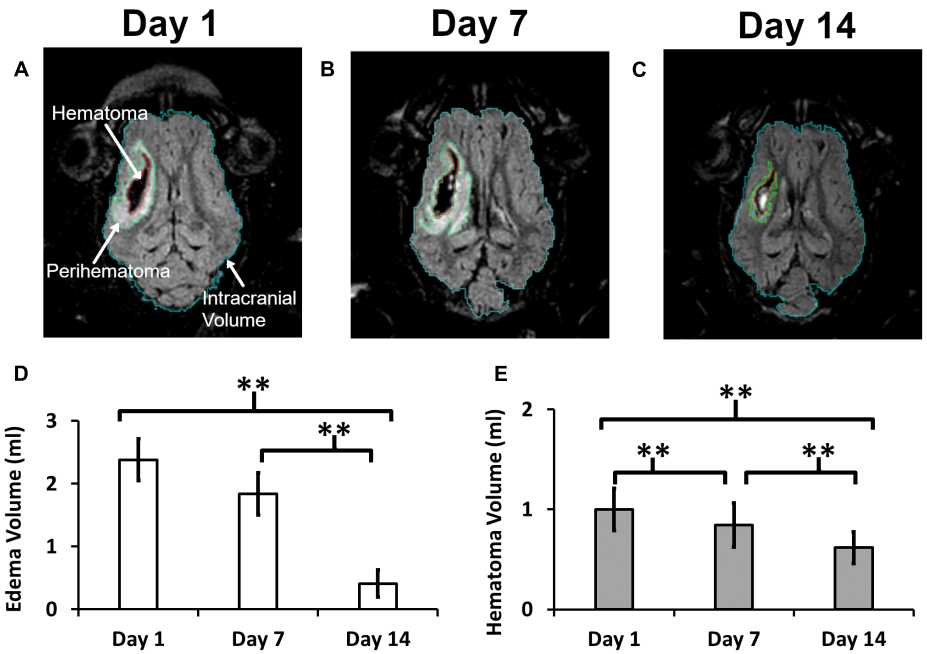

FIGURE 1 | A quantitative summary of the change in hematoma and edema volume in a post-ICH pig brain. Panels **(A–C)** illustrate a representative MRI image showing outlined boundaries of intracranial volume, perihematoma, and hematoma at days 1, 7, and 14, respectively. Panels **(D,E)** show Perihematoma edema **(D)** and hematoma **(E)** volumes. A double asterisk (**) denotes the significant temporal ipsilesional difference between the time point ($p < 0.05$). The error bars represent standard error in the mean.

for ATNE) 14 days after ICH as compared to contralesional tissue that was not affected by ICH (9.43 ± 2.2 mM vs. 10.7 ± 2.3 mM, $p = 0.08$).

Cho concentrations in the PHE and ATNE were also sharply reduced as determined on day 1 and 7 after ICH ($p < 0.001$), compared to the contralesional side (**Figure 3C**). The Cho levels were restored by day 14 in the PHE, but no signs of recovery were seen at this time point in ATNE. Cho concentration was unchanging in the contralesional side throughout the experiment.

There was no significant correlation between hematoma and edema volume with NAA, Cr, and Cho in all three spectroscopic voxel locations. No change was seen in the ratio of water signals between PHE, ATNE, and the contralesional side over time (P = NS), suggesting that the observed patterns of metabolic alterations are not due to changes in the reference tissue water content.

DISCUSSION

It is generally accepted that autologous blood infusion animal models provide a strong translational platform for studying the pathogenesis of ICH and testing therapeutic approaches (Wagner et al., 1999; Andaluz et al., 2002; Gu et al., 2009). The present study evaluated temporal metabolic changes in the perihematoma region using MRS in a piglet model of ICH. As compared to the rodent models of ICH, the larger brain size of piglets and thus ability to generate larger hematoma aids in the more qualitative and quantitative analyses of the changes in the perihematomal regions. Our present study compared metabolic heterogeneity in the perihematomal/ICH-adjacent tissue, sampled to capture metabolites within the edema-affected tissue (PHE) and the location devoid of edema (ATNE). We found that the concentrations of three measured metabolites (NAA, Cho and Cr) were reduced as early as day 1 after ICH in both PHE and ATNE regions. However, over the course of 14 days these metabolites were largely restored in the PHE, but not in the ATNE. These data suggest the potential of MR spectroscopy to identify salvageable tissue around the hematoma. Since perihematomal tissue demonstrating edema recovered more effectively from metabolic disturbances, our data may suggest that edema could play a homeostatic role regarding integrity of perihematomal tissue.

NAA and *N*-Acetylaspartylglutamate (NAAG) are both synthetized by neurons in the brain and upon secretion are internalized and metabolized by glial cells (Baslow, 2010). Both NAA and NAAG produce overlapping magnetic resonance spectral peaks at 2.01 ppm, not permitting differentiation between the individual metabolites. The consensus is that NAA concentration is a total (NAA ++ NAAG) concentration. Reduction of NAA concentration typically reflects some types of neuronal dysfunction or direct neuronal loss. Since ICH is known to produce extensive brain damage either through mass effect-mediated injury or through biochemical-mediated injury via toxic products of blood, blood-brain-barrier disruption, and brain edema (Aronowski and Zhao, 2011; Keep et al., 2012b; Bobinger et al., 2018), neurons surrounding the hematoma are

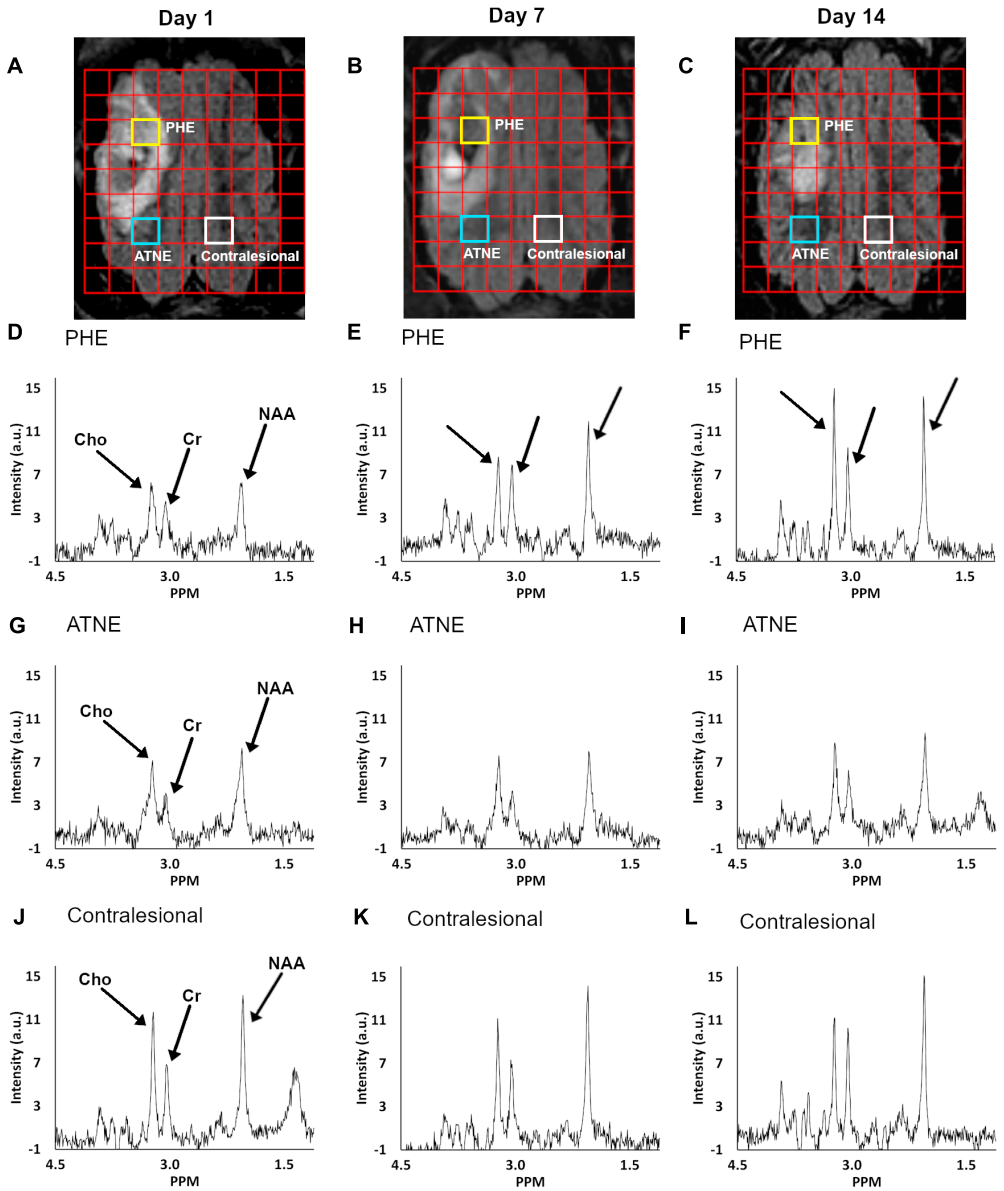

FIGURE 2 | Serial FLAIR MRI images overlaid with a multi-voxel grid of corresponding temporal spectra with highlighted voxels of interest **(A–C)**. Panels **(A–C)** show the PHE, ATNE, and contralesional voxel location at day 1, 7, and 14, respectively, from which the metabolite spectra were measured. MR spectroscopy graphs at days 1, 7, and 14 (columns) are shown for voxels from the PHE **(D–F)**, ATNE **(G–I)**, and the contralesional regions **(J–L)**.

adversely affected by ICH. Thus, it is not surprising that NAA levels in tissue close to the hematoma both in areas with and without edema show significant reduction at day 1 after ICH. However, the essential question is whether this early neuronal injury is transient and associated with reversible damage. Our results indicate that NAA gradually recovered in the PHE but not in the ATNE. Ultimately, these results suggest that neural tissue integrity, at least in the PHE region, is retained after ICH. The irreversible decline of NAA in the ATNE suggests more permanent metabolic dysfunction or neuronal loss. Our data also raise the possibility that the presence of edema could provide a protective cushioning from irreversible damage.

Creatine is a key molecule in the regulation of energy metabolism in the brain and is responsible for re-synthesis of ATP in glial cells (Rackayova et al., 2017). Here we found a significant loss of Cr levels in both the PHE and ATNE regions, suggesting either higher cellular energy demand-mediated depletion of (increased catabolism) Cr and/or its reduced synthesis. In contrast to the transient nature of NAA reduction in the PHE region, the Cr level decline was more sustained and still significantly reduced in both the PHE and ATNE regions at 14 days after ICH. However, over time a weak increasing trend of Cr concentration in both the PHE and ATNE regions suggests regional variance in metabolic dysfunction around the

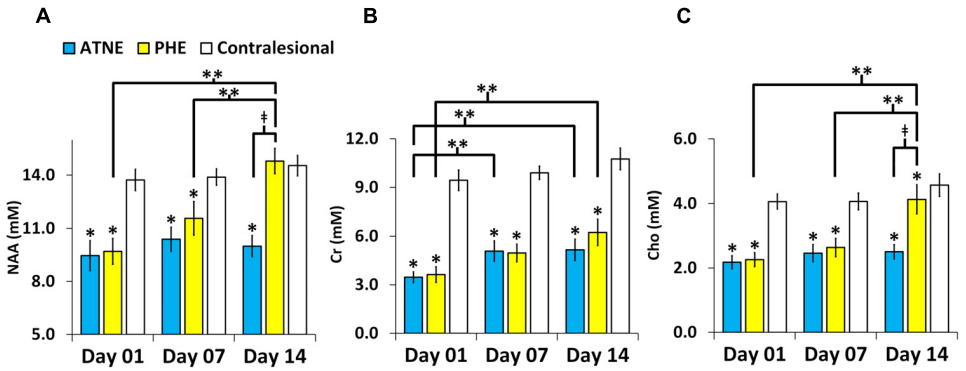

FIGURE 3 | Metabolite concentration in the perihematomal edema (PHE), adjacent tissues with no edema (ATNE), and contralesional voxels over two week follow-up post ICH. **(A–C)** Represent serial NAA, Cr, and Cho concentrations, respectively. The asterisk (*) denotes significant ($p < 0.001$) hemispheric differences, the double asterisk (**) denotes significant ($p < 0.001$) temporal difference and (‡) denotes significant ($p < 0.001$) change between PHE and ATNE. The error bars represent standard error in the mean.

injury. Often, Cr levels are presumed to be constant and have been utilized as a normalizing factor in reporting metabolite concentrations. While this assumption is valid for a healthy brain, under certain pathological conditions Cr levels are altered (Burklen et al., 2006; Andres et al., 2008), including in our study. Thus, appropriate caution must be taken using Cr as a constant value under pathological conditions and reporting metabolite concentrations relative to Cr.

Unlike other pathologies where an elevated concentration of choline has been recognized as a marker of progressive pathologies (Fayed et al., 2008; Karaszewski et al., 2010), here we are reporting a significant reduction in choline in both the PHE and ATNE during the first 7 days after ICH onset. By day 14, choline is restored in the PHE but not in the ATNE region, suggesting transient and sustainable metabolic dysfunction, respectively. Choline, which is localized in all types of cells, serves as a marker for overall membrane integrity, and as such in reference to our study, suggests that the integrity of cell membranes varies around brain tissue surrounding the hematoma. Previously in ischemic stroke animal studies an inverse relation between regional cerebral blood flow (CBF) and choline concentration had been documented (Scremin and Jenden, 1991). The relation between regional metabolic variation and CBF in the ICH model will be further investigated in the future. In addition, the changes in all three metabolite concentrations over time in the PHE, as compared to the absence of changes in the contralesional hemisphere, not only validate the methodology but also suggests a hemispheric rather than global compromise in response to ICH in this model.

In our piglet ICH model, we attempted to generate a modest size hematoma that results in a modest level of edema, which did not result in midline shift or cause too severe mass effect that inflicts irreversible injury and morbidity, as it happens in many humans with large bleeds. This approach allowed for more "uncontaminated" probing of the metabolic characteristics in the perihematomal zone, specifically edema-affected brain tissue vs. perihematomal non-edematous brain tissue. Here, we unexpectedly found the more effective reversal of metabolite levels in the PHE regions as compared to the non-edematous tissue. We certainly predict that the mild edema is beneficial and not detrimental compared to larger degrees of peri-hematoma edema, which leads to compression of local microvasculature resulting in hypoperfusion and compression of white matter tract resulting in anomalous nerve conduction. Collectively, this data may suggest potential beneficial function for mild edema in re-establishing homeostasis in peri-hematoma tissue after ICH.

Our study is limited by a small sample size and will need to be reproduced in larger studies. Another limitation is the variation in edema volume among animals induces partial volume effects in the PHE voxels with normal appearing tissues. In addition, the evolution of hematoma over time also complicates voxel placement and induces partial volume effects. Validation of our findings will require additional studies including PHE tissue histology and *in vitro* metabolite concentration measurements using mass spectrometry or High Performance Liquid Chromatography (HPLC).

In conclusion, this study demonstrated the possible application of MR spectroscopy in monitoring the sub-acute phase of ICH to identify salvageable tissue in the perihematoma region. Also, reversible metabolic recovery in the PHE as compared to the tissue adjacent to the injury without edema, suggesting the potentially beneficial role of edema.

DATA AVAILABILITY

The datasets generated for this study are available on request to the corresponding author.

ETHICS STATEMENT

Animal studies were approved by our institution's Animal Welfare Committee. The studies followed the guidelines outlined in the Guide for the Care and Use of Laboratory Animals from the National Institutes of Health.

AUTHOR CONTRIBUTIONS

MH designed the study, carried out MRI quantitative analysis, and drafted the manuscript. RG wrote Matlab code for spectral integration and assisted in optimizing MRI acquisition. XiZ induced hematoma and supervised the surgery. SG and SB performed regions of interest analysis and generated final plots and figures. KH provided qualitative and quantitative quality assurance of data analysis. XuZ performed statistical analysis. S-MT and GS performed animal surgery. SS supervised the study, edited manuscript, and provided necessary resources. JA is the PI of the study.

FUNDING

This work was supported by National Institute of Health/National Institute of Neurological Disorders and Stroke 5R42NS090650-03.

ACKNOWLEDGMENTS

The authors thank Dr. Christopher Smith and veterinarian team for surgical and technical assistance and Mr. Vipulkumar Patel for help with MRI experiments.

REFERENCES

Al-Shahi Salman, R., Frantzias, J., Lee, R. J., Lyden, P. D., Battey, T. W. K., Ayres, A. M., et al. (2018). Absolute risk and predictors of the growth of acute spontaneous intracerebral haemorrhage: a systematic review and meta-analysis of individual patient data. *Lancet Neurol.* 17, 885–894. doi: 10.1016/S1474-4422(18)30253-9

Andaluz, N., Zuccarello, M., and Wagner, K. R. (2002). Experimental animal models of intracerebral hemorrhage. *Neurosurg. Clin. N Am.* 13, 385–393. doi: 10.1016/s1042-3680(02)00006-2

Andres, R. H., Ducray, A. D., Schlattner, U., Wallimann, T., and Widmer, H. R. (2008). Functions and effects of creatine in the central nervous system. *Brain Res. Bull.* 76, 329–343. doi: 10.1016/j.brainresbull.2008.02.035

Aronowski, J., and Hall, C. E. (2005). New horizons for primary intracerebral hemorrhage treatment: experience from preclinical studies. *Neurol. Res.* 27, 268–279. doi: 10.1179/016164105x25225

Aronowski, J., and Zhao, X. (2011). Molecular pathophysiology of cerebral hemorrhage: secondary brain injury. *Stroke* 42, 1781–1786. doi: 10.1161/STROKEAHA.110.596718

Babu, R., Bagley, J. H., Di, C., Friedman, A. H., and Adamson, C. (2012). Thrombin and hemin as central factors in the mechanisms of intracerebral hemorrhage-induced secondary brain injury and as potential targets for intervention. *Neurosurg. Focus* 32:E8. doi: 10.3171/2012.1.FOCUS11366

Bakhshayesh, B., Hosseininezhad, M., Saadat, S. N., Ansar, M. M., Ramezani, H., and Saadat, S. M. (2014). Iron overload is associated with perihematoma edema growth following intracerebral hemorrhage that may contribute to in-hospital mortality and long-term functional outcome. *Curr. Neurovasc. Res.* 11, 248–253. doi: 10.2174/1567202611666140530124855

Baslow, M. H. (2010). Evidence that the tri-cellular metabolism of N-acetylaspartate functions as the brain's "operating system": how NAA metabolism supports meaningful intercellular frequency-encoded communications. *Amino Acids* 39, 1139–1145. doi: 10.1007/s00726-010-0656-6

Bernstein, J. E., Savla, P., Dong, F., Zampella, B., Wiginton, J. G. T., Miulli, D. E., et al. (2018). Inflammatory markers and severity of intracerebral hemorrhage. *Cureus* 10:e3529. doi: 10.7759/cureus.3529

Bivard, A., Krishnamurthy, V., Stanwell, P., Yassi, N., Spratt, N. J., Nilsson, M., et al. (2014). Spectroscopy of reperfused tissue after stroke reveals heightened metabolism in patients with good clinical outcomes. *J. Cereb. Blood Flow Metab.* 34, 1944–1950. doi: 10.1038/jcbfm.2014.166

Bobinger, T., Burkardt, P., Huttner, B. H., and Manaenko, A. (2018). Programmed cell death after intracerebral hemorrhage. *Curr. Neuropharmacol.* 16, 1267–1281. doi: 10.2174/1570159X15666170602112851

Burklen, T. S., Schlattner, U., Homayouni, R., Gough, K., Rak, M., Szeghalmi, A., et al. (2006). The creatine kinase/creatine connection to Alzheimer's disease: CK-inactivation. APP-CK complexes and focal creatine deposits. *J. Biomed Biotechnol.* 2006:35936. doi: 10.1155/JBB/2006/35936

Carhuapoma, J. R., Wang, P., Beauchamp, N. J., Hanley, D. F., and Barker, P. B. (2005). Diffusion-perfusion MR evaluation and spectroscopy before and after surgical therapy for intracerebral hemorrhage. *Neurocrit. Care* 2, 23–27. doi: 10.1385/NCC:2:1:023

Carhuapoma, J. R., Wang, P. Y., Beauchamp, N. J., Keyl, P. M., Hanley, D. F., and Barker, P. B. (2000). Diffusion-weighted MRI and proton MR spectroscopic imaging in the study of secondary neuronal injury after intracerebral hemorrhage. *Stroke* 31, 726–732. doi: 10.1161/01.str.31.3.726

Castejon, O. J., Castellano, A., Arismendi, G. J., and Medina, Z. (2005). The inflammatory reaction in human traumatic oedematous cerebral cortex. *J. Submicrosc. Cytol. Pathol.* 37, 43–52.

Cherubini, A., Ruggiero, C., Polidori, M. C., and Mecocci, P. (2005). Potential markers of oxidative stress in stroke. *Free Radic. Biol. Med.* 39, 841–852. doi: 10.1016/j.freeradbiomed.2005.06.025

Ernst, T., Lee, J. H., and Ross, B. D. (1993). Direct 31P imaging in human limb and brain. *J. Comput. Assist. Tomogr.* 17, 673–680. doi: 10.1097/00004728-199309000-00001

Falcone, G. J., Biffi, A., Brouwers, H. B., Anderson, C. D., Battey, T. W., Ayres, A. M., et al. (2013). Predictors of hematoma volume in deep and lobar supratentorial intracerebral hemorrhage. *JAMA Neurol.* 70, 988–994. doi: 10.1001/jamaneurol.2013.98

Fayed, N., Davila, J., Medrano, J., and Olmos, S. (2008). Malignancy assessment of brain tumours with magnetic resonance spectroscopy and dynamic susceptibility contrast MRI. *Eur. J. Radiol.* 67, 427–433. doi: 10.1016/j.ejrad.2008.02.039

Feigin, V. L., Lawes, C. M., Bennett, D. A., Barker-Collo, S. L., and Parag, V. (2009). Worldwide stroke incidence and early case fatality reported in 56 population-based studies: a systematic review. *Lancet Neurol.* 8, 355–369. doi: 10.1016/S1474-4422(09)70025-0

Felber, S. R., Luef, G. J., Birbamer, G. G., Aichner, F. T., and Gerstenbrand, F. (1992). Magnetic resonance studies in stroke. *Lancet* 339, 879–880. doi: 10.1016/0140-6736(92)90328-z

Fenstermacher, M. J., and Narayana, P. A. (1990). Serial proton magnetic resonance spectroscopy of ischemic brain injury in humans. *Invest. Radiol.* 25, 1034–1039. doi: 10.1097/00004424-199009000-00016

Grunwald, Z., Beslow, L. A., Urday, S., Vashkevich, A., Ayres, A., Greenberg, S. M., et al. (2017). Perihematomal edema expansion rates and patient outcomes in deep and lobar intracerebral hemorrhage. *Neurocrit. Care* 26, 205–212. doi: 10.1007/s12028-016-0321-3

Gu, Y., Hua, Y., Keep, R. F., Morgenstern, L. B., and Xi, G. (2009). Deferoxamine reduces intracerebral hematoma-induced iron accumulation and neuronal death in piglets. *Stroke* 40, 2241–2243. doi: 10.1161/STROKEAHA.108.539536

Haque, M. E., Gabr, R. E., Zhao, X., Hasan, K. M., Valenzuela, A., Narayana, P. A., et al. (2018). Serial quantitative neuroimaging of iron in the intracerebral hemorrhage pig model. *J. Cereb. Blood Flow Metab.* 38, 375–381. doi: 10.1177/0271678X17751548

Hemphill, J. C., Greenberg, S. M., Anderson, C. S., Becker, K., Bendok, B. R., Cushman, M., et al. (2015). Guidelines for the management of spontaneous intracerebral hemorrhage: a guideline for healthcare professionals from the American heart Association/American Stroke Association. *Stroke* 46, 2032–2060. doi: 10.1161/str.0000000000000069

Kang, D. W., Roh, J. K., Lee, Y. S., Song, I. C., Yoon, B. W., and Chang, K. H. (2000). Neuronal metabolic changes in the cortical region after subcortical infarction: a proton MR spectroscopy study. *J. Neurol. Neurosurg. Psychiatry* 69, 222–227. doi: 10.1136/jnnp.69.2.222

Karaszewski, B., Thomas, R. G., Chappell, F. M., Armitage, P. A., Carpenter, T. K., Lymer, G. K., et al. (2010). Brain choline concentration. Early quantitative marker of ischemia and infarct expansion?. *Neurology* 75, 850–856. doi: 10.1212/WNL.0b013e3181f11bf1

Keep, R. F., Hua, Y., and Xi, G. (2012a). Brain water content. A misunderstood measurement? *Transl. Stroke Res.* 3, 263–265. doi: 10.1007/s12975-012-0152-2

Keep, R. F., Hua, Y., and Xi, G. (2012b). Intracerebral haemorrhage: mechanisms of injury and therapeutic targets. *Lancet Neurol.* 11, 720–731. doi: 10.1016/s1474-4422(12)70104-7

Klahr, A. C., Kate, M., Kosior, J., Buck, B., Shuaib, A., Emery, D., et al. (2018). Early hematoma retraction in intracerebral hemorrhage is uncommon and does not predict outcome. *PLoS One* 13:e0205436. doi: 10.1371/journal.pone.0205436

Kobayashi, M., Takayama, H., Suga, S., and Mihara, B. (2001). Longitudinal changes of metabolites in frontal lobes after hemorrhagic stroke of basal ganglia: a proton magnetic resonance spectroscopy study. *Stroke* 32, 2237–2245. doi: 10.1161/hs1001.096621

Kreis, R., Ernst, T., and Ross, B. D. (1993). Development of the human brain: in vivo quantification of metabolite and water content with proton magnetic resonance spectroscopy. *Magn. Reson. Med.* 30, 424–437. doi: 10.1002/mrm.1910300405

Lim-Hing, K., and Rincon, F. (2017). Secondary hematoma expansion and perihemorrhagic edema after intracerebral hemorrhage: from bench work to practical aspects. *Front. Neurol.* 8:74. doi: 10.3389/fneur.2017.00074

Littell, R. C., Henry, P. R., and Ammerman, C. B. (1998). Statistical analysis of repeated measures data using SAS procedures. *J. Anim. Sci.* 76, 1216–1231. doi: 10.2527/1998.7641216x

Liu, R., Li, H., Hua, Y., Keep, R. F., Xiao, J., Xi, G., et al. (2019). Early Hemolysis within human intracerebral hematomas: an MRI study. *Transl. Stroke Res.* 10, 52–56. doi: 10.1007/s12975-018-0630-2

Madhavarao, C. N., and Namboodiri, A. M. (2006). NAA synthesis and functional roles. *Adv. Exp. Med. Biol.* 576, 49–66. doi: 10.1007/0-387-30172-0_4

Murthy, S. B., Urday, S., Beslow, L. A., Dawson, J., Lees, K., Kimberly, W. T., et al. (2016). Rate of perihaematomal oedema expansion is associated with poor clinical outcomes in intracerebral haemorrhage. *J. Neurol. Neurosurg. Psychiatry* 87, 1169–1173. doi: 10.1136/jnnp-2016-313653

Ozdinc, S., Unlu, E., Karakaya, Z., Turamanlar, O., Dogan, N., Isler, Y., et al. (2016). Prognostic value of perihematomal edema area at the initial ED presentation in patients with intracranial hematoma. *Am. J. Emerg. Med.* 34, 1241–1246. doi: 10.1016/j.ajem.2016.03.048

Prado, M. A., Reis, R. A., Prado, V. F., De Mello, M. C., Gomez, M. V., and De Mello, F. G. (2002). Regulation of acetylcholine synthesis and storage. *Neurochem. Int.* 41, 291–299. doi: 10.1016/s0197-0186(02)00044-x

Qureshi, A. I., Ling, G. S., Khan, J., Suri, M. F., Miskolczi, L., Guterman, L. R., et al. (2001). Quantitative analysis of injured, necrotic, and apoptotic cells in a new experimental model of intracerebral hemorrhage. *Crit. Care Med.* 29, 152–157. doi: 10.1097/00003246-200101000-00030

Rackayova, V., Cudalbu, C., Pouwels, P. J. W., and Braissant, O. (2017). Creatine in the central nervous system: from magnetic resonance spectroscopy to creatine deficiencies. *Anal. Biochem.* 529, 144–157. doi: 10.1016/j.ab.2016.11.007

Reyngoudt, H., De Deene, Y., Descamps, B., Paemeleire, K., and Achten, E. (2010). (1)H-MRS of brain metabolites in migraine without aura: absolute quantification using the phantom replacement technique. *MAGMA* 23, 227–241. doi: 10.1007/s10334-010-0221-z

Rigotti, D. J., Inglese, M., and Gonen, O. (2007). Whole-brain N-acetylaspartate as a surrogate marker of neuronal damage in diffuse neurologic disorders. *AJNR Am. J. Neuroradiol.* 28, 1843–1849. doi: 10.3174/ajnr.a0774

Rodriguez-Luna, D., Coscojuela, P., Rubiera, M., Hill, M. D., Dowlatshahi, D., Aviv, R. I., et al. (2016). Ultraearly hematoma growth in active intracerebral hemorrhage. *Neurology* 87, 357–364. doi: 10.1212/WNL.0000000000002897

Scremin, O. U., and Jenden, D. J. (1991). Time-dependent changes in cerebral choline and acetylcholine induced by transient global ischemia in rats. *Stroke* 22, 643–647. doi: 10.1161/01.str.22.5.643

Selim, M., and Norton, C. (2018). Perihematomal edema: Implications for intracerebral hemorrhage research and therapeutic advances. *J. Neurosci. Res.* doi: 10.1002/jnr.24372 [Epub ahead of print].

Selim, M., and Sheth, K. N. (2015). Perihematoma edema: a potential translational target in intracerebral hemorrhage? *Transl. Stroke Res.* 6, 104–106. doi: 10.1007/s12975-015-0389-7

Volbers, B., Giede-Jeppe, A., Gerner, S. T., Sembill, J. A., Kuramatsu, J. B., Lang, S., et al. (2018). Peak perihemorrhagic edema correlates with functional outcome in intracerebral hemorrhage. *Neurology* 90, e1005–e1012. doi: 10.1212/WNL.0000000000005167

Wagner, K. R., Sharp, F. R., Ardizzone, T. D., Lu, A., and Clark, J. F. (2003). Heme and iron metabolism: role in cerebral hemorrhage. *J. Cereb. Blood Flow Metab.* 23, 629–652. doi: 10.1097/01.wcb.0000073905.87928.6d

Wagner, K. R., Xi, G., Hua, Y., Zuccarello, M., De Courten-Myers, G. M., Broderick, J. P., et al. (1999). Ultra-early clot aspiration after lysis with tissue plasminogen activator in a porcine model of intracerebral hemorrhage: edema reduction and blood-brain barrier protection. *J. Neurosurg.* 90, 491–498. doi: 10.3171/jns.1999.90.3.0491

Wagner, M., Jurcoane, A., Hildebrand, C., Guresir, E., Vatter, H., Zanella, F. E., et al. (2013). Metabolic changes in patients with aneurysmal subarachnoid hemorrhage apart from perfusion deficits: neuronal mitochondrial injury? *AJNR Am. J. Neuroradiol.* 34, 1535–1541. doi: 10.3174/ajnr.A3420

Xi, G., Hua, Y., Bhasin, R. R., Ennis, S. R., Keep, R. F., and Hoff, J. T. (2001). Mechanisms of edema formation after intracerebral hemorrhage: effects of extravasated red blood cells on blood flow and blood-brain barrier integrity. *Stroke* 32, 2932–2938. doi: 10.1161/hs1201.099820

Yang, J., Li, Q., Wang, Z., Qi, C., Han, X., Lan, X., et al. (2017). Multimodality MRI assessment of grey and white matter injury and blood-brain barrier disruption after intracerebral haemorrhage in mice. *Sci. Rep.* 7:40358. doi: 10.1038/srep40358

Yin, X., Zhang, X., Wang, W., Chang, L., Jiang, Y., and Zhang, S. (2006). Perihematoma damage at different time points in experimental intracerebral hemorrhage. *J. Huazhong. Univ. Sci. Technolog. Med. Sci.* 26, 59–62. doi: 10.1007/bf02828039

Zhang, Z., Zhang, Z., Lu, H., Yang, Q., Wu, H., and Wang, J. (2017). Microglial polarization and inflammatory mediators after intracerebral hemorrhage. *Mol. Neurobiol.* 54, 1874–1886. doi: 10.1007/s12035-016-9785-6

Zhao, X., Sun, G., Zhang, J., Strong, R., Song, W., Gonzales, N., et al. (2007). Hematoma resolution as a target for intracerebral hemorrhage treatment: role for peroxisome proliferator-activated receptor gamma in microglia/macrophages. *Ann. Neurol.* 61, 352–362. doi: 10.1002/ana.21097

Zhao, X., Ting, S. M., Liu, C. H., Sun, G., Kruzel, M., Roy-O'reilly, M., et al. (2017). Neutrophil polarization by IL-27 as a therapeutic target for intracerebral hemorrhage. *Nat. Commun.* 8:602. doi: 10.1038/s41467-017-00770-7

Conflict of Interest Statement: The authors declare that the research was conducted in the absence of any commercial or financial relationships that could be construed as a potential conflict of interest.

Copyright © 2019 Haque, Gabr, George, Zhao, Boren, Zhang, Ting, Sun, Hasan, Savitz and Aronowski. This is an open-access article distributed under the terms of the Creative Commons Attribution License (CC BY). The use, distribution or reproduction in other forums is permitted, provided the original author(s) and the copyright owner(s) are credited and that the original publication in this journal is cited, in accordance with accepted academic practice. No use, distribution or reproduction is permitted which does not comply with these terms.

frontiers in Neurology

SYSTEMATIC REVIEW
published: 27 August 2019
doi: 10.3389/fneur.2019.00924

The Potential of Biomaterial-Based Approaches as Therapies for Ischemic Stroke: A Systematic Review and Meta-Analysis of Pre-clinical Studies

Faye Bolan[1†], *Irene Louca*[1†], *Calvin Heal*[2] *and Catriona J. Cunningham*[1*]

[1] Division of Neuroscience and Experimental Psychology, Faculty of Biology, Medicine and Health, School of Biological Sciences, University of Manchester, Manchester, United Kingdom, [2] Faculty of Biology, Medicine and Health, Centre for Biostatistics, Academic Health Sciences Centre, University of Manchester, Manchester, United Kingdom

OPEN ACCESS

Edited by:
Johannes Boltze,
University of Warwick,
United Kingdom

Reviewed by:
Claire Gibson,
University of Nottingham,
United Kingdom
Jialing Liu,
University of California, San Francisco,
United States

***Correspondence:**
Catriona J. Cunningham
catriona.cunningham@
manchester.ac.uk

[†]These authors have contributed equally to this work

Specialty section:
This article was submitted to Stroke, a section of the journal Frontiers in Neurology

Received: 29 March 2019
Accepted: 09 August 2019
Published: 27 August 2019

Citation:
Bolan F, Louca I, Heal C and Cunningham CJ (2019) The Potential of Biomaterial-Based Approaches as Therapies for Ischemic Stroke: A Systematic Review and Meta-Analysis of Pre-clinical Studies. Front. Neurol. 10:924. doi: 10.3389/fneur.2019.00924

Background: In recent years pre-clinical stroke research has shown increased interest in the development of biomaterial-based therapies to promote tissue repair and functional recovery. Such strategies utilize biomaterials as structural support for tissue regeneration or as delivery vehicles for therapeutic agents. While a range of biomaterials have been tested in stroke models, currently no overview is available for evaluating the benefit of these approaches. We therefore performed a systematic review and meta-analysis of studies investigating the use of biomaterials for the treatment of stroke in experimental animal models.

Methods: Studies were identified by searching electronic databases (PubMed, Web of Science) and reference lists of relevant review articles. Studies reporting lesion volume and/or neurological score were included. Standardized mean difference (SMD) and 95% confidence intervals were calculated using DerSimonian and Laird random effects. Study quality and risk of bias was assessed using the CAMARADES checklist. Publication bias was visualized by funnel plots followed by trim and fill analysis of missing publications.

Results: A total of 66 publications were included in the systematic review, of which 44 (86 comparisons) were assessed in the meta-analysis. Overall, biomaterial-based interventions improved both lesion volume (SMD: −2.98, 95% CI: −3.48, −2.48) and neurological score (SMD: −2.3, 95% CI: −2.85, −1.76). The median score on the CAMARADES checklist was 5.5/10 (IQR 4.25-6). Funnel plots of lesion volume and neurological score data revealed pronounced asymmetry and publication bias. Additionally, trim and fill analysis estimated 19 "missing" studies for the lesion volume outcome adjusting the effect size to −1.91 (95% CI: −2.44, −1.38).

Conclusions: Biomaterials including scaffolds and particles exerted a positive effect on histological and neurological outcomes in pre-clinical stroke models. However, heterogeneity in the field, publication bias and study quality scores which may be another source of bias call for standardization of outcome measures and improved study reporting.

Keywords: systematic review, meta-analysis, stroke, biomaterials, tissue engineering, hydrogels, nanoparticles, regenerative medicine

INTRODUCTION

Stroke is a global health problem with limited treatment options. The World Health Organization reports stroke as the second leading cause of death worldwide accounting for around 6.7 million deaths annually (1). For patients surviving stroke, close to two thirds will have a disability (2). Despite the major societal impact, the only widely available therapy for ischaemic stroke is tissue plasminogen activator (tPA). However, due to the narrow time window of administration (<4.5 h of symptom onset), only around 12% of patients in the UK are eligible for treatment (3). In recent years, great advances have been made in the development of endovascular thrombectomy as an alternative treatment (4, 5). While clinical trials have demonstrated thrombectomy is effective up to 6 h after stroke onset, it has been estimated that only 10% of patients would be eligible even with national coverage in the UK, which is presently not the case (6). Both thrombolysis and thrombectomy aim to restore reperfusion and limit further damage to the ischaemic brain and there are currently no approved regenerative medicine therapies available for promoting repair and regeneration.

In recent years, interest in regenerative medicine approaches to increase neuronal tissue repair following ischaemic stroke has increased. Notably, over 20 early phase clinical trials have been conducted assessing the safety of cell therapies including mesenchymal stem cells (MSCs) (7), neural stem cells (NSCs) (8), and haematopoietic stem cells (9). A number of studies have used cell-based therapies and growth factors to promote endogenous brain repair or tissue replacement in animal models of stroke with limited success. For this reason, biomaterials are now being investigated as potential agents to enhance the therapeutic efficacy of such interventions as scaffolds for tissue regeneration or vehicles for drug release (10, 11). For example, cell transplantation in the brain may be facilitated by the use of engineered scaffolds, which mimic native extracellular matrix (ECM) properties and provide adhesion sites for native cell attachment, aiding graft cell retention in the infarct cavity (12, 13). Alternatively, scaffolds may be used to aid recruitment and survival of endogenous stem cell populations for tissue restoration. Examples of scaffolds studied for cell delivery in stroke models include natural and synthetic hydrogels, electrospun fibers, sponges, and glue. Particulates are another class of biomaterials commonly used as delivery systems for targeted and controlled release of therapeutic agents. A wide variety of particulates have been tested for ischaemic stroke repair including nanoparticles, microparticles, micelles, liposomes, nanocarriers, and microspheres (14, 15).

To date, there is no systematic review or meta-analysis available investigating the potential of biomaterial-based approaches in pre-clinical models of ischaemic stroke. Given that biomaterial-based interventions are currently attracting great interest it is timely therefore to provide such a review, with the hope of averting the "translational roadblock" (16) and poor predictive validity of previous studies of neuroprotective agents for stroke (17, 18). Our systematic review and meta-analysis aims to assess the methodological quality of current research into biomaterial-based interventions for ischaemic stroke repair and to determine the efficacy of such approaches, helping to inform future research directions.

MATERIALS AND METHODS

Search Strategy

We searched PubMed and Web of Science for (stroke OR cerebral ischemia OR cerebral ischemia) AND (biomaterial OR tissue engineering OR hydrogel$ OR scaffold$ OR *particle$ OR sponge$). No restrictions were placed on date of publication and the last search was conducted on 4 February 2019. We also searched reference lists of review articles for additional articles. Titles and abstracts were initially screened by two authors (CC and FB).

Data Sources, Studies Selections, and Data Extraction

Full texts of the identified publications were screened (CC, FB, and IL) for studies assessing the efficacy of biomaterial-based strategies in pre-clinical models of cerebral ischemia. Studies were included if lesion volume and/or neurological score were reported as outcome measures. Studies in which the method of induction of cerebral ischemia was not stated were excluded. After screening full texts for suitability, study design information was extracted from each publication (CC and FB). Information extracted included the species and stroke model used, type of biomaterial investigated and whether the material was combined with another therapeutic agent (such as growth factors or a drug), the time of administration and any functional tests conducted.

The risk of bias of each publication was assessed using the CAMARADES (Collaborative Approach to Meta-analysis and Review of Animal Data in Experimental Studies) study quality checklist (19): (1) peer reviewed publication; (2) control of temperature; (3) random allocation to treatment or control; (4) blinded induction of ischemia; (5) blinded assessment of outcome; (6) use of anesthetic without significant intrinsic neuroprotective activity; (7) animal model (aged, diabetic, or hypertensive); (8) sample size calculation; (9) compliance with animal welfare regulations; and (10) statement of potential conflict of interests. All information extracted was independently cross-checked by a second reviewer (CC, FB, and IL).

For both lesion volume and neurological score, mean values, ± standard deviation (SD) or standard error of the mean (SEM), and group sizes for treatment and control groups were extracted. Publications that did not specify specific group sizes and reported variance as SEM or did not include control groups were excluded from the meta-analysis. Where variance was reported as SEM, this was converted to SD in Microsoft Excel in order to calculate standardized mean difference (SMD) for analysis. Since the effect of biomaterial administration on stroke recovery was the main focus of this analysis, control groups chosen for comparisons were either stroke only or vehicle. In cases where the material was combined with additional therapeutic agents, stroke or vehicle were also used as controls. In two cases (20, 21), the control

group was biomaterial alone so these papers were excluded from the meta-analysis.

Two publications which presented lesion volumes and neurological scores as median ± interquartile range (IQR), were also excluded from the meta-analysis (22, 23). One paper expressed the neurological score inversely to the convention (higher scores indicate a higher degree of impairment) so the data were inverted relative to the stated baseline measure (24). Where multiple treatments were assessed, we selected the treatment identified by authors in the publications as the primary focus. When publications reported multiple outcome measures from multiple timepoints, the data for the final end point was chosen. Where publications included multiple administration timepoints, data from each group was extracted separately.

Where possible, raw values were extracted from the text of the publication. When data was presented only graphically, the online tool WebPlotDigitizer (https://automeris.io/WebPlotDigitizer/) was used to estimate mean and variance from graphs. Estimate measures were independently cross-checked by a second reviewer and any conflicts (>10% difference) were resolved by a third reviewer (CC, FB, and IL). For analysis of effect size, the publications were split into subgroups by type of biomaterial (scaffolds and particles). The scaffolds subgroup included publications using hydrogels, extracellular matrix scaffolds, fibrin glue, and sponges. The particles subgroup included publications using nanoparticles, microparticles, nanocarriers, microspheres, liposomes, nanoemulsions, nanotubes, and micelles. The selected publications were also

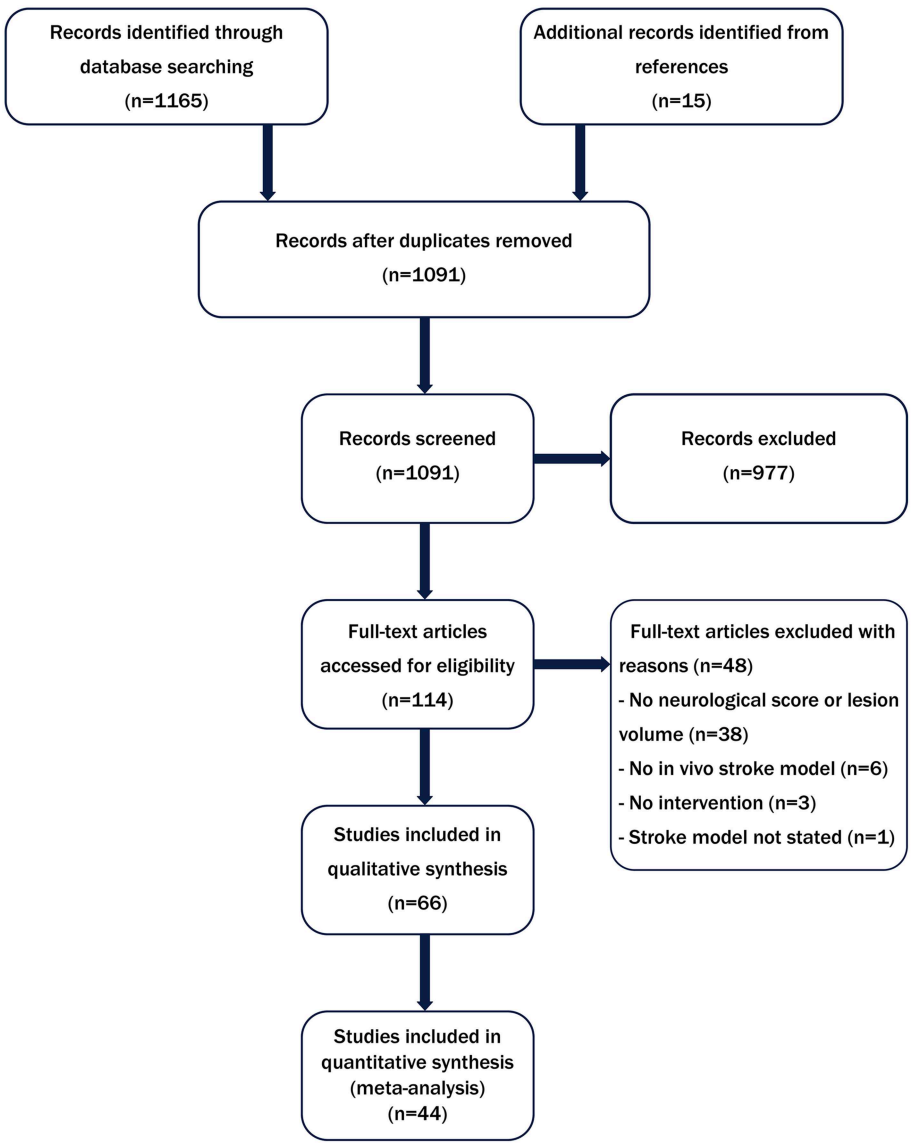

FIGURE 1 | Flow diagram summarizing the literature search strategy and number of studies included in the systematic review and meta-analysis.

divided into subgroups according to the time of administration. The groups were as follows: administration prior to stroke and up to time of reperfusion; from reperfusion to 24 h post-stroke; >24 h to 1 week post-stroke; >1–3 weeks post-stroke and multiple administrations spanning these timepoints.

Statistical Analysis

For both the lesion volume and neurological score outcomes, the SMD between the trial arms and accompanying 95% confidence intervals were calculated using DerSimonian and Laird random effects meta-analysis. Studies were weighted based on animal number. The presence of heterogeneity in the data sets was assessed using the I^2 statistic. Due to very high heterogeneity in the data ($I^2 = 82.8$ and 84.3% for lesion volume and neurological score, respectively), random effects were chosen. Forest plots were used to visually present the results. The analysis was stratified by type of biomaterial and time of administration although for brevity, only the former are presented graphically. The extent of publication bias was assessed graphically using funnel plots and confirmed with Egger's regression test. The trim and fill approach was also used to estimate an effect size accounting for publication bias. Stata 15 (StataCorp, USA) was used for all statistical analyses with the exception of the trim and fill analysis which was conducted in RStudio version 1.1.463 (RStudio Inc., USA) using the metafor package (http://www.metafor-project.org/doku.php).

RESULTS

Study Selection and Characteristics

As shown in **Figure 1**, 1,091 publications were identified from our literature search of which 66 met the inclusion

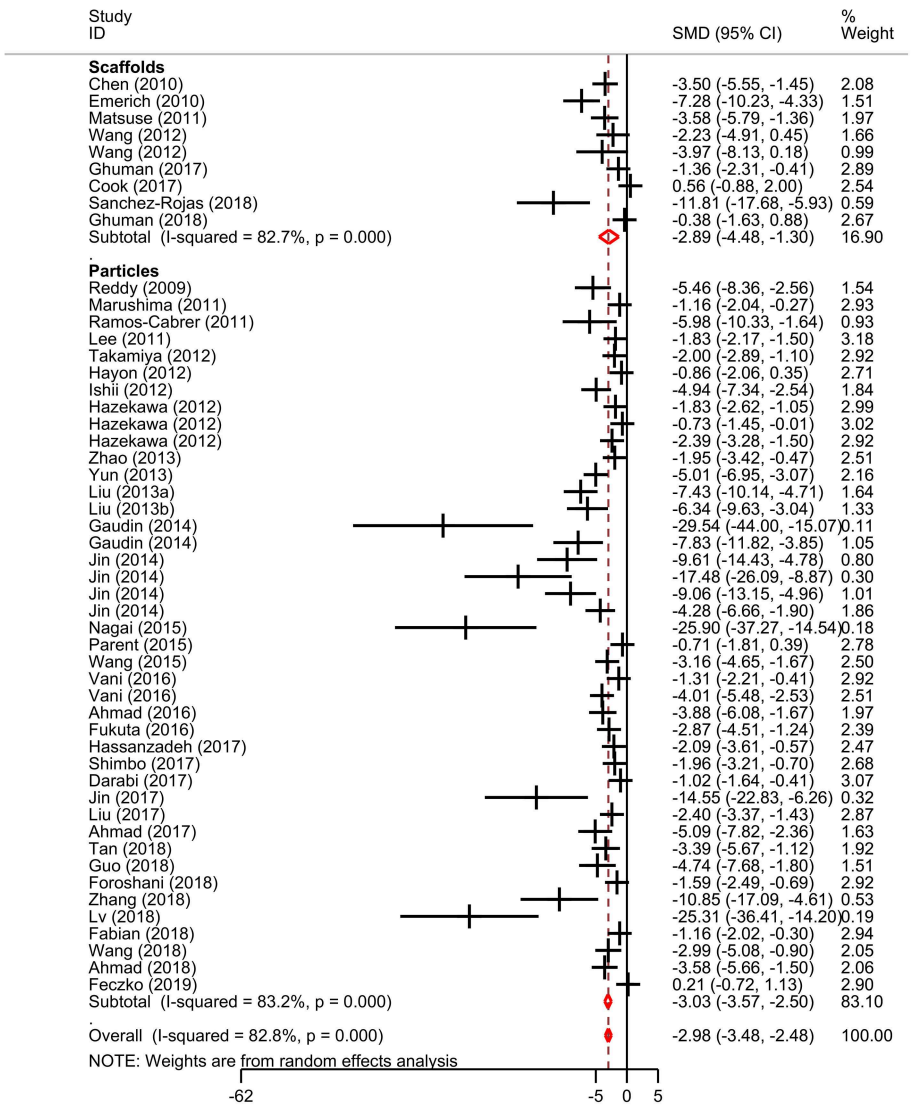

FIGURE 2 | Effect sizes for biomaterial-based interventions for lesion volume. Forest plot of standardized mean difference and 95% CI. CI, confidence interval; SMD, standardized mean difference.

criteria for the systematic review. The characteristics of these studies including stroke model, animal numbers and type of biomaterial intervention are shown in **Supplementary Table 1**. All of the included studies were conducted in rats ($n = 49$) or mice ($n = 16$) or both rats and mice ($n = 1$). The most commonly used model was the transient intraluminal filament model of middle cerebral artery occlusion (MCAO) ($n = 46$). Only two studies used comorbid animals. Hayon et al. (25) used spontaneously hypertensive rats and Fabian et al. (26) induced acute hyperglycemia in Sprague-Dawley rats using streptozotocin. As shown in **Supplementary Table 1**, there was high variation in the functional outcome measures employed (23 different behavioral tests). Furthermore, several different neurological scores were reported including modified neurological severity score (both 14 and 18 points), Bederson, modified Bederson and Longa (27, 28). A total of 44 studies including 1,075 animals (control $n = 522$, treatment $n = 553$) were then included in the meta-analysis reporting 86 comparisons. Of these, 51 assessed lesion volume and 35 assessed neurological score. There was

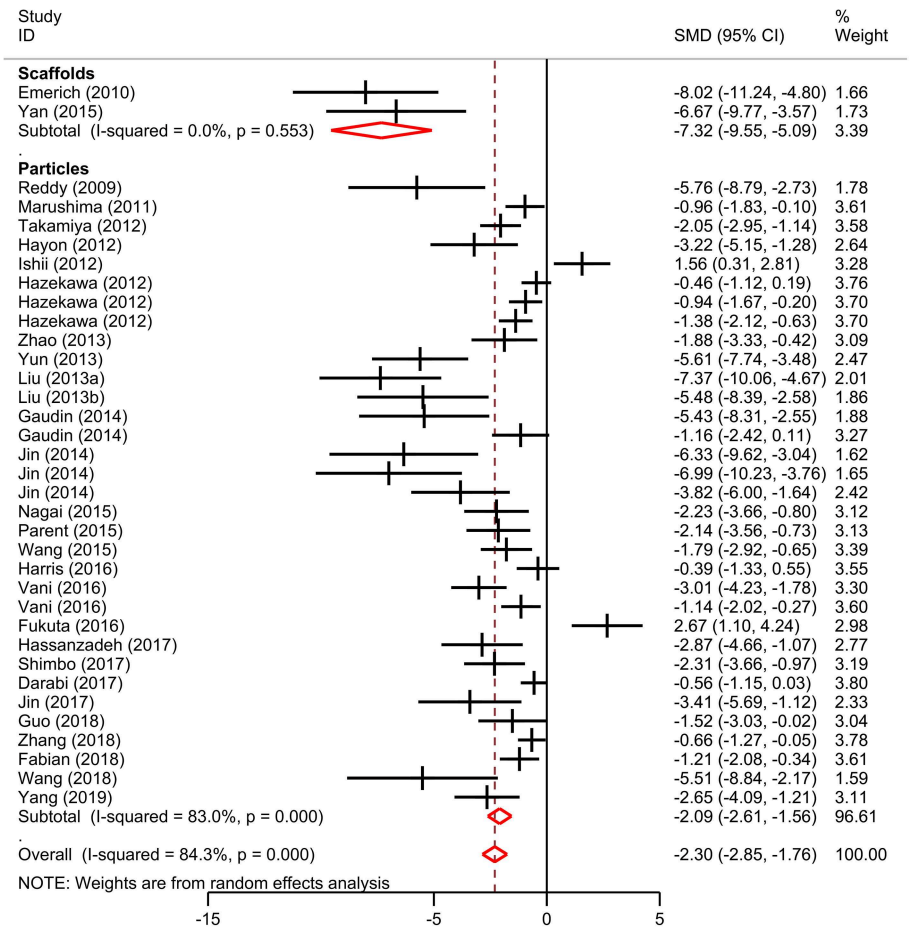

FIGURE 3 | Effect size for biomaterial-based interventions for neurological score. Forest plot of mean standard difference and 95% CI. CI, confidence interval; SMD, standardized mean difference.

TABLE 1 | Subgroup meta-analysis comparing time of intervention on lesion volume and neurological score outcomes.

	Lesion volume			Neurological score		
Time of intervention	**Comparisons**	**Effect size (95% CI)**	**I^2, p-value**	**Comparisons**	**Effect size (95% CI)**	**I^2, p-value**
Pre-treatment–0 h	25	−3.15 (−3.76, −2.55)	79.7%, <0.001	18	−3.03 (−4.10, −1.96)	89.2%, <0.001
>0–24 h	15	−3.94 (−5.19, −2.69)	87.1%, <0.001	13	−1.84 (−2.48, −1.21)	75.3%, <0.001
>24 h–1 week	5	−2.15 (−4.43, −0.14)	85.5%, 0 < 001	0	N/A	N/A
>1–3 weeks	3	−1.14 (−2.27, −0.00)	41.1%, 0.183	0	N/A	N/A
Multiple timepoints	3	−3.51 (−6.75, 0.27)	78.5%, 0.010	4	−1.32 (−2.18, −0.45)	56.5%, 0.075

TABLE 2 | Summary of study quality assessed by study compliance to the CAMARADES risk of bias checklist.

	Overall	Scaffolds	Particles
(1) Peer-reviewed publication (%)	100	100	100
(2) Control of temperature (%)	50	42.1	53.2
(3) Random allocation to treatment or control (%)	56.1	52.6	57.4
(4) Blinded induction of ischemia (%)	34.9	42.1	31.9
(5) Blinded assessment of outcome (%)	50	52.6	48.9
(6) Use of anesthetic without significant intrinsic neuroprotective activity (%)	83.3	89.5	80.9
(7) Animal model (aged, diabetic, or hypertensive) (%)	3	0	4.26
(8) Sample size calculation (%)	9.1	15.8	6.4
(9) Compliance with animal welfare regulations (%)	93.9	89.5	95.7
(10) Statement of potential conflict of interests (%)	62.1	73.7	57.4
Median quality (/10) (IQR)	5.5 (4.25–6)	6 (4–7)	5 (4–6)

substantial heterogeneity in the datasets from both lesion volume and neurological score outcomes (I^2 = 82.8 and 84.3%, respectively).

Synthesized Findings

Meta-analysis was performed on lesion volume and neurological score data. Overall, treatment with biomaterial-based interventions led to improvements in lesion volume (SMD: −2.98, 95% CI: −3.48, −2.48). Both the scaffolds (SMD: −2.89, 95% CI: −4.48, −1.30) and particles subgroups (SMD: −3.03, 95% CI: −3.57, −2.50) had comparable effect sizes (**Figure 2**). There was high variability in the reported effect sizes in the particles groups ranging from –29.54 to −0.21. Similarly, biomaterial-based approaches were also associated with overall improvements in neurological score (SMD: −2.3, 95% CI: −2.85, −1.76; **Figure 3**). Administration of the biomaterial-based therapies within 24 h of stroke onset appeared to be most effective leading to the most marked improvement in lesion volume (SMD: −3.94, 95% CI: −5.19, −2.69; **Table 1**).

Risk of Bias and Study Quality

Risk of bias was assessed using the CAMARADES checklist (19). Overall, the median score was 5.5/10 (IQR 4.25-6). Studies within the scaffolds (6/10, IQR 4-7) and particles (5/10, IQR 4-6) subgroups had very similar scores (**Table 2**). Reporting of randomization (56%), blinding (35% to stroke and 50% to outcome) and sample size calculations (9%) was low.

Publication bias was then assessed. From visual inspection of the funnel plot for lesion volume (**Figure 4**), there was pronounced asymmetry denoting publication bias. This was confirmed by Egger's regression test ($p < 0.001$). Similarly, there was asymmetry in the funnel plot of neurological score ($p < 0.001$; **Figure 4**). Trim and fill analysis estimated 19 "missing" studies on the right side of the funnel plot of lesion volume outcome (**Figure 5**) which adjusted the effect size to −1.91 (95% CI: −2.44, −1.38). Conversely, trim and fill analysis did not report any "missing" studies for neurological score.

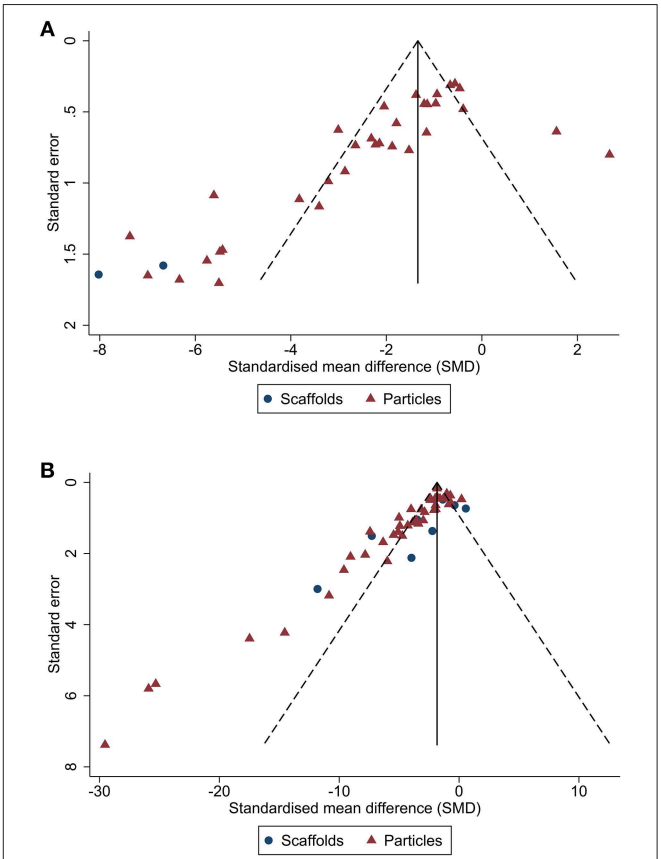

FIGURE 4 | Publication bias analysis for biomaterial-based interventions by type. Funnel plots with pseudo 95% CI for publication bias of lesion volume **(A)** and neurological score **(B)**.

DISCUSSION

Summary of Findings

In this study we assessed the efficacy of biomaterial-based approaches in pre-clinical models of ischaemic stroke. A total of 66 publications met our inclusion criteria for the systematic

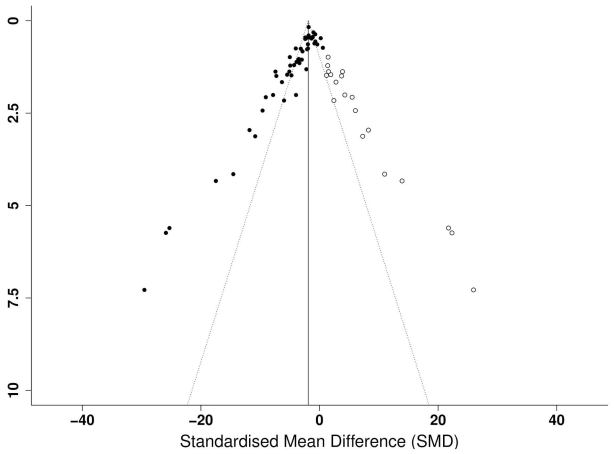

FIGURE 5 | Trim and fill analysis of lesion volume showing published studies (filled circles) and estimated unpublished studies (unfilled circles). The solid vertical line indicates the adjusted effect size.

review with 44 studies (86 comparisons) included in the meta-analysis. Overall, our findings show that biomaterial-based interventions improved both lesion volume and neurological score. Treatment within 24 h of stroke onset appeared to be the most effective timepoint. We next assessed risk of bias using the CAMARADES checklist (19) and showed the median score was 5.5/10. We also identified pronounced asymmetry in the funnel plots of both the lesion volume and neurological score dataset, indicating publication bias. Trim and fill analysis indicated there were 19 "missing" studies reporting negative or neutral lesion volume data which when adjusted for, greatly reduced the effect size.

Variability in Outcome Measures

In agreement with a recent systematic review on animal models of stroke and vascular cognitive impairment (29), we reported very high variability in the choice of functional outcome measures. A limitation of the pre-clinical stroke field is the lack of consensus on the optimal test or battery of tests for assessing functional recovery (30). We selected neurological score as one of our outcome measures as it is by far the most widely used assessment of recovery (29). While there are a number of advantages including being fast to perform and requiring no specialist equipment, a large drawback of neurological scores is that they are highly subjective (31). Additionally, we noted there was no standardization in the scale used and a number of publications neglected to report the scoring system used. A further limitation is that as rodents have a great capacity for spontaneous recovery, simpler assessments such as neurological scores often cannot detect deficits at later timepoints (30). These scores may therefore have limited use in studies where scaffold materials are administered at chronic timepoints after stroke (1–2 weeks) (32–34). In addition, neurological scores are not able to adequately distinguish compensatory strategies from true motor recovery (35) which as previously suggested, could lead to false positives (36, 37). Future studies should therefore aim to use tasks such as skilled reaching and gait analysis which can differentiate between the two.

Additionally, we noted that all but two publications identified in our systematic review reported neurological score as mean ± SD/SEM. This is surprising given that these data are ordinal and thus should be expressed as median ± IQR. The calculated effect sizes of individual studies should therefore be approached with caution. Nevertheless, given that the central limit theory states that the mean of a large number of observations will tend toward a normal distribution, our overall effect size for neurological score are robust.

Lesion volume was also chosen as an outcome measure in our meta-analysis given its wide use in the pre-clinical stroke field. The vast majority of the included studies assessing the efficacy of nanoparticles chose acute end points (24–48 h) with lesion volume as the primary outcome measure of neuroprotection. However, most studies assessing the capacity of scaffolds to promote brain regeneration elect to administer during the sub-acute and chronic phase of stroke. In these instances, it is currently unclear whether lesion volume assessment at chronic timepoints is a measure of tissue atrophy, repair or a combination of the two (33, 38, 39). Future work should therefore focus on developing standardized methods for evaluating tissue regeneration. For example, Ghuman and colleagues have chosen to focus on host cell infiltration into ECM hydrogels as an outcome measure (32, 38). Furthermore, it is worth noting that many studies that focused solely on material characterization or assessment of administration at the tissue level were excluded from our systematic review and meta-analysis as lesion volume and neurological scores were not included as outcome measures.

Both histological techniques (including 2,3,5-triphenyltetrazolium chloride (TTC), cresyl violet or haematoxylin & eosin (H&E) stains) and magnetic resonance imaging (MRI) were used to measure lesion volume. The variation in choice of method likely reflects the availability of MR scanners or preference of researchers toward a certain method. However, this may introduce inter-study variability into lesion volume measurements. A meta-analysis comparing measurements obtained from T2-weighted MR images and histological sections found a strong correlation between the two methods ($p < 0.001$) (40). Nevertheless, lesion volume measurements from MR images were larger than for histology and there was considerable variation in the reporting and use of MR methods (40). Despite this, as our study compares the SMD of treatment and control group measurements obtained using the same method, the differences in methodology is unlikely to have an effect on the conclusions of our study.

Study Quality and Risk of Bias

To improve the quality of pre-clinical research, a number of guidelines have been published in recent years including the National Centre for the Replacement, Refinement and Reduction of Animals (NC3Rs) published the Animal Research: Reporting of *in vivo* Experiments (ARRIVE) guidelines (41). This consists of a checklist of 20 items which should be reported including full details of allocation to experimental groups, sample size calculations and reporting of exact animal numbers. While most

of the studies included in our systematic review were published after the ARRIVE guidelines (2011 onwards), reporting of these items remained low. This is in agreement with a recent position paper which shows compliance with the guidelines so far has been low (42). We noted that several publications had extremely large effect sizes (SMD >-10) of which a number reported >80% reductions in lesion volume following treatment. Previous systematic reviews of *in vivo* studies have shown that studies reporting the greatest efficacies often have the lowest compliance with such checklists (43). It is possible that limitations in study design could account for an overestimation in effect size and reduced reliability of the results. It has been suggested that the lack of blinding and randomization has led to false positives in neuroprotection studies or over-estimates of efficacy which may have contributed to the translational roadblock in the field (16).

As previously mentioned, our results indicated the presence of publication bias. In particular, trim and fill analysis predicted there was a substantial number of "missing" unpublished studies reporting neutral or negative lesion volume outcomes. Publication bias is an issue not limited to pre-clinical stroke research (19, 44, 45) which can lead to overestimation of efficacy. For example, a number of studies has shown that conference abstracts reporting positive results are more likely to be published later (46–48). To avoid another translational roadblock, greater emphasis should be placed on publishing negative and neutral data.

Limitations

This systematic review and meta-analysis is the first to collate the pre-clinical literature on biomaterials for ischaemic stroke. As such, we believe the synthesized findings and conclusions are important for the field. Nevertheless, there are a number of limitations. Firstly, only summary data obtained from the publications was used for the meta-analysis and in many cases, values had to be estimated from graphs. As such, our measurements may differ marginally to the raw values. However, we did not contact authors to obtain these data. A study by the Cochrane Library compared meta-analyses using summary or "aggregate" data to those using raw data and found the difference in results and conclusions to be minimal (49). As our aim was to provide a succinct summary of the current field, we reason that the use of summary data for meta-analysis has negligible impact on the conclusions of the review.

Additionally, the considerable heterogeneity in the types of biomaterials used made identifying suitable subgroups problematic. We reasoned that all of the publications could be classified broadly as either scaffolds (administered at the lesion site for *in situ* tissue engineering in the sub-acute to chronic phase of stroke) or as particles (usually delivered systemically before or acutely after stroke). We acknowledge the wide range of material types within the chosen subgroups and an alternative option may have been to include a greater number of specific subgroups. However, we reasoned that this would decrease the statistical power of the meta-analysis and the main objective was to give an overview of the efficacy of biomaterial-based approaches in pre-clinical stroke.

We acknowledge our search criteria only identified studies relating to ischaemic stroke. A separate search containing the keywords intracerebral hemorrhage and subarachnoid hemorrhage, returned seven relevant publications (50–56). Based on the small number of publications and the heterogeneity in outcome measures used, we chose not to include these studies. Given our findings concerning risk of bias and study quality, a future systematic review and meta-analysis should investigate this in the emerging field of biomaterial therapies for hemorrhagic stroke.

CONCLUSIONS

Our meta-analysis revealed that studies assessing biomaterial-based interventions for ischaemic stroke report overall positive results leading to reductions in lesion volume and neurological improvements in rodent models. Additionally, our systematic review regarding study quality showed CAMARADES checklist score was 5.5/10. Our findings provide insight into the field of biomaterials for stroke therapeutics and the quality of studies conducted. We believe the results highlight the need for improved study design and reporting to ultimately support translation of biomaterial-based therapies to the clinical setting.

DATA AVAILABILITY

All datasets generated for this study are included in the manuscript and/or the **Supplementary Files**.

AUTHOR CONTRIBUTIONS

CC: conception. CC, FB, and IL: design, literature search, study screening, data extraction, and manuscript writing. CH and CC: data analysis. CC, CH, FB, and IL: interpretation.

FUNDING

This work was supported by an Engineering and Physical Sciences Research Council (EPSRC) Doctoral Prize Fellowship grant EP/N509565/1 and EPSRC and Medical Research Council (MRC) Centre for Doctoral Training in Regenerative Medicine studentship grant EP/L014904/1.

ACKNOWLEDGMENTS

The authors would like to thank Dr. Emily Sena (University of Edinburgh) and Dr. Raymond Wong (University of Manchester) for their advice on data extraction. We would also like to thank Dr. Jack Rivers-Auty (University of Manchester) for his advice on statistical analysis. We also acknowledge the contribution to study design and manuscript editing by Dr. Catherine Lawrence, Dr. Emmanuel Pinteaux, and Prof. Stuart Allan, who are also supervisors of CC, FB, and IL.

SUPPLEMENTARY MATERIAL

The Supplementary Material for this article can be found online at: https://www.frontiersin.org/articles/10.3389/fneur.2019.00924/full#supplementary-material

REFERENCES

1. World Health Organisation. *Global Status Report on Noncommunicable Diseases 2014*. Geneva (2014).
2. Stroke Association. *State of the Nation Stroke Statistics*. London (2018).
3. Royal College of Physicians Intercollegiate Stroke Working Party. *Sentinel Stroke National Audit Programme (SSNAP) Clinical Audit April 2017—July 2017 Public Report*. London (2017).
4. Campbell BCV, Mitchell PJ, Kleinig TJ, Dewey HM, Churilov L, Yassi N, et al. Endovascular therapy for ischemic stroke with perfusion-imaging selection. *N Engl J Med.* (2015) 372:1009–18. doi: 10.1056/NEJMoa1414792
5. Goyal M, Demchuk AM, Menon BK, Eesa M, Rempel JL, Thornton J, et al. Randomized assessment of rapid endovascular treatment of ischemic stroke. *N Engl J Med.* (2015) 372:1019–30. doi: 10.1056/NEJMoa1414905
6. McMeekin P, White P, James MA, Price CI, Flynn D, Ford GA. Estimating the number of UK stroke patients eligible for endovascular thrombectomy. *Eur Stroke J.* (2017) 2:319–26. doi: 10.1177/2396987317733343
7. Bhasin A, Kumaran SS, Bhatia R, Mohanty S, Srivastava MVP. Safety and feasibility of autologous mesenchymal stem cell transplantation in chronic stroke in Indian patients. A four-year follow up. *J Stem Cells Regen Med.* (2017) 13:14–19.
8. Kalladka D, Sinden J, Pollock K, Haig C, McLean J, Smith W, et al. Human neural stem cells in patients with chronic ischaemic stroke (PISCES): a phase 1, first-in-man study. *Lancet.* (2016) 388:787–96. doi: 10.1016/S0140-6736(16)30513-X
9. Banerjee S, Bentley P, Hamady M, Marley S, Davis J, Shlebak A, et al. Intra-arterial immunoselected CD34+ stem cells for acute ischemic stroke. *Stem Cells Transl Med.* (2014) 3:1322–30. doi: 10.5966/sctm.2013-0178
10. Marquardt LM, Heilshorn SC. Design of injectable materials to improve stem cell transplantation. *Curr Stem Cell Rep.* (2016) 2:207–20. doi: 10.1007/s40778-016-0058-0
11. Boisserand LSB, Kodama T, Papassin J, Auzely R, Moisan A, Rome C, et al. Biomaterial applications in cell-based therapy in experimental stroke. *Stem Cells Int.* (2016) 2016:1–14. doi: 10.1155/2016/6810562
12. Tuladhar A, Payne SL, Shoichet MS. Harnessing the potential of biomaterials for brain repair after stroke. *Front Mater.* (2018) 5:14. doi: 10.3389/fmats.2018.00014
13. Pakulska MM, Ballios BG, Shoichet MS. Injectable hydrogels for central nervous system therapy. *Biomed Mater.* (2012) 7:24101. doi: 10.1088/1748-6041/7/2/024101
14. Vidu R, Rahman M, Mahmoudi M, Enachescu M, Poteca TD, Opris I. Nanostructures: a platform for brain repair and augmentation. *Front Syst Neurosci.* (2014) 8:91. doi: 10.3389/fnsys.2014.00091
15. Vieira DB, Gamarra LF. Getting into the brain: liposome-based strategies for effective drug delivery across the blood-brain barrier. *Int J Nanomed.* (2016) 11:5381–414. doi: 10.2147/IJN.S117210
16. Dirnagl U, Macleod MR. Stroke research at a road block: the streets from adversity should be paved with meta-analysis and good laboratory practice. *Br J Pharmacol.* (2009) 157:1154–6. doi: 10.1111/j.1476-5381.2009.00211.x
17. Minnerup J, Wersching H, Schilling M, Schäbitz WR. Analysis of early phase and subsequent phase III stroke studies of neuroprotectants: outcomes and predictors for success. *Exp Transl Stroke Med.* (2014) 6:2. doi: 10.1186/2040-7378-6-2
18. Chamorro Á, Dirnagl U, Urra X, Planas AM. Neuroprotection in acute stroke: targeting excitotoxicity, oxidative and nitrosative stress, and inflammation. *Lancet Neurol.* (2016) 15:869–81. doi: 10.1016/S1474-4422(16)00114-9
19. Macleod MR, O'Collins T, Howells DW, Donnan GA. Pooling of animal experimental data reveals influence of study design and publication bias. *Stroke.* (2004) 35:1203–8. doi: 10.1161/01.STR.0000125719.25853.20
20. George PM, Oh B, Dewi R, Hua T, Cai L, Levinson A, et al. Engineered stem cell mimics to enhance stroke recovery. *Biomaterials.* (2018) 178:63–72. doi: 10.1016/j.biomaterials.2018.06.010
21. George PM, Bliss TM, Hua T, Lee A, Oh B, Levinson A, et al. Electrical preconditioning of stem cells with a conductive polymer scaffold enhances stroke recovery. *Biomaterials.* (2017) 142:31–40. doi: 10.1016/j.biomaterials.2017.07.020
22. Saraiva C, Talhada D, Rai A, Ferreira R, Ferreira L, Bernardino L, et al. MicroRNA-124-loaded nanoparticles increase survival and neuronal differentiation of neural stem cells in vitro but do not contribute to stroke outcome *in vivo*. *PLoS ONE.* (2018) 13:e0193609. doi: 10.1371/journal.pone.0193609
23. Quittet M-S, Touzani O, Sindji L, Cayon J, Fillesoye F, Toutain J, et al. Effects of mesenchymal stem cell therapy, in association with pharmacologically active microcarriers releasing VEGF, in an ischaemic stroke model in the rat. *Acta Biomater.* (2015) 15:77–88. doi: 10.1016/j.actbio.2014.12.017
24. Shimbo D, Abumiya T, Kurisu K, Osanai T, Shichinohe H, Nakayama N, et al. Superior microvascular perfusion of infused liposome-encapsulated hemoglobin prior to reductions in infarctions after transient focal cerebral ischemia. *J Stroke Cerebrovasc Dis.* (2017) 26:2994–3003. doi: 10.1016/j.jstrokecerebrovasdis.2017.07.026
25. Hayon Y, Dashevsky O, Shai E, Brill A, Varon D, Leker RR. Platelet microparticles induce angiogenesis and neurogenesis after cerebral ischemia. *Curr Neurovasc Res.* (2012) 9:185–92. doi: 10.2174/156720212801619018
26. Fabian RH, Derry PJ, Rea HC, Dalmeida WV, Nilewski LG, Sikkema WKA, et al. Efficacy of novel carbon nanoparticle antioxidant therapy in a severe model of reversible middle cerebral artery stroke in acutely hyperglycemic rats. *Front Neurol.* (2018) 9:199. doi: 10.3389/fneur.2018.00199
27. Bederson JB, Pitts LH, Tsuji M, Nishimura MC, Davis RL, Bartkowski H. Rat middle cerebral artery occlusion: evaluation of the model and development of a neurologic examination. *Stroke.* (1986) 17:472–6. doi: 10.1161/01.STR.17.3.472
28. Longa EZ, Weinstein PR, Carlson S, Cummins R. Reversible middle cerebral artery occlusion without craniectomy in rats. *Stroke.* (1989) 20:84–91. doi: 10.1161/01.STR.20.1.84
29. Hietamies TM, Ostrowski C, Pei Z, Feng L, McCabe C, Work LM, et al. Variability of functional outcome measures used in animal models of stroke and vascular cognitive impairment – a review of contemporary studies. *J Cereb Blood Flow Metab.* (2018) 38:1872–84. doi: 10.1177/0271678X18799858
30. Balkaya MG, Trueman RC, Boltze J, Corbett D, Jolkkonen J. Behavioral outcome measures to improve experimental stroke research. *Behav Brain Res.* (2017)161–71. doi: 10.1016/j.bbr.2017.07.039
31. Schönfeld L-M, Dooley D, Jahanshahi A, Temel Y, Hendrix S. Evaluating rodent motor functions: Which tests to choose? *Neurosci Biobehav Rev.* (2017) 83:298–312. doi: 10.1016/j.neubiorev.2017.10.021
32. Ghuman H, Mauney C, Donnelly J, Massensini AR, Badylak SF, Modo M. Biodegradation of ECM hydrogel promotes endogenous brain tissue restoration in a rat model of stroke. *Acta Biomater.* (2018) 80:66–84. doi: 10.1016/j.actbio.2018.09.020
33. Payne SL, Tuladhar A, Obermeyer JM, Varga BV, Teal CJ, Morshead CM, et al. Initial cell maturity changes following transplantation in a hyaluronan-based hydrogel and impacts therapeutic success in the stroke-injured rodent brain. *Biomaterials.* (2019) 192:309–22. doi: 10.1016/j.biomaterials.2018.11.020
34. Cook DJ, Nguyen C, Chun HN, Llorente LI, Chiu AS, Machnicki M, et al. Hydrogel-delivered brain-derived neurotrophic factor promotes tissue repair and recovery after stroke. *J Cereb Blood Flow Metab.* (2017) 37:1030–45. doi: 10.1177/0271678X16649964
35. Boltze J, Lukomska B, Jolkkonen J, MEMS–IRBI consortium for the M. Mesenchymal stromal cells in stroke: improvement of motor recovery or functional compensation? *J Cereb Blood Flow Metab.* (2014) 34:1420–1. doi: 10.1038/jcbfm.2014.94
36. Cui L, Golubczyk D, Jolkkonen J. Top 3 behavioral tests in cell therapy studies after stroke. *Stroke.* (2017) 48:3165–7. doi: 10.1161/STROKEAHA.117.018950
37. Hicks A, Schallert T, Jolkkonen J. Cell-based therapies and functional outcome in experimental stroke. *Cell Stem Cell.* (2009) 5:139–40. doi: 10.1016/j.stem.2009.07.009
38. Ghuman H, Gerwig M, Nicholls FJ, Liu JR, Donnelly J, Badylak SF, et al. Long-term retention of ECM hydrogel after implantation into a sub-acute stroke cavity reduces lesion volume. *Acta Biomater.* (2017) 63:50–63. doi: 10.1016/j.actbio.2017.09.011

39. Sanchez-Rojas L, Gómez-Pinedo U, Benito-Martin MS, León-Espinosa G, Rascón-Ramirez F, Lendinez C, et al. Biohybrids of scaffolding hyaluronic acid biomaterials plus adipose stem cells home local neural stem and endothelial cells: Implications for reconstruction of brain lesions after stroke. *J Biomed Mater Res B Appl Biomater.* (2018) 107:1598–606 doi: 10.1002/jbm.b.34252
40. Xenios M, Marshall I, Macleod MR, Sena ES. Magnetic resonance imaging in experimental stroke and comparison with histology. *Stroke.* (2015) 46:843–51. doi: 10.1161/STROKEAHA.114.007560
41. Kilkenny C, Browne WJ, Cuthill IC, Emerson M, Altman DG. Improving bioscience research reporting: the ARRIVE guidelines for reporting animal research. *PLoS Biol.* (2010) 8:e1000412. doi: 10.1371/journal.pbio.1000412
42. Percie du Sert N, Hurst V, Ahluwalia A, Alam S, Altman DG, Avey MT, et al. Revision of the ARRIVE guidelines: rationale and scope. *BMJ Open Sci.* (2018) 2:e000002. doi: 10.1136/bmjos-2018-000002
43. Macleod MR, Lawson McLean A, Kyriakopoulou A, Serghiou S, de Wilde A, Sherratt N, et al. Risk of bias in reports of *in vivo* research: a focus for improvement. *PLoS Biol.* (2015) 13:e1002273. doi: 10.1371/journal.pbio.1002273
44. Landis SC, Amara SG, Asadullah K, Austin CP, Blumenstein R, Bradley EW, et al. A call for transparent reporting to optimize the predictive value of preclinical research. *Nat 2012.* (2012) 490:187–91. doi: 10.1038/nature11556
45. Sena ES, van der Worp HB, Bath PMW, Howells DW, Macleod MR. Publication bias in reports of animal stroke studies leads to major overstatement of efficacy. *PLoS Biol.* (2010) 8:e1000344. doi: 10.1371/journal.pbio.1000344
46. Meyer C, Fuller K, Scott J, Vassar M. Is publication bias present in gastroenterological research? An analysis of abstracts presented at an annual congress. *PeerJ.* (2018) 6:e4995. doi: 10.7717/peerj.4995
47. Callaham ML, Wears RL, Weber EJ, Barton C, Young G. Positive-outcome bias and other limitations in the outcome of research abstracts submitted to a scientific meeting. *JAMA.* (1998) 280:254–7. doi: 10.1001/jama.280.3.254
48. Scherer RW, Langenberg P, von Elm E. Full publication of results initially presented in abstracts. *Cochrane Database Syst Rev.* (2007) 2:MR000005. doi: 10.1002/14651858.MR000005.pub3
49. Tudur Smith C, Marcucci M, Nolan SJ, Iorio A, Sudell M, Riley R, et al. Individual participant data meta-analyses compared with meta-analyses based on aggregate data. *Cochrane Database Syst Rev.* (2016) 9:MR000007. doi: 10.1002/14651858.MR000007.pub3
50. Galho AR, Cordeiro MF, Ribeiro SA, Marques MS, Antunes MFD, Luz DC, et al. Protective role of free and quercetin-loaded nanoemulsion against damage induced by intracerebral haemorrhage in rats. *Nanotechnology.* (2016) 27:175101. doi: 10.1088/0957-4484/27/17/175101
51. Vaquero J, Otero L, Bonilla C, Aguayo C, Rico MA, Rodriguez A, et al. Cell therapy with bone marrow stromal cells after intracerebral hemorrhage: impact of platelet-rich plasma scaffolds. *Cytotherapy.* (2013) 15:33–43. doi: 10.1016/j.jcyt.2012.10.005
52. Sang LY-H, Liang Y-X, Li Y, Wong W-M, Tay DK-C, So K-F, et al. A self-assembling nanomaterial reduces acute brain injury and enhances functional recovery in a rat model of intracerebral hemorrhage. *Nanomed Nanotechnol Biol Med.* (2015) 11:611–20. doi: 10.1016/j.nano.2014.05.012
53. Zhang N, Luo Y, He L, Zhou L, Wu W. A self-assembly peptide nanofibrous scaffold reduces inflammatory response and promotes functional recovery in a mouse model of intracerebral hemorrhage. *Nanomed Nanotechnol Biol Med.* (2016) 12:1205–17. doi: 10.1016/j.nano.2015.12.387
54. Sakai H, Okamoto M, Ikeda E, Horinouchi H, Kobayashi K, Tsuchida E. Histopathological changes of rat brain after direct injection of Hb-vesicles (artificial oxygen carriers) and neurological impact in an intracerebral hemorrhage model. *J Biomed Mater Res Part.* (2009) 90A:1107–19. doi: 10.1002/jbm.a.32164
55. Luo T, Guo T, Yang Q, Hao S, Wang J, Cheng Z, et al. *In situ* hydrogels enhancing postoperative functional recovery by reducing iron overload after intracerebral haemorrhage. *Int J Pharm.* (2017) 534:179–89. doi: 10.1016/j.ijpharm.2017.10.010
56. Park J, Kim JY, Choi S-K, Kim JY, Kim JH, Jeon WB, et al. Thermo-sensitive assembly of the biomaterial REP reduces hematoma volume following collagenase-induced intracerebral hemorrhage in rats. *Nanomed Nanotechnol Biol Med.* (2017) 13:1853–62. doi: 10.1016/j.nano.2017.04.001
57. Hazekawa M, Sakai Y, Yoshida M, Haraguchi T, Uchida T. Single injection of ONO-1301-loaded PLGA microspheres directly after ischaemia reduces ischaemic damage in rats subjected to middle cerebral artery occlusion. *J Pharm Pharmacol.* (2012) 64:353–359. doi: 10.1111/j.2042-7158.2011.01416.x
58. Marushima A, Suzuki K, Nagasaki Y, Yoshitomi T, Toh K, Tsurushima H, et al. Newly synthesized radical-containing nanoparticles enhance neuroprotection after cerebral ischemia-reperfusion injury. *Neurosurgery.* (2011) 68:1418–26. doi: 10.1227/NEU.0b013e31820c02d9
59. Nagai N, Yoshioka C, Ito Y, Funakami Y, Nishikawa H, Kawabata A. Intravenous administration of cilostazol nanoparticles ameliorates acute ischemic stroke in a cerebral ischemia/reperfusion-induced injury model. *Int J Mol Sci.* (2015) 16:29329–44. doi: 10.3390/ijms161226166
60. Jin Q, Cai Y, Li S, Liu H, Zhou X, Lu C, et al. Edaravone-encapsulated agonistic micelles rescue ischemic brain tissue by tuning blood-brain barrier permeability. *Theranostics.* (2017) 7:884–98. doi: 10.7150/thno.18219
61. Zhang T, Li C-Y, Jia J-J, Chi J-S, Zhou D, Li J-Z, et al. Combination therapy with LXW7 and ceria nanoparticles protects against acute cerebral ischemia/reperfusion injury in rats. *Curr Med Sci.* (2018) 38:144–52. doi: 10.1007/s11596-018-1858-5
62. Emerich DF, Silva E, Ali O, Mooney D, Bell W, Yu SJ, et al. Injectable VEGF hydrogels produce near complete neurological and anatomical protection following cerebral ischemia in rats. *Cell Transplant.* (2010) 19:1063–71. doi: 10.3727/096368910X498278
63. Feczkó T, Piiper A, Ansar S, Blixt FW, Ashtikar M, Schiffmann S, et al. Stimulating brain recovery after stroke using theranostic albumin nanocarriers loaded with nerve growth factor in combination therapy. *J Control Release.* (2019) 293:63–72. doi: 10.1016/j.jconrel.2018.11.017
64. Moon SU, Kim J, Bokara KK, Kim JY, Khang D, Webster TJ, et al. Carbon nanotubes impregnated with subventricular zone neural progenitor cells promotes recovery from stroke. *Int J Nanomed.* (2012) 7:2751–65. doi: 10.2147/IJN.S30273
65. Hu J, Huang S, Zhu L, Huang W, Zhao Y, Jin K, et al. Tissue plasminogen activator-porous magnetic microrods for targeted thrombolytic therapy after ischemic stroke. *ACS Appl Mater Interfaces.* (2018) 10:32988–97. doi: 10.1021/acsami.8b09423
66. Zhang H, Sun F, Wang J, Xie L, Yang C, Pan M, et al. Combining injectable plasma scaffold with mesenchymal stem/stromal cells for repairing infarct cavity after ischemic stroke. *Aging Dis.* (2017) 8:203–14. doi: 10.14336/AD.2017.0305
67. Lee HJ, Park J, Yoon OJ, Kim HW, Lee DY, Kim DH, et al. Amine-modified single-walled carbon nanotubes protect neurons from injury in a rat stroke model. *Nat Nanotechnol.* (2011) 6:121–5. doi: 10.1038/nnano.2010.281
68. Hettiaratchi MH, O'Meara MJ, Teal CJ, Payne SL, Pickering AJ, Shoichet MS. Local delivery of stabilized chondroitinase ABC degrades chondroitin sulfate proteoglycans in stroke-injured rat brains. *J Control Release.* (2019) 297:14–25. doi: 10.1016/j.jconrel.2019.01.033
69. Reddy MK, Labhasetwar V. Nanoparticle-mediated delivery of superoxide dismutase to the brain: an effective strategy to reduce ischemia-reperfusion injury. *FASEB J.* (2009) 23:1384–95. doi: 10.1096/fj.08-116947
70. Ramos-Cabrer P, Agulla J, Argibay B, Pérez-Mato M, Castillo J. Serial MRI study of the enhanced therapeutic effects of liposome-encapsulated citicoline in cerebral ischemia. *Int J Pharm.* (2011) 405:228–33. doi: 10.1016/j.ijpharm.2010.12.014
71. Matsuse D, Kitada M, Ogura F, Wakao S, Kohama M, Kira J, et al. Combined transplantation of bone marrow stromal cell-derived neural progenitor cells with a collagen sponge and basic fibroblast growth factor releasing microspheres enhances recovery after cerebral ischemia in rats. *Tissue Eng Part A.* (2011) 17:1993–2004. doi: 10.1089/ten.tea.2010.0585
72. Liu Y, Ai K, Ji X, Askhatova D, Du R, Lu L, et al. Comprehensive insights into the multi-antioxidative mechanisms of melanin nanoparticles and their application to protect brain from injury in ischemic stroke. *JACS.* (2017) 139:856–62. doi: 10.1021/jacs.6b11013
73. Fukuta T, Asai T, Sato A, Namba M, Yanagida Y, Kikuchi T, et al. Neuroprotection against cerebral ischemia/reperfusion injury by intravenous administration of liposomal fasudil. *Int J Pharm.* (2016) 506:129–37. doi: 10.1016/j.ijpharm.2016.04.046

74. Jin Y-C, Kim S-W, Cheng F, Shin J-H, Park J-K, Lee S, et al. The effect of biodegradable gelatin microspheres on the neuroprotective effects of high mobility group box 1 A box in the postischemic brain. *Biomaterials.* (2011) 32:899–908. doi: 10.1016/j.biomaterials.2010.09.054
75. Joachim E, Kim I-D, Jin Y, Kim K, Lee J-K, Choi H. Gelatin nanoparticles enhance the neuroprotective effects of intranasally administered osteopontin in rat ischemic stroke model. *Drug Deliv Transl Res.* (2014) 4:395–9. doi: 10.1007/s13346-014-0208-9
76. Moshayedi P, Nih LR, Llorente IL, Berg AR, Cinkornpumin J, Lowry WE, et al. Systematic optimization of an engineered hydrogel allows for selective control of human neural stem cell survival and differentiation after transplantation in the stroke brain. *Biomaterials.* (2016) 105:145–55. doi: 10.1016/j.biomaterials.2016.07.028
77. Ahmad N, Ahmad R, Naqvi AA, Alam MA, Ashafaq M, Abdur Rub R, et al. Intranasal delivery of quercetin-loaded mucoadhesive nanoemulsion for treatment of cerebral ischaemia. *Artif Cells Nanomed Biotechnol.* (2018) 46:717–29. doi: 10.1080/21691401.2017.1337024
78. Yang X, Xu L, Zhou J, Ge Y, Wu S, Huang J, et al. Integration of phospholipid-complex nanocarrier assembly with endogenous N-oleoylethanolamine for efficient stroke therapy. *J Nanobiotechnol.* (2019) 17:8. doi: 10.1186/s12951-019-0442-x
79. Klose D, Laprais M, Leroux V, Siepmann F, Deprez B, Bordet R, et al. Fenofibrate-loaded PLGA microparticles: effects on ischemic stroke. *Eur J Pharm Sci.* (2009) 37:43–52. doi: 10.1016/j.ejps.2008.12.016
80. Darabi S, Mohammadi MT. Fullerenol nanoparticles decrease ischaemia-induced brain injury and oedema through inhibition of oxidative damage and aquaporin-1 expression in ischaemic stroke. *Brain Inj.* (2017) 31:1142–50. doi: 10.1080/02699052.2017.1300835
81. Harris NM, Ritzel R, Mancini NSN, Jiang Y, Yi X, Manickam DS, et al. Nanoparticle delivery of brain derived neurotrophic factor after focal cerebral ischemia reduces tissue injury and enhances behavioral recovery. *Pharmacol Biochem Behav.* (2016) 150–151:48–56. doi: 10.1016/j.pbb.2016.09.003
82. Tan L, Liang C, Wang Y, Jiang Y, Zeng S, Tan R. Pharmacodynamic effect of luteolin micelles on alleviating cerebral ischemia reperfusion injury. *Pharmaceutics.* (2018) 10:E248. doi: 10.3390/pharmaceutics10040248
83. Liu X, An C, Jin P, Liu X, Wang L. Protective effects of cationic bovine serum albumin-conjugated PEGylated tanshinone IIA nanoparticles on cerebral ischemia. *Biomaterials.* (2013) 34:817–30. doi: 10.1016/j.biomaterials.2012.10.017
84. Bao Q, Hu P, Xu Y, Cheng T, Wei C, Pan L, et al. Simultaneous blood-brain barrier crossing and protection for stroke treatment based on edaravone-loaded ceria nanoparticles. *ACS Nano.* (2018) 12:6794–805. doi: 10.1021/acsnano.8b01994
85. Bible E, Chau DYS, Alexander MR, Price J, Shakesheff KM, Modo M. The support of neural stem cells transplanted into stroke-induced brain cavities by PLGA particles. *Biomaterials.* (2009) 30:2985–94. doi: 10.1016/j.biomaterials.2009.02.012
86. Gaudin A, Yemisci M, Eroglu H, Lepetre-Mouelhi S, Turkoglu OF, Dönmez-Demir B, et al. Squalenoyl adenosine nanoparticles provide neuroprotection after stroke and spinal cord injury. *Nat Nanotechnol.* (2014) 9:1054–62. doi: 10.1038/nnano.2014.274
87. Ishii T, Asai T, Oyama D, Fukuta T, Yasuda N, Shimizu K, et al. Amelioration of cerebral ischemia–reperfusion injury based on liposomal drug delivery system with asialo-erythropoietin. *J Control Release.* (2012) 160:81–7. doi: 10.1016/j.jconrel.2012.02.004
88. Wang Y, Cooke MJ, Morshead CM, Shoichet MS. Hydrogel delivery of erythropoietin to the brain for endogenous stem cell stimulation after stroke injury. *Biomaterials.* (2012) 33:2681–92. doi: 10.1016/j.biomaterials.2011.12.031
89. Ravina K, Briggs DI, Kislal S, Warraich Z, Nguyen T, Lam RK, et al. Intracerebral delivery of brain-derived neurotrophic factor using HyStem®-C hydrogel implants improves functional recovery and reduces neuroinflammation in a rat model of ischemic stroke. *Int J Mol Sci.* (2018) 19:3782. doi: 10.3390/ijms19123782
90. Yan F, Yue W, Zhang Y, Mao G, Gao K, Zuo Z, et al. Chitosan-collagen porous scaffold and bone marrow mesenchymal stem cell transplantation for ischemic stroke. *Neural Regen Res.* (2015) 10:1421–6. doi: 10.4103/1673-5374.163466
91. Guo X, Deng G, Liu J, Zou P, Du F, Liu F, et al. Thrombin-responsive, brain-targeting nanoparticles for improved stroke therapy. *ACS Nano.* (2018) 12:8723–32. doi: 10.1021/acsnano.8b04787
92. Yu H, Cao B, Feng M, Zhou Q, Sun X, Wu S, et al. Combinated transplantation of neural stem cells and collagen type I promote functional recovery after cerebral ischemia in rats. *Anat Rec.* (2010) 293:911–7. doi: 10.1002/ar.20941
93. Ahmad N, Ahmad R, Naqvi AA, Alam MA, Ashafaq M, Samim M, et al. Rutin-encapsulated chitosan nanoparticles targeted to the brain in the treatment of Cerebral Ischemia. *Int J Biol Macromol.* (2016) 91:640–55. doi: 10.1016/j.ijbiomac.2016.06.001
94. Lv W, Xu J, Wang X, Li X, Xu Q, Xin H. Bioengineered boronic ester modified dextran polymer nanoparticles as reactive oxygen species responsive nanocarrier for ischemic stroke treatment. *ACS Nano.* (2018) 12:5417–26. doi: 10.1021/acsnano.8b00477
95. Liu X, Ye M, An C, Pan L, Ji L. The effect of cationic albumin-conjugated PEGylated tanshinone IIA nanoparticles on neuronal signal pathways and neuroprotection in cerebral ischemia. *Biomaterials.* (2013) 34:6893–905. doi: 10.1016/j.biomaterials.2013.05.021
96. Yun X, Maximov VD, Yu J, Zhu G, Vertegel AA, Kindy MS. Nanoparticles for targeted delivery of antioxidant enzymes to the brain after cerebral ischemia and reperfusion injury. *J Cereb Blood Flow Metab.* (2013) 33:583–92. doi: 10.1038/jcbfm.2012.209
97. Zhao L, Liu A, Yu S, Wang Z, Lin X, Zhai G, et al. The permeability of puerarin loaded poly(butylcyanoacrylate) nanoparticles coated with polysorbate 80 on the blood–brain barrier and its protective effect against cerebral ischemia/reperfusion injury. *Biol Pharm Bull.* (2013) 36:1263–70. doi: 10.1248/bpb.b12-00769
98. Jin Y, Kim I-Y, Kim I-D, Lee H-K, Park J-Y, Han P-L, et al. Biodegradable gelatin microspheres enhance the neuroprotective potency of osteopontin via quick and sustained release in the post-ischemic brain. *Acta Biomater.* (2014) 10:3126–35. doi: 10.1016/j.actbio.2014.02.045
99. Chen S-J, Chang C-M, Tsai S-K, Chang Y-L, Chou S-J, Huang S-S, et al. Functional improvement of focal cerebral ischemia injury by subdural transplantation of induced pluripotent stem cells with fibrin glue. *Stem Cells Dev.* (2010) 19:1757–67. doi: 10.1089/scd.2009.0452
100. Nih LR, Gojgini S, Carmichael ST, Segura T. Dual-function injectable angiogenic biomaterial for the repair of brain tissue following stroke. *Nat Mater.* (2018) 17:642–51. doi: 10.1038/s41563-018-0083-8
101. Hassanzadeh P, Atyabi F, Dinarvand R, Dehpour A-R, Azhdarzadeh M, Dinarvand M. Application of nanostructured lipid carriers: the prolonged protective effects for sesamol in *in vitro* and *in vivo* models of ischemic stroke via activation of PI3K signalling pathway. *DARU J Pharm Sci.* (2017) 25:25. doi: 10.1186/s40199-017-0191-z
102. Parent M, Boudier A, Perrin J, Vigneron C, Maincent P, Violle N, et al. *In situ* microparticles loaded with S-nitrosoglutathione protect from stroke. *PLoS ONE.* (2015) 10:e0144659. doi: 10.1371/journal.pone.0144659
103. Jin K, Mao X, Xie L, Galvan V, Lai B, Wang Y, et al. Transplantation of human neural precursor cells in matrigel scaffolding improves outcome from focal cerebral ischemia after delayed postischemic treatment in rats. *J Cereb Blood Flow Metab.* (2010) 30:534–44. doi: 10.1038/jcbfm.2009.219
104. Mdzinarishvili A, Sutariya V, Talasila PK, Geldenhuys WJ, Sadana P. Engineering triiodothyronine (T3) nanoparticle for use in ischemic brain stroke. *Drug Deliv Transl Res.* (2013) 3:309–17. doi: 10.1007/s13346-012-0117-8
105. Vani JR, Mohammadi MT, Foroshani MS, Jafari M. Polyhydroxylated fullerene nanoparticles attenuate brain infarction and oxidative stress in rat model of ischemic stroke. *EXCLI J.* (2016) 15:378–90. doi: 10.17179/excli2016-309
106. Takamiya M, Miyamoto Y, Yamashita T, Deguchi K, Ohta Y, Abe K. Strong neuroprotection with a novel platinum nanoparticle against ischemic stroke- and tissue plasminogen activator-related brain damages in mice. *Neuroscience.* (2012) 221:47–55. doi: 10.1016/j.neuroscience.2012.06.060
107. Ahmad N, Ahmad R, Abbas Naqvi A, Ashafaq M, Alam MA, Ahmad FJ, et al. The effect of safranal loaded mucoadhesive nanoemulsion on oxidative stress markers in cerebral ischemia. *Artif Cells Nanomed Biotechnol.* (2017) 45:775–87. doi: 10.1080/21691401.2016.1228659

108. Sarami Foroshani M, Sobhani ZS, Mohammadi MT, Aryafar M. Fullerenol nanoparticles decrease blood-brain barrier interruption and brain edema during cerebral ischemia-reperfusion injury probably by reduction of interleukin-6 and matrix metalloproteinase-9 transcription. *J Stroke Cerebrovasc Dis.* (2018) 27:3053–65. doi: 10.1016/j.jstrokecerebrovasdis.2018.06.042
109. Wang Y, Li S-Y, Shen S, Wang J. Protecting neurons from cerebral ischemia/reperfusion injury via nanoparticle-mediated delivery of an siRNA to inhibit microglial neurotoxicity. *Biomaterials.* (2018) 161:95–105. doi: 10.1016/j.biomaterials.2018.01.039
110. Wang Z, Zhao Y, Jiang Y, Lv W, Wu L, Wang B, et al. Enhanced anti-ischemic stroke of ZL006 by T7-conjugated PEGylated liposomes drug delivery system. *Sci Rep.* (2015) 5:12651. doi: 10.1038/srep12651

Conflict of Interest Statement: The authors declare that the research was conducted in the absence of any commercial or financial relationships that could be construed as a potential conflict of interest.

Copyright © 2019 Bolan, Louca, Heal and Cunningham. This is an open-access article distributed under the terms of the Creative Commons Attribution License (CC BY). The use, distribution or reproduction in other forums is permitted, provided the original author(s) and the copyright owner(s) are credited and that the original publication in this journal is cited, in accordance with accepted academic practice. No use, distribution or reproduction is permitted which does not comply with these terms.

frontiers in Aging Neuroscience

ORIGINAL RESEARCH
published: 27 August 2019
doi: 10.3389/fnagi.2019.00228

New Perspective for Non-invasive Brain Stimulation Site Selection in Mild Cognitive Impairment: Based on Meta- and Functional Connectivity Analyses

Jiao Liu, Binlong Zhang, Georgia Wilson, Jian Kong and the Alzheimer's Disease Neuroimaging Initiative†*

Department of Psychiatry, Harvard Medical School, Massachusetts General Hospital, Boston, MA, United States

OPEN ACCESS

Edited by:
Johannes Boltze, The University of Warwick, United Kingdom

Reviewed by:
Gabriel Gonzalez-Escamilla, Johannes Gutenberg University Mainz, Germany
Ramesh Kandimalla, Texas Tech University Health Sciences Center, United States

****Correspondence:***
Jian Kong
kongj@nmr.mgh.harvard.edu

† Data used in preparation of this article were obtained from the Alzheimer's Disease Neuroimaging Initiative (ADNI) database (adni.loni.usc.edu). As such, the investigators within the ADNI contributed to the design and implementation of ADNI and/or provided data but did not participate in analysis or writing of this report. A complete listing of ADNI investigators can be found at: http://adni.loni.usc.edu/wp-content/uploads/how_to_apply/ADNI_Acknowledgement_List.pdf

Received: *12 April 2019*
Accepted: *09 August 2019*
Published: *27 August 2019*

Citation:
Liu J, Zhang B, Wilson G, Kong J and the Alzheimer's Disease Neuroimaging Initiative (2019) New Perspective for Non-invasive Brain Stimulation Site Selection in Mild Cognitive Impairment: Based on Meta- and Functional Connectivity Analyses. Front. Aging Neurosci. 11:228. doi: 10.3389/fnagi.2019.00228

Background: Non-invasive brain stimulation (NIBS) has been widely used to treat mild cognitive impairment (MCI). However, there exists no consensus on the best stimulation sites.

Objective: To explore potential stimulation locations for NIBS treatment in patients with MCI, combining meta- and resting state functional connectivity (rsFC) analyses.

Methods: The meta-analysis was conducted to identify brain regions associated with MCI. Regions of interest (ROIs) were extracted based on this meta-analysis. The rsFC analysis was applied to 45 MCI patients to determine brain surface regions that are functionally connected with the above ROIs.

Results: We found that the dorsolateral prefrontal cortex (DLPFC) and inferior frontal gyrus (IFG) were the overlapping brain regions between our results and those of previous studies. In addition, we recommend that the temporoparietal junction (including the angular gyrus), which was found in both the meta- and rsFC analysis, should be considered in NIBS treatment of MCI. Furthermore, the bilateral orbital prefrontal gyrus, inferior temporal gyrus, medial superior frontal gyrus, and right inferior occipital gyrus may be potential brain stimulation sites for NIBS treatment of MCI.

Conclusion: Our results provide several potential sites for NIBS, such as the DLFPC and IFG, and may shed light on the locations of NIBS sites in the treatment of patients with MCI.

Keywords: mild cognitive impairment, non-invasive brain stimulation, stimulation site, meta-analysis, resting state functional connectivity

INTRODUCTION

Mild cognitive impairment (MCI) is defined as subjective memory impairment without dementia or loss of function (Bruscoli and Lovestone, 2004). Literature suggests that MCI can be the early expression of Alzheimer's disease (AD) and that up to 14.9% of MCI patients older than 65 will develop dementia. However, pharmacologic treatment for MCI is far from satisfactory (Petersen et al., 2018).

Recently, non-invasive brain stimulation (NIBS), such as repetitive transcranial magnetic stimulation (rTMS) and transcranial direct/alternating current stimulation (tDCS/tACS), has been widely used in the treatment of MCI (Brunoni et al., 2014; Nardone et al., 2014; Birba et al., 2017; Padala et al., 2018; Rajji, 2019). While most NIBS studies have targeted brain areas such as the dorsolateral prefrontal cortex (DLPFC), inferior frontal gyrus (IFG), inferior parietal lobule (IPL), and superior temporal gyrus (STG) (Elder and Taylor, 2014; Cappon et al., 2016; Birba et al., 2017), no stimulation location has been universally agreed upon (Pievani et al., 2017).

With the aid of cutting edge brain-imaging tools, investigators have found that many brain regions and networks are involved in the pathology of MCI (Cai et al., 2017; Melrose et al., 2018). These findings provide a basis for exploring new stimulation locations for NIBS. However, some of these regions pose a challenge for NIBS application, as they are located beneath the brain surface and are therefore difficult to access (Pievani et al., 2017).

In past decades, resting state functional connectivity (rsFC) has been widely used in brain research and in identifying NIBS locations. Functional connectivity is defined as the temporal correlation or coherence of a neurophysiological index measured in different brain areas that may show similar functional properties among these brain regions (Friston et al., 1993; Biswal et al., 1997). In a previous study, Fox used a connectivity-based approach to explore the underlying mechanisms of different TMS targets, which demonstrated the potential of using a connectivity-based targeting strategy to optimize TMS locations and increase clinical response (Fox et al., 2012).

In this study, we combined brain imaging meta- and rsFC analyses to explore brain locations for NIBS treatment of MCI. Specifically, we first performed a meta-analysis to identify surface brain areas associated with MCI and then selected these regions as potential NIBS targets. Further, we selected the key MCI-associated brain areas (including both superficial and deep structures) as regions of interest (ROIs) based on the meta-analysis. These ROIs were then used as seeds in the following rsFC analysis to further identify the functionally connected brain regions that are proximal to brain surface cortex in a cohort of MCI patients. We hypothesized that areas on the brain surface that are functionally connected with the deep brain structures involved in MCI pathology (meta-analysis map) may also be used as NIBS target locations in MCI treatment.

MATERIALS AND METHODS

In the present study, we first used Neurosynth[1] to conduct a forward inference meta-analysis at the threshold of $p < 0.01$ FDR-corrected and identify key brain regions involved in the pathophysiology of MCI. Neurosynth is a platform for automatically synthesizing the results of many different neuroimaging studies. Using the Neurosynth framework, a researcher can conduct large-scale automated neuroimaging meta-analyses of broad psychological concepts. The ability of Neurosynth to quantitatively distinguish forward inference from reverse inference allows researchers to assess the specificity of mappings between neural and cognitive functions (Yarkoni et al., 2011).

We then used three different pipelines (methods) to explore potential locations for NIBS in MCI patients. In Pipeline 1, we directly selected clusters on the brain surface of the original forward inference map from the meta-analysis as potential NIBS target regions. In Pipelines 2 and 3, we applied seed-based rsFC analysis to further explore the potential brain surface locations for NIBS in MCI patients. To do this, we first chose 20 ROIs from the meta-analysis map. In Pipeline 2, the group-level correlation maps of each ROI were saved to a binary mask (with positive and negative functional connectivity separated). The 20 positive and 20 negative correlation maps were added to obtain third level maps, and 4–6 surface clusters were selected from the third level maps as potential stimulation locations. In Pipeline 3, after 20 ROIs were picked, we combined them into a single ROI. The group-level seed-based functional connectivity map was created, and 4–6 surface clusters were chosen as potential stimulation locations.

Meta-Analysis (Pipeline 1)

In the Neurosynth platform, we used "MCI" as the search term to conduct forward inference analysis on all neuroimaging studies in the database that were available until February 2018. The forward brain maps were downloaded from the platform. Potential NIBS locations were chosen based on the report, and they were visually confirmed using BrainNet view[2](Xia et al., 2013), as well as MRcon_GL and MRcron_ice toolboxes. These potential locations were mapped onto a standard brain map and standard head map with the international 10–20 system in MNI space (Cutini et al., 2011).

Resting State Functional Connectivity Analysis

fMRI Data Acquisition

The structural and resting state functional MRI data of MCI patients used in the present study were obtained from large multicenter Alzheimer's Disease Neuroimaging Initiative (ADNI) studies[3]. The ADNI was launched in 2003 as a public-private partnership, led by Principal Investigator Michael W. Weiner, MD. The primary goal of ADNI has been to test whether serial magnetic resonance imaging (MRI), positron emission tomography (PET), other biological markers, and clinical and neuropsychological assessments can be combined to measure the progression of MCI and early AD. A total of 45 MCI patients were included.

The inclusion and exclusion criteria for MCI patients are available at: http://adni.loni.usc.edu/methods/documents/ (ADNI 1 Procedures Manual). Inclusion criteria was as follows: memory complaint by subject or study partner that is verified by a study partner; abnormal memory function documented by scoring below the education-adjusted cutoff on the logical

[1]http://neurosynth.org/

[2]https://www.nitrc.org/projects/bnv/

[3]http://adni.loni.usc.edu/

memory II subscale (delayed paragraph recall) from the Wechsler memory scale-revised (the maximum score is 25): (a) less than or equal to 8 for 16 or more years of education, (b) less than or equal to 4 for 8–15 years of education, (c) less than or equal to 2 for 0–7 years of education; mini-mental state exam score between 24 and 30 (inclusive) (Exceptions may be made for subjects with less than 8 years of education at the discretion of the project director); clinical dementia rating = 0.5 Memory Box score must be at least 0.5; General cognition and functional performance sufficiently preserved such that a diagnosis of AD cannot be made by the site physician at the time of the screening visit."

The data of Mild cognitive impairment patients from 55 to 90 years old with the same fMRI scanning parameters (TR = 3000 ms, TE = 30 ms, phases = 140 with eyes opened) was used in the present study. Eligibility criteria included MCI at any stage.

Resting State Functional Connectivity Analysis

Seed-to-voxel correlational analysis were calculated in MATLAB by applying the functional connectivity (CONN) toolbox v17.C[4]. Similar to our previous studies (Tao et al., 2016, 2019; Liu et al., 2019a,b), the images were preprocessed with slice timing, realigned, co-registered to subjects' respective structural images, normalized, and smoothed with a 6 mm full width at half maximum kernel. Segmentation of gray matter, white matter, and cerebrospinal fluid for the removal of temporal confounding factors was employed. Band-pass filtering was performed with a frequency window of 0.01 to 0.089 Hz.

To eliminate correlations caused by head motion and artifacts, we identified outlier time points in the motion parameters and global signal intensity using ART[5]. We treated images as outliers if the composite movement from a preceding image exceeded 0.5 mm or if the global mean intensity was greater than three standard deviations from the mean image intensity. In addition, the 12 motion regressions (three rotation and three translation parameters plus six first-order temporal derivatives) were used in the preprocessing of BOLD time courses. Outliers were included as regressors in the first level general linear model along with motion parameters (Tao et al., 2016; Wang et al., 2017).

Based on the results of the meta-analysis, we chose the key peak MNI coordinates from the brain map (see details in section "Results" and **Table 2**) as ROIs. To ensure only voxels that were part of the original Neurosynth map were included, and to maintain regional specificity within the mentioned peak coordinates, the mask was derived by taking the overlap of the original forward inference Neurosynth map and a 6 mm radius spherical mask centered on the identified peak coordinates. This methodology is similar to that of a previous study conducted by Goldstein-Piekarski et al. (2018). The ROIs were further defined and refined by WFU-Pick Atlas software (Maldjian et al., 2003, 2004) to ensure that the regions were within the specific structure identified. The BOLD time course from these ROIs was then extracted, and Pearson's correlation coefficients were computed between that time course and the time courses of all other voxels in the brain. Correlation coefficients were Fisher transformed into *Z* scores.

Before the rsFC group analysis, we created a brain cortex mask to exclude sub-cortex brain regions from the AAL template using WFU-Pick Atlas software. The mask included bilateral pre and postcentral, superior and middle frontal, superior and inferior and middle occipital, superior and inferior parietal, supramarginal, angular, superior temporal, superior temporal pole, middle temporal, middle temporal pole, inferior temporal, oper inferior frontal, oper Rolandic, tri inferior frontal, superior medial frontal, calcarine, orbital middle and superior and inferior frontal, orbital medial frontal, supplementary motor area, paracentral lobule, precuneus, and cuneus.

Pipeline 2

For every seed in the subject-level correlation maps, the residual BOLD time course was extracted for each subject, and Pearson's correlation coefficients were computed between ROIs and all other brain voxels. The resulting correlation coefficients were subsequently transformed into *Z* scores to increase normality and thus conform to the assumptions of generalized linear models. In the group-level seed-to-voxel analysis, all subject-level seed maps of seed-to-voxel connectivity were included in a one sample *t*-test to obtain a group-level correlation map (positive and negative separated; *Z* values greater than or less than zero). A threshold of voxel-wise $p < 0.001$ uncorrected and cluster-level $p < 0.05$ family-wise error (FWE) corrected were applied within the cortex mask in data analysis.

After all whole-brain rsFC results of all ROIs above threshold had been extracted (binary mask), we calculated the sum of all brain masks using DPABI[6] to form a correlation map. The intensity of this correlation map represented the number of ROIs, and a higher intensity indicated a greater number of overlapping ROIs in the brain region. The 4 to 6 clusters on the brain surface with the largest peak intensity based on the report, visually confirmed using BrainNet view (Xia et al., 2013) and MRconGL and MRcron_ice toolboxes, were identified as potential stimulation locations.

Pipeline 3

We also calculated group functional connectivity using the seed that combined all above seeds into one seed. A threshold of voxel-wise $p < 0.001$ uncorrected and cluster-level $p < 0.05$ FWE corrected were applied within the cortex mask in data analysis.

RESULTS

Patient Demographics and Characteristics

Demographic and clinical characteristics of the study group are summarized in **Table 1**. Of the 45 enrolled MCI patients (24 female), the score of mini mental state examination (MMSE), clinical dementia rating-sum of boxes, and Alzheimer's disease assessment scale-cognition 12 (ADAS-Cog 12) were 27.64 (1.88), 0.95 (0.78), and 8.68 (3.66), respectively [mean (SD)], with

[4]http://www.nitrc.org/projects/conn

[5]http://www.nitrc.org/projects/artifact_detect

[6]http://rfmri.org/dpabi

33.33% APOE4 positive. The average age of MCI patients was 69.32 with a standard deviation of 8.07.

Meta-Analysis Results (Pipeline 1)

A total of 67 studies were included in the meta-analysis, and 20 clusters had a size greater than 30 continuous voxels. With the BrainNet viewing software, we visually determined that the left orbital IFG (F7) and left angular gyrus (P3) are proximal to the brain surface and can thereby serve as brain stimulation sites directly (**Figures 1B,C**, **Table 2**, and **Supplementary Figure S1A**).

Seed-to-Voxel rsFC Results

To further investigate potential surface locations of brain stimulation, we selected the peak coordinates from the meta-analysis maps as ROIs (seeds) (**Supplementary Figure S2**) and performed a rsFC analysis. The 20 seeds of MNI coordinates (*X*, *Y*, and *Z*) are shown in **Table 2**.

We used the above 20 seeds and applied rsFC analysis separately. The brain surface regions that showed overlap positively correlated with seed regions are listed in **Figures 1B,C**, **Table 3**, and **Supplementary Figure S1B**. These regions include the left inferior temporal gyrus, right inferior temporal gyrus, bilateral medial orbital frontal gyrus, right middle temporal gyrus/temporoparietal junction (TPJ), left middle occipital gyrus/TPJ, and left DLPFC. The left inferior temporal gyrus (T3), right supramarginal gyrus (between C4 and P4), and bilateral medial superior frontal gyrus (T3 and T4) were found to be negatively associated with seed regions applied in this study (**Figures 1B,C**, **Table 3**, and **Supplementary Figure S1C**; Pipeline 2).

When combining all seeds into one large seed, we only found positive rsFC with the right inferior occipital gyrus (between T6 and O2) proximal to the brain surface (**Figures 1B,C**, **Table 3**, and **Supplementary Figure S1D**; Pipeline 3).

DISCUSSION

In this study, we combined a meta-analysis and rsFC analysis to explore potential stimulation locations at the brain surface in patients with MCI. Our results suggest that the left DLPFC, left inferior orbital frontal gyrus, bilateral inferior temporal gyrus, TPJ, medial superior frontal gyrus, medial orbital prefrontal gyrus, right middle temporal gyrus, and inferior occipital gyrus should be considered as potential brain stimulation sites for MCI.

Location is a critical component in the treatment of MCI via NIBS (Fox and Greicius, 2010; Bergmann et al., 2016). In a previous study, Birba et al. (2017) used a meta-analysis method to test the effects of NIBS techniques on patients with MCI. They found that the DLPFC and IFG are brain stimulation areas commonly used in studies (**Figure 1A**). These findings are consistent with our results, indicating that these regions should be preferentially selected in the treatment of MCI with NIBS.

In further support of the important role of the DLPFC in patients with MCI, Yang et al. (2009) found that the BOLD response of the DLPFC is weaker in patients with MCI when compared with normally aging individuals. This finding suggests that a functional abnormality of the DLPFC may be an early indicator of the disease. In addition, results from neuroimaging studies suggest that the IFG plays an important role in cognitive functions such as memory processing (Thompson-Schill et al., 1997). For instance, Bell reported that, compared with amnestic MCI patients, patients with MCI-multiple cognitive domain had significantly reduced volume of the right IFG

TABLE 1 | Baseline characteristics.

Characteristics	Mean (SD) *n* = 45
Age	69.32 (8.07)
Gender (female/male)	24/21
Education (years)	15.71 (2.71)
MMSE	27.64 (1.88)
APOE4+	33.33%
CDR-SOB	0.95 (0.78)
ADAS-Cog12	8.68 (3.66)

MMSE, mini mental state examination; CDR-SOB, clinical dementia rating – sum of boxes; ADAS-Cog12, Alzheimer's disease assessment scale-cognition 12.

TABLE 2 | Results of meta-analysis (*indicates cluster on the brain surface).

Cluster	Voxel	Peak intensity	Peak MNI coordinate			Brain region
			x	*y*	*z*	
1	519	6.88	−22	−22	−16	L hippocampus
2	442	10.84	24	−10	−20	R hippocampus
3	80	5.90	−54	−6	−20	L middle temporal gyrus
4	94	6.88	40	−54	−20	R fusiform gyrus
5*	101	6.88	−36	26	−8	L orbital inferior frontal gyrus
6	85	5.90	34	26	−6	R orbital inferior frontal gyrus
7	37	4.91	−12	62	−12	L superior orbital frontal gyrus
8	48	4.91	−6	−58	2	L lingual gyrus
9	39	4.91	6	−18	8	R thalamus
10	436	8.86	0	−54	28	L post cingulum cortex
11	31	7.91	44	34	16	R tri inferior frontal gyrus
12	101	5.90	−50	12	26	L oper inferior frontal gyrus
13	59	5.90	0	54	30	L medial superior frontal gyrus
14	31	4.91	−34	−78	40	L inferior parietal gyrus
15	77	6.88	−42	−46	40	L inferior parietal gyrus
16*	41	5.90	−44	−64	40	L angular gyrus
17	59	6.88	46	−4	44	R precentral gyrus
18	47	5.90	−14	−68	50	L superior parietal gyrus
19	54	5.90	34	−58	50	R angular gyrus
20	43	6.88	10	14	50	R supplementary motor area

L: left; R: right.

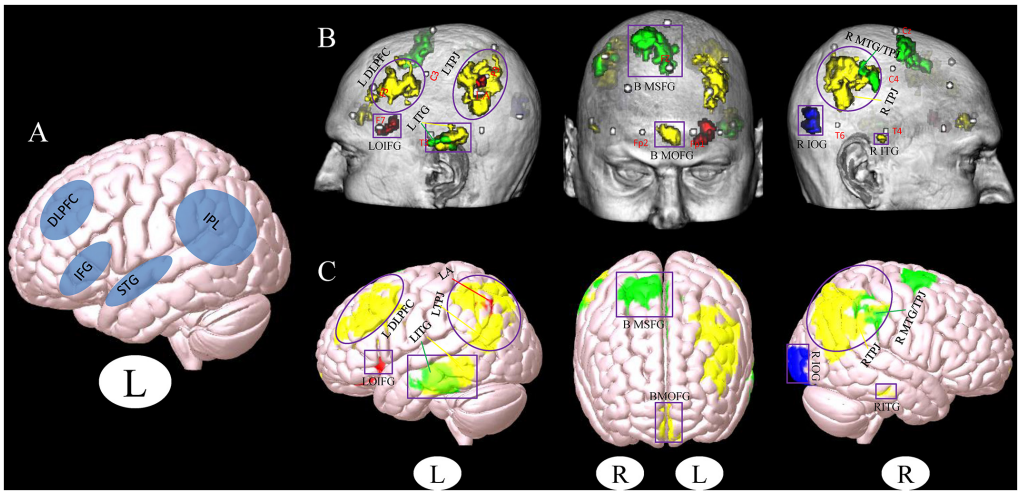

FIGURE 1 | (A) Stimulation location setup from a previous review study (Birba et al., 2017). **(B,C)** Cluster associated with the brain surface based on the results of meta- and functional connectivity analyses **(B)**, the template of chris_t1.nii.gz was used from Mricro_GL software. **(C)** The template of mni152.2009.mz 3 was used from Surf_Ice software. Red, results from the meta-analysis; Yellow, results from the positive rsFC; Green, results from the negative rsFC; Blue, results from the combination of all ROIs rsFC; Gray, MNI coordinates of 10–20 scalp positions found by Cutini et al. (2011). Purple box indicates the different brain regions between the results of a previous study (Birba et al., 2017) and our present results. Purple circle indicates the overlapping brain regions between the results of a previous study (Birba et al., 2017) and our present results (L, left and R, right). LDLPFC, left dorsolateral prefrontal cortex; LTPJ, left temporoparietal junction; LOIFG, left orbital inferior frontal gyrus; LITG, left inferior temporal gyrus; BMOFG, bilateral medial orbital frontal gyrus; BMSFG, bilateral medial superior frontal gyrus; RMTG/TPJ, right middle temporal gyrus and right temporoparietal junction; RITG, right inferior temporal gyrus; RIOG, right inferior occipital gyrus; LA: left angular.

TABLE 3 | Resting state functional connectivity results of regions on the brain surface.

Seed	Brain region	Cluster	Peak intensity	Peak MNI coordinate			Positive rsFC	Negative rsFC
				X	*Y*	*Z*		
20 seeds from meta-analysis	L inferior temporal gyrus	526	6	−54	−48	−18	✓	
	R inferior temporal gyrus	34	5	58	−22	20	✓	
	Bilateral medial orbital frontal gyrus	216	6	−2	58	−8	✓	
	R middle temporal gyrus/TPJ	2023	8	54	−60	14	✓	
	L middle occipital gyrus/TPJ	1879	8	−32	−70	28	✓	
	L DLPFC	1093	9	−42	4	38	✓	
	L inferior temporal gyrus	315	4	−52	−28	−18		✓
	R supramarginal gyrus	340	4	58	−28	32		✓
	Bilateral medial superior frontal gyrus	1066	4	−2	18	42		✓
Combinate seeds	R inferior occipital gyrus	277	4	38	−90	−14	✓	

L: left; R: right; TPJ: temporoparietal junction; DLPFC: dorsolateral prefrontal cortex.

(Bell-McGinty et al., 2005). Lin found that IFG activities may protect the memory function of individuals with MCI (Lin et al., 2017). These studies demonstrate the functional alterations of the DLPFC and inferior prefrontal gyrus in MCI and provide support for using these regions as treatment targets.

The temporal gyrus/TPJ was an overlapping brain region of both the meta-analysis and rsFC analysis, suggesting that it may be another important stimulation site for patients with MCI. A previous study reported that, compared with healthy elderly subjects, amnesiac MCI (aMCI) patients showed increased ALFF values in the left TPJ (Xi et al., 2013). The TPJ has been implicated across a broad range of cognitive areas, such as attention, social cognition, decision making, and episodic memory reconsolidation (Simon et al., 2017). Olichney reported that there was a significant suppression in amplitude of the late positive potential in the TPJ during a 3-choice vigilance task in individuals with MCI, and this change in amplitude may be a potential biomarker for early dementia (Olichney et al., 2011). Further, a study from Griffith et al. (2010) reported that the volume of the angular gyrus, a brain area within the TPJ, can predict cognitive function in MCI patients. Herholz also found that non-pharmacological interventions like recreational activity can yield an increase in cortical thickness of the right angular gyrus in patients with early stage AD (Herholz et al., 2013).

Our results suggest that the bilateral orbital prefrontal gyrus, inferior temporal gyrus, medial superior frontal gyrus, and right inferior occipital gyrus are potential stimulation sites based on rsFC analysis. Previous studies have suggested that the

orbitofrontal cortex is important in cognitive processes such as learning, decision making (Wilson et al., 2014), and maintaining appropriate social behavior (Jonker et al., 2015). Sacuiu showed that cortical atrophy in the frontal lobe, including the orbital prefrontal gyrus, can hasten the conversion of MCI to AD (Sacuiu et al., 2016).

In addition, studies suggest that the inferior temporal gyrus plays an important role in verbal fluency processing (Scheff et al., 2011) and serial visual recognition (Baylis and Rolls, 1987). For instance, investigators found that synaptic loss in the inferior temporal gyrus is a prominent pathological defect in the early stages of AD, and individuals with aMCI have significantly fewer synapses compared to those with no cognitive impairment (Scheff et al., 2011). The current literature suggests that increased activity of the superior frontal gyrus may be closely related to attentional shift between object features (Nagahama et al., 1999), cognitive control, working memory, and execution (Zhang et al., 2012).

Moreover, the medial superior frontal is an important node within the default mode network (DMN). Zhou et al. (2015) found several important nodes within the DMN that are involved in MCI, including the medial superior frontal gyrus. Huang et al. (2016) suggested that the DMN may indeed be a crucial target for interventions of MCI. Fink et al. (1996) found that the left inferior occipital cortex was activated in a local directed attention task, and Belleville suggested that attentional control deficits occur in patients with MCI (Belleville et al., 2007). Taken together, these studies provide further support for the aforementioned brain regions as targets for MCI treatment with NIBS.

It is worth noting that identifying these locations may also help to advance other interventions such as scalp acupuncture. Unlike traditional acupuncture, where needles are inserted into acupuncture points, scalp acupuncture stimulates the area of scalp corresponding to brain regions believed to be involved in the pathology of the disorders (Hao and Hao, 2012). Thus, results obtained from this study may facilitate the development of acupuncture and therapeutic modalities such as transcutaneous electrical nerve stimulation for the treatment of MCI.

Further, the aim of this preliminary study was to investigate potential stimulation locations for NIBS treatment using a unique approach that combined meta- and functional connectivity analyses. However, different stimulation techniques may have different intensities and reach different depth. How to apply and optimize these different treatment modalities to target the brain areas identified in our study is beyond the scope of this manuscript. Investigators should consider the characteristics of different tools when attempting to stimulate these areas.

CONCLUSION

Our results suggest that the DLPFC, IFG, and TPJ should be preferentially recommended as locations for NIBS treatment of MCI. Furthermore, the bilateral orbital prefrontal gyrus, inferior temporal gyrus, medial superior frontal gyrus, and right inferior occipital gyrus may also be potential brain stimulation sites. Our results ultimately shed light on possible NIBS sites in the treatment of MCI and other cases of age-related cognitive decline.

LIMITATIONS

There are several limitations to our study. First, while we provide several potential stimulation sites for NIBS treatment, we cannot predict the specific effects of such stimulation. For instance, we do not know whether the effect of the stimulation will be excitatory or inhibitory in nature. Another limitation is that the results of the connectivity analysis were strictly functional in the present study (i.e., rsFC). Future studies combining anatomical and functional connectivity analyses may yield stronger evidence for stimulation sites. Furthermore, our present study provided only a starting point for brain stimulation location selection via meta- and rsFC analysis methods. Determining the best brain region for NIBS remains a challenge. One option is to apply stimulation to multiple regions simultaneously. Stimulation paradigms are beyond the scope of this manuscript, and future studies are needed to explore these paradigms based on the specific NIBS modalities and, most importantly, the condition of the individual. In addition, due to the database limitation, we included patients within the age range of 55–90. Future studies with a smaller age range should be conducted to reduce the effects of standard deviation of age.

DATA AVAILABILITY

All datasets generated for this study are included in the manuscript and/or the **Supplementary Files**.

ETHICS STATEMENT

Data used in preparation of this article were obtained from the Alzheimer's disease ADNI database (adni.loni.usc.edu). As such, the investigators within the ADNI contributed to the design and implementation of ADNI and/or provided data but did not participate in analysis or writing of this report. A complete listing of ADNI investigators can be found at: http://adni.loni.usc.edu/wp-content/uploads/how_to_apply/ADNI_Acknowledgement_List.pdf.

AUTHOR CONTRIBUTIONS

JK designed the experiments. JL, BZ, and JK analyzed and interpreted the data. JL and GW prepared the manuscript. All authors prepared the manuscript, and read and approved the final manuscript.

FUNDING

JK was supported by grants R01 AT008563, R33 AT009310, R33AT009341, R34DA046635, and R21AT008707 from NIH. JL was supported by the Science and Technology Platform Construction project of Fujian Science and Technology Department (Grant No. 2015Y2001). Data collection and sharing for this project was funded by the Alzheimer's Disease

Neuroimaging Initiative (ADNI) (National Institutes of Health Grant U01 AG024904) and DOD ADNI (Department of Defense award number W81XWH-12-2-0012). ADNI was funded by the National Institute on Aging, the National Institute of Biomedical Imaging and Bioengineering, and through generous contributions from the following: AbbVie, Alzheimer's Association, Alzheimer's Drug Discovery Foundation, Araclon Biotech, BioClinica, Inc., Biogen; Bristol-Myers Squibb Company, CereSpir, Inc., Cogstate, Eisai Inc., Elan Pharmaceuticals, Inc., Eli Lilly and Company, EuroImmun, F. Hoffmann-La Roche Ltd. and its affiliated company Genentech, Inc., Fujirebio, GE Healthcare, IXICO Ltd., Janssen Alzheimer Immunotherapy Research & Development, LLC., Johnson & Johnson Pharmaceutical Research & Development LLC., Lumosity, Lundbeck, Merck & Co., Inc., Meso Scale Diagnostics, LLC., NeuroRx Research, Neurotrack Technologies, Novartis Pharmaceuticals Corporation, Pfizer Inc., Piramal Imaging, Servier, Takeda Pharmaceutical Company, and Transition Therapeutics. The Canadian Institutes of Health Research is providing funds to support ADNI clinical sites in Canada. Private sector contributions are facilitated by the Foundation for the National Institutes of Health (www.fnih.org). The grantee organization is the Northern California Institute for Research and Education, and the study is coordinated by the Alzheimer's Therapeutic Research Institute at the University of Southern California. ADNI data are disseminated by the Laboratory for Neuro Imaging at the University of Southern California.

SUPPLEMENTARY MATERIAL

The Supplementary Material for this article can be found online at: https://www.frontiersin.org/articles/10.3389/fnagi.2019.00228/full#supplementary-material

FIGURE S1 | (A) Results from the meta-analysis. **(B)** Results from the positive rsFC based on Pipeline 2 analysis. **(C)** Results from the negative rsFC based on Pipeline 2 analysis. **(D)** Results from the combination of all ROIs based on Pipeline 3 analysis.

FIGURE S2 | ROIs used for the functional connectivity analysis.

REFERENCES

Baylis, G. C., and Rolls, E. T. (1987). Responses of neurons in the inferior temporal cortex in short term and serial recognition memory tasks. *Exp. Brain Res.* 65, 614–622. doi: 10.1007/BF00235984

Belleville, S., Chertkow, H., and Gauthier, S. (2007). Working memory and control of attention in persons with Alzheimer's disease and mild cognitive impairment. *Neuropsychology* 21, 458–459. doi: 10.1037/0894-4105.21.4.458

Bell-McGinty, S., Lopez, O. L., Meltzer, C. C., Scanlon, J. M., Whyte, E. M., DeKosky, S. T., et al. (2005). Differential cortical atrophy in subgroups of mild cognitive impairment. *Arch. Neurol.* 62, 1393–1397. doi: 10.1001/archneur.62.9.1393

Bergmann, T. O., Karabanov, A., Hartwigsen, G., Thielscher, A., and Siebner, H. R. (2016). Combining non-invasive transcranial brain stimulation with neuroimaging and electrophysiology: current approaches and future perspectives. *NeuroImage* 140, 4–19. doi: 10.1016/j.neuroimage.2016.02.012

Birba, A., Ibáñez, A., Sedeño, L., Ferrari, J., García, A. M., and Zimerman, M. (2017). Non-invasive brain stimulation: a new strategy in mild cognitive impairment? *Front. Aging Neurosci.* 9:16. doi: 10.3389/fnagi.2017.00016

Biswal, B. B., Van Kylen, J., and Hyde, J. S. (1997). Simultaneous assessment of flow and BOLD signals in resting-state functional connectivity maps. *NMR Biomed.* 10, 165–170. doi: 10.1002/(sici)1099-1492(199706/08)10:4/5<165::aid-nbm454>3.0.co;2-7

Brunoni, A. R., Boggio, P. S., De Raedt, R., Bensenor, I. M., Lotufo, P. A., Namur, V., et al. (2014). Cognitive control therapy and transcranial direct current stimulation for depression: a randomized, double-blinded, controlled trial. *J. Affective Disord.* 162, 43–49. doi: 10.1016/j.jad.2014.03.026

Bruscoli, M., and Lovestone, S. (2004). Is MCI really just early dementia? A systematic review of conversion studies. *Int. Psychogeriatr.* 19, 129–140. doi: 10.1017/s1041610204000092

Cai, S., Chong, T., Peng, Y., Shen, W., Li, J., von Deneen, K. M., et al. (2017). Altered functional brain networks in amnestic mild cognitive impairment: a resting-state fMRI study. *Brain Imaging Behav.* 11, 619–631. doi: 10.1007/s11682-016-9539-0

Cappon, D., Jahanshahi, M., and Bisiacchi, P. (2016). Value and efficacy of transcranial direct current stimulation in the cognitive rehabilitation: a critical review since 2000. *Front. Neurosci.* 10:157. doi: 10.3389/fnins.2016.00157

Cutini, S., Scatturin, P., and Zorzi, M. (2011). A new method based on ICBM152 head surface for probe placement in multichannel fNIRS. *NeuroImage* 54, 919–927. doi: 10.1016/j.neuroimage.2010.09.030

Elder, G. J., and Taylor, J. P. (2014). Transcranial magnetic stimulation and transcranial direct current stimulation: treatments for cognitive and neuropsychiatric symptoms in the neurodegenerative dementias? *Alzheimers Res. Ther.* 6:74. doi: 10.1186/s13195-014-0074-1

Fink, G. R., Halligan, P. W., Marshall, J. C., Frith, C. D., Frackowiak, R. S. J., and Dolan, R. J. (1996). Where in the brain does visual attention select the forest and the trees? *Nature* 382, 626–629. doi: 10.1038/382626a0

Fox, M. D., Buckner, R. L., White, M. P., Greicius, M. D., and Pascual-Leone, A. (2012). Efficacy of TMS targets for depression is related to intrinsic functional connectivity with the subgenual cingulate. *Biol. Psychiatry* 72, 595–603. doi: 10.1016/j.biopsych.2012.04.028

Fox, M. D., and Greicius, M. (2010). Clinical applications of resting state functional connectivity. *Front. Syst. Neurosci.* 4:19. doi: 10.3389/fnsys.2010.00019

Friston, K. J., Frith, C. D., Liddle, P. F., and Frackowiak, R. S. J. (1993). Functional connectivity: the principal-component analysis of large (PET) data sets. *J. Cereb. Blood Flow Metab.* 13, 5–14. doi: 10.1038/jcbfm.1993.4

Goldstein-Piekarski, A. N., Staveland, B. R., Ball, T. M., Yesavage, J., Korgaonkar, M. S., and Williams, L. M. (2018). Intrinsic functional connectivity predicts remission on antidepressants: a randomized controlled trial to identify clinically applicable imaging biomarkers. *Transl. Psychiatry* 8:57. doi: 10.1038/s41398-018-0100-3

Griffith, R., Stewart, C., Stoeckel, L., Okonkwo, O., Den, J., Martin, R., et al. (2010). Magnetic resonance imaging volume of the angular gyri predicts financial skill deficits in people with amnestic mild cognitive impairment. *J. Am. Geriatr. Soc.* 58, 265–274. doi: 10.1111/j.1532-5415.2009.02679.x

Hao, J. J., and Hao, L. L. (2012). Review of clinical applications of scalp acupuncture for paralysis: an excerpt from chinese scalp acupuncture. *Glob. Adv. Health Med.* 1, 102–121. doi: 10.7453/gahmj.2012.1.1.017

Herholz, S. C., Herholz, R. S., and Herholz, K. (2013). Non-pharmacological interventions and neuroplasticity in early stage Alzheimer's disease. *Expert Rev. Neurother.* 13, 1235–1245. doi: 10.1586/14737175.2013.845086

Huang, P., Fang, R., Li, B. Y., and Chen, S. D. (2016). Exercise-related changes of networks in aging and mild cognitive impairment brain. *Front. Aging Neurosci.* 8:47. doi: 10.3389/fnagi.2016.00047

Jonker, F. A., Jonker, C., Scheltens, P., and Scherder, E. J. A. (2015). The role of the orbitofrontal cortex in cognition and behavior. *Rev. Neurosci.* 26, 1–11. doi: 10.1515/revneuro-2014-43

Lin, F., Ren, P., Lo, R. Y., Chapman, B. P., Jacobs, A., Baran, T. M., et al. (2017). Insula and inferior frontal gyrus' activities protect memory performance against Alzheimer's disease pathology in old age. *J. Alzheimers Dis.* 55, 669–678. doi: 10.3233/JAD-160715

Liu, J., Chen, L., Chen, X., Hu, K., Tu, Y., Lin, M., et al. (2019a). Modulation effects of different exercise modalities on the functional connectivity of the periaqueductal grey and ventral tegmental area in patients with knee osteoarthritis – a randomized multi-modal MRI study. *Br. J. Anesth.* doi: 10.1016/j.bja.2019.06.017 [Epub ahead of print].

Liu, J., Tao, J., Liu, W., Huang, J., Xue, X., Li, M., et al. (2019b). Different modulation effects of tai chi chuan and baduanjin on resting state functional connectivity of the default mode network in older adults. *Soc. Cogn. Affect. Neurosci.* 14, 217–224. doi: 10.1093/scan/nsz001

Maldjian, J. A., Laurienti, P. J., and Burdette, J. H. (2004). Precentral gyrus discrepancy in electronic versions of the talairach atlas. *NeuroImage* 21, 450–455. doi: 10.1016/j.neuroimage.2003.09.032

Maldjian, J. A., Laurienti, P. J., Kraft, R. A., and Burdette, J. H. (2003). An automated method for neuroanatomic and cytoarchitectonic atlas-based interrogation of fMRI data sets. *NeuroImage* 19, 1233–1239. doi: 10.1016/S1053-8119(03)00169-1

Melrose, R. J., Jimenez, A. M., Riskin-Jones, H., Weissberger, G., Veliz, J., Hasratian, A. S., et al. (2018). Alterations to task positive and task negative networks during executive functioning in mild cognitive impairment. *NeuroImage* 19, 970–981. doi: 10.1016/j.nicl.2018.06.014

Nagahama, Y., Okada, T., Katsumi, Y., Hayashi, T., Yamauchi, H., Sawamoto, N., et al. (1999). Transient neural activity in the medial superior frontal gyrus and precuneus time locked with attention shift between object features. *NeuroImage* 10, 193–199. doi: 10.1006/nimg.1999.0451

Nardone, R., Tezzon, F., Höller, Y., Golaszewski, S., Trinka, E., and Brigo, F. (2014). Transcranial magnetic stimulation (TMS)/repetitive TMS in mild cognitive impairment and Alzheimer's disease. *Acta Neurol. Scand.* 129, 351–366. doi: 10.1111/ane.12223

Olichney, J. M., Yang, J. C., Taylor, J., and Kutas, M. (2011). Cognitive event-related potentials: biomarkers of synaptic dysfunction across the stages of Alzheimer's disease. *Adv. Alzheimers Dis.* 2, 421–434.

Padala, P. R., Padala, K. P., Lensing, S. Y., Jackson, A. N., Hunter, C. R., Parkes, C. M., et al. (2018). Repetitive transcranial magnetic stimulation for apathy in mild cognitive impairment: a double-blind, randomized, sham-controlled, cross-over pilot study. *Psychiatry Res.* 261, 312–318. doi: 10.1016/j.psychres.2017.12.063

Petersen, R. C., Lopez, O., Armstrong, M. J., Getchius, T. S. D., Ganguli, M., Gloss, D., et al. (2018). Practice guideline update summary: mild cognitive impairment: report of the guideline development, dissemination, and implementation subcommittee of the american academy of neurology. *Neurology* 90, 126–135. doi: 10.1212/WNL.0000000000004826

Pievani, M., Pini, L., Ferrari, C., Pizzini, F. B., Boscolo Galazzo, I., Cobelli, C., et al. (2017). Coordinate-based meta-analysis of the default mode and salience network for target identification in non-invasive brain stimulation of Alzheimer's disease and behavioral variant frontotemporal dementia networks. *J. Alzheimers Dis.* 57, 825–843. doi: 10.3233/JAD-161105

Rajji, T. K. (2019). Impaired brain plasticity as a potential therapeutic target for treatment and prevention of dementia. *Expert Opin. Ther. Targets* 23, 21–28. doi: 10.1080/14728222.2019.1550074

Sacuiu, S., Insel, P. S., Mueller, S., Tosun, D., Mattsson, N., Jack, C. R., et al. (2016). Chronic depressive symptomatology in mild cognitive impairment is associated with frontal atrophy rate which hastens conversion to Alzheimer dementia. *Am. J. Geriatr. Psychiatry* 24, 126–135. doi: 10.1016/j.jagp.2015.03.006

Scheff, S. W., Price, D. A., Schmitt, F. A., Scheff, M. A., and Mufson, E. J. (2011). Synaptic loss in the inferior temporal gyrus in mild cognitive impairment and Alzheimer disease. *J. Alzheimers Dis.* 24, 547–557. doi: 10.3233/JAD-2011-101782

Simon, K. C. N. S., Gómez, R. L., Nadel, L., and Scalf, P. E. (2017). Brain correlates of memory reconsolidation: a role for the TPJ. *Neurobiol. Learn. Mem.* 142, 154–161. doi: 10.1016/j.nlm.2017.03.003

Tao, J., Liu, J., Chen, X., Xia, R., Li, M., Huang, M., et al. (2019). Mind-body exercise improves cognitive function in patients with mild cognitive impairment and centrally modulates the hippocampus/ACC: a multi-modal MRI study. *NeuroImage* 23:101834. doi: 10.1016/j.nicl.2019.101834

Tao, J., Liu, J., Egorova, N., Chen, L., Sun, S., Xue, H., et al. (2016). Increased hippocampus–medial prefrontal cortex resting state functional connectivity and memory function after tai chi chuan practice in elder adults. *Front. Aging Neurosci.* 8:25. doi: 10.3389/fnagi.2016.00025

Thompson-Schill, S. L., D'Esposito, M., Aguirre, G. K., and Farah, M. J. (1997). Role of left inferior prefrontal cortex in retrieval of semantic knowledge: a reevaluation. *Proc. Natl. Acad. Sci. U.S.A.* 94, 14792–14797. doi: 10.1073/pnas.94.26.14792

Wang, Z., Wang, X., Liu, J., Chen, J., Liu, X., Nie, G., et al. (2017). Acupuncture treatment modulates the corticostriatal reward circuitry in major depressive disorder. *J. Psychiatr. Res.* 84, 18–26. doi: 10.1016/j.jpsychires.2016.09.014

Wilson, R. C., Takahashi, Y. K., Schoenbaum, G., and Niv, Y. (2014). Orbitofrontal cortex as a cognitive map of task space. *Neuron* 81, 267–278. doi: 10.1016/j.neuron.2013.11.005

Xi, Q., Zhao, X. H., Wang, P. J., Guo, Q. H., and He, Y. (2013). Abnormal intrinsic brain activity in amnestic mild cognitive impairment revealed by amplitude of low-frequency fluctuation: a resting-state functional magnetic resonance imaging study. *Chin. Med. J.* 126, 2912–2917. doi: 10.3760/cma.j.issn.0366-6999.20130431

Xia, M., Wang, J., and He, Y. (2013). BrainNet viewer: a network visualization tool for human brain connectomics. *PLoS One* 8:e68910. doi: 10.1371/journal.pone.0068910

Yang, Y. H., Liang, P. P., Lu, S. F., Li, K. C., and Zhong, N. (2009). The role of the DLPFC in inductive reasoning of MCI patients and normal agings: an fMRI study. *Sci. Chin. C* 52, 789–795. doi: 10.1007/s11427-009-0089-1

Yarkoni, T., Poldrack, R. A., Nichols, T. E., Van Essen, D. C., and Wager, T. D. (2011). Large-scale automated synthesis of human functional neuroimaging data. *Nat. Methods* 8, 665–670. doi: 10.1038/nmeth.1635

Zhang, S., Ide, J. S., and Li, C. S. R. (2012). Resting-state functional connectivity of the medial superior frontal cortex. *Cereb. Cortex* 22, 99–111. doi: 10.1093/cercor/bhr088

Zhou, B., Yao, H., Wang, P., Zhang, Z., Zhan, Y., Ma, J., et al. (2015). Aberrant functional connectivity architecture in Alzheimer's disease and mild cognitive impairment: a whole-brain, data-driven analysis. *BioMed. Res. Int.* 2015, 1–9. doi: 10.1155/2015/495375

Conflict of Interest Statement: JK has a disclosure to report (holding equity in a startup company, MNT, and pending patents to develop a new brain stimulation device) but declares no conflict of interest.

The remaining authors declare that the research was conducted in the absence of any commercial or financial relationships that could be construed as a potential conflict of interest.

Copyright © 2019 Liu, Zhang, Wilson, Kong and the Alzheimer's Disease Neuroimaging Initiative. This is an open-access article distributed under the terms of the Creative Commons Attribution License (CC BY). The use, distribution or reproduction in other forums is permitted, provided the original author(s) and the copyright owner(s) are credited and that the original publication in this journal is cited, in accordance with accepted academic practice. No use, distribution or reproduction is permitted which does not comply with these terms.

frontiers in Cellular Neuroscience

BRIEF RESEARCH REPORT
published: 03 September 2019
doi: 10.3389/fncel.2019.00394

Stem Cell-Derived Exosomes Protect Astrocyte Cultures From *in vitro* Ischemia and Decrease Injury as Post-stroke Intravenous Therapy

Xiaoyun Sun[1], Ji-Hye Jung[2,3], Oiva Arvola[1], Michelle R. Santoso[2], Rona G. Giffard[1], Phillip C. Yang[2,3] and Creed M. Stary[1]**

[1] Department of Anesthesiology, Perioperative and Pain Medicine, Stanford University School of Medicine, Stanford, CA, United States, [2] Division of Cardiovascular Medicine, Department of Medicine, Stanford University School of Medicine, Stanford, CA, United States, [3] Stanford Cardiovascular Institute, Stanford University School of Medicine, Stanford, CA, United States

OPEN ACCESS

Edited by:
Gregory Jaye Bix, University of Kentucky, United States

Reviewed by:
Cesar V. Borlongan, University of South Florida, United States
Alison Willing, University of South Florida, United States

***Correspondence:**
Phillip C. Yang
phillip@stanford.edu
Creed M. Stary
cstary@stanford.edu

Specialty section:
This article was submitted to Cellular Neuropathology, a section of the journal Frontiers in Cellular Neuroscience

Received: *06 March 2019*
Accepted: *13 August 2019*
Published: *03 September 2019*

Citation:
Sun X, Jung J-H, Arvola O, Santoso MR, Giffard RG, Yang PC and Stary CM (2019) Stem Cell-Derived Exosomes Protect Astrocyte Cultures From in vitro Ischemia and Decrease Injury as Post-stroke Intravenous Therapy. Front. Cell. Neurosci. 13:394. doi: 10.3389/fncel.2019.00394

In the present study, we assessed efficacy of exosomes harvested from human and mouse stem cell cultures in protection of mouse primary astrocyte and neuronal cell cultures following *in vitro* ischemia, and against ischemic stroke *in vivo*. Cell media was collected from primary mouse neural stem cell (NSC) cultures or from human induced pluripotent stem cell-derived cardiomyocyte (iCM) cultures. Exosomes were extracted and purified by polyethylene glycol complexing and centrifugation, and exosome size and concentration were determined with a NanoSite^{TM} particle analyzer. Exosomes were applied to primary mouse cortical astrocyte or neuronal cultures prior to, and/or during, combined oxygen-glucose deprivation (OGD) injury. Cell death was assessed *via* lactate dehydrogenase (LHD) and propidium iodide staining 24 h after injury. NSC-derived exosomes afforded marked protection to astrocytes following OGD. A more modest (but significant) level of protection was observed with human iCM-derived exosomes applied to astrocytes, and with NSC-derived exosomes applied to primary neuronal cultures. In subsequent experiments, NSC-derived exosomes were injected intravenously into adult male mice 2 h after transient (1 h) middle cerebral artery occlusion (MCAO). Gross motor function was assessed 1 day after reperfusion and infarct volume was assessed 4 days after reperfusion. Mice treated post-stroke with intravenous NSC-derived exosomes exhibited significantly reduced infarct volumes. Together, these results suggest that exosomes isolated from mouse NSCs provide neuroprotection against experimental stroke possibly *via* preservation of astrocyte function. Intravenous NSC-derived exosome treatment may therefore provide a novel clinical adjuvant for stroke in the immediate post-injury period.

Keywords: glia, iCM, iPSC, pluripotent, MCAO, cerebral ischemia

INTRODUCTION

Stroke remains the second-leading cause of death worldwide, with ischemic/embolic stroke accounting for ∼87% of total stroke occurrence (Benjamin et al., 2019). To date, early restoration of cerebral blood flow with thrombolytics remains the only effective intervention to minimize the evolution of injury. The failure to develop novel adjuvant therapies may lie in a historical focus on genes and cell-signaling pathways that are predominant in terminally differentiated cells. Neural progenitor cells persist in the adult brain and recent evidence (Peron and Berninger, 2015) describes latent neurogenic pathways re-activated after ischemic injury that act to preserve and restore neuronal function. Stem-cell targeted therapies have more recently been studied intensely as a therapeutic option to translate the developmental capacity of embryogenesis to treat a wide array of adult diseases and injuries. However, early promising results with directly transplanted stem cell lines (Hao et al., 2014) have been offset by immune-rejection, and tumorigenesis (Solter, 2006; Kawai et al., 2010). Most recently, in the setting of stroke therapy, the beneficial outcomes of stem cell therapy have been localized to their paracrine effects, and not mediated by cell replacement or transplanted cell differentiation (Chen et al., 2014; Xin et al., 2014). Therefore, a more immediate focus has been delineating the cellular mechanisms of the stem cell *secretome*.

Exosomes are nanoscale vesicles (≈30–130 nm in diameter) released by most cell types after multivesicular bodies (MVBs) fuse with the plasma membrane (Colombo et al., 2014). Exosomes are present in the circulation and contain a variety of proteins, nucleic acids and lipids derived from their host cells, facilitating intercellular communication and regulating recipient cell function (Robbins et al., 2016). Exosomes can cross the blood-brain barrier (BBB), and are transported into brain cells *via* pinocytosis, direct fusion with the plasma membrane, or binding to cell surface proteins and cell adhesion molecules (Colombo et al., 2014). Recent work utilizing exosomes for ischemic stroke therapy have attributed improved functional outcome to their cargoes, which includes microRNAs, DNAs, lipids, proteins and RNAs (Chen and Chopp, 2018). Deng et al. (2018) recently demonstrated that human neural stem cell (NSC)-derived exosomes had the best effect on neuronal recovery after *in vitro* ischemia compared to exosomes derived from terminally differentiated neurons or glia. These observations suggest that application of NSC-derived exosomes may be a promising new avenue for stroke therapy, however, their cellular targets remains poorly defined. Specifically, whether there are species-, organ- or cell-type specific effects of stem cell-derived exosomes on neuroprotection remains a critical gap impeding therapeutic implementation.

Notably, re-activation of latent embryonic pathways in the brain following ischemic injury have been shown to be regulated by astrocytes (Gotz et al., 2015), specialized glia critical in maintaining neuronal homeostasis in health and in response to injury (Clarke and Barres, 2013). Our lab and others have demonstrated that preserving astrocyte survival and function can translate to neuronal protection and reduced injury (Ouyang et al., 2013; Stary and Giffard, 2015), further supporting their potential as therapeutic targets for stroke. Therefore, in the present study, we assessed the effect of exosomes derived from mouse NSC cultures on primary mouse astrocyte and neuronal cultures subjected to *in vitro* ischemic injury. To assess inter-species exosome protection we also assessed the effect of exosomes derived from human induced pluripotent stem cell-derived cardiomyocytes (iCM) on primary mouse astrocyte cultures subjected to *in vitro* ischemic injury. After observing marked protection primarily by mouse NSC-derived exosomes in primary mouse astrocyte cultures, we then assessed their efficacy with post-injury intravenous application in an *in vivo* model of ischemic stroke.

MATERIALS AND METHODS

Primary Mouse Neural Stem Cell Cultures

All animal experiments were approved by Stanford University Animal Care and Use Committee (Stanford, CA, United States) and conducted according to the National Institutes of Health guidelines for animal welfare. Mouse NSCs were isolated from newborn mice within 24 h as previously described (Sun et al., 2015) (**Figure 1**). In brief, brains were removed, freed of meninges, and diced with a sterile razor blade in dissociation buffer [DMEM (Thermo Fisher Scientific, Waltham, MA, United States) containing 2.5 U/ml papain, 250 U/ml DNase I (Thermo Fisher Scientific), and 1 U/ml Dispase II (Roche Diagnostics, Indianapolis, IN, United States)]. After 1 h incubation the cells were washed three times with DMEM plus 10% fetal bovine serum (FBS, HyClone, Logan, UT, United States). The cells were then resuspended in plating medium, Neurobasal A (Thermo Fisher Scientific), with 2 mM L-glutamine, 100 U/ml penicillin, and 100 ug/ml streptomycin (Thermo Fisher Scientific), B-27 without vitamin A (Thermo Fisher Scientific), 20 ng/ml fibroblast growth factor-2 (Peprotech, Rocky Hill, NJ, United States), and 20 ng/ml epidermal growth factor (Peprotech), and plated at a density of one brain per six-well plate. Neural precursor cells proliferated and started to form neurosphere morphology (NSCs) in 2–3 days.

Human Induced Pluripotent Stem Cell-Derived Cardiomyocytes

Human induced pluripotent stem cell (iPSC)-derived cardiomyocytes (iCMs) were generated from human amniotic mesenchymal stem cells (hAMSCs), as previously described (Ge et al., 2012) (**Figure 1**). In brief, human placental tissue was obtained from healthy subjects at the Stanford Healthcare Center. All donors provided written informed consent before collection. Placental tissue underwent serial enzymatic digestion with trypsin-EDTA (Thermo Fisher Scientific) in phosphate-buffered saline and HBSS (Thermo Fisher Scientific) containing 50 mg type I collagenase (Thermo Fisher Scientific), 0.01% papain (Sigma, St. Louis, MO, United States), and 10% FBS (HyClone). After digestion, the suspension was filtered and the cells were collected by centrifugation at 200 g for 5 min.

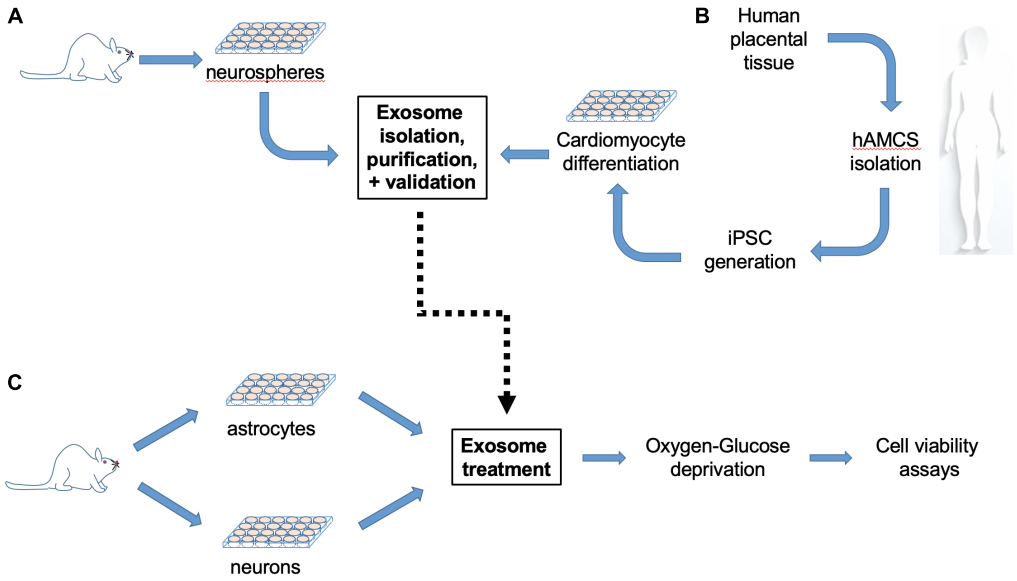

FIGURE 1 | Experimental workflow. **(A)** Mouse neural stem cells (NPCs) isolated from newborn mice were cultured for 2–3 days until proliferation to neurospheres, and then processed for exosome extraction, purification and size validation. **(B)** In parallel, exosomes were isolated from cultured human induced pluripotent stem cell (iPSC)-derived cardiomyocytes (iCMs) generated from human amniotic mesenchymal stem cells (hAMSCs). **(C)** Primary cerebral cortical astrocyte cultures were prepared from post-natal day 1–3 mice, plated for 21 days and then subjected to 6 h combined oxygen/glucose deprivation (OGD) with or without exosome treatment, followed by 24 h reperfusion prior cell viability assay. Neuronal cultures prepared from the cortices of embryonic day 15–16 mouse fetuses were plated for 12–13 days and then subjected to 70 min OGD with or without exosome treatment, followed by 24 h reperfusion prior to cell viability assay.

hAMSCs were seeded in 6-well plates and infected with 150 μL of pHAGE2-EF1α-OKSM (courtesy of Mostoslavsky, G, Ph.D., Boston University) virus in the presence of polybrene (10 mg/mL; Sigma). On day 6 post-infection, the cells were trypsinized (trypLE; Thermo Fisher Scientific), and pre-seeded with irradiated mouse embryonic fibroblasts (MEF-irr; GlobalStem). The resulting iPSCs were identified and verified as spontaneous colonies forming in human embryonic stem cell (hESC) culture media. iPSCs were then differentiated toward cardiac lineage with small molecules as previously described (Tachibana et al., 2017).

Exosome Extraction and Characterization

Exosome extraction was performed using a modified protocol by Chen et al. (2013). Briefly, Cell culture supernatant was centrifuged at 300 g for 10 min and passed through 0.2 um pore bottle top filter (BD Falcon, #352340, Thermo Fisher Scientific). One quarter volume of PEG (polyethylene glycol 8000, Thermo Fisher Scientific) stock solution [(20 g PEG8000 in 20 ml 0.5 NaCl phosphate-buffered saline (PBS, Sigma)] was added, then the total volume was brought to 50 ml with deionized H_2O and incubated overnight at 4°C. Samples were then centrifuged at 1500 g for 30 min, then at 300 g for 5 min after removal of most supernatant. The final pellet was then resuspended in PBS. Protein concentrations were determined *via* the bicinchoninic acid method (BCA Protein Assay Kit; Pierce, Rockford, IL, United States). The Malvern Panalytical NanoSight^{TM} instrument (which utilizes Nanoparticle Tracking Analysis to characterize nanoparticles from 10 to 2000 nm) was used to define exosome size and concentration.

Primary Mouse Astrocyte Cultures and Neuronal Cultures

Primary cerebral cortical astrocyte cultures were prepared from postnatal days 1–3 Swiss Webster mice (Charles River, Wilmington, MA, United States) as previously described (Dugan et al., 1995). Briefly, cortices freed of meninges were incubated in 0.05% trypsin/EDTA (Thermo Fisher Scientific) for 30 min at 37°C, mechanically dissociated, and plated in Falcon Primaria 24-well plates (Becton Dickinson, Lincoln, IL, United States) at 1–2 hemispheres per plate, in Eagle's minimal essential medium, high glucose (Glutamic, Thermo Fisher Scientific) supplemented with 10% fetal bovine serum, (Hyclone, Logan, UT, United States), 100 u/ml penicillin, 100 ug/ml streptomycin (Thermo Fisher Scientific). Cultures were maintained at 37°C in 5% CO_2, and medium was changed every 2 days before cell confluence, then twice/week after confluence, and utilized at day-*in-vitro* (DIV) 21. Relatively pure neuronal cultures, containing <1% astrocytes (Dugan et al., 1995), were prepared from the cortices of embryonic day (ED) 15 or 16 Swiss Webster mice. Cortices collected in ice-cold Eagle's minimal essential medium (Thermo Fisher Scientific) were digested with 0.05% trypsin/EDTA for 15 min at 37°C, triturated, then plated in medium containing 5% FBS and 5% ES (Hyclone). The culture medium was replaced with glial-conditioned medium containing 5% ES and 2% B-27 (Thermo Fisher Scientific). Cytosine arabinoside (3 mol/liter, Sigma) was added 24 h after plating to

inhibit glial proliferation. Cultures were used after 12–13 days (DIV 12,13) for oxygen-glucose deprivation (OGD) experiments.

Cell Culture Injury and Exosome Treatment

Combined OGD was employed as *in vitro* ischemic injury as we have previously done (Volobouева et al., 2008). Briefly, primary astrocyte and neuronal cultures were transferred to an anaerobic chamber (Coy Laboratory Products Inc., Grass Lake, MI, United States) with atmosphere gas partial pressure maintained of 5% CO_2, 5% H_2, and 90% N_2. The culture medium was replaced by three washes with deoxygenated, glucose-free balanced salt solution (BSS0), pH 7.4, containing phenol red (10 mg/liter) and (in mM) NaCl 116, $CaCl_2$ 1.8, $MgSO_4$ 0.8, KCl 5.4, NaH_2PO_4 1, $NaHCO_3$ 14.7, HEPES 10. BSS5.5 contains 25 mM glucose in BSS0 and is the medium used for wash controls. Cultures were kept at 37°C in the anaerobic chamber for 6 h for astrocyte cultures (Sun et al., 2013) and 70 min for neuronal cultures (Wang et al., 2004). Oxygen tension was monitored with an oxygen electrode (Microelectrodes, Bedford, NH, United States) and was kept under 0.02%. OGD was terminated by adding glucose to the culture medium to a final concentration of 5.5 mM and returning the cultures to the normoxic incubator for 24 h prior to assessment of cell death. In separate (unpublished) results, we have observed protection by iPSC-derived exosomes in cardiomyocytes at doses of at 10, 25, 50, 100, 200, 500 μg with an optimal dose at 50 μg. In the present study, we assessed doses *in vitro* of 30, 60, and 90 μg.

Cell Viability Assays

Extracellular release of lactate dehydrogenase (LHD) was measured to assess the extent of cell death as we routinely perform (Stary et al., 2017). LDH is an intracellular enzyme that catalyzes the conversion of lactate to pyruvate with the reduction of NAD to NADH which can be detected fluorescently (Decker and Lohmann-Matthes, 1988). LDH activity in the medium was assessed at 24 h of reperfusion and compared with maximum LDH release in medium after cells were frozen/thawed. The percentage death (% of LDH release) was calculated by dividing the experimental time point by the maximum LDH release values ×100. In parallel experiments propidium iodide (PI, 1 mg/ml) and Hoechst33258 (Sigma, 1 mg/ml) fluorescence were used to determine the percentage of cell death (Stary et al., 2017). Automated fluorescent image capture was performed at 200× using a Lumascope^{TM} 720 (Etaluma, Carlsbad, CA, United States) as we have previously performed (Xia et al., 2018). The number of PI-positive and Hoechst-positive cells were quantified using ImageJ software (v1.49b, National Institutes of Health, United States) and expressed as percentage of total cells.

In vivo Transient Focal Cerebral Ischemia and Exosome Treatment

All experimental protocols using animals were performed according to protocols approved by the Stanford University Animal Care and Use Committee and in accordance with the NIH guide for the care and use of laboratory animals. Adult male CB57/B6 mice (n = 16, 25–30 g from Jackson Lab) were anesthetized with 2% isoflurane in balance O_2 by facemask and focal cerebral ischemia was produced by 1 h of middle cerebral artery occlusion (MCAO) using a silicone-coated 6-monofilament (Doccol Co. Redlands, CA, United States) followed by reperfusion as we have previously performed (Stary et al., 2015, 2017). Rectal temperature was maintained at 37 ± 0.5°C controlled by a homeothermic blanket control unit (Harvard Apparatus, Holliston, MA, United States). Temperature and respiratory rate were monitored continuously. Mice were randomized to surgery, and mice with evidence of hemorrhage (n = 1 each group) were excluded from analysis and further treatment. Mice received treatment 2 h after reperfusion, a time point similar to when most stroke patients receive intervention (144 mins, (Saver et al., 2013)). Animals were re-anesthetized and either exosomes (10 ug total protein diluted in 100 μl saline, n = 7) or sterile saline alone (10 μl, n = 7) was administered into the surgically re-exposed internal jugular vein. This dose was chosen based on a prior study by Otero-Ortega et al. (2018) which administered 100 mg IV to rats, and scaled down to mice by body weight. Neurological status was assessed by neurologic deficit score 24 h after reperfusion (Xiong et al., 2011) using the following scoring system: 0 – no observable neurological deficits, 1 – failure to extend right forepaw; 2 – circling to the right; 3 – falling to the right; and 4 – cannot walk spontaneously. Cerebral infarction volume was determined after 4 days with 2,3,5-triphenyltetrazolium chloride (TTC, Sigma) staining of brains. Four sections/mouse were analyzed by a blinded observer and corrected for edema as described previously (Han et al., 2009) using ImageJ (v1.49b). Percent brain infarction was calculated as the area of the contralateral hemisphere minus the ipsilateral heather portion/contralateral hemisphere × 100, averaged for the sections.

Statistical Analysis

All values are presented as mean ± SD. For comparisons with more than two groups (i.e., **Figures 2**, **3**), one-way ANOVA was used. For comparison of two groups (i.e., **Figure 4**), student's t-test was used; Bonferroni *post-hoc* analysis was applied for statistical significance. GraphPad Prism 7.0 was used for statistical analysis and to plot graphs.

RESULTS

To investigate whether exosomes-derived from human or mouse stem cells had any effect on astrocytic cell death induced by OGD-reperfusion, we applied exosomes from either human iCMs or mouse NSC cultures immediately prior to and during OGD to confluent primary mouse astrocyte cultures. Both exosomes from human iCMs (**Figure 2A**) and exosomes from mouse NSCs (**Figure 2B**) exerted a neuroprotective effect. Exosomes derived from human iCMs reduced astrocytic LDH release from 47 to 32.9% at 30 ug/well, and then significantly ($p < 0.05$) reduced injury to 23.8% at 60 ug/well and to 21.6% in 90 ug/well. Comparatively, mouse NSC-derived exosomes treatment significantly ($p < 0.0005$) reduced LDH release

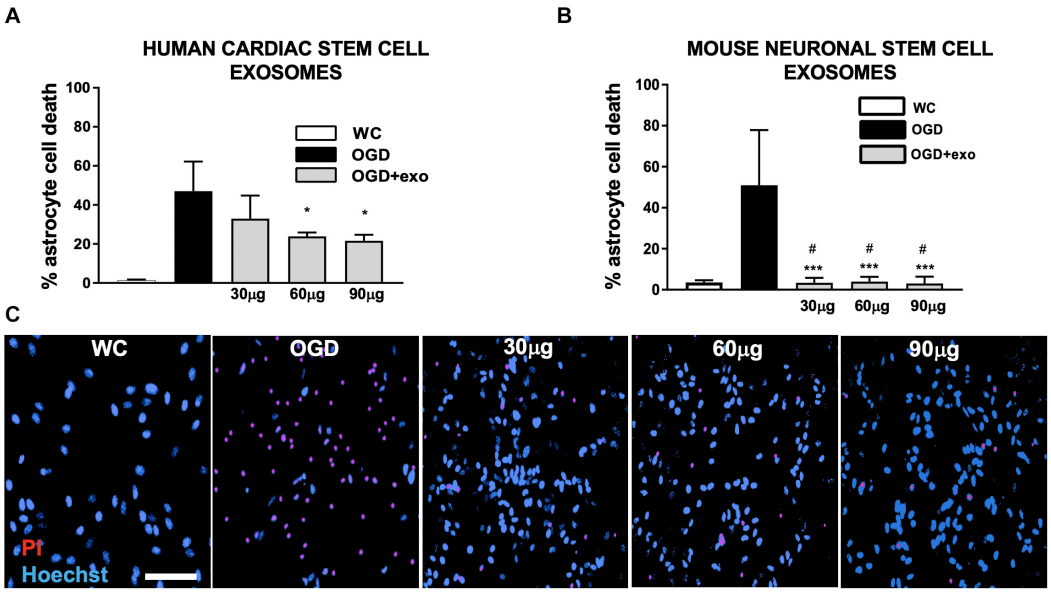

FIGURE 2 | Protection of mouse primary astrocytes against ischemic injury with exosomes derived from human iCMs and exosomes derived from mouse NSCs. **(A)** Cell death assessed by lactate dehydrogenase (LDH) release from mouse primary astrocyte cultures after oxygen/glucose deprivation injury (OGD) with/without exosomes derived from human iCMs. **(B)** Cell death assessed by LDH in mouse primary astrocyte cultures after OGD with/without exosomes derived from mouse NSCs. **(C)** Examples of astrocyte cultures stained to assess cell death with propidium iodide (PI, red) after OGD and treated with varying concentrations of exosomes derived from mouse neuronal stem cells. Cells are counterstained with Hoechst (blue) which stains all nuclei. Data are expressed as mean ± SD, all graphs represent pooled data from three individual experiments (n = 4–6 per treatment group for each individual experiment). *$p < 0.05$, ***$p < 0.0005$, compared with the control group. $^{\#}p < 0.05$ versus same dose exosomes derived from human iCMs. WC = wash control.

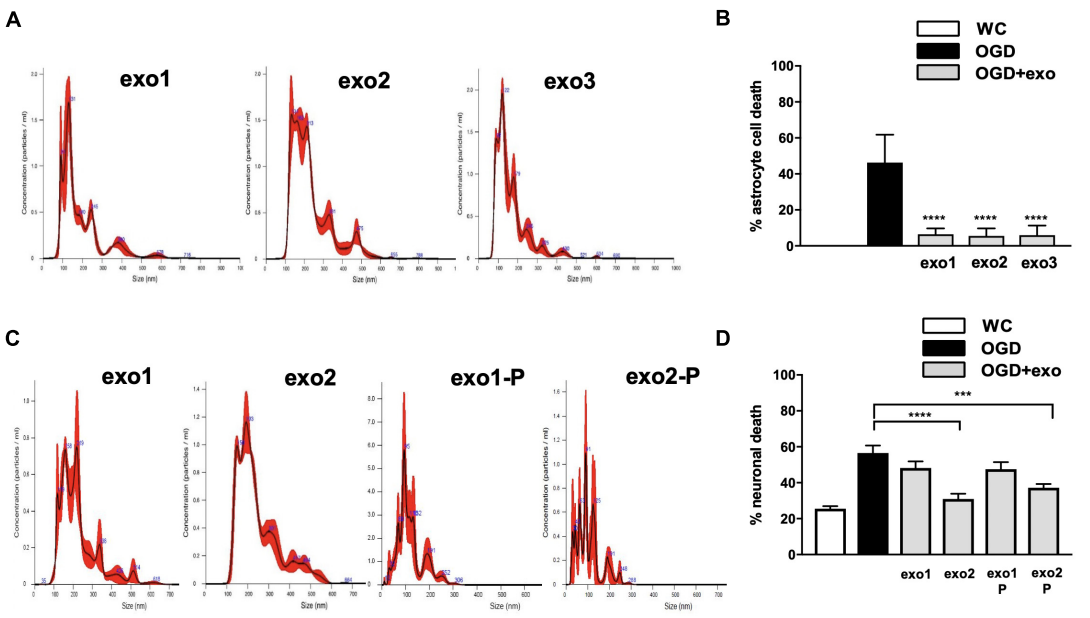

FIGURE 3 | Protection with mouse neural stem cell (NSC)-derived exosome in primary mouse astrocyte cultures and mouse primary mouse neuronal cultures after ischemic injury. **(A)** Microparticle size distribution analysis of exosomes isolated from three separate mouse NSC cultures. **(B)** Astrocyte cell death with exosomes isolated from three separate mouse NSC cultures applied at 60 ug/well during oxygen/glucose deprivation (OGD), assessed by lactate dehydrogenase (LDH) release. **(C)** Microparticle size distribution analysis of exosomes derived from two separate mouse NSC cultures with standard purification ("exo1" and "exo2") or an additional purification step ("exo1-P" and "exo2-P") to remove residual polyethylene glycol (PEG) beads. **(D)** Neuronal cell death after OGD with exosomes derived from two separate mouse NSC cultures with either standard purification or an additional purification step applied at 60 ug/well. Data are expressed as mean ± SD, graphs represent pooled data from three individual experiments, (n = 4–6 per treatment group for each individual experiment). ***$p < 0.0005$, ****$p < 0.0001$. WC = wash control.

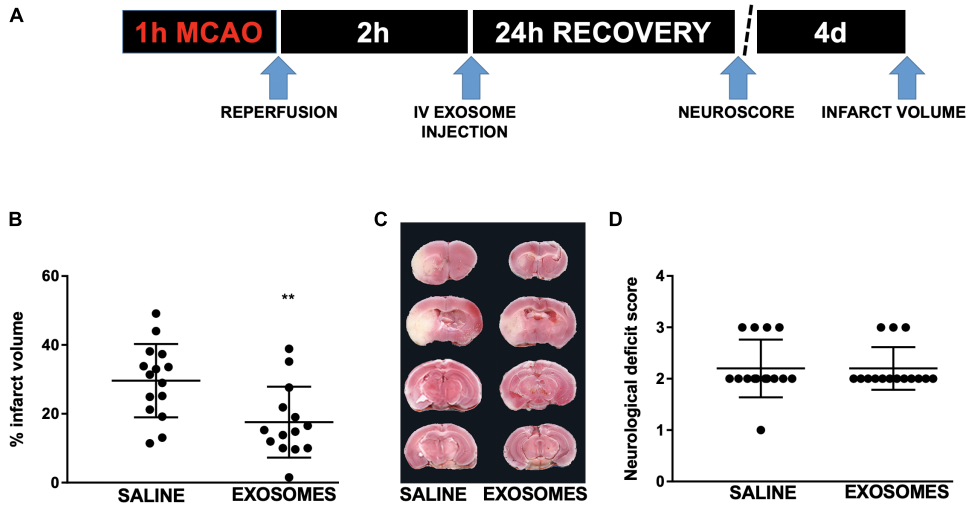

FIGURE 4 | Effect of post-injury intravenous treatment with exosomes from mouse NSCs on *in vivo* injury from transient middle cerebral artery occlusion (MCAO). **(A)** Injury and treatment workflow. Mice were subjected to 1 h MCAO and treated after 2 h reperfusion with either intravenous (IV) saline or exosomes derived from mouse NSCs. **(B)** Quantification of infarct volume 4 days after MCAO in mice treated with either saline or mouse NSC-derived exosomes. **(C)** Representative TTC-stained brain sections with saline or exosome treatment (infarcted areas are lighter in color). **(D)** Neurological deficit 24 h following MCAO in mice treated with saline or NSC-derived exosomes. Data are expressed as mean ± SD, $^{**}p < 0.0046$ versus saline (control) and exosome; n = 15–14/treatment group. TTC = 2,3,5-Triphenyltetrazolium chloride.

from astrocyte cultures at all doses: from 50.9 to 3.34% with 30 ug/well, 3.9% with 60 ug/well and 3% with 90 ug/well. In comparison with the same dose human iCM-derived exosomes, mouse NSC-derived exosomes provided significantly ($p < 0.05$) greater protection against *in vitro* ischemia in these astrocyte cultures. Protection was confirmed in parallel *via* propidium iodide/Hoescht co-staining (**Figure 2C**).

To further validate these observations, we tested the protective effect of exosomes isolated from three additional culture dissections of mouse NSCs. Exosome quality and concentration from each dissection were first independently validated (**Figure 3A**) and were similarly significantly protective when applied at 60 ug/well during OGD, as assessed either by LDH release (**Figure 3B**: 46.32 to 6.5% for exosome 1, 5.53% for exosome 2 and 5.93% for exosome 3) or PI/Hoescht staining (data not shown).

Next, to assess whether protection by stem cell-derived exosomes is cell-type specific, we assessed their effect in primary neuronal cultures subjected to OGD. We observed that while NSC-derived exosomes were protective neuronal cultures were sensitive to trace amounts of the purification agent PEG 8000 and required an additional purification step (**Figure 3C**). Treatment with 60 ug/well NSC-derived exosomes during OGD reduced neuronal cell death significantly ($p < 0.05$) only when subjected to additional purification: from 56.58% to 30.97 for exo1-P, and to 37.18 by exo2-P (**Figure 3D**). We failed to observe any significant protection in primary neuronal cultures treated with human iCM-derived exosomes (data not shown).

Finally, to advance the clinical application of NSC-derived exosomes we assessed the effect of post-injury application in a mouse model of ischemic stroke. Mice were treated 2 h after reperfusion following 1 h of MCAO with an intravenous injection of NSC-derived exosomes (**Figure 4A**) or with saline alone. Relative to saline control, NSC-derived exosome treatment resulted in a significantly reduced infarct volume from 29.62 ± 2.755 to 17.59 ± 2.75% ($p < 0.005$; **Figures 4B,C**) 4 days after injury. However, we did not observe a significant difference in neurological deficit score (**Figure 4D**) at 24 h reperfusion.

DISCUSSION

In the present study, we first assessed *in vitro* the protective effect of mouse NSC- and human cardiac iCM-derived exosomes in primary mouse astrocyte cultures subjected to ischemic injury. Interestingly, we observed that application of human cardiac iCM-derived exosomes was protective in primary mouse astrocytes. These observations validate the clinical utility of utilizing rodent models of cerebral ischemia for pre-clinical testing human-derived exosomes, which will likely be available for clinical therapy in the near future, and also highlight that xenotransplantation of exosomes derived from other species may be a possible therapeutic route for human neuroprotection. However, comparatively, treatment with mouse NSC-derived exosomes resulted in near-perfect preservation of mouse astrocyte viability. Subsequently, we observed that mouse NSC-derived exosomes applied to mouse primary neuronal cultures also had a more modest (but significantly) protective effect against *in vitro* ischemia compared with the marked protection of NSC-derived exosomes applied to primary astrocyte cultures. Together these findings suggest that *in vivo* exosome-mediated neuroprotection may be primarily mediated by astrocytes in a species and/or organ-dependent manner.

Astrocytes play a key role in neuroprotection by maintaining cellular ion homeostasis and pH, sequestering excess neurotransmitter, and in neuronal synaptic signaling (Clarke and Barres, 2013; Liu et al., 2017). Astrocytes also mediate neuronal energy homeostasis by providing energy substrate and regulating neuronal mitochondrial biogenesis and degradation (Davis et al., 2014). Notably Hayakawa et al. (2016) recently demonstrated that astrocytes are capable of direct transfer of functional mitochondria to neurons, and that suppression of this process worsens ischemic injury. Relevant to the results from the present study, Xin et al. (2017) recently demonstrated that improved functional recovery after MCAO from *in vivo* treatment with exosomes derived from microRNA 133b-overexpressing mesenchymal stem cells was dependent on secondary exosome release from astrocytes. Both embryonic and adult neurogenesis is an astrocyte-mediated process (Sultan et al., 2015; Platel and Bordey, 2016), and specific to stroke, reactive astrocytes have been observed to behave as neural progenitor cells, an effect tied to latent activation of embryonic neurotrophic pathways in astrocytes (Gotz et al., 2015). Building on our observations from the present study of enhanced astrocyte protection with NSC-derived exosome, future investigations should assess *in vivo* whether NSC-derived exosome administration can recapitulate astrocyte-mediated neuro-restoration after stroke.

Exosomes are also central to embryonic intercellular communication in the developing nervous system and play a major role in brain development and function (Sharma et al., 2013). Exosomes released by glia regulate neuronal signaling and plasticity (Wang et al., 2012a; Fruhbeis et al., 2013; Gosselin et al., 2013) and astrocyte-derived exosomes have been demonstrated to promote neurite outgrowth and neuronal survival after oxidative stress (Wang et al., 2011). Xin et al. (2013a) originally demonstrated that systemic treatment of stroke with cell-free exosomes derived from mesenchymal stem cells significantly improved neurologic outcome and contributed to neurovascular remodeling. They noted that exosome-based therapies represented a safer therapeutic approach than cell-based therapies, as exogenously administered cells have the potential to generate emboli and to self-replicate (Wang et al., 2012b), and that protection and enhanced recovery of stem cell-based therapies are mediated by exosomal trafficking (Xin et al., 2012, 2013b). One aim of the present study was to demonstrate proof-of-principle whether clinical administration of exosomes derived from NSCs could minimize the evolution of injury from stroke. We observed that NSC-derived exosomes provided significant protection against ischemic stroke injury when given as post-MCAO IV therapy. Clinically, approximately 65–70% of stroke patients receive care within 3.5 h after onset of stroke symptoms to be treated with thrombolysis (Saver et al., 2013; Benjamin et al., 2019). The results from the present study with IV exosome treatment at 2 h post-stroke represents a realistic clinical scenario whereby exosomes could be co-administered as an adjuvant therapy with thrombolytics. Future investigations should extend these observations to assess the efficacy of direct (intracerebroventricular or intrathecal) NSC-derived exosome therapy on both acute and extended injury phases and clinical outcomes, with and without thrombolytic therapy.

One limitation of the present study was that we did not see improvement in gross motor function at 24 h post-MCAO with exosome treatment. This may be related to the short interval between post-injury exosome intervention (2 h) and our assessment of post-injury neuroscore (24 h), and/or the relative insensitivity of a 4-point test of gross motor function, although we have utilized this test to reliably demonstrate neuroprotection at 24 h in the past (Xiong et al., 2011; Xia et al., 2018). Another contributing factor may have been organ sequestration of circulating exosomes given IV or possibly secondary to inadequate dosing, however, in this mouse ischemic stroke model we employed a similar dosing regimen scaled to prior studies in rats (Xin et al., 2013b, 2017). Future studies would benefit from assessing long-term neurobehavioral outcome with repeated IV exosome dosing to more accurately assess the clinical potential of NSC-derived exosome therapy.

Another caveat is that we did not demonstrate the presence of the exosomes within the brain with IV treatment, leaving the possibility that protection from systemic exosome administration may have been mediated by systemic responses, possibly immune-mediated. Indeed, recent studies (Zagrean et al., 2018) indicate that altered immune system signaling in response to stroke may be communicated *via* exosome-mediated glial-neuronal crosstalk. Future studies should seek to develop methods to assess cell-type specific and sub-regional localization of exogenously applied exosomes which would provide additional insight into their therapeutic mechanism of action and expand their potential as a novel adjuvant stroke therapy.

Finally, in order to advance clinical relevance future pre-clinical studies should fully implement the stroke therapy academic industry roundtable (STAIR) and the stem cell therapies as an emerging paradigm in stroke (STEPS) recommendations (Lapchak et al., 2013). Combined, these recommendations include: randomized and blinded studies; efficacy in two or more laboratories; replication in a second species; consideration of age and gender; consideration of route of administration, and useful therapeutic window and dose response; defining inclusion/exclusion criteria; conducting full power analysis and sample size calculations; disclosing potential conflicts of interest; extended functional outcome (minimum of 1 month); and stratifying ischemic and hemorrhagic stroke subgroups. While the present study employed several of these criteria (randomization and blinding, clinical route of administration, etc.), future studies should assess exosome efficacy in females and in aged animals, with a focus on extended functional recovery.

DATA AVAILABILITY

The datasets generated for this study are available on request to the corresponding author.

ETHICS STATEMENT

All animal experiments were approved by Stanford University Animal Care and Use Committee (Stanford, CA, United States)

and conducted according to the National Institutes of Health guidelines for animal welfare.

AUTHOR CONTRIBUTIONS

XS performed experiments and acquired the data. J-HJ prepared biological reagents and the manuscript. OA prepared the manuscript. MS prepared biological reagents. RG and PY assisted in experimental design and data analysis and provided funding. CS assisted in experimental design and data analysis, prepared the manuscript, and provided funding.

FUNDING

This work was supported by the National Institutes of Health (NIH) grant NS 084396 to RG, NIH grant HL113456, NIH grant HL130553, and California Institute for Regenerative Medicine grant DISC1-08650 to PY, and American Heart Association grant 14FTF19970029 to CS.

REFERENCES

Benjamin, E. J., Muntner, P., Alonso, A., Bittencourt, M. S., Callaway, C. W., Carson, A. P., et al. (2019). Heart disease and stroke statistics-2019 update: a report from the american heart association. *Circulations* 139, e56–e528. doi: 10.1161/CIR.0000000000000659

Chen, J., and Chopp, M. (2018). Exosome therapy for stroke. *Stroke J. Cereb. Circ.* 49, 1083–1090. doi: 10.1161/STROKEAHA.117.018292

Chen, J., Venkat, P., Zacharek, A., and Chopp, M. (2014). Neurorestorative therapy for stroke. *Front. Hum. Neurosci.* 8:382. doi: 10.3389/fnhum.2014.00382

Chen, L., Wang, Y., Pan, Y., Zhang, L., Shen, C., Qin, G., et al. (2013). Cardiac progenitor-derived exosomes protect ischemic myocardium from acute ischemia/reperfusion injury. *Biochem. Biophys. Res. Commun.* 431, 566–571. doi: 10.1016/j.bbrc.2013.01.015

Clarke, L. E., and Barres, B. A. (2013). Emerging roles of astrocytes in neural circuit development. *Nat. Rev. Neurosci.* 14, 311–321. doi: 10.1038/nrn3484

Colombo, M., Raposo, G., and Thery, C. (2014). Biogenesis, secretion, and intercellular interactions of exosomes and other extracellular vesicles. *Annu. Rev. Cell Dev. Biol.* 30, 255–289. doi: 10.1146/annurev-cellbio-101512-122326

Davis, C. H., Kim, K. Y., Bushong, E. A., Mills, E. A., Boassa, D., Shih, T., et al. (2014). Transcellular degradation of axonal mitochondria. *Proc. Natl. Acad. Sci. U.S.A.* 111, 9633–9638. doi: 10.1073/pnas.1404651111

Decker, T., and Lohmann-Matthes, M. L. (1988). A quick and simple method for the quantitation of lactate dehydrogenase release in measurements of cellular cytotoxicity and tumor necrosis factor (TNF) activity. *J. Immunol. Methods* 115, 61–69. doi: 10.1016/0022-1759(88)90310-9

Deng, M., Xiao, H., Peng, H., Yuan, H., Xu, Y., Zhang, G., et al. (2018). Preservation of neuronal functions by exosomes derived from different human neural cell types under ischemic conditions. *Eur. J. Neurosci.* 47, 150–157. doi: 10.1111/ejn.13784

Dugan, L. L., Bruno, V. M., Amagasu, S. M., and Giffard, R. G. (1995). Glia modulate the response of murine cortical neurons to excitotoxicity: glia exacerbate AMPA neurotoxicity. *J. Neurosci.* 15, 4545–4555. doi: 10.1523/jneurosci.15-06-04545.1995

Fruhbeis, C., Frohlich, D., Kuo, W. P., and Kramer-Albers, E. M. (2013). Extracellular vesicles as mediators of neuron-glia communication. *Front. Cell Neurosci.* 7:182. doi: 10.3389/fncel.2013.00182

Ge, X., Wang, I. N., Toma, I., Sebastiano, V., Liu, J., Butte, M. J., et al. (2012). Human amniotic mesenchymal stem cell-derived induced pluripotent stem cells may generate a universal source of cardiac cells. *Stem Cells Dev.* 21, 2798–2808. doi: 10.1089/scd.2011.0435

Gosselin, R. D., Meylan, P., and Decosterd, I. (2013). Extracellular microvesicles from astrocytes contain functional glutamate transporters: regulation by protein kinase C and cell activation. *Front. Cell Neurosci.* 7:251. doi: 10.3389/fncel.2013.00251

Gotz, M., Sirko, S., Beckers, J., and Irmler, M. (2015). Reactive astrocytes as neural stem or progenitor cells: in vivo lineage, in vitro potential, and Genome-wide expression analysis. *Glia* 63, 1452–1468. doi: 10.1002/glia.22850

Han, R. Q., Ouyang, Y. B., Xu, L., Agrawal, R., Patterson, A. J., and Giffard, R. G. (2009). Postischemic brain injury is attenuated in mice lacking the beta2-adrenergic receptor. *Anesth. Analg.* 108, 280–287. doi: 10.1213/ane.0b013e318187ba6b

Hao, L., Zou, Z., Tian, H., Zhang, Y., Zhou, H., and Liu, L. (2014). Stem cell-based therapies for ischemic stroke. *Biomed. Res. Int.* 2014:468748. doi: 10.1155/2014/468748

Hayakawa, K., Esposito, E., Wang, X., Terasaki, Y., Liu, Y., Xing, C., et al. (2016). Transfer of mitochondria from astrocytes to neurons after stroke. *Nature* 535, 551–555. doi: 10.1038/nature18928

Kawai, H., Yamashita, T., Ohta, Y., Deguchi, K., Nagotani, S., Zhang, X., et al. (2010). Tridermal tumorigenesis of induced pluripotent stem cells transplanted in ischemic brain. *J. Cereb. Blood Flow Metab.* 30, 1487–1493. doi: 10.1038/jcbfm.2010.32

Lapchak, P. A., Zhang, J. H., and Noble-Haeusslein, L. J. (2013). RIGOR guidelines: escalating STAIR and STEPS for effective translational research. *Transl. Stroke Res.* 4, 279–285. doi: 10.1007/s12975-012-0209-2

Liu, B., Teschemacher, A. G., and Kasparov, S. (2017). Neuroprotective potential of astroglia. *J. Neurosci. Res.* 95, 2126–2139. doi: 10.1002/jnr.24140

Otero-Ortega, L., Gomez de Frutos, M. C., Laso-Garcia, F., Rodriguez-Frutos, B., Medina-Gutierrez, E., Lopez, J. A., et al. (2018). Exosomes promote restoration after an experimental animal model of intracerebral hemorrhage. *J. Cereb. Blood Flow Metab.* 38, 767–779. doi: 10.1177/0271678X17708917

Ouyang, Y. B., Stary, C. M., Yang, G. Y., and Giffard, R. (2013). microRNAs: innovative targets for cerebral ischemia and stroke. *Curr. Drug Targets* 14, 90–101. doi: 10.2174/138945013804806424

Peron, S., and Berninger, B. (2015). Reawakening the sleeping beauty in the adult brain: neurogenesis from parenchymal glia. *Curr. Opin. Genet. Dev.* 34, 46–53. doi: 10.1016/j.gde.2015.07.004

Platel, J. C., and Bordey, A. (2016). The multifaceted subventricular zone astrocyte: from a metabolic and pro-neurogenic role to acting as a neural stem cell. *Neuroscience* 323, 20–28. doi: 10.1016/j.neuroscience.2015.10.053

Robbins, P. D., Dorronsoro, A., and Booker, C. N. (2016). Regulation of chronic inflammatory and immune processes by extracellular vesicles. *J. Clin. Invest.* 126, 1173–1180. doi: 10.1172/JCI81131

Saver, J. L., Fonarow, G. C., Smith, E. E., Reeves, M. J., Grau-Sepulveda, M. V., Pan, W., et al. (2013). Time to treatment with intravenous tissue plasminogen activator and outcome from acute ischemic stroke. *JAMA* 309, 2480–2488. doi: 10.1001/jama.2013.6959

Sharma, P., Schiapparelli, L., and Cline, H. T. (2013). Exosomes function in cell-cell communication during brain circuit development. *Curr. Opin. Neurobiol.* 23, 997–1004. doi: 10.1016/j.conb.2013.08.005

Solter, D. (2006). From teratocarcinomas to embryonic stem cells and beyond: a history of embryonic stem cell research. *Nat. Rev. Genet.* 7, 319–327. doi: 10.1038/nrg1827

Stary, C. M., and Giffard, R. G. (2015). Advances in astrocyte-targeted approaches for stroke therapy: an emerging role for mitochondria and microRNAS. *Neurochem. Res.* 40, 301–307. doi: 10.1007/s11064-014-1373-4

Stary, C. M., Xu, L., Li, L., Sun, X., Ouyang, Y. B., Xiong, X., et al. (2017). Inhibition of miR-181a protects female mice from transient focal cerebral ischemia by targeting astrocyte estrogen receptor-alpha. *Mol. Cell Neurosci.* 82, 118–125. doi: 10.1016/j.mcn.2017.05.004

Stary, C. M., Xu, L., Sun, X., Ouyang, Y. B., White, R. E., Leong, J., et al. (2015). MicroRNA-200c contributes to injury from transient focal cerebral ischemia by targeting Reelin. *Stroke J. Cereb. Circ.* 46, 551–556. doi: 10.1161/STROKEAHA.114.007041

Sultan, S., Li, L., Moss, J., Petrelli, F., Casse, F., Gebara, E., et al. (2015). Synaptic Integration of adult-born hippocampal neurons is locally controlled by astrocytes. *Neuron* 88, 957–972. doi: 10.1016/j.neuron.2015.10.037

Sun, X., Budas, G. R., Xu, L., Barreto, G. E., Mochly-Rosen, D., and Giffard, R. G. (2013). Selective activation of protein kinase C in mitochondria is neuroprotective in vitro and reduces focal ischemic brain injury in mice. *J. Neurosci. Res.* 91, 799–807. doi: 10.1002/jnr.23186

Sun, X., Voloboueva, L. A., Stary, C. M., and Giffard, R. G. (2015). Physiologically normal 5% O2 supports neuronal differentiation and resistance to inflammatory injury in neural stem cell cultures. *J. Neurosci. Res.* 93, 1703–1712. doi: 10.1002/jnr.23615

Tachibana, A., Santoso, M. R., Mahmoudi, M., Shukla, P., Wang, L., Bennett, M., et al. (2017). Paracrine effects of the pluripotent stem cell-derived cardiac myocytes salvage the injured myocardium. *Circ. Res.* 121, e22–e36. doi: 10.1161/CIRCRESAHA.117.310803

Voloboueva, L. A., Duan, M., Ouyang, Y., Emery, J. F., Stoy, C., and Giffard, R. G. (2008). Overexpression of mitochondrial Hsp70/Hsp75 protects astrocytes against ischemic injury in vitro. *J. Cereb. Blood Flow Metab.* 28, 1009–1016. doi: 10.1038/sj.jcbfm.9600600

Wang, G., Dinkins, M., He, Q., Zhu, G., Poirier, C., Campbell, A., et al. (2012a). Astrocytes secrete exosomes enriched with proapoptotic ceramide and prostate apoptosis response 4 (PAR-4): potential mechanism of apoptosis induction in Alzheimer disease (AD). *J. Biol. Chem.* 287, 21384–21395. doi: 10.1074/jbc.M112.340513

Wang, J., Bright, R., Mochly-Rosen, D., and Giffard, R. G. (2004). Cell-specific role for epsilon- and betaI-protein kinase C isozymes in protecting cortical neurons and astrocytes from ischemia-like injury. *Neuropharmacology* 47, 136–145. doi: 10.1016/j.neuropharm.2004.03.009

Wang, S., Cesca, F., Loers, G., Schweizer, M., Buck, F., Benfenati, F., et al. (2011). Synapsin I is an oligomannose-carrying glycoprotein, acts as an oligomannose-binding lectin, and promotes neurite outgrowth and neuronal survival when released via glia-derived exosomes. *J. Neurosci.* 31, 7275–7290. doi: 10.1523/JNEUROSCI.6476-10.2011

Wang, Y., Han, Z. B., Song, Y. P., and Han, Z. C. (2012b). Safety of mesenchymal stem cells for clinical application. *Stem Cells Int.* 2012:652034. doi: 10.1155/2012/652034

Xia, Y., Sun, X., Luo, Y., and Stary, C. M. (2018). Ferroptosis contributes to isoflurane neurotoxicity. *Front. Mol. Neurosci.* 11:486. doi: 10.3389/fnmol.2018.00486

Xin, H., Li, Y., Buller, B., Katakowski, M., Zhang, Y., Wang, X., et al. (2012). Exosome-mediated transfer of miR-133b from multipotent mesenchymal stromal cells to neural cells contributes to neurite outgrowth. *Stem Cells* 30, 1556–1564. doi: 10.1002/stem.1129

Xin, H., Li, Y., and Chopp, M. (2014). Exosomes/miRNAs as mediating cell-based therapy of stroke. *Front. Cell Neurosci.* 8:377. doi: 10.3389/fncel.2014.00377

Xin, H., Li, Y., Cui, Y., Yang, J. J., Zhang, Z. G., and Chopp, M. (2013a). Systemic administration of exosomes released from mesenchymal stromal cells promote functional recovery and neurovascular plasticity after stroke in rats. *J. Cereb. Blood Flow Metab.* 33, 1711–1715. doi: 10.1038/jcbfm.2013.152

Xin, H., Li, Y., Liu, Z., Wang, X., Shang, X., Cui, Y., et al. (2013b). MiR-133b promotes neural plasticity and functional recovery after treatment of stroke with multipotent mesenchymal stromal cells in rats via transfer of exosome-enriched extracellular particles. *Stem Cells* 31, 2737–2746. doi: 10.1002/stem.1409

Xin, H., Wang, F., Li, Y., Lu, Q. E., Cheung, W. L., Zhang, Y., et al. (2017). Secondary release of exosomes from astrocytes contributes to the increase in neural plasticity and improvement of functional recovery after stroke in rats treated with exosomes harvested from MicroRNA 133b-overexpressing multipotent mesenchymal stromal cells. *Cell Transplant.* 26, 243–257. doi: 10.3727/096368916X693031

Xiong, X., Barreto, G. E., Xu, L., Ouyang, Y. B., Xie, X., and Giffard, R. G. (2011). Increased brain injury and worsened neurological outcome in interleukin-4 knockout mice after transient focal cerebral ischemia. *Stroke J. Cereb. Circ.* 42, 2026–2032. doi: 10.1161/strokeaha.110.593772

Zagrean, A. M., Hermann, D. M., Opris, I., Zagrean, L., and Popa-Wagner, A. (2018). Multicellular crosstalk between exosomes and the neurovascular unit after cerebral ischemia. therapeutic implications. *Front. Neurosci.* 12:811. doi: 10.3389/fnins.2018.00811

Conflict of Interest Statement: The authors declare that the research was conducted in the absence of any commercial or financial relationships that could be construed as a potential conflict of interest.

Copyright © 2019 Sun, Jung, Arvola, Santoso, Giffard, Yang and Stary. This is an open-access article distributed under the terms of the Creative Commons Attribution License (CC BY). The use, distribution or reproduction in other forums is permitted, provided the original author(s) and the copyright owner(s) are credited and that the original publication in this journal is cited, in accordance with accepted academic practice. No use, distribution or reproduction is permitted which does not comply with these terms.

frontiers in Neuroscience

ORIGINAL RESEARCH
published: 06 September 2019
doi: 10.3389/fnins.2019.00935

Neurons Induced From Fibroblasts of c9ALS/FTD Patients Reproduce the Pathology Seen in the Central Nervous System

Peter O. Bauer[1,2,3], Judith H. Dunmore[1], Hiroki Sasaguri[1] and Vaclav Matoska[3]*

[1] Department of Neuroscience, Mayo Clinic, Jacksonville, FL, United States, [2] Bioinova, Ltd., Prague, Czechia, [3] Department of Clinical Biochemistry, Hematology and Immunology, Na Homolce Hospital, Prague, Czechia

Amyotrophic lateral sclerosis (ALS) and frontotemporal dementia (FTD) are incurable neurodegenerative conditions. A non-coding hexanucleotide (GGGGCC) repeat expansion in the *c9orf72* gene is the most common genetic cause of ALS/FTD. We present a cellular model of c9ALS/FTD where induced neurons (iNeurons) are generated within 2 weeks by direct conversion of patients' dermal fibroblasts through down-regulation of polypyrimidine-tract-binding protein 1 (PTB1). While sense (S) and anti-sense (AS) intranuclear RNA foci were observed in both fibroblasts and iNeurons, the accumulation of (S) and (AS) repeat-associated non-ATG translation (RANT) products were detected only in iNeurons. Importantly, anti-sense oligonucleotides (ASOs) against the (S) repeat transcript lead to decreased (S) RNA foci staining and a reduction of the corresponding RANT products without affecting its (AS) counterparts. ASOs treatment also rescued the cell viability upon stressful stimulus. The results indicate that iNeurons is an advantageous model that not only recapitulates c9ALS/FTD hallmark features but can also help uncover promising therapeutics.

Keywords: amyotrophic lateral sclerosis, c9ALS/FTD, c9orf72 expansion, induced neurons, iNeurons, RNA foci, repeat-associated non-ATG translation, anti-sense oligonucleotides

OPEN ACCESS

Edited by:
Gregory Jaye Bix,
University of Kentucky, United States

Reviewed by:
Patrizia Longone,
Fondazione Santa Lucia (IRCCS), Italy
Johnathan Cooper-Knock,
The University of Sheffield,
United Kingdom

****Correspondence:***
Peter O. Bauer
peter.bauer@bioinova.cz

Specialty section:
This article was submitted to Neurodegeneration, a section of the journal Frontiers in Neuroscience

Received: *25 January 2019*
Accepted: *20 August 2019*
Published: *06 September 2019*

Citation:
Bauer PO, Dunmore JH, Sasaguri H and Matoska V (2019) Neurons Induced From Fibroblasts of c9ALS/FTD Patients Reproduce the Pathology Seen in the Central Nervous System. Front. Neurosci. 13:935. doi: 10.3389/fnins.2019.00935

INTRODUCTION

Amyotrophic lateral sclerosis (ALS) and frontotemporal dementia (FTD) are devastating neurodegenerative diseases with significant genetic, neuropathological, and clinical overlap (Lillo and Hodges, 2009; Walsh and Hochedlinger, 2010). ALS is characterized by selective degeneration of upper and lower motor neurons causing muscle weakness, spasticity, atrophy, and death within 1–5 years after disease onset (Cleveland and Rothstein, 2001; Bruijn et al., 2004). FTD is one of the most common early onset dementias (Ratnavalli et al., 2002) characterized by neuronal degeneration in the frontal and temporal lobes causing a progressive deterioration of behavior, language, and personality (Bozeat et al., 2000). An expanded non-coding hexanucleotide repeat expansion [r(GGGGCC)$_{exp}$] in the chromosome 9 open reading frame 72 (*c9orf72*) gene has been identified as the most common genetic cause underlying FTD and ALS (c9ALS/FTD) (DeJesus-Hernandez et al., 2011; Renton et al., 2011). Normal length is considered less between 2 and 30 hexanucleotides while 65 repeats are regarded as the limit for the pathogenic range [r(GGGGCC)$_{exp}$] (Loy et al., 2014; Van Mossevelde et al., 2017). Approximately 40% of

FTD patients develop motor neuron dysfunction (MND) (Lomen-Hoerth et al., 2003) and as approximately 15% of ALS patients also meet the criteria for FTD (Giordana et al., 2011; Phukan et al., 2012) while up to 50% of cases displaying frontotemporal dysfunction features (Montuschi et al., 2015).

The repeat expansion may cause c9ALS/FTD through three potential pathomechanisms. Firstly, RNA transcripts containing the expansion of sense (S) r(GGGGCC)$_{exp}$ or anti-sense (AS) r(CCCCGG)$_{exp}$ can form nuclear foci in the CNS of c9ALS/FTD patients (Gendron et al., 2013; Lagier-Tourenne et al., 2013; Taylor et al., 2016; Liu et al., 2017) which may lead to RNA-mediated toxicity by sequestering RNA-binding proteins (RBP) impairing their ability to interact with their physiological RNA targets (Lee et al., 2013; Gendron et al., 2014). Secondly, (S) and (AS) RNA transcripts can be processed by repeat associated non-ATG translation (c9RANT) resulting in dipeptide repeat proteins (S: poly GP, GA, GR; AS: poly PR, PA, GP) production that are prone to form neuronal inclusions in the CNS (Ash et al., 2013; Gendron et al., 2013; Mori et al., 2013). Thirdly, reduction of *c9orf72* mRNA levels in brain and other tissues of repeat expansion carriers were first reported in 2011 (DeJesus-Hernandez et al., 2011; Renton et al., 2011) in which several other groups and we subsequently have reported this reduction may largely due to histones hypermethylation in the vicinity of the *c9orf72* gene (Belzil et al., 2013), indicating that loss of yet unknown function of the C9orf72 protein may also play a role in disease pathogenesis (Belzil et al., 2014; Bauer, 2016; Shi et al., 2018). The haploinsufficiency of the C9orf72 protein, however, seems to be not sufficient to cause the disease, as has been shown in a C9orf72 knock out mouse model (Koppers et al., 2015; Sudria-Lopez et al., 2016). Nevertheless, it is thought to affect the inflammatory response during the disease course (O'Rourke et al., 2016).

Several cellular models of c9ALS/FTD have been generated, however, most of them have limitations. For example, although overexpression of the expansion results in robust RNA foci formation and c9RANT products accumulation (Wen et al., 2014; Molliex et al., 2015; Webster et al., 2016; Gendron et al., 2017), it does not result in reduced expression of *c9orf72* mRNA and protein as seen in c9ALS/FTD patients (DeJesus-Hernandez et al., 2011; Renton et al., 2011). It may also bypass potentially important events resulting from the presence of the repeat in genomic DNA. Moreover, it is very challenging to clone repeat sequences with lengths similar to those in patients.

So far, the most accurate cellular models have been considered neurons generated from induced pluripotent stem cells (iPSCs) derived from c9ALS/FTD patients. In these cells, RNA foci and accumulation of inclusions composed of c9RAN proteins, mainly poly GP, have been observed while maintaining the reduction of *C9orf72* mRNA (Almeida et al., 2013; Donnelly et al., 2013; Sareen et al., 2013). Although robust, the preparation of this type of cell model can be costly and time-consuming. Here we present a method involving direct conversion of human dermal fibroblasts (HDFs) into induced neurons (iNeurons). We used a previously described vector encoding short hairpin RNA targeting polypyrimidine-tract-binding protein 1 (PTB1) (Xue et al., 2013). PTB1 has been shown to inhibit neuronal differentiation triggered by miR-124 while miR-124 can reduce PTB1 resulting in a cascade including proneuronal alternative splicing events (Makeyev et al., 2007). Xue et al. (2013) generated neurons from different types of cells including HeLa, NT2, Neuro2a, or mouse embryonic fibroblasts (Xue et al., 2013). We developed a modified protocol for direct transformation of HDFs to iNeurons within 2 weeks compared to 12–16 weeks through conventional iPSC differentiation. Characterization of these iNeurons generated from c9ALS/FTD patients showed expression of all six (S) and (AS)-c9RANT products detected by polyclonal antibodies against each individual protein addition to the presence of intranuclear (S) and (AS) RNA foci in all tested cell lines. Moreover, the usefulness of iNeurons in *in vitro* modeling of ALS has been shown recently (Lim et al., 2016). In this study, iNeurons generated from fibroblasts of three ALS patients with mutations in fused in sarcoma (FUS) gene recapitulated all key features of FUS pathology found in the patient brain and spinal cord motor neurons.

Several groups have recently shown that anti-sense oligonucleotides (ASOs) therapy targeting the r(GGGGCC)$_{exp}$ RNA sequence in iPSC differentiated neurons can significantly reduce (S) RNA foci and mitigate cellular toxicity with little effect on c9RAN products detected with a polyclonal antibody preferentially detecting poly GP (Donnelly et al., 2013; Sareen et al., 2013). Therefore, we tested antisense oligonucleotides (ASOs) targeting the sense transcript containing repeat expansion r(GGGGCC)$_{exp}$ in our model and observed significant reduction of (S) RNA foci and c9RANT products accumulation without affecting (AS) RNA foci and c9RANT products. Thus, our c9ALS/FTD iNeuron model may be an efficient tool for validating therapeutic screenings.

MATERIALS AND METHODS

Standard Protocol Approvals, Registrations, and Patient Consents

Protocols were approved by the Mayo Clinic Institutional Review Board and Ethics Committee on human experimentation. Skin biopsies were collected after the participants gave written informed consent.

Human Samples

Punch skin biopsies were performed on the anterior aspect of the forearm from six individuals visiting Department of Neurology of Mayo Clinic, which included three control participants (control 1: female diagnosed with sixth nerve palsy, 61 years old at the time of biopsy; control 2: healthy female, 64 years; control 3: healthy female, 38 years) and three repeat expansion carriers (carrier 1: female, asymptomatic, 28 years old; carrier 2: female diagnosed with ALS at 49 years of age, 50 years; carrier 3: male diagnosed with ALS/FTD at 41 years of age, 43 years). Fibroblasts were generated by ReGen Theranostics Inc., (Rochester, MN). The presence or absence of the *c9orf72* repeat expansion was determined by PCR method as previously described (DeJesus-Hernandez et al., 2011). These studies were approved by

Institutional Review Board and all participants provided written informed consent.

Cell Culture and Differentiation of iNeurons

Fibroblasts were maintained in Dulbecco's modified Eagle's medium (DMEM; Lonza) supplemented with 10% heat-inactivated fetal bovine serum (Sigma), 100 units/ml penicillin, and 100 μg/ml streptomycin (Gibco) at 37°C, in an atmosphere containing 5% CO2 and 95% air. The shRNA against human PTB1 (shPTB) cloned into lentiviral plasmid pLKO.1 was a kind gift from Dr. Fu (University of California, San Diego, CA, United States). Both shPTB and non-silencing shRNA in the pLKO.1 vector (Sigma) were packaged in HEK293FT cells using Virapower (Invitrogen). Viral particles were collected 48 and 72 h after transfection.

For iNeurons production, our previously modified method (Su et al., 2014) was further optimized. Fibroblasts were seeded on a poly-D-lysine-coated surface and were transduced with lentiviral particles with shPTB for 16–18 h in the presence of 5 μg/ml polybrene. We selected the infected cells with 1.5 μg/ml puromycin for 48 h starting 2 days after transduction. At day 5, 10 ng/ml basic fibroblast growth factor (bFGF; GenScript) was added to the medium for 2 days. Cells were then maintained in DMEM/F12 medium containing 5% FBS (reduced to 2% after 2 days), 25 mg/ml insulin, 100 nM putrescine, 50 mg/ml transferrin, 30 nM sodium selenite (all Sigma), and 15 ng/ml bFGF. After 4 days, we added B27 supplement (Gibco) and 10 ng/ml each of brain-derived neurotrophic factor (BDNF), glial cell-derived neurotrophic factor (GDNF; both R&D Systems), neurotensin-3 (NT3; Peprotech), and ciliary neurotrophic factor (CNTF; Sigma). The cells were used for experiments 2–4 days later.

Immunocytochemistry

Cells were fixed with 4% paraformaldehyde, permeabilized with 0.5% Triton X-100/PBS and blocked with 5% skim milk in TBS-Tween20 (TBS-T) buffer. All antibodies were diluted in 5% skim milk/TBS-T. For neuronal markers analysis, following antibodies were used: mouse anti-MAP2 (Sigma; 1:2,000 dilution), mouse anti-Neurofilament H (Smi-32; 1:2,000), mouse anti-neuronal nuclei (NeuN; 1:500), rabbit anti-Synapsin 1 (Syn1; 1:500), rabbit anti-MAP2 (all Millipore; 1:2,000), mouse anti-Tuj1 (Cell Signaling, 1:2,000), rabbit anti-postsynaptic density protein 95 (PSD95; 1:250), rabbit anti-Drebrin (both Abcam; 1:500), rabbit anti-pan voltage-gated Na2 + channels (pan Nav; Alomone; 1:250), anti-vesicular glutamate transporter 1 (vGlut1; Synaptic Systems; 1:500), and goat polyclonal anti-PTB1 (Abcam; 1:200). Rabbit antibodies against c9RANT products, anti-poly(GP), anti-poly(GA), anti-poly(GR), anti-poly(PA), and anti-poly(PR), were generated as described previously (Gendron et al., 2013; Mann et al., 2013) and used at 1:1,000 dilutions. Secondary fluorescent antibodies (Invitrogen) were used at 1:1000 dilutions. Nuclei were stained with Hoechst 33258 (Invitrogen). Confocal microscopy was performed using Zeiss LSM 510 microscope.

Western Blot Analysis

Fibroblasts were transduced with shPTB1 or non-silencing control shRNA. Cells were collected and lysed 5 days later and the samples were run on 4–20% Tris–glycine polyacrylamide gel. Proteins were then transferred from the gel to nitrocellulose membranes following standard protocols and the immunoblot was completed using goat polyclonal anti-PTB1 (1:1,000) and mouse monoclonal anti-β-actin (Sigma; 1:10,000).

Cell Treatment

Control anti-sense oligonucleotides (ctrl ASO; sequence: CCTTCCCTGAAGGTTCCTCC) and ASOs targeting the $r(GGGGCC)_{exp}$ (ASOs; sequence: CCGGCCCCGGCCCCGGCCCC) (Donnelly et al., 2013) in final concentration of 5 μM were added to the cells at day 5, after the puromycin selection. Modified 2′ *O*-methyl RNA/DNA ASOs were generated by Integrated DNA Technologies (IDT). For quantification experiments, iNeurons were induced in 96-well plates and serial pictures were generated with BD Pathway Bio-imager (BD Biosciences). For each cell line and condition, the percentage of cells containing c9RANT inclusions was calculated from 6 wells in 4 independent experiments.

RNA Fluorescence *in situ* Hybridization (FISH)

RNA FISH on fibroblasts and iNeurons to detect RNA foci consisting of the sense (S) transcript was performed using a modified method described previously (Lagier-Tourenne et al., 2013). Briefly, cells on coverslips were fixed in 4% PFA/DEPC-PBS, permeabilized with 0.2% Triton X-100/DEPC-PBS and washed twice with DEPC-PBS. The samples were then dehydrated by 70 and 100% ethanol and air dried. This step was followed by incubation in hybridization buffer (10% dextran sulfate, 50% formamide, 50 mM sodium phosphate buffer (pH 7), 2xSSC) at 66°C for 20–60 min. Prior to use, the locked nucleic acid (LNA) probe (5′TYE563-CCCCGGCCCCGGCCCC-3′, Batch #612968, Exiqon) was denatured at 80°C for 75 s and diluted to 40 nM with hybridization buffer. The hybridization with probe was performed in a sealed, light-protected chamber at 66°C for 16–24 h. RNA FISH of fibroblasts and iNeurons to detect RNA foci consisting of the (AS) transcript were performed as above with slight modifications. The incubation with hybridization buffer (10% dextran sulfate, 50% formamide, 50 mM lithium phosphate buffer (pH 7), 2xSSC) changed to 60°C for 16–24 h with LNA probe (5′TYE563-GGGGCCGGGGCCGGGG, batch #614784, Exiqon). The coverslips were subsequently washed with 0.1% Tween-20/2xSSC for 5 min followed by three 10 min stringency washes in 0.1xSSC at 66°C. The cells were stained with Hoechst 33258, rinsed with DEPC-treated water, dehydrated through 70 and 100% ethanol and air dried. Coverslips were then mounted with Prolong Gold anti-fade reagent (Life Technologies) and the RNA foci were visualized and quantified using a Zeiss Axiovert Fluorescence Microscope with apotome module. For each cell line, three experiments were performed with three fields consisting of at least 100 cells each were randomly selected per condition.

For each field, the number of foci-positive nuclei and the total number of nuclei were counted to determine the average percentage of foci-positive cells.

Cell Toxicity Assay

The iNeurons were grown in 96-well plates and treated with increasing concentrations of tunicamycin (Sigma) for 24 h or 10 μM glutamate (Sigma) for 8 h. Medium was collected and lactate dehydrogenase (LDH) levels using Cyto-tox 96 (Promega) were measured with Spectra Max M5e Microplate Reader (Molecular Devices).

Statistical Analysis

We used paired student's *t*-test for comparison between two sample groups. Two-way ANOVA Fisher's test was used for multiple comparisons with a 95% confidence level. We considered the difference between comparisons to be significant when $P < 0.05$ for all the statistical analyses.

RESULTS

Knock-Down of PTB1 in Human Dermal Fibroblasts Leads to Induction of Neural Phenotype

Effect of PTB1 downregulation in several cell types has been shown to result in direct conversion to neuron-like cells (Xue et al., 2013). In an attempt to develop human neuronal disease models with endogenous mutation, we extended this finding to adult human dermal fibroblasts (HDFs). HDFs obtained by skin biopsies were transduced with pLKO.1-shPTB1 packaged into lentiviral particles. Interestingly, cells started to acquire neuron-like morphology as early as 4 days after transduction and with further differentiation process, the cells continued to develop into iNeurons (**Figure 1A**). The iNeurons with down-regulated PTB1 (**Figure 1B**) also expressed neuronal marker MAP2 (**Figure 1C**). In addition, differentiated cells expressed multiple neuron-specific markers including cytoskeletal, synaptic, nuclear, and other markers after 12–14 days after transduction (**Figure 1D**). Of note, HDFs transduced with non-silencing shRNA did not exhibit neurite outgrowth or neuronal markers expression.

iNeurons Derived From c9ALS/FTD Patients Form RNA Foci and Accumulate RANT Products

To see whether iNeurons could serve as a useful cellular model for *c9orf72*-related pathologies, we analyzed them for the presence of RNA foci, usually found in c9ALS/FTD patients. As reported previously, HDFs of c9ALS/FTD patients contain intranuclear RNA foci (Lagier-Tourenne et al., 2013). (S) and (AS) foci were detected in both fibroblasts and iNeurons by RNA fluorescent *in situ* hybridization (RNA FISH) by utilizing fluorescently labeled locked nucleic acid (LNA) oligonucleotides probes against the (S) and (AS) repeat RNA expansion (**Figure 2**). RNA foci were not detected in non-c9orf72 (C9-) HDF cell lines. The fraction of cells containing intranuclear (S) foci varied between ∼20% and 30% in HDFs whereas after differentiation into iNeurons, the fraction of cells containing (S) foci varied between ∼30 and 50% among the three c9ALS/FTD patient cell lines (**Figures 2C,D**). Interestingly Patient 3 had more than 50% of the cells accumulating intranuclear (AS) RNA foci in HDFs (**Figure 2C**) but is reduced by half in iNeurons. Majority of the c9ALS/FTD fibroblasts and iNeurons had 1 to 4 (S) or (AS) foci per cell with less than 5% exhibiting more than 10 nuclear foci (**Supplementary Figure 1**). The percentage of cells with 5–10 (S) foci/cell increased whereas the numbers of >20 (AS) foci/cell decreased in iNeurons compared to HDFs (**Supplementary Figure 1**). The variability of RNA foci observed in our three iNeurons cell lines generated from *c9orf72* expansion carriers (C9 +) are consistent with results previously reported in iPSC derived neurons from *c9orf72* ALS fibroblasts (Donnelly et al., 2013; Sareen et al., 2013).

In contrast to the RNA foci, we were not able to detect RANT products in HDFs (**Figure 3A**). We were curious whether we could detect some of the RANT products in iNeurons. Surprisingly, we observed all RANT products from the (S) [poly-(GA) and -(GR)], or (AS) repeat [poly-(PR) and -(PA)]; poly-(GP) is translated from both strands (**Figure 3B**). Interestingly, different RANT peptides displayed distinct distribution and pattern of inclusions (**Figure 3C**). Moreover, partial translocation of TAR DNA-binding protein 43 (TDP-43) from its normal nuclear location to cytoplasm of the C9 + iNeurons was observed (**Supplementary Figure 2**). These results indicate that C9 + iNeurons recapitulate main pathological hallmarks of c9ALS/FTD and can be used as an accurate cellular model obtainable quickly and easily.

RNA Foci Staining and RANT Is Reduced by Antisense Oligonucleotides Treatment

To examine, whether our iNeuron model could be utilized as a tool for research related to experimental therapies, we treated the cells with ASOs. Specifically designed antisense oligonucleotides have been proven to mediate the target RNA molecules degradation through RNase H-based mechanism. Previously, it has been shown that a 3-day treatment with ASOs efficiently reduced the RNA foci formation, however, did not significantly affect poly(GP) accumulation (Donnelly et al., 2013).

Control ASO or ASOs (5 μM) were applied to the cells 4 days post-transduction. Further differentiation steps including the media changes remained unmodified. ASOs reduced the staining of RNA foci formed from the (S) strand by more than 90% in three different C9 + iNeuron lines (**Figures 4A,B**). The RNA foci staining from the (AS) strand, on the other hand, was not inhibited (**Figures 4A,B**). Similar effects of ASOs were observed in the fibroblasts (**Supplementary Figure 3**).

Importantly, we also observed effect on c9RANT products translated from the (S) strand. The quantification was performed by counting cells containing inclusions by BD Pathway Bio-imager. In case of poly(GR) and poly(GA) peptides, the peptides translated only from the (S) strand, the inclusion formation was reduced by more than 85 and 75%, respectively, in all three C9 + iNeuron lines (**Figures 4C,D**). Accordingly to (AS) RNA

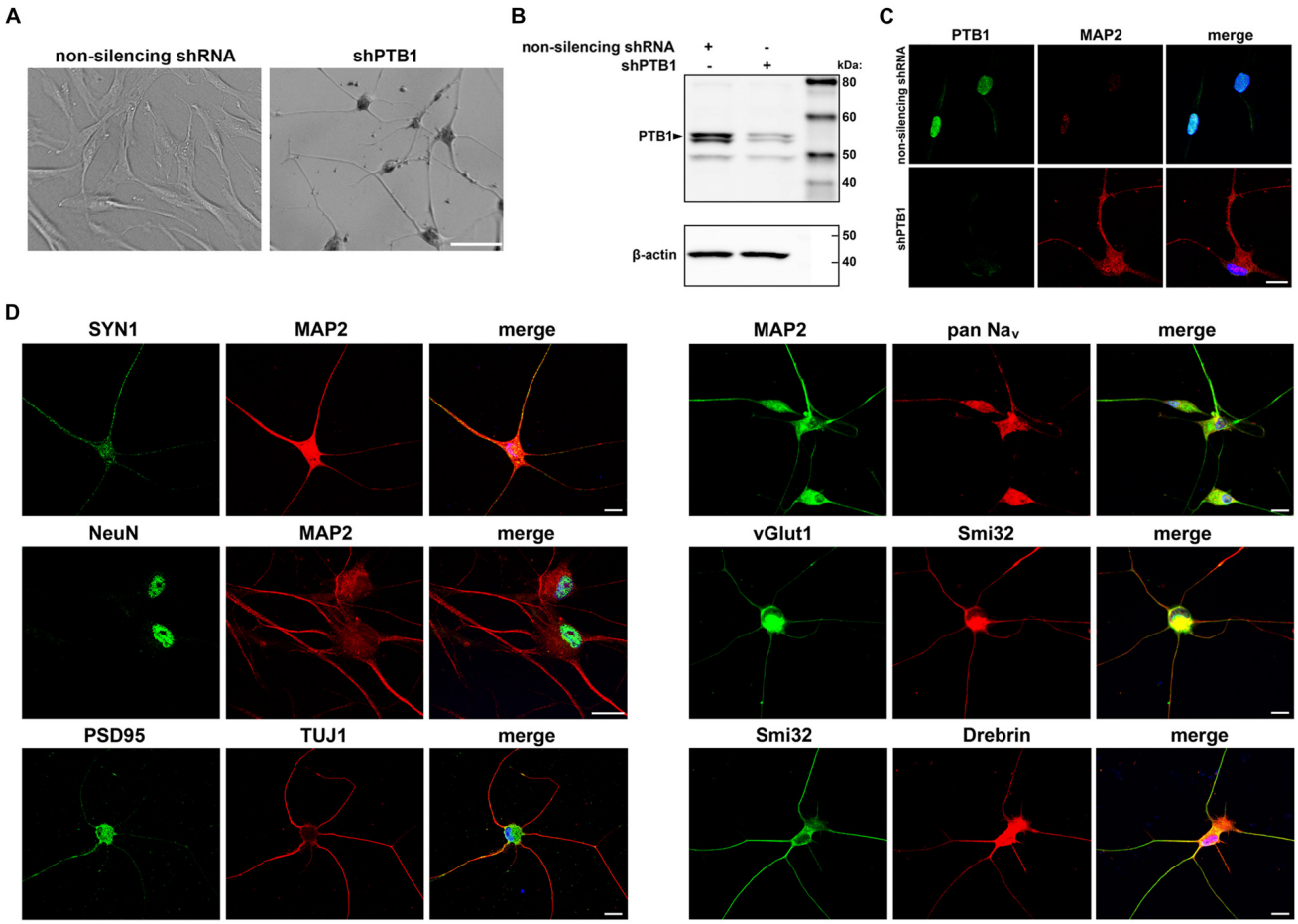

FIGURE 1 | Generation and characterization of c9ALS/FTD patient-specific induced neurons (iNeurons). **(A)** Representative bright field images show cell morphology upon non-silencing shRNA and shPTB1 transduction of human fibroblasts. While the cells infected with control shRNA retained their fibroblast-like shape, shPTB1-transduction induced a neuronal morphology with reduced size of cell soma, and neurite outgrowth. Scale bar, 400 μm. **(B)** Western blot analysis of fibroblasts transduced or not with shPTB1. **(C)** Immunofluorescence staining of cells transduced with non-silencing shRNA or shPTB1 for PTB1 and the neuronal marker, MAP2. Scale bar, 20 μm. **(D)** Expression of cytoskeletal (MAP2, TUJ1, Smi32), synaptic (SYN1, PSD95) and other neuronal markers in iNeurons. These cells also express Drebrin, which plays a role in the formation and maintenance of dendritic spines in neurons. Scale bars, 20 μm.

foci, the inclusion formed by (AS) c9RANT products were not affected by ASOs treatment. Poly(GP) inclusions were reduced only by about 52–54% likely due to the fact that it is translated from both (S) and (AS) repeat sequence.

Solely the presence of the r(GGGGCC)$_{exp}$ did not cause cytotoxicity in iNeurons. However, the C9 + cells were more sensitive to the treatment with a well-known endoplasmic reticulum stress inducer, tunicamycin (**Figure 4E** and **Supplementary Figure 4**). This is similar to a previous study showing no difference in cell viability in iPSC-derived neurons with or without r(GGGGCC)$_{exp}$. The C9 + iPSC-derived neurons were, however, more sensitive to the proteotoxic stress (Haeusler et al., 2014). Importantly, ASOs treatment was able to reduce the toxicity of tunicamycin, as determined by LDH test and by propidium iodide staining (**Figure 4E** and **Supplementary Figure 4**). Similar effect of ASOs was observed in C9 + iNeurons treated with glutamate (**Supplementary Figure 5**), that has previously been shown to be more toxic to C9 + iPSC-derived neurons (Donnelly et al., 2013). Our results suggest, that blocking the (S) RNA strand leading to reduction of c9RANT products accumulation represents a promising therapeutic strategy for c9ALS/FTD.

These results confirm that iNeurons are a suitable cellular disease model system for screening and performing experimental therapies for c9ALS/FTD.

DISCUSSION

In this study, we characterize a cellular model of c9ALS/FTD and provide evidence that this model is suitable for experimental therapeutic attempts. Studying neurological diseases is very challenging as compared to other medical fields due to the inaccessibility of the CNS neurons affected by diseases. Most of the human brain studies in neurological patients have been performed on post-mortem tissues often depicting the

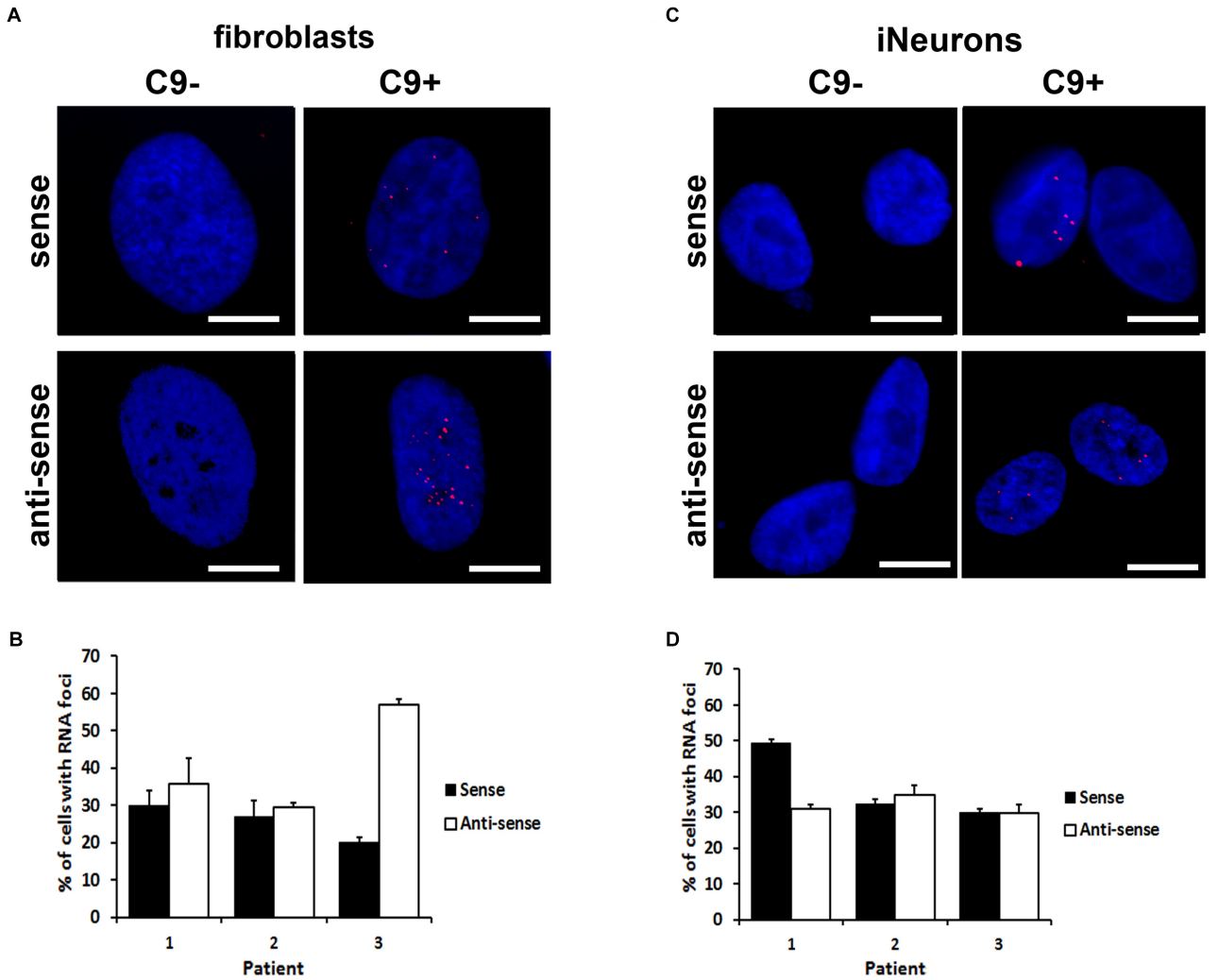

FIGURE 2 | Formation of sense and anti-sense (AS) RNA foci. **(A)** RNA foci in fibroblasts. Blue staining: Hoechst 33258. Scale bars, 20 μm. **(B)** Quantification of fibroblasts with RNA foci. Data represents mean ± standard deviation (SD; *n* = 3, see "Materials and Methods"). **(C)** RNA foci in iNeurons. Blue staining: Hoechst 33258. Scale bars, 20 μm. **(D)** Quantification of iNeurons with RNA foci. Data represents mean ± standard deviation (SD; *n* = 3, see "Materials and Methods").

end-stage of the disease. With improving cellular and animal models of the GGGGCC repeat expansion, we can uncover the pathomechanism related to c9ALS/FTD. Traditional approaches in modeling disease have multiple limitations often due to overexpression of the disease gene. Moreover, cellular and animal models often partially imitate the disease leading to limited phenotypic correlations between the genetic models and human diseases. Consequently, most of the successful experimental treatments fail to be introduced to clinics.

New approaches in disease modeling are not only vital to recapitulate human neuropathologic conditions but also can reveal unknown aspects, which could greatly improve the benefits for patients. It is particularly true in disorders without definitive causative genes and mutations (e.g., sporadic cases of AD, PD, ALS) as well as in sporadic neurological disorders caused by interactions of environmental and (multi)genetic risk factors. Another category comprises disorders where the cloning of the causing genes is problematic (e.g., CG-rich sequence, repeat expansions). The cell reprograming technology for producing iPSCs allows studying the development and progression of neurological diseases in human systems with the disease-specific pathways investigated before and during disease onset. Several reports have been published on employing iPSC technology in modeling neurological diseases, including PD, AD, spinal muscular atrophy or familial dysautonomia (Yung et al., 2013).

Direct conversion of somatic cells bypassing the iPSC stage is an alternative approach which considerably shortens the process patient-specific neurons generation. There have been several methods published using various cocktails of transcription factors (e.g., Ascl1, Brn2, or Myt1l, etc.) (Qiang et al., 2013). These methods appear to be more efficient with as much as 10% of cells conversion rate when compared with those involving iPSC generation (Pfisterer et al., 2011). The strategy of direct conversion has been even more simplified after the discovery of

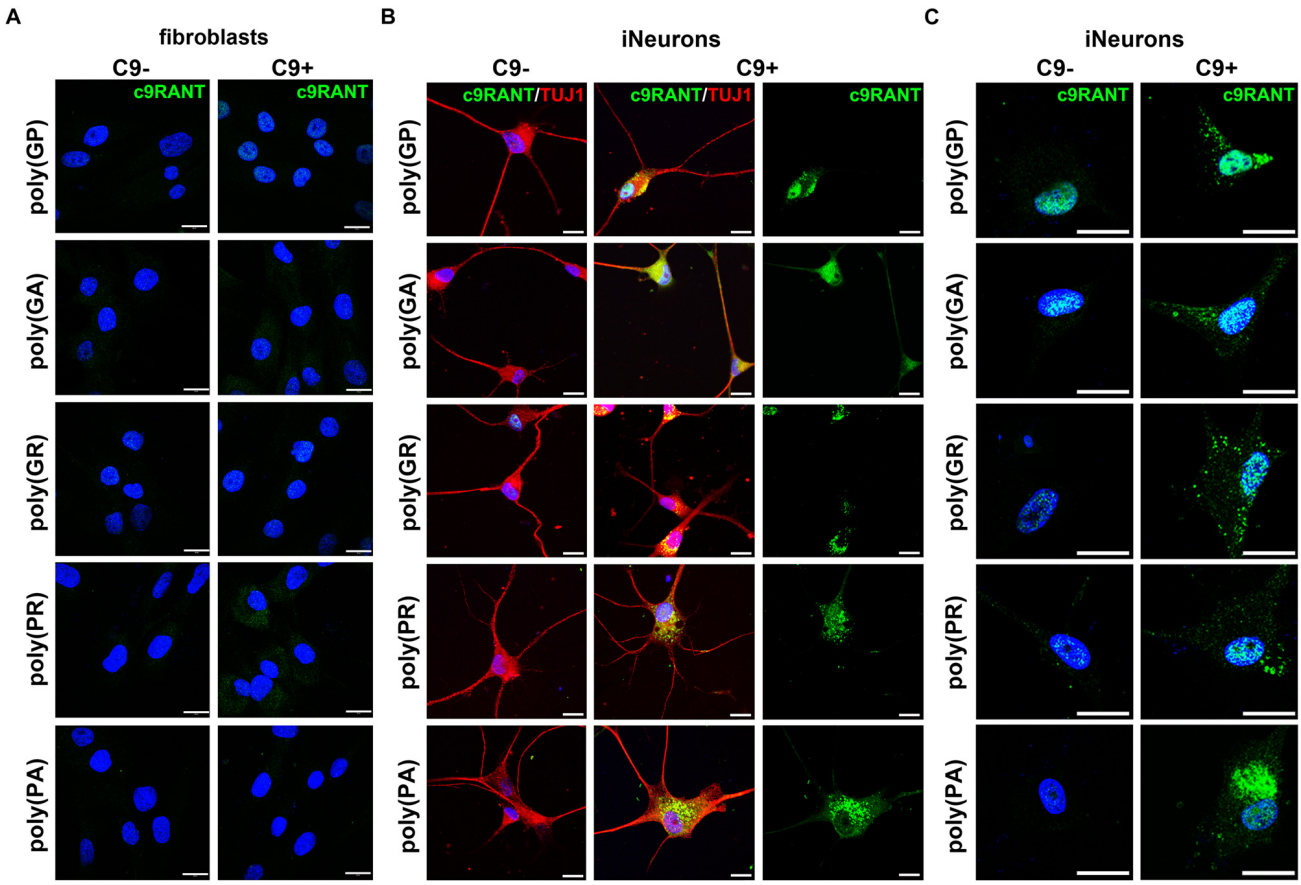

FIGURE 3 | iNeurons express c9RANT products. **(A)** c9ALS/FTD patients' fibroblasts do not accumulate RANT peptides. **(B)** Accumulation of c9RANT products can be detected in iNeurons generated from c9ALS/FTD patients. **(C)** Distribution of c9RANT products in iNeurons generated from c9ALS/FTD patients. Blue staining: Hoechst 33258. Scale bars, 20 μm.

miR-124 (a microRNA highly expressed in neurons which plays an important role in neural development) being able to efficiently contribute to induction of neurons (Ambasudhan et al., 2011) and that the down-regulation of PTB1 by shRNA, leading to an activation of miR-124-related proneuronal expression cascade, was sufficient to transdifferentiate multiple cell lines to neurons (Xue et al., 2013). The delivery of a single factor to the cells enables an extremely simple strategy in changing the fate of differentiated cells.

We extended this finding and used shPTB1 in HDFs obtained from c9ALS/FTD patients. Within 2 weeks, we were able to generate iNeurons which expressed multiple neuronal markers (**Figure 1**). Importantly, iNeurons displayed both main pathological hallmarks seen in c9ALS/FTD patients: accumulation of RNA foci and c9RANT products (**Figures 2, 3**). Inclusions formed by c9RANT products were present only in the C9 + iNeurons while not detected in the C9 + fibroblasts (**Figure 3**). These findings are consistent with our prior observation that poly(GP) inclusions are restricted to neurons in c9ALS/FTD patients (Ash et al., 2013). We also observed a partial translocation of TDP-43 from nucleus to the cytoplasm in the C9 + iNeurons (**Supplementary Figure 2**). The presence of the repeat expansion did not appear to interfere with the neuronal differentiation process and did not lead to decreased viability of the iNeurons. With additional stressful stimuli, the vulnerability of iNeurons was exposed and displayed increased cytotoxicity associated with $r(GGGGCC)_{exp}$ (**Figure 4E**). To test the suitability of our model for experimental therapeutic testing, we treated the cells with ASOs targeting the (S) repeat sequence (Donnelly et al., 2013). We found that ASOs the c9RANT products accumulation (**Figures 4A–D**). Importantly, the viability of the ASOs-treated C9 + iNeurons also increased after treatment with tunicamycin (**Figure 4E** and **Supplementary Figure 4**) and glutamate (**Supplementary Figure 5**).

Reduction of the *c9orf72* mRNA has been shown to be one of the pathological hallmarks of the c9ALS/FTD disease (DeJesus-Hernandez et al., 2011; Renton et al., 2011), probably affecting the inflammatory response (O'Rourke et al., 2016). We have previously observed such reduction in fibroblasts from patients with *c9orf72* mutation, including those involved in this study (Belzil et al., 2013).

The simplicity of the direct conversion strategy enables rapid production of iNeurons, as the whole procedure routinely takes 2–3 weeks. As the primary fibroblast cultures from

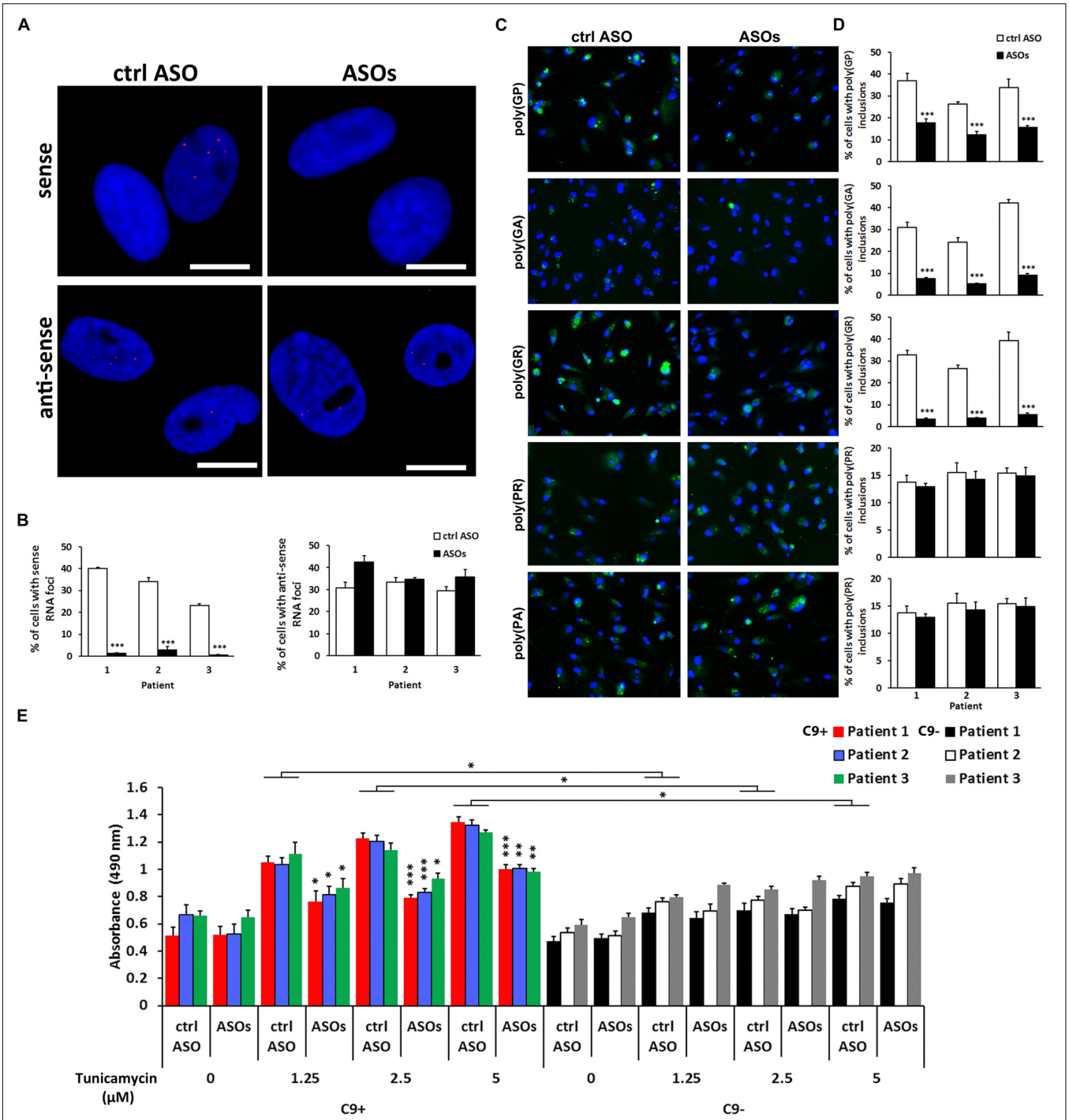

FIGURE 4 | Effect of anti-sense oligonucleotides(ASOs) targeting the sense strand of the c9orf72 repeat, r(GGGGCC)$_{exp}$, on RNA foci staining, c9RANT products accumulation and cell viability. **(A)** ASOs reduced the number of iNeurons with visualized sense but not anti-sense RNA foci. Magnification, 20 ×. **(B)** Quantification of iNeurons containing RNA foci. Data represents mean ± standard error of the mean (SEM; $n = 4$, each with at least 300 cells from 12 wells in 96-well plates). (***$p < 0.001$). **(C)** Treatment with ASOs reduced the number of cells with inclusions formed by sense RANT peptides: poly(GP),(GA), and (GR) while products translated only from the anti-sense strand, poly(PR) and (PA), remained unchanged. Blue staining: Hoechst 33258. Scale bars, 20 μm. **(D)** Quantification of iNeurons containing inclusions formed by RANT products. Data represents mean ± standard deviation (SD; $n = 3$). (***$p < 0.001$). **(E)** ASOs reduce the dose-dependent tunicamycin toxicity in C9 + iNeurons. Data represents mean ± standard error of the mean (SEM; $n = 4$, each with data from two wells). (*$p < 0.05$, **$p < 0.005$, ***$p < 0.001$).

punch biopsies can be established in 4–6 weeks, the patient-specific iNeurons can be generated within 2 months after the patient's visit. Therefore, this model represents a powerful tool not only for accurately recapitulating the pathology of c9ALS/FTD but also for individualized testing of potentially effective drugs in the future.

AUTHOR CONTRIBUTIONS

POB conceived and designed the experiments. POB, JHD, and HS performed the experiments. POB and VM analyzed the data. POB and VM wrote the manuscript.

FUNDING

This work was supported by Amyotrophic Lateral Sclerosis Association (POB; No. 2137) and Center for Regenerative Medicine, Mayo Clinic (POB, HS; No. FP00076246).

ACKNOWLEDGMENTS

We are grateful to all the patients who agreed to donate skin samples. We thank Dr. Leonard Petrucelli for the valuable discussions and providing materials. We acknowledge the expert technical assistance of Dr. Jeannie Chew for the help with FISH.

SUPPLEMENTARY MATERIAL

The Supplementary Material for this article can be found online at: https://www.frontiersin.org/articles/10.3389/fnins.2019.00935/full#supplementary-material

REFERENCES

Almeida, S., Gascon, E., Tran, H., Chou, H. J., Gendron, T. F., Degroot, S., et al. (2013). Modeling key pathological features of frontotemporal dementia with C9ORF72 repeat expansion in iPSC-derived human neurons. *Acta Neuropathol.* 126, 385–399. doi: 10.1007/s00401-013-1149-y

Ambasudhan, R., Talantova, M., Coleman, R., Yuan, X., Zhu, S., Lipton, S. A., et al. (2011). Direct reprogramming of adult human fibroblasts to functional neurons under defined conditions. *Cell Stem Cell* 9, 113–118. doi: 10.1016/j.stem.2011.07.002

Ash, P. E., Bieniek, K. F., Gendron, T. F., Caulfield, T., Lin, W. L., DeJesus-Hernandez, M., et al. (2013). Unconventional translation of C9ORF72 GGGGCC expansion generates insoluble polypeptides specific to c9ALS/FTD. *Neuron* 77, 639–646. doi: 10.1016/j.neuron.2013.02.004

Bauer, P. O. (2016). Methylation of C9orf72 expansion reduces RNA foci formation and dipeptide-repeat proteins expression in cells. *Neurosci. Lett.* 612, 204–209. doi: 10.1016/j.neulet.2015.12.018

Belzil, V. V., Bauer, P. O., Gendron, T. F., Murray, M. E., Dickson, D., and Petrucelli, L. (2014). Characterization of DNA hypermethylation in the cerebellum of c9ALS/FTD patients. *Brain Res.* 1584, 15–21. doi: 10.1016/j.brainres.2014.02.015

Belzil, V. V., Bauer, P. O., Prudencio, M., Gendron, T. F., Stetler, C. T., Yan, I. K., et al. (2013). Reduced C9orf72 gene expression in c9ALS/FTD is caused by histone trimethylation, an epigenetic event detectable in blood. *Acta Neuropathol.* 126, 895–905. doi: 10.1007/s00401-013-1199-1

Bozeat, S., Gregory, C. A., Ralph, M. A., and Hodges, J. R. (2000). Which neuropsychiatric and behavioural features distinguish frontal and temporal variants of frontotemporal dementia from Alzheimer's disease? *J. Neurol. Neurosurg. Psychiatry* 69, 178–186.

Bruijn, L. I., Miller, T. M., and Cleveland, D. W. (2004). Unraveling the mechanisms involved in motor neuron degeneration in ALS. *Annu. Rev. Neurosci.* 27, 723–749. doi: 10.1146/annurev.neuro.27.070203.144244

Cleveland, D. W., and Rothstein, J. D. (2001). From Charcot to Lou Gehrig: deciphering selective motor neuron death in ALS. *Nat. Rev. Neurosci.* 2, 806–819. doi: 10.1038/35097565

DeJesus-Hernandez, M., Mackenzie, I. R., Boeve, B. F., Boxer, A. L., Baker, M., Rutherford, N. J., et al. (2011). Expanded GGGGCC hexanucleotide repeat in noncoding region of C9ORF72 causes chromosome 9p-linked FTD and ALS. *Neuron* 72, 245–256. doi: 10.1016/j.neuron.2011.09.011

Donnelly, C. J., Zhang, P. W., Pham, J. T., Heusler, A. R., Mistry, N. A., Vidensky, S., et al. (2013). RNA toxicity from the ALS/FTD C9ORF72 expansion is mitigated by antisense intervention. *Neuron* 80, 415–428. doi: 10.1016/j.neuron.2013.10.015

Gendron, T. F., Belzil, V. V., Zhang, Y. J., and Petrucelli, L. (2014). Mechanisms of toxicity in C9FTLD/ALS. *Acta Neuropathol.* 127, 359–376. doi: 10.1007/s00401-013-1237-z

Gendron, T. F., Bieniek, K. F., Zhang, Y. J., Jansen-West, K., Ash, P. E., Caulfield, T., et al. (2013). Antisense transcripts of the expanded C9ORF72 hexanucleotide repeat form nuclear RNA foci and undergo repeat-associated non-ATG translation in c9ALS/FTD. *Acta Neuropathol.* 126, 829–844. doi: 10.1007/s00401-013-1192-8

Gendron, T. F., Chew, J., Stankowski, J. N., Hayes, L. R., Zhang, Y. J., Prudencio, M., et al. (2017). Poly(GP) proteins are a useful pharmacodynamic marker for C9ORF72-associated amyotrophic lateral sclerosis. *Sci. Transl. Med.* 9:eaai7866. doi: 10.1126/scitranslmed.aai7866

Giordana, M. T., Ferrero, P., Grifoni, S., Pellerino, A., Naldi, A., and Montuschi, A. (2011). Dementia and cognitive impairment in amyotrophic lateral sclerosis: a review. *Neurol. Sci.* 32, 9–16. doi: 10.1007/s10072-010-0439-6

Haeusler, A. R., Donnelly, C. J., Periz, G., Simko, E. A., Shaw, P. G., Kim, M. S., et al. (2014). C9orf72 nucleotide repeat structures initiate molecular cascades of disease. *Nature* 507, 195–200. doi: 10.1038/nature13124

Koppers, M., Blokhuis, A. M., Westeneng, H.-J., Terpstra, M. L., Zundel, C. A. C., Vieira de Sá, R., et al. (2015). C9orf72 ablation in mice does not cause motor neuron degeneration or motor deficits. *Ann. Neurol.* 78, 426–438. doi: 10.1002/ana.24453

Lagier-Tourenne, C., Baughn, M., Rigo, F., Sun, S., Liu, P., Li, H. R., et al. (2013). Targeted degradation of sense and antisense C9orf72 RNA foci as therapy for ALS and frontotemporal degeneration. *Proc. Natl. Acad. Sci. U.S.A.* 110, E4530–E4539. doi: 10.1073/pnas.1318835110

Lee, Y. B., Chen, H. J., Peres, J. N., Gomez-Deza, J., Attig, J., Stalekar, M., et al. (2013). Hexanucleotide repeats in ALS/FTD form length-dependent RNA foci, sequester RNA binding proteins, and are neurotoxic. *Cell Rep.* 5, 1178–1186. doi: 10.1016/j.celrep.2013.10.049

Lillo, P., and Hodges, J. R. (2009). Frontotemporal dementia and motor neurone disease: overlapping clinic-pathological disorders. *J. Clin. Neurosci.* 16, 1131–1135. doi: 10.1016/j.jocn.2009.03.005

Lim, S. M., Choi, W. J., Oh, K. W., Xue, Y., Choi, J. Y., Kim, S. H., et al. (2016). Directly converted patient-specific induced neurons mirror the neuropathology of FUS with disrupted nuclear localization in amyotrophic lateral sclerosis. *Mol. Neurodegener.* 22:8. doi: 10.1186/s13024-016-0075-6

Liu, J., Hu, J., Ludlow, A. T., Pham, J. T., Shay, J. W., Rothstein, J. D., et al. (2017). c9orf72 disease-related foci are each composed of one mutant expanded repeat RNA. *Cell Chem. Biol.* 24, 141–148. doi: 10.1016/j.chembiol.2016.12.018

Lomen-Hoerth, C., Murphy, J., Langmore, S., Kramer, J. H., Olney, R. K., and Miller, B. (2003). Are amyotrophic lateral sclerosis patients cognitively normal? *Neurology* 60, 1094–1097.

Loy, C. T., Schofield, P. R., Turner, A. M., and Kwok, J. B. (2014). Genetics of dementia. *Lancet* 383, 828–840. doi: 10.1016/S0140-6736(13)60630-3

Makeyev, E. V., Zhang, J., Carrasco, M. A., and Maniatis, T. (2007). The MicroRNA miR-124 promotes neuronal differentiation by triggering brain-specific alternative pre-mRNA splicing. *Mol. Cell* 27, 435–448. doi: 10.1016/j.molcel.2007.07.015

Mann, D. M., Rollinson, S., Robinson, A., Bennion Callister, J., Thompson, J. C., Snowden, J. S., et al. (2013). Dipeptide repeat proteins are present in the p62 positive inclusions in patients with frontotemporal lobar degeneration and motor neurone disease associated with expansions in C9ORF72. *Acta Neuropathol. Commun.* 1:68. doi: 10.1186/2051-5960-1-68

Molliex, A., Temirov, J., Lee, J., Coughlin, M., Kanagaraj, A. P., Kim, H. J., et al. (2015). Phase separation by low complexity domains promotes stress granule assembly and drives pathological fibrillization. *Cell* 163, 123–133. doi: 10.1016/j.cell.2015.09.015

Montuschi, A., Iazzolino, B., Calvo, A., Moglia, C., Lopiano, L., Restagno, G., et al. (2015). Cognitive correlates in amyotrophic lateral sclerosis: a population-based study in Italy. *J. Neurol. Neurosurg. Psychiatry* 86, 168–173. doi: 10.1136/jnnp-2013-307223

Mori, K., Weng, S. M., Arzberger, T., May, S., Rentzsch, K., Kremmer, E., et al. (2013). The C9orf72 GGGGCC repeat is translated into aggregating dipeptide-repeat proteins in FTLD/ALS. *Science* 339, 1335–1338. doi: 10.1007/s00401-013-1189-3

O'Rourke, J. G., Bogdanik, L., Yanez, A., Lall, D., Wolf, A. J., Muhammad, A. K., et al. (2016). C9orf72 is required for proper macrophage and microglial function in mice. *Science* 351, 1324–1329. doi: 10.1126/science.aaf1064

Pfisterer, U., Kirkeby, A., Torper, O., Wood, J., Nelander, J., Dufour, A., et al. (2011). Direct conversion of human fibroblasts to dopaminergic neurons. *Proc. Natl. Acad. Sci. U.S.A.* 108, 10343–10348. doi: 10.1073/pnas.1105135108

Phukan, J., Elamin, M., Bede, P., Jordan, N., Gallagher, L., Byrne, S., et al. (2012). The syndrome of cognitive impairment in amyotrophic lateral sclerosis: a population-based study. *J. Neurol. Neurosurg. Psychiatry* 83, 102–108. doi: 10.1136/jnnp-2011-300188

Qiang, L., Fujita, R., and Abeliovich, A. (2013). Remodeling neurodegeneration: somatic cell reprogramming-based models of adult neurological disorders. *Neuron* 78, 957–969. doi: 10.1016/j.neuron.2013.06.002

Ratnavalli, E., Brayne, C., Dawson, K., and Hodges, J. R. (2002). The prevalence of frontotemporal dementia. *Neurology* 58, 1615–1621.

Renton, A. E., Majounie, E., Waite, A., Simon-Sanchez, J., Rollinson, S., Gibbs, J. R., et al. (2011). A hexanucleotide repeat expansion in C9ORF72 is the cause of chromosome 9p21-linked ALS-FTD. *Neuron* 72, 257–268. doi: 10.1016/j.neuron.2011.09.010

Sareen, D., O'Rourke, J. G., Meera, P., Muhammad, A. K., Grant, S., Simpkinson, M., et al. (2013). Targeting RNA foci in iPSC-derived motor neurons from ALS patients with a C9ORF72 repeat expansion. *Sci. Transl. Med.* 5:208ra149. doi: 10.1126/scitranslmed.3007529

Shi, Y., Lin, S., Staats, K. A., Li, Y., Chang, W. H., Hung, S. T., et al. (2018). Haploinsufficiency leads to neurodegeneration in C9ORF72 ALS/FTD human induced motor neurons. *Nat. Med.* 24, 313–325. doi: 10.1038/nm.4490

Su, Z., Zhang, Y., Gendron, T. F., Bauer, P. O., Chew, J., Yang, W. Y., et al. (2014). Discovery of a biomarker and lead small molecules to target r(GGGGCC)-associated defects in c9ALS/FTD. *Neuron* 83, 1043–1050. doi: 10.1016/j.neuron.2014.07.041

Sudria-Lopez, E., Koppers, M., de Wit, M., van der Meer, C., Westeneng, H. J., Zundel, C. A., et al. (2016). Full ablation of C9orf72 in mice causes immune system-related pathology and neoplastic events but no motor neuron defects. *Acta Neuropathol.* 132, 145–147. doi: 10.1007/s00401-016-1581-x

Taylor, J. P., Brown, R. H. Jr., and Cleveland, D. W. (2016). Decoding ALS: from genes to mechanism. *Nature* 539, 197–206. doi: 10.1038/nature20413

Van Mossevelde, S., van der Zee, J., Cruts, M., and Van Broeckhoven, C. (2017). Relationship between C9orf72 repeat size and clinical phenotype. *Curr. Opin. Genet. Dev.* 44, 117–124. doi: 10.1016/j.gde.2017.02.008

Walsh, R. M., and Hochedlinger, K. (2010). Modeling Rett syndrome with stem cells. *Cell* 143, 499–500. doi: 10.1016/j.cell.2010.10.037

Webster, C. P., Smith, E. F., Bauer, C. S., Moller, A., Hautbergue, G. M., Ferraiuolo, L., et al. (2016). The C9orf72 protein interacts with Rab1a and the ULK1 complex to regulate initiation of autophagy. *EMBO J.* 35, 1656–1676. doi: 10.15252/embj.201694401

Wen, X., Tan, W., Westergard, T., Krishnamurthy, K., Markandaiah, S. S., Shi, Y., et al. (2014). Antisense proline-arginine RAN dipeptides linked to C9ORF72-ALS/FTD form toxic nuclear aggregates that initiate in vitro and in vivo neuronal death. *Neuron* 84, 1213–1225. doi: 10.1016/j.neuron.2014.12.010

Xue, Y., Ouyang, K., Huang, J., Zhou, Y., Ouyang, H., Li, H., et al. (2013). Direct conversion of fibroblasts to neurons by reprogramming PTB-regulated microRNA circuits. *Cell* 152, 82–96. doi: 10.1016/j.cell.2012.11.045

Yung, J. S., Tam, P. K., and Ngan, E. S. (2013). Pluripotent stem cell for modeling neurological diseases. *Exp. Cell Res.* 319, 177–184. doi: 10.1016/j.yexcr.2012.11.007

Conflict of Interest Statement: POB is employed by the company Bioinova, Ltd.

The remaining authors declare that the research was conducted in the absence of any commercial or financial relationships that could be construed as a potential conflict of interest.

Copyright © 2019 Bauer, Dunmore, Sasaguri and Matoska. This is an open-access article distributed under the terms of the Creative Commons Attribution License (CC BY). The use, distribution or reproduction in other forums is permitted, provided the original author(s) and the copyright owner(s) are credited and that the original publication in this journal is cited, in accordance with accepted academic practice. No use, distribution or reproduction is permitted which does not comply with these terms.

frontiers in Neurology

MINI REVIEW
published: 24 September 2019
doi: 10.3389/fneur.2019.01020

Small Vessel Disease

Antoine M. Hakim [1,2,3]*

[1] Ottawa Hospital Research Institute, Ottawa, ON, Canada, [2] Faculty of Medicine, Brain and Mind Research Institute, University of Ottawa, Ottawa, ON, Canada, [3] Division of Neurology, University of Ottawa, Ottawa, ON, Canada

Small vessel disease (SVD) refers to conditions where damage to arterioles and capillaries is predominant, leading to reduced, or interrupted perfusion of the affected organ. Data suggest that when this condition is evident in any organ, it is already systemic in its occurrence and consequences. SVD affects primarily organs that receive significant portions of cardiac output such as the brain, the kidney, and the retina. Thus, SVD is a major etiologic cause in debilitating conditions such as renal failure, blindness, lacunar infarcts, and dementia. The factors that lead to this devastating condition include all the known vascular risk factors when they are not strictly controlled, but lifestyles that include sedentary existence, obesity, and poor sleep patterns are also recognized drivers of SVD. In addition, depression is now recognized as a vascular risk factor. Inflammation is a mediator of SVD, but it is not known which factor(s) predominate in its etiology. This article emphasizes the need for more investigations to define this link further and suggests clinical and societal responses that might reduce the major impacts of this condition on populations.

Keywords: SVD, vascular risk factors, inflammation, dementia, lifestyle

OPEN ACCESS

Edited by:
Gregory Jaye Bix,
University of Kentucky, United States

Reviewed by:
Costantino Iadecola,
Cornell University, United States
Kaori Miwa,
National Cerebral and Cardiovascular Center, Japan
Kazuo Kitagawa,
Tokyo Women's Medical University, Japan

***Correspondence:**
Antoine M. Hakim
ahakim@ohri.ca

Specialty section:
This article was submitted to Stroke, a section of the journal Frontiers in Neurology

Received: *15 February 2019*
Accepted: *09 September 2019*
Published: *24 September 2019*

Citation:
Hakim AM (2019) Small Vessel Disease. Front. Neurol. 10:1020. doi: 10.3389/fneur.2019.01020

INTRODUCTION

Small vessel disease (SVD) refers to any pathologic process that damages small end arteries, arterioles, venules, and brain capillaries (1). Although this condition was described pathologically more than a century ago (2), its pervasive nature and its association with clinically relevant conditions have been increasingly appreciated as imaging technologies advanced and became more accessible (3).

PATHOLOGY AND PATHOPHYSIOLOGY OF SVD

The main target of SVD is the endothelium, the organ that is a barrier between circulating blood and the vessel wall. Healthy endothelial cells control vascular permeability to components in plasma, limit aggregation of platelets and leucocytes, and regulate vascular tone, all of which is essential if blood flow will match metabolic demand (4). The main task of the endothelial cells is therefore to integrate information scanned constantly from the vessel wall, the blood flowing through the arterioles, and from the physiological parameters defining vascular health, and respond by varying vasomotor tone in the arterioles and maintaining an adequate antithrombotic surface.

While the endothelial cells are the main contributors to the properties of the blood brain barrier, their capabilities are induced and maintained by their interactions with mural cells (pericytes and vascular smooth muscle cells), immune cells, and glial cells—predominantly astrocytes (5). As a result, SVD results in lipohyalinosis and arteriolosclerosis.

Several animal models have been studied to shed light on the physiological processes leading to and accompanying SVD, and most involve sustained hypoperfusion of the brain as a result of bilateral stenosis of the common carotid arteries (6). This results in multiple small infarcts and hemosiderin-like regions in subcortical nuclei, with the eventual appearance of cerebral atrophy.

INFLAMMATION AND SVD

There is a growing appreciation that endothelial cells may become damaged when the environment is inflammatory (7). Inflammatory markers have been associated with periventricular white matter hyperintensities (WMH), the main MRI signature of SVD in the brain (8). Reports have linked a number of abnormalities in the interleukin (IL) pathways to SVD including IL-1beta, tumor necrosis factor, IL-10, IL-21, and IL-23 (9), confirming earlier findings by Flex et al. linking proinflammatory gene polymorphisms to one of the major consequences of SVD, dementia (10). C-reactive protein (CRP), a non-specific marker of inflammation, is considered an endothelial toxin, and CRP is both predictive of SVD and is elevated when the condition is evident (11). A relationship between midlife systemic inflammation and late-life SVD has also been reported (12).

NEUROIMAGING OF SVD

The damage caused by SVD impacts both deep gray and white matter structures in the brain (13). While CT scans can reveal the presence of SVD, the ideal method for visualizing the full spectrum of SVD is structural MRI. This includes FLAIR, T1 and T2-weighted as well as gradient echo MRI sequences (14). More recently, whole-brain magnetic resonance spectroscopy has also been used to study markers of brain inflammation (15). These brain imaging modalities reveal in SVD recent small subcortical infarcts, hyperintensities in the periventricular and deep white matter, lacunes, microbleeds, and enlarged perivascular spaces, located predominantly in the basal ganglia and the subcortical white matter (16). As well, the blood-brain barrier is impaired in small vessel disease (17). Eventually, brain atrophy becomes evident (18). Combining MRI studies with measurements of cerebral blood flow and metabolism using positron emission tomography is allowing new insights linking the progression of physiological and imaging abnormalities to the development of cognitive deficits (19, 20).

HEALTH CONSEQUENCES OF SMALL VESSEL DISEASE

In 2016 a report from experts in the field sponsored by the National Institutes of Neurological Diseases and Stroke titled: "Small Blood Vessels: Big Health Problems," highlighted the systemic nature of the disease and its neurological consequences (21). The current review unequivocally confirms the conclusion that the presence of SVD in any organ implies that the patient is suffering from a "systemic" condition.

In the brain, SVD is strongly associated with stroke (22), and the presence of SVD in the brain hampers recovery in patients who have suffered a stroke (23). SVD in the brain is also associated with declines in psychiatric (24), and gait functions (25). As might be expected from these statements, and as already noted, SVD is a major etiologic factor in dementia (26).

If brain imaging modalities reveal SVD, there is a high probability that the condition is also affecting in variable combinations the retina (27), the kidneys (28–31), the heart (32), the lungs (33), and the musculoskeletal system (34)—in fact, every organ that is perfused at a high rate of flow. Although it is possible that all these organs are impacted by the same vascular risk factors, there is nonetheless multi-organ involvement with SVD, and the link appears multidirectional. Thus, it was reported recently that retinal neurodegeneration can predict cognitive impairment (35, 36), and small vessel disease as well as retinal microvascular abnormalities are now confirmed to be associated with an increased risk of renal failure (30, 31). Consequently, in addition to damaging the brain, SVD is perhaps the main etiology for blindness, renal dysfunction, and cardiac insufficiency, making it the etiology for major medical, and neurological conditions.

WHO IS A CANDIDATE FOR SVD?

A paper published in 2007 by Vermeer et al. outlined the conditions associated with MRI-defined silent brain infarcts (37). The highest associations were noted with prior stroke, cardiovascular risk factors, and the presence of renal failure (37). This article also identified depression as having a strong association with silent brain infarcts, a link that has been confirmed subsequently (38). A 2014 study that specifically tested the association of total SVD score with vascular risk factors confirmed that smoking, hypertension, male sex, and advancing age were conditions that promoted brain SVD (39). In a separate study, SVD was observed in 3% of 40–49-year-olds but 18.9% of 70-year-olds, highlighting the association of SVD with aging (40).

In terms of the cardiovascular risk factors, hypertension is a major driver of SVD (41), and ambulatory measurements of blood pressure are better predictors of WMH than self-reported measurements (42). In the setting of hypertension, the risk of accumulating WMH rises rapidly above a resting systolic blood pressure of approximately 120 mmHg (43). Systolic blood pressure sustained above this threshold also predicts a growing risk for dementia and strokes (42, 44). Despite this overwhelming evidence in favor of maintaining at-rest systolic blood pressure at 120 mmHg, concern is often expressed that this may lead to increased mortality in the elderly, perhaps contributed to by falls and hip fractures due to orthostatic hypotension and dizziness (45). The implications of these new guidelines and the challenges they represent merited an entire issue of Circulation Research (46). It is important to note that in the SPRINT trial, among patients aged 75 or older, primary outcomes of myocardial infarction, acute coronary syndrome, stroke, congestive heart failure and cardiovascular death were all significantly lower in

those whose systolic blood pressures were maintained at or below 120 mmHg (47). Despite this, Canada's hypertension guidelines still define hypertension as systolic blood pressure of more than 135 mm Hg (48).

Obesity's impact on the development of brain small vessel disease is now well-documented (49). A 2017 review concluded that obesity and its comorbidities were associated with impaired cognitive performance, accelerated cognitive decline and dementia in later life (50), confirming the conclusion of a systematic review by Pedditzi et al., published a year earlier (51). In the setting of obesity there is a significant rise in the factors promoting inflammation, leading to the conclusion that accumulated fat, particularly in its abdominal location, is a source for inflammatory cytokines (52). It is perhaps not surprising therefore that obesity has been associated with smaller brain volumes (53).

Another reason for referring to obesity's negative impact on brain function is its high prevalence in our societies. In the United States, in 2010, 35.5% of men and 35.8% of women satisfied the criteria for obesity (Body Mass Index (BMI) of 30 or more) (54), with a clear trend for increasing prevalence of abdominal obesity between 1999 and 2012 in both men and women (55). In 2009, 24% of Canadian men and women satisfied the criteria for obesity (56).

Several other vascular risk factors have been associated with greater occurrence of SVD. These include prediabetes (57), untreated diabetes (58, 59), and hyperlipidemia (60, 61). In diabetes, microvascular complications are associated with proinflammatory cytokines and with both vascular and intracellular cell adhesion molecules (62). It is now also clear that gut microbiota can impact brain health through immune influences that can lead to cerebral endothelial dysfunction. In this context, new evidence suggests that dietary salt may promote neurovascular and cognitive dysfunction through a gut-initiated TH17 response (63).

A newly emphasized risk factor for SVD is a poor sleep pattern (64). Those who chronically cheat themselves out of sufficient sleep suffer from increased systemic inflammation (65) and are at risk for SVD and eventually develop cortical atrophy (66). The most likely reason for this is that metabolic clearance from the brain occurs preferentially during sleep (67). Unfortunately, it is estimated that a large segment of the population lives daily with inadequate sleep (68), particularly in school aged children (69).

As noted above, depression was identified by Vermeer as a factor promoting silent brain infarcts (37), and depression has been confirmed to be associated specifically with SVD (70, 71). The importance of this association arises from the disturbing statistics about the prevalence of loneliness in society, a state of mind that is highly correlated with depression (72). In the United States, it has been estimated that 40% of Americans felt lonely (73), and a survey by Statistics Canada in 2012 reported that 20% of older people declared feeling lonely (74). Thus, several societal factors associated with loneliness and depression may be promoting SVD.

SVD AND THE RISK FOR DEMENTIA

Since the prevalence of SVD increases with age, it is the consensus that the prevalence of dementia will increase over time as life expectancy lengthens (75). SVD is associated with both a reduction in cerebral blood flow (CBF) (76), and impaired CBF autoregulation (77), making it a key player in the etiologic mix that leads to dementia. Alzheimer's disease, where beta-amyloid and tau proteins accumulate in the brain, does lead to dementia, but the genetically inherited Alzheimer's variant becomes apparent early and impacts patients in their 50's and 60's. When individuals live past that age with normal cognitive function, the physiological profile that leads to dementia is very different. As mentioned above, data from the ADNI cohort (Alzheimer's Disease Neuroimaging Initiative) have clearly shown that when individuals are still cognitively intact, the sequence of pathophysiologic events that eventually leads to a decline in cognitive function starts with a reduction in cerebral blood flow (20), an association that was confirmed in a population-based study (78). This results in both reduced energy supply and reduced ability to clear accumulated waste. The important point to remember is that the reduction in CBF occurs before glucose dysregulation, before the abnormal accumulation of A-beta and other molecular biomarkers in the CSF, and before any impairment in cognition is evident. This new appreciation for the role of cerebral blood flow in delivering energy to the brain and removing the accumulated toxic molecules is perhaps one explanation for the failure of drugs designed to improve symptoms of cognitive decline by reducing the cerebral load of beta-amyloid (79, 80). Consequently, protecting CBF from decline and securing the brain's energy supply are crucial to our ability to defend against dementia.

The powerful message in all of this is that we need to explore the premise that individuals and societies may succeed in lowering their risk for dementia by reducing vascular risk factors and changing potentially harmful lifestyles. A review of advances in stroke research accomplished during 2018 confirms the impact of adverse lifestyle exposures on brain health and on cognition (81). Decades ago the lesson was established that a successful cure is dwarfed in its societal impact by a reduction in risk, and books intended for the public are now available with advice on how to achieve the goal of reducing the risk for dementia (82, 83).

SVD DESERVES MORE RESEARCH ATTENTION

Because SVD represents a major and growing threat to vascular health, it deserves more focused research attention. Addressing the specific pathophysiology of SVD is urgently needed. Several endothelial toxins associated with SVD are already known (84), but if we knew which played predominant roles, then it might be possible to test in SVD therapeutic tools to decrease the concentration of the most harmful inflammatory molecules. Another approach may arise from our knowledge that sustained activation of certain pro-angiogenic signaling factors studied in cancer biology can promote the generation of new blood vessels

(85). Could one or more of these factors be tested as repair paradigms in the setting of SVD?

IDEAL RESPONSE TO SVD AT THE CLINICAL LEVEL

The patient with SVD keeps many subspecialists occupied. He or she sees the neurologist for failing memory function and for other consequences of lacunar infarcts, the ophthalmologist for failing vision, the nephrologist for failing kidney function, the cardiologist for heart failure, and the family physician and geriatrician for control of vascular risk factors. Each specialist is focused on how to protect his or her subspecialty organ from damage. As a result, there is enormous duplication of effort, when a centralized "Vascular Clinic" that focusses on optimizing the function of the small blood vessels may be effective. In addition to monitoring and treating the vascular risk factors, such a clinic would also help patients with the lifestyle changes they need to bring about to reduce further SVD and provide support to accomplish these goals.

IDEAL SOCIETAL RESPONSE

SVD puts a very heavy burden on our individual and national health care budgets. Add to that the unpaid labor of caregivers to patients afflicted by the consequences of SVD, and the cost increases further. Society needs to respond with a cohesive and integrated set of actions.

When we became convinced that smoking was the cause of some lung cancers, clinicians, and scientists developed a discourse with our patients and the public emphasizing the serious consequences of smoking. Eventually society took on the industry—and it was not easy. To reduce the incidence of SVD we need to regenerate that energy, educate the public by talking about the damaging consequences of untreated high blood pressure and all the other vascular risk factors we know. Like there was in smoking, there are industries that will oppose us. Focused taxation may be one solution as it is now proven to limit the consumption of items known to contribute to SVD (86).

CONCLUSION

We now recognize that small vessel disease is a major health threat, aggravated by the current lifestyle trends in our society. We need to understand the disease better and mobilize energies to improve its prevention and treatment.

AUTHOR CONTRIBUTIONS

The author confirms being the sole contributor of this work and has approved it for publication.

REFERENCES

1. Poggesi A, Salvadori E, Pantoni L, Pracucci G, Cesari F, Chiti A, et al. Risk and determinants of dementia in patients with mild cognitive impairment and brain subcortical vascular changes: a study of clinical neuroimaging, and biological markers-the VMCI-tuscany study: rationale, design, and methodology. *Int J Alzheimers Dis*. (2012) 2012:608013. doi: 10.1155/2012/608013
2. Durand-Fardel CLM. *Traité pratique des Maladies des Vieillards*. Paris: Baillère (1873) (see also W. Hughes, 'Origin of lacunes', Lancet, 1965, ii, 19–21).
3. Cannistraro RJ, Badi M, Eidelman BH, Dickson DW, Middlebrooks EH, Meschia JF. CNS small vessel disease: a clinical review. *Neurology*. (2019) 92:1146–56. doi: 10.1212/WNL.0000000000007654
4. Persson PB. The multiple functions of the endothelium: more than just wallpaper. *Acta Physiol.* (2015) 13:7847–9. doi: 10.1111/apha.12464
5. Daneman R, Prat A. The blood-brain barrier. *Cold Spring Harb Perspect Biol.* (2015) 7:a020412. doi: 10.1101/cshperspect.a020412
6. Holland PR, Searcy JL, Salvadores N, Scullion G, Chen G, Lawson G, et al. Gliovascular disruption and cognitive deficits in a mouse model with features of small vessel disease. *J Cereb Blood Flow Metab*. (2015) 35:1005–14. doi: 10.1038/jcbfm.2015.12
7. Steyers CM III, Miller FJ Jr. Endothelial dysfunction in chronic inflammatory diseases. *Int J Mol Sci.* (2014) 15:11324–49. doi: 10.3390/ijms150711324
8. Rosano C, Marsland AL, Gianaros PJ. Maintaining brain health by monitoring inflammatory processes: a mechanism to promote successful aging. *Aging Dis.* (2012) 3:16–33.
9. Swardfager W, Yu D, Ramirez J, Cogo-Moreira H, Szilagyi G, Holmes MF, et al. Peripheral inflammatory markers indicate microstructural damage within periventricular white matter hyperintensities in Alzheimer's disease: a preliminary report. *Alzheimers Dement.* (2017) 7:56–60. doi: 10.1016/j.dadm.2016.12.011
10. Flex A, Giovannini S, Biscetti F, Liperoti R, Spalletta G, Straface G, et al. Effect of proinflammatory gene polymorphisms on the risk of Alzheimer's disease. *Neurodegener Dis.* (2014) 13:230–6. doi: 10.1159/000353395
11. Mitaki S, Nagai A, Oguro H, Yamaguchi S. C-reactive protein levels are associated with cerebral small vessel-related lesions. *Acta Neurol Scand.* (2016) 133:68–74. doi: 10.1111/ane.12440
12. Walker KA, Power MC, Hoogeyeen RC, Folsom AR, Ballantyne CM, Knopman DS, et al. Midlife systemic inflammation, late-life white matter integrity, and cerebral small vessel disease: the atherosclerosis risk in communities study. *Stroke*. (2017) 48:3196–202. doi: 10.1161/STROKEAHA.117.018675
13. Blair GW, Hernandez MV, Thrippleton MJ, Doubal FN, Wardlaw JM. Advanced neuroimaging of cerebral small vessel disease. *Curr Treat Options Cardio Med.* (2017) 19:56. doi: 10.1007/s11936-017-0555-1
14. Cuadrado-Godia E, Dwivedi P, Sharma S, Ois Santiago A, Roquer Gonzalez J, Balcells M, et al. Cerebral small vessel disease: a review focusing on pathophysiology, biomarkers, and machine learning strategies. *J Stroke*. (2018) 20:302–20. doi: 10.5853/jos.2017.02922
15. Mueller C, Lin JC, Sheriff S, Maudsley AA, Younger JW. Evidence of widespread metabolite abnormalities in Myalgic encephalomyelitis/chronic fatigue syndrome: assessment with whole-brain magnetic resonance spectroscopy. *Brain Imaging Behav.* (2019). doi: 10.1007/s11682-018-0029-4. [Epub ahead of print].
16. Wardlaw JM, Smith C, Dichgans M. Mechanisms underlying sporadic cerebral small vessel disease: insights from neuroimaging. *Lancet Neurol.* (2013) 12:483–97. doi: 10.1016/S1474-4422(13)70060-7
17. Wong SM, Jansen JFA, Zhang CE, Hoff EI, Staals J, van Oostenbrugge RJ, et al. Blood-brain barrier impairment and hypoperfusion are linked in cerebral small vessel disease. *Neurology*. (2019) 92:e1669–77. doi: 10.1212/WNL.0000000000007263
18. Nylander R, Fahlstrom M, Rostrup, Kullberrg J, Damangir S, Ahlstrom H, et al. Quantitative and qualitative MRI evaluation of cerebral small vessel

disease in an elderly population: a longitudinal study. *Acta Radiol.* (2018) 59:612–8. doi: 10.1177/0284185117727567
19. Iadecola C, Duering M, Hachinski V, Joutel A, Pendlebury ST, Schneider JA, et al. Vascular cognitive impairment and dementia: JACC scientific expert panel. *J Am Coll Cardiol.* (2019) 73:3326–44. doi: 10.1016/j.jacc.2019.04.034
20. Iturria-Medina Y, Sotero RC, Tussaint PJ, Mateos-Perez JM, Evans AC. Alzheimer's disease neuroimaging initiative. *Nat Commun.* (2016) 7:11934. doi: 10.1038/ncomms11934
21. Bosetti F, Galis ZS, Bynoe MS, Charette M, Cipolla MJ, Del Zoppo GJ, et al. "Small blood vessels: big health problems" workshop participants. "small blood vessels: big health problems?" scientific recommendations of the national institutes of health workshop. *J AM Heart Assoc.* (2016) 5:e004389. doi: 10.1161/JAHA.116.004389
22. Ostergaard L, Engedal TS, Moreton F, Hansen MB, Wardlaw JM, Dalkara T, et al. Cerebral small vessel disease: capillary pathways to stroke and cognitive decline. *J Cereb Blood Flow Metab.* (2016) 36:302–25. doi: 10.1177/0271678X15606723
23. Liang Y, Chen Y-K, Deng M, Mok VCT, Wang D-F, Ungvari GS, et al. Association of cerebral small vessel disease burden and health-related quality of life after acute ischemic stroke. *Front. Aging Neurosci.* (2017) 9:372. doi: 10.3389/fnagi.2017.00372
24. Kim HJ, Kang SJ, Kim C, Kim GH, Jeon S, Lee JM, et al. The effects of small vessel disease and amyloid burden on neuropsychiatric symptoms: a study among patients with subcortical vascular cognitive impairments. *Neurobiol Aging.* (2013) 34:1913–20. doi: 10.1016/j.neurobiolaging.2013.01.002
25. Pinter D, Ritchie SJ, Doubal F, Gattringer T, Morris Z, Bastin ME, et al. Impact of small vessel disease in the brain on gait and balance. *Sci Rep.* (2017) 7:41637. doi: 10.1038/srep41637
26. van Uden IW, van der Hoist, HM, Tuladhar AM, van Norden AG, de Laat KE, Rutten-Jacobs LC, et al. White matter and hippocampal volume predict the risk of dementia in patients with cerebral small vessel disease: the RUN DMC study. *J Alzheimers Dis.* (2016) 49:863–73. doi: 10.3233/JAD-150573
27. Ahsan H. Diabetic retinopathy—biomolecules and multiple pathophysiology. *Diabetes Metab Syndr.* (2015) 9:51–4. doi: 10.1016/j.dsx.2014.09.011
28. Makin SD, Cook FA, Dennis MS, Wardlaw JM. Cerebral small vessel disease and renal function: systematic review and meta-analysis. *Cerebrovasc Dis.* (2015) 39:39–52. doi: 10.1159/000369777
29. Ikram MA, Vernooij MW, Hofman A, Niessen WJ, van der Lugt A, Breteler MMB. Kidney function is related to cerebral small vessel disease. *Stroke.* (2008) 39:55–61. doi: 10.1161/STROKEAHA.107.493494
30. Vogels SC, Emmelot-Vonk MH, Verhaar HJ, Koek HL. The association of chronic kidney disease with brain lesions on MRI or CT. A systematic review. *Maturitas.* (2012) 71:331–6. doi: 10.1016/j.maturitas.2012.01.008
31. Yip W, Sabanayagam C, Teo BW, Tay WT, Ikram MK, Tai ES, et al. Retinal microvascular abnormalities and risk of renal failure in Asian populations. *PLoS ONE.* (2015) 10:e0118076. doi: 10.1371/journal.pone.0118076
32. Kim BJ, Lee SH, Kim CK, Ryu WS, Kwon HM, Choi SY, et al. Advanced coronary artery calcification and cerebral small vessel diseases in the healthy elderly. *Cir J.* (2011) 75:451–6. doi: 10.1253/circj.CJ-10-0762
33. Seto-Yukimura R, Ogawa E, Hisamatsu T, Torii S, Shiino A, Nozaki K, et al. Reduced lung function and cerebral small vessel disease in japanese men: the shiga epidemiological study of subclinical atherosclerosis (SESSA). *J Atheroscler Thromb.* (2018) 25:1009–21. doi: 10.5551/jat.42127
34. Schroder JM, Zuchner S, Dichgans M, Nagy Z, Molnar MJ. Peripheral nerve and skeletal muscle involvement in CADASIL. *Acta Neuropathol.* (2005) 110:587–99. doi: 10.1007/s00401-005-1082-9
35. Mutlu U, Colijn JM, Ikram MA, Bonnemaijer PWM, Licher S, Wolters FJ, et al. Association of retinal neurodegeneration on optical coherence tomography with dementia: a population-based study. *JAMA Neurol.* (2018) 75:1256–63. doi: 10.1001/jamaneurol.2018.1563
36. O'Bryhim BE, Apte RS, Kung N, Coble D, Van Stavern G. Association of preclinical Alzheimer disease with optical coherence tomographic angiography findings. *JAMA Ophthalmol.* (2018) 136:1242–8. doi: 10.1001/jamaophthalmol.2018.3556
37. Vermeer SE, Longstreth WT, Koudstaal PJ. Silent brain infarcts: a systematic review. *Lancet Neurol.* (2007) 6:611–9. doi: 10.1016/S1474-4422(07)70170-9
38. Brookes RL, Herbert V, Lawrence AJ, Morris RG, Markus HS. Depression in small-vessel disease relates to white matter ultrastructural damage, not disability. *Neurology.* (2014) 83:1417–23. doi: 10.1212/WNL.0000000000000882
39. Staals J, Makin SDJ, Doubal FN, Dennis MS, Wardlaw JM. Stroke subtype, vascular risk factors, and total MRI brain small-vessel disease burden. *Neurology.* (2014) 83:1228–34. doi: 10.1212/WNL.0000000000000837
40. Smith EE, O'Donnell M, Dagenais G, Lear SA, Wielgosz A, Sharma M, et al. Early cerebral small vessel disease and brain volume, cognition, and gait. *Ann Neurol.* (2015) 77:251–61. doi: 10.1002/ana.24320
41. Abraham HMA, Wolfson L, Moscufo N, Guttmann CRG, Kaplan RF, White WB. Cardiovascular risk factors and small vessel disease of the brain: blood pressure, white matter lesions, and functional decline in older persons. *J Cereb Blood Flow Metab.* (2016) 36:132–42. doi: 10.1038/jcbfm.2015.121
42. Abell JG, Kivimaki M, Dugravot A, Tabak AG, Fayosse A, Shipley M, et al. Association between systolic blood pressure and dementia in the Whitehall II cohort study: role of age, duration, and threshold used to define hypertension. *Eur Heart J.* (2018) 39:3119–25. doi: 10.1093/eurheartj/ehy288
43. The SPRINT MIND Investigators for the SPRINT Research Group, Nasrallah IM, Pajewski NM, Auchus AP, Chelune G, Cheung AK, et al. Association of intensive vs. standard blood pressure control with cerebral white matter lesions. *JAMA.* (2019) 322:524–34. doi: 10.1001/jama.2019.10551
44. Egan BM, Li J, Wagner CS. Systolic blood pressure intervention trial (SPRINT) and target systolic blood pressure in future hypertension guidelines. *Hypertension.* (2016) 68:318–23. doi: 10.1161/HYPERTENSIONAHA.116.07575
45. Birns J, Markus H, Kaira L. Blood pressure reduction for vascular risk: is there a price to be paid? *Stroke.* (2005) 36:1308–13. doi: 10.1161/01.STR.0000165901.38039.5f
46. Iadecola, Gottesman RF. Neurovascular and cognitive dysfunction in hypertension: epidemiology, pathobiology, and treatment. *Circul Res.* (2019) 124:1025–44. doi: 10.1161/CIRCRESAHA.118.313260
47. Wright JT Jr, Williamson JD, Whelton PK, Snyder JK, Sink KM, Rocco MV, et al. A randomized trial of intensive versus standard blood pressure control. SPRINT research group. *N Engl J Med. Nov.* (2015) 373:2103–216. doi: 10.1056/NEJMoa1511939
48. Nerenberg KA, Zarnke KB, Leung AA, Dasgupta K, Butalia S, McBrien K, et al. Hypertension Canada's 2018 guidelines for diagnosis, risk assessment, prevention, and treatment of hypertension in adults and children. *Can J Cardiol.* (2018) 34:506–25. doi: 10.1016/j.cjca.2018.02.022
49. Yamashiro K, Tanaka R, Tanaka Y, Miyamoto N, Shimada Y, Ueno Y, et al. Visceral fat accumulation is associated with cerebral small vessel disease. *Eur J Neurol.* (2014) 21:667–73. doi: 10.1111/ene.12374
50. Dye L, Boyle NB, Champ C, Lawton C. The relationship between obesity and cognitive health and decline. *Proc Nutr Soc.* (2017) 76:443–54. doi: 10.1017/S0029665117002014
51. Pedditzi E, Peters R, Beckett N. The risk of overweight/obesity in mid-life and late life for the development of dementia: a systematic review and meta-analysis of longitudinal studies. *Age Ageing.* (2016) 45:14–21. doi: 10.1093/ageing/afv151
52. Shaley D, Arbuckle MR. Metabolism and memory: obesity, diabetes, and dementia. *Biol Psychiatry.* (2017) 82:e81–3. doi: 10.1016/j.biopsych.2017.09.025
53. Brey RL. Long-term obesity is linked to loss of brain tissue. *Neurology.* (2004) 63:E19–20. doi: 10.1212/01.wnl.0000148952.71557.bf
54. Flegal KM, Carroll MD, Kit BK, Ogden CL. Prevalence of obesity and trends in the distribution of body mass index among US adults, 1999–2010. *JAMA.* (2012) 307:491–7. doi: 10.1001/jama.2012.39
55. Ford ES, Maynard LM, Li C. Trends in mean waist circumference and abdominal obesity among US adults, 1999–2012. *JAMA.* (2014) 312:1073–5. doi: 10.1001/jama.2014.8362
56. Shields M, Carroll MD, Ogden CL. Adult obesity prevalence in Canada and the United States. *NCHS Data Brief.* (2011) 56:1–8. doi: 10.3945/an.111.000497
57. Sorensen BM, Houben AJ, Berendschot TT, Schouten JS, Kroon AA, van der Kallen CJ, et al. Prediabetes and type 2 diabetes are associated with generalized microvascular dysfunction: the maastricht study. *Circulation.* (2016) 134:1339–52. doi: 10.1161/CIRCULATIONAHA.116.023446
58. Sanahuja J, Alonso N, Diez J, Ortega E, Rubinat E, Traveset A, et al. Increased burden of cerebral small vessel disease in patients with type 2

diabetes and retinopathy. *Diabetes Care*. (2016) 39:1614–20. doi: 10.2337/dc15-2671
59. Karapanayiotides T, Piechowski-Jozwiak B, van Melle G, Bogousslavsky J, Devuyst G. Stroke patterns, etiology, and prognosis in patients with diabetes mellitus. *Neurology*. (2004) 62:1558–62. doi: 10.1212/01.WNL.0000123252.55688.05
60. Staszewski J, Piusinska-Macoch R, Brodacki B, Skrobowska E, Stepien A. Association between hemostatic markers, serum lipid fractions and progression of cerebral small vessel disease: a 2-years follow-up study. *Neurol Neurochir Pol*. (2018) 52:54–63. doi: 10.1016/j.pjnns.2017.11.005
61. Kraft P, Schuhmann MK, Garz C, Jandke S, Urlaub D, Menci S, et al. Hypercholesterolemia induced cerebral small vessel disease. *PLoS ONE*. (2017) 12:e0182822. doi: 10.1371/journal.pone.0182822
62. Kaul K, Hodgkinson A, Tarr JM, Kohner EM, Chibber R. Is inflammation a common retinal-renal-nerve pathogenic link in diabetes? *Curr Diabetes Rev*. (2010) 6:294–303. doi: 10.2174/157339910793360851
63. Faraco G, Brea D, Garcia-Bonilla L, Wang G, Racchumi G, Chang H, et al. Dietary salt promotes neurovascular and cognitive dysfunction through a gut-initiage TH17 response. *Nat Neurosci*. (2018) 21:240–9. doi: 10.1038/s41593-017-0059-z
64. Gelber RP, Redline S, Ross GW, Petrovitch H, Sonnen JA, Zarow C, et al. Associations of brain lesions at autopsy with polysomnography features before death. *Neurology*. (2015) 84:296–303. doi: 10.1212/WNL.0000000000001163
65. Irwin MR, Olmstead R, Carroll JE. Sleep disturbance, sleep duration, and inflammation: a systematic review and meta-analysis of cohort studies and experimental sleep deprivation. *Biol Psychiatry*. (2016) 80:40–52. doi: 10.1016/j.biopsych.2015.05.014
66. Sexton CE, Storsve AB, Walhovd KB, Johansen-Berg H, Fjell AM. Poor sleep quality is associated with increased cortical atrophy in community-dwelling adults. *Neurology*. (2014) 83:967–73. doi: 10.1212/WNL.0000000000000774
67. Xie L, Kang H, Xu Q, Chen MJ, Liao Y, Thiyagarajan M, et al. Sleep drives metabolite clearance from the adult brain. *Science*. (2013) 342:373.7. doi: 10.1126/science.1241224
68. Jean-Louis G, Grandner MA, Youngstedt SD, Williams NJ, Zizi F, Sarpong DF, et al. Differential increase in prevalence estimates of indadequate sleep among black and white Americans. *BMC Public Health*. (2015) 15:1185. doi: 10.1186/s12889-015-2500-0
69. Owens JA, Spirito A, McGuinn M, Nobile C. Sleep habits and sleep disturbance in elementary school-aged children. *J Dev Behav Pediatr*. (2000) 21:27–36. doi: 10.1097/00004703-200002000-00005
70. Rensma SP, van Sloten TT, Launer LJ, Stehouwer CDA. Cerebral small vessel disease and risk of incident stroke, dementia and depression, and all-cause mortality: a systematic review and meta-analysis. *Neurosci Biobehav Rev*. (2018) 90:164–73. doi: 10.1016/j.neubiorev.2018.04.003
71. van Sloten TT, Mitchell GF, Sigurdsson S, van Buchem MA, Jonsson PV, Garcia ME, et al. Associations between arterial stiffness, depressive symptoms and cerebral small vessel disease: cross-sectional findings from the AGES-Reykjavik Study. *J Psychiatry Neurosci*. (2016) 41:162–8. doi: 10.1503/jpn.140334
72. Cacioppo JT, Hawkley LC, Thisted RA. Perceived social isolation makes me sad: 5-year cross-lagged analyses of loneliness and depressive symptomatology in the Chicago Health Aging, and Social Relations Study. *Psychol Aging*. (2010) 25:453–63. doi: 10.1037/a0017216
73. Hawkley LC, Cacioppo JT. Loneliness matters: a theoretical and empirical review of consequences and mechanisms. *Ann Behav Med*. (2010) 40:218–27. doi: 10.1007/s12160-010-9210-8
74. Gilmour H. Social participation and the health and well-being of Canadian seniors. *Health Rep*. (2012) 23:23−32.
75. Grammas P. Neurovascular dysfunction inflammation and endothelial activation: implications for the pathogenesis of Alzheimer's disease. *J Neuroinf*. (2011) 8:26. doi: 10.1186/1742-2094-8-26
76. Shi Y, Thrippleton MJ, Makin SD, Marshall L, Geerlings MI, de Craen AJM, et al. Cerebral blood flow in small vessel disease: a systematic review and meta-analysis. *J Cereb Blood Flow Metab*. (2016) 36:1653–67. doi: 10.1177/0271678X16662891
77. Brickman AM, Guzman VA, Gonzalez-Castellon M, Razlighi Q, Gu Y, Narkhede A, et al. Cerebral autoregulation, beta amyloid, and white matter hyperintensities are interrelated. *Neurosci Lett*. (2015) 592:54–8. doi: 10.1016/j.neulet.2015.03.005
78. Wolters FJ, Zonneveld HI, Hofman A, van der Lugt A, Koudstaal PJ, Vernooij MV, et al. Cerebral perfusion and the risk of dementia: a population-based study. *Circulation*. (2017) 136:719–28. doi: 10.1161/CIRCULATIONAHA.117.027448
79. Mehta D, Jackson R, Paul G, Shi J, Sabbagh M. Why do trials for Alzheimer's disease drugs keep failing? A discontinued drug perspective for 2010-2015. *Expert Opin Investig Drugs*. (2017) 26:735–9. doi: 10.1080/13543784.2017.1323868
80. Ricciarelli R, Fedele E. The amyloid cascade hypothesis in Alzheimer's disease: it's time to change our mind. *Curr Neuropharmacol*. (2017) 15:926–35. doi: 10.2174/1570159X15666170116143743
81. Wardlaw JM, Bath PM. Stroke research in 2018: extended time windows, refined benefit, and lifestyle prevention targets. *Lancet Neurol*. (2019) 18:2–3. doi: 10.1016/S1474-4422(18)30457-5
82. Hakim A. *Save Your Mind. Seven Rules to Avoid Dementia*. Toronto, ON: Barlow Publishing (2017).
83. Sherzai D, Sherzai A. *The Alzheimer's Solution: A Breakthrough Program to Prevent and Reverse the Symptoms of Cognitive Decline at Every Age*. New York, NY: Harper Collins Publishers (2017).
84. Poggesi A, Pasi M, Pescini F, Pantoni L, Inzitari D. Circulating biologic markers of endothelial dysfunction in cerebral small vessel disease: a review. *J Cereb Blood Flow Metab*. (2016) 36:72–94. doi: 10.1038/jcbfm.2015.116
85. Fraineau S, PalIi CG, McNeil B, Ritso M, Prasain SN, Chu A, et al. Epigenetic activation of pro-angiogenic signaling pathways in human endothelial progenitors increases vasculogenesis. *Stem Cell Rep*. (2017) 9:1573–87. doi: 10.1016/j.stemcr.2017.09.009
86. Cabrera Escobar MA, Veerman JL, Tollman SM, Bertram MY, Hofman KJ. Evidence that a tax on sugar sweetened beverages reduces the obesity rate: a meta-analysis. *BMC Public Health*. (2013) 13:072. doi: 10.1186/1471-2458-13-1072

Conflict of Interest: The author declares that the research was conducted in the absence of any commercial or financial relationships that could be construed as a potential conflict of interest.

Copyright © 2019 Hakim. This is an open-access article distributed under the terms of the Creative Commons Attribution License (CC BY). The use, distribution or reproduction in other forums is permitted, provided the original author(s) and the copyright owner(s) are credited and that the original publication in this journal is cited, in accordance with accepted academic practice. No use, distribution or reproduction is permitted which does not comply with these terms.

frontiers in Neuroscience

ORIGINAL RESEARCH
published: 26 September 2019
doi: 10.3389/fnins.2019.01033

Enzymatic Digestion of Hyaluronan-Based Brain Extracellular Matrix *in vivo* Can Induce Seizures in Neonatal Mice

*Alena Balashova[1], Vladimir Pershin[1,2], Olga Zaborskaya[1,2], Natalia Tkachenko[1,2], Andrey Mironov[1,2], Evgeny Guryev[1,2], Leonid Kurbatov[3], Murat Gainullin[2,4] and Irina Mukhina[1,2]**

[1] Laboratory for Brain Extracellular Matrix Research, N. I. Lobachevsky State University of Nizhny Novgorod, Nizhny Novgorod, Russia, [2] Cell Technology Group, Privolzhsky Research Medical University, Nizhny Novgorod, Russia, [3] V. N. Orekhovich Institute of Biomedical Chemistry, Russian Academy of Medical Sciences, Moscow, Russia, [4] Norwegian PSC Research Center and Institute of Clinical Medicine, Oslo University Hospital and University of Oslo, Oslo, Norway

It is well-known that hyaluronic acid (HA) as a component of brain extracellular matrix (ECM) plays a pivotal role in the nervous system and is involved in synaptic plasticity changes in vascular cognitive impairment and dementia. HA breakdown is a feature of the acute stage of stroke injury and may be detrimental through enhancement of the inflammatory response. Recent studies have shown that knockout mice lacking hyaluronic acid synthetase demonstrates epileptic phenotype *in vivo* and removal of HA leads to delayed development of epileptiform activity in cultured hippocampal neurons *in vitro*. Here, we studied whether digestion of hyaluronic acid in the hippocampus in early postnatal period can trigger seizures. Hyaluronidase (Hyal) (5 U/μl) was bilaterally injected into C57BL/6j mice (P17) CA1 field of hippocampus using the stereotaxic method to remove hyaluronan-based ECM. Transcriptome analysis of hippocampal tissue 2 h after enzymatic digestion of hyaluronan-based brain ECM revealed increased gene expression of proteins involved in inflammation reactions (TLR2, CCL2,3,5), neuroinflammation, axonal guidance and ephrin receptor signaling, versus the vehicle group. Mice injected with hyaluronidase exhibited delayed audiogenic seizures and improvement in working memory 72 h after injection, while there were no changes in locomotor activity, anxious level and exploratory behavior due to the open field test. The obtained results point to a link between the activation of neuroinflammation by enzymatic digestion of hyaluronan-based brain ECM during the neonatal period and their subsequent reactivity to seizures, which may play an important role in the functional features of the developing brain, including its seizure propensity.

Keywords: brain extracellular matrix, hyaluronic acid, seizure, behavioral tests, transcriptome analysis, neuroinflammation

OPEN ACCESS

Edited by:
Emmanuel Pinteaux, The University of Manchester, United Kingdom

Reviewed by:
Xingchun Gou, Xi'an Medical University, China
Veronica Perez de la Cruz, National Institute of Neurology and Neurosurgery (INNN), Mexico

***Correspondence:**
Irina Mukhina
mukhinaiv@mail.ru

Specialty section:
This article was submitted to Neurodegeneration, a section of the journal Frontiers in Neuroscience

Received: *15 May 2019*
Accepted: *12 September 2019*
Published: *26 September 2019*

Citation:
Balashova A, Pershin V, Zaborskaya O, Tkachenko N, Mironov A, Guryev E, Kurbatov L, Gainullin M and Mukhina I (2019) Enzymatic Digestion of Hyaluronan-Based Brain Extracellular Matrix in vivo Can Induce Seizures in Neonatal Mice. Front. Neurosci. 13:1033. doi: 10.3389/fnins.2019.01033

INTRODUCTION

Brain extracellular matrix (ECM) is a multicomponent complex. Members of the lectican family, chondroitin sulfate proteoglycans (CSPGs) such as neurocan, brevican, versican, and aggrecan with tenascins are anchored on hyaluronic acid (HA) backbone. HA is a unique non-sulfated glycosaminoglycan. It has a lot of physiological and biochemical properties including providing

biomechanical integrity, altering tissue hydration and facilitating tissue assembly which are dependent on its size, concentration, and localization (George and Geller, 2018).

Hyaluronic acid is distributed throughout the ECM but the highest density of HA is detected around neuronal bodies and myelinated fibers (Perkins et al., 2017). ECM in the brain has two main states: (1) diffuse ECM, which is represented throughout the brain, and (2) densely packed matrix, forming so-called perineural networks (PNNs) (George and Geller, 2018). In the adult brain, PNNs generally surround parvalbumin-expressing GABA-ergic neurons by forming a lattice structure around synapses on the body and proximal dendrites, which may affect the development and stabilization of synapses in neonatal period (McRae et al., 2012). Moreover, depending on the proteoglycan component, PNNs prevent the formation of new synaptic connections by inhibiting axonal growth (Ueno et al., 2019). There is evidence that PNNs can also protect neurons from oxidative stress and glutamate-stimulated excitotoxicity (Ueno et al., 2019).

The formation of PNNs is a long activity-dependent process. *In vitro* studies have shown that formation of PNNs requires the activity of alpha-amino-3-hydroxy-5-methyl-4-isoxazole-propionic acid (AMPA) receptors and L-type voltage-dependent calcium channels (L-VDCC). During the period from the second to the third week after birth, the expression of crucial molecules of immature ECM such as tenascin-C and neurocan decreases, whereas expression of CSPGs such as aggrecan, brevican, versican V2, phosphacan, as well as tenascin-R and hyaluronan-binding protein Hapln1, are increased (Song and Dityatev, 2018). Rowlands et al. (2018) recently found that mice with knock-out of a gene responsible for aggrecan synthesis (*Acan*) has a significantly lower level of aggrecan, as well as phosphacan, neurocan, brevican, versican, and tenascin-R together with the reduced density of PNNs. This finding points to the crucial role of aggrecan in the formation of functional perineuronal nets.

Hyaluronic acid plays a pivotal role in synaptic plasticity during vascular cognitive impairment and dementia (Dityatev et al., 2009). Extracellular remodeling is a common response to different types of injuries and diseases. Upregulation of HA synthases (Has1 and 2) and hyaluronidases (Hyal1 and 2) in the cells from both stroke and peri-infarcted regions of the brain were demonstrated (Sherman et al., 2015). Recent studies have shown that knockout mice lacking hyaluronic acid synthase demonstrates epileptic phenotype (Arranz et al., 2014).

For most types of epilepsy, it is unknown how the hippocampus becomes hyperexcitable and how hyperexcitable cells integrate into a pathological circuit, resulting in the generation of spontaneous recurrent seizures. Subsequent transcriptional and translation alterations can induce changes in neuronal circuits, which predispose to development of seizures (Kim et al., 2017). Assessing the role of particular genes and pathways through the analysis of genome-wide gene expression is a promising tool to identify key trigger genes or pathways of epileptogenesis and other neurologic conditions (Younus and Reddy, 2017).

Previously, we have found that enzymatic digestion of hyaluronic acid by exogenous enzyme Hyal leads to the delayed development of epileptiform activity in cultured hippocampal neurons *in vitro* (Vedunova et al., 2013). In this study, we performed behavioral tests to identify seizure-like activity following Hyal intrahippocampal injections in C57BL/6j mice (P17). The ability for learning was assessed with a fear conditioning test. Open field exploratory test was used to estimate locomotor activity, anxiety and exploratory behavior. Transcriptome analysis of hippocampal tissue was carried out 2 h after enzymatic digestion of hyaluronan-based brain ECM to reveal changes in gene expression of different proteins. Immunohistochemical staining with anti-aggrecan antibodies was carried out to assess the integrity of PNNs.

MATERIALS AND METHODS

Animals

Animals were housed in a specific pathogen-free animal facility at 20 ± 2°C with 60% humidity, a 12 h/12 h light/dark cycle, and *ad libitum* access to food and tap water until the surgery procedures. Animals were transferred into animal cages after surgery and maintained at the same environment with their male-littermates for 2–9 days. All experiments were carried out with an effort to minimize the number of animals used and the suffering caused by study procedures.

Ethics Statement

All animals were treated in strict accordance with ethical animal research standards defined by the Russian law and approved by the Ethical Committee on Animal Health and Care of Lobachevsky State University and Privolzhsky Research Medical University of the Nizhny Novgorod.

Hyaluronidase Injection

17-day-old C57BL/6J mice were divided among two groups: hyaluronidase-treated (Hyal) and phosphate-buffered saline (PBS) treated (Vehicle). Animals were deeply anesthetized with 1.5% isoflurane and the scalp was incised. For hyaluronidase injection, a 1 mm diameter portion of the skull was removed with a drill bit at stereotactic coordinates −2.06 mm anterio–posterior, 1.89 mm medio-lateral relative to bregma. 1.25 mm diameter glass capillary with open tip 5–10 μm diameter were used for injections. The glass capillary tip was placed 1.8 mm dorso-ventral to the skull surface. The speed of the liquid flow was maintained at 3–4 nl/s. The coordinates of the injection were calculated individually for each animal based on the ratio of the distance between bregma and lambda from those mentioned above. Animals in the experimental group (Hyal) were injected with 1 μl of Hyaluronidase from bovine testis (Sigma) diluted in 0.1 M phosphate buffered saline (PBS) at a concentration of 5 U/μl. Animals in vehicle group were injected with equal volume of 0.1 M PBS.

Behavioral Tests

All the behavioral tests (n = 10/group) were carried out on second and third days after hyaluronidase injection.

Open Field Exploration Test

Mouse was placed in an open field chamber or arena (PanLab, Spain) and allowed to explore freely for 5 min. The locomotor activity (such as mean and max speed and traveled distance) in the whole arena was monitored and analyzed by an automated system (Smart v.3.0, PanLab, Spain). The distance traveled and the time spent in different parts of the arena (center and periphery) were estimated in a same way.

Anxiety (the duration of rearing and grooming in both compartments) was made in open field test.

Passive Avoidance Test

The short-term memory of experimental animals was evaluated by Passive Avoidance test (PanLab, Spain). The Passive Avoidance test is a behavioral model of conditioned reflex, consisting of the stages of training and reproduction of the reflex. The equipment was "Shuttle Box" divided into a dark and light compartment. Assessment of acquisition and retention of the passive avoidance task was carried out using identical illuminated and non-illuminated compartments containing a 50 W bulb. In brief, the animals underwent two separate trials: an acquisition trial and a retention trial, conducted 24 h after the acquisition trial. For the acquisition trial, the mouse was initially placed in the light compartment; the door between the two compartments was opened. When the mouse entered the dark compartment, the door automatically closed and an electrical foot shock (0.5 mA, 3 s) was delivered through the grid floor. The time before entering the dark room (latency) was registered. For the retention trial, the mice were placed in the light compartment as well as in acquisition trial and the time taken to enter the dark compartment was recorded again. If the mouse did not enter the dark compartment within 180 s, it was assumed that the mouse remembered the foot shock from the acquisition trial. The difference in time spent by an animal before entering dark chamber during retention and acquisition trials (delta time) was calculated.

Audiogenic Stimulus Assay

The animals were placed individually in the chamber (a glass cylinder 15 cm diameter, 25 cm height and video camera were placed a sound-proofing box) and were habituated for 5 min. Audiogenic stimulus was performed by a bell sound (100 dB) inside of box∼15 cm above the test subject. The stimulus lasted 60 s or until tonic-clonic seizure was observed visually. The behavior of the animal was recorded in three categories: wild running, tonic-clonic seizures, and death. If an animal displays the single wild run bout and stopped, thus displaying the low intensity fit score (Krushinsky–Molodkina, or KM, arbitrary unit "1"). The last stage of seizures goes through wild run which is followed first by clonic and then by tonic/clonic and tonic "full" seizure with extension of extremities and death (KM arbitrary unit "6").

Immunohistochemistry

Staining

The animals were transcardially perfused with 0.1 M PBS (pH = 7.4) at 2 h, 2 and 3 days after surgery, and subsequently followed by 4% paraformaldehyde (PFA) in PBS. Brains were then removed and fixed overnight in PFA, washed in PBS and dehydrated through a series of graded ethanol baths, and then infiltrated with paraffin; infiltrated tissues were embedded into paraffin blocks. Sections from paraffin blocks 5 um thick were made with semi-automated rotary microtome (Leica Biosystems, Germany). Every third slice was placed on an adhesive slide and dried. Paraffin sections were deparaffinized, rehydrated, treated with antigen retrieval buffer and washed in tris-buffered saline (TBS) (pH = 7.4). Permeabilization were made with 0.2% Triton X-100 (Sigma 93443-100ML) solution in TBS and was followed by blocking in 10% fetal cow serum (FCS), 1% bovine serum albumin (BSA) in TBS for 2 h. After that, sections were incubated overnight at 4°C with primary antibodies. The next day, sections were incubated with the appropriate species-specific fluoroconjugated secondary antibodies (Alexa Fluor 647 and Alexa Fluor 488; 1:400; Abcam) for 1 h. Primary antibodies used were rabbit polyclonal anti Aggrecan (ab36861; 1:100; Abcam), and chicken polyclonal anti NeuN as a neuronal marker (266006; 1:100; Synaptic Systems). The secondary antibody was goat polyclonal secondary antibody to rabbit IgG – H&L (Alexa Fluor® 488) (ab150077; 1:400; Abcam) and goat polyclonal secondary antibody to chicken IgY – H&L (Alexa Fluor® 647) (ab150171; 1:400; Abcam). Stained sections were mounted using Fluoroshield Mounting Medium with DAPI (ab104139, Abcam) and examined by fluorescence microscopy using a ZEISS LSM 880. Images were acquired controlling for equal exposure times using Zen 2.1 SP3 software. 1.2 Pl-Apo objective, pinhole 0.8 μm. Data from three channels (DAPI 405, Alexa Fluor 488, and Alexa Fluor 647) were collected by sequential scanning. Single confocal planes were analyzed to determine co-localization of signals in tissue sections.

We assessed the fluorescence intensity of anti-aggrecan antibody to assess the integrity of PNNs in four 212.5 × 212.5 μm fields of view from each slice. The average cell area and average area of extracellular space was also estimated using ImageJ. $N = 3$ animals/group, three slices from each animal.

RNA Extraction

For RNA extractions, hippocampi were dissected on ice 2 h after injections and immediately frozen via liquid nitrogen with subsequent transfer into −80°C freezer.

Total RNA was extracted from hippocampi of animals from both Hyal and Vehicle groups. RNA extraction was performed with the RNeasy mini kit (Qiagen, Valencia, CA, United States). A NanoDrop® NP-1000 spectrophotometer (NanoDrop Technologies, Wilmington, DE, United States) was used to measure the quantity of the RNA samples. The quality of the RNA samples was checked using a 2100 Bioanalyzer (Agilent Technologies Inc., Santa Clara, CA, United States), RNA integrity of each sample was assessed using ratio of 18S/28S RNA and RNA integrity number (RIN).

Agilent Microarray Analysis

The synthesis of cDNA followed by the synthesis of cRNA with fluorescent labels was performed using the Agilent Low RNA Input Fluorescent Linear Amplification Kit (Agilent

Technologies Inc., Santa Clara, CA, United States). 3-CTP or 5-CTP nucleotides with fluorescent labels (Agilent Technologies Inc., Santa Clara, CA, United States) were used for detection.

After determining the concentration of cRNA and evaluating the efficiency of fluorescent labels incorporating, the samples (750 ng each) were mixed in one tube and fragmented using reagents from the *in situ* Hybridization kit-plus kit (Agilent Technologies Inc., Santa Clara, CA, United States). After the end of fragmentation, 500 μl of the mixture was applied to Sure Print G3 Mouse Gene Expression v2 8 K× 60K Microarray Kit (Agilent Technologies Inc., Santa Clara, CA, United States) expression chips. These microchips contain 60,000 of 60 nucleotide probes immobilized on a glass and designed to analyze gene expression of the complete mouse genome (annotated genes with known and unknown function) in a given volume. Hybridization was performed in a rotary incubator (Agilent Technologies Inc., Santa Clara, CA, United States) at 65°C for 17 h. The chips were washed in an SSC buffer with the addition of Triton X102 according to the protocol of the manufacturer, then chips were scanned on a G2505B confocal laser scanner (Agilent) with a resolution of 10 μm. Extraction of DNA chip data and their primary processing were performed using the Feature Extraction 9.1 (Agilent Technologies Inc., Santa Clara, CA, United States) program.

The background signal was calculated and the fluorescence intensity in the red and green channels was calculated for each sample (spot). After determining the background signal level, all genes which are not expressed both in the Vehicle and Hyal samples were excluded from further analysis. Finally, the degree of difference in the signal of certain genes in different samples was evaluated (Vehicle, $n = 4$; Hyal, $n = 4$).

Microarray Analysis

A microarray analysis was performed using BRB-ArrayTools[1] to identify probe intensity values developed by Dr. Richard Simon and the BRB-ArrayTools Development Team that were significantly affected by hyaluronan digestion. Intra-array LOWESS normalizations were performed. The BRB-ArrayTools "Random Variance Model" option was used.

To identify the direct effect of hyaluronidase injection we compare Vehicle and Hyal groups. For this analysis two-sample *t*-test were used and *q*-value was 0.05 this resulted in 25 genes passed this filter (0.089%).

Pathway Analysis

Ingenuity pathway analysis (IPA, Qiagen, Valencia, CA, United States) was used to perform "Core Analysis" to discover biological pathways that were significantly affected by hyaluronidase treatment. Data from microarray analysis were first uploaded into Qiagen's IPA system for core analysis and then overlaid with the global molecular network in the Ingenuity Pathway Knowledge Base (IPKB).

Ingenuity pathway analysis was performed to identify canonical pathways, functions, upstream regulators that are most significant to microarray outcomes and to categorize differentially expressed genes in pathways and upstream regulators.

Establishment of Protein–Protein Interaction Network

Search Tool for the Retrieval of Interacting Genes/Proteins (STRING) database[2] was used to analyze protein interactions (Szklarczyk et al., 2014). We modeled a network of 22 genes where the interaction scores above 0.4 was considered as *de facto* interaction with the high confidence (≥0.700). After modeling the interactions network, we performed the *k*-means clustering (number of clusters = 3).

Statistical Analysis

All data quantification is presented as the mean ± standard error of the mean (SEM). Statistical analysis was performed using GraphPad Prism 6.0. Normality test was performed using Shapiro–Wilk criterion. The Mann–Whitney test and 2-way ANOVA multiple comparison test with Bonferroni's correction were used to quantify behavioral test results. The difference between groups was considered significant if the p value was less than 0.05.

RESULTS

Locomotor Activity, Anxiety, and Exploratory Behavior

Hyal animals in Open field test were shown neither increase nor decrease in anxiety and exploratory behavior versus vehicle group on time points 2 and 3 days. Locomotor activity wasn't changed after hyaluronidase injection as well (**Figures 1**, **2**).

Short-Termed Memory Changes

At the following time point: 48 h after hyaluronidase injection, animals from the Hyal group remembered foot shock in 90% of cases, while animals from Vehicle group remembered aversive stimuli only in 60% of cases. However, the difference between latency time before entering the dark room in acquisition and retention sessions (delta time) in two groups were not significantly different. 100% of animals in Hyal group avoided entering the dark chamber during retention trial versus 70% of animals in Vehicle group, delta time were significantly higher in Hyal group (Mann–Whitney test, $p < 0.05$). Delta time for both time points is shown in **Figure 3**.

Audiogenic Seizures

It was shown that hyaluronidase injection can promote audiogenic seizures in neonatal animals. 20% of animals in Hyal group demonstrated wild running, 10% showed nearly complete tonic extension except hind feet (KM arbitrary unit "4"), and 10% of animals underwent all the stages of KM scale and died (KM arbitrary unit "6") after audiogenic stimuli at the time point of 48 h. In the vehicle group, 10% of animals demonstrated wild running during stimulation.

[1] http://brb.nci.nih.gov/BRB-ArrayTools

[2] http://string-db.org/

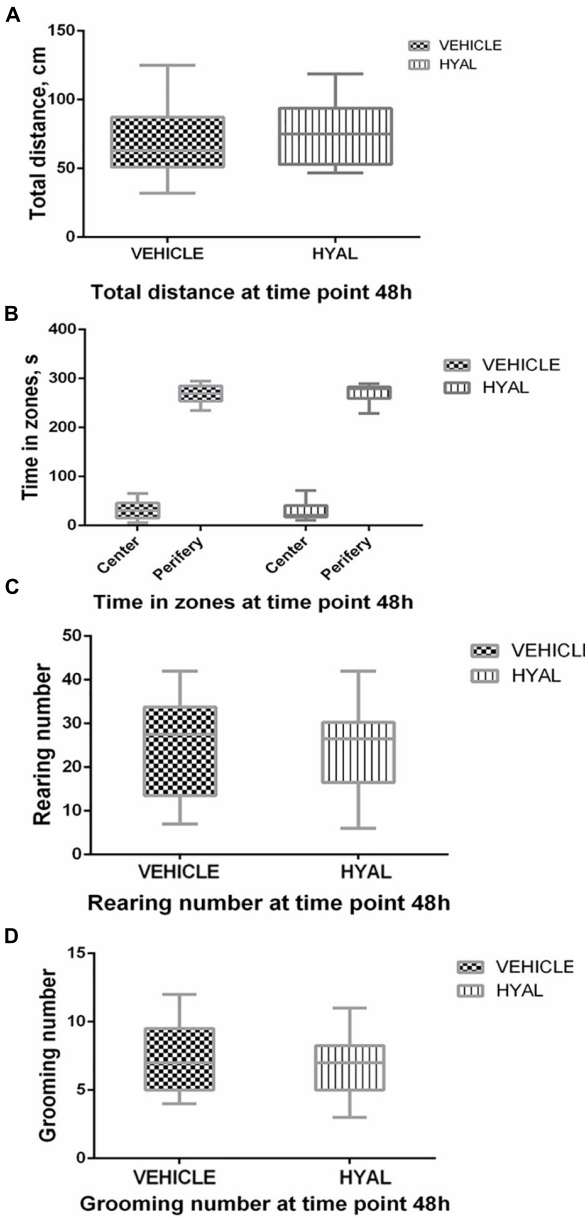

FIGURE 1 | Open field test results at the time point 48 h. Hyal animals in Open field test show neither increase nor decrease in anxiety and exploratory behavior versus vehicle group on time points of 48 h. There was no difference in locomotor activity of animals as indicated by traveled distance **(A)**. Time spent by animals in center and periphery of Open field didn't differ as well **(B)**. Anxiety level of Hyal animals didn't differ refer to Vehicle group as was shown by rearing and grooming analysis **(C,D)**. Figures show mean ± SEM, $N = 10$ per group. Two-way ANOVA and Mann–Whitney test didn't reveal any significant difference ($p > 0.05$).

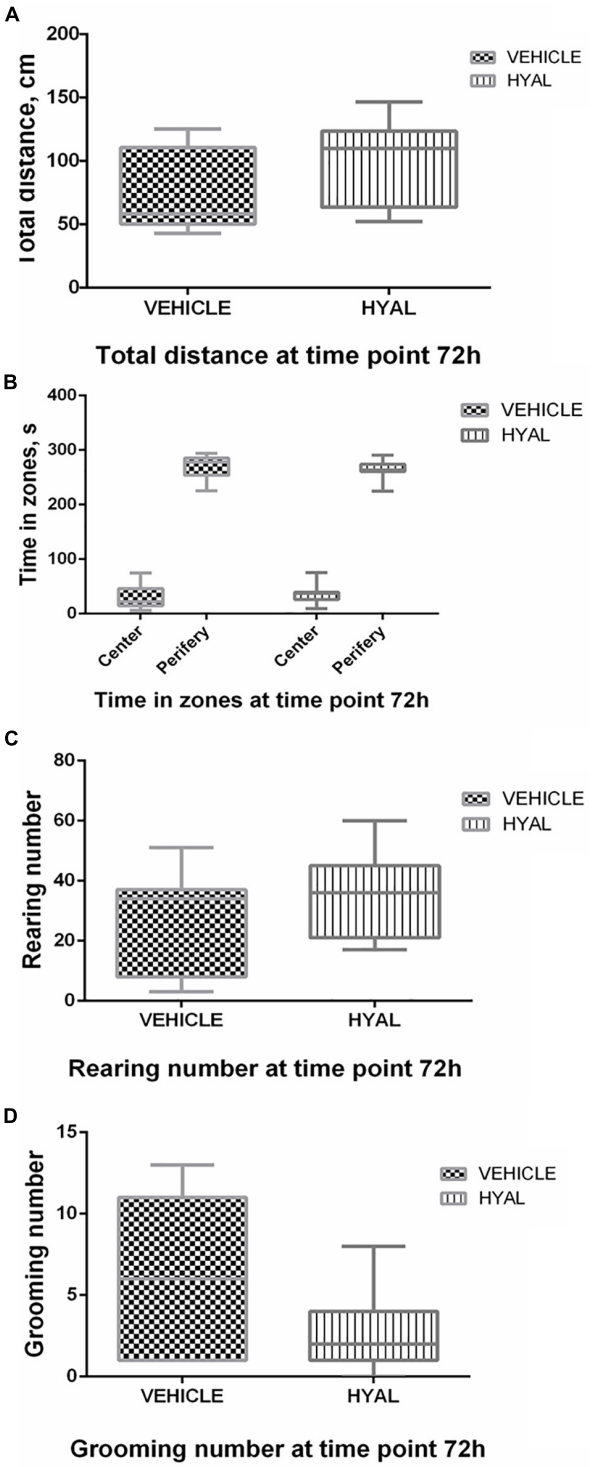

FIGURE 2 | Open field test results at the time point 72 h. There was no difference in locomotor activity of animals as was shown by traveled distance **(A)**. Hyal animals exhibited normal aversion to brightly lit open areas as well as Vehicle animals did, as was shown by time spent by animals in center and periphery of Open field **(B)**. Anxiety level of Hyal animals didn't differ refer to Vehicle group as was shown by rearing and grooming analysis **(C,D)**. Figures show mean ± SEM, $p < 0.05$. $N = 10$ per group. Two-way ANOVA and Mann–Whitney test didn't reveal any significant difference.

The number of animals with audiogenic seizures was even higher at the time point of 72 h in the Vehicle group; 40% of animals demonstrated wild running and 10% of animals demonstrated seizures of KM arbitrary unit "4," while in Vehicle group situation stayed the same (**Figure 4**).

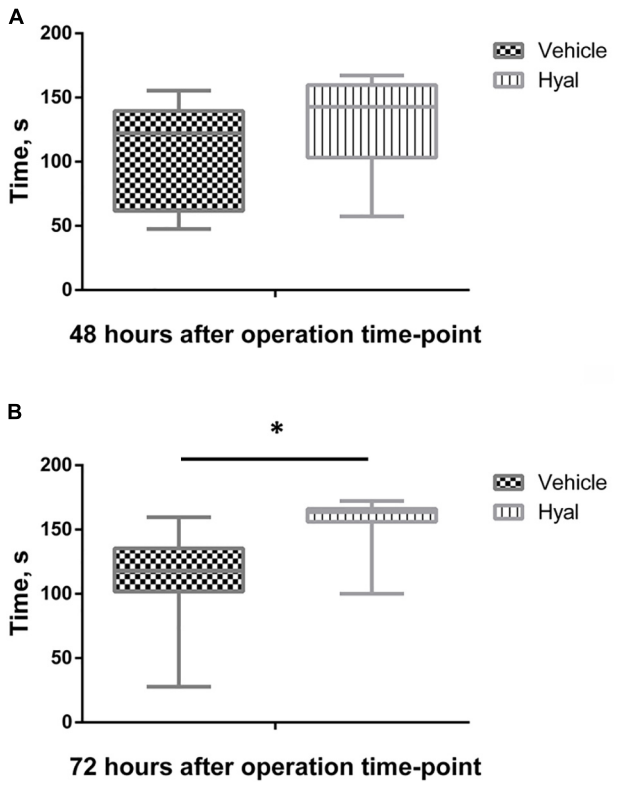

FIGURE 3 | Passive avoidance test results. Time before enter dark compartment in acquisition and retention trials at time points of 48 h **(A)** and 72 h **(B)**. *Y* axis indicates the difference between latency time before entering the dark room in acquisition and retention sessions (delta time). All the animals entering dark compartment during acquisition trial. At the time point of 48 h after hyaluronidase injection animals from Hyal group remembered foot shock in 90% cases, while animals from Vehicle group remembered aversive stimuli only in 60% cases, but Mann–Whitney test showed no significant difference. At the time point of 72 h 100% of animals in Hyal group avoided entering the dark compartment during retention trial versus 70% of animals in Vehicle group, delta time in two groups significantly differs. Figures show mean ± SEM, $N = 10$ per group, $^*p < 0.05$.

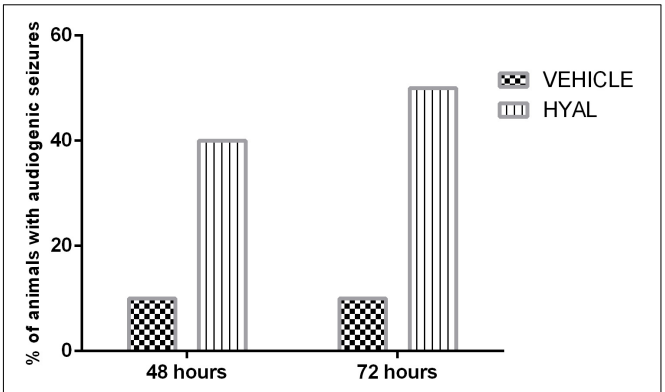

FIGURE 4 | Audiogenic seizures test results. Data shown in the diagram represents the percent of animals demonstrating audiogenic seizures. $N = 10$. The percent of animals in Vehicle group demonstrating wild running during audiogenic stimuli stayed at the level of 10% on the time points of 48 and 72 h. 40% of animals in Hyal group in total demonstrated audiogenic seizures at the time point of 48 h. 20% of animals demonstrated wild running, 10% showed nearly complete tonic extension except hind feet (KM arbitrary unit "4") and 10% of animals underwent all the stages of KM scale and died (KM arbitrary unit "6") after audiogenic stimuli at the time point of 48 h. At the time point of 72 h in vehicle group number of animals with audiogenic seizure was even higher – 50% in total. 40% of animals demonstrated wild running and 10% of animals demonstrated seizures of KM arbitrary unit "4."

PNN Immunostaining

It was shown that, 2 h after hyaluronidase injection, there was no detectable aggrecan agglomerates surrounding pyramidal neurons in hippocampal regions of injections in Hyal group in comparison with the Vehicle group. The trend persisted in both Hyal and Vehicle groups 48 and 72 h after injection (**Figures 5A,B**). The analysis of the area of extracellular space and an average cell area didn't reveal any significant differences between Hyal and Vehicle groups (**Figures 5C,D**). Fluorescence intensity analysis showed that the level of aggrecan in Hyal group reached its minimum at the 48 h after injection (**Figure 5E**) and started to restore at 72 h time point.

Analysis of Differential Expressed Genes and Their Interactions

The data expression matrix was processed with BRB-array tools, whole gene expression data presented in **Figure 6**.

According to the heat map (**Figure 7**), hyaluronidase treatment resulted in strong difference in comparison to vehicle control (PBS). The total number of DEGs were 25 (FDR = 0.05, *P* value ≤ 0.05, Benjamini–Hochberg correction).

Data from the STRING database revealed that several of the genes interacted with each other. In total, 25 genes were used to form the network complex (**Figure 8**). The network contained 27 nodes and 70 edges. Among them, seven nodes were the most significant (node degree ≥ 5). These were CCL2, CCL4, CCL5, CXCL1, CXCL10, CCR5, and TNF. Among seven nodes, TNF exhibited the highest node degree ($n = 10$).

Functional Analysis

To obtain an elementary investigation of the molecular mechanisms underlying disruption of hyaluronan matrix, microarray data were submitted to IPA core analysis. The differentially expressed genes were categorized to related canonical pathways based on IPKB. The top enriched categories of canonical pathways with *P* value < 0.05 are listed in **Figure 9**. Among pathways with $-\log_{10}$ *P* value, 3 include the Axonal guidence signaling, Neuroinflammation signaling pathway and Ephrin signaling pathway (Yu et al., 2016).

As hyaluronidase-treatment changed the profile of DEGs and signaling pathways, upstream regulators can also be changed. To investigate this issue, we tested DEGs identified upon Hyal treatment for enrichment of known key transcriptional regulators using the Upstream Regulator Analysis within the IPA Knowledgebase contains information about known regulators targets and can predict which transcriptional regulators are

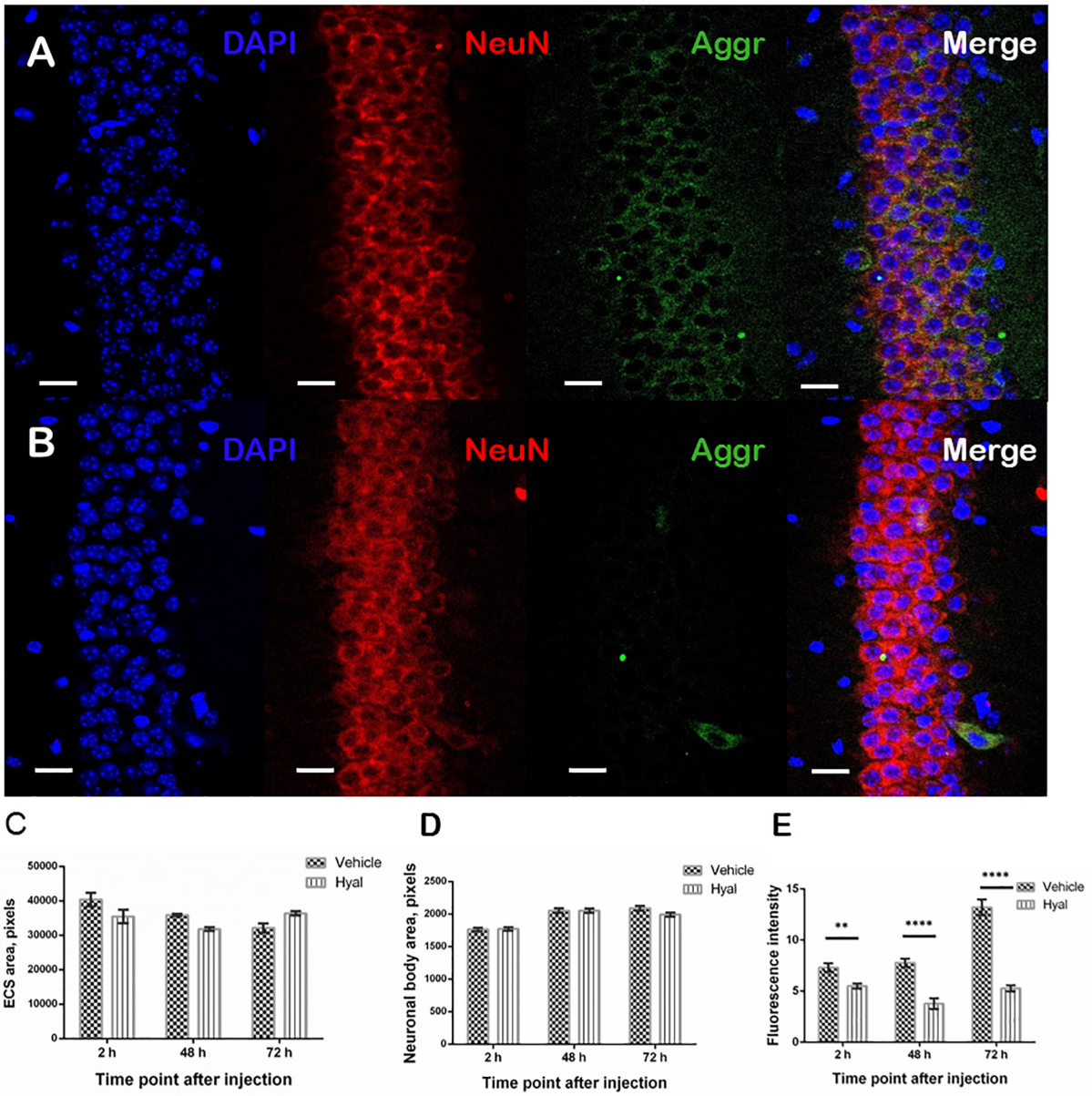

FIGURE 5 | Immunohistochemical staining of paraffin embedded brain slices. Images obtained by fluorescence microscopy at the 48 h after injection time point from Vehicle **(A)** and Hyal **(B)** animals brain slices. The nuclear marker DAPI is shown in blue. Aggrecan, the component of perineuronal nets, is shown in green, neuronal marker NeuN is shuwn in red. The scale is 20 μm. We measured ECS area **(C)** and average neuronal body area **(D)** at the 2, 48, and 72 h after injection time points. Mann–Whitney test didn't reveal any differences. The presence of aggrecan was measured by fluorescence intensity of green channel **(E)**. There is significant decrease in aggrecan component at all the time points but the minimum was fixed 48 h after injections. At the time point of 72 h the level of aggrecan starts to restore. $^{**}p < 0.005$, $^{****}p < 0.0001$.

responsible for certain biological processes or it can suggest pathways and the potential impact regulators may have on those pathways.

Analysis identified five genes upregulated in hyaluronidase-treated hippocampal tissues (**Figure 10**) with a significant number of their targets ($p < 10^{-5}$) changed in a direction which indicates an activated regulator status on a protein level (positive Z-score > 2).

DISCUSSION

Epilepsy is a most common neurological disorder all around the world. There are a lot of people suffering secondary epilepsy after brain infections or non-infectious (sterile) inflammatory response, traumatic brain injury or brain tumors (for review see Lowenstein, 2009; Vezzani et al., 2016). There is a large amount of mechanisms leading to seizure appearance and lots of it needs

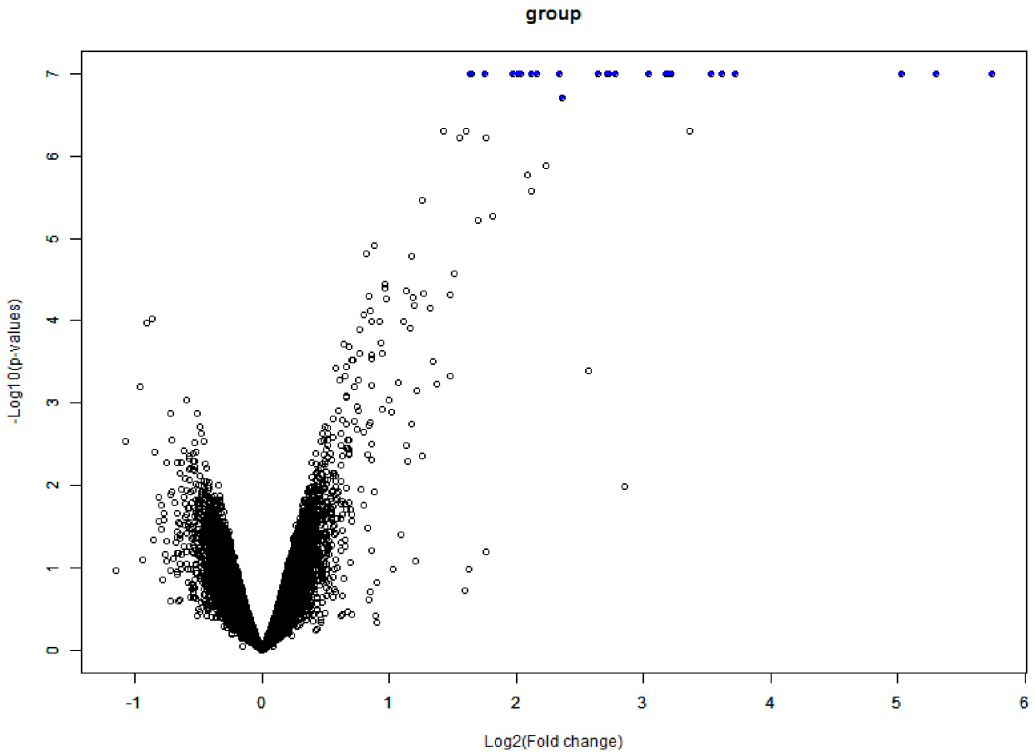

FIGURE 6 | Volcano plot of DEGs. The *x*-axis is logFC and the *y*-axis represents –log10 (adjusted *P*-value). The blue dots represent the DEGs, while the black dots represent genes that were not differentially expressed. DEGs, differentially expressed genes; FC, fold change.

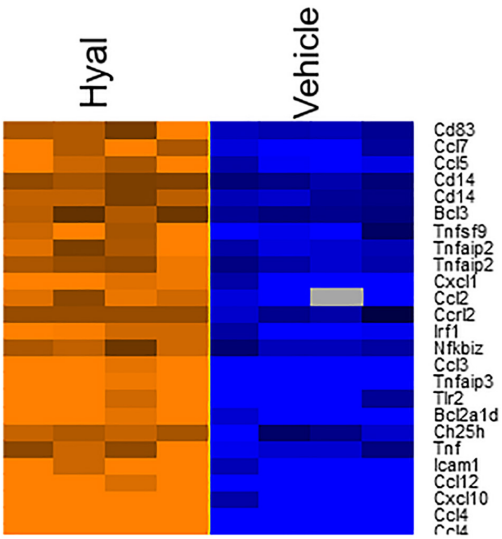

FIGURE 7 | Heatmap of genes involved in response to hyaluronan digestion. The expression levels of genes were indicated by the color bar above the heatmap. Orange color indicates the increased expression whereas blue color indicates the decreased expression. Data $\log_2$ normalized.

further investigation (Klein et al., 2018). The reasons for seizure occurrence in early postnatal development is the less studied subject in the field.

Brain ECM was shown to affect the maturation of central nervous system during early developmental stages (McRae et al., 2012; Ueno et al., 2019). We assumed that the destruction of ECM molecules during the early postnatal period may lead to the occurrence of some pathological states. Indeed, it was shown that 40 and 50% of animals after bilateral intrahippocampal hyaluronidase injections at the 48 and 72 h time points, respectively, exhibited seizures. The mechanism of epileptogenesis after ECM digestion during early development is not known so we decided to make a full transcriptomic analysis to unveil the possible pathways and detect target molecules for a further correction. Our transcriptomic analysis with further analysis of interacting genes/proteins revealed activation of a number of genes implicated in inflammatory responses (as far as cytokine-cytokine receptor interaction pathway was activated) in the Hyal group. Enzymatic digestion of hyaluronan produces a lot of low molecular weight fragments (<500 kDa), which can trigger an inflammatory response. During the inflammation, chemokines such as CCL2, CCL3, and CCL 5 can activate pathways leading to status epilepticus (Arisi et al., 2015; Cerri et al., 2016; Tian et al., 2017). In the current study, transcriptomic analysis showed the activation of the chemokine pathway due to upregulation of TLR2. Activation of TLR2 by short fragments of hyaluronan and disruption of CD44 can induce an inflammatory response (Jiang et al., 2011). Signals from these receptors can be transmitted through NF-κB transcription factor upregulating the expression of chemokines (CCL2,3,4,5,7,10,12, CXCL 1,10), which can act through $ERK_{1,2}$ enhancing the production of

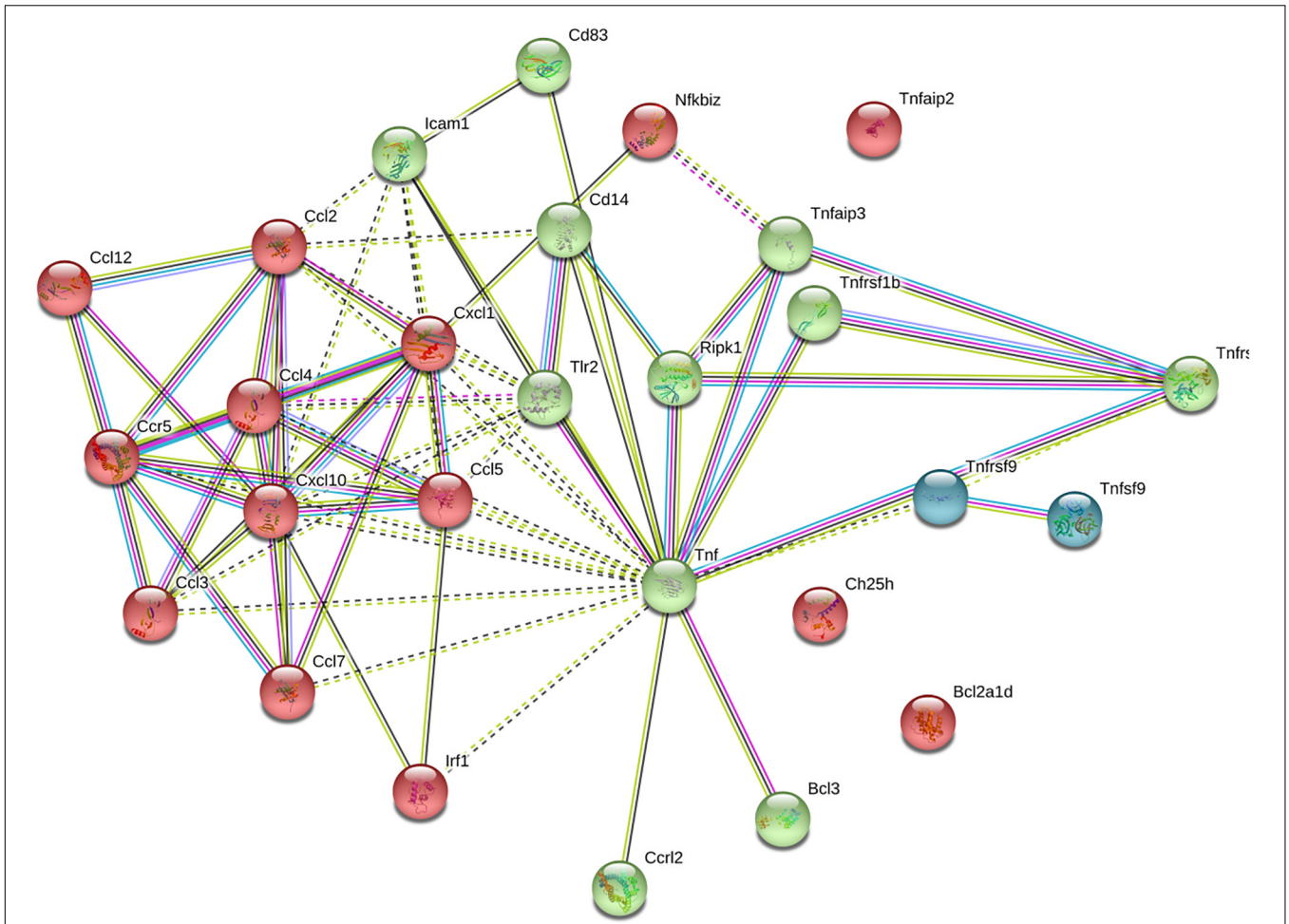

FIGURE 8 | Protein–protein interaction networks of differentially expressed genes upon hyaluronidase treatment. Using STRING database 25 genes were used to construct the PPI network. PPI, protein–protein interactions. Colors of nodes indicate result of clustering. Nodes represent proteins, edges represent protein–protein associations. Dotted lines indicate insignificant link, solid lines indicate significant interactio, pink lines indicate experimentally determined interaction, blue lines from curated database, black lines indicate co-expression, yellow lines indicate text mining, and gray lines indicate protein homology.

TNF and activating CREB1 expression (Bose and Cho, 2013; Cekanaviciute and Buckwalter, 2016). Activation of CREB and glial-mediated production of TNF-α may led to enhancing the release of glutamate. Imbalance of glutamate production can cause excitotoxicity and seizures (Li and Ransohoff, 2008; Vezzani et al., 2016). These findings coincide with the opinion that at least 40% of all epilepsies have structural or metabolic causes as a consequence of diverse brain injuries and the most common risk is inflammation during infections and sterile inflammation during stroke and autoimmune encephalitis (Vezzani et al., 2016).

However, animals in the Hyal group didn't show any differences in locomotor activity and anxiety level. This finding correlates with the previously made by Hosseini et al. (2018) where the overexpression of inflammatory factors didn't affect the activity of animals in open field test, although the chronic inflammation can lead to a memory loss (Zhou et al., 2016). In contrast, we demonstrate that hyaluronidase-treated animals showed elicited ability for learning. At the time point of 48 h after surgery, 90% of animals in Hyal group learnt aversive stimuli versus 60% of animals in Vehicle group. The percentage of animals that learnt the task 72 h after surgery was 100 and 70, respectively, although Mann–Whitney test revealed the significant difference in delta time only at the 72 h time point. According to transcriptome analysis, this memory improvement might be due to an activation of *BCL3* and *IRF1* genes directly interacting with CREB, which is tightly connected with long-term potentiation and memory (Silva et al., 1998). Facilitation of working memory can also be explained by the fact that ECM modification leads to the formation of a new structural and functional connections between neurons, changes the ratio of inhibitory and excitatory neurons leading to changes of plasticity (Morellini et al., 2010). It had also been shown that some matrix proteins have a particular importance for the behavior, spatial, and contextual memory. For example, decreased expression of reelin is a common characteristic among neurological and mental

FIGURE 9 | Significantly enriched pathways of significant genes in response to hyaluronan digestion. Green bars represent number of downregulated genes, red bars represent number of upregulated genes, gray bars represent no change of expression, orange curve with dots represent ($-\log_{10}$ (*P* value) – FDR), numbers in right border reflect number of genes including in canonical pathway.

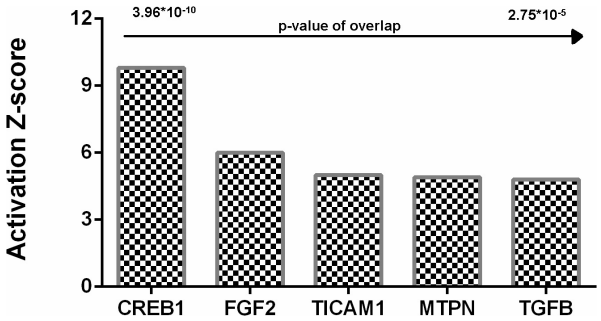

FIGURE 10 | Upstream regulators identified by Ingenuity Pathway analysis for hyaluronidase dependent treatment. Positive activation *Z*-score (>2) indicates activation of these upstream regulators. CREB1, cAMP response element-binding protein; FGF2, fibroblast growth factor 2; TICAM1, TIR domain-containing adaptor molecule 1; MTPN, myotrophin; TGFB, Transforming growth factor beta.

disorders such as autism, schizophrenia, depression and bipolar disorder (Ferrer-Ferrer and Dityatev, 2018), and knock-out mice lacking aggrecan demonstrated improvement in memory in spontaneous object recognition test (Rowlands et al., 2018).

There are pathways activated after several types of cerebral insults, which are associated with epileptogenesis or epilepsy progression such as Janus Kinase/Signal Transducer and Activator of Transcription (JAK/STAT) and mammalian Target of Rapamycin Complex (mTORC) (Klein et al., 2018). These signaling pathways mediate cellular physiological mechanisms that are critical for memory formation, long-term depression (LTD) and long-term potentiation (LTP). The JAK/STAT pathway is activated after many types of epileptogenic injuries in experimental models, including TBI, SE and stroke (Satriotomo et al., 2006; Lund et al., 2008; Zhao et al., 2011). It regulates expression of genes critical for multiple essential functions including cell proliferation, differentiation, neurogenesis, learning and memory. We found the elevation in *NFKBIZ*, *IRF1*, and *BCL3* genes, which tightly interact with members of the JAK/STAT pathway. Structural or dysplastic lesions associated with infantile spasms in rodents or humans also demonstrate overactivation of the mTORC1 pathway in the epileptogenic area (Galanopoulou et al., 2012). We found an upregulation of TNF, which is involved in this pathway and TLR2, TNFAIP3, and CD14, which directly interact with other members of mTORC1 signaling pathways.

Brain tumors are the other pathological process that can cause seizures. One of the factors which contribute to peritumoral seizures is glioma-released glutamate, which presumably acts through chronic overactivation of neuronal glutamate receptors enhancing the excitatory drive in the cortex (Buckingham et al., 2011; Yuen et al., 2012). A recent study demonstrates that seizures can appear as a result of the loss of fast-spiking interneurons concomitant with a significantly reduced firing rate of those that remain due to the degradation of PNNs that surround fast-spiking interneurons, resulting in alterations of its membrane capacities (Tewari et al., 2018). It also should be noted that treatment with a GM6001, a broad-spectrum inhibitor of MMPs, leads to retention of the PNN's structure and, most importantly, membrane properties of FSNs in GM6001-treated mice were essentially identical to the control group. The alteration of membrane capacities may also contribute to epileptogenesis after hyaluronidase injections.

There is an idea that seizures appearing in mice with ECM deficiency are linked with the reduction of ECS (Arranz et al., 2014). However, our immunohistochemical

analysis didn't reveal any significant differences in ECS area and in average neuronal body area at all time points, which means that seizures appeared after digestion of HA during postnatal stages were not a result of changes in osmotic parameters of cell environment.

Brain ECM is known to play a pivotal role in the functioning of the nervous system, especially during ontogenesis, but some of mechanisms by which it regulates neuronal activity are still hidden from the scientist's eye. Therefore, our study provides new insight into the mechanisms of epilepsy development in early postnatal period, showing the role of hyaluronic acid in the stabilization of morphology and neural network activity. These mechanisms can become potential targets for the correction of seizures during early postnatal development. Proteomic analysis is needed to reveal the precise mechanism of epileptogenesis in neonatal animals after ECM digestion. It also remains unknown how long the hyperexcitable state of the brain is preserved after hyaluronan digestion.

DATA AVAILABILITY STATEMENT

The datasets generated for this study are available on request to the corresponding author.

ETHICS STATEMENT

The animal study was reviewed and approved by the Ethical Committee on Animal Health and Care of N. I. Lobachevsky State University of Nizhny Novgorod and Privolzhsky Research Medical University, Nizhny Novgorod.

AUTHOR CONTRIBUTIONS

IM initiated the study. AB, VP, and MG generated a detailed plan of the experiments and supervised the research. AB, OZ, NT, and AM performed the behavioral and immunocytochemistry experiments. VP, EG, LK, and MG performed the transcriptome analysis. AB, VP, MG, and IM analyzed the data and wrote the first draft. All authors edited the manuscript.

FUNDING

The reported study was funded by RFBR (research project No. 18-44-520016) and the state project "Provision of scientific research" (No. 6.6379.2017/8.9).

REFERENCES

Arisi, G. M., Foresti, M. L., Katki, K., and Shapiro, L. A. (2015). Increased CCL2, CCL3, CCL5, and IL-1β cytokine concentration in piriform cortex, hippocampus, and neocortex after pilocarpine-induced seizures. *J. Neuroinflamm.* 12:129. doi: 10.1186/s12974-015-0347-z

Arranz, A. M., Perkins, K. L., Irie, F., Lewis, D. P., Hrabe, J., Xiao, F., et al. (2014). Hyaluronan deficiency due to Has3 knock-out causes altered neuronal activity and seizures via reduction in brain extracellular space. *J. Neurosci.* 34, 6164–6176. doi: 10.1523/JNEUROSCI.3458-13.2014

Bose, S., and Cho, J. (2013). Role of chemokine CCL2 and its receptor CCR2 in neurodegenerative diseases. *Arch. Pharm. Res.* 36, 1039–1050. doi: 10.1007/s12272-013-0161-z

Buckingham, S. C., Campbell, S. L., Haas, B. R., Montana, V., Robel, S., Ogunrinu, T., et al. (2011). Glutamate release by primary brain tumors induces epileptic activity. *Nat. Med.* 17, 1269–1274. doi: 10.1038/nm.2453

Cekanaviciute, E., and Buckwalter, M. S. (2016). Astrocytes: integrative regulators of neuroinflammation in stroke and other neurological diseases. *Neurotherapeutics* 13, 685–701. doi: 10.1007/s13311-016-0477-8

Cerri, C., Genovesi, S., Allegra, M., Pistillo, F., Püntener, U., Guglielmotti, A., et al. (2016). The chemokine CCL2 mediates the seizure-enhancing effects of systemic inflammation. *J. Neurosci.* 36, 3777–3788. doi: 10.1523/JNEUROSCI.0451-15.2016

Dityatev, A., Irintchev, A., Morellini, F., and Schachner, M. (2009). "Extracellular matrix molecules: synaptic plasticity and learning," in *The Encyclopedia of Neuroscience*, ed. L. R. Squire (Cambridge, MA: Academic Press), 149–156. doi: 10.1016/b978-008045046-9.00793-2

Ferrer-Ferrer, M., and Dityatev, A. (2018). Shaping synapses by the neural extracellular matrix. *Front. Neuroanat.* 12:40. doi: 10.3389/fnana.2018.00040

Galanopoulou, A. S., Gorter, J. A., and Cepeda, C. (2012). Finding a better drug for epilepsy: the mTOR pathway as an antiepileptogenic target. *Epilepsia* 53, 1119–1130. doi: 10.1111/j.1528-1167.2012.03506.x

George, N., and Geller, H. M. (2018). Extracellular matrix and traumatic brain injury. *J. Neurosci. Res.* 96, 573–588. doi: 10.1002/jnr.24151

Hosseini, S., Wilk, E., Michaelsen-Preusse, K., Gerhauser, I., Baumgärtner, W., Geffers, R., et al. (2018). Long-term neuroinflammation induced by influenza A virus infection and the impact on hippocampal neuron morphology and function. *J Neurosci.* 38, 3060–3080. doi: 10.1523/JNEUROSCI.1740-17.2018

Jiang, D., Liang, J., and Noble, P. W. (2011). Hyaluronan as an immune regulator in human diseases. *Physiol. Rev.* 91, 221–264. doi: 10.1152/physrev.00052.2009

Kim, H., Choi, Y., Joung, H.-Y., Choi, Y. S., Kim, H. J., Joo, Y., et al. (2017). Structural and functional alterations at pre-epileptic stage are closely associated with epileptogenesis in pilocarpine-induced epilepsy model. *Exp. Neurobiol.* 26, 287–294. doi: 10.5607/en.2017.26.5.287

Klein, P., Dingledine, R., Aronica, E., Bernard, C., Blümcke, I., Boison, D., et al. (2018). Commonalities in epileptogenic processes from different acute brain insults: do they translate? *Epilepsia* 59, 37–66. doi: 10.1111/epi.13965

Li, M., and Ransohoff, R. M. (2008). Multiple roles of chemokine CXCL12 in the central nervous system: a migration from immunology to neurobiology. *Prog. Neurobiol.* 84, 116–131. doi: 10.1016/j.pneurobio.2007.11.003

Lowenstein, D. H. (2009). Epilepsy after head injury: an overview. *Epilepsia* 50, 4–9. doi: 10.1111/j.1528-1167.2008.02004.x

Lund, I. V., Hu, Y., Raol, Y. H., Benham, R. S., Faris, R., Russek, S. J., et al. (2008). BDNF selectively regulates GABAA receptor transcription by activation of the JAK/STAT pathway. *Sci. Signal.* 1:ra9. doi: 10.1126/scisignal.1162396

McRae, P. A., Baranov, E., Rogers, S. L., and Porter, B. E. (2012). Persistent decrease in multiple components of the perineuronal net following status epilepticus. *Eur. J. Neurosci.* 36, 3471–3482. doi: 10.1111/j.1460-9568.2012.08268.x

Morellini, F., Sivukhina, E., Stoenica, L., Oulianova, E., Bukalo, O., Jakovcevski, I., et al. (2010). Improved reversal learning and working memory and enhanced reactivity to novelty in mice with enhanced GABAergic innervation in the dentate gyrus. *Cereb. Cortex* 20, 2712–2727. doi: 10.1093/cercor/bhq017

Perkins, K. L., Arranz, A. M., Yamaguchi, Y., and Hrabetova, S. (2017). Brain extracellular space, hyaluronan, and the prevention of epileptic seizures. *Rev. Neurosci.* 28, 869–892. doi: 10.1515/revneuro-2017-0017

Rowlands, D., Lensjø, K. K., Dinh, T., Yang, S., Andrews, M. R., Hafting, T., et al. (2018). Aggrecan directs extracellular matrix-mediated neuronal plasticity. *J. Neurosci.* 38, 10102–10113. doi: 10.1523/JNEUROSCI.1122-18.2018

Satriotomo, I., Bowen, K. K., and Vemuganti, R. (2006). JAK2 and STAT3 activation contributes to neuronal damage following transient focal cerebral ischemia. *J. Neurochem.* 98, 1353–1368. doi: 10.1111/j.1471-4159.2006.04051.x

Sherman, L., Matsumoto, S., Weiping, S., Srivastava, T., and Back, S. (2015). Hyaluronan synthesis, catabolism, and signaling in neurodegenerative diseases. *Int. J. Cell Biol.* 2015:368584. doi: 10.1155/2015/368584

Silva, A. J., Kogan, J. H., Frankland, P. W., and Kida, S. (1998). CREB and memory. *Annu. Rev. Neurosci.* 21, 127–148. doi: 10.1146/annurev.neuro.21.1.127

Song, I., and Dityatev, A. (2018). Crosstalk between glia, extracellular matrix and neurons. *Brain Res. Bull.* 136, 101–108. doi: 10.1016/j.brainresbull.2017.03.003

Szklarczyk, D., Franceschini, A., Wyder, S., Forslund, K., Heller, D., Huerta-Cepas, J., et al. (2014). STRING v10: protein–protein interaction networks, integrated over the tree of life. *Nucleic Acids Res.* 43, D447–D452. doi: 10.1093/nar/gku1003

Tewari, B. P., Chaunsali, L., Campbell, S. L., Patel, D. C., Goode, A. E., and Sontheimer, H. (2018). Perineuronal nets decrease membrane capacitance of peritumoral fast spiking interneurons in a model of epilepsy. *Nat. Commun.* 9:4724. doi: 10.1038/s41467-018-07113-0

Tian, D. S., Peng, J., Murugan, M., Feng, L. J., Liu, J. L., Eyo, U. B., et al. (2017). Chemokine CCL2–CCR2 signaling induces neuronal cell death via STAT3 activation and IL-1β production after status epilepticus. *J. Neurosci.* 37, 7878–7892. doi: 10.1523/JNEUROSCI.0315-17.2017

Ueno, H., Suemitsu, S., Murakami, S., Kitamura, N., Wani, K., Matsumoto, Y., et al. (2019). Layer-specific expression of extracellular matrix molecules in the mouse somatosensory and piriform cortices. *IBRO Rep.* 6, 1–17. doi: 10.1016/j.ibror.2018.11.006

Vedunova, M., Sakharnova, T., Mitroshina, E., Perminova, M., Pimashkin, A., Zakharov, Y., et al. (2013). Seizure-like activity in hyaluronidase-treated dissociated hippocampal cultures. *Front. Cell. Neurosci.* 7:149. doi: 10.3389/fncel.2013.00149

Vezzani, A., Fujinami, R. S., White, H. S., Preux, P. M., Blümcke, I., Sander, J. W., et al. (2016). Infections, inflammation and epilepsy. *Acta Neuropathol.* 131, 211–234. doi: 10.1007/s00401-015-1481-5

Younus, I., and Reddy, D. S. (2017). Epigenetic interventions for epileptogenesis: a new frontier for curing epilepsy. *Pharmacol. Ther.* 177, 108–122. doi: 10.1016/j.pharmthera.2017.03.002

Yu, J., Gu, X., and Yi, S. (2016). Ingenuity pathway analysis of gene expression profiles in distal nerve stump following nerve injury: insights into wallerian degeneration. *Front. Cell Neurosci.* 10:274. doi: 10.3389/fncel.2016.00274

Yuen, T. I., Morokoff, A. P., Bjorksten, A., D'Abaco, G., Paradiso, L., Finch, S., et al. (2012). Glutamate is associated with a higher risk of seizures in patients with gliomas. *Neurology.* 79, 883–889. doi: 10.1212/WNL.0b013e318266fa89

Zhao, J. B., Zhang, Y., Li, G. Z., Su, X. F., and Hang, C. H. (2011). Activation of JAK2/STAT pathway in cerebral cortex after experimental traumatic brain injury of rats. *Neurosci. Lett.* 498, 147–152. doi: 10.1016/j.neulet.2011.05.001

Zhou, M., Greenhill, S., Huang, S., Silva, T. K., Sano, Y., Wu, S., et al. (2016). CCR5 is a suppressor for cortical plasticity and hippocampal learning and memory. *eLife* 5:e20985. doi: 10.7554/eLife.20985

Conflict of Interest: The authors declare that the research was conducted in the absence of any commercial or financial relationships that could be construed as a potential conflict of interest.

Copyright © 2019 Balashova, Pershin, Zaborskaya, Tkachenko, Mironov, Guryev, Kurbatov, Gainullin and Mukhina. This is an open-access article distributed under the terms of the Creative Commons Attribution License (CC BY). The use, distribution or reproduction in other forums is permitted, provided the original author(s) and the copyright owner(s) are credited and that the original publication in this journal is cited, in accordance with accepted academic practice. No use, distribution or reproduction is permitted which does not comply with these terms.

frontiers in Neuroscience

ORIGINAL RESEARCH
published: 04 October 2019
doi: 10.3389/fnins.2019.01055

Visualization and Quantification of Post-stroke Neural Connectivity and Neuroinflammation Using Serial Two-Photon Tomography in the Whole Mouse Brain

Katherine Poinsatte[1†], Dene Betz[1†], Vanessa O. Torres[1†], Apoorva D. Ajay[1], Shazia Mirza[1], Uma M. Selvaraj[1], Erik J. Plautz[1], Xiangmei Kong[1], Sankalp Gokhale[1], Julian P. Meeks[1,2], Denise M. O. Ramirez[1], Mark P. Goldberg[1†] and Ann M. Stowe[1,3*†]*

[1] Department of Neurology and Neurotherapeutics, UT Southwestern Medical Center, Peter O'Donnell Jr. Brain Institute, Dallas, TX, United States, [2] Department of Neuroscience, UT Southwestern Medical Center, Dallas, TX, United States, [3] Department of Neurology, University of Kentucky, Lexington, KY, United States

Whole-brain volumetric microscopy techniques such as serial two-photon tomography (STPT) can provide detailed information on the roles of neuroinflammation and neuroplasticity throughout the whole brain post-stroke. STPT automatically generates high-resolution images of coronal sections of the entire mouse brain that can be readily visualized in three dimensions. We developed a pipeline for whole brain image analysis that includes supervised machine learning (pixel-wise random forest models via the "ilastik" software package) followed by registration to a standardized 3-D atlas of the adult mouse brain (Common Coordinate Framework v3.0; Allen Institute for Brain Science). These procedures allow the detection of cellular fluorescent signals throughout the brain in an unbiased manner. To illustrate our imaging techniques and automated image quantification, we examined long-term post-stroke motor circuit connectivity in mice that received a motor cortex photothrombotic stroke. Two weeks post-stroke, mice received intramuscular injections of pseudorabies virus (PRV-152), a trans-synaptic retrograde herpes virus driving expression of green fluorescent protein (GFP), into the affected contralesional forelimb to label neurons in descending tracts to the forelimb musculature. Mice were sacrificed 3 weeks post-stroke. We also quantified sub-acute neuroinflammation in the post-stroke brain in a separate cohort of mice following a 60 min transient middle cerebral artery occlusion (tMCAo). Naive e450^{+}-labeled splenic CD8^{+} cytotoxic T cells were intravenously injected at 7, 24, 48, and 72 h post-tMCAo. Mice were sacrificed 4 days after stroke. Detailed quantification of post-stroke neural connectivity and neuroinflammation indicates a role for remote brain regions in stroke pathology and recovery. The workflow described herein, incorporating STPT and automated quantification of fluorescently labeled features of interest, provides a framework by which one can objectively evaluate labeled neuronal or

OPEN ACCESS

Edited by:
Paulo Henrique Rosado-de-Castro, D'Or Institute for Research and Education (IDOR), Brazil

Reviewed by:
Hong-bing Xiang, Huazhong University of Science and Technology, China
Pavel Osten, Cold Spring Harbor Laboratory, United States

***Correspondence:**
Mark P. Goldberg
mark.goldberg@utsouthwestern.edu
Ann M. Stowe
ann.stowe@uky.edu

[†]These authors have contributed equally to this work

Specialty section:
This article was submitted to Brain Imaging Methods, a section of the journal Frontiers in Neuroscience

Received: *15 May 2019*
Accepted: *19 September 2019*
Published: *04 October 2019*

Citation:
Poinsatte K, Betz D, Torres VO, Ajay AD, Mirza S, Selvaraj UM, Plautz EJ, Kong X, Gokhale S, Meeks JP, Ramirez DMO, Goldberg MP and Stowe AM (2019) Visualization and Quantification of Post-stroke Neural Connectivity and Neuroinflammation Using Serial Two-Photon Tomography in the Whole Mouse Brain. Front. Neurosci. 13:1055. doi: 10.3389/fnins.2019.01055

lymphocyte populations in healthy and injured brains. The results provide region-specific quantification of neural connectivity and neuroinflammation, which could be a critical tool for investigating mechanisms of not only stroke recovery, but also a wide variety of brain injuries or diseases.

Keywords: stroke, serial two-photon tomography, whole brain imaging, neural connectivity, neuroinflammation, CD8 T cells, pseudorabies virus, corticospinal tract

INTRODUCTION

In the United States, nearly 800,000 people have a stroke annually, making it the 5th leading cause of death and the leading cause of adult disability (Benjamin et al., 2018). More than half of all stroke survivors experience persistent motor deficits that impair daily function, underscoring the significant need for a better understanding of the mechanisms of injury and repair after stroke (Dobkin, 2005). Spontaneous recovery of function is associated with a higher capacity for neuroplasticity in homologous brain regions after stroke (Brown et al., 2009). These regions, which are both remote and adjacent to the infarcted tissue, undergo changes in order to assume the functions of the lost neuronal networks (Furlan et al., 1996). Preclinical models of stroke have been instrumental in understanding the complexity of post-stroke responses and how they relate to functional recovery (Nudo, 2007). Using these models, plasticity which underlies circuit remodeling has been repeatedly shown to be correlated with improved recovery from stroke (Jones and Adkins, 2015). These forms of circuit plasticity involve recruitment of homologous neuronal pathways, inhibition of aberrant electrical signaling, and formation of new connections through synaptogenesis and axonal sprouting throughout the brain and spinal cord (Murphy and Corbett, 2009). However, in some cases, post-stroke neuroplasticity can impede recovery. The degree of functional recovery is heavily dependent on the regions in which the plasticity occurs (Dancause et al., 2005; Kim et al., 2005), emphasizing the need for pre-clinical studies that investigate changes in axonal connectivity in the whole brain after stroke.

In addition to alterations in brain architecture after stroke, the immune system plays a major role in post-stroke pathology and recovery. In particular, the critical role of the immune system in both the acute and chronic phases of post-stroke recovery is becoming increasingly apparent (Jin et al., 2013). Within hours of the onset of injury, damage-associated molecular patterns (DAMPS) are released from dying neurons, astrocytes, and endothelial cells, recruiting immune cells to the brain (Rubartelli and Lotze, 2007). Blood-brain barrier (BBB) disruption, upregulation of cell adhesion molecules, and activation of resident microglia enhance the post-stroke neuro-immune interactions (Abulrob et al., 2008; Patel et al., 2013). Within 24 h of stroke onset, adaptive immune cells, including T cells, can be detected in the ipsilesional hemisphere (Gelderblom et al., 2009). Migration of these cells peaks around 3–4 days post-stroke, but helper $CD4^+$ and cytotoxic $CD8^+$ T cells persist in the perilesional tissue for weeks after injury, implicating this leukocyte subset in long-term recovery (Xie et al., 2018). Many of these studies rely on flow cytometry, a technique that requires the dissociation of brain tissue, and therefore the loss of information of spatial dynamics of leukocyte diapedesis. Even research using spatially-sensitive techniques like immunohistochemistry often overlook the possibility of recruitment of immune cells into remote brain areas. Given that leukocytes modulate axonal growth after injury through the secretion of cytokines and growth factors (Wang et al., 2018), it is possible that migration of immune cells, such as $CD8^+$ T cells, to remote brain regions could affect post-stroke plasticity far from the stroke lesion. This highlights the need to understand where neuroplasticity and neuroinflammation occur in the brain after stroke, and if the two phenomena are interconnected. To visualize post-stroke responses that directly involve neuroplasticity or occur on the larger scale, systematic analysis of the entire brain must be incorporated into preclinical studies of stroke recovery.

Advances in the field of functional imaging have greatly enhanced the ability to study global post-stroke alterations in brain connectivity (Bauer et al., 2014). However, few studies currently exist which incorporate the use of high resolution, whole brain volumetric microscopy techniques to assess changes in brain architecture in the context of stroke (Lugo-Hernandez et al., 2017). In the current study, we used serial two-photon tomography (STPT) (Ragan et al., 2012; Oh et al., 2014; Amato et al., 2016; Kim et al., 2016; Whitesell et al., 2018; Ramirez et al., 2019), a block-face automated imaging technique, to acquire volumetric image datasets comprising entire mouse brains. A custom-developed image analysis pipeline incorporating supervised machine learning (ML)-based methods to isolate relevant fluorescent signals of interest and registration of the images into the Allen Institute Common Coordinate Framework version 3.0 (CCF 3.0) was then employed to quantify stroke-induced neural connectivity and neuroinflammation throughout the mouse brain. We found robust changes in connectivity in the corticospinal tract, as well as $CD8^+$ T cell migration into motor and somatosensory brain regions affected by stroke. Taken together, our results indicate that mesoscale whole-brain imaging reveals important information about region-specific changes in both neural connectivity and neuroinflammation that may be key to developing long-term therapies to promote functional recovery after stroke.

METHODS

Animal Approval

Experiments involving corticospinal tract tracing with PRV-152 used 8–11-week old adult, male C57BL/6 (wild type; WT) mice from Jackson Laboratories. For neuroinflammation experiments involving $CD8^+$ T cells, 10–15-week-old male WT mice were

randomized for the isolation of donor $CD8^+$ T cells or to receive the donor T cells following stroke. Animals were housed in a 12 h light/dark cycle with access to food and water *ad libitum*. All protocols were approved by the University of Texas Southwestern Medical Center Institutional Animal Care and Use Committee.

Photothrombotic (PT) Stroke

Cortical stroke was induced using the photothrombotic stroke model previously described (Yanev et al., 2019). Mice ($n = 6$) were anesthetized using 1–4% isoflurane, 0.7% nitric oxide, and 0.3% oxygen and temperature and breathing rates were monitored. Mice were placed on a stereotaxic frame and an incision was made down the midline of the scalp. Mice were administered 1.5 mg of Rose Bengal (Sigma Aldrich, St. Louis, MO, USA) dissolved in 0.3 cc of saline via intraperitoneal injection. One minute later, we aimed a 45 mW laser (Coherent Sapphire, Santa Clara, CA, USA; 561 nm; 2.7 mm collimated beam diameter) 1.7 mm lateral to Bregma as the forelimb representation of the motor cortex for 15 min. Buprenorphine was administered post-operation for pain management, and moist food was provided for the first 24 h following stroke. All mice that received a PT stroke had a successful surgery.

Transient Middle Cerebral Artery Occlusion (tMCAo)

Mice ($n = 7$) were anesthetized (2% isoflurane/ 70% NO_2/30% O_2) and their body temperatures were maintained at 37°C while the left middle cerebral artery (MCA) was exposed for transcranial Laser Doppler flowmetry (TSI, Inc.) as previously described (Monson et al., 2014; Ortega et al., 2015). A blunted suture (6.0-gauge nylon, 12 mm) was advanced to block the MCA (>80% reduction relative to baseline blood flow) by surgeons blinded to condition, between 8 and 14:00 h. Animals were placed in an incubator (34°C), re-anesthetized after 60 min, and suture withdrawn. Flowmetry confirmed reperfusion (CBF > 50% baseline) and animals were monitored. All animals met blood flow criteria and were included in analysis.

Intramuscular Injections of Pseudorabies Virus (PRV)

An incision was made on ulnar border of forelimb on anesthetized mice using a standard scalpel (Liu et al., 2009). After the forelimb flexor muscle was identified, mice were given an intramuscular injection using a 27 G needle and 10 μL syringe of PRV-152, a generous gift from Dr. Lynn Enquist (Princeton University, Princeton, NJ), a trans-synaptic pseudorabies virus expressing green fluorescent protein (GFP). PRV-152 injections were divided into multiple injections of 2 μL of virus in multiple locations in the forelimb flexor muscle (Ganzer et al., 2018). All standard viral handling precautions were followed during this procedure. Animals recovered in a standard recovery chamber. A single administration (0.2 ml) of subcutaneous buprenorphine (0.05 mg/kg) and lidocaine was given immediately after the procedure for pain relief. Mice that were injected with PRV that received a stroke had a 50% morality rate (3/6 mice) while mice that received a sham surgery all survived (6/6 mice) to the 6-day sacrifice time point.

Sample Preparation for Imaging on TissueCyte 1000

All mice were transcardially perfused with 1X Phosphate Buffered Saline (PBS) followed by 4% paraformaldehyde (PFA) to fix brain tissues. Extracted tissues were further post-fixed in 4% PFA at 4°C for 24 h and transferred to 0.01% NaN_3 in 1X PBS for storage at 4°C until embedding. 4.5% (w/v) agarose (Type 1A, low EEO, Sigma #A0169) solution in 50 mM phosphate buffer was first prepared and oxidized by adding 10 mM $NaIO_4$ (Sigma #S1878) while stirring gently for 2 to 3 h in the dark. The agarose solution was filtered with vacuum suction and washed 3 times with 50 mM phosphate buffer. The washed agarose was resuspended in the appropriate volume of phosphate buffer to make a 4.5% agarose solution. The oxidized agarose solution was heated to boiling in a microwave, then transferred to a stirring plate and allowed to cool to 60–65°C. Brains were embedded by filling a cryoembedding mold (VWR #15560-215) with oxidized agarose, placing the filled mold on a flat frozen ice pack, and then quickly submerging the brain using forceps into the bottom of the block with the cerebellum touching the bottom of the block (olfactory bulbs facing upward). The agarose block was allowed to fully solidify on a frozen ice pack in the dark. Once the agarose blocks were fully hardened, the agarose blocks including the specimens were removed from the molds and placed in small glass jars, where they were treated overnight at 4°C in the dark in sodium borohydride buffer (50 mM sodium borohydride, 50 mM borax, 50 mM boric acid, pH 9.0–9.5). After overnight crosslinking, the agarose blocks were transferred to phosphate buffer for storage at 4°C until TissueCyte imaging.

Serial Two-Photon Tomography

The agarose blocks containing the brain samples were attached to a custom magnetic slide with superglue and placed on a magnetized stage within an imaging chamber filled with phosphate buffer. STPT imaging is a block-face imaging technique in which a series of 2-dimensional (2-D) mosaic images in the coronal plane is acquired just below the cut surface of the brain (within ∼100 μm), followed by physical sectioning with a built-in vibrating microtome to cut away the imaged tissue, preparing a new cut surface for imaging (Ragan et al., 2012). For this study, three optical planes were imaged at 25, 50, and 75 μm below the cut surface, followed by a vibrating microtome cut at 75 μm (blade vibration frequency of 70 Hz, advancement velocity 0.5 mm/s). The excitation laser (MaiTai DeepSee, SpectraPhysics/Newport, Santa Clara, CA) wavelength was tuned to either 920 nm to excite GFP (PRV experiments) or 850 nm to excite e450 ($CD8^+$ T cell experiments). Three image channels of emission fluorescence (pre-set bandpass filters encompassing red, green, and blue fluorophores) were collected with a predetermined photomultiplier tube voltage of 700 V. This process produced 190 physical sections and 570 2-D stitched coronal section images (9 by 13 mosaic collected for each coronal section) with a lateral resolution of 0.875 μm/pixel and axial resolution of 25 μm (∼280 gigabytes of raw data per brain). The

raw image tiles were first trimmed and subjected to flat field correction, then stitched into 2-D mosaic coronal section images using the Autostitcher software (TissueVision, Inc.).

Image Analysis Pipeline

We used an automated pipeline (as described in Ramirez et al., 2019) to analyze and extract quantitative results from raw STPT-generated data. The image analysis pipeline is depicted in **Figure 1** and consists of three main components: image registration, pixel classification and numerical quantification. The red channel 2-D stitched images are used to register the dataset into the Allen Institute Common Coordinate Framework (CCF 3.0) using SimpleElastix (an extension of SimpleITK that combines elastix and transformix) (Lowekamp et al., 2015). A multi-step registration process was chosen using rigid, affine, and b-spline registration components. At each step, optimization was performed on a 6-resolution multi-grid (pyramid) schedule, with Mattes Mutual Information as the optimization metric. To balance local/global optimization across the whole dataset, the "Random Coordinate" Image Sampler was used with sample regions of $2 \times 2 \times 4$ mm. Final b-spline grid dimensions were $0.5 \times 0.5 \times 0.5$ mm. The optimized registration parameters identified for the red channel images were then applied to the other raw image channels and ilastik probability maps using transformix.

Relevant signals of interest were identified in the images using the "Pixel Classification" plugin for the Interactive Learning and Segmentation Toolkit (ilastik), which implements a random forest supervised machine learning (ML) classifier (Somner et al., 2011). To support the supervised ilastik training, a maximum intensity projection (MIP) was first created for each physical section from its three optical planes and the resultant MIP image was downsampled to a pixel size of $1.5\,\mu m \times 1.5\,\mu m$ in the x-y dimension. This resulted in a set of 16-bit 3-color compressed

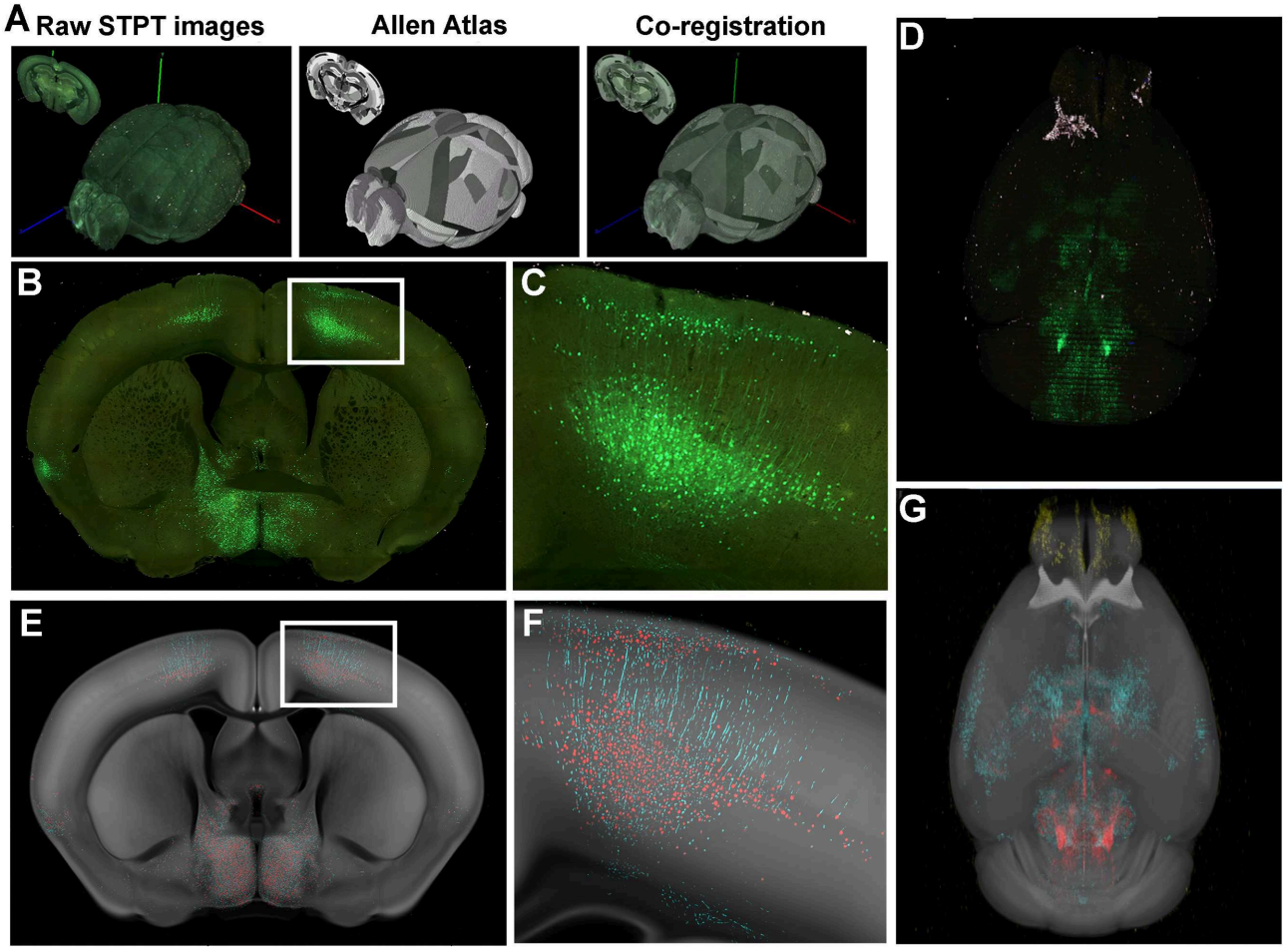

FIGURE 1 | Serial two-photon tomography of the whole mouse brain. **(A)** Overview of serial two-photo tomography (STPT) data acquisition and registration. **(B)** Representative coronal section raw fluorescence image, with **(C)** expansion of areas identified in white box in B showing GFP+ neuronal cell bodies and processes. **(D)** Coronal images are stacked into a 3D representation and co-registered to the Common Coordinate Framework (CCF 3.0; Allen Institute for Brain Science) Atlas. **(E)** Probability map output of the same section shown in **(B)** depicting pixels classified via machine learning (ML) as either GFP+ cell bodies (red) or GFP+ neuronal processes (cyan) overlaid onto the corresponding section from the atlas (CCF 3.0 average template) shown in gray. **(F)** Enlarged image of boxed area in **(E)** showing fine detail and accurate classification of neuronal cell bodies and processes corresponding to the raw fluorescence image shown in **(C)**. **(G)** 3-D rendering of the probability maps corresponding to the raw fluorescence images of the brain shown in D. GFP^+ cell bodies, red, GFP^+ neuronal processes, cyan, atlas images, gray.

TIFF images with the same number of images as physical sections in the STPT image (190). At least three representative sections containing examples of fluorescent signals of interest (e.g., GFP^- expressing neurons or e450-labeled T cells) were selected from each sample. The random forest ML model was trained on these selected sections by assigning labels including as fluorescent cell bodies, tissue autofluorescence, stroke, and other features (e.g., microbubbles surrounding the olfactory bulbs). After completing the initial training, each of the sample images was iteratively updated until visible misclassifications were minimized. Each cohort of brains (PRV injected or T cell injected) was used to train an independent model for classification, and every section from every brain in the cohort was subjected to the same model. Ilastik predictions were exported as an 8-bit "probability map" TIFF for each trained label, with the pixel value of 0 mapping to 0% probability and 255 100% probability of a pixel belonging to the label. The resulting TIFF stacks were warped to the CCF 3.0 using the transformation parameters identified by elastix via transformix. The summed intensity of all voxels lying within CCF 3.0 annotated regions were quantified using custom MATLAB software, producing a matrix of signal intensity for each sample, label, and brain region.

Image Analysis Validation

To assess the performance of the ilastik-based image analysis pipeline, three independent observers (i.e., different than the individual that trained the ilastik model) selected at least 8 random 1-megapixel subregions from at least two brains from each experimental condition (8 brains total, 4 from $CD8^+$ T cell cohort, 4 from PRV −152 cohort) for manual annotation of critical labels (e.g., fluorescent cell bodies, stroke). Each observer utilized Adobe Photoshop tools to create binary masks for each test label, as well as autofluorescence and black background labels. These observer-generated binary masks were considered the reference set, with the ilastik probability maps as the test set. Custom MATLAB software was used to compare each reference image to the corresponding test image while varying the segmentation thresholds in the test image (i.e., to convert the 8-bit range of the probability map to a complementary binary map). From these comparisons the true positive, false negative, false positive, and false negative rates were calculated for each threshold. These values were calculated on a voxel basis to match the values quantified in these studies. For the critical test labels (fluorescent cell bodies and stroke) the ilastik model achieved very low false positive rates even when a segmentation threshold at 5% of the 8-bit range ($CD8^+$ T cell bodies: 0.008 ± 0.001%; PRV GFP^+ cell bodies: 2.0 ± 0.5%; stroke: 0.10 ± 0.03%; $n = 8$ subregions each from 2, 4, and 4 brains, respectively). In control samples for the $CD8^+$ T cell experiments (samples lacking labeled T cells), observers noted rare blue spots in the tissue that roughly resembled the small T cell bodies and annotated them. The false positive rate for T cell-negative samples was even lower than for the labeled T cell samples (0.0006 ± 0.0003%, 8 subregions from 2 brains). True positive rates at these thresholds were not saturated ($CD8^+$ T cell bodies: 57.0 ± 4.8%; PRV GFP^+ cell bodies: 84.6 ± 4.4%; stroke: 48.2 ± 0.5%; 2, 4, and 2 brains, respectively). F1 score (scale 0 to 1 with 1 being best performance), a common measurement of model accuracy, indicated strong performance for PRV GFP^+ cell bodies and adequate performance for $CD8^+$ T cell bodies and stroke voxels ($CD8^+$ T cell bodies: 0.72 ± 0.13; PRV GFP^+ cell bodies 0.90 ± 0.03; stroke 0.73 ± 0.04; $n = 2$, 4, and 2 brains, respectively). The Matthews Correlation Coefficient, an alternative metric (ranging from −1, worse than chance, to 0 for chance, to 1 for optimal), showed similar results to the F1 score ($CD8^+$ T cell bodies: 0.63 ± 0.04; PRV GFP^+ cell bodies: 0.84 ± 0.4; stroke 0.64 ± 0.4, $n = 2$, 4, and 2 brains, respectively).

These validation studies indicate that the ilastik model was conservative (prioritized low false positive rates at the expense of true positives) for the labels quantified in these studies.

In order to further validate the ilastik STPT quantification, we manually counted cell bodies in the primary motor cortex (MOp), primary somatosensory cortex (SSp), and supplemental motor cortex (MOs) in both the right and left hemispheres in STPT sections. We counted cells within a range of 71 coronal slices. The initial slice was identified by the morphology of the hippocampus, size of lateral ventricles, and the presence of the fasiculus retroflexus. The final slice in the range was determined from the size of the olfactory bulb. The images used for manual quantification were identical to those used for automated quantification. We classified a cell as a circular object with GFP signal that was clearly distinguishable from the background. Manual quantification of neuronal processes was not performed.

$CD8^+$ T Cell Isolation, Labeling, and Intravenous Injections

Using magnetic CD8 T cell isolation kits (STEMCELL Cat. 19853), donor CD8 T cells were isolated from the spleens of naïve, adult donor WT mice ($n = 8$). A small aliquot of cells was assessed before and after enrichment by flow cytometry to ensure purity of the isolated CD8 T cells. CD8 T cells were then labeled with a fluorescent proliferation dye according to manufacturer's protocol (e450; eBioscience 65-0842-85) and resuspended in 1XPBS immediately prior to injection. On average, $\sim 3.2 \times 10^6$ $CD8^+$ T cells were intravenous injected into the tail veins of WT recipient mice. Brains were extracted and further post-fixed overnight in 4% PFA at 4°C, transferred to 1X PBS + 0.01% NaN_3 and stored at 4°C until embedding. Peripheral migration of T cells into secondary lymphoid organs (i.e., spleen and cervical lymph nodes) was confirmed using flow cytometry. Briefly, single cell suspensions were generated from secondary lymphoid organs, and 1×10^6 cells were used for the fluorescent antibody staining to specific leukocyte (CD45-APC-Cy7) and T cell (TCRβ-711, CD4-PE/Dazzle 594, CD8-APC) markers for 30 min. at 4°C and subsequently washed and fixed in 1% paraformaldehyde. Flow cytometric data were acquired using a BD LSRFortessa using FACS Diva 6.0 software and FlowJo 9.0 software was used to subset leukocytes according to gating strategy shown in **Supplementary Figure 1**.

Statistics

Statistical differences were analyzed using unpaired parametric two-sample Student's *t*-test, ratio paired student's *t*-test, two-way

repeated measures ANOVA where appropriate and indicated in the text (Graph Pad Prism 6.0). Manual cell counts and ML probability values were correlated using a linear regression analysis (Graph Pad Prism 6.0). Values of $p < 0.05$ were considered significant. All experimenters were blinded to condition, and all animal were randomly assigned to group.

RESULTS

Whole Brain Visualization of Post-stroke Neural Connectivity

Previous studies utilizing traditional and viral retrograde tracers demonstrated robust descending connections from the brain to the skeletal muscle (Kerman et al., 2003, 2006; Lee et al., 2007). Furthermore, many studies demonstrate that stroke induces widespread changes in neuronal connectivity. Much attention has been given to remodeling of the corticospinal and corticorubral tracts (Ishida et al., 2016; Okabe et al., 2017), including increased corticospinal innervation of the stroke-impaired forelimb from the uninjured contralesional motor cortex (Bachmann et al., 2014). One recent study showed that connectivity in the brainstem also undergoes dynamic changes after a photothrombotic (PT) stroke in the primary motor cortex, highlighting the importance of global interrogation of circuitry (Bachmann et al., 2014). Imaging techniques, such as *in vivo* magnetic resonance imaging (MRI), can be used in mice to quantify whole-brain changes in connectivity after stroke (Dijkhuizen et al., 2012; Bauer et al., 2014). However, such techniques do not offer sufficient resolution to visualize cell bodies or axonal processes. Microscopy methods such as STPT can visualize and quantify these fine details, making these techniques vital in developing an understanding of connectivity on a mesoscale.

To demonstrate how STPT can be used to elucidate post-stroke changes in neural connectivity, 8–11-week-old C57/B6 mice received either a PT focal stroke in the right primary motor cortex (MOp) or a sham surgery. Two weeks later, mice received an intramuscular left forelimb injection of pseudorabies virus (PRV-152) carrying GFP, an effective trans-synaptic retrograde tracer that labels motor tracks which project to distal musculature (Kerman et al., 2003) Following STPT processing of the brains, the resultant images were analyzed using the custom-developed automated pipeline (**Figure 1A**). During the process of training the ML-based pixel classification algorithm, the random forest classifier was trained to recognize multiple structures of interest including cell bodies, neuronal processes, and areas of infarction. **Figure 1** shows raw STPT data of GFP^+ cell bodies and processes (**Figures 1B–D**), as well as the probability maps generated from the STPT data for automated identification of cell bodies and processes in the healthy mouse brain (**Figures 1E–G**). We also generated 3-D videos of these data from an uninjured brain, with fly-through and rotational videos of raw STPT data (**Supplementary Videos 1, 2**), as well as fly-through and rotation videos of corresponding probability maps (**Supplementary Videos 3, 4**).

The probability maps of these cortical regions show that neuronal cell bodies and their processes in both the left and right motor and somatosensory cortices (SS) of uninjured animals have been accurately identified by the trained ML algorithm, with more cells in the right cortex compared to the left (**Figures 2A–D**). In addition to the cell bodies and processes of layer 5 neurons, second-order neurons in layer 2 and 3 of the motor cortex and axons passing in the corpus callosum were also visible in labeled data set. The probability maps clearly demonstrate the widespread robust viral labeling, indicating a large number of descending connections to the left forelimb from the predicted motor cortex regions, as well as remote regions in the midbrain and brainstem. In mice that received a stroke, the ML algorithm detected some cells in the contralesional left motor cortex, albeit fewer than observed in uninjured animals (**Figures 2E–H**). ML classified bright autofluorescent signal in the ipsilesional right motor cortex as infarcted tissue (**Figure 2G**). While the ML algorithm did not classify all pixels within the lesion as infarcted tissue, it still offered excellent spatial resolution of most of the lesioned tissue and provided detailed visualization of where the PT stroke was induced in the brain (**Figure 2H**). The 3-D videos of stroke-injured brains clearly identify the PT stroke in both the fly-through and rotational videos of raw STPT data (**Supplementary Videos 5, 6**), as well as fly-through and rotation videos of corresponding probability maps (**Supplementary Videos 7, 8**).

In uninjured mice, nearly all cortical sensory and motor areas were labeled in the right hemisphere. Cortical sensory and motor areas had many GFP^+ cell bodies and processes and therefore, a robust fluorescent signal in these areas in the absence of injury. The highest fluorescent signal was observed in the layer 5 neurons in the right primary motor cortex (MOp5) and in neurons in the primary somatosensory area associated with the lower limb (SSp-ll), an area adjacent to the primary motor cortex (**Figure 2C**). Fewer PRV^+ cells were detected in left MOp5 neurons and SSp-ll neurons in these uninjured animals, suggesting that there was greater innervation of the left forelimb flexor from the right cortical motor regions in the absence of stroke (**Figures 2I,J**). After stroke, we observed that there were fewer GFP^+ MOp5 neurons in the right (i.e., lesioned) motor cortex, decreasing the fluorescent signal in this region and indicating a disruption in the corticospinal tract due to injury. Uninjured animals had significantly higher fluorescent signal in the right MOp (80,536 pixels/mm^3) compared to the left MOp (33,519 pixels/mm^3; $p < 0.001$; **Figure 2I**). After stroke, there was a dramatic decrease in the fluorescence intensity in the right ipsilesional MOp (to 665,2 pixels/mm^3) compared to the right MOp of mice that received a sham surgery ($p < 0.0001$), indicating the expected loss of descending connections from the MOp to the forelimb after ischemic injury.

Previous studies found that contralesional plasticity, as detected by injections of PRV into the forelimb flexor, was associated with improved functional recovery after stroke (Liu et al., 2009). Therefore, we hypothesized that we would observe contralesional plasticity after stroke and predicted that after a focal ischemic injury, descending connections from the left contralesional MOp to the affected forelimb would increase in mice that received a stroke compared to uninjured mice. However, we did not observe any significant differences in the fluorescent signal of neuronal cell bodies compared to our control

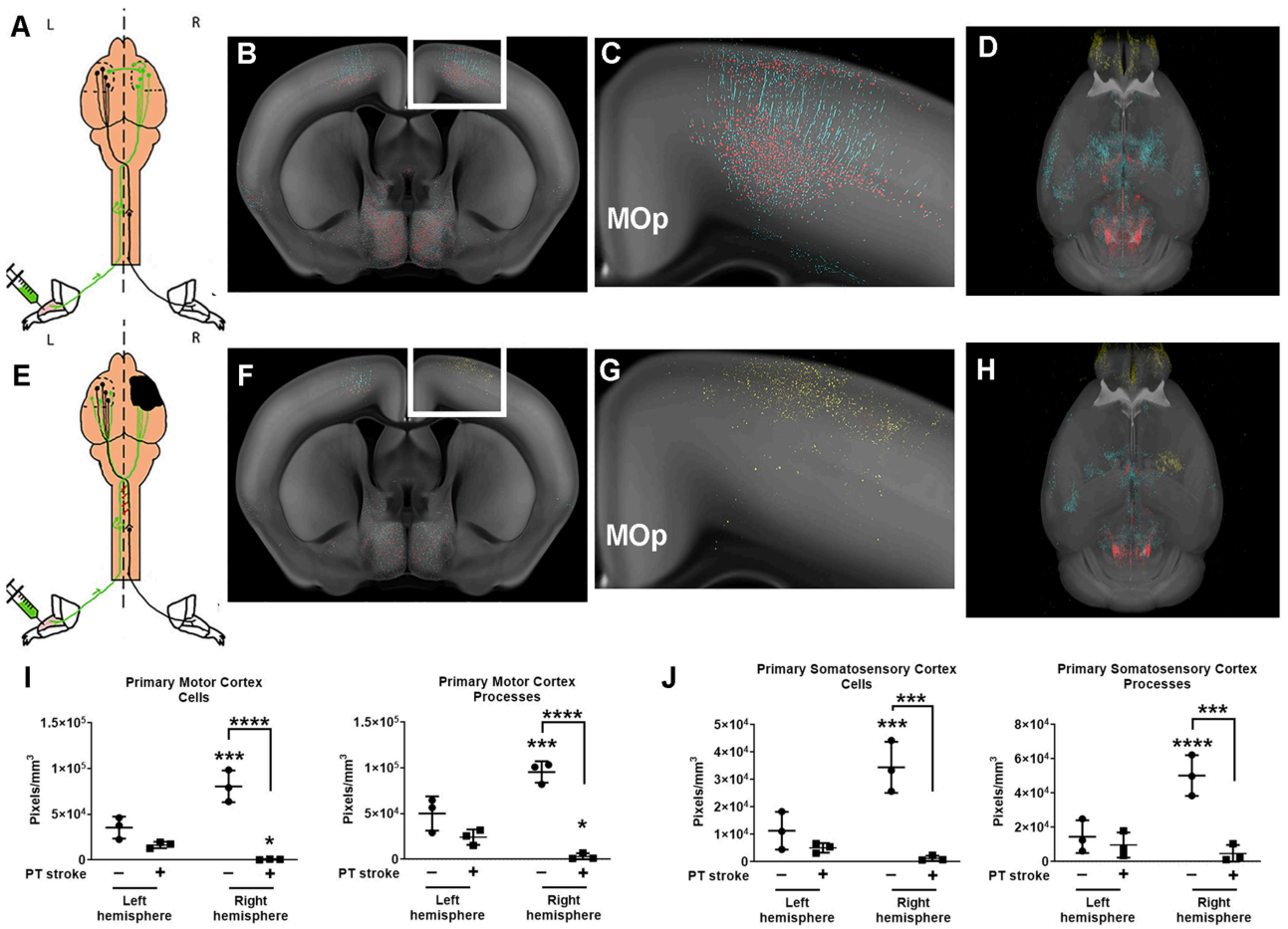

FIGURE 2 | Quantification of changes in forelimb innervation after stroke. **(A)** Schematic of pseudorabies virus (PRV) injection in healthy mice, with **(B)** corresponding coronal section of the probability maps from a representative animal overlaid onto the CCF 3.0 average template (gray) at the level of the primary motor cortex (MOp) **(C)** Enlargement of white boxed area shown in **(B)** depicts pixels classified as cell bodies (red) and neuronal processes (cyan). **(D)** 3-D rendering of the whole brain probability map (images from this animal also shown in **Figure 1**) **(E)** Schematic of PRV injections after stroke (black area, right hemisphere). **(F)** Corresponding coronal section of the probability maps from a representative post-stroke animal overlaid onto the CCF 3.0 average template (gray) at the level of the primary motor cortex. **(G)** Enlargement of white boxed area shown in **(F)** depicts pixels predominantly classified as infarction (yellow) in the right hemisphere. **(H)** 3-D probability map shows area of infarction in the right hemisphere. **(I,J)** Quantification of cell bodies and processes in **(I)** primary motor cortex (MOp) and **(J)** primary somatosensory cortex (SSp) for both left and right hemispheres of uninjured (circles) and post-stroke (square) cohorts. Data shown are pixels/mm^3 for each area. $^*p < 0.05$, $^{***}p < 0.001$, $^{****}p < 0.0001$ vs. left hemisphere unless otherwise indicated by brackets.

cohort ($p = 0.1$). Analysis with two-way ANOVA determined there was a significant effect of both group (stroke vs. no stroke; $p < 0.01$) and hemisphere (right vs. left; $p < 0.01$) on post-stroke neural connectivity in the MOp. Furthermore, there was a significant interaction between group and hemisphere on fluorescence intensity per mm^3 in the MOp ($p < 0.001$).

Because neuroplasticity has also been shown in regions neighboring the ischemic lesion, we quantified changes in fluorescence intensity in the primary somatosensory cortex (SSp) (Bachmann et al., 2014). Similar to the MOp, there was a higher density of fluorescent pixels in the right SSp compared to the left SSp of uninjured mice ($p < 0.001$). Stroke diminished the fluorescent signal in the right SSp ($p < 0.001$). There was no significant difference between the left and right SSp in mice that received a stroke and no difference in fluorescence intensity in the left SSp of injured and uninjured mice.

We also quantified the fluorescent signal in neuronal processes (e.g., axons, dendrites). While the fluorescent signal in virally labeled cell bodies was brighter than that of neuronal processes, as expected, there was still robust labeling of the proximal axons and dendrites in the left and right hemisphere of mice with and without strokes. These data complement the findings observed when quantifying GFP$^+$ cell bodies, showing fluorescent processes in the same regions in which we found cells (i.e., MOp5, SSp-ll). There was unilateral cortical labeling in primary motor and sensory areas, particularly in the MOp5 and SSp-ll, in uninjured mice. Fluorescent processes, predominantly apical dendrites, were identified in both the left (50,099 pixels/mm^3) and right (95,526 pixels/mm^3) hemisphere with significantly more labeling in the right hemisphere (**Figure 2J**; $p < 0.001$). In the stroke cohort, there was sparse labeling of axons in any primary motor or sensory areas, with the

exception of one mouse that showed faint axonal labeling in the left contralesional MOp5 and SSp-II regions (right MOp−3,094 pixels/mm^3). Additionally, there was moderate fluorescent signal in bilateral mid- and hindbrain nuclei in both healthy and injured mice, supporting our findings of robust labeling of neuronal cell bodies in these brain areas.

We also trained our model to identify tissue regions affected by ischemic injury. The PT model produces a small permanent focal lesion in the primary motor cortex. Fluorescent signal corresponding to damaged tissue was identified in the 3 mice that received PT strokes (**Figure 2G**, **Supplementary Videos 7, 8**). All 3 mice that received a stroke exhibited autofluorescent tissue in the MOp, our target region. Damage, albeit to a lesser extent, was also observed in the SSP-ll, a region immediately adjacent to the MOp. The control cohort of mice did not exhibit any fluorescent signal indicative of ischemic tissue in their cortical sensory and motor regions. These data confirm successful induction of stroke in the primary sensory and motor cortices.

In addition to detailed, region-specific visualization of connectivity in the post-stroke brain, our methodology is also able to provide global quantification of alterations in brain architecture after injury. We generated heat maps that visually represent which brain regions contain pixels classified as one of our fluorescent signals of interest, which allowed us to compare probability values between brain regions, between animals, and between the stroke and no stroke cohorts. We selected 52 brain regions to analyze, particularly focusing on regions that were associated with motor or sensory function and/or undergo dynamic changes after stroke (Bachmann et al., 2014). We also selected "control" regions that we predicted would not innervate the forelimb [e.g., hippocampal formation (HPF), olfactory areas (OLF)]. There were high fluorescent signals in many brain regions, albeit with moderate variability between mice. Fluorescence labeling from cell bodies (**Figure 3**) and neuronal processes (**Supplementary Figure 1**) was higher in the mice that did not receive a stroke. The most robust labeling for the cell bodies and neuronal processes was observed in the midbrain and hindbrain, and this labeling was largely bilateral. The brain regions with the most consistently high fluorescent signal appeared to be the medulla, behavioral state related (MY-sat) and the magnocellular reticular nucleus (MARN), a medullary motor-related nuclei, in both the uninjured (left) and injured (right) hemispheres.

Comparison of Automated and Manual Counting

In order to confirm that our ML algorithm had correctly classified pixels as neuronal cell bodies, we manually counted cell bodies in 70 coronal sections in one uninjured mouse (# 439, **Figure 3**). Several cortical regions were quantified: SSp, MOp, and supplemental motor cortex (MOs; **Figure 4A**). Our ML algorithm identified higher fluorescent signal in the right hemisphere of all regions examined, with the highest probability of classification in the MOp5 (**Figure 4B**). Manual counting confirmed that there was a greater number of GFP$^+$ cell bodies in each of these ipsilesional right brain areas (**Figure 4C**). The largest number of cells was located in the right MOp, followed by the SSp, and lastly, the MOs (**Figure 4D**). Similar distributions of cells were observed in the left hemisphere, albeit with fewer cell bodies labeled (**Figure 4E**). There was a significant correlation between the normalized probability values obtained from our ML algorithm and our manual counting ($R^2 = 0.77$; $p < 0.05$; **Figure 4F**). These data support the classification accuracy of the ML algorithm and registration to regions of interest.

Whole Brain Visualization of Post-stroke Neuroinflammation

In addition to neural connectivity, we were also interested in whether STPT and our automated imaged analysis pipeline could quantify immune cell diapedesis after stroke. We focused on the migration patterns of cytotoxic CD8$^+$ T cells within the brain. Early studies confirm migration of CD8$^+$ T cells into the brain (Gelderblom et al., 2009), but with little to no examination of specific brain regions targeted by these cells outside of the area of injury. In order to examine this phenomenon, 13–15-week-old WT mice were given a left transient middle cerebral artery occlusion (tMCAo) and were randomly assigned to experimental groups that would either receive serial intravenous (i.v.) tail injections of either PBS or e450$^+$-labeled CD8$^+$ T cells. We confirmed the presence of viable e450$^+$-labeled cells in the both spleens and cervical lymph nodes of recipient mice (**Supplementary Figure 2**). Flow cytometry confirmed the purity of e450$^+$-labeled cells, as these cells were primarily CD8$^+$ T cells that were present only in the CD8$^+$ T cell recipient group shown both by percentage (**Supplemental Figures 2B,C**) and absolute cell number (**Supplemental Figures 2D,E**), but not the PBS controls.

We trained the ML algorithm to identify e450$^+$ fluorescent cells in representative sections throughout the whole brain, and observed CD8$^+$ T cells within the brain tissue, traveling through blood vessels, and interestingly, along the meninges (**Supplementary Videos 9, 10**). CD8$^+$ T cell diapedesis occurred throughout the brain, including ipsilesional somatosensory cortices (SS; **Figures 5A–C**) and sensory-related midbrain regions (MBsen; **Figures 5D–F**). 3-D renderings of our probability maps and associated videos were generated, demonstrating the bilateral movement of cells throughout the whole brain. After applying the ML algorithm to the entire cohort, a heat map was generated with 41 brain regions that were pre-selected as regions of interest for immune cell diapedesis (**Figure 6**). Similar to the heat maps in the neural connectivity studies (**Figure 3**), these heat maps allow for the comparison of the fluorescence intensity of e450$^+$-labeled CD8$^+$ T cells across multiple brain regions, between groups and animals. As expected, the PBS group showed low fluorescent signal in many of the brain regions, although "background" fluorescence was detected, potentially due to increased autofluorescence in dead or injured ischemic tissue secondary to the tMCAo model. Additionally, some variability was observed in the amount of CD8$^+$ diapedesis between animals of the T cell-recipient group, with high diapedesis into two brain regions in particular, the behavioral state-related midbrain (MBsta) and sensory

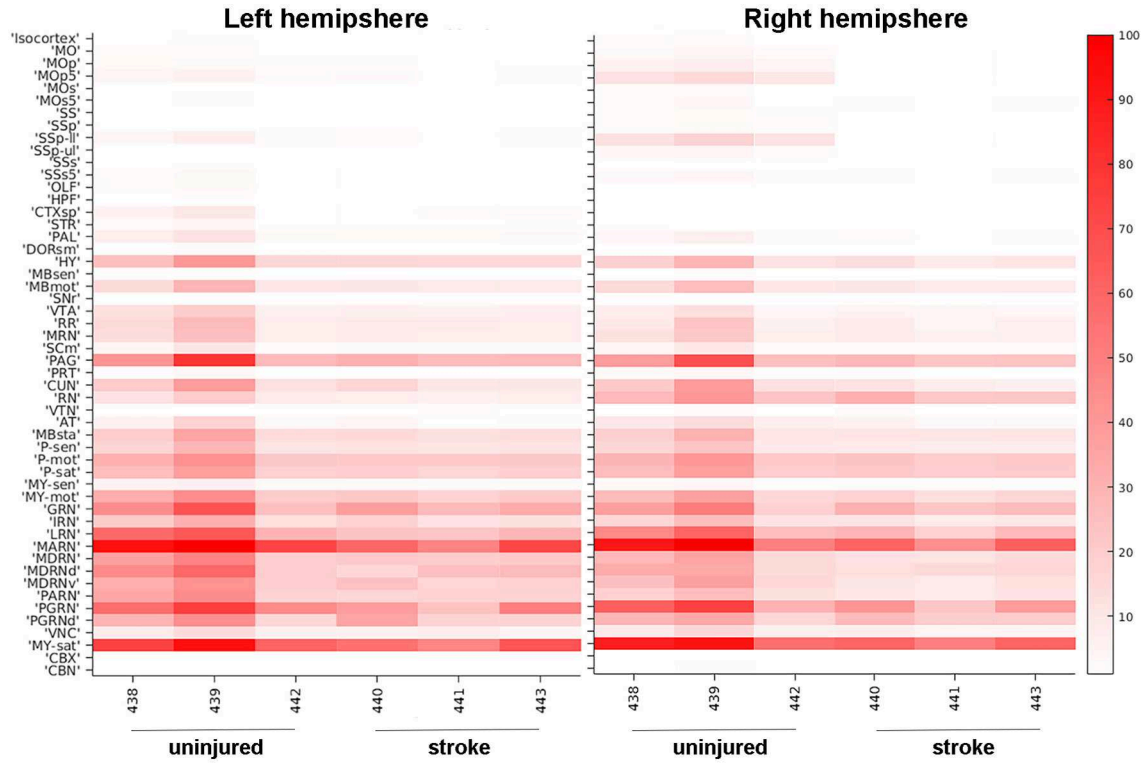

FIGURE 3 | Heat map of neuronal cell body quantification in cortical and other areas. The signal intensities for pixels classified via machine learning as neuronal cell bodies in various cortical areas are shown for uninjured and stroke animals in both left hemisphere (left panel) and right hemisphere (right panel). Each brain area analyzed is listed on the left Y-axis according to the nomenclature used in the CCFv3.0 and individual animals (#, x-axis) are grouped by uninjured and stroke-injured cohorts. The intensity scale is shown on the right Y-axis and corresponds to the number of pixels classified as neuronal cell bodies normalized per region volume (pixels/mm^3). MO, somatomotor areas; MOp, primary motor cortex; MOp5, primary motor cortex, Layer 5; MOs, supplemental motor cortex; MOs5, supplemental motor cortex, Layer 5; SS, somatosensory areas; SSp, primary somatosensory cortex; SSp-ll, primary somatosensory cortex, lower limb; SSp-ul, primary somatosensory cortex, upper limb; SSs, supplemental somatosensory cortex; SSs5, supplemental somatosensory cortex, layer 5; OLF, olfactory areas; HPF, hippocampal formation; CTXsp, cortical subplate; STR, striatum; PAL, pallidum; DORsm, thalamus, sensory motor-related; HY, hypothalamus; MBsen, midbrain, sensory-related; MBmot, midbrain, motor-related; SNr, substantia nigra, reticular part; VTA, ventral tegmental area; RR, midbrain reticular nucleus, retrorubral area; MRN, midbrain reticular nucleus; SCm, superior colliculus, motor-related; PAG, periaqueductal gray; PRT, pretectal nucleus; CUN, cuneiform nucleus; RN, red nucleus; VTN, ventral tegmental nucleus; AT, anterior tegmental area; MBsta, midbrain, behavioral state-related; P-sen, pons, sensory-related; P-mot, pons, motor-related; P-sat, pons, behavioral state-related; MY-sen, medulla, sensory-related; MY-mot, medulla, motor-related; GRN, gigantocellular reticular nucleus; IRN, intermediate reticular nucleus; LRN, lateral reticular nucleus; MARN, magnocellular reticular nucleus; MDRN, medullary reticular nucleus; MDRNd, medullary reticular nucleus, dorsal part; MDRNv, medullary reticular nucleus, ventral part; PARN, parvicellular reticular nucleus; PGRN, paragigantocellular reticular nucleus; PGRNd, paragigantocellular reticular nucleus, dorsal part; VNC, vestibular nuclei; MY-sat, medulla, behavioral state-related; CBX, cerebellar cortex; CBN, cerebellar nuclei.

motor-related thalamus (DORsm). Our ML algorithm was not trained to detect ischemic tissue in these animals.

Overall, CD8$^+$ T cells migrated into many areas of the brain of all animals 4 days after stroke, with greater diapedesis apparent in the left injured hemisphere compared to the right uninjured hemisphere. CD8$^+$ T cells targeted the left ipsilesional SSp and secondary somatosensory cortex (SSs), with significantly more cells detected in the left SSp compared to PBS controls ($p < 0.05$; **Figure 5G**) and more cells in the left SSs ($p < 0.01$; **Figure 5H**). The left ipsilesional MOp was also infiltrated by CD8$^+$ T cells, with more cells in the ipsilesional MOp than the corresponding contralateral MOp ($p < 0.05$; **Figure 5J**). Given the nature of a tMCAo injury, which affects motor and sensory cortices, it is likely these cells were targeting regions damaged by the stroke. In addition to these cortical motor and sensory regions, there was bilateral movement of CD8$^+$ T cells into remote brain regions associated with motor and sensory function, namely the midbrain (**Figures 5D–F,I**) and the pons (**Figures 5K,L**). One region, corpus callosum (cc), exhibited higher contralesional CD8$^+$ T cell diapedesis compared to ipsilesional cc ($p < 0.05$; **Figure 5M**). CD8$^+$ T cells did not significantly infiltrate behavioral-state related regions in either the midbrain or the pons (data not shown) or the hippocampus (**Figure 5N**). Our data demonstrate that 4 days following tMCAo, CD8$^+$ T cells migrate into the brain, targeting both sensory- and motor-related regions of the cortex, midbrain, and pons. In some regions, such as the MBsen and P-sen, this movement is bilateral, with cells detected in both the ipsilesional and contralesional hemisphere relative to PBS controls. In other regions, including the SSp, there is preferential migration into the ipsilesional hemisphere compared to the corresponding contralesional brain regions in CD8$^+$ T cell recipients. Together, these results illustrate how STPT can

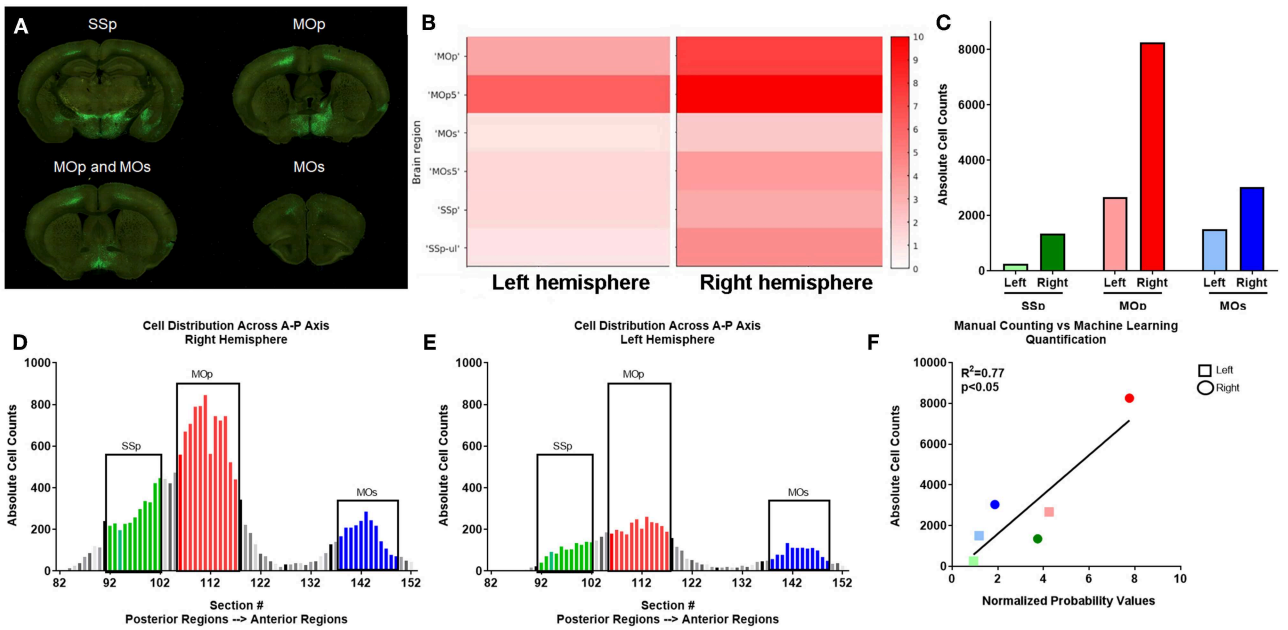

FIGURE 4 | Verification of automated quantification via manual counting. **(A)** PRV labeled neurons are identified by GFP expression in serial two-photon coronal section images, including primary somatosensory (SSp), primary motor (MOp), and supplemental motor (MOs) areas. **(B)** ML identified fluorescent intensity (right y axis in heat map) in the indicated subregions (noted in the left y axis) for left and right hemispheres corresponding to the coronal sections shown in **(A)** for this uninjured mouse. Heat map show visual depiction of the summed probabilities of pixels classified as neuronal cell bodies from the ML data set, with highest intensity shown as red. **(C)** Manual quantification of PRV+ cell bodies in each region. **(D,E)** Manual quantification of PRV+ cell bodies in all coronal sections with PRV+ cell bodies for a representative uninjured brain, shown in a posterior to anterior orientation (left to right on the graph) for SSp (green), MOp (red), and MOs (blue) regions in both the **(D)** right and **(E)** left hemispheres. **(F)** Linear regression analysis of ML data (x axis) and manual counts (y axis) demonstrate a correlation between the two data sets.

be utilized to quantify region-specific diapedesis of immune cells into the ischemic brain.

DISCUSSION

While much research has been performed on post-stroke neuroplasticity and neuroinflammation (Gelderblom et al., 2009; Bachmann et al., 2014), these studies have been limited by conventional imaging methods. STPT, a modern microscopy technique that produces large-scale, 3-D images of intact, uncleared brain tissue, is expanding the capacity to investigate brain-wide circuit mechanisms associated with brain injury, as well as models of neurological and psychiatric disorders. Our work establishes this technique as a reliable method to quantify whole brain neural connectivity and neuroinflammation after stroke to understand region-specific mechanisms of injury and repair. STPT provides many advantages over traditional slide-based methods of mesoscale brain imaging. While automated slide scanning instruments improved our ability to image large numbers of serial sections at high resolution, sectioning and mounting artifacts such as tissue folding and tearing are unavoidable using traditional sectioning methods. These artifacts lead to inaccurate 3-D reconstruction of the whole brain. Additionally, traditional sectioning studies are often limited in scope to discrete brain regions or small numbers of whole brains due to the amount of processing and imaging time needed. STPT, through its use of automated block face imaging and sectioning, overcomes these issues. Optical clearing has also become a popular method to develop 3-D models of neuronal circuits that allows one to acquire volumetric images of the whole brain without physical sectioning (Cai et al., 2019). STPT, however, uses standard perfusion fixed brains and as such avoids a potential pitfall of optical clearing: namely, morphological changes such as increases or decreases in organ size that may distort neuronal circuits in a non-uniform way and reduce the accuracy of brain wide circuit analyses. Despite these advantages, STPT is not without its limitations. One drawback of the method is that it requires tissue to have an inherent fluorescent signal. While this is compatible with viral tracers and fluorescently labeled cells as used in our study, as well as many strains of transgenic mice with expression of fluorescent reporter proteins, it does not allow for staining with traditional primary antibodies, an accessible and commonly used technique in most laboratories. Additionally, STPT is a time-consuming method for whole brain imaging. Data could be more quickly acquired using newer technologies such as high-throughput light tomography (HTLP) (Yang et al., 2018). Future studies should utilize HTLP and other volumetric imaging techniques to confirm our findings regarding changes in axonal connectivity and $CD8^+$ T cell diapedesis after stroke. Another issue to consider when using STPT or any volumetric imaging strategy is the effect of stroke on atlas registration. Missing tissue or swelling around the site of injury could lead to inappropriate designation of anatomical regions. This problem is

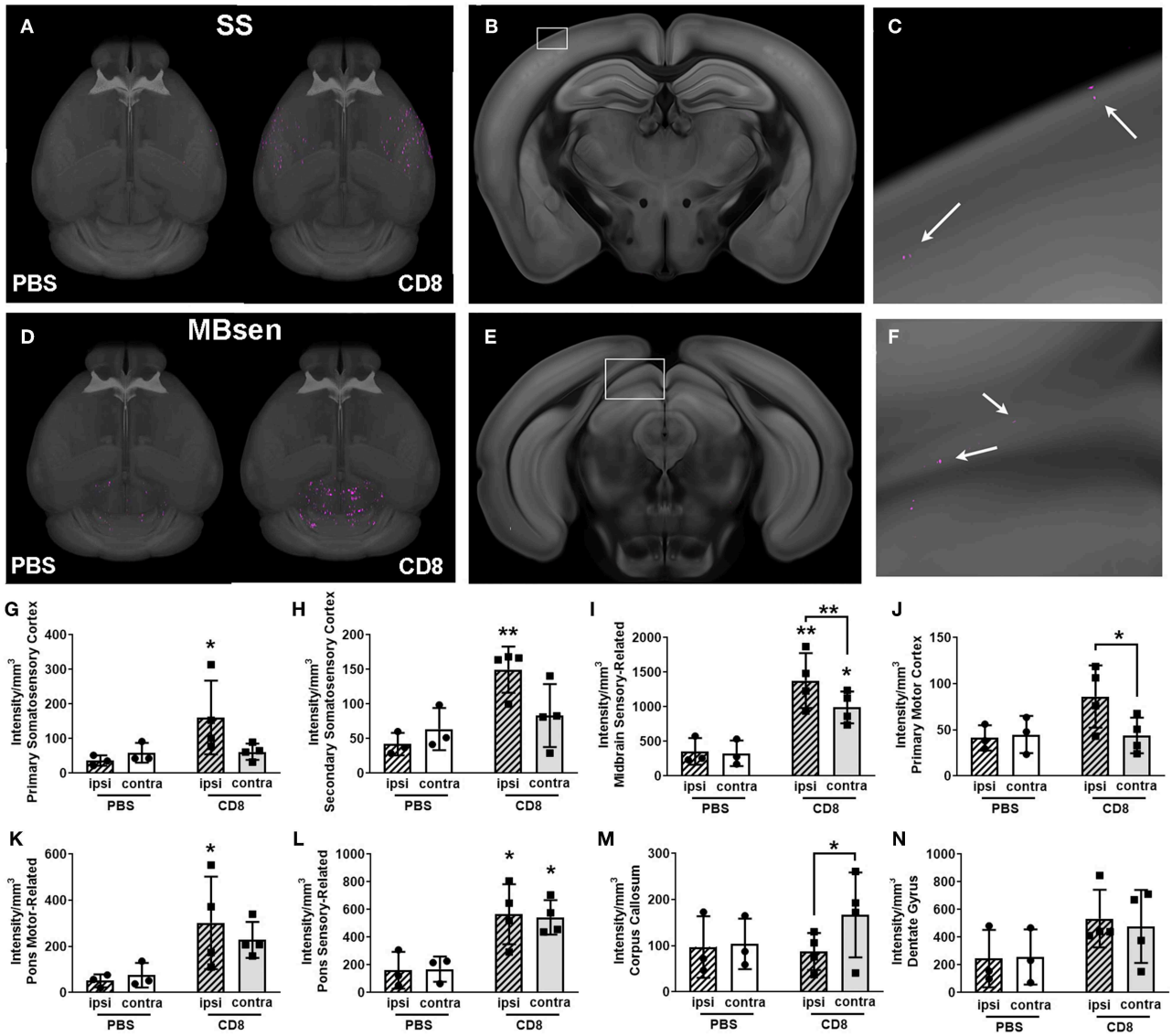

FIGURE 5 | Visualization of quantification of CD8$^+$ T cell diapedesis in the whole brain after stroke. **(A)** Masked 3-D probability map images of somatosensory areas only from a representative CD8$^+$-treated animal (right brain) overlaid onto the CCF 3.0 average template (gray) shows pixels classified as CD8$^+$ T cell (magenta) which have migrated into somatosensory areas (SS). Minimal magenta pixels are present in the PBS-treated brain (left) **(B)** Coronal section with white box highlighting part of the primary somatosensory area from the brain shown in A, with **(C)** enlargement of white boxed area showing several magenta areas classified as CD8$^+$ T cells (white arrows). **(D)** 3-D probability maps from the same brains as in **(A)** but masked to show pixels classified as CD8$^+$ T cells in the midbrain, sensory-related (MBsen) shows high CD8$^+$ T cell diapedesis (magenta) in both hemispheres, though PBS-treated mice (left brain) also have some background level of pixels classified as fluorescently labeled CD8$^+$ T cells. **(E)** Coronal section with white box highlighting MBsen from the brain shown in C, with **(F)** enlargement of white boxed area showing several magenta areas classified as CD8$^+$ T cells (white arrows). **(G–N)** Bar graph shows ipsilesional (hatched bars) and contralesional (plain bars) diapedesis into selected regions in CD8$^+$-treated mice (black squares, right columns) and PBS controls (black circles, left columns). Ipsilesional CD8$^+$ T cell diapedesis also occurs in **(G)** primary somatosensory cortex, **(H)** supplemental somatosensory, **(I)** MBsen, **(J)** primary motor cortex, and **(I)** motor-related pons. **(L)** Sensory-related pons exhibits bilateral diapedesis, while **(M)** the corpus callosum is predominantly contralesional. **(N)** There is no significant CD8$^+$ T cell diapedesis into the dentate gyrus. $^*p < 0.05$, $^{**}p < 0.01$ vs. PBS control unless otherwise indicated by brackets.

not limited to studies of stroke. Indeed, automated quantification of STPT or any type of volumetric images of mouse models of brain injury or neurodegeneration could be similarly impaired by improper tissue warping and atlas registration due to abnormal presentation of the brain tissue.

In this study, we used STPT to examine neural connectivity and neuroinflammation. In order to study of neural connectivity we utilized PRV-152, a viral retrograde tracer. Because PRV is a trans-synaptic virus, this method allows labeling from specific muscles, to spinal interneurons and motor neurons, and ultimately to motor projection neurons in the brainstem and cerebral cortex. However, because it is a trans-synaptic tracer, one downside to this method is that we cannot distinguish between first-, second-, and third-order

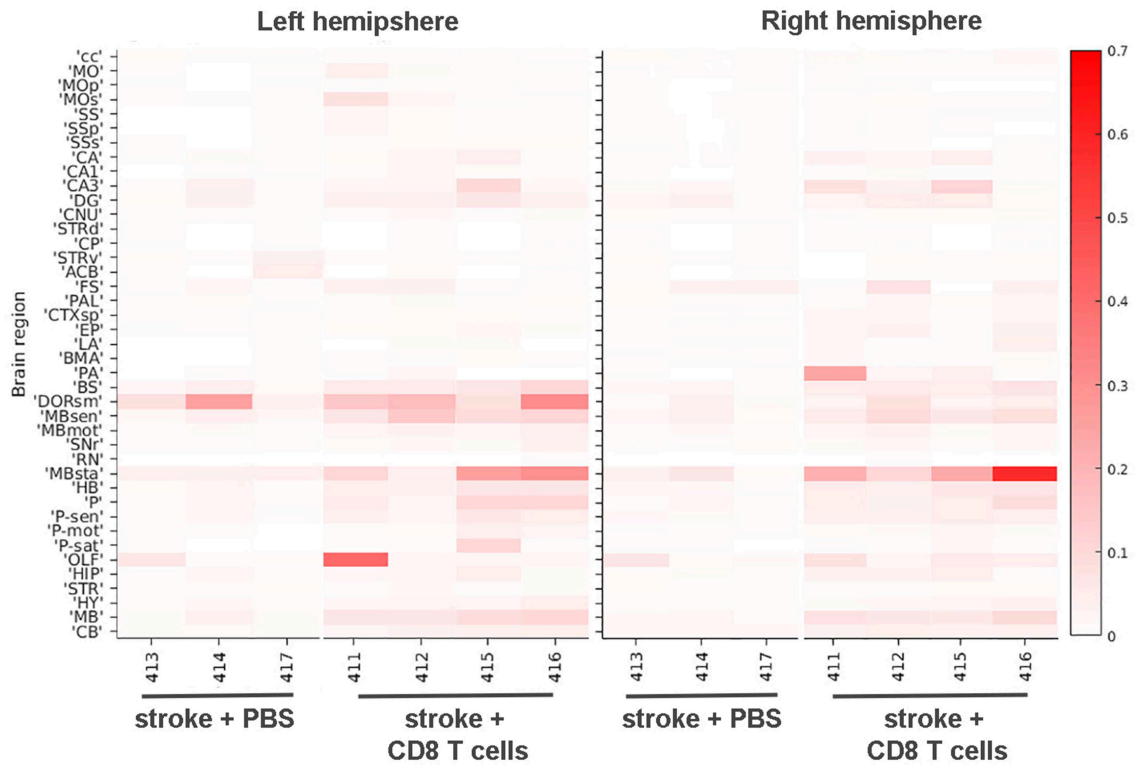

FIGURE 6 | Heat map of CD8$^+$ T cell diapedesis in cortical and other areas. The signal intensities for pixels classified via ML as e450-labeled CD8$^+$ T cells in various cortical and other brain areas are shown for stroke animals either injected with PBS or CD8$^+$ T cells in both left hemisphere (left panel) and right hemisphere (right panel). Each brain area analyzed is listed on the left Y-axis according to the nomenclature used in the CCF 3.0 and individual animals (#, x-axis) are grouped by PBS and T cell injected cohorts. The intensity scale is shown on the right Y-axis and corresponds to the number of pixels classified as CD8$^+$ T cells normalized per region volume (pixels/mm^3). cc, corpus callosum; MO, somatomotor areas; MOp, primary motor cortex; SS, somatosensory areas; SSp, primary somatosensory cortex; SSs, supplemental somatosensory cortex; CA, Ammon's horn, CA1, field CA1; CA3, field CA3; DG, dentate gyrus; CNU, cerebral nuclei; STRd, striatum, dorsal region; CP, caudate putamen; STRv, striatum, ventral region; ACB, nucleus accumbens; FS, fundus of the striatum; PAL, pallidum; CTXsp, cortical subplate; EP, endopiriform nucleus; LA, lateral amygdalar nucleus; BMA, basomedial amygdalar nucleus; PA, posterior amygdalar nucleus; BS, bed nuclei of stria terminalis; DORsm, thalamus, sensory motor-related; MBsen, midbrain, sensory-related; MBmot, midbrain, motor-related; SNr, substantia nigra, reticular part; RN, red nucleus; MBsta, midbrain, behavioral state-related; HB, hindbrain; P, pons; P-sen, pons, sensory-related; P-mot, pons, motor-related; P-sat, pons, behavioral state-related; OLF, olfactory areas; HIP, hippocampal region; STR, striatum, HY, hypothalamus, MB, midbrain, CB, cerebellum.

connections to the forelimb. New viral monosynaptic tracers, such as glycoprotein-deleted rabies virus, and traditional monosynaptic chemical tracers like FastBlue could allow us to look specifically at first-order connections, although this would require direct injections into spinal cord or brain. Furthermore, PRV is a lethal virus, inducing significant cell death and neuronal dysfunction, and ultimately killing the animal (McCarthy et al., 2009). We had a 50% mortality rate in the PT stroke cohort, while all mice that received sham surgeries survived, suggesting a detrimental synergistic effect of ischemic injury and PRV-induced cytotoxicity at 6 days after peripheral intramuscular injection. The newer viral tracers have sought to reduce or eliminate this toxicity with the promising new development of a self-inactivating glycoprotein-deleted rabies virus that allows for life-long labeling of circuits (Ciabatti et al., 2017).

It is well-established that immune cells diapedese into the infarct and penumbral regions after stroke (Xie et al., 2018), but it is less clear where and when immune cells traffic into remote brain regions that support functional recovery. Furthermore, post-stroke diapedesis has never been characterized in 3-D, making this study the first whole-brain quantification of CD8 trafficking from the periphery following stroke. One of the limitations of our study is that CD8 T cells may diapedese from the ventricles and the meninges before they reach their targeted brain tissue after stroke (Benakis et al., 2018; Yanev et al., 2019). Not all of the meningeal lymphatics are removed during sample preparation, and the ventricles are adjacent to several analyzed brain regions. Thus, it is possible that these areas could be warped and registered into the atlas, giving the false positive impression of parenchymal penetration of CD8$^+$ T cells when in actuality, they are traveling through the meningeal lymphatics or ventricles to another location. It may be necessary to visually inspect coronal sections on a case by case basis, particularly if larger immune cell populations are quantified in a similar manner.

Modern techniques such as STPT and other new imaging methods further our understanding of post-stroke pathology and repair. Our data demonstrate that rapid whole brain microscopy

followed by large-scale automated analyses can provide new insight into neural connectivity and neuroinflammation post-stroke in an unbiased, region-specific manner that is difficult, if not impossible, with current conventional techniques. Future studies should use these techniques to further investigate neuroplasticity and neuroinflammation following stroke, as well as other diseases and injuries with global effects on the brain.

DATA AVAILABILITY STATEMENT

All datasets generated for this study are included in the manuscript/**Supplementary Files**. All raw data is immediately available upon request.

ETHICS STATEMENT

The animal study was reviewed and approved by University of Texas Southwestern Medical Center Institutional Animal Care and Use Committee.

AUTHOR CONTRIBUTIONS

MG, KP, and DB designed the neural connectivity experiments. KP, DB, SM, XK, and SG acquired data for neural connectivity experiments. AS and VT designed the neuroinflammation experiments. US isolated $CD8^+$ T cells for neuroinflammation experiments. VT and XK acquired data for neuroinflammation experiment. EP performed all stroke surgeries. AA, JM, and DR acquired all STPT data and conducted pipeline analyses. KP, DB, VT, and AS analyzed final STPT results. All authors edited the manuscript.

FUNDING

This study was funded by grants to AS from NIH/NINDS (NS088555), to AS from the Dana Foundation David Mahoney Neuroimaging Program, to VT from the NIH Intergrative Immunology Training Program (5T32AI005284-40) the Haggerty Center for Brain Injury and Repair, and the Texas Institute for Brain Injury and Repair (TIBIR) (UTSW). SG was supported by the National Center for Advancing Translational Sciences of the National Institutes of Health under award Number KL2TR001103. PRV-152 was generously provided by Dr. Lynn Enquist (Princeton University, Princeton, NJ) through the Center for Neuroanatomy with Neurotropic Viruses (NIH P40 OD010996).

ACKNOWLEDGMENTS

The authors acknowledge the Moody Foundation Flow Cytometry Facility at the Children's Research Institute and the Neuro-Models Facility at UT Southwestern.

SUPPLEMENTARY MATERIAL

The Supplementary Material for this article can be found online at: https://www.frontiersin.org/articles/10.3389/fnins.2019.01055/full#supplementary-material

Supplementary Figure 1 | Heat map of neuronal processes quantification in cortical and other areas.

Supplementary Figure 2 | Verification of live e450-labeled CD8 T cells in recipient mice.

Supplementary Video 1 | Non-stroke mouse, fly-through of raw data of GFP fluorescence.

Supplementary Video 2 | Non-stroke mouse, rotation of raw data of GFP fluorescence.

Supplementary Video 3 | Non-stroke mouse, fly-through of probability maps for axons and soma of GFP fluorescence.

Supplementary Video 4 | Non-stroke mouse, rotation of probability maps for axons and soma of GFP fluorescence.

Supplementary Video 5 | Stroke mouse, fly-through of raw data of GFP fluorescence.

Supplementary Video 6 | Stroke mouse, rotation of raw data of GFP fluorescence.

Supplementary Video 7 | Stroke mouse, fly-through of probability maps for axons and soma of GFP fluorescence.

Supplementary Video 8 | Stroke mouse, rotation of probability maps for axons and soma of GFP fluorescence.

Supplementary Video 9 | Stroke mouse, fly-through of raw data of CD8 T cell fluorescence.

Supplementary Video 10 | Stroke mouse, fly-through of probability map for CD8 T cell fluorescence.

REFERENCES

Abulrob, A., Brunette, E., Slinn, J., Baumann, E., and Stanimirovic, D. (2008). Dynamic analysis of the blood-brain barrier disruption in experimental stroke using time domain *in vivo* fluorescence imaging. *Mol. Imaging* 7, 248–262. doi: 10.2310/7290.2008.00025

Amato, S. P., Pan, F., Schwartz, J., and Ragan, T., M. (2016). Whole brain imaging with serial two-photon tomography. *Front. Neuroanat.* 10:31. doi: 10.3389/fnana.2016.00031

Bachmann, L. C., Lindau, N T., Felder, P., and Schwab, M. E. (2014). Sprouting of brainstem-spinal tracts in response to unilateral motor cortex stroke in mice. *J. Neurosci.* 34, 3378–3389. doi: 10.1523/JNEUROSCI.4384-13.2014

Bauer, A. Q., Kraft, A. W., Wright, P. W., Snyder, A. Z., Lee, J. M., and Culver, J. P. (2014). Optical imaging of disrupted functional connectivity following ischemic stroke in mice. *Neuroimage* 99, 388–401. doi: 10.1016/j.neuroimage.2014.05.051

Benakis, C., Llovera, G., and Liesz, A. (2018). The meningeal and choroidal infiltration routes for leukocytes in stroke. *Ther. Adv. Neurol. Disord.* 11:1756286418783708. doi: 10.1177/1756286418783708

Benjamin, E. J., Virani, S. S., Callaway, C. W., Chamberlain, A. M., Chang, A. R., Cheng, S., et al. (2018). Heart disease and stroke statistics-2018 update: a report from the American Heart Association. *Circulation* 137, e67–e492. doi: 10.1161/CIR.0000000000000558

Brown, C. E., Aminoltejari, K., Erb, H., Winship, I. R., and Murphy, T. H. (2009). *In vivo* voltage-sensitive dye imaging in adult mice reveals that somatosensory maps lost to stroke are replaced over weeks by new structural and functional circuits with prolonged modes of activation within both the peri-infarct zone and distant sites. *J. Neurosci.* 29, 1719–1734. doi: 10.1523/JNEUROSCI.4249-08.2009

Cai, R., Pan, C., Ghasemigharagoz, A., Todorov, M. I., Forstera, B., Zhao, S., et al. (2019). Panoptic imaging of transparent mice reveals whole-body neuronal

projections and skull-meninges connections. *Nat. Neurosci.* 22, 317–327. doi: 10.1038/s41593-018-0301-3

Ciabatti, E., Gonzalez-Rueda, A., Mariotti, L., Morgese, F., and Tripodi, M. (2017). Life-long genetic and functional access to neural circuits using self-inactivating rabies virus. *Cell* 170, 382–392.e314. doi: 10.1016/j.cell.2017.06.014

Dancause, N., Barbay, S., Frost, S. B., Plautz, E. J., Chen, D., Zoubina, E. V., et al. (2005). Extensive cortical rewiring after brain injury. *J. Neurosci.* 25, 10167–10179. doi: 10.1523/JNEUROSCI.3256-05.2005

Dijkhuizen, R. M., van der Marel, K., Otte, W. M., Hoff, E. I., van der Zijden, J. P., van der Toorn, A., et al. (2012). Functional MRI and diffusion tensor imaging of brain reorganization after experimental stroke. *Transl. Stroke Res.* 3, 36–43. doi: 10.1007/s12975-011-0143-8

Dobkin, B. H. (2005). Clinical practice. Rehabilitation after stroke. *N. Engl. J. Med.* 352, 1677–1684. doi: 10.1056/NEJMcp043511

Furlan, M., Marchal, G., Viader, F., Derlon, J. M., and Baron, J. C. (1996). Spontaneous neurological recovery after stroke and the fate of the ischemic penumbra. *Ann. Neurol.* 40, 216–226. doi: 10.1002/ana.410400213

Ganzer, P. D., Darrow, M. J., Meyers, E. C., Solorzano, B. R., Ruiz, A. D., Robertson, N. M., et al. (2018). Closed-loop neuromodulation restores network connectivity and motor control after spinal cord injury. *Elife* 7:e32058. doi: 10.7554/eLife.32058

Gelderblom, M., Leypoldt, F., Steinbach, K., Behrens, D., Choe, C. U., Siler, D. A., et al. (2009). Temporal and spatial dynamics of cerebral immune cell accumulation in stroke. *Stroke* 40, 1849–1857. doi: 10.1161/STROKEAHA.108.534503

Ishida, A., Isa, K., Umeda, T., Kobayashi, K., Kobayashi, K., Hida, H., et al. (2016). Causal link between the cortico-rubral pathway and functional recovery through forced impaired limb use in rats with stroke. *J. Neurosci.* 36, 455–467. doi: 10.1523/JNEUROSCI.2399-15.2016

Jin, R., Liu, L., Zhang, S., Nanda, A., and Li, G. (2013). Role of inflammation and its mediators in acute ischemic stroke. *J. Cardiovasc. Transl. Res.* 6, 834–851. doi: 10.1007/s12265-013-9508-6

Jones, T. A., and Adkins, D. L. (2015). Motor system reorganization after stroke: stimulating and training toward perfection. *Physiology* 30, 358–370. doi: 10.1152/physiol.00014.2015

Kerman, I. A., Akil, H., and Watson, S. J. (2006). Rostral elements of sympatho-motor circuitry: a virally mediated transsynaptic tracing study. *J. Neurosci.* 26, 3423–3433. doi: 10.1523/JNEUROSCI.5283-05.2006

Kerman, I. A., Enquist, L. W., Watson, S. J., and Yates, B. J. (2003). Brainstem substrates of sympatho-motor circuitry identified using trans-synaptic tracing with pseudorabies virus recombinants. *J. Neurosci.* 23, 4657–4666. doi: 10.1523/JNEUROSCI.23-11-04657.2003

Kim, Y., Perova, Z., Mirrione, M. M., Pradhan, K., Henn, F. A., Shea, S., et al. (2016). Whole-brain mapping of neuronal activity in the learned helplessness model of depression. *Front. Neural Circuits* 10:3. doi: 10.3389/fncir.2016.00003

Kim, Y. R., Huang, I. J., Lee, S. R., Tejima, E., Mandeville, J. B., van Meer, M. P., et al. (2005). Measurements of BOLD/CBV ratio show altered fMRI hemodynamics during stroke recovery in rats. *J. Cereb. Blood Flow Metab.* 25, 820–829. doi: 10.1038/sj.jcbfm.9600084

Lee, T. K., Lois, J. H., Troupe, J. H., Wilson, T. D., and Yates, B. J. (2007). Transneuronal tracing of neural pathways that regulate hindlimb muscle blood flow. *Am. J. Physiol. Regul. Integr. Comp. Physiol.* 292, 1532–1541. doi: 10.1152/ajpregu.00633.2006

Liu, Z., Zhang, R. L., Li, Y., Cui, Y., and Chopp, M. (2009). Remodeling of the corticospinal innervation and spontaneous behavioral recovery after ischemic stroke in adult mice. *Stroke* 40, 2546–2551. doi: 10.1161/STROKEAHA.109.547265

Lowekamp, B., gabehart, Blezek, D., Ibanez, L., and McCormick, M. (2015). *SimpleElastix v0.9.0*. Available online at: https://zenodo.org/record/19049#.XYwFbChKhhE

Lugo-Hernandez, E., Squire, A., Hagemann, N., Brenzel, A., Sardari, M., Schlechter, J., et al. (2017). 3D visualization and quantification of microvessels in the whole ischemic mouse brain using solvent-based clearing and light sheet microscopy. *J. Cereb. Blood Flow Metab.* 37, 3355–3367. doi: 10.1177/0271678X17698970

McCarthy, K. M., Tank, D. W., and Enquist, L. W. (2009). Pseudorabies virus infection alters neuronal activity and connectivity *in vitro*. *PLoS Pathog.* 5:e1000640. doi: 10.1371/journal.ppat.1000640

Monson, N. L., Ortega, S. B., Ireland, S. J., Meeuwissen, A. J., Chen, D., Plautz, E. J., et al. (2014). Repetitive hypoxic preconditioning induces an immunosuppressed B cell phenotype during endogenous protection from stroke. *J. Neuroinflammation* 11:22. doi: 10.1186/1742-2094-11-22

Murphy, T. H., and Corbett, D. (2009). Plasticity during stroke recovery: from synapse to behaviour. *Nat. Rev. Neurosci.* 10, 861–872. doi: 10.1038/nrn2735

Nudo, R. J. (2007). Postinfarct cortical plasticity and behavioral recovery. *Stroke* 38(Suppl. 2), 840–845. doi: 10.1161/01.STR.0000247943.12887.d2

Oh, S. W., Harris, J. A., Ng, L., Winslow, B., Cain, N., Mihalas, S., et al. (2014). A mesoscale connectome of the mouse brain. *Nature* 508, 207–214. doi: 10.1038/nature13186

Okabe, N., Narita, K., and Miyamoto, O. (2017). Axonal remodeling in the corticospinal tract after stroke: how does rehabilitative training modulate it? *Neural Regen. Res.* 12, 185–192. doi: 10.4103/1673-5374.200792

Ortega, S. B., Noorbhai, I., Poinsatte, K., Kong, X., Anderson, A., Monson, N., et al. (2015). Stroke induces a rapid adaptive autoimmune response to novel neuronal antigens. *Discov. Med.* 19, 381–392.

Patel, A. R., Ritzel, R., McCullough, L. D., and Liu, F. (2013). Microglia and ischemic stroke: a double-edged sword. *Int. J. Physiol. Pathophysiol. Pharmacol.* 5, 73–90.

Ragan, T., Kadiri, L. R., Venkataraju, K. U., Bahlmann, K., Sutin, J., Taranda, J., et al. (2012). Serial two-photon tomography for automated *ex vivo* mouse brain imaging. *Nat. Methods* 9, 255–258. doi: 10.1038/nmeth.1854

Ramirez, D. M. O., Ajay, D. A., Goldberg, M. P., and Meeks, J. (2019). "Serial multiphoton tomography and analysis of volumetric images of the mouse brain," in *Multiphoton Microscopy, Neuromethods Series*, ed E. Hartveit (Totowa, NJ: Springer Nature; Humana Press).

Rubartelli, A., and Lotze, M. T. (2007). Inside, outside, upside down: damage-associated molecular-pattern molecules (DAMPs) and redox. *Trends Immunol.* 28, 429–436. doi: 10.1016/j.it.2007.08.004

Somner, C., Straehle, C., Kothe, U., and Hamprecht, F. A. (2011). "*Ilastik: Interactive Learning and Segmentation Toolkit*," in *Proceedings of the Eighth IEEE International Symposium on Biomedical Imaging, ISBI* (Chicago, IL). doi: 10.1109/ISBI.2011.5872394

Wang, X., Xuan, W., Zhu, Z. Y., Li, Y., Zhu, H., Zhu, L., et al. (2018). The evolving role of neuro-immune interaction in brain repair after cerebral ischemic stroke. *CNS Neurosci. Ther.* 24, 1100–1114. doi: 10.1111/cns.13077

Whitesell, J. D., Buckley, A. R., Knox, J. E., Kuan, L., Graddis, N., Pelos A., et al. (2018). Whole brain imaging reveals distinct spatial patterns of amyloid beta deposition in three mouse models of Alzheimer's disease. *J. Comp. Neurol.* 527, 2122–2145. doi: 10.1002/cne.24555

Xie, L., Li, W., Hersh, J., Liu, R., and Yang, S. H. (2018). Experimental ischemic stroke induces long-term T cell activation in the brain. *J. Cereb. Blood Flow Metab.* 271678X18792372. doi: 10.1177/0271678X18792372

Yanev, P., Poinsatte, K., Hominick, D., Khurana, N., Zuurbier, K. R., Berndt, M., et al. (2019). Impaired meningeal lymphatic vessel development worsens stroke outcome. *J. Cereb. Blood Flow Metab.* 271678X18822921. doi: 10.1177/0271678X18822921

Yang, X., Zhang, Q., Huang, F., Bai, K., Guo, Y., Zhang, Y., et al. (2018). High-throughput light sheet tomography platform for automated fast imaging of whole mouse brain. *J. Biophotonics* 11:e201800047. doi: 10.1002/jbio.201800047

Conflict of Interest: The authors declare that the research was conducted in the absence of any commercial or financial relationships that could be construed as a potential conflict of interest.

Copyright © 2019 Poinsatte, Betz, Torres, Ajay, Mirza, Selvaraj, Plautz, Kong, Gokhale, Meeks, Ramirez, Goldberg and Stowe. This is an open-access article distributed under the terms of the Creative Commons Attribution License (CC BY). The use, distribution or reproduction in other forums is permitted, provided the original author(s) and the copyright owner(s) are credited and that the original publication in this journal is cited, in accordance with accepted academic practice. No use, distribution or reproduction is permitted which does not comply with these terms.

frontiers in Neuroscience

ORIGINAL RESEARCH
published: 11 October 2019
doi: 10.3389/fnins.2019.01092

A Safe and Effective Magnetic Labeling Protocol for MRI-Based Tracking of Human Adult Neural Stem Cells

Albrecht Stroh[1,2], Jenny Kressel[3,4], Roland Coras[5], Antje Y. Dreyer[6], Wenke Fröhlich[6], Annette Förschler[3], Donald Lobsien[7], Ingmar Blümcke[5], Saida Zoubaa[8], Jürgen Schlegel[8], Claus Zimmer[3] and Johannes Boltze[6,9]*

[1] Institute for Pathophysiology, Mainz University, Mainz, Germany, [2] German Resilience Center, Mainz, Germany, [3] Department of Neuroradiology, Technical University Munich, Munich, Germany, [4] Helmholtz Center Munich, Institute for Biological and Medical Imaging, Munich, Germany, [5] Department of Neuropathology, University Hospital Erlangen, Erlangen, Germany, [6] Translational Center for Regenerative Medicine, Fraunhofer Institute for Cell Therapy and Immunology, University of Leipzig, Leipzig, Germany, [7] Department of Neuroradiology, University Hospital Leipzig, Leipzig, Germany, [8] Division of Neuropathology, Institute of Pathology, Technical University of Munich, Munich, Germany, [9] School of Life Sciences, University of Warwick, Coventry, United Kingdom

OPEN ACCESS

Edited by:
Yogesh Rathi, Harvard Medical School, United States

Reviewed by:
Uwe Himmelreich, University of Leuven, Belgium
Pavla Jendelova, Institute of Experimental Medicine (ASCR), Czechia

***Correspondence:**
Albrecht Stroh
albrecht.stroh@unimedizin-mainz.de

Specialty section:
This article was submitted to Brain Imaging Methods, a section of the journal Frontiers in Neuroscience

Received: *15 May 2019*
Accepted: *27 September 2019*
Published: *11 October 2019*

Citation:
Stroh A, Kressel J, Coras R, Dreyer AY, Fröhlich W, Förschler A, Lobsien D, Blümcke I, Zoubaa S, Schlegel J, Zimmer C and Boltze J (2019) A Safe and Effective Magnetic Labeling Protocol for MRI-Based Tracking of Human Adult Neural Stem Cells. Front. Neurosci. 13:1092. doi: 10.3389/fnins.2019.01092

Magnetic resonance imaging (MRI) provides a unique tool for *in vivo* visualization and tracking of stem cells in the brain. This is of particular importance when assessing safety of experimental cell treatments in the preclinical or clinical setup. Yet, specific imaging requires an efficient and non-perturbing cellular magnetic labeling which precludes adverse effects of the tag, e.g., the impact of iron-oxide-nanoparticles on the critical differentiation and integration processes of the respective stem cell population investigated. In this study we investigated the effects of very small superparamagnetic iron oxide particle (VSOP) labeling on viability, stemness, and neuronal differentiation potential of primary human adult neural stem cells (haNSCs). Cytoplasmic VSOP incorporation massively reduced the transverse relaxation time T2, an important parameter determining MR contrast. Cells retained cytoplasmic label for at least a month, indicating stable incorporation, a necessity for long-term imaging. Using a clinical 3T MRI, 1×10^3 haNSCs were visualized upon injection in a gel phantom, but detection limit was much lower (5×10^4 cells) in layer phantoms and using an imaging protocol feasible in a clinical scenario. Transcriptional analysis and fluorescence immunocytochemistry did not reveal a detrimental impact of VSOP labeling on important parameters of cellular physiology with cellular viability, stemness and neuronal differentiation potential remaining unaffected. This represents a pivotal prerequisite with respect to clinical application of this method.

Keywords: human adult stem cells, magnetic labeling, MRI, cell tracking, CNS – disorder

INTRODUCTION

Stem cell transplantation represents one of the most promising strategies for the restoration of lost cells or tissue including their functions, or at least for delaying the pathogenic progress in neurodegenerative diseases (Janowski et al., 2015). The question whether adult or embryonic stem cells are best suited for clinical applications remains open (Modo et al., 2002;

Dietrich and Kempermann, 2006), yet adult stem cells show reduced probability of teratoma formation, and thereby represent a promising candidate for clinical translation (Dietrich and Kempermann, 2006; Bellenchi et al., 2013). In humans, adult neural stem cells are present in the subventricular zone and in the subgranular zone of the hippocampal dentate gyrus (Zimmer et al., 1995; Stroh et al., 2005, 2009). These cells can be isolated from patients with intractable temporal lobe epilepsy subjected to neurosurgical intervention (Hoehn et al., 2002). Stem cells tracking and long term monitoring is demanded for thorough development of safe and efficient transplantation protocols and to further our understanding about therapeutic modes of action in both the preclinical and clinical setting.

To date, magnetic resonance imaging (MRI) of magnetically labeled stem cells represents the only clinically applicable imaging method for highly sensitive, non-invasive detection and long-term tracking of transplanted stem cells over extended periods of time (Modo et al., 2002; Stroh et al., 2005, 2009). Citrate-coated very small superparamagnetic iron oxide particles (VSOP) are widely used for pre-transplantation stem cell labeling. These particles are incorporated via endocytosis, aggregate and ultimately get stored in intracytoplasmic vesicles (Zimmer et al., 1995; Stroh et al., 2005). Incorporation of VSOP can be enhanced by lipofection to enhance the percentage of strongly labeled cells (Hoehn et al., 2002). Superparamagnetic iron oxide particles also seem to be biodegradable (Weissleder et al., 1989) and can even be utilized by the cells in iron metabolism pathways (Pouliquen et al., 1991).

However, the incorporation of iron oxide particles may lead to distinct changes in stem cell physiology (Stroh et al., 2004; Guzman et al., 2007; Focke et al., 2008; Neri et al., 2008). Moreover, superparamagnetic iron oxide/poly-L-lysine-labeling of a mouse neural stem cell line was reported to induce changes in expression of genes responsible for iron homeostasis, despite apoptotic pathways were not upregulated in that particular study (Walczak et al., 2006). Further, iron oxide particles have been shown to cause transient oxidative stress, closely linked to the free iron during incubation (Stroh et al., 2004), and most likely due to degradation and release of ferric ions into the acidic endolysosomal compartments (Soenen et al., 2011). Thus, evaluating the safety and impact of VSOP labeling on the differentiation potential of highly sensitive human adult stem cells is an important prerequisite for clinical translation (Gupta et al., 2007). Finally, the intended labeling protocol needs to be tailored to the respective stem cell population to ensure an acceptable balance between labeling intensity/efficacy and safety (Boltze et al., 2015).

Our study investigates describe the long term efficacy of human adult human neural stem cell (haNSC) VSOP labeling and its impact on viability, expansion, and neuronal differentiation potential for the first time. We analyzed both non-differentiated haNSCs as well as mature haNSCs-derived neurons, with murine embryonic stem cells (mESC) serving as cellular controls. We also assessed cell detection limit *in vitro* MRI with different modalities including one being close to a potential clinical application.

RESULTS

Safety of Cell Labeling With VSOP

To assess safety of haNSC preparation, cryopreservation, and labeling (0.5 mM), or to detect any donor-dependent differences, cell viability was tested in the first step. No significant donor-dependent differences in cell viability between cells which underwent the labeling procedure with 0.5 mM (85–89%) and non-labeled control cells (91%, sample pooled from all patients) could be detected 1 day after labeling (**Figure 1A**). All samples could be included in onward experiments according to preset viability criteria (>80%). Next, cell viability of haNSCs and mESCs was compared 8 and 48 h after labeling with 0.5 and 1.5 mM VSOP, respectively (**Figure 1B**). Again, no significant differences in haNSCs viability between non-labeled control cells (95%), as well as 8 (87.5%) and 48 h (94.5%) after labeling became apparent. Viability of mESCs decreased slightly to 89% at 8 h and to 93.5% at 48 h after labeling. No viability differences were observed between 0.5 and 1.5 mM VSOP concentration.

Efficacy of Magnetic Cell Labeling

Incubation of haNSCs with 0.5 mM VSOP alone ("simple") and additional lipofection resulted in a substantial uptake of magnetic label (**Figure 2**). Prussian blue staining revealed a homogenous ferric ion distribution in the cytoplasm, excluding the nuclei (**Figures 2a,b**). Prussian blue signals remained unchanged from day 2 to day 28 post simple incubation (**Figures 2c,d**), indicating a stable vesicular incorporation of VSOP for at least 1 month. This ratio did not differ significantly between day 2 and day 28. No apparent increase in iron-oxide particle uptake was observed upon visual inspection in lipofected cells (**Figures 2e,f**), which was confirmed by counting labeled cells. Overall, 96–100% of haNSCs were labeled. Labeling efficacy could not be improved significantly at any time point by additional lipofection (+L) (**Figure 2g**), so lipofection was omitted in all further experiments.

Proliferation Assays

We next conducted a proliferation assay of labeled and non-labeled haNSCs. Over the course of 8 days, an exponential increase in cell number could be observed, yet, notably, no significant difference could be detected between the proliferation curves on non-labeled and haNSCs incubated with 0.5 and 1.5 mM VSOP (**Figure 2h**).

Magnetic Resonance Properties

Next, the impact of 0.5 and 1.5 mM VSOP-labeling of both stem cell populations on magnetic resonance properties was determined after 8 and 48 h via NMR relaxometry (**Figures 3a,b**). Unlabeled cells had a T2 time of 2110 ms (mESCs) and 1948 ms (haNSCs), revealing no significant difference between both protocols. In contrast, VSOP-labeling with 0.5 mM and 8 h incubation time led to a significant reduction of T2 time to 10% of control values (mESCs: 218 ms, haNSCs: 227 ms, **Figure 3a**, $P < 0.01$). 48 h after incubation, T2 time ranged at 15% of control values (mESCs: 298 ms, haNSCs: 408 ms, **Figure 3b**). Further increasing VSOP concentrations to 1.5 mM resulted in

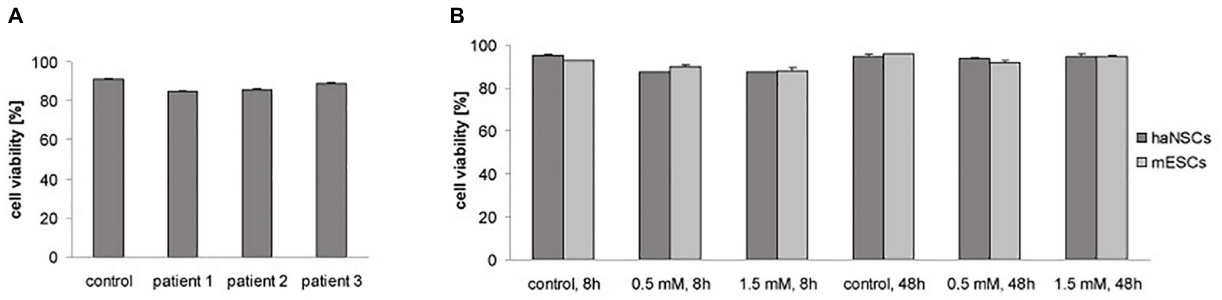

FIGURE 1 | Cell viability of magnetically labeled haNSCs and mESCs (n = 3 with 3 technical replicates each). **(A)** Trypan blue exclusion test showed no significant differences in viability of three different patient samples (labeling with 0.5 mM). **(B)** Trypan blue exclusion test 8 and 48 h after labeling showed no decrease in cell viability due to the labeling procedure.

an additional reduction of average T2 time which, however, was not statistically significant from that after 0.5 mM incubation.

In vitro MR Imaging

To assess clinical applicability of the labeling protocol, gradient echo MR images of gel phantoms with injected cells were acquired (**Figures 3c,g**). On the T2*-weighted images two needle tracks on the gel surface can be delineated as hyperintense signal changes (**Figure 3c**) in injection phantoms. On the left side of the phantom 1×10^3 magnetically labeled haNSCs were injected, whereas 1×10^3 unlabeled control haNSCs where placed on the right side. The T2*-weighted images clearly showed hyperintense signal changes only in the left injection track deposit of 1×10^3 labeled haNSCs (**Figures 3d,e**). Cell detectability was lower in layer phantoms imaged at 3T SWI with a protocol that could be applied on hypothetical patient. Only 5×10^4 labeled cells were detectable with the applied imaging protocol (**Figures 3f,g**).

Characterization of Non-differentiated VSOP Labeled Stem Cells

Cells were magnetically labeled and subsequently analyzed by RT-PCR and Western Blotting (**Figure 4a**). Non-labeled haNSCs and mESCs served as cellular controls. After culturing in the appropriate expansion media, all cells except the HT22 expressed the mRNA for the stemness markers Oct4 and Sox2, and the neural progenitor marker nestin. haNSCs and mESCs loaded with 0.5 mM VSOP (VSOP) or VSOP plus lipofection agent (VSOP + L) revealed the same mRNA expression pattern. No difference between stem cells incubated with (L) and without lipofectin became apparent.

Analysis of haNSCs using fluorescent immunocytochemistry showed that 99% of cells express the intermediate filament protein nestin (**Figure 4b**). 65% co-expressed the nuclear proliferation marker Ki-67 (**Figures 4c,d**). 99% of haNSCs, which underwent the VSOP-labeling procedure and subsequently had a high cytoplasmatic iron loading, expressed nestin while 64% of cells were found positive for Ki-67 (**Figures 4e–g**). Substantial differences between control cells and VSOP labeled haNSCs from all three donors could not be observed (**Figure 4h**). Analysis of nestin and Ki-67 co-expression revealed no impact of VSOP labeling (**Figure 4i**). However, we found a significant effect on relative numbers of cells co-expressing nestin and Ki-67 in the three patients ($P < 0.01$).

Differentiation Potential of VSOP-Labeled Stem Cells

Figure 4j illustrates the analysis of stem cells that were magnetically labeled and subsequently neuronally differentiated over 15 days. Non-labeled, but neuronally differentiated haNSCs and mESCs served as controls. To characterize the transition from neural progenitors to mature neurons, mRNA expression levels of β-tubulin III, doublecortin (DCX), neural cell adhesion molecule 1 (NCAM-1) as well as microtubule associated phosphoprotein 2 (MAP-2) were investigated. RT-PCR analysis indicated neural progenitors and immature neurons in control cell populations as well as in magnetically loaded cell populations. No differences in expression patterns were observed.

DISCUSSION

In this study, we were able to show that labeling of haNSC with iron-oxide-particles, required for a high-resolution MR Imaging, is both safe and efficient. Labeling efficiency using 0.5 mM VSOP was found up to 100% and resulted in stable cell labeling for at least 1 month. Trypan blue exclusion tests at different time points and comparison of different patient samples demonstrated that VSOP-labeling had no effect on overall haNSCs viability. Using clinical 3T MRI, we visualized 1×10^3 labeled cells in an injection phantom, modeling the *in vivo* situation under optimal imaging conditions. Moreover, 3T SWI MRI of layer phantoms with layers containing up to 5×10^4 labeled cells was performed, applying an imaging protocol taking 41:00 min. This is short enough to be applied in a hypothetical clinical scenario, but on the upper limit what could be performed in critically ill patients. The protocol settings were chosen on optimal detectability in VSOP-labeled mesenchymal stem cells (Stroh et al., 2011). The analysis of Oct4 and Sox2 mRNA-expression in addition to the quantitative fluorescence immunocytochemistry analysis of Ki-67 and nestin co-expression as stem cell markers and indicators of proliferation activity showed no impact of VSOP labeling, but

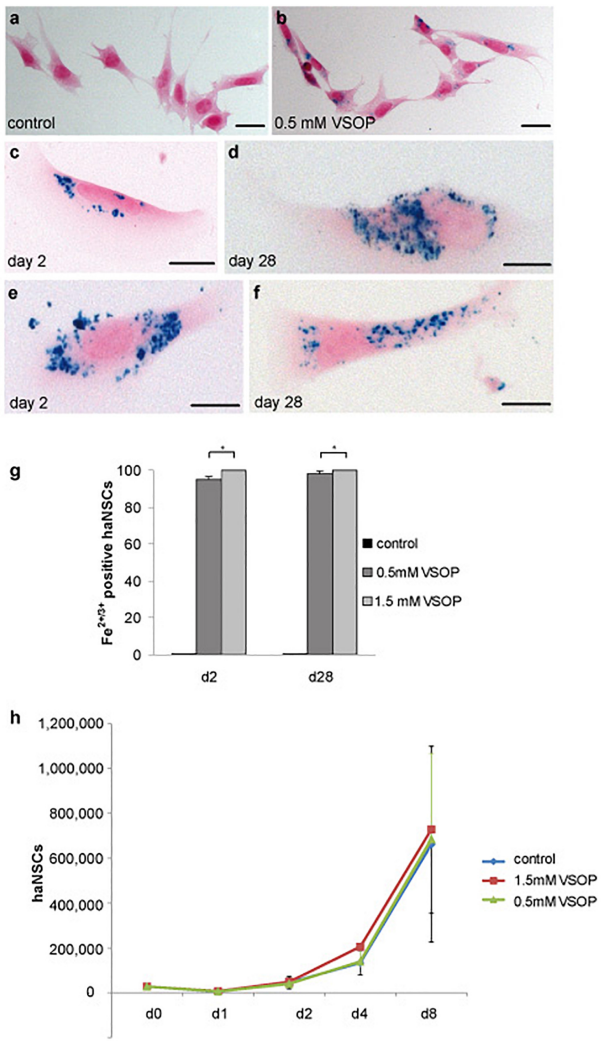

FIGURE 2 | Cytological analysis of magnetically labeled haNSCs (n = 3 with 3 technical replicates each). **(a)** Unlabeled control cells and **(b)** intracytoplasmic VSOP uptake by haNSCs following incubation with 0.5 mM VSOP. **(c–f)** Cells were fixed with 4% phosphate-buffered saline-buffered paraformaldehyde and intracellular iron was visualized using Prussian blue staining on day 2 as shown in **(c,e)** and on day 28 as provided in **(d,f)** after labeling. **(g)** Cell counting revealed that labeling efficacy at any time point could not be enhanced significantly by lipofection. **(h)** Proliferation analysis of VSOP-labeled haNSC (1.5 mM) revealed no statistically significant difference in the proliferation abilities of unlabeled haNSC and haNSCs labeled with 0.5 mM VSOP, respectively. Scale bars in **(a–f)** represent 10 μm. $^*p < 0.01$.

significant differences in haNSC samples from different donors. Furthermore, neuronal differentiation potential and neuronal marker expression were not affected by the labeling procedure.

Prussian blue staining resulted in a homogenous ferric ion distribution in the cytoplasm, but not in the nucleus. This is in line with previous findings from our group, showing a direct relation between VSOP incubation, intracellular iron load as measured by atomic absorption spectroscopy, and T2 time reduction (Stroh et al., 2005). Prussian blue staining was found stable after 48 h and 28 days, indicating a transfer of VSOP onto daughter cells during cytokinesis for proliferating cells. Our data indicate no difference in labeling efficiency and stability between incubation with VSOP and additional lipofection. One explanation of the efficient incorporation with VSOP alone could be the small diameter and the negative surface charge of the citrate coating, already allowing efficient uptake without additional lipofection. Albeit lipofection did not raise a safety concern in our study, off-target effects and immune response caused by transfection reagents have been described (Bauer et al., 2006). Thus, sufficient labeling with VSOP but omitting lipofection may represent a clear advantage for subsequent *in vivo* and clinical applications.

It is known that citrate coating may interact with the extracellular domain of integrins and triggers their activation and subsequently intracellular signaling cascades (Miller et al., 2010). Furthermore, VSOP can induce increased levels of transferrin receptor-1. VSOP incubation can also result in a fast increase and high level of reactive oxygen species (ROS), most likely due to degradation and release of ferric ions into the acidic endolysosomal compartments (Soenen et al., 2011). Although no detrimental influence has been shown in the present study, the overall impact of these potential alterations should be carefully controlled after *in vivo* transplantation. While measures of T2 relaxation times provide an indication of the cellular iron uptake, a direct measure of iron content, as conducted in previous studies of ours using the same iron-oxide particles, yet in different cells, would be desirable (Stroh et al., 2005, 2009). We were not able to conduct these assays due to the scarcity of the cellular material. Also, iron-oxide particles have shown to induce oxidative stress (Stroh et al., 2004), potentially leading to oxidative damage to proteins, lipids and even DNA, also at low concentrations of the label (Novotna et al., 2012). Viability assays, as conducted here, might not be sensitive toward these molecular changes, but again, we were not able to conduct these assays due to the limited availability of the cells.

Potential effects of iron oxide on the neuronal differentiation potential of haNSC and mESC, were analyzed on the gene transcription level. The present data indicates that VSOP-labeled haNSCs and mESCs can be expanded without affecting their potential for both neurogenesis, as represented by the pluripotency markers Sox2 (Suh et al., 2007) and Oct4 (Nichols et al., 1998), or their ability for neuronal differentiation. Magnetic labeling had also no impact on mRNA transcription of nestin and Ki-67 expression even after 14 days in culture. In this study, we used iron-oxide nanoparticles, which are presumably taken up by the cells by endocytosis (Stroh et al., 2004). This means, that in contrast to genetically encoded labels, the concentration of particles in the cells will diminish over time, both due to cell proliferation, and also due to particle degradation. This limits the time window, in which these cells will be detectable by MRI. What is more, we provided data on RNA level on the differentiation potential of these labeled cells, but this does not prove a functional stable differentiation into a given neuronal subtype. For that, additional assays on protein level and ultimately electrophysiological evidence need to be conducted (Stroh et al., 2011).

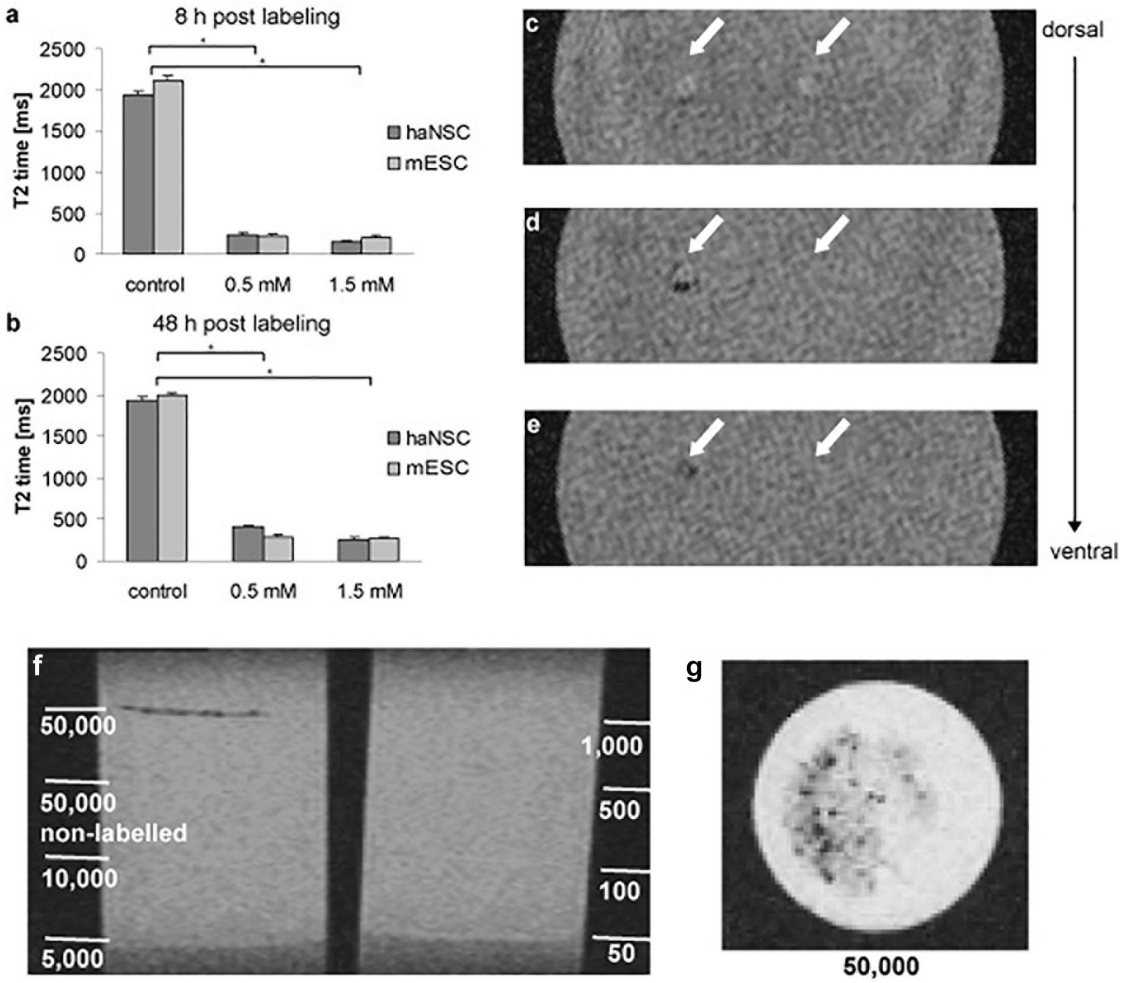

FIGURE 3 | NMR relaxometry and gradient echo MR images of gel phantoms containing haNSCs (n = 3 or more). **(a,b)** Efficiency of VSOP-labeling was determined after 8 **(a)** and 48 h **(b)** using NMR relaxometry. All data were analyzed and presented as mean ± SEM. Differences were considered significant at $P < 0.01$. **(c)** Coronal section at gel surface showing two needle tracks as hyperintense signal change. 1×10^3 VSOP labeled haNSCs were injected on the left side; on the right side 1×10^3 unlabeled control haNSCs were injected. **(d)** Slice 4.5 mm ventral of **(c)**. In the left injection track an area of signal loss can be visualized, due to clusters of magnetically labeled haNSCs. No signal change in the right injection track was observed. **(e)** Slice 5 mm ventral of **(c)**. The left injection track again shows an area of signal loss, no signal change in the right injection track. **(f,g)** layer phantoms investigated in 3T SWI MRI. Only 5×10^4 labeled haNSCs were detectable with an imaging protocol being short enough (41:00 min) to be applicable in a hypothetical clinical scenario. *$p < 0.01$.

1×10^3 VSOP-labeled haNSC were easily identified in a gel phantom, reliably modeling the situation upon stereotactic transplantation *in vivo* (Stroh et al., 2005). This detection range is more than sufficient to monitor cell migration in clinical scenarios where 20 to 300×10^3 or even more cells are transplanted (Kondziolka et al., 2004; Stover et al., 2005). Nevertheless, the detection limit is rather high compared to other studies that repeatedly shown single cell detectability. A direct comparison is difficult though. For instance, some studies employed ultra-high field strengths (11.7T) and imaging protocols optimized for that purpose (Hinds et al., 2003). Others used long imaging times and different cell types such MDA-MB-231BR breast cancer cells or J774 macrophages (Heyn et al., 2006). Both cell types are much larger (up to 25 μm diameter and up to 100 μm in length for MDA-MB-231BR) than neural stem cells and therefore can store much higher amounts of VSOP, while macrophages are particularly efficient in uptaking VSOPs. We also had to apply relatively long scanning times to visualize 1×10^3 labeled cells. Moreover, ultra long-term *in vivo* imaging at 3T may necessitate higher cell concentrations as cell loss or dilution of intracellular iron content due to *in vivo* proliferation may reduce the overall signal obtained. It should be noted though that cell detectability is different in gel phantom and *in vivo* imaging, the latter commonly associated with higher detection limits.

On the other hand, 3T SWI with a short-term protocol optimized for cell detectability was only able to detect 5×10^4 cells in a layer phantom, modeling wide-spread cell distribution as can be observed after systemic transplantation or migration. Apart from the shorter imaging time and the lower number of

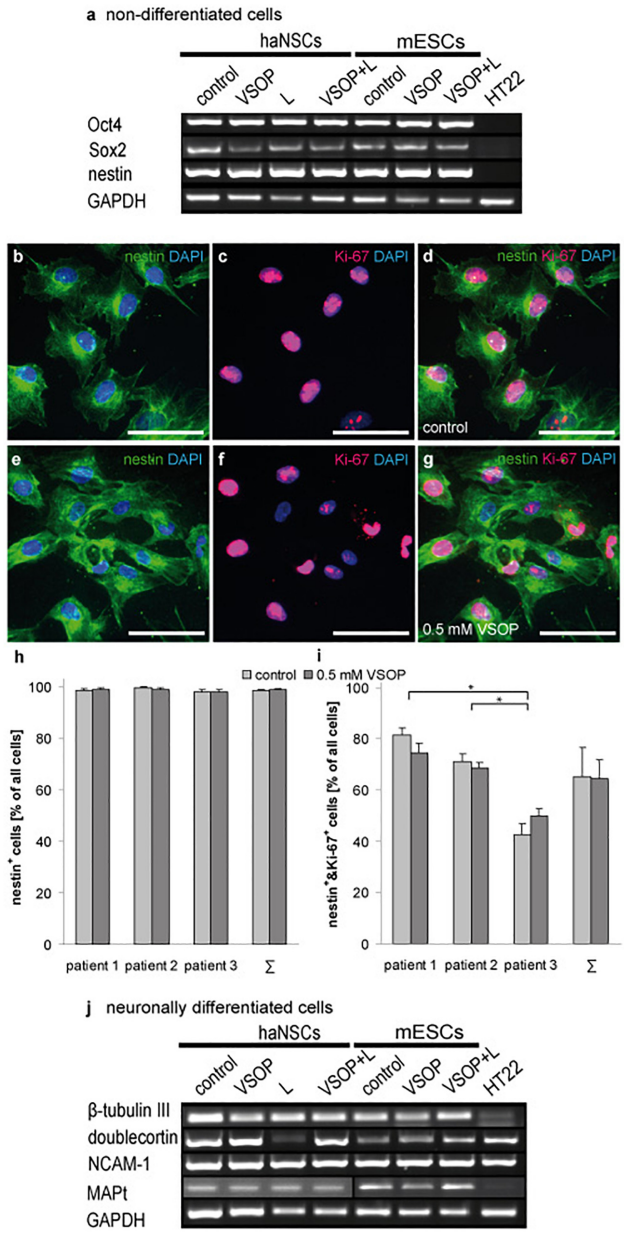

FIGURE 4 | Transcriptional and immunohistochemical analysis of stemness and neuronal differentiation (n = 6 to 10). **(a)** VSOP-labeling and lipofection of non-differentiated stem cells; RT-PCR analysis of pluripotency markers revealed no impact on stemness, and transcribed nestin. 99% of haNSCs expressed the intermediate filament protein nestin, and 65% co-express the nuclear proliferation marker Ki-67. No significant difference between control cells and VSOP labeled haNSCs could be detected. **(b–d)** show unlabeled control cells, and **(e–g)** give the VSOP labeled pendant. **(h)** Nestin expression of haNSCs from three different patients was compared, showing that there is neither a significant difference between patients nor between control cells or labeled cells. **(i)** 65% of haNSCs co-express nestin and Ki-67, but significant differences between the three patients become apparent. **(j)** Subsequent neuronal differentiation (n = 6 to 10) resulted in a neuronal phenotype transcribing β-tubulin III, doublecortin, N-CAM1, and MAP-2. Mature mouse hippocampal cells HT22 served as a negative control for pluripotency markers and as a positive control for mature neuronal markers. Scale bars represent 50 μm. *$p < 0.01$.

averages, the higher detection limit might have two potential reasons. First, layer phantoms represent the cell distribution seen after systemic (intraarteriell or intravenous) cell injection. Systemic cell injection is believed to be more feasible for clinical applications and is therefore used predominantly in ongoing clinical trials (Cui et al., 2019). The density of cells is lower than in injection phantoms that represent the situation after stereotactic cell implantation procedures, being reserved for a targeted approach requiring local cell deposits. Second, the imaging protocol applied for layer phantom imaging was developed for mesenchymal stem cells which are larger than haNSCs and might therefore incorporate more VSOP leading to better detectability. 7T MRI, which is being introduced into clinical imaging, and allowing for detection of small local concentrations of labeled cells while the feature of VSOP to further reduce the longitudinal (T1) and transverse (T2) relaxation time may provide much better cell detectability at high filed strengths in future applications (Klug et al., 2010).

In summary, our study strongly suggests that in the clinical setting, cell tracking using magnetic VSOP labeling represents a safe method, capable of addressing three key issues vital for effective transplantation strategies: location, migration, and viability.

MATERIALS AND METHODS

Ethics Statement

Human adult neural stem cells were obtained from patients with temporal lobe epilepsy submitted to epilepsy surgery. Informed and written consent was given for additional scientific investigations approved by the local ethics committee of the University of Erlangen, in accordance with the Declaration of Helsinki.

Human Adult Neural Stem Cell and Murine Embryonic Stem Cell Cultures

Composition of expansion and differentiation media is given in **Table 1**. After surgical en bloc resection, the dentate gyrus was micro-dissected and dissociated mechanically followed by enzymatic digestion as described previously (Hoehn et al., 2002). Of the obtained cells, haNSC from passage 5 to 11 were cryopreserved, shipped to the primary investigation site and used for all experiments. Cells were plated on poly-L-ornithine (250 μg/mL)-/laminin (15 μg/mL, both Sigma-Aldrich, Munich, Germany)-coated cell culture dishes (Sarstedt, Nuembrecht, Germany) and grown in expansion medium at 37°C and 5% CO_2. Medium was changed every second day. Cells were detached with accutase (PAA, Cölbe, Germany) at 80% confluence, and split. Culturing over at least five passages selected for proliferating cells.

Previously cryopreserved mouse embryonic stem cells (mESCs, CRL-1934, ATCC, Manassas, United States) were cultured in expansion medium (**Table 1**) at 37°C and 5% CO_2 on mouse fibroblasts (CRL-1503, ATCC, Manassas, United States) inactivated by mitomycin C (Sigma-Aldrich). Stem cells were

TABLE 1 | Expansion and differentiation media.

haNSC		mESC				
Basic cell culture medium				**mESC-derived nestin+ neural progenitors**		
Knockout-DMEM and Ham's F12, 5% knockout serum replacement, 2 mM L-glutamine, 1% penicillin-streptomycin, 1% MEM non-essential amino acids, and 1% N2 supplement (all Invitrogen, Karlsruhe, Germany)						
Expansion medium	**Differentiation medium**	**Expansion medium**	**Differentiation medium**	**Selection medium (from mESC)**	**Expansion medium**	**Differentiation medium**
Basic cell culture medium	Basic cell culture medium	Basic cell culture medium	Basic cell culture medium	Knockout-DMEM and Ham's F12	haNSC/mESC basic cell culture medium	Expansion medium
+10 ng/mL basic fibroblast growth factor (bFGF, Invitrogen)	+2% B-27 supplement	+0.1 mM 2-mercaptoethanol	Embryoid body formation in bacterial dishes for 6 days, final differentiation in gelatine-coated dishes	+1 % ITS supplement (insulin-transferrin-selenium, Invitrogen)	+10% knockout serum replacement	- N2 supplement
+10 ng/mL epidermal growth factor (EGF, Invitrogen)	+200 ng/mL sonic hedgehog (SHH)	+15 ng/mL LIF			+10 ng/mL bFGF	- bFGF
+2.5 μg/mL bovine pituitary extract (BPE, Sigma-Aldrich)	+100 ng/mL fibroblast growth factor-8 (FGF-8)	On mouse fibroblasts (CRL-1503, Sigma)				+20 ng/mL nerve growth factor (NGF) (Invitrogen)
+15 ng/mL leukemia inhibitory factor (LIF, Sigma-Aldrich)	+2 mM ascorbic acid					+1× B-27 supplement (Invitrogen)
+2 μg/mL heparin						

separated from the fibroblast layer at 60% confluence by detaching them with accutase, and transferred to gelatin-coated cell culture dishes with daily medium changes. mESCs were detached and transferred every other day. A fibroblast-free mESCs culture was obtained after three passages.

Magnetic Cell Labeling and Viability Assessment

Sterile VSOP (C200, Ferropharm, Teltow, Germany), consisting of a 5nm iron oxide core coated with monomer citrate, resulting in a hydrodynamic diameter of 11 nm and a negative charge were used for labeling at 0.5 and 1.5 mM with or without additional lipofection agent (lipofectin, Invitrogen) for 4 h as described previously (Gupta et al., 2007). These molarities were chosen based on previous findings showing that VSOP labeling causes transient oxidative stress or even irreversible cell damage (Stroh et al., 2004, 2009). Transient oxidative stress is already observed at 1.5 mM, and higher incubation molarities such as 3.0 or 6.0 mM cause more intensive stress or even increase apoptosis and necrosis. In turn, higher VSOP incubation molarities not necessarily shortens T2 relaxation times or increases detectability, particularly in smaller cells (Stroh et al., 2009).

Control specimens were incubated in Opti-MEM I for 4 h instead. First, potential donor-specific viability differences were assessed 20 h after labeling with 0.5 mM VSOP. Only cells samples with >80% viability after labeling were defined acceptable for further investigation. Next, cell viability in relation to incubation molarities was assessed 8 and 48 h after VSOP incubation by the Trypan Blue (Sigma-Aldrich) exclusion test on 10 randomly selected regions per coverslip.

Labeling Efficacy Assessment and haNSC Proliferation Experiments

Uptake of VSOP was evaluated using Prussian blue staining 48 h and 28 days after VSOP labeling by phase contrast microscopy of 10 regions per coverslip. The relative labeling efficacy was displayed as a ratio of Prussian blue positive cells to all cells identified by nuclear counterstaining.

After labeling with 0.5 μM or 1.5 μM VSOP (see above), haNSCs were seeded on 12-well-plates covered with poly-L-ornithine-covered (Sigma-Aldrich) at a density of 7,500 cells/cm^2 (28,500 cells/well) on expansion medium. Unlabeled haNSCs served as controls. Proliferation of haNSCs was monitored over 8 days, and cell culture medium was exchanged every second day. Cell numbers were assessed on days 1, 2, 4, and 8 in three wells for each VSOP concentration and on each day. Experiments were performed with using a total of six haNSC lines derived from three different patients ($n = 3$).

NMR Relaxometry

Further, nuclear magnetic resonance (NMR) relaxometry was performed to determine the T2 time (transverse relaxation time). 9×10^5 cells were suspended in 3 mL PBS and measured in a NMR-Relaxometer Minispec 0.47T/20MHz (Bruker, Ettlingen, Germany). Data analysis was performed using the ORIGIN Pro 8G software (OriginLab Corporation, Northampton, MA,

United States). All samples have been analyzed in three independent experiments.

Clinical MR Imaging at 3 Tesla

Detectability of VSOP labeled haNSCs was assessed by *in vitro* MRI. Two different types of agarose gel phantoms, cell injection and cell layer phantoms, were used. For injection phantoms, 1×10^3 magnetically labeled haNSCs (1.5 μM VSOP) were injected into air bubble-free gel phantoms as described previously (Soenen et al., 2011). Briefly, 1×10^3 magnetically labeled haNSCs were injected on one side of the phantom, and 1×10^3 non-labeled haNSCs on the other.

Injection phantom MRI was performed on a clinical 3 Tesla scanner (Achieva 3T, Philips Medical Systems, Best, Netherlands) under conditions optimized for cell imaging. A 3T solenoid rat coil (RX SN 1116, Philips) with a coil diameter of 55 mm was used. 2D gradient echo sequences were applied, with TE/TR 13.8/50 ms, a flip angle of the excitation pulse of 15°, yielding images that were T2* (effective transverse relaxation time) weighted. Both a coronal as well as a sagittal data set was acquired covering the entire gel phantom. The slice thickness was 0.3 mm, the interslice distance 0.15 mm, with a 20 mm field of view, and a 288 × 288 matrix, resulting in an inplane resolution of 69 μm and a voxel size of $69 \times 69 \times 300\ \mu m^3$.

Layer gel phantoms were produced as described elsewhere (Lobsien et al., 2013). Two phantoms were produced, each containing four layers in which unlabeled or VSOP-labeled haNSCs (1.5 μM) were embedded. Layer phantom 1 contained layers with 5×10, 1×10^2, 5×10^2, and 1×10^3 VSOP-labeled haNSCs, respectively. Layer phantom 2 contained layers with 5×10^3, 1×10^4, and 5×10^4 VSOP-labeled haNSCs, as well as a layer containing 5×10^4 unlabeled haNSCs.

Layer phantom MRI was performed on a clinical 3 Tesla Scanner (Magnetom Trio, Siemens, Erlangen, Germany) equipped with a standard 8ch knee coil. The imaging protocol was not particularly optimized for cellular imaging but rather to reflect a clinical situation. 3D Susepctibility-weighted images (SWI) were obtained with TE/TR 20/60 ms at a flip-angle FA of 15°. A voxel size of $560\ \mu m^3 \times 490\ \mu m^3 \times 250\ \mu m^3$ was achieved. Acquisition time TA was 41:00 min. SWI sequences were processed by vendor-specific software of the MRI scanner (Syngo B15, Siemens, Erlangen, Germany) and analyzed without further post-processing.

RT-PCR Analysis

Cells were harvested before and after magnetic labeling, and neuronal differentiation (see below), respectively. RNA species >200 nt were extracted using Mini RNeasy kit. cDNA synthesis with integrated removal of genomic DNA contamination was performed on 1 μg RNA using QuantiTect Reverse Transkription kit (both Qiagen, Hilden, Germany). PCR was performed on 2 μl of cDNA using Taq-DNA-Polymerase all inclusive kit (Peqlab, Erlangen, Germany). **Table 2** shows the primer sequences used in this experiment. All samples were analyzed in at least three independent experiments. Mature mouse hippocampal cells HT22 were used as a negative control for pluripotency and neural progenitor markers.

TABLE 2 | List of primers.

Gene	Primer forward	Primer reverse
Oct4	5′- CTCCTGAAGCAGA AGAGGATCAC-3′	5′-CTTCTGGCGCCGG TTACAGAACCA-3′
Sox2	5′-TGCAGTACAACT CCATGACCA-3′	5′-GTGCTGGGACATGT GAAGTCG-3′
nestin	5′-CAGCGTTGGAACAG AGGTTG-3′	5′-GCTGGCACAGG TGTCTCAAG-3′
β_3-tubulin	5′-GCAAGGCCTTCC TGCACT-3′	5′-GCGTCCTGGTACT GCTGGTA-3′
DCX	5′-GACAGCCCACTCT TTTGAGC-3′	5′-GCGTAGAGATGGGA GACTGC-3′
NCAM1	5′-TATCCCAGTGCCA CGATCTC-3′	5′-TGGCTTCCTTGGC ATCATAC-3′
MAP-2 (*mus musculus*)	5′-GGTGGCAAGGTGC AGATAAT-3′	5′-CTTTGGCATTCTCC CTGAAG-3′
MAP-2 *(homo sapiens)*	5′-GTGGGGGTTGTC ACAGAGG-3′	5′-GCTCTCCCAGCG GCAAGG-3′
GAPDH	5′-CAACGAATTTGGC TACAGCA-3′	5′-AGGGGTCTACATG GCAACTG-3′

Fluorescence Immunocytochemistry and Characterization

For characterization of cultured haNSCs and for determining effects of magnetic labeling on stemness, cells were fixed in PBS-buffered paraformaldehyde (4%). Processing, immunocytochemistry and quantitative evaluation were performed as described elsewhere (Heyn et al., 2006). Mouse-anti-Ki67 (Dako, 1:100, proliferation marker), and rabbit-anti-nestin (Millipore, 1:200, neural progenitor cell marker) were used as primary antibodies, and Alexa Fluor 555 or 488 (both Invitrogen, 1:100) served as secondary antibodies. Nuclei were labeled by 4′,6-Diamidino-2-phenylindole dihydrochloride (DAPI, Sigma-Aldrich, 1.1000). For analysis, 10 randomly selected regions per coverslip were counted. Percentage was determined as the number of nestin$^+$, Ki-67$^+$, or Ki-67$^+$/nestin$^+$ cells compared to total cells identified by nuclear DAPI counterstaining.

Neuronal Differentiation of haNSCs and mESC

The possible interference of VSOP-labeling or lipofectin on neuronal differentiation was also assessed. haNSC were differentiated for 15 days in haNSC differentiation medium (**Table 1**), which was changed every second day. Six independent experiments were conducted, containing at least three technical replicates each.

mESCs-differentiation was performed as described elsewhere (Bibel et al., 2004) with some modifications. For embryoid body formation expanded mESCs were transferred into bacterial dishes and LIF was removed. After 6 days cells had aggregated and formed embryoid bodies, which were carefully transferred to gelatine-coated dishes. During the following 2–3 days, the heterogeneous bodies adhered and migrating cells started to form a monolayer. Neural progenitor cells were selected for 3 days and then expanded in neural progenitor expansion medium

(**Table 1**) for 10 days. RT-PCR analysis and Prussian blue staining were performed as described above. Ten independent experiments were conducted.

Statistical Analysis

Statistical analysis was conducted using SPSS (Chicago, IL, United States) software. First, data sets from all conditions were tested for normal distribution using the parameter free one-sample Kolmogorov-Smirnov test. In cases where normal distribution of data was confirmed, the parametric two-tailed Student's *t*-test was employed to compare means. *P*-values <0.01 were considered statistically significant. All data are presented as mean ± standard error of the mean (SEM).

DATA AVAILABILITY STATEMENT

The datasets generated for this study are available on request to the corresponding author.

ETHICS STATEMENT

Human adult neural stem cells were obtained from patients with temporal lobe epilepsy submitted to epilepsy surgery. Informed and written consent was given for additional scientific investigations approved by the local ethics committee of the University of Erlangen, in accordance with the Declaration of Helsinki.

AUTHOR CONTRIBUTIONS

AS, JK, IB, JS, CZ, and JB: conception and design. AS, JK, RC, AD, WF, and SZ: collection of data. AF and DL: collection of data, and data analysis and interpretation. AS, JK, and JB: data analysis and interpretation, and manuscript writing. All authors have approved the final manuscript.

FUNDING

VSOP were kindly provided by Herbert Pilgrimm, Ferropharm. This work was supported by the Bavarian State Ministry of Sciences, Research and the Arts ("ForNeuroCell").

ACKNOWLEDGMENTS

The authors thank Vasilis Ntziachristos, AF, and Birte Rings for expert technical support.

REFERENCES

Bauer, M., Kristensen, B. W., Meyer, M., Gasser, T., Widmer, H. R., Zimmer, J., et al. (2006). Toxic effects of lipid-mediated gene transfer in ventral mesencephalic explant cultures. *Basic Clin. Pharmacol. Toxicol.* 98, 395–400. doi: 10.1111/j.1742-7843.2006.pto_310.x

Bellenchi, G. C., Volpicelli, F., Piscopo, V., Perrone-Capano, C., and di Porzio, U. (2013). Adult neural stem cells: an endogenous tool to repair brain injury? *J. Neurochem.* 124, 159–167. doi: 10.1111/jnc.12084

Bibel, M., Richter, J., Schrenk, K., Tucker, K. L., Staiger, V., Korte, M., et al. (2004). Differentiation of mouse embryonic stem cells into a defined neuronal lineage. *Nat. Neurosci.* 7, 1003–1009. doi: 10.1038/nn1301

Boltze, J., Arnold, A., Walczak, P., Jolkkonen, J., Cui, L., and Wagner, D. C. (2015). The dark side of the force - constraints and complications of cell therapies for stroke. *Front. Neurol.* 6:155. doi: 10.3389/fneur.2015.00155

Cui, L. L., Golubczyk, D., Tolppanen, A. M., Boltze, J., and Jolkkonen, J. (2019). Cell therapy for ischemic stroke: are differences in preclinical and clinical study design responsible for the translational loss of efficacy? *Ann. Neurol.* 86, 5–16.

Dietrich, J., and Kempermann, G. (2006). Role of endogenous neural stem cells in neurological disease and brain repair. *Adv. Exp. Med. Biol.* 557, 191–220. doi: 10.1007/0-387-30128-3_12

Focke, A., Schwarz, S., Foerschler, A., Scheibe, J., Milosevic, J., Zimmer, C., et al. (2008). Labeling of human neural precursor cells using ferromagnetic nanoparticles. *Magn. Reson. Med.* 60, 1321–1328. doi: 10.1002/mrm.21745

Gupta, A. K., Naregalkar, R. R., Vaidya, V. D., and Gupta, M. (2007). Recent advances on surface engineering of magnetic iron oxide nanoparticles and their biomedical applications. *Nanomedicine* 2, 23–39. doi: 10.2217/17435889.2.1.23

Guzman, R., Uchida, N., Bliss, T. M., He, D., Christopherson, K. K., Stellwagen, D., et al. (2007). Long-term monitoring of transplanted human neural stem cells in developmental and pathological contexts with MRI. *Proc. Natl. Acad. Sci. U.S.A.* 104, 10211–10216. doi: 10.1073/pnas.0608519104

Heyn, C., Ronald, J. A., Mackenzie, L. T., MacDonald, I. C., Chambers, A. F., Rutt, B. K., et al. (2006). In vivo magnetic resonance imaging of single cells in mouse brain with optical validation. *Magn. Reson. Med.* 55, 23–29. doi: 10.1002/mrm.20747

Hinds, K. A., Hill, J. M., Shapiro, E. M., Laukkanen, M. O., Silva, A. C., Combs, C. A., et al. (2003). Highly efficient endosomal labeling of progenitor and stem cells with large magnetic particles allows magnetic resonance imaging of single cells. *Blood* 102, 867–872. doi: 10.1182/blood-2002-12-3669

Hoehn, M., Kustermann, E., Blunk, J., Wiedermann, D., Trapp, T., Wecker, S., et al. (2002). Monitoring of implanted stem cell migration *in vivo*: a highly resolved in vivo magnetic resonance imaging investigation of experimental stroke in rat. *Proc. Natl. Acad. Sci. U.S.A.* 99, 16267–16272. doi: 10.1073/pnas.242435499

Janowski, M., Wagner, D. C., and Boltze, J. (2015). Stem cell-based tissue replacement after stroke: factual necessity or notorious fiction? *Stroke* 46, 2354–2363. doi: 10.1161/strokeaha.114.007803

Klug, G., Kampf, T., Bloemer, S., Bremicker, J., Ziener, C. H., Heymer, A., et al. (2010). Intracellular and extracellular T1 and T2 relaxivities of magneto-optical nanoparticles at experimental high fields. *Magn. Reson. Med.* 64, 1607–1615. doi: 10.1002/mrm.22557

Kondziolka, D., Steinberg, G. K., Cullen, S. B., and McGrogan, M. (2004). Evaluation of surgical techniques for neuronal cell transplantation used in patients with stroke. *Cell Transplant.* 13, 749–754. doi: 10.3727/000000004783983350

Lobsien, D., Dreyer, A. Y., Stroh, A., Boltze, J., and Hoffmann, K. T. (2013). Imaging of VSOP labeled stem cells in agarose phantoms with susceptibility weighted and T2* weighted MR imaging at 3T: determination of the detection limit. *PLoS One* 8:e62644. doi: 10.1371/journal.pone.0062644

Miller, I. S., Lynch, I., Dowling, D., Dawson, K. A., and Gallagher, W. M. (2010). Surface-induced cell signaling events control actin rearrangements and motility. *J. Biomed Mater. Res. A* 93, 493–504. doi: 10.1002/jbm.a.32530

Modo, M., Cash, D., Mellodew, K., Williams, S. C., Fraser, S. E., Meade, T. J., et al. (2002). Tracking transplanted stem cell migration using bifunctional, contrast agent-enhanced, magnetic resonance imaging. *Neuroimage.* 17, 803–811. doi: 10.1016/s1053-8119(02)91194-8

Neri, M., Maderna, C., Cavazzin, C., Deidda-Vigoriti, V., Politi, L. S., Scotti, G., et al. (2008). Efficient in vitro labeling of human neural precursor cells with

superparamagnetic iron oxide particles: relevance for in vivo cell tracking. *Stem Cells* 26, 505–516. doi: 10.1634/stemcells.2007-0251

Nichols, J., Zevnik, B., Anastassiadis, K., Niwa, H., Klewe-Nebenius, D., Chambers, I., et al. (1998). Formation of pluripotent stem cells in the mammalian embryo depends on the POU transcription factor Oct4. *Cell* 95, 379–391. doi: 10.1016/s0092-8674(00)81769-9

Novotna, B., Jendelova, P., Kapcalova, M., Rossner, P. Jr., Turnovcova, K., Bagryantseva, Y., et al. (2012). Oxidative damage to biological macromolecules in human bone marrow mesenchymal stromal cells labeled with various types of iron oxide nanoparticles. *Toxicol. Lett.* 210, 53–63. doi: 10.1016/j.toxlet.2012.01.008

Pouliquen, D., Le Jeune, J. J., Perdrisot, R., Ermias, A., and Jallet, P. (1991). Iron oxide nanoparticles for use as an MRI contrast agent: pharmacokinetics and metabolism. *Magn. Reson. Imaging* 9, 275–283. doi: 10.1016/0730-725x(91)90412-f

Soenen, S. J., Himmelreich, U., Nuytten, N., and De Cuyper, M. (2011). Cytotoxic effects of iron oxide nanoparticles and implications for safety in cell labelling. *Biomaterials* 32, 195–205. doi: 10.1016/j.biomaterials.2010.08.075

Stover, N. P., Bakay, R. A., Subramanian, T., Raiser, C. D., Cornfeldt, M. L., Schweikert, A. W., et al. (2005). Intrastriatal implantation of human retinal pigment epithelial cells attached to microcarriers in advanced Parkinson disease. *Arch. Neurol.* 62, 1833–1837.

Stroh, A., Boltze, J., Sieland, K., Hild, K., Gutzeit, C., Jung, T., et al. (2009). Impact of magnetic labeling on human and mouse stem cells and their long-term magnetic resonance tracking in a rat model of Parkinson disease. *Mol. Imaging* 8, 166–178.

Stroh, A., Faber, C., Neuberger, T., Lorenz, P., Sieland, K., Jakob, P. M., et al. (2005). In vivo detection limits of magnetically labeled embryonic stem cells in the rat brain using high-field (17.6 T) magnetic resonance imaging. *Neuroimage.* 24, 635–645. doi: 10.1016/j.neuroimage.2004.09.014

Stroh, A., Tsai, H. C., Wang, L. P., Zhang, F., Kressel, J., Aravanis, A., et al. (2011). Tracking stem cell differentiation in the setting of automated optogenetic stimulation. *Stem Cells* 29, 78–88. doi: 10.1002/stem.558

Stroh, A., Zimmer, C., Gutzeit, C., Jakstadt, M., Marschinke, F., Jung, T., et al. (2004). Iron oxide particles for molecular magnetic resonance imaging cause transient oxidative stress in rat macrophages. *Free Radic. Biol. Med.* 36, 976–984. doi: 10.1016/j.freeradbiomed.2004.01.016

Suh, H., Consiglio, A., Ray, J., Sawai, T., D'Amour, K. A., and Gage, F. H. (2007). In vivo fate analysis reveals the multipotent and self-renewal capacities of Sox2+ neural stem cells in the adult hippocampus. *Cell Stem Cell* 1, 515–528. doi: 10.1016/j.stem.2007.09.002

Walczak, P., Ruiz-Cabello, J., Kedziorek, D. A., Gilad, A. A., Lin, S., Barnett, B., et al. (2006). Magnetoelectroporation: improved labeling of neural stem cells and leukocytes for cellular magnetic resonance imaging using a single FDA-approved agent. *Nanomedicine* 2, 89–94. doi: 10.1016/j.nano.2006.01.003

Weissleder, R., Stark, D. D., Engelstad, B. L., Bacon, B. R., Compton, C. C., White, D. L., et al. (1989). Superparamagnetic iron oxide: pharmacokinetics and toxicity. *Am. J. Roentgenol.* 152, 167–173. doi: 10.2214/ajr.152.1.167

Zimmer, C., Weissleder, R., Poss, K., Bogdanova, A., Wright, S. C. Jr., and Enochs, W. S. (1995). MR imaging of phagocytosis in experimental gliomas. *Radiology* 197, 533–538. doi: 10.1148/radiology.197.2.7480707

Conflict of Interest: The authors declare that the research was conducted in the absence of any commercial or financial relationships that could be construed as a potential conflict of interest.

Copyright © 2019 Stroh, Kressel, Coras, Dreyer, Fröhlich, Förschler, Lobsien, Blümcke, Zoubaa, Schlegel, Zimmer and Boltze. This is an open-access article distributed under the terms of the Creative Commons Attribution License (CC BY). The use, distribution or reproduction in other forums is permitted, provided the original author(s) and the copyright owner(s) are credited and that the original publication in this journal is cited, in accordance with accepted academic practice. No use, distribution or reproduction is permitted which does not comply with these terms.

frontiers in Neurology

REVIEW
published: 18 October 2019
doi: 10.3389/fneur.2019.01103

Thyroid Hormones in the Brain and Their Impact in Recovery Mechanisms After Stroke

Daniela Talhada[1,2,3], *Cecília Reis Alves Santos*[2], *Isabel Gonçalves*[2] *and Karsten Ruscher*[1,3]*

[1] *Laboratory for Experimental Brain Research, Division of Neurosurgery, Department of Clinical Sciences, Lund University, Lund, Sweden,* [2] *CICS-UBI-Health Sciences Research Centre, Faculdade de Ciências da Saúde, Universidade da Beira Interior, Covilha, Portugal,* [3] *LUBIN Lab-Lunds Laboratorium för Neurokirurgisk Hjärnskadeforskning, Division of Neurosurgery, Department of Clinical Sciences, Lund University, Lund, Sweden*

Thyroid hormones are of fundamental importance for brain development and essential factors to warrant brain functions throughout life. Their actions are mediated by binding to specific intracellular and membranous receptors regulating genomic and non-genomic mechanisms in neurons and populations of glial cells, respectively. Among others, mechanisms include the regulation of neuronal plasticity processes, stimulation of angiogenesis and neurogenesis as well modulating the dynamics of cytoskeletal elements and intracellular transport processes. These mechanisms overlap with those that have been identified to enhance recovery of lost neurological functions during the first weeks and months after ischemic stroke. Stimulation of thyroid hormone signaling in the postischemic brain might be a promising therapeutic strategy to foster endogenous mechanisms of repair. Several studies have pointed to a significant association between thyroid hormones and outcome after stroke. With this review, we will provide an overview on functions of thyroid hormones in the healthy brain and summarize their mechanisms of action in the developing and adult brain. Also, we compile the major thyroid-modulated molecular pathways in the pathophysiology of ischemic stroke that can enhance recovery, highlighting thyroid hormones as a potential target for therapeutic intervention.

Keywords: brain, recovery, stroke, thyroid hormones, 3,5,3′,5′-tetraiodo-L-thyronine (T_4), 3,5,3′-triiodo-L-thyronine (T_3)

OPEN ACCESS

Edited by:
Stephan Schilling, Fraunhofer Society (FHG), Germany

Reviewed by:
Steffen Rossner, Leipzig University, Germany
Tobias Bobinger, University Hospital Erlangen, Germany

***Correspondence:**
Karsten Ruscher
karsten.ruscher@med.lu.se

Specialty section:
This article was submitted to Stroke, a section of the journal Frontiers in Neurology

Received: *29 May 2019*
Accepted: *02 October 2019*
Published: *18 October 2019*

Citation:
Talhada D, Santos CRA, Gonçalves I and Ruscher K (2019) Thyroid Hormones in the Brain and Their Impact in Recovery Mechanisms After Stroke. Front. Neurol. 10:1103. doi: 10.3389/fneur.2019.01103

INTRODUCTION

Thyroid hormones (TH), 3,5,3′,5′-tetraiodo-L-thyronine (T_4) and 3,5,3′-triiodo-L-thyronine (T_3), are important for brain development in mammals, during embryonic and fetal stages, regulating processes of neuronal proliferation, migration and differentiation, neurite outgrowth, synaptic plasticity, dendritic branching, and myelination (1–5). Also, after birth, TH are crucial for normal brain function throughout the entire life. Specifically for the central nervous system (CNS) the active form T_3 is a key regulator for normal metabolism in humans and rodents (1, 6, 7).

Availability of T_3 to the developing and adult brain is tightly controlled by mechanisms regulating TH secretion, free fraction unbound to thyroxine binding globulins (TBG), transmembrane transporters and the activity of iodothyronine deiodinases (DIO). The pattern of these regulatory processes may vary according to the developmental stage and in the adult brain. T_3 plays an essential role for neurological functions, and minimal disturbances of these mechanisms may have consequences for normal brain development and function (1, 8).

Dependence of the CNS on T_3 at all stages of development prompted us to review the actions of TH and the relevance of these mechanisms for processes of recovery after ischemic stroke. We will begin to provide an overview on TH signaling in the brain during development and throughout adult life. Thereafter, we will focus on molecules involved in TH signaling after stroke. TH actions at specific time points after the insult, that are dependent of carrier proteins, transmembrane transporters, DIO activity, thyroid hormone receptors (TR) and co-factors, may provide information on underlying molecular and cellular mechanisms that enhance functional recovery of lost neurological functions. Moreover, we will discuss which mechanisms of action of TH in the brain may contribute to enhance functional outcome in stroke patients.

THYROID HORMONE TRANSPORT AND AVAILABILITY TO THE HUMAN AND RODENT BRAIN

In the adult, TH originate in the thyroid gland that secretes ∼93% as T_4 and 7% as T_3. Once secreted to plasma, TH binding proteins play an important role to maintain TH homeostasis and distribution into tissues, and <0.1% of TH circulate free in the blood (9, 10). In humans, 65% of TH bind to TBG, 20% to albumin and about 15% to transthyretin (TTR) (11, 12) while in rodents TTR is the main protein carrier in the blood circulation (13, 14). TH also bind to lipoproteins to a less extent (15, 16).

In contrary to processes during brain development, a different fraction of T_3 in the adult brain is provided from free T_3 available in the blood circulation and in the cerebrospinal fluid (CSF) (17, 18). Most of TH provided to the brain crosses the blood brain barrier (BBB) and around 20% the blood cerebrospinal fluid barrier (BCSFB) (19, 20). This passage is mediated by transmembrane transporter proteins with overlapping specificity that were identified in endothelial cells of brain microvessels that constitute the BBB and epithelial cells of the choroid plexus (CP) of humans and rodents. These transporters are also important for brain development, and include monocarboxylate transporter (MCT), organic anion transporting polypeptide (OATP), large neutral aminoacid transporter (LAT) and sodium/taurocholate co-transporting polypeptide (SLC10A1) families (17, 21–31). Among those, MCT8 is of particular importance for T_3 (21, 26, 29), and in mice deficient for this transporter, T_3 uptake is compromised (32). In humans, MCT10 also facilitates uptake and efflux of TH, in particular for T_3 (33). The gene that encodes MCT8 (*Slc16a2*) is also present in membranes of neurons, astrocytes, tanycytes and oligodendrocyte precursor cells and OATP1C1 mRNA has been found in astrocytes (34), mediating intracellular TH transport. In addition, it has been proposed that either T_4 or T_3 or both are captured via gaps at the endfeet of astrocytes covering brain microvessels (35, 36).

In contrast to the rodent, MCT8 deficiency in humans results in low T_3 levels in the brain and high levels in the serum due to TH transport deficiency. Thus, the development of the cerebral cortex is impaired accompanied with severe neurological impairment (37–40). The lack of alternative TH transporters such as OATP1C1 (28) and MCT10 (41) in the adult human brain to compensate the transport of T_3, may contribute to the neurological deficits observed in humans with MCT8 mutations. The activity of DIO2 and DIO3 in the brain is important to balance neuronal intracellular T_3 levels in the adult brain, according to the developmental stage and brain region (42–44). DIO enzymes catalyze and remove specific iodine atoms from iodothyronine molecules. In rodents, ∼50% of T_3 levels localized in the brain relies on local deiodination of T_4 in astrocytes and tanycytes by DIO2 (45). T_3 produced in glial cells is able to promote T_3 driven transcriptional activity in neurons, demonstrated by *in vitro* experiments in co-cultures of H4 human glioma cells expressing DIO2 and neuroblastoma cells (46). Homeostasis of T_3 in the CNS is also controlled by DIO3 activity in neurons, that converts T_4 into 3,3′,5′ reverse triiodo-L-thyronine (rT_3) and inactivates T_3 into 3,3′-diiodo-L-thyronine (T_2) (43, 47, 48).

Other compensatory mechanisms to maintain sufficient T_3 levels in the rodent brain include the reduction of DIO3 activity and consequently T_3 degradation, the increase of DIO2 activity in astrocytes (17, 32, 49) and the increase of *Dio2* expression in interneurons in the cerebral cortex (50).

THYROID HORMONES IN BRAIN DEVELOPMENT

It has been shown that mechanisms of brain development might be re-activated in processes of brain reorganization following stroke (51) involving cascades regulated by TH. Therefore, knowledge of TH actions critical and specific for each step of brain development is instrumental to understand their functions following stroke. Epidemiological and clinical studies in humans clearly show that several conditions that compromise maternal TH availability to the fetus impair brain development and are associated with neurological disorders and structural defects, most of them irreversible. A detailed review about TH transport, metabolism and function in the developing brain was recently published (52).

Despite epidemiological and clinical studies have demonstrated the demand of TH during brain development, animal experimental models are of high relevance to identify molecular mechanisms and detailed morphological changes of their biological function during brain development (53). Processes of neurogenesis, proliferation, migration, and maturation show different temporal profiles between humans and rodents, however, basic mechanisms and pathways that regulate brain development are similar (54, 55) allowing the extrapolation of TH deficiency mediated effects in rodents to abnormal TH signaling in humans. Maternal TH are crucial for early cortical neurogenesis, neuronal migration and maturation, during the first trimester of gestation, when fetal brain development occurs (1, 56–58). Both T_4 and T_3 are detected in the human brain embryo even before fetal thyroid gland maturation (59) that occurs at 11–12th week of gestation and starts to secrete TH at week 16 (60).

Also in the rat, the embryo is exposed to maternal TH after embryonic day 11 (E11), before the start of thyroid gland development at E17 (61–64). Experimental hypothyroxinemia induced in rats during this period (before E18) causes abnormal neurogenesis in the cortex and hippocampus, leading to impairment of synaptic plasticity and cognitive deficits (65–67), processes of high relevance in mechanisms of recovery after stroke.

Most of TH dependent processes during brain development are due to the interaction of T_3 with nuclear receptors and regulation of gene expression (68). Increasing levels of protein and mRNA encoding TR alpha and beta (TRα and TRβ) isoforms in the cerebrum and cerebellum start from the 8th to 10th week and increase over gestational time (69, 70) and in rodents there is expression of nuclear TR protein before thyroid gland functioning (71) suggesting transcriptional activity of TH. Several TH dependent genes expressed in the fetal rat brain and neuronal cultures, such as cytoskeletal proteins, are involved in mechanisms of neuronal migration and maturation, branching in neurons and astrocytes (1, 72–74). In both human and rodent species, mutations at the *TRα* and *TRβ* result in several neurological disorders (75–79).

The expression pattern of TR in the brain changes during CNS development. TRα1 is the predominant isoform with mRNA and protein expression in the entire brain, in rodents from E14 (80, 81) and in humans from 8th week of gestation (82, 83) onwards, importantly the expression decreases during brain development (84). TRβ1 is expressed at later stages of brain development and in contrary to TRα, TRβ1 mRNA levels do not decrease over gestational time (80, 84, 85). These studies indicate that gene transcription mediated by nuclear TR has spatiotemporal expression patterns and, therefore, TH actions are distinct in all stages of brain development.

In an *in vitro* model of differentiating mouse embryonic stem cell line (ES-E14TG2a) T_3 treatment (1 nM) enhanced the number of nestin-positive neuronal progenitors, accelerated differentiation and increased survival of pyramidal neurons (86). T_3 mediated differentiation was associated with the regulation of genes involved in corticogenesis namely *nestin*, empty spiracles homeobox 1 *(Emx1)*, T-box brain gene 1 *(Tbr1)*, Calmodulin kinase 4 *(Camk4),* and RC3/Neurogranin *(Nrgn)* (86). Regulation of gene expression during differentiation seems to be inversely correlated with levels of chicken ovalbumin upstream-transcription factor 1 (COUP-TF1) (86), that is crucial for adequate neuronal development (87).

MECHANISMS OF THYROID HORMONES ACTIONS IN THE ADULT BRAIN

Cellular actions of TH in the adult brain can be mediated by nuclear receptors and transcriptional activity, and also by non-genomic actions (85, 88, 89). Here we will elaborate in relevant TH actions described in the literature, and below we will delineate TH actions that might be involved in neurorepair processes.

Genomic Actions of TH

Actions of T_3 in the brain are mainly dependent on transcription mediated by T_3 binding to the nuclear receptors and formation of regulatory complexes (85, 88–91). In the presence of TH, TR are regulated by corepressors (CoR) and coactivators (CoA), proteins, that repress or activate transcription, respectively (36, 85, 88, 89, 92) (**Figure 1**).

In mammals, there are four isoforms of TR (TRα1, TRα2, TRβ1, and TRβ2) encoded by genes alpha (*Thra*) and beta (*Thrb*), which expression and distribution is different to the developmental brain (93). These isoforms are differently distributed in the tissues, regulate the transcription of different genes and exert different biological actions (94).

TRα1 and TRβ1 are the predominant isoforms in the CNS. TRα1 mRNA and protein accounts to 70–80% of TR expression in the brain (36, 95, 96). Thus, genomic actions of T_3 in the brain are mainly, but not exclusively, dependent of TRα1 signaling (97). The analysis of brains from TRα1—green fluorescent protein (GFP) mice revealed that this receptor is expressed in all NeuN positive neurons, especially in the nucleus (83). TRα1 is expressed in both excitatory glutamatergic and inhibitory GABAergic neurons in several brain regions including the striatum, cerebral cortex, hippocampus and dentate gyrus, hypothalamus and cerebellum (83, 98). This isoform of TR is also found in tanycytes lining the third ventricle and oligodendrocytes in the hypothalamus, but not in the striatum, somatosensory cortex or hippocampus (83, 99). Its presence in astrocytes is not completely clear (100), however may be dependent on the activation status. Although lower concentration of the receptor is found in cultured rat astrocytes (101), it is not expressed in glial fibrillary acidic protein (GFAP) positive astrocytes in the naïve rat and mouse brain (83, 99). TRα1 is absent in Purkinje cells in the cerebellum (83). Levels of TRα2, a non T_3 binding isoform, is also detected in the adult brain in a similar pattern as TRα1 (98).

TRβ1 is expressed in the neocortex, and mainly expressed in the pyramidal cell layers of the hippocampus, granule cells of dentate gyrus and paraventricular hypothalamic nucleus (102). It is also expressed in myelin basic protein positive oligodendrocytes (99). In contrary to TRα1, this isoform is highly expressed in Purkinje neurons (94). The TRβ2 isoform is restricted to the anterior pituitary gland and hypothalamus (102–105). As for TRα isoforms, TRβ1 and TRβ2 were not observed in positive GFAP positive astrocytes in the rat brain (99).

Although TR are mainly localized in the cell nucleus and nuclear membrane, TRα1 and TRβ1 isoforms have also been found in the cytoplasm of neurons and astroglia, and this shuttle may increase the rate of T_3 nuclear import (106). It has been suggested that T_4 may also exert genomic actions in the brain through binding to TRα1, that is more susceptible to T_4 than TRβ1 (36), however we did not find experimental studies supporting this hypothesis. So far, a total of 4,108 genes, of which 734 have been identified as being repeatedly regulated by T_3 in the rodents' brain by microarray analysis (72). In this review, we provide an overview on T_3-modulated genes that might be involved in brain repair mechanisms (**Table 1**). Hence, different

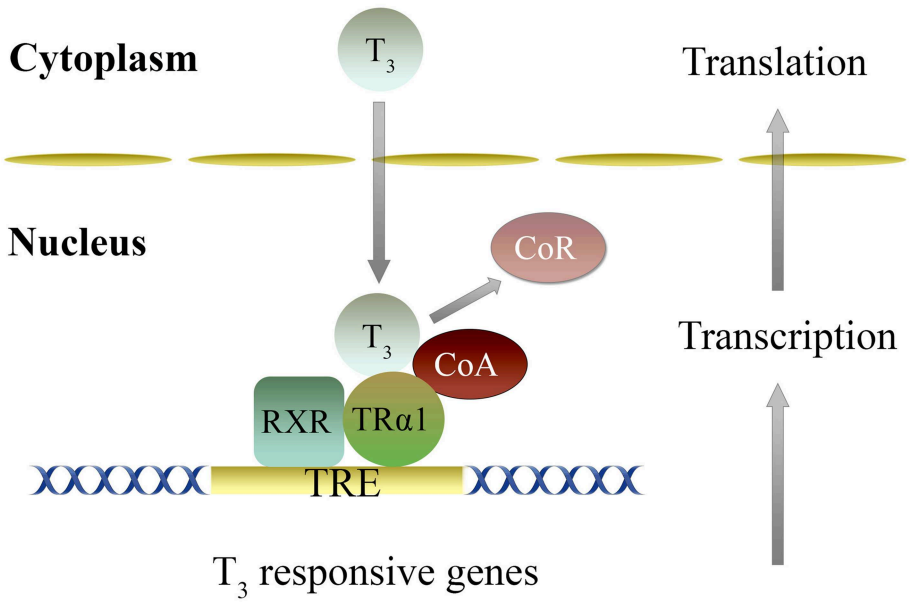

FIGURE 1 | Genomic mechanisms of thyroid hormones action in the brain. Genomic actions of T_3 are dependent on gene transcription mediated by its binding to nuclear TRα and TRβ, and the formation of heterodimer complex with RXR (RXR-TR) that binds to a TRE, located at the regulatory region of T_3 target genes. This activity is regulated by an exchange of CoR for CoA. CoA, Co-activator; CoR, Co-repressor; RXR, Retinoid X receptor; TR, Thyroid hormone receptor; TRE, Thyroid response element; T_3, 3,5,3′-triiodo-L-thyronine.

T_3–dependent transcriptional activities have been observed in different cell types and brain regions.

Non-genomic Actions of TH

TH non-genomic actions that do not require TH binding to nuclear receptors are well-described in the literature (127–130). Actions are immediate and include several interactions of TH with extranuclear receptors, including TRα and TRβ, located in the cytoplasm, cellular membrane, cytoskeleton and mitochondria, modulating several intracellular pathways.

The following points summarize relevant non-genomic actions of TH binding to membranous and cytoplasmic receptors (i–iii), cytoplasmic TH binding proteins affecting ion pumps activity (iv) and the action of TH on the cytoskeleton (v) (**Figure 2**). (i) T_3 complexed to TRβ1 in the cytoplasm interacts with p85α subunit of phosphatidylinositol 3-kinase (PI3K), resulting in phosphorylation and activation of protein kinase (PK) B/Akt signal transduction pathway, rapamycin (mTOR) and phosphorylation of $p70^{S6K}$ (131–136). (ii) T_3 is able to bind to integrin αvβ3 S1 domain in plasma membranes and activates PI3K via Src kinase. T_4 and T_3 interact with integrin αvβ3 S2 domain and activate mitogen-activated protein kinase 1/2 (MAPK 1/2) signaling cascade, through phospholipase C (PLC) and PKC (127, 133, 137–140). Subsequently, it results in an nuclear translocation of TRβ1 (141), estrogen receptor α (142), signal transducing and activator of transcription (STAT) 1α, interferon gamma (IFN-γ) (143) and CoA protein Trip230 (144). In addition, hormone activated MAPK 1/2 phosphorylates TRβ1 at Ser-142, leading to recruitment of CoA proteins (145). (iii) T_4 non-gnomically activates MAPK 1/2 in HeLa and CV-1 cultured cells (146, 147) and phosphorylation of p53 (148) and STAT3 (147). (iv) T_3 modulates Na^+/H^+ exchanger in myoblasts (149); Na-K-ATPase activity in alveolar epithelial cells (150–152), embryonal hepatocytes (153), and synaptosomes (154, 155) through either the PI3K or MAPK pathways (152, 156); the Ca-ATPase activity in erythrocytes (88), the sarcoplasmic reticulum in the heart (157) and in cerebrocortical synaptosomes (158). (v) T_4 and rT_3 stimulate polymerization of actin components of the cytoskeleton neuronal and astrocyte cell cultures, through TH binding to an extranuclear truncated form of TRα1 (TRΔα1) (159–162).

THYROID HORMONES IN THE AGING BRAIN AND ISCHEMIC STROKE

The complex process of aging is associated with changes in TH metabolism and action in all tissues. During aging, the disruption of circadian rhythm leads to a reduction in thyroid stimulating hormone (TSH) secretion (163–165) and circulating TH levels, in particular T_3, in humans (166, 167) and rodents (168). Nevertheless, TH signaling is well-preserved in the aging brain, as demonstrated in mouse models of aging (169).

TABLE 1 | List of genes regulated by thyroid hormones involved in their transport into the brain, mechanisms of tissue repair, and neuronal plasticity following ischemic stroke.

Genes human/rodent	Gene name	Function	Tissue/cultured cells	References
SLC16A2/Slc16a2	MCT8	TH transport	Brain	(107)
DIO2/Dio2	DIO2	TH deiodination		
DIO3/Dio3	DIO3			
Bcl2	Bcl2	Neuronal survival, neurogenesis and neurotrophic factors	Brain cortex	(107–109)
Vegfa	VEGFA			
Sox2	SRY-box2			
Ntf	Neurotrophin			
Nos2	NOS2			
HIF2α	HIF2α		Neuroblastoma cell line	(107)
VEGF	VEGF			
c-JUN	c-Jun			
ENO2	Enolase-2			
Emx1	empty spiracles homeobox 1		mES cell line	(86)
Tbr1	T-box brain gene 1			
Bdnf	Brain derived neurotrophic factor		Hippocampal slices	(110)
Slc12a5	KCC2			
NRGN/Nrgn	Neurogranin	Synaptic plasticity	Hippocampus and forebrain/mES cell line	(86, 111–113)
CAMK4/Camk4	Calmodulin kinase 4		Brain/Neurons/mES cell line	(86, 114–117)
Reln	Reelin		Brain	(118–120)
Srg1	Synaptotagmin-related gene 1		Brain	(121)
Nefh	Neurofilament heavy polypeptide		Neurons	(122)
Nefm	Neurofilament medium polypeptide			(122)
GFAP	GFAP		Astrocytes	(123)
Vim	Vimentin		Mesenchimal cells	(122)
Nes	Nestin		Neurons	(86, 122)
Vegf	VEGF	Angiogenesis	Brain	(124–126)
Angpt2	Angiopoietin-2			

However, hypothyroidism and decreased TH availability to the brain has been considered a risk factor for the development of neurodegenerative diseases (170, 171) and acute ischemic stroke (172, 173). In addition, recent epidemiological studies have associated low levels of T_3 with poor functional outcome after acute ischemic stroke (174–179). Interestingly, lower total T_3 levels is not related with poor functional recovery after ischemic stroke in patients below 65 years of age, suggesting that the association between levels of T_3 and stroke recovery may be clinically important in older patients (180). Non-thyroidal illness syndrome also impairs functional recovery after stroke (181). Besides, stroke patients with thyroid dysfunction (lower levels of TSH and higher levels of free T_4) are associated with poorer clinical outcome (182). Together, studies point toward the need for a systemic assessment of thyroid dysfunction and stroke outcome.

Some reports suggest neuroprotective effects of hypothyroidism prior to brain ischemia in humans (183, 184), as well as experimental studies in rodents (185, 186). In a recent systematic review, stroke patients with subclinical hypothyroidism (higher levels of TSH and normal levels of free T_4 within the reference range) were more prone to suffer a non-fatal stroke and minor adverse events (182). However, we lack mechanistic studies how systemic levels of TH exactly influence processes in the postischemic brain. It is likely that hypothyroid episodes prior to stroke only delayed neuronal death, due to decreased metabolic demand of neurons, decreased glutamate production and delayed oxidative stress (185, 187). There is no evidence from experimental studies that show beneficial effects in hypothyroid animals after stroke. A recent animal study suggested that daily intravenous administrations of rT_3, an inactive form of T_3, prevents ischemic-reperfusion injury in rats subjected to transient MCAO, however authors did not evaluate if rT_3 induced an hypothyroid state (188). Similarly, in rats subjected to permanent middle cerebral artery occlusion (MCAO), TH serum levels are reduced 14 days after injury correlated with increased neurological impairment (189).

On the other hand, hyperthyroidism has been associated with an increased risk for ischemic stroke in humans (190–192). However, the population-based study was performed in patients

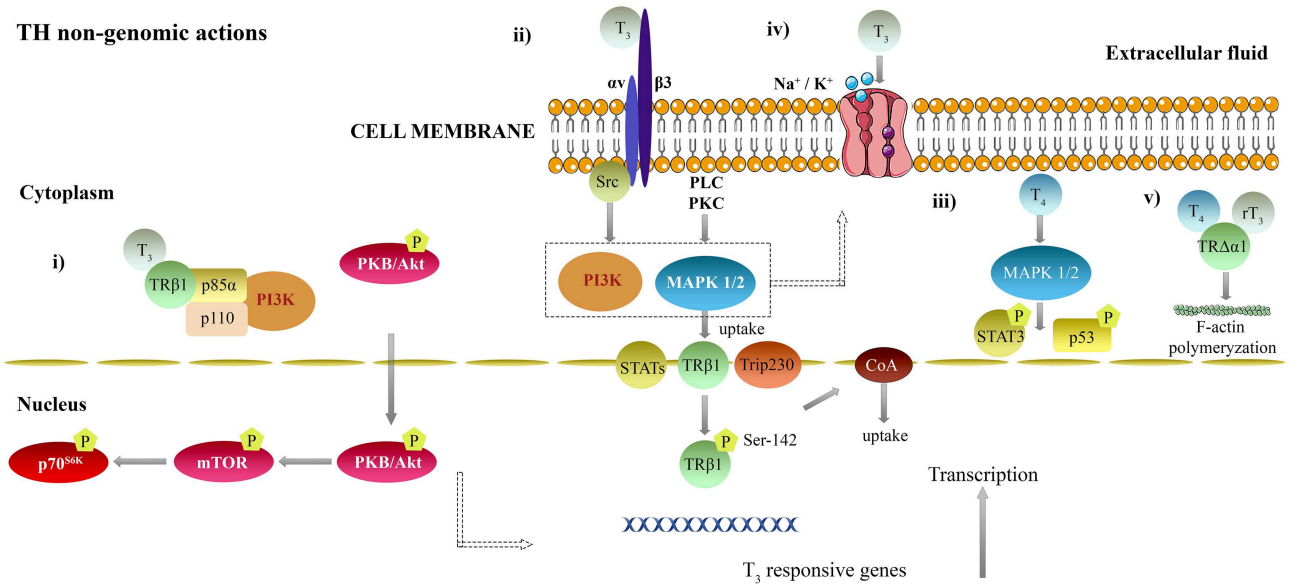

FIGURE 2 | Non-genomic mechanisms of thyroid hormones action in the brain. T_3 can also modulate other genes not containing TRE, by non-genomic actions. **(i)** T_3 complexed to TRβ1 in the cytoplasm interacts with p85α subunit of PI3K, resulting in phosphorylation and activation of PKB/Akt signal transduction pathway, mTOR and phosphorylation of $p70^{S6K}$ (131–136). **(ii)** T_3 is able to bind to integrin αvβ3 S1 domain in plasma membranes and activates PI3K via Src kinase. T_4 and T_3 interact with integrin αvβ3 S2 domain and activate MAPK 1/2 signaling cascade, PLC and PKC (127, 133, 137–140). Subsequently, it results in an nuclear translocation of TRβ1 (141), estrogen receptor α (142), STAT1α, IFN-γ (143) and CoA protein Trip230 (144). In addition, hormone activated MAPK 1/2 phosphorylates TRβ1 at Ser-142, leading to recruitment of CoA proteins (145). **(iii)** T_4 non-gnomically activates MAPK 1/2 in HeLa and CV-1 cultured cells (146, 147) and phosphorylation of p53 (148) and STAT3 (147). **(iv)** T_3 modulates Na^+/H^+ exchanger in myoblasts (149); Na-K-ATPase activity in alveolar epithelial cells (150–152), embryonal hepatocytes (153) and synaptosomes (154, 155) through either the PI3K or MAPK pathways (152, 156) the Ca-ATPase activity in erythrocytes (88), the sarcoplasmic reticulum in the heart (157) and in cerebrocortical synaptosomes (158). **(v)** T_4 and rT_3 stimulate polymerization of actin components of the cytoskeleton neuronal and astrocyte cell cultures, through TH binding to an extranuclear truncated form of TRα1 (TRΔα1) (159–162). IFN-γ, interferon gamma; MAPK 1/2, mitogen-activated protein kinase 1/2; PLC, phospholipase C; PI3K, phosphatidylinositol 3-kinase; PK - protein kinase; mTOR – rapamycin; STAT - signal transducing and activator of transcription; TH, Thyroid hormones; TR, Thyroid hormone receptor; TRE, Thyroid response element; T_4, 3,5,3′,5′-tetraiodo-L-thyronine; T_3, 3,5,3′-triiodo-L-thyronine.

aged 18–44 years. Hence, this study has not been adjusted for other risk factors such as hypertension and atrial fibrillation that may independently contribute for stroke. Larger infarct volumes also have been found in hyperthyroid rats after transient MCAO (193). Hence, hyperthyroid rats (oral administration of TH for 4 weeks) showed profound effects on the cardiovascular system including hypertension and tachyarrhythmia and treatment resulted in a catabolic metabolism (193).

Interestingly, increased mRNA expression of *Dio2* has been found in astrocytes during the first 72 h after transient MCAO (194). Together with modulation of *Thrb* expression, that is reduced in the infarct core and increased in the peri-infarct area, it suggests a local action of T_3 (189). Repeated daily administrations of T_4, before and on days one, two and three after stroke, decrease neuronal damage in the cornu ammonis CA1 pyramidal cells in the hippocampus (195). In an animal model of MCAO, intraperitoneal injection of T_4 (11 μg/kg, 1 h after ischemia and 6 h after reperfusion) reduced cortical and striatal infarct volume 24 h after stroke, with a reduction of GFAP, Iba-1, PKC, and MAPK 1/2 expression (196). Treatment with levothyroxine (25 μg/kg intraperitoneal) 1 h after traumatic brain injury stimulated mRNA expression of genes encoding MCT8, DIO2, and DIO3; genes related with neuronal survival and neurogenesis, namely *Bcl2*, vascular endothelial growth factor A (*Vegfa*), *Sox2,* and neurotrophin (*Ntf*) in the cortex, and of inducible nitrite oxide synthase 2 (*Nos2*) (107).

Moreover, intraperitoneal administration of T_3 at 12 μg/kg 1 h after traumatic brain injury reduced lesion size and inflammation (197). T_3 treatment 25 μg/kg 30 min after transient MCAO also reduced volume of stroke damage in mice through stimulation of fatty acid oxidation by astrocytes (198). A combination therapy of bone marrow stromal cells, daily injections of T_3 200 μg/kg and mild exercise was related to reduce ischemic damage 7 days after transient MCAO in rats (199). Likewise, intraperitoneal administration of thyroxine derivates, 3-iodothyronamine and thyronamine, 50 mg/kg 1 h after MCAO in mice, also reduced infarct volume (200). Neuroprotective action of 3-iodothyronamine administered 2 days before MCAO was associated with hypothermia (200). Although molecular mechanisms have not been evaluated, these studies suggest that non-genomic actions of TH contribute to neuroprotection in the acute phase following stroke. In addition, T_3 treatment prior to brain ischemia (25 μg/kg intravenous) has prevented edema through suppression of aquaporin-4 (AQP4) water channel expression and thereby reducing infarct volume and improving neurological outcome after transient MCAO (109), effects that

were enhanced when T_3 was administrated in nanoparticles at equivalent doses (108). Recently, it has been demonstrated that T_3 modulates AQP4 expression dependent on developmental stage of the CNS. Treatment of mice with T_3 at 1 μg/g increased AQP4 expression in astrocytes in the cerebral cortex until the 60th postnatal day. In contrast, whereas in glioblastoma cell lines stimulation with T_3 (50 nM) treatment was downregulating the expression of AQP4 (201).

Few experimental studies have been performed to identify the mechanisms of TH actions in neuroprotection. Treatment of mouse hippocampal slices lesioned between CA3 and CA1 with T_4 increases levels K-Cl cotransporter (KCC2) mRNA in a brain derived neurotrophic factor (BDNF) dependent manner, that promoted survival and regeneration of damaged neurons in the CA1 region (110). Moreover, it has been demonstrated that treatment with T_3 has a protective effect against glutamate toxicity in cultured astrocytes and neurons (202, 203). This action has been linked to non-genomic actions of TH on Na^+/H^+ exchange activity and glutamate transport (204). Also, T_3 treatment stimulated the expression of *HIF2α*, *VEGF*, *c-JUN,* and Enolase-2 (*ENO2*) in the neuroblastoma in an *in vitro* hypoxia model (107). Although only a few scattered studies have been performed, they indicate an involvement of T_3 in pathways that promote neuronal protection and recovery, through genomic or non-genomic actions.

The expression of TR in the human brain after ischemic stroke have not been studied. Also in experimental models, TR expression has not been investigated, and we found only one experimental study reporting TR expression after permanent MCAO (189). Interestingly, TRα1 expression is increased in microglial cells in the infarct core and in neurons in the peri-infarct area. Astrocytes mildly express nuclear TRα1 and expression of TRβ1 is strongly expressed in the astrocytic scar. If TRα1 and TRβ1 play a crucial role for recovery after brain stroke, in humans and rodents, it remains to be investigated. In fact, TRα1 have been demonstrated to play a crucial role for cardiomyocyte survival after myocardial infarction (205) Therefore, the idea that TRα1 could be a target to promote stroke recovery definitively needs to be further investigated.

MECHANISMS OF THYROID HORMONES THAT MAY ENHANCE MECHANISMS OF RECOVERY AFTER STROKE

Beyond the acute phase after stroke, the brain shows the capacity of spontaneous recovery of lost neurological functions albeit to a limited extent. This process remains slow, however, the intrinsic mechanisms are present and patients may benefit from enhancing those. TH regulate several pathways that are involved in neurorepair, namely regulation of processes of neuronal plasticity, neurogenesis, angiogenesis, and glutamate toxicity. Adjuvant therapies that modulate those processes may improve recovery of function after stroke, in particular when applied in combination with physiotherapy in stroke patients or an enriched environment in rodent models of stroke (206, 207).

Neuronal Plasticity

Neuronal reorganization occurs during the recovery phase of stroke and is initiated by cellular responses to degeneration. Cell death in the infarct core results in synaptic degeneration, instigating regenerative responses among surviving neurons, as the formation of new synaptic connections (208). Neuronal plasticity includes all mechanisms involved in modulation of dendritic and axonal arborization, dendritic spine density and neuronal density that will determine the formation of new synaptic connections and neuronal networks (209, 210).

Neuroplasticity occurs spontaneously during stroke recovery and TH have been identified as a modulator of several genes that may stimulate endogenous neuroplasticity and therefore contributing to facilitate recovery (**Table 1**).

In rodents, T_3 regulates neuron specific RC3/Neurogranin gene (*Nrgn*), that encodes a calmodulin binding protein (112) which binds to calmodulin in the absence of calcium distribution in spines and enhances synaptic plasticity (211). *Nrgn* is highly expressed in dendritic spines in the hippocampus and forebrain and deficiency of *Nrgn* in mice has been reported to induce deficits in spatial learning and anxiety-like tendencies (113). In the human, the homolog gene NRGN is also a direct TH target, during development and in the adult brain (111). TH also regulates *Reelin* (*Reln*) expression during brain development (118). Administration of T_3 increases *Reln* expression in the hippocampus of adult rats (212). Reelin is involved in the migration of multipolar neurons in the developing neocortex (120) and in the adult brain interacts with apoliprotein E receptors and regulates synaptic plasticity and neurogenesis (119).

During brain development, T_3 regulates genes related with the calcium/Calmodulin-activated kinase 4—cAMP responsive element-binding protein 1 (CaMK4/Creb1) signaling pathway, as demonstrated in cultured fetal neurons (213), a mouse embryonic stem cell line (86) and *in vivo* studies (114–117). The CaMK4/Creb1 pathway regulates calcium influx and dendritic growth during development (214), inhibits apoptosis through phosphorylation of Creb and increases anti-apoptotic gene expression. Synaptotagmin-related gene 1 (*Srg1*) is also a TH responsive gene during brain development, that has a putative role as a mediator of synaptic structure and activity (121).

Reorganization of spine cytoskeleton, principally microtubules and actin filaments, can be dynamically modulated and consequently change the pattern of synaptic activity (215). Several studies have shown that TH modulate tubulins (216, 217), microtubule associated proteins (218) and Tau protein (219) in the cytoskeleton during brain development and in the adult brain. TH has also been demonstrated to modulate transcription of genes of intermediate filaments, namely neurofilaments (*Nefh* and *Nefm*), GFAP in mature astrocytes, vimentin in mesenchymal cells and nestin (116, 122). Experiments in cerebral cortex slices suggest that TH activates phosphorylation of cytoskeletal proteins mediated by GABAergic signaling dependent on PKA and PKCaMII activity (220). Studies conducted in cultured glial cells also suggests that TH reorganize the cytoskeleton

through GFAP phosphorylation mediated by RhoA signaling pathway (221).

Actions of TH in the cytoskeleton are particularly important during brain development, to guarantee proper cell migration and to foster neurite outgrowth (160). T_3 also regulates transcription of genes involved in cytoskeleton formation in neurons and astrocytes, during fetal and postnatal brain development (74). Hypothyroidism leads to impaired actin cytoskeleton formation in neurons and astrocytes, affecting neuronal migration and neurite outgrowth. Both rT_3 or T_4 administration can restore polymerization of intracellular filaments F-actin (222, 223) and laminin (223, 224), but this effect was not observed by T_3 administration. Also in neuronal and astrocyte cultures, T_4 and rT_3 stimulate polymerization of the actin cytoskeleton, as already mentioned above (**Figure 2**) (159, 160, 162). As during brain development, basic transcription element-binding protein is upregulated by TH and this protein may play a role in neuronal outgrowth, modulating changes in the cytoskeleton, and cell differentiation (225, 226).

Studies also demonstrate that TH signaling is critical to proper functioning of short term (227) and long term synaptic plasticity (228). Induced hypothyroidism has been related with disruption in synaptic plasticity (229, 230) and long term potentiation in the CA1 neonatal (231, 232) and adult (233) rat hippocampus. Hyperthyroidism has been also related to detrimental effects in dendritic spines. Intraperitoneal injection of T_3 750 μg/kg during 5 consecutive days in adult rats significantly decreased dendritic spine density in CA1 pyramidal cells in the hippocampus (234) and thyroxine induced hyperthyroidism impairs special learning and synaptic plasticity in rats (235).

On the cellular level, TH genomic or non-genomic actions may modulate the activity of ion pumps that are important for normal excitable cell function. Particularly in brain tissues affected by ischemia, directly or indirectly, adapted function of ion pumps is required to avoid intracellular overload of H^+ and Ca^{2+}, preventing cell acidosis and excitotoxicity. T_3 has been shown to decrease the activity of Na, K-ATPase (154, 155) and to stimulate the Na^+/H^+ exchanger (149) and Ca^{2+}/Mg^{2+} ATPase pump activity (158) in cerebrocortical synaptosomes. T_3 increases the transcription of SR Ca^{2+}-ATPase gene (ATP2A2) in the sarcoplasmic reticulum (157). In addition, T_3 has been demonstrated to be benefical in *in vitro* and *in vivo* experimental myocardial ischemia preventing excessive intracellular Ca^{2+} accumulation (236, 237).

Also, T3 contributes to glutamate uptake by astrocytes, protecting neurons from intracellular calcium toxicity and death (203). Neuroprotective effect was attributed to an increased expression of mRNA and protein levels of GLT-1 and GLAST in the astrocytes. It also has been demonstrated that T3 decreases N-methyl-d-aspartate (NMDA)-evoked currents and prevent glutamate-induced neuronal death in hippocampal neurons (202). Together, these actions might be beneficial to prevent cell dysfunction or death of principal neurons during the acute phase after ischemic stroke. Conversely, these mechanisms might be involved to reduce the activity of inhibitory neurons in critical periods of plasticity during the first weeks after stroke. Hence, these actions most likely will dependent on receptor expression profiles in different neuron populations.

The balance between excitation and inhibition is of particular importance for neuronal plasticity processes potentially relevant for recovery. During development, TH increases the level of γ-aminobutyric acid (GABA) in the brain, while the opposite effect is observed in the adult brain. In the developing brain, hypothyroidism impairs the generation of interneurons including reduced proliferation and delayed differentiation of precursor cells in the cerebellum and their migration to the cerebellar cortex (238). These effects could be antagonized by administration of T_3 binding to the TRα1. Likewise, deletion of TRα1 reduced cerebellar GAT-1 expression and Pax-2 precursor cell proliferation (238). TH also affect the release and uptake of GABA from the neuron into the synapse. T_3 stimulates depolarization and release of GABA in synaptosomes from rat cerebral cortex (239). In the adult brain, hypothyroidism is reported to increase glutamic acid decarboxylase (GAD) activity and GABA reuptake, from cerebral cortex homogenates (240, 241) while hyperthyroidism has no effect on GABA uptake (241). In addition, T_3 administration inhibits GABA-induced Cl^- currents, which may affect $GABA_A$ receptors in the cerebral cortex, by non-genomic mechanisms (242).

Adult Neurogenesis

TH signaling is crucial for proper neurogenesis during brain development (1). Several studies have demonstrated that neurogenic events in the adult brain are dependent on TH actions (243–250) and have been reviewed in detail (251, 252). Particularly T_3 is involved in mechanisms of proliferation, survival, differentiation and maturation of neuronal precursors in the adult brain (246, 251). With potential contribution of TH NSPCs from the SVZ may proliferate, migrate and differentiate into neurons, astrocytes or oligodendrocytes in the damaged region and thereby contribute to brain plasticity after ischemic stroke or other brain injury (253, 254). Stem cell therapy and neurogenesis have been explored as a potential therapeutic strategy for neuronal repair after ischemic stroke (255).

Angiogenesis

Therapeutic angiogenesis has been used to enhance brain repair promoting the formation of new blood vessels and restoration of blood flow in the damaged area (256–258). Angiogenic effects of TH have been demonstrated in infarcted tissue of the myocardium (259). Moreover, an increased number of new blood vessels has been found in the brain of hypothyroid rats after administration of 3,5-diiothyroprionic acid (a thyroid hormone analog) or T_4 (260). The proangiogenic effects of TH are apparently mediated by non-genomic actions, through binding to integrin αvβ3 resulting in activation of MAPK 1/2 and STAT3. TH binding to αvβ3 directs transcription of genes that promote angiogenesis, namely fibroblast factors, VEGF and angiopoietin-2 (124–126, 137, 147, 261, 262). To our knowledge, so far no experimental studies have been performed to investigate pro-angiogenic effects of TH after stroke.

TRANSLATION TO CLINICAL STUDIES

Current epidemiological studies in humans and experimental evidence from rodents strongly suggest that TH signaling plays a crucial for stroke recovery. In particular T_3, the active form in the brain, exerts genomic and non-genomic actions that may foster functional outcome after stroke.

Although several epidemiological studies have associated low levels of TH with poor outcome, no clinical trials have been performed to evaluate the recovery promoting effects of TH in stroke patients. At the current stage the first step of translational studies will be to understand exact mechanisms underlying beneficial action of TH after stroke in animal models, in particular T_3. Based on knowledge about mechanisms of action, exact treatment regimens with specific targets can be developed and tested during critical windows of stroke recovery. In this context, the development of cell-specific approaches to target TH signaling in the postischemic brain may result in specific treatments in experimental stroke models, that later, might be translated into clinical studies.

CONCLUSIONS

Several mechanisms in the brain are tightly regulated by TH and T_3 availability to the brain is dependent on factors including (i) maternal TH release before fetus thyroid gland development; (ii) TSH levels and TH release by thyroid gland; (iii) passage of TH through placenta in the fetus; (iv) control of free fraction of TH determined by TH binding proteins; (v) TH transmembrane transport into the cytoplasm; (vi) local activity of iodothyronine deiodinases; (vii) expression and distribution of TR; (viii) and translational activity and non-genomic actions of TH in the brain. Disruption in these mechanisms compromise TH availability and actions in the brain and may result in impairments of neurological functions. There is clinical and preclinical evidence that TH are involved in mechanisms of neuronal plasticity and function of glial cells after ischemic stroke. Further understanding and targeting those might be exploited in future therapies to enhance functional recovery in stroke patients.

AUTHOR CONTRIBUTIONS

DT conceptualized and wrote the review, under supervision of KR. KR, CS, and IG revised the manuscript. All authors approved the final version of the manuscript for submission and publication.

FUNDING

This work was supported by funds from the Health Sciences Research Center (CICS-UBI) through National Funds by FCT—Foundation for Science and Technology (UID/Multi/00709/2019); by a doctoral fellowship (SFRH/BD/104679/2014) from Fundação para a Ciência e Tecnologia; partially supported by Programa Operacional do Centro, Centro 2020 through the funding of the ICON project (Interdisciplinary Challenges on Neurodegeneration; CENTRO-01-0145-FEDER-000013); the Swedish Brain Fund; the Crafoord Foundation, Sveriges Stroke Riksförbundet; the Hans-Gabriel and Alice Wachtmeister Foundation, Sparbanksstiftelsen Färs & Frosta and the Stiftelsen Sven-Olof Jansons livsverk.

REFERENCES

1. Bernal J. Thyroid hormones in brain development and function. In: Feingold KR, Anawalt B, Boyce A, editors. *Endotext.* South Dartmouth, MA: MDText.com, Inc. (2000) 1–136.
2. Gothié JD, Demeneix B, Remaud S. Comparative approaches to understanding thyroid hormone regulation of neurogenesis. *Mol Cell Endocrinol.* (2017) 459:104–15. doi: 10.1016/j.mce.2017.05.020
3. Hartley MD, Banerji T, Tagge IJ, Kirkemo LL, Chaudhary P, Calkins E, et al. Myelin repair stimulated by CNS-selective thyroid hormone action. *JCI Insight.* (2019) 4:e126329. doi: 10.1172/jci.insight.126329
4. Moog NK, Entringer S, Heim C, Wadhwa PD, Kathmann N, Buss C. Influence of maternal thyroid hormones during gestation on fetal brain development. *Neuroscience.* (2017) 342:68–100. doi: 10.1016/j.neuroscience.2015.09.070
5. Morreale de Escobar G, Obregon MJ, Escobar del Rey F. Role of thyroid hormone during early brain development. *Eur J Endocrinol.* (2004) 151:U25–37. doi: 10.1530/EJE.0.151U025
6. Bárez-López S, Guadaño-Ferraz A. Thyroid hormone availability and action during brain development in rodents. *Front Cell Neurosci.* (2017) 11:240. doi: 10.3389/fncel.2017.00240
7. Mullur R, Liu YY, Brent GA. Thyroid hormone regulation of metabolism. *Physiol Rev.* (2014) 94:355–82. doi: 10.1152/physrev.00030.2013
8. Ahmed OM, El-Gareib AW, El-bakry AM, Abd El-Tawab SM, Ahmed RG. Thyroid hormones states and brain development interactions. *Int J Dev Neurosci.* (2008) 26:147–209. doi: 10.1016/j.ijdevneu.2007.09.011
9. Mendel CM, Weisiger RA, Jones AL, Cavalieri RR. Thyroid hormone-binding proteins in plasma facilitate uniform distribution of thyroxine within tissues: a perfused rat liver study. *Endocrinology.* (1987) 120:1742–9. doi: 10.1210/endo-120-5-1742
10. Palha JA. Transthyretin as a thyroid hormone carrier: function revisited. *Clin Chem Lab Med.* (2002) 40:1292–300. doi: 10.1515/CCLM.2002.223
11. Refetoff S. Thyroid hormone serum transport proteins. In: Feingold KR, Anawalt B, Boyce A, editors. *Endotext.* South Dartmouth. MA: MDText.com, Inc. (2015). p. 1–13.
12. Schreiber G, Richardson SJ. The Evolution of Gene Expression, Structure and Function of Transthyretin. *Comp Biochem Physiol Part B Biochem Mol Biol.* (1997) 116:137–60. doi: 10.1016/S0305-0491(96)00212-X
13. Vranckx R, Rouaze M, Savu L, Nunez EA, Beaumont C, Flink IL. The hepatic biosynthesis of rat thyroxine binding globulin (TBG): demonstration, ontogenesis, and UP-regulation in experimental hypothyroidism. *Biochem Biophys Res Commun.* (1990) 167:317–22. doi: 10.1016/0006-291X(90)91767-M
14. Vranckx R, Savu L, Maya M, Nunez EA. Characterization of a major development-regulated serum thyroxine-binding globulin in the euthyroid mouse. *Biochem J.* (1990) 271:373–9. doi: 10.1042/bj2710373
15. Benvenga S, Cahnmann HJ, Robbins J. Localization of the thyroxine binding sites in apolipoprotein B-100 of human low density lipoproteins. *Endocrinology.* (1990) 127:2241–6. doi: 10.1210/endo-127-5-2241
16. Benvenga S, Lapa D, Trimarchi F. Re-evaluation of the thyroxine binding to human plasma lipoproteins using three techniques. *J Endocrinol Invest.* (2001) 24:RC16–8. doi: 10.1007/BF03343863

17. Bernal J, Guadaño-Ferraz A, Morte B. Thyroid hormone transporters—functions and clinical implications. *Nat Rev Endocrinol.* (2015) 11:1–12. doi: 10.1038/nrendo.2015.66
18. Morte B, Bernal J. Thyroid hormone action: astrocyte-neuron communication. *Front Endocrinol.* (2014) 5:82. doi: 10.3389/fendo.2014.00082
19. Chanoine JP, Alex S, Fang SL, Stone S, Leonard JL, Korhle J, et al. Role of transthyretin in the transport of thyroxine from the blood to the choroid plexus, the cerebrospinal fluid, and the brain. *Endocrinology.* (1992) 130:933–8. doi: 10.1210/endo.130.2.1733735
20. Richardson SJ, Wijayagunaratne RC, D'Souza DG, Darras VM, Van Herck SLJ. Transport of thyroid hormones via the choroid plexus into the brain: the roles of transthyretin and thyroid hormone transmembrane transporters. *Front. Neurosci.* (2015) 9:66. doi: 10.3389/fnins.2015.00066
21. Friesema EC, Ganguly S, Abdalla A, Manning Fox JE, Halestrap AP, Visser TJ. Identification of monocarboxylate transporter 8 as a specific thyroid hormone transporter. *J Biol Chem.* (2003) 278:40128–35. doi: 10.1074/jbc.M300909200
22. Friesema EC, Jansen J, Milici C, Visser TJ. Thyroid hormone transporters. *Vitam Horm.* (2005) 70:137–67. doi: 10.1016/S0083-6729(05)70005-4
23. Hagenbuch B. Cellular entry of thyroid hormones by organic anion transporting polypeptides. *Best Pract Res Clin Endocrinol Metab.* (2007) 21:209–21. doi: 10.1016/j.beem.2007.03.004
24. Halestrap AP. The monocarboxylate transporter family-Structure and functional characterization. *IUBMB Life.* (2012) 64:1–9. doi: 10.1002/iub.573
25. Halestrap AP, Wilson MC. The monocarboxylate transporter family-Role and regulation. *IUBMB Life.* (2012) 64:109–19. doi: 10.1002/iub.572
26. Jansen J, Friesema EC, Milici C, Visser TJ. *Thyroid* Hormone Transporters in Health and Disease. *Thyroid.* (2005) 15:757–68. doi: 10.1089/thy.2005.15.757
27. Kinne A, Schülein R, Krause G. Primary and secondary thyroid hormone transporters. *Thyroid Res.* (2011) 4:S7. doi: 10.1186/1756-6614-4-S1-S7
28. Roberts LM, Woodford K, Zhou M, Black DS, Haggerty JE, Tate EH, et al. Expression of the thyroid hormone transporters monocarboxylate transporter-8 (*SLC16A2*) and organic ion transporter-14 (*SLCO1C1*) at the blood-brain barrier. *Endocrinology.* (2008) 149:6251–61. doi: 10.1210/en.2008-0378
29. Van Der Deure WM, Peeters RP, Visser TJ. Molecular aspects of thyroid hormone transporters, including MCT8, MCT10, and OATPs, and the effects of genetic variation in these transporters. *J Mol Endocrinol.* (2010) 44:1–11. doi: 10.1677/JME-09-0042
30. Visser WE, Friesema EC, Jansen J, Visser TJ. Thyroid hormone transport by monocarboxylate transporters. *Best Pract Res Clin Endocrinol Metab.* (2007) 21:223–36. doi: 10.1016/j.beem.2007.03.008
31. Visser WE, Friesema EC, Visser TJ. Minireview: thyroid hormone transporters: the knowns and the unknowns. *Mol Endocrinol.* (2011) 25:1–14. doi: 10.1210/me.2010-0095
32. Trajkovic M, Visser TJ, Mittag J, Horn S, Lukas J, Darras VM, et al. Abnormal thyroid hormone metabolism in mice lacking the monocarboxylate transporter 8. *J Clin Invest.* (2007) 117:627–35. doi: 10.1172/JCI28253
33. Friesema EC, Jansen J, Jachtenberg J, Visser WE, Kester MHA, Visser TJ. Effective cellular uptake and efflux of thyroid hormone by human monocarboxylate transporter 10. *Mol Endocrinol.* (2008) 22:1357–69. doi: 10.1210/me.2007-0112
34. Zhang Y, Chen K, Sloan SA, Bennett ML, Scholze AR, O'Keeffe S, et al. An RNA-sequencing transcriptome and splicing database of glia, neurons, and vascular cells of the cerebral cortex. *J Neurosci.* (2014) 34:11929–47. doi: 10.1523/JNEUROSCI.1860-14.2014
35. Mathiisen TM, Lehre KP, Danbolt NC, Ottersen OP. The perivascular astroglial sheath provides a complete covering of the brain microvessels: an electron microscopic 3D reconstruction. *Glia.* (2010) 58:1094–103. doi: 10.1002/glia.20990
36. Schroeder AC, Privalsky ML. Thyroid hormones, T3 and T4, in the brain. *Front Endocrinol.* (2014) 5:40. doi: 10.3389/fendo.2014.00040
37. Dumitrescu AM, Liao XH, Best TB, Brockmann K, Refetoff S. A novel syndrome combining thyroid and neurological abnormalities is associated with mutations in a monocarboxylate transporter gene. *Am J Hum Genet.* (2004) 74:168–75. doi: 10.1086/380999
38. Friesema EC, Grueters A, Biebermann H, Krude H, Von Moers A, Reeser M, et al. Association between mutations in a thyroid hormone transporter and severe X-linked psychomotor retardation. *Lancet.* (2004) 364:1435–7. doi: 10.1016/S0140-6736(04)17226-7
39. López-Espíndola D, Morales-Bastos C, Grijota-Martínez C, Liao XH, Lev D, Sugo E, et al. Mutations of the thyroid hormone transporter MCT8 cause prenatal brain damage and persistent hypomyelination. *J Clin Endocrinol Metab.* (2014) 99:E2799–E2804. doi: 10.1210/jc.2014-2162
40. Schwartz CE, May MM, Carpenter NJ, Rogers RC, Martin J, Bialer MG, et al. Allan-Herndon-Dudley syndrome and the monocarboxylate transporter 8 (MCT8) gene. *Am J Hum Genet.* (2005) 77:41–53. doi: 10.1086/431313
41. Kim DK, Kanai Y, Chairoungdua A, Matsuo H, Cha SH, Endou H. Expression cloning of a Na+-independent aromatic amino acid transporter with structural similarity to H+/monocarboxylate transporters. *J Biol Chem.* (2001) 276:17221–8. doi: 10.1074/jbc.M009462200
42. Bianco AC. Minireview: cracking the metabolic code for thyroid hormone signaling. *Endocrinology.* (2011) 152:3306–11. doi: 10.1210/en.2011-1104
43. Bianco AC, Kim BW. Deiodinases: implications of the local control of thyroid hormone action. *J Clin Invest.* (2006) 116:2571–9. doi: 10.1172/JCI29812
44. Dentice M, Marsili A, Zavacki A, Larsen PR, Salvatore D. The deiodinases and the control of intracellular thyroid hormone signaling during cellular differentiation. *Biochim Biophys Acta Gen Subj.* (2013) 1830:3937–45. doi: 10.1016/j.bbagen.2012.05.007
45. Tu HM, Kim SW, Salvatore D, Bartha T, Legradi G, Larsen PR, et al. Regional distribution of type 2 thyroxine deiodinase messenger ribonucleic acid in rat hypothalamus and pituitary and its regulation by thyroid hormone. *Endocrinology.* (1997) 138:3359–68. doi: 10.1210/endo.138.8.5318
46. Freitas BC, Gereben B, Castillo M, Kalló I, Zeöld A, Egri P, et al. Paracrine signaling by glial cell-derived triiodothyronine activates neuronal gene expression in the rodent brain and human cells. *J Clin Invest.* (2010) 120:2206–17. doi: 10.1172/JCI41977
47. Gereben B, Zavacki AM, Ribich S, Kim BW, Huang SA, Simonides WS, et al. Cellular and molecular basis of deiodinase-regulated thyroid hormone signaling. *Endocr Rev.* (2008) 29:898–938. doi: 10.1210/er.2008-0019
48. Tu HM, Legradi G, Bartha T, Salvatore D, Lechan RM, Larsen PR. Regional expression of the type 3 iodothyronine deiodinase messenger ribonucleic acid in the rat central nervous system and its regulation by thyroid hormone. *Endocrinology.* (1999) 140:784–90. doi: 10.1210/endo.140.2.6486
49. Dumitrescu AM, Liao XH, Weiss RE, Millen K, Refetoff S. Tissue-specific thyroid hormone deprivation and excess in monocarboxylate transporter (Mct) 8-deficient mice. *Endocrinology.* (2006) 147:4036–43. doi: 10.1210/en.2006-0390
50. Guadaño-Ferraz A, Obregón MJ, St Germain DL, Bernal J, Obregon MJ, StGermain DL. The type 2 iodothyronine deiodinase is expressed primarily in glial cells in the neonatal rat brain. *Proc Natl Acad Sci USA.* (1997) 94:10391–6. doi: 10.1073/pnas.94.19.10391
51. Cramer SC, Chopp M. Recovery recapitulates ontogeny. *Trends Neurosci.* (2000) 23:265–71. doi: 10.1016/S0166-2236(00)01562-9
52. Stepien BK, Huttner WB. Transport, metabolism, and function of thyroid hormones in the developing mammalian brain. *Front Endocrinol.* (2019) 10:209. doi: 10.3389/fendo.2019.00209
53. Anderson GW, Schoonover CM, Jones SA. Control of thyroid hormone action in the developing rat brain. *Thyroid.* (2003) 13:1039–56. doi: 10.1089/105072503770867219
54. Clancy B, Finlay BL, Darlington RB, Anand KJ. Extrapolating brain development from experimental species to humans. *Neurotoxicology.* (2007) 28:931–7. doi: 10.1016/j.neuro.2007.01.014
55. Semple BD, Blomgren K, Gimlin K, Ferriero DM, Noble-Haeusslein LJ. Brain development in rodents and humans: identifying benchmarks of maturation and vulnerability to injury across species. *Prog Neurobiol.* (2013) 106–107:1–16. doi: 10.1016/j.pneurobio.2013.04.001
56. Berbel P, Mestre JL, Santamaría A, Palazón I, Franco A, Graells M, et al. Delayed neurobehavioral development in children born to pregnant women with mild hypothyroxinemia during the first month of gestation: the importance of early iodine supplementation. *Thyroid.* (2009) 19:511–9. doi: 10.1089/thy.2008.0341

57. Carreón-Rodríguez A, Perez-Martínez L. Clinical implications of thyroid hormones effects on nervous system development. *Pediatr Endocrinol Rev.* (2012) 9:644–9.
58. Downing S, Halpern L, Carswell J, Brown RS. Severe maternal hypothyroidism corrected prior to the third trimester is associated with normal cognitive outcome in the offspring. *Thyroid.* (2012) 22:625–30. doi: 10.1089/thy.2011.0257
59. Contempré B, Jauniaux E, Calvo R, Jurkovic D, Campbell S, de Escobar GM. Detection of thyroid hormones in human embryonic cavities during the first trimester of pregnancy. *J Clin Endocrinol Metab.* (1993) 77:1719–22. doi: 10.1210/jcem.77.6.8263162
60. Obregon M, Calvo R, Escobar Del Rey F, Morreale De Escobar G. Ontogenesis of thyroid function and interactions with maternal function. *Endocr Dev.* (2007) 10:86–98. doi: 10.1159/000106821
61. Obregon MJ, Mallol J, Pastor R, Morreale de Escobar G, Escobar Del Rey F. L-thyroxine and 3,5,3'-triiodo-L-thyronine in rat embryos before onset of fetal thyroid function. *Endocrinology.* (1984) 114:305–7. doi: 10.1210/endo-114-1-305
62. Porterfield SP, Hendrich CE. Tissue iodothyronine levels in fetuses of control and hypothyroid rats at 13 and 16 days gestation. *Endocrinology.* (1992) 131:195–200. doi: 10.1210/endo.131.1.1611997
63. Woods RJ, Sinha AK, Ekins RP. Uptake and metabolism of thyroid hormones by the rat foetus in early pregnancy. *Clin Sci.* (1984) 67:359–63.
64. Morreale De Escobar GMD, Pastor R, Obregon MJ, Del Rey FE. Effects of maternal hypothyroidism on the weight and thyroid hormone content of rat embryonic tissues, before and after onset of fetal thyroid function. *Endocrinology.* (1985) 117:1890–900. doi: 10.1210/endo-117-5-1890
65. Ausó E, Lavado-Autric R, Cuevas E, Escobar Del Rey F, Morreale De Escobar G, Berbel P. A moderate and transient deficiency of maternal thyroid function at the beginning of fetal neocorticogenesis alters neuronal migration. *Endocrinology.* (2004) 145:4037–47. doi: 10.1210/en.2004-0274
66. Gilbert ME, Goodman JH, Gomez J, Johnstone AFM, Ramos RL. Adult hippocampal neurogenesis is impaired by transient and moderate developmental thyroid hormone disruption. *Neurotoxicology.* (2017) 59:9–21. doi: 10.1016/j.neuro.2016.12.009
67. Mohan V, Sinha RA, Pathak A, Rastogi L, Kumar P, Pal A, et al. Maternal thyroid hormone deficiency affects the fetal neocorticogenesis by reducing the proliferating pool, rate of neurogenesis and indirect neurogenesis. *Exp Neurol.* (2012) 237:477–88. doi: 10.1016/j.expneurol.2012.07.019
68. Bernal J. Thyroid hormone receptors in brain development and function. *Nat Clin Pract Endocrinol Metab.* (2007) 3:249–59. doi: 10.1038/ncpendmet0424
69. Bernal J, Pekonen F. Ontogenesis of the nuclear 3,5,3'-triiodothyronine receptor in the human fetal brain. *Endocrinology.* (1984) 114:677–9. doi: 10.1210/endo-114-2-677
70. Kilby MD, Gittoes N, McCabe C, Verhaeg J, Franklyn JA. Expression of thyroid receptor isoforms in the human fetal central nervous system and the effects of intrauterine growth restriction. *Clin Endocrinol.* (2000) 53:469–77. doi: 10.1046/j.1365-2265.2000.01074.x
71. Perez-Castillo A, Bernal J, Ferreiro B, Pans T. The early ontogenesis of thyroid hormone receptor in the rat fetus. *Endocrinology.* (1985) 117:2457–61. doi: 10.1210/endo-117-6-2457
72. Chatonnet F, Flamant F, Morte B. A temporary compendium of thyroid hormone target genes in brain. *Biochim Biophys Acta Gene Regul Mech.* (2015) 1849:122–9. doi: 10.1016/j.bbagrm.2014.05.023
73. Horn S, Heuer H. Thyroid hormone action during brain development: more questions than answers. *Mol Cell Endocrinol.* (2010) 315:19–26. doi: 10.1016/j.mce.2009.09.008
74. Sampson D, Pickard MR, Sinha AK, Evans IM, Leonard AJ, Ekins RP. Maternal thyroid status regulates the expression of neuronal and astrocytic cytoskeletal proteins in the fetal brain. *J Endocrinol.* (2000) 167:439–45. doi: 10.1677/joe.0.1670439
75. Bochukova E, Schoenmakers N, Agostini M, Schoenmakers E, Rajanayagam O, Keogh JM, et al. A mutation in the thyroid hormone receptor alpha gene. *N Engl J Med.* (2012) 366:243–9. doi: 10.1056/NEJMoa1110296
76. Forrest D, Golarai G, Connor J, Curran, T. Genetic analysis of thyroid hormone receptors in development and disease. *Recent Prog Horm Res.* (1996) 51:1–22.
77. Jones I, Srinivas M, Ng L, Forrest D. The thyroid hormone receptor beta gene: structure and functions in the brain and sensory systems. *Thyroid.* (2003) 13:1057–68. doi: 10.1089/105072503770867228
78. Refetoff S, Dumitrescu AM. Syndromes of reduced sensitivity to thyroid hormone: genetic defects in hormone receptors, cell transporters and deiodination. *Best Pract Res Clin Endocrinol Metab.* (2007) 21:277–305. doi: 10.1016/j.beem.2007.03.005
79. van Mullem AA, Visser TJ, Peeters RP. Clinical consequences of mutations in thyroid hormone receptor-alpha1. *Eur Thyroid J.* (2014) 3:17–24. doi: 10.1159/000360637
80. Bradley DJ, Towle HC, Young WS. Spatial and temporal expression of alpha- and beta-thyroid hormone receptor mRNAs, including the beta 2-subtype, in the developing mammalian nervous system. *J Neurosci.* (1992) 12:2288–302.
81. Forrest D, Hallböök F, Persson H, Vennström B. Distinct functions for thyroid hormone receptors alpha and beta in brain development indicated by differential expression of receptor genes. *EMBO J.* (1991) 10:269–75.
82. Iskaros J, Pickard M, Evans I, Sinha A, Hardiman P, Ekins R. Thyroid hormone receptor gene expression in first trimester human fetal brain. *J Clin Endocrinol Metab.* (2000) 85:2620–3. doi: 10.1210/jcem.85.7.6766
83. Wallis K, Dudazy S, van Hogerlinden M, Nordström K, Mittag J, Vennström B. The thyroid hormone receptor α1 protein is expressed in embryonic postmitotic neurons and persists in most adult neurons. *Mol Endocrinol.* (2010) 24:1904–16. doi: 10.1210/me.2010-0175
84. Hodin RA, Lazar MA, Chin WW. Differential and tissue-specific regulation of the multiple rat c-erbA messenger RNA species by thyroid hormone. *J Clin Invest.* (1990) 85:101–5. doi: 10.1172/JCI114398
85. Sinha R, Yen PM. Cellular action of thyroid hormone. In: Feingold KR, Anawalt B, Boyce A, editors. *Endotext.* South Dartmouth, MA: MDTextcom, Inc. (2013). p. 1–27. doi: 10.1089/105072502760143827
86. Teng X, Lin YY, Teng W, Brent GA. COUP-TF1 modulates thyroid hormone action in an embryonic stem-cell model of cortical pyramidal neuronal differentiation. *Thyroid.* (2018) 28:667–78. doi: 10.1089/thy.2017.0256
87. Faedo A, Tomassy GS, Ruan Y, Teichmann H, Krauss S, Pleasure SJ, et al. COUP-TFI coordinates cortical patterning, neurogenesis, and laminar fate and modulates MAPK/ERK, AKT, and beta-catenin signaling. *Cereb Cortex.* (2008) 18:2117–31. doi: 10.1093/cercor/bhm238
88. Cheng SY, Leonard JL, Davis PJ. Molecular aspects of thyroid hormone actions. *Endocr Rev.* (2010) 31:139–70. doi: 10.1210/er.2009-0007
89. Yen PM. Physiological and molecular basis of thyroid hormone action. *Physiol Rev.* (2001) 81:1097–142. doi: 10.1152/physrev.2001.81.3.1097
90. Bernal J. Action of thyroid hormone in brain. *J Endocrinol Invest.* (2002) 25:268–88. doi: 10.1007/BF03344003
91. Harvey CB, Williams GR. Mechanism of thyroid hormone action. *Thyroid.* (2002) 12:441–6. doi: 10.1089/105072502760143791
92. McKenna NJ, Lanz RB, O'Malley BW. Nuclear receptor coregulators: cellular and molecular biology. *Endocr Rev.* (1999) 20:321–44. doi: 10.1210/edrv.20.3.0366
93. Brent GA. Mechanisms of thyroid hormone action. *J Clin Invest.* (2012) 122:3035–43. doi: 10.1172/JCI60047
94. Flamant F, Gauthier K. Thyroid hormone receptors: the challenge of elucidating isotype-specific functions and cell-specific response. *Biochim Biophys Acta Gen Subj.* (2013) 1830:3900–7. doi: 10.1016/j.bbagen.2012.06.003
95. Chan IH, Privalsky ML. Isoform-specific transcriptional activity of overlapping target genes that respond to thyroid hormone receptors alpha1 and beta1. *Mol Endocrinol.* (2009) 23:1758–75. doi: 10.1210/me.2009-0025
96. Schwartz HL, Strait KA, Ling NC, Oppenheimer JH. Quantitation of rat tissue thyroid hormone binding receptor isoforms by immunoprecipitation of nuclear triiodothyronine binding capacity. *J Biol Chem.* (1992) 267:11794–9.
97. Gil-Ibañez P, Morte B, Bernal J. Role of thyroid hormone receptor subtypes α and β on gene expression in the cerebral cortex and striatum of postnatal mice. *Endocrinology.* (2013) 154:1940–7. doi: 10.1210/en.2012-2189
98. Constantinou C, Margarity M, Valcana T. Region-specific effects of hypothyroidism on the relative expression of thyroid hormone receptors in adult rat brain. *Mol Cell Biochem.* (2005) 278:93–100. doi: 10.1007/s11010-005-6934-z

99. Carlson DJ, Strait KA, Schwartz HL, Oppenheimer JH. Immunofluorescent localization of thyroid hormone receptor isoforms in glial cells of rat brain. *Endocrinology*. (1994) 135:1831–6. doi: 10.1210/endo.135.5.7525253
100. Mohácsik P, Zeöld A, Bianco AC, Gereben B. Thyroid hormone and the neuroglia: Both source and target. *J Thyroid Res.* (2011) 2011:16. doi: 10.4061/2011/215718
101. Yusta B, Besnard F, Ortiz-Caro J, Pascual A, Aranda A, Sarlieve L. Evidence for the presence of nuclear 3,5,3'- triiodothyronine receptors in secondary cultures of pure rat oligodendrocytes. *Endocrinology*. (1988) 122:2278–84. doi: 10.1210/endo-122-5-2278
102. Bradley DJ, Young WS, Weinberger C. Differential expression of alpha and beta thyroid hormone receptor genes in rat brain and pituitary. *Proc Natl Acad Sci USA*. (1989) 86:7250–4. doi: 10.1073/pnas.86.18.7250
103. Cook CB, Kakucska I, Lechan RM, Koenig RJ. Expression of thyroid hormone receptor beta 2 in rat hypothalamus. *Endocrinology*. (1992) 130:1077–9. doi: 10.1210/endo.130.2.1733708
104. Lechan RM, Qi Y, Berrodin TJ, Davis KD, Schwartz HL, Strait KA, et al. Immunocytochemical delineation of thyroid hormone receptor beta 2-like immunoreactivity in the rat central nervous system. *Endocrinology*. (1993) 132:2461–9. doi: 10.1210/endo.132.6.7684976
105. Williams GR. Cloning and characterization of two novel thyroid hormone receptor beta isoforms. *Mol Cell Biol*. (2000) 20:8329–42. doi: 10.1128/MCB.20.22.8329-8342.2000
106. Anyetei-Anum CS, Roggero VR, Allison LA. Thyroid hormone receptor localization in target tissues. *J Endocrinol*. (2018) 237:R19–34. doi: 10.1530/JOE-17-0708
107. Li J, Donangelo I, Abe K, Scremin O, Ke S, Li F, et al. Thyroid hormone treatment activates protective pathways in both *in vivo* and *in vitro* models of neuronal injury. *Mol Cell Endocrinol*. (2017) 452:120–30. doi: 10.1016/j.mce.2017.05.023
108. Mdzinarishvili A, Sutariya V, Talasila PK, Geldenhuys WJ, Sadana P. Engineering triiodothyronine (T3) nanoparticle for use in ischemic brain stroke. *Drug Deliv Transl Res*. (2013) 3:309–17. doi: 10.1007/s13346-012-0117-8
109. Sadana P, Coughlin L, Burke J, Woods R, Mdzinarishvili A. Anti-edema action of thyroid hormone in MCAO model of ischemic brain stroke: possible association with AQP4 modulation. *J Neurol Sci*. (2015) 354:37–45. doi: 10.1016/j.jns.2015.04.042
110. Shulga A, Blaesse A, Kysenius K, Huttunen HJ, Tanhuanpää K, Saarma M, et al. Thyroxin regulates BDNF expression to promote survival of injured neurons. *Mol Cell Neurosci*. (2009) 42:408–18. doi: 10.1016/j.mcn.2009.09.002
111. De Arrieta CM, Morte B, Coloma A, Bernal J. The human RC3 gene homolog, NRGN contains a thyroid hormone-responsive element located in the first intron. *Endocrinology*. (1999) 140:335–43. doi: 10.1210/en.140.1.335
112. Iniguez MA, De Lecea L, Guadano-Ferraz A, Morte B, Gerendasy D, Sutcliffe JG, et al. Cell-specific effects of thyroid hormone on RC3/neurogranin expression in rat brain. *Endocrinology*. (1996) 137:1032–41. doi: 10.1210/endo.137.3.8603571
113. Miyakawa T, Yared E, Pak JH, Huang FL, Huang KP, Crawley JN. Neurogranin null mutant mice display performance deficits on spatial learning tasks with anxiety related components. *Hippocampus*. (2001) 11:763–75. doi: 10.1002/hipo.1092
114. Krebs J, Honegger P. Calmodulin kinase IV: Expression and function during rat brain development. *Biochim Biophys Acta Mol Cell Res*. (1996) 1313:217–22. doi: 10.1016/0167-4889(96)00092-4
115. Liu YY, Brent GA. Thyroid hormone-dependent gene expression in differentiated embryonic stem cells and embryonal carcinoma cells: identification of novel thyroid hormone target genes by deoxyribonucleic acid microarray analysis. *Endocrinology*. (2005) 146:776–83. doi: 10.1210/en.2004-1177
116. Morte B, Díez D, Ausó E, Belinchón MM, Gil-Ibáñez P, Grijota-Martínez C, et al. Thyroid hormone regulation of gene expression in the developing rat fetal cerebral cortex: prominent role of the Ca2+/calmodulin-dependent protein kinase IV pathway. *Endocrinology*. (2010) 151:810–20. doi: 10.1210/en.2009-0958
117. Navarro D, Alvarado M, Morte B, Berbel D, Sesma J, Pacheco P, et al. Late maternal hypothyroidism alters the expression of CAMK4 in neocortical subplate neurons: a comparison with nurr1 labeling. *Cereb Cortex*. (2014) 24:2694–706. doi: 10.1093/cercor/bht129
118. Alvarez-Dolado M, Ruiz M, Del Río JA, Alcántara S, Burgaya F, Sheldon M, et al. Thyroid hormone regulates reelin and dab1 expression during brain development. *J. Neurosci*. (1999) 19:6979–93.
119. Herz J, Chen Y. Reelin, lipoprotein receptors and synaptic plasticity. *Nat Rev Neurosci*. (2006) 7:850–9. doi: 10.1038/nrn2009
120. Jossin Y, Cooper JA. Reelin, Rap1 and N-cadherin orient the migration of multipolar neurons in the developing neocortex. *Nat Neurosci*. (2011) 14:697–703. doi: 10.1038/nn.2816
121. Thompson CC, Potter GB. Thyroid hormone action in neural development. *Cereb Cortex*. (2000) 10:939–45. doi: 10.1093/cercor/10.10.939
122. Morte B, Ceballos A, Diez D, Grijota-Martínez C, Dumitrescu AM, Di Cosmo C, et al. Thyroid hormone-regulated mouse cerebral cortex genes are differentially dependent on the source of the hormone: a study in monocarboxylate transporter-8- and deiodinase-2-deficient mice. *Endocrinology*. (2010) 151:2381–7. doi: 10.1210/en.2009-0944
123. Morte B, Gil-Ibáñez P, Bernal J. Regulation of gene expression by thyroid hormone in primary astrocytes: factors influencing the genomic response. *Endocrinology*. (2018) 159:2083–92. doi: 10.1210/en.2017-03084
124. Davis FB, Mousa SA, O'Connor L, Mohamed S, Lin HY, Cao HJ, et al. Proangiogenic action of thyroid hormone is fibroblast growth factor-dependent and is initiated at the cell surface. *Circ Res*. (2004) 94:1500–6. doi: 10.1161/01.RES.0000130784.90237.4a
125. Liu X, Zheng N, Shi YN, Yuan J, Li L. Thyroid hormone induced angiogenesis through the integrin αvβ3/protein kinase D/histone deacetylase 5 signaling pathway. *J Mol Endocrinol*. (2014) 52:245–54. doi: 10.1530/JME-13-0252
126. Luidens MK, Mousa SA, Davis FB, Lin HY, Davis PJ. Thyroid hormone and angiogenesis. *Vascul Pharmacol*. (2010) 52:142–5. doi: 10.1016/j.vph.2009.10.007
127. Davis PJ, Leonard JL, Davis FB. Mechanisms of nongenomic actions of thyroid hormone. *Front Neuroendocrinol*. (2008) 29:211–8. doi: 10.1016/j.yfrne.2007.09.003
128. Davis PJ, Goglia F, Leonard JL. Nongenomic actions of thyroid hormone. *Nat Rev Endocrinol*. (2016) 12:111–21. doi: 10.1038/nrendo.2015.205
129. Hiroi Y, Kim HH, Ying H, Furuya F, Huang Z, Simoncini T, et al. Rapid nongenomic actions of thyroid hormone. *Proc Natl Acad Sci USA*. (2006) 103:14104–9. doi: 10.1073/pnas.0601600103
130. Osmak-Tizon L, Poussier M, Cottin Y, Rochette L. Non-genomic actions of thyroid hormones: molecular aspects. *Arch Cardiovasc Dis*. (2014) 107:207–11. doi: 10.1016/j.acvd.2014.02.001
131. Cao X, Kambe F, Moeller LC, Refetoff S, Seo H. Thyroid hormone induces rapid activation of Akt/protein kinase B-mammalian target of rapamycin-p70S6K cascade through phosphatidylinositol 3-kinase in human fibroblasts. *Mol Endocrinol*. (2005) 19:102–12. doi: 10.1210/me.2004-0093
132. Furuya F, Guigon CJ, Zhao L, Lu C, Hanover JA, Cheng S. Nuclear receptor corepressor is a novel regulator of phosphatidylinositol 3-kinase signaling. *Mol Cell Biol*. (2007) 27:6116–26. doi: 10.1128/MCB.00900-07
133. Lin HY, Sun M, Tang HY, Lin C, Luidens MK, Mousa SA, et al. L-Thyroxine vs. 3,5,3'-triiodo-L-thyronine and cell proliferation: activation of mitogen-activated protein kinase and phosphatidylinositol 3-kinase. *Am J Physiol Cell Physiol*. (2009) 296:C980–91. doi: 10.1152/ajpcell.00305.2008
134. Martin NP, Marron De Velasco E, Mizuno F, Scappini EL, Gloss B, Erxleben C, et al. A rapid cytoplasmic mechanism for PI3 kinase regulation by the nuclear thyroid hormone receptor, TRβ, and genetic evidence for its role in the maturation of mouse hippocampal synapses *in vivo*. *Endocrinology*. (2014) 155:3713–24. doi: 10.1210/en.2013-2058
135. Moeller LC, Cao X, Dumitrescu AM, Seo H, Refetoff S. Thyroid hormone mediated changes in gene expression can be initiated by cytosolic action of the thyroid hormone receptor beta through the phosphatidylinositol 3-kinase pathway. *Nucl Recept Signal*. (2006) 4:e020. doi: 10.1621/nrs.04020
136. Storey NM, Gentile S, Ullah H, Russo A, Muessel M, Erxleben C, et al. Rapid signaling at the plasma membrane by a nuclear receptor for thyroid hormone. *Proc Natl Acad Sci USA*. (2006) 103:5197–201. doi: 10.1073/pnas.0600089103
137. Bergh JJ, Lin HY, Lansing L, Mohamed SN, Davis FB, Mousa S, et al. Integrin alphaVbeta3 contains a cell surface receptor site for thyroid hormone that

is linked to activation of mitogen-activated protein kinase and induction of angiogenesis. *Endocrinology*. (2005) 146:2864–71. doi: 10.1210/en.2005-0102
138. Davis PJ, Davis FB, Cody V. Membrane receptors mediating thyroid hormone action. *Trends Endocrinol Metab.* (2005) 16:429–35. doi: 10.1016/j.tem.2005.09.007
139. Davis PJ, Davis FB, Mousa SA, Luidens MK, Lin HY. Membrane receptor for thyroid hormone: physiologic and pharmacologic implications. *Annu Rev Pharmacol Toxicol.* (2011) 51:99–115. doi: 10.1146/annurev-pharmtox-010510-100512
140. Kalyanaraman H, Schwappacher R, Joshua J, Zhuang S, Scott BT, Klos M, et al. Nongenomic thyroid hormone signaling occurs through a plasma membrane-localized receptor. *Sci Signal.* (2014) 7:ra48. doi: 10.1126/scisignal.2004911
141. Cao HJ, Lin HY, Luidens MK, Davis FB, Davis PJ. Cytoplasm-to-nucleus shuttling of thyroid hormone receptor-β1 (TRβ1) is directed from a plasma membrane integrin receptor by thyroid hormone. *Endocr Res.* (2009) 34:31–42. doi: 10.1080/07435800902911810
142. Lin HY, Tang HY, Shih A, Keating T, Cao G, Davis PJ, et al. Thyroid hormone is a MAPK-dependent growth factor for thyroid cancer cells and is anti-apoptotic. *Steroids.* (2007) 72:180–7. doi: 10.1016/j.steroids.2006.11.014
143. Lin HY, Martino LJ, Wilcox BD, Davis FB, Gordinier JK, Davis PJ. Potentiation by thyroid hormone of human IFN-gamma-induced HLA-DR expression. *J Immunol.* (1998) 161:843–9.
144. Chen Y, Chen PL, Chen CF, Sharp ZD, Lee WH. Thyroid hormone, T3-dependent phosphorylation and translocation of Trip230 from the Golgi complex to the nucleus. *Proc Natl Acad Sci USA.* (1999) 96:4443–8. doi: 10.1073/pnas.96.8.4443
145. Davis PJ, Shih A, Lin HY, Martino LJ, Davis FB. Thyroxine promotes association of mitogen-activated protein kinase and nuclear thyroid hormone receptor (TR) and causes serine phosphorylation of TR. *J Biol Chem.* (2000) 275:38032–9. doi: 10.1074/jbc.M002560200
146. Lin HY, Davis FB, Gordinier JK, Martino LJ, Davis PJ. Thyroid hormone induces activation of mitogen-activated protein kinase in cultured cells. *Am J Physiol Physiol.* (1999) 276:C1014–24. doi: 10.1152/ajpcell.1999.276.5.C1014
147. Lin HY, Shih A, Davis FB, Davis PJ. Thyroid hormone promotes the phosphorylation of STAT3 and potentiates the action of epidermal growth factor in cultured cells. *Biochem J.* (1999) 338(Pt 2):427–32. doi: 10.1042/0264-6021:3380427
148. Shih A, Lin HY, Davis FB, Davis PJ. Thyroid hormone promotes serine phosphorylation of p53 by mitogen-activated protein kinase. *Biochemistry.* (2001) 40:2870–8. doi: 10.1021/bi001978b
149. Incerpi S, Luly P, De Vito P, Farias RN. Short-term effects of thyroid hormones on the Na/H antiport in L-6 myoblasts: high molecular specificity for 3,3',5-triiodo-L-thyronine. *Endocrinology.* (1999) 140:683–9. doi: 10.1210/endo.140.2.6535
150. Bhargava M, Lei J, Mariash CN, Ingbar DH. Thyroid hormone rapidly stimulates alveolar Na,K-ATPase by activation of phosphatidylinositol 3-kinase. *Curr Opin Endocrinol Diabetes Obes.* (2007) 14:416–20. doi: 10.1097/MED.0b013e3282f02ae8
151. Lei J, Mariash CN, Ingbar DH. 3,3',5-Triiodo-L-thyronine up-regulation of Na,K-ATPase activity and cell surface expression in alveolar epithelial cells is Src kinase- and phosphoinositide 3-kinase-dependent. *J Biol Chem.* (2004) 279:47589–600. doi: 10.1074/jbc.M405497200
152. Lei J, Mariash CN, Bhargava M, Wattenberg EV, Ingbar DH. T3 increases Na-K-ATPase activity via a MAPK/ERK1/2-dependent pathway in rat adult alveolar epithelial cells. *Am J Physiol Lung Cell Mol Physiol.* (2008) 294:L749–54. doi: 10.1152/ajplung.00335.2007
153. Scapin S, Leoni S, Spagnuolo S, Fiore AM, Incerpi S. Short-term effects of thyroid hormones on Na+-K+-ATPase activity of chick embryo hepatocytes during development: focus on signal transduction. *Am J Physiol Cell Physiol.* (2009) 296:C4–12. doi: 10.1152/ajpcell.90604.2007
154. Sarkar PK, Biswas A, Ray AK, Martin, JV. Mechanisms of L-triiodothyronine-induced inhibition of synaptosomal na(+)-k(+)-ATPase activity in young adult rat brain cerebral cortex. *J Thyroid Res.* (2013) 2013:457953. doi: 10.1155/2013/457953
155. Sarkar PK, Ray AK. Specific binding of L-triiodothyronine modulates Na+-K+-ATPase activity in adult rat cerebrocortical synaptosomes. *Neuroreport.* (1998) 9:1149–52.
156. Davis PJ, Zhou M, Davis FB, Lansing L, Mousa SA, Lin HY. Mini-review: cell surface receptor for thyroid hormone and nongenomic regulation of ion fluxes in excitable cells. *Physiol Behav.* (2010) 99:237–9. doi: 10.1016/j.physbeh.2009.02.015
157. Kahaly GJ, Dillmann WH. Thyroid hormone action in the heart. *Endocr Rev.* (2005) 26:704–28. doi: 10.1210/er.2003-0033
158. Chakrabarti N, Ray, AK. Stimulation of Ca2+/Mg2+-ATPase activity in adult rat cerebrocortical synaptosomes by 3-5-3′-L-triiodothyronine. *Neurosci Res Commun.* (2002) 31:193–201. doi: 10.1002/nrc.10052
159. Farwell AP, Lynch RM, Okulicz WC, Comi AM, Leonard JL. The actin cytoskeleton mediates the hormonally regulated translocation of type II iodothyronine 5'-deiodinase in astrocytes. *J Biol Chem.* (1990) 265:18546–553.
160. Farwell AP, Dubord-tomasetti SA, Pietrzykowski AZ, Stachelek SJ, Leonard JL. Regulation of cerebellar neuronal migration and neurite outgrowth by thyroxine and 3,3′,5′-triiodothyronine. *Dev Brain Res.* (2005) 154:121–35. doi: 10.1016/j.devbrainres.2004.07.016
161. Leonard JL, Farwell AP. *Thyroid.* hormone-regulated actin polymerization in brain. *Thyroid.* (1997) 7:147–51. doi: 10.1089/thy.1997.7.147
162. Siegrist-Kaiser CA, Juge-Aubry C, Tranter MP, Ekenbarger DM, Leonard JL. Thyroxine-dependent modulation of actin polymerization in cultured astrocytes. A novel, extranuclear action of thyroid hormone. *J Biol Chem.* (1990) 265:5296–302.
163. Campos Costa I, Nogueira Carvalho H, Fernandes L. Aging, circadian rhythms and depressive disorders: a review. *Am J Neurodegener Dis.* (2013) 2:228–46.
164. Froy O. Circadian rhythms, aging, and life span in mammals. *Physiology.* (2011) 26:225–35. doi: 10.1152/physiol.00012.2011
165. Morris CJ, Aeschbach D, Scheer FA. Circadian system, sleep and endocrinology. *Mol Cell Endocrinol.* (2012) 349:91–104. doi: 10.1016/j.mce.2011.09.003
166. Bensenor IM, Olmos RD, Lotufo PA. Hypothyroidism in the elderly: diagnosis and management. *Clin Interv Aging.* (2012) 7:97–111. doi: 10.2147/CIA.S23966
167. Chakraborti S, Chakraborti T, Mandal M, Das S, Batabyal SK. Hypothalamic-pituitary-thyroid axis status of humans during development of ageing process. *Clin Chim Acta.* (1999) 288:137–45. doi: 10.1016/S0009-8981(99)00061-3
168. Cao L, Jiang W, Wang F, Yang QG, Wang C, Chen YP, et al. The reduced serum free triiodothyronine and increased dorsal hippocampal SNAP-25 and Munc18-1 had existed in middle-aged CD-1 mice with mild spatial cognitive impairment. *Brain Res.* (2013) 1540:9–20. doi: 10.1016/j.brainres.2013.09.034
169. Visser WE, Bombardieri CR, Zevenbergen C, Barnhoorn S, Ottaviani A, Van Der Pluijm I, et al. Tissue-specific suppression of thyroid hormone signaling in various mouse models of aging. *PLoS ONE.* (2016) 11:1–25. doi: 10.1371/journal.pone.0149941
170. Fu AL, Zhou CY, Chen X. Thyroid hormone prevents cognitive deficit in a mouse model of Alzheimer's disease. *Neuropharmacology.* (2010) 58:722–9. doi: 10.1016/j.neuropharm.2009.12.020
171. Villanueva I, Alva-Sánchez C, Pacheco-Rosado J. The role of thyroid hormones as inductors of oxidative stress and neurodegeneration. *Oxid Med Cell Longev.* (2013) 2013:218145. doi: 10.1155/2013/218145
172. Qureshi AI, Suri FK, Nasar A, Kirmani JF, Divani AA, Giles WH. Free thyroxine index and risk of stroke: results from the National Health and Nutrition Examination Survey Follow-up Study. *Med Sci Monit.* (2006) 12:CR501–6.
173. Remmel KS, Wanahita A, Moore K, Gruenthal M. Acute ischemic stroke and hypothyroidism. *J Ky Med Assoc.* (2006) 104:191–3.
174. Dhital R, Poudel DR, Tachamo N, Gyawali B, Basnet S, Shrestha P, et al. Ischemic stroke and impact of thyroid profile at presentation: a systematic review and meta-analysis of observational studies. *J Stroke Cerebrovasc Dis.* (2017) 26:2926–34. doi: 10.1016/j.jstrokecerebrovasdis.2017.07.015
175. Jiang X, Xing H, Wu J, Du R, Liu H, Chen J, et al. Prognostic value of thyroid hormones in acute ischemic stroke – a meta analysis. *Sci Rep.* (2017) 7:16256. doi: 10.1038/s41598-017-16564-2
176. Lamba N, Liu C, Zaidi H, Broekman MLD, Simjian T, Shi C, et al. A prognostic role for Low tri-iodothyronine syndrome in acute stroke

patients: a systematic review and meta-analysis. *Clin Neurol Neurosurg.* (2018) 169:55–63. doi: 10.1016/j.clineuro.2018.03.025
177. Liu J, Wang D, Xiong Y, Yuan R, Tao W, Liu M. Low free triiodothyronine levels are related to symptomatic intracranial hemorrhage and poor functional outcomes after intravenous thrombolysis in acute ischemic stroke patients. *Neurol Res.* (2016) 38:429–33. doi: 10.1080/01616412.2016.1178480
178. O'Keefe LM, Conway SE, Czap A, Malchoff CD, Benashski S, Fortunato G, et al. Thyroid hormones and functional outcomes after ischemic stroke. *Thyroid Res.* (2015) 8:9. doi: 10.1186/s13044-015-0021-7
179. Suda S, Muraga K, Kanamaru T, Okubo S, Abe A, Aoki J, et al. Low free triiodothyronine predicts poor functional outcome after acute ischemic stroke. *J Neurol Sci.* (2016) 368:89–93. doi: 10.1016/j.jns.2016.06.063
180. Li LQ, Xu XY, Li WY, Hu XY, Lv W. The prognostic value of total T3 after acute cerebral infarction is age-dependent: a retrospective study on 768 patients. *BMC Neurol.* (2019) 19:54. doi: 10.1186/s12883-019-1264-z
181. Hama S, Kitaoka T, Shigenobu M, Watanabe A, Imura I, Seno H, et al. Malnutrition and nonthyroidal illness syndrome after stroke. *Metabolism.* (2005) 54:699–704. doi: 10.1016/j.metabol.2004.11.016
182. Chaker L, Baumgartner C, Den Elzen WPJ, Collet TH, Ikram MA, Blum MR, et al. Thyroid function within the reference range and the risk of stroke: an individual participant data analysis. *J Clin Endocrinol Metab.* (2016) 101:4270–82. doi: 10.1210/jc.2016-2255
183. Akhoundi FH, Ghorbani A, Soltani A, Meysamie A. Favorable functional outcomes in acute ischemic stroke patients with subclinical hypothyroidism. *Neurology.* (2011) 77:349–54. doi: 10.1212/WNL.0b013e3182267ba0
184. Alevizaki M, Synetou M, Xynos K, Alevizaki CC, Vemmos KN. Hypothyroidism as a protective factor in acute stroke patients. *Clin Endocrinol.* (2006) 65:369–72. doi: 10.1111/j.1365-2265.2006.02606.x
185. Rastogi L, Godbole MM, Ray M, Rathore P, Rathore P, Pradhan S, et al. Reduction in oxidative stress and cell death explains hypothyroidism induced neuroprotection subsequent to ischemia/reperfusion insult. *Exp Neurol.* (2006) 200:290–300. doi: 10.1016/j.expneurol.2006.02.013
186. Shuaib A, Ijaz S, Mazagri R, Kalra J, Hemmings S, Senthilsvlan A, et al. Hypothyroidism protects the brain during transient forebrain ischemia in gerbils. *Exp Neurol.* (1994) 127:119–25. doi: 10.1006/exnr.1994.1085
187. Lee CH, Yoo KY, Hwang IK, Choi JH, Park OK, Li H, et al. Hypothyroid state does not protect but delays neuronal death in the hippocampal CA1 region following transient cerebral ischemia: focus on oxidative stress and gliosis. *J Neurosci Res.* (2010) 88:2661–8. doi: 10.1002/jnr.22436
188. Rastogi L, Godbole MM, Sinha RA, Pradhan S. Reverse triiodothyronine (rT3) attenuates ischemia-reperfusion injury. *Biochem Biophys Res Commun.* (2018) 506:597–603. doi: 10.1016/j.bbrc.2018.10.031
189. Lourbopoulos A, Mourouzis I, Karapanayiotides T, Nousiopoulou E, Chatzigeorgiou S, Mavridis T, et al. Changes in thyroid hormone receptors after permanent cerebral ischemia in male rats. *J Mol Neurosci.* (2014) 54:78–91. doi: 10.1007/s12031-014-0253-3
190. Bengtsson D, Brudin L, Wanby P, Carlsson M. Previously unknown thyroid dysfunction in patients with acute ischemic stroke. *Acta Neurol Scand.* (2012) 126:98–102. doi: 10.1111/j.1600-0404.2011.01604.x
191. Sheu JJ, Kang JH, Lin HC, Lin HC. Hyperthyroidism and risk of ischemic stroke in young adults: a 5-year follow-up study. *Stroke.* (2010) 41:961–6. doi: 10.1161/STROKEAHA.109.577742
192. Wollenweber FA, Zietemann V, Gschwendtner A, Opherk C, Dichgans M. Subclinical hyperthyroidism is a risk factor for poor functional outcome after ischemic stroke. *Stroke.* (2013) 44:1446–8. doi: 10.1161/STROKEAHA.113.000833
193. Keshavarz S, Dehghani GA. Cerebral ischemia/reperfusion injury in the hyperthyroid rat. *Iran J Med Sci.* (2017) 42, 48–56.
194. Margaill I, Royer J, Lerouet D, Ramaugé M, Le Goascogne C, Li WW, et al. Induction of type 2 iodothyronine deiodinase in astrocytes after transient focal cerebral ischemia in the rat. *J Cereb Blood Flow Metab.* (2005) 25:468–76. doi: 10.1038/sj.jcbfm.9600041
195. Rami A, Krieglstein J. Thyroxine attenuates hippocampal neuronal damage caused by ischemia in the rat. *Life Sci.* (1992) 50:645–50. doi: 10.1016/0024-3205(92)90251-J
196. Genovese T, Impellizzeri D, Ahmad A, Cornelius C, Campolo M, Cuzzocrea S, et al. Post-ischaemic thyroid hormone treatment in a rat model of acute stroke. *Brain Res.* (2013) 1513:92–102. doi: 10.1016/j.brainres.2013.03.001
197. Crupi R, Paterniti I, Campolo M, Di Paola R, Cuzzocrea S, Esposito E. Exogenous T3 administration provides neuroprotection in a murine model of traumatic brain injury. *Pharmacol Res.* (2013) 70:80–9. doi: 10.1016/j.phrs.2012.12.009
198. Sayre NL, Sifuentes M, Holstein D, Cheng SY, Zhu X, Lechleiter JD. Stimulation of astrocyte fatty acid oxidation by thyroid hormone is protective against ischemic stroke-induced damage. *J Cereb Blood Flow Metab.* (2017) 37:514–27. doi: 10.1177/0271678X16629153
199. Akhoundzadeh K, Vakili A, Sameni HR, Vafaei AA, Rashidy-Pour A, Safari M, et al. Effects of the combined treatment of bone marrow stromal cells with mild exercise and thyroid hormone on brain damage and apoptosis in a mouse focal cerebral ischemia model. *Metab Brain Dis.* (2017) 32:1267–77. doi: 10.1007/s11011-017-0034-0
200. Doyle KP, Suchland KL, Ciesielski TMP, Lessov NS, Grandy DK, Scanlan TS, et al. Novel thyroxine derivatives, thyronamine and 3-iodothyronamine, induce transient hypothermia and marked neuroprotection against stroke injury. *Stroke.* (2007) 38:2569–76. doi: 10.1161/STROKEAHA.106.480277
201. Costa LES, Clementino-Neto J, Mendes CB, Franzon NH, De Oliveira Costa E, Moura-Neto V, et al. Evidence of aquaporin 4 regulation by thyroid hormone during mouse brain development and in cultured human glioblastoma multiforme cells. *Front Neurosci.* (2019) 13:317. doi: 10.3389/fnins.2019.00317
202. Losi G, Garzon G, Puia G. Nongenomic regulation of glutamatergic neurotransmission in hippocampus by thyroid hormones. *Neuroscience.* (2008) 151:155–63. doi: 10.1016/j.neuroscience.2007.09.064
203. Mendes-de-Aguiar CBN, Alchini R, Decker H, Alvarez-Silva M, Tasca CI, Trentin, AG. Thyroid hormone increases astrocytic glutamate uptake and protects astrocytes and neurons against glutamate toxicity. *J Neurosci Res.* (2008) 86:3117–25. doi: 10.1002/jnr.21755
204. Guo ZH, Li F, Wang WZ. The mechanisms of brain ischemic insult and potential protective interventions. *Neurosci Bull.* (2009) 25:139–52. doi: 10.1007/s12264-009-0104-3
205. Pantos C, Mourouzis I. Thyroid hormone receptor α1 as a novel therapeutic target for tissue repair. *Ann Transl Med.* (2018) 6:254. doi: 10.21037/atm.2018.06.12
206. Madinier A, Quattromani MJ, Sjölund C, Ruscher K, Wieloch T. Enriched housing enhances recovery of limb placement ability and reduces aggrecan-containing perineuronal nets in the rat somatosensory cortex after experimental stroke. *PLoS ONE.* (2014) 9:e93121. doi: 10.1371/journal.pone.0093121
207. Quattromani MJ, Cordeau P, Ruscher K, Kriz J, Wieloch T. Enriched housing down-regulates the Toll-like receptor 2 response in the mouse brain after experimental stroke. *Neurobiol Dis.* (2014) 66:66–73. doi: 10.1016/j.nbd.2014.02.010
208. Wieloch T, Nikolich K. Mechanisms of neural plasticity following brain injury. *Curr Opin Neurobiol.* (2006) 16:258–64. doi: 10.1016/j.conb.2006.05.011
209. Pekna M, Pekny M, Nilsson M. Modulation of neural plasticity as a basis for stroke rehabilitation. *Stroke.* (2012) 43:2819–28. doi: 10.1161/STROKEAHA.112.654228
210. Sharma N, Classen J, Cohen LG. Neural plasticity and its contribution to functional recovery. *Handb Clin Neurol.* (2013) 110:3–12. doi: 10.1016/B978-0-444-52901-5.00001-0
211. Zhong L, Gerges NZ. Neurogranin targets calmodulin and lowers the threshold for the induction of long-term potentiation. *PLoS ONE.* (2012) 7:e41275. doi: 10.1371/journal.pone.0041275
212. Sui L, Ren WW, Li BM. Administration of thyroid hormone increases reelin and brain-derived neurotrophic factor expression in rat hippocampus *in vivo*. *Brain Res.* (2010) 1313:9–24. doi: 10.1016/j.brainres.2009.12.010
213. Krebs J, Means RL, Honegger P. Induction of calmodulin kinase IV by the thyroid hormone during the development of rat brain. *J Biol Chem.* (1996) 271:11055–8. doi: 10.1074/jbc.271.19.11055
214. Redmond L, Kashani AH, Ghosh A. Calcium regulation of dendritic growth via CaM kinase IV and CREB-mediated transcription. *Neuron.* (2002) 34:999–1010. doi: 10.1016/S0896-6273(02)00737-7
215. Gordon-Weeks PR, Fournier AE. Neuronal cytoskeleton in synaptic plasticity and regeneration. *J Neurochem.* (2014) 129:206–12. doi: 10.1111/jnc.12502

216. Aniello F, Couchie D, Gripois D, Nunez J. Regulation of five tubulin isotypes by thyroid hormone during brain development. *J Neurochem.* (1991) 57:1781–6. doi: 10.1111/j.1471-4159.1991.tb06381.x
217. Lorenzo PI, Ménard C, Miller FD, Bernal J. Thyroid hormone-dependent regulation of Talpha1 alpha-tubulin during brain development. *Mol Cell Neurosci.* (2002) 19:333–43. doi: 10.1006/mcne.2001.1087
218. Silva JE, Rudas P. Effects of congenital hypothyroidism on microtubule-associated protein-2 expression in the cerebellum of the rat. *Endocrinology.* (1990) 126:1276–82. doi: 10.1210/endo-126-2-1276
219. Aniello F, Couchie D, Bridoux AM, Gripois D, Nunez J. Splicing of juvenile and adult tau mRNA variants is regulated by thyroid hormone. *Proc Natl Acad Sci USA.* (1991) 88:4035–9. doi: 10.1073/pnas.88.9.4035
220. Zamoner A, Funchal C, Heimfarth L, Silva FR, Pessoa-Pureur R. Short-term effects of thyroid hormones on cytoskeletal proteins are mediated by GABAergic mechanisms in slices of cerebral cortex from young rats. *Cell Mol Neurobiol.* (2006) 26:209–24. doi: 10.1007/s10571-006-9027-y
221. Zamoner A, Funchal C, Jacques-Silva MC, Gottfried C, Barreto Silva FR, Pessoa-Pureur R. Thyroid hormones reorganize the cytoskeleton of glial cells through Gfap phosphorylation and Rhoa-dependent mechanisms. *Cell Mol Neurobiol.* (2007) 27:845–65. doi: 10.1007/s10571-006-9084-2
222. Faivre-Sarrailh C, Rabié A. Developmental study of factors controlling microtubule *in vitro* cold-stability in rat cerebrum. *Dev Brain Res.* (1988) 42:199–204. doi: 10.1016/0165-3806(88)90238-6
223. Farwell AP, Dubord-Tomasetti SA, Pietrzykowski AZ, Leonard JL. Dynamic nongenomic actions of thyroid hormone in the developing rat brain. *Endocrinology.* (2006) 147:2567–74. doi: 10.1210/en.2005-1272
224. Farwell AP, Dubord-Tomasetti SA. Thyroid hormone regulates the expression of laminin in the developing rat cerebellum. *Endocrinology.* (1999) 140:4221–7. doi: 10.1210/endo.140.9.7007
225. Cayrou C, Denver RJ, Puymirat J. Suppression of the basic transcription element-binding protein in brain neuronal cultures inhibits thyroid hormone-induced neurite branching. *Endocrinology.* (2002) 143:2242–9. doi: 10.1210/en.143.6.2242
226. Martel J, Cayrou C, Puymirat J. Identification of new thyroid hormone-regulated genes in rat brain neuronal cultures. *Neuroreporte.* (2002) 13:1849–51. doi: 10.1097/00001756-200210280-00003
227. Vara H, Martínez B, Santos A, Colino A. Thyroid hormone regulates neurotransmitter release in neonatal rat hippocampus. *Neuroscience.* (2002) 110:19–28. doi: 10.1016/S0306-4522(01)00541-3
228. Liu W, Dong J, Wang Y, Xi Q, Chen J. Developmental iodine deficiency and hypothyroidism impaired *in vivo* synaptic plasticity and altered PKC activity and GAP-43 expression in rat hippocampus. *Nutr Neurosci.* (2010) 11:50. doi: 10.1179/147683010x12611460764525
229. Dong J, Yin H, Liu W, Wang P, Jiang Y, Chen J. Congenital iodine deficiency and hypothyroidism impair LTP and decrease c-fos and c-jun expression in rat hippocampus. *Neurotoxicology.* (2005) 26:417–26. doi: 10.1016/j.neuro.2005.03.003
230. Sui L, Gilbert ME. Pre- and postnatal propylthiouracil-induced hypothyroidism impairs synaptic transmission and plasticity in area CA1 of the neonatal rat hippocampus. *Endocrinology.* (2003) 144:4195–203. doi: 10.1210/en.2003-0395
231. Gerges NZ, Alkadhi KA. Hypothyroidism impairs late LTP in CA1 region but not in dentate gyrus of the intact rat hippocampus: MAPK involvement. *Hippocampus.* (2004) 14:40–5. doi: 10.1002/hipo.10165
232. Niemi WD, Slivinski K, Audi J, Rej R, Carpenter DO. Propylthiouracil treatment reduces long-term potentiation in area CA1 of neonatal rat hippocampus. *Neurosci Lett.* (1996) 210:127–9. doi: 10.1016/0304-3940(96)12676-8
233. Gilbert ME. Alterations in synaptic transmission and plasticity in area CA1 of adult hippocampus following developmental hypothyroidism. *Dev Brain Res.* (2004) 148:11–8. doi: 10.1016/j.devbrainres.2003.09.018
234. Gould E, Allan MD, McEwen BS. Dendritic spine density of adult hippocampal pyramidal cells is sensitive to thyroid hormone. *Brain Res.* (1990). doi: 10.1016/0006-8993(90)90884-E
235. Taşkin E, Artis AS, Bitiktas S, Dolu N, Liman N, Süer C. Experimentally induced hyperthyroidism disrupts hippocampal long-term potentiation in adult rats. *Neuroendocrinology.* (2011) 94:218–27. doi: 10.1159/000328513
236. Forini F, Kusmic C, Nicolini G, Mariani L, Zucchi R, Matteucci M, et al. Triiodothyronine prevents cardiac ischemia/reperfusion mitochondrial impairment and cell loss by regulating miR30a/p53 axis. *Endocrinology.* (2014) 155:4581–90. doi: 10.1210/en.2014-1106
237. Zinman T, Shneyvays V, Tribulova N, Manoach M, Shainberg A. Acute, nongenomic effect of thyroid hormones in preventing calcium overload in newborn rat cardiocytes. *J Cell Physiol.* (2006) 207:220–31. doi: 10.1002/jcp.20562
238. Manzano J, Cuadrado M, Morte B, Bernal J. Influence of thyroid hormone and thyroid hormone receptors in the generation of cerebellar γ-aminobutyric acid-ergic interneurons from precursor cells. *Endocrinology.* (2007) 148:5746–51. doi: 10.1210/en.2007-0567
239. Hashimoto H, Walker CH, Prange AJJ, Mason GA. The effects of thyroid hormones on potassium-stimulated release of 3H-GABA by synaptosomes of rat cerebral cortex. *Neuropsychopharmacology.* (1991) 5:49–54.
240. Kalaria RN, Prince AK. Effects of thyroid deficiency on the development of cholinergic, GABA, dopaminergic and glutamate neuron markers and DNA concentrations in the rat corpus striatum. *Int J Dev Neurosci.* (1985) 3:655–66. doi: 10.1016/0736-5748(85)90056-5
241. Mason GA, Walker CH, Prange AJ, Bondy SC. GABA uptake is inhibited by thyroid hormones: implications for depression. *Psychoneuroendocrinology.* (1987) 12:53–9. doi: 10.1016/0306-4530(87)90022-9
242. Martin JV, Williams DB, Fitzgerald RM, Im HK, Vonvoigtlander PF. Thyroid hormonal modulation of the binding and activity of the GABA(A) receptor complex of brain. *Neuroscience.* (1996) 73:705–13. doi: 10.1016/0306-4522(96)00052-8
243. Ambrogini P, Cuppini R, Ferri P, Mancini C, Ciaroni S, Voci A, et al. Thyroid hormones affect neurogenesis in the dentate gyrus of adult rat. *Neuroendocrinology.* (2005) 81:244–53. doi: 10.1159/000087648
244. Desouza LA, Ladiwala U, Daniel SM, Agashe S, Vaidya RA, Vaidya VA. Thyroid hormone regulates hippocampal neurogenesis in the adult rat brain. *Mol Cell Neurosci.* (2005) 29:414–26. doi: 10.1016/j.mcn.2005.03.010
245. Fanibunda SE, Desouza LA, Kapoor R, Vaidya RA, Vaidya VA. Thyroid hormone regulation of adult neurogenesis. *Vitam Horm.* (2017) 106:211–51. doi: 10.1016/bs.vh.2017.04.006
246. Kapoor R, Desouza LA, Nanavaty IN, Kernie SG, Vaidya VA. Thyroid hormone accelerates the differentiation of adult hippocampal progenitors. *J Neuroendocrinol.* (2012) 24:1259–71. doi: 10.1111/j.1365-2826.2012.02329.x
247. Lemkine GF, Raj A, Alfama G, Turque N, Hassani Z, Alegria-Prévot O, et al. Adult neural stem cell cycling *in vivo* requires thyroid hormone and its alpha receptor. *FASEB J.* (2005) 19:863–5. doi: 10.1096/fj.04-2916fje
248. López-Juárez A, Remaud S, Hassani Z, Jolivet P, Pierre Simons J, Sontag T, et al. Thyroid hormone signaling acts as a neurogenic switch by repressing Sox2 in the adult neural stem cell niche. *Cell Stem Cell.* (2012) 10:531–43. doi: 10.1016/j.stem.2012.04.008
249. Montero-Pedrazuela A, Venero C, Lavado-Autric R, Fernández-Lamo I, García-Verdugo JM, Bernal J, et al. Modulation of adult hippocampal neurogenesis by thyroid hormones: implications in depressive-like behavior. *Mol Psychiatry.* (2006) 11:361–71. doi: 10.1038/sj.mp.4001802
250. Zhang L, Blomgren K, Kuhn HG, Cooper-Kuhn CM. Effects of postnatal thyroid hormone deficiency on neurogenesis in the juvenile and adult rat. *Neurobiol Dis.* (2009) 34:366–74. doi: 10.1016/j.nbd.2009.02.006
251. Kapoor R, Fanibunda SE, Desouza LA, Guha SK, Vaidya VA. Perspectives on thyroid hormone action in adult neurogenesis. *J Neurochem.* (2015) 133:599–616. doi: 10.1111/jnc.13093
252. Remaud S, Gothié JD, Morvan-Dubois G, Demeneix BA. Thyroid hormone signaling and adult neurogenesis in mammals. *Front Endocrinol.* (2014) 5:62. doi: 10.3389/fendo.2014.00062
253. Christie KJ, Turnley AM. Regulation of endogenous neural stem/progenitor cells for neural repair—factors that promote neurogenesis and gliogenesis in the normal and damaged brain. *Front Cell Neurosci.* (2013) 6:70. doi: 10.3389/fncel.2012.00070
254. Ming GL, Song H. Adult neurogenesis in the mammalian brain: significant answers and significant questions. *Neuron.* (2011) 70:687–702. doi: 10.1016/j.neuron.2011.05.001
255. Lu J, Manaenko A, Hu Q. Targeting adult neurogenesis for poststroke therapy. *Stem Cells Int.* (2017) 2017:5868632. doi: 10.1155/2017/5868632

256. Angels Font M, Arboix A, Krupinski J. Angiogenesis, neurogenesis and neuroplasticity in ischemic stroke. *Curr Cardiol Rev.* (2010) 6:238–44. doi: 10.2174/157340310791658802
257. Arai K, Jin G, Navaratna D, Lo EH. Brain angiogenesis in developmental and pathological processes: neurovascular injury and angiogenic recovery after stroke. *FEBS J.* (2009) 276:4644–52. doi: 10.1111/j.1742-4658.2009.07176.x
258. Arenillas JF, Sobrino T, Castillo J, Dávalos A. The role of angiogenesis in damage and recovery from ischemic stroke. *Curr Treat Options Cardiovasc Med.* (2007) 9:205–12. doi: 10.1007/s11936-007-0014-5
259. Tomanek RJ, Zimmerman MB, Suvarna PR, Morkin E, Pennock GD, Goldman S. A thyroid hormone analog stimulates angiogenesis in the post-infarcted rat heart. *J Mol Cell Cardiol.* (1998) 30:923–32. doi: 10.1006/jmcc.1998.0671
260. Schlenker EH, Hora M, Liu Y, Redetzke RA, Morkin E, Gerdes AM. Effects of thyroidectomy, T4, and DITPA replacement on brain blood vessel density in adult rats. *AJP Regul Integr Comp Physiol.* (2008) 294:R1504–9. doi: 10.1152/ajpregu.00027.2008
261. Davis PJ, Sudha T, Lin HY, Mousa SA. Thyroid hormone, hormone analogs, and angiogenesis. *Compr Physiol.* (2016) 6:353–62. doi: 10.1002/cphy.c150011
262. Mousa SA, O'Connor LJ, Bergh JJ, Davis FB, Scanlan TS, Davis PJ. The proangiogenic action of thyroid hormone analogue GC-1 is initiated at an integrin. *J Cardiovasc Pharmacol.* (2005) 46:356–60. doi: 10.1097/01.fjc.0000175438.94906.a0

Conflict of Interest: The authors declare that the research was conducted in the absence of any commercial or financial relationships that could be construed as a potential conflict of interest.

Copyright © 2019 Talhada, Santos, Gonçalves and Ruscher. This is an open-access article distributed under the terms of the Creative Commons Attribution License (CC BY). The use, distribution or reproduction in other forums is permitted, provided the original author(s) and the copyright owner(s) are credited and that the original publication in this journal is cited, in accordance with accepted academic practice. No use, distribution or reproduction is permitted which does not comply with these terms.

frontiers in Neurology

CASE REPORT
published: 22 October 2019
doi: 10.3389/fneur.2019.01102

Behcet's Disease With Cerebral Artery Infarction Caused by Cerebral Arteritis as an Early Symptom Only With Elevated Interleukin-8

Hao Yin[1,2], *Yun Song*[1,2], *Meimei Zheng*[1,2], *Ju Han*[1,2] *and Jiyou Tang*[1,2]*

[1] *Shandong Provincial Qianfoshan Hospital, Shandong University, Jinan, China,* [2] *The First Affiliated Hospital of Shandong First Medical University, Jinan, China*

Background: Behcet's disease (BD) is multi-systemic vasculitis, which generally is repeated oral and genital ulcerations as well as ocular and skin lesions. Today, the pathogenesis of BD remains mostly unknown. It is also suggested that the disease is probably related to autoinflammatory and autoimmune disorders, and innate immunity damages were perceived as key in its pathologic process. Only 5% of BD patients have neurological involvement, and it usually occurs in 4–6 years after the initial symptoms. Early onset of neurological impairment makes it difficult to diagnose and treat definitely.

Case Presentation: A 38-year-old man was admitted to our hospital with numbness and weakness of the left extremities. Diffusion magnetic resonance imaging (MRI) revealed focal infarction in the posterior limb of the internal capsule. Skin pathology suggested small vessel vasculitis, and high-resolution MRI revealed intracranial arteritis. The patient had a negative skin pathery test and then developed a scar at the venous puncture site at the early stage of disease. Laboratory examination showed that interleukin 8 (IL-8) increased. The patient was treated with an immunosuppressive agent including mycophenolate mofetil, hydroxychloroquine, and colchicine. All symptoms were alleviated after half a year's treatment. There was neither stroke nor recurrence of oral ulcer thereafter.

Conclusion: This case demonstrates that neurological involvement might be an early symptom of BD. IL-8 could act as a novel target for the treatment of BD theoretically and probably play a key role in disease recovery.

Keywords: Behcet's disease, neuro-Behcet's disease, cerebral infarction, cerebral arteritis, IL-8

OPEN ACCESS

Edited by:
Johannes Boltze, University of Warwick, United Kingdom

Reviewed by:
Giuseppe Lopalco, Interdisciplinary Department of Medicine, Italy
Alexander Tsiskaridze, Tbilisi State University, Georgia

***Correspondence:**
Jiyou Tang
jytang001@sohu.com

Specialty section:
This article was submitted to Stroke, a section of the journal Frontiers in Neurology

Received: *04 June 2019*
Accepted: *01 October 2019*
Published: *22 October 2019*

Citation:
Yin H, Song Y, Zheng M, Han J and Tang J (2019) Behcet's Disease With Cerebral Artery Infarction Caused by Cerebral Arteritis as an Early Symptom Only With Elevated Interleukin-8. Front. Neurol. 10:1102. doi: 10.3389/fneur.2019.01102

INTRODUCTION

Behcet's disease (BD) is recognized as a multi-systemic disease characterized by possible inflammatory lesions of any-size vessels (1). Although the etiopathogenesis has not yet been clarified, it is generally believed that immunological factors play an important role (2–4). It is also suggested that the disease is probably related to autoinflammatory and autoimmune disorders, and innate immunity damages were perceived as having a key role in its pathologic process (5–7). The diagnosis is established by clinical criteria only (8). The international criteria for BD (ICBD) allow for earlier recognition, thus leading to earlier and accurate diagnosis and treatment with salutary results (9).

Involvement of central nervous system symptoms is reported in 3.2–49%, mostly about 5%, in BD patients (10, 11), which is known as neuro-Behcet's disease (NBD).Nervous system impairment mostly occurs in 4–6 years after the onset of BD (12). However, some of the patients have neurological symptoms at the same time as or even before the classical BD symptoms, which may lead to diagnostic confusion and may result in there being more BD patients than actually reported (13).

In this kind of patient, the pathological feature is various types of arteriovenous vasculitis, which mainly affects small vessels in multiple systems. It appears as focal or multiple brain parenchymal damage in the central nervous system (14, 15). Artery involvement is rare compared with venous involvement, manifesting as arterial stenosis and aneurysm formation, which often lead to arterial infarction or intracranial and/or subarachnoid hemorrhage (16–18).

CASE PRESENTATION

A 38-year-old man was admitted to our hospital with numbness and weakness of the left extremities. Diffusion-weighted imaging (DWI) revealed focal infarction in the posterior limb of the internal capsule, and cranial and cervical magnetic resonance angiography was normal (**Figure 1**).

The patient had recurrent multiple and painful oral ulcers after 2 months; meanwhile, he suffered pain in both knees and the left shoulder joint. The physical examination revealed that the old and new *acneiform folliculitis* were alternated on the face and back and behind the ears (**Figure 2**); also, a scar was shown at the venous puncture site (**Figure 3**). The patient had no other risk factors for cerebral atherosclerotic disease and is also not a smoker. Blood routine, serologic etiology test (including syphilis, AIDS, and other pathogens), lipid profile, plasma glucose, plasma and urine homocysteine levels (indicating the possibility of a genetic predisposition to thrombosis), proteins C and S deficiency, antithrombin III deficiency, activated protein C resistance, antiphospholipid antibody (hypercoagulability markers), anticardiolipin immunoglobulin G (IgG) and immunoglobulin M (IgM), antineutrophilic cytoplasmic antibody, C-reactive protein (CRP), erythrocyte sedimentation rate, and rheumatoid factor were performed, and all of them were within normal range. Transesophageal echocardiography, contrasted transthoracic echocardiography, and 24-h dynamic electrocardiogram were normal. Interleukin 8 (IL-8) was increased to 252 pg/ml (normal value: <62 pg/ml), but IL-6, tumor necrosis factors (TNF), and other cytokines were maintained at normal levels. No cardiogenic embolism, cardiac structure and rhythm abnormalities were found.

High-resolution magnetic resonance imaging (HRMRI) of the brain suggested that some blood vessel walls were slightly thickened, including the terminal portion of the left internal carotid artery, V4 segment of the bilateral vertebral artery, P2 segment of the right posterior cerebral artery (**Figure 4**), the terminal portion of M1 segment of the right middle cerebral artery (MCA), M2 and M3 segments of bilateral MCA, and A2 segment of the bilateral anterior cerebral artery. The enhancement scanning showed a double-track-like change and a narrowed vascular lumen, which suggested multiple intracranial arteritis. Hip magnetic resonance imaging (MRI) showed a long and flaky T1-weighted and T2 high fat-suppression signal on the lateral of the left femoral head, which suggested degenerative changes. Pathological biopsy of the skin lesion showed that some regions were infiltrated by extensively perivascular inflammatory cells, suggesting small vessel vasculitis (**Figure 5**). Genetic testing also was performed to analyze hereditary cerebrovascular disease elements (detected by Golden Field Medical, Inc., using analysis of missense mutations and alternative splicing; this lab has gotten the accreditation of the College of American Pathologists), and the result *did not* show pathogenic variation. Based on the above testing results and related to a history of genital ulcers of the patient, this case was diagnosed as BD under the direction of diagnostic criteria. The patient could not use azathioprine (AZP) to thiopurine S-methyltransferase (TPMT) mutation, and this could be checked by gene detection, which indicated that there was TPMT*3C (A719G) in this patient. Meanwhile, the patient refused to use cyclophosphamide after acquainting with its side effects (nephrotoxicity etc.) and its cumulative toxicity with long-term use (19).

Therefore, the patient was treated with mycophenolate mofetil dispersible tablets (Seccopin), hydroxychloroquine tablets (Flush), and colchicine tablets. After half a year's treatment, the patient's skin rash gradually was alleviated, and the symptoms of oral ulcer and nervous system damage did not recur.

DISCUSSION AND CONCLUSIONS

Our patient fulfilled the diagnostic criteria of ICBD; he had recurrent oral ulcers (2 points), skin lesions (1 point), central nervous system lesions (1 point), vascular symptoms (1 point), and a positive pathergy test (1 point).

The patient initially consulted for acute cerebral infarction. This patient did not show risk factors for cerebral atherosclerotic disease other than smoking and also had no abnormalities in the gene test of hereditary cerebrovascular disease and other common causes, for example, hypercoagulability. According to his medical history, laboratory tests, and examination results, vasculitis caused by syphilitic vasculitis, rheumatoid arthritis, systemic lupus erythematosus, and Sjogren's syndrome can be excluded. The high-resolution MRI (HRMRI) of the brain showed intimal thickening in the wall of the intracranial and cervical arteries, which suggested arteritis. However, carotid

Abbreviations: IL-8, interleukin 8; NBD, neuro-Behcet's disease; BD, Behcet's disease; ICBD, international criteria for Behcet's disease; AZP, azathioprine; MMF, mycophenolate mofetil; IL-1, interleukin 1; IgG, immunoglobulin G; IgM, immunoglobulin M; DWI, diffusion-weighted imaging; MRI, magnetic resonance imaging; HRMRI, high-resolution MRI; MCA, middle cerebral artery; CRP, C-reactive protein; ESR, erythrocyte sedimentation rate; TPMT, thiopurine S-methyltransferase; FMF, familial Mediterranean fever.

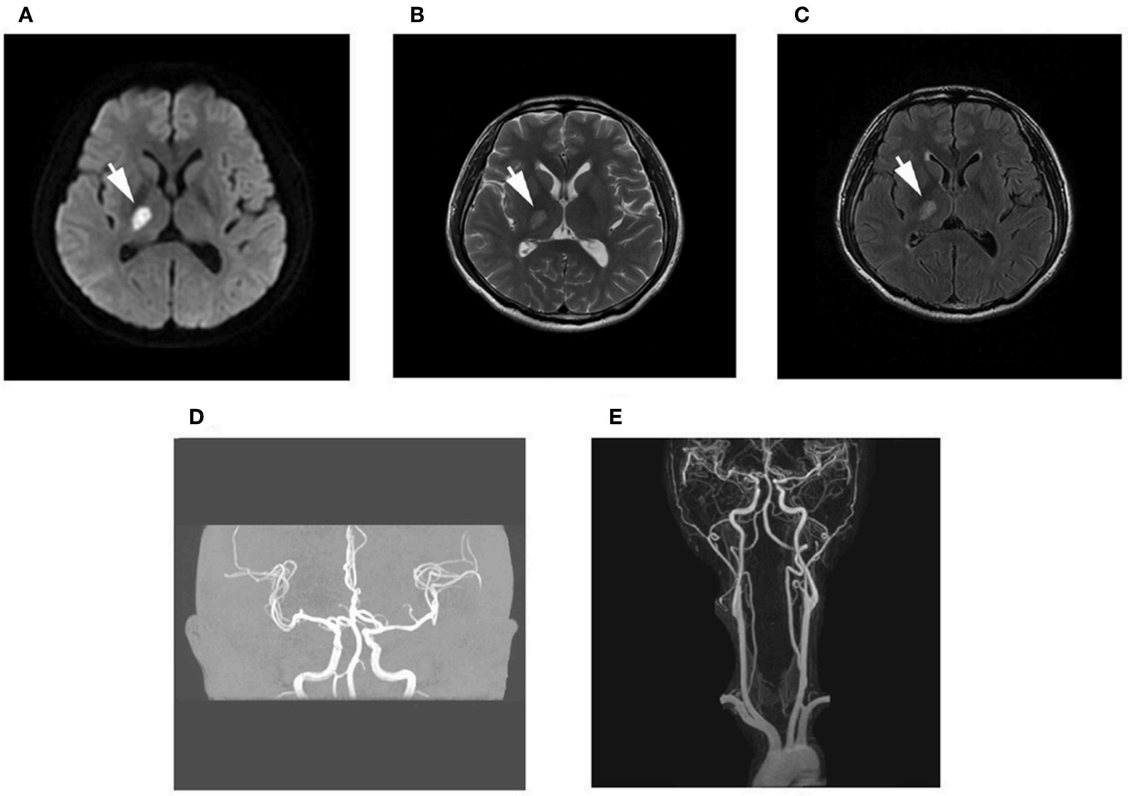

FIGURE 1 | Brain magnetic resonance imaging (MRI). **(A–C)** Diffusion-weighted imaging (DWI) and T2 fluid-attenuated inversion recovery (FLAIR) imaging showed high signal, while long signal was shown in T1-weighted imaging and T2-weighted imaging of the posterior limb of the internal capsule. **(D,E)** Magnetic resonance angiography examination of the intracranial and cervical vascular was normal.

dissection or Moyamoya symptoms *were not* shown. The new internal capsule lesion seen on MRI was consistent with the occlusion regions resulting from arteritis of the MCA deep perforator branches. In conclusion, the patient was diagnosed with BD.

Vasculitis is the central pathological process of BD. In this case, skin pathology was a representation of vasculitis, and it was verified by HRMRI as cerebral arteritis. Venipuncture is an inflammatory lesion of the skin, and it is similar to spontaneous skin lesions seen in the disease. Our patient had a negative skin pathery test, which developed a scar at the venous puncture site for the intravenous fluid infusion at the early stage of disease, but we have not observed the whole process of scar formation. The investigation results revealed that the presence of a positive reaction was irrelevant to the clinical manifestations of the disease (20, 21). However, the pathery reaction (PR) was reported to be significantly associated with vascular involvement (22). Chang et al. described that the intravenous Pathergy test seemed to be superior to the skin Pathergy test on specificity, sensitivity, and positive rate. Pathergy test reactions usually occur during active periods of BD as well (23). Although no peripheral vascular pathological examination was performed, the case was tested by negative classic PR, and the results suggested that the scar formation at the venipuncture site was caused by peripheral venous vasculitis.

Different immunologic abnormalities in the etiopathogenesis of BD have been reported. Increased Th1-associated cytokines such as IL-12, interferon-γ (IFN-γ), and tumor necrosis factor-α (TNF-α), as well as IL-2, IL-8, and IL-6, have been documented in BD patients (24). Many studies have reported that increased serum IL-8 plays an important role in BD (25–31). One recent report even implied that serum IL-8 could be a more credible marker of disease activity than CRP or erythrocyte sedimentation rate (ESR) (32). Durmazlar et al. found that IL-8 is positively correlated with the activity of BD and also closely related with the BD activity index and numbers of disease clinical manifestations. IL-8, known as neutrophil activating factor, is substantially produced by granulocytes, T cells, macrophages, and endothelial cells. A small amount of IL-8 can also be induced in keratinocytes, fibroblasts, chondrocytes, and hepatocytes (31, 33, 34). It strongly attracts and activates leukocytes. It has been supposed to establish a prominent connection between immune system activation and endothelial alterations involved in the conversion of mononuclear to granulocytic infiltration and causes raised adhesion of peripheral blood leukocytes to endothelial cells in BD. It has been found that the significant increase of IL-8 is associated with different clinical manifestations

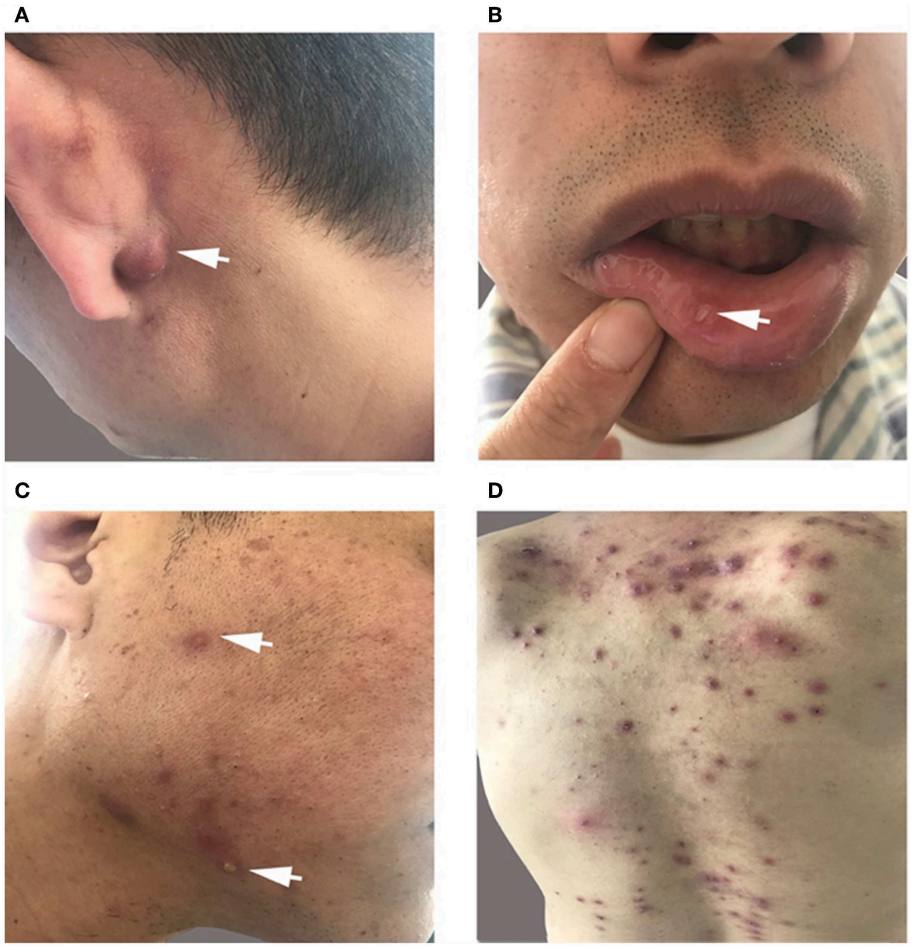

FIGURE 2 | (A,C,D) Old and new acneiform folliculitis behind the ears **(A)** and on the face **(C)** and back **(D)**. **(B)** Recurrent multiple and painful oral ulcers.

in BD, such as skin lesions, oral lesions, and ocular manifestations in one study (31). Moreover, compared with the active patient group without vascular involvement, the levels of IL-8 in patients with vascular involvement were markedly increased. On the basis of the patients' pathology and imaging, active BD patients with vascular involvement were found to possess pretty enhanced IL-8 in serum levels, which supported that endothelial cells may be partly responsible for secretion of IL-8 in the active phase of BD (35), since an IL-8 increase of fourfold in the active phase may represent endothelial injury in any part of the body. HRMRI results suggested central nervous system vasculitis. It is considered to be largely associated with a high IL-8 level, resulting in vascular endothelial destruction.

BD *is not* generally received as a cerebral vasculitis introducer compared with other systemic diseases known to lead to vasculitis. Only 1–5% arterial involvement is seen throughout the course of BD. The pattern of cerebral infarction and cerebral vasculitis represents a specific and uncommon form of neuro-Behcet's manifestation, and only two cases have been reported so far (10, 36). In one case, neurological deficits were considered to be infarction in the deep perforating branch of MCA, but it did not show specific change in brain imaging. The other case was an autopsy study, and it showed clearly that the infarction area was consistent with the occlusion regions resulting from arteritis of the MCA branches (37). Vascular involvement is a fatal complication for BD patients, so early diagnosis is very important.

Fortunately, for this case, the above conditions could be excluded according to the result that there was extensive cerebral artery intimal thickening from HRMRI. So we could clearly diagnose this case as BD with cerebral arterial infarction caused by cerebral arteritis, which led to early nervous system symptoms. In addition, we found that plasma IL-8 level was significantly elevated at the early stage of this case, while ESR, CRP, and other indicators have no obvious abnormalities. IL-6 is a key cytokine involved in NBD, especially since this inflammatory marker has been found to be increased also in the cerebrospinal fluid of patients with BD. However, IL-6 was not changed in the patient's plasma, which suggested that IL-8 is a dominant factor in the BD process.

AZP is the preferred treatment for BD. It commonly causes myelosuppression, presenting as megaloblastic anemia, leukopenia, severe hair loss, macrocytosis, pancytopenia, and thrombocytopenia (38–40). Leukopenia and severe hair loss are

strongly associated with mutations in TPMT and NUDT15, which are widespread in the Asian population (41). Gene detection indicated that there was TPMT*3C (A719G) in this patient, so we did not choose AZP to treat patients. Mycophenolate mofetil is used in organ transplantation, multiple sclerosis, Crohn's disease and other immune-related diseases. Borhani Haghighi and Safari divide the anti-NBD armamentarium into first-line, second-line, and experimental drugs. Mycophenolate mofetil is classified as a second-line drug (42). The International Neuro-Behcet's Advisory Group has developed a consensus on NBD, which refers to mycophenolate mofetil as an alternative drug for NBD (43). Colchicine is used for the treatment of gout (44), as well as specific inflammatory conditions such as familial Mediterranean fever (FMF) (45), recurrent pericarditis (46) and BD (47). It seems to inhibit neutrophil chemotaxis and reduce plasma levels of cytokine, thereby reducing the occurrence and the duration of mucocutaneous (oral ulcers, erythema nodosum, genital) and articular manifestations of the disease (47). Hydroxychloroquine is proven to have a relatively benign toxicity profile and a low incidence of infections as an immunosuppressive agent (48, 49). A large cohort study has reported the successful empiric use of hydroxychloroquine to treat BD (50).

Considering the choice of patients and the drugs, the inflammatory activity was controlled followed by treatment with mycophenolate mofetil dispersible tablets (Seccopin), hydroxychloroquine tablets (Flush), and colchicine tablets. The clinical symptoms were ameliorated, such as suppressing oral

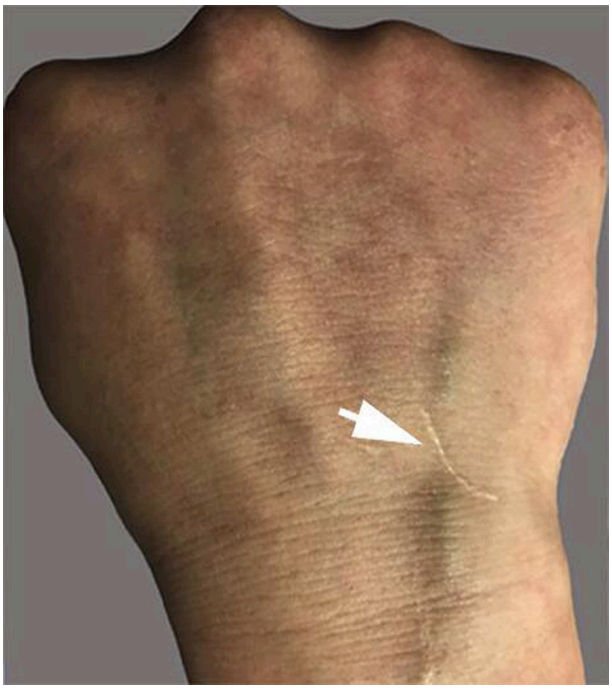

FIGURE 3 | Scar at the venous puncture site.

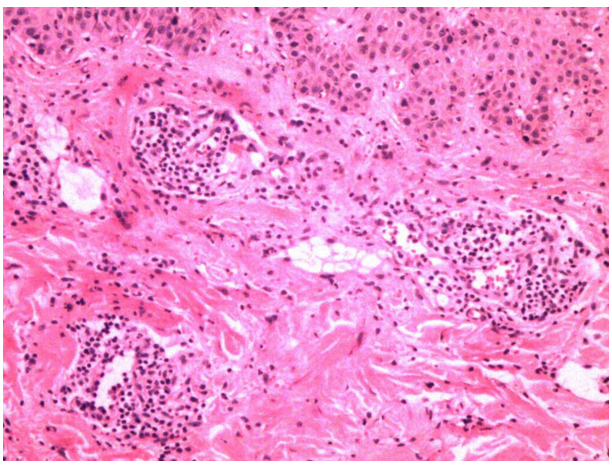

FIGURE 5 | Extensively perivascular inflammatory cell infiltration with pathological biopsy of the skin lesion.

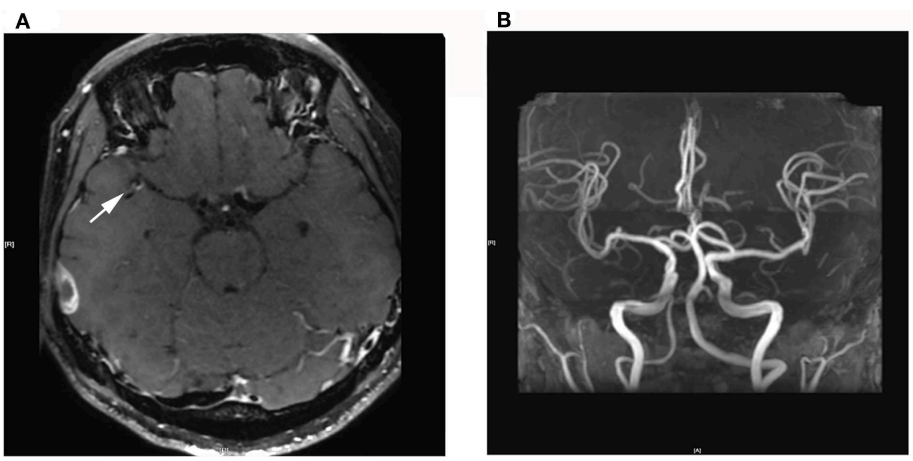

FIGURE 4 | (A) 3D Cube T1 enhancement shows slightly thickened walls of the terminal portion of the M1 segment of the right middle cerebral artery. **(B)** 3D-TOF-MRA shows no abnormalities.

immunity, preventing relapses in skin lesions and progressive neurological disease, as well as settling the systemic disease. However, it is unclear whether long-term immunosuppression might also work well in central nervous system (CNS) vasculitis. That is to say, the risk of recurrent cerebral infarcts remains to be elucidated in the future. Therefore, seeking new medicine targets becomes an urgent issue. IL-8, a major chemoattractant and activator of neutrophils, could act as a novel target for the treatment of BD theoretically and perhaps prove to be the key to recovery.

DATA AVAILABILITY STATEMENT

Publicly available datasets were analyzed in this study. This data can be found here: hospital ID: 000444000, Shandong Povincial Qianfoshan Hospital.

ETHICS STATEMENT

The studies involving human participants were reviewed and approved by the ethics committee of Qianfoshan Hospital. The patients/participants provided their written informed consent to participate in this study. Written informed consent was obtained from the individual(s) for the publication of any potentially identifiable images or data included in this article.

AUTHOR CONTRIBUTIONS

HY, YS, and MZ made substantial contributions to conception and design. HY and MZ collected the data. HY, YS, MZ, and JH contributed to analysis and interpretation of the data. HY, JH, and JT have been involved in drafting the manuscript or revising it critically for important intellectual content. All authors have given final approval of the version to be published. Each author should have participated sufficiently in the work to take public responsibility for appropriate portions of the content. All authors agreed to be accountable for all aspects of the work in ensuring that questions related to the accuracy or integrity of any part of the work are appropriately investigated and resolved.

REFERENCES

1. Yazici H. Behcet's syndrome: an update. *Curr Rheumatol Rep*. (2003) 5:195–9. doi: 10.1007/s11926–003-0066–9
2. Kural-Seyahi E, Fresko I, Seyahi N, Ozyazgan Y, Mat C, Hamuryudan V, et al. The long-term mortality and morbidity of Behcet syndrome: a 2-decade outcome survey of 387 patients followed at a dedicated center. *Medicine*. (2003) 82:60–76. doi: 10.1097/00005792–200301000-00006
3. Tsuruta D, Dainichi T, Hamada T, Ishii N, Hashimoto T. Molecular diagnosis of autoimmune blistering diseases. *Methods Mol Biol*. (2013) 961:17–32. doi: 10.1007/978–1-62703–227-8_2
4. Direskeneli H. Behcet's disease: infectious aetiology, new autoantigens, and HLA-B51. *Ann Rheum Dis*. (2001) 60:996–1002. doi: 10.1136/ard.60.11.996
5. McGonagle D, McDermott MF. A proposed classification of the immunological diseases. *PLoS Med*. (2006) 3:e297. doi: 10.1371/journal.pmed.0030297
6. Cantarini L, Lopalco G, Vitale A, Coladonato L, Rigante D, Lucherini OM, et al. Paradoxical mucocutaneous flare in a case of Behcet's disease treated with tocilizumab. *Clin Rheumatol*. (2015) 34:1141–3. doi: 10.1007/s10067–014-2589-z
7. Vitale A, Rigante D, Lopalco G, Selmi C, Galeazzi M, Iannone F, et al. Interleukin-1 Inhibition in Behcet's disease. *Isr Med Assoc J*. (2016) 18:171–6.
8. Criteria for diagnosis of Behcet's disease. International Study Group for Behcet's Disease. *Lancet*. (1990) 335:1078–80. doi: 10.1016/0140–6736(90)92643-V
9. The International Criteria for Behcet's Disease (ICBD): a collaborative study of 27 countries on the sensitivity and specificity of the new criteria. *J Eur Acad Dermatol Venereol*. (2014) 28:338–47. doi: 10.1111/jdv.12107
10. Akman-Demir G, Serdaroglu P, Tasci B. Clinical patterns of neurological involvement in Behcet's disease: evaluation of 200 patients. The Neuro-Behcet Study Group. *Brain*. (1999) 122 (Pt 11):2171–82. doi: 10.1093/brain/122.11.2171
11. Siva A, Kantarci OH, Saip S, Altintas A, Hamuryudan V, Islak C, et al. Behcet's disease: diagnostic and prognostic aspects of neurological involvement. *J Neurol*. (2001) 248:95–103. doi: 10.1007/s004150170242
12. Serdaroglu P. Behcet's disease and the nervous system. *J Neurol*. (1998) 245:197–205. doi: 10.1007/s004150050205
13. Kidd D, Steuer A, Denman AM, Rudge P. Neurological complications in Behcet's syndrome. *Brain*. (1999) 122 (Pt 11):2183–94. doi: 10.1093/brain/122.11.2183
14. Reynolds N. Vasculitis in Behcet's syndrome: evidence-based review. *Curr Opin Rheumatol*. (2008) 20:347–52. doi: 10.1097/BOR.0b013e3282ff0d51
15. Mendes D, Correia M, Barbedo M, Vaio T, Mota M, Goncalves O, et al. Behcet's disease–a contemporary review. *J Autoimmun*. (2009) 32:178–88. doi: 10.1016/j.jaut.2009.02.011
16. Hamza M. Large artery involvement in Behcet's disease. *J Rheumatol*. (1987) 14:554–9.
17. Zelenski JD, Capraro JA, Holden D, Calabrese LH. Central nervous system vasculitis in Behcet's syndrome: angiographic improvement after therapy with cytotoxic agents. *Arth Rheum*. (1989) 32:217–20. doi: 10.1002/anr.1780320217
18. Pannone A, Lucchetti G, Stazi G, Corvi F, Ferguson TL, Massucci M, et al. Internal carotid artery dissection in a patient with Behcet's syndrome. *Ann Vasc Surg*. (1998) 12:463–7. doi: 10.1007/s1001699 00185
19. Shugaiv E, Tuzun E, Mutlu M, Kiyat-Atamer A, Kurtuncu M, Akman-Demir G. Mycophenolate mofetil as a novel immunosuppressant in the treatment of neuro-Behcet's disease with parenchymal involvement: presentation of four cases. *Clin Exp Rheumatol*. (2011) 29 (Suppl. 67):S64–7.
20. Davies PG, Fordham JN, Kirwan JR, Barnes CG, Dinning WJ. The pathergy test and Behcet's syndrome in Britain. *Ann Rheum Dis*. (1984) 43:70–3. doi: 10.1136/ard.43.1.70
21. Krause I, Molad Y, Mitrani M, Weinberger A. Pathergy reaction in Behcet's disease: lack of correlation with mucocutaneous manifestations and systemic disease expression. *Clin Exp Rheumatol*. (2000) 18:71–4.
22. Koc Y, Gullu I, Akpek G, Akpolat T, Kansu E, Kiraz S, et al. Vascular involvement in Behcet's disease. *J Rheumatol*. (1992) 19:402–10.
23. Chang HK, Cheon KS. The clinical significance of a pathergy reaction in patients with Behcet's disease. *J Korean Med Sci*. (2002) 17:371–4. doi: 10.3346/jkms.2002.17.3.371
24. Ben Ahmed M, Houman H, Miled M, Dellagi K, Louzir H. Involvement of chemokines and Th1 cytokines in the pathogenesis of mucocutaneous lesions of Behcet's disease. *Arth Rheum*. (2004) 50:2291–5; doi: 10.1002/art.20334
25. Itoh R, Takenaka T, Okitsu-Negishi S, Matsushima K, Mizoguchi M. Interleukin 8 in Behcet's disease. *J Dermatol*. (1994) 21:397–404. doi: 10.1111/j.1346–8138.1994.tb01762.x
26. Ozoran K, Aydintug O, Tokgoz G, Duzgun N, Tutkak H, Gurler A. Serum levels of interleukin-8 in patients with Behcet's disease. *Ann Rheum Dis*. (1995) 54:610. doi: 10.1136/ard.54.7.610
27. Bardak Y, Aridogan BC. The demonstration of serum interleukin 6–8, tumor necrosis factor-alpha, complement, and immunoglobulin levels in Behcet's

disease with ocular involvement. *Ocul Immunol Inflamm*. (2004) 12:53–8. doi: 10.1076/ocii.12.1.53.28062
28. Kaburaki T, Fujino Y, Kawashima H, Merino G, Numaga J, Chen J, et al. Plasma and whole-blood chemokine levels in patients with Behcet's disease. *Graefes Arch Clin Exp Ophthalmol*. (2003) 241:353–8. doi: 10.1007/s00417–003-0668-y
29. Freire Ade L, Bertolo MB, de Pinho AJ Jr, Samara AM, Fernandes SR. Increased serum levels of interleukin-8 in polyarteritis nodosa and Behcet's disease. *Clin Rheumatol*. (2004) 23:203–5. doi: 10.1007/s10067–003-0851-x
30. Evereklioglu C, Er H, Turkoz Y, Cekmen M. Serum levels of TNF-alpha, sIL-2R, IL-6, and IL-8 are increased and associated with elevated lipid peroxidation in patients with Behcet's disease. *Mediators Inflamm*. (2002) 11:87–93. doi: 10.1080/09629350220131935
31. Gur-Toy G, Lenk N, Yalcin B, Aksaray S, Alli N. Serum interleukin-8 as a serologic marker of activity in Behcet's disease. *Int J Dermatol*. (2005) 44:657–60. doi: 10.1111/j.1365–4632.2004.02184.x
32. Katsantonis J, Adler Y, Orfanos CE, Zouboulis CC. Adamantiades-Behcet's disease: serum IL-8 is a more reliable marker for disease activity than C-reactive protein and erythrocyte sedimentation rate. *Dermatology*. (2000) 201:37–9. doi: 10.1159/000018426
33. Durmazlar SP, Ulkar GB, Eskioglu F, Tatlican S, Mert A, Akgul A. Significance of serum interleukin-8 levels in patients with Behcet's disease: high levels may indicate vascular involvement. *Int J Dermatol*. (2009) 48:259–64. doi: 10.1111/j.1365–4632.2009.03905.x
34. Pineton de Chambrun M, Wechsler B, Geri G, Cacoub P, Saadoun D. New insights into the pathogenesis of Behcet's disease. *Autoimmun Rev*. (2012) 11:687–98. doi: 10.1016/j.autrev.2011.11.026
35. Zouboulis CC, Katsantonis J, Ketteler R, Treudler R, Kaklamani E, Hornemann S, et al. Adamantiades-Behcet's disease: interleukin-8 is increased in serum of patients with active oral and neurological manifestations and is secreted by small vessel endothelial cells. *Arch Dermatol Res*. (2000) 292:279–84. doi: 10.1007/s004030000128
36. Krespi Y, Akman-Demir G, Poyraz M, Tugcu B, Coban O, Tuncay R, et al. Cerebral vasculitis and ischaemic stroke in Behcet's disease: report of one case and review of the literature. *Eur J Neurol*. (2001) 8:719–22. doi: 10.1046/j.1468–1331.2001.00300.x
37. Nishimura M, Satoh K, Suga M, Oda M. Cerebral angio- and neuro-Behcet's syndrome: neuroradiological and pathological study of one case. *J Neurol Sci*. (1991) 106:19–24. doi: 10.1016/0022–510X(91)90188-D
38. Gisbert JP, Gomollon F. Thiopurine-induced myelotoxicity in patients with inflammatory bowel disease: a review. *Am J Gastroenterol*. (2008) 103:1783–800. doi: 10.1111/j.1572–0241.2008.01848.x
39. Gisbert JP, Gonzalez-Lama Y, Mate J. Thiopurine-induced liver injury in patients with inflammatory bowel disease: a systematic review. *Am J Gastroenterol*. (2007) 102:1518–27. doi: 10.1111/j.1572–0241.2007.01187.x
40. Dubinsky MC, Lamothe S, Yang HY, Targan SR, Sinnett D, Theoret Y, et al. Pharmacogenomics and metabolite measurement for 6-mercaptopurine therapy in inflammatory bowel disease. *Gastroenterology*. (2000) 118:705–13. doi: 10.1016/S0016–5085(00)70140–5
41. Sato T, Takagawa T, Kakuta Y, Nishio A, Kawai M, Kamikozuru K, et al. NUDT15, FTO, and RUNX1 genetic variants and thiopurine intolerance among Japanese patients with inflammatory bowel diseases. *Intest Res*. (2017) 15:328–37. doi: 10.5217/ir.2017.15.3.328
42. Borhani Haghighi A, Safari A. Proposing an algorithm for treatment of different manifestations of neuro-Behcet's disease. *Clin Rheumatol*. (2010) 29:683–6. doi: 10.1007/s10067–010-1414–6
43. Kalra S, Silman A, Akman-Demir G, Bohlega S, Borhani-Haghighi A, Constantinescu CS, et al. Diagnosis and management of Neuro-Behcet's disease: international consensus recommendations. *J Neurol*. (2014) 261:1662–76. doi: 10.1007/s00415–013-7209–3
44. Slobodnick A, Shah B, Pillinger MH, Krasnokutsky S. Colchicine: old and new. *Am J Med*. (2015) 128:461–70. doi: 10.1016/j.amjmed.2014.12.010
45. Akar S, Yuksel F, Tunca M, Soysal O, Solmaz D, Gerdan V, et al. Familial Mediterranean fever: risk factors, causes of death, and prognosis in the colchicine era. *Medicine*. (2012) 91:131–6. doi: 10.1097/MD.0b013e3182561a45
46. Adler Y, Charron P, Imazio M, Badano L, Baron-Esquivias G, Bogaert J, et al. 2015 ESC Guidelines for the diagnosis and management of pericardial diseases: the task force for the diagnosis and management of pericardial diseases of the European Society of Cardiology (ESC)Endorsed by: The European Association for Cardio-Thoracic Surgery (EACTS). *Eur Heart J*. (2015) 36:2921–64. doi: 10.1093/eurheartj/ehv318
47. Yurdakul S, Mat C, Tuzun Y, Ozyazgan Y, Hamuryudan V, Uysal O, et al. A double-blind trial of colchicine in Behcet's syndrome. *Arth Rheum*. (2001) 44:2686–92. doi: 10.1002/1529-0131(200111)44:11<2686::aid-art448>3.0.co;2-h
48. Louyot P, Gaucher A, Mathieu J. [Intermittent hydarthrosis of the knee as a component in the picture of Behcet's disease. Apparent cure of the recurrent articular effusion using chloroquine]. *Ann Med Nancy*. (1962) 1:241–9.
49. Gonzalez-Echavarri C, Capdevila O, Espinosa G, Suarez S, Marin-Ballve A, Gonzalez-Leon R, et al. Infections in newly diagnosed Spanish patients with systemic lupus erythematosus: data from the RELES cohort. *Lupus*. (2018) 27:2253–61. doi: 10.1177/0961203318811598
50. Muruganandam M, Rolle NA, Sibbitt WL Jr, Cook GB, Emil NS, Fangtham M, et al. Characteristics of Behcet's Disease in the American Southwest. *Semin Arthritis Rheum*. (2019) 49:296–302. doi: 10.1016/j.semarthrit.2019.03.003

Conflict of Interest: The authors declare that the research was conducted in the absence of any commercial or financial relationships that could be construed as a potential conflict of interest.

Copyright © 2019 Yin, Song, Zheng, Han and Tang. This is an open-access article distributed under the terms of the Creative Commons Attribution License (CC BY). The use, distribution or reproduction in other forums is permitted, provided the original author(s) and the copyright owner(s) are credited and that the original publication in this journal is cited, in accordance with accepted academic practice. No use, distribution or reproduction is permitted which does not comply with these terms.

frontiers in Neurology

ORIGINAL RESEARCH
published: 22 October 2019
doi: 10.3389/fneur.2019.01074

Metabolic Changes in Focal Brain Ischemia in Rats Treated With Human Induced Pluripotent Stem Cell-Derived Neural Precursors Confirm the Beneficial Effect of Transplanted Cells

Daniel Jirak[1,2,3], Natalia Ziolkowska[1,2], Karolina Turnovcova[4], Kristyna Karova[4], Eva Sykova[5†], Pavla Jendelova[4,6] and Nataliya Romanyuk[4*]*

[1] MR Unit, Department of Diagnostic and Interventional Radiology, Institute for Clinical and Experimental Medicine, Prague, Czechia, [2] First Faculty of Medicine, Institute of Biophysics and Informatics, Charles University, Prague, Czechia, [3] Faculty of Health Studies, Technical University of Liberec, Liberec, Czechia, [4] Department of Neuroregeneration, Institute of Experimental Medicine, Czech Academy of Sciences, Prague, Czechia, [5] Department of Neuroscience, Institute of Experimental Medicine, Czech Academy of Sciences, Prague, Czechia, [6] Department of Neuroscience, Second Faculty of Medicine, Charles University, Prague, Czechia

OPEN ACCESS

Edited by:
Marietta Zille,
Universität zu Lübeck, Germany

Reviewed by:
Axel Montagne,
University of Southern California, United States
Poonam Rana,
Defence Research and Development Organisation (DRDO), India

***Correspondence:**
Pavla Jendelova
pavla.jendelova@iem.cas.cz
Nataliya Romanyuk
nataliya.romanyuk@iem.cas.cz

†Present address:
Eva Sykova,
Institute of Neurobiology,
Slovak Academy of Science,
Bratislava, Slovakia

Specialty section:
This article was submitted to Stroke, a section of the journal Frontiers in Neurology

Received: 12 April 2019
Accepted: 23 September 2019
Published: 22 October 2019

Citation:
Jirak D, Ziolkowska N, Turnovcova K, Karova K, Sykova E, Jendelova P and Romanyuk N (2019) Metabolic Changes in Focal Brain Ischemia in Rats Treated With Human Induced Pluripotent Stem Cell-Derived Neural Precursors Confirm the Beneficial Effect of Transplanted Cells. Front. Neurol. 10:1074. doi: 10.3389/fneur.2019.01074

There is currently no treatment for restoring lost neurological function after stroke. A growing number of studies have highlighted the potential of stem cells. However, the mechanisms underlying their beneficial effect have yet to be explored in sufficient detail. In this study, we transplanted human induced pluripotent stem cell-derived neural precursors (iPSC-NPs) in rat temporary middle cerebral artery occlusion (MCAO) model. Using magnetic resonance imaging (MRI) and magnetic resonance spectroscopy (MRS) we monitored the effect of cells and assessed lesion volume and metabolite changes in the brain. We monitored concentration changes of myo-inositol (Ins), Taurine (Tau), Glycerophosphocholine+Phosphocholine (GPC+PCh), N-acetyl-aspartate+N-acetyl-aspartyl-glutamate (NAA+NAAG), Creatine+Phosphocreatine (Cr+PCr), and Glutamate+Glutamine (Glu+Gln) in the brains of control and iPSC-NP-transplanted rats. Based on initial lesion size, animals were divided into small lesion and big lesion groups. In the small lesion control group (SCL), lesion size after 4 months was three times smaller than initial measurements. In the small lesion iPSC-NP-treated group, lesion volume decreased after 1 month and then increased after 4 months. Although animals with small lesions significantly improved their motor skills after iPSC-NP transplantation, animals with big lesions showed no improvement. However, our MRI data demonstrate that in the big lesion iPSC-NP-treated (BTL) group, lesion size increased only up until 1 month after MCAO induction and then decreased. In contrast, in the big lesion control group, lesion size increased throughout the whole experiment. Significantly higher concentrations of Ins, Tau, GPC+PCh, NAA+NAAG, Cr+PCr, and Glu+Gln were found in in contralateral hemisphere in BTL animals 4 months after cell injection. Lesion volume decreased at this time point. Spectroscopic results of metabolite concentrations in lesion correlated with volumetric measurements of lesion,

with the highest negative correlation observed for NAA+NAAG. Altogether, our results suggest that iPSC-NP transplantation decreases lesion volume and regulates metabolite concentrations within the normal range expected in healthy tissue. Further research into the ability of iPSC-NPs to differentiate into tissue-specific neurons and its effect on the long-term restoration of lesioned tissue is necessary.

Keywords: iPSC-NPs, stroke, magnetic resonance, metabolic changes, IMR, MRS

INTRODUCTION

Stroke is a neurodegenerative disorder and the leading cause of disability in adult humans. One in six people worldwide will have at least one stroke in their lifetime (1). There is currently no treatment for restoring lost neurological function after stroke. A growing number of studies have highlighted the potential of stem cell transplantation and more differentiated neural cell transplantation as intriguing therapeutic approaches to post-stroke reparation. Cells from different sources (fetal cortical- and striatal-derived neural precursors, subventricular zone precursors, neuroepithelial stem cells, bone marrow stromal cells, hESC-derived neural precursors, etc.) have been tested for their ability to reconstruct the forebrain and improve function after transplantation in animals with stroke (2–5). As an autologous, multifunctional cell therapy for stroke, induced pluripotent stem cell-derived neural precursors (iPSC-NPs) have significant potential. Several studies have demonstrated the beneficial effect of iPSC-NPs in ischemia treatment using animal models (6–9). It has been shown that transplantation of human iPSC-derived cells is a safe and efficient approach to promoting recovery after stroke, supplying the injured brain with new neurons for replacement (6). In one rat model study, pluripotent stem cells were shown to differentiate into more specific cortical neuronal progenitors, in turn differentiating into functional neurons, and improving neurological outcomes after intracortical implantation (10). Grafted human iPSCs-NPs have been shown to survive, differentiate into neurons and ameliorate functional deficits in stroke-injured neonatal (11), and aged brains (7). Their strong therapeutic potential has also been demonstrated in large animal models (9). However, the mechanisms of iPSC-NPs in stroke treatment have yet to be investigated in sufficient detail.

Magnetic resonance imaging and spectroscopy (MRI/MRS) are powerful non-invasive diagnostic tools used to provide anatomical and biochemical information. MRI is an optimal imaging modality for ischemic lesion visualization. MRS is a technique used in preclinical and clinical studies to obtain metabolic information of the brain parenchyma under experimental conditions. Although MRS cannot directly localize the area of transplanted cells, it can provide information on the metabolic processes of the brain following cell transplantation. The most frequently assessed metabolites in proton magnetic resonance spectroscopy (^{1}H-MRS) are lactate, which accumulates as the end product of anaerobic glycolysis, and N-acetyl-aspartate (NAA), which is considered a predominantly neuronal marker (12, 13). Thus, reduction of NAA is often acknowledged as an indicator of neuron loss (14). However, alternative explanations, such as the metabolic degradation and redistribution of NAA, warrant further analysis (15).

In this study, we transplanted human induced pluripotent stem cell (IMR90)-derived neural precursors in a rat temporary middle cerebral artery occlusion (MCAO) model. As previously demonstrated in our laboratory, grafted cells successfully survive and provide trophic support to host brain tissue, leading to the recovery of sensorimotor, and motor functions (16). It should be noted, however, that these effects were mainly demonstrated in animals with small lesions, while animals with big lesions showed no improvement.

The aim of this study was to determine metabolic changes by ^{1}H-MRS in the striatal tissue region of the rat brain within 4 months after focal brain ischemia. We studied the effect of transplanted iPSC-NPs on metabolite concentrations at measured time points (1 month and 4 months) by comparing changes in ischemic lesion size. The results presented here may help to elucidate the biochemical changes that occur during early stages of ischemic stroke, distinguish at-risk individuals, benefit early diagnosis, and improve our understanding of the dynamic pathogenesis of early cerebral ischemia (17).

MATERIALS AND METHODS

Animals and Study Groups

All animal experiments were performed in accordance with EU Directive 2010/63/EU on the protection of animals used for scientific purposes, and approved by the ethics committees of the Institute of Experimental Medicine, the Czech Academy of Sciences, and the Institute for Clinical and Experimental Medicine.

The study group consisted of 35 ten-week-old female Sprague-Dawley rats, including healthy controls ($n = 3$). Body weight ranged from 280 to 350 g to minimize differences in body size. All animals were pre-trained in the tape removal test for 3–4 days and tested for both behavioral tests the day before MCAO. Six days after MCAO, rats were randomly divided into control ($n = 12$) and transplanted groups ($n = 20$) and the last group began to receive the immunosuppression. Cells were transplanted 7 days after induction of the lesion. First MRI was performed 7 days after transplantation. According to its results, two existing groups were divided as follows: small control lesions without transplantation (SCL; $n = 6$), small lesions treated with iPSC-NPs (STL; $n = 10$), big control lesions without transplantation (BCL; $n = 6$), and big lesions treated with iPSC-NPs (BTL; $n = 10$). All these animals underwent MRI/MRS and behavioral tests according to the timeline shown in **Figure 1**, and immunohistochemical

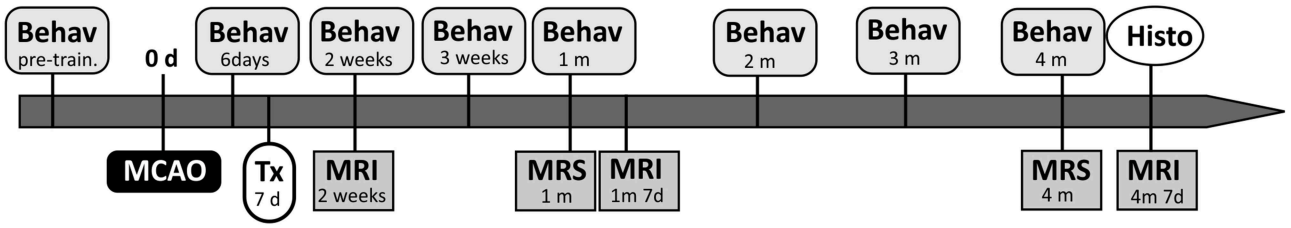

FIGURE 1 | Schematic timeline of the experiments. The day when MCAO have been performed was taken as day 0. Animals were transplanted (Tx) with iPSC-NPs 7 days after lesion and were followed by magnetic resonance imaging (MRI), magnetic resonance spectroscopy (MRS), behavioral tests (Behav) over 4 months. Histological data (Histo) were acquired in the end of the experiment. D, days; m, months.

analysis was used at the end of the study of brain tissue. However, MRS data of several rats were excluded from the statistical analysis in accordance with the rules, which are described in the MRS section below.

Human Induced Pluripotent Stem Cell-Derived Neural Precursors

The human iPSC line was derived from female fetal lung fibroblasts (IMR90 line, ATCC, USA) transduced with a lentivirus-mediated combination of OCT4, SOX2, NANOG, and LIN28 human cDNA [see (18)]. Clone selection, validation of the iPSC line and derivation of neuronal precursors are described in detail in Polentes et al. (16). Human induced pluripotent stem cell-derived neural precursors (iPSC-NPs) were routinely cultured in tissue culture flasks coated with poly-L-ornithine (0.002% in distilled water) and laminin (10 μg/ml in DMEM:F12), both obtained from Sigma (St. Louis, MO). Growth media comprising DMEM:F12 and neurobasal medium (1:1), B27 supplement (1:50), N2 supplement (1:100) (GIBCO, Life Technologies, Grand Island, NY), L-glutamine (2 mM) (Sigma), penicillin and streptomycin (50 U/ml) (GIBCO), FGF (10 ng/ml), EGF (10 ng/ml), and BDNF (20 ng/ml) (PeproTech, London, UK) were changed 3 times per week. Prior to implantation, the neural precursors were pre-differentiated in the same medium (omitting FGF and EGF) for 7 days.

Antibodies and Immunocytochemistry

Pre-differentiated iPSC-NPs plated on poly-L-ornithine and laminin-coated chamber slides were washed in PBS and fixed with 4% paraformaldehyde in PBS for 15 min. Fixed cells were washed twice with PBS before staining. To identify neural precursors and differentiated neurons, antibodies directed against βIII-tubulin (1:100), Olig2 (1:400), nestin (1:200), chondroitin sulfate proteoglycan (NG2, 1:400), NF70 (1:200) (all Sigma-Aldrich), and Ki-67 (1:50) (Abcam) were used. To visualize primary antibodies, goat anti-mouse IgG conjugated with Alexa-Fluor 488 (1:400) and goat anti-rabbit IgG conjugated with Alexa-Fluor 594 (1:400) (Molecular Probes, Eugene, OR) were used. To visualize cell nuclei, DAPI was used. Confocal images were taken with the Zeiss LSM 5 Duo confocal microscope (Carl Zeiss AG). The index of the mitotic activity of the cells was evaluated as the ratio of Ki-67 positive cells to the total number of cells in the 10 randomly selected fields of view.

Middle Cerebral Artery Occlusion Model and Cell Transplantation

Animals were anesthetised with 2.5% isoflurane (Forane®, Abbott Laboratories, Queenborough, UK). Transient focal cerebral ischemia was induced by intraluminal right middle cerebral artery occlusion (MCAO) using a nylon thread (0.08 mm diameter) and terminal cylinder of silicon (3 mm length, 0.24 mm diameter) for 90 min. Animals were then re-anesthetised for reperfusion and divided into control ($n = 12$) and transplanted ($n = 20$) groups. Based on volumetry results obtained by MRI, groups were further categorized according to lesion size.

Cell-treated animals were transplanted 7 days after ischemia induction. The control group was left untreated. Using an aseptic technique, a small hole was drilled into the skull above the lesion (0.5 mm anterior to the bregma, 3 mm lateral to the midline). Next, using a Hamilton syringe with its tip placed 4.5–5 mm deep from the cortical surface, 3 μl of a cell suspension (100 000 cells/μl) was slowly injected over a 5-min period into the lesion. Triple drug immunosuppression was used to prevent graft rejection. Sandimmun (10 mg/kg; intraperitoneal) (Novartis, East Hanover, NJ), Imuran (4 mg/kg; intraperitoneal) (Aspen Pharma Trading Ltd., Dublin, Ireland), and Solu-Medrol (2 mg/kg; intramuscular) (Pfizer Inc., New York, NY) were administered throughout the experiment (for 1 or 4 months). Immunosuppression administration started 1 day before cell transplantation and then was applied each second day (or three times per week).

Behavioral Testing

The adhesive tape removal test (sensorimotor integration) was performed on iPSC-NP-transplanted animals and controls. A sticky colored paper dot (12 mm in diameter) was placed over the rat's left paw and fingers, and the time taken to remove the dot was measured. Rats were pre-trained for 3–4 days before MCAO and tested 3 times per week until the end of the experiment.

Apomorphine-induced rotation (motor dysfunction, pharmacological) was performed on all groups and quantified for 30 min after an intra-peritoneal injection of 1 mg/kg apomorphine in saline. Deficits were quantified using a formula modified from Arvidsson et al. (19): Score = IspiCyl+(2xIpsiHslf)-ContrCyl-(2xContrHslf) with IpsiCyl: rotation ipsilateral to the lesion around the central cylinder; IpsiHslf: rotation ipsilateral on itself; ContrCyl: rotation

contralateral to the lesion around the central cylinder; ContrHslf: rotation contralateral on itself.

Magnetic Resonance

MRI measurements were performed using a 4.7 T Bruker equipped with a custom-made surface coil. Rats were anesthetised by passive inhalation of 1.5–2.5% isoflurane in air. Breathing was monitored during the measurements. For imaging, a T_2-weighted turbo spin-echo sequence (Rapid Acquisition with Relaxation Enhancement—RARE) was used. Sequence parameters were as follows: repetition time TR = 3,000 ms, effective echo time TE = 36.0 ms, turbo factor = 8, number of acquisitions AC = 8, field of view FOV = 3.5 cm, matrix 256 × 256, slice thickness 0.85 mm, number of slices = 29 (covering whole brain), voxel resolution 0.0159 μl, acquisition time 9 min 36 s. Imaging was performed 7 days, 1 and 4 months following iPSC-NP transplantation in treated groups. For the control groups the same time span was used for the unification, even if no transplantation procedure was carried out. Acquired images were used for anatomy reference and localization of spectra.

Following the imaging protocol, magnetic resonance spectroscopy was performed 1 and 4 months after MCAO. ^{1}H-MR spectra were obtained from the striatal tissue of both hemispheres in all groups. They were then measured by the single-voxel PRESS MRS sequence with water suppression using the variable pulse power and optimized relaxation delays (VAPOR) technique according to the following parameters: TR = 2,500 ms, TE = 13.2 ms, AC = 512, acquisition time 21 min 30 s. The volume of interest was FOV = 4 × 4 × 4 mm^3 (0.064 ml) for each hemisphere. Shimming for correction of magnetic in homogeneities was performed using an automated mapshim procedure. To get as robust data as possible, we had strict rules for data used in following imaging and spectroscopic analyses. Animal data were excluded if (1) there was movement artifacts due to breathing problems; (2) the half-width of water signal was 14 Hz or higher; (3) Cramér-Rao lower bounds (CRLB) was 25% and higher. To assess metabolic profiles of striatal tissue in both hemispheres, spectra were evaluated using the LC Model v 6.1 (20) to obtain metabolite concentrations. This software takes unsuppressed water as a reference. No corrections of calculated metabolite concentration for relaxation times were performed.

Concentrations of the following brain metabolites were used for analysis: Ins—a glial-specific marker (21) connected with cell metabolism and signaling pathways (22), it is also an osmolyte and essential requirement for cell growth (23); Tau—an osmoregulator and neuroprotectant with antioxidative properties that stabilizes the membrane, regulates cytoplasmic calcium levels, and reduces proinflammation (24, 25); GPC+PCh—are associated with membrane breakdown, myelinization/demyelinization or inflammation in brain diseases and were released in the brain with calcium overload (26); NAA+NAAG—markers of neuronal viability (27); Cr+PCr—PCr acts as a reservoir for the generation of ATP (23), this pair is also involved in antioxidative mechanisms and cellular bioenergetics (28); Glu+Gln—glutamate is the brain's major neurotransmitter and during ischemia acts as an important mediator of neuronal degeneration (29), also Glu+Gln pair decreased signals reflect glutamate-glutamine cycle dysfunction, while increased levels are connected with higher neurotoxicity and cell death in stroke (25, 30). Some metabolite values are presented together, as overlapping peaks from some of the spectra results made them difficult to distinguish.

Volumetry and Experimental Groups

Images obtained by MRI were used for lesion volumetry analysis. Lesion volume was assessed by manually marking MR images using ImageJ software (version 1.46r, National Institutes of Health, USA) (31). According to initial lesion size measurements (14 days after MCAO and 7 days after iPSC-NP transplantation), animals were divided into two groups in both control and treated groups, with the dividing threshold at 0.027 ml (small lesion <0.027 ml <big lesion). Groups were divided into small control lesions without transplanted cells (SCL; $n = 5$), small lesions treated with transplanted cells (STL; $n = 3$), big control lesions without transplanted cells (BCL; $n = 6$), and big lesions treated with transplanted cells (BTL; $n = 10$). To make results more precise, lesion size was calculated as the mean value of the axial and coronal areas segmented in MR images.

Histological Analysis

To analyse the fate of grafted iPSC-NPs, rats were sacrificed 4 months after transplantation. For the control groups the same time span was used for the unification, even if no transplantation procedure was carried out. The anesthetised animals were perfused with 4% paraformaldehyde in PBS (pH 7.4). Fixed brains were dissected and immersed in PBS with 30% sucrose. Frozen coronal sections (40 μm) were cut through the areas of interest. To identify human neural precursors transplanted into the rat brain, antibodies directed against human mitochondria (MTC02, 1:125) (Abcam) and against human nuclei (HuNu 1:40) (Chemicon, Temecula, CA) were used. For volumetric measurements, six sections were selected at 1-mm intervals along the craniocaudal axis, and whole images of the brain were taken with an Axioskop 2 plus microscope (Carl Zeiss AG, Oberkochen, Germany) and analyzed by ImageJ software (31). To follow the fate of the transplanted iPSC-NPs, antibodies directed against MAP2 (1:500), DARPP32 (1:500), Ki67 (1:50) (all Abcam), NeuN (1:100), TH (1:1,000) (Millipore, Billerica, MA), and GFAP (1:200) (Sigma-Aldrich) were used. To visualize primary antibody reactivity, the following appropriate secondary antibodies were used: goat anti-mouse IgG conjugated with Alexa-Fluor 488 (1:400) and goat anti-rabbit IgG conjugated with Alexa-Fluor 594 (1:400) (Molecular Probes, Eugene, OR). To visualize cell nuclei, DAPI was used. Confocal images were taken with the Zeiss LSM 5 Duo confocal microscope (Carl Zeiss AG). The index of the cell mitotic activity was calculated as the ratio of Ki-67-positive cells to the total number of surviving cells positive for HuNu. Cells were counted in the samples from 4 animals using at least 10 randomly selected fields of view for each animal. The total volume of the transplanted cell mass was estimated as described in Romanyuk et al. (32).

Statistical Analysis

Statistical analysis was performed using GraphPad Prism 7 software. The following parameters were evaluated using non-parametric Wilcoxon matched paired test: metabolite concentration measurements of lesion and contralateral hemispheres at 1 and 4 months and comparisons of volumetry results at all-time points. To compare control and treated groups the non-parametric Kruskal-Wallis multiple comparison test with Dunn's multiple comparisons were used. Non-parametric Spearman correlation was estimated between lesion volume and metabolite concentrations from both time points and both hemispheres separately. For correlation and volume changes the Bonferroni correction was applied. Statistical analysis of RT-qPCR data was performed based on $\Delta\Delta$Ct values using GraphPad Prism software (GraphPad Prism 5, La Jolla, CA, USA). For all analyses $p \leq 0.05$ was considered significant.

RESULTS

Human Induced Pluripotent Stem Cell-Derived Neural Precursors Before and After Transplantation

In order to prepare iPSC-NPs for transplantation, cells were pre-differentiated over 7 days in a regular culture medium omitting FGF and EGF. According to immunocytochemical staining, the majority of pre-differentiated neural precursors were positive for nestin, βIII-tubulin, NG2, NF-68, and Olig2. Only 23.8 + 3.2% were positive for Ki67 (**Figure 2**). These data confirm their neural phenotypes prior to transplantation. For more detailed antigens and gene expression characteristics of pre-differentiated iPSC (IMR90)-NPs, see Romanyuk et al. (32).

Human iPSC-NPs in the ischemic rat brain were evaluated for survival and differentiation into neuronal and glial phenotypes 4 months after transplantation. The engrafted cells were identified by immunohistochemical staining for the human-specific markers HuNu and MTC02 (**Figure 3**). The severe necrotic processes occurring in big lesions complicated the quantitative estimation of the number of surviving grafted cells. Graphical information on transplant survival is presented in **Supplementary Figure 1**. Histological analysis of the survival, proliferation and differentiation of transplanted cells was performed in all transplanted animals where the graft survived ($n = 12$). Two of them are not presented in **Supplementary Figure 1**, because the graft survival was very poor. The total volume of the transplanted cell mass was 1.16 ± 0.12 mm^3 for animals with big lesion and 0.70 ± 0.09 mm^3 for animals with small lesion. Some grafted cells differentiated into more mature and tissue-specific neurons, such as NeuN-, MAP2- and DARPP32-positive cells (**Figures 3E–G**). A small portion of transplanted cells were positive for GFAP

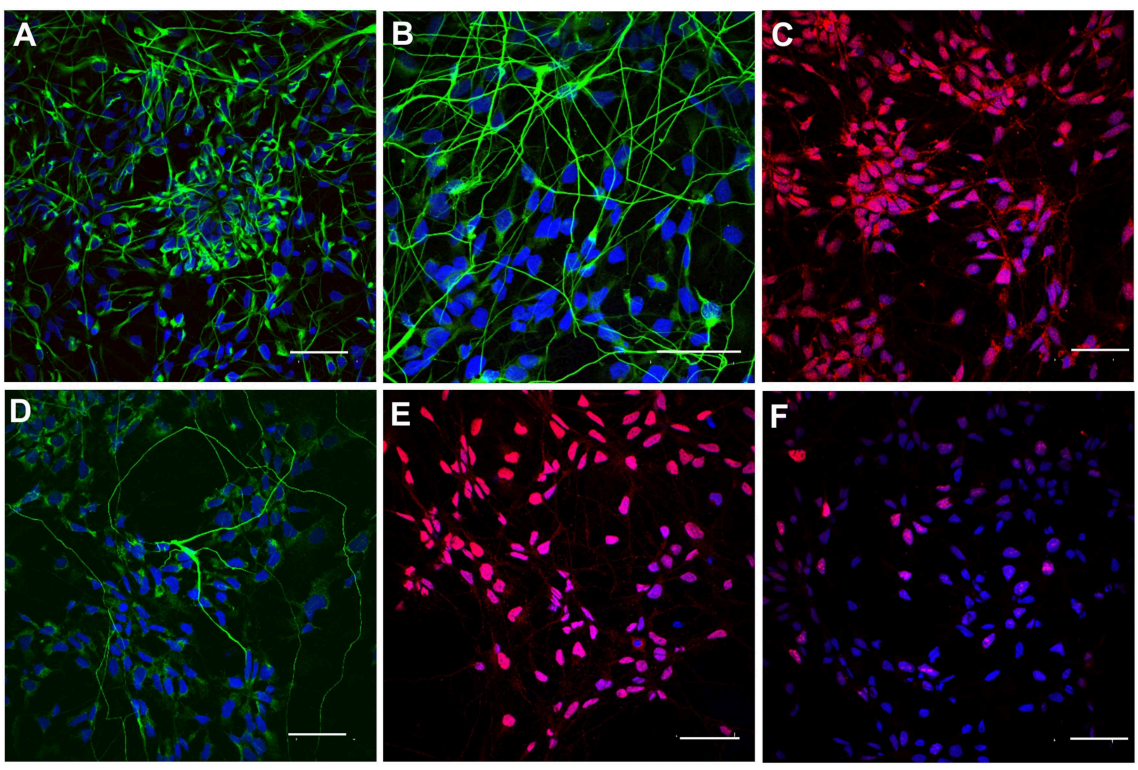

FIGURE 2 | Immunocytochemical staining of pre-differentiated iPSC-NPs prior to transplantation. **(A)** Nestin, **(B)** βIII-tubulin, **(C)** NG2, **(D)** NF-68, **(E)** Olig2, **(F)** Ki67; magnification −20 μm.

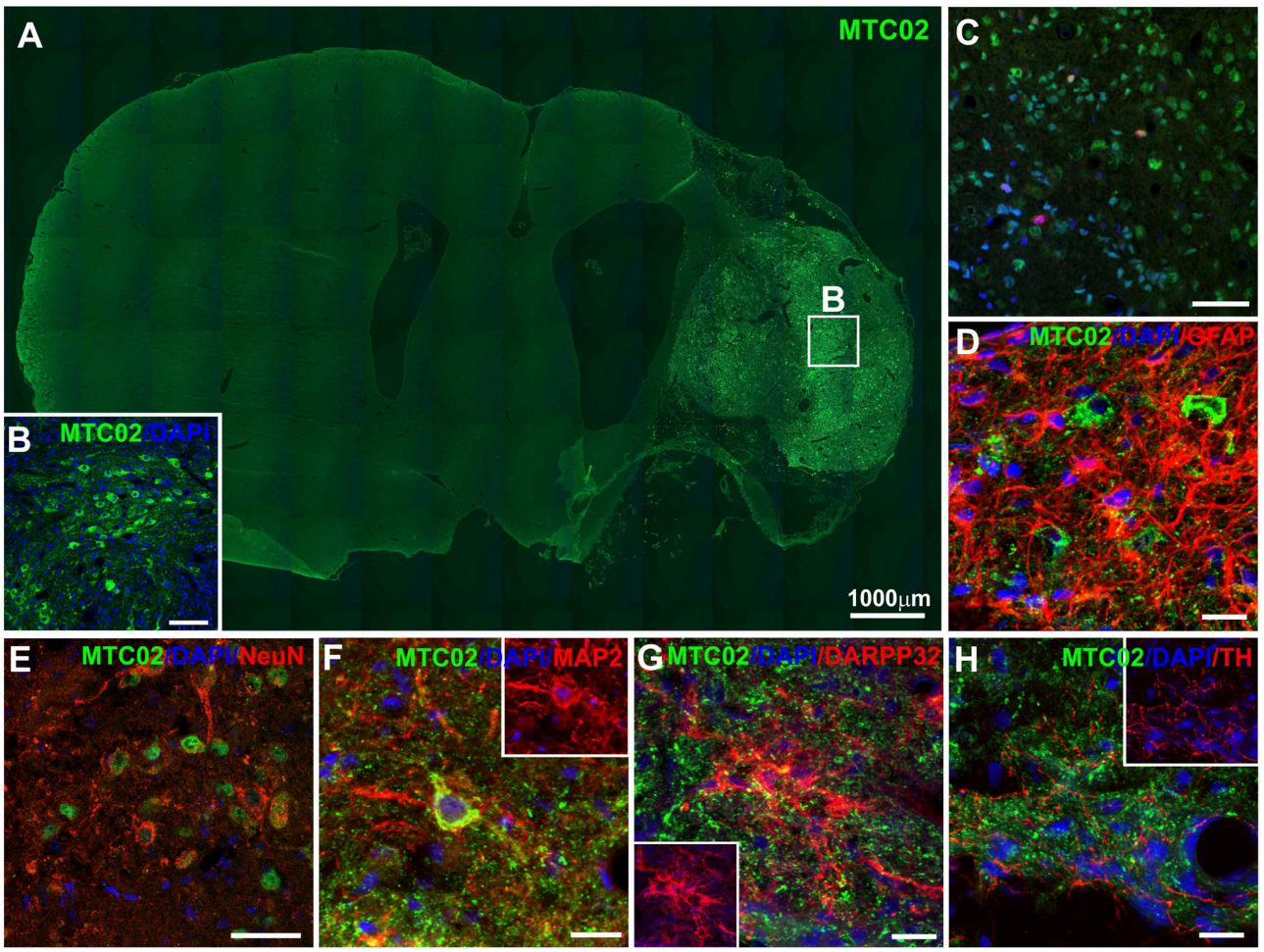

FIGURE 3 | Immunohistochemical staining of ischemic rat brain tissue 4 months after iPSC-NP transplantation. Grafted neural precursors survived and migrated toward the lesion area **(A,B)**, differentiated into NeuN- **(E)**, MAP2- **(F)**, and DARPP32- **(G)** positive cells, actively integrated into the lesioned host tissue **(D,H)** and decreased their Ki67 index **(C)** to 3.2–0.8%.

(**Figure 3D**), while transplants infiltrated by host cells were positive for GFAP or thyroxine hydroxylase (**Figures 3G,H**). Quantification of mitotic activity with Ki-67 immunoreactivity identified 2.53 ± 0.54% dividing cells, which was similar to the index shown previously for these cells (16, 32). Histological analysis of transplanted iPSC-NPs in animals with small lesions is presented on **Supplementary Figure 2**. No tumor formation was observed throughout the whole experiment. The survival of iPSC-NPs grafted in the rat brain was estimated from serial cross sections.

Behavioral Testing

To evaluate functional improvement after iPSC-NP transplantation in animals with big ischemic lesions, behavioral tests—the tape removal test and apomorphine test—were performed starting from the fifth day after lesions appeared (2 days before transplantation). Grafted animals showed almost no significant improvement compared to control animals with big lesions. Whereas, in animals with small lesions transplantation of iPSC-NP rescued functional impairment (**Figure 4**).

Magnetic Resonance Imaging and Volumetry

Images obtained by MRI confirmed the effect of MCAO on brain tissue. Ischemic lesions were localized and assessed for both size and changes caused by iPSC transplantation at different time points. MR images were used in volumetric lesion measurements and for MRS localization.

Focal brain ischemia volume measurements were performed at three time points: 7 days, 1 month, and 4 months after cells transplantation in the treated animals and at the same time points for the control groups. Lesion volume changes were observed at all-time points and in all groups. In the BCL group, lesion sizes increased and, especially between 1 and 4 months, signal became more homogenous. In the BTL group, lesion sizes increased at first (between 7 days and 1 month) but then decreased between 1 and 4 months. In the SCL group,

lesions decreased throughout the experiment, reaching a value three times smaller than initial sizes after 4 months. In the STL group, lesion sizes decreased at first (between 7 days and 1 month) to a value three times smaller than initial sizes but then increased after 4 months. The volumetry results are summarized in **Table 1**. MR images representative for average results obtained from all time points in presented groups are contained in **Figure 5**.

Magnetic Resonance Spectroscopy

^{1}H-MR spectroscopy (^{1}H-MRS) was employed to determine metabolic changes in the striatal tissue region of the rat brain over 4 months after focal brain ischemia. CRLB was usually around 10% in our study. Unfortunately, sometimes there was problem with shimming. It resulted in wide Full Width Half Maximum (FWHM) of the water signal. Linewidths of <0.1 ppm are considered essential for ^{1}H-MRS *in vivo*; for 4.7T it is 20 Hz (33). We excluded data if FWHM > 14 Hz); usually FWHM was around 10 Hz in our study. The spectroscopy results are summarized in **Tables 2A,B**, with typical spectra given in **Figure 6**.

MRS results from big lesion groups 1 and 4 months after MCAO revealed significant ($p < 0.05$) or at the limit of statistical significance ($p = 0.0625$) differences in metabolite concentrations [IU] between ipsi- and contralateral hemispheres. Significant differences were observed in MRS measurement 4 months post-MCAO in BTL group (**Figure 7**) in the following metabolites: Tau ($p = 0.0039$), NAA+NAAG ($p = 0.0039$), Cr+PCr ($p = 0.0039$), Glu+Gln ($p = 0.0039$). These changes are thought to occur due to the extent of ischemic injury. In the same group metabolite changes (Tau, GPC+PCh, NAA+NAAG, Cr+PCr, Glu+Gln) were observed to be on the limit of

TABLE 1 | Volumetric measurement results.

Group	Time point	Lesion volume [ml]
SCL	7 days	0.012 ± 0.009
	1 month	0.006 ± 0.003
	4 months	0.004 ± 0.003
BCL	7 days	0.104 ± 0.06
	1 month	0.125 ± 0.07
	4 months	0.145 ± 0.09
STL	7 days	0.006 ± 0.009
	1 month	0.002 ± 0.0008
	4 months	0.011 ± 0.007
BTL	7 days	0.062 ± 0.06
	1 month	0.147 ± 0.02
	4 months	0.119 ± 0.06

Data are expressed as the lesion mean [ml] ± std; SCL, small control lesions; BCL, big control lesions; STL, small treated lesions; BTL, big treated lesions.

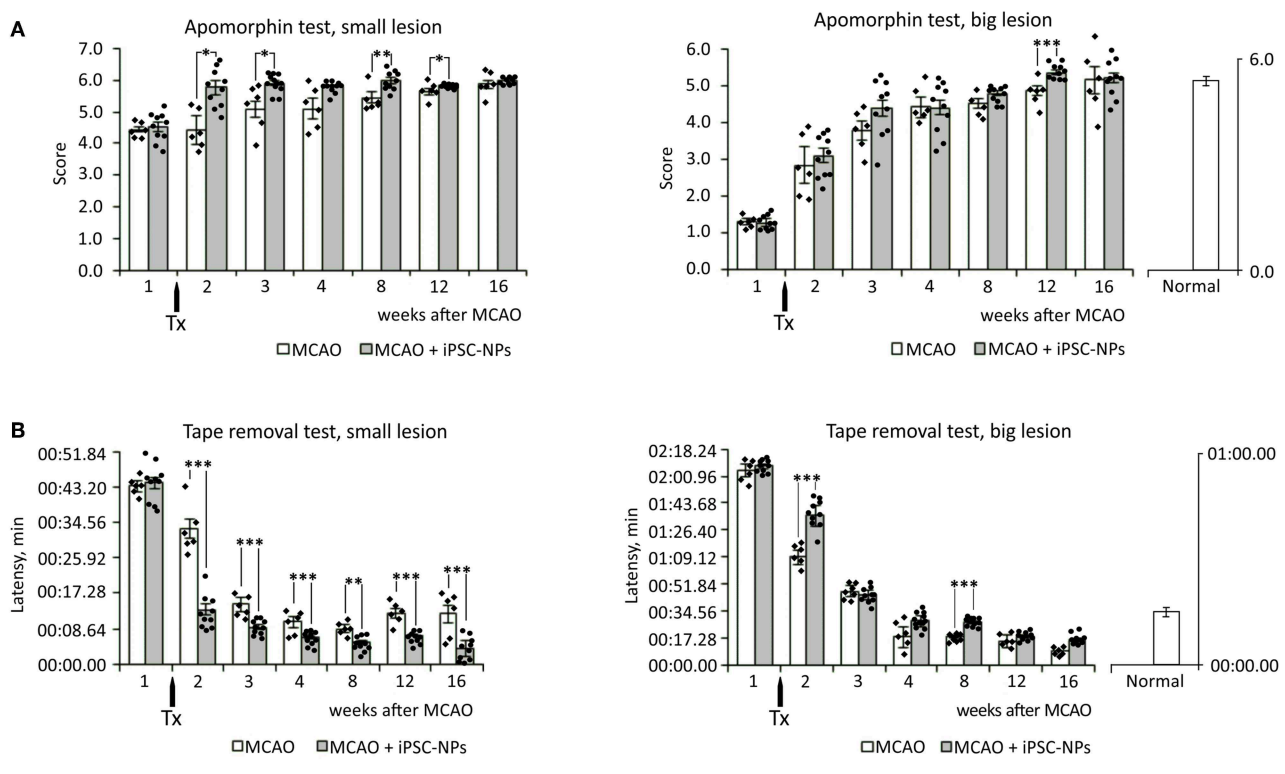

FIGURE 4 | Transplantation of neural precursors improves functional recovery in animals with small lesion size. **(A)** Apomorphin-induced rotation test in non-grafted animals and animals grafted with iPSC-NPs. **(B)** Adhesive tape removal test in non-grafted animals and animals grafted with iPSC-NPs. Tx, transplantation. ***$p < 0.001$,**$p < 0.01$, *$p < 0.05$.

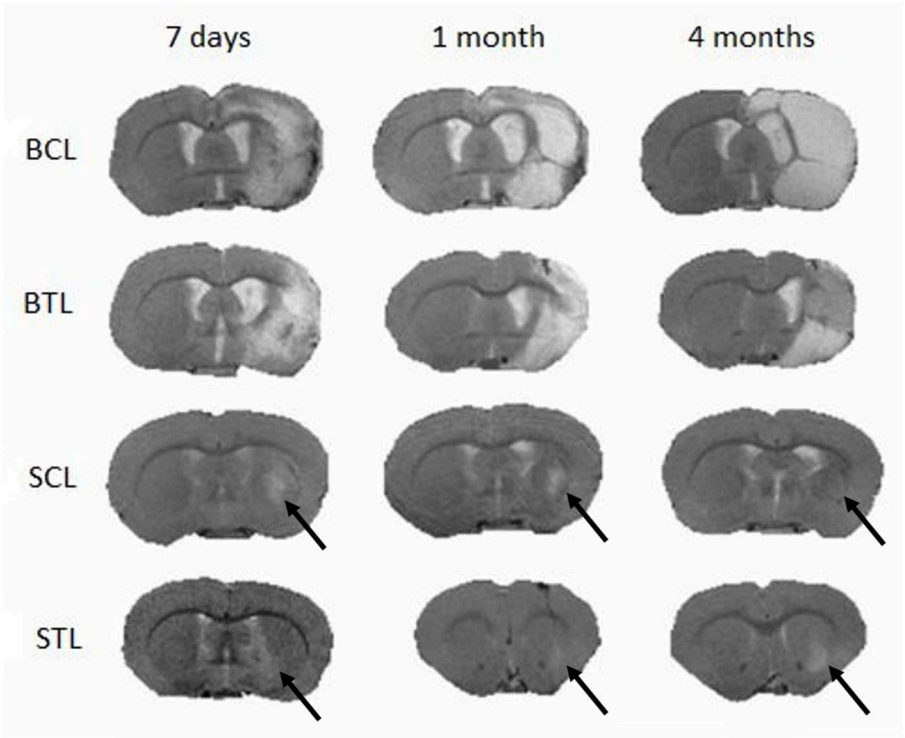

FIGURE 5 | Typical MR images of lesions in the brain induced by MCAO following cell transplantation at three imaging time points (7 days, 1 month, and 4 months); SCL, small control lesions; BCL, big control lesions; STL, small treated lesions; BTL, big treated lesions. To present images representative for each time point lesion average size, not in all groups images are taken from one animal.

statistical significance ($p = 0.0625$) 1 month after occlusion was performed. Also in the BCL group results on the limit of statistical significance ($p = 0.0625$) were observed. Four out of six measured metabolite concentrations differed between ipsilesional and contralateral brain tissue in this group: Tau (4 months), NAA+NAAG (4 months), Cr+PCr (1 month and 4 months), and Glu+Gln (1 month and 4 months). In all four groups, metabolite concentrations were lower on the lesion side. The metabolite concentrations did not differ significantly between healthy animals and contralateral hemisphere in SCL group with MCAO and without iPSC transplantation. The absolute concentration of selected metabolites obtained from healthy animals were: Ins = 6.4 ± 0.9 IU, Tau = 8.0 ± 0.1 IU, GPC+PCh = 1.9 ± 0.3 IU, NAA+NAAG = 11.4 ± 2.4 IU, Cr+PCr = 9.8 ± 1.4 IU, Glu+Gln = 19.2 ± 4.9 IU (**Supplementary Figure 3**).

Metabolite concentrations changes between 1 and 4 months after MCAO were calculated using Wilcoxon matched paired test. In the BTL group significant results were observed on the contralateral side for Ins ($p = 0.0156$), Tau ($p = 0.0156$), GPC+PCh ($p = 0.0156$), NAA+NAAG ($p = 0.0313$), Cr+PCr ($p = 0.0156$), Glu+Gln ($p = 0.0156$) (**Figure 8**).

Spectroscopic results from all groups were compared, separately for both time points and both hemispheres using the Kruskal-Wallis multiple comparison tests with Dunn's multiple comparison test (**Tables 2A,B**). After 1 month, groups were observed to be significantly heterogeneous in results from all measured metabolites and in both hemispheres. The highest significant heterogeneity was obtained from NAA+NAAG ($p < 0.0001$) 1 month after MCAO on the lesion side. From this time point also between-groups significant differences were found. On the lesion side almost all metabolites (Tau, NAA+NAAG, Cr+PCr, Glu+Gln) concentrations were observed to differ between SCL vs. BTL groups using Dunn's multiple comparisons test. On the contralateral side this difference was found for all metabolites. Four months after lesion, results from ipsilateral hemisphere of MCAO groups were significantly inhomogeneous in NAA+NAAG and Cr+PCr, while no inhomogeneity was found on the contralateral hemisphere at this time point. There were no significant differences found between the control and treated groups with the same lesion sizes. Although the mean metabolite concentrations between BCL and BTL groups from the lesion side were all higher in the BCL animals after 1 month and then in the BTL after 4 months. The same regularity was observed for the contralateral side. In small lesions the mean metabolite concentration was higher in SCL for all metabolites in both hemispheres after 1 month. After 4 months all concentrations were higher in SCL only on the contralateral side and NAA+NAAG, Cr+PCr, Glu+Gln on the lesion side. The rest of the metabolites (Ins, Tau, GPC+PCh) were found to have higher mean concentration in STL group.

TABLE 2 | MRS results of absolute metabolite concentrations in the striatal tissue: small lesions **(A)** and big lesions **(B)** groups.

Small lesions		Ins	Tau	GPC+PCh	NAA+NAAG	Cr+PCr	Glu+Gln
(A)							
1 month	C_C	5.5 ± 1.6*§§§	7.2 ± 1.8**§§§	1.8 ± 0.5**§§§	10.0 ± 2.2**§§§	8.8 ± 2.2**§§§	15.1 ± 4.1**§§§
	C_L	5.6 ± 2.1	5.0 ± 1.5*§§§	1.7 ± 0.6	7.8 ± 2.2**§§§	7.2 ± 2.5*§§§	12.7 ± 3.5*§§§**§§§§
	iPS_C	2.9 ± 0.8	5.0 ± 0.2	1.0 ± 0.0	6.0 ± 0.4	5.0 ± 0.2	9.2 ± 0.8
	iPS_L	4.1 ± 1.2	4.3 ± 0.7	1.2 ± 0.2	4.4 ± 0.6	4.7 ± 0.2	7.4 ± 0.4
4 months	C_C	5.3 ± 2.0	7.1 ± 2.5	1.4 ± 0.5	10.4 ± 4.4	8.2 ± 3.1	13.3 ± 5.5
	C_L	5.9 ± 2.3	4.2 ± 1.5	1.4 ± 0.5	7.8 ± 2.2	6.9 ± 2.3	10.1 ± 2.6
	iPS_C	3.4 ± 2.5	3.9 ± 3.1	1.0 ± −0.6	5.9 ± 4.2	5.1 ± 3.3	9.3 ± 6.5
	iPS_L	7.3 ± 7.0	5.1 ± 3.9	2.1 ± 1.3	4.9 ± 2.8	5.6 ± 2.6	10.0 ± 7.2
Big lesions		**Ins**	**Tau**	**GPC+PCh**	**NAA+NAAG**	**Cr+PCr**	**Glu+Gln**
(B)							
1 month	C_C	3.1 ± 0.6	4.6 ± 1.0	1.0 ± 0.2	5.9 ± 0.5	5.1 ± 0.4	8.2 ± 1.0
	C_L	2.7 ± 0.9	1.8 ± 0.5	0.6 ± 0.2	2.8 ± 1.2	2.1 ± 1.1	3.7 ± 1.8
	iPS_C	1.9 ± 0.9*§§	3.0 ± 1.2*§§	0.7 ± 0.2*§§	4.2 ± 1.6*§§	3.6 ± 1.2*§§	5.9 ± 1.6*§§
	iPS_L	2.0 ± 1.0	1.5 ± 1.0	0.5 ± 0.3	1.8 ± 1.2	1.7 ± 1.2	3.2 ± 1.6
4 months	C_C	3.3 ± 0.3	4.7 ± 0.6	0.8 ± 0.1	5.9 ± 0.7	5.2 ± 0.5	8.1 ± 1.1
	C_L	2.5 ± 1.0	1.6 ± 0.2	0.6 ± 0.2	2.7 ± 1.0	2.3 ± 0.8	4.0 ± 1.3
	iPS_C	4.7 ± 2.0	5.3 ± 1.3**§	1.3 ± 0.5	7.6 ± 2.6**§	6.5 ± 2.1**§	11.4 ± 4.4**§
	iPS_L	4.4 ± 4.2	2.9 ± 1.9	1.1 ± 0.8	2.8 ± 2.4	3.4 ± 2.8	5.6 ± 3.7

*Data are expressed as the mean [IU] ± std. C_C: spectra from the contralateral hemisphere in animals with MCAO and without iPSC transplantation; C_L: spectra from lesions in animals with MCAO and without iPSC transplantation; iPS_C: spectra from the contralateral hemisphere in animals with MCAO and with iPSC transplantation; iPS_L: spectra from lesions in animals with MCAO and with iPSC transplantation; Wilcoxon matched paired test and Kruskal—Wallis tests were performed: *p < 0.05, **p < 0.01, ***p < 0.001, § contralateral/lesion, §§ 1/4 months, §§§ SCL vs. BTL, §§§§ SCL vs. BCL; asterisks are informing about the tests significance while the rest of the signs are referring to the used comparison tests; asterisks denoting significance level indicate the first of the compared cells.*

Correlation Between Lesion Size Changes and Metabolic Profiles in the Ischemic Rat Brain

The aim of this part of the experiment was to determine a possible correlation between volume changes and metabolic profiles in lesioned and contralateral areas over a 4-months period after occlusion and cell injection. These changes at different time points were compared using non-parametric Spearman correlation test. Spectroscopic results from lesion side correlated with volumetric measurements with the highest correlation observed in both time points for NAA+NAAG (1 month: $r = -0.83$, $p = 0.0002$; 4 months: $r = -0.87$, $p = 0.000002$) (**Figure 9**). Other metabolites on the lesion side significantly correlating with lesion volume were Ins (4 months: $r = -0.61$, $p = 0.0067$), Tau (1 month: $r = -0.72$, $p = 0.003$), GPC+PCh (1 month: $r = -0.71$, $p = 0.003$), Cr+PCr (1 month: $r = -0.75$, $p = 0.001$; 4 months: $r = -0.76$, $p = 0.0003$), and Glu+Gln (1 month: $r = -0.77$, $p = 0.0007$; 4 months: $r = -0.74$, $p = 0.0005$). No correlation was found between spectroscopic results from contralateral side and lesion volume.

DISCUSSION

A large number of iPSC-differentiated derivatives have already been obtained and successfully used in experimental models of different disorders (34–37), including different stroke models (6, 8, 9). The data in this study may be valuable in elucidating the action mechanisms of neural precursors derived from human iPSCs in stroke models. Using a rat MCAO model, we previously demonstrated that iPSC-NPs (IMR90) successfully alleviate stroke-induced dysfunction. Transplanted neural precursors reversed stroke-induced sensorimotor and motor deficits and also dramatically protected the host substantia nigra from atrophy (16). However, these effects applied only to rats with small lesions, whereas animals with big lesions demonstrated no functional improvement. In this current study, we confirm the promising use of human iPSC-NPs for post-ischemic tissue repair in animals with big lesions. Our histology analysis reveals that transplanted cells survived and migrated toward the lesion area during the 4 month-period after transplantation. They then integrated into the striatal tissue and underwent further differentiation into more mature and tissue-specific neurons. No tumor formation was observed throughout the entire experiment.

Potential recovery and/or other changes were also quantified by volumetric measurements and metabolic changes. The biggest changes in lesion volume means per group were in the small lesion groups. In the SCL group, the volume of ischemic brain lesions decreased throughout the experiment (7 days, 1 month, 4 months), becoming almost invisible on MR images (0.004 ± 0.003 ml) 4 months after MCAO. This effect may be connected with spontaneous recovery of less extensively damaged brain tissue not subjected to invasive transplantation. In STL subjects

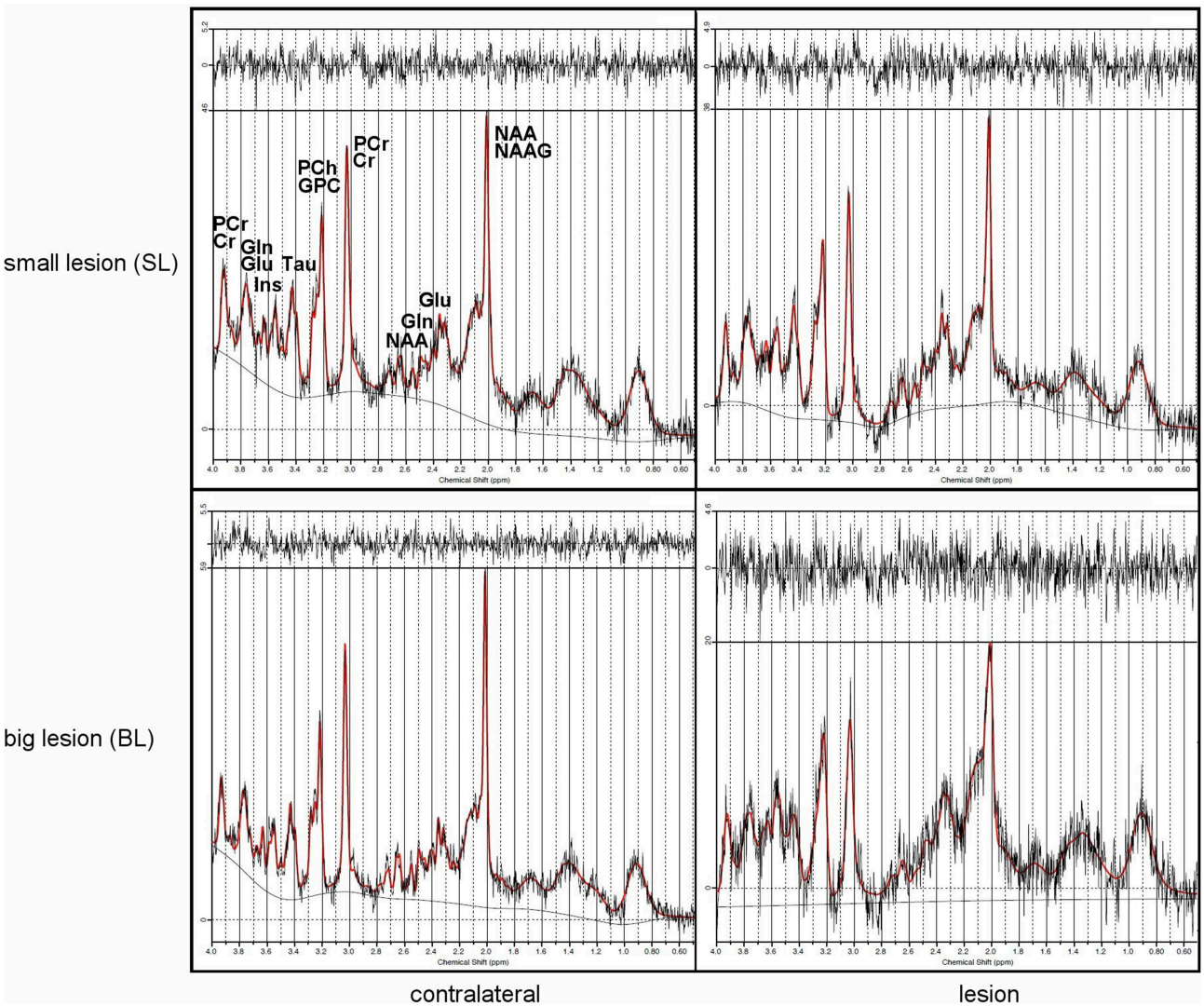

FIGURE 6 | Typical MRS rat brain spectra showing lesions (right) and contralateral sides (left) from small (top) and big (bottom) lesions with signal intensities scaled to the highest signal in the spectrum.

that did undergo the transplantation procedure, lesion volume also decreased during the first part of the experiment (between 7 days and 1 month: 0.006 ± 0.009−0.002 ± 0.0008) but then increased (between 1 and 4 months: 0.002 ± 0.0008–0.011 ± 0.007). The reason for this difference may be a secondary effect of brain tissue damage arising from cell transplantation and/or inflammation. In the big lesion groups, lesion volume changes were more variable. In BCL animals, lesion sizes increased, with signals becoming more stable between 1 and 4 months (0.125 ± 0.07–0.145 ± 0.09), which may have been caused by a greater range of tissue damage or anoxic depolarization (38). In the BTL group, lesion sizes increased at the beginning but then decreased, with the restoration of the brain cells functions perhaps attributable to cell grafts integrating into the tissue at this time point. Our hypothesis to explain the initial lesion size increase followed by a decrease is that the necrotic processes are slowing down in time and grafted cells need time to incorporate to the lesioned tissue, maybe more time points would standardize these results. All of these results suggest that, in the case of big lesions, spontaneous recovery and compensation of ischemic damage in the brain is limited.

Spectroscopy is a non-invasive method used to precisely determine biochemical changes in damaged tissue. In addition to lesion volume alterations, we also observed changes in metabolite concentrations in our animal model. As with volumetry analysis, results were again more variable in the case of big lesions. The first round of statistical analysis involved obtaining data on metabolite concentrations from the ipsilesional and contralateral hemispheres as a control for themselves. In the BTL group, a significant difference ($p < 0.01$) in Tau, NAA+NAAG, Cr+PCr, Glu+Gln concentrations were observed 4 months after MCAO, with higher values on the contralateral side. According to the

literature, taurine has the ability to maintain neuronal calcium homeostasis and prevent neuronal cell death due to necrosis or apoptosis (24). Taurine may also be used in ischemic stroke, during which intracellular free calcium increases. Levels of taurine are understood to increase in patients after stroke (25, 39). An increase in glutamate concentration is considered toxic, as it binds to ionotropic N-methyl-D-aspartate (NMDA) and α-amino-3-hydroxy-5-methyl-4-isoxazolepropionic acid (AMPA) receptors. This in turn promotes a major influx of calcium, which triggers phospholipases and proteases that degrade essential membranes and proteins (40). Tissue necrosis may have been suppressed with the neuroprotective influence from Tau, NAA+NAAG and Cr+PCr. Confirming these findings in our study, we observed a decrease in lesion volume co-occurring with higher metabolite concentrations after 4 months in both hemispheres. Previous studies have identified lower concentrations of the neuronal marker NAA (27) in lesions (41) and the ability of Cr to protect the brain from neurotoxicity (28). All mentioned metabolites had also higher (on the limit of statistical significance) concentrations on the contralateral side 1 month after MCAO. Here additional might be the functional improvement induced by GPC, already mentioned in models of ischemic damage (42).

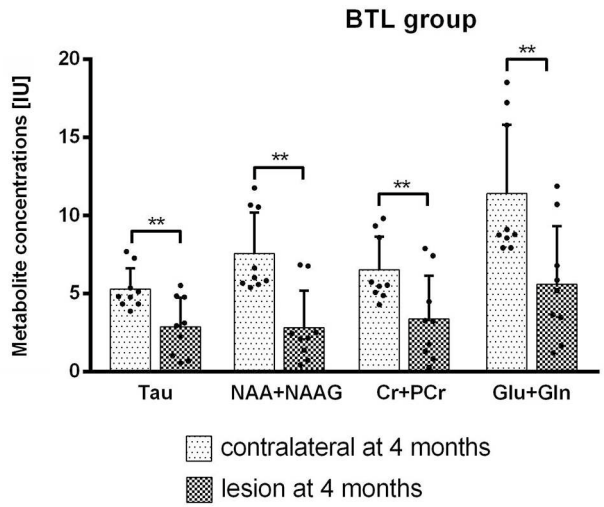

FIGURE 7 | Metabolite concentrations from both hemispheres were compared using Wilcoxon matched paired test. BTL group at 4 months after MCAO. Significant results ($p = 0.0039$) were observed for Tau, NAA+NAAG, Cr+PCr, and Glu+Gln concentrations [IU].

In the BCL group results which reflect the direction of changes (1 month: Cr+PCr, Glu+Gln; 4 months: Tau, NAA+NAAG, Cr+PCr, Glu+Gln) were found, all with concentrations higher on the contralateral side. In all four groups in our study, metabolite concentrations were lower on the lesion side.

In the second round of statistical analysis, differences occurring over time on both contralateral and lesion sides were measured. In BLT group metabolites concentrations changed—this time on the contralateral side, with significant results in all metabolites. In our study, the contralateral side probably compensated for the decrease in lesion metabolites concentration and may have influenced the decrease in lesion volume, as we observed in BTL and SCL groups. Here we can point out also trend of results observed in the BTL group, with Cr+PCr concentrations higher on the lesion side 4 months after MCAO compared to the initial

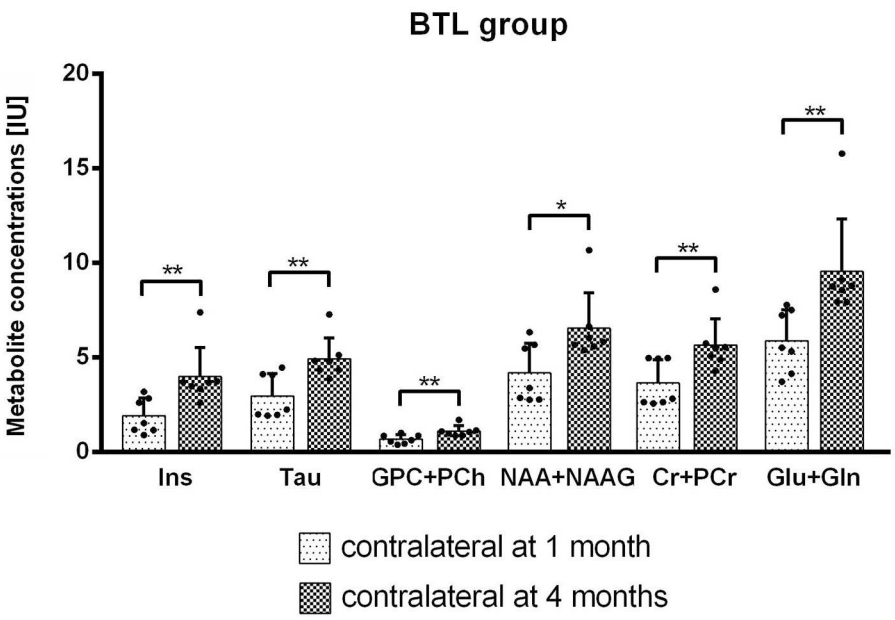

FIGURE 8 | Metabolite concentrations [IU] for the contralateral hemisphere in time were compared using Wilcoxon matched paired test. BTL group from between 1 and 4 months after MCAO on the contralateral side. Significant results were observed for Ins ($p = 0.0156$), Tau ($p = 0.0156$), GPC+PCh ($p = 0.0156$), NAA+NAAG ($p = 0.0313$), Cr+PCr ($p = 0.0156$), Glu+Gln ($p = 0.0156$) concentrations [IU].

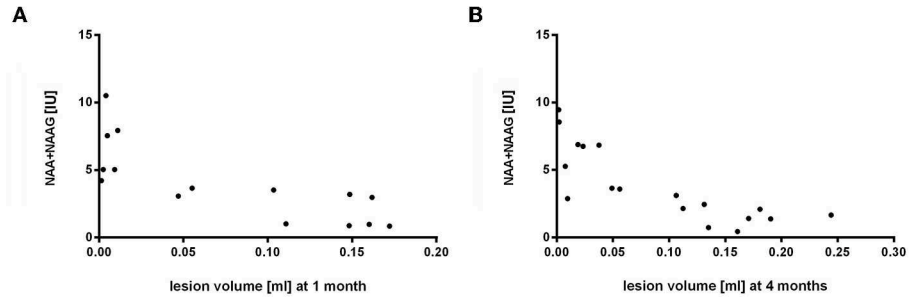

FIGURE 9 | Correlation of volumetry to spectroscopy results from the lesion side 1 and 4 months after MCAO. Lesion volume [ml] and NAA+NAAG concentrations [IU] were compared by Spearman correlation (1 month: $r = -0.83$, $p = 0.0002$; 4 months: $r = -0.87$, $p = 0.000002$).

measurement. This may have influenced the recovery of brain tissue, as lesion volume also decreased during this time. The functions of creatine and phosphocreatine in improving cerebrovascular function and reducing lesion have been previously reported (43).

Based on group comparisons, the biggest differences in metabolites were found 1 month following transplantation. However, no significant results in metabolite concentrations between same lesion size groups was obtained, in the BTL group all metabolite concentrations from both hemispheres were lower than those in the BCL group after 1 month and all higher after 4 months. In the STL group, the same trend was observed on the lesion side for Ins, Tau and GPC+PCh.

The glutamate concentrations are higher on the contralateral side possibly because there is no tissue necrosis in this hemisphere after 1 and 4 months and as there is healthier neural tissue, we can observe higher glutamate levels. If the measurement would be performed in shorter period after the MCAO procedure was carried out, there would be probably more glutamate measured on the lesion side, as the changes in the tissue structure were not so drastic. Our results show that bigger mean differences between hemispheres in glutamate concentrations were observed in big lesions (**Table 2B**), what could support our hypothesis.

The lower metabolite concentrations in treated animals we observed were probably due to the inherent fluctuation of transplanted cells and the injections, an invasive procedure that can lead to biochemical changes. In all animals, in which lesion volume decreased at the onset of ischemic damage, the protective function of the penumbra could be observed (44). Its possible influence highlights the importance of introducing additional measurements during early stages of lesion development.

Based on our literature search, our data are not in contradiction with published MRS results (45). However, it should be mentioned that published MRS data are usually obtained from MR scanners with higher magnetic field (45), which affect significantly relaxation times, or from different species (46). Therefore, concentration of metabolites can be slightly different.

The findings of this study have to be seen in light of some limitations. The first is the absence of sham operated group of animals and group of animals transplanted with vehicle. Our interpretation of the above results is possibly limited by the small group sizes and the time discrepancy between measurements of MRS (taken 1 and 4 months after MCAO) and MRI (initially taken 14 days after MCAO). Even the smallest changes in time can have a crucial influence on stroke, a factor that may reflect our results. It is necessary to mention that metabolite concentrations were assessed by LCModel without T1, T2 correction factor. TR = 2,500 ms was chosen as a compromise between accuracy and scan time (to minimize passing of animal during scanning). If we look at the relaxation times of metabolites [for example (47) or (48)], we can roughly estimate that real absolute metabolite concentration would be about 20% higher. Higher effect has T1 relaxation time, attenuation of MRS signal due to T2 is not high because T2 relaxation times of metabolites are much higher than used TE (13 ms) (47, 48). Due to the technical reasons, we were not able to quantify the numbers of surviving and differentiated grafted iPSC-NP cells.

CONCLUSION

We confirm the beneficial effect of induced pluripotent stem cell-derived neural precursors on post-ischemic tissue repair in animals with small lesions (demonstrated previously) as well as in those with big lesions. We suggest that iPSC-NP transplantation leads to a decrease in lesion volume and helps to regulate metabolite concentrations within the normal range expected in healthy nervous tissue. These results may add to the current store of knowledge on the biochemical processes occurring during early stages of ischemic stroke. Studying the correlation of lesion volume changes with spectroscopic changes over time may improve our understanding of how metabolite concentrations change after occlusion and how they are linked to lesion volume, leading to better predictions of stroke outcomes. This may in turn benefit early diagnosis and elucidate the dynamic pathogenesis of early cerebral ischemia. The decrease in lesion volume we observed in animals with big lesions indicates that iPSC-NP transplantation may indeed be a safe tool for cell transplantation therapy in stroke and a promising tool for restoring neurological function. However, how the differentiation of iPSC-NPs into tissue-specific neurons leads to the long-term restoration of lesioned tissue precisely needs to be researched in more details.

As most of the major changes occur at stroke onset, particular attention should be given to the metabolite and morphologic changes that occur during early stages of stroke.

DATA AVAILABILITY STATEMENT

All datasets generated for this study are available on request.

ETHICS STATEMENT

All animal experiments were performed in accordance with EU Directive 2010/63/EU on the protection of animals used for scientific purposes, and approved by the ethics committees of the Institute of Experimental Medicine, the Czech Academy of Sciences, and the Institute for Clinical and Experimental Medicine.

AUTHOR CONTRIBUTIONS

DJ: performance and coordination of experiments, MRI and MRS measurements, spectroscopy data processing, statistical analysis, and manuscript writing. NZ: volumetry and MRI and MRS statistical analysis. KT: animal surgery (MCAO), behavioral testing, and data and statistical analysis. KK: RNA isolation, PCR, and data and statistical analysis. ES: financial support and project management. PJ: experimental design, project management, critical reading, and correction of the manuscript. NR: experimental design, performance and coordination of experiments, iPSC-NP culturing and grafting, immunocytochemical analysis, animal surgery (MCAO), immunohistochemical analysis, confocal imaging, data and statistical analysis, and manuscript writing.

FUNDING

This study was supported by the Operational Research, Development and Education Programme, the Center of Reconstructive Neuroscience (CZ.02.1.01/0.0./0.0/15_003/0000419), the National Sustainability Programme (LO1309), and the project EATRIS-CZ (LM2015064). As members of BIOCEV (CZ.1.05/1.1.00/02.0109), PJ, KK, and NR were supported by the Ministry of Education, Youth and Sports of the CR under National Sustainability Programme II (LQ1604) (BIOCEV-FAR Project).

ACKNOWLEDGMENTS

We wish to acknowledge the Imaging Methods Core Facility at BIOCEV supported by Czech BioImaging's large RI projects LM2015062 and CZ.02.1.01/0.0/0.0/16_013/0001775 funded by the MEYS CR. We also wish to thank the Advanced Bioimaging of Living Tissues project (CZ.2.16/3.1.00/21527) financed by the European Regional Development Fund and public expenditure of the Czech Republic through the Operational Prague Competitiveness Programme. MR experiments were funded by the Ministry of Health of the Czech Republic (Institute for Clinical and Experimental Medicine IKEM, Project IN 00023001). We thank Brigitte Onteniente for providing iPSC-NP cell line within project STEMS. We thank Vera Lanska for consultion on statistical analysis.

SUPPLEMENTARY MATERIAL

The Supplementary Material for this article can be found online at: https://www.frontiersin.org/articles/10.3389/fneur.2019.01074/full#supplementary-material

Methods

RNA Extraction and Quantitative PCR Analysis of Gene Expression

Brain tissue was dissected from animals of two different groups: control animals with big lesions that underwent the MCAO procedure only ($n = 4$) and animals with big lesions grafted with iPSC-NPs ($n = 4$) sacrificed 4 months after transplantation. Total RNA was extracted from rat brain tissue (frozen sections) using the High Pure RNA Paraffin Kit (Roche, Penzberg, Germany) according to the manufacturer's instructions. Reverse transcription was performed using the T100™ Thermal Cycler (Bio-Rad, Hercules, CA, USA) and the Transcriptor Universal cDNA Master (Roche, Penzberg, Germany).

Expressions of the rat (Rattus norvegicus) target genes Bdnf, Ngf, Vegf, Fgf8, Dcx, Syp, Ppp1r1b, Drd1, Drd2, Gap43, and Actb were determined by quantitative real-time reverse transcription polymerase chain reaction (qPCR) using StepOnePlus™ (Life Technologies, Carlsbad, CA, USA), the FastStart Universal Probe Master (Roche, Penzberg, Germany) and TaqMan Gene Expression Assays (4331182) [Rn02531967_s1/Bdnf/, Rn01533872_m1/Ngf/, Rn01511601_m1/Vegfa/, Rn00590996_m1/Fgf8/, Rn00670390_m1/Dcx/, Rn01528256_m1/Syp/, Rn01452984_m1/Ppp1r1b/, Rn03062203_s1/Drd1/, Rn00561126_m1/Drd2/, Rn01474579_m1/Gap43/, Rn00667869_m1/Actb/]. The final reaction volume amounted to 10 μL containing 25 ng of extracted RNA. The following thermal profile was used: a single cycle to prevent carryover contamination for 2 min at 50°C and 10 min at 95°C for DNA polymerase activation, followed by 40 cycles of denaturation at 95°C for 15 s and annealing and extension at 60°C for 1 min. The results were analyzed using integrated StepOnePlus® software (Life Technologies, Carlsbad, CA, USA). Each data set was normalized with an appropriate TaqMan endogenous control selected by NormFinder. Actb [Rn00667869_m1] was chosen as the housekeeping gene. Finally, data were recalculated to relative quantities and transformed to a $\log_2$ scale.

Results

To evaluate the effect of transplanted iPSC-NPs on endogenous regenerative processes, we examined the gene expression of several neurotrophic factors and the neurospecific genes Bdnf, Ngf, Vegfa, Fgf8, Dcx, Syp, Ppp1r1b, Drd1, Drd2, and Gap43 separately in the right (lesioned) and left hemispheres of control and transplanted animals 4 months after cell grafting using qPCR. This analysis was performed only for

animals with big lesions; similar results for animals with small lesions are presented in Polentes et al. (16). We found no significant differences in the expression of listed genes in transplanted animals vs. control animals with big lesions (**Supplementary Figure 4**).

Supplementary Figure 1 | Graft survival and localization in rat ischemic brains with small and big lesions showing immunohistochemical staining with MTC02, a marker of human mitochondria; magnification −1 mm.

Supplementary Figure 2 | Immunohistochemical staining of ischemic rat brain tissue with small lesion size 4 months after iPSC-NP transplantation. Grafted human neural precursors were identified by the staining for MTC02 **(A,B)**. They differentiated into NeuN- **(E)**, MAP2- **(F)** and DARPP32- **(D)** positive cells, actively integrated into the lesioned host tissue **(C,G)**.

Supplementary Figure 3 | Metabolite concentrations [IU] ± std for healthy animals.

Supplementary Figure 4 | Effect of transplanted iPSC-NPs on rat gene expression 4 months after MCAO.

REFERENCES

1. Bushnell CD. Stroke in women: risk and prevention throughout the lifespan. *Neurol Clin*. (2008) 26, 1161–76, xi. doi: 10.1016/j.ncl.2008.05.009
2. Darsalia V, Kallur T, Kokaia Z. Survival, migration and neuronal differentiation of human fetal striatal and cortical neural stem cells grafted in stroke-damaged rat striatum. *Eur J Neurosci*. (2007) 26:605–14. doi: 10.1111/j.1460-9568.2007.05702.x
3. Takahashi K, Yasuhara T, Shingo T, Muraoka K, Kameda M, Takeuchi A, et al. Embryonic neural stem cells transplanted in middle cerebral artery occlusion model of rats demonstrated potent therapeutic effects, compared to adult neural stem cells. *Brain Res*. (2008) 1234:172–82. doi: 10.1016/j.brainres.2008.07.086
4. Honmou O, Onodera R, Sasaki M, Waxman SG, Kocsis JD. Mesenchymal stem cells: therapeutic outlook for stroke. *Trends Mol Med*. (2012) 18:292–7. doi: 10.1016/j.molmed.2012.02.003
5. Huang W, Mo X, Qin C, Zheng J, Liang Z, Zhang C. Transplantation of differentiated bone marrow stromal cells promotes motor functional recovery in rats with stroke. *Neurol Res*. (2013) 35:320–8. doi: 10.1179/1743132812Y.0000000151
6. Oki K, Tatarishvili J, Wood J, Koch P, Wattananit S, Mine Y, et al. Human-induced pluripotent stem cells form functional neurons and improve recovery after grafting in stroke-damaged brain. *Stem Cells*. (2012) 30:1120–33. doi: 10.1002/stem.1104
7. Tatarishvili J, Oki K, Monni E, Koch P, Memanishvili T, Buga AM, et al. Human induced pluripotent stem cells improve recovery in stroke-injured aged rats. *Restor Neurol Neurosci*. (2014) 32:547–58. doi: 10.3233/RNN-140404
8. Qin J, Ma X, Qi H, Song B, Wang Y, Wen X, et al. Transplantation of induced pluripotent stem cells alleviates cerebral inflammation and neural damage in hemorrhagic stroke. *PLoS ONE*. (2015) 10:e0129881. doi: 10.1371/journal.pone.0129881
9. Baker EW, Platt SR, Lau VW, Grace HE, Holmes SP, Wang L, et al. Induced pluripotent stem cell-derived neural stem cell therapy enhances recovery in an ischemic stroke pig model. *Sci Rep*. (2017) 7:10075. doi: 10.1038/s41598-017-10406-x
10. Tornero D, Wattananit S, Gronning Madsen M, Koch P, Wood J, Tatarishvili J, et al. Human induced pluripotent stem cell-derived cortical neurons integrate in stroke-injured cortex and improve functional recovery. *Brain*. (2013) 136(Pt 12):3561–77. doi: 10.1093/brain/awt278
11. Chau MJ, Deveau TC, Song M, Gu X, Chen D, Wei L. iPSC Transplantation increases regeneration and functional recovery after ischemic stroke in neonatal rats. *Stem Cells*. (2014) 32:3075–87. doi: 10.1002/stem.1802
12. Birken DL, Oldendorf WH. N-acetyl-L-aspartic acid: a literature review of a compound prominent in 1H-NMR spectroscopic studies of brain. *Neurosci Biobehav Rev*. (1989) 13:23–31. doi: 10.1016/S0149-7634(89)80048-X
13. Simmons ML, Frondoza CG, Coyle JT. Immunocytochemical localization of N-acetyl-aspartate with monoclonal antibodies. *Neuroscience*. (1991) 45:37–45. doi: 10.1016/0306-4522(91)90101-S
14. Bruhn H, Frahm J, Gyngell ML, Merboldt KD, Hanicke W, Sauter R. Cerebral metabolism in man after acute stroke: new observations using localized proton NMR spectroscopy. *Magn Reson Med*. (1989) 9:126–31. doi: 10.1002/mrm.1910090115
15. Weber R, Ramos-Cabrer P, Hoehn M. Present status of magnetic resonance imaging and spectroscopy in animal stroke models. *J Cereb Blood Flow Metab*. (2006) 26:591–604. doi: 10.1038/sj.jcbfm.9600241
16. Polentes J, Jendelova P, Cailleret M, Braun H, Romanyuk N, Tropel P, et al. Human induced pluripotent stem cells improve stroke outcome and reduce secondary degeneration in the recipient brain. *Cell Transplant*. (2012) 21:2587–602. doi: 10.3727/096368912X653228
17. Wang H, Li Y, Jiang N, Chen X, Zhang Y, Zhang K, et al. Protective effect of oxysophoridine on cerebral ischemia/reperfusion injury in mice. *Neural Regen Res*. (2013) 8:1349–59. doi: 10.3969/j.issn.1673-5374.2013.15.001
18. Yu J, Vodyanik MA, Smuga-Otto K, Antosiewicz-Bourget J, Frane JL, Tian S, et al. Induced pluripotent stem cell lines derived from human somatic cells. *Science*. (2007) 318:1917–20. doi: 10.1126/science.1151526
19. Arvidsson A, Kirik D, Lundberg C, Mandel RJ, Andsberg G, Kokaia Z, et al. Elevated GDNF levels following viral vector-mediated gene transfer can increase neuronal death after stroke in rats. *Neurobiol Dis*. (2003) 14:542–56. doi: 10.1016/j.nbd.2003.08.002
20. Provencher SW. Estimation of metabolite concentrations from localized *in vivo* proton NMR spectra. *Magn Reson Med*. (1993) 30:672–9. doi: 10.1002/mrm.1910300604
21. Rumpel H, Lim WE, Chang HM, Chan LL, Ho GL, Wong MC, et al. Is myo-inositol a measure of glial swelling after stroke? A magnetic resonance study. *J Magn Reson Imaging*. (2003) 17:11–9. doi: 10.1002/jmri.10233
22. Yu W, Ye C, Greenberg ML. Inositol hexakisphosphate kinase 1. (IP6K1) regulates inositol synthesis in mammalian cells. *J Biol Chem*. (2016) 291:10437–44. doi: 10.1074/jbc.M116.714816
23. Govindaraju V, Young K, Maudsley AA. Proton NMR chemical shifts and coupling constants for brain metabolites. *NMR Biomed*. (2000) 28:923–24. doi: 10.1002/1099-1492(200005)13:3<129::AID-NBM619>3.0.CO;2-V
24. Kumari N, Prentice H, Wu JY. Taurine and its neuroprotective role. *Adv Exp Med Biol*. (2013) 775:19–27. doi: 10.1007/978-1-4614-6130-2_2
25. Menzie J, Prentice H, Wu JY. Neuroprotective mechanisms of taurine against ischemic stroke. *Brain Sci*. (2013) 3:877–907. doi: 10.3390/brainsci3020877
26. Bustillo JR, Jones T, Chen H, Lemke N, Abbott C, Qualls C, et al. Glutamatergic and neuronal dysfunction in gray and white matter: a spectroscopic imaging study in a large schizophrenia sample. *Schizophr Bull*. (2017) 43:611–19. doi: 10.1093/schbul/sbw122
27. Pomares FB, Funck T, Feier NA, Roy S, Daigle-Martel A, Ceko M, et al. Histological underpinnings of grey matter changes in fibromyalgia investigated using multimodal brain imaging. *J Neurosci*. (2017) 37:1090–101. doi: 10.1523/JNEUROSCI.2619-16.2016
28. Smith RN, Agharkar AS, Gonzales EB. A review of creatine supplementation in age-related diseases: more than a supplement for athletes. *F1000Res*. (2014) 3:222. doi: 10.12688/f1000research.5218.1
29. Campos F, Sobrino T, Ramos-Cabrer P, Argibay B, Agulla J, Pérez-Mato M, et al. Neuroprotection by glutamate oxaloacetate transaminase in ischemic stroke: an experimental study. *J Cereb Blood Flow Metab*. (2011) 31:1378–86. doi: 10.1038/jcbfm.2011.3
30. Jeitner TM, Battaile K, Cooper AJ. Critical evaluation of the changes in glutamine synthetase activity in models of cerebral stroke. *Neurochem Res*. (2015) 40:2544–56. doi: 10.1007/s11064-015-1667-1
31. Schneider CA, Rasband WS, Eliceiri KW. NIH Image to ImageJ: 25 years of image analysis. *Nature Methods*. (2012) 9:671–5. doi: 10.1038/nmeth.2089

32. Romanyuk N, Amemori T, Turnovcova K, Prochazka P, Onteniente B, Sykova E, et al. Beneficial effect of human induced pluripotent stem cell-derived neural precursors in spinal cord injury repair. *Cell Transplant*. (2015) 24:1781–97. doi: 10.3727/096368914X684042
33. Forster D, Davies K, Williams S. Magnetic resonance spectroscopy in vivo of neurochemicals in a transgenic model of Alzheimer's disease: a longitudinal study of metabolites, relaxation time, and behavioral analysis in TASTPM and wild-type mice. *Magn Reson Med*. (2013) 69:944–55. doi: 10.1002/mrm.24349
34. Hanna J, Wernig M, Markoulaki S, Sun CW, Meissner A, Cassady JP, et al. Treatment of sickle cell anemia mouse model with iPS cells generated from autologous skin. *Science*. (2007) 318:1920–3. doi: 10.1126/science.1152092
35. Dimos JT, Rodolfa KT, Niakan KK, Weisenthal LM, Mitsumoto H, Chung W, et al. Induced pluripotent stem cells generated from patients with ALS can be differentiated into motor neurons. *Science*. (2008) 321:1218–21. doi: 10.1126/science.1158799
36. Karakikes I, Ameen M, Termglinchan V, Wu JC. Human induced pluripotent stem cell-derived cardiomyocytes: insights into molecular, cellular, and functional phenotypes. *Circ Res*. (2015) 117:80–8. doi: 10.1161/CIRCRESAHA.117.305365
37. Shahjalal HM, Abdal Dayem A, Lim KM, Jeon TI, Cho SG. Generation of pancreatic beta cells for treatment of diabetes: advances and challenges. *Stem Cell Res Therapy*. (2018) 9:355. doi: 10.1186/s13287-018-1099-3
38. Anderson TR, Jarvis CR, Biedermann AJ, Molnar C, Andrew RD. Blocking the anoxic depolarization protects without functional compromise following simulated stroke in cortical brain slices. *J Neurophysiol*. (2005) 93:963–79. doi: 10.1152/jn.00654.2004
39. Ghandforoush-Sattari M, Mashayekhi SO, Nemati M, Ayromlou H. Changes in plasma concentration of taurine in stroke. *Neurosci Lett*. (2011) 496:172–5. doi: 10.1016/j.neulet.2011.04.010
40. Xing C, Arai K, Lo EH, Hommel M. Pathophysiologic cascades in ischemic stroke. *Int J Stroke*. (2012) 7:378–85. doi: 10.1111/j.1747-4949.2012.00839.x
41. Saunders DE. MR spectroscopy in stroke. *Br Med Bull*. (2000) 56:334–45. doi: 10.1258/0007142001903256
42. Jadavji NM, Emmerson JT, MacFarlane AJ, Willmore WG, Smith PD. B-vitamin and choline supplementation increases neuroplasticity and recovery after stroke. *Neurobiol Dis*. (2017) 103:89–100. doi: 10.1016/j.nbd.2017.04.001
43. Prass K, Royl G, Lindauer U, Freyer D, Megow D, Dirnagl U, et al. Improved reperfusion and neuroprotection by creatine in a mouse model of stroke. *J Cereb Blood Flow Metab*. (2007) 27:452–9. doi: 10.1038/sj.jcbfm.9600351
44. McCabe C, Arroja MM, Reid E, Macrae IM. Animal models of ischaemic stroke and characterisation of the ischaemic penumbra. *Neuropharmacology*. (2018) 134(Pt B):169–77. doi: 10.1016/j.neuropharm.2017.09.022
45. Pfeuffer J, Tkac I, Provencher SW, Gruetter R. Toward an *in vivo* neurochemical profile: quantification of 18 metabolites in short-echo-time. (1)H NMR spectra of the rat brain. *J Magn Reson*. (1999) 141:104–20. doi: 10.1006/jmre.1999.1895
46. Petroff OA, Ogino T, Alger JR. High-resolution proton magnetic resonance spectroscopy of rabbit brain: regional metabolite levels and postmortem changes. *J Neurochem*. (1988) 51:163–71. doi: 10.1111/j.1471-4159.1988.tb04850.x
47. de Graaf RA, Brown PB, McIntyre S, Nixon TW, Behar KL, Rothman DL. High magnetic field water and metabolite proton T1 and T2 relaxation in rat brain *in vivo*. *Magn Reson Med*. (2006) 56:386–94. doi: 10.1002/mrm.20946
48. Kettunen MI, Gröhn OH, Kauppinen RA. Quantitative T1 NMR spectroscopy of rat cerebral metabolites *in vivo*: effects of global ischemia. *Magn Reson Med*. (2004) 51:875–80. doi: 10.1002/mrm.20099

Conflict of Interest: The authors declare that the research was conducted in the absence of any commercial or financial relationships that could be construed as a potential conflict of interest.

Copyright © 2019 Jirak, Ziolkowska, Turnovcova, Karova, Sykova, Jendelova and Romanyuk. This is an open-access article distributed under the terms of the Creative Commons Attribution License (CC BY). The use, distribution or reproduction in other forums is permitted, provided the original author(s) and the copyright owner(s) are credited and that the original publication in this journal is cited, in accordance with accepted academic practice. No use, distribution or reproduction is permitted which does not comply with these terms.

frontiers in Neuroscience

ORIGINAL RESEARCH
published: 25 October 2019
doi: 10.3389/fnins.2019.01127

ApoA-I Mimetic Peptide Reduces Vascular and White Matter Damage After Stroke in Type-2 Diabetic Mice

Xiaohui Wang[1†], Rongwen Li[1], Alex Zacharek[1], Julie Landschoot-Ward[1], Michael Chopp[1,2], Jieli Chen[1] and Xu Cui[1*]*

[1] Department of Neurology, Henry Ford Hospital, Detroit, MI, United States, [2] Department of Physics, Oakland University, Rochester, MI, United States

OPEN ACCESS

Edited by:
Emmanuel Pinteaux, The University of Manchester, United Kingdom

Reviewed by:
Xingshun Xu, Second Affiliated Hospital of Soochow University, China
Ken Arai, Massachusetts General Hospital and Harvard Medical School, United States

***Correspondence:**
Jieli Chen
jieli@neuro.hfh.edu
Xu Cui
xcui1@hfhs.org

†Present address:
Xiaohui Wang, Department of Pathology, Shanxi Medical Science University, Shanxi, China

Specialty section:
This article was submitted to Neurodegeneration, a section of the journal Frontiers in Neuroscience

Received: *01 May 2019*
Accepted: *04 October 2019*
Published: *25 October 2019*

Citation:
Wang X, Li R, Zacharek A, Landschoot-Ward J, Chopp M, Chen J and Cui X (2019) ApoA-I Mimetic Peptide Reduces Vascular and White Matter Damage After Stroke in Type-2 Diabetic Mice. Front. Neurosci. 13:1127. doi: 10.3389/fnins.2019.01127

Diabetes leads to an elevated risk of stroke and worse functional outcome compared to the general population. We investigate whether L-4F, an economical ApoA-I mimetic peptide, reduces neurovascular and white-matter damage in db/db type-2 diabetic (T2DM) stroke mice. L-4F (16 mg/kg, subcutaneously administered initially 2 h after stroke and subsequently daily for 4 days) reduced hemorrhagic transformation, decreased infarct-volume and mortality, and treated mice exhibited increased cerebral arteriole diameter and smooth muscle cell number, decreased blood-brain barrier leakage and white-matter damage in the ischemic brain as well as improved neurological functional outcome after stroke compared with vehicle-control T2DM mice ($p < 0.05$, $n = 11$/group). Moreover, administration of L-4F mitigated macrophage infiltration, and reduced the level of proinflammatory mediators tumor necrosis factor alpha (TNFα), high-mobility group box-1 (HMGB-1)/advanced glycation end-product receptor (RAGE) and plasminogen activator inhibitor-1 (PAI-1) in the ischemic brain in T2DM mice ($p < 0.05$, $n = 6$/group). *In vitro*, L-4F treatment did not increase capillary-like tube formation in mouse-brain endothelial cells, but increased primary artery explant cell migration derived from C57BL/6-aorta 1 day after middle cerebral artery occlusion (MCAo), and enhanced neurite-outgrowth after 2 h of oxygen-glucose deprivation and axonal-outgrowth in primary cortical neurons derived from the C57BL/6-embryos subjected to high-glucose condition. This study suggests that early treatment with L-4F provides a potential strategy to reduce neuroinflammation and vascular and white-matter damage in the T2DM stroke population.

Keywords: diabetes, stroke, blood–brain barrier (BBB), white matter (WM), inflammation

INTRODUCTION

Diabetes mellitus (DM) is a major risk factor for ischemic and hemorrhagic stroke. Stroke patients with DM exhibit a worse neurovascular prognosis and white-matter (WM) lesion and neurological function than non-DM stroke patients. Therefore, development of therapeutic approaches for the DM-stroke population are urgently needed.

Type-2 diabetes (T2DM) constitutes 90% of the DM population. DM patients have low levels of blood high-density lipoprotein (HDL) (Maron, 2000; Sharrett et al., 2001; Gotto and Brinton, 2004; Bonora, 2006) and impairment of HDL function such as the antioxidative capacity of HDL

(Bonora, 2006; Kontush and Chapman, 2006; Anan et al., 2010; Kruit et al., 2010; Mulder et al., 2011; Scheffer et al., 2011; Dullaart et al., 2012). Improved HDL functionality may contribute to maintenance of pancreas beta-cell function in subjects with well-controlled T2DM (Dullaart et al., 2012). Impairment of HDL anti-oxidative function in T2DM contributes to enhanced formation of oxidative stress products, such as advanced glycation end products (AGEs) (Mulder et al., 2011; Scheffer et al., 2011). Dysfunction of HDL also promotes inflammatory effects (Kruit et al., 2010) and increases proinflammatory factor activation, such as tumor necrosis factor alpha (TNFα) (Igarashi et al., 2008; Nayak et al., 2010; Gomez-Banoy et al., 2016), high-mobility group box 1 (HMGB1) and AGE receptor (RAGE) (Williams and Nadler, 2007; Ye et al., 2011), and plasminogen activator inhibitor-1 (PAI-1) (Scarabin et al., 1998; Bonora, 2006; Williams and Nadler, 2007; Al-Hamodi et al., 2011; Ye et al., 2011; Costa and Soares, 2013; Gorska-Ciebiada et al., 2016), which can exacerbate vascular and WM damage after stroke in T2DM. Therefore, improving HDL function through modification of its lipid and/or protein content maybe a therapeutic target for the treatment of stroke in T2DM.

In human, the circulating blood contains only about 40% of the total amount of HDL, with most of HDL particles present in human interstitial fluids including the arterial intimal fluid (Miller et al., 2013). The HDL particles in plasma contain either a single copy or multiple copies of apolipoprotein A-I (ApoA-I). ApoA-I has been shown to possess several atheroprotective functions, including inhibition of inflammation. However, ApoA-I is a selective target for oxidation by myeloperoxidase, which results in impaired HDL function (Imaizumi et al., 2011). 4F is an economical 18 amino acid peptide mimetic the tertiary structure of ApoA-I. There are two 4F species, D-4F (right hand) and L-4F (left hand). When administered subcutaneously, D-4F and L-4F are equally efficacious, D-4F is orally efficacious but L-4F is digested by gut proteases (Navab et al., 2009). Both of them have remarkable anti-inflammatory properties based on their ability to preferentially bind proinflammatory oxidized lipids and decrease serum oxidized low-density lipoprotein (LDL) level (Van Lenten et al., 2008; Liu et al., 2014; Yao et al., 2015), improve HDL function (Ou et al., 2005; Van Lenten et al., 2008; Yu et al., 2008; Navab et al., 2009; Nandedkar et al., 2011; Qin et al., 2012), and increase cholesterol efflux (Navab et al., 2004; Sherman et al., 2010). Our previous studies show that D-4F treatment of wild-type mice subjected to stroke reduces vascular and WM damage as well as improves recovery of neurological function 14 days after stroke (Cui et al., 2016). Rats with type-1 diabetes and subjected to stroke receiving orally administered D-4F initiated at 2 h after stroke, and subsequently at 24 and 48 h after stroke exhibit significantly decreased neuroinflammation (Ning et al., 2017). However, to our knowledge, there are no studies investigating whether L-4F has a therapeutic effect on stroke-induced vascular and WM damage in T2DM mice. In this study, we therefore investigated the hypothesis that anti-inflammation may play an important role in L-4F treatment of stroke induced neuroprotection and reduction of WM damage in a clinically relevant stroke model using db/db T2DM mice.

MATERIALS AND METHODS

Animal Stroke Model and Experimental Groups

The number of animals for the *in vivo* study was calculated *a priori* by power analysis. For blood biochemistry, lesion volume, and histochemical/immunohisto-staining measurement, 11 mice per group survival stroke animals were targeted to achieve a power of 0.83 at a significance level of < 0.05, assuming 25% difference in mean, a 20% standard deviation at the 95% confidence level. For Western-blot (WB) and real time-quantitative PCR (RT-qPCR) assays, 6 stroke mice per group were needed. To meet these experimental targets, a total of 90 adult male T2DM mice (BKS.Cg-$m + / + Lepr^{db}$/J, db/db mice, 3 month old, Jackson Laboratory, Wilmington, MA, United States) were used. For middle cerebral artery occlusion (MCAo) surgery, animals were anesthetized with 2% isoflorane in a jar for pre-anesthetic, and spontaneously respired with 1.5% isoflurane in 2:1 N_2O:O_2 mixture using a facemask connected and regulated with a modified FLUOTEC 3 Vaporizer (Fraser Harlake). Rectal temperature was maintained at 37°C throughout the surgical procedure using a feedback regulated water heating system. Transient right MCAo was induced for 1 h by advancing a 6-0 surgical nylon suture (8.0–9.0 mm), determined by the animal weight, with its tip rounded by heating near a flame, to block the origin of the MCA, using a method of intraluminal vascular occlusion modified in our laboratory (Liu et al., 2007). One hour after MCAo, reperfusion was performed by withdrawal of the suture. Two hours after suture withdrawal mice were randomly separated into three groups by drawing different colored balls:

(1) Sham-control group: mice were subjected to the same procedures as the MCAo without insertion of filament ($n = 4$ mice).
(2) MCAo group: mice were subcutaneously administered saline daily for 4 days ($n = 52$ mice).
(3) L-4F treatment group: mice were administered L-4F (BioMatik, Cambridge, ON, Canada) 16 mg/kg ($n = 34$ mice) and subsequently daily for 4 days. All survival animals were sacrificed 4 days after MCAo.

Functional Tests

To evaluate neurological functional deficits and recovery after stroke, all animals were evaluated on the modified neurological severity score (mNSS, the total score is 12) and left foot-fault test before MCAo (as the baseline) and at 1, 3, and 4 days after MCAo, as previously described (Chen et al., 2001; Shehadah et al., 2014). Functional analyses were performed by an investigator blinded to the experimental groups.

Blood Biochemistry Measurement

To test blood biochemistry, the animals were fasted overnight and blood was collected from tail vein before MCAo as the baseline and prior to sacrifice. Blood levels of glucose were measured using glucose test strips in a glucose analyzer (Accu-Chek Compact System; Roche Diagnostics, Basel, Switzerland), and the levels of HDL, total-cholesterol (T-CH) and triglyceride were tested using

CardioChek P●A analyzer (Polymer Technology System, Inc., Indianapolis, IN, United States), following the manufacturer's instructions. Each sample was tested in triplicate and the data are presented as mg/dl values.

Cerebral Hemorrhagic Transformation, Lesion Volume, and Survival Rate Measurement

All brains were fixed by transcardial-perfusion with saline, followed by perfusion and immersion in 4% paraformaldehyde and were then embedded in paraffin. Using a mouse brain matrix (Activational Systems Inc., Warren, MI, United States), the cerebral tissues were cut into seven equally spaced (1 mm) coronal blocks, and a series of adjacent 6 μm thick sections were cut from each block. Seven coronal sections of tissue were processed and stained with hematoxylin and eosin (HE). For calculation of brain hemorrhage volume, the percentage areas of petechial and gross hemorrhage were measured in each histological section and summed. For lesion volume measurement, the indirect lesion area was calculated, in which the intact area of the ipsilateral hemisphere was subtracted from the area of the contralateral hemisphere. Lesion volume is presented as a volume percentage of the lesion compared with the contralateral hemisphere (Swanson et al., 1990). For evaluation of mortality, all animals were counted daily. The total number of dead animals in each group was counted within the 4 days after MCAo. The survival rate is presented as a percentage of the total number of stroke animals in each group.

Histochemical and Immuno-Staining

For histochemical/immunostaining, a standard paraffin block was obtained from the center of the lesion (bregma −1 to +1 mm). A series of 6-μm thick sections were cut from the block. Every 10^{th} coronal section for a total of five sections was used. Histochemical-staining for Bielshowsky silver (BS, an axon marker) and Luxol fast blue (LFB, a myelin marker), or histoimmino-staining for antibodies against albumin (BBB leakage marker, 1:500; Abcam), von Willebrand Factor (vWF, a vessel marker, 1:400; Dako), α-smooth muscle actin (αSMA, a smooth muscle cell-SMC marker, 1:800, Dako), SMI31 (a marker of phosphorylated-neurofilament, 1:1000, Covance), platelet-derived growth factor receptor alpha (PDGFRα, a marker of oligodendrocyte progenitor cells-OPCs, 1:100, Chemicon), and HMGB1 (1:800, Abcam) were performed. For immunostaining measurement, five sections with each section containing 8 fields of view within the cortex and striatum from the ischemic boundary zone (IBZ), defined as the area surrounding the lesion, which morphologically differs from the surrounding normal tissue, were digitized using a 40X objective (Olympus BX40) using a 3-CCD color video camera (Sony DXC-970MD) interfaced with an MCID computer imaging analysis system (Imaging Research, St. Catharines, ON, Canada).

BBB Leakage Measurement

Cerebral infiltration of albuminuria, which is associated with DM, has been flagged as a predictor for cerebrovascular events (Anan et al., 2008) and as an index of BBB permeability (Wallin et al., 2000). In this study, to test whether L-4F treatment enhances BBB-integrity after stroke in T2DM mice, the albumin density in the ischemic brain was measured. The positive area of albumin in the ischemic border area is presented.

Vascular Density, Perimeter/Diameter, and Cell Number Measurement

vWF-immunoreactivity was employed to identify vascular vessels, and αSMA was used as a marker of arterioles (Ho et al., 2006). The density and perimeter of vWF-coated vessels, and the number and diameter of αSMA-positive arterioles (have only one to two layers of SMCs, diameter 10–20 μm) were analyzed in the IBZ. The diameter is presented as the average of a total 10 largest arteries in the IBZ.

WM Density and OPC Number Measurement

For measurement of WM-density, the BS, LFB, or SMI31 -positive area in the WM bundles of striatum and the total number of PDGFRα^{+}-OPCs in the IBZ of the striatum were measured in each referenced coronal section using the MCID computer imaging analysis system.

Real-Time RT-PCR Assay

Tissues from the ischemic area of the ipsilateral hemisphere from both vehicle-control and L-4F-treatment T2DM mice were isolated 4 days after MCAo. Total RNA was isolated using a standard protocol. Quantitative PCR was performed on an ABI 7000 PCR instrument (Applied Biosystems, Foster City, CA, United States) using three-stage program parameters provided by the manufacturer. Each sample was tested in triplicate, and analysis of relative gene expression data using the $2^{-\Delta\Delta CT}$ method. The following primers for RT-PCR were designed using Primer Express software (ABI). TNFα: Fwd: TACTCCCAGGTTCTCTTCAAGG, Rev: GAGGTTGACTTTCTCCTGGTA; PAI-1: Fwd: GTCTTTCCG ACCAAGAGCAG.

Rev: ATCACTTGGCCCATGAAGAG; GAPDH: Fwd: AGA ACA TCA TCC CTG CAT CC, Rev: CAC ATT GGG GGT AGG AAC AC.

Western Blot (WB) Assay

Equal amounts of brain-tissue lysate from the ischemic area of the ipsilateral hemisphere were subjected to WB analysis. Specific proteins were visualized using a SuperSignal West Pico chemiluminescence kit (Pierce). The following primary antibodies were used: anti-RAGE (1:1000, rat, R&D MAB1179), anti-HMGB1 (1:1000, rabbit, Abcam ab18256), anti-TNFα (1: 1000, Abcam ab9755), anti-PAI-1 (1:500, rabbit, Santa Cruz sc-8979), anti-ED1 (CD68, 1:800, Bio-rad, MCA341, a single chain glycoprotein of 90–110 kDa, is the widely used pan-macrophage marker), and anti-β-actin (1:2000; Santa Cruz sc-1616) for 16 h at 4°C. The membranes were washed with blocking buffer without milk, and then incubated with horseradish peroxidase-conjugated secondary antibody in blocking buffer.

Mouse Brain Cerebral Endothelial Cell (bEnd.3) Culture and Capillary-Like Tube Formation Assay

The bEnd.3 cell line (ATCC, cat# CRL02299) was used. Briefly, 0.1 ml growth factor reduced Matrigel (Becton Dickinson) was added per well of a 96 well plate, and cells (2×10^4 cells) were seeded in Matrigel and cultured with serum free DMEM medium. The cells were divided into four groups (n = 6 wells/group), and treated with: (1) normal-glucose (12.5 mM glucose) as control; (2) high-glucose (HG, 37.5 mM glucose); (3) HG + L-4F (50 ng/ml); (4) HG + L-4F (100 ng/ml). Cells were incubated for 5 h and the capillary tube formation measurement was performed. For quantitative measurements of capillary tube formation, Matrigel wells were digitized under a 4X objective (Olympus BX40). Tracks of cells organized into networks of cellular cords (tubes) were counted and averaged in randomly selected three microscopic fields, and the total tube length of capillary tube formation was measured using a video camera (Sony DXC-970MD) interfaced with the MCID image analysis system.

Primary Artery Cell Migration Measurement

To investigate whether L-4F treatment promotes arterial cell migration in hyperglyceridemia, a primary artery explant culture model was employed (Cui et al., 2011). The aorta was surgically removed from adult C57BL/6 wild-type mice (6–8 weeks, purchased from Jaxson Lab) 24 h after MCAo. The artery explant was cut to 1 mm^3 and placed in Matrigel and cultured with DMEM medium containing 2% B27. The artery explants were divided into four groups as follows: (1) normal glucose (12.5 mM) as a control; (2) HG (37.5 mM glucose); (3) HG + L-4F (50 ng/ml); (4) HG + L-4F (100 ng/ml). Arterial explant cultures were allowed to grow for 5 days before being photographed and the 10 longest distances of outgrowth were measured under a microscope at 4X magnification, processed with the MCID and averaged. n = 6/group.

Primary Cortical Neuron (PCN) Culture and Neurite/Axonal Outgrowth Measurements

The PCNs derived from E15 C57BL/6 embryos were employed, as previously described (Cui et al., 2016). Briefly, embryos were removed, and the cerebral cortex was dissected out, stripped of meninges, and dissociated by a combination of Ca^{2+}- and Mg^{2+}-free Hanks balance salt solution (HBSS) containing 0.125% trypsin digestion and mechanical trituration. The dissociated cell suspensions were seeded into poly-L-lysine precoated plates in a density of 10^5 cells/cm^2. The cells were grown in Dulbecco's Modified Eagle Medium (DMEM, Invitrogen, Carlsbad, CA, United States) supplemented with 5% fetal bovine serum (FBS, GIBCO, Grand Island, NY, United States) at 37°C with 5% CO_2. After 24 h, the cell cultures were switched to incubate with serum-free neurobasal medium (Invitrogen) with 2% B27 supplement (GIBCO), 0.5 mM L-glutamine, and 1% antibiotic-antimycotic media.

To test whether L-4F dose-dependently increases neurite-outgrowth in hyperglycemia after ischemia, the PCN cultures were subjected to 2 h of oxygen and glucose deprivation (OGD) on day-*in vitro* 4 (DIV4) followed by 24 h of reperfusion. The DIV5 OGD-PCNs were randomly divided into (n = 6 wells/group): (1) normal glucose control; (2) HG; (3) + L-4F 50 ng/ml; (4) + L-4F 100 ng/ml for 24 h. The PCN cultures were then stained with TUJ1 (a phenotypic marker of neural cells, 1:1000, Covance) with Cy3 and photographed using a 10 × objective fluorescent microscope (Zeiss). The average length of the 20 longest neurites in each well was calculated (Cui et al., 2016).

For testing whether L-4F increases axonal-outgrowth in HG condition, the axonal-outgrowth was measured using a microfluidic axonal growth model (Standard Neuron Device; catalog No SND450, Xona Microfluidics) (Cui et al., 2016). On DIV4, the PCN cultures were divided into four groups (n = 6 well/group): (1) normal glucose control; (2) HG; (3) + L-4F 50 ng/ml; (4) + L-4F 100 ng/ml. All axon-cultures were allowed to grow for an additional 48 h and were subjected to TUJ-1 immunostaining, and the axonal-outgrowth was measured on DIV6. The average length of the 10 longest axons in each well was calculated.

Statistical Analysis

One-way ANOVA followed by Tukey *Post Hoc* Test were used for analysis of the differences among the three or four groups of sham, MCAo and L-4F treatment *in vivo* or *in vitro* experiments. $p < 0.05$ was set as a significant difference, and all data are presented as mean ± Standard Error (SE).

RESULTS

L-4F-Treatment Deceases Hemorrhage/Lesion Volume and Mortality Rate, and Improves Functional Outcome After Stroke in T2DM Mice

There were no significant differences in the levels of blood glucose, HDL, T-CH, and triglyceride among animals of sham-control (n = 4) and MCAo groups treated with or without L-4F (n = 11/group) 4 days after MCAo, respectively (**Figures 1A,B**). However, L-4F treatment of MCAo mice significantly decreased hemorrhage volume (**Figure 1C**, n = 11/group), and reduced lesion volume (**Figure 1D**, n = 11/group) and mortality rate (**Figure 1E**, n = 52 in MCAo-control group, n = 34 in L-4F treatment group) compared to the MCAo-control group ($p < 0.05$).

Stroke induced significant functional deficits as indicated by significantly increased mNSS and left foot-fault at 1, 3, and 4 days in T2DM mice in the MCAo-control group (n = 11) compared with non-stroke T2DM mice in the sham-control group (n = 4, $p < 0.05$). L-4F treatment significantly improved neurological functional outcome 4 days after MCAo in T2DM-stroke mice

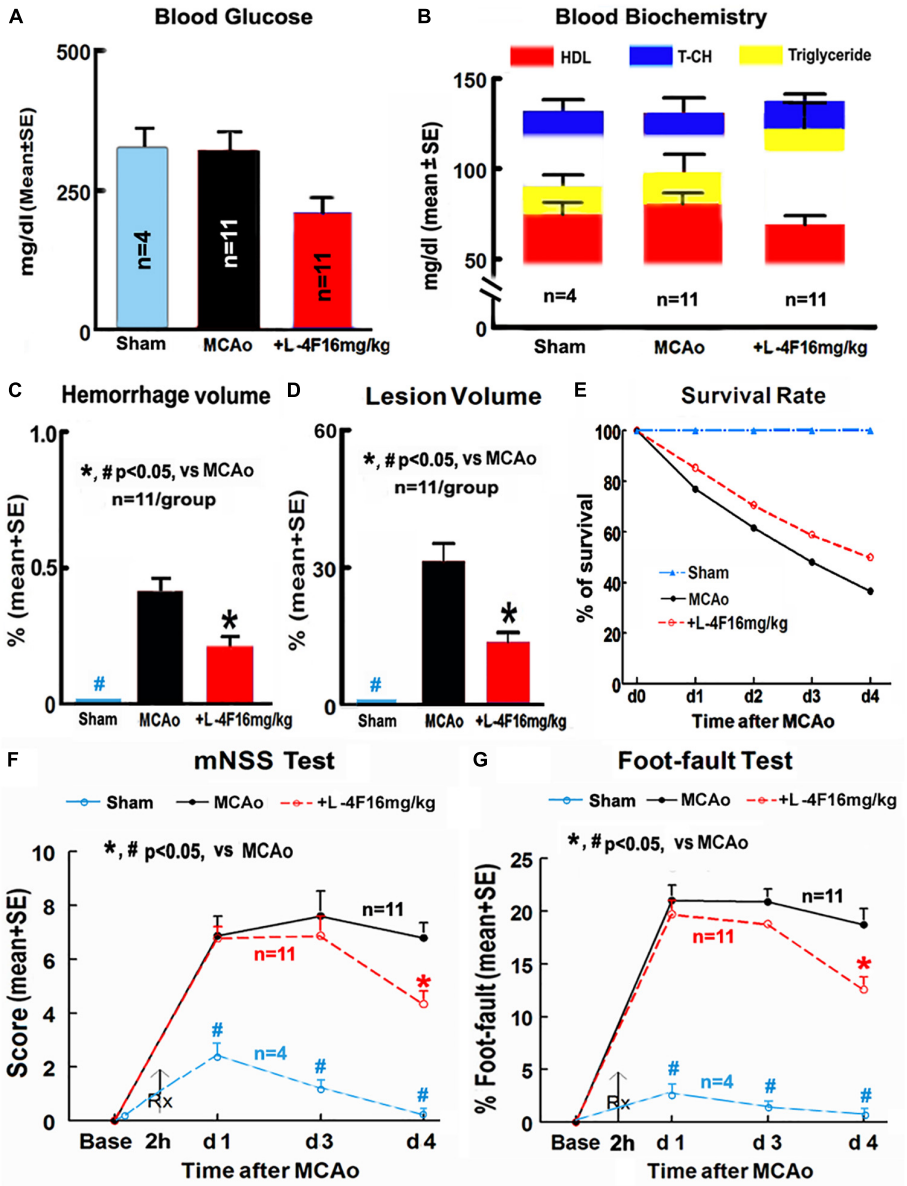

FIGURE 1 | L-4F treatment did not change blood biochemistry, but decreases hemorrhage/lesion volumes in the ischemic brain and reduces mortality, and improves functional outcome in T2DM mice 4 days after MCAo. **(A)** Blood levels of glucose; **(B)** blood level of HDL, T-CH, and triglyceride; **(C)** hemorrhage volume; **(D)** lesion volumes; **(E)** survival rate; **(F,G)** functional outcome.

(**Figures 1F,G**, $p < 0.05$, $n = 11$/group). These data indicate that L-4F significantly decreases cerebral hemorrhagic transformation and reduces lesion volume and mortality as well as improves neurological functional outcome, independently of blood HDL and glucose level.

L-4F Treatment Reduces Vascular Damage in the Ischemic Brain in T2DM Mice

There was no albumin infiltration in the non-stroke brains ($n = 4$). However, albumin infiltration was observed in the ischemic core area in the T2DM-stroke brains, and the albumin density was significantly decreased in the L-4F treatment group compared with MCAo-control group (**Figure 2A**, $p < 0.05$, $n = 11$/group). These data indicate that the integrity of the BBB was compromised in the ischemic brain in T2DM stroke mice, and early L-4F treatment protects BBB integrity in the ischemic brain after stroke in T2DM mice. These data (i.e., BBB disruption as measured using albumin) are consistent with our previous study that D-4F enhances BBB-integrity as detected by Evans blue (EB) dye infiltration detection in the ischemic brain in C57BL/6 wild type mice after stroke (Cui et al., 2016).

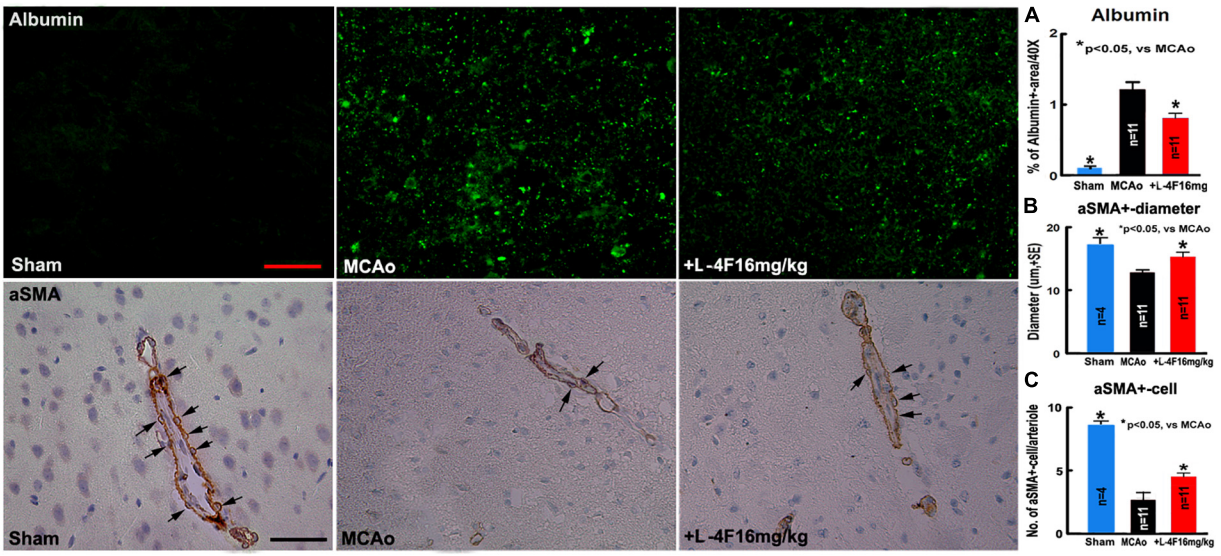

FIGURE 2 | L-4F treatment decreases BBB-leakage, increases SMC number and arteriolar diameter in the ischemic brain in T2DM mice 4 days after MCAo; **(A)** albumin-immunostaining and quantitative data; **(B)** αSMA-immunostaining and quantitative data. **(C)** Numbers of αSMA^+-cells in the arteriolar walls. Scale bar = 25 μm; n = 4 in sham-control group, n = 11 in MCAo-control and L-4F treatment group.

Using vascular density, diameter and perimeter to indicate vascular structure changes, we found that there is no difference in the density/perimeter of vWF^+-vessels among the sham-control, MCAo-control and L-4F treatment groups, and no differences in the density of αSMA^+-arterioles between sham-control and MCAo-control groups. However, both the diameter of αSMA^+-arterioles and the number of αSMA^+-SMCs were significantly decreased in the MCAo-control group (n = 11) compared with sham-control group (n = 4), and the diameter of αSMA^+-arterioles (**Figure 2B**) and the number of αSMA^+-SMCs (**Figure 2C**) in the IBZ significantly increased in the L-4F treatment group compared with MCAo-control group ($p < 0.05$, n = 11/group). These data indicate that vascular structure was damaged in ischemic brain in T2DM stroke mice, and early L-4F treatment has a vascular protective effect on the ischemic brain after stroke in T2DM mice.

L-4F Treatment Decreases WM-Damage and OPC Loss in the Ischemic Brain in T2DM Mice

To investigate whether L-4F reduces WM-damage and OPC loss after stroke, we measured the densities of BS^+ (axon marker, **Figure 3A**), $\alpha SMI31^+$ (phosphorylated-neurofilament marker, **Figure 3B**), LFB^+ (myelin marker, **Figure 3C**) and the number of PDGFR(+-OPCs (**Figure 3D**) in the IBZ of striatum in the ischemic ipsilateral hemisphere, respectively. Compared with sham-control mice (n = 4), the MCAo-control mice (n = 11) exhibited a significant decrease in the densities of axons, phosphorylated-neurofilament, myelin and the number of OPCs 4 days after MCAo ($p < 0.05$). However, L-4F treatment significantly increased the densities of axons, phosphorylated-neurofilaments, myelin and the number of OPCs 4 days after MCAo compared with MCAo-control group ($p < 0.05$, n = 11/group). These data indicate that L-4F treatment decreases WM damage and OPC loss after stroke in T2DM mice.

L-4F Treatment Reduces Macrophage Infiltration and Decreases RAGE/HMGB1 and PAI-1 Expression in the Ischemic Brain After Stroke in T2DM Mice

To investigate the mechanism underlying L-4F treatment-induced neuroprotection in T2DM, the macrophage infiltration was measured by ED1 protein level, and the protein and mRNA levels of HMGB1, RAGE, TNFα, and PAI-1 were measured by using immunostaining, WB or RT-PCR assay, respectively. The data show that L-4F treatment significantly decreases HMGB1 protein levels measured by immunostaining (**Figures 4A–D**, n = 11/group) and reduces RAGE/ED/HMGB1 level measured by WB (**Figures 4E,F**, n = 6/group). Moreover, L-4F treatment significantly decreases TNFα and PAI-1 protein and mRNA level (**Figures 4G–I**) in the ischemic ipsilateral brain compared to MCAo-control group ($p < 0.05$, n = 6/group).

L-4F Treatment Does Not Change Capillary-Like Tube Formation, but Increases Artery Explant Cell Migration Under HG Condition

To confirm the *in vivo* findings, *in vitro* capillary-like tube formation assay for angiogenesis and primary artery explant cell migration for artery function test were employed. L-4F treatment at concentrations of 50 or 100 ng/ml did not increase capillary tube formation under HG conditions compared to non-treatment control (**Figure 5A**). However, L-4F treatment

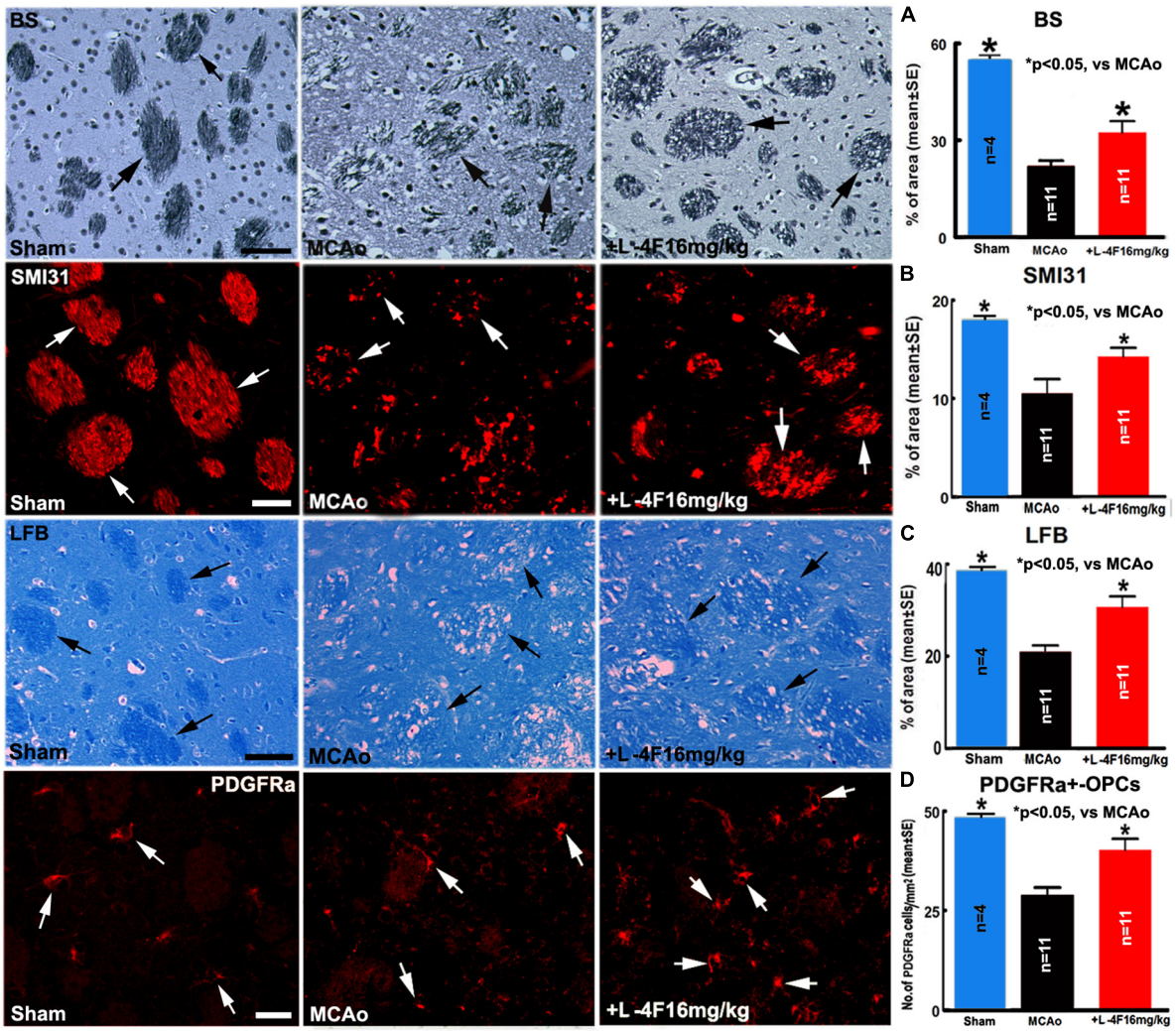

FIGURE 3 | L-4F treatment increases WM density and OPC numbers in the ischemic brain in T2DM mice 4 days after stroke. **(A)** BS^{+} -axon and quantitative data; **(B)** SMI31^{+} -neurofilament and quantitative data; **(C)** LFB^{+} -myelin and quantitative data; **(D)** PDGFRα^{+} -OPCs and quantitative data. Scale bar in **(A,C)** = 40 μm; in **(B,D)** = 20 μm. *$p < 0.05$, $n = 4$ in sham-control group, $n = 11$ in MCAo-control and L-4F treatment group.

significantly increases artery explant cell migration at both 50 and 100 ng/ml concentration in HG media (**Figure 5B**, $p < 0.05$, $n = 6$/group) compared to non-treatment control, respectively. These data suggest that L-4F does not change angiogenesis, but increases arterial function in HG condition.

L-4F Treatment Increases Neurite/Axonal Outgrowth in HG Condition

To confirm the *in vivo* findings that L-4F treatment protects WM damage, we measured the neurite and axonal outgrowth under HG conditions. To mimic *in vivo* ischemia, the PCNs were subjected to 2 h of OGD. The data show that HG decreases PCN neurite outgrowth, but L-4F treatment (both 50 and 100 ng/ml) significantly increases PCN neurite outgrowth after ischemia (**Figure 6A**). In addition, L-4F (50 and 100 ng/ml) also increases and axonal outgrowth in HG condition compared with non-treatment control group (**Figure 6B**, $p < 0.05$, $n = 6$ wells/group).

DISCUSSION

T2DM confers increased micro- and macro- vascular complications and amplifies of morbidity and mortality after ischemic stroke (Basu et al., 2005; Madonna and De Caterina, 2011). Compared to non-DM stroke patients, T2DM stroke patients have chronic states of oxidative stress and inflammation, which accompany long-term endothelial dysfunction and impaired vasodilation, and increased vasogenic edema, BBB damage, and secondary hemorrhage transformation (Capes et al., 2001; Kruger et al., 2005; Ergul et al., 2007; Peterson et al., 2007; Ding et al., 2015). WM-damage is an important prognostic factor for the development of functional deficits after

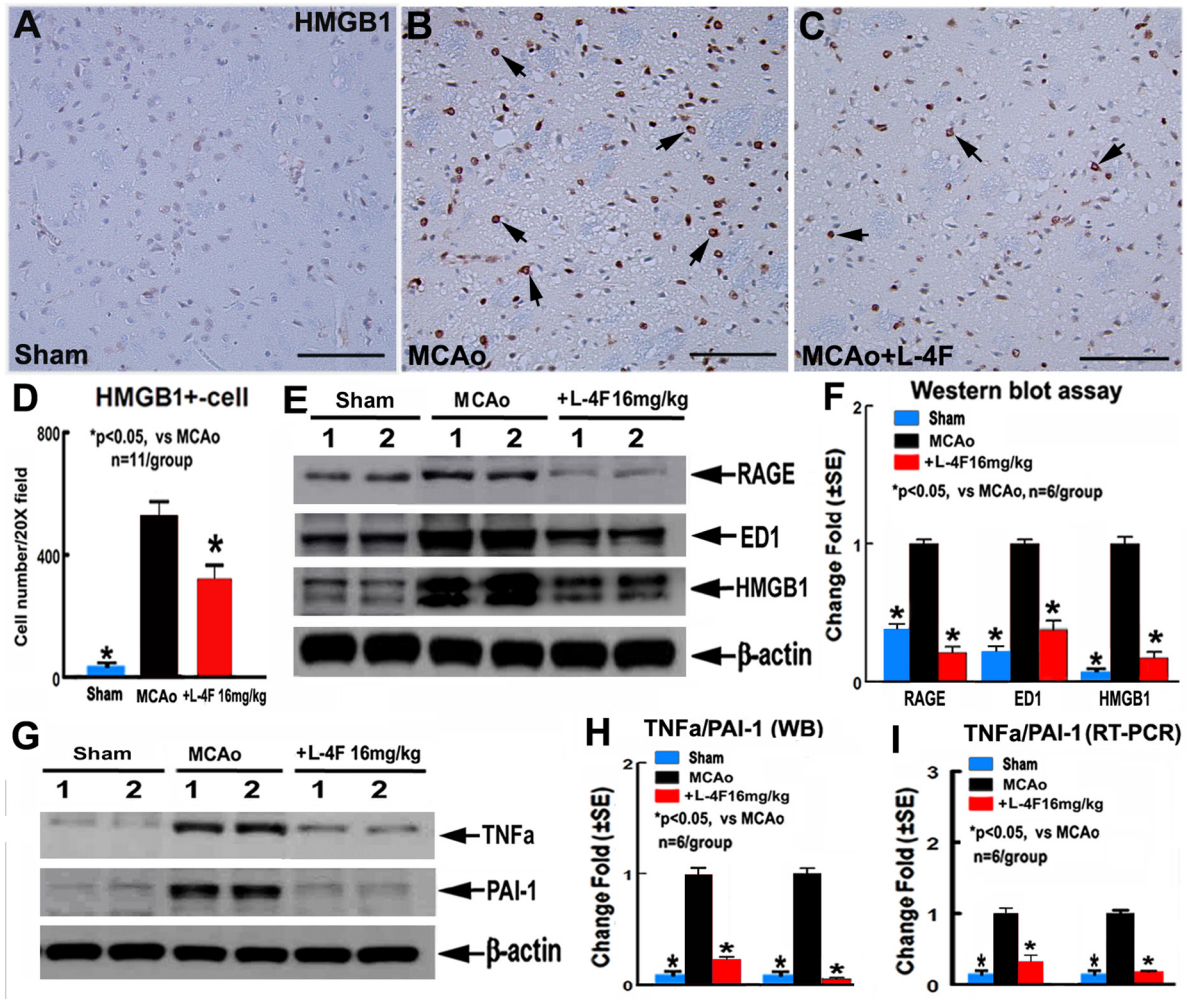

FIGURE 4 | L-4F treatment decreases RAGE/ED1/HMGB-1, and PAI-1 in the ischemic brain in T2DM mice 4 days after MCAo. **(A–D)** HMGB-1 immunostaining and quantitative data; **(E,F)** RAGE/ED1/HMGB-1 WB assay and quantitative data; **(G,H)** TNFα/PAI-1 WB assay and quantitative data; **(I)** TNFα/PAI-1 RT-PCR data. Scale bar in **(A–C)** = 50 μm; *$p < 0.05$, n = 11/group in **(A–D)**; n = 6/group in **(A–I)**.

stroke (Anan et al., 2008), BBB and WM damage which are associated with enlarged infarct volume and worse functional outcome after stroke is found in both the experimental T2DM rodents and T2DM patients (Mooradian et al., 2005; Ennis and Keep, 2007; Anan et al., 2010). D-4F increases arterial concentrations of hemeoxygenase-1 and superoxide dismutase, decreases superoxide levels and endothelial cell fragmentation, and restores arterial vasoreactivity to normal in DM animal models (Ou et al., 2003, 2005; Kruger et al., 2005; Sherman et al., 2010). In a mouse model of systemic sclerosis, D-4F functioned to improve vasodilation and angiogenic potential, while reducing myocardial inflammation and oxidative stress (Sherman et al., 2010). In addition, L-4F dramatically improves impaired vasodilation in LDL receptor knockout (Ldlr−/−) mice, via decreased oxidative damage to endothelium (Ou et al., 2003). In our previous study, using a dose-dependent effect on MCAo model in wild type mice, an elevated concentration of D-4F (32 mg/kg) did not provide increased benefit on neurovascular and WM remodeling compared to treatment with a reduced concentration (16 mg/kg) (Cui et al., 2016). D-4F and L-4F have similar anti-inflammatory properties (Van Lenten et al., 2008; Liu et al., 2014; Yao et al., 2015). Therefore, in the present study, the dose of 16 mg/kg L-4F, the same as the optimal dose of D-4F identified from our previous study was used. db/db mice are gene knockout mice which mimic features of human T2DM and have been widely used to investigate diabetic stroke (Vannucci et al., 2001; Kumari et al., 2010; Chen et al., 2011; Cui et al., 2011; Kumari et al., 2011; Sims-Robinson et al., 2012). The db/db stroke mice exhibit increased neurovascular and WM damage and hemorrhagic/mortality rate compared with non-DM stroke mice (Chen et al., 2011; Cui et al., 2011; Ye et al., 2011). In the current study, db/db mice were employed as the T2DM model. We found that L-4F treatment initiated from 2 h post-stroke onset significantly decreased animal mortality rate and hemorrhage/infarct volume, decreased BBB leakage and WM damage, as well as increased vascular SMC

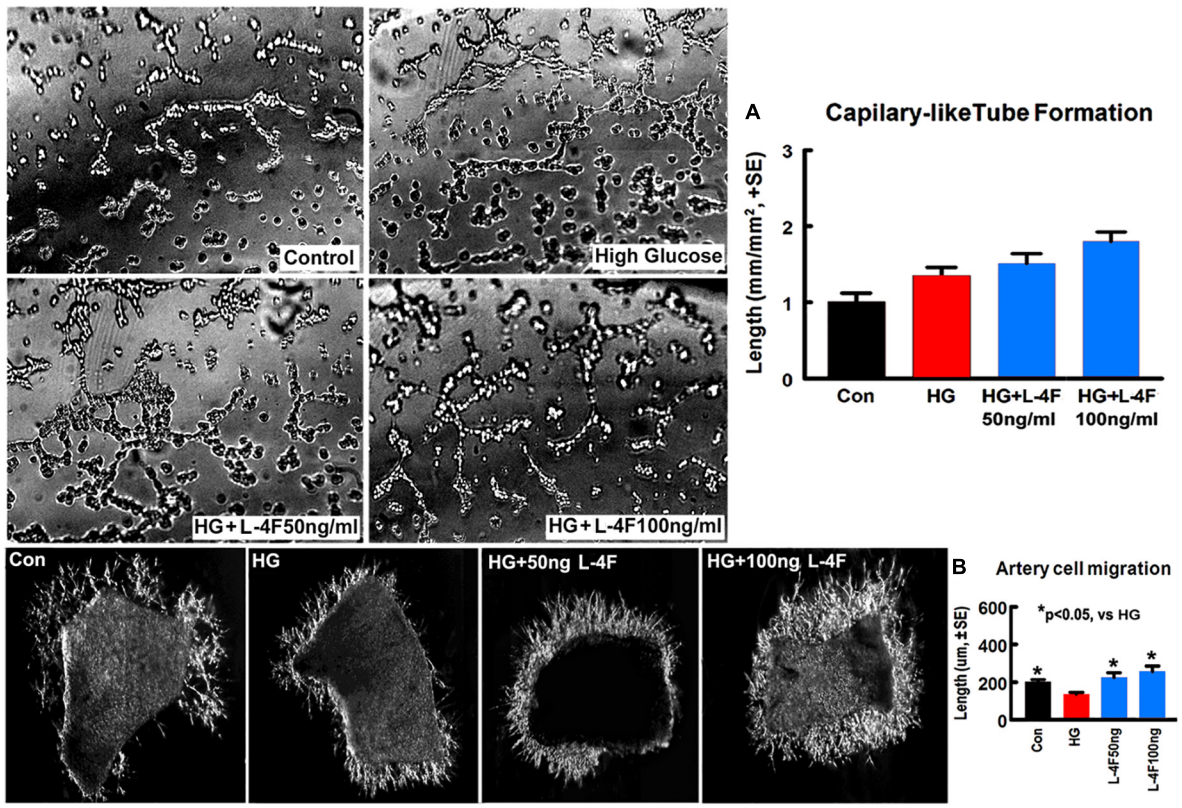

FIGURE 5 | L-4F treatment does not change capillary-like tube formation, but increases artery cell migration in normal and HG condition. **(A)** *In vitro* capillary-like tube formation and quantitative data; **(B)** primary cultured artery cell migration and quantitative data in normal and high glucose condition. $*p < 0.05$, $n = 6$ well/group.

and OPC numbers and enlarged arteriolar diameter in the ischemic brain 4 days after stroke. *In vitro* study shows that L-4F treatment did not change angiogenesis of mouse cerebral endothelial cells, but increased artery explant cell migration and neurite/axon outgrowth under HG condition. These data suggest that improving vascular integrity and retaining vasodilation as well as protecting WM damage, but not necessarily angiogenesis may play important role in L-4F induced neuroprotective effects.

In the brain of both T2DM patients and animal models, the extensive vascular and WM damage are highly associated with and are a consequence of inflammation (Golay et al., 1987; Williams and Nadler, 2007; Anan et al., 2010; Doll et al., 2015). Under normal physiology, RAGE is expressed at low levels, but it is highly upregulated in T2DM under chronic inflammation states because of the accumulation of various RAGE ligands such as AGEs and HMGB1. Blocking RAGE signaling in cell and animal models has revealed that targeting RAGE impairs inflammation and progression of DM vascular complications (Hudson and Lippman, 2018). M1-phage macrophages ($ED1^+$) constitute about 70% of infiltrating cells and exert a major inflammatory function in the brain lesions (Tran et al., 1998). HMGB1 is mainly released from activated immune cells, such as the peripherally infiltrating immune cells (e.g., macrophage/monocytes) in the ischemic brain (Wang et al., 2010; Qin and Crews, 2012; Crews and Vetreno, 2014). HMGB-1 functions also as a proinflammatory factor, promotes cell toxicity and cell death, regulates clot-promoting properties which propagate further inflammation and coagulation (Semeraro et al., 2012), and contributes to the initiation and progression of stroke (Hu et al., 2016). In the present study, L-4F treatment significantly reduced macrophage infiltration and HMGB1/RAGE level. These data suggest that L-4F treatment suppresses neuroinflammation in the ischemic brain, which may contribute to L-4F induced neuroprotective effects in T2DM stroke mice.

High stroke risk in T2DM patients is often related to their accelerated endothelial dysfunction which is accompanied by an array of abnormalities, including altered endothelial-dependent vasodilation, and an imbalance between local pro- and anticlotting factors (Scarabin et al., 1998; Bonora, 2006; Al-Hamodi et al., 2011; Costa and Soares, 2013; Gorska-Ciebiada et al., 2016). The AGE/RAGE signaling pathway not only promotes inflammation such as TNFα and cell death, but also increases endothelial activation biomarker PAI-1 expression in cultured endothelial cells (He et al., 2003; Gregorio et al., 2018). Moreover, TNFα also exerted a stimulatory effect on PAI-1 protein release and increased PAI-1 mRNA levels in T2DM (Birgel et al., 2000; de Carvalho et al., 2006). Recombinant

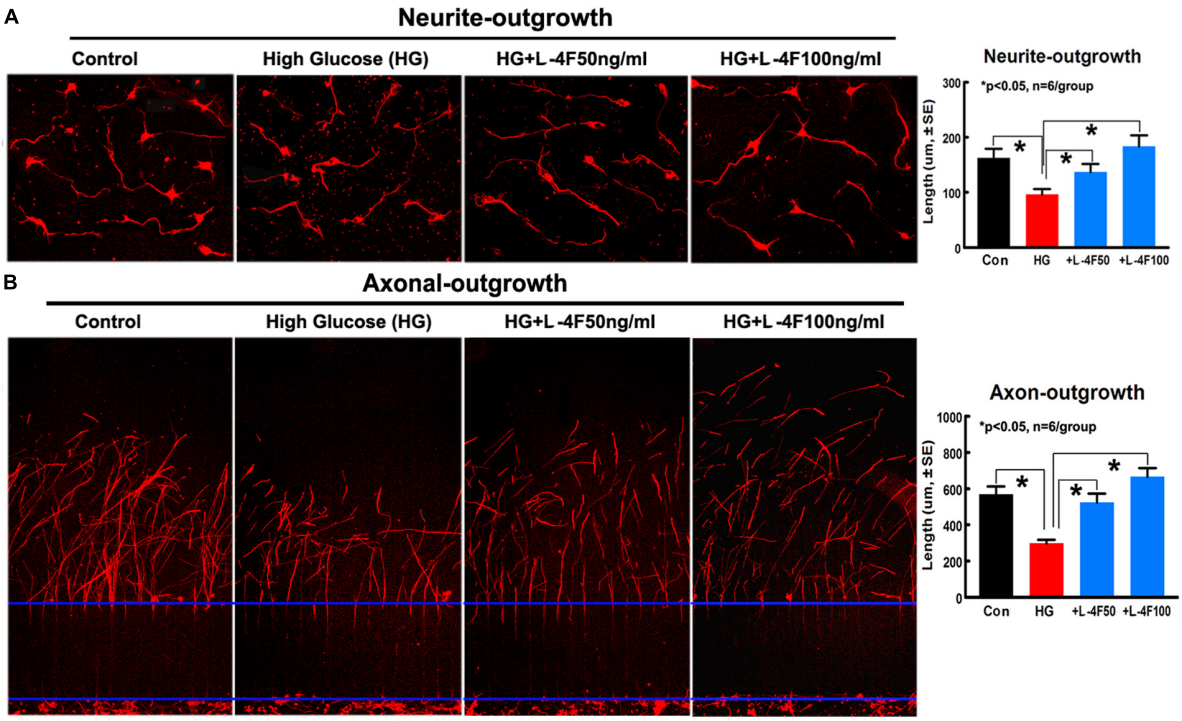

FIGURE 6 | L-4F treatment increases neurite and axonal outgrowth under HG condition. **(A)** *In vitro* neurite outgrowth and quantitative data. **(B)** Axonal-outgrowth and quantitative data. *$p < 0.05$, $n = 6$ well/group.

human HMGB1 increases the secretion of PAI-1 and tissue plasminogen activator (tPA) in cultured human endothelial cells, and elicits proinflammatory responses of endothelial cells and may contribute to alterations in endothelial cell function in human inflammation (Fiuza et al., 2003). HMGB-1 can bind to both tPA and plasminogen, and enhance tPA-dependent fibrinolytic activity, while PAI-1 is a key negative regulator of fibrinolysis through inhibition of plasminogen and tPA (Scarabin et al., 1998; Bonora, 2006; Al-Hamodi et al., 2011; Costa and Soares, 2013; Gorska-Ciebiada et al., 2016). Moreover, PAI-1 exerts various cellular effects independently of fibrinolysis, such as insulin resistance, metabolic abnormalities and endothelial dysfunction as well as pro-inflammatory effects (Cheng and Daskalakis, 2015; Kaji, 2016). PAI-1 is significantly increased in DM subjects compared with non-DM subjects with or without cardiovascular disease (Scarabin et al., 1998; Bonora, 2006; Al-Hamodi et al., 2011; Costa and Soares, 2013; Gorska-Ciebiada et al., 2016). In the present study, L-4F treatment significantly decreases TNFα and PAI-1 expression in the ischemic brain which may partially contribute to L-4F treatment-induced vascular and WM protection in T2DM stroke mice.

Plasma levels of HDL and glucose are highly associated with WM lesions in T2DM patients not receiving insulin treatment (Anan et al., 2010). Moreover, severe vascular and WM damage and neurological functional deficits in diabetic stroke populations are highly associated with dysfunction of HDL in the plasma (Anan et al., 2010; Kruit et al., 2010). Using ApoE-null (ApoE-/-) mice, administration of L-4F (20 mg/kg body weight, once daily subcutaneously) increases HDL level and ApoA-I concentration at 72 h post initial dosing (Chen et al., 2009). However in our study, T2DM mice subjected to stroke and treated with L-4F for 4 days did not exhibit significant changes in blood HDL cholesterol, triglyceride and glucose levels. Our data are consistent with others that D-4F or L-4F have no effect on blood T-CH or HDL concentrations (Navab et al., 2004, 2006, 2009; Kruger et al., 2005; Ou et al., 2005; Bloedon et al., 2008; Van Lenten et al., 2008; Yu et al., 2008; Morgantini et al., 2010; Sherman et al., 2010; Nandedkar et al., 2011). Other studies show that D-4F or L-4F reduces proinflammatory HDL levels and changes HDL function, increases cholesterol efflux, reduces lipoprotein oxidation and improves arterial vasoreactivity in T2DM patients, and in DM mice and rats (Navab et al., 2004, 2006, 2009; Kruger et al., 2005; Ou et al., 2005; Bloedon et al., 2008; Van Lenten et al., 2008; Yu et al., 2008; Morgantini et al., 2010; Sherman et al., 2010; Nandedkar et al., 2011). In addition, high levels of blood PAI-1 are associated with decreased functional HDL in T2DM patients (Bonora, 2006; Al-Hamodi et al., 2011; Gorska-Ciebiada et al., 2016). HDL can also regulate inflammatory responses in various types of cells that have been activated by proinflammatory stimuli in the arterial wall cells including endothelial cells and vascular SMCs (Mineo and Shaul, 2013). Therefore, we speculate that L-4F treatment may improve HDL function and decrease neuroinflammation, and thereby lessens vascular and WM damage after stroke in db/db T2DM mice.

CONCLUSION

This study demonstrates that L-4F, an economical ApoA-I mimetic peptide, reduces neurovascular and WM damage via reducing proinflmammatory factors RAGE/HMGB-1 and TNFα/PAI-1 in the ischemic brain in db/db T2DM stroke mice. These provide a proof-of-concept that treatment with L-4F is a potential strategy to reduce neuroinflammation in the T2DM stroke population.

DATA AVAILABILITY STATEMENT

The raw data supporting the conclusions of this manuscript will be made available by the authors, without undue reservation, to any qualified researcher.

ETHICS STATEMENT

Our animal use protocols were approved by the Guide for the Institute of Animal Care and Use Committee of the Henry Ford health System and in accordance with the standards of the Institutional Animal Care and Use Committee, National Institutes of Health. Adult male db/db mice (3 month old) were used.

AUTHOR CONTRIBUTIONS

XC, JC, and MC conceived and designed the study. XW, RL, AZ, JL-W, and XC acquisition of data and statistical analysis. XW and XC drafted the manuscript. JC and MC critical revision of the manuscript for intellectual content.

FUNDING

This study was supported by National Institute of Neurological Disorders and Stroke Grants R01NS097747 (JC).

ACKNOWLEDGMENTS

We thank Qinge Lu and Sutapa Santra for technical assistance, and Yisheng Cui for performing behavioral functional tests.

REFERENCES

Al-Hamodi, Z., Ismail, I. S., Saif-Ali, R., Ahmed, K. A., and Muniandy, S. (2011). Association of plasminogen activator inhibitor-1 and tissue plasminogen activator with type 2 diabetes and metabolic syndrome in Malaysian subjects. *Cardiovasc. Diabetol.* 10:23. doi: 10.1186/1475-2840-10-23

Anan, F., Masaki, T., Iwao, T., Eto, T., Shimomura, T., Umeno, Y., et al. (2008). The role of microalbuminuria and insulin resistance as significant risk factors for white matter lesions in Japanese type 2 diabetic patients. *Curr. Med. Res. Opin.* 24, 1561–1567. doi: 10.1185/03007990802061818

Anan, F., Masaki, T., Kikuchi, H., Iwao, T., Shimomura, T., Umeno, Y., et al. (2010). Association between plasma high-sensitivity C-reactive protein and insulin resistance and white matter lesions in Japanese type 2 diabetic patients. *Diabetes. Res. Clin. Pract.* 87, 233–239. doi: 10.1016/j.diabres.2009.10.017

Basu, A. K., Pal, S. K., Saha, S., Bandyopadhyay, R., Mukherjee, S. C., and Sarkar, P. (2005). Risk factor analysis in ischaemic stroke: a hospital-based study. *J. Indian Med. Assoc.* 103, 588.

Birgel, M., Gottschling-Zeller, H., Rohrig, K., and Hauner, H. (2000). Role of cytokines in the regulation of plasminogen activator inhibitor-1 expression and secretion in newly differentiated subcutaneous human adipocytes. *Arterioscler. Thromb. Vasc. Biol.* 20, 1682–1687. doi: 10.1161/01.atv.20.6.1682

Bloedon, L. T., Dunbar, R., Duffy, D., Pinell-Salles, P., Norris, R., DeGroot, B. J., et al. (2008). Safety, pharmacokinetics, and pharmacodynamics of oral apoA-I mimetic peptide D-4F in high-risk cardiovascular patients. *J. Lipid Res.* 49, 1344–1352. doi: 10.1194/jlr.P800003-JLR200

Bonora, E. (2006). The metabolic syndrome and cardiovascular disease. *Ann. Med.* 38, 64–80.

Capes, S. E., Hunt, D., Malmberg, K., Pathak, P., and Gerstein, H. C. (2001). Stress hyperglycemia and prognosis of stroke in nondiabetic and diabetic patients: a systematic overview. *Stroke* 32, 2426–2432. doi: 10.1161/hs1001.096194

Chen, J., Cui, X., Zacharek, A., Cui, Y., Roberts, C., and Chopp, M. (2011). White matter damage and the effect of matrix metalloproteinases in type 2 diabetic mice after stroke. *Stroke* 42, 445–452. doi: 10.1161/STROKEAHA.110.596486

Chen, J., Sanberg, P. R., Li, Y., Wang, L., Lu, M., Willing, A. E., et al. (2001). Intravenous administration of human umbilical cord blood reduces behavioral deficits after stroke in rats. *Stroke* 32, 2682–2688. doi: 10.1161/hs1101.098367

Chen, X., Burton, C., Song, X., McNamara, L., Langella, A., Cianetti, S., et al. (2009). An apoA-I mimetic peptide increases LCAT activity in mice through increasing HDL concentration. *Int. J. Biol. Sci.* 5, 489–499. doi: 10.7150/ijbs.5.489

Cheng, C., and Daskalakis, C. (2015). Association of adipokines with insulin resistance, microvascular dysfunction, and endothelial dysfunction in healthy young adults. *Mediators Inflamm.* 2015:594039. doi: 10.1155/2015/594039

Costa, P. Z., and Soares, R. (2013). Neovascularization in diabetes and its complications. Unraveling the angiogenic paradox. *Life Sci.* 92, 1037–1045. doi: 10.1016/j.lfs.2013.04.001

Crews, F. T., and Vetreno, R. P. (2014). Neuroimmune basis of alcoholic brain damage. *Int. Rev. Neurobiol.* 118, 315–357. doi: 10.1016/B978-0-12-801284-0.00010-5

Cui, X., Chopp, M., Zacharek, A., Cui, C., Yan, T., Ning, R., et al. (2016). D-4F decreases white matter damage after stroke in mice. *Stroke* 47, 214–220. doi: 10.1161/STROKEAHA.115.011046

Cui, X., Chopp, M., Zacharek, A., Ye, X., Roberts, C., and Chen, J. (2011). Angiopoietin/Tie2 pathway mediates type 2 diabetes induced vascular damage after cerebral stroke. *Neurobiol. Dis.* 43, 285–292. doi: 10.1016/j.nbd.2011.04.005

de Carvalho, M. H., Colaco, A. L., and Fortes, Z. B. (2006). Cytokines, endothelial dysfunction, and insulin resistance. *Arq. Bras. Endocrinol. Metabol.* 50, 304–312.

Ding, G., Yan, T., Chen, J., Chopp, M., Li, L., Li, Q., et al. (2015). Persistent cerebrovascular damage after stroke in type two diabetic rats measured by magnetic resonance imaging. *Stroke* 46, 507–512. doi: 10.1161/STROKEAHA.114.007538

Doll, D. N., Hu, H., Sun, J., Lewis, S. E., Simpkins, J. W., and Ren, X. (2015). Mitochondrial crisis in cerebrovascular endothelial cells opens the blood-brain barrier. *Stroke* 46, 1681–1689. doi: 10.1161/STROKEAHA.115.009099

Dullaart, R. P., Annema, W., de Boer, J. F., and Tietge, U. J. (2012). Pancreatic beta-cell function relates positively to HDL functionality in well-controlled type 2 diabetes mellitus. *Atherosclerosis* 222, 567–573. doi: 10.1016/j.atherosclerosis.2012.03.037

Ennis, S. R., and Keep, R. F. (2007). Effect of sustained-mild and transient-severe hyperglycemia on ischemia-induced blood-brain barrier opening. *J. Cereb. Blood Flow Metab.* 27, 1573–1582. doi: 10.1038/sj.jcbfm.9600454

Ergul, A., Elgebaly, M. M., Middlemore, M. L., Li, W., Elewa, H., Switzer, J. A., et al. (2007). Increased hemorrhagic transformation and altered infarct size and localization after experimental stroke in a rat model type 2 diabetes. *BMC Neurol.* 7:33.

Fiuza, C., Bustin, M., Talwar, S., Tropea, M., Gerstenberger, E., Shelhamer, J. H., et al. (2003). Inflammation-promoting activity of HMGB1 on human

microvascular endothelial cells. *Blood* 101, 2652–2660. doi: 10.1182/blood-2002-05-1300

Golay, A., Zech, L., Shi, M. Z., Chiou, Y. A., Reaven, G. M., and Chen, Y. D. (1987). High density lipoprotein (HDL) metabolism in noninsulin-dependent diabetes mellitus: measurement of HDL turnover using tritiated HDL. *J. Clin. Endocrinol. Metab.* 65, 512–518. doi: 10.1210/jcem-65-3-512

Gomez-Banoy, N., Cuevas, V., Higuita, A., Aranzalez, L. H., and Mockus, I. (2016). Soluble tumor necrosis factor receptor 1 is associated with diminished estimated glomerular filtration rate in colombian patients with type 2 diabetes. *J. Diabetes Complications* 30, 852–857. doi: 10.1016/j.jdiacomp.2016.03.015

Gorska-Ciebiada, M., Saryusz-Wolska, M., Borkowska, A., Ciebiada, M., and Loba, J. (2016). Plasma levels of thrombomodulin, plasminogen activator inhibitor-1 and fibrinogen in elderly, diabetic patients with depressive symptoms. *Aging Clin. Exp. Res. Oct* 28, 843–851. doi: 10.1007/s40520-015-0504-3

Gotto, A. M. Jr., and Brinton, E. A. (2004). Assessing low levels of high-density lipoprotein cholesterol as a risk factor in coronary heart disease: a working group report and update. *J. Am. Coll. Cardiol.* 43, 717–724. doi: 10.1016/j.jacc.2003.08.061

Gregorio, P. C., Favretto, G., Sassaki, G. L., Cunha, R. S., Becker-Finco, A., Pecoits-Filho, R., et al. (2018). Sevelamer reduces endothelial inflammatory response to advanced glycation end products. *Clin. Kidney J.* 11, 89–98. doi: 10.1093/ckj/sfx074

He, G., Bruun, J. M., Lihn, A. S., Pedersen, S. B., and Richelsen, B. (2003). Stimulation of PAI-1 and adipokines by glucose in human adipose tissue in vitro. *Biochem. Biophys. Res. Commun.* 310, 878–883. doi: 10.1016/j.bbrc.2003.09.091

Ho, T. K., Rajkumar, V., Black, C. M., Abraham, D. J., and Baker, D. M. (2006). Increased angiogenic response but deficient arteriolization and abnormal microvessel ultrastructure in critical leg ischaemia. *Br. J. Surg.* 93, 1368–1376. doi: 10.1002/bjs.5496

Hu, J., Liu, B., Zhao, Q., Jin, P., Hua, F., Zhang, Z., et al. (2016). Bone marrow stromal cells inhibits HMGB1-mediated inflammation after stroke in type 2 diabetic rats. *Neuroscience* 324, 11–19. doi: 10.1016/j.neuroscience.2016.02.058

Hudson, B. I., and Lippman, M. E. (2018). Targeting RAGE signaling in inflammatory disease. *Annu. Rev. Med.* 69, 349–364. doi: 10.1146/annurev-med-041316-085215

Igarashi, M., Hirata, A., Yamaguchi, H., Jimbu, Y., and Tominaga, M. (2008). Pioglitazone reduces atherogenic outcomes in type 2 diabetic patients. *J. Atheroscler. Thromb.* 15, 34–40. doi: 10.5551/jat.e528

Imaizumi, S., Navab, M., Morgantini, C., Charles-Schoeman, C., Su, F., Gao, F., et al. (2011). Dysfunctional high-density lipoprotein and the potential of apolipoprotein A-1 mimetic peptides to normalize the composition and function of lipoproteins. *Circ. J.* 75, 1533–1538. doi: 10.1253/circj.cj-11-0460

Kaji, H. (2016). Adipose tissue-derived plasminogen activator inhibitor-1 function and regulation. *Compr Physiol.* 6, 1873–1896. doi: 10.1002/cphy.c160004

Kontush, A., and Chapman, M. J. (2006). Functionally defective high-density lipoprotein: a new therapeutic target at the crossroads of dyslipidemia, inflammation, and atherosclerosis. *Pharmacol. Rev.* 58, 342–374. doi: 10.1124/pr.58.3.1

Kruger, A. L., Peterson, S., Turkseven, S., Kaminski, P. M., Zhang, F. F., Quan, S., et al. (2005). D-4F induces heme oxygenase-1 and extracellular superoxide dismutase, decreases endothelial cell sloughing, and improves vascular reactivity in rat model of diabetes. *Circulation* 111, 3126–3134. doi: 10.1161/circulationaha.104.517102

Kruit, J. K., Brunham, L. R., Verchere, C. B., and Hayden, M. R. (2010). HDL and LDL cholesterol significantly influence beta-cell function in type 2 diabetes mellitus. *Curr. Opin. Lipidol.* 21, 178–185. doi: 10.1097/MOL.0b013e328339387b

Kumari, R., Willing, L. B., Patel, S. D., Baskerville, K. A., and Simpson, I. A. (2011). Increased cerebral matrix metalloprotease-9 activity is associated with compromised recovery in the diabetic db/db mouse following a stroke. *J. Neurochem.* 119, 1029–1040. doi: 10.1111/j.1471-4159.2011.07487.x

Kumari, R., Willing, L. B., Patel, S. D., Krady, J. K., Zavadoski, W. J., Gibbs, E. M., et al. (2010). The PPAR-gamma agonist, darglitazone, restores acute inflammatory responses to cerebral hypoxia-ischemia in the diabetic ob/ob mouse. *J. Cereb. Blood Flow Metab.* 30, 352–360. doi: 10.1038/jcbfm.2009.221

Liu, J., Yao, S., Wang, S., Jiao, P., Song, G., Yu, Y., et al. (2014). D-4F, an apolipoprotein A-I mimetic peptide, protects human umbilical vein endothelial cells from oxidized low-density lipoprotein-induced injury by preventing the downregulation of pigment epithelium-derived factor expression. *J. Cardiovasc. Pharmacol.* 63, 553–561. doi: 10.1097/FJC.0000000000000080

Liu, X. S., Zhang, Z. G., Zhang, R. L., Gregg, S. R., Meng, H., and Chopp, M. (2007). Comparison of in vivo and in vitro gene expression profiles in subventricular zone neural progenitor cells from the adult mouse after middle cerebral artery occlusion. *Neuroscience* 146, 1053–1061. doi: 10.1016/j.neuroscience.2007.02.056

Madonna, R., and De Caterina, R. (2011). Cellular and molecular mechanisms of vascular injury in diabetes–part I: pathways of vascular disease in diabetes. *Vasc. Pharmacol.* 54, 68–74. doi: 10.1016/j.vph.2011.03.005

Maron, D. J. (2000). The epidemiology of low levels of high-density lipoprotein cholesterol in patients with and without coronary artery disease. *Am. J. Cardiol.* 86, 11L–14L.

Miller, N. E., Olszewski, W. L., Hattori, H., Miller, I. P., Kujiraoka, T., Oka, T., et al. (2013). Lipoprotein remodeling generates lipid-poor apolipoprotein A-I particles in human interstitial fluid. *Am. J. Physiol. Endocrinol. Metab.* 304, E321–E328. doi: 10.1152/ajpendo.00324.2012

Mineo, C., and Shaul, P. W. (2013). Regulation of signal transduction by HDL. *J. Lipid Res.* 54, 2315–2324. doi: 10.1194/jlr.R039479

Mooradian, A. D., Haas, M. J., Batejko, O., Hovsepyan, M., and Feman, S. S. (2005). Statins ameliorate endothelial barrier permeability changes in the cerebral tissue of streptozotocin-induced diabetic rats. *Diabetes Metab. Res. Rev.* 54, 2977–2982. doi: 10.2337/diabetes.54.10.2977

Morgantini, C., Imaizumi, S., Grijalva, V., Navab, M., Fogelman, A. M., and Reddy, S. T. (2010). Apolipoprotein A-I mimetic peptides prevent atherosclerosis development and reduce plaque inflammation in a murine model of diabetes. *Diabetes Metab. Res. Rev.* 59, 3223–3228. doi: 10.2337/db10-0844

Mulder, D. J., de Boer, J. F., Graaff, R., de Vries, R., Annema, W., Lefrandt, J. D., et al. (2011). Skin autofluorescence is inversely related to HDL anti-oxidative capacity in type 2 diabetes mellitus. *Atherosclerosis* 218, 102–106. doi: 10.1016/j.atherosclerosis.2011.05.011

Nandedkar, S. D., Weihrauch, D., Xu, H., Shi, Y., Feroah, T., Hutchins, W., et al. (2011). D-4F, an apoA-1 mimetic, decreases airway hyperresponsiveness, inflammation, and oxidative stress in a murine model of asthma. *J. Lipid Res.* 52, 499–508. doi: 10.1194/jlr.M012724

Navab, M., Anantharamaiah, G. M., Reddy, S. T., and Fogelman, A. M. (2006). Apolipoprotein A-I mimetic peptides and their role in atherosclerosis prevention. *Nat. Clin. Pract. Cardiovasc. Med.* 3, 540–547. doi: 10.1038/ncpcardio0661

Navab, M., Anantharamaiah, G. M., Reddy, S. T., Hama, S., Hough, G., Grijalva, V. R., et al. (2004). Oral D-4F causes formation of pre-beta high-density lipoprotein and improves high-density lipoprotein-mediated cholesterol efflux and reverse cholesterol transport from macrophages in apolipoprotein E-null mice. *Circulation* 109, 3215–3220. doi: 10.1161/01.cir.0000134275.90823.87

Navab, M., Ruchala, P., Waring, A. J., Lehrer, R. I., Hama, S., Hough, G., et al. (2009). A novel method for oral delivery of apolipoprotein mimetic peptides synthesized from all L-amino acids. *J. Lipid Res.* 50, 1538–1547. doi: 10.1194/jlr.M800539-JLR200

Nayak, B. S., Ramsingh, D., Gooding, S., Legall, G., Bissram, S., Mohammed, A., et al. (2010). Plasma adiponectin levels are related to obesity, inflammation, blood lipids and insulin in type 2 diabetic and non-diabetic Trinidadians. *Prim. Care Diabetes* 4, 187–192. doi: 10.1016/j.pcd.2010.05.006

Ning, R., Venkat, P., Chopp, M., Zacharek, A., Yan, T., Cui, X., et al. (2017). D-4F increases microRNA-124a and reduces neuroinflammation in diabetic stroke rats. *Oncotarget* 8, 95481–95494. doi: 10.18632/oncotarget.20751

Ou, J., Ou, Z., Jones, D. W., Holzhauer, S., Hatoum, O. A., Ackerman, A. W., et al. (2003). L-4F, an apolipoprotein A-1 mimetic, dramatically improves vasodilation in hypercholesterolemia and sickle cell disease. *Circulation* 107, 2337–2341. doi: 10.1161/01.cir.0000070589.61860.a9

Ou, J., Wang, J., Xu, H., Ou, Z., Sorci-Thomas, M. G., Jones, D. W., et al. (2005). Effects of D-4F on vasodilation and vessel wall thickness in hypercholesterolemic LDL receptor-null and LDL receptor/apolipoprotein A-I double-knockout mice on Western diet. *Cir. Res.* 97, 1190–1197. doi: 10.1161/01.res.0000190634.60042.cb

Peterson, S. J., Husney, D., Kruger, A. L., Olszanecki, R., Ricci, F., Rodella, L. F., et al. (2007). Long-term treatment with the apolipoprotein A1 mimetic peptide

increases antioxidants and vascular repair in type I diabetic rats. *J. Pharmacol. Exp. Ther.* 322, 514–520. doi: 10.1124/jpet.107.119479

Qin, L., and Crews, F. T. (2012). Chronic ethanol increases systemic TLR3 agonist-induced neuroinflammation and neurodegeneration. *J. Neuroinflam.* 9:130. doi: 10.1186/1742-2094-9-130

Qin, S., Kamanna, V. S., Lai, J. H., Liu, T., Ganji, S. H., Zhang, L., et al. (2012). Reverse D4F, an apolipoprotein-AI mimetic peptide, inhibits atherosclerosis in ApoE-null mice. *J. Cardiovasc. Pharmacol. Ther.* 17, 334–343. doi: 10.1177/1074248411434598

Scarabin, P. Y., Aillaud, M. F., Amouyel, P., Evans, A., Luc, G., Ferrieres, J., et al. (1998). Associations of fibrinogen, factor VII and PAI-1 with baseline findings among 10,500 male participants in a prospective study of myocardial infarction–the PRIME Study. Prospective epidemiological study of myocardial infarction. *Thromb. Haemost.* 80, 749–756. doi: 10.1055/s-0037-1615353

Scheffer, P. G., Tushuizen, M. E., Vermue, H. P., Schindhelm, R. K., Rustemeijer, C., and Diamant, M. (2011). Effect of three consecutive meals on the physicochemical properties of HDL and LDL in individuals with the metabolic syndrome and patients with type 2 diabetes. *Eur. J. Clin. Nutr.* 65, 1242–1249. doi: 10.1038/ejcn.2011.114

Semeraro, N., Ammollo, C. T., Semeraro, F., and Colucci, M. (2012). Sepsis, thrombosis and organ dysfunction. *Thromb. Res.* 129, 290–295. doi: 10.1016/j.thromres.2011.10.013

Sharrett, A. R., Ballantyne, C. M., Coady, S. A., Heiss, G., Sorlie, P. D., Catellier, D., et al. (2001). Coronary heart disease prediction from lipoprotein cholesterol levels, triglycerides, lipoprotein(a), apolipoproteins A-I and B, and HDL density subfractions: the atherosclerosis risk in communities (ARIC) study. *Circulation* 104, 1108–1113. doi: 10.1161/hc3501.095214

Shehadah, A., Chen, J., Pal, A., He, S., Zeitlin, A., Cui, X., et al. (2014). Human placenta-derived adherent cell treatment of experimental stroke promotes functional recovery after stroke in young adult and older rats. *PLoS One* 9:e86621. doi: 10.1371/journal.pone.0086621

Sherman, C. B., Peterson, S. J., and Frishman, W. H. (2010). Apolipoprotein A-I mimetic peptides: a potential new therapy for the prevention of atherosclerosis. *Cardiol. Rev.* 18, 141–147. doi: 10.1097/CRD.0b013e3181c4b508

Sims-Robinson, C., Zhao, S., Hur, J., and Feldman, E. L. (2012). Central nervous system endoplasmic reticulum stress in a murine model of type 2 diabetes. *Diabetologia* 55, 2276–2284. doi: 10.1007/s00125-012-2573-6

Swanson, R. A., Morton, M. T., Tsao-Wu, G., Savalos, R. A., Davidson, C., and Sharp, F. R. (1990). A semiautomated method for measuring brain infarct volume. *J. Cereb. Blood Flow Metab.* 10, 290–293. doi: 10.1038/jcbfm.1990.47

Tran, E. H., Hoekstra, K., van Rooijen, N., Dijkstra, C. D., and Owens, T. (1998). Immune invasion of the central nervous system parenchyma and experimental allergic encephalomyelitis, but not leukocyte extravasation from blood, are prevented in macrophage-depleted mice. *J. Immunol.* 161, 3767–3775.

Van Lenten, B. J., Wagner, A. C., Jung, C. L., Ruchala, P., Waring, A. J., Lehrer, R. I., et al. (2008). Anti-inflammatory apoA-I-mimetic peptides bind oxidized lipids with much higher affinity than human apoA-I. *J. Lipid Res.* 49, 2302–2311. doi: 10.1194/jlr.M800075-JLR200

Vannucci, S. J., Willing, L. B., Goto, S., Alkayed, N. J., Brucklacher, R. M., Wood, T. L., et al. (2001). Experimental stroke in the female diabetic, db/db, mouse. *J. Cereb. Blood Flow Metab.* 21, 52–60. doi: 10.1097/00004647-200101000-00007

Wallin, A., Sjogren, M., Edman, A., Blennow, K., and Regland, B. (2000). Symptoms, vascular risk factors and blood-brain barrier function in relation to CT white-matter changes in dementia. *Eur. Neurol.* 44, 229–235. doi: 10.1159/000008242

Wang, H., Li, W., Zhu, S., Li, J., D'Amore, J., Ward, M. F., et al. (2010). Peripheral administration of fetuin-A attenuates early cerebral ischemic injury in rats. *J. Cereb. Blood Flow Metab.* 30, 493–504. doi: 10.1038/jcbfm.2009.247

Williams, M. D., and Nadler, J. L. (2007). Inflammatory mechanisms of diabetic complications. *Curr. Diab. Rep* 7, 242–248. doi: 10.1007/s11892-007-0038-y

Yao, S., Tian, H., Miao, C., Zhang, D. W., Zhao, L., Li, Y., et al. (2015). D4F alleviates macrophage-derived foam cell apoptosis by inhibiting CD36 expression and ER stress-CHOP pathway. *J. Lipid Res.* 56, 836–847. doi: 10.1194/jlr.M055400

Ye, X., Chopp, M., Liu, X., Zacharek, A., Cui, X., Yan, T., et al. (2011). Niaspan reduces high-mobility group box 1/receptor for advanced glycation endproducts after stroke in type-1 diabetic rats. *Neuroscience* 190, 339–345. doi: 10.1016/j.neuroscience.2011.06.004

Yu, R., Yekta, B., Vakili, L., Gharavi, N., Navab, M., Marelli, D., et al. (2008). Proatherogenic high-density lipoprotein, vascular inflammation, and mimetic peptides. *Curr. Atheroscler. Rep.* 10, 171–176. doi: 10.1007/s11883-008-0025-z

Conflict of Interest: The authors declare that the research was conducted in the absence of any commercial or financial relationships that could be construed as a potential conflict of interest.

Copyright © 2019 Wang, Li, Zacharek, Landschoot-Ward, Chopp, Chen and Cui. This is an open-access article distributed under the terms of the Creative Commons Attribution License (CC BY). The use, distribution or reproduction in other forums is permitted, provided the original author(s) and the copyright owner(s) are credited and that the original publication in this journal is cited, in accordance with accepted academic practice. No use, distribution or reproduction is permitted which does not comply with these terms.

frontiers in Cellular Neuroscience

BRIEF RESEARCH REPORT
published: 25 October 2019
doi: 10.3389/fncel.2019.00461

Transcranial Current Stimulation Alters the Expression of Immune-Mediating Genes

*Monika Rabenstein[1], Marcus Unverricht-Yeboah[2], Meike Hedwig Keuters[1,3,4], Anton Pikhovych[1,3], Joerg Hucklenbroich[1,5], Sabine Ulrike Vay[1], Stefan Blaschke[1,3,5], Anne Ladwig[1,3], Helene Luise Walter[1], Magdalena Beiderbeck[1], Gereon Rudolf Fink[1,5], Michael Schroeter[1,3,5], Ralf Kriehuber[2] and Maria Adele Rueger[1,3,5]**

[1] Department of Neurology, University Hospital of Cologne, Cologne, Germany, [2] Radiation Biology Unit, Department of Safety and Radiation Protection, Research Centre Jülich, Jülich, Germany, [3] Max Planck Institute for Metabolism Research, Cologne, Germany, [4] A.I. Virtanen Institute for Molecular Sciences, University of Eastern Finland, Kuopio, Finland, [5] Cognitive Neuroscience, Institute of Neuroscience and Medicine (INM-3), Research Centre Jülich, Jülich, Germany

OPEN ACCESS

Edited by:
Johannes Boltze,
University of Warwick,
United Kingdom

Reviewed by:
Tino Zaehle,
Otto von Guericke University
Magdeburg, Germany
Thomas Polak,
University Clinic of Wüerzburg,
Germany

***Correspondence:**
Maria Adele Rueger
maria.rueger@uk-koeln.de

Specialty section:
This article was submitted to
Cellular Neurophysiology,
a section of the journal
Frontiers in Cellular Neuroscience

Received: 25 July 2019
Accepted: 27 September 2019
Published: 25 October 2019

Citation:
Rabenstein M,
Unverricht-Yeboah M, Keuters MH,
Pikhovych A, Hucklenbroich J,
Vay SU, Blaschke S, Ladwig A,
Walter HL, Beiderbeck M, Fink GR,
Schroeter M, Kriehuber R and
Rueger MA (2019) Transcranial
Current Stimulation Alters
the Expression of Immune-Mediating
Genes. Front. Cell. Neurosci. 13:461.
doi: 10.3389/fncel.2019.00461

Despite its extensive use in clinical studies, the molecular mechanisms underlying the effects of transcranial direct current stimulation (tDCS) remain to be elucidated. We previously described subacute effects of tDCS on immune- and stem cells in the rat brain. To investigate the more immediate effects of tDCS regulating those cellular responses, we treated rats with a single session of either anodal or cathodal tDCS, and analyzed the gene expression by microarray; sham-stimulated rats served as control. Anodal tDCS increased expression of several genes coding for the major histocompatibility complex I (MHC I), while cathodal tDCS increased the expression of the immunoregulatory protein osteopontin (OPN). We confirmed the effects of gene upregulation by immunohistochemistry at the protein level. Thus, our data show a novel mechanism for the actions of tDCS on immune- and inflammatory processes, providing a target for future therapeutic studies.

Keywords: direct transcranial current stimulation, gene expression, microarray, MHC-I, osteopontin, transcriptome

INTRODUCTION

Transcranial direct current stimulation (tDCS) has been applied in experimental and clinical settings for more than 20 years and may facilitate rehabilitation after stroke as suggested by clinical data (Hummel et al., 2005; Sparing et al., 2009). Moreover, tDCS is used as experimental therapy for various neurological and psychiatrical diseases, e.g., multiple sclerosis, Parkinson's, depression, dementia, evaluated by Lefaucheur et al. (2017). TDCS leads to changes of the cortical excitability in animals and humans (Bindman et al., 1962; Nitsche and Paulus, 2000), promoting changes in long-term potentiation and synaptic plasticity via NMDA-receptors

Abbreviations: DAVID, database for annotation visualization and integrated discovery 6.8; FDR, false discovery rate; Iba1, ionized calcium binding adaptor molecule 1; MHC I, major histocompatibility complex class I; OPN, osteopontin; tDCS, transcranial direct current stimulation; SVZ, subventricular zone.

(Bolin et al., 2002; Nitsche et al., 2003; Fritsch et al., 2010; Monte-Silva et al., 2013; Kronberg et al., 2017). As tDCS can be applied either using anodal or a cathodal current polarity, anodal tDCS increases cortical excitability while cathodal tDCS results in its decrease (Fritsch et al., 2010; Stagg and Nitsche, 2011; Lafon et al., 2017).

Intriguingly, tDCS evokes various cellular effects on neural stem cells, neurons, astrocytes, oligodendrocytes, and microglia exceeding its primary neurophysiological actions: In the healthy rat brain, tDCS increases proliferation and migration of endogenous neural stem cells and activates microglia as the brain-resident immune cells (Rueger et al., 2012a; Keuters et al., 2015). Both anodal and cathodal tDCS induce neurogenesis, both in healthy animals (Braun et al., 2016) as well as after experimental stroke (Braun et al., 2016; Pikhovych et al., 2016). Cathodal tDCS recruits oligodendrocyte precursors toward an ischemic lesion while supporting polarization of microglia toward a pro-inflammatory M1-phenotype (Braun et al., 2016). Depending on the current density, tDCS downregulates inflammatory mediators (Peruzzotti-Jametti et al., 2013) and the constitutive expression of ionized calcium binding adaptor molecule 1 (Iba1) by activated microglia (Spezia Adachi et al., 2012; Peruzzotti-Jametti et al., 2013; Pikhovych et al., 2016). These data suggest that – depending on current density and polarity – tDCS possesses distinct immunomodulatory effects and supports stem cell-mediated regeneration in the brain. Further knowledge of the patterns of action of the different polarities is still warranted. Cellular effects of tDCS occur from acute effects within hours to subacute and longterm effects within days and weeks after stimulation (Rueger et al., 2012b; Spezia Adachi et al., 2012; Peruzzotti-Jametti et al., 2013; Braun et al., 2016; Pikhovych et al., 2016). It is yet unknown how they are regulated and altered over time. Expression changes on the transcriptome can be expected after a few hours after a stimulus, therefore we chose to investigate the acute tDCS-induced transcriptome in an unbiased microarray approach 6 h after tDCS.

MATERIALS AND METHODS

Animals and Surgery

All animal procedures followed the German Laws for Animal Protection and were approved by the local animal care committee as well as local governmental authorities (Landesamt für Natur, Umwelt und Verbraucherschutz North Rhine-Westphalia, LANUV). To exclude putative influences of hormonal changes on the findings, only male rats were used.

Spontaneously breathing 10–11 weeks old male Wistar rats weighing 260–310 g were anesthetized with 5% isoflurane and maintained with 2.5% isoflurane in 65%/35% nitrous oxide/oxygen. Throughout surgical procedures, body temperature was maintained at 37.0°C with a thermostatically controlled heating pad.

Transcranial Direct Current Stimulation

Twenty-four rats were subjected to a single tDCS session as described previously by our group (Rueger et al., 2012a; Braun et al., 2016). In brief, an epicranial electrode holder made of plastic (self-manufactured) with a defined contact area of 3.5 mm^2 was mounted onto the intact skull over the right hemisphere using non-toxic glass ionomer luting cement (Ketac Cem Plus, 3M-ESPE, Germany) at bregma AP + 2.0 mm, ML + 2.0 mm, and left in place for the entire experiment. The skin around the electrode holder was closed with sutures after the placement. The holder was left in place for the entire experiment. Animals were randomized to receive tDCS with either anodal (n = 8) or cathodal (n = 8) polarity; the control group received a sham-stimulation (n = 8) (**Table 1**).

For transcranial direct current stimulation, an argentic electrode was placed in the electrode holder, and 0.9% sodium chloride was added to buffer electrochemical changes. The counter electrode, a 1.5 cm × 2 cm silver-coated sensor electrode (#DENIS01526; Spes Medica, Genova, Italy), was placed on the rat's ventral thorax.

Transcranial direct current stimulation was applied continuously for 15 min at 500 μA using a constant current stimulator (CX-6650, Schneider-Electronics, Germany) under isoflurane anesthesia, resulting in a charge density of 128 kC/m2. Charge density was calculated as charge (A × s) per area, according to Liebetanz et al., 2009. For sham stimulation, rats were treated equally to the tDCS group with isoflurane anesthesia for 15 min, but were not connected to the current stimulator during this time. tDCS was performed under anesthesia to avoid dislocation of the cable.

After tDCS, animals were allowed to recover in their home cages with access to food and water *ad libitum*.

RNA-Extraction

Six hours after tDCS, four rats of each stimulation group were deeply anesthetized and decapitated. The brains were rapidly removed and the sensorimotor cortices of each hemisphere were isolated. 20mg cortical tissue of each hemisphere was crushed and stabilized overnight in PurifyLater Tissue Stabilizer (BioEcho, Dormagen, Germany). On the next day, the total RNA was isolated using the GenUP^{TM} Total RNA Kit (Biotechrabbit, Henningsdorf, Germany) according to the manufacturer's guidelines. RNA quantification was carried out using a NanoDrop-1000 spectrophotometer (Peqlab, Erlangen, Germany), and RNA quality was monitored by agarose gel separation and with the Agilent 2100 Bioanalyzer (Agilent, Böblingen, Germany). All extracted RNA samples were

TABLE 1 | Overview of the experimental groups.

	Microarray	Immunohistochemistry
Sham	n = 4	n = 4
Anodal	n = 4	n = 4
Cathodal	n = 4	n = 4

found to be of good quality. RNA integrity numbers (RINs) ranged from 9.8 to 10.

DNA Microarray Hybridization

DNA microarray experiments were performed according to the manufacturer's manual and as previously described (Unverricht-Yeboah et al., 2018). Of the total RNA, 400 ng was transcribed into cDNA with an oligo-dT primer, followed by transcription into cRNA labeled with cyanine 3-CTP (Quick-Amp Labeling Kit, One-color, Agilent, Santa Clara, CA, United States). cRNA purification was performed with the RNeasy Mini Kit (Qiagen). cRNA yield and the dye incorporation were measured with the NanoDrop-1000 spectrophotometer. Labeled cRNA samples were hybridized for 17 h to 44 k Whole Rat Genome DNA microarrays (G2519F, Agilent) using a hybridization oven (Agilent). After hybridization and washing, DNA microarrays were scanned with the Microarray Scanner (G2505 B, Agilent) as recommended by Agilent.

Data Analysis

Images of the scanned microarrays were processed with the Agilent Feature Extraction software. Gene expression data were processed, normalized, and analyzed using the GeneSpring GX software (Agilent) and Excel (Microsoft Corperation, Redmond, WA, United States). By data filtering, non-uniform outliers were excluded, as well as signals that were not significantly above the background intensity in at least 25% of the samples. To indicate the significantly regulated genes, the *p*-values were adjusted using the method of Benjamini and Hochberg to calculate the false discovery rate (FDR). Genes with non-FDR adjusted *p*-values were considered for the filtering process to increase the number of potential candidate genes. The criteria for candidate genes were: a significant expression change (>2.0 fold), a FDR $\leq$ 0.16 after filtering, and a *p*-value $<$ 0.05 (**Table 2**). Protein expression of selected candidate genes was analyzed by immunohistochemistry.

Functional Analysis of Significantly Regulated Genes

The significantly expressed genes after anodal and cathodal tDCS were functionally categorized using the Database for Annotation Visualization and Integrated Discovery 6.8 (DAVID) (Huang et al., 2009). To assign the significantly altered genes to affected biological processes and pathways, we used the gene ontology analysis feature.

TABLE 2 | Numbers of significantly regulated genes after tDCS with a fold change > 2.

Groups	Significantly regulated genes (fold change > 2.0, $p < 0.05$, FDR $\leq$ 0.16)
Cathodal ipsilateral vs. Sham	20
Anodal ipsilateral vs. Sham	14
Cathodal contralateral vs. Sham	0
Anodal contralateral vs. Sham	0
Cathodal ipsilateral vs. Cathodal contralateral	1
Anodal ipsilateral vs. Anodal contralateral	0

Immunohistochemistry

Six hours after tDCS, four rats of each stimulation group were deeply anesthetized with isoflurane and decapitated. Brains were rapidly removed, frozen in isopentane, and stored at −80°C before further processing. Serial coronal brain sections of 10 μm were cut throughout each brain at 500 μm intervals. For immunohistochemistry, primary antibodies included: MHC Class I Antibody (Ox18) (1:500 cat# NB120-6405, Novus Biological, Littleton, CO, United States) and anti-Osteopontin-Antibody (1:500 cat# ab8448, Abcam, Cambridge, United Kingdom), Iba1 Antibody (1:1000 cat# 019-19741WAKO, Osaka, Japan), and NeuN Antibody (1:200, cat# MAB377 Merck, Kenilworth, NJ, United States). For visualization of the MHC I-antibody, the ABC-Elite kit (Vector Laboratories, United States) with diaminobenzidine (Sigma, Germany) as the final reaction product was used. For visualization of the other antibodies, fluorescent-labeled secondary antibodies were used (1:500, cat#A11001 Alexa-Fluor–488 and cat#A11036 Alexa-Fluor–568, Invitrogen, Thermo Fisher Scientific, Waltham, MA, United States). Sections were counterstained with Hoechst to label all nuclei (Hoechst 33,342, Thermo Fisher Scientific, Massachusetts, United States).

Representative pictures were taken with an inverted fluorescence phase-contrast microscope (Keyence BZ-9000E, Keyence, Osaka, Japan).

To determine the amount of MHC Class I-positive cells, the size of the subventricular zone (SVZ) was quantified for each animal by measuring the area in μm^2 covered by MHC Class I-positive cells with a predefined length at 100 μm multiplied with the width in μm of the area covered with MHC + cells [as previously described by our group for doublecortin stainings (Klein et al., 2014)], and calculated as the mean of three coronal sections at 500 μm intervals of each animal.

To determine the number of OPN-positive, NeuN-positive, and Iba1-positive cells in the cortex, three coronal sections at 500 μm intervals were stained with the respective antibody. Using a Keyence microscope with a 40× objective, images of representative fields of view (measuring 746 μm × 557 μm) of the sensorimotor cortex of the ipsilateral, stimulated hemisphere were taken of each section. The numbers of positive cells of each antibody staining were counted manually and calculated as the mean of three coronal sections.

Immunohistochemical quantifications of MHC Class I and OPN positive cells were performed by a blinded evaluator (MS).

Descriptive statistics were performed with Graph Pad Prism (GraphPad Software Inc.). For comparison of multiple groups, One Way Analysis of Variance (ANOVA) and Tukey's *post hoc* tests were performed with the same software. Statistical significance was set at the <5% level ($p < 0.05$).

RESULTS

Gene Expression Changes Following Different tDCS Polarities

Six hours after cathodal ipsilateral tDCS (compared to sham stimulation), 20 genes were significantly up- or downregulated (10 genes up-, 10 genes downregulated, cmp. **Supplementary Table S1A**). After anodal ipsilateral tDCS (compared to sham stimulation), 14 genes were significantly up- or downregulated (9 genes up-, 5 genes downregulated, cmp. **Supplementary Table S1B**). Of all the other groups, comparing ipsilaterally stimulated to contralaterally stimulated hemispheres, or contralaterally stimulated hemispheres to sham stimulation, only cathodal ipsilateral tDCS compared to cathodal contralateral stimulation resulted in a significant difference of one gene that was downregulated (**Supplementary Table S1C**).

The effects of tDCS were lateralized in comparison to sham but not in comparison to the unstimulated hemisphere. Given the small size of a rat brain, tDCS stimulation was not assumed to be restricted to one hemisphere. Therefore, tDCS effects will also reflect in the unstimulated hemisphere, albeit to a lower extent, which explains the lack of significant changes between the unstimulated hemisphere and sham. Thus, the "unstimulated" hemisphere cannot function as control. We therefore used sham control animals, specifically from the same hemisphere that was stimulated in the tDCS group.

Biological Processes and Pathways Affected by Different tDCS Polarities

We functionally categorized the upregulated genes, using DAVID (Huang et al., 2009), to examine biological processes and pathways affected by the different tDCS polarities (**Supplementary Figure S1**). Six hours after anodal tDCS, the categories "antigen presentation via MHC I" and "immune response" were significantly upregulated, both consisting of the same 5 different genes coding for RT1 Class (MHC I), thus strongly suggesting an upregulation of MHC I coding genes after anodal tDCS (**Supplementary Figure S1A**).

After cathodal tDCS, the categories "osteoblast differentiation," "positive regulation of angiogenesis," "cellular response to mechanical stimuli," "ossification," and "response to activity" were significantly upregulated (**Supplementary Figure S1B**). For the downregulated genes in cathodal and anodal tDCS no functional categories could be detected.

Identification of Candidate Genes for Immunomodulation

To confirm the effects of upregulated genes seen in the microarray analysis by immunohistochemistry, we selected candidate genes for each stimulation polarity. Given the strong effects of tDCS on neuroinflammation found in earlier studies of our group (Rueger et al., 2012a; Braun et al., 2016; Pikhovych et al., 2016), we focused on genes coding for immunomodulating processes. After anodal tDCS, we identified a cluster of 5 upregulated genes coding for RT1 Class as part of the MHC I complex (RT1-CE2, RT1-CE15, RT1-CE16, Rt1.aa, and RT1-EC2) that we singled out as candidate genes. We performed immunohistochemical stainings for MHC I on brain slices from animals that had been identically treated as the microarray group. Quantification showed more MHC I + cells in the ipsilateral subventricular zone (SVZ) of animals treated with anodal tDCS compared to controls by trend (anodal tDCS 7533,75 ± 881,41 MHC I + cells/μm^2 vs. sham stimulation 6758,33 ± 675,57 MHC I + cells/μm^2). Results are displayed as mean ± SEM (**Figure 1**).

Intriguingly, cathodal tDCS led to upregulation of Spp1 encoding for the phosphoprotein osteopontin (OPN), possessing pleiotropic immunoregulatory properties after cerebral ischemia as well as beneficial effects on endogenous neural stem cells (Rabenstein et al., 2015, 2016; Ladwig et al., 2017). To validate the involvement of OPN, we performed immunohistochemical stainings in animals that had been identically treated as the microarray group. Quantification showed more OPN + cells in ipsilateral the cortex of animals treated with cathodal tDCS compared to sham-treated controls by trend (cathodal tDCS 54.89 ± 1.29% OPN + cells vs. sham stimulation 51.02 ± 2.16% OPN + cells/total cell count). Results are displayed as mean ± SEM (**Figure 2A**). Co-staining OPN with either NeuN for neurons or Iba1 for microglia revealed that OPN was almost exclusively expressed by neurons (**Figures 2B,C**).

Other Genes of Interest

In cathodal tDCS, the Slitrk6 inhibitor of neurite outgrowth was significantly downregulated (Aruga and Mikoshiba, 2003). While bone morphogenic protein 6 (bmp-6), a secreted extracellular matrix (ECM)-associated component with important functions in development, was upregulated, its antagonist Sostdc1 was downregulated (Brazil et al., 2015). Sostdc 1 was also significantly downregulated after anodal tCDS, but without upregulation of bone morphogenic protein.

Both cathodal and anodal tDCS upregulated Wisp2 (Ohkawa et al., 2011) that leads to the facilation of neurite formation. Wisp2 is part of the Wnt signaling pathway involved in neural stem cell development (Bengoa-Vergniory and Kypta, 2015).

Together, both in cathodal and anodal tDCS, neurite growth and stem cell development were enhanced, while extracellular developmental processes were enhanced after cathodal tDCS only.

DISCUSSION

A single session of tDCS led to significant changes in gene expression after 6 h, which were accompanied by concordant changes at the protein level as detected immunohistochemically. The rationale behind this short interval after tDCS was to observe the acute of effects tDCS within the first hours.

Changes in protein upregulation were not statistically significant, most likely since their expression maximum occurred at later time points (Jansen and Pfaffelhuber, 2015). Moreover, increased protein synthesis may not necessarily lead to an

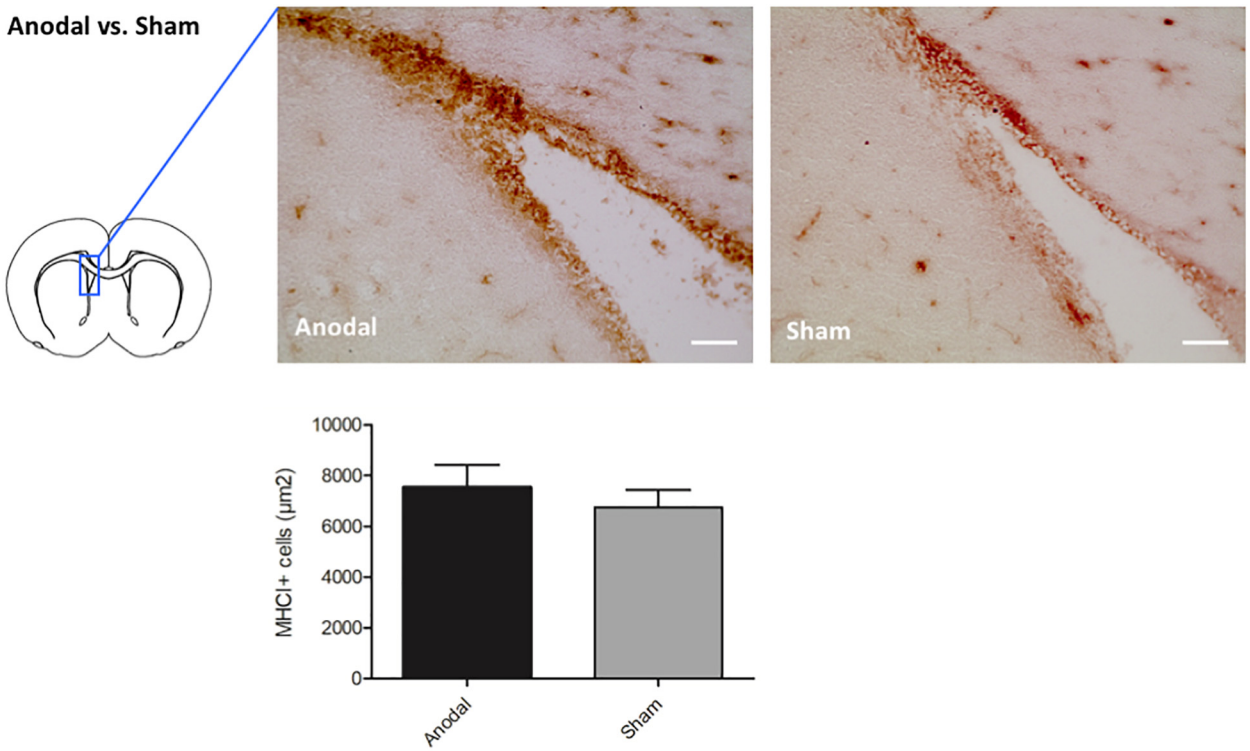

FIGURE 1 | Effects of anodal tDCS on protein expression. Representative immunohistochemical images of Ox18 + cells in the SVZ ipsilateral to anodal tDCS or sham stimulation. Staining for Ox18 (MHC I) in the ipsilateral SVZ revealed more Ox18 + cells in animals treated by anodal tDCS (left panel) compared to sham stimulation (right panel) by trend (scale bars = 100 μm). Results are displayed as mean ± SEM.

increased number of positive cells, but to an increased amount of gene product per cell. Further studies are warranted to address the issue of induced protein expression.

After anodal tDCS, five genes involved in MHC I expression were upregulated. In the healthy brain, MHC-I is expressed at the synapses of neurons (Shatz, 2009; Needleman et al., 2010). It is generally associated with negative regulation of neural plasticity (Datwani et al., 2009; Shatz, 2009; Elmer and McAllister, 2012); on the other hand, decreased MHC I signaling impairs axonal repair (Thams et al., 2008). After brain damage such as stroke, MHC-I is upregulated, and MHC-I presenting cells are recognized by cytotoxic T-cells, supporting neuroinflammation (Schroeter et al., 1994; Piehl and Lidman, 2001). Interestingly, MHC-I is upregulated after kainate-induced seizure and downregulated after activity-blockage (Corriveau et al., 1998). Thus, upregulation of genes coding for MHC-I by anodal tDCS – potentially inducing cortical excitability – is in line with previous reports linking altered neuronal activity directly to MHC I expression (Neumann et al., 1995, 1997). Data suggest that the increase in neuroinflammation seen after tDCS (Rueger et al., 2012a; Braun et al., 2016; Pikhovych et al., 2016) may result from an upregulation of MHC-I that tags neurons to surveillance of microglia, the immunocompetent cells of the CNS. Together, anodal tDCS may act by upregulating MHC I expression through an increase in cortical excitability, leading to an augmented neuroinflammatory response.

Cathodal tDCS led to an upregulation of OPN as an endogenous phosphoglycoprotein with essential roles in tissue homeostasis, wound healing, immune regulation, and stress responses (Denhardt et al., 2001; Brown, 2012). OPN acts as a negative feedback regulator for the synthesis of nitric oxide (Hwang et al., 1994; Rollo et al., 1996), suggesting key immunoregulatory functions. OPN increases survival, proliferation, migration, and neuronal differentiation of endogenous neural stem cells in culture, and enhances proliferation and migration of neuronal precursors *in vivo* after cerebral ischemia (Rabenstein et al., 2015). Additionally, OPN seems to polarize microglia to a neuroprotective subtype in an inflammation setting (Rabenstein et al., 2016). Thus, upregulating OPN by cathodal tDCS may provide an easily accessible non-pharmacological approach to enhance OPN synthesis in order to harness its beneficial effects, e.g., after a stroke. In conclusion, we speculate that cathodal tDCS leads to a multitude of regulatory neuroinflammatory and neuroplastic effects through upregulation of OPN.

As yet, only Holmes et al. conducted an RNA-sequencing study after tDCS (Holmes et al., 2016). They analyzed gene expression only minutes after a single session of anodal tDCS using three different currents (250, 500, and 2,000 μA),

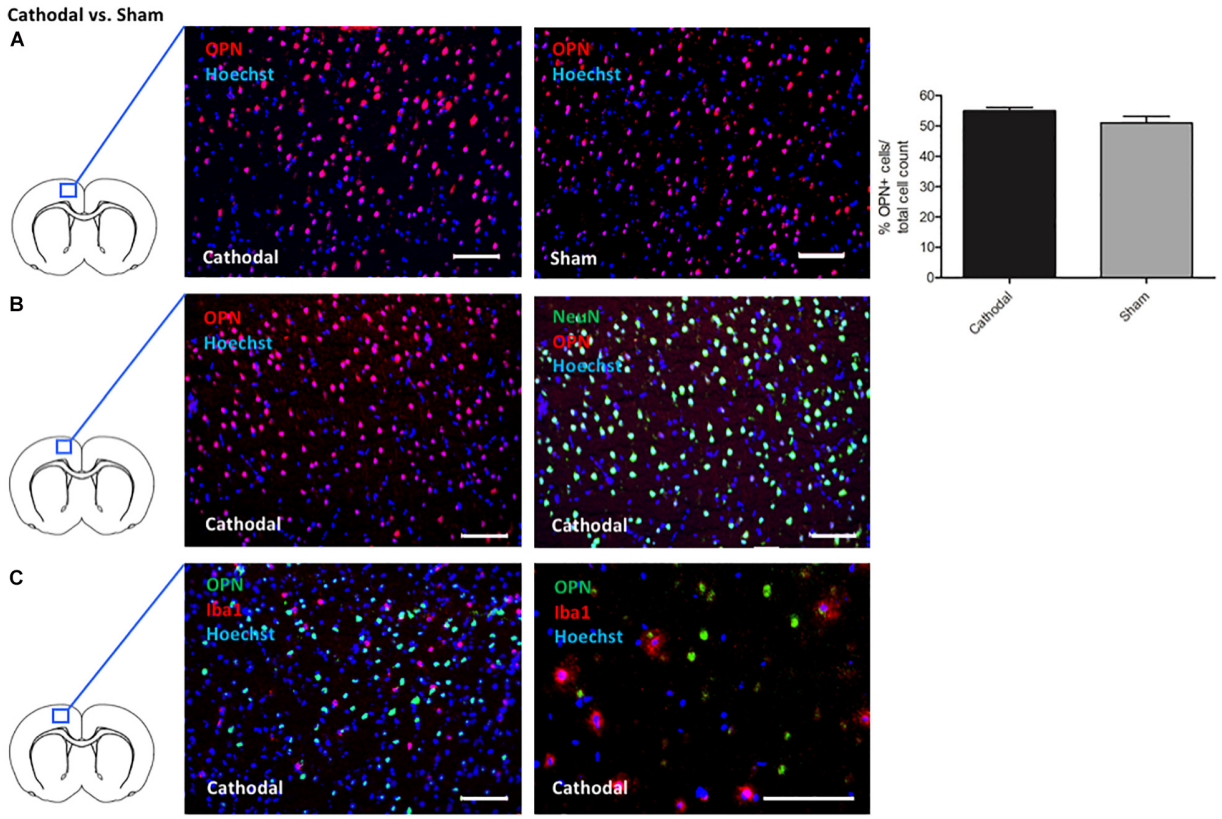

FIGURE 2 | Effects of cathodal tDCS on protein expression. **(A)** Representative immunohistochemical images of OPN + cells (red) in the cortex ipsilateral to cathodal tDCS or sham stimulation, co-stained with a nuclear marker (Hoechst; blue). Staining for OPN revealed more OPN + cells in the cortex of animals treated by cathodal tDCS (left panel) compared to sham stimulation (right panel) by trend (right panel; scale bars = 100 μm). Results are displayed as mean ± SEM. **(B)** Representative immunohistochemical images of OPN + cells co-stained with NeuN (green) in the cortex ipsilateral to cathodal tDCS. All images were co-stained with a cell nucleus marker/DNA dye (Hoechst; blue). OPN + cells almost exclusively co-expressed NeuN (left panel and right panel represent the same picture with and without NeuN fluorescence signal, scale bars = 100 μm). **(C)** Representative immunohistochemical images of OPN + cells (green) co-stained with Iba1 (red) in the cortex ipsilateral to cathodal tDCS. All images were co-stained with a cell nucleus marker/DNA dye (Hoechst; blue). OPN + cells did not express Iba1 (left panel and right panel represent different magnifications, scale bars = 100 μm).

equivalent to charge densities of 132, 264, and 1,057 kC/m^2), while our study was performed 6 h after tDCS of either anodal or cathodal polarity at 128 kC/m^2. For each charge density, Holmes et al. found about 1000 genes differentially up- and downregulated, especially from inflammatory, antidepressant-related, and receptor signaling pathways. In contrast to our study, they chose a fold change of 1.2 with adjusted p-value < 0.1 as the cut-off for significantly regulated genes, while we used a more conservative approach with only >2-fold changes, explaining the larger number of differentially regulated genes in their study. At 132 kC/m^2, similar to the charge density in our study, cellular response to stress- and B-cell activation-clusters, and only at 1,057 kC/m^2 – far above the published lesion threshold (Liebetanz et al., 2009; Rueger et al., 2012a) - a favorable adjustment of immune system regulation clusters was found.

As previously suggested by Liebetanz et al. (2009), another recent study found that subtle lesions can possibly occur even below the current intensity used in our study (Jackson et al., 2017). While this certainly needs to be kept in mind for future studies, we here did not detect any tissue lesions by immunohistochemistry using the current stimulation parameters.

Further studies are warranted to establish the effects of tDCS on gene expression not only in relation to timing but also to charge density and polarity, as well as in awake stimulated animals.

CONCLUSION

Anodal tDCS enhanced expression of several genes coding for MHC-I, affecting inflammation and synaptic plasticity, while cathodal tDCS increased expression of the gene encoding for the immunoregulatory protein OPN linking tDCS treatment to beneficial effects on regeneration after stroke or cerebral hemorrhage (Yan et al., 2009; Wu et al., 2011; Rabenstein et al., 2015; Ladwig et al., 2017; Rogall et al., 2018). Overall, specific modulation of neuroinflammatory processes by non-invasive brain stimulation constitutes a promising therapeutic option with immediate translational relevance.

DATA AVAILABILITY STATEMENT

Microarray data can be found on ArrayExpress (accession E-MTAB-8318).

ETHICS STATEMENT

The animal study was reviewed and approved by the Landesamt für Natur, Umwelt und Verbraucherschutz North Rhine-Westphalia.

AUTHOR CONTRIBUTIONS

MR performed the microarray analyses, gene ontology analyses, and immunohistochemical stainings, and drafted the manuscript. AP and MK carried out the surgery. SV, MB, SB, AL, and HW helped with the immunohistochemical stainings. MR and JH performed the RNA isolation. MU-Y performed the microarray and helped with statistical analyses. GF, RK, and MS participated in the design and coordination of the study, and helped to draft and critically revised the manuscript. MAR conceived of, designed, and coordinated the study, helped with the statistical analyses, and finalized the manuscript.

FUNDING

This research work was supported by the "Marga-und-Walter-Boll-Foundation" (#210-12-12 and #210-10-15) and the "Köln Fortune Program", Faculty of Medicine, University of Cologne, Germany (#345/2018).

SUPPLEMENTARY MATERIAL

The Supplementary Material for this article can be found online at: https://www.frontiersin.org/articles/10.3389/fncel.2019.00461/full#supplementary-material

FIGURE S1 | Effects of tDCS on gene regulation. Genes significantly expressed 6 h after anodal tDCS (A) respectively, cathodal tDCS (B) were functionally categorized. Affected biological processes and pathways as well as the respective enrichment p-values are shown.

TABLE S1 | Significantly up- and downregulated genes after tDCS.

REFERENCES

Aruga, J., and Mikoshiba, K. (2003). Identification and characterization of Slitrk, a novel neuronal transmembrane protein family controlling neurite outgrowth. *Mol. Cell. Neurosci* 24, 117–129. doi: 10.1016/S1044-7431(03)00129-5

Bengoa-Vergniory, N., and Kypta, R. M. (2015). Canonical and noncanonical Wnt signaling in neural stem/progenitor cells. *Cell. Mol. Life Sci.* 72, 4157–4172. doi: 10.1007/s00018-015-2028-6

Bindman, L. J., Lippold, O. C. J., and Redfearn, J. W. T. (1962). Long-lasting changes in the level of the electrical activity of the cerebral cortex produced by polarizing currents. *Nature* 196, 584–585. doi: 10.1038/196584a0

Bolin, L. M., Strycharska-Orczyk, I., Murray, R., Langston, J. W., and Di Monte, D. (2002). Increased vulnerability of dopaminergic neurons in MPTP-lesioned interleukin-6 deficient mice. *J. Neurochem.* 83, 167–175. doi: 10.1046/j.1471-4159.2002.01131.x

Braun, R., Klein, R., Walter, H. L., Ohren, M., Freudenmacher, L., Getachew, K., et al. (2016). Transcranial direct current stimulation accelerates recovery of function, induces neurogenesis and recruits oligodendrocyte precursors in a rat model of stroke. *Exp. Neurol.* 279, 127–136. doi: 10.1016/j.expneurol.2016.02.018

Brazil, D. P., Church, R. H., Surae, S., Godson, C., and Martin, F. (2015). BMP signalling: agony and antagony in the family. *Trends Cell Biol.* 25, 249–264. doi: 10.1016/j.tcb.2014.12.004

Brown, A. (2012). Osteopontin: a key link between immunity, inflammation and the central nervous system. *Transl. Neurosci.* 3, 288–293. doi: 10.2478/s13380-012-0028-7

Corriveau, R. A., Huh, G. S., and Shatz, C. J. (1998). Regulation of class I MHC gene expression in the developing and mature CNS by neural activity. *Neuron* 21, 505–520. doi: 10.1016/S0896-6273(00)80562-0

Datwani, A., McConnell, M. J., Kanold, P. O., Micheva, K. D., Busse, B., Shamloo, M., et al. (2009). Classical MHCI molecules regulate retinogeniculate refinement and limit ocular dominance plasticity. *Neuron* 64, 463–470. doi: 10.1016/j.neuron.2009.10.015

Denhardt, D. T., Noda, M., O'Regan, A. W., Pavlin, D., and Berman, J. S. (2001). Osteopontin as a means to cope with environmental insults: regulation of inflammation, tissue remodeling, and cell survival. *J. Clin. Invest.* 107, 1055–1061. doi: 10.1172/JCI12980

Elmer, B. M., and McAllister, A. K. (2012). Major histocompatibility complex class I proteins in brain development and plasticity. *Trends Neurosci.* 35, 660–670. doi: 10.1016/j.tins.2012.08.001

Fritsch, B., Reis, J., Martinowich, K., Schambra, H. M., Ji, Y., Cohen, L. G., et al. (2010). Direct current stimulation promotes BDNF-dependent synaptic plasticity: potential implications for motor learning. *Neuron* 66, 198–204. doi: 10.1016/j.neuron.2010.03.035

Holmes, B., Jung, S. H., Lu, J., Wagner, J. A., Rubbi, L., Pellegrini, M., et al. (2016). Transcriptomic modification in the cerebral cortex following noninvasive brain stimulation: RNA-sequencing approach. *Neural. Plast.* 2016:5942980. doi: 10.1155/2016/5942980

Huang, D. W., Sherman, B. T., and Lempicki, R. A. (2009). Systematic and integrative analysis of large gene lists using DAVID bioinformatics resources. *Nat. Protoc.* 4, 44–57. doi: 10.1038/nprot.2008.211

Hummel, F., Celnik, P., Giraux, P., Floel, A., Wu, W. H., Gerloff, C., et al. (2005). Effects of non-invasive cortical stimulation on skilled motor function in chronic stroke. *Brain* 128(Pt 3), 490–499. doi: 10.1093/brain/awh369

Hwang, S. M., Lopez, C. A., Heck, D. E., Gardner, C. R., Laskin, D. L., Laskin, J. D., et al. (1994). Osteopontin inhibits induction of nitric oxide synthase gene expression by inflammatory mediators in mouse kidney epithelial cells. *J. Biol. Chem.* 269, 711–715.

Jackson, M. P., Truong, D., Brownlow, M. L., Wagner, J. A., McKinley, R. A., Bikson, M., et al. (2017). Safety parameter considerations of anodal transcranial direct current stimulation in rats. *Brain. Behav. Immun.* 64, 152–161. doi: 10.1016/j.bbi.2017.04.008

Jansen, M., and Pfaffelhuber, P. (2015). Stochastic gene expression with delay. *J. Theor. Biol.* 364, 355–363. doi: 10.1016/j.jtbi.2014.09.031

Keuters, M. H., Aswendt, M., Tennstaedt, A., Wiedermann, D., Pikhovych, A., Rotthues, S., et al. (2015). Transcranial direct current stimulation promotes the mobility of engrafted NSCs in the rat brain. *NMR Biomed.* 28, 231–239. doi: 10.1002/nbm.3244

Klein, R., Blaschke, S., Neumaier, B., Endepols, H., Graf, R., Keuters, M., et al. (2014). The synthetic NCAM mimetic peptide FGL mobilizes neural stem cells in vitro and in vivo. *Stem Cell Rev. Rep.* 10, 539–547. doi: 10.1007/s12015-014-9512-5

Kronberg, G., Bridi, M., Abel, T., Bikson, M., and Parra, L. C. (2017). Direct current stimulation modulates LTP and LTD: activity dependence and dendritic effects. *Brain Stimul.* 10, 51–58. doi: 10.1016/j.brs.2016.10.001

Ladwig, A., Walter, H. L., Hucklenbroich, J., Willuweit, A., Langen, K. J., Fink, G. R., et al. (2017). Osteopontin auzgments M2 microglia response and separates M1- and M2-polarized microglial activation in permanent Focal Cerebral Ischemia. *Mediators Inflamm.* 2017:7189421. doi: 10.1155/2017/7189421

Lafon, B., Rahman, A., Bikson, M., and Parra, L. C. (2017). Direct current stimulation alters neuronal input/output function. *Brain Stimul.* 10, 36–45. doi: 10.1016/j.brs.2016.08.014

Lefaucheur, J. P., Antal, A., Ayache, S. S., Benninger, D. H., Brunelin, J., Cogiamanian, F., et al. (2017). Evidence-based guidelines on the therapeutic use of transcranial direct current stimulation (tDCS). *Clin. Neurophysiol.* 128, 56–92. doi: 10.1016/j.clinph.2016.10.087

Liebetanz, D., Koch, R., Mayenfels, S., König, F., Paulus, W., and Nitsche, M. A. (2009). Safety limits of cathodal transcranial direct current stimulation in rats. *Clin. Neurophysiol.* 120, 1161–1167. doi: 10.1016/j.clinph.2009.01.022

Monte-Silva, K., Kuo, M. F., Hessenthaler, S., Fresnoza, S., Liebetanz, D., Paulus, W., et al. (2013). Induction of late LTP-like plasticity in the human motor cortex by repeated non-invasive brain stimulation. *Brain Stimul.* 128, 56–92. doi: 10.1016/j.brs.2012.04.011

Needleman, L. A., Liu, X.-B., El-Sabeawy, F., Jones, E. G., and McAllister, A. K. (2010). MHC class I molecules are present both pre- and postsynaptically in the visual cortex during postnatal development and in adulthood. *Proc. Natl. Acad. Sci. U.S.A.* 107, 16999–17004. doi: 10.1073/pnas.1006087107

Neumann, H., Cavalié, A., Jenne, D. E., and Wekerle, H. (1995). Induction of MHC class I genes in neurons. *Science* 269, 549–552. doi: 10.1126/science.7624779

Neumann, H., Schmidt, H., Cavalié, D., Jenne, D., and Wekerle, H. (1997). Major histocompatibility complex (MHC) class I gene expression in single neurons of the central nervous system : differential regulation by interferon (IFN)-gamma and tumor necrosis factor (TNF)-alpha. *J. Exp. Med.* 185, 305–316. doi: 10.1084/jem.185.2.305

Nitsche, M. A., Fricke, K., Henschke, U., Schlitterlau, A., Liebetanz, D., Lang, N., et al. (2003). Pharmacological modulation of cortical excitability shifts induced by transcranial direct current stimulation in humans. *J. Physiol.* 553(Pt 1), 293–301. doi: 10.1113/jphysiol.2003.049916

Nitsche, M. A., and Paulus, W. (2000). Excitability changes induced in the human motor cortex by weak transcranial direct current stimulation. *J. Physiol.* 527(Pt 3)), 633–639. doi: 10.1111/j.1469-7793.2000.t01-1-00633.x

Ohkawa, Y., Ohmi, Y., Tajima, O., Yamauchi, Y., Furukawa, K., and Furukawa, K. (2011). Wisp2/CCN5 up-regulated in the central nervous system of GM3-only mice facilitates neurite formation in Neuro2a cells via integrin-Akt signaling. *Biochem. Biophys. Res. Commun.* 411, 483–489. doi: 10.1016/j.bbrc.2011.06.118

Peruzzotti-Jametti, L., Cambiaghi, M., Bacigaluppi, M., Gallizioli, M., Gaude, E., Mari, S., et al. (2013). Safety and efficacy of transcranial direct current stimulation in acute experimental ischemic stroke. *Stroke* 44, 3166–3174. doi: 10.1161/STROKEAHA.113.001687

Piehl, F., and Lidman, O. (2001). Neuroinflammation in the rat - CNS cells and their role in the regulation of immune reactions. *Immunol. Rev.* 184, 212–225. doi: 10.1034/j.1600-065x.2001.1840119.x

Pikhovych, A., Stolberg, N. P., Jessica Flitsch, L., Walter, H. L., Graf, R., Fink, G. R., et al. (2016). Transcranial direct current stimulation modulates neurogenesis and microglia activation in the mouse brain. *Stem Cells Int.* 2016, 1–9. doi: 10.1155/2016/2715196

Rabenstein, M., Hucklenbroich, J., Willuweit, A., Ladwig, A., Fink, G. R., Schroeter, M., et al. (2015). Osteopontin mediates survival, proliferation and migration of neural stem cells through the chemokine receptor CXCR4. *Stem Cell Res. Ther.* 6, 1–12. doi: 10.1186/s13287-015-0098-x

Rabenstein, M., Vay, S. U., Flitsch, L. J., Fink, G. R., Schroeter, M., and Rueger, M. A. (2016). Osteopontin directly modulates cytokine expression of primary microglia and increases their survival. *J. Neuroimmunol.* 299, 130–138. doi: 10.1016/j.jneuroim.2016.09.009

Rogall, R., Rabenstein, M., Vay, S., Bach, A., Pikhovych, A., Baermann, J., et al. (2018). Bioluminescence imaging visualizes osteopontin-induced neurogenesis and neuroblast migration in the mouse brain after stroke. *Stem Cell Res. Ther.* 9, 1–12. doi: 10.1186/s13287-018-0927-9

Rollo, E. E., Laskin, D. L., and Denhardt, D. T. (1996). Osteopontin inhibits nitric oxide production and cytotoxicity by activated RAW264.7 macrophages. *J. Leukoc. Biol.* 60, 397–404. doi: 10.1002/jlb.60.3.397

Rueger, M. A., Keuters, M. H., Walberer, M., Braun, R., Klein, R., Sparing, R., et al. (2012a). Multi-session transcranial direct current stimulation (tDCS) elicits inflammatory and regenerative processes in the rat brain. *PLoS One* 7:e43776. doi: 10.1371/journal.pone.0043776

Rueger, M. A., Muesken, S., Walberer, M., Jantzen, S. U., Schnakenburg, K., Backes, H., et al. (2012b). Effects of minocycline on endogenous neural stem cells after experimental stroke. *Neuroscience* 215, 174–183. doi: 10.1016/j.neuroscience.2012.04.036

Schroeter, M., Jander, S., Witte, O. W., and Stoll, G. (1994). Local immune responses in the rat cerebral cortex after middle cerebral artery occlusion. *J. Neuroimmunol.* 55, 195–203. doi: 10.1016/0165-5728(94)90010-8

Shatz, C. J. (2009). MHC class I: an unexpected role in neuronal plasticity. *Neuron.* 64, 40–45. doi: 10.1016/j.neuron.2009.09.044

Sparing, R., Thimm, M., Hesse, M. D., Küst, J., Karbe, H., and Fink, G. R. (2009). Bidirectional alterations of interhemispheric parietal balance by non-invasive cortical stimulation. *Brain* 132(Pt 11), 3011–3020. doi: 10.1093/brain/awp154

Spezia Adachi, L. N., Caumo, W., Laste, G., Fernandes Medeiros, L., Ripoll Rozisky, J., De Souza, A., et al. (2012). Reversal of chronic stress-induced pain by transcranial direct current stimulation (tDCS) in an animal model. *Brain Res.* 1489, 17–26. doi: 10.1016/j.brainres.2012.10.009

Stagg, C. J., and Nitsche, M. A. (2011). Physiological basis of transcranial direct current stimulation. *Neuroscientist* 17, 37–53. doi: 10.1177/1073858410386614

Thams, S., Oliveira, A., and Cullheim, S. (2008). MHC class I expression and synaptic plasticity after nerve lesion. *Brain Res. Rev.* 57, 265–269. doi: 10.1016/j.brainresrev.2007.06.016

Unverricht-Yeboah, M., Giesen, U., and Kriehuber, R. (2018). Comparative gene expression analysis after exposure to 123I-iododeoxyuridine, γ- and α-radiation—potential biomarkers for the discrimination of radiation qualities. *J. Radiat. Res.* 59, 411–429. doi: 10.1093/jrr/rry038

Wu, B., Ma, Q., Suzuki, H., Chen, C., Liu, W., Tang, J., et al. (2011). Recombinant osteopontin attenuates brain injury after intracerebral hemorrhage in mice. *Neurocrit. Care* 14, 109–117. doi: 10.1007/s12028-010-9372-z

Yan, Y. P., Lang, B. T., Vemuganti, R., and Dempsey, R. J. (2009). Persistent migration of neuroblasts from the subventricular zone to the injured striatum mediated by osteopontin following intracerebral hemorrhage. *J. Neurochem.* 109, 1624–1635. doi: 10.1111/j.1471-4159.2009.06059.x

Conflict of Interest: The authors declare that the research was conducted in the absence of any commercial or financial relationships that could be construed as a potential conflict of interest.

Copyright © 2019 Rabenstein, Unverricht-Yeboah, Keuters, Pikhovych, Hucklenbroich, Vay, Blaschke, Ladwig, Walter, Beiderbeck, Fink, Schroeter, Kriehuber and Rueger. This is an open-access article distributed under the terms of the Creative Commons Attribution License (CC BY). The use, distribution or reproduction in other forums is permitted, provided the original author(s) and the copyright owner(s) are credited and that the original publication in this journal is cited, in accordance with accepted academic practice. No use, distribution or reproduction is permitted which does not comply with these terms.

frontiers in Neuroscience

ORIGINAL RESEARCH
published: 29 October 2019
doi: 10.3389/fnins.2019.01133

The Delta-Subunit Selective $GABA_A$ Receptor Modulator, DS2, Improves Stroke Recovery via an Anti-inflammatory Mechanism

*Silke Neumann[1,2†], Lily Boothman-Burrell[2†], Emma K. Gowing[2], Thomas A. Jacobsen[3], Philip K. Ahring[4], Sarah L. Young[1], Karin Sandager-Nielsen[3] and Andrew N. Clarkson[2]**

[1] Department of Pathology, Dunedin School of Medicine, University of Otago, Dunedin, New Zealand, [2] Department of Anatomy, Brain Health Research Centre, Brain Research New Zealand, University of Otago, Dunedin, New Zealand, [3] Saniona A/S, Copenhagen, Denmark, [4] School of Pharmacy, University of Sydney, Sydney, NSW, Australia

OPEN ACCESS

Edited by:
Johannes Boltze,
University of Warwick,
United Kingdom

Reviewed by:
Karsten Ruscher,
Lund University, Sweden
Miroslav M. Savic,
University of Belgrade, Serbia

***Correspondence:**
Andrew N. Clarkson
andrew.clarkson@otago.ac.nz

[†]These authors have contributed equally to this work

Specialty section:
This article was submitted to Neurodegeneration, a section of the journal Frontiers in Neuroscience

Received: 30 March 2019
Accepted: 07 October 2019
Published: 29 October 2019

Citation:
Neumann S, Boothman-Burrell L, Gowing EK, Jacobsen TA, Ahring PK, Young SL, Sandager-Nielsen K and Clarkson AN (2019) The Delta-Subunit Selective $GABA_A$ Receptor Modulator, DS2, Improves Stroke Recovery via an Anti-inflammatory Mechanism. Front. Neurosci. 13:1133. doi: 10.3389/fnins.2019.01133

Inflammatory processes are known to contribute to tissue damage in the central nervous system (CNS) across a broad range of neurological conditions, including stroke. Gamma amino butyric acid (GABA), the main inhibitory neurotransmitter in the CNS, has been implicated in modulating peripheral immune responses by acting on $GABA_A$ receptors on antigen-presenting cells and lymphocytes. Here, we investigated the effects and mechanism of action of the delta-selective compound, DS2, to improve stroke recovery and modulate inflammation. We report a decrease in nuclear factor (NF)-κB activation in innate immune cells over a concentration range *in vitro*. Following a photochemically induced motor cortex stroke, treatment with DS2 at 0.1 mg/kg from 1 h post-stroke significantly decreased circulating tumor necrosis factor (TNF)-α, interleukin (IL)-17, and IL-6 levels, reduced infarct size and improved motor function in mice. Free brain concentrations of DS2 were found to be lower than needed for robust modulation of central $GABA_A$ receptors and were not affected by the presence and absence of elacridar, an inhibitor of both P-glycoprotein and breast cancer resistance protein (BCRP). Finally, as DS2 appears to dampen peripheral immune activation and only shows limited brain exposure, we assessed the role of DS2 to promote functional recovery after stroke when administered from 3-days after the stroke. Treatment with DS2 from 3-days post-stroke improved motor function on the grid-walking, but not on the cylinder task. These data highlight the need to further develop subunit-selective compounds to better understand change in GABA receptor signaling pathways both centrally and peripherally. Importantly, we show that GABA compounds such as DS2 that only shows limited brain exposure can still afford significant protection and promote functional recovery most likely via modulation of peripheral immune cells and could be given as an adjunct treatment.

Keywords: stroke, inflammation, GABA, immune response, neuroinflammation, functional recovery, neuroimmunology

INTRODUCTION

Stroke is the leading cause of lasting disability, with patients experiencing varied levels of functional recovery, and with more than 50% of survivors being discharged into care (Dobkin, 2008; Go et al., 2014). Changes in neuronal excitability, loss of gamma amino butyric acid (GABA) inhibition, enhanced glutamatergic signaling, and changes in neuronal connections and plasticity all contribute to impairment after stroke (Wittenberg and Schaechter, 2009; Clarkson et al., 2010, 2011, 2015, 2019; Carmichael, 2012; Krakauer et al., 2012). In addition, it is well documented that the full expansion of the infarction and ongoing impairment in the weeks to months following a stroke is underpinned by inflammation and the infiltration of peripheral immune cells that cross the blood–brain-barrier (BBB) (Gelderblom et al., 2009, 2015; Doyle et al., 2015). To date, drug therapies have attempted to minimize the extent of cell death, however, all drug therapies that have been trialled have failed to translate into the clinic. Therefore, new drug therapies need to be developed in order to support the recovery of stroke patients.

Changes in inflammatory processes is a hallmark for many pathologies including obesity, diabetes and stroke. Although acute inflammation is beneficial for the repairing and healing process, chronic inflammation contributes to tissue damage. Immune cells play a critical role in contributing to brain damage initiated by ischemic stroke. As a consequence of stroke, immune cells migrate to the brain in response to danger signals (damage-associated molecular patterns, DAMPs), in an effort to repair the damage (Brait et al., 2010; Gelderblom et al., 2015). However, these cells can also promote further inflammation and damage. In addition, the injured brain has an immune-suppressive effect that promotes life-threating infections, which threaten the survival of stroke patients (Liesz et al., 2015).

Traditionally considered a disease refined to the brain, it is becoming increasingly clear that the immune system heavily impacts the pathology of stroke. Local microglia, endothelial cells, neurons, and astrocytes recognize danger signals released from dying cells, which in turn stimulate the production of pro-inflammatory cytokines that attract circulating immune cells to migrate to the central nervous system (Offner et al., 2006; Gelderblom et al., 2009). Together, local and infiltrating cells, contribute to further neural cell death by producing pro-inflammatory cytokines, reactive oxygen species and by activating matrix metalloproteinases (Amantea et al., 2015). In particular, microglia have been shown to be chronically activated even when the initial DAMPs have been cleared (Huh et al., 2003; McGeer et al., 2003). This results in prolonged neuroinflammation that is associated with delayed recovery in stroke patients (Liguz-Lecznar and Kossut, 2013), and impaired memory, sensory learning and plasticity (Greifzu et al., 2011; Doyle et al., 2015).

Gamma amino butyric acid, known for its role as inhibitory neurotransmitter in the CNS, has a similar inhibiting effect on immune cells thereby creating a link between the CNS and the peripheral inflammatory response (Reyes-Garcia et al., 2007). Both, innate and adaptive immune cells express functional GABA receptors and possess enzymes to synthesize and catabolize GABA (Wheeler et al., 2011; Fuks et al., 2012). This includes microglia, macrophages, dendritic cells and T-cells. GABA signals through $GABA_A$ and $GABA_B$ receptors, both of which are expressed on immune cells (Kuhn et al., 2004; Wheeler et al., 2011; Fuks et al., 2012). The composition of the five subunits that make up $GABA_A$ receptors likely varies for the various immune cells, which in turn will account for differences in potency and efficacy of drug treatments targeting GABA receptors and GABA itself (Fuks et al., 2012). GABA is known to act on $GABA_A$ receptors in both millimolar and nanomolar to micromolar concentrations depending on the location (synaptic versus extrasynaptic) and functional composition of the receptors (Mody, 2001; Semyanov et al., 2003; Glykys and Mody, 2007). Of importance, submicromolar GABA concentrations have not only been found around neurons in the brain, but have also been detected in blood and hormone-producing cells in the intestine (Petty et al., 1999; Braun et al., 2004; Wendt et al., 2004). In addition to being exposed to chronic low levels of GABA, these peripheral tissues and receptors are likely to also be modulated following treatment with various GABA modulators. With the development of subunit specific GABA modulators, we may be able to find and develop compounds that could selectively regulate the function of peripheral immune cells.

Extrasynaptic $GABA_A$ receptors, which are located outside the synapse typically contain either the δ- or α5-subunit and are highly sensitive to low GABA concentrations (Mody, 2001). Recent evidence has shown that modulation of extrasynaptic $GABA_A$ receptors plays an important role in minimizing the extent of damage when given early (within hours) to increase tonic GABA currents after a stroke. In addition, this modulation can also facilitate an improvement in motor function when treatment is initiated at a delay (days) to dampen tonic GABA currents after the initial insult (Clarkson et al., 2010, 2019). As little is known about the role of δ-containing $GABA_A$ receptor after stroke, we were interested in testing the therapeutic effects of the δ-subunit-selective $GABA_A$ receptor modulator DS2 (4-chloro-N-[2-(2-thienyl)imidazo[1,2-a]pyridin-3-yl]benzamide). DS2 positively modulates δ-containing $GABA_A$ receptors (Wafford et al., 2009), however, DS2 has not been investigated in a clinical disease model. Therefore, we aimed to assess the potential of DS2 to improve stroke recovery and to modulate inflammatory responses in innate immune cells. Herein, we show that positive allosteric modulation of δ-containing $GABA_A$ receptors with DS2 affords significant protection and improves motor function in a mouse model of stroke. Investigation into a potential mechanism of action revealed that DS2 reduces the activation of NF-κB in LPS-stimulated macrophages and reduces the expression of activation markers on bone marrow-derived dendritic cells (BMDCs). Interestingly, we show that DS2 only has limited brain exposure, indicating that DS2-mediated effects *in vivo* are most likely attributed to modulation of peripheral immune cells.

MATERIALS AND METHODS

Materials

Lipopolysaccharides from *Escherichia coli* 055:B5 (LPS) were ordered from Sigma-Aldrich (St. Louis, MO, United States); Dulbecco's Modified Eagle Medium (DMEM), 2-Mercaptoethanol, Penicillin/Streptomycin, and Roswell Park Memorial Institute Medium (RPMI) were ordered from Life Technologies (Auckland, New Zealand); foetal calf serum (FCS) was purchased from Moregate Biotech (Hamilton, New Zealand), DS2 from Tocris Bioscience (Bristol, United Kingdom), Zeocin™ from Invitrogen (Auckland, New Zealand) and Quantiblue™ from InvivoGen (CA, United States). The LIVE/DEAD® Fixable Near-IR Dead Cell Stain was purchased from Thermo Fisher Scientific (MA, United States); Granulocyte-macrophage colony-stimulating factor (GM-CSF) and flow antibodies MHCII FITC, CD80 PE, CD86 PE-Cy7, CD11c BV421, and CD40 APC came from BioLegend (Auckland, New Zealand). The reagents for real-time PCR (qPCR) were purchased from the following suppliers: RNeasy® Plus Mini kit from Qiagen (Austin, TX, United States), DNA-free™ kit from Life Technologies Corporation (Carlsbad, CA, United States), SensiFAST cDNA Synthesis Kit and SYBR Green kit from Bioline (London, United Kingdom) and primers ordered from Integrated DNA Technologies (Singapore).

Cell Culture of RAWblue™ Macrophage Cells

RAWblue™ macrophages were cultured in DMEM supplemented with heat-inactivated FCS (10%) and 200 μg/mL Zeocin™ (antibiotic selection) as previously described (Clarkson et al., 2019). For experiments, 5×10^4 RAWblue macrophages were added to a 96-well plate (flat-bottom) in the absence of Zeocin, and left untreated for 16 h. Increasing concentrations of DS2 (10^{-6} to 10^{-3} M) were added for 30 min before LPS (2.5 ng/mL) was added. The supernatant was collected after 6 h and the levels of the secreted embryonic alkaline phosphatase (SEAP) determined using the Quantiblue™ assay. For this, 80 μL of the Quantiblue solution and 30 μL of the cell culture supernatant were combined, left at 37°C for 3 h and the absorbance read at 620 nm. Three independent experiments were performed in triplicate each.

Generation and Stimulation of Bone Marrow-Derived Dendritic Cells

Bone marrow-derived dendritic cells were generated from bone marrow cells obtained from C57Bl/6J mice as described previously (Scheicher et al., 1992). Briefly, bone marrow cells were isolated from the hind legs of mice and processed into single cell suspensions. Bone marrow cells were re-suspended in IMDM supplemented with 5% FCS, 20 ng/mL GM-CSF, 1% streptomycin/penicillin and 0.1% 2-mercapto ethanol, plated at a density of 5×10^5 cells/mL and maintained at 37°C for 6 days. Half of the media was refreshed on days 3 and 5 of the culture. On day 6, BMDCs were seeded to a 96 well plate at 2×10^5 cells/mL and either pre-incubated with DS2 (10^{-8} to 10^{-4} M) for 30 min or left untreated before stimulation with LPS (100 ng/mL). BMDCs were harvested and stained with antibodies against cell surface markers: CD11c BV421, MHCII FITC, CD80 PE, CD86 PE-Cy7, and CD40 APC after unspecific binding was blocked by using the CD16/32 antibody. Dead cells were excluded by gating on LIVE/DEAD® Fixable Near-IR-negative cells. Fluorescence minus one controls for each fluorophore were used to distinguish positive from background staining.

Quantitative Polymerase Chain Reaction (qPCR)

RAWblue macrophages were grown to approximately 80% confluency in 6-well plates and detached using a cell scraper. Cells were spun down to remove residual cDMEM and total RNA was extracted using the RNeasy® Plus Mini kit as previously described (Clarkson et al., 2019). Total RNA was incubated with DNase using the DNA-free™ kit before reverse transcription into cDNA was performed on a ThermoCycler using the SensiFAST cDNA Synthesis Kit (25°C for 10 min, 42°C for 15 min, and 85°C for 5 min). All kits were used according to the manufacturer's instructions and the cDNA was stored at −20°C until further processing. qPCR samples were prepared by mixing the SYBR green master mix with RNAfree water and primers in a 96-well plate. All primers are listed in **Table 1**. qPCR was performed on a Roche LightCycler® (30 s at 95°C, 40 cycles of 5 min at 95°C, 15 s at 60°C and 10 s at 72°C) and the LightCycler 480® software was used to determine *Ct* values. A dissociation curve analysis was performed and the differences in *Ct* values was calculated using the following equation: $2^{(\text{Ctreference} - \text{CTtarget})}$ (Schmittgen et al., 2000). *Ct* values were normalized against the house keeping gene SDHA. Dissociation curve analysis was performed for all samples (60 s at 95°C, 30 s at 55°C, and 30 s at 95°C).

Photothrombosis Model of Focal Ischemia

The University of Otago Animal Ethics Committee approved all animal experiments. Focal stroke was induced in the left hemisphere in either adult (2–3 month old, for protection studies) or aged (22 month old, for recovery studies) male C57BL/6J mice weighing 25–27 g (2–3 month old) or 32–40 g (22 month old) using the photothrombosis method (Clarkson et al., 2010, 2019). Briefly, mice were anesthetized and placed in a stereotactic apparatus, a midline incision was performed to expose the skull, which was subsequently cleared of connective tissue and dried. The cold light source (KL1500 LCD, Zeiss) was attached to a 40× objective to give a 2 mm diameter illumination and was positioned 1.5 mm lateral from Bregma. Rose Bengal solution (0.2 mL, Sigma; 10 g/L in normal saline, i.p.) was administered and the brain illuminated through the intact skull for 15 min after a 5 min lag period. The color temperature intensity used for all experiments to induce a stroke was 3300 K. Mice had unrestricted access to water and food and were housed under a 12-h light/dark cycle.

Drug Administration

DS2 (0.01, 0.1, 1 or 4 mg/kg in DMSO) or vehicle (DMSO) was injected i.p., 1 h after stroke. A second dose was given 24 h

TABLE 1 | Primer sequences for GABA receptor subunits and transporters as determined by qPCR.

Target gene	Primer sequences (5′–3′)	Amplicon length
α1	F: CATGACAGTGCTCCGGCTAA	136
	R: GCCATCCTCTGTGATACGCA	
α2	F: TTCAAAGCCACTGGAGGAAAAC	107
	R: GCAGCAGAGACCATACATTGC	
α3	F: TCCTGCTGAGACCAAGACCT	361
	R: GGCTCAATCCAAGCAATGTT	
α4	F: GCCAAACCCTGGTAAAGGGA	99
	R: CGGGTCAGCGACTTCAAAAC	
α5	F: GCTGACCCATCCTCCAAACA	71
	R: TGGAGACTGTGGGTGCATTC	
α6	F: GGTGACCGGGCATCCCAGTGA	197
	R: TGTTACAGCACCCCCAAATCCTGGC	
β1	F: ATCGAGAGAGTTTGGGGCTTC	80
	R: GCTGGGTTCATTGGAGCTGT	
β2	F: TAGTGGGCACGACGGTTAGA	111
	R: ATGACGATCCACCACAGCAG	
β3	F: TCTGAGCCCAGCAGCGTAAA	133
	R: TGTTCATCCCCACGCAGAC	
δ	F: AGGAACGCCATCGTCCTTTT	73
	R: CTTGACGACGGGAGATAGCC	
ε	F: ACTGCGCCCTGGCATTGGAG	70
	R: AGGCCCGAGGCTGTTGACAA	
γ1	F: CTCAGTTCTGCTGGGAGTCG	111
	R: CCCCAAGCACAGAGTTTTGC	
γ2	F: CTGAGCTGACGCTTTGATGG	120
	R: TGCCTCTAGTAGGTCCCGTC	
γ3	F: ATTACATCCAGATTCCACAAGATG	149
	R: CAC AGG TGT CCT CAA ATT CCT	
ρ1	F: CTTCTCACGGCTTCTTGGGA	98
	R: ACCCATCCCCACCACAAAAG	
ρ2	F: GAAGATTCGAAGACCTCCACCTCAGTC	120
	R: GTCTTTGTCCAGCTCTGTGATCTTCATTC	
ρ3	F: CAACTCAACAGGAGGGGAAA	101
	R: TCCACATCAGTCTCGCTGTC	
pi	F: TCGGTGGTGACCCAGTTCGGAT	115
	R: TCTGTCCAACGCTGCCGGAG	
σ	F: GCTGGAGGTGGAGAGCTATGGCT	115
	R: CCCCAGGTACGTGTACTGAGGGA	
GAT1	F: GCTTTCGGAAGTTGGGTGTG	135
	R: GTTGGACTGGAAAGGTGGTCT	
GAT3	F:TGTGCGGGCATCTTCATCTT	81
	R: GCCCCAAGCAGGATATGTGT	
BGT1	F: TTCTGGGAGAGACGGGTTTTG	158
	R: GCTGTGAAGTAAACAACCTTGC	
NKCC1	F: TCCTTCTCGGTGGACTGGTGGT	95
	R: AAGAGCTCGTCCTCATCGTCGC	
NKCC2 isoform A	F: GGTAACCTCTATCACTGGGT	154
	R: GTCATTGGTTGGATCCACCA	
KCC1	F: AACGAGGTCATTGTCACGCGCT	147
	R: ACGCACCAACAACACCCGTT	
KCC2	F: GTTCCATGTCCATCCAGGTGA	110
	R: ATTGCATTGCCCTGCACATAG	
KCC3	F: AGTGAAGATGCTCGCGCTTGGA	170
	R: AGCATGCCCCCATCATGCACAA	
KCC4	F: AACTGGCGTCCACGCTTCAAGT	122
	R: CCGGCAATGAGCATGGCGAAAA	
GABABR1	F: ATTTCCGATGTGACCCCGAC	102
	R: TTCGATTCACCTGGCAGTGG	
GABABR2	F: TCCGGAACGGGGAAAGAATG	136
	R: TCCGACCCCTGGAACCTTAT	
SDHA	F: GCCCATGCCAGGGAAGATTA	92
	R: TGTTCCCCAAACGGCTTCTT	
RPL13a	F: ATTGTGGCCAAGCAGGTACT	142
	R: CTCGGGAGGGGTTGGTATTC	
Ppia	F: CGCGTCTCCTTCGAGCTGTTTG	150
	R: TGTAAAGTCACCACCCTGGCACAT	

later by an independent experimenter not involved in any other experiments in order to randomize the animals and minimize bias. For recovery studies, DS2 (10 mM) was loaded into ALZET 1002 mini-pumps and implanted subcutaneously from 3-days post-stroke. Mini-pumps were replaced after 2 week with new pumps to allow for continuous treatment for 28-days after stroke. The treatment groups were assigned randomly post-stroke.

Behavioral Assessment

The baseline performance of animals was established 1 week prior to surgery, both, on the grid-walking and cylinder tasks. One week after stroke induction, animals were tested for motor function at the end of their dark cycle. For recovery studies, behavioral assessments were performed on weeks 1, 2, 4, and 6 post-stroke. Observers, blinded to the treatment group, scored the behaviors as previously described (Clarkson et al., 2010, 2019).

Stroke Volume

Animals were anesthetized seven or 42 days post-stroke, and subsequently transcardially perfused with 4% paraformaldehyde, brains extracted and processed histologically. Cresyl violet staining was used to quantify stroke volumes as reported previously (Clarkson et al., 2010, 2011, 2019; Overman et al., 2012).

Assessment of Circulating Pro-inflammatory Cytokine Levels

Three days post-stroke, blood samples were collected into EDTA treated tubes and centrifuged at 1000 × *g* for 10 min, 4°C. Plasma was collected and then stored at −80°C until required for analysis. A multiplex bead assay was performed using the Luminex 100^{TM} analyzer (Luminex Corporation, Austin, TX, United States). Cytokines IL-1β, TNF-α, IL-6, and IL-17 were analyzed with a BioPlex mouse cytokine assay kit (Bio-Rad Laboratories Inc., New Zealand), according to the manufacturer's instructions. For each cytokine, a minimum of 100 events were collected. Cytokine concentrations were automatically calculated

from median fluorescence intensities (MFI), based on standard curve data (detectable range of 2–32,000 pg/ml) using Bio-Plex Manager™ software.

Brain Accumulation of DS2 in Combination With Elacridar

Male black 6 mice (C57/BL/6Ntac, Taconic, Denmark) received i.v. administration of either elacridar (5 mg/kg, 1 mg/ml, in a dose volume of 5 ml/kg, dissolved in dimethyl acetamide/PEG400/30%/(2-hydroxypropyl)-beta-cyclodextrin (HPbCD) (10/40/50)) or vehicle. Thirty minutes later, DS2 [10 mg/kg, 1 mg/ml, in a dose volume of 10 ml/kg, dissolved in 5% dimethylsulfoxide (DMSO) + 30% HPbCD in demineralized water] was administered to mice orally. Animals were sacrificed and blood and brains were isolated at either 0.5 or 1 h post DS2 administration. DS2 concentrations in, plasma and brain tissue homogenates were determined using liquid chromatography-tandem mass spectrometry assay.

Statistical Analysis

All data are expressed as mean ± SD. One-way analysis of variances (ANOVA) and Newman–Keuls' multiple pair-wise comparisons for *post hoc* comparisons were applied for histological, biochemical DS2 brain/plasma levels and behavioral assessments post-stroke. For behavioral assessments in the recovery study, a two-way ANOVA following Tukey's multiple pairwise comparisons performed. Five mice were used per treatment group for histological and seven mice per group for behavioral assessments. $P < 0.05$ was considered significant. Samples sizes were based on prior publications (Clarkson et al., 2010, 2013, 2019). To detect differences in infarct size in vehicle and DS2-treated mice, an $n = 3$ mice/group is sufficient for achieving a power of 80%, when using the following parameters: $\alpha = 0.05$ (type 1 error rate); $\beta = 0.2$ (type 2 error rate); q1 = 0.5 (proportion of mice in vehicle group); q2 = 0.5 (proportion of mice in DS2 treated group); E = 2.94 (effect size, magnitude of difference); and S = 1.26 (Standard deviation).

RESULTS

DS2 Is Neuroprotective and Improves Functional Recovery After Focal Ischemia

It has previously been shown that reduction of extrasynaptic GABAergic signaling from 3 days after stroke improves functional recovery (Clarkson et al., 2010). In contrast, treatment with the flavonoid, 2'MeO6MF, which was shown to stimulate an increase in extrasynaptic GABA signaling, early after stroke affords significant neuroprotection (Clarkson et al., 2019). To further investigate the role of delta-containing $GABA_A$ receptors as a potential target for stroke, we tested the delta-selective compound, DS2, for its ability to afford neuroprotection after stroke. The protective effects of DS2 were investigated in a focal photothrombosis model of stroke. The reperfusion component is minimal in this model and it is in general more difficult to protect against cell death. Mice were injected i.p. with DS2 (0.01-4 mg/kg) or vehicle 1 and 24 h post-stroke. Body temperature was stable (data not shown) and mice did not show signs of sedation. The stroke volume was assessed 7-days post-stroke and demonstrated that treatment with DS2 resulted in a decrease in infarct volume [$F(4,20) = 6.912$; $P < 0.0012$: vehicle, 2.28 ± 0.26 mm^3 versus DS2 (0.01 mg/kg), 1.78 ± 0.58 mm^3, $P > 0.05$; DS2 (0.1 mg/kg), 0.77 ± 0.27 mm^3, $P < 0.01$, DS2 (1 mg/kg), 2.01 ± 0.62 mm^3, $P > 0.05$, and DS2 (4 mg/kg) 1.96 ± 0.62 mm^3, $P > 0.05$: $n = 5$/group; **Figures 1A,B**].

Next mice were tested for grid-walking (forelimb function) and cylinder (forelimb asymmetry) tasks. Consistent with what we have previously reported, mice had increased numbers of foot-faults on the grid-walking test ($n = 5$ per group; **Figure 1C**) and an increase in spontaneous forelimb asymmetry in the cylinder task ($n = 5$ per group; **Figure 1D**) was detected 7-days post-stroke (Clarkson et al., 2010, 2013, 2019). Treatment with DS2 decreased the number of foot-faults on the grid-walking task ($F(4,20) = 4.06$, $P = 0.0144$) and an improved forelimb asymmetry in the cylinder task ($F(4,20) = 5.858$, $P = 0.0027$). *Post hoc* analysis revealed that only treatment with 0.1 mg/kg DS2 significantly improved motor function on either the grid-walking ($P = 0.0094$) or cylinder ($P = 0.0022$) tasks, compared to vehicle-treated controls.

DS2 Modulates Inflammatory Pathways

Inflammation is crucially involved in contributing to modulation and progression of tissue damage induced by the stroke. Inflammation contributes to the induction of apoptotic processes (Downes and Crack, 2010), and stimulates tonic GABA signaling (Wang et al., 2012), which hinders regaining function after stroke (Clarkson et al., 2010). To confirm that innate immune cells express GABA receptor subunits, necessary for responding directly to DS2, qPCR was performed on unstimulated RAWblue macrophages for the following $GABA_A$ receptor subunits (α1, α2, α3, α4, α5, α6, β1, β2, β3, δ, ε, γ1, γ2, γ3, ρ1, ρ2, ρ3, π, θ), GABAB receptor subunits (GABAB1, GABAB2) and GABA transporters (GAT1, GAT3, BGT1, NKCC1, NKCC2, KCC1, KCC2, KCC3, KCC4) involved in GABA signaling. The relative mRNA levels were investigated by qPCR using the specific primers listed in **Table 1**. We detected several $GABA_A$ receptor subunits, with β_1, α_5, α_6, and δ showing the highest relative expression (**Figure 2A**). mRNA levels for the subunits β_2, π, and ρ_2 were lower in comparison but higher than the levels of the low-expressing subunits β_3, ε, γ_{1-2}, and ρ_3. In addition, high levels of transcripts for the betaine/GABA receptor (BGT1), the K^+-Cl^- co-transporters KCC3 and KCC4 and the Na^+ K^+ Cl^- co-transporter NKCC1 were found in RAWblue macrophages (**Figure 2B**). The mRNA levels of GABA receptor subunits and transporters were not significantly changed upon stimulation with LPS for either 6 or 24 h (data not shown).

Next, we assessed the efficacy of DS2 to decrease NF-kB activity, a common measure of inflammation. RAWblue macrophages, stimulated with LPS (2.5 ng/mL), showed a marked increase in NF-kB activity ($P < 0.001$; **Figure 2C**),

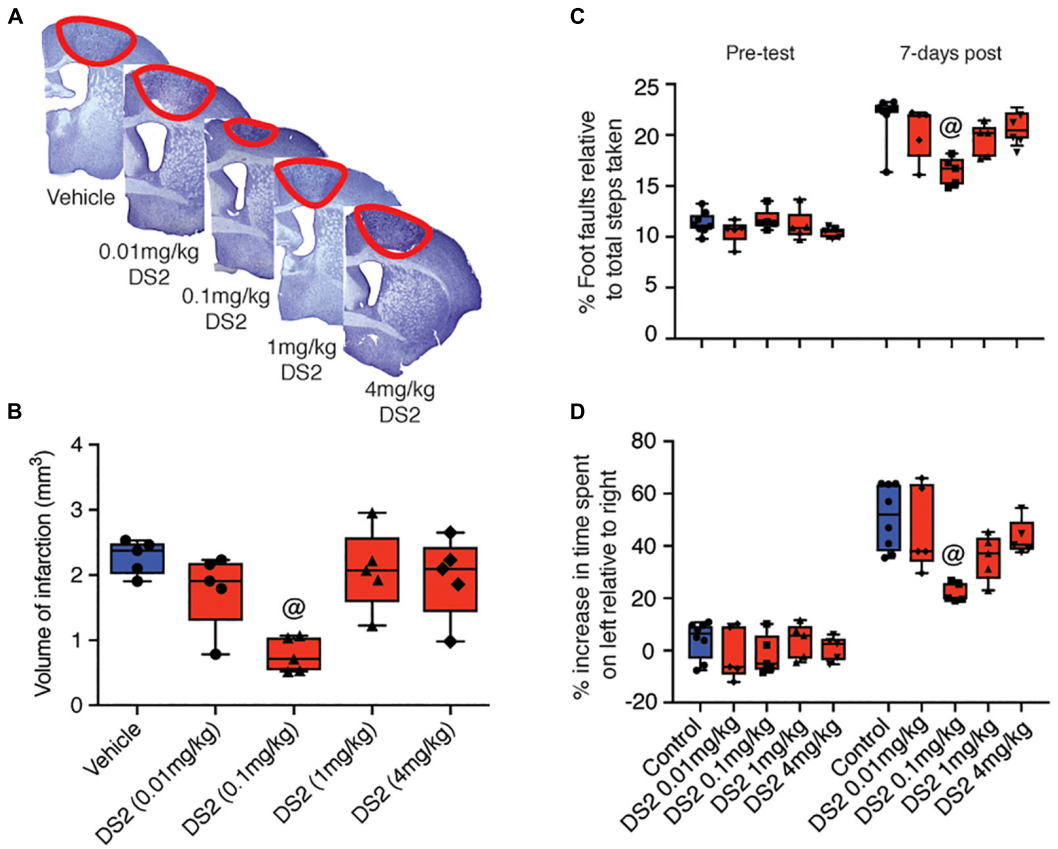

FIGURE 1 | Treatment with DS2 reduces infarct volume and improves functional outcomes post-stroke. Mice were subjected to focal stroke and injected intraperitoneally with either DS2 (0.01, 0.1, 1 or 4 mg/kg) or vehicle 1 and 24 h after the surgery. The brains were collected 7 days later, stained with cresyl violet and the stroke volume was calculated. **(A)** Representative cresyl violet-stained sections of animals treated with vehicle or three different concentrations of DS2. **(B)** Mice injected with 0.1 mg/kg DS2 had significantly smaller strokes than untreated animals. Baseline motor function was established by grid-walking and cylinder test 1 week prior stroke surgery. Mice treated with either vehicle or DS2 (0.01 0.1, 1, and 4 mg/kg) at 1 and 24 h post-stroke induction were assessed in the **(C)** grid-walking (foot-faults) and **(D)** cylinder task (forelimb asymmetry). Data are expressed as mean ± SD for n = 5-7 per group. $^{@}P < 0.01$ compared with vehicle control.

which did not change upon addition of the vehicle (2.5% DMSO). LPS-stimulated macrophages, pre-incubated with DS2 (10^{-3} to 10^{-4} M) showed a significant decrease in NF-kB activity ($P < 0.001$; **Figure 2C**) with levels being similar to unstimulated macrophages.

To confirm the anti-inflammatory effect of DS2, observed in the immortalized RAWblue macrophage cell line, we next tested DS2 using LPS-stimulated primary innate immune cells. For this experiment we generated BMDCs from bone marrow precursor cells by adding GM-CSF to the culture medium. Resulting $CD11c^{+}$ $MHCII^{+}$ BMDCs have previously been shown to closely resemble migratory DCs found *in vivo* (Helft et al., 2015), which makes them an interesting population to study in the stroke context. BMDCs were pre-incubated with varying concentrations of DS2 before LPS was added for 24 h. BMDCs were harvested and the expression of CD40, CD80, and CD86 determined by flow cytometry. BMDCs pre-incubated with the highest dose of DS2 (10^{-4} M) demonstrated a significant decrease in CD40, CD80 ($P < 0.01$) but not CD86 expression when stimulated with LPS (**Figures 2D–F**). Treatment with DS2 did not affect the viability of RAWblue macrophages and BMDCs (data not shown). This data further confirms that DS2 is having a positive effect to dampen the immune response.

DS2 Dampens Stroke-Induced Cytokine Production *in vivo*

Next, we investigated the effects of DS2 on inflammation post-stroke *in vivo*. As reported previously, we show that cerebral ischemia significantly increases peripheral cytokine levels of IL-1β (sham control versus stroke + vehicle: 109.91 ± 20.08 pg/mL versus 209.24 ± 54.05 pg/mL; $P < 0.01$, **Figure 3A**), TNF-α (sham control versus stroke + vehicle: 594.02 ± 97.44 pg/mL versus 960.98 ± 125.63 pg/mL; $P < 0.001$, **Figure 3B**), IL-6 (sham control: 185.33 ± 20.17 pg/mL versus stroke + vehicle: 299.50 ± 41.52 pg/mL; $P < 0.001$, **Figure 3C**), and IL-17 (sham control: 2145.31 ± 124.27 pg/mL, versus stroke + vehicle: 2934.50 ± 204.76 pg/mL; $P < 0.05$, **Figure 3D**). Treatment with DS2 significantly decreased circulating IL-6 (0.1 mg/kg,

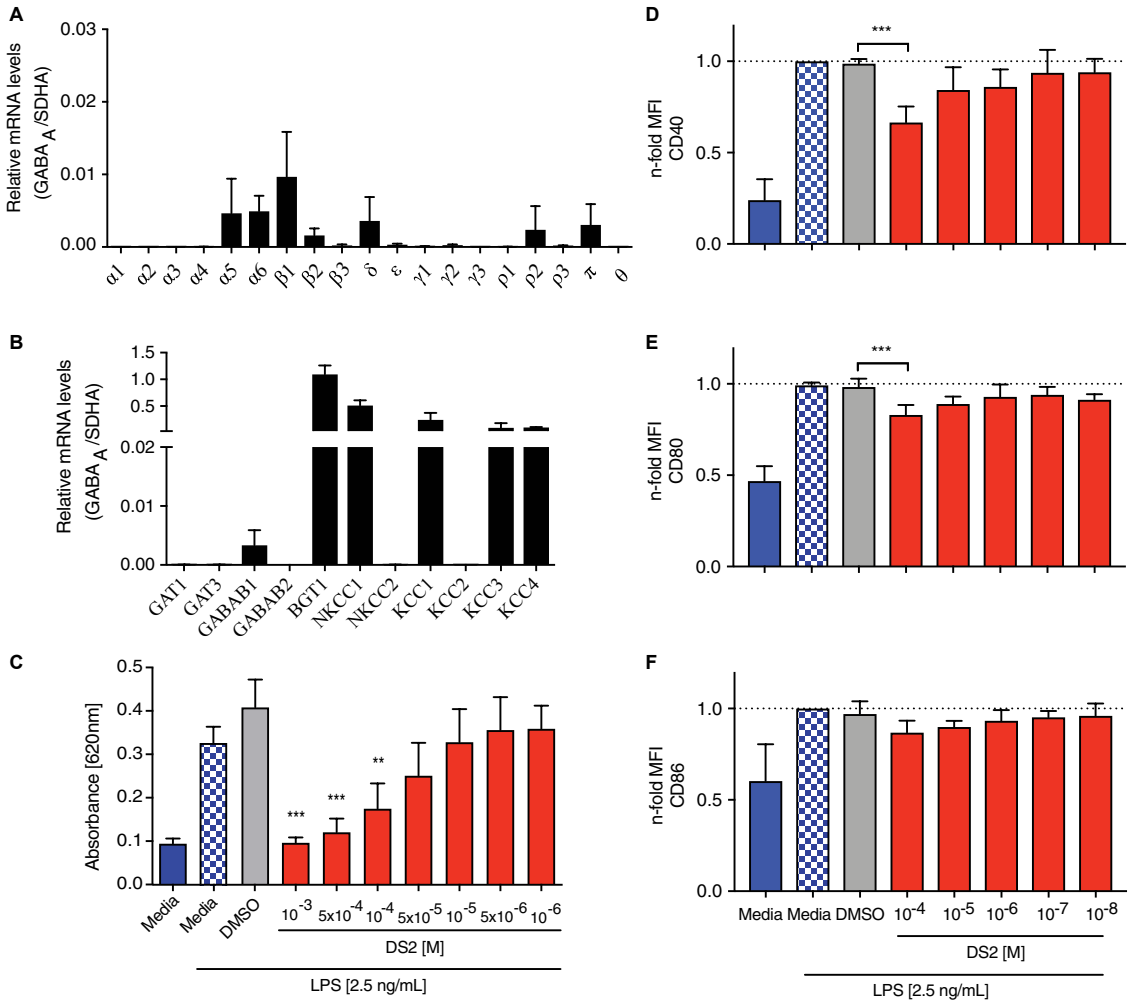

FIGURE 2 | DS2 dampens activation of innate immune cells after an inflammatory stimulus. **(A,B)** Expression of GABA receptor subunits by RAWblue macrophages was analyzed by qPCR. Relative mRNA levels of **(A)** GABA receptor subunits and **(B)** transporters involved in GABA signaling on unstimulated RAWblue macrophages in relation to the reference gene succinate dehydrogenase complex subunit A (SDHA) are shown. **(C)** RAWblue macrophages (5×10^4 cells/well) were either pre-treated with DS2 (10^{-3} to 10^{-6} M) or DMSO (2.5%) for 30 min or left un-treated before stimulation with LPS (2.5 ng/mL) for 6 h. Cell supernatants were collected and the extent of NF-κB activation was determined by quantifying the reporter protein SEAP with the Quantiblue™ assay. **(D–F)** BMDCs were incubated with decreasing concentrations of DS2 (10^{-4} to 10^{-8} M) for 30 min prior to the addition of LPS (100 ng/mL) to the cultures. BMDCs were harvested 24 h later and expression of cell surface markers CD40, CD80 and CD86 on live, $CD11c^+$ $MHCII^+$ BMDCs was determined by flow cytometry. MFI shown as n-fold increase over LPS-treated cells. Results are the mean ± SD of three independent experiments with three replicates each. $^{***}P < 0.001$ and $^{**}P < 0.01$.

$P < 0.01$; 1 and 4 mg/kg, $P < 0.05$), IL-17 and TNF-α levels ($P < 0.05$ and $P < 0.001$, respectively following treatment) at 3-days post-stroke. Treatment however, with DS2 did not have any effect on IL-1β levels with levels remaining similar to stroke + vehicle controls. These data suggest that DS2 can dampen an NF-kB-mediated pro-inflammatory response that is most likely occurring via δ-containing $GABA_A$ receptors located on immune cells.

DS2 Shows Limited Brain Exposure Following Systemic Administration

To correlate our *in vitro* data with our *in vivo* data, we assessed the ability of DS2 to cross the mouse BBB. We found that injection of a single dose of DS2 (i.p.,10 mg/kg), resulted in robust plasma, but only marginal brain exposure at either 0.5 or 1 h following dosing (**Table 2**). The free fraction of DS2 in brain tissue is very low (1.2% unbound, Saniona, unpublished data), corresponding to 54 and 64 nM free at 0.5 and 1 h following dosing respectively, which does not cover the ED50 for potentiating the effect of GABA at the α4β3δ receptors in L(tk-) cells (Wafford et al., 2009). As DS2 was speculated to act as a P-glycoprotein substrate, which could block the entry of DS2 into the brain, we next assessed if co-administration of DS2 with elacridar, an inhibitor of both p-glycoprotein and breast cancer resistance protein (BCRP) (Cutler et al., 2006), would increase brain DS2 levels. Assessment of both brain and plasma DS2 levels in the presence of elacridar revealed similar levels at both 0.5 and

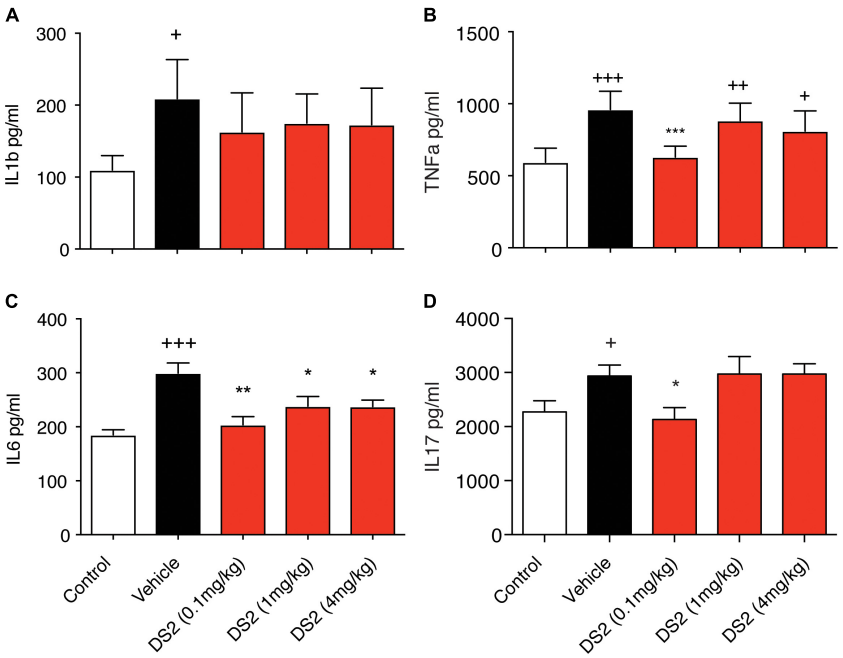

FIGURE 3 | DS2 decreases pro-inflammatory cytokine production post-stroke. Mice were injected i.p. with vehicle or DS2 (0.1, 1 or 4 mg/kg) 1 and 24 h after induction of stroke and peripheral blood collected from the tail vein of mice 3-days post-stroke. Sera were analyzed for **(A)** IL-β, **(B)** TNF-α, **(C)** IL-6, and **(D)** IL-17 concentrations using a BioPlex kit. Data are expressed as mean ± SD for $n = 5$ per group. $^{***}P < 0.001$, $^{**}P < 0.01$, $^{*}P < 0.05$ compared to vehicle. $^{+++}P < 0.001$, $^{++}P < 0.01$, $^{+}P < 0.05$ compared to sham control.

TABLE 2 | Brain and plasma concentrations following DS2 administration and co-treatment with or without elacridar.

		Plasma (P)		Brain (B)		P ratio	B ratio	B/P ration	
		Without ng/ml (μM)	With ng/ml (μM)	Without ng/ml (μM)	With ng/ml (μM)			Without	With
DS2	0.5 h	12,205	12,262	1587	1696	1.0	1.1	0.13	0.14
		(34.5)	(34.7)	(4.5)	(4.8)				
	1 h	15,231	13,928	1874	1957	0.9	1.0	0.12	0.13
		(43.2)	(39.5)	(5.3)	(5.5)				

Data is expressed as both ng/ml and (μM) concentrations.

1 h following DS2 dosing as levels reported without elacridar, indicating that brain penetrance by DS2 is not restricted by active efflux by p-glycoprotein or BCRP (**Table 2**). These results suggest that DS2, in the dose tested, does not lead to sufficient free brain concentrations needed to activate the α4β3δ receptors indicating that the protective effects of DS2 most likely occur via modulation of the peripheral immune response or some as yet unknown mechanism. We also acknowledge that the BBB is leaky after stroke and more so in animals relative to humans, which could lead to mildly higher brain concentrations. However, in a recent study using a GABA modulator, we did not observe this (Clarkson et al., 2019).

DS2 Improves Functional Recovery When Administered at a Delay

Finally, as DS2 appears to dampen peripheral immune activation and only showed limited brain exposure, we assessed the role of DS2 to promote functional recovery after focal stroke to the motor cortex when administered at a delay of 3 days. DS2 was administered continuously from 3 to 28-days post-stroke, a critical period for neuroplasticity in rodents post-stroke (Corbett et al., 2017). This is also a period where we have previously reported that starting treatment with GABA modulators can aid in improving functional recovery without affecting stroke volume (Clarkson et al., 2010; Lie et al., 2017). Throughout the 42 day observation period, we detected marked forelimb motor deficits in the grid-walking and cylinder tasks in mice treated with vehicle only. Vehicle-treated mice showed limited spontaneous recovery (**Figures 4A,B**).

Chronic delayed treatment with DS2 improved motor performance of the affected forelimb on days 7, 14, and 28 post-stroke on the grid-walking task (**Figure 4A**). However, upon discontinuation of treatment, the DS2 treated animals showed a decrease in the recovery, such that no difference was observed in grid-walking performance at 42-days post-stroke compared with

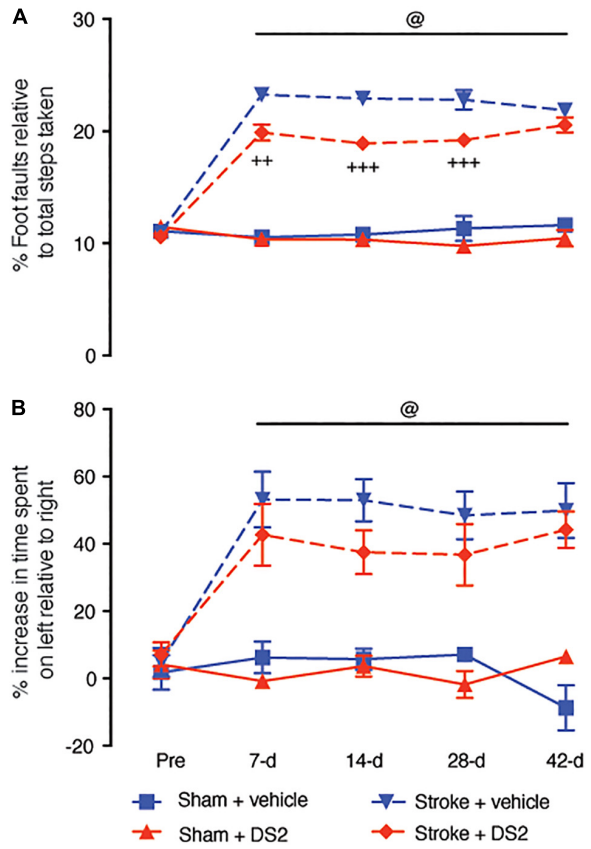

FIGURE 4 | Delayed administration of DS2 from day-3 post-stroke improves functional outcomes when continuously administered. Mice were subjected to focal stroke or sham surgery and DS2 (10 mM, red) or vehicle (blue) were loaded into ALZET 1002 mini-pumps and implanted subcutaneously from 3-days post-stroke. Mini-pumps were replaced after 2 week with new pumps to allow for continuous treatment for 28-days after stroke. Mice were assessed for functional deficits using the **(A)** grid-walking (foot-faults) and **(B)** cylinder task (forelimb asymmetry). Data are expressed as mean ± SD for $n = 7$ per group. $^{+++}P < 0.001$, $^{++}P < 0.01$ compared to stroke vehicle control. $^{@}P < 0.001$ compared to sham controls.

the vehicle-treated controls recovering from the stroke. Analysis of cylinder task performance showed no significant improvement in the presence of DS2 compared to vehicle treated controls (**Figure 4B**). However, it should be noted that some animals did show an improvement.

Delayed DS2 treatment did not induce any obvious signs of seizures or seizure-like behaviors in any of the mice throughout the 42 days. In addition, delayed treatment had no effect on infarct volumes (data not shown).

DISCUSSION

It is currently not fully understood how GABAergic compounds promote neuroprotection after stroke. $GABA_A$ receptor subtype-selective agonists, such as DS2 provide an opportunity to investigate the mechanism of action more thoroughly. Receptor subtype-selective compounds are more likely to have an effect and have therefore been investigated clinically for treating diseases, such as schizophrenia, Downs syndrome and autism (Rudolph and Knoflach, 2011; Rudolph and Mohler, 2014). Furthermore, using subtype selective GABAergic compounds will allow us to increase our understanding of GABA signaling post-stroke. In addition to the positive allosteric $GABA_A$ modulator described here, we have previously reported that negative modulation of $GABA_A$ receptors can improve stroke recovery when administered three days post-stroke (Clarkson et al., 2010). Within this timeframe, the infarct is fully developed and pharmaceutical treatments aimed to improve cortical excitability do not necessarily change the infarct size (Clarkson et al., 2010, 2011). These findings have led to pharmaceuticals companies developing compounds that aim to normalize extrasynaptic $GABA_A$ inhibition, and assess these for stroke in human Phase II clinical trials (ClinicalTrials.gov ID: Hoffman La-Roche – NCT02928393; Servier RESTORE BRAIN Study – NCT02877615).

Activation of $GABA_A$ receptors can mediate both synaptic and extrasynaptic inhibitory currents depending on the receptor composition (Sieghart, 1995). α5- or δ-subunits are crucial components of extrasynaptic $GABA_A$ receptors in the hippocampus, cortex and thalamus (Glykys and Mody, 2007; Olsen and Sieghart, 2009). Antagonism of α5- or δ-subunits facilitates pyramidal neuron signaling to afferent inputs (Drasbek and Jensen, 2006; Glykys and Mody, 2007), and enhances neuronal network excitability (Walker and Semyanov, 2008). Since extrasynaptic $GABA_A$ receptors play an important role in shaping neuronal excitability, modulation of α5- or δ-subunits early could offer a viable treatment for reducing the glutamate-mediated hyperexcitability, which we have recently reported following treatment with the flavonoid, 2'MeO6MF (Clarkson et al., 2019). As flavonoids can have multiple modes of action it is good to assess the mechanistic function of δ-subunit-mediated protection using other δ-subunits modulators, such as DS2 (Wafford et al., 2009) or AA29504 (Vardya et al., 2012).

Prior studies have shown that DS2 binds to and modulates δ-subunit containing extrasynaptic $GABA_A$ receptors in neuronal cell culture systems (Wafford et al., 2009; Jensen et al., 2013; Lee et al., 2016). DS2 enhances the maximum GABA response at α4/6βxδ $GABA_A$ receptors while only a minimal response is observed at α4/6βxγ2 $GABA_A$ receptors, clearly indicating a δ-subunit preference of DS2. While the potency of DS2 is influenced by which α-subunit is present in the receptor complex (α4/6βxδ > α1βxδ >> γ2-GABAA receptors), the type of β-subunit does not affect the potency as much (Wafford et al., 2009; Ahring et al., 2016). Our findings suggest that the effects of DS2 on macrophages are most likely mediated via binding to α6β1/2δ $GABA_A$ receptors. Previously, α6βδ-subunit containing $GABA_A$ receptors have been identified in cerebellar granule cells (Nusser et al., 1998) whereas α4βδ receptors were found in hippocampal interneurons (Barnard et al., 1998).

Our study is one of the first to assess the biological efficacy of DS2 *in vivo*, and in doing so confirm the observation by Jensen et al. (2013) that DS2 has a limited ability to cross the BBB. In the studies by Jensen and colleagues, treatment with DS2, even at doses 10-fold higher than what we used in

the current study, DS2 failed to show any biological response when assessed for gross behavior, psychosis and pain. While the brain concentration we report of 1587 ng/ml (4.5 μM) following a single 10 mg/kg i.p. dose appears modest, the free fraction is only 1.2% of this and therefore, equates to a 45 nM dose equivalent to an ED1-ED5 for potentiating the effect of GABA at the α4β3δ receptors. In our studies, we observed a significant reduction of stroke infarct size and an improvement of functional outcomes after administration of two doses of 0.1 mg/kg DS2. According to our pharmacokinetic studies it can be expected that this dose would result in a total and free plasma concentration of 345 and 4.1 nM, respectively. The total and free DS2 brain concentration are estimated to be 45 and 0.54 nM after a dose of 0.1 mg/kg DS2. Such low brain concentrations are unlikely to elicit a biological effect. It still remains to be determined whether these low concentrations of DS2 can exert a local effect on extrasynaptic $GABA_A$ receptors. The lack of efficacy of DS2 at higher doses could be due to a couple of reasons: (1) potentially desensitization of the delta subunit at these slightly higher doses, which means DS2 may switch from having an agonist effect to having an antagonist effect, but most likely (2) the biphasic dose response is due to hormesis (Calabrese et al., 2017). The term hormesis, which means "to excite," was first described when researchers found some fungi from Red Cedar trees displayed a stimulatory effect at low-doses whilst having an inhibitory effect at high-dose for cell metabolism and survival (Calabrese et al., 2017). Such hormetic dose-responses have been reported previous for stroke, but mainly in a neuroprotective/preconditioning setting (Bradley et al., 2014). In addition, similar hormetic responses have also been extensively reported for cancer and inflammatory conditions (Calabrese, 2005). The mechanisms that underpin hormetic responses is poorly understood, but it is known that changes in intracellular signaling pathways are also altered and it could be an intrinsic cellular response that ensures neuronal activity does not get too out of balance. This is clearly an area that requires much needed work, especially when it comes to drug receptor interactions and pharmacokinetic responses.

In this study, we demonstrate that DS2 can act by dampening immune cell activation and inflammation, offering this as a novel mechanism of action for DS2. Innate and adaptive immune cells produce functional $GABA_A$ receptors (Fuks et al., 2012) where binding of GABA has been demonstrated to reduce inflammation (Reyes-Garcia et al., 2007). Mechanistically this has been linked to a GABA-mediated decrease in IL-1β, IL-6, and IL-12 production following LPS-stimulation of innate immune cells, including peritoneal macrophages (Reyes-Garcia et al., 2007; Bhat et al., 2010). Here we add to these observations by showing that the δ-subunit preferring $GABA_A$ agonist, DS2, reduced LPS-induced NF-kB activation in a murine macrophage cell line and decreased expression of co-stimulatory molecules in primary BMDCs. The influx of DCs into the brain increases dramatically post-stroke and is associated with elevated expression of co-stimulatory molecules MHCII, CD40, and CD80 (Gelderblom et al., 2009; Posel et al., 2014). The induction of these co-stimulatory molecules occurs following exposure to DAMPs that are derived from dying and necrotic cells in the post-ischemic hemisphere (Offner et al., 2006; Gelderblom et al., 2009; Felger et al., 2010). Mature DCs are able to present antigens on MHC molecules to T-cells (signal 1) and provide co-stimulation through CD40, CD80, and CD86 expression (signal 2) and cytokine secretion (signal 3). The initiation of an adaptive immune response has been linked to development of autoimmunity and worse outcomes in stroke patients (Becker et al., 2011). Reduced expression of the co-stimulatory markers seen after treatment of BMDCs with DS2 may therefore translate into decreased ability of DCs to stimulate autoimmune responses in the post-ischemic brain. Since administration of the δ-subunit-selective compound, DS2, led to a decreased inflammatory response in murine macrophages and BMDCs, it is tempting to speculate that the δ-subunit is a crucial component for elucidating anti-inflammatory responses through $GABA_A$ receptors. This is supported by studies showing good expression levels of the δ-subunit in a range of murine and human innate immune cells, such as peritoneal macrophages (Reyes-Garcia et al., 2007), human peripheral blood mononuclear cells (Alam et al., 2006), monocytes and immortalized monocytic cell lines (Wheeler et al., 2011).

Interestingly, expression of $GABA_A$ receptors and in particular the δ-subunit has also been found in resting, activated and encephalitogenic T-cells (Tian et al., 2004; Bjurstom et al., 2008). Even though it remains to be determined if DS2 has a direct effect on T-cells it is likely that DS2 modulates T-cells indirectly. Bhat et al. (2010) have previously demonstrated a direct effect of GABAergic agents on innate immune cells, which did not affect cytokine production or proliferation of T-cells directly. However, cytokines secreted by innate immune cells altered the function of T-cell, which was associated with delayed onset and reduced severity in an animal model of multiple sclerosis. This links a reduced activity of innate immune cells with downstream T-cell responses, known to have a major impact on neurological diseases (Brait et al., 2012; Anderson et al., 2014).

The production of pro-inflammatory cytokines and expression of activation markers on innate immune cells has been previously observed to impact the priming of naïve T-cells and drives the polarization of T-cells toward a distinct effector function (Martin-Fontecha et al., 2003; Joffre et al., 2009). In particular, polarization of γδ T-cells and αβ T-cells toward IL-17-producing subsets has been shown to negatively impact stroke recovery (Shichita et al., 2009). T-cells, producing IL-17 have been found in increased numbers in the blood of patients early after stroke onset and has also been observed in post-mortem brain tissue of stroke patients (Kostulas et al., 1999; Gelderblom et al., 2012). IL-17 also contributes to disruption of BBB tight junctions and neutrophil recruitment into the brain, resulting in further tissue damage (Kebir et al., 2007; Wang et al., 2009; Gelderblom et al., 2012). We report here that systemic administration of DS2 decreases blood cytokine levels of, IL-6, TNF-α, and IL-17, three days post-stroke, which suggests that DS2-mediated suppression of innate immune cell activation could be associated with reduced numbers of Il-17 producing cells infiltrating the brain. It should be noted however, that not all cytokines are suppressed, as IL-1β is still elevated indicating

that part of the innate immune system is most likely still active, the extent of which requires further investigation.

In addition to influencing immune cell phenotypes, inflammatory cytokines, such as TNF-α are able control the extent of immune cell entry into the CNS at the choroid plexus epithelium (Kunis et al., 2013). Here, TNF-α and interferon-γ synergistically promote the expression of trafficking molecules that promote the entry of leukocytes into the CNS under conditions of inflammation. Based on our data, it is possible to assume that the dampened systemic TNF-α levels following treatment with DS2, may inhibit the trafficking of immune cells through the choroid plexus and into the CNS. The reduction in systemic cytokine levels may also be interesting in the context of the recent discovery that innate immune cells originate from the skull bone marrow and migrate to the brain after ischemic injury (Herisson et al., 2018). The skull bone marrow can be reached by the systemic blood supply, containing drugs, such as DS2 and thus potentially impact the trafficking of leukocytes via modulation of cytokine and chemokine expression.

We show here that administration of DS2 attenuates peripheral cytokine levels, associated with inflammation. Recent work demonstrated that pro-inflammatory cytokines, such IL-1β affect the surface expression of $GABA_A$ receptor subunits, such as α_5, which impaired memory (Wang et al., 2012). We observed using DS2 that this also applies to δ-containing $GABA_A$ receptors. Increased cytokine levels could drive a delayed increase in extrasynaptic GABA signaling post-stroke (Clarkson et al., 2010). The relationship between blood cytokine levels and changes in extrasynaptic GABA currents has been reported, however, the mechanisms linking the two remain poorly understood. This could be happening in part via Phosphatidylinositol 3-Kinase/Akt signaling (Serantes et al., 2006). A change in cytokine production would most likely be mediated by the compound acting on immune cells directly and reducing the secretion of cytokines and not via alterations in GABA signaling. In support of this, we report that, DS2 show only limited brain exposure, and most likely dampens NF-kB activity in immune leading to reduced release of cytokines. This in turn could prevent the infiltration of immune cell and release of cytokines in the brain to alter GABA inhibitory currents. Increasing extrasynaptic GABA signaling does not trigger inflammatory processes, however, increased blood cytokine levels can elevate extrasynaptic GABA signaling. For this reason, compounds reducing cytokine production can be used within a day of stroke onset to reduce tissue damage. In addition, as the immune cell/inflammatory cascade is elevated across a protracted time window, starting treatment from day 3 post-stroke also modestly improve functional recovery. Interestingly, DS2 failed to dampen all pro-inflammatory cytokines, so the elevated IL-1β levels still present could possibly have an effect tonic inhibitory currents and still impair some recovery from happening.

In summary, we show here that increasing $GABA_A$ signaling early provides protection, improves motor function and reduces peripheral cytokine levels associated with inflammation. In addition, delaying treatment until 3-days post-stroke resulted in a modest effect to improve functional recovery. In summary, our results identify $GABA_A$ receptors containing the δ subunit as a novel target for stroke therapy and suggest peripheral inflammation as an important factor in driving cell death and impairing recovery post-stroke. However, it should be noted that dosing at these sites does appear to illicit a hormetic dose-response and the mechanisms that underpin this are yet to be ascertained.

DATA AVAILABILITY STATEMENT

The datasets generated for this study are available on request to the corresponding author.

AUTHOR CONTRIBUTIONS

SN, LB-B, EG, TJ, and AC acquired and analyzed the data, and critically revised the manuscript. SN, PA, KS-N, SY, and AC designed the experiments, analyzed the data, and prepared and edited the manuscript. All authors reviewed and approved the final version of the manuscript and have also agreed to be accountable for the content of the work.

FUNDING

This work was supported by a Health Research Council and Royal Society of New Zealand Project grants (AC). This publication was drafted during a New Zealand Lottery Health Postdoctoral Fellowship (SN).

ACKNOWLEDGMENTS

We thank Dr. Zabeen Lateef for technical advice on growing the RAW Blue cells and Professor Vernon Ward for providing these cells.

REFERENCES

Ahring, P. K., Bang, L. H., Jensen, M. L., Strobaek, D., Hartiadi, L. Y., Chebib, M., et al. (2016). A pharmacological assessment of agonists and modulators at alpha4beta2gamma2 and alpha4beta2delta GABAA receptors: the challenge in comparing apples with oranges. *Pharmacol. Res.* 111, 563–576. doi: 10.1016/j.phrs.2016.05.014

Alam, S., Laughton, D. L., Walding, A., and Wolstenholme, A. J. (2006). Human peripheral blood mononuclear cells express GABAA receptor subunits. *Mol. Immunol.* 43, 1432–1442. doi: 10.1016/j.molimm.2005.07.025

Amantea, D., Micieli, G., Tassorelli, C., Cuartero, M. I., Ballesteros, I., Certo, M., et al. (2015). Rational modulation of the innate immune system for neuroprotection in ischemic stroke. *Front. Neurosci.* 9:147. doi: 10.3389/fnins.2015.00147

Anderson, K. M., Olson, K. E., Estes, K. A., Flanagan, K., Gendelman, H. E., and Mosley, R. L. (2014). Dual destructive and protective roles of adaptive immunity in neurodegenerative disorders. *Transl. Neurodegener.* 3:25. doi: 10.1186/2047-9158-3-25

Barnard, E. A., Skolnick, P., Olsen, R. W., Mohler, H., Sieghart, W., Biggio, G., et al. (1998). International union of pharmacology. XV. Subtypes of gamma-aminobutyric acidA receptors: classification on the basis of subunit structure and receptor function. *Pharmacol. Rev.* 50, 291–313.

Becker, K. J., Kalil, A. J., Tanzi, P., Zierath, D. K., Savos, A. V., Gee, J. M., et al. (2011). Autoimmune responses to the brain after stroke are associated with worse outcome. *Stroke* 42, 2763–2769. doi: 10.1161/STROKEAHA.111.619593

Bhat, R., Axtell, R., Mitra, A., Miranda, M., Lock, C., Tsien, R. W., et al. (2010). Inhibitory role for GABA in autoimmune inflammation. *Proc. Natl. Acad. Sci. U.S.A.* 107, 2580–2585. doi: 10.1073/pnas.0915139107

Bjurstom, H., Wang, J., Ericsson, I., Bengtsson, M., Liu, Y., Kumar-Mendu, S., et al. (2008). GABA, a natural immunomodulator of T lymphocytes. *J. Neuroimmunol.* 205, 44–50. doi: 10.1016/j.jneuroim.2008.08.017

Bradley, E., Zhao, X., Wang, R., Brann, D., Bieberich, E., and Wang, G. (2014). Low dose Hsp90 inhibitor 17AAG protects neural progenitor cells from ischemia induced death. *J. Cell Commun. Signal* 8, 353–362. doi: 10.1007/s12079-014-0247-5

Brait, V. H., Arumugam, T. V., Drummond, G. R., and Sobey, C. G. (2012). Importance of T lymphocytes in brain injury, immunodeficiency, and recovery after cerebral ischemia. *J. Cereb. Blood Flow Metab.* 32, 598–611. doi: 10.1038/jcbfm.2012.6

Brait, V. H., Jackman, K. A., Walduck, A. K., Selemidis, S., Diep, H., Mast, A. E., et al. (2010). Mechanisms contributing to cerebral infarct size after stroke: gender, reperfusion, T lymphocytes, and Nox2-derived superoxide. *J. Cereb. Blood Flow Metab.* 30, 1306–1317. doi: 10.1038/jcbfm.2010.14

Braun, M., Wendt, A., Birnir, B., Broman, J., Eliasson, L., Galvanovskis, J., et al. (2004). Regulated exocytosis of GABA-containing synaptic-like microvesicles in pancreatic beta-cells. *J. Gen. Physiol.* 123, 191–204. doi: 10.1085/jgp.200308966

Calabrese, E. J. (2005). Hormetic dose-response relationships in immunology: occurrence, quantitative features of the dose response, mechanistic foundations, and clinical implications. *Crit. Rev. Toxicol.* 35, 89–295. doi: 10.1080/10408440590917044

Calabrese, E. J., Calabrese, V., and Giordano, J. (2017). The role of hormesis in the functional performance and protection of neural systems. *Brain Circ.* 3, 1–13. doi: 10.4103/2394-8108.203257

Carmichael, S. T. (2012). Brain excitability in stroke: the yin and yang of stroke progression. *Arch. Neurol.* 69, 161–167. doi: 10.1001/archneurol.2011.1175

Clarkson, A. N., Boothman-Burrell, L., Dosa, Z., Nagaraja, R. Y., Jin, L., Parker, K., et al. (2019). The flavonoid, 2'-methoxy-6-methylflavone, affords neuroprotection following focal cerebral ischaemia. *J. Cereb. Blood Flow Metab.* 39, 1266–1282. doi: 10.1177/0271678X18755628

Clarkson, A. N., Huang, B. S., Macisaac, S. E., Mody, I., and Carmichael, S. T. (2010). Reducing excessive GABA-mediated tonic inhibition promotes functional recovery after stroke. *Nature* 468, 305–309. doi: 10.1038/nature09511

Clarkson, A. N., Lopez-Valdes, H. E., Overman, J. J., Charles, A. C., Brennan, K. C., and Thomas Carmichael, S. (2013). Multimodal examination of structural and functional remapping in the mouse photothrombotic stroke model. *J. Cereb. Blood Flow Metab.* 33, 716–723. doi: 10.1038/jcbfm.2013.7

Clarkson, A. N., Overman, J. J., Zhong, S., Mueller, R., Lynch, G., and Carmichael, S. T. (2011). AMPA receptor-induced local brain-derived neurotrophic factor signaling mediates motor recovery after stroke. *J. Neurosci.* 31, 3766–3775. doi: 10.1523/jneurosci.5780-10.2011

Clarkson, A. N., Parker, K., Nilsson, M., Walker, F. R., and Gowing, E. K. (2015). Combined ampakine and BDNF treatments enhance poststroke functional recovery in aged mice via AKT-CREB signaling. *J. Cereb. Blood Flow Metab.* 35, 1272–1279. doi: 10.1038/jcbfm.2015.33

Corbett, D., Carmichael, S. T., Murphy, T. H., Jones, T. A., Schwab, M. E., Jolkkonen, J., et al. (2017). Enhancing the alignment of the preclinical and clinical stroke recovery research pipeline: consensus-based core recommendations from the stroke recovery and rehabilitation roundtable translational working group. *Int. J. Stroke* 12, 462–471. doi: 10.1177/1747493017711814

Cutler, L., Howes, C., Deeks, N. J., Buck, T. L., and Jeffrey, P. (2006). Development of a P-glycoprotein knockout model in rodents to define species differences in its functional effect at the blood-brain barrier. *J. Pharm. Sci.* 95, 1944–1953. doi: 10.1002/jps.20658

Dobkin, B. H. (2008). Training and exercise to drive poststroke recovery. *Nat. Clin. Pract. Neurol.* 4, 76–85. doi: 10.1038/ncpneuro0709

Downes, C. E., and Crack, P. J. (2010). Neural injury following stroke: are toll-like receptors the link between the immune system and the CNS? *Br. J. Pharmacol.* 160, 1872–1888. doi: 10.1111/j.1476-5381.2010.00864.x

Doyle, K. P., Quach, L. N., Sole, M., Axtell, R. C., Nguyen, T. V., Soler-Llavina, G. J., et al. (2015). B-lymphocyte-mediated delayed cognitive impairment following stroke. *J. Neurosci.* 35, 2133–2145. doi: 10.1523/JNEUROSCI.4098-14.2015

Drasbek, K. R., and Jensen, K. (2006). THIP, a hypnotic and antinociceptive drug, enhances an extrasynaptic GABAA receptor-mediated conductance in mouse neocortex. *Cereb. Cortex* 16, 1134–1141. doi: 10.1093/cercor/bhj055

Felger, J. C., Abe, T., Kaunzner, U. W., Gottfried-Blackmore, A., Gal-Toth, J., Mcewen, B. S., et al. (2010). Brain dendritic cells in ischemic stroke: time course, activation state, and origin. *Brain Behav. Immun.* 24, 724–737. doi: 10.1016/j.bbi.2009.11.002

Fuks, J. M., Arrighi, R. B., Weidner, J. M., Kumar Mendu, S., Jin, Z., Wallin, R. P., et al. (2012). GABAergic signaling is linked to a hypermigratory phenotype in dendritic cells infected by Toxoplasma gondii. *PLoS Pathog.* 8:e1003051. doi: 10.1371/journal.ppat.1003051

Gelderblom, M., Leypoldt, F., Steinbach, K., Behrens, D., Choe, C. U., Siler, D. A., et al. (2009). Temporal and spatial dynamics of cerebral immune cell accumulation in stroke. *Stroke* 40, 1849–1857. doi: 10.1161/STROKEAHA.108.534503

Gelderblom, M., Sobey, C. G., Kleinschnitz, C., and Magnus, T. (2015). Danger signals in stroke. *Ageing Res. Rev.* 24, 77–82. doi: 10.1016/j.arr.2015.07.004

Gelderblom, M., Weymar, A., Bernreuther, C., Velden, J., Arunachalam, P., Steinbach, K., et al. (2012). Neutralization of the IL-17 axis diminishes neutrophil invasion and protects from ischemic stroke. *Blood* 120, 3793–3802. doi: 10.1182/blood-2012-02-412726

Glykys, J., and Mody, I. (2007). Activation of GABAA receptors: views from outside the synaptic cleft. *Neuron* 56, 763–770. doi: 10.1016/j.neuron.2007.11.002

Go, A. S., Mozaffarian, D., Roger, V. L., Benjamin, E. J., Berry, J. D., Blaha, M. J., et al. (2014). Heart disease and stroke statistics–2014 update: a report from the American Heart Association. *Circulation* 129, e28–e292.

Greifzu, F., Schmidt, S., Schmidt, K. F., Kreikemeier, K., Witte, O. W., and Lowel, S. (2011). Global impairment and therapeutic restoration of visual plasticity mechanisms after a localized cortical stroke. *Proc. Natl. Acad. Sci. U.S.A.* 108, 15450–15455. doi: 10.1073/pnas.1016458108

Helft, J., Bottcher, J., Chakravarty, P., Zelenay, S., Huotari, J., Schraml, B. U., et al. (2015). GM-CSF mouse bone marrow cultures comprise a heterogeneous population of CD11c(+)MHCII(+) macrophages and dendritic cells. *Immunity* 42, 1197–1211. doi: 10.1016/j.immuni.2015.05.018

Herisson, F., Frodermann, V., Courties, G., Rohde, D., Sun, Y., Vandoorne, K., et al. (2018). Direct vascular channels connect skull bone marrow and the brain surface enabling myeloid cell migration. *Nat. Neurosci.* 21, 1209–1217. doi: 10.1038/s41593-018-0213-2

Huh, Y., Jung, J. W., Park, C., Ryu, J. R., Shin, C. Y., Kim, W. K., et al. (2003). Microglial activation and tyrosine hydroxylase immunoreactivity in the substantia nigral region following transient focal ischemia in rats. *Neurosci. Lett.* 349, 63–67. doi: 10.1016/s0304-3940(03)00743-2

Jensen, M. L., Wafford, K. A., Brown, A. R., Belelli, D., Lambert, J. J., and Mirza, N. R. (2013). A study of subunit selectivity, mechanism and site of action of the delta selective compound 2 (DS2) at human recombinant and rodent native GABA(A) receptors. *Br. J. Pharmacol.* 168, 1118–1132. doi: 10.1111/bph.12001

Joffre, O., Nolte, M. A., Sporri, R., Reis, E., and Sousa, C. (2009). Inflammatory signals in dendritic cell activation and the induction of adaptive immunity. *Immunol. Rev.* 227, 234–247. doi: 10.1111/j.1600-065X.2008.00718.x

Kebir, H., Kreymborg, K., Ifergan, I., Dodelet-Devillers, A., Cayrol, R., Bernard, M., et al. (2007). Human TH17 lymphocytes promote blood-brain barrier disruption and central nervous system inflammation. *Nat. Med.* 13, 1173–1175. doi: 10.1038/nm1651

Kostulas, N., Pelidou, S. H., Kivisakk, P., Kostulas, V., and Link, H. (1999). Increased IL-1beta, IL-8, and IL-17 mRNA expression in blood mononuclear cells observed in a prospective ischemic stroke study. *Stroke* 30, 2174–2179. doi: 10.1161/01.str.30.10.2174

Krakauer, J. W., Carmichael, S. T., Corbett, D., and Wittenberg, G. F. (2012). Getting neurorehabilitation right: what can be learned from animal models? *Neurorehabil. Neural Repair* 26, 923–931. doi: 10.1177/1545968312440745

Kuhn, S. A., Van Landeghem, F. K., Zacharias, R., Farber, K., Rappert, A., Pavlovic, S., et al. (2004). Microglia express GABA(B) receptors to modulate interleukin release. *Mol. Cell Neurosci.* 25, 312–322. doi: 10.1016/j.mcn.2003.10.023

Kunis, G., Baruch, K., Rosenzweig, N., Kertser, A., Miller, O., Berkutzki, T., et al. (2013). IFN-gamma-dependent activation of the brain's choroid plexus for CNS immune surveillance and repair. *Brain* 136, 3427–3440. doi: 10.1093/brain/awt259

Lee, H. J., Absalom, N. L., Hanrahan, J. R., Van Nieuwenhuijzen, P., Ahring, P. K., and Chebib, M. (2016). A pharmacological characterization of GABA, THIP and DS2 at binary alpha4beta3 and beta3delta receptors: GABA activates beta3delta receptors via the beta3(+)delta(-) interface. *Brain Res.* 1644, 222–230. doi: 10.1016/j.brainres.2016.05.019

Lie, M. E., Gowing, E. K., Johansen, N. B., Dalby, N. O., Thiesen, L., Wellendorph, P., et al. (2017). GAT3 selective substrate l-isoserine upregulates GAT3 expression and increases functional recovery after a focal ischemic stroke in mice. *J. Cereb. Blood Flow Metab.* 39, 74–88. doi: 10.1177/0271678X17744123

Liesz, A., Dalpke, A., Mracsko, E., Antoine, D. J., Roth, S., Zhou, W., et al. (2015). DAMP Signaling is a key pathway inducing immune modulation after brain injury. *J. Neurosci.* 35, 583–598. doi: 10.1523/JNEUROSCI.2439-14.2015

Liguz-Lecznar, M., and Kossut, M. (2013). Influence of inflammation on poststroke plasticity. *Neural Plast.* 2013:258582. doi: 10.1155/2013/258582

Martin-Fontecha, A., Sebastiani, S., Hopken, U. E., Uguccioni, M., Lipp, M., Lanzavecchia, A., et al. (2003). Regulation of dendritic cell migration to the draining lymph node: impact on T lymphocyte traffic and priming. *J. Exp. Med.* 198, 615–621. doi: 10.1084/jem.20030448

McGeer, P. L., Schwab, C., Parent, A., and Doudet, D. (2003). Presence of reactive microglia in monkey substantia nigra years after 1-methyl-4-phenyl-1,2,3,6-tetrahydropyridine administration. *Ann. Neurol.* 54, 599–604. doi: 10.1002/ana.10728

Mody, I. (2001). Distinguishing between GABA(A) receptors responsible for tonic and phasic conductances. *Neurochem. Res.* 26, 907–913.

Nusser, Z., Sieghart, W., and Somogyi, P. (1998). Segregation of different GABAA receptors to synaptic and extrasynaptic membranes of cerebellar granule cells. *J. Neurosci.* 18, 1693–1703. doi: 10.1523/jneurosci.18-05-01693.1998

Offner, H., Subramanian, S., Parker, S. M., Afentoulis, M. E., Vandenbark, A. A., and Hurn, P. D. (2006). Experimental stroke induces massive, rapid activation of the peripheral immune system. *J. Cereb. Blood Flow Metab.* 26, 654–665. doi: 10.1038/sj.jcbfm.9600217

Olsen, R. W., and Sieghart, W. (2009). GABA A receptors: subtypes provide diversity of function and pharmacology. *Neuropharmacology* 56, 141–148. doi: 10.1016/j.neuropharm.2008.07.045

Overman, J. J., Clarkson, A. N., Wanner, I. B., Overman, W. T., Eckstein, I., Maguire, J. L., et al. (2012). A role for ephrin-A5 in axonal sprouting, recovery, and activity-dependent plasticity after stroke. *Proc. Natl. Acad. Sci. U.S.A.* 109, E2230–E2239. doi: 10.1073/pnas.1204386109

Petty, F., Fulton, M., Kramer, G. L., Kram, M., Davis, L. L., and Rush, A. J. (1999). Evidence for the segregation of a major gene for human plasma GABA levels. *Mol. Psychiatry* 4, 587–589. doi: 10.1038/sj.mp.4000569

Posel, C., Uri, A., Schulz, I., Boltze, J., Weise, G., and Wagner, D. C. (2014). Flow cytometric characterization of brain dendritic cell subsets after murine stroke. *Exp. Transl. Stroke Med.* 6:11. doi: 10.1186/2040-7378-6-11

Reyes-Garcia, M. G., Hernandez-Hernandez, F., Hernandez-Tellez, B., and Garcia-Tamayo, F. (2007). GABA (A) receptor subunits RNA expression in mice peritoneal macrophages modulate their IL-6/IL-12 production. *J. Neuroimmunol.* 188, 64–68. doi: 10.1016/j.jneuroim.2007.05.013

Rudolph, U., and Knoflach, F. (2011). Beyond classical benzodiazepines: novel therapeutic potential of GABAA receptor subtypes. *Nat. Rev. Drug Discov.* 10, 685–697. doi: 10.1038/nrd3502

Rudolph, U., and Mohler, H. (2014). GABAA receptor subtypes: therapeutic potential in down syndrome, affective disorders, schizophrenia, and autism. *Annu. Rev. Pharmacol. Toxicol.* 54, 483–507. doi: 10.1146/annurev-pharmtox-011613-135947

Scheicher, C., Mehlig, M., Zecher, R., and Reske, K. (1992). Dendritic cells from mouse bone marrow: in vitro differentiation using low doses of recombinant granulocyte-macrophage colony-stimulating factor. *J. Immunol. Methods* 154, 253–264. doi: 10.1016/0022-1759(92)90199-4

Schmittgen, T. D., Zakrajsek, B. A., Mills, A. G., Gorn, V., Singer, M. J., and Reed, M. W. (2000). Quantitative reverse transcription-polymerase chain reaction to study mRNA decay: comparison of endpoint and real-time methods. *Anal. Biochem.* 285, 194–204. doi: 10.1006/abio.2000.4753

Semyanov, A., Walker, M. C., and Kullmann, D. M. (2003). GABA uptake regulates cortical excitability via cell type-specific tonic inhibition. *Nat. Neurosci.* 6, 484–490. doi: 10.1038/nn1043

Serantes, R., Arnalich, F., Figueroa, M., Salinas, M., Andres-Mateos, E., Codoceo, R., et al. (2006). Interleukin-1beta enhances GABAA receptor cell-surface expression by a phosphatidylinositol 3-kinase/Akt pathway: relevance to sepsis-associated encephalopathy. *J. Biol. Chem.* 281, 14632–14643. doi: 10.1074/jbc.m512489200

Shichita, T., Sugiyama, Y., Ooboshi, H., Sugimori, H., Nakagawa, R., Takada, I., et al. (2009). Pivotal role of cerebral interleukin-17-producing gammadeltaT cells in the delayed phase of ischemic brain injury. *Nat. Med.* 15, 946–950. doi: 10.1038/nm.1999

Sieghart, W. (1995). Structure and pharmacology of gamma-aminobutyric acidA receptor subtypes. *Pharmacol. Rev.* 47, 181–234.

Tian, J., Lu, Y., Zhang, H., Chau, C. H., Dang, H. N., and Kaufman, D. L. (2004). Gamma-aminobutyric acid inhibits T cell autoimmunity and the development of inflammatory responses in a mouse type 1 diabetes model. *J. Immunol.* 173, 5298–5304. doi: 10.4049/jimmunol.173.8.5298

Vardya, I., Hoestgaard-Jensen, K., Nieto-Gonzalez, J. L., Dosa, Z., Boddum, K., Holm, M. M., et al. (2012). Positive modulation of delta-subunit containing GABA(A) receptors in mouse neurons. *Neuropharmacology* 63, 469–479. doi: 10.1016/j.neuropharm.2012.04.023

Wafford, K. A., Van Niel, M. B., Ma, Q. P., Horridge, E., Herd, M. B., Peden, D. R., et al. (2009). Novel compounds selectively enhance delta subunit containing GABA a receptors and increase tonic currents in thalamus. *Neuropharmacology* 56, 182–189. doi: 10.1016/j.neuropharm.2008.08.004

Walker, M. C., and Semyanov, A. (2008). Regulation of excitability by extrasynaptic GABA(A) receptors. *Results Probl. Cell Differ.* 44, 29–48. doi: 10.1007/400_2007_030

Wang, D. D., Zhao, Y. F., Wang, G. Y., Sun, B., Kong, Q. F., Zhao, K., et al. (2009). IL-17 potentiates neuronal injury induced by oxygen-glucose deprivation and affects neuronal IL-17 receptor expression. *J. Neuroimmunol.* 212, 17–25. doi: 10.1016/j.jneuroim.2009.04.007

Wang, D. S., Zurek, A. A., Lecker, I., Yu, J., Abramian, A. M., Avramescu, S., et al. (2012). Memory deficits induced by inflammation are regulated by alpha5-subunit-containing GABAA receptors. *Cell Rep.* 2, 488–496. doi: 10.1016/j.celrep.2012.08.022

Wendt, A., Birnir, B., Buschard, K., Gromada, J., Salehi, A., Sewing, S., et al. (2004). Glucose inhibition of glucagon secretion from rat alpha-cells is mediated by GABA released from neighboring beta-cells. *Diabetes* 53, 1038–1045. doi: 10.2337/diabetes.53.4.1038

Wheeler, D. W., Thompson, A. J., Corletto, F., Reckless, J., Loke, J. C., Lapaque, N., et al. (2011). Anaesthetic impairment of immune function is mediated via GABA(A) receptors. *PLoS One* 6:e17152. doi: 10.1371/journal.pone.0017152

Wittenberg, G. F., and Schaechter, J. D. (2009). The neural basis of constraint-induced movement therapy. *Curr. Opin. Neurol.* 22, 582–588. doi: 10.1097/WCO.0b013e3283320229

Conflict of Interest: TJ and KS-N are employed by Saniona A/S.

The remaining authors declare that the research was conducted in the absence of any commercial or financial relationships that could be construed as a potential conflict of interest.

Copyright © 2019 Neumann, Boothman-Burrell, Gowing, Jacobsen, Ahring, Young, Sandager-Nielsen and Clarkson. This is an open-access article distributed under the terms of the Creative Commons Attribution License (CC BY). The use, distribution or reproduction in other forums is permitted, provided the original author(s) and the copyright owner(s) are credited and that the original publication in this journal is cited, in accordance with accepted academic practice. No use, distribution or reproduction is permitted which does not comply with these terms.

frontiers in Neuroscience

ORIGINAL RESEARCH
published: 07 November 2019
doi: 10.3389/fnins.2019.01180

Opposite Effects of Neuroprotective Cannabinoids, Palmitoylethanolamide, and 2-Arachidonoylglycerol on Function and Morphology of Microglia

*Urszula Hohmann†, Markus Pelzer†, Joshua Kleine, Tim Hohmann, Chalid Ghadban and Faramarz Dehghani**

Department of Anatomy and Cell Biology, Medical Faculty, Martin Luther University Halle-Wittenberg, Halle (Saale), Germany

OPEN ACCESS

Edited by:
Johannes Boltze, University of Warwick, United Kingdom

Reviewed by:
Livio Luongo, Second University of Naples, Italy
Meliha Karsak, University Medical Center Hamburg-Eppendorf, Germany
Natsuo Ueda, Kagawa University, Japan

***Correspondence:**
Faramarz Dehghani
Faramarz.Dehghani@medizin.uni-halle.de

†These authors have contributed equally to this work

Specialty section:
This article was submitted to Neurodegeneration, a section of the journal Frontiers in Neuroscience

Received: *15 May 2019*
Accepted: *18 October 2019*
Published: *07 November 2019*

Citation:
Hohmann U, Pelzer M, Kleine J, Hohmann T, Ghadban C and Dehghani F (2019) Opposite Effects of Neuroprotective Cannabinoids, Palmitoylethanolamide, and 2-Arachidonoylglycerol on Function and Morphology of Microglia. Front. Neurosci. 13:1180. doi: 10.3389/fnins.2019.01180

Various studies performed in cultured cells and in *in vivo* models of neuronal damage showed that cannabinoids exert a neuroprotective effect. The increase in cannabinoids and cannabinoid like substances after stroke has been postulated to limit the content of neuronal injury. As well-accepted, inflammation, and neuronal damage are coupled processes and microglial cells as the main intrinsic immunological effector within the brain play a central role in their regulation. Treatment with the endocannabinoid, 2-arachidonoylglycerol (2-AG) or the endocannabinoid-like substance, palmitoylethanolamide (PEA) affected microglial cells and led to a decrease in the number of damaged neurons after excitotoxical lesion in organotypic hippocampal slice cultures (OHSC). 2-AG activated abnormal cannabidiol (abn-CBD) receptor, PEA was shown to mediate neuroprotection via peroxisome proliferator-activated receptor (PPAR)α. Despite the known neuroprotective and anti-inflammatory properties, the potential synergistic effect, namely possible entourage effect after treatment with the combination of these two protective cannabinoids has not been examined yet. After excitotoxical lesion OHSC were treated with PEA, 2-AG or a combination of both and the number of damaged neurons was evaluated. To investigate the role of microglial cells in PEA and 2-AG mediated protection, primary microglial cell cultures were treated with lipopolysaccharide (LPS) and 2-AG, PEA or a combination of those. Thereafter, we measured NO production, ramification index, proliferation and PPARα distribution in microglial cells. While PEA or 2-AG alone were neuroprotective, their co-application vanished the protective effect. This behavior was independent of microglial cells. Furthermore, PEA and 2-AG had contrary effects on ramification index and on NO production. No significant changes were observed in the proliferation rate of microglial cells after treatment. The expression of PPARα was not changed upon stimulation with PEA or 2-AG, but the distribution was significantly altered. 2-AG and

PEA mediated neuroprotection was abolished when co-applied. Both cannabinoids exert contrary effects on morphology and function of microglial cells. Co-application of both cannabinoids with different targets did not lead to a positive additive effect as expected, presumably due to the contrary polarization of microglial cells.

Keywords: 2-arachidonoylglycerol, palmitoylethanolamide, peroxisome proliferator-activated receptor, neuroprotection, microglial cells

INTRODUCTION

Traumatic brain injury affects a high number of young adults and their hospitalization is still a significant public challenge (Meaney et al., 2014). During neuronal damage a complex series of mechanisms becomes activated (Dirnagl et al., 2003; Kunz et al., 2010). Energy failure leads to calcium overload, depolarization of neurons and release of neurotransmitters with consecutive excitotoxicity, induced through overstimulation from excitatory receptors like NMDA receptor. This cascade is followed by activation of proteolytic enzymes and release of reactive oxygen species, damaging mitochondria, followed by apoptosis and neuronal death (Bruce et al., 1995; Kunz et al., 2010). Injured neuronal tissue releases pro-inflammatory cytokines leading to migration of inflammatory cells to the damaged site and inflammation (Jassam et al., 2017). Microglial cells play a crucial role during this process of secondary neuronal damage since they are the immunocompetent cells of the central nervous system (Kettenmann et al., 2011).

Cannabinoids positively affect cellular and molecular processes during ischemic, excitotoxical, or traumatic brain injury and were shown to be protective in different models mostly via microglial cells. All kind, plant-derived (isolated from *Cannabis sativa*), endo- (animal-derived) and synthetic cannabinoids were shown to affect neuronal damage (Kreutz et al., 2007, 2009; Mechoulam and Shohami, 2007; Koch et al., 2011a,b; Grabiec et al., 2012; Fernández-Ruiz et al., 2015; Guida et al., 2017; Belardo et al., 2019; Impellizzeri et al., 2019). Using the model of excitotoxically lesioned OHSC the number of damaged neurons was significantly reduced after treatment with endocannabinoids, like *N*-arachidonoyl dopamine, 2-arachidonoylglycerol (2-AG) or PEA associated with altered microglial cell number but not the phytocannabinoid, Δ-9-tetrahydrocannabinol (Kreutz et al., 2007; Koch et al., 2011a; Grabiec et al., 2012).

2-AG was shown to induce protection after neuronal lesion and to reduce the amount of tumor necrosis factor α released from LPS activated microglial cells (Facchinetti et al., 2003). Both, PEA and 2-AG are produced in the central nervous system and upregulated after neuronal damage (Kondo et al., 1998; Panikashvili et al., 2001; Franklin et al., 2003) and were shown to exhibit neuroprotection in several *in vivo* and *in vitro* models (Koch et al., 2011a; Beggiato et al., 2018; Herrera et al., 2018). Anti-inflammatory effects of PEA were associated with PPARα activation (LoVerme et al., 2005; Koch et al., 2011a; Citraro et al., 2013), and induction of PPARα expression was related in parallel to protective effects (Genovese et al., 2008; Koch et al., 2011a). A recent study demonstrated the presence of PPARα in different brain regions on neurons, astrocytes and microglial cells (Warden et al., 2016). Effects of 2-AG were abolished by O-1918 and cannabidiol (CBD), both antagonists of the abn-CBD sensitive receptor (abn-CBDR) (Kreutz et al., 2009). Evidence for functional abn-CBDR in the brain was pharmacologically found on microglial cells (Franklin and Stella, 2003; Walter et al., 2003; Kreutz et al., 2009). Consequently, 2-AG mediated protection depends on the presence of microglial cells as confirmed by microglial cells depletion (Kohl et al., 2003; Kreutz et al., 2009).

2-AG mediated protective properties were demonstrated in a variety of animal models of degenerative neurological disorders including multiple sclerosis, Parkinson's disease, and Alzheimer's disease (Scotter et al., 2010; Pertwee, 2014; Mounsey et al., 2015) and *in vitro* in astrocytes exposed to oxygen-glucose deprivation (Wang et al., 2015, 2018). 2-AG is the most abundant endocannabinoid in the brain and known to bind and activate CB_1 and CB_2 receptors. The treatment with exogenous 2-AG attenuated neuronal damage *in vivo* partly via CB_1 and mimicked the effects reported after aplication of synthetic CB_2 agonists. Some effects were absent in $CB_1^{-/-}$ mice (Mechoulam and Shohami, 2007; Magid et al., 2019). Furthermore, Carrier et al. (2004) observed that 2-AG affected microglial cells via CB_2. However, in rat OHSC and after NMDA damage effects of 2-AG were not blocked by CB_1 or CB_2 antagonists but inhibited by abnormal cannabidiol sensitive receptor (abn-CBDR) antagonists. These results make an involvement of CB_1 or CB_2 in 2-AG mediated neuroprotection unlikely (Kreutz et al., 2009). Application of PEA improved neuronal survival *in vitro* in primary mouse cortical astrocyte-neuron co-cultures (Beggiato et al., 2018) and in cortical neurons after hypoxia (Portavella et al., 2018). PEA possessed further beneficial properties in animal models of degenerative neurological disorders including vascular dementia (Siracusa et al., 2017). PEA and anandamide, if administrated together reduced the pain response 100-fold more potently than both substances alone and induced stronger vascular effects (Calignano et al., 1998; Ho et al., 2008). Such a co-application of two active cannabinoids increased their efficacy via the so called entourage effect, which is an endogenous cannabinoid molecular regulation route (Ben-Shabat et al., 1998). Ben-Shabat et al. (1998) demonstrated for the first time, that two inactive compounds, namely 2-linoleoylglycerol and 2-palmitoylglycerol potentiate the binding of 2-AG to the CB_1 and thereby its effects. Additionally, 2-linoleoylglycerol significantly inhibited the inactivation of 2-AG. Similarly, PEA was reported to prevent the inactivation of anandamide (Jonsson et al., 2001;

Abbreviations: 2-AG, 2-arachidonoylglycerol; abn-CBD, abnormal cannabidiol; abn-CBDR, abn-CBD-sensitive receptor; CB, cannabinoid receptor; CBD, cannabidiol; div, day *in vitro*; iNOS, inducible nitric oxide synthase; LPS, lipopolysaccharide; NMDA, *N*-methyl-D -aspartate, NO, nitric oxide; OHSC, organotypic hippocampal slice cultures; PEA, palmitoylethanolamide; PPAR, peroxisome proliferator-activated receptor.

Ho et al., 2008) indicating possible entourage effect. Microglial cells, the main immune cell of the central nervous system, has a ramified morphology and is stationary, surveying its surrounding if in an undamaged and non-inflammatory state (Smith et al., 2012). In pathologies, like neuropathic pain CB_2 expression increased in parallel to appearance of activated microglial cells. CB_2 ligands significantly alleviated the pain indicating that microglial cells are a main target of cannabinoids (Zhang et al., 2003; Luongo et al., 2010). During neuronal damage microglial cells become amoeboid, migrate to the lesion site, proliferate and can be affected by cannabinoids, as for example PEA potentiates microglial cell motility (Franklin et al., 2003; Vinet et al., 2012). Microglial cells mediate neuroprotection, but can also contribute to the damage, e.g., by upregulation of iNOS, an enzyme producing toxic amounts of NO from L-arginine (Garry et al., 2015). 2-AG was shown to induce the iNOS expression and NO production (Lipina and Hundal, 2017) and to stimulate NO release in invertebrate immune cells via CB_1 (Stefano et al., 2000). Contrary, NO donors were found to be neuroprotective (Kakizawa et al., 2007). Little is known about the influence of endocannabinoids on arginase, which inhibits the production of NO as a competing regulatory enzyme in the arginase-NO-synthase regulatory system in microglial cells. In peripheral immune cells Δ-9-tetrahydrocannabinol and AM1241, an CB_2 agonist induced arginase 1 expression (Hegde et al., 2010; Ma et al., 2015).

Earlier studies consistently reported about increased levels of endocannabinoids, such as PEA or 2-AG after neuronal injury. A question is raised why the secondary neuronal damage can't be prevented despite the high presence of neuroprotective substances. Since both endocannabinoids 2-AG and PEA if applied exogenously were shown to be neuroprotective via abn-CBDR or PPARα respectively, we asked whether the neuroprotective potential of both is additive. To assess a potential entourage effect between 2-AG and PEA on neuroprotective properties OHSC were excitotoxically lesioned and treated with PEA, 2-AG or combination of both. As mentioned, PEA and 2-AG target microglial cells. Therefore, their effects on function and morphology of primary microglial cells were investigated in untreated or LPS stimulated cultures. Ramification index, NO production, proliferation index, and temporal PPARα distribution were determined overtime.

MATERIALS AND METHODS

All experiments involving animal material were performed in accordance with the directive 2010/63/EU of the European Parliament and the Council of the European Union (22.09.2010) and approved by local authorities of the State of Saxony-Anhalt (permission number: I11M18, date: 01.12.2012) protecting animals and regulating tissue collection used for scientific purposes.

Materials

2-Arachidonylglycerol (2-AG, 10 nM, stock solved in DMSO; Tocris, Minneapolis, MN, United States, cat No. 1298), Clodronate (100 μg/ml, stock solved in Aqua; Bayer Vital GmbH GB; PZN: 04299668), Palmitoylethanolamide (PEA, 10 nM, stock solved in DMSO, Tocris, cat No. 0879), LPS (10 ng/ml, stock solved in Aqua; Sigma-Aldrich, cat No. L8274) and NMDA (50 μM, stock solved in Aqua bidest., Sigma-Aldrich, cat No. M3262) were used and applied to the culture medium according to treatment protocol.

Cell Culture

Primary microglia astrocyte co-cultures were prepared from 1 day old Wistar rats and cultured, as described earlier (Kohl et al., 2003; Grabiec et al., 2012). Briefly brains were treated with 0.5 mg/mL DNAse (Worthington, Bedford, MA, United States) and 4 mg/mL trypsin (Merck Millipore, Billerica, MA, United States) solved in Hank's balanced salts solution (Invitrogen, Carlsbad, CA, United States). Cells were cultured in DMEM (Invitrogen, cat No. 41965-062) with 10% FBS (Invitrogen, cat No. 10500-062) and 1 ml streptomycin/penicillin (Invitrogen). After 10 days microglial cells were isolated from astrocytic monolayer and seeded into well plates.

For immunocytochemical analysis 50,000 cells were placed on glass cover slips coated with poly-L-lysin and allowed to attach for 3 h. Cannabinoids were applied for 48 h to determine the microglial cells morphology. Bromodeoxyuridine (BrdU) (0.01 mM, Sigma-Aldrich) was added to the culture medium 16 h before the fixation to assess proliferation. Intracellular distribution of PPARα was analyzed 1, 6, and 24 h after treatment. The cells were fixed with 4% paraformaldehyde (Sigma-Aldrich, Munich, Germany) for 10 min and stored in 0.02M PBS at 4°C for further analysis.

For NO measurement supernatant of 50,000 cells treated for 72 h with cannabinoids was collected and stored at −80°C until further analysis.

Organotypic Hippocampal Slice Cultures (OHSC)

Organotypic hippocampal slice cultures were prepared from 7 to 9 day old Wistar rats as reported earlier (Grabiec et al., 2012, 2017; Hagemann et al., 2013; Hohmann et al., 2017, 2019) and kept at 35°C in a fully humidified atmosphere with 5% (v/v) CO_2. Culture medium was changed every other day. After 6 days *in vitro* experiments were started. All slices despite the control groups were treated with NMDA (50 μM) for 4 h. OHSC were treated with PEA (10 nM) or 2-AG (10 nM) or their combination for 72 h. The NMDA treated set of excitotoxically damaged OHSC was supplemented with 2-AG, PEA or combination of both or left untreated to asses an effect on neuronal damage in region of dentate gyrus.

To investigate the role of microglial cells OHSC were incubated with 100 μg/ml clodronate from 1 to 6 day *in vitro* (div). Clodronic acid, a bisphosphonate, affects only cells of the monocytic lineage and leads to apoptosis of microglia and macrophages (Kohl et al., 2003) (**Figures 1**, **2A**).

All slice cultures were treated with propidium iodide (PI; Merck Millipore, cat No. 537059) 2 h prior to fixation to visualize

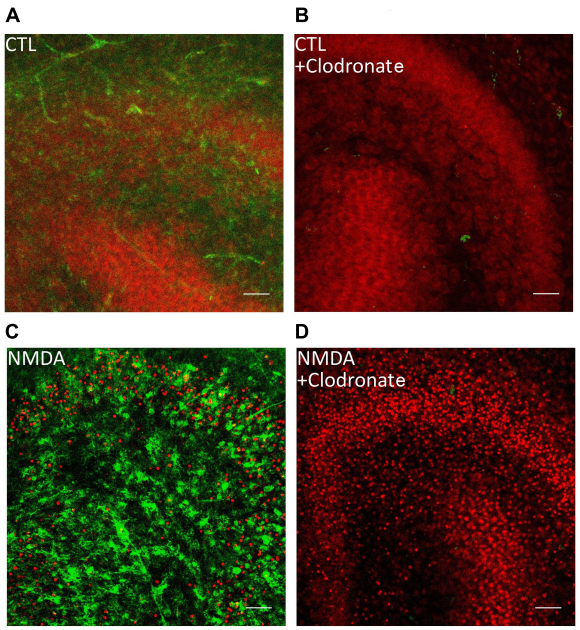

FIGURE 1 | Clodronate depletes microglial cells from OHSC. **(A)** PI labeled control OHSC with dentate gyrus and CA3. No PI positive nuclei (red) and ramified IB_4 (green) labeled microglial cells are visible. **(B)** Application of clodronate to CTL slices removed IB_4 positive microglial cells without damaging the neurons. **(C)** Treatment with NMDA led to massive increase in PI positive cells and IB_4 positive microglia. **(D)** Depletion of microglial cells led to exacerbation of neuronal damage after NMDA treatment in OHSC. Scale bar = 50 μm.

degenerated neurons (Ebrahimi et al., 2010; Grabiec et al., 2012, 2017; Hezel et al., 2012).

Immuno-, Lectinhistochemistry and Staining

All antibodies and lectins and conditions used are listed in **Table 1**. For labeling of incorporated BrdU fixed microglial cells were incubated with 2 mol/l HCl for 1 h, washed three times with PBS/Triton and pre-incubated with normal horse serum (Gibco BRL, Life Technologies, Eggenstein, Germany, cat No. 31874, dilution 1:20) in PBS/Triton. Afterward anti-BrdU antibody (**Table 1**) was applied for 1 h, followed by incubation with Alexa 488 conjugated goat anti-mouse antibody for 1 h. Cells were washed three times with PBS/Triton and incubated with 4′,6-diamidino-2-phenylindole (DAPI, Sigma-Aldrich, Munich, Germany, cat No. D9542).

Organotypic hippocampal slice cultures were stained with Alexa 488 conjugated IB_4 (Molecular Probes). All fluorescence stained slides were washed with PBS/Triton and Aqua dest. before covering with mounting medium (DAKO, Agilent Technologies, Inc., Santa Clara, CA, United States).

For measurement of ramification index biotin labeled IB_4 was used. To measure the PPARα distribution, an anti-PPARα antibody was applied as characterized before (Koch et al., 2011a). After washing with PBS, biotinylated goat anti-rabbit antibody

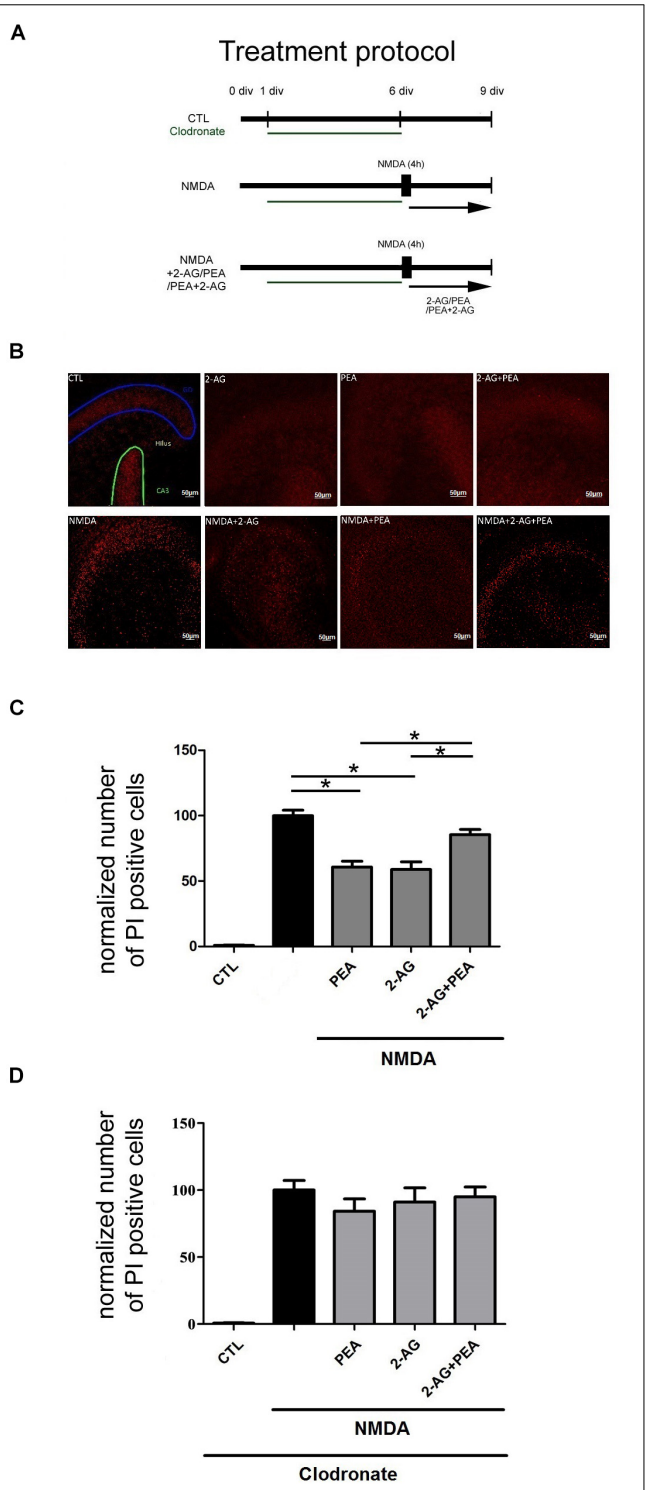

FIGURE 2 | Effects of 2-AG and PEA in excitotoxically damaged OHSC. 2-AG and PEA did not further decrease the number of PI positive degenerated neurons in comparison to OHSC treated with 2-AG or PEA alone.
(A) Treatment protocol. Control OHSC (CTL), were kept in culture medium and served as negative controls. The NMDA treated group function as positive control (NMDA). For microglial cells depleted groups clodronate (green) was applied from 1 div until 6 div. Cannabinoids were added alone on day 6 *in vitro*

(Continued)

FIGURE 2 | Continued
(div) to OHSC or following 4 h incubation with NMDA (NMDA+2-AG/PEA/PEA+2-AG). The fixation was performed on 9 div. **(B)** Representative images of the dentate gyrus in OHSC stained with PI (in red). After NMDA damage a massive increase in the number of damaged neurons occurred in comparison to control group (CTL), PEA, and 2-AG significantly reduced the neurodegeneration, but combination of both did not significantly reduce the number of PI positive nuclei. Dentate gyrus (GD) is highlighted in blue, Cornu ammonis (CA) 3 in green. Scale bar = 50 μm. **(C)** Quantitative analysis of PI positive nuclei in treated groups. The number of PI positive neurons increased significantly after treatment with NMDA (n_{NMDA} = 42) in comparison to control group (n_{CTL} = 42). 2-AG, PEA alone or combination of both had no effect on viability of OHSC (n_{PEA} = 12, n_{2-AG} = 12, $n_{2-AG+PEA}$ = 10). Treatment with PEA ($n_{NMDA+PEA}$ = 23) or 2-AG ($n_{NMDA+2-AG}$ = 20) of excitotoxically damaged OHSC reduced significantly the number of PI positive cells. The combination of 2-AG and PEA after NMDA damage induced no significant protective effect ($n_{NMDA+2-AG+PEA}$ = 34). **(D)** Treatment of microglia depleted OHSC with NMDA induced a massive neuronal damage (n_{CTL} = 15, n_{NMDA} = 18). The application of PEA, 2-AG or combination of both to clodronate treated NMDA damaged OHSC had no significant effect on the number of PI positive cells ($n_{CLO+NMDA+2-AG}$ = 12, $n_{CLO+NMDA+PEA}$ = 12, $n_{CLO+NMDA+2-AG+PEA}$ = 14). Statistics was performed using a One-Way ANOVA with Bonferroni *post hoc* analysis and significance was chosen for $p < 0.05$. The asterisk denotes significant results regarding the respective measurement indicated with the bar. The values are served as a mean with standard error of the mean.

was applied for 1 h. The following subsequent steps were the same as for IB_4 staining: the cells were washed tree times with PBS and incubated with ExtrAvidin-Peroxidase for 1 h. After washing with PBS and Tris buffer, the slides were stained with 3,3′-Diaminobenzidine (DAB) (Sigma-Aldrich, cat No. D8001) and covered with Entallan (Merck Millipore, Darmstadt, Germany, cat No. 107960).

Microscopy and Analysis

For analysis of proliferation index, ramification index and PPARα staining five areas per cover slip were recorded with Leica DMi8 (Wetzlar, Germany) or Axioplan (Zeiss, Oberkochen, Germany) microscopes.

Proliferation index was represented as the ratio of BrdU positive cells to all DAPI positive cells. The BrdU positive cells were counted using image J v1.46r (National Institutes of Health, Laboratory for Optical and Computational Instrumentation, University of Wisconsin, Madison, WI, United States).

To evaluate the ramification of microglial cells, the surface of microglia was stained with IB_4 and the outlining of the cell was divided by the smallest convex hull around the cell. Values close to 1 correspond to strongly amoeboid cells while lower numbers represent ramified cells. The analysis was performed automatically using a self-written MatLab script (The MathWorks, Natick, MA, United States).

Next, the translocation of PPARα from the cytoplasm to the nucleus or vice versa was assessed after treatment with cannabinoids. PPARα staining was performed and manually evaluated by counting cells that showed a nuclear or/and cytoplasmic staining or were free of PPARα labeling. Results are presented as proportion of cells with a specific expression pattern relative to the total number of cells. For the calculation of the standard error of the mean in these experiments we used bootstrapping to calculate empirical standard deviations. Therefore all measurements were used and resampled 10,000 times. Afterward, the proportion of nuclear, cytoplasmic, nuclear+cytoplasmic location or no expression was calculated for each resampling and an empirical standard deviation and standard error of the mean was calculated.

The imaging of the fixed OHSC was performed using a confocal laser scanning microscope (LSM 510 Meta, Zeiss) with an excitation wavelength of 488 nm for IB_4 and 543 nm for PI. Emission was detected using a band-pass filter with $\Delta\lambda$ = 510–550 nm (IB_4) and $\Delta\lambda$ = 610–720 nm (PI). The dentate gyrus was visualized with a 20x objective, as a z-stack with a step width of 2 μm (Grabiec et al., 2012). The number of PI positive death cells in the obtained image stacks was analyzed using the maximal intensity projection and quantified using a self-written Matlab script.

Nitrite Assay

A standard solution was prepared by solving sodium nitrite in medium up to concentrations of 100, 50, 25, 12.5, 6.25, 3.125, and 1.5625 μM. The measured values were used for calculation of a standard curve. 50 μl of the standard solutions or 50 μl of the collected samples were analyzed in duplicate. After applying 50 μl of Griess reagent (Sigma-Aldrich) the extinction was measured after 15 min at 540 nm in a microplate reader (SynergyTM Mx, BioTek Instruments, Winooski, VT, United States). The nitrite concentrations for the samples were interpolated from the standard curves.

Statistical Analysis

Statistics was performed using the one-way ANOVA with Bonferroni post-test and significance was chosen for $p < 0.05$. All *p*-values refer to the respective controls of the same parameter of the same cell line or to the treatment with agonist for the respective receptor. All groups were normalized to the positive

TABLE 1 | Antibodies.

Name	Company	Number	Dilution	Antibody ID
Biotinylated goat anti-rabbit antibody	Sigma-Aldrich	B7389	1:100	
BrdU	DAKO	M0744	1:100	
Alexa 488 conjugated IB_4	Molecular Probes, Life Technologies, Eggenstein, Germany	I21411	1:500	AB_2314662
Biotin labeled IB_4	Vector Laboratories, Burlingame, CA, United States	B-1205	1:100	AB_2314661
ExtrAvidin-Peroxidase	Sigma-Aldrich	E2886	1:100	
PPARα	Thermo Fisher, Waltham, MA, United States	PA1-822A	1:500	AB_2165595

control. Statistics for cellular PPARα was performed using a Chi Square test and significance was chosen for $p < 0.05$. The values are served as a mean with standard error of the mean. The asterisk denotes significant results regarding the respective measurement indicated with the bar.

RESULTS

2-AG and PEA Do Not Further Decrease the Number of PI Positive Degenerated Neurons

The application of NMDA led to an increase in the number of PI positive cells in OHSC (100.0 ± 4.24%) in comparison to control group (0.86 ± 0.28%, **Figures 2B,C**).

Treatment of NMDA lesioned OHSC with PEA (60.64 ± 4.52%) or 2-AG (58.78 ± 5.94%) induced a significant reduction of neuronal damage. Combination of 2-AG and PEA (85.46 ± 3.92%) in excitotoxically damaged OHSC did not decrease the number of dead cells in a significant manner (**Figures 2B,C**). Notably the values were not significantly different when compared to NMDA group, but significantly higher when compared to NMDA+2-AG or NMDA+ PEA groups.

Depletion of Microglial Cells Leads to Loss of Neuroprotection

The application of NMDA to microglia depleted OHSC (**Figure 1**) led to a significant increase in the number of PI positive cells (100.0 ± 7.12%) in comparison to control group (0.74 ± 0.17%, **Figure 2D**). The depletion of microglial cells was controlled through IB_4 staining (**Figure 1**).

Neither the application of PEA (84.19 ± 9.29%) nor 2-AG (91.04 ± 10.68%) to NMDA damaged microglia depleted OHSC induced a significant neuroprotective effect. Also, the combination of 2-AG and PEA (94.93 ± 7.42%) to excitotoxically damaged microglia depleted OHSC showed any significant effect on the number of dead neurons (**Figure 2D**).

Effects of 2-AG and PEA Treatment on Ramification Index

Application of PEA (0.72 ± 0.01) or 2-AG (0.75 ± 0.02) had no impact on ramification index in comparison to control group (0.73 ± 0.01). Treatment with LPS (0.89 ± 0.01) led to a more amoeboid morphology of cells. Co-application of LPS and PEA reduced the ramification index significantly (0.76 ± 0.03) making cells more ramified. Incubation with 2-AG did not change the ramification index (0.84 ± 0.01) in comparison to LPS. However, PEA and 2-AG application together with LPS induced significant reduction in ramification index (0.76 ± 0.02) (**Figures 3A,C**).

Effects of 2-AG and PEA on Nitrite Concentration

Application of PEA (0.19 ± 0.1%), 2-AG (0.14 ± 0.06%), or PEA+2-AG (0.76 ± 0.30%) did not change the nitrite concentration in comparison to control group (0.48 ± 0.22%). Treatment with LPS (100.0 ± 2.24%) led to an increased concentration of nitrite. Whereas co-application of LPS and PEA reduced the nitrite concentration significantly (81.06 ± 4.6%), incubation with 2-AG increased the nitrite concentration (128.2 ± 5.52%) in comparison to LPS. The same increase was detected for application of 2-AG+ PEA+ LPS (134.5 ± 7.11%) (**Figure 3E**).

Effect of 2-AG and PEA on Proliferation of Primary Microglial Cells

After incubation with LPS (0.07 ± 0.01), PEA (0.13 ± 0.04), or 2-AG (0.12 ± 0.05) no significant changes in proliferation were detected in comparison to control group (0.097 ± 0.02). The results for PEA+2-AG (0.07 ± 0.02); LPS+PEA (0.07 ± 0.019); LPS+2-AG (0.09 ± 0.05); and LPS+PEA+2-AG (0.07 ± 0.03) were not significantly altered after treatment (**Figures 3B,D**). The overall test showed no significant differences between the groups.

PPARα Distribution and Cellular Localization After Incubation With 2-AG and PEA

The evaluation of the localization of the PPARα receptor was significantly altered for treated groups overtime (1, 6, 24 h) (**Figures 4A–E**). The positive staining was localized in the cytoplasm and in the nucleus. The subcellular location was scored in 483 (1 h), 362 (6 h), and 337 (24 h) cells by light microscopy and presented as percentage. Each independent experiment was repeated at least three times (n = 3). The number of cells expressing nuclear as compared to cytoplasmic PPARα was significantly different between groups. Treatment with PEA; 2-AG; and LPS induced a significant shift in PPARα distribution after 1 and 6 h from nuclear to cytoplasmic and from cytoplasmic to nuclear localization. PEA and LPS changed significantly the localization of the receptor after 24 h (**Figures 4A–C**). The distribution was significantly different between 2-AG (Nucleus, N: 36%, Cytoplasm, C:21%, Both, B:33%, No signal, None:10%) and 2-AG co-applied with PEA (N:50%, C:4%, B:43%, None:4%) after 1 h, between PEA (N:49%, C:11%, B:38%, None:2%) and 2-AG+PEA (N:22%, C:11%, B:51%, None:16%) after 6 h and between PEA (N:51%, C:3%, B:36%, None:10%) or 2-AG (N:11%, C:7%, B:83%, None:0%) and 2-AG+PEA (N:29%, C:2%, B:66%, None:2%) after 24 h. PEA ($N_{1\ h}$:51%, $C_{1\ h}$:5%, $B_{1\ h}$:17%, $None_{1\ h}$:27%; $N_{6\ h}$:61%, $C_{6\ h}$:7%, $B_{6\ h}$:18%, $None_{6\ h}$:14%), 2-AG ($N_{1\ h}$:67%, $C_{1\ h}$:3%, $B_{1\ h}$:29%, $None_{1\ h}$:1%; $N_{6\ h}$:30%, $C_{6\ h}$:11%, $B_{6\ h}$:34%, $None_{6\ h}$:26%) and PEA+2-AG ($N_{1\ h}$:54%, $C_{1\ h}$:14%, $B_{1\ h}$:20%, $None_{1\ h}$:12%; $N_{6\ h}$:21%, $C_{6\ h}$:21%, $B_{6\ h}$:35%, $NS_{6\ h}$:23%) changed significantly the localization of PPARα after 1 and 6 h in combination with LPS (vs. LPS; $N_{1\ h}$:25%, $C_{1\ h}$:15%, $B_{1\ h}$:53%, $None_{1\ h}$:7%; $N_{6\ h}$:67%, $C_{6\ h}$:10%, $B_{6\ h}$:20%, $None_{6\ h}$:3%). No effect could be observed for LPS+PEA (N: 22%, C: 3%, B: 69%, None: 6%) in comparison to LPS (N: 28%, C: 2%, B: 56%, None: 14%) after 24 h, but 2-AG (N: 27%, C: 2%, B: 69%, None: 2%) and 2-AG+PEA (N: 20%, C: 0%, B: 80%, None: 0%) if co-applied

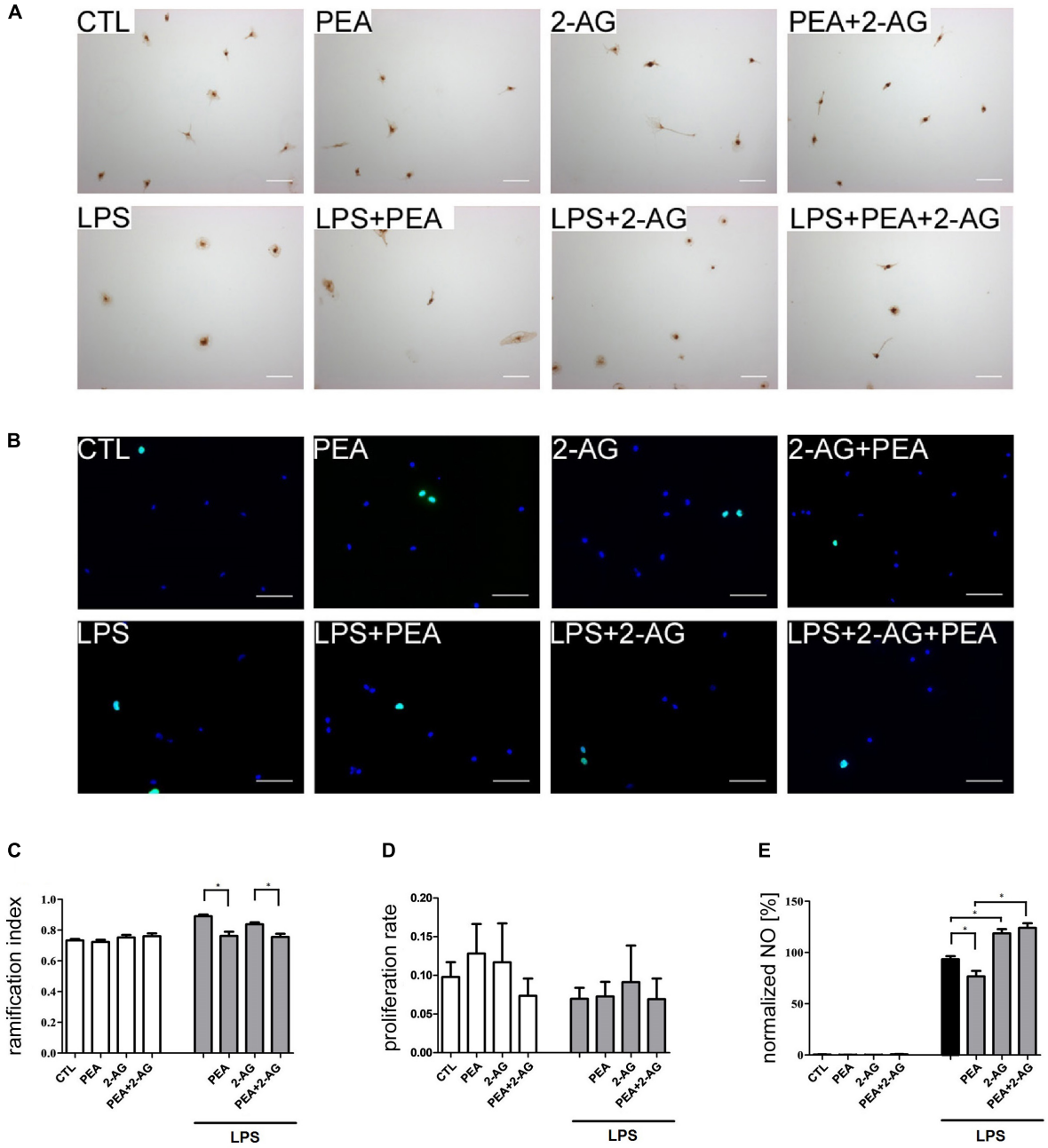

FIGURE 3 | Effect of 2-AG and PEA on ramification index, proliferation index and nitrite concentration of primary rat microglia. Representative pictures of stained microglia for **(A)** ramification index (IB_4) and **(B)** proliferation rate (BrdU in green, DAPI in blue). Scale bar = 50 μm. **(C)** Effects of 2-AG and PEA on ramification index. Application of LPS (n_{LPS} = 22) led to an increase in the ramification index in comparison to control group (CTL; n_{CTL} = 22). Whereas PEA co-applied with LPS ($n_{LPS+PEA}$ = 23) reduced the ramification index significantly, 2-AG ($n_{LPS+2-AG}$ = 23) had no effect. 2-AG, PEA, or combination of both applied alone (n_{PEA} = 19, n_{2-AG} = 22, $n_{2-AG+PEA}$ = 22) had no effect on ramification index. The combination of LPS, 2-AG and PEA ($n_{LPS+2-AG+PEA}$ = 22) led to decrease in the ramification index in comparison to the groups treated with LPS and 2-AG. **(D)** No effect of 2-AG and PEA with/or without LPS on proliferation of primary microglia cells could be observed (n_{CTL} = 12, n_{LPS} = 12, n_{PEA} = 11, n_{2-AG} = 11, $n_{2-AG+PEA}$ = 12, $n_{LPS+PEA}$ = 12, $n_{LPS+2-AG}$ = 11, $n_{LPS+2-AG+PEA}$ = 12). **(E)** Effects of 2-AG and PEA on nitrite concentration after 72 h. PEA, 2-AG, or PEA combined with 2-AG had no effect on the nitrite concentration in primary microglia (n_{CTL} = 18, n_{PEA} = 18, n_{2-AG} = 18, $n_{2-AG+PEA}$ = 18). After administration of LPS, nitrite concentration increased significantly. PEA co-applied with LPS ($n_{LPS+PEA}$ = 18) decreased the NO production in comparison to LPS (n_{LPS} = 18). 2-AG+LPS ($n_{LPS+2-AG}$ = 18) and also 2-AG+PEA+LPS ($n_{LPS+2-AG+PEA}$ = 18) treated microglia produced significantly more NO in comparison to LPS. Statistics was performed using a one-way ANOVA test with Bonferroni correction and significance was chosen for $p < 0.05$. The asterisk denotes significant results regarding the respective measurement indicated with the bar. The values are served as a mean with standard error of the mean.

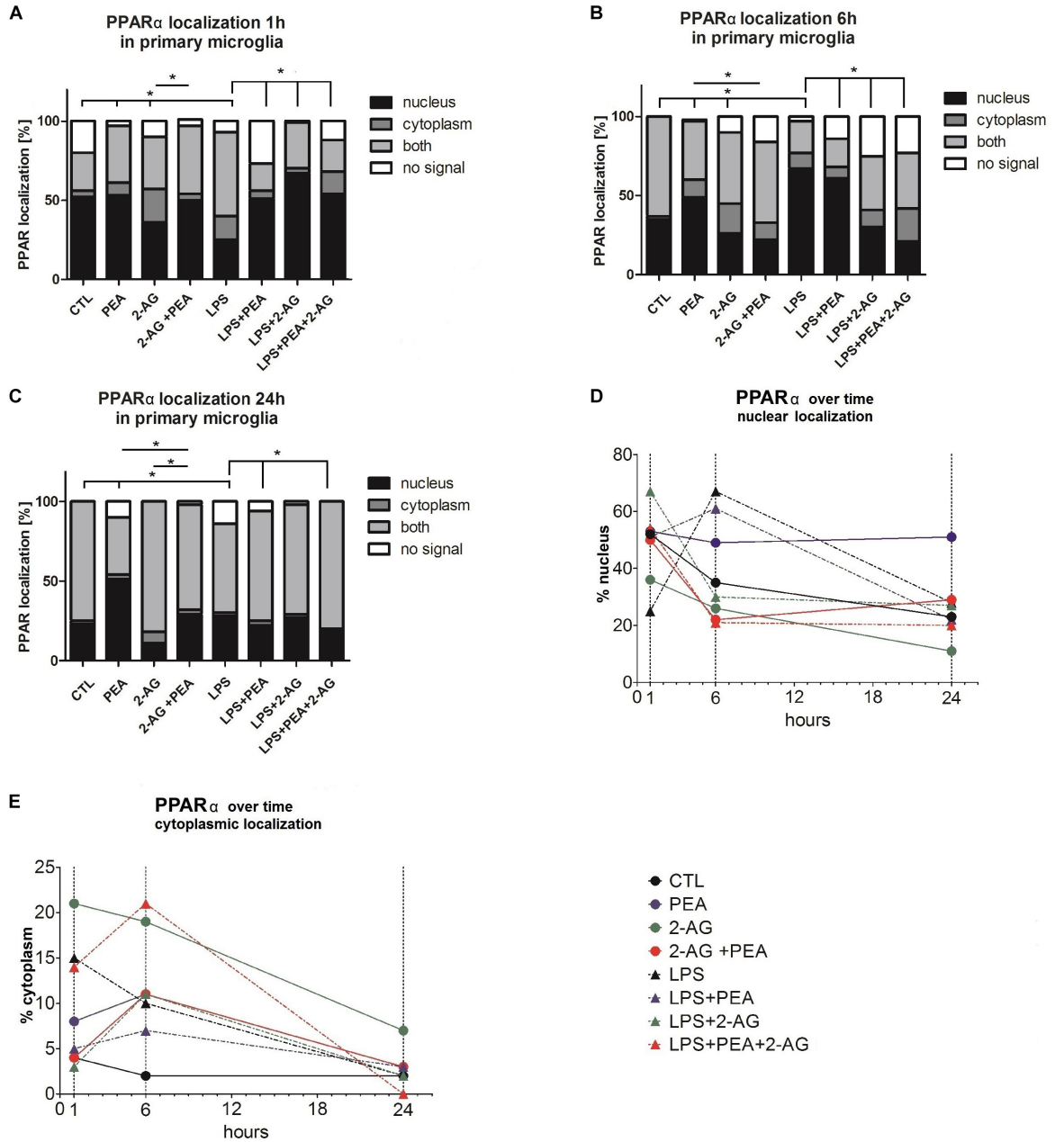

FIGURE 4 | PPARα subcellular distribution and cellular localization after incubation with 2-AG and PEA in primary microglial cells. The localization of PPARα was analyzed over time by the use of staining **(A–C)** 1, 6, and 24 h after treatment, **(D)** nuclear, **(E)** cytoplasmic localization (1, 6, and 24 h after treatment). The number of cells which did not or expressed PPARα in the nucleus or/and cytoplasm was counted. In graphs **(A–E)** the subcellular location was scored in 483 (1 h), 362 (6 h), and 337 (24 h) cells by light microscopy and presented as percentage. Each independent experiment was repeated at least three times. The same data are displayed in two different ways to point out the differences in the distribution **(A–C)** between the time points for cytoplasmic and nuclear localization **(D,E)**. Statistics was performed using a Chi Square test and significance was chosen for $p < 0.05$. The asterisk denotes significant results regarding the respective measurement indicated with the bar. The values are served as a mean with standard error of the mean.

with LPS altered significantly the distribution (**Figures 4A–C** and **Table 2**).

Lipopolysaccharide alone induced a shift to nuclear localization after 6 h, whereas LPS+PEA+2-AG after 6 h led to more cytoplasmic expression, similar to 2-AG and PEA alone (**Figures 4D,E**).

DISCUSSION

Reduction of neuronal damage in injured patients is a main contributor to sustain quality of life, for this reason its improvement and new approaches are needed. Evidence has accumulated that endocannabinoids can be beneficial for

TABLE 2 | PPARα subcellular distribution and cellular localization after incubation with 2-AG and PEA in primary microglial cells.

	Mean	SEM	Mean	SEM	Mean	SEM	Mean	SEM	Mean	SEM	Mean	SEM	Mean	SEM
Localization	**CTL**		**PEA**		**2-AG**		**2-AG+PEA**		**LPS**		**LPS+PEA**		**LPS+2-AG**		**LPS+2-AG+PEA**	
1 h																
Nucleus	0.53	0.01	0.39	0.01	0.30	0.01	0.34	0.01	0.18	0.01	0.26	0.02	0.65	0.01	0.38	0.01
Cytoplasm	0.04	0.00	0.06	0.00	0.18	0.01	0.03	0.01	0.10	0.00	0.03	0.01	0.03	0.00	0.10	0.00
Both	0.24	0.01	0.26	0.01	0.28	0.01	0.29	0.01	0.36	0.01	0.09	0.01	0.29	0.01	0.14	0.01
No signal	0.20	0.01	0.03	0.00	0.09	0.00	0.03	0.01	0.05	0.00	0.14	0.01	0.01	0.00	0.09	0.00
6 h																
Nucleus	0.35	0.01	0.51	0.01	0.22	0.01	0.20	0.01	0.51	0.01	0.53	0.01	0.27	0.01	0.18	0.01
Cytoplasm	0.02	0.00	0.12	0.01	0.16	0.01	0.10	0.01	0.08	0.01	0.06	0.01	0.10	0.01	0.18	0.01
Both	0.63	0.01	0.39	0.01	0.37	0.01	0.45	0.01	0.16	0.01	0.16	0.01	0.31	0.01	0.29	0.01
No signal	0.00	0.00	0.02	0.00	0.08	0.01	0.14	0.01	0.02	0.00	0.12	0.01	0.24	0.01	0.20	0.01
24 h																
Nucleus	0.23	0.01	0.50	0.01	0.13	0.01	0.30	0.01	0.30	0.01	0.18	0.01	0.35	0.01	0.23	0.01
Cytoplasm	0.03	0.00	0.03	0.00	0.08	0.01	0.03	0.00	0.03	0.00	0.03	0.01	0.03	0.00	0.00	0.00
Both	0.75	0.01	0.35	0.01	0.95	0.01	0.68	0.01	0.60	0.01	0.55	0.01	0.90	0.01	0.90	0.01
No signal	0.00	0.00	0.10	0.01	0.00	0.00	0.03	0.00	0.15	0.01	0.05	0.01	0.03	0.00	0.00	0.00

Rounded mean values (two positions) and SEM.

treatment of patients with brain injury (Fernandez-Ruiz et al., 2010). Cannabinoids, as shown before have different targets and are potential therapeutics, but first it is necessary to better understand the molecular and cellular mechanisms of cannabinoid action.

The Protective Effects of 2-AG and PEA Are Abolished, When Both Are Applied Together

In this study, we focused on excitotoxicity, a main factor of neuronal damage as described before (Kunz et al., 2010; Lau and Tymianski, 2010). To investigate the intrinsic responses and to exclude interfering influences such as blood flow and infiltrating peripheral immune cells the well-established model of excitotoxic lesioned OHSC was chosen. Both, PEA and 2-AG were shown to be protective with microglia participation in NMDA lesioned OHSC before. In our previous studies we extensively examined the involvement of cannabinoid receptors in PEA and 2-AG mediated actions. Whereas PEA and the synthetic PPARα agonist Wy-14,643 protected dentate gyrus granule cells, treatment with the PPARα antagonist GW6471 blocked PEA-mediated neuroprotection. Selective activation or inhibition of PPARγ displayed no positive effect (Koch et al., 2011a). Interestingly, 2-AG induced neuroprotection was inhibited by cannabidiol (CBD) and O-1918 and mimicked by abn-CBD indicating the involvement of abn-CBDR. The 2-AG effects were not blocked by the specific CB_2 receptor antagonist (AM630). Depletion of microglial cells abolished the neuroprotection mediated by 2-AG or abn-CBD raising the hypothesis that the neuroprotective effects of 2-AG were abn-CBDR and microglia dependent (Kreutz et al., 2007, 2009). The abn-CBDR is a pharmacologically characterized non-CB_1/non-CB_2 receptor and has been first described on endothelial cells of rat mesenteric blood vessels (Járai et al., 1999; Pertwee et al., 2010), and has not been identified yet. PEA, 2-AG or their analogs were also protective in other models like moderate traumatic injury and reduced neuroinflammation (Panikashvili et al., 2001; Genovese et al., 2008; D'Agostino et al., 2012; Esposito et al., 2012; Mounsey et al., 2015; Guida et al., 2017; Belardo et al., 2019; Impellizzeri et al., 2019). In PPARα$^{-/-}$ mice PEA induced neuroprotection after spinal cord trauma was abolished, however involvement of further PPARs was suggested (Paterniti et al., 2013). The application of PEA was found to trigger the synthesis of 2-AG in human and canine plasma and enhance its effects on transient receptor potential cation channel subfamily V member 1 (TRPV1) in HEK-293 cells (Petrosino et al., 2016). In striatum PEA triggered the synthesis of 2-AG via GPR55 (Musella et al., 2017). These effects were referred to an entourage effect, which might be mediated through TRPV1 activation or inhibition of fatty acid amide hydrolase, with PEA as its substrate or activation of GPR55 (Jonsson et al., 2001; Smart et al., 2002). A further possible explanation is an allosteric modulation, which could explain that 2-AG and PEA abolished their neuroprotective properties in the OHSC model and reduced ramification index at PEA level. While TRPV1 was not found in OHSC, GPR55

was expressed in slices and was associated with neuroprotection (Grabiec et al., 2012; Kallendrusch et al., 2013). Consequently, GPR55 might be involved in the PEA mediated actions observed here. Furthermore, PEA was also shown to enhance the CB_2 expression via PPARα activation in macrophages (Guida et al., 2017). Increased number of CB_2 next to abn-CBDR can be activated by 2-AG and induce further effects. PEA at cellular level reduced ramification index, making cells more ramified whereas 2-AG had no impact on morphology of microglial cells. The decrease in neuroprotection mediated by co-treatment with both cannabinoids might be attributable to their effects on cellular level, especially on microglial cells, the conductor of the neuroprotective properties of 2-AG and PEA. An entourage effect with PEA as enhancer of the anti-inflammatory and anti-nociceptive activity of other endogenous compounds by potentiating their affinity for a receptor or by inhibiting their metabolic degradation (Skaper and Facci, 2014) is missing in OHSC in the context of neuroprotection.

Effects of PEA and 2-AG Are Microglia Dependent

Neuroprotective capabilities of microglial cells include synaptic stripping, induction of neurogenesis, phagocytosis, and maintenance of central nervous system homeostasis (Chen and Trapp, 2016). On the other hand microglial cells are also able to suppress neuroinflammation, protect nerve tissue by producing anti-inflammatory and tissue-repairing cytokines and factors (Colton, 2009). Microglial cells can contribute to neuronal damage via inflammation and release of cytotoxic substances as described earlier and are associated with neurodegenerative diseases, cognitive dysfunction in aging and dementia, epilepsy, and other conditions leading to brain inflammation and neuronal lesion (Ekdahl et al., 2003; Smith et al., 2012; Chhor et al., 2013). Cannabinoids were shown to interact with microglial cells in further pathological states and to change the morphology, activation and number of the cells (Zhang et al., 2003; Luongo et al., 2010; Guida et al., 2017).

After microglia depletion in OHSC with the bisphosphonate clodronate PEA and 2-AG lost their neuroprotective effects supporting the hypothesis that 2-AG, PEA exert their neuroprotective effects via microglial cells. PEA was shown before to induce migration and increase of motility of BV2 microglial cell line (Franklin et al., 2003; Guida et al., 2017). Notably, microglial cells produce both 2-AG and PEA (Muccioli et al., 2007; Muccioli and Stella, 2009) and their levels were found to be increased after focal cerebral ischemia (Franklin et al., 2003).

PEA and 2-AG Mediate Opposite Effects on Nitric Oxide Synthesis in Primary Microglial Cells

Endocannabinoids, which are in part produced by microglia, affect the ability of microglia cells to proliferate, phagocytize, and produce NO (Stella, 2009). NO production occurs enzymatically via a conversion of L-arginine to L-citrulline by NO synthase, competing with arginase for L-arginine as a substrate. iNOS is not expressed in healthy brain tissue under physiological conditions but its expression can be induced in astrocytes and microglial cells through trauma. iNOS induction starts several hours before NO is generated and involves transcription of mRNA and novel protein synthesis. iNOS is mainly expressed under inflammatory conditions and after transient ischemic periods and is known as an antimicrobial defense mechanism of the immune system (Vincent et al., 1998). The increase in NO driven by iNOS might be neurotoxic as it forms reactive nitrogen oxide species like peroxynitrite (Garry et al., 2015). It was reported that 2-AG alone stimulates the release of NO from human immune and vascular tissues and from invertebrate immune cells via CB_1 activation (Stefano et al., 2000). Contrary, in our study 2-AG or PEA applied alone had no effect on NO production by microglial cells after 72 h. However, LPS in combination with 2-AG increased NO concentration, although 2-AG was protective after NMDA damage. PEA was able to reduce NO production by microglial cells after LPS treatment. In accordance to this study PEA significantly inhibited the NO release induced by LPS in murine macrophage cell line RAW264.7, which was not sensitive to pertussis toxin treatment, indicating a G-protein independent mode of action (Ross et al., 2000). Pre-treatment of LPS-stimulated primary mouse microglial cells with PPARα agonists also resulted in inhibition of NO production (Xu et al., 2005). In similarity to PEA in murine macrophage cell line RAW264.7, WIN55,212, a neuroprotective cannabinoid decreased NO level when applied together with LPS via CB_2 receptor (Ross et al., 2000; Koch et al., 2011b). Furthermore, PEA reduced iNOS expression in spinal cord 6 h after paw edema induction (D'Agostino et al., 2007). The results presented in our study are in accordance with previous investigations and strengthen the hypothesis that PEA mediates neuroprotection via microglial cells. The neuroprotective effects observed here in the OHSC model underline the intrinsic positive effects of cannabinoids as influences through alterations in cerebral blood flow and infiltration of peripheral cells are missing (Grabiec et al., 2017), making the inhibition of NO produced by microglial cells one possible explanation for neuroprotection. In agreement with our work and previous studies LPS induces NO production mainly in microglial cells in models of excitotoxicity or during transient ischemic periods (Nakamura et al., 1999; Genovese et al., 2008; Yao et al., 2017). Further endocannabinoids were shown to decrease iNOS activity in rat microglial cells, e.g., CP55940 exerted a dose-dependent inhibition of interferon gamma /LPS-inducible NO production (Cabral et al., 2001) Little is known about the influence of endocannabinoids on arginase, in peripheral immune cells and in microglial N9 cells Δ-9- tetrahydrocannabinol and CB_2 agonist induced arginase 1 expression, what reduce NO production (Hegde et al., 2010; Ma et al., 2015).

Through combination treatment of both PEA and 2-AG, NO production was significantly elevated and neuroprotective properties were diminished. It leads to the hypothesis that PEA may be neuroprotective through reduction of NO present after brain injury. On the other hand, 2-AG significantly elevated NO production while still exerting neuroprotective effects similar

to NO donors (Kakizawa et al., 2007), 2-AG acts probably via another targets and mechanisms.

Changes in Morphology and Phenotypes of Primary Microglial Cells After Treatment

In vivo, *ex vivo,* and *in vitro* a broad spectrum of differentiation stages of microglial cells has been observed (Dubbelaar et al., 2018). Under physiological conditions microglial cells are ramified and constantly scanning their surroundings (Nimmerjahn et al., 2005). Upon damage or inflammation, they become amoeboid, move to the site of neuronal lesion and remove cell debris. However, this morphological change of microglia upon a shift in activation state does not seem to be uniform, but it can be best mimicked by administration of LPS. The morphology ranges from amoeboid-like shapes during inflammation to highly ramified ones and includes many intermediate forms that are often associated with the activation status of microglial cells (Zhou et al., 2017; Dubbelaar et al., 2018). According to the phenotype microglial cells were often described as anti-inflammatory or neuroprotective or proinflammatory and neurotoxic. However, there is no binary system of phenotypes for microglia and they may possess multiple context dependent properties at the same time (Ransohoff, 2016; Dubbelaar et al., 2018).

In synopsis with NO reduction, the administration of PEA to LPS stimulated microglial cells induced a more ramified morphology; these anti-inflammatory properties of PEA may mediate its neuroprotective effects. 2-AG did not alter the LPS induced amoeboid state of microglial cells but increased the NO concentration, indicating that the neuroprotective properties of 2-AG are mediated through other microglial cell dependent mechanisms than those involving NO. However, *in vivo* and in acute experimental autoimmune encephalomyelitis 2-AG increased the ramification of microglia (Lourbopoulos et al., 2011). In excitotoxically lesioned OHSC 2-AG reduced the number of microglial cells (Kreutz et al., 2007). It is plausible that the absence of changes is model dependent or that 2-AG influenced other properties of microglia, which were not examined in this study, like phagocytosis, motility, and alterations in extracellular signaling.

The combination of 2-AG and PEA induced a ramification of microglial cells in comparison to 2-AG and abolished PEA mediated NO concentration decrease. This may indicate that the anti-inflammatory properties of PEA are lost if co-incubated with 2-AG, since decrease in the number of damaged neurons in OHSC was missing and therefore neuroprotection. 2-AG and PEA exert contrary effects on microglial cells and it is plausible, that co-application of both led to their abolishment. Expected entourage effect is missing in case of this model and those substances.

It will be necessary to verify how 2-AG exerts neuroprotection at a cellular level and whether this process is microglia dependent only, since 2-AG was found protective in isolated neuronal cultures (Zhang and Chen, 2008). Interestingly, proliferation of pure microglial cell cultures was not affected in this study, whereas the number of microglial cells was significantly decreased in dentate gyrus in OHSC after excitotoxical damage and treatment with PEA or 2-AG, this effect was mimicked by PPARα agonists and blocked by its antagonists (Kreutz et al., 2007; Koch et al., 2011a). Since microglial cells in culture proliferate very slowly without astrocytes, it seems plausible that the effects observed in OHSC might be the result of PEA actions on astrocytes, microglia, possibly neurons in the network and/or their cross-talk, since all cell types express the PPARα receptor (Xu et al., 2006; Warden et al., 2016).

PPARα Expression and Localization Changed After Incubation With Cannabinoids

Peroxisome proliferator-activated receptors predominantly are localized in the nucleus, theirs activity is modulated via phosphorylation and PPARα undergoes ligand-dependent nucleo-cytoplasmic shuttling (Burns and Vanden Heuvel, 2007; Umemoto and Fujiki, 2012). The amount of PPARα was shown to increase in microglial cells in nucleus after 6 h and to decrease after 24 h after PEA treatment. PPARs are ligand-activated transcription factors, and their biological role is coupled to the function of their target genes. In immunocytochemical staining a translocation of PPARα into the nucleus was seen. Neuroprotective effects of PEA are known to be mediated by PPARα. On the one hand, the nuclear localization of the receptor induces specific PEA related effects; its shift into the cytoplasm reduces the amount of available receptor in the nucleus. On the other hand the cytoplasmic localization of PPARα may favor the binding of other ligands and mediate different actions (Guida et al., 2017). The lower levels of PPARα in nuclei of microglial cells after simultaneous treatment with 2-AG and PEA with or without LPS might be a possible explanation for the missing neuroprotection in OHSC. It also indicates an interference between 2-AG and PEA signaling pathways with a more dominant role of 2-AG and inhibitory actions on PPARs translocation into the nucleus. Specific activation of central PPARα controls inflammation in the spinal cord as well as in the periphery (D'Agostino et al., 2007), when the amount of receptor decreased no effect could be induced. Additionally, fatty acid oxygenase metabolism products of 2-AG were able to activate PPARα receptor in human undifferentiated epidermal keratinocytes and stimulation of PPARα and its downstream target genes led to cell differentiation (Kömüves et al., 2000; Kozak et al., 2002). It is plausible that 2-AG and PEA interact directly on PPARα receptor in the opposite way.

CONCLUSION

While endocannabinoids are promising regarding treatment of neuronal diseases, and their neuroprotective properties are known for a while, little is known how they are mediated. 2-AG and PEA are both protective agents with different targets. Their positive effect is not enhanced by co-incubation. The understanding of interactions between signaling pathways of

different endocannabinoids will help to elucide the in part conflicting results reported in the literature.

DATA AVAILABILITY STATEMENT

All datasets generated for this study are included in the article/supplementary material.

ETHICS STATEMENT

The animal study was reviewed and approved by the local authorities of the State of Saxony-Anhalt (permission number: I11M18, date: 01.12.2012) protecting animals and regulating tissue collection used for scientific purposes.

AUTHOR CONTRIBUTIONS

FD and UH: conceptualization, supervision, and project administration. MP, UH, TH, and JK: methodology and formal analysis. TH: software and data curation. MP, UH, TH, and FD: validation. MP, UH, JK, TH, and CG: investigation. FD: resources. UH and MP: visualization and writing original draft. UH, TH, JK, and FD: writing review and editing. All authors contributed to the manuscript revision, and read and approved the submitted version.

FUNDING

We acknowledge the financial support within the funding program Open Access Publishing by the German Research Foundation (DFG).

REFERENCES

Beggiato, S., Borelli, A. C., Ferraro, L., Tanganelli, S., Antonelli, T., and Cristina Tomasini, M. (2018). Palmitoylethanolamide blunts activation and improves neuronal survival in primary mouse cortical astrocytes-neuron co-cultures. *J. Alzheimer's Dis.* 61, 389–399. doi: 10.3233/JAD-170699

Belardo, C., Iannotta, M., Boccella, S., Rubino, R. C., Ricciardi, F., Infantino, R., et al. (2019). Oral cannabidiol prevents allodynia and neurological dysfunctions in a mouse model of mild traumatic brain injury. *Front. Pharmacol.* 10:352. doi: 10.3389/fphar.2019.00352

Ben-Shabat, S., Fride, E., Sheskin, T., Tamiri, T., Rhee, M.-R., Vogel, Z., et al. (1998). An entourage effect: inactive endogenous fatty acid glycerol esters enhance 2-arachidonoyl-glycerol cannabinoid activity. *Eur. J. Pharmacol.* 353, 23–31. doi: 10.1016/s0014-2999(98)00392-6

Bruce, A. J., Sakhi, S., Schreiber, S. S., and Baudry, M. (1995). Development of kainic acid and N-methyl-d-aspartic acid toxicity in organotypic hippocampal cultures. *Exp. Neurol.* 132, 209–219. doi: 10.1016/0014-4886(95)90026-8

Burns, K. A., and Vanden Heuvel, J. P. (2007). Modulation of PPAR activity via phosphorylation. *Biochim. Biophys. Acta* 1771, 952–960. doi: 10.1016/j.bbalip.2007.04.018.Modulation

Cabral, G. A., Harmon, K. N., and Carlisle, S. J. (2001). "Cannabinoid-mediated inhibition of inducible nitric oxide production by rat microglial cells: evidence for receptor participation," in *Neuroimmune Circuits, Drugs of Abuse, and Infectious Diseases*, eds H. Friedman, T. W. Klein, and J. J. Madden (Boston, MA: Springer), 207–214. doi: 10.1007/0-306-47611-8_24

Calignano, A., Rana, G., La Giuffrida, A., and Piomelli, D. (1998). Control of pain initiation by endogenous cannabinoids. *Nature* 394, 277–281. doi: 10.1038/28393

Carrier, E. J., Kearn, C. S., Barkmeier, A. J., Breese, N. M., Yang, W., Nithipatikom, K., et al. (2004). Cultured rat microglial cells synthesize the endocannabinoid 2-arachidonylglycerol, which increases proliferation via a CB 2 receptor-dependent mechanism. *Mol. Pharmacol.* 65, 999–1007. doi: 10.1124/mol.65.4.999

Chen, Z., and Trapp, B. D. (2016). Microglia and neuroprotection. *J. Neurochem.* 136, 10–17. doi: 10.1111/jnc.13062

Chhor, V., Le, T., Lebon, S., Oré, M.-V., Celador Lara, I., Josserand, J., et al. (2013). Brain, behavior, and immunity characterization of phenotype markers and neuronotoxic potential of polarised primary microglia *in vitro*. *Brain Behav. Immun.* 32, 70–85. doi: 10.1016/j.bbi.2013.02.005

Citraro, R., Russo, E., Scicchitano, F., Rijn, C. M., Van Cosco, D., Avagliano, C., et al. (2013). Neuropharmacology Antiepileptic action of N - palmitoylethanolamine through CB1 and PPAR- a receptor activation in a genetic model of absence epilepsy. *Neuropharmacology* 69, 115–126. doi: 10.1016/j.neuropharm.2012.11.017

Colton, C. A. (2009). Heterogeneity of microglial activation in the innate immune response in the brain. *J. Neuroimmune. Pharmacol.* 4, 399–418. doi: 10.1007/s11481-009-9164-4

D'Agostino, G., Rana, G., La Russo, R., Sasso, O., Iacono, A., Esposito, E., et al. (2007). Acute intracerebroventricular administration of palmitoylethanolamide, an endogenous peroxisome proliferator-activated receptor-alpha agonist, modulates carrageenan-induced paw edema in mice. *J. Pharmacol. Exp. Ther.* 332, 1137–1143. doi: 10.1124/jpet.107.123265

D'Agostino, G. D., Russo, R., Avagliano, C., Cristiano, C., Meli, R., and Calignano, A. (2012). Palmitoylethanolamide protects against the amyloid- B 25-35-induced learning and memory impairment in mice, an experimental model of alzheimer disease. *Neuropsychopharmacology* 37, 1784–1792. doi: 10.1038/npp.2012.25

Dirnagl, U., Simon, R. P., and Hallenbeck, J. M. (2003). Ischemic tolerance and endogenous neuroprotection. *Trends Neurosci.* 26, 248–254. doi: 10.1016/S0166-2236(03)00071-7

Dubbelaar, M. L., Kracht, L., Eggen, B. J. L., and Boddeke, E. W. G. M. (2018). The kaleidoscope of microglial phenotypes. *Front. Immunol.* 9:1753. doi: 10.3389/fimmu.2018.01753

Ebrahimi, F., Hezel, M., Koch, M., Ghadban, C., Korf, H. W., and Dehghani, F. (2010). Analyses of neuronal damage in excitotoxically lesioned organotypic hippocampal slice cultures. *Ann. Anat.* 192, 199–204. doi: 10.1016/j.aanat.2010.06.002

Ekdahl, C. T., Claasen, J., Bonde, S., Kokaia, Z., and Lindvall, O. (2003). Inflammation is detrimental for neurogenesis in adult brain. *PNAS* 100, 13632–13637.

Esposito, E., Impellizzeri, D., Mazzon, E., Paterniti, I., and Cuzzocrea, S. (2012). Neuroprotective activities of palmitoylethanolamide in an animal model of parkinson ' s disease. *PLoS One* 7:e41880. doi: 10.1371/journal.pone.0041880

Facchinetti, F., Del Giudice, E., Furegato, S., Passarotto, M., and Leon, A. (2003). Cannabinoids ablate release of TNFalpha in rat microglial cells stimulated. *Glia* 41, 161–168. doi: 10.1002/glia.10177

Fernandez-Ruiz, J., Garcia, C., Sagredo, O., Gomez-Ruiz, M., and de Lago, E. (2010). The endocannabinoid system as a target for the treatment of neuronal damage. *Expert Opin. Ther. Targets* 14, 387–404. doi: 10.1517/14728221003709792

Fernández-Ruiz, J., Moro, M. A., and Martínez-Orgado, J. (2015). Cannabinoids in neurodegenerative disorders and stroke / brain trauma: from preclinical models to clinical applications. *Neurotherapeutics* 12, 793–806. doi: 10.1007/s13311-015-0381-7

Franklin, A., Parmentier-batteur, S., Walter, L., Greenberg, D. A., and Stella, N. (2003). Palmitoylethanolamide increases after focal cerebral ischemia and

potentiates microglial cell motility. *J. Neurosci.* 23, 7767–7775. doi: 10.1523/jneurosci.23-21-07767.2003

Franklin, A., and Stella, N. (2003). Arachidonylcyclopropylamide increases microglial cell migration through cannabinoid CB 2 and abnormal-cannabidiol-sensitive receptors. *Eur. J. Pharmacol.* 474, 195–198. doi: 10.1016/S0014-2999(03)02074-0

Garry, P. S., Ezra, M., Rowland, M. J., Westbrook, J., and Pattinson, K. T. S. (2015). The role of the nitric oxide pathway in brain injury and its treatment — From bench to bedside. *Exp. Neurol.* 263, 235–243. doi: 10.1016/j.expneurol.2014.10.017

Genovese, T., Esposito, E., Mazzon, E., Paola, R., Di Meli, R., Bramanti, P., et al. (2008). Effects of palmitoylethanolamide on signaling pathways implicated in the development of spinal cord injury. *J. Pharmacol. Exp. Ther.* 326, 12–23. doi: 10.1124/jpet.108.136903.recent

Grabiec, U., Hohmann, T., Hammer, N., and Dehghani, F. (2017). Organotypic hippocampal slice cultures as a model to study neuroprotection and invasiveness of tumor cells. *J. Vis. Exp.* 126:e55359. doi: 10.3791/55359

Grabiec, U., Koch, M., Kallendrusch, S., Kraft, R., Hill, K., Merkwitz, C., et al. (2012). The endocannabinoid N-arachidonoyldopamine (n.d.) exerts neuroprotective effects after excitotoxic neuronal damage via cannabinoid receptor 1 (CB 1). *Neuropharmacology* 62, 1797–1807. doi: 10.1016/j.neuropharm.2011.11.023

Guida, F., Luongo, L., Boccella, S., Giordano, M. E., Romano, R., Bellini, G., et al. (2017). Palmitoylethanolamide induces microglia changes associated with increased migration and phagocytic activity: involvement of the CB2 receptor. *Sci. Rep.* 7:375. doi: 10.1038/s41598-017-00342-1

Hagemann, C., Fuchs, S., Monoranu, C. M., Herrmann, P., Smith, J., Hohmann, T., et al. (2013). Impact of MACC1on human malignant glioma progression and patients' unfavorable prognosis. *Neuro. Oncol.* 15, 1696–1709. doi: 10.1093/neuonc/not136

Hegde, V. L., Nagarkatti, M., and Nagarkatti, P. S. (2010). Cannabinoid receptor activation leads to massive mobilization of myeloid-derived suppressor cells with potent immunosuppressive properties. *Eur J Immunol.* 40, 3358–3371. doi: 10.1002/eji.201040667.Cannabinoid

Herrera, M. I., Udovin, L. D., Toro-urrego, N., and Kusnier, C. F. (2018). Palmitoylethanolamide ameliorates hippocampal damage and behavioral dysfunction after perinatal asphyxia in the immature rat brain. *Front Neurosci.* 12:145. doi: 10.3389/fnins.2018.00145

Hezel, M., Ebrahimi, F., Koch, M., and Dehghani, F. (2012). Propidium iodide staining: a new application in fluorescence microscopy for analysis of cytoarchitecture in adult and developing rodent brain. *Micron* 43, 1031–1038. doi: 10.1016/j.micron.2012.04.006

Ho, W.-S., Barrett, D., and Randall, M. (2008). " Entourage " effects of N -palmitoylethanolamide and N -oleoylethanolamide on vasorelaxation to anandamide occur through TRPV1 receptors. *Br. J. Pharmocol.* 155, 837–846. doi: 10.1038/bjp.2008.324

Hohmann, T., Feese, K., Greither, T., Ghadban, C., Jäger, V., Dehghani, F., et al. (2019). Synthetic cannabinoids influence the invasion of glioblastoma cell lines in a cell- and receptor-dependent manner. *Cancers* 11, 1–20. doi: 10.3390/cancers11020161

Hohmann, T., Grabiec, U., Ghadban, C., Feese, K., and Dehghani, F. (2017). The influence of biomechanical properties and cannabinoids on tumor invasion. *Cell Adh. Migr.* 11, 54–67. doi: 10.1080/19336918.2016.1183867

Impellizzeri, D., Siracusa, R., Cordaro, M., Peritore, A. F., Gugliandolo, E., D'Amico, R., et al. (2019). N-Palmitoylethanolamine-oxazoline (PEA-OXA): a new therapeutic strategy to reduce neuroinflammation, oxidative stress associated to vascular dementia in an experimental model of repeated bilateral common carotid arteries occlusion. *Neurobiol. Dis* 125, 77–91. doi: 10.1016/j.nbd.2019.01.007

Járai, Z., Wagner, J. A., Varga, K., Lake, K. D., Compton, D. R., Martin, B. R., et al. (1999). Cannabinoid-induced mesenteric vasodilation through an endothelial site distinct from CB1 or CB2 receptors. *Proc. Natl. Acad. Sci. U.S.A.* 96, 14136–14141. doi: 10.1073/pnas.96.24.14136

Jassam, Y. N., Izzy, S., Whalen, M., Mcgavern, D. B., and El Khoury, J. (2017). Review neuroimmunology of traumatic brain injury: time for a paradigm shift. *Neuron* 95, 1246–1265. doi: 10.1016/j.neuron.2017.07.010

Jonsson, K.-O., Vandevoorde, S., Lambert, D. M., Tiger, G., and Fowler, C. J. (2001). Effects of homologues and analogues of palmitoylethanolamide upon the inactivation of the endocannabinoid anandamide. *Br. J. Pharmocology* 133, 1263–1275. doi: 10.1038/sj.bjp.0704199

Kakizawa, H., Matsui, F., Tokita, Y., Hirano, K., Okumura, A., Kojima, S., et al. (2007). Neuroprotective effect of nipradilol, an NO donor, on hypoxic – ischemic brain injury of neonatal rats. *Early Hum. Dev.* 83, 535–540. doi: 10.1016/j.earlhumdev.2006.10.003

Kallendrusch, S., Kremzow, S., Nowicki, M., Grabiec, U., Winkelmann, R., Benz, A., et al. (2013). The G protein-coupled receptor 55 Ligand L - a -lysophosphatidylinositol exerts after excitotoxic lesion. *Glia* 61, 1822–1831. doi: 10.1002/glia.22560

Kettenmann, H., Hanisch, U.-K., Noda, M., and Verkhratsky, A. (2011). Physiology of microglia. *Physiol. Rev.* 91, 461–553. doi: 10.1152/physrev.00011.2010

Koch, M., Kreutz, S., Boettger, C., Benz, A., Maronde, E., Ghadban, C., et al. (2011a). Palmitoylethanolamide protects dentate gyrus granule cells via peroxisome proliferator-activated receptor-alpha. *Neurotox. Res.* 19, 330–340. doi: 10.1007/s12640-010-9166-2

Koch, M., Kreutz, S., Böttger, C., Grabiec, U., Ghadban, C., Korf, H. W., et al. (2011b). The cannabinoid WIN 55,212-2-mediated protection of dentate gyrus granule cells is driven by CB1 receptors and modulated by TRPA1 and Ca v2.2 channels. *Hippocampus* 21, 554–564. doi: 10.1002/hipo.20772

Kohl, A., Dehghani, F., Korf, H., and Hailer, N. P. (2003). The bisphosphonate clodronate depletes microglial cells in excitotoxically injured organotypic hippocampal slice cultures. *Exp. Neurol.* 181, 1–11. doi: 10.1016/S0014-4886(02)00049-3

Kömüves, L. G., Hanley, K., Lefebvre, A.-M., Man, M.-Q., Ng, D. C., Bikle, D. D., et al. (2000). Stimulation of PPAR a promotes epidermal keratinocyte differentiation *In Vivo*. *J. Invest. Dermatol.* 115, 353–360. doi: 10.1046/j.1523-1747.2000.00073.x

Kondo, S., Kondo, H., Nakane, S., Kodaka, T., Tokumura, A., Waku, K., et al. (1998). 2-Arachidonoylglycerol, an endogenous cannabinoid receptor agonist: identification as one of the major species of monoacylglycerols in various rat tissues, and evidence for its generation through Ca2+‡ -dependent and -independent mechanisms. *FEBS Lett.* 429, 152–156. doi: 10.1016/s0014-5793(98)00581-x

Kozak, K. R., Gupta, R. A., Moody, J. S., Ji, C., Boeglin, W. E., Dubois, R. N., et al. (2002). 15-Lipoxygenase metabolism of 2-Arachidonylglycerol. *J. Biol. Chem.* 277, 23278–23286. doi: 10.1074/jbc.M201084200

Kreutz, S., Koch, M., Böttger, C., Ghadban, C., Korf, H. W., and Dehghani, F. (2009). 2-Arachidonoylglycerol elicits neuroprotective effects on excitotoxically lesioned dentate gyrus granule cells via abnormal-cannabidiol-sensitive receptors on microglial cells. *Glia* 57, 286–294. doi: 10.1002/glia.20756

Kreutz, S., Koch, M., Ghadban, C., Korf, H., and Dehghani, F. (2007). Cannabinoids and neuronal damage: differential effects of THC, AEA and 2-AG on activated microglial cells and degenerating neurons in excitotoxically lesioned rat organotypic hippocampal slice cultures. *Exp. Neurol.* 203, 246–257. doi: 10.1016/j.expneurol.2006.08.010

Kunz, A., Dirnagl, U., and Mergenthaler, P. (2010). Acute pathophysiological processes after ischaemic and traumatic brain injury. *Best Pract. Res. Clin. Anaesthesiol.* 24, 495–509. doi: 10.1016/j.bpa.2010.10.001

Lau, A., and Tymianski, M. (2010). Glutamate receptors, neurotoxicity and neurodegeneration. *Pflugers Arch. Eur. J. Physiol.* 460, 525–542. doi: 10.1007/s00424-010-0809-1

Lipina, C., and Hundal, H. S. (2017). The endocannabinoid system: " NO " longer anonymous in the control of nitrergic signalling? *J. Mol. Cell Biol.* 9, 91–103. doi: 10.1093/jmcb/mjx008

Lourbopoulos, A., Grigoriadis, N., Lagoudaki, R., Touloumi, O., Polyzoidou, E., Mavromatis, I., et al. (2011). Administration of 2-arachidonoylglycerol ameliorates both acute and chronic experimental autoimmune encephalomyelitis. *Brain Res.* 1390, 126–141. doi: 10.1016/j.brainres.2011.03.020

LoVerme, J., La Rana, G., Russo, R., Calignano, A., and Piomelli, D. (2005). The search for the palmitoylethanolamide receptor. *Life Sci.* 77, 1685–1698. doi: 10.1016/j.lfs.2005.05.012

Luongo, L., Palazzo, E., Tambaro, S., Giordano, C., Gatta, L., Scafuro, M. A., et al. (2010). 1-(2′,4′-dichlorophenyl)-6-methyl-N-cyclohexylamine-1,4-dihydroindeno[1,2-c] pyrazole-3-carboxamide, a novel CB2 agonist, alleviates neuropathic pain through functional microglial changes in mice. *Neurobiol. Dis.* 37, 177–185. doi: 10.1016/j.nbd.2009.09.021

Ma, L., Jia, J., Liu, X., Bai, F., Wang, Q., and Xiong, L. (2015). Biochemical and Biophysical Research Communications Activation of murine microglial N9 cells is attenuated through cannabinoid receptor CB2 signaling. *Biochem. Biophys. Res. Commun.* 458, 92–97. doi: 10.1016/j.bbrc.2015.01.073

Magid, L., Heymann, S., Elgali, M., Avram, L., Cohen, Y., Liraz-zaltsman, S., et al. (2019). The Role of CB 2 Receptor in the Recovery of Mice after Traumatic Brain Injury. *J. Neurotrauma* 36, 1836–1846. doi: 10.1089/neu.2018.6063

Meaney, D. F., Morrison, B., and Bass, C. D. (2014). The mechanics of traumatic brain Injury: a review of what we know and what we need to know for reducing its societal burden. *J. Biomech. Eng.* 136:021008. doi: 10.1115/1.4026364

Mechoulam, R., and Shohami, E. (2007). Endocannabinoids and traumatic brain injury. *Mol. Neurobiol.* 36, 68–74. doi: 10.1007/s12035-007-8008-6

Mounsey, R. B., Mustafa, S., Robinson, L., Ross, R. A., Riedel, G., Pertwee, R. G., et al. (2015). Increasing levels of the endocannabinoid 2-AG is neuroprotective in the Parkinson ' s disease. *Exp. Neurol.* 273, 36–44. doi: 10.1016/j.expneurol.2015.07.024

Muccioli, G. G., and Stella, N. (2009). Microglia produce and hydrolyze palmitoylethanolamide. *Neuropharmacology* 54, 16–22. doi: 10.1016/j.neuropharm.2007.05.015

Muccioli, G. G., Xu, C., Odah, E., Cudaback, E., Cisneros, J. A., Lambert, D. M., et al. (2007). Identification of a Novel Endocannabinoid-Hydrolyzing Enzyme Expressed by Microglial Cells. *J. Neurosci.* 27, 2883–2889. doi: 10.1523/JNEUROSCI.4830-06.2007

Musella, A., Fresegna, D., Rizzo, F. R., Gentile, A., Bullitta, S., and De Vito, F. (2017). A novel crosstalk within the endocannabinoid system controls GABA transmission in the striatum. *Sci. Rep.* 7, 1–8. doi: 10.1038/s41598-017-07519-8

Nakamura, Y., Si, Q. S., and Kataoka, K. (1999). Lipopolysaccharide-induced microglial activation in culture: temporal profiles of morphological change and release of cytokines and nitric oxide. *Neurosci. Res.* 35, 95–100. doi: 10.1016/s0168-0102(99)00071-1

Nimmerjahn, A., Kirchhoff, F., and Helmchen, F. (2005). Resting microglial cells are highly dynamic surveillants of brain parenchyma *In Vivo*. *Science* 308, 1314–1319.

Panikashvili, D., Simeonidou, C., Ben-shabat, S., Breuer, A., Mechoulam, R., and Shohami, E. (2001). An endogenous cannabinoid (2-AG) is neuroprotective after brain injury. *Nature* 413, 527–531. doi: 10.1038/35097089

Paterniti, I., Impellizzeri, D., Crupi, R., Morabito, R., Campolo, M., Esposito, E., et al. (2013). Molecular evidence for the involvement of PPAR- δ and PPAR- γ in anti-inflammatory and neuroprotective activities of palmitoylethanolamide after spinal cord trauma. *J. Neuroinflammation* 10, 1–13. doi: 10.1186/1742-2094-10-20

Pertwee, R. G. (2014). Elevating endocannabinoid levels: pharmacological strategies and potential therapeutic applications. *Proc. Nutr. Soc.* 73, 96–105. doi: 10.1017/S0029665113003649

Pertwee, R. G., Howlett, A. C., Abood, M. E., Alexander, S. P. H., Marzo, V., Di Elphick, M. R., et al. (2010). International union of basic and clinical pharmacology . LXXIX . cannabinoid receptors and their ligands: beyond CB 1 and CB 2. *Pharmacol. Rev.* 62, 588–631.

Petrosino, S., Moriello, A. S., Cerrato, S., Fusco, M., Puigdemont, A., De Petrocellis, L. X., et al. (2016). The anti-inflammatory mediator palmitoylethanolamide enhances the levels of 2-arachidonoyl-glycerol and potentiates its actions at TRPV1 cation channels. *Br. J. Pharmocol.* 173, 1154–1162. doi: 10.1111/bph.13084

Portavella, M., Rodriguez-espinosa, N., Galeano, P., Blanco, E., and Romero, J. I. (2018). Oleoylethanolamide and Palmitoylethanolamide Protect Cultured Cortical Neurons Against Hypoxia. *Cannabis Cannabinoid Res.* 3, 171–178. doi: 10.1089/can.2018.0013

Ransohoff, R. M. (2016). A polarizing question: do M1 and M2 microglia exist? *Nat. Neurosci.* 19, 987–991. doi: 10.1038/nn.4338

Ross, R. A., Brockie, H. C., and Pertwee, R. G. (2000). Inhibition of nitric oxide production in RAW264.7 macrophages by cannabinoids and palmitoylethanolamide. *Eur. J. Pharmacol.* 401, 121–130. doi: 10.1016/s0014-2999(00)00437-4

Scotter, E. L., Abood, M. E., and Glass, M. (2010). The endocannabinoid system as a target for the treatment of neurodegenerative disease. *Br. J. Pharmocology* 160, 480–498. doi: 10.1111/j.1476-5381.2010.00735.x

Siracusa, R., Impellizzeri, D., Cordaro, M., Crupi, R., and Cuzzocrea, S. (2017). Anti-inflammatory and neuroprotective effects of Co-UltraPEALut in a mouse model of vascular dementia. *Front. Neurol.* 8:233. doi: 10.3389/fneur.2017.00233

Skaper, S. D., and Facci, L. (2014). Mast cells, glia and neuroinflammation: partners in crime? *Immunology* 141, 314–327. doi: 10.1111/imm.12170

Smart, D., Jonsson, K.-O., Vandevoorde, S., Lambert, D. M., and Fowler, C. J. (2002). ' Entourage ' effects of N -acyl ethanolamines at human vanilloid receptors . Comparison of e € ects upon anandamide-induced vanilloid receptor activation and upon anandamide metabolism. *Br. J. Pharmocology* 136, 452–458. doi: 10.1038/sj.bjp.0704732

Smith, J. A., Das, A., Ray, S. K., and Banik, N. L. (2012). Role of pro-inflammatory cytokines released from microglia in neurodegenerative diseases. *Brain Res. Bull.* 87, 10–20. doi: 10.1016/j.brainresbull.2011.10.004

Stefano, G. B., Bilfinger, T. V., Rialas, C. M., and Dale, G. (2000). 2-arachidonyl-glycerol stimulates nitric oxide release from human immune and vascular tissues and invertebrate immunocytes by cannabinoid receptor 1. *Pharmacol. Res.* 42, 317–322. doi: 10.1006/phrs.2000.0702

Stella, N. (2009). Endocannabinoid signaling in microglial cells. *Neuropharmacology* 56, 244–253. doi: 10.1016/j.neuropharm.2008.07.037. Endocannabinoid

Umemoto, T., and Fujiki, Y. (2012). Ligand-dependent nucleo-cytoplasmic shuttling of peroxisome proliferator-activated receptors, PPAR a and PPAR c. *Genes Cells* 17, 576–596. doi: 10.1111/j.1365-2443.2012.01607.x

Vincent, V. A. M., Tilders, F. J. H., and Van Dam, A.-M. (1998). Production, regulation and role of nitric oxide in glial cells. *Mediators Inflamm.* 7, 239–255. doi: 10.1080/09629359890929

Vinet, J., van Weering, H. R., Heinrich, A., Kälin, R. E., Wegner, A., Brouwer, N., et al. (2012). Neuroprotective function for ramified microglia in hippocampal excitotoxicity. *J. Neuroinflamm.* 9:27. doi: 10.1186/1742-2094-9-27

Walter, L., Franklin, A., Witting, A., Wade, C., Xie, Y., Kunos, G., et al. (2003). Nonpsychotropic cannabinoid receptors regulate microglial cell migration. *J. Neurosci.* 23, 1398–1405. doi: 10.1002/glia.20813

Wang, F., Li, M., Li, X., Kinden, R., Zhou, H., Guo, F., et al. (2015). 2-AG protects primary astrocytes exposed to oxygen-glucose deprivation through a blockade of NDRG2 signaling and STAT3 phosphorylation. *Exp. Neurol.* 273, 1–25. doi: 10.1089/rej.2015.1703

Wang, S., Zhang, H., Geng, B., Xie, Q., Li, W., Deng, Y., et al. (2018). 2-arachidonyl glycerol modulates astrocytic glutamine synthetase via p38 and ERK1 / 2 pathways. *J. Neuroinflamm.* 15, 1–10. doi: 10.1186/s12974-018-1254-x

Warden, A., Truitt, J., Merriman, M., Ponomareva, O., Jameson, K., Ferguson, L. B., et al. (2016). Localization of PPAR isotypes in the adult mouse and human brain. *Sci. Rep.* 6, 1–15. doi: 10.1038/srep27618

Xu, J., Chavis, J. A., Racke, M. K., and Drew, P. D. (2006). Peroxisome proliferator-activated receptor- a and retinoid X receptor agonists inhibit inflammatory responses of astrocytes. *J. Neuroimmunol.* 176, 95–105. doi: 10.1016/j.jneuroim.2006.04.019

Xu, J., Storer, P. D., Chavis, J. A., Racke, M. K., Drew, P. D., and Rock, L. (2005). Agonists for the peroxisome proliferator- activated receptor- a and the retinoid X receptor inhibit inflammatory responses of microglia. *J. Neurosci. Res.* 411, 403–411. doi: 10.1002/jnr.20518

Yao, X., Liu, S., Ding, W., Yue, P., Jiang, Q., Zhao, M., et al. (2017). TLR4 signal ablation attenuated neurological de fi cits by regulating microglial M1 / M2 phenotype after traumatic brain injury in mice. *J. Neuroimmunol.* 310, 38–45. doi: 10.1016/j.jneuroim.2017.06.006

Zhang, J., and Chen, C. (2008). Endocannabinoid 2-arachidonoylglycerol protects neurons by limiting COX-2 elevation. *J. Biol. Chem. Biol. Chem.* 283, 22601–22611. doi: 10.1074/jbc.M800524200

Zhang, J., Hoffert, C., Vu, H. K., Groblewski, T., Ahmad, S., Donnell, D. O., et al. (2003). Induction of CB2 receptor expression in the rat spinal cord of neuropathic but not in ¯ ammatory chronic pain models. *Eur. J. Neurosci.* 17, 2750–2754. doi: 10.1046/j.1460-9568.2003.02704.x

Zhou, T., Huang, Z., Sun, X., Zhu, X., Zhou, L., Li, M., et al. (2017). Microglia polarization with M1 / M2 phenotype changes in rd1 mouse model of retinal degeneration. *Front. Neuroanat.* 11:77. doi: 10.3389/fnana.2017.00077

Conflict of Interest: The authors declare that the research was conducted in the absence of any commercial or financial relationships that could be construed as a potential conflict of interest.

Copyright © 2019 Hohmann, Pelzer, Kleine, Hohmann, Ghadban and Dehghani. This is an open-access article distributed under the terms of the Creative Commons Attribution License (CC BY). The use, distribution or reproduction in other forums is permitted, provided the original author(s) and the copyright owner(s) are credited and that the original publication in this journal is cited, in accordance with accepted academic practice. No use, distribution or reproduction is permitted which does not comply with these terms.

frontiers in Neuroscience

REVIEW
published: 07 November 2019
doi: 10.3389/fnins.2019.01156

Bioscaffold-Induced Brain Tissue Regeneration

Michel Modo[1,2,3,4]*

[1] McGowan Institute for Regenerative Medicine, University of Pittsburgh, Pittsburgh, PA, United States, [2] Center for the Neural Basis of Cognition, University of Pittsburgh, Pittsburgh, PA, United States, [3] Department of Bioengineering, University of Pittsburgh, Pittsburgh, PA, United States, [4] Department of Radiology, University of Pittsburgh, Pittsburgh, PA, United States

Brain tissue lost after a stroke is not regenerated, although a repair response associated with neurogenesis does occur. A failure to regenerate functional brain tissue is not caused by the lack of available neural cells, but rather the absence of structural support to permit a repopulation of the lesion cavity. Inductive bioscaffolds can provide this support and promote the invasion of host cells into the tissue void. The putative mechanisms of bioscaffold degradation and its pivotal role to permit invasion of neural cells are reviewed and discussed in comparison to peripheral wound healing. Key differences between regenerating and non-regenerating tissues are contrasted in an evolutionary context, with a special focus on the neurogenic response as a *conditio sine qua non* for brain regeneration. The pivotal role of the immune system in biodegradation and the formation of a neovasculature are contextualized with regeneration of peripheral soft tissues. The application of rehabilitation to integrate newly forming brain tissue is suggested as necessary to develop functional tissue that can alleviate behavioral impairments. Pertinent aspects of brain tissue development are considered to provide guidance to produce a metabolically and functionally integrated *de novo* tissue. Although little is currently known about mechanisms involved in brain tissue regeneration, this review outlines the various components and their interplay to provide a framework for ongoing and future studies. It is envisaged that a better understanding of the mechanisms involved in brain tissue regeneration will improve the design of biomaterials and the methods used for implantation, as well as rehabilitation strategies that support the restoration of behavioral functions.

Keywords: extracellular matrix, stroke, regeneration, tissue repair, biodegradation, biomaterial, scaffold, physical therapy

OPEN ACCESS

Edited by:
Johannes Boltze, University of Warwick, United Kingdom

Reviewed by:
Ludwig Aigner, Paracelsus Medical University, Austria
Jukka Jolkkonen, University of Eastern Finland, Finland

***Correspondence:**
Michel Modo
mmm154@pitt.edu

Specialty section:
This article was submitted to Neurodegeneration, a section of the journal Frontiers in Neuroscience

Received: *15 May 2019*
Accepted: *14 October 2019*
Published: *07 November 2019*

Citation:
Modo M (2019) Bioscaffold-Induced Brain Tissue Regeneration. Front. Neurosci. 13:1156. doi: 10.3389/fnins.2019.01156

INTRODUCTION

Acute brain injury and progressive neurodegenerative disease represent some of the most challenging medical conditions. The financial burden of these conditions in the US alone amounts to nearly $800 billion per year (Gooch et al., 2017). With an aging population, this cost will continue to rise, especially considering the lack of effective treatment options. There are currently no approved therapies to limit or revert cell loss. In a few conditions, such as Parkinson's disease, pharmacological agents can compensate for the loss of a specific neurotransmitter (e.g., dopamine). However, the continued cell loss due to neurodegeneration is not reversed. This continued loss of

cells produces a tissue atrophy that gradually shrinks brain tissue. In contrast to tissue atrophy, acute brain injuries, such as a stroke and penetrating traumatic brain injuries, produce a volumetric tissue loss that is characterized by cavitation, i.e., cell and matrix loss (Moreau et al., 2012). Tissues surrounding this cavitation are also damaged and typically undergo an acute and sub-acute neuronal loss associated with reactive gliosis and angiogenesis. Atrophy in peri-cavity damaged tissue can also occur. Pharmacological therapies, such as neuroprotective agents, are primarily focused on rescuing acutely dying neurons, whereas anti-inflammatory agents target the immune system's response to the inflicted damage, aiming to reduce secondary tissue damage (Neuhaus et al., 2017). Neither approach replaces lost cells or tissues.

In contrast to these pharmacological interventions, biological interventions aim to replace cellular components that have been lost (Modo et al., 2018). For example, in the case of Parkinson's disease, ectopic transplantation of dopaminergic cells attempts to restore the local neurotransmitter tone, whereas in Huntington's disease the goal is to replace lost neurons and to integrate these new neurons into existing neuronal circuitry (Barker and TRANSEURO consortium, 2019). In the case of acute brain injuries, two paradigms have found clinical translation, with one focused on influencing the immune response using intravenous or intra-arterial injections of mesenchymal stem cells during the acute phase of injury, whereas the other focuses on intracerebral implantation of cells into damaged tissue in the sub-acute to chronic phase by supplementing endogenous repair mechanism (Ghuman et al., 2018; Borlongan, 2019). Emerging evidence suggests that brain regeneration is feasible if the appropriate conditions are engineered (Ghuman et al., 2018; Nih et al., 2018; Modo and Badylak, 2019). An endogenous repair response to tissue damage and injury is crucial for this process and replicates certain aspects of peripheral wound healing. Herein, we review putative mechanisms involved in brain tissue regeneration and contrast these mechanisms with peripheral soft tissue regeneration following injury.

TISSUE REPAIR VERSUS REGENERATION

Progressive neurodegeneration or acute brain injury lead to cell death by several mechanisms, including apoptosis, necrosis, oncosis, autophagy, and pyroptosis. The resulting cell debris activates resident immune cells, such as microglia, and is associated with reactive astrocytes that change morphology and function (Donnelly and Popovich, 2008; Chapman et al., 2015; Gabel et al., 2016). These cell and tissue responses mitigate the impact on surrounding healthy cells and tissues. In the case of penetrative and ischemic injuries, liquefactive necrosis occurs in the core of the injured tissue, with an associated loss of the tissue structure itself. The liquefactive debris, including cell debris and the disrupted extracellular matrix, are removed, leaving behind a tissue cavity. These events occur in up to 94% of patients with an ischemic stroke (Moreau et al., 2012). Still, tissue cavitation remains a poorly understood phenomenon with location and time post-injury being key factors. Some species, such as rat and human, are more prone to this process than others, such as mice (Surey et al., 2014). Inflammation may play a key role in this process and explain differences between species, as well as location (Chung et al., 2018). The liquefactive debris is itself neurotoxic upon permeation into peri-cavity tissue (Zbesko et al., 2018) and might provoke a pro-inflammatory response. The tissue inflammatory response eventually results in a structural barrier in the form of gliosis and scarring that prevents the spread of neurotoxic debris to limit further tissue damage.

In addition to the formation of a glial scar, local astrocytes and oligodendrocyte progenitor cells proliferate to produce an expanded cell population that can support tissue function. A small proportion of these cells may have the potential to replace lost neurons (Donnelly and Popovich, 2008; Chapman et al., 2015; Gabel et al., 2016), but evidence for this remains controversial. The local vasculature also responds to tissue damage with the formation of new small blood vessels that improve nutrient supply to hypoxic tissue containing dying or at-risk cells (Manoonkitiwongsa et al., 2001; Senior, 2001).

The brain possesses a neurogenic potential that is involved in maintaining tissue homeostasis during normal aging. However, recent evidence suggests that neurogenesis in adult human brain is very limited (Kempermann et al., 2018). After injury or during ongoing neurodegeneration, neurogenic regions, such as the subventricular zone (SVZ) upregulate the proliferation of progenitor cells, which then migrate toward the area of damage (**Figure 1A**) (Lindvall and Kokaia, 2015). This repair response is still active more than 1 year after a stroke (Kazanis et al., 2013), but survival and integration of newly generated cells is generally considered poor (Magavi et al., 2000; Arvidsson et al., 2002), potentially due to a non-permissive environment. New blood vessels might serve as a guidance conduit toward areas of damage (Kojima et al., 2010). Intraparenchymal cell transplants aim to supplement this endogenous tissue repair response (**Figure 1B**), without replacing lost tissue (Smith et al., 2012). For the present review, we define tissue repair to consist of the changes that occur in and around damaged tissue without the replacement of any lost brain tissue (**Table 1**).

Tissue regeneration or replacement of lost tissue requires the infiltration and organization of functional neurons, glial cells and support structures (e.g., vascularization). Infiltration of cells into the lesion cavity requires the presence of a matrix substrate to facilitate cell migration. Provision of inductive bioscaffolds, such as those composed of extracellular matrix (ECM) derived from decellularized tissues, can facilitate endogenous tissue regeneration in the brain (**Figure 1C**). Other materials, such as cross-linked hyaluronic acid might serve the same function (Nih et al., 2018). *In vitro* morphogenesis of brain tissue, i.e., organoids, have also been reported to spontaneously arrange into structures that resemble cortical layers. This further indicates that there is an inherent potential in brain cells to structurally organize into tissue if the appropriate conditions are provided (Mansour et al., 2018). A further example of this tissue morphogenesis is provided by the co-implantation of a dense mixture of NSCs and endothelial cells (ECs) into a stroke cavity (Nicholls et al., 2015). Implantation of essential brain tissue components (i.e.,

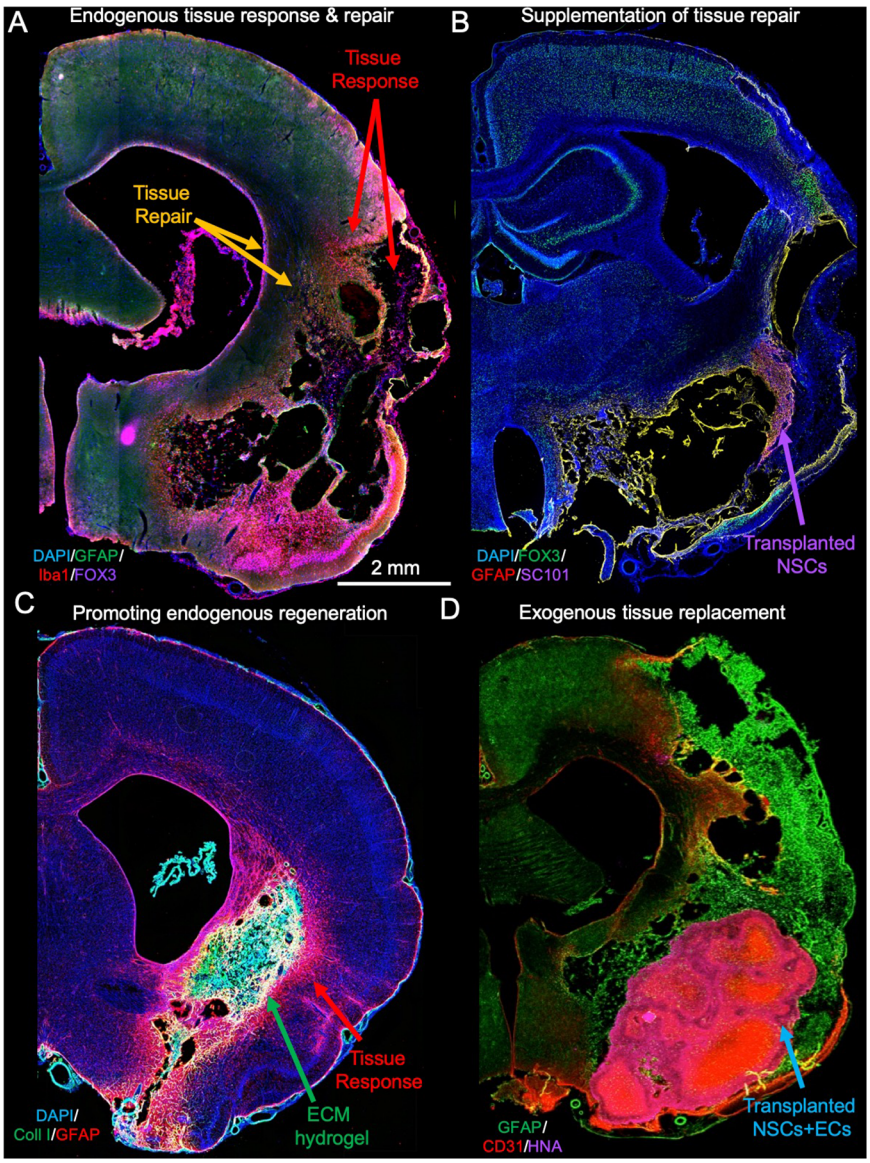

FIGURE 1 | Tissue response, repair, and regenerative response. **(A)** After acute brain injuries, such as stroke, astrocytes and microglia get activated to respond to tissue damage that at its core eventually produce a loss of cells, as well as the extracellular matrix, leaving behind a cavity. The glial scar is aimed at providing structural support but also preventing neurotoxic fluid to permeate into the peri-infarct tissue. In addition to this tissue response, the brain mounts reparative activities, which include an upregulation of neurogenesis in the subventricular zone. **(B)** To supplement the endogenous repair response, neural stem cells (NSCs) can be transplanted into damaged tissue where these differentiate and integrate with host cells, but they also increase local angiogenesis providing a better blood supply to poorly perfused tissues (Smith et al., 2012). **(C)** In contrast to cell transplantation, implantation of inductive extracellular matrix (ECM) bioscaffolds promotes a restoration of tissue inside the lesion cavity from endogenous cells that invade the material (Ghuman et al., 2018). **(D)** An alternative approach to tissue regeneration using an inductive bioscaffolds is to implant a mixture of NSCs and ECs that spontaneously organize into a vascular and neuropil compartment, potentially accelerating the restoration process and overcoming the potential limitation of the reservoir of endogenous cells (Nicholls et al., 2015).

NSCs, ECs, ECM) could therefore provide an alternative or supplementation to endogenous tissue regeneration (**Figure 1D**).

THE BRAIN'S FAILURE TO REGENERATE

Ramon y Cajal professed that "*In adult centers the nerve paths are something fixed, ended, immutable. Everything may die, nothing may be regenerated. It is key for the science of the future to change, if possible, this decree*" (Ramon y Cajal, 1928). The discovery of neurogenic zones in the adult mammalian brain and their participation in response to tissue injury partially refuted this long-held dogma that neurons in the brain cannot be replaced (Kempermann et al., 2018). However, the belief that the brain cannot regenerate (i.e., form new functional tissue) has mostly remained unchallenged (Fry, 2001;

TABLE 1 | Terminology used to define different aspects associated with tissue regeneration.

Terminology	Description
Angiogenesis	The process of a new artery branching out from an existing artery
Anastomosis	Establishment of a cross-connection between two blood vessels to create a new supply network
Arteriogenesis	The process of creating a new artery, including engineering of engraftable arteries
Axonogenesis	The formation of new axons
Behavioral Recovery	Improvements observed in solving behavioral tasks (e.g., walking)
Cell Replacement	Replacement of cells lost due to injury either through endogenous processes or through cell implantation
De novo tissue	Tissue that has newly formed where there was none, includes tissue that is established through endogenous means (i.e., regeneration) or through implantation (e.g., cells plus bioscaffold)
Developing tissue	Tissue that is undergoing development, i.e., cells invade and mature
Functional Recovery	Re-establishment of an electrophysiological connectivity (e.g., evoked potential between motor and somatosensory cortex)
Functional Tissue	The establishment of a tissue that supports brain activity (e.g., metabolic response to glucose)
In situ tissue engineering	Creating a new tissue through use of cells and biomaterials in the location where it is needed
Neovascularization	Formation of new blood vessels in a tissue void of vasculature, as in the case of tissue regeneration
Neuro/Gliogenesis	The formation of new neurons and glial cells
Tissue Response	Biological activity in tissue that responds to injury (e.g., glial scarring, cavitation)
Primitive tissue	Tissue that is not completely formed (e.g., tissue containing cells, but lacking appropriate cytoarchitecture or connectivity)
Revascularization	Re-establishing a vascular supply in a tissue that was lacking it, as in poorly perfused peri-infarct tissue
Synaptogenesis	The formation of new synapses
Tissue construct	A pre-formed *ex vivo* tissue that can be implanted
Tissue neogenesis	Newly developing tissue in a cavity, as opposed to damaged tissue being repaired to establish a functional tissue again
Tissue Regeneration	Establishment of a new tissue in a cavity through endogenous cells, including axonal connections
Tissue Repair	Cellular response to tissue damage trying to restore function (e.g., neurogenesis, angiogenesis)
Tissue Restoration	Establishment of a new tissue in a cavity through endogenous or exogenous means
Tissue engineering	Use of cells and biomaterials to create a new tissue *in vivo*, *ex vivo*, or *in vitro*
Vasculogenesis	The process of creating a new vasculature, including veins
Veterate tissue	Organ tissue that is established and remained after injury (e.g., peri-infarct tissue), as opposed to partially formed or newly forming tissue

Bechmann, 2005; Illis, 2012). By many, regeneration of brain tissue is considered the ultimate challenge for regenerative medicine (Obernier et al., 2014): by others, it is considered a biological impossibility (Price, 2011). Essentially, two main arguments are postulated as to why brain tissue regeneration is impossible: (1) The central nervous system of adult mammals is an inhibitory environment that "irreversibly" seals off tissue cavities to protect the remaining brain and consequently prevent tissue regeneration; and (2) The brain arises through a complex interplay between cells during development to form long-distance connections within and between brain regions, which cannot be recreated in the adult. Both viewpoints have merit, but do not consider the possibility that certain engineering strategies could overcome the scarring around the tissue cavity, or that functional brain tissue can develop via alternative mechanisms from normal brain development. Indeed, most tissue regeneration (e.g., liver) utilizes certain developmental processes, but does not strictly recapitulate fetal development.

When considering tissue regeneration across multiple organ systems and species, it is evident that tissue regeneration is reduced as a function of age and the complexity of the organ system (**Figure 2A**). Less complicated organ systems, such as the hematopoietic system, readily replenish. With increasing tissue complexity, as evidenced in most solid organs, there is less replenishing of cells during homeostasis, less cell replacement after injury and more limited regeneration after tissue loss compared to the hematopoietic system. A notable exception is the liver, which can completely regenerate from only 25% of remaining tissue (Michalopoulos and DeFrances, 1997). However, the reasons for a disparate regenerative potential of tissues and organs remains unknown at the present time.

A differential capacity to regenerate complex tissue exists across the evolutionary ladder (Tanaka and Ferretti, 2009; Ferretti, 2011), with species such as zebrafish and newts able to "regenerate" brain tissue after ablation (Kroehne et al., 2011; Urata et al., 2018). Inflammation at the site of injury and the invasion of macrophages are increasingly emerging as a key signaling axis to initiate and regulate this tissue regeneration (Kyritsis et al., 2012; Godwin et al., 2013). In the brain, the presence of neurogenic regions is considered a *conditio sine qua non-for* tissue repair and regeneration (Ferretti, 2011). Indeed, the size of the neurogenic reservoir directly correlated with the degree of tissue regeneration in carp (Kirsche and Kirsche, 1961). Large neurogenic regions persist into zebrafish adulthood, which respond to ablations in nearby brain regions (Kizil et al., 2012). The requirement for adequate neurogenic tissue would suggest that the proximity to a neurogenic region will be a determining factor in promoting tissue repair and regeneration. Relative distances in larger mammalian brains might hence be more difficult to bridge than those in smaller brains.

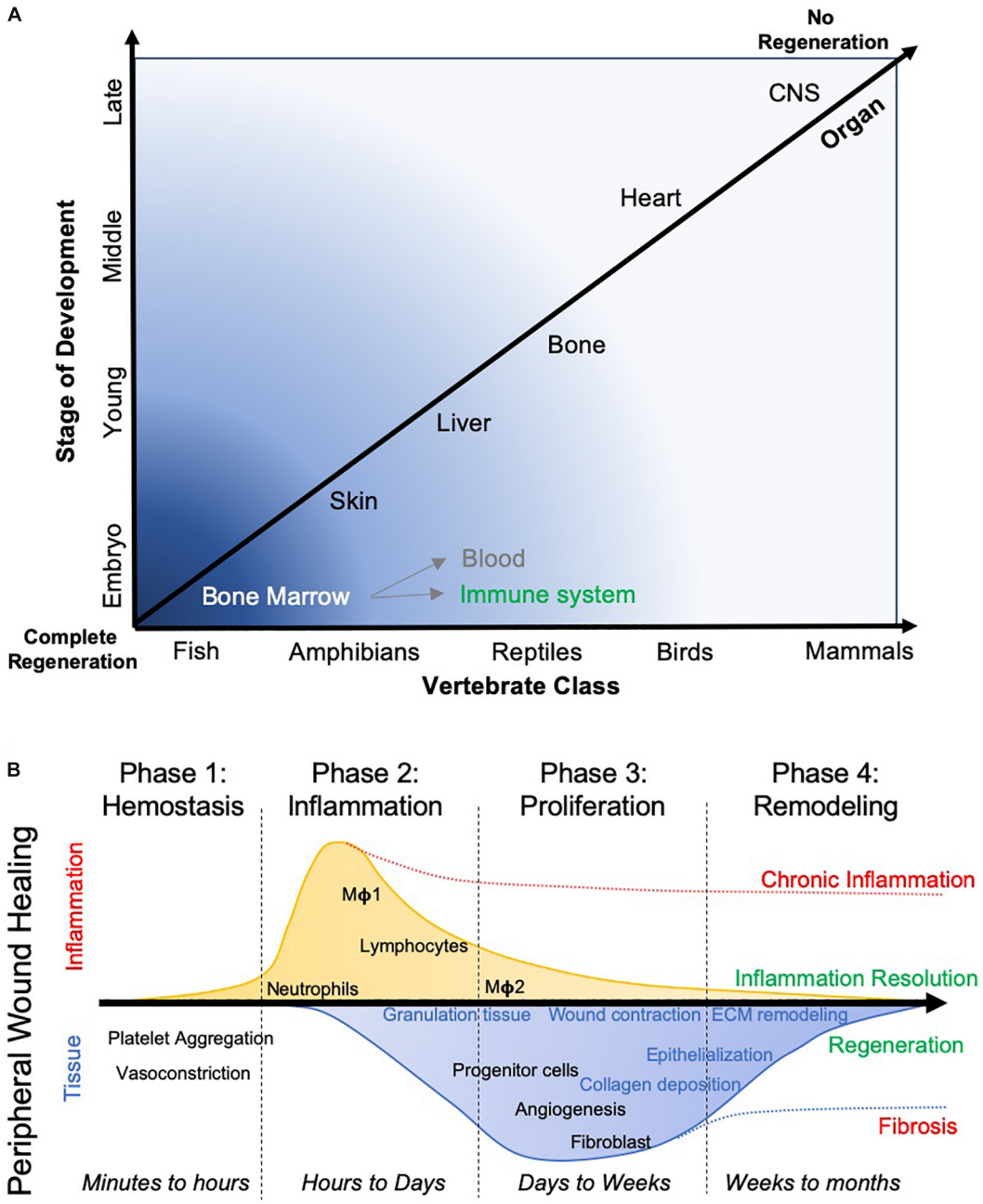

FIGURE 2 | Evolutionary aspects of tissue regeneration. **(A)** The capacity of different species to regenerate different organ tissue over their lifespan widely varies. Anatomical complexity of the species, as well as tissues, is a major factor in their ability to regenerate. Lower species more readily regenerate more complex tissue, whereas more complex species, such as mammals, are only able to regenerate very few organs. It is pertinent to contrast a replenishing of blood and immune system from the bone marrow, which essentially restitutes single cells, from constructing a tissue that involves multiple cell lineages and the deposition of ECM to create a geometric arrangement of cells. **(B)** In wound healing, where a cut in a tissue, such as the skin, restores tissue integrity, typically follows 4 phases. These phases are characterized by a major difference in inflammation, which peaks in phase 2, but also by changes in tissue characteristics, with the deposition of a transient granulation tissue that is being remodeled by the infiltration of host tissue cells. The formation of blood vessels and epithelization of the tissue are further key events required to ensure that a seamless wound closure occurs. Depending on which process is interrupted, a wound breakdown can occur or scarring occurs that limits tissue function. This process can take months to complete.

Alternatively, this required cellular reservoir may be supplied through implantation, as is the case in the transplantation of neural stem cells (NSCs). The neurogenic region's supply of NSCs and neural progenitors that can participate in tissue repair and regeneration is therefore a crucial element in brain tissue regeneration.

Time is a separate factor to consider, with a "perfect" tissue replacement being a slow process (>1 year) and dependent on wound closure through a tubular arrangement of ependymoglia cells (Urata et al., 2018). In axolotls and newts, true tissue regeneration after a volumetric defect can occur (Amamoto et al., 2016; Urata et al., 2018). However, alterations in cytoarchitecture and a failure to re-establish long-distance connections can happen in regenerated tissue in adult axolotls, even though cells were electrophysiologically appropriate for the tissue (Amamoto et al., 2016). It is nevertheless unclear if an altered cytoarchitectural arrangement will not allow the tissue to function as needed. Anomalies in spontaneously regenerated tissue were evident in axolotls (Amamoto et al., 2016) and zebrafish (Kroehne et al., 2011; Kaslin et al., 2017), whereas adult newt exhibit a more complete structural and cellular regeneration (Urata et al., 2018). Studies in neuro-regenerative species can therefore provide unique insights into the key factors that are required to engineer functional brain tissue regeneration in adult mammals.

WOUND HEALING VERSUS TISSUE REGENERATION

In adult mammals, healing of the skin is often considered a key example of how adult tissue can regenerate. Typically, four phases are recognized in this "regenerative process": (1) Hemostasis; (2) Inflammation; (3) Proliferation and tissue growth; and (4) Remodeling and maturation (**Figure 2B**). During injury to the skin, blood vessels are disrupted and platelets are released in the area of damage (Eming et al., 2014). The adherent platelet plug assumes an amorphous shape covering the lesion. Fibrin acts as "glue" that bridges the edges of tissue, essentially restoring the physical support for the next phase of wound repair, the invasion of inflammatory cells. Neutrophils and mast cells are among the first cells invading the clot and initiate a cascade of cytokines and chemokines that promote further cell invasion (e.g., macrophages), eventually leading to the removal of the cellular debris and the clot. The cytokine milieu also facilitates the recruitment of tissue-specific cells to repopulate the area of damage. During this proliferation phase new tissue is gradually assembled, including a restoration of vascular supply and deposition of tissue-specific ECM. Granulation tissue is formed, but is remodeled and replaced during the tissue maturation process. It is important to note the sequence of events, as these are dependent on each other for a successful wound healing process. A delay in blood clotting or a lack of re-epithelization will result in scar formation and prevent wound healing (Martin and Nunan, 2015).

It has been proposed that the repair of CNS injury resembles peripheral tissue wound healing, with the key difference being that in the CNS an insufficient resolution of pro-inflammatory events occurs (Shechter and Schwartz, 2013). The brain's response to injury therefore is akin to an unresolved wound healing process, in which a lack of a timely re-epithelization leads to scar formation. Scar formation is commonly seen as the main obstacle to the repair and regeneration of CNS tissues (Silver and Miller, 2004). However, it is also notable that peripheral tissue wound healing typically occurs following an acute disruption of tissue due to a cut or a superficial wound. The injuries typically involve a shallow loss of cell layers (i.e., more of a repair than regenerative response) or a very narrow disruption between layers occurs. Typically, these injuries do not involve a major volumetric loss of tissue. This is comparable to traumatic brain injury caused by penetration of a sharp object, such as a knife or an injection tract. We here argue that this type of injury and its associated repair response is quite different from what is required to regenerate a large volumetric tissue loss, as would occur after a stroke or removal of parts of the liver. The wound healing paradigm is therefore useful to understand how a reparative response is mounting to a particular type of tissue injury, but it fails to account for major tissue loss, which might require additional strategies to re-grow lost tissue.

The best known example of tissue regeneration in adult mammals is liver tissue regeneration (Cordero-Espinoza and Huch, 2018). A liver can regenerate within 5–7 days in a mouse and 8–15 days in humans (Michalopoulos, 2007). Tissue regeneration occurs in cases of volumetric tissue loss, as exemplified by a partial hepatectomy, but not in cases of certain types of liver disease, such as liver cirrhosis, further showing a difference between a tissue repair and regenerative response. Regeneration of tissue occurs from undamaged lobes by creating new tissue rather than expanding existing tissue. Akin to the inflammation phase in wound healing, macrophages resident in the liver (i.e., Kupffer cells), as well as those recruited from the blood, initiate an inflammatory cascade that stimulates hepatocyte progenitor proliferation and migration.

Myofibroblasts deposit matrix at the tissue boundary. This is degradable by matrix metalloproteinases (MMPs) and replaced by ECM deposited from stromal cells that integrate into the matrix. Upon integration, cells differentiate into appropriate phenotypes. The creation of a transitional ECM is similar to the formation of granulation tissue in wound healing and might indicate that remodeling of a temporary matrix is a key component of actual tissue creation. In addition to progenitor cell proliferation, de-differentiation and re-differentiation of stromal cells occurs. This cell pool is an important contributor to re-populate the regenerating tissue (Gilgenkrantz and Collin de l'Hortet, 2018). The extent of tissue regeneration might hence depend on the available cellular pool that can supply sufficient cells to regrow the needed tissue.

However, in the brain the pool of cells being able to replace lost tissue is thought to be restricted to neurogenic regions in the subventricular zone (SVZ) and the subgranular zone (SGZ) of the hippocampus (Ming and Song, 2011). This restricted endogenous neurogenic potential of brain tissue might therefore need to be complemented. Implantation of fetal tissue that can develop into site-appropriate brain tissue potentially provides all the required elements to

regenerate lost brain tissue and complement the endogenous tissue repair process.

FETAL CNS TISSUE TRANSPLANTS AND BRAIN DEVELOPMENT

Transplantation of fetal brain tissue is providing a substrate that contains all required elements to construct brain tissue, notably neural cells, a vasculature, microglia, as well as ECM. To ensure optimal survival, post-lesion implantation time and the age of the donor are two crucial variables. Implantable tissue should be derived from the neurogenic period of the developing brain (E11-17 in mice/rats, GW8-30 in humans) (van den Ameele et al., 2014). Earlier tissues are likely to still contain embryonic stem cells that could form teratocarcinomas, whereas more developed tissues will contain partially differentiated neurons, which are likely to die due to axotomy that results in apoptosis. The neurogenic phase is followed by the gliogenic phase (>E18), which produces astrocytes and oligodendrocytes, limiting the yield of neurons required to support function (Sauvageot and Stiles, 2002). The neurogenic tissue hence provides appropriate conditions to produce new brain tissue after implantation into a tissue cavity. A 2–3 weeks post-lesion time frame is considered to be a favorable pro-repair environment for fetal tissue transplants into a cavity, whereas integration and survival at later time points is potentially reduced by the maturation of a glial scar limiting access to host tissue (Grabowski et al., 1994).

Preclinical rodent studies using fetal tissue implanted into the stroke cavity showed the formation of new tissue that filled the cavity (Grabowski et al., 1992b, 1994; Hadani et al., 1992). This fetal tissue developed a vasculature that integrated with the host vasculature and afforded normal metabolic functioning of the tissue (Miyoshi et al., 1995a,b). However, grafts were easily identifiable and distinguishable from host tissue. A tissue mass was created in the cavity, rather than developing a homogenous transition of cytoarchitecture between the host and grafted tissues (Sorensen et al., 1996). A distinct scar separates host and graft highlighting limits to integration (Zeng et al., 1999). Still, implanted tissue fragments matured with neuronal differentiation that led to efferent and afferent axonal projections (Grabowski et al., 1992a, 1993; Sorensen et al., 1996). Although tissue grafts improved behavioral deficits (Grabowski et al., 1995), it remains unclear if this efficacy was due to neuronal connections being formed or if it was mainly due to a trophic factor support reducing secondary degeneration (Mattsson et al., 1997). Nevertheless, these studies demonstrated that new brain tissue can develop in a cavity formed after a stroke.

A regional specificity is observed with brain tissue implants. Cortical grafts implanted into the striatum developing as cortical rather than striatal tissue (Wictorin et al., 1991). This result reflects the positional specification of different brain regions during development (**Figure 3**). Cortical tissues typically develop from the pallium through Pax6-dependent positional specification, whereas the striatum (i.e., caudate-putamen) develop from the lateral and medial ganglionic eminence (LGE and MGE) (Campbell, 2003). The LGE is specified by Gsx2 and Ascl1, whereas the MGE is defined by both Gsx2 and Nkx2.1 (Evans et al., 2012). In the adult, this positional specification is mostly restricted to the SVZ with the dorsal element reflecting the pallial specification (i.e., Pax6 and Emx1/2), the middle section expressing Gsx2 and the ventral part Nkx2.1 (Chaker et al., 2016; Delgado and Lim, 2017). Neurogenesis in the SVZ in the adult therefore produces progenitors that contain some positional specification, which can affect their potential to repair site-appropriate tissue.

NEURAL STEM CELLS: FROM TISSUE REPAIR TO REGENERATION

The differential expression of positional specification in the adult SVZ has profound implications for tissue repair and regeneration. If the neural progenitors are already pre-specified to develop into cortical or striatal phenotypes, their migration across the corpus callosum could direct these into heterologous tissues (**Figure 3**). Commonly, only the SVZ region affected by damage is mounting a repair response with a transient proliferation of NSCs and a more prolonged activation (>1 year) of neural progenitors (Kazanis et al., 2013). If only a restricted portion of the SVZ is responding to tissue injury, this might limit the type of cells available for tissue regeneration. It remains to be determined if this positional specification can be re-specified upon final differentiation. Although fetal tissue experiments suggest that cortical cells will develop into cortex even if implanted into the striatum (Wictorin et al., 1991), these transplants are considerably different from individual cells migrating and interacting with a striatal environment. It is also unclear what the functional effects of differentiated cortical neurons in striatal tissue would be. Cortical NSCs implanted into the stroke-damaged striatum integrate positionally into peri-infarct tissue, in some cases extensive (17%) neuronal differentiation is observed (Darsalia et al., 2007), whereas in others only very few transplanted cells (<2%) actually become neurons (Smith et al., 2012). It therefore remains unclear to what degree the tissue region influences individual transplanted NSCs. For instance, typically striatal projection neurons are produced by cells from the LGE, whereas striatal GABAergic and cholinergic interneurons are derived from the MGE (Marin et al., 2000). Neuroblasts responding to stroke co-express markers for striatal projection neurons (i.e., Pbx and Meis2), indicating their regional specificity stemming from the LGE region (Arvidsson et al., 2002). Hence, both a contribution of MGE and LGE regions of the SVZ are required to produce a functional striatal tissue. Multiple SVZ regions therefore need to respond to striatal tissue damage to reconstruct functional circuitries. In the case of tissue damage encompassing both striatal and cortical tissue, it is further tantalizing to speculate that cortical and striatal cells would sort themselves into their respective territories to restore a pallio-subpallial boundary. Some local cell proliferation is occurring and participating in the tissue response, for instance, glial scarring, but also by producing a small number of neural progenitors (Buffo et al., 2008; Gabel et al., 2016). Astrocytes from the

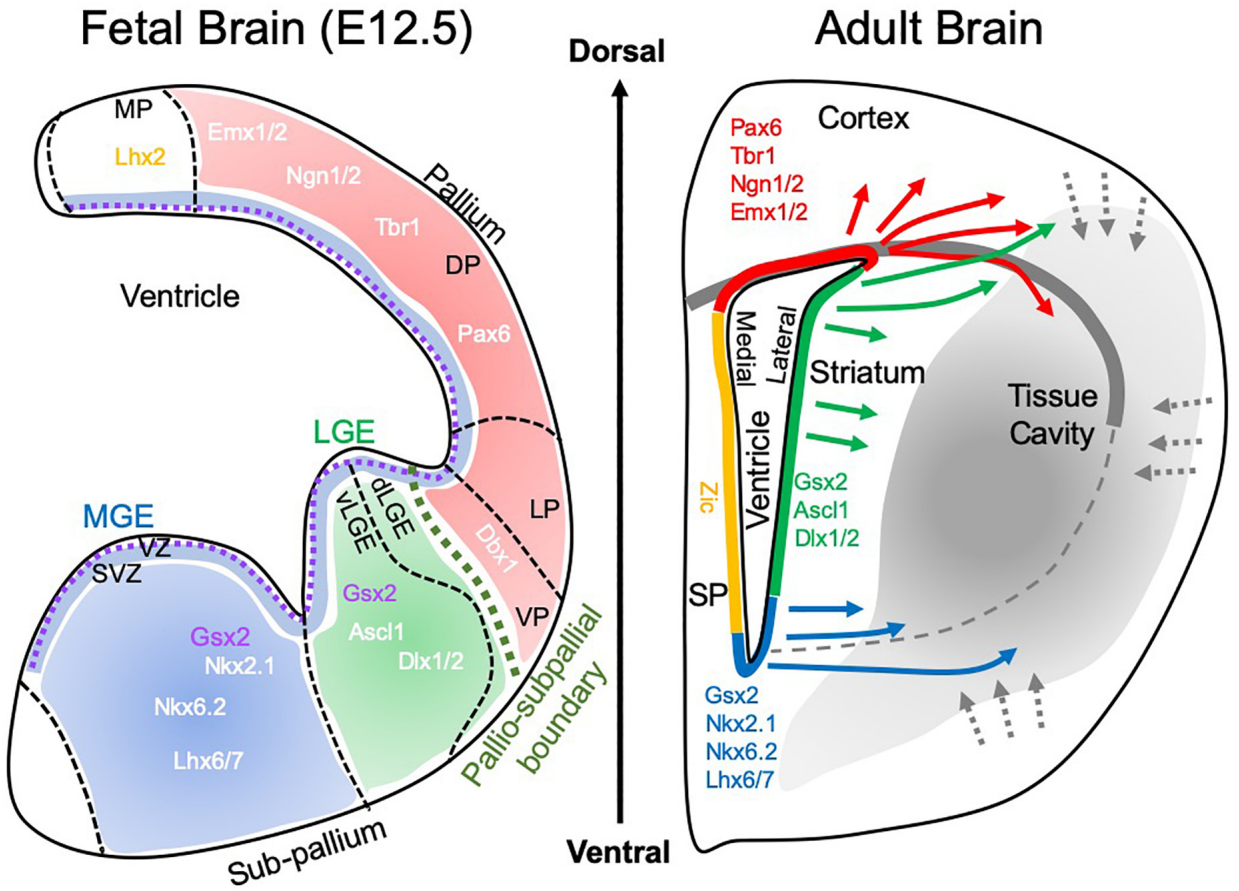

FIGURE 3 | Brain development and tissue repair. During brain development, the pallio-subpallial boundary defines the divide between regions that mature into cortical and striatal tissues. The subventricular zone (SVZ) lies beneath the ventricular zone (VZ) and during development is the birthplace for cells that colonize tissue by migrating along radial glia. Within these tissues, particular gene expressions define the positional specifications of cells to become neurons that characterize the functions of individual regions. The medial ganglionic eminence (MGE) produces striatal interneurons (i.e., calretinin, paravalbumin, calbindin, cholinergic positive), whereas the lateral ganglionic eminence (LGE) is the main source of striatal projection neurons, which constitute 90% of neurons in the striatum. Of these 98% are DARPP-32 positive neurons. A further sub-division of the LGE into the ventral (vLGE) and dorsal (dLGE) has emerged, with vLGE producing a subset of projection neurons. The dLGE is thought to be the main source of interneurons in the olfactory bulb. In contrast, the pallium (a.k.a. telencephalon) is giving rise to the cortex with subdivisions of the ventral pallium (VP), lateral pallium (LP), deep pallium (DP) and medial pallium (MP). These regions produce different subdivision of the cortex, such as the motor cortex and somatosensory cortex. In the adult brain, this positional specification is retained within the subventricular zone (SVZ), the site of adult endogenous neurogenesis. Neurons born along different segments of the SVZ therefore contain a certain positional specification to produce region-specific cells. In response to acute brain injury. These cells respond and migrate through damaged tissue. In the context of tissue regeneration, the SVZ is the main source of cells to replenish lost cells. It remains currently unclear if these cells will cross the pallio-subpallial division that is defined by the lateral corpus callosum in adults. It also remains unknown if cells can change their positional specification and what functional consequence ensue if cells are not expressing a site-appropriate neuron differentiation.

lesion environment gain the potential to produce neurons *in vitro* (Buffo et al., 2008), but *in vivo* the restrictive non-permissive environment suppresses this potential (Seidenfaden et al., 2006; Costa et al., 2010; Robel et al., 2011). This local response is therefore not considered a major source of neuronal replacement in damaged tissue, but these cells are in a position to rapidly invade a cavity and initiate tissue regeneration.

An enhanced proliferation and mobilization of neuroblasts is likely to be advantageous to promote a more extensive tissue repair, but will be essential to produce a sufficient cell pool to replace lost tissue. Intracerebral infusion of growth factors, such as glial cell line derived neurotrophic factor (GDNF), enhanced striatal neurogenesis in the SVZ, but also improved the survival of cells migrating into the stroke-damaged striatum (Kobayashi et al., 2006). A continued infusion of growth factors, such as EGF or betacellulin (Gomez-Gaviro et al., 2012), into the lateral ventricle can hence increase the proliferation of NSCs and/or neuroblast to improve invasion into the damaged striatum and cortex. However, at present it is unclear if these different SVZ sub-regions can be stimulated separately to control tissue specificity of neural progenitors. Proliferating peri-infarct cells could also provide a source of cells that can be expanded to provide a cellular population

that can promote tissue regeneration. Stimulation of the progenitor pool prior to tissue regeneration could be important to ensure that a sufficient invasion of progenitors is available in the damaged tissue to afford invasion into the cavity to replace lost tissue.

INDUCTIVE BIOSCAFFOLDS TO PROMOTE BRAIN TISSUE REGENERATION

The tissue repair response mediated by endogenous neurogenesis, however, does not lead to an invasion of progenitors into the lesion cavity to replace lost tissue. The tissue boundary is undergoing an injury response that seals off the cavity and aims to preserve viable tissue from ill effects of liquefactive necrosis. Unlike in wound healing, no substrate, such as a granulation tissue, is available in the cavity that can sustain the migration of brain cells to repopulate tissue. Indeed, this is evident in the peri-infarct area, where the repair response is using the available tissue substrate for migration and guides cells into position. A physical substrate to sustain cells within the cavity is therefore needed. Akin to fetal tissue transplants, experimentally this principle was demonstrated by implanting NSCs on scaffolds into a tissue cavity formed by a stroke. Provision of a structural support afforded a primitive *de novo* tissue formation by NSCs (Park et al., 2002; Bible et al., 2009, 2012a), although vascularization of this tissue was an issue (Bible et al., 2012b). It was also noted that large degradable solid microparticles produced a spiderweb-like tissue (Bible et al., 2009), hence producing an unfavorable condition to produce a homogenous tissue that integrates with the host. In contrast, implantation of NSCs in a hydrogel made out of ECM from decellularized urinary bladder matrix (UBM) and brain tissue resulted in an excellent cell survival in the tissue cavity, while producing a homogenous tissue that was distinct from host brain tissue (Bible et al., 2012a). These experiments indicated that a hydrogel formulation of a bioscaffold is favorable for replacing brain tissue. The hydrogel bioscaffold readily conforms to the cavity topology if a magnetic resonance imaging (MRI) guided injection-drainage approach is adopted (Massensini et al., 2015).

ECM scaffolds are widely used in peripheral soft tissue repair, including bladder (Santucci and Barber, 2005; Pearlman et al., 2018), dermis (Tchanque-Fossuo et al., 2017; Jeon and Kim, 2018), muscle (Sicari et al., 2014; Zhao and Bass, 2018), heart (Badylak et al., 2006; Khalil et al., 2018), and peripheral nerve (Nectow et al., 2012; Prest et al., 2018). These biomaterials can be sourced from different organs, such as the UBM (Freytes et al., 2008; Crapo et al., 2012, 2014; Dziki et al., 2017; Faust et al., 2017), umbilical cord (Koci et al., 2017), peripheral nervous system (Prest et al., 2018), spinal cord (Tukmachev et al., 2016), as well as the brain (Crapo et al., 2012; Medberry et al., 2013; Faust et al., 2017). It is important to note that the bioscaffolds are natural products that contain soluble (e.g., VEGF-A, BDNF) and juxtracrine factors (e.g., vitronectin, laminin), as well as structural proteins (e.g., collagen, hyaluronic acid) that can affect cellular functions (Saldin et al., 2017). The relative composition is dependent on the organ of origin, rather than being specifically designed, as in the case of synthetic materials (Wolf et al., 2015). Sheets of ECM are often used in peripheral tissue regeneration, but a minimally invasive implantable approach through narrow needles is desirable for brain applications, as this reduces damage to tissues overlying the cavity (Massensini et al., 2015). The formulation of ECM as a lyophilized digest that is reformulated as hydrogel serves this purpose (Freytes et al., 2008; Badylak et al., 2009) and affords reconstitution at different protein concentrations that determine bioscaffold stiffness (Massensini et al., 2015) and biodegradation (Ghuman et al., 2018).

Pre-gel ECM preparations are cytocompatible, while enhancing proliferation and migration of neural progenitors (Crapo et al., 2012; Crapo et al., 2014). Differentiation and neurite outgrowth of neural progenitors with UBM-ECM was higher compared to central nervous system (CNS)-derived ECM (Crapo et al., 2012; Faust et al., 2017), potentially demonstrating that non-CNS scaffolds might be favorable to induce tissue regeneration (Chan and Leong, 2008). In the spinal cord for instance, UBM-ECM performed as well as spinal cord-derived ECM, but provided favorable degradation kinetics (Tukmachev et al., 2016). Non-gelling UBM- and brain-ECM injections after traumatic brain injury revealed improvements in behavioral deficits, further highlighting their potential for therapeutic CNS applications (Zhang et al., 2013; Wu et al., 2016), but no tissue regeneration was reported due to the low concentration and small volume of injectate in these studies. However, these materials might have created a more favorable environment in damaged tissues to promote the survival of newly generated endogenous neural progenitors. Sourcing of homologous CNS tissues also poses a challenge due its low yield (Faust et al., 2017). It is important to point out that these acellular bioscaffolds are used to induce a host regenerative response and not to replicate the existing ECM that is found in a target organ. Heterologous organ sources therefore potentially exert a greater pro-repair effect than CNS-derived ECM.

IMMUNE SYSTEM RESPONSE TO IMPLANTATION

The initial inductive event after ECM implantation remains essentially unknown. It is conceivable that the physical implantation of a bioscaffold into a damaged tissue induces a pressure gradient that provokes a pro-inflammatory response from the immune system. Mechanotransduction in host tissue has also been associated with a good outcome in wound healing, but is generally neglected as an initiating event (Barnes et al., 2018). Invasion of cells needs to occur through existing tissue, as there are no blood vessels in the cavity that could support an invasion into the scaffold. Neutrophils and macrophages are dominant cell types acutely invading these scaffolds in peripheral tissues (Brown et al., 2009; Valentin et al., 2009), as well as the brain (Ghuman et al., 2016, 2018). However, cells resident within veterate tissue could provide the first response with low concentrations of ECM hydrogel permeating into damaged tissue (Massensini et al., 2015). The presence of juxtacrine

and/or paracrine factors, as well as nanovesicles, released from the scaffold into tissue are potentially factors that induce an immune response in peri-cavity tissues (Sciari et al., 2014; Slivka et al., 2014; Dziki et al., 2017; Huleihel et al., 2017a). The acute invasion of immune cells is likely a reflection of innate immunity. This arm of the immune system involves neutrophils, eosinophils, basophils, dendritic cells, as well as macrophages (**Figure 4A**).

However, the acute immune response to inductive bioscaffolds in the brain remains poorly understood. The main focus has been on the role of macrophages, which constitute 23% of all cells found within ECM hydrogel implanted into the brain (Ghuman et al., 2016). Still, 66% of cells in the hydrogel at this time point have not been associated with a particular cell phenotype (**Figure 4B**) and could reflect other immune cells (i.e., neutrophils) contributing to a rapid innate response (Ghuman et al., 2018). It is unclear if macrophages found in the ECM hydrogel in the brain are derived from peripheral macrophages or if these are mostly brain-resident microglia that respond. More detailed studies of the mode of action (i.e., cellular level) involved in this early phase are required to gain a better understanding of the factors (i.e., mechanisms of action) that elicit the initial response and provoke a regenerative cascade (Badylak and Gilbert, 2008). Understanding this process is especially important for the design of synthetic bioscaffolds aiming to replicate the tissue regeneration achieved with natural materials (Drury and Mooney, 2003; Zhu and Marchant, 2011; Aurand et al., 2012).

Immune cell recruitment is most likely mediated through soluble factors that can diffuse through a large volume of tissue, although it is influenced by tissue density and other structures (e.g., scarring) that provide barriers (Nicholson, 2001). Notch and PI3K/Akt signaling in ECM bioscaffolds, for instance, have been associated with the phagocytic activity of immune cells (Slivka et al., 2014). The migration of macrophages is dependent on monocyte chemoattractant protein-1 (MCP-1/CCL2), which guides cells to their target (Deshmane et al., 2009). During the acute phase of macrophage invasion, most of these monocytes (>35%) exhibit an M1-like phenotype (CD86+), but by 14 days this proportion is reduced and mostly (>20%) M2-like (CD206+) characteristics are found (Ghuman et al., 2018). This shift in macrophage phenotype is also thought to affect the differentiation of organ-specific cells, such as neurons, in the case of the brain (Faust et al., 2017). In wound healing, a shift toward an M2-like phenotype is thought to be influenced by lymphocytes (i.e., T and B cells) that invade as part of the adaptive immune response (**Figure 4C**). IL-4 is commonly associated with this shift in macrophage phenotype, but juxtacrine factors, such as MEK/ERK and integrin signaling are also known to decrease phagocytic activity and promote a repair phenotype (Slivka et al., 2014). There is also recent evidence that ECM bioscaffolds produce a macrophage activation that might be distinct from the characteristics associated with M0, M1 or M2 activation (Huleihel et al., 2017b), but this might merely be a reflection of the activating signals rather than the cells' function (Novak and Koh, 2013). Other classifications, such as division of macrophages into pro-fibrotic and pro-repair phenotypes have also been proposed to be more relevant to the processes involved in tissue repair and regeneration (Sadtler et al., 2019).

Although macrophage activity within ECM bioscaffolds has been extensively investigated, their interaction with other cells remains poorly understood, especially in the context of an adaptive (delayed) immune response (**Figure 5A**), which has also been reported to participate in tissue regeneration (Strbo et al., 2014; Sadtler et al., 2019). The use of xenogenic matrix grafts raises the question of the role of an adaptive immune response to foreign proteins. The blood-brain barrier (BBB) produces an immune-privileged tissue environment, but drainage of solutes through the glymphatic system leads to a sensitization of B and T cells in the cervical lymph nodes (Verheggen et al., 2018). There is evidence that T helper cells respond to xenogenic proteins in ECM bioscaffolds, suggesting that a specific immune response develops (Allman et al., 2001). Still, it remains unclear if an "adaptive immune response" is an indication of an incomplete decellularization, which might lead to remnants of cells being retained with the bioscaffold to produce a sensitization of the immune system. It is generally thought that ECM molecules by themselves do not elicit an adaptive immune response. Still, the complexity of molecules contained within decellularized materials (e.g., microvesicular bodies) can provide a range of targets for an adaptive immune response that is distinct from the ECM molecules *per se*. An adaptive immune response to even endogenous proteins can follow an innate immune response, as in the case of stroke for instance (Rayasam et al., 2018). The division between an innate and adaptive immune response is based on infection studies and might therefore not be an adequate description of the response observed after tissue damage and repair (Sadtler et al., 2019). A greater focus on the role of the immune system in these conditions is likely to provide a more adequate understanding and conceptualization of the role inflammation plays in modulating a tissue response toward repair and regeneration.

BIODEGRADATION OF SCAFFOLDS

The recognition that the same immune cells can exert different functions is part of this evolving conceptualization. For instance, the polarization toward an M2-like phenotype is thought to be crucial for the repair response, even though M1-like macrophages persist for 90 days and are thought to play an essential role in the degradation of the bioscaffold (Ghuman et al., 2018). Ablation of peripheral macrophages prevents structural remodeling of ECM bioscaffolds, further highlighting their crucial role in this process (Valentin et al., 2009). Macrophages secrete proteases that degrade cross-linked collagen scaffolds (Yahyouche et al., 2011; Madsen et al., 2013), as is the case with ECM hydrogel. Especially, MMP-2 and MMP-9 (**Table 2**) are upregulated after acute brain injuries, such as stroke, by secretion from brain microglia reacting to the tissue insult (del Zoppo et al., 2007), but so are MMP-3, MMP-7, MMP-10, and MMP-11 (Rempe et al., 2016). UBM-ECM hydrogel is especially high in collagen I (Saldin et al., 2017), which is primarily degraded by MMP-1, MMP-2, MMP-8, MMP-12, and MMP-13 (Webster and Crowe, 2006;

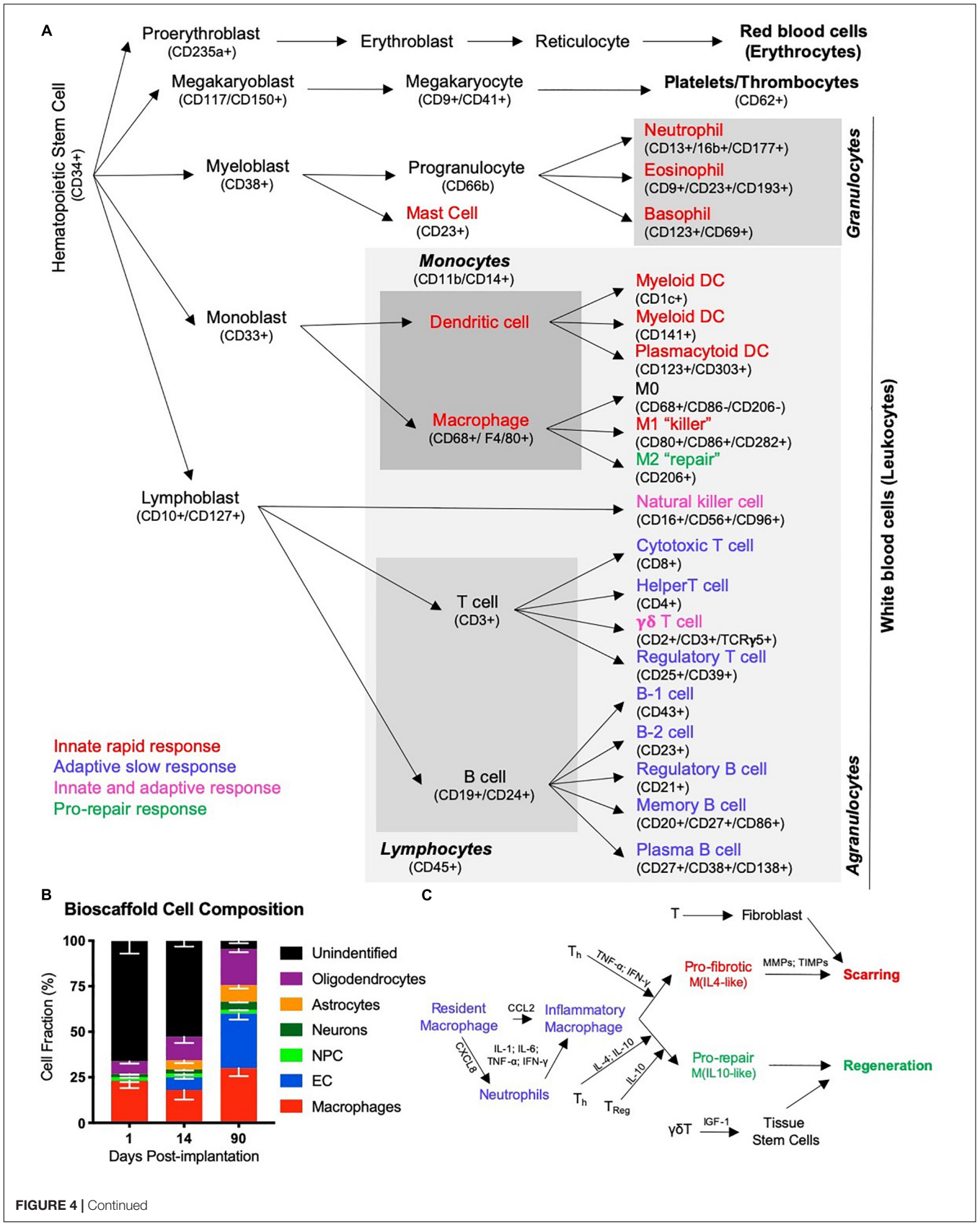

FIGURE 4 | Continued

FIGURE 4 | The immune response in tissue regeneration. **(A)** The inflammatory response is driven by the immune system. Although the immune system is a complex network of circulating and tissue-resident cells, these originate from a hematopoietic stem cell. Traditionally the immune system was characterized in studies of infection and cells have therefore been divided into those that contribute to an innate rapid response versus those that produce an adaptive slow response. Only a few types of cells, such as natural killer cells and γδT cells, have been thought to contribute to both. However, more recently the importance of inflammation in tissue repair and regeneration has revealed distinct phenotypic changes in cells, such as macrophages, that questions the traditional division into an innate and adaptive immune response to recognize a pro-repair response of the immune system. It is likely that a range of immune cells are involved in this pro-repair response, but that the function of cells might be different to their role in response to an infection. **(B)** A characterization of cells infiltrating an ECM bioscaffold implanted into a stroke cavity revealed that >75% of cells (mean – standard deviation) at 1 day post-implantation are not of a brain origin (Ghuman et al., 2018). Although the majority of these are currently unidentified phenotypes, it is likely that these are of an immune origin, such as neutrophils and eosinophils, which respond rapidly, but also transiently, to tissue changes. **(C)** Inflammation in wound healing is thought to be initiated by resident macrophages that release inflammatory cytokines (IL-1; IL-6, TNF-; IFN-) in response to detection of an injury. The chemokine CXCL8 is released and drives the rapid invasion of neutrophils into the damaged tissue from the blood. A secondary invasion response is recruiting inflammatory macrophages, as well as lymphocytes, such as helper (T_h), regulatory (T_{reg}) and γδT cells. T cells are thought to play a key role in modulating macrophage activity and promoting a pro-fibrotic response that results in tissue scarring or a pro-repair response that leads to tissue regeneration.

Lu et al., 2011). In contrast, MMP-9 is mostly associated with degradation of the basement membrane around blood vessels, which is rich in collagen IV, laminin, and vitronectin (Fukuda et al., 2004; Underly et al., 2017). Neutrophils also produce MMP-9 and are known to be involved in ischemic tissue regeneration in peripheral limbs (Heissig et al., 2010). Other proteases, such as A Disintegrin And Metalloproteinases (ADAMs) and Meprins, are also likely involved in ECM remodeling, but their role remains poorly understood, especially in the context of tissue regeneration (Bonnans et al., 2014). How different immune cells and their activation state drive protease production and bioscaffold degradation also requires more mechanistic studies to understand their role in initiating the tissue regeneration process.

Although collagen I is considered a major structural target for biodegradation, the role of the biodegradation of other ECM molecules remains poorly understood. In ECM hydrogels implanted into the brain, for instance, fibronectin and chondroitin sulfate were mostly degraded within a week, even though collagen I was still abundantly present (Jin et al., 2017). Laminin, collagen IV and hyaluronic acid (HA) were also present at 1 day post-implantation (Massensini et al., 2015), but it remains unclear if these molecules are rapidly degraded or if the degradation profile of the ECM molecules is equivalent to collagen I. Less abundant molecules could be degraded faster than more abundant one's, even though the rate of biodegradation is the same. A quantitative comparison between different ECM molecules and their degradation is needed to address these key questions. While bioscaffolds from different sources are thought to exert similar regenerative effects (Keane and Badylak, 2015; Tukmachev et al., 2016), their biodegradation is likely to be influenced by their composition. Understanding how individual ECM molecules are degraded and lead to the release of other factors (e.g., VEGF-A) will be essential to design novel biomaterials that afford a greater control over biodegradation (Sridharan et al., 2015; Kelly et al., 2017).

Biodegradation of ECM bioscaffolds in the brain potentially follows a different dynamic than in peripheral organs. Stiffer ECM hydrogel (8 mg/mL) undergoes a slow degradation in the brain, with only a 32% reduction in volume by 90 days, whereas softer bioscaffolds (3 and 4 mg/mL) were almost completely absorbed (>95%) (Ghuman et al., 2017, 2018). Stiffer brain-compliant 8 mg/mL UBM-ECM hydrogel was rapidly invaded by macrophages compared to the weaker gels, but the density of cells inside the scaffold decreased over time indicating that a poor biodegradation occurred (Ghuman et al., 2018). Softer gels produced a more consistent cell density (∼4000 cells/μL) with a vasculature forming, which was absent in stiffer material. Although these differences indicate a potential mode of action for biodegradation, it remains unclear how stiffness or the higher protein concentration adversely affected biodegradation, considering that there was an extensive cellular response at 1-day post-implantation in the bioscaffold that did not readily degrade (Ghuman et al., 2016). In peripheral tissues, a complete replacement with host tissue between 75 and 90 days has been associated with tissue regeneration (Record et al., 2001; Gilbert et al., 2007; Valentin et al., 2009; Carey et al., 2014; Dearth et al., 2016) and is consistent with the time course observed with softer gels in the brain (Ghuman et al., 2018). However, in peripheral tissues most biodegradation studies investigate the use of ECM sheets, rather than hydrogel. It is therefore unclear if ECM hydrogel will follow a similar time course in peripheral tissues. Crucially, the lack of biodegradation in the brain did not lead to tissue regeneration (Ghuman et al., 2017), whereas biodegradation of the scaffold produced *de novo* tissue (Ghuman et al., 2018). Biodegradation gradually removed the bioscaffold and provided the structural basis for new cells to invade the cavity. These newly invading cells showed assembly in and inbetween the ECM hydrogel to initiate the formation of new tissue. This process is very similar to that described in peripheral tissues, where biodegradation or the remodeling of a "transient" ECM is a key step to replace lost tissues (Swinehart and Badylak, 2016).

NEURAL TISSUE FORMATION AND CONNECTIVITY

Tissue-specificity is determined by the cells that invade from the host organ into the degrading bioscaffold. The continued proliferation and response of the SVZ to brain injury (Kazanis et al., 2013; Chang et al., 2016) provides a ready supply of local (i.e., peri-cavity) neural progenitors that can respond to the implantation of a bioscaffold. Inflammatory factors released from microglia and invading immune cells provide a trail of ligands, such as CCL2 (a.k.a. monocyte

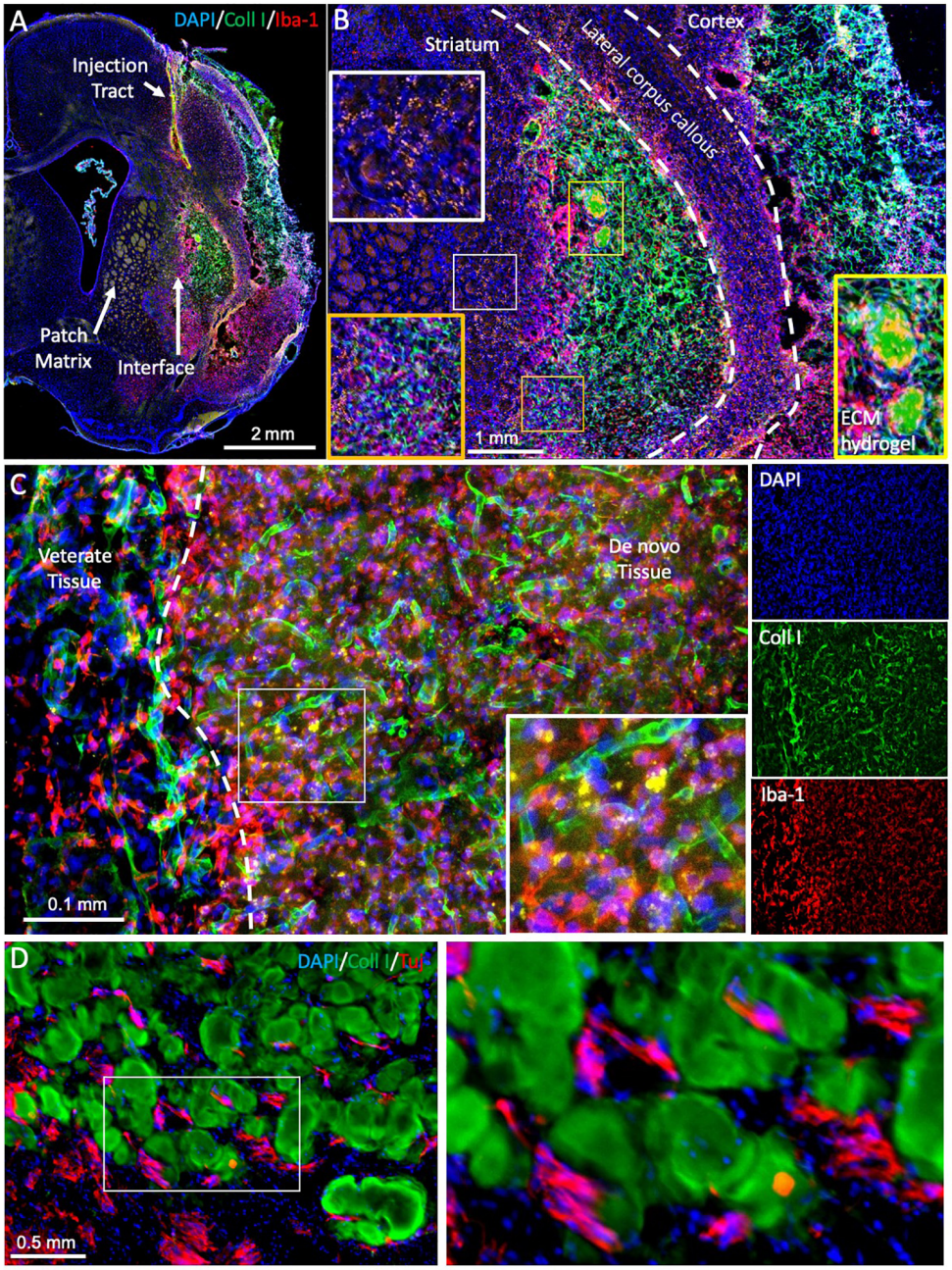

FIGURE 5 | Evaluating brain tissue regeneration. **(A)** A bioscaffold is implanted into the lesion cavity through a narrow bore needle that produces an injection tract and defines the trajectory of the injection. The aim of the procedure is to fill the tissue cavity and to produce a close-fitting interface with host tissue that affords invasion of cells into the scaffold and produces a seamless integration between veterate and *de novo* brain tissue (Ghuman et al., 2018). *De novo* tissue growing inside the cavity can be identified based on collagen I staining of the ECM hydrogel and the neovasculature, surrounded by veterate tissue, as indicated by the peri-infarct area and a dense presence of microglia (Iba1 + cells). **(B)** At 90 days post-implantation, the bioscaffold is almost completely degraded. In this case, two small remnants of the ECM hydrogel, characterized by a dense collagen I content are still undergoing cell invasion and degradation (yellow box). However, the rest of the scaffold is degraded and replaced with *de novo* tissue, in which blood vessels contain a higher level of collagen I compared to host tissue. Regenerated tissue (orange box) has blood vessels high in collagen I, but a dense tissue structure is evident with a reduced number of Iba-1 positive microglia/macrophages. It was also noted that in *de novo* tissue, some particulates were present that were not evident in veterate brain (white box). **(C)** In regenerating tissue, the bioscaffold is degraded, but there is still a higher collagen I background compared to host brain. Morphologically it is also distinct with a higher content of microglia/macrophages and strongly collagen I positive blood vessels. Nevertheless, more robust unique identifiable markers are desirable to contrast these different microenvironments. **(D)** In between patches of ECM bioscaffold, tissue is developing that contains neurons (Tuj) at a higher density than within the bioscaffold. However, at present there are no robust markers that allow a reliable identification of this as *de novo* tissue, complicating the quantification of the regenerative process.

TABLE 2 | Matrix metalloproteinases (MMPs).

Family Member	Aliases	Activators	Collagen Targets											Other ECM Targets
			I	II	III	IV	V	VI	VII	VIII	IX	X	XI	XIV	
MMP-1 (1) secreted	Collagenase-I Interstitial Collagenase	MMP-3 MMP-10 Plasmin Kallikrein Chymase	*	*	*			*	*			*			Aggrecan Entactin Gelatin Perlecan Tenascin
MMP-2 *(2) secreted*	Gelatinase A	MMP-1 MMP-7 MMP-13 MMP-14 MMP-15 MMP-16 MMP-24 MMP-25 Plasmin	*		*	*	*		*			*	*	*	Aggrecan Elastin Fibronectin Gelatin Laminin
MMP-3 *(1) secreted*	Stromelysin-I	Plasmin Kallikrein Chymase Tryptase			*	*					*	*	*		Aggrecan Decorin Fibronectin Gelatin Laminin Perlecan Tenascin
MMP-7 *(3) secreted*	Matrilysin-1 PUMP-1	MMP-3 MMP-10 Plasmin				*						*			Aggrecan Decorin Elastin Fibronectin Gelatin Laminin
MMP-8 (1) *secreted*	Collagenase-2 Neutrophil collagenase	MMP-3 MMP-10 Plasmin	*	*	*		*		*	*		*			Aggrecan Gelatin
MMP-9 *(2) secreted*	Gelatinase B	MMP-2 MMP-3 MMP-10 MMP-13 Plasmin				*	*		*			*		*	Aggrecan Decorin Elastin Gelatin Fibrin Laminin Vitronectin
MMP-10 *(1) secreted*	Stromelysin-2	Plasmin Kallikrein Chymase Tryptase			*	*	*		*		*	*			Aggrecan Fibronectin Laminin
MMP-11 *(1) secreted*	Stromelysin-3	Furin Plasmin													Aggrecan Fibronectin Gelatin Laminin
MMP-12 (1) *secreted*	Macrophage Metalloelastase	n.d.	*			*									Aggrecan Elastin Fibronectin Laminin Nidogen Osteonectin
MMP-13 (1) *secreted*	Collagenase-3	MMP-2 MMP-14 Plasmin Kallikrein Chymase Tryptase	*	*	*	*			*		*	*		*	Aggrecan Fibronectin Laminin Osteonectin Perlecan Tenascin

(Continued)

TABLE 2 | Continued

Family Member	Aliases	Activators	Collagen Targets												Other ECM Targets
			I	II	III	IV	V	VI	VII	VIII	IX	X	XI	XIV	
MMP-14 (4) membrane	MT1-MMP	Furin	*	*	*										Aggrecan Fibrin Fibronectin Gelatin Laminin
MMP-15 (4) membrane	MT2-MMP	Furin													Aggrecan Fibronectin Laminin Nidogen Perlecan Tenascin
MMP-16 (4) membrane	MT3-MMP	Furin			*										Fibronectin Gelatin
MMP-17 (4) membrane	MT4-MMP	Furin													Fibrinogen Gelatin
MMP-18	Collagenase-4 XCol4 Xenopus Collagenase	n.d.	*												n.d.
MMP-19	Stromelysin-4 RASI-I	n.d.	*			*									Fibronectin Gelatin Laminin
MMP-20 secreted	Enamelysin	n.d.													Aggrecan
MMP-21 (1) secreted	XMMP	n.d.													n.d.
MMP-23 membrane	CA-MMP	n.d.													Gelatin
MMP-24 (4) membrane	MT5-MMP	n.d.													Fibrin Gelatin
MMP-25 (4) membrane	MT6-MMP	n.d.				*									Gelatin Fibrin Fibronectin Laminin
MMP-26 (3)	Matrylisin-2 Endometase	n.d.				*									Gelatin Fibronectin
MMP-27 (1)	MMP-22 Chick embryo-MMP	n.d.													Gelatin
MMP-28 secreted	Epilysin	n.d.													n.d.

MMPs can be divided into several sub-domains consisting of MMPs with basic domains (i.e., prodomain + catalytic domain + hemopexin-containing ancillary domain) (1); MMPs with minimal domains (i.e., prodomain + catalytic domain) (3), MMPs with fibronectin-domain inserts (2), Membrane-bound MMP anchored by GPI or a transmembrane domain (4). There is a further distinction in MMPs either being secreted or membrane-associated. A variety of aliases have been used to refer to different MMPs, depending on their original discovery. MMPs typically also act as activators of other MMPs, further enhancing their potential to degrade different types of collagen, as well as other types of ECM molecules. A few MMPs have been associated with acute brain injury, as indicated by italics, but other have been found to be upregulated in different types of neurodegenerative disease, as well as synaptic plasticity. MMPs therefore serve important roles in maintaining a healthy brain environment, as well as being propagators of tissue damage in disease conditions (n.d., not defined).

chemoattractant protein 1) and CXCL12 (a.k.a. stromal-derived factor-1α), for neural progenitors to follow (Bye et al., 2012; Kaneko et al., 2017). Some local proliferation might also occur in response to factors, such as bFGF (FGF2) and VEGF-A, released by activated astrocytes (Gabel et al., 2016). Release of these factors can occur from the ECM bioscaffold and lead to the initial cell invasion of neural progenitors and astrocytes observed within 1 day in implanted gels (Ghuman et al., 2016). However, the continued recruitment of neural progenitors from veterate brain is likely dependent on the secretion of appropriate factors, such as CCL2 and CXCL12, from microglia and/or macrophages that are degrading the scaffold. It can be surmised that in the case of the 8 mg/mL ECM hydrogel implanted into a stroke, the very slow biodegradation associated with very few macrophages present in the scaffold provided insufficient chemokines to drive host cell invasion, including blood vessels (Ghuman et al., 2018). Blood vessels are likely to play a triple role. Their formation in the scaffold affords a direct route for macrophage invasion to accelerate biodegradation, but they also provide

a migration substrate for neural progenitors and are required to meet the metabolic demands of a newly forming tissue (Serbo and Gerecht, 2013).

The cellular composition inside the bioscaffold shifts from predominantly immune cells, such as macrophages, being present to endothelial cells, as well as neural cells, such as oligodendrocytes, neurons, neural progenitor cells, and astrocytes. These constitute over 70% of cells at 90 days (**Figure 4B**) (Ghuman et al., 2018). This suggests that some cellular composition required for *de novo* tissue formation precedes the degradation of the implanted ECM. This is consistent with new ECM being deposited by site-appropriate cells, rather than immune cells. Still, the density of neurons (6% of cells) inside the hydrogel is considerably lower at 90 days compared to intact tissue (42%) (Ghuman et al., 2018). This is also the case during development, where radial glia provide the substrate for neuron progenitors to migrate into position and gradually produce the neuronal density of an adult brain (Malatesta and Gotz, 2013). Astrocytes present within the bioscaffold, however, do not morphologically or topologically resemble radial glia (Ghuman et al., 2016). The transitional microenvironment in the bioscaffold, where neural cells are found, does not contain strands of radial glia along which neural progenitors migrate.

Regenerating tissue produces unique microenvironments not present in development. Notably, intact brain tissue borders on peri-cavity damaged tissue, with this damaged tissue transitioning into *de novo* tissue (**Figure 5A**). This *de novo* tissue borders in turn on the bioscaffold still undergoing constructive remodeling. The cytoarchitecture within the bioscaffold does not reflect the density of *de novo* or damaged tissue (**Figure 5B**). Identification of neural cells inside the bioscaffold is facilitated by visualizing the ECM hydrogel, traces of which often remain even at a low concentration (**Figure 5C**). However, a definition of *de novo* tissue, which can develop in between patches of degrading bioscaffolds (**Figure 5D**), is more challenging. Its cytoarchitecture and composition therefore currently remains unknown. To contrast *de novo* from damaged peri-cavity veterate tissue is challenging, as there are no specific markers for these microenvironments. Positional specification markers might provide some guidance to identify the differentiation of site-appropriate cells, but these are likely to be expressed inside the bioscaffold, damaged and *de novo* tissue. Deposition of ECM molecules might have greater potential to distinguish these different microenvironments. For instance, the formation of new blood vessels follows a sequential deposition of vitronectin, fibronectin, laminin, collagen I and collagen IV (Chou and Modo, 2016). Establishing a similar deposition pattern for the interstitial ECM could lead to a better characterization of microenvironments. The use of specific tags for the bioscaffold would further afford a distinction from veterate tissue that does not rely on the abundancy of ECM molecules in the hydrogel (Park et al., 2019).

Akin to the transplantation of fetal tissue, the integration between newly forming and veterate tissue will be a key aspect to produce behavioral recovery that is dependent on neuronal circuitry. Axons containing neurofilament are found within ECM hydrogel implanted in a stroke, as well as in *de novo* tissue forming in between patches of remaining scaffold (Ghuman et al., 2018). Oligodendrocytes were the most abundant neural cell phenotype within the ECM hydrogel, but it remains unclear if these myelinate axons. Implantation of angiogenic HA hydrogel indicated axonal regeneration through a cortical cavity along newly forming blood vessels (Nih et al., 2018). Wider connectivity with veterate tissue or the formation of neuronal circuitry in *de novo* forming tissue remain to be investigated. Extensive work on axon regeneration has been focused on the spinal cord (Anderson et al., 2018), but a more complex topology of connections is required to establish neuronal circuitries in the brain, as well as to establish a functional integration between *de novo* and veterate tissue. Although fetal tissue transplants and implantation of HA hydrogel indicate that new axonal connections can be formed in or through cavities, it is unclear if guidance to newly forming connections is required to ensure the appropriate development of neuronal circuitry. So far, no epileptic fits have been reported, potentially suggesting that spontaneously appropriate connections are formed or that there is a lack of functional integration (Modo and Badylak, 2019). The use of conductive hydrogels and specific stimulation might provide a new perspective to promote an integration of newly forming tissues (Oh and George, 2019). The time course of establishing axonal connections and their potential underpinning of behavioral functions remain to be investigated, but it is expected that neuronal differentiation in *de novo* tissue formation precedes axonogenesis.

CELL-BIOSCAFFOLDS AND ENGINEERED MICRO-TISSUE CONSTRUCTS FOR REPAIR AND REGENERATION

Endogenous tissue regeneration is preferable, as it will use the patients' own cells and avoid potential immune rejection. However, endogenous tissue regeneration is a lengthy process, potentially taking over 1 year to complete. Moreover, the reservoir of neural progenitors in the brain might be insufficient to supply sufficient neurons to repopulate a large *de novo* tissue. Alternative engineering strategies therefore need to be considered to expand the neural substrate required for tissue restoration (Chen et al., 2016). Implantation of allogenic neural cells in a biomaterial can potentially increase the neural substrate required to restore lost tissue. Most studies to date have focused on the use of biomaterials, such as hydrogels, to improve the delivery of cells to the brain (Ho et al., 2019). Only a few studies have aimed at restoring tissue inside the cavity. Bioscaffolds combined with neural stem cells will provide the structural support to retain cells in the cavity and allow them to differentiate (Park et al., 2002; Bible et al., 2009, 2012a). Implantation of fetal-derived neural stem cells has the potential to produce a cell substrate that is positionally specified to be striatal or cortical tissue (Bible et al., 2012a,b), but so far no evidence for the generation of region-specific tissue has been reported. Induced pluripotent stem cells

(iPS) will require positional specification *ex vivo* or *in vivo*. Implantation of NSCs requires the invasion of host endothelial cells to form a vasculature, as well as microglia to provide their support function. NSCs implanted with a non-angiogenic bioscaffold do not facilitate a neovascularization (Bible et al., 2009) and require additional instructive signals, such as release of VEGF-A, to ensure a re-vascularization (Bible et al., 2012b). Moreover, implantation of NSCs can exert an anti-inflammatory effect that prevents or reduces the infiltration of microglia. In the case of inductive bioscaffolds, this could lead to a reduction in bioscaffold degradation (Bible et al., 2012a). The inductive properties of the bioscaffold are, however, less important in this approach. In contrast to endogenous brain regeneration, implanted cells should provide a rapid replacement of tissue and hence a site-appropriate ECM might be more important. It is noteworthy that neural stem cells in brain ECM accelerate the formation of neuronal circuitry (Lam et al., 2019).

A rapid tissue restoration might therefore require the key "ingredients" for brain tissue, notably NSCs, ECs and ECM. The ratio between NSCs and ECs is crucial to promote the formation of a vasculature *in vitro* (Chou et al., 2014; Chou and Modo, 2016), as well as *in vivo* after implantation into a stroke cavity (Nicholls et al., 2015). ECs are highly immunogenic and upon formation of a vasculature in *de novo* tissue will lead to exposure of the endothelial wall to circulating immune cells, as in the case of fetal tissue or whole organ transplants. This will require a continued immunosuppression that potentially compromises the quality of life of patients. However, it is not expected that immunosuppression, such as cyclosporin A, will affect the regenerative response *per se*, as these pharmacological agents affect the indirect chronic immune response mediated through lymphocyte stimulation and not microglia/macrophages (Karam and Wali, 2015). The low immunogenicity of NSCs does not raise this issue, with good survival in the absence of immunosuppression (Modo et al., 2002, 2003). In contrast, implantation of microglia could potentially cause greater concerns, as these are highly immunogenic, and could mount a graft-versus-host response (Nassereddine et al., 2017), where implanted microglia would attack host cells. Cellular sourcing hence will be an issue with the co-implantation of cells that are immunogenic. iPS cells can circumvent these issues, but the protracted time to grow sufficient cells *ex vivo* would be a concern that would need to be balanced against the time course of endogenously induced tissue regeneration.

Beyond the co-implantation of NSCs and ECs to "spontaneously" form a tissue *in situ*, the *ex vivo* construction of micro-tissues is also considered a potential therapeutic intervention aimed at replacing lost tissue. Stem cell niches can be engineered for implantation to provide a continuous supply of new cells to repair or reconstruct brain tissue (Lampe and Heilshorn, 2012). Preformed neurovascular units can also be envisaged for implantation (Potjewyd et al., 2018). *Ex vivo* growing of brain organoids for transplantation can potentially accelerate *in vivo* tissue growth, as an essential cytoarchitecture and rudimentary connectivity can be pre-established (Mansour et al., 2018). Larger constructs with pre-formed axonal projection can also be envisaged (Struzyna et al., 2015, 2017) and in some cases be designed to specifically replace a major fiber tract, such as the nigrostriatal pathway, which is almost completely lost in Parkinson's disease (Struzyna et al., 2018). Pre-assembly of micro-tissue is potentially an exciting approach to pre-define an cytoarchitecture using bio-printing to produce homologous constructs more rapidly than spontaneously forming tissue (de la Vega et al., 2019). Delivery of these complex constructs will, nevertheless, be more challenging through a narrow bore needle without deforming or destroying the construct (Wahlberg et al., 2018). Creating a tight interface with veterate tissue also needs considering to ensure integration, as the topology is very different between subjects. Preformed connections could adversely affect cell viability, if these connections are cut or damaged during the implantation process, similar to fetal tissue transplants in Parkinson's disease (Schierle et al., 1999). Implantation of tissue constructs is therefore likely to be a more complex procedure to achieve, especially in terms of intracerebral delivery and cell sourcing.

TRAINING OF FUNCTIONAL CIRCUITRY

Axonal projections lead to connectivity between regions, but synaptic connectivity is required to avoid synaptic pruning and a potential die-back of axons. To avoid synapse pruning, functional synapses need to be established between axons and dendrites (Butz et al., 2009). Synaptogenesis will establish connections, but it is their activation through a common input that renders these functionally dependent and avoids pruning. These so called Hebbian synapses underpin plasticity in the damaged brain, which is exploited during rehabilitation training (Dalise et al., 2014; Takeuchi and Izumi, 2015). Transplantation of NSCs and their functional integration into neuronal circuits is also dependent on synaptic integration between grafted and host cells (Tornero et al., 2013, 2017). However, mapping these connections across a whole brain poses a formidable challenge (Doerr et al., 2017). Although day-to-day activities lead to some functional recovery, this is further enhanced by providing an enriched environment to animals to increase activity and improve the establishment of functional synapses. An enriched environment leads to diverse changes in function, as well as anatomical markers of grafted cells (Dobrossy and Dunnett, 2001). However, introduction of a rehabilitation paradigm does not always lead to an improvement in graft-mediated recovery (Hicks et al., 2009). Only a few studies have investigated the interaction between rehabilitation after intra-striatal grafting of fetal tissue into striatal lesions modeling Huntington's disease (Dobrossy and Dunnett, 2004, 2008) or stem cells after a stroke (Hicks et al., 2007, 2008, 2009). Although the effects of rehabilitation on synapse formation in transplanted cells is potentially profound, our current state of knowledge about these interactions is unsatisfactory and requires more extensive studies that define appropriate rehabilitation paradigms and how these differ from interventions without cell therapy (Ghuman et al., 2018). Establishing optimal intervention periods for when these programs should be administered, as well as how long a rehabilitation program is needed in conjunction

with "regenerative therapies" to achieve a maximal integration requires detailed investigations to ensure clinical efficacy (Savitz et al., 2014; Ross et al., 2016).

The role of training new tissue in the context of brain tissue regeneration remains unaddressed. However, there is evidence from ECM bioscaffolds regenerating muscle tissue that rehabilitation training is an essential element to produce functional tissue (Gentile et al., 2014; Sicari et al., 2014). Rehabilitation tasks are likely to be dependent on behavioral deficits after brain injury, as these are dependent on the regional location of damage (Feys et al., 2000). The rehabilitation paradigm will therefore need to adapt depending on the functional deficit (Kreber and Griesbach, 2016), which will complicate group-wise comparisons as no one rehabilitation paradigm will be suitable for all subjects (Gentile et al., 2014). In the case of damaged tissue, neuronal progenitors from the SVZ will integrate and supplement existing neuronal networks to improve their function. In contrast with tissue regeneration, a complete new set of neuronal networks is created that needs to form a functional circuit based on a behavioral input. Tissue replacement is expected to restore function of lost tissue, but akin to learning in development it can be expected that new tissue needs to be trained to function appropriately (Dobrossy and Dunnett, 2001; Dobrossy and Nikkhah, 2012). In conventional rehabilitation, plasticity of existing networks can be induced by exercise (Dobkin, 2008), which leads to the release of growth factors, such as BDNF, that support synaptogenesis (Dalise et al., 2017). To ensure a functional synapses formation, task integration is required (Rensink et al., 2009). In animal models, behavioral testing can be considered a form of task integration. However, ideally a separate task will be used to integrate and evaluate functional effects (Ghuman et al., 2018). Compensation (i.e., solving the same task using an alternative strategy) might occur, which will confound the assessment of efficacy. Extensive testing on a particular behavioral task could increase compensation effects, as the animal is learning novel ways to solve the task (Boltze et al., 2014). Separating training and testing should therefore be considered the gold standard for a behavioral evaluation of tissue regeneration and the use of rehabilitation to train *de novo* tissues.

CRITERIA TO EVALUATE FUNCTIONAL BRAIN TISSUE REGENERATION

The evaluation of behavioral effects of brain tissue regeneration needs to be performed in contrast to subjects that only experienced brain injury, as some spontaneous recovery of deficits occurs. Learning and compensatory strategies could be adopted to improve performance that would not reflect a therapeutic benefit. Inclusion of appropriate non-injured controls is required to establish a performance baseline over time, as well as an effect size for the deficit and potential recovery. Considering the invasiveness of the procedure to deliver a bioscaffold, appropriate surgical controls (e.g., needle implantation, vehicle injection) need to be evaluated, but only need to be included consistently in studies if there are significant behavioral effects. Eventually, more detailed studies are required to determine the influence of biological variables (e.g., age, sex) on brain tissue regeneration. Specifically, subject age is known to affect inflammation, ECM composition and its potential to induce a regenerative response (Brown et al., 2017; Hachim et al., 2017; LoPresti and Brown, 2018). Inflammation is another biological variable that is known to be affected by age and sex, but little is known about regenerative differences between sexes. To gain a robust mechanistic understanding, effects of all these variables need to be accounted for.

Although improvements in behavioral deficits are the ultimate aim of this approach, it cannot be expected that initial studies defining the important variables to achieve tissue regeneration will reveal behavioral improvements. Initial studies should aim to achieve a robust and reproducible tissue formation by defining key rules, such as the formation of a tissue cavity prior to bioscaffold implantation etc. (**Table 3**). Histological analyses need to establish robust methods that can contrast damaged tissue from regenerating tissue. Particular ECM molecules might provide differential markers for this purpose, but need to be validated. In the absence of this validation, it is possible that mechanistic interventions will target damaged veterate brain, rather than regenerated brain. This would lead to erroneous interpretations of functions in regenerated brain tissue.

A distinction between behavioral and functional effects is made to differentiate overt observations related to performing a specific task (i.e., behavior) from brain activity and tissue metabolism (i.e., function). We further propose that the claim of establishing a *de novo* functional brain tissue should be provided by non-invasive imaging techniques, such as MRI. A pre-implant image of the tissue cavity and the host brain should be provided with further images charting how the cavity is transformed by tissue regeneration (Ghuman et al., 2017). This *in vivo* time-lapse in combination with histology should

TABLE 3 | Emerging rules for an induced brain tissue regeneration.

Rules	Description
1	The adult mammalian brain does not spontaneously restore lost tissue.
2	Preserved neurogenic regions are required to produce endogenous neurons.
3	Distance of neurogenic regions to areas of damage is crucial to induce a response.
4	Extent of cellular reservoir in neurogenic regions is crucial to produce sufficient cells to promote repair and regeneration.
5	Neurogenic regions need to produce cells with site-appropriate positional specification.
6	A tissue substrate needs to be introduced to provide support for cell invasion.
7	A continuous interface between scaffold and tissue is required to ensure a homogenous tissue integration.
8	Formation of a mature glial scar prior to introducing a tissue substrate will complicate tissue regeneration and integration.
9	A rapid invasion of cells is required to ensure a regenerative cascade is initiated.
10	The tissue substrate needs to be degraded to >90% within 3–4 weeks to allow *de novo* tissue to form.

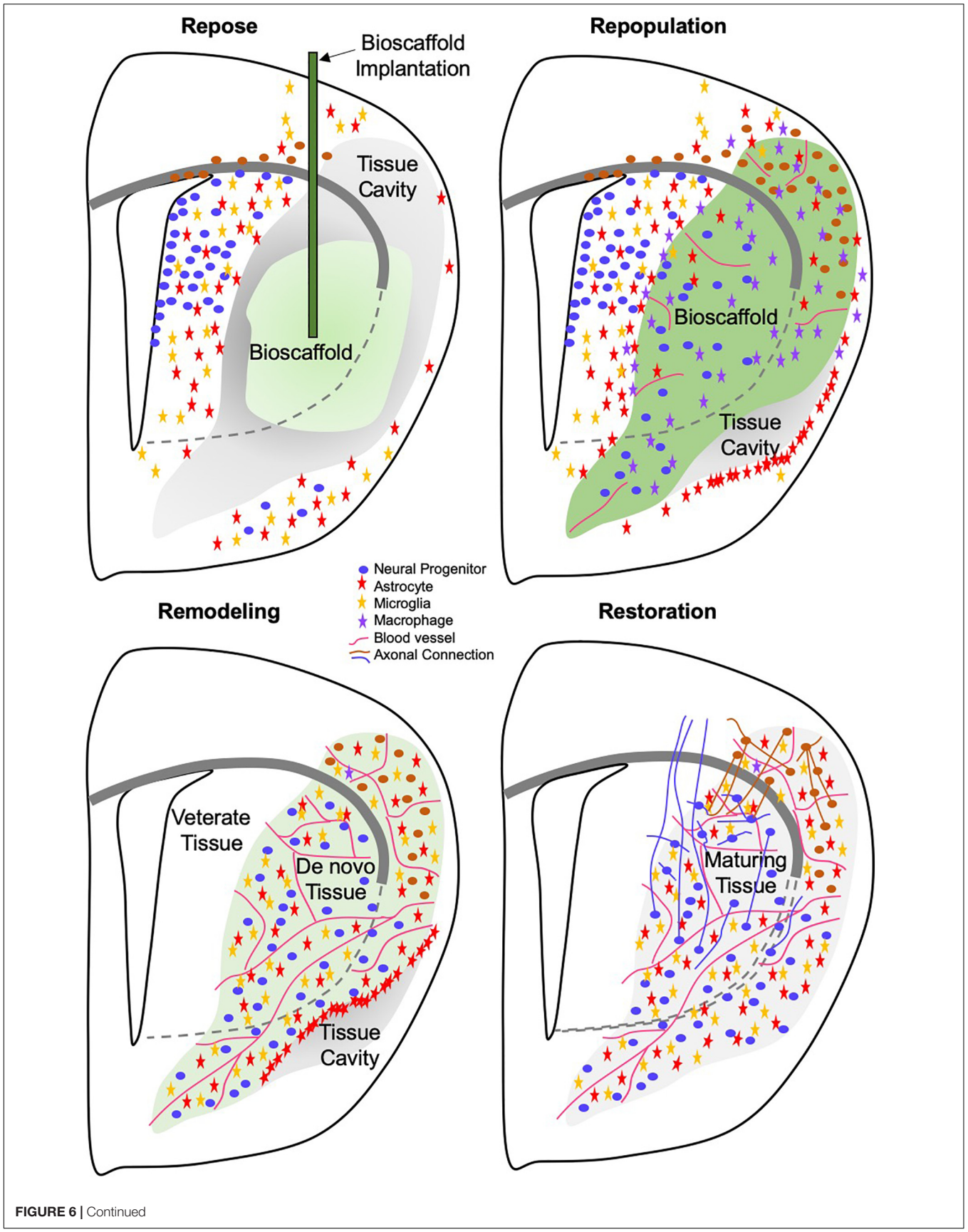

FIGURE 6 | Continued

FIGURE 6 | Four phase of brain tissue regeneration. Phase 1: The repose phase is characterized by tissue loss being mostly complete and a repair response having been instigated. Although gliosis is ongoing, no defining scar along the tissue cavitation has emerged. During this phase, a bioscaffold can be implanted to initiate the tissue regeneration process. In the absence of an introduction of a bioscaffold a scar is forming around the cavity. Phase 2: During the repopulation phase, host cells are invading the bioscaffold. Even during the acute invasion phase, brain derived cells, such as neural progenitors and astrocytes, are infiltrating the biomaterial, but immune cells are more rapidly invading and provide additional soluble and juxtracrine signaling to recruit host brain cells to repopulate the tissue cavity. Phase 3: Invading cells deposit transient matrix molecules and take-up positions inside the bioscaffold that leads to a gradual degradation of the scaffold. Blood vessel formation during this phase plays a key role to promote biodegradation, but also to remodel individual compartments that will develop into neuropil. Within the vascular compartment, cells are depositing appropriate matrix molecules, such as vitronectin, laminin and collagen. In the neuropil, neural cells deposit matrix molecules, such as laminin, aggrecan, decorin, thrombospondin that are involved in maintaining structure and juxtracrine signaling. At the end of this phase, the bioscaffold is completed degraded and replaced with host matrix. Phase 2 and Phase 3 overlap within different parts of the cavity. Phase 4: Once host brain cells are in position and formed a neuropil in between blood vessels, tissue maturation is occurring with terminal differentiation of neurons through interaction with astrocytes, oligodendrocytes and ECM molecules. It can be anticipated that *de novo* tissue formation in phase 3 and maturation processes, such as axonal and dendritic branching, can occur side-by-side. Axonal and dendritic processes are required to form a functional neuronal circuitry.

be the gold standard to accept claims of tissue restoration. The cytoarchitectural organization of *de novo* tissue should be contrasted with intact brain tissue, as well as the phenotypes of cells within the bioscaffold. These two microenvironments provide benchmarks that contrast regenerating and target tissue. Proof of tissue dynamics and a restorative process occurring over time are required to substantiate the processes involved in brain tissue regeneration, eventually leading to mode and mechanism of action studies.

To this end, we further suggest that proof of the bioscaffold's presence, retention, distribution and degradation are required to indicate their pivotal role in tissue regeneration. Although a reliance on morphological and protein concentration difference can serve at early time points post-implantation to identify the bioscaffold (Massensini et al., 2015), as these materials are degraded, protein concentrations are increasingly similar to veterate brain and regenerating tissue is morphologically increasingly similar to damaged or intact brain tissue (Ghuman et al., 2016; Jin et al., 2017). Ideally, unique identification strategies for bioscaffolds are implemented (e.g., labeling) without affecting the biological activity of the material (Park et al., 2019). This should allow the identification of even small quantities of bioscaffold that might still undergo degradation or be incorporated into the new tissue. *In vivo* monitoring of the bioscaffold (Liang et al., 2015; Jin et al., 2017; Piejko et al., 2019), as well as cells (Nicholls et al., 2015, 2016) would further improve our understanding of how biomaterials and cells interact to form an integrated brain tissue.

Finally, it is important to develop a framework that will define the sequence of cellular dynamics (e.g., neutrophils invade first and facilitate macrophage recruitment) that drive different phases of brain tissue regeneration. Are these events dependent on each other? What happens if we interfere with individual processes? Does this lead to a disruption of the regenerative cascade or does it lead to a different type of tissue? In contrast to wound healing, which mainly focuses on reintegrating adjoining tissues, we here propose that (1) brain tissue needs to repose (i.e., cavitation needs to be mostly complete without maturation of a surrounding glial scar) to receive an inductive bioscaffold; (2) the lack of scarring permits the rapid invasion of immune and neural cells to repopulate the tissue void: (3) a remodeling of the bioscaffold and newly deposited ECM is required (4) to allow the establishment of a tissue architecture that matures and restores function (**Figure 6**). However, these phases merely provide a general descriptive framework that needs to be refined by detailed mechanistic studies to elucidate how each cell type influences the overall process. Considering the range and dynamics of molecules each cell produces, this poses a formidable challenge.

CONCLUSION

With the discovery of adult neurogenesis, Ramon y Cajal's decree on the lack of regeneration in the CNS has been undergoing a rigorous reassessment. Although spontaneous tissue regeneration does not occur in the mammalian CNS (Illis, 2012), engineering strategies are gradually overcoming the biological and physical challenges imposed by brain injury through harnessing the potential of endogenous neurogenesis (Modo and Badylak, 2019). In this context, it is important to contrast conditions with volumetric tissue loss (i.e., a chunk of tissue is missing) versus neurological disease in which tissue gradually shrinks (i.e., tissue atrophy). We here described putative mechanisms involved in tissue regeneration after a volumetric loss of brain tissue. Some of these strategies, such as enhancing endogenous neurogenesis, can potentially provide benefits to both scenarios, but provision of, for instance, a scaffold, will only be amenable to conditions in which a tissue cavity formed. In a clinical scenario, it can be expected that a patient will receive rehabilitation training shortly after a stroke and this could be combined with an enhancement of neurogenesis. Bioscaffold implantation would only occur after cavitation is complete, with concomitant neurogenesis and rehabilitation training being required to yield an optimal outcome. Although the aim is to define specific modes and mechanisms of action, we have to recognize that these at present can merely be putative. Investigations first have to define zero and first orders of approximation of the variables and conditions required to produce brain tissue regeneration. Consequently, the therapeutic value of restoring lost tissue currently remains unclear. Although fetal tissue transplant suggest that *de novo* brain tissue can integrate into the host and reduce behavioral impairments, we currently have a poor understanding of what cellular substrates are required to support behavioral changes. Studies in axolotl suggest that regenerated tissue is unlikely to exactly replicate the tissue structure that emerged through brain development, but might support restoration of function. Still, a

functional tissue requires integration with veterate brain regions to support behavior and cognition. The utility of brain tissue regeneration is not to perfectly restore the damaged brain, but to produce a sufficient tissue substrate that can reduce behavioral deficits. It is expected that this review provides the context for future studies to improve engineering strategies that will produce a robust regeneration of brain tissue.

AUTHOR CONTRIBUTIONS

The author confirms being the sole contributor of this work and has approved it for publication.

FUNDING

This study was supported by the NINDS (R01 NS08226), NIBIB (R01 EB016629), ReNeuron Ltd., ACell, Vertex Pharmaceuticals, and C. R. Bard. None of the funders had a role in the design of the studies.

ACKNOWLEDGMENTS

The author gratefully acknowledges Dr. Stephen Badylak who provided useful discussions and crucial insights to the topic of tissue regeneration.

REFERENCES

Allman, A. J., Mcpherson, T. B., Badylak, S. F., Merrill, L. C., Kallakury, B., Sheehan, C., et al. (2001). Xenogeneic extracellular matrix grafts elicit a TH2-restricted immune response. *Transplantation* 71, 1631–1640.

Amamoto, R., Huerta, V. G., Takahashi, E., Dai, G., Grant, A. K., Fu, Z., et al. (2016). Adult axolotls can regenerate original neuronal diversity in response to brain injury. *eLife* 5:e13998. doi: 10.7554/eLife.13998

Anderson, M. A., O'shea, T. M., Burda, J. E., Ao, Y., Barlatey, S. L., Bernstein, A. M., et al. (2018). Required growth facilitators propel axon regeneration across complete spinal cord injury. *Nature* 561, 396–400. doi: 10.1038/s41586-018-0467-6

Arvidsson, A., Collin, T., Kirik, D., Kokaia, Z., and Lindvall, O. (2002). Neuronal replacement from endogenous precursors in the adult brain after stroke. *Nat. Med.* 8, 963–970.

Aurand, E. R., Lampe, K. J., and Bjugstad, K. B. (2012). Defining and designing polymers and hydrogels for neural tissue engineering. *Neurosci. Res.* 72, 199–213. doi: 10.1016/j.neures.2011.12.005

Badylak, S. F., Freytes, D. O., and Gilbert, T. W. (2009). Extracellular matrix as a biological scaffold material: structure and function. *Acta Biomater.* 5, 1–13. doi: 10.1016/j.actbio.2008.09.013

Badylak, S. F., and Gilbert, T. W. (2008). Immune response to biologic scaffold materials. *Semin. Immunol.* 20, 109–116.

Badylak, S. F., Kochupura, P. V., Cohen, I. S., Doronin, S. V., Saltman, A. E., Gilbert, T. W., et al. (2006). The use of extracellular matrix as an inductive scaffold for the partial replacement of functional myocardium. *Cell Transplant.* 15(Suppl 1), S29–S40.

Barker, R. A., and TRANSEURO consortium (2019). Designing stem-cell-based dopamine cell replacement trials for Parkinson's disease. *Nat. Med.* 25, 1045–1053.

Barnes, L. A., Marshall, C. D., Leavitt, T., Hu, M. S., Moore, A. L., Gonzalez, J. G., et al. (2018). Mechanical forces in cutaneous wound healing: emerging therapies to minimize scar formation. *Adv. Wound Care* 7, 47–56. doi: 10.1089/wound.2016.0709

Bechmann, I. (2005). Failed central nervous system regeneration: a downside of immune privilege? *Neuromol. Med.* 7, 217–228.

Bible, E., Chau, D. Y., Alexander, M. R., Price, J., Shakesheff, K. M., and Modo, M. (2009). The support of neural stem cells transplanted into stroke-induced brain cavities by PLGA particles. *Biomaterials* 30, 2985–2994. doi: 10.1016/j.biomaterials.2009.02.012

Bible, E., Dell'acqua, F., Solanky, B., Balducci, A., Crapo, P. M., Badylak, S. F., et al. (2012a). Non-invasive imaging of transplanted human neural stem cells and ECM scaffold remodeling in the stroke-damaged rat brain by (19)F- and diffusion-MRI. *Biomaterials* 33, 2858–2871. doi: 10.1016/j.biomaterials.2011.12.033

Bible, E., Qutachi, O., Chau, D. Y., Alexander, M. R., Shakesheff, K. M., and Modo, M. (2012b). Neo-vascularization of the stroke cavity by implantation of human neural stem cells on VEGF-releasing PLGA microparticles. *Biomaterials* 33, 7435–7446. doi: 10.1016/j.biomaterials.2012.06.085

Boltze, J., Lukomska, B., Jolkkonen, J., and Consortium, M. -I. (2014). Mesenchymal stromal cells in stroke: improvement of motor recovery or functional compensation? *J. Cereb. Blood Flow Metab.* 34, 1420–1421. doi: 10.1038/jcbfm.2014.94

Bonnans, C., Chou, J., and Werb, Z. (2014). Remodelling the extracellular matrix in development and disease. *Nat. Rev. Mol. Cell Biol.* 15, 786–801. doi: 10.1038/nrm3904

Borlongan, C. V. (2019). Concise review: stem cell therapy for stroke patients: are we there yet? *Stem Cells Transl. Med.* 8, 983–988. doi: 10.1002/sctm.19-0076

Brown, B. N., Haschak, M. J., Lopresti, S. T., and Stahl, E. C. (2017). Effects of age-related shifts in cellular function and local microenvironment upon the innate immune response to implants. *Semin. Immunol.* 29, 24–32. doi: 10.1016/j.smim.2017.05.001

Brown, B. N., Valentin, J. E., Stewart-Akers, A. M., Mccabe, G. P., and Badylak, S. F. (2009). Macrophage phenotype and remodeling outcomes in response to biologic scaffolds with and without a cellular component. *Biomaterials* 30, 1482–1491. doi: 10.1016/j.biomaterials.2008.11.040

Buffo, A., Rite, I., Tripathi, P., Lepier, A., Colak, D., Horn, A. P., et al. (2008). Origin and progeny of reactive gliosis: a source of multipotent cells in the injured brain. *Proc. Natl. Acad. Sci. U.S.A.* 105, 3581–3586. doi: 10.1073/pnas.0709002105

Butz, M., Van Ooyen, A., and Worgotter, F. (2009). A model for cortical rewiring following deafferentation and focal stroke. *Front. Comput. Neurosci.* 3:10. doi: 10.3389/neuro.10.010.2009

Bye, N., Turnley, A. M., and Morganti-Kossmann, M. C. (2012). Inflammatory regulators of redirected neural migration in the injured brain. *Neurosignals* 20, 132–146. doi: 10.1159/000336542

Campbell, K. (2003). Dorsal-ventral patterning in the mammalian telencephalon. *Curr. Opin. Neurobiol.* 13, 50–56.

Carey, L.E., Dearth, C.L., Johnson, S.A., Londono, R., Medberry, C.J., Daly, K.A., et al. (2014). In vivo degradation of 14C-labeled porcine dermis biologic scaffold. *Biomaterials* 35, 8297–8304. doi: 10.1016/j.biomaterials.2014.06.015

Chaker, Z., Codega, P., and Doetsch, F. (2016). A mosaic world: puzzles revealed by adult neural stem cell heterogeneity. *Wiley Interdiscip. Rev. Dev. Biol.* 5, 640–658. doi: 10.1002/wdev.248

Chan, B. P., and Leong, K. W. (2008). Scaffolding in tissue engineering: general approaches and tissue-specific considerations. *Eur. Spine J.* 17(Suppl 4), 467–479. doi: 10.1007/s00586-008-0745-3

Chang, E. H., Adorjan, I., Mundim, M. V., Sun, B., Dizon, M. L., and Szele, F. G. (2016). Traumatic brain injury activation of the adult subventricular zone neurogenic niche. *Front. Neurosci.* 10:332. doi: 10.3389/fnins.2016.00332

Chapman, K. Z., Ge, R., Monni, E., Tatarishvili, J., Ahlenius, H., Arvidsson, A., et al. (2015). Inflammation without neuronal death triggers striatal neurogenesis comparable to stroke. *Neurobiol. Dis.* 83, 1–15. doi: 10.1016/j.nbd.2015.08.013

Chen, H. I., Jgamadze, D., Serruya, M. D., Cullen, D. K., Wolf, J. A., and Smith, D. H. (2016). Neural substrate expansion for the restoration of brain function. *Front. Syst. Neurosci.* 10:1. doi: 10.3389/fnsys.2016.00001

Chou, C. H., and Modo, M. (2016). Human neural stem cell-induced endothelial morphogenesis requires autocrine/paracrine and juxtacrine signaling. *Sci. Rep.* 6:29029. doi: 10.1038/srep29029

Chou, C.H., Sinden, J.D., Couraud, P.O., and Modo, M. (2014). In vitro modeling of the neurovascular environment by coculturing adult human brain endothelial cells with human neural stem cells. *PLoS One* 9:e106346. doi: 10.1371/journal.pone.0106346

Chung, A. G., Frye, J. B., Zbesko, J. C., Constantopoulos, E., Hayes, M., Figueroa, A. G., et al. (2018). Liquefaction of the brain following stroke shares a similar molecular and morphological profile with atherosclerosis and mediates secondary neurodegeneration in an osteopontin-dependent mechanism. *eNeuro* 5:ENEURO.0076-18.2018.

Cordero-Espinoza, L., and Huch, M. (2018). The balancing act of the liver: tissue regeneration versus fibrosis. *J. Clin. Invest.* 128, 85–96. doi: 10.1172/JCI93562

Costa, M. R., Gotz, M., and Berninger, B. (2010). What determines neurogenic competence in glia? *Brain Res. Rev.* 63, 47–59. doi: 10.1016/j.brainresrev.2010.01.002

Crapo, P. M., Medberry, C. J., Reing, J. E., Tottey, S., Van Der Merwe, Y., Jones, K. E., et al. (2012). Biologic scaffolds composed of central nervous system extracellular matrix. *Biomaterials* 33, 3539–3547. doi: 10.1016/j.biomaterials.2012.01.044

Crapo, P. M., Tottey, S., Slivka, P. F., and Badylak, S. F. (2014). Effects of biologic scaffolds on human stem cells and implications for CNS tissue engineering. *Tissue Eng. Part A* 20, 313–323. doi: 10.1089/ten.TEA.2013.0186

Dalise, S., Ambrosio, F., and Modo, M. (2014). Brain plasticity and recovery in preclinical models of stroke. *Arch. Ital. Biol.* 152, 190–215. doi: 10.12871/00039829201442

Dalise, S., Cavalli, L., Ghuman, H., Wahlberg, B., Gerwig, M., Chisari, C., et al. (2017). Biological effects of dosing aerobic exercise and neuromuscular electrical stimulation in rats. *Sci. Rep.* 7:10830. doi: 10.1038/s41598-017-11260-7

Darsalia, V., Kallur, T., and Kokaia, Z. (2007). Survival, migration and neuronal differentiation of human fetal striatal and cortical neural stem cells grafted in stroke-damaged rat striatum. *Eur. J. Neurosci.* 26, 605–614.

de la Vega, L., Lee, C., Sharma, R., Amereh, M., and Willerth, S. M. (2019). 3D bioprinting models of neural tissues: the current state of the field and future directions. *Brain Res. Bull.* 150, 240–249.

Dearth, C. L., Slivka, P. F., Stewart, S. A., Keane, T. J., Tay, J. K., Londono, R., et al. (2016). Inhibition of COX1/2 alters the host response and reduces ECM scaffold mediated constructive tissue remodeling in a rodent model of skeletal muscle injury. *Acta Biomater* 31, 50–60. doi: 10.1016/j.actbio.2015.11.043

del Zoppo, G. J., Milner, R., Mabuchi, T., Hung, S., Wang, X., Berg, G. I., et al. (2007). Microglial activation and matrix protease generation during focal cerebral ischemia. *Stroke* 38, 646–651.

Delgado, R. N., and Lim, D. A. (2017). Maintenance of positional identity of neural progenitors in the embryonic and postnatal telencephalon. *Front. Mol. Neurosci.* 10:373. doi: 10.3389/fnmol.2017.00373

Deshmane, S. L., Kremlev, S., Amini, S., and Sawaya, B. E. (2009). Monocyte chemoattractant protein-1 (MCP-1): an overview. *J. Interferon. Cytokine. Res.* 29, 313–326. doi: 10.1089/jir.2008.0027

Dobkin, B. H. (2008). Training and exercise to drive poststroke recovery. *Nat. Clin. Pract. Neurol.* 4, 76–85. doi: 10.1038/ncpneuro0709

Dobrossy, M. D., and Dunnett, S. B. (2001). The influence of environment and experience on neural grafts. *Nat. Rev. Neurosci.* 2, 871–879.

Dobrossy, M. D., and Dunnett, S. B. (2004). Environmental enrichment affects striatal graft morphology and functional recovery. *Eur. J. Neurosci.* 19, 159–168.

Dobrossy, M. D., and Dunnett, S. B. (2008). Environmental housing and duration of exposure affect striatal graft morphology in a rodent model of Huntington's disease. *Cell Transplant.* 17, 1125–1134.

Dobrossy, M. D., and Nikkhah, G. (2012). Role of experience, training, and plasticity in the functional efficacy of striatal transplants. *Prog. Brain Res.* 200, 303–328. doi: 10.1016/B978-0-444-59575-1.00014-4

Doerr, J., Schwarz, M. K., Wiedermann, D., Leinhaas, A., Jakobs, A., Schloen, F., et al. (2017). Whole-brain 3D mapping of human neural transplant innervation. *Nat. Commun.* 8:14162. doi: 10.1038/ncomms14162

Donnelly, D. J., and Popovich, P. G. (2008). Inflammation and its role in neuroprotection, axonal regeneration and functional recovery after spinal cord injury. *Exp. Neurol.* 209, 378–388.

Drury, J. L., and Mooney, D. J. (2003). Hydrogels for tissue engineering: scaffold design variables and applications. *Biomaterials* 24, 4337–4351.

Dziki, J. L., Wang, D. S., Pineda, C., Sicari, B. M., Rausch, T., and Badylak, S. F. (2017). Solubilized extracellular matrix bioscaffolds derived from diverse source tissues differentially influence macrophage phenotype. *J. Biomed. Mater. Res. A* 105, 138–147. doi: 10.1002/jbm.a.35894

Eming, S. A., Martin, P., and Tomic-Canic, M. (2014). Wound repair and regeneration: mechanisms, signaling, and translation. *Sci. Transl. Med.* 6:265sr266.

Evans, A. E., Kelly, C. M., Precious, S. V., and Rosser, A. E. (2012). Molecular regulation of striatal development: a review. *Anat. Res. Int.* 2012:106529. doi: 10.1155/2012/106529

Faust, A., Kandakatla, A., Van Der Merwe, Y., Ren, T., Huleihel, L., Hussey, G., et al. (2017). Urinary bladder extracellular matrix hydrogels and matrix-bound vesicles differentially regulate central nervous system neuron viability and axon growth and branching. *J. Biomater. Appl.* 31, 1277–1295. doi: 10.1177/0885328217698062

Ferretti, P. (2011). Is there a relationship between adult neurogenesis and neuron generation following injury across evolution? *Eur. J. Neurosci.* 34, 951–962. doi: 10.1111/j.1460-9568.2011.07833.x

Feys, H., Hetebrij, J., Wilms, G., Dom, R., and De Weerdt, W. (2000). Predicting arm recovery following stroke: value of site of lesion. *Acta Neurol. Scand.* 102, 371–377.

Freytes, D. O., Martin, J., Velankar, S. S., Lee, A. S., and Badylak, S. F. (2008). Preparation and rheological characterization of a gel form of the porcine urinary bladder matrix. *Biomaterials* 29, 1630–1637. doi: 10.1016/j.biomaterials.2007.12.014

Fry, E. J. (2001). Central nervous system regeneration: mission impossible? *Clin. Exp. Pharmacol. Physiol.* 28, 253–258.

Fukuda, S, Fini, CA, Mabuchi, T, Koziol, JA, Eggleston, LL Jr., del, Zoppo, GJ. (2004). Focal cerebral ischemia induces active proteases that degrade microvascular matrix. *Stroke* 35, 998–1004.

Gabel, S., Koncina, E., Dorban, G., Heurtaux, T., Birck, C., Glaab, E., et al. (2016). Inflammation promotes a conversion of astrocytes into neural progenitor cells via nf-kappab activation. *Mol. Neurobiol.* 53, 5041–5055. doi: 10.1007/s12035-015-9428-3

Gentile, N. E., Stearns, K. M., Brown, E. H., Rubin, J. P., Boninger, M. L., Dearth, C. L., et al. (2014). Targeted rehabilitation after extracellular matrix scaffold transplantation for the treatment of volumetric muscle loss. *Am. J. Phys. Med. Rehabil.* 93, S79–S87. doi: 10.1097/PHM.0000000000000145

Ghuman, H., Gerwig, M., Nicholls, F. J., Liu, J. R., Donnelly, J., Badylak, S. F., et al. (2017). Long-term retention of ECM hydrogel after implantation into a sub-acute stroke cavity reduces lesion volume. *Acta Biomater.* 63, 50–63. doi: 10.1016/j.actbio.2017.09.011

Ghuman, H., Massensini, A. R., Donnelly, J., Kim, S. M., Medberry, C. J., Badylak, S. F., et al. (2016). ECM hydrogel for the treatment of stroke: characterization of the host cell infiltrate. *Biomaterials* 91, 166–181. doi: 10.1016/j.biomaterials.2016.03.014

Ghuman, H., Mauney, C., Donnelly, J., Massensini, A. R., Badylak, S. F., and Modo, M. (2018). Biodegradation of ECM hydrogel promotes endogenous brain tissue restoration in a rat model of stroke. *Acta Biomater.* 80, 66–84. doi: 10.1016/j.actbio.2018.09.020

Gilbert, T. W., Stewart-Akers, A. M., and Badylak, S. F. (2007). A quantitative method for evaluating the degradation of biologic scaffold materials. *Biomaterials* 28, 147–150.

Gilgenkrantz, H., and Collin de l'Hortet, A. (2018). Understanding liver regeneration: from mechanisms to regenerative medicine. *Am. J. Pathol.* 188, 1316–1327.

Godwin, J. W., Pinto, A. R., and Rosenthal, N. A. (2013). Macrophages are required for adult salamander limb regeneration. *Proc. Natl. Acad. Sci. U.S.A.* 110, 9415–9420. doi: 10.1073/pnas.1300290110

Gomez-Gaviro, M. V., Scott, C. E., Sesay, A. K., Matheu, A., Booth, S., Galichet, C., et al. (2012). Betacellulin promotes cell proliferation in the neural stem cell niche and stimulates neurogenesis. *Proc. Natl. Acad. Sci. U.S.A.* 109, 1317–1322. doi: 10.1073/pnas.1016199109

Gooch, C. L., Pracht, E., and Borenstein, A. R. (2017). The burden of neurological disease in the United States: a summary report and call to action. *Ann. Neurol.* 81, 479–484.

Grabowski, M., Brundin, P., and Johansson, B. B. (1992a). Fetal neocortical grafts implanted in adult hypertensive rats with cortical infarcts following a middle cerebral artery occlusion: ingrowth of afferent fibers from the host brain. *Exp. Neurol.* 116, 105–121.

Grabowski, M., Brundin, P., and Johansson, B. B. (1993). Functional integration of cortical grafts placed in brain infarcts of rats. *Ann. Neurol.* 34, 362–368.

Grabowski, M., Christofferson, R. H., Brundin, P., and Johansson, B. B. (1992b). Vascularization of fetal neocortical grafts implanted in brain infarcts in spontaneously hypertensive rats. *Neuroscience* 51, 673–682.

Grabowski, M., Johansson, B. B., and Brundin, P. (1994). Survival of fetal neocortical grafts implanted in brain infarcts of adult rats: the influence of postlesion time and age of donor tissue. *Exp. Neurol.* 127, 126–136.

Grabowski, M., Sorensen, J. C., Mattsson, B., Zimmer, J., and Johansson, B. B. (1995). Influence of an enriched environment and cortical grafting on functional outcome in brain infarcts of adult rats. *Exp. Neurol.* 133, 96–102.

Hachim, D., Wang, N., Lopresti, S. T., Stahl, E. C., Umeda, Y. U., Rege, R. D., et al. (2017). Effects of aging upon the host response to implants. *J. Biomed. Mater. Res. A* 105, 1281–1292. doi: 10.1002/jbm.a.36013

Hadani, M., Freeman, T., Munsiff, A., Young, W., and Flamm, E. (1992). Fetal cortical cells survive in focal cerebral infarct after permanent occlusion of the middle cerebral artery in adult rats. *J. Neurotrauma* 9, 107–112.

Heissig, B., Nishida, C., Tashiro, Y., Sato, Y., Ishihara, M., Ohki, M., et al. (2010). Role of neutrophil-derived matrix metalloproteinase-9 in tissue regeneration. *Histol. Histopathol.* 25, 765–770. doi: 10.14670/HH-25.765

Hicks, A. U., Hewlett, K., Windle, V., Chernenko, G., Ploughman, M., Jolkkonen, J., et al. (2007). Enriched environment enhances transplanted subventricular zone stem cell migration and functional recovery after stroke. *Neuroscience* 146, 31–40.

Hicks, A. U., Lappalainen, R. S., Narkilahti, S., Suuronen, R., Corbett, D., Sivenius, J., et al. (2009). Transplantation of human embryonic stem cell-derived neural precursor cells and enriched environment after cortical stroke in rats: cell survival and functional recovery. *Eur. J. Neurosci.* 29, 562–574. doi: 10.1111/j.1460-9568.2008.06599.x

Hicks, A. U., Maclellan, C. L., Chernenko, G. A., and Corbett, D. (2008). Long-term assessment of enriched housing and subventricular zone derived cell transplantation after focal ischemia in rats. *Brain Res.* 1231, 103–112. doi: 10.1016/j.brainres.2008.07.041

Ho, M. T., Teal, C. J., and Shoichet, M. S. (2019). A hyaluronan/methylcellulose-based hydrogel for local cell and biomolecule delivery to the central nervous system. *Brain Res. Bull.* 148, 46–54. doi: 10.1016/j.brainresbull.2019.03.005

Huleihel, L., Bartolacci, J. G., Dziki, J. L., Vorobyov, T., Arnold, B., Scarritt, M. E., et al. (2017a). Matrix-bound nanovesicles recapitulate extracellular matrix effects on macrophage phenotype. *Tissue Eng. Part A* 23, 1283–1294. doi: 10.1089/ten.TEA.2017.0102

Huleihel, L., Dziki, J. L., Bartolacci, J. G., Rausch, T., Scarritt, M. E., Cramer, M. C., et al. (2017b). Macrophage phenotype in response to ECM bioscaffolds. *Semin. Immunol.* 29, 2–13.

Illis, L. S. (2012). Central nervous system regeneration does not occur. *Spinal Cord* 50, 259–263.

Jeon, M., and Kim, S. Y. (2018). Application of a paste-type acellular dermal matrix for coverage of chronic ulcerative wounds. *Arch. Plast. Surg.* 45, 564–571. doi: 10.5999/aps.2018.00605

Jin, T., Nicholls, F. J., Crum, W. R., Ghuman, H., Badylak, S. F., and Modo, M. (2017). Diamagnetic chemical exchange saturation transfer (diaCEST) affords magnetic resonance imaging of extracellular matrix hydrogel implantation in a rat model of stroke. *Biomaterials* 113, 176–190. doi: 10.1016/j.biomaterials.2016.10.043

Kaneko, N., Sawada, M., and Sawamoto, K. (2017). Mechanisms of neuronal migration in the adult brain. *J. Neurochem.* 141, 835–847.

Karam, S., and Wali, R. K. (2015). Current state of immunosuppression: past, present, and future. *Crit. Rev. Eukaryot. Gene. Expr.* 25, 113–134.

Kaslin, J., Kroehne, V., Ganz, J., Hans, S., and Brand, M. (2017). Distinct roles of neuroepithelial-like and radial glia-like progenitor cells in cerebellar regeneration. *Development* 144, 1462–1471. doi: 10.1242/dev.144907

Kazanis, I., Gorenkova, N., Zhao, J. W., Franklin, R. J., Modo, M., and Ffrench-Constant, C. (2013). The late response of rat subependymal zone stem and progenitor cells to stroke is restricted to directly affected areas of their niche. *Exp. Neurol.* 248, 387–397. doi: 10.1016/j.expneurol.2013.06.025

Keane, T. J., and Badylak, S. F. (2015). The host response to allogeneic and xenogeneic biological scaffold materials. *J. Tissue Eng. Regen. Med.* 9, 504–511. doi: 10.1002/term.1874

Kelly, S. H., Shores, L. S., Votaw, N. L., and Collier, J. H. (2017). Biomaterial strategies for generating therapeutic immune responses. *Adv. Drug Deliv. Rev.* 114, 3–18. doi: 10.1016/j.addr.2017.04.009

Kempermann, G., Gage, F. H., Aigner, L., Song, H., Curtis, M. A., Thuret, S., et al. (2018). Human adult neurogenesis: evidence and remaining questions. *Cell Stem Cell* 23, 25–30. doi: 10.1016/j.stem.2018.04.004

Khalil, H. H., Kalkat, M., Malahias, M. N., Rhobaye, S., Ashour, T., Djearaman, M. G., et al. (2018). Chest wall reconstruction with porcine acellular dermal matrix (Strattice) and autologous tissue transfer for high risk patients with chest wall tumors. *Plast. Reconstr. Surg. Glob. Open.* 6:e1703. doi: 10.1097/GOX.0000000000001703

Kirsche, W., and Kirsche, K. (1961). [Experimental studies on the problem of regeneration and function of the tectum opticum of Carassium carassium L]. *Z. Mikrosk. Anat. Forsch.* 67, 140–182.

Kizil, C., Kaslin, J., Kroehne, V., and Brand, M. (2012). Adult neurogenesis and brain regeneration in zebrafish. *Dev. Neurobiol.* 72, 429–461. doi: 10.1002/dneu.20918

Kobayashi, T., Ahlenius, H., Thored, P., Kobayashi, R., Kokaia, Z., and Lindvall, O. (2006). Intracerebral infusion of glial cell line-derived neurotrophic factor promotes striatal neurogenesis after stroke in adult rats. *Stroke* 37, 2361–2367.

Koci, Z., Vyborny, K., Dubisova, J., Vackova, I., Jager, A., Lunov, O., et al. (2017). Extracellular matrix hydrogel derived from human umbilical cord as a scaffold for neural tissue repair and its comparison with extracellular matrix from porcine tissues. *Tissue Eng. Part C Methods* 23, 333–345. doi: 10.1089/ten.TEC.2017.0089

Kojima, T., Hirota, Y., Ema, M., Takahashi, S., Miyoshi, I., Okano, H., et al. (2010). Subventricular zone-derived neural progenitor cells migrate along a blood vessel scaffold toward the post-stroke striatum. *Stem Cells* 28, 545–554. doi: 10.1002/stem.306

Kreber, L. A., and Griesbach, G. S. (2016). The interplay between neuropathology and activity based rehabilitation after traumatic brain injury. *Brain Res.* 1640, 152–163. doi: 10.1016/j.brainres.2016.01.016

Kroehne, V., Freudenreich, D., Hans, S., Kaslin, J., and Brand, M. (2011). Regeneration of the adult zebrafish brain from neurogenic radial glia-type progenitors. *Development* 138, 4831–4841. doi: 10.1242/dev.072587

Kyritsis, N., Kizil, C., Zocher, S., Kroehne, V., Kaslin, J., Freudenreich, D., et al. (2012). Acute inflammation initiates the regenerative response in the adult zebrafish brain. *Science* 338, 1353–1356. doi: 10.1126/science.1228773

Lam, D., Enright, H. A., Cadena, J., Peters, S. K. G., Sales, A. P., Osburn, J. J., et al. (2019). Tissue-specific extracellular matrix accelerates the formation of neural networks and communities in a neuron-glia co-culture on a multi-electrode array. *Sci. Rep.* 9:4159. doi: 10.1038/s41598-019-40128-1

Lampe, K. J., and Heilshorn, S. C. (2012). Building stem cell niches from the molecule up through engineered peptide materials. *Neurosci. Lett.* 519, 138–146. doi: 10.1016/j.neulet.2012.01.042

Liang, Y., Bar-Shir, A., Song, X., Gilad, A. A., Walczak, P., and Bulte, J. W. (2015). Label-free imaging of gelatin-containing hydrogel scaffolds. *Biomaterials* 42, 144–150. doi: 10.1016/j.biomaterials.2014.11.050

Lindvall, O., and Kokaia, Z. (2015). Neurogenesis following stroke affecting the adult brain. *Cold Spring Harb. Perspect. Biol.* 7:a019034. doi: 10.1101/cshperspect.a019034

LoPresti, S. T., and Brown, B. N. (2018). Effect of source animal age upon macrophage response to extracellular matrix biomaterials. *J. Immunol. Regen. Med.* 1, 57–66. doi: 10.1016/j.regen.2018.03.004

Lu, P., Takai, K., Weaver, V. M., and Werb, Z. (2011). Extracellular matrix degradation and remodeling in development and disease. *Cold Spring Harb. Perspect. Biol.* 3:a005058. doi: 10.1101/cshperspect.a005058

Madsen, D. H., Leonard, D., Masedunskas, A., Moyer, A., Jurgensen, H. J., Peters, D. E., et al. (2013). M2-like macrophages are responsible for collagen degradation through a mannose receptor-mediated pathway. *J. Cell Biol.* 202, 951–966. doi: 10.1083/jcb.201301081

Magavi, S. S., Leavitt, B. R., and Macklis, J. D. (2000). Induction of neurogenesis in the neocortex of adult mice. *Nature* 405, 951–955.

Malatesta, P., and Gotz, M. (2013). Radial glia - from boring cables to stem cell stars. *Development* 140, 483–486. doi: 10.1242/dev.085852

Manoonkitiwongsa, P. S., Jackson-Friedman, C., Mcmillan, P. J., Schultz, R. L., and Lyden, P. D. (2001). Angiogenesis after stroke is correlated with increased numbers of macrophages: the clean-up hypothesis. *J. Cereb. Blood Flow Metab.* 21, 1223–1231.

Mansour, A. A., Goncalves, J. T., Bloyd, C. W., Li, H., Fernandes, S., Quang, D., et al. (2018). An in vivo model of functional and vascularized human brain organoids. *Nat. Biotechnol.* 36, 432–441.

Marin, O., Anderson, S. A., and Rubenstein, J. L. (2000). Origin and molecular specification of striatal interneurons. *J. Neurosci.* 20, 6063–6076.

Martin, P., and Nunan, R. (2015). Cellular and molecular mechanisms of repair in acute and chronic wound healing. *Br. J. Dermatol.* 173, 370–378. doi: 10.1111/bjd.13954

Massensini, A. R., Ghuman, H., Saldin, L. T., Medberry, C. J., Keane, T. J., Nicholls, F. J., et al. (2015). Concentration-dependent rheological properties of ECM hydrogel for intracerebral delivery to a stroke cavity. *Acta Biomater.* 27, 116–130. doi: 10.1016/j.actbio.2015.08.040

Mattsson, B., Sorensen, J. C., Zimmer, J., and Johansson, B. B. (1997). Neural grafting to experimental neocortical infarcts improves behavioral outcome and reduces thalamic atrophy in rats housed in enriched but not in standard environments. *Stroke* 28, 1225-1231.

Medberry, C. J., Crapo, P. M., Siu, B. F., Carruthers, C. A., Wolf, M. T., Nagarkar, S. P., et al. (2013). Hydrogels derived from central nervous system extracellular matrix. *Biomaterials* 34, 1033–1040. doi: 10.1016/j.biomaterials.2012.10.062

Michalopoulos, G. K. (2007). Liver regeneration. *J. Cell Physiol.* 213, 286–300.

Michalopoulos, G. K., and DeFrances, M. C. (1997). Liver regeneration. *Science* 276, 60–66.

Ming, G. L., and Song, H. (2011). Adult neurogenesis in the mammalian brain: significant answers and significant questions. *Neuron* 70, 687–702. doi: 10.1016/j.neuron.2011.05.001

Miyoshi, Y., Date, I., and Ohmoto, T. (1995a). Neovascularization of rat fetal neocortical grafts transplanted into a previously prepared cavity in the cerebral cortex: a three-dimensional morphological study using the scanning electron microscope. *Brain Res.* 681, 131–140.

Miyoshi, Y., Date, I., and Ohmoto, T. (1995b). Three-dimensional morphological study of microvascular regeneration in cavity wall of the rat cerebral cortex using the scanning electron microscope: implications for delayed neural grafting into brain cavities. *Exp. Neurol.* 131, 69–82.

Modo, M., and Badylak, S. F. (2019). A roadmap for promoting endogenous in situ tissue restoration using inductive bioscaffolds after acute brain injury. *Brain Res. Bull.* 150, 136–149. doi: 10.1016/j.brainresbull.2019.05.013

Modo, M., Mellodew, K., and Rezaie, P. (2003). In vitro expression of major histocompatibility class I and class II antigens by conditionally immortalized murine neural stem cells. *Neurosci. Lett.* 337, 85–88.

Modo, M., Rezaie, P., Heuschling, P., Patel, S., Male, D. K., and Hodges, H. (2002). Transplantation of neural stem cells in a rat model of stroke: assessment of short-term graft survival and acute host immunological response. *Brain Res.* 958, 70–82.

Modo, M. M., Jolkkonen, J., Zille, M., and Boltze, J. (2018). Future of animal modeling for poststroke tissue repair. *Stroke* 49, 1099–1106.

Moreau, F., Patel, S., Lauzon, M. L., Mccreary, C. R., Goyal, M., Frayne, R., et al. (2012). Cavitation after acute symptomatic lacunar stroke depends on time, location, and MRI sequence. *Stroke* 43, 1837–1842. doi: 10.1161/STROKEAHA.111.647859

Nassereddine, S., Rafei, H., Elbahesh, E., and Tabbara, I. (2017). Acute graft versus host disease: a comprehensive review. *Anticancer Res.* 37, 1547–1555.

Nectow, A. R., Marra, K. G., and Kaplan, D. L. (2012). Biomaterials for the development of peripheral nerve guidance conduits. *Tissue Eng. Part B Rev.* 18, 40–50. doi: 10.1089/ten.TEB.2011.0240

Neuhaus, A. A., Couch, Y., Hadley, G., and Buchan, A. M. (2017). Neuroprotection in stroke: the importance of collaboration and reproducibility. *Brain* 140, 2079–2092. doi: 10.1093/brain/awx126

Nicholls, F. J., Ling, W., Ferrauto, G., Aime, S., and Modo, M. (2015). Simultaneous MR imaging for tissue engineering in a rat model of stroke. *Sci. Rep.* 5:14597. doi: 10.1038/srep14597

Nicholls, F. J., Rotz, M. W., Ghuman, H., Macrenaris, K. W., Meade, T. J., and Modo, M. (2016). DNA-gadolinium-gold nanoparticles for in vivo T1 MR imaging of transplanted human neural stem cells. *Biomaterials* 77, 291–306. doi: 10.1016/j.biomaterials.2015.11.021

Nicholson, C. (2001). Diffusion and related transport mechanisms in brain tissue. *Rep. Prog. Phys.* 64, 815–884.

Nih, L. R., Gojgini, S., Carmichael, S. T., and Segura, T. (2018). Dual-function injectable angiogenic biomaterial for the repair of brain tissue following stroke. *Nat. Mater.* 17, 642–651. doi: 10.1038/s41563-018-0083-8

Novak, M. L., and Koh, T. J. (2013). Macrophage phenotypes during tissue repair. *J. Leukoc. Biol.* 93, 875–881. doi: 10.1189/jlb.1012512

Obernier, K., Tong, C. K., and Alvarez-Buylla, A. (2014). Restricted nature of adult neural stem cells: re-evaluation of their potential for brain repair. *Front. Neurosci.* 8:162. doi: 10.3389/fnins.2014.00162

Oh, B., and George, P. (2019). Conductive polymers to modulate the post-stroke neural environment. *Brain Res. Bull.* 148, 10–17. doi: 10.1016/j.brainresbull.2019.02.015

Park, G. K., Kim, S. H., Kim, K., Das, P., Kim, B. G., Kashiwagi, S., et al. (2019). Dual-channel fluorescence imaging of hydrogel degradation and tissue regeneration in the brain. *Theranostics* 9, 4255–4264. doi: 10.7150/thno.35606

Park, K. I., Teng, Y. D., and Snyder, E. Y. (2002). The injured brain interacts reciprocally with neural stem cells supported by scaffolds to reconstitute lost tissue. *Nat. Biotechnol.* 20, 1111–1117.

Pearlman, A. M., Mujumdar, V., Mcabee, K. E., and Terlecki, R. P. (2018). Outcomes of adult urethroplasty with commercially available acellular matrix. *Ther. Adv. Urol.* 10, 351–355. doi: 10.1177/1756287218790370

Piejko, M., Walczak, P., Li, X., Bulte, J.W.M., and Janowski, M. (2019). In vitro assessment of fluorine nanoemulsion-labeled hyaluronan-based hydrogels for precise intrathecal transplantation of glial-restricted precursors. *Mol. Imaging Biol.* doi: 10.1007/s11307-019-01341-6 [Epub ahead of print]

Potjewyd, G., Moxon, S., Wang, T., Domingos, M., and Hooper, N. M. (2018). Tissue engineering 3D neurovascular units: a biomaterials and bioprinting perspective. *Trends Biotechnol.* 36, 457–472. doi: 10.1016/j.tibtech.2018.01.003

Prest, T. A., Yeager, E., Lopresti, S. T., Zygelyte, E., Martin, M. J., Dong, L., et al. (2018). Nerve-specific, xenogeneic extracellular matrix hydrogel promotes recovery following peripheral nerve injury. *J. Biomed. Mater. Res. A* 106, 450–459. doi: 10.1002/jbm.a.36235

Price, J. (2011). Reconstructing brains: a biological impossibility? *Biosciences* 6, 299–322.

Ramon y Cajal, S. (1928). *Degeneration and Regeneration of the Nervous System*. New York, NY: Haffner Publishing.

Rayasam, A., Hsu, M., Kijak, J. A., Kissel, L., Hernandez, G., Sandor, M., et al. (2018). Immune responses in stroke: how the immune system contributes to damage and healing after stroke and how this knowledge could be translated to better cures? *Immunology* 154, 363–376. doi: 10.1111/imm.12918

Record, R.D., Hillegonds, D., Simmons, C., Tullius, R., Rickey, F.A., Elmore, D., et al. (2001). In vivo degradation of 14C-labeled small intestinal submucosa (SIS) when used for urinary bladder repair. *Biomaterials* 22, 2653–2659.

Rempe, R. G., Hartz, A. M. S., and Bauer, B. (2016). Matrix metalloproteinases in the brain and blood-brain barrier: versatile breakers and makers. *J. Cereb. Blood Flow Metab.* 36, 1481–1507. doi: 10.1177/0271678X16655551

Rensink, M., Schuurmans, M., Lindeman, E., and Hafsteinsdottir, T. (2009). Task-oriented training in rehabilitation after stroke: systematic review. *J. Adv. Nurs.* 65, 737–754. doi: 10.1111/j.1365-2648.2008.04925.x

Robel, S., Berninger, B., and Gotz, M. (2011). The stem cell potential of glia: lessons from reactive gliosis. *Nat. Rev. Neurosci.* 12, 88–104. doi: 10.1038/nrn2978

Ross, H. H., Ambrosio, F., Trumbower, R. D., Reier, P. J., Behrman, A. L., and Wolf, S. L. (2016). Neural stem cell therapy and rehabilitation in the central nervous system: emerging partnerships. *Phys. Ther.* 96, 734–742. doi: 10.2522/ptj.20150063

Sadtler, K., Wolf, M. T., Ganguly, S., Moad, C. A., Chung, L., Majumdar, S., et al. (2019). Divergent immune responses to synthetic and biological scaffolds. *Biomaterials* 192, 405–415. doi: 10.1016/j.biomaterials.2018.11.002

Saldin, L. T., Cramer, M. C., Velankar, S. S., White, L. J., and Badylak, S. F. (2017). Extracellular matrix hydrogels from decellularized tissues: structure and function. *Acta Biomater.* 49, 1–15. doi: 10.1016/j.actbio.2016.11.068

Santucci, R. A., and Barber, T. D. (2005). Resorbable extracellular matrix grafts in urologic reconstruction. *Int. Braz. J. Urol.* 31, 192–203.

Sauvageot, C. M., and Stiles, C. D. (2002). Molecular mechanisms controlling cortical gliogenesis. *Curr. Opin. Neurobiol.* 12, 244–249.

Savitz, S. I., Cramer, S. C., Wechsler, L., and Consortium, S. (2014). Stem cells as an emerging paradigm in stroke 3: enhancing the development of clinical trials. *Stroke* 45, 634–639.

Schierle, G. S., Hansson, O., Leist, M., Nicotera, P., Widner, H., and Brundin, P. (1999). Caspase inhibition reduces apoptosis and increases survival of nigral transplants. *Nat. Med.* 5, 97–100.

Sciari, B., Dziki, J. L., Siu, B. F., Medberry, C. J., Dearth, C. L., and Badylak, S. F. (2014). The promotion of a constructive macrophage phenoytype by solubilized extracellular matrix. *Biomaterials* 35, 8605–8612 doi: 10.1016/j.biomaterials.2014.06.060

Seidenfaden, R., Desoeuvre, A., Bosio, A., Virard, I., and Cremer, H. (2006). Glial conversion of SVZ-derived committed neuronal precursors after ectopic grafting into the adult brain. *Mol. Cell Neurosci.* 32, 187–198.

Senior, K. (2001). Angiogenesis and functional recovery demonstrated after minor stroke. *Lancet* 358:817.

Serbo, J. V., and Gerecht, S. (2013). Vascular tissue engineering: biodegradable scaffold platforms to promote angiogenesis. *Stem Cell Res. Ther.* 4:8. doi: 10.1186/scrt156

Shechter, R., and Schwartz, M. (2013). CNS sterile injury: just another wound healing? *Trends Mol. Med.* 19, 135–143. doi: 10.1016/j.molmed.2012.11.007

Sicari, B. M., Rubin, J. P., Dearth, C. L., Wolf, M. T., Ambrosio, F., Boninger, M., et al. (2014). An acellular biologic scaffold promotes skeletal muscle formation in mice and humans with volumetric muscle loss. *Sci. Transl Med.* 6:234ra258.

Silver, J., and Miller, J. H. (2004). Regeneration beyond the glial scar. *Nat. Rev. Neurosci.* 5, 146–156.

Slivka, P. F., Dearth, C. L., Keane, T. J., Meng, F. W., Medberry, C. J., Riggio, R. T., et al. (2014). Fractionation of an ECM hydrogel into structural and soluble components reveals distinctive roles in regulating macrophage behavior. *Biomater. Sci.* 2, 1521–1534. doi: 10.1039/c4bm00189c

Smith, E. J., Stroemer, R. P., Gorenkova, N., Nakajima, M., Crum, W. R., Tang, E., et al. (2012). Implantation site and lesion topology determine efficacy of a human neural stem cell line in a rat model of chronic stroke. *Stem Cells* 30, 785–796. doi: 10.1002/stem.1024

Sorensen, J. C., Grabowski, M., Zimmer, J., and Johansson, B. B. (1996). Fetal neocortical tissue blocks implanted in brain infarcts of adult rats interconnect with the host brain. *Exp. Neurol.* 138, 227–235.

Sridharan, R., Cameron, A. R., Kelly, D. J., Kearney, C. J., and O"Brien, F. J. C. (2015). Biomaterial based modulation of macrophage polarization: a review and suggested design principles. *Mater. Today* 18, 313–325.

Strbo, N., Yin, N., and Stojadinovic, O. (2014). Innate and adaptive immune responses in wound epithelialization. *Adv. Wound Care* 3, 492–501.

Struzyna, L. A., Adewole, D. O., Gordián-Vélez, W. J., Grovola, M. R., Burrell, J. C., Katiyar, K. S., et al. (2017). Anatomically inspired three-dimensional micro-tissue engineered neural networks for nervous system reconstruction, modulation, and modeling. *J. Vis. Exp.* 123:e55609. doi: 10.3791/55609

Struzyna, L. A., Browne, K. D., Brodnik, Z. D., Burrell, J. C., Harris, J. P., Chen, H. I., et al. (2018). Tissue engineered nigrostriatal pathway for treatment of Parkinson's disease. *J. Tissue Eng. Regen. Med.* 12, 1702–1716. doi: 10.1002/term.2698

Struzyna, L. A., Wolf, J. A., Mietus, C. J., Adewole, D. O., Chen, H. I., Smith, D. H., et al. (2015). Rebuilding brain circuitry with living micro-tissue engineered neural networks. *Tissue Eng. Part A* 21, 2744–2756. doi: 10.1089/ten.TEA.2014.0557

Surey, S., Berry, M., Logan, A., Bicknell, R., and Ahmed, Z. (2014). Differential cavitation, angiogenesis and wound-healing responses in injured mouse and rat spinal cords. *Neuroscience* 275, 62–80. doi: 10.1016/j.neuroscience.2014.06.003

Swinehart, I. T., and Badylak, S. F. (2016). Extracellular matrix bioscaffolds in tissue remodeling and morphogenesis. *Dev. Dyn.* 245, 351–360.

Takeuchi, N., and Izumi, S. (2015). Combinations of stroke neurorehabilitation to facilitate motor recovery: perspectives on Hebbian plasticity and homeostatic metaplasticity. *Front. Hum. Neurosci.* 9:349. doi: 10.3389/fnhum.2015.00349

Tanaka, E. M., and Ferretti, P. (2009). Considering the evolution of regeneration in the central nervous system. *Nat. Rev. Neurosci.* 10, 713–723. doi: 10.1038/nrn2707

Tchanque-Fossuo, C. N., Dahle, S. E., Lev-Tov, H., Li, C. S., and Isseroff, R. R. (2017). Cellular versus acellular grafts for diabetic foot ulcers: altering the protocol to improve recruitment to a comparative efficacy trial. *Cutis* 100, E18–E21.

Tornero, D., Tsupykov, O., Granmo, M., Rodriguez, C., Gronning-Hansen, M., Thelin, J., et al. (2017). Synaptic inputs from stroke-injured brain to grafted human stem cell-derived neurons activated by sensory stimuli. *Brain* 140, 692–706. doi: 10.1093/brain/aww347

Tornero, D., Wattananit, S., Gronning Madsen, M., Koch, P., Wood, J., Tatarishvili, J., et al. (2013). Human induced pluripotent stem cell-derived cortical neurons integrate in stroke-injured cortex and improve functional recovery. *Brain* 136, 3561–3577. doi: 10.1093/brain/awt278

Tukmachev, D., Forostyak, S., Koci, Z., Zaviskova, K., Vackova, I., Vyborny, K., et al. (2016). Injectable extracellular matrix hydrogels as scaffolds for spinal cord injury repair. *Tissue Eng. Part A* 22, 306–317. doi: 10.1089/ten.TEA.2015.0422

Underly, R. G., Levy, M., Hartmann, D. A., Grant, R. I., Watson, A. N., and Shih, A. Y. (2017). Pericytes as inducers of rapid, matrix metalloproteinase-9-dependent capillary damage during ischemia. *J. Neurosci.* 37, 129–140. doi: 10.1523/JNEUROSCI.2891-16.2016

Urata, Y., Yamashita, W., Inoue, T., and Agata, K. (2018). Spatio-temporal neural stem cell behavior leads to both perfect and imperfect structural brain regeneration in adult newts. *Biol. Open.* 7:bio033142. doi: 10.1242/bio.033142

Valentin, J. E., Stewart-Akers, A. M., Gilbert, T. W., and Badylak, S. F. (2009). Macrophage participation in the degradation and remodeling of extracellular matrix scaffolds. *Tissue Eng. Part A* 15, 1687–1694. doi: 10.1089/ten.tea.2008.0419

van den Ameele, J., Tiberi, L., Vanderhaeghen, P., and Espuny-Camacho, I. (2014). Thinking out of the dish: what to learn about cortical development using pluripotent stem cells. *Trends Neurosci.* 37, 334–342. doi: 10.1016/j.tins.2014.03.005

Verheggen, I. C. M., Van Boxtel, M. P. J., Verhey, F. R. J., Jansen, J. F. A., and Backes, W. H. (2018). Interaction between blood-brain barrier and glymphatic system in solute clearance. *Neurosci. Biobehav. Rev.* 90, 26–33. doi: 10.1016/j.neubiorev.2018.03.028

Wahlberg, B., Ghuman, H., Liu, J. R., and Modo, M. (2018). Ex vivo biomechanical characterization of syringe-needle ejections for intracerebral cell delivery. *Sci. Rep.* 8:9194. doi: 10.1038/s41598-018-27568-x

Webster, N. L., and Crowe, S. M. (2006). Matrix metalloproteinases, their production by monocytes and macrophages and their potential role in HIV-related diseases. *J. Leukoc. Biol.* 80, 1052–1066.

Wictorin, K., Lagenaur, C. F., Lund, R. D., and Bjorklund, A. (1991). Efferent projections to the host brain from intrastriatal striatal mouse-to-rat grafts: time course and tissue-type specificity as revealed by a mouse specific neuronal marker. *Eur. J. Neurosci.* 3, 86–101.

Wolf, M. T., Dearth, C. L., Sonnenberg, S. B., Loboa, E. G., and Badylak, S. F. (2015). Naturally derived and synthetic scaffolds for skeletal muscle reconstruction. *Adv. Drug Deliv. Rev.* 84, 208–221. doi: 10.1016/j.addr.2014.08.011

Wu, Y., Wang, J., Shi, Y., Pu, H., Leak, R. K., Liou, A. K., et al. (2016). Implantation of brain-derived extracellular matrix enhances neurological recovery after traumatic brain injury. *Cell Transplant.* 26, 1224–1234 doi: 10.1177/0963689717714090

Yahyouche, A., Zhidao, X., Czernuszka, J. T., and Clover, A. J. (2011). Macrophage-mediated degradation of crosslinked collagen scaffolds. *Acta Biomater.* 7, 278–286. doi: 10.1016/j.actbio.2010.08.005

Zbesko, J. C., Nguyen, T. V., Yang, T., Frye, J. B., Hussain, O., Hayes, M., et al. (2018). Glial scars are permeable to the neurotoxic environment of chronic stroke infarcts. *Neurobiol. Dis.* 112, 63–78. doi: 10.1016/j.nbd.2018.01.007

Zeng, J., Zhao, L. R., Nordborg, C., Mattsson, B., and Johansson, B. B. (1999). Are neuronal markers and neocortical graft-host interface influenced by housing conditions in rats with cortical infarct cavity? *Brain Res. Bull.* 48, 165–171.

Zhang, L., Zhang, F., Weng, Z., Brown, B. N., Yan, H., Ma, X. M., et al. (2013). Effect of an inductive hydrogel composed of urinary bladder matrix upon functional recovery following traumatic brain injury. *Tissue Eng. Part A* 19, 1909–1918. doi: 10.1089/ten.TEA.2012.0622

Zhao, J. Y., and Bass, K. D. (2018). Skeletal muscle regeneration by extracellular matrix biological scaffold: a case report. *J. Wound Care* 27, S11–S14. doi: 10.12968/jowc.2018.27.Sup9.S11

Zhu, J., and Marchant, R. E. (2011). Design properties of hydrogel tissue-engineering scaffolds. *Expert Rev. Med. Devices* 8, 607–626. doi: 10.1586/erd.11.27

Conflict of Interest: The author declares that the research was conducted in the absence of any commercial or financial relationships that could be construed as a potential conflict of interest.

Copyright © 2019 Modo. This is an open-access article distributed under the terms of the Creative Commons Attribution License (CC BY). The use, distribution or reproduction in other forums is permitted, provided the original author(s) and the copyright owner(s) are credited and that the original publication in this journal is cited, in accordance with accepted academic practice. No use, distribution or reproduction is permitted which does not comply with these terms.

frontiers in Neuroscience

REVIEW
published: 12 November 2019
doi: 10.3389/fnins.2019.01178

Brain–Immune Interactions and Neuroinflammation After Traumatic Brain Injury

Virginie Dinet[1]*, *Klaus G. Petry*[1] and *Jerome Badaut*[2,3]*

[1] INSERM U1029, Angiogenesis and Neuroinflammation Group, University of Bordeaux, Bordeaux, France, [2] CNRS UMR 5287, INCIA, Brain molecular Imaging Team, University of Bordeaux, Bordeaux, France, [3] Department of Basic Sciences, Loma Linda University School of Medicine, Loma Linda, CA, United States

Traumatic brain injury (TBI) is the principal cause of death and disability in children and young adults. Clinical and preclinical research efforts have been carried out to understand the acute, life-threatening pathophysiological events happening after TBI. In the past few years, however, it was recognized that TBI causes significant morbidity weeks, months, or years after the initial injury, thereby contributing substantially to the overall burden of TBI and the decrease of life expectancy in these patients. Long-lasting sequels of TBI include cognitive decline/dementia, sensory-motor dysfunction, and psychiatric disorders, and most important for patients is the need for socio-economic rehabilitation affecting their quality of life. Cerebrovascular alterations have been described during the first week after TBI for direct consequence development of neuroinflammatory process in relation to brain edema. Within the brain–immune interactions, the complement system, which is a family of blood and cell surface proteins, participates in the pathophysiology process. In fact, the complement system is part of the primary defense and clearance component of innate and adaptive immune response. In this review, the complement activation after TBI will be described in relation to the activation of the microglia and astrocytes as well as the blood–brain barrier dysfunction during the first week after the injury. Considering the neuroinflammatory activity as a causal element of neurological handicaps, some major parallel lines of complement activity in multiple sclerosis and Alzheimer pathologies with regard to cognitive impairment will be discussed for chronic TBI. A better understanding of the role of complement activation could facilitate the development of new therapeutic approaches for TBI.

Keywords: traumatic brain injury, neuroinflammation, complement, blood-brain barrier, astrocyte

OPEN ACCESS

Edited by:
Emmanuel Pinteaux, University of Manchester, United Kingdom

Reviewed by:
Rodolfo Gabriel Gatto, University of Illinois at Chicago, United States
Lisa Anne Brenner, University of Colorado Anschutz Medical Campus, United States

***Correspondence:**
Virginie Dinet
virginie.dinet@inserm.fr
Jerome Badaut
jerome.badaut@u-bordeaux.fr

Specialty section:
This article was submitted to Neurodegeneration, a section of the journal Frontiers in Neuroscience

Received: *27 July 2019*
Accepted: *18 October 2019*
Published: *12 November 2019*

Citation:
Dinet V, Petry KG and Badaut J (2019) Brain–Immune Interactions and Neuroinflammation After Traumatic Brain Injury. Front. Neurosci. 13:1178. doi: 10.3389/fnins.2019.01178

TRAUMATIC BRAIN INJURY

Traumatic brain injury (TBI) is a consequence of a direct or indirect external mechanical impact on the brain inducing the disruption of the normal structure and function of the brain. Despite its simple mechanical definition, TBI is a very complex and heterogeneous injury with various severities graded in clinic. The severity of TBI is predicated on alteration of consciousness, organized according to the Glasgow Coma Scale (GCS) for assessment of neurological function and neuroimaging as mild, moderate, or severe (Maas et al., 2008).

TBI is a major burden worldwide, and in the United States, it represents more than 30% of all injury-related deaths (Faul et al., 2010). In Europe, it is about 75,000 deaths each year (Maas et al., 2015), and it affects all ages. It is important to underline that pediatric and elderly populations are more vulnerable than adults (Faul et al., 2010). Therefore, TBI has an economic toll on the society that includes medical expenses and losses of productivity (Corso et al., 2006; Gustavsson et al., 2011). A widespread research on TBI pathophysiology is still sparse compared to other brain diseases such as Alzheimer's disease (AD) and the progressive chronicity of multiple sclerosis (MS).

Pathophysiology following TBI is grouped into the following: (1) The primary acute event is the mechanical injury that can give extracranial and intracranial complications like epidural hematoma, subarachnoid hemorrhage, or hypoxia. Thus, TBI is particularly heterogeneous depending on the primary injury severity, location, and the age and sex of the patient. Important in the TBI pathogenesis is that the functional outcomes may deteriorate over time after initial admission of the patient (Baethmann et al., 1988). For example, the patient can communicate early after TBI and then worsen with loss of consciousness, with an early small contusion that becomes a much larger injury the day after. This evolution is due to the secondary injury events (Plesnila, 2016). (2) The secondary injury cascade includes the following landmarks: glutamatergic excitotoxicity, calcium overload, vascular dysfunction, and inflammation/neuroinflammation. Inflammation/neuroinflammation can last for several months and could contribute to chronic TBI (Plesnila, 2016). The pattern of "chronic brain disease" has been leading the concept of accelerating of brain aging post-TBI (Johnson et al., 2010; Pop and Badaut, 2011; Smith et al., 2013). Patients can present long-lasting behavioral dysfunctions including some psychiatric disorders after TBI (Smith et al., 2013). Very recently, a nationwide population cohort study was done in Denmark to monitor individuals who had TBI from 1977 to 2013. Over the study period, 4.7% of recruited people had at least one TBI, and about 112,218 (85.0%) of 132,093 individuals had a mild TBI for their first TBI diagnosis; those people were 24% more likely to develop dementia than those without a history of TBI. Additionally, the younger the person was at the time of the injury, the higher the risk of dementia development over time (Fann et al., 2018).

Several animal models have been developed in order to extend our understanding of the cellular and molecular mechanisms in post-TBI secondary injuries (Prins and Hovda, 2003; Petraglia et al., 2014). Having a wide variety of preclinical models is a good sketch to mimic the heterogeneity in human TBI. However, it is important to highlight that the definition of the degree of TBI severity differs between animal models, and it is difficult to compare findings between models (Badaut et al., 2019). Sometimes, it is challenging to make the translation with clinical severities. The molecular and cellular mechanisms of secondary injuries are dependent on injury severity and brain location. The post-TBI outcome is more severe for younger patients; therefore, it is important to consider the age of the animal in the preclinical models (McMillan and Teasdale, 2007; Himanen et al., 2011; Pop and Badaut, 2011). In fact, neuroinflammation/inflammation response will vary in function of the location and severity of the impact as well as the age of the animal. The review focuses on some of the cerebrovascular alterations and the importance of the inflammation through the exploration of the complement system as a new potential mechanism. Actually, the role of the complement pathway in TBI pathogenesis is not yet well-understood.

NEUROVASCULATURE IMPAIRMENT POST-TBI

The neurovascular unit (NVU) is composed of neurons, a vascular tree with endothelial cells, smooth muscle cells, pericytes, astrocytes, and microglia (Zhang et al., 2012). Immune cells have been included as part of this physiological unit (Zhang et al., 2012). Cognitive impairments in AD as well as in healthy aging have been paralleled with NVU alterations (Iadecola, 2004; Raz et al., 2016). Similarly, NVU alteration is a typical landmark of the secondary injuries after TBI with, for example, a decrease of blood–brain perfusion with consequences on the good operation of the neurons (Pop and Badaut, 2011; Jullienne et al., 2016). In fact, preclinical TBI models unveil blood–brain barrier (BBB) disruption, hemorrhage, and cerebral blood flow alterations with hypo-perfusion, which are illustrations of the NVU alterations (Golding, 2002; DeWitt and Prough, 2003; Pop and Badaut, 2011). Cerebrovascular dysfunction has been described for almost two decades as a poor prognostic outcome. In fact, early decrease of the cerebral blood flow (CBF) post-injury induces hypoxic events in the brain tissue that directly contribute to the loss of neurons. In addition, the changes in BBB permeability play a role in edema formation with disruption of brain homeostasis. It exacerbates the cascade of secondary injury events including excitotoxicity (glutamate release and resulting higher metabolic demand) and inflammation (with the complement pathway, see below). TBI is a chronic brain disorder with molecular changes at the BBB several months after the initial injury (Jullienne et al., 2016). As it has been suggested in AD, the long-term alterations at the blood–brain interface could therefore be associated with premature aging of the brain after TBI (Pop and Badaut, 2011; Keightley et al., 2014; Jullienne et al., 2016).

Brain Perfusion Alterations

Early decrease of CBF is a landmark of the pathophysiology post-TBI and its recovery represents a prognostic factor for outcome post-TBI (Bouma et al., 1991, 1992; DeWitt and Prough, 2003). Preclinical models appropriately reproduce CBF changes observed in clinic. Decreased CBF is observed after TBI using controlled cortical impact (CCI) and lateral fluid percussion (LFP) injury models and it is described up to 8 months after injury in adult rats (Bouma et al., 1991; Bryan et al., 1995; Plesnila et al., 2003; Hayward et al., 2010), which probably feeds the inflammatory process. Even for mild TBI, a decrease of CBF has also been described (Villapol et al., 2014; Long et al., 2015). In a mild CCI model, the reduction of CBF was described with restoration at 30 days post-TBI in young adult

mice (Villapol et al., 2015). Importantly, hypo-perfusion adds to the development of the secondary injuries after TBI by decreasing glucose and oxygen delivery. Moreover, an ischemic event could be aggravated by the presence of cell hyper-metabolism during the first 6 h after concussion in rats (Yoshino et al., 1991). Consequently, decreased CBF and hyper-metabolism occurring early after TBI result in a mismatch between demand and supply, known as uncoupling of CBF and glucose metabolism, with direct consequence and aggravation of the secondary injuries and directly feeding the inflammation and neuroinflammation process. At the time, dysfunction in vascular perfusion is paralleled with BBB hyper-permeability and edema process.

BBB Dysfunction Post-TBI

The presence of hemorrhage is a marker of acute vascular dysfunction, and it is frequently observed in moderate and severe TBI. BBB and cerebral blood vessel alterations are frequently shadowed by edema formation with dramatic consequences on morbidity and mortality because it induces intracranial hypertension and contributes to the vicious cycle of the secondary injury cascade (Unterberg et al., 2004). Even for mild TBI characterized by the absence of major bleeding, the BBB structure can be damaged or altered during the acute period after the injury. Very importantly, the BBB dysfunction is not only an acute event; it could also be observed several months and years after the traumatic event in human post-mortem tissue (Hay et al., 2015) and in preclinical models (Pop et al., 2013; Jullienne et al., 2014).

The consequences of primary injury on the BBB properties significantly differ according to the age, the type, and the severity of the lesion. The "opening" of the BBB can be observed as early as 3 min after injury in a model of concussion (Povlishock et al., 1978). The "opening" of BBB can be characterized with the presence of two types of lesions on the luminal surface of pial arterioles: crater-shaped indentations and dome-shaped projections of the endothelial cell surface, suggesting necrotic cells (Wei et al., 1980). The tight junction protein complex is potentially altered after TBI. In fact, pial, and intracerebral blood vessels demonstrate decreased claudin-5 and occludin expressions early after injury (Nag et al., 2007). Similar changes in tight junction protein complex have been described in rodent models of mild TBI induced by blast shock waves, with specifically decreased expression in occludin, claudin-5, and *zonula occludens* protein-1 at 6 h and 24 h post-TBI (Abdul-Muneer et al., 2013). The changes in tight junction proteins have been paralleled with an increase of immunoglobulin G extravasation from 5 min to 48 h post-injury (Yeoh et al., 2013; Shetty et al., 2014). However, it is important to underline that tight junction complexes appear intact under electron microscopy during the first hours after a mild TBI; then, the expression of the tight junction protein is altered (Rafols et al., 2007). Therefore, the changes in expression of the tight junction proteins and increased IgG extravasation are not directly linked with physical rupture of the tight junctions in electron microscopy (Knowland et al., 2014; Haley and Lawrence, 2017). Similarly, IgG extravasation is increased close to the site of impact and surrounding tissue in the absence of a direct relation with changes in claudin-5 expression in a model of juvenile CCI (Pop and Badaut, 2011; Badaut et al., 2015). Similarly, IgG extravasation has been observed in the corpus callosum at 24 h after mild closed head injury, suggesting BBB hyper-permeability even for mild injury (Rodriguez-Grande et al., 2018).

Changes of expression of the tight junction proteins are accompanied by up-regulation of various matrix metalloproteases (MMPs), which have been involved in BBB alteration. In fact, MMP-9 and MMP-2 increase acutely after TBI in rodents (Wang et al., 2000; Zhang et al., 2010). MMP-3 activity is increased chronically after TBI and possibly plays a role in synaptic remodeling (Zhang et al., 2010). Up-regulation of MMPs alters proteins of the extracellular matrix and participates in BBB alteration and neurovascular unit dysfunction.

In summary, it is important to highlight that neurovascular unit disturbance, encompassing BBB and blood flow changes, fuels the inflammation and neuroinflammation process.

Astrogliosis, Neuroinflammation, and Consequences on Blood Perfusion and BBB

Astrocyte endfeet wrap the blood vessels and they play a key role in BBB properties in collaboration with pericytes (Zhang et al., 2012). Astrocytes become "reactive" and proliferate to form a glial scar in various severe brain injury models (Burda and Sofroniew, 2014). Depending on the timeline of the pathological process after injury, astrogliosis can be both beneficial and detrimental to the brain tissue adjacent to the lesion (Sofroniew, 2009). Astrocytes have various physiological functions such as providing energy substrates for neurons, regulating ion and neurotransmitter homeostasis, participating in synapse development and transmission, and regulation of CBF. Then, transformation of astrocyte in "reactive astrocyte" can have a direct and weighty impact on the brain functions on the post-injury outcomes (Sofroniew and Vinters, 2010). Astrocytes are among the first responder brain cells to TBI, and the mechanical forces of the primary injury trigger reactive astrocyte or astrogliosis (Burda et al., 2016). In fact, stretch injury or shear stress involves a rapid calcium influx in the astrocytes (Rzigalinski et al., 1998; Maneshi et al., 2015), by potential activation of astrocytic mechano-receptive channels (Burda et al., 2016). In parallel, activation of the astrocyte potentially contributes to the release of vasoactive substances (Howarth, 2014). In fact, release of isoprostanes (Hoffman et al., 1997, 2000) and endothelin 1 (Ostrow et al., 2000), powerful vasoconstrictors, have been described to increase after TBI in preclinical models (Petrov and Rafols, 2001; Armstead and Kreipke, 2011; Armstead and Raghupathi, 2011). Then, any changes in the calcium concentration within astrocytes could have a direct or indirect consequence on the regulation of CBF and perfusion post-injury. Then, calcium changes in astrocytes could contribute to the NVU dysfunction post-TBI with the increase of vasoconstrictor molecules.

Astrocytes play an important role in the integrity of the BBB (Abbott et al., 2006). Cytokines and inflammatory mediators are released by the astrocytes after injury with consequences

on BBB properties (Chodobski et al., 2011; Sofroniew, 2014). For example, chemokines (Chodobski et al., 2011) and three isoforms of transforming growth factor–β (TGF- β) (Constam et al., 1992), potentially released by the astrocytes, have been implicated the BBB alterations after TBI (Shen et al., 2011). Very interestingly, increased TGF-β expression has been observed in patients with severe TBI where it parallels BBB dysfunction (Morganti-Kossmann et al., 1999). As already discussed, MMPs disturb the structure of the BBB after TBI and they are extensively produced by reactive astrocytes (Chen and Swanson, 2003). In the vicinity of the perivascular astrocyte endfoot, the water channel aquaporin 4 expression is altered after TBI, which is related to the formation of cerebral edema (Badaut et al., 2014; Gatto et al., 2015; Zhang et al., 2015). Increased aquaporin expression associated to edema brain formation event is also described in earlier stages of several neurodegenerative diseases (Sun et al., 2016; Yang et al., 2016; Gatto et al., 2018). There is a correlation between the level of aquaporin 4 expression and disruption of BBB (Fukuda and Badaut, 2012). The astrocyte endfeet play a critical role in the BBB integrity, and very interestingly, the physical interaction between astrocyte endfeet and the brain vasculature can also be altered after TBI (Villapol et al., 2014), with a direct contribution to the vascular dysfunction after injury.

Altogether, astrocyte phenotypic transformation can feed forward the brain-vascular pathology observed after TBI in relation to neuroinflammation and the complement pathway. In addition, the neurodegeneration proposed after TBI could be a result of astrocyte activation and chronic inflammation (Faden and Loane, 2015). Interestingly, astrocyte plays a potential role in immune response in the brain with expression of the specific receptors to complement proteins (see *part 3*). Therefore, it may be important to consider the contribution of reactive astrocytes into the long-term consequences of vascular dysfunction and a target of the activation of the complement pathway. This pathway could represent a new avenue for drug development targeting the NVU.

GENERAL DESCRIPTION OF THE COMPLEMENT PATHWAY

The complement system is part of an innate and adaptive immune response after infection acting as a primary defense and mechanism of clearance in order to preserve the organ against pathogens. It includes a wide collection of blood and cell surface proteins (C3, C5, CFB, CFD, CFH, C1q, etc.), whose activation results in a self-amplifying cascade of proteolytic reactions (Walport, 2001). Most of the plasmatic complement proteins (90%) are produced by the hepatocytes in the liver (C3, C5, CFB, CFH), released in the bloodstream to circulate as inactive forms. However, a local expression of complement proteins is also observed in cells (microglia/macrophages/astrocytes and neuronal cells) in the brain and the eye, mainly for C3 and its cleavage regulators (CFH and CFB).

The complement system is a key molecular pathway in various cellular and molecular activities, ranging from cell lysis to increase in the local inflammatory response. The complement activation is composed of three main pathways: classical, lectin, and alternate. They converge to the common effector pathway by forming the membrane attack complex (MAC) as illustrated in **Figure 1**.

The Classical Pathway

The classical pathway activation is antibody-dependent. It happens when the complement protein C1 complex, formed by C1q, C1r, and C1s proteins, interacts with antigen–IgM or aggregated antigen–IgG complex, or is antibody-independent. It also happens when poly-anions (e.g., heparin, protamine, DNA and RNA from apoptotic cells), gram-negative bacteria, or bound C-reactive protein reacts directly with the C1 complex. Once the C1 complex is activated, then C1s cleave C4 and C2 into C4a/C4b and C2a/C2b, respectively, and forms the C3 convertase of the classical pathway (C4b2a). C4b2a cleaves C3 into C3a and C3b fragments. The classical pathway is regulated by C1 inhibitor (C1-INH).

The Lectin Pathway

The lectin pathway is activated when mannose-binding lectin (MBL), a serum protein, binds to mannose or fructose groups on bacterial cell walls, yeast walls, or viruses, independently of the antibody complex. The lectin pathway shares similarities with the classical pathway.

The Alternative Pathway

The alternative pathway is activated after cleavage of a small amount of complement compound C3 caused by microbial cell surfaces or immunoglobulin. This pathway is functionally present in physiological situation, with a spontaneous (hydrolysis) cleavage of C3 to C3a/C3b. The C3b product is rapidly inactivated by its binding to proteins complement factor H (CFH) and associated with complement factor I (CFI) as a co-factor, and then its opsonization functions (tagging pathogens, immune complexes apoptotic cells for phagocytosis) are aborted. After injury, C3b product binds to complement factor B (CFB) and its co-factor complement factor D (CFD) to form a molecular complex "C3bBb," called C3 convertase complex, which acts on additional C3 to form more C3b and C3a products (**Figure 1**). This function of C3b contributes to a positive feedback loop and amplifies a first C3 cleavage that is induced by either the classical pathway or both classical and alternative pathways, in order to produce high-level C3b and C3a proteins. It is important to highlight that each complement pathway (classical, lectin, and alternative pathways) activation ends up into the cleavage of C3.

Complement Cleavage Products Functions

Once activated, the complement pathway produces a high concentration of anaphylactic C3a/C5a and opsin C3b proteins (**Figure 1**). The receptors of these complement proteins (C3aR, C5aR, and CD11b, respectively) are expressed on cell membranes in various cerebral cell types such as endothelial cells, microglia/macrophage cells, and astrocytes. The wide distribution of the complement receptors underlines the variety of cellular functions to this system. Importantly, the complement system makes the link between the innate and acquired immunity

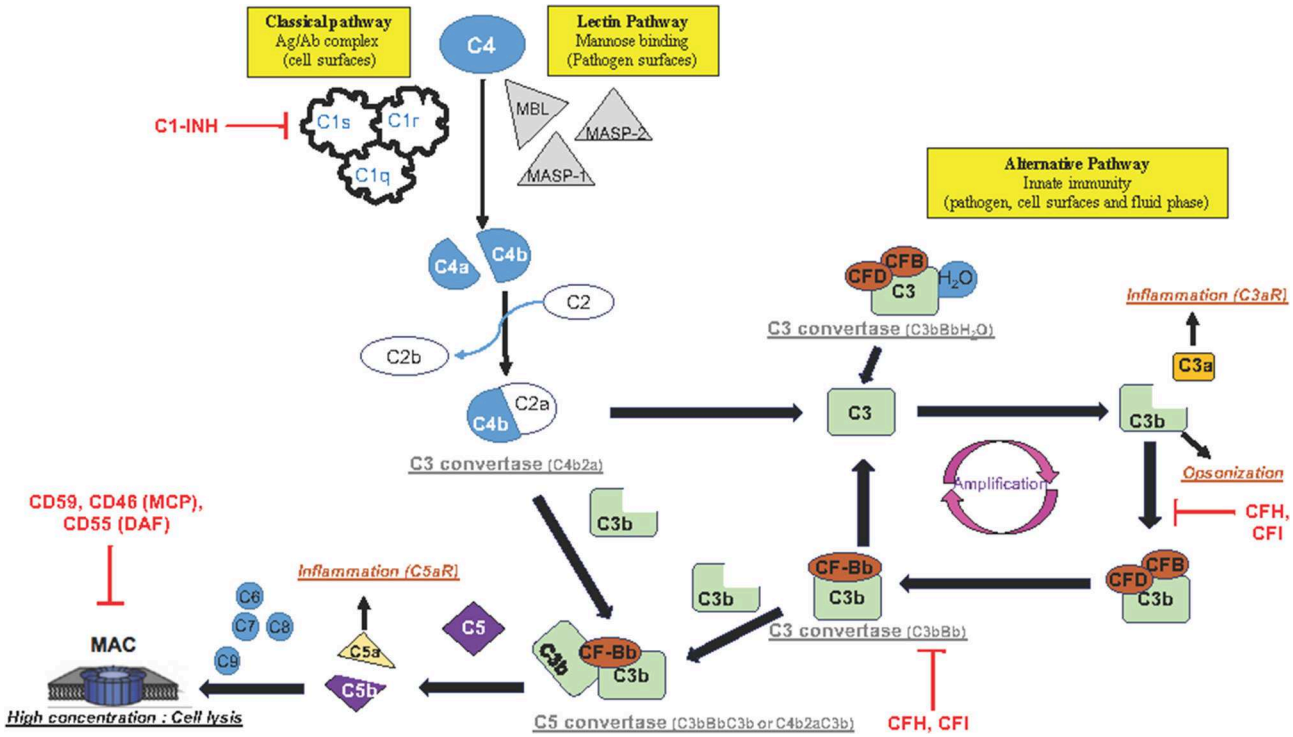

FIGURE 1 | Schematic representation of complement activation pathways: The complement system is composed of three pathways (classical, lectin, and alternative pathway) that involve a collection of blood and cell surface proteins to eliminate pathogens from organism or damaged cells. This system consists of a series of proteins that interact with one another in a highly regulated manner. The classical pathway helps antibodies and phagocytic cells to clear pathogens or damaged cells. The lectin pathway is activated when MBL binds to mannose residues on the pathogen surface. This pathway is very similar to the classical pathway. The alternative pathway is an important part of innate immune system in which proteins cleave one another to form enzymatic complex able to initiate amplification of further cleavages and finally promotes inflammation by production of anaphylactic fragments. The final product of each activated complement pathway is the formation of the MAC in the target cell membrane. Once activated, the complement system has several major functions: lysis of pathogens or damaged cells, activation of inflammation, opsonization, and immune clearance.

by (a) enhancing antibody response and immunologic memory, (b) lysing the pathogens, and (c) clearing immune complexes and apoptotic cells.

The anaphylactic C3a molecule has a remote result because it diffuses away to play the role of an inflammation and chemotactic factor. In contrast, the produced C3b binds to the C3 convertase complex (C3bBb) to form a C5 convertase complex (C3bBbC3b). The C5 convertase complex is located in the cell membrane or in the bloodstream and cleaves complement 5 (C5) into C5b and C5a fragments. Similarly to C3a, the C5a product is described in the bloodstream to act remotely as an anaphylactic protein inducing a general inflammatory reaction. In contrast, C5b initiates the MAC in the cell membrane (**Figure 1**). Sequentially, C5b interacts successively with C6, C7, and C8 complement proteins, and finally with a number of C9 complement proteins to form MAC. Importantly, MAC is organized in a circle with, in its center, a pore that produces a hole in the cell membrane. High concentration of MAC induces lysis of the foreign cell (such as microbes or bacteria) or apoptosis (of host cell).

Very interestingly, MAC has been found to contribute to secondary damages in various preclinical models of human brain diseases (Leinhase et al., 2006; Stahel et al., 2009; Fluiter et al., 2014; Ruseva et al., 2015). However, depending on the level of expression of MAC, opposite physiological responses can be observed. In fact, a low level of the MAC (C5b9) complex on the cell surface promotes cell-cycle progression instead of cell lysis or apoptosis (Fosbrink et al., 2005). The role of MAC in cell-cycle progression is due to the transactivation of receptor tyrosine kinases, a regulator of cytosolic free Ca^{2+} concentration (Cybulsky et al., 1999), and activation of protein kinase C and cytosolic phospholipase A_2-α (Cybulsky et al., 1995; Panesar et al., 1997).

It is important to have a fine-tuned regulation of MAC formation with a full panel of specific inhibitor proteins. Many of the complement regulator proteins are found in the blood plasma and on the cell membranes, and among them, CFH acts on the activity of the upstream C3 convertase complex (C3bBb) in the blood and on the cell surface. CFH removes "Bb fragment" from the C3 convertase enzymatic complex and inactivates C3 cleavage by competition with CFB for binding C3b; it stops the main amplification loop of the alternative complement pathways (**Figure 1**). Downstream, CD55 (or DAF: decay accelerating factor), CD46 (or MCP: membrane cofactor protein), and CD59 (known as protectin) have also been described as inhibitors of

MAC formation in the cell membrane for both classical and alternative complement pathways (**Figure 1**).

INVOLVEMENT OF COMPLEMENT PATHWAY IN TBI PATHOPHYSIOLOGY

The secondary injury events post-TBI include inflammatory mechanisms with early activation of the innate immune system, and then the chronic inflammation post-injury possibly contributes to the progressive neurodegenerative process (Francis et al., 2003; Schmidt et al., 2005; Stahel and Barnum, 2006).

The complement pathway represents a key element in the inflammatory response, and it contributes to neuronal cell death, edema, and infiltration of inflammatory cells after injury using rodent models of moderate and severe TBI (Kaczorowski et al., 1995; Ruseva et al., 2015; Rich et al., 2016). Involvement of the complement pathway observed in rodent TBI models has been confirmed with up-regulation of CFB (Kossmann et al., 1997), C3, C1q, and C4 (Stahel et al., 1998), and increase of soluble terminal complement complex C5b9 has been detected in ventricular cerebrospinal fluid (CSF) of severe TBI patients for up to 10 days after trauma, possibly due to the alteration of the BBB integrity (Stahel et al., 2001). CSF increase of complement proteins is paralleled by higher concentration of complement proteins in blood plasma of TBI patients (Manek et al., 2018). Expression of complement protein C3 and C9 has been described up to 6 months post-injury (Bao et al., 2018) in patients, suggesting a continuous complement pathway activation in the chronic TBI. Very interestingly, similar observations have been found in various preclinical rodent models, with higher levels of C9 and CFB in serum of rat during the first days after TBI (Thelin et al., 2018). Deposits of C3 have also been described in the peri-lesion tissue, while C9 protein has been reported in damaged neurons after cortical contusion in the adult rat (Bellander et al., 1996). Thus, a similar change in activation of the complement pathway has been described in clinical and in preclinical rodent models.

As presented above, C3 protein is common to the three complement pathways. In this line with the complement pathway inhibition in TBI, $C3^{-/-}$ mice exhibit less brain edema and microglia activation/infiltration compared to WT after TBI, suggesting a role of the complement pathways in the secondary injury cascade (Sewell et al., 2004; Yang et al., 2006) and inhibition of C3 could be a therapeutic strategy. Interestingly, severe TBI swine resuscitation with valproic acid (a histone deacetylase inhibitor) induces a down-regulation of the complement system activation, resulting in a significant decrease of lesion size after resuscitation (Dekker et al., 2014a,b; Bambakidis et al., 2016). Similarly, inhibition of MAC has been proposed to be protective. In fact, over-exuberant MAC formation contributes to neuronal cell death after severe TBI injury in mice lacking CD59, an inhibitor of MAC formation on the membrane cells (**Figure 1**) (Stahel et al., 2009). The inhibition of MAC formation using C6 antisense oligonucleotide or an inhibitor of C5 convertase complex reduces not only MAC deposition but also accumulation of microglia/macrophages, neuronal death, and axonal loss and enhances neurologic performances as compared to the placebo-treated TBI group (Fluiter et al., 2014).

The current paradigm is that MAC formation is predominantly implicated in development of post-TBI process neuropathology and neuroinflammation, but it is not excluded that C3 cleavage inhibition could prevent inflammation and/or cell death. Then, C3 and MAC would be good therapeutic targets to reduce TBI damage. Studies show that inhibition of C3 cleavage reduces post-injury of microglial and astrocyte activations, C3 deposits, and the extent of neuron cell death, and then triggers improvements in cognitive and functional recovery (Rich et al., 2016; Alawieh et al., 2018). It demonstrates a critical role of the complement system and mainly of the alternative pathway in the TBI neuropathology process.

Targeted deletion of *cfb* gene expression, the activator of alternate complement pathway by activation of C3 convertase, in transgenic mice clearly reveals a significant decrease of neuronal cell death post-TBI (Leinhase et al., 2006). In support to these results in transgenic mice, inhibition of the CFB by injection of anti-CFB monoclonal antibody attenuates both inflammation and cell death in TBI animals (Leinhase et al., 2007), confirming a key role of the alternative complement system in TBI.

Both the classical and lectin pathways have also been assessed in preclinical TBI models and human studies: (1) C1-inhibitor injection after TBI mitigates motor deficits, cognitive dysfunction, and contusion volumes (Longhi et al., 2009), arguing for a role of the classical complement pathway in TBI secondary injuries. (2) Activation of the lectin complement pathway has been shown to be involved in secondary ischemic/inflammatory injury after severe TBI along with an increase of MBL protein in plasma of patients at 48 h post-injury (Osthoff et al., 2017). However, there is no correlation between lectin complement pathway activation and mortality/consciousness after severe TBI (Osthoff et al., 2017). In human and mice, MBL is expressed in the injured cortex from 30 min and persists up to 1 week post-TBI (Longhi et al., 2014). The inactivation of the lectin complement pathway induces a decrease of cortical cell death (Longhi et al., 2014), arguing that this deletion has a protective effect in TBI damages. Until now, no specific pharmacological compound has been found to limit TBI damages, but targeting complement pathway would be a novel therapeutic way.

CHRONIC TBI AND NEURODEGENERATIVE LANDMARKS

Neurodegenerative Landmarks After TBI

Brain vasculature alterations and inflammatory processes implicating complement pathways are very likely hand in hand in the early secondary events post-injury. Several works clearly indicate that TBI is a chronic brain disorder with development of neurodegenerative disease landmarks such as accumulation of the amyloid-β (Aβ) (Johnson et al., 2010; Pop and Badaut, 2011; Pop et al., 2013). We and other groups have shown changes in the

brain vasculature and their involvement in functional outcome after TBI, with BBB dysfunctions several months and years after the injury (Pop et al., 2013; Hay et al., 2015). We previously described increase of claudin-5 expression in large blood vessels, decrease of the efflux pump P-glycoprotein (P-gp), and increase of the perivascular matrix proteins perlecan and fibronectin up to 6 months post-injury in a juvenile TBI model (Pop et al., 2013; Jullienne et al., 2014). The matrix changes observed up to 6 months after juvenile TBI (Jullienne et al., 2014) have also been described in AD patients (Lepelletier et al., 2017). Changes in the matrix properties possibly participate in neurodegenerative processes by leading to the accumulation of Aβ, decreasing its clearance and its perivascular drainage (Pop et al., 2013; Jullienne et al., 2014). P-gp has been suggested to be a key player in Aβ clearance from the brain parenchyma. P-gp knock-out models have increased Aβ deposition after injection of Aβ in the brain compared to the wild type (Cirrito et al., 2005). Moreover, P-gp expression is decreased on endothelial cells in aged human and AD brains as well as in aged rodents (Silverberg et al., 2010). In addition to the vascular dysfunction, the presence of Aβ deposition could contribute to amplify the pathophysiology with activation of the complement pathways around the Aβ deposition, and the vicious cycle of chronic inflammation would accelerate the brain aging.

Complement Pathway Activation in Neurodegenerative Disease

A number of chronic neurodegenerative diseases of the central nervous system (CNS) are characterized by prominent neuroinflammation marked by activated astrogliosis and microgliosis. In AD and MS affections of CNS, similar to what is seen in TBI, there is strong evidence of complement involvement in the pathogenesis that arises from a confluence of histochemical, genetic, and model data. The involvement of the complement system in the AD process comes from the identification of complement receptor 1, the C3b receptor expressed on macrophage/erythrocyte or monocyte cells, as a genetic risk to develop this neurodegenerative disease (Lambert et al., 2009; Crehan et al., 2012). In fact, erythrocyte cells capture complement-opsonized Aβ through CR1 receptor expressed on their membrane and facilitate clearance mechanism, which is relevant in AD pathophysiology (Brubaker et al., 2017). On the other hand, Aβ deposition promotes complement pathway activation by inhibition of CFI enzymatic activity, a cofactor of CFH (Lashkari et al., 2018). Thus, accumulation of Aβ contributes to increase C3 complement protein and ends up giving rise to the anaphylactic C3a/C5a proteins and MAC formation (Bradt et al., 1998; Lian et al., 2015). In fact, accumulation of these complement proteins generates damaged neurons, increases numbers of activated glial cells (Bradt et al., 1998), and, through neuronal C3a/C3aR signaling, disrupts dendritic morphology and network function (Lian et al., 2015). The Aβ-induced neuroinflammation response is also exaggerated by C5a/C5aR signaling (An et al., 2018), demonstrating another link between Aβ and complement activation. Similarly, the role of the complement pathway has been investigated in the context of the neuroinflammatory autoimmune neurodegenerative disease MS. Comparatively, these studies would help to understand the potential role of complement pathways in the long-term outcomes after TBI. With the aim to better understand the cause of MS, a demyelinating and neurodegenerative disease of the CNS, several investigations defined and quantified complement compounds in the blood circulation and CSF. In relation to the inflammatory activity of MS, to define potential biomarkers of the various MS disease forms, levels of C3, C4, and C9 were mostly investigated, providing convincing evidence of the role of complement compounds in MS disease development. The data obtained from various cohorts of patients, however, generated controversies. Indeed, early studies in patients with progressive MS revealed elevated levels of C4 in MS-serum and reduced C4 levels in MS-CSF (Jans et al., 1984). These findings were, however, not supported by others (Jongen et al., 2000). A more recent study defined elevated plasma C4a levels and elevated C3 levels in CSF of patients with active relapsing-remitting MS (RRMS) potentially providing furthermore follow-up markers for therapeutic efficacy (Tatomir et al., 2017). The levels of C9 compound and terminal complement complex (MAC) in CSF and/or blood also give heterogeneous quantitative data found to be reduced, unchanged, or increased (Ingram et al., 2009). Differences in the presence of the complement compounds in the CSF and blood circulation might be related to the modulation of the BBB by the inflammatory disease activity at the various disease MS forms. Histophathological post-mortem investigations of MS brain tissues revealed complement deposition and activation. Activated microglia is commonly observed in contact with axons suffering from demyelination. In brain tissue from patients with progressive MS, a combined immunohistopathology and *in situ* hybridization study showed the local expression of compounds of the complement activation pathways. Both transcripts for C1qA, activation fragment and opsonin C3b, and immunostained proteins C1q of the classical complement pathway and the activation CFB-fragment Bb of the alternative complement pathway were observed in neurons and/or glia within and in the vicinity of cortical and deep gray matter lesions. Furthermore, activated microglia expressing complement *anaphylatoxin receptor* were observed in these lesions in post-mortem brain tissue (Watkins et al., 2016). The deposits of activated C3 fragment on microglia in such chronic cortical lesions, but not in acute disease, indicate that C3 could function as a mediator for the removal of damaged nervous cells in the MS animal model of the relapsing experimental autoimmune encephalomyelitis (EAE) (Michailidou et al., 2017). The formation of MAC as a final complement product has been reported in acute and chronic white matter lesions of MS and would have a direct impact on nervous tissue destruction (Compston et al., 1989; Storch et al., 1998). Many experimental animal studies of MS support the complement-mediated role of nervous tissue degeneration. Further evidence for MAC in the inflammatory disease progression is documented in the EAE mouse model by the systemic curative administration of MAC inhibitors that prevents relapses after a first clinical attack (Michailidou et al., 2018). In EAE gray matter neurodegeneration, a significant synapse loss in the CA1 statum radiatum of the hippocampus reflecting cognitive impairment is caused by increased complement production and deposition of Cq1 and C3d that could make

TABLE 1 | Summary of complement effects on the TBI process in animals models and human studies.

Human	Complement analysis	Complement levels	References
Severe TBI	C3/CFB	↑CSF	Kossmann et al., 1997
Severe TBI	C3/C1q/C4	↑CSF	Stahel et al., 1998
Severe TBI	C5b9	↑CSF	Stahel et al., 2001
Severe TBI	C3/C9	↑Plasma	Bao et al., 2018
Severe TBI	MBL	↑Plasma	Osthoff et al., 2017
Animal models	**Complement target**	**Complement biologic effects**	**References**
Cortical impact (severe TBI)	C9/CFB	↑Serum	Thelin et al., 2018
Cortical contusion (severe TBI)	C3	↑Deposits (peri-lesion tissue)	Bellander et al., 1996
Cortical contusion (severe TBI)	C9	↑Deposits (damaged neurons)	Bellander et al., 1996
Intra-cerebral hemorrhage	*C3*$^{-/-}$ mice	↓Brain edema ↓Microglia activation/infiltration	Sewell et al., 2004; Yang et al., 2006
Severe TBI swine resuscitation	CD59/C1q	↓Complement system activation associated to a decrease of lesion size	Dekker et al., 2014a,b; Bambakidis et al., 2016
Cortical impact (severe TBI)	CD59$^{-/-}$ mice	↑Neuronal cell death	Stahel et al., 2009
Severe closed head injury mice	C6 antisense oligonucleotide Or C5 convertase inhibition	↓C5b9 deposits/axon loss ↓Microglia/macrophage accumulation ↓Neuronal cells death ↑Neurologic perfomances	Fluiter et al., 2014
Cortical impact (severe TBI)	C3 cleavage inhibition	↓Microglial/astrocyte activations ↓C3 deposits/neuron cells death ↑Cognitive/functional recovery	Rich et al., 2016; Alawieh et al., 2018
Focal trauma (severe TBI)	*cfb*$^{-/-}$ mice	↓Neuronal cell death	Leinhase et al., 2006
Focal trauma (severe TBI)	Anti-CFB antibody	↓Inflammation/cell death	Leinhase et al., 2007
Cortical impact (severe TBI)	C1q inhibitor	↓Cognitive dysfunction/contusion volumes	Longhi et al., 2009
Cortical impact (severe TBI)	MBL	↑MBL deposits (injured cortex)	Longhi et al., 2014
Cortical impact (severe TBI)	*mbl*$^{-/-}$ mice	↑Cortical cell death	Longhi et al., 2014

CSF, CerebroSpinal Fluid; MBL, Mannose Binding Lectin protein.

synapses vulnerable to phagocytosis by microglia. In particular, C3 mediates microglial activation and EAE motor impairments (Hammond et al., 2019). Altogether, there is convincing evidence that the complement activation is involved in MS disease development and the cerebral complement over-activation in inflammatory CNS lesions may be essential for the irreversible progression of MS. The knowledge gathered on the role of the complement pathway activation in MS patients and animal model of MS can be useful for understanding the chronic brain disorders post-TBI. The presence of the complement in serum can serve as a biomarker in TBI patients, and the potential inhibition of the complement can be a therapeutic strategy for the long-term consequences of TBI.

CONCLUDING REMARKS

Complement pathway activation is present early after TBI and can contribute to the development of the secondary injuries by inducing neuronal cell loss and synapse pruning (**Table 1**). Very likely, the complement activation is still present in the long term after TBI (**Table 1**). The knowledge on complement activation in AD and MS strongly suggests that the activation of the complement pathways in the long term after TBI could be an interesting mechanism in order to develop new therapeutic approaches for chronic TBI. It is possible that the pruning of synapses by complement-mediated microglia activation causes long-term neurological handicaps including cognitive impairment in various models of neurodegenerative diseases such as Alzheimer's disease, viral encephalitis, TBI, and MS and potentially contributes to schizophrenia (Stevens et al., 2007; Paolicelli et al., 2011; Ingram et al., 2014; Hong et al., 2016; Sekar et al., 2016; Vasek et al., 2016; Alawieh et al., 2018; Hammond et al., 2019). Therefore, inhibition of the long-term complement activation could improve TBI outcomes.

AUTHOR CONTRIBUTIONS

VD and JB contributed to the design and concept of the review manuscript. VD, KP, and JB wrote and revised the manuscript.

ACKNOWLEDGMENTS

This work was supported by grants from the Eranet neuron consortia TRAINS (JB), TRAIL-Labex ANR (JB), ANR-17-CE37-0011, Nanospace (JB), INSERM (VD and KP), and ANR (KP).

REFERENCES

Abbott, N. J., Rönnbäck, L., and Hansson, E. (2006). Astrocyte-endothelial interactions at the blood-brain barrier. *Nat. Rev. Neurosci.* 7, 41–53. doi: 10.1038/nrn1824

Abdul-Muneer, P. M., Schuetz, H., Wang, F., Skotak, M., Jones, J., Gorantla, S., et al. (2013). Induction of oxidative and nitrosative damage leads to cerebrovascular inflammation in an animal model of mild traumatic brain injury induced by primary blast. *Free Radic. Biol. Med.* 60, 282–291. doi: 10.1016/j.freeradbiomed.2013.02.029

Alawieh, A., Langley, E. F., Weber, S., Adkins, D., and Tomlinson, S. (2018). Identifying the role of complement in triggering neuroinflammation after traumatic brain injury. *J. Neurosci.* 38, 2519–2532. doi: 10.1523/JNEUROSCI.2197-17.2018

An, X.-Q., Xi, W., Gu, C.-Y., and Huang, X. (2018). Complement protein C5a enhances the β-amyloid-induced neuro-inflammatory response in microglia in Alzheimer's disease. *Med. Sci.* 34, 116–120. doi: 10.1051/medsci/201834f120

Armstead, W. M., and Kreipke, C. W. (2011). Endothelin-1 is upregulated after traumatic brain injury: a cross-species, cross-model analysis. *Neurol. Res.* 33, 133–136. doi: 10.1179/016164111X12881719352174

Armstead, W. M., and Raghupathi, R. (2011). Endothelin and the neurovascular unit in pediatric traumatic brain injury. *Neurol. Res.* 33, 127–132. doi: 10.1179/016164111X12881719352138

Badaut, J., Adami, A., Huang, L., and Obenaus, A. (2019). Noninvasive magnetic resonance imaging stratifies injury severity in a rodent model of male juvenile traumatic brain injury. *J. Neurosci. Res.* doi: 10.1002/jnr.24415. [Epub ahead of print].

Badaut, J., Ajao, D. O., Sorensen, D. W., Fukuda, A. M., and Pellerin, L. (2015). Caveolin expression changes in the neurovascular unit after juvenile traumatic brain injury: signs of blood-brain barrier healing? *Neuroscience* 285, 215–226. doi: 10.1016/j.neuroscience.2014.10.035

Badaut, J., Fukuda, A. M., Jullienne, A., and Petry, K. G. (2014). Aquaporin and brain diseases. *Biochim. Biophys. Acta* 1840, 1554–1565. doi: 10.1016/j.bbagen.2013.10.032

Baethmann, A., Maier-Hauff, K., Kempski, O., Unterberg, A., Wahl, M., and Schürer, L. (1988). Mediators of brain edema and secondary brain damage. *Crit. Care Med.* 16, 972–978. doi: 10.1097/00003246-198810000-00008

Bambakidis, T., Dekker, S. E., Sillesen, M., Liu, B., Johnson, C. N., Jin, G., et al. (2016). Resuscitation with valproic acid alters inflammatory genes in a porcine model of combined traumatic brain injury and hemorrhagic shock. *J. Neurotrauma* 33, 1514–1521. doi: 10.1089/neu.2015.4163

Bao, W., He, F., Yu, L., Gao, J., Meng, F., Ding, Y., et al. (2018). Complement cascade on severe traumatic brain injury patients at the chronic unconscious stage: implication for pathogenesis. *Expert Rev. Mol. Diagn.* 18, 761–766. doi: 10.1080/14737159.2018.1471985

Bellander, B. M., von Holst, H., Fredman, P., and Svensson, M. (1996). Activation of the complement cascade and increase of clusterin in the brain following a cortical contusion in the adult rat. *J. Neurosurg.* 85, 468–475. doi: 10.3171/jns.1996.85.3.0468

Bouma, G. J., Muizelaar, J. P., Choi, S. C., Newlon, P. G., and Young, H. F. (1991). Cerebral circulation and metabolism after severe traumatic brain injury: the elusive role of ischemia. *J. Neurosurg.* 75, 685–693. doi: 10.3171/jns.1991.75.5.0685

Bouma, G. J., Muizelaar, J. P., Stringer, W. A., Choi, S. C., Fatouros, P., and Young, H. F. (1992). Ultra-early evaluation of regional cerebral blood flow in severely head-injured patients using xenon-enhanced computerized tomography. *J. Neurosurg.* 77, 360–368. doi: 10.3171/jns.1992.77.3.0360

Bradt, B. M., Kolb, W. P., and Cooper, N. R. (1998). Complement-dependent proinflammatory properties of the Alzheimer's disease beta-peptide. *J. Exp. Med.* 188, 431–438. doi: 10.1084/jem.188.3.431

Brubaker, W. D., Crane, A., Johansson, J. U., Yen, K., Garfinkel, K., Mastroeni, D., et al. (2017). Peripheral complement interactions with amyloid β peptide: erythrocyte clearance mechanisms. *Alzheimers Dement.* 13, 1397–1409. doi: 10.1016/j.jalz.2017.03.010

Bryan, R. M., Cherian, L., and Robertson, C. (1995). Regional cerebral blood flow after controlled cortical impact injury in rats. *Anesth. Analg.* 80, 687–695. doi: 10.1213/00000539-199504000-00007

Burda, J. E., Bernstein, A. M., and Sofroniew, M. V. (2016). Astrocyte roles in traumatic brain injury. *Exp. Neurol. 275 Pt* 3, 305–315. doi: 10.1016/j.expneurol.2015.03.020

Burda, J. E., and Sofroniew, M. V. (2014). Reactive gliosis and the multicellular response to CNS damage and disease. *Neuron* 81, 229–248. doi: 10.1016/j.neuron.2013.12.034

Chen, Y., and Swanson, R. A. (2003). Astrocytes and brain injury. *J. Cereb. Blood Flow Metab.* 23, 137–149. doi: 10.1097/01.WCB.0000044631.80210.3C

Chodobski, A., Zink, B. J., and Szmydynger-Chodobska, J. (2011). Blood-brain barrier pathophysiology in traumatic brain injury. *Transl Stroke Res.* 2, 492–516. doi: 10.1007/s12975-011-0125-x

Cirrito, J. R., Deane, R., Fagan, A. M., Spinner, M. L., Parsadanian, M., Finn, M. B., et al. (2005). P-glycoprotein deficiency at the blood-brain barrier increases amyloid-beta deposition in an Alzheimer disease mouse model. *J. Clin. Invest.* 115, 3285–3290. doi: 10.1172/JCI25247

Compston, D. A., Morgan, B. P., Campbell, A. K., Wilkins, P., Cole, G., Thomas, N. D., et al. (1989). Immunocytochemical localization of the terminal complement complex in multiple sclerosis. *Neuropathol. Appl. Neurobiol.* 15, 307–316. doi: 10.1111/j.1365-2990.1989.tb01231.x

Constam, D. B., Philipp, J., Malipiero, U. V., ten Dijke, P., Schachner, M., and Fontana, A. (1992). Differential expression of transforming growth factor-beta 1, -beta 2, and -beta 3 by glioblastoma cells, astrocytes, and microglia. *J. Immunol.* 148, 1404–1410.

Corso, P., Finkelstein, E., Miller, T., Fiebelkorn, I., and Zaloshnja, E. (2006). Incidence and lifetime costs of injuries in the United States. *Inj. Prev.* 12, 212–218. doi: 10.1136/ip.2005.010983

Crehan, H., Holton, P., Wray, S., Pocock, J., Guerreiro, R., and Hardy, J. (2012). Complement receptor 1 (CR1) and Alzheimer's disease. *Immunobiology* 217, 244–250. doi: 10.1016/j.imbio.2011.07.017

Cybulsky, A. V., Monge, J. C., Papillon, J., and McTavish, A. J. (1995). Complement C5b-9 activates cytosolic phospholipase A2 in glomerular epithelial cells. *Am. J. Physiol.* 269, F739-749. doi: 10.1152/ajprenal.1995.269.5.F739

Cybulsky, A. V., Takano, T., Papillon, J., and McTavish, A. J. (1999). Complement C5b-9 induces receptor tyrosine kinase transactivation in glomerular epithelial cells. *Am. J. Pathol.* 155, 1701–1711. doi: 10.1016/S0002-9440(10)65485-5

Dekker, S. E., Bambakidis, T., Sillesen, M., Liu, B., Johnson, C. N., Jin, G., et al. (2014a). Effect of pharmacologic resuscitation on the brain gene expression profiles in a swine model of traumatic brain injury and hemorrhage. *J Trauma Acute Care Surg.* 77, 906–912. doi: 10.1097/TA.0000000000000345

Dekker, S. E., Sillesen, M., Bambakidis, T., Andjelkovic, A. V., Jin, G., Liu, B., et al. (2014b). Treatment with a histone deacetylase inhibitor, valproic acid, is associated with increased platelet activation in a large animal model of traumatic brain injury and hemorrhagic shock. *J. Surg. Res.* 190, 312–318. doi: 10.1016/j.jss.2014.02.049

DeWitt, D. S., and Prough, D. S. (2003). Traumatic cerebral vascular injury: the effects of concussive brain injury on the cerebral vasculature. *J. Neurotrauma* 20, 795–825. doi: 10.1089/089771503322385755

Faden, A. I., and Loane, D. J. (2015). Chronic neurodegeneration after traumatic brain injury: Alzheimer disease, chronic traumatic encephalopathy, or persistent neuroinflammation? *Neurotherapeutics* 12, 143–150. doi: 10.1007/s13311-014-0319-5

Fann, J. R., Ribe, A. R., Pedersen, H. S., Fenger-Grøn, M., Christensen, J., Benros, M. E., et al. (2018). Long-term risk of dementia among people with traumatic brain injury in Denmark: a population-based observational cohort study. *Lancet Psychiatry* 5, 424–431. doi: 10.1016/S2215-0366(18)30065-8

Faul, M., Xu, L., Wald, M. M., and Coronado, V. G. (2010). *Traumatic Brain Injury in the United States: Emergency Department Visits, Hospitalizations, and Deaths, 2002–2006*. Atlanta, GA: CDC.

Fluiter, K., Opperhuizen, A. L., Morgan, B. P., Baas, F., and Ramaglia, V. (2014). Inhibition of the membrane attack complex of the complement system reduces secondary neuroaxonal loss and promotes neurologic recovery after traumatic brain injury in mice. *J. Immunol.* 192, 2339–2348. doi: 10.4049/jimmunol.1302793

Fosbrink, M., Niculescu, F., and Rus, H. (2005). The role of c5b-9 terminal complement complex in activation of the cell cycle and transcription. *Immunol. Res.* 31, 37–46. doi: 10.1385/IR:31:1:37

Francis, K., van Beek, J., Canova, C., Neal, J. W., and Gasque, P. (2003). Innate immunity and brain inflammation: the key role of complement. *Expert Rev. Mol. Med.* 5, 1–19. doi: 10.1017/S1462399403006252

Fukuda, A. M., and Badaut, J. (2012). Aquaporin 4: a player in cerebral edema and neuroinflammation. *J Neuroinflammation* 9:279. doi: 10.1186/1742-2094-9-279

Gatto, R., Chauhan, M., and Chauhan, N. (2015). Anti-edema effects of rhEpo in experimental traumatic brain injury. *Restor. Neurol. Neurosci.* 33, 927–941. doi: 10.3233/RNN-150577

Gatto, R. G., Amin, M. Y., Deyoung, D., Hey, M., Mareci, T. H., and Magin, R. L. (2018). Ultra-high field diffusion MRI reveals early axonal pathology in spinal cord of ALS mice. *Transl. Neurodegener* 7:20. doi: 10.1186/s40035-018-0122-z

Golding, E. M. (2002). Sequelae following traumatic brain injury. The cerebrovascular perspective. *Brain Res. Brain Res. Rev.* 38, 377–388. doi: 10.1016/S0165-0173(02)00141-8

Gustavsson, A., Svensson, M., Jacobi, F., Allgulander, C., Alonso, J., Beghi, E., et al. (2011). Cost of disorders of the brain in Europe 2010. *Eur. Neuropsychopharmacol.* 21, 718–779. doi: 10.1016/j.euroneuro.2011.08.008

Haley, M. J., and Lawrence, C. B. (2017). The blood-brain barrier after stroke: structural studies and the role of transcytotic vesicles. *J. Cereb. Blood Flow Metab.* 37, 456–470. doi: 10.1177/0271678X16629976

Hammond, J. W., Bellizzi, M. J., Ware, C., Qiu, W. Q., Saminathan, P., Li, H., et al. (2019). Complement-dependent synapse loss and microgliosis in a mouse model of multiple sclerosis. *bioRxiv [preprint]* 720649. doi: 10.1101/720649

Hay, J. R., Johnson, V. E., Young, A. M. H., Smith, D. H., and Stewart, W. (2015). Blood-brain barrier disruption is an early event that may persist for many years after traumatic brain injury in humans. *J. Neuropathol. Exp. Neurol.* 74, 1147–1157. doi: 10.1093/jnen/74.12.1147

Hayward, N. M. E. A., Immonen, R., Tuunanen, P. I., Ndode-Ekane, X. E., Gröhn, O., and Pitkänen, A. (2010). Association of chronic vascular changes with functional outcome after traumatic brain injury in rats. *J. Neurotrauma* 27, 2203–2219. doi: 10.1089/neu.2010.1448

Himanen, L., Portin, R., Hämäläinen, P., Hurme, S., Hiekkanen, H., and Tenovuo, O. (2011). Risk factors for reduced survival after traumatic brain injury: a 30-year follow-up study. *Brain Inj.* 25, 443–452. doi: 10.3109/02699052.2011.556580

Hoffman, S. W., Moore, S., and Ellis, E. F. (1997). Isoprostanes: free radical-generated prostaglandins with constrictor effects on cerebral arterioles. *Stroke* 28, 844–849. doi: 10.1161/01.STR.28.4.844

Hoffman, S. W., Rzigalinski, B. A., Willoughby, K. A., and Ellis, E. F. (2000). Astrocytes generate isoprostanes in response to trauma or oxygen radicals. *J. Neurotrauma* 17, 415–420. doi: 10.1089/neu.2000.17.415

Hong, S., Beja-Glasser, V. F., Nfonoyim, B. M., Frouin, A., Li, S., Ramakrishnan, S., et al. (2016). Complement and microglia mediate early synapse loss in Alzheimer mouse models. *Science* 352, 712–716. doi: 10.1126/science.aad8373

Howarth, C. (2014). The contribution of astrocytes to the regulation of cerebral blood flow. *Front. Neurosci.* 8:103. doi: 10.3389/fnins.2014.00103

Iadecola, C. (2004). Neurovascular regulation in the normal brain and in Alzheimer's disease. *Nat. Rev. Neurosci.* 5, 347–360. doi: 10.1038/nrn1387

Ingram, G., Hakobyan, S., Robertson, N. P., and Morgan, B. P. (2009). Complement in multiple sclerosis: its role in disease and potential as a biomarker. *Clin. Exp. Immunol.* 155, 128–139. doi: 10.1111/j.1365-2249.2008.03830.x

Ingram, G., Loveless, S., Howell, O. W., Hakobyan, S., Dancey, B., Harris, C. L., et al. (2014). Complement activation in multiple sclerosis plaques: an immunohistochemical analysis. *Acta Neuropathol. Commun.* 2:53. doi: 10.1186/2051-5960-2-53

Jans, H., Heltberg, A., Zeeberg, I., Kristensen, J. H., Fog, T., and Raun, N. E. (1984). Immune complexes and the complement factors C4 and C3 in cerebrospinal fluid and serum from patients with chronic progressive multiple sclerosis. *Acta Neurol. Scand.* 69, 34–38. doi: 10.1111/j.1600-0404.1984.tb07777.x

Johnson, V. E., Stewart, W., and Smith, D. H. (2010). Traumatic brain injury and amyloid-β pathology: a link to Alzheimer's disease? *Nat. Rev. Neurosci.* 11, 361–370. doi: 10.1038/nrn2808

Jongen, P. J., Doesburg, W. H., Ibrahim-Stappers, J. L., Lemmens, W. A., Hommes, O. R., and Lamers, K. J. (2000). Cerebrospinal fluid C3 and C4 indexes in immunological disorders of the central nervous system. *Acta Neurol. Scand.* 101, 116–121. doi: 10.1034/j.1600-0404.2000.101002116.x

Jullienne, A., Obenaus, A., Ichkova, A., Savona-Baron, C., Pearce, W. J., and Badaut, J. (2016). Chronic cerebrovascular dysfunction after traumatic brain injury. *J. Neurosci. Res.* 94, 609–622. doi: 10.1002/jnr.23732

Jullienne, A., Roberts, J. M., Pop, V., Paul Murphy, M., Head, E., Bix, G. J., et al. (2014). Juvenile traumatic brain injury induces long-term perivascular matrix changes alongside amyloid-beta accumulation. *J. Cereb. Blood Flow Metab.* 34, 1637–1645. doi: 10.1038/jcbfm.2014.124

Kaczorowski, S. L., Schiding, J. K., Toth, C. A., and Kochanek, P. M. (1995). Effect of soluble complement receptor-1 on neutrophil accumulation after traumatic brain injury in rats. *J. Cereb. Blood Flow Metab.* 15, 860–864. doi: 10.1038/jcbfm.1995.107

Keightley, M. L., Sinopoli, K. J., Davis, K. D., Mikulis, D. J., Wennberg, R., Tartaglia, M. C., et al. (2014). Is there evidence for neurodegenerative change following traumatic brain injury in children and youth? A scoping review. *Front. Hum. Neurosci.* 8:139. doi: 10.3389/fnhum.2014.00139

Knowland, D., Arac, A., Sekiguchi, K. J., Hsu, M., Lutz, S. E., Perrino, J., et al. (2014). Stepwise recruitment of transcellular and paracellular pathways underlies blood-brain barrier breakdown in stroke. *Neuron* 82, 603–617. doi: 10.1016/j.neuron.2014.03.003

Kossmann, T., Stahel, P. F., Morganti-Kossmann, M. C., Jones, J. L., and Barnum, S. R. (1997). Elevated levels of the complement components C3 and factor B in ventricular cerebrospinal fluid of patients with traumatic brain injury. *J. Neuroimmunol.* 73, 63–69. doi: 10.1016/S0165-5728(96)00164-6

Lambert, J.-C., Heath, S., Even, G., Campion, D., Sleegers, K., Hiltunen, M., et al. (2009). Genome-wide association study identifies variants at CLU and CR1 associated with Alzheimer's disease. *Nat. Genet.* 41, 1094–1099. doi: 10.1038/ng.439

Lashkari, K., Teague, G., Chen, H., Lin, Y.-Q., Kumar, S., McLaughlin, M. M., et al. (2018). A monoclonal antibody targeting amyloid β (Aβ) restores complement factor I bioactivity: potential implications in age-related macular degeneration and Alzheimer's disease. *PLoS ONE* 13:e0195751. doi: 10.1371/journal.pone.0195751

Leinhase, I., Holers, V. M., Thurman, J. M., Harhausen, D., Schmidt, O. I., Pietzcker, M., et al. (2006). Reduced neuronal cell death after experimental brain injury in mice lacking a functional alternative pathway of complement activation. *BMC Neurosci.* 7:55. doi: 10.1186/1471-2202-7-55

Leinhase, I., Rozanski, M., Harhausen, D., Thurman, J. M., Schmidt, O. I., Hossini, A. M., et al. (2007). Inhibition of the alternative complement activation pathway in traumatic brain injury by a monoclonal anti-factor B antibody: a randomized placebo-controlled study in mice. *J Neuroinflammation* 4:13. doi: 10.1186/1742-2094-4-13

Lepelletier, F.-X., Mann, D. M. A., Robinson, A. C., Pinteaux, E., and Boutin, H. (2017). Early changes in extracellular matrix in Alzheimer's disease. *Neuropathol. Appl. Neurobiol.* 43, 167–182. doi: 10.1111/nan.12295

Lian, H., Yang, L., Cole, A., Sun, L., Chiang, A. C.-A., Fowler, S. W., et al. (2015). NFκB-activated astroglial release of complement C3 compromises neuronal morphology and function associated with Alzheimer's disease. *Neuron* 85, 101–115. doi: 10.1016/j.neuron.2014.11.018

Long, J. A., Watts, L. T., Li, W., Shen, Q., Muir, E. R., Huang, S., et al. (2015). The effects of perturbed cerebral blood flow and cerebrovascular reactivity on structural MRI and behavioral readouts in mild traumatic brain injury. *J. Cereb. Blood Flow Metab.* 35, 1852–1861. doi: 10.1038/jcbfm.2015.143

Longhi, L., Orsini, F., De Blasio, D., Fumagalli, S., Ortolano, F., Locatelli, M., et al. (2014). Mannose-binding lectin is expressed after clinical and experimental traumatic brain injury and its deletion is protective. *Crit. Care Med.* 42, 1910–1918. doi: 10.1097/CCM.0000000000000399

Longhi, L., Perego, C., Ortolano, F., Zanier, E. R., Bianchi, P., Stocchetti, N., et al. (2009). C1-inhibitor attenuates neurobehavioral deficits and reduces contusion volume after controlled cortical impact brain injury in mice. *Crit. Care Med.* 37, 659–665. doi: 10.1097/CCM.0b013e318195998a

Maas, A. I. R., Menon, D. K., Steyerberg, E. W., Citerio, G., Lecky, F., Manley, G. T., et al. (2015). Collaborative European NeuroTrauma Effectiveness Research in Traumatic Brain Injury (CENTER-TBI): a prospective longitudinal observational study. *Neurosurgery* 76, 67–80. doi: 10.1227/NEU.0000000000000575

Maas, A. I. R., Stocchetti, N., and Bullock, R. (2008). Moderate and severe traumatic brain injury in adults. *Lancet Neurol.* 7, 728–741. doi: 10.1016/S1474-4422(08)70164-9

Manek, R., Moghieb, A., Yang, Z., Kumar, D., Kobessiy, F., Sarkis, G. A., et al. (2018). Protein biomarkers and neuroproteomics characterization of microvesicles/exosomes from human cerebrospinal fluid following traumatic brain injury. *Mol. Neurobiol.* 55, 6112–6128. doi: 10.1007/s12035-017-0821-y

Maneshi, M. M., Sachs, F., and Hua, S. Z. (2015). A threshold shear force for calcium influx in an astrocyte model of traumatic brain injury. *J. Neurotrauma* 32, 1020–1029. doi: 10.1089/neu.2014.3677

McMillan, T. M., and Teasdale, G. M. (2007). Death rate is increased for at least 7 years after head injury: a prospective study. *Brain* 130, 2520–2527. doi: 10.1093/brain/awm185

Michailidou, I., Jongejan, A., Vreijling, J. P., Georgakopoulou, T., de Wissel, M. B., Wolterman, R. A., et al. (2018). Systemic inhibition of the membrane attack complex impedes neuroinflammation in chronic relapsing experimental autoimmune encephalomyelitis. *Acta Neuropathol. Commun.* 6:36. doi: 10.1186/s40478-018-0536-y

Michailidou, I., Naessens, D. M. P., Hametner, S., Guldenaar, W., Kooi, E.-J., Geurts, J. J. G., et al. (2017). Complement C3 on microglial clusters in multiple sclerosis occur in chronic but not acute disease: implication for disease pathogenesis. *Glia* 65, 264–277. doi: 10.1002/glia.23090

Morganti-Kossmann, M. C., Hans, V. H., Lenzlinger, P. M., Dubs, R., Ludwig, E., Trentz, O., et al. (1999). TGF-beta is elevated in the CSF of patients with severe traumatic brain injuries and parallels blood-brain barrier function. *J. Neurotrauma* 16, 617–628. doi: 10.1089/neu.1999.16.617

Nag, S., Venugopalan, R., and Stewart, D. J. (2007). Increased caveolin-1 expression precedes decreased expression of occludin and claudin-5 during blood-brain barrier breakdown. *Acta Neuropathol.* 114, 459–469. doi: 10.1007/s00401-007-0274-x

Osthoff, M., Walder, B., Delhumeau, C., Trendelenburg, M., and Turck, N. (2017). Association of lectin pathway protein levels and genetic variants early after injury with outcomes after severe traumatic brain injury: a prospective cohort study. *J. Neurotrauma* 34, 2560–2566. doi: 10.1089/neu.2016.4941

Ostrow, L. W., Langan, T. J., and Sachs, F. (2000). Stretch-induced endothelin-1 production by astrocytes. *J. Cardiovasc. Pharmacol.* 36, S274-277. doi: 10.1097/00005344-200036001-00081

Panesar, M., Papillon, J., McTavish, A. J., and Cybulsky, A. V. (1997). Activation of phospholipase A2 by complement C5b-9 in glomerular epithelial cells. *J. Immunol.* 159, 3584–3594.

Paolicelli, R. C., Bolasco, G., Pagani, F., Maggi, L., Scianni, M., Panzanelli, P., et al. (2011). Synaptic pruning by microglia is necessary for normal brain development. *Science* 333, 1456–1458. doi: 10.1126/science.1202529

Petraglia, A. L., Dashnaw, M. L., Turner, R. C., and Bailes, J. E. (2014). Models of mild traumatic brain injury: translation of physiological and anatomic injury. *Neurosurgery* 75 (Suppl. 4), S34–S49. doi: 10.1227/NEU.0000000000000472

Petrov, T., and Rafols, J. A. (2001). Acute alterations of endothelin-1 and iNOS expression and control of the brain microcirculation after head trauma. *Neurol. Res.* 23, 139–143. doi: 10.1179/016164101101198479

Plesnila, N. (2016). The immune system in traumatic brain injury. *Curr. Opin. Pharmacol.* 26, 110–117. doi: 10.1016/j.coph.2015.10.008

Plesnila, N., Friedrich, D., Eriskat, J., Baethmann, A., and Stoffel, M. (2003). Relative cerebral blood flow during the secondary expansion of a cortical lesion in rats. *Neurosci. Lett.* 345, 85–88. doi: 10.1016/S0304-3940(03)00396-3

Pop, V., and Badaut, J. (2011). A neurovascular perspective for long-term changes after brain trauma. *Transl Stroke Res.* 2, 533–545. doi: 10.1007/s12975-011-0126-9

Pop, V., Sorensen, D. W., Kamper, J. E., Ajao, D. O., Murphy, M. P., Head, E., et al. (2013). Early brain injury alters the blood-brain barrier phenotype in parallel with β-amyloid and cognitive changes in adulthood. *J. Cereb. Blood Flow Metab.* 33, 205–214. doi: 10.1038/jcbfm.2012.154

Povlishock, J. T., Becker, D. P., Sullivan, H. G., and Miller, J. D. (1978). Vascular permeability alterations to horseradish peroxidase in experimental brain injury. *Brain Res.* 153, 223–239. doi: 10.1016/0006-8993(78)90404-3

Prins, M. L., and Hovda, D. A. (2003). Developing experimental models to address traumatic brain injury in children. *J. Neurotrauma* 20, 123–137. doi: 10.1089/08977150360547053

Rafols, J. A., Kreipke, C. W., and Petrov, T. (2007). Alterations in cerebral cortex microvessels and the microcirculation in a rat model of traumatic brain injury: a correlative EM and laser Doppler flowmetry study. *Neurol. Res.* 29, 339–347. doi: 10.1179/016164107X204648

Raz, L., Knoefel, J., and Bhaskar, K. (2016). The neuropathology and cerebrovascular mechanisms of dementia. *J. Cereb. Blood Flow Metab.* 36, 172–186. doi: 10.1038/jcbfm.2015.164

Rich, M. C., Keene, C. N., Neher, M. D., Johnson, K., Yu, Z.-X., Ganivet, A., et al. (2016). Site-targeted complement inhibition by a complement receptor 2-conjugated inhibitor (mTT30) ameliorates post-injury neuropathology in mouse brains. *Neurosci. Lett.* 617, 188–194. doi: 10.1016/j.neulet.2016.02.025

Rodriguez-Grande, B., Obenaus, A., Ichkova, A., Aussudre, J., Bessy, T., Barse, E., et al. (2018). Gliovascular changes precede white matter damage and long-term disorders in juvenile mild closed head injury. *Glia* 66, 1663–1677. doi: 10.1002/glia.23336

Ruseva, M. M., Ramaglia, V., Morgan, B. P., and Harris, C. L. (2015). An anticomplement agent that homes to the damaged brain and promotes recovery after traumatic brain injury in mice. *Proc. Natl. Acad. Sci. U.S.A.* 112, 14319–14324. doi: 10.1073/pnas.1513698112

Rzigalinski, B. A., Weber, J. T., Willoughby, K. A., and Ellis, E. F. (1998). Intracellular free calcium dynamics in stretch-injured astrocytes. *J. Neurochem.* 70, 2377–2385. doi: 10.1046/j.1471-4159.1998.70062377.x

Schmidt, O. I., Heyde, C. E., Ertel, W., and Stahel, P. F. (2005). Closed head injury–an inflammatory disease? *Brain Res. Brain Res. Rev.* 48, 388–399. doi: 10.1016/j.brainresrev.2004.12.028

Sekar, A., Bialas, A. R., de Rivera, H., Davis, A., Hammond, T. R., Kamitaki, N., et al. (2016). Schizophrenia risk from complex variation of complement component 4. *Nature* 530, 177–183. doi: 10.1038/nature16549

Sewell, D. L., Nacewicz, B., Liu, F., Macvilay, S., Erdei, A., Lambris, J. D., et al. (2004). Complement C3 and C5 play critical roles in traumatic brain cryoinjury: blocking effects on neutrophil extravasation by C5a receptor antagonist. *J. Neuroimmunol.* 155, 55–63. doi: 10.1016/j.jneuroim.2004.06.003

Shen, W., Li, S., Chung, S. H., Zhu, L., Stayt, J., Su, T., et al. (2011). Tyrosine phosphorylation of VE-cadherin and claudin-5 is associated with TGF-β1-induced permeability of centrally derived vascular endothelium. *Eur. J. Cell Biol.* 90, 323–332. doi: 10.1016/j.ejcb.2010.10.013

Shetty, A. K., Mishra, V., Kodali, M., and Hattiangady, B. (2014). Blood brain barrier dysfunction and delayed neurological deficits in mild traumatic brain injury induced by blast shock waves. *Front. Cell Neurosci.* 8:232. doi: 10.3389/fncel.2014.00404

Silverberg, G. D., Messier, A. A., Miller, M. C., Machan, J. T., Majmudar, S. S., Stopa, E. G., et al. (2010). Amyloid efflux transporter expression at the blood-brain barrier declines in normal aging. *J. Neuropathol. Exp. Neurol.* 69, 1034–1043. doi: 10.1097/NEN.0b013e3181f46e25

Smith, D. H., Johnson, V. E., and Stewart, W. (2013). Chronic neuropathologies of single and repetitive TBI: substrates of dementia? *Nat. Rev. Neurol.* 9, 211–221. doi: 10.1038/nrneurol.2013.29

Sofroniew, M. V. (2009). Molecular dissection of reactive astrogliosis and glial scar formation. *Trends Neurosci.* 32, 638–647. doi: 10.1016/j.tins.2009.08.002

Sofroniew, M. V. (2014). Multiple roles for astrocytes as effectors of cytokines and inflammatory mediators. *Neuroscientist* 20, 160–172. doi: 10.1177/1073858413504466

Sofroniew, M. V., and Vinters, H. V. (2010). Astrocytes: biology and pathology. *Acta Neuropathol.* 119, 7–35. doi: 10.1007/s00401-009-0619-8

Stahel, P. F., and Barnum, S. R. (2006). The role of the complement system in CNS inflammatory diseases. *Expert Rev. Clin. Immunol.* 2, 445–456. doi: 10.1586/1744666X.2.3.445

Stahel, P. F., Flierl, M. A., Morgan, B. P., Persigehl, I., Stoll, C., Conrad, C., et al. (2009). Absence of the complement regulatory molecule CD59a leads to exacerbated neuropathology after traumatic brain injury in mice. *J. Neuroinflammation* 6:2. doi: 10.1186/1742-2094-6-2

Stahel, P. F., Morganti-Kossmann, M. C., and Kossmann, T. (1998). The role of the complement system in traumatic brain injury. *Brain Res. Brain Res. Rev.* 27, 243–256. doi: 10.1016/S0165-0173(98)00015-0

Stahel, P. F., Morganti-Kossmann, M. C., Perez, D., Redaelli, C., Gloor, B., Trentz, O., et al. (2001). Intrathecal levels of complement-derived soluble membrane attack complex (sC5b-9) correlate with blood-brain barrier dysfunction in patients with traumatic brain injury. *J. Neurotrauma* 18, 773–781. doi: 10.1089/089771501316919139

Stevens, B., Allen, N. J., Vazquez, L. E., Howell, G. R., Christopherson, K. S., Nouri, N., et al. (2007). The classical complement cascade mediates CNS synapse elimination. *Cell* 131, 1164–1178. doi: 10.1016/j.cell.2007.10.036

Storch, M. K., Piddlesden, S., Haltia, M., Iivanainen, M., Morgan, P., and Lassmann, H. (1998). Multiple sclerosis: *in situ* evidence for antibody- and complement-mediated demyelination. *Ann. Neurol.* 43, 465–471. doi: 10.1002/ana.410430409

Sun, H., Liang, R., Yang, B., Zhou, Y., Liu, M., Fang, F., et al. (2016). Aquaporin-4 mediates communication between astrocyte and microglia: implications of neuroinflammation in experimental Parkinson's disease. *Neuroscience* 317, 65–75. doi: 10.1016/j.neuroscience.2016.01.003

Tatomir, A., Talpos-Caia, A., Anselmo, F., Kruszewski, A. M., Boodhoo, D., Rus, V., et al. (2017). The complement system as a biomarker of disease activity and response to treatment in multiple sclerosis. *Immunol. Res.* 65, 1103–1109. doi: 10.1007/s12026-017-8961-8

Thelin, E. P., Just, D., Frostell, A., Häggmark-Månberg, A., Risling, M., Svensson, M., et al. (2018). Protein profiling in serum after traumatic brain injury in rats reveals potential injury markers. *Behav. Brain Res.* 340, 71–80. doi: 10.1016/j.bbr.2016.08.058

Unterberg, A. W., Stover, J., Kress, B., and Kiening, K. L. (2004). Edema and brain trauma. *Neuroscience* 129, 1021–1029. doi: 10.1016/j.neuroscience.2004.06.046

Vasek, M. J., Garber, C., Dorsey, D., Durrant, D. M., Bollman, B., Soung, A., et al. (2016). A complement-microglial axis drives synapse loss during virus-induced memory impairment. *Nature* 534, 538–543. doi: 10.1038/nature18283

Villapol, S., Balarezo, M. G., Affram, K., Saavedra, J. M., and Symes, A. J. (2015). Neurorestoration after traumatic brain injury through angiotensin II receptor blockage. *Brain* 138, 3299–3315. doi: 10.1093/brain/awv172

Villapol, S., Byrnes, K. R., and Symes, A. J. (2014). Temporal dynamics of cerebral blood flow, cortical damage, apoptosis, astrocyte-vasculature interaction and astrogliosis in the pericontusional region after traumatic brain injury. *Front. Neurol.* 5:82. doi: 10.3389/fneur.2014.00082

Walport, M. J. (2001). Complement. First *of two parts. N. Engl. J. Med.* 344, 1058–1066. doi: 10.1056/NEJM200104053441406

Wang, X., Jung, J., Asahi, M., Chwang, W., Russo, L., Moskowitz, M. A., et al. (2000). Effects of matrix metalloproteinase-9 gene knock-out on morphological and motor outcomes after traumatic brain injury. *J. Neurosci.* 20, 7037–7042. doi: 10.1523/JNEUROSCI.20-18-07037.2000

Watkins, L. M., Neal, J. W., Loveless, S., Michailidou, I., Ramaglia, V., Rees, M. I., et al. (2016). Complement is activated in progressive multiple sclerosis cortical grey matter lesions. *J. Neuroinflammation* 13:161. doi: 10.1186/s12974-016-0611-x

Wei, E. P., Dietrich, W. D., Povlishock, J. T., Navari, R. M., and Kontos, H. A. (1980). Functional, morphological, and metabolic abnormalities of the cerebral microcirculation after concussive brain injury in cats. *Circ. Res.* 46, 37–47. doi: 10.1161/01.RES.46.1.37

Yang, C., Huang, X., Huang, X., Mai, H., Li, J., Jiang, T., et al. (2016). Aquaporin-4 and Alzheimer's Disease. *J. Alzheimers Dis.* 52, 391–402. doi: 10.3233/JAD-150949

Yang, S., Nakamura, T., Hua, Y., Keep, R. F., Younger, J. G., He, Y., et al. (2006). The role of complement C3 in intracerebral hemorrhage-induced brain injury. *J. Cereb. Blood Flow Metab.* 26, 1490–1495. doi: 10.1038/sj.jcbfm.9600305

Yeoh, S., Bell, E. D., and Monson, K. L. (2013). Distribution of blood-brain barrier disruption in primary blast injury. *Ann. Biomed. Eng.* 41, 2206–2214. doi: 10.1007/s10439-013-0805-7

Yoshino, A., Hovda, D. A., Kawamata, T., Katayama, Y., and Becker, D. P. (1991). Dynamic changes in local cerebral glucose utilization following cerebral conclusion in rats: evidence of a hyper- and subsequent hypometabolic state. *Brain Res.* 561, 106–119. doi: 10.1016/0006-8993(91)90755-K

Zhang, C., Chen, J., and Lu, H. (2015). Expression of aquaporin-4 and pathological characteristics of brain injury in a rat model of traumatic brain injury. *Mol. Med. Rep.* 12, 7351–7357. doi: 10.3892/mmr.2015.4372

Zhang, H., Adwanikar, H., Werb, Z., and Noble-Haeusslein, L. J. (2010). Matrix metalloproteinases and neurotrauma: evolving roles in injury and reparative processes. *Neuroscientist* 16, 156–170. doi: 10.1177/1073858409355830

Zhang, J. H., Badaut, J., Tang, J., Obenaus, A., Hartman, R., and Pearce, W. J. (2012). The vascular neural network–a new paradigm in stroke pathophysiology. *Nat. Rev. Neurol.* 8, 711–716. doi: 10.1038/nrneurol.2012.210

Conflict of Interest: The authors declare that the research was conducted in the absence of any commercial or financial relationships that could be construed as a potential conflict of interest.

Copyright © 2019 Dinet, Petry and Badaut. This is an open-access article distributed under the terms of the Creative Commons Attribution License (CC BY). The use, distribution or reproduction in other forums is permitted, provided the original author(s) and the copyright owner(s) are credited and that the original publication in this journal is cited, in accordance with accepted academic practice. No use, distribution or reproduction is permitted which does not comply with these terms.

frontiers in Neurology

ORIGINAL RESEARCH
published: 14 November 2019
doi: 10.3389/fneur.2019.01113

Development of a Routinely Applicable Imaging Protocol for Fast and Precise Middle Cerebral Artery Occlusion Assessment and Perfusion Deficit Measure in an Ovine Stroke Model: A Case Study

Andrea Maria Herrmann[1,2†], Giorgio Franco Maria Cattaneo[3†], Sebastian Alexander Eiden[1], Manuela Wieser[1], Elias Kellner[4], Christoph Maurer[5], Jörg Haberstroh[6], Christoph Mülling[2], Wolf-Dirk Niesen[7], Horst Urbach[2], Johannes Boltze[8,9], Stephan Meckel[2†] and Mukesch Johannes Shah[10†]*

[1] Department of Neuroradiology, Faculty of Medicine, Medical Center – University of Freiburg, University of Freiburg, Freiburg, Germany, [2] Faculty of Veterinary Medicine, Institute of Veterinary Anatomy, Histology and Embryology, Leipzig University, Leipzig, Germany, [3] Institute for Biomedical Engineering, University of Stuttgart, Stuttgart, Germany, [4] Department of MR Physics, Faculty of Medicine, Medical Center – University of Freiburg, University of Freiburg, Freiburg, Germany, [5] Department of Diagnostic and Interventional Neuroradiology, University Hospital Augsburg, Augsburg, Germany, [6] Department of Experimental Surgery, CEMT-FR, Faculty of Medicine, Medical Center – University of Freiburg, University of Freiburg, Freiburg, Germany, [7] Department of Neurology, Faculty of Medicine, Medical Center – University of Freiburg, University of Freiburg, Freiburg, Germany, [8] Fraunhofer Research Institution for Marine Biotechnology and Institute for Medical and Marine Biotechnology, University of Lübeck, Lübeck, Germany, [9] School of Life Sciences, University of Warwick, Coventry, United Kingdom, [10] Department of Neurosurgery, Faculty of Medicine, Medical Center – University of Freiburg, University of Freiburg, Freiburg, Germany

OPEN ACCESS

Edited by:
Rick M. Dijkhuizen, University Medical Center Utrecht, Netherlands

Reviewed by:
Norbert Nighoghossian, Université Claude Bernard Lyon 1, France
Heleen M. M. Van Beusekom, Erasmus Medical Center, Netherlands

***Correspondence:**
Stephan Meckel
stephanmeckel@gmail.com

[†] These authors have contributed equally to this work

Specialty section:
This article was submitted to Stroke, a section of the journal Frontiers in Neurology

Received: *11 April 2019*
Accepted: *04 October 2019*
Published: *14 November 2019*

Citation:
Herrmann AM, Cattaneo GFM, Eiden SA, Wieser M, Kellner E, Maurer C, Haberstroh J, Mülling C, Niesen W-D, Urbach H, Boltze J, Meckel S and Shah MJ (2019) Development of a Routinely Applicable Imaging Protocol for Fast and Precise Middle Cerebral Artery Occlusion Assessment and Perfusion Deficit Measure in an Ovine Stroke Model: A Case Study. Front. Neurol. 10:1113. doi: 10.3389/fneur.2019.01113

Temporary middle cerebral artery occlusion (MCAO) in sheep allows modeling of acute large vessel occlusion stroke and subsequent vessel recanalization. However, rapid and precise imaging-based assessment of vessel occlusion and the resulting perfusion deficit during MCAO still represents an experimental challenge. Here, we tested feasibility and suitability of a strategy for MCAO verification and perfusion deficit assessment. We also compared the extent of the initial perfusion deficit and subsequent lesion size for different MCAO durations. The rete mirabile prevents reliable vascular imaging investigation of middle cerebral artery filling status. Hence, computed tomography perfusion imaging was chosen for indirect confirmation of MCAO. Follow-up infarct size evaluation by diffusion-weighted magnetic resonance imaging revealed fluctuating results, with no apparent relationship of lesion size with MCAO at occlusion times below 4 h, potentially related to the variable collateralization of the MCA territory. This underlines the need for intra-ischemic perfusion assessment and future studies focusing on the correlation between perfusion deficit, MCAO duration, and final infarct volume. Temporary MCAO and intra-ischemic perfusion imaging nevertheless has the potential to be applied for the simulation of novel recanalization therapies, particularly those that aim for a fast reperfusion effect in combination with mechanical thrombectomy in a clinically realistic scenario.

Keywords: CT perfusion, DSA, MCAO, reperfusion, sheep stroke model, cerebral ischemia, translational research, brain imaging

INTRODUCTION

Several recent randomized-controlled trials have shown that endovascular mechanical thrombectomy is highly beneficial for patients with acute ischemic stroke and large vessel occlusion (LVO) (1). This breakthrough in acute stroke treatment has led to steadily increasing numbers of patients undergoing endovascular treatment with recanalization, providing options for novel combined treatment strategies. For instance, companion neuroprotective therapies are believed to augment the beneficial impact of recanalization therapies in future settings (2, 3).

Although ischemia/reperfusion rodent models exist, these models have limitations in simulating endovascular approaches under conditions which are similar to a clinical intervention in humans. The major limitation are the much smaller vessels which, for instance, would not allow to test intravascular test devices used for or to support thrombectomy. Large animal models can fill this gap by providing a suitable vascular anatomy and size for preclinical evaluation of new endovascular or combination treatment concepts for LVO stroke (4). Non-human primate and canine stroke models are restricted by ethical concerns and high mortality in the acute and subacute stages after stroke, preventing long-term assessment of functional outcome and final lesion size as the most important clinical endpoints. Alternatively applied porcine and ovine models are more suitable to monitor long-term impact of an intervention, but exhibit a rete mirabile which does not allow direct endovascular access to the middle cerebral artery (MCA) for occlusion (MCAO). Stroke models using these species therefore require surgical access to the MCA. Recently, ovine permanent and transient MCAO stroke models were established (5, 6). Effective occlusion of the MCA main trunk or its branches was reported to depend on the qualitative visual assessment of the operating surgeon, but this may only be predictive in permanent occlusion studies. In reperfusion studies, the individual extent and capacity of collaterals can cause significant variations in final lesion volume similarly to the situation in human LVO stroke. Thus, a reliable, rapid and unbiased estimation of the perfusion deficit during MCAO is an important prerequisite for acute and long-term MCA recanalization studies. Investigating how the initial diffusion deficit corresponds to final infarct size is another important aspect awaiting clarification.

In this feasibility study, we tested several imaging modalities for application in acute ovine MCAO modeling human LVO stroke. We specifically aimed to assess (i) the reliability to confirm successful transient MCAO, (ii) MCA territory hypoperfusion, and (iii) feasibility of the imaging strategy in an experimental MCAO setting only offering a short imaging time window between vessel occlusion and reopening. This work is also intended to report pitfalls and challenges we faced during this development. We finally want to share the experience we have gained with other groups in the field, or trying to access it.

MATERIALS AND METHODS

Animal Baseline Data

The study involved 10 merino sheep half breed (age, 1–3 years; weight, 80.2 ± 7.4 kg), kept in the CEMT-FR (Center for Experimental Models and Transgenic Service, Freiburg, Germany) under following conditions: straw boxes, daily grazing, water and hay *ad libitum*, concentrated feed pellets as reward and to foster human familiarization.

Anesthesia

Anesthesia was prepared by intramuscular injection of midazolam [0.5 mg/kg bodyweight (BW)] and ketamine hydrochloride (20 mg/kg BW), and was induced by intravenous propofol administration (2–4 mg/kg BW). Following endotracheal intubation, 12–15 breaths/min were provided by a volume-controlled ventilator at a 10–15 mL/kg BW tidal volume and 5-mbar positive end-expiratory pressure. Settings were adjusted to normalize oxygen and carbon dioxide tension, and pH values.

Anesthesia for surgical and endovascular procedures was maintained by isoflurane in oxygen/air ($FiO_2 > 0.4$), intravenous ketamine (10 mg/kg BW/h) and fentanyl (2–3 μg/kg BW/h) administration. For CT perfusion and CT angiography as well as brain MRI and angiography anesthesia was maintained by intravenous propofol (15–18 mg/kg/h).

Fluid homeostasis was maintained by intravenous infusion of Ringer solution (10 mg/kg BW/h). Electrocardiogram and blood pressure were monitored continuously. A postsurgical antibiotic (dihydrostreptomycin sulfate 12.9 mg/kg, benzylpenicillin-procaine 8 mg/kg) and analgesic (carprofen 4 mg/kg) treatment was performed.

Surgical MCA Preparation, Occlusion, and Recanalization

Sheep were placed in the supine position slightly elevating the right shoulder. The head was then tilted to the left by ninety degrees. The wool between the ear and eye was shorn, and sterile draping was applied to cover the surgical field.

Two different approaches to the MCA were performed. MCAO surgery in the first series of experiments (series a, cases 1–3) was carried out as described by Wells et al. (6), with the following modifications (**Figure 1B**). A 5 cm vertical incision was made, terminating at the zygomatic arch. Temporal and other mastication muscles were divided and stripped from the coronoid process of the mandible. Partial removal of the coronoid process was omitted when accessing the proximal MCA. The remaining masticators were then divided and stripped from the outer table as far rostral as the fibrous ring attaching the posterior orbit to the concave border of the parietal bone. Thereafter, a small craniectomy over the junction of the parietal and squamous temporal bones was performed using an electric high-speed drill (microspeed, Aesculap, Tuttlingen, Germany) to access the floor of the middle cranial fossa directly behind the orbita. The dura was then opened carefully. A 3 Head VM-900 surgical microscope (Möller-Wedel, Wedel, Germany) was used for surgical preparation of the proximal MCA and terminal ICA. The proximal MCA was occluded by a Yasargil temporary titanium clip (Aesculap) for 2 h.

Surgery in the second series (series b, cases 4–10) was carried out as described by Boltze et al. (5) (**Figure 1C**). The skin between the eye and ear was incised at 5–7 cm along the superior

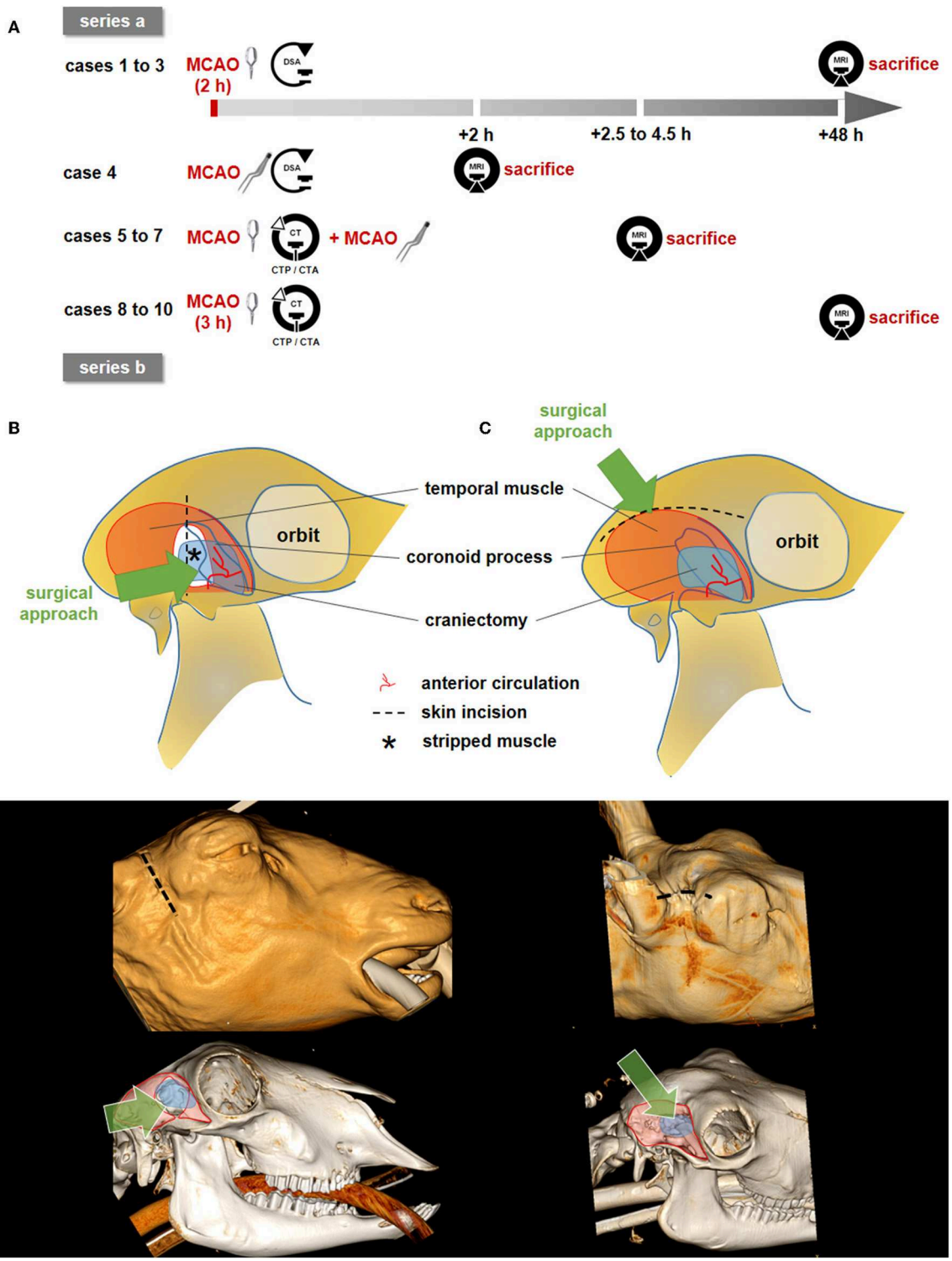

FIGURE 1 | Study design and surgical approaches. **(A)** Overview on study design with two experimental series. Clip pictograms indicate (transient) MCAO by vessel clipping whereas the forceps indicate MCAO by electrocoagulation. **(B,C)**: Schematic illustration of the surgical approaches (top), 3D-Reconstruction showing the skin incision (middle), 3D-bony-reconstruction with muscle (red), and craniectomy (blue) overlays (bottom). **(B)** The surgical approach according to Wells et al. (series a). The proximal MCA and terminal ICA were reached easily. Bony CT reconstruction shows the partial removal of the coronoid process. **(C)** Approach according to Boltze et al. (series b), in which the distal branches of the MCA were followed proximally until the optic nerve and the terminal internal carotid artery (ICA) had been identified. A partial resection of the coronoid process was not necessary (CT reconstruction). Dotted lines: skin incision; blue areas: craniectomy; *: muscle dissection (series a only). The green arrows describes the surgeon's approach and the approximate line of vision.

temporal fossa. The fascia of the temporal muscle was opened and the muscle was stripped away in lateral manner to expose the temporal fossa. During this maneuver, the coronoid process was lateralized and thereafter kept laterally with a self-holding spreader. The remaining masticators were then stripped from the outer table of the cranium as far rostral as the fibrous ring attaching the posterior orbit to the concave border of the parietal bone.

Craniectomy was performed as described for series a. The distal branches of the MCA were followed proximally until the optic nerve and the terminal internal carotid artery (ICA) had been identified. The MCA was permanently occluded using an electrocoagulation device (KLS Martin, Mühlheim, Germany) in case 4. This was performed to control for the influence of the exact occlusion site. In cases 5–7, a clip was placed on the MCA and left in place during CT imaging. The clip was then removed and the vessel was immediately electrocoagulated at the same location (**Figure 1A**). MCAO varied between 2.5 and 4.5 h depending on the particular research question to be addressed in each case. In cases 8–10, the clip was placed on the MCA and removed after 3.0 h without subsequent electrocoagulation (**Figure 1A**).

Endovascular Procedure

MCAO was immediately followed by surgical cut down of the femoral artery for introduction of a 12F sheath by an experienced veterinarian (J.H.). An 8F 90-cm sheath (Flexor Shuttle Guiding Sheath; Cook, Bloomington, Indiana, USA) was then inserted into the right common carotid artery (CCA) using a coaxial 125 cm 5F vertebral or Simmons-2 shaped inner catheter for vessel selection by an experienced interventional neuroradiologist (S.M., C.M.). Selective digital subtraction angiography (DSA) with injections of contrast media (Solutrast 300, Bracco Imaging Deutschland, Konstanz, Germany) into the right CCA that was performed using a C-arm monoplanar angiography system (XA BV300, Philips Health Systems, Hamburg, Germany). Angiographic imaging for visualization of the clip-occluded right MCA was performed in variable angulations.

Brain MRI and MR Angiography

Magnetic resonance imaging (MRI) was performed on a 3T MRI Scanner (Trio, Siemens, Erlangen Germany) using a combined 12-channel head/neck coil. The MRI protocol included sequences as shown in **Table 1**.

Volumetric analysis of ischemic volume (on coronal DWI) and volume of edema (ischemic area plus surrounding edema on coronal T2w) was based on manual segmentations using the medical imaging platform NORA (http://www.nora-imaging.org). Ischemic areas were classified as such after correlation with generated ADC maps. Image evaluation and infarct localization was performed by an experienced neuroradiologist (S.M., C.M.) on a PACS station.

CT Perfusion and CT Angiography

Cases 5 to 10 in series b were transferred to a 16-slice computed tomography (CT) scanner (Somatom Sensation 16, Siemens) immediately after surgical clip placement. Plain CT of the brain was performed in coronary plane sequential acquisition (5-mm slice thickness) to localize the surgical clip and to rule out intracranial hemorrhage. Then, a CT perfusion (CTP) scan was performed covering a 2.4 cm slab of the sheep brain which was centered on the tips of the MCAO clip within the MCA territory (four slices; 6-mm slice thickness). Post-processing of standard perfusion maps (CBV, CBF, and Tmax) was conducted using a dedicated commercial software package (SyngoVia, Siemens). These perfusion maps were rated by an experienced neuroradiologist (S.M.) for presence and degree of MCA territory hypoperfusion using the following semiquantitative score: 0 = no lesion visible on Tmax/CBF/CBV, 1 = lesion visible on Tmax only, 2 = lesion visible on Tmax and partially visible on CBF/CBV, 3 = lesion visible on Tmax/CBF and partially on CBV. Finally, thin-section CT angiography of the craniocervical arterial vasculature (slice thickness; 0.75 mm) was performed with arterial bolus tracking. Assessment of CTA 3D datasets was conducted by an experienced neuroradiologist (S.M., C.M.) on a PACS station.

End of Experiments

Sheep were killed in deep anesthesia by an intravenous potassium chloride overdose at the end of each experiment (after MRI acquisition on day 2 in cases 1–3 and 8–10 and on day 0 in cases 4–7). Death by cardiac arrest was certified by an independent veterinarian.

RESULTS

All procedures were performed without major complications. No sheep suffered from any clinical complications except for neurological deficits after MCAO. Physiological parameters were continuously monitored before and directly after MCAO, and were in normal ranges throughout the experiments. Mean arterial blood pressure (MAP, median [IQR]) was 93 [82.25–103.75] mmHg/92 [82–107] mmHg, and pulse rate was 78 [71–99] beats/min/81 [73–97] beats/min before/after MCAO, respectively. Both parameters did not differ significantly between pre- and intraischemic measurements ($p = 0.903$ for MAP and $p = 0.451$ for pulse rate). Imaging results from all experiments are summarized in **Table 2**.

Results From Series a

Case 1

DWI and T2w MRI on day 2 after MCAO showed a small ischemic lesion (1.7 mL; **Figure 2A**) in right thalamic and midbrain regions after 2 h of transient clip MCAO. The midbrain ischemia suggested an erroneous confusion of the MCA main trunk (M1 segment) with the terminal ICA, resulting in occlusion of terminal ICA and thus of perforating and choroidal artery branches with mesencephalic supply. This appears likely since the proximal segment of the MCA trunk forms a steep 180° curvature with an almost parallel course to the terminal ICA at the anterior skull base of sheep (please also see case 2, **Figure 2B**; and case 4, **Figure 4**).

TABLE 1 | Summary of 3 Tesla MRI sequence parameters.

MRI sequence	Sequence parameters	Orientation	Voxel size	Acquisition time
3D FLAIR	TE/TR, 395 ms/5,000 ms; TI, 1,800 ms; FA, 15°; NA, 1; IPAT, 2	sagittal	1.0 × 1.0 × 1.0 mm	5.52 min
3D MPRAGE	TE/TR, 2.15 ms/1,400 ms; FA, 15°; NA, 1; IPAT, 2	sagittal	1.0 × 1.0 × 1.0 mm	3:27 min
TSE T2	TE/TR, 95 ms/4,090 ms; FA, 140°; IPAT, 2; NA, 1	axial	0.4 × 0.4 × 0.4 mm	2:29 min
TSE T2	TE/TR, 102 ms/5,660 ms; FA, 140°; IPAT 2; NA, 1	sagittal	0.7 × 0.7 × 3.0 mm	2:23 min
TSE T2	TE/TR, 95 ms/4,911 ms; FA, 140°; NA, 1	coronal	0.4 × 0.4 × 3.0 mm	4:51 min
3D TOF MRA	TE/TR, 3.85 ms/23 ms; FA, 18°; 3D slabs, 3; NA, 2; IPAT, 2	coronal	0.5 × 0.4 × 0.6 mm	11:14 min
DWI	TE/TR, 87 ms/4,700 ms; NA, 3; IPAT, 2	coronal	1.3 × 1.3 × 3.0 mm	1:12 min
DWI	TE/TR, 86 ms/3500 ms; NA, 3; IPAT, 2	axial	1.3 × 1.3 × 3.0 mm	1:12 min

DWI, diffusion weighted imaging; FA, flip angle; FLAIR, Fluid-attenuated inversion recovery; IPAT, integrated parallel imaging techniques; MPRAGE, Magnetization Prepared Rapid Acquisition GRE (gradient echo); NA, number of averages; TE, echo time; TOF MRA, time-of-flight MR angiography; TR, repetition time; TSE, turbo spin echo.

TABLE 2 | Summary of MCAO technique, MRI findings, and visualization of MCAO with various imaging modalities.

Animal No.	MCAO		MRI findings				Visibility of MCAO on vascular imaging modalities			
	Surgical technique	Duration of ischemia* [hours]	Day of MRI	DWI lesion volume [ml]	T2 lesion volume [ml]	Location of ischemia/ surrounding edema	TOF MRA#	CT Angiography	CT Perfusion – hypoperfusion score§	DSA of CCA/rete mirabile
1	Clip	2	2	1.7	4.8	Midbrain/No	NA	NA	NA	NA/NA
2	Clip	2	2	25.6	17.0	Large MCA infarct/No	NA	NA	NA	NV/NA
3	Clip	2	2	0.5	3.6	Small MCA infarct/Yes	NA	NA	NA	NV/NA
4	Coagulation	2	0	13.3	5.8	Large MCA ischemia/No	Visible	NA	NA	NV/NV
5	Clip for CTP - coagulation for MRI	2.5	0	2.2	0	Medium MCA ischemia/No	Visible	NV	1	NA/NA
6	Clip for CTP - coagulation for MRI	4.5	0	14.5	11.3	Large MCA ischemia/No	Visible	NV	NV - Artifacts	NA/NA
7	Clip for CTP - coagulation for MRI	4.0	0	16.8	0.2	Large MCA ischemia/No	Visible	NV	3	NV/NA
8	Clip	3.0	2	6.0	5.4	Medium MCA ischemia/No	NA	NV	1	NV/NA
9	Clip	3.0	2	8.5	9.2	Medium MCA ischemia/minimal	NA	NV	3	NV/NA
10	Clip	3.0	2	0.9	3.9	Small MCA infarct/Yes	NA	NV	2 - clip Artifacts	Partially visible/NA

**refers to time interval from start of MCAO until MRI DWI was performed in cases 4–7 (vessel coagulation). § refers to semiquantitative visual assessment of hypoperfusion in MCA territory: 0, no lesion on Tmax/CBF/CBV; 1, lesion visible on Tmax only; 2, lesion visible on Tmax and partially visible on CBF/CBV; 3, lesion fully visible on Tmax/CBF and partially on CBV.*

NV, not visible; NA, not available.

Case 2

Transient clip MCAO was performed for 2 h. Selective DSA of the CCA could not unequivocally demonstrate MCA main trunk occlusion despite variable angulations of the DSA images during angiography (**Figure 2B**). MRI on day 2 showed a large-sized MCA territory infarct (**Figure 3**, upper panels) with recanalized MCA on 3D TOF MRA.

Case 3

Transient clip MCAO was performed for 2 h. Selective DSA of CCA during MCAO again failed to demonstrate MCA main trunk occlusion despite variable angulations of the DSA images during angiography. MRI on day 2 showed no relevant ischemia on DWI (DWI lesion volume, 0.5 ml). A small area of vasogenic edema with scattered and small hemorrhagic foci was found in the area of the surgical access to the MCAO (**Figure 3**, lower

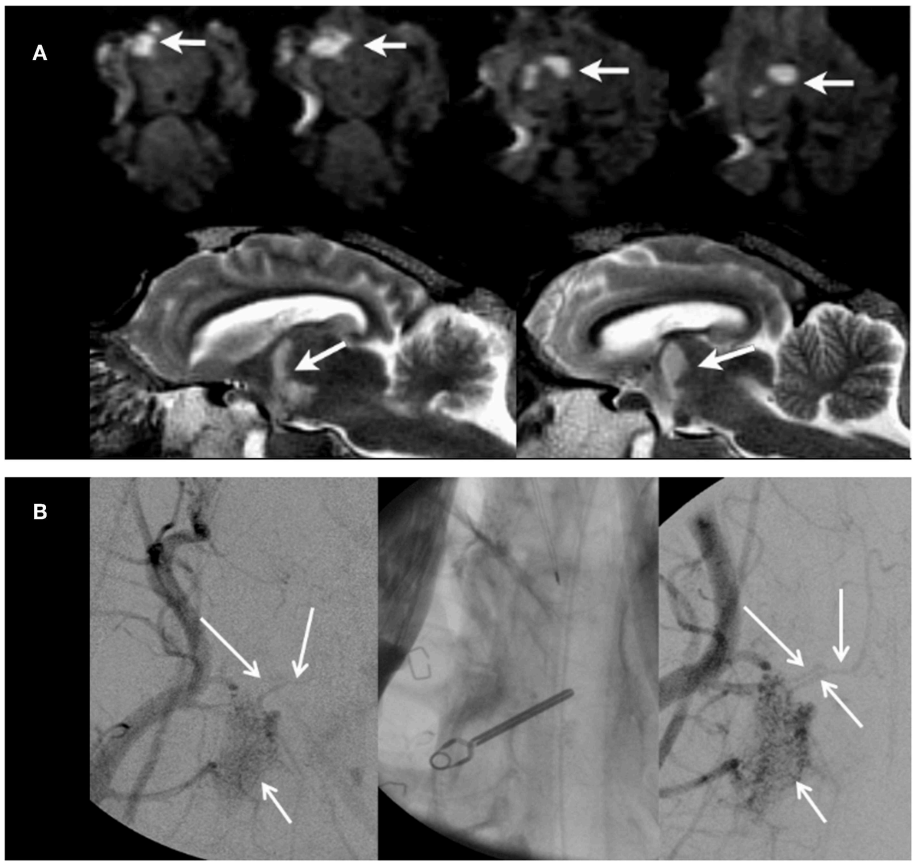

FIGURE 2 | Results from case 1. **(A)** MRI images on day 2 after MCAO from case 1. Upper panels show DWI images in coronal view with ischemic lesions of the midbrain tegmental area within the right crus cerebri and right thalamus (white arrows). Lower panels show consecutive edema on T2w images in mid-sagittal views. **(B)** CCA DSA images before and after clip MCAO. After clip MCAO, no clear cut-off of MCA main trunk was visible with possible faint MCA filling (DSA image in left panel) at the clip level (unsubtracted image in mid panel). After clip removal (DSA image in right panel), filling of the main MCA trunk was visible. However, the distal MCA branch vasculature was not seen due to vessel overlap from rete mirabile and larger extracranial arteries.

panels). The MCA showed a normal flow signal on 3D TOF-MRA images at day 2 after temporary clip occlusion. The neuro-deficit of the animal was light.

The chosen approach in series a (cases 1–3) resulted in a highly variable infarct configuration for two potential reasons. First, the vessel location for the surgical clip placement was inappropriate in case 1 (resulting in mid brain infarcts). Second and similar to the human situation, there might be a variable extent of MCA vessel collateral flow resulting in highly different infarct sizes between cases 2 and 3. Thus, we decided to modify the surgical approach in series b. We further tested whether the chosen MCAO location was correct by using an optimized imaging algorithm during the ischemia phase.

Results From Series b

Case 4

In this case, we tested whether DSA of the CCA with additional superselective views from injection of the right rete mirabile is capable of proofing MCAO. For immediate comparative assessment of the vessel status after MCAO on 3D TOF MRA, the MCA main trunk was electrocoagulated to avoid MRI artifacts emerging from the clip. A 0.021 inch microcatheter (Prowler Select Plus, Codman & Shurtleff, Inc., Raynham, USA) was introduced into the largest inferior arterial branch supplying the rete mirabile via long sheath endovascular access to right CCA directly after MCAO. Despite multiple angulated vessel views on superselective DSA (**Figure 4**, left panel), MCAO could not be correctly visualized. Further distal microcatheter navigation toward the rete mirabile led to subsequent vasospasm with impaired demonstration of downstream vasculature. MRI was performed directly at 2 h following vessel occlusion. MRA visualized the MCAO site at the MCA main trunk (**Figure 4**, right panel). The resulting early MCA territory infarct was visible on DWI images (DWI lesion volume 13.3 ml) with beginning edematous change on T2w images (T2 lesion volume 5.8 ml).

Case 5

Since DSA (including superselective views used in case 4) failed to demonstrate adequate vessel occlusion, we decided to further amend the imaging protocol by introducing CTA with CTP imaging in cases 5–7. Since electrocoagulation is not a feasible technique for transient MCAO, we decided to first perform

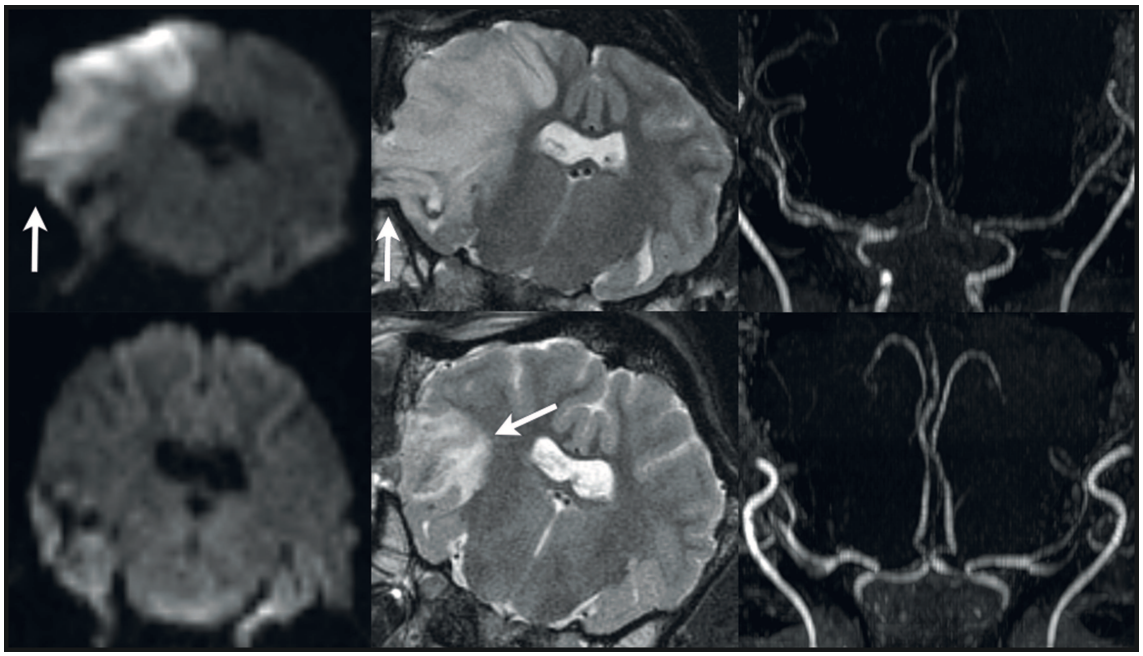

FIGURE 3 | Results from cases 2 and 3. MRI images of case 2 **(upper panels)** and case 3 **(lower panels)** on day 2 after 2 h of transient MCAO. DWI and T2w images show a large right MCA territory infarct lesion (DWI lesion volume, 25.6 ml) with swelling and mild herniation through the craniectomy site (arrows in **upper left** and **mid panels**). MRA **(upper right panel)** demonstrates adequate MCA recanalization after right temporary MCAO. In case 3, no relevant MCA territory ischemia is seen on DWI images (**lower left panel**; DWI lesion volume, 0.5 ml), whereas T2w images exhibit vasogenic edema in the area of the craniectomy with mild hemorrhagic foci (arrow in **lower middle panel**). Again, MRA demonstrates adequate MCA vessel recanalization after right temporary MCAO **(lower right panel)**.

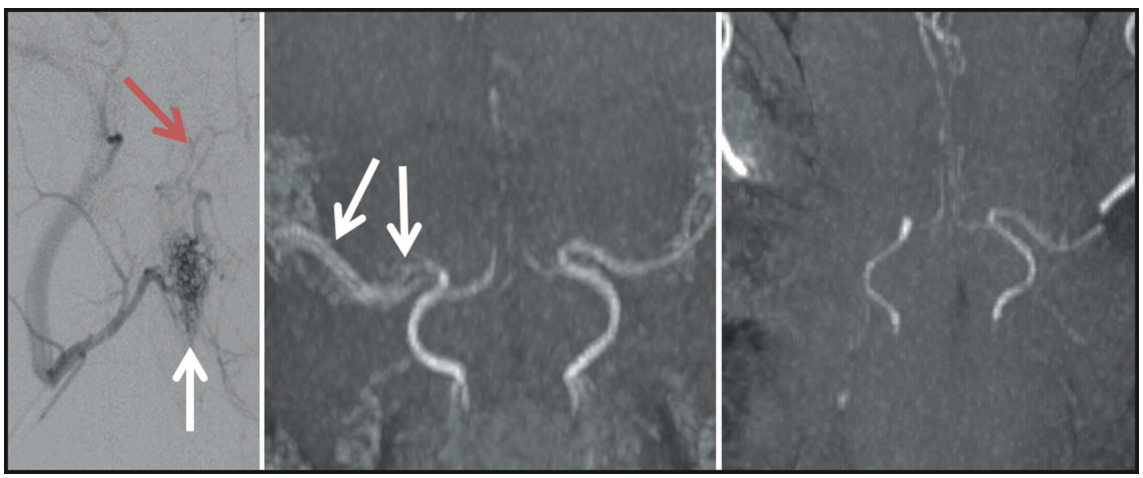

FIGURE 4 | Results from case 4. DSA image **(left panel)** showing superselective rete mirabile injection (red arrow) after permanent MCAO (animal 4) without clear evidence of MCA main trunk occlusion (red arrow). 3T TOF MRA showing duplicated right MCA main trunk post temporary MCAO (**mid panel**, arrows) and clear evidence of right MCA occlusion after permanent MCAO **(right panel)**.

MCAO with a clip followed by immediate transfer to CTA/CTP imaging. Thereafter, the clip was removed and the vessel was occluded in the same location by electrocoagulation in order to perform subsequent MRI without clip-borne artifacts. Thus, CTP findings could be correlated with the results of MRI simulating a temporary MCAO with ischemia duration of 2.5 h (time interval from initial vessel occlusion to MRI acquisition).

On CTP, a large area of right MCA territory hypoperfusion was seen on Tmax, whereas CBF and CBV maps showed no areas hypoperfusion (perfusion score 1; **Figure 5**). Missing flow signal of the MCA main trunk was seen on 3D TOF MRA. Visualization of the MCAO at the main trunk was not possible on CTA images due to beam hardening artifacts originating from skull bone and the clip. On DWI, signs of a small infarct in the MCA territory

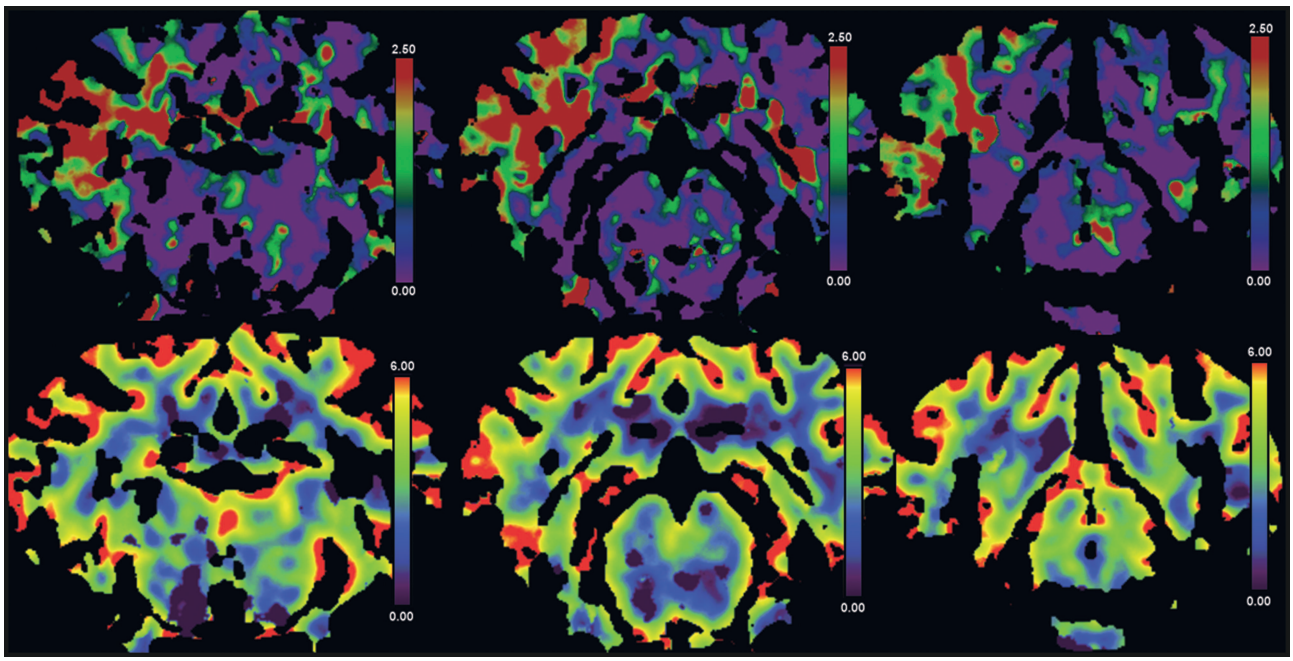

FIGURE 5 | Results from case 5. CTP images from case 5. Directly after clip MCAO profound hypoperfusion is visible on Tmax maps **(upper panels)** without reduction in CBV **(lower panels)**. False color scale indicates Tmax from 0 (purple) to 2.5 s (red) in upper panels and CBV from 0 ml/100 g (purple) to 6 ml/100 g (red) in lower panels, respectively.

were detected (lesion volume 2.2 ml) without edematous change on T2w images. In this case, evidence of correct temporary MCAO at the main trunk by visualization of CTP hypoperfusion during the time window of clip occlusion was first demonstrated with good correspondence to findings in immediate MRI. Hence, duration of MCAO for 2.5 h may still have been too short to detect a fully evolved infarct.

Case 6

MCAO and imaging procedures were performed as described in case 5 except for the longer (4.5 h) duration of ischemia at the time of the MRI measurements in order to avoid a small final infarct due to premature recanalization. Perfusion in the right hemisphere could not be evaluated on CTP due to major streak artifacts from extensive jugular venous contrast media reflux. Correct MCA main trunk occlusion could be reliably demonstrated using 3D TOF MRA, but CTA again failed to do so due to beam hardening artifacts. Four and a half hours of ischemia led to a rather large-sized MCA infarct that was seen on DWI MRI (lesion volume 14.5 ml) with resulting early edematous changes on T2w images.

Case 7

MCAO was performed as described in case 5 and 6 except for a modification in the positioning of the animal during CTP acquisition in order to avoid streak artifacts originating from contrast media reflux into the jugular veins. To this end, the animal was placed in left anterior-lateral position on the CT scanner table to relieve paunch-related increase in central venous pressure. DSA was also added directly after CTP and before removal of the clip, and subsequent permanent electrocogaluation of the MCA. However, as in the previous cases, DSA images could not clearly demonstrate correct vessel occlusion. MRI was performed at 4.0 h after MCAO. MRA was able to correctly visualize MCA main trunk trunk occlusion. On CTP, a large area of MCA territory hypoperfusion was seen on and on CBF maps with hypoperfusion also visible on CBV maps (perfusion score 3). There were no major artifacts on CTP images. However, MCAO was not visible on CTA images due to beam hardening artifacts similar to cases 5 and 6. Likewise, a rather large-sized MCA territory infarct was seen on MRI (DWI volume, 16.8 ml) without significant early edematous change on T2w images after 4 h of ischemia.

Cases 8–10

During an interim summary of cases 5–7, the utilization of CT perfusion for demonstrating MCA territory hypoperfusion as an indicator of correct MCAO was found successful except for extensive beam hardening artifacts in case 6, caused by jugular venous reflux. Thus, we planned to gain further experience with this CT perfusion protocol (applied with modified animal positioning as described in case 7) in combination with the modified surgical approach of series b. However, we decided to continue by performing a transient clip MCAO only (omitting electrocoagulation) and infarct size measurement by MRI on day 2. The latter modifications were chosen in order to establish an imaging-based MCAO model which is designed for testing novel combined endovascular approaches of LVO stroke therapy in the future. Such transient MCAO stroke model should not only allow for ultra-early MRI but also for delayed imaging assessment

of final infarct evolution and clinical follow-up as additional outcome measures.

The clip was removed after an ischemic period of 3.0 h. CTP imaging was performed directly after clip placement with modified animal positioning on the scanner table as described in case 7. Ultra-early MRI scanning was skipped and animals were allowed to wake-up and recover from the procedure. Infarct size measurement was performed on MRI at day 2 after MCAO in all three cases. On CTP, MCA territory hypoperfusion was visible on Tmax in all three cases. In addition, CBF reduction 9 and mild CBV reduction within the MCA territory was found in case 9 (perfusion score 3). In case 10, there were streak artifacts within the MCA territory from clip placement which, however, did not severely impair visibility of hypoperfusion (perfusion score 2). The MCAO was again not visible at all on DSA of the CCA in cases 8 and 9 after clip placement, and only poorly visible in case 10. On MRI at day 2, medium-sized MCA territory infarcts were evident on both DWI and T2w images (DWI volume, 6–8.5 ml) in cases 8 and 9. In contrast, the MCA territory infarction was rather small-sized (DWI volume, 0.9 ml) despite proved MCA territory hypoperfusion on CTP in case 10. This surprising result was explained by MRA on day 2 showing an early duplication of the MCA vessels as a normal variation in this case (**Figure 4**, mid panel). This variant may be a source for strongly improved collateralization within the MCA territory in some individuals. Identification and occlusion of the duplicate MCA main trunk can be challenging as it could be located deeply within a cerebral sulcus or the brain parenchyma.

DISCUSSION

The aim of this case study was to establish a feasible imaging modality for MCA territory hypoperfusion assessment in an ovine transient MCAO model, and to document our experience collected on the way toward this aim. Final infarct size on MRI represents a meaningful efficacy surrogate in experiments on acute stroke therapeutic interventions. However, in studies using transient MCAO this is only valid when the extent of brain hypoperfusion and thus the expected final lesion size without reperfusion or therapeutic intervention is known in order to compare it to the final lesion volume with recanalization and/or accompanying therapeutic intervention.

We evaluated different imaging protocols for both intra-ischemic and post-ischemic perfusion and infarct assessment, and performed a step-wise amendment of the imaging procedures and protocols. The finally resulting imaging strategy was feasible to demonstrate temporary MCA territory hypoperfusion during clip occlusion prior to vessel reopening in the intra-ischemic phase of temporary MCAO. Furthermore, we performed a "two-step" occlusion by MCA clipping prior to CTP, and electrocoagulation after CTP at the exact same vessel location to validate the results by means of TOF MRA without the risk of clip-derived artifacts.

We also determined CTP using standard post-processed image maps (Tmax, CBF, and CBV). This imaging technique was feasible to confirm hypoperfusion and thus the correct clip placement during MCAO. Such confirmation is an important quality assurance method when later removing the clip to model successful recanalization. Although derived from a relatively small number of animals undergoing CTP, our results indicate that final infarct size may be highly variable at least within a time window of 3–4.5 h of MCAO. These results are in-line with previous experiments done by Wells et al. (7) that demonstrated DWI volumes ranging from 7 to 15% of whole brain tissue after 2 h of ischemia with proximal clip MCAO in six animals. In principle, this variability may arise from incomplete MCA occlusion or a variable extent of collateral circulation to the MCA territory. Although a definite conclusion is hard to make, we argue for the latter as the most likely explanation due to numerous reasons. First, the Yasargil clips used in our experiments are also used in humans and exhibit closing forces (>150 g, 1.47 N) that should be absolutely sufficient to occlude the ovine MCA. Complete vessel coverage by the clip was confirmed after thorough visual inspection by the surgeon (M.J.S.). Of note, the ovine MCA is smaller than the vessels Yarsagil clips are usually placed on, so it is not difficult to cover it entirely. Second, we report cases of considerable infarcts (e.g., cases 2, 8, and 9). This points at a factor being different between individual subjects rather than a technical failure. Indeed, the extent of collateral circulation determines the extent of the core infarct size very early after onset of human LVO stroke of the MCA (8, 9), and the situation can be similar in sheep. If this assumption was right, it would underpin the translational value of the model described herein, but also calls for pretest assessment of collateral status to exclude extreme outcomes. In the sheep model, collateral circulation of the MCA may further be enhanced by dedicated variants of the ovine cerebral arteries such as a duplicated MCA main trunk (see case 10). Permanent MCAO by electrocoagulation as employed in our study was previously reported to result in reproducible infarct volumes throughout a 7 week surveillance period, starting 24 h after MCAO (5). Similar findings were reported for swine (10). This might come in line with our assumption, as the initially tissue-preserving effects of collateralization will become less prominent over time in case a critical hypoperfusion/complete blood flow disruption is present. During the acute stage, however, individual differences in collateralization capacity would result in much more variable lesion volumes.

The volume of hypoperfused brain tissue at early time points of vessel occlusion may be later correlated to the final lesion size. In our series, some cases that demonstrated profound hypoperfusion at the time of vessel occlusion (score 3) showed rather large-sized infarct volumes on follow-up DWI MRI. However, owing to the small number of cases with well-evaluable CTP images ($n = 4$) we were not able to clearly prove a suggested association between the extent of hypoperfusion early after clip application and final infarct on DWI by using a semiquantitative analysis of perfusion deficits. In order to provide a robust estimation of final infarcts, more data from CTP before clip removal (simulating the endovascular recanalization) should be compared to final infarct size on MRI or infarct histology in future studies.

Surgical Approach

Reproducible and reliable infarcts could not be induced in series a, and effective occlusion depended on qualitative visual assessment by the surgeon. Due to the basal approach, the proximal MCA and terminal ICA could be reached easily. However, the narrow loop between the terminal ICA and the proximal MCA may have led to erroneous terminal ICA occlusion, resulting in brain stem infarct presumably from associated choroidal vessel occlusion with the absence of any MCA territory ischemia (case 2). Surgical knowledge of this dedicated anatomy being different to human basal brain arteries is crucial to avoid such complication. Moreover, duplication of MCA main trunk (M1 segment, see case 10 and **Figure 4**) represents a relatively frequently observed anatomical variant in sheep, and is also supposed to be the source for of a high degree of collateralization within the MCA territory. Such duplication may not be entirely visible during neurosurgical exposure.

According to the impression from our experienced vascular neurosurgeon (M.J.S.), the surgical approach chosen in series b was technically more suitable for MCAO, as long as possible early duplication of the MCA was ruled out and the proximal MCA (vascular loop near the optic nerve) was clearly identified.

MCAO Imaging

DSA, superselective DSA of vessels supplying the rete mirabile, and CTA were not suitable to confirm correct MCAO. This was presumably due to the tiny caliber of intracranial arteries distal to the rete mirabile on superselective DSA and CTA, and many overlapping large-sized extracranial branches of the carotid artery on non-selective DSA, respectively. 3D rotational DSA might be an alternative option to visualize the occlusion of the MCA main trunk which was however not possible due to limited technical capabilities of our experimental angiography suite. Imaging of leptomeningeal collateral status in MCAO may be of interest as it could serve as an estimate for clinical outcome and final infarct size. However, the same methodological limitations of DSA and CTA as in the confirmation of correct MCAO may also account for the poor visualization of the tiny pial vessels in the sheep brain that impair a sufficient analysis of collaterals. However, in analogy to human large vessel occlusion stroke, CT perfusion penumbral imaging may also provide indirect information on the presence or absence of collaterals (11, 12). Non-human primate (NHP) models of ischemic stroke [for review see (4)] might be advantageous when assessing small-caliber intracerebral vessels and the cranial anatomy in NHPs is even closer to the human situation. However, the use of NHPs is ethically restricted in many contains, and costs related to using the species by far exceed those of other large animal stroke models. In turn, this restricts sample sizes and often severely limits endpoints that can be addressed quantitatively.

Beam-hardening metal artifacts were visible on CTA during temporary MCAO induced by titanium clip application. 3D TOF MRA at 3T reliably showed MCAO, but required (permanent) occlusion by electrocoagulation to avoid clip-borne artifacts (13). This issue might be mitigated by the use of newly developed and improved, but extremely expensive MRI-compatible clips. These are made of special titanium based alloys or Phynox, an alloy composed of cobalt, chrome, nickel, and molybdenum (e.g., Aesculap Yasargil mini clips) and cause only minimal artifacts. However, in transient MCAO, this imaging modality may be less efficient and also difficult to apply during a short ischemic time window between two neurosurgical procedures for clip placement and subsequent removal. This is particularly relevant for experiments that add additional time for endovascular procedures, e.g., for intra-arterial neuroprotective therapy, which necessitate additional navigation and placement of a catheter into the brain supplying arteries. Nevertheless, MRI-compatible clips might allow perfusion-weighted imaging sequences to assess the perfusion deficit during occlusion.

Positron emission tomography (PET) has been reported as a gold standard for experimental perfusion deficit assessment and is applicable in sheep (14, 15). Moreover, PET imaging is hardly susceptible to metal artifacts from a placed clip. However, PET imaging requires a dedicated infrastructure while its application and in particular full data analysis may be too time-consuming to be applied in acute experimental settings during a short time window of temporary vessel occlusion.

We found that CT perfusion reliably provided indirect evidence of MCAO by demonstrating MCA territory hypoperfusion already in a small number of cases. Importantly, it was the most feasible modality that could be applied in a time-efficient manner during temporary neurosurgical clip MCAO among the tested imaging techniques. In our experience, streak artifacts related to venous reflux into the internal jugular vein may be reduced by placing the animal in a left anterior-lateral position on the CT scanner table to relieve paunch-related venous pressure. This finally resulted in good diagnostic quality of the CTP images.

Study Limitations

In this pilot study with small number of consecutive animals, no complete blinding or randomization could be performed which may potentially bias the analysis of study outcomes. However, the investigators who performed the volumetric analysis of infarct volume on MRI images were blinded to the respective animals' treatment protocols. Detailed information derived on correlation of infarct size with hypoperfusion volume could not be obtained due to variable imaging protocols and the small number of animals that finally underwent CTP, warranting additional research on this aspect. Consequently, further studies with a fixed CTP imaging protocol and ischemic time window of temporary MCAO are necessary.

DATA AVAILABILITY STATEMENT

The datasets generated and/or analyzed during the current study are available from the corresponding author on request.

ETHICS STATEMENT

This study was carried out in accordance with the recommendations of the German animal protection law

and the animal care guidelines of the European Community (2010/63/EU). The protocol was approved by the local ethics committee (Regierungspräsidium Freiburg, Germany; reference numbers #35-9185.81/G-14/85 and #39-9185.81/G-15/38). Study design is illustrated in **Figure 1A**. ARRIVE guidelines were followed as applicable for a pilot study.

AUTHOR CONTRIBUTIONS

AH: significant contribution to study design, to data acquisition, analysis of data, to article drafting, critical review of intellectual contents, and approval of final version. GC: significant contribution to study design, to article drafting, critical review of intellectual contents, and approval of final version. SE: significant contribution to data acquisition, analysis and interpretation of data, and to critical review of intellectual contents, and approval of final version. MW, EK, and CMa: significant contribution to data acquisition, analysis of data, and to critical review of intellectual contents, and approval of final version. JH: significant contribution to concept and study design, to data acquisition, and to critical review of intellectual contents, and approval of final version. CMü and HU: significant contribution to concept and study design, and to critical review of intellectual contents, and approval of final version. W-DN: significant contribution to data acquisition, and to critical review of intellectual contents, and approval of final version. JB: significant contribution to concept and study design, to data interpretation, and to article drafting, critical review of intellectual contents, and approval of final version. SM: significant contribution to experimental design image analysis, data acquisition and analysis and interpretation of data, article drafting, critical review of intellectual contents, and approval of final version. MS: significant contribution to experimental design, to article drafting, critical review of intellectual contents, and approval of final version.

FUNDING

This work was supported by Federal Ministry of Education and Research, Germany (grant #13GW0015B).

ACKNOWLEDGMENTS

We thank our research technician Hansjörg Mast for valuable support with the MRI measurements of all animals. We thank Acandis GmbH (Pforzheim, Germany) for the collaboration in the frame of the joint granted project 13GW0015B.

REFERENCES

1. Goyal M, Menon BK, van Zwam WH, Dippel DWJ, Mitchell PJ, Demchuk AM, et al. Endovascular thrombectomy after large-vessel ischaemic stroke: a meta-analysis of individual patient data from five randomised trials. *Lancet.* (2016) 387:1723–31. doi: 10.1016/S0140-6736(16)00163-X
2. Linfante I, Cipolla MJ. Improving reperfusion therapies in the era of mechanical thrombectomy. *Transl Stroke Res.* (2016) 7:294–302. doi: 10.1007/s12975-016-0469-3
3. Savitz SI, Baron, J.-C., Yenari MA, Sanossian N, Fisher M. Reconsidering neuroprotection in the reperfusion era. *Stroke.* (2017) 48:3413–9. doi: 10.1161/STROKEAHA.117.017283
4. Herrmann AM, Meckel S, Gounis MJ, Kringe L, Motschall E, Mülling C, et al. Large animals in neurointerventional research: a systematic review on models, techniques and their application in endovascular procedures for stroke, aneurysms and vascular malformations. *J Cereb Blood Flow Metab.* (2019) 39:375–94. doi: 10.1177/0271678X19827446
5. Boltze J, Förschler A, Nitzsche B, Waldmin D, Hoffmann A, Boltze CM, et al. Permanent middle cerebral artery occlusion in sheep: a novel large animal model of focal cerebral ischemia. *J Cereb Blood Flow Metab.* (2008) 28:1951–64. doi: 10.1038/jcbfm.2008.89
6. Wells AJ, Vink R, Blumbergs PC, Brophy BP, Helps SC, Knox SJ, et al. A surgical model of permanent and transient middle cerebral artery stroke in the sheep. *PLoS ONE.* (2012) 7:e42157. doi: 10.1371/journal.pone.0042157
7. Wells AJ, Vink R, Helps SC, Knox SJ, Blumbergs PC, Turner RJ. Elevated intracranial pressure and cerebral edema following permanent MCA occlusion in an ovine model. *PLoS ONE.* (2015) 10:e0130512. doi: 10.1371/journal.pone.0130512
8. Wheeler HM, Mlynash M, Inoue M, Tipirnini A, Liggins J, Bammer R, et al. The growth rate of early DWI lesions is highly variable and associated with penumbral salvage and clinical outcomes following endovascular reperfusion. *Int J Stroke.* (2015) 10:723–9. doi: 10.1111/ijs.12436
9. Maurer CJ, Egger K, Dempfle, A.-K., Reinhard M, Meckel S, Urbach H. Facing the time window in acute ischemic stroke: the infarct core. *Clin Neuroradiol.* (2016) 26:153–8. doi: 10.1007/s00062-016-0501-8
10. Imai H, Konno K, Nakamura M, Shimizu T, Kubota C, Seki K, et al. A new model of focal cerebral ischemia in the miniature pig. *J Neurosurg.* (2006) 104:123–32. doi: 10.3171/ped.2006.104.2.123
11. Vagal A, Menon BK, Foster LD, Livorine A, Yeatts SD, Qazi E, et al. Association between CT angiogram collaterals and CT perfusion in the interventional management of stroke III trial. *Stroke.* (2016) 47:535–8. doi: 10.1161/STROKEAHA.115.011461
12. Lu S-S., Zhang X, Xu X-Q, Cao Y-Z, Zhao LB, Liu Q-H, et al. Comparison of CT angiography collaterals for predicting target perfusion profile and clinical outcome in patients with acute ischemic stroke. *Eur Radiol.* (2019) 29:4922–9. doi: 10.1007/s00330-019-06027-9
13. Steiger HJ, van Loon JJ. Virtues and drawbacks of titanium alloy aneurysm clips. *Acta Neurochirurg.* (1999) 72:81–8.
14. Terpolilli NA, Kim S-W, Thal SC, Kataoka H, Zeisig V, Nitzsche B, et al. Inhalation of nitric oxide prevents ischemic brain damage in experimental stroke by selective dilatation of collateral arterioles. *Circ Res.* (2012) 110:727–38. doi: 10.1161/CIRCRESAHA.111.253419
15. Werner P, Saur D, Zeisig V, Ettrich B, Patt M, Sattler B, et al. Simultaneous PET/MRI in stroke: a case series. *J Cereb Blood Flow Metab.* (2015) 35:1421–5. doi: 10.1038/jcbfm.2015.158

Conflict of Interest: GC was engineer at the company Acandis GmbH until August 2019. SM received fees and travel grants as member of scientific advisory board of company Acandis GmbH.

The remaining authors declare that the research was conducted in the absence of any commercial or financial relationships that could be construed as a potential conflict of interest.

Copyright © 2019 Herrmann, Cattaneo, Eiden, Wieser, Kellner, Maurer, Haberstroh, Mülling, Niesen, Urbach, Boltze, Meckel and Shah. This is an open-access article distributed under the terms of the Creative Commons Attribution License (CC BY). The use, distribution or reproduction in other forums is permitted, provided the original author(s) and the copyright owner(s) are credited and that the original publication in this journal is cited, in accordance with accepted academic practice. No use, distribution or reproduction is permitted which does not comply with these terms.

frontiers in Neuroscience

REVIEW
published: 15 November 2019
doi: 10.3389/fnins.2019.01142

Proteostasis in Cerebral Small Vessel Disease

*Christof Haffner**

Institute for Stroke and Dementia Research, Klinikum der Universität München, Ludwig-Maximilians-Universität München, Munich, Germany

Maintaining the homeostasis of proteins (proteostasis) by controlling their synthesis, folding and degradation is a central task of cells and tissues. The gradual decline of the capacity of the various proteostasis machineries, frequently in combination with their overload through mutated, aggregation-prone proteins, is increasingly recognized as an important catalyst of age-dependent pathologies in the brain, most prominently neurodegenerative disorders. A dysfunctional proteostasis might also contribute to neurovascular disease as indicated by the occurrence of excessive protein accumulation or massive extracellular matrix expansion within vessel walls in conditions such as cerebral small vessel disease (SVD), a major cause of ischemic stroke, and cerebral amyloid angiopathy. Recent advances in brain vessel isolation techniques and mass spectrometry methodology have facilitated the analysis of cerebrovascular proteomes and fueled efforts to determine the proteomic signatures associated with neurovascular disease. In several studies in humans and mice considerable differences between healthy and diseased vessel proteomes were observed, emphasizing the critical contribution of an impaired proteostasis to disease pathogenesis. These findings highlight the important role of a balanced proteostasis for cerebrovascular health.

Keywords: CADASIL, CARASIL, cerebral amyloid angiopathy, HTRA1, Notch3, proteomics, chaperone

OPEN ACCESS

Edited by:
Emmanuel Pinteaux, The University of Manchester, United Kingdom

Reviewed by:
Masafumi Ihara, National Cerebral and Cardiovascular Center, Japan
Steven M. Greenberg, Harvard University, United States

***Correspondence:**
Christof Haffner
christof.haffner@med.uni-muenchen.de

Specialty section:
This article was submitted to Neurodegeneration, a section of the journal Frontiers in Neuroscience

Received: *07 May 2019*
Accepted: *10 October 2019*
Published: *15 November 2019*

Citation:
Haffner C (2019) Proteostasis in Cerebral Small Vessel Disease. Front. Neurosci. 13:1142. doi: 10.3389/fnins.2019.01142

INTRODUCTION

Proteome homeostasis or proteostasis refers to the maintenance of all proteins of an organism in a conformation, concentration, and location that is required for their correct function (Balch et al., 2008). Safeguarding proteostasis under a wide range of environmental and metabolic conditions is a fundamental task of cells and tissues and ensured by a proteostasis network, which controls protein synthesis, folding, trafficking, and degradation/clearance (Hipp et al., 2019). The surveillance of protein folding is a particularly challenging problem, since incompletely folded and misfolded proteins are common byproducts of the cell metabolism and represent a considerable risk due to their high aggregation potential. Molecular chaperones counteract aggregation by facilitating the folding/refolding of proteins on a physiological timescale or by initiating the degradation of terminally misfolded proteins through the ubiquitin–proteasome or the autophagosome–lysosome system (Hartl et al., 2011). Chaperones shield hydrophobic amino acid residues and unpaired β-strands of incorrectly folded proteins from the aqueous cellular environment and abolish the formation of intermolecular contacts between non-native protein states. Yet, excessive protein misfolding due to increased environmental stress or genetic mutations is a frequent cause of pathological conditions (Wyatt et al., 2013; Chiti and Dobson, 2017). These

proteinopathies are characterized by an overload and failure of the proteostasis network and a subsequent predominance of aggregation-mediated proteotoxicity over aggregate clearance inside and/or outside the cell. Prominent examples are degenerative disorders of the brain associated with protein aggregates adopting well-ordered structures referred to as amyloid. The progressivity of these conditions with age is likely linked to the age-dependent decline of the proteostasis network capacity (Labbadia and Morimoto, 2015; Hipp et al., 2019). How protein aggregates cause toxicity and cellular dysfunction is only partially understood, but once aggregation has been initiated a further collapse in proteostasis is likely to occur due to the sequestration of chaperones and other proteostasis components into pathologic inclusions (Balchin et al., 2016).

While the molecular details of intracellular proteostasis have been investigated extensively, our understanding of the mechanisms maintaining proteostasis in the extracellular space is limited. The discovery of a small but growing number of constitutively secreted chaperones has advanced our knowledge about processes counteracting extracellular proteotoxicity (Wyatt et al., 2013). These chaperones share functional similarities with the family of intracellular small heat shock proteins in that they recognize targets via exposed hydrophobic regions and serve as sensors as well as disposal mediators of misfolded proteins. However, they lack ATPase activity and cannot refold proteins, limiting their role in safeguarding against proteotoxicity to protein degradation and aggregate removal. The clearance of misfolded proteins from the brain parenchyma is a particular challenging task and believed to occur to a substantial extent via transport along glymphatic/perivascular routes (Morris et al., 2016; Rasmussen et al., 2018). The impairment of this process is likely to facilitate protein aggregation and deposition within the brain vasculature and to promote the development of cerebrovascular pathologies (Carare et al., 2013; Weller et al., 2015). Two important examples are cerebral amyloid angiopathy (CAA), an important cause of intracerebral hemorrhage, and cerebral autosomal-dominant arteriopathy with subcortical infarcts and leukoencephalopathy (CADASIL), the most prevalent monogenic form of lacunar (ischemic) stroke in adults. Both are characterized by excessive protein accumulation in brain vessel walls highlighting the importance of a balanced extracellular proteome for brain health.

CEREBRAL SMALL VESSEL DISEASE

Cerebrovascular disease resulting in vascular cognitive impairment (VCI)/vascular dementia (VD) is increasingly recognized as important cause of dementia in the elderly and has become a major challenge for aging societies (Iadecola, 2013). It can occur in "pure" form without concomitant cerebral pathologies or, much more frequently, in "mixed" form together with pathologies of neurodegenerative disorders, most prominently Alzheimer's disease (AD) or Parkinson's disease (Jellinger, 2013). Cerebral small vessel disease (SVD), a major cause of VCI, describes a heterogeneous group of conditions affecting small arteries, arterioles, capillaries and sometimes venules of the brain and comprises CAA as well as non-amyloid arteriopathies (Pantoni, 2010; Kalaria, 2018; Vinters et al., 2018). CAA is clinically characterized by microbleeds, microinfarcts and hemorrhagic stroke and histologically clearly defined by the accumulation of insoluble amyloid-β (Aβ) peptides in the walls of small, mainly cortical and leptomeningeal vessels (Charidimou et al., 2017). In contrast, non-amyloid SVD results in both lacunar stroke as well as intracerebral hemorrhage and encompasses common sporadic pathologies such as small vessel arteriosclerosis, lipohyalinosis and arteriolosclerosis as well as rare hereditary syndromes (Pantoni, 2010; Wardlaw et al., 2019). Histopathological features include concentric hyaline vessel wall thickening, luminal stenosis, accumulation of amorphous proteinaceous material and plasma proteins in the vessel matrix as well as loss of mural cells [vascular smooth muscle cells (VSMC), pericytes] from the tunica media (Grinberg and Thal, 2010; Pantoni, 2010). Some insight into the underlying molecular mechanisms has been gained from hereditary SVD forms with defined genetic etiology and the analysis of the biology and physiology of the underlying genes (Haffner et al., 2016; Tan et al., 2017; Yamamoto and Ihara, 2017). The following sections provide an overview of the molecular etiologies and pathological features of the SVD forms relevant for the topic of this review.

CADASIL AND CARASIL

Cerebral autosomal-dominant arteriopathy with subcortical infarcts and leukoencephalopathy is the most common heritable cause of stroke and VCI in adults (Chabriat et al., 2009; Joutel, 2011). It is a progressive neurological syndrome associated with ischemic events and cognitive decline affecting young or middle-aged individuals and leading to a terminal stage of being bedridden and demented within a mean of 25 years. In magnetic resonance imaging (MRI) patients display the typical signs of chronic small artery disease of the brain such as white matter damage, lacunar infarcts and dilated perivascular spaces (Chabriat et al., 2009). Histological analysis of vessels shows a marked thickening of the walls of small and medium-sized, leptomeningeal and penetrating arteries, luminal stenosis and the presence of ultrastructural, non-amyloid protein deposits termed granular osmiophilic material (GOM) in the extracellular space of the tunica media (Kalimo et al., 2002; Tikka et al., 2014). Although a structural and functional impairment of mural cells of the vessel wall has been reported (Ghosh et al., 2015; Capone et al., 2016b), many aspects of the pathophysiological processes leading to vessel degeneration and dysfunction are still unknown. CADASIL is caused by mutations in the *NOTCH3* gene (Chabriat et al., 2009; Rutten et al., 2014), which encodes a signaling receptor essential for VSMC survival, blood vessel integrity, blood-brain barrier function and regulation of vascular tone (Henshall et al., 2015; Kofler et al., 2015). Notch3 is a large, single-pass transmembrane protein with an extracellular domain ($Notch3^{ECD}$) mainly consisting of 34 tandem epidermal growth factor (EGF)-like repeats and an intracellular domain acting as a transcriptional coactivator when proteolytically released from the membrane-bound receptor upon ligand-mediated activation

(Siebel and Lendahl, 2017). Although a loss of Notch3 function cannot be completely ruled out as driving force for CADASIL pathogenesis (Machuca-Parra et al., 2017; Coupland et al., 2018), a gain of toxic function is currently widely accepted as disease mechanism (Joutel, 2011; Haffner et al., 2016). Typical CADASIL mutations are missense variants in the Notch3^{ECD} causing a gain or loss of cysteine residues and resulting in a disruption of the highly conserved disulfide bond pattern characteristic for EGF repeats (Chabriat et al., 2009). As a consequence, mutant receptors are likely to engage via unpaired sulfhydryl groups in abnormal intermolecular interactions leading to Notch3^{ECD} aggregation (Duering et al., 2011) and the formation of focal protein deposits corresponding to the ultrastructural GOM (Joutel, 2011). Notch3^{ECD} aggregates are believed to confer toxicity by dysregulating ECM homeostasis, but the underlying molecular processes are largely unknown (Joutel et al., 2016).

Another monogenic SVD related to CADASIL is CARASIL (cerebral autosomal-recessive arteriopathy with subcortical infarcts and leukoencephalopathy), a rare familial form of non-hypertensive SVD with an age of onset in the second or third decade of life (Fukutake, 2011; Nozaki et al., 2014). As the acronym implies, it shows an overlap in clinical and histopathological features with CADASIL, with cardinal neurological features being early onset lacunar stroke primarily in the basal ganglia or brainstem, extensive white matter abnormalities and premature cognitive decline. Clinically, it can be differentiated from CADASIL mainly due to the recessive inheritance pattern and the extraneurological symptoms such as premature baldness and spondylosis. Histological analysis typically reveals extensive pathological alterations of the cerebral vasculature including vessel wall thickening, vessel lumen narrowing, elastic lamina splitting and VSMC loss (Oide et al., 2008; Tikka et al., 2014). CARASIL is caused by mutations in the conserved serine protease HTRA1 (high temperature requirement A1) through a loss-of-function mechanism attributed to a reduction of its proteolytic capacity or to mRNA instability (Hara et al., 2009; Shiga et al., 2011; Beaufort et al., 2014; Nozaki et al., 2014). Heterozygous HTRA1 mutations were further found to cause a dominant, late-onset form of SVD with a milder phenotype (Verdura et al., 2015), but whether this condition results from haploinsufficiency or a dominant-negative effect is an unresolved issue (Nozaki et al., 2016). HTRA1 is a primarily secreted protease and a member of a conserved protein family, which has well documented roles in cellular quality control processes in bacteria and plants (Clausen et al., 2011). The function of human HTRA1 is less clear, but findings over the last decade including the proteomic studies described below indicate a crucial role in balancing the extracellular proteome.

CEREBRAL AMYLOID ANGIOPATHY

Cerebral amyloid angiopathy is a brain condition frequently associated with Alzheimer's disease (AD) and characterized by the accumulation of Aβ peptides in the cerebral vasculature (Charidimou et al., 2017). Its major clinical presentations are spontaneous intracerebral hemorrhage, cognitive impairment and dementia, with MRI signatures including multiple, strictly lobar cerebral microbleeds, white matter hyperintensities, cortical microinfarcts and enlarged perivascular spaces. Despite its close molecular and clinical relationship with AD, CAA remains clinically distinct (Viswanathan and Greenberg, 2011). The overall cognitive profile of CAA patients, which primarily comprises executive dysfunction and impaired processing speed with relatively preserved episodic memory, is more similar to that seen in classic VCI (Charidimou et al., 2017). The vasculopathic changes include fibrinoid necrosis, VSMC loss and vessel wall thickening (Attems et al., 2011), degenerative processes also observed in ischemic SVD. Nevertheless, CAA differs from non-amyloid SVD in various aspects: First, it preferentially affects small arterioles and capillaries of the leptomeninges and cerebral cortex, without necessarily involving white matter vessels; second, it lacks association with hypertension, arteriosclerosis and other common vascular risk factors; and third, it is mainly observed in posterior lobar brain regions (especially the occipital lobes), whereas basal ganglia and brainstem are usually spared (Reijmer et al., 2016). Two different types of CAA can be distinguished, with type 1 (capillary CAA) being characterized by Aβ deposition in capillaries (with or without involvement of larger vessels), and type 2 showing Aβ pathology exclusively in leptomeningeal and cortical arteries (Attems et al., 2011). Current evidence suggests that cerebrovascular Aβ accumulation is largely driven by a failure to efficiently clear parenchymal Aβ via perivascular routes (Carare et al., 2013; Weller et al., 2015). While the molecular mechanisms leading to the arteriopathy are largely unknown, alterations in ECM structure and composition, similar to ischemic SVD, likely play a critical role (Morris et al., 2014).

PROTEOMIC STUDIES IN SVD

Liquid chromatography/tandem mass spectrometry (LC-MS/MS) has become an invaluable technology for global proteomic analyses of tissues under physiological and pathophysiological conditions, allowing the elucidation of disease-relevant molecular processes and pathways (Aebersold and Mann, 2016). In recent years a number of proteomic studies have been conducted on cerebrovascular tissue isolated from CADASIL and CAA post-mortem samples to determine the disease-specific proteome profiles and revealed a distinct set of proteins enriched in both disorders with unexpected consistency (**Table 1**). In two of the four CADASIL studies, laser-capture microdissection was used to isolate brain artery material, resulting in the identification of a relatively low total number of proteins (Arboleda-Velasquez et al., 2011; Nagatoshi et al., 2017). Arboleda-Velasquez et al. (2011) used subcortical white matter tissue from two patients and two healthy control individuals and semiquantitative evaluation based on peptide counts revealed a small set of proteins enriched in patients. One of the most strongly accumulating proteins was clusterin, an extracellular chaperone with functional features similar to heat shock proteins (see below). Clusterin enrichment was confirmed by immunohistochemistry and shown to also occur in the cerebrovasculature of a CADASIL

TABLE 1 | Summary of major proteins with increased abundance in proteomic SVD studies.

Disease	Study	Tissue/vessel type	Proteins					
			SAP	TIMP3	VTN	APOE	CLU	HTRA1
CADASIL	Arboleda-Velasquez et al., 2011	Autopsy, laser-microdissected subcortical arterioles	ND	ND	ND	ND	↑	ND
	Monet-Lepretre et al., 2013	Autopsy, enriched GOM from isolated brain vessels	↑	↑	↑	↑	↑	↑
	Nagatoshi et al., 2017	Autopsy, biopsy, laser-microdissected leptomeningeal vessels	↑	=	↑	ND	=	=
	Zellner et al., 2018	Autopsy, isolated cortical and subcortical vessels	↑	↑	↑	↑	↑	↑
CAA	Manousopoulou et al., 2017	Autopsy, Isolated leptomeningeal vessels	↑	↑	↑	↑	↑	ND
	Inoue et al., 2017	Autopsy, laser-microdissected leptomeningeal vessels	=	=	↑	↑	↑	ND
	Hondius et al., 2018	Autopsy, laser-microdissected brain vessels	↑	ND	ND	↑	↑	↑
	Endo et al., 2019	Biopsy, laser-microdissected leptomeningeal and cortical vessels	ND	=	↑	↑	↑	ND

↑ Increased abundance = no significant abundance difference ND not detected or data not available. Proteins investigated in more detail in individual studies are highlighted. SAP, serum amyloid P component; TIMP3, tissue inhibitor of metalloproteinases 3; VTN, vitronectin; APOE, apolipoprotein E; CLU, clusterin; HTRA1, high temperature requirement A1 protease.

mouse model (Arboleda-Velasquez et al., 2011). Furthermore, immuno-electron microscopy analysis suggested its presence in human GOM deposits. An independent histological analysis of a larger number of post-mortem samples confirmed the clusterin enrichment in patient vessels, especially in white matter arteries, but a colocalization with GOM deposits could not be observed (Craggs et al., 2016). In the proteomic study by Nagatoshi et al. (2017) leptomeningeal arteries from two autopsied patients and the superficial temporal artery from one biopsied patient were used, but LC-MS/MS analysis yielded only a few proteins consistently detected in both the patient and control group. Label-free quantification revealed serum amyloid P component (SAP), annexin A2, and periostin as most strongly enriched proteins, but only SAP accumulation could be confirmed by immunohistochemistry. It was further shown to colocalize with Notch3^{ECD} aggregates in patient brain tissue sections and to interact with a recombinant Notch3^{ECD} fragment *in vitro* indicating involvement in GOM formation. The plasma protein SAP is a well-known universal constituent of human amyloid deposits and might be a general component of extracellular protein aggregates (see below) (Pepys, 2018).

In the study by Monet-Lepretre et al. (2013) the proteomics work on CADASIL was extended by establishing a method to isolate brain vessels from human autopsy material and by enriching GOM using a biochemical fractionation procedure. After nanoLC-MS/MS performed on material from one CADASIL patient and one control subject and subsequent quantification by peptide counting, a number of proteins with increased abundance were identified including clusterin and SAP. Enrichment was also observed for the two matrisomal proteins tissue inhibitor of metalloproteinases 3 (TIMP3) and vitronectin as well as for HTRA1, the serine protease genetically associated with CARASIL (see above). TIMP3 and vitronectin were shown to colocalize with GOM deposits, to bind to Notch3^{ECD} *in vitro* and to also accumulate in brain vessels of a CADASIL mouse model. From these and other studies (Kast et al., 2014; Lee et al., 2014; Zhang et al., 2015), it became increasingly clear, that the accumulation of ECM proteins represents a critical step in CADASIL pathogenesis likely causing a dysregulation of ECM homeostasis and multifactorial toxicity (Joutel et al., 2016). To provide further support for this hypothesis in a larger cohort and with increased proteome depth, Zellner et al. (2018) conducted label-free quantitative LC-MS/MS on brain vessels from six patients carrying five different Notch3 mutations and six age-matched healthy controls. For the first time, a truly quantitative comparison in combination with meaningful statistical evaluation of protein abundance changes in CADASIL was performed. An improved protocol of the brain vessel isolation technique published by Monet-Lepretre et al. (2013) was used, but no fractionation applied, resulting in the determination of a proteomic whole-vessel profile, in which matrisomal components were strongly overrepresented. The set of significantly enriched proteins included clusterin, TIMP3, vitronectin, SAP as well as HTRA1. Accumulation of HTRA1 was confirmed by quantitative immunoblotting, and its colocalization with Notch3^{ECD} deposits demonstrated by confocal immunofluorescence microscopy (Zellner et al., 2018). In addition, enrichment of several ECM proteins previously reported as HTRA1 substrates was noticed, suggesting reduced HTRA1 activity in the cerebrovasculature of CADASIL patients. To further substantiate this finding, the brain vessel proteome from HTRA1 knockout mice was determined to obtain a definite HTRA1 deficiency profile. Proteins accumulating in this profile were considered likely HTRA1 substrates and thus indicators for a loss of catalytic function. The comparison with the CADASIL profile indeed revealed a significant overlap which included clusterin, TIMP3, vitronectin and a number of other, mostly matrisomal proteins. Several previously uncharacterized, putative substrates were shown to be processed by HTRA1 in an *in vitro* assay (Zellner et al., 2018). These findings indicated the presence of a HTRA1 loss-of-function signature in the CADASIL vessel proteome and provided an unexpected mechanistical link between CADASIL and HTRA1-related SVDs. Proteomic analyses in CARASIL patients with genetically compromised HTRA1 activity have so far not been reported, likely due to the rareness of the disease. The discovery of affected heterozygous

mutation carriers might facilitate the realization of such studies in the future (Verdura et al., 2015).

Proteomic approaches have also been applied in CAA to determine protein abundance changes associated with excessive vascular Aβ deposition (**Table 1**). Manousopoulou et al. (2017) performed quantitative LC-MS on leptomeningeal vessels isolated from autopsy tissue of four patients with severe arterial and capillary CAA. From the set of proteins with increased abundance, clusterin and TIMP3 were selected for immunohistochemistry analysis and shown to be enriched in leptomeningeal, but not cortical arteries and to largely colocalize with Aβ deposits. In the study by Inoue et al. (2017) laser capture microdissection was used to isolate vascular material from leptomeningeal arteries and neocortical arterioles from eight cases with severe CAA. Quantitative LC/MS-MS revealed enrichment of a variety of proteins including apolipoprotein E (APOE), vitronectin and clusterin. Sushi repeat-containing protein X-linked 1 (SRPX1), an apoptosis inducer in tumor cells previously described as SRPX, was investigated in more detail and shown in brain sections to co-accumulate with vascular Aβ deposits. SRPX mRNA levels were found to be increased in patient vessels and in primary cultures of cerebrovascular smooth muscle cells treated with Aβ peptides, indicating a transcriptional effect as cause of the observed enrichment (Inoue et al., 2017). SRPX was further shown to bind Aβ peptides *in vitro* and to enhance Aβ-induced caspase activity in cultured VSMCs. It was therefore proposed to promote Aβ-induced cerebrovascular degeneration in CAA. SRPX1 was not found to be enriched in most of the other proteomic studies and is therefore not further discussed.

The study by Hondius et al. (2018) investigated capillary (type I) CAA as a frequent comorbidity in AD and compared the proteomic profiles of microdissected gray matter material (including vessels) from AD cases with and without vascular amyloid pathology. After label-free quantification clusterin emerged as most significantly enriched protein in the CAA group extending the results of an earlier histological investigation (Verbeek et al., 1998). CAA-specific accumulation was also observed for norrin (NDP) and collagen α2(VI) (COL6A2) and colocalization with perivascular Aβ deposits demonstrated by immunohistochemistry. In contrast, APOE and SAP were found to be enriched in both the CAA and the AD group. HTRA1 was detected in none of the control samples and in only one AD sample, but in all CAA samples prompting the authors to claim its CAA-specific accumulation (Hondius et al., 2018). In partial agreement with this, immunohistochemistry staining associated with Aβ deposits was more intense in CAA than in AD tissue sections, a finding confirming the results of an earlier study (Grau et al., 2005). Vascular APOE and HTRA1 accumulation was also reported in Tg-SwDI mice, a CAA model carrying three human amyloid precursor protein (APP) mutations (Swedish, Dutch and Iowa) (Searcy et al., 2014). A quantitative comparison of the proteomic profiles of older mice exhibiting prominent vascular amyloid pathology with younger mice showing minimal Aβ deposition revealed APOE and HTRA1 as the proteins with the largest abundance increase. For both, the accumulation was confirmed by immunohistochemistry, but no clear colocalization with Aβ deposits could be observed. In the proteomic study by Endo et al. (2019) quantitative analysis was performed on biopsied, microdissected samples of leptomeningeal and cortical vessels obtained from six CAA patients who had underwent surgery for large lobar hemorrhages. Clusterin and APOE were most strongly enriched and their effects on Aβ aggregation investigated using an *in vitro* model of CAA recapitulating the intramural periarterial drainage process. Physiological concentrations of APOE and clusterin delayed the initiation time of Aβ aggregation kinetics in a concentration-dependent manner and thus, both were proposed to represent extracellular chaperones inhibiting vascular Aβ deposition.

EXTRACELLULAR PROTEOSTASIS IN SVD

Despite the substantial differences in sensitivity, depth and quantification methodology of the described proteomic studies in CADASIL and CAA, they yielded a shared set of proteins showing enrichment with a relatively high consistency (**Table 1**). However, these proteins differ substantially in structure and function and are thus likely to contribute to disease pathogenesis in different ways (**Figure 1**). SAP, TIMP3 and vitronectin might associate with pathologic protein deposits primarily for structural reasons resulting in aggregate stabilization and/or growth. SAP is an abundant plasma protein of the pentraxin family and has gained a great deal of attention through its role as universal constituent of human amyloid deposits of all types including senile plaques in AD and vascular Aβ deposits in CAA (Pepys, 2018). It has been shown to avidly bind to and stabilize amyloid fibrils, possibly in an attempt to opsonize them for phagocytosis. Its depletion from the blood circulation was reported to result in the destabilization of amyloid deposits leading to the initiation of clinical trials in systemic amyloidosis and AD to investigate its therapeutic potential (Richards et al., 2015). SAP was also found to inhibit the heat-induced formation of amorphous aggregates, an activity believed to be relevant in protein misfolding during inflammatory processes (Ozawa et al., 2016). A role in non-amyloid protein aggregation is now further suggested by its accumulation observed in three of the four proteomic CADASIL studies as well as by its colocalization with $Notch3^{ECD}$ deposits and its binding to $Notch3^{ECD}$ *in vitro* (Nagatoshi et al., 2017).

Tissue inhibitor of metalloproteinases 3 (TIMP3) is a matrisomal protein well known for its role in ECM homeostasis. It controls the activity of proteases degrading matrix components and catalyzing the shedding of ectodomains from cell surface proteins (Arpino et al., 2015). Although TIMP3 enrichment was found in only one of the CAA studies, the presented immunohistochemistry results clearly support the conclusion of Aβ-associated accumulation (Manousopoulou et al., 2017). Similarly, TIMP3 was shown to colocalize with $Notch3^{ECD}$ deposits in CADASIL-affected vessels (Monet-Lepretre et al., 2013). Moreover, increased TIMP3 levels were also observed in a CADASIL mouse model and follow-up experiments suggested an impairment of a signaling cascade regulating arterial smooth

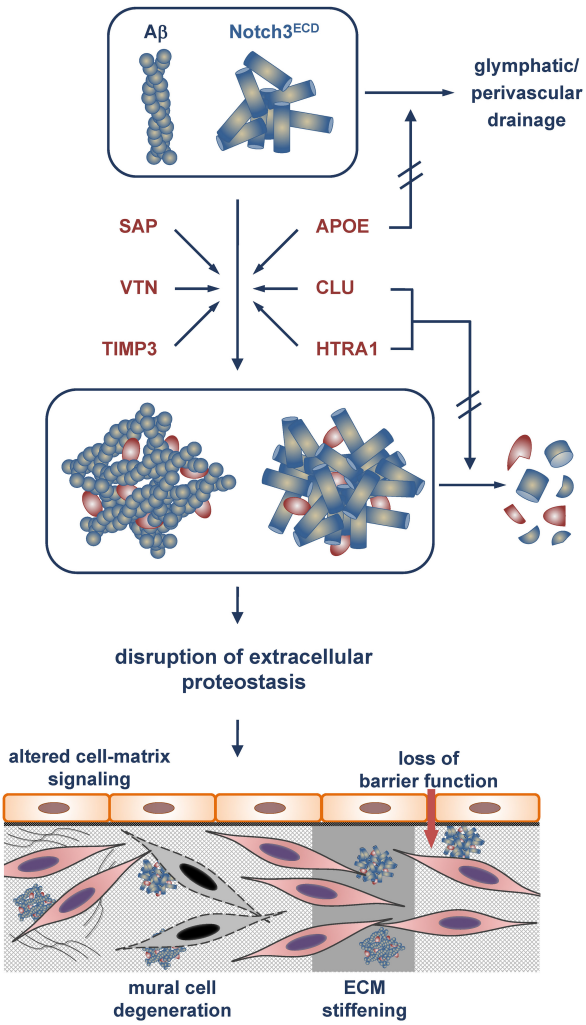

FIGURE 1 | Model of Aβ and Notch3^{ECD} aggregate formation and proteostasis disruption in the brain vessel wall. Incorporation of the metastable proteins SAP, vitronectin (VTN) and TIMP3 with an increased tendency toward misfolding stabilizes Aβ and Notch3^{ECD} aggregates and/or accelerates aggregate growth. Excessive recruitment of the chaperones/clearance factors APOE, clusterin (CLU) and HTRA1 results in their depletion from the proteostasis network and a reduction or even loss of their activity. While APOE is impaired in its role in clearing of Aβ (and other misfolded proteins) from the brain (e.g., via glymphatic/perivascular pathways), clusterin and HTRA1 are compromised in their tasks to promote aggregate removal or degradation. The eventual disruption of extracellular proteostasis initiates a variety of pathophysiological processes including dysregulation of cell-matrix signaling, mural cell degeneration, alteration of physical ECM properties such as stiffness and loss of barrier function.

muscle cell activity leading to cerebral blood flow deficits (Capone et al., 2016b), a symptom known to occur early in CADASIL pathogenesis. Genetic mutations in the *TIMP3* gene result in Sorsby fundus dystrophy (SFD) (Anand-Apte et al., 2019), a rare, dominantly inherited, adult-onset retinal dystrophy clinically and histopathologically related to age-related macular degeneration, the most common cause of blindness in adults. SFD is characterized by the presence of drusen, extracellular deposits located below the basement membrane of the retinal pigment epithelium. TIMP3 shows a striking structural similarity to Notch3 in that its primary sequence contains an even number of cysteines all forming disulfide bonds (Anand-Apte et al., 2019). Very similar to CADASIL mutations SFD-causing variants are typically missense mutations altering the number of cysteine residues and enhancing TIMP3 multimerization/aggregation. It is thus conceivable that the recruitment of TIMP3 to Aβ and Notch3^{ECD} aggregates promotes TIMP3 misfolding resulting in a further enhancement of the aggregation process. Also vitronectin is a well-known ECM component and a major adhesive protein of the extracellular environment (Leavesley et al., 2013). It interacts with a multitude of proteins and promotes cell adhesion, spreading, and migration. Its accumulation in three of the four proteomic CAA studies extends previous histological studies which showed enrichment in the senile plaques of AD patients (Shin et al., 2008; Winter et al., 2015). Vitronectin was furthermore reported to be able to form spherical oligomers as well as typical amyloid fibrils *in vitro* which are toxic for cultured cells (Shin et al., 2008). Its role in Notch3^{ECD} aggregation has not been investigated yet, but its genetic reduction in a CADASIL mouse model led to a reversal of white matter pathology, although the underlying molecular mechanisms remained unclear (Capone et al., 2016a). Thus, SAP, TIMP3 and vitronectin might represent metastable proteins, whose tendency toward misfolding and multimerization is enhanced upon recruitment to Notch3^{ECD} or Aβ deposits.

In contrast, APOE, clusterin and HTRA1 accumulation in CADASIL and CAA is likely to follow a different mechanism due to their established or presumed ability to act as molecular chaperones. APOE has long been known for its role in modulating AD and CAA risk (depending on the combination of the three human isoforms APOE2, APOE3 and APOE4) and for its ability to bind Aβ peptides and to be recruited to amyloid deposits (Yu et al., 2014). It has been suggested to modulate Aβ deposition in a variety of ways: (1) acceleration of Aβ aggregation and deposition, (2) facilitation of Aβ uptake by microglia, astrocytes and neurons, (3) enhancement of enzymatic Aβ degradation, and (4) facilitation of Aβ clearance via transport across the blood-brain barrier or by drainage via the interstitial fluid or the perivasculature. The identification of APOE as major accumulating factor in all the proteomic CAA studies as well as in the Tg-SwDI mouse model extends previous histological analyses (Verbeek et al., 1998) and provides further support for an important role of APOE in CAA pathogenesis. Some insight into a potential mechanism was gained in the study by Endo et al. (2019) in which an *in vitro* model of CAA recapitulating the intramural periarterial drainage pathway was used and an inhibitory role of APOE on the early phase of vascular Aβ deposition reported. The impact of APOE on Notch3^{ECD} in CADASIL is more difficult to assess, since no follow-up studies have been published to date. The influence of the APOE genotype on clinical CADASIL features was investigated in two studies, but while in one increased white matter hyperintensity volumes in *APOE2*, but not *APOE4* carriers were reported (Gesierich et al., 2015), in the other no association with MRI lesion volumes or disease phenotype (age of onset, presence of stroke) could

be detected (Singhal et al., 2004). Interestingly, two studies demonstrated proteolytic APOE processing by HTRA1 (Chu et al., 2016; Munoz et al., 2018) providing a potential link to HTRA1-related SVDs.

Clusterin is a ubiquitously and constitutively expressed protein present in a wide range of tissues and body fluids (Wilson and Zoubeidi, 2017). It is involved in a number of cellular processes including inhibition of the complement system, lipid transport, regulation of cell survival and cell death pathways and has often been referred to as an extracellular chaperone. Its accumulation reported in all four CAA proteome studies is in agreement with earlier histological findings (Verbeek et al., 1998; Craggs et al., 2016) and its well-established link to AD (Foster et al., 2019). Clusterin is able to bind a wide range of Aβ oligomers (from dimers to 50-mers) and to interfere with Aβ peptide aggregation and amyloid fibril formation *in vitro* (Narayan et al., 2012). It further promotes Aβ clearance in a variety of experimental settings (Wojtas et al., 2017; Endo et al., 2019). From these observations, an anti-amyloidogenic role of clusterin due to its chaperone function was deduced, but studies on clusterin knockout mice have not provided clear answers on its neuroprotective function and fueled the ongoing controversy about its beneficial role in amyloid diseases (Foster et al., 2019). The detection of clusterin enrichment in three of the four proteomic CADASIL studies suggests a role also in non-amyloid protein aggregation. However, conflicting results have been reported about its precise colocalization with Notch3^{ECD} aggregates. Whereas Arboleda-Velasquez et al. (2011) reported the presence of clusterin in GOM deposits, Craggs et al. (2016) were unable to confirm this finding and even showed a clear separation of clusterin and Notch3 immunofluorescence staining patterns in patient vessels. They nevertheless observed a correlation between clusterin levels and white matter pathology scores, not only in CADASIL, but also in other leukoencephalopathies, suggesting a more general role of clusterin in ischemic SVD.

The proteomic results on the serine protease HTRA1 might have the most far-reaching impact on our understanding of SVD pathomechanisms. Its involvement in cerebrovascular disease had first become clear with the discovery of its genetic association with monogenic recessive and dominant hereditary SVD forms (Hara et al., 2009; Verdura et al., 2015). The realization of the loss-of-function nature of pathogenic HTRA1 mutations indicated a critical role of its catalytic activity for normal cerebrovascular function. However, the substrates involved in SVD pathogenesis as well as the molecular processes affected by HTRA1 deficiency including a possible dysregulation of TGFβ signaling have not yet been clearly determined (Hara et al., 2009; Shiga et al., 2011; Beaufort et al., 2014). The accumulation of HTRA1 in CADASIL and the high degree of colocalization with Notch3^{ECD} deposits *in vivo* provided further support of its key role in the brain microvasculature (Monet-Lepretre et al., 2013; Zellner et al., 2018). Moreover, the phenotypic similarities between CADASIL and the HTRA1-related SVDs as well as the extensive overlap between the proteomic CADASIL signature and the murine HTRA1 loss-of-function profile strongly suggest a role of HTRA1-mediated substrate processing also in CADASIL (Monet-Lepretre et al., 2013; Zellner et al., 2018). APOE, vitronectin and TIMP3 have all been shown in earlier studies to be processed by HTRA *in vitro*, and for APOE even isoform-specific differences were reported, with APOE4 more efficiently cleaved compared to APOE3 (An et al., 2010; Chu et al., 2016; Munoz et al., 2018). Thus, a loss in HTRA1 catalytic activity might contribute to the accumulation of these proteins under pathophysiological conditions. A link between HTRA1 and Aβ metabolism was first indicated by the demonstration of HTRA1-mediated degradation of Aβ peptides *in vitro* and the colocalization of HTRA1 with parenchymal and perivascular Aβ deposits (Grau et al., 2005). In subsequent studies, HTRA1 was shown to also degrade tau protein in monomeric and fibrillar form (Tennstaedt et al., 2012). The degradation of tau fibrils was furthermore reported to involve the disintegration of the fibrillar core structure and the subsequent solubilization of fibrils allowing productive interaction of aggregated polypeptides with the active site of HTRA1 for rapid degradation (Poepsel et al., 2015). Thus, HTRA1 apparently combines chaperone and protease activity in a single polypeptide and might be able to efficiently dissolve and degrade pathological protein aggregates thereby antagonizing neurodegeneration caused by excessive protein aggregation (Shorter, 2017). The proteomic findings in CAA patients and the Tg-SwDI mouse model, most importantly those of the Hondius et al. (2018) study, showing preferential HTRA1 accumulation in vascular Aβ deposits, suggest that its function might especially be important in cerebrovascular Aβ biology.

CONCLUSION

Proteomic studies on human cerebrovascular tissue have identified several extracellular proteins accumulating with unexpected consistency in CADASIL and CAA, two neurovascular conditions caused by protein misfolding and aggregation. The enrichment of the same set of proteins in two different types of protein deposits suggests the contribution of shared pathways to pathogenesis. A search for these proteins within the mouse brain vasculome, a previously determined transcriptome of cerebral endothelial cells (Guo et al., 2012), revealed only a marginal overlap, arguing against this cell type as a major source of the accumulating proteins. Although the molecular details of cerebrovascular protein aggregation are still largely unknown, the identified proteins might facilitate disease progression by two different mechanisms (**Figure 1**). SAP, TIMP3 and vitronectin appear to be incorporated into preexisting protein deposits mainly due to their metastability, thus contributing directly to aggregate stabilization or growth and exerting a gain-of-toxic-function effect. In contrast, APOE, clusterin and HTRA1 are possibly actively recruited to pathological protein aggregates due to their chaperone function within the extracellular proteostasis network. Under physiological conditions they facilitate the refolding of misfolded proteins or promote their removal either by degradation or

by clearance via vascular routes. The permanent encroachment of chaperone capacity under pathophysiological conditions, e.g., during aging or due to genetic mutations, will inevitably result in a network overload. This process is aggravated by the excessive recruitment of chaperones to protein deposits resulting in their sequestration and depletion, tantamount to a loss-of-function mechanism (Balchin et al., 2016). Thus, cerebrovascular disease might be the result of a combination of a gain-of-toxic-function and loss-of-function effect, similar to scenarios discussed in neurodegenerative disorders such as Parkinson's disease (Winklhofer et al., 2008; Benskey et al., 2016). The consequences of a disruption of extracellular proteostasis on the functionality of cerebral vessels are largely unknown, but they are likely to include the dysregulation of cell-matrix signaling, the degeneration of mural cells, alterations of physical ECM properties such as stiffness, and loss of barrier function (**Figure 1**). Whether impaired extracellular proteostasis might also contribute to pathologies of the brain microvasculature not associated with excessive protein aggregation such as arteriolosclerosis is currently difficult to assess, largely due to the lack of appropriate proteomic studies. While substantial alterations in the vessel architecture are a key pathological finding in sporadic SVD, a causal link to disrupted proteostasis has so far not been established. The further elucidation of proteostasis mechanisms will undoubtedly advance our understanding of the physiological and pathophysiological processes underlying brain health and disease.

AUTHOR CONTRIBUTIONS

CH wrote the manuscript and prepared the figure.

FUNDING

This work was supported by the German Research Foundation (DFG) (HA 2448/6-1).

REFERENCES

Aebersold, R., and Mann, M. (2016). Mass-spectrometric exploration of proteome structure and function. *Nature* 537, 347–355. doi: 10.1038/nature19949

An, E., Sen, S., Park, S. K., Gordish-Dressman, H., and Hathout, Y. (2010). Identification of novel substrates for the serine protease HTRA1 in the human RPE secretome. *Invest. Ophthalmol. Vis. Sci.* 51, 3379–3386. doi: 10.1167/iovs.09-4853

Anand-Apte, B., Chao, J. R., Singh, R., and Stohr, H. (2019). Sorsby fundus dystrophy: insights from the past and looking to the future. *J. Neurosci. Res.* 97, 88–97. doi: 10.1002/jnr.24317

Arboleda-Velasquez, J. F., Manent, J., Lee, J. H., Tikka, S., Ospina, C., Vanderburg, C. R., et al. (2011). Hypomorphic Notch 3 alleles link Notch signaling to ischemic cerebral small-vessel disease. *Proc. Natl. Acad. Sci. U.S.A.* 108, E128–E135. doi: 10.1073/pnas.1101964108

Arpino, V., Brock, M., and Gill, S. E. (2015). The role of TIMPs in regulation of extracellular matrix proteolysis. *Matrix Biol.* 4, 247–254. doi: 10.1016/j.matbio.2015.03.005

Attems, J., Jellinger, K., Thal, D. R., and Van Nostrand, W. (2011). Review: sporadic cerebral amyloid angiopathy. *Neuropathol. Appl. Neurobiol.* 37, 75–93. doi: 10.1111/j.1365-2990.2010.01137.x

Balch, W. E., Morimoto, R. I., Dillin, A., and Kelly, J. W. (2008). Adapting proteostasis for disease intervention. *Science* 319, 916–919. doi: 10.1126/science.1141448

Balchin, D., Hayer-Hartl, M., and Hartl, F. U. (2016). In vivo aspects of protein folding and quality control. *Science* 353:aac4354. doi: 10.1126/science.aac4354

Beaufort, N., Scharrer, E., Kremmer, E., Lux, V., Ehrmann, M., Huber, R., et al. (2014). Cerebral small vessel disease-related protease HtrA1 processes latent TGF-beta binding protein 1 and facilitates TGF-beta signaling. *Proc. Natl. Acad. Sci. U.S.A.* 111, 16496–16501. doi: 10.1073/pnas.1418087111

Benskey, M. J., Perez, R. G., and Manfredsson, F. P. (2016). The contribution of alpha synuclein to neuronal survival and function - Implications for Parkinson's disease. *J. Neurochem.* 137, 331–359. doi: 10.1111/jnc.13570

Capone, C., Cognat, E., Ghezali, L., Baron-Menguy, C., Aubin, D., Mesnard, L., et al. (2016a). Reducing Timp3 or vitronectin ameliorates disease manifestations in CADASIL mice. *Ann. Neurol.* 79, 387–403. doi: 10.1002/ana.24573

Capone, C., Dabertrand, F., Baron-Menguy, C., Chalaris, A., Ghezali, L., Domenga-Denier, V., et al. (2016b). Mechanistic insights into a TIMP3-sensitive pathway constitutively engaged in the regulation of cerebral hemodynamics. *eLife* 5:e17536. doi: 10.7554/eLife.17536

Carare, R. O., Hawkes, C. A., Jeffrey, M., Kalaria, R. N., and Weller, R. O. (2013). Review: cerebral amyloid angiopathy, prion angiopathy, CADASIL and the spectrum of protein elimination failure angiopathies (PEFA) in neurodegenerative disease with a focus on therapy. *Neuropathol. Appl. Neurobiol.* 39, 593–611. doi: 10.1111/nan.12042

Chabriat, H., Joutel, A., Dichgans, M., Tournier-Lasserve, E., and Bousser, M. G. (2009). CADASIL. *Lancet Neurol.* 8, 643–653. doi: 10.1016/s1474-4422(09)70127-9

Charidimou, A., Boulouis, G., Gurol, M. E., Ayata, C., Bacskai, B. J., Frosch, M. P., et al. (2017). Emerging concepts in sporadic cerebral amyloid angiopathy. *Brain* 140, 1829–1850. doi: 10.1093/brain/awx047

Chiti, F., and Dobson, C. M. (2017). Protein misfolding, amyloid formation, and human disease: a summary of progress over the last decade. *Annu. Rev. Biochem.* 86, 27–68. doi: 10.1146/annurev-biochem-061516-45115

Chu, Q., Diedrich, J. K., Vaughan, J. M., Donaldson, C. J., Nunn, M. F., Lee, K. F., et al. (2016). HtrA1 proteolysis of ApoE in vitro is allele selective. *J. Am. Chem. Soc.* 138, 9473–9478. doi: 10.1021/jacs.6b03463

Clausen, T., Kaiser, M., Huber, R., and Ehrmann, M. (2011). HTRA proteases: regulated proteolysis in protein quality control. *Nat. Rev. Mol. Cell Biol.* 12, 152–162. doi: 10.1038/nrm3065

Coupland, K., Lendahl, U., and Karlstrom, H. (2018). Role of NOTCH3 mutations in the cerebral small vessel disease cerebral autosomal dominant arteriopathy with subcortical infarcts and leukoencephalopathy. *Stroke* 49, 2793–2800. doi: 10.1161/STROKEAHA.118.021560

Craggs, L., Taylor, J., Slade, J. Y., Chen, A., Hagel, C., Kuhlenbaeumer, G., et al. (2016). Clusterin/apolipoprotein J immunoreactivity is associated with white matter damage in cerebral small vessel diseases. *Neuropathol. Appl. Neurobiol.* 42, 194–209. doi: 10.1111/nan.12248

Duering, M., Karpinska, A., Rosner, S., Hopfner, F., Zechmeister, M., Peters, N., et al. (2011). Co-aggregate formation of CADASIL-mutant NOTCH3: a single-particle analysis. *Hum. Mol. Genet.* 20, 3256–3265. doi: 10.1093/hmg/ddr237

Endo, Y., Hasegawa, K., Nomura, R., Arishima, H., Kikuta, K. I., Yamashita, T., et al. (2019). Apolipoprotein E and clusterin inhibit the early phase of amyloid-beta aggregation in an in vitro model of cerebral amyloid angiopathy. *Acta Neuropathol. Commun.* 7:12. doi: 10.1186/s40478-019-0662-1

Foster, E. M., Dangla-Valls, A., Lovestone, S., Ribe, E. M., and Buckley, N. J. (2019). Clusterin in Alzheimer's Disease: mechanisms, genetics, and lessons from other pathologies. *Front. Neurosci.* 13:164. doi: 10.3389/fnins.2019.00164

Fukutake, T. (2011). Cerebral autosomal recessive arteriopathy with subcortical infarcts and leukoencephalopathy (CARASIL): from discovery to gene identification. *J. Stroke Cerebrovasc. Dis.* 20, 85–93. doi: 10.1016/j.jstrokecerebrovasdis.2010.11.008

Gesierich, B., Opherk, C., Rosand, J., Gonik, M., Malik, R., Jouvent, E., et al. (2015). APOE varepsilon2 is associated with white matter hyperintensity volume

in CADASIL. *J. Cereb. Blood Flow Metab.* 36, 199–203. doi: 10.1038/jcbfm.2015.85

Ghosh, M., Balbi, M., Hellal, F., Dichgans, M., Lindauer, U., and Plesnila, N. (2015). Pericytes are involved in the pathogenesis of cerebral autosomal dominant arteriopathy with subcortical infarcts and leukoencephalopathy. *Ann. Neurol.* 78, 887–900. doi: 10.1002/ana.24512

Grau, S., Baldi, A., Bussani, R., Tian, X., Stefanescu, R., Przybylski, M., et al. (2005). Implications of the serine protease HtrA1 in amyloid precursor protein processing. *Proc. Natl. Acad. Sci. U.S.A.* 102, 6021–6026. doi: 10.1073/pnas.0501823102

Grinberg, L. T., and Thal, D. R. (2010). Vascular pathology in the aged human brain. *Acta Neuropathol.* 119, 277–290. doi: 10.1007/s00401-010-0652-7

Guo, S., Zhou, Y., Xing, C., Lok, J., Som, A. T., Ning, M., et al. (2012). The vasculome of the mouse brain. *PLoS One* 7:e52665. doi: 10.1371/journal.pone.0052665

Haffner, C., Malik, R., and Dichgans, M. (2016). Genetic factors in cerebral small vessel disease and their impact on stroke and dementia. *J. Cereb. Blood Flow Metab.* 36, 158–171. doi: 10.1038/jcbfm.2015.71

Hara, K., Shiga, A., Fukutake, T., Nozaki, H., Miyashita, A., Yokoseki, A., et al. (2009). Association of HTRA1 mutations and familial ischemic cerebral small-vessel disease. *N. Engl. J. Med.* 360, 1729–1739. doi: 10.1056/NEJMoa0801560

Hartl, F. U., Bracher, A., and Hayer-Hartl, M. (2011). Molecular chaperones in protein folding and proteostasis. *Nature* 475, 324–332. doi: 10.1038/nature10317

Henshall, T. L., Keller, A., He, L., Johansson, B. R., Wallgard, E., Raschperger, E., et al. (2015). Notch3 is necessary for blood vessel integrity in the central nervous system. *Arterioscler. Thromb. Vasc. Biol.* 35, 409–420. doi: 10.1161/ATVBAHA.114.304849

Hipp, M. S., Kasturi, P., and Hartl, F. U. (2019). The proteostasis network and its decline in ageing. *Nat. Rev. Mol. Cell Biol.* 20, 421–435. doi: 10.1038/s41580-019-0101-y

Hondius, D. C., Eigenhuis, K. N., Morrema, T. H. J., van der Schors, R. C., van Nierop, P., Bugiani, M., et al. (2018). Proteomics analysis identifies new markers associated with capillary cerebral amyloid angiopathy in Alzheimer's disease. *Acta Neuropathol. Commun.* 6:46. doi: 10.1186/s40478-018-0540-2

Iadecola, C. (2013). The pathobiology of vascular dementia. *Neuron* 80, 844–866. doi: 10.1016/j.neuron.2013.10.008

Inoue, Y., Ueda, M., Tasaki, M., Takeshima, A., Nagatoshi, A., Masuda, T., et al. (2017). Sushi repeat-containing protein 1: a novel disease-associated molecule in cerebral amyloid angiopathy. *Acta Neuropathol.* 134, 605–617. doi: 10.1007/s00401-017-1720-z

Jellinger, K. A. (2013). Pathology and pathogenesis of vascular cognitive impairment-a critical update. *Front. Aging Neurosci.* 5:17. doi: 10.3389/fnagi.2013.00017

Joutel, A. (2011). Pathogenesis of CADASIL: transgenic and knock-out mice to probe function and dysfunction of the mutated gene, Notch3, in the cerebrovasculature. *Bioessays* 33, 73–80. doi: 10.1002/bies.201000093

Joutel, A., Haddad, I., Ratelade, J., and Nelson, M. T. (2016). Perturbations of the cerebrovascular matrisome: a convergent mechanism in small vessel disease of the brain? *J. Cereb. Blood Flow Metab.* 36, 143–157. doi: 10.1038/jcbfm.2015.62

Kalaria, R. N. (2018). The pathology and pathophysiology of vascular dementia. *Neuropharmacology* 134(Pt B), 226–239. doi: 10.1016/j.neuropharm.2017.12.030

Kalimo, H., Ruchoux, M. M., Viitanen, M., and Kalaria, R. N. (2002). CADASIL: a common form of hereditary arteriopathy causing brain infarcts and dementia. *Brain Pathol.* 12, 371–384. doi: 10.1111/j.1750-3639.2002.tb00451.x

Kast, J., Hanecker, P., Beaufort, N., Giese, A., Joutel, A., Dichgans, M., et al. (2014). Sequestration of latent TGF-beta binding protein 1 into CADASIL-related Notch3-ECD deposits. *Acta Neuropathol. Commun.* 2:96. doi: 10.1186/s40478-014-0096-8

Kofler, N. M., Cuervo, H., Uh, M. K., Murtomaki, A., and Kitajewski, J. (2015). Combined deficiency of Notch1 and Notch3 causes pericyte dysfunction, models CADASIL, and results in arteriovenous malformations. *Sci. Rep.* 5:16449. doi: 10.1038/srep16449

Labbadia, J., and Morimoto, R. I. (2015). The biology of proteostasis in aging and disease. *Annu. Rev. Biochem.* 84, 435–464. doi: 10.1146/annurev-biochem-060614-33955

Leavesley, D. I., Kashyap, A. S., Croll, T., Sivaramakrishnan, M., Shokoohmand, A., Hollier, B. G., et al. (2013). Vitronectin–master controller or micromanager? *IUBMB Life* 65, 807–818. doi: 10.1002/iub.1203

Lee, S. J., Zhang, X., and Wang, M. M. (2014). Vascular accumulation of the small leucine-rich proteoglycan decorin in CADASIL. *Neuroreport* 25, 1059–1063. doi: 10.1097/WNR.0000000000000230

Machuca-Parra, A. I., Bigger-Allen, A. A., Sanchez, A. V., Boutabla, A., Cardona-Velez, J., Amarnani, D., et al. (2017). Therapeutic antibody targeting of Notch3 signaling prevents mural cell loss in CADASIL. *J. Exp. Med.* 214, 2271–2282. doi: 10.1084/jem.20161715

Manousopoulou, A., Gatherer, M., Smith, C., Nicoll, J. A. R., Woelk, C. H., Johnson, M., et al. (2017). Systems proteomic analysis reveals that clusterin and tissue inhibitor of metalloproteinases 3 increase in leptomeningeal arteries affected by cerebral amyloid angiopathy. *Neuropathol. Appl. Neurobiol.* 43, 492–504. doi: 10.1111/nan.12342

Monet-Lepretre, M., Haddad, I., Baron-Menguy, C., Fouillot-Panchal, M., Riani, M., Domenga-Denier, V., et al. (2013). Abnormal recruitment of extracellular matrix proteins by excess Notch3 ECD: a new pathomechanism in CADASIL. *Brain* 136, 1830–1845. doi: 10.1093/brain/awt092

Morris, A. W., Carare, R. O., Schreiber, S., and Hawkes, C. A. (2014). The cerebrovascular basement membrane: role in the clearance of beta-amyloid and cerebral amyloid angiopathy. *Front. Aging Neurosci.* 6:251. doi: 10.3389/fnagi.2014.00251

Morris, A. W., Sharp, M. M., Albargothy, N. J., Fernandes, R., Hawkes, C. A., Verma, A., et al. (2016). Vascular basement membranes as pathways for the passage of fluid into and out of the brain. *Acta Neuropathol.* 131, 725–736. doi: 10.1007/s00401-016-1555-z

Munoz, S. S., Li, H., Ruberu, K., Chu, Q., Saghatelian, A., Ooi, L., et al. (2018). The serine protease HtrA1 contributes to the formation of an extracellular 25-kDa apolipoprotein E fragment that stimulates neuritogenesis. *J. Biol. Chem.* 293, 4071–4084. doi: 10.1074/jbc.RA117.001278

Nagatoshi, A., Ueda, M., Ueda, A., Tasaki, M., Inoue, Y., Ma, Y., et al. (2017). Serum amyloid P component: a novel potential player in vessel degeneration in CADASIL. *J. Neurol. Sci.* 379, 69–76. doi: 10.1016/j.jns.2017.05.033

Narayan, P., Meehan, S., Carver, J. A., Wilson, M. R., Dobson, C. M., and Klenerman, D. (2012). Amyloid-beta oligomers are sequestered by both intracellular and extracellular chaperones. *Biochemistry* 51, 9270–9276. doi: 10.1021/bi301277k

Nozaki, H., Kato, T., Nihonmatsu, M., Saito, Y., Mizuta, I., Noda, T., et al. (2016). Distinct molecular mechanisms of HTRA1 mutants in manifesting heterozygotes with CARASIL. *Neurology* 86, 1964–1974. doi: 10.1212/WNL.0000000000002694

Nozaki, H., Nishizawa, M., and Onodera, O. (2014). Features of cerebral autosomal recessive arteriopathy with subcortical infarcts and leukoencephalopathy. *Stroke* 45, 3447–3453. doi: 10.1161/strokeaha.114.004236

Oide, T., Nakayama, H., Yanagawa, S., Ito, N., Ikeda, S., and Arima, K. (2008). Extensive loss of arterial medial smooth muscle cells and mural extracellular matrix in cerebral autosomal recessive arteriopathy with subcortical infarcts and leukoencephalopathy (CARASIL). *Neuropathology* 28, 132–142. doi: 10.1111/j.1440-1789.2007.00864.x

Ozawa, D., Nomura, R., Mangione, P. P., Hasegawa, K., Okoshi, T., Porcari, R., et al. (2016). Multifaceted anti-amyloidogenic and pro-amyloidogenic effects of C-reactive protein and serum amyloid P component in vitro. *Sci. Rep.* 6:29077. doi: 10.1038/srep29077

Pantoni, L. (2010). Cerebral small vessel disease: from pathogenesis and clinical characteristics to therapeutic challenges. *Lancet Neurol.* 9, 689–701. doi: 10.1016/S1474-4422(10)70104-6

Pepys, M. B. (2018). The Pentraxins 1975-2018: serendipity, diagnostics and drugs. *Front. Immunol.* 9:2382. doi: 10.3389/fimmu.2018.02382

Poepsel, S., Sprengel, A., Sacca, B., Kaschani, F., Kaiser, M., Gatsogiannis, C., et al. (2015). Determinants of amyloid fibril degradation by the PDZ protease HTRA1. *Nat. Chem. Biol.* 11, 862–869. doi: 10.1038/nchembio.1931

Rasmussen, M. K., Mestre, H., and Nedergaard, M. (2018). The glymphatic pathway in neurological disorders. *Lancet Neurol.* 17, 1016–1024. doi: 10.1016/S1474-4422(18)30318-1

Reijmer, Y. D., van Veluw, S. J., and Greenberg, S. M. (2016). Ischemic brain injury in cerebral amyloid angiopathy. *J. Cereb. Blood Flow Metab.* 36, 40–54. doi: 10.1038/jcbfm.2015.88

Richards, D. B., Cookson, L. M., Berges, A. C., Barton, S. V., Lane, T., Ritter, J. M., et al. (2015). Therapeutic clearance of amyloid by antibodies to serum amyloid p component. *N. Engl. J. Med.* 373, 1106–1114. doi: 10.1056/NEJMoa1504942

Rutten, J. W., Haan, J., Terwindt, G. M., van Duinen, S. G., Boon, E. M., and Lesnik Oberstein, S. A. (2014). Interpretation of NOTCH3 mutations in the diagnosis of CADASIL. *Expert Rev. Mol. Diagn.* 14, 593–603. doi: 10.1586/14737159.2014.922880

Searcy, J. L., Le Bihan, T., Salvadores, N., McCulloch, J., and Horsburgh, K. (2014). Impact of age on the cerebrovascular proteomes of wild-type and Tg-SwDI mice. *PLoS One* 9:e89970. doi: 10.1371/journal.pone.0089970

Shiga, A., Nozaki, H., Yokoseki, A., Nihonmatsu, M., Kawata, H., Kato, T., et al. (2011). Cerebral small-vessel disease protein HTRA1 controls the amount of TGF-beta1 via cleavage of proTGF-beta1. *Hum. Mol. Genet.* 20, 1800–1810. doi: 10.1093/hmg/ddr063

Shin, T. M., Isas, J. M., Hsieh, C. L., Kayed, R., Glabe, C. G., Langen, R., et al. (2008). Formation of soluble amyloid oligomers and amyloid fibrils by the multifunctional protein vitronectin. *Mol. Neurodegener.* 3:16. doi: 10.1186/1750-1326-3-16

Shorter, J. (2017). Designer protein disaggregases to counter neurodegenerative disease. *Curr. Opin. Genet. Dev.* 44, 1–8. doi: 10.1016/j.gde.2017.01.008

Siebel, C., and Lendahl, U. (2017). notch signaling in development, tissue homeostasis, and disease. *Physiol. Rev.* 97, 1235–1294. doi: 10.1152/physrev.00005.2017

Singhal, S., Bevan, S., Barrick, T., Rich, P., and Markus, H. S. (2004). The influence of genetic and cardiovascular risk factors on the CADASIL phenotype. *Brain* 127(Pt 9), 2031–2038. doi: 10.1093/brain/awh223

Tan, R., Traylor, M., Rutten-Jacobs, L., and Markus, H. (2017). New insights into mechanisms of small vessel disease stroke from genetics. *Clin. Sci.* 131, 515–531. doi: 10.1042/CS20160825

Tennstaedt, A., Popsel, S., Truebestein, L., Hauske, P., Brockmann, A., Schmidt, N., et al. (2012). Human high temperature requirement serine protease A1 (HTRA1) degrades tau protein aggregates. *J. Biol. Chem.* 287, 20931–20941. doi: 10.1074/jbc.M111.316232

Tikka, S., Baumann, M., Siitonen, M., Pasanen, P., Poyhonen, M., Myllykangas, L., et al. (2014). CADASIL and CARASIL. *Brain Pathol.* 24, 525–544. doi: 10.1111/bpa.12181

Verbeek, M. M., Otte-Holler, I., Veerhuis, R., Ruiter, D. J., and De Waal, R. M. (1998). Distribution of A beta-associated proteins in cerebrovascular amyloid of Alzheimer's disease. *Acta Neuropathol.* 96, 628–636.

Verdura, E., Herve, D., Scharrer, E., Amador Mdel, M., Guyant-Marechal, L., Philippi, A., et al. (2015). Heterozygous HTRA1 mutations are associated with autosomal dominant cerebral small vessel disease. *Brain* 138, 2347–2358. doi: 10.1093/brain/awv155

Vinters, H. V., Zarow, C., Borys, E., Whitman, J. D., Tung, S., Ellis, W. G., et al. (2018). Review: vascular dementia: clinicopathologic and genetic considerations. *Neuropathol. Appl. Neurobiol.* 44, 247–266. doi: 10.1111/nan.12472

Viswanathan, A., and Greenberg, S. M. (2011). Cerebral amyloid angiopathy in the elderly. *Ann. Neurol.* 70, 871–880. doi: 10.1002/ana.22516

Wardlaw, J. M., Smith, C., and Dichgans, M. (2019). Small vessel disease: mechanisms and clinical implications. *Lancet Neurol.* 18, 684–696. doi: 10.1016/S1474-4422(19)30079-1

Weller, R. O., Hawkes, C. A., Kalaria, R. N., Werring, D. J., and Carare, R. O. (2015). White matter changes in dementia: role of impaired drainage of interstitial fluid. *Brain Pathol.* 25, 63–78. doi: 10.1111/bpa.12218

Wilson, M. R., and Zoubeidi, A. (2017). Clusterin as a therapeutic target. *Expert Opin. Ther. Targets* 21, 201–213. doi: 10.1080/14728222.2017.1267142

Winklhofer, K. F., Tatzelt, J., and Haass, C. (2008). The two faces of protein misfolding: gain- and loss-of-function in neurodegenerative diseases. *EMBO J.* 27, 336–349. doi: 10.1038/sj.emboj.7601930

Winter, M., Tholey, A., Kruger, S., Schmidt, H., and Rocken, C. (2015). MALDI-mass spectrometry imaging identifies vitronectin as a common constituent of amyloid deposits. *J. Histochem. Cytochem.* 63, 772–779. doi: 10.1369/0022155415595264

Wojtas, A. M., Kang, S. S., Olley, B. M., Gatherer, M., Shinohara, M., Lozano, P. A., et al. (2017). Loss of clusterin shifts amyloid deposition to the cerebrovasculature via disruption of perivascular drainage pathways. *Proc. Natl. Acad. Sci. U.S.A.* 114, E6962–E6971. doi: 10.1073/pnas.1701137114

Wyatt, A. R., Yerbury, J. J., Ecroyd, H., and Wilson, M. R. (2013). Extracellular chaperones and proteostasis. *Annu. Rev. Biochem.* 82, 295–322. doi: 10.1146/annurev-biochem-072711-163904

Yamamoto, Y., and Ihara, M. (2017). Disruption of transforming growth factor-beta superfamily signaling: a shared mechanism underlying hereditary cerebral small vessel disease. *Neurochem. Int.* 107, 211–218. doi: 10.1016/j.neuint.2016.12.003

Yu, J. T., Tan, L., and Hardy, J. (2014). Apolipoprotein E in Alzheimer's disease: an update. *Annu. Rev. Neurosci.* 37, 79–100. doi: 10.1146/annurev-neuro-071013-14300

Zellner, A., Scharrer, E., Arzberger, T., Oka, C., Domenga-Denier, V., Joutel, A., et al. (2018). CADASIL brain vessels show a HTRA1 loss-of-function profile. *Acta Neuropathol.* 136, 111–125. doi: 10.1007/s00401-018-1853-8

Zhang, X., Lee, S. J., Young, M. F., and Wang, M. M. (2015). The small leucine-rich proteoglycan BGN accumulates in CADASIL and binds to NOTCH3. *Transl. Stroke Res.* 6, 148–155. doi: 10.1007/s12975-014-0379-1

Conflict of Interest: The author declares that the research was conducted in the absence of any commercial or financial relationships that could be construed as a potential conflict of interest.

Copyright © 2019 Haffner. This is an open-access article distributed under the terms of the Creative Commons Attribution License (CC BY). The use, distribution or reproduction in other forums is permitted, provided the original author(s) and the copyright owner(s) are credited and that the original publication in this journal is cited, in accordance with accepted academic practice. No use, distribution or reproduction is permitted which does not comply with these terms.

frontiers in Neuroscience

REVIEW
published: 19 November 2019
doi: 10.3389/fnins.2019.01194

Successes and Hurdles in Stem Cells Application and Production for Brain Transplantation

Daniel Henriques[1,2†], Ricardo Moreira[1,2†], Jens Schwamborn[3], Luís Pereira de Almeida[1,2,4‡] and Liliana S. Mendonça[1,2*‡]*

[1] Center for Neuroscience and Cell Biology, University of Coimbra, Coimbra, Portugal, [2] Center for Innovative Biomedicine and Biotechnology, University of Coimbra, Coimbra, Portugal, [3] Luxembourg Centre for Systems Biomedicine, University of Luxembourg, Esch-sur-Alzette, Luxembourg, [4] Faculty of Pharmacy, University of Coimbra, Coimbra, Portugal

OPEN ACCESS

Edited by:
Johannes Boltze,
The University of Warwick,
United Kingdom

Reviewed by:
Aurel Popa-Wagner,
Essen University Hospital, Germany
Miroslaw Janowski,
Johns Hopkins University,
United States

***Correspondence:**
Luís Pereira de Almeida
luispa@cnc.uc.pt;
lpereiradealmeida@gmail.com
Liliana S. Mendonça
liliana.mendonca@cnc.uc.pt;
liliana.s.mendonca@gmail.com

[†] These authors have contributed equally to this work and share first authorship
[‡] These authors have contributed equally to this work and share senior authorship

Specialty section:
This article was submitted to Neurodegeneration, a section of the journal Frontiers in Neuroscience

Received: 28 June 2019
Accepted: 21 October 2019
Published: 19 November 2019

Citation:
Henriques D, Moreira R, Schwamborn J, Pereira de Almeida L and Mendonça LS (2019) Successes and Hurdles in Stem Cells Application and Production for Brain Transplantation. Front. Neurosci. 13:1194. doi: 10.3389/fnins.2019.01194

Brain regenerative strategies through the transplantation of stem cells hold the potential to promote functional rescue of brain lesions caused either by trauma or neurodegenerative diseases. Most of the positive modulations fostered by stem cells are fueled by bystander effects, namely increase of neurotrophic factors levels and reduction of neuroinflammation. Nevertheless, the ultimate goal of cell therapies is to promote cell replacement. Therefore, the ability of stem cells to migrate and differentiate into neurons that later become integrated into the host neuronal network replacing the lost neurons has also been largely explored. However, as most of the preclinical studies demonstrate, there is a small functional integration of graft-derived neurons into host neuronal circuits. Thus, it is mandatory to better study the whole brain cell therapy approach in order to understand what should be better comprehended concerning graft-derived neuronal and glial cells migration and integration before we can expect these therapies to be ready as a viable solution for brain disorder treatment. Therefore, this review discusses the positive mechanisms triggered by cell transplantation into the brain, the limitations of adult brain plasticity that might interfere with the neuroregeneration process, as well as some strategies tested to overcome some of these limitations. It also considers the efforts that have been made by the regulatory authorities to lead to better standardization of preclinical and clinical studies in this field in order to reduce the heterogeneity of the obtained results.

Keywords: stem cells transplantation, brain, neuronal integration and survival, adult brain plasticity, regulatory framework

INTRODUCTION

In 1868, the German biologist Haeckel coined the term "stem cell" (Haeckel, 1868), proposing in Natural Creation Story (Natürliche Schöpfungsgeschichte) that each organism came from one cell. Since then, many authors have contributed to the growing knowledge of the stem cell research field. Dunn's (1917) study is credited as the first clear evidence of successful transplantation of central nervous system (CNS) tissue into the brain of adult mammals, with clear survival of the transplanted neonatal cortex tissue (Dunn, 1917). Others followed her steps, providing more evidence of the successful introduction of new brain cells into the adult mammalian brain.

Nevertheless, the prevailing dogma at the time that the adult brain is devoid of plasticity would impair a real paradigm change, and therefore the field of cell transplantation into the brain would have to wait until the 1970s and 1980s to be really launched (reviewed in Bjorklund and Stenevi, 1985; Dunnett, 2010).

A remarkable study in the field of neural cells transplantation has been the work conducted by Perlow et al. (1979), producing the first robust evidence of functional recovery upon rat fetal brain tissue implantation in rat adult brain whose dopaminergic input to the caudate had been destroyed. Additionally, in the same year, Beebe et al. (1979) demonstrated for the first time that transplants of embryonic brain tissue originate extensive axonal networks forming synaptic connections with the host brain. Other landmark studies were the improvements in motor function of patients with Parkinson's disease (PD) observed by Lindvall et al. (1990), promoted by transplantation of grafts of fetal dopaminergic neurons (Lindvall et al., 1992), as well as the more recent observation that a patient with PD, 24 years upon being transplanted with human cells derived from embryonic ventral mesencephalon, presented graft-derived dopaminergic reinnervation of the putamen (Li et al., 2016).

Moreover, in the last decades important studies promoted the development of new sources of stem cells prone to be tested for human transplantation, such as the establishment of lines of human embryonic stem cells (ESC), and cell reprograming that culminated in the development of induced pluripotent stem cells (iPSC) and their derived cells (Gurdon, 1962; Gurdon et al., 1975; Davis et al., 1987; Thomson et al., 1998; Takahashi and Yamanaka, 2006).

These studies carried us to the concept of stem cell-based personalized medicines and to the possibility of generating potentially any type of cell from a specialized cell by reprograming it. Thus, presently, we must ask what should be the next steps to keep moving forward. Certainly, there is much to know about the stem cells' potential and safety as regenerative approaches, but there is much more to know about the limitations caused by the restricted plasticity of the adult brain, hampering the migration and functional integration of enough new graft-derived neurons, and glial cells to promote strong neuroregeneration upon brain injury. Moreover, the standardization of preclinical and clinical studies enabling comparison of results obtained in different studies and triggering a faster development of cell-based therapies is also essential.

CELL-BASED THERAPY FOR BRAIN REGENERATION

Cell therapy consists of the use of cells or cell-based products in order to replace dead or defective cells with the purpose of restoring the tissue or organ functions lost in the disease or trauma process (Lindvall et al., 2004; Kim and de Vellis, 2009). There are different types of cells to be considered as a source of cells or as precursors of neural progenitors to be used in brain regeneration (**Figure 1**), namely, ESC obtained from the inner cell mass of the embryo's blastocyst, iPSC obtained by cell reprograming, and neural stem cells that can be isolated from the nervous system at different stages of development, such as fetal and adult neural stem cells (Rippon and Bishop, 2004; Takahashi and Yamanaka, 2006; Kim and de Vellis, 2009). All of these cell types have strengths and drawbacks (Lo and Parham, 2009; Mendonca et al., 2018) and have been tested in different preclinical studies that proved them to be effective in the treatment of PD (Bjorklund et al., 2002; Wernig et al., 2008; Hargus et al., 2010), Huntington's disease (HD) (Dunnett et al., 1998; Johann et al., 2007), and Machado-Joseph disease (MJD) (Mendonca et al., 2015). Importantly, some clinical trials have also demonstrated the great potential of these therapies in diseases like PD (Piccini et al., 1999; Olanow et al., 2003; Li et al., 2016; Bjorklund and Lindvall, 2017) and HD (Freeman et al., 2000). Despite the large number of preclinical studies and some clinical assays, describing positive results with cell therapy approaches for brain transplantation, the mechanisms behind such positive modulation as well as the types of cells promoting it are not fully understood.

Understanding the Mechanism of Recovery Promoted by Stem Cell Transplantation

It has been described that the transplanted cells improve disease symptoms through the integration of new cells derived from the graft, provide trophic support to endogenous cells, and trigger immunomodulation (**Figure 2A**; Pluchino et al., 2005; Xu et al., 2011; Steinbeck and Studer, 2015). Nevertheless, the exact contribution of each of these positive mechanisms in the general improvements observed is unknown.

The functional integration of the graft-derived neurons into the host neuronal networks holds the potential to fully repair the damaged brain areas and rescue behavioral impairments. In fact, it has been suggested in different preclinical studies that the observed behavioral recovery is in part a result of the establishment of new synaptic connections between the brain and the graft (Clarke and Dunnett, 1993; Thompson et al., 2008; Cardoso et al., 2018), and clinical data support this evidence. In a remarkable study, cells derived from human embryonic ventral mesencephalon were transplanted in a PD patient, and 24 years upon the transplantation, authors observed graft-derived dopaminergic reinnervation of the putamen (Li et al., 2016). Nevertheless, most studies indicate that only a small number of graft-derived new neurons functionally integrate into the neuronal network (Cossetti et al., 2012; Forraz et al., 2013; Dunnett and Rosser, 2014). Additionally, given the described glia impairments in various conditions such as stroke, multiple sclerosis (MS), amyotrophic lateral sclerosis (ALS), PD, and Alzheimer's disease (AD) (Miller et al., 2004; Lindvall and Kokaia, 2006; Dzamba et al., 2016; Kokaia et al., 2018), promoting the replacement of these cells has been tested and resulted in important positive outcomes (Windrem et al., 2004; Ericson et al., 2005) (described in more detail in section "Glial Cells Transplantation").

Grafted cells are capable of increasing the survival and recovery of the host neurons by secreting neurotrophic factors

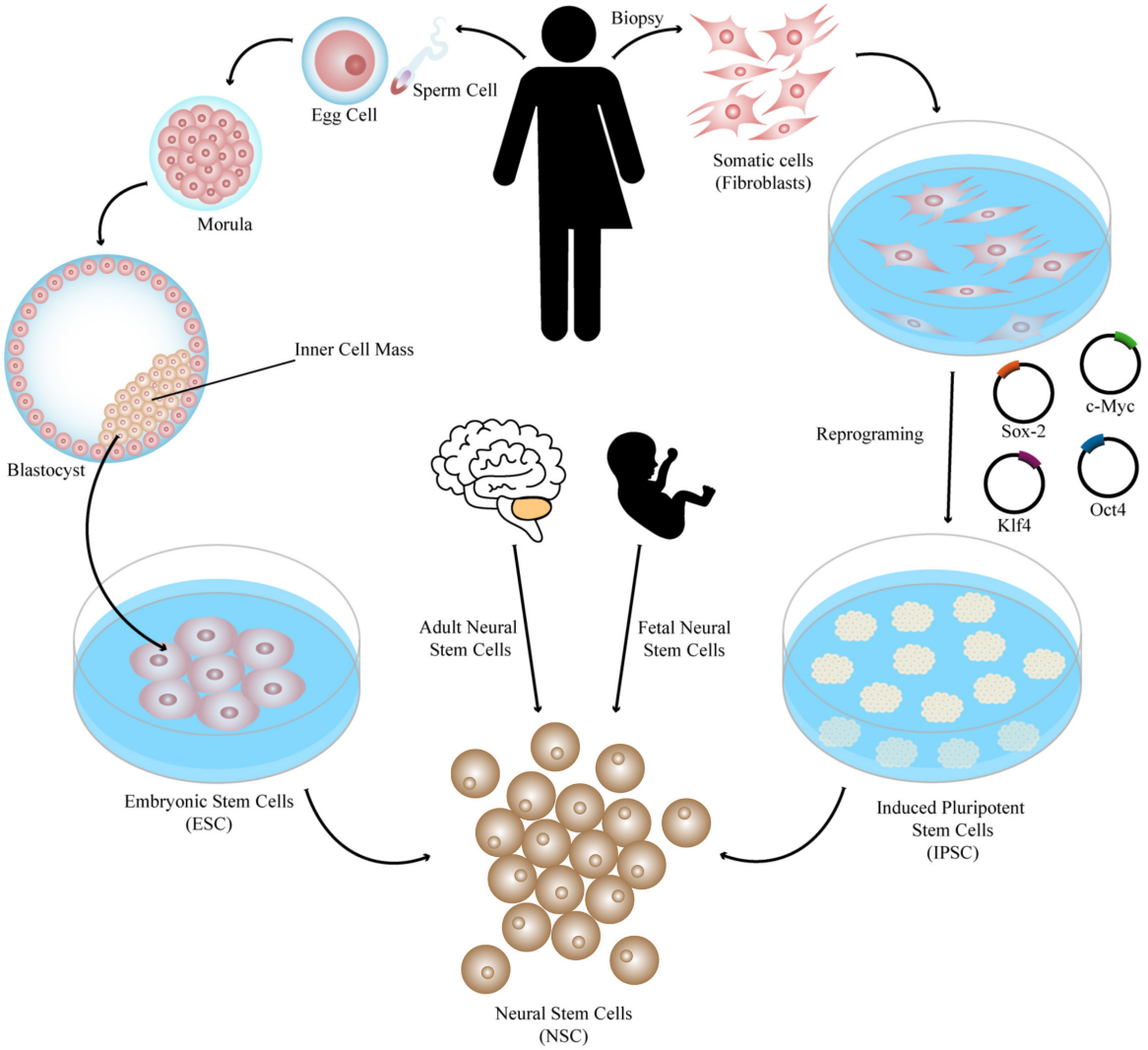

FIGURE 1 | Different sources of stem cells to be used in brain regeneration. Pluripotent stem cells such as ESC obtained from the inner cell mass of the embryo's blastocyst and iPSC obtained by cell reprograming of somatic cells by several protocols, such as expression of the reprograming factors Sox-2, Klf4, c-Myc, and Oct4, can be patterned and differentiated into different types of neural cells to be transplanted such as neural stem cells, which can also be isolated from the nervous system at different stages of development (fetal and adult neural stem cells).

such as brain-derived neurotrophic factor (BDNF), nerve growth factor (NGF), and glial cell-derived neurotrophic factor (GDNF) (Wang et al., 2013; Mendonca et al., 2015; **Figure 2B**), known to positively impact neural cells by promoting survival of host neurons, and survival, migration, and differentiation of the transplanted cells (Kamei et al., 2007; Xu et al., 2011; Ma et al., 2012).

The crosstalk between transplanted stem cells and the immune system (**Figure 2C**) in the brain is another important therapeutic mechanism (Kokaia et al., 2012). In fact, some studies demonstrated that transplanted stem cells decrease neuroinflammation, reducing neuronal death. The work of Pluchino et al. (2005, 2009) provided evidence that replacement of the affected or dead cells might not necessarily be the main mechanism behind the observed recovery upon stem cells transplantation, and it is instead the immune regulation that plays an important role in the observed improvements.

Thus, the transplantation of stem cells into the brain triggers several therapeutic mechanisms, and it would be of great importance to understand which cell type produces the positive effects, how these mechanisms are regulated, and to comprehend which features might be hindering better outcomes, namely in neuronal migration and integration in neuronal circuits of adult brain.

Migration of Transplanted Cells

The brain is an organ with highly complex tissues composed of numerous different types of cells precisely organized. When damaged by trauma or disease, tissue regeneration involves complex processes. For instance, it is necessary that the

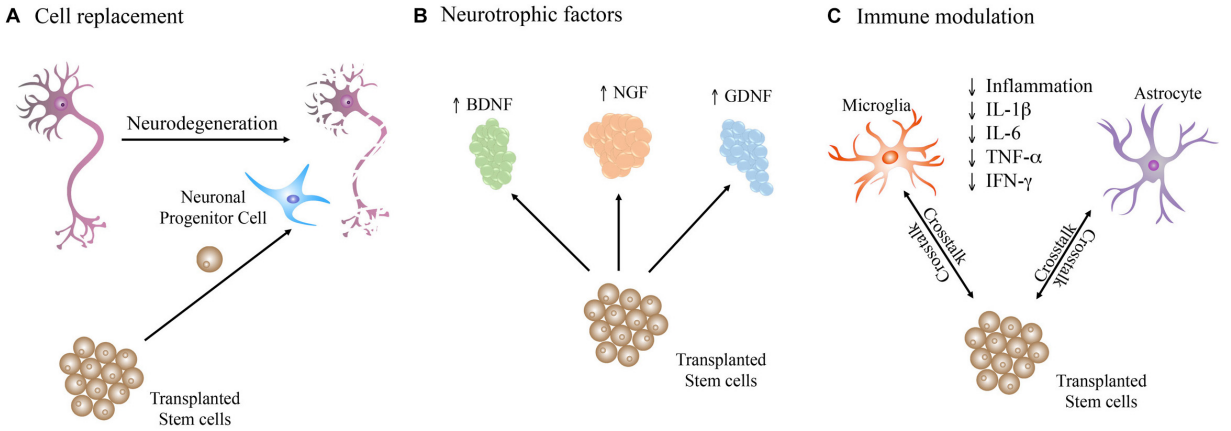

FIGURE 2 | Therapeutic mechanisms triggered by stem cells upon transplantation in the diseased brain. Stem cells may act by **(A)** directly replacing the dead and impaired neurons in the neuronal network. **(B)** Production of neurotrophic factors that support the brain cells homeostasis. **(C)** Crosstalk with brain cells, such as astrocytes and microglia, which play important roles in immune regulation, leading to a reduction in inflammation through decrease of pro-inflammatory cytokines such as IL-1β, IL-6, TNF-α, and IFN-γ.

transplanted cells be able to migrate to the affected areas in order to reach the proper and desired place and to be integrated (Fricker et al., 1999). The brain presents a limited capacity of structural repair after damage, not being able to fully recover from injuries. And in many cases, even if any amelioration of disease symptoms is visible, when the graft is analyzed it is perceived that transplanted cells into the adult brain tend to form clusters close to the site of transplantation demonstrating the low capacity of migration, thus limiting its regenerative capacity (Ladewig et al., 2014). To explain the lack of migration of the transplanted cells and also the low integration into the host brain, many several hypotheses have been suggested and investigated.

The maturity of the donor cells at the time of transplantation is an important aspect of the engraftment success. Different studies have achieved different rates of success when the transplanted cells presented different maturity. Ganat et al. (2012) used three mouse ESC cell lines, modified through the induction of specific cell stage transcription factors that mimic the *in vivo* progression of midbrain dopaminergic neuron development, namely early (Hes5), middle (Nurr1), and late (Pitx3) differentiation. These cells were transplanted into the striatum of adult unilateral 6-OHDA-lesioned immunocompromised mice, a PD mouse model. Authors observed that all cell lines, including the control cell line (parental cell line), originated robust tyrosine hydroxylase positive neurons. Nevertheless, the cell line corresponding to the earlier stage of development (Hes5) had a slightly lower yield than the other two cell lines. Nurr1 cells promoted more robust improvements on behavioral tests, indicating that cells in the middle stage of differentiation were ideal for ESC-derived dopaminergic neuron engraftment (Ganat et al., 2012). In a similar study performed by Payne et al. (2018), cortically specified neuroepithelial stem cells (cNESC) derived from iPSC were transplanted into a stroke-injured rat model 7 days post-injury, and transplantation success was analyzed 7 days later. Similarly to the previous study, the authors attempted to mimic three different stages of cell development. The cNESC were submitted to *in vitro* differentiation, promoted by the withdrawal of factors that maintained the immature state, plus BSA fraction V addition to the culture medium, establishing three different stages of cell maturation: early-differentiated cells at day 0, mid-differentiated at day 16, and late-differentiated stage at day 32 of differentiation. A higher number of graft-derived cells was observed in rats transplanted with the early and mid-differentiated cell groups. The higher number of cells observed was attributed to the survival of the initial transplanted population, demonstrating the importance of cell maturity for cell therapy success. Ladewig et al. (2014) also demonstrated that purified neurons presented increased migratory potential as opposed to neurons transplanted together with neural precursor cells. The authors found that factors such as FGF2 and VEGF expressed by neural progenitor cells, and not by mature neurons, acted as chemoattractants and were responsible for attracting neurons, reducing their migration. Authors demonstrated that chemoattraction inhibition through the pretreatment of cells to be transplanted with FGF2 and VEGF tyrosine kinase receptor inhibitor, the small molecule BIBF1120, or with neutralizing antibodies of FGF2 or receptor-blocking VEGF antibodies resulted in better migration. Furthermore, pretreated cells transplanted into the striatum of adult mice showed an increased extension of the graft, further spreading and generation of a less packed engraftment 1 week after transplantation (Ladewig et al., 2014).

Another hypothesis for the limited cell migration in the adult brain after transplantation lies in the differences between the developing and the adult brain. Looking at the nervous system dynamic composition during development, the role played by radial glial cells in this process is widely known. These cells are highly present during brain development but only a few persist in the adult brain (Barry et al., 2014) making them obvious targets of inquiry concerning possible altered processes in adult brain hindering cell migration. Briefly, the development of the CNS begins as an epithelial sheet that bends and forms

the neural tube, composed by neuroepithelial cells, and then it expands at different rates to form the different areas of the CNS. Afterward, neuroepithelial cells change into radial glial cells retaining epithelial characteristics but becoming highly elongated. Radial glial cells then either directly generate neurons or other radial glial-like cells (intermediate progenitors and basal radial glia), which might later become neurons themselves. When neurons are produced in this stage, they migrate following the radial glia fascicles as a guide from their birthplace to their final locations. Radial glial cells ultimately differentiate into astrocytes and oligodendrocytes, and only a few remain in the adult brain in neurogenic niches (Merkle et al., 2004; Bonfanti and Peretto, 2007). Therefore, radial glial cells are crucial for the correct development of the brain and play a critical role on the migration of new neurons to their right locations (Nulty et al., 2015; Kelava and Lancaster, 2016). Besides the difference in the number of radial glial cells, the environment is also totally different (Gotz et al., 2016). During embryonic development, the surrounding environment promotes neurogenesis, inhibiting gliogenesis, while in the adult brain the predominant fate is gliogenesis (Kempermann et al., 2004; Miller and Gauthier, 2007). The impact of some extrinsic neurogenesis regulators change from the developing to the adult brain, for example, in the adult brain elements such as the blood-brain barrier, astrocytes, oligodendrocytes, and neuronal networks are elements that were absent during early development, which leads to different responses to extrinsic factors like neurotransmitters and growth factors by radial glial cells. This is the case for neurotransmitters like GABA and Glutamate that show opposing effects in the embryo and in the adult brain (Haydar et al., 2000; Nakamichi et al., 2009; Giachino et al., 2014; Gotz et al., 2016).

Other structures that play a role in the limited adult brain plasticity are the perineuronal nets (PNNs), described as a layer of lattice-like extracellular matrix aggregates surrounding the soma and proximal axons and dendrites of some neurons in different locations in the CNS such as the visual cortex (Pizzorusso et al., 2002), deep cerebellar nuclei (Carulli et al., 2006), substantia nigra (Bruckner et al., 2008), and hippocampus (Hylin et al., 2013). These PNNs are composed of different extracellular matrix molecules strongly present in the nervous system, namely chondroitin sulfate proteoglycans (CSPGs), hyaluronan, and link proteins (Kwok et al., 2011). These structures appear after neurodevelopment and are thought to contribute to the stabilization of synapses, limiting neuroplasticity. Nevertheless, PNNs can be modulated (in response to learning, stress or CNS injury/diseases), usually by the action of CSPG-degrading proteases (Lemarchant et al., 2016). A study has shown that degrading PNNs using chondroitinases ABC that remove chondroitin sulfate glycoaminoglycans (side chains attached to CSPG) can render the environment of the damaged CNS more permissive to axon regeneration (Moon et al., 2001). Thus, it is important to better understand the complete role of PNNs and if modulating its function might improve the migration and integration of newborn neurons after transplant.

The limited migratory capacity of the transplanted cells might be a result of a cocktail of conditions hindering cell migration, such as the inadequate maturation stage of the transplanted cells, the absence of guiding cues, and the presence of a supporting extracellular matrix in the adult brain that blocks cell migration. Thus, it is necessary to better comprehend the role played by these processes in the restricted migration that is usually observed in cell-based therapies and to exploit ways to mitigate these issues.

Integration and Survival of New Neurons

The correct integration of graft-derived neurons into the host neuronal circuits is necessary to restore tissue functionality (Isacson et al., 1986; Steinbeck and Studer, 2015). Moreover, the transplanted cells must be capable of extending their neurites over long distances (Quadrato et al., 2014), which is quite demanding in the adult brain. Therefore, one aspect that has been addressed to increase graft integration is the axonal outgrowth, i.e., the projection of axons from the cell body to the target cells. This process is still present in the adult brain but is weakened as compared to the young brain and might contribute to the smaller regenerative capacity of the adult brain (Scheff et al., 1980; Ronn et al., 2000).

Therefore, several strategies have been tested to improve axonal outgrowths, such as genetically modifying the cells to be transplanted to overexpress described factors, exposure of donor cells to modulating compounds (**Table 1**) or making the host more prone to cell migration and axonal outgrowth (Steinbeck and Studer, 2015). Glaser et al. (2007) demonstrated that overexpression of polysialic acid (PSA) in embryonic stem cell-derived glial precursors enhances the cells' sensitivity to migration guidance cues, and recent studies also tested the effect of PSA in axonal outgrowth. PSA is a carbohydrate expressed by neural precursors in both embryonic and adult brain (Hoffman and Edelman, 1983; Rutishauser and Landmesser, 1996) and has a major involvement in important steps of brain development, such as neural precursors migration, neuronal guidance, and synapse formation (Rothbard et al., 1982; Di Cristo et al., 2007; Jiang et al., 2016). Thus, its ability to reduce cell-to-cell interactions has been explored, which, consequently, promotes tissue plasticity (Battista et al., 2014). Battista et al. (2014) observed that the overexpression of the enzymes responsible for PSA synthesis, the polysialyltransferases (PST), resulting in higher PSA levels, led to an increase in axonal growth and enhanced behavioral recovery upon cell transplantation in a PD mouse model. In fact, ESC-derived dopaminergic neuron precursor cells overexpressing PST (Nurr1/PST) and control cells were transplanted into the striatum of 6-OHDA-lesioned mice. Control cells failed to produce any behavioral recovery, whereas with augmented PSA expression, the same number of cells produced significant recovery on PD motor impairments. Two months post-transplantation Nurr1/PST cells presented higher graft survival, more dopaminergic neuronal processes (dendrites and axons), increased axonal outgrowth, and increased synaptic marker synapsin that was correlated with functional recovery. Overall, these data demonstrate the crucial role of axonal outgrowth and graft-host innervation in the behavioral recovery.

Axonal growth in the CNS is often inhibited by molecules associated with adult myelin such as Nogo (Chen et al., 2000), myelin-associated glycoprotein (MAG)

TABLE 1 | Targets and mechanisms of cell replacement modulation.

Target	Strategy	Outcomes	References
Neurotrophic factors (BDNF, NGF, and GDNF)	Expression of Neurotrophic factors by transplanted cells	Survival of host neurons, Survival, migration, and differentiation of transplanted cells	Kamei et al., 2007; Xu et al., 2011; Ma et al., 2012
Cell maturation	Transplant cells with the ideal maturity stage	Increase cell therapy success	Ganat et al., 2012; Payne et al., 2018
Neuroinflammation	Transplantation of cells to decrease neuroinflammation	Reduction of neuronal death	Pluchino et al., 2005, 2009
FGF2 and VEGF	Receptor inhibition; Neutralizing antibodies/receptor-blocking	Enhanced migration	Ladewig et al., 2014
Perineuronal nets (PNNs)	PNNs degradation with CSPGs*-degrading proteases	Render CNS more permissive to axon regeneration	Moon et al., 2001; Lemarchant et al., 2016
Polysialic acid (PSA)	Increase PSA levels: Overexpression of PSA or Overexpression of the enzymes responsible for PSA synthesis	Increased axonal growth	Glaser et al., 2007; Battista et al., 2014
Myelin	Knockdown of Cdh1 to revert myelin associated inhibition of axonal growth	Increased axonal growth	Konishi et al., 2004; Poplawski et al., 2018

CSPGs, chondroitin sulfate proteoglycans.

(McKerracher et al., 1994), and oligodendrocyte myelin glycoprotein (OMgp) (Kottis et al., 2002). Poplawski et al. (2018) recently investigated the interaction of adult myelin with axons extending from stem cell grafts. Plating different types of cells in different substrates, they confirmed that neurite growth from adult dorsal root ganglion (DRG) is inhibited by myelin and increased by laminin. Thus, different studies explored the potential of neutralizing these interactions in order to increase axonal outgrowth. Konishi et al. (2004) showed that inhibiting the anaphase-promoting complex (APC – highly expressed in postmitotic neurons and essential for cell cycle transition) by knockdown of Cdh1 (required for APC activity) enhanced axonal growth in primary cerebellar granule cells from postnatal day 6. Furthermore, they tested these cells' ability to grow axons over myelin substrate. Here, axonal growth in control cells was significantly inhibited whereas the knockdown of Cdh1 reverted the myelin inhibition on axonal growth.

Lipid rafts have also been investigated when it comes to axonal growth and guidance. Lipid rafts are membrane microdomains enriched in cholesterol, glycosphingolipids and many proteins, namely proteins involved in cell signaling (Pike, 2003). As these lipid rafts are important for signaling transduction, they also play a role in neural development, namely the spatial and temporal control mediated by extracellular signals on axonal growth and guidance refereed by extracellular cues (Guirland et al., 2004; Kamiguchi, 2006; Guirland and Zheng, 2007). Age-associated loss of cholesterol in plasma membranes leads to loss of membrane lipid rafts, and consequently a decrease in its function (Egawa et al., 2016). Thus, it is important to investigate whether the age-related loss of membrane lipid rafts might play a critical role in axonal growth and guidance of the transplanted cells in the adult brain. Overall, different approaches have been tested to improve axonal elongation while trying to increase the success of cell-based therapies.

Besides the modulators assessed in this review (**Table 1**), several other molecules and mechanisms play an important role in neuronal migration and integration, such as neurotransmitters (Platel et al., 2010), neurotrophic factors (Waterhouse et al., 2012), and even pathological situations such as neuroinflammation (Whitney et al., 2009; Ryan and Nolan, 2016), which should also be taken into consideration.

Glial Cells Transplantation

Glial cells are crucial for maintaining brain homeostasis, providing support and protection to neurons. Thus, cell therapies aiming at cell replacement in the brain, besides integration of new neurons into the neuronal network, should also consider promoting glial cells replacement, given the aforementioned impairment of these cells in several diseases (Miller et al., 2004; Lindvall and Kokaia, 2006; Dzamba et al., 2016; Kokaia et al., 2018) and also because upon transplantation glial cells promote brain functional recovery, namely by increasing axonal myelination, clearing aggregated proteins, reducing reactive oxygen species, and increasing survival, proliferation, and neural differentiation (Almad and Maragakis, 2012; Kokaia et al., 2018).

Brain trauma and diseases like MS, AD, PD, and leukodystrophy impair the production of new oligodendrocytes and their mediated axonal remyelination process (Bartzokis, 2004, 2011; Braak and Del Tredici, 2004; Franklin and Goldman, 2015). Windrem et al. (2004) showed that after oligodendrocyte progenitor cells transplantation into the forebrains of a leukodystrophy mouse model, the transplanted cells were capable of wide migration and differentiation into astrocytes and oligodendrocytes, showing increased myelin production and axonal myelination 12 weeks post-transplantation, resulting in phenotype improvement. Moreover, Piao and collaborators demonstrated that human ESC-derived oligodendrocytes upon transplantation into the brain of a rat model of radiation-induced demyelination are capable of migrating throughout white matter tracts, resulting in both structural and functional recovery (Piao et al., 2015).

In AD, astrocytes promote neuroprotection by reducing nitric oxide production mediated by microglia (Vincent et al., 1997) and by capturing and degrading Aβ plaques (Koistinaho et al., 2004). Nevertheless, the inability to

continuously degrade these species confers aberrant and cytotoxic properties to astrocytes. Pihlaja and colleagues demonstrated that the transplantation of astrocytes into AD mice expressing human Aβ mediated a 70% reduction of Aβ plaques (Pihlaja et al., 2008) through proteolytic mechanisms (Pihlaja et al., 2011), demonstrating the ability of astrocytes transplantation to reduce the burden of Aβ plaques in the brain of AD mice. Moreover, the transplantation of glia restricted precursors (GRP) in the spinal cord of an ALS rat model, expressing human mutant SOD1, resulted in successful migration, differentiation, and integration of mature astrocytes. These increased the mice lifespan and survival of the motor neurons by neuroprotection mediated in part by the primary astrocyte glutamate transporter GLT1 (Lepore et al., 2008), demonstrating the potential therapeutic potential of astrocytes transplantation for ALS treatment. The transplantation of glial cell progenitors into spinal cord has also been shown to trigger neuroprotection in ALS by Haidet-Phillips and Maragakis (2015). Moreover, the co-transplantation of NSC with astrocytes into the ischemic striatum of a mouse model of stroke (middle cerebral artery occlusion) resulted in better outcomes when compared to transplantation of NSC alone, namely higher survival, proliferation, and neural differentiation of the transplanted NSC (Luo et al., 2017).

In a different approach, Thomsen et al. (2018) targeted cortical neurons through the transplantation of human cortical-derived neural progenitor cells engineered to secrete GDNF into the cortex of a transgenic mouse model of ALS ($SOD1^{G93A}$). The transplanted cells migrated and differentiated into GDNF-releasing astrocytes, which resulted in motor neuron protection, delayed pathology, and extended animal lifespan. Ericson et al. (2005) have previously employed a similar strategy for PD treatment through the transplantation of rat astrocytes, transduced with lentivirus encoding for GDNF, into the striatum or substantia nigra of an adult rat model of PD. Results indicate that GDNF-expressing astrocytes maintained GDNF expression for 12 weeks and promoted neuroprotective effects on nigral tyrosine hydroxylase-positive cells. Moreover, Lundberg et al. (1996) also demonstrated that the transplantation of DOPA-secreting astrocytes into the striatum of a PD rat model (6-hydroxydopamine unilaterally lesioned rats) resulted in significant reduction of motor impairments 2 weeks post-transplantation, providing evidence of the therapeutic potential of *ex vivo* modifying glia to secrete L-DOPA, a keystone neurotransmitter in PD treatment, before transplantation.

Altogether, it has been demonstrated that the transplantation of glia and glial progenitors to improve the survival of other transplanted cells and trigger neuroprotective mechanisms has the potential to be used in the treatment of neurodegenerative diseases.

Impact of Comorbidities in Stem Cell-Based Therapy Outcomes

Most preclinical studies using cell-based therapies have been performed without taking into account comorbidities, which might influence the outcomes of therapeutic strategies (Hermann et al., 2013; Sandu et al., 2015; Pradillo et al., 2017). Evidence indicates that neuroinflammation is one possible common pathway to several diseases, being fueled by conditions such as hypertension, diabetes, atherosclerosis, PD, HD, AD, and aging (Nguyen et al., 2002; Denes et al., 2012; Sandu et al., 2015). Aging is one of the most common risk factors for CNS-related diseases affecting brain function (Mattson and Arumugam, 2018). As the brain ages, several cellular and molecular functions become impaired (Niccoli and Partridge, 2012), leading to multiple modifications such as extensive neuronal loss, decreased neurotransmitters and their receptors levels, impaired myelination, reduced neurotrophic factors levels (Yang et al., 2012; Roozbehi et al., 2015), increased neuroinflammation (Currais, 2015; Deleidi et al., 2015), and decreased neurogenesis (Jinno, 2016) and brain plasticity (Badan et al., 2003). Considering that cell therapies applied to the treatment of brain diseases are frequently used to treat age-related diseases, such as neurodegenerative diseases with late-onset and stroke, aging effects in the therapeutic outcomes must be considered. As described above, the microenvironment of the aged brain is refractory for cell migration, proliferation, and differentiation, hindering the success of the transplanted cells (Della Porta et al., 2014; Conboy et al., 2015). Thus, in order for cell-based therapy preclinical tests to be clinically relevant, they must also be performed in aged animals so as to better predict the *in vivo* efficacy and capacity of the transplanted cells to promote beneficial effects (Popa-Wagner et al., 2014; Tatarishvili et al., 2014; Sandu et al., 2017).

Impact of Combined Therapies in Stem Cell-Based Therapies Outcomes

Given that diseases are frequently multifactorial, combining different therapeutic strategies directed to different molecular and cellular targets may potently improve outcomes. Therefore, a promising therapeutic strategy is the combination of cell transplantation with drugs that act at comorbidities or enhance graft integration and corresponding brain regeneration. An interesting example is the combination of cell transplantation with the growth factor granulocyte colony-stimulating factor (G-CSF) that induces stem cell mobilization. Popa-Wagner et al. (2010) have shown that G-CSF administration after stroke in aged rats enhances neurogenesis and motor function parameters. Balseanu et al. (2014) demonstrated in a stroke rat model that daily intravenous injection of G-CSF led to robust and consistent improvement of neurological functions, which in combination with a single intravenous administration of mesenchymal stromal cells (MSC) resulted in significantly higher density of new blood vessels in the infarct core. However, the combination of G-CSF with bone marrow-derived mononuclear cells (BM MNC) also for stroke treatment led to no advantage over G-CSF treatment alone, suggesting that different outcomes might be achieved depending on the type of cells used (Buga et al., 2015). Sanchez-Ramos et al. (2009) tested G-CSF combination with human umbilical cord blood cell transplantation in a transgenic mouse model of

AD and observed increased neurogenesis, reduced expression of amyloid proteins and inflammation, which resulted in an overall improvement of cognition in these animals. Similarly, another group tested the effect of G-CSF combined with human umbilical cord blood cells (hUCB) on traumatic brain injury (TBI), which reduced neuroinflammation and hippocampal cell loss, enhanced endogenous neurogenesis, and improved motor function, attaining better results than hUCB or G-CSF treatments alone (Acosta et al., 2014). Finally, the combination of statins, such as atorvastatin or simvastatin [promoting reduction of oxidative stress in the brain and clearing disease-causing proteins (Barone et al., 2011; Schultz et al., 2018)], with bone marrow stromal cells and MSC in a rat model of TBI, also resulted in increased cellular proliferation and differentiation, enhanced vascular density and neurological improvements, and behavioral amelioration (Mahmood et al., 2007, 2008).

Overall, the results obtained with combined therapies, including cell transplantation for brain regeneration and neuroprotection, indicate that better outcomes can be attained with this strategy.

STANDARDIZATION OF PRECLINICAL AND CLINICAL STUDIES – THE REGULATORY FRAMEWORK IN THE PARTICULAR CASE OF CELL-BASED THERAPIES

The heterogeneous results obtained upon cell transplantation in some patients (Bachoud-Lévi et al., 2006; Cicchetti et al., 2009; Keene et al., 2009; Mendonca et al., 2018) and the increasing notion that the standardization of the procedures in cell transplantation field would accelerate development and guarantee the safety of new therapeutics (Bachoud-Lévi and Perrier, 2014) resulted in the establishment of several guidelines.

Cellular and gene therapies as well as tissue-engineered products, commonly known as advanced therapy medicinal products (ATMPs), are complex pharmaceutical products that represent a unique and challenging scientific and regulatory framework. Accordingly, to the regulatory framework scope, a cell-based medicinal product must contain viable human cells (of allogenic or autologous origins) that underwent a manufacturing process and may be combined with non-cellular components (such as scaffolds or matrixes) or be genetically modified (CHMP, 2008a). The major concern of regulators is to ensure the safety of these products for the patients, the population, and the environment, as well as to guarantee the efficacy of such treatments and their rapid entry into clinical practice to treat diseases that very often have no other therapeutic alternative (Lapteva et al., 2018).

The creation of regulations and guidance regarding ATMPs are under the responsibility of the European medicines agency (EMA) and the food and drug administration (FDA), in Europe and the United States, respectively. In particular, the advanced therapies are regulated by the committee for advanced therapies (CAT) and the office of cellular, tissue and gene therapies (OCTGT), from the EMA and FDA, respectively. Despite some differences, there are efforts for the harmonization of procedures between all markets under the international council for harmonization (ICH) of technical requirements for pharmaceuticals for human use, composed by the EMA, FDA, and the Japanese regulatory agency (Gee, 2018).

In this section, we review the processes and regulatory particularities regarding cellular and gene therapy from early manufacturing setting, to the definition of non-clinical profiling, and extrapolation to clinical assessments. The inclusion in this review of regulatory guidelines regarding gene therapy is justified by the common use of genetic modifications in cell-based products.

Risk Evaluation

The complexity of these products makes the creation of a single regulatory strategy for the evaluation of risk difficult. Both the EMA and FDA recommend a risk-based approach and a case-by-case analysis for each product regarding their risk assessment. Not only the cellular nature but also the *ex vivo* manipulation, storage and shipment conditions, and pre-application procedures are a source of variability. Thus, EMA suggests that the risk analysis should cover the entire manufacture and non-clinical and clinical assessment of the product. The risk posed by cell-based therapies is dependent on the origin of the cells, the manufacturing process, the non-cellular components, and the therapeutic application, namely the action mechanism of the final product. The risk of cross-contamination of the product in any stage of manufacture is of utmost importance since it can threaten the quality of the final product. In addition, the environmental impact of the reagents used in cell culture must also be assessed (CHMP, 2008b; CAT/CPWP, 2013). The data presented when submitting a clinical trial application or a marketing authorization application must have in consideration the risks presented in risk management plan so that the safety of the product is assured (EMA, 2018).

From a clinical point of view, the main concern regarding cell-based medicinal products is the risk of tumor formation. Hence, cells must not be transplanted in a pluripotent state, which is associated with increased tumor formation. The *in vivo* microenvironment may also induce the cells to acquire tumor-like characteristics and, in turn, cells might induce host-derived tumors. The use of cells with short cell culturing periods is encouraged, given that cell manipulation may cause mutations responsible for tumor formation or loss of therapeutic potential. Moreover, the use of viral vectors for cell reprograming and gene correction might be responsible for the activation of oncogenes, depending on the site of gene insertion. The administration route of the cells is also crucial; intravenous administration is discouraged since cells can aggregate, causing emboli, or can accumulate in undesired peripheral organs, such as lungs, spleen or liver. The immune activation promoted by the cells is also a major issue that needs to be evaluated. Taken together, these represent risks associated with the use of cell-based products that strongly impact the success of these

therapies (Herberts et al., 2011). The type of tests used to characterize the cells and their effects is a critical issue as well. For example, the establishment of tests for the evaluation of a cell's potency, i.e., their biological activity, is particularly demanding given the frequent multiple action mechanisms of the cell-based products that might differ from product to product, and therefore regulatory entities adopted a flexible strategy. EMA, for example, allows the establishment of a product development adapted to its specificities, without a rigid framework with predefined requirements, and the FDA released technical recommendations although they are not mandatory (CBER, 2011; Pimpaneau et al., 2015).

Manufacturing Process

It is often difficult to make the manufacturing process of cell-based medicinal products comply with the regulatory good manufacturing practices (GMP); nevertheless, these processes should be able to characterize, as full as possible, the product at several stages of manufacture and ensure product quality and yield at defined stages. The development of standard operating procedures (SOPs) is critical and the creation of in-process checkpoints to validate product quality and consistency is crucial (CBER, 2008; Carpenter, 2017; EC, 2017, 2018).

For example, in the manufacture of iPSC-derived products, the reprograming *per se* already represents a considerable manipulation of the cells, and it requires the use of manufacturing grade (instead of research grade) reagents that should also be used in the expansion and differentiation steps. The safety testing for infections, such as human immunodeficiency virus (HIV), of the starting materials is essential. For iPSC, the interclone variability after the reprograming should also be taken into consideration, and therefore the selection of the adequate clone for production is crucial since the reprograming could lead to severe karyotype abnormalities and mutations,

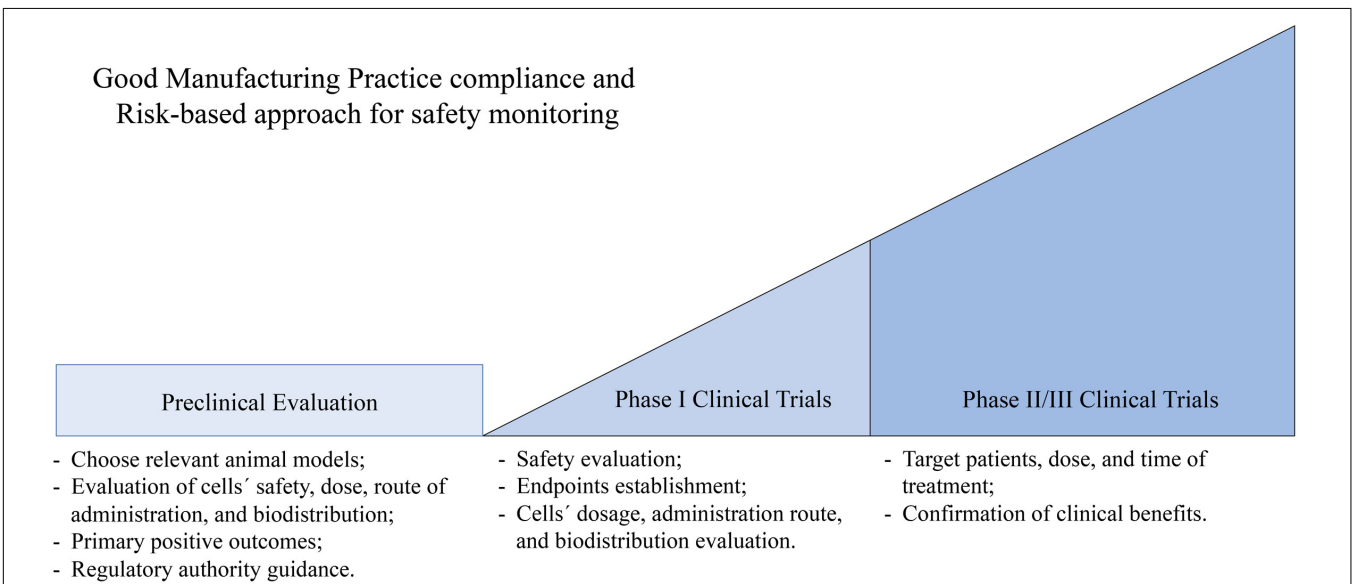

FIGURE 3 | Illustration of some golden checkpoints in the preclinical and clinical evaluation process of cell-based therapies. At a preclinical level when testing cell-based therapies it is important to (i) choose a relevant disease model, (ii) assess cells' safety, dose, biodistribution, and ideal route of administration, (iii) establish primary positive outcomes, and (iv) enter conversations with the regulatory authority. Considering phase I clinical trials, the key points are (i) safety evaluation, (ii) establishment of clearly defined endpoints, and (iii) cells' dosage, administration route, and biodistribution evaluation. In phase II/III clinical trials it is important to establish (i) target patients, dose, and time of the treatment, (ii) clear primary and secondary endpoints, and (iii) sample size should provide statistical power to the endpoint evaluations.

TABLE 2 | Clinical trials using pluripotent stem cells-derived cells in nervous system.

CT	Condition/phase	Title	Type of cells	Sponsors and collaborators
NCT03482050	Amyotrophic lateral sclerosis phase I/IIa	A study to evaluate transplantation of astrocytes derived from human embryonic stem cells in patients with amyotrophic lateral sclerosis (ALS)	AstroRx: Astrocytes derived from human embryonic stem cells	Kadimastem
NCT03119636	Parkinson's disease phase I/II	Safety and efficacy study of human ESC-derived neural precursor cells in the treatment of Parkinson's disease	Embryonic stem cells-derived neural precursor cells	Chinese Academy of Sciences
NCT02452723	Parkinson's disease phase I	A study to evaluate the safety of neural stem cells in patients with Parkinson's disease	Parthenogenetic neural stem cells*	Cyto Therapeutics Pty Limited
NCT02302157	Spinal cord injury phase I/IIa	Dose escalation study of AST-OPC1 in spinal cord injury	Embryonic stem cell-derived oligodendrocyte progenitor cells	Asterias Biotherapeutics, Inc.

*CT, clinical trial number; *, derived from unfertilized oocytes; AST-OPC1, asterias -oligodendrocyte progenitor cell 1.*

which may interfere with the efficiency and safety of the final product. Thus, extensive characterization of phenotype, karyotype, and genotype of these cells is mandatory to ensure compliance with GMP. Furthermore, the expansion, cryopreservation, and differentiation protocols may also affect the quality, safety, and efficacy of the final product. Thus, valid biomarkers for each cell state are imperative; nevertheless, these biomarkers are not yet specified for any cell type used and strongly depend on a case-by-case analysis and on the desired characteristics of the final product (Carpenter, 2017; Stacey et al., 2018).

Non-clinical Evaluation

Non-clinical evaluation of any medicinal product is a crucial step in their development to establish important clinical features such as pharmacodynamics, pharmacokinetics, or toxicology. These tests should be designed in order to establish the initial safe cell doses to be used in humans, the ideal route of administration, the biodistribution of the cells (accessing the organs more susceptible to the therapy/toxicity), and to assess potential side effects (CHMP, 2008a; CBER, 2013b; **Figure 3**).

The correct design of non-clinical testing for cellular therapies should start with the selection of a relevant animal model, which should mimic as closely as possible the pathology in humans, and should allow precise characterization of the treatment. The use of at least two different animal models, desirably from different species, is strongly encouraged. For a clear-cut assessment, animals from the Hominidae family may represent a good model to be used. Nevertheless, the use of the animal model must be clearly justified from a scientific point of view and the limitations of the use of such a model must be acknowledged (Salmikangas et al., 2015).

Another important aspect to be evaluated at this stage is the tumorigenicity of the cell therapy *in vivo*. The ability of the cells to migrate, uncontrollably grow or to differentiate should be defined. The non-clinical studies must also determine the long-term survival of the cells, their capacity to induce long-term toxicity, genotoxicity, and reproductive/developmental toxicity. In this regard, there are no specific recommended tests, and the analysis should depend on the product, its intent, and the risk management plan (Salmikangas et al., 2015).

Overall, this stage of testing of the cell-based medicinal product must, above all, indicate the safe use of this therapy in humans. Moreover, signs of its efficacy may be given, which can be demonstrated by the correct localization of the cells *in vivo*, their correct differentiation on the cell type desired, the improvement of the pathological characteristics of the disease (such as reduction of neuronal loss in neurodegenerative diseases), and by the alleviation of the animal's phenotype (Salmikangas et al., 2015; Lapteva et al., 2018; Stacey et al., 2018).

The preclinical testing of a medicinal product may be quite costly. Thus, the initiation of an early conversation with regulatory authorities to seek their recommendation and input on the study design, as well as desired endpoint evaluations, becomes of the highest importance. Noteworthy is the fact that, at this point, the EMA and FDA have some regulatory differences. The EMA requires full compliance of GMP by the time the cell therapy is ready for Phase I human clinical trials. As for FDA regulations, their flexibility allows products not to be fully GMP compliant at early stage clinical trials (Carpenter, 2017).

Clinical Studies

The complexity and invasive nature of cellular therapies define that all clinical testing must be performed in patients. The phase I trials should be designed taking into consideration the limitations of the preclinical tests performed and enroll a minimal number of patients sufficient to confirm the safety and efficacy. Standardization of all medical procedures, including administration route, dosage, and evaluation parameters, should be established at this stage and maintained throughout the clinical trial. Furthermore, the assessment of the cell's behavior in the human body regarding its migration and differentiation capacity is also important. The results obtained at this stage must support and justify the testing of the medicinal product in a larger cohort of patients (CBER, 2013a; Salmikangas et al., 2015). Phase II/III clinical trials must clearly define the target population, dose and time of the treatment, the primary and secondary endpoints to be assessed during the clinical trial, and patient specificities, such as concomitant medication allowed. Moreover, the sample size must be sufficient to give statistical power to the observations and the endpoint evaluation enough to justify the attribution of marketing authorization by the regulatory authority (Salmikangas et al., 2015).

Several clinical trials using ESC- or iPSC-derived cells to treat a wide range of conditions are currently ongoing. **Table 2** summarizes ongoing clinical trials using these types of cells in nervous system conditions. To this day, the approval of cellular therapies is somehow limited and, when granted, cases of withdrawal after short periods of time occurred (Carpenter, 2017).

CONCLUSION

Presently, there are different types of stem cells and their derived neural progenitors prone to being tested in cell-based therapies for brain disorders treatment. Preclinical studies have demonstrated the undeniable potential of these cells to promote functional recovery of neurodegenerative diseases as well as other brain conditions through cell replacement and neuroprotection. Nevertheless, the integration of new functional neurons into adult neuronal circuits is a demanding and not yet fully understood process. A better comprehension of the modulating factors of the route taken by the graft-derived neurons during the migration, differentiation, and integration into the adult brain is of great importance in order to identify potential players and mechanisms that might be hindering a wider integration of new neurons and the restoration of neuronal circuits.

On the other hand, the higher complexity of cell-based products represents a challenge, since the manufacturing process becomes more difficult to standardize as compared with the

classical chemical compounds or even with biologic products with more straightforward manufacturing processes and simpler therapeutic mechanisms. Nevertheless, the EMA and FDA have established a regulatory framework guiding procedures of preclinical and clinical assays to reduce heterogeneity, which is expected to enable comparison of results between studies.

Great hopes are set in cell-based therapies applied to neuroregenerative medicine, and although many questions are still to be answered these therapies have the potential to become the next generation of medicinal products.

AUTHOR CONTRIBUTIONS

All authors listed have made a substantial, direct and intellectual contribution to the work, and approved it for publication.

FUNDING

This work was supported by the European Union through the Regional Operational Program CENTRO2020, the Competitiveness Factors Operational Program (COMPETE 2020), and the National Funds through FCT (Foundation for Science and Technology) – projects Brain Health 2020 (CENTRO-01-0145-FEDER-000008), POCI-01-0145-FEDER-016719, POCI-01-0145-FEDER-029716, and PTDC/BTM-ORG/30737/2017 (POCI-01-0145-FEDER-030737). This work was also funded by the National Ataxia Foundation, the French Muscular Dystrophy Association (AFM-Téléthon), Trampoline Grant #20126, SynSpread, Model PolyQ and ESMI: under the EU Joint Program – Neurodegenerative Disease Research (JPND), and the Richard Chin and Lily Lock Machado-Joseph Disease Research Fund.

REFERENCES

Acosta, S. A., Tajiri, N., Shinozuka, K., Ishikawa, H., Sanberg, P. R., Sanchez-Ramos, J., et al. (2014). Combination therapy of human umbilical cord blood cells and granulocyte colony stimulating factor reduces histopathological and motor impairments in an experimental model of chronic traumatic brain injury. *PLoS One* 9:e90953. doi: 10.1371/journal.pone.0090953

Almad, A. A., and Maragakis, N. J. (2012). Glia: an emerging target for neurological disease therapy. *Stem Cell Res. Ther.* 3:37. doi: 10.1186/scrt128

Bachoud-Lévi, A. C., Gaura, V., Brugières, P., Lefaucheur, J. P., Boissé, M. F., Maison, P., et al. (2006). Effect of fetal neural transplants in patients with Huntington;s disease 6 years after surgery: a long-term follow-up study. *Lancet Neurol.* 5, 303–309. doi: 10.1016/S1474-4422(06)70381-7

Bachoud-Lévi, A. C., and Perrier, A. L. (2014). Regenerative medicine in Huntington's disease: current status on fetal grafts and prospects for the use of pluripotent stem cell. *Rev. Neurol.* 170, 749–762. doi: 10.1016/j.neurol.2014.10.007

Badan, I., Platt, D., Kessler, C., and Popa-Wagner, A. (2003). Temporal dynamics of degenerative and regenerative events associated with cerebral ischemia in aged rats. *Gerontology* 49, 356–365. doi: 10.1159/000073763

Balseanu, A. T., Buga, A. M., Catalin, B., Wagner, D. C., Boltze, J., Zagrean, A. M., et al. (2014). Multimodal approaches for regenerative stroke therapies: combination of granulocyte colony-stimulating factor with bone marrow mesenchymal stem cells is not superior to G-CSF alone. *Front. Aging Neurosci.* 6:130. doi: 10.3389/fnagi.2014.00130

Barone, E., Cenini, G., Di Domenico, F., Martin, S., Sultana, R., Mancuso, C., et al. (2011). Long-term high-dose atorvastatin decreases brain oxidative and nitrosative stress in a preclinical model of Alzheimer disease: a novel mechanism of action. *Pharmacol. Res.* 63, 172–180. doi: 10.1016/j.phrs.2010.12.007

Barry, D. S., Pakan, J. M., and McDermott, K. W. (2014). Radial glial cells: key organisers in CNS development. *Int. J. Biochem. Cell Biol.* 46, 76–79. doi: 10.1016/j.biocel.2013.11.013

Bartzokis, G. (2004). Age-related myelin breakdown: a developmental model of cognitive decline and Alzheimer's disease. *Neurobiol. Aging* 25, 5–18. doi: 10.1016/j.neurobiolaging.2003.03.001

Bartzokis, G. (2011). Alzheimer's disease as homeostatic responses to age-related myelin breakdown. *Neurobiol. Aging* 32, 1341–1371. doi: 10.1016/j.neurobiolaging.2009.08.007

Battista, D., Ganat, Y., El Maarouf, A., Studer, L., and Rutishauser, U. (2014). Enhancement of polysialic acid expression improves function of embryonic stem-derived dopamine neuron grafts in Parkinsonian mice. *Stem Cells Transl. Med.* 3, 108–113. doi: 10.5966/sctm.2013-0084

Beebe, B. K., Mollgard, K., Bjorklund, A., and Stenevi, U. (1979). Ultrastructural evidence of synaptogenesis in the adult rat dentate gyrus from brain stem implants. *Brain Res.* 167, 391–395. doi: 10.1016/0006-8993(79)90833-3

Bjorklund, A., and Lindvall, O. (2017). Replacing dopamine neurons in Parkinson's disease: how did it happen? *J. Parkinsons Dis.* 7, S21–S31. doi: 10.3233/JPD-179002

Bjorklund, A., and Stenevi, U. (eds) (1985). *Intracerebral Neural Grafting: a Historical Perspective. In: Neural Grafting in the Mammalian CNS*. Amesterdam: Elsevier, 3–14.

Bjorklund, L. M., Sánchez-Pernaute, R., Chung, S., Andersson, T., Chen, I. Y., McNaught, K. S., et al. (2002). Embryonic stem cells develop into functional dopaminergic neurons after transplantation in a Parkinson rat model. *Proc. Natl. Acad. Sci. U.S.A.* 99, 2344–2349. doi: 10.1073/pnas.022438099

Bonfanti, L., and Peretto, P. (2007). Radial glial origin of the adult neural stem cells in the subventricular zone. *Prog. Neurobiol.* 83, 24–36. doi: 10.1016/j.pneurobio.2006.11.002

Braak, H., and Del Tredici, K. (2004). Poor and protracted myelination as a contributory factor to neurodegenerative disorders. *Neurobiol. Aging* 25, 19–23. doi: 10.1016/j.neurobiolaging.2003.04.001

Bruckner, G., Morawski, M., and Arendt, T. (2008). Aggrecan-based extracellular matrix is an integral part of the human basal ganglia circuit. *Neuroscience* 151, 489–504. doi: 10.1016/j.neuroscience.2007.10.033

Buga, A. M., Scheibe, J., Moller, K., Ciobanu, O., Posel, C., Boltze, J., et al. (2015). Granulocyte colony-stimulating factor and bone marrow mononuclear cells for stroke treatment in the aged brain. *Curr. Neurovasc. Res.* 12, 155–162. doi: 10.2174/1567202612666150311112550

Cardoso, T., Adler, A. F., Mattsson, B., Hoban, D. B., Nolbrant, S., Wahlestedt, J. N., et al. (2018). Target-specific forebrain projections and appropriate synaptic inputs of hESC-derived dopamine neurons grafted to the midbrain of parkinsonian rats. *J. Comp. Neurol.* 526, 2133–2146. doi: 10.1002/cne.24500

Carpenter, M. K. (2017). Regulatory considerations for pluripotent stem cell therapies. *Prog. Brain Res.* 230, 151–163. doi: 10.1016/bs.pbr.2016.12.008

Carulli, D., Rhodes, K. E., Brown, D. J., Bonnert, T. P., Pollack, S. J., Oliver, K., et al. (2006). Composition of perineuronal nets in the adult rat cerebellum and the cellular origin of their components. *J. Comp. Neurol.* 494, 559–577. doi: 10.1002/cne.20822

CAT/CPWP, (2013). *Guideline on the Risk-Based Approach According to Annex I, part IV of Directive 2001/83/EC Applied to Advanced Therapy Medicinal Products*. Amsterdam: EMA.

CBER, (2008). *Guidance for FDA Reviewers and Sponsors: Content and Review of Chemistry, Manufacturing, and Control (CMC) Information for Human Somatic Cell Therapy Investigational New Drug Applications (INDs)*. Silver Spring, MD: FDA.

CBER, (2011). *Guidance for Industry: Potency Tests for Cellular and Gene Therapy Products*. Silver Spring, MD: FDA.

CBER, (2013b). *Preclinical Assessment of Investigational Cellular and Gene Therapy Products: Final Guidance*. Silver Spring, MD: FDA.

CBER, (2013a). *Guidance for Industry: Considerations for the Design of Early-Phase Clinical Trials of Cellular and Gene Therapy Products*. Silver Spring, MD: FDA.

Chen, M. S., Huber, A. B., van der Haar, M. E., Frank, M., Schnell, L., Spillmann, A. A., et al. (2000). Nogo-A is a myelin-associated neurite outgrowth inhibitor and an antigen for monoclonal antibody IN-1. *Nature* 403, 434–439. doi: 10.1038/35000219

CHMP, (2008a). *Guideline on Human Cell-Based Medicinal Products. EMEA/CHMP/410869/2006, EMA*. Amsterdam: European Medicines Agency.

CHMP, (2008b). *Guideline on Safety and Efficacy Follow-up Risk Management of Advanced Therapy Medicinal Products. EMEA/149995/2008*. London: EMA.

Cicchetti, F., Saporta, S., Hauser, R. A., Parent, M., Saint-Pierre, M., Sanberg, P. R., et al. (2009). Neural transplants in patients with Huntington's disease undergo disease-like neuronal degeneration. *Proc. Natl. Acad. Sci. U.S.A.* 106, 12483–12488. doi: 10.1073/pnas.0904239106

Clarke, D. J., and Dunnett, S. B. (1993). Synaptic relationships between cortical and dopaminergic inputs and intrinsic GABAergic systems within intrastriatal striatal grafts. *J. Chem. Neuroanat.* 6, 147–158. doi: 10.1016/0891-0618(93)90024-X

Conboy, I. M., Conboy, M. J., and Rebo, J. (2015). Systemic problems: a perspective on stem cell aging and rejuvenation. *Aging* 7, 754–765. doi: 10.18632/aging.100819

Cossetti, C., Alfaro-Cervello, C., Donegà, M., Tyzack, G., and Pluchino, S. (2012). New perspectives of tissue remodelling with neural stem and progenitor cell-based therapies. *Cell Tissue Res.* 349, 321–329. doi: 10.1007/s00441-012-1341-8

Currais, A. (2015). Ageing and inflammation - A central role for mitochondria in brain health and disease. *Ageing Res. Rev.* 21, 30–42. doi: 10.1016/j.arr.2015.02.001

Davis, R. L., Weintraub, H., and Lassar, A. B. (1987). Expression of a single transfected cDNA converts fibroblasts to myoblasts. *Cell* 51, 987–1000. doi: 10.1016/0092-8674(87)90585-x

Deleidi, M., Jaggle, M., and Rubino, G. (2015). Immune aging, dysmetabolism, and inflammation in neurological diseases. *Front. Neurosci.* 9:172. doi: 10.3389/fnins.2015.00172

Della Porta, M. G., Alessandrino, E. P., Bacigalupo, A., van Lint, M. T., Malcovati, L., Pascutto, C., et al. (2014). Predictive factors for the outcome of allogeneic transplantation in patients with MDS stratified according to the revised IPSS-R. *Blood* 123, 2333–2342. doi: 10.1182/blood-2013-12-542720

Denes, A., Drake, C., Stordy, J., Chamberlain, J., McColl, B. W., Gram, H., et al. (2012). Interleukin-1 mediates neuroinflammatory changes associated with diet-induced atherosclerosis. *J. Am. Heart Assoc.* 1:e002006. doi: 10.1161/JAHA.112.002006

Di Cristo, G., Chattopadhyaya, B., Kuhlman, S. J., Fu, Y., Bélanger, M. C., Wu, C. Z., et al. (2007). Activity-dependent PSA expression regulates inhibitory maturation and onset of critical period plasticity. *Nat. Neurosci.* 10, 1569–1577. doi: 10.1038/nn2008

Dunn, E. (1917). Primary and secondary findings in a series of attempts to transplant cerebral cortex in the albino rat. *J. Comp. Neurol.* 27, 565–582. doi: 10.1002/cne.900270403

Dunnett, S. B. (2010). Chapter 55: neural transplantation. *Handb. Clin. Neurol.* 95, 885–912. doi: 10.1016/S0072-9752(08)02155-6

Dunnett, S. B., Carter, R. J., Watts, C., Torres, E. M., Mahal, A., Mangiarini, L., et al. (1998). Striatal transplantation in a transgenic mouse model of Huntington's disease. *Exp. Neurol.* 154, 31–40. doi: 10.1006/exnr.1998.6926

Dunnett, S. B., and Rosser, A. E. (2014). Challenges for taking primary and stem cells into clinical neurotransplantation trials for neurodegenerative disease. *Neurobiol. Dis.* 61, 79–89. doi: 10.1016/j.nbd.2013.05.004

Dzamba, D., Harantova, L., Butenko, O., and Anderova, M. (2016). Glial cells - the key elements of Alzheimer s disease. *Curr. Alzheimer Res.* 13, 894–911. doi: 10.2174/1567205013666160129095924

EC, (2017). *Guidelines on Good Manufacturing Practice Specific to Advanced Therapy Medicinal Products*. Brussels: European Comission.

EC, (2018). *EU Guidelines for Good Manufacturing Practice for Medicinal Products for Human and Veterinary Use: Annex 2: Manufacture of Biological Active Substances and Medicinal Products for Human Use. In: EudraLex - Volume 4*, Chap. Brussels. European Comission.

Egawa, J., Pearn, M. L., Lemkuil, B. P., Patel, P. M., and Head, B. P. (2016). Membrane lipid rafts and neurobiology: age-related changes in membrane lipids and loss of neuronal function. *J. Physiol.* 594, 4565–4579. doi: 10.1113/JP270590

EMA, (2018). *Guidance on the Format of the Risk Management Plan (RMP) in the EU – in Integrated Format*. Amsterdam: EMA.

Ericson, C., Georgievska, B., and Lundberg, C. (2005). Ex vivo gene delivery of GDNF using primary astrocytes transduced with a lentiviral vector provides neuroprotection in a rat model of Parkinson's disease. *Eur. J. Neurosci.* 22, 2755–2764. doi: 10.1111/j.1460-9568.2005.04503.x

Forraz, N., Wright, K. E., Jurga, M., and McGuckin, C. P. (2013). Experimental therapies for repair of the central nervous system: stem cells and tissue engineering. *J. Tissue Eng. Regen. Med.* 7, 523–536. doi: 10.1002/term.552

Franklin, R. J., and Goldman, S. A. (2015). Glia disease and repair-remyelination. *Cold Spring Harb. Perspect. Biol.* 7:a020594. doi: 10.1101/cshperspect.a020594

Freeman, T. B., Cicchetti, F., Hauser, R. A., Deacon, T. W., Li, X. J., Hersch, S. M., et al. (2000). Transplanted fetal striatum in Huntington's disease: phenotypic development and lack of pathology. *Proc. Natl. Acad. Sci. U.S.A.* 97, 13877–13882. doi: 10.1073/pnas.97.25.13877

Fricker, R. A., Carpenter, M. K., Winkler, C., Greco, C., Gates, M. A., and Bjorklund, A. (1999). Site-specific migration and neuronal differentiation of human neural progenitor cells after transplantation in the adult rat brain. *J. Neurosci.* 19, 5990–6005. doi: 10.1523/JNEUROSCI.19-14-05990.1999

Ganat, Y. M., Calder, E. L., Kriks, S., Nelander, J., Tu, E. Y., Jia, F., et al. (2012). Identification of embryonic stem cell-derived midbrain dopaminergic neurons for engraftment. *J. Clin. Invest.* 122, 2928–2939. doi: 10.1172/JCI58767

Gee, A. P. (2018). Regulation of regenerative medicine products. *Adv. Exp. Med. Biol.* 1098, 189–198. doi: 10.1007/978-3-319-97421-7_10

Giachino, C., Barz, M., Tchorz, J. S., Tome, M., Gassmann, M., Bischofberger, J., et al. (2014). GABA suppresses neurogenesis in the adult hippocampus through GABAB receptors. *Development* 141, 83–90. doi: 10.1242/dev.102608

Glaser, T., Brose, C., Franceschini, I., Hamann, K., Smorodchenko, A., Zipp, F., et al. (2007). Neural cell adhesion molecule polysialylation enhances the sensitivity of embryonic stem cell-derived neural precursors to migration guidance cues. *Stem Cells.* 25, 3016–3025. doi: 10.1634/stemcells.2007-0218

Gotz, M., Nakafuku, M., and Petrik, D. (2016). Neurogenesis in the developing and adult brain-similarities and key differences. *Cold Spring Harb. Perspect. Biol.* 8:a018853. doi: 10.1101/cshperspect.a018853

Guirland, C., Suzuki, S., Kojima, M., Lu, B., and Zheng, J. Q. (2004). Lipid rafts mediate chemotropic guidance of nerve growth cones. *Neuron* 42, 51–62. doi: 10.1016/s0896-6273(04)00157-6

Guirland, C., and Zheng, J. Q. (2007). Membrane lipid rafts and their role in axon guidance. *Adv. Exp. Med. Biol.* 621, 144–155. doi: 10.1007/978-0-387-76715-4_11

Gurdon, J. B. (1962). The developmental capacity of nuclei taken from intestinal epithelium cells of feeding tadpoles. *J. Embryol. Exp. Morphol.* 10, 622–640.

Gurdon, J. B., Laskey, R. A., and Reeves, O. R. (1975). The developmental capacity of nuclei transplanted from keratinized skin cells of adult frogs. *J. Embryol. Exp. Morphol.* 34, 93–112.

Haeckel, E. (1868). *Natürliche Schöpfungsgeschichte*. Berlin: Verlag von Georg Reimer.

Haidet-Phillips, A. M., and Maragakis, N. J. (2015). Neural and glial progenitor transplantation as a neuroprotective strategy for amyotrophic lateral sclerosis (ALS). *Brain Res.* 1628, 343–350. doi: 10.1016/j.brainres.2015.06.035

Hargus, G., Cooper, O., Deleidi, M., Levy, A., Lee, K., Marlow, E., et al. (2010). Differentiated Parkinson patient-derived induced pluripotent stem cells grow in the adult rodent brain and reduce motor asymmetry in Parkinsonian rats. *Proc. Natl. Acad. Sci. U.S.A.* 107, 15921–15926. doi: 10.1073/pnas.1010209107

Haydar, T. F., Wang, F., Schwartz, M. L., and Rakic, P. (2000). Differential modulation of proliferation in the neocortical ventricular and subventricular zones. *J. Neurosci.* 20, 5764–5774. doi: 10.1523/JNEUROSCI.20-15-05764.2000

Herberts, C. A., Kwa, M. S., and Hermsen, H. P. (2011). Risk factors in the development of stem cell therapy. *J. Transl. Med.* 9:29. doi: 10.1186/1479-5876-9-29

Hermann, D. M., Buga, A. M., and Popa-Wagner, A. (2013). Enabling brain plasticity and neurological recovery in the ischemic brain: effect of age and vascular risk factors as confounders. *Rom. J. Morphol. Embryol.* 54, 687–693.

Hoffman, S., and Edelman, G. M. (1983). Kinetics of homophilic binding by embryonic and adult forms of the neural cell adhesion molecule. *Proc. Natl. Acad. Sci. U.S.A.* 80, 5762–5766. doi: 10.1073/pnas.80.18.5762

Hylin, M. J., Orsi, S. A., Moore, A. N., and Dash, P. K. (2013). Disruption of the perineuronal net in the hippocampus or medial prefrontal cortex impairs fear conditioning. *Learn. Mem.* 20, 267–273. doi: 10.1101/lm.030197.112

Isacson, O., Dunnett, S. B., and Bjorklund, A. (1986). Graft-induced behavioral recovery in an animal model of Huntington disease. *Proc. Natl. Acad. Sci. U.S.A.* 83, 2728–2732. doi: 10.1073/pnas.83.8.2728

Jiang, X., Lachance, M., and Rossignol, E. (2016). Involvement of cortical fast-spiking parvalbumin-positive basket cells in epilepsy. *Prog. Brain Res.* 226, 81–126. doi: 10.1016/bs.pbr.2016.04.012

Jinno, S. (2016). Aging affects new cell production in the adult hippocampus: a quantitative anatomic review. *J. Chem. Neuroanat.* 76, 64–72. doi: 10.1016/j.jchemneu.2015.10.009

Johann, V., Schiefer, J., Sass, C., Mey, J., Brook, G., Kruttgen, A., et al. (2007). Time of transplantation and cell preparation determine neural stem cell survival in a mouse model of Huntington's disease. *Exp. Brain Res.* 177, 458–470. doi: 10.1007/s00221-006-0689-y

Kamei, N., Tanaka, N., Oishi, Y., Hamasaki, T., Nakanishi, K., Sakai, N., et al. (2007). BDNF, NT-3, and NGF released from transplanted neural progenitor cells promote corticospinal axon growth in organotypic cocultures. *Spine* 32, 1272–1278. doi: 10.1097/BRS.0b013e318059afab

Kamiguchi, H. (2006). The region-specific activities of lipid rafts during axon growth and guidance. *J. Neurochem.* 98, 330–335. doi: 10.1111/j.1471-4159.2006.03888.x

Keene, C. D., Chang, R. C., Leverenz, J. B., Kopyov, O., Perlman, S., Hevner, R. F., et al. (2009). A patient with Huntington's disease and long-surviving fetal neural transplants that developed mass lesions. *Acta Neuropathol.* 117, 329–338. doi: 10.1007/s00401-008-0465-0

Kelava, I., and Lancaster, M. A. (2016). Stem cell models of human brain development. *Cell Stem Cell.* 18, 736–748. doi: 10.1016/j.stem.2016.05.022

Kempermann, G., Jessberger, S., Steiner, B., and Kronenberg, G. (2004). Milestones of neuronal development in the adult hippocampus. *Trends Neurosci.* 27, 447–452. doi: 10.1016/j.tins.2004.05.013

Kim, S. U., and de Vellis, J. (2009). Stem cell-based cell therapy in neurological diseases: a review. *J. Neurosci. Res.* 87, 2183–2200. doi: 10.1002/jnr.22054

Koistinaho, M., Lin, S., Wu, X., Esterman, M., Koger, D., Hanson, J., et al. (2004). Apolipoprotein E promotes astrocyte colocalization and degradation of deposited amyloid-beta peptides. *Nat. Med.* 10, 719–726. doi: 10.1038/nm1058

Kokaia, Z., Llorente, I. L., and Carmichael, S. T. (2018). Customized brain cells for stroke patients using pluripotent stem cells. *Stroke* 49, 1091–1098. doi: 10.1161/STROKEAHA.117.018291

Kokaia, Z., Martino, G., Schwartz, M., and Lindvall, O. (2012). Cross-talk between neural stem cells and immune cells: the key to better brain repair? *Nat. Neurosci.* 15, 1078–1087. doi: 10.1038/nn.3163

Konishi, Y., Stegmuller, J., Matsuda, T., Bonni, S., and Bonni, A. (2004). Cdh1-APC controls axonal growth and patterning in the mammalian brain. *Science* 303, 1026–1030. doi: 10.1126/science.1093712

Kottis, V., Thibault, P., Mikol, D., Xiao, Z. C., Zhang, R., Dergham, P., et al. (2002). Oligodendrocyte-myelin glycoprotein (OMgp) is an inhibitor of neurite outgrowth. *J. Neurochem.* 82, 1566–1569. doi: 10.1046/j.1471-4159.2002.01146.x

Kwok, J. C., Dick, G., Wang, D., and Fawcett, J. W. (2011). Extracellular matrix and perineuronal nets in CNS repair. *Dev. Neurobiol.* 71, 1073–1089. doi: 10.1002/dneu.20974

Ladewig, J., Koch, P., and Brustle, O. (2014). Auto-attraction of neural precursors and their neuronal progeny impairs neuronal migration. *Nat. Neurosci.* 17, 24–26. doi: 10.1038/nn.3583

Lapteva, L., Vatsan, R., and Purohit-Sheth, T. (2018). Regenerative medicine therapies for rare diseases. *Transl. Sci. Rare Dis.* 3, 121–132. doi: 10.3233/TRD-180030

Lemarchant, S., Wojciechowski, S., and Koistinaho, J. (2016). Perineuronal nets in neurodegeneration. *Oncotarget* 7, 78224–78225. doi: 10.18632/oncotarget.13420

Lepore, A. C., Rauck, B., Dejea, C., Pardo, A. C., Rao, M. S., Rothstein, J. D., et al. (2008). Focal transplantation-based astrocyte replacement is neuroprotective in a model of motor neuron disease. *Nat. Neurosci.* 11, 1294–1301. doi: 10.1038/nn.2210

Li, W., Englund, E., Widner, H., Mattsson, B., van Westen, D., Latt, J., et al. (2016). Extensive graft-derived dopaminergic innervation is maintained 24 years after transplantation in the degenerating parkinsonian brain. *Proc. Natl. Acad. Sci. U.S.A.* 113, 6544–6549. doi: 10.1073/pnas.1605245113

Lindvall, O., Brundin, P., Widner, H., Rehncrona, S., Gustavii, B., Frackowiak, R., et al. (1990). Grafts of fetal dopamine neurons survive and improve motor function in Parkinson's disease. *Science* 247, 574–577. doi: 10.1126/science.2105529

Lindvall, O., and Kokaia, Z. (2006). Stem cells for the treatment of neurological disorders. *Nature* 441, 1094–1096. doi: 10.1038/nature04960

Lindvall, O., Kokaia, Z., and Martinez-Serrano, A. (2004). Stem cell therapy for human neurodegenerative disorders-how to make it work. *Nat. Med.* 10, S42–S50. doi: 10.1038/nm1064

Lindvall, O., Widner, H., Rehncrona, S., Brundin, P., Odin, P., Gustavii, B., et al. (1992). Transplantation of fetal dopamine neurons in Parkinson's disease: one-year clinical and neurophysiological observations in two patients with putaminal implants. *Ann. Neurol.* 31, 155–165. doi: 10.1002/ana.410310206

Lo, B., and Parham, L. (2009). Ethical issues in stem cell research. *Endocr. Rev.* 30, 204–213. doi: 10.1210/er.2008-0031

Lundberg, C., Horellou, P., Mallet, J., and Bjorklund, A. (1996). Generation of DOPA-producing astrocytes by retroviral transduction of the human tyrosine hydroxylase gene: in vitro characterization and in vivo effects in the rat Parkinson model. *Exp. Neurol.* 139, 39–53. doi: 10.1006/exnr.1996.0079

Luo, L., Guo, K., Fan, W., Lu, Y., Chen, L., Wang, Y., et al. (2017). Niche astrocytes promote the survival, proliferation and neuronal differentiation of co-transplanted neural stem cells following ischemic stroke in rats. *Exp. Ther. Med.* 13, 645–650. doi: 10.3892/etm.2016.4016

Ma, H., Yu, B., Kong, L., Zhang, Y., and Shi, Y. (2012). Neural stem cells over-expressing brain-derived neurotrophic factor (BDNF) stimulate synaptic protein expression and promote functional recovery following transplantation in rat model of traumatic brain injury. *Neurochem. Res.* 37, 69–83. doi: 10.1007/s11064-011-0584-1

Mahmood, A., Goussev, A., Lu, D., Qu, C., Xiong, Y., Kazmi, H., et al. (2008). Long-lasting benefits after treatment of traumatic brain injury (TBI) in rats with combination therapy of marrow stromal cells (MSCs) and simvastatin. *J. Neurotrauma* 25, 1441–1447. doi: 10.1089/neu.2007.0495

Mahmood, A., Lu, D., Qu, C., Goussev, A., and Chopp, M. (2007). Treatment of traumatic brain injury with a combination therapy of marrow stromal cells and atorvastatin in rats. *Neurosurgery* 60, 546–553. doi: 10.1227/01.NEU.0000255346.25959.99

Mattson, M. P., and Arumugam, T. V. (2018). Hallmarks of brain aging: adaptive and pathological modification by metabolic states. *Cell Metab.* 27, 1176–1199. doi: 10.1016/j.cmet.2018.05.011

McKerracher, L., David, S., Jackson, D. L., Kottis, V., Dunn, R. J., and Braun, P. E. (1994). Identification of myelin-associated glycoprotein as a major myelin-derived inhibitor of neurite growth. *Neuron* 13, 805–811. doi: 10.1016/0896-6273(94)90247-x

Mendonca, L. S., Nóbrega, C., Hirai, H., Kaspar, B. K., and Pereira de Almeida, L. (2015). Transplantation of cerebellar neural stem cells improves motor coordination and neuropathology in Machado-Joseph disease mice. *Brain* 138, 320–335. doi: 10.1093/brain/awu352

Mendonca, L. S., Onofre, I., Miranda, C. O., Perfeito, R., Nóbrega, C., and de Almeida, L. P. (2018). Stem cell-based therapies for polyglutamine diseases. *Adv. Exp. Med. Biol.* 1049, 439–466. doi: 10.1007/978-3-319-71779-1_21

Merkle, F. T., Tramontin, A. D., García-Verdugo, J. M., and Alvarez-Buylla, A. (2004). Radial glia give rise to adult neural stem cells in the subventricular zone. *Proc. Natl. Acad. Sci. U.S.A.* 101, 17528–17532. doi: 10.1073/pnas.0407893101

Miller, D. W., Cookson, M. R., and Dickson, D. W. (2004). Glial cell inclusions and the pathogenesis of neurodegenerative diseases. *Neuron Glia Biol.* 1, 13–21. doi: 10.1017/s1740925x04000043

Miller, F. D., and Gauthier, A. S. (2007). Timing is everything: making neurons versus glia in the developing cortex. *Neuron* 54, 357–369. doi: 10.1016/j.neuron.2007.04.019

Moon, L. D., Asher, R. A., Rhodes, K. E., and Fawcett, J. W. (2001). Regeneration of CNS axons back to their target following treatment of adult rat brain with chondroitinase ABC. *Nat. Neurosci.* 4, 465–466. doi: 10.1038/87415

Nakamichi, N., Takarada, T., and Yoneda, Y. (2009). Neurogenesis mediated by gamma-aminobutyric acid and glutamate signaling. *J. Pharmacol. Sci.* 110, 133–149. doi: 10.1254/jphs.08r03cr

Nguyen, M. D., Julien, J. P., and Rivest, S. (2002). Innate immunity: the missing link in neuroprotection and neurodegeneration? *Nat. Rev. Neurosci.* 3, 216–227. doi: 10.1038/nrn752

Niccoli, T., and Partridge, L. (2012). Ageing as a risk factor for disease. *Curr. Biol.* 22, R741–R752. doi: 10.1016/j.cub.2012.07.024

Nulty, J., Alsaffar, M., and Barry, D. (2015). Radial glial cells organize the central nervous system via microtubule dependant processes. *Brain Res.* 1625, 171–179. doi: 10.1016/j.brainres.2015.08.027

Olanow, C. W., Goetz, C. G., Kordower, J. H., Stoessl, A. J., Sossi, V., Brin, M. F., et al. (2003). A double-blind controlled trial of bilateral fetal nigral transplantation in Parkinson's disease. *Ann. Neurol.* 54, 403–414. doi: 10.1002/ana.10720

Payne, S. L., Anandakumaran, P. N., Varga, B. V., Morshead, C. M., Nagy, A., and Shoichet, M. S. (2018). In vitro maturation of human iPSC-derived neuroepithelial cells influences transplant survival in the stroke-injured rat brain. *Tissue Eng. Part A.* 24, 351–360. doi: 10.1089/ten.TEA.2016.0515

Perlow, M. J., Freed, W. J., Hoffer, B. J., Seiger, A., Olson, L., and Wyatt, R. J. (1979). Brain grafts reduce motor abnormalities produced by destruction of nigrostriatal dopamine system. *Science* 204, 643–647. doi: 10.1126/science.571147

Piao, J., Major, T., Auyeung, G., Policarpio, E., Menon, J., Droms, L., et al. (2015). Human embryonic stem cell-derived oligodendrocyte progenitors remyelinate the brain and rescue behavioral deficits following radiation. *Cell Stem Cell.* 16, 198–210. doi: 10.1016/j.stem.2015.01.004

Piccini, P., Brooks, D. J., Bjorklund, A., Gunn, R. N., Grasby, P. M., Rimoldi, O., et al. (1999). Dopamine release from nigral transplants visualized in vivo in a Parkinson's patient. *Nat. Neurosci.* 2, 1137–1140. doi: 10.1038/16060

Pihlaja, R., Koistinaho, J., Kauppinen, R., Sandholm, J., Tanila, H., and Koistinaho, M. (2011). Multiple cellular and molecular mechanisms are involved in human Abeta clearance by transplanted adult astrocytes. *Glia* 59, 1643–1657. doi: 10.1002/glia.21212

Pihlaja, R., Koistinaho, J., Malm, T., Sikkila, H., Vainio, S., and Koistinaho, M. (2008). Transplanted astrocytes internalize deposited beta-amyloid peptides in a transgenic mouse model of Alzheimer's disease. *Glia* 56, 154–163. doi: 10.1002/glia.20599

Pike, L. J. (2003). Lipid rafts: bringing order to chaos. *J. Lipid Res.* 44, 655–667. doi: 10.1194/jlr.R200021-JLR200

Pimpaneau, V., Gianelli, F., Trouvin, J. H., and Poiseau, A. D. (2015). *The Challenges of Potency Assay Development for Cell-Based Medicinal Products in Europe*, Vol. 12. Bangalore: Voisin Consulting Life Sciences.

Pizzorusso, T., Medini, P., Berardi, N., Chierzi, S., Fawcett, J. W., and Maffei, L. (2002). Reactivation of ocular dominance plasticity in the adult visual cortex. *Science* 298, 1248–1251. doi: 10.1126/science.1072699

Platel, J. C., Dave, K. A., Gordon, V., Lacar, B., Rubio, M. E., and Bordey, A. (2010). NMDA receptors activated by subventricular zone astrocytic glutamate are critical for neuroblast survival prior to entering a synaptic network. *Neuron* 65, 859–872. doi: 10.1016/j.neuron.2010.03.009

Pluchino, S., Gritti, A., Blezer, E., Amadio, S., Brambilla, E., Borsellino, G., et al. (2009). Human neural stem cells ameliorate autoimmune encephalomyelitis in non-human primates. *Ann. Neurol.* 66, 343–354. doi: 10.1002/ana.21745

Pluchino, S., Zanotti, L., Rossi, B., Brambilla, E., Ottoboni, L., Salani, G., et al. (2005). Neurosphere-derived multipotent precursors promote neuroprotection by an immunomodulatory mechanism. *Nature* 436, 266–271. doi: 10.1038/nature03889

Popa-Wagner, A., Buga, A. M., Doeppner, T. R., and Hermann, D. M. (2014). Stem cell therapies in preclinical models of stroke associated with aging. *Front. Cell Neurosci.* 8:347. doi: 10.3389/fncel.2014.00347

Popa-Wagner, A., Stocker, K., Balseanu, A. T., Rogalewski, A., Diederich, K., Minnerup, J., et al. (2010). Effects of granulocyte-colony stimulating factor after stroke in aged rats. *Stroke* 41, 1027–1031. doi: 10.1161/STROKEAHA.109.575621

Poplawski, G. H. D., Lie, R., Hunt, M., Kumamaru, H., Kawaguchi, R., Lu, P., et al. (2018). Adult rat myelin enhances axonal outgrowth from neural stem cells. *Sci. Transl. Med.* 10:eaa12563. doi: 10.1126/scitranslmed.aal2563

Pradillo, J. M., Murray, K. N., Coutts, G. A., Moraga, A., Oroz-Gonjar, F., Boutin, H., et al. (2017). Reparative effects of interleukin-1 receptor antagonist in young and aged/co-morbid rodents after cerebral ischemia. *Brain Behav. Immun.* 61, 117–126. doi: 10.1016/j.bbi.2016.11.013

Quadrato, G., Elnaggar, M. Y., and Di Giovanni, S. (2014). Adult neurogenesis in brain repair: cellular plasticity vs. cellular replacement. *Front. Neurosci.* 8:17. doi: 10.3389/fnins.2014.00017

Rippon, H. J., and Bishop, A. E. (2004). Embryonic stem cells. *Cell Prolif.* 37, 23–34. doi: 10.1111/j.1365-2184.2004.00298.x

Ronn, L. C., Berezin, V., and Bock, E. (2000). The neural cell adhesion molecule in synaptic plasticity and ageing. *Int. J. Dev. Neurosci.* 18, 193–199. doi: 10.1016/s0736-5748(99)00088-x

Roozbehi, A., Joghataei, M. T., Bakhtiyari, M., Mohammadi, J., Rad, P., and Delaviz, H. (2015). Age-associated changes on axonal regeneration and functional outcome after spinal cord injury in rats. *Acta Med. Iran.* 53, 281–286.

Rothbard, J. B., Brackenbury, R., Cunningham, B. A., and Edelman, G. M. (1982). Differences in the carbohydrate structures of neural cell-adhesion molecules from adult and embryonic chicken brains. *J. Biol. Chem.* 257, 11064–11069.

Rutishauser, U., and Landmesser, L. (1996). Polysialic acid in the vertebrate nervous system: a promoter of plasticity in cell-cell interactions. *Trends Neurosci.* 19, 422–427. doi: 10.1016/0166-2236(96)10041-2

Ryan, S. M., and Nolan, Y. M. (2016). Neuroinflammation negatively affects adult hippocampal neurogenesis and cognition: can exercise compensate? *Neurosci. Biobehav. Rev.* 61, 121–131. doi: 10.1016/j.neubiorev.2015.12.004

Salmikangas, P., Schuessler-Lenz, M., Ruiz, S., Celis, P., Reischl, I., Menezes-Ferreira, M., et al. (2015). Marketing regulatory oversight of advanced therapy medicinal products (ATMPs) in Europe: the EMA/CAT perspective. *Adv. Exp. Med. Biol.* 871, 103–130. doi: 10.1007/978-3-319-18618-4_6

Sanchez-Ramos, J., Song, S., Sava, V., Catlow, B., Lin, X., Mori, T., et al. (2009). Granulocyte colony stimulating factor decreases brain amyloid burden and reverses cognitive impairment in Alzheimer's mice. *Neuroscience* 163, 55–72. doi: 10.1016/j.neuroscience.2009.05.071

Sandu, R. E., Balseanu, A. T., Bogdan, C., Slevin, M., Petcu, E., and Popa-Wagner, A. (2017). Stem cell therapies in preclinical models of stroke. Is the aged brain microenvironment refractory to cell therapy?. *Exp. Gerontol.* 94, 73–77. doi: 10.1016/j.exger.2017.01.008

Sandu, R. E., Buga, A. M., Uzoni, A., Petcu, E. B., and Popa-Wagner, A. (2015). Neuroinflammation and comorbidities are frequently ignored factors in CNS pathology. *Neural Regen. Res.* 10, 1349–1355. doi: 10.4103/1673-5374.165208

Scheff, S. W., Benardo, L. S., and Cotman, C. W. (1980). Decline in reactive fiber growth in the dentate gyrus of aged rats compared to young adult rats following entorhinal cortex removal. *Brain Res.* 199, 21–38. doi: 10.1016/0006-8993(80)90227-9

Schultz, B. G., Patten, D. K., and Berlau, D. J. (2018). The role of statins in both cognitive impairment and protection against dementia: a tale of two mechanisms. *Transl. Neurodegener.* 7:5. doi: 10.1186/s40035-018-0110-3

Stacey, G., Andrews, P., Asante, C., Barbaric, I., Barry, J., Bisset, L., et al. (2018). Science-based assessment of source materials for cell-based medicines: report of a stakeholders workshop. *Regen. Med.* 13, 935–944. doi: 10.2217/rme-2018-0120

Steinbeck, J. A., and Studer, L. (2015). Moving stem cells to the clinic: potential and limitations for brain repair. *Neuron* 86, 187–206. doi: 10.1016/j.neuron.2015.03.002

Takahashi, K., and Yamanaka, S. (2006). Induction of pluripotent stem cells from mouse embryonic and adult fibroblast cultures by defined factors. *Cell* 126, 663–676. doi: 10.1016/j.cell.2006.07.024

Tatarishvili, J., Oki, K., Monni, E., Koch, P., Memanishvili, T., Buga, A. M., et al. (2014). Human induced pluripotent stem cells improve recovery in stroke-injured aged rats. *Restor. Neurol. Neurosci.* 32, 547–558. doi: 10.3233/RNN-140404

Thompson, L. H., Kirik, D., and Bjorklund, A. (2008). Non-dopaminergic neurons in ventral mesencephalic transplants make widespread axonal connections in the host brain. *Exp. Neurol.* 213, 220–228. doi: 10.1016/j.expneurol.2008.06.005

Thomsen, G. M., Avalos, P., Ma, A. A., Alkaslasi, M., Cho, N., Wyss, L., et al. (2018). Transplantation of neural progenitor cells expressing glial cell line-derived neurotrophic factor into the motor cortex as a strategy to treat amyotrophic lateral sclerosis. *Stem Cells* 36, 1122–1131. doi: 10.1002/stem.2825

Thomson, J. A., Itskovitz-Eldor, J., Shapiro, S. S., Waknitz, M. A., Swiergiel, J. J., Marshall, V. S., et al. (1998). Embryonic stem cell lines derived from human blastocysts. *Science* 282, 1145–1147. doi: 10.1126/science.282.5391.1145

Vincent, V. A., Tilders, F. J., and Van Dam, A. M. (1997). Inhibition of endotoxin-induced nitric oxide synthase production in microglial cells by the presence of astroglial cells: a role for transforming growth factor beta. *Glia* 19, 190–198. doi: 10.1002/(sici)1098-1136(199703)19:3<190::aid-glia2>3.0.co;2-3

Wang, Z., Yao, W., Deng, Q., Zhang, X., and Zhang, J. (2013). Protective effects of BDNF overexpression bone marrow stromal cell transplantation in rat models of traumatic brain injury. *J. Mol. Neurosci.* 49, 409–416. doi: 10.1007/s12031-012-9908-0

Waterhouse, E. G., An, J. J., Orefice, L. L., Baydyuk, M., Liao, G. Y., Zheng, K., et al. (2012). BDNF promotes differentiation and maturation of adult-born neurons through GABAergic transmission. *J. Neurosci.* 32, 14318–14330. doi: 10.1523/JNEUROSCI.0709-12.2012

Wernig, M., Zhao, J. P., Pruszak, J., Hedlund, E., Fu, D., Soldner, F., et al. (2008). Neurons derived from reprogrammed fibroblasts functionally integrate into the fetal brain and improve symptoms of rats with Parkinson's disease. *Proc. Natl. Acad. Sci. U.S.A.* 105, 5856–5861. doi: 10.1073/pnas.0801677105

Whitney, N. P., Eidem, T. M., Peng, H., Huang, Y., and Zheng, J. C. (2009). Inflammation mediates varying effects in neurogenesis: relevance to the pathogenesis of brain injury and neurodegenerative disorders. *J. Neurochem.* 108, 1343–1359. doi: 10.1111/j.1471-4159.2009.05886.x

Windrem, M. S., Nunes, M. C., Rashbaum, W. K., Schwartz, T. H., Goodman, R. A., McKhann, G. II, et al. (2004). Fetal and adult human oligodendrocyte progenitor cell isolates myelinate the congenitally dysmyelinated brain. *Nat. Med.* 10, 93–97. doi: 10.1038/nm974

Xu, L., Shen, P., Hazel, T., Johe, K., and Koliatsos, V. E. (2011). Dual transplantation of human neural stem cells into cervical and lumbar cord ameliorates motor neuron disease in SOD1 transgenic rats. *Neurosci. Lett.* 494, 222–226. doi: 10.1016/j.neulet.2011.03.017

Yang, S., Lu, W., Zhou, D. S., and Tang, Y. (2012). Enriched environment and white matter in aging brain. *Anat. Rec. (Hoboken)* 295, 1406–1414. doi: 10.1002/ar.22526

Conflict of Interest: The authors declare that the research was conducted in the absence of any commercial or financial relationships that could be construed as a potential conflict of interest.

Copyright © 2019 Henriques, Moreira, Schwamborn, Pereira de Almeida and Mendonça. This is an open-access article distributed under the terms of the Creative Commons Attribution License (CC BY). The use, distribution or reproduction in other forums is permitted, provided the original author(s) and the copyright owner(s) are credited and that the original publication in this journal is cited, in accordance with accepted academic practice. No use, distribution or reproduction is permitted which does not comply with these terms.

frontiers in Cellular Neuroscience

REVIEW
published: 22 November 2019
doi: 10.3389/fncel.2019.00519

Pericytes in Cerebrovascular Diseases: An Emerging Therapeutic Target

Xiaojuan Su[1,2], Lingyi Huang[3], Yi Qu[1,2], Dongqiong Xiao[1,2] and Dezhi Mu[1,2]*

[1] Department of Paediatrics, West China Second University Hospital, Sichuan University, Chengdu, China, [2] Key Laboratory of Birth Defects and Related Diseases of Women and Children, Sichuan University, Ministry of Education, Chengdu, China, [3] West China College of Stomatology, Sichuan University, Chengdu, China

Pericytes are functional components of the neurovascular unit (NVU) that are located around the blood vessels, and their roles in the regulation of cerebral health and diseases has been reported. Currently, the potential properties of pericytes as emerging therapeutic targets for cerebrovascular diseases have attracted considerable attention. Nonetheless, few reviews have comprehensively discussed pericytes and their roles in cerebrovascular diseases. Therefore, in this review, we not only summarized and described the basic characteristics of pericytes but also focused on clarifying the new understanding about the roles of pericytes in the pathogenesis of cerebrovascular diseases, including white matter injury (WMI), hypoxic–ischemic brain damage, depression, neovascular insufficiency disease, and Alzheimer's disease (AD). Furthermore, we summarized the current therapeutic strategies targeting pericytes for cerebrovascular diseases. Collectively, this review is aimed at providing a comprehensive understanding of pericytes and new insights about the use of pericytes as novel therapeutic targets for cerebrovascular diseases.

Keywords: pericytes, angiogenesis, basement membrane, blood brain barrier, cerebrovascular disease

OPEN ACCESS

Edited by:
Emmanuel Pinteaux, The University of Manchester, United Kingdom

Reviewed by:
Jerome Badaut, UMR5287 Institut de Neurosciences Cognitives et Intégratives d'Aquitaine (INCIA), France
Germano Guerra, University of Molise, Italy

****Correspondence:***
Yi Qu
quyi712002@163.com

Specialty section:
This article was submitted to Cellular Neuropathology, a section of the journal Frontiers in Cellular Neuroscience

Received: *13 May 2019*
Accepted: *05 November 2019*
Published: *22 November 2019*

Citation:
Su X, Huang L, Qu Y, Xiao D and Mu D (2019) Pericytes in Cerebrovascular Diseases: An Emerging Therapeutic Target. Front. Cell. Neurosci. 13:519. doi: 10.3389/fncel.2019.00519

INTRODUCTION

Pericytes are among the major components of vascular composition. They are located along the capillary walls at intervals and possess numerous biological functions and characteristics. In particular, pericytes exhibit migratory, immune, phagocytic, and cytoprotective functions as well as stem cell potential and are involved in tissue repair (Attwell et al., 2016). In the CNS, pericytes participate in brain self-regulation, which is vital for blood vessel formation, maintenance of BBB integrity, regulation of cerebral blood flow, and coagulation (Santos et al., 2018). Additionally, pericytes are involved in the pathogenesis and development of various diseases. For instance, under ischemic conditions, pericytes constrict the capillaries in rigidity and hinder the flow of blood cells, which eventually prevents microcirculatory reperfusion even if the plaque has been removed in

Abbreviations: α-SMA, alpha smooth muscle actin; AD, Alzheimer's disease; BBB, blood–brain barrier; CNS, central nervous system; ICAM-1, intercellular adhesion molecule 1; IL-6, interleukin 6; MMP3, matrix metallopeptidase 3; MMP9, matrix metallopeptidase 9; NG2, chondroitin sulfate proteoglycan; NVU, neurovascular unit; PAR1, protease-activated receptor-1; PAR4, protease-activated receptor-4; PDGFR-α, β, platelet-derived growth factor α, β receptors; RGS5, regulators of G protein signaling 5; TGF-β, transforming growth factor; TNF-α, tumor necrosis factor α; WMI, brain white matter injury.

stroke disorders (Beazley-Long et al., 2018). Furthermore, studies have indicated that pericytes are associated with other neurovascular disorders, including WMI, cerebral hemorrhage, and hypoxic–ischemic brain damage (Hill et al., 2014). Therefore, after gaining a comprehensive understanding of the characteristics of pericytes and the in-depth studies on their relationship with diseases, scientists have regarded pericytes as good targets for the treatment of diseases. Although pericytes have been the subject matter of various studies, only few reviews have focused on discussing pericytes in cerebrovascular diseases, and data on the characteristics of pericytes and their use as therapeutic targets remain insufficient (Lange et al., 2013). Thus, we decided to conduct a review that firstly provided sufficient knowledge about this topic.

To provide a comprehensive understanding of pericytes, in this review, we summarized the biological characteristics of pericytes in detail, including their research history, distribution, isolation and culture methods, identification strategies, and biological functions. In addition, we elucidated the roles of pericytes in the pathogenesis of cerebrovascular diseases, including hemorrhagic brain injury, WMI, hypoxic–ischemic brain damage and other neurovascular dysfunctions, and clarified the progress in the treatment of cerebrovascular diseases targeted to pericytes.

BIOLOGICAL CHARACTERISTICS OF PERICYTES

Research History of Pericytes

The research history of pericytes covers several centuries. In 1873, pericytes were first discovered by Charles Rouget, who was investigating on capillary contractility. Later in 1923, Krogh named them "Rouget cells." In 1929, the concept of pericytes was formally proposed by Zimmerman, who described their relevant biological characteristics. In the 1960s, Majino et al. showed that pericytes are derived from the mesenchyme of the mesoderm and are widely distributed in the capillaries of vertebrates (**Figure 1**; Dore-Duffy and Cleary, 2011). Subsequently, accumulating studies had investigated the source and destination of pericytes. Majino et al. indicated that CNS pericytes are mainly derived from the mesenchymal stem cells of the mesoderm and the neural crest cells of neuroepithelial origin (Faal et al., 2019). Cell transplantation experiments on chicken embryos have revealed that the pericytes of the forebrain are mainly differentiated from neuroepithelial cells (Etchevers et al., 2001), whereas the pericytes of the midbrain, brainstem, and spinal cord are derived from the mesoderm (Kumar et al., 2017). Moreover, human brain pericytes also contain a large amount of acid phosphatase and have a phagocytic function, suggesting that pericytes could be originated from macrophages (Barreto et al., 2019). Further studies have shown that pericytes have rich destinations, which can differentiate into fat, muscle, cartilage, and bone cells as well as other types, indicating that pericytes have stem cell characteristics (Ahmed and El-Badri, 2018). Collectively, overall findings indicate that pericytes can be derived from various origins and are capable of producing diverse cells.

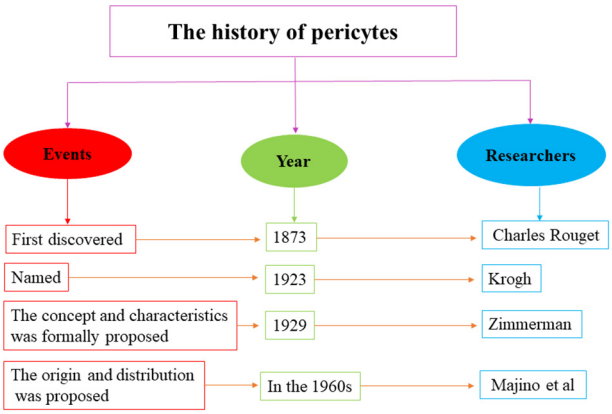

FIGURE 1 | The research history of pericytes. The research history of pericytes covers several centuries, which ranges from first discovery in 1873 to further study in the 1960s.

Morphology, Distribution, and Communication of Pericytes

Pericytes are polymorphic and usually appear as star-shaped or flat cells. The cell body of pericytes is spherical or oval and contains a large, round nucleus. The cytoplasm of pericytes contains a large number of organelles and mitochondria that can synthesize proteins, in addition to several lysosomes, which make the outer surface of pericytes appear to be granular (Jindatip et al., 2012). Studies have revealed that pericytes are constricted cells that spaced apart on capillary walls and closely linked to capillary endothelial cells. Besides, pericytes are widely distributed in the large blood vessels of the entire body, which located between the intima and adventitia of the microvascular and capillary walls, and mainly cover the capillaries, arterioles, and venules (Mazurek et al., 2017). Although pericytes are distributed throughout all organs, the number of CNS pericytes, which are important cellular components of the NVU and the BBB, is higher than that of pericytes in other organs (Armulik et al., 2011). In capillaries, pericytes are located between the endothelial cells and basement membrane, together with the endothelial cells, pericytes form a barrier between the blood vessels and interstitial space, such as the BBB, retinal blood barrier, and the like (Hall et al., 2014). Pericytes extend long protrusions along the longitudinal axis of the blood vessels that branch into two or three longitudinal and annular protrusions surrounding the blood vessels. The longitudinal protrusions are distributed along the longitudinal axis of the blood vessels, whereas the annular protrusions are perpendicular to the longitudinal axis. The neurites extended by pericytes contain large amounts of tubulin, whereas those on the surface of cell membranes that contact the endothelial cells contain dense microfilament-rich bands (Sava et al., 2017). However, when observed under a transmission electron microscope, pericytes are almost invisible, and the pericytes in mature capillaries have a disc-shaped nucleus surrounded by a small amount of cytoplasm (Liu et al., 2016). Based on the distribution and morphological

characteristics of pericytes, the transmission of information between pericytes, and other cells requires the formation of specific structures. For instance, the communication between pericytes and endothelial cells requires the formation of gap junctions, adhesion plaques, and structures such as peg–socket boxes (periosteal cells forming staples and wrapped by nail grooves formed by endothelial cells). The discontinuity of the basement membrane and the incomplete coverage of pericytes allow the endothelial cells to form a broad connection with the glial border membrane, which in turn interacts with astrocytes, and together they form the NVU (Hartmann et al., 2015). In addition, *in vitro* studies showed that pericytes could express occludin, claudin-12, and zona occludens-1 and -2 on the cell border, suggesting that tight junctions can be formed between pericytes (Shimizu et al., 2008).

Identification of Pericytes

Pericytes express a series of protein molecules, including α-SMA (Alarcon-Martinez et al., 2018), nestin (Muñoz-Fernández et al., 2018), vimentin (Bandopadhyay et al., 2001), NG2 (Sato et al., 2016), aminopeptidases A and N (Winkler et al., 2018), intercellular adhesion molecule-1 (ICAM-1) (Fan et al., 2019), vascular cell adhesion molecule-1 (Winkler et al., 2018), platelet-derived growth factor alpha and beta receptors (PDGFR-α and -β) (Wilson et al., 2018), CD34, CD146 (MCAM), CD4, CD11b (Wang et al., 2019), regulator of G-protein signaling 5 (RGS5) (Berger et al., 2005), stem cell antigen-1 (Kunisaki, 2019), and major histocompatibility complex classes I and II (Rink et al., 2017), without the expression of von Willebrand factor (Yin et al., 2019), platelet endothelial cell adhesion molecule (Nikolajsen et al., 2016), and glial fibrillary acidic protein (Winkler et al., 2018). Brain pericytes also express ATP-sensitive potassium channel protein Kir6.1 (**Table 1**; Bondjers et al., 2006).

TABLE 1 | The markers of pericytes.

Markers	References
α-SMA	Alarcon-Martinez et al., 2018
Nestin	Muñoz-Fernández et al., 2018
Vimentin	Bandopadhyay et al., 2001
NG2	Sato et al., 2016
Aminopeptidase A and N	Winkler et al., 2018
ICAM-1	Fan et al., 2019
VCAM-1	Winkler et al., 2018
PDGF-α,β	Wilson et al., 2018
CD34/CD146/CD4/CD11b	Wang et al., 2019
RGS-5	Berger et al., 2005
Sca-1	Kunisaki, 2019
MHC-I/II	Rink et al., 2017
Kir6.1	Bondjers et al., 2006

α-SMA, alpha smooth muscle actin; NG2, chondroitin sulfate proteoglycan; ICAM-1, intercellular adhesion molecule-1; VCAM-1, vascular cell adhesion molecule-1; PDGF-α, β (platelet-derived growth factor α, β receptors); RGS-5, regulators of G protein signaling 5; Sca-1, spinocerebellar ataxia 1; MHC-I/II, major histocompatibility Complex-I and II; Kir6.1, ATP-sensitive potassium channel protein.

Nonetheless, due to the heterogeneity of pericytes, the surface markers of pericytes may be different even in different areas of the same tissue and even in different stages of differentiation or different pathophysiological states of the same pericytes (Dias Moura Prazeres et al., 2017). In addition, the surface markers of pericytes may not be specific for pericytes. For example, PDGFR, the common marker for pericytes, can also be expressed in fibroblasts and smooth muscle cells (Muñoz-Fernández et al., 2018). Therefore, in view of the deficiency of specific immunological molecular markers for pericytes, current approaches to pericytes identification are mainly based on morphology and the combined application of a series of positive and negative immunological markers. For instance, to identify musculoskeletal pericytes of vascular origin, researchers use combined detection of markers for CD146, NG2, α-SMA, and PDGFR expression without CD31, CD34, CD45, and CD144 (Tonlorenzi et al., 2017).

Culture of Pericytes

The heterogeneity of pericytes makes their identification complicated and difficult. It is easy to mix other cells (e.g., adventitial cells) with pericytes after isolation. The traditional methods for pericytes isolation include sequential sieve technique and immunomagnetic bead sorting. With the sequential sieve technique, the brain tissue is first converted into a cell suspension and sequentially passes through a sieve with different pores to separate the pericytes. This method requires initial separation of the microvascular fragments, which is cumbersome. Moreover, the grinding time is difficult to control, which may result in physical damage to the microvessels. Additionally, the separated microvascular fragments are usually not conducive to progeny cells climbing out, and cell viability is weak (Boroujerdi et al., 2014). In contrast, immunomagnetic bead sorting uses antibodies for the markers of pericytes linking to the magnetic beads to separate pericytes from other cells. The commonly used markers of pericytes include NG2, α-SMA, desmin, and PDGFR-β, which vary depending on the species, tissues, and developmental stages of the origin. Similarly, this method consists of a complicated process and is costly. Moreover, the effect of separation and culture is not ideal (Primo and Arboleda-Velasquez, 2016).

Considering that traditional culture approaches have their advantages and disadvantages, recent investigations have improved the technique of separating the pulmonary microvascular pericytes through the use of mechanical shearing, enzymatic digestion, mesh filtration, and lysis by red blood cell lysate to obtain a purer microvascular fragment. Given that pericytes can secrete TGF-β to inhibit endothelial cell growth, researchers have acquired pulmonary microvascular progeny cells with a purity of 100% by extending the natural purification time. Compared with the two former methods, this method avoids damage to the microvascular fragments during grinding and has a simpler operation process, thereby reducing the procedural time and cost. Additionally, the progeny cells are easily derived from the microvascular fragments, and cell survival probability is increased. Moreover, this approach solves endothelial cell contamination, which is the main problem when isolating pericytes by using microvascular fragments

(Wertheim et al., 2019). Currently, isolation and *in vitro* culture technologies for the retinal, spinal, lung, and brain microvascular pericytes are relatively mature.

FUNCTION OF PERICYTES

As one of the most important components of the blood vessels, pericytes carry out various physiological functions. The functions of pericytes can be roughly summarized as follows.

Regulation of Vascular Genesis and Microecology

Studies have shown that the formation of new blood vessels and the maintenance of vessel wall stability require a sufficient number of pericytes (Bergers and Song, 2005). Pericytes are the dominant cells in regulating angiogenesis, primarily via secretion of different signals. The process of angiogenesis involves four major steps (Diaz-Flores et al., 2017). In the initial stage of angiogenesis, pericytes promote endothelial cell maturation and neovascular sprouting by secreting vascular endothelial growth factor and interleukin-6 (IL-6) (Eilken et al., 2017). During the stage of shaping and prolongation of blood vessels, pericytes contribute to the migration, proliferation, aggregation, and differentiation of endothelial cells by secreting vascular endothelial growth factor and fibroblast growth factor (Cross and Claesson-Welsh, 2001). In the process of generation, connection, and termination of new blood vessels, an active interaction exists between pericytes, and endothelial cells. For instance, PDGFR-β secreted by endothelial cells should firstly bind to endothelium-derived heparan sulfate proteoglycan, which promotes pericytes recruitment around the blood vessels and facilitates peripheral cell proliferation and migration by interacting with the PDGFR-β receptor on the surface of pericytes (Cuervo et al., 2017). In the last stage of angiogenesis, pericytes divide and proliferate rapidly to generate the extracellular matrix, accelerate the maturation of neovascularization, and participate in the modification and reinforcement of new blood vessels (**Figure 2**; Marchand et al., 2018).

Pericytes signals are also involved in the construction of vascular microecology after ischemia. For example, in brain tissues, brain pericytes are capable of secreting angiopoietin-1, and stromal cell-derived factor-1. Angiopoietin-1 binds to Tie2 expressed by endothelial cells and promotes Tie2 auto-phosphorylation (activation), which in turn recruits peripheral cells, such as smooth muscle cells and pericytes, to support endothelial cells in forming intact blood vessel walls, promote vascular remodeling and maturation, maintain vascular integrity, and regulate vascular function (Fukuhara et al., 2010). At the same time, stromal cell-derived factor-1 and its specific receptor CXCR4 promote endothelial cell migration, adult blood vessel formation, nerve development, and neuronal migration (**Figure 2**; Cui et al., 2013).

Regulation of Brain Blood Vessels

Pericytes have different subtypes and multiple functions. Pericytes located near the end of the capillary arteriole express more α-SMA and participate in the reflow process. These contractile pericytes contract the capillaries when ischemia occurs and are preferentially involved in the regulation of cerebral blood flow. Targeting these pericytes can reduce the no-reflux phenomenon after ischemic brain injury (Fernandez-Klett and Priller, 2015). The contraction of pericytes is involved in the following four mechanisms: (1) the endothelial cells surrounded by blood vessels show a flaky-fold structure with high and low undulations; (2) the ultrastructure of pericytes has a cytoskeletal structure capable of finely regulating cell contraction; (3) pericytes can express contractile proteins, such as α-SMA and troponin, and the expression levels of contractile proteins are distinct in different blood vessels; and (4) pericytes have some molecular receptors, such as endothelin receptors, which interact with angiotensin II and norepinephrine, causing rapid contraction of pericytes. Pericytes in the middle of capillaries express lower α-SMA and are preferentially involved in the maintenance of the BBB. Targeting these pericytes may reduce BBB damage after ischemic brain injury (Cai et al., 2017). However, the pericytes located at the end of the capillary venules are preferred to regulate the entry of immune cells into the brain parenchyma, and the amount of immune cells that enters into the brain parenchyma is significantly increased after ischemic brain injury (Navarro et al., 2016). Additionally, pericytes are capable of regulating blood pressure and coagulation. Angiotensin II secreted by endothelial cells can bind to its receptors on pericytes, causing contraction of the systemic arterioles, and elevation of arterial blood pressure, whereas vasoactive intestinal peptide secreted by endothelial cells can bind to its receptors on pericytes and has a vasodilating effect in lowering blood pressure (Fransen et al., 2016). Endothelin-1 is an endogenous vasoconstrictor regulator that is also present on pericytes (Dore-Duffy et al., 2011). During vascular injury or reconstruction, pericytes can secrete tissue factors, activate other coagulation factors, and form a positive feedback for the exogenous coagulation pathway, thereby regulating the prothrombin complex and participating in the whole coagulation process. At the same time, pericytes can also provide the necessary membrane surface for prothrombin complexes and promote the formation of thrombin with the help of coagulation factors Va and Xa. For example, human choroidal pericytes not only produce and regulate procoagulant complex but also support the functionally activated tissue factors present on its surface, which form a functional complex by binding to factor VIIa, thereby activating factors IX and X (**Figure 2**; Luo et al., 2018).

Collectively, pericytes regulate blood vessels by contracting themselves, controlling the size of capillary lumens, preventing excessive expansion of blood vessels, and maintaining homeostasis and metabolic balance of tissues.

Regulation of BBB

Pericytes are one of the constituent cells of the NVU and play an important role in regulating the permeability of the BBB. Hypoxia can lead to increased permeability of monolayer endothelial cells, and co-culture with pericytes can reduce sensitivity to hypoxia and permeability of endothelial cells (Yamamizu et al., 2017).

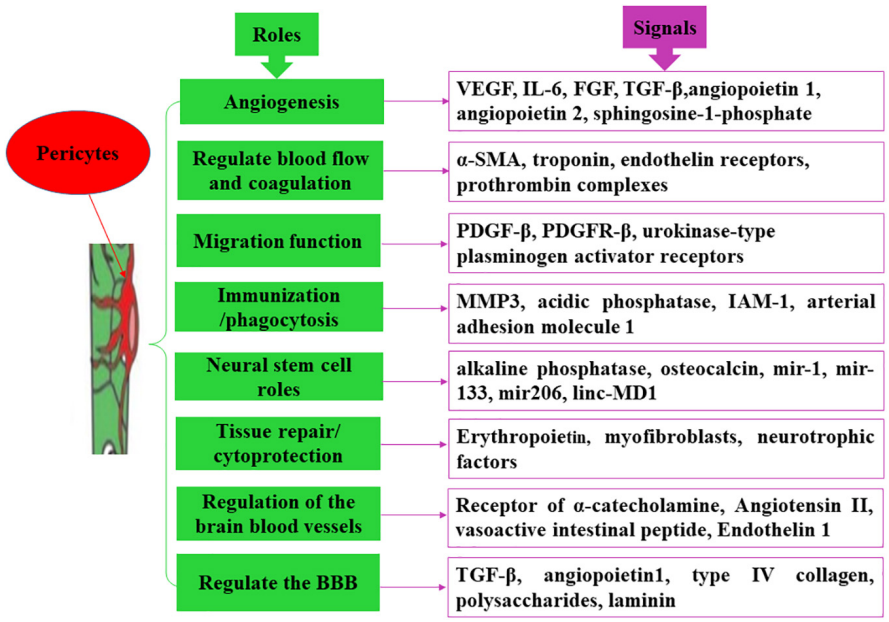

FIGURE 2 | Main functions of pericytes. Pericytes exert divers functions via secreting different molecules.

In addition, pericytes and brain microvascular endothelial cells communicate through gap junctions, tight junctions, focal adhesions, and some soluble factors, which in turn secrete growth factors to regulate the formation of tight junctions and permeability of endothelial cells that are important for the remodeling and maintenance of the vascular system (Ma et al., 2018). At the same time, pericytes can also regulate the proliferation, migration, and differentiation of endothelial cells (Zhou et al., 2016). Moreover, type IV collagen, polysaccharides, and laminin synthesized by the mouse kidney pericytes have been reported to have an effect on the formation of basement membrane (Wnuk et al., 2017). Hence, it can be speculated that pericytes are involved in the formation and maintenance of the BBB (**Figure 2**).

Migration Function

During arterial vascular development, endothelial-derived PDGF-β and PDGF-β receptors expressed by pericytes mediate pericytes migration to the endothelial cells (Thijssen et al., 2018). *In vitro* experiments that mimic capillary structures of the human BBB have shown the migration of pericytes to endothelial cells (Campisi et al., 2018). In addition, cortical pericytes can rapidly respond under brain hypoxic conditions or during brain trauma, wherein approximately 40% of pericytes migrate to the perivascular site, which may be mediated by urokinase-type plasminogen activator receptors expressed by pericytes, and exacerbate BBB damage and increase BBB permeability, leading to cerebral edema (**Figure 2**; Castejon, 2011).

Immunization and Phagocytosis

Pericytes have been reported to express matrix metalloproteinase 3 (MMP3); mice with MMP3 mutations exhibit a lower inflammatory response and a decrease in the number of permeable neutrophils, suggesting that pericytes are immunologically active in the inflammatory response (Kennedy-Lydon, 2017). At the same time, pericytes are capable of delivering antigens to T lymphocytes and participate in the immune response (Pober et al., 2017). Studies in the developing brain have revealed that lysosomes in pericytes can extensively express acidic phosphatase and exhibit phagocytic activity and that some pericytes can be directly transformed from macrophages (Prazeres et al., 2018). Furthermore, *in vitro* study found that cultured brain capillary pericytes can express a small number of adhesion molecules (such as ICAM-1 and arterial adhesion molecule-1) under the induction of inflammatory cytokines and can actively absorb and eliminate harmful small molecule particles (Pieper et al., 2014). These results indicated that pericytes have a phagocytic function that is similar to that of macrophages (**Figure 2**).

Potentiality of Neural Stem Cell

Pericytes isolated from different tissues can differentiate into other types of cells. For example, when cultured *in vitro*, the expression levels of alkaline phosphatase and osteocalcin in pericytes are increased, aggregated, and calcified, and pericytes demonstrate certain osteogenic ability (Gaceb et al., 2018). Pericytes can also differentiate into odontoblasts (Farahani et al., 2012). Furthermore, when pericytes extracted from skeletal muscle vessels are implanted into rats with muscle dysfunction, they can differentiate into skeletal muscle cells, thereby producing a large number of muscle tubules, and inducing muscle remodeling (Pierantozzi et al., 2016). When pericytes extracted from bovine renal microvessels are transplanted into the rats, they can differentiate into cartilages and

adipocytes (Konig et al., 2016; Vidhya et al., 2018). In addition, in hemorrhagic cerebral infarction, brain pericytes can differentiate into glial cells (Cheng et al., 2018). For different cell-derived and subtype pericytes, their differentiation and repair ability are not alike. For example, skeletal muscle-derived pericytes express three major myogenic RNA (mir-1, mir-133, and mir206) and unencoded myogenic RNA (linc-MD1), and their myogenic capacity was significantly higher than that of adipose-derived pericytes (**Figure 2**; Gautam and Yao, 2019).

Tissue Repair and Cytoprotection

Pericytes are involved in the repair and regeneration of various tissues and organs. Under physiological conditions, renal pericytes can produce erythropoietin to maintain microvascular stability. However, during renal injury, pericytes are exfoliated from the blood vessels, migrating, aggregating, and proliferating toward the injury, where they differentiate into other types of cells (such as myofibroblasts) to promote capillary regeneration at the site of injury and prevent the loss of capillaries (Shaw et al., 2018). Additionally, brain pericytes can express neurotrophic factors to promote neuronal survival when hypoxia occurs (Li et al., 2017). In the cardiovascular system, pericytes are involved in angiogenesis and affect the stability of arterial plaques. For instance, arterial plaques contain a large number of new blood vessels; when pericytes are absent, the permeability and fragility of new blood vessels increase, leading to plaque instability (Kennedy-Lydon, 2017). Pericytes also control effective myocardial perfusion by regulating the contractility of myocardial capillaries and participate in the reconstruction process after myocardial infarction (Costa et al., 2018). However, during the process of tissue repair, pericytes can cause excessive fibrosis. When repairing renal damage, pericytes may reduce the stability of the glomerular microvasculature, resulting in chronic hypoxia in the tubular and interstitial cells, and in turn leading to renal fibrosis (Venkatachalam and Weinberg, 2017). Pericytes can also cause pulmonary fibrosis and hepatic fibrosis. Along with increasing age, the activity of pericytes decreases and some special receptors are also lost, hindering the related signaling pathways for differentiation into other tissues, and thereby reducing the regeneration function for tissue repair (**Figure 2**; Birbrair et al., 2015).

PERICYTES AND CEREBROVASCULAR DISEASES

The neurovascular unit is a dynamic functional module composed of various members, such as neurons, glial cells, and pericytes. Studies have shown that NVU dysfunction is involved in the development of various cerebrovascular diseases, including hypoxic–ischemic brain damaged, brain WMI, and cerebral hemorrhage (Hill et al., 2014). Pericytes can regulate nerve and blood vessel events. For example, brain pericytes are involved in the regulation of cerebral blood flow, neurovascular growth, homeostasis of the NVU, and development and integrity of the BBB, and they have the potential activity of immune phagocytosis and stem cells (Sa-Pereira et al., 2012). In addition, studies on PDGFR-β-deficient rats reported that loss of brain pericytes might cause nerve damage through a reduction in chronic hypoperfusion and hypoxia by decreasing the level of brain microcirculation and through massive accumulation of plasma proteins and neurotoxic substances owing to damage to BBB integrity (Sauer et al., 2017). Both processes are related to the activity of pericytes.

Pericytes and Cerebral Hemorrhage

After cerebral hemorrhage, thrombin induces the release of MMP9, and its expression in brain pericytes is higher than that in other BBB-constituting cells, which may be related to the higher expression of thrombin receptors PAR1 and PAR4 in brain pericytes (Underly et al., 2017). Among proteins, PAR1 is the most abundant in brain pericytes, and the use of PAR1 inhibitor SCH79797 can prevent the release of MMP9 from brain pericytes, suggesting the important role of the thrombin–PAR1–MMP9 axis of brain pericytes in the pathological process of cerebral hemorrhage (Machida et al., 2017). Further studies have shown that thrombin stimulates PAR1 in brain pericytes after cerebral hemorrhage, activates PKCh-Akt and PKCd-ERK1/2 signaling pathways, and subsequently releases MMP9, leading to BBB damage, and aggravating brain damage (**Table 2**; Wang et al., 2018).

Pericytes and Hypoxic–Ischemic Brain Damage

Cerebral hypoxic–ischemic damage triggers the activity of pericytes. However, whether the activation of pericytes

TABLE 2 | The pericytes with cerebrovascular disease.

Cerebrovascular disease	Pericytes signals/ function	References
Cerebral hemorrhage	PAR1 PAR4 MMP9	Machida et al., 2017; Underly et al., 2017; Wang et al., 2018
Hypoxia-ischemic brain damage	Calcium overload Pericyte excessive contraction TGF-β1/AP-1 Collagen IV/laminin/hyaluronic acid	Kose et al., 2007; Zechariah et al., 2013; Rustenhoven et al., 2016; Cai et al., 2017
White matter injury	Notch 3 Kir6.1/ATP	Thomzig et al., 2005; Kofler et al., 2015
Neovascular deficiency disease	PHD2 VEGF PDGFβ RGS5 SPARC Sema3A/Nrp-1	Hamzah et al., 2008; Dhar et al., 2010; Bai et al., 2015; Svensson et al., 2015; Urrutia et al., 2016; Thijssen et al., 2018

PAR1, protease-activated receptor-1; PAR4, protease-activated receptor-4; MMP9, matrix metallopeptidase 9; AP-1, activator protein-1; PHD2, proline hydroxylase 2; VEGF, vascular endothelial growth factor; PDGFβ, platelet-derived growth factor β; RGS5, regulators of G protein signaling 5; SPARC, protein acidic and rich in cysteine; Sema3A, axon guiding molecule 3; Nrp-1, neurociliary protein 1.

is beneficial or harmful depends on the specific tissue microenvironment, degree of activation, type of stimulation, and existing factors (Schneider et al., 2015). For instance, pericytes take on various tasks in different stages of ischemic stroke (Cai et al., 2017). (1) In the hyper-acute phase of stroke, the intracellular calcium concentration is enhanced, the number of ATP molecules is insufficient, and oxygen and nitrogen free radicals are formed in the microvasculature, leading to the contraction and death of pericytes, which finally cause no-reflow phenomenon in the capillaries of the brain. (2) In the acute phase, pericytes are stripped from microvessels and participate in inflammatory and immune responses, leading to BBB damage and cerebral edema. (3) During the late recovery phase of stroke, pericytes contribute to angiogenesis and neurogenesis, thereby promoting nerve recovery. In addition, pericytes are abnormally active and exhibit quantitative, structural, and functional changes when stimulated by certain extracellular noxious stimuli (such as acidosis, high glucose level, and reactive oxygen species), which cause pericytes dysfunction and excessive contraction, hinder red blood cells from passing through the vessels, and subsequently lead to microcirculatory disorders. For example, in a rat model of cerebral ischemia, oxidation-nitrous stress can induce constant contraction of retinopathy pericytes, and result in the disturbance of microcirculation and blood flow (Fu et al., 2016). In focal ischemic rat models, the contraction of pericytes occurred during cerebral artery occlusion and persisted even after the blood flow was restored (Zechariah et al., 2013). Thus, excessive and continuous contraction of pericytes after cerebral ischemia may be the cause of local microcirculation disorder, which may also be an important pathological mechanism of cerebral ischemia–reperfusion injury (**Table 2**).

Nevertheless, pericytes also provide benefits for neuroprotection in hypoxic–ischemic brain damage by protecting the endothelium, stabilizing BBB permeability, and releasing neurotrophins (Ishitsuka et al., 2012). For example, in the *in vitro* BBB model with mixed endothelial cells, pericytes, and astrocytes, the researchers found that the permeability of monolayer endothelial cells was significantly attenuated due to the presence of pericytes. Similarly, when co-cultured with pericytes, the sensitivity of endothelial cells to hypoxia was significantly reduced (Wang et al., 2016). Under continuous hypoxic conditions, TGF-β1 and angiopoietin-1 expressed by pericytes contributed to the maintenance of the tight junction of the BBB (Rustenhoven et al., 2016), whereas type IV collagen, laminin, and hyaluronic acid secreted by pericytes are involved in the construction of the basement membrane (Kose et al., 2007). In addition, when observing the brain tissue of rats with minimal cerebral hemorrhage via electron microscopy, researchers found that ions, and plasma components exist in the cytoplasm of pericytes (Jindatip et al., 2018). Therefore, when the tight binding of the BBB was disrupted, pericytes might act as phagocytes to play a remedial role (**Table 2**).

Pericytes and Brain White Matter Injury

Brain WMI can be induced by hypoxic–ischemia, infection, and so on (Duerden et al., 2019). Pericytes dysfunction is involved in the pathogenesis of WMI (Montagne et al., 2018). Numerous studies have confirmed that human *Notch3* gene is mainly expressed in the arterial smooth muscle cells and pericytes and that its mutations cause capillary blood flow dysregulation, thereby triggering impaired cerebrovascular reactivity and WMI disorders such as hereditary multi-infarct dementia (cerebral autosomal dominant arteriopathy with subcortical infarcts and leukoencephalopathy) (Kofler et al., 2015). Furthermore, the observation of cerebral microvessels in patients with cerebral autosomal dominant arteriopathy with subcortical infarcts and leukoencephalopathy via electron microscopy indicated that pericytes showed degeneration, the nuclei were swollen, and the basement membrane between pericytes and endothelial cells was thickened with a large amount of osmiophilic granules (Craggs et al., 2015). In rats with chronic cerebral hypoperfusion-induced WMI, the pericytes were damaged and its biomarker Kir6.1/Kir6.2 was expressed in heterogeneity, suggesting that the Kir6.1/K-ATP channel might be involved in the pathological process of chronic WMI (**Table 2**; Thomzig et al., 2005).

Pericytes and Neovascular Deficiency Disease

Pericytes maintain vascular osmotic pressure and morphology and participate in vascular genesis and maturation via signal transmissions with endothelial cells and extracellular matrix (Ferland-McCollough et al., 2017). The insufficiency of pericytes always leads to the occurrence and development of neovascular deficiency disease (Bergers and Song, 2005). The neovascular deficiency disease refers to a category of disorder which is caused by the shortage of formation or immaturities of new blood vessels, including tumors, atherosclerosis, diabetic retinopathy, and the like. Besides, neovascular deficiency often occurs following different types of brain damage such as hypoxic ischemic encephalopathy and WMI, which in turn attenuated the recovery of brain injury. Generally, this category of disorder shares the following characteristics: (1) the morphology of endothelial cells is abnormal, showing overlapping growth, and the connection between endothelial cells is reduced; (2) the morphology of pericytes is abnormal, the function is inadequate, and the coverage is decreased; and (3) the basement membrane is incomplete or missing, with uneven thickness or thinness, and is distributed in sheets (Davis et al., 2015). Studies have shown that these neovascular immaturity diseases are associated with various signaling pathways. For example, the excessive activation of angiogenic signaling pathways, such as proline hydroxylase-2 (Urrutia et al., 2016) and vascular endothelial growth factor (Bai et al., 2015), leads to excessive angiogenesis. On the other hand, the recruitment and proliferation of pericytes are inhibited and the decomposition of the basement membrane is excessive, ultimately inhibiting the maturation of new blood vessels (Cheng et al., 2018). In addition, the signals secreted by pericytes such as PDGF-β (Thijssen et al., 2018), RGS5 (Hamzah et al., 2008), secreted protein acidic and rich in cysteine (Svensson et al., 2015), and axon guidance molecule 3/neurociliary protein 1 (Sema3A/Nrp-1) (Dhar et al., 2010)

are also closely related to the occurrence of neovascularization immaturity (**Table 2**).

PERICYTES AND NON-VASCULAR BRAIN DISORDERS

Pericytes and Depression

Depression is a type of neuropsychiatric disease caused by NVU dysfunction, which is closely related to neuroinflammation that can affect serotonin levels (Liu et al., 2015). Depression is also associated with NVU dysfunction caused by abnormally high BBB permeability. For example, studies have shown that the BBB integrity in patients with depression is disrupted, and the pericytes coverage of the cortical and hippocampal capillary networks is significantly reduced (Liu et al., 2019). In addition, *in vitro* study indicated that brain pericytes secrete various cytokines, including ICAM-1, IL-6, tumor necrosis factor-α (TNF-α), and MMP, which disrupt BBB integrity and aggravate brain inflammatory factors (Dohgu et al., 2019). Numerous studies have shown that inflammatory factors such as IL-6, IL-1, and TNF-α can trigger acute pro-inflammatory effects and that the downregulation of these factors can induce depression-like behavior (Chu et al., 2019). However, the upregulation of IL-6, IL-1β, and TNF-α has been shown to impair nerve cell regeneration and aggravate cell death, leading to neurodegenerative diseases (Zou et al., 2018). In addition, neuropathological studies have reported that patients with depression have abnormally elevated ICAM-1 in the prefrontal cortex and white matter. Antidepressant treatment reduces the expression of vascular cell adhesion molecule-1 and ICAM-1 in serum. These effects are triggered primarily by the interference of these cytokines secreted by pericytes, which disrupt cell survival signaling pathways and caspase-dependent cascades, and altering the function of major receptors (Dewispelaere et al., 2015).

Pericytes and Alzheimer's Disease

Alzheimer's disease, triggered by chronic inflammation as well as the pathological accumulation of beta-amyloid (Aβ) and neurofibrillary tangles in the brain, is related to pericytes dysfunction (Yamazaki and Kanekiyo, 2017). In transgenic animals with AD pathology, researchers found that circulating white blood cells penetrate the BBB to interact with NVU components and disrupt their structural integrity and function (Zuo et al., 2017). In addition, Aβ receptors such as LRP1, LDLR, RAGE, and CD36 are expressed on pericytes in the brain of AD patients, and these receptors are involved in Aβ-mediated cerebral perivascular cell death (Miners et al., 2018). Mice with depleted pericytes showed deposition of Aβ plaques in the brain parenchyma and blood vessels, as well as an accumulation of hyper phosphorylated tau protein, suggesting that pericytes deficiency contributed to the development of tau pathology (Sagare et al., 2013).

TARGETING PERICYTES AS A THERAPEUTIC STRATEGY FOR CEREBROVASCULAR DISEASES

Pericytes play an important role in the maintenance of normal functions of blood vessels in the brain and are involved in the pathogenesis of several cerebrovascular diseases. Therefore, targeting pericytes is a potential therapeutic strategy for cerebrovascular diseases.

Regulator of G-protein signaling 5, which regulates vascular development, showed a perivascular expression pattern and was identified as a marker for brain pericytes (Bondjers et al., 2003). In a mouse model of permanent midbrain occlusion, when knocking out *RGS5* gene, the amount of pericytes and endothelial coverage were increased, and the BBB injury was also significantly attenuated. Furthermore, loss of *RGS5* in pericytes alleviated vascular leakage, maintained tight junction integrity and aquaporin-4 levels, reduced cerebral hypoxia, and protected neurons in the infarcted area (Ozen et al., 2018). Therefore, targeting pericytes RGS5 might be effective in the treatment of ischemic stroke.

In a mouse model of cerebral ischemia, when TGF-β was used, it continuously stimulated the formation of extracellular matrix and the transformation of mesenchymal cells to vascular pericytes, thereby strengthening the blood vessels, preventing the leakage of new blood vessels, and promoting the maturation of blood vessels (Dhandapani and Brann, 2003). Therefore, TGF-β might be an effective agent to treat neovascular deficiency disease.

In a rat model of cerebral ischemia–reperfusion injury, pericytes were observed to migrate from the vessel wall at an early stage, the microvascular basement membrane structure was disordered, and the BBB function was impaired. When ischemic post-conditioning was performed, the MMP9 expression of pericytes was reduced. As MMP9 is a critical factor regulating pericytes migration, the downregulation of MMP9 after post-conditioning inhibited pericytes migration after ischemia–reperfusion, and maintained the integrity of BBB structure and function (Underly et al., 2017).

DISCUSSION

As components of the NVU, pericytes play an important role in the regulation of physiological and pathological processes of the CNS and have currently attracted considerable interest (Geranmayeh et al., 2019). This review primarily discussed the basic characteristics and research dynamics of pericytes in cerebrovascular diseases, aiming to provide a comprehensive understanding of pericytes and new insights about the use of pericytes as novel therapeutic targets for cerebrovascular diseases.

AUTHOR CONTRIBUTIONS

XS and YQ contributed to the conception and design of the review and drafting the manuscript. LH and DX

participated in the table making work. YQ and DM contributed to approving the final version of the manuscript submitted for publication.

FUNDING

This work was supported by the National Natural Science Foundation of China (81971433, 81971428, 81630038, 81771634, and 81842011), the Science and Technology Project of Sichuan Province (2016TD0002), and the National Key Project of Neonatal Children (1311200003303).

ACKNOWLEDGMENTS

We would like to thank Editage (www.editage.cn) for English language editing.

REFERENCES

Ahmed, T. A., and El-Badri, N. (2018). Pericytes: the role of multipotent stem cells in vascular maintenance and regenerative medicine. *Adv. Exp. Med. Biol.* 1079, 69–86. doi: 10.1007/5584-2017-138

Alarcon-Martinez, L., Yilmaz-Ozcan, S., Yemisci, M., Schallek, J., Kilic, K., Can, A., et al. (2018). Capillary pericytes express alpha-smooth muscle actin, which requires prevention of filamentous-actin depolymerization for detection. *eLife* 7:e34861. doi: 10.7554/eLife.34861

Armulik, A., Genove, G., and Betsholtz, C. (2011). Pericytes: developmental, physiological, and pathological perspectives, problems, and promises. *Dev. Cell.* 21, 193–215. doi: 10.1016/j.devcel.2011.07.001

Attwell, D., Mishra, A., Hall, C. N., O'Farrell, F. M., and Dalkara, T. (2016). What is a pericyte? *J. Cereb. Blood Flow Metab.* 36, 451–455. doi: 10.1177/0271678X15610340

Bai, Y., Zhu, X., Chao, J., Zhang, Y., Qian, C., Li, P., et al. (2015). Pericytes contribute to the disruption of the cerebral endothelial barrier via increasing VEGF expression: implications for stroke. *PLoS One* 10:e0124362. doi: 10.1371/journal.pone.0124362

Bandopadhyay, R., Orte, C., Lawrenson, J. G., Reid, A. R., De Silva, S., and Allt, G. (2001). Contractile proteins in pericytes at the blood-brain and blood-retinal barriers. *J. Neurocytol.* 30, 35–44. doi: 10.1023/a:1011965307612

Barreto, R. S. N., Romagnolli, P., Cereta, A. D., Coimbra-Campos, L. M. C., Birbrair, A., and Miglino, M. A. (2019). Pericytes in the placenta: role in placental development and homeostasis. *Adv. Exp. Med. Biol.* 1122, 125–151. doi: 10.1007/978-3-030-11093-2_8

Beazley-Long, N., Durrant, A. M., Swift, M. N., and Donaldson, L. F. (2018). The physiological functions of central nervous system pericytes and a potential role in pain. *F1000Res* 7:341. doi: 10.12688/f1000research.13548.1

Berger, M., Bergers, G., Arnold, B., Hammerling, G. J., and Ganss, R. (2005). Regulator of G-protein signaling-5 induction in pericytes coincides with active vessel remodeling during neovascularization. *Blood* 105, 1094–1101. doi: 10.1182/blood-2004-06-2315

Bergers, G., and Song, S. (2005). The role of pericytes in blood-vessel formation and maintenance. *Neuro. Oncol.* 7, 452–464. doi: 10.1215/S1152851705000232

Birbrair, A., Zhang, T., Wang, Z. M., Messi, M. L., Mintz, A., and Delbono, O. (2015). Pericytes at the intersection between tissue regeneration and pathology. *Clin. Sci.* 128, 81–93. doi: 10.1042/CS20140278

Bondjers, C., He, L., Takemoto, M., Norlin, J., Asker, N., Hellstrom, M., et al. (2006). Microarray analysis of blood microvessels from PDGF-B and PDGF-Rbeta mutant mice identifies novel markers for brain pericytes. *FASEB J.* 20, 1703–1705. doi: 10.1096/fj.05-4944fje

Bondjers, C., Kalen, M., Hellstrom, M., Scheidl, S. J., Abramsson, A., Renner, O., et al. (2003). Transcription profiling of platelet-derived growth factor-B-deficient mouse embryos identifies RGS5 as a novel marker for pericytes and vascular smooth muscle cells. *Am. J. Pathol.* 162, 721–729. doi: 10.1016/S0002-9440(10)63868-0

Boroujerdi, A., Tigges, U., Welser-Alves, J. V., and Milner, R. (2014). Isolation and culture of primary pericytes from mouse brain. *Methods Mol. Biol.* 1135, 383–392. doi: 10.1007/978-1-4939-0320-7-31

Cai, W., Liu, H., Zhao, J., Chen, L. Y., Chen, J., Lu, Z., et al. (2017). Pericytes in brain injury and repair after ischemic stroke. *Transl. Stroke Res.* 8, 107–121. doi: 10.1007/s12975-016-0504-4

Campisi, M., Shin, Y., Osaki, T., Hajal, C., Chiono, V., and Kamm, R. D. (2018). 3D self-organized microvascular model of the human blood-brain barrier with endothelial cells, pericytes and astrocytes. *Biomaterials* 180, 117–129. doi: 10.1016/j.biomaterials.2018.07.014

Castejon, O. J. (2011). Ultrastructural pathology of cortical capillary pericytes in human traumatic brain oedema. *Folia Neuropathol.* 49, 162–173.

Cheng, J., Korte, N., Nortley, R., Sethi, H., Tang, Y., and Attwell, D. (2018). Targeting pericytes for therapeutic approaches to neurological disorders. *Acta Neuropathol.* 136, 507–523. doi: 10.1007/s00401-018-1893-0

Chu, A. L., Stochl, J., Lewis, G., Zammit, S., Jones, P. B., and Khandaker, G. M. (2019). Longitudinal association between inflammatory markers and specific symptoms of depression in a prospective birth cohort. *Brain Behav. Immun.* 76, 74–81. doi: 10.1016/j.bbi.2018.11.007

Costa, M. A., Paiva, A. E., Andreotti, J. P., Cardoso, M. V., Cardoso, C. D., Mintz, A., et al. (2018). Pericytes constrict blood vessels after myocardial ischemia. *J. Mol. Cell Cardiol.* 116, 1–4. doi: 10.1016/j.yjmcc.2018.01.014

Craggs, L. J., Fenwick, R., Oakley, A. E., Ihara, M., and Kalaria, R. N. (2015). Immunolocalization of platelet-derived growth factor receptor-beta (PDGFR-beta) and pericytes in cerebral autosomal dominant arteriopathy with subcortical infarcts and leukoencephalopathy (CADASIL). *Neuropathol. Appl. Neurobiol.* 41, 557–570. doi: 10.1111/nan.12188

Cross, M. J., and Claesson-Welsh, L. (2001). FGF and VEGF function in angiogenesis: signalling pathways, biological responses and therapeutic inhibition. *Trends Pharmacol. Sci.* 22, 201–207. doi: 10.1016/s0165-6147(00)01676-x

Cuervo, H., Pereira, B., Nadeem, T., Lin, M., Lee, F., Kitajewski, J., et al. (2017). PDGFRbeta-P2A-CreER(T2) mice: a genetic tool to target pericytes in angiogenesis. *Angiogenesis* 20, 655–662. doi: 10.1007/s10456-017-9570-9

Cui, L., Qu, H., Xiao, T., Zhao, M., Jolkkonen, J., and Zhao, C. (2013). Stromal cell-derived factor-1 and its receptor CXCR4 in adult neurogenesis after cerebral ischemia. *Restor. Neurol. Neurosci.* 31, 239–251. doi: 10.3233/RNN-120271

Davis, G. E., Norden, P. R., and Bowers, S. L. (2015). Molecular control of capillary morphogenesis and maturation by recognition and remodeling of the extracellular matrix: functional roles of endothelial cells and pericytes in health and disease. *Connect. Tissue Res.* 56, 392–402. doi: 10.3109/03008207.2015.1066781

Dewispelaere, R., Lipski, D., Foucart, V., Bruyns, C., Frere, A., Caspers, L., et al. (2015). ICAM-1 and VCAM-1 are differentially expressed on blood-retinal barrier cells during experimental autoimmune uveitis. *Exp. Eye Res.* 137, 94–102. doi: 10.1016/j.exer.2015.06.017

Dhandapani, K. M., and Brann, D. W. (2003). Transforming growth factor-beta: a neuroprotective factor in cerebral ischemia. *Cell Biochem. Biophys.* 39, 13–22. doi: 10.1385/CBB:39:1:13

Dhar, K., Dhar, G., Majumder, M., Haque, I., Mehta, S., Van Veldhuizen, P. J., et al. (2010). Tumor cell-derived PDGF-B potentiates mouse mesenchymal stem cells-pericytes transition and recruitment through an interaction with NRP-1. *Mol. Cancer* 9:209. doi: 10.1186/1476-4598-9-209

Dias Moura Prazeres, P. H., Sena, I. F. G., Borges, I. D. T., de Azevedo, P. O., Andreotti, J. P., de Paiva, A. E., et al. (2017). Pericytes are heterogeneous in their origin within the same tissue. *Dev. Biol.* 427, 6–11. doi: 10.1016/j.ydbio.2017.05.001

Diaz-Flores, L., Gutierrez, R., Garcia-Suarez, M. P., Saez, F. J., Gutierrez, E., Valladares, F., et al. (2017). Morphofunctional basis of the different types of angiogenesis and formation of postnatal angiogenesis-related secondary structures. *Histol. Histopathol.* 32, 1239–1279. doi: 10.14670/hh-11-923

Dohgu, S., Takata, F., Matsumoto, J., Kimura, I., Yamauchi, A., and Kataoka, Y. (2019). Monomeric alpha-synuclein induces blood-brain barrier dysfunction through activated brain pericytes releasing inflammatory mediators in vitro. *Microvasc. Res.* 124, 61–66. doi: 10.1016/j.mvr.2019.03.005

Dore-Duffy, P., and Cleary, K. (2011). Morphology and properties of pericytes. *Methods Mol. Biol.* 686, 49–68. doi: 10.1007/978-1-60761-938-3-2

Dore-Duffy, P., Wang, S., Mehedi, A., Katyshev, V., Cleary, K., Tapper, A., et al. (2011). Pericyte-mediated vasoconstriction underlies TBI-induced hypoperfusion. *Neurol. Res.* 33, 176–186. doi: 10.1179/016164111X12881719352372

Duerden, E. G., Halani, S., Ng, K., Guo, T., Foong, J., Glass, T. J. A., et al. (2019). White matter injury predicts disrupted functional connectivity and microstructure in very preterm born neonates. *Neuroimage Clin.* 21:101596. doi: 10.1016/j.nicl.2018.11.006

Eilken, H. M., Dieguez-Hurtado, R., Schmidt, I., Nakayama, M., Jeong, H. W., Arf, H., et al. (2017). Pericytes regulate VEGF-induced endothelial sprouting through VEGFR1. *Nat. Commun.* 8:1574. doi: 10.1038/s41467-017-01738-3

Etchevers, H. C., Vincent, C., Le Douarin, N. M., and Couly, G. F. (2001). The cephalic neural crest provides pericytes and smooth muscle cells to all blood vessels of the face and forebrain. *Development* 128, 1059–1068.

Faal, T., Phan, D. T. T., Davtyan, H., Scarfone, V. M., Varady, E., Blurton-Jones, M., et al. (2019). Induction of mesoderm and neural crest-derived pericytes from human pluripotent stem cells to study blood-brain barrier interactions. *Stem Cell Rep.* 12, 451–460. doi: 10.1016/j.stemcr.2019.01.005

Fan, Q., Tao, Z., Yang, H., Shi, Q., Wang, H., Jia, D., et al. (2019). Modulation of pericytes by a fusion protein comprising of a PDGFR beta-antagonistic affibody and TNFalpha induces tumor vessel normalization and improves chemotherapy. *J. Control. Release* 302, 63–78. doi: 10.1016/j.jconrel.2019.03.018

Farahani, R. M., Sarrafpour, B., Simonian, M., Li, Q., and Hunter, N. (2012). Directed glia-assisted angiogenesis in a mature neurosensory structure: pericytes mediate an adaptive response in human dental pulp that maintains blood-barrier function. *J. Comp. Neurol.* 520, 3803–3826. doi: 10.1002/cne.23162

Ferland-McCollough, D., Slater, S., Richard, J., Reni, C., and Mangialardi, G. (2017). Pericytes, an overlooked player in vascular pathobiology. *Pharmacol. Ther.* 171, 30–42. doi: 10.1016/j.pharmthera.2016.11.008

Fernandez-Klett, F., and Priller, J. (2015). Diverse functions of pericytes in cerebral blood flow regulation and ischemia. *J. Cereb. Blood Flow Metab.* 35, 883–887. doi: 10.1038/jcbfm.2015.60

Fransen, P., Van Hove, C. E., Leloup, A. J., Schrijvers, D. M., De Meyer, G. R., and De Keulenaer, G. W. (2016). Effect of angiotensin II-induced arterial hypertension on the voltage-dependent contractions of mouse arteries. *Pflugers Arch.* 468, 257–267. doi: 10.1007/s00424-015-1737-x

Fu, D., Yu, J. Y., Yang, S., Wu, M., Hammad, S. M., Connell, A. R., et al. (2016). Survival or death: a dual role for autophagy in stress-induced pericyte loss in diabetic retinopathy. *Diabetologia* 59, 2251–2261. doi: 10.1007/s00125-016-4058-5

Fukuhara, S., Sako, K., Noda, K., Zhang, J., Minami, M., and Mochizuki, N. (2010). Angiopoietin-1/Tie2 receptor signaling in vascular quiescence and angiogenesis. *Histol Histopathol.* 25, 387–396. doi: 10.14670/HH-25.387

Gaceb, A., Barbariga, M., Ozen, I., and Paul, G. (2018). The pericyte secretome: potential impact on regeneration. *Biochimie* 155, 16–25. doi: 10.1016/j.biochi.2018.04.015

Gautam, J., and Yao, Y. (2019). Pericytes in skeletal muscle. *Adv. Exp. Med. Biol.* 1122, 59–72. doi: 10.1007/978-3-030-11093-2-4

Geranmayeh, M. H., Rahbarghazi, R., and Farhoudi, M. (2019). Targeting pericytes for neurovascular regeneration. *Cell Commun. Signal.* 17:26. doi: 10.1186/s12964-019-0340-8

Hall, C. N., Reynell, C., Gesslein, B., Hamilton, N. B., Mishra, A., Sutherland, B. A., et al. (2014). Capillary pericytes regulate cerebral blood flow in health and disease. *Nature* 508, 55–60. doi: 10.1038/nature13165

Hamzah, J., Jugold, M., Kiessling, F., Rigby, P., Manzur, M., Marti, H. H., et al. (2008). Vascular normalization in Rgs5-deficient tumours promotes immune destruction. *Nature* 453, 410–414. doi: 10.1038/nature06868

Hartmann, D. A., Underly, R. G., Grant, R. I, Watson, A. N., Lindner, V., and Shih, A. Y. (2015). Pericyte structure and distribution in the cerebral cortex revealed by high-resolution imaging of transgenic mice. *Neurophotonics* 2:041402. doi: 10.1117/1.NPh.2.4.041402

Hill, J., Rom, S., Ramirez, S. H., and Persidsky, Y. (2014). Emerging roles of pericytes in the regulation of the neurovascular unit in health and disease. *J. Neuroimmune. Pharmacol.* 9, 591–605. doi: 10.1007/s11481-014-9557-x

Ishitsuka, K., Ago, T., Arimura, K., Nakamura, K., Tokami, H., Makihara, N., et al. (2012). Neurotrophin production in brain pericytes during hypoxia: a role of pericytes for neuroprotection. *Microvasc. Res.* 83, 352–359. doi: 10.1016/j.mvr.2012.02.009

Jindatip, D., Fujiwara, K., Kouki, T., and Yashiro, T. (2012). Transmission and scanning electron microscopy study of the characteristics and morphology of pericytes and novel desmin-immunopositive perivascular cells before and after castration in rat anterior pituitary gland. *Anat. Sci. Int.* 87, 165–173. doi: 10.1007/s12565-012-0144-z

Jindatip, D., Fujiwara, K., Sarachana, T., Mutirangura, A., and Yashiro, T. (2018). Characteristics of pericytes in diethylstilbestrol (DES)-induced pituitary prolactinoma in rats. *Med. Mol. Morphol.* 51, 147–155. doi: 10.1007/s00795-018-0180-4

Kennedy-Lydon, T. (2017). Immune functions and properties of resident cells in the heart and cardiovascular system: pericytes. *Adv. Exp. Med. Biol.* 1003, 93–103. doi: 10.1007/978-3-319-57613-8-5

Kofler, N. M., Cuervo, H., Uh, M. K., Murtomaki, A., and Kitajewski, J. (2015). Combined deficiency of Notch1 and Notch3 causes pericyte dysfunction, models CADASIL, and results in arteriovenous malformations. *Sci. Rep.* 5:16449. doi: 10.1038/srep16449

Konig, M. A., Canepa, D. D., Cadosch, D., Casanova, E., Heinzelmann, M., Rittirsch, D., et al. (2016). Direct transplantation of native pericytes from adipose tissue: a new perspective to stimulate healing in critical size bone defects. *Cytotherapy* 18, 41–52. doi: 10.1016/j.jcyt.2015.10.002

Kose, N., Asashima, T., Muta, M., Iizasa, H., Sai, Y., and Terasaki, T. (2007). Altered expression of basement membrane-related molecules in rat brain pericyte, endothelial, and astrocyte cell lines after transforming growth factor-beta1 treatment. *Drug Metab. Pharmacokinet.* 22, 255–266. doi: 10.2133/dmpk.22.255

Kumar, A., D'Souza, S. S., Moskvin, O. V., Toh, H., Wang, B., Zhang, J., et al. (2017). Specification and diversification of pericytes and smooth muscle cells from mesenchymoangioblasts. *Cell Rep.* 19, 1902–1916. doi: 10.1016/j.celrep.2017.05.019

Kunisaki, Y. (2019). Pericytes in bone marrow. *Adv. Exp. Med. Biol.* 1122, 101–114. doi: 10.1007/978-3-030-11093-2-6

Lange, S., Trost, A., Tempfer, H., Bauer, H. C., Bauer, H., Rohde, E., et al. (2013). Brain pericyte plasticity as a potential drug target in CNS repair. *Drug Discov. Today* 18, 456–463. doi: 10.1016/j.drudis.2012.12.007

Li, Y., Lucas-Osma, A. M., Black, S., Bandet, M. V., Stephens, M. J., and Vavrek, R. (2017). Pericytes impair capillary blood flow and motor function after chronic spinal cord injury. *Nat. Med.* 23, 733–741. doi: 10.1038/nm.4331

Liu, J., Wang, Y. H., Li, W., Liu, L., Yang, H., Meng, P., et al. (2019). Structural and functional damage to the hippocampal neurovascular unit in diabetes-related depression. *Neural. Regen Res.* 14, 289–297. doi: 10.4103/1673-5374.244794

Liu, M. Y., Ren, Y. P., Wei, W. L., Tian, G. X., and Li, G. (2015). Changes of Serotonin (5-HT), 5-HT2A receptor, and 5-HT transporter in the sprague-dawley rats of depression, myocardial infarction and myocardial infarction co-exist with depression. *Chin. Med. J.* 128, 1905–1909. doi: 10.4103/0366-6999.160526

Liu, Y. H., Wang, Y. P., Wang, Y., Ma, K. T., Si, J. Q., and Li, L. (2016). [Study on the electrophysiological properties in the stria vascularis pericytes in cochlear of guinea pig]. *Zhonghua Er Bi Yan Hou Tou Jing Wai Ke Za Zhi.* 51, 600–605. doi: 10.3760/cma.j.issn.1673-0860.2016.08.008

Luo, X., Yang, S., Liang, J., Zhai, Y., Shen, M., Sun, J., et al. (2018). Choroidal pericytes promote subretinal fibrosis after experimental photocoagulation. *Dis. Model Mech.* 11:dmm032060. doi: 10.1242/dmm.032060

Ma, Q., Zhao, Z., Sagare, A. P., Wu, Y., Wang, M., Owens, N. C., et al. (2018). Blood-brain barrier-associated pericytes internalize and clear aggregated amyloid-beta42 by LRP1-dependent apolipoprotein E isoform-specific mechanism. *Mol. Neurodegener.* 13:57. doi: 10.1186/s13024-018-0286-0

Machida, T., Dohgu, S., Takata, F., Matsumoto, J., Kimura, I., Koga, M., et al. (2017). Role of thrombin-PAR1-PKCtheta/delta axis in brain pericytes in

thrombin-induced MMP-9 production and blood-brain barrier dysfunction *in vitro*. *Neuroscience* 350, 146–157. doi: 10.1016/j.neuroscience.2017.03.026

Marchand, M., Monnot, C., Muller, L., and Germain, S. (2018). Extracellular matrix scaffolding in angiogenesis and capillary homeostasis. *Semin. Cell Dev. Biol.* 89, 147–156. doi: 10.1016/j.semcdb.2018.08.007

Mazurek, R., Dave, J. M., Chandran, R. R., Misra, A., Sheikh, A. Q., and Greif, D. M. (2017). Vascular cells in blood vessel wall development and disease. *Adv. Pharmacol.* 78, 323–350. doi: 10.1016/bs.apha.2016.08.001

Miners, J. S., Schulz, I., and Love, S. (2018). Differing associations between Ab accumulation, hypoperfusion, blood-brain barrier dysfunction and loss of PDGFRB pericyte marker in the precuneus and parietal white matter in Alzheimer's disease. *J. Cereb. Blood Flow Metab.* 38, 103–115. doi: 10.1177/0271678X17690761

Montagne, A., Nikolakopoulou, A. M., Zhao, Z., Sagare, A. P., Si, G., Lazic, D., et al. (2018). Pericyte degeneration causes white matter dysfunction in the mouse central nervous system. *Nat. Med.* 24:326. doi: 10.1038/nm.4482

Muñoz-Fernández, R., de, la Mata C, Prados, A., Perea, A., Ruiz-Magaña, M. J., Llorca, T., et al. (2018). Human predecidual stromal cells have distinctive characteristics of pericytes: cell contractility, chemotactic activity, and expression of pericyte markers and angiogenic factors. *Placenta* 61, 39–47. doi: 10.1016/j.placenta.2017.11.010

Navarro, R., Compte, M., Alvarez-Vallina, L., and Sanz, L. (2016). Immune regulation by pericytes: modulating innate and adaptive immunity. *Front. Immunol.* 7:480. doi: 10.3389/fimmu.2016.00480

Nikolajsen, G. N., Jensen, M. S., and West, M. J. (2016). A zinc fixative for 3D visualization of cerebral capillaries and pericytes. *J. Neurosci. Methods* 257, 1–6. doi: 10.1016/j.jneumeth.2015.09.016

Ozen, I., Roth, M., Barbariga, M., Gaceb, A., Deierborg, T., Genove, G., et al. (2018). Loss of regulator of G-protein signaling 5 leads to neurovascular protection in stroke. *Stroke* 49, 2182–2190. doi: 10.1161/STROKEAHA.118.020124

Pieper, C., Marek, J. J., Unterberg, M., Schwerdtle, T., and Galla, H. J. (2014). Brain capillary pericytes contribute to the immune defense in response to cytokines or LPS in vitro. *Brain Res.* 1550, 1–8. doi: 10.1016/j.brainres.2014.01.004

Pierantozzi, E., Vezzani, B., Badin, M., Curina, C., Severi, F. M., Petraglia, F., et al. (2016). Tissue-specific cultured human pericytes: perivascular cells from smooth muscle tissue have restricted mesodermal differentiation ability. *Stem Cells Dev.* 25, 674–686. doi: 10.1089/scd.2015.0336

Pober, J. S., Merola, J., Liu, R., and Manes, T. D. (2017). Antigen presentation by vascular cells. *Front. Immunol.* 8:1907. doi: 10.3389/fimmu.2017.01907

Prazeres, P., Almeida, V. M., Lousado, L., Andreotti, J. P., Paiva, A. E., Santos, G. S. P., et al. (2018). Macrophages generate pericytes in the developing brain. *Cell Mol. Neurobiol.* 38, 777–782. doi: 10.1007/s10571-017-0549-2

Primo, V. A., and Arboleda-Velasquez, J. F. (2016). Isolation and transfection of primary culture bovine retinal pericytes. *Methods Mol. Biol.* 1430, 107–117. doi: 10.1007/978-1-4939-3628-1-7

Rink, B. E., Amilon, K. R., Esteves, C. L., French, H. M., Watson, E., Aurich, C., et al. (2017). Isolation and characterization of equine endometrial mesenchymal stromal cells. *Stem Cell Res Ther.* 166. doi: 10.1186/s13287-017-0616-0

Rustenhoven, J., Aalderink, M., Scotter, E. L., Oldfield, R. L., Bergin, P. S., Mee, E. W., et al. (2016). TGF-beta1 regulates human brain pericyte inflammatory processes involved in neurovasculature function. *J Neuroinflamm.* 13:37. doi: 10.1186/s12974-016-0503-0

Sagare, A. P., Bell, R. D., Zhao, Z., Ma, Q. Y., Winkler, E. A., Ramanathan, A., et al. (2013). Pericyte loss influences Alzheimer-like neurodegeneration in mice. *Nat. Commun.* 4:2932. doi: 10.1038/ncomms3932

Santos, G. S. P., Magno, L. A. V., Romano-Silva, M. A., Mintz, A., and Birbrair, A. (2018). Pericyte plasticity in the brain. *Neurosci. Bull.* 35, 551–560. doi: 10.1007/s12264-018-0296-5

Sa-Pereira, I., Brites, D., and Brito, M. A. (2012). Neurovascular unit: a focus on pericytes. *Mol. Neurobiol.* 45, 327–347. doi: 10.1007/s12035-012-8244-2

Sato, S., Tang, Y. J., Wei, Q., Hirata, M., Weng, A., Han, I., et al. (2016). Mesenchymal tumors can derive from ng2/cspg4-expressing pericytes with beta-catenin modulating the neoplastic phenotype. *Cell Rep.* 16, 917–927. doi: 10.1016/j.celrep.2016.06.058

Sauer, R. S., Kirchner, J., Yang, S., Hu, L., Leinders, M., Sommer, C., et al. (2017). Blood-spinal cord barrier breakdown and pericyte deficiency in peripheral neuropathy. *Ann. N. Y. Acad. Sci.* 1405, 71–88. doi: 10.1111/nyas.13436

Sava, P., Ramanathan, A., Dobronyi, A., Peng, X., Sun, H., Ledesma-Mendoza, A., et al. (2017). Human pericytes adopt myofibroblast properties in the microenvironment of the IPF lung. *JCI Insight.* 2:e96352. doi: 10.1172/jci.insight.96352

Schneider, G., Bubel, M., Pohlemann, T., and Oberringer, M. (2015). Response of endothelial cells and pericytes to hypoxia and erythropoietin in a co-culture assay dedicated to soft tissue repair. *Mol. Cell. Biochem.* 407, 29–40. doi: 10.1007/s11010-015-2451-x

Shaw, I., Rider, S., Mullins, J., Hughes, J., and Peault, B. (2018). Pericytes in the renal vasculature: roles in health and disease. *Nat. Rev. Nephrol.* 14, 521–534. doi: 10.1038/s41581-018-0032-4

Shimizu, F., Sano, Y., Maeda, T., Abe, M. A., Nakayama, H., Takahashi, R., et al. (2008). Peripheral nerve pericytes originating from the blood-nerve barrier expresses tight junctional molecules and transporters as barrier-forming cells. *J. Cell. Physiol.* 217, 388–399. doi: 10.1002/jcp.21508

Svensson, A., Ozen, I., Genove, G., Paul, G., and Bengzon, J. (2015). Endogenous brain pericytes are widely activated and contribute to mouse glioma microvasculature. *PLoS One* 10:e0123553. doi: 10.1371/journal.pone.0123553

Thijssen, V. L., Paulis, Y. W., Nowak-Sliwinska, P., Deumelandt, K. L., Hosaka, K., Soetekouw, P. M., et al. (2018). Targeting PDGF-mediated recruitment of pericytes blocks vascular mimicry and tumor growth. *J. Pathol.* 246, 447–458. doi: 10.1002/path.5152

Thomzig, A., Laube, G., Pruss, H., and Veh, R. W. (2005). Pore-forming subunits of K-ATP channels, Kir6.1 and Kir6.2, display prominent differences in regional and cellular distribution in the rat brain. *J. Comp. Neurol.* 484, 313–330. doi: 10.1002/cne.20469

Tonlorenzi, R., Rossi, G., and Messina, G. (2017). Isolation and characterization of vessel-associated stem/progenitor cells from skeletal muscle. *Methods Mol. Biol.* 1556, 149–177. doi: 10.1007/978-1-4939-6771-1-8

Underly, R. G., Levy, M., Hartmann, D. A., Grant, R. I., Watson, A. N., and Shih, A. Y. (2017). Pericytes as inducers of rapid, matrix metalloproteinase-9-dependent capillary damage during ischemia. *J. Neurosci.* 37, 129–140. doi: 10.1523/JNEUROSCI.2891-16.2016

Urrutia, A. A., Afzal, A., Nelson, J., Davidoff, O., Gross, K. W., and Haase, V. H. (2016). Prolyl-4-hydroxylase 2 and 3 coregulate murine erythropoietin in brain pericytes. *Blood* 128, 2550–2560. doi: 10.1182/blood-2016-05-713545

Venkatachalam, M. A., and Weinberg, J. M. (2017). Pericytes Preserve Capillary Integrity to Prevent Kidney Hypoxia. *J. Am. Soc. Nephrol.* 28, 717–719. doi: 10.1681/ASN.2016111157

Vidhya, S., Ramya, R., Coral, K., Sulochana, K. N., and Bharathidevi, S. R. (2018). Free amino acids hydroxyproline, lysine, and glycine promote differentiation of retinal pericytes to adipocytes: a protective role against proliferative diabetic retinopathy. *Exp. Eye Res.* 173, 179–187. doi: 10.1016/j.exer.2018.05.004

Wang, J. D., Khafagy el, S., Khanafer, K., Takayama, S., and ElSayed, M. E. (2016). Organization of endothelial cells, pericytes, and astrocytes into a 3D microfluidic *in vitro* model of the blood-brain barrier. *Mol. Pharm.* 13, 895–906. doi: 10.1021/acs.molpharmaceut.5b00805

Wang, Q., Tang, Y., Wang, T., Yang, H. L., Wang, X., Ma, H., et al. (2018). EPCR promotes MGC803 human gastric cancer cell tumor angiogenesis *in vitro* through activating ERK1/2 and AKT in a PAR1-dependent manner. *Oncol. Lett.* 16, 1565–1570. doi: 10.3892/ol.2018.8869

Wang, Y., Xu, J., Chang, L., Meyers, C. A., Zhang, L., and Broderick, K. (2019). Relative contributions of adipose-resident CD146(+) pericytes and CD34(+) adventitial progenitor cells in bone tissue engineering. *NPJ Regen Med.* 4:1. doi: 10.1038/s41536-018-0063-2

Wertheim, B. M., Lin, Y. D., Zhang, Y. Y., Samokhin, A. O., Alba, G. A., Arons, E., et al. (2019). Isolating pulmonary microvascular endothelial cells ex *vivo*: implications for pulmonary arterial hypertension, and a caution on the use of commercial biomaterials. *PLoS One* 14:e0211909. doi: 10.1371/journal.pone.0211909

Wilson, C. L., Stephenson, S. E., Higuero, J. P., Feghali-Bostwick, C., Hung, C. F., and Schnapp, L. M. (2018). Characterization of human PDGFR-beta-positive pericytes from IPF and non-IPF lungs. *Am. J. Physiol. Lung. Cell Mol. Physiol.* 315, L991–L1002. doi: 10.1152/ajplung.00289.2018

Winkler, E. A., Birk, H., Burkhardt, J. K., Chen, X., Yue, J. K., Guo, D., et al. (2018). Reductions in brain pericytes are associated with arteriovenous

malformation vascular instability. *J. Neurosurg.* 129, 1464–1474. doi: 10.3171/2017.6.JNS17860

Wnuk, M., Anderegg, M. A., Graber, W. A., Buergy, R., Fuster, D. G., and Djonov, V. (2017). Neuropilin1 regulates glomerular function and basement membrane composition through pericytes in the mouse kidney. *Kidney Int.* 91, 868–879. doi: 10.1016/j.kint.2016.10.010

Yamamizu, K., Iwasaki, M., Takakubo, H., Sakamoto, T., Ikuno, T., and Miyoshi, M. (2017). *In Vitro* modeling of blood-brain barrier with human iPSC-derived endothelial cells, pericytes, neurons, and astrocytes via notch signaling. *Stem Cell Rep.* 8, 634–647. doi: 10.1016/j.stemcr.2017.01.023

Yamazaki, Y., and Kanekiyo, T. (2017). Blood-brain barrier dysfunction and the pathogenesis of alzheimer's disease. *Int. J. Mol. Sci.* 18:E1965.

Yin, G. N., Ock, J., Choi, M. J., Song, K. M., Ghatak, K., Nguyen, N. M., et al. (2019). A simple and nonenzymatic method to isolate human corpus cavernosum endothelial cells and pericytes for the study of erectile dysfunction. *World J. Mens Health* 37:e11. doi: 10.5534/wjmh.180091

Zechariah, A., ElAli, A., Doeppner, T. R., Jin, F., Hasan, M. R., Helfrich, I., et al. (2013). Vascular endothelial growth factor promotes pericyte coverage of brain capillaries, improves cerebral blood flow during subsequent focal cerebral ischemia, and preserves the metabolic penumbra. *Stroke* 44, 1690–1697. doi: 10.1161/STROKEAHA.111.000240

Zhou, Z., Pausch, F., Schlotzer-Schrehardt, U., Brachvogel, B., and Poschl, E. (2016). Induction of initial steps of angiogenic differentiation and maturation of endothelial cells by pericytes in vitro and the role of collagen IV. *Histochem. Cell Biol.* 145, 511–525. doi: 10.1007/s00418-015-1398-z

Zou, W., Feng, R., and Yang, Y. (2018). Changes in the serum levels of inflammatory cytokines in antidepressant drug-naive patients with major depression. *PLoS One* 13:e0197267. doi: 10.1371/journal.pone.0197267

Zuo, Z. J., Qi, F. F., Yang, J. H., Wang, X., Wu, Y. Y., Wen, Y. R., et al. (2017). Immunization with bacillus calmette-guerin (BCG) alleviates neuroinflammation and cognitive deficits in APP/PS1 mice via the recruitment of inflammation-resolving monocytes to the brain. *Neurobiol. Dis.* 101, 27–39. doi: 10.1016/j.nbd.2017.02.001

Conflict of Interest: The authors declare that the research was conducted in the absence of any commercial or financial relationships that could be construed as a potential conflict of interest.

Copyright © 2019 Su, Huang, Qu, Xiao and Mu. This is an open-access article distributed under the terms of the Creative Commons Attribution License (CC BY). The use, distribution or reproduction in other forums is permitted, provided the original author(s) and the copyright owner(s) are credited and that the original publication in this journal is cited, in accordance with accepted academic practice. No use, distribution or reproduction is permitted which does not comply with these terms.

frontiers in Neuroscience

ORIGINAL RESEARCH
published: 04 December 2019
doi: 10.3389/fnins.2019.01261

A Pilot Study Investigating Changes in Capillary Hemodynamics and Its Modulation by Exercise in the APP-PS1 Alzheimer Mouse Model

*Xuecong Lu[1,2], Mohammad Moeini[3], Baoqiang Li[4], Yuankang Lu[1,2], Rafat Damseh[1,2], Philippe Pouliot[1,2], Éric Thorin[2,5] and Frédéric Lesage[1,2]**

[1] Biomedical Engineering Institute, École Polytechnique de Montréal, Montreal, QC, Canada, [2] Montreal Heart Institute, Research Center, Montreal, QC, Canada, [3] Department of Biomedical Engineering, Amirkabir University of Technology (Tehran Polytechnic), Tehran, Iran, [4] Athinoula A. Martinos Center for Biomedical Imaging, Massachusetts General Hospital, Harvard Medical School, Charlestown, MA, United States, [5] Department of Surgery, Faculty of Medicine, Université de Montréal, Montreal, QC, Canada

Dysfunction in neurovascular coupling that results in a mismatch between cerebral blood flow and neuronal activity has been suggested to play a key role in the pathogenesis of Alzheimer's disease (AD). Meanwhile, physical exercise is a powerful approach for maintaining cognitive health and could play a preventive role against the progression of AD. Given the fundamental role of capillaries in oxygen transport to tissue, our pilot study aimed to characterize changes in capillary hemodynamics with AD and AD supplemented by exercise. Exploiting two-photon microscopy, intrinsic signal optical imaging, and magnetic resonance imaging, we found hemodynamic alterations and lower vascular density with AD that were reversed by exercise. We further observed that capillary properties were branch order-dependent and that stimulation-evoked changes were attenuated with AD but increased by exercise. Our study provides novel indications into cerebral microcirculatory disturbances with AD and the modulating role of voluntary exercise on these alterations.

Keywords: Alzheimer's disease, capillary hemodynamics, voluntary exercise, two-photon imaging, neural stimulation

OPEN ACCESS

Edited by:
Marietta Zille,
Universität zu Lübeck, Germany

Reviewed by:
Ana Margarida Ledo,
University of Coimbra, Portugal
Cátia Lourenço Marques,
University of Coimbra, Portugal

****Correspondence:***
Frédéric Lesage
frederic.lesage@polymtl.ca

Specialty section:
This article was submitted to Neurodegeneration, a section of the journal Frontiers in Neuroscience

Received: *28 March 2019*
Accepted: *06 November 2019*
Published: *04 December 2019*

Citation:
Lu X, Moeini M, Li B, Lu Y, Damseh R, Pouliot P, Thorin É and Lesage F (2019) A Pilot Study Investigating Changes in Capillary Hemodynamics and Its Modulation by Exercise in the APP-PS1 Alzheimer Mouse Model. Front. Neurosci. 13:1261. doi: 10.3389/fnins.2019.01261

INTRODUCTION

Alzheimer's disease (AD) is the most common cause of cognitive impairment in the elderly (Iadecola, 2010; Toledo et al., 2013). Dysfunction in neurovascular coupling, resulting in a mismatch between cerebral blood flow and neuronal activity, has long been suggested to play a part in the pathogenesis of AD (Iadecola, 2004, 2010; Zlokovic, 2011; Kisler et al., 2017). AD also shares many risk factors with cardiovascular diseases (Østergaard et al., 2013; Nielsen et al., 2017) and is associated with alterations in vascular function (Iadecola, 2010). Capillaries are the vessels most proximal to neurons (Stefanovic et al., 2008) and thus play a significant role in modulating oxygen extraction to support neuronal activity (Østergaard et al., 2013; Hall et al., 2014; Nielsen et al., 2017). Characterizing microvascular (dys)function in AD is of vital importance, as compromised capillary networks may lead to hypoxia, which, in turn, damages neurons and precipitates Aβ amyloid retention (Nielsen et al., 2017). The first aim of this pilot study was to quantify the changes in capillary red blood cell (RBC) dynamics with AD to provide insights into these issues.

Beyond characterizing hemodynamic dysfunction in microvessels, it is also critical to explore how to mitigate the negative impacts of AD on microcirculation. Physical exercise is a powerful approach for maintaining cognitive health and is hypothesized to play a preventive role against the progression of AD (Radak et al., 2010). Regular aerobic exercise has been found to inhibit the progression of amyloid-related neuropathology in mouse models of AD (Adlard et al., 2005) and to enhance cognitive performance in humans (Pereira et al., 2007; Brown et al., 2010; Hayes et al., 2014). Voluntary exercise has also been shown to improve vascular function in a mouse model of atherosclerosis (Shing et al., 2015). Oxidative stress associated with aging has been found to be reduced with exercise in both humans (Pialoux et al., 2009) and rodents (Durrant et al., 2009). Notwithstanding, the hemodynamic changes in microvascular networks in response to physical exercise with the onset of AD have yet to be studied. Despite a number of hypotheses that indicate the beneficial role of exercise, we still do not have a clear quantification of these changes, which can now be carried out with *in vivo* optical imaging techniques. The second aim of this study was, thus, to quantify the modulatory effect of exercise on cerebral capillaries in AD.

To address these questions, we applied multiple imaging techniques, including two-photon microscopy, intrinsic optical signal imaging (IOSI), and magnetic resonance imaging (MRI), to measure hemodynamic changes at different spatial scales. We found capillary hemodynamic alterations and lower vascular density with AD that were modulated by exercise. We further observed that capillary RBC flow properties were branch order-dependent and that the stimulation-evoked changes were decreased with AD but increased by exercise.

MATERIALS AND METHODS

Animal Groups

Animals were handled according to the Animal Research: Reporting *in vivo* Experiments (ARRIVE) guidelines and the recommendations of the Canadian Council on Animal Care. The protocol was approved by the Ethics Committee of the Research Center of the Montreal Heart Institute. An APP/PS1 mouse model (generous gift from Dr. Bernard Levy, France) and wild-type (WT) mice were genotyped by standard PCR analysis of genomic DNA isolated from ear clips to select both hemizygous APP/PS1 males and their non-transgenic control (WT) male littermates, as previously described (Radde et al., 2006). Mice were kept under standard conditions (24°C; 12-h:12-h light/dark cycle) and were fed *ad libitum* with regular chow (2019S; Harlan Laboratories, Madison, WI, United States). Initially housed four per cage, they were separated and housed one per cage following the surgeries detailed below.

Experimental Design

Experiments were performed in male wild-type mice at 6 months old (WT6: $n = 4$), transgenic Amyloid Precursor Protein Presenilin-1 (APP/PS1) mice at 6 months old (AD6: $n = 4$), and APP/PS1 mice at 6 months old for which voluntary exercise was initiated at 3 months old (AD6&EX: $n = 4$). Previous work showed a clear onset of cognitive symptoms in APP/PS1 mice at 4.5 months old (Cifuentes et al., 2015) and established at 6 months old (de Montgolfier et al., 2019), and thus, we conducted imaging at 6 months old and investigated the hemodynamic changes in this relatively early stage of AD. For the AD6&EX group, exercise was voluntary. Mice in the exercise group were housed individually from 3 months old forward in separate cages to which a running wheel was attached with a rotation counter. Mice started running on wheels at 3 months old and continued the daily exercise until 6 months old, when imaging data were recorded. The wheel (diameter 15 cm, recorded by an easyMATRIX 16 EMKA) was mounted outside the home cage, and the total number of wheel rotations was recorded daily on an LE907 individual counter. The running distance averaged across mice ranged from ∼2 to ∼4 km per day in the 3-month exercising period.

Multiple imaging techniques were used for the data collection, as shown in **Figure 1**. The order of procedures was as follows. At 6 months old, mice were imaged with MRI in anesthetized (1h30, isoflurane) condition. Ten days later, two-photon imaging was conducted to collect capillary properties in awake animals. One day later, intrinsic signal optical imaging (ISOI) was performed to collect data on changes in hemoglobin, again in awake animals. Each mouse was included in all of these experiments.

Two-Photon Imaging

For two-photon imaging, a craniotomy was performed, and mice were familiarized with the awake imaging device. On the day of cranial surgery, animals were anesthetized with isoflurane (1.5–2.0% in pure oxygen), with their physiological parameters monitored in real time. A fixation bar was attached for awake imaging. At the same time as bar fixation, a cranial imaging window was prepared to allow for two-photon imaging of the cortex following well-established guidelines (Shih et al., 2012). A cranial window with a 3-mm diameter was made over the left barrel cortex (0.5 mm posterior to bregma, 3.5 mm lateral to the midline). Agarose in artificial cerebral spinal fluid (ACSF) was placed over the exposed skull, and then a three-layer cover glass was glued onto the skull to generate a transparent cranial window. Ketoprofen (5 mg/kg, Merial, Canada) and buprenorphine (0.05 mg/kg, Reckitt Benckiser Healthcare, United Kingdom) were injected before the surgery for analgesic and antipyretic effects. Baytril (5 mg/kg, Bayer, Germany) was injected after the surgery and repeated one day after the surgery. To adapt to the device during imaging, animals were trained on the imaging wheel in four fixation-training sessions beginning after 3 days of recovery following the cranial surgery. The length of fixation time gradually increased from 10 to 45 min over the four sessions.

A home-built two-photon microscope was used to record functional capillary data and vascular density. The MaiTai-BB laser oscillator (Newport Corporation, United States) of the two-photon microscope generated a sequence of 820 nm, 80 MHz, 150 fs pulses modulated by an acousto-optic modulator for power control. The fluorescent dye (dextran-FITC) was injected through the tail vein to distinguish plasma (in bright colors) and RBCs (appearing as dark shadows) in the recorded

FIGURE 1 | Timeline of imaging experiments.

images. The line scans were performed both perpendicularly and longitudinally to each measured capillary over 250-ms time intervals to generate space-time images. In consecutive longitudinal scans, the dark shadows move toward the right or left of the scanning beam because of the movement of RBCs, resulting in tilted dark streaks in the space-time image (Kleinfeld et al., 1998). The angle of these dark streaks was used to quantify RBC velocity, with streaks closer to horizontal orientation associated with higher velocity. In perpendicular line scans, the signal is dark when an RBC is passing through the optical focus, and RBC flux can be assessed. Following line scanning, 3D angiograms were obtained over four overlapping 600 × 600 μm (400 × 400 pixels) regions at depths of 100–550 μm with 5-μm steps at a frame rate of 0.5 Hz. During all measurements, animals were awake, with the head fixed by a titanium bar and limbs free to move on the rotating wheel (Moeini et al., 2018, 2019).

Measurement of Capillary Properties

The spacetime images were used to obtain the following capillary parameters, following (Moeini et al., 2018): (1) diameter, by fitting the perpendicular scans with a Gaussian function with estimated diameter at half maximum of the distribution; (2) RBC velocity from the angle of the streaks in longitudinal scanning; (3) RBC flux, calculated by the number of dark shadows divided by the acquisition time of the images (the flux was obtained from the average of values in longitudinal and perpendicular scans); and (4) hematocrit, calculated by RBC flux × RBC volume/capillary volumetric flow [capillary volumetric flow = RBC velocity × capillary cross-sectional area; RBC volume assumed to be 55 μm^3 for C57Bl/6 mice (Wirth-Dzięciołowska et al., 2009)]. The angiogram images were used to compute the vascular density using a deep-learning segmentation approach based on the FC-Densenets architecture (Damseh et al., 2018a,b). The vascular density was quantified with each slice of the segmented two-photon angiograms by restricting the analysis to vessels with a diameter of less than 8 um.

We also divided the capillaries based on branching order. The artery region, with the diving arteriole, precapillary arteriole, and capillaries, was labeled with respect to branching order A1, A2, and A3, with A1 branching off directly from the precapillary arterioles. The vein region, with the surfacing venule and post-capillary venule, was labeled with the branching order V1, V2, and V3, with V1 linking directly to veins. In our recordings, the capillary segments ranged from 6 to 12 branch orders. We only labeled and defined the first three branch orders from arterioles (A1, A2, and A3) and venules (V1, V2, and V3). When a capillary path had more than six branching orders, these additional branch orders were merged into V3, thus enabling consistent numbering for all capillaries observed.

Magnetic Resonance Imaging (MRI)

Anatomical and perfusion MRI scanning was performed with a 30 cm 7T horizontal MR scanner (Agilent, Palo Alto, CA, United States) before two-photon imaging. The mice were in a prone position and imaged with a gradient insert coil (12-cm inner diameter, gradient strength 600 mT/m, and rise time 130 ms). The brain was imaged with a 2-channel receive-only surface coil and a quadrature transmit/receive birdcage coil (69-mm internal diameter) (RAPID Biomedical, Germany), while the animal was anesthetized with 1.4–2.2% isoflurane in air with 30% oxygen, with the body temperature kept at 37.0°C using a warm air fan (SA Instruments, Stony Brook, NY, United States). Respiration was monitored with a target of ∼100 bpm, adjusting the level of isoflurane only whenever the rate was outside 80–120 bpm. Heart rate was monitored with a pulse oximeter.

Anatomical images were recorded with a 3D true free induction with steady-state precession (TFISP) sequence (Bowen et al., 2006) at a 100-μm isotropic resolution (TR = 5.0 ms, TE = 2.5 ms, 16 frequencies, 22-min scan time). A 3D amplitude-modulated continuous arterial spin labeling scan (amCASL) was then acquired (TR = 3.0 s, labeling duration = 1.0 s, 60 × 54 × 48 matrix, 300 μm × 333 μm × 333 μm resolution, 23-min scan time).

The anatomical recordings were first aligned manually to a previously produced anatomic template using ITK-SNAP and then co-registered non-linearly with the advanced normalization tools (ANTs) (Avants et al., 2010, 2011), thus producing the ANT transformations to co-register the perfusion scans to a common referential. Perfusion was calculated voxel-by-voxel as described in Chugh et al. (2012), with assumed parameters of brain/blood partition coefficient = 0.9 mL/g, mouse arterial blood transit time = 0.08 s, tagging efficacy = 0.67, T_{1b} = 2.3 s, T_1 = 1.53 s, T_{1sat} = 0.57 s, and $M_a^z(w)$ = 0.48 s. The MarsBar toolbox in SPM was also used to extract the average perfusion data (Delafontaine-Martel et al., 2018).

Intrinsic Signal Optical Imaging (ISOI)

An ISOI system (Labeo Technologies, Inc.) was used to investigate the stimulus-evoked hemodynamic responses in all

experimental groups. Whiskers of mice were deflected at a rate of 10 Hz to activate the somatosensory cortex, with a 5-s stimulation time and a 15-s post-stimulus period. Illumination using green and red lights was positioned to illuminate the exposed skull of the mouse head. Images were acquired by a camera at a rate of 5 Hz per wavelength over a period spanning 10 stimulation repetitions. We computed changes in oxy-hemoglobin concentration (Δ[HBO](t)), deoxy-hemoglobin concentration (Δ[HBR](t)), and total hemoglobin concentration (Δ[HBT](t)), as was done in Dubeau et al. (2011a,b).

Statistical Analysis

The results are presented as mean ± SEM. Non-parametric Kruskal–Wallis tests were applied with follow-up tests for multiple group comparisons. Statistical significance was assigned at $^{+}p < 0.1$, $^{*}p < 0.05$, $^{**}p < 0.01$, $^{***}p < 0.001$.

RESULTS

Capillary RBC Flow Is Altered by AD and Modulated by Exercise

To better understand the role of exercise and AD on capillary RBC flow properties, we assessed the values of the resting capillary diameter, RBC velocity, RBC flux, and capillary hematocrit in all groups and their coefficient of variation (CV) using two-photon microscopy.

In **Figure 2A**, we observed that the capillary diameter had an increasing trend from the WT6 group (4.67 ± 0.06 μm) to the AD6 group (4.98 ± 0.07 um, $p = 0.09$) and significantly increased from the WT6 group to the AD6&EX group (5.15 ± 0.08 μm, $p = 0.011$). A decreasing trend of RBC velocity from WT6 (0.87 ± 0.03 mm/s) to AD6 (0.79 ± 0.03 mm/s) was also observed (see **Figure 2A**). RBC velocity increased significantly with exercise (velocity in the AD6&EX group: 0.91 ± 0.04 mm/s, $p = 0.04$, **Figure 2A**). However, there were no significant differences in RBC flux between groups (**Figure 2A**). Finally, the capillary hematocrit had a decreasing trend from the WT6 group (39.57 ± 1.15%) to the AD6 group (35.15 ± 1.30%, $p = 0.09$) (see **Figure 2A**). Exercise elevated the hematocrit (AD6&EX group, 37.32 ± 1.19%), as expected from physiology (see **Figure 2A**).

Given the hypothesis that capillary heterogeneity is a key element in oxygen delivery, we also computed the CV of these parameters. The CV represents the variations of each property within a capillary as a function of time. In **Figure 2B**, we show the CV of each parameter to explore the influence of AD and exercise on capillary heterogeneity. We observed significant variations in the velocity CV, flux CV, and hematocrit CV (see **Figure 2B**), while we did not find significant differences regarding the diameter CV in different groups. The velocity CV decreased significantly from the AD6 group (24.63 ± 1.92%) to the WT6 group (18.69 ± 1.33%, $p = 0.049$). The flux CV increased ($p = 0.01$) from the WT6 group (29.17 ± 1.25%) to the AD6 group (40.63 ± 2.13%) (see **Figure 2B**). Exercise trended to decrease the flux CV from AD6 to AD6&EX (35.50 ± 1.58%) (see **Figure 2B**). Finally, hematocrit CV increased from WT6 (14.65 ± 0.79%) to AD6 (20.95 ± 1.41%, $p = 0.008$), while exercise trended toward a reduction of the hematocrit CV from AD6 to AD6&EX (18.42 ± 1.08%, see **Figure 2B**). Taken together, the capillary velocity flux and hematocrit were reduced with AD, associated with increased variations over time, while exercise regularized parameters toward values found in WT mice. Capillary diameter was the exception to this. Given the increased heterogeneity in RBC velocity, RBC flux, and hematocrit with AD, we also analyzed the variations of these properties as a function of branch order of capillaries to explore how they varied from the upstream to the downstream segments. The results of this analysis are provided in the **Appendix**.

High Temporal Fluctuations in Capillary RBC Velocity and Flux Were More Frequent With AD

Previous studies observed spontaneous stalls in capillary RBC flux in individual capillary segments (Erdener et al., 2017; Hernández et al., 2019). We thus analyzed our data to capture the presence of highly fluctuating RBC properties in capillaries by quantifying the fraction of capillaries with outlier standard deviations of RBC flux or speed within a 5-s recording window (see **Figures 3A,B**). Although stalling was not characterized in our experiments, these capillary outliers tend to display highly fluctuating flux and velocity, which may influence oxygen extraction (Gutiérrez-Jiménez et al., 2016; Østergaard et al., 2016). Examples for capillary outliers with temporally high self-fluctuation of RBC flux and velocity were shown in **Figures 3A,B**, respectively.

We further calculated and compared the fraction of outliers in all groups and found that the proportion with high temporal self-fluctuating RBC velocity was highest in the AD6 group (10.43%, 48 outliers in 460 capillaries), followed by the AD6&EX group (9.45%, 48 outliers in 508 capillaries), and was lowest in the WT6 group (8.19%, 46 outliers in 562 capillaries) (see **Figure 3C**). We did the same analysis for RBC flux (see **Figure 3D**). We again found that the proportion with high temporal self-fluctuating RBC flux was highest in the AD6 group (18.70%, 86 outliers in 460 capillaries), followed by the AD6&EX group (15.35%, 78 outliers in 508 capillaries), and was lowest in the WT6 group (13.17%, 74 outliers in 562 capillaries) (see **Figure 3D**).

Higher Vascular Density Peak Value and Lower Average Vascular Density in the AD Group

We calculated the vascular density from two-photon angiograms (see **Figure 4A**) after binary segmentation. Interestingly, all experimental groups reached their peak values of vascular density at a depth of ∼220 μm and the values then gradually decreased with increasing depth beneath the brain surface (see **Figure 4B**). The AD groups (both AD6 and AD6&EX) had significantly higher peak values (AD: 14.60 ± 0.98%; AD6&EX: 14.48 ± 1.09%) when compared with the peak value of the WT6 group (12.74 ± 0.70%) (see **Figure 4B**). Voluntary exercise did not significantly change the peak value of vascular density (see **Figure 4B**). When integrating across depths, the AD6 group

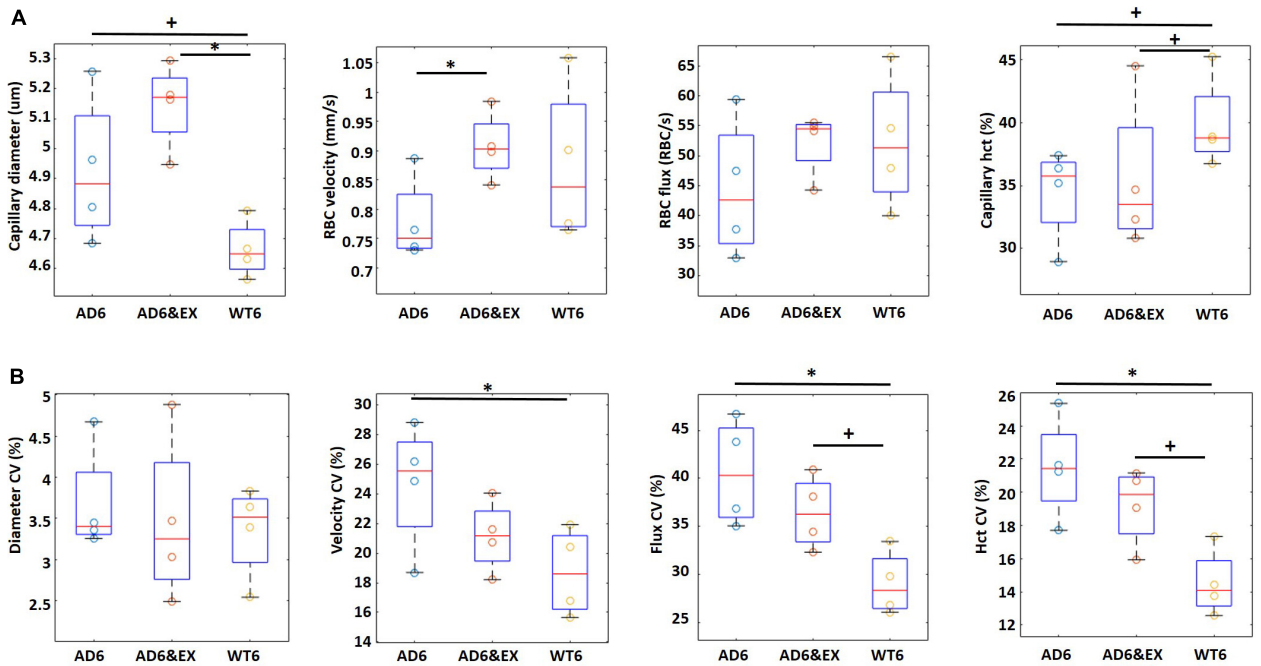

FIGURE 2 | Capillary RBC flow characteristics in different groups (four mice per group). **(A)** Capillary diameter, RBC velocity, flux, and hematocrit in different experimental groups. **(B)** Coefficient of variation (CV) for all capillary parameters. The CV in each capillary was computed based on multiple frames recorded each 0.25 s within a 5-s time window. Thus, CV represents the temporal variations of each property within a capillary. CV was computed as the standard deviation divided by the mean. $^{*}p < 0.05$ and $^{+}p < 0.1$.

showed a trend toward a lower average value (8.16 ± 0.37%) compared to the WT6 group (8.85 ± 0.29%) (see **Figure 4C**). With voluntary exercise, the AD6&EX group (8.64 ± 0.34%) exhibited a trend of higher vascular density than the AD6 group (see **Figure 4C**). Overall, higher vascular density peak values and lower average vascular densities were observed in the AD groups.

AD Reduced Brain Perfusion and Task-Related Changes, With the Latter Modulated by Exercise

We used MRI to quantify brain perfusion in each group (see **Figures 5A,B**). We observed that brain perfusion decreased from the WT6 group (2.69 ± 0.15 ml/g/min) to the AD6 group (2.16 ± 0.10 ml/g/min, $p = 0.06$) (see **Figure 5C**). However, exercise did not significantly modulate brain perfusion in AD groups (AD6&EX: 2.13 ± 0.16 ml/g/min) (see **Figure 5C**).

Intrinsic signal optical imaging was also used to investigate the response to stimulation to investigate task-related changes in hemoglobin concentration (see **Figures 5D,E**). The whiskers of mice were deflected to activate the somatosensory cortex, with a 5-s stimulation time and a 15-s post-stimulus period. We observed increased HBO with stimulation for all groups, while HBO had higher peak values in the WT6 group and the AD6&EX group when compared to the AD6 group, as shown in **Figure 5D**. We found that the Δ[HBO](t) in the AD6 group (10.75 ± 0.64 μM) was lower ($p = 0.03$) than that in the WT6 group (15.00 ± 0.85 μM). However, exercise tended to increase the Δ[HBO](t) from the AD6 group to the AD6&EX group (12.69 ± 0.85 μM, see **Figure 5F** upper panel). Finally, there were no significant differences regarding Δ[HBR](t) between groups (see **Figure 5F** lower panel).

DISCUSSION

In this study, we aimed to quantify the hemodynamic properties of and modulatory role of exercise on cerebral capillaries in AD due to the important role of microcirculation in cognitive health (Østergaard et al., 2016; Erdener et al., 2017; Zhang et al., 2017; Hernández et al., 2019). Exploiting awake microscopic vascular imaging and a transgenic mouse model of AD, we found that in this model (APP-PS1), AD is associated with hemodynamic disruption in capillaries. Voluntary exercise was seen to decrease capillary hemodynamic heterogeneity, although exercise did not increase the global cerebral blood flow in the cortex.

Capillary Flow Property Changes Due to AD and Exercise

Blood flow was slightly reduced in the AD6 group compared with WT6 mice but tended to increase with exercise in the AD6&EX group compared with the AD6 group. Specifically, RBC velocity tended to decrease with AD, with moderate modulation by exercise. The disrupted RBC velocity could

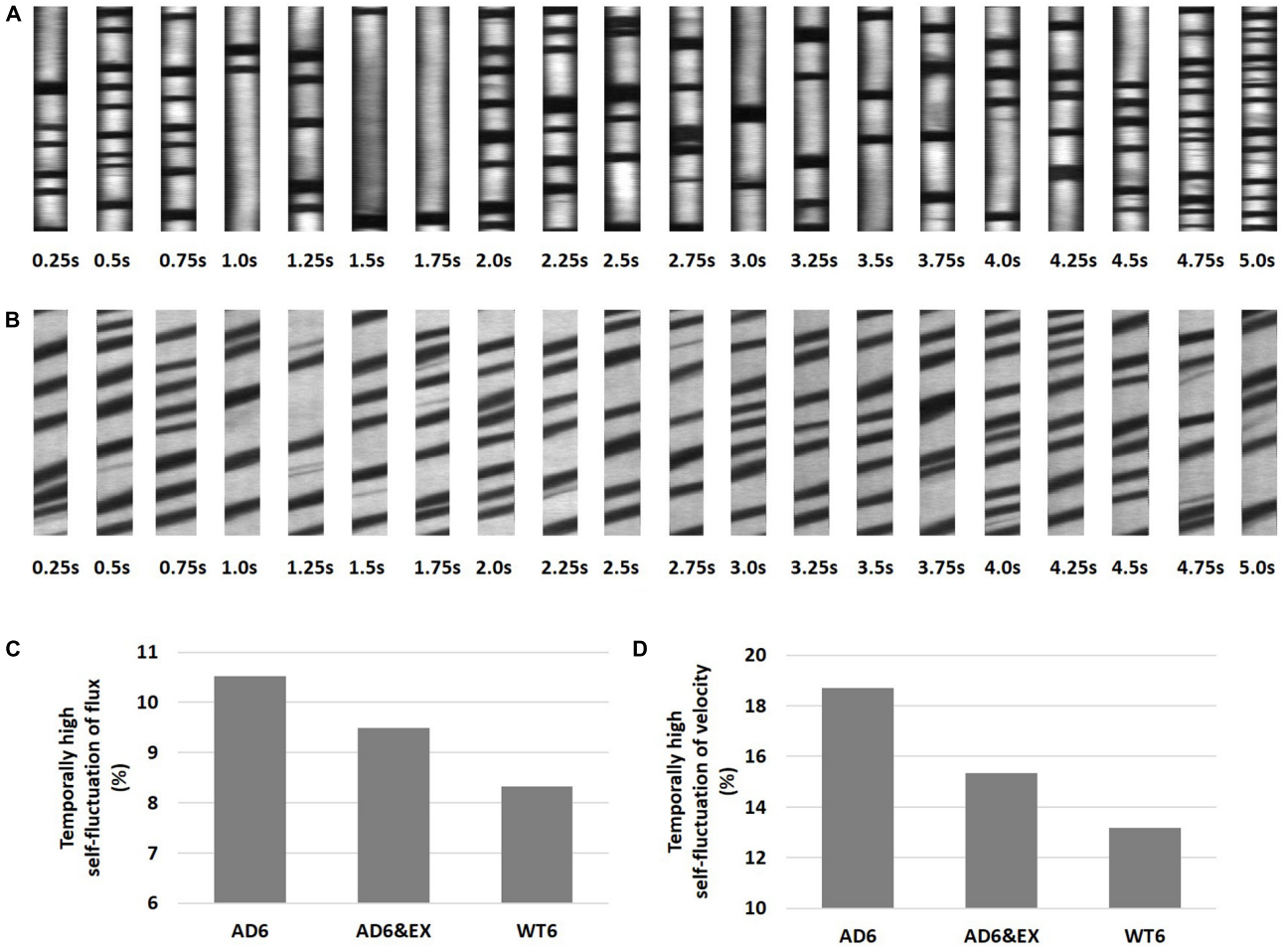

FIGURE 3 | High temporal capillary fluctuations of RBC velocity and RBC flux. **(A)** Representative space-time images with higher fluctuations of RBC flux as a function of time, with 0.25 s intervals during a 5-s recording window. The flux was obtained using both longitudinal and perpendicular scans, and the average value was used. **(B)** Longitudinal equivalent RBC velocity was calculated from the angle of dark streaks in a specific recording frame. **(C)** The percentage of capillaries with high temporal fluctuations of RBC velocity in all groups. The "isoutlier" method in MATLAB was applied to detect outliers with a standard deviation of RBC velocity exceeding three standard deviations from the mean. **(D)** Same for RBC flux.

result from the occlusion of vessels due to amyloid deposition (Arbel-Ornath et al., 2013). In another study (Lu et al., 2019), we gathered immunohistological evidence showing increased amyloid deposition with AD with a moderate, but significant, reduction due to exercise. Future research may consider immunohistological markers such as inflammation to shed light on the impact of AD on capillary properties more directly. The reduced RBC velocity could, in turn, lead to compromised perfusion in the mouse cortex, further slowing the clearance of amyloid and increasing its deposition (Kisler et al., 2017). We further observed that hematocrit was reduced with AD compared with the WT mice, with an increasing trend with exercise. A previous study (Moeini et al., 2018) found reduced hematocrit in healthy aging, thus disrupting capillary oxygen delivery efficiency. The prior literature has also observed miscrocirculation flow disruption in other cardiovascular diseases, such as stroke (Kazmi et al., 2013) and hypertension (Pialoux et al., 2009), and in even healthy aging (Dubeau et al., 2011b). The microvascular flow alterations observed in our study suggest that AD does share many similar microvessel disruptions with cardiovascular pathologies and aging. These microvessel problems could be alleviated by exercise, as is the case in other cardiovascular diseases (Pialoux et al., 2009; Brown et al., 2010).

We also found that RBC properties, especially velocity and flux, were branch order-dependent for all experimental groups. Prior study (Sakadžić et al., 2014) suggests that oxygen is in good proportion extracted in the first few branches after the precapillary arteriole in normal physiological conditions. Our results were related to previous findings and showed that RBC velocity and flux decreased from the upstream capillaries to the downstream capillaries for all groups to allow for oxygen delivery. Capillaries are responsible for transporting oxygen and nutrients to brain tissue and clearing metabolic end products from the brain to venous circulation (Kisler et al., 2017). In

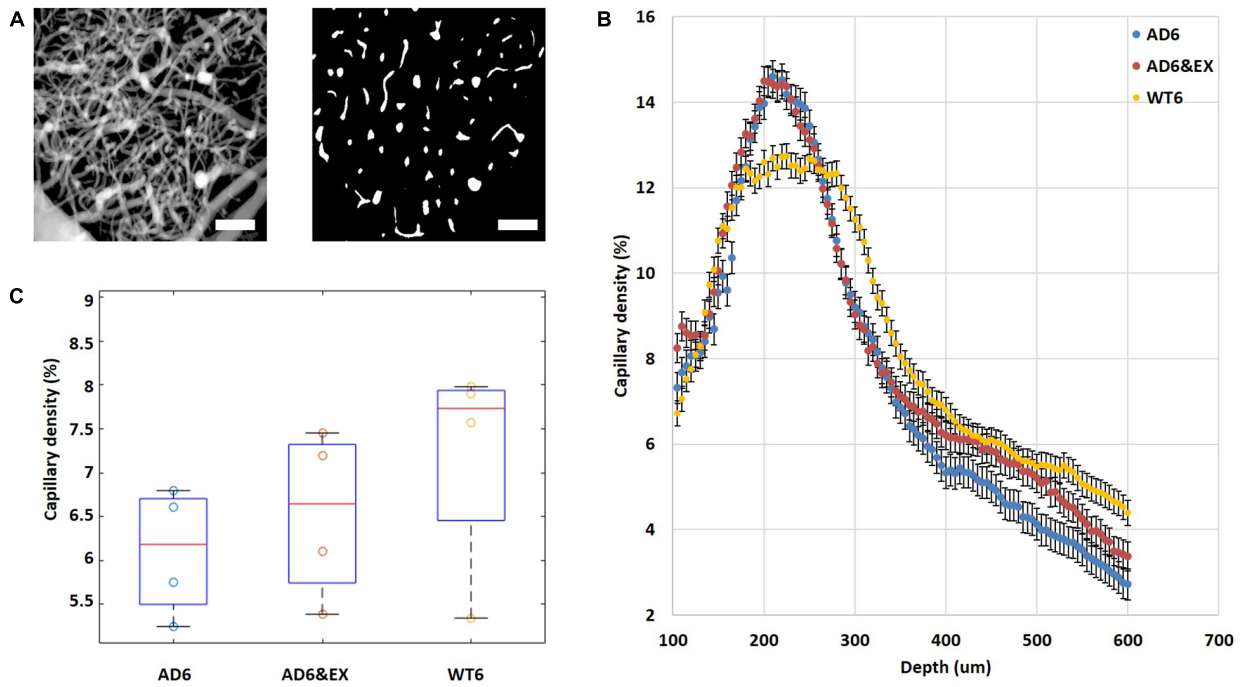

FIGURE 4 | Vascular distribution in different experimental groups and at different depths. **(A)** Binarization of microvascular angiograms was applied to calculate the vascular density. Left: MIP image with depths ranging from 100 to 550 μm under the brain surface with 5 μm steps. Right: an example of a binary segmentation of a single *en face* slice after removing the large horizontal vessels at a depth of 120 um (scale bar: 100 μm). **(B)** Average vascular density in different experimental groups as a function of depth from 100 to 550 μm under the brain surface. **(C)** Estimated vascular density (volume%). Results are presented as box plots with the median value (red line).

another paper (Lu et al., 2019), we found that indeed, tissue oxygen was reduced and more heterogeneous in mice with AD, consistent with this study. In capillary segments close to arterioles, capillaries were observed to have larger RBC velocity and flux, potentially enabling the delivery of oxygen and energy metabolites to the brain tissues. Future research may further explore the functioning of different capillary branches and investigate whether AD could lead to differentiated impacts on these segments.

Capillary obstruction due to flow dysfunction and tissue inflammation has been observed in animal models and has been shown to contribute to the development of neuron pathology and disease (Santisakultarm et al., 2014; Erdener et al., 2017; Hernández et al., 2019). Inflammation and flow disruption are well-recognized features of AD (Gaugler et al., 2018). Inflammation triggers reactive oxygen species, which lead to obstruction in capillaries (Park et al., 2008). Meanwhile, amyloid deposition may also lead to vessel occlusion by disrupting the interstitial fluid drainage pathway (Arbel-Ornath et al., 2013). Although we only focused on non-stalling capillaries in this study, the highly fluctuating RBC velocity and flux could indicate potential microvascular flow problems. We found a higher fraction of capillaries with high self-fluctuations of RBC velocity and flux in AD, slightly decreased with exercise. Previous research suggests that capillary flow patterns should homogenize to support metabolic demands, whereas heterogenous velocities across the capillary network diminish the oxygen extraction capabilities (Stefanovic et al., 2008; Gutiérrez-Jiménez et al., 2016). Our results suggest more heterogeneous flow distribution in the AD group when compared to WT but a reduced heterogeneity in the AD&EX group compared with the AD group, which may underly the benefits of exercise in AD.

Vascular Morphology Alterations in AD

Studies on morphological abnormalities of capillaries in AD have reported lower capillary densities due to deposition of Aβ amyloid (Kitaguchi et al., 2007). Previous work indicated a more rapid loss of vascular density with age, leading to compromised cerebral perfusion (Farkas and Luiten, 2001). Our results indicate that AD is associated with lower vascular density, which could contribute to reduced cerebral perfusion. This should be set against other studies that showed spatial and age-related variations in these vascular density differences between WT and APP/PS1 mice (Delafontaine-Martel et al., 2018). Here, the observed reduction in the somatosensory cortex could be potentially mitigated by exercise. Several previous studies have demonstrated the capacity of exercise to improve cognitive function (Hamer and Chida, 2008; Durrant et al., 2009; Mekari et al., 2015). Here, our data partially support the positive role of voluntary exercise on the maintenance of healthy vascular density. One intriguing observation was that at a depth of 200 um, the vascular density was higher in AD mice than in controls. The vascular density in this AD model (and others)

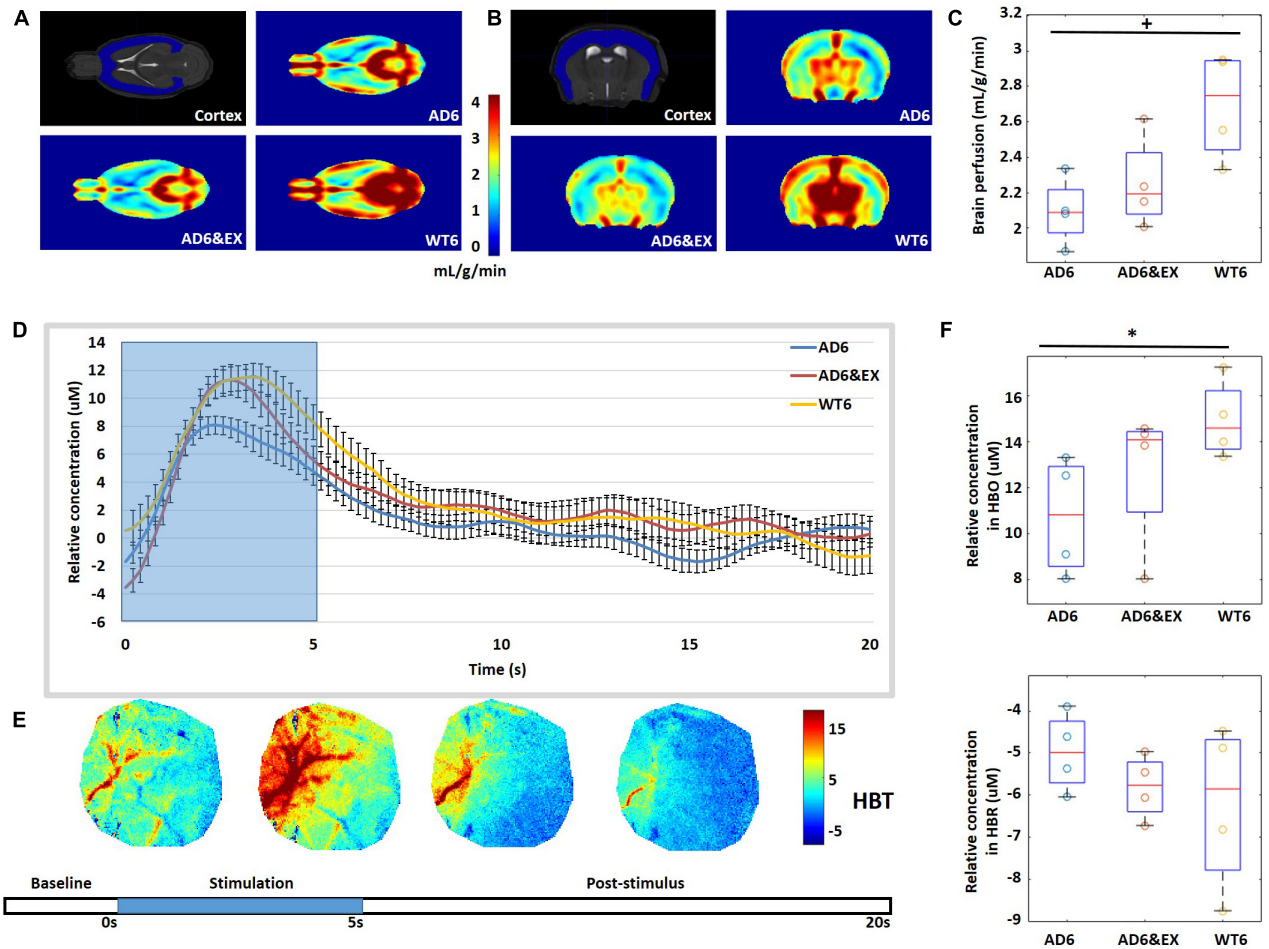

FIGURE 5 | (A,B) Typical 7-T MRI images, with coronal and axial views of the cortex. **(C)** Quantification of cerebral perfusion (ml/g/min) by MRI. **(D)** Averaged temporal response of oxy-hemoglobin (HBO) for all groups with 5-s stimulation (blue background). **(E)** Temporal dynamics of total hemoglobin (HBT) response to whisker stimulation. Stimulation lasted for 5 s, followed by a 15-s rest. **(F)** Averaged results for change in HBO (Δ[HBO](t)) and change in HBR (Δ[HBR](t)) over all mice. $^{*}p < 0.05$ and $^{+}p < 0.1$.

is age-dependent, and previous work has documented higher vascular density in AD mice when compared to WT (Cifuentes et al., 2015) in the cortex but not in the hippocampus. This indicates a potential complex distribution of vascular changes that cannot be accounted for by a single local observation. AD could also influence capillary diameter constriction and dilation, which respond to brain demands (Iadecola, 2017). Prior studies have shown that pericytes, the multi-functional cells wrapping around the capillaries, are able to influence capillary diameter to adjust oxygenation levels (Østergaard et al., 2013; Iadecola, 2017). Minimal changes in capillary diameter could produce large changes in oxygen delivery, since capillaries are closest to neurons in the vascular network and have large surface areas. Interestingly, we observed increased capillary diameters in the AD group and the exercise group. This change in diameters could be due to the compromised flow in AD groups, with the diameters dilating to compensate for the hypoperfusion. Another possible reason for the dilation of capillaries could be the occlusion of capillaries in AD due to amyloid deposition or inflammation (Park et al., 2008; Arbel-Ornath et al., 2013), as occlusion of vessels was shown to lead to vessel dilation in upstream capillaries in stroke disease (Nguyen et al., 2011).

Reduced Cerebral Perfusion and Functional Responses in AD

Using ISOI, we measured the functional hemodynamic response to stimulation (Sheth et al., 2005). Prior studies used ISOI to investigate pathological departures of neurovascular coupling in diseases such as focal epileptic seizures that exhibit an elevation in HBO (Schwartz et al., 2011). Another study applied ISOI and observed that functional connectivity strength was reduced in patients with AD, in cognitively normal elderly with elevated amyloid deposition, and in advanced aging (Bero et al., 2012). Our results corroborate previous findings showing a lower response amplitude in AD, suggesting neuro-vascular coupling changes. In contrast, the HBO response

further increased with voluntary exercise, suggesting that exercise may increase the regional oxygen delivery efficiency in capillaries but not through global increases in CBF. This finding was supported by MRI results suggesting decreased overall cerebral perfusion in both AD groups. Beyond the mesoscopic hemodynamic response to stimulation, future studies may consider characterizing the hemodynamic response to whisker stimulation at the capillary level directly using two-photon microscopy.

Limitations of the Study

The major limitation of our study is the small sample size used for the analyses, which may lead to potential type I (characterized as false-positive results) and type II (characterized as false-negative results) errors (Hackshaw, 2008). We admit that the associations we found were from a hypothesis-generating study, and a larger confirmatory study is needed in future. Additionally, the individual housing condition of the AD&EX group may cause some extent of social deprivation, which may mitigate the benefits of exercise. Future studies may need to find a balance between the social inclusion factors and the validity of voluntary exercise.

CONCLUSION

Our study provides novel insights into the hemodynamic mechanisms of cerebral microcirculatory disturbances in AD and the modulatory effects of voluntary exercise on these hemodynamic alterations. Our work suggests therapeutic targets that may alleviate microvascular complications observed in AD.

DATA AVAILABILITY STATEMENT

The datasets generated for this study are available on request to the corresponding author.

ETHICS STATEMENT

Animals were handled according to the Animal Research: Reporting *in vivo* Experiments (ARRIVE) guidelines and the recommendations of the Canadian Council on Animal Care. The protocol was approved by the Ethics Committee of the Research Center of the Montreal Heart Institute.

AUTHOR CONTRIBUTIONS

XL designed the study, carried out the experiments, analyzed the data, and drafted the manuscript. MM and PP carried out the experiments. MM, BL, YL, RD, and PP analyzed the data. ET participated in the designing of the study. FL conceived, designed, and coordinated the study, and revised the manuscript. All authors gave final approval for publication.

FUNDING

This study was funded by a Canadian Institutes of Health Research (CIHR, 299166) operating grant and a Natural Sciences and Engineering Research Council of Canada (NSERC, 239876-2011) discovery grant to FL.

ACKNOWLEDGMENTS

The authors thank Marc-Antoine Gillis and Natacha Duquette (Montreal Heart Institute) for their help with animal preparations. The authors are grateful to Sava Sakadzic (Harvard Medical School) for discussions on the pO_2 results, Sergei Vinogradov (University of Pennsylvania) for useful comments on PtP-C343 probe synthesis and calibrating the probe for us. The authors also thank the RQRV (Réseau Québécois de Recherche sur le Vieillissement, in part funded by the Fonds de Recherche du Québec-Santé) for its valued contribution to this study.

REFERENCES

Adlard, P. A., Perreau, V. M., Pop, V., and Cotman, C. W. (2005). Voluntary exercise decreases amyloid load in a transgenic model of Alzheimer's disease. *J. Neurosci.* 25, 4217–4221. doi: 10.1523/jneurosci.0496-05.2005

Arbel-Ornath, M., Hudry, E., Eikermann-Haerter, K., Hou, S., Gregory, J. L., Zhao, L., et al. (2013). Interstitial fluid drainage is impaired in Ischemic Stroke and Alzheimer's disease mouse models. *Acta Neuropathol.* 126, 353–364. doi: 10.1007/s00401-013-1145-2

Avants, B. B., Tustison, N. J., Song, G., Cook, P. A., Klein, A., and Gee, J. C. (2011). A reproducible evaluation of ANTs similarity metric performance in brain image registration. *NeuroImage* 54, 2033–2044. doi: 10.1016/j.neuroimage.2010.09.025

Avants, B. B., Yushkevich, P., Pluta, J., Minkoff, D., Korczykowski, M., Detre, J., et al. (2010). The optimal template effect in hippocampus studies of diseased populations. *NeuroImage* 49, 2457–2466. doi: 10.1016/j.neuroimage.2009.09.062

Bero, A. W., Bauer, A. Q., Stewart, F. R., White, B. R., Cirrito, J. R., Raichle, M. E., et al. (2012). Bidirectional relationship between functional connectivity and amyloid- deposition in mouse brain. *J. Neurosci.* 32, 4334–4340. doi: 10.1523/JNEUROSCI.5845-11.2012

Bowen, C. V., Gati, J. S., and Menon, R. S. (2006). Robust prescan calibration for multiple spin-echo sequences: application to FSE and b-SSFP. *Magn. Reson. Imaging* 24, 857–867. doi: 10.1016/j.mri.2006.04.008

Brown, A. D., McMorris, C. A., Longman, R. S., Leigh, R., Hill, M. D., Friedenreich, C. M., et al. (2010). Effects of cardiorespiratory fitness and cerebral blood flow on cognitive outcomes in older women. *Neurobiol. Aging* 31, 2047–2057. doi: 10.1016/j.neurobiolaging.2008.11.002

Chugh, B. P., Bishop, J., Zhou, Y. Q., Wu, J., Henkelman, R. M., and Sled, J. G. (2012). Robust method for 3D arterial spin labeling in mice. *Magn. Reson. Med.* 68, 98–106. doi: 10.1002/mrm.23209

Cifuentes, D., Poittevin, M., Dere, E., Broquères-You, D., Bonnin, P., Benessiano, J., et al. (2015). Hypertension accelerates the progression of Alzheimer-like pathology in a mouse model of the disease. *Hypertension* 65, 218–224. doi: 10.1161/HYPERTENSIONAHA.114.04139

Damseh, R., Cheriet, F., and Lesage, F. (2018a). Fully convolutional DenseNets for segmentation of microvessels in two-photon microscopy. *Proc. Annu. Int. Conf. IEEE Eng. Med. Biol. Soc.* 2018, 661–665. doi: 10.1109/EMBC.2018.8512285

Damseh, R., Pouliot, P., Gagnon, L., Sakadzic, S., Boas, D., Cheriet, F., et al. (2018b). Automatic graph-based modeling of brain microvessels captured with two-photon microscopy. *IEEE J. Biomed. Health* 23, 2551–2562. doi: 10.1109/JBHI.2018.2884678

de Montgolfier, O., Pinçon, A., Pouliot, P., Gillis, M., Bishop, J., Sled, J., et al. (2019). High systolic blood pressure induces cerebral microvascular endothelial dysfunction, neurovascular unit damage, and cognitive decline in mice. *Hypertension* 73, 217–228. doi: 10.1161/HYPERTENSIONAHA.118.12048

Delafontaine-Martel, P., Lefebvre, J., Tardif, P., Lévy, B., Pouliot, P., and Lesage, F. (2018). Whole brain vascular imaging in a mouse model of Alzheimer's disease with two-photon microscopy. *J. Biomed. Opt.* 23, 1–10.

Dubeau, S., Desjardins, M., Pouliot, P., Beaumont, E., Gaudreau, P., Ferland, G., et al. (2011a). Biophysical model estimation of neurovascular parameters in a rat model of healthy aging. *NeuroImage* 57, 1480–1491. doi: 10.1016/j.neuroimage.2011.04.030

Dubeau, S., Ferland, G., Gaudreau, P., Beaumont, E., and Lesage, F. (2011b). Cerebrovascular hemodynamic correlates of aging in the Lou/c rat: a model of healthy aging. *NeuroImage* 56, 1892–1901. doi: 10.1016/j.neuroimage.2011.03.076

Durrant, J. R., Seals, D. R., Connell, M. L., Russell, M. J., Lawson, B. R., Folian, B. J., et al. (2009). Voluntary wheel running restores endothelial function in conduit arteries of old mice: direct evidence for reduced oxidative stress, increased superoxide dismutase activity and down-regulation of NADPH oxidase. *J. Physiol.* 587, 3271–3285. doi: 10.1113/jphysiol.2009.169771

Erdener, S. E., Tang, J. B., Sajjadi, A., Kılıç, K., Kura, S., Schaffer, C. B., et al. (2017). Spatio-temporal dynamics of cerebral capillary segments with stalling red blood cells. *J. Cereb. Blood Flow Metab.* 39, 886–900. doi: 10.1177/0271678X17743877

Farkas, E., and Luiten, P. (2001). Cerebral microvascular pathology in aging and Alzheimer's disease. *Prog. Neurobiol.* 64, 575–611. doi: 10.1016/s0301-0082(00)00068-x

Gaugler, J., James, B., Johnson, T., Scholz, K., and Weuve, J. (2018). 2018 Alzheimer's disease facts and figures. *Alzheimers Dement.* 12, 459–509. doi: 10.1016/j.jalz.2016.03.001

Gutiérrez-Jiménez, E., Cai, C., Mikkelsen, I., Rasmussen, P., Angleys, H., Merrild, M., et al. (2016). Effect of electrical forepaw stimulation on capillary transit-time heterogeneity (CTH). *J. Cereb. Blood Flow Metab.* 36, 2072–2086. doi: 10.1177/0271678x16631560

Hackshaw, A. (2008). Small studies: strengths and limitations. *Eur. Respir. J.* 32, 1141–1143. doi: 10.1183/09031936.00136408

Hall, C., Reynell, C., Gesslein, B., Hamilton, N., Mishra, A., Sutherland, B., et al. (2014). Capillary pericytes regulate cerebral blood flow in health and disease. *Nature* 508, 55–60. doi: 10.1038/nature13165

Hamer, M., and Chida, Y. (2008). Physical activity and risk of neurodegenerative disease: a systematic review of prospective evidence. *Psychol. Med.* 39, 3–11. doi: 10.1017/S0033291708003681

Hayes, S., Alosco, M., and Forman, D. (2014). The effects of aerobic exercise on cognitive and neural decline in aging and cardiovascular disease. *Curr. Geriatr. Rep.* 3, 282–290. doi: 10.1007/s13670-014-0101-x

Hernández, J., Bracko, O., Kersbergen, C., Muse, V., Haft-Javaherian, M., Berg, M., et al. (2019). Neutrophil adhesion in brain capillaries reduces cortical blood flow and impairs memory function in Alzheimer's disease mouse models. *Nat. Neurosci.* 22, 413–420. doi: 10.1038/s41593-018-0329-4

Iadecola, C. (2004). Neurovascular regulation in the normal brain and in Alzheimer's disease. *Nat. Rev. Neurosci.* 5, 347–360. doi: 10.1038/nrn1387

Iadecola, C. (2010). The overlap between neurodegenerative and vascular factors in the pathogenesis of dementia. *Acta Neuropathol.* 120, 287–296. doi: 10.1007/s00401-010-0718-6

Iadecola, C. (2017). The neurovascular unit coming of age: a journey through neurovascular coupling in health and disease. *Neuron* 96, 17–42. doi: 10.1016/j.neuron.2017.07.030

Kazmi, S., Parthasarthy, A., Song, N., Jones, T., and Dunn, A. (2013). Chronic imaging of cortical blood flow using multi-exposure speckle imaging. *J. Cereb. Blood Flow Metab.* 33, 798–808. doi: 10.1038/jcbfm.2013.57

Kisler, K., Nelson, A., Montagne, A., and Zlokovic, B. (2017). Cerebral blood Flow regulation and neurovascular dysfunction in Alzheimer disease. *Nat. Rev. Neurosci.* 18, 419–434. doi: 10.1038/nrn.2017.48

Kitaguchi, H., Ihara, M., Saiki, H., Takahashi, R., and Tomimoto, H. (2007). Capillary beds are decreased in Alzheimer's disease, but not in Binswanger's disease. *Neurosci. Lett.* 417, 128–131. doi: 10.1016/j.neulet.2007.02.021

Kleinfeld, D., Mitra, P., Helmchen, F., and Denk, W. (1998). Fluctuations and stimulus-induced changes in blood flow observed in individual capillaries in layers 2 through 4 of rat neocortex. *Proc. Natl. Acad. Sci. U.S.A.* 95, 15741–15746. doi: 10.1073/pnas.95.26.15741

Lu, X., Moeini, M., Li, B., Montgolfier, O., Lu, Y., Bélanger, S., et al. (2019). *Voluntary Exercise Increases Brain Tissue Oxygenation and Spatially Homogenizes Oxygen Delivery in a Mouse Model of Alzheimer's Disease. Imaging Cerebral Oxygenation Alterations in an Alzheimer Mouse Model.* Ph.D. thesis, Polytechnique Montréal, Montreal, QC. Available at: https://publications.polymtl.ca/3930/

Mekari, S., Fraser, S., Bosquet, L., Bonnéry, C., Labelle, V., Pouliot, P., et al. (2015). The relationship between exercise intensity, cerebral oxygenation and cognitive performance in young adults. *Eur. J. Appl. Physiol.* 115, 2189–2197. doi: 10.1007/s00421-015-3199-4

Moeini, M., Lu, X., Avti, P. K., Damseh, R., Bélanger, S., Picard, F., et al. (2018). Compromised microvascular oxygen delivery increases brain tissue vulnerability with age. *Sci. Rep.* 8:8219. doi: 10.1038/s41598-018-26543-w

Moeini, M., Lu, X., Bélanger, S., Picard, F., Boas, D., Kakkar, A., et al. (2019). Cerebral tissue pO2 response to stimulation is preserved with age in awake mice. *Neurosci. Lett.* 699, 160–166. doi: 10.1016/j.neulet.2019.02.007

Nguyen, J., Nishimura, N., Fetcho, R., Iadecola, C., and Schaffer, C. (2011). Occlusion of cortical ascending venules causes blood flow decreases, reversals in flow direction, and vessel dilation in upstream capillaries. *J. Cereb. Blood Flow Metab.* 31, 2243–2254. doi: 10.1038/jcbfm.2011.95

Nielsen, R., Egefjord, L., Angleys, H., Mouridsen, K., Gejl, M., Møller, A., et al. (2017). Capillary dysfunction is associated with symptom severity and neurodegeneration in Alzheimer's disease. *Alzheimers Dement.* 13, 1143–1153. doi: 10.1016/j.jalz.2017.02.007

Østergaard, L., Aamand, R., Gutiérrez-Jiménez, E., Ho, Y., Blicher, J., Madsen, S., et al. (2013). The capillary dysfunction hypothesis of Alzheimer's disease. *Neurobiol. Aging* 34, 1018–1031. doi: 10.1016/j.neurobiolaging.2012.09.011

Østergaard, L., Engedal, T., Moreton, F., Hansen, M., Wardlaw, J., Dalkara, T., et al. (2016). Cerebral small vessel disease: capillary pathways to stroke and cognitive decline. *J. Cereb. Blood Flow Metab.* 36, 302–325. doi: 10.1177/0271678X15606723

Park, L., Zhou, P., Pitstick, R., Capone, C., Anrather, J., Norris, E., et al. (2008). Nox2-derived radicals contribute to neurovascular and behavioral dysfunction in mice overexpressing the amyloid precursor protein. *Proc. Natl. Acad. Sci. U.S.A.* 105, 1347–1352. doi: 10.1073/pnas.0711568105

Pereira, A. C., Huddleston, D. E., Brickman, A. M., Sosunov, A. A., Hen, R., McKhann, G. M., et al. (2007). An in vivo correlate of exercise-induced neurogenesis in the adult dentate gyrus. *Proc. Natl. Acad. Sci. U.S.A.* 104, 5638–5643.

Pialoux, V., Brown, A. D., Leigh, R., Friedenreich, C. M., and Poulin, M. J. (2009). Effect of cardiorespiratory fitness on vascular regulation and oxidative stress in postmenopausal women. *Hypertension* 54, 1014–1020. doi: 10.1161/HYPERTENSIONAHA.109.138917

Radak, Z., Hart, N., Sarga, L., Koltai, E., Atalay, M., Ohno, H., et al. (2010). Exercise plays a preventive role against Alzheimer's disease. *J. Alzheimers Dis.* 20, 777–783. doi: 10.3233/JAD-2010-091531

Radde, R., Bolmont, T., Kaeser, S. A., Coomaraswamy, J., Lindau, D., Stoltze, L., et al. (2006). Aβ42-driven cerebral amyloidosis in transgenic mice reveals early and robust pathology. *EMBO Rep.* 7, 940–946. doi: 10.1038/sj.embor.7400784

Sakadžić, S., Mandeville, E., Gagnon, L., Musacchia, J., Yaseen, M., Yucel, M., et al. (2014). Large arteriolar component of oxygen delivery implies a safe margin of oxygen supply to cerebral tissue. *Nat. Comm.* 5:5734. doi: 10.1038/ncomms6734

Santisakultarm, T. P., Paduano, C. Q., Stokol, T., Southard, T. L., Nishimura, N., Skoda, R. C., et al. (2014). Stalled cerebral capillary blood flow in mouse models of essential thrombocythemia and polycythemia vera revealed by in vivo two-photon imaging. *J. Thromb. Haemost.* 12, 2120–2130. doi: 10.1111/jth.12738

Schwartz, T. H., Hong, S. B., Bagshaw, A. P., Chauvel, P., and Bénar, C. G. (2011). Preictal changes in cerebral haemodynamics: review of findings and insights from intracerebral EEG. *Epilepsy. Res.* 97, 252–266. doi: 10.1016/j.eplepsyres.2011.07.013

Sheth, S. A., Nemoto, M., Guiou, M. W., Walker, M. A., and Toga, A. W. (2005). Spatiotemporal evolution of functional hemodynamic changes and their

relationship to neuronal activity. *J. Cereb. Blood Flow Metab.* 25, 830–841. doi: 10.1038/sj.jcbfm.9600091

Shih, A. Y., Mateo, C., Drew, P. J., Tsai, P. S., and Kleinfeld, D. (2012). A polished and reinforced thinned-skull window for long-term imaging of the mouse brain. *J. Vis. Exp.* 61, 4–9. doi: 10.3791/3742

Shing, C. M., Fassett, R. G., Peake, J. M., and Coombes, J. S. (2015). Voluntary exercise decreases atherosclerosis in nephrectomised ApoE knockout mice. *PLoS One* 10:e0120287. doi: 10.1371/journal.pone.0120287

Stefanovic, B., Hutchinson, E., Yakovleva, V., Schram, V., Russell, J. T., Belluscio, L., et al. (2008). Functional reactivity of cerebral capillaries. *J. Cereb. Blood Flow Metab.* 28, 961–972. doi: 10.1038/sj.jcbfm.9600590

Toledo, J. B., Arnold, S. E., Raible, K., Brettschneider, J., Xie, S. X., Grossman, M., et al. (2013). Contribution of cerebrovascular disease in autopsy confirmed neurodegenerative disease cases in the national Alzheimer's coordinating centre. *Brain* 136, 2697–2706. doi: 10.1093/brain/awt188

Wirth-Dzięciołowska, E., Karaszewska, J., Pyśniak, K., Smolińska, M., and Gajewska, M. (2009). Selected peripheral blood cell parameters in twelve inbred strains of laboratory mice. *Anim. Sci. Pap. Rep.* 27, 69–77.

Zhang, C., Tabatabaei, M., Bélanger, S., Girouard, H., Moeini, M., Lu, X., et al. (2017). Astrocytic endfoot Ca2+ correlates with parenchymal vessel responses during 4-AP induced epilepsy: an *in vivo* two-photon lifetime microscopy study. *J. Cereb. Blood Flow Metab.* 39, 260–271. doi: 10.1177/0271678X17725417

Zlokovic, B. V. (2011). Neurovascular pathways to neurodegeneration in Alzheimer's disease and other disorders. *Nat. Rev. Neurosci.* 12, 723–738. doi: 10.1038/nrn3114

Conflict of Interest: FL reports a minority ownership in LabeoTech, Inc.

The remaining authors declare that the research was conducted in the absence of any commercial or financial relationships that could be construed as a potential conflict of interest.

Copyright © 2019 Lu, Moeini, Li, Lu, Damseh, Pouliot, Thorin and Lesage. This is an open-access article distributed under the terms of the Creative Commons Attribution License (CC BY). The use, distribution or reproduction in other forums is permitted, provided the original author(s) and the copyright owner(s) are credited and that the original publication in this journal is cited, in accordance with accepted academic practice. No use, distribution or reproduction is permitted which does not comply with these terms.

APPENDIX

Branch Dependent Investigation of Capillary RBC Properties

We used the 3D angiogram to distinguish different branching orders in capillaries (see **Appendix Figure 1a**). We investigated how capillary hemodynamics varied in different branching orders for all groups.

We observed that the average diameter showed a slight decreasing trend in WT6 group, while its value remained stable in the AD6 group (see **Appendix Figure 1b** first from the left). With exercise, the AD group remained relatively stable with a dip in the downstream capillaries (see **Appendix Figure 1b** first from the left). The smaller diameter in downstream capillaries could be linked to the stalling occuring more in the downstream capillaries (Erdener et al., 2017). The average RBC velocity showed sharp decrease in the upstream capillaries for all groups (see **Appendix Figure 1b** second from the left). The average RBC flux also had sharp reduction in all branches for the AD groups, but had a moderate decrease in the WT group (see **Appendix Figure 1b** third from the left). Finally, all groups showed increasing trends of hematocrit from upper to lower streams (see **Appendix Figure 1b** the fourth from the left).

Due to the larger reduction in the first three branching orders of capillary RBC velocity and flux, we further calculated the RBC property differences among the initial three orders for each group to explore the differences across branches. We observed that for the initial three orders (from A1 to A3), the RBC velocity dropped at least 62% [calculated by (A1-V3)/A1] (67.28, 67.70, and 62.25% for AD6, AD6&EX, and WT6, respectively), suggesting that the RBC velocity was largely modulated in the upper stream of capillaries. Additionally, for the average RBC flux, we observed that in the initial three orders (from A1 to A3), the flux dropped ~ 32% over three groups [calculated by (A1-V3)/A1] (32.74, 31.87, and 34.83% for AD6, AD6&EX, and WT6, respectively), indicating that the RBC flux modulation in the upper orders still largely contributed to the variance of overall RBC flux across all capillaries.

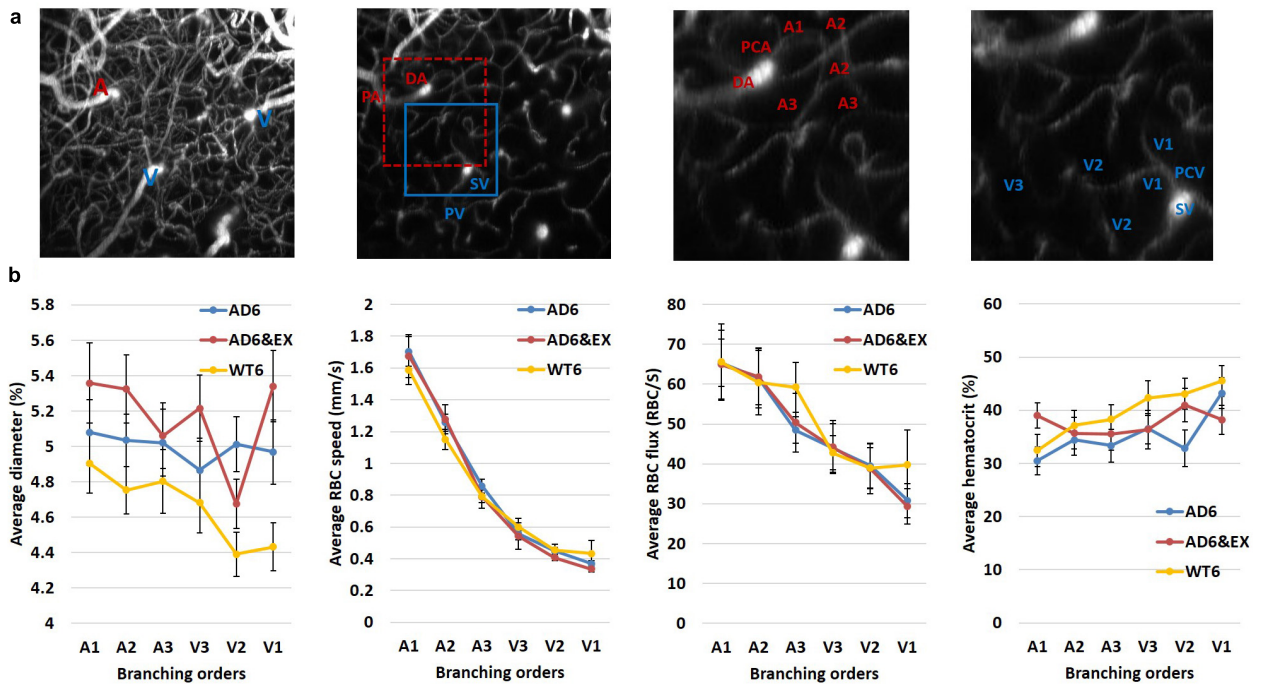

FIGURE A1 | Capillary property changes with branching orders. **(a)** Left: a maximum intensity projection image of the angiogram. Second from the left: an *en face* slice at the depth of ~100 μm. The red square indicates the area used to calculate branching orders from arterioles, and the blue square indicates the area used to calculate branching orders from venules. Third from left: the enlarged artery region with diving arteriole, precapillary arteriole, and capillaries labeled with branching orders. Fourth from left: the enlarged vein region with surfacing venule and postcapillary venule, labeled with the branching orders. **(b)** The changes of capillary diameter/velocity/flux/hematocrit as a function of branching order (460, 508, and 562 capillaries measured in the AD6, AD6&EX, and WT6 groups, respectively).

frontiers in Neuroscience

ORIGINAL RESEARCH
published: 05 December 2019
doi: 10.3389/fnins.2019.01306

Viability and Contractility of Rat Brain Pericytes in Conditions That Mimic Stroke; an *in vitro* Study

*Mohammed Heyba†, Lulwa Al-Abdullah†, Andreas W. Henkel, Zeinab Sayed, Slava A. Malatiali and Zoran B. Redzic**

Department of Physiology, Faculty of Medicine, Kuwait University, Kuwait City, Kuwait

Reopening of the cerebral artery after occlusion often results in "no-reflow" that has been attributed to the death and contraction (*rigor mortis*) of pericytes. Since this hypothesis still needs to be confirmed, we explored the effects of oxygen glucose deprivation (OGD) on viability and cell death of primary rat pericytes, in the presence or absence of neurovascular unit-derived cytokines. Two morphodynamic parameters, single cell membrane mobility (SCMM) and fractal dimension (D_f), were used to analyze the cell contractions and membrane complexity before and after OGD. We found a marginal reduction in cell viability after 2–6 h OGD; 24 h OGD caused a large reduction in viability and a large increase in the number of apoptotic and dead cells. Application of erythropoietin (EPO), or a combination of EPO and endothelial growth factor ($VEGF_{A1-165}$) during OGD significantly reduced cell viability; application of Angiopoietin 1 (Ang1) during OGD caused a marginal, insignificant increase in cell viability. Simultaneous application of EPO, $VEGF_{A1-165}$, and Ang1 significantly increased cell viability during 24 h OGD. Twenty minutes and one hour OGD both significantly reduced SCMM compared to pre-OGD values, while no significant difference was seen in SCMM before and after 3 h OGD. There was a significant decrease in membrane complexity (D_f) at 20 min during the OGD that disappeared thereafter. In conclusion, OGD transiently affected cell mobility and shape, which was followed by apoptosis in cultured pericytes. Ang1 may have a potentiality for preventing from the OGD-induced apoptosis. Further studies could clarify the relationship between cell contraction and apoptosis during OGD.

Keywords: pericytes, stroke, no-reflow, cytokines, viability, contractility, oxygen glucose deprivation

OPEN ACCESS

Edited by:
Christoph Harms, Charité Medical University of Berlin, Germany

Reviewed by:
Zahoor A. Shah, University of Toledo, United States
Kuniyuki Nakamura, Kyushu University, Japan

****Correspondence:***
Zoran B. Redzic
redzic@hsc.edu.kw

†These authors have contributed equally to this work

Specialty section:
This article was submitted to Neurodegeneration, a section of the journal Frontiers in Neuroscience

Received: *31 March 2019*
Accepted: *21 November 2019*
Published: *05 December 2019*

Citation:
Heyba M, Al-Abdullah L, Henkel AW, Sayed Z, Malatiali SA and Redzic ZB (2019) Viability and Contractility of Rat Brain Pericytes in Conditions That Mimic Stroke; an in vitro Study. Front. Neurosci. 13:1306. doi: 10.3389/fnins.2019.01306

INTRODUCTION

Pericytes wrap capillaries and express contractile proteins, so they could potentially regulate capillary diameter by constricting or relaxing their processes (Winkler et al., 2017). Whether or not they really control cerebral blood flow (CBF) *in vivo* is not clear. Local CBF is controlled by changes in smooth muscle tone around cerebral arterioles (Attwell et al., 2010). A concept has emerged from an *in vivo*/*in situ* study by Hall et al. (2014), which demonstrated that an increase in neuronal activity dilated neighboring capillaries before dilating arterioles and was accompanied by morphological changes in pericytes' shapes that were consistent with relaxation. A study that used loss-of-function pericyte-deficient mice has shown that pericyte degeneration reduces capillary blood flow responses to neuronal activity (Kisler et al., 2017). These findings have been challenged

by studies, which revealed that brain pericytes were not able to contract since the contractile proteins, such as alpha smooth muscle actin (aSMA), was only present in vascular smooth muscle cells (Hartmann et al., 2015; Hill et al., 2015; Wei et al., 2016).

Conflicting evidence exists regarding the role of pericytes in "no-reflow" following reperfusion of the occluded artery. Peppiatt et al. (2006) found that brain pericytes in mice remained contracted after the middle cerebral artery (MCA) was reopened, following 2 h occlusion. Hall et al. (2014) reported that brain pericytes die rapidly following cerebral ischemia and their processes subsequently contract (*rigor mortis*), which causes constriction of the capillaries.

To clarify whether or not conditions that occur during cerebral ischemia *in vivo* cause rapid death and/or a long contraction of brain pericytes, we cultured primary rat pericytes and then measured their viability and motility at different time points during oxygen glucose deprivation (OGD).

MATERIALS AND METHODS

Animals

Primary cultures of pericytes were obtained from 1 to 2-month-old male and female Sprague Dawley rats weighting 200–220 g. Animals were supplied by Animal Resource Center (ARC), Health Science Center (HSC), Kuwait University.

The study was carried out in accordance with the guidelines of laboratory animal care in HSC, Kuwait University, which are based on principles of the Office of Laboratory Animal Welfare, National Institutes of Health[1], and on Animal Research: Reporting of *in vivo* Experiments recommendations[2].

Primary Culture of Rat Brain Pericytes

Primary pericyte cultures were generated according to a protocol for rat brain endothelial cells (BECs) isolation (Abbott et al., 2012). For details on how this protocol was amended to produce pericytes, see **Supplemental Figure 1**. Experiments that tested cell viability were performed on >90% confluent cultures, while experiments that analyzed contractility of pericytes were performed on cultures at <50% confluence.

Immunocytochemistry

Unless stated otherwise all antibodies were from Abcam, UK. Following fixation, permeabilization and blocking, cells were incubated overnight at 4°C with the following six primary antibodies (1:100 dilution) in PBS/0.1% Tween20/1% FCS: (1) Rabbit polyclonal antibody raised against purified rat NG2 chondroitin sulfate proteoglycan; (2) Mouse monoclonal antibody raised against 22–112 sequence of human SMA, which cross-reacts with rat (DAKO-Millipore); (3) Rabbit polyclonal antibody raised against native anti-Von Willebrand factor from human plasma and also recognizes the rat homolog; (4) Rabbit monoclonal antibody raised against a recombinant fragment 400–600 of mouse CD31 and cross reacts with the rat homolog; (5) Rabbit monoclonal antibody raised against the intracellular C-terminus of the human platelet-derived growth factor receptor beta (PDGFRβ) receptor, homologous to rat; (6) Rabbit polyclonal to Tie2 receptor, raised against synthetic peptide within human TIE2 amino acid 450–500 and cross reacts with rat, mouse, and human TIE2.

After washing, the cultures were incubated for 2 h at room temperature with the following secondary antibodies (1/200–1/500 dilution), solubilized in 2 ml of PBS with 0.1% Tween20, 1% FCS: (1) goat anti-rabbit IgG conjugated to fluorescein-isothiocyanate (FITC); (2) goat anti-mouse IgG conjugated to cyanine Cy5; (3) goat anti-mouse IgG conjugated to Cy3; (4) Donkey anti-rabbit IgG conjugated to Alexa Fluor 555.

Flasks were then washed and 4′, 6-diamidino-2-phenylindole (DAPI) was added to stain the nuclei. The cells were then examined under a fluorescence microscope Zeiss Axiovert 40 CFL or Zeiss AxioObserver A1 fitted with AxioCam HRc and AxioCam MRm cameras, respectively. For Alexa Fluor 555 staining analysis, images were further processed with self-written SynoQuant Ver. 10.69 software (for details see Henkel et al., 2019). The images were deblurred with a non-linear algorithm ("Level background") that removed specifically homogenous stain corresponding to background staining, while enhancing structured any objects. The separation between background and structures was based on a local intensity standard deviation.

Oxygen Glucose Deprivation Protocols

A glove box (Plas BY Labs, Lansing, MI, USA) was maintained with 0% O_2, 5% CO_2, and 5% H_2 in N_2 at 37°C (for the justification of gas composition see Al-Sarraf et al., 2018). All cell culture media and buffers were kept in the glove box for at least 24 h prior to OGD experiments. Cell cultures were incubated in glucose- and pyruvate-free DMEM (Invitrogen) that did not contain other supplements (OGD medium) for 2–24 h. For control experiments, cultures were incubated for 2–24 h in supplement-free DMEM that contained 5 mM glucose and 1.25 mM pyruvate (control medium) in 5% CO_2 in air at 37°C.

In some cases, the following cytokines were added to the cell culture medium prior to the start of the experiments: (1) Rat recombinant EPO (rrEPO, R&D Systems, UK), 5 IU/mL, corresponding to ≈40 ng/ml; (2) Rat recombinant vascular endothelial growth factor ($rrVEGF_{A1-165}$, Abcam, UK) 10 ng/ml; (3) Rat recombinant Angiopoietin 1 (rrAng1, My BioSource, UK) 40 ng/mL.

The rationale behind choosing these cytokines was that they have been shown to be the three main cytokines released from cells of the neurovascular unit during hypoxia (Augustin et al., 2009; Becerra-Calixto and Cardona-Gómez, 2017; Hu et al., 2017). Final concentrations of these three cytokines were selected based on the available data. The concentration of rrEPO was selected according to its determined ED_{50} value for the induction of erythroleukemic TF-1 cell line proliferation (Krejci et al., 2009) and on its concentration in the cerebrospinal

[1]Available at https://olaw.nih.gov/sites/default/files/GuideBook.pdf

[2]Available at https://www.nc3rs.org.uk/sites/default/files/documents/Guidelines/Responsibility%20in%20the%20use%20of%20animals%20in%20bioscience%20research-%20expectations%20of%20the%20major%20research%20councils%20and%20charitable%20funding%20bodies%20April%202017.pdf

fluid (Janik et al., 2010). The concentration of rrAng1 was selected according to the manufacturer's recommendation, Ang1 activation of Tie2 receptor (Bogdanovic et al., 2006) and on Ang1-induced proliferation of endothelial cells (Kanda et al., 2005). Concentration of rrVEGF$_{A1-165}$ was chosen according to the manufacturer's recommendations, dose-dependent effects of VEGF$_{A1-165}$ on BECs (Mayhan, 1999) and on its concentrations in the rat CSF (Jones et al., 2003). Also, observed effects of these cytokines on cell viability and apoptosis (Koblizek et al., 1998; Kwak et al., 1999; Papapetropoulos et al., 2000) were taken into consideration.

Assessment of Cell Viability and Apoptosis

Following completion of anoxia or control protocols, cells were detached, stained with Annexin–V PE and 7-aminoactinomycin D (7-AAD) and analyzed using Epics XL flow cytometer (Beckman Coulter, USA). Based on the staining cells were considered as viable, apoptotic or dead (see **Supplemental Figure 2**). A marginal fraction of the cells in every sample was 7-AAD-positive/Annexin PE-negative; since this fraction was independent of experimental procedure it was excluded from the analysis.

Assessment of Cell Contractility and Motility Speed

We measured the membrane dynamics and the overall contraction/relaxation of pericytes. The measurements were done on digitally segmented single cells or small connected cell groups (<3 cells). **Figure 3E** and **Supplemental Figure 3** show representative examples of pericytes in contracted and relaxed states. Additionally, we quantified the overall motility speed upon various experimental interventions in order to determine if the cellular movement apparatus was affected by the treatments. The **Supplemental Video 1** shows the typical morpho-dynamics of a small connected group of pericytes. Contraction and dynamics of large processes are quantified by the area/perimeter ratio (A/PR), while small membrane movements could be measured by the fractal dimension (D_f) of the cellular perimeter (red border around cells in **Supplemental Figure 3**). The mobility speed was quantified by spatial intensity difference changes between successive image frames; this protocol was described in detail previously (Henkel et al., 2019).

Primary cultures in flasks were transferred to a temperature–controlled (37°C) incubation microscope (Cell Observer, Zeiss, Germany). Image sections for morpho-dynamic analysis were selected, if they contained preferentially single cells, covering not more than 50% of the area. Control images were recorded at a rate of 1 per 5 min for 15 h. The culture flasks were then transferred to the glove box and exposed to OGD for variable time periods (20 min−6 h). The flasks were then transferred back to the cell observer and the same cells that were imaged before OGD were monitored again. Thus, during this second imaging protocol, cells were exposed to control conditions. Image stacks of 11–22 cells from different flasks were obtained for each experimental group before and after OGD for statistical analysis.

Image Acquisition, Processing, and Quantification

Details of all procedures have been described previously (Henkel et al., 2019). The following parameters were measured: single cell membrane mobility (SCMM), Area/Perimeter ratio (A/PR), which corresponds to cell surface–cell volume ratio and is well-suited to monitor cell process dynamics. Finally, the fractal dimension (D_f) was calculated using the segmented cell perimeter as an object, which provided a quantitative approximation of the cellular plasma membrane complexity (Popescu et al., 2010).

Co-localization of immune-stained proteins (green and red channels) was measured with SynoQuant's build in "Co-localization module" that included a background subtraction algorithm, which was based on structure elements in the image. Essentially, the analysis employed the Pearson's correlation coefficient between the red and green channels (Dunn et al., 2011) to calculate coincidental appearances of proteins inside a cell and cell structures.

Statistical Analysis

The value distribution was assessed by Shapiro-Wilk's test for normality (Shapiro and Wilk, 1965; Villaseñor and González-Estrada, 2009). Differences between experimental groups were pre-assessed by one-way or two-way ANOVA to determine the effects of OGD, cytokine presence, and viability of pericytes. The homogeneity of variances was assessed by Levene's test for equality of variances (Levene, 1960). Whenever the data was not normally distributed, the Kruskal-Wallis test was used instead of ANOVA.

For assessment of the contractility, statistical significance was calculated by paired *t*-tests between control and experimental groups, since the same cells were imaged before and after OGD. A $p < 0.05$ was considered statistically significant. Effect sizes between controls and experimental groups were calculated as Cohen's D (Cohen, 1988).

RESULTS

Purity of Primary Cultures

Overall, rat brain pericytes in culture revealed heterogeneous phenotypes and were the largely dominant cell type, while VSMCs were only marginally present.

Figure 1A shows that the majority of cells were NG2-positive (FITC), and many NG2-positive cells were also positive for SMA (Cy5). The Pearson's coefficient for cellular co-localization of both markers, after background correction, was ≈0.7, which corresponds to a colocalization of ≈48–50%. Cells with a typical pericyte-like morphology that were positive for NG2 and marginally positive for SMA could be observed in all cultures (dashed arrows). Cells that were positive for SMA and marginally positive for NG2, and thus could represent vascular smooth muscle cells (dotted arrows). Rarely, cells showed no immune-reactivity for either NG2 or SMA (solid arrows); these were possibly fibroblasts or macrophages. Since expression of SMA by pericytes largely depends on their localization, pericytes from capillaries that branch directly from arterioles and venules

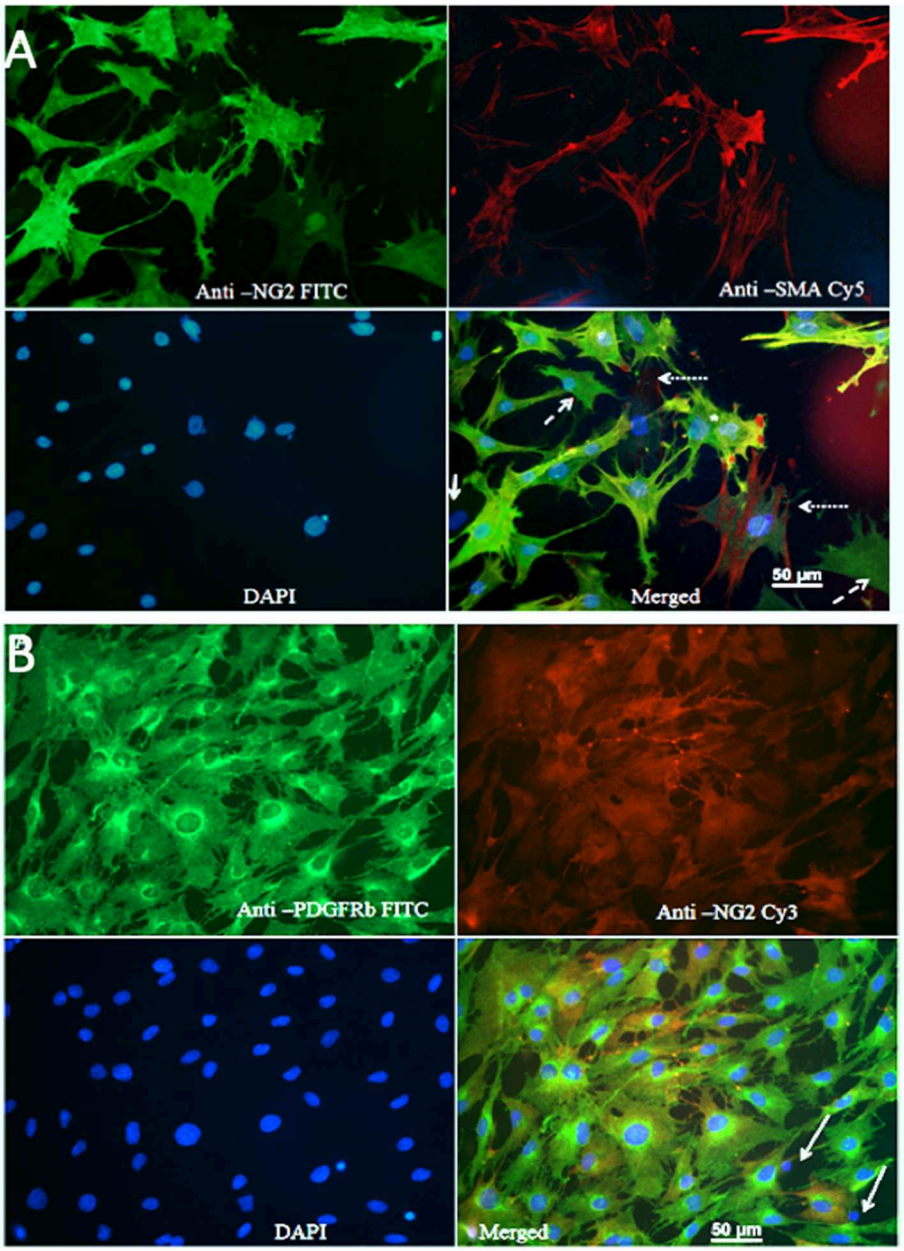

FIGURE 1 | (A) Staining of primary cultures with anti-NG2 (FITC, green channel)/anti-SMA antibodies (Cy5, red channel). These images show polygonal, pericyte-like cells with processes. Anti-NG2 was mostly diffuse diffusely, while staining with anti SMA revealed fibrillary structures, which most likely corresponded to actin filaments. Cells that were poorly stained with both NG2 and SMA could be observed rarely (arrows); some cells were positive only for NG2 (dashed arrows), while some cells were mainly SMA positive (dotted arrow). **(B)** Immunostaining for PDGFRβ. A typical image showing staining of primary cultures with anti PDGFRβ (FITC, green)/anti-NG2 antibodies (Cy3, red).

express more SMA than those in mid-capillary regions (Nehls and Drenckhahn, 1991). This may account for the absence or low abundance of SMA in pericytes from these areas. Contamination of primary cultures with BECs was marginal, which was confirmed by immunostaining with anti-Von Willebrand factor antibody and CD31 antibody (**Supplemental Figure 4**).

Since brain pericytes can be distinguished from VSMCs by PDGFRb as marker (Hutter-Schmid and Humpel, 2016), we stained primary cultures with anti-PDGFRb (FITC, green channel) and anti-NG2 (Cy3, red channel) antibodies (**Figure 1B**). The vast majority of cells were PDGFR-positive; the Pearson's coefficient for co-localization of both markers after background correction was ≈0.7, which corresponded to a co-localization of ≈48–50%. PDGFRb positive–NG2 negative cells were present in all cell cultures. A small fraction of the cells was NG2 positive but PDGFRb

negative, presumably VSMCs. Isolated pyknotic nuclei were also observed (arrows).

Viability of Pericytes During OGD and Effects of NVU-Derived Cytokines

Two and six hours OGD caused small but significant ($p < 0.05$) reduction in pericyte viability (**Supplemental Figure 5A**), which was accompanied by a small increase in the number of apoptotic (**Supplemental Figure 5B**) and dead cells (**Supplemental Figure 5C**). However, 24 h exposure to OGD caused a large reduction in viability, to 27% ($p < 0.001$ vs. control, **Figure 2A**), which was accompanied by a large and significant increase in the number of apoptotic cells (**Figure 2B**) and a moderate and significant increase in the number of dead cells (**Figure 2C**).

Presence of rrEPO in in the medium did not exert any effect on cell survival either during 2 and 6 h OGD or in control conditions during 2, 6, and 24 h (**Figure 2A** and **Supplemental Figure 5A**). However, it caused a large decrease in cell viability after 24 h OGD from 27% (OGD without rrEPO) to 8% ($p < 0.01$, **Figure 2A**). The number of apoptotic cells significantly decreased under these conditions to 35% ($p < 0.05$ vs. OGD without rrEPO, **Figure 2B**), but the number of dead cells increased significantly to 55% ($p < 0.01$ vs. OGD without rrEPO, **Figure 2C**). Interestingly, presence of rrAng1 in in the medium caused a marginal and significant reduction in cell viability in control conditions ($p < 0.05$ vs. control without any cytokine, **Figure 2A**), which was

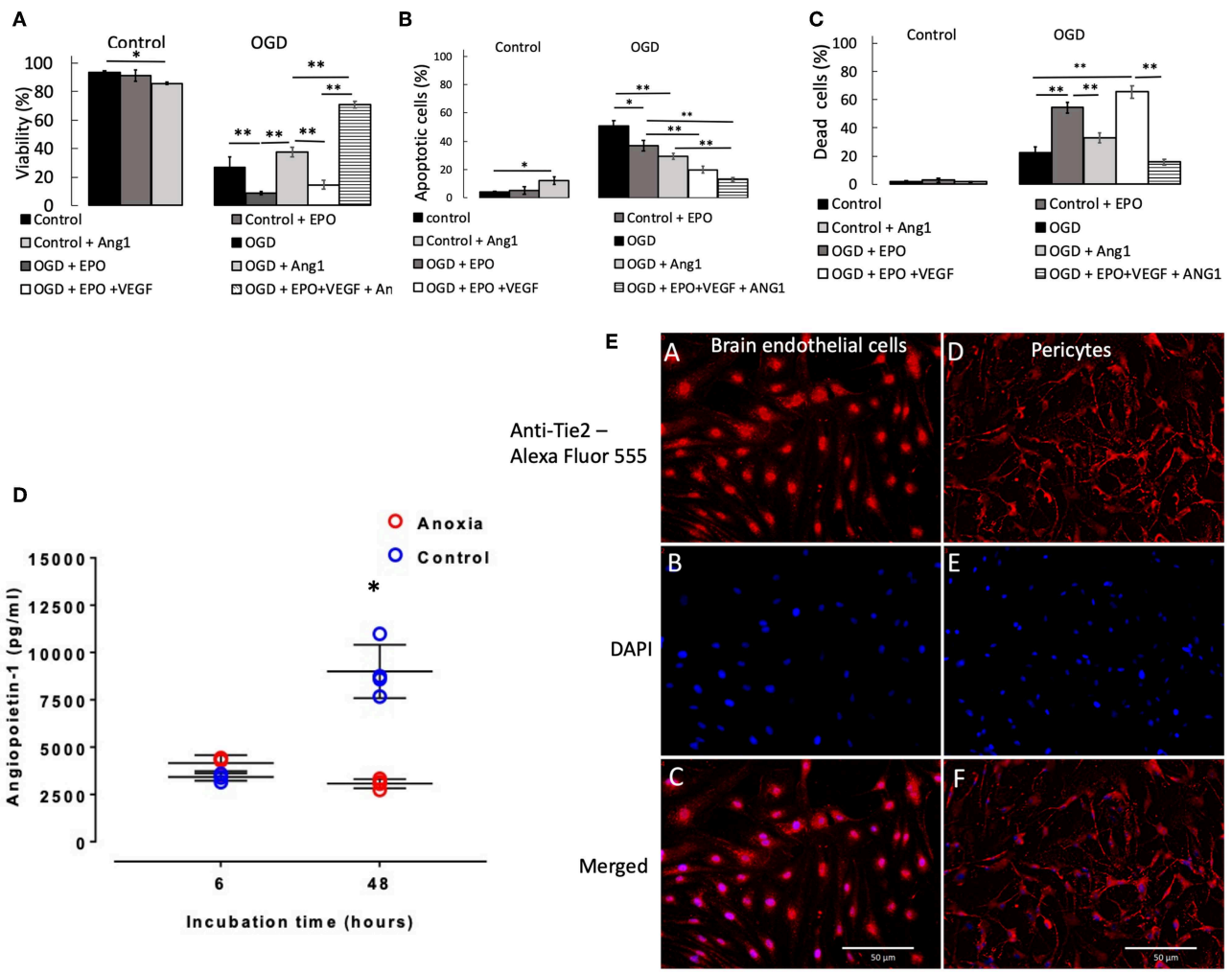

FIGURE 2 | Percentage of pericytes that were viable **(A)**, apoptotic **(B)**, and dead **(C)**, respectively after 24 h control or OGD protocols. Data were presented as mean ± SD, $n = 4$–8. Symbols indicate: $^{*}p < 0.05$, $^{**}p < 0.01$. **(D)** Angiopoietin-1 secretion by pericytes in culture during anoxia and control conditions. Values from each sample are presented as separate points. In some cases, data overlap and hence may appear to be <4 samples. The mean of the four values and SD were calculated; the latter ones being presented with solid lines. In some cases, SDs were marginal, so they appear as a single line. Symbol [*] indicates that values in anoxic groups were lower ($p < 0.05$) vs. values during normoxia (control). **(E)** Staining of rat primary brain endothelial cells (left column of images, A–C) and rat primary pericytes (right column of images, D,E) for Tie2 receptor. (A,D) Anti-Tie2 receptor staining, labeled with Alexa Fluor 555; (B,E) DAPI stain; (C,F) overlay of anti-Tie2 receptor and DAPI staining.

mainly due to a significant increase in the number of apoptotic cells (**Figure 2B**). This finding requires further investigation of the mechanism behind it, however, this was beyond the scope of the current study. Presence of rrAng1 in in the medium caused a marginal and insignificant increase in cell viability during 24 h OGD, when compared to OGD without any cytokine added ($p = 0.247$, **Figure 2A**). When $rrVEGF_{A1-165}$ and rrEPO were added together to the cell culture medium, there was a decrease in viability of pericytes after 2 h OGD to 71% ($p < 0.01$ vs. OGD and vs. OGD + rrEPO, **Supplemental Figure 5A**) and an increase in cell viability after 6 h OGD to 95% ($p < 0.05$ vs. OGD and vs. OGD + rrEPO), while after 24 h OGD cell viability under these conditions was only 14%, which was significantly lower than after 24 h OGD without any cytokine added ($p < 0.01$, **Figure 2A**). This was mainly due to a large increase in the number of dead cells (**Figure 2C**). Addition of rrEPO, $rrVEGF_{A1-165}$ and rrAng1 to the cell culture medium before exerted only small effects on cell viability after 2 and 6 h but were strongly protective to pericytes after 24 h OGD, with a cell viability exceeding 70% ($p < 0.001$ vs. OGD without cytokines, **Figure 2A**). This was due to a large reduction in the number of apoptotic cells (<13%, **Figure 2B**) and dead cells (<16%, **Figure 2C**). This observation suggests that a large number of pericytes could survive as long as 24 h without oxygen, glucose and pyruvate in the presence of these three NVU-derived cytokines. Since pericytes normally secrete Ang1 we speculated on why this secretion could not exert protective effects when primary pericytes were exposed to OGD with rrEPO and $rrVEGF_{A1-165}$, i.e., why was the difference in the survival between these two groups (rrEPO and $rrVEGF_{A1-165}$ vs. rrEPO, $rrVEGF_{A1-165}$ and Ang1) so large. To clarify this, we used ELISA kit (Boster biological technology, USA) to measure concentrations of Ang1 in cell culture media collected from the conditioned pericytes. These results are presented in **Figure 2D**. In the presence of oxygen, pericytes secreted Ang1 in the medium and there was an almost linear increase in the concentration between 6 and 24 h in the control groups. However, when they were deprived of oxygen, there was no significant increase in Ang1 concentrations between 6 and 48 h ($p > 0.05$); the concentration after 48 h was significantly lower than in controls ($p < 0.01$).

After staining for Tie2 receptor, immunofluorescence showed punctate staining on the membrane in both brain endothelial cells, which were used as a control, and in primary pericytes (**Figure 2E**). There was some nuclear staining that was more prominent in endothelial than in pericyte cells. Pericyte processes were more intense stained than cell somata, while endothelial cells showed a more homogeneous distribution and smaller puncta.

Effects of OGD Protocols on Pericytes' Morpho-Dynamics

To confirm that the reduction in SCMM actually represented contraction of the contractile filaments in pericytes, 22 cells were imaged before and after application of the vasoactive drug endothelin-1 (ET-1, 50 nM) (Rubanyi and Polokoff, 1994). The result is presented in **Figure 3A**, first bar; 19 out of 22 cells exhibited a reduced SCMM ($p < 0.01$, $n = 22$).

Exposure of pericytes to 20 min ($n = 11$) and 1 h ($n = 16$) OGD produced a similar effect as the presence of ET-1, which was a pronounced reduction of pericytes' SCMM when compared to the corresponding pre-OGD control period (**Figure 3A**, $p < 0.05$ for both time points). The effect sizes (Cohen's D) after 20 min and 1 h OGD, were 0.65 and 0.9, respectively, corresponding to medium and large effects. After 3 and 6 h OGD, the overall motility speed of their processes did not change significantly, when compared to the pre-OGD period ($n = 22$, $p = 0.02$ and $n = 16$, $p = 0.46$, respectively). In both cases the effect sizes were small (Cohen's $D < 0.4$).

The ratio between cell area and cell perimeter (A/PR) was used to check if the protrusions and process formation was affected by OGD. Initially, the A/PR increased after 20 min OGD (**Figure 3B**, $n = 25$, $p < 0.01$), which indicated that the cell became rounder and that the processes grew shorter. Later on, there were either no changes detectable (1 h, $n = 22$), or a slight decrease (3 h, $n = 18$, $p < 0.05$) compared to controls. The exposure to 6 h OGD caused a significant increase in A/PR ($n = 20$, $p < 0.01$), pointing to the retraction of processes and protrusions. In summary, the pericytes became rounder after 20 min and 6 h OGD.

Generally, we could not detect differences in pericytes' membrane complexity estimated by fractal dimension D_f (**Figure 3C**) between images taken before and after OGD, except when cells were exposed to 1 h OGD, when D_f was significantly decreased ($p < 0.05$ compared to controls, $n = 54$). In order to verify that this reduction was associated with contraction of cellular processes, we measured D_f before and after addition of ET-1 (50 nM). Despite heterogenous behavior of pericytes, ET-1 caused a significant reduction in D_f from (mean ± SD) 1.28 ± 0.04 before OGD to 1.25 ± 0.05 after OGD ($n = 65$, $p < 0.01$).

In most pericytes the plasma membrane motility was very dynamic, but on a slow time scale. **Figure 3D** (modified from Henkel et al., 2019) shows a representative A/PR trace with transient contractions and relaxations, occurring over the course of ≈15 h. At the end, most pericytes remained rounder than at the start of the experiment. The 4 insets show the segmented cell plasma membrane, acquired at corresponding times (arrows) of the experiment.

DISCUSSION

Pericytes Were Resistant to OGD

The data from this study suggest that pericytes in primary culture represented a heterogenous population of cells; they could survive OGD for relatively long periods of time, if rrEPO, rrVEGF, and rrAng1 were added in the cell culture medium. The only source of glucose during OGD could be from glycogen. In the presence of NVU-derived cytokines, astrocytes store substantial amounts of glycogen and metabolize it by glycolysis (Rischke et al., 1992; Thoren et al., 2006). Pericytes have been shown to store glycogen *in vivo* (Cataldo and Broadwell, 1986); our findings suggest that the available glucose quantity is apparently sufficient to supply ATP in the absence of oxygen.

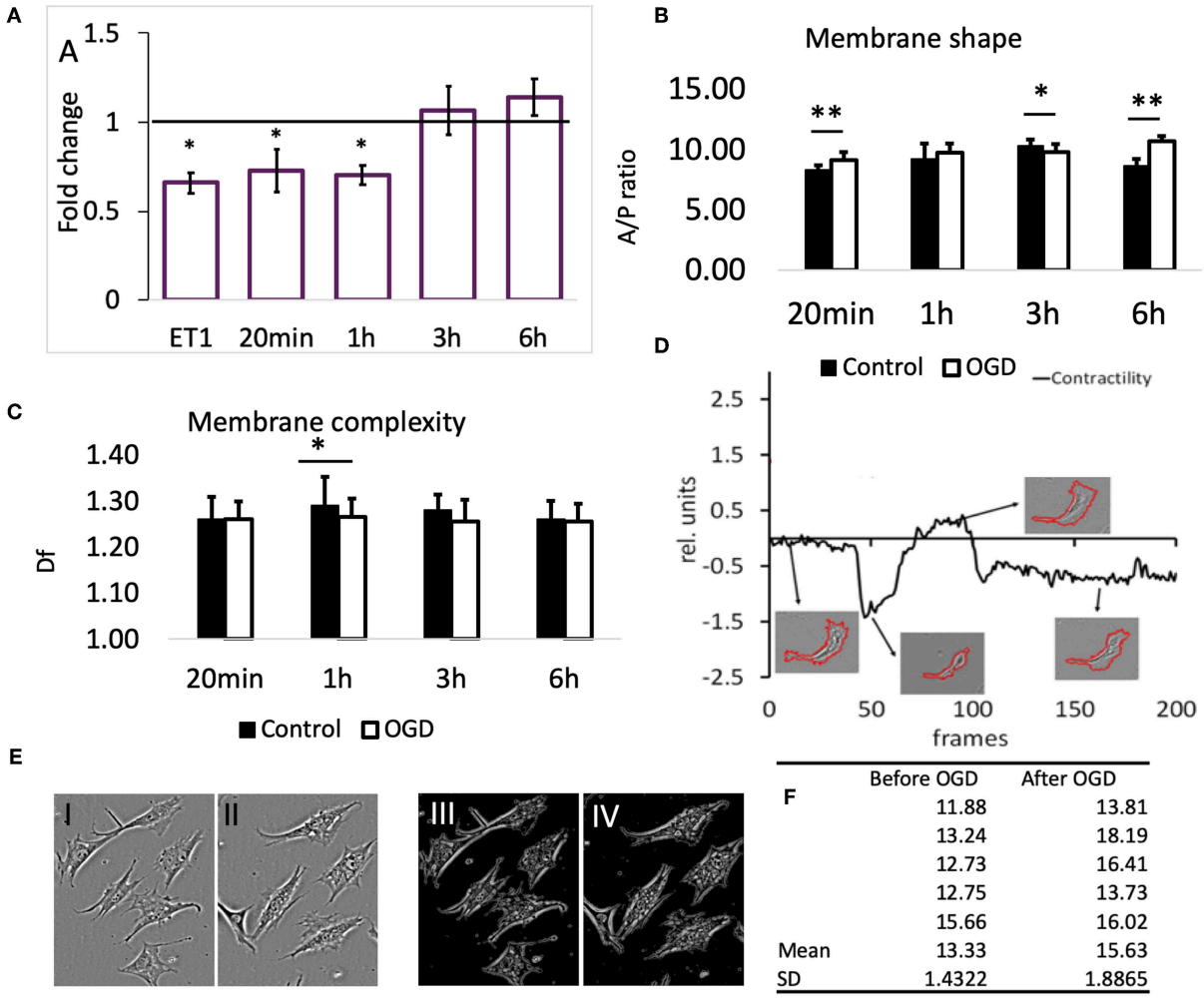

F	Before OGD	After OGD
	11.88	13.81
	13.24	18.19
	12.73	16.41
	12.75	13.73
	15.66	16.02
Mean	13.33	15.63
SD	1.4322	1.8865

FIGURE 3 | (A) Effects of OGD protocols on cell membrane mobility. The bars represent the fold-change compared to controls of motility speed after exposure to OGD for the indicated time periods. ET1 serves as a positive control for motility speed reduction. Data are presented as mean ± SD from the following number of cells: 22 (ET-1), 11 (20 min), 16 (1 h), 22 (3 h), and 16 (6 h). **(B)** Membrane shape of pericytes before and after OGD quantified by area/perimeter ratio (A/PR) at indicated OGD exposure times. The values were obtained from the following number of single cells: 25 (20 min), 22 (1 h), 18 (3 h), 20 (6 h). **(C)** Membrane complexity (membrane roughness) of pericytes, represented by D_f, before and after OGD protocols. Asterisk indicates significance level to corresponding controls (set to 1) $^*p < 0.05$, $^{**}p < 0.01$. **(D)** Example of a contractility time series derived from a contraction-expansion cycle of a single pericyte. The insets show the outlines of pericyte plasma membranes at the indicated time points in the contractility trace. **(E)** An example of a partial retractions of cell processes after OGD. I and III show a typical visual field under phase contrast microscope with 6 pericytes before, while II and IV show the remaining 5 pericytes after 6 h OGD. Images III and IV represent structure enhanced images I and II, respectively. **(F)** Using protocol that has been described already (Henkel et al., 2019), the A/P ratio for every cell in images shown in E has been calculated and then the mean and SD estimated. These data reveal that A/P ratio for each of the five cells in this particular visual field has increased, i.e., cells have partially retracted processes becoming more "round." Paired *t*-test revealed statistically significant difference ($p < 0.05$).

NVU-Derived Cytokines Exerted Differential Effects on Pericytes During OGD

EPO exerted detrimental effects on pericytes after 24 h OGD, which could be either due to a reduced ability of these cells to generate sufficient amounts of ATP through glycolysis, or to an increase in energy expenditure. These effects were similar to those observed on rat astrocytes and rat BECs during anoxia (Al-Sarraf et al., 2018) and contradict the classical concept that EPO signaling is neuroprotective during hypoxia (Mallet and Ryou, 2017). Astrocytes are the main source of endogenous EPO in the hypoxic brain (Chavez et al., 2006). Clinical trials have revealed either no effects or damaging effects of exogenous EPO in stroke patients (Souvenir et al., 2015). Cerebral glucose metabolic rate was significantly increased in constitutively EPO-overexpressing transgenic mice (Frietsch et al., 2007). This suggests that EPO enhances energy demands in brain cells. EPO is also one of the cytokines that could affect cellular metabolism through a 5′ AMP-activated protein kinase (AMPK–EC 2.7.11.31)—dependent pathway (Wang et al., 2013). AMPK

activation in pericytes enhances glucose uptake by increasing the expression of GLUT-1 and GLUT-4 and ATP production through glucose utilization (Carlsson et al., 2018). This could enhance glucose utilization beyond the minimum required and, therefore, could reduce ability of pericytes to survive OGD for a longer period of time. Activation of AMPK was detrimental to neurons during ischemia-reperfusion, while AMPK inhibition was neuroprotective (Ronnett et al., 2009). VEGF can also activate AMPK (Baufeld et al., 2017; Zibrova et al., 2017) and pericytes express VEGF receptor 1 (Eilken et al., 2017). Thus, it is likely that the detrimental effects of simultaneous application of VEGF and EPO on pericytes during OGD could be due to enhanced AMPK activation, which in turn enhances glycolysis, and depletes available energy substrate (i.e., glycogen) more rapidly, while increasing lactate production. An increase in lactate inhibits Na^+/Ca^{2+} exchangers (Yamanishi et al., 2006), which triggers Ca^{++} overload and apoptosis.

The presence of rrAng1 in the medium, though it significantly reduced the number of dead cells (**Figure 2C**), exerted only marginal and insignificant increase in viability of pericytes during 24 h OGD. On the other hand, presence of rrEPO, $rrVEGF_{A1-165}$, and rrAng1 in the cell culture medium exerted protective effects on pericytes during 24 h OGD. It is not clear why this protective effect was so different, when compared to the effects observed in the presence of rrEPO alone, rrAng1 alone or rrEPO and rrVEGF. One of the explanations could be that pericytes secrete Ang1 during hypoxia, but in the absence of oxygen pericytes cannot continue to produce Ang1 for a longer period of time (**Figure 2D**); thus, the protective effect appeared only when rrAng1 was added to the medium. Ang1 exerts its effects by binding to the Tie2 receptor tyrosine kinase (Augustin et al., 2009; Reiss et al., 2015), which is primarily expressed in endothelial cells (Sato et al., 1995), but this study (**Figure 2E**) confirmed previous findings that it was also expressed in pericytes (Teichert et al., 2017). The only common intracellular mechanism that is activated by EpoR, VEGFR, and Tie2 is the phosphatidylinositol 3-kinase pathway (PI3K, EC 2.7.1.137). Subsequent stimulation of 3-phosphoinositide-dependent kinase 1, activates RAC-alpha serine/threonine-protein kinase (AKT1). The resulting phosphorylation suppresses apoptosis by inhibiting the Bcl-2-associated death promoter through the p53 protein. It has been shown that a well-known β-adrenergic receptor agonist that exerts protective effects on retinal pericytes in diabetes patients is mediated *via* Akt activation (Yun et al., 2018). Thus, we can assume that simultaneous activation of the PI3K pathway by the three cytokines, mentions above, reduces apoptosis of pericytes during OGD, similar to earlier findings that have shown PI3K/Akt dependent apoptosis reduction in retinal pericytes (Haribalaganesh et al., 2009).

Do Pericytes Contract During OGD?

In this study, we have video-imaged pericytes, exposed them to OGD of various durations and then video-imaged the same cells again in normal conditions, which partially mimicked conditions that occur during the reperfusion *in vivo*.

Addition of ET-1 to primary cultures caused changes in SCMM and D_f that corresponded to cell contractions, which confirms that the vast majority of pericytes in primary cultures, regardless of their heterogeneity, possess the necessary cellular apparatus to contract. OGD protocols that lasted for 20 min and for 1 h caused changes in pericytes' morphology similar to changes caused by addition of ET-1. However, they did not persist after 3 and 6 h, though the latter data was not conclusive, since changes in D_f were consistent with contraction of processes. We observed that 20 min OGD protocol caused a significant reduction in cell mobility. This was even more pronounced after 1 h OGD protocol. These effects disappeared after 3 and 6 h OGD, which suggests that the mobility of the cells was transiently impaired by OGD. The A/PR increased after 20 min and 6 h OGD, indicating rounder cells with fewer processes. Interestingly, since 1 and 3 h long exposure to OGD had no apparent effects on process formation, it appears likely that two independent molecular mechanisms may control the membrane shape. Overall, it appears that brain pericytes do contract after 20 min and possibly 1 h OGD protocols, but not after 3 h and also most likely after 6 h OGD protocols.

LIMITATIONS AND CONCLUSIONS

Our results revealed that OGD transiently affected cell mobility and cell shape, which was followed by cell apoptosis in cultured pericytes. Angiopoietin-1 may have a potentiality for preventing from the OGD-induced apoptosis. However, further analysis is required to clarify the relationship between cell contraction and cell apoptosis during OGD. The main limitation of this study was that it was an *in vitro* study, hence these findings should be applied to *in vivo* conditions with caution. Also, SCMM has not been determined in the presence of Ang1, VEGF, and/or EPO. If the time pattern of pericytes' survival and contraction *in vivo* is the same as revealed in our *in vitro* study, for which we have no evidence so far, then it is unlikely that rapid death and contraction of pericytes are the cause of no-reflow in the brain.

DATA AVAILABILITY STATEMENT

The datasets generated for this study are available on request to the corresponding author.

ETHICS STATEMENT

The details of the experimental protocol were approved by the Animal Ethics Committee, HSC.

AUTHOR CONTRIBUTIONS

MH performed the study of pericytes' viability and apoptosis during OGD and analyzed these data. LA-A performed the study of pericytes' motility and contractility after OGD and analyzed these data. AH developed the software to

analyse motility and contractility data, supervised data analysis, and partially wrote the manuscript together with ZR. ZS participated in all cell culture work and performed NG2/SMA/PDGFRb staining. SM performed staining for Tie2 receptor in pericytes and BECs. ZR designed and supervised the study, provided funding, supervised data analysis, directed other contributors, and drafted the manuscript together with AH.

FUNDING

This study was generously supported by Kuwait University College of Graduate Studies and Kuwait University Research Sector General Facility Grant No. SRUL02/13.

ACKNOWLEDGMENTS

We acknowledge Mrs. Mini Verkey and Mrs. Deepa Varghese for their excellent technical assistance. We acknowledge the help of Dr. Suleiman Al-Sabah and Miss. Sofija Redzic in improving language, style, and clarity of the manuscript.

SUPPLEMENTARY MATERIAL

The Supplementary Material for this article can be found online at: https://www.frontiersin.org/articles/10.3389/fnins.2019.01306/full#supplementary-material

Supplementary Video 1 | Time lapse video of contracting and expanding pericyte in primary culture.

REFERENCES

Abbott, J., Dolman, D., Drndarski, S., and Fredriksson, S. (2012). An improved *in vitro* blood-brain barrier model: rat brain endothelial cells co-cultured with astrocytes. *Methods Mol. Biol.* 814, 415–430. doi: 10.1007/978-1-61779-452-0_28

Al-Sarraf, H., Malatiali, S., Al-Awadi, M., and Redzic, Z. (2018). Effects of erythropoietin on astrocytes and brain endothelial cells in primary culture during anoxia depend on simultaneous signaling by other cytokines and on duration of anoxia. *Neurochem. Int.* 113, 34–45. doi: 10.1016/j.neuint.2017.11.014

Attwell, D., Buchan, A.M., Charpak, S., Lauritzen, M., Macvicar, B.A., and Newman, E.A. (2010). Glial and neuronal control of brain blood flow. *Nature* 468, 232–243. doi: 10.1038/nature09613

Augustin, H.G., Koh, G.Y., Thurston, G., and Alitalo, K. (2009). Control of vascular morphogenesis and homeostasis through the angiopoietin-Tie system. *Nat. Rev. Mol. Cell Biol.* 10, 165–177. doi: 10.1038/nrm2639

Baufeld, A., Koczan, D., and Vanselow, J. (2017). Induction of altered gene expression profiles in cultured bovine granulosa cells at high cell density. *Reprod. Biol. Endocrinol.* 15:3. doi: 10.1186/s12958-016-0221-6

Becerra-Calixto, A., and Cardona-Gómez, G. P. (2017). The role of astrocytes in neuroprotection after brain stroke: potential in cell therapy. *Front. Mol. Neurosci.* 10:88. doi: 10.3389/fnmol.2017.00088

Bogdanovic, E., Nguyen, V.P., and Dumont, D.J. (2006). Activation of Tie2 by angiopoietin-1 and angiopoietin-2 results in their release and receptor internalization. *J. Cell Sci.* 119(Pt 17), 3551–3560. doi: 10.1242/jcs.03077

Carlsson, R., Ozen, I., Barbariga, M., Gaceb, A., Roth, M., and Paul, G. (2018). STAT3 precedes HIF1alpha transcriptional responses to oxygen and oxygen and glucose deprivation in human brain pericytes. *PLoS ONE* 13:e0194146. doi: 10.1371/journal.pone.0194146

Cataldo, A.M., and Broadwell, R.D. (1986). Cytochemical identification of cerebral glycogen and glucose-6-phosphatase activity under normal and experimental conditions. II. Choroid plexus and ependymal epithelia, endothelia and pericytes. *J. Neurocytol.* 15, 511–524. doi: 10.1007/BF01611733

Chavez, J.C., Baranova, O., Lin, J., and Pichiule, P. (2006). The transcriptional activator hypoxia inducible factor 2 (HIF-2/EPAS-1) regulates the oxygen-dependent expression of erythropoietin in cortical astrocytes. *J. Neurosci.* 26, 9471–9481. doi: 10.1523/JNEUROSCI.2838-06.2006

Cohen, J. E. (1988). Estimating the effects of successful malarial control programmes on mortality. *Popul. Bull. UN* 25, 6–26.

Dunn, K.W., Kamocka, M.M., and McDonald, J.H (2011). A practical guide to evaluating colocalization in biological microscopy. *Am. J. Physiol. Cell. Physiol.* 300, C723–C742. doi: 10.1152/ajpcell.00462.2010

Eilken, H.M., Diéguez-Hurtado, R., Schmidt, I., Nakayama, M., Jeong, H.-W., Arf, H., et al. (2017). Pericytes regulate VEGF-induced endothelial sprouting through VEGFR1. *Nat. Commun.* 8:1574. doi: 10.1038/s41467-017-01738-3

Frietsch, T., Maurer, M.H., Vogel, J., Gassmann, M., Kuschinsky, W., and Waschke, K.F. (2007). Reduced cerebral blood flow but elevated cerebral glucose metabolic rate in erythropoietin overexpressing transgenic mice with excessive erythrocytosis. *J. Cereb. Blood Flow Metab.* 27, 469–476. doi: 10.1038/sj.jcbfm.9600360

Hall, C.N., Reynell, C., Gesslein, B., Hamilton, N.B., Mishra, A., Sutherland, B.A., et al. (2014). Capillary pericytes regulate cerebral blood flow in health and disease. *Nature* 508, 55–60. doi: 10.1038/nature13165

Haribalaganesh, R., Sheikpranbabu, S., Elayappan, B., Venkataraman, D., and Gurunathan, S. (2009). Pigment-epithelium-derived factor down regulates hyperglycemia-induced apoptosis via PI3K/Akt activation in goat retinal pericytes. *Angiogenesis* 12, 381–389. doi: 10.1007/s10456-009-9159-z

Hartmann, D.A., Underly, R.G., Grant, R.I., Watson, A.N., Lindner, V., and Shih, A.Y. (2015). Pericyte structure and distribution in the cerebral cortex revealed by high-resolution imaging of transgenic mice. *Neurophotonics* 2:041402. doi: 10.1117/1.NPh.2.4.041402

Henkel, A.W., Al-Abdullah, L., Al-Qallaf, M.S., and Redzic, Z.B. (2019). Quantitative determination of cellular-and neurite motility speed in dense cell cultures. *Front. Neuroinform.* 13:15. doi: 10.3389/fninf.2019.00015

Hill, R.A., Tong, L., Yuan, P., Murikinati, S., Gupta, S., and Grutzendler, J. (2015). Regional blood flow in the normal and ischemic brain is controlled by arteriolar smooth muscle cell contractility and not by capillary pericytes. *Neuron* 87, 95–110. doi: 10.1016/j.neuron.2015.06.001

Hu, X., De Silva, T.M., Chen, J., and Faraci, F.M. (2017). Cerebral vascular disease and neurovascular injury in ischemic stroke. *Circ. Res.* 120, 449–471. doi: 10.1161/CIRCRESAHA.116.308427

Hutter-Schmid, B., and Humpel, C. (2016). Platelet-derived growth factor receptor-beta is differentially regulated in primary mouse pericytes and brain slices. *Curr. Neurovasc. Res.* 13, 127–134. doi: 10.2174/1567202613666160219120411

Janik, P., Kwiecinski, H., Sokolowska, B., and Niebroj-Dobosz, I. (2010). Erythropoietin concentration in serum and cerebrospinal fluid of patients with amyotrophic lateral sclerosis. *J. Neural. Transm.* 117, 343–347. doi: 10.1007/s00702-009-0354-2

Jones, K.L., Krous, H.F., Nadeau, J., Blackbourne, B., Zielke, H.R., and Gozal, D. (2003). Vascular endothelial growth factor in the cerebrospinal fluid of infants who died of sudden infant death syndrome: evidence for antecedent hypoxia. *Pediatrics* 111, 358–363. doi: 10.1542/peds.111.2.358

Kanda, S., Miyata, Y., Mochizuki, Y., Matsuyama, T., and Kanetake, H. (2005). Angiopoietin 1 is mitogenic for cultured endothelial cells. *Cancer. Res.* 65, 6820–6827. doi: 10.1158/0008-5472.CAN-05-0522

Kisler, K., Nelson, A.R., Rege, S.V., Ramanathan, A., Wang, Y., Ahuja, A., et al. (2017). Pericyte degeneration leads to neurovascular uncoupling and limits oxygen supply to brain. *Nat. Neurosci.* 20, 406–416. doi: 10.1038/nn.4489

Koblizek, T.I., Weiss, C., Yancopoulos, G.D., Deutsch, U., and Risau, W. (1998). Angiopoietin-1 induces sprouting angiogenesis *in vitro*. *Curr. Biol.* 8, 529–532. doi: 10.1016/S0960-9822(98)70205-2

Krejci, P., Prochazkova, J., Bryja, V., Jelinkova, P., Pejchalova, K., Kozubik, A., et al. (2009). Fibroblast growth factor inhibits interferon gamma-STAT1 and interleukin 6-STAT3 signaling in chondrocytes. *Cell. Signal.* 21, 151–160. doi: 10.1016/j.cellsig.2008.10.006

Kwak, H.J., So, J.N., Lee, S.J., Kim, I., and Koh, G.Y. (1999). Angiopoietin-1 is an apoptosis survival factor for endothelial cells. *FEBS Lett.* 448, 249–253. doi: 10.1016/S0014-5793(99)00378-6

Levene, H. (1960). "Robust tests for equality of variances," in *Contributions to Probability and Statistics: Essays in Honor of Harold Hotelling*, eds I. Olkin and H. Hotelling (Stanford University Press), 278–292.

Mallet, R.T., and Ryou, M.G. (2017). Erythropoietin: endogenous protection of ischemic brain. *Vitam. Horm.* 105, 197–232. doi: 10.1016/bs.vh.2017.01.002

Mayhan, W.G. (1999). VEGF increases permeability of the blood-brain barrier via a nitric oxide synthase/cGMP-dependent pathway. *Am. J. Physiol.* 276, C1148–1153. doi: 10.1152/ajpcell.1999.276.5.C1148

Nehls, V., and Drenckhahn, D. (1991). Heterogeneity of microvascular pericytes for smooth muscle type alpha-actin. *J. Cell Biol.* 113, 147–154. doi: 10.1083/jcb.113.1.147

Papapetropoulos, A., Fulton, D., Mahboubi, K., Kalb, R.G., O'Connor, D.S., Li, F., et al. (2000). Angiopoietin-1 inhibits endothelial cell apoptosis via the Akt/survivin pathway. *J. Biol. Chem.* 275, 9102–9105. doi: 10.1074/jbc.275.13.9102

Peppiatt, C.M., Howarth, C., Mobbs, P., and Attwell, D. (2006). Bidirectional control of CNS capillary diameter by pericytes. *Nature* 443, 700–704. doi: 10.1038/nature05193

Popescu, D.P., Flueraru, C., Mao, Y., Chang, S., and Sowa, M.G. (2010). Signal attenuation and box-counting fractal analysis of optical coherence tomography images of arterial tissue. *Biomed. Opt. Express.* 1, 268–277. doi: 10.1364/BOE.1.000268

Reiss, Y., Scholz, A., and Plate, K.H. (2015). "The angiopoietin—Tie system: common signaling pathways for angiogenesis, cancer, and inflammation," in *Endothelial Signaling in Development and Disease,* eds. M. H. H. Schmidt, and S. Liebner (New York, NY: Springer New York), 313–328. doi: 10.1007/978-1-4939-2907-8_13

Rischke, R., Rami, A., Bachmann, U., Rabie, A., and Krieglstein, J. (1992). Activated astrocytes, but not pyramidal cells, increase glucose utilization in rat hippocampal CA1 subfield after ischemia. *Pharmacology* 45, 142–153. doi: 10.1159/000138992

Ronnett, G. V., Ramamurthy, S., Kleman, A. M., Landree, L. E., and Aja, S. (2009). AMPK in the brain: its roles in energy balance and neuroprotection. *J. Neurochem.* 109(Suppl. 1): 17–23. doi: 10.1111/j.1471-4159.2009.05916.x

Rubanyi, G.M., and Polokoff, M.A. (1994). Endothelins: molecular biology, biochemistry, pharmacology, physiology, and pathophysiology. *Pharmacol. Rev.* 46, 325–415.

Sato, T.N., Tozawa, Y., Deutsch, U., Wolburg-Buchholz, K., Fujiwara, Y., Gendron-Maguire, M., et al. (1995). Distinct roles of the receptor tyrosine kinases Tie-1 and Tie-2 in blood vessel formation. *Nature* 376, 70–74. doi: 10.1038/376070a0

Shapiro, S. S., and Wilk, M. B. (1965). An analysis of variance test for normality (complete samples). *Biometrika* 52, 591–611. doi: 10.2307/2333709

Souvenir, R., Doycheva, D., Zhang, J.H., and Tang, J. (2015). Erythropoietin in stroke therapy: friend or foe. *Curr. Med. Chem.* 22, 1205–1213. doi: 10.2174/0929867322666150114152134

Teichert, M., Milde, L., Holm, A., Stanicek, L., Gengenbacher, N., Savant, S., et al. (2017). Pericyte-expressed Tie2 controls angiogenesis and vessel maturation. *Nat. Commun.* 8:16106. doi: 10.1038/ncomms16106

Thoren, A.E., Helps, S.C., Nilsson, M., and Sims, N.R. (2006). The metabolism of C-glucose by neurons and astrocytes in brain subregions following focal cerebral ischemia in rats. *J. Neurochem.* 97, 968–978. doi: 10.1111/j.1471-4159.2006.03778.x

Villaseñor, J. A., and González-Estrada, E. (2009). Generalization of Shapiro–Wilk's test for multivariate normality. *Commun. Stat. - Theory M.* 38, 1870–1883. doi: 10.1080/03610920802474465

Wang, L., Jia, Y., Rogers, H., Suzuki, N., Gassmann, M., Wang, Q., et al. (2013). Erythropoietin contributes to slow oxidative muscle fiber specification via PGC-1alpha and AMPK activation. *Int. J. Biochem. Cell Biol.* 45, 1155–1164. doi: 10.1016/j.biocel.2013.03.007

Wei, H. S., Kang, H., Rasheed, I. D., Zhou, S., Lou, N., Gershteyn, A., et al. (2016). Erythrocytes are oxygen-sensing regulators of the cerebral microcirculation. *Neuron* 91, 851–862. doi: 10.1016/j.neuron.2016.07.016

Winkler, E.A., Rutledge, W.C., Kalani, M.Y.S., and Rolston, J.D. (2017). Pericytes regulate cerebral blood flow and neuronal health at a capillary level. *Neurosurgery* 81, N37–N38. doi: 10.1093/neuros/nyx457

Yamanishi, S., Katsumura, K., Kobayashi, T., and Puro, D.G. (2006). Extracellular lactate as a dynamic vasoactive signal in the rat retinal microvasculature. *Am. J. Physiol. Heart Circ. Physiol.* 290, H925–H934. doi: 10.1152/ajpheart.01012.2005

Yun, J.H., Jeong, H.S., Kim, K.J., Han, M.H., Lee, E.H., Lee, K., et al. (2018). β-Adrenergic receptor agonists attenuate pericyte loss in diabetic retinas through Akt activation. *Faseb J.* 32, 2324–2338. doi: 10.1096/fj.201700570RR

Zibrova, D., Vandermoere, F., Goransson, O., Peggie, M., Marino, K.V., Knierim, A., et al. (2017). GFAT1 phosphorylation by AMPK promotes VEGF-induced angiogenesis. *Biochem. J.* 474, 983–1001. doi: 10.1042/BCJ20160980

Conflict of Interest: The authors declare that the research was conducted in the absence of any commercial or financial relationships that could be construed as a potential conflict of interest.

Copyright © 2019 Heyba, Al-Abdullah, Henkel, Sayed, Malatiali and Redzic. This is an open-access article distributed under the terms of the Creative Commons Attribution License (CC BY). The use, distribution or reproduction in other forums is permitted, provided the original author(s) and the copyright owner(s) are credited and that the original publication in this journal is cited, in accordance with accepted academic practice. No use, distribution or reproduction is permitted which does not comply with these terms.

frontiers in Neurology

ORIGINAL RESEARCH
published: 10 December 2019
doi: 10.3389/fneur.2019.01274

Mean Platelet Volume-To-Lymphocyte Ratio Predicts Poor Functional Outcomes Among Ischemic Stroke Patients Treated With Intravenous Thrombolysis

*Si-Yan Chen, Yuan-Shao Lin, Yi-Fan Cheng, Hong Wang, Xiao-Ting Niu and Wan-Li Zhang**

Department of Neurology, The First Affiliated Hospital of Wenzhou Medical University, Wenzhou, China

OPEN ACCESS

Edited by:
Johannes Boltze, University of Warwick, United Kingdom

Reviewed by:
Piotr Sobolewski, Jan Kochanowski University in Kielce, Poland
Lili Cui, University of Eastern Finland, Finland

***Correspondence:**
Wan-Li Zhang
zhangwanli36@126.com

Specialty section:
This article was submitted to Stroke, a section of the journal Frontiers in Neurology

Received: *16 June 2019*
Accepted: *18 November 2019*
Published: *10 December 2019*

Citation:
Chen S-Y, Lin Y-S, Cheng Y-F, Wang H, Niu X-T and Zhang W-L (2019) Mean Platelet Volume-To-Lymphocyte Ratio Predicts Poor Functional Outcomes Among Ischemic Stroke Patients Treated With Intravenous Thrombolysis. Front. Neurol. 10:1274. doi: 10.3389/fneur.2019.01274

Background and Purpose: According to previous studies, the mean platelet volume-to-lymphocyte ratio (MPVLR) represents a novel marker of a poor short-term prognosis in patients with a myocardial infarction who underwent primary percutaneous coronary intervention. We aimed to evaluate the association between MPVLR and clinical outcomes of patients with acute ischemic stroke who were treated with intravenous thrombolysis.

Methods: Two hundred forty-one patients with ischemic stroke receiving intravenous thrombolysis were prospectively enrolled in this study. Blood samples for MPVLR were obtained at admission and at 18–24 h after treatment with intravenous thrombolysis. A poor functional outcome was defined as a modified Rankin scale score of 3–6 at 3 months after stroke.

Results: At admission, the area under the curve of MPVLR to predict poor functional outcomes at 3 months was 0.613 [95% confidence interval (CI), 0.541–0.686; $P = 0.003$), and the best predictive MPVLR value was 5.8. Patients with an MPVLR $\geq$5.8 had a 3.141-fold increased risk of a poor outcome at 3 months (95% CI, 1.491–6.615; $P = 0.003$) compared to patients with an MPVLR <5.8. At 18–24 h after treatment with intravenous thrombolysis, the area under the curve of MPVLR to predict a poor outcome at 3 months was 0.697 (95% CI, 0.630–0.765, $P < 0.001$), and the best predictive MPVLR value was 6.9. The inclusion of MPVLR as a continuous (odds ratio, 1.145; 95% CI, 1.044–1.256, $P = 0.004$) and categorical variable (odds ratio, 6.555; 95% CI, 2.986–14.393, $P < 0.001$) was independently associated with poor outcomes at 3 months.

Conclusions: Both the values of MPVLR at admission and 18–24 h after intravenous thrombolysis were independently associated with poor functional outcomes. MPVLR may serve as an activity marker for a poor prognosis in patients with acute ischemic stroke receiving intravenous thrombolysis.

Keywords: ischemic stroke, mean platelet volume, MPVLR, thrombolysis, outcomes

INTRODUCTION

Intravenous administration of recombinant tissue plasminogen activator (rt-PA) is recommended as the primary treatment for patients with acute ischemic stroke within 4.5 h from symptom onset (1, 2). However, approximately half of the participants were not independent or died at 3 months, despite the administration of intravenous thrombolytic therapy (3). Since the factors related to the functional outcomes of patients with ischemic stroke who are treated with intravenous alteplase have not been well identified (3, 4), the detection of new risk factors is always important.

Hemocyte variables have been reported to predict the risk and prognosis of ischemic stroke, particularly in patients treated with intravenous thrombolysis (5–8). Platelets play an important role in inducing inflammation and contributing to thrombus formation in cardiovascular disease (9, 10). The mean platelet volume (MPV) is an indicator of platelet function, reflecting platelet size, and activity (11). According to Greisenegger et al. an increased MPV is associated with poor functional outcomes in patients with acute ischemic stroke (12). However, the association between MPV and stroke outcomes remains controversial (13, 14). The pathophysiological pathways induced by cerebral ischemia mainly include the immune response, neuroinflammation, and the accumulation of leukocytes, such as lymphocytes, monocytes, and neutrophils (4, 15). Lower lymphocyte counts are independently associated with an increased probability of a poor functional outcome (7). Recently, the MPV-to-lymphocyte ratio (MPVLR) was considered a novel marker of a poor short-term prognosis in patients with myocardial infarction who underwent a primary percutaneous coronary intervention (16). Based on this information, we were prompted to explore the prognostic value of MPVLR in acute ischemic stroke. Therefore, the objective of our study was to explore whether MPVLR was associated with the functional outcomes of patients with acute ischemic stroke who were treated with intravenous thrombolysis.

MATERIALS AND METHODS

Study Population

We performed a prospective, hospital-based observational study. The study consecutively enrolled patients with ischemic stroke who were treated with intravenous thrombolysis from March 2013 to Oct 2017 in the First Affiliated Hospital of Wenzhou Medical University. Each patient received intravenous alteplase at a dose of 0.9 mg/kg. Notably, 10% of the total dosage was administered as a bolus within 4.5 h of stroke onset, followed by a continuous intravenous infusion of the remaining dose over a period of 1 h. The inclusion criteria for intravenous thrombolysis were as follows: (1) older than 18 years, (2) a diagnosis of acute ischemic stroke by neurologists according to the recommendations from World Health Organization (17), and (3) an onset-to-treatment time within 4.5 h. The exclusion criteria were defined according to the 2013 American Heart Association/American Stroke Association Guidelines (18). The present study was approved by the Ethics Committee of the First Affiliated Hospital of Wenzhou Medical University. All patients or their relatives provided written informed consent and agreed to participate in the study.

Clinical Protocol and Laboratory Tests

The severity of neurological impairment was assessed using the National Institutes of Health Stroke Scale (NIHSS) at admission and at 24 h after intravenous thrombolysis. Baseline information about age, sex, onset-to-treatment time, systolic, and diastolic blood pressure, medical history, including potential stroke risk factors and ongoing antiplatelet therapy, and electrocardiographs were obtained at admission and in the inpatient department. We collected the following poststroke infection parameters within 48 h: pneumonia, tracheobronchitis, urinary tract infections, and other defined infections. In addition, the blood glucose level was measured in the emergency room at admission. All patients were subjected to a routinely performed computed tomographic scan at admission and a follow-up scan at 24 h after thrombolysis, or any other time when the patient's neurological deterioration was noted. We also collected information about the symptomatic intracerebral hemorrhage according to the Safe Implementation of Thrombolysis in Stroke-Monitoring Study definition: a local or remote type 2 parenchymal hemorrhage on imaging 24 h after thrombolysis or earlier if the computed tomographic scan was performed due to neurological deterioration combined with an increase in the NIHSS score of 4 points from baseline or a stroke resulting in death within 24 h (19).

Data were obtained from blood tests performed at admission and at 18–24 h after treatment with intravenous thrombolysis. A complete blood count was determined using the automated hematology analyzer (XE-2100, Sysmex Company, Japan) within 60 min after blood sample collection. The MPVLR was calculated as the ratio of MPV to lymphocytes, the unit of MPVLR is $fl/10^9/L$. The platelet-to-lymphocyte ratio (PLR) was calculated as the platelet count divided by the lymphocyte count.

Outcome Measures

The main outcomes of all patients were evaluated based on the modified Rankin scale (mRS) score recorded in the outpatient department or via a telephone follow-up interview conducted by a trained neurologist. A poor functional outcome was defined as a mRS score of 3–6 at 3 months after stroke. The second endpoint was early neurological improvement (ENI). ENI was defined as a reduction in the NIHSS score $\geq$8 from baseline or an NIHSS score that decreased to 0 or 1 at 24 h after treatment (20).

Statistical Analyses

Statistical analyses were performed with the SPSS 22.0 package for Windows (SPSS Inc., Chicago, USA, RRID:SCR_002865). A $P < 0.05$ was considered statistically significant. Continuous variables are reported as the means with standard deviations or medians with interquartile ranges. Categorical variables are reported as percentages. Statistical analyses were performed using Student's *t*-tests and the Kruskal–Wallis test for continuous data or the chi-square test or Fisher's exact test for categorical data.

Receiver operating characteristic (ROC) curves were constructed to assess the predictive value of MPV, lymphocyte, PLR, and MPVLR for poor outcomes at 3 months. The method of an optimal cutoff was applied to transform the MPVLR into a categorical variable. We divided the participants into two groups according to the MPVLR cutoff at admission and compared the differences in baseline characteristics between these groups. We also compared the differences in characteristics between the poor and good outcome group. We employed different multivariate logistic regression models to evaluate the associations between MPV, lymphocyte counts, PLR, MPVLR, and poor functional outcomes at 3 months.

RESULTS

Among the 266 patients, 12 patients with missing data for the complete blood count at 18–24 h after rt-PA were excluded. Among the remaining patients, four patients with no data on hematological parameters at admission and nine patients who were lost to follow-up were also excluded. Finally, we enrolled 241 patients in this study (**Figure 1**). A detailed description of the baseline clinical characteristics of the study population is provided in **Table 1**. The mean age of all patients was 66.5 ± 12.0 years, and 163 patients (67.6%) were male. The median NIHSS score at admission was 9 points. The mean value of the MPVLR for the entire population of participants was 6.7 ± 3.6 $fl/10^9/L$ at admission and 8.8 ± 4.7 $fl/10^9/L$ at 18–24 h after rt-PA. Among the 241 patients, 25 (10.4%) died, 29 (12.0%) presented ENI, and 105 (43.6%) presented poor functional outcomes at 3 months.

An ROC curve analysis was performed to assess the predictive values of MPV, lymphocyte counts, PLR, and MPVLR for poor outcomes at 3 months (**Table 2**). At admission, the area under the curve (AUC) of MPVLR was 0.613 [95% confidence interval (CI), 0.541–0.686; $P = 0.003$), and the best predictive MPVLR value was 5.8. Furthermore, the predictive value of MPVLR for functional outcomes was better than PLR. Accordingly, at 18–24 h after rt-PA infusion, the AUC of MPVLR to predict a poor outcome at 3 months was 0.697 (95% CI, 0.630–0.765, $P < 0.001$), and the best predictive MPVLR value was 6.9.

The baseline and clinical characteristics of the study cohort stratified according to MPVLR cutoff at admission are listed in **Table 3**. Patients presenting with an MPVLR ≥5.8 were older, had a higher NIHSS score at 24 h after intravenous thrombolysis, and longer onset to treatment time than patients with an MPVLR <5.8. Otherwise, ENI and hyperlipidemia were more prevalent in patients with an MPVLR <5.8. Patients with an MPVLR ≥5.8 more frequently presented with a history of previous stroke/transient ischemic attack (TIA) and atrial fibrillation than patients with an MPVLR <5.8.

The distribution of functional outcomes at 3 months stratified according to the MPVLR cutoff value is shown in **Figures 2**, **3**. Regardless of whether outcomes were measured at admission or at 18–24 h after rt-PA infusion, a poor functional outcome was more common in the higher MPVLR group stratified by cutoff value. However, ENI was less common in the higher MPVLR group stratified by cutoff value (**Table 4**). The blood tests and the baseline characteristics were compared between patients with poor and good functional outcomes, and the results are shown in **Table 1**. Patients with poor functional outcomes at 3 months after stroke were older, had higher NIHSS scores, and

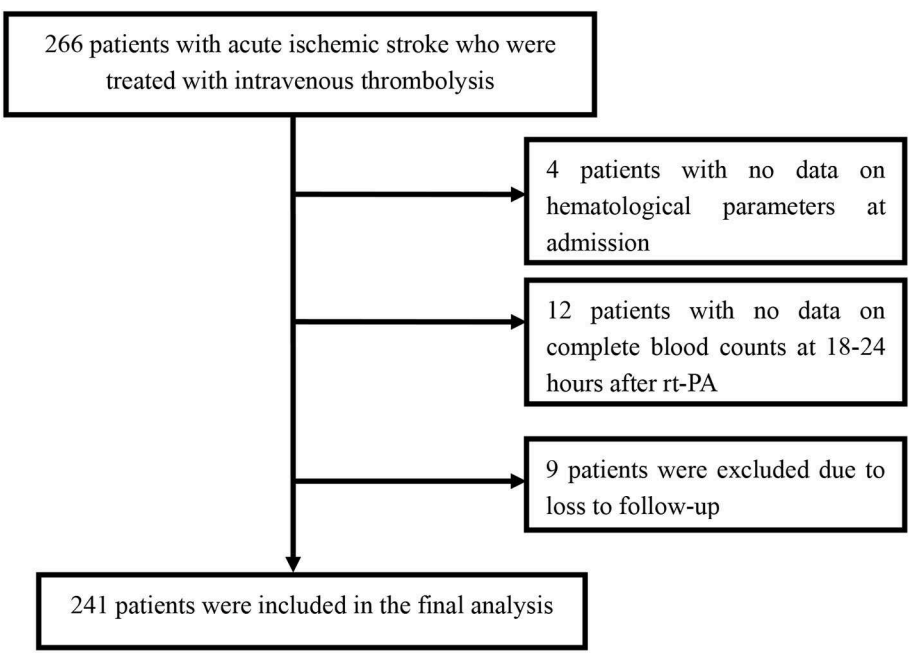

FIGURE 1 | Flow diagram showing the patient selection process.

TABLE 1 | Comparison of the baseline characteristics between patients with poor and good functional outcomes.

Characteristics	Total ($n = 241$)	Good outcome ($n = 136$)	Poor outcome ($n = 105$)	*P*-value
Age (year), mean ± SD	66.5 ± 12.0	63.6 ± 12.2	70.2 ± 10.6	0.000
Gender, male, *n* (%)	163 (67.6)	95 (69.9)	68 (64.8)	0.402
Baseline NIHSS score, median (IQR)	9 (5,13)	7 (4,10)	12 (9,17)	0.000
24 h NIHSS score, median (IQR)	7 (4,13)	5 (3,7)	14 (10,18)	0.000
History of smoking, *n* (%)	90 (37.3)	54 (39.7)	36 (34.3)	0.388
Coronary artery disease, *n* (%)	22 (9.1)	9 (6.6)	13 (12.4)	0.123
Hypertension, *n* (%)	166 (68.9)	87 (64.0)	79 (75.2)	0.061
Diabetes, *n* (%)	51 (21.2)	29 (21.3)	22 (21.0)	0.944
Hyperlipidemia, *n* (%)	125 (51.9)	71 (52.2)	54 (51.4)	0.905
Previous stroke/TIA, *n* (%)	31 (12.9)	14 (10.3)	17 (16.2)	0.175
Atrial fibrillation, *n* (%)	79 (32.8)	35 (25.7)	44 (41.9)	0.008
Ongoing antiplatelet therapy, *n* (%)	23 (9.5)	11 (8.1)	12 (11.4)	0.382
Systolic BP (mmHg), mean ± SD	151.0 ± 20.0	149.8 ± 18.8	152.6 ± 21.5	0.277
Diastolic BP (mmHg), mean ± SD	85.8 ± 14.5	86.3 ± 13.6	85.1 ± 15.7	0.510
Glucose level at admission (mmol/l), mean ± SD	7.9 ± 2.8	7.7 ± 2.8	8.0 ± 2.8	0.378
Onset to treatment time, min, mean ± SD	214.0 ± 57.3	209.4 ± 59.7	220.1 ± 53.9	0.153
Hemorrhagic transformation, *n* (%)	56 (23.2)	23 (16.9)	33 (31.4)	0.008
SICH, *n* (%)	14 (5.8)	2 (1.5)	12 (11.4)	0.001
Poststroke infection, *n* (%)	65 (27.0)	17 (12.5)	48 (45.7)	0.000
Cell count at admission				
WBC, $\times 10^9$/L, mean ± SD	8.4 ± 2.8	8.3 ± 2.9	8.4 ± 2.7	0.933
Lymphocytes, $\times 10^9$/L, mean ± SD	1.7 ± 0.8	1.8 ± 0.8	1.6 ± 0.8	0.022
MPV, fl, mean ± SD	9.3 ± 1.4	9.2 ± 1.4	9.5 ± 1.5	0.105
PLT, $\times 10^9$/L, mean ± SD	207.1 ± 70.0	216.0 ± 76.5	195.5 ± 59.0	0.024
MPVLR, fl/10^9/L, mean ± SD	6.7 ± 3.6	6.0 ± 3.1	7.5 ± 4.1	0.002
PLR, mean ± SD	140.1 ± 66.5	134.9 ± 60.6	146.7 ± 73.3	0.173
Cell count at 18–24 H after rt-PA				
WBC, $\times 10^9$/L, mean ± SD	8.7 ± 3.0	7.9 ± 2.2	9.8 ± 3.5	0.000
Lymphocytes, $\times 10^9$/L, mean ± SD	1.5 ± 0.6	1.6 ± 0.5	1.2 ± 0.5	0.000
MPV, fl, mean ± SD	10.6 ± 1.4	10.7 ± 1.3	10.6 ± 1.5	0.935
PLT, $\times 10^9$/L, mean ± SD	208.8 ± 65.2	216.7 ± 68.1	198.6 ± 59.9	0.032
MPVLR, fl/10^9/L, mean ± SD	8.8 ± 4.7	7.5 ± 3.3	10.5 ± 5.6	0.000
PLR, mean ± SD	165.4 ± 85.4	148.4 ± 78.9	187.5 ± 88.6	0.000

NIHSS, National Institute of Health Stroke Scale; TIA, transient ischemic attack; BP, blood pressure; rt-PA, recombinant tissue plasminogen activator; SICH, symptomatic intracerebral hemorrhage; WBC, white blood cell; MPV, mean platelet volume; PLT, platelet; MPVLR, mean platelet volume-to-lymphocyte ratio; PLR, platelet-to-lymphocyte ratio; SD, standard deviation; IQR, interquartile range.

more frequently suffered from atrial fibrillation and hemorrhagic transformation than patients with good functional outcomes. Before the rt-PA treatment, patients in the poor functional outcome group at admission had lower lymphocyte and platelet counts but higher MPVLR levels than patients in the good functional outcome group. At 18–24 h after rt-PA infusion, white blood cell counts, MPVLR, and PLR were significantly higher in patients with poor functional outcomes than in patients with good functional outcomes. In addition, lower lymphocyte and platelet counts were observed in the poor than in the good functional outcome group.

Table 5 shows the results of the binary logistic regression analysis of MPV, lymphocyte counts, PLR, MPVLR, and poor outcomes. At admission, the inclusion of the MPVLR level as a dichotomous variable was independently associated with a higher risk of poor outcomes at 3 months, with an adjusted odds ratio (OR) of 2.600 (95% CI, 1.396–4.843; $P = 0.003$) after adjustment for age, sex, and baseline NIHSS score (model 1) and 3.141 (95% CI, 1.491–6.615, $P = 0.003$) after further adjustment for the variables included in model 1 plus variables such as hypertension, coronary artery disease, previous stroke/TIA, atrial fibrillation, onset-to-treatment time, diabetes, hyperlipidemia, poststroke infection, and symptomatic intracerebral hemorrhage that were identified as having $P < 0.2$ in **Tables 1**, **3** (model 2), respectively. The predictive value of MPVLR as a continuous variable at admission for poor outcomes tended to become significant, regardless of whether it was included in model 1 or 2. At 18–24 h after rt-PA infusion, regardless of whether model 1 or

TABLE 2 | Receiver operating characteristic curves identifying the predictive value of PLR and MPVLR for poor outcomes at 3 months.

	AUC (95% CI)	*P*-value
Cell count at admission		
PLR	0.538 (0.464–0.611)	0.318
MPVLR	0.613 (0.541–0.686)	0.003
MPV	0.553 (0.479–0.627)	0.160
Lymphocyte	0.400 (0.327–0.472)	0.008
Cell count at 18–24 H after rt-PA		
PLR	0.651 (0.580–0.721)	0.000
MPVLR	0.697 (0.630–0.765)	0.000
MPV	0.504 (0.429–0.579)	0.908
Lymphocyte	0.292 (0.225–0.358)	0.000

PLR, platelet-to-lymphocyte ratio; MPVLR, mean platelet volume-to-lymphocyte ratio; MPV, mean platelet volume; AUC, area under the curve; CI, confidence interval; rt-PA, recombinant tissue plasminogen activator.

2 was used, an increased MPVLR level maintained its predictive accuracy as either continuous or categorical variable.

DISCUSSION

To our knowledge, this study is the first to investigate the prognostic value of the MPVLR in patients with ischemic stroke who were treated with intravenous thrombolysis. When analyzed either pre- or postthrombolysis, the MPVLR was independently associated with increased risks of poor functional outcomes at 3 months. The prethrombolysis value of the MPVLR exhibited a better prediction ability than the PLR. In addition, the best discriminating values of the MPVLR for predicting poor outcomes were determined in this study.

Platelet activation plays an important role in thrombosis and inflammation (21). The size of platelets represents their activity, and larger-sized platelets are functionally more active (22). The MPV is a readily available marker due to the automatic analysis when blood tests were performed. A study including 776 patients with acute ischemic stroke or TIA revealed an adverse effect of a higher MPV son clinical outcome (12). Another study examining patients with ischemic stroke who were receiving intravenous thrombolysis suggested that the MPV was an independent predictor of a poor functional outcome (23), which contradicts the findings from our study. Our study did not observe an association between the MPV and functional outcome. This discrepancy may be due to the use of different designs and outcome measures compared to our study. Furthermore, Ntaios et al. reported that the MPV measured within 24 h after onset was not associated with functional outcomes in patients with ischemic stroke (3).

The inflammatory response after stroke plays an important role in ischemic brain pathobiology (4). The effect of lymphocyte activation on the prognosis of ischemic stroke remains unclear (24). According to the results of some animal experiments, lymphocytes exert a deleterious effect on infarcted brain tissues (5). Another study observed a protective role for regulatory T lymphocytes after experimental brain ischemia (6). Our clinical evidence indicated that lower lymphocyte counts were associated with poor functional outcomes in patients with acute cerebral infarction after rt-PA treatment, consistent with the results reported by Kim et al. (7). Lower lymphocyte counts may be attributed to an increase in inflammation-related lymphocyte apoptosis that predisposes an individual to ischemic stroke.

The PLR predicts clinical outcomes in patients with acute ischemic stroke undergoing thrombectomy (16). However, the

TABLE 3 | Comparison of the baseline characteristics between subgroups based on the MPVLR cutoff at admission.

Characteristics	MPVLR ≥5.8 (*n* = 122)	MPVLR <5.8 (*n* = 119)	*P*-value
Age (year), mean ± SD	69.1 ± 10.8	63.8 ± 12.5	0.000
Gender, male, *n* (%)	87 (71.3)	76 (63.9)	0.217
Baseline NIHSS score, median (IQR)	9 (5.5, 13)	8 (5,13)	0.497
24 h NIHSS score, median (IQR)	8 (4, 14.5)	5 (3,13)	0.026
History of smoking, *n* (%)	46 (37.7)	44 (37)	0.907
Coronary artery disease, *n* (%)	12 (9.8)	10 (8.4)	0.699
Hypertension, *n* (%)	81 (66.4)	85 (71.4)	0.399
Diabetes, *n* (%)	30 (24.6)	21 (17.6)	0.187
Hyperlipidemia, *n* (%)	54 (44.3)	71 (59.7)	0.017
Previous stroke/TIA, *n* (%)	21 (17.2)	10 (8.4)	0.041
Atrial fibrillation, *n* (%)	49 (40.2)	30 (25.2)	0.013
Ongoing antiplatelet therapy, *n* (%)	12 (9.8)	11 (9.2)	0.876
Systolic BP (mmHg), mean ± SD	149.8 ± 20.4	152.3 ± 19.6	0.331
Diastolic BP (mmHg), mean ± SD	85.2 ± 15.1	86.4 ± 13.9	0.547
Glucose level at admission (mmol/L), mean ± SD	8.0 ± 2.8	7.7 ± 2.8	0.341
Onset-to-treatment time, min, mean ± SD	228.4 ± 53.6	199.3 ± 57.5	0.000
Hemorrhagic transformation, *n* (%)	31 (25.4)	25 (21.0)	0.419
SICH, *n* (%)	8 (6.6)	6 (5.0)	0.615
Poststroke infection, *n* (%)	39 (32.0)	26 (21.8)	0.077
Cell count at admission			
WBC, $\times 10^9$/L, mean ± SD	8.5 ± 3.2	8.2 ± 2.3	0.306
Lymphocytes, $\times 10^9$/L, mean ± SD	1.2 ± 0.4	2.3 ± 0.8	0.000
MPV, fl, mean ± SD	9.9 ± 1.3	8.8 ± 1.4	0.000
PLT, $\times 10^9$/L, mean ± SD	185.0 ± 52.2	229.6 ± 78.5	0.000
MPVLR, fl/10^9/L, mean ± SD	9.1 ± 3.6	4.2 ± 1.1	0.000
PLR, mean ± SD	168.5 ± 70.4	110.9 ± 47.2	0.000
Cell count at 18–24 H after rt-PA			
WBC, $\times 10^9$/L, mean ± SD	8.9 ± 3.5	8.5 ± 2.4	0.258
Lymphocytes, $\times 10^9$/L, mean ± SD	1.2 ± 0.5	1.7 ± 0.6	0.000
MPV, fl, mean ± SD	11.0 ± 1.4	10.3 ± 1.3	0.000
PLT, $\times 10^9$/L, mean ± SD	190.9 ± 51.7	226.9 ± 72.3	0.000
MPVLR, fl/10^9/L, mean ± SD	10.7 ± 5.3	6.9 ± 3.0	0.000
PLR, mean ± SD	179.7 ± 88.9	150.9 ± 79.3	0.008

NIHSS, National Institute of Health Stroke Scale; TIA, transient ischemic attack; BP, blood pressure; rt-PA, recombinant tissue plasminogen activator; SICH, symptomatic intracerebral hemorrhage; WBC, white blood cell; MPV, mean platelet volume; PLT, platelet; MPVLR, mean platelet volume-to-lymphocyte ratio; PLR, platelet-to-lymphocyte ratio; SD, standard deviation; IQR, interquartile range.

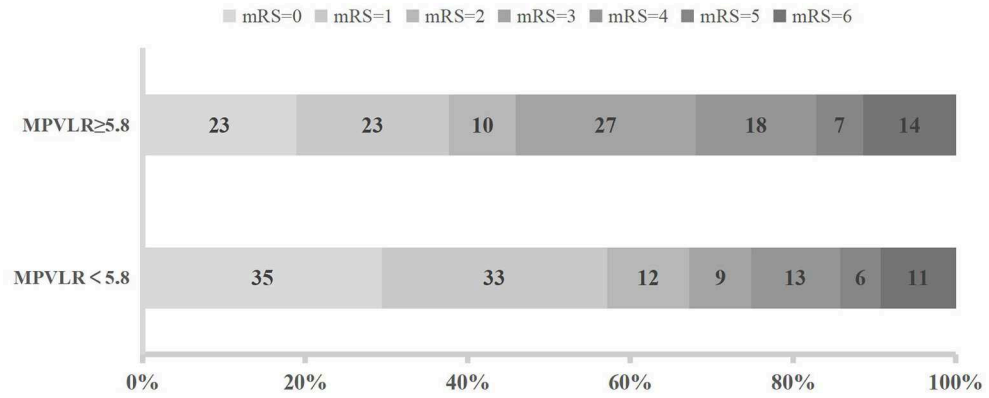

FIGURE 2 | Functional outcomes at 3 months in groups stratified according to the cutoff value of mean platelet volume-to-lymphocyte ratio (MPVLR) at admission.

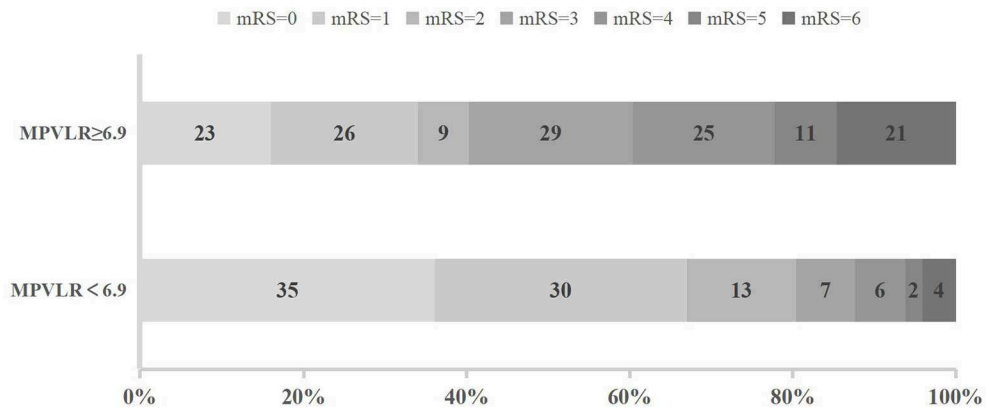

FIGURE 3 | Functional outcomes at 3 months in groups stratified according to the cutoff value of mean platelet volume-to-lymphocyte ratio (MPVLR) at 18–24 h after recombinant tissue plasminogen activator (rt-PA).

platelet size reflects function and activation more accurately than the platelet count (8). In addition, an increased MPVLR has been introduced as a predictor of no-reflow and a poor prognosis in patients with acute myocardial infarction (8, 16). In the present study, an elevated MPVLR was associated with less ENI and worse functional outcomes in patients with ischemic stroke who were treated with intravenous alteplase, suggesting that increased platelet activity and inflammation may be associated with a poor prognosis. The rate of poststroke infection was up to 30%, and the infection might influence hematological parameters, including the lymphocyte count and MPV. We adjusted for poststroke infection in the multivariate regression models, which did not attenuate the risk of poor outcomes associated with MPVLR (25). We also confirmed that the dynamic monitoring of MPVLR at admission and 18–24 h after rt-PA infusion was prospectively associated with poor functional outcomes. In particular, the MPVLR proved to exhibit a better predictive value for poor functional outcomes than the PLR in ROC analyses. The adjusted OR value of MPVLR was also larger than the PLR. We presume that MPVLR may synthetically reflect the degree of thrombosis and inflammation. A potential mechanism is proposed in which an elevated MPVLR may activate platelets by releasing platelet activators from ischemic/necrotic tissue, leading to increased thrombosis (16). However, the present study is not able to confirm a causative role of the MPVLR in the pathophysiology of ischemic stroke. Prospective studies are needed to explore the exact mechanism of this phenomenon.

The current study has certain limitations. First, the MPVLR level and follow-up data were not acquired from 25 patients included in this study. However, no significant differences in the baseline characteristics were observed between the excluded and included patients. Second, the study was only performed at a single center, and thus, the results may not be generalizable to all other patients with ischemic stroke. In addition, the best discriminating values must be further verified in other studies and populations. Furthermore, other platelet markers and inflammatory markers were not evaluated in the study.

CONCLUSIONS

Despite the limitations mentioned above, we report the first study focusing on the predictive value of MPVLR in patients with

TABLE 4 | Comparison of outcomes between subgroups stratified according to the MPVLR cutoff.

Outcomes	Cell count at admission		*P*-value	Cell count at 18–24 h after rt-PA		*P*-value
	MPVLR ≥5.8 (*n* = 122)	MPVLR <5.8 (*n* = 119)		MPVLR ≥6.9 (*n* = 144)	MPVLR <6.9 (*n* = 97)	
ENI, *n* (%)	9 (7.4)	20 (16.8)	0.024	11 (7.6)	18 (18.6)	0.011
mRS score, median (IQR)	3 (1,4)	1 (0, 4)	0.009	3 (1,4)	1 (0, 2)	0.000
mRS score of 3–6, *n* (%)	66(54.1)	39 (32.8)	0.001	86 (59.7)	19 (19.6)	0.000

MPVLR, mean platelet volume-to-lymphocyte ratio; rt-PA, recombinant tissue plasminogen activator; ENI, early neurology improvement; mRS, modified Rankin Scale; IQR, interquartile range.

TABLE 5 | Multivariate logistic regression analysis of the associations between MPV, lymphocyte, MPVLR, and poor outcome.

		Multivariate adjusted model (model 1)	*P*-value		Multivariate adjusted model (model 2)	*P*-value
	OR	95% CI		OR	95% CI	
Cell count at admission						
MPV	1.100	0.891–1.358	0.377	1.119	0.886–1.412	0.345
lymphocyte	0.748	0.499–1.120	0.159	0.764	0.481–1.214	0.255
MPVLR	1.092	0.999–1.193	0.053	1.102	0.997–1.217	0.057
MPVLR≥5.8	2.600	1.396–4.843	0.003	3.141	1.491–6.615	0.003
PLR	1.004	0.999–1.009	0.097	1.003	0.998–1.008	0.207
Cell count at 18–24 H After rt-PA						
MPV	1.040	0.836–1.295	0.723	1.083	0.848–1.384	0.523
lymphocyte	0.337	0.181–0.626	0.001	0.305	0.148–0.627	0.001
MPVLR	1.134	1.044–1.232	0.003	1.145	1.044–1.256	0.004
MPVLR ≥ 6.9	5.521	2.754–11.067	0.000	6.555	2.986–14.393	0.000
PLR	1.006	1.002–1.009	0.005	1.005	1.001–1.009	0.021

Model 1, adjusted for age, sex, and National Institutes of Health Stroke Scale score.
*Model 2, adjusted for the variables included in model 1 plus the variables hypertension, coronary artery disease, previous stroke/TIA, atrial fibrillation, onset-to-treatment time, diabetes, hyperlipidemia, poststroke infection, and symptomatic intracerebral hemorrhage that were identified as having a P < 0.2 in **Tables 1**, **3**.*
MPV, mean platelet volume; MPVLR, mean platelet volume-to-lymphocyte ratio; PLR, platelet-to-lymphocyte ratio; OR, odds ratio; CI, confidence interval; rt-PA, recombinant tissue plasminogen activator.

stroke after intravenous thrombolysis. Moreover, we assessed the MPVLR at admission and at 18–24 h after intravenous thrombolysis, and both values were independently associated with poor functional outcomes. The MPVLR is easy to monitor and therefore might serve as an activity marker for an unfavorable prognosis in patients with acute ischemic stroke receiving intravenous thrombolysis.

DATA AVAILABILITY STATEMENT

The datasets generated for this study are available on request to the corresponding author.

ETHICS STATEMENT

The studies involving human participants were reviewed and approved by this study was approved by the ethics committee of the First Affiliated Hospital of Wenzhou Medical University. The patients/participants provided their written informed consent to participate in this study.

AUTHOR CONTRIBUTIONS

S-YC and W-LZ conceived and designed the study. Y-SL, Y-FC, and HW organized the database. X-TN performed the statistical analysis. S-YC and W-LZ wrote the paper. S-YC, W-LZ, and X-TN reviewed and edited the manuscript. All authors read and approved the manuscript.

FUNDING

This study was supported by the Wenzhou Science and Technology Bureau (Grant No. Y20180632).

REFERENCES

1. Emberson J, Lees KR, Lyden P, Blackwell L, Albers G, Bluhmki E, et al. Effect of treatment delay, age, and stroke severity on the effects of intravenous thrombolysis with alteplase for acute ischaemic stroke: a meta-analysis of individual patient data from randomised trials. *Lancet.* (2014) 384:1929–35. doi: 10.1016/S0140-6736(14)60584-5
2. Hacke W, Kaste M, Bluhmki E, Brozman M, Davalos A, Guidetti D, et al. Thrombolysis with alteplase 3 to 4.5 hours after acute ischemic stroke. *N Engl J Med.* (2008) 359:1317–29. doi: 10.1056/NEJMoa0804656
3. Ntaios G, Gurer O, Faouzi M, Aubert C, Michel P. Mean platelet volume in the early phase of acute ischemic stroke is not associated with severity or functional outcome. *Cerebrovasc Dis.* (2010) 29:484–9. doi: 10.1159/000297964
4. Kim JY, Park J, Chang JY, Kim SH, Lee JE. Inflammation after ischemic stroke: the role of leukocytes and glial cells. *Exp Neurobiol.* (2016) 25:241–51. doi: 10.5607/en.2016.25.5.241
5. Becker K, Kindrick D, Relton J, Harlan J, Winn R. Antibody to the alpha4 integrin decreases infarct size in transient focal cerebral ischemia in rats. *Stroke.* (2001) 32:206–11. doi: 10.1161/01.str.32.1.206
6. Liesz A, Suri-Payer E, Veltkamp C, Doerr H, Sommer C, Rivest S, et al. Regulatory T cells are key cerebroprotective immunomodulators in acute experimental stroke. *Nat Med.* (2009) 15:192–9. doi: 10.1038/nm.1927
7. Kim J, Song TJ, Park JH, Lee HS, Nam CM, Nam HS, et al. Different prognostic value of white blood cell subtypes in patients with acute cerebral infarction. *Atherosclerosis.* (2012) 222:464–7. doi: 10.1016/j.atherosclerosis.2012.02.042
8. Hudzik B, Szkodzinski J, Lekston A, Gierlotka M, Polonski L, Gasior M. Mean platelet volume-to-lymphocyte ratio: a novel marker of poor short- and long-term prognosis in patients with diabetes mellitus and acute myocardial infarction. *J Diabetes Complications.* (2016) 30:1097–102. doi: 10.1016/j.jdiacomp.2016.04.010
9. Fuentes QE, Fuentes QF, Andres V, Pello OM, Font de Mora J, Palomo GI. Role of platelets as mediators that link inflammation and thrombosis in atherosclerosis. *Platelets.* (2013) 24:255–62. doi: 10.3109/09537104.2012.690113
10. Hvas AM. Platelet function in thrombosis and hemostasis. *Semin Thromb Hemost.* (2016) 42:183–4. doi: 10.1055/s-0036-1572329
11. Noris P, Melazzini F, Balduini CL. New roles for mean platelet volume measurement in the clinical practice? *Platelets.* (2016) 27:607–12. doi: 10.1080/09537104.2016.1224828
12. Greisenegger S, Endler G, Hsieh K, Tentschert S, Mannhalter C, Lalouschek W. Is elevated mean platelet volume associated with a worse outcome in patients with acute ischemic cerebrovascular events? *Stroke.* (2004) 35:1688–91. doi: 10.1161/01.STR.0000130512.81212.a2
13. D'Erasmo E, Aliberti G, Celi FS, Romagnoli E, Vecci E, Mazzuoli GF. Platelet count, mean platelet volume and their relation to prognosis in cerebral infarction. *J Intern Med.* (1990) 227:11–4.
14. Butterworth RJ, Bath PM. The relationship between mean platelet volume, stroke subtype and clinical outcome. *Platelets.* (1998) 9:359–64. doi: 10.1080/09537109876429
15. Vidale S, Consoli A, Arnaboldi M, Consoli D. Postischemic inflammation in acute stroke. *J Clin Neurol.* (2017) 13:1–9. doi: 10.3988/jcn.2017.13.1.1
16. Kurtul A, Acikgoz SK. Usefulness of mean platelet volume-to-lymphocyte ratio for predicting angiographic no-reflow and short-term prognosis after primary percutaneous coronary intervention in patients with ST-segment elevation myocardial infarction. *Am J Cardiol.* (2017) 120:534–41. doi: 10.1016/j.amjcard.2017.05.020
17. Stroke—1989. Recommendations on stroke prevention, diagnosis, and therapy. Report of the WHO task force on stroke and other cerebrovascular disorders. *Stroke.* (1989) 20:1407–31. doi: 10.1161/01.str.20.10.1407
18. Jauch EC, Saver JL, Adams HP, Jr, Bruno A, Connors JJ, Demaerschalk BM, et al. Guidelines for the early management of patients with acute ischemic stroke: a guideline for healthcare professionals from the American Heart Association/American Stroke Association. *Stroke.* (2013) 44:870–947. doi: 10.1161/STR.0b013e318284056a
19. Mazya M, Egido JA, Ford GA, Lees KR, Mikulik R, Toni D, et al. Predicting the risk of symptomatic intracerebral hemorrhage in ischemic stroke treated with intravenous alteplase: safe Implementation of Treatments in Stroke (SITS) symptomatic intracerebral hemorrhage risk score. *Stroke.* (2012) 43:1524–31. doi: 10.1161/STROKEAHA.111.644815.
20. Kharitonova T, Mikulik R, Roine RO, Soinne L, Ahmed N, Wahlgren N. Safe Implementation of Thrombolysis in Stroke Investigators. Association of early National Institutes of Health Stroke Scale improvement with vessel recanalization and functional outcome after intravenous thrombolysis in ischemic stroke. *Stroke.* (2011) 42:1638–43. doi: 10.1161/STROKEAHA.110.606194.
21. Wagner DD, Burger PC. Platelets in inflammation and thrombosis. *Arterioscler Thromb Vasc Biol.* (2003) 23:2131–7. doi: 10.1161/01.ATV.0000095974.95122.EC
22. Thompson CB, Eaton KA, Princiotta SM, Rushin CA, Valeri CR. Size dependent platelet subpopulations: relationship of platelet volume to ultrastructure, enzymatic activity, and function. *Br J Haematol.* (1982) 50:509–19.
23. Xie D, Xiang W, Weng Y, Li J, Xu L, Zhang X, et al. Platelet volume indices for the prognosis of acute ischemic stroke patients with intravenous thrombolysis. *Int J Neurosci.* (2018):1–6. doi: 10.1080/00207454.2018.1536054
24. Saino O, Taguchi A, Nakagomi T, Nakano-Doi A, Kashiwamura S, Doe N, et al. Immunodeficiency reduces neural stem/progenitor cell apoptosis and enhances neurogenesis in the cerebral cortex after stroke. *J Neurosci Res.* (2010) 88:2385–97. doi: 10.1002/jnr.22410
25. Westendorp WF, Nederkoorn PJ, Vermeij JD, Dijkgraaf MG, van de Beek D. Post-stroke infection: a systematic review and meta-analysis. *BMC Neurol.* (2011) 11:110. doi: 10.1186/1471-2377-11-110

Conflict of Interest: The authors declare that the research was conducted in the absence of any commercial or financial relationships that could be construed as a potential conflict of interest.

Copyright © 2019 Chen, Lin, Cheng, Wang, Niu and Zhang. This is an open-access article distributed under the terms of the Creative Commons Attribution License (CC BY). The use, distribution or reproduction in other forums is permitted, provided the original author(s) and the copyright owner(s) are credited and that the original publication in this journal is cited, in accordance with accepted academic practice. No use, distribution or reproduction is permitted which does not comply with these terms.

frontiers in Neurology

CLINICAL TRIAL
published: 22 January 2020
doi: 10.3389/fneur.2019.01402

Effects of Transcranial Direct Current Stimulation (tDCS) and Exercises Treadmill on Autonomic Modulation of Hemiparetic Patients Due To Stroke—Clinic Test, Controlled, Randomized, Double-Blind

*Glauber Heinz[1], Katia De Angelis[2], Simone Dal Corso[1], Maria Helena Gomes De Sousa[1], Ariane Viana[2], Fernando Dos Santos[3], João Carlos Ferrari Corrêa[1] and Fernanda Ishida Corrêa[1]**

[1] Doctorate and Master Program in Rehabilitation Science of University Nove de Julho, UNINOVE, São Paulo, Brazil, [2] Doctorate and Master Program in Medicine School of University Nove de Julho, UNINOVE, São Paulo, Brazil, [3] Arterial Hypertension Unit, Instituto do Coração (InCor), Medical School of Universidade de São Paulo, São Paulo, Brazil

OPEN ACCESS

Edited by:
Johannes Boltze,
University of Warwick,
United Kingdom

Reviewed by:
Maria Adele Rueger,
University Hospital of Cologne, Germany
Vitor E. Valenti,
São Paulo State University, Brazil

***Correspondence:**
Fernanda Ishida Corrêa
fecorrea@uninove.br

Specialty section:
This article was submitted to Stroke, a section of the journal Frontiers in Neurology

Received: 23 October 2019
Accepted: 20 December 2019
Published: 22 January 2020

Citation:
Heinz G, De Angelis K, Dal Corso S, Sousa MHGD, Viana A, Dos Santos F, Corrêa JCF and Corrêa FI (2020) Effects of Transcranial Direct Current Stimulation (tDCS) and Exercises Treadmill on Autonomic Modulation of Hemiparetic Patients Due To Stroke—Clinic Test, Controlled, Randomized, Double-Blind. Front. Neurol. 10:1402. doi: 10.3389/fneur.2019.01402

Background: After a Stroke, there is an autonomic nervous system (ANS) changes. Transcranial Direct Current Stimulation (tDCS) can promote the reorganization of the affected circuits.

Objective: To evaluate the effects of tDCS applied before a session of physical activity on the treadmill, in the modulation of the autonomic nervous system of post-stroke patients.

Methodology: Cross-over study, were randomized 12 adult hemiparetic subjects in 2 groups, Group 1 (active tDCS before exercise on the treadmill) and Group 2 (sham tDCS before exercise on the treadmill). Stimulation times were 20 min; treadmill time was 20 min. The heart rate variability (HRV) and Variability of Systolic Blood Pressure (VSBP) were evaluated for 15 min, in 3 periods (pre and post tDCS and during exercise recovery on the treadmill).

Results: There was no difference in the VSBP and the HRV between the groups, compared with the baseline data; however, in the intragroup analysis, the parasympathetic modulation after active tDCS increased by 18% over baseline by the RMSSD with IC 95% (−7.85 to −0.34). In group 1, the post-tDCS active and post-exercise periods presented a value of variance above baseline, indicating a better prognosis. In group 2, there was a significant reduction of 38% of Variance values ($p = 0.003$) after tDCS sham.

Conclusion: tDCS does not generate immediate effects on HRV and VSBP, except for intragroup comparison, which has greater participation in parasympathetic modulation in the group receiving active tDCS.

Keywords: stroke, autonomic modulation, transcranial direct current stimulation, exercise treadmill, hemiparetic patients

INTRODUCTION

One of the most serious causes of stroke reoccurrence is the alteration in the Autonomic Nervous System (ANS) function that leads to a reduction of heart rate variability (HRV). This was due to the disbalance to the homeostasis of the autonomic control, based on cardiac interbeat intervals analyzed by the physiological information, which can lead to myocardial infarction and sudden death (1–3).

Damages to ANS can also affect the control of blood pressure (BP). McLaren et al. (4) conducted a case-control cross-study in which compared the autonomic function of patients that had a stroke, not-treated, with resident controls in the Community and observed that the blood pressure alteration was maintained several months after the stroke.

Although the mechanisms of this cardiovascular autonomic dysregulation have not been fully understood, several studies (3, 5–7) suggest an anatomical-functional asymmetry between the right and left cerebral hemispheres in ANS modulation activity. Dutsch et al. (8) observed that stroke survivors whose infarction occurred on the right side had increased sympathetic cardiac modulation and parasympathetic cardiac deficit. The changes after the stroke in autonomic nervous system showed that favor increased tonus sympathetic and reduced parasympathetic appear to be independent to the both hemisphere injury (1). Macey et al. (7) and Al-Qudah et al. (3) reported that an important area in autonomic control is the insular cortex, with the right lobe insular cortex related to sympathetic modulation and the insular cortex of left lobe responsible for parasympathetic modulation. The insular cortex is located topographically in the neocortex region below the parietal, temporal and frontal cortex (5).

Upon the importance of the ANS in cardiovascular control, some studies have researched the effects of Transcranial Direct Current Stimulation (tDCS) over the left temporal cortex in the ANS modulation. One of them is the study from Montenegro et al. (6) that applied the tDCS in healthy athlete and none athlete individuals. They observed a reduction in the improved HRV in rest and quicker recovery from the exercise for athlete individuals. Another study is from Okano et al. (9) that observed a better parasympathetic action and decrease in the effort sensation and fatigue of healthy individuals during the exercise with cycle ergometer. Cogiamanian et al. (10) observed that the modulation of cortical excitability by tDCS might be used as a possible tool for human artery hypertension treatment.

The use of tDCS in individuals with stroke is safe and may be used during the rehabilitation to promote the reorganization of circuits affected by the lesion (11). However, its effects were not researched in the modulation of ANS by the temporal area in these individuals.

With the increase in surviving patients from stroke events, it is important to expand the comprehension of the lesions' chronic effects and that interferences in this sense, when positive, will enable better prognosis of cardiac autonomic function, reducing the possibility of a stroke relapse and sudden death and providing also better quality of daily living.

Therefore, the main objective of the study was to evaluate the HRV and the Variability of Systolic Blood Pressure (VSBP) in hemiparetic patients due to stroke in basal conditions (rest), immediately after the application of active tDCS and sham (pre-exercise) and during the exercise recovery on the treadmill. As a secondary outcome, the performance of the exercise, and perception of stress was evaluated, with the cardiac parameters (cardiac rate, modified Borg for dyspnea and fatigue, distance traveled).

METHODOLOGY

This study consists of an original cross-sectional, randomized, controlled, double-blind trial study of 12 adult hemiparetic stroke patients. The study followed the norms set by the Consort.

Survey participants included those with stroke hemiparesis for more than 6 months (12); from 21 to 74 years old; with mild or moderate lower limb motor impairment [between 20 and 31 points on the Fugl-Meyer lower limb scale (13)]; which presented comfortable walking speed between 0.3 and 1.15 m/s (14); walk at least 50 meters (15) without difficulty; agreeing to sign a consent and informed form.

Those with cognitive impairment (Mini-Mental State Examination-MMSE) with a score below 24 points (16) were excluded so that they could understand the study protocol; visual alteration that would prevent the execution of the protocol; severe heart problems (congestive heart failure, angina, peripheral vascular disease). Use of pacemaker; contraindications to the use of tDCS (brain metal clip implant near the region to be stimulated, history of recurrent seizure, recurrent epilepsy, brain tumors, brain pacemaker, and opening in the skullcap); women who had an irregular menstrual cycle or who were in the menstrual cycle during the evaluation; without medical clearance for treadmill exercise testing.

This study was performed at University Nove de Julho at unit Vergueiro and approved by Ethics Committee of University Nove de Julho (protocol CAAE: 57314716.7.0000.5511), São Paulo, Brazil and registered in Clinical Trial (NCT02956096) https://clinicaltrials.gov/ct2/show/NCT02956096.

INTERVENTION

The patients were submitted to two intervention protocols crossover (active tDCS and sham tDCS) (**Figure 1**):

1- Evaluation of basal HRV (15 min), followed by active direct current transcranial stimulation (tDCS) (20 min). Immediately at tDCS, 15 min of HRV assessment followed by 20 min of treadmill walking, and finally another 15 min of HRV during exercise recovery.
2- Evaluation of basal HRV (15 min), followed by sham direct current transcranial stimulation (tDCS) (20 min). Immediately at tDCS, 15 min of HRV assessment followed by 20 min of treadmill walking, and finally another 15 min of HRV during exercise recovery.

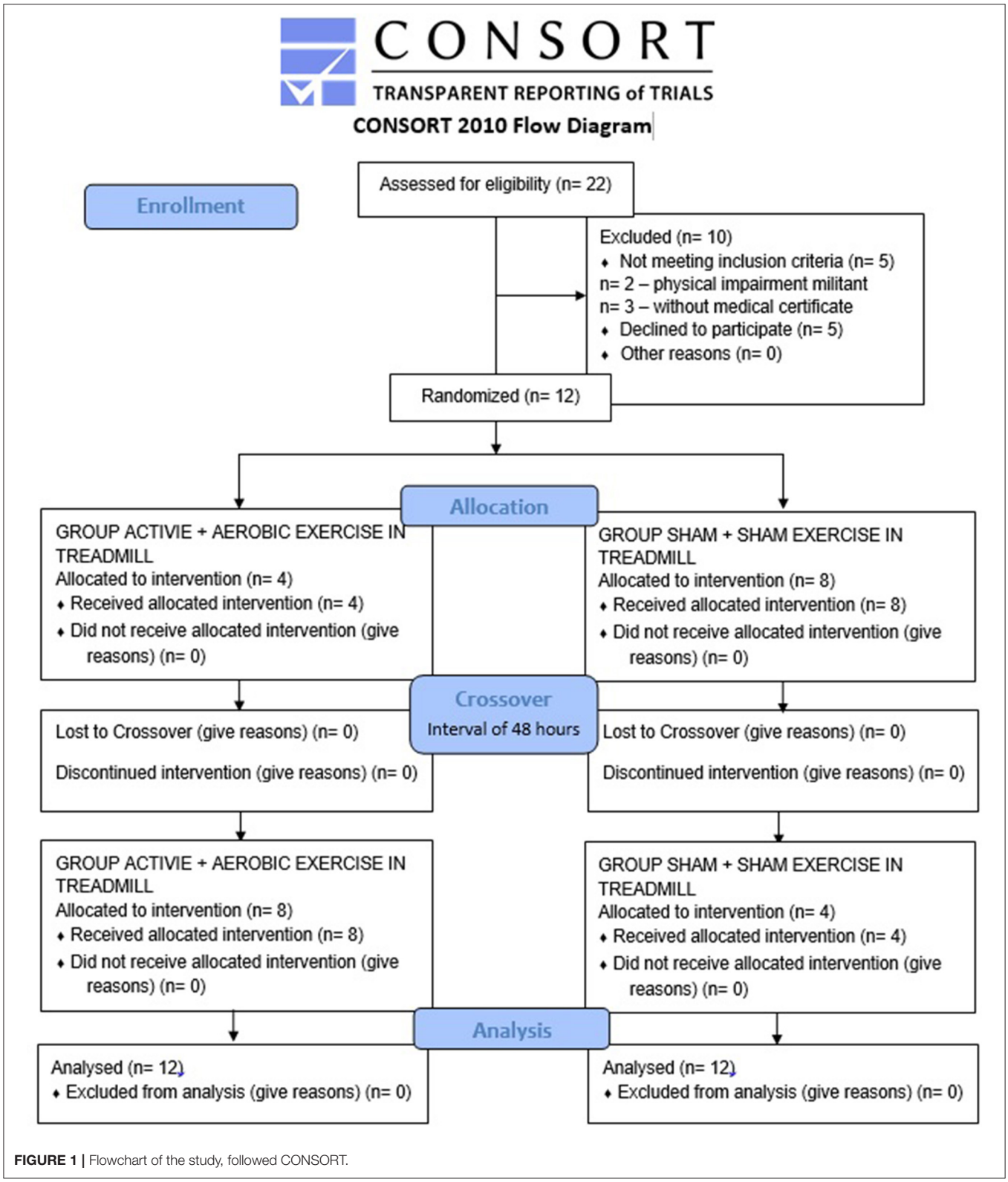

FIGURE 1 | Flowchart of the study, followed CONSORT.

Protocols (active tDCS or sham tDCS) were randomized to the first day of treatment only. On the second day (after 48 h) (17), the crossover was performed to be different from the first day.

Randomization was performed by lottery with brown, sealed envelopes to ensure reliability. The contents of each envelope determined which protocol the patient would initiate.

TRANSCRANIAL DIRECT CURRENT STIMULATION (tDCS)

The investigators responsible for the evaluation procedures and the patients were blinded to the treatment being applied (active tDCS or sham tDCS).

The patient was seated to receive the stimulus. Stimulation was performed with the NeuroConn tDCS DC-Stimulator Plus device using two 5 × 5 cm^2 (non-metallic) surface electrodes, wrapped in a moist saline sponge with a 2 mA current for 20 min before exercise in running machine.

The anode electrode was positioned over the left temporal cortex (T3) and the cathode electrode over the middle deltoid muscle contralateral to the anode. In placebo stimulation, all lead positioning procedures were performed equally to the active tDCS procedure, but the stimulator was maintained on for 30 seconds (according to the fake device program). The patient was informed that he would feel a slight initial tingling, but would reduce, disappear or stay for 20 min after application. Thus, the patients had the initial feeling, but did not receive any stimulus in the remaining time. This procedure is a valid form of control in transcranial direct current stimulation studies (18).

ACUTE AEROBIC EXERCISE ON THE TREADMILL

After 20 min of tDCS in a sitting position, the patients were positioned standing on the treadmill. To avoid possible falls, at least two physical therapists followed the exercise next to the patient. Cardiorespiratory parameters were monitored, such as heart rate, blood pressure, and oxygen saturation. Should these parameters be changed that put them at risk or if they expressed an interest in withdrawing from intervention, this would be immediately discontinued.

The velocity and inclination of each individual were determined by a previous exercise stress test using the modified Harbor protocol (14). Speed was kept constant and comfortable as determined by the individual and the treadmill inclination was increased by 2.5% every 2 min (19) until the patient reached 60–70% of the reserve heart rate (20). The inclination, therefore, was calculated to 60–80% of the maximum obtained in the ergometric test.

The electrocardiographic trace was acquired by (CPX Ultima, MedGraphics); heart rate (HR), oxygen saturation (SpO_2) and blood pressure (BPA) were continuously recorded every 2 min of exercise. Dyspnea scores and perception of lower limb fatigue were measured at rest and immediately after an exercise session by the modified Borg scale (21).

EVALUATION OF HEART RATE VARIABILITY (HRV) AND VARIABILITY OF SYSTOLIC BLOOD PRESSURE (VSBP), OBTAINED BY FINOMETER EQUIPMENT

HRV and VSBP were collected in three moments (basal, immediately after the tDCS and after the exercise on the treadmill, during the exercise recovery). The data HRV were evaluated immediately after exercise for 15 min (during the exercise recovery). For this, the patient was positioned in seated and told not to move or speak.

For this, a Finometer hemodynamic meter (Finomiter® Pro/Finapres Medical Systems incorporates Modelflow technology) was used. It consists of equipment used to continuously monitor non-invasive cardiac pressure, which uses the technique of digital infrared photoplethysmography. For this procedure, an inflatable cuff is used around the middle finger phalanx.

Hemodynamic variables such as systolic (SBP), diastolic (DBP), mean (MBP), blood pressure (BP), cardiac output (CD) and total peripheral resistance (RPF) were assessed by beating and recorded in BeatScope software., based on values derived from the blood pressure curve and information on age, gender, weight, and height.

The data collection of blood pressure and its derivations such as the intervals R-R, observing the waves of high frequency (HF), low frequency (LF), and the low frequency interrelation with high frequency (HF/LF), were collected continuously in the basal periods and during the recovery from acute exercise for 15 min.

Data Analysis of HRV and VSBP

The HRV analysis followed the Task Force's short-term spectral analysis in the time and frequency domain (22).

The cardiac modulation evaluation was performed by the register of interval R-R (ms) with the software *BeatScope*. The data were converted and stored in *Excel* files, used posteriorly for spectral analysis. A verification by visual inspection was performed by software *CardioSeries*, to identify and/or correct some premature or affected ectopic beats, using the linear interpolation to remove undesirable transients that alter the signal stationarity. The variations of Pulse Interval (PI) were evaluated in the time domain and the frequency domain by the linear method.

The linear methods were analyzed in the time domain and the frequency domain. Therefore, each RR interval was measured during a determined time interval, as described in the heart rate variability, calculating the floating transducer indexes of cardiac cycles.

RR intervals were collected in three periods: pretreatment (basal condition) for 15 min, immediately after tDCS application was completed (for 15 min) and during recovery from treadmill exercise (15 min).

In all three periods, the patient remained seated, without speaking or moving. Only 5 min of each patient's data were used for visual inspection by CardioSeries software to identify and/or correct some premature ectopic beats or artifacts, using linear interpolation to remove unwanted transients that could alter the signal stationarity of these patients analyzes in each period.

The indexes obtained by the determination of RR intervals by the time domain were the average of pulse interval RR through the absolute Variance and RMSSD that is the square root of the squared mean of the difference between the adjacent normal RR interval, in a time interval expressed in ms^2 and is better correlated with the vagal modulation. But by the frequency

domain, data were analyzed were through the high band (0.15 and 0.4 Hz), and low frequency (0.04 and 0.15 Hz) in its absolute values, and the sympathetic vagal balance.

STATISTICAL ANALYSIS

The data were analyzed in the statistic program, *SPSSR* version 17.0 according to the distributed nature of variables, the central tendency measures, and the dispersion to be used as the averages and standard-deviation (parametric) or median and interquartile interval (non-parametric). HRV and BPV data are presented as mean ± SD or median and interquartile interval. For comparison between the applications, parametric tests (ANOVA of two repeated measure ways) and for the none-parametric tests were used (Friedman followed by the post-test Wilcoxon). $P < 0.05$ was considered statistically significant.

OUTCOMES

Twenty-two patients were selected, 10 were excluded (two due to physical impairment that prevented them from performing the exercise, three for not having medical authorization for exercise testing and five for dropout (this dropout was reported for different reasons, such as disliking the exercise test (two patients), disliking having to stand still and not talking during HRV analysis (two patients), and unable to return to another assessment (Crossover) (one patient), thus constituting a sample of 12 patients.

To describe the demographic data of the patients, data were collected on age (years and months), topographic diagnosis of stroke, time of injury, classification (hemorrhagic or ischemic), affected hemisphere, weight (kg), height (cm), body mass index (BMI–kg/m²), blood pressure (BP), motor classification according to Fulg Meyer (mild, moderate, striking and severe).

All patients were instructed to appear always at 2:00 p.m. on assessment days, to avoid the influence of the circadian cycle. The prior recommendations were: continue with the use of medications on the respective hours, eat light diet on the test days, abstain from caffeine and ingestion of alcoholic beverages and/or smoking, avoid moderate or excessive effort on the previous day and the test day. The study procedures were performed in 6 moments.

The sample size was calculated using the mean of the three periods (baseline, post tDCS, and exercise recovery) of five individuals from the active tDCS group and five individuals from the tDCS sham group (crossover) from the pilot study.

To make the total average of the standard deviation, the sum of all deviations was calculated and divided by 6, which represents the total number of periods of the two groups.

To calculate the effect size (0.2453323), these values were entered in the G * Power 3.1.9.2 program and applied *F* tests, with a repeated-measures ANOVA statistical test between two factors with an $\alpha = 0.05$, $\beta = 0.80$, and sample correlation of 0.5 giving an $n = 90$.

The clinic-demographic characteristics of patients are presented in **Table 1**.

TABLE 1 | Descriptive characteristics of the sample.

Variables	*N* = 12
Age (year)	59 ± 7.00
Gender (F/M)	12 (4/8)
Injury in right hemisphere	5 (41.7%)
Injury in left hemisphere	7 (58.3%)
Injury time (months)	65.45 ± 54.86
Ischemic stroke	9 (75%)
Hemorrhagic stroke	3 (25%)
Use of blockers	6 (50%)
Use of diuretics	2 (17%)
Use of calcium channel blockers	3 (25%)
Use of ECA inhibitors	2 (17%)
Use of angiotensin receiver blockers	6 (50%)
Use of type 2 diabetes medication	3 (25%)
Use of medication for cholesterol	3 (25%)
Use of medication for arthrosis	1 (8%)
Use of medication for spasticity	1 (8%)
FulgMeyer	77.27 ± 20.36
FulgMeyer MMII	25.58 ± 3.48
Light	3
Moderate	1
Marking	6
Severe	2
MEEM	24.33 ± 3.60
BMI (kg/m^2)	26.52 ± 3.47
Weight (kg)	72.25 ± 11.03
Height (cm)	165 ± 9.92
HR basal (bpm)	71.42 ± 10.70
SBP basal (mmHg)	130 ± 8.42
DBP basal (mmHg)	76 ± 9.30
Comorbidities:	17
Diabetes	3
Hypertension	10
Positive HIV	1
Cholesterol	3

Data expressed in average ± DP and frequency and percentage (%);F, Female; M, Male; MEEM, Mini exam of mental state, BMI, Body mass index; HR, Heart Rate; SBP, Systolic Blood Pressure; DBP, Diastolic Blood Pressure.

Table 1 presents the demographic data for patients evaluated. The average body mass index (BMI) was 26.52 ± 3.47 kg/m² with the average weight 72.25 ± 11.03 kg and an average height of 165 ± 9.92 cm, showing that the patients of the sample were overweight.

The heart rate average in rest was in (71 ± 10.70 bpm) within the normality and the SBP (130 ± 8.42 mmHg) and DBP (76 ± 9.30 mmHg) indicating stage 1 hypertension. All hypertense patients (83%) took medication for arterial hypertension, showing, therefore, a resistance hypertension degree.

Metabolic deficits such as diabetes or thyroid dysfunction were also not exclusion criteria, and of the 12 subjects participating in the study, three had drug-controlled type two diabetes.

TABLE 2 | Values of HRV and VSBP of hemiparetic patients due to stroke in basal conditions.

Groups (1 or 2)	Variance (ms)	RMSSD (ms)	HF abs (ms^2)	LF abs (ms^2)	LF/HF	Variance (mmHg)	LF ($mmHg^2$)	α-LF
Group 1	695.86 ± 326.28	17.89 ± 7.65	84.75 (13.84–157.03)	175.93 ± 119.34	2.29 ± 1.41	30.10 (19.82–45.96)	5.12 (2.82–10.66)	1.74 (0.94–2.20)
Group 2	852.24 ± 336.39	19.57 ± 8.28	135.81 (60.39–236.61)	213.56 ± 142.91	1.64 ± 1.10	26.04 (19.75–42.58)	5.61 (3.18–9.73)	1.73 (1.39–2.86)
Difference of averages	−0.89	−0.23	–	−1.45	0.94	–	–	–
IC 95%	(−416.17 to 181.32)	(−7.25 to 5.90)	–	(−190.58 to 40.04)	(−0.98 to 2.27)	–	–	–
P	0.40	0.82	0.51	0.18	0.38	0.48	0.58	0.39
Z	–	–	−0.65	–	–	−0.71	−0.55	−0.87

*Variance, Total variability; RMSSD, Square root of the square mean of the difference between adjacent normal RR intervals; HF, High frequency band; LF, Low frequency band; abs, absolute; LF/HF, Balance sympathovagal; ms^2, milliseconds to square; $mmHg^2$, millimeters of mercury to square; α-LF, Low frequency alpha index; Mean ± Standard Deviation; Median (minimum-maximum); *$p < 0.05$.*

TABLE 3 | Values of VSBP of hemiparetic patients, in time and frequency domain, in the period's basal, post-tDCS, and post-exercise, of Groups 1 and 2.

Groups (1 or 2)	Variance (mmHg)	LF ($mmHg^2$)	α-LF
Group 1 basal	30.10 (19.82–45.96)	5.12 (2.82–10.66)	1.74 (0.94–2.20)
Group 2 basal	26.04 (19.75–42.58)	5.61 (3.18–9.73)	1.73 (1.39–2.86)
Group 1 post-tDCS	33.07 (18.63–48.83)	9.81 (2.91–12.43)	1.54 (0.99–2.65)
Group 2 post-tDCS	35.86 (26.70–43.82)	8.82 (4.04–12.95)	1.94 (1.09–2.48)
Group 1 post-exercise	30.71 (25.75–41.70)	5.76 (4.27–10.71)	1.18 (0.63–1.88)
Group 2 post-exercise	31.25 (19.12–45.78)	5.76 (4.27–10.71)	1.45 (0.70–1.66)
P (Group 1)	0.78	0.78	0.74
P (Group 2)	0.53	0.37	0.53
Z	–	–	–

Variance, Total variability; LF, Low frequency band; $mmHg^2$, Millimeters of mercury to square; α-LF, Low frequency alpha index; Median (minimum-maximum).

All patients in the sample were overweight, as can be seen in **Table 1**, but after analyzing the baseline data between the groups, no differences were observed between the means as shown in **Table 2**.

Table 2 presents the results of Heart Rate Variability (HRV) and Variability of Systolic Blood Pressure (VSBP) in basal conditions (pre active tDCS and sham tDCS) of hemiparetic patients due to stroke.

The result presented in **Table 2** demonstrates that there was no difference in HRV and VSBP of patients due to stroke, in the basal condition of the two protocols. These data demonstrates that the patients found themselves in the same pre-test conditions.

In **Table 3** are presented the resulted of VSBP in time and frequency domain in the periods basal, pos-tDCS and during the exercise recovery in the treadmill of Group 1 and 2.

The results of **Table 3** show that there was no difference between the active groups and sham (1 and 2) in VSBP, in both the time domain and frequency domain in all periods analyzed.

Table 4 is presented the results of HRV in time and frequency domain in periods basal, pos-tDCS, and during the recovery from acute aerobic exercise post-exercise of Group 1 and 2.

The results of HRV in **Table 4** demonstrate that there was no difference between the active tDCS groups and sham in the following variables: Total variability (Variance), Square root of the square mean of the difference between adjacent normal RR intervals (RMSSD); Low frequency band absolute (LF abs) High frequency band absolute (HF abs).

In the period's post, tDCS and post-exercise in the linear analysis of time-domain of HRV intra-Group were observed that the variance value in the period post active tDCS increased in respect to the basal values, but did not maintain this increase in the post-exercise period. However, in the analysis intra-Group in the period post tDCS sham is also observed an increase in the variance value in respect to the basal values; however, in the period post-exercise of the group sham, there was a significant reduction in respect to the basal values.

Moreover, in the analysis intra-Groups, it was observed that RMSSD after active tDCS increased significantly and reduced after the exercise recovery period, but not significantly. In tDCS sham Groups, there was no significant difference in RMSSD.

In the frequency domain, it was observed an increase of Low-frequency band after the application of tDCS active and a reduction of the low-frequency band in the period post-exercise. However, in Group tDCS sham is observed the same Standard of high and low-frequency bands of active Group.

The effect size of active tDCS on intragroup HRV between post-tDCS periods compared to baseline HRV was calculated. As a result, an average effect size of ($d = 0.44$) was observed. There was no effect of active tDCS on HRV during the recovery period compared to baseline HRV.

In **Table 5** are presented the short term analysis (1 min) for RMSSD for post-exercise recovery.

Table 5 demonstrate that there was no difference between the active tDCS and sham groups. Intra-group post-exercise period, short-term linear analysis (1 min) for RMSSD demonstrated reduction of RMMSD in active and sham tDCS groups.

An analysis of the effects of tDCS by subgroups of left hemispheric lesions vs. right were generated (**Table 6**) and shows that both the active tDCS and sham tDCS group did not show differences in HRV between the injured hemisphere, regardless of the three periods (baseline, post-tDCS and exercise recovery).

TABLE 4 | Values of HRV in time and frequency domain between pre and post-tDCS periods and post-exercise, of Groups 1 and 2 (active and sham).

Groups (1 or 2)	Variance (ms)	RMSSD (ms)	HF abs (ms^2)	LF abs (ms^2)
Group 1 basal	695.86 ± 326.28*	17.89 ± 7.65*	84.75 (13.84–157.03)*	175.93 ± 119.34*
Group 2 basal	852.24 ± 336.39*	19.57 ± 8.28	135.81 (60.39–236.61)	213.56 ± 142.91
Group 1 post-tDCS	1104.89 ± 95.15*	21.99 ± 10.75*	172.13 (50.30–366.73)*	329.90 ± 233.93*
Group 2 post-tDCS	1475.80 ± 632.90*	22.18 ± 9.08	146.01 (89.99–415.33)*	355.90 ± 249.83*
Group 1 post-exercise	751.50 ± 368.07	16.60 ± 5.70	65.01 (17.73–127.20)*	152.00 ± 122.65*
Group 2 post-exercise	852.81 ± 559.16*	16.18 ± 6.72	74.14 (21.07–139.18)*	168.00 ± 123.15*
Difference of Averages pre-post tDCS active	−409.02*	−4.10*	–	−165.59*
Difference of averages pre-post tDCS sham	−623.56*	−2.61	–	−142.34
Difference of averages basal—post-exercise active	−55.64	1.29*	–	2.39
Difference of averages basal—post-exercise sham	−0.57	3.38	–	45.50
Difference of averages post-tDCS–post-exercise active	353.38	5.39	–	167.98*
Difference of averages post-tDCS—post-exercise sham	622.99*	6.00	–	187.84*
IC 95% pre-post tDCS active	(−813.24 to −4.81)	(−7.85 to −0.34)	–	(−323.66 to −7.53)
IC 95% pre-post tDCS sham	(−1047.50 to −199.62)	(−6.54 to 1.31)	–	(−300.41 to 15.73)
IC 95% basal—post-exercise active	(−505.21 to 393.92)	(−4.76 to 7.35)	–	(−131.74 to 136.51)
IC 95% basal—post-exercise sham	(−472.07 to 470.94)	(−2.94 to 9.71)	–	(−88.63 to 179.63)
IC 95% post-tDCS—post-exercise active	(−126.58 to 833.30)	(−2.04 to 12.81)	–	(4.58–331.40)
IC 95% post-tDCS—post-exercise sham	(119.60–1126.38)	(−1.76 to 13.75)	–	(24.44–351.24)
Z pre-post tDCS active	–	–	−2.50*	–
Z pre-post tDCS sham	–	–	−1.72	–
Z basal—post-exercise active	–	–	−0.46	–
Z basal—post-exercise sham	–	–	−1.84	–
Z post-tDCS—post-exercise active	–	–	−2.50*	–
Z post-tDCS—post-exercise sham	–	–	−2.43*	–

*tDCS, Transcranial Direct Current Stimulation; Variance, Total variability; RMSSD, Square root of the square mean of the difference between adjacent normal RR intervals; HF, High-frequency band; LF, Low-frequency band; abs, absolute; ms^2, milliseconds to square; Mean ± Standard Deviation; Median (Minimum-Maximum); *p < 0.05 vs. adjusted for several comparisons of table: Bonferroni in parametric data and Wilcoxon in non-parametric.*

TABLE 5 | Result of HRV in the time domain of 1-min RMSSD Wave Analysis between the basal period, post-tDCS and post-Exercise of Groups 1 and 2 (active and sham).

	Group 1	Group 2
RMSSD (ms)-basal Period	16.33 ± 7.52	17.50 ± 8.78
RMSSD (ms)-Post-tDCS Period	17.83 ± 7.25	18.83 ± 8.00
RMSSD (ms)-Post-Exercise Period	12.92 ± 4.64	13.92 ± 6.54
Difference of averages basal and Post-tDCS	−1.50	−1.33
Difference of averages basal and Post-exercise	3.42	3.58
Difference of averages Post-tDCS and Post-exercise	4.92*	4.92*
IC95% lower–top basal and Post-tDCS	(−4.42/1.42)	(−4.25/1.59)
IC95% lower–top basal and Post-exercise	(−1.24/8.08)	(−1.08/8.24)
IC95% lower–top Post-tDCS and Post-exercise	(0.50/9.33)	(0.50/9.33)
p-Value of averages basal and Post-tDCS	0.591	0.749
p-Value of averages basal and Post-exercise	0.212	0.177
p-Value of averages Post-tDCS and Post-exercise	0.026	0.026

*HRV, Heart Rate Variability; tDCS, Transcranial Direct Current Stimulation; RMSSD, Square root of the square mean of the difference between adjacent RR intervals; Mean Standard Deviation; Median (lower-top); *p < 0.05 adjusted for the various comparisons in the table; Bonferroni in the parametric data.*

Table 7 presents the results after active and sham tDCS of treadmill exercise time performance in minutes (min), distance covered in kilometers (Km) and degree of effort of lower limb fatigue and respiratory exhaustion by the modified BORG.

Observed in **Table 7** that the active Group presented a significant increase of 90 m in the distance traveled in comparison with Group sham and the permanency time on the treadmill was greater in active Group (1 min), but not significant.

No difference was observed between the active Groups and sham in the perception of effort.

DISCUSSION

Considering the increase in patients surviving stroke events, it is important to increase knowledge regarding the mechanisms involved in the progression of lesions, as well as possible strategies for the management of this population, reducing the possibility of relapse and sudden death and providing a better quality of daily life. In this study, we evaluated the effects of a single exercise session, associated or not with prior tDCS stimulation, on BPPV and HRV in stroke survivors. Our results demonstrated that: there was no difference in VSBP and HRV between groups compared to baseline data; there was a reduction in time domain RMSSD band exercise recovery (short period linear analysis) in the groups with and without tDCS; however, in intragroup analysis, parasympathetic modulation after active tDCS increased the RMSSD by 18% from baseline, and the post-tDCS active and post-exercise periods had a variation value above baseline and, finally, and Importantly, there was better physical

TABLE 6 | Difference between sides of injury (right and left hemisphere) in baseline heart rate variability, post-TDCS and during exercise recovery.

HRV active or sham at baseline, post-tDCS and exercise recovery	Right hemisphere injury	Left hemisphere injury	95% Confidence Interval for Difference	*F*	*p*
Variance active at baseline	666.16 ± 153.23	720.61 ± 139.88	(−523.78/414.88)	0.069	0.799
Variance sham at baseline	892.21 ± 158.31	812.27 ± 158.31	(−436.32/596.21)	0.128	0.730
Variance active at post-tDCS	1117.08 ± 233.35	1094.73 ± 213.02	(−692.40/737.11)	0.005	0.945
Variance sham at post-tDCS	1559.15 ± 297.30	1392.45 ± 297.30	(−802.85/1136.26)	0.157	0.702
Variance active at exercise recovery	885.38 ± 162.65	639.94 ± 148.48	(−252.76/743.63)	1.242	0.294
Variance sham at exercise recovery	1134.87 ± 224.63	570.75 ± 224.63	(−168.44/1296.68)	3.153	0.114
RMSSD active at baseline	16.74 ± 3.55	18.72 ± 3.00	(−12.35/8.39)	0.181	0.679
RMSSD sham at baseline	22.73 ± 3.63	16.93 ± 3.32	(−5.33/16.92)	1.386	0.269
RMSSD active at post-tDCS	21.30 ± 5.03	22.48 ± 4.25	(−15.87/13.50)	0.032	0.861
RMSSD sham at post-tDCS	25.71 ± 3.97	19.24 ± 3.63	(−5.71/18.64)	1.442	0.260
RMSSD active at exercise recovery	16.28 ± 2.67	16.83 ± 2.26	(−8.35/7.24)	0.025	0.877
RMSSD sham at exercise recovery	20.19 ± 2.60	12.84 ± 2.37	(−0.61/15.31)	4.363	0.066
LF active at baseline	161.78 ± 36.10	118.72 ± 32.95	(−67.52/153.63)	0.776	0.401
LF sham at baseline	181.58 ± 65.81	240.22 ± 60.07	(−260.21/142.92)	0.433	0.527
LF active at post-tDCS	306.38 ± 106.47	301.81 ± 97.19	(−321.54/330.68)	0.001	0.975
LF sham at post-tDCS	415.12 ± 114.70	306.56 ± 104.71	(−242.77/459.88)	0.489	0.502
LF active at exercise recovery	142.48 ± 59.28	130.43 ± 54.12	(−169.54/193.64)	0.023	0.884
LF sham at exercise recovery	216.42 ± 53.80	127.78 ± 49.11	(−76.14/253.43)	1.481	0.255
HF active at baseline	89.44 ± 51.25	122.00 ± 51.25	(−199.69/134.56)	0.202	0.665
HF sham at baseline	175.13 ± 53.31	131.10 ± 59.61	(−145.07/233.12)	0.303	0.599
HF active at post–tDCS	172.28 ± 72.71	221.11 ± 72.71	(−285.95/188.28)	0.226	0.648
HF sham at post-tDCS	234.59 ± 84.86	194.98 ± 94.88	(−261.41/340.62)	0.097	0.765
HF active at exercise recovery	100.86 ± 30.75	61.29 ± 30.75	(−60.72/139.87)	0.828	0.389
HF sham at exercise recovery	132.82 ± 38.29	43.86 ± 42.81	(−46.86/224.79)	2.399	0.165
LF/HF active at baseline	2.63 ± 0.67	1.59 ± 0.55	(−0.97/3.04)	1.428	0.266
LF/HF sham at baseline	1.82 ± 0.55	1.60 ± 0.45	(−1.43/1.88)	0.098	0.762
LF/HF active at post-tDCS	2.13 ± 0.88	2.90 ± 0.72	(−3.40/1.85)	0.466	0.514
LF/HF sham at post-tDCS	1.79 ± 0.35	1.62 ± 0.28	(−0.86/1.21)	0.146	0.712
LF/HF active at exercise recovery	1.43 ± 0.54	2.23 ± 0.44	(−2.40/0.80)	1.329	0.282
LF/HF sham at exercise recovery	1.89 ± 0.98	3.21 ± 0.80	(−4.23/1.59)	1.099	0.325

tDCS, Transcranial Direct Current Stimulation; Variance, Total variability; RMSSD, Square root of the square mean of the difference between adjacent normal RR intervals; HF, High-frequency band; LF, Low-frequency band; LF/HF, (high frequency/low frequency) ratio; Mean ± Standard Deviation; adjusted for several comparisons of table: Bonferroni in parametric data.

performance, as assessed by the increased distance covered in the active tDCS group, suggesting a better prognosis.

The research was composed of patients of both sexes (**Table 1**), with 83% of the sample presenting drug-controlled hypertension, but not yet classified as stage 1 hypertension (23). Hypertension is an important risk factor for stroke patients and is aggravated by the aging of this population (24). As a characteristic, patients were also overweight, which increases cardiovascular risk due to aortic stiffness (23).

The results in **Table 2** showed that baseline HRV and VSBP values between the active groups and time domain and frequency domain simulation showed no differences, which demonstrates that the patients were in the same baseline conditions. Therefore, we show that the 48-h interval period was sufficient to avoid the effect of therapy addition (active or farce tDCS), corroborating with Nitsche and Paulus (25), who report that a 48-h interval between single session protocols is sufficient. to avoid possible effects additions.

The values of band LF absolute, in basal condition, suggested that the sympathetic system is already increased, what is already mentioned in the literature by Constantinescu et al. (26), Sander and Klingelhöfer (27), and Orlandi et al. (28), that describes that an acute ischemic stroke causes an autonomic unbalance capable of increasing the sympathetic cardiac activity, reduce HRV, and increase the risks of cardiac arrhythmia. It is important to remind the limitation about LF band of HRV and LF/HF ratio, sympatho-vagal balance, to provide indexes of the sympathetic activity. In these sense, there are evidences that LF band of HRV is modulated by the sympathetic and the parasympathetic nervous systems, thus LF band does not an index of sympathetic activity and the rationale for use LF/HF ratio, despite used as a cardiac sympatho-vagal balance, can be questioned (29).

TABLE 7 | Values of performance in the treadmill, time, distance elapsed, and the fatigue stress degree of lower limbs and breathing exhaustions by *BORG* modified od patients due to stroke.

Groups (1 or 2)	Time in the treadmill (min)	Distance traveled (Km)	*BORG* modified final breathing	*BORG* modified final MMII
Group tDCS active (1)	14.17 ± 5.08	0.61 ± 0.31	3.17 ± 1.40	3.50 ± 1.78
Group tDCS sham (2)	12.83 ± 5.37	0.52 ± 0.27	3.12 ± 1.76	3.67 ± 1.82
Difference of averages	0.96	2.18	0.11	−0.45
IC 95%	(−1.73 to −0.001)	(0.20–4.40)	(−0.82 to 0.90)	(−0.97 to 0.64)
P	0.36	0.05	0.92	0.66

*min, Minute; Km, Kilometer; BORG, Subjective perception scale of effort; MMII, Lower limbs; Mean ± Deviation-Standard, *p < 0.05.*

In **Table 3**, the results of VSBP shows that the band of LF absolute of SBP was reduced in the basal condition, presenting an approximate value of 5 $mmHg^2$. The normal values, of healthy individuals, present a mean LF band value of SBP around 17 $mmHg^2$. This data suggests an exacerbated reduction of vascular sympathetic modulation, characteristic of sympathetic hyperactivity situations (30).

In respect to the results of VSBP after active tDCS and tDCS sham, no differences were found between the Groups and in the evaluation moments. However, we believe that the vascular sympathetic modulation may be reestablished, at least in part, post active tDCS. That was observed by the value of LF (of SBP) that increased ∼48% (despite not significant) in respect to the basal values. These results corroborate with the studies of immediate effects of anodic tDCS described by Cogiamania et al. (10) and Piccirillo et al. (31) about the autonomic modulation. However, this was demonstrated in healthy individuals, reporting that the techniques no invasive of brain stimulation that effectively modulate the human cortical function may influence the blood pressure.

Piccirillo et al. (31) observed an improvement of temporal dispersion of myocardium, reduction in sympathetic sinus control, and increased vagal modulation in healthy elderly, after the single application of tDCS for 15 min, intensity 2 mA, over the left temporal area (T3) associated to breathing exercises. This differentiation of results observed in our study may have occurred for being a different population, and that already presents an autonomic modulation alteration, as described by Dutsch et al. (8) that report that independent of the ischemia side, the patient's post sever stroke present a parasympathetic cardiac deficit.

In respect to HRV (**Table 4**), our results demonstrate that there were no differences between the variables analyzed between the Groups active tDCS and sham, both post tDCS as well as during the exercise recovery. But, in the analysis of variables between the moment's basal, post tDCS and exercise recovery of each Group, a significant increase was observed of IP Variance in the time domain, between the moments basal and post tDCS in two Groups. However, only in Group sham, the post-exercise values were significantly reduced, demonstrating a domain of sympathetic activation and reduction of vagal modulation, already expected after an acute physical activity. The fact that there was no significant reduction of variance, that expresses the total variability after active tDCS, leads us to suggest that tDCS could maintain a greater parasympathetic modulation post-acute exercise and, therefore, a possible sympathetic regulation by a parasympathetic activation.

We also observed an increase in the RMSSD variable only in the Group active tDCS, showing a possible parasympathetic modulation by tDCS. These findings corroborate with the findings of de Paula et al. (32) that compare HRV and baroreflex sensitivity to aerobic resistance to acute exercise, on men with autonomic dysfunction, showing an increase of sympathovagal balance and a late standard of recovery of baroreflex sensitivity, what delays an abrupt sympathetic reduction.

In the HVR frequency domain of linear mode, still in **Table 4**, we have shown an increase in LF band in its absolute values only in Group active tDCS after stimulation. Furthermore, after acute exercise, was observed a reduction in both Groups, active tDCS, and sham. This reduction is unexpected, being a normal reaction after acute stress from exercise (33). The absolute HF variable shows a significant reduction after acute exercise in both groups, but only in Group active tDCS, there was an increase of this band after active tDCS, showing a possible action of tDCS in the cardiac parasympathetic modulation.

Another important data observed in this study was a significant increase of the distance traveled on the treadmill after active tDCS when compared to the tDCS sham, results that corroborate with the findings Okano et al. (9) and CICCONE et al. (34) that observed the increase of performance in healthy individuals when compared to Group sham.

The literature has demonstrated that tDCS may modify the autonomic responses in healthy individuals Vandermeeren et al. (35) and Clancy et al. (36), in healthy athletes Montenegro et al. (6) and Okano et al. (9). This is the first study that has as purpose to assess the effects of tDCS over the left temporal lobe, in HRV in individuals with stroke sequel. The region where the electrodes were placed in our study differ from Vandermeeren et al. (35) that stimulate frontal cortex, and the reference electrode was extracephalic. Clancy et al. (36) stimulate the primary motor cortex (M1) of none dominant hemisphere placing anode in C3 or C4 (international system 10/20 of EEG) and the cathode electrode over the supraorbital area contralateral to the anode electrode; Montenegro et al. (6) and Okano et al. (9) stimulate left temporal cortex (T3), and the cathode electrode was placed in the supraorbital area (Fp2) contralateral to anode electrode.

We opted to stimulate T3 to be the area closest to the insular cortex, responsible for autonomic control (37) and used by

Montenegro et al. (6) and Okano et al. (9) with positive results in sympathetic modulation, observed by reduction and stability of heart rate of healthy athletes. These athletes performed better during a maximum incremental test, being 4% more efficient than their control group.

We performed more one analysis to see if the side of the lesion would affect our results (**Table 6**), since tDCS stimulation was only applied to the left temporal cortex, regardless of the side of the lesion, and the results showed no difference between groups, corroborating with Korpelainen et al. (38); Tokgözoglu et al. (39); Harms et al. (40); Constantinescu et al. (26) who report that neurovascular diseases such as ischemic stroke present changes in autonomic modulation with sympathetic hyperactivity, regardless of stroke lateralization.

Regarding the positioning of the reference electrode (cathode) we opted for the extracephalic (deltoid) positioning once according to Noetscher et al. (41) and removing the influence of cathode electrode action on the frontal cortex. Vandermeeren et al. (35), when studying the use of tDCS in the frontal cortex with an extracephalic reference electrode, under continuous cardiorespiratory monitoring and sympathovagal balance of healthy subjects, observed that subjects had a progressive reduction in respiratory rate, a constant increase in blood pressure over time, in which HR remained stable. However, regarding HRV, there was a trend of progressive change in sympathovagal balance, benefiting sympathetic tone, even when there is no significant difference between anode groups and cathode when compared with the tDCS sham, but proving to be a safe fit in healthy humans. Clancy et al. (36) observed autonomic modulation after active tDCS in M1 of healthy individuals.

There were no analyzes of all these data in our study regarding age. However, studies show that age alone is a cardiovascular risk factor (42). Aging promotes the reduction of vagal tone, favoring sympathetic predominance (42, 43).

Bonnemeier et al. (44) evaluated healthy individuals between 27 and 57 years old to verify the relationship of age with all HRV parameters and demonstrated that the parameters with the highest correlation with age were SDNNi, SNN50, and rMSSD; noting a decrease in vagal control as they get older, being more prominent among women.

In addition, systolic and diastolic blood pressure tends to increase with increasing age, especially in women, along with changes in peripheral and central mechanisms that help maintain adequate brain flow (45).

However, it should be considered that in our study we evaluated fewer women than men who would have more influence on age. Moreover, the presence of established hypertension and drug use in all research subjects, besides being stroke survivors, certainly have a greater impact on cardiovascular autonomic modulation than age. However, this can be considered a limiting factor in our study.

FINAL CONSIDERATIONS

This study supplies evidence that a single stimulation with tDCS over the left temporal cortex (T3) of hemiparetic patients due to stroke may improve the cardiac parasympathetic response (RMSSD and HF band of IP). However, significant differences were not observed in the other parameters studied. These results may provide the base for future perspectives of researches about the autonomic modulation after tDCS in stroke.

This study is one of the first studies purposes for evaluating the effects of tDCS over the autonomic modulation in hemiparetic patients due to stroke. Therefore, such opens a path for the betterment of a protocol purpose of verifying the best positioning of electrodes, best stimulation moment, as well as the best aerobic training protocol to be associated to electric stimulation over the cerebral cortex. We consider being important the continuity of the researches in this field for the improvement of knowledge and development of this treatment method considering the advantages listed.

STUDY LIMITATIONS

We consider some topics as limitations of our study:

Difficulty in recruiting patients due to their limited mobility;

Some patients had insecurity to walk on the treadmill. This fear may have influenced the increase in stress and, consequently, a greater parasympathetic action;

Absence of other neurophysiological evaluations such as electroencephalogram or lipid analysis, to better understand the effects of treatment.

Absence of complementary exams for an accurate diagnosis regarding the location and extent of the lesion. Patients with metabolic deficits such as diabetes or thyroid dysfunction were not excluded.

Study data were not analyzed by age. All patients were overweight.

DATA AVAILABILITY STATEMENT

Requests for data can be directed to Glauber Heinz, glauber.heinz@hotmail.com.

ETHICS STATEMENT

The studies involving human participants were reviewed and approved by the proposed study complies with the principles of the Declaration of Helsinki and the Regulating Norms and Directives for Research Involving Human Subjects formulated by the Brazilian National Health Council established in October 1996. The study received approval from the ethics committee of Universidade Nove de Julho (São Paulo, Brazil) under protocol CAAE: 57314716.7.0000.5511 and is registered with the International Registry of Clinical Trials (ClinicalTrials.gov–NCT02956096). The participating institutions have provided a declaration of participation and will be allowed to abandon the study at any time with no negative repercussions. The patients/participants provided their written informed consent to participate in this study.

AUTHOR CONTRIBUTIONS

GH and FC conceived and planned the theory and drafted the manuscript. GH and MS carried out the experiment. KD, SD, AV, FD, and JC helped supervise the project. GH, MS, and FC conceived the original idea. GH, MS, AV, and FD developed the theoretical formalism and participated in the design of the study. SD participated the performed the statistical analysis. FC oriented the project and the authors KD and SD coordinated the project. All the authors have made substantive contributions to the manuscript and assume full responsibility for its content, conceived of the study, participated in its design and coordination and helped to draft the manuscript, read and approved the final manuscript. All authors agree to be accountable for the content of the work.

FUNDING

This work was supported by Coordenação de Aperfeiçoamento de Nível Superior (CAPES) support and Nove de Julho University (UNINOVE) scholarship.

ACKNOWLEDGMENTS

The authors are grateful to University Nove de Julho for supporting the present study.

REFERENCES

1. Dorrance AM, Fink G. Effects of stroke on the autonomic nervous system. In: Prakash YS, editor. *Comprehensive Physiology*. Hoboken, NJ: John Wiley & Sons, Inc. (2015). p. 1241–63.
2. Xiong L, Leung H, Chen XY, Han JH, Leung T, Soo Y, et al. Preliminary findings of the effects of autonomic dysfunction on functional outcome after acute ischemic stroke. *Clin Neurol Neurosurg*. (2012). 114:316–20. doi: 10.1016/j.clineuro.2011.10.037
3. Al-Qudah ZA, Yacoub HA, Souayah N. Disorders of the autonomic nervous system after hemispheric cerebrovascular disorders: an update. *J Vasc Interv Neurol*. (2015). 8:43–52.
4. McLaren A, Kerr S, Allan L, Steen IN, Ballard C, Allen J, et al. Autonomic function is impaired in elderly stroke survivors. *Stroke*. (2005). 36:1026–30. doi: 10.1161/01.STR.0000160748.88374.ce
5. Shura RD, Hurley RA, Taber KH. Insular cortex: structural and functional neuroanatomy. *J Neuropsychiatry Clin Neurosci*. (2014). 26:276–82. doi: 10.1176/appi.neuropsych.260401
6. Montenegro RA, Farinatti P de TV, Fontes EB, Soares PP da S, Cunha FA da, Gurgel JL, et al. Transcranial direct current stimulation influences the cardiac autonomic nervous control. *Neurosci Lett*. (2011). 497:32–6. doi: 10.1016/j.neulet.2011.04.019
7. Macey PM, Wu P, Kumar R, Ogren JA, Richardson HL, Woo MA, et al. Differential responses of the insular cortex gyri to autonomic challenges. *Auton Neurosci Basic Clin*. (2012). 168:72–81. doi: 10.1016/j.autneu.2012.01.009
8. Dutsch M, Burger M, Dorfler C, Schwab S, Hilz MJ. Cardiovascular autonomic function in poststroke patients. *Neurology*. (2007). 69:2249–55. doi: 10.1212/01.wnl.0000286946.06639.a7
9. Okano AH, Fontes EB, Montenegro RA, De Tarso Veras Farinatti P, Cyrino ES, Li LM, et al. Brain stimulation modulates the autonomic nervous system, rating of perceived exertion and performance during maximal exercise. *Br J Sports Med*. (2015). 49:1213–8. doi: 10.1136/bjsports-2012-091658
10. Cogiamanian F, Brunoni AR, Boggio PS, Fregni F, Ciocca M, Priori A. Non-invasive brain stimulation for the management of arterial hypertension. *Med Hypotheses*. (2010). 74:332–6. doi: 10.1016/j.mehy.2009.08.037
11. Brunoni AR, Amadera J, Berbel B, Volz MS, Rizzerio BG, Fregni F. A systematic review on reporting and assessment of adverse effects associated with transcranial direct current stimulation. *Int J Neuropsychopharmacol*. (2011). 14:1133–45. doi: 10.1017/S1461145710001690
12. Bernhardt J, Hayward KS, Kwakkel G, Ward NS, Wolf SL, Borschmann K, et al. Agreed definitions and a shared vision for new standards in stroke recovery research: the stroke recovery and rehabilitation roundtable taskforce. *Neurorehabil Neural Repair*. (2017). 31:793–9. doi: 10.1177/1545968317732668
13. Fugl-Meyer AR, Jääskö L, Leyman I, Olsson S, Steglind S. The post-stroke hemiplegic patient. 1. a method for evaluation of physical performance. *Scand J Rehabil Med*. (1975). 7:13–31.
14. Ovando AC, Michaelsen SM, Carvalho T de, Herber V. Avaliação da aptidão cardiopulmonar em indivíduos com hemiparesia após acidente vascular encefálico. *Arq Bras Cardiol*. (2011). 96:140–7. doi: 10.1590/S0066-782X2011005000001
15. Graham HK, Harvey A, Rodda J, Nattrass GR, Pirpiris M. The functional mobility scale (FMS). *J Pediatr Orthop*. (2004). 24:514–20. doi: 10.1097/01241398-200409000-00011
16. Almeida OP. Mini mental state examination and the diagnosis of dementia in brazil. *Arq Neuropsiquiatr*. (1998). 56:605–12. doi: 10.1590/S0004-282X1998000400014
17. Adeyemo BO, Simis M, Macea DD, Fregni F. Systematic review of parameters of stimulation, clinical trial design characteristics, and motor outcomes in non-invasive brain stimulation in stroke. *Front Psychiatry*. (2012). 3:88. doi: 10.3389/fpsyt.2012.00088
18. Mendonça M, Fregni F. Neuromodulação com estimulação cerebral não invasiva: aplicação no acidente vascular encefálico, doença de Parkinson e dor crônica ASSIS RD. In: Manole M, editor. *Condutas Práticas em Fisioterapia Neurológica*. São Paulo: R.D Manole (2012). p. 307–39.
19. van de Port IGL, Kwakkel G, Wittink H. Systematic review of cardiopulmonary exercise testing post stroke: are we adhering to practice recommendations? *J Rehabil Med*. (2015). 47:881–900. doi: 10.2340/16501977-2031
20. Macko RF, Ivey FM, Forrester LW, Hanley D, Sorkin JD, Katzel LI, et al. Treadmill exercise rehabilitation improves ambulatory function and cardiovascular fitness in patients with chronic stroke: a randomized, controlled trial. *Stroke*. (2005). 36:2206–11. doi: 10.1161/01.STR.0000181076.91805.89
21. Borg GA. Psychophysical bases of perceived exertion. *Med Sci Sports Exerc*. (1982). 14:377–81. doi: 10.1249/00005768-198205000-00012
22. Schlosser J. 'Wall Street' clearances in review. *Broadcast Cable*. (1999). 129:31.
23. Whelton PK, Carey RM, Aronow WS, Casey DE, Collins KJ, Dennison Himmelfarb C, et al. 2017 ACC/AHA/AAPA/ABC/ACPM/AGS/APhA/ASH/ASPC/NMA/PCNA guideline for the prevention, detection, evaluation, and management of high blood pressure in adults: a report of the American College of Cardiology/American Heart Association Task Force on clinical practice guidelines. *Hypertens*. (2017). 71:1269–324. doi: 10.1161/HYP.0000000000000066
24. Kernan WN, Ovbiagele B, Black HR, Bravata DM, Chimowitz MI, Ezekowitz MD, et al. Guidelines for the prevention of stroke in patients with stroke and transient ischemic attack: a guideline for healthcare professionals from the American Heart Association/American Stroke Association. *Stroke*. (2014). 45:2160–236. doi: 10.1161/STR.0000000000000024
25. Nitsche MA, Paulus W. Sustained excitability elevations induced by transcranial DC motor cortex stimulation in humans. *Neurology*. (2001). 57:1899–901. doi: 10.1212/WNL.57.10.1899
26. Constantinescu V, Matei D, Costache V, Cuciureanu D, Arsenescu-Georgescu C. Linear and nonlinear parameters of heart rate variability

in ischemic stroke patients. *Neurol Neurochir Pol*. (2018). 52:194–206. doi: 10.1016/j.pjnns.2017.10.002
27. Sander D, Klingelhöfer J. Changes of circadian blood pressure patterns and cardiovascular parameters indicate lateralization of sympathetic activation following hemispheric brain infarction. *J Neurol*. (1995). 242:313–8. doi: 10.1007/BF00878874
28. Orlandi G, Fanucchi S, Strata G, Pataleo L, Landucci Pellegrini L, Prontera C, et al. Transient autonomic nervous system dysfunction during hyperacute stroke. *Acta Neurol Scand*. (2000). 102:317–21. doi: 10.1034/j.1600-0404.2000.102005317.x
29. Billman GE. The LF/HF ratio does not accurately measure cardiac sympatho-vagal balance. *Front Physiol*. (2013). 4:1–5. doi: 10.3389/fphys.2013.00026
30. Sociedade Brasileira de Cardiologia. [Review of the II Guidelines of the Sociedade Brasileira de Cardiologia for the diagnosis and treatment of heart failure]. *Arq Bras Cardiol*. (2002). 79(Suppl 4):1–30.
31. Piccirillo G, Ottaviani C, Fiorucci C, Petrocchi N, Moscucci F, Di Iorio C, et al. Transcranial direct current stimulation improves the QT variability index and autonomic cardiac control in healthy subjects older than 60 years. *Clin Interv Aging*. (2016). 11:1687–95. doi: 10.2147/CIA.S116194
32. de Paula T, Neves MF, da Silva Itaborahy A, Monteiro W, Farinatti P, Cunha FA. Acute effect of aerobic and strength exercise on heart rate variability and baroreflex sensitivity in men with autonomic dysfunction. *J Strength Cond Res*. (2017). 33:2743–52. doi: 10.1519/JSC.0000000000002372
33. Gupt AAM, Kumar M, Sharma RK, Misra R, Gupt AAM, Madan Gupt A, et al. Original article effect of moderate aerobic exercise training on autonomic functions and its correlation with the antioxidant status. *J Physiol Pharmacol*. (2015). 59:162–9.
34. Ciccone AB, Deckert JA, Schlabs CR, Tilden MJ, Herda TJ, Gallagher PM, et al. Transcranial direct current stimulation of the temporal lobe does not affect high intensity work capacity. *J Strength Cond Res*. (2018). 33:2074–86. doi: 10.1519/JSC.0000000000002561
35. Vandermeeren Y, Jamart J, Ossemann M. Effect of tDCS with an extracephalic reference electrode on cardio-respiratory and autonomic functions. *BMC Neurosci*. (2010). 11:38. doi: 10.1186/1471-2202-11-38
36. Clancy JA, Johnson R, Raw R, Deuchars SA, Deuchars J. Anodal transcranial direct current stimulation (tDCS) over the motor cortex increases sympathetic nerve activity. *Brain Stimul*. (2014). 7:97–104. doi: 10.1016/j.brs.2013.08.005
37. Augustine JR. Full-length review Circuitry and fimctional aspects of the insular lobe in primates including humans. *Brain Res Rev*. (1996) 22:229–44. doi: 10.1016/S0165-0173(96)00011-2
38. Korpelainen JT, Sotaniemi KA, Myllyla V V. Asymmetric sweating in stroke. *Neurology*. (1993). 43:1211–4. doi: 10.1212/WNL.43.6.1211
39. Tokgözoglu SL, Batur MK, Topçuoglu MA, Saribas O, Kes S, Oto A. Effects of stroke localization on cardiac autonomic balance and sudden death. *Stroke*. (1999). 30:1307–11. doi: 10.1161/01.STR.30.7.1307
40. Harms H, Reimnitz P, Bohner G, Werich T, Klingebiel R, Meisel C, et al. Influence of stroke localization on autonomic activation, immunodepression, and post-stroke infection. *Cerebrovasc Dis*. (2011). 32:552–60. doi: 10.1159/000331922
41. Noetscher GM, Yanamadala J, Makarov SN, Pascual-Leone A. Comparison of cephalic and extracephalic montages for transcranial direct current stimulation–a numerical study. *IEEE Trans Biomed Eng*. (2014). 61:2488–98. doi: 10.1109/TBME.2014.2322774
42. Abell JG, Kivimäki M, Dugravot A, Tabak AG, Fayosse A, Shipley M, et al. Association between systolic blood pressure and dementia in theWhitehall II cohort study: role of age, duration, and threshold used to define hypertension. *Eur Heart J*. (2018). 39:3119–25. doi: 10.1093/eurheartj/ehy288
43. Abhishekh HA, Nisarga P, Kisan R, Meghana A, Chandran S, Trichur Raju, et al. Influence of age and gender on autonomic regulation of heart. *J Clin Monit Comput*. (2013). 27:259–64. doi: 10.1007/s10877-012-9424-3
44. Bonnemeier H, Wiegand UKH, Brandes A, Kluge N, Katus HA, Richardt G, et al. Circadian profile of cardiac autonomic nervous modulation in healthy subjects: differing effects of aging and gender on heart rate variability. *J Cardiovasc Electrophysiol*. (2003). 14:791–9. doi: 10.1046/j.1540-8167.2003.03078.x
45. Teixeira SC, Madureira JB, Azevedo EI, Castro PM. Ageing affects the balance between central and peripheral mechanisms of cerebrovascular regulation with increasing influence of systolic blood pressure levels. *Eur J Appl Physiol*. (2019). 119:519–29. doi: 10.1007/s00421-018-4036-3

Conflict of Interest: The authors declare that the research was conducted in the absence of any commercial or financial relationships that could be construed as a potential conflict of interest.

Copyright © 2020 Heinz, De Angelis, Dal Corso, Sousa, Viana, Dos Santos, Corrêa and Corrêa. This is an open-access article distributed under the terms of the Creative Commons Attribution License (CC BY). The use, distribution or reproduction in other forums is permitted, provided the original author(s) and the copyright owner(s) are credited and that the original publication in this journal is cited, in accordance with accepted academic practice. No use, distribution or reproduction is permitted which does not comply with these terms.

frontiers in Neuroscience

ORIGINAL RESEARCH
published: 04 February 2020
doi: 10.3389/fnins.2020.00046

Acute Treatment With Gleevec Does Not Promote Early Vascular Recovery Following Intracerebral Hemorrhage in Adult Male Rats

*Mohammed Abbas[1], Elizabeth Haddad[2], Mary Hamer[2], Derek Nowrangi[3], John Zhang[3,4,5], William J. Pearce[6], Jiping Tang[3] and Andre Obenaus[1,2]**

[1] Department of Pediatrics, Loma Linda University, Loma Linda, CA, United States, [2] Department of Pediatrics, University of California, Irvine, Irvine, CA, United States, [3] Department of Physiology and Pharmacology, Loma Linda University, Loma Linda, CA, United States, [4] Department of Anesthesiology, Loma Linda University, Loma Linda, CA, United States, [5] Department of Neurosurgery, Loma Linda University, Loma Linda, CA, United States, [6] Center for Perinatal Biology, Loma Linda University, Loma Linda, CA, United States

OPEN ACCESS

Edited by:
Emmanuel Pinteaux, University of Manchester, United Kingdom

Reviewed by:
DaZhi Liu, University of California, Davis, United States
Guodong Cao, University of Pittsburgh, United States

***Correspondence:**
Andre Obenaus
obenausa@uci.edu

Specialty section:
This article was submitted to Neurodegeneration, a section of the journal Frontiers in Neuroscience

Received: *20 August 2019*
Accepted: *13 January 2020*
Published: *04 February 2020*

Citation:
Abbas M, Haddad E, Hamer M, Nowrangi D, Zhang J, Pearce WJ, Tang J and Obenaus A (2020) Acute Treatment With Gleevec Does Not Promote Early Vascular Recovery Following Intracerebral Hemorrhage in Adult Male Rats. Front. Neurosci. 14:46. doi: 10.3389/fnins.2020.00046

Intracerebral hemorrhage (ICH) remains one of the most debilitating types of stroke and is characterized by a sudden bleeding from a ruptured blood vessel. ICH often results in high mortality and in survivors, permanent disability. Most studies have focused on neuroprotective strategies designed to minimize secondary consequences and prevent further pathology. Lacking is an understanding of how ICH acutely affects cerebrovascular components and their response to therapeutic interventions. We hypothesized that ICH alters cortical vessel complexity in the parenchyma adjacent to site of the initial vascular disruption and that vascular abnormalities would be mitigated by administration of the PDGFR inhibitor, Imatinib mesylate (Gleevec). Briefly, ICH was induced in male adult rats by injection of collagenase into basal ganglia, followed by Gleevec administration (60 mg/kg) 1 h after injury. Rats were then perfused using vessel painting methodology (Salehi et al., 2018b) to stain whole brain vascular networks at 1 day post-ICH. Axial and coronal wide field fluorescence microscopy was performed. Analyses for vascular features were undertaken and fractal analysis for vascular complexity. Data were collected from four groups of rats: Sham + Vehicle; Sham + Gleevec; ICH + Vehicle; ICH + Gleevec. Microscopy revealed that cortical vessels in both ipsi- and contralateral hemispheres exhibited significantly reduced density and branching by 22 and 34%, respectively. Fractal measures confirmed reduced complexity as well. Gleevec treatment further reduced vascular parameters, including reductions in vessel density in tissues adjacent to the ICH. The reductions in brain wide vascular networks after Gleevec in the current study after ICH is contrasted by previous reports of improved behavioral outcomes and decreased ICH lesion volumes Reductions in the vascular network after Gleevec may be involved in long-term repair mechanisms by pruning injured vessels to ultimately promote new vessel growth.

Keywords: cerebrovasculature, vessels, vessel painting, magnetic resonance imaging, edema, fractal

INTRODUCTION

Spontaneous intracerebral hemorrhage (ICH) is defined as a sudden bleeding from ruptured cerebral blood vessels. It accounts for about 10–20% of all strokes (Feigin et al., 2009) and is associated with higher mortality and morbidity leading often to worse outcomes compared to other strokes (Broderick et al., 1999). ICH occurs primarily when a hematoma rapidly accumulates within brain parenchyma (Aronowski and Zhao, 2011) with a persistent expansion over 6–24 h (Aguilar and Brott, 2011). This leads to further mechanical disruption of the normal parenchymal anatomy (Aronowski and Zhao, 2011) followed by subsequent tissue compression effects and increased intracranial pressure (Qureshi et al., 2009). This expansion of the hematoma is highly predictive of neurological deterioration, poor functional outcome and mortality (Broderick et al., 1993; Kazui et al., 1996, 1997; Leira et al., 2004). The hemorrhagic expansion can be attributed to leakage or rebleeding from secondary mechanical shearing of vessels surrounding hematoma (Fisher, 1971) but other cellular processes are also known to contribute including, but not limited to: (a) initiation by thrombin of the coagulation cascade leading to activated microglia (Wagner et al., 2002; Nakamura et al., 2005; Nakamura et al., 2006; Xi et al., 2006), (b) hematoma breakdown-products such as hemoglobin (Mracsko and Veltkamp, 2014), and (c) a robust inflammatory response (Wang and Dore, 2007; Yang et al., 2016). These secondary outcomes lead to a disrupted BBB resulting in significant brain edema (Hua et al., 2007) that are strongly predictive of functional outcomes (Gebel et al., 2002). While neuroinflammation and other secondary injury cascades in the context of ICH have been well studied previously (Yang et al., 2016), little has been reported on the how ICH modifies cerebrovascular integrity and morphology. We have previously reported that ICH results in a modified cerebral vascular smooth muscle phenotype (Pearce et al., 2016). However, the morphological features of the injured cerebrovasculature including integrity of the neurovascular unit are critical features that are poorly understood. Clinically, the microvascular integrity has been cited as a potential key factor in hematoma expansion in one third of ICH patients (Chen et al., 2017). Thus, a more complete understanding of how the vasculature is altered following ICH is warranted.

To our knowledge, there are no comprehensive studies examining the vascular morphology of parenchymal vessels following ICH nor the vasoprotective effects Gleevec. Thus, we set out to investigate the microvascular morphological changes adjacent to perihematomal parenchyma and in cortical regions remote from the site of the ICH lesion. To examine whole brain vessel morphology, we applied our novel vessel painting technique as we have reported in other models of acquired brain injury (Obenaus et al., 2017; Salehi et al., 2018b). This approach allows whole brain staining of the vasculature and is amenable to confocal microscopy for derivation of vascular morphological details. In the present study we first investigated how ICH modifies vascular morphological features followed by assessment of how Gleevec treatment could maintain vascular morphology acutely after ICH. We examined the vascular plexus in cortex and basal ganglia closely and analyzed their features in both hemispheres.

Gleevec or Imatinib Mesylate was developed to treat chronic myelogenous leukemia (CML) and is known to have multiple roles (Soverini et al., 2018). Gleevec has been shown to minimize stroke damage by its actions on the vasculature (Su et al., 2008). More recently we and others have identified that Gleevec antagonism of the platelet-derived growth factor receptor-β (PDGFR-β) on vascular elements. We reported that vascular smooth muscle phenotype is modified after ICH and that Gleevec mitigates this phenotypic switch (Pearce et al., 2016; Yang et al., 2016). Others have also shown that PDGF and its family play an important role in vascular protection using the retina as a model system (He et al., 2014). We investigated the role of Gleevec (Imatinib), a PDGFR-β antagonist, on vessels and how it influenced vascular measures acutely (1 day) after ICH. Thus, this study reports that ICH induces vascular loss, locally at the site of ICH and in regions distant from the injury. Moreover, acute assessment of Gleevec treatment found no significant protection of the cerebrovasculature during the acute assessment period.

MATERIALS AND METHODS

Animals

All animal experiments and care were in compliance with federal regulations and approved by the Loma Linda University Institutional Animal Care and Use Committee. Thirty male Sprague Dawley rats weighing 250–300 g (2–5 months old) were housed in a temperature controlled animal facility on a 12 h light-dark cycle and were allowed free access to food and water. Animals were randomly assigned to experimental groups. Aseptic techniques were used for all surgeries. No rats died or were excluded from the study due adverse outcomes from intracerebral hemorrhage injury (ICH).

Experimental Groups

All drug administration was performed by within 1 h following ICH induction, where vehicle (PBS and 0.1% DMSO) or 60 mg/kg Gleevec were injected intraperitoneally. Rats were subdivided randomly into four groups (n = 6/group): (a) Sham + vehicle, (b) sham + Gleevec, (c) ICH + vehicle, (d) ICH + Gleevec. Neurological function and behavior were assessed 24 h after ICH induction.

Intracerebral Hemorrhage Injury (ICH) Model

ICH was induced using the Bacterial Collagenase injection model as previously described (Pearce et al., 2016). Rats underwent isoflurane anesthesia (4% induction with 2% maintenance in 70% medical air and 30% O_2) and then were secured prone onto a stereotactic frame (David Kopf Instruments, Tujunga, CA, United States). Body temperature was maintained at 37.0°C ± 0.5°C using a thermostat-controlled heating blanket throughout the entire surgical procedure. The following stereotactic coordinates were used to localize the right basal

ganglia: 0.2 mm anterior, 5.6 mm ventral, and 2.9 mm lateral to the bregma. An incision was then made over the scalp and a posterior cranial burr hole (1 mm) was drilled over the right cerebral hemisphere into which a 27-gauge needle was inserted at a rate of 1 mm/min. A micro infusion pump (Harvard Apparatus, Holliston, MA, United States) infused the bacterial collagenase Type VII-S (0.2 U/μL; Sigma-Aldrich, St. Louis, MO, United States) through a Hamilton syringe at a rate of 0.2 μL/min. The needle remained in place for 10 min to prevent back-leakage before being slowly withdrawn (1 mm/min). The borehole was then sealed with bone wax, the incision sutured closed and the animals were monitored during the recovery period. Sham animals received the identical manipulations but instead of collagenase injection they received vehicle infusion. Food, water, and post-operative supportive care were provided, as is routinely done. Animals were euthanized 24 h after surgery for assessment of vascular morphology.

Vessel Painting and Tissue Fixation

Animals were sacrificed via transcranial perfusion 24 h after ICH for vessel painting and for tissue fixation (Salehi et al., 2018b). Briefly, rats were anesthetized by intraperitoneal injection of ketamine (90 mg/kg) and xylazine (10 mg/kg), then perfused for vessel painting and finally tissue fixation. Our vessel painting protocol stains the vascular network using DiI (1,1′-dioctadecyl-3,3,3′,3′-tetramethylindocarbocyanine perchlorate) (Life Technologies, Carlsbad, CA, United States) which has been commonly used for labeling cell membranes (Schlessinger et al., 1977) and neuronal tissues (Honig and Hume, 1986; Godement et al., 1987). The lipophilic properties of DiI allow direct vascular staining. The perfusion device consisted of a 25- gauge butterfly needle and syringes for phosphate-buffered saline (PBS), DiI solution and Paraformaldehyde (PFA). After exposure of the heart a butterfly needle was inserted into the left ventricle. Heparin (0.02 mg/g, Sagent Pharmaceuticals) and sodium nitroprusside (0.075 mg/gm, Sigma-Aldrich, St. Louis, MO, United States) were injected followed by serial injections of 150 ml of PBS, 50 ml of DiI (13ug/ml) in diluent solution and 200 ml of 4% PFA. Care was taken to ensure that no air was trapped within the perfusion system. Brains were extracted from the cranium, rinsed in PFA and post-fixed for 24 h. Thereafter, vessel painted brains were stored in PBS until MRI or wide-field microscopy were undertaken. Individual photographs of vessel-stained brains were acquired to document the labeling efficacy. In this study, vessel painting was successful in 71% of animals wherein vascular staining was uniform (**Figure 1**).

Magnetic Resonance Imaging Acquisition and Analysis

High resolution MRI was undertaken using an 11.7T Bruker Avance instrument (Bruker Biospin, Billerica, MA, United States) running with the Paravision software (version 5.1, Bruker Biospin) to assess brain injury volumes. T2-weighted images [T2WI; repetition time (TR)/echo time (TE): 2395 ms/10 ms, 20 × 1 mm slices] were acquired and collected on a 256 × 256 matrix with a 2 cm field of view to quantitate edema and extravascular blood.

Volumetric analysis of hematoma size and quantification of surrounding edema was performed on T2WI coronal slices using Cheshire image processing software (Hayden Image/Processing Group, Waltham, MA, United States, version 4.3). Investigators who were blind to treatment groups manually defined the region of interest (ROI) on each slice that included whole brain, hematoma (hypointensity), and edema (hyperintensity). Hematoma and edema area on each slice affected by the ICH injury were delineated based on the differentiation of hyper-/hypo- intensive regions of injury relative to surrounding normative tissue conditions. Any blood or edema on or below the corpus callosum was classified as subcortical injury, whereas any injury above the corpus callosum was classified as cortical injury. Whole brain analysis started where the olfactory bulb begins to merge with the cortex and spanned the entire cerebrum. To obtain edema volumes the hematoma volume was subtracted as the edematous region typically encased the hematoma. Cortical injury was analyzed separately and also combined with subcortical injury for total ICH injury volumes. All data were organized and summarized in Microsoft Excel.

Vessel Painting Image Acquisition and Analyses

Vessel painted brains were imaged using Keyence BZ-9000 fluorescent microscope (Keyence BZ-X700; Keyence Corp., Osaka, Japan). Whole brains were gently positioned between 2 glass slides and lightly compressed to eliminate bubbles and improve visibility. Whole brain axial views were imaged at 2X with z-stacks using 60 μm steps with 50 slices resulting in 3 mm slab. After axial views were collected, the brains were bisected into 2 coronal segments with an anterior and posterior face at the level of the ICH lesion using MRI data as a guide. Coronal images were then scanned at the same resolution by gently fixing the anterior half of the brain on a single glass slide, examined at 2X, z-stacked at 60 μm with 30 slices resulting in 1.8 mm sections. Z-stacks for both axial and coronal were merged into full focus images using the BZ-II analyzer software (Keyence Corp., Version 1.2.0.1.). Finally, the software haze reduction feature (Blur/Brightness/Reduction: 10/10/1) was applied on the resultant images to remove any background and enhance the vascular network.

Classical vascular analysis was undertaken using the Image J plugin, Angiotool (RRID:SCR_016393) (Zudaire et al., 2011). Originally developed to assess spatial features of the angiogenic vasculature in the retina we have adapted this software for use in evaluating whole brain cortical vessels after traumatic brain injury (Obenaus et al., 2017; Salehi et al., 2018b). Angiotool features used in the current study were structural parameters such as vessel density and length, branch points and lacunarity (space without vessels).

Similar to our previous studies (Obenaus et al., 2017; Salehi et al., 2018b), we utilized fractal analysis to determine vascular complexity. Fractals have been widely used to describe structural

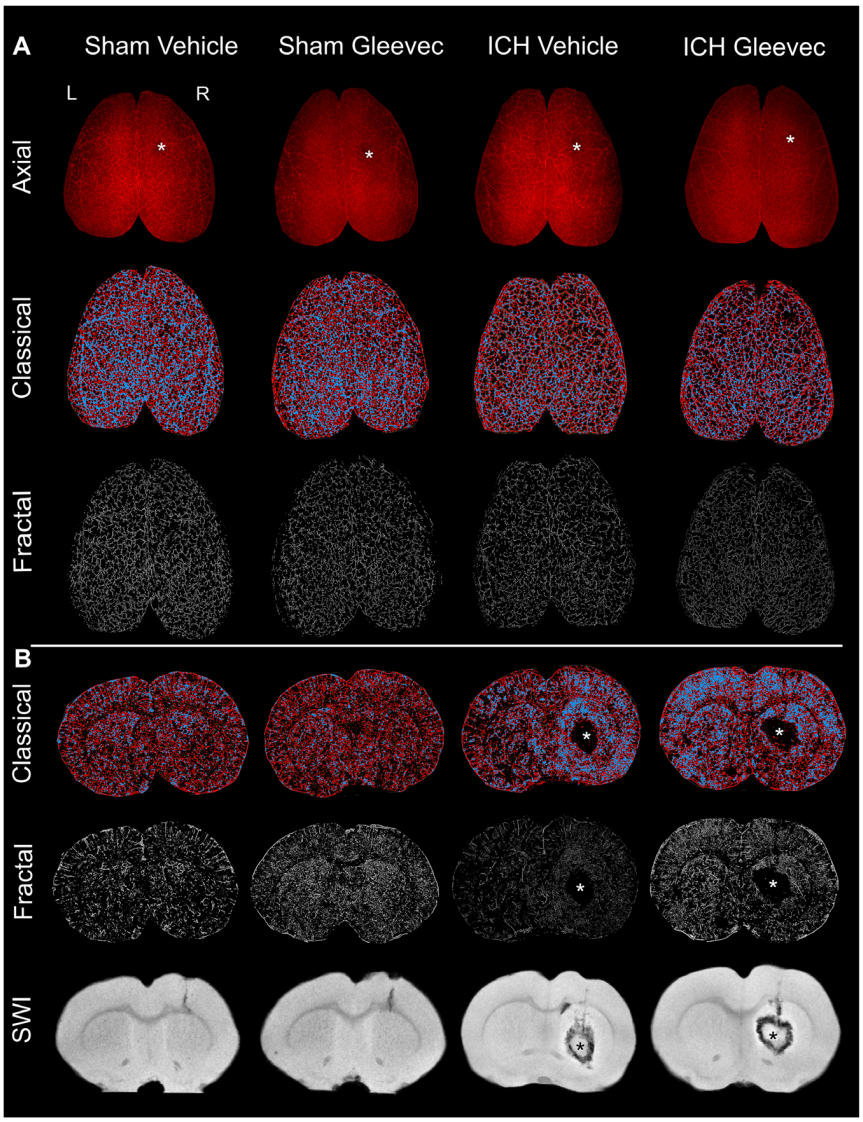

FIGURE 1 | Intracerebral hemorrhage (ICH) results in cerebral vascular decrements at 24 h after injury or treatment. **(A)** Axial: The top row illustrates representative axial vessel painted whole brains in ICH animals with and without Gleevec treatment (* = injection site). The middle row are sample classical vascular analysis maps where red denotes vessels and blue demarcates vessel junctions. The third row displays fractal maps utilized for analysis of vascular complexity. **(B)** Coronal: Classical vascular analysis of coronal sections from all experimental groups wherein the ICH lesion in the striatum can be visualized in the injured rats (*). Middle row are the corresponding fractal analysis maps. The last row of coronal images are from susceptibility weighted magnetic resonance imaging (SWI MRI) which was utilized to monitor the extent of the hematoma and edema after ICH induction. Sham animals exhibited minimal vascular alterations from needle insertion whereas ICH animals have prominent and extensive areas of vessel disruption at the site of the ICH. All images in each column are from the same animal.

complexity of various tissues, including the microvasculature of retina (Cheung et al., 2012), pituitary (Di Ieva et al., 2007), microglial complexity (Karperien et al., 2013) and cortical vessels (Obenaus et al., 2017). The ramified and irregular pattern of vessels after injury has made their evaluation by standard tools inaccurate and difficult. As we have done previously, we utilized the Fraclac ImageJ plugin (RRID:SCR_003070) to optimize quantification of vessels in cortex and basal ganglia (Schneider et al., 2012; Karperien et al., 2013). Briefly, binary images were analyzed by measuring the total number of pixels locally connected in a box of increasing size ε using the slope of the log regression line for pixel mass against scale (Karperien et al., 2013). The Local connected Fractal Dimension (DLC) is extracted and is calculated similar to the mass Fractal Dimension:

$$D_{Bmass} = \lim_{\varepsilon \to 0} \left\lceil {\ln(\mu_\varepsilon)}/{\ln(\varepsilon)} \right\rceil$$

Where με is the mean pixels per box at some size ε. The pixel mass is calculated from concentrically placed sampling units using a connected set at each pixel to produce a distribution

of local variation in complexity in data as previously described (Obenaus et al., 2017).

We used ImageJ analysis software to convert vessel painted images into binary images. First, we outlined our area of interest on each image then we ran Fraclac DLC analysis for each brain and saved the results. The distribution of DLC (also denoted as local fractal dimension, LFD) for each brain was then further processed for kurtosis, skewness, peak fractal frequency and local fractal dimension (LFD) for group comparisons. The LFD represents patterns at different scales and is often used to represent complexity of the subject. Skewness and kurtosis of the fractal histograms offer additional measures on how uniformly the fractal dimensions were distributed and how (peaked) the fractal distribution appears, respectively. Analyzed images were colorized based on fractal dimension using a default LUT color coding.

Laser Confocal Microscopy

Whole vessel painted brains and their coronal sections were imaged on the laser scanning confocal microscope Zeiss LSM 710 (Jena, Germany) to evaluate at high resolution vascular structures. Images were obtained (10X objective lens, excitation wavelength Abs: 549 nm, Ems: 565 nm) of the ipsilateral ICH hemisphere. Zeiss software (Zen) was used to process the z-stacks (28.4 μm steps) for resultant maximum intensity projections.

Statistics

All data was tested for normal distribution and comparisons were made using *t*-test (unpaired). If samples did not have normal distributions data were evaluated using a Mann–Whitney test. All graphical and statistical analysis used GraphPad Prism 7 software (GraphPad Prism, San Diego, CA, United States; RRID: SCR_002798). All calculations were achieved without knowledge of group. All data are presented as mean ± SEM with statistical significance reported at $p < 0.05$.

RESULTS

The results are comprised of two components: (a) first we report the novel findings of how ICH impacts the cortical and basal ganglia vasculature following ICH, and (b) we then describe the results of how Gleevec treatment after ICH may modify the cortical and basal ganglia vessels. Representative axial and coronal vessel painted brains and the classical and fractal vessel analysis maps as well as magnetic resonance imaging (MRI) are illustrated in **Figure 1**. It is readily apparent that ICH results in vascular modifications.

Vascular Modifications in the Cortex and Basal Ganglia 24 h After ICH

Visual examination of the wide field axial microscopic images of Sham + Vehicle ($n = 9$) and ICH + Vehicle ($n = 9$) vessel painted brains revealed a lack of overt gross cortical vascular changes (**Figure 1A**). Mild vascular disruptions at the injection sites on the cortex were visible in both Sham and ICH vessel painted brains (**Figure 1A** – denoted by *). However, in coronal images for classical vascular analysis maps, there was a visible apparent increase in junctional density after ICH, often adjacent to the hematoma (*) (**Figure 1B**, blue dots). Quantitative analysis was undertaken to evaluate the effects of ICH on cortical and basal ganglia vessels. Multiple vascular morphological parameters were quantified including: (1) vessel density (% vessel/total area), (2) branching index (branch points or junctions/unit area), (3) total vessel length, and (4) lacunarity, which describe areas that do not have vascular elements.

Axial Cortex Analysis

The morphological features of cortical vessels were derived from the whole axial cortical surface cortex, the ipsilateral (injection side) and contralateral (intact) cortex. Whole brain cortical (both hemispheres) vessel density of Sham + Vehicle animals was 26.94 ± 0.98 compared to 21.09 ± 0.85 in ICH + Vehicle rats (**Figure 2A**). This reduction in vessel density was significantly decreased by 21.7% ($p < 0.01$) in ICH + Vehicle compared to Sham + Vehicle rats. Similarly, vessel density of ipsilateral axial cortex in ICH + Vehicle rats was significantly decreased by 19.4% ($p < 0.01$) compared to Sham + Vehicle, with Sham + Vehicle having a vessel density of 27.30 ± 1.21 compared to 21.99 ± 0.87 in the ICH + Vehicle animals. Interestingly, contralateral axial cortical vessel density was also significantly decreased by 17.4% ($p < 0.01$) in ICH + Vehicle, where Sham + Vehicle animals had a vessel density of 27.47 ± 0.92 in the contralateral axial cortex compared to 22.69 ± 1.17 in ICH + Vehicle animals.

However, cortical vascular branching (branching index; junctions/mm^2) followed a similar pattern where ICH + Vehicle animals exhibited significant decreases of 34.2% ($p < 0.01$), 32.8% ($p < 0.03$), 31.6% ($p < 0.01$), respectively across the whole brain, in the ipsilateral hemisphere and in contralateral hemisphere (**Figure 2B**). As would be expected, lacunarity features were also increased with decreasing vessel density (**Figure 2C**). In the whole cortex and in the ipsilateral cortex, lacunarity was significantly increased in ICH + Vehicle animals by 21% ($p < 0.05$) and by 23% ($p < 0.01$) compared to Sham + Vehicle rats, respectively. Unexpectedly, the contralateral axial cortex of ICH + Vehicle rats did not exhibit increased lacunarity compared to Sham + Vehicle animals, despite reductions in vessel density and branching indices. Quantitative measurement of the total vessel length of the whole, ipsilateral and contralateral axial cortical vessels revealed no significant differences between the ICH vehicle and sham vehicle groups (data not shown).

Coronal Cortex and Basal Ganglia Analysis

Following axial cortical data collection, the brains were cut through the ICH lesion resulting in an anterior and posterior portion of the brain. Wide field fluorescent microscopic images were acquired from the anterior face of the vessel painted brains (**Figure 1B**). Ipsilateral coronal hemispheric analysis excluded the hematoma. The rationale for these coronal analyses was that it could reveal parenchymal vascular alterations in regions that encompassed cortical and deep gray matter structures such as the basal ganglia.

Coronal vessel density measures of the whole coronal slab in ICH + Vehicle rats was significantly decreased by 38.7%

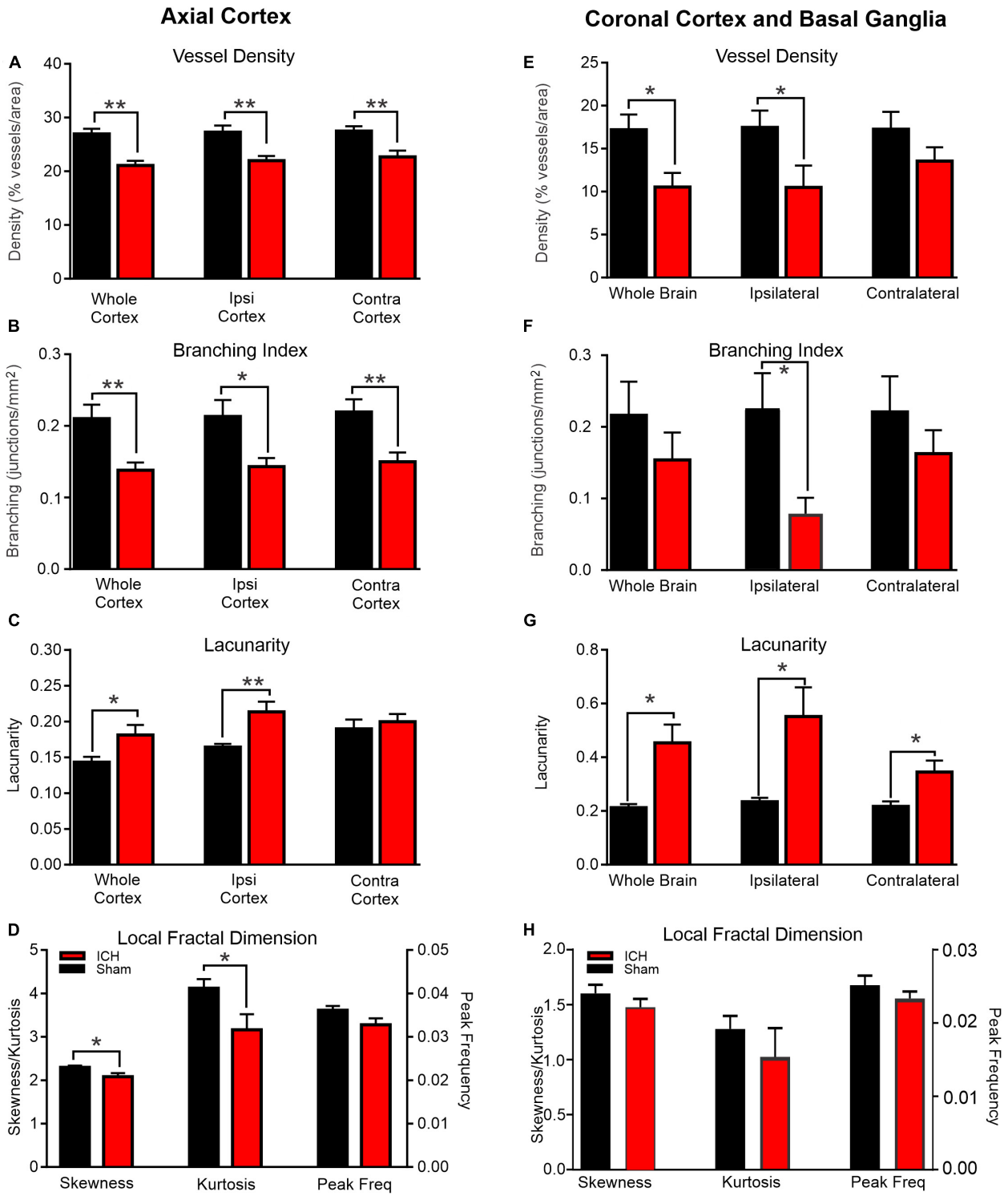

FIGURE 2 | ICH induces modification of vascular features at 24 h post-injury. Axial Cortex: Classical vascular analysis of the entire axial cortex, ipsilateral (Ipsi) and contralateral (Contra) cortical hemispheres resulted in significant reductions in vessel density **(A)** and branching index **(B)** after ICH compared to shams. There was a concomitant increase in lacunarity **(C)** but not in the contralateral hemisphere. Fractal derived vascular complexity of the ipsilateral cortex using local fractal dimension histograms (LFD) **(D)** exhibited significant decrements in skewness and kurtosis between shams and ICH animals. Coronal Cortex and Basal Ganglia: Classical vascular analysis of coronal vessel painted sections at the level of the ICH lesion revealed significant reductions in vessel density **(E)** and reduced branching indices **(F)**. There was a dramatic increase in lacunarity **(G)**. Quantitative analysis of the LFD histograms from the ipsilateral cortex and basal ganglia exhibited no significant changes in skewness, kurtosis or peak frequency **(H)** in ICH vehicle compared to sham vehicle animals (*t*-test $^{**}p < 0.03$, $^{*}p < 0.05$).

($p < 0.03$) compared to Sham + Vehicle rats (**Figure 2E**). The vessel density was 17.20 ± 1.78 in Sham + Vehicle rats compared to 10.53 ± 1.65 in the ICH + Vehicle animals. Similarly, vessel density in the ipsilateral coronal hemisphere of ICH + Vehicle animals were significantly decreased by 39.8% ($p < 0.05$) compared to Sham + Vehicle animals. Sham + Vehicle animals had a vessel density of 17.46 ± 1.97 compared to 10.50 ± 2.53 in the ICH + Vehicle animals. The vessel density of contralateral coronal sections had a 21.4% reduction in ICH + Vehicle compared to Sham + Vehicle animals but was not significantly different ($p = 0.17$).

The branching indices showed considerable variance in the coronal sections which is not overly surprising given differences in the vascular networks between cortical and basal ganglia brain regions (**Figure 2F**). Only the ipsilateral coronal section exhibited a significant ($p < 0.03$) reduction in vascular branching in ICH + Vehicle compared to Sham + Vehicle animals. Coronal total vessel length measures were not significantly different between ICH + Vehicle and Sham + Vehicle animals, similar to axial total vessel lengths (data not shown).

Lacunarity measures from coronal brain slices were significantly increased by 53.2% ($p < 0.03$), 57.4% ($p < 0.03$) and 37.2% ($p < 0.03$) in whole brain, ipsilateral, coronal and contralateral sections respectively (**Figure 2G**). In whole brain slices, lacunarity in ICH + Vehicle animals was 0.45 ± 0.09 compared to 0.21 ± 0.014 in sham vehicle rats. The lacunarity of ipsilateral coronal sections of ICH + Vehicle rats were reduced compared to Sham + Vehicle animals at 0.55 ± 0.11 and 0.23 ± 0.015, respectively. Even the lacunarity of contralateral coronal sections were reduced in ICH + Vehicle animals compared to Sham + Vehicle animals (ICH: 0.35 ± 0.04; Sham: 0.22 ± 0.02).

Fractal Analysis

Global measures of axial vascular complexity also revealed reductions similar to and validating our classical angiographic measures (**Figures 1**, **2D**). Analysis of the ipsilateral axial cortex found that skewness and kurtosis of ICH + Vehicle animals were significantly ($p < 0.05$) reduced by 9.37 and 23.2% respectively compared to Sham + Vehicle animals. Peak frequency of the local frequency dimension (LFD) histograms which is a measure of the number of vessels was also reduced by 10% in ICH + Vehicle compared to Sham + Vehicle animals but did not reach significance ($p = 0.09$).

Skewness, kurtosis and peak frequency of the LFD histograms of the ipsilateral coronal basal ganglia and cortex showed no significant differences (**Figure 2H**). ICH resulted in reduced kurtosis and peak frequency of the LFD histograms of ipsilateral coronal basal ganglia and cortex by 46.9% ($p = 0.42$) and 8.2% ($p = 0.28$) respectively in ICH + Vehicle compared to Sham + Vehicle animals. In the automated fractal analyses we were unable to exclude the hematoma from the analysis and likely contributed to the non-significant findings.

In summary, vascular features of the cortex were predominately reduced with the induction of ICH compared to Sham + Vehicle animals. Both axial and coronal assessments yielded similar reductions, further validating our analyses. Interestingly, ICH in many measures also resulted in reductions in contralateral vessel parameters at 24 h after injury. Acutely, other studies of acquired neurological injury have reported similar contralateral effects on the cerebrovasculature.

Effects of Gleevec on the Vasculature

Axial Cortex Analysis

Gleevec (Imantinib) has been reported to be anti-inflammatory and alter the structure of the vasculature following ICH (Soverini et al., 2018; Su et al., 2008). We undertook a more direct measure of the vasculature after Gleevec treatment on vascular features for the ipsilateral hemisphere. For these analyses our comparisons were made between Sham + Vehicle, Sham + Gleevec, ICH + Vehicle and ICH + Gleevec.

The density of the axial cerebrovasculature was significantly reduced in ICH + Vehicle and ICH + Gleevec rats compared to Sham + Vehicle (ANOVA, $p = 0.002$, *post hoc* multiple comparisons $p < 0.01$) (**Figure 3A**). The reduction between Sham + Vehicle compared to ICH + Gleevc was 28.2%. Identical reductions were observed in the branching index (ANOVA, $p = 0.005$, *post hoc* multiple comparisons $p < 0.01$) with a 35.6% reduction in junctions between Sham + Vehicle and ICH + Gleevec groups (**Figure 3B**). As would be expected with reduced vessel density, lacunarity was significantly increased in Sham + Gleevec, ICH + Vehicle and ICH + Gleevec compared to Sham + Vehicle rats (ANOVA, $p = 0.002$, *post hoc* multiple comparisons $p < 0.01$) (**Figure 3C**). Lacunarity was significantly increased in Sham + Gleevec by 49.2% ($p < 0.01$) compared to Sham + Vehicle animals. Thus, classical vascular measures of the axial cortex did not show improvement in Gleevec treated ICH animals with treatment at 24 h after ICH induction.

Alternatively, we also undertook a less conservative statistical analysis of just Sham + Vehicle and Sham + Gleevec groups and their vessel characteristics (**Supplementary Figure S1**) and found that lacunarity was increased significantly ($p < 0.001$) in Sham + Gleevec rats compared to Sham + Vehicle (**Supplementary Figure S1C**). No significant differences were observed in ICH rats between ICH + Vehicle and ICH + Gleevec groups. Fractal measures were significantly decreased in Sham + Vehicle and Sham + Gleevec rats (**Supplementary Figure S1D**) but no differences were observed between ICH + Vehicle and ICH + Gleevec groups.

Coronal Cortex and Basal Ganglia Analysis

We further investigated whether Gleevec had any effect on parenchymal vascular parameters in coronal brain samples (**Figure 1B**). Specifically, we examined vessels in the ipsilateral hemisphere (injured) that included the basal ganglia (peri-hematoma, but excluding the hematoma) and adjacent cortex.

Similar to our axial cortical findings (**Figure 3A**) we observed a significant reduction in vessel density (ANOVA, $p = 0.002$, Tukey's *post hoc* multiple comparisons $p < 0.05$) (**Figure 3E**). In ICH + Vehicle and ICH + Gleevec rats there were significant reductions compared to Sham + Vehicle rats, 39.8 and 57.3%, respectively. Total vessel length was unchanged with no differences between groups (data not shown). Branching index trended toward a reduction, like vessel density (ANOVA,

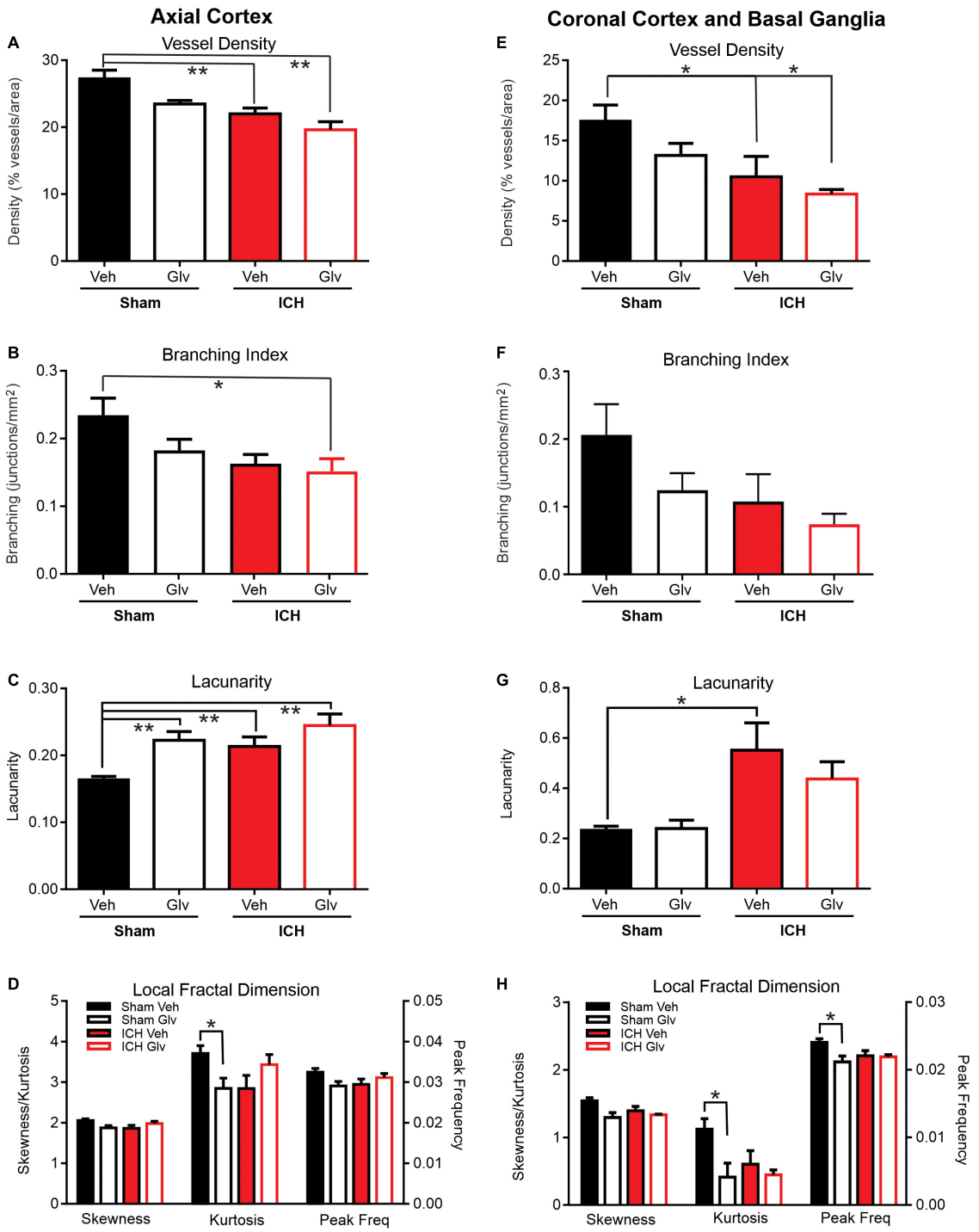

FIGURE 3 | Gleevec treatment does not improve ICH parenchymal vascular measures. Axial Cortex: Ipsilateral cortical vascular analysis revealed no significant changes in vessel density **(A)** or branching index **(B)** between Vehicle nor ICH Gleevec treated rats. However, significant reductions in vessel density were observed between sham vehicle and ICH + Vehicle and ICH + Gleevec rats. Vascular branching was significantly reduced between Sham + Vehicle and ICH + Gleevec rats. Lacunarity **(C)** was only increased in all groups relative to sham vehicle treated rats. Quantitative analysis of the distribution of LFD histograms **(D)** exhibited no significant reductions in skewness, and peak frequency in sham + Gleevec compared to sham + Vehicle animals. Kurtosis was significantly reduced between sham groups. Coronal Cortex and Basal Ganglia: Classical vascular analysis of ipsilateral cortex and basal ganglia revealed a progressively significant decrement in vessel density **(E)** across all groups. *Post-hoc* testing found significant differences between Sham + Vehicle and ICH groups (Vehicle, Gleevec). Branching index **(F)** and lacunarity **(G)** in sham nor ICH animals were not altered, except for a significant increase in lacunarity between sham + Vehicle and ICH + Vehicle rats. The distribution of LFD histograms **(H)** exhibited significant decreases in skewness, kurtosis and peak frequency across groups ($p < 0.05$) but *post-hoc* testing observed significant decreases only in sham groups. (one way Anova with Tukey's multiple comparisons, $^{**}p < 0.03$, $^{*}p < 0.05$).

p = 0.08) (**Figure 3F**). Again, the largest reductions were in the ICH + Gleevec rats. Lacunarity was increased in ICH animals where a significant increase in lacunarity was observed in ICH + Vehicle rats compared to Sham + Vehicle (ANOVA, p = 0.02, Tukey's *post hoc* multiple comparisons $p < 0.05$) (**Figure 3G**). Coronal analyses further substantiated a lack of Gleevec in mitigating the acute vascular consequences of ICH on basal ganglia and cortical vessels.

A similar less conservative statistical approach was applied to the coronal cortex and basal ganglia vascular measures (**Supplementary Figure S2**). No significant differences between Sham + Vehicle and Sham + Gleevec nor ICH + Vehicle and ICH + Gleevec groups were reported for classical vessel features. However, we found fractal measures were significantly decreased in Sham + Vehicle and Sham + Gleevec rats (**Supplementary Figure S2D**) with no differences observed between ICH + Vehicle and ICH + Gleevec groups. Again, the ANOVA and the *t*-tests for group differences essentially reported similar results.

Fractal Analysis

In the axial hemisphere fractal measures, skewness, kurtosis and peak frequency of the local fractal dimensions, were determined. Analysis of the ipsilateral axial cortex found that skewness, kurtosis and peak frequency were significantly reduced ($p < 0.05$) (**Figure 3D**). In the axial cortex Gleevec caused significant reductions ($p < 0.03$) in both skewness and kurtosis of the LFD histograms by 8.6 and 23.1% respectively in Sham + Gleevec compared to Sham + Vehicle animals (**Figure 3D**). Peak frequency of the local frequency dimension (LFD) histograms, which is a measure of the number of vessels, was also reduced by 10.3% in ICH + Vehicle compared to Sham + Vehicle animals but did not reach significance (p = 0.09). Gleevec resulted in no significant differences in fractal measures between the ICH groups (ICH + Vehicle vs. ICH + Gleevec).

Analysis of skewness, kurtosis and peak frequency of the LFD histograms of the ipsilateral coronal basal ganglia and cortex found significant differences when compared across all groups (**Figure 3H**) ($p < 0.05$). *Post hoc* analysis of ipsilateral coronal basal ganglia and cortical regions showed that Gleevec resulted in significant reductions ($p < 0.03$; *t*-test) in skewness, kurtosis and peak frequency of the LFD histograms by 15.9, 63.2, and 12.0% respectively in Sham + Gleevec compared to Sham + Vehicle animals. Gleevec resulted in no differences in fractal measures between the ICH groups (ICH + Vehicle vs. ICH + Gleevec), although post-hoc analyses observed significant changes between the sham groups ($^*p < 0.05$). These findings match those of the ipsilateral axial cortex (**Figure 3D**).

The Gleevec fractal results suggest possible alterations in ipsilateral vascular complexity compared to otherwise intact animals (Shams) at 24 h after ICH. These reductions in vascular complexity could play a role in the reported cerebral edema caused by Gleevec in patients with CML4 (Soverini et al., 2018).

Confocal Vascular Features

The effects of Gleevec on the cerebral vasculature were assessed from axial and coronal confocal images derived from vessel painted brains (**Figure 4**). All confocal images were acquired adjacent to the site of injection. As can be readily appreciated by visual inspection, Gleevec resulted in reductions in vascular density in ICH rats compared to ICH + Vehicle treated rats (**Figures 4A,B**). Vessel density was significantly reduced (p = 0.05) in ICH + Gleevec compared to ICH + Vehicle rats in axial cortex (**Figure 5A**). Branching index was also reduced with a trend to significance (p = 0.052) as was mean vessel length (p = 0.06) but lacunarity was significantly increased in

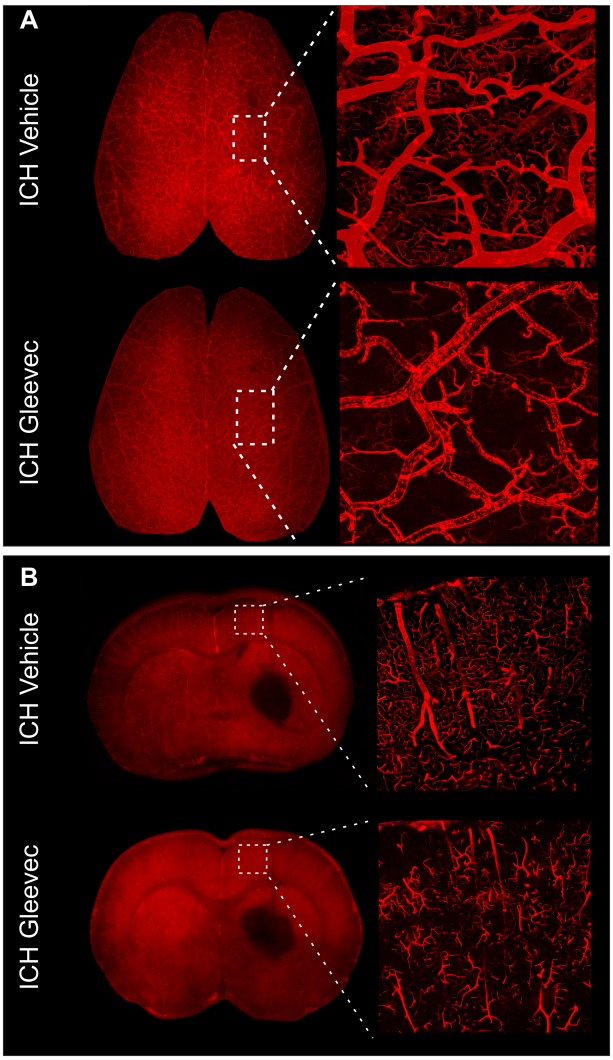

FIGURE 4 | Gleevec treatment does not improve the morphology of the cortical vasculature. **(A)** Vessel painted brains from the axial surface were imaged using confocal microscopy and then subjected to classical vascular analysis. ICH vehicle and ICH Gleevec animals exhibited uniform staining of large, intermediate and small vessels within the cortex. Note the apparent loss of fine branching vessels in the ICH + Gleevec rats. **(B)** In coronal sections from vessel painted brains, the cortical vessels descending into the cortex exhibited a dense plexus of vessels in ICH Vehicle treated rats. In contrast, ICH Gleevec treated rats showed a reduced vascular plexus with fragmented vessels and regions with overt loss of vasculature (see **Figure 5** for quantification).

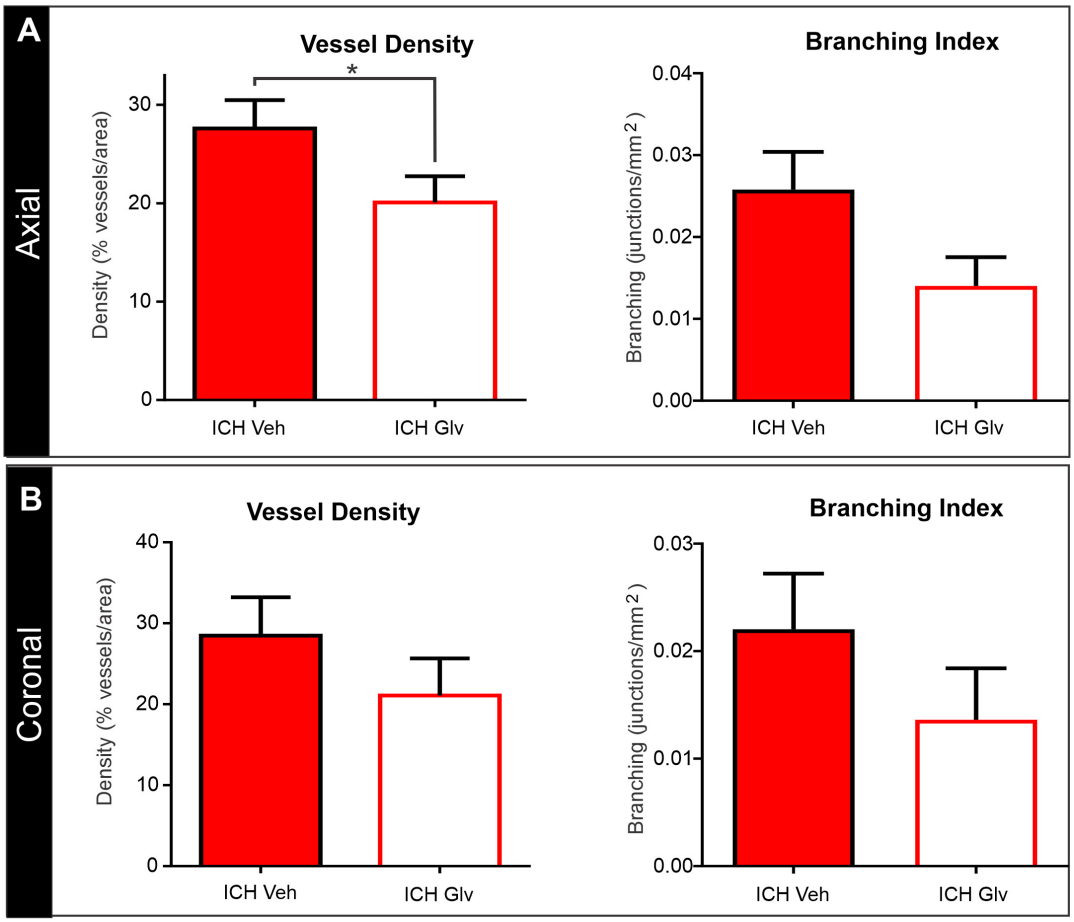

FIGURE 5 | Confocal vascular analysis also demonstrated that Gleevec treatment does not improve vascular density. **(A)** Quantitative assessment of axial cortical vascular features adjacent to the ICH injection site, revealed significant decrements in vascular density and trending decreases in vessel branching after Gleevec treatment. **(B)** Vascular features from cortical sections from coronal tissues also showed decreased vascular density and branching but did not reach significance. Note that both cortical assessments (axial vs. coronal) had similar relative decreases in vascular features (see **Figure 4** for images) (*$p < 0.05$).

ICH + Gleevec treated rats compared to ICH + Vehicle controls ($p = 0.03$). In the coronal cortex, no significant differences in vessel density ($p = 0.14$), branching index ($p = 0.13$), total vessel length ($p = 0.09$) nor lacunarity ($p = 0.06$) were observed, although some features were trending (**Figure 5B**).

We also examined vascular features in the basal ganglia adjacent to the hematoma (**Figure 6**). As can be seen in the confocal microscopy images there was an overt reduction in vessel density in Gleevec treated rats (**Figure 6A**). Quantification demonstrated a significant decrease in vessel density ($p = 0.05$) in ICH + Gleevec compared to ICH + vehicle treated rats (**Figure 6B**). Lacunarity in the ICH + Gleevec rats was also significantly increased ($p = 0.04$) compared to ICH + Vehicle controls. No significant differences were found in branching index ($p = 0.09$) nor total vessel length ($p = 0.70$) (data not shown).

Magnetic Resonance Imaging (MRI)

High resolution *ex vivo* MRI was undertaken to assess hematoma (SWI) and edema (T2WI) volumes (T2WI) (**Figure 7**). Hematoma volumes were outlined from ICH + Vehicle and ICH + Gleevec rats as shown in **Figure 7A** (red dotted line). There were no statistical differences for hematoma volumes between the two groups (**Figure 7B**), where hematoma volumes for ICH + Vehicle rats were 2.30 ± 0.23% of brain volumes and ICH + Gleevec rats had 1.96 ± 0.21% ($p = 0.31$). Similarly, for edema volumes there were no significant differences between groups (**Figure 7C**). Edema volumes corrected for brain volumes were 2.14 ± 0.28% and 2.22 ± 0.38% in ICH + Vehicle and ICH + Gleevec rats, respectively.

To assess relationship between vascular features and MRI lesion (hematoma + edema) volumes, we correlated vascular complexity measures (skewness, kurtosis, peak LFD value, and peak frequency) to total ICH lesion volumes (**Figure 7D**). In ICH + Vehicle treated rats, lesion volume (right hemisphere) was significantly correlated to skewness ($R^2 = 0.6725$, $p = 0.0127$), kurtosis ($R^2 = 0.6665$, $p = 0.0134$), and peak frequency ($R^2 = 0.6290$, $p = 0.0189$), but not for maximum LFD ($R^2 = 0.1194$, $p = 0.4019$) (**Figure 7D**). We

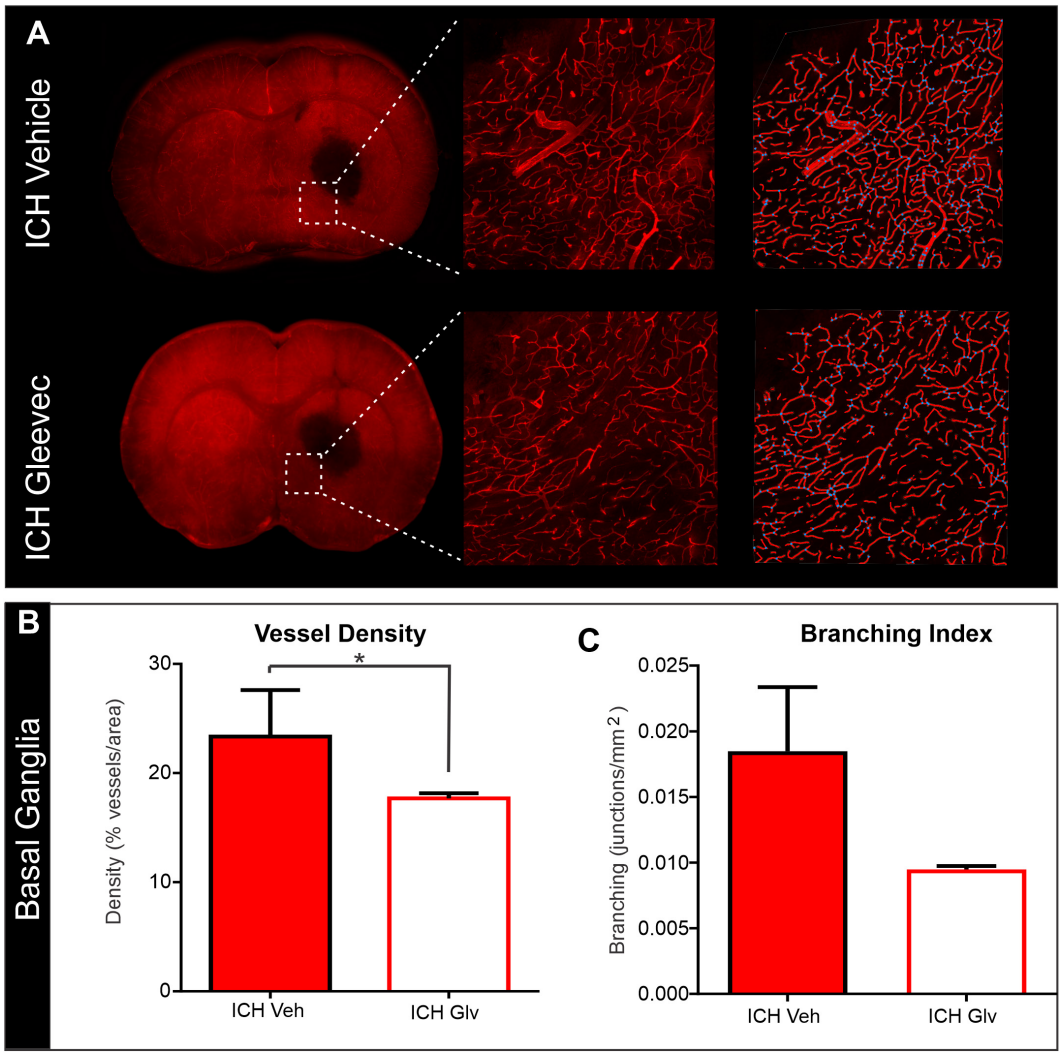

FIGURE 6 | Confocal analysis of the basal ganglia vasculature revealed no improvement with Gleevec treatment. **(A)** The basal ganglia vasculature was assessed for morphological characteristics adjacent to the ICH site. As in the cortex, there was reduced vascular density with loss of fine vascular structures, including branch points. Far right pane illustrates the analysis that derived vessel density (red) and branching (blue dots). **(B)** Quantification of vascular metrics confirmed the visual observations with significantly reduced vascular density ($p = 0.05$) and trending decreases in **(C)** vessel branching ($p = 0.09$) in Gleevec treated compared to Vehicle treated rats.

did not observe any such correlations in ICH + Gleevec treated rats (**Table 1**). **Table 1** outlines a number of additional correlations that were undertaken with respect to whole brain and lesion volumes (cortical vs. subcortical). Interestingly, axial cortical measures of vascular density also did not yield any significant correlations to MRI derived volumes (**Table 1**).

In summary, at 24 h post-ICH there were no significant differences in hematoma, edema nor total lesion volumes as derived from MRI. However, MRI volumes did reflect alterations in vascular complexity but only in ICH vehicle rats. These results further suggest that Gleevec treatment alters vascular phenotype acutely after ICH.

DISCUSSION

A comprehensive examination of the morphological vascular features after ICH is lacking and prior to evaluation of putative neuroprotective compounds a more complete understanding of how ICH modifies the cerebrovasculature is required. Toward filling this knowledge gap, we now report that ICH resulted in decrements of vascular features acutely following ICH. Specifically, the novel findings we report are, (a) the application of our unique vessel painting methodology to the ICH model, (b) significant reductions in classical vessel features including vessel density and branching, (c) these reductions in vascular morphology are present even distant from the ICH lesion (i.e., cortex, contralateral brain tissues), and (d)

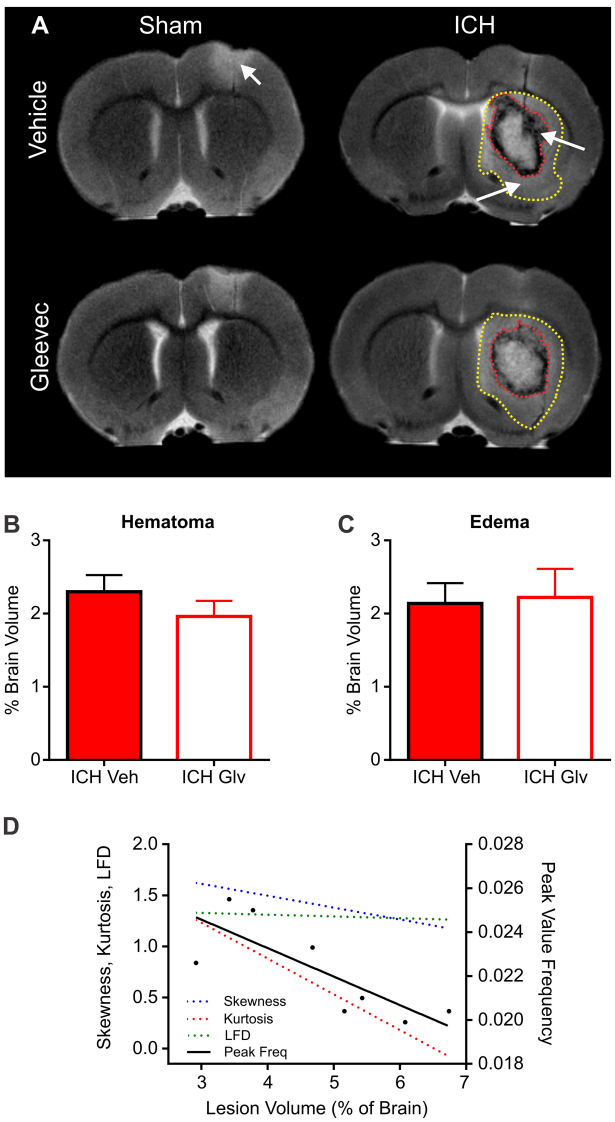

FIGURE 7 | Lesion and hemorrhage volumes were not modified by Gleevec treatment 24 h after ICH. **(A)** Representative MR images from Vehicle and Gleevec treatment rats. Shams exhibited cortical edema (white arrow) at the site of needle insertion. In ICH animals there were hypo- and hyperintense regions visible in the basal ganglia, consistent with blood (red dotted line) and edema (yellow dotted line), respectively (white arrows). **(B)** Subcortical hematoma volumes were not significantly altered between shams and Gleevec treated rats. **(C)** Volume of subcortical edema volumes was not significantly different following Gleevec treatment. **(D)** Correlations of total ICH lesion (blood + edema) volumes compared to ipsilateral fractal properties of ICH vehicle treated rat's revealed significant correlations. The lesion volume was strongly correlated to fractal skewness (R^2 = 0.6725, p = 0.0127), kurtosis (R^2 = 0.6665, p = 0.0134), and peak frequency (R^2 = 0.6290, p = 0.0189), but not for LFD (R^2 = 0.1194, p = 0.4019). See **Table 1** for additional correlations.

measures of vessel complexity using fractal analyses also report decrements. In addition, we used Gleevec to restore or blunt these vessel morphological decrements. Gleevec did not result in improvements but resulted additional vascular reductions in the cortex and in the basal ganglia. Thus, ICH leads to loss of vessels and morphology at 1 day post-injury and Gleevec induces a further exacerbation of vascular density loss.

The effects of ICH on cerebral vessels and blood flow in animal models and in human subjects have been previously described (Zazulia et al., 2001; Xie et al., 2012) and detailed in a recent review (Keep et al., 2014). Most studies investigating the vascular effects of ICH focused on the components of the neurovascular unit (NVU), endothelia, astrocytes and pericytes, with an eye toward blood brain barrier (BBB) breakdown. The disruption of the BBB by ICH leads to numerous downstream (secondary) events including increased bleeding, neuroinflammation and edema formation (Yang et al., 1994; Chen-Roetling et al., 2015; Leclerc et al., 2018; Xu et al., 2019). An 11% reduction in vessel density and volume was reported adjacent to the ICH lesion using high resolution micro-computed tomography (Xie et al., 2012). Functionally, Zazuila and colleagues found a 44% decrease in cerebral blood flow adjacent to the ICH clot within 24 h, consistent with our results that showed a decrease in vascular density and edema at the same time point (Zazulia et al., 2001). Thus, whilst preservation of the BBB is important following ICH, a more thorough understanding of how the morphology of vessels are modified by ICH is clearly warranted prior to studies targeted to improving the vasculature.

We undertook in the present study a quantitative evaluation of the alterations in vessel morphology acutely after ICH. We report a dramatic ∼20% reduction in vessel density in the whole cortex as well as the ipsilateral and contralateral cortices. The observed reduction was distant from the ICH site of injury and in the basal ganglia we observed a 39% decrement in vascular density. Other vascular metrics such as vessel branching were similarly reduced at 24 h post-ICH induction. The marked reduction in vessel density within the basal ganglia would be expected based on the reported mass effects (Brouwers et al., 2014), ferroptosis (Wan et al., 2019) and associated redox activities known to occur after ICH (Chen-Roetling et al., 2015; reviewed in Keep et al., 2014). What was surprising were the global (ipsi- vs. contralateral) cortical reductions in vessel features (density, branching, etc.). In the acute stages of ICH (<24 h) numerous mechanisms could contribute to distant modifications of brain vessels (Aronowski and Zhao, 2011; Ren et al., 2014; Schlunk and Greenberg, 2015). Indeed, we have reported on a yet unidentified diffusible factor after ICH that can alter the structure of vessels distant from the injury site that likely modifies vessel morphology as well as function (Pearce et al., 2016).

We suggest that a combination of factors contribute to the reductions in vessel features we observed following ICH. Firstly, as we and others have reported there is a significant edematous response within the basal ganglia surrounding the perihematomal region (Yang et al., 1994; Belayev et al., 2003; Xu et al., 2019). This robust disruption of the vasculature and subsequent BBB leads to increased vascular permeability and edema formation (see **Figure 7**) in the collagenase model of ICH. Secondly, the deposition of red blood cells and subsequent lysis increase iron and thrombin at the ICH lesion site (Hua et al., 2007; Wan et al., 2019). This results in a neuroinflammatory cascade that certainly further exacerbates existing vessels and might play a significant role in subsequent lesion expansion. A number of

TABLE 1 | Summary of correlations between MRI derived lesion volumes and fractal vascular features where strong correlations (green) are color coded, as are *p*-values.

	Skewness		Kurtosis		LFD		Peak frequency	
ICH Vehicle	R^2	*p*	R^2	*p*	R^2	*p*	R^2	*p*
Total les vs. coronal RH	0.6725	**0.0127**	0.6665	**0.0134**	0.1194	0.4019	0.629	**0.0189**
Total les vs. coronal LH	0.6085	0.0672	0.5436	0.0945	0.6653	0.0478	0.01111	0.8425
Total les vs. coronal WB	0.6491	**0.0158**	0.5881	**0.0264**	0.3343	0.1333	0.4267	0.079
Sub-cort les vs. coronal RH	0.5532	**0.0344**	0.5389	**0.0381**	0.07283	0.518	0.5002	**0.0498**
Sub-Cort Les vs. Coronal LH	0.567	0.084	0.5252	0.1033	0.00957	0.8537	0.577	0.0797
Sub-Cort Les vs. Coronal WB	0.7231	**0.0075**	0.6517	**0.0154**	0.4752	0.0586	0.4573	0.0656
Cort les vs. axial RH	0.09392	0.4225	0.08223	0.4544	0.1859	0.2466	0.1527	0.2984
Cort les vs. axial LH	0.1099	0.3835	0.1081	0.3876	0.3016	0.1257	0.1279	0.3447
Cort les vs. axial WB	0.0979	0.4123	0.09031	0.432	0.1273	0.3459	0.1821	0.252
ICH Gleevec								
Total les vs. coronal RH	0.8509	0.0775	0.00443	0.9334	0.1853	0.5695	0.09991	0.6839
Total les vs. coronal LH	0.06086	0.6375	0.04209	0.6966	0.00248	0.9254	0.02985	0.7434
Total les vs. coronal WB	0.01243	0.8335	0.00467	0.8976	0.01133	0.8409	0.02128	0.7827
Sub-cort les vs. coronal RH	0.7422	0.1385	0.0002	0.986	0.1096	0.6689	0.1348	0.6329
Sub-cort les vs. coronal LH	0.02626	0.7591	0.01368	0.8254	0.00023	0.977	0.00856	0.8616
Sub-cort les vs. coronal WB	0.0289	0.7475	0.02346	0.7721	0.3841	0.1894	0.01456	0.8199
Cort les vs. axial RH	0.3401	0.2244	0.3328	0.2306	0.2258	0.3408	0.2603	0.3011
Cort les vs. axial LH	0.01057	0.8463	0.00215	0.9305	0.2705	0.2902	0.00046	0.968
Cort les vs. axial WB	0.0791	0.5892	0.08711	0.5701	0.2529	0.3092	0.0671	0.6201

*The red to green spectrum indicates the strength of the correlation, where red is poor and green a strong correlation. Lesion = total lesion volume comprised of hematoma + edema (see **Figure 7**). Total Les, total lesion volume; Sub-Cort, sub-cortical; Cort, cortical; RH, right hemisphere (ipsilateral); LH, left hemisphere (contralateral); WB, whole brain. Bolded values indicate statistical significance ($p < 0.05$).*

key proteins involved in inflammation, necrosis and apoptosis, have been shown to be upregulated acutely after ICH induction (Ren et al., 2014). Thirdly, a number of endothelial junction proteins and regulatory mechanisms that act synergistically to maintain vascular integrity are known to be impacted by ICH and have been comprehensively reviewed recently (Keep et al., 2018). Thus, a wide range of cellular and molecular mechanisms could directly impact vessel morphology both at the ICH lesion and surrounding tissues and also at distant cortical structures. Further research is needed to clarify the mechanisms that impact the cerebrovascular network after ICH.

A range of interventions have been applied to mitigate the neurobiological effects of ICH and its subsequent poor outcomes (Hatakeyama et al., 2013; Chen-Roetling et al., 2015; Yang et al., 2016; Leclerc et al., 2018; Xu et al., 2019). However, most of the interventions for ICH to date have been neuro-centric, that is, focused on neuroprotection. While protection of cellular elements such as neurons is important, an intact vascular network is critical for neuroprotection with the delivery of nutrients and removal of waste products. There is increasing recognition that platelet-derived growth factor (PDGF; a sub-family of tyrosine kinase receptors) and its various ligands and receptors are critical for the health and stability of endothelial cells and pericytes (Kazlauskas, 2017; Heldin et al., 2018). PDGFs and their isoforms have also provided new treatment options, particularly for manipulating angiogenesis in cancer (Paulsson et al., 2014; Heldin et al., 2018). Foundational studies developed therapeutic interventions targeting tyrosine kinase in vessels to inhibit tumor growth by targeting angiogenic processes, including those associated with PDGFs (Soverini et al., 2018).

As noted above, we and others have targeted PDGF receptors as a therapeutic option for ICH using Gleevec (imatinib mesylate) (Ma et al., 2011; Pearce et al., 2016; Yang et al., 2016). We found that Gleevec treatment following ICH blunts the phenotypic transformation of smooth muscle surrounding arteries (Pearce et al., 2016), reduced BBB disruption leading to improved outcomes (Ma et al., 2011) and mitigated plasmin induced vascular inflammation (Yang et al., 2016). Many of the beneficial effects of Gleevec were found to occur acutely (<24 h) with long term improvements but the direct effects on vascular morphology have not been reported upon.

While arterial smooth muscle phenotypes are rescued by Gleevec, likely through modulation of neuroinflammation, there have been no direct studies examining the vascular morphology after Gleevec treatment. We sought to examine the effectiveness of Gleevec treatment delivered within 1 h after ICH in preventing the vascular alterations observed after lesion induction. Much to our surprise, in general, we found no improvements in cortical vascular morphology after Gleevec treatment 24 h after ICH. ICH + Gleevec rats had significant reductions in vascular measures compared to Sham + Vehicle treated rats, but statistical analyses of group measures found no statistically significant differences between ICH + Gleevec and ICH + Vehicle rats (see **Figure 3**). When comparisons were made for both axial and coronal vessel painted brain sections of the cortex, a modest but significant reduction in vessel density was reported (**Figure 5**). Despite statistically insignificant

reductions in vascular parameters there appeared to be an overall trend for continued decrements following ICH + Gleevec treatment compared to ICH + Vehicle treated rats in both visual assessments and quantitative findings (**Figures 3–5**). The perihematomal region also had statistically significant reductions in vessel density but not vessel junctions (**Figure 6**). Gleevec also did not modify edema nor blood volumes at 24 h after ICH. Overall, Gleevec did not directly improve vascular morphological features at 24 h after treatment. In fact, in some measures there appeared to be a modest further reduction in vascular elements.

Initially, we were surprised by the lack and perhaps enhanced detrimental effects of Gleevec. There are several factors that could be responsible for the lack of therapeutic effectiveness on the vessels. One clear possibility is that we assessed vessel morphology during the early acute phase of the ICH injury, a period during which many molecular processes are being activated (Ren et al., 2014). The prevention of acute changes in vascular smooth muscle we previously reported appeared to be due in part to probable reductions in neuroinflammatory processes (Yang et al., 2016). Further, in CD163−/− mice there was a decreased acute (3 days) inflammatory response to ICH (Leclerc et al., 2018). Similarly, heme oxygenase 1 (HO-1) activation and overexpression in astrocytes improved BBB disruption after ICH, acutely (Chen-Roetling et al., 2015). HO-1 has also been shown to have a vasoprotective effect on vessels in the retina (He et al., 2014). Thus, inflammatory mediators in conjunction with coagulopathic mechanisms that are known to be active during ICH may acutely inhibit vascular remodeling necessary for long-term neurological improvements (Ren et al., 2014; Liu et al., 2018). It is also possible that Gleevec treatment modified vessel staining while using the vessel painting method. However, we do not believe that Gleevec resulted in adverse vessel labeling as we utilized a potent vasodilator, sodium nitroprusside, at the time of perfusion (see methods). Further, several reports have reported a suppression of vascular contractility following Gleevec treatment (Gur et al., 2013; Tang, 2015) including our own findings (Pearce et al., 2016).

PDGF is well known to have angiogenic activities and differential roles for its isoforms have been noted including recruitment of pericytes (Zhang et al., 2009). Tan and colleagues reported increased angiogenesis around the hematoma at 7–14 days after ICH likely via a vascular endothelial growth factor (VEGF) mechanisms (Tang et al., 2007) and confirmed in subsequent reports (Zhou et al., 2012). This vascular repair timeline is very similar to what we have reported in traumatic brain injury, albeit via a Wnt/β-catenin mechanism (Salehi et al., 2018a). In stroke, Gleevec protected the BBB, as well as "normalized" vessels within the brain early (1 h) post-injury (Su et al., 2008). It is likely that in our acute ICH study we did not observe any angiogenic potential due to Gleevec treatment, as this repair mechanism under baseline conditions appears to take several days. In future studies we will evaluate the previously reported spontaneous angiogenesis and whether this might be accelerated by Gleevec treatment.

Gleevec and subsequent generation tyrosine kinase inhibitors are known to act at BCR-ABL and c-KIT sites that can regulate the response of the cerebrovasculature following brain injury (see Rossari et al., 2018, review). However, adverse vascular events have been reported in patients treated with Gleevec or other related tyrosine kinase inhibitors (Pasvolsky et al., 2015). It is intriguing to speculate that the early lack of effect on vascular morphology seen in our study could be related to downstream effects of Gleevec on BCR-ABL on Wnt/β-catenin cascades (Cilloni and Saglio, 2012) which we have previously reported is involved in late vascular remodeling following traumatic brain injury (Salehi et al., 2018a).

Neuroimaging using clinically relevant modalities such as computed tomography and magnetic resonance imaging (MRI) are potent methods for non-invasively assessing the degree of hemorrhage and edema in patients and in preclinical models (Belayev et al., 2003; Goh et al., 2015; Heit et al., 2017). In our present study we also acquired T2 weighted MRI for edema and susceptibility weighted (SWI) MRI for blood content to assess if there was a correlation between vessel features and clinically relevant MRI. No correlations were observed between classical vascular measures (density, etc.) and lesion volumes. However, as noted in **Table 1** and in **Figure 7** there were several strong correlations between total lesion volumes and vessel features derived from fractal measures of vascular complexity in ICH + Vehicle treated rats. We observed that vascular complexity was reduced after ICH but not in ICH + Gleevec rats. For example, as lesion volume (edema + hematoma) increases, vascular complexity was reduced (**Figure 7D**, peak frequency reductions). Similar, reductions in vascular complexity using fractal analysis was observed at 1d post-traumatic brain injury (Obenaus et al., 2017). Interestingly, Gleevec treatment resulted in a loss of significant correlations between lesion characteristics and fractal features of complexity (**Table 1**). While it is difficult to ascertain what the underlying mechanism(s) might be for Gleevec in modulating vascular complexity, it is clear that many of the smaller vessels appear to be lost after treatment (see **Figure 4**). It is possible that the global reduction in vascular complexity due to Gleevec treatment could further disrupt fractal measures leading to loss of correlative measures. Interestingly, fractal analysis of ICH lesions from computed tomography were found to be a good predictor of outcomes (Klis et al., 2018). Thus, MRI-derived hematoma and edema volumes can reflect the relative loss of vascular complexity, but additional research is needed to corroborate these findings.

CONCLUSION

In conclusion, this study for the first-time reports on quantitative measures of the vascular network within 24 h after ICH induction using a novel vessel painting methodology (Salehi et al., 2018b). The acute reductions in vessel density (and other features) after ICH were not reversed by treatment with Gleevec. While previous reports have suggested a restorative effect on vessels with Gleevec treatment, these studies did not directly assess vessel morphology but rather constituents of the BBB and/or artery smooth muscle phenotypes (Pearce et al., 2016; Yang et al., 2016). Inhibition of inflammatory mediators appears to restore the neurovascular unit and

limit BBB disruption but in our hands Gleevec did not appreciably alter the morphology of the vascular network (Wang and Dore, 2007; Mracsko and Veltkamp, 2014). BBB improvements and PDGF modulation of neuroinflammation are likely independent of vessel morphology. Vascular morphology has at least two important components, (a) number of arteries/capillaries and (b) structure of arteries/capillaries. While loosely related modification in one aspect does not necessarily lead to alterations in the other. Smooth muscle can also upregulate and downregulate expression of membrane receptors and ion channels, without any obvious change in structure. From this perspective, our observed changes in vessels are a somewhat crude assessment of vascular response. While it was not examined in the present study, future studies should examine vascular reactivity and perfusion as they are important in understanding the cellular and molecular underpinnings for the vascular morphological changes we observed. Finally, MRI derived hematoma measures related to vascular complexity in ICH + Vehicle but not ICH + Gleevec treated rats. More research is required to better understand the relationship between the vascular network's response to ICH and how putative therapies may enhance vessel structure and function. Thus, vascular morphology is an important outcome measure in assessing future therapies for treatment of ICH.

DATA AVAILABILITY STATEMENT

The datasets generated for this study are available on request to the corresponding author.

ETHICS STATEMENT

The animal study was reviewed and approved by Loma Linda University Institutional Animal Care and Use, Loma Linda University.

AUTHOR CONTRIBUTIONS

All authors had full access to all the data in the study and take responsibility for the integrity of the data and the accuracy of the data analysis. MA, MH, JT, WP, JZ, and AO: conceptualization. MA, MH, DN, and AO: investigation. MA, MH, and EH: formal analysis. MA, MH, and AO: writing – original draft. MA, MH, JT, WP, JZ, and AO: writing – review and editing. MA, MH, EH, and AO: visualization. AO: supervision. JZ, JT, WP, and AO: funding acquisition.

FUNDING

This work was supported by the NIH Program Project Grant from NINDS 1PO1NS082184, Projects 2, 3.

ACKNOWLEDGMENTS

A portion of this research used resources in the Loma Linda University School of Medicine Advanced Imaging and Microscopy Core, a facility that is supported in part by the National Science Foundation through the Major Research Instrumentation program of the Division of Biological Infrastructure Grant No. 0923559 and the Loma Linda University School of Medicine.

SUPPLEMENTARY MATERIAL

The Supplementary Material for this article can be found online at: https://www.frontiersin.org/articles/10.3389/fnins.2020.00046/full#supplementary-material

REFERENCES

Aguilar, M. I., and Brott, T. G. (2011). Update in intracerebral hemorrhage. *Neurohospitalist* 1, 148–159. doi: 10.1177/1941875211409050

Aronowski, J., and Zhao, X. (2011). Molecular pathophysiology of cerebral hemorrhage: secondary brain injury. *Stroke* 42, 1781–1786. doi: 10.1161/STROKEAHA.110.596718

Belayev, L., Saul, I., Curbelo, K., Busto, R., Belayev, A., Zhang, Y., et al. (2003). Experimental intracerebral hemorrhage in the mouse: histological, behavioral, and hemodynamic characterization of a double-injection model. *Stroke* 34, 2221–2227. doi: 10.1161/01.str.0000088061.06656.1e

Broderick, J. P., Adams, H. P., Barsan, W., Feinberg, W., Feldmann, E., Grotta, J., et al. (1999). Guidelines for the management of spontaneous intracerebral hemorrhage - a statement for healthcare professionals from a special writing group of the stroke council, American Heart Association. *Stroke* 30, 905–915. doi: 10.1161/01.str.30.4.905

Broderick, J. P., Brott, T. G., Duldner, J. E., Tomsick, T., and Huster, G. (1993). Volume of intracerebral hemorrhage. A powerful and easy-to-use predictor of 30-day mortality. *Stroke* 24, 987–993. doi: 10.1161/01.str.24.7.987

Brouwers, H. B., Chang, Y., Falcone, G. J., Cai, X., Ayres, A. M., Battey, T. W., et al. (2014). Predicting hematoma expansion after primary intracerebral hemorrhage. *JAMA Neurol.* 71, 158–164. doi: 10.1001/jamaneurol.2013.5433

Chen, S., Zhao, B., Wang, W., Shi, L., Reis, C., and Zhang, J. (2017). Predictors of hematoma expansion predictors after intracerebral hemorrhage. *Oncotarget* 8, 89348–89363. doi: 10.18632/oncotarget.19366

Chen-Roetling, J., Song, W., Schipper, H. M., Regan, C. S., and Regan, R. F. (2015). Astrocyte overexpression of heme oxygenase-1 improves outcome after intracerebral hemorrhage. *Stroke* 46, 1093–1098. doi: 10.1161/STROKEAHA.115.008686

Cheung, C. Y., Thomas, G. N., Tay, W., Ikram, M. K., Hsu, W., Lee, M. L., et al. (2012). Retinal vascular fractal dimension and its relationship with cardiovascular and ocular risk factors. *Am. J. Ophthalmol.* 154, 663–674.e1. doi: 10.1016/j.ajo.2012.04.016

Cilloni, D., and Saglio, G. (2012). Molecular pathways: BCR-ABL. *Clin. Cancer Res.* 18, 930–937. doi: 10.1158/1078-0432.CCR-10-1613

Di Ieva, A., Grizzi, F., Ceva-Grimaldi, G., Russo, C., Gaetani, P., Aimar, E., et al. (2007). Fractal dimension as a quantitator of the microvasculature of normal and adenomatous pituitary tissue. *J. Anat.* 211, 673–680. doi: 10.1111/j.1469-7580.2007.00804.x

Feigin, V. L., Lawes, C. M., Bennett, D. A., Barker-Collo, S. L., and Parag, V. (2009). Worldwide stroke incidence and early case fatality reported in 56 population-based studies: a systematic review. *Lancet Neurol.* 8, 355–369. doi: 10.1016/S1474-4422(09)70025-0

Fisher, C. M. (1971). Pathological observations in hypertensive cerebral hemorrhage. *J. Neuropathol. Exp. Neurol.* 30, 536–550. doi: 10.1097/00005072-197107000-00015

Gebel, J. M., Jauch, E. C., Brott, T. G., Khoury, J., Sauerbeck, L., Salisbury, S., et al. (2002). Relative edema volume is a predictor of outcome in patients with hyperacute spontaneous intracerebral hemorrhage. *Stroke* 33, 2636–2641. doi: 10.1161/01.str.0000035283.34109.ea

Godement, P., Vanselow, J., Thanos, S., and Bonhoeffer, F. (1987). A study in developing visual systems with a new method of staining neurones and their processes in fixed tissue. *Development* 101, 697–713.

Goh, S. Y., Irimia, A., Torgerson, C. M., Tubi, M. A., Real, C. R., Hanley, D. F., et al. (2015). Longitudinal quantification and visualization of intracerebral haemorrhage using multimodal magnetic resonance and diffusion tensor imaging. *Brain Inj.* 29, 438–445. doi: 10.3109/02699052.2014.989907

Gur, S., Sikka, S. C., Abdel-Mageed, A. B., Abd Elmageed, Z. Y., Rezk, B., Pankey, E., et al. (2013). Imatinib mesylate (Gleevec) induces human corpus cavernosum relaxation by inhibiting receptor tyrosine kinases (RTKs): identification of new RTK targets. *Urology* 82, 745.e11–745.e16. doi: 10.1016/j.urology.2013.04.030

Hatakeyama, T., Okauchi, M., Hua, Y., Keep, R. F., and Xi, G. H. (2013). Deferoxamine reduces neuronal death and hematoma lysis after intracerebral hemorrhage in aged rats. *Transl. Stroke Res.* 4, 546–553. doi: 10.1007/s12975-013-0270-5

He, C., Zhao, C., Kumar, A., Lee, C., Chen, M., Huang, L., et al. (2014). Vasoprotective effect of PDGF-CC mediated by HMOX1 rescues retinal degeneration. *Proc. Natl. Acad. Sci. U.S.A.* 111, 14806–14811. doi: 10.1073/pnas.1404140111

Heit, J. J., Iv, M., and Wintermark, M. (2017). Imaging of intracranial hemorrhage. *J. Stroke* 19, 11–27. doi: 10.5853/jos.2016.00563

Heldin, C. H., Lennartsson, J., and Westermark, B. (2018). Involvement of platelet-derived growth factor ligands and receptors in tumorigenesis. *J. Intern. Med.* 283, 16–44. doi: 10.1111/joim.12690

Honig, M. G., and Hume, R. I. (1986). Fluorescent carbocyanine dyes allow living neurons of identified origin to be studied in long-term cultures. *J. Cell Biol.* 103, 171–187. doi: 10.1083/jcb.103.1.171

Hua, Y., Keep, R. F., Hoff, J. T., and Xi, G. H. (2007). Brain injury after intracerebral hemorrhage - the role of thrombin and iron. *Stroke* 38, 759–762. doi: 10.1161/01.str.0000247868.97078.10

Karperien, A., Ahammer, H., and Jelinek, H. F. (2013). Quantitating the subtleties of microglial morphology with fractal analysis. *Front. Cell. Neurosci.* 7:3. doi: 10.3389/fncel.2013.00003

Kazlauskas, A. (2017). PDGFs and their receptors. *Gene* 614, 1–7. doi: 10.1016/j.gene.2017.03.003

Kazui, S., Minematsu, K., Yamamoto, H., Sawada, T., and Yamaguchi, T. (1997). Predisposing factors to enlargement of spontaneous intracerebral hematoma. *Stroke* 28, 2370–2375. doi: 10.1161/01.str.28.12.2370

Kazui, S., Naritomi, H., Yamamoto, H., Sawada, T., and Yamaguchi, T. (1996). Enlargement of spontaneous intracerebral hemorrhage. Incidence and time course. *Stroke* 27, 1783–1787. doi: 10.1161/01.str.27.10.1783

Keep, R. F., Andjelkovic, A. V., Xiang, J., Stamatovic, S. M., Antonetti, D. A., Hua, Y., et al. (2018). Brain endothelial cell junctions after cerebral hemorrhage: changes, mechanisms and therapeutic targets. *J. Cereb. Blood Flow Metab.* 38, 1255–1275. doi: 10.1177/0271678X18774666

Keep, R. F., Zhou, N., Xiang, J., Andjelkovic, A. V., Hua, Y., and Xi, G. (2014). Vascular disruption and blood-brain barrier dysfunction in intracerebral hemorrhage. *Fluids Barriers CNS.* 11:18. doi: 10.1186/2045-8118-11-18

Klis, K. M., Krzyzewski, R. M., Kwinta, B. M., Stachura, K., and Gasowski, J. (2018). Computer-assisted analysis of intracerebral hemorrhage shape and density. *World Neurosurg.* 120, e863–e869. doi: 10.1016/j.wneu.2018.08.178

Leclerc, J. L., Lampert, A. S., Loyola Amador, C., Schlakman, B., Vasilopoulos, T., Svendsen, P., et al. (2018). The absence of the CD163 receptor has distinct temporal influences on intracerebral hemorrhage outcomes. *J. Cereb. Blood Flow Metab.* 38, 262–273. doi: 10.1177/0271678X17701459

Leira, R., Davalos, A., Silva, Y., Gil-Peralta, A., Tejada, J., Garcia, M., et al. (2004). Early neurologic deterioration in intracerebral hemorrhage: predictors and associated factors. *Neurology* 63, 461–467. doi: 10.1212/01.wnl.0000133204.81153.ac

Liu, T., Zhou, J., Cui, H., Li, P., Li, H., Wang, Y., et al. (2018). Quantitative proteomic analysis of intracerebral hemorrhage in rats with a focus on brain energy metabolism. *Brain Behav.* 8:e01130. doi: 10.1002/brb3.1130

Ma, Q., Huang, B., Khatibi, N., Rolland, W. II, Suzuki, H., Zhang, J. H., et al. (2011). PDGFR-alpha inhibition preserves blood-brain barrier after intracerebral hemorrhage. *Ann. Neurol.* 70, 920–931. doi: 10.1002/ana.22549

Mracsko, E., and Veltkamp, R. (2014). Neuroinflammation after intracerebral hemorrhage. *Front. Cell. Neurosci.* 8:388. doi: 10.3389/fncel.2014.00388

Nakamura, T., Keep, R. F., Hua, Y., Nagao, S., Hoff, J. T., and Xi, G. (2006). Iron-induced oxidative brain injury after experimental intracerebral hemorrhage. *Acta Neurochir. Suppl.* 96, 194–198. doi: 10.1007/3-211-30714-1_42

Nakamura, T., Xi, G. H., Park, J. W., Hua, Y., Hoff, J. T., and Keep, R. F. (2005). Holo-transferrin and thrombin can interact to cause brain damage. *Stroke* 36, 348–352. doi: 10.1161/01.str.0000153044.60858.1b

Obenaus, A., Ng, M., Orantes, A. M., Kinney-Lang, E., Rashid, F., Hamer, M., et al. (2017). Traumatic brain injury results in acute rarefication of the vascular network. *Sci. Rep.* 7:239. doi: 10.1038/s41598-017-00161-4

Pasvolsky, O., Leader, A., Iakobishvili, Z., Wasserstrum, Y., Kornowski, R., and Raananni, P. (2015). Tyrosine kinase inhibitor associated vascular toxicity in chronic myeloid leukemia. *Cardiooncology* 1:5.

Paulsson, J., Ehnman, M., and Ostman, A. (2014). PDGF receptors in tumor biology: prognostic and predictive potential. *Future Oncol.* 10, 1695–1708. doi: 10.2217/fon.14.83

Pearce, W. J., Doan, C., Carreon, D., Kim, D., Durrant, L. M., Manaenko, A., et al. (2016). Imatinib attenuates cerebrovascular injury and phenotypic transformation after intracerebral hemorrhage in rats. *Am. J. Physiol. Regul. Integr. Comp. Physiol.* 311, R1093–R1104. doi: 10.1152/ajpregu.00240.2016

Qureshi, A. I., Mendelow, A. D., and Hanley, D. F. (2009). Intracerebral haemorrhage. *Lancet* 373, 1632–1644. doi: 10.1016/S0140-6736(09)60371-8

Ren, C., Guingab-Cagmat, J., Kobeissy, F., Zoltewicz, S., Mondello, S., Gao, M., et al. (2014). A neuroproteomic and systems biology analysis of rat brain post intracerebral hemorrhagic stroke. *Brain Res. Bull.* 102, 46–56. doi: 10.1016/j.brainresbull.2014.02.005

Rossari, F., Minutolo, F., and Orciuolo, E. (2018). Past, present, and future of Bcr-Abl inhibitors: from chemical development to clinical efficacy. *J. Hematol. Oncol.* 11:84. doi: 10.1186/s13045-018-0624-2

Salehi, A., Jullienne, A., Baghchechi, M., Hamer, M., Walsworth, M., Donovan, V., et al. (2018a). Up-regulation of Wnt/beta-catenin expression is accompanied with vascular repair after traumatic brain injury. *J. Cereb. Blood Flow Metab.* 38, 274–289. doi: 10.1177/0271678X17744124

Salehi, A., Jullienne, A., Wendel, K. M., Hamer, M., Tang, J., Zhang, J. H., et al. (2018b). A novel technique for visualizing and analyzing the cerebral vasculature in rodents. *Transl. Stroke Res.* doi: 10.1007/s12975-018-0632-0 [Epub ahead of print].

Schlessinger, J., Axelrod, D., Koppel, D. E., Webb, W. W., and Elson, E. L. (1977). Lateral transport of a lipid probe and labeled proteins on a cell membrane. *Science* 195, 307–309. doi: 10.1126/science.556653

Schlunk, F., and Greenberg, S. M. (2015). The pathophysiology of intracerebral hemorrhage formation and expansion. *Transl. Stroke Res.* 6, 257–263. doi: 10.1007/s12975-015-0410-1

Schneider, C. A., Rasband, W. S., and Eliceiri, K. W. (2012). NIH Image to ImageJ: 25 years of image analysis. *Nat. Methods* 9, 671–675. doi: 10.1038/nmeth.2089

Soverini, S., Mancini, M., Bavaro, L., Cavo, M., and Martinelli, G. (2018). Chronic myeloid leukemia: the paradigm of targeting oncogenic tyrosine kinase signaling and counteracting resistance for successful cancer therapy. *Mol. Cancer* 17:49. doi: 10.1186/s12943-018-0780-6

Su, E. J., Fredriksson, L., Geyer, M., Folestad, E., Cale, J., Andrae, J., et al. (2008). Activation of PDGF-CC by tissue plasminogen activator impairs blood-brain barrier integrity during ischemic stroke. *Nat. Med.* 14, 731–737. doi: 10.1038/nm1787

Tang, D. D. (2015). Critical role of actin-associated proteins in smooth muscle contraction, cell proliferation, airway hyperresponsiveness and airway remodeling. *Respir. Res.* 16:134. doi: 10.1186/s12931-015-0296-1

Tang, T., Liu, X. J., Zhang, Z. Q., Zhou, H. J., Luo, J. K., Huang, J. F., et al. (2007). Cerebral angiogenesis after collagenase-induced intracerebral hemorrhage in rats. *Brain Res.* 1175, 134–142. doi: 10.1016/j.brainres.2007.08.028

Wagner, K. R., Packard, B. A., Hall, C. L., Smulian, A. G., Linke, M. J., De Courten-Myers, G. M., et al. (2002). Protein oxidation and heme oxygenase-1 induction in porcine white matter following intracerebral infusions of whole blood or plasma. *Dev. Neurosci.* 24, 154–160. doi: 10.1159/000065703

Wan, J., Ren, H., and Wang, J. (2019). Iron toxicity, lipid peroxidation and ferroptosis after intracerebral haemorrhage. *Stroke Vasc. Neurol.* 4, 93–95. doi: 10.1136/svn-2018-000205

Wang, J., and Dore, S. (2007). Inflammation after intracerebral hemorrhage. *J. Cereb. Blood Flow Metab.* 27, 894–908.

Xi, G., Keep, R. F., and Hoff, J. T. (2006). Mechanisms of brain injury after intracerebral haemorrhage. *Lancet Neurol.* 5, 53–63. doi: 10.1016/s1474-4422(05)70283-0

Xie, B., Miao, P., Sun, Y., Wang, Y., and Yang, G. Y. (2012). Micro-computed tomography for hemorrhage disruption of mouse brain vasculature. *Transl. Stroke Res.* 3, 174–179. doi: 10.1007/s12975-012-0164-y

Xu, F., Shen, G., Su, Z., He, Z., and Yuan, L. (2019). Glibenclamide ameliorates the disrupted blood-brain barrier in experimental intracerebral hemorrhage by inhibiting the activation of NLRP3 inflammasome. *Brain Behav.* 9:e01254. doi: 10.1002/brb3.1254

Yang, G. Y., Betz, A. L., Chenevert, T. L., Brunberg, J. A., and Hoff, J. T. (1994). Experimental intracerebral hemorrhage: relationship between brain edema, blood flow, and blood-brain barrier permeability in rats. *J. Neurosurg.* 81, 93–102. doi: 10.3171/jns.1994.81.1.0093

Yang, P., Manaenko, A., Xu, F., Miao, L., Wang, G., Hu, X., et al. (2016). Role of PDGF-D and PDGFR-beta in neuroinflammation in experimental ICH mice model. *Exp. Neurol.* 283, 157–164. doi: 10.1016/j.expneurol.2016.06.010

Zazulia, A. R., Diringer, M. N., Videen, T. O., Adams, R. E., Yundt, K., Aiyagari, V., et al. (2001). Hypoperfusion without ischemia surrounding acute intracerebral hemorrhage. *J. Cereb. Blood Flow Metab.* 21, 804–810. doi: 10.1097/00004647-200107000-00005

Zhang, J., Cao, R., Zhang, Y., Jia, T., Cao, Y., and Wahlberg, E. (2009). Differential roles of PDGFR-alpha and PDGFR-beta in angiogenesis and vessel stability. *FASEB J.* 23, 153–163. doi: 10.1096/fj.08-113860

Zhou, H. J., Tang, T., Cui, H. J., Yang, A. L., Luo, J. K., Lin, Y., et al. (2012). Thrombin-triggered angiogenesis in rat brains following experimental intracerebral hemorrhage. *J. Neurosurg.* 117, 920–928. doi: 10.3171/2012.8.JNS112152

Zudaire, E., Gambardella, L., Kurcz, C., and Vermeren, S. (2011). A computational tool for quantitative analysis of vascular networks. *PLoS One* 6:e27385. doi: 10.1371/journal.pone.0027385

Conflict of Interest: The authors declare that the research was conducted in the absence of any commercial or financial relationships that could be construed as a potential conflict of interest.

Copyright © 2020 Abbas, Haddad, Hamer, Nowrangi, Zhang, Pearce, Tang and Obenaus. This is an open-access article distributed under the terms of the Creative Commons Attribution License (CC BY). The use, distribution or reproduction in other forums is permitted, provided the original author(s) and the copyright owner(s) are credited and that the original publication in this journal is cited, in accordance with accepted academic practice. No use, distribution or reproduction is permitted which does not comply with these terms.

frontiers in Neuroscience

ORIGINAL RESEARCH
published: 06 February 2020
doi: 10.3389/fnins.2020.00084

Hierarchical Clustering Analyses of Plasma Proteins in Subjects With Cardiovascular Risk Factors Identify Informative Subsets Based on Differential Levels of Angiogenic and Inflammatory Biomarkers

*Zachary Winder[1,2], Tiffany L. Sudduth[1], David Fardo[1,3], Qiang Cheng[4], Larry B. Goldstein[5], Peter T. Nelson[1,6], Frederick A. Schmitt[1,5], Gregory A. Jicha[1,5] and Donna M. Wilcock[1,2]**

[1] Sanders-Brown Center on Aging, University of Kentucky, Lexington, KY, United States, [2] Department of Physiology, University of Kentucky, Lexington, KY, United States, [3] Department of Biostatistics, University of Kentucky, Lexington, KY, United States, [4] Department of Computer Science, University of Kentucky, Lexington, KY, United States, [5] Department of Neurology, University of Kentucky, Lexington, KY, United States, [6] Department of Pathology, University of Kentucky, Lexington, KY, United States

OPEN ACCESS

Edited by:
Emmanuel Pinteaux, The University of Manchester, United Kingdom

Reviewed by:
Hilario Blasco-Fontecilla, Puerta de Hierro University Hospital, Spain
Fanny M. Elahi, University of California, San Francisco, United States

***Correspondence:**
Donna M. Wilcock
donna.wilcock@uky.edu

Specialty section:
This article was submitted to Neurodegeneration, a section of the journal Frontiers in Neuroscience

Received: *15 May 2019*
Accepted: *21 January 2020*
Published: *06 February 2020*

Citation:
Winder Z, Sudduth TL, Fardo D, Cheng Q, Goldstein LB, Nelson PT, Schmitt FA, Jicha GA and Wilcock DM (2020) Hierarchical Clustering Analyses of Plasma Proteins in Subjects With Cardiovascular Risk Factors Identify Informative Subsets Based on Differential Levels of Angiogenic and Inflammatory Biomarkers. Front. Neurosci. 14:84. doi: 10.3389/fnins.2020.00084

Agglomerative hierarchical clustering analysis (HCA) is a commonly used unsupervised machine learning approach for identifying informative natural clusters of observations. HCA is performed by calculating a pairwise dissimilarity matrix and then clustering similar observations until all observations are grouped within a cluster. Verifying the empirical clusters produced by HCA is complex and not well studied in biomedical applications. Here, we demonstrate the comparability of a novel HCA technique with one that was used in previous biomedical applications while applying both techniques to plasma angiogenic (FGF, FLT, PIGF, Tie-2, VEGF, VEGF-D) and inflammatory (MMP1, MMP3, MMP9, IL8, TNFα) protein data to identify informative subsets of individuals. Study subjects were diagnosed with mild cognitive impairment due to cerebrovascular disease (MCI-CVD). Through comparison of the two HCA techniques, we were able to identify subsets of individuals, based on differences in VEGF ($p < 0.001$), MMP1 ($p < 0.001$), and IL8 ($p < 0.001$) levels. These profiles provide novel insights into angiogenic and inflammatory pathologies that may contribute to VCID.

Keywords: hierarchical clustering analysis, vascular cognitive impairment and dementia, mild cognitive impairment, VEGF, MMP1, IL8

INTRODUCTION

Vascular cognitive impairment and dementia (VCID) is an active area in dementia research (Murphy et al., 2016) and is described as "encompassing all the cognitive disorders associated with cerebrovascular disease (CVD), from dementia to mild cognitive deficits" (Gorelick et al., 2011). VCID is estimated to occur in roughly 20% of the cases of dementia; however, the exact prevalence in the population is unknown with varying estimates in the literature (Rizzi et al., 2014; Corriveau et al., 2016). Much of the uncertainty in assessing the prevalence of VCID is due to varied diagnostic criteria (Harrison et al., 2016). In addition, there is substantial overlap in cognitive manifestations of cerebrovascular and neurodegenerative pathologies [such as Alzheimer's disease (AD)] that can culminate in clinical dementia (Kapasi and Schneider, 2016), which further complicates our

understanding of VCID. Further, both pathologies commonly co-exist in the same individual, yet some autopsy studies suggest that there is a significant increase in dementia risk due to vascular factors when Alzheimer pathology is low (Abner et al., 2017; Dodge et al., 2017).

Currently, magnetic resonance imaging (MRI) and cerebrospinal fluid (CSF) biomarkers are used to differentiate VCID from AD and monitor the progression of VCID (Cipollini et al., 2019; Wardlaw et al., 2019). Plasma biomarkers are currently being investigated as a lower cost and less invasive alternative approach. The current study is focused on exploring the potential clustering of plasma biomarkers using hierarchical clustering analysis (HCA) in participants with VCID who have mild cognitive impairment (MCI) due to CVD (MCI-CVD) to identify unique plasma profiles of disease (Winblad et al., 2004). Persons with MCI-CVD are of particular interest as they are at an increased risk of developing dementia and already have cognitive decline (Petersen et al., 1999). We evaluated angiogenic (FGF, FLT, PIGF, Tie-2, VEGF, VEGF-D) and inflammatory (MMP1, MMP3, MMP9, IL8, TNFα) protein plasma biomarkers in these participants using the highly sensitive meso-scale discoveries (MSD) platform. Angiogenic and inflammatory markers are of particular interest due to their roles in endothelial dysfunction, which has been shown to play a role in the pathogenesis of CVD (Poggesi et al., 2016; Mahoney et al., 2019). Presently, studies have demonstrated mixed results in the association of angiogenic and inflammatory biomarkers with VCID; however, it is suspected that this is due to the inconsistency in both the patient populations and the analytical measures (Cipollini et al., 2019).

Agglomerative HCA is an unsupervised machine learning technique commonly used to determine similar subsets within a larger population (Xu and Wunsch, 2010). HCA can be used to identify subsets within a variety of different patient populations. The accuracy of this technique is difficult to quantify, as most studies rely on *post hoc* analysis of the clusters produced by HCA to determine their validity. We propose a unique methodology for validating clusters produced by HCA. This method relies on using two unique HCA models on the same dataset and evaluates congruencies between the two models by comparing a novel HCA model to one that is widely used (Wallin et al., 2010; Damian et al., 2013; Nettiksimmons et al., 2014; Racine et al., 2016). Before applying both HCA models to our dataset, we tested the accuracy of each model on various distributions of data and compared them to each other using the adjusted rand index (ARI). After demonstrating the interchangeability of the two HCA models in the simulated data distribution comparable to our dataset, we tested both models on our dataset and compared the underlying components of each cluster produced by the HCA models.

MATERIALS AND METHODS

Participants

Plasma samples were collected from a cohort of adult research volunteers enrolled in a randomized behavioral intervention study for MCI-CVD (N = 80, NCT01924312). Inclusion criteria for the parent study include age older than 55 years, Montreal Cognitive Assessment score < 29, and at least one uncontrolled vascular risk factor. Risk factors included poorly controlled hypertension, poorly controlled cholesterol, cardiomyopathy/CHF, diabetes with a fasting glucose > 110 or HbA1c > 7%, homocysteine > 12, history of transient ischemic attack, tobacco use > 30 pack-years, and BMI > 30. Potential subjects were excluded from this cohort if they had dementia, evidence of a non-CVD cause of cognitive decline, evidence of a non-CVD neurologic disease, or any focal motor, sensory, visual, or auditory deficits. For the current study, participants were also excluded if they had an incomplete panel of markers as measured via MSD assays as described below (n = 7).

Plasma Collection and Quantification

Plasma samples were collected by venous puncture using 10 mL EDTA Vacutainer tubes. Plasma was aliquot into cryo-tubes at 500 mL volumes. Quantification of plasma samples was accomplished using MSD Multi-Spot V-PLEX assays [Angiogenesis Panel 1 (human) and Proinflammatory Panel 1 (human)] and Ultra-Sensitive assays (MMP 2-Plex and MMP 3-Plex). Plasma did not undergo any freeze-thaw cycles after the initial thawing of the aliquot. Assays were performed using plate specific protocols as followed with analysis performed in the MSD Discovery Workbench 4.0 software.

MMP 2-Plex and MMP 3-Plex

MMP plates were brought to room temperature for approximately 30 min and then loaded with 25 μL of diluent, covered (protect from light), and incubated at room temperature for 30 min while shaking at 600 r/min. After incubation, plates were removed from the shaker and 25 μL of calibrator was added to the assigned wells in duplicate with 5 μL of undiluted sample and 20 μL of diluent. Plates were covered and incubated at room temperature while shaking at 600 r/min. After incubation, plates were removed from the shaker and washed three times with 300 μL of wash buffer. Plates were turned upside down and tapped against paper towels to ensure the removal of all wash buffer from the wells. 25 μL of the antibody mix was loaded into each well, covered (protect from light), and incubated at room temperature for 2 h shaking at 600 r/min. After incubation, plates were removed from the shaker and the wash steps were repeated from above; 150 μL of read buffer was loaded into each well and read on the MSD Quickplex SQ 120 machine.

Proinflammatory Panel 1

Proinflammatory plates were brought to room temperature for approximately 30 min and washed three times with 300 μL of wash buffer. Plates were turned upside down and tapped against paper towels to ensure the removal of all wash buffer from the wells; 50 μL of calibrator was added to the assigned wells in duplicate with 50 μL of undiluted sample and covered (protect from light). Plates were incubated at 4°C overnight while shaking at 600 r/min. In the morning, plates were removed from 4°C and incubated at room temperature for 1 h while shaking at 600 r/min. After incubation, plated were removed from the shaker and the wash steps were repeated from above; 25 μL of the antibody mix was added into each well, covered (protect

from light), and incubated at room temperature for 2 h shaking at 600 r/min. After incubation, plates were removed from the shaker and wash steps were repeated from above; 150 μL of read buffer was loaded into each well and read on the MSD Quickplex SQ 120 machine.

Angiogenesis Panel 1

Angiogenesis plates were brought to room temperature for approximately 30 min and then loaded with 150 μL of diluent, covered (protect from light), and incubated at room temperature for 1 h while shaking at 600 r/min. After incubation, plates were removed from the shaker and washed three times with 300 μL of wash buffer. Plates were turned upside down and tapped against paper towels to ensure the removal of all wash buffer from the wells; 50 μL of calibrator was added to the assigned wells in duplicate with 25 μL of undiluted sample and 25 μL of diluent. Plates were covered (protect from light) and incubated at 4°C overnight while shaking at 600 r/min. In the morning, plates were removed from 4°C and incubated at room temperature for one hour while shaking at 600 r/min. After incubation, plates were removed from the shaker and wash steps were repeated from above; 25 μL of the antibody mix was added into each well, covered (protect from light), and incubated at room temperature for 2 h shaking at 600 r/min. After incubation, plates were removed from the shaker and wash steps were repeated from above; 150 μL of read buffer was loaded into each well and read on the MSD Quickplex SQ 120 machine.

Samples were run in duplicate and three pooled control samples were run on each plate to measure inter- and intra-plate variability. MSD quantification was performed on a table stabilizer in order to reduce error in MSD plate readings.

Plasma Sample Analysis

Protein markers measured through MSD assays were subjected to intra- and inter-plate variability tests. Intra-plate variability was assessed through two distinct methods. The first method calculated the percentage of samples for each marker that had a coefficient of variation, as determined by the duplicate runs for each sample, greater than or equal to 0.25. Markers that contained 20% of samples above this threshold were removed from further analysis. The second method ran three pooled control sample twice on the same plate (two samples each run in duplicate) to ensure consistency in final quantifications. The coefficient of variation for each of the three controls measured for each marker was then averaged together. Markers with an average coefficient of variation greater than 0.25 were excluded from the analysis. Markers that passed both criteria were included in the final analysis. Inter-plate variability was accounted for using the three pooled control samples run on each plate. Each plate control value was divided by the control mean and all three of these values for each marker were averaged together to provide a plate-scaling factor. Each value was then divided by this factor to adjust for inter-plate variability. The resulting measures were log-transformed to scale each marker to a common order of magnitude, which is required in clustering algorithms to provide equal weighting of markers. Grubb's test was lastly applied to the data to remove outliers (Grubbs, 1950). Individual samples containing one or more outliers in the measured markers were excluded from further analysis (n = 7) due to their effects on clustering techniques. The final dataset consisted of 66 patient plasma samples, which were quantified for 11 plasma markers (FGF, FLT, PLGF, Tie-2, VEGF, VEGFD, MMP1, MMP3, MMP9, IL8, TNFα).

Hierarchical Clustering Analysis

All HCAs were performed using the Matlab Statistics and Machine Learning Toolbox functions *pdist*, *linkage*, and *cluster*. Previously described HCA models were comprised of three different algorithms, distance, linkage, and clustering (Wallin et al., 2010; Damian et al., 2013; Nettiksimmons et al., 2014; Racine et al., 2016). The conventional HCA model consists of a Euclidean distance algorithm, which calculates the distance between two samples using the Euclidean distance formula (a special case of the generalized Minkowski distance formula), where the distance between observations s and t in a sample with n markers equals d_{st}:

$$d_{st} = \sqrt{\sum_{j=1}^{n} |X_{sj} - X_{tj}|^2}$$

The linkage algorithm used was Ward's Linkage, which calculates the incremental increase in within-cluster sum of squares and links samples one at a time until all samples are combined into a single cluster (Xu and Wunsch, 2010). This method combines similar samples until all samples fall within one cluster (i.e., agglomerative hierarchical clustering). The final algorithm in the conventional HCA model used a standard agglomerative clustering approach (Racine et al., 2016).

The novel proposed HCA model uses consensus clustering as presented by Fred and Jain (2002) to combine HCA models with different distance and clustering algorithms. The distance algorithms used the Minkowski distance formula with p ranging from 0.1 to 2.0 in increments of 0.1. The distance between observations s and t in a sample with n markers equals d_{st}:

$$d_{st} = \sqrt[p]{\sum_{j=1}^{n} |X_{sj} - X_{tj}|^p}$$

Each distance algorithm's data were then used with the weighted average linkage algorithm, which combines samples

TABLE 1 | Means ± standard deviation for age, MMSE, and MoCA for the MCI-CVD cohort population in addition to percent of female participants.

	Mean ± SDev	Range
Age (years)	75.07 ± 8.14	(56.99–89.22)
MMSE	26.86 ± 2.95	(18–30)
MoCA	22.11 ± 3.74	(11–28)
Systolic blood pressure (mmHg)	141.33 ± 15.31	(102–185)
Hemoglobin A1c (%)	6.18 ± 1.31	(4.3–11.8)
LDL cholesterol (mg/dL)	97.44 ± 42.63	(22–299)
Sex	47% Female	

into clusters that have the smallest distance between them and determines that distance using a recursive function which treats the subset of linkages equally (Xu and Wunsch, 2010).

Lastly, data from each linkage algorithm were clustered using an inconsistency clustering algorithm. This algorithm calculates an inconsistency coefficient of a new linkage using the mean and standard deviation of the linkage heights for a specified depth (*dep*) of sub linkages within each new linkage. Clusters were formed when the inconsistency coefficient for each linkage and all sub linkages were less than a specified cutoff (*cut*) value. Each linkage algorithm output was run through multiple iterations of the inconsistency clustering algorithm with values for depth (*dep*) from 2 to 6 in increments of 1, whereas cutoff (*cut*) values were adjusted from 1.0 to 3.0 in increments of 0.1. All iterations of depth and cutoff were evaluated, and if only one cluster was formed, then that iteration was not used in the consensus clustering model. Once each clustering model was established, distances between samples were calculated based on the percentage of models in which two samples shared a cluster. Samples that shared no clusters were given a distance of 1 and, samples that were paired in the same cluster in each model were given a distance of 0. Plots of each clustering model were created using the dimensionality reduction function, t-distributed stochastic neighbor embedding (t-sne), with a random number generation seed of 10 to maintain reproducibility (Maaten, 2008). Clinical data were excluded from the clustering algorithm to avoid clusters based on clinical findings as this study sought to identify clusters of participants based on a differential level of fluid biomarkers.

Simulated Data Generation and Analysis

Simulated data generation was performed using the Matlab Statistics and Machine Learning Toolbox function *mvnrnd*. Each simulated data experiment was run with 35 trials and each trial was initiated with a unique random number generation seed to maintain reproducibility. Generated data contained 11 variables and 100 samples per group, obtained from known distributions with the mean and sigma of each distribution differing depending on the experiment. **Supplementary Tables S1–S3** detail the mean and sigma for each group within each experiment. The ARI was used to evaluate the accuracy of each clustering model by comparing each clustering result to the known cluster assignment. The ARI has a maximum value of 1 indicating that the clustering result matches perfectly to the known cluster assignment. An ARI of 0 indicates that the clustering model assigns observations to the correct cluster assignment with an equal probability as random chance. An ARI below 0 demonstrates that the clustering model is less effective than random chance at assigning observations to the correct cluster assignment (McComb, 2015).

Statistical Analysis

Statistical analysis was performed using the Matlab Statistics and Machine Learning Toolbox and SPSS. A two-sample *t*-test using the Matlab function *ttest2* was conducted to compare the ARI

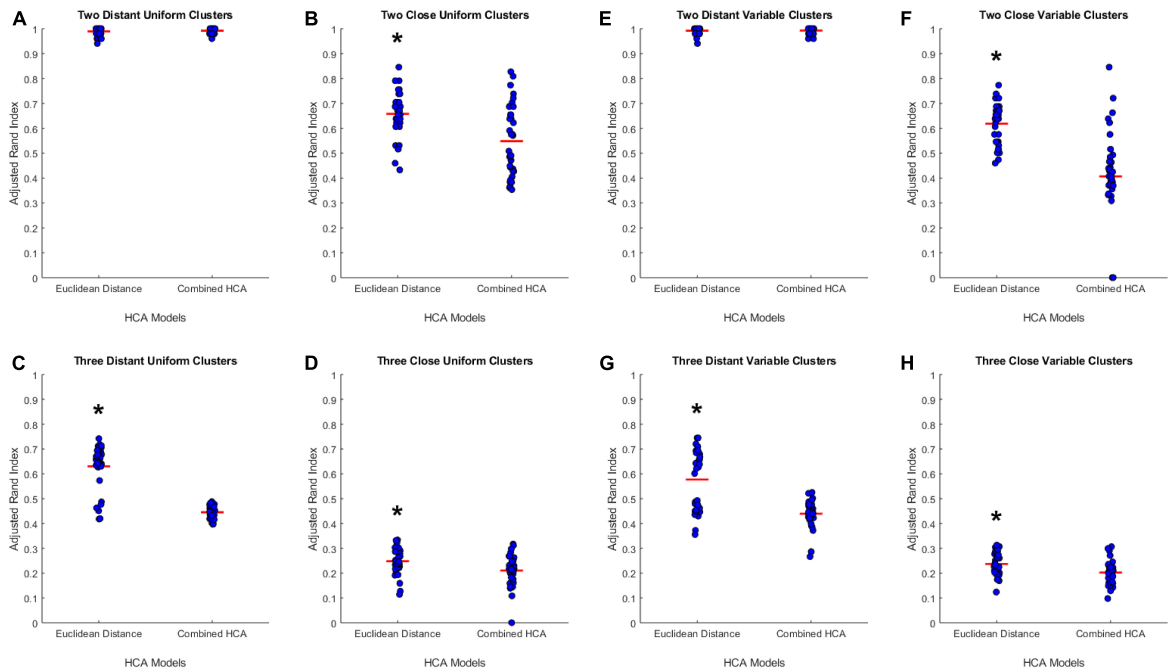

FIGURE 1 | Compares the combined HCA model to the Euclidean distance model in eight different datasets. Each dataset was produced using the *mvnrnd*. The accuracy of each model was assessed using the adjusted rand index (ARI). Datasets used in **A**–**D** have identical means for each variable in each cluster. Datasets used in **E**–**H** have the same means for the first six variables and means of opposite signs for the other five variables. Means and standard deviations for each dataset are shown in **Supplementary Table S1**. Red horizontal lines indicate means for each model. Stars (*) indicate statistical significance between groups using an independent samples *t*-test ($p < 0.05$).

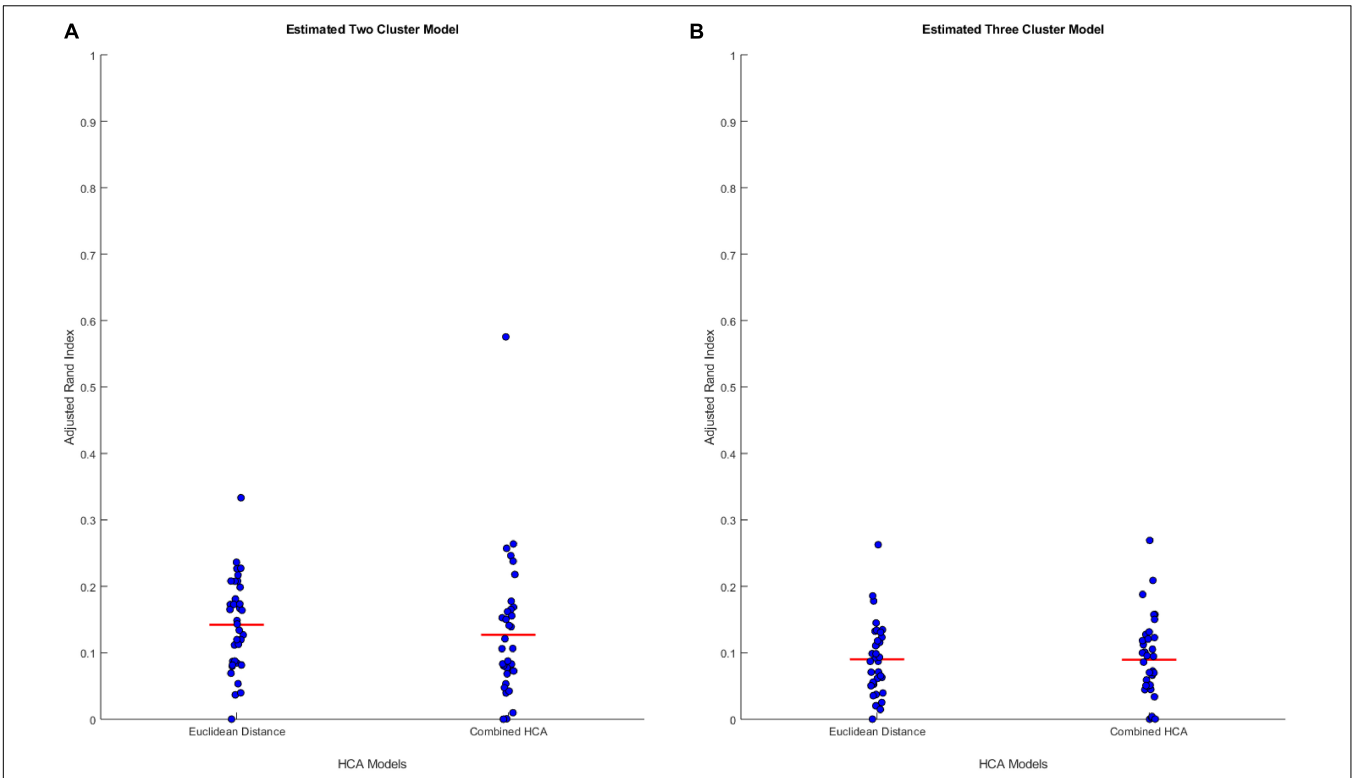

FIGURE 2 | Compares the combined HCA model to the Euclidean distance model in two predicted distributions. Each dataset was produced using *mvnrnd*. The accuracy of each model was assessed using the adjusted rand index (ARI). Means and covariance matrix for each dataset are shown in **Supplementary Tables S2**, **S3**. Red horizontal lines indicate means for each model. Stars (*) indicate statistical significance between groups using an independent samples *t*-test ($p < 0.05$). **(A)** Shows estimated two cluster model, and **(B)** shows estimated three cluster model.

means of the two HCA models for all simulated data experiments. SPSS was used for the remaining statistical tests to determine differences between clusters for each log-transformed protein marker. Levene's test for equality of variances was performed before each two-sample *t*-test, and Satterthwaite's *t*-test was used for any marker found to have significantly different variances. Levene's test for homogeneity of variances based on the mean was also conducted before performing an ANOVA test for each marker and a Welch's test for equality of means was performed for markers with non-homogeneous variances. *Post hoc* analysis was then conducted on markers which had a significant *p*-value for an ANOVA or Welch's test. Tukey's HSD was used for significant ANOVA tests and Dunnett T3 was used for significant Welch's test.

RESULTS

Study Population Description

Demographic and neurocognitive evaluations were obtained in 65/66 participants within our MCI-CVD cohort (**Table 1**). The mean age of the participants was 75.07 ± 8.14 with a female population of 47%. MMSE scores ranged from 18 to 30 with a mean of 26.86 ± 2.95, while MoCA scores ranged from 11 to 28 with a mean of 22.11 ± 3.74. Vascular risk factors including systolic blood pressure, hemoglobin A1C, and LDL cholesterol were also evaluated in our cohort (**Table 1**). Mean systolic blood pressure was found to be 141.33 ± 15.31 mmHg, hemoglobin A1c 6.18 ± 1.31%, and LDL cholesterol 97.44 ± 42.63 mg/dL.

Simulated Data Analysis

To test the applicability of the novel combined HCA model, we tested its accuracy in eight unique simulated datasets (detailed in **Supplementary Table S1**). We tested the novel model against an established HCA model using the ARI to measure the accuracy of each model (**Figure 1**). In our first experiment, we studied the accuracy of both models in a dataset with two distant uniform clusters (**Figure 1A**). The established HCA model using Euclidean distance showed no difference in ARI compared to the novel combined HCA model (Euclidean: 0.9892 ± 0.0029, Novel: 0.9920 ± 0.0019, $p = 0.413$). A similar result was found in a dataset with two distant variable clusters (Euclidean: 0.9920 ± 0.0023, Novel: 0.9926 ± 0.0020, $p = 0.857$) (**Figure 1E**). These results demonstrate that both models were able to assign each distribution to its own cluster. Next, we tested both models on a dataset with three distant uniform clusters (**Figure 1C**) and three distant variable clusters (**Figure 1G**). The established HCA model had a significantly increased ARI over the novel HCA model in both of these experiments (Euclidean: 0.6186 ± 0.0139, Novel: 0.4067 ± 0.0320, $p < 0.001$,

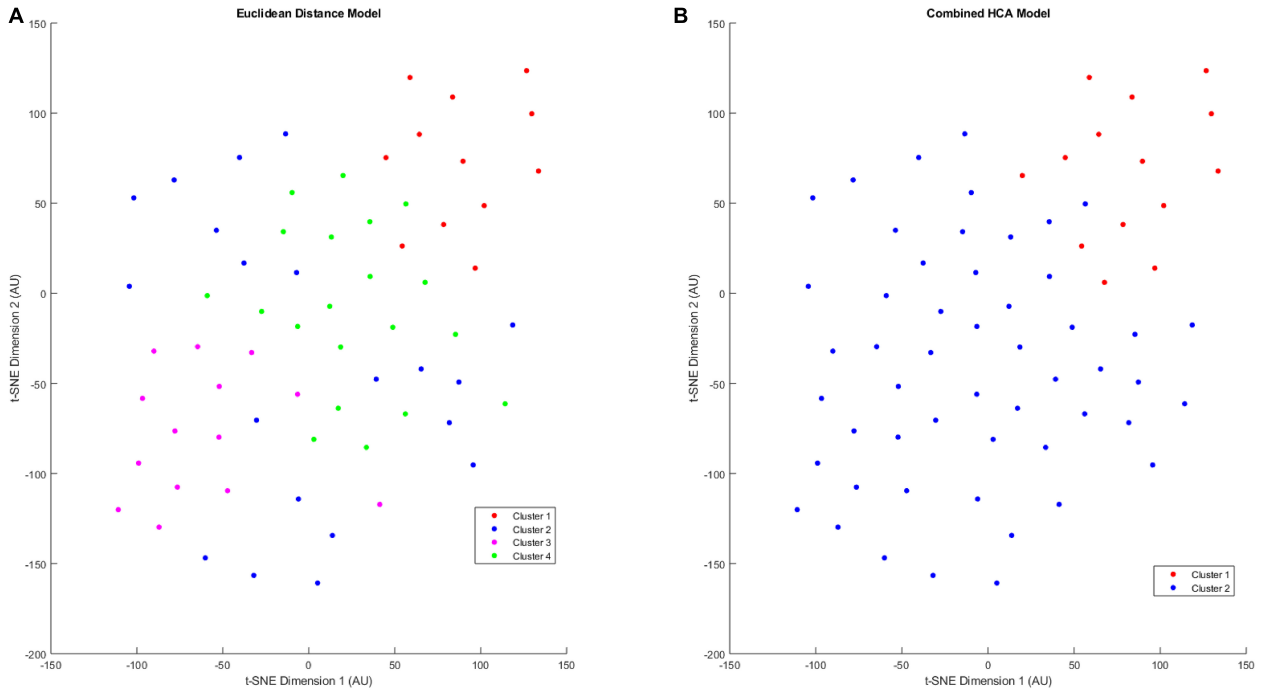

FIGURE 3 | T-SNE dimensionality reduction plot of clustered data. Data were clustered using the Euclidean distance model **(A)** and the Combined HCA model **(B)**. The dataset was produced by measuring 11 inflammatory (MMP1, MMP3, MMP9, IL8, TNFα) and angiogenic proteins of interest (FGF, FLT, PIGF, Tie-2, VEGF, VEGF-D) from 66 participant plasma samples.

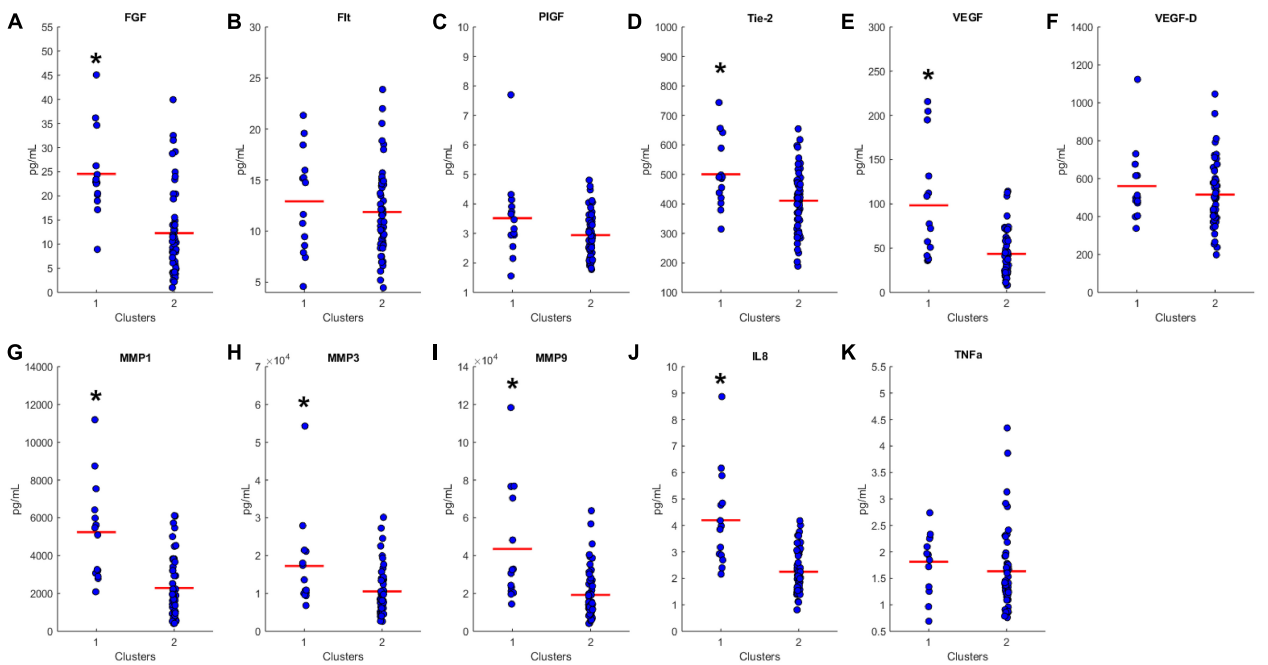

FIGURE 4 | Compares clusters 1 and 2 produced from the Combined HCA model in each inflammatory and angiogenic protein measured. **(A–K)** Show mean and scatter of FGF **(A)**, FLt **(B)**, PIGF **(C)**, Tie-2 **(D)**, VEGF **(E)**, VEGF-D **(F)**, MMP1 **(G)**, MMP3 **(H)**, MM9 **(I)**, IL8 **(J)**, and TNFa **(K)**. Red horizontal lines indicate the means for each cluster. Stars (*) indicate statistical significance between groups as calculated by the log transform of the data shown using an independent samples *t*-test ($p < 0.05$). Means ± SEM are shown in **Table 2**.

TABLE 2 | Means ± SEM for clusters 1 and 2 produced by the combined HCA model.

Biomarker	*p*-value	Cluster 1 (pg/mL)	Cluster 2 (pg/mL)
FGF	<0.001	24.56 ± 2.39	12.27 ± 1.22
FLT	0.568	12.92 ± 1.35	11.87 ± 0.59
PIGF	0.093	3.52 ± 0.38	2.94 ± 0.11
Tie-2	0.013	500.55 ± 31.69	411.09 ± 14.77
VEGF	<0.001	98.39 ± 17.46	43.55 ± 3.63
VEGFD	0.350	560.73 ± 52.17	515.59 ± 24.35
MMP1	<0.001	5244.74 ± 700.11	2292.86 ± 219.55
MMP3	0.005	17275.46 ± 3267.49	10547.71 ± 856.39
MMP9	<0.001	43561.18 ± 8177.19	19232.98 ± 1851.63
IL8	<0.001	4.20 ± 0.49	2.25 ± 0.11
TNFa	0.283	1.81 ± 0.15	1.63 ± 0.10

*Statistical significance between groups was determined using the log transform of the data shown in **Figure 4** in an independent samples t-test ($p < 0.05$).*

Figure 1C) (Euclidean: 0.5767 ± 0.0200, Novel: 0.4393 ± 0.0092, $p < 0.001$, **Figure 1G**). These results show that the established HCA model has a higher accuracy when separating three distant clusters of normally distributed data. We then tested if the models performed differently on distributions that had more overlapping characteristics. The first experiments of these distributions were with two close uniform clusters (**Figure 1B**) and two close variable clusters (**Figure 1F**). In both experiments, the established HCA model had a higher accuracy compared to the novel HCA model (Euclidean: 0.6579 ± 0.0150, Novel: 0.5482 ± 0.0237, $p < 0.001$, **Figure 1B**) (Euclidean: 0.6186 ± 0.0139, Novel: 0.4067, $p < 0.001$, **Figure 1F**). This difference continued in the final set of experiments which used three close uniform clusters (Euclidean: 0.2477 ± 0.0087, Novel: 0.2103 ± 0.0103, $p < 0.007$, **Figure 1D**) and three distant variable clusters (Euclidean: 0.2370 ± 0.0080, Novel: 0.2023 ± 0.0078, $p < 0.003$, **Figure 1H**). These experiments show that as the distributions progressively overlap the accuracy for both models decrease and the difference between the accuracy of the models decreases as well.

Predicted Distribution Analysis

We hypothesized that clusters, if any, in our empirical dataset would overlap more and thus be more difficult to differentiate than those used in the previous experiments. To test the accuracy of each model in this distribution, we generated simulated data from predicted distributions based on analysis from our collaborators (detailed in **Supplementary Tables S2**, **S3**). The first experiment was based on a two-cluster model within our sample population (**Figure 2A**). This experiment showed no differences between the established Euclidean HCA model and the novel HCA model (Euclidean: 0.1422 ± 0.0118, Novel: 0.1270 ± 0.0181, $p = 0.486$, **Figure 2A**). In addition, we tested a three cluster model for our sample population and found similar results with no differences between the two models in this study (Euclidean: 0.0902 ± 0.0092, Novel: 0.0895 ± 0.0105, $p = 0.962$, **Figure 2B**). The data from these two experiments demonstrate the interchangeability of these two models when studying datasets with extensive overlapping distributions.

Application of Models to Dataset

After validating the novel combined HCA model using predicted distributions, we applied both HCA models to our 66 patient sample (**Figure 3**). When the Euclidean distance HCA model was applied to our dataset, four clusters emerged (**Figure 3A**). Clusters 1, 3, and 4 appear to be more compact in the 2-D t-SNE dimensionality reduction plot, while cluster 2 exists along the periphery of the plot in a more scattered manner. We continued this experiment and applied the novel combined HCA model to the same dataset and uncovered two clusters (**Figure 3B**). Cluster 1 contains 14 samples of which 12 also appear in cluster 1 of the Euclidean distance HCA model. The other 52 samples appear in cluster 2, which is comprised of clusters 2–4 from the Euclidean distance HCA model. The similarity of these two results emphasizes the underlying distributions within this dataset.

Characterizing Cluster Differences

We proceeded to analyze the differences that drive cluster differentiation. First, we examined the clusters produced by

TABLE 3 | Means ± SEM for clusters 1–4 produced by the Euclidean distance model.

Biomarker	*p*-value	Cluster 1 (pg/mL)	Cluster 2 (pg/mL)	Cluster 3 (pg/mL)	Cluster 4 (pg/mL)
FGF	<0.001	24.90 ± 2.78	5.16 ± 0.60	12.70 ± 1.37	20.11 ± 1.97
FLT	0.340	12.77 ± 1.56	13.08 ± 0.82	11.05 ± 1.44	11.42 ± 0.82
PIGF	0.342	3.53 ± 0.45	2.94 ± 0.17	2.79 ± 0.28	3.10 ± 0.16
Tie-2	0.040	512.42 ± 35.98	437.13 ± 25.44	384.29 ± 26.72	405.64 ± 21.72
VEGF	<0.001	106.97 ± 19.29	49.97 ± 6.65	27.69 ± 4.39	48.56 ± 5.14
VEGFD	0.258	563.88 ± 60.58	579.18 ± 46.39	469.25 ± 36.56	487.25 ± 32.33
MMP1	<0.001	5605.20 ± 769.82	3061.39 ± 356.41	736.27 ± 71.84	2692.85 ± 285.62
MMP3	0.096	17517.09 ± 3822.29	10666.69 ± 1443.84	9646.52 ± 1192.19	11587.35 ± 1561.28
MMP9	<0.001	46055.29 ± 9378.94	25868.67 ± 3771.38	17474.83 ± 2787.13	14764.34 ± 1748.47
IL8	<0.001	4.49 ± 0.52	2.32 ± 0.18	1.78 ± 0.12	2.53 ± 0.18
TNFα	0.362	1.86 ± 0.16	1.52 ± 0.16	1.51 ± 0.10	1.83 ± 0.21

*Statistical significance between groups was determined using the log transform of the data shown in **Figure 5** in an ANOVA followed by Tukey's HSD for post hoc analysis ($p < 0.05$). Results of the ANOVA omnibus are shown in p-value.*

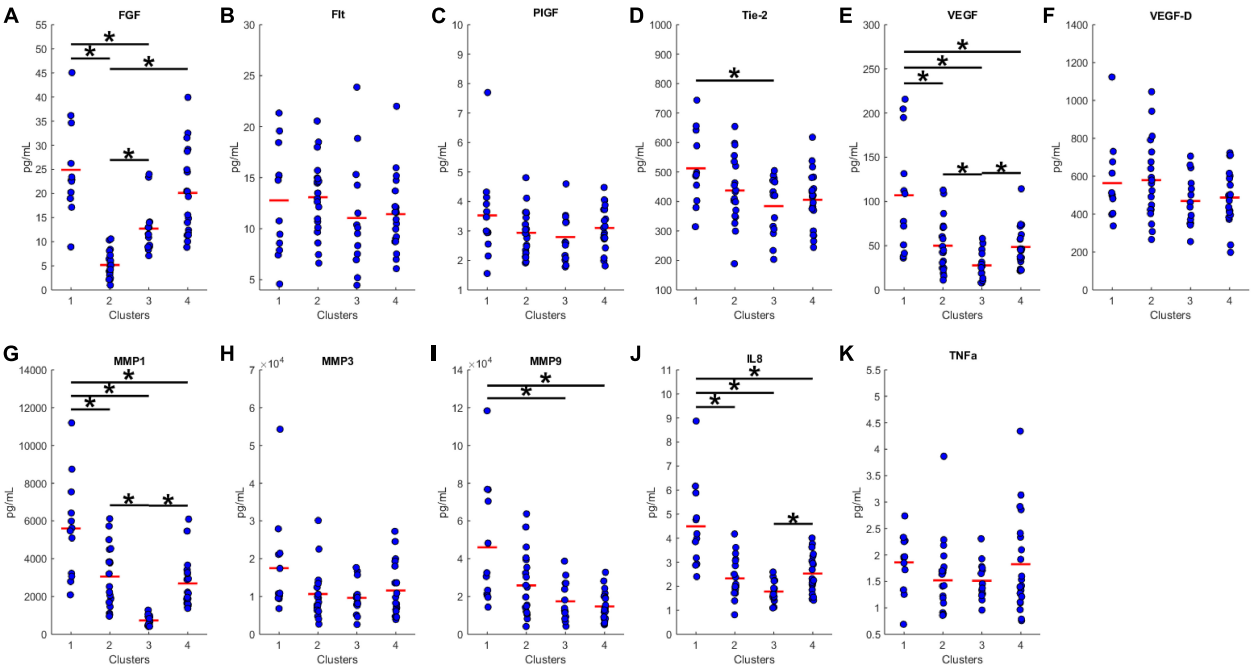

FIGURE 5 | Compares clusters 1–4 produced from the Euclidean distance model in each inflammatory and angiogenic protein measured. **(A–K)** Show mean and scatter of FGF **(A)**, FLt **(B)**, PlGF **(C)**, Tie-2 **(D)**, VEGF **(E)**, VEGF-D **(F)**, MMP1 **(G)**, MMP3 **(H)**, MM9 **(I)**, IL8 **(J)**, and TNFa **(K)**. Red horizontal lines indicate the means for each cluster. Stars (*) indicate statistical significance between groups as calculated by the log transform of the data shown using ANOVA followed by Tukey's HSD for *post hoc* analysis ($p < 0.05$). Means ± SEM are shown in **Table 3**.

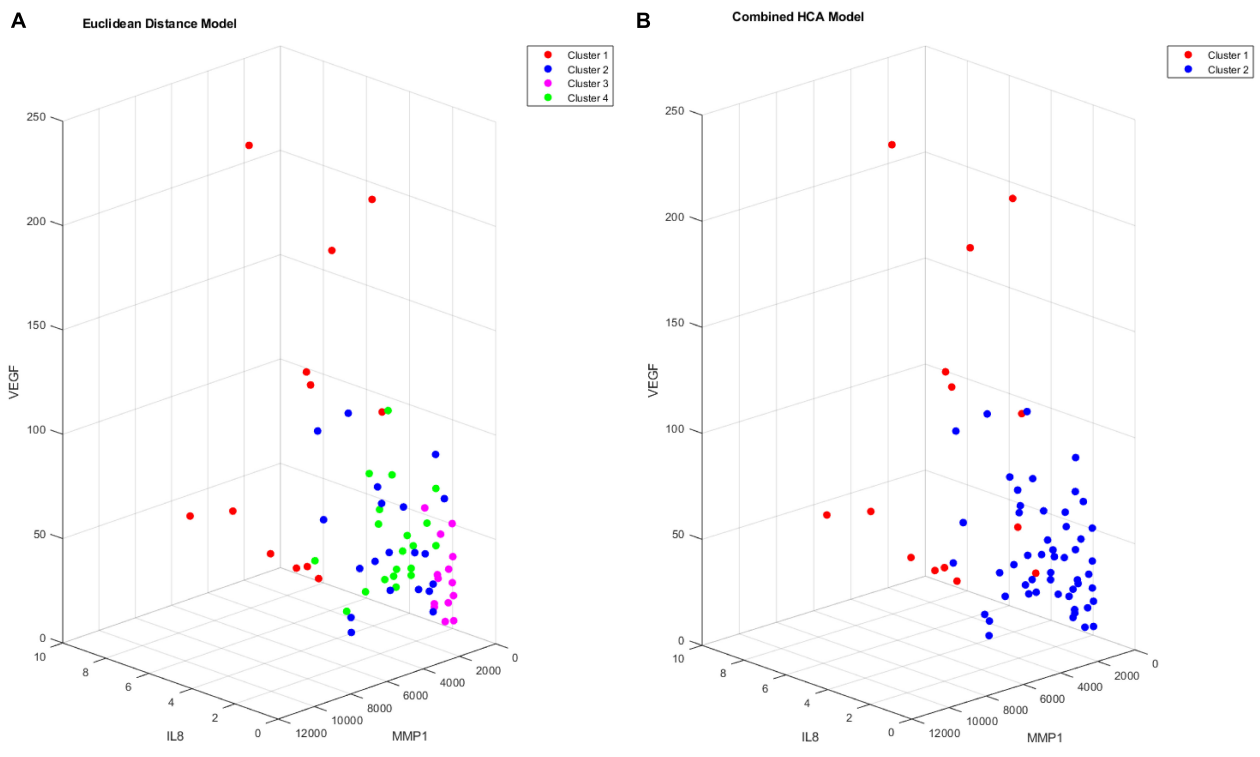

FIGURE 6 | Cluster comparison of VEGF (pg/mL), MMP1 (pg/mL), and IL8 (pg/mL) for data clustered using the Euclidean distance model **(A)** and the combined HCA model **(B)** from 66 participant plasma samples.

the novel HCA model (**Figure 4**), and found that cluster 1 was increased compared to cluster 2 in FGF ($p < 0.001$), Tie-2 ($p = 0.013$), VEGF ($p < 0.001$), MMP1 ($p < 0.001$), MMP3 ($p = 0.005$), MMP9 ($p < 0.001$), and IL8 ($p < 0.001$) (**Table 3**). When the clusters produced from the Euclidean distance HCA model were analyzed (**Figure 5**), we found a similar pattern of clusters. In this model, cluster 1 was increased compared to clusters 2–4 in VEGF ($p = 0.006$, $p < 0.001$, $p = 0.013$), MMP1 ($p = 0.003$, $p < 0.001$, $p = 0.001$), and IL8 ($p < 0.001$, $p < 0.001$, $p < 0.001$), respectively. Cluster 1 was also increased in FGF ($p = 0.004$), Tie-2 ($p = 0.033$), and MMP9 ($p = 0.003$) compared to cluster 3. The elevated level of these proteins in cluster 1 agrees with the characteristics of cluster 1 established previously with both models demonstrating a subset with significant increases in VEGF, MMP1, and IL8 compared to the other subsets (**Figure 6**). However, the Euclidean distance HCA model does show differences between clusters 2 and 4, which were not seen in the novel HCA model. Clusters 2 and 4 were similar in their makeup, both increased over cluster 3 in MMP1 ($p < 0.001$ and $p < 0.001$) and VEGF ($p = 0.032$ and $p = 0.016$), respectively, but different levels of FGF ($p < 0.001$). These differences lead to the possibility of four disease profiles within the MCI-CVD patient population.

DISCUSSION

The results of this study provide evidence supporting the use of the novel combined HCA model in datasets with extensive overlapping distributions. The results of the first set of experiments demonstrate that the Euclidean distance HCA model outperforms the novel combined HCA model in datasets with a moderate amount of overlapping distributions (**Figures 1B–D,F–H**). This difference is reduced as the distributions progressively increase in overlap and eventually disappears entirely in our second set of experiments involving the more complex datasets with predicted distributions (**Figure 2**).

It is important to note that the capacity of the two HCA models to accurately cluster data into their known distributions decreases as the datasets become more complex. In our experiments involving two distant distributions of data, both models were able to separate each distribution with an ARI approximately equal to 1 (**Figures 1A,E**). In experiments using our predicted distributions, the average ARI decreased to approximately 0.13 and 0.09 for the two and three cluster models, respectively (**Figure 2**). These findings demonstrate the limits of reliability in both HCA models and provide a measure to compare additional HCA models to in future experiments. Accounting for this accuracy is crucial when interpreting HCA results because clusters produced by the HCA model may not correspond to any true unique distribution and may simply be a subset within the normal variation of a larger distribution. Therefore, it is important to compare multiple HCA models on an unknown dataset in order to elucidate which clusters are in fact unique distributions within the dataset. Overall, results from our experiments support the interchangeability of HCA models in datasets similar to those shown in **Supplementary Tables S2**, **S3**, which allows for the use of both models in assessing clustering distributions within our dataset.

Both the Euclidean distance HCA model and the novel combined HCA model resulted in similar disease profiles within our cohort of MCI-CVD patients (**Figure 3**). In this study, both models classified participants into a cluster that had elevated levels of VEGF, MMP1, and IL8 compared to the other clusters (**Figures 4**, **5**). We suspect that this disease profile seen in cluster 1 may be involved in a more active VCID process resulting in increased pathology due to the increased level of angiogenic and inflammatory markers. Clusters 2–4 in the Euclidean distance HCA model may also be clinically relevant in terms of disease pathology but require future studies to understand how these profiles may contribute to progression of VCID in a population of individuals with MCI-CVD.

CONCLUSION

The usage of both the novel HCA model and a Euclidean distance HCA model identified a novel subset of patients within the MCI-CVD population. This study provides insight into a potential underlying inflammatory and angiogenic profile of disease in patients with VCID. Defining subsets of patients within this population with different disease profiles continues to be a key research objective. These profiles can provide a more complete understanding of disease progression and allow physicians and researchers to identify patients undergoing different rates of pathologic change in a prospective cohort. In the future, we hope to further clarify these profiles by combining plasma and MRI imaging biomarkers that can also be used in clinical trials as key outcome measures to determine the efficacy of novel therapeutics.

DATA AVAILABILITY STATEMENT

The datasets generated for this study are available on request to the corresponding author.

ETHICS STATEMENT

The studies involving human participants were reviewed and approved by the University of Kentucky Institutional Review Board. The patients/participants provided their written informed consent to participate in this study.

AUTHOR CONTRIBUTIONS

ZW designed and executed the analyses. TS performed the assessment of analytes using MSD. DF and QC consulted on study design. LG consulted on clinical readouts. PN provided samples. FS consulted on neuropsychological assessments. GJ

assessed the patients and collected all samples. DW oversaw the studies and assisted in the development of hypotheses and data interpretation.

ACKNOWLEDGMENTS

The authors gratefully acknowledge the Sanders-Brown Center on Aging Clinic team for their support in participant recruitment and evaluations, Dr. Erin Abner for her assistance in study design, the NIH [NINR: 4R01NR014189-05 (GJ), NIA: 5UH2NS100606-02 (DW and GJ), NCATS: UL1TR001998, NIA: 5P30AG028383], and the participants of this study for their time and commitment.

SUPPLEMENTARY MATERIAL

The Supplementary Material for this article can be found online at: https://www.frontiersin.org/articles/10.3389/fnins.2020.00084/full#supplementary-material

REFERENCES

Abner, E. L., Kryscio, R. J., Schmitt, F. A., Fardo, D. W., Moga, D. C., Ighodaro, E. T., et al. (2017). Outcomes after diagnosis of mild cognitive impairment in a large autopsy series. *Ann. Neurol.* 81, 549–559. doi: 10.1002/ana.24903

Cipollini, V., Troili, F., and Giubilei, F. (2019). Emerging biomarkers in vascular cognitive impairment and dementia: from pathophysiological pathways to clinical application. *Int. J. Mol. Sci.* 20:2812 doi: 10.3390/ijms20112812

Corriveau, R. A., Bosetti, F., Emr, M., Gladman, J. T., Koenig, J. I., Moy, C. S., et al. (2016). The science of vascular contributions to cognitive impairment and dementia (VCID): a framework for advancing research priorities in the cerebrovascular biology of cognitive decline. *Cell Mol. Neurobiol.* 36, 281–288. doi: 10.1007/s10571-016-0334-7

Damian, M., Hausner, L., Jekel, K., Richter, M., Froelich, L., Almkvist, O., et al. (2013). Single-domain amnestic mild cognitive impairment identified by cluster analysis predicts Alzheimer's disease in the european prospective DESCRIPA study. *Dement. Geriatr. Cogn. Disord.* 36, 1–19. doi: 10.1159/000348354

Dodge, H. H., Zhu, J., Woltjer, R., Nelson, P. T., Bennett, D. A., Cairns, N. J., et al. (2017). Risk of incident clinical diagnosis of Alzheimer's disease-type dementia attributable to pathology-confirmed vascular disease. *Alzheimers Dement.* 13, 613–623. doi: 10.1016/j.jalz.2016.11.003

Fred, A., and Jain, A. K. (2002). "Data clustering using evidence accumulation," in *Proceedings of the International Conference Pattern Recognition*, Quebec, 276–280.

Gorelick, P. B., Scuteri, A., Black, S. E., Decarli, C., Greenberg, S. M., Iadecola, C., et al. (2011). Vascular contributions to cognitive impairment and dementia: a statement for healthcare professionals from the american heart association/american stroke association. *Stroke* 42, 2672–2713. doi: 10.1161/str.0b013e3182299496

Grubbs, F. E. (1950). Sample criteria for testing outlying observations. *Ann. Math. Statist.* 21, 27–58. doi: 10.1214/aoms/1177729885

Harrison, S. L., Tang, E. Y., Keage, H. A., Taylor, J. P., Allan, L., Robinson, L., et al. (2016). A systematic review of the definitions of vascular cognitive impairment. No dementia in cohort studies. *Dement. Geriatr. Cogn. Disord.* 42, 69–79. doi: 10.1159/000448213

Kapasi, A., and Schneider, J. A. (2016). Vascular contributions to cognitive impairment, clinical Alzheimer's disease, and dementia in older persons. *Biochim. Biophys. Acta* 1862, 878–886. doi: 10.1016/j.bbadis.2015.12.023

Maaten, L. (2008). Visualizing data using t-SNE. *J. Mach. Learn. Res.* 9:2579.

Mahoney, E. R., Dumitrescu, L., Moore, A. M., Cambronero, F. E., De Jager, P. L., Koran, M. E. I., et al. (2019). Brain expression of the vascular endothelial growth factor gene family in cognitive aging and alzheimer's disease. *Mol. Psychiatry* [Epub ahead of print]. doi: 10.1038/s41380-019-0458-5

McComb, C. (2015). *Adjusted RAND INDEX*, 1.0.0.0 Edn. Natick, MA: MATLAB Central File Exchange.

Murphy, M. P., Corriveau, R. A., and Wilcock, D. M. (2016). Vascular contributions to cognitive impairment and dementia (VCID). *Biochim. Biophys. Acta* 1862, 857–859. doi: 10.1016/j.bbadis.2016.02.010

Nettiksimmons, J., Decarli, C., Landau, S., Beckett, L., and Alzheimer's Disease Neuroimaging Initiative, (2014). Biological heterogeneity in ADNI amnestic mild cognitive impairment. *Alzheimers Dement.* 10:511-521.e1. doi: 10.1016/j.jalz.2013.09.003

Petersen, R. C., Smith, G. E., Waring, S. C., Ivnik, R. J., Tangalos, E. G., and Kokmen, E. (1999). Mild cognitive impairment: clinical characterization and outcome. *Arch. Neurol.* 56, 303–308.

Poggesi, A., Pasi, M., Pescini, F., Pantoni, L., and Inzitari, D. (2016). Circulating biologic markers of endothelial dysfunction in cerebral small vessel disease: a review. *J. Cereb. Blood Flow Metab.* 36, 72–94. doi: 10.1038/jcbfm.2015.116

Racine, A. M., Koscik, R. L., Berman, S. E., Nicholas, C. R., Clark, L. R., Okonkwo, O. C., et al. (2016). Biomarker clusters are differentially associated with longitudinal cognitive decline in late midlife. *Brain* 139, 2261–2274. doi: 10.1093/brain/aww142

Rizzi, L., Rosset, I., and Roriz-Cruz, M. (2014). Global epidemiology of dementia: Alzheimer's and vascular types. *Biomed. Res. Int.* 2014:908915. doi: 10.1155/2014/908915

Wallin, A. K., Blennow, K., Zetterberg, H., Londos, E., Minthon, L., and Hansson, O. (2010). CSF biomarkers predict a more malignant outcome in Alzheimer disease. *Neurology* 74, 1531–1537. doi: 10.1212/WNL.0b013e3181dd4dd8

Wardlaw, J. M., Smith, C., and Dichgans, M. (2019). Small vessel disease: mechanisms and clinical implications. *Lancet Neurol.* 18, 684–696. doi: 10.1016/S1474-4422(19)30079-1

Winblad, B., Palmer, K., Kivipelto, M., Jelic, V., Fratiglioni, L., Wahlund, L. O., et al. (2004). Mild cognitive impairment–beyond controversies, towards a consensus: report of the International working group on mild cognitive impairment. *J. Intern. Med.* 256, 240–246.

Xu, R., and Wunsch, D. C. II (2010). Clustering algorithms in biomedical research: a review. *IEEE Rev. Biomed. Eng.* 3, 120–154. doi: 10.1109/RBME.2010.2083647

Conflict of Interest: The authors declare that the research was conducted in the absence of any commercial or financial relationships that could be construed as a potential conflict of interest.

Copyright © 2020 Winder, Sudduth, Fardo, Cheng, Goldstein, Nelson, Schmitt, Jicha and Wilcock. This is an open-access article distributed under the terms of the Creative Commons Attribution License (CC BY). The use, distribution or reproduction in other forums is permitted, provided the original author(s) and the copyright owner(s) are credited and that the original publication in this journal is cited, in accordance with accepted academic practice. No use, distribution or reproduction is permitted which does not comply with these terms.

frontiers in Cellular Neuroscience

ORIGINAL RESEARCH
published: 11 February 2020
doi: 10.3389/fncel.2020.00018

Subarachnoid Hemorrhage Induces Dynamic Immune Cell Reactions in the Choroid Plexus

*Peter Solár[1,2], Ilona Klusáková[1], Radim Jančálek[2], Petr Dubový[1] and Marek Joukal[1]**

[1] Department of Anatomy, Cellular and Molecular Neurobiology Research Group, Faculty of Medicine, Masaryk University, Brno, Czechia, [2] Department of Neurosurgery, Faculty of Medicine, Masaryk University and St. Anne's University Hospital Brno, Brno, Czechia

Subarachnoid hemorrhage (SAH) is a specific form of hemorrhagic stroke that frequently causes intracranial hypertension. The choroid plexus (CP) of the brain ventricles is responsible for producing cerebrospinal fluid and forms the blood – cerebrospinal fluid barrier. The aim of the current study was to determine whether SAH induces an immune cell reaction in the CP and whether the resulting increase in intracranial pressure (ICP) itself can lead to cellular changes in the CP. SAH was induced by injecting non-heparinized autologous blood to the cisterna magna. Artificial cerebrospinal fluid (ACSF) instead of blood was used to assess influence of increased ICP alone. SAH and ACSF animals were left to survive for 1, 3, and 7 days. SAH induced significantly increased numbers of M1 (ED1+, CCR7+) and M2 (ED2+, CD206+) macrophages as well as MHC-II+ antigen presenting cells (APC) compared to naïve and ACSF animals. Increased numbers of ED1+ macrophages and APC were found in the CP only 3 and 7 days after ACSF injection, while ED2+ macrophage number did not increase. CD3+ T cells were not found in any of the animals. Following SAH, proliferation activity in the CP gradually increased over time while ACSF application induced higher cellular proliferation only 1 and 3 days after injection. Our results show that SAH induces an immune reaction in the CP resulting in an increase in the number of several macrophage types in the epiplexus position. Moreover, we also found that increased ICP due to ACSF application induced both an immune reaction and increased proliferation of epiplexus cells in the CP. These findings indicate that increased ICP, and not just blood, contributes to cellular changes in the CP following SAH.

Keywords: subarachnoid hemorrhage, choroid plexus, intracranial hypertension, macrophages, blood-cerebrospinal fluid barrier

OPEN ACCESS

Edited by:
Johannes Boltze, University of Warwick, United Kingdom

Reviewed by:
Nicole A. Terpolilli, Ludwig Maximilian University of Munich, Germany
Fernanda Marques, University of Minho, Portugal

****Correspondence:***
Marek Joukal
mjoukal@med.muni.cz

Specialty section:
This article was submitted to Non-Neuronal Cells, a section of the journal Frontiers in Cellular Neuroscience

Received: *01 November 2019*
Accepted: *23 January 2020*
Published: *11 February 2020*

Citation:
Solár P, Klusáková I, Jančálek R, Dubový P and Joukal M (2020) Subarachnoid Hemorrhage Induces Dynamic Immune Cell Reactions in the Choroid Plexus. Front. Cell. Neurosci. 14:18. doi: 10.3389/fncel.2020.00018

INTRODUCTION

Subarachnoid hemorrhage (SAH) is a specific form of hemorrhagic stroke that is recorded in up to 10 cases per 100,000 people annually, and has a combined morbidity and mortality of more than 50% (King, 1997; Rincon et al., 2013). More than 80% of these cases are due to the rupture of a cerebral aneurysm with bleeding into the subarachnoid cisterns and fissures (Fisher et al., 1980; van Gijn and Rinkel, 2001). In the first few seconds following aneurysm rupture, intracranial pressure (ICP) rises rapidly and brain tissue gets compressed. This sudden

rise in ICP may reach values up to diastolic blood pressure but later falls to slightly above the baseline (Prunell et al., 2003).

The extent to which ICP rises is correlated with early onset brain injury and mortality (Zoerle et al., 2015). The inflammatory cascade that gets activated within minutes after SAH comprises adhesion molecules, cytokines, migration of leukocytes, and complement activation (Sehba et al., 2011). Early inflammation seems to play an important role in development of delayed cerebral ischemia and affects the outcome after SAH (Sercombe et al., 2002; Miller et al., 2014).

The choroid plexus (CP) of the brain ventricles is responsible for producing almost 60 – 80% cerebrospinal fluid (CSF) by volume. The CP comprises a highly vascularized stroma containing loose connective tissue, fenestrated capillaries and immune cells. The stroma is covered by a layer of cuboidal epithelial cells linked by tight junctions that is one of the fundamental components of the blood–cerebrospinal fluid (B-CSF) barrier. Kolmer cells (KC) of the epiplexus adhere to the ventricular side of these cuboidal epithelial cells and are in direct contact with CSF (Hosoya and Fujita, 1973; Segal and Pollay, 1977; McMenamin et al., 2003; Wolburg and Paulus, 2009).

There is a growing body of evidence that implicates changes in the CP (due to extravasated blood into the CSF following SAH) in hypersecretion of CSF leading to the development of post-hemorrhagic hydrocephalus (Simard et al., 2011; Xiang et al., 2017). It is believed that post-hemorrhagic hydrocephalus results when CSF flow within the ventricular system is impaired or there is a structural blockage of CSF drainage in the arachnoid villi (Yong et al., 2010). It has been suggested that SAH may also lead to hypersecretion of CSF by the CP. Aydin et al. (2014) showed that increased CSF secretion seems to be triggered by the petrous ganglion of the glossopharyngeal nerve and the numerous water-filled vesicles in the early stages of SAH. Similarly, Kanat et al. (2013) observed increased CSF secretion caused by fluid filled vesicles in the CP following SAH and concluded that hypersecretion of CSF contributes to the development of post-hemorrhagic hydrocephalus.

It has been found that SAH increases the number of macrophages in the epiplexus position of the CP (Liszczak et al., 1984). However, the type of macrophages and other immune cells that increase and proliferate after SAH remains a mystery. Further, the dynamics of these cell changes is also unclear. There is very little known about the effect of elevated ICP and inflammation on the SAH-affected CP.

The aim of our study was to investigate and specify cellular changes in the CP following SAH by monitoring the different subpopulations of macrophages, antigen presenting cells (APC), T lymphocytes as well as cellular proliferation over time. A further objective was to clarify whether these changes are caused mainly by blood degradation products or whether increased intracranial pressure after SAH also has an effect. We found that SAH induced increases in the number of several subpopulations of immune cells predominantly in the epiplexus position and enhanced their proliferation in the CP. Moreover, artificial cerebrospinal fluid (ACSF) application also induced similar increases in immune cell numbers in the CP. The results indicate that immune cell changes in the CP can be induced not only by blood and blood degradation products but also by increased ICP.

MATERIALS AND METHODS

Animals and Surgical Procedures

Experiments were performed on 54 adult male rats (Wistar 200 – 250 g; Animal Breeding Facility, Masaryk University, Czechia). All experimental procedures were carried out aseptically and according to protocols approved by the Ethical Committee of Masaryk University, Brno and the Departmental Committee of the Ministry of Education, Youth and Sports, Czechia. The rats were anesthetized with a mixture of 5% ketamine (100 mg/kg) and 2% xylazine (10 mg/kg) administrated intraperitoneally.

Subarachnoid hemorrhage was induced by the application of non-heparinized autologous arterial blood into the cisterna magna following the standardized method originally published by Solomon et al. (1985) and modified by other authors (d'Avella et al., 1996; Matz et al., 1996). Briefly, cannulation of the caudal artery was performed (SAH group) and a midline suboccipital incision was made to expose the arch of the atlas, the occipital bone and the atlanto-occipital membrane. Then, the animal was placed in a stereotaxic apparatus (Kopf Instruments, Tujunga, CA, United States), the atlanto-occipital membrane was cleared of connective tissue, and a syringe with 30G needle was placed on the manipulating arm of the stereotaxic frame tilted at 60° from horizontal plane. Under the high magnification of a surgical microscope the arachnoid was penetrated by the needle and 200 μl of non-heparinized autologous blood taken from the caudal artery was injected within 60 s into the cisterna magna (SAH group).

Two hundred μl of ACSF containing 130 mmol/l NaCl, 3.0 mmol/l KCl, 1.2 mmol/l NaH_2PO_4, 20 mmol/l $NaHCO_3$, 1.3 mmol/l $MgCl_2$, 2.4 mmol/l $CaCl_2$, 10 mmol/l Glucose (Hylden and Wilcox, 1980) instead of blood was injected within 60 s into the cisterna magna to the animals of ACSF group.

The needle was slowly withdrawn 2 min after injection to prevent leakage of blood or ACSF from the cisterna magna and the membrane puncture was closed by gelatin sponge. The muscles and the skin were closed by 4-0 silk suture.

Rats exposed to blood (SAH group) or ACSF (ACSF group) were left to survive for 1, 3, and 7 days (n = 8 SAH; n = 8 ACSF for each time point).

Rats of SAH and ACSF groups as well as a naive group (n = 6) were sacrificed using CO_2, perfused transcardially with 500 ml heparinized (1000 units/500 ml) phosphate–buffered saline (PBS; pH 7.4) followed by 500 ml of Zamboni's fixative (Zamboni and de Martino, 1967).

Then, brains were promptly removed and assessed for successful injection. In the SAH group, brains from animals with expressed SAH (presence of the blood in the subarachnoid cisterns and basal surface of the brain after full blood volume injection) and brains with no SAH from the ACSF group (no blood in the subarachnoid space, full ACSH volume injection) were included. After macroscopic assessment, the brains were immersed in Zamboni's fixative for 3 days, washed in 10%

sucrose and embedded in Tissue-Tek OCT compound (Miles, Elkhart, IN, United States). Coronal cryostat sections were cut (20 μm sections; Leica 1800 cryostat; Leica Microsystem, Wetzlar, Germany) and mounted onto chrome-alum covered microscope slides.

Immunohistochemical Staining

To detect subpopulations of macrophages, the brain sections of naive, SAH and ACSF groups were immunostained under identical conditions with anti-CD68 (activated ED1+ macrophages), anti-CD163 (resident ED2+ macrophages), anti-CCR7 and anti-CD206 antibodies. M1 macrophages are characterized by expression of CD68 (ED1) and CCR7 besides other antigens (Badylak et al., 2008; Ma et al., 2010). The expression of CD163 (ED2) and CD206 antigens marks the M2 macrophage phenotype (Kigerl et al., 2009). APC were detected using an anti-major histocompatibility complex class II (MHC II) antibody (Dijkstra and Damoiseaux, 1993), and T lymphocytes with anti-CD3 antibody (Mason et al., 1989). Proliferation activity was assessed using Ki-67 immunostaining (Gerdes et al., 1984).

Sections were washed with PBS containing 0.3% bovine serum albumin and 0.1% Tween-20, treated with 3% normal serum for 30 min. and then incubated with the primary antibody at room temperature. Primary antibody sources and incubation conditions are listed in **Table 1**. Affinity purified Cy5- or FITC conjugated donkey anti-rabbit or anti-mouse secondary antibodies (Jackson, 1:100) were applied at room temperature for 90 min. Control sections were incubated in parallel omitting the primary antibodies. Positive immunostaining of CD3 antibody was confirmed in sections of the spleen. Immunostained sections were rinsed, stained with Hoechst 33342 (Sigma, St. Louis, MO, United States) to locate cell nuclei, and mounted in Vectashield aqueous mounting medium (Vector Laboratories, Burlingame, CA, United States). Immunofluorescence was observed and analyzed using a Nikon Eclipse NI-E epifluorescence microscope, equipped with a Nikon DS-Ri1 camera (Nikon, Prague, Czechia).

Double Immunohistochemical Staining

Proliferation activity of APC and macrophages in the CP was monitored using double immunostaining for MHC II, ED1 or ED2 and Ki-67. A subset of sections was incubated with rabbit polyclonal anti-Ki-67 antibody and treated with FITC-conjugated donkey anti-rabbit secondary antibody for 90 min. After thorough washing, primary MHC II, ED1 or ED2 antibody was applied overnight followed by Cy5-conjugated secondary antibody. Sections were mounted and analyzed as above.

Image and Statistical Analysis

Images (magnification 200x) were acquired from at least 10 sections cut at 60 μm intervals through the brain ventricles containing the CP for each group of animals. CP area was determined in the images, manually edited when needed, and measured using the NIS-Elements AR Analysis software (version 4.20.00, Nikon, Prague, Czechia). ED1, ED2, CCR7, CD206, MHC II, and CD3 immunopositive cells (ED1+, ED2+, CCR7+, CD206+, MHC II+, and CD3+) were correlated using the positions of cell nuclei and counted manually in the defined CP area. The analysis was performed in a randomized fashion by an investigator who was blinded to the group of animals. The number of positive cells for every 1 mm^2 of CP area was expressed as mean ± standard deviation (SD).

To detect cellular proliferation, double immunostaining (ED1, ED2 or MHC II and Ki67) was analyzed in the colocalization module of NIS Elements software (Nikon, Czechia). The percentage of ED1+/Ki-67+, ED2+/Ki-67+, and MHC II+/Ki-67+ cells (to total Ki-67+ cell number) was expressed as mean ± standard deviation (SD).

The data of naive, ACSF and SAH groups were compared pairwise using the Mann–Whitney *U*-test in STATISTICA 5.5 software (StatSoft, Tulsa, OK, United States).

RESULTS

All animals that underwent application of blood (SAH group; $n = 24$) or ACSF ($n = 24$) survived the experiments and the injection was successful (scored as the presence of blood in the subarachnoid space in the SAH group and no blood in the ACSF group).

Position and Number of Immune Cells in the CP

Activated (ED1+) and resident (ED2+) macrophages as well as CCR7+ and CD206+ cells were found mainly on the ventricular side of the cuboidal epithelial cells in the epiplexus position (**Figures 1–4**).

The number of ED1+ macrophages in the CP of SAH and ACSF animals increased over time in our experiments. One day after SAH, the numbers of ED1+ macrophages in the CP was slightly increased compared to CP of naïve control ($n = 147.2 \pm 36.5/mm^2$). A significant increase, compared to the CP of naïve rats, in the number of ED1+ macrophages was found 3 days ($n = 265 \pm 70/mm^2$; $p < 0.01$) and 7 days ($n = 339.1 \pm 85.9/mm^2$; $p < 0.01$) after SAH as well as 3 days ($n = 215.8 \pm 49.4/mm^2$; $p < 0.05$) and 7 days ($n = 228.2 \pm 51.8/mm^2$; $p < 0.05$) after ACSF injection. The number of ED1 + macrophages after 7 days was significantly higher in the CP of the SAH animals ($n = 339.1 \pm 85.9/mm^2$; $p < 0.05$) compared to the ACSF group ($n = 228.2 \pm 51.8/mm^2$; **Figure 5A**).

Immunoquantification showed a similar significant increase in the number of ED2+ macrophages at 1 ($n = 24.5 \pm 9.3/mm^2$; $p < 0.05$), 3 ($n = 23.3 \pm 1.5/mm^2$; $p < 0.05$) and 7 days ($n = 25.8 \pm 9.6/mm^2$; $p < 0.05$) following SAH compared to naïve rats ($n = 6.8 \pm 4.5/mm^2$). Strikingly, the number of ED2+ macrophages was significantly increased 1, 3, and 7 days following SAH, also when compared to ACSF animals at the same time points ($n = 7.3 \pm 7.9/mm^2$; $n = 8.85 \pm 4.95/mm^2$; $n = 11.5 \pm 2.4/mm^2$, respectively). No significant changes in the number of ED2+ cells were found in the CP of the ACSF animals when compared to naïve controls (**Figure 5B**).

The number of CCR7+ cells was significantly increased, compared to CP of naïve controls, in the CP of animals 1

TABLE 1 | List of primary antibodies used, their dilutions, incubation times and suppliers.

Name	Type of antibody	Dilution	Incubation time	Supplier
ED1	Mouse monoclonal	1:200	240 min	Serotec
ED2	Mouse monoclonal	1:200	16 hrs	Serotec
Ki-67	Rabbit polyclonal	1:500	240 min	Vector Laboratories
MHC II	Mouse monoclonal	1:100	Overnight	Serotec
CCR7	Rabbit polyclonal	1:50	Overnight	Acris
CD206	Rabbit polyclonal	1:50	Overnight	Santa Cruz
CD3	Rabbit monoclonal	1:100	Overnight	Abcam

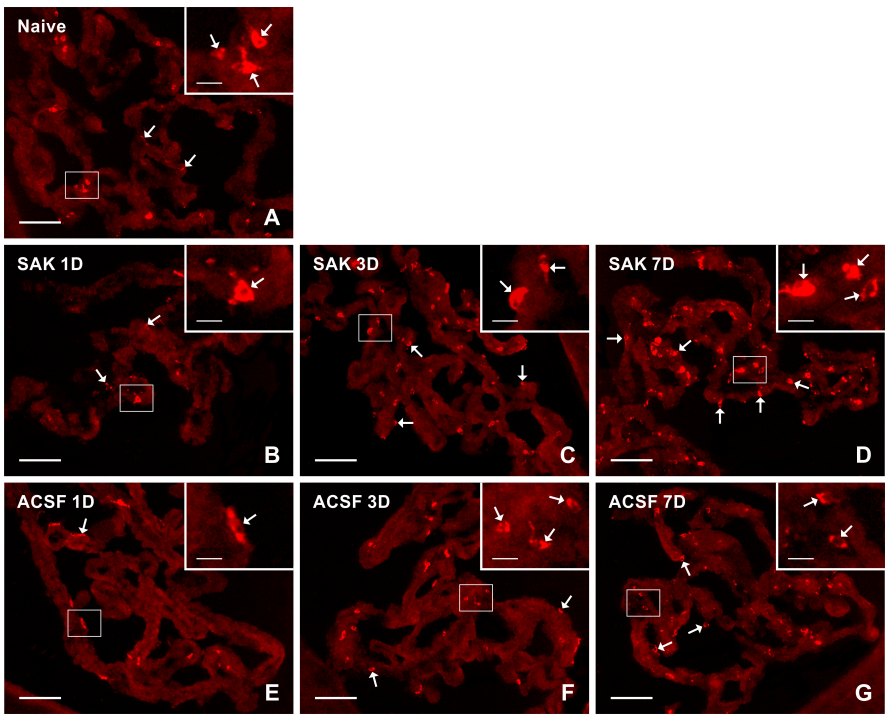

FIGURE 1 | Representative pictures showing results of immunostaining with ED1 antibody in cryostat sections of the CP from naïve **(A)**, SAH **(B–D),** and ACSF **(E–G)** rats at 1, 3 and 7 days (1D, 3D, and 7D) after operation. SAH induced an increase in the number of ED1+ cells 3 and 7 days after operation. Increased numbers of ED1+ cells were also found 3 and 7 days after application of ACSF. Arrows indicate ED1+ cells predominantly in the epiplexus position of the CP. Insets show a higher magnification of regions marked by the boxes. Scale bars = 80 μm (main image); 10 μm (insets).

($n = 45 \pm 8.4/mm^2$; $p < 0.01$) and 3 days ($n = 23.1 \pm 8.1/mm^2$; $p < 0.05$) following SAH ($n = 3.6 \pm 1.8/mm^2$). The number of CCR7+ cells in the CP of the SAH and ACSF group decreased over time and dropped to normal at 7 days. Moreover, the CP of the ACSF group showed a significantly higher CCR7 + cell number ($n = 58.9 \pm 23/mm^2$; $p < 0.05$), compared to CP of naïve rats only after 1 day following ACSF application ($n = 3.6 \pm 1.8/mm^2$; **Figure 5C**).

Immunostaining showed a significantly higher number, compared to naïve controls (n = $21.6 \pm 3.4/mm^2$), of anti-inflammatory CD206+ cells in the CP 1 ($n = 46.4 \pm 8.5/mm^2$; $p < 0.05$), 3 ($n = 90.5 \pm 12.4/mm^2$; $p < 0.001$) and 7 days ($n = 90.4 \pm 11.6/mm^2$; $p < 0.001$) after SAH. However, the number of CD206 + cells in the CP of the ACSF group decreased over time following ACSF injection; it was significantly increased compared to CP of naïve animals ($n = 21.6 \pm 3.4/mm^2$) at 1 ($n = 58.9 \pm 6.1/mm^2$; $p < 0.001$) and 3 days ($n = 40.2 \pm 3.2/mm^2$; $p < 0.01$), but dropped to normal at 7 days. SAH significantly increased the number of CD206+ cells in the CP 3 ($n = 90.5 \pm 12.4/mm^2$; $p < 0.01$) and 7 days ($n = 90.4 \pm 11.6/mm^2$; $p < 0.001$) when compared to ACSF at the same time points ($n = 40.2 \pm 3.1/mm^2$ and $n = 26.7 \pm 3.6/mm^2$, respectively; **Figure 5D**).

MHC II+ APC displayed a range of shapes from oval to ramified and were found in the epiplexus position as well as in the stromal core of the CP (**Figure 6**). The APC population of the CP showed a progressive increase in number following SAH over the duration of our experiment. Significantly increased numbers of APC were found 3 ($n = 647.6 \pm 85.1/mm^2$; $p < 0.01$) and 7 days ($n = 766.2 \pm 111.1/mm^2$; $p < 0.05$) following SAH as well as 3 ($n = 639.5 \pm 77.6/mm^2$; $p < 0.05$) and 7 days ($n = 651 \pm 75.6/mm^2$; $p < 0.05$) following ACSF injection when

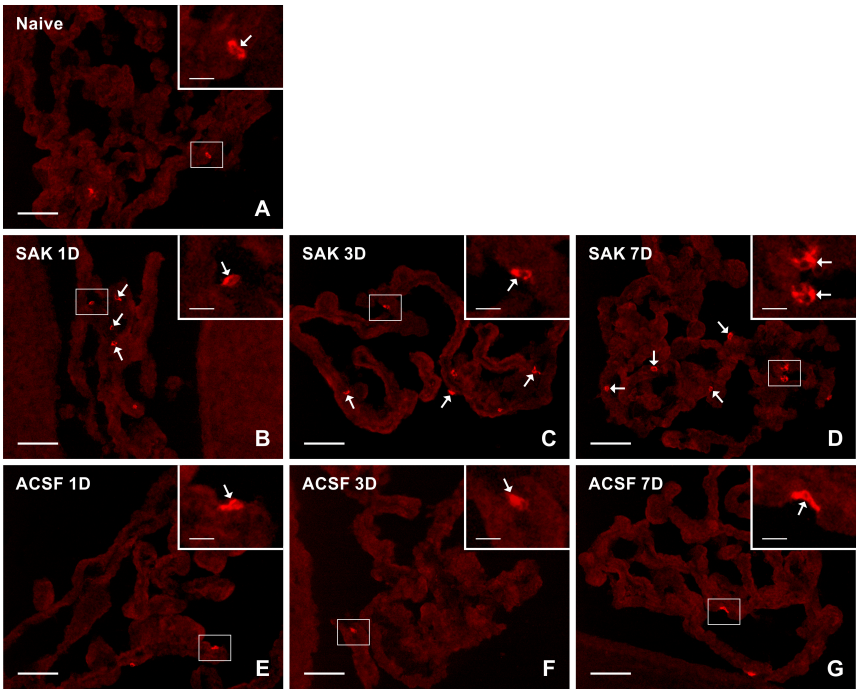

FIGURE 2 | Representative pictures of cryostat sections through the CP showing immunostaining with ED2 antibody from naïve **(A)**, SAH (**B–D**), and ACSF **(E–G)** rats at 1, 3 and 7 days (1D, 3D, and 7D) after operation. SAH led to increased numbers of ED2+ cells at 1, 3, and 7 days after operation. The number of ED2+ cells in CP of ACSF animals did not increase at any time point after ACSF administration. Arrows indicate ED2+ cells in the epiplexus position of the CP. Insets show a higher magnification of regions marked by the boxes. Scale bars = 80 μm (main image); 10 μm (insets).

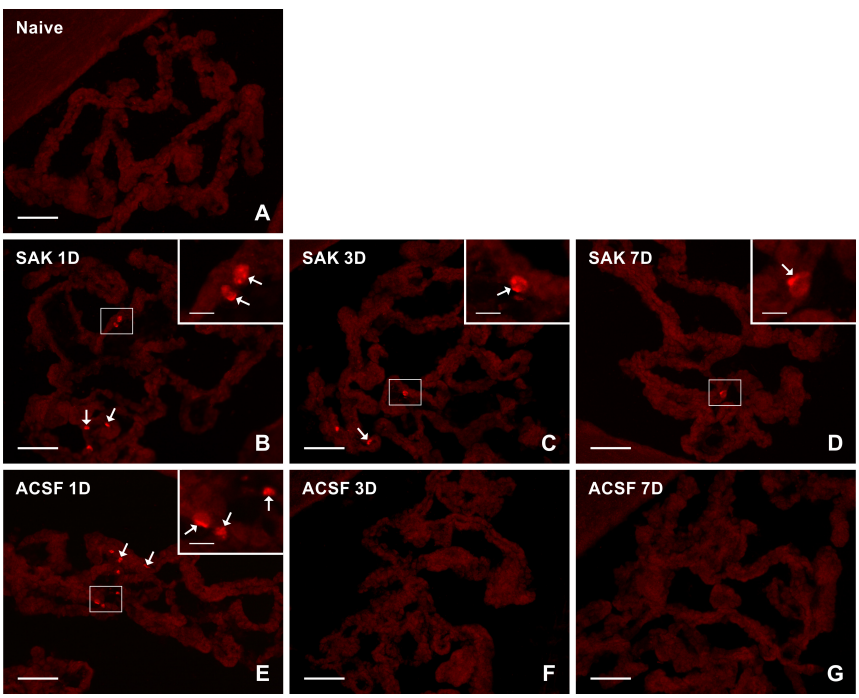

FIGURE 3 | Representative pictures showing results of immunostaining with CCR7 antibody in cryostat sections of the CP from naïve **(A)**, SAH **(B–D)**, and ACSF **(E–G)** rats at 1, 3 and 7 days (1D, 3D, and 7D) after operation. The number of CCR7+ cells was increased 1 and 3 days following induction of SAH and 1 day after ACSF administration. Arrows indicate CCR7+ cells in the epiplexus position of the CP. Insets show a higher magnification of regions marked by the boxes. Scale bars = 80 μm (main image); 10 μm (insets).

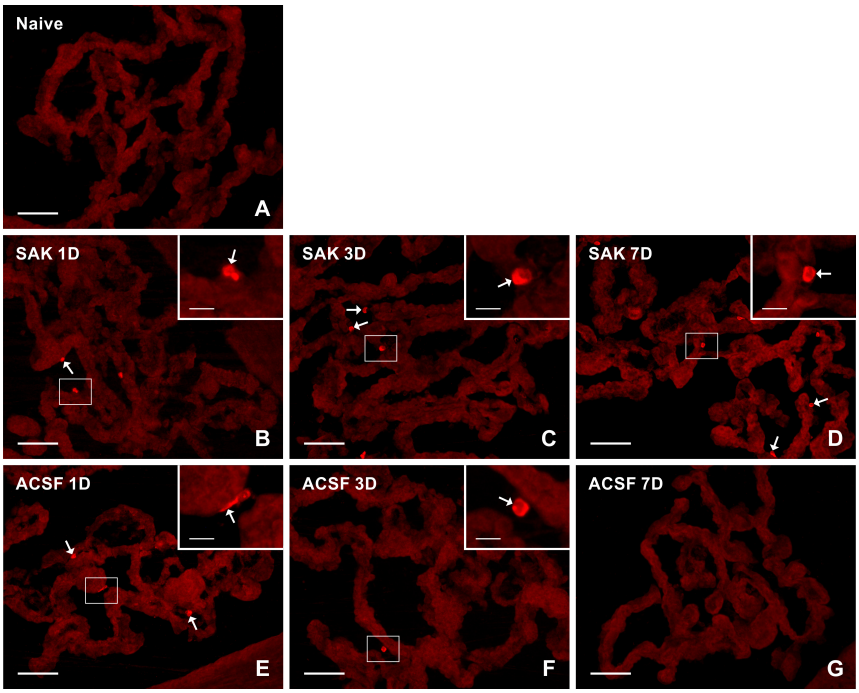

FIGURE 4 | Representative pictures of cryostat sections through the CP showing immunostaining with CD206 antibody from naïve **(A)**, SAH **(B–D),** and ACSF **(E–G)** rats at 1, 3, and 7 days (1D, 3D, and 7D) after operation. Increased numbers of CD206+ cells were found 1, 3, and 7 days following induction of SAH. ACSF application led to an increase in the number of CD206+ cells 1 and 3 days following injection. Arrows indicate CD206+ cells in epiplexus position of the CP. Insets show a higher magnification of regions marked by the boxes. Scale bars = 80 μm (main image); 10 μm (insets).

compared to naïve rats (n = 495.7 ± 98.7/mm^2). The number of MHC II+ APC in the CP was significantly increased 7 days (n = 766 ± 111.1/mm^2; $p < 0.05$) after SAH compared to ACSF animals (n = 651 ± 75.6/mm^2; **Figure 5E**). CD3 immunostaining did not reveal T cells in the CP of any group of the animals (not shown).

Assessment of Proliferation Activity in the CP

Immunostaining for Ki-67 revealed proliferating cells in the epiplexus position (**Figure 7**). Significantly increased proliferation of epiplexus KC was found 1 (n = 63.3 ± 6.8/mm^2; $p < 0.05$), 3 (n = 79.3 ± 12.3/mm^2; $p < 0.01$) and 7 days (n = 86.1 ± 13.8/mm^2; $p < 0.05$) following SAH, compared to the number of Ki-67 positive cells in the CP of naïve animals (n = 37.6 ± 9.4/mm^2). Moreover, the proliferation showed a tendency to increase. Significantly increased proliferation of KC was also found in the CP of the ACSF group 1 (n = 64 ± 12.6/mm^2; $p < 0.05$) and 3 days (n = 58.2 ± 8.3/mm^2; $p < 0.05$) after ACSF injection compared to naïve animals (n = 37.6 ± 9.4/mm^2). KC proliferation activity returned to normal 7 days after ACSF application. The number of Ki-67+ cells was significantly increased 7 days (n = 86.1 ± 13.8/mm^2; $p < 0.01$) after SAH compared to the control group 7 days after ACSF application (n = 19.6 ± 5.2/mm^2) (**Figure 5F**).

Double immunostaining of MHC II+ and Ki67+ cells revealed that all proliferating cells in the CP were APC in all animals (**Figures 8A–C**). Double immunostaining for ED1+ and Ki-67+ (**Figures 8D–F**) cells did not reveal significant changes in the percentage of proliferating activated macrophages in the CP following either SAH or ACSF application (**Figure 8J**). In contrast, double immunostaining for ED2+ and Ki-67+ cells (**Figures 8G–I**) displayed a significantly higher percentage of proliferating ED2+ cells 7 days (n = 38.4 ± 9.4%; $p < 0.05$) following SAH, but at 3 days (n = 17.2 ± 3.5%) the number was lower compared to ACSF animals. Surprisingly, the number of proliferating ED2+ cells in the CP was significantly higher, compared to naïve animals (n = 17.2 ± 3.5%), 3 days (n = 29.6 ± 4.2%; $p < 0.05$) after ACSF application. The proliferation of ED2+ cells was significantly increased 3 days following ACSF application (n = 29.6 ± 4.2/mm^2; $p < 0.01$), when compared to 3 days after SAH induction (n = 17.2 ± 1.2%), whereas it was reversed at 7 days following SAH, being significantly higher (n = 38.4 ± 9.4%; $p < 0.01$) when compared to CP of the ACSF group (n = 15.9 ± 4.1%; **Figure 8K**).

DISCUSSION

Subarachnoid Hemorrhage Induced Inflammatory Reaction in the Choroid Plexus

Subarachnoid hemorrhage from a ruptured intracranial aneurysm results in an initial increase of ICP which together with

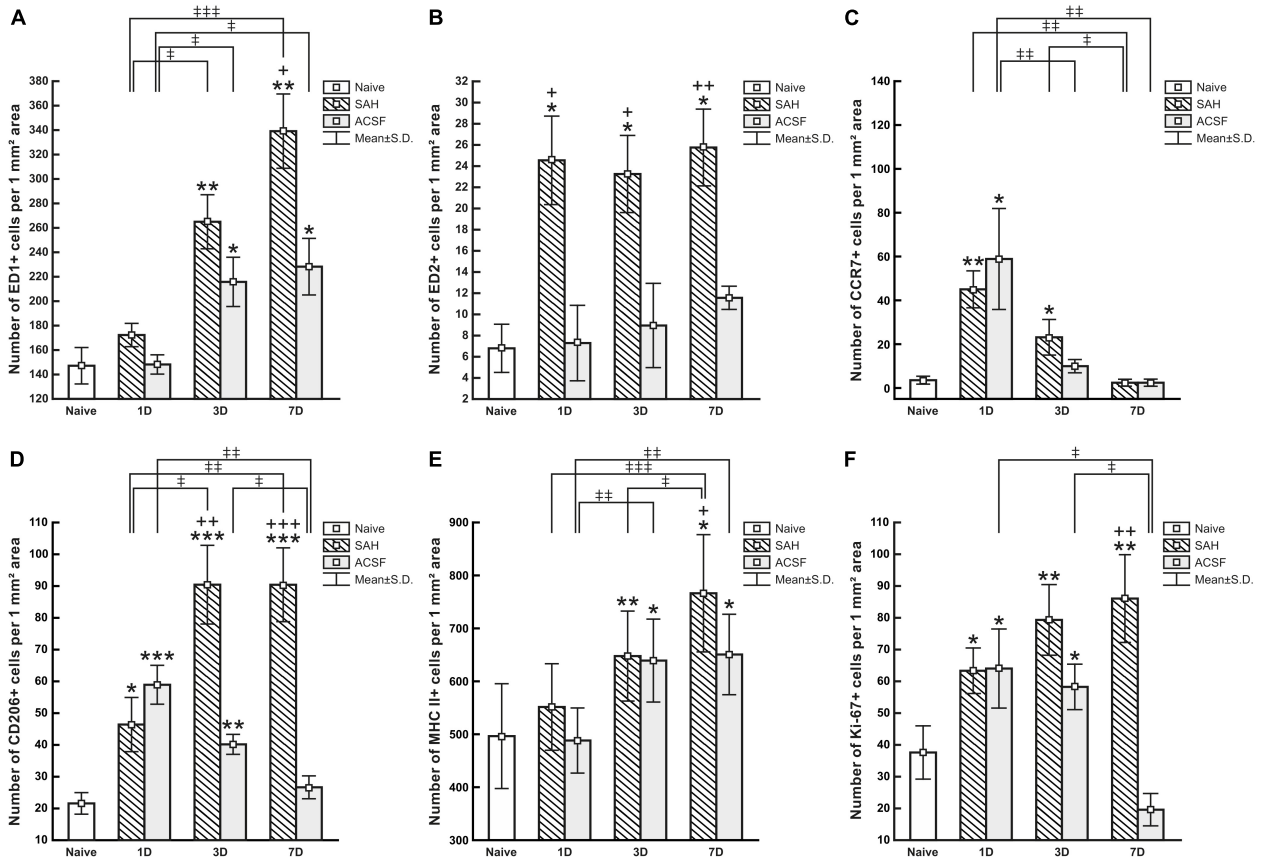

FIGURE 5 | Numbers of ED1+ **(A)**, ED2+ **(B)**, CCR7+ **(C)**, CD206+ **(D)**, MHC II+ **(E)** and Ki67+ **(F)** cells per mm^2 of CP from naive, ACSF and SAH rats at 1, 3, and 7 days after operation. Error bars indicate SD. *Indicates a significant difference when compared to CP from naïve rats (*$p < 0.05$; **$p < 0.01$; ***$p < 0.001$). +Indicates a significant difference when compared to CP from ACSF rats ($^{+}p < 0.05$; $^{++}p < 0.01$; $^{+++}p < 0.001$). ‡Indicates a significant difference between the individual time points of survival ($^{‡}p < 0.05$; $^{‡‡}p < 0.01$; $^{‡‡‡}p < 0.001$).

subsequent blood degradation products produce further clinical complications (Grote and Hassler, 1988; Kamp et al., 2013). The main pathophysiological changes like early brain injury, cerebrovascular inflammation and alteration/disturbance of the blood-brain barrier occur during the first several days after SAH (Germanò et al., 2000; Sercombe et al., 2002; Cahill et al., 2006).

In our experiments, we used the technique of volume infusion, a well-established model of SAH originally published by Solomon et al. (1985) where a constant volume of blood or ACSF is injected into the cisterna magna. Volume infusion is a standardized model with very low mortality in animals (0% in our experiments) and produces a similar change in ICP as well as in cerebral blood flow in all animals. It has been found that application of 200 μl of autologous arterial blood or ACSF into the subarachnoid cistern induced a sudden increase in ICP from 7 ± 1 to 107 ± 5 mmHg (102 ± 7 mmHg, respectively) within 15 s with a drop to near-normal levels within 2.5 min. Moreover, compared to other models, the volume infusion model is more valuable for late SAH changes (Prunell et al., 2002). We injected blood or ACSF within 60 s. It has been found that injection speed plays a crucial role in ICP dynamics, cerebral blood flow and autoregulation. Rapid injection (within 60 s), compared to slow injection (10, 30, or 60 min), produces the highest ICP peaks, autoregulation impairment and neuronal loss resulting in early brain injury (Conzen et al., 2019). In our experiments we did not assess behavioral changes because 7 days is too short a time for evaluating functional outcomes. Nevertheless, it has been found that blood injection into the cisterna magna induces motor impairment compared to saline injection (Germanò et al., 1994).

It is generally accepted that the products of heme catabolism, e.g., free ferrous iron, CO or biliverdin/bilirubin are biologically active substances that may exert profound effects on cellular differentiation, proliferation, physiology and death (Schipper, 2004). Therefore, it is reasonable to assume that the formation and subsequent degradation of a blood clot may lead to the alteration of macrophage numbers and increased cellular proliferation in the CP.

Our experimental study demonstrated that SAH induced an increase in the number of epiplexus macrophages with ED1, ED2, CCR7, CD206 and MHC immunophenotypes and caused their proliferation in the CP. These findings corroborate the findings of Liszczak et al. (1984), where increased KC numbers were seen in the CP 1 week after SAH, but they did not evaluate cellular specification, nor did they monitor earlier time points.

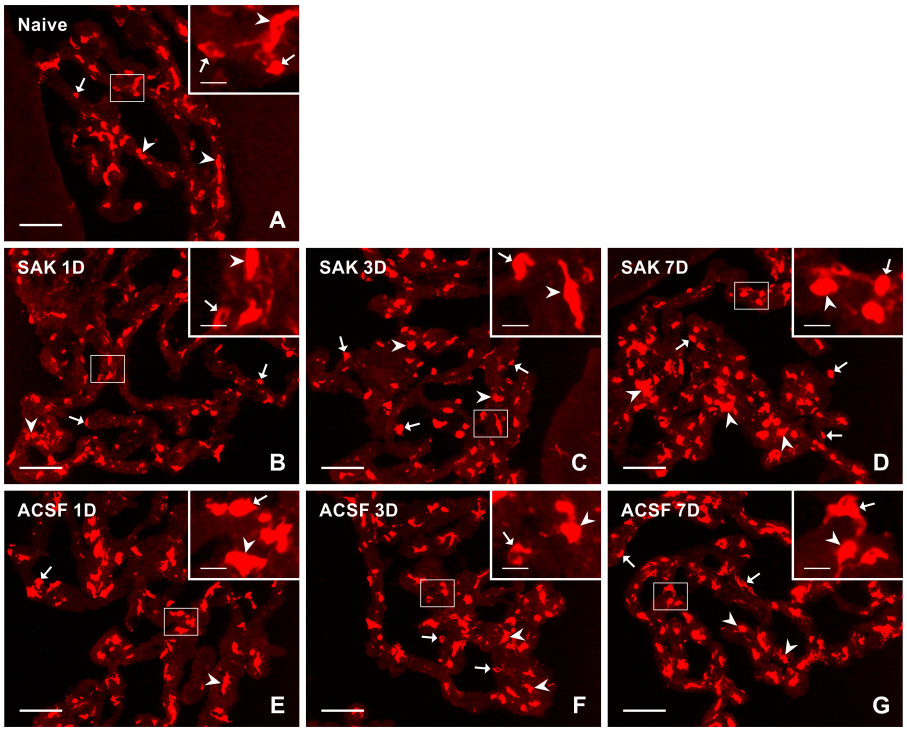

FIGURE 6 | Representative pictures of cryostat sections through the CP showing immunostaining with MHC II antibody from naïve **(A)**, SAH **(B–D),** and ACSF **(E–G)** rats at 1, 3, and 7 days (1D, 3D, and 7D) after operation. Arrows indicate MHC II+ cells in the epiplexus position and arrowheads in the stroma of CP. Insets show a higher magnification of regions marked by the boxes. Scale bars = 80 μm (main image); 10 μm (insets).

Immunostaining revealed higher numbers of activated (ED1+) macrophages and MHC II+ immune cells in the epiplexus position over the period of survival following SAH. This is probably linked to similar cellular specificity of the ED1 antibody and that recognizing MHC II. The ED1 antibody is produced against a 110-kD the lysosomal/endosomal-associated membrane glycoprotein (CD68) highly expressed by monocytes and tissue macrophages. This protein is a member of the scavenger receptor family involved in the clearance of cellular debris and the promotion of phagocytosis in activated macrophages (Juniantito et al., 2010; Zeibig et al., 2019). The ED1 monoclonal antibody of the same clone was specified and used by many other authors as a marker of macrophages with activated phagocytosis (Dijkstra et al., 1985; Hu et al., 2007; Lee and Zhang, 2012). Similarly, MHC-II is strongly expressed in activated and phagocytic macrophages (Lee and Zhang, 2012). Our results are in line with earlier reports showing a high level of MHC-II in epiplexus macrophages (Li and Barres, 2018). There is growing body of recent evidence that inflammation in CP leads to CSF hypersecretion following the intraventricular hemorrhage (Karimy et al., 2017). Moreover, epiplexus cell activation in rat CP characterized by increased number of CD68+ and Iba-1+ cells as well as Iba-1+ cell soma size was associated with the development of hydrocephalus 24 h after SAH induction (Wan et al., 2019). Similarly, inflammation in the CP may lead to hypersecretion of CSF and thus contribute to the development of post-hemorrhagic hydrocephalus.

It has been reported that the recruitment of monocytes after SAH is stimulated by the pro-inflammatory and chemotactic molecules of the CP via activation of toll like receptor 4 (TLR-4; Meeker et al., 2012; Gram et al., 2014). Moreover, upregulation of TLR-4 by heme leads to increased TNF-α expression, inducing alterations in tight junction proteins like zonula occludens-1 (Zeni et al., 2007; Simard et al., 2009, 2011; Aveleira et al., 2010; Lin et al., 2012). Since the percentage of proliferating ED1+ cells was approximately the same in the CP of the SAH, ACSF and naïve groups, it can be assumed that their increased number in the epiplexus position probably arises from recruited monocytes. Moreover, we found a significantly increased percentage of proliferating (Ki-67+) ED2+ macrophages in the epiplexus position 7 days after SAH, but the number of ED2+ macrophages was approximately the same at all time-points. Therefore, activation and proliferation of resident ED2+ macrophages may be another source of increased number of ED1+ activated macrophages 7 days after SAH as has been previously described after nerve injury, focal brain ischemia and traumatic brain injury (Hu and McLachlan, 2003; Hu et al., 2012; Wang et al., 2013). It was demonstrated that circulating monocytes migrate through the fenestrated capillaries into the connective tissue of the CP and pass through epithelial cells by "emperipolesis" to become KC (Ling et al., 1998). Blood circulation in meningeal vessels could be another source of the increased number of epiplexus macrophages (Wilson et al., 2010).

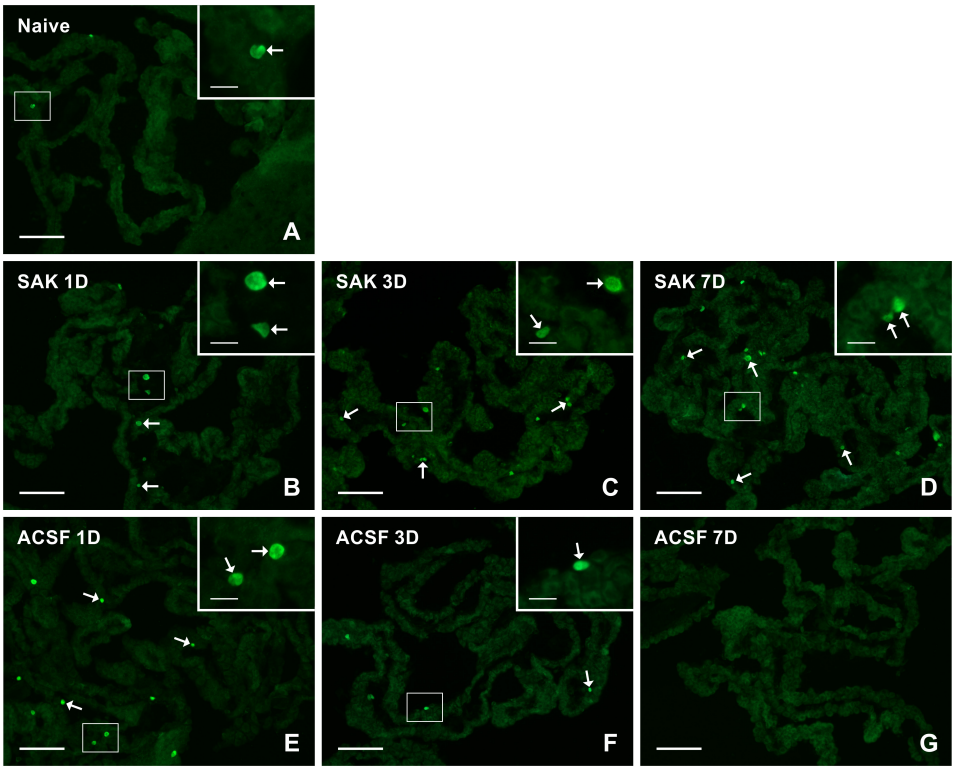

FIGURE 7 | Representative pictures of cryostat sections through the CP showing immunostaining with Ki67 antibody from naïve **(A)**, SAH **(B–D)**, and ACSF **(E–G)** rats at 1, 3, and 7 days (1D, 3D, and 7D) after operation. SAH induced a progressive increase in the number of proliferating cells 1, 3, and 7 days after injection of blood. ACSF application led to an increase in the number of KI67+ cells 1 and 3 days after operation. Arrows indicate Ki67+ cells in the epiplexus position of the CP. Insets show a higher magnification of regions marked by the boxes. Scale bars = 80 μm (main image); 10 μm (insets).

In general, the distinct functional macrophage phenotypes are designated as M1 and M2 (Demeestere et al., 2015). M1 macrophages are characterized by expression of CD68 (ED1) and CCR7 besides other antigens (Badylak et al., 2008; Ma et al., 2010). In contrast, the expression of CD163 (ED2) and CD206 antigens are indicative of the M2 macrophage phenotype (Kigerl et al., 2009). The pro-inflammatory M1 macrophages are associated with the initial phases of acute inflammation, while anti-inflammatory M2 macrophages are associated with tissue repair and regeneration (Chazaud, 2014; Demeestere et al., 2015). It is known that modulation of immune-cell phenotype and function in the CP acts as a "checkpoint" for peripheral immune cells invading into the central nervous system (CNS) in a variety of neurological diseases (Brendecke and Prinz, 2015; Goldmann et al., 2016). Moreover, the CP has been described as the entry point for anti-inflammatory M2 macrophages into the injured spinal cord while the pro-inflammatory M1 macrophages were determined to arise from the adjacent spinal cord leptomeninges (Shechter et al., 2013). However, almost all macrophages in the CP following a cortical ischemic stroke, expressed M1-like markers indicating their pro-inflammatory immunophenotyping (Ge et al., 2017).

In our experiments, we found an increased number of CCR7+ cells (approximately one fourth of all ED1+ cells) in the CP mainly 1 day after SAH, while the cell number dropped back to that of naïve animals 7 days. In contrast, CD206+ cells gradually increased over the period of survival with a peak between 3 and 7 days. This difference in the numbers of CCR7+ and CD206+ cells is probably associated with the acute inflammatory reaction in the CP immediately after and the initiation of regenerative processes in later periods after SAH. This gradual phenotypic shift toward anti-inflammatory and cytoprotective CD206+ cells in later stages after SAH could be mediated by the induction of heme oxygenase-1 (HO-1) stimulated by hemoglobin-degradation products (Abraham and Drummond, 2006; Naito et al., 2014).

Increased Intracranial Pressure Contributes to Immune Cell Changes in the Choroid Plexus

Increased ICP following the application of ACSF mimics aneurysmal subarachnoid hemorrhage (Prunell et al., 2002). ACSF application is widely used as a control for intrathecal drug application and experimental models of inflammatory diseases without any evidence of immunogenicity (Hylden and Wilcox, 1980; Hernangómez et al., 2016). Cellular changes found in the CP after ACSF application are therefore most likely induced by increased ICP. Our quantitative analysis revealed similarly increased numbers of ED1+ and MHC II+

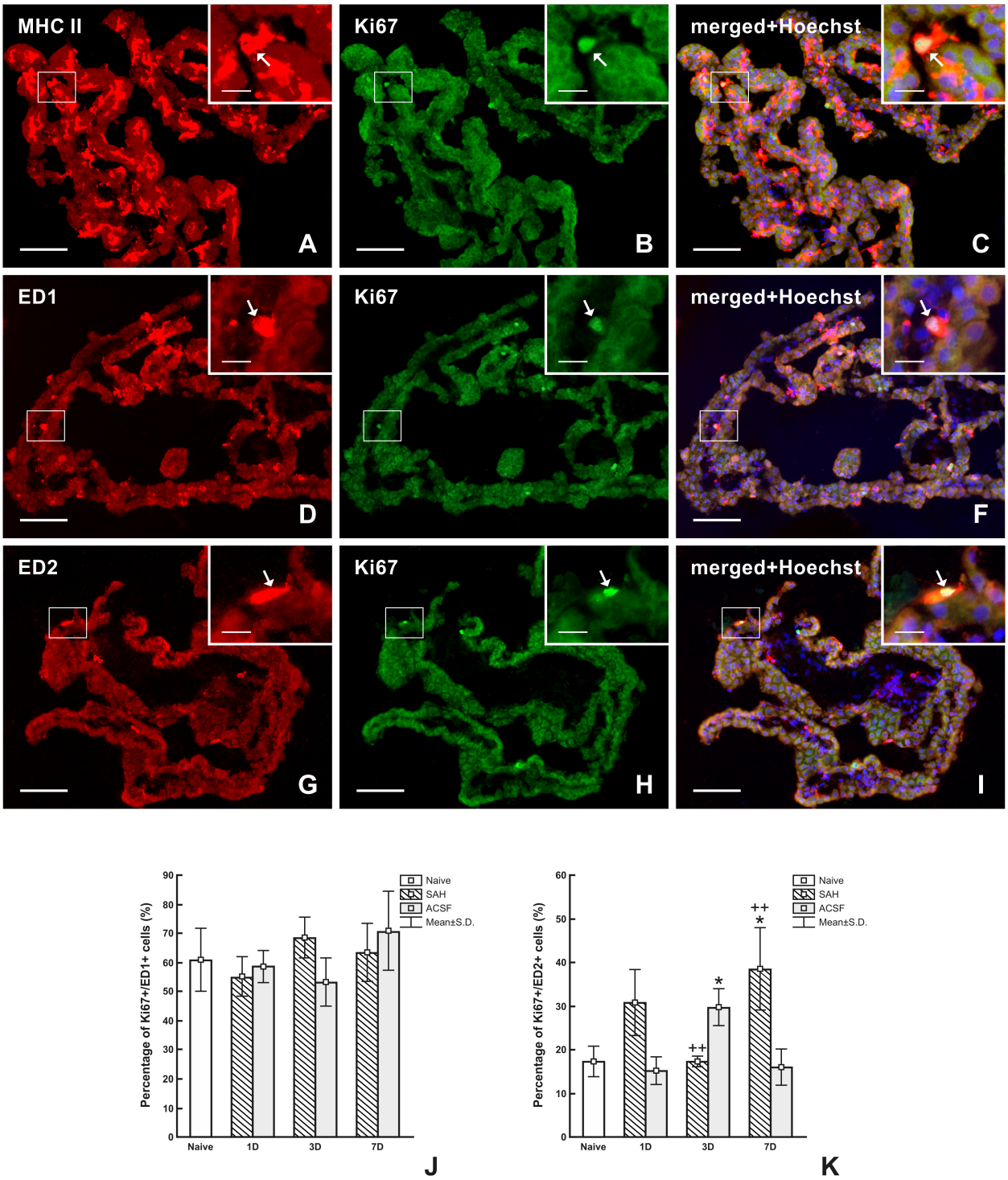

FIGURE 8 | Representative images of double immunostaining to detect MHC II+, ED1+, and ED2+ macrophages as well as Ki67+ cells in the CP 7 days after SAH. Double immunostaining for MHC II and Ki-67 **(A–C)** showed that all proliferating cells are antigen presenting cells *(arrows)*. Simultaneous reaction for ED1 and Ki67 **(D–F)** proved that most proliferating cells are activated macrophages *(arrows)*. Double immunostaining reaction for ED2 and Ki-67 **(G–I)** showed that approximately one-third of proliferating cells are resident macrophages *(arrows)*. Merged figures **(C,F,I)** include a merge with Hoechst-stained nuclei. Scale bars – main images 80 μm; insets 20 μm. Percentage of ED1+/Ki-67+ cells **(J)** and ED2+/Ki67+ cells **(K)** in the CP of naïve, SAH and ACSF rats at 1, 3, and 7 days after operation. *Indicates a significant difference when compared to CP from naïve rats ($p < 0.05$). $^{++}$Indicates a significant difference when compared to CP from control rats ($p < 0.01$).

cells following ACSF application as those seen in SAH animals. On the other hand, the initial increase in CCR7+ and CD206+ cell number followed by a decrease at later time points is probably a reaction to the surgical procedure. These results indicate that the reaction of epiplexus cells after SAH can also be affected by increased intracranial pressure. However, blood application (SAH group) induced a stronger immune reaction as expressed by increased number of ED2+, CD206+ cells and increased proliferation of ED2+ cells. This clearly indicates that blood and/or blood degradation products contributes to strong immune reaction in the later phase (3 and 7 days) following SAH compared to ACSF application. Since anti-inflammatory M2 macrophages (ED2+, CD206+) are associated with tissue repair and regeneration (Chazaud, 2014; Demeestere et al., 2015) we assume that this reaction may contribute to phagocytosis of the blood clot and restoration of brain homeostasis. Moreover, in contrast to the CP of naïve rats, ACSF application into the subarachnoid space elicits significantly increased epiplexus cell proliferation in the initial stages (1 and 3 days after ACSF application), but returns to normal 7 days after injection. We can assume that increased ICP may also affect the number of epiplexus immune cells in the CP by modulating cell proliferation early as an acute reaction. However, based on our results we assume that increased intracranial pressure itself does not have the ability to induce long-lasting changes in the CP.

Interestingly, we did not find CD3+ cells in any animal group even after sensitive CD3 immunofluorescence staining using cryostat sections and image analysis. In addition, positive immunostaining of spleen sections confirmed the function of the anti-CD3 antibody used. Absence of CD3+ cells in our CP samples is consistent with the finding that only a few CD3+ cells are located to the CP of naïve mice (Petito and Adkins, 2005) and indicate no recruitment of CD3+ cells following SAH or ACSF application. In addition, absence of CD3+ cells in CP following SAH might be explained by inhibitory mechanisms of T cell activation and proliferation that get triggered. It is well known that degradation of heme leads to the induction of HO-1 expression in macrophages and dendritic cells. Moreover, overexpression of HO-1 downregulates co-stimulatory molecules of dendritic cells that are necessary for the activation of T lymphocytes (Chauveau et al., 2005; Hull et al., 2014).

CONCLUSION

Our experimental results demonstrate increased numbers of immune cells with diverse immunophenotypes predominantly in the epiplexus position of the CP in response to SAH. Moreover, this increased epiplexus cell number was also found in the CP of the ACSF group, indicating that not only blood, but also increased ICP contributes to cellular changes in the CP. Immune cell changes in the CP may alter the B-CSF barrier with the consequent development of hydrocephalus in response to SAH. On the other hand, SAH triggers the recruitment of epiplexus macrophages that may ingest the blood clot by phagocytosis and may thus contribute to the restoration of brain homeostasis.

DATA AVAILABILITY STATEMENT

The datasets generated for this study are available on request to the corresponding author.

ETHICS STATEMENT

The animal study was reviewed and approved by the Animal Investigation Committee of the Faculty of Medicine, Masaryk University, Brno.

AUTHOR CONTRIBUTIONS

PS and MJ designed the research, performed the experiments, and wrote the manuscript. IK performed the experiments, prepared the samples for immunohistochemistry, and wrote the manuscript. PD and RJ analyzed the data and wrote the manuscript.

FUNDING

This work was supported by the Internal Grant Agency of the Masaryk University (Grant Nos. MUNI/A/1086/2018 and MUNI/A/0908/2017).

ACKNOWLEDGMENTS

The authors thank Ms. Marta Lněníčková, Ms. Jitka. Mikulášková, Mgr. Jana Vachová, and Mr. Lumír Trenčanský for their skillful technical assistance.

REFERENCES

Abraham, N. G., and Drummond, G. (2006). CD163-mediated hemoglobin-heme uptake activates macrophage HO-1, providing an antiinflammatory function. *Circ. Res.* 99, 911–914. doi: 10.1161/01.RES.0000249616.10603.d6

Aveleira, C. A., Lin, C.-M., Abcouwer, S. F., Ambrósio, A. F., and Antonetti, D. A. (2010). TNF-α signals through PKCζ/NF-κB to alter the tight junction complex and increase retinal endothelial cell permeability. *Diabetes* 59, 2872–2882. doi: 10.2337/db09-1606

Aydin, M. D., Kanat, A., Turkmenoglu, O. N., Yolas, C., Gundogdu, C., and Aydın, N. (2014). Changes in number of water-filled vesicles of choroid plexus in early and late phase of experimental rabbit subarachnoid hemorrhage model: the role of petrous ganglion of glossopharyngeal nerve. *Acta Neurochir.* 156, 1311–1317. doi: 10.1007/s00701-014-2088-7

Badylak, S. F., Valentin, J. E., Ravindra, A. K., McCabe, G. P., and Stewart-Akers, A. M. (2008). Macrophage phenotype as a determinant of biologic scaffold remodeling. *Tissue Eng. Part A* 14, 1835–1842. doi: 10.1089/ten.tea.2007.0264

Brendecke, S. M., and Prinz, M. (2015). Do not judge a cell by its cover–diversity of CNS resident, adjoining and infiltrating myeloid cells in inflammation. *Semin. Immunopathol.* 37, 591–605. doi: 10.1007/s00281-015-0520-6

Cahill, W. J., Calvert, J. H., and Zhang, J. H. (2006). Mechanisms of early brain injury after subarachnoid hemorrhage. *J. Cereb. Blood Flow Metab.* 26, 1341–1353. doi: 10.1038/sj.jcbfm.9600283

Chauveau, C., Rémy, S., Royer, P. J., Hill, M., Tanguy-Royer, S., Hubert, F.-X., et al. (2005). Heme oxygenase-1 expression inhibits dendritic cell maturation and proinflammatory function but conserves IL-10 expression. *Blood* 106, 1694–1702. doi: 10.1182/blood-2005-02-0494

Chazaud, B. (2014). Macrophages: supportive cells for tissue repair and regeneration. *Immunobiology* 219, 172–178. doi: 10.1016/j.imbio.2013.09.001

Conzen, C., Becker, K., Albanna, W., Weiss, M., Bach, A., Lushina, N., et al. (2019). The acute phase of experimental subarachnoid hemorrhage: intracranial pressure dynamics and their effect on cerebral blood flow and autoregulation. *Transl. Stroke Res.* 10, 566–582. doi: 10.1007/s12975-018-0674-3

d'Avella, D., Cicciarello, R., Zuccarello, M., Albiero, F., Romano, A., Angileri, F. F., et al. (1996). Brain energy metabolism in the acute stage of experimental subarachnoid haemorrhage: local changes in cerebral glucose utilization. *Acta Neurochir.* 138, 737–744. doi: 10.1007/BF01411481

Demeestere, D., Libert, C., and Vandenbroucke, R. E. (2015). Clinical implications of leukocyte infiltration at the choroid plexus in (neuro)inflammatory disorders. *Drug Discov. Today* 20, 928–941. doi: 10.1016/j.drudis.2015.05.003

Dijkstra, C. D., and Damoiseaux, J. G. M. C. (1993). Macrophage heterogenity established by immunocytochemistiry. *Prog. Histochem. Cytochem.* 27, III–65. doi: 10.1016/S0079-6336(11)80067-7

Dijkstra, C. D., Döpp, E. A., Joling, P., and Kraal, G. (1985). "The heterogeneity of mononuclear phagocytes in lymphoid organs: distinct macrophage subpopulations in rat recognized by monoclonal antibodies ED1, ED2 and ED3," in *Microenvironments in the Lymphoid System*, ed. G. G. B. Klaus (New York, NY: Springer), 409–419. doi: 10.1007/978-1-4613-2463-8_50

Fisher, C. M., Kistler, J. P., and Davis, J. M. (1980). Relation of cerebral vasospasm to subarachnoid hemorrhage visualized by computerized tomographic scanning. *Neurosurgery* 6, 1–9. doi: 10.1227/00006123-198001000-00001

Ge, R., Tornero, D., Hirota, M., Monni, E., Laterza, C., Lindvall, O., et al. (2017). Choroid plexus-cerebrospinal fluid route for monocyte-derived macrophages after stroke. *J. Neuroinflammation* 14:153. doi: 10.1186/s12974-017-0909-3

Gerdes, J., Lemke, H., Baisch, H., Wacker, H. H., Schwab, U., and Stein, H. (1984). Cell cycle analysis of a cell proliferation-associated human nuclear antigen defined by the monoclonal antibody Ki-67. *J. Immunol.* 133, 1710–1715.

Germanò, A., D'avella, D., Imperatore, C., Caruso, G., and Tomasello, F. (2000). Time-course of blood-brain barrier permeability changes after experimental subarachnoid haemorrhage. *Acta Neurochir. Wien* 142, 575–580; discussion 580–581. doi: 10.1007/s007010050472

Germanò, A. F., Dixon, C. E., d'Avella, D., Hayes, R. L., and Tomasello, F. (1994). Behavioral deficits following experimental subarachnoid hemorrhage in the rat. *J. Neurotrauma* 11, 345–353. doi: 10.1089/neu.1994.11.345

Goldmann, T., Wieghofer, P., Jordão, M. J. C., Prutek, F., Hagemeyer, N., Frenzel, K., et al. (2016). Origin, fate and dynamics of macrophages at central nervous system interfaces. *Nat. Immunol.* 17, 797–805. doi: 10.1038/ni.3423

Gram, M., Sveinsdottir, S., Cinthio, M., Sveinsdottir, K., Hansson, S. R., Mörgelin, M., et al. (2014). Extracellular hemoglobin - mediator of inflammation and cell death in the choroid plexus following preterm intraventricular hemorrhage. *J. Neuroinflammation* 11:200. doi: 10.1186/s12974-014-0200-9

Grote, E., and Hassler, W. (1988). The critical first minutes after subarachnoid hemorrhage. *Neurosurgery* 22, 654–661. doi: 10.1227/00006123-198804000-00006

Hernangómez, M., Klusáková, I., Joukal, M., Hradilová-Svíženská, I., Guaza, C., and Dubový, P. (2016). CD200R1 agonist attenuates glial activation, inflammatory reactions, and hypersensitivity immediately after its intrathecal application in a rat neuropathic pain model. *J. Neuroinflammation* 13:43. doi: 10.1186/s12974-016-0508-8

Hosoya, Y., and Fujita, T. (1973). Scanning electron microscope observation of intraventricular macrophages (kolmer cells) in the rat brain. *Arch. Histol. Jpn.* 35, 133–140. doi: 10.1679/aohc1950.35.133

Hu, P., Bembrick, A. L., Keay, K. A., and McLachlan, E. M. (2007). Immune cell involvement in dorsal root ganglia and spinal cord after chronic constriction or transection of the rat sciatic nerve. *Brain Behav. Immun.* 21, 599–616. doi: 10.1016/j.bbi.2006.10.013

Hu, P., and McLachlan, E. M. (2003). Distinct functional types of macrophage in dorsal root ganglia and spinal nerves proximal to sciatic and spinal nerve transections in the rat. *Exp. Neurol.* 184, 590–605. doi: 10.1016/S0014-4886(03)00307-8

Hu, X., Li, P., Guo, Y., Wang, H., Leak, R. K., Chen, S., et al. (2012). Microglia/macrophage polarization dynamics reveal novel mechanism of injury expansion after focal cerebral ischemia. *Stroke* 43, 3063–3070. doi: 10.1161/STROKEAHA.112.659656

Hull, T. D., Agarwal, A., and George, J. F. (2014). The mononuclear phagocyte system in homeostasis and disease: a role for heme oxygenase-1. *Antioxid. Redox Signal.* 20, 1770–1788. doi: 10.1089/ars.2013.5673

Hylden, J. L., and Wilcox, G. L. (1980). Intrathecal morphine in mice: a new technique. *Eur. J. Pharmacol.* 67, 313–316. doi: 10.1016/0014-2999(80)90515-4

Juniantito, V., Izawa, T., Yamamoto, E., Kuwamura, M., and Yamate, J. (2010). The kinetics and distribution of different macrophage populations in the developing rat skin. *Histol. Histopathol.* 25, 985–994. doi: 10.14670/HH-25.985

Kamp, M. A., Dibué, M., Etminan, N., Steiger, H.-J., Schneider, T., and Hänggi, D. (2013). Evidence for direct impairment of neuronal function by subarachnoid metabolites following SAH. *Acta Neurochir.* 155, 255–260. doi: 10.1007/s00701-012-1559-y

Kanat, A., Turkmenoglu, O., Aydin, M. D., Yolas, C., Aydin, N., Gursan, N., et al. (2013). Toward changing of the pathophysiologic basis of acute hydrocephalus after subarachnoid hemorrhage: a preliminary experimental study. *World Neurosurg.* 80, 390–395. doi: 10.1016/j.wneu.2012.12.020

Karimy, J. K., Zhang, J., Kurland, D. B., Theriault, B. C., Duran, D., Stokum, J. A., et al. (2017). Inflammation-dependent cerebrospinal fluid hypersecretion by the choroid plexus epithelium in posthemorrhagic hydrocephalus. *Nat. Med.* 23, 997–1003. doi: 10.1038/nm.4361

Kigerl, K. A., Gensel, J. C., Ankeny, D. P., Alexander, J. K., Donnelly, D. J., and Popovich, P. G. (2009). Identification of two distinct macrophage subsets with divergent effects causing either neurotoxicity or regeneration in the injured mouse spinal cord. *J. Neurosci.* 29, 13435–13444. doi: 10.1523/JNEUROSCI.3257-09.2009

King, J. T. Jr. (1997). Epidemiology of aneurysmal subarachnoid hemorrhage. *Neuroimaging Clin. N. Am.* 7, 659–668.

Lee, S., and Zhang, J. (2012). Heterogeneity of macrophages in injured trigeminal nerves: cytokine/chemokine expressing vs. phagocytic macrophages. *Brain Behav. Immun.* 26, 891–903. doi: 10.1016/j.bbi.2012.03.004

Li, Q., and Barres, B. A. (2018). Microglia and macrophages in brain homeostasis and disease. *Nat. Rev. Immunol.* 18, 225–242. doi: 10.1038/nri.2017.125

Lin, S., Yin, Q., Zhong, Q., Lv, F.-L., Zhou, Y., Li, J.-Q., et al. (2012). Heme activates TLR4-mediated inflammatory injury via MyD88/TRIF signaling pathway in intracerebral hemorrhage. *J. Neuroinflammation* 9:46. doi: 10.1186/1742-2094-9-46

Ling, E. A., Kaur, C., and Lu, J. (1998). Origin, nature, and some functional considerations of intraventricular macrophages, with special reference to the epiplexus cells. *Microsc. Res. Tech.* 41, 43–56. doi: 10.1002/(sici)1097-0029(19980401)41:1<43::aid-jemt5>3.0.co;2-v

Liszczak, T. M., Black, P. M., Tzouras, A., Foley, L., and Zervas, N. T. (1984). Morphological changes of the basilar artery, ventricles, and choroid plexus after experimental SAH. *J. Neurosurg.* 61, 486–493. doi: 10.3171/jns.1984.61.3.0486

Ma, J., Liu, L., Che, G., Yu, N., Dai, F., and You, Z. (2010). The M1 form of tumor-associated macrophages in non-small cell lung cancer is positively associated with survival time. *BMC Cancer* 10:112. doi: 10.1186/1471-2407-10-112

Mason, D. Y., Cordell, J., Brown, M., Pallesen, G., Ralfkiaer, E., Rothbard, J., et al. (1989). Detection of T cells in paraffin wax embedded tissue using antibodies against a peptide sequence from the CD3 antigen. *J. Clin. Pathol.* 42, 1194–1200. doi: 10.1136/jcp.42.11.1194

Matz, P., Turner, C., Weinstein, P. R., Massa, S. M., Panter, S. S., and Sharp, F. R. (1996). Heme-oxygenase-1 induction in glia throughout rat brain following experimental subarachnoid hemorrhage. *Brain Res.* 713, 211–222. doi: 10.1016/0006-8993(95)01511-6

McMenamin, P. G., Wealthall, R. J., Deverall, M., Cooper, S. J., and Griffin, B. (2003). Macrophages and dendritic cells in the rat meninges and choroid plexus: three-dimensional localisation by environmental scanning electron microscopy

and confocal microscopy. *Cell Tissue Res.* 313, 259–269. doi: 10.1007/s00441-003-0779-0

Meeker, R. B., Williams, K., Killebrew, D. A., and Hudson, L. C. (2012). Cell trafficking through the choroid plexus. *Cell Adh. Migr.* 6, 390–396. doi: 10.4161/cam.21054

Miller, B. A., Turan, N., Chau, M., and Pradilla, G. (2014). Inflammation, vasospasm, and brain injury after subarachnoid hemorrhage. *Biomed Res. Int.* 2014:384342. doi: 10.1155/2014/384342

Naito, Y., Takagi, T., and Higashimura, Y. (2014). Heme oxygenase-1 and anti-inflammatory M2 macrophages. *Arch. Biochem. Biophys.* 564, 83–88. doi: 10.1016/j.abb.2014.09.005

Petito, C. K., and Adkins, B. (2005). Choroid plexus selectively accumulates T-lymphocytes in normal controls and after peripheral immune activation. *J. Neuroimmunol.* 162, 19–27. doi: 10.1016/j.jneuroim.2004.12.020

Prunell, G. F., Mathiesen, T., Diemer, N. H., and Svendgaard, N.-A. (2003). Experimental subarachnoid hemorrhage: subarachnoid blood volume, mortality rate, neuronal death, cerebral blood flow, and perfusion pressure in three different rat models. *Neurosurgery* 52, 165–175; discussion 175–176. doi: 10.1097/00006123-200301000-00022

Prunell, G. F., Mathiesen, T., and Svendgaard, N.-A. (2002). A new experimental model in rats for study of the pathophysiology of subarachnoid hemorrhage. *Neuroreport* 13, 2553–2556. doi: 10.1097/01.wnr.0000052320.62862.37

Rincon, F., Rossenwasser, R. H., and Dumont, A. (2013). The epidemiology of admissions of nontraumatic subarachnoid hemorrhage in the United States. *Neurosurgery* 73, 217–223. doi: 10.1227/01.neu.0000430290.93304.33

Schipper, H. M. (2004). Heme oxygenase expression in human central nervous system disorders. *Free Radic. Biol. Med.* 37, 1995–2011. doi: 10.1016/j.freeradbiomed.2004.09.015

Segal, M. B., and Pollay, M. (1977). The secretion of cerebrospinal fluid. *Exp. Eye Res.* 25, 127–148. doi: 10.1016/S0014-4835(77)80012-2

Sehba, F. A., Pluta, R. M., and Zhang, J. H. (2011). Metamorphosis of subarachnoid hemorrhage research: from delayed vasospasm to early brain injury. *Mol. Neurobiol.* 43, 27–40. doi: 10.1007/s12035-010-8155-z

Sercombe, R., Dinh, Y. R. T., and Gomis, P. (2002). Cerebrovascular inflammation following subarachnoid hemorrhage. *Jpn. J. Pharmacol.* 88, 227–249. doi: 10.1254/jjp.88.227

Shechter, R., Miller, O., Yovel, G., Rosenzweig, N., London, A., Ruckh, J., et al. (2013). Recruitment of beneficial M2 macrophages to injured spinal cord is orchestrated by remote brain choroid plexus. *Immunity* 38, 555–569. doi: 10.1016/j.immuni.2013.02.012

Simard, J. M., Geng, Z., Woo, S. K., Ivanova, S., Tosun, C., Melnichenko, L., et al. (2009). Glibenclamide reduces inflammation, vasogenic edema, and caspase-3 activation after subarachnoid hemorrhage. *J. Cereb. Blood Flow Metab.* 29, 317–330. doi: 10.1038/jcbfm.2008.120

Simard, P. F., Tosun, C., Melnichenko, L., Ivanova, S., Gerzanich, V., and Simard, J. M. (2011). Inflammation of the choroid plexus and ependymal layer of the ventricle following intraventricular hemorrhage. *Transl. Stroke Res.* 2, 227–231. doi: 10.1007/s12975-011-0070-8

Solomon, R. A., Antunes, J. L., Chen, R. Y., Bland, L., and Chien, S. (1985). Decrease in cerebral blood flow in rats after experimental subarachnoid hemorrhage: a new animal model. *Stroke* 16, 58–64. doi: 10.1161/01.STR.16.1.58

van Gijn, J., and Rinkel, G. J. (2001). Subarachnoid haemorrhage: diagnosis, causes and management. *Brain J. Neurol.* 124, 249–278. doi: 10.1093/brain/124.2.249

Wan, Y., Hua, Y., Garton, H. J. L., Novakovic, N., Keep, R. F., and Xi, G. (2019). Activation of epiplexus macrophages in hydrocephalus caused by subarachnoid hemorrhage and thrombin. *CNS Neurosci. Ther.* 25, 1134–1141. doi: 10.1111/cns.13203

Wang, G., Zhang, J., Hu, X., Zhang, L., Mao, L., Jiang, X., et al. (2013). Microglia/macrophage polarization dynamics in white matter after traumatic brain injury. *J. Cereb. Blood Flow Metab.* 33, 1864–1874. doi: 10.1038/jcbfm.2013.146

Wilson, E. H., Weninger, W., and Hunter, C. A. (2010). Trafficking of immune cells in the central nervous system. *J. Clin. Invest.* 120, 1368–1379. doi: 10.1172/JCI41911

Wolburg, H., and Paulus, W. (2009). Choroid plexus: biology and pathology. *Acta Neuropathol.* 119, 75–88. doi: 10.1007/s00401-009-0627-8

Xiang, J., Routhe, L. J., Wilkinson, D. A., Hua, Y., Moos, T., Xi, G., et al. (2017). The choroid plexus as a site of damage in hemorrhagic and ischemic stroke and its role in responding to injury. *Fluids Barriers CNS* 14:8. doi: 10.1186/s12987-017-0056-3

Yong, C. I., Hwang, S.-K., and Kim, S.-H. (2010). The role of lumbar drainage to prevent shunt-dependent hydrocephalus after coil embolization for aneurysmal subarachnoid hemorrhage in good-grade patients. *J. Korean Neurosurg. Soc.* 48, 480–484. doi: 10.3340/jkns.2010.48.6.480

Zamboni, L., and de Martino, C. (1967). Buffered picric acid-formaldehyde: a new, rapid fixative for electron microscopy. *J. Cell Biol.* 35:148a.

Zeibig, S., Büttcher, M., Goebel, S., Pauli, J., Hunger, A., Ungerer, M., et al. (2019). The scavenger receptor CD68 regulates platelet mediated oxidized low-density lipoprotein (oxLDL) deposition in atherosclerotic vessels at an early stage of atherosclerosis in LDLR-/-/ApoBec-/- mice. *Cell. Physiol. Biochem.* 52, 681–695. doi: 10.33594/000000048

Zeni, P., Doepker, E., Topphoff, U. S., Huewel, S., Tenenbaum, T., and Galla, H.-J. (2007). MMPs contribute to TNF-α-induced alteration of the blood-cerebrospinal fluid barrier in vitro. *Am. J. Physiol. Cell Physiol.* 293, C855–C864. doi: 10.1152/ajpcell.00470.2006

Zoerle, T., Lombardo, A., Colombo, A., Longhi, L., Zanier, E. R., Rampini, P., et al. (2015). Intracranial pressure after subarachnoid hemorrhage. *Crit. Care Med.* 43, 168–176. doi: 10.1097/CCM.0000000000000670

Conflict of Interest: The authors declare that the research was conducted in the absence of any commercial or financial relationships that could be construed as a potential conflict of interest.

Copyright © 2020 Solár, Klusáková, Jančálek, Dubový and Joukal. This is an open-access article distributed under the terms of the Creative Commons Attribution License (CC BY). The use, distribution or reproduction in other forums is permitted, provided the original author(s) and the copyright owner(s) are credited and that the original publication in this journal is cited, in accordance with accepted academic practice. No use, distribution or reproduction is permitted which does not comply with these terms.

frontiers in Neuroscience

ORIGINAL RESEARCH
published: 03 March 2020
doi: 10.3389/fnins.2020.00129

Platelets in Amyloidogenic Mice Are Activated and Invade the Brain

Kathrin M. Kniewallner[1,2†], Diana M. Bessa de Sousa[1,2†], Michael S. Unger[1,2], Heike Mrowetz[1,2] and Ludwig Aigner[1,2,3]*

[1] *Institute of Molecular Regenerative Medicine, Paracelsus Medical University, Salzburg, Austria,* [2] *Spinal Cord Injury and Tissue Regeneration Center Salzburg (SCI-TReCS), Paracelsus Medical University, Salzburg, Austria,* [3] *Austrian Cluster for Tissue Regeneration, Vienna, Austria*

Alzheimer's disease (AD) is a neurodegenerative disease with a complex and not fully understood pathogenesis. Besides brain-intrinsic hallmarks such as abnormal deposition of harmful proteins, i.e., amyloid beta in plaques and hyperphosphorylated Tau in neurofibrillary tangles, blood-derived elements, in particular, platelets have been discussed to be involved in AD pathogenesis. The underlying mechanisms, however, are rather unexplored. Here, we investigate a potential role of platelets in an AD transgenic animal model with severe amyloid plaque formation, the APP-PS1 transgenic mice, and analyzed the presence, spatial location and activation status of platelets within the brain. In APP-PS1 mice, a higher number of platelets were located within the brain parenchyma, i.e., outside the cerebral blood vessels compared to WT controls. Such platelets were activated according to the expression of the platelet activation marker CD62P and to morphological hallmarks such as membrane protrusions. In the brain, platelets were in close contact exclusively with astrocytes suggesting an interaction between these two cell types. In the bloodstream, although the percentage of activated platelets did not differ between transgenic and age-matched control animals, APP-PS1 blood-derived platelets showed remarkable ultrastructural peculiarities in platelet-specific organelles such as the open canalicular system (OCS). This work urges for further investigations on platelets and their yet unknown functional roles in the brain, which might go beyond AD pathogenesis and be relevant for various age-related neurodegenerative diseases.

Keywords: platelets, Alzheimer's disease, aging, vascular pathology, astrocytes

OPEN ACCESS

Edited by:
Stephan Schilling, Fraunhofer Society (FHG), Germany

Reviewed by:
Henri Van Der Heyde, La Jolla Institute for Immunology, United States
Ling Li, University of Minnesota Twin Cities, United States

***Correspondence:**
Ludwig Aigner
ludwig.aigner@pmu.ac.at

† These authors have contributed equally to this work

Specialty section:
This article was submitted to Neurodegeneration, a section of the journal Frontiers in Neuroscience

Received: *31 July 2019*
Accepted: *31 January 2020*
Published: *03 March 2020*

Citation:
Kniewallner KM, de Sousa DMB, Unger MS, Mrowetz H and Aigner L (2020) Platelets in Amyloidogenic Mice Are Activated and Invade the Brain. Front. Neurosci. 14:129. doi: 10.3389/fnins.2020.00129

INTRODUCTION

Worldwide, approximately 50 million people live with dementia, a large number that is expected to triplicate by 2050 as the world population grows and the lifespan increases (International Alzheimer's Disease [IAD], 2015). In about 60 to 70% of the patients, dementia is due to Alzheimer's disease (AD), which makes AD not only the most common cause of dementia but also a major economic and social burden (International Alzheimer's Disease [IAD], 2015; Van Cauwenberghe et al., 2015). Nevertheless, and more than a century after its first description, the exact etiology of AD pathology is still not understood (Piaceri et al., 2013). Moreover, there are currently no drugs available that can stop or reverse AD progression, and the approved therapeutics merely ameliorate symptomatology (Frozza et al., 2018).

Drug development in AD over the last decades repeatedly tried to target brain-intrinsic hallmarks of the pathology. These included neuroprotective approaches and attempts to reduce

the load of harmful proteinaceous deposits in the brain, such as amyloid beta (Aβ) in plaques and hyperphosphorylated Tau in neurofibrillary tangles. So far, these approaches failed in the late clinical phases (Michael et al., 2019). Therefore, the amyloid cascade and the tau hypotheses as being causative in AD pathogenesis are increasingly questioned (De Strooper and Karran, 2016). In addition, novel concepts consider that the brain is not an isolated organ but is strongly influenced by systemic factors, which might contribute to brain degeneration or alternatively function as protective and/or self-regenerative mechanisms to compensate CNS damages. Along this line, increasing evidence illustrates that blood components are contributing to brain aging (Villeda et al., 2011; Smith et al., 2018) and that components present in young blood might be developed as therapeutics to treat AD (Middeldorp et al., 2016).

In the context of brain aging and neurodegeneration, blood-derived elements with therapeutic potential are platelets. Platelets have repeatedly been hypothesized to play a role in AD pathology (Li et al., 1998; Evin et al., 2003), in particular, in cerebral amyloid angiopathy (CAA) (Gowert et al., 2014; Jarre et al., 2014; Donner et al., 2016; Kniewallner et al., 2016, 2018). Platelets are small anuclear blood cells, which store a plethora of bioactive factors in specialized cytoplasmic compartments (Rumbaut and Thiagarajan, 2010). Upon activation, these factors are released to the extracellular space, allowing platelets to participate in diverse physiological and pathological processes (Rivera et al., 2016). In AD, vascular abnormalities, such as disrupted microvascular integrity or microbleedings, might trigger platelet activation in an attempt to restore vascular integrity. Once activated, platelets release among other substances Aβ peptides and several inflammatory mediators (e.g., IL-1β, CD40L, Thromboxane A2) (Arman et al., 2015; Canobbio et al., 2015; Heijnen and Korporaal, 2017; Humpel, 2017; Kniewallner et al., 2018). Thus, platelets might contribute to the deposition of Aβ peptides in the wall of cerebral blood vessels as well as to an inflammatory environment, which ultimately translates into vascular degeneration (Kniewallner et al., 2018). Whereas the involvement of platelets in the formation of cerebral amyloid angiopathy deposits has been a matter of extensive study, less is known concerning the general role of platelets in AD (Gowert et al., 2014).

Here, we investigated platelets in APP-PS1 transgenic mice with a severe amyloid plaque formation but no CAA pathology in the brain. We analyzed the spatial location of platelets in the brain with respect to their location within or outside blood vessels. We also studied blood-circulating platelets for their activation status by flow cytometry (FC) and analyzed their ultrastructure using electron microscopy.

MATERIALS AND METHODS

Animals

Female and male APP Swedish PS1 dE9 mice (reviewed in Jankowsky et al., 2001) expressing a chimeric mouse/human mutant amyloid precursor protein (Mo/HuAPP695swe) and a mutant human presenilin 1 (PS1-dE9) both directed to CNS neurons under the prion protein promoter (Jackson Laboratory)[1] were used. Mice were housed at the Paracelsus Medical University Salzburg in groups under standard conditions at a temperature of 22°C and a 12-h light/dark cycle with *ad libitum* access to standard food and water. Animal care, handling, genotyping, and experiments were approved by local ethical committees (BMWFW-66.019/0011-WF/V/3b/2016) and conducted accordingly to the Declaration of Helsinki. For brain histology, FC and transmission electron microscopy (TEM) mice were analyzed at 14 months of age. Age-matched non-transgenic mice derived from the breeding of APP-PS1 were used as control animals (WT).

Tissue Processing

Mice were anesthetized with a solution of ketamine (20.5 mg/mL; Ketamidor; Richter Pharma), xylazine (5.36 mg/mL; Chanazine; Chanelle), and acepromacine (0.27 mg/mL; Vanastress 10 mg/mL; Vana GmbH) in 0.9% sodium chloride. In order to retain blood in the blood vessels, brains were extracted without being perfused and post-fixed with 4% paraformaldehyde in sodium phosphate buffer (0.1 M; pH = 7.4) overnight at 4°C. The brains were cryoprotected and transferred into 30% sucrose in 0.1 M sodium phosphate buffer (pH = 7.4). Sagittal sections of 40 μm were cut on dry ice, using a sliding microtome.

Preparation of Washed Platelets

Upon thoracotomy, blood was collected by cardiac puncture using ethylenediaminetetraacetic acid (EDTA; 0.1 M; Promega) coated syringes. To further prevent coagulation, EDTA (0.1 M) was added to all blood samples. Anticoagulated blood samples were centrifuged at 200 × *g* for 20 min at room temperature (RT) to obtain platelet-rich plasma (PRP). PRP fractions were collected into new tubes, and 1 μM Prostaglandin E1 (Sigma-Aldrich #P55115-1MG) was added to avoid platelet aggregation, before centrifugation at 800 × *g*, for 20 min, RT. The supernatant was discarded and platelet pellets resuspended in Tyrode's buffer (134 mM NaCl, 12 mM $NaHCO_3$, 2.9 mM KCl, 1 mM $MgCl_2$, 0.34 mM Na_2HPO_4, 10 mM Hepes solution). Before use, washed platelets in Tyrode's buffer were allowed to rest for approximately 1 h, to minimize artificial platelet activation.

Immunohistochemistry

Fluorescence immunohistochemistry of mouse tissue was performed on free-floating sections as previously described (Marschallinger et al., 2015; Unger et al., 2016, 2018). Antigen retrieval was performed depending on the used primary antibody by steaming the sections for 15–20 min in citrate buffer (pH = 6.0, Sigma). The following primary antibodies were used: rat anti-CD41 (1:300; Abcam), mouse anti-CD62P (1:300; Abcam), rabbit anti-collagen IV (1:50; Abcam), guinea pig anti-GFAP (1:500; Progen), goat anti-Iba1 (1:500; Abcam), guinea pig anti-NeuN (1:500; Millipore), rabbit anti-Olig2 (1:500; Merck), goat anti-PDGFRβ (1:100; R&D Systems). Incubation with primary antibodies occurred either overnight at RT or for 72 h at 4°C. After incubation with primary antibodies, sections were

[1]http://www.jax.org/strain/005864

extensively washed in PBS and incubated for 3 h at RT in secondary antibodies (all at 1:1,000). The following secondary antibodies were used: donkey anti-goat Alexa Fluor 568, donkey anti-guinea pig Alexa Fluor 647, donkey anti-mouse Alexa Fluor 647, donkey anti-rabbit Alexa Fluor 488 and 568, donkey anti-rat Alexa Fluor 488, goat anti-rat Alexa Fluor 568 (all Invitrogen or Molecular Probes). For amyloid-β plaque staining, Thioflavin S (1 mg/mL; 1:625; Sigma-Aldrich) was added to the secondary antibody solution. Nucleus counterstaining was performed with 4′,6′-diamidino-2-phenylindole dihydrochloride hydrate (DAPI; 1 mg/mL; 1:2,000; Sigma-Aldrich).

Electron Microscopy

Transmission electron microscopy (TEM) was used for morphological characterization of blood isolated platelets from APP-PS1 and WT age-matched controls (n = 3/group). Platelets dissolved in Tyrode's buffer were fixed for 10 min with Cell Fix (BD Biosciences, 1:4). Upon centrifugation at 800 × g, for 20 min, at RT, platelet pellets were post-fixed in 2.5% glutaraldehyde (Agar Scientific), 4% PFA in phosphate buffer solution overnight. Upon centrifugation at 800 × g for 10 min, pelleted platelets were incubated in 1% osmium tetroxide (Electron Microscopy Sciences) in PBS Dulbecco (Merck) for 45 min in the dark. Following centrifugation at 800 × g for 10 min, pellets were washed twice in distilled water for 5 min. Between washes, platelets were centrifuged at 800 × g for 5 min. A third fixation step was carried out for 10 min in uranyl acetate replacement stain (1:10 in water; Electron Microscopy Sciences). Fixative solution was removed by centrifugation at 800 × g for 5 min, and platelets were washed as described previously. Washed pellets were dehydrated in a graded series of ethanol solutions, by incubation in ethanol 25% (5 min), 50% (5 min), 70% (5 min), 96% (5 min), and 100% (10 min). To finally complete dehydration, platelets were transferred to acetone (10 min), before being embedded in DurcupanTM ACM (four-component resin; Sigma-Aldrich). Resin curation was carried out at 37°C overnight and subsequently at 60°C for 72 h. Plastic blocks were trimmed to a trapezoid shape and sectioned using an ultramicrotome (Reichert-Jung Ultracut E, Austria). Semithin sections (0.5 μm) were generated with a glass knife and stained with 1% toluidine blue to confirm specimen exposure. After identification of stained cells, ultrathin sections (approximately 60 nm) were prepared using a diamond knife (Diatome Histo). Sections were flattened with chloroform and subsequently mounted on cooper grids (G75-Cu; Electron Microscopy Science), pre-coated with 0.2% Formvar. Transmission electron micrographs were obtained using a Leo 912 Omega transmission electron microscope (Carl Zeiss, Germany), at an operating voltage of 100 kV and magnification of 20,000×.

Flow Cytometry Analysis

To investigate the basal activation level of circulating platelets in APP-PS1 and WT age-matched mice (n = 7/group), we performed two-color FC analysis in washed platelets. Before staining, a 50 μL aliquot of each sample was incubated with rat anti-mouse BD CD16/CD32 Fc Block TM (1:100; #553142; BD Biosciences) for 5 min at RT in FC buffer [2% bovine serum albumin (Sigma), 2 mM EDTA (Promega) in PBS Dulbecco (Merck)] to block unspecific binding sites. Thereafter, samples were stained with allophycocyanin (APC)-labeled anti-mouse CD41 (1:100; #133913; BioLegend) and fluorescein isothiocyanate (FITC)-labeled rat anti-mouse CD62P (1:100; #553744; BD Pharmingen) antibodies for 30 min in the dark. An aliquot of washed platelets incubated with thrombin from bovine plasma (0.25 U/mL; #1.12374; Sigma-Aldrich) and the respective antibodies, served as positive control for platelet activation. Additionally, isotype IgG staining was performed using FITC-rat IgG1λ isotype control (1:100; #553995; BD Pharmingen). Staining reaction was stopped with FC buffer, and samples were centrifuged at 800 × g for 10 min. Platelet pellets were resuspended in FC buffer and immediately analyzed with BD Accuri TM C6 Plus Flow Cytometer (BD Biosciences).

Platelet population was defined based on their pattern of forward and side scattering on a logarithmic scale and by positive staining for CD41, commonly used as a pan-platelet marker. Cell doublets were discriminated and excluded from the analysis. Per sample, at least 5,000 $CD41^+$ single events were recorded. To determine the activation level of platelets, $CD41^+$ cells were gated for $CD62P^+$ expression. CD62P, also known as P-selectin, is a transmembrane glycoprotein mainly stored in platelet α-granules, which rapidly translocates onto the platelet surface upon activation (Rumbaut and Thiagarajan, 2010; Yun et al., 2016). The percentage of $CD62P^+$ platelets was calculated relatively to the number of $CD41^+$ platelets present in each sample. To compensate for non-specific immunofluorescence, the percentage of positive platelets detected in the isotype control staining for CD62P was subtracted from the percentage of $CD62P^+$ platelets determined in each sample. For data presentation, FC plots were generated with Kaluza Analysis Software (Beckman Coulter).

Microscopy, Visualization, and Image Processing

For qualitative and quantitative microscopic analysis of mouse tissue, confocal laser scanning microscopy was performed using a LSM 710 from Zeiss. Representative images were taken at 20×, 40×, and 63× magnification as confocal z-stack images and imported into the Imaris software (version 9.1.2, Bitplane) for 3D surface rendering and image analysis.

Quantitative and Qualitative Analysis of Immunohistochemical Data

To analyze platelet distribution in the brain, four confocal images from the cortex and hippocampus of each animal (n = 6/group) were used for 3D modeling. Localization of platelets, visualized by CD41 staining, was assessed in relation to cerebral blood vessels, stained for collagen IV. The number of platelets located in the intra- and extraluminal spaces as well as their volume were determined. To study platelet activation *in vivo*, expression of CD62P was investigated in 100 $CD41^+$ platelets present in the brain per animal, regardless of their location in relation to blood vessels (n = 6/group). To evaluate the occurrence of cellular interactions between platelets and

Thioflavin S^+ amyloid plaques (n = 2/group) and other cells of the neurovascular niche (n = 3/group), confocal Z-stacks from randomly selected visual fields of the hippocampus and cortex were employed for 3D surface rendering. Three-dimensional projection models were rotated around different angles in order to seek surface co-localizations. To quantify platelet–astrocyte interactions, four confocal images of the hippocampus were collected per animal (n = 3/group) and processed for 3D imaging in order to determine the number of $CD41^+$ cells co-localizing with $GFAP^+$ cells.

Quantitative Analysis of Electron Microscopy Data

Per genotype, the surface and OCS areas of 90 randomly selected platelets (30 platelets/animal, three animals/genotype) were assessed using the Image J software (version 1.44p). The platelet surface area and OCS area of single platelets were analyzed, and the number of every analyzed platelet per genotype was used for statistical analysis. In order to determine the OCS area, the area of all white vacuole and tubular sections within the cell was measured. Relative OCS area was calculated accordingly to the formula:

$$\text{Relative OCS Area (\%)} = \frac{\text{OCS measured area} \times 100}{\text{Platelet measured area}}$$

Statistical Analysis

Statistical analysis was performed using GraphPad Prism (GraphPad Software, version 6). Data was tested for normality using the Shapiro–Wilk normality test. To compare values between two groups, unpaired Student's t-test was used for normally distributed data and Mann–Whitney test for non-normally distributed data. For multiple comparisons between groups, two-way ANOVA with Tukey's multiple comparison test was used. For statistical analysis of quantitative electron microscopy data, the ROUT method (Q = 1%) was used to identify outliers. Two outliers were identified and removed in the platelet area data set and one in the OCS relative area data set. Values of $p < 0.0001$ (****) were considered most significant, $p < 0.01$ (**) highly significant, and $p < 0.05$ (*) significant. Values were expressed as mean ± standard error of the mean (SEM).

RESULTS

Platelets in APP-PS1 Mice Invade the Brain Parenchyma

First, we investigated platelet localization in the hippocampus and cortex of 14-month-old APP-PS1 transgenic mice and age-matched WT controls by immunohistochemical staining for CD41. We have selected APP-PS1 mice with the age of 14 months, as at this time point the animals present a full spectrum of pathology, showing severe amyloid plaque deposition in the hippocampus and cortex, high levels of microgliosis and astrogliosis, vascular alterations, and cognitive deficits (Jankowsky et al., 2004; Lalonde et al., 2005; Janota et al., 2015; Unger et al., 2016). To discriminate between platelets being completely inside or exposed to the outside of the blood vessels, we modeled the vessel structure in 3D with different levels of transparency, using the Imaris software. This allowed us to visualize platelets located within the vessels. In WT and APP-PS1 mice, $CD41^+$ platelets were mainly located in the intraluminal space of blood vessels, or at least within the blood vessel's basement membrane, which was outlined by collagen IV immunoreactivity (**Figures 1A,B**). Besides that, and more pronounced in APP-PS1 mice, platelets spread through the vessel wall, partially transposing into the extraluminal space (**Figures 1A,B**). Moreover, in APP-PS1 mice, platelets were also found completely outside the blood vessels in the brain parenchyma (**Figures 1A,B**), being in this case mostly located in the vicinity of a blood vessel (**Figure 1B**). Quantitative analysis in hippocampal and cortical brain regions revealed that APP-PS1 mice had a higher total number of platelets per brain section in comparison to WT controls (**Figure 1C**). As similar observations were made in the hippocampus and cortex (**Figure 1C**), we did no further discrimination between these two brain regions in subsequent analyses and pooled the data from both brain regions. A significantly higher percentage of platelets was found outside blood vessels in the extraluminal space in APP-PS1 compared to WT brains (22.18 ± 1.37% vs. 6.81 ± 0.92%), and vice versa; a significantly lower percentage of platelets were inside the vessels in APP-PS1 brains (77.83 ± 1.37% vs. 93.20 ± 0.92%) (**Figure 1D**).

Characterization of Blood Circulating Platelets in APP-PS1 and WT Age-Matched Control Mice

The presence of platelets in brains with an AD amyloid pathology raises various questions such as their molecular profile and identity, their activation status, and their functional role in the brain parenchyma. As a first urging question, we addressed whether platelets are activated once they enter the brain parenchyma or whether they are already activated in the bloodstream. To that, we used FC to analyze the surface expression of CD62P, a widely used marker for platelet activation, as well as TEM for ultrastructural analysis of platelets isolated from the blood of APP-PS1 and WT mice. To assess CD62P expression by FC, we first gated the platelet population based on its pattern for forward and side light scattering and CD41 expression, and further defined the activated platelet population as $CD62P^+/CD41^+$ (**Figures 2A,B**). Up to 70% of $CD41^+$ platelets expressed CD62P when stimulated *ex vivo* with thrombin as a positive control, and only very few $CD62P^+/CD41^+$ platelets were detected under native conditions (**Figure 2B**) indicating that the vast majority of platelets in the blood are not activated. Quantitative analysis revealed only a slight, but not significant, difference between the percentage of activated platelets in the bloodstream of APP-PS1 compared to WT mice (**Figures 2C,D**). TEM ultrastructural analysis (**Figure 2E**) revealed that WT platelets presented a round or discoid shape with smooth plasma membrane, although some WT platelets also showed small elongations and protrusions of the membrane, most likely being pseudopods. In APP-PS1 platelets, the plasma membrane was

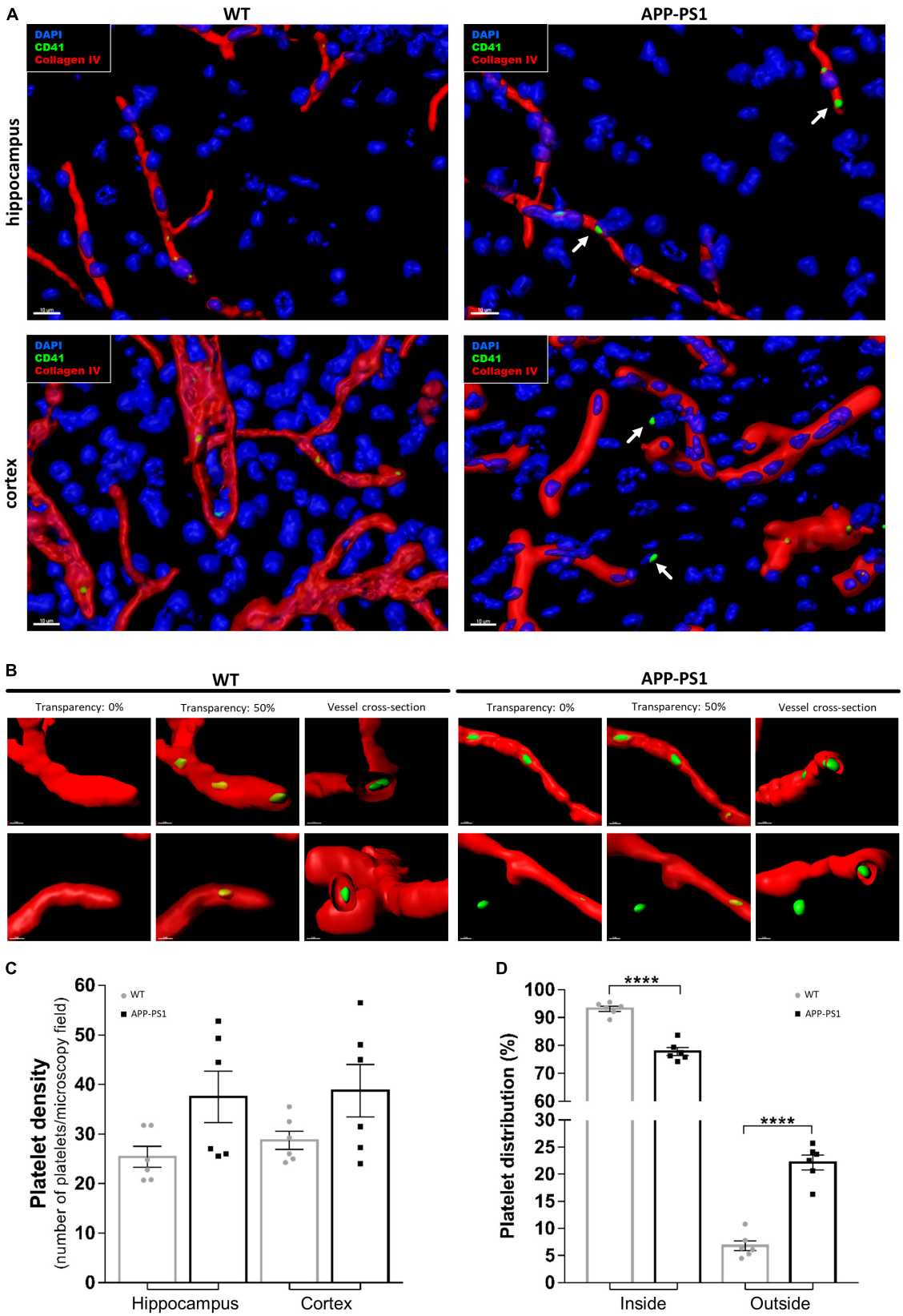

FIGURE 1 | Continued

FIGURE 1 | Immunohistochemical analysis of platelet distribution in the brain of APP-PS1 mice. Brain sections from APP-PS1 mice and age-matched WT controls were stained with collagen IV (red) for blood vessels and CD41 (green) for platelets. 4′,6′-diamidino-2-phenylindole dihydrochloride hydrate (DAPI; blue) was used as nucleus stain. Confocal microscopy images, from randomly selected hippocampal and cortical regions, were processed for 3D imaging. Platelets from WT and APP-PS1 mice were mainly located within the cerebral blood vessels **(A,B)**, whereas platelets from APP-PS1 mice were frequently seen in the brain parenchyma or at the blood vessel wall, suggesting extravasation **(A**—arrows, **B**—right**)**. Overall, APP-PS1 mice seem to have higher platelet densities in the hippocampus and cortex in comparison with WT controls **(C)**. Moreover, quantification of platelets located inside (blood vessel) and outside (parenchyma/vessel wall) cerebral blood vessels revealed that APP-PS1 mice have a significantly higher percentage of platelets outside the blood vessels compared to WT controls **(D)**. Data shown as mean ± SEM. Statistical analysis was performed by two-way ANOVA with Tukey's multiple comparison test (n = 6/group; including WT: six females and APP-PS1: three females and three males); $^{****}p < 0.0001$. Scale: 10 μm **(A)** and 3 μm **(B)**.

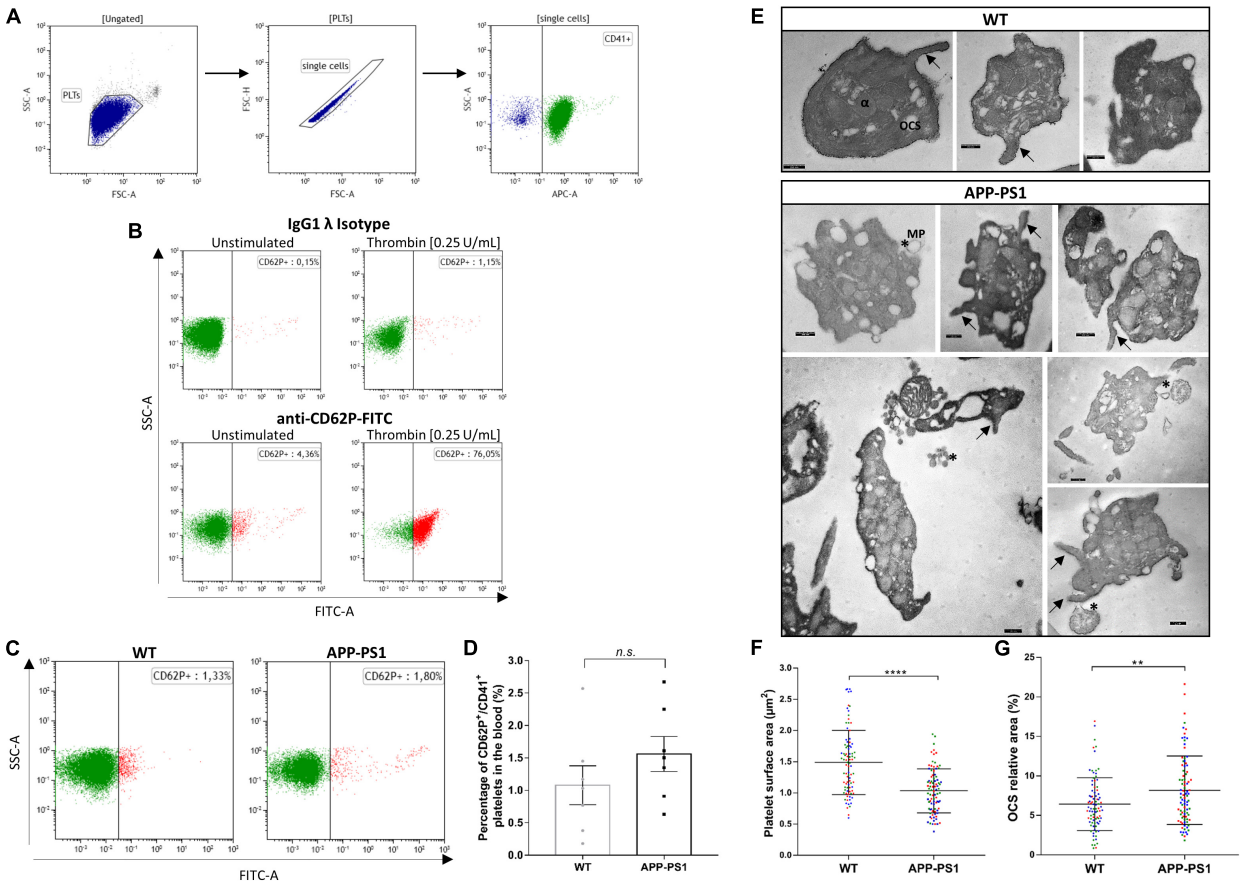

FIGURE 2 | Activation status and ultrastructure analysis of peripheral blood platelets in APP-PS1 mice. Surface expression of CD62P by CD41$^+$ platelets was assessed by flow cytometry to determine the activation status of blood-isolated platelets. Gating strategy for single CD41$^+$ platelets **(A)**. Positive control for platelet activation: Unstimulated or thrombin-stimulated platelets were stained with CD62P or respective IgG isotype control antibody **(B)**. Both APP-PS1 and WT animals showed CD62P$^+$/CD41$^+$ platelets under unstimulated conditions **(C)**, but the percentage of activated platelets in the bloodstream of APP-PS1 and WT were not significantly different **(D)**. However, TEM analysis revealed ultrastructural differences between APP-PS1 and WT blood-isolated platelets. APP-PS1 platelets presented a more irregular cell membrane, with formation of membrane elongations (arrows), and released microparticles (asterisks, *), the last two being signs of platelet activation **(E)**. APP-PS1 platelets also exhibited a significantly smaller surface area **(F)** and an enlarged OCS **(G)** compared with WT platelets. The annotated structures are α-granules (α), open canalicular system (OCS), and microparticule (MP). Scale: 250 nm **(E)**. Graph bars represent mean ± SEM. Statistical analysis was performed by unpaired Student's t test (**B:** n = 7/group; including three females and four males per group) and Mann–Whitney test **(F** and **G:** n = 90 platelets/genotype, including WT: three females and APP-PS1: two females and one male, with the 30 platelets analyzed per animal being color coded**)**. $^{****}p < 0.0001$; $^{**}p < 0.01$.

more irregular, with invaginations and protrusions. Some APP-PS1 platelets presented a microparticle formation (**Figure 2E**, asterisks), showing either microparticles under the process of budding off or already completely located in the extracellular space. Quantification of the platelet area showed that APP-PS1 platelets had an approximately 30% smaller surface in comparison with WT platelets (**Figure 2F**). Moreover, when compared to WT, APP-PS1 platelets presented an enlarged OCS (**Figure 2G**), a specific platelet organelle that appears as cytoplasmic vacuoles and thin tubular structures. In summary, our FC and TEM data suggests that APP-PS1 mice might possess a population of blood-circulating platelets exhibiting classical

signs of activation, with a highly altered cell morphology and increased microparticle formation.

Activated Platelets Are Present in the Brain of APP-PS1 Transgenic Mice

Even though we took special care to avoid platelet activation during the isolation procedure, we cannot exclude the possibility that some of the analyzed activation hallmarks were artificially induced. Therefore, and to investigate the activation status of brain platelets, we stained non-perfused brain sections for CD41, CD62P, and Collagen IV. We further used the IMARIS software to characterize platelets located inside and outside the blood vessels in more detail regarding their CD62P expression. Using 3D models with different levels of transparency, we could allocate platelets inside or outside the blood vessels. By setting the transparency level of the reconstructed vessels at 0%, only platelets exposed to the outside of the vessel can be seen, whereas at 50% transparency, platelets are visible regardless of their location, i.e., inside or outside the vessel. As a result, some of the platelets within APP-PS1 and WT (not shown) cerebral blood vessels were $CD62P^+$ and had cellular protrusions (**Figure 3A**), indicating the presence of activated platelets within the cerebral bloodstream. Similarly, platelets in the process of penetrating the vessel wall, i.e., partially visualized at 0% transparency and fully visible in the 50% transparent situation, expressed CD62P in WT and APP-PS1 mice (**Figure 3A**) indicating activation. At the quantitative level, the percentage of platelets that carry the activation marker CD62P was significantly higher in APP-PS1 compared to WT mice (**Figure 3B**). Taken together, these data suggest that platelets in the brain of APP-PS1 mice are activated.

A crucial hallmark of platelet function, at least in homeostasis, is platelet aggregation. Therefore, we raised the question whether platelets present in the brain parenchyma of APP-PS1 and WT mice might be aggregated. We used the IMARIS software to measure the volume of 3D modeled $CD41^+$ structures. We further categorized these structures as single platelets when the volume was smaller than 10 fL or as platelet aggregates for volumes bigger than 10 fL. This threshold was set accordingly to the current knowledge on platelet size (Everds, 2004). In the brain of APP-PS1 mice, where a higher number of platelets were present, there was a clear shift from single platelets to small aggregates (**Figure 3C**).

Platelets in the Brain Parenchyma Tightly Associate With Astrocytes

In the context of CAA, platelets have been shown to accumulate at cerebrovascular Aβ deposits, where they seem to fuel Aβ deposition (Gowert et al., 2014; Kniewallner et al., 2015, 2016). To assess whether intra-parenchymal platelets might promote similar effects, we analyzed the localization of $CD41^+$ platelets within the brain with respect to Thioflavin S^+ amyloid plaques. However, an association between platelets and amyloid plaques in the brain of APP-PS1 mice was not observed (**Figure 4**). We further investigated the putative cellular interaction partners within the brain, assessing potential interactions with astrocytes, pericytes, microglia, neurons, and oligodendrocytes. In APP-PS1 mice (**Figure 5**), and similarly in WT animals (data not shown), brain-located $CD41^+$ platelets were found in tight association with $GFAP^+$ astrocytes, as revealed by 3D surface rendering and co-localization analysis of GFAP and CD41 signals showing astrocyte processes covering platelet surfaces (**Figure 5A**, magenta showing co-localization, and **Supplementary Videos**). No interactions were detected with $PDGFR\beta^+$ pericytes (**Figure 5B**), $Iba1^+$ microglia (**Figure 5C**), $NeuN^+$ neurons (**Figure 5D**), or $Oligo2^+$ oligodendrocytes (**Figure 5E**). Approximately 60% of the platelets in the brain of APP-PS1 and WT mice were associated with astrocytes, whereas the other 40% did not associate with any other cell type analyzed ($59.91 \pm 5.76\%$ vs. $40.08 \pm 5.76\%$; $p = 0.0352$).

DISCUSSION

The current work reveals the presence of a significantly higher number of platelets in the brain parenchyma of APP-PS1 compared to WT mice. Platelets in the brain were more likely to be activated compared to the blood-circulating platelets, regardless of the genotype. In APP-PS1 mouse brains, the relative amount of activated platelets was significantly higher compared to WT. Platelets presumably invaded the brain and were found in tight association with astrocytes suggesting that these two cell types might interact, and that this interaction might contribute and shape AD pathology.

There is increasing evidence for blood-born elements influencing molecular, cellular, structural, and functional features of the brain in aging and in de- and regeneration in CNS diseases such as AD (Villeda et al., 2011, 2014; Middeldorp et al., 2016; Smith et al., 2018). In this context, blood components of emerging interest are platelets. For example, platelets are actively involved in the onset and development of cerebral amyloid angiopathy (CAA), a vascular pathology common among AD patients, which is characterized by platelet-derived Aβ depositions (Gowert et al., 2014; Jarre et al., 2014; Kniewallner et al., 2016, 2018). Interestingly, injections of platelets isolated from APP-Swedish Dutch Iowa mice, which is an AD transgenic mouse model with CAA pathology, into healthy age-matched control mice caused vessel damage, whereas WT platelet injection failed to do so (Kniewallner et al., 2018). Thus, we hypothesized that platelets in AD are intrinsically altered or dysfunctional, actively contributing to vascular damages (Kniewallner et al., 2018). To determine whether this kind of "aggressive or invasive" phenotype described for APP-Swedish Dutch Iowa mice is a general phenomenon in AD, we investigated platelets in a CAA-independent AD transgenic mouse model, the APP-PS1 (Jankowsky et al., 2001, 2004; Liu et al., 2004).

Here, we show that APP-PS1 mice contained a significantly higher number of platelets in the brain parenchyma compared to age-matched WT controls. Approximately 20% of the platelets present in the APP-PS1 brain invaded the intraparenchymal space, whereas in WT animals, only approximately 6% of the platelets were found within the brain parenchyma. Interestingly, brain intraparenchymal platelets appeared as single platelets as well as small aggregates, with APP-PS1 mice presenting a higher number of aggregated platelets compared to WT animals. Therefore, as the quantitative analysis of platelet

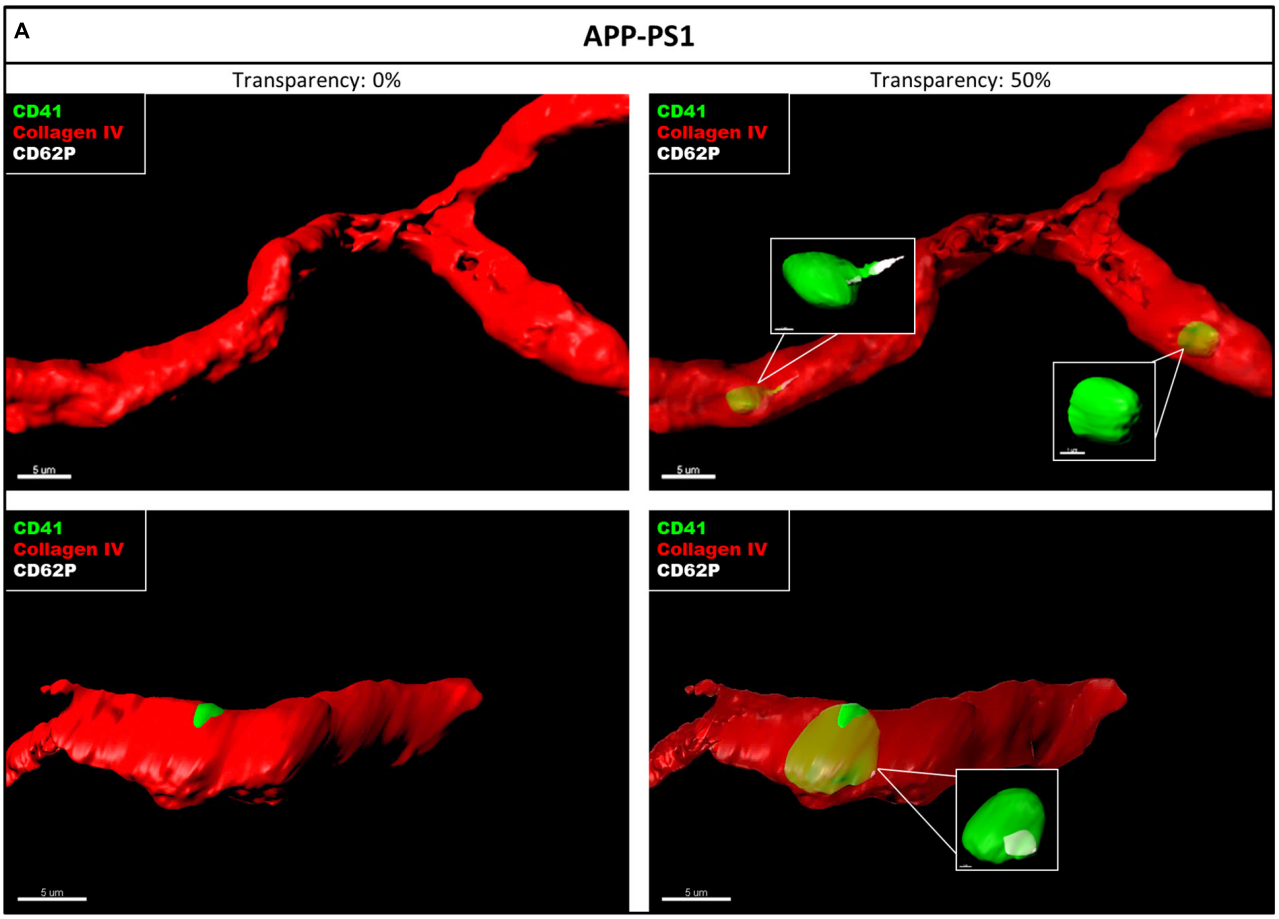

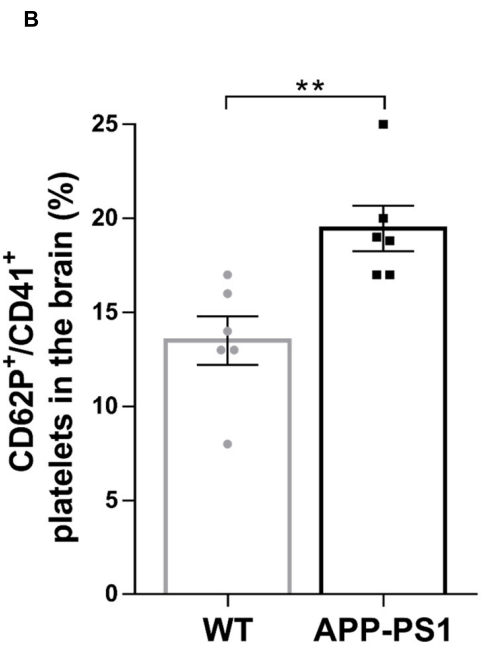

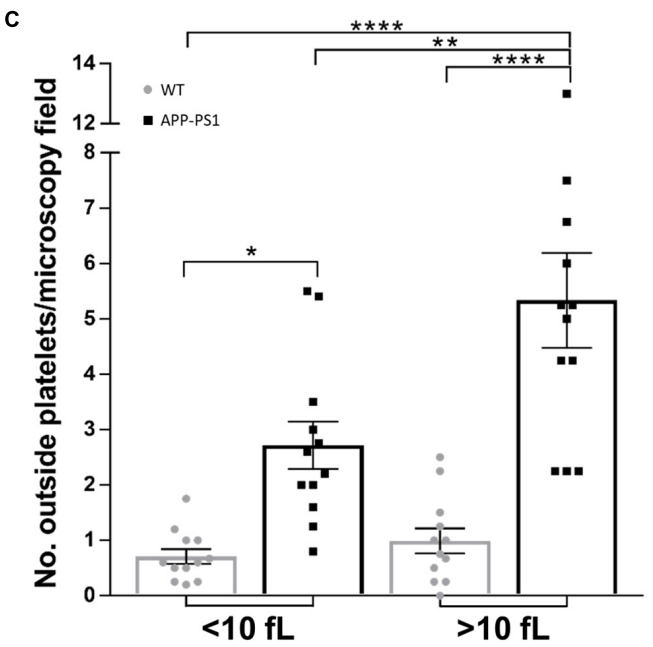

FIGURE 3 | Continued

FIGURE 3 | Activation status of platelets located in the brain of APP-PS1 mice. Immunohistochemical analysis revealed that $CD41^+$ platelets (green) expressing the activation marker CD62P (white) circulate within cerebral blood vessels (red) in APP-PS1 mice **(A**, upper row**)**. Similarly, platelets in the process of fenestrating the vessel wall also expressed CD62P **(A**, lower row**)**. Quantitative analysis showed that APP-PS1 mice have a significantly higher percentage of $CD62P^+/CD41^+$ platelets in the brain compared to WT animals **(B)**. Moreover, in APP-PS1 mice, extravascular platelets exhibit a shift from single cells (<10 fL) to aggregates (>10 fL). Graph bars represent mean ± SEM (n = 6/group including WT: six females and APP-PS1: three females and three males). Statistical analysis was performed by unpaired Student's t test **(B)** or two-way ANOVA with Tukey's multiple comparison test **(C)**. *$p < 0.05$; **$p < 0.01$; and ****$p < 0.0001$. Scale: 5 μm **(A)** and 1 μm (**A**—zoom in).

density presented in **Figure 1** did not differentiate between single platelets or platelet aggregates due to methodological limitations, putative aggregates might have been counted as individual platelets leading ultimately to an underestimation of the overall platelet load of APP-PS1 brains. Whether platelets penetrate the brain parenchyma actively or passively is still an ongoing question. We previously demonstrated that penetration of APP-Swedish Dutch Iowa platelets into the brain parenchyma is accompanied by release of platelet-derived matrix metalloproteinases, which promotes blood vessel disruption (Kniewallner et al., 2018). A similar mechanism might mediate the invasion of individual platelets into the brain of animals with subarachnoid hemorrhage (Doczi et al., 1986; Friedrich et al., 2010). In this model, platelets enter the brain parenchyma via "platelet-sized holes" in the basement membrane, possibly originated by platelet-derived proteases such as metalloproteinases-2 and -9 (Friedrich et al., 2010). Alternatively, platelets in AD might invade the brain parenchyma through a disrupted blood–brain barrier (BBB), as at the age of analysis (14 months) APP-PS1 mice present a comprised BBB (Janota et al., 2015).

The Fate and Function of Platelets in the Brain?

Besides the penetration of platelets through the vessel wall, crucial questions are: What is the fate of platelets once they enter the brain parenchyma? What is their functional role in the brain? Are platelets able to home back to the circulation, for example, after discharging their contents? The latter has recently been shown in a mouse model of systemic shock, where platelets entered the brain parenchyma, released pathogenic levels of serotonin, and thereafter returned to the bloodstream (Cloutier et al., 2018). Alternatively, they might become simply eliminated from the brain parenchyma through phagocytosis by, for example, microglia, perivascular-macrophages, or astrocytes. Nevertheless, platelets, as long as they are within the CNS parenchyma, might communicate with certain cell types, modulate their functions, and shape certain pathogenic processes.

Various CNS lesions, e.g., neurotrauma, subarachnoid hemorrhage, demyelination, or experimental autoimmune encephalomyelitis show extravascular platelets in the brain, which are linked to the onset of either beneficial or detrimental responses in the brain (Pluta and Amek, 2008; Friedrich et al., 2010; Hayon et al., 2013; Sotnikov et al., 2013; Au et al., 2014; Kazanis et al., 2015; Rivera et al., 2016). One possible function of platelets in the brain seems to be the impact on neuroinflammation. This has been demonstrated in the context of experimental autoimmune encephalomyelitis (Sotnikov et al., 2013) and chronic hypertension (Bhat et al., 2017), where platelets promote neuroinflammation. In the context of AD, APP-Swedish Dutch Iowa platelets recruit and activate microglia to the penetrated vessels, leading to enhanced levels of tumor-necrosis-factor-alpha and supporting an inflammatory environment (Kniewallner et al., 2018). In the present work, we show that intra-parenchymal platelets are in tight and exclusive association with astrocytes, and this interaction might influence the astrocyte responses in the context of neuroinflammation or plaque load. Platelet–astrocyte interaction was previously reported in experimental autoimmune encephalomyelitis, an established model of neuroinflammation, demyelination, and neurodegeneration (Sotnikov et al., 2013), and in an experimental chronic hypertension rat model (Bhat et al., 2017), the latter being a well-known predisposing factor for vascular dementia and AD (Birkenhäger and Staessen, 2006). In both cases, platelet–astrocyte interactions were associated with enhanced neuroinflammation and neuronal injury (Sotnikov et al., 2013; Bhat et al., 2017). Whether platelet–astrocyte interaction is also promoting neuroinflammation and neurodegeneration in AD remains speculative, and it is a matter of further investigations. Of course, platelet–astrocyte interaction might occur as part of a

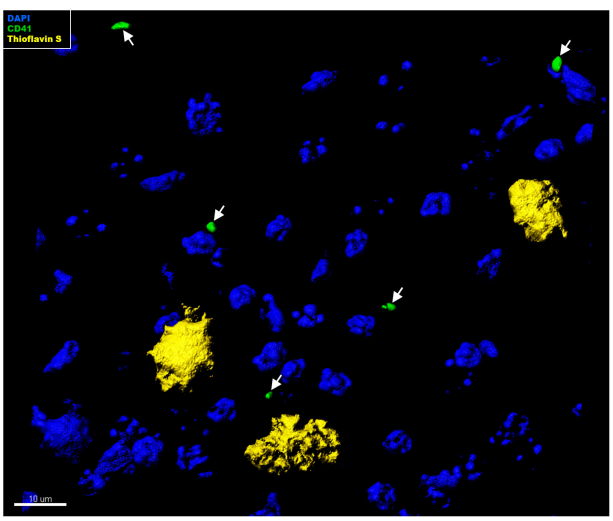

FIGURE 4 | Immunohistochemical analysis of platelet interaction with amyloid plaques in the brain of APP-PS1 mice. Brain sections from APP-PS1 mice (n = 1/gender) were co-stained for platelets (green) and Thioflavin S (yellow). DAPI (blue) was used as nucleus stain. Representative confocal images were 3D modeled for co-localization analysis. In APP-PS1 mice, $CD41^+$ platelets were not associated with Thioflavin S^+ amyloid plaques.

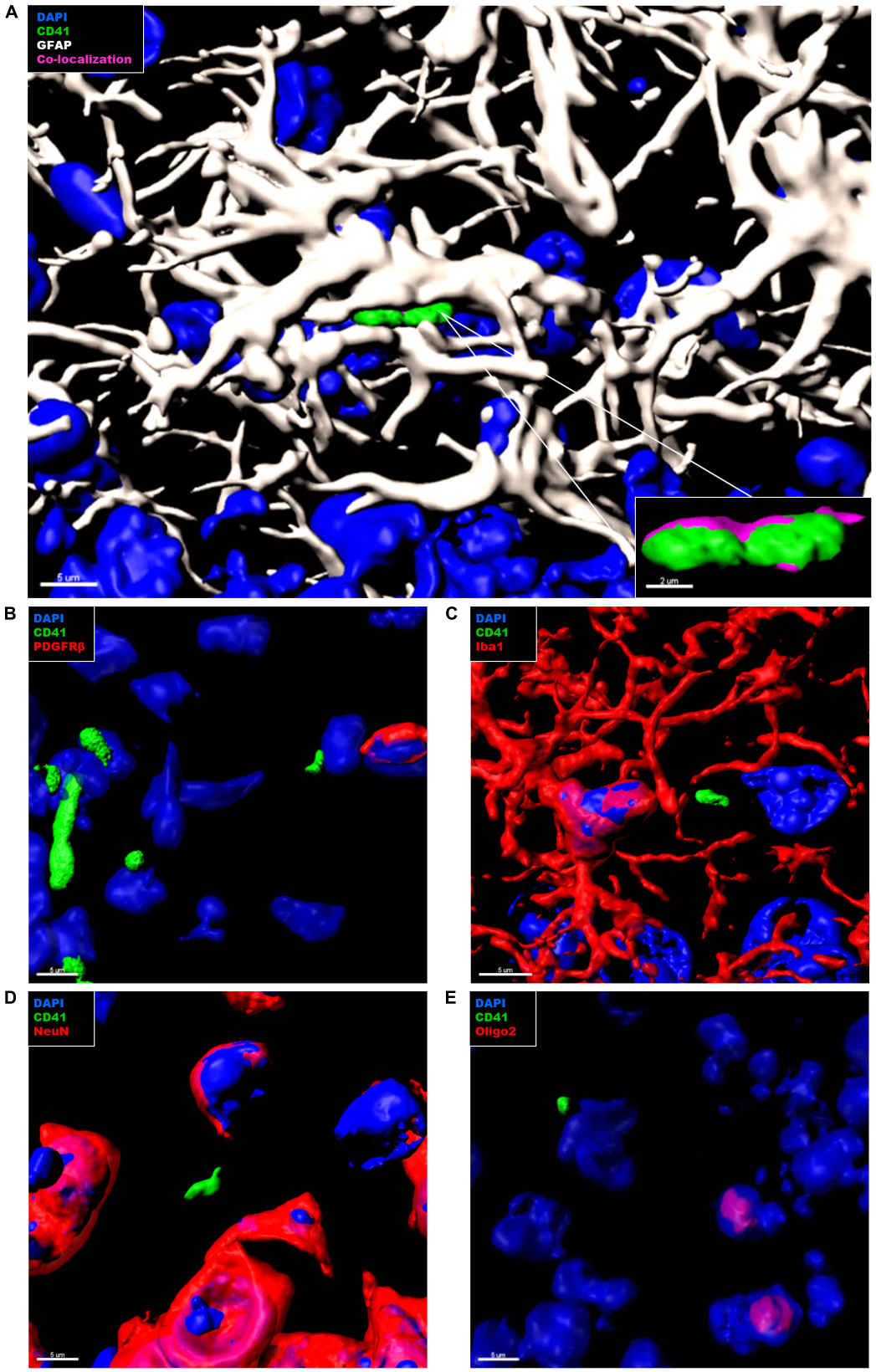

FIGURE 5 | Continued

FIGURE 5 | Immunohistochemical analysis of platelet interaction with neurovascular niche cellular components in the brain of APP-PS1 mice. Brain sections from APP-PS1 mice (n = 3, including two females and one male) were co-stained for platelets (CD41), **(A–E**, green**)**, and one of the following cell types: astrocytes (GFAP) **(A**, white**)**; pericytes (PDGFRβ) **(B**, red**)**, microglia (Iba-1) **(C**, red**)**, neurons (NeuN) **(D**, red**)**, or oligodendrocytes (Oligo2) **(E**, red**)**. DAPI (blue) was used as nucleus stain. Representative confocal images were selected for 3D surface projection and co-localization analysis. In APP-PS1 mice, platelets were found in tight association with astrocytes **(A)**. Co-localization of CD41 and GFAP signals is depicted in magenta **(A**, zoom in**)**. No further interactions were observed between $CD41^+$ platelets and other immunolabeled cells **(B)**. Scale: 5 μm **(A,B)**, 2 μm **(B**—zoom in**)**.

clearance strategy, and platelets might simply be phagocytosed by astrocytes. However, the platelet–astrocyte association was not exclusively observed in APP-PS1 mice but also in age-matched WT animals (data not shown). Nevertheless, the load of platelets and the number of activated platelets was higher in the brain of APP-PS1 mice, and therefore, the impact on astrocytes might be different at the quantitative level.

Platelets might not only have detrimental functions in the brain but also beneficial ones. For example, it has recently been demonstrated that the exercise-induced stimulatory effects on adult hippocampal neurogenesis are partially mediated through platelets (Leiter et al., 2019). In the context of stroke and of demyelinating lesions, platelet-derived factors promote neurogenesis and neuroprotection (Hayon et al., 2013; Au et al., 2014; Kazanis et al., 2015). A long-term perspective might be to exploit the beneficial effects and to inhibit the detrimental effects of platelets in a therapeutic context. This could be achieved through pharmacological means, through cell therapies such as infusion of regeneration-promoting platelets, or through the use of platelet-derived factors.

Platelets Are Activated in the Brain of APP-PS1 Mice but Not in the Bloodstream

Increased platelet activation in the blood has been previously reported in AD patients and in animal models of AD (Sevush et al., 1998; Ciabattoni et al., 2007; Stellos et al., 2010; Jarre et al., 2014; Canobbio et al., 2015, 2016). In AD, the activation status of platelets correlates with the rate of cognitive decline (Stellos et al., 2010; Canobbio et al., 2015), indicating that platelet activation might be functionally related to AD pathogenesis. In the APP-PS1 mice, we observed only a slight but not significantly higher platelet activation status in the bloodstream. Nevertheless, at the ultrastructural level, APP-PS1 mouse platelets showed clear signs of activation in cell morphology, i.e., significantly smaller size, membrane protrusions, and microparticle release. As a hypothesis, in AD, platelets might be either primed or even activated in the by bloodstream and become fully activated once entering the brain parenchyma. Regardless, a more detailed understanding of platelet activation as well as their underlying molecular mechanisms, especially in the context of CNS pathologies, is required.

Alterations in the OCS of APP-PS1 Mouse Platelets

Abnormalities in the internal membrane system of platelets in AD have been previously described (Zubenko et al., 1987a,b, Hajimohammadreza et al., 1990; Piletz et al., 1991). In AD patients, 10–25% of platelets are atypical, exhibiting an extensive system of membrane-bounded "trabeculated cisternae" (Zubenko et al., 1987a,b; Hajimohammadreza et al., 1990). In our ultrastructural characterization, we observed that in APP-PS1 mouse platelets, vacuolar and tubular structures occupy a significantly wider area of the cytoplasm in comparison to WT controls. We considered these structures as being part of the platelet OCS, a system of interconnected and tortuous membrane-bound channels that spans through the platelet interior (Rumbaut and Thiagarajan, 2010; White, 2013; Selvadurai and Hamilton, 2018). Further analysis using specific dyes for the OCS, such as ruthenium red (Heijnen and Korporaal, 2017; Selvadurai and Hamilton, 2018), or morphological characterization of platelets using 3D electron microscopy are needed to determine whether the structures we observed are, indeed, part of the platelet OCS. Interestingly, abnormalities in platelet ultrastructure are common to other neurological disorders such as Parkinson's disease, where platelets display an enlarged OCS (Factor et al., 1994), amyotrophic lateral sclerosis (Shrivastava et al., 2011), or major depression (Mendoza-Sotelo et al., 2010). Therefore, it is important to understand whether alterations in the platelet ultrastructure might directly affect the CNS environment and, in particular, to discern whether and how the enlargement of platelet OCS can be related with the pathological processes occurring in AD.

Platelets in the Aging Brain

Even though most of the effects that we observed in the present study were more pronounced in APP-PS1 mice, they were also detected at a lower level in 14-month-old WT mice. Therefore, it will be crucial in future experiments to dissect the aging from the disease-specific effects. It is already well-known that platelet activity and function are altered with advanced age in humans as well as in mice (Zahavi et al., 1980; Kasjanovova and Balaz, 1986; Bastyr et al., 1990; Gleerup and Winther, 1995; Cowman et al., 2015; Jones, 2016). Nevertheless, since aging is the main risk factor for AD and various other neurodegenerative diseases, platelets might be a very promising target for the future development of therapeutic strategies to prevent brain aging and to prevent or treat age-related neurodegenerative diseases.

CONCLUSION

Platelets are an emerging topic in brain aging and neurodegenerative diseases. The functional role of platelets in the brain and the underlying molecular and cellular mechanisms

remain elusive, but platelets might have beneficial as well as detrimental functions in the brain. This requires further investigations, especially since platelets are a very promising and feasible target for cellular and pharmacological interventions, and targeting platelets might be a therapeutic approach to repair, regenerate, or even rejuvenate the aged and diseased brain.

DATA AVAILABILITY STATEMENT

The datasets generated for this study are available on request to the corresponding author.

ETHICS STATEMENT

The animal study was reviewed and approved by BMWFW.

AUTHOR CONTRIBUTIONS

KK and DS designed the study, performed the experiments, and wrote the manuscript. MU designed the experiments and wrote the manuscript. HM designed and performed the experiments. LA designed the study and wrote the manuscript.

FUNDING

This work was supported by the PMU Rise Project (PMU-FFF) R-17/04/097-KNI and the PMU Postgraduate Students Support Program DISCITE! (D-19/01/008-BES).

ACKNOWLEDGMENTS

The authors thank the microscopy core facility of SCI-TReCS (Spinal Cord Injury and Tissue Regeneration Center Salzburg) and Pia Zaunmaier for the support with the animal work.

SUPPLEMENTARY MATERIAL

The Supplementary Material for this article can be found online at: https://www.frontiersin.org/articles/10.3389/fnins.2020.00129/full#supplementary-material

VIDEO S1 | 3D animation created by surface rendering upon immunohistochemical stained APP-PS1 brain tissue showing $CD41^+$ platelets (green) in tight association with $GFAP^+$ astrocyte processes (white). Cell nuclei can be visualized in blue (DAPI staining).

VIDEO S2 | 3D animation created by surface rendering upon immunohistochemical stained WT brain tissue showing $CD41^+$ platelets (green) in tight association with $GFAP^+$ astrocyte processes (white). Cell nuclei can be visualized in blue (DAPI staining).

REFERENCES

Arman, M., Holly, P., Ponomaryov, T., and Brill, A. (2015). "Role of platelets in inflammation," in *The Non-Thrombotic Role of Platelets in Health and Disease*, eds S. W. Kerrigan, and N. Moran (London: Intechopen).

Au, A. E. L., Sashindranath, M., Borg, R. J., Kleifeld, O., Andrews, R. K., Gardiner, E. E., et al. (2014). Activated platelets rescue apoptotic cells via paracrine activation of EGFR and DNA-dependent protein kinase. *Cell Death Dis.* 5:e1410. doi: 10.1038/cddis.2014.373

Bastyr, E. J., Kadrofske, M. M., and Vinik, A. I. (1990). Platelet activity and phosphoinositide turnover increase with advancing age. *Am. J. Med.* 88, 601–606. doi: 10.1016/0002-9343(90)90525-i

Bhat, S. A., Goel, R., Shukla, R., and Hanif, K. (2017). Platelet CD40L induces activation of astrocytes and microglia in hypertension. *Brain Behav. Immun.* 59, 173–189. doi: 10.1016/j.bbi.2016.09.021

Birkenhäger, W. H., and Staessen, J. A. (2006). Progress in cardiovascular diseases: cognitive function in essential hypertension. *Prog. Cardiovasc. Dis.* 49, 1–10.

Canobbio, I., Abubaker, A. A., Visconte, C., Torti, M., and Pula, G. (2015). Role of amyloid peptides in vascular dysfunction and platelet dysregulation in Alzheimer's disease. *Front. Cell. Neurosci.* 9:65. doi: 10.3389/fncel.2015.00065

Canobbio, I., Visconte, C., Oliviero, B., Guidetti, G., Zara, M., Pula, G., et al. (2016). Increased platelet adhesion and thrombus formation in a mouse model of Alzheimer's disease. *Cell. Signall.* 28, 1863–1871. doi: 10.1016/j.cellsig.2016.08.017

Ciabattoni, G., Porreca, E., Di Febbo, C., Di Iorio, A., Paganelli, R., Bucciarelli, T., et al. (2007). Determinants of platelet activation in Alzheimer's disease. *Neurobiol. Aging* 28, 336–342.

Cloutier, N., Allaeys, I., Marcoux, G., Machlus, K. R., Mailhot, B., Zufferey, A., et al. (2018). Platelets release pathogenic serotonin and return to circulation after immune complex-mediated sequestration. *Proc. Natl. Acad. Sci. U.S.A.* 115, E1550–E1559.

Cowman, J., Dunne, E., Oglesby, I., Byrne, B., Ralph, A., Voisin, B., et al. (2015). Age-related changes in platelet function are more profound in women than in men. *Sci. Rep.* 5, 12235–12235.

De Strooper, B., and Karran, E. (2016). The cellular phase of Alzheimer's disease. *Cell* 164, 603–615.

Doczi, T., Joo, F., Adam, G., Bozoky, B., and Szerdahelyi, P. (1986). Blood-brain barrier damage during the acute stage of subarachnoid hemorrhage, as exemplified by a new animal model. *Neurosurgery* 18, 733–739. doi: 10.1227/00006123-198606000-00010

Donner, L., Falker, K., Gremer, L., Klinker, S., Pagani, G., Ljungberg, L. U., et al. (2016). Platelets contribute to amyloid-beta aggregation in cerebral vessels through integrin alphaIIbbeta3-induced outside-in signaling and clusterin release. *Sci. Signal.* 9:ra52. doi: 10.1126/scisignal.aaf6240

Everds, N. (2004). "Chapter 17 – Hematology of the mouse," in *The Laboratory Mouse*, ed. G. Bullock (London: Academic Press), 271–286. doi: 10.1016/b978-012336425-8/50070-4

Evin, G., Zhu, A., Holsinger, R. M. D., Masters, C. L., and Li, Q.-X. (2003). Proteolytic processing of the Alzheimer's disease amyloid precursor protein in brain and platelets. *J. Neurosci. Res.* 74, 386–392.

Factor, S. A., Ortof, E., Dentinger, M. P., Mankes, R., and Barron, K. D. (1994). Platelet morphology in Parkinson's disease: an electron microscopic study. *J. Neurol. Sci.* 122, 84–89. doi: 10.1016/0022-510x(94)90056-6

Friedrich, V., Flores, R., Muller, A., and Sehba, F. A. (2010). Escape of intraluminal platelets into brain parenchyma after subarachnoid hemorrhage. *Neuroscience* 165, 968–975. doi: 10.1016/j.neuroscience.2009.10.038

Frozza, R. L., Lourenco, M. V., and De Felice, F. G. (2018). Challenges for Alzheimer's disease therapy: insights from novel mechanisms beyond memory defects. *Front. Neurosci.* 12:37. doi: 10.3389/fnins.2018.00037

Gleerup, G., and Winther, K. (1995). The effect of ageing on platelet function and fibrinolytic activity. *Angiology* 46, 715–718. doi: 10.1177/000331979504600810

Gowert, N. S., Donner, L., Chatterjee, M., Eisele, Y. S., Towhid, S. T., Münzer, P., et al. (2014). Blood platelets in the progression of Alzheimer's disease. *PLoS ONE* 9:e90523. doi: 10.1371/journal.pone.0090523

Hajimohammadreza, I., Brammer, M. J., Eagger, S., Burns, A., and Levy, R. (1990). Platelet and erythrocyte membrane changes in Alzheimer's disease. *Biochim. Biophys. Acta (BBA) – Biomembranes* 1025, 208–214. doi: 10.1016/0005-2736(90)90099-a

Hayon, Y., Dashevsky, O., Shai, E., Varon, D., and Leker, R. R. (2013). Platelet lysates stimulate angiogenesis, neurogenesis and neuroprotection after stroke. *Thrombosis Haemostasis* 110, 323–330. doi: 10.1160/th12-11-0875

Heijnen, H. F. G., and Korporaal, S. J. A. (2017). "Platelet morphology and ultrastructure," in *Platelets in Thrombotic and Non-Thrombotic Disorders: Pathophysiology, Pharmacology and Therapeutics: an Update*, eds P. Gresele, N. S. Kleiman, J. A. Lopez, and C. P. Page (Cham: Springer International Publishing), 21–37. doi: 10.1007/978-3-319-47462-5_3

Humpel, C. (2017). Platelets: their potential contribution to the generation of beta-amyloid plaques in Alzheimer's disease. *Curr. Neurovasc. Res.* 14, 290–298.

International Alzheimer's Disease [IAD] (2015). *World Alzheimer Report 2015: The Global Impact of Dementia*. London: Alzheimer's Disease International.

Jankowsky, J. L., Fadale, D. J., Anderson, J., Xu, G. M., Gonzales, V., Jenkins, N. A., et al. (2004). Mutant presenilins specifically elevate the levels of the 42 residue β-amyloid peptide in vivo: evidence for augmentation of a 42-specific γ secretase. *Hum. Mol. Genet.* 13, 159–170. doi: 10.1093/hmg/ddh019

Jankowsky, J. L., Slunt, H. H., Ratovitski, T., Jenkins, N. A., Copeland, N. G., and Borchelt, D. R. (2001). Co-expression of multiple transgenes in mouse CNS: a comparison of strategies. *Biomol. Eng.* 17, 157–165. doi: 10.1016/s1389-0344(01)00067-3

Janota, C. S., Brites, D., Lemere, C. A., and Brito, M. A. (2015). Glio-vascular changes during ageing in wild-type and Alzheimer's disease-like APP/PS1 mice. *Brain Res.* 1620, 153–168. doi: 10.1016/j.brainres.2015.04.056

Jarre, A., Gowert, N. S., Donner, L., Munzer, P., Klier, M., Borst, O., et al. (2014). Pre-activated blood platelets and a pro-thrombotic phenotype in APP23 mice modeling Alzheimer's disease. *Cell. Signall.* 26, 2040–2050. doi: 10.1016/j.cellsig.2014.05.019

Jones, C. I. (2016). Platelet function and ageing. *Mamm. Genome* 27, 358–366. doi: 10.1007/s00335-016-9629-8

Kasjanovova, D., and Balaz, V. (1986). Age-related changes in human platelet function in vitro. *Mechan. Ageing Dev.* 37, 175–182. doi: 10.1016/0047-6374(86)90074-6

Kazanis, I., Feichtner, M., Lange, S., Rotheneichner, P., Hainzl, S., Öller, M., et al. (2015). Lesion-induced accumulation of platelets promotes survival of adult neural stem/progenitor cells. *Exp. Neurol.* 269, 75–89. doi: 10.1016/j.expneurol.2015.03.018

Kniewallner, K. M., Ehrlich, D., Kiefer, A., Marksteiner, J., and Humpel, C. (2015). Platelets in the Alzheimer's disease brain: do they play a role in cerebral amyloid angiopathy? *Curr. Neurovasc. Res.* 12, 4–14. doi: 10.2174/1567202612666150102124703

Kniewallner, K. M., Foidl, B. M., and Humpel, C. (2018). Platelets isolated from an Alzheimer mouse damage healthy cortical vessels and cause inflammation in an organotypic ex vivo brain slice model. *Sci. Rep.* 8:15483.

Kniewallner, K. M., Wenzel, D., and Humpel, C. (2016). Thiazine Red(+) platelet inclusions in Cerebral Blood Vessels are first signs in an Alzheimer's disease mouse model. *Sci. Rep.* 6:28447.

Lalonde, R., Kim, H. D., Maxwell, J. A., and Fukuchi, K. (2005). Exploratory activity and spatial learning in 12-month-old APP(695)SWE/co+PS1/DeltaE9 mice with amyloid plaques. *Neurosci. Lett.* 390, 87–92. doi: 10.1016/j.neulet.2005.08.028

Leiter, O., Seidemann, S., Overall, R. W., Ramasz, B., Rund, N., Schallenberg, S., et al. (2019). Exercise-induced activated platelets increase adult hippocampal precursor proliferation and promote neuronal differentiation. *Stem Cell Rep.* 12, 667–679. doi: 10.1016/j.stemcr.2019.02.009

Li, Q.-X., Cappai, R., Evin, G., Tanner, J. E., and Gray, C. W. (1998). Products of the Alzheimer's disease amyloid precursor protein generated by,β-secretase are present in human platelets, and secreted upon degranulation. *Am. J. Alzheimer's Dis.* 13, 236–244. doi: 10.1177/153331759801300504

Liu, L., Herukka, S.-K., Minkeviciene, R., van Groen, T., and Tanila, H. (2004). Longitudinal observation on CSF Aβ42 levels in young to middle-aged amyloid precursor protein/presenilin-1 doubly transgenic mice. *Neurobiol. Dis.* 17, 516–523. doi: 10.1016/j.nbd.2004.08.005

Marschallinger, J., Sah, A., Schmuckermair, C., Unger, M., Rotheneichner, P., Kharitonova, M., et al. (2015). The L-type calcium channel Cav1.3 is required for proper hippocampal neurogenesis and cognitive functions. *Cell Calcium* 58, 606–616. doi: 10.1016/j.ceca.2015.09.007

Mendoza-Sotelo, J., Torner, C., Alvarado-Vásquez, N., Lazo-Langner, A., López, G., Arango, I., et al. (2010). Ultrastructural changes and immunolocalization of P-selectin in platelets from patients with major depression. *Psychiatry Res.* 176, 179–182. doi: 10.1016/j.psychres.2009.07.021

Michael, J., Marschallinger, J., and Aigner, L. (2019). The leukotriene signaling pathway: a druggable target in Alzheimer's disease. *Drug Discov. Today* 24, 505–516. doi: 10.1016/j.drudis.2018.09.008

Middeldorp, J., Lehallier, B., Villeda, S. A., Miedema, S. S., Evans, E., Czirr, E., et al. (2016). Preclinical assessment of young blood plasma for Alzheimer disease. *JAMA Neurol.* 73, 1325–1333.

Piaceri, I., Nacmias, B., and Sorbi, S. (2013). Genetics of familial and sporadic Alzheimer's disease. *Front. Biosci. (Elite Ed.)* 5, 167–177. doi: 10.2741/e605

Piletz, J. E., Sarasua, M., Whitehouse, P., and Chotani, M. (1991). Intracellular membranes are more fluid in platelets of Alzheimer's disease patients. *Neurobiol. Aging* 12, 401–406. doi: 10.1016/0197-4580(91)90064-q

Pluta, R., and Amek, M. U. (2008). Brain ischemia and ischemic blood-brain barrier as etiological factors in sporadic Alzheimer's disease. *Neuropsychiatr. Dis. Treat.* 4, 855–864.

Rivera, F. J., Kazanis, I., Ghevaert, C., and Aigner, L. (2016). Beyond clotting: a role of platelets in CNS repair? *Front. Cell. Neurosci.* 9:511. doi: 10.3389/fncel.2015.00511

Rumbaut, R. E., and Thiagarajan, P. (2010). "Chapter 2: General characteristics of platelets ," in *Platelet-Vessel Wall Interactions in Hemostasis and Thrombosis* eds D. N. Granger and J. P. Granger (San Rafael, CA: Morgan & Claypool Life Sciences).

Selvadurai, M. V., and Hamilton, J. R. (2018). Structure and function of the open canalicular system – The platelet's specialized internal membrane network. *Platelets* 29, 319–325. doi: 10.1080/09537104.2018.1431388

Sevush, S., Jy, W., Horstman, L. L., Mao, W. W., Kolodny, L., and Ahn, Y. S. (1998). Platelet activation in Alzheimer disease. *Arch. Neurol.* 55, 530–536.

Shrivastava, M., Das, T. K., Behari, M., Pati, U., and Vivekanandhan, S. (2011). Ultrastructural variations in platelets and platelet mitochondria: a novel feature in amyotrophic lateral sclerosis. *Ultrastruct. Pathol.* 35, 52–59. doi: 10.3109/01913123.2010.541985

Smith, L. K., White, C. W. III, and Villeda, S. A. (2018). The systemic environment: at the interface of aging and adult neurogenesis. *Cell Tissue Res.* 371, 105–113. doi: 10.1007/s00441-017-2715-8

Sotnikov, I., Veremeyko, T., Starossom, S. C., Barteneva, N., Weiner, H. L., and Ponomarev. (2013). Platelets recognize brain-specific glycolipid structures, respond to neurovascular damage and promote neuroinflammation. *PLoS One* 8:e58979. doi: 10.1371/journal.pone.0058979

Stellos, K., Panagiota, V., Kögel, A., Leyhe, T., Gawaz, M., and Laske, C. (2010). Predictive value of platelet activation for the rate of cognitive decline in Alzheimer's disease patients. *J. Cereb. Blood Flow Metabol.* 30, 1817–1820. doi: 10.1038/jcbfm.2010.140

Unger, M. S., Marschallinger, J., Kaindl, J., Hofling, C., Rossner, S., Heneka, M. T., et al. (2016). Early changes in hippocampal neurogenesis in transgenic mouse models for Alzheimer's disease. *Mol. Neurobiol.* 53, 5796–5806. doi: 10.1007/s12035-016-0018-9

Unger, M. S., Schernthaner, P., Marschallinger, J., Mrowetz, H., and Aigner, L. (2018). Microglia prevent peripheral immune cell invasion and promote an anti-inflammatory environment in the brain of APP-PS1 transgenic mice. *J. Neuroinflammation* 15, 274.

Van Cauwenberghe, C., Van Broeckhoven, C., and Sleegers, K. (2015). The genetic landscape of Alzheimer disease: clinical implications and perspectives. *Genet. Med.* 18:421. doi: 10.1038/gim.2015.117

Villeda, S. A., Luo, J., Mosher, K. I., Zou, B., Britschgi, M., Bieri, G., et al. (2011). The ageing systemic milieu negatively regulates neurogenesis and cognitive function. *Nature* 477, 90–94. doi: 10.1038/nature10357

Villeda, S. A., Plambeck, K. E., Middeldorp, J., Castellano, J. M., Mosher, K. I., Luo, J., et al. (2014). Young blood reverses age-related impairments in cognitive function and synaptic plasticity in mice. *Nat. Med.* 20, 659–663. doi: 10.1038/nm.3569

White, J. G. (2013). "Chapter 7 – Platelet structure," in *Platelets*, Third Edn, ed. A. D. Michelson (Cambridge, MA: Academic Press), 117–144.

Yun, S.-H., Sim, E.-H., Goh, R.-Y., Park, J.-I., and Han, J.-Y. (2016). Platelet activation: the mechanisms and potential biomarkers. *BioMed. Res. Int.* 2016, 9060143–9060143.

Zahavi, J., Jones, N. A. G., Leyton, J., Dubiel, M., and Kakkar, V. V. (1980). Enhanced in vivo platelet "release reaction" in old healthy individuals. *Thrombosis Res.* 17, 329–336. doi: 10.1016/0049-3848(80)90067-5

Zubenko, G. S., Cohen, B. M., Boller, F., Malinakova, I., Keefe, N., and Chojnacki, B. (1987a). Platelet membrane abnormality in Alzheimer's disease. *Ann. Neurol.* 22, 237–244. doi: 10.1002/ana.410220208

Zubenko, G. S., Malinakova, I., and Chojnacki, B. (1987b). Proliferation of internal membranes in platelets from patients with Alzheimer's disease. *J. Neuropathol. Exp. Neurol.* 46, 407–418. doi: 10.1097/00005072-198707000-00001

Conflict of Interest: The authors declare that the research was conducted in the absence of any commercial or financial relationships that could be construed as a potential conflict of interest.

Copyright © 2020 Kniewallner, de Sousa, Unger, Mrowetz and Aigner. This is an open-access article distributed under the terms of the Creative Commons Attribution License (CC BY). The use, distribution or reproduction in other forums is permitted, provided the original author(s) and the copyright owner(s) are credited and that the original publication in this journal is cited, in accordance with accepted academic practice. No use, distribution or reproduction is permitted which does not comply with these terms.

frontiers in Neurology

ORIGINAL RESEARCH
published: 05 March 2020
doi: 10.3389/fneur.2020.00131

Influence of Age-Related Complications on Clinical Outcome in Patients With Small Ruptured Cerebral Aneurysms

*Jianfeng Zheng, Xiaochuan Sun and Xiaodong Zhang**

Department of Neurosurgery, The First Affiliated Hospital of Chongqing Medical University, Chongqing, China

Background: Small ruptured cerebral aneurysms (≤5 mm) account for the majority of aneurysmal subarachnoid hemorrhages, and its clinical management remains a challenge. The aim of this study was to identify the effect of age-related complications on the outcome of patients with small ruptured aneurysm.

Methods: A retrospective review was performed in patients with small ruptured aneurysms who underwent microsurgical clipping or endovascular coiling from September 2012 to December 2018. According to their ages, the patients were divided into the elderly group and the non-elderly group. Baseline characteristics, clinical complications, and outcome of patients were analyzed between the two groups. A multivariate logistic regression analysis was used to determine the risk factors associated with the poor outcome of the elderly patients.

Results: In the elderly group, 83 patients were treated with clipping and 50 were treated with coiling. In the non-elderly group, 188 patients were treated with clipping and 117 were treated with coiling. The incidence of neurological complications with neurologic deficit in the elderly group was significantly higher compared with that in the non-elderly group ($P = 0.006$). The elderly patients had a longer hospital stay ($P = 0.032$) and a poorer outcome ($P = 0.001$) compared with the non-elderly patients. A multivariate analysis showed that irregular aneurysms ($P = 0.045$) and ischemic events ($P < 0.001$) were independent risk factors associated with poor outcome in the elderly.

Conclusions: Neurological complications with neurologic deficit, especially ischemic complications, were clearly more common in the elderly patients. Irregular small aneurysms or postoperative ischemic events should be paid attention as the higher risk of poor outcome in the elderly.

Keywords: small ruptured aneurysm, age, complication, treatment, outcome

OPEN ACCESS

Edited by:
Johannes Boltze,
University of Warwick,
United Kingdom

Reviewed by:
Dale Ding,
University of Louisville, United States
Wengui Yu,
University of California, Irvine,
United States

****Correspondence:***
Xiaodong Zhang
dr_zxd@yeah.net

Specialty section:
This article was submitted to Stroke, a section of the journal Frontiers in Neurology

Received: *10 November 2019*
Accepted: *05 February 2020*
Published: *05 March 2020*

Citation:
Zheng J, Sun X and Zhang X (2020) Influence of Age-Related Complications on Clinical Outcome in Patients With Small Ruptured Cerebral Aneurysms. Front. Neurol. 11:131. doi: 10.3389/fneur.2020.00131

INTRODUCTION

A growing number of patients with aneurysmal subarachnoid hemorrhage (aSAH) caused by small ruptured cerebral aneurysms have been treated with microsurgical clipping or endovascular coiling (1–3). Compared with the younger patients, the elderly patients may have more underlying comorbidities, poorer physical condition, and higher operation risk (4–6). It is generally agreed

that the outcome of the patients is largely determined by the severity of the initial aSAH and subsequent complications associated with neurologic deficit (7, 8). Old age is reported to be one of the significant risk factors that affect the severity of aSAH (7, 9, 10), and the elderly patients with poor cerebrovascular reserve function are more likely to suffer from severe neurological dysfunction after aSAH. Few previous studies have focused on comparing the clinical outcome of patients with small ruptured aneurysms according to age, and most of these previous studies have focused on the treatment outcome of coiling or clipping for patients with small ruptured aneurysms (3, 11–14). It is unclear whether age itself increases the risk of complications in patients during small cerebral aneurysm treatment. Therefore, this study was a desire to investigate the incidence of complications in elderly patients treated for small ruptured aneurysms and to determine whether age-related complications affected the treatment outcome.

TABLE 1 | Baseline characteristics of patients with small ruptured aneurysms.

	Overall	Non-elderly ($n = 305$)	Elderly ($n = 133$)	*P*-value
Age (year)	53.4 ± 9.8	48.2 ± 6.5	65.3 ± 4.1	<0.001
Sex (female)	310 (70.8%)	210 (68.9%)	100 (75.2%)	0.209
Tobacco smoking	94 (21.5%)	69 (22.6%)	25 (18.8%)	0.448
Alcohol consumption	76 (17.4%)	58 (19.0%)	18 (13.5%)	0.173
Hypertension	210 (47.9%)	129 (42.3%)	81 (60.9%)	<0.001
Diabetes	27 (6.2%)	12 (3.9%)	15 (11.3%)	<0.001
Cardiopulmonary diseases	24 (5.5%)	8 (2.6%)	16 (12.0%)	<0.001
Hunt–Hess Grade 4 or 5	59 (13.5%)	30 (9.8%)	29 (21.8%)	0.001
Modified Fisher Grade 3 or 4	180 (41.1%)	120 (39.3%)	60 (45.1%)	0.291

Results with P < 0.05 were considered to indicate statistical significance.

METHODS

We retrospectively analyzed the clinical record of 438 patients with small ruptured cerebral aneurysms who were treated with microsurgical clipping or endovascular coiling from September 2012 to December 2018. All of the patients were divided into two groups according to age: the elderly group (those 60 years of age or older) and the non-elderly group (those younger than 60 years). The data of each patient were collected in detail including age, sex, smoking history, drinking history, hypertension, diabetes, cardiopulmonary disease, clinical grade, location, number and shape of aneurysm, treatment modality, clinical complications, and outcomes.

Three-dimensional (3D) rotational angiography was used to examine small aneurysms in all of the patients, and the maximum diameter of the aneurysms as measured by 3D angiography was ≤5 mm. With the use of 3D rotational angiography, the shape and the location of the aneurysms were determined by an experienced neuroradiologist. For patients with multiple small aneurysms, the most likely source of bleeding can be judged by the subarachnoid hemorrhage (SAH) distribution on a CT scan.

Informed consent for the operation was signed after full consideration by the patient or his or her family. The modality of treatment for small aneurysms was determined by the cerebrovascular group composed of experienced neurointerventionists and neurosurgeons. The neurological complications were assessed by two professional neurosurgeons; hemorrhagic event, ischemia event, hydrocephalus, and seizure were recorded. Bleeding events include intraoperative bleeding and postoperative hematoma. Ischemic events include intraoperative thrombosis and postoperative delayed cerebral ischemia. Delayed cerebral ischemia was defined as new or worsening neurological deficits after the exclusion of other possible causes. Hydrocephalus was defined as neurological deterioration accompanied by an enlargement of the temporal horns of more than 2 mm. Cardiopulmonary complications were evaluated by the relevant department physicians, such as arrhythmia, pulmonary infection, and pulmonary embolism. Before discharge, CT angiography or magnetic resonance angiography was performed to evaluate the degree of small aneurysm occlusion and the patency of the parent artery. Each patient's follow-up information was supplemented by imaging reviews and telephone interviews. Based on the Glasgow Outcome Scale (GOS) at the last follow-up, the outcome of each patient was rated and then classified into good outcome (GOS scores of 4 or 5) or poor outcome (GOS scores of 1–3).

Statistical Analysis

All data in this study were analyzed using SPSS V.22 software (IBM Corp., Armonk, New York, USA). Data related to categorical variables are presented as percentages, and Fisher exact test or Pearson χ^2 test was used to compare female, smoking, drinking, hypertension, diabetes, cardiopulmonary diseases, clinical grade, location of aneurysms, irregular and multiple aneurysms, complications, and outcome. Data related to continuous variables are presented as mean ± SD, and Student *t*-test or Mann–Whitney *U*-test was used to compare age and hospital days. All clinical variables with $P < 0.1$ were entered into the multivariate analysis models, and odds ratios (ORs) with 95% confidence intervals (CIs) were calculated.

RESULTS

A total of 133 (30.4%) patients were in the elderly group and 305 (69.6%) were in the non-elderly group, with an average age of 53 years (range, 23–77 years). In the elderly group, the prevalence of hypertension (60.9 vs. 42.3%; $P < 0.001$), diabetes (11.3 vs. 3.9%; $P < 0.001$), and cardiopulmonary disease (12.0 vs. 2.6%; $P < 0.001$) were significantly increased. More Hunt–Hess grade 4 or 5 cases were observed in the elderly group (21.8 vs. 9.8%; $P = 0.001$), but there was no significant difference in the modified Fisher grade 3 or 4. The other baseline characteristics of the two groups are shown in **Table 1**.

TABLE 2 | Location and characteristics of the small ruptured aneurysms.

	Overall	Non-elderly ($n = 305$)	Elderly ($n = 133$)	*P*-value
Aneurysm location				
AcomA	158 (36.1%)	120 (39.3%)	38 (28.6%)	0.031
PcomA	145 (33.1%)	87 (28.5%)	58 (43.6%)	0.003
MCA	55 (12.6%)	35 (11.5%)	20 (15.0%)	0.347
ACA	17 (3.9%)	15 (4.9%)	2 (1.5%)	0.109
ICA	52 (11.9%)	39 (12.8%)	13 (9.8%)	0.424
PC	11 (2.5%)	9 (3.0%)	2 (1.5%)	0.516
Aneurysm characteristics				
Irregular	67 (15.3%)	46 (15.1%)	21 (15.8%)	0.885
Multiple	65 (14.8%)	35 (11.5%)	30 (22.6%)	0.005

AcomA, anterior communicating artery; PcomA, posterior communicating artery; MCA, middle cerebral artery; ACA, anterior cerebral artery; ICA, internal carotid artery; PC, posterior circulation. Results with P < 0.05 were considered to indicate statistical significance.

There were 158 small ruptured aneurysms located in the anterior communicating artery (AcomA), 145 in the posterior communicating artery (PcomA), 55 in the middle cerebral artery (MCA), 17 in the anterior cerebral artery (ACA), 52 in the internal carotid artery (ICA), and 11 in the posterior circulation (PC). The non-elderly patients have more ruptured small aneurysms in the location of the AcomA (39.3 vs. 28.6%; $P = 0.031$), while the elderly patients have more ruptured small aneurysms in the location of the PcomA (43.6 vs. 28.5%; $P = 0.003$). It was observed that the elderly patients had significantly more multiple aneurysms than the non-elderly patients (22.6 vs. 11.5%; $P = 0.005$). The irregularly shaped aneurysms were similar between the two groups (**Table 2**).

Clinical Complications and Outcome

There was no significant difference in treatment modality and intraoperative strategy between the elderly group and the non-elderly group (**Table 3**). Common neurological complications included hemorrhage events in 13 cases (3.0%), ischemic events in 98 cases (22.4%), hydrocephalus in 69 cases (15.8%), and seizure in 15 cases (3.4%). Hemorrhage events included intraoperative rebleeding in six patients (1.4%) and postoperative rebleeding in seven patients (1.6%). The ischemic events included intraoperative thrombosis in three patients (0.7%) and postoperative delayed cerebral ischemia in 95 (21.7%) patients. Temporary clipping was performed in 80 cases (31.1%) and was not associated with hemorrhage events ($P = 0.238$) or ischemic events ($P = 0.963$). Stent-assisted coiling was performed in 113 (25.8%) patients and balloon-assisted coiling was performed in four patients (1.0%). Neither stent-assisted nor balloon-assisted strategy was associated with hemorrhage events ($P = 0.389$ and $P = 1.000$, respectively) or ischemic events ($P = 0.106$ and $P = 0.999$, respectively). Common cardiopulmonary complications included arrhythmia in 30 cases (6.8%), pulmonary infection in 147 cases (33.6%), and pulmonary embolism in five cases (1.1%).

Compared with the non-elderly group, the incidence of ischemic events (28.6 vs. 19.7%; $P = 0.046$), cardiopulmonary complications (44.4 vs. 33.1%; $P = 0.031$), and pulmonary infections (42.9 vs. 29.5%; $P = 0.008$) was significantly higher in the elderly group. The total neurological complications (31.6 vs. 23.3%; $P = 0.075$) and the neurological complications without neurological deficits (15.0 vs. 15.7%; $P = 0.887$) did not vary significantly with the increase of patient age (**Figure 1**). However, compared with the non-elderly patients, the more elderly patients suffered from neurological complications with neurologic deficit (16.5 vs. 7.5%; $P = 0.006$). As a result of complications, the length of stay in the elderly group was significantly longer than that in the non-elderly group (23.2 ± 14.1 vs. 20.3 ± 9.0; $P = 0.032$) (**Table 3**).

After 3–60 months of follow-up (17 months on average), 88.1% of the patients had a good outcome (GOS 4 or 5). Compared with the non-elderly group, poor outcome occurred at a significantly greater rate in the elderly group (20.3 vs. 8.2%; $P = 0.001$). Whether treated by microsurgical clipping or endovascular coiling, the outcome of the patients with small ruptured aneurysms was worse with the increase of age (**Figure 2**). Only the elderly patients were considered, and the risk factors of poor outcome were analyzed. A univariate analysis showed that hypertension ($P = 0.022$), Hunt–Hess grade 4 or 5 ($P < 0.001$), modified Fisher grade 3 or 4 ($P = 0.001$),

TABLE 3 | Complications and outcomes of patients with small ruptured aneurysms.

	Overall	Non-elderly ($n = 305$)	Elderly ($n = 133$)	*P*-value
Clipping	271 (61.9%)	188 (61.6%)	83 (62.4%)	0.915
Coiling	167 (38.1%)	117 (38.4%)	50 (37.6%)	
Balloon-assisted	4 (1.0%)	2 (0.6%)	2 (1.6%)	0.516
Stent-assisted	113 (25.8%)	78 (25.6%)	35 (26.3%)	0.906
Temporary clipping used	80 (18.3%)	58 (19.0%)	22 (16.5%)	0.592
Neurological complications	113 (25.8%)	71 (23.3%)	42 (31.6%)	0.075
Hemorrhagic event	13 (3.0%)	10 (3.3%)	3 (2.3%)	0.762
Ischemic event	98 (22.4%)	60 (19.7%)	38 (28.6%)	0.046
Hydrocephalus	69 (15.8%)	44 (14.4%)	25 (18.8%)	0.256
Seizure	15 (3.4%)	10 (3.3%)	5 (3.8%)	0.780
Cardiopulmonary complications	166 (36.5%)	101 (33.1%)	59 (44.4%)	0.031
Arrhythmia	30 (6.8%)	16 (5.2%)	14 (10.5%)	0.062
Pulmonary infection	147 (33.6%)	90 (29.5%)	57 (42.9%)	0.008
Pulmonary embolism	5 (1.1%)	1 (0.3%)	4 (3.0%)	0.031
Length of stay (day)	21.1 ± 10.9	20.3 ± 9.0	23.2 ± 14.1	0.032
Good outcome (GOS 4 or 5)	386 (88.1%)	280 (91.8%)	106 (79.7%)	0.001
Poor outcome (GOS 1 or 3)[a]	52 (11.9%)	25 (8.2%)	27 (20.3%)	

GOS, Glasgow Outcome Scale. Results with P < 0.05 were considered to indicate statistical significance. [a]After adjustment for smoking, hypertension, cardiopulmonary disease, Hunt–Hess grade, modified Fisher grade, multiple aneurysms, irregular aneurysms, and treatment modality, a multivariate analysis showed that the elderly was independently associated with poor outcome [OR, 2.025 (1.015–4.040); P = 0.045].

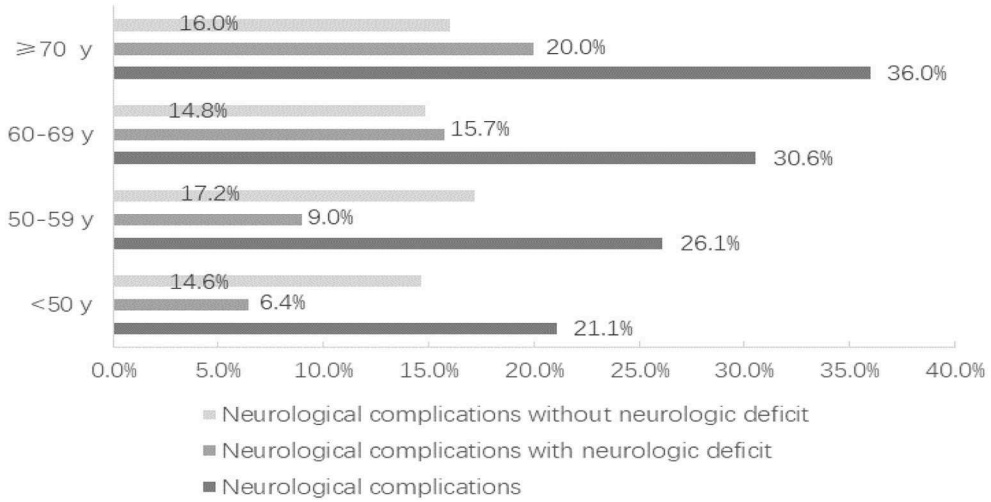

FIGURE 1 | The distribution of neurological complications according to the age of the patients, divided into those with neurologic deficit and those without neurologic deficit.

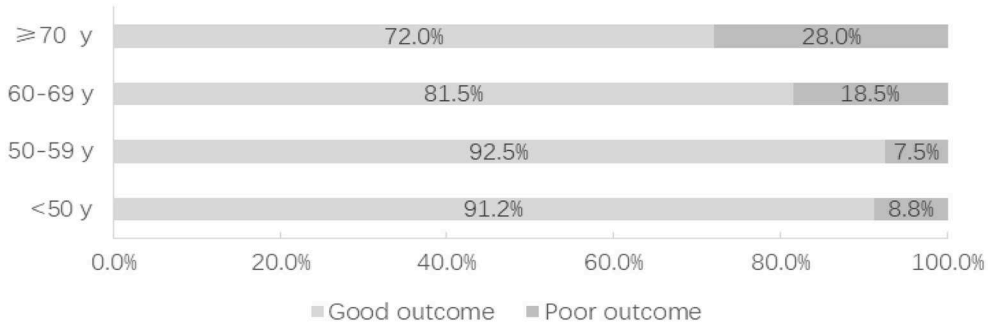

FIGURE 2 | The distribution of functional outcome according to the age of the patients, divided into those with good outcome and poor outcome.

irregular aneurysms ($P < 0.001$), multiple aneurysms ($P = 0.019$), ischemic events ($P < 0.001$), seizure ($P = 0.047$), and cardiopulmonary complications ($P = 0.033$) were significantly associated with the poor outcome of the elderly patients with small ruptured aneurysm. A multivariate analysis showed that irregular aneurysms [OR, 4.465 (1.032–19.310); $P = 0.045$] and ischemic events [OR, 13.532 (4.128–44.364); $P < 0.001$] were independent predictive factors of poor outcome in the elderly patients (**Table 4**).

DISCUSSION

We presented a large number of patients with small ruptured cerebral aneurysms to compare the effect of age-related complications on the functional outcome. The incidence of neurological complications associated with neurological deficit, especially ischemic events, was obviously higher in the elderly patients than in the non-elderly patients. As a result of age-related complications, the outcome of the elderly patients is significantly worse compared with that of the non-elderly patients.

With the advances in medical imaging facilities and techniques, a growing number of small cerebral aneurysms in the world have been detected and treated (1–3, 7, 11, 14). A retrospective study of 223 small unruptured aneurysms by Oishi et al. (11) reported that endovascular treatment is effective with low morbidity and mortality. Feng et al. (14) thought that the coil embolization of small unruptured aneurysms can be performed safely and achieve a low rate of recurrence. Chalouhi et al. (15) reported that patients with small ruptured aneurysms were treated with a pipeline embolization device, and these patients had a good outcome. Although endovascular coiling was technically feasible, smaller aneurysms were reported to be significantly associated with a higher risk of procedural aneurysm rupture (16). Mitchell et al. (17) believed that a small aneurysm size is a significant risk factor for intraoperative rupture in ruptured aneurysms rather than in unruptured aneurysms. In our study of 438 small ruptured cerebral aneurysms, six patients suffer from intraoperative rebleeding. The incidence of intraoperative aneurysm rupture was similar between the elderly and the non-elderly patients, and these did not lead to serious neurological dysfunctions.

TABLE 4 | Risk factors of poor outcome in elderly patients with small ruptured aneurysms.

	Univariate analysis		Multivariable analysis	
	P-value	OR (95% CI)	*P*-value	OR (95% CI)
Hypertension	0.022	3.373 (1.187–9.584)	0.404	–
Hunt–Hess Grade 4 or 5	<0.001	8.214 (3.194–21.126)	0.248	–
Modified Fisher Grade 3 or 4	0.001	4.714 (1.830–12.142)	0.487	–
Irregular aneurysms	<0.001	6.600 (2.412–18.062)	0.045	4.465 (1.032–19.310)
Multiple aneurysms	0.019	2.956 (1.191–7.336)	0.535	–
Ischemic event	<0.001	18.324 (6.443–52.108)	<0.001	13.532 (4.128–44.364)
Seizure	0.047	6.500 (1.029–41.068)	0.848	–
Cardiopulmonary complications	0.033	2.590 (1.082–6.200)	0.637	

Variables with P < 0.1 according to univariate analysis were entered into the multivariate analysis model. OR, odds ratio; CI, confidence interval. Results with P < 0.05 were considered to indicate statistical significance.

However, due to the smaller size and the weaker wall of the aneurysm, and the more difficult operation, the risk of postoperative ischemic complications was significantly increased. Delayed cerebral ischemia is reported to occur in about 30% of patients with aSAH and leads to higher morbidity and mortality (18, 19). Our study on small ruptured aneurysm showed that the incidence of delayed cerebral ischemia was 21.7%, which was obviously higher in the elderly patients than that in the non-elderly patients. Wachter et al. (20) believes that the elderly patients seem to be more vulnerable to aSAH, plus the complications are more problematic. The severe aSAH after rupture together with the subsequent operation on the surrounding anatomical structures such as parent arteries, perforators, brain parenchyma, and veins will cause cerebral vasospasm, which can be further aggravated by the decline of the cerebrovascular regulatory function in the elderly. In our study, although there was no significant difference in the high modified Fisher grade, the high Hunt-Hess grade in the elderly patients was more significant than in the non-elderly patients. This may mean that the elderly patients with poor cerebrovascular reserve capacity are more likely to suffer from severe brain damage after aSAH, even if the aneurysm size is small. The elderly patients have more comorbidities such as hypertension, diabetes, and cardiopulmonary disease, which makes the treatment risk of this special elderly population higher. Differently from our results, another aSAH study (20) reported a lower incidence of delayed cerebral ischemia in the elderly patients than in the non-elderly patients due to arteriosclerosis. The outcome of the study by Lai et al. (21) is consistent with our results that older women are at obviously greater risk of cerebral vasospasm, cerebral infarction, and clinical deterioration. Since the majority (75.2%) of the elderly patients in our study are female, female hormones could play a very important role in the development of ischemic complications in aSAH patients (21).

The total mortality rate of our patients with small ruptured aneurysms was 3.2%, higher than 0.91% of patients with small unruptured aneurysms as reported by Feng et al. (14). It should be noted that a more aggressive treatment performed before the rupture status of small cerebral aneurysms may reduce the mortality, but older age also needs to be considered, which is a very important factor affecting the incidence of complications associated with functional outcome. A study of in-patient samples (22) showed that the mortality rate of patients over 65 years old was obviously higher than that of patients younger than 65 years. Several other studies (23–25) have suggested that the outcome was worse with the increase of age in patients treated with clipping or coiling, but no emphasis has been placed on the influence of age-related complications on functional outcome. Similarly, in our study, the poor outcome occurred at an obviously greater rate in the patients aged 60 years and over compared with the patients under 60 years old, while the outcome of patients over 70 years old was the worst. The neurological complications have a greater impact on the neurological function of the elderly patients.

In the past 10 years of cerebral aneurysm research, the proportion of small ruptured aneurysms has increased to nearly 50% (26–28). Kim et al. believed that a sidewall aneurysm found with multiple aneurysms or an AcomA aneurysm found from a patient with hypertension may be prone to rupture at smaller sizes. In a prospective study in Japan (29), patient age and PcomA were reported to be significant risk factors for rupture in the elderly patients. Similarly, our results show that small ruptured cerebral aneurysms at the location of the PcomA are more common and the proportion of multiple aneurysms is higher in the elderly patients compared with those in the non-elderly patients. A recent survey (30) indicated that 42–76% of surgeons suggested treating the small anterior circulation aneurysms with a SAH history and most of the surgeons stop treating the unruptured aneurysms in patients who are 70–80 years old. Therefore, in order to avoid over-intervention as well as in consideration of the higher aneurysm rupture risk and the age-related complication risk, more preventive treatment is suitable for the younger patients with small unruptured communicating segment (PcomA/AcomA) aneurysms or with multiple aneurysms.

LIMITATIONS

There are several limitations in the current study. The interpretation of these final conclusions needs to take into account our single-center retrospective design. Firstly, since there is no prospective randomized intervention for the small ruptured aneurysms, potential selection bias may affect the efficacy of the treatment. However, the aim of our study was to ascertain the relationship between age-related complications and clinical outcomes rather than simply comparing the outcomes of the different treatment modalities. Secondly, due to the underdevelopment of the economy and the medical level in Western China, fewer patients over the age of 70 received operation and none over the age of 80 received intervention. Thirdly, we define the elderly as patients aged 60 and over, while

other studies have used a different age cutoff, so the overall morbidity and mortality may be different from other research data.

CONCLUSIONS

This study provides some useful data for the clinical management of elderly patients with small ruptured aneurysm. Based on our findings, we conclude that neurological complications associated with neurologic deficit were clearly more common in the elderly patients than in the non-elderly patients. The preoperative irregular small aneurysms or the postoperative ischemic events should be paid attention as the higher risk of poor outcome in elderly patients.

DATA AVAILABILITY STATEMENT

The raw data supporting the conclusions of this article will be made available by the authors, without undue reservation, to any qualified researcher.

ETHICS STATEMENT

The studies involving human participants were reviewed and approved by Ethics committee of the First Affiliated Hospital of Chongqing Medical University. The patients/participants provided their written informed consent to participate in this study.

AUTHOR CONTRIBUTIONS

JZ was involved in the acquisition of the data, the analysis and interpretation of the data, the drafting of the article, and the final approval of the version to be published. XS and XZ critically revised the article for intellectual content and gave final approval of the version to be published.

FUNDING

This study was supported by the National Key Research Development Program (grant no. 2016YFC1300800).

REFERENCES

1. Griessenauer CJ, Ogilvy CS, Foreman PM, Chua MH, Harrigan MR, He L, et al. Pipeline embolization device for small intracranial aneurysms: evaluation of safety and efficacy in a multicenter cohort. *Neurosurgery*. (2017) 80:579–87. doi: 10.1227/NEU.0000000000001377
2. Chalouhi N, Zanaty M, Whiting A, Yang S, Tjoumakaris S, Hasan D, et al. Safety and efficacy of the pipeline embolization device in 100 small intracranial aneurysms. *J Neurosurg*. (2015) 122:1498–502. doi: 10.3171/2014.12.JNS14411
3. Li J, Su L, Ma J, Kang P, Ma L, Ma L. Endovascular coiling versus microsurgical clipping for patients with ruptured very small intracranial aneurysms: management strategies and clinical outcomes of 162 cases. *World Neurosurg*. (2017) 99:763–9. doi: 10.1016/j.wneu.2015.11.079
4. Ryttlefors M, Howells T, Ronne-Engström E, Nilsson P, Enblad P. Neurointensive care is justified in elderly patients with severe subarachnoid hemorrhage–an outcome and secondary insults study. *Acta Neurochir*. (2010) 152:241–9. doi: 10.1007/s00701-009-0496-x
5. Degos V, Gourraud PA, Tursis VT, Whelan R, Colonne C, Korinek AM, et al. Elderly age as a prognostic marker of 1-year poor outcome for subarachnoid hemorrhage patients through its interaction with admission hydrocephalus. *Anesthesiology*. (2012) 117:1289–99. doi: 10.1097/ALN.0b013e318267395b
6. Bekelis K, Gottlieb D, Su Y, O'Malley AJ, Labropoulos N, Goodney P, et al. Surgical clipping versus endovascular coiling for elderly patients presenting with subarachnoid hemorrhage. *J Neurointerv Surg*. (2016) 8:913–8. doi: 10.1136/neurintsurg-2015-011890
7. Zheng J, Xu R, Guo Z, Sun X. Small ruptured intracranial aneurysms: the risk of massive bleeding and rebleeding. *Neurol Res*. (2019) 41:312–8. doi: 10.1080/01616412.2018.1563737
8. De Marchis GM, Lantigua H, Schmidt JM, Lord AS, Velander AJ, Fernandez A, et al. Impact of premorbid hypertension on haemorrhage severity and aneurysm rebleeding risk after subarachnoid haemorrhage. *J Neurol Neurosurg Psychiatry*. (2014) 85:56–9. doi: 10.1136/jnnp-2013-305051
9. Brawanski N, Kunze F, Bruder M, Tritt S, Senft C, Berkefeld J, et al. Subarachnoid hemorrhage in advanced age: comparison of patients aged 70-79 years and 80 years and older. *World Neurosurg*. (2017) 106:139–44. doi: 10.1016/j.wneu.2017.06.056
10. Da Silva IR, Gomes JA, Wachsman A, Rodriguez de Freitas G, Provencio JJ. Effect of age on transcranial doppler velocities in patients with aneurysmal subarachnoid hemorrhage. *Eur Neurol*. (2016) 76:261–6. doi: 10.1159/000452273
11. Oishi H, Yamamoto M, Shimizu T, Yoshida K, Arai H. Endovascular therapy of 500 small asymptomatic unruptured intracranial aneurysms. *AJNR Am J Neuroradiol*. (2012) 33:958–64. doi: 10.3174/ajnr.A2858
12. Bruneau M, Amin-Hanjani S, Koroknay-Pal P, Bijlenga P, Jahromi BR, Lehto H, et al. Surgical clipping of very small unruptured intracranial aneurysms: a Multicenter International Study. *Neurosurgery*. (2016) 78:47–52. doi: 10.1227/NEU.0000000000000991
13. Rahmanian A, Ghaffarpasand F, Alibai E, Choque-Velasquez J, Jahromi BR, Hernesniemi J. Surgical outcome of very small intracranial aneurysms utilizing the double clip technique. *World Neurosurg*. (2018) 110:e605–11. doi: 10.1016/j.wneu.2017.11.060
14. Feng X, Wang L, Guo E, Zhang B, Qian Z, Liu P, et al. Progressive occlusion and recanalization after endovascular treatment for 287 unruptured small aneurysms (<5mm): a single-center 6-year experience. *World Neurosurg*. (2017) 103:576–83. doi: 10.1016/j.wneu.2017.04.017
15. Chalouhi N, Zanaty M, Whiting A, Tjoumakaris S, Hasan D, Ajiboye N, et al. Treatment of ruptured intracranial aneurysms with the pipeline embolization device. *Neurosurgery*. (2015) 76:165–72. doi: 10.1227/NEU.0000000000000586
16. van Rooij WJ, Keeren GJ, Peluso JP, Sluzewski M. Clinical and angiographic results of coiling of 196 very small (< or = 3 mm) intracranial aneurysms. *AJNR Am J Neuroradiol*. (2009) 30:835–9. doi: 10.3174/ajnr.A1429
17. Mitchell PJ, Muthusamy S, Dowling R, Yan B. Does small aneurysm size predict intraoperative rupture during coiling in ruptured and unruptured aneurysms? *J Stroke Cerebrovasc Dis*. (2013) 22:1298–303. doi: 10.1016/j.jstrokecerebrovasdis.2012.10.017
18. Lee H, Perry JJ, English SW, Alkherayf F, Joseph J, Nobile S, et al. Clinical prediction of delayed cerebral ischemia in aneurysmal subarachnoid hemorrhage. *J Neurosurg*. (2018) 1:1–8. doi: 10.3171/2018.1.JNS172715
19. Yu Z, Zheng J, Ma L, Li H, You C, Jiang Y. Predictive value of cerebral autoregulation impairment for delayed cerebral ischemia in aneurysmal subarachnoid hemorrhage: a meta-analysis. *World Neurosurg*. (2019) 126:e853–9. doi: 10.1016/j.wneu.2019.02.188
20. Wachter D, Hans F, Kreitschmann-Andermahr I, Rohde V. Lower incidence of transcranial Doppler and symptomatic vasospasm after aneurysmal subarachnoid hemorrhage and aneurysm clipping in the elderly patient? *Neurosurgery*. (2011) 69:261–6. doi: 10.1227/NEU.0b013e31821d2b49
21. Lai PMR, Gormley WB, Patel N, Frerichs KU, Aziz-Sultan MA, Du R. Age-dependent radiographic vasospasm and delayed cerebral ischemia in women after aneurysmal subarachnoid hemorrhage. *World Neurosurg*. (2019) 130:e230–5. doi: 10.1016/j.wneu.2019.06.040

22. Brinjikji W, Rabinstein AA, Lanzino G, Kallmes DF, Cloft HJ. Effect of age on outcomes of treatment of unruptured cerebral aneurysms: a study of the National Inpatient Sample 2001-2008. *Stroke*. (2011) 42:1320–4. doi: 10.1161/STROKEAHA.110.607986
23. Qureshi AI, Chaudhry SA, Tekle WG, Suri MF. Comparison of long-term outcomes associated with endovascular treatment vs surgical treatment among medicare beneficiaries with unruptured intracranial aneurysms. *Neurosurgery*. (2014) 75:380–6. doi: 10.1227/NEU.0000000000000450
24. Alshekhlee A, Mehta S, Edgell RC, Vora N, Feen E, Mohammadi A, et al. Hospital mortality and complications of electively clipped or coiled unruptured intracranial aneurysm. *Stroke*. (2010) 41:1471–6. doi: 10.1161/STROKEAHA.110.580647
25. Mahaney KB, Brown RD Jr, Meissner I, Piepgras DG, Huston J 3rd, Zhang J, et al. Age-related differences in unruptured intracranial aneurysms: 1-year outcomes. *J Neurosurg*. (2014) 121:1024–38. doi: 10.3171/2014.6.JNS121179
26. Froelich JJ, Neilson S, Peters-Wilke J, Dubey A, Thani N, Erasmus A, et al. Size and location of ruptured intracranial aneurysms: a 5-year clinical survey. *World Neurosurg*. (2016) 91:260–5. doi: 10.1016/j.wneu.2016.04.044
27. Bender MT, Wendt H, Monarch T, Beaty N, Lin LM, Huang J, et al. Small aneurysms account for the majority and increasing percentage of aneurysmal subarachnoid hemorrhage: a 25-year, single institution Study. *Neurosurgery*. (2018) 83:692–9. doi: 10.1093/neuros/nyx484
28. Kim BJ, Kang HG, Kwun BD, Ahn JS, Lee J, Lee SH, et al. Small versus large ruptured intracranial aneurysm: concerns with the site of aneurysm. *Cerebrovasc Dis*. (2017) 43:139–44. doi: 10.1159/000452347
29. Hishikawa T, Date I, Tokunaga K, Tominari S, Nozaki K, Shiokawa Y, et al. Risk of rupture of unruptured cerebral aneurysms in elderly patients. *Neurology*. (2015) 85:1879–85. doi: 10.1212/WNL.0000000000002149
30. Fargen KM, Soriano-Baron HE, Rushing JT, Mack W, Mocco J, Albuquerque F, et al. A survey of intracranial aneurysm treatment practices among United States physicians. *J Neurointerv Surg*. (2018) 10:44–9. doi: 10.1136/neurintsurg-2016-012808

Conflict of Interest: The authors declare that the research was conducted in the absence of any commercial or financial relationships that could be construed as a potential conflict of interest.

Copyright © 2020 Zheng, Sun and Zhang. This is an open-access article distributed under the terms of the Creative Commons Attribution License (CC BY). The use, distribution or reproduction in other forums is permitted, provided the original author(s) and the copyright owner(s) are credited and that the original publication in this journal is cited, in accordance with accepted academic practice. No use, distribution or reproduction is permitted which does not comply with these terms.

frontiers in Neuroscience

ORIGINAL RESEARCH
published: 10 March 2020
doi: 10.3389/fnins.2020.00210

In vivo Two-Photon Imaging Reveals Acute Cerebral Vascular Spasm and Microthrombosis After Mild Traumatic Brain Injury in Mice

Xinjia Han[1,2,3,4], Zhi Chai[5], Xingjie Ping[1,2], Li-Juan Song[5], Cungen Ma[5], Yiwen Ruan[4,6] and Xiaoming Jin[1,2]**

[1] Spinal Cord and Brain Injury Research Group, Stark Neurosciences Research Institute, Indiana University School of Medicine, Indianapolis, IN, United States, [2] Department of Anatomy and Cell Biology, Indiana University School of Medicine, Indianapolis, IN, United States, [3] Department of Obstetrics and Gynecology, Guangzhou Women and Children's Medical Center, Guangzhou Medical University, Guangzhou, China, [4] GHM Institute of CNS Regeneration (GHMICR), Jinan University, Guangzhou, China, [5] Neurobiology Research Center, Shanxi Key Laboratory of Innovative Drugs for Serious Illness, College of Basic Medicine, Shaanxi University of Chinese Medicine, Jinzhong, China, [6] Co-innovation Center of Neuroregeneration, Nantong University, Nantong, China

OPEN ACCESS

Edited by:
Emmanuel Pinteaux, University of Manchester, United Kingdom

Reviewed by:
Sava Sakadzic, Massachusetts General Hospital and Harvard Medical School, United States
Jinyuan Zhou, Johns Hopkins University, United States

***Correspondence:**
Yiwen Ruan
tyiwen@jnu.edu.cn;
yiwenruan@yahoo.com
Xiaoming Jin
xijin@iupui.edu

Specialty section:
This article was submitted to Brain Imaging Methods, a section of the journal Frontiers in Neuroscience

Received: *16 November 2019*
Accepted: *25 February 2020*
Published: *10 March 2020*

Citation:
Han X, Chai Z, Ping X, Song L-J, Ma C, Ruan Y and Jin X (2020) In vivo Two-Photon Imaging Reveals Acute Cerebral Vascular Spasm and Microthrombosis After Mild Traumatic Brain Injury in Mice. Front. Neurosci. 14:210. doi: 10.3389/fnins.2020.00210

Mild traumatic brain injury (mTBI), or concussion, is reported to interfere with cerebral blood flow and microcirculation in patients, but our current understanding is quite limited and the results are often controversial. Here we used longitudinal *in vivo* two-photon imaging to investigate dynamic changes in cerebral vessels and velocities of red blood cells (RBC) following mTBI. Closed-head mTBI induced using a controlled cortical impact device resulted in a significant reduction of dwell time in a Rotarod test but no significant change in water maze test. Cerebral blood vessels were repeatedly imaged through a thinned skull window at baseline, 0.5, 1, 6 h, and 1 day following mTBI. In both arterioles and capillaries, their diameters and RBC velocities were significantly decreased at 0.5, 1, and 6 h after injury, and recovered in 1 day post-mTBI. In contrast, decreases in the diameter and RBC velocity of venules occurred only in 0.5–1 h after mTBI. We also observed formation and clearance of transient microthrombi in capillaries within 1 h post-mTBI. We concluded that *in vivo* two-photon imaging is useful for studying earlier alteration of vascular dynamics after mTBI and that mTBI induced reduction of cerebral blood flow, vasospasm, and formation of microthrombi in the acute stage following injury. These changes may contribute to early brain functional deficits of mTBI.

Keywords: cerebral cortex, vasculature, blood circulation, mild traumatic brain injury, two-photon imaging

INTRODUCTION

Traumatic brain injury (TBI) is increasingly being recognized as a significant problem of public health. Mild traumatic brain injury (mTBI), or concussion, which accounts for 70–90% of the TBI patient population, often occurs in falls, motor vehicle accidents and sports-related injury (Cassidy et al., 2004; McCrory et al., 2005; Chiu et al., 2007). Although mTBI is known to cause chronic post-concussive syndrome with symptoms such as memory and thinking impairments, headache, anxiety, and sleep disorders that significantly affect the quality of life and long-term outcomes, the injury rarely causes specific neurological deficits or brain structural damages that are detectable in clinical imaging (Levin et al., 1987; Bramlett and Dietrich, 2004; McCrory et al., 2009). This lack

of evidence of brain structural and functional damage represents a major challenge in understanding the mechanism of this disease and finding effective therapeutics (Margulies, 2000; Boake et al., 2005).

The cerebral vasculature consists of a complicated network of arteries, veins and capillaries, and plays an essential role in sustaining energy supply and metabolism of the cortex by delivering glucose and oxygen (Sunwoo et al., 2011; Shih et al., 2012a). Abnormal cerebral circulation is known to occur not only in patients with moderate to severe TBI but also in patients of mTBI during the acute and chronic stages (Bonne et al., 2003; Werner and Engelhard, 2007; Len and Neary, 2011). A strong correlation exists between microvascular dysfunction and TBI outcome, supporting that damage to the microvasculature may be a key contributor to secondary complications, including ischemia and increased intracranial pressure (Golding et al., 1999). Studies in animal models of mTBI found that pathophysiological alterations of cerebral vasculature include increase or decrease in cerebral blood flow, disruption of blood brain barrier, endothelial damage, and loss or altered vascular reactivity to various vasodilators (DeWitt et al., 1986; Wei et al., 2009; Zweckberger et al., 2010; Buckley et al., 2015). However, little information is available about acute dynamic changes in brain vessels and circulation after mTBI, particularly at the microscopic level. Given the critical importance of cerebral perfusion and oxygenation to normal brain function and its role in subsequent secondary injury and recovery, understanding cerebral microcirculation at the acute stage will be fundamental for understanding the mechanism of mTBI and its short- and long-term outcomes.

The recent two-photon imaging technique provides a powerful tool for studying longitudinal changes in cerebral vasculature and blood flow after brain ischemia and brain injuries (Schaffer et al., 2006; Drew et al., 2010a). To better mimic clinical situation of concussion in which most patients have no skull fracture or brain penetration and no positive findings in their neuroimaging examination (Alexander, 1995; McCrory et al., 2009), we used a closed-head mTBI preparation for *in vivo* two-photon longitudinal imaging of the cerebral vasculature and for revealing potential pathological changes in cerebral blood flow. Our results showed that mTBI resulted in decreases in the diameters of cerebral blood vessels as well as the velocities of red blood cells (RBCs), which is attributable to reduced cerebral blood flow and microthrombosis in capillaries.

MATERIALS AND METHODS

Animals

Male C57BL/6J mice or the same background Thy1-YFP transgenic mice were used in this study. For imaging, mice at the ages between 8 and 10 weeks old were divided into a sham group (11 mice) and an mTBI group (15 mice). The animals were kept on a 12 h light/dark cycle with sufficient food and water. The experiment was performed according to a protocol approved by the Institutional Animal Care and Use Committee (IACUC) of the Indiana University School of Medicine.

Thinned-Skull Window Preparation

Reinforced thinned-skull imaging windows were prepared based on a technique described previously (Drew et al., 2010b; Shih et al., 2012b). The mice were anesthetized with an intraperitoneal (i.p.) injection of ketamine/xylazine (87.7/12.3 mg/kg), and the scalp skin was removed to expose the skull. A 2 × 2 mm skull thinning area was prepared on the left parietal cortex, with the rostral edge being 2 mm posterior to the bregma and medial edge being 2–3 mm lateral from the middle line (**Figure 1A**). At the beginning of the surgery, a microdrill was used to thin a 1–2 mm diameter circular skull region to about a half of the thickness, then a 10# surgical blade was used to slowly and carefully thin the skull until surface blood vessels on the cerebral cortex were clearly visible under a light microscope. During this process, 0.9% physiological saline was added to the skull surface from time to time to reduce heat. After the thinned skull became dry, a small drop of thin cyanoacrylate glue (Ted Pella, Inc., Cat# 1003) was applied and a small piece of coverglass (1–1.5 × 1–1.5 mm size) was placed onto the thinned skull. The remaining area of the skull was covered with a layer of cyanoacrylate glue. The mice were allowed to recover for least 2 days before starting imaging sessions.

Preparation of Closed-Head mTBI

Following initial imaging of cerebral vasculature to record baseline conditions, a mouse model of closed-head mTBI was created on the left hemisphere by using a controlled cortical impact device, modified from a previously described technique (Creed et al., 2011). After the mice were anesthetized with ketamine/xylazine (87.7/12.3 mg/kg, i.p.) injection, their heads were stabilized on a stereotaxic apparatus by using a pair of ear rods with the tips enclosed in a piece of sponge. To avoid rigidly holding the head, the incisor hook of the stereotaxic device was not used. The skull orientation was adjusted to make sure it was in a horizontal position and perpendicular to the impactor tip. A 3 mm diameter impactor tip was used to strike the head at 5.0 m/s to a depth of 1.0 mm with a dwell time of 10 ms (Creed et al., 2011). The posterior edge of the impactor tip was targeted to an area ∼1 mm rostral to the anterior edge of the imaging window (**Figure 1A**). The mice of the sham injury group were subjected to the same procedures without receiving an impact. All animals were allowed to recover on a heating pad and were returned to their home cages after recovering from anesthesia. Of 13 and 20 mice of the sham and mTBI groups, 2 and 5 mice were used for *in vivo* imaging, respectively due to poor quality of cranial windows.

Behavioral Testing

To determine the effect of mTBI on cognitive and motor functions in this model, another set of mice were randomly assigned to a sham group ($n = 12$) and a mild TBI group ($n = 10$).

Rotarod Test

Motor coordination was assessed with a Rotarod apparatus (IITC Life Science Inc., CA, United States). Mice were placed on a spinning cylindrical rod accelerating from 0 to 30 rpm and the time to fall off was recorded. The maximum latency if a mouse

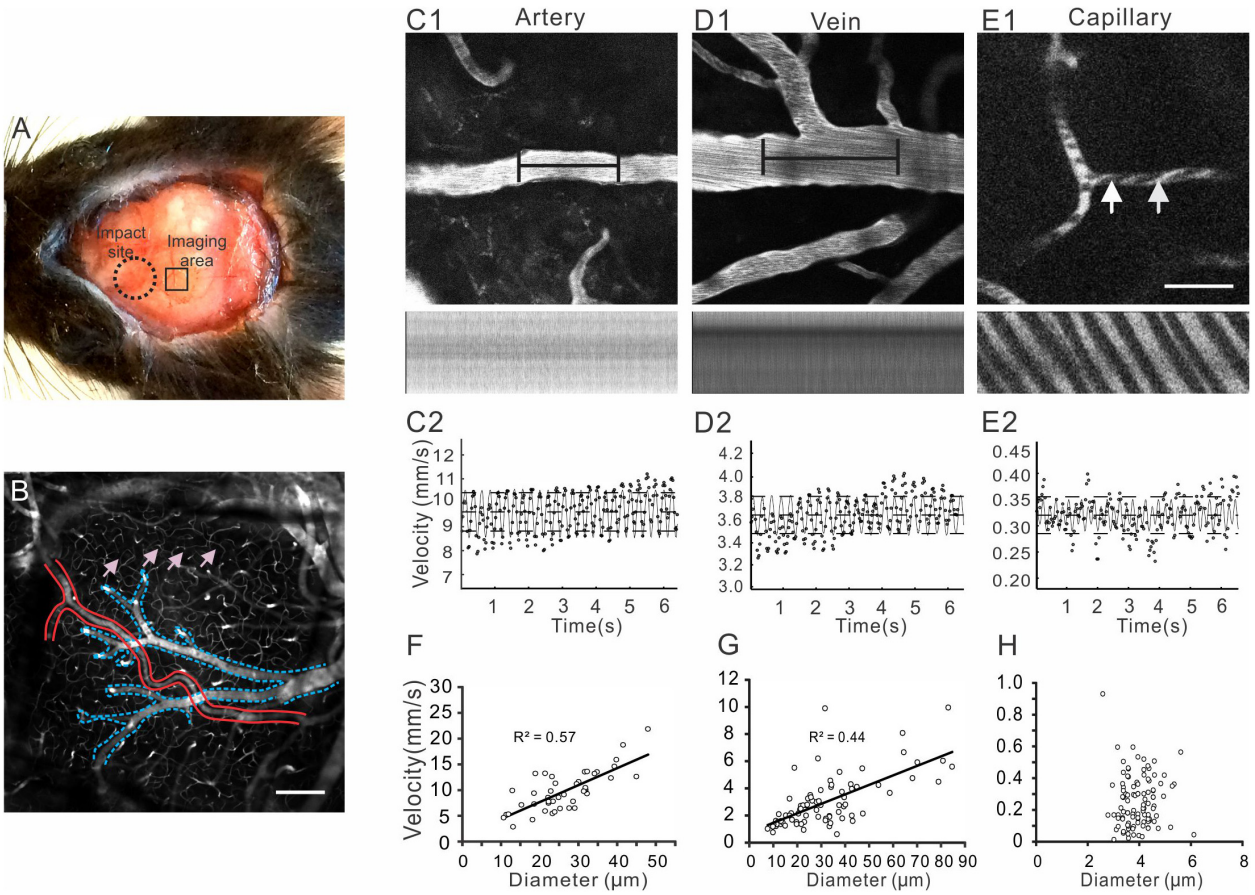

FIGURE 1 | *In vivo* two-photon microscopy for imaging cerebral vasculature and measuring blood flow through a thinned-skull window. **(A)** The skull above left parietal cortex of a mouse was thinned and strengthened by gluing a piece of square coverglass (~ 1.5 × 1.5 mm) for *in vivo* imaging (small square). Closed-head mTBI was induced by using a controlled cortical impact (CCI) device with a 3 mm diameter tip to strike on an area that was about 1 mm rostral to the anterior edge of the imaging window (large dotted circle). **(B)** A representative image of Z series projection of cerebral vessels reveals arteries (delineated in red), veins (delineated in blue), and networks of capillaries (pink arrows). **(C–E)** A segment of arteriole **(C1)**, venule **(D1)**, or capillary **(E1)** was oriented in a horizontal direction (top row) and imaged in line scan mode at 1 ms/line, which generated dark stripes (second row). The measurements were obtained from a single vessel. Velocity of red blood cells (RBC) in each vessel was calculated based on the line scan using a Matlab script **(C2–E2)**; the resulting velocities at different moments (small dots in **C2–E2**) were fitted to a second-order Fourier series (oscillating solid lines); the dashed horizontal lines represented time-averaged velocities. **(F–H)** Analyses of the relationships between RBC velocities and vessel diameters revealed positive correlations in arterioles and venules **(F,G)**, but not in capillaries **(H)**. Scale bars in B and E1 for C1-E1: 50 μm.

did not fall was 120 s. Before injury, each mouse received three training trials per day with inter-trial intervals of 20–30 min, and the latency to fall on the third day was recorded as baseline (day 0). Then the mice were split randomly into the sham and the mild TBI groups, and were tested on days 2, 4, 6, 8, and 10 after sham or mild TBI surgery. The mean latencies to fall off the Rotarod at each time point were used for result analysis.

Morris Water Maze

The water maze was performed in a circular tank (110 cm in diameter) filled with 22°C water, which was made opaque by adding non-toxic white paint. A hidden platform (10 cm in diameter) was placed in the southwestern quadrant 1 cm below the water surface. External cues for spatial reference were attached on the inner walls of the tank. Mice were released into the tank from a random starting point and trained to find the hidden platform for four trials per day. The maximum time for each trial was 60 s. Mice that didn't find the platform within 60 s were manually guided to it and allowed to sit on the platform for 30 s. Escape latency, and swimming distance and velocity were recorded by automated tracking software TopScan (CleverSys). Animals were trained on days 1, 3, 5, 7, and 9 after sham or mild TBI surgery, and the average latency to reach the platform on each training day was computed by averaging the four trials.

In vivo Two-Photon Imaging and Measurements of Red Blood Cell (RBC) Velocity and Blood Vessel Diameters

The mice were anesthetized with ketamine/xylazine (87.7/12.3 mg/kg, i.p.) injection, and received an i.p. injection of 0.1 ml Rhodamine B sothiocyanate-dextran solution (70 KDa,

3 mg/ml in distilled water) at least 15 min before imaging to label blood plasma. The mice were placed on a miniature stereotaxic apparatus and the head position was adjusted so that the cortical surface was horizontal to the microscope objective. The mice were placed on a heating pad to maintain their body temperature, and the arterial blood pressure and heart rate were monitored via the tails using a non-invasive Volume Pressure Recording (VPR) system (CODA Surgical Monitor, Kent Scientific Corporation, CT). To obtain consistent measurements of blood pressure, the animals were placed in position for 5 min prior to obtaining pressure measurements and the tail cuff was positioned to the base of the tail. At each time, at least three measurements were made for each mouse for calculating mean values of diastolic and systolic pressures.

Imaging was made with a two-photon microscope (Ultima Multiphoton Imaging System, Bruker, United States) (Xiong et al., 2017). Excitation was provided by a Maitai diode laser source pumping a Tsunami Ti: sapphire laser (Spectra-Physics, Mountain View, CA, United States) tuned to 870 nm wavelength. Band-pass-filtered fluorescence (560–660 nm) was collected by photo-multiplier tubes of the Prairie View Ultima system. Images (512 × 512 pixels, 0.15 μm/pixel in the *x*- and *y*-axes) or line scans were acquired using Prairie View software (**Figures 1C–E**). The mice were imaged at baseline, and at 0.5, 1, 6 h, and 1 day after mTBI. A Z-series of blood vessel images within 100–200 μm of the pial surface were first captured under a 10X objective. Then an Olympus SUPER 20X water immersion objective was used to image individual blood vessels and take line scan images along the central axis of a vessel at 3X optical zoom. The orientation of a segment of blood vessel (∼35 μm) was adjusted so that it paralleled the direction of the line scan. Typically, each session of line scan consisted of 5000 lines with a spatial resolution of 0.7 μm per pixel and at a speed of about 1 ms per line. The line scan parameters were automatically recorded in the Prairie View software.

For longitudinal imaging, the same imaging fields and segments of line-scanned vessels at different time points after initial baseline imaging were identified based on the location and patterns of vessels. The depth and orientation of the vessels were carefully adjusted so that the same vessels were imaged with the same imaging parameters including pixel size and scanning speed. Each experimental session took 20–30 min. From baseline to 0.5 and 1 h imaging, anesthesia and labeling of blood plasma were carried out only once. For 6 h and 1 day imaging sessions, anesthesia and labeling of blood plasma were done separately. The animals were allowed to recover after each imaging on a heating pad and then returned to their home cages after being awake. Images of microthrombosis were captured in two mice after mTBI. Because the microthrombosis was transient and sporadic, the RBC velocities and diameters of the involved capillaries were not measured.

Imaging analyses were made with Metlab and NIH ImageJ software. Maximal intensity projections of image stacks were made for identifying and confirming imaged vasculature in regions of interest. RBC velocities were calculated from line-scan images using a Metlab script written according to previous work of line-scanning particle image velocimetry developed by Kim et al. (2012). Briefly, this technique determines RBC displacements between pairs of line-scans using spatial cross-correlation analysis. The shift from the origin to the peak center of the cross-correlation was a measure of the distance traveled by RBCs between image frames. After the peak was fitted with a Gaussian distribution to improve calculation accuracy, the shift in pixels was converted to microns and velocity was calculated. The resulting velocities at different moments were fitted to a second-order Fourier series (**Figures 2C2–E2**), time-averaged velocities were obtained (**Figures 2C2–E2**). The diameters of line-scanned blood vessels were determined in ImageJ by manually measuring the maximal widths at the middle of the scanned vessel segment that was filled with fluorescence dye. For each vessel at each time point, three measurements were made and averaged. For measuring vessel diameters at different time points, efforts were taken to make diameter measurements at the same spots as close as possible.

Statistics

The data were averaged among animals in each group and all data are presented as mean ± standard error of the mean (SE). Because of the large variability of the imaged vessels in size and its corresponding blood flow, vessel diameters and RBI velocities are expressed as percent change from baseline. For comparisons of diameters and velocities at different time points between the sham and mTBI groups, data were analyzed with a two-way repeated measures ANOVA using Origin Pro 9.1 software, followed by pairwise comparisons using Bonferroni test. A p value less than 0.05 ($p < 0.05$) was considered statistically significant. Graphs of the data were obtained using GraphPad Prism 5 software.

RESULTS

Imaging Cerebral Blood Vessels Through a Thinned-Skull Window *in vivo*

In this *in vivo* imaging study, we used a thinned skull window preparation, because preparing these windows were less invasive (without exposing the brain) and they usually sustained the physical impacts generated from a CCI device during mTBI model preparation. **Table 1** summarized numbers of measured vessels and numbers of animals in each experimental group. Occasionally, mice with damaged or deteriorating windows were excluded from further experiment and data analysis. As shown in **Figure 1A**, the posterior edge of an impact site was about 1 mm from the anterior edge of an imaging window, which would allow us to observe changes in cerebral vessels after the relatively diffuse brain injury (Drew et al., 2010b; Shih et al., 2012b).

Cerebral vessels including arteries, capillaries, and veins were clearly visible within ∼400 μm below the pial surface (**Figure 1B**). The fluorescence dye (Rhodamine B) revealed the serum in bright red and the RBCs as dark dots due to their impermeability to the dye. RBC velocities of different vessels, which typically represent the velocities of blood flow, were measured using line scan and calculated from the dark strips (**Figures 1C–E**; Drew et al., 2010a; Shih et al., 2012a). The mean velocity at baseline was calculated by combining data from the

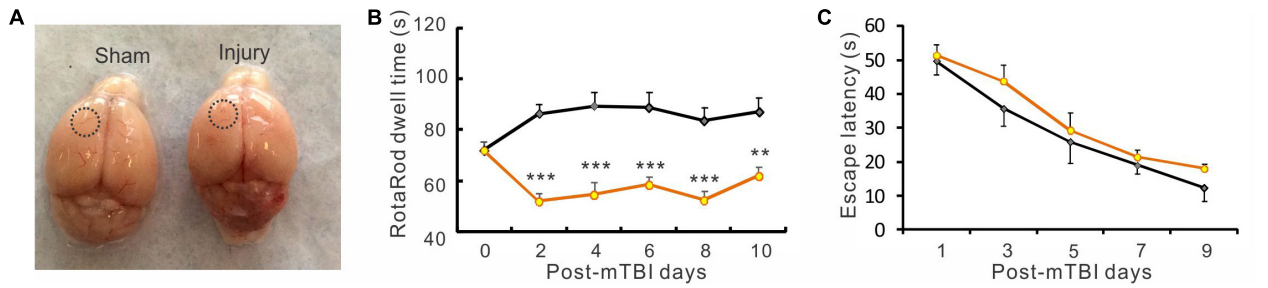

FIGURE 2 | Closed-head mTBI resulted in impaired motor function. **(A)** Morphology of freshly dissected mouse brains from sham injured (left) and mTBI (right) mice. There was no obvious difference between them in gross brain structure. The dotted circles indicate approximate regions of sham or actual cortical impact. **(B)** In repeated RotaRod tests, the dwell times of the mTBI group were highly significantly less than those of the sham group between days 1 and 10 post-mTBI ($F_{(1,100)} = 106.47$, $^{**}p < 0.01$, $^{***}p < 0.001$, two-way ANOVA followed by Bonferroni post-test), suggesting an impaired motor function in these mice. **(C)** The escape latency in water maze test had no significant change after mTBI. (all $p > 0.05$. $n = 12$ in sham and $n = 10$ in mTBI).

shame group and mTBI groups. Arterials were differentiated from veins based on their smaller sizes, smoother vessel walls, fewer branches, and faster RBC velocities. RBC velocities of most arteries were between 5 and 20 mm/s, the velocities of veins ranged between 1 and 10 mm/s, and the velocities of capillaries were less than 1 mm/s with a mean value of 0.25 ± 0.02 mm/s.

We analyzed the relationships between vessel diameters and RBC velocities in arteries, veins, and capillaries. As expected, there were positive correlations between RBC velocities and diameters of arteries and veins, with the correlation coefficients being 0.57 and 0.44 for arteries and veins, respectively (**Figures 1F,G**). In contrast, the diameters of capillaries had no correlation with RBC velocities (**Figure 1H**).

mTBI Induced Motor Deficit but Did Not Impair Learning and Memory Function

Closed-head mTBI induced by the modified CCI technique produced little gross brain structure damage. We observed freshly dissected mouse brains and found that closed-head mTBI induced by the modified CCI technique produced little gross brain structure damage (**Figure 2A**). However, behavioral tests revealed that the mTBI model produced motor behavioral deficits, as indicated by a significant reduction of dwell time in a Rotarod test in the mTBI group than the sham group during a 10-day period after injury (**Figure 2B**. $p < 0.01$ or $p < 0.001$, two-way ANOVA followed by Bonferroni post-test). In contrast, in the water maze test there was no significant difference in the latency of finding the hidden platform between the two groups (**Figure 2C**, $p > 0.05$), indicating that this type of mTBI preparation didn't significantly impair spatial learning and memory in the mice.

TABLE 1 | The number of imaged vessels and animals for each experimental group.

Group	Artery		Vein		Capillary	
	mice	vessels	mice	vessels	mice	vessels
Diameter and velocity relationship	19	44	21	79	16	104
Sham group	11	29	11	54	11	49
mTBI group	15	19	15	41	15	48

No Significant Changes in Arterial Blood Pressure After mTBI

To monitor whether mTBI affected systemic blood pressure, systolic blood pressure (SBP) and diastolic blood pressure (DBP) of mouse tail were measured in the sham and injury groups using a tail cuff. Repeated measurements were carried out in each animal at each imaging time point (**Figures 3A,B**). In the sham group, the SBP and DBP were between 105.1 ± 2.5 and 108.9 ± 3.0 mmHg and between 79.9 ± 2.0 and 82.8 ± 4.0 mmHg, respectively. In the mTBI group, the SBP and DBP were between 107.9 ± 3.0 and 113.0 ± 9.0 mmHg and between 76.5 ± 5.8 and 81.9 ± 9.1 mmHg, respectively. There were no significant differences between the two groups at different time points (all $p > 0.05$).

Significant Decreases in Diameters and RBC Velocities of Arterioles After mTBI

Morphological changes of arterioles at different time points in sham and mTBI groups are shown in **Figure 4A**. In the sham group, arterioles maintained stable morphology overtimes. However, spasm of arterioles was markedly visible at 0.5, 1, and 6 h following closed-head mTBI. Quantitative analysis showed that normalized arterial diameters were 101% ± 2, 101% ± 1, 97% ± 2, and 100% ± 1 at 0.5, 1, 6 h, and 1 day in the sham group (**Figure 4B**, $p > 0.05$). However, the diameter of arterioles decreased significantly at 0.5, 1, and 6 h post-injury (94% ± 3, 93% ± 3, and 93% ± 2, respectively, all $p < 0.05$ when compared with the sham group) and partially recovered at 1 day after mTBI (96% ± 3, $p > 0.05$ when compared with the sham group). The RBC velocities of the sham group were 97% ± 3, 102% ± 4, 100% ± 5, 100% ± 3 at 0.5, 1, 6 h, and 1 day, respectively. It was also significantly reduced at 30 min, 1, and 6 h after injury (**Figure 4C** 79% ± 6, 84% ± 5, and 84% ± 5, respectively, all $p < 0.05$ when compared with the sham group) and recovered partially at 1 day following mTBI

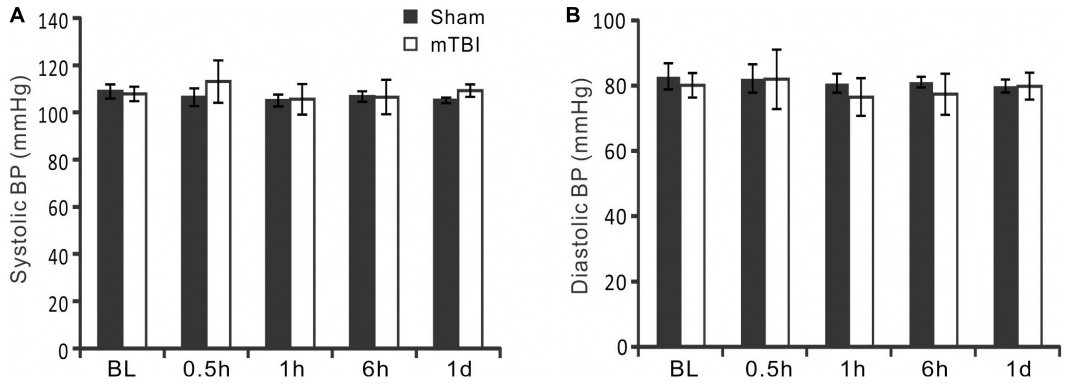

FIGURE 3 | Measurement of systematic blood pressures. **(A,B)** Blood pressure (BP) was monitored by measuring tail artery BP throughout the duration of the imaging experiment. There were no significant changes in systolic BP and diastolic BP at baseline and different times after mTBI ($p > 0.05$, repeated measure ANOVA).

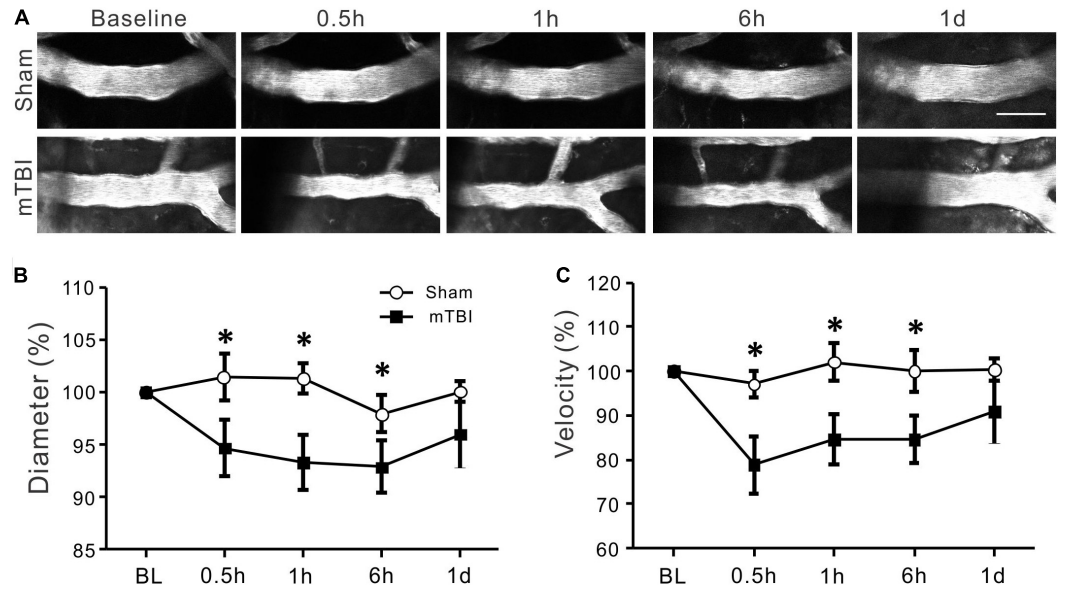

FIGURE 4 | Reduced arterial diameter and RBC velocity after mTBI. **(A)** Changes in cerebral arterial morphology at different time points after mTBI in sham and injury groups. In comparison to the sham group, arteries of the mTBI group showed obvious constriction between 0.5 and 6 h post-mTBI. **(B)** Arterial diameters became smaller between 0.5 and 6 h post-injury ($p < 0.05$ at all time points when compared with the same time points of the sham groups, repeated measure ANOVA), and partially recovered to baseline level at one day post-mTBI ($p > 0.05$). **(C)** Consistent with the reduced diameter, arterial RBC velocity also significantly decreased between 0.5 and 6 h and recover to thebaseline level at 1 day following mTBI (*$p < 0.05$).

(91% ± 4, $p > 0.05$ when compared with the sham group). The data suggest that both the diameter and blood flow of arterials decreased significantly during 0.5–6 h after mTBI and partially recovered in 1 day after mTBI.

Acute Reduction but Earlier Recovery in Diameter and RBC Velocity of Venules After mTBI

The morphology of small veins remained relatively stable at different time points in both sham group and injury group (**Figure 5A**). Quantitative analysis revealed that both diameter and velocity of venules underwent significant reduction in diameter at 1 h (95% ± 3, $p < 0.05$) and in velocity at 30 min (87% ± 6, $p < 0.05$) after mTBI when compared with the sham group at the corresponding time points (**Figures 5B,C**). However, these two parameters gradually recovered close to the normal level from 6 h after mTBI (**Figures 5B,C**).

Decreased Diameter and RBC Velocity and Formation of Microthrombi of Capillaries After mTBI

The movement of individual RBCs in capillaries were quite slow (**Figure 1H**, ∼0.05–0.93 mm/s) and clearly discernible under two-photon imaging (**Figure 6A**). While the capillaries of the

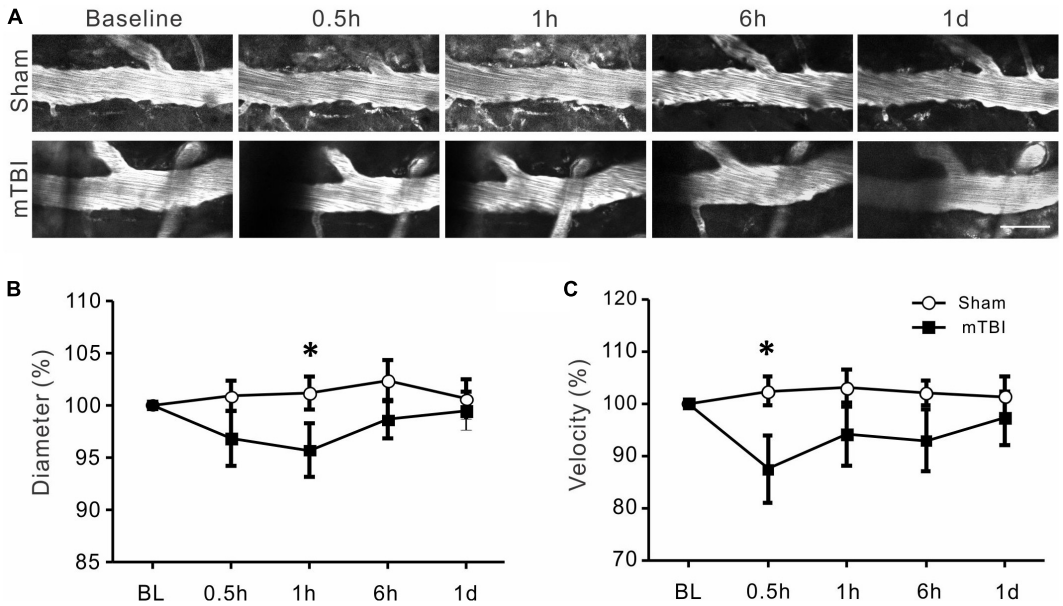

FIGURE 5 | Changes in venous diameter and RBC velocity after mTBI. **(A)** Representative images of cerebral veins at different time points after mTBI of the sham and injury groups. There seems a small decrease in vein diameter within 0.5–1 h post-mTBI, which recovered to baseline level in one day. **(B)** There was a significant decrease in venous diameter at 1 h after mTBI ($p < 0.05$), but insignificant changes at other time points ($p > 0.05$). **(C)** The changes in venous RBC velocity were similar with the changes in vein diameter: a significant decrease in venous RBC velocity occurred at 0.5 h ($p < 0.05$) post-mTBI, which recovered in 1 h to 1 day post-mTBI. *$p < 0.05$.

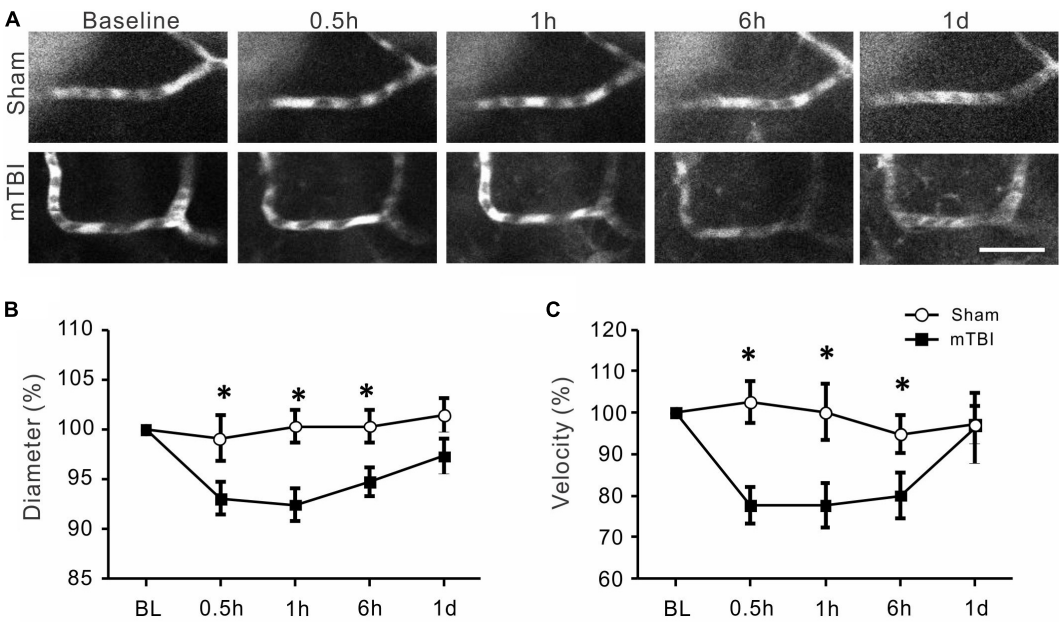

FIGURE 6 | Reduced capillary diameter and RBC velocity after mTBI. **(A)** Representative images of capillary segments at different time points after mTBI of the sham and injury groups. Individual RBCs are discernable as single dark spots inside the capillaries. Scale bar: 25 μm. **(B)** Capillary diameters became smaller between 0.5 and 6 h post-injury ($p < 0.05$ at all time points), and recovered at 1 d post-mTBI ($p > 0.05$). **(C)** Changes in capillary RBC velocity were similar to that of capillary diameter: it decreased during 0.5–6 h post-mTBI and recovered at 1 d post-mTBI. *$p < 0.05$.

sham group maintained relatively stable diameter and RBC velocity, there was a small yet significant decrease in diameters of capillaries at 0.5, 1, and 6 h after mTBI (**Figure 6B**. 94% ± 2, 92% ± 2, and 94% ± 1, respectively, all $p < 0.05$ when compared with the sham group at the corresponding time points), which partially recovered to baseline level at 1 day after mTBI. There

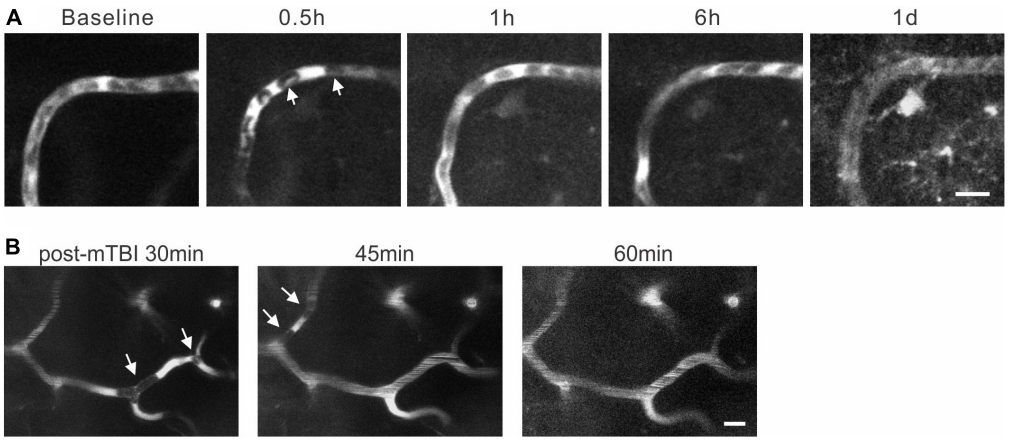

FIGURE 7 | Formation and clearance of transient microthrombi following mTBI. **(A)**. At 0.5 h post-mTBI, RBCs in a segment of capillary (arrows) stopped moving and the fluorescent dye accumulated locally. This type of RBC accumulation was removed at 1 h post-mTBI and smooth blood flow recovered. **(B)** Images of cerebral capillaries between 30 and 60 min after mTBI. At 30 min, formation of microthrombi (white arrows in the left image) completely stopped blood flow in a segment of capillary. The original microthrombi disappeared at 45 min, but new ones formed (white arrows in the middle image) in different locations, which were cleared at 60 min post-mTBI (right image). Scale bars: 10 μm.

were more dramatic decreases in RBC velocity of capillaries at 0.5, 1, and 6 h after mTBI (**Figure 6C**. 78% ± 4, 78% ± 5, 80% ± 5, respectively, all $p < 0.05$ when compared the sham group at the corresponding time points), which also increased to baseline level at 1 day after mTBI.

We also found that mTBI induced transient formation of microthrombi or microthrombus-like structures inside capillaries. These microthrombi consisted of a few RBCs in capillaries and partially or totally blocked blood circulation in the particular segments of capillaries. They appeared as early as 30 min after injury and sustained for a short time period (∼10–30 min) before clearance and re-perfusion of the capillaries (**Figures 7A,B**, $n = 2$ mice). Formation and clearance of the microthrombi occurred simultaneously at multiple locations: while a microthrombus was being cleared in one location (**Figure 7B**, left and middle images), a new microthrombus formed in a nearby capillary, which again disappeared in ∼15 min (**Figure 7B**, the middle and right images). Accompanying with microthrombosis was a reversal of blood flow direction in some capillaries, which changed back once a microthrombus was cleared.

DISCUSSION

In this study, we used *in vivo* two-photon microscopy in a closed-head mTBI model to study longitudinal changes in diameters and blood flow of cerebral arteries, veins, and capillaries within one day after injury. Repeated measurements of vessel diameter and centerline RBC velocity were made before and at different time points after closed-head mTBI. To our best knowledge, this is the first attempt to examine real-time longitudinal dynamics of cerebral vasculature and microcirculation at a vessel-by-vessel level in a closed-head concussion model. The technique convincingly demonstrated that cerebral arteries and capillaries had significant decreases in vessel diameter and RBC velocity from 30 min to 6 h post-mTBI and partially recovered to baseline values at one day post-mTBI. The diameter and RBC velocity of veins underwent reduction in a short time window 0.5–1 h after mTBI. We also observed formation of transient microthrombi and their subsequent clearance. These results suggest that mTBI causes acute spasm of cerebral blood vessels, reduction of blood flow, and impairment of capillary microcirculation.

We used an established closed-head mTBI model that mimics human concussion, the most common type of TBI. Consistent with published results (Schaffer et al., 2006; Drew et al., 2010b), the model induced transient loss of consciousness and impairment of motor behavior in the Rotarod test. Although the escape latency in the water maze test of the mTBI group was not significantly longer than that of the sham group, a trend of longer escape latency existed, particularly in the first 3 d after mTBI (**Figure 2C**), which is consistent with a previous observation of impaired spatial acquisition in 1–3 days but no change in 4–6 days after mTBI (Schaffer et al., 2006).

This model of mTBI not only mimics key features of human concussion such as closed-head injury, subtle yet diffuse structural damages, and behavioral deficits, but also is suitable for *in vivo* two-photon imaging of brain structural damage at the cellular level, including dynamics of cerebral vasculature and microcirculation. A major concern about using *in vivo* two-photon imaging for longitudinal study of mTBI is that the physical impact generated from an impact device will damage the cranial window and make it impossible to follow dynamic changes in structures of neurons, glial cells, or vasculature. By targeting the impactor tip to an area next to a small thinned skull window, we found it feasible to create an mTBI model without damaging the imaging window. We only experienced an occasional crack of window glass or leak of air into the windows. Although the physical impact from an impact device is focal, its effect on the brain is diffuse, including more distant

brain regions, as was validated from our morphological data and behavioral testing results. Thus, the thinned-skull window preparation can sustain the impact of a CCI device and allow longitudinal imaging studies on dynamic changes in neuronal structures as well as vascular structures and blood circulation. This approach may also be used for testing longitudinal effects of therapeutic and rehabilitative interventions on cellular structures and activities after mTBI.

Moderate or severe TBI is known to induce a significant decrease in the cerebral blood flow (CBF) in patients during the acute stage (less than 3 h after head injury) and chronic stage (at least 3 months after TBI), as measured by transcranial Doppler (TCD) ultrasound or arterial spin labeling perfusion fMRI techniques (McQuire et al., 1998; Shi et al., 2010). Cerebral hypoperfusion also appears in rat TBI models with severe damage in the early stage (4 h after cortical contusion) and late stage (9 months after lateral fluid-percussion injury) using arterial spin labeling (ASL) MRI technique or Laser Doppler Flowmetry (LDF) measurement (Thomale et al., 2002; Hayward et al., 2010, 2011). Besides lower CBF, reduction in carotid artery blood flow was also observed after a rapid head rotational injury (Clevenger et al., 2015).

Reduced CBF after mTBI is observed in both animal and human studies. In acute sports-related concussion patients, ASL MRI techniques showed decreased CBF in several brain regions in 24–48 h after injury (Wang et al., 2018). Furthermore, the decrease in CBF in 8 d after injury was more severe and diffuse than at 24 h after injury (Wang et al., 2016). In a rat model of blast-induced mild TBI, a reduction in cerebral perfusion was found with LDF within 2 h after injury (Kawoos et al., 2016). In a mouse closed-head mTBI model, a single concussion caused CBF reduction by $35 \pm 4\%$ at 4 h, which returned to preinjury levels by 24 h (Buckley et al., 2015). These results are generally consistent with our observation that RBC velocity was decreased between 30 min to 6 h after mTBI, before recovering to about baseline level at 24 h. In contrast, an investigation on 14 patients with mTBI using an ASL technique showed increases in regional CBF in the striatum and frontal and occipital cortex in 3 h to 10 days after injury, which was accompanied by high level of oxygen in veins (Doshi et al., 2015). Similarly, increases in cerebral blood flow and pial arteriolar diameter were observed in a fluid percussion model of TBI (Wei et al., 1980, 1981). This discrepancy may originate from the wide range of post-concussion time periods of the patients in that human study (Doshi et al., 2015), or from the difference in injury model and severity as well as animal species (Wei et al., 1980, 1981). Although our results showed recovery of vessel diameter and RBC velocity to baseline level at 1 day after mTBI, such recovery may not be complete and stable. Changes in chronic post-concussion period need to be further determined in future.

There is apparent discrepancy between changes in the diameters and velocities in arterials and venous (**Figures 4**, **5**). Because many other factors also contribute to the blood flow volume, including numbers and lengths of arteries and veins, velocity changes, and extracellular space, it would be difficult to estimate the volume of blood flow by imaging diameter and velocity of a small numbers of vessels of the brain. On the other hand, an assumption that total inflow of blood should equal to outflow may not be true, particularly under pathological conditions such as TBI. Disturbed cerebral microcirculation participated in the pathological process of neurological disease; changes in diameter and velocity of arteries and veins can be quite different in various pathological conditions. For example, in 60 min after subarachnoid hemorrhage, arterioles become dilated but venules do not change (Ishikawa et al., 2016). In diabetic mice, there was no significant change in the blood velocity of arterioles while there was a significant decline in those of venules (Huang et al., 2014). Middle cerebral artery occlusion in diabetic mice can cause the blood velocities of both arterioles and venules to decrease (Huang et al., 2014). Changes of velocities and diameters of arterioles and venules also showed potential discrepancy in recovery one day after mTBI induction in the present study. Gattinoni et al. have proposed that venous and arterial base excess difference is closely related to physiological reality (Lang and Zander, 2002; Gattinoni and Busana, 2019).

The present study showed that the mean RBC velocity in all animals at baseline was 0.25 mm/s (0.05–0.93 mm/s) and the mean value from each animal varied from 0.10 to 0.44 mm/s. In contrast, the mean capillary RBC velocities were within the scopes of 0.1∼1.6 mm/s and 0.05∼0.9 mm/s as reported by Emmanuelle (Chaigneau et al., 2003) and Stefanovic et al. (2008). In some other studies, the velocities in both anesthetized and awake mice were calculated to be approximately 0.7 or 1.3 mm/s (Huang et al., 2014; Wei et al., 2016; Li et al., 2019; Lu et al., 2019). Comparing to these values, our data seemed to be lower. One possible reason may be due to the relatively smaller capillaries (with a mean diameter of 3.96 μm) we imaged than those imaged in prior studies (with mean diameters of 4.7 to 6 μm) (Li et al., 2019; Lu et al., 2019). Small vessels usually have lower RBC velocity. Another possible reason may be due to different effects of anesthetic agents on blood vessel diameters (Slupe and Kirsch, 2018). For example, ketamine has been shown to cause constriction of microvessels (Small et al., 2014).

The mechanism of mTBI-induced decrease in cerebral blood flow may involve vasospasm, edema, and neuroinflammation. A body of studies have reported post-TBI vasospasm (Kramer et al., 2013; Fehnel et al., 2014; Perrein et al., 2015; Ogami et al., 2017). In severe TBI, post- traumatic vasospasm is detected in 30–40% of patients (Perrein et al., 2015). Vasospasm appears in the early stage after TBI and is considered related to delayed ischemic neurological deficit, which contributes to the formation of subarachnoid hemorrhage (DeWitt and Prough, 2003). In the present study, direct measurement of decreased arteriole diameter between 0.5 and 6 h post-mTBI provides strong evidence of vasospasm during the early time period after the injury. A decrease in vein diameter after mTBI was also observed. Since the diameters of cerebral arteries and veins are positively correlated to their RBC velocity (**Figures 1F–H**), the decreased vessel diameters after mTBI likely contribute to the reduced CBF. Mechanistically, calponin phosphorylation and carbon dioxide ($Pa\,CO_2$) may be factors involved in regulation of cerebrovascular reactivity to TBI (Shen et al., 2007; Len et al., 2011). Increases in the level of NO and Ca^{++} in endothelium after TBI are also considered major factors in stimulating vasospasm of cerebral

arteries (Villalba et al., 2014). In addition, we also observed early reductions of diameters and RBC velocity of capillaries in 0.5–6 h after mild TBI in our study. Because cerebral blood flows in the capillary and arteriole are regulated through different signaling cascades (Biesecker et al., 2016; Mishra et al., 2016), it would be interesting to investigate whether different molecular mechanisms are involved in the regulation of blood flow in arteries and capillaries after mTBI.

Edema is known to develop after moderate to severe TBI and contribute to increased intracranial pressure (ICP) (Bolouri et al., 2012). An increase of ICP from tissue edema is thought to be one of the major mechanisms of blood flow loss (Nortje and Menon, 2004). However, increase in ICP after TBI varies considerably in different TBI models as well as in different animal species (Reid et al., 2010). Particularly, TBI alone does not cause significant increase of ICP in either lateral fluid percussion or impact acceleration induced injury in rats (Gabrielian et al., 2011) and closed-head mTBI is shown not to cause edema in a weight drop model in mice (Garcia et al., 1994; Kane et al., 2012). Therefore, edema may not make a significant contribution to the reduced RBC velocity in our mTBI mice.

Microthrombosis resulting from abnormal platelet activation occurs in the early stage after moderate and severe TBI, which can lead to perfusion loss in the peri-contusional cortex (Dietrich et al., 1994; Maeda et al., 1997; Bramlett and Dietrich, 2004). There is a positive correlation between the number of microthrombi and the degree of neuronal necrosis (Stein et al., 2004). In the present study, the observed microthrombi in capillaries seem different from typical microthrombi that occur after more severe TBI. Among all the capillaries being imaged, we observed only three cases of microthrombus formation in the mTBI brain and none in sham brain. Given the rare and transient nature of microthrombosis in this particular model of mTBI, it was not possible to quantify them. These capillary microthrombi were transient and reversible, lasting for only minutes to tens of minutes. They may be regarded as a mild type of microthrombi. Given the transient and microscopic nature of the microthrombi, it would be difficult to capture them using conventional imaging techniques such as CT scan or even tissue histology. Their pathological significance is unclear. In controlled cortical impact and fluid percussion models of TBI, factors that may induce or facilitate microthrombosis include endothelial damage and release of procoagulant molecules such as cardiolipin (Kontos et al., 1981; Zhao et al., 2016; Hall et al., 2017), and release of platelet activating factor and platelet aggregation (Rosenblum et al., 1982; Maeda et al., 1997). While a high density of microthrombi is associate with more severe selective neuronal necrosis (Deng et al., 2005), the transient microthrombi we observed after mTBI may not be severe enough to cause neuronal death. However, their interference with capillary microcirculation likely contributes to exacerbating brain ischemia and acute functional deficits.

In summary, we used an *in vivo* two-photon imaging technique to study acute changes in cerebral vasculature and blood circulation in a model of closed-head mTBI. Our results provide direct evidence that mTBI caused acute decreases in the diameter and blood flow of cerebral arterioles, veins, and capillaries to different degrees within 0.5 to 6 h after injury. These decreases mostly recovered to baseline levels at 24 h after injury. The mTBI also caused microthrombosis in capillaries, which were transient and cleared in a short time period. These vascular changes may contribute to acute brain ischemia and functional impairments and may guide therapeutic development for mTBI.

DATA AVAILABILITY STATEMENT

All datasets generated for this study are included in the article/supplementary material.

ETHICS STATEMENT

The animal study was reviewed and approved by the Institutional Animal Care and Use Committee (IACUC) of the Indiana University School of Medicine.

AUTHOR CONTRIBUTIONS

XJ and YR conceived and designed the experiments. XH and XP performed the experiments:. XH, XP, ZC, L-JS, and CM analyzed the data. XH, ZC, L-JS, CM, XJ, and YR wrote, revised, and commented on the manuscript.

FUNDING

This work was supported in part by the Indiana Spinal Cord and Brain Injury Research Fund from the Indiana State Department of Health (A70-1-079438, A70-3-079971, and A70-4-079956) to XJ. This work was also supported by funding from the China's National 111 project (Grant number B14036) to YR and postdoctoral research start-up funding (3001008-04) from Guangzhou Women and Children's Medical Center.

REFERENCES

Alexander, M. P. (1995). Mild traumatic brain injury: pathophysiology, natural history, and clinical management. *Neurology* 45, 1253–1260. doi: 10.1212/wnl.45.7.1253

Biesecker, K. R., Srienc, A. I., Shimoda, A. M., Agarwal, A., Bergles, D. E., Kofuji, P., et al. (2016). Glial cell calcium signaling mediates capillary regulation of blood flow in the retina. *J. Neurosci.* 36, 9435–9445. doi: 10.1523/JNEUROSCI.1782-16.2016

Boake, C., McCauley, S. R., Levin, H. S., Pedroza, C., Contant, C. F., Song, J. X., et al. (2005). Diagnostic criteria for postconcussional syndrome after mild to moderate traumatic brain injury. *J. Neuropsychiatry Clin. Neurosci.* 17, 350–356. doi: 10.1176/jnp.17.3.350

Bolouri, H., Saljo, A., Viano, D. C., and Hamberger, A. (2012). Animal model for sport-related concussion; ICP and cognitive function. *Acta Neurol. Scand.* 125, 241–247. doi: 10.1111/j.1600-0404.2011.01614.x

Bonne, O., Gilboa, A., Louzoun, Y., Kempf-Sherf, O., Katz, M., Fishman, Y., et al. (2003). Cerebral blood flow in chronic symptomatic mild traumatic

brain injury. *Psychiatry Res.* 124, 141–152. doi: 10.1016/s0925-4927(03)00109-4

Bramlett, H. M., and Dietrich, W. D. (2004). Pathophysiology of cerebral ischemia and brain trauma: similarities and differences. *J. Cereb. Blood Flow Metab.* 24, 133–150. doi: 10.1097/01.WCB.0000111614.19196.04

Buckley, E. M., Miller, B. F., Golinski, J. M., Sadeghian, H., McAllister, L. M., Vangel, M., et al. (2015). Decreased microvascular cerebral blood flow assessed by diffuse correlation spectroscopy after repetitive concussions in mice. *J. Cereb. Blood Flow Metab.* 35, 1995–2000. doi: 10.1038/jcbfm.2015.161

Cassidy, J. D., Carroll, L. J., Peloso, P. M., Borg, J., von Holst, H., Holm, L., et al. (2004). Incidence, risk factors and prevention of mild traumatic brain injury: results of the WHO collaborating centre task force on mild traumatic brain injury. *J. Rehabil. Med.* 43(Suppl.), 28–60. doi: 10.1080/16501960410023732

Chaigneau, E., Oheim, M., Audinat, E., and Charpak, S. (2003). Two-photon imaging of capillary blood flow in olfactory bulb glomeruli. *Proc. Natl. Acad. Sci. U.S.A.* 100, 13081–13086. doi: 10.1073/pnas.2133652100

Chiu, W. T., Huang, S. J., Tsai, S. H., Lin, J. W., Tsai, M. D., Lin, T. J., et al. (2007). The impact of time, legislation, and geography on the epidemiology of traumatic brain injury. *J. Clin. Neurosci.* 14, 930–935. doi: 10.1016/j.jocn.2006.08.004

Clevenger, A. C., Kilbaugh, T., and Margulies, S. S. (2015). Carotid artery blood flow decreases after rapid head rotation in piglets. *J. Neurotrauma* 32, 120–126. doi: 10.1089/neu.2014.3570

Creed, J. A., DiLeonardi, A. M., Fox, D. P., Tessler, A. R., and Raghupathi, R. (2011). Concussive brain trauma in the mouse results in acute cognitive deficits and sustained impairment of axonal function. *J. Neurotrauma* 28, 547–563. doi: 10.1089/neu.2010.1729

Deng, P., Pang, Z. P., Zhang, Y., and Xu, Z. C. (2005). Increase of delayed rectifier potassium currents in large aspiny neurons in the neostriatum following transient forebrain ischemia. *Neuroscience* 131, 135–146. doi: 10.1016/j.neuroscience.2004.11.004

DeWitt, D. S., Jenkins, L. W., Wei, E. P., Lutz, H., Becker, D. P., and Kontos, H. A. (1986). Effects of fluid-percussion brain injury on regional cerebral blood flow and pial arteriolar diameter. *J. Neurosurg.* 64, 787–794. doi: 10.3171/jns.1986.64.5.0787

DeWitt, D. S., and Prough, D. S. (2003). Traumatic cerebral vascular injury: the effects of concussive brain injury on the cerebral vasculature. *J. Neurotrauma* 20, 795–825. doi: 10.1089/089771503322385755

Dietrich, W. D., Alonso, O., and Halley, M. (1994). Early microvascular and neuronal consequences of traumatic brain injury: a light and electron microscopic study in rats. *J. Neurotrauma* 11, 289–301. doi: 10.1089/neu.1994.11.289

Doshi, H., Wiseman, N., Liu, J., Wang, W., Welch, R. D., O'Neil, B. J., et al. (2015). Cerebral hemodynamic changes of mild traumatic brain injury at the acute stage. *PLoS ONE* 10:e0118061. doi: 10.1371/journal.pone.0118061

Drew, P. J., Blinder, P., Cauwenberghs, G., Shih, A. Y., and Kleinfeld, D. (2010a). Rapid determination of particle velocity from space-time images using the Radon transform. *J. Comput. Neurosci.* 29, 5–11. doi: 10.1007/s10827-009-0159-1

Drew, P. J., Shih, A. Y., Driscoll, J. D., Knutsen, P. M., Blinder, P., Davalos, D., et al. (2010b). Chronic optical access through a polished and reinforced thinned skull. *Nat. Methods* 7, 981–984. doi: 10.1038/nmeth.1530

Fehnel, C. R., Wendell, L. C., Potter, N. S., Klinge, P., and Thompson, B. B. (2014). Severe cerebral vasospasm after traumatic brain injury. *R I Med. J. (2013)* 97, 45–46.

Gabrielian, L., Willshire, L. W., Helps, S. C., van den Heuvel, C., Mathias, J., and Vink, R. (2011). Intracranial pressure changes following traumatic brain injury in rats: lack of significant change in the absence of mass lesions or hypoxia. *J. Neurotrauma* 28, 2103–2111. doi: 10.1089/neu.2011.1785

Garcia, J. H., Liu, K. F., Yoshida, Y., Chen, S., and Lian, J. (1994). Brain microvessels: factors altering their patency after the occlusion of a middle cerebral artery (Wistar rat). *Am. J. Pathol.* 145, 728–740.

Gattinoni, L., and Busana, M. (2019). Venous and arterial base excess difference: methodological error or physiological reality? *Intensive Care Med.* 45, 1686–1687. doi: 10.1007/s00134-019-05695-x

Golding, E. M., Robertson, C. S., and Bryan, R. M. Jr. (1999). The consequences of traumatic brain injury on cerebral blood flow and autoregulation: a review. *Clin. Exp. Hypertens.* 21, 299–332. doi: 10.3109/10641969909068668

Hall, A. A., Mendoza, M. I., Zhou, H., Shaughness, M., Maudlin-Jeronimo, E., McCarron, R. M., et al. (2017). Repeated low intensity blast exposure is associated with damaged endothelial glycocalyx and downstream behavioral deficits. *Front. Behav. Neurosci.* 11:104. doi: 10.3389/fnbeh.2017.00104

Hayward, N. M., Immonen, R., Tuunanen, P. I., Ndode-Ekane, X. E., Grohn, O., and Pitkanen, A. (2010). Association of chronic vascular changes with functional outcome after traumatic brain injury in rats. *J. Neurotrauma* 27, 2203–2219. doi: 10.1089/neu.2010.1448

Hayward, N. M., Tuunanen, P. I., Immonen, R., Ndode-Ekane, X. E., Pitkanen, A., and Grohn, O. (2011). Magnetic resonance imaging of regional hemodynamic and cerebrovascular recovery after lateral fluid-percussion brain injury in rats. *J. Cereb. Blood Flow Metab.* 31, 166–177. doi: 10.1038/jcbfm.2010.67

Huang, J. Y., Li, L. T., Wang, H., Liu, S. S., Lu, Y. M., Liao, M. H., et al. (2014). In vivo two-photon fluorescence microscopy reveals disturbed cerebral capillary blood flow and increased susceptibility to ischemic insults in diabetic mice. *CNS Neurosci. Ther.* 20, 816–822. doi: 10.1111/cns.12268

Ishikawa, M., Kajimura, M., Morikawa, T., Tsukada, K., Tsuji, T., Kusaka, G., et al. (2016). Cortical microcirculatory disturbance in the super acute phase of subarachnoid hemorrhage – In vivo analysis using two-photon laser scanning microscopy. *J. Neurol. Sci.* 368, 326–333. doi: 10.1016/j.jns.2016.06.067

Kane, M. J., Angoa-Perez, M., Briggs, D. I., Viano, D. C., Kreipke, C. W., and Kuhn, D. M. (2012). A mouse model of human repetitive mild traumatic brain injury. *J. Neurosci. Methods* 203, 41–49. doi: 10.1016/j.jneumeth.2011.09.003

Kawoos, U., Gu, M., Lankasky, J., McCarron, R. M., and Chavko, M. (2016). Effects of exposure to blast overpressure on intracranial pressure and blood-brain barrier permeability in a rat model. *PLoS ONE* 11:e0167510. doi: 10.1371/journal.pone.0167510

Kim, T. N., Goodwill, P. W., Chen, Y., Conolly, S. M., Schaffer, C. B., Liepmann, D., et al. (2012). Line-scanning particle image velocimetry: an optical approach for quantifying a wide range of blood flow speeds in live animals. *PLoS ONE* 7:e38590. doi: 10.1371/journal.pone.0038590

Kontos, H. A., Wei, E. P., and Povlishock, J. T. (1981). Pathophysiology of vascular consequences of experimental concussive brain injury. *Trans Am. Clin. Climatol. Assoc.* 92, 111–121.

Kramer, D. R., Winer, J. L., Pease, B. A., Amar, A. P., and Mack, W. J. (2013). Cerebral vasospasm in traumatic brain injury. *Neurol. Res. Int.* 2013:415813. doi: 10.1155/2013/415813

Lang, W., and Zander, R. (2002). The accuracy of calculated base excess in blood. *Clin. Chem. Lab. Med.* 40, 404–410. doi: 10.1515/CCLM.2002.065

Len, T. K., and Neary, J. P. (2011). Cerebrovascular pathophysiology following mild traumatic brain injury. *Clin. Physiol. Funct. Imaging* 31, 85–93. doi: 10.1111/j.1475-097X.2010.00990.x

Len, T. K., Neary, J. P., Asmundson, G. J., Goodman, D. G., Bjornson, B., and Bhambhani, Y. N. (2011). Cerebrovascular reactivity impairment after sport-induced concussion. *Med. Sci. Sports Exerc.* 43, 2241–2248. doi: 10.1249/MSS.0b013e3182249539

Levin, H. S., Mattis, S., Ruff, R. M., Eisenberg, H. M., Marshall, L. F., Tabaddor, K., et al. (1987). Neurobehavioral outcome following minor head injury: a three-center study. *J. Neurosurg.* 66, 234–243. doi: 10.3171/jns.1987.66.2.0234

Li, B., Esipova, T. V., Sencan, I., Kilic, K., Fu, B., Desjardins, M., et al. (2019). More homogeneous capillary flow and oxygenation in deeper cortical layers correlate with increased oxygen extraction. *Elife* 8:e42299. doi: 10.7554/eLife.42299

Lu, X., Moeini, M., Li, B., Lu, Y., Damseh, R., Pouliot, P., et al. (2019). A pilot study investigating changes in capillary hemodynamics and its modulation by exercise in the APP-PS1 alzheimer mouse model. *Front. Neurosci.* 13:1261. doi: 10.3389/fnins.2019.01261

Maeda, T., Katayama, Y., Kawamata, T., Aoyama, N., and Mori, T. (1997). Hemodynamic depression and microthrombosis in the peripheral areas of cortical contusion in the rat: role of platelet activating factor. *Acta Neurochir. Suppl.* 70, 102–105. doi: 10.1007/978-3-7091-6837-0_32

Margulies, S. (2000). The postconcussion syndrome after mild head trauma: is brain damage overdiagnosed? Part 1. *J. Clin. Neurosci.* 7, 400–408. doi: 10.1054/jocn.1999.0681

McCrory, P., Johnston, K., Meeuwisse, W., Aubry, M., Cantu, R., Dvorak, J., et al. (2005). Summary and agreement statement of the 2nd international conference on concussion in Sport, Prague 2004. *Clin. J. Sport Med.* 15, 48–55. doi: 10.1097/01.jsm.0000159931.77191.29

McCrory, P., Meeuwisse, W., Johnston, K., Dvorak, J., Aubry, M., Molloy, M., et al. (2009). Consensus statement on concussion in sport–the 3rd International Conference on concussion in sport, held in Zurich, November 2008. *J. Clin. Neurosci.* 16, 755–763. doi: 10.1016/j.jocn.2009.02.002

McQuire, J. C., Sutcliffe, J. C., and Coats, T. J. (1998). Early changes in middle cerebral artery blood flow velocity after head injury. *J. Neurosurg.* 89, 526–532. doi: 10.3171/jns.1998.89.4.0526

Mishra, A., Reynolds, J. P., Chen, Y., Gourine, A. V., Rusakov, D. A., and Attwell, D. (2016). Astrocytes mediate neurovascular signaling to capillary pericytes but not to arterioles. *Nat. Neurosci.* 19, 1619–1627. doi: 10.1038/nn.4428

Nortje, J., and Menon, D. K. (2004). Traumatic brain injury: physiology, mechanisms, and outcome. *Curr. Opin. Neurol.* 17, 711–718. doi: 10.1097/00019052-200412000-00011

Ogami, K., Dofredo, M., Moheet, A. M., and Lahiri, S. (2017). Early and severe symptomatic cerebral vasospasm after mild traumatic brain injury. *World Neurosurg.* 101, 813.e13–813.e14. doi: 10.1016/j.wneu.2017.03.039

Perrein, A., Petry, L., Reis, A., Baumann, A., Mertes, P., and Audibert, G. (2015). Cerebral vasospasm after traumatic brain injury: an update. *Minerva Anestesiol.* 81, 1219–1228.

Reid, W. M., Rolfe, A., Register, D., Levasseur, J. E., Churn, S. B., and Sun, D. (2010). Strain-related differences after experimental traumatic brain injury in rats. *J. Neurotrauma* 27, 1243–1253. doi: 10.1089/neu.2010.1270

Rosenblum, W. I., Wei, E. P., and Kontons, H. A. (1982). Platelet aggregation in cerebral arterioles after percussive brain trauma. *Tex Heart Inst. J.* 9, 345–348.

Schaffer, C. B., Friedman, B., Nishimura, N., Schroeder, L. F., Tsai, P. S., Ebner, F. F., et al. (2006). Two-photon imaging of cortical surface microvessels reveals a robust redistribution in blood flow after vascular occlusion. *PLoS Biol.* 4:e22. doi: 10.1371/journal.pbio.0040022

Shen, Y., Kou, Z., Kreipke, C. W., Petrov, T., Hu, J., and Haacke, E. M. (2007). In vivo measurement of tissue damage, oxygen saturation changes and blood flow changes after experimental traumatic brain injury in rats using susceptibility weighted imaging. *Magn. Reson. Imaging* 25, 219–227. doi: 10.1016/j.mri.2006.09.018

Shi, Y., Kim, S., Huff, T. B., Borgens, R. B., Park, K., Shi, R., et al. (2010). Effective repair of traumatically injured spinal cord by nanoscale block copolymer micelles. *Nat. Nanotechnol.* 5, 80–87. doi: 10.1038/nnano.2009.303

Shih, A. Y., Driscoll, J. D., Drew, P. J., Nishimura, N., Schaffer, C. B., and Kleinfeld, D. (2012a). Two-photon microscopy as a tool to study blood flow and neurovascular coupling in the rodent brain. *J. Cereb. Blood Flow Metab.* 32, 1277–1309. doi: 10.1038/jcbfm.2011.196

Shih, A. Y., Mateo, C., Drew, P. J., Tsai, P. S., and Kleinfeld, D. (2012b). A polished and reinforced thinned-skull window for long-term imaging of the mouse brain. *J. Vis. Exp.* 3742. doi: 10.3791/3742

Slupe, A. M., and Kirsch, J. R. (2018). Effects of anesthesia on cerebral blood flow, metabolism, and neuroprotection. *J. Cereb. Blood Flow Metab.* 38, 2192–2208. doi: 10.1177/0271678X18789273

Small, D. M., Sanchez, W. Y., Roy, S., Hickey, M. J., and Gobe, G. C. (2014). Multiphoton fluorescence microscopy of the live kidney in health and disease. *J. Biomed. Opt.* 19:020901. doi: 10.1117/1.JBO.19.2.020901

Stefanovic, B., Hutchinson, E., Yakovleva, V., Schram, V., Russell, J. T., Belluscio, L., et al. (2008). Functional reactivity of cerebral capillaries. *J. Cereb. Blood Flow Metab.* 28, 961–972. doi: 10.1038/sj.jcbfm.9600590

Stein, S. C., Graham, D. I., Chen, X. H., and Smith, D. H. (2004). Association between intravascular microthrombosis and cerebral ischemia in traumatic brain injury. *Neurosurgery* 54, 687–691;discussion691.

Sunwoo, J., Cornelius, N. R., Doerschuk, P. C., and Schaffer, C. B. (2011). Estimating brain microvascular blood flows from partial two-photon microscopy data by computation with a circuit model. *Conf. Proc. IEEE Eng. Med. Biol. Soc.* 2011, 174–177. doi: 10.1109/IEMBS.2011.6089922

Thomale, U. W., Kroppenstedt, S. N., Beyer, T. F., Schaser, K. D., Unterberg, A. W., and Stover, J. F. (2002). Temporal profile of cortical perfusion and microcirculation after controlled cortical impact injury in rats. *J. Neurotrauma* 19, 403–413. doi: 10.1089/08977150252932361

Villalba, N., Sonkusare, S. K., Longden, T. A., Tran, T. L., Sackheim, A. M., Nelson, M. T., et al. (2014). Traumatic brain injury disrupts cerebrovascular tone through endothelial inducible nitric oxide synthase expression and nitric oxide gain of function. *J. Am. Heart Assoc.* 3, e001474. doi: 10.1161/JAHA.114.001474

Wang, Y., Nelson, L. D., LaRoche, A. A., Pfaller, A. Y., Nencka, A. S., Koch, K. M., et al. (2016). Cerebral blood flow alterations in acute sport-related concussion. *J. Neurotrauma* 33, 1227–1236. doi: 10.1089/neu.2015.4072

Wang, Y., Nencka, A. S., Meier, T. B., Guskiewicz, K., Mihalik, J. P., Alison Brooks, M., et al. (2018). Cerebral blood flow in acute concussion: preliminary ASL findings from the NCAA-DoD CARE consortium. *Brain Imaging Behav.* 13, 1375–1385. doi: 10.1007/s11682-018-9946-5

Wei, E. P., Dietrich, W. D., Povlishock, J. T., Navari, R. M., and Kontos, H. A. (1980). Functional, morphological, and metabolic abnormalities of the cerebral microcirculation after concussive brain injury in cats. *Circ Res.* 46, 37–47. doi: 10.1161/01.res.46.1.37

Wei, E. P., Hamm, R. J., Baranova, A. I., and Povlishock, J. T. (2009). The long-term microvascular and behavioral consequences of experimental traumatic brain injury after hypothermic intervention. *J. Neurotrauma* 26, 527–537. doi: 10.1089/neu.2008.0797

Wei, E. P., Kontos, H. A., Dietrich, W. D., Povlishock, J. T., and Ellis, E. F. (1981). Inhibition by free radical scavengers and by cyclooxygenase inhibitors of pial arteriolar abnormalities from concussive brain injury in cats. *Circ Res.* 48, 95–103. doi: 10.1161/01.res.48.1.95

Wei, H. S., Kang, H., Rasheed, I. D., Zhou, S., Lou, N., Gershteyn, A., et al. (2016). Erythrocytes Are Oxygen-Sensing Regulators of the Cerebral Microcirculation. *Neuron* 91, 851–862. doi: 10.1016/j.neuron.2016.07.016

Werner, C., and Engelhard, K. (2007). Pathophysiology of traumatic brain injury. *Br. J. Anaesth.* 99, 4–9. doi: 10.1093/bja/aem131

Xiong, W., Ping, X., Ripsch, M. S., Chavez, G. S. C., Hannon, H. E., Jiang, K., et al. (2017). Enhancing excitatory activity of somatosensory cortex alleviates neuropathic pain through regulating homeostatic plasticity. *Sci. Rep.* 7:12743.

Zhao, Z., Wang, M., Tian, Y., Hilton, T., Salsbery, B., Zhou, E. Z., et al. (2016). Cardiolipin-mediated procoagulant activity of mitochondria contributes to traumatic brain injury-associated coagulopathy in mice. *Blood* 127, 2763–2772. doi: 10.1182/blood-2015-12-688838

Zweckberger, K., Simunovic, F., Kiening, K. L., Unterberg, A. W., and Sakowitz, O. W. (2010). Anticonvulsive effects of the dopamine agonist lisuride maleate after experimental traumatic brain injury. *Neurosci. Lett.* 470, 150–154. doi: 10.1016/j.neulet.2009.12.075

Conflict of Interest: The authors declare that the research was conducted in the absence of any commercial or financial relationships that could be construed as a potential conflict of interest.

Copyright © 2020 Han, Chai, Ping, Song, Ma, Ruan and Jin. This is an open-access article distributed under the terms of the Creative Commons Attribution License (CC BY). The use, distribution or reproduction in other forums is permitted, provided the original author(s) and the copyright owner(s) are credited and that the original publication in this journal is cited, in accordance with accepted academic practice. No use, distribution or reproduction is permitted which does not comply with these terms.

frontiers in Aging Neuroscience

ORIGINAL RESEARCH
published: 10 March 2020
doi: 10.3389/fnagi.2020.00054

Hypoxia-Inducible Factor 1α and 2α Have Beneficial Effects in Remote Ischemic Preconditioning Against Stroke by Modulating Inflammatory Responses in Aged Rats

Xiangnan Du[1†], Jian Yang[2†], Cuiying Liu[2], Sainan Wang[2], Chencheng Zhang[2], Heng Zhao[3], Huishan Du[1] and Xiaokun Geng[1,2]**

[1]Department of Neurology, Beijing Luhe Hospital, Capital Medical University, Beijing, China, [2]China-America Institute of Neuroscience, Department of Neurology, Beijing Luhe Hospital, Capital Medical University, Beijing, China, [3]Department of Neurosurgery, School of Medicine, Stanford University, Stanford, CA, United States

OPEN ACCESS

Edited by:
Piotr Walczak,
Johns Hopkins Medicine,
United States

Reviewed by:
Carsten Culmsee,
University of Marburg, Germany
Ana I. Duarte,
University of Coimbra, Portugal

***Correspondence:**
Huishan Du
dhs13106@126.com
Xiaokun Geng
xgeng@ccmu.edu.cn

†These authors have contributed equally to this work

Received: 12 September 2019
Accepted: 18 February 2020
Published: 10 March 2020

Citation:
Du X, Yang J, Liu C, Wang S, Zhang C, Zhao H, Du H and Geng X (2020) Hypoxia-Inducible Factor 1α and 2α Have Beneficial Effects in Remote Ischemic Preconditioning Against Stroke by Modulating Inflammatory Responses in Aged Rats. Front. Aging Neurosci. 12:54. doi: 10.3389/fnagi.2020.00054

Limb remote ischemic preconditioning (RIPC) has been proven to alleviate stroke injury in young rats, but its protective effect and its mechanism in aged rats are still unclear. Hypoxia-inducible factor (HIF) is one of the important markers of stroke, and its high expression plays an important role in the pathogenesis of stroke. In this study, we tested the hypothesis that RIPC could regulate the expression of HIF, leading to reduced inflammatory responses in aged rats. Stroke was induced by transient middle cerebral artery occlusion (MCAo) in aged rats, and RIPC was conducted in both hind limbs. The HIF-1α and HIF-2α mRNA and protein were examined by real-time RT-PCR and western blotting (WB). Inflammatory cytokines in the peripheral blood and brain were measured using AimPlex multiplex immunoassays. The protein levels of p-Akt, Akt, p-ERK, and ERK were examined by WB. We investigated that RIPC reduced the infarct size, improved neurological functions, and decreased the expression of HIF-1α and HIF-2α in the ischemic brain. RIPC reduced the levels of IL-1β, IL-6 and IFN-γ in the peripheral blood and the levels of IL-1β and IFN-γ in the ischemic brain 48 h post-stroke. Moreover, intraperitoneal injection of the HIF inhibitor, acriflavine hydrochloride (ACF), abolished the protection of RIPC with respect to infarct size and neurological functions and neutralized the downregulation of pro-inflammatory IL-1β, IL-6 and IFN-γ. ACF also reversed the activation of the Akt signaling pathway induced by RIPC following stroke. HIF may play a key role in RIPC, which was likely mediated by the Akt signaling pathway and systemic modulation of the inflammatory response in aged rats.

Keywords: cerebral ischemia, remote ischemic preconditioning, hypoxia-inducible factor, Akt signaling pathway, inflammatory cytokines

INTRODUCTION

Ischemic stroke is considered to be the third most lethal and disabling disease in the world. Aging, above all risk factors of stroke, accounts for a large proportion of stroke-related mortality (Mozaffarian et al., 2015). According to the World Health Organization (WHO) statistics, twelve million people will suffer from stroke in the coming decade (Krishnamurthi et al., 2013). At present, however, no alternative neuroprotective agent has been approved by the FDA except for thrombolytic recombinant tissue plasminogen activator (tPA), which is only administrated to a small number of patients. Given the increase of the senior citizen and the aggravating of the associated stroke burden, it is urgent to find effective treatments for this disease. In recent years, remote ischemic preconditioning (RIPC) has become a feasible therapeutic strategy for stroke and has been proven to provide a protective effect on young experimental animals (Wei et al., 2012; Liu et al., 2016; Yang et al., 2018) and in clinical trials (Mi et al., 2016; Zhao S. C. et al., 2017). Nevertheless, its protective effect and its mechanism in the elderlies are still unclear.

Age is an important risk factor for pre-clinical studies on ischemic stroke, which has been largely overlooked. Previous studies have suggested that aged rats, compared with younger ones, represent a more clinically relevant model of ischemic stroke (Mayhan et al., 2008; Modrick et al., 2009). Advanced age increases the expression of immune cells including T cells, neutrophils, macrophages, and dendritic cells in middle cerebral artery occlusion (MCAo) mice, which may be responsible for the exacerbated behavioral deficits in the aged (Manwani et al., 2013). Age also stimulates the activation of macrophages and the expression of inflammatory cytokines in MCAo mice (Zhao S. C. et al., 2017). Although most experimental stroke studies have been conducted on healthy young animals, accumulating evidence points to age-related differences in gene expression and cytokine production (Kuzumaki et al., 2010; Semple et al., 2013; Orre et al., 2014; Suenaga et al., 2015); thus, applying aged animals as models may increase the clinical relevance of the experimental results.

Hypoxia-inducible factor (HIF) is the most crucial regulator of oxygen balance in mammals, and it has been shown to promote tolerance to acute ischemia (Semenza, 2012). HIF-1α and HIF-2α, as the HIF-α subunits, combine with HIF-β to regulate target gene transcription under hypoxic conditions. They share 48% identical DNA binding regions in structure, but each has its own unique biological effects. HIF can easily degrade under normal oxygen conditions within 5 min, while under hypoxia, its stability and transcriptional activity are significantly increased, which induces the expression of its downstream target genes. Because of its particularity of function, HIF is critically related to ischemic stroke (Sharp and Bernaudin, 2004; Ogle et al., 2012). Previous studies showed that suppressing the expression of basal HIF-2α, but not that of HIF-1α, was sufficient to accelerate cell death in nerve growth factor (NGF)-stimulated neurons (Lomb et al., 2009). In addition, the HIF-α subunits HIF-1α, HIF-2α and HIF-3α can be regulated by the phosphoinositide 3-kinase (PI3K) pathway in the brain of MCAo rats (Wei et al., 2017). The interaction between RIPC and HIF has been explored by some studies, where HIF was required for RIPC in protecting heart function in young animal models (Cai et al., 2013; Martin-Puig et al., 2015). Our previous study showed that HIF-1α was indispensable for RIPC against stroke by modulating inflammation in a young rat model of MCAo. Accumulating data provide indications for the roles of HIF-α in neuroprotection of RIPC against ischemia, but there is still a lack of solid evidence of its involvement in an aged model of stroke with RIPC.

After a stroke, systemic inflammation contributes to brain injury, as neuroinflammation occurs not only in the brain but also in the peripheral organs (Nguyen et al., 2016; Shim and Wong, 2016; Yamashiro et al., 2017). RIPC could reduce neuroinflammation in ischemic stroke through modulating the upregulated expression of HIF-1α (Yang et al., 2018), improving the peripheral immune cell response (Liu et al., 2016), activating the adenosine A1 receptor and affecting redox status (Hu et al., 2012), and changing the activation of signaling pathways such as Akt and ERK. All of these findings have focused on young animal models, whereas whether RIPC can regulate neuroinflammation in aged animals remains unclear.

In this study, we aimed to provide insights into the roles of HIF-1α and HIF-2α in RIPC protection in aged stroke rats and explore the regulatory mechanism of inflammatory cytokines. First, we defined the protection of RIPC on aged MCAo rats. Then, we tested the expression of HIF-1α and HIF-2α in penumbra tissue and measured the levels of multiple inflammatory cytokines in the peripheral blood and brain. Furthermore, we used the HIF inhibitor, acriflavine hydrochloride (ACF), to determine the role of HIF in modulating the protective effects of RIPC against stroke. Finally, we studied the activation of the Akt and ERK signaling pathways in this process.

MATERIALS AND METHODS

All procedures in this study were conducted according to ethical standards and in accordance with the Declaration of Helsinki and with national and international guidelines and have been approved by the authors' institutional review board. Male Sprague–Dawley (SD) rats, age-matched 19–20 months, were purchased from Vital River Laboratory Animal Technology Company Limited (Beijing, China). They were housed in a controlled room at a temperature of 24°C with a standard 12-h light/dark cycle, had free access to food and water and were randomly distributed into different groups. The number of animals in each group was 6–8.

Middle Cerebral Artery Occlusion (MCAo)

Most pre-clinical stroke studies exclusively examined the response to stroke in young male animals. This is in part due to the difficulty of performing the surgeries, the high costs, and the poor survival rates in aged animals. In our experiment, rats were anesthetized with 3–5% isoflurane in 70% nitrous oxide and 30% oxygen and then maintained with 1–3% isoflurane. For the MCAo model, ischemia and reperfusion were established as previously described (Ren et al., 2011; Yang et al., 2018). As the aged rat weight was higher than that of younger ones, we chose

a silica gel-coated nylon suture that was appropriate for rats up 450 g. The suture was withdrawn after 90 min of occlusion to allow for the re-opening of the MCA. Rat rectal temperature was maintained at 37 ± 0.5°C during the entire procedure. The cerebral blood flow (CBF) during the surgery before and after occlusion were measured by laser Doppler perfusion monitoring with a laser Doppler probe (PeriFlux System 5000, Perimed AB, Sweden) interfaced to a laptop equipped with the PeriSoft data acquisition software (PeriSoft Systems, Inc., Sweden) as previously described (Chen et al., 2018). The blood gas ($PaCO_2$, PaO_2 [mmHg] and pH) and blood sugar (mmol/L) were also examined during the surgery. The rats in the sham group were subjected to the surgical procedure without MCA occlusion.

Remote Ischemic Preconditioning (RIPC)

RIPC was established as previously described (Yang et al., 2018). Briefly, 24 h before MCAo, RIPC was conducted on both hind limbs of rats anesthetized with 1–3% isoflurane by non-invasive occlusion of hind limb blood flow with a gauge bandage, in contrast to an invasive, direct femoral artery occlusion. The two hind limbs were simultaneously tied with a bandage to occlude blood circulation for 10 min and then released for 10 min to allow for reperfusion. The occlusion/reperfusion cycle was repeated three times.

Behavioral Testing

Behavioral tests were conducted as described previously (Zhao et al., 2005; Yang et al., 2018). The behavioral tests were conducted to evaluate neurological functions after stroke in aged rats, including the tail hang test, home cage, and postural reflex. All behavioral tests were performed by a person who was blinded to the experimental conditions. We handled the rats for 3 days before surgery and tested their baseline on the day before surgery. All behavioral tests were then conducted 48 h after stroke onset.

For the tail hang test, the rat was hung by its tail approximately 10 cm above the floor. Stroke rats will turn to the contralateral side (left) of the ischemic hemisphere, and a head-turn of more than 90° was counted. Each time the rat was hung for no more than 5 s and each rat was hung for a total of 20 times. The percentage of head turns was calculated.

For the home cage limb test, the rat uses its forelimbs to explore the cage edge, and we counted the number of the times the ipsilateral, contralateral or both forelimbs touched the cage wall. A total of 20 contacts were recorded. The percentage of times that the ipsilateral forelimb was used was calculated using the formula: [ipsilateral + (both/2)] × 100%.

In the postural reflex test, the rat was placed on a table, its tail was held by one hand and the other hand was used to push its shoulder by nearly 20 cm three times. Non-ischemic rats gripped the table vigorously during the push, which was given a 0 score. A rat that showed less resistance and become stiff during the push was given a 1 score. A score of 2 was given if the rat had no resistance.

We also measured neurological deficits to evaluate stroke outcomes at 48 h after reperfusion using the method of the Longa scoring system, in which the scores were based on the following criteria: 0 = no deficit, 1 = failure to extend the left forepaw, 2 = circling to the left, 3 = falling to the left, 4 = failure to walk spontaneously and loss of consciousness, 5 = death.

Drug Injections

To study the role of HIF in RIPC, a HIF inhibitor was used. Acriflavine hydrochloride (ACF, A8251, Sigma) was dissolved in phosphate-buffered saline (PBS), adjusted to a concentration of 2 mmol/L with additional PBS, and stored at 4°C. The ACF solution was given by intraperitoneal injection at a dose of 1.5 mg/kg, 24 h before stroke onset and every 24 h thereafter until euthanized (Ogle et al., 2012; Yang et al., 2018).

Infarct Size Measurement

2,3,5-triphenyl-2H-tetrazolium chloride (TTC) staining was used for measuring the infarct size 48 h after reperfusion when the animals were euthanized. The non-ischemic hemisphere and the non-ischemic region in the ischemic hemisphere were measured, from which the infarct size was calculated according to the following formula: [(area of the non-ischemic hemisphere—area of the non-ischemic region in the ischemic hemisphere)/area of the non-ischemic hemisphere] × 100%. The detailed protocol has been described previously (Ren et al., 2009; Yang et al., 2018).

Quantitative RT-PCR Analysis

To measure HIF-1α and HIF-2α mRNA expression, total RNA was isolated from the cortical penumbra, which was collected on ice and stored at −80°C immediately after the animals were euthanized. RNA was extracted with TRIzol reagent (Cat# 15596-026, Life Technologies, Carlsbad, CA, USA) according to the manufacturer's instructions. The purified RNA was then reverse-transcribed into cDNA using the Reverse Transcription System (Cat# E6300S, New England BioLabs® Inc., Ipswich, MA, USA). Quantitative RT-PCR analysis of the mRNA level of HIF-1α (HIF-1α F, GATGAATCAAAAGCAGTGACGAAGG, HIF-1α R, ATGCCTTAGCAGTGGTCATTTCTTG; HIF-2α F, ATCT TCCAGCCGCTCACC, HIF-2α R, GCCCACAGACCACTTCG TA) was performed using the SYBR Green Prime Script kit (RR420A, TAKARA). GAPDH (GAPDH F, TTCCTACCCCC AATGTATCCG; GAPDH R, CCACCCTGTTGCTGTAGCCAT A) was chosen as the housekeeping gene. The real-time PCR program steps were: 95°C for 5 min, 45 cycles at 95°C for 5 s, 60°C for 5 s, and 72°C for 10 s, followed by 72°C for 1 min.

Western Blotting

The cortical penumbra was collected on ice and stored at −80°C immediately after the animals were euthanized. Protein extractions were prepared with lysis buffer (50 mM Tris-HCl, pH 7.4, 150 mM NaCl, 5 mM EDTA, 0.5% NP-40, 0.1% Triton X-100, 0.1% SDS, 1 mM PMSF, 1× protein inhibitor mix Complete Mini). Then, 20 mg of protein per lane were separated by 10% polyacrylamide gel electrophoresis and transferred to nitrocellulose membranes for 2 h. The membranes were blocked with 5% skimmed milk for 1 h and then incubated overnight at 4°C with the primary antibody. Membranes were washed with TBST and incubated with the secondary antibody for 1 h. The signal was visualized by enhanced chemiluminescence. The primary antibodies used were

anti-GAPDH (1:1000; Cat# 5174, Cell Signaling Technology, Inc., Danvers, MA, USA), anti-HIF-1α (1:1000; Cat# 14179, Cell Signaling Technology, Inc., Danvers, MA, USA), anti-HIF-2α (1:500; ab199, Abcam, Cambridge, MA, USA), anti-Akt (1:1,000, Cat# 4691, Cell Signaling Technology, Inc., Danvers, MA, USA), anti-p-Akt (1:1,000, Ser473, Cat# 4060, Cell Signaling Technology, Inc., Danvers, MA, USA), anti-ERK (1:1,000, Cat# 4695, Cell Signaling Technology, Inc., Danvers, MA, USA), and anti-p-ERK (1:1,000, Cat# 4370, Cell Signaling Technology, Inc., Danvers, MA, USA).

AimPlex Multiplex Immunoassays

Peripheral blood and penumbra tissue were collected from the heart and the cortex of the ischemic brain, and an AimPlex rat inflammation assay kit (Beijing Quantobio, China) was used to detect multiple inflammatory cytokines in these samples. Six cytokines: IL-1β, IL-6, TNFα, IFN-γ, IL-4 and IL-10 were measured. The procedure was conducted according to the manufacturer's instructions and as discussed previously (Yang et al., 2018). Briefly, 45 μl of capture bead working suspension and a 45 μl sample were sequentially shaken 750 times per minute for 60 min in the dark, followed by three washings in 100 μl washing buffer. The biotin-conjugated antibodies (25 μl) were added and the wells were sealed and shaken for 30 min in the dark. After washing three times with washing buffer, streptavidin-PE was added and they were shaken for 20 min in the dark. Finally, 100–200 μl 1 × Reading buffer was added to each well and the fluorescence signals of the samples were acquired using a flow cytometer (NovoCyte, ACEA Biosciences, Inc., San Diego, CA, USA), and the levels of the inflammatory factors were analyzed with FCAP Array 3.0 software.

Statistical Analysis

Statistical analysis was performed using Prism 6 (GraphPad Software, Inc., La Jolla, CA, USA). Values are presented as means ± SEM. Differences between experimental groups were analyzed by Student's *t*-test or one-way ANOVA with Newman-Keuls Multiple Comparison test as a *post hoc* test. A value of $P < 0.05$ was considered statistically significant. Before statistical analysis, data were checked for the Gaussian distribution and fitted the normal distribution.

RESULTS

RIPC Protected Against Stroke in Aging Rats

In the previous study, we confirmed that RIPC was neuroprotective in young rats. In the current study, we used the same method we have used previously to detect the neuroprotective ability of RIPC in aged rats. The TTC staining results showed that RIPC induced a 34.64% significantly reduction of infarct size from 38.85 ± 1.15% to 25.39 ± 1.12% compared with MCAo (**Figure 1A** and

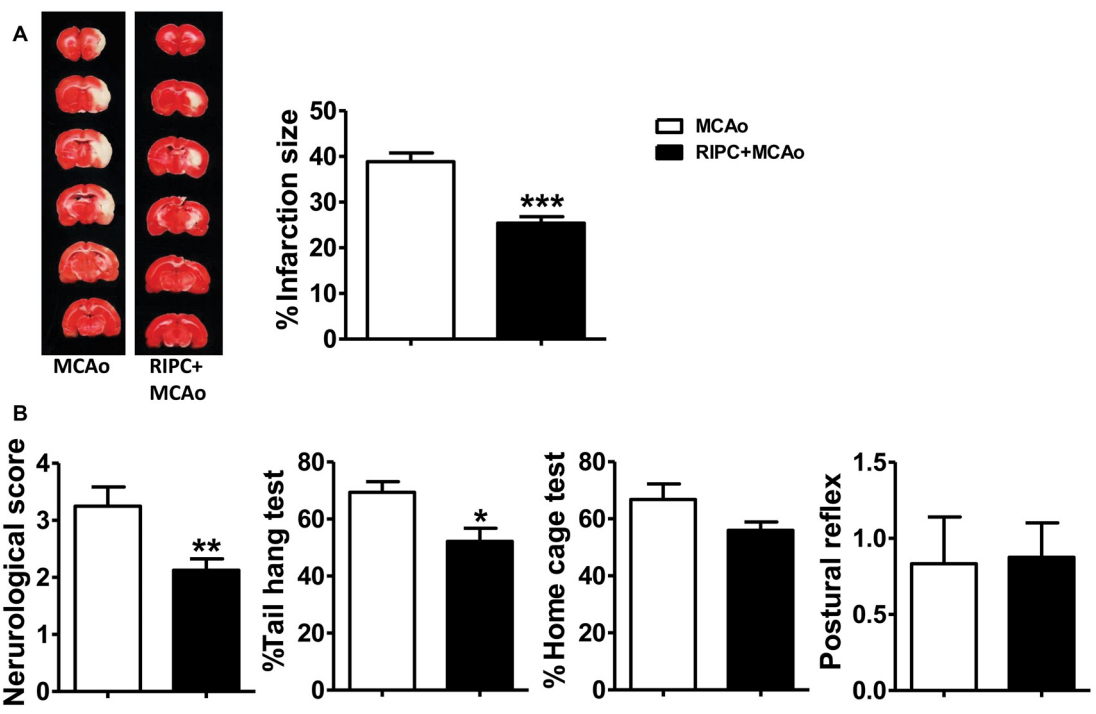

FIGURE 1 | Remote ischemic preconditioning (RIPC) reduced infarct size and improved neurological function and the behavioral test after stroke in aged rats. **(A)** Representative images and infarct volume of 2,3,5-triphenyl-2H-tetrazolium chloride (TTC) staining in the MCAo and RIPC+MCAo group in aged rats. **(B)** Neurological score and behavior tests. Statistical analysis was performed by ANOVA. *,**,*** vs. MCAo, $p < 0.05$, 0.01, 0.001, respectively (N = 8–10 per group). MCAo, middle cerebral artery occlusion; RIPC, remote ischemic preconditioning.

Supplementary Figure S2), attenuated neurological scores (**Figure 1B**), and improved behavioral performance in the tail hang test (**Figure 1B**). Although there was no significant difference in the home cage test, RIPC showed a trend towards the promotion of functional recovery in aged rats. There was no significant difference in the postural reflex test (**Figure 1B**). Meanwhile, CBF detected during MCAo surgery had no change between MCAo and RIPC+MCAo group. It was reduced by nearly 80% of baseline during ischemia and reestablished to 78% of baseline following reperfusion (**Supplementary Figure S1**). There were no differences in blood gas and blood sugar between groups, either (**Supplementary Tables S1**, **S2**). These findings confirm that RIPC triggers structural and functional protection against stroke in aged rats.

RIPC Decreased the Expression of HIF in the Ischemic Brain at 48 h Post-stroke

To test whether RIPC could regulate the expression of HIF-1α and HIF-2α in the ischemic tissue in aged rats, we measured HIF-1α and HIF-2α mRNA and protein levels in the penumbra tissue. The real-time RT-PCR results showed that mRNA expression of HIF-1α and HIF-2α were more than 3-fold upregulated 48 h post-stroke in the ischemic brain (**Figure 2A**), whereas RIPC decreased nearly 50% of HIF-1α and 60% of HIF-2α mRNA expression (**Figure 2A**). Similarly, the western blotting (WB) results (**Figure 2B**) and the statistical data showed that RIPC attenuated the protein expression of HIF-1α and HIF-2α in the ischemic brain 48 h post-stroke (**Figure 2B**).

RIPC Downregulated Pro-inflammatory Factors in the Peripheral Blood and Brain

To test if the inflammatory status were regulated by RIPC in aged rats after MCAo, we measured the effect of RIPC on the protein levels of the anti-inflammatory cytokines, IL-4 and IL-10, and that of the pro-inflammatory cytokines, IL-1β, IL-6, TNFα and IFN-γ in the peripheral blood and brain tissue. The results showed that MCAo increased the levels of pro-inflammatory cytokines while RIPC significantly decreased the levels of pro-inflammatory IL-1β, IL-6 and IFN-γ in the peripheral blood (**Figure 3A**) and that of IL-1β and IFN-γ in penumbra tissue (**Figure 3B**) 48 h post-stroke in aged rats. Taken together, these results suggest that RIPC reverses the increase

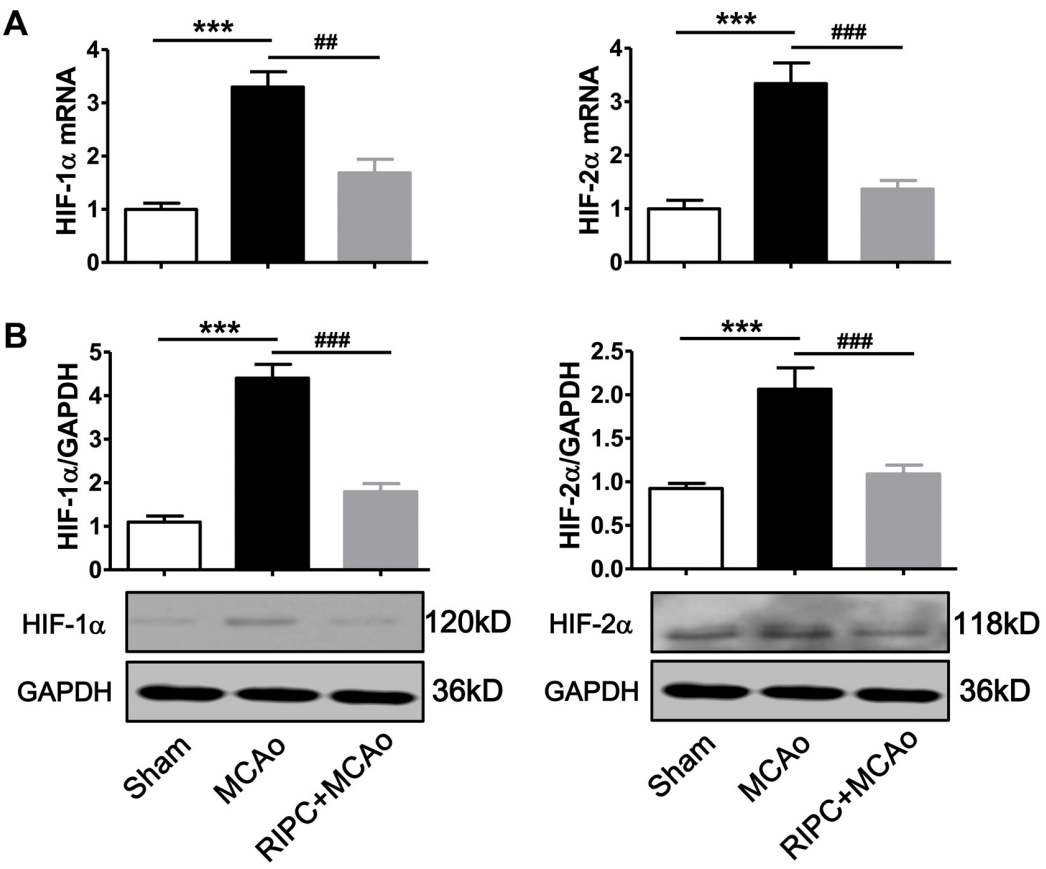

FIGURE 2 | The expression of HIF-1α and HIF-2α in penumbra tissues. **(A)** The mRNA level of HIF-1α and HIF-2α was assessed by real-time RT-PCR. **(B)** Statistical data and representative images of western blot of HIF-1α and HIF-2α protein levels in penumbra tissues in the Sham, MCAo and RIPC+MCAo group. (N = 5–6 per group) Statistical analysis was performed by ANOVA. *** vs. Sham, $p < 0.001$, ##,### vs. MCAo, $p < 0.01$, 0.001, respectively.

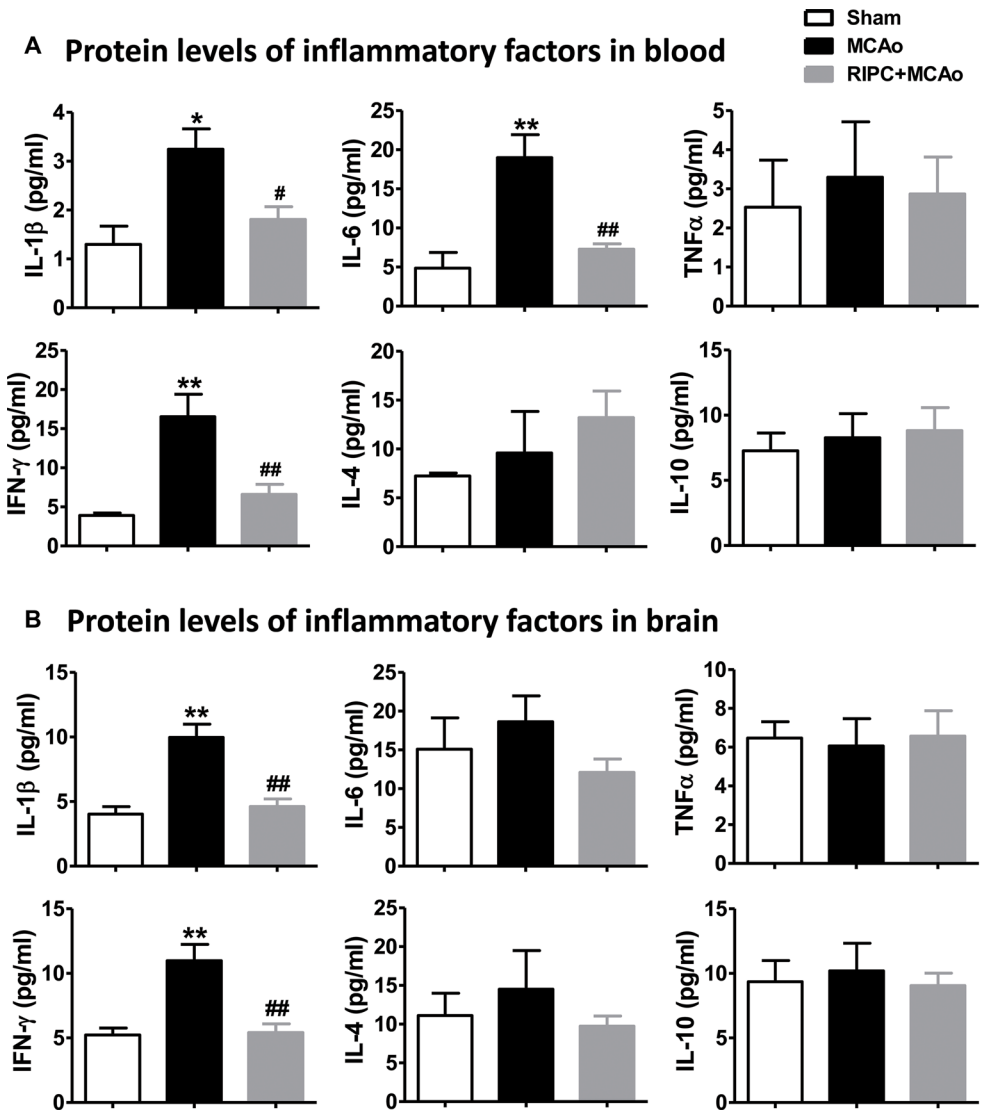

FIGURE 3 | The effects of RIPC on inflammatory cytokines in the peripheral blood and brain. **(A)** Protein levels of the pro-inflammatory cytokines IL-1β, IL-6, TNFα and IFN-γ and anti-inflammatory cytokines IL-4 and IL-10, respectively, in the peripheral blood. A total of three groups were evaluated: Sham, MCAo, RIPC+MCAo. **(B)** Protein levels of IL-1β, IL-6, TNFα IFN-γ IL-4 and IL-10, in the ischemic brain. All samples were collected 48 h after stroke (N = 5–6 per group). *,** vs. Sham, $p < 0.05$, 0.01, $^{\#,\#\#}$ vs. MCAo, $p < 0.05$, 0.01, respectively.

in HIF expression caused by stroke and improves the level of inflammation in the ischemic and peripheral areas.

HIF Inhibition Abolished the Protection of RIPC

If HIF was necessary for the brain protection of RIPC in aged rats, inhibiting HIF activity would contribute to brain injuries induced by stroke. TTC staining results showed that the HIF inhibitor, ACF, abolished the protection of RIPC which ACF induced a 27.02% increase of the infarct size from 25.39 ± 1.12% to 32.25 ± 1.65% compared with RIPC (**Figure 4A** and **Supplementary Figure S2**). In addition, ACF also abolished the protective effects of RIPC as measured by neurological scores and behavioral performance including the tail hang test (**Figure 4B**). The initial decrease in CBF during ischemia and the restoration of CBF during reperfusion, the changes between groups were similar. Blood gas and blood sugar values had no differences between groups (**Supplementary Figure S1** and **Supplementary Tables S1**, **S2**).

HIF Inhibition Neutralized the Downregulation of Inflammatory Cytokines Induced by RIPC

After examining the antagonistic effect of the HIF inhibitor with RIPC on brain injury, we further assessed its effect on inflammatory factors in aged rats. The results of the

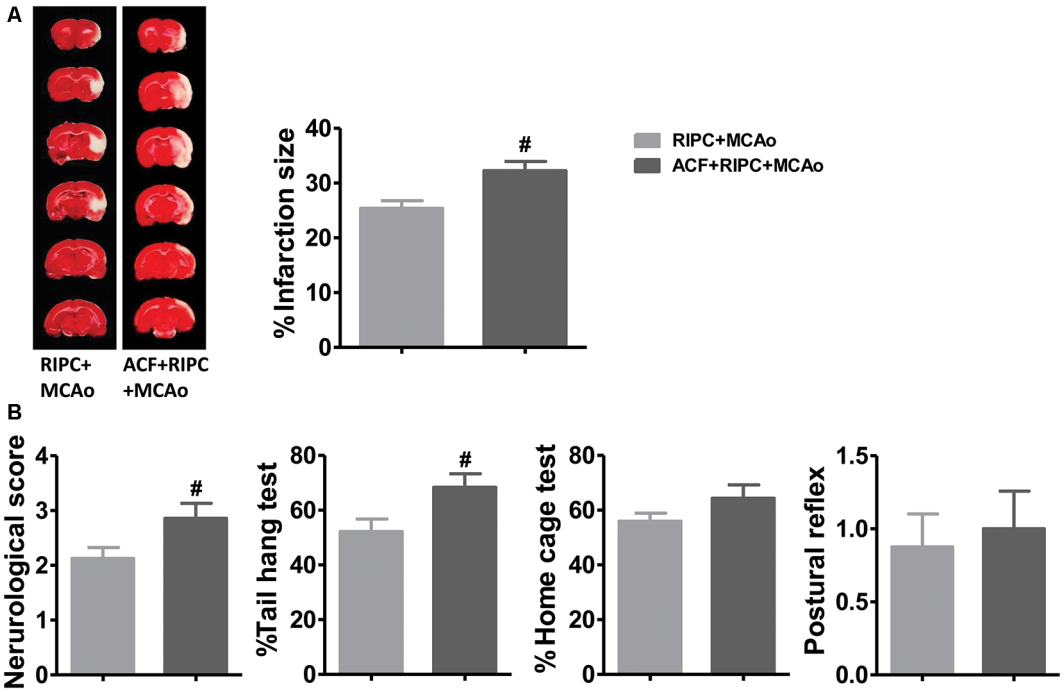

FIGURE 4 | The effects of hypoxia-inducible factor (HIF) antagonist ACF on stroke outcomes in aged stroke animals treated with RIPC. **(A)** Representative images of TTC staining and the statistical results of infarct volume in the RIPC+MCAo and ACF+RIPC+MCAo group in aged rats. **(B)** Neurological score and behavioral tests of the tail hang test, home cage test, and postural reflex test (N = 8–10 per group). $^{\#}P < 0.05$, vs. RIPC+MCAo. ACF, acriflavine hydrochloride, HIF inhibitor.

AimPlex multiplex immunoassays showed that in the peripheral blood, the HIF inhibitor ACF had an antagonist effect on IL-6 and IFN-γ (**Figure 5A**). ACF+RIPC+MCAo increased the expression of IL-6 and IFN-γ at the protein level compared with the RIPC+MCAo group. In addition, ACF had an antagonist effect on IL-1β and IFN-γ in the brain (**Figure 5B**). These results suggest that inhibition of HIF abolished the structural and functional protection of RIPC and neutralized the downregulation of inflammatory responses.

RIPC Activated the Akt Signaling Pathway, While ACF Abolished It

Several studies have demonstrated that under ischemic conditions, the activation of the PI3k/Akt or EKR signaling pathway can be regulated by the expression of HIF, and signaling pathway activation can regulate inflammatory responses. We, therefore, investigated whether the Akt or ERK signaling pathway was involved in the action of RIPC to inhibit cerebral inflammation. Penumbra tissue was collected from the cortex of the ischemic brain. The results showed that the ratios of p-Akt/Akt (**Figure 6A**) and p-ERK/ERK (**Figure 6B**) were decreased 48 h post-stroke, whereas RIPC upregulated the expression of p-Akt not p-ERK (**Figure 6**). RIPC had no effect on the total expression of Akt and ERK. Moreover, ACF decreased the ratios of both p-Akt/Akt and p-ERK/ERK (**Figure 6**). These collective findings suggest that RIPC reverses the reduced expression of p-Akt following a stroke, while inhibition of HIF abolishes the reversion.

DISCUSSION

In the current study, first, we demonstrated that RIPC reduced the infarction size and improved neurological function in aged rats. Second, RIPC has been shown to decrease the expression of HIF-1α and HIF-2α in the ischemic brain and to decrease the protein levels of pro-inflammatory cytokines IL-1β and IFN-γ in both the blood and brain 48 h post-stroke. Third, the HIF-1α inhibitor, ACF, abolished the protective effects of RIPC on infarction and neurological function. Additionally, ACF inhibited the downregulation of pro-inflammatory factors induced by RIPC, including IL-6 and IFN-γ in blood and IL-1β and IFN-γ in the brain. Fourth, RIPC increased the ratio of p-Akt to total Akt, while ACF abolished the activation of the Akt signaling pathway in the brain. Collectively, these data showed that HIF-1α and HIF-2α played key roles in the protective effect of RIPC by modulating inflammatory responses likely mediated by the Akt signaling pathway in the brain and peripheral blood circulation in aged rats.

The success of most stroke models has not been well transformed into clinical practice. One potential reason for this failure is that stroke predominantly afflicts the elderly. Aging is a very important factor in stroke, and it has been found that there are many differences in stroke models between young and old animals such as infarction size, behavior, and expression and distribution of immune cells (Kuzumaki et al., 2010; Manwani et al., 2013; Orre et al., 2014; Zhao W. B. et al., 2017). In the previous study, we demonstrated that HIF-1α played a critical

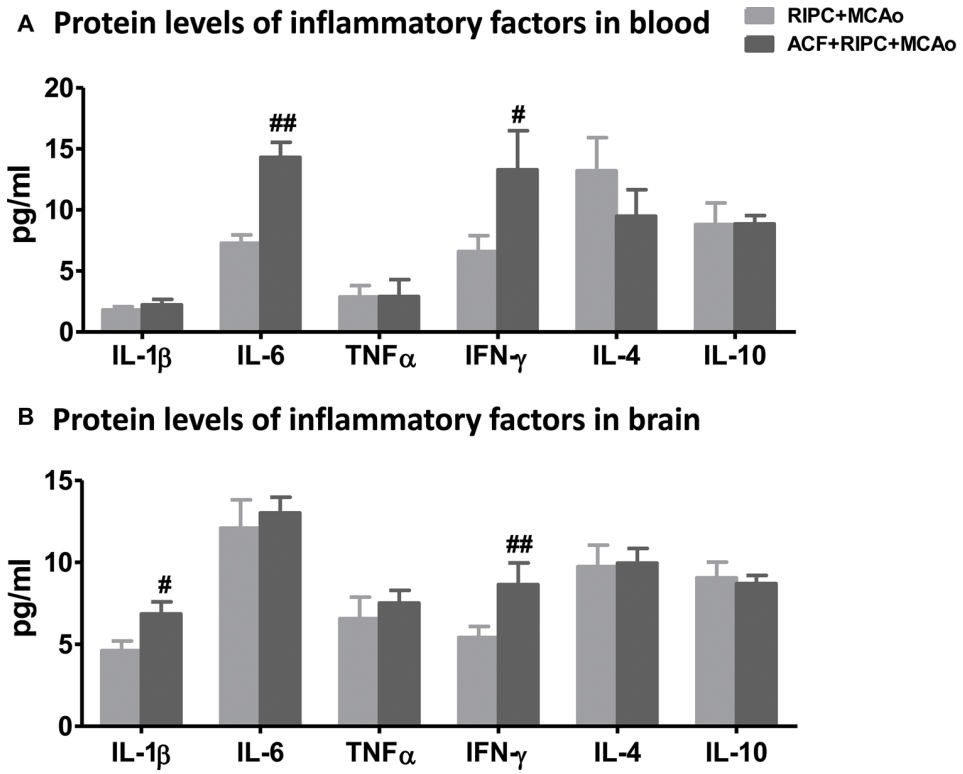

FIGURE 5 | The effect of ACF on protein levels of inflammatory cytokines in aged stroke animals receiving RIPC. **(A)** Protein levels of the pro-inflammatory cytokines IL-1β, IL-6, TNFα and IFN-γ and anti-inflammatory cytokines IL-4 and IL-10 in the peripheral blood, respectively in RIPC+MCAo and ACF+RIPC+MCAo group in aged rats. **(B)** Protein levels of IL-1β, IL-6, TNFα, IFN-γ, IL-4 and IL-10 in the ischemic brain, respectively (N = 5–6 per group). $^{\#,\#\#}$, vs. RIPC+MCAo, $p < 0.05$, 0.01, respectively.

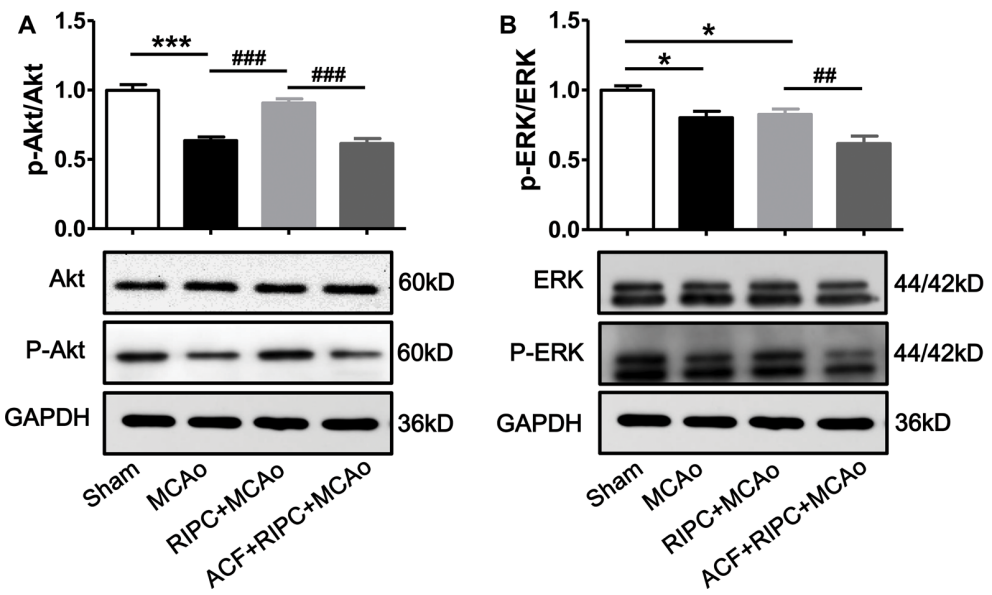

FIGURE 6 | The effect of RIPC and ACF on the activation of Akt and ERK signaling pathway. **(A)** Statistical data of the ratio of p-Akt to total Akt and representative images of western blot of total Akt and p-Akt. A total of 4 groups were assessed: Sham, MCAo, RIPC+MCAo, ACF+RIPC+MCAo. **(B)** Statistical data of the ratio of p-ERK to total ERK and representative images of western blot of total ERK and p-ERK in penumbra tissues (N = 5–6 per group). Statistical analysis was performed by ANOVA. *,*** vs. Sham, $p < 0.05$, 0.001 respectively, $^{\#\#,\#\#\#}$ vs. MCAo, RIPC+MCAo, $p < 0.01$, 0.001, respectively.

role in the protective effect of RIPC against stroke, which was likely achieved by modulating neuroinflammation in young rats (Yang et al., 2018). However, whether HIF plays a key role in RIPC in aged stroke is not addressed. Based on these, we chose an aged rats MCAo model and studied the protection and mechanism of RIPC post-stroke. We verified the infarction size was smaller in aged rats but there was worse neurological function than young rats. Further, our data suggested that RIPC protected against stroke not only in young rats but also in aged rats. RIPC reduced the infarction size and improved neurological function and behavior (**Figure 1**).

The HIF protein is a transcriptional factor that exists just a few minutes under normal oxygen levels but accumulates in hypoxic and ischemic cells (Ogle et al., 2012). Previous studies have shown that the neuroprotection against focal cerebral ischemia provided by various agents is mediated through the regulation of HIF (Doeppner et al., 2012; Wang et al., 2012; Meller and Simon, 2015). In the current study, we showed that MCAo upregulated the expression of HIF-1α and HIF-2α mRNA and protein levels in the ischemic brain of aged rats (**Figure 2**), which the evidence has been described in young animals in other reports (Zhong et al., 2012; Zhao et al., 2015; Zong et al., 2015). Further, we found that RIPC reversed this MCAo-induced upregulation of HIFs (**Figure 2**). It was suggested that RIPC improved the regional ischemia in the brain 48 h post-stroke in aged rats. Previous evidence showed that RIPC could regulate the expression of HIF, such as HIF-1α and HIF-2α, and played key roles in ischemic tissue including in the brain and heart in young experimental animals (Cai et al., 2008, 2013; Kapitsinou et al., 2014; Yang et al., 2018). To examine whether HIF also plays an important role in the neuroprotection of RIPC in aged rats, we used the heterodimer inhibitor, ACF, to inhibit HIF activity. The data showed that the injection of ACF abolished the structural and functional protection of RIPC on infarction size, neurological function and the tail hang test, one of the behavioral tests (**Figure 4**). These results demonstrated that HIF-1α and HIF-2α are key factors in the protection of RIPC in aged rats.

HIF is an inflammation mediator and can be stabilized by TNFα and IL-1β (Sharp and Bernaudin, 2004). It has been shown that IL-10 is the main target of HIF-1α in cardiomyocytes of circulating hypoxia-reoxygenation mice. RIPC can increase the plasma concentration of IL-10 and promote the subsequent remote activation of Akt signals in the heart (Cai et al., 2013). These findings are based on young animal models, and the changes in aged animals remain unclear. Our data showed that RIPC reduced the levels of pro-inflammatory cytokines IL-1β, IL-6 and IFN-γ in the blood, and IL-1β and IFN-γ in the brain in aged rats 48 h post-stroke (**Figure 3**), while the changes that were neutralized by the HIF inhibitor (**Figure 5**).

Several reports have identified under ischemic conditions, the activation of the Akt or EKR signaling pathway can be regulated by the expression of HIF (Hausenloy and Yellon, 2007; Cai et al., 2013; Martin-Puig et al., 2015; Meller and Simon, 2015; Ong et al., 2015). However, if HIF is directly affected by RIPC and further regulate the activity of Akt or EKR signaling pathway is unknown. Interestingly, in our study, we found that RIPC activated the Akt but not the ERK signaling pathway and that inhibition of HIF abolished the activation of Akt in aged rats following stroke (**Figure 6**). It suggested that HIF played key roles in RIPC reversed the reduced expression of p-Akt.

In the current study, there are several limitations. First, inhibitors of inflammatory cytokines and signaling pathways were not used. Thus, future studies should examine the infarct size when the inhibitors of inflammatory cytokines and signaling pathways are used; and come to a convincing conclusion the inflammatory responses and Akt/ERK signaling pathway is the cause of the reduced infarct size. Second, RIPC is an endogenous protective mechanism through which short-term sub-lethal ischemia in a remote organ can protect the major organ from further severe ischemia. However, due to the unpredictability of cerebral infarction, its clinical application is limited. Unlike ischemic preconditioning, ischemic postconditioning is a relatively novel concept, which follows reperfusion of a vessel and effectively inhibits inflammatory responses and delays cell death. So many researchers believe that ischemic postconditioning is more suitable for clinical transformation. However, to date, the evidence of cerebral ischemia postconditioning is limited to preclinical studies. Therefore, future studies will address the mechanism of remote ischemic postconditioning in the protection against cerebral ischemia, stimulate the clinical transformation of remote ischemic postconditioning.

CONCLUSION

Our study provided strong evidence that RIPC protected against stroke in aged rats by modulating the expression of HIF-1α and HIF-2α in ischemic tissue, not only affecting the activation of the Akt pathway but also reducing the expression of pro-inflammatory cytokines in the peripheral blood and brain.

DATA AVAILABILITY STATEMENT

All datasets generated for this study are included in the article/**Supplementary Material**.

ETHICS STATEMENT

The animal study was reviewed and approved by Capital Medical University Animal Review Committee.

AUTHOR CONTRIBUTIONS

XG, HD, and HZ: study concept and design. XD and JY: acquisition of data and wrote the draft. CL: made the figure and statistical analysis. SW and CZ: made a model. All authors contributed to the critical revision of the manuscript and have approved the final version of this review article.

FUNDING

This study was supported by the National Natural Science Foundation of China Grant No. 81701154 and Tong Zhou District Science and Technology Project Grant Nos. KJ2019CX014-31 and KJ2019CX004-03.

ACKNOWLEDGMENTS

We thank Xuan Liu and Haiteng Ji for their long-term feeding of experimental animals.

SUPPLEMENTARY MATERIAL

The Supplementary Material for this article can be found online at: https://www.frontiersin.org/articles/10.3389/fnagi.2020.00054/full#supplementary-material.

FIGURE S1 | Cerebral blood flow during the MCAo surgery. Cerebral blood flow was measured at four time-points, baseline, 1 and 5 min of ischemia and reperfusion in the MCAo, RIPC+MCAo and ACF+RIPC+MCAo groups. Data were normalized to baseline and expressed as percentages.

FIGURE S2 | Images of TTC staining. All the panels and representative images of TTC staining were presented. **(A)** MCAo group. **(B)** RIPC+MCAo group. **(C)** ACF+RIPC+MCAo group.

TABLE S1 | Arterial blood gas parameter before and immediately after MCAo.

TABLE S2 | Blood sugar value after surgery in each group.

REFERENCES

Cai, Z. Q., Luo, W. B., Zhan, H. W., and Semenza, G. L. (2013). Hypoxia-inducible factor 1 is required for remote ischemic preconditioning of the heart. *Proc. Natl. Acad. Sci. U S A* 110, 17462–17467. doi: 10.1073/pnas.1317158110

Cai, Z. Q., Zhong, H., Bosch-Marce, M., Fox-Talbot, K., Wang, L., Wei, C. M., et al. (2008). Complete loss of ischaemic preconditioning-induced cardioprotection in mice with partial deficiency of HIF-1α. *Cardiovasc. Res.* 77, 463–470. doi: 10.1093/cvr/cvm035

Chen, C., Jiang, W., Liu, Z. J., Li, F. W., Yang, J., Zhao, Y. L., et al. (2018). Splenic responses play an important role in remote ischemic preconditioning-mediated neuroprotection against stroke. *J. Neuroinflmmation* 15:167. doi: 10.1186/s12974-018-1190-9

Doeppner, T. R., Mlynarczuk-Bialy, I., Kuckelkorn, U., Kaltwasser, B., Herz, J., Hasan, M. R., et al. (2012). The novel proteasome inhibitor BSc2118 protects against cerebral ischemia through HIF1A accumulation and enhanced angioneurogenesis. *Brain* 135, 3282–3297. doi: 10.1093/brain/aws269

Hausenloy, D. J., and Yellon, D. M. (2007). Reperfusion injury salvage kinase signalling: taking a RISK for cardioprotection. *Heart Fail. Rev.* 12, 217–234. doi: 10.1007/s10741-007-9026-1

Hu, S., Dong, H. L., Zhang, H. P., Wang, S. Q., Hou, L. C., Chen, S. Y., et al. (2012). Noninvasive limb remote ischemic preconditioning contributes neuroprotective effects *via* activation of adenosine A1 receptor and redox status after transient focal cerebral ischemia in rats. *Brain Res.* 1459, 81–90. doi: 10.1016/j.brainres.2012.04.017

Kapitsinou, P. P., Sano, H., Michael, M., Kobayashi, H., Davidoff, O., Bian, A., et al. (2014). Endothelial HIF-2 mediates protection and recovery from ischemic kidney injury. *J. Clin. Invest.* 124, 2396–2409. doi: 10.1172/JCI69073

Krishnamurthi, R. V., Feigin, V. L., Forouzanfar, M. H., Mensah, G. A., Connor, M., Bennett, D. A., et al. (2013). Global and regional burden of first-ever ischemic and haemorrhagic stroke during 1990–2010: findings from the Global Burden of Disease Study 2010. *Lancet Glob. Health* 5, e259–e281. doi: 10.1016/S2214-109X(13)70089-5

Kuzumaki, N., Ikegami, D., Imai, S., Narita, M., Tamura, R., Yajima, M., et al. (2010). Enhanced IL-1α production in response to the activation of hippocampal glial cells impairs neurogenesis in aged mice. *Synapse* 64, 721–728. doi: 10.1002/syn.20800

Liu, Z. J., Chen, C., Li, X. R., Ran, Y. Y., Xu, T., Zhang, Y., et al. (2016). Remote ischemic preconditioning-mediated neuroprotection against stroke is associated with significant alterations in peripheral immune responses. *CNS Neurosci. Ther.* 22, 43–52. doi: 10.1111/cns.12448

Lomb, D. J., Desouza, L. A., Franklin, J. L., and Freeman, R. S. (2009). Prolyl hydroxylase inhibitors depend on extracellular glucose and hypoxia-inducible factor (HIF)-2 to inhibit cell death caused by nerve growth factor (NGF) deprivation: evidence that HIF-2 has a role in NGF-promoted survival of sympathetic neurons. *Mol. Pharmacol.* 75, 1198–1209. doi: 10.1124/mol.108.053157

Manwani, B., Liu, F., Scranton, V., Hammond, M. D., Sansing, L. H., and McCullough, L. D. (2013). Differential effects of aging and sex on stroke induced inflammation across the lifespan. *Exp. Neurol.* 249, 120–131. doi: 10.1016/j.expneurol.2013.08.011

Martin-Puig, S., Tello, D., and Aragonés, J. (2015). Novel perspectives on the PHD-HIF oxygen sensing pathway in cardioprotection mediated by IPC and RIPC. *Front. Physiol.* 6:137. doi: 10.3389/fphys.2015.00137

Mayhan, W. G., Arrick, D. M., Sharpe, G. M., and Sun, H. (2008). Age-related alterations in reactivity of cerebral arterioles: role of oxidative stress. *Microcirculation* 15, 225–236. doi: 10.1080/10739680701641421

Meller, R., and Simon, R. P. (2015). A critical review of mechanisms regulating remote preconditioning-induced brain protection. *J. Appl. Physiol.* 119, 1135–1142. doi: 10.1152/japplphysiol.00169.2015

Mi, T. M., Yu, F., Ji, X. M., Sun, Y. X., and Qu, D. M. (2016). The interventional effect of remote ischemic preconditioning on cerebral small vessel disease: a pilot randomized clinical trial. *Eur. Neurol.* 76, 28–34. doi: 10.1159/000447536

Modrick, M. L., Didion, S. P., Sigmund, C. D., and Faraci, F. M. (2009). Role of oxidative stress and AT1 receptors in cerebral vascular dysfunction with aging. *Am. J. Physiol. Heart Circ. Physiol.* 296, H1914–H1919. doi: 10.1152/ajpheart.00300.2009

Mozaffarian, D., Benjamin, E. J., Go, A. S., Arnett, D. K., Blaha, M. J., Cushman, M., et al. (2015). Heart disease and stroke statistics—2015 update: a report from the american heart association. *Circulation* 131, e29:e322. doi: 10.1161/CIR.0000000000000152

Nguyen, T. V., Frye, J. B., Zbesko, J. C., Stepanovic, K., Hayes, M., Urzua, A., et al. (2016). Multiplex immunoassay characterization and species comparison of inflammation in acute and non-acute ischemic infarcts in human and mouse brain tissue. *Acta Neuropathol. Commun.* 4:100. doi: 10.1186/s40478-016-0371-y

Ogle, M. E., Gu, X., Espinera, A. R., and Wei, L. (2012). Inhibition of prolyl hydroxylases by dimethyloxaloylglycine after stroke reduces ischemic brain injury and requires hypoxia inducible factor-1α. *Neurobiol. Dis.* 45, 733–742. doi: 10.1016/j.nbd.2011.10.020

Ong, S. B., Hall, A. R., Dongworth, R. K., Kalkhoran, S., Pyakurel, A., Scorrano, L., et al. (2015). Akt protects the heart against ischaemia-reperfusion injury by modulating mitochondrial morphology. *Thromb. Haemost.* 113, 513–521. doi: 10.1160/TH14-07-0592

Orre, M., Kamphuis, W., Osborn, L. M., Melief, J., Kooijman, L., Huitinga, I., et al. (2014). Acute isolation and transcriptome characterization of cortical astrocytes and microglia from young and aged mice. *Neurobiol. Aging* 35, 1–14. doi: 10.1016/j.neurobiolaging.2013.07.008

Ren, C. H., Gao, M. Q., Dornbos, D., Ding, Y. C., Zeng, X. W., Luo, Y. M., et al. (2011). Remote ischemic post-conditioning reduced brain damage in experimental ischemia/reperfusion injury. *Neurol. Res.* 33, 514–519. doi: 10.1179/016164111x13007856084241

Ren, C. C., Yan, Z. M., Wei, D. T., Gao, X. W., Chen, X. Y., and Zhao, H. (2009). Limb remote ischemic postconditioning protects against focal ischemia in rats. *Brain Res.* 1288, 88–94. doi: 10.1016/j.brainres.2009.07.029

Semenza, G. L. (2012). Hypoxia-inducible factors in physiology and medicine. *Cell* 148, 399–408. doi: 10.1016/j.cell.2012.01.021

Semple, B. D., Blomgren, K., Gimlin, K., Ferriero, D. M., and Noble-Haeusslein, L. J. (2013). Brain development in rodents and humans: identifying benchmarks of maturation and vulnerability to injury across species. *Prog. Neurobiol.* 106–107, 1–16. doi: 10.1016/j.pneurobio.2013.04.001

Sharp, F. R., and Bernaudin, M. (2004). HIF-1 and oxygen sensing in the brain. *Nat. Rev.* 5, 437–448. doi: 10.1515/bc.2004.016

Shim, R., and Wong, C. H. (2016). Ischemia, immunosuppression and infection—tackling the predicaments of post-stroke complications. *Int. J. Mol. Sci.* 17:E64. doi: 10.3390/ijms17010064

Suenaga, J., Hu, X., Pu, H., Shi, Y., Hassan, S. H., Xu, M., et al. (2015). White matter injury and microglia/macrophage polarization are strongly linked with

age-related long-term deficits in neurological function after stroke. *Exp. Neurol.* 272, 109–119. doi: 10.1016/j.expneurol.2015.03.021

Wang, C. H., Wang, Z. H., Zhang, X. J., Zhang, X. L., Dong, L. P., Xing, Y. X., et al. (2012). Protection by silibinin against experimental ischemic stroke: upregulated pAkt, pmTOR, HIF-1α and Bcl-2, down-regulated Bax, NF-κB expression. *Neurosci. Lett.* 1, 45–50. doi: 10.1016/j.neulet.2012.08.078

Wei, Y. C., Hong, H. M., Zhang, X. Q., Lai, W. F., Wang, Y. Z., Chu, K. D., et al. (2017). Salidroside inhibits inflammation through PI3K/Akt/HIF signaling after focal cerebral ischemia in rats. *Inflammation* 40, 1297–1309. doi: 10.1007/s10753-017-0573-x

Wei, D. T., Ren, C. C., Chen, X. Y., and Zhao, H. (2012). The chronic protective effects of limb remote preconditioning and the underlying mechanisms involved in inflammatory factors in rat stroke. *PLoS One* 7:e30892. doi: 10.1371/journal.pone.0030892

Yamashiro, K., Tanaka, R., Urabe, T., Ueno, Y., Yamashiro, Y., Nomoto, K., et al. (2017). Gut dysbiosis is associated with metabolism and systemic inflammation in patients with ischemic stroke. *PLoS One* 12:e0171521. doi: 10.1371/journal.pone.0171521

Yang, J., Liu, C. Y., Du, X. N., Liu, M. L., Ji, X. M., Du, H. S., et al. (2018). Hypoxia inducible factor 1α plays a key role in remote ischemic preconditioning against stroke by modulating inflammatory responses in rats. *J. Am. Heart Assoc.* 7:e007589. doi: 10.1161/JAHA.117.007589

Zhao, Y., Deng, B., Li, Y., Zhou, L., Yang, L., Gou, X., et al. (2015). Electroacupuncture pretreatment attenuates cerebral ischemic injury *via* notch pathway-mediated up-regulation of hypoxia inducible factor-1α in rats. *Cell Mol. Neurobiol.* 35, 1093–1103. doi: 10.1007/s10571-015-0203-9

Zhao, W. B., Meng, R., Ma, C., Hou, B. J., Jiao, L. Q., Zhu, F. S., et al. (2017). Safety and efficacy of remote ischemic preconditioning in patients with severe carotid artery stenosis before carotid artery stenting: a proof-of-concept, randomized controlled trial. *Circulation* 135, 1325–1335. doi: 10.1161/circulationaha.116.024807

Zhao, H., Shimohata, T., Wang, J. Q., Sun, G., Schaal, D. W., Sapolsky, R. M., et al. (2005). Akt contributes to neuroprotection by hypothermia against cerebral ischemia in rats. *J. Neurosci.* 25, 9794–9806. doi: 10.1523/JNEUROSCI.3163-05.2005

Zhao, S. C., Wang, C., Xu, H., Wu, W. Q., Chu, Z. H. C., Ma, L. S., et al. (2017). Age-related differences in interferon regulatory factor-4 and -5 signaling in ischemic brains of mice. *Acta Pharmacol. Sin.* 38, 1425–1434. doi: 10.1038/aps.2017.122

Zhong, Q., Zhou, Y. F., Ye, W. B., Cai, T., Zhang, X. Q., and Deng, D. Y. (2012). Hypoxia-inducible factor 1-a-AA-modified bone marrow stem cells protect PC12 cells from hypoxia-induced apoptosis, partially through VEGF/PI3K/Akt/FoxO1 pathway. *Stem Cells Dev.* 21, 2703–2717. doi: 10.1089/scd.2011.0604

Zong, Y. H., Jiang, L., Zhang, M. X., Zhou, F. F., Qi, W. Q., Li, S., et al. (2015). Limb remote ischemic postconditioning protects cerebral ischemia from injury associated with expression of HIF-1α in rats. *BMC Neurosci.* 16:97. doi: 10.1186/s12868-015-0235-6

Conflict of Interest: The authors declare that the research was conducted in the absence of any commercial or financial relationships that could be construed as a potential conflict of interest.

Copyright © 2020 Du, Yang, Liu, Wang, Zhang, Zhao, Du and Geng. This is an open-access article distributed under the terms of the Creative Commons Attribution License (CC BY). The use, distribution or reproduction in other forums is permitted, provided the original author(s) and the copyright owner(s) are credited and that the original publication in this journal is cited, in accordance with accepted academic practice. No use, distribution or reproduction is permitted which does not comply with these terms.

frontiers in Neuroscience

ORIGINAL RESEARCH
published: 02 April 2020
doi: 10.3389/fnins.2020.00280

Gene Expression Dynamics at the Neurovascular Unit During Early Regeneration After Cerebral Ischemia/Reperfusion Injury in Mice

Roxane-Isabelle Kestner[1,2], Franziska Mayser[1,2], Rajkumar Vutukuri[2], Lena Hansen[2], Stefan Günther[3], Robert Brunkhorst[1], Kavi Devraj[2,4†] and Waltraud Pfeilschifter[1†]*

[1] Department of Neurology, University Hospital Frankfurt, Goethe University, Frankfurt am Main, Germany, [2] Department of General Pharmacology and Toxicology, Pharmazentrum Frankfurt, University Hospital Frankfurt, Goethe University, Frankfurt am Main, Germany, [3] Department of Cardiac Development and Remodeling, Max Planck Institute for Heart and Lung Research, Bad Nauheim, Germany, [4] Institute of Neurology (Edinger Institute), University Hospital Frankfurt, Goethe University, Frankfurt am Main, Germany

OPEN ACCESS

Edited by:
Christoph Harms, Charité – Universitätsmedizin Berlin, Germany

Reviewed by:
Dominik Michalski, Leipzig University, Germany
Yongting Wang, Shanghai Jiao Tong University, China

****Correspondence:***
Roxane-Isabelle Kestner
roxane-isabelle.kestner@kgu.de

† These authors have contributed equally to this work

Specialty section:
This article was submitted to Neurodegeneration, a section of the journal Frontiers in Neuroscience

Received: *25 November 2019*
Accepted: *11 March 2020*
Published: *02 April 2020*

Citation:
Kestner R-I, Mayser F, Vutukuri R, Hansen L, Günther S, Brunkhorst R, Devraj K and Pfeilschifter W (2020) Gene Expression Dynamics at the Neurovascular Unit During Early Regeneration After Cerebral Ischemia/Reperfusion Injury in Mice. Front. Neurosci. 14:280. doi: 10.3389/fnins.2020.00280

With increasing distribution of endovascular stroke therapies, transient middle cerebral artery occlusion (tMCAO) in mice now more than ever depicts a relevant patient population with recanalized M1 occlusion. In this case, the desired therapeutic effect of blood flow restauration is accompanied by breakdown of the blood-brain barrier (BBB) and secondary reperfusion injury. The aim of this study was to elucidate short and intermediate-term transcriptional patterns and the involved pathways covering the different cellular players at the neurovascular unit after transient large vessel occlusion. To achieve this, male C57Bl/6J mice were treated according to an intensive post-stroke care protocol after 60 min occlusion of the middle cerebral artery or sham surgery to allow a high survival rate. After 24 h or 7 days, RNA from microvessel fragments from the ipsilateral and the contralateral hemispheres was isolated and used for mRNA sequencing. Bioinformatic analyses allowed us to depict gene expression changes at two timepoints of neurovascular post-stroke injury and regeneration. We validated our dataset by quantitative real time PCR of BBB-associated targets with well-characterized post-stroke dynamics. Hence, this study provides a well-controlled transcriptome dataset of a translationally relevant mouse model 24 h and 7 days after stroke which might help to discover future therapeutic targets in cerebral ischemia/reperfusion injury.

Keywords: stroke, blood-brain barrier, high-throughput nucleotide sequencing, matrix metalloproteinases, reperfusion injury, translational medical research

INTRODUCTION

Over the past decades, management of ischemic stroke has improved dramatically. The "penumbra" concept has given rise to pharmacological and mechanical recanalization therapies which are able to rescue ischemic brain tissue if applied early enough. Unfortunately, only a fraction of all stroke patients benefits from those therapies due to a narrow time window for optimal treatment and relevant contraindications. Additionally, after successful recanalization reperfusion-associated

brain injury occurs due to secondary impairment of the blood-brain barrier (BBB) (Choi and Pile-Spellman, 2018). Despite intensive experimental research, promising drug candidates for acute and postacute stroke treatment have failed to translate into new therapeutic strategies (O'Collins et al., 2006). Better understanding of the processes at the BBB and their temporal dynamics is critical to overcome this "translational roadblock."

Target of many of these experimental approaches is the neurovascular unit (NVU) which comprises brain capillaries as well as adjacent pericytes, astrocytes, along with their extracellular matrix (ECM) in addition to microglia and neurons (Iadecola, 2017). The specialized endothelium of those capillaries forms the BBB, a highly polarized and tightly regulated interface of the brain microvasculature and CNS tissue. The interplay of an unfenestrated network of tight junctions and specialized transporters allows a selective permeability to water and nutrients yet keeping toxins and pathogens out (Cummins, 2012; Knowland et al., 2014).

Ischemic strokes are caused by an acute occlusion of a cerebral vessel leading to oxygen and glucose deprivation in the dependent brain tissue. Due to a consecutive breakdown of the neuronal ionic balance release of glutamate and induction of glutamate-mediated pathways occurs and triggers cell death by massive calcium influx. This so-called glutamate excitotoxicity is one of the first phenomena to take place in the ischemic lesion leading to extensive cell death (Szydlowska and Tymianski, 2010). In parallel, lack of oxygen causes a failure of the respiratory chain and mitochondrial function so that pH is reduced and free radicals expand the local tissue damage (Lipton, 1999). Subsequently, a sterile inflammatory reaction going along with a hyperacute imbalance of matrix metallopeptidases (MMPs), especially MMP-9, and their endogenous counterplayers, tissue inhibitor of metallopeptidases (TIMP)-1 and -2 (Barr et al., 2010; Lenglet et al., 2014) triggers the destruction of the crucial endothelial-ECM interface of the BBB (Edwards and Bix, 2018). On the other hand, a step-wise degradation of endothelial cells in the oxygen-deprived area has been observed in the context of permanent and reperfused stroke even without disintegration of tight junction molecules (Krueger et al., 2015). Altogether, BBB function is disrupted and allows invasion of immune cells and pathogenic factors.

Unfortunately, re-establishment of blood-flow in the occluded vessel does not simply reverse those effects. MMPs stay upregulated after reperfusion and free radicals have been reported to even increase in this context as degraded lipid components serve as substrates for further production of reactive oxidative species (Bai and Lyden, 2015). In combination with a transient hyperemia which can last for hours or even days after recanalization treatment (Kidwell et al., 2001) patients are at risk for secondary vasogenic edema and hemorrhagic transformation of the infarcted area (Yang et al., 2007; Strbian et al., 2008; Sun et al., 2017). This so-called cerebral ischemia/reperfusion (I/R) injury hampers the clinical benefit of recanalization therapies and is target of experimental treatment strategies.

Previous experimental studies have shown a neuroprotective effect of acute MMP-9 inhibition in stroke (Asahi et al., 2000) whereas MMP-9 inhibition in the early recovery phase exacerbated stroke-induced brain damage (Zhao et al., 2006). Several other pathophysiological processes have shown a similar unexpected biphasic function after stroke (Ma et al., 2017; Sandvig et al., 2018). Only long-term observations of cohorts with acceptable survival rates allow to assess the full picture of post-ischemic vascular inflammation, its resolution and tissue repair.

We therefore performed a transcriptomic analysis of brain microvessels of a carefully monitored mouse population at 24 h and 7 days post transient middle cerebral artery occlusion (tMCAO) to depict an early timepoint after transient vessel occlusion, dominated by cytotoxic, protein degrading and inflammatory pathways as well as a later one, displaying first regenerative processes amid persisting immune cell infiltration and cytotoxic conditions. By this, we obtained comprehensive and unbiased insights on the complex molecular changes that occur at the BBB in the first days after cerebral I/R injury in mice.

MATERIALS AND METHODS

Animals

A total of 95 male 10–12 weeks old C57Bl/6J mice (25–30 g) were purchased from Charles River Laboratories (Sulzfeld, Germany) and housed on a 12 h/12 h light/dark cycle with *ad libitum* access to food and water. Due to fight wounds, three mice were excluded before intervention. Experiments were performed in compliance with the ARRIVE guidelines for animal research, in accordance with the German Protection of Animals Act and the guidelines for care and use of laboratory animals by the local committee (Regierungspräsidium Darmstadt, approval number FU/1143).

Transient Middle Cerebral Artery Occlusion and Post-stroke Care

The right middle cerebral artery was occluded as described previously (Pfeilschifter et al., 2012). Briefly, mice were anesthetized with 1.5% isoflurane and kept on a temperature-controlled heating mat throughout surgeries. After ligation of the right common and external carotid arteries, a standard silicone rubber-coated monofilament (6-0 medium, Doccol, Sharon, MA, United States) was advanced until the branching point of the middle cerebral artery, allowing reperfusion after 60 min. In sham controls, the filament was retracted immediately after reaching the branching point. Analgesia was achieved by i.p. injections of buprenorphine (0.1 mg/kg bodyweight) 30 min before surgery and in 8 h-intervals during the first 48 h. Mice were housed in groups of 3–5 animals and cages kept on a heating mat (Beurer, Ulm, Germany). Daily monitoring included body weight, rectal temperature and clinical signs of pain, subarachnoid hemorrhage (SAH) or brain herniation. Experimental design is summarized in **Figure 1A**. On day 1, 3, and 7 after surgery, neurological and general deficits were assessed using the Experimental Stroke Scale (ESS) established by Lourbopoulos et al. (2017). Food and water were supplied adapted to the individual animal's need according to the maximized post-stroke support protocol described there. This procedure included daily monitoring of weight and body temperature and, according to the hereby identified condition of the animals, oral feeding of 1–3 mL of dissolved food pellets

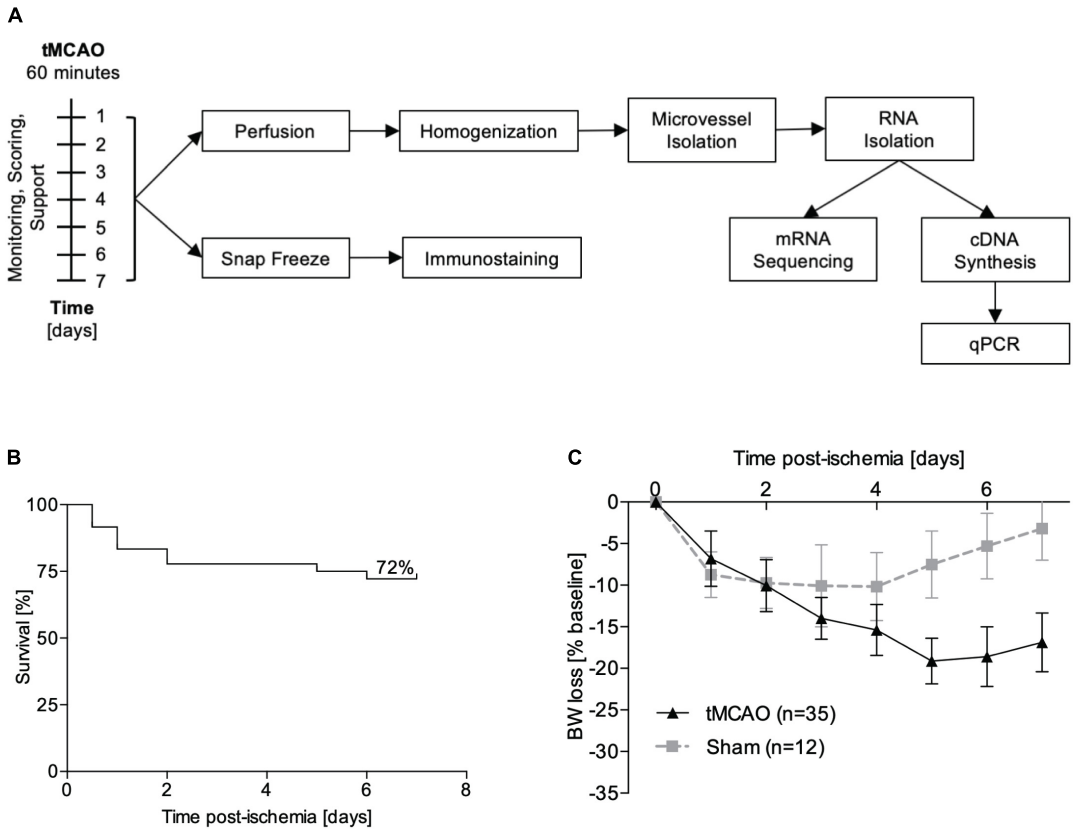

FIGURE 1 | Experimental design. **(A)** Male C57Bl/6 mice underwent tMCAO or sham surgery and were supported for either 24 h or 7 days. For RNA sequencing, perfused microvessels from the ipsi- and contralateral hemispheres were isolated and pooled (n = 3 hemibrains per sample, n = 3 samples per group). For immunofluorescence staining, brains were snap frozen and cut into 10 μm sections. **(B)** Kaplan–Meier plot for survival of animals after tMCAO (n = 35). **(C)** Weight loss after sham (gray line, n = 12) and tMCAO surgery (black line, n = 35) presented as percentage reduction from preoperative body weight ± SD.

per day. Liquids were provided by subcutaneous application of 2–4 mL warmed 0.9% saline given in two doses per day. Additionally, jelly food and food pellets were kept on the cage floor to be easily accessible for recovering individuals. Animals were sacrificed either 24 h or 7 days post-stroke. Stroke-related mortality was 12% in the 24 h- and 28% in the 7 day-cohort. Four mice were excluded from the study and calculation of stroke related mortality: three animals due to proof of artificial SAH in post-mortem autopsy and one sham-operated animal due to stroke symptoms.

Isolation of Mouse Brain Microvessels

Isolation of mouse brain microvessels (MBMVs) were isolated as indicated in **Figure 2A** using a previously described protocol (Gurnik et al., 2016). All steps were performed at 4°C or on ice. In brief, post anesthesia, mice were transcardially perfused with sterile phosphate buffered saline (PBS; Gibco, Thermo Fisher Scientific) for 10 min using a peristaltic pump (Ismatec, Cole-Parmer, Wertheim, Germany). Brains were macroscopically checked for broad cortical infarction and collected in microvessel buffer (MVB: 15 mM HEPES, 147 mM NaCl, 4 mM KCl, 3 mM $CaCl_2$, 1.2 mM MgCl2, 5 mM glucose, and 0.5% BSA, pH 7.4) on ice. Individual stroke volumes could not be quantified during the isolation process without risking loss of vital material and artificial tissue reactions. Medium stroke sizes in our surgery setup covering about 60% of the hemisphere have been reported before (Friedländer et al., 2017). To estimate stroke volumes in the present study, male C57B/6J mice were operated by RK under same conditions as the mice used for mRNA sequencing. After 24 h, mice were sacrificed, brains removed carefully from the skull and cut into 1 mm sections. Subsequently, brain slices were stained in 2% 2,3,5-Triphenyl-tetrazolium chloride (TTC) at 37°C for 5 min and imaged on a flatbed color scanner (CanoScan LiDE 100; Canon, Tokyo, Japan). The hereby obtained Photoshop images were used for semi-automatical stroke volume calculation by an ImageJ macro established by Friedländer et al. (2017). Individual results are summarized in **Supplementary Figure IV** (mean stroke volume 57.2%, median 55.6%).

After removal of the cerebellum, brain stem and olfactory lobes, meninges were peeled off by rolling the cerebrum on autoclaved Whatman filter paper (Schleicher & Schuell, München, Germany). Hemispheres were separated and pooled (from three animals). Tissue was homogenized in MVB using a Dounce homogenizer (Wheaton, 0.025 mm clearance) attached to an electrical overhead stirrer (2000 rpm, VOS 14, VWR) and centrifuged at 400 × g for 10 min. Myelin fat was separated

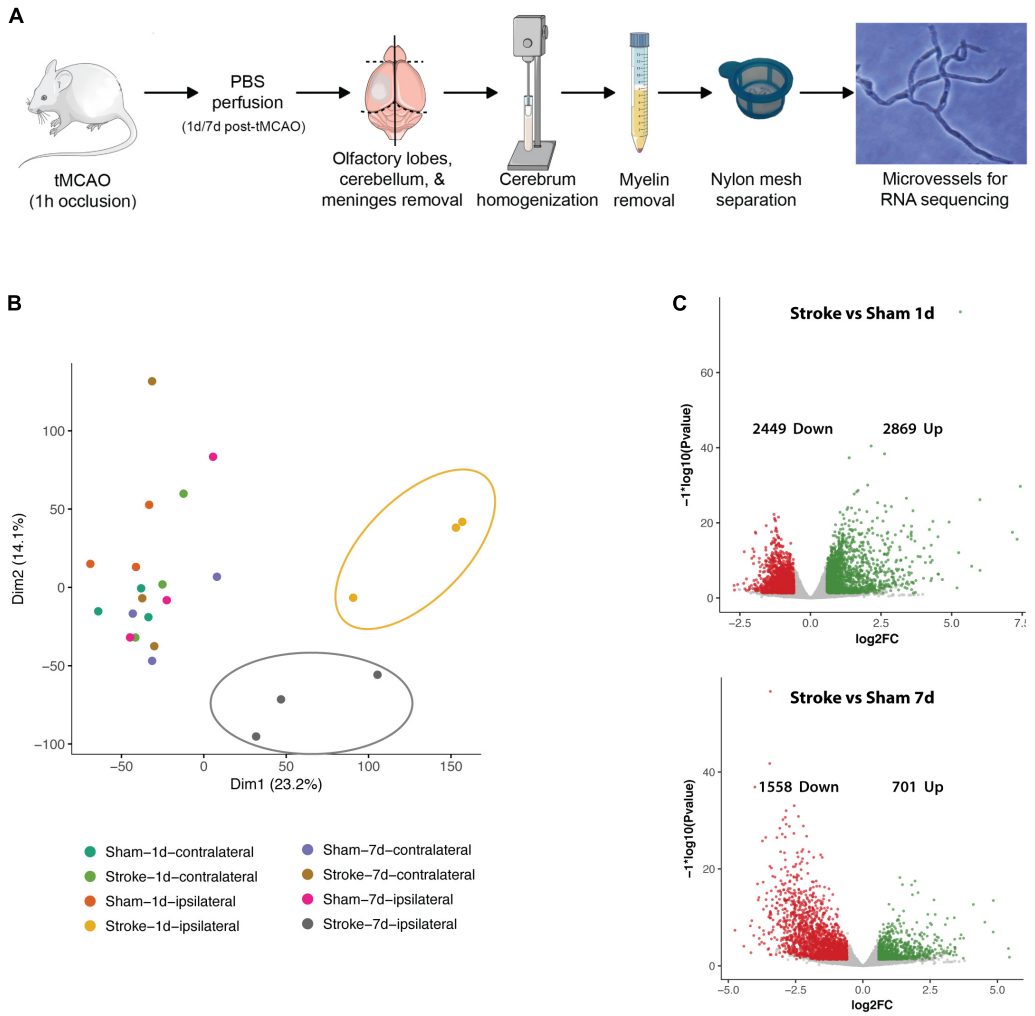

FIGURE 2 | Basic characteristics post-stroke transcriptomics in microvessels. **(A)** Microvessel isolation protocol. **(B)** PCA plot of all samples. Distinct clusters are highlighted (yellow/upper right circle: ipsilateral hemispheres 24 h after tMCAO, gray/central circle: ipsilateral hemispheres 7 days after tMCAO). **(C)** Volcano plots of regulated genes in comparison 5 (stroke ipsilateral versus sham ipsilateral 24 h) and 6 (stroke ipsilateral versus sham ipsilateral 7 days). Transcripts accepted as regulated: mean > 5 counts, $\log_2$fc <> ±0.585, FDR ≤ 0.05.

by resuspension of the pellet in 25% BSA and centrifugation at 2000 × *g* for 30 min. Subsequently, the cell pellet was resuspended in MVB and filtered through a 100 μm cell strainer (Falcon, Corning, NY, United States) to remove large vessel fragments and tissue clusters. The flow-through was filtered through a 40 μm cell strainer (Falcon, Corning, NY, United States) to be cleared from erythrocytes, dead cell nuclei and cell debris. Microvessels were harvested directly from the 40 μm mesh in RLT buffer (Qiagen, Düsseldorf, Germany) containing Dithiothreitol (DTT, 40 mM; Roche Diagnostics, Indianapolis, IN, United States) and stored at −80°C until RNA isolation. Successful isolation of microvessel fragments was verified by light microscopy assessment.

A total of 32 MBMV samples were generated and included into 8 groups (sham ipsilateral 24 h, sham contralateral 24 h, tMCAO ipsilateral 24 h, tMCAO contralateral 24 h, sham ipsilateral 7 days, sham contralateral 7 days, tMCAO ipsilateral 7 days, tMCAO contralateral 7 days). One group consisted of $n = 4$ samples each. One sample was generated by pooling three hemispheres of the same kind after brain removal and separation of ipsi- and contralateral hemispheres. Analysis identified four samples as outliers and further analysis was performed on $n = 3$ samples per group. In total, one group contains brain hemispheres of 3 × 3 = 9 animals. The work flow and experimental design is shown in **Figure 1A**.

mRNA Sequencing From MBMVs

RNA was extracted from MBMVs using Qiagen RNeasy plus Micro Kit (Qiagen, Düsseldorf, Germany) following the instructions provided by the manufacturer. RNA concentration measured by Qubit fluorometer (Thermo Fisher Scientific) did not differ significantly within the samples [mean 24 h 22.24 (ng/μL) ± SD 4.55 (ng/μL), mean 7 d 27.82 (ng/μL) ± SD 2.51 (ng/μL), mean total 25.03 (ng/μL) ± SD 9.05 (ng/μL)].

Samples were deep frozen (−80°C) and transferred to the mRNA sequencing facility at Max Planck Institute for Heart and Lung Research Bad Nauheim.

After verification of RNA quality (LabChip Gx Touch 24, Perkin Elmer), equal amounts of RNA from each sample were subjected to mRNA sequencing using a NextSeq 500 sequencer (Illumina, San Diego, CA, United States). FastQC tool (Babraham Bioinformatics, 2010) was used to verify signal quality, adaptor content and duplication rate. Adapters were removed and data trimmed; reads of a length between 30 and 150 base pairs were accepted for further analysis. Using STAR 2.4.0a, results were aligned to the murine mm10 genome (Ensembl) with maximum ratio of mismatches to mapped length set to 10%. Reads matching multiple genes or regions were excluded.

Quantitative Real Time PCR

Part of the total RNA (40 ng) from each sample was subjected to cDNA synthesis using RevertAid Reverse Transcriptase Kit (Thermo Fisher Scientific, Darmstadt, Germany). Quantitative Real Time PCR (qRT-PCR) was performed using TaqMan Gene Expression Assays in Applied Biosystems 96-well PCR plates (Thermo Fisher Scientific). Plates were sealed with Clear Seal Diamond Heat Sealing Film (Thermo Fisher Scientific) and run in an AB7500 fast system (Applied Biosystems, Thermo Fisher Scientific, Foster City, CA, United States). TaqMan probes (Thermo Fisher Scientific) were used to quantify transcripts of hypoxanthine phosphoribosyltransferase 1 (HPRT, Mm03024075_m1), matrix metalloproteinase 9 (MMP9, Mm00442991_m1) and tissue inhibitor of metalloproteinases 1 (TIMP1, Mm01341361_m1).

Immunohistochemical Staining on Cryosections

After sacrificing the animals, brains were extracted and natively frozen in Tissue TEK O.C.T. Compound (Sakura Finetek, Torrance, CA, United States) on dry ice and stored at −80°C. Coronal 10 μm sections were fixed in 4% PFA for 10 min and blocked in 10% fetal bovine serum in TBS-TritonX 0.3%. Tissue was incubated with primary antibodies (mouse-anti-mouse occludin, Invitrogen/Thermo Fisher Scientific #OC-3F10, 1:200; rat-anti-mouse CD31, BD Biosciences #BD553370, 1:200) for 2 h at room temperature followed by 1 h-incubation using fluorescence-conjugated secondary antibodies (donkey-anti-rat Alexa Fluor 488, donkey-antimouse Alexa Fluor 568, 1:400). After counter-staining for nucleic acids with 4',6-diamidino-2-phenylindole (DAPI, Sigma-Aldrich, St. Louis, MO, United States, 1:1000) sections were mounted with fluorescent mounting medium (Dako, Agilent, Santa Clara, CA, United States). Images were acquired at 40× magnification with a Nikon 80i microscope and quantified using NIS elements software (Nikon, Düsseldorf, Germany). Exposure time and LUTs settings were maintained at same values for all samples.

Statistical Methods

Reads obtained by *mRNA sequencing* were normalized and differentially analyzed using DESeq2 package version 1.14.1 (Love et al., 2014). To define genes as significantly regulated, a logarithmic fold change of at least ± 0.585, a mean value higher than 5 and p-value lower than 0.05 adjusted by Benjamini–Hochberg procedure for multiple comparisons was required.

For *qRT-PCR* validation cDNA levels were normalized to HPRT as this gene was identified as being unchanged between samples from ischemic and non-ischemic hemispheres. Differential expression was calculated by the $2^{-\Delta CT}$ method. Assuming a normally distributed population we used a t-test for separate comparison of sample pairs (sham ipsilateral 24 h versus tMCAO ipsilateral 24 h, sham ipsilateral 7 days versus tMCAO ipsilateral 7 days). A p-value below 0.05 was accepted as significant.

For *IHC* validation on cryosections we normalized occludin staining to CD31 positive vessels. To achieve this, we defined binaries for both antibodies by signal intensity in NIS elements software and measured the respective areas were measured. Afterward, the percentage of the CD31 + occludin-positive fraction from the total CD31-positive area was calculated. Separate comparison of sample pairs (core ipsilateral versus periinfarct ipsilateral 24 h, core ipsilateral versus core contralateral 24 h, core ipsilateral versus periinfarct ipsilateral 7 days, core ipsilateral versus core contralateral 7 days), was performed by t-test. A p-value below 0.05 was accepted as significant.

RESULTS

Establishment of the Post-stroke Care Protocol

Using the post-stroke care protocol of Lourbopoulos et al. (2017) that we established in our facility, we achieved similar survival rates in the tMCAO model as previously reported. With optimized monitoring and feeding support, the mortality at 7 days post-stroke was reduced to 28% (**Figure 1B**) from an expected mortality of at least 59%. The weight loss curve reached the nadir at day 3 for sham operated mice and at day 5 for animals which underwent tMCAO. From day 6 onward, weight either stabilized or started to recover (**Figure 1C**).

Expression Dynamics After Cerebral I/R Injury

Of a total of 141,136 reads in protein coding sequences 12,690 show significant regulation in altogether 7 comparisons (1: stroke ipsi- versus contralateral 24 h, 2: stroke ipsi- versus contralateral 7 days, 3: sham ipsi- versus contralateral 24 h, 4: sham ipsi- versus contralateral 7 days, 5: stroke ipsilateral versus sham ipsilateral 24 h, 6: stroke ipsilateral versus sham ipsilateral 7 days, and 7: stroke ipsilateral 24 h versus 7 days). Principal component analysis (PCA) revealed that all control samples (contralateral hemispheres of mice 24 h and 7 days post-stroke as well as both hemispheres of sham operated animals) cluster together. As no major differences were seen between the different controls we decided to continue analysis on comparisons 5–7. Heatmaps and pathway analyses of comparisons 1 and 2 can be seen

in **Supplementary Figure I**. The ipsilateral hemispheres 24 h post-stroke form a distinctive cluster farthest from the controls. Ipsilateral hemispheres 7 days post-stroke cluster between the acutely ischemic tissue and the controls indicating post-stroke recovery (**Figure 2B**). Volcano plots (significance versus fold-change) show 2869 up- and 2449 downregulated genes in the ipsilateral hemisphere of tMCAO- compared to sham-operated animals 24 h post-surgery and 701 genes up- and 1558 downregulated 7 days post-surgery (**Figure 2C**).

Figure 3 shows top 25 up- and downregulated genes at 24 h and 7 days post-stroke and their bioinformatic pathway analyses using KOBAS (Xie et al., 2011). Several genes belonging to the ECM-receptor interaction such as TIMP1 and cell adhesion molecules are dysregulated at 24 h post-stroke indicating an acute BBB breakdown. Metabolic and inflammatory pathways are highly regulated indicating the ischemic injury and the ensuing immune response (**Figure 3A**). At day 7, cell adhesion molecules and ECM-receptor interaction pathways are still dysregulated compared to sham control indicating BBB impairment also in the postacute phase.

Quantitative Validation of Transcriptional Changes in Proteinases

As a measure of representativeness of the observed dynamics, we aimed to validate the well characterized post-ischemic changes in the MMP/TIMP system. MMP9 expression is dramatically increased after 24 h and still significantly upregulated after 7 days when compared to sham animals. qPCR measurements confirmed the acute overshoot of MMP9 (**Figure 4A**). Similarly, for TIMP1 a massive increase could be detected by RNA sequencing and reproduced by qPCR validation (**Figure 4B**).

Changes in MMP/TIMP expression are paralleled by breakdown of tight junction markers. By immunohistochemical staining (IHC), occludin signal was reduced at both time points within the stroke region in comparison to CD31 staining reaching significance on 7 days post-stroke. Representative images of the stroke core and corresponding area in the contralateral hemisphere as well as quantification of occludin staining fraction of CD31 positive vessels are shown in **Supplementary Figure II**.

Expression Dynamics in the Early Regeneration Phase Post-stroke

In order to characterize the intermediate-term expression dynamics post-stroke, we compared the gene expression pattern relative to sham controls at 24 h post-stroke with that of 7 days post-stroke. We defined four groups, namely resolved, induced, unresolved, and biphasic for further analyses as shown in the Venn diagrams of **Figure 5A**. Genes that are regulated at 24 h but not anymore at 7 days post-stroke belong to the resolved group (771 genes). Genes that are not regulated at 24 h but only at 7 days post-stroke belong to the induced group (131 genes). Genes that are upregulated at both time points (201 genes) along with genes that are downregulated at both time points (796 genes) belong to the unresolved group (201 + 796 = 997 genes). Finally, genes that are upregulated at 24 h but downregulated at 7 days (26 genes) and vice-versa (51 genes) are categorized into the biphasic group (26 + 51 = 77 genes).

Top 25 regulated genes in each direction for all the groups are summarized by heatmaps (**Figure 5B**). Top 20 pathways identified by gene set enrichment analysis (KOBAS KEGG) are shown in **Figure 5C** for all the groups. Several transcripts belonging to metabolic pathways such as PINK1 are resolved at day 7. This is accompanied by induction of pathways of angiogenic/ECM-remodeling (e.g., HIF-1- and proteoglycan-associated pathways) and inflammation at day 7 including genes of innate immunity (e.g., SAMHD1). However, some genes are unresolved by 7 days post-stroke comprising primarily cell adhesion and ECM-endothelial interaction molecules such as ITGB2, ITGA5 indicating persistent disruption of the BBB but also glutamatergic pathways as a hint for ongoing cytotoxicity.

The biphasic group represents genes that are counter-regulated by 7 days compared to 24 h post-stroke potentially in a compensatory manner for neurovascular regeneration. Wnt signaling is one of the major pathways regulated in such a biphasic manner at the NVU (**Figure 5C**). Wnt family members 5A (WNT5a) and 11 (WNT11) are significantly decreased 24 h and strongly induced 7 days after tMCAO. This is paralleled by induction of transcription factor SRY-Box 17 (SOX17) on day 7. Transcripts of LDL receptor related proteins 5 (LRP5) and 6 (LRP 6) which represent direct actors in the Wnt/β-catenin signaling cascade are acutely reduced (**Supplementary Figure III**).

DISCUSSION

The struggle for translation from bench to bedside in preclinical stroke research was paralleled by significant clinical advances that occurred rather independently. To date, patients benefit from effective recanalization therapies (Berkhemer et al., 2015; Lees et al., 2016) and the stroke unit concept which includes close monitoring, treatment of complications and rehabilitation (Indredavik et al., 1991; Stroke Unit Trialists' Collaboration, 2013). Those innovations have changed stroke patients' populations and needs while post-stroke care for mice has not been adapted accordingly.

Brain reperfusion injury after vessel occlusion and recanalization is best modeled by tMCAO but should go along with understanding and careful consideration of surgery-associated side effects. In a recent study, Lourbopoulos et al. (2017) set out to overcome technical confounders and mortality bias of this model by establishing a stroke unit-like post-stroke care protocol. They achieved a relevant increase in survival rates making this model now practicable for long-term observations. From our point of view, this is a fine example of translation from the clinic to the laboratory to make experimental models more reliable which may in turn facilitate translation from the laboratory to the clinic.

Since we are interested in time-dependent transcriptome changes at the NVU to identify potential therapeutic targets beyond the narrow time window of current recanalization-focused interventions, we chose this model to obtain a translationally relevant sample. The recorded transcriptomic

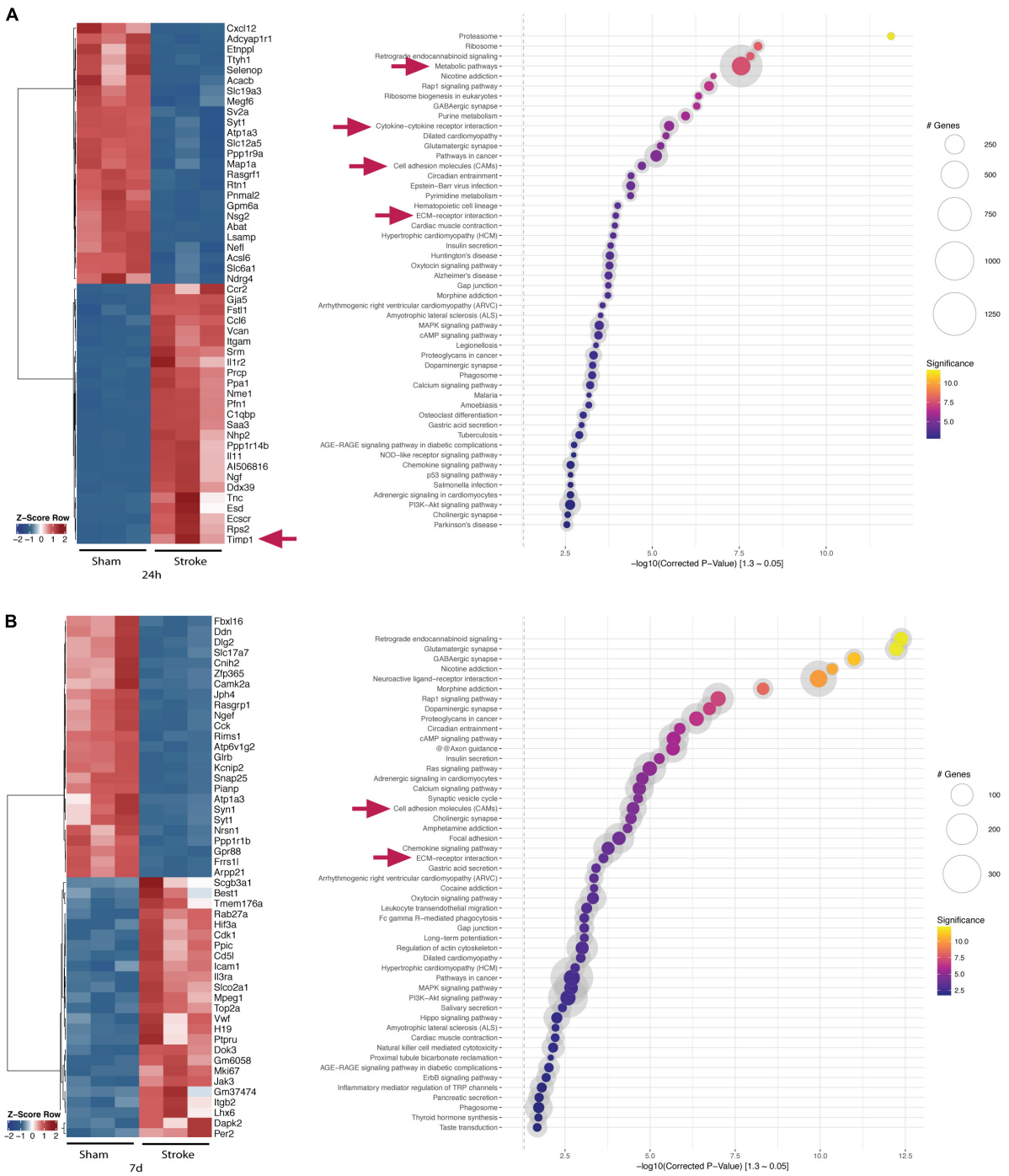

FIGURE 3 | Top-regulated genes and pathways in the acute and postacute stage post-stroke after DESEQ2 normalization. **(A)** *Z*-score of top 25 up- and top 25 downregulated genes in the ipsilateral hemisphere of tMCAO- versus sham-operated animals 24 h post-surgery and gene set enrichment within the identified genes. **(B)** Z-score of top 25 up- and top 25 downregulated genes in the ipsilateral hemisphere of tMCAO- versus sham-operated animals 7 days post-surgery and gene set enrichment within the identified genes. Transcripts accepted as regulated: mean > 5 counts, $\log_2$fc <> ±0.585, FDR ≤ 0.05. Exemplary genes and gene sets are highlighted (arrows).

dynamics representatively reflect inflammatory response at the brain microvasculature at an early and a late timepoint, its imbalance of cell adhesion and matrix components, the associated messengers and enzymes and the take-over by regenerative processes. PCA revealed that most dramatic transcriptomic changes occur at 24 h after stroke and already

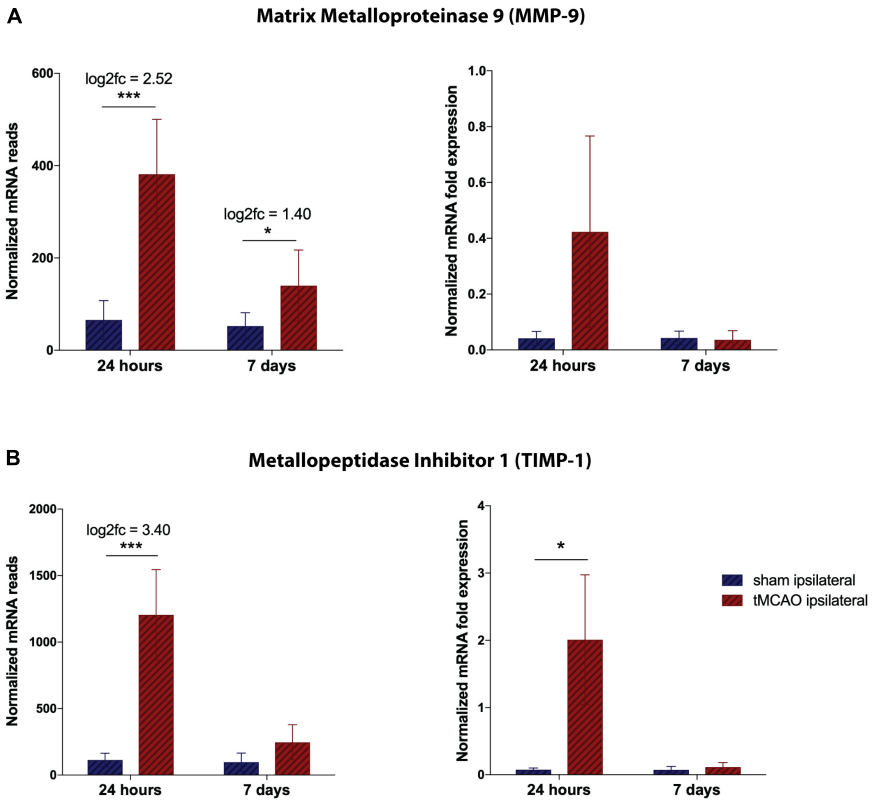

FIGURE 4 | Validation of RNA sequencing dataset by qRT-PCR for proteinases at the NVU. **(A)** Total mRNA reads for TIMP-1 and MMP-9, normalized by DESEQ2. Presented as mean counts per group ± SD, logarithmic fold change and summarized *p*-value ($n = 3$ per group). **(B)** Quantitative validation by qPCR on remaining RNA and freshly isolated samples, normalized to HPRT. Presented as mean $2^{-\Delta CT}$ values per group ± SD and summarized *p*-value ($n = 3$ per group). $^{*}p$-value < 0.05, $^{***}p$-value < 0.0005.

begin to resolve after 1 week. As acute I/R injury-associated breakdown of the BBB, leading to enhanced vascular edema and risk of hemorrhagic transformation gained increasing importance in the light of current stroke treatment, the focus of our study was on the brain microvasculature. Targeting the cellular and extracellular interplay within this compartment might help to overcome present therapeutic limitations (Gurnik et al., 2016; Manley et al., 2000). Exemplarily and as a validation of our dataset, we analyzed MMP-9 and TIMP-1 by quantitative PCR and could confirm the previously observed dramatic imbalance of MMPs and their inhibitors (Lenglet et al., 2014) in our samples.

In order to identify central regulatory pathways that emerge within the first week post-stroke at the BBB, we compared the gene expression patterns at 24 h and 7 days. Gene expression and bioinformatic pathway analyses indicate resolution of several pathways including metabolic and apoptotic signaling cascades by 7 days while – rather surprisingly – glutamatergic pathways remain unresolved (indicated by KEGG pathway terms "glutamatergic synapse" but also "nicotine addiction" and "morphine addiction") (Kegg Pathway Maps, 2020). Late induction of PINK1, a mitophagy regulator to clear damaged mitochondria, indicates potential resolution of mitochondrial dysfunction and repair of I/R injury as shown previously in cardiac and renal ischemia (Siddall et al., 2013; Tang et al., 2018). The role of mitophagy in ischemic stroke is however not fully understood (Guan et al., 2018).

Furthermore, induction of HIF-1- and proteoglycan-associated pathways at 7 days indicate angiogenic remodeling. Mutations in SAMHD1, a dNTPase known to be important for innate immunity, have been shown to lead to cerebral vasculopathy and early onset stroke (Xin et al., 2011). Along this line, our dataset shows an induction of SAMHD1 in the postacute phase suggesting a potential role for SAMHD1 in post-stroke vascular repair and regeneration. However, several genes are unresolved 7 days after tMCAO especially cell-adhesion molecules such as integrins ITGB2 and ITGA5 as reported previously to be dysregulated in the acute phase (Edwards and Bix, 2018). Previous studies support the therapeutic significance of this group for integrin-based therapeutics (Ley et al., 2016).

A unique feature achieved by intermediate-term observation after stroke is the identification of biphasically regulated genes which might otherwise be misinterpreted. These genes are regulated in one direction at 24 h and in the opposite direction at 7 days post-stroke and potentially represent compensatory mechanisms essential for post-stroke recovery. As an intriguing example, actors of the Wnt signaling cascade, namely WNT5a, WNT11 and – as a downstream target of canonical Wnt

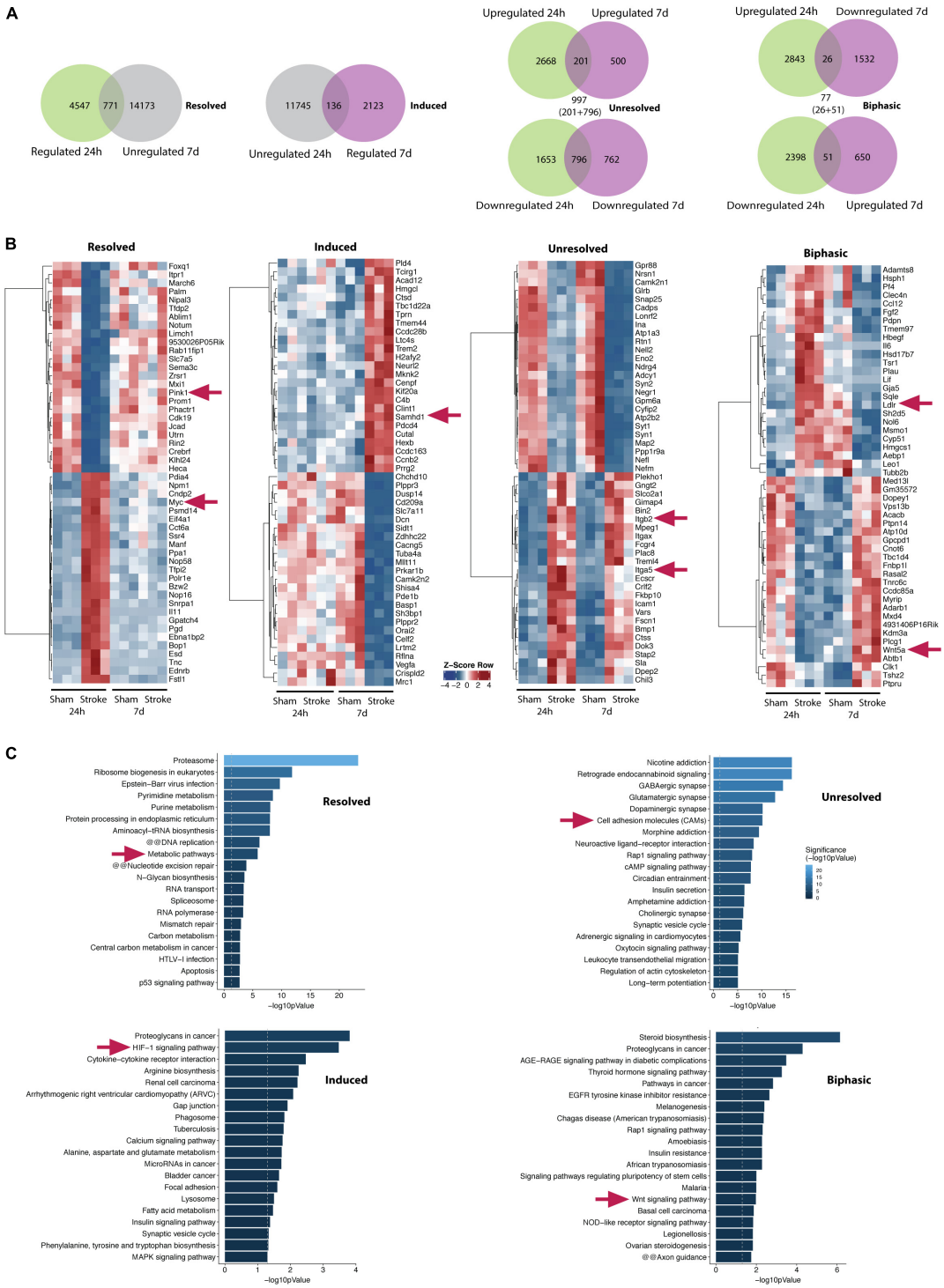

FIGURE 5 | Transcriptomic dynamics at the NVU within one week after stroke. **(A)** Venn diagrams show numbers of genes which are regulated 24 h (first from left, green/left circle) and genes which are not regulated 7 days post-stroke in the ipsilateral hemisphere (first from left, gray/right circle). A total of 771 genes belonging to both groups are defined as resolved (first from left, overlap). A total of 136 genes (second from left, overlap) which are regulated 7 days (second from left, violet/right circle) and not regulated 24 h post-stroke (second from left, gray/left circle) are defined as induced. A total of 997 genes (second from right, sum of overlapping genes) which are either up- or downregulated at both time points are defined as unresolved. A total of 77 genes (first from right, sum of overlapping genes) which are oppositely regulated at both time points are defined as biphasic. **(B)** *Z*-score of top 25 up- and top 25 downregulated genes of induced, resolved and unresolved genes. For biphasic genes top 25 toward each direction are shown (first half: upregulated 24 h and downregulated 7 days post-stroke, second half: downregulated 24 h and upregulated 7 days post-stroke). **(C)** Corresponding bar graphs summarize gene set enrichment within the identified genes. Exemplary genes and gene sets are highlighted (arrows).

signaling – SOX17 show such an expression pattern. While these factors and their direct responders LRP5 and LRP6 are significantly reduced in the acute phase, they show an induction 7 days after tMCAO. This finding is of special interest as Wnt/β-catenin signaling has recently been shown to conduct its crucial role in brain angiogenesis and BBB formation at the NVU (Liebner et al., 2008; Reis et al., 2012) potentially via SOX17 induction (Corada et al., 2018). Furthermore, pharmacological induction of β-Catenin by CHIR99021 was able to reactivate matured cardiomyocytes and therefore suggested as a future approach for regeneration after myocardial infarction (Fan et al., 2018). The same compound has been reported to suppress MMP9 release from macrophages *in vitro* (Kim et al., 2015) which also implies a potential use in BBB protection after cerebral I/R injury. Our current results might help in designing future *in vivo* assessment of this approach according to the biphasic regulation of the Wnt signaling cascade.

Previous RNA sequencing approaches after cerebral I/R injury used either the complete tissue of the affected hemisphere or focused on a specific cell type. Recently, a genome-wide analysis of brain tissue of rats 4.5 and 24 h post tMCAO depicted the acute and hyperacute transcriptional changes within the subcortex of the stroke hemisphere (Dergunova et al., 2018). They identified transcription factors, cytokines and hormones as being regulated already within the first hours after stroke onset and a shift within the expressed cytokine classes until 24 h post-stroke. KEGG pathway analysis showed some common regulations with our dataset e.g., in calcium signaling, MAPK signaling, and ECM-receptor interaction. Interestingly, oxytocine signaling was found to be regulated already at 4.5 h post-stroke which our analysis of microvessels after tMCAO in mice revealed to be unresolved over the first 7 days (**Figure 5C**). In another study by Duan et al. (2019) the affected hemisphere of rats was isolated 4 days after tMCAO and used to identify long non-coding (lnc)RNA transcripts as potential regulators of apoptosis-associated gene expression. They suggest important lncRNA to be co-expressed in KEGG pathway analysis with calcium signaling, TNF and EBV signaling which mainly comprises pro-inflammatory cytokines as well as PI3K-Akt signaling. Our dataset adds the prolonged scope of transcription dynamics with an explicit focus on the NVU including all its cellular compartments which is why in our study BBB-associated gene transcripts are much more prominent than in the aforementioned works.

Isolating microvessel fragments allows us to picture the dynamics in most components of the NVU (mainly endothelial cells, but to a lesser extent also pericytes, astrocytic endfeet, adjacent microglia and neurons). But it also goes along with certain limitations as it does not allow to pinpoint the specific cellular source of the observed changes. To keep contamination by peripheral blood cells to a minimum, all mice underwent thorough transcardial perfusion before brain isolation. Nevertheless, some immune cells might have been trapped in the microvasculature. From our point of view, this is not necessarily a weakness as immune cells play a crucial role in the vascular pathophysiology after I/R injury and contribute to the transcriptional pattern including cytokine-cytokine receptor interactions and expression of cell adhesion molecules. The contralateral hemispheres of the affected mice and both hemispheres of sham operated animals separately served as controls for stroke-associated changes.

Due to the hereby-caused complexity of the dataset our study is limited to a standard ischemia duration of 60 min and two investigated timepoints. Future studies are needed to investigate (a) shorter occlusion times to capture processes in primarily subcortical/minor strokes, (b) permanent filament insertion to assess differential dynamics between cerebral ischemia with and without reperfusion injury, (c) earlier (e.g., 72 h post-stroke, focusing on first- versus second-line inflammatory reaction) and later timepoints (e.g., 1 month after stroke to assess chronic repair processes), and (d) gene expression data from complete hemispheric tissue in relation to data specifically derived from microvessels of the ischemic hemisphere. Another limitation of our approach is that we isolated microvessels from the whole hemispheres as otherwise the material yield would have been too low for representative mRNA sequencing analysis. Therefore, it has to be kept in mind that our results stem from infarcted, peri-infarct and partly from intact brain regions. By this, genes of interest have to be validated subsequently on the spatial level. Exemplarily, we chose immunofluorescence staining to assess the differential expression of occludin in ischemic and non-ischemic vasculature. We found that within the infarct area, occludin expression was still significantly downregulated after 7 days while staining was normalized in the periinfarct cortex at this time point, in accordance with previous reports (Sun et al., 2017).

CONCLUSION

In summary, we provide a well-controlled transcriptome dataset of a translationally relevant mouse cohort after tMCAO. Keeping the above-mentioned limitations in mind, this dataset may help to identify future therapeutic targets in post-stroke inflammation and repair processes including acute BBB alterations, glial scar formation, angiogenesis and neuroregeneration.

DATA AVAILABILITY STATEMENT

The authors declare that all supporting data are available within the article and **Supplementary Material**. The RNA sequencing dataset has been uploaded to GEO (record GSE131193).

ETHICS STATEMENT

The animal study was reviewed and approved by the Regierungspräsidium Darmstadt.

AUTHOR CONTRIBUTIONS

RB, WP, and KD conceived of the presented idea and developed the experimental design together with R-IK. R-IK carried out the surgeries, post-stroke survival care, microvessel and mRNA isolation under support of RV, LH, and KD. SG performed the

mRNA sequencing and supplied the respective graphs upon joined the data analysis with R-IK, FM, KD, WP, and RB. R-IK and FM were carried out the staining and qPCR validation. R-IK, WP, and KD prepared the manuscript.

FUNDING

R-IK, RB, and WP received funding from the Fondation Leducq (SphingoNet) and the German Research Foundation (SFB 1039/TP B08). R-IK was supported by a stipend from the Medical Faculty of Goethe University ("Patenschaftsmodell").

ACKNOWLEDGMENTS

We would like to acknowledge Ricardo Mamede Figueiredo and Elif Fidan for their support in data analysis.

SUPPLEMENTARY MATERIAL

The Supplementary Material for this article can be found online at: https://www.frontiersin.org/articles/10.3389/fnins.2020.00280/full#supplementary-material

REFERENCES

Asahi, M., Asahi, K., Jung, J. C., del Zoppo, G. J., Fini, M. E., and Lo, E. H. (2000). Role for matrix metalloproteinase 9 after focal cerebral ischemia: effects of gene knockout and enzyme inhibition with BB-94. *J. Cereb. Blood. Flow. Metab.* 20, 1681–1689. doi: 10.1097/00004647-200012000-00007

Babraham Bioinformatics (2010). *Babraham Bioinformatics*. Available online at: https://www.bioinformatics.babraham.ac.uk/projects/fastqc (accessed November 24, 2019).

Bai, J., and Lyden, P. D. (2015). Revisiting cerebral postischemic reperfusion injury: new insights in understanding reperfusion failure, hemorrhage, and edema. *Int. J. Stroke* 10, 143–152. doi: 10.1111/ijs.1243

Barr, T. L., Latour, L. L., Lee, K. Y., Schaewe, T. J., Luby, M., Chang, G. S., et al. (2010). Blood-brain barrier disruption in humans is independently associated with increased matrix metalloproteinase-9. *Stroke* 41, e123–e128. doi: 10.1161/STROKEAHA.109.570515

Berkhemer, O. A., Fransen, P. S. S., Beumer, D., van den Berg, L. A., Lingsma, H. F., Yoo, A. J., et al. (2015). A randomized trial of intraarterial treatment for acute ischemic stroke. *N. Engl. J. Med.* 372, 11–20. doi: 10.1056/NEJMoa1411587

Choi, J. H., and Pile-Spellman, J. (2018). Reperfusion changes after stroke and practical approaches for neuroprotection. *Neuroimag. Clin. N. Am.* 28, 663–682. doi: 10.1016/j.nic.2018.06.008

Corada, M., Orsenigo, F., Bhat, G. P., Conze, L. L., Breviario, F., Cunha, S. I., et al. (2018). Fine tuning of sox17 and canonical wnt coordinates the permeability properties of the blood-brain barrier. *Circ. Res.* 0, 1–20. doi: 10.1161/CIRCRESAHA.118.313316

Cummins, P. M. (2012). Occludin: one protein. *Many Forms. Mol. Cell. Biol.* 32, 242–250. doi: 10.1128/MCB.06029-11

Dergunova, L. V., Filippenkov, I. B., Stavchansky, V. V., Denisova, A. E., Yuzhakov, V. V., Mozerov, S. A., et al. (2018). Genome-wide transcriptome analysis using RNA-Seq reveals a large number of differentially expressed genes in a transient MCAO rat model. *BMC Genom.* 19:655. doi: 10.1186/s12864-018-5039-5

Duan, X., Han, L., Peng, D., Peng, C., Xiao, L., Bao, Q., et al. (2019). Bioinformatics analysis of a long non-coding RNA and mRNA regulation network in rats with middle cerebral artery occlusion based on RNA sequencing. *Mol. Med. Rep.* 20, 417–432. doi: 10.3892/mmr.2019.10300

Edwards, D. N., and Bix, G. J. (2018). Roles of blood-brain barrier integrins and extracellular matrix in stroke. *Am. J. Physiol. Cell. Physiol.* 316, C252–C263. doi: 10.1152/ajpcell.00151.2018

Fan, Y., Ho, B. X., Pang, J. K. S., Pek, N. M. Q., Hor, J. H., Ng, S. Y., et al. (2018). Wnt/β-catenin-mediated signaling re-activates proliferation of matured cardiomyocytes. *Stem Cell Res. Ther.* 9:338. doi: 10.1186/s13287-018-1086-8

Friedländer, F., Bohmann, F., Brunkhorst, M., Chae, J. H., Devraj, K., Köhler, Y., et al. (2017). Reliability of infarct volumetry: its relevance and the improvement by a software-assisted approach. *J. Cereb. Blood Flow Metab.* 37, 3015–3026. doi: 10.1177/0271678X16681311

Guan, R., Zou, W., Dai, X., Yu, X., Liu, H., Chen, Q., et al. (2018). Mitophagy a potential therapeutic target for stroke. *J. Biomed. Sci.* 25:87. doi: 10.1186/s12929-018-0487-4

Gurnik, S., Devraj, K., Macas, J., Yamaji, M., Starke, J., Scholz, A., et al. (2016). Angiopoietin-2-induced blood-brain barrier compromise and increased stroke size are rescued by VE-PTP-dependent restoration of Tie2 signaling. *Acta Neuropathol.* 131, 753–773. doi: 10.1007/s00401-016-1551-3

Iadecola, C. (2017). The neurovascular unit coming of age: a journey through neurovascular coupling in health and disease. *Neuron* 96, 17–42. doi: 10.1016/j.neuron.2017.07.030

Indredavik, B., Bakke, F., Solberg, R., Rokseth, R., Haaheim, L. L., and Holme, I. (1991). Benefit of a stroke unit: a randomized controlled trial. *Stroke* 22, 1026–1031. doi: 10.1161/01.str.22.8.1026

Kegg Pathway Maps (2020). *Last visited on 20th January 2020*. Available online at: https://www.kegg.jp/kegg-bin/get_htext?query=04728&htext=br08901.keg&option=-a (accessed November 24, 2019).

Kidwell, C. S., Saver, J. L., Matiello, J., Starkman, S., Vinuela, F., Duckwiler, G., et al. (2001). Diffusion-perfusion MRI characterization of post-recanalization hyperperfusion in humans. *Neurology* 57, 2015–2021. doi: 10.1212/WNL.57.11.2015

Kim, S., Bong, N., Kim, O. S., Jin, J., Kim, D. E., and Lee, D. K. (2015). Lithium chloride suppresses LPS mediated matrix metalloproteinase-9 expression in macrophages through phosphorylation of GSK-3β. *Cell Biol. Int.* 2, 177–184. doi: 10.1002/cbin.10352

Knowland, D., Arac, A., Sekiguchi, K. J., Hsu, M., Lutz, S. E., Perrino, J., et al. (2014). Stepwise recruitment of transcellular and paracellular pathways underlies blood-brain barrier breakdown in stroke. *Neuron* 82, 603–617. doi: 10.1016/j.neuron.2014.03.003

Krueger, M., Bechmann, I., Immig, K., Reichenbach, A., Härtig, W., and Michalski, D. (2015). Blood-brain barrier breakdown involves four distinct stages of vascular damage in various models of experimental focal cerebral ischemia. *J. Cereb. Blood Flow Metab.* 35, 292–303. doi: 10.1038/jcbfm.2014.199

Lees, K. R., Emberson, J., Blackwell, L., Bluhmki, E., Davis, S. M., Donnan, G. A., et al. (2016). Effects of alteplase for acute stroke on the distribution of functional outcomes. A pooled analysis of 9 trials. *Stroke* 47, 2373–2379. doi: 10.1161/STROKEAHA.116.013644

Lenglet, S., Montecucco, F., Mach, F., Schaller, K., Gasche, Y., and Copin, J. C. (2014). Analysis of the expression of nine secreted matrix metalloproteinases and their endogenous inhibitors in the brain of mice subjected to ischaemic stroke. *Thromb. Haemost.* 112, 363–378. doi: 10.1160/TH14-01-0007

Ley, K., Rivera-Nieves, J., Sandborn, W. J., and Shattil, S. (2016). Integrin-based therapeutics: biological basis, clinical use and new drugs. *Nat. Rev. Drug Discov.* 15, 173–183. doi: 10.1038/nrd.2015.10

Liebner, S., Corada, M., Bangsow, T., Babbage, J., Taddei, A., Czupalla, C. J., et al. (2008). Wnt/β-catenin signaling controls development of the blood-brain barrier. *J. Cell. Biol.* 183, 409–417. doi: 10.1083/jcb.200806024

Lipton, P. (1999). Ischemic cell death in brain neurons. *Physiol. Rev.* 79, 1431–1586. doi: 10.1152/physrev.1999.79.4.1431

Lourbopoulos, A., Mamrak, U., Roth, S., Balbi, M., Shrouder, J., Liesz, A., et al. (2017). Inadequate food and water intake determine mortality following stroke in mice. *J. Cereb. Blood. Flow. Metab.* 37, 2084–2097. doi: 10.1177/0271678X16660986

Love, M. I., Huber, W., and Anders, S. (2014). Moderated estimation of fold change and dispersion for RNA-seq data with DESeq2. *Genome Biol.* 15:550. doi: 10.1186/s13059-014-0550-8

Ma, Y., Wang, J., Wang, Y., and Yang, G. Y. (2017). The biphasic function of microglia in ischemic stroke. *Prog. Neurobiol.* 157, 247–272. doi: 10.1016/j.pneurobio.2016.01.005

Manley, G. T., Fujimura, M., Ma, T., Noshita, N., Filiz, F., Bollen, A. W., et al. (2000). Aquaporin-4 deletion in mice reduces brain edema after acute water intoxication and ischemic stroke. *Nat. Med.* 6, 159–163. doi: 10.1038/72256

O'Collins, V. E., Macleod, M. R., Donnan, G. A., Horky, L. L., van der Worp, B. H., and Howells, D. W. (2006). 1,026 experimental treatments in acute stroke. *Ann. Neurol.* 59, 467–477. doi: 10.1002/ana.20741

Pfeilschifter, W., Bohmann, F., Baumgarten, P., Mittelbronn, M., Pfeilschifter, J., Lindhoff−Last, E., et al. (2012). Thrombolysis with recombinant tissue plasminogen activator under dabigatran anticoagulation in experimental stroke. *Ann. Neurol.* 71, 624–633. doi: 10.1002/ana.23558

Reis, M., Czupalla, C. J., Ziegler, N., Devraj, K., Zinke, J., Seidel, S., et al. (2012). Endothelial Wnt//β-catenin signaling inhibits glioma angiogenesis and normalizes tumor blood vessels by inducing PDGF-B expression. *J. Exp. Med.* 209, 1611–1627. doi: 10.1084/jem.20111580

Sandvig, I., Augestad, I. L., Håberg, A. K., and Sandvig, A. (2018). Neuroplasticity in stroke recovery. The role of microglia in engaging and modifying synapses and networks. *Eur. J. Neurosci.* 47, 1414–1428. doi: 10.1111/ejn.13959

Siddall, H. K., Yellon, D. M., Ong, S. B., Mukherjee, U. A., Burke, N., Hall, A. R., et al. (2013). Loss of PINK1 increases the heart's vulnerability to ischemia-reperfusion injury. *PLoS One* 8:e62400. doi: 10.1371/journal.pone.0062400

Strbian, D., Durukan, A., Pitkonen, M., Marinkovic, I., Tatlisumak, E., Pedrono, E., et al. (2008). The blood–brain barrier is continuously open for several weeks following transient focal cerebral ischemia. *Neuroscience* 153, 175–181. doi: 10.1016/j.neuroscience.2008.02.012

Stroke Unit Trialists' Collaboration (2013). Organised inpatient (stroke unit) care for stroke. *Cochrane Database Syst. Rev.* 17:CD000197.

Sun, J., Yu, L., Huang, S., Lai, X., Milner, R., Li, L., et al. (2017). Vascular expression of Angiopoietin1, a5B1 integrin and tight junction proteins is tightly regulated during vascular remodeling in the post-ischemic brain. *Neuroscience* 362, 248–256. doi: 10.1016/j.neuroscience.2017.08.040

Szydlowska, K., and Tymianski, M. (2010). Calcium, ischemia and excitotoxicity. *Cell Calcium* 47, 122–129. doi: 10.1016/j.ceca.2010.01.003

Tang, C., Han, H., Yan, M., Zhu, S., Liu, J., Liu, Z., et al. (2018). PINK1-PRKN/PARK2 pathway of mitophagy is activated to protect against renal ischemia-reperfusion injury. *Autophagy* 14, 880–897. doi: 10.1080/15548627.2017.1405880

Xie, C., Mao, X., Huang, J., Ding, Y., Wu, J., Dong, S., et al. (2011). KOBAS 2.0: a web server for annotation and identification of enriched pathways and diseases. *Nucleic Acids Res.* 39, W316–W322. doi: 10.1093/nar/gkr483

Xin, B., Jones, S., Puffenberger, E. G., Hinze, C., Bright, A., Tan, H., et al. (2011). Homozygous mutation in SAMHD1 gene causes cerebral vasculopathy and early onset stroke. *Proc. Natl. Acad. Sci. U.S.A.* 108, 5372–5377. doi: 10.1073/pnas.1014265108

Yang, Y., Estrada, E. Y., Thompson, J. F., Liu, W., and Rosenberg, G. A. (2007). Matrix metalloproteinase-mediated disruption of tight junction proteins in cerebral vessels is reversed by synthetic matrix metalloproteinase inhibitor in focal ischemia in rat. *J. Cereb. Blood. Flow. Metab.* 27, 697–709. doi: 10.1038/sj.jcbfm.9600375

Zhao, B. Q., Wang, S., Kim, H. Y., Storrie, H., Rosen, B. R., Mooney, D. J., et al. (2006). Role of matrix metalloproteinases in delayed cortical responses after stroke. *Nat. Med.* 12, 441–445. doi: 10.1038/nm1387

Conflict of Interest: The authors declare that the research was conducted in the absence of any commercial or financial relationships that could be construed as a potential conflict of interest.

Copyright © 2020 Kestner, Mayser, Vutukuri, Hansen, Günther, Brunkhorst, Devraj and Pfeilschifter. This is an open-access article distributed under the terms of the Creative Commons Attribution License (CC BY). The use, distribution or reproduction in other forums is permitted, provided the original author(s) and the copyright owner(s) are credited and that the original publication in this journal is cited, in accordance with accepted academic practice. No use, distribution or reproduction is permitted which does not comply with these terms.

frontiers in Cellular Neuroscience

METHODS
published: 09 April 2020
doi: 10.3389/fncel.2020.00084

Isolation of Mouse Cerebral Microvasculature for Molecular and Single-Cell Analysis

*Hallel C. Paraiso[1], Xueqian Wang[2], Ping-Chang Kuo[3], Destin Furnas[3], Barbara A. Scofield[3], Fen-Lei Chang[4], Jui-Hung Yen[3] and I-Chen Yu[1]**

[1]Department of Anatomy, Cell Biology, and Physiology, Indiana University School of Medicine, Fort Wayne, IN, United States, [2]Department of Pharmacology and Toxicology, Indiana University School of Medicine, Fort Wayne, IN, United States, [3]Department of Microbiology and Immunology, Indiana University School of Medicine, Fort Wayne, IN, United States, [4]Department of Neurology, Indiana University School of Medicine, Fort Wayne, IN, United States

Brain microvasculature forms a specialized structure, the blood-brain barrier (BBB), to maintain homeostasis and integrity of the central nervous system (CNS). The BBB dysfunction is emerging as a critical contributor to multiple neurological disorders, including stroke, traumatic brain injury, autoimmune multiple sclerosis, and neurodegenerative diseases. The brain microvasculature exhibits highly cellular and regional heterogeneity to accommodate dynamic changes of microenvironment during homeostasis and diseases. Thus, investigating the underlying mechanisms that contribute to molecular or cellular changes of the BBB is a significant challenge. Here, we describe an optimized protocol to purify microvessels from the mouse cerebral cortex using mechanical homogenization and density-gradient centrifugation, while maintaining the structural integrity and functional activity of the BBB. We show that the isolated microvessel fragments consist of BBB cell populations, including endothelial cells, astrocyte end-feet, pericytes, as well as tight junction proteins that seal endothelial cells. Furthermore, we describe the procedures to generate single-cell suspensions from isolated microvessel fragments. We demonstrate that cells in the single-cell suspensions are highly viable and suitable for single-cell RNA-sequencing analysis. This protocol does not require transgenic mice and cell sorting equipment to isolate fluorescence-labeled endothelial cells. The optimized procedures can be applied to different disease models to generate viable cells for single-cell analysis to uncover transcriptional or epigenetic landscapes of BBB component cells.

Keywords: blood-brain barrier, endothelial cells, brain capillaries, single-cell isolation, microvasculature damage

OPEN ACCESS

Edited by:
Emmanuel Pinteaux, University of Manchester, United Kingdom

Reviewed by:
Hector Rosas-Hernandez, National Center for Toxicological Research (FDA), United States
Leyre Mestre, Cajal Institute (CSIC), Spain

****Correspondence:***
I-Chen Yu
ivoyu@iu.edu

Specialty section:
This article was submitted to Cellular Neuropathology, a section of the journal Frontiers in Cellular Neuroscience

Received: *23 December 2019*
Accepted: *20 March 2020*
Published: *09 April 2020*

Citation:
Paraiso HC, Wang X, Kuo P-C, Furnas D, Scofield BA, Chang F-L, Yen J-H and Yu I-C (2020) Isolation of Mouse Cerebral Microvasculature for Molecular and Single-Cell Analysis. Front. Cell. Neurosci. 14:84. doi: 10.3389/fncel.2020.00084

INTRODUCTION

The brain vasculature is a complex system composed of endothelial cells, pericytes, astrocytes, smooth muscle cells, and extracellular matrix components, forming the unique blood-brain barrier (BBB), which lies at the interface between circulating blood and the neural tissue (Abbott and Friedman, 2012; Obermeier et al., 2013). The BBB tightly regulates the transport of ions and nutrients necessary for neuronal health and function. It also prevents harmful substances or cells

from entering into the central nervous system (CNS). Previous literature suggests that the BBB disruption can lead to neuronal injury mediated through peripheral immune cells or harmful agents that enter into the CNS in multiple neurological disorders, such as Alzheimer's disease (AD; Sweeney et al., 2018; Nation et al., 2019), ischemic stroke (Kassner and Merali, 2015), multiple sclerosis (Ortiz et al., 2014), and traumatic brain injury (Alluri et al., 2015). Despite the importance of BBB highlighted in many neurological disorders, the molecular and cellular mechanisms that lead to BBB dysfunction or disruption in these disease conditions remain largely unknown. Therefore, it is vital to develop a method to isolate brain microvasculature with preserved structural integrity to identify subtle aberrations of the BBB in disease animal models. Here, we describe an optimized protocol that would allow isolating brain microvessels that closely resemble *in vivo* structures suitable for downstream applications of molecular and single-cell analyses to characterize molecular signatures of BBB component cells.

MATERIALS AND EQUIPMENTS

Animals

C57BL/6 and *db*/*db* mice were purchased from the Jackson Laboratory and bred at the animal facility of Indiana University School of Medicine. Mice were housed and maintained at 25°C under a 12 h light/ 12 h dark cycle with ad libitum access to food and water. Adult female mice aged 12–16 weeks or 9 months were used for the present study. All animal procedures in this study were conducted following the National Institutes of Health (NIH) Guide for the Care and Use of Laboratory Animals and approved by Purdue Animal Care and Use Committee.

Reagents

(1) Sigma–Aldrich Potassium Chloride (SKU: P9541-500G)
(2) Baker Analyzed® Potassium Phosphate Monobasic, Crystal (CAS: 7778-77-0)
(3) Fisher Sodium Chloride (CAS: 7647-14-5)
(4) Fisher Sodium Phosphate Dibasic Anhydrous (CAS: 7558-79-4)
(5) Fisher Calcium Chloride Dihydrate (CAS: 10035-04-8)
(6) Fisher Magnesium Chloride (CAS: 7791-18-6)
(7) Sigma Aldrich D-(+)-glucose (SKU: G8270-100G)
(8) Sigma–Aldrich Sodium Pyruvate (Product number: P2256)
(9) Thermo Fisher Scientific GE Healthcare Ficoll PM400 (Catalog number: 45-001-745)
(10) Elko Filtering Co 30 micron nylon mesh (Catalog number: NC0478162)
(11) Sefar, 03-100/32, Nylon Mesh Filtering Screen 100 Micron—Open Area %: 32— Width: 38 in, Natural Color (1 Yard; Part number: 3A03-0100-098-00)
(12) Alkali Scientific Inc. 100 micron strainer (Catalog number: TS100)
(13) Thermo Fisher Scientific Sartorius™ glass beads (0.4 mm–0.6 mm; Catalog number: BBI-8541701)
(14) Sigma–Aldrich Bovine Serum Albumin (BSA; Catalog number: A2153)
(15) Sigma–Aldrich Collagenase (Catalog number: C5138)
(16) Sigma–Aldrich DNase I (Catalog number: DN25)
(17) BioLegend APC/Cy7 anti-mouse CD45 (clone: 30-F11)
(18) BioLegend Alexa Fluor 488 anti-mouse CD31 (clone: MEC13.3)
(19) BioLegend 7-AAD Viability Staining
(20) Miltenyi Biotec APC anti-mouse ACSA2 (clone: IH3-18A3)
(21) Miltenyi Biotec FcR blocking reagent—mouse
(22) BioLegend anti-mouse CD140b (clone: APB5)
(23) BD Bioscience anti-mouse CD31 (clone: MEC13.3)
(24) Sigma–Aldrich Rabbit anti-Aqp4 (Catalog number: HPA014784)
(25) Thermo Fisher Scientific Rabbit anti-ZO-1 (Catalog number: 61-7300)
(26) Proteintech Rabbit anti-Occludin (Catalog number: 13409-1-AP)
(27) BD Bioscience Mouse anti-actin (Catalog number: 612656)
(28) Sigma–Aldrich Phosphate Buffered Saline with 10% Bovine Albumin (BSA; Catalog number: SRE0036)
(29) Anaspec HiLyte™ Fluor 488 labeled human amyloid beta-peptide 1–42 (Catalog number: AS-60479-01)
(30) Sigma–Aldrich PSC833 (Catalog number: SML0572)

Isolation Equipment

(1) Milwaukee $\frac{1}{2}$ in (13 mm) drill (Catalog number: 0299-20)
(2) Wheaton Dounce homogenizer—7 ml (Catalog number: 3432T40)
(3) Staco Energy Products Variable Autotransformer (Model: 3PN1010B)
(4) Beckman Coulter Avanti J-E centrifuge
(5) Beckman JA-20 rotor (20,000 rpm)
(6) Fotodyne Stovall The Belly Dancer Hybridization Water Bath (SKU: 7121211)
(7) Eppendorf 5810 R Centrifuge

Analysis Equipment and Software

(1) BD FACSVerse™
(2) Olympus FV10i confocal microscope
(3) Olympus DP72 light microscope
(4) Applied Biosystems StepOne Plus real-time PCR system
(5) NIH ImageJ software
(6) Prism 8

STEP-BY-STEP PROCEDURES

Day Before Experiment

(1) Prepare modified phosphate-buffered saline (PBS, 2.7 mmol/L KCl, 1.5 mmol/L KH_2PO_4, 136.8 mmol/L NaCl, 4.3 mmol/L Na_2HPO_4, 0.7 mmol/L $CaCl_2$, 0.5 mmol/L $MgCl_2$, pH 7.4). The volume of 500 ml modified PBS would be used for 3–5 mice.
(2) Prepare 8 ml of 40% Ficoll solution in modified PBS per group.
(3) Store both the modified PBS and the 40% Ficoll in 4°C.

Day of Experiment

(1) Add D-glucose (5 mmol/L) and sodium pyruvate (1 mmol/L) to the modified PBS.

(2) Prepare 1% BSA in modified PBS.
(3) Place all buffers on ice and pre-cool all tools and centrifuges.

Brain Microvessel Fragments for Molecular Assays

(1) Anesthetize mice using isoflurane. When the animals are asleep, sterilize the animals with 70% ethanol, and decapitate the animals. Extract brains as described in **Figure 2** and transfer brains to a Petri dish containing ice-cold modified PBS. Carefully remove the thin slices of subdural meninges (SDM) on the dorsal surface of the brain. Use the dissecting microscope to validate the removal of SDM quickly. Keep the brain on ice.
(2) Using the brain matrix, remove olfactory bulbs and cerebellum. Cut the brain in half horizontally. Using Needle blade, separate the cortex from the corpus callosum. Place cortices in a glass tube containing 7 ml ice-cold modified PBS.
(3) In a 4°C cold room, homogenize cortices for 35 strokes using an electrical drill (Milwaukee drill connected to the Staco Energy Products Autotransformer)
    (a) Speed for the first 20 strokes: 18
    (b) Speed for the last 15 strokes: 20
    (c) Transfer homogenates to Dounce homogenizer and homogenize manually for additional 10 strokes.
(4) Mix brain homogenate with an equal volume of 40% Ficoll solution to a final concentration of 20% Ficoll PM 400. Shake tubes before centrifuge.
(5) The homogenate will be spun at 5,800× *g*, 4°C for 20 min.
(6) Discard supernatant and vacuum the myelin layer at the top.
(7) The pellet containing enriched microvessels can then be used for molecular assays such as RNA extraction or Western blot analysis. Add the appropriate volume of Trizol or RIPA buffer to the pellet and re-suspend it gently for downstream analyses.

Purification of Brain Capillaries for Imaging/Functional Assays

(1) In a 4°C cold room, take the pellet containing enriched microvessels from the previous step and re-suspend it into 1 ml of 1% BSA/modified PBS.
(2) Filter the solution with 300 μm nylon mesh and wash the mesh with 10 ml of 1% BSA/modified PBS and save the flow-through.
(3) Filter the flow through with 30 μm strainer very slowly by using a 7 ml transfer pipet. The speed of the droplet is 1 drop every 2 s. Capillaries will be captured on top of the strainer.
(4) Carefully invert the 30 μm strainer and wash with 10 ml of 1% BSA/modified PBS.
(5) Prepare an enrichment column in a 4°C room and add a volume of 15 ml glass beads to a 30 ml syringe supported by a 30 μm nylon mesh.
(6) Rinse the column with 10 ml of 1% BSA/modified PBS before adding the capillary solution.
(7) Transfer the capillary solution into the syringe by using a 7 ml transfer pipet.
(8) Gently agitate the beads, but do not touch the bottom 5 ml of beads.
(9) Adjust the flow rate so that the speed of the droplet is 1 drop per every 2 s.
(10) Rinse with 10 ml of 1% BSA/modified PBS one time, gently agitating the beads after adding the buffer.
(11) Rinse with 10 ml of BSA-free PBS twice, gently agitating the beads after adding the buffer.
(12) Brain capillaries will be bound by the glass beads. Collect capillaries by pouring the beads into a sterile glass beaker.
(13) Add 50 ml of BSA-free modified PBS and gently agitate by aspirating the beads with a 25 ml serological pipet.
(14) Filter the solution into a clean 50 ml Falcon tube supported by a 100 μm strainer to capture the glass beads.
(15) Repeat the wash step of glass beads one time with an additional 50 ml of BSA-free modified PBS and filter the solution into another clean 50 ml Falcon tube.
(16) Centrifuge 50 ml Falcon tubes at 1,100 rpm, 4°C for 5 min. At the end of the centrifugation, remove supernatant and combine the pellets into one tube.
(17) Wash the pellet with 50 ml BSA-free modified PBS for an additional two times.
(18) Re-suspend the pellet in 250 μl 1% BSA/modified PBS. The enriched capillaries can be examined by light microscopy.
(19) For imaging, load 20 μl of re-suspended capillaries on a glass coverslip, spreading in a Z-shaped manner gently.
(20) Let the capillaries attach to the glass coverslip at room temperature for 30 min.
(21) Wash with 1 ml of 1% BSA/modified PBS. After wash, the capillaries can be fixed with 2% paraformaldehyde and subjected to immunostaining analyses.

Generation of Single-Cell Suspensions of Brain Microvessels

(1) After the glass bead purification step, the capillary pellet can be used to generate single-cell suspensions. Re-suspend the enriched capillary pellet in 2 ml of 1× $HBSS^{-/-}$ buffer and transfer to a new 50 ml Falcon tube.
(2) Add 0.5 mg/ml collagenase, and incubate the solution in a water bath set to 37°C with gentle shaking for 15 min. Swirl the tube gently every 5 min.
(3) At the end of the incubation period, add 2 μg/ml DNase, and gently pipet up and down with a 1 ml wide-bore tip until aggregate is dissociated.
(4) Incubate the mixture in the hybridization water bath at 37°C for 5 min.
(5) At the end of the incubation period, immediately add 13 ml pre-warmed RPMI-164 media with 10% fetal bovine serum to quench the enzyme activity.
(6) Pass a total of 15 ml of the mixture through a 70 μm strainer and transfer to a new 50 ml Falcon tube. Centrifuge mixture at 1,100 rpm, 4°C for 5 min.
(7) Remove the supernatant carefully using a pipette and re-suspend the cell pellet with ice-cold buffer. Pass cell suspensions through a 40 μm FLOWMI strainer.

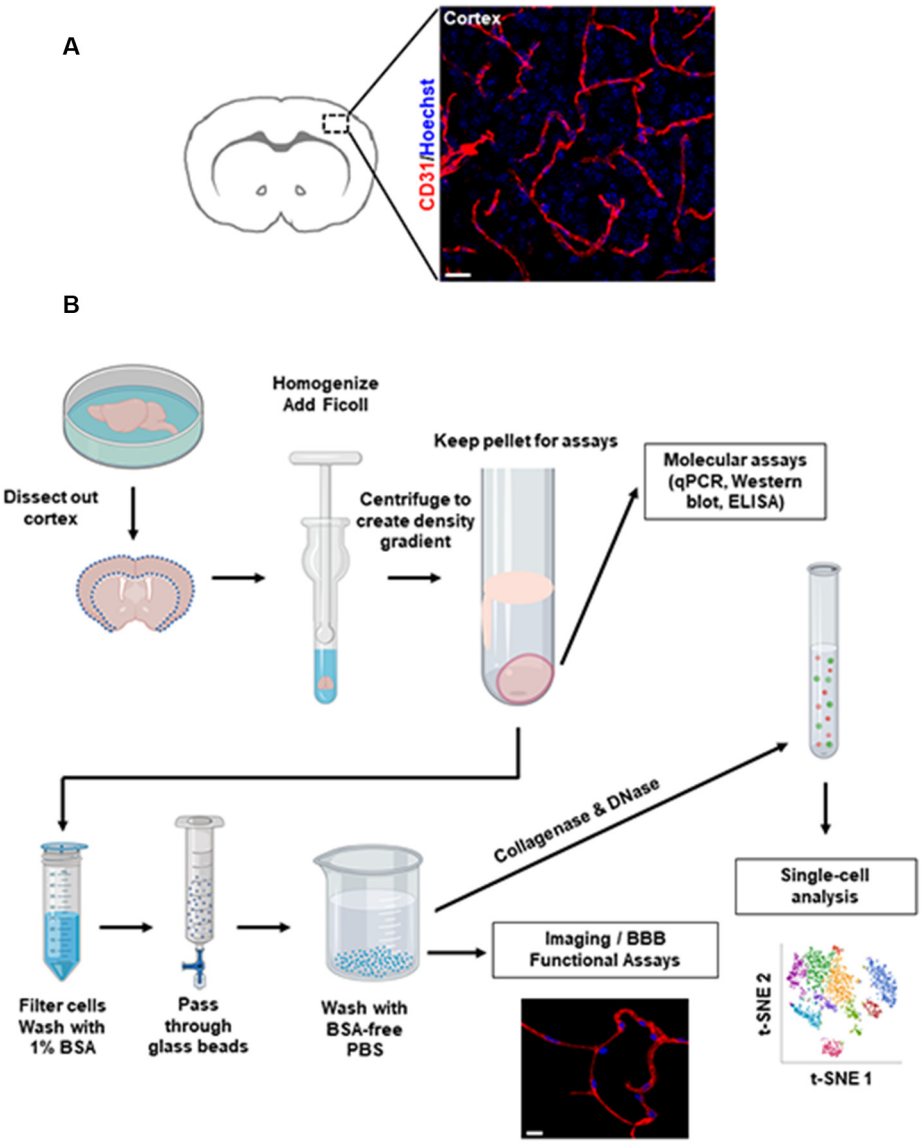

FIGURE 1 | Overview of brain microvessel purification protocol. **(A)** Representative images of microvessels in the mouse cerebral cortex labeled by immunofluorescence staining. Scale bar, 20 μm. **(B)** Flowchart of the isolation procedures. This diagram depicts the major steps to isolate microvessels from freshly harvested mouse brain. Scale bar, 10 μm. Representative single-cell t-SNE plot shows different colored clusters to identify different cell types.

(8) The viability and cell yield can be examined. At this point, the cells are ready for downstream applications, such as single-cell analyses.

RESULTS

To isolate microvessels from the mouse cerebral cortex, as shown in **Figure 1A**, we adapted the protocol initially described by Miller, Bauer, and Hartz groups (Miller et al., 2000; Hartz et al., 2004, 2018b; Wang et al., 2010, 2014). The isolated microvessel fragments using mechanical homogenization described by Miller et al. (2000) retain P-glycoprotein, an ATP-dependent efflux transporter of the BBB and maintain the functional transport activity (Hartz et al., 2010, 2018b; Wang et al., 2010, 2014). We modified the Ficoll density-gradient and homogenization strokes to obtain optimal sizes of microvessel fragments from a pool of dissected cortices. The isolation protocol is overviewed in **Figure 1B**. The procedures described in **Figure 2** yielded intact microvessel fragments as examined under a light microscope, although there was some brain parenchymal debris observed (**Figures 3A,B**). We validated the purity of isolated microvessels by examining the unique mRNAs expressed in different cell types. The isolated microvessels showed a 30-fold enrichment of endothelial cell-specific genes, *Pecam1*, *Cldn5*, and *Cdh5*, compared to other cell types, such as astrocytes, neurons, and microglia (**Figure 3C**). When compared to protein

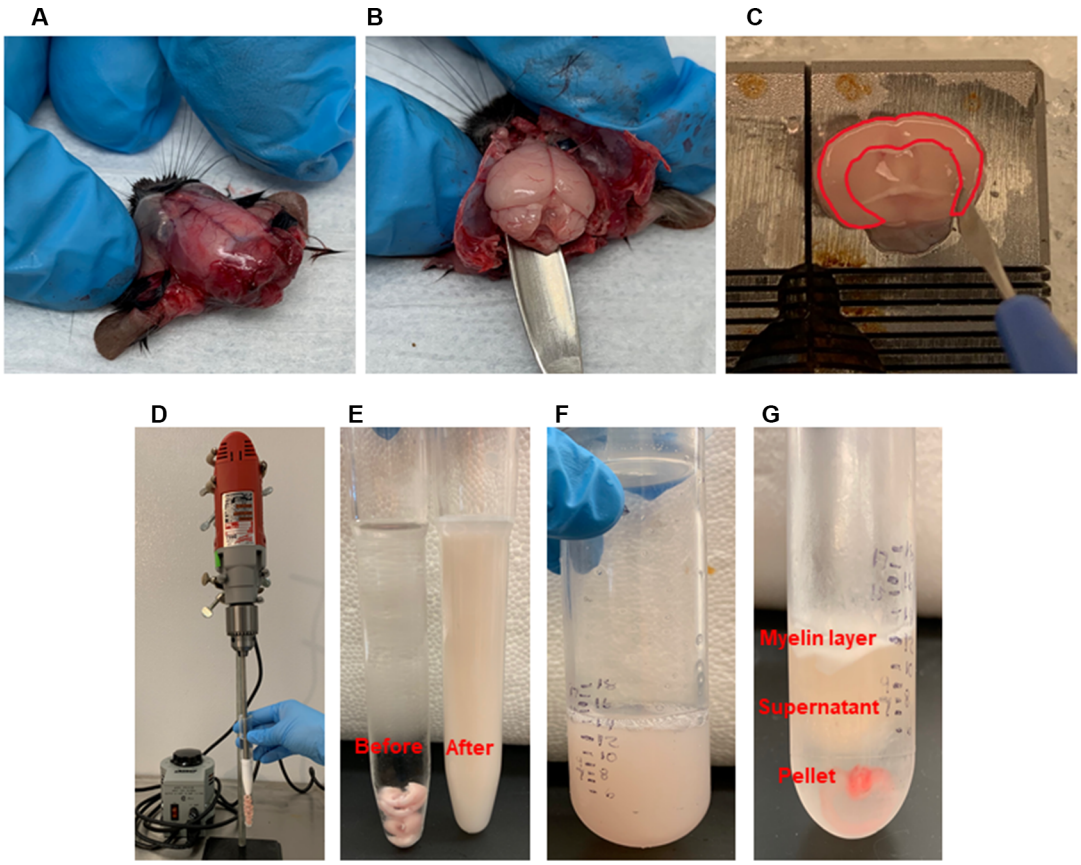

FIGURE 2 | Brain microvessel enrichment. **(A–C)** Tissue harvest and dissection. After head decapitation, peeling the skin to reveal the skull. Extracting the brain with a spatula. After transferring the whole brain into a Petri dish containing modified phosphate buffered saline (PBS) on ice, dissecting the brain regions on ice. Dissecting the cerebral cortex was shown. Highlighted area showed the cortex which is cut out using a needle blade. **(D–G)**. Homogenization and Ficoll gradient enrichment. **(D)** Multi-speed drill homogenizes collected cortices. **(E)** Before and after homogenization. **(F)** An equal amount of 40% Ficoll is added to the homogenates and transferred to a centrifuge tube. **(G)** Post-centrifugation shows the myelin layer at the top and the pellet at the bottom, which contains the brain microvessels.

homogenates of the cerebral cortex, the isolated microvessels showed enrichment of tight junction protein, Zonula Occludens (ZO-1) and Occludin, indicating the intact barrier structure of microvessel fragments (**Figure 3D**). At this point, the isolated microvessel fragments can be used for molecular or biochemical assays to examine changes of tight junction proteins in a disease model. We examined a well-characterized model of human obesity and type 2 diabetes, which carries the mutated leptin receptor (*db*) alleles (Bahary et al., 1990). The *db*/*db* mouse has been reported exhibiting comorbid phenotypes of obesity, diabetes, and cognitive deficits (Erion et al., 2014; Stranahan et al., 2016; Cope et al., 2018). The cerebral vascular abnormalities and BBB damage were suggested contributing to the impairment of cognition observed (Niedowicz et al., 2014; Stranahan et al., 2016). We used this model as our validation studies for this isolation protocol. We isolated brain microvessels from *db*/*db* mice as procedures described above and examined the tight junction protein, Occludin (**Figure 3E**). The levels of Occludin in the microvessel fragments of *db*/*db* mice were significantly reduced compared to the controls. These results demonstrated the applications of this protocol to examine the vascular pathology in a dementia mouse model.

To exclude unwanted cellular debris, further purification of the enriched microvessel fragments was accomplished *via* the filtration through the glass beads column as shown in **Figures 4A–E**. We examined the diameters of the microvessel fragments using a bright-field light microscope. The majority of the microvessel fragments captured were less than 10 μm in diameter (**Figures 4F,G**). We observed that 75.7% of fragments were less than 5 μm, and 21.6% of fragments were between 5 and 10 μm (**Figure 4H**). The results suggested that most of the purified microvessel fragments are brain parenchymal capillaries. This filtration facilitated obtaining stretched and untangled capillaries that are suitable for imaging analyses (**Figure 5A**). We performed immunostaining to characterize the morphology of purified capillaries. Using the immunostaining of endothelial cell marker, CD31, we were able to visualize homogeneously labeled endothelial cells within the intact structure of capillaries (**Figure 5B**). Also, the tight junction protein, ZO-1, was

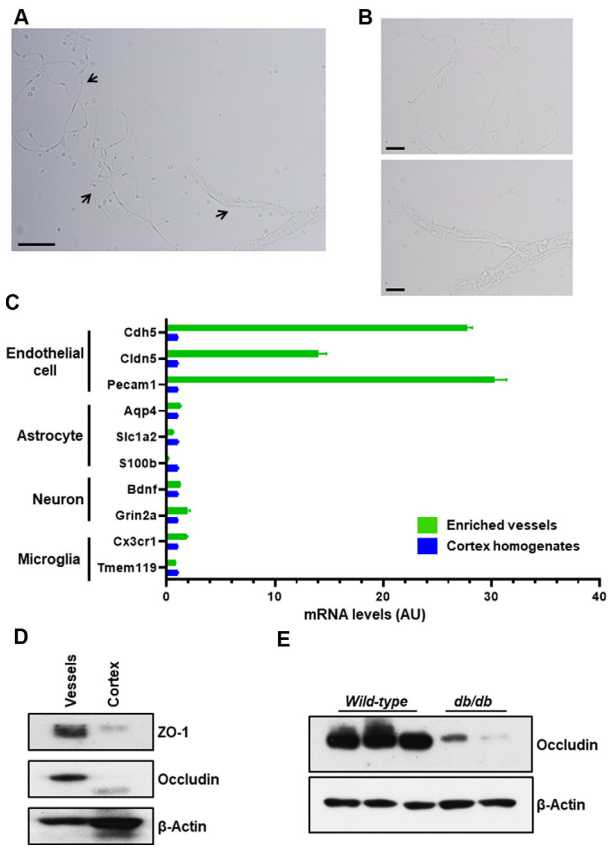

FIGURE 3 | Purity of enriched brain microvessels. The enriched microvessels were examined by light microscope, bright-field directly after isolation and resuspension. **(A)** 100× magnification. Arrows indicate different sizes of microvessel fragments isolated. Scale bar, 50 μm. **(B)** 400× magnification. Top insert depicts a single stretched out capillary. The bottom insert depicts a capillary network attached to smooth muscle cells. Scale bar, 20 μm. **(C)** Endothelial cell markers (Cdh5, Cldn5, and Pecam1), astrocyte markers (Aqp4, Slc1a2 m, and S100b), neuron markers (Bdnf and Grin2a), and microglia markers (Cx3cr1 and Tmem119) were compared between the enriched brain microvessels and the cortex homogenates using qPCR quantification. Data are mean ± SEM, $n = 2$ mice per experiment from two independent experiments. **(D)** Representative Western blot shows that tight junction proteins, ZO-1 and Occludin, were enriched in isolated microvessel fragments compared to the cortex homogenates. The cytoskeletal β-actin was used as a control. Ten microgram of total protein preparation was examined. Data presented are from four independent experiments. **(E)** Representative Western blot of enriched brain microvessels isolated from wild-type C57BL/6 female mice (three samples) and *db/db* female mice (two samples) at age of 9 months. The tight junction protein, Occludin, was diminished in the *db/db* group. $n = 2$ mice per experiment from two independent experiments.

co-labeled with CD31+ endothelial cells with no apparent discontinuity, suggesting that the structure of endothelial tight junctions were preserved in our capillary preparation. The surface of brain capillaries is covered by pericytes and astrocyte end-feet that seals the BBB entirely resulting in the unique characteristics of the cerebrovascular system (Daneman et al., 2010). We performed immunostaining of pericytes and astrocyte end-feet using makers, PDGFRβ and Aquaporin-4 (App4) respectively, to examine the sheathing of isolated capillaries. The PDGFRβ+ pericytes were shown adhered to the surface of isolated capillaries (**Figure 5C**). The water channel Aqp4 is concentrated at the astrocyte end-feet membrane, serving as an influx route of water to maintain homeostasis (Papadopoulos and Verkman, 2013; Camassa et al., 2015). We found that the Aqp4+ end-feet membrane outlined the wall of isolated capillaries (**Figure 5D**). Together, these results suggest that our optimized protocol using mechanical homogenization, but not enzymatic digestion, preserves the structure of the BBB that closely mimic *in vivo* situations.

The purified capillaries using this protocol can be applied for functional transport assays to test small-molecule drugs (Wang et al., 2010, 2014). AD is an age-associated neurodegenerative disorder characterized by the buildup of amyloid-β (Aβ) plaques. The accumulation of Aβ as the result of unbalanced Aβ generation subsequent clearance is reported to contribute to the pathogenesis of AD (Bell et al., 2007; Mawuenyega et al., 2010; Zlokovic, 2011). We used the transport of human $A\beta_{42}$ peptide to validate the function of the purified microvessel fragments (**Figure 6A**). We first used freshly isolated capillaries to examine the transport of $A\beta_{42}$ (Hartz et al., 2010). We incubated HiLyte-Fluor 488 labeled $A\beta_{42}$ peptide ($A\beta_{42-488}$) or non-labeled $A\beta_{42}$ peptide with purified capillaries in modified PBS at room temperature for 1.5 h. We observed the accumulated fluorescence of $A\beta_{42-488}$ in the luminal space of capillaries, compared to non-labeled $A\beta_{42}$ peptide. The P-glycoprotein inhibitor, PSC833, to suppress the transport of $A\beta_{42-488}$ was shown. We tested the ability of purified capillaries to transport $A\beta_{42-488}$ at 4h after purification (**Figure 6B**). The purified capillaries were incubated with modified PBS at room temperature for 4 h and then subjected to the transport assay for 1.5 h as described above. The reduction of $A\beta_{42-488}$ fluorescence in the luminal space suggested that the purified capillaries have reduced function and viability at 5.5 h after purification, as suggested in previous studies (Bauer et al., 2008; Hartz et al., 2010, 2018b). We also found that the CD31 immunostaining signal in purified capillaries is reduced at 4 h and almost diminished at 7 h after purification (**Figure 6C**). Together, these results suggested that the purified capillaries retain the transport function of BBB as *in vivo*, and the viability of purified capillaries can be preserved at modified PBS for up to 5 h.

Transcriptional profiling of the brain vascular endothelial cells provides new insights into the molecular mechanisms of vascular function in health and diseases at a whole-genome level (Guo et al., 2012; Zhang et al., 2014; Sabbagh et al., 2018). The fluorescence-activated cell sorting (FACS) technique enables to purify pre-defined cell populations based on the expression of surface markers or fluorescent reporters (Crouch and Doetsch, 2018; Jung et al., 2018; Munji et al., 2019). The selection of appropriate markers is often challenging, as some common markers being shared among BBB component cells and other types of brain parenchymal cells, such as oligodendrocyte progenitor cells. The enzymatic tissue dissociation before FACS purification is a critical step, as some epitopes required for immunostaining are degraded in a time-dependent manner during tissue dissociation (Crouch and Doetsch, 2018).

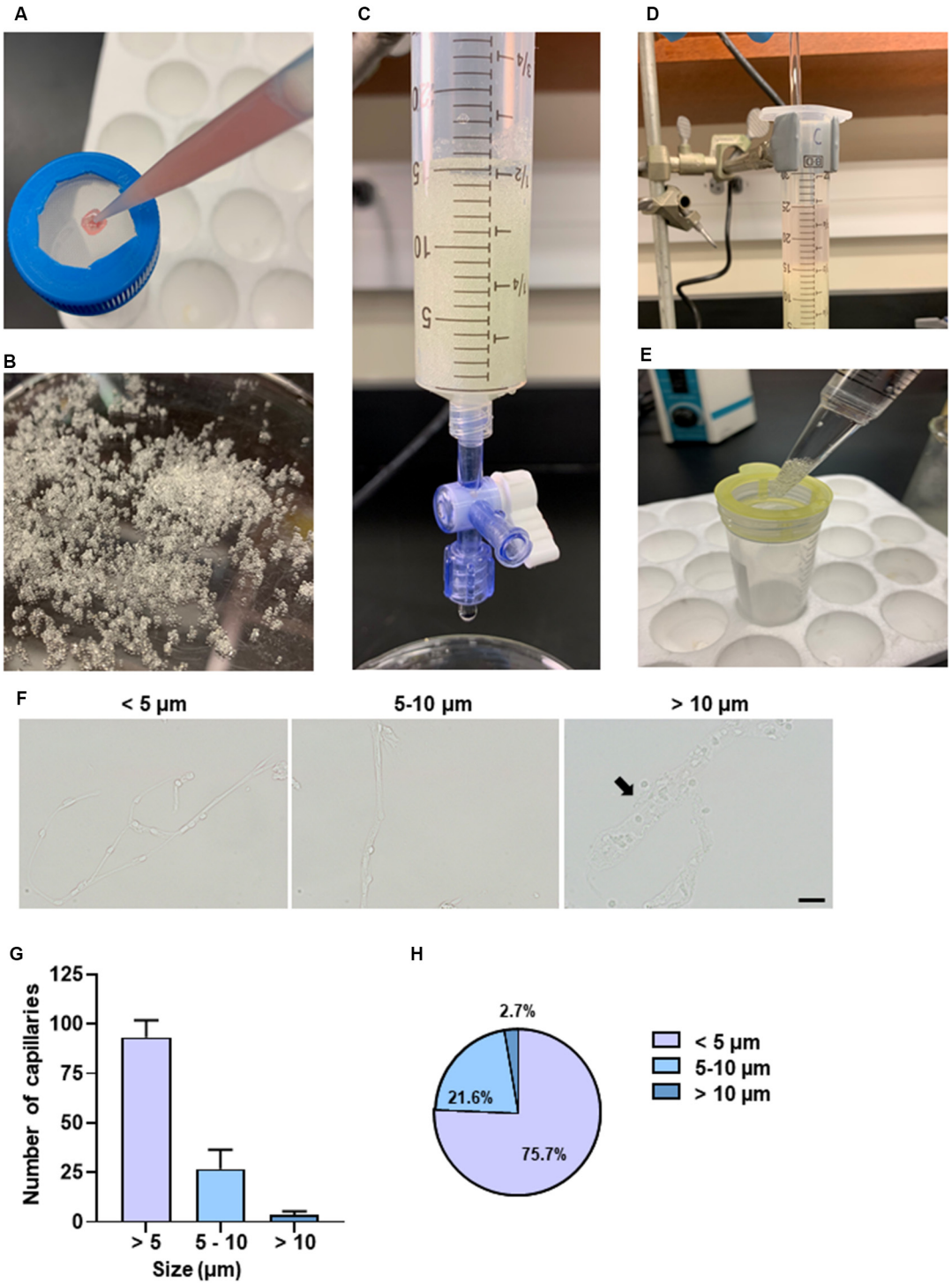

FIGURE 4 | Purification of brain capillaries and characterization of capillary size. **(A)** Passing pellet resuspensions through a 300 µm nylon mesh. **(B)** Example of glass beads used. **(C)** Collection syringe with adjustable flow rate has 15 ml glass beads supported by a 30 µm nylon mesh. **(D)** Gentle agitation using a glass stirrer is necessary for microvessels to adhere to glass beads. **(E)** Filtering solution with a 100 µm filter to remove excess glass beads. **(F)** Representative bright-field images of different sizes of capillaries. The diameters of the capillaries were measured. A total of 70–120 capillaries was examined per experiment. Three independent experiments were performed. Arrow points to the representative capillary with a size between 10 and 20 µm. **(G)** The size of the capillaries was examined from each experimental preparation. Data are mean ± SEM $n = 5$ mice per experiment from three independent experiments. **(H)** Percentages of capillaries based on size. Data are mean ± SEM $n = 5$ mice per experiment from three independent experiments.

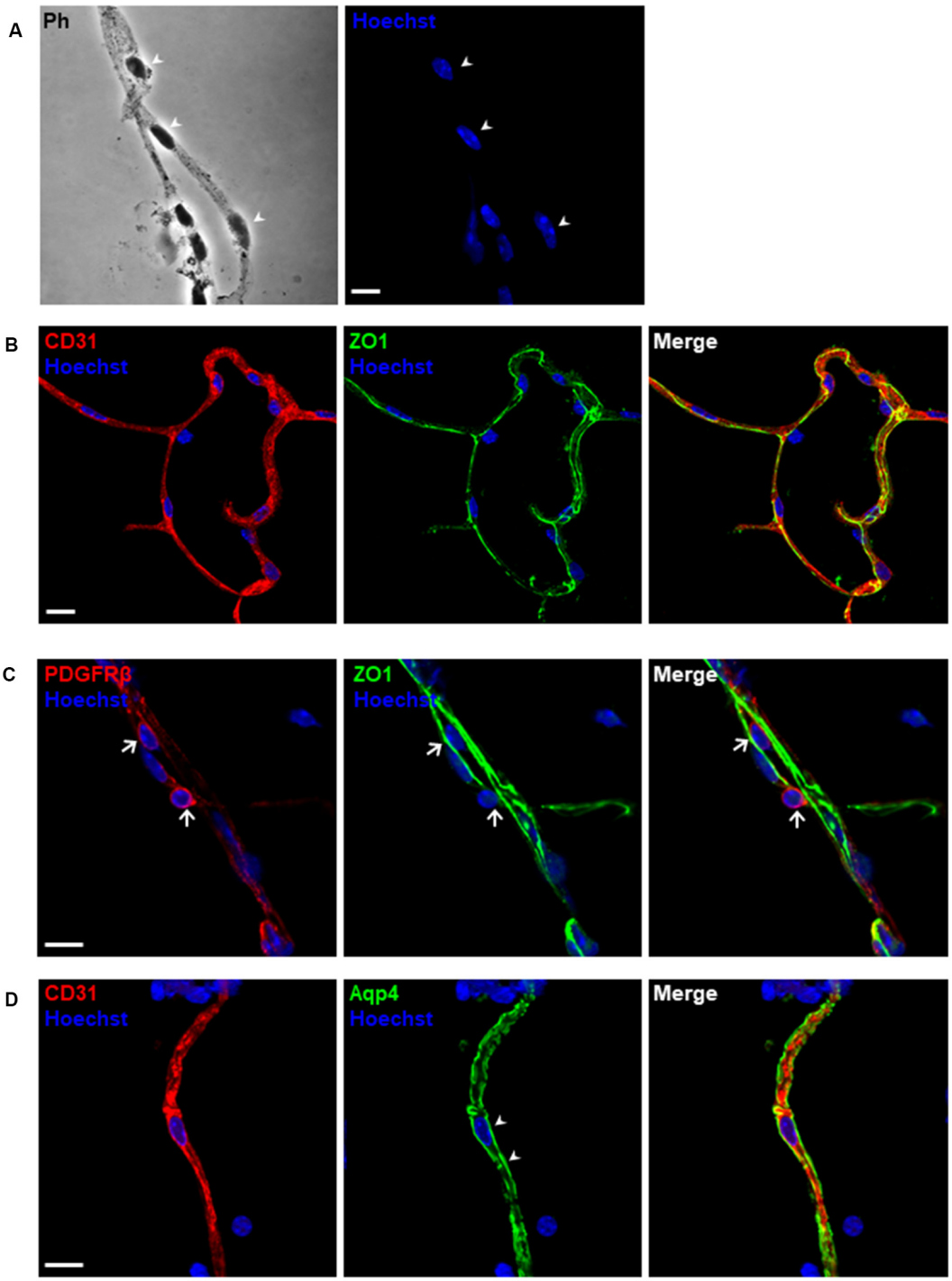

FIGURE 5 | Morphological characterization of purified microvessels. Confocal images of immunostaining for different markers of blood-brain barrier (BBB) cell components. **(A)** Phase-contrast (Ph) image of microvessels. The cell nuclei shown by arrowheads are depicted as blue using Hoechst 33342 staining (1 μg/ml). **(B–D)** Isolated microvessels retain most of the *in situ* structure. **(B)** Endothelial markers, CD31 (red) and tight junction proteins, ZO-1 (green) were detected. **(C)** Pericyte markers, PDGFRβ (red) were detected adhering to the surface of an isolated capillary, as shown by arrows. **(D)** Astrocyte end-feet membranes, pointed by arrowheads, remain attached to the microvessel fragment. Scale bar, 10 μm. The data presented are from three independent experiments.

The development of single-cell technologies opens the opportunity to map cellular heterogeneity within BBB component cells and to unravel the molecular signatures of previously unrecognized cell populations or functional states in

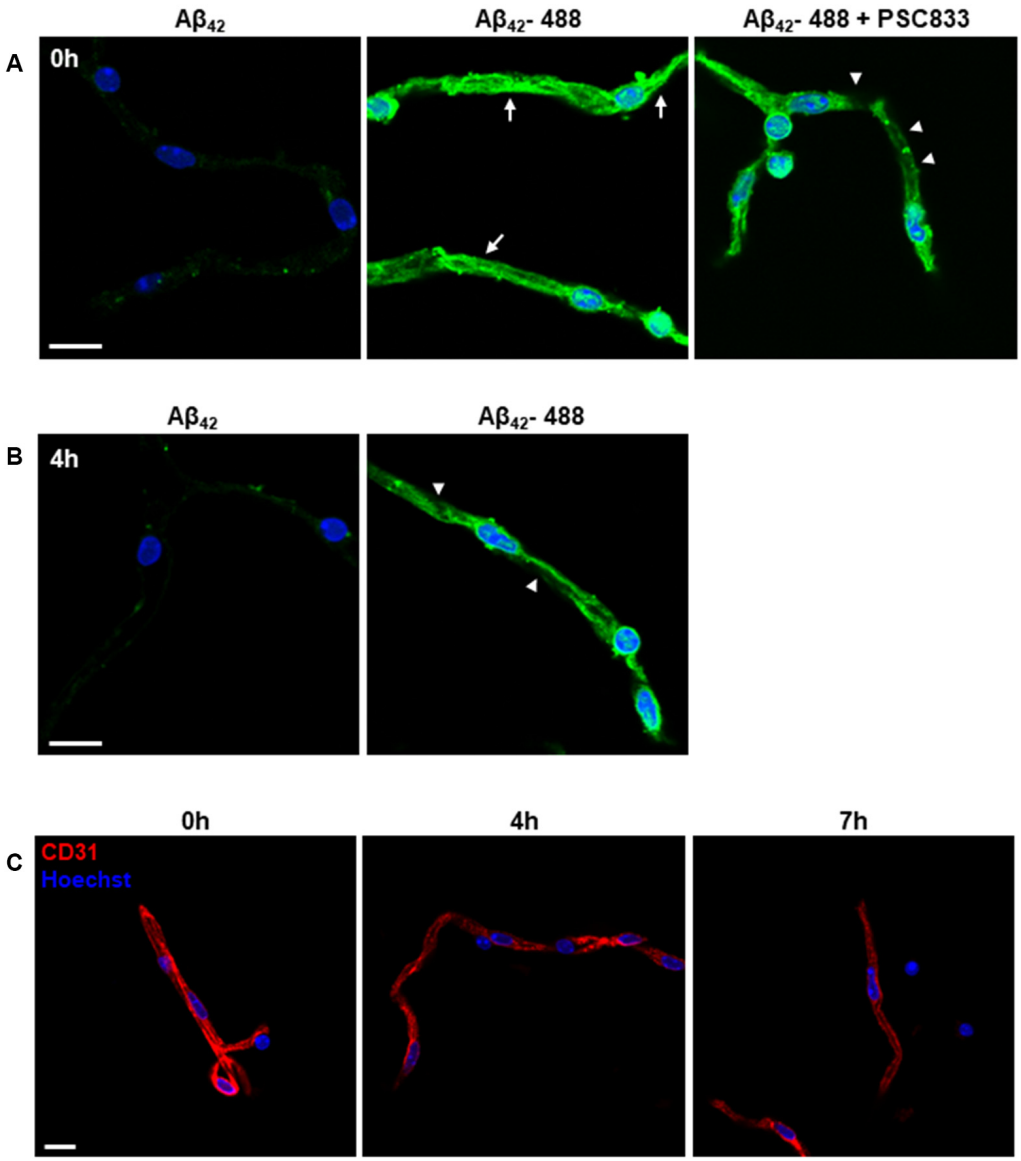

FIGURE 6 | Functional transport characterization of purified microvessels. **(A,B)** Confocal images of $A\beta_{42}$ transport in purified capillaries. **(A)** Freshly prepared capillaries were incubated with 5 μM HiLyte Fluor-488 $A\beta_{42}$ ($A\beta_{42-488}$) peptide or non-labeled $A\beta_{42}$ peptide (as control) in modified PBS at room temperature for 1.5 h. After incubation, capillaries were washed and processed for imaging analysis. Capillary luminal fluorescence (green) of $A\beta_{42-488}$ was examined using a confocal microscope. Cell nuclei are shown as blue using Hoechst 33342 staining (1 μg/ml). A P-glycoprotein inhibitor, PSC833, was co-incubated with $A\beta_{42-488}$ to suppress the transport of $A\beta_{42-488}$ mediated by the P-glycoprotein. Representative images from four independent experiments are shown. $n = 5$ mice per experiment. Arrows indicate the transport of $A\beta_{42-488}$ into the capillary luminal space. Arrowheads indicate the reduced green fluorescence in the capillary luminal space. Scale bar, 10 μm. **(B)** Transport of $A\beta_{42-488}$ in capillaries at 4 h after purification. The assay condition was the same as described in **(A)**. Arrowheads indicate decreased capillary luminal green fluorescence. **(C)** Endothelial markers, CD31, was used to examine the viable endothelial cells in purified capillaries at 0 h, 4 h, and 7 h after purification. The cell nuclei are shown as blue using Hoechst 33342 staining (1 μg/ml). Scale bar, 10 μm.

various subregions of the brain (Saliba et al., 2014; Cembrowski, 2019; Kalluri et al., 2019). Yousef and colleagues recently applied enzymatic digestion procedures following flow cytometry sorting to characterize the molecular phenotype of brain endothelial cells in the aging mouse brain (Czupalla et al., 2018; Yousef et al., 2018, 2019). Since we obtained the structurally and functionally intact brain capillaries, we further optimized the procedures to generate single-cell suspensions with relatively shortened time (15 vs. 50 min) and lowered dose of collagenase (0.5 mg/ml vs. 1 mg/ml) digestion step to minimize the potential of cell activation compared with other methods (Czupalla et al., 2018; Yousef et al., 2018; Kalluri et al., 2019). We used 10% fetal bovine serum to inactivate collagenase activity and stabilize cells rapidly during collection procedures. Following the procedures

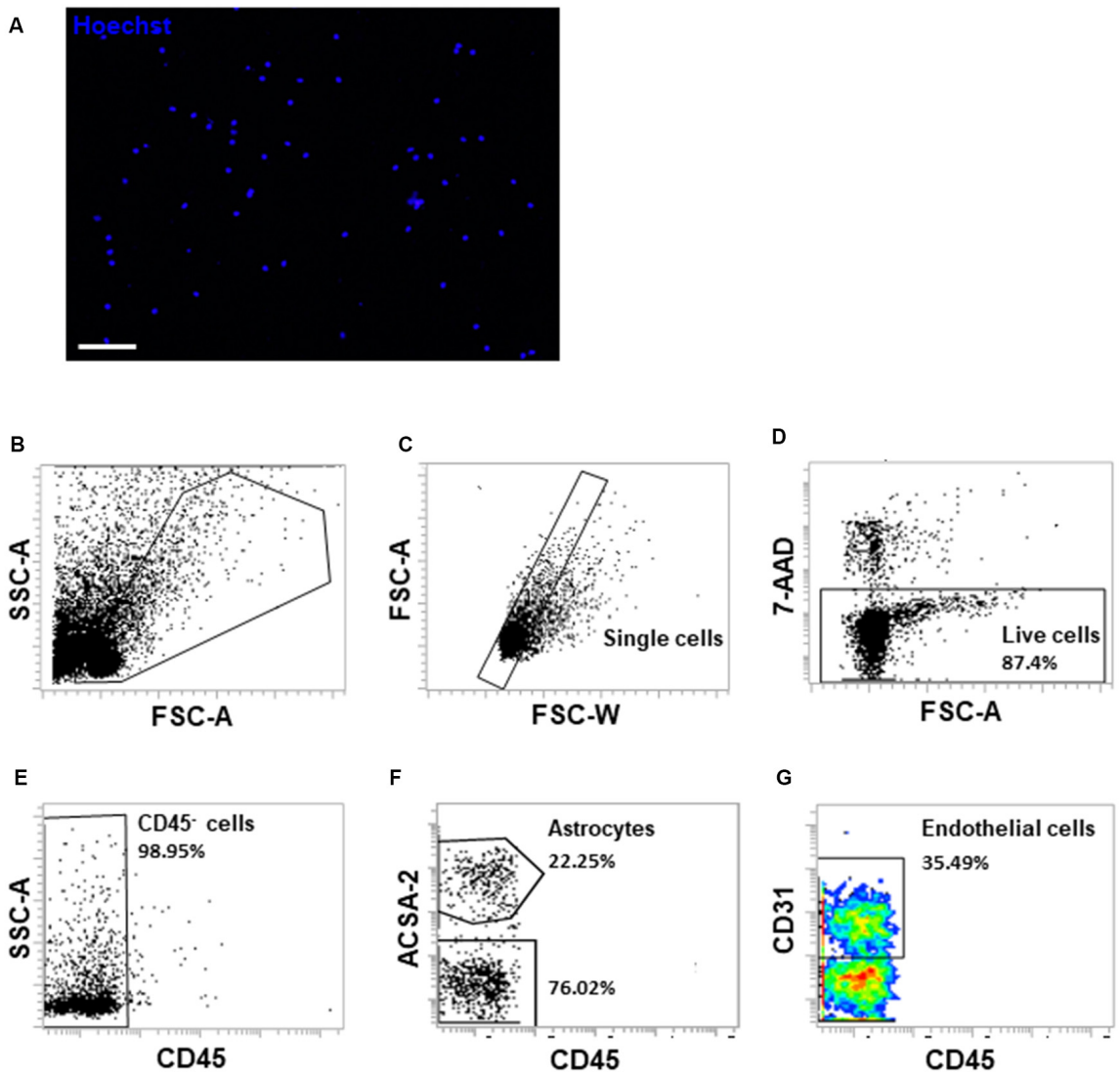

FIGURE 7 | Fluorescence-activated cell sorting (FACS) analysis of single-cell suspensions of isolated brain microvessels. **(A)** Single-cell suspensions were examined under a fluorescent microscope immediately after resuspension. The cell nuclei were stained with Hoechst 33342 (1 μg/ml). Scale bar, 50 μm. **(B)** Single-cell suspensions were gated on FSC-A and SSC-A to exclude cell debris. **(C)** Cells were gated on FSC-W and FSC-A to exclude cell doublets or aggregates. **(D)** 7-AAD uptake indicates dead cells, which account for approximately 13% of cells. **(E)** CD45- cells were gated to exclude monocytes/macrophages and brain resident microglial cells. **(F,G)** ACSA-2 and CD31 staining were applied to examine different cell types within the single-cell suspensions generated from isolated microvessel fragments. Representative FACS images were from three to four independent experiments.

described, we were able to generate single-cell suspensions as examined under a fluorescence microscope (**Figure 7A**). The viable cells accounted for approximately 87% of the total single cells using 7-AAD uptake analysis (**Figures 7B–D**). We observed heterogeneous cell populations with minimal contamination of 2% CD45+ immune cell populations (**Figure 7E**). As we observed astrocyte end-feet covered the wall of isolated brain capillaries, we used astrocyte cell surface antigen-2 (ACSA-2) and CD31 to characterize BBB component cell types within the single-cell suspensions (**Figures 7F,G**). Cumulatively, this protocol is highly reproducible. We were able to yield an average of 4–6 $\times$ 10^5 cells from a pool of cerebral cortices collected from four to five adult mice.

Potential Pitfalls and Troubleshooting

This protocol describes the relative ease in isolating the microvessels from the adult mouse brain. Here, we list several conditions that will facilitate the preservation of cellular interactions between microvascular endothelial cells and mural cells, which is critical for maintaining the molecular phenotypes of BBB component cells.

- Keep all tools and buffers ice-cold to maintain a high viability (>80%). Also, performing the majority of the steps in a 4°C cold room will help keeping the cells viable.
- Each isolation of cerebral microvascular fragments should include experimental and control groups. The number of mice to use per group depends on downstream analyses. The protocol described above, especially the volume of Ficoll, is good for 3–5 mice per group. For biochemical analyses, such as RNA or protein quantifications, a pool of dissected cortices from two young mice (3–4-month-old male or female) is the amount required. For imaging of functional assays and single-cell analyses, a pool of dissected cortices from four to five young mice (3–4-month-old male or female) is the amount required.
- To maintain the high viability and functionality, the maximum number of groups that can be isolated at one time is two sets of mice (4–8 mice total). Increasing the total time for the procedure is detrimental to the procedure. We found that once the cells are in a single-cell suspension, the cells will begin loss of viability after 30 min and will affect the results.
- Modified PBS and the Ficoll must be made the day before the experiment and not any longer. Also, the sodium pyruvate and the glucose can only be added on the day of the experiment and must be used within the day of the experiment. Likewise, the 1% BSA solution is made right after the sodium pyruvate and the glucose are added to the modified PBS.
- The flow rate during the glass beads section is critical for the microvessel fragments to attach to the glass beads. If the flow rate is too fast, the capillaries will not adhere to the glass beads.
- The glass beads can be reused up to five times before brain parenchyma will contaminate the beads, preventing the capillary segments from adhering to the beads. Upon completion of the experiment, the glass beads can be washed by adding deionized water first followed by 95% ethanol to the glass beads, swirling first, then dumping the excess ethanol out. Rinse the glass beads twice with deionized water. Dry beads by immersing them in 100% ethanol overnight. The glass beads must be fully dry before being used again.

DISCUSSION

This protocol will be of significant interest in investigating molecular mechanisms that lead to BBB dysfunction. It describes in detail how to isolate brain microvessels while the isolated fragments retain the structural and functional integrity of the BBB. Freshly isolated microvessels can be used to characterize barrier dysfunction or capillary permeability if a disease mouse model is applied (Hartz et al., 2012). We validated the application of this protocol using a mouse model exhibiting BBB damage and cognitive impairment. Importantly, this protocol describes procedures to generate single-cell suspensions from isolated microvessels. The procedures require approximately 3–3.5 h in total depending on the experiment groups of mice used. The shorten time required from the described protocol can significantly improve the quality of RNA obtained. Moreover, the purified microvessel fragments were demonstrated retaining the *in vivo* structure and function of transport. The highly viable single-cell suspensions obtained from microvessels that retain *in situ* structure provide a valuable resource for identifying unique subpopulations of BBB component cells that might be associated with disease progression using single-cell analyses, such as RNA-sequencing (Yousef et al., 2019), DNA methylation (Hui et al., 2018), or ATAC-sequencing (Lalonde et al., 2019).

This protocol is optimized for the isolation of microvessel fragments and capillaries from the cerebral cortex of the adult mouse brain. However, it is crucial to consider that the dissection of the brain region of interest is required. If other brain sub-regions, such as sub-ventricular zone containing neurogenic niche or highly vascularized hippocampus, are of interest, the microdissection skill, fine forceps, and a dissection microscope will be required. The procedures described during brain harvest remove the thin slices from the dorsal surface of the brain, which contains the subdural meninges. Since we were unable to peel off the pia/arachnoid mater within the brain parenchyma, the isolated microvessels do not contain extra-parenchymal meningeal or large vessels on the surface of the brain as demonstrated in the size characterization of purified fragments. For the study interest of meningeal vessels, other methods should be followed (Park et al., 2011; Faraco et al., 2019).

CONCLUSION

Developing a protocol to isolate microvessel fragments is vital to generate a model to study the BBB dysfunction in diseases. Since the capillaries make up for roughly 1% of the whole brain in humans, using crude brain homogenates will most likely generate weak signals to study the BBB dysfunction as shown in our results and reported literature (Bauer et al., 2008; Hartz et al., 2018a). Here, we show that enrichment of the cerebral capillaries *via* a density gradient and glass beads opens the door for future experiments to examine and characterize the neurovascular unit through various assays and molecular characterization, such as single-cell analysis.

DATA AVAILABILITY STATEMENT

All datasets generated for this study are included in the article.

ETHICS STATEMENT

The animal study was reviewed and approved by Purdue Animal Care and Use Committee.

AUTHOR CONTRIBUTIONS

J-HY and I-CY conceived the study. HP, XW, and I-CY designed the experiments. HP, XW, P-CK, DF, and BS performed the experiments and analyzed the data. HP wrote the manuscript. J-HY, F-LC, and I-CY reviewed and edited the manuscript.

FUNDING

This project was supported, in part, with support from the Indiana Clinical and Translational Sciences Institute, funded in part by Grant Number UL1TR002529 from the NIH, National Center for Advancing Translational Sciences, Clinical and Translational Sciences Award. The Indiana Clinical and Translation Sciences Award was to I-CY. J-HY was supported by NIH R01NS102449.

REFERENCES

Abbott, N. J., and Friedman, A. (2012). Overview and introduction: the blood-brain barrier in health and disease. *Epilepsia* 53, 1–6. doi: 10.1111/j.1528-1167.2012.03696.x

Alluri, H., Wiggins-Dohlvik, K., Davis, M. L., Huang, J. H., and Tharakan, B. (2015). Blood-brain barrier dysfunction following traumatic brain injury. *Metab. Brain Dis.* 30, 1093–1104. doi: 10.1007/s11011-015-9651-7

Bahary, N., Leibel, R. L., Joseph, L., and Friedman, J. M. (1990). Molecular mapping of the mouse db mutation. *Proc. Natl. Acad. Sci. U S A* 87, 8642–8646. doi: 10.1073/pnas.87.21.8642

Bauer, B., Hartz, A. M., Lucking, J. R., Yang, X., Pollack, G. M., and Miller, D. S. (2008). Coordinated nuclear receptor regulation of the efflux transporter, Mrp2, and the phase-II metabolizing enzyme, GSTpi, at the blood-brain barrier. *J. Cereb. Blood Flow Metab.* 28, 1222–1234. doi: 10.1038/jcbfm.2008.16

Bell, R. D., Sagare, A. P., Friedman, A. E., Bedi, G. S., Holtzman, D. M., Deane, R., et al. (2007). Transport pathways for clearance of human Alzheimer's amyloid β-peptide and apolipoproteins E and J in the mouse central nervous system. *J. Cereb. Blood Flow Metab.* 27, 909–918. doi: 10.1038/sj.jcbfm.9600419

Camassa, L. M. A., Lunde, L. K., Hoddevik, E. H., Stensland, M., Boldt, H. B., De Souza, G. A., et al. (2015). Mechanisms underlying AQP4 accumulation in astrocyte endfeet. *Glia* 63, 2073–2091. doi: 10.1002/glia.22878

Cembrowski, M. S. (2019). Single-cell transcriptomics as a framework and roadmap for understanding the brain. *J. Neurosci. Methods* 326:108353. doi: 10.1016/j.jneumeth.2019.108353

Cope, E. C., LaMarca, E. A., Monari, P. K., Olson, L. B., Martinez, S., Zych, A. D., et al. (2018). Microglia play an active role in obesity-associated cognitive decline. *J. Neurosci.* 38, 8889–8904. doi: 10.1523/JNEUROSCI.0789-18.2018

Crouch, E. E., and Doetsch, F. (2018). FACS isolation of endothelial cells and pericytes from mouse brain microregions. *Nat. Protoc.* 13, 738–751. doi: 10.1038/nprot.2017.158

Czupalla, C. J., Yousef, H., Wyss-Coray, T., and Butcher, E. C. (2018). Collagenase-based single cell isolation of primary murine brain endothelial cells using flow cytometry. *Bio Protoc.* 8:e3092. doi: 10.21769/bioprotoc.3092

Daneman, R., Zhou, L., Kebede, A. A., and Barres, B. A. (2010). Pericytes are required for blood-brain barrier integrity during embryogenesis. *Nature* 468, 562–566. doi: 10.1038/nature09513

Erion, J. R., Wosiski-Kuhn, M., Dey, A., Hao, S., Davis, C. L., Pollock, N. K., et al. (2014). Obesity elicits interleukin 1-mediated deficits in hippocampal synaptic plasticity. *J. Neurosci.* 34, 2618–2631. doi: 10.1523/JNEUROSCI.4200-13.2014

Faraco, G., Hochrainer, K., Segarra, S. G., Schaeffer, S., Santisteban, M. M., Menon, A., et al. (2019). Dietary salt promotes cognitive impairment through tau phosphorylation. *Nature* 574, 686–690. doi: 10.1038/s41586-019-1688-z

Guo, S., Zhou, Y., Xing, C., Lok, J., Som, A. T., Ning, M., et al. (2012). The vasculome of the mouse brain. *PLoS One* 7:e52665. doi: 10.1371/journal.pone.0052665

Hartz, A. M., Bauer, B., Fricker, G., and Miller, D. S. (2004). Rapid regulation of P-glycoprotein at the blood-brain barrier by endothelin-1. *Mol. Pharmacol.* 66, 387–394. doi: 10.1124/mol.104.001503

Hartz, A. M., Bauer, B., Soldner, E. L., Wolf, A., Boy, S., Backhaus, R., et al. (2012). Amyloid-β contributes to blood-brain barrier leakage in transgenic human amyloid precursor protein mice and in humans with cerebral amyloid angiopathy. *Stroke* 43, 514–523. doi: 10.1161/strokeaha.111.627562

Hartz, A. M., Miller, D. S., and Bauer, B. (2010). Restoring blood-brain barrier P-glycoprotein reduces brain amyloid-β in a mouse model of Alzheimer's disease. *Mol. Pharmacol.* 77, 715–723. doi: 10.1124/mol.109.061754

Hartz, A. M. S., Schulz, J. A., Sokola, B. S., Edelmann, S. E., Shen, A. N., Rempe, R. G., et al. (2018a). Isolation of cerebral capillaries from fresh human brain tissue. *J. Vis. Exp.* 139:e57346. doi: 10.3791/57346

Hartz, A. M. S., Zhong, Y., Shen, A. N., Abner, E. L., and Bauer, B. (2018b). Preventing P-gp ubiquitination lowers aβ brain levels in an Alzheimer's disease mouse model. *Front. Aging Neurosci.* 10:186. doi: 10.3389/fnagi.2018.00186

Hui, T., Cao, Q., Wegrzyn-Woltosz, J., O'Neill, K., Hammond, C. A., Knapp, D., et al. (2018). High-resolution single-cell DNA methylation measurements reveal epigenetically distinct hematopoietic stem cell subpopulations. *Stem Cell Reports* 11, 578–592. doi: 10.1016/j.stemcr.2018.07.003

Jung, B., Arnold, T. D., Raschperger, E., Gaengel, K., and Betsholtz, C. (2018). Visualization of vascular mural cells in developing brain using genetically labeled transgenic reporter mice. *J. Cereb. Blood Flow Metab.* 38, 456–468. doi: 10.1177/0271678x17697720

Kalluri, A. S., Vellarikkal, S. K., Edelman, E. R., Nguyen, L., Subramanian, A., Ellinor, P. T., et al. (2019). Single-cell analysis of the normal mouse aorta reveals functionally distinct endothelial cell populations. *Circulation* 140, 147–163. doi: 10.1161/circulationaha.118.038362

Kassner, A., and Merali, Z. (2015). Assessment of blood-brain barrier disruption in stroke. *Stroke* 46, 3310–3315. doi: 10.1161/strokeaha.115.008861

Lalonde, S., Codina-Fauteux, V. A., de Bellefon, S. M., Leblanc, F., Beaudoin, M., Simon, M. M., et al. (2019). Integrative analysis of vascular endothelial cell genomic features identifies AIDA as a coronary artery disease candidate gene. *Genome Biol.* 20:133. doi: 10.1186/s13059-019-1749-5

Mawuenyega, K. G., Sigurdson, W., Ovod, V., Munsell, L., Kasten, T., Morris, J. C., et al. (2010). Decreased clearance of CNS β-amyloid in Alzheimer's disease. *Science* 330:1774. doi: 10.1126/science.1197623

Miller, D. S., Nobmann, S. N., Gutmann, H., Toeroek, M., Drewe, J., and Fricker, G. (2000). Xenobiotic transport across isolated brain microvessels studied by confocal microscopy. *Mol. Pharmacol.* 58, 1357–1367. doi: 10.1124/mol.58.6.1357

Munji, R. N., Soung, A. L., Weiner, G. A., Sohet, F., Semple, B. D., Trivedi, A., et al. (2019). Profiling the mouse brain endothelial transcriptome in health and disease models reveals a core blood-brain barrier dysfunction module. *Nat. Neurosci.* 22, 1892–1902. doi: 10.1038/s41593-019-0497-x

Nation, D. A., Sweeney, M. D., Montagne, A., Sagare, A. P., D'Orazio, L. M., Pachicano, M., et al. (2019). Blood-brain barrier breakdown is an early biomarker of human cognitive dysfunction. *Nat. Med.* 25, 270–276. doi: 10.1038/s41591-018-0297-y

Niedowicz, D. M., Reeves, V. L., Platt, T. L., Kohler, K., Beckett, T. L., Powell, D. K., et al. (2014). Obesity and diabetes cause cognitive dysfunction in the absence of accelerated β-amyloid deposition in a novel murine model of mixed or vascular dementia. *Acta Neuropathol. Commun.* 2:64. doi: 10.1186/2051-5960-2-64

Obermeier, B., Daneman, R., and Ransohoff, R. M. (2013). Development, maintenance and disruption of the blood-brain barrier. *Nat. Med.* 19, 1584–1596. doi: 10.1038/nm.3407

Ortiz, G. G., Pacheco-Moisés, F. P., Macias-Islas, M. Á., Flores-Alvarado, L. J., Mireles-Ramirez, M. A., Gonzalez-Renovato, E. D., et al. (2014). Role of the blood-brain barrier in multiple sclerosis. *Arch. Med. Res.* 45, 687–697. doi: 10.1016/j.arcmed.2014.11.013

Papadopoulos, M. C., and Verkman, A. S. (2013). Aquaporin water channels in the nervous system. *Nat. Rev. Neurosci.* 14, 265–277. doi: 10.1038/nrn3468

Park, L., Wang, G., Zhou, P., Zhou, J., Pitstick, R., Previti, M. L., et al. (2011). Scavenger receptor CD36 is essential for the cerebrovascular oxidative stress and neurovascular dysfunction induced by amyloid-β. *Proc. Natl. Acad. Sci. U S A* 108, 5063–5068. doi: 10.1073/pnas.1015413108

Sabbagh, M. F., Heng, J. S., Luo, C., Castanon, R. G., Nery, J. R., Rattner, A., et al. (2018). Transcriptional and epigenomic landscapes of CNS and non-CNS vascular endothelial cells. *Elife* 7:e36187. doi: 10.7554/eLife.36187

Saliba, A. E., Westermann, A. J., Gorski, S. A., and Vogel, J. (2014). Single-cell RNA-seq: advances and future challenges. *Nucleic Acids Res.* 42, 8845–8860. doi: 10.1093/nar/gku555

Stranahan, A. M., Hao, S., Dey, A., Yu, X., and Baban, B. (2016). Blood-brain barrier breakdown promotes macrophage infiltration and cognitive impairment in leptin receptor-deficient mice. *J. Cereb. Blood Flow Metab.* 36, 2108–2121. doi: 10.1177/0271678x16642233

Sweeney, M. D., Kisler, K., Montagne, A., Toga, A. W., and Zlokovic, B. V. (2018). The role of brain vasculature in neurodegenerative disorders. *Nat. Neurosci.* 21, 1318–1331. doi: 10.1038/s41593-018-0234-x

Wang, X., Campos, C. R., Peart, J. C., Smith, L. K., Boni, J. L., Cannon, R. E., et al. (2014). Nrf2 upregulates ATP binding cassette transporter expression and activity at the blood-brain and blood-spinal cord barriers. *J. Neurosci.* 34, 8585–8593. doi: 10.1523/JNEUROSCI.2935-13.2014

Wang, X., Sykes, D. B., and Miller, D. S. (2010). Constitutive androstane receptor-mediated up-regulation of ATP-driven xenobiotic efflux transporters at the blood-brain barrier. *Mol. Pharmacol.* 78, 376–383. doi: 10.1124/mol.110.063685

Yousef, H., Czupalla, C. J., Lee, D., Butcher, E. C., and Wyss-Coray, T. (2018). Papain-based single cell isolation of primary murine brain endothelial cells using flow cytometry. *Bio Protoc.* 8:e3091. doi: 10.21769/bioprotoc.3091

Yousef, H., Czupalla, C. J., Lee, D., Chen, M. B., Burke, A. N., Zera, K. A., et al. (2019). Aged blood impairs hippocampal neural precursor activity and activates microglia *via* brain endothelial cell VCAM1. *Nat. Med.* 25, 988–1000. doi: 10.1038/s41591-019-0440-4

Zhang, Y., Chen, K., Sloan, S. A., Bennett, M. L., Scholze, A. R., O'Keeffe, S., et al. (2014). An RNA-sequencing transcriptome and splicing database of glia, neurons, and vascular cells of the cerebral cortex. *J. Neurosci.* 34, 11929–11947. doi: 10.1523/JNEUROSCI.1860-14.2014

Zlokovic, B. V. (2011). Neurovascular pathways to neurodegeneration in Alzheimer's disease and other disorders. *Nat. Rev. Neurosci.* 12, 723–738. doi: 10.1038/nrn3114

Conflict of Interest: The authors declare that the research was conducted in the absence of any commercial or financial relationships that could be construed as a potential conflict of interest.

Copyright © 2020 Paraiso, Wang, Kuo, Furnas, Scofield, Chang, Yen and Yu. This is an open-access article distributed under the terms of the Creative Commons Attribution License (CC BY). The use, distribution or reproduction in other forums is permitted, provided the original author(s) and the copyright owner(s) are credited and that the original publication in this journal is cited, in accordance with accepted academic practice. No use, distribution or reproduction is permitted which does not comply with these terms.

frontiers in Neurology

ORIGINAL RESEARCH
published: 15 April 2020
doi: 10.3389/fneur.2020.00254

Effects of Periprocedural Tirofiban vs. Oral Antiplatelet Drug Therapy on Posterior Circulation Infarction in Patients With Acute Intracranial Atherosclerosis-Related Vertebrobasilar Artery Occlusion

Xuan Sun[1†], *Huijun Zhang*[2†], *Xu Tong*[1], *Feng Gao*[1], *Gaoting Ma*[1] *and Zhongrong Miao*[1*]

[1] Department of Interventional Neuroadiology, Beijing Tiantan Hospital, Capital Medical University, Beijing, China,
[2] Department of Neurology, Tong Ren Hospital Shanghai Jiaotong University School of Medicine, Shanghai, China

OPEN ACCESS

Edited by:
Jean-Claude Baron,
University of Cambridge,
United Kingdom

Reviewed by:
Beom Joon Kim,
Seoul National University Bundang Hospital, South Korea
Johannes Boltze,
University of Warwick,
United Kingdom

***Correspondence:**
Zhongrong Miao
miaozhongrong123@126.com

[†]These authors have contributed equally to this work

Specialty section:
This article was submitted to Stroke, a section of the journal Frontiers in Neurology

Received: 19 July 2019
Accepted: 17 March 2020
Published: 15 April 2020

Citation:
Sun X, Zhang H, Tong X, Gao F, Ma G and Miao Z (2020) Effects of Periprocedural Tirofiban vs. Oral Antiplatelet Drug Therapy on Posterior Circulation Infarction in Patients With Acute Intracranial Atherosclerosis-Related Vertebrobasilar Artery Occlusion. Front. Neurol. 11:254. doi: 10.3389/fneur.2020.00254

Background and purpose: Tirofiban and oral antiplatelet drugs can be used to inhibit reocclusion and restore microvascular reperfusion during endovascular treatment (EVT). This study compared recanalization rates, symptomatic intracranial hemorrhage (SICH), 90 day mortality, and functional outcomes between periprocedural tirofiban and antiplatelet therapy in patients with acute intracranial atherosclerosis-related vertebrobasilar artery occlusion.

Methods: A total of 105 consecutive patients with acute intracranial atherosclerosis-related vertebrobasilar artery occlusion who underwent EVT + tirofiban + oral antiplatelet or EVT + oral antiplatelet therapy at the Beijing Tiantan Hospital between January 2012 and July 2018 were included. Baseline characteristics, procedural parameters, and functional outcomes were assessed.

Results: Among the 105 patients, 74 underwent EVT + tirofiban + oral antiplatelet therapy, while 31 underwent EVT + oral antiplatelet drug therapy. EVT + tirofiban + oral antiplatelet therapy resulted in higher recanalization rates compared to EVT + oral antiplatelet drug therapy (93.24% vs. 77.42%; $p = 0.038$), whereas the risk for SICH, 90 day mortality, and functional independence outcomes did not differ between the groups. Logistic regression analysis revealed that EVT + tirofiban + oral antiplatelet therapy had an increased probability of higher recanalization rates (OR 0.18 [95% confidence interval (CI) 1.24–24.39]; $p = 0.025$). There were no differences in SICH (OR 0.00 [95% CI 0.00–Inf]; $p = 0.998$), 90 day mortality (OR 1.19 [95% CI 0.17–4.05]; $p = 0.826$), or functional independence (modified Rankin score 0 to ≤ 2) (OR 1.43 [95% CI 0.23–2.17]; $p = 0.538$) between the groups.

Conclusions: Ninety day functional outcomes of EVT + tirofiban + oral antiplatelet therapy were not superior to those of EVT + oral antiplatelet drug therapy; however, the recanalization rate was higher and the risks for SICH and 90 day mortality were lower.

Keywords: endovascular treatment, tirofiban, antiplatelet, intracranial atherosclerosis-related vertebrobasilar artery occlusion, vertebrobasilar artery occlusion

INTRODUCTION

Many randomized trials have demonstrated the improved efficacy of endovascular treatment (EVT) compared with standard medical care in patients with acute ischemic stroke (AIS) caused by arterial occlusion in the anterior circulation (1–5). For patients with acute ischemia due to basilar artery occlusion, the rates of death or dependency are 76–78% (6), even when these patients are treated with intravenous or intra-arterial thrombolysis agents. Different case scenarios have shown that stent-retriever thrombectomy is a safe and feasible treatment technique in patients with acute basilar artery occlusion (BAO) (7–10). However, for acute intracranial atherosclerosis-related occlusion (ICASO), which is more common in Asia (11–14), salvage therapies (15), such as balloon angioplasty and stent angioplasty, are necessary to increase the rate of successful and complete reperfusion. The associated risks, such as perforator occlusion (16), endothelial damage (17, 18), microvascular dysfunction (19), and reocclusion of recanalized vessels (20–22), may cause intracranial hemorrhage or even worse outcomes.

Many studies have investigated methods to prevent the negative events caused by antithrombotic EVT, either in the anterior or the posterior circulation. A *post hoc* analysis from the Multicenter Randomized Clinical Trial of Endovascular Treatment for Acute Ischemic Stroke from the Netherlands reported that patients on a previous oral antiplatelet drug regimen were twice as likely to experience a favorable functional outcome (23). Injection of low-dose tirofiban combined with EVT can enhance recanalization rates (24–26). However, there have been no studies confirming which method is safer and/or more effective. The aim of the present study, therefore, was to compare outcomes in patients who underwent EVT plus tirofiban (EVT + tirofiban) therapy vs. those who underwent EVT in conjunction with oral antiplatelet drug therapy.

METHODS

Study Design

Consecutive patients presenting with ICAS-related acute BAO who underwent EVT + tirofiban + oral antiplatelet or EVT + oral antiplatelet drug therapy at Beijing Tiantan Hospital (Beijing, China) between January 2012 and July 2018 were included in this retrospective study. Intravenous thrombolysis with tissue plasminogen activator was allowed prior to EVT, consistent with current guidelines (27). The details of patient selection and grouping are presented in **Figure 1** according to previous studies (28–30). Tirofiban was considered for application in the following situations/parameters: (1) rescue treatment with emergency stenting for residual artery stenosis or failed thrombectomy; (2) rescue treatment with emergency balloon angioplasty for residual artery stenosis or failed thrombectomy; (3) local new thrombosis or vascular dissection of the responsible vessel; and (4) severe atherosclerosis lesions with a high possibility of reocclusion after being recanalized. Informed consent was obtained from all participants or their relatives, and the protocol was approved by the Institutional Review Board of Beijing Tiantan Hospital.

Plain computed tomography (CT) of the brain was performed first to exclude intracranial bleeding. Magnetic resonance imaging (MRI) was used to exclude large brainstem infarctions. CT angiography (CTA) or magnetic resonance angiography (MRA) was used to confirm the presence of acute BAO. The clinical and radiological data of these patients were retrospectively collected and analyzed and included age; sex; stroke risk factors, including hypertension, diabetes mellitus, hypercholesterolemia, and current smoking status; initial stroke severity, as reflected by the National Institutes of Health Stroke Scale (NIHSS) score; initial imaging modality; previous intravenous thrombolysis; type of EVT device(s); onset to puncture time; procedure duration; onset to recanalization time; and collateral status.

EVT

The decision to perform EVT was made by a stroke neurologist and a neuroradiologist based on the CT, CTA, or MRA results of the patient. All EVT procedures were performed by a neurointerventionalist with sufficient experience in neurovascular intervention in mechanical thrombectomy for AIS (>50 cases). Cerebral angiography and EVT were performed under general anesthesia or conscious sedation after evaluation by a dedicated anesthesiology team. A stent retriever or aspiration was used first, with a possible switch to another strategy in the case of recanalization failure (mTICI grade = 0–2a) with the first approach. Underlying ICAS was determined when significant stenosis was seen on the initial diagnostic angiography or on follow-up angiography after a mechanical thrombectomy procedure (31). Causes of acute BAO were classified based on our previous research (32). ICAS was defined as significant fixed focal stenosis that could be resolved by means of angioplasty or stent insertion at the site of occlusion. Significant stenosis was defined as (1) fixed stenosis ≥70% or (2) fixed stenosis ≥50% in addition to either angiographical evidence of impaired perfusion or evidence of reocclusion after sufficient treatment with a stent retriever. The cause of acute BAO was classified as embolism based on the following: (1) after clot retrieval, there was no focal stenosis; (2) an embolus was removed with a stent retriever; or (3) MRA or CTA performed within 1 week after the procedure showed lack of stenosis in the responsible artery. In cases of recanalization failure (mTICI grade 0–2a after mechanical thrombectomy within 10 min), intracranial angioplasty or stenting was performed. All patients immediately received a loading dose of 300 mg of aspirin and 300 mg of clopidogrel orally. Patients with daily aspirin (100 mg) or/and clopidogrel (75 mg) medication before the intervention did not receive a loading dose. Alternatively, tirofiban therapy (Grand Pharmaceutical Co Ltd, China) was applied. Standard procedure was to administer 5 mg of tirofiban diluted in 100 ml

Abbreviations: EVT, endovascular treatment; SICH, symptomatic intracranial hemorrhage; AIS, acute ischemic stroke; ICASO, intracranial atherosclerosis-related occlusion; tPA, tissue plasminogen activator; CT, computed tomography; CTA, computed tomography angiography; MRI, magnetic resonance imaging; MRA, magnetic resonance angiography; NIHSS, National Institutes of Health Stroke Scale; mTICI, modified Thrombolysis in Cerebral Infarction; mRS, modified Rankin Scale; ORs, odds ratios.

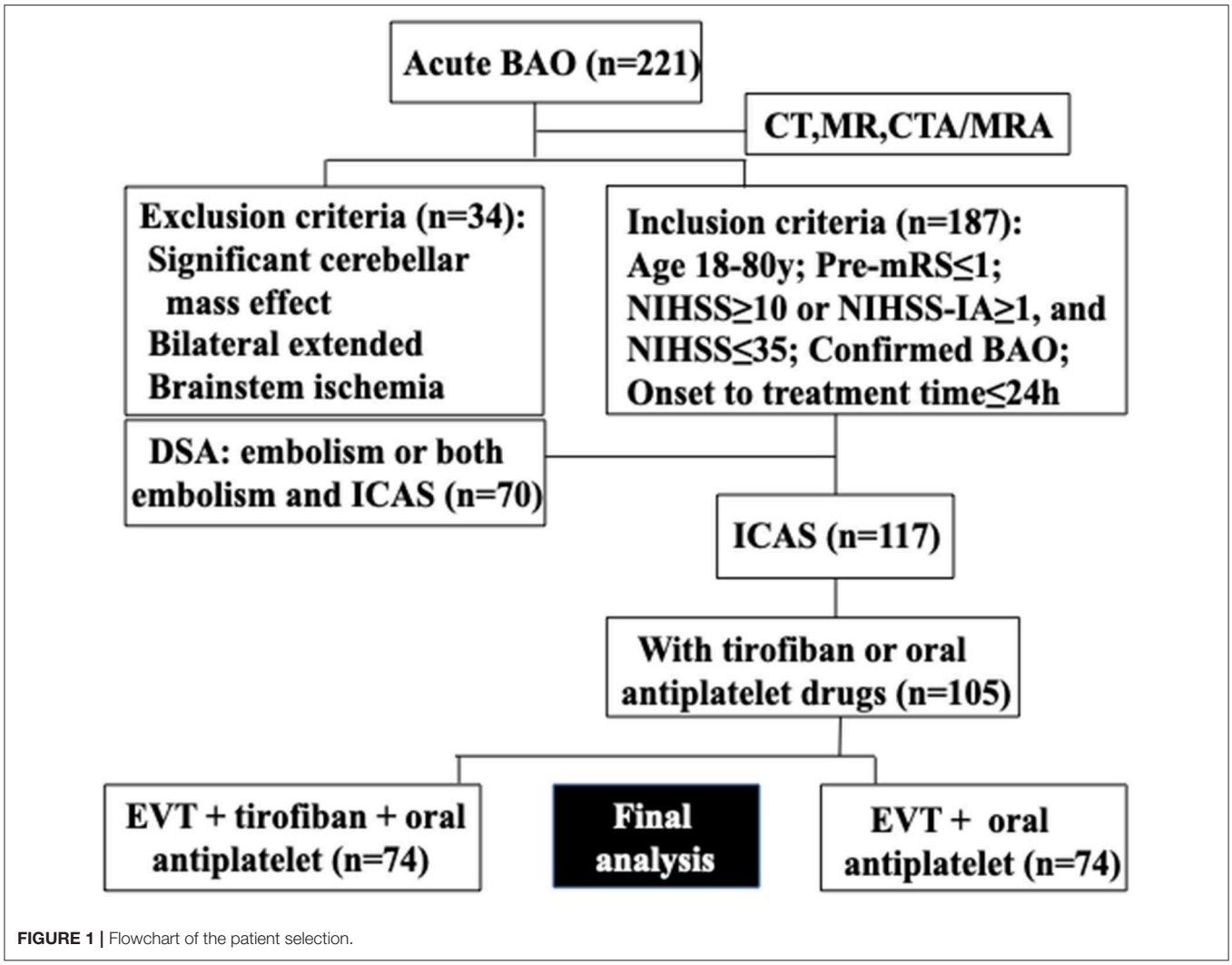

FIGURE 1 | Flowchart of the patient selection.

of normal saline and infused with a 6- to 8-ml (0.3–0.4 mg) loading dose via a catheter at a rate of 1 ml/min. Intravenous tirofiban was continued at a rate of 0.15 μg/kg/min for the next 24 h. Intravenous tirofiban was continued at a rate of 0.15 μg/kg/min for the next 24 h. If there were no hemorrhagic complications seen on the head CT scan, aspirin and clopidogrel (one tablet each) were used with overlap for 4–6 h during the operation. If CT performed 24 h after the operation revealed no dynamic bleeding or hemorrhagic transformation, dual antiplatelet therapy was maintained for at least 3 months after the procedure, followed by lifelong aspirin or clopidogrel monotherapy thereafter.

Image Interpretation

Diffusion-weighted images were assessed using the pons-midbrain index (using the posterior communicating artery) and the American Society of Interventional and Therapeutic Neuroradiology/Society of Interventional Radiology (ASITN/SIR) (29, 33) grading system. All images were analyzed retrospectively by two neurologists blinded to the patient information and study protocol. If no consensus was reached, a third neurointerventionalist with 20 years of experience made the final decision.

Outcome Measures

For primary effectiveness, outcomes were assessed according to the BASICS definition (34). Functional independence and a favorable outcome were defined as mRS $\leq$ 2 and mRS $\leq$ 3, respectively. Other effectiveness outcome measures included the rates of successful recanalization [modified treatment for cerebral infarction (mTICI) = 2b−3] and complete recanalization (mTICI = 3) (35).

The safety outcome measures included 90 day mortality and rates of intracerebral hemorrhage and symptomatic intracerebral hemorrhage (SICH) within 24 h according to the criteria described in the European Cooperative Acute Stroke Study III (ECASS III) (36).

Statistical Analysis

Study data were collected on standard forms, evaluated for completeness, and double keyed into an EpiData statistics data document. Statistical analysis was performed using R

(http://www.R-project.org, The R Foundation for Statistical Computing, Vienna, Austria) and EmpowerStats (http://www.empowerstats.com, X&Y Solutions, Inc., Boston, MA, USA). Continuous variables are expressed as medians and interquartile ranges (IQRs) and as absolute numbers and percentages, while categorical variables are expressed as the means and standard deviations (SDs). Shapiro–Wilk test, histogram, and QQ chart were used to confirm normal distribution of data. The chi-squared test was used to compare categorical variables, *t*-tests were used to compare continuous variables, and the Mann–Whitney *U* test was used to compare scores. Logistic regression was performed to estimate odds ratios (ORs) for 90 day mortality and primary effectiveness outcomes (mRS $\leq$ 2 and $\leq$ 3). Variables including the NIHSS score, sex, standard preoperative intravascular tissue plasminogen activator, general anesthesia, stent thrombectomy, and intraoperative heparinization were entered into a logistic regression model. All tests were two-tailed, and statistical significance was determined at a *P* level of 0.05.

RESULTS

Of 105 patients, 71 [mean ($\pm$ SD) age, 60.0 $\pm$ 8 years; 86.49% men] underwent EVT + tirofiban + oral antiplatelet drug therapy, whereas 34 (mean age, 60.0 $\pm$ 10 years; 83.87% men) underwent EVT + oral antiplatelet drug therapy.

A comparison of the baseline data and treatment procedures between the two groups is shown in **Table 1**. The NIHSS score was higher in patients who underwent EVT + tirofiban + oral antiplatelet drug therapy (25 [IQR 13–35] vs. 12 [IQR 10–23]; $p = 0.005$) than in those who underwent EVT + oral antiplatelet drug therapy (**Table 1**). More patients in the EVT + tirofiban + oral antiplatelet drug therapy group required stent thrombectomy (77.03% vs. 45.16%; $p = 0.001$) than patients in the EVT + oral antiplatelet drug therapy group, and fewer patients required intraoperative heparinization (40.54% vs. 70.97%; $p = 0.004$), which may have been related to differences in the severity of neurological deficits at the time of admission between the two groups.

A comparison of higher recanalization rates, 90 day mortality, SICH, and functional outcomes between the two groups is summarized in **Table 2**. In both groups, there was a higher rate of successful recanalization (mTICI 2b-3) among patients who underwent EVT + tirofiban + oral antiplatelet drug therapy (93.24% vs. 77.42%; $p = 0.038$). After comparing the two groups, the functional independence outcome rate (mRS 0 to $\leq$ 2) at 90 days (32.43% vs. 51.61%, $p = 0.065$), 7 day intracerebral hemorrhage (16.22% vs. 6.45%, $p = 0.223$), 90 day mortality (16.22% vs. 9.68%, $p = 0.544$), 7 day SICH (4.05% vs. 0.00%, $p = 0.553$), and 30 day responsible artery reocclusion (16.22% vs. 12.90%, $p = 0.773$) was not significantly different. The favorable outcome rate (mRS 0 to $\leq$3) in the EVT + tirofiban + oral antiplatelet drug therapy group was higher than that in the EVT + oral antiplatelet drug therapy group, owing to the differences in severe neurological deficits at admission.

Adjusted logistic regression analysis revealed that treatment with EVT + tirofiban + oral antiplatelet drug therapy was associated with an increased rate of successful recanalization (OR 0.18 [95% confidence interval (CI) 1.24–24.39]; $p = 0.025$), whereas no differences were found in SICH (OR 0.00 [95% CI 0.00–Inf]; $p = 0.998$), 90 day mortality (OR 1.19 [95% CI 0.17–4.05]; $p = 0.826$), or functional independence outcomes (mRS 0 to $\leq$ 2) (OR 1.43 [95% CI 0.23–2.17]; $p = 0.538$) between the groups (**Table 3**).

TABLE 1 | Comparison of baseline data and treatment procedures between patients who underwent ET +tirofiban + oral antiplatelet and those who underwent ET + oral antiplatelet drug therapy.

Baseline characteristics, treatment procedures, and outcomes	Treatment		*P*-value
	ET + Tirofiban+ oral antiplatelet (*n* = 74)	ET + oral antiplatelet drug (*n* =31)	
Age, mean (SD)	60 (8)	60 (10)	0.944
Male sex (%)	64 (86.49%)	26 (83.87%)	0.764
NIHSS, median, points (IQR)	25 (13–35)	12 (10–23)	0.005
Door to needle, median, min (IQR)	420 (300–540)	450 (307–705)	0.165
Operative time, median, min (IQR)	90 (60–120)	60 (60–120)	0.224
Medical history			
Previous stroke	18 (24.32%)	7 (22.58%)	>0.999
Hypertension	54 (72.97%)	25 (80.65%)	0.446
Diabetes mellitus	19 (25.68%)	10 (32.26%)	0.485
Hyperlipidemia	19 (25.68%)	8 (25.81%)	>0.999
Previous smoking	30 (40.54%)	11 (35.48%)	0.628
Coronary heart disease	7 (9.46%)	2 (6.45%)	>0.999
Affected position			0.749
Proximal BA (including intracranial VA)	50 (67.57%)	23 (74.19%)	
Middle BA	23 (31.08%)	8 (25.81%)	
Distal BA	1 (1.35%)	0 (0.00%)	
Tandem occlusions	0 (0.00%)	1 (3.23%)	0.295
ASITN/SIR collateral score			0.262
Score of 0 or 1	28 (37.84%)	16 (51.61%)	
Score of 2	39 (52.70%)	11 (35.48%)	
Score of 3 or 4	7 (9.46%)	4 (12.90%)	
Standard IV rt-PA preoperative	18 (24.32%)	2 (6.45%)	0.054
General anesthesia	64 (86.49%)	22 (70.97%)	0.093
Stent thrombectomy	57 (77.03%)	14 (45.16%)	0.001
Intra-arterial thrombolysis	15 (20.27%)	10 (32.26%)	0.214
Intraoperative Heparinization	30 (40.54%)	22 (70.97%)	0.004
Intracranial angioplasty	62 (83.58%)	21 (67.74%)	0.125
Balloon angioplasty alone	15 (20.27%)	7 (22.58%)	
Stent implantation	47 (63.51%)	14 (45.16%)	

Values are numbers with percentages in parentheses, unless indicated otherwise. IQR, interquartile range; NIHSS, National Institutes of Health Stroke Scale; SD, standard deviation; ASITN/SIR, American Society of Interventional and Therapeutic Neuroradiology/Society of Interventional Radiology.

DISCUSSION

ICAS occlusion is more common in the posterior than in the anterior circulation, especially among the Asian population (22, 37). Therefore, rescue therapies such as emergency angioplasty

TABLE 2 | Comparison of higher recanalization rates, mortality at 90 days, symptomatic intracerebral hemorrhage (SICH), and function outcomes between EVT + tirofiban + oral antiplatelet and EVT + oral antiplatelet drug therapy.

Outcome measures	Treatment		*P* value
	ET + tirofiban+ oral antiplatelet (*n* = 74)	ET + oral antiplatelet drug (*n* =31)	
Angiographic outcome (mTICI)			
2b-3	69 (93.24%)	24 (77.42%)	0.038
Good Outcome (mRS 0–≤ 2)	24 (32.43%)	16 (51.61%)	0.065
mRS 0–≤ 3	35 (47.30%)	22 (70.97%)	0.026
90 days mortality	12 (16.22%)	3 (9.68%)	0.544
7 days intracerebral hemorrhage	12 (16.22%)	2 (6.45%)	0.223
7 days SICH	3 (4.05%)	0 (0.00%)	0.553
30 days responsible artery reocclusion	12 (16.22%)	4 (12.90%)	0.773

Values are numbers with percentages in parentheses, unless indicated otherwise.
mRS, modified Rankin Scale; mTICI, modified Thrombolysis in Cerebral Infarction; SICH, symptomatic intracerebral hemorrhage, tPA, tissue plasminogen activator.

TABLE 3 | Univariate and multivariate logistic regression analysis.

Outcome measures	Univariate Logistic Regression Analysis	Multivariate Logistic Regression Analysis
Angiographic outcome (mTICI 2b-3)		
ET + tirofiban + oral antiplatelet	1.0	1.0
ET + oral antiplatelet	0.25 (0.07, 0.86) 0.028	0.18 (0.04, 0.81) 0.025
Good Outcome (mRS 0–≤ 2)		
ET + tirofiban + oral antiplatelet	1.0	1.0
ET + oral antiplatelet	2.22 (0.94, 5.23) 0.068	1.43 (0.46, 4.42) 0.538
mRS 0–≤ 3		
ET + tirofiban + oral antiplatelet	1.0	1.0
ET + oral antiplatelet	2.72 (1.11, 6.70) 0.029	1.45 (0.48, 4.35) 0.509
90 days mortality		
ET + tirofiban + oral antiplatelet	1.0	1.0
ET + oral antiplatelet	0.55 (0.14, 2.12) 0.388	1.19 (0.25, 5.77) 0.826
7 days intracerebral hemorrhage		
ET + tirofiban + oral antiplatelet	1.0	1.0
ET + oral antiplatelet	0.36 (0.07, 1.70) 0.195	0.59 (0.11, 3.31) 0.553
7 days SICH		
ET + tirofiban + oral antiplatelet	1.0	1.0
ET + oral antiplatelet	0.00 (0.00, Inf) 0.996	0.00 (0.00, Inf) 0.998
30 days responsible artery reocclusion		
ET + tirofiban + oral antiplatelet	1.0	1.0
ET + oral antiplatelet	0.77 (0.23, 2.59) 0.667	0.56 (0.14, 2.24) 0.409

Data: OR (95% CI) P-value.
mRS, modified Rankin Scale; mTICI, modified Thrombolysis in Cerebral Infarction; SICH, symptomatic intracerebral hemorrhage; tPA, tissue plasminogen activator.

or stenting are often required when treating these patients with EVT (15, 21), thereby inducing the removal of *in situ* thrombi (17), instability in the ICAS endothelium (38), and the "snowplow" effect (21). These steps result in perforator occlusion, microvascular dysfunction, and reocclusion of recanalized vessels. Many treatment strategies, including EVT + tirofiban + oral antiplatelet drug therapy (23) and EVT + oral antiplatelet drug therapy (24, 25), have been performed on patients with anterior and posterior circulation infarction in previous studies to prevent these drawbacks.

Due to the disparate characteristics of patients with posterior circulation cerebral infarction, intravascular tirofiban is more convenient than oral antiplatelet drug therapy. First, most patients with posterior circulation infarction exhibit consciousness disorders and difficulty swallowing. Oral antiplatelet drugs need to be administered through a gastric tube, the insertion of which is time-consuming. Second, it is important to differentiate an ICAS occlusion from an intracranial embolism before operating on patients without a clear history of intracranial artery stenosis. For these patients, intravascular tirofiban has the advantage of a rapid onset. Therefore, the present study compared the safety and outcomes in patients who underwent EVT+ tirofiban drug therapy vs. those who underwent EVT + oral antiplatelet drug therapy.

Our study found that acute intracranial atherosclerosis-related vertebrobasilar artery occlusion treated with EVT + tirofiban + oral antiplatelet drug therapy was associated with an increased rate of successful recanalization (OR 0.18 [95% (CI) 1.24–24.39]; $p = 0.025$), whereas no differences were found in SICH (OR 0.00 [95% CI 0.00–Inf]; $p = 0.998$) or 90 day mortality (OR 1.19 [95% CI 0.17–4.05]; $p = 0.826$). Functional independence outcomes at 90 days (mRS 0 to ≤2) were not significantly different (OR 1.43 [95% CI 0.23–2.17]; $p = 0.538$), which may be attributed to the severity of the neurological deficits between the groups at the time of admission and the small sample size. Since the investigation was an observational one based on a single-center prospective registry study, there are several limitations. First, the administration route, dose, and duration of tirofiban used in this study were pragmatic. Furthermore, inherent bias because of the retrospective and monocentric study design was inevitable. Compared to patients with EVT + oral antiplatelet drug therapy, those with EVT + tirofiban + oral antiplatelet drug therapy had a higher NIHSS score at baseline and a more frequent application of stent thrombectomy and intraoperative heparinization. However, after adjusting for potential confounders and conducting a multivariate analysis, we presume that this bias probably had little influence on our results. A multicenter study involving a larger sample size or a randomized controlled trial is needed to verify this result.

CONCLUSIONS

In summary, for patients who have trouble swallowing and those without a clear history of intracranial artery stenosis,

intravascular tirofiban treatment can be performed to save time. Our results demonstrated that EVT + tirofiban + oral antiplatelet drug therapy was not superior to EVT + oral antiplatelet drug therapy in terms of the functional independence outcomes at 90 days. Therefore, a more effective perioperative administration route, time, and dosage await further study.

DATA AVAILABILITY STATEMENT

The datasets generated for this study are available on request to the corresponding author.

ETHICS STATEMENT

All procedures performed in studies involving human participants were in accordance with the ethical standards of Beijing Tiantan Hospital, Capital Medical University medical ethics committee and with the 1964 Helsinki declaration and its later amendments or comparable ethical standards.

AUTHOR CONTRIBUTIONS

ZM designed the research and wrote the manuscript. XS and HZ designed the research. XS, HZ, and ZM performed the research. XT, FG, and GM analyzed the data.

FUNDING

This study was supported by the National Key Research and Development Program of China (Grant number 2016YFC1301501).

ACKNOWLEDGMENTS

We thank all relevant clinicians, statistician, and imaging technicians.

REFERENCES

1. Berkhemer OA, Fransen PS, Beumer D, van den Berg LA, Lingsma HF, Yoo AJ, et al. A randomized trial of intraarterial treatment for acute ischemic stroke. *N Engl J Med*. (2015) 372:11–20. doi: 10.1056/NEJMoa1411587
2. Campbell BC, Mitchell PJ, Kleinig TJ, Dewey HM, Churilov L, Yassi N, et al. Endovascular therapy for ischemic stroke with perfusion-imaging selection. *N Engl J Med*. (2015) 372:1009–18. doi: 10.1056/NEJMoa1414792
3. Goyal M, Demchuk AM, Menon BK, Eesa M, Rempel JL, Thornton J, et al. Randomized assessment of rapid endovascular treatment of ischemic stroke. *N Engl J Med*. (2015) 372:1019–30. doi: 10.1056/NEJMoa1414905
4. Molina CA, Chamorro A, Rovira A, de Miquel A, Serena J, Roman LS, et al. REVASCAT: a randomized trial of revascularization with solitaire FR device vs. Best medical therapy in the treatment of acute stroke due to anterior circulation large vessel occlusion presenting within eight-hours of symptom onset. *Int J Stroke*. (2015) 10:619–26. doi: 10.1111/ijs.12157
5. Saver JL, Goyal M, Bonafe A, Diener HC, Levy EI, Pereira VM, et al. Stent-retriever thrombectomy after intravenous t-pa vs. T-pa alone in stroke. *N Engl J Med*. (2015) 372:2285–95. doi: 10.1056/NEJMoa1415061
6. Yeung JT, Matouk CC, Bulsara KR, Sheth KN. Endovascular revascularization for basilar artery occlusion. *Interv Neurol*. (2015) 3:31–40. doi: 10.1159/000368968
7. Gory B, Eldesouky I, Sivan-Hoffmann R, Rabilloud M, Ong E, Riva R, et al. Outcomes of stent retriever thrombectomy in basilar artery occlusion: an observational study and systematic review. *J Neurol Neurosurg Psychiatry*. (2016) 87:520–5. doi: 10.1136/jnnp-2014-310250
8. Mohlenbruch M, Stampfl S, Behrens L, Herweh C, Rohde S, Bendszus M, et al. Mechanical thrombectomy with stent retrievers in acute basilar artery occlusion. *AJNR Am J Neuroradiol*. (2014) 35:959–64. doi: 10.3174/ajnr.A3796
9. Baek JM, Yoon W, Kim SK, Jung MY, Park MS, Kim JT, et al. Acute basilar artery occlusion: outcome of mechanical thrombectomy with solitaire stent within 8 hours of stroke onset. *Am J Neuroradiol*. (2014) 35:989–93. doi: 10.3174/ajnr.A3813
10. Yoon W, Kim SK, Heo TW, Baek BH, Lee YY, Kang HK. Predictors of good outcome after stent-retriever thrombectomy in acute basilar artery occlusion. *Stroke*. (2015) 46:2972–5. doi: 10.1161/STROKEAHA.115.010840
11. Lee JS, Hong JM, Lee KS, Suh HI, Demchuk AM, Hwang YH, et al. Endovascular therapy of cerebral arterial occlusions: intracranial atherosclerosis versus embolism. *J Stroke Cerebrovasc Dis*. (2015) 24:2074–80. doi: 10.1016/j.jstrokecerebrovasdis.2015.05.003
12. De Silva DA, Woon FP, Lee MP, Chen CP, Chang HM, Wong MC. South Asian patients with ischemic stroke: intracranial large arteries are the predominant site of disease. *Stroke*. (2007) 38:2592–4. doi: 10.1161/STROKEAHA.107.484584
13. Lee SJ, Cho SJ, Moon HS, Shon YM, Lee KH, Kim DI, et al. Combined extracranial and intracranial atherosclerosis in Korean patients. *Arch Neurol*. (2003) 60:1561–4. doi: 10.1001/archneur.60.11.1561
14. Wang Y, Zhao X, Liu L, Soo YO, Pu Y, Pan Y, et al. Prevalence and outcomes of symptomatic intracranial large artery stenoses and occlusions in China: the Chinese intracranial atherosclerosis (cicas) study. *Stroke*. (2014) 45:663–9. doi: 10.1161/STROKEAHA.113.003508
15. Gao F, Lo WT, Sun X, Mo DP, Ma N, Miao ZR. Combined use of mechanical thrombectomy with angioplasty and stenting for acute basilar occlusions with underlying severe intracranial vertebrobasilar stenosis: preliminary experience from a single Chinese center. *AJNR Am J Neuroradiol*. (2015) 36:1947–52. doi: 10.3174/ajnr.A4364
16. Yoon W, Kim SK, Park MS, Kim BC, Kang HK. Endovascular treatment and the outcomes of atherosclerotic intracranial stenosis in patients with hyperacute stroke. *Neurosurgery*. (2015) 76:680–6. doi: 10.1227/NEU.0000000000000694
17. Gory B, Bresson D, Kessler I, Perrin ML, Guillaudeau A, Durand K, et al. Histopathologic evaluation of arterial wall response to 5 neurovascular mechanical thrombectomy devices in a swine model. *AJNR Am J Neuroradiol*. (2013) 34:2192–8. doi: 10.3174/ajnr.A3531
18. Arai D, Ishii A, Chihara H, Ikeda H, Miyamoto S. Histological examination of vascular damage caused by stent retriever thrombectomy devices. *J Neurointerv Surg*. (2016) 8:992–5. doi: 10.1136/neurintsurg-2015-011968
19. Dalkara T, Arsava EM. Can restoring incomplete microcirculatory reperfusion improve stroke outcome after thrombolysis? *J Cereb Blood Flow Metab*. (2012) 32:2091–9. doi: 10.1038/jcbfm.2012.139
20. Heo JH, Lee KY, Kim SH, Kim DI. Immediate reocclusion following a successful thrombolysis in acute stroke: a pilot study. *Neurology*. (2003) 60:1684–7. doi: 10.1212/01.WNL.0000063323.23493.98
21. Kang DH, Kim YW, Hwang YH, Park SP, Kim YS, Baik SK. Instant reocclusion following mechanical thrombectomy of *in situ* thromboocclusion and the role of low-dose intra-arterial tirofiban. *Cerebrovasc Dis*. (2014) 37:350–5. doi: 10.1159/000362435
22. Lee JS, Hong JM, Lee KS, Suh HI, Choi JW, Kim SY. Primary stent retrieval for acute intracranial large artery occlusion due to atherosclerotic disease. *J Stroke*. (2016) 18:96–101. doi: 10.5853/jos.2015.01347
23. Mulder MJ, Berkhemer OA, Fransen PS, van den Berg LA, Lingsma HF, den Hertog HM, et al. Does prior antiplatelet treatment improve functional outcome after intra-arterial treatment for acute ischemic stroke? *Int J Stroke*. (2017) 12:368–76. doi: 10.1177/1747493016677842

24. Goh DH, Jin SC, Jeong HW, Ha SY. Mechanical solitaire thrombectomy with low-dose booster tirofiban injection. *Neurointervention*. (2016) 11:114–9. doi: 10.5469/neuroint.2016.11.2.114
25. Seitz RJ, Hamzavi M, Junghans U, Ringleb PA, Schranz C, Siebler M. Thrombolysis with recombinant tissue plasminogen activator and tirofiban in stroke: preliminary observations. *Stroke*. (2003) 34:1932–5. doi: 10.1161/01.STR.0000080535.61188.A6
26. Seitz RJ, Siebler M. Platelet gpiib/iiia receptor antagonists in human ischemic brain disease. *Curr Vasc Pharmacol*. (2008) 6:29–36. doi: 10.2174/157016108783331303
27. Powers WJ, Rabinstein AA, Ackerson T, Adeoye OM, Bambakidis NC, Becker K, et al. 2018 guidelines for the early management of patients with acute ischemic stroke: a guideline for healthcare professionals from the American Heart Association/American Stroke Association. *Stroke*. (2018). 49:e46–110. doi: 10.1161/STR.0000000000000172
28. Sun X, Tong X, Gao F, Lao H, Miao Z. Endovascular treatment for acute basilar artery occlusion: a single center retrospective observational study. *BMC Neurol*. (2019) 19:315. doi: 10.1186/s12883-019-1551-8
29. van der Hoeven Erik JRJ, Schonewille Wouter J, Vos Jan, Algra Ale, Audebert Heinrich J, Berge Eivind, et al. The Basilar Artery International Cooperation Study (BASICS): study protocol for a randomised controlled trial. *Trials*. (2013) 14:200. doi: 10.1186/1745-6215-14-200
30. Writing Group for the BASILAR Group, Zi W, Qiu Z, Wu D, Li F, Liu H, et al. Assessment of endovascular treatment for acute basilar artery occlusion via a nationwide prospective registry. *JAMA Neurol*. (2020) 72:1295–303. doi: 10.1001/jamaneurol.2020.0156
31. Samuels OB, Joseph GJ, Lynn MJ, Smith HA, Chimowitz MI. A standardized method for measuring intracranial arterial stenosis. *Am J Neuroradiol*. (2000) 21:643–6. doi: 10.1016/S0925-4927(99)00050-5
32. Zhang H, Sun X, Huang Q, Wang XM, Yue YH, Ju MF, et al. Intracranial atherosclerotic disease-related acute middle cerebral artery occlusion can be predicted by diffusion-weighted imaging. *Front Neurosci*. (2019) 13:903. doi: 10.3389/fnins.2019.00903
33. Goyal N, Tsivgoulis G, Nickele C, Doss VT, Hoit D, Alexandrov AV, et al. Posterior circulation CT angiography collaterals predict outcome of endovascular acute ischemic stroke therapy for basilar artery occlusion. *J Neurointerv Surg*. (2016) 8:783–6. doi: 10.1136/neurintsurg-2015-011883
34. Singer OC, Berkefeld J, Nolte CH, Bohner G, Haring HP, Trenkler J, et al. Mechanical recanalization in basilar artery occlusion: the endostroke study. *Ann Neurol*. (2015) 77:415–24. doi: 10.1002/ana.24336
35. Zaidat OO, Yoo AJ, Khatri P, Tomsick TA, von Kummer R, Saver JL, et al. Recommendations on angiographic revascularization grading standards for acute ischemic stroke: a consensus statement. *Stroke*. (2013) 44:2650–63. doi: 10.1161/STROKEAHA.113.001972
36. Hacke W, Kaste M, Bluhmki E, Brozman M, Davalos A, Guidetti D, et al. Thrombolysis with alteplase 3 to 4.5 hours after acute ischemic stroke. *N Engl J Med*. (2008) 359:1317–29. doi: 10.1056/NEJMoa0804656
37. Lee JS, Hong JM, Kim JS. Diagnostic and therapeutic strategies for acute intracranial atherosclerosis-related occlusions. *J Stroke*. (2017) 19:143–51. doi: 10.5853/jos.2017.00626
38. Suwanwela NC, Chutinetr A. Risk factors for atherosclerosis of cervicocerebral arteries: intracranial versus extracranial. *Neuroepidemiology*. (2003) 22:37–40. doi: 10.1159/000067112

Conflict of Interest: The authors declare that the research was conducted in the absence of any commercial or financial relationships that could be construed as a potential conflict of interest.

Copyright © 2020 Sun, Zhang, Tong, Gao, Ma and Miao. This is an open-access article distributed under the terms of the Creative Commons Attribution License (CC BY). The use, distribution or reproduction in other forums is permitted, provided the original author(s) and the copyright owner(s) are credited and that the original publication in this journal is cited, in accordance with accepted academic practice. No use, distribution or reproduction is permitted which does not comply with these terms.

frontiers in Neuroscience

HYPOTHESIS AND THEORY
published: 21 April 2020
doi: 10.3389/fnins.2020.00272

Hypothesis and Theory: A Pathophysiological Concept of Stroke-Induced Acute Phase Response and Increased Intestinal Permeability Leading to Secondary Brain Damage

Fabienne Ferrara[1], Vilia Zeisig[2], Sören Pietsch[3], Rita Rütten[1], Antje Y. Dreyer[1], Laura Pieper[4], Ann-Kathrin Schatzl[1], Damian D. McLeod[5,6], Henryk Barthel[2], Johannes Boltze[7], Wieland Schrödl[8] and Björn Nitzsche[2]*

[1] Fraunhofer Institute for Cell Therapy and Immunology (IZI), Leipzig, Germany, [2] Clinic and Policlinic for Nuclear Medicine, University of Leipzig, Leipzig, Germany, [3] Klinik und Poliklinik für Kinder und Jugendmedizin, Universitätsklinikum Leipzig, Leipzig, Germany, [4] Institut für Veterinär-Epidemiologie und Biometrie, Freie Universität Berlin, Berlin, Germany, [5] OncoRay - National Center for Radiation Research in Oncology, Faculty of Medicine and University Hospital CG Carus, TU Dresden, HZDR, Dresden, Germany, [6] School of Biomedical Sciences and Pharmacy, Faculty of Health and Medicine, and Hunter Medical Research Institute, The University of Newcastle, Callaghan, NSW, Australia, [7] School of Life Sciences, Faculty of Science, University of Warwick, Coventry, United Kingdom, [8] Faculty of Veterinary Medicine, Institute of Bacteriology and Mycology, University of Leipzig, Leipzig, Germany

OPEN ACCESS

Edited by:
Christian Gonzalez-Billault, University of Chile, Chile

Reviewed by:
Bogdan A. Stoica, University of Maryland, United States
Alba Di Pardo, Mediterranean Neurological Institute (IRCCS), Italy

***Correspondence:**
Fabienne Ferrara
fabienne_ferrara@gmx.de

Specialty section:
This article was submitted to Neurodegeneration, a section of the journal Frontiers in Neuroscience

Received: *17 May 2019*
Accepted: *10 March 2020*
Published: *21 April 2020*

Citation:
Ferrara F, Zeisig V, Pietsch S, Rütten R, Dreyer AY, Pieper L, Schatzl A-K, McLeod DD, Barthel H, Boltze J, Schrödl W and Nitzsche B (2020) Hypothesis and Theory: A Pathophysiological Concept of Stroke-Induced Acute Phase Response and Increased Intestinal Permeability Leading to Secondary Brain Damage. Front. Neurosci. 14:272. doi: 10.3389/fnins.2020.00272

Gut integrity impairment leading to increased intestinal permeability (IP) is hypothesized to be a trigger of critically illness. Approximately 15–20% of human ischemic stroke (IS) victims require intensive care, including patients with impaired level of consciousness or a high risk for developing life-threatening cerebral edema. Local and systemic inflammatory reactions are a major component of the IS pathophysiology and can significantly aggravate brain tissue damage. Intracerebral inflammatory processes following IS have been well studied. Until now, less is known about systemic inflammatory responses and IS consequences apart from a frequently observed post-IS immunosuppression. Here, we provide a hypothesis of a crosstalk between systemic acute phase response (APR), IP and potential secondary brain damage during acute and subacute IS stages supported by preliminary experimental data. Alterations of the acute phase proteins (APPs) C-reactive protein and lipopolysaccharide-binding protein and serum level changes of antibodies directed against *Escherichia coli*-cell extract antigen (IgA-, IgM-, and IgG-anti-*E. coli*) were investigated at 1, 2, and 7 days following IS in ten male sheep. We found an increase of both APPs as well as a decrease of all anti-*E. coli* antibodies within 48 h following IS. This may indicate an early systemic APR and increased IP, and underlines the importance of the increasingly recognized gut-brain axis and of intestinal antigen release for systemic immune responses in acute and subacute stroke stages.

Keywords: ischemic stroke, immune response, intestinal permeability, acute phase proteins, systemic inflammation, large animal stroke models, cerebral ischemia, gut-brain axis

INTRODUCTION

Gut integrity (GI) plays an important role in balancing permeable gut functions required for the uptake of nutritional components versus preventive functions such as forming a barrier against pathogen egress (Doig et al., 1998; Otani and Coopersmith, 2019). GI impairment and subsequently increased intestinal permeability (IP) are believed to be a major pathophysiological elements in a number of severe conditions. They have been described in chronic heart failure (Doig et al., 1998; Sandek et al., 2014), complications in intensive care unit (ICU) patients (Klehmet et al., 2009) and in individuals undergoing cardiopulmonary bypass (Riddington et al., 1996), as well as after traumatic brain injury (Bansal et al., 2009). GI impairment and increased IP are supposed to be related to inadequate mucosal perfusion (Doig et al., 1998; Klehmet et al., 2009; Sandek et al., 2014) or a potential epithelial disruption by proinflammatory cytokines such as TNF-α (Triantafilou and Triantafilou, 2002). Decreased intestinal blood flow and increased proliferation of mucosal bacteria were correlated with a higher level of systemic anti-lipopolysaccharide (LPS) IgA in patients with critical chronic heart failure (Sandek et al., 2014).

Despite the recent advances in acute ischemic stroke (IS) management and care (Saver et al., 2016), IS is still a leading cause of chronic disability and death (Zazulia, 2009). Next to primary ischemic and secondary neuroinflammatory brain damage, IS patients also suffer from systemic stroke sequelae such as stroke-induced systemic immune suppression (SIIS) leading to pneumonia or severe gut alterations including dysmotility, microbiotic dysbiosis, and bleedings (Arya and Hu, 2018). While SIIS and related pulmonary infections have been investigated decently (Prass et al., 2003; Dirnagl et al., 2007; Klehmet et al., 2009), not much is known about intestinal epithelial barrier dysfunction following IS. Since GI and increased IP could serve as an important systemic immunological and inflammation trigger, they have recently been discussed as potential elements of systemic IS pathophysiology and as potential therapeutic targets (Zazulia, 2009; Wen and Wong, 2017). Based on a set of preliminary experimental data, we hypothesize that an impaired GI with increased IP can emerge after IS and could potentially pave the way for endogenous gut-borne infections, or fuel reciprocal immune responses leading to secondary brain damage.

INTESTINAL PERMEABILITY AND STROKE MODELS

Recent investigations on the role of the microbiome in mouse IS models suggested a protective function of bacteria in the conventional gut flora as intestinal dysbiosis was associated with poor outcome (Winek et al., 2016; Sadler et al., 2017). However, rodent data on disturbed GI and increased IP following IS are controversial. Some studies report bacterial translocation and sepsis after IS in rats and aged mice (Crasper et al., 2016), while others did not find evidence for increased IP and bacterial translocation 3 days after transient middle cerebral artery occlusion (Oyama et al., 2018). This may raise the question whether these findings from rodent IS models might be breed-, supplier- or even model-specific.

The Stroke Treatment Academic Industry Roundtable (STAIR) expert consortium recommends the additional use of suitable gyrencephalic models of focal cerebral ischemia to increase the validity of experimental findings (Fisher et al., 2009). Due to a closer similarity to humans regarding neuroanatomical and physiological features, large animal models are believed to mimic the clinical situation of human stroke patients realistically (Dirnagl et al., 2013). In particular, large animals might be useful to investigate GI breakdown and increased IP after IS. Ruminants, for which IS models are available (Boltze et al., 2008; Wells et al., 2012), possess a much larger gastrointestinal tract than rodents and humans in both absolute and relative terms, and a higher physiological bacteria load, what may be an advantage when aiming to detect potential systemic immunological consequences.

HYPOTHESIS: STROKE-INDUCED ACUTE PHASE RESPONSE AND INCREASED INTESTINAL PERMEABILITY LEAD TO SECONDARY BRAIN DAMAGE

The mechanism behind a potential GI impairment and increased IP after IS remain poorly understood. Hypothetically, impaired GI and increased IP can be caused by inadequate mucosal perfusion or epithelial breakdown mediated by proinflammatory cytokines such as TNF-α or zonulin. This has been described in the context of ischemic diseases and reduced organ motility (Rahman et al., 2018). Indeed, inflammatory cytokines can compromise intestinal mucosa integrity by affecting endothelial (gate) and tight junction (fence) functions (Bruewer et al., 2003).

Within minutes, IS leads to a four-step process of ischemia-related blood-brain barrier breakdown (BBB) in peri-infarct regions (Ballabh et al., 2004; Sandoval and Witt, 2008; Krueger et al., 2015), accompanied by endothelial cell damage and loss (Krueger et al., 2015). BBB disruption then facilitates exchange of blood components and brain antigens such as brain myelin basic protein (del Zoppo and Mabuchi, 2003; Offner et al., 2006; Krueger et al., 2015). Inflammatory cytokines are released into the circulation in large amounts after IS and hence could inflict "off-site" damage to the intestinal mucosa. Moreover, inflammatory cytokines induce the production of acute phase proteins (APPs) in the liver, but interestingly also in intestinal epithelium (Molmenti et al., 1993; Wang et al., 1998). Some APPs, such as serum amyloid A (SAA) stimulate inflammatory cytokine production themselves, providing a positive feedback mechanism. SAA, once present in the circulation, also increases the recruitment of immune cells to inflammatory sites. Other APPs, such as coagulation factors and plasminogen activator-inhibitor foster coagulation and might negatively affect perfusion, contributing to thromboinflammation in cerebral and intestinal capillaries. A vicious circle finally leading to increased secondary brain damage might evolve (**Figure 1**).

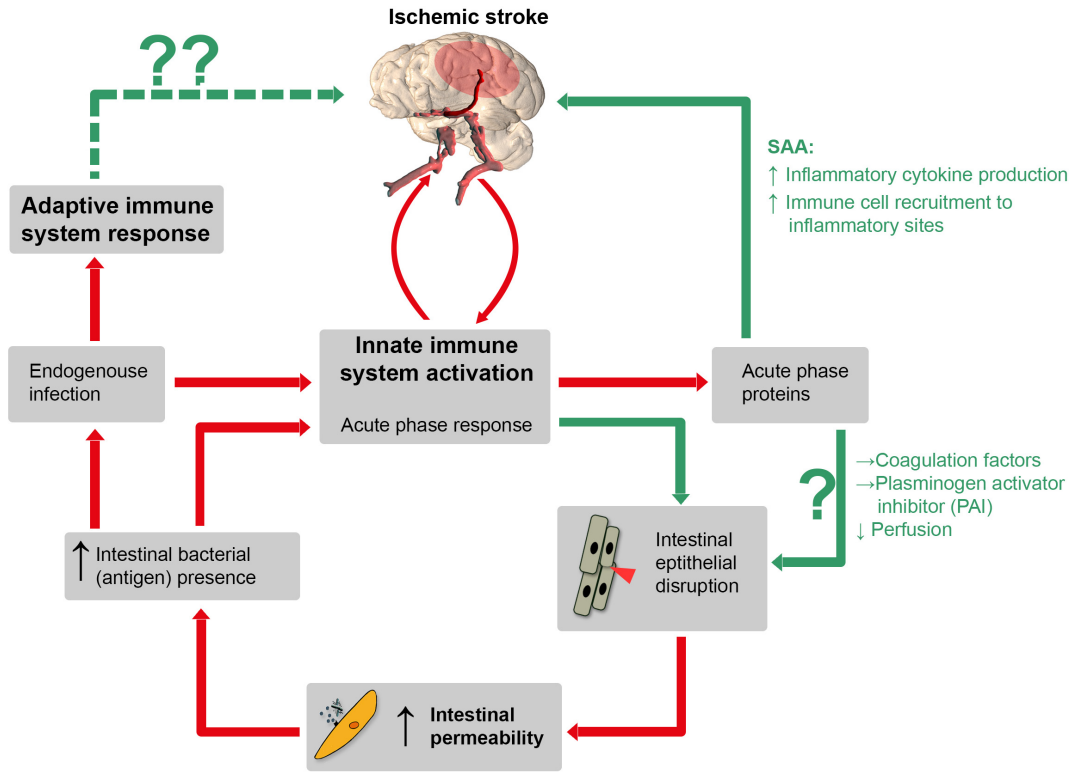

FIGURE 1 | Schematic illustration of a hypothetical pathophysiological cascade following ischemic stroke (IS): the innate immune system is activated by cerebral ischemia due to release of inflammatory cytokines after blood-barrier-breakdown. Hence, these cytokines could directly inflict "off-site" damage to the intestinal mucosa and induce the production of APPs such as serum amyloid A (SAA), coagulation factor and plasminogen activator inhibitor (PAI). SAA itself stimulates further inflammatory cytokine production via positive feedback stimulation. Other APPs, such as coagulation factors and PAI can impair capillary perfusion and, importantly, increase IP which is associated with bacterial translocation. Consequently, both pathways increase the amount of pro-inflammatory mediators, which leads to a prolonged inflammatory stage following IS. Red lines: established mechanisms, green lines: potential mechanisms (according to our hypothesis). Whether or not adaptive immune processes, augmented by the translocation of bacteria and bacterial antigens from the gut, can inflict secondary brain damage is entirely speculative (dotted green line, upper left).

STATEMENT OF HYPOTHESIS

Collection of Preliminary Data to Support the Hypothesis

In order to find support for abovementioned hypothesis, we took advantage of a running experiment in an ovine IS model in which peripheral blood samples were collected at days 1, 2, and 7 following IS. We focused on signs for potential (i) acute phase response (APR), (ii) IP alterations, and (iii) interaction between intestinal antigen translocation and systemic inflammation. Specifically, we determined levels of the APPs C-reactive protein (CRP), lipopolysaccharide-binding protein (LBP), and of and IgA-, IgM-, and IgG-anti-*E. coli* antibodies 1, 2, and 7d following IS. *E. coli* belongs to the physiological adhesive intestinal flora in sheep (Wang et al., 1998), but does not egress from the intestine in the steady state. Hence, changes of IgA-, IgM-, and IgG-anti-*E. coli* antibody levels could reflect IP alterations following IS. Animals were subjected to permanent middle cerebral artery occlusion (pMCAO) as described elsewhere (Boltze et al., 2008). Please refer to the **Supplementary Material** for methodological details.

All animals were considered clinically healthy prior to surgery (for further details see **Supplementary Tables S1** and **Supplementary Tables S2**). Animal health was assessed one day after pMCAO and every second day thereafter. No clinical signs of infection (e.g., fever) were observed. A standardized anesthesia and medication scheme was performed in all animals (see **Supplementary Table S3**). However, two animals with massive strokes were sacrificed 1d post IS due to severe neurological dysfunction and rapid worsening of general condition. These animals were excluded from further analysis. Stroke induction failed in one animal (no IS at day 1). Since this particular animal underwent the same procedure as other pMCAO animals, it was kept and served as a sham reference to control for surgery-related effects in APR.

Findings

Imaging Findings

Combined positron-emission tomography and magnetic resonance (PET/MR) imaging confirmed a perfusion deficit corresponding to the ischemic area within the MCA territory at day 1 after pMCAO in all but the sham reference animal

(**Supplementary Figure SF1B**). Details on the lesion and lesion size (t2w TSE defect volume in ml) at days 1 and 7 post pMCAO are given in **Supplementary Figure SF1** and **Supplementary Table S4**.

Systemic Acute Phase Protein Levels

Average CRP plasma levels tended to increase on day 1 after pMCAO as compared to baseline (p = 0.067), but not on day 2 (p = 0.213) and day 7 (p = 0.241, **Figure 2**). Statistically significantly increased levels of mean LBP were detected on day 1 (p = 0.002) and day 2 (p < 0.001) when compared to baseline (**Figure 2**). At each time point (baseline/1d/2d/7d), a relatively high inter-individual variability could be detected for CRP (39.6%/41.3%/35.7%/43.2%) and LBP (39.5%/41.7%/19.7%/101.5%). Baseline-corrected values showed a significant increase of CRP on day 1 (p = 0.028), while LBP was increased on day 1 (p = 0.002) and 2 (p < 0.001; all **Figure 3**). Baseline APP values in the sham reference animal were higher than in other subjects, but followed a similar kinetic except for a slight decrease of CRP values at d1 (**Figure 2**, green crosses).

IgA-, IgM-, and IgG-Anti-*Escherichia coli* Antibodies

Average plasma levels of IgA-, IgM-, and IgG-anti-*E. coli* antibodies decreased within the first 2 days after pMCAO, followed by an minor increase on day 7 (**Figure 3**). In detail, mean IgG-anti-*E. coli* antibody levels were significantly decreased on day 2 (p = 0.0012), and a significant (p = 0.048) drop of IgM-anti-*E. coli* antibodies levels was observed on day 1 post pMCAO. Additionally, IgA-anti-*E. coli* antibodies were significantly decreased at day 1 (p = 0.006) and day 2 (p = 0.001). Since the coefficient of variation for IgG-anti-*E. coli* (41.3%/55.7%/48.1%/35.4%), IgM-anti-*E. coli* (42.2%/40.0%/45.9%/33.7%) and IgA-anti-*E. coli* (42.8%/48.5%/49.7%/48.6%) was high at each time point, baseline-corrected values were analyzed (**Figure 3**). Values relative to baseline for IgG-anti-*E. coli* significantly decreased on day 1 (p = 0.048), and those for IgM- and IgA-anti-*E.coli* on days 1 (p = 0.008, p = 0.002) and 2 (p = 0.045, p < 0.001) post pMCAO (**Figure 3**). Antibody levels remained almost constant in the sham reference samples, apart from an isolated increase of IgA-anti-*E.coli* on day 2.

Correlation With Ischemic Brain Damage

A negative correlation (r = −0.700, p = 0.036) was found between LBP and IgA-anti-*E. coli* values 1d post pMCAO. Moreover, the levels of IgM-anti-*E. coli* correlated positively with rCBF values (r = 0.927, p = 0.003) 1d after pMCAO. In addition, a negative correlation (r = -0.901, p = 0.014) was detected between total brain volume (excluding IS lesion) 7d following pMCAO and IgG-anti-*E. coli* 2d post pMCAO. We found no further significant correlations between any measured parameters. Detailed results of all correlation analyses are given in **Supplementary Tables S5–S8**.

APP Response Following IS

CRP and LBP are relevant APPs in humans (Schumann and Zweigner, 1999) and sheep (Schroedl et al., 2001; Ulutas and Ozpinar, 2006). In fact, clinical investigations revealed that blood-borne markers of peripheral inflammation, including increased CRP, IL-6 or white cell counts, are present within the first week following IS in human patients, thus providing evidence of early and sustained inflammatory conditions (Emsley et al., 2003). Elevated CRP levels in cardiovascular ischemia are hypothesized to increase myocardial damage in the infarct area, likely by activating the complement cascade (Nijmeijer et al., 2003). Additional myocardial damage can in turn increase CRP levels, forming a part of the rational basis for our hypothesis that a similar mechanism might exist in stroke. This vicious circle is thought to contribute to poor outcome (Gill et al., 2004; Pepys et al., 2006; Slagman et al., 2011). CRP is normally absent from serum, but typically rises within 6 h of inflammation onset in humans with serum levels increasing up to 1000-fold within 24 h in cases of severe inflammation (Roudbary et al., 2011). LBP plays an essential role for the innate immune response against bacterial infection (Triantafilou and Triantafilou, 2002; Worthmann et al., 2015) and is capable of binding bacterial LPS. It activates macrophages and monocytes via CD14 and toll-like receptors (TLR), leading to release of pro-inflammatory cytokines (Schumann and Zweigner, 1999). In healthy humans, LBP serum values fluctuate between 5–10 μg/ml, and can increase up to 10-fold during the acute stage of severe inflammatory processes (Myc et al., 1997). LBP mean levels in our data set increased from 6 up to 47 μg/ml at day 1 after pMCAO, quantitatively resembling the situation in humans. LBP is usually produced in the liver, but can also be produced extrahepatically under pro-inflammatory conditions. For instance, LBP production was observed in murine and human intestinal epithelium in cases of severe systemic inflammation (Vreugdenhil et al., 1999, 2000). High amounts of ruminant LBP is also expressed within the forestomach, small intestine crypts and colon glands, at which it likely plays an important role in mucosal innate pathogen defense (Rahman et al., 2010). The data may further indicate an early increase of local gastrointestinal LBP production in sheep under pro-inflammatory conditions as previously assumed (Rahman et al., 2010). This might indicate a systemic APR in the early stage of experimental IS in sheep, thus supporting the reference of IS-triggered cascade of systemic immunoreactions observed in rodents (Offner et al., 2006) and humans (Emsley et al., 2003).

Connecting APP Response, IP, and Secondary Brain Damage

Ruminants possess a much larger gastrointestinal tract than rodents and humans. The continuous physiological presence of bacteria such as *E. coli* ensures that a "baseline" antibody titer is maintained in the sheep blood. Interestingly, levels of all tested anti-*E. coli* antibodies were reduced during the first 48 h post IS, but recovered to baseline levels 7d post IS. Theoretically, decreased antibody levels may be related to changes of intestinal barrier integrity. We hypothesize that the decreased antibody levels are related to a suddenly increased presence of bacterial antigens in plasma, as a result of translocation through the gut wall, thus leading to initial anti-*E. coli* antibody consumption.

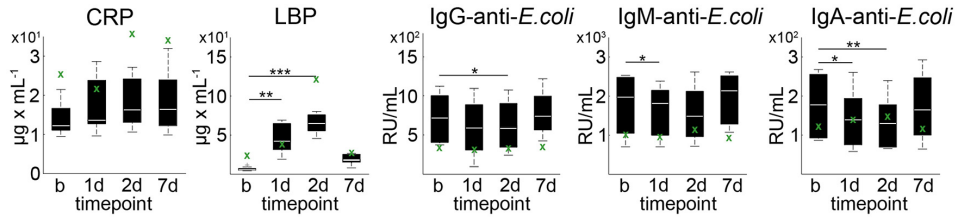

FIGURE 2 | Acute phase proteins and anti-*E. coli* antibodies in plasma. CRP, LBP as well as IgA-, IgM- and IgG-anti-*E. coli* antibodies exhibited a high inter-individual variance at baseline (b) and 1, 2, and 7 days post pMCAO. Boxplots indicate the mean at each time point (white bar), 1st and 3rd quartiles, and 95% confidence intervals. Significance level of paired two-sample *t*-test against baseline were $p < 0.05$ (*), $p < 0.01$ (**), and $p < 0.001$ (***). The green crosses (x) indicate sole data points from the animal with failed pMCAO (no stroke at day 1) serving as a sham reference for surgery-related effects.

Our hypothesis is underpinned by the simultaneously increased LBP levels as well as by a negative correlation between LBP and anti-*E. coli* antibodies within 24 h post IS. Local LBP expression might be increased by pro-inflammatory factors such as LPS (Su et al., 1994; Dentener et al., 2000; Bruewer et al., 2003). However, our results could also be related to SIIS in general. Hence, to substantiate our hypothesis, further investigations should be performed, including measurement of cytokine (e.g., TNF-α) as well as measurements of the sympathetic nervous system status (e.g., catecholamine and cortisol), in order to explore the entire inflammatory and immunosuppression process.

Enhanced IP may enable antigen fluxes through the intestinal wall or could activate the local intestinal immune system. Both events could increase the amount of inflammatory mediators such as intestinal factors including *i*-PAMPs (pathogen associated molecular pattern, e.g., *E. coli* lipopolysaccharide: F-, K-, or H-antigens) F-, K-, or H-antigens or cytokines within the circulation. In summary, increased IP could hypothetically lead to a prolonged inflammatory stage following IS, which may further aggravate IS outcome. We found some indirect indication for a potential relationship between increased IP and a systemic immune reaction. We detected that higher free anti-*E. coli* antibody levels at day 2 were related to smaller lesions (rCBF deficits) 1d following IS (see **Supplementary Table S8**). In turn, higher levels of IgA-anti-*E. coli* (2d post IS) are related to reduced post-stroke total brain volume (indicating post-IS tissue loss) 7d following IS (see **Supplementary Table S8**). This may imply that increased IP could amplify or modify systemic-adaptive and-innate immune reaction patterns, cumulating in secondary brain damage. Subsequent studies must be performed to investigate this assumption, e.g., determination of bacterial antigen, cytokine or endotoxin measurements, histological assessment and CFU content determination in blood, gut lymph nodes, spleen, liver, and lung.

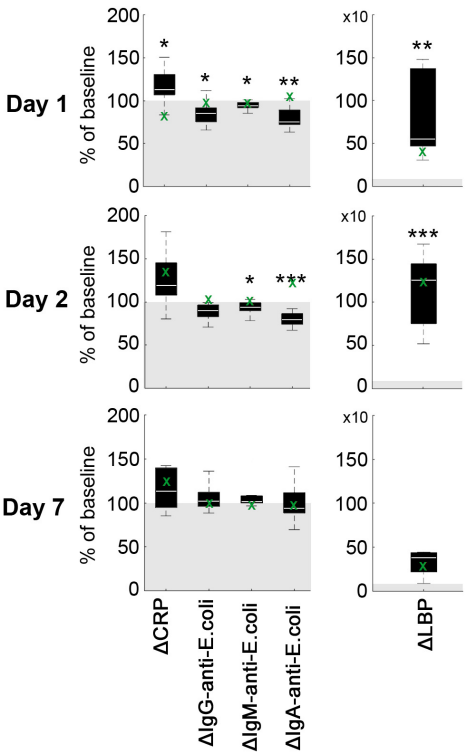

FIGURE 3 | Difference of acute phase proteins ΔCRP and ΔLBP as well as IgA-, IgM- and IgG-anti-*E.coli* antibodies. Values are given as percentage of baseline (gray area). Boxplots indicate the mean difference at each time point (white bar), 1st and 3rd quartiles, and 95% confidence intervals. Significance level of one-sample *t*-test against 100 (baseline) is indicated by $p < 0.05$ (*), $p < 0.01$ (**) and $p < 0.001$ (***). The green crosses (x) indicate sole data points from an animal with failed pMCAO (no stroke at day 1) serving as a sham reference for surgery-related effects.

Critical Appraisal of Preliminary Data and Hypothesis

Rodent brain structure and size, genetic homogeneity, and differences in immunobiology may limit the translation of experimental findings from rodent models to the human patients. Large animal IS models are potentially useful for IP investigations following IS. However, outcome variability is often higher than in rodent models (Herrmann et al., 2019), what may reflect the inter-individual variations observed in human stroke patients. Accordingly, we found a relatively high inter-individual variation for all measured blood parameters, but overall data indeed indicate increased IP after IS.

A limitation of the supporting data is the small statistical sample size and the existence of only one sham case. In consequence, general effects of the surgical procedure, anesthesia

or medication on evaluated blood markers cannot be excluded. The responses of CRP and LBP in the sham subject with identical surgical intervention except for MCA occlusion show a relative similar pattern than that in other animals, apart from a drop in CRP value at day 1 (**Figure 2**). These APPs would be expected to generally increase after tissue trauma (Baumann and Gauldie, 1994; Nijmeijer et al., 2003) as for instance exerted by the invasive MCAO model (trepanation). However, antibody titers relative to baseline remained almost constant in this animal over the course of the experiment. This makes it less likely that the changes observed in the other subjects are simply caused by the surgical intervention itself, supporting our hypothesis.

Potentially, there might be an interaction between medication and post-stroke immune system responses, i.e., clinical signs of infection following pMCAO could be masked by medication. However, there is no evidence of relevant impact of butorphanol-, cyclooxigenase inhibitor flunixin-, or antibiotic treatment (enrofloxacin) on CRP and LBP levels in contemporary literature (Löscher et al., 2014; Henke et al., 2015). However, systemic antibiotic therapy was given in a uniform scheme as required by the experimental protocol of the study these cases were derived from. This may have counteracted some of the consequences of potential *E. coli* traffic across intestinal barriers and on inflammatory response, but post-stroke changes in antibody and APP levels were nevertheless large enough to be statistically significant despite the small sample sizes.

CONCLUSION

We initially characterized the modification of the APR and the interactions between the systemic immune system and IP following IS in an ovine IS model. Our findings confirm the reaction patterns of CRP and LBP as APPs following IS, and revealed preliminary indications for alterations of intestinal barrier functions. In addition, we found indirect indications of IP enhancement in the early stage of IS in sheep. To our knowledge, this was first explored in a large animal model. Further confirmatory investigations, e.g., direct identification of bacterial antigens, endotoxin measurements, histological assessment and colony forming unit (CFU) determination in blood, gut lymph nodes, spleen, liver, or lung, need to be performed. Measurements of inflammatory cytokines as well as potential interaction with the sympathetic nervous system (e.g., catecholamine and cortisol determination) should be conducted to gain a more holistic picture of the entire pathophysiological cascade. Moreover, any effect of antibiotic treatment should be excluded by a carefully planned study design.

DATA AVAILABILITY STATEMENT

All raw data are available upon reasonable request.

ETHICS STATEMENT

The animal study was reviewed and approved by the Experimental Animal Committee of the Regional Council of Leipzig, Germany (animal protocol number 09-11).

AUTHOR CONTRIBUTIONS

FF designed the study, performed the experiments, obtained and analyzed the data, drafted, and reviewed the manuscript. VZ obtained and analyzed the data and reviewed the manuscript. SP helped in performing the experiments and the obtained data. RR and DM performed the experiments and reviewed the manuscript. AD performed the experiments and obtained the data. LP analyzed the data. A-KS helped in performing the experiments. HB obtained and analyzed the data. JB analyzed the data, drafted, and reviewed the manuscript. WS analyzed the data and reviewed the manuscript. BN obtained and analyzed the data, drafted, and reviewed the manuscript. All authors acknowledged the final version of the manuscript.

FUNDING

Parts of this work was supported by the German Federal Ministry of Education and Research (grant number 0315920).

ACKNOWLEDGMENTS

We wish to thank Kerstin Klimke for technical assistance (ELISA), the cyclotron and PET/MR imaging crew members for excellent technical support during the PET/MR investigations. Furthermore, we would also like to thank Franziska Schwarz (Scivisto) for providing graphic tools.

SUPPLEMENTARY MATERIAL

The Supplementary Material for this article can be found online at: https://www.frontiersin.org/articles/10.3389/fnins.2020.00272/full#supplementary-material

REFERENCES

Arya, A. K., and Hu, B. (2018). Brain-gut axis after stroke. *Brain Circ.* 4, 165–173. doi: 10.4103/bc.bc_32_18

Ballabh, P., Braun, A., and Nedergaard, M. (2004). The blood-brain barrier an overview: structure, regulation, and clinical implications. *Neurobiol. Dis.* 16, 1–13.

Bansal, V., Costantini, T., Kroll, L., Peterson, C., Loomis, W., Eliceiri, B., et al. (2009). Traumatic brain injury and intestinal dysfunction: uncovering the neuro-enteric axis. *J. Neurotrauma* 26, 1353–1359. doi: 10.1089/neu.2008-0858

Baumann, H., and Gauldie, J. (1994). The acute phase response. *Immunol. Today.* 5, 74–80.

Boltze, J., Förschler, A., Nitzsche, B., Waldmin, D., Hoffmann, A., Boltze, C. M., et al. (2008). Permanent middle cerebral artery occlusion in sheep: a novel

large animal model of focal cerebral ischemia. *J. Cereb. Blood Flow Metab.* 28, 1951–1964. doi: 10.1038/jcbfm.2008.89

Bruewer, M., Luegering, A., Kucharzik, T., Parkos, C. A., Madara, J. L., Hopkins, A. M., et al. (2003). Proinflammatory cytokines disrupt epithelial barrier function by apoptosis-independent mechanisms. *J. Immunol.* 171, 6164–6172.

Crasper, J., Ritzel, R., Verma, R., Venna, V. R., Lui, F., Chauhan, A., et al. (2016). Ischemic stroke inducec gut permeability and enhances bacterial translocation leading to sepsis in aged mice. *Aging* 8, 1049–1063.

del Zoppo, G. J., and Mabuchi, T. (2003). Cerebral microvessel responses to focal ischemia. *J. Cereb. Blood Flow Metab.* 23, 879–894.

Dentener, M. A., Vreugdenhil, A. C., Hoet, P. H., Vernooy, J. H., Nieman, F. H., Heumann, D., et al. (2000). Production of the acute-phase protein lipopolysaccharide-binding protein by respiratory type II epithelial cells: implications for local defense to bacterial endotoxin. *Am. J. Respir. Cell Mol. Biol.* 23, 146–153.

Dirnagl, U., Hakim, A., Macleod, M., Fisher, M., Howells, D., Alan, S. M., et al. (2013). A concerted appeal for international cooperation in preclinical stroke research. *Stroke* 44, 1754–1760.

Dirnagl, U., Klehmet, J., Braun, J. S., Harms, H., Meisel, C., Ziemssen, T., et al. (2007). Stroke-induced immunodepression: experimental evidence and clinical relevance. *Stroke* 38(2 Suppl.), 770–773.

Doig, C. J., Sutherland, L. R., Sandham, J. D., Fick, G. H., Verhoef, M., and Meddings, J. B. (1998). Increased intestinal permeability is associated with the development of multiple organ dysfunction syndrome in critically ill ICU patients. *Am. J. Respir. Crit. Care Med.* 158, 444–451.

Emsley, H. C., Smith, C. J., Gavin, C. M., Georgiou, R. F., Vail, A., Barberan, E. M., et al. (2003). An early and sustained peripheral inflammatory response in acute ischaemic stroke: relationships with infection and atherosclerosis. *J. Neuroimmunol.* 139, 93–101.

Fisher, M., Feuerstein, G., Howells, D. W., Hurn, P. D., Kent, T. A., Savitz, S. I., et al. (2009). Update of the stroke therapy academic industry roundtable preclinical recommendations. *Stroke. Jun* 40, 2244–2250. doi: 10.1161/STROKEAHA.108.541128

Gill, R., Kemp, J. A., Sabin, C., and Pepys, M. B. (2004). Human C-reactive protein increases cerebral infarct size after middle cerebral artery occlusion in adult rats. *J. Cereb. Blood Flow Metab.* 24, 1214–1218.

Henke, J., Haberstroh, J., Sager, M., Becker, K., Eberspächer, E., Bergadano, A., et al. (2015). *Pain Management for Laboratory Animals. Committee on Anaesthesia of GV-SOLAS (German society for laboratory Animal Science)*. Available online at: http://www.gv-solas.de/fileadmin/user_upload/pdf_publikation/Anaest._Analgesie/Schmerztherapie_Mai2015_e.pdf (accessed January 9, 2020).

Herrmann, A. M., Meckel, S., Gounis, M. J., Kringe, L., Motschall, E., Mülling, C., et al. (2019). Large animals in neurointerventional research: a systematic review on models, techniques and their application in endovascular procedures for stroke, aneurysms and vascular malformations. *J. Cereb. Blood Flow Metab. Mar.* 39, 375–394. doi: 10.1177/0271678X19827446

Klehmet, J., Harms, H., Richter, M., Prass, K., Volk, H. D., Dirnagl, U., et al. (2009). Stroke-induced immunosuppression and post-stroke infections: lessons from the preventive antibacterial therapy in stroke trial. *Neuroscience* 158, 1184–1193. doi: 10.1016/j.neuroscience.2008.07.044

Krueger, M., Bechmann, I., Immig, K., Reichenbach, A., Härtig, W., and Michalski, D. (2015). Blood-brain barrier breakdown involves four distinct stages of vascular damage in various models of experimental focal cerebral ischemia. *J. Cereb. Blood Flow Metab.* 5, 292–303. doi: 10.1038/jcbfm.2014.199

Löscher, W., Richter, A., and Potschka, H. (2014). *Pharmakotherapie bei Haus- und Nutztieren. 9*. Enke Verlag: Aktualisierte und Erweiterte Auflage.

Molmenti, E. P., Ziambaras, T., and Perlmutter, D. H. (1993). Evidence for an acute phase response in human intestinal epithelial cells. *J. Biol. Chem.* 268, 14116–14124.

Myc, A., Buck, J., Gonin, J., Reynolds, B., Hammerling, U., and Emanuel, D. (1997). The level of lipopolysaccharide-binding protein is significantly increased in plasma in patients with the systemic inflammatory response syndrome. *Clin. Diagn. Lab. Immunol.* 42, 113–116.

Nijmeijer, R., Lagrand, W. K., Lubbers, Y. T. P., Visser, C. A., Meijer, C. J. L. M., Niessen, H. W. M., et al. (2003). C-reactive protein activates complement in infarcted h33.u*man myocardium*. *Am. J. Pathol.* 163, 269–275.

Offner, H., Subramanian, S., Parker, S. M., Afentoulis, M. E., Vandenbark, A. A., and Hurn, P. D. (2006). Experimental stroke induces massive, rapid activation of the peripheral immune system. *J. Cereb. Blood Flow Metab.* 26, 654–665. doi: 10.1038/sj.jcbfm.9600217

Otani, S., and Coopersmith, C. M. (2019). Gut integrity in critical illness. *J. Intensive Care.* 2:17.

Oyama, N., Winek, K., Bäcker-Koduah, P., Zhang, T., Dames, C., Werich, M., et al. (2018). Exploratory investigation of intestinal function and bacterial translocation after focal cerebral ischemia in the mouse. *Front. Neurol.* 19:937. doi: 10.3389/fneur.2018.00937

Pepys, M. B., Hirschfield, G. M., Tennent, G. A., Gallimore, J. R., Melvyn, C. K., Bellotti, V., et al. (2006). Targeting C-reactive protein for the treatment of cardiovascular disease. *Nature* 440, 1217–1221. doi: 10.1038/nature04672

Prass, K., Meisel, C., Höflich, C., Braun, J., Halle, E., Wolf, T., et al. (2003). Stroke-induced immunodeficiency promotes spontaneous bacterial infections and is mediated by sympathetic activation reversal by poststroke T helper cell type 1–like immunostimulation. *J. Exp. Med.* 198, 725–736.

Rahman, M. M., Lecchi, C., Avallone, G., Roccabianca, P., Sartorelli, P., and Ceciliani, F. (2010). Lipopolysaccharide-binding protein: Local expression in bovine extrahepatic tissues. *Vet. Immunol. Immunopathol.* 137, 28–35. doi: 10.1016/j.vetimm.2010.04.006

Rahman, M. T., Ghosh, C., Hossain, M., Linfield, D., Rezaee, F., Janigro, D., et al. (2018). IFN-γ, IL-17A, or zonulin rapidly increase the permeability of the blood-brain and small intestinal epithelial barriers: Relevance for neuro-inflammatory diseases. *Biochem. Biophys. Res. Commun.* 507, 274–279. doi: 10.1016/j.bbrc.2018.11.021

Riddington, D. W., Venkatesh, B., Boivin, C. M., Bonser, R. S., Elliott, T. S., Marshall, T., et al. (1996). Intestinal permeability, gastric intramucosal pH, and systemic endotoxemia in patients undergoing cardiopulmonary bypass. *JAMA* 275, 1007–1012.

Roudbary, S. A., Saadat, F., Forghanparast, K., and Sohrabnejad, R. (2011). Serum C-reactive protein level as a biomarker for differentiation of ischemic from hemorrhagic stroke. *Acta Med. Iran.* 49, 149–152.

Sadler, R., Singh, V., Benakis, C., Garzetti, D., Brea, D., Stecher, B., et al. (2017). Microbiota differences between commercial breeders impacts the post-stroke immune response. *Brain Behav. Immun.* 66, 23–30. doi: 10.1016/j.bbi.2017.03.011

Sandek, A., Swidsinski, A., Schroedl, W., Watson, A., Valentova, M., Herrmann, R., et al. (2014). Intestinal blood flow in patients with chronic heart failure: a link with bacterial growth, gastrointestinal symptoms, and cachexia. *J. Am. Coll Cardiol.* 64, 1092–1102. doi: 10.1016/j.jacc.2014.06.1179

Sandoval, K. E., and Witt, K. A. (2008). Blood-brain barrier tight junction permeability and ischemic stroke. *Neurobiol. Dis.* 32, 200–219. doi: 10.1016/j.nbd.2008.08.005

Saver, J. L., Goyal, M., van der Lugt, A., Menon, B. K., Majoie, C. B., Dippel, D. W., et al. (2016). Time to treatment with endovascular thrombectomy and outcomes from ischemic stroke: a meta-analysis. *JAMA* 316, 1279–1288. doi: 10.1001/jama.2016.13647

Schroedl, W., Fuerll, B., Reinhold, P., Krueger, M., and Schuett, C. (2001). A novel acute phase marker in cattle: lipopolysaccharide binding protein (LBP). *J. Endotoxin. Res.* 7, 49–52.

Schumann, R. R., and Zweigner, J. (1999). A novel acute-phase marker: lipopolysaccharide binding protein (LBP). *Clin. Chem. Lab. Med.* 37, 271–274.

Slagman, A. C., Bock, C., Abdel-Aty, H., Vogt, B., Gebauer, F., Janelt, G., et al. (2011). Specific removal of C-reactive protein by apheresis in a porcine cardiac infarction Model. *Blood Purif.* 31, 9–17. doi: 10.1159/000320763

Su, G. L., Freeswick, P. D., Geller, D. A., Wang, Q., Shapiro, R. A., Wan, Y. H., et al. (1994). Molecular cloning, characterization, and tissue distribution of rat lipopolysaccharide binding protein. Evidence for extrahepatic expression. *J. Immunol.* 153, 743–752.

Triantafilou, M., and Triantafilou, K. (2002). Lipopolysaccharide recognition: CD14. TLRs and the LPS-activation cluster. *Trends Immunol.* 23, 301–304.

Ulutas, P. A., and Ozpinar, A. (2006). Effect of mannheimia (Pasteurella) haemolytica infection on acute-phase proteins and some mineral levels in colostrum–breast milk-fed or colostrum–breast milk-deprived sheep. *Vet. Res. Commun.* 30, 485–495.

Vreugdenhil, A. C., Dentener, M. A., Snoek, A. M., Greve, J. W., and Buurman, W. A. (1999). Lipopolysaccharide binding protein, and serum amyloid A

secretion by human intestinal epithelial cells during the acute phase response. *J. Immunol.* 163, 2792–2798.

Vreugdenhil, A. C., Snoek, A. M., Greve, J. W., and Buurman, W. A. (2000). Lipopolysaccharide-binding protein is vectorially secreted and transported by cultured intestinal epithelial cells and is present in the intestinal mucus of mice. *J. Immunol.* 165, 4561–4566.

Wang, Q., Wang, J. J., Fischer, J. E., and Hasselgren, P. O. (1998). Mucosal production of complement C3 and serum amyloid A is differentially regulated in different parts of the gastrointestinal tract during endotoxemia in mice. *J. Gastrointest. Surg.* 2, 537–546.

Wells, A. J., Vink, R., Blumbergs, P. C., Brophy, B. P., Helps, S. C., Knox, S. J., et al. (2012). A surgical model of permanent and transient middle cerebral artery stroke in the sheep. *PLoS One* 7:e42157. doi: 10.1371/journal.pone.0042157

Wen, S. W., and Wong, C. H. Y. (2017). An unexplored brain-gut microbiota axis in stroke. *Gut. Microbes.* 8, 601–606. doi: 10.1080/19490976.2017.1344809

Winek, K., Engel, O., Koduah, P., Heimesaat, M. M., Fischer, A., Bereswill, S., et al. (2016). Depletion of cultivatable gut microbiota by broad-spectrum antibiotic pretreatment worsens outcome after murine stroke. *Stroke* 47, 1354–1363. doi: 10.1161/STROKEAHA.115.011800

Worthmann, H., Tryc, A. B., Dirks, M., Schuppner, R., Brand, K., Klawonn, F., et al. (2015). Lipopolysaccharide binding protein, interleukin-10, interleukin-6 and C-reactive protein blood levels in acute ischemic stroke patients with post-stroke infection. *J. Neuroinflammation* 12:13. doi: 10.1186/s12974-014-0231-2

Zazulia, A. R. (2009). Critical care management of acute ischemic stroke. *Continuum Lifelong Learn. Neurol.* 15, 68–82.

Conflict of Interest: The authors declare that the research was conducted in the absence of any commercial or financial relationships that could be construed as a potential conflict of interest.

Copyright © 2020 Ferrara, Zeisig, Pietsch, Rütten, Dreyer, Pieper, Schatzl, McLeod, Barthel, Boltze, Schrödl and Nitzsche. This is an open-access article distributed under the terms of the Creative Commons Attribution License (CC BY). The use, distribution or reproduction in other forums is permitted, provided the original author(s) and the copyright owner(s) are credited and that the original publication in this journal is cited, in accordance with accepted academic practice. No use, distribution or reproduction is permitted which does not comply with these terms.

frontiers in Neuroscience

BRIEF RESEARCH REPORT
published: 12 May 2020
doi: 10.3389/fnins.2020.00453

Reduced Post-ischemic Brain Injury in *Transient Receptor Potential Vanilloid 4* Knockout Mice

*Koji Tanaka[1], Shoji Matsumoto[2], Takeshi Yamada[3], Ryo Yamasaki[1], Makoto Suzuki[4], Mizuho A. Kido[5] and Jun-Ichi Kira[1]**

[1] Department of Neurology, Neurological Institute, Graduate School of Medical Sciences, Kyushu University, Fukuoka, Japan, [2] Department of Comprehensive Strokology, School of Medicine, Fujita Health University, Toyoake, Japan, [3] Department of Neurology, Saiseikai Fukuoka General Hospital, Fukuoka, Japan, [4] Department of Pharmacology, Division of Molecular Pharmacology, Jichi Medical University, Shimotsuke, Japan, [5] Department of Anatomy and Physiology, Faculty of Medicine, Saga University, Saga, Japan

OPEN ACCESS

Edited by:
Mathias Gelderblom, University Medical Center Hamburg-Eppendorf, Germany

Reviewed by:
Juan C. Saez, Pontifical Catholic University of Chile, Chile
Zahoor A. Shah, The University of Toledo, United States

***Correspondence:**
Jun-Ichi Kira
kira@neuro.med.kyushu-u.ac.jp

Specialty section:
This article was submitted to Neuroenergetics, Nutrition and Brain Health, a section of the journal Frontiers in Neuroscience

Received: *23 November 2019*
Accepted: *14 April 2020*
Published: *12 May 2020*

Citation:
Tanaka K, Matsumoto S, Yamada T, Yamasaki R, Suzuki M, Kido MA and Kira J-I (2020) Reduced Post-ischemic Brain Injury in Transient Receptor Potential Vanilloid 4 Knockout Mice. Front. Neurosci. 14:453. doi: 10.3389/fnins.2020.00453

Background and Purpose: In the acute phase of ischemia-reperfusion, hypoperfusion associated with ischemia and reperfusion in microvascular regions and disruption of the blood–brain barrier (BBB) contribute to post-ischemic brain injury. We aimed to clarify whether brain injury following transient middle cerebral artery occlusion (tMCAO) is ameliorated in *Transient receptor potential vanilloid 4* knockout (*Trpv4*$^{-/-}$) mice.

Methods: tMCAO was induced in wild-type (WT) and *Trpv4*$^{-/-}$ mice aged 8–10 weeks. Ischemia-induced lesion volume was evaluated by 2,3,5-triphenyltetrazolium chloride staining at 24 h post-tMCAO. Tissue water content and Evans blue leakage in the ipsilateral hemisphere and a neurological score were evaluated at 48 h post-tMCAO. Transmission electron microscopy (TEM) was performed to assess the morphological changes in microvasculature in the ischemic lesions at 6 h post-tMCAO.

Results: Compared with WT mice, *Trpv4*$^{-/-}$ mice showed reduced ischemia-induced lesion volume and reduced water content and Evans blue leakage in the ipsilateral hemisphere alongside milder neurological symptoms. The loss of zonula occludens-1 and occludin proteins in the ipsilateral hemisphere was attenuated in *Trpv4*$^{-/-}$ mice. TEM revealed that parenchymal microvessels in the ischemic lesion were compressed and narrowed by the swollen endfeet of astrocytes in WT mice, but these effects were markedly ameliorated in *Trpv4*$^{-/-}$ mice.

Conclusion: The present results demonstrate that TRPV4 contributes to post-ischemic brain injury. The preserved microcirculation and BBB function shortly after reperfusion are the key neuroprotective roles of TRPV4 inhibition, which represents a promising target for the treatment of acute ischemic stroke.

Keywords: ischemic stroke, transient receptor potential vanilloid 4, knockout mice, brain edema, blood–brain barrier

INTRODUCTION

Acute ischemic stroke secondary to large artery occlusion is a common and devastating condition that results in death or long-term disability in a high proportion of patients. Recent advances in revascularization therapies, including mechanical thrombectomy, have enabled rapid and effective recanalization for large artery occlusions in patients with acute ischemic stroke (Goyal et al., 2016). However, despite the high rates of early recanalization, some patients still experience poor outcomes. In these cases, lack of reperfusion due to blockade of the microcirculation leading to hypoperfusion associated with ischemia and reperfusion and disruption of the blood–brain barrier (BBB) may contribute to post-ischemic brain injury (Molina and Alvarez-Sabín, 2009).

Transient receptor potential vanilloid 4 (TRPV4), a member of the TRP vanilloid subfamily, is a non-selective cation channel permeable to Ca^{2+}, Na^{+}, and Mg^{2+} ions (Ramsey et al., 2006). TRPV4 was first described as a cellular osmotic sensor that detects extracellular hypo-osmolarity, and was subsequently shown to be activated by multiple stimuli. TRPV4 is widely expressed in the central nervous system (Nilius and Voets, 2013), and its localization on astrocyte endfeet plays an essential role in the regulation of vascular tone in brain microvessels (Dunn et al., 2013; Filosa et al., 2013). Enrichment of TRPV4 and aquaporins at the endfeet of astrocytes ensures that even small changes in conditions, such as extracellular ion concentrations, result in astroglial swelling, volume regulation, and reorganization of downstream signaling pathways (Ryskamp et al., 2015; Iuso and Križaj, 2016). Pharmacological blockade of TRPV4 results in reduction of brain ischemia-induced lesion volume through inhibition of matrix metalloprotease (MMP) activation, thereby providing protection against BBB disruption following transient focal cerebral ischemia (Li et al., 2013; Jie et al., 2015a,b, 2016). Moreover, TRPV4 contributes to Ca^{2+} influx in both astrocytes and neurons and to extracellular glutamate accumulation during peri-infarct depolarizations (Rakers et al., 2017). These findings indicate that TRPV4 has a large influence on ischemia-induced brain injury and indicate that inhibition of TRPV4 has a neuroprotective role in acute ischemic stroke. However, a recent report demonstrated exacerbation of ischemia-induced brain edema formation in *Trpv4* knockout ($Trpv4^{-/-}$) mice (Pivonkova et al., 2018). Specifically, $Trpv4^{-/-}$ mice showed larger T2-hyperintensity lesions following transcranial permanent middle cerebral artery occlusion (pMCAO) compared with wild-type (WT) mice. Moreover, the report described a minimal involvement of TRPV4 in astrocyte volume regulation *in vivo*. Thus, the mechanism for the neuroprotective effects of TRPV4 in acute ischemic stroke remains inconclusive. Given this context, we aimed to investigate the differences in post-ischemic brain injury between $Trpv4^{-/-}$ and WT mice, and to clarify the mechanism for any identified differences using a transient MCAO (tMCAO) model in the C57BL/6N mouse strain.

MATERIALS AND METHODS

Ethics Statement

The animal experiments were conducted in accordance with the National Institutes of Health Guide for the Care and Use of Laboratory Animals, and all procedures were approved by the Animal Ethics Committee of Kyushu University (Approval Nos. A28-08-4, A30-138-2, 26-60, and 1-48).

Animals

$Trpv4^{-/-}$ mice were transferred from Jichi Medical University (Suzuki et al., 2003). C57BL/6N mice were purchased from Kyudo (Fukuoka, Japan). The $Trpv4^{-/-}$ mouse strain had been backcrossed with the C57BL/6N strain for >10 generations. Inbred adult male mice at 8–10 weeks of age (median [interquartile range] weight: 23.3 [21.7–24.9] g for WT mice and 24.1 [20.8–26.2] g for $Trpv4^{-/-}$ mice) were maintained in a temperature-controlled (22–25°C) specific pathogen-free animal facility on a 12-h/12-h light/dark cycle with free access to food and water.

tMCAO Surgery

tMCAO was performed using a previously described method with modifications (Engel et al., 2011). Mice were anesthetized with 1.5–2.0% isoflurane (Escain; Mylan Seiyaku, Tokyo, Japan) in 30% oxygen-mixed gas under spontaneous respiration. Focal cerebral ischemia was induced by a silicone-coated 6-0 monofilament (#602356; Doccol, Redlands, CA, United States) inserted through a small incision in the right common carotid artery and then advanced through the internal carotid artery to occlude the origin of the MCA. The filament was withdrawn to allow reperfusion of the ischemic hemisphere. Regional cerebral blood flow in the right MCA territory was monitored by laser Doppler flowmetry (Omegaflo FLO-C1; Omegawave, Tokyo, Japan) to confirm vessel occlusion, shown by a rapid and dramatic decrease in brain perfusion (mean reduction: 70–80%) that remained stable until reperfusion. Body temperature was maintained at 37°C based on the rectal temperature. In sham-operated animals, the same procedure was performed except for insertion of the intraluminal filament. The optimal time of tMCAO was determined by a preliminarily experiment in which tMCAO was induced in WT mice for 15, 30, or 45 min. The lesion size at 24 h post-tMCAO became larger and more stable while the mortality rate increased with longer tMCAO induction (≈0% mortality for 15 min, ≈10% for 30 min, ≈20% for 45 min tMCAO). Based on the lesion size and mortality rate, 30 min tMCAO was used in this study.

2,3,5-Triphenyltetrazolium Chloride (TTC) Staining

Transient focal cerebral ischemia was induced in 12 $Trpv4^{-/-}$ and 12 WT mice. At 24 h post-tMCAO, mice were transcardially perfused with cold saline. The brain was removed immediately and cut into serial 1-mm-thick coronal sections. The sections

were incubated in a 2% solution of TTC (Sigma-Aldrich Japan, Tokyo, Japan) for 15 min at 37°C. Images were captured with a Nikon D7100 digital camera (Nikon, Tokyo, Japan). Unstained areas were measured in TTC-stained sections using ImageJ software, version 1.46r (National Institutes of Health, Bethesda, MD, United States) to calculate the infarct volume.

Tissue Water Content

Transient focal cerebral ischemia was induced in 12 *Trpv4*$^{-/-}$ and 12 WT mice. At 48 h post-tMCAO, mice were decapitated under anesthesia and the olfactory bulb, cerebellum, and brainstem were removed from each dissected brain. The ipsilateral and contralateral hemispheres were separated and their wet weights immediately recorded. The dry weights were determined after drying the tissues to a constant weight at 100°C for 48 h. Tissue water content was calculated as % H_2O = (1 − dry weight/wet weight) × 100%.

Evans Blue (EB) Extravasation

Transient focal cerebral ischemia was induced in 12 *Trpv4*$^{-/-}$ and 12 WT mice. At 46 h post-tMCAO, 2% EB dye (Sigma-Aldrich Japan) in normal saline was injected intraperitoneally at a dose of 4 ml/kg body weight. Subsequently, the mice were perfused with cold saline at 48 h post-tMCAO. The ipsilateral hemisphere was collected and incubated with 500 μl formamide (Sigma-Aldrich Japan) at room temperature for 24 h to extract EB. The concentration of dye in the extract was calculated by reference to a standard curve of EB in formamide quantified at 620 nm by spectrofluorophotometry (PerkinElmer Ensight; PerkinElmer, Waltham, MA, United States).

Neurological Scoring

Neurological scores were evaluated at 24 and 48 h post-tMCAO in the *Trpv4*$^{-/-}$ and WT mice subjected to evaluation of tissue water content and EB leakage (n = 24 per group) using a scoring system modified from a neurological scoring system for sensorimotor deficits (Garcia et al., 1995). The highest possible score of 18 indicated no neurological deficit and the lowest score of 3 indicated the most severe impairment.

Western Blot Analysis

Transient focal cerebral ischemia was induced or a sham operation performed in 9 *Trpv4*$^{-/-}$ and 9 WT mice. At 48 h post-tMCAO, mice were transcardially perfused with cold saline and a 1-mm coronal slice of the ipsilateral hemisphere at 4 mm posterior to the olfactory bulb was collected. The brain slice was homogenized in RIPA buffer (50 mM Tris-HCl pH 7.4, 150 mM NaCl, 5 mM EDTA, 1% Nonidet P-40, 1% sodium deoxycholate, 0.1% SDS, 1% aprotinin, 50 mM NaF, 0.1 mM Na_3VO_4, 1% Triton-X100) containing anti-phosphatase PhoSTOP (Roche, Mannheim, Germany) and then centrifuged at 10,000 × g for 10 min at 4°C. The protein sample was separated by 4–15% SDS-PAGE and transferred to a polyvinylidene fluoride membrane. The membrane was incubated with anti-zonula occludens (ZO)-1 (61-7300; Zymed Laboratories, San Francisco, CA, United States; 1:1,000 dilution), anti-occludin (ab167161; Abcam, Cambridge, MA, United States; 1:2,000 dilution), or anti-β-actin (A5441; Sigma-Aldrich Japan; 1:20,000 dilution) primary antibodies at 4°C overnight. After washing in Tris-buffered saline with 0.5% Tween-20, the membrane was incubated with a horseradish peroxidase-labeled secondary antibody (Abcam). Antibody-bound protein bands were visualized by enhanced chemiluminescence (ECL prime; Amersham Biosciences, Piscataway, NJ, United States). The protein levels were quantitatively analyzed using a ChemiDoc Touch Imaging System (Bio-Rad, Hercules, CA, United States) and Image Lab software version 5.2.1 (Bio-Rad). The amount of occludin was defined as the sum of the amounts of its dimeric (120 kDa) and monomeric (64 kDa) forms (Yanai et al., 2017). The protein levels of ZO-1 and occludin were normalized by those of β-actin. One mouse without surgery was used as an external control.

Reverse Transcription-Quantitative Polymerase Chain Reaction (RT-qPCR)

Five *Trpv4*$^{-/-}$ and five WT mice without surgery were evaluated for their baseline gene expression levels of *Trpv4*, *Aqp4*, and *Kcnj10*. The mice were transcardially perfused with cold saline and a 1-mm-thick coronal slice of the hemisphere at 4 mm posterior to the olfactory bulb was collected. Total RNA was extracted using an RNeasy Mini Kit (Qiagen, Valencia, CA, United States). The A260/A280 ratio was measured using a spectrophotometer (Nanodrop 2000; Thermo Fisher Scientific, Wilmington, DE, United States) to determine the purity and concentration of the RNA. Complementary DNA was synthesized from the total RNA using ReverTra Ace reverse transcriptase (Toyobo, Osaka, Japan). Subsequently, RT-qPCR analysis was performed in a 7500 Fast Real-Time PCR System (Applied Biosystems, Foster City, CA, United States) using TaqMan Fast Universal PCR master mixture and TaqMan probes (Applied Biosystems) for *Trpv4* (Hs01099348_m1), *Aqp4* (Hs00242342_m1), *Kcnj10* (Hs01922935_s1), and *Gapdh* (Sp03785097_s1) under standard reaction conditions recommended by the manufacturer. The mRNA levels were normalized by those of *Gapdh*.

Transmission Electron Microscopy (TEM)

Transient focal cerebral ischemia was induced in one *Trpv4*$^{-/-}$ and one WT mouse. At 6 h post-tMCAO (Kurisu et al., 2016), mice were transcardially perfused with 4% paraformaldehyde with 3.4% sucrose. Brain slices including the right striatum were fixed with 2.5% glutaraldehyde in 0.1 M cacodylate buffer at 4°C overnight, post-fixed with 1% OsO_4 in 0.1 M cacodylate buffer on ice for 2 h, dehydrated in a graded ethanol series and propylene oxide, and embedded in epoxy resin. Ultrathin sections were cut at 80-nm thickness with an EM UC7 ultramicrotome (Leica Microsystems, Wetzlar, Germany) and stained with 2% uranyl acetate followed by a mixture of lead nitrate-lead acetate-lead citrate. The sections were observed with a Tecnai 20 electron microscope (FEI Co., Eindhoven, Netherlands) operated at an accelerating voltage of 200 kV and micrographs were recorded at a magnification of 5,000× for at least 10 microvasculatures.

Statistical Analysis

Statistical analyses were performed using JMP version 9.0 software (SAS Institute, Cary, NC, United States). Data are expressed as the median and interquartile range. Statistically significant differences were evaluated by the Wilcoxon rank-sum test or the Kruskal–Wallis test with *post hoc* comparison by Dunn's multiple comparison test. Values of $p < 0.05$ were considered to indicate statistical significance.

RESULTS

Brain Injury After tMCAO Is Reduced in *Trpv4*$^{-/-}$ Mice

To assess the ischemia-induced lesion volume, TTC staining was performed at 24 h post-tMCAO. The ischemia-induced lesion volume was significantly reduced in *Trpv4*$^{-/-}$ mice compared with WT mice ($p = 0.002$; **Figures 1A,B**). Because brain edema progressed to the maximum level on the second and third days, the tissue water content in the ipsilateral hemisphere was measured at 48 h post-tMCAO. The increase in tissue water in the ipsilateral hemisphere was significantly decreased in *Trpv4*$^{-/-}$ mice compared with WT mice ($p = 0.004$; **Figure 1C**). To assess the BBB function, EB leakage in the ipsilateral hemisphere was measured at 48 h post-tMCAO. The extent of EB leakage was significantly smaller in *Trpv4*$^{-/-}$ mice compared with WT mice ($p = 0.002$; **Figure 1D**). To assess the sensorimotor performance, the neurological score was evaluated at 24 and 48 h post-tMCAO in the two types of mice. Performance was impaired in both *Trpv4*$^{-/-}$ and WT mice after tMCAO with no significant difference between the groups at 24 h (12 [11–13] vs. 12 [10–12], $p = 0.307$; **Figure 1E**). However, *Trpv4*$^{-/-}$ mice showed significantly milder symptoms than WT mice at 48 h post-tMCAO (12 [10–13] vs. 10 [9–11], $p = 0.009$).

Preservation of Tight Junction Proteins After tMCAO in *Trpv4*$^{-/-}$ Mice

To assess protein levels in tight junctions of the BBB, western blotting was performed at 48 h post-tMCAO (**Figures 2A,B**). The occludin and ZO-1 protein levels in the ipsilateral hemisphere were significantly lower in WT mice after tMCAO than after sham operation ($p = 0.044$ and $p = 0.019$, respectively), while these changes were not statistically significant in *Trpv4*$^{-/-}$ mice ($p = 0.400$ and $p = 0.535$, respectively).

RT-qPCR Analysis of WT and *Trpv4*$^{-/-}$ Mouse Brains

The expression levels of *Trpv4* and genes associated with astrocyte volume regulation (*Aqp4* and *Kcnj10*) were evaluated by

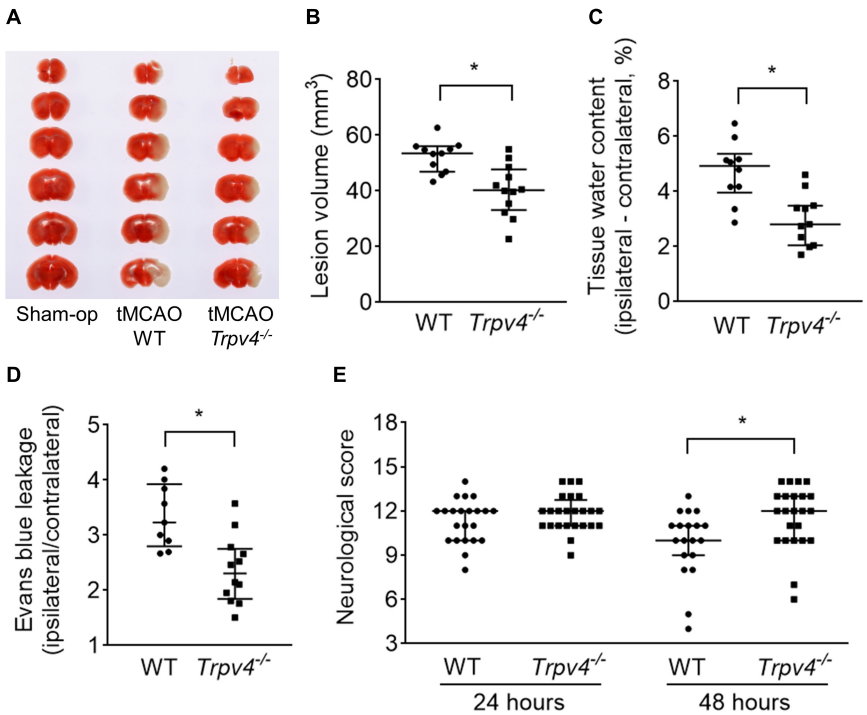

FIGURE 1 | Effects of *Trpv4*$^{-/-}$ on neurological and pathophysiological findings. **(A,B)** Evaluation of ischemia-induced lesion volumes at 24 h post-tMCAO (one WT mouse died within 24 h; therefore, $n = 11$ for WT mice and $n = 12$ for *Trpv4*$^{-/-}$ mice). **(C)** Evaluation of tissue water content by subtraction of the contralateral hemisphere from the ipsilateral hemisphere at 48 h post-tMCAO (two WT mice and one *Trpv4*$^{-/-}$ mice died within 48 h; therefore, $n = 10$ for WT mice and $n = 11$ for *Trpv4*$^{-/-}$ mice). **(D)** Evans blue leakage presented as the ratio of leakage in the ipsilateral hemisphere to that in the contralateral hemisphere at 48 h post-tMCAO (three WT mice died within 48 h; therefore, $n = 9$ for WT mice and $n = 12$ for *Trpv4*$^{-/-}$ mice). **(E)** Evaluation of neurological scores at 24 and 48 h post-tMCAO ($n = 22$ for WT mice and $n = 24$ for *Trpv4*$^{-/-}$ mice at 24 h post-tMCAO; $n = 19$ for WT mice and $n = 23$ for *Trpv4*$^{-/-}$ mice at 48 h post-tMCAO). *$p < 0.05$.

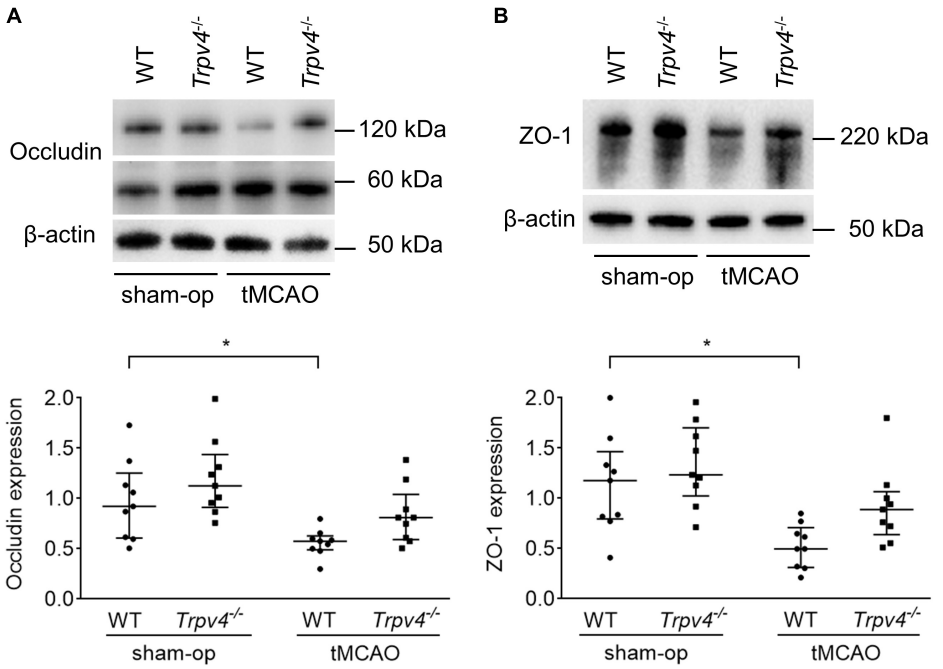

FIGURE 2 | Effects of *Trpv4*$^{-/-}$ on changes in tight junction proteins. **(A,B)** Western blot analysis of occludin **(A)** and ZO-1 **(B)** protein levels in the ipsilateral hemisphere at 48 h after tMCAO or sham operation in WT and *Trpv4*$^{-/-}$ mice. Each group contained nine mice. Protein levels were corrected by β-actin. *$p < 0.05$.

RT-qPCR. The data revealed significantly decreased expression of *Trpv4* in the *Trpv4*$^{-/-}$ mouse brain compared with the WT mouse brain ($p = 0.009$), while *Aqp4* and *Kcnj10* showed no differences ($p = 0.347$ and $p = 0.465$, respectively; **Figure 3**).

Reduction in Astrocyte Endfeet Swelling in Microvessels After tMCAO in *Trpv4*$^{-/-}$ Mice

Given the highly polarized localization of TRPV4 in the astrocyte endfeet surrounding brain capillaries, microvascular morphological changes in the ischemic lesion were analyzed by TEM at 6 h post-tMCAO. As shown in **Figure 4**, there was evidence of widespread endfeet swelling of pericapillary astrocytes in most of the microvasculature in the ischemic lesion. The cytoplasm was expanded, and mitochondria in the endfeet were enlarged and degenerated with swollen cristae. The residual lumen of microvessels was narrowed through compression by the extensive swollen endfeet of perivascular astrocytes in WT mice, but this was markedly suppressed in *Trpv4*$^{-/-}$ mice.

DISCUSSION

This study demonstrated that *Trpv4*$^{-/-}$ mice showed reduced brain ischemia-induced lesion size and preserved BBB compared with WT mice in the acute phase. Astrocyte endfeet swelling and microvascular narrowing shortly after reperfusion were markedly suppressed in *Trpv4*$^{-/-}$ mice.

Previous research using ischemia-reperfusion animal models demonstrated decreased capillary blood flow with narrowed capillary diameters (Hauck et al., 2004). This microvessel narrowing was caused by swelling of perivascular astrocyte endfeet shortly after ischemia-reperfusion (Ito et al., 2011; Kurisu et al., 2016). Furthermore, the astrocyte endfeet swelling was markedly ameliorated by *Aqp4* knockout (Manley et al., 2000) or infusion of cold saline or mannitol (Ito et al., 2014; Kurisu et al., 2016), leading to reduced infarct volumes. Shimbo et al. (2017) demonstrated that infusion of hemoglobin-encapsulating liposomes, which were smaller than red blood cells and could

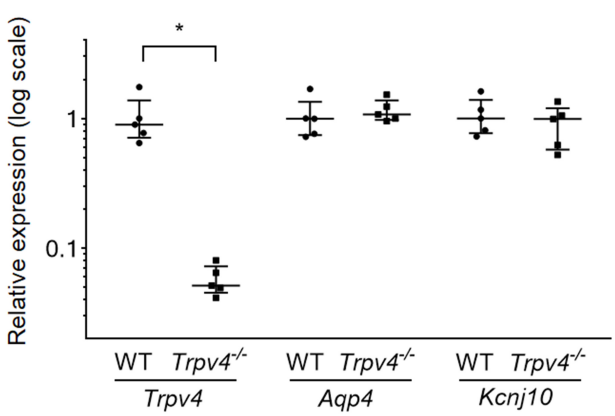

FIGURE 3 | Expression levels of *Trpv4*, *Aqp4*, and *Kcnj10* in WT and *Trpv4*$^{-/-}$ mouse brains. RT-qPCR analyses were performed to measure the mRNA levels of *Trpv4*, *Aqp4*, and *Kcnj10* in the brains of WT and *Trpv4*$^{-/-}$ mice. Expression levels were corrected by *Gapdh*. Each group contained five mice. *$p < 0.05$.

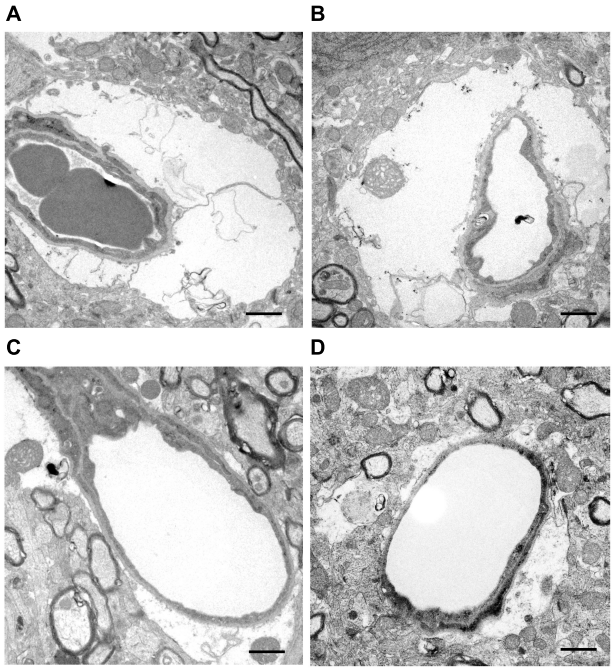

FIGURE 4 | Representative images of microvascular morphological changes evaluated by TEM. **(A,B)** Microvessels are compressed and narrowed by swollen astrocyte endfeet in WT mice. **(C,D)** By contrast, the astrocyte endfeet swelling is milder and the residual vascular lumen is well-preserved in *Trpv4*$^{-/-}$ mice. One WT mouse and one *Trpv4*$^{-/-}$ mouse were assessed. Scale bars = 1 μm.

pass through narrowed blood vessels, reduced the infarction size. These reports indicate that microvascular narrowing may contribute to hypoperfusion associated with ischemia and reperfusion. The mechanism for astrocyte endfeet swelling in acute ischemia was assumed to involve upregulated expression and polarized localization of AQP4 at astrocyte endfeet shortly after reperfusion (Steiner et al., 2012; Kurisu et al., 2016). The present study found similar mRNA expression patterns of *Aqp4* and *Kcnj10* between WT and *Trpv4*$^{-/-}$ mouse brains, in accordance with a previous study (Pivonkova et al., 2018). Blockade of TRPV4 altered hypothermia-induced surface localization of AQP4, despite there being no change in total protein expression levels (Salman et al., 2017). Thus, TRPV4 deficiency may reduce astrocyte endfeet swelling by inhibiting the AQP4 surge or AQP4 surface localization at astrocyte endfeet after ischemia-reperfusion.

This study demonstrated preserved BBB function shortly after reperfusion in *Trpv4*$^{-/-}$ mice, which was similar to that observed after pharmacological blockade of TRPV4 (Jie et al., 2015b). TRPV4-mediated Ca^{2+} influx led to activation of MMPs in lung tissue (Villalta et al., 2014), with subsequent disruption of tight junctions among alveolar epithelial cells (Dagenais et al., 2018). Therefore, TRPV4 deficiency may maintain the BBB via MMP inhibition to preserve tight junction proteins. A TRPV4 antagonist, GSK2798745, is currently being administered to patients in a phase II clinical trial for treatment of congestive heart failure-induced pulmonary edema (NTC02497937) (Stewart et al., 2020). EB leakage might have occurred because of BBB disruption and also because of ischemia-induced opening of connexin hemichannels in neurovascular unit constituent cells, making them permeable to EB dye (Orellana et al., 2013); however, TRPV4 has potential as a therapeutic target for post-ischemic brain injury from the perspective of BBB protection.

An important concern against clinical application of TRPV4 inhibition is that it may lead to increased lesion volumes (Pivonkova et al., 2018). However, this was inconsistent with the findings of the present study. The difference between the two studies may be because of the different model used (pMCAO vs. tMCAO). Although recanalization is considered the most important event, development of collateral circulation is another major determinant for severity of ischemic stroke with large artery occlusions. Dilation of leptomeningeal arteries occurs as early as 6 h after pMCAO via increased phosphorylation of endothelial nitric oxide synthase (eNOS) in response to shear stress (Iwasawa et al., 2018). Meanwhile, *Trpv4*$^{-/-}$ mice exhibited loss of shear stress-induced vasodilatation of the carotid artery (Hartmannsgruber et al., 2007), and endothelial downregulation of TRPV4 was shown to contribute to impairment of eNOS-mediated relaxation of the mesenteric artery (Boudaka et al., 2019). These findings suggest that TRPV4 deficiency may exacerbate ischemic brain injury through impairment of acute collateral development in cases of recanalization failure, such as the pMCAO model.

The neuroprotective effects of TRPV4 inhibition may not be solely derived from astrocytic TRPV4 as suggested in a previous report (Pivonkova et al., 2018), because TRPV4 is also expressed in endothelial cells and neutrophils. TRPV4 deficiency prevented neutrophil responses to proinflammatory stimuli, including formation of reactive oxygen species (ROS), adhesion, chemotaxis to break the alveolar–capillary barrier, and development of acute lung injury (Yin et al., 2016). Neutrophils play an important role in acute stroke pathology, wherein reperfusion provides neutrophils with access to the vulnerable brain (Stowe et al., 2009). TRPV4 deficiency or blockade may suppress neutrophil activation to break the BBB. Moreover, free radical damage was shown to play a key role in ischemia-reperfusion injury (Sun et al., 2018). Activation of TRPV4 enhanced oxidative stress in hippocampal neurons (Hong et al., 2016), and TRPV4 was simultaneously activated by ROS (Badr et al., 2016; Suresh et al., 2018). These observations indicate that TRPV4 and free radicals form a positive feedback loop that is involved in neurotoxicity. Thus, blockade of TRPV4 may have other neuroprotective effects in terms of ROS-mediated brain injury.

This study has several limitations. First, the mouse groups were not randomized for surgery and other tests because of the study design, which may have caused some selection biases. Second, in the TEM analysis, we could not perform a statistical evaluation because of a shortage in the number of detected microvessels in our data. Therefore, we qualitatively described the main observed findings in terms of microvascular morphological changes. Third, the neuroprotective effects in *Trpv4*$^{-/-}$ mice

were only assessed in the acute phase of transient focal cerebral ischemia because most of the mice showed continuous body weight loss that exceeded 20% by 48 h post-tMCAO and thus met the humane endpoint for laboratory animals (Science Council of Japan, 2006). Therefore, the effects of *Tprv4* deficiency on chronic ischemia and delayed ischemic neurological deficits remain to be established. Activation of TRPV4 via 4α-phorbol 12,13-didecanoate was reported to contribute to functional recovery through angiogenesis and neurogenesis at 5 days post-tMCAO (Chen et al., 2018). Further investigations are needed to confirm whether long-term inhibition of TRPV4 in the subacute to convalescent phases plays a neuroprotective role. Finally, we only examined the expression of two genes that regulate astrocyte volume, *Aqp4* and *Kcnj10* (Iuso and Križaj, 2016); therefore, further unbiased gene expression studies using microarray methodology are necessary to reveal any gene expression changes that contribute to ischemia-resistance due to knockout of *Trpv4*.

CONCLUSION

TRPV4 contributes to post-ischemic brain injury following transient focal cerebral ischemia. The preserved BBB function and microcirculation shortly after reperfusion are the key neuroprotective roles of TRPV4 inhibition, which represents a promising target for the treatment of acute ischemic stroke.

DATA AVAILABILITY STATEMENT

The datasets generated for this study are available on request to the corresponding author.

ETHICS STATEMENT

The animal study was reviewed and approved by Animal Ethics Committee of Kyushu University.

AUTHOR CONTRIBUTIONS

KT, SM, and TY made substantial contributions to the concept and design of the study and analysis and interpretation of data. KT acquired data and drafted the manuscript. SM, TY, MS, MK, RY, and J-IK revised the manuscript critically for important intellectual content. KT approved the version to be published.

FUNDING

This study was supported by a Japan Society for the Promotion of Science Grant-in-Aid for Scientific Research (grant number 16K10727) and a Grant-in-Aid for Research Activity Start-up (grant number 19K21303).

ACKNOWLEDGMENTS

We appreciate the technical assistance from The Research Support Center, Research Center for Human Disease Modeling, Kyushu University. We thank Mr. Ryo Ugawa, Laboratory for Technical Support, Medical Institute of Bioregulation, Kyushu University for electron microscopy. We also thank Alison Sherwin, Ph.D., from Edanz Group (www.edanzediting.com/ac) for editing a draft of this manuscript.

REFERENCES

Badr, H., Kozai, D., Sakaguchi, R., Numata, T., and Mori, Y. (2016). Different contribution of redox-sensitive transient receptor potential channels to acetaminophen-induced death of human hepatoma cell line. *Front. Pharmacol.* 7:19. doi: 10.3389/fphar.2016.00019

Boudaka, A., Al-Suleimani, M., Al-Lawati, I., Baomar, H., Al-Siyabi, S., and Zadjali, F. (2019). Downregulation of endothelial transient receptor potential vanilloid type 4 channel underlines impaired endothelial nitric oxide-mediated relaxation in the mesenteric arteries of hypertensive rats. *Physiol. Res.* 68, 219–231. doi: 10.33549/physiolres.933952

Chen, C. K., Hsu, P. Y., Wang, T. M., Miao, Z. F., Lin, R. T., and Juo, S. H. (2018). TRPV4 activation contributes functional recovery from ischemic stroke via angiogenesis and neurogenesis. *Mol. Neurobiol.* 55, 4127–4135. doi: 10.1007/s12035-017-0625-0

Dagenais, A., Desjardins, J., Shabbir, W., Roy, A., Filion, D., Sauvé, R., et al. (2018). Loss of barrier integrity in alveolar epithelial cells downregulates ENaC expression and activity via Ca2+ and TRPV4 activation. *Pflugers. Arch.* 470, 1615–1631. doi: 10.1007/s00424-018-2182-4

Dunn, K. M., Hill-Eubanks, D. C., Liedtke, W. B., and Nelson, M. T. (2013). TRPV4 channels stimulate Ca2+-induced Ca2+ release in astrocytic endfeet and amplify neurovascular coupling responses. *Proc. Natl. Acad. Sci. U.S.A.* 110, 6157–6162. doi: 10.1073/pnas.1216514110

Engel, O., Kolodziej, S., Dirnagl, U., and Prinz, V. (2011). Modeling stroke in mice - middle cerebral artery occlusion with the filament model. *J. Vis. Exp.* 47:2423. doi: 10.3791/2423

Filosa, J. A., Yao, X., and Rath, G. (2013). TRPV4 and the regulation of vascular tone. *J. Cardiovasc. Pharmachol.* 61, 113–119. doi: 10.1097/FJC.0b013e318279ba42

Garcia, J. H., Wagner, S., Liu, K. F., and Hu, X. J. (1995). Neurological deficit and extent of neuronal necrosis attributable to middle cerebral artery occlusion in rats. Statistical validation. *Stroke* 26, 627–634. doi: 10.1161/01.str.26.4.627

Goyal, M., Menon, B. K., van Zwam, W. H., Dippel, D. W., Mitchell, P. J., Demchuk, A. M., et al. (2016). Endovascular thrombectomy after large-vessel ischaemic stroke: a meta-analysis of individual patient data from five randomised trials. *Lancet* 387, 1723–1731. doi: 10.1016/S0140-6736(16)00163-X

Hartmannsgruber, V., Heyken, W. T., Kacik, M., Kaistha, A., Grgic, I., Harteneck, C., et al. (2007). Arterial response to shear stress critically depends on endothelial TRPV4 expression. *PLoS One* 2:e827. doi: 10.1371/journal.pone.0000827

Hauck, E. F., Apostel, S., Hoffmann, J. F., Heimann, A., and Kempski, O. (2004). Capillary flow and diameter changes during reperfusion after global cerebral ischemia studied by intravital video microscopy. *J. Cereb. Blood Flow Metab.* 24, 383–391. doi: 10.1097/00004647-200404000-00003

Hong, Z., Tian, Y., Yuan, Y., Qi, M., Li, Y., Du, Y., et al. (2016). Enhanced oxidative stress is responsible for TRPV4-induced neurotoxicity. *Front. Cell Neurosci.* 10:232. doi: 10.3389/fncel.2016.00232

Ito, U., Hakamata, Y., Kawakami, E., and Oyanagi, K. (2011). Temporary cerebral ischemia results in swollen astrocytic end-feet that compress microvessels and lead to delayed focal cortical infarction. *J. Cereb. Blood Flow Metab.* 31, 328–338. doi: 10.1038/jcbfm.2010.97

Ito, U., Hakamata, Y., Watabe, K., and Oyanagi, K. (2014). Mannitol infusion immediately after reperfusion suppresses the development of focal cortical

infarction after temporary cerebral ischemia in gerbils. *Neuropathology* 34, 360–369. doi: 10.1111/neup.12113

Iuso, A., and Križaj, D. (2016). TRPV4-AQP4 interactions 'turbocharge' astroglial sensitivity to small osmotic gradients. *Channels* 10, 172–174. doi: 10.1080/19336950.2016.1140956

Iwasawa, E., Ishibashi, S., Suzuki, M., Li, F., Ichijo, M., Miki, K., et al. (2018). Sphingosine-1-phosphate receptor 1 activation enhances leptomeningeal collateral development and improves outcome after stroke in mice. *J. Stroke Cerebrovasc. Dis.* 27, 1237–1251. doi: 10.1016/j.jstrokecerebrovasdis.2017.11.040

Jie, P., Lu, Z., Hong, Z., Li, L., Zhou, L., Li, Y., et al. (2016). Activation of transient receptor potential vanilloid 4 is involved in neuronal injury in middle cerebral artery occlusion in mice. *Mol. Neurobiol.* 53, 8–17. doi: 10.1007/s12035-014-8992-2

Jie, P., Hong, Z., Tian, Y., Li, Y., Lin, L., Zhou, L., et al. (2015a). Activation of transient receptor potential vanilloid 4 induces apoptosis in hippocampus through downregulating PI3K/Akt and upregulating p38 MAPK signaling pathways. *Cell Death Dis.* 6:e1775. doi: 10.1038/cddis.2015.146

Jie, P., Tian, Y., Hong, Z., Li, L., Zhou, L., Chen, L., et al. (2015b). Blockage of transient receptor potential vanilloid 4 inhibits brain edema in middle cerebral artery occlusion mice. *Front. Cell Neurosci.* 9:141. doi: 10.3389/fncel.2015.00141

Kurisu, K., Abumiya, T., Nakamura, H., Shimbo, D., Shichinohe, H., Nakayama, N., et al. (2016). Transarterial regional brain hypothermia inhibits acute aquaporin-4 surge and sequential microvascular events in ischemia/reperfusion injury. *Neurosurgery* 79, 125–134. doi: 10.1227/NEU.0000000000001088

Li, L., Qu, W., Zhou, L., Lu, Z., Jie, P., Chen, L., et al. (2013). Activation of transient receptor potential vanilloid 4 increases NMDA-activated current in hippocampal pyramidal neurons. *Front. Cell Neurosci.* 7:17. doi: 10.3389/fncel.2013.00017

Manley, G. T., Fujimura, M., Ma, T., Noshita, N., Filiz, F., Bollen, A. W., et al. (2000). Aquaporin-4 deletion in mice reduces brain edema after acute water intoxication and ischemic stroke. *Nat. Med.* 6, 159–163. doi: 10.1038/72256

Molina, C. A., and Alvarez-Sabín, J. (2009). Recanalization and reperfusion therapies for acute ischemic stroke. *Cerebrovasc. Dis.* 27(Suppl. 1), 162–167. doi: 10.1159/000200455

Nilius, B., and Voets, T. (2013). The puzzle of TRPV4 channelopathies. *EMBO Rep.* 14, 152–163. doi: 10.1038/embor.2012.219

Orellana, J. A., Martinez, A. D., and Retamal, M. A. (2013). Gap junction channels and hemichannels in the CNS: regulation by signaling molecules. *Neuropharmacology* 75, 567–582. doi: 10.1016/j.neuropharm.2013.02.020

Pivonkova, H., Hermanova, Z., Kirdajova, D., Awadova, T., Malinsky, J., Valihrach, L., et al. (2018). The contribution of TRPV4 channels to astrocyte volume regulation and brain edema formation. *Neuroscience* 394, 127–143. doi: 10.1016/j.neuroscience.2018.10.028

Rakers, C., Schmid, M., and Petzold, G. C. (2017). TRPV4 channels contribute to calcium transients in astrocytes and neurons during peri-infarct depolarizations in a stroke model. *Glia* 65, 1550–1561. doi: 10.1002/glia.23183

Ramsey, I. S., Delling, M., and Clapham, D. E. (2006). An introduction to TRP channels. *Annu. Rev. Physiol.* 68, 619–647. doi: 10.1146/annurev.physiol.68.040204.100431

Ryskamp, D. A., Iuso, A., and Križaj, D. (2015). TRPV4 links inflammatory signaling and neuroglial swelling. *Channels* 9, 70–72. doi: 10.1080/19336950.2015.1017998

Salman, M. M., Kitchen, P., Woodroofe, M. N., Brown, J. E., Bill, R. M., Conner, A. C., et al. (2017). Hypothermia increases aquaporin 4 (AQP4) plasma membrane abundance in human primary cortical astrocytes via a calcium/transient receptor potential vanilloid 4 (TRPV4)- and calmodulin-mediated mechanism. *Eur. J. Neurosci.* 46, 2542–2547. doi: 10.1111/ejn.13723

Science Council of Japan (2006). *Guidelines for Proper Conduct of Animal Experiments*. Available online at: http://www.scj.go.jp/ja/info/kohyo/pdf/kohyo-20-k16-2e.pdf (accessed October 23, 2019).

Shimbo, D., Abumiya, T., Kurisu, K., Osanai, T., Shichinohe, H., Nakayama, N., et al. (2017). Superior microvascular perfusion of infused liposome-encapsulated hemoglobin prior to reductions in infarctions after transient focal cerebral ischemia. *J. Stroke Cerebrovasc. Dis.* 26, 2994–3003. doi: 10.1016/j.jstrokecerebrovasdis.2017.07.026

Steiner, E., Enzmann, G. U., Lin, S., Ghavampour, S., Hannocks, M. J., Zuber, B., et al. (2012). Loss of astrocyte polarization upon transient focal brain ischemia as a possible mechanism to counteract early edema formation. *Glia* 60, 1646–1659. doi: 10.1002/glia.22383

Stewart, G. M., Johnson, B. D., Sprecher, D. L., Reddy, Y. N. V., Obokata, M., Goldsmith, S., et al. (2020). Targeting pulmonary capillary permeability to reduce lung congestion in heart failure: a randomized, controlled pilot trial. *Eur. J. Heart Fail.* doi: 10.1002/ejhf.1809 [Epub ahead of print].

Stowe, A. M., Adair-Kirk, T. L., Gonzales, E. R., Perez, R. S., Shah, A. R., Park, T. S., et al. (2009). Neutrophil elastase and neurovascular injury following focal stroke and reperfusion. *Neurobiol. Dis.* 35, 82–90. doi: 10.1016/j.nbd.2009.04.006

Sun, M. S., Jin, H., Sun, X., Huang, S., Zhang, F. L., Guo, Z. N., et al. (2018). Free radical damage in ischemia-reperfusion injury: an obstacle in acute ischemic stroke after revascularization therapy. *Oxid. Med. Cell Longev.* 2018:3804979. doi: 10.1155/2018/3804979

Suresh, K., Servinsky, L., Jiang, H., Bigham, Z., Yun, X., Kliment, C., et al. (2018). Reactive oxygen species induced Ca2+ influx via TRPV4 and microvascular endothelial dysfunction in the SU5416/hypoxia model of pulmonary arterial hypertension. *Am. J. Physiol. Lung Cell Mol. Physiol.* 314, L893–L907. doi: 10.1152/ajplung.00430.2017

Suzuki, M., Mizuno, A., Kodaira, K., and Imai, M. (2003). Impaired pressure sensation in mice lacking TRPV4. *J. Biol. Chem.* 278, 22664–22668. doi: 10.1074/jbc.M302561200

Villalta, P. C., Rocic, P., and Townsley, M. I. (2014). Role of MMP2 and MMP9 in TRPV4-induced lung injury. *Am. J. Physiol. Lung Cell Mol. Physiol.* 307, L652–L659. doi: 10.1152/ajplung.00113.2014

Yanai, S., Toyohara, J., Ishiwata, K., Ito, H., and Endo, S. (2017). Long-term cilostazol administration ameliorates memory decline in senescence-accelerated mouse prone 8 (SAMP8) through a dual effect on cAMP and blood-brain barrier. *Neuropharmacology* 116, 247–259. doi: 10.1016/j.neuropharm.2016.12.006

Yin, J., Michalick, L., Tang, C., Tabuchi, A., Goldenberg, N., Dan, Q., et al. (2016). Role of Transient receptor potential vanilloid 4 in neutrophil activation and acute lung injury. *Am. J. Respir. Cell Mol. Biol.* 54, 370–383. doi: 10.1165/rcmb.2014-0225OC

Conflict of Interest: The authors declare that the research was conducted in the absence of any commercial or financial relationships that could be construed as a potential conflict of interest.

Copyright © 2020 Tanaka, Matsumoto, Yamada, Yamasaki, Suzuki, Kido and Kira. This is an open-access article distributed under the terms of the Creative Commons Attribution License (CC BY). The use, distribution or reproduction in other forums is permitted, provided the original author(s) and the copyright owner(s) are credited and that the original publication in this journal is cited, in accordance with accepted academic practice. No use, distribution or reproduction is permitted which does not comply with these terms.

frontiers in Neurology

ORIGINAL RESEARCH
published: 19 May 2020
doi: 10.3389/fneur.2020.00352

Serum-Based Proteomics Reveals Lipid Metabolic and Immunoregulatory Dysregulation in Cervical Artery Dissection With Stroke

*Yongtao Yang[1], Jing Peng[2], Suxia Wang[3], Jialu Huang[3], Hong Ran[3], Kangning Chen[3] and Zhenhua Zhou[3]**

[1] Department of Neurology, Chongqing Renji Hospital, University of Chinese Academy of Sciences, Chongqing, China, [2] Department of Geriatrics, Sichuan Second Hospital of Traditional Chinese Medicine, Chengdu, China, [3] Department of Neurology, Southwest Hospital, Third Military Medical University, Chongqing, China

Cervical artery dissection (CAD) is an important causal factor for stroke in young and middle-aged individuals and presents a great burden to the individual stroke victim. However, the pathophysiological mechanisms underlying CAD remain unknown. Here, an iTRAQ (isobaric tagging for relative and absolute quantitation)–based quantitative proteomic approach was performed, to identify differentially expressed proteins in serum samples obtained from spontaneous CAD and non-CAD ischemic stroke subjects. Differential protein expression was analyzed for Kyoto Encyclopedia of Genes and Genomes (KEGG) pathway overrepresentation, and six differential proteins were selected for enzyme-linked immunosorbent assay validation. Through KEGG analysis, the significantly differentiated proteins were primarily involved in immunoregulation, blood coagulation, and lipid metabolism. For the first time, differential expressions of apolipoprotein B, apolipoprotein C-I, lipopolysaccharide-binding protein, vascular cell adhesion molecule 1, fibulin-1, and ficolin-2 were confirmed as being significantly upregulated in CAD as compared to non-CAD ischemic stroke subjects. In conclusion, proteomic analysis reveals that early perturbation of immunoregulation and lipid metabolism may be involved in the pathophysiology of CAD. Specifically, the panel of six proteins identified is promising as serum-based biomarkers for the detection of increased CAD risk in stroke subjects.

Keywords: cervical artery dissection, stroke, serum, immunoregulation, lipid metabolism

OPEN ACCESS

Edited by:
Johannes Boltze, University of Warwick, United Kingdom

Reviewed by:
Anna Swierzko, Institute for Medical Biology (PAN), Poland
Xiao-Lian Zhang, Wuhan University, China

***Correspondence:**
Zhenhua Zhou
exploiter001@126.com

Specialty section:
This article was submitted to Stroke, a section of the journal Frontiers in Neurology

Received: *03 June 2019*
Accepted: *08 April 2020*
Published: *19 May 2020*

Citation:
Yang Y, Peng J, Wang S, Huang J, Ran H, Chen K and Zhou Z (2020) Serum-Based Proteomics Reveals Lipid Metabolic and Immunoregulatory Dysregulation in Cervical Artery Dissection With Stroke. Front. Neurol. 11:352. doi: 10.3389/fneur.2020.00352

INTRODUCTION

Cervical artery dissection (CAD) is an important cause of cerebral ischemia in young and middle-aged patients. Although accounting for only 2% of all ischemic strokes, CAD accounts for 8–25% of strokes in patients younger than 45 years (1). Such a high incidence of stroke presents a great burden not only to the individual stroke victim but also to their family, society, and the economy (2). A lack of clinical symptoms associated with CAD is regarded as the main cause of missed diagnoses. Thanks to the development of advanced imaging techniques, CAD has been increasingly

recognized in the past few years as involved in at least some aspects of this disease. However, the underlying pathogenesis responsible for spontaneous CAD is unknown, making the diagnosis of CAD more challenging.

Unfortunately, the search for clinically useful predictors for stroke risk has been inconclusive. One study found that hyperhomocysteinemia and elevated peripheral leukocyte counts have been reported previously in patients with CAD. However, these factors have yielded poor results and lack specificity as a biomarker (3, 4). Currently, the candidate biomarkers for CAD risk that have shown promise include fibrillin-1 (5), serum neurofilament light chain (6), extracellular matrix (ECM)–regulating enzymes (7), and plasma TT MTHFR genotype (8). These factors, however, are neither standardized nor clinically practical as they exhibit low sensitivity and variable specificity.

To address this challenge, several lines of evidence suggest that the peripheral circulation may be adversely affected in individuals at risk of CAD and therefore may serve as a source of useful biomarkers for this disorder (9). Proteomics, the analysis of protein expression in biological samples, can improve our understanding of the pathophysiological mechanisms and aid in diagnostic tool development (10). We hypothesize that a proteomic signature for CAD can be detected in human serum.

In this study, serum samples from spontaneous CAD and non-CAD stroke subjects with ischemic events were analyzed using a quantitative proteomic approach based on isobaric tags for relative and absolute quantitation (iTRAQ) and multidimensional liquid chromatography–tandem mass spectrometry (LC-MS/MS). Differentially expressed proteins were further validated by enzyme-linked immunosorbent assay (ELISA) and analyzed by cluster Profiler R package bioinformatics resources. This proteomic approach may ultimately contribute to a better understanding of the pathophysiology underlying CAD.

MATERIALS AND METHODS

Subjects and Ethics Statement

Fifteen patients with spontaneous CAD admitted to the Department of Neurology, Southwest Hospital, Army Medical University, from February 2014 to December 2016 were prospectively enrolled, all having symptoms of cerebral ischemia. Thirteen age- and sex-matched patients with ischemic stroke unrelated to CAD were admitted to our department during the same period for comparisons. The diagnosis of CAD was based on widely accepted criteria as previously described (11). Symptomatic patients with ischemic stroke within 15 days after the first symptom onset represented the acute stage. Patients with a recent history of head or neck trauma were excluded. Stroke severity was assessed based on the National Institutes of Health Stroke Scale (NIHSS) score. Dual antiplatelet treatment or anticoagulation therapy was utilized in all patients. The study was approved by the local ethics committee. Written informed consent was obtained from each patient or from an authorized family member.

Sample Collection

All blood samples were obtained from non-fasting patients in the morning between 8:00 and 10:00 AM. Serum samples were collected in 10-cc separator tubes (BD Vacutainers, catalog no. 367820; Becton, Dickinson & Co., Franklin Lakes, New Jersey, NJ, USA) and were kept at 4°C for 1 h and then centrifuged at 3,000 revolutions/min for 10 min at 4°C. The serum samples were distributed into 400-μL aliquots and stored at −80°C until use.

Protein Digestion and iTRAQ Labeling

Each sample consisted of a pool of serum from 15 CAD and 13 non-CAD stroke subjects. The proteins in each sample were denatured, reduced, alkylated, and digested with sequencing-grade modified trypsin with a protein-to-enzyme ratio of 20:1 at 37°C overnight and then labeled with the following iTRAQ reagent tags in duplicate: 113 and 116 for CAD, and 115 and 118 for the non-CAD ischemic stroke subjects.

LC-MS/MS Analysis for Peptide Identification and Sequence Database Search

The iTRAQ-labeled peptides were mixed and fractionated by 16 SCX chromatography using the AKTA Purifier system (GE Healthcare, Pittsburgh, PA, USA) and then for LC-MS/MS analysis using Q Exactive mass spectrometer (Thermo Fisher Scientific, Waltham, MA, USA). Desalted peptide mixture were loaded onto a Acclaim PePmap C18-reversed phase column (75 μm × 2 cm, 3 μm, 100 *Å*; Thermo Fisher Scientific, Waltham, MA, USA) and separated with reversed phase C18column (75 μm × 10 cm, 5 μm, 300 *Å*; Agela Technologies, Torrance, CA, USA) mounted onto a Dionex ultimate 3000 nano LC system (Thermo Fisher Scientific, Waltham, MA, USA). Peptides were eluted using a gradient of 5% to 80% (vol/vol) acetonitrile in 0.1% formic acid over 65 min at a flow rate of 400 nL min^{-1} combined with a Q Exactive mass spectrometer (Thermo Fisher Scientific, Waltham, MA, USA). The eluates were directly entered Q-Exactive MS (Thermo Fisher Scientific), setting in positive ion mode and data-dependent manner with full MS scan from 350 to 2,000 m/z, full scan resolution at 70,000, MS/MS scan resolution at 17,500. MS/MS scan with minimum signal threshold 1E+5, isolation width at 2 Da. To evaluate the performance of this mass spectrometry on the iTRAQ-labeled samples, two MS/MS acquisition modes, higher collision energy dissociation (HCD) was employed. And to optimize the MS/MS acquisition efficiency of HCD, normalized collision energy was systemically examined 28, stepped 20%.

All LC-MS/MS data were processed using Proteome Discoverer Software 1.3 (Thermo Fisher Scientific, Waltham, MA, USA). MS/MS spectra were searched using MASCOT engine (Matrix Science, London, UK; version 2.3) against the 2019-uniprot-human9606.fasta (downloaded 2011-11-11). For protein identification, the following options were used: peptide mass tolerance, 15 ppm; MS/MS tolerance, 20 mmu; enzyme, trypsin; max missed cleavage, 1; fixed modification, carbamidomethyl (C); variable modification, Oxidation(M) CGln→Pyro-Glu (N-term Q), iTRAQ8plex (K), iTRAQ 8 plex

(Y), iTRAQ8plex (N-term); variable modification, oxidation (M); and decoy database pattern, reverse, and false discovery rate (FDR) <0.01.

Gene Ontology and Pathway Analysis

To obtain ENTREZ Gene IDs, the org.Hs.eg.db R package of Bioconductor was used to search ENTREZ Gene IDs with UniProtKB accession and gene name. Then, using ENTREZ Gene IDs, gene ontology (GO) functional classification and enrichment analyses were performed to identify GO terms that were significantly enriched in differentially expressed proteins using the clusterProfiler R package (12). Furthermore, Kyoto Encyclopedia of Genes and Genomes (KEGG) pathway enrichment analysis was also performed to obtain enriched pathways using the clusterProfiler R package. To obtain further KEGG pathway information, a bioconductor package for pathway-based data integration and visualization was used (13).

Enzyme-Linked Immunosorbent Assay Validation

A total of 28 individual serum samples consisting of CAD ($n = 15$) and non-CAD ischemic stroke ($n = 13$) subjects were employed in the ELISA validation. Six proteins including lipopolysaccharide-binding protein (LBP), vascular cell adhesion molecule 1 (VCAM1), ficolin-2 (FCN2), fibulin-1 (FBLN1), apolipoprotein C-I (APOC-I), and apolipoprotein B (APOB) were analyzed using commercially available kits (Wuhan Colorful Gene Biological Technology, Wuhan, China) following the manufacturers' instructions.

The reason why we selected the six proteins is that mounting evidence suggests a close association between these six proteins and key biological processes underlying CAD. In addition, we should consider the following factors: first, there is a statistically significant difference in expression level of these proteins between CAD and non-CAD group. Second, the result of MS/MS is very reliable. Third, the result from bioinformatics analysis indicated that six proteins might play key role in CAD. Every protein was analyzed in duplicate.

Statistical Analysis

Statistical analysis was performed using the Statistical Package of Social Science (SPSS) for Windows v21.0 (SPSS, Chicago, IL, USA). Data are expressed as mean ± SD. The Student *t* test was applied to identify proteins with significant differences in abundance between the CAD and non-CAD ischemic stroke subjects. All the tests were two-tailed, and the significance threshold was set at $P < 0.05$.

We further evaluated the classification performance and the robustness of panel identification, as well as the six selected proteins using leave-one-out (LOO) cross-validation to alleviate overfitting of classifier training on small size data set. At each step of this procedure, one sample was left out for test, and the remaining 27 samples were used to build the LR classifiers. This process was repeated until all samples were selected as the test set once. So, these processes were cycled for 28 times. In the meantime, the predicted probabilities for each sample being CAD were obtained, from which we draw the receiver operating characteristic (ROC) curves (14). The optimal cutoff points were selected based on the Youden index and should be larger than 0.5.

TABLE 1 | The basic demographic and clinical characteristics of subjects.

	CAD ($n = 15$)	Non-CAD ($n = 13$)	*P*-value
Age, mean ± SD, years	45.27 ± 3.87	48.87 ± 2.68	0.45
Male sex, *n* (%)	11 (73.3)	9 (60.0)	0.46
Hypertension, *n* (%)	5 (33.3)	8 (53.3)	0.28
Diabetes mellitus, *n* (%)	1 (6.7)	4 (26.7)	0.15
Hyperlipidemia, *n* (%)	3 (20)	6 (40)	0.25
Smoking, *n* (%)	4 (26.7)	7 (46.7)	0.27
Symptoms at onset, *n* (%)			
Headache or neck pain	7 (46.7)	3 (20)	0.13
Horner sign	2 (13.3)	1 (6.7)	0.56
Stroke	15(100)	13 (100)	0.27
NIHSS score on admission	4.07±1.14	6.53±0.71	0.07
Site of dissection, *n* (%)			
Internal carotid artery	9 (60)	n/a	
Vertebral artery	5 (33.3)	n/a	
Multiple dissections	1 (6.7)	n/a	
Time to serum sampling, days	13.40 ± 3.21	9.93±1.96	0.12

n/a, not applicable; multiple dissection includes: ICA and VA, bilateral ICA and bilateral VA; ICA, internal carotid artery; VA, vertebral artery.

RESULTS

Subject Characteristics

Demographic and clinical data obtained from patients with CAD ($n = 15$) and patients with non-CAD ischemic stroke ($n = 13$) are provided in **Table 1**. The two groups of subjects were not distinguishable by key demographic characteristics, including age and sex. Patients with CAD had a lower prevalence of traditional vascular risk factors. Headache and Horner syndrome were seen more frequently in the CAD group compared to the non-CAD ischemic stroke group. However, differences were not statistically significant. The frequency of internal carotid artery dissection (nine patients representing, 60%) was higher than vertebral artery dissection (five patients representing 33.3%). In addition, bilateral internal carotid artery dissection was found in one patient. No significant difference was found in the meantime from symptom onset to blood removal between the group of patients with CAD (13.40 ± 3.21 days) and the group of patients with non-CAD ischemic stroke (9.93 ± 1.96 days).

Qualitative Results

The immunodepleted protein fractions were then profiled using iTRAQ coupled to an LC-MS/MS–based approach. The identified proteins in the CAD subjects were used for non-CAD ischemic stroke comparisons. The FDR calculated by searching the data against a decoy database was 1%. Data from the two MS repetitions identified 438 unique proteins according to the parameters set as described above. Differentially regulated

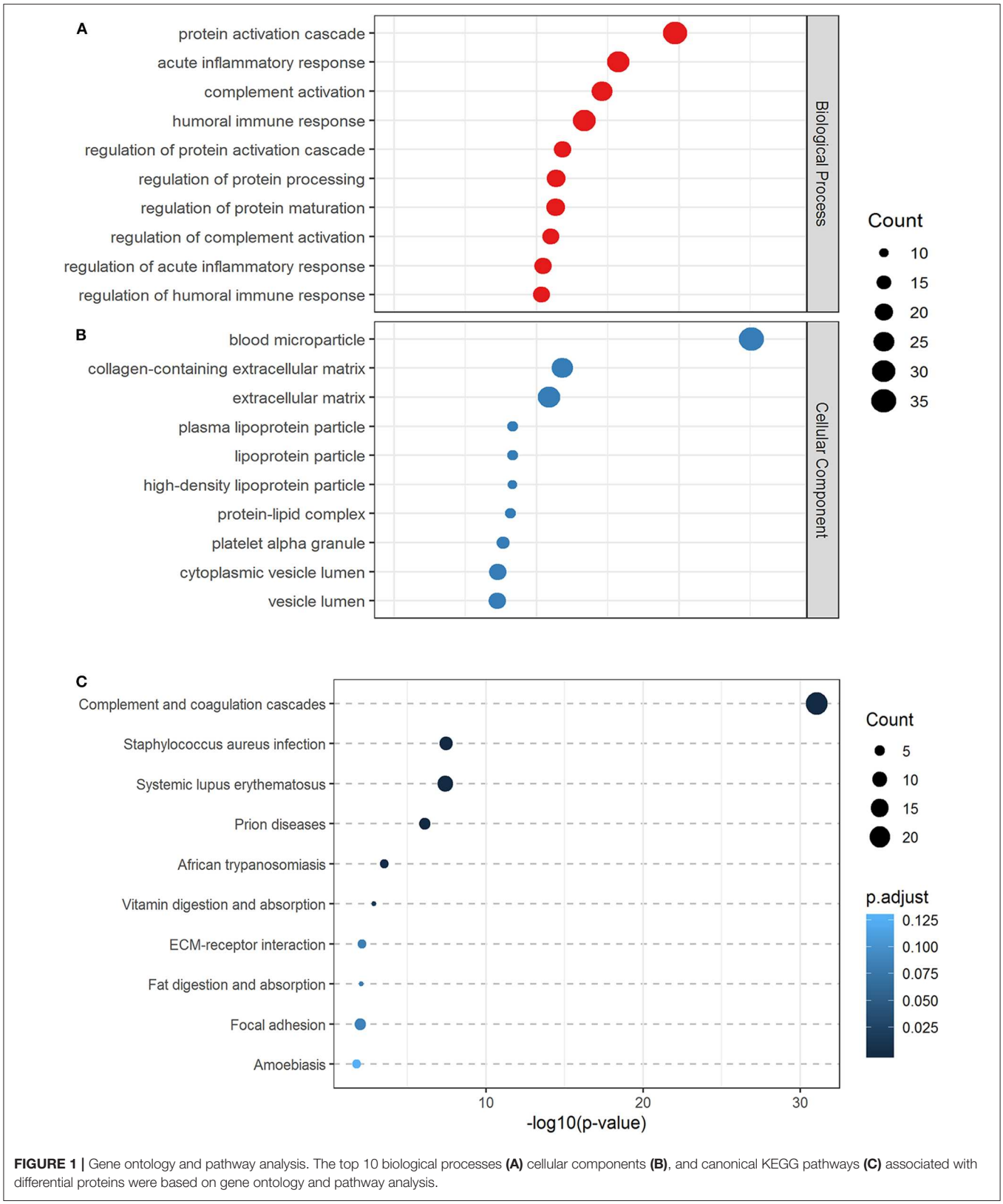

FIGURE 1 | Gene ontology and pathway analysis. The top 10 biological processes **(A)** cellular components **(B)**, and canonical KEGG pathways **(C)** associated with differential proteins were based on gene ontology and pathway analysis.

proteins (1.2-fold change with $P < 0.05$) were selected for further analysis. These cutoffs were selected based on a literature search of the reproducibility of iTRAQ TM quantification (15). One hundred thirty proteins were found to be differentially expressed in the CAD as compared to non-CAD ischemic stroke subjects (**Supplementary Table 1**).

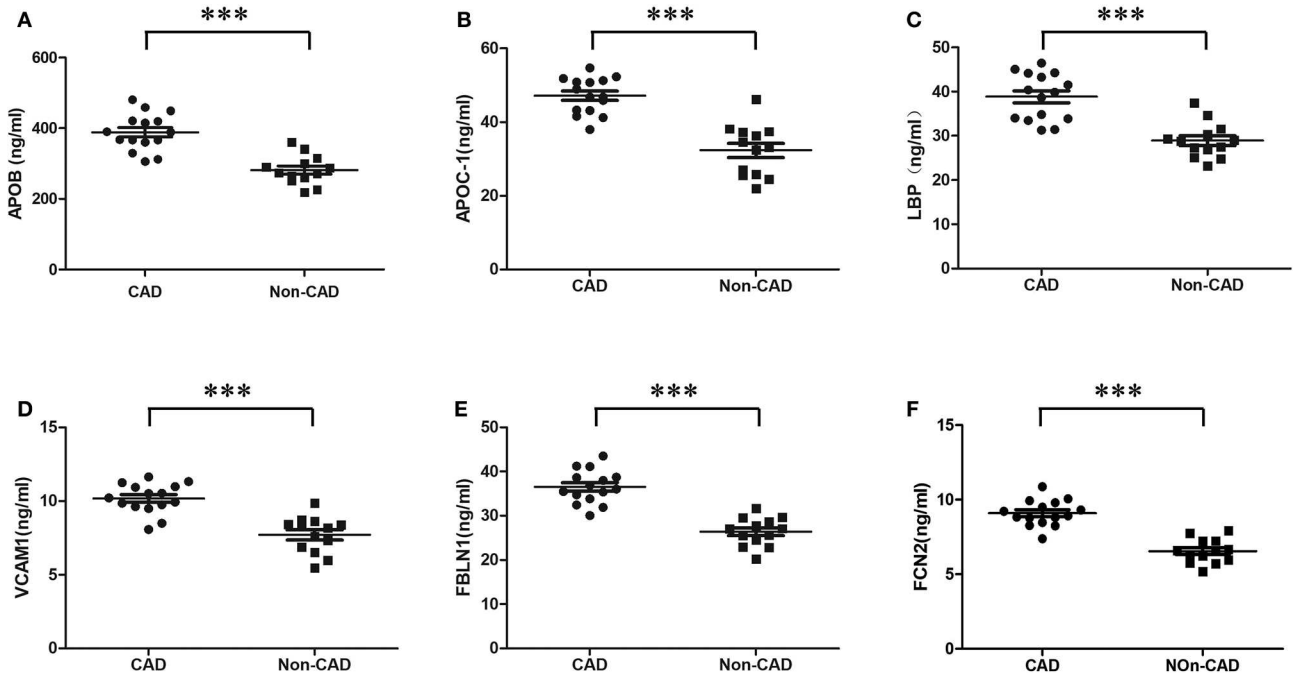

FIGURE 2 | Enzyme-linked immunosorbent assay validation of differential proteins. Six proteins analyzed by ELISA displayed significant changes between CAD ($n = 15$) and non-CAD ischemic stroke ($n = 13$) subjects. **(A)** APOB, **(B)** APOC1, **(C)** LBP, **(D)** VCAM1, **(E)** FBLN1, and **(F)** FCN2 were significantly upregulated in CAD subjects compared to non-CAD ischemic stroke subjects. Statistical analysis was performed using the Statistical Package of Social Science (SPSS) for Windows v21.0. The Student *t* test was applied to identify proteins with significant differences in abundance between the CAD and non-CAD ischemic stroke subjects. All the tests were two-tailed, and the significance threshold was set at $P < 0.05$. $^{***}P = 0.000$. ELISA, enzyme-linked immunosorbent assay; CAD, cerebral artery dissection; APOB, apolipoprotein B; APOC-1, apolipoprotein C-I; LBP, lipopolysaccharide-binding protein; VCAM1, vascular cell adhesion molecule 1; FBLN1, fibulin-1; FCN2, ficolin-2.

Annotation of Identified Proteins

The significantly differentiated proteins were categorized by biological function such as acute inflammatory response, humoral immune response, complement activation, and cellular component (blood microparticle, platelet alpha granule, plasma lipoprotein particle, lipoprotein particle, protein–lipid complex). The biologic processes (**Figure 1A**) and cellular component (**Figure 1B**) attributed to the differentially expressed proteins are displayed.

Altered Biological Pathways Identified by KEGG

The 130 differentially expressed proteins were analyzed for KEGG overrepresentation of pathways. Inflammatory processes were the most statistically overrepresented, including complement and coagulation cascades ranking highest ($P < 0.001$) (**Figure 1C**).

Detection of Differentially Expressed Proteins by ELISA

Six candidate proteins (LBP, VCAM1, FCN2, FBLN1, APOC-I, and APOB) were assessed using individual samples from the CAD and non-CAD ischemic stroke subjects. Consistent with our proteomic findings, the expression levels of all proteins were significantly upregulated in CAD as compared to non-CAD ischemic stroke subjects (**Figure 2**).

Diagnostic Performance

Based on ELISA results, all the six differentially expressed proteins were selected to form a biomarker panel. By LOO cross-validation, we got 28 formulas and 28 prediction scores listed in **Supplementary Table 2**. Receiver operating characteristic curves were constructed, in which the area under the curve (AUC) was 0.954, 0.964, 0.933, 0.931, 0.995, 0.990, and 1 for APOB, APOC-I, LBP, VCAM1, FBLN1, FCN2, and the whole panel, respectively (**Figure 3**). The whole panel exhibited a higher sensitivity (100%) and specificity (100%) than the six proteins individually: APOB (80.0%, 92.3%), APOC-I (93.3%, 92.3%), LBP (86.7%, 84.6%), VCAM1 (86.7%, 92.3%), FBLN1 (93.3%, 92.3%), and FCN2 (93.3%, 92.3%) (**Table 2**).

DISCUSSION

This study is the first reported proteomic-based study investigating putative peripheral biomarkers for CAD. Our analysis revealed immunoregulatory, coagulation, and lipid metabolic dysregulation in CAD, and the potential of using the panel of the six increased proteins with 100% sensitivity and 100% specificity shows to be promising for the detection of increased CAD risk in stroke subjects.

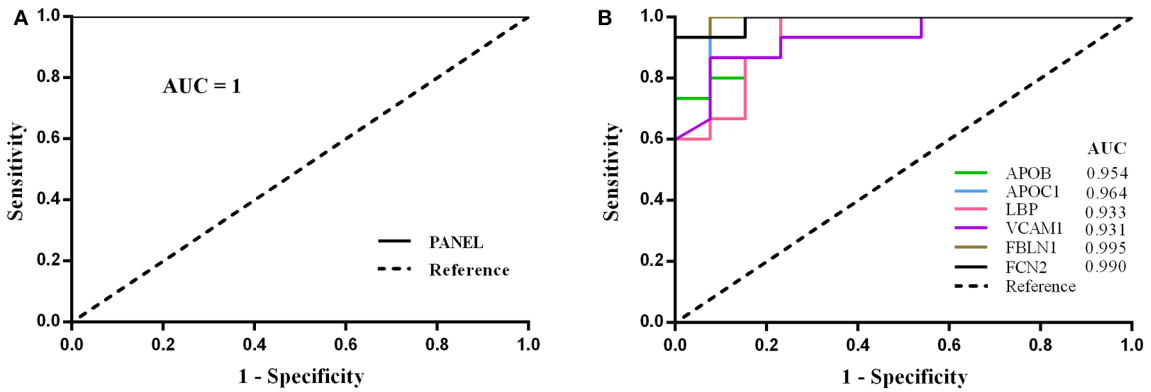

FIGURE 3 | Receiver operating characteristic analyses showing the combined diagnostic utility of the panel including APOB, APOC1, LBP, VCAM1, FBLN1, and FCN2 in CAD. By leave-one-out (LOO) cross-validation, ELISA-based ROC analyses of combined quantitation of APOB, APOC1, LBP, VCAM1, FBLN1, and FCN2 showing promising for the detection of increased CAD risk in stroke subjects (PANEL = APOB + APOC1 + LBP + VCAM1 + FBLN1 + FCN2). The AUC of panel **(A)** was 1, and the panel exhibited a higher sensitivity (100%) and specificity (100%) than the six proteins individually **(B)**.

TABLE 2 | Statistics of ROC curves.

Variables	AUC	Cutoff	*P*-value	Sensitivity	Specificity	95% confidence interval	
						Lower bound	Upper bound
PANEL	1	0.500	0.000007	1	1	1	1
APOB	0.954	0.752	0.000046	0.800	0.923	0.886	1
APOC-I	0.964	0.4643	0.000031	0.933	0.923	0.898	1
LBP	0.933	0.469	0.000099	0.867	0.846	0.844	1
VCAM1	0.931	0.573	0.000109	0.867	0.923	0.838	1
FBLN1	0.995	0.483	0.000009	0.933	0.923	0.978	1
FCN2	0.990	0.701	0.000011	0.933	0.923	0.963	1

ROC, receiver operating characteristic; AUC, area under the curve; APOB, apolipoprotein B; APOC-1, apolipoprotein C-I; LBP, lipopolysaccharide-binding protein; VCAM1, vascular cell adhesion molecule 1; FBLN1, fibulin-1; FCN2, ficolin-2; PANEL, APOB + APOC1 + LBP + VCAM1 + FBLN1 + FCN2.

Inflammatory Response

The complement and coagulation cascade were identified as a significantly altered pathway by KEGG analysis. Gene ontology annotation analysis demonstrated that the inflammatory response was identified as significantly altered ($P < 0.01$). Consistent with our findings, substantial evidence supported the view that dysfunction of the inflammatory response was well established in CAD. In the prospective multicenter CADISP (cervical artery dissection and ischemic stroke patients) trial, acute CAD was associated with particularly high white blood cell counts (4). An elevated leucocyte count was also described by Forster et al. (16) in a retrospective case control study comparing patients with CAD and traumatic CAD. Imaging studies have revealed signs of local inflammation around the affected vessels of patients with CAD, but not in those with traumatic CAD (17). However, the mechanism underlying the association between inflammation and occurrence of CAD remains speculative. It is proposed that inflammation in addition to constitutional connective tissue defects may increase the risk of arterial wall disintegration in CAD (4).

Lipopolysaccharide-binding protein, as a type I acute phase response protein, was considered as a marker for infections in stroke-associated pneumonia but with no data presented on microbiological findings (18). The present study demonstrated for the first time significantly increased levels of LBP in CAD compared to non-CAD ischemic stroke subjects, which were consistent with infection and inflammation as an important risk factor causing a transient arteriopathy linked to spontaneous CAD (19). Furthermore, we speculated that significantly increased LBP in CAD revealed the underlying imbalance of the immune system and increased the risk of infection in CAD subjects. However, the mechanism needs further study.

Vascular cell adhesion molecule 1, as a proinflammatory marker, plays a crucial role in the initiation of inflammatory mechanisms soon after cerebral damage and promotes migration of immune cells across the blood–brain barrier within the cerebral parenchyma (20). Vascular cell adhesion molecule 1 has been reported to be increased early after stroke (21) and may influence peripheral mechanisms such as cell adhesion–regulated processes and may lower nitric oxide (NO) release in the vessels, thereby contributing to decreased vascular endothelial function. Furthermore, VCAM1 has also been found to be associated with impaired endothelial dependent dilation in cerebral artery vasoreactivity, early after stroke with poor prognoses (22). In

our study, the early increased level of VCAM1 may indicate an enhanced inflammatory state and more serious damage to endothelial function in CAD.

Human FCN2 is synthesized in the liver and secreted into the bloodstream where it is one of the few molecules known to activate the lectin pathway of complement (23) and may link complement to the coagulation system (24). Watanabe et al., have observed that serum levels of FCN2 in patients with systemic lupus erythematosus were significantly lower when compared to healthy controls, which is associated with thrombocytopenia (25). Although clinical research involving FCN2 is still in its infancy, evidence is emerging that suggests insufficiency of FCN2 may increase susceptibility to respiratory infections. In the present work, FCN2 was found to be upregulated in CAD subjects, demonstrating more susceptible to infection in the pathophysiology of CAD.

Blood Coagulation

Gene ontology annotation analysis showed that coagulation-related components (blood microparticles and platelet alpha granule) were identified as significantly altered ($P < 0.01$). Inflammation may also impact on the coagulation system resulting in a hypercoagulable state, which may be responsible for ischemic events. Specifically, the physiological crosstalk between inflammation and coagulation may facilitate the formation of arterial and venous thrombosis, not only in the microcirculation, but also in larger vessels, a process that may be further aggravated by a preexisting or newly occurring vessel wall damage, as is the case in CAD (26). Pelz et al. (27) found evidence for a hypercoagulable state in patients with CAD as indicated by a shortened activated partial thromboplastin time, which was associated with a trend to an increased leucocyte count at the same time. Furthermore, the results strengthened the hypothesis that inflammation critically impacts on the occurrence of CAD and linked this condition to a marked effect on the coagulation system.

Fibulin-1, as an ECM protein, was found to be significantly upregulated in CAD as compared to stroke subjects in this study. In addition, FBLN1 has been found to bind to the plasma protein fibrinogen (FG) and to incorporate into fibrin clots formed *in vitro* and *in vivo* (28). It is possible that following vascular injury FBLN1 may be present in the extracellular matrix of the vessel wall and therefore may interact with plasma FG and promote platelet adhesion, leading to the formation of a platelet plug, and could therefore serve as a participant in the earliest events of thrombus formation (29). Mohamed et al. (30) showed that downregulation of FBLN1 may weaken extracellular components in the aorta and/or interfere with the transmission of cellular signals and eventually cause acute aortic dissection. Taken together, our findings supported the hypothesis that increased expression of FBLN1 may represent more serious blood vessel damage and a hypercoagulable state, which would be more likely to cause a more severe ischemic event in CAD subjects.

Lipid Metabolism

Several studies have demonstrated that perturbation of lipid metabolism may be involved in the pathophysiology of both CAD (31) and stroke (32). Our bioinformatics analysis showed that lipid-related components (plasma lipoprotein particle, lipoprotein particle, protein–lipid complex) were identified as significantly altered ($P < 0.01$). This study was the first to report that APOB and APOC-I levels were significantly increased in CAD as compared to stroke subjects, indicating that the dysregulation of lipid metabolism may play an important role in the pathophysiology of CAD.

Apolipoprotein B present in very low-density lipoprotein (VLDL), intermediate-density lipoproteins, large buoyant low-density lipoprotein (LDL), and small dense LDL reflects the total number of atherogenic particles and leads to entrapment of these lipoproteins in the arterial wall. Recent reports suggest that the higher value of the APOB/APOA1 ratio, the more cholesterol is likely to be deposited in the arterial wall, thereby enhancing atherogenesis and increasing vascular risk (33). An additional study has supported the clinical utility of oxidized phospholipids-APOB as a biomarker for the prediction of recurrent fatal or nonfatal stroke, which have augmented proinflammatory responses and enhanced uptake of monocytes into the vessel wall (34). Here, the increased expression of APOB in CAD may indicate an enhanced vascular risk and more severe ischemic events.

Apolipoprotein C-I is a secreted plasma protein present in the circulation in association with LDL and VLDL and is produced by the liver. Kolmkova et al. (35) have shown that APOC-I and APOC-I–enriched high-density lipoprotein activated the neutral sphingomyelinase–ceramide signaling pathway, leading to apoptosis in human aortic smooth muscle cells, which may lead to plaque rupture *in vivo*. However, the potential physiological role and clinical significance of APOC-I in stroke have recently emerged. Allard et al. (36) first reported that APOC-I may be the plasma biomarker capable of accurately distinguishing between ischemic and hemorrhagic stroke in a small number of patients. Recent reports have shown that CAD-related infarcts are likely to be large when the vessel occludes and responds poorly to conventional treatment with antithrombotics, anticoagulants, or intravenous thrombolysis (37). In our study, we were the first to report increased APOC-I in CAD subjects, which may accelerate the plaque rupture, leading to a more severe stroke.

Finally, we conducted an LOO cross-validation to determine the predictive value of the panel combined with six proteins. This method enables ROC analysis to be performed even with the small sample sizes used in our study. We found the greatest predictive utility when combining measurements from our six upregulated proteins, resulting in high sensitivity (100%) and specificity (100%). However, the predicted performance had some limitations which were principally due to the small sample size. But the research gives us a hint that the panel of six proteins identified is promising for the detection of increased CAD risk in stroke subjects. We expect that, with further validation and research using a larger sample size, this panel will provide an early sensitive and specific predictor of CAD with stroke and will open a new avenue for the diagnosis of this disease.

Limitations

The present study had some limitations. First, given the relatively small sample size of the study, some confounding effects could

not be controlled, and this raised the risk of chance findings. Furthermore, the diagnostic efficiency of the model was reduced by the small sample size. Research with larger sample sizes and using healthy controls is necessary for a better comparison. Second, the timeline for this study was limited to acute dissection; subacute and chronic dissections were neglected. In future studies, a longer timeline, such as a 3 months' follow-up after acute stroke, should be implemented. Third, CAD subjects singly manifested with local signs (Horner syndrome and cranial nerve palsy), pain (cervical pain and headache), and transient ischemic attack (TIA) should be included for increased model diagnostic power. Furthermore, to elucidate the pathogenesis, subgroup analysis is necessary. In future studies, patients should be subdivided further on the basis of the following: clinical severity assessed with the (NIHSS) score; radiologic severity, based on the number of dissected arteries and luminal changes for each vessel; different therapeutic approaches with respect to strokes; delayed stroke upon CAD; dissection with and without ischemic events; and patients presented with ischemic events and hemorrhagic strokes. Further studies are needed to understand the mechanism(s) underlying CAD and to develop more diagnostically accurate biomarkers for stroke.

CONCLUSION

In this study, 130 differentially expressed proteins were found in serum sampled from CAD and non-CAD ischemic stroke subjects using an iTRAQ-based proteomic approach. Most of these proteins were associated with inflammatory reactions, lipid metabolism, and coagulation cascades, suggesting that these processes were involved in the pathophysiology of CAD. Through ELISA validation, six differentially expressed proteins were found to be significantly upregulated in CAD relative to non-CAD ischemic stroke subjects. The panel containing the six proteins showed a higher sensitivity and specificity for the prediction of CAD. Further investigation of these proteins in a larger cohort of patients is now needed in order to better understand the underlying pathophysiology of CAD.

DATA AVAILABILITY STATEMENT

The raw data supporting the conclusions of this article will be made available by the authors, without undue reservation.

ETHICS STATEMENT

The studies involving human participants were reviewed and approved by The Ethical Committee of Third Military Medical University. The patients/participants provided their written informed consent to participate in this study.

AUTHOR CONTRIBUTIONS

ZZ conceived and designed the research. YY did the statistical analysis and wrote the manuscript. JP made subject recruitment and collected the clinical data. JH collected the blood samples of patients and stored the serum samples. HR and SW performed the ELISA validations. KC made the LC-MS/MS analysis and annotated the functions of differentially expressed proteins. All authors reviewed the manuscript before submission.

FUNDING

This work was supported by National Natural Science Foundation of China (Grant No. 81471194) and the clinical novel technology program of military medicine and injury treatment of Southwest Hospital (SWH2016JSTSYB-23, SWH2016JHJC-03).

ACKNOWLEDGMENTS

Thanks was extended to Hong Yu (Shanghai Shengzi biotechnology Ltd., Co.) for his assistance with bioinformatics analysis. We graciously thank Yujie Lin and Qian Zhou (Shanghai Omicsspace Biotechnology Ltd., Co.) for mass spectrometric analysis. We also thank International Science Editing (http://www.internationalscienceediting.com) for editing this manuscript. All authors are entirely responsible for the scientific content of the paper.

SUPPLEMENTARY MATERIAL

The Supplementary Material for this article can be found online at: https://www.frontiersin.org/articles/10.3389/fneur.2020.00352/full#supplementary-material

REFERENCES

1. Schwartz NE, Vertinsky AT, Hirsch KG, Albers GW. Clinical and radiographic natural history of cervical artery dissections. *J Stroke Cerebrovasc Dis*. (2009) 18:416–23. doi: 10.1016/j.jstrokecerebrovasdis.2008.11.016
2. Arnold M, Kappeler L, Georgiadis D, Berthet K, Keserue B, Bousser MG, et al. Gender differences in spontaneous cervical artery dissection. *Neurol*. (2006) 67:1050–2. doi: 10.1212/01.wnl.0000237341.30854.6a
3. Gallai V, Caso V, Paciaroni M, Cardaioli G, Arning E, Bottiglieri T, et al. Mild hyperhomocyst(e)inemia: a possible risk factor for cervical artery dissection. *Stroke*. (2001) 32:714–8. doi: 10.1161/01.STR.32.3.714
4. Grond-Ginsbach C, Giossi A, Aksay SS, Engelter ST, Lyrer PA, Metso TM, et al. Elevated peripheral leukocyte counts in acute cervical artery dissection. *Eur J Neurol*. (2013) 20:1405–10. doi: 10.1111/ene.12201
5. Zhu Z, Tang W, Ge L, Han X, Dong Q. The value of plasma fibrillin-1 level in patients with spontaneous cerebral artery dissection. *Neurology*. (2018) 90:e732–7. doi: 10.1212/WNL.0000000000005027
6. Traenka C, Disanto G, Seiffge DJ, Gensicke H, Hert L, Grond-Ginsbach C, et al. Serum neurofilament light chain levels are associated with clinical characteristics and outcome in patients with cervical artery dissection. *Cerebrovasc Dis*. (2015) 40:222–7. doi: 10.1159/000440774
7. Guillon B, Peynet J, Bertrand M, Benslamia L, Bousser MG, Tzourio C. Do extracellular matrix-regulating enzymes play a role in cervical artery dissection?. *Cerebrovasc Dis*. (2007) 23:299–303. doi: 10.1159/000098331

8. Pezzini A, Del Zotto E, Archetti S, Negrini R, Bani P, Albertini A, et al. Plasma homocysteine concentration, C677T MTHFR genotype, and 844ins68bp CBS genotype in young adults with spontaneous cervical artery dissection and atherothrombotic stroke. *Stroke*. (2002) 33:664–9. doi: 10.1161/hs0302.103625
9. Rubinstein SM, Peerdeman SM, van Tulder MW, Riphagen I, Haldeman S. A systematic review of the risk factors for cervical artery dissection. *Stroke*. (2005) 36:1575–80. doi: 10.1161/01.STR.0000169919.73219.30
10. Huang JT, Leweke FM, Oxley D, Wang L, Harris N, Koethe D, et al. Disease biomarkers in cerebrospinal fluid of patients with first-onset psychosis. *PLoS Med*. (2006) 3:e428. doi: 10.1371/journal.pmed.0030428
11. Engelter ST, Traenka C, Von Hessling A, Lyrer PA. Diagnosis and treatment of cervical artery dissection. *Neurol Clin*. (2015) 33:421–41. doi: 10.1016/j.ncl.2014.12.002
12. Yu G, Wang LG, Han Y, He QY. Cluster Profiler: An R package for comparing biological themes among gene clusters. *OMICS: J Integr Biol*. (2012) 16:284–7. doi: 10.1089/omi.2011.0118
13. Luo W, Brouwer C. Pathview: an R/Bioconductor package for pathway-based data integration and visualization. *Bioinformatics*. (2013) 29:1830–1. doi: 10.1093/bioinformatics/btt285
14. Fischer R, Trudgian DC, Wright C, Thomas G, Bradbury LA, Brown MA, et al. Discovery of candidate serum proteomic and metabolomic biomarkers in Ankylosing Spondylitis. *Mol Cell Proteomics*. (2012) 11:M111013904. doi: 10.1074/mcp.M111.013904
15. Moulder R, Lönnberg T, Elo LL, Filén JJ, Rainio E, Corthals G, et al. Quantitative proteomics analysis of the nuclear fraction of human CD4+ cells in the early phases of IL-4-induced Th2 differentiation. *Mol Cell Proteomics*. (2010) 9:1937–53. doi: 10.1074/mcp.M900483-MCP200
16. Forster K, Poppert H, Conrad B, Sander D. Elevated inflammatory laboratory parameters in spontaneous cervical artery dissection as compared to traumatic dissection: a retrospective case-control study. *J. Neurol*. (2006) 253:741–5. doi: 10.1007/s00415-006-0109-z
17. Pfefferkorn T, Saam T, Rominger A, Habs M, Gerdes LA, Schmidt C, et al. Vessel wall inflammation in spontaneous cervical artery dissection: a prospective, observational positron emission tomography, computed tomography, and magnetic resonance imaging study. *Stroke*. (2011) 42:1563–8. doi: 10.1161/STROKEAHA.110.599548
18. Hannawi Y, Hannawi B, Rao CP, Suarez JI, Bershad EM. Stroke-associated pneumonia: major advances and obstacles. *Cerebrovasc*. (2013) 35:430–43. doi: 10.1159/000350199
19. Schievink W, Mokri B, O'Fallon WM. Recurrent spontaneous cervical-artery dissection. *N Engl J Med*. (1994) 330:393–7. doi: 10.1056/NEJM199402103300604
20. Wang HC, Lin WC, Lin YJ, Rau CS, Lee TH, Chang WN, et al. The association between serum adhesion molecules and outcome in acute spontaneous intracerebral hemorrhage. *Crit Care*. (2011) 15:R284. doi: 10.1186/cc10568
21. Billinger SA, Sisante JV, Mattlage AE, Alqahtani AS, Abraham MG, Rymer MM, et al. The relationship of pro-inflammatory markers to vascular endothelial function after acute stroke. *Int J Neurosci*. (2017) 27, 486–492. doi: 10.1080/00207454.2016.1198344
22. Tchalla AE, Wellenius GA, Travison TG, Gagnon M, Iloputaife I, Dantoine T, et al. Circulating vascular cell adhesion molecule-1 is associated with cerebral blood flow dysregulation, mobility impairment, and falls in older adults. *Hypertension*. (2015) 66:340–6. doi: 10.1161/HYPERTENSIONAHA.115.05180
23. Matsushita M, Endo Y, Fujita T. Cutting edge: complement-activating complex of ficolin and mannose binding lectin-associated serine protease. *J Immunol*. (2000) 164:2281–4. doi: 10.4049/jimmunol.164.5.2281
24. Presanis JS, Hajela K, Ambrus G, Gál P, Sim RB. Differential substrate and inhibitor profiles for human MASP-1 and MASP-2. *Mol Immunol*. (2004) 40:921–9. doi: 10.1016/j.molimm.2003.10.013
25. Watanabe H, Saito R, Asano T, Sato S, Iwadate H, Kobayashi H, et al. Serum L-ficolin levels in patients with systemic lupus erythematosus. *Mod Rheumatol*. (2012) 22:899–902. doi: 10.3109/s10165-012-0616-y
26. Foley JH, Conway E. Cross talk pathways between coagulation and inflammation. *Circ Res*. (2016) 118:1392–408. doi: 10.1161/CIRCRESAHA.116.306853
27. Pelz JO, Harms K, Metze M, Michalski D. Spontaneous cervical artery dissection is accompanied by a hypercoagulable state and simultaneous inflammatory condition. *J Neurol*. (2018) 265:308–14. doi: 10.1007/s00415-017-8696-4
28. Tran H, Tanaka A, Litvinovich SV, Medved LV, Haudenschild CC, Argraves WS. The interaction of fibulin-1 with fibrinogen: a potential role in hemostasis and thrombosis. *J Biol Chem*. (1995) 270:19458–64. doi: 10.1074/jbc.270.33.19458
29. Godyna S, Diaz-Ricart M, Argraves WS. Fibulin-1 mediates platelet adhesion via a bridge of fibrinogen. *Blood*. (1996) 88:2569–77. doi: 10.1182/blood.V88.7.2569.bloodjournal8872569
30. Mohamed SA, Sievers HH, Hanke T, Richardt D, Schmidtke C, Charitos EI, et al. Pathway analysis of differentially expressed genes in patients with acute aortic dissection. *Biomark Insights*. (2009) 6:81–90. doi: 10.4137/BMI.S2530
31. Putaala J, Strbian D, Mustanoja S, Haapaniemi E, Kaste M, Tatlisumak T. Functional outcome in young adult ischemic stroke: impact of lipoproteins. *Acta Neurol Scand*. (2013) 12:761–9. doi: 10.1111/j.1600-0404.2012.01683.x
32. Lorenzano S. Oxidized low-density lipoprotein A plasma biomarker predicting stroke recurrence. *Neurology*. (2018) 91:443. doi: 10.1212/WNL.0000000000006127
33. Tian YF, Zhou YP, Zhong CK, Buren B, Xu T, Li HM, et al. C-reactive protein level, apolipoprotein B-to-apolipoprotein A-1 ratio, and risks of ischemic stroke and coronary heart disease among inner mongolians in China. *Biomed Environ Sci*. (2016) 29:467–74. doi: 10.3967/bes2016.062
34. Byun YS, Yang X, Bao W, DeMicco D, Laskey R, Witztum JL, et al. Oxidized phospholipids on apolipoprotein B-100 an recurrent ischemic events following stroke or transient ischemic attack. *J Am Coll Cardiol*. (2017) 69:147–58. doi: 10.1016/j.jacc.2016.10.057
35. Kolmkova A, Kwiterovich P, Vlaupovic P, Virgil D, Alaupovic P, Knight-Gibson C, et al. Apolipoprotein C-I induces apoptosis in human aortic smooth muscle cells via recruiting neutral sphingomyelinase. *Arterioscler Thromb Vasc Biol*. (2004) 24:264–9. doi: 10.1161/01.ATV.0000112036.72200.ac
36. Allard L, Lescuyer P, Burgess J, Leung KY, Ward M, Walter N, et al. ApoC-I and ApoC-III as potential plasmatic markers to distinguish between ischemic and hemorrhagic stroke. *Proteomics*. (2004) 4:42242–51. doi: 10.1002/pmic.200300809
37. Putaala J, Metso TM, Metso AJ, Mäkelä E, Haapaniemi E, Salonen O, et al. Thrombolysis in young adults with ischemic stroke. *Stroke*. (2009) 40:2085–91. doi: 10.1161/STROKEAHA.108.541185

Conflict of Interest: The authors declare that the research was conducted in the absence of any commercial or financial relationships that could be construed as a potential conflict of interest.

Copyright © 2020 Yang, Peng, Wang, Huang, Ran, Chen and Zhou. This is an open-access article distributed under the terms of the Creative Commons Attribution License (CC BY). The use, distribution or reproduction in other forums is permitted, provided the original author(s) and the copyright owner(s) are credited and that the original publication in this journal is cited, in accordance with accepted academic practice. No use, distribution or reproduction is permitted which does not comply with these terms.

frontiers in Neuroscience

ORIGINAL RESEARCH
published: 19 May 2020
doi: 10.3389/fnins.2020.00335

New PAR1 Agonist Peptide Demonstrates Protective Action in a Mouse Model of Photothrombosis-Induced Brain Ischemia

*Maksim Galkov[1,2], Ekaterina Kiseleva[2,3], Mikhail Gulyaev[4], Maria Sidorova[5] and Liubov Gorbacheva[1,2]**

[1] Faculty of Biology, Lomonosov Moscow State University, Moscow, Russia, [2] Electrophysiology Laboratory, Translational Medicine Institute, Pirogov Russian National Research Medical University, Moscow, Russia, [3] Department of Cell Biology, Koltzov Institute of Developmental Biology of Russian Academy of Sciences, Moscow, Russia, [4] Faculty of Fundamental Medicine, Lomonosov Moscow State University, Moscow, Russia, [5] Laboratory of Peptide Synthesis, Institute of Experimental Cardiology, National Medical Research Center for Cardiology of Russian Ministry of Health, Moscow, Russia

OPEN ACCESS

Edited by:
Emmanuel Pinteaux, University of Manchester, United Kingdom

Reviewed by:
Xu Cui, Henry Ford Hospital, United States
Veronica Perez de la Cruz, Instituto Nacional de Neurología y Neurocirugía Manuel Velasco Suárez, Mexico

***Correspondence:**
Liubov Gorbacheva
LyubovGorbacheva@gmail.com; gorbi67@mail.ru

Specialty section:
This article was submitted to Neurodegeneration, a section of the journal Frontiers in Neuroscience

Received: *24 December 2019*
Accepted: *20 March 2020*
Published: *19 May 2020*

Citation:
Galkov M, Kiseleva E, Gulyaev M, Sidorova M and Gorbacheva L (2020) New PAR1 Agonist Peptide Demonstrates Protective Action in a Mouse Model of Photothrombosis-Induced Brain Ischemia. Front. Neurosci. 14:335. doi: 10.3389/fnins.2020.00335

Protease-activated receptors (PARs) are involved not only in hemostasis but also in the development of ischemic brain injury. In the present work, we examined *in vivo* effects of a new peptide (AP9) composing Asn^{47}-$Phen^{55}$ of PAR1 "tethered ligand" generated by activated protein C. We chose a mouse model of photothrombosis (PT)-induced ischemia to assess AP9 effects *in vivo*. To reveal the molecular mechanism of AP9 action, mice lacking β-arrestin-2 were used. AP9 was injected intravenously once 10 min before PT at doses of 0.2, 2, or 20 mg/kg, or twice, that is, 10 min before and 1 h after PT at a dose of 20 mg/kg. Lesion volume was measured by magnetic resonance imaging and staining of brain sections with tetrazolium salt. Neurologic deficit was estimated using the cylinder and the grid-walk tests. Blood–brain barrier (BBB) disruption was assessed by Evans blue dye extraction. Eosin-hematoxylin staining and immunohistochemical staining were applied to evaluate the number of undamaged neurons and activated glial cells in the penumbra. A single administration of AP9 (20 mg/kg), as well as its two injections (20 mg/kg), decreased brain lesion volume. A double administration of AP9 also reduced BBB disruption and neurological deficit in mice. We did not observe the protective effect of AP9 in mice lacking β-arrestin-2 after PT. Thus, we demonstrated for the first time protective properties of a PAR1 agonist peptide, AP9, *in vivo*. β-Arrestin-2 was required for the protective action of AP9 in PT-induced brain ischemia.

Keywords: protease-activated receptor 1 (PAR1), PAR1 agonist peptide, protein C, β-arrestin-2, photothrombosis-induced focal ischemia

INTRODUCTION

Vessel wall damage and hemostatic balance disturbances lead to changes in tissue blood flow and, as a result, to the development of ischemic conditions (Khoshnam et al., 2017). Activation of endothelial cells is a key factor for initiating thrombus formation. A wide range of receptors, which regulate the state of the endothelium and platelets, is involved not only in hemostasis but also in the development of ischemic brain injury. Protease-activated receptors (PARs) are ones of these receptors. PARs belong to the family of G-protein-coupled receptors (GPCRs) and regulate cellular and physiological processes in normal and pathological conditions (Ossovskaya and Bunnett, 2004; Coughlin, 2005).

The mechanism of PAR activation was revealed and thoroughly studied for PAR1 (Vu et al., 1991) and other PAR subtypes (Coughlin, 2005). Proteases cleave the receptor at the specific site of the exodomain that results in formation of a novel N-terminus ("tethered ligand"). This N-terminal sequence interacts with the second extracellular loop and activates the receptor (Ossovskaya and Bunnett, 2004; Coughlin, 2005). It was shown that serine proteases of the blood coagulation system, thrombin and activated protein C (APC), exert multidirectional effects during excitotoxicity and neuroinflammation via PAR1 activation (Suo et al., 2004; Gorbacheva et al., 2008; Griffin et al., 2015).

Thrombin demonstrates procoagulant effects and increases expression of proinflammatory and proapoptotic factors in the nervous tissue (Suo et al., 2004; Coughlin, 2005). APC, in contrast to thrombin, protects neurons and endothelium, stabilizes the endothelial barrier, and controls cytokine gene expression in brain injury (Riewald and Ruf, 2005; Minhas et al., 2009; Zlokovic and Griffin, 2011; Griffin et al., 2015; Roy et al., 2016). Earlier we have shown PAR1-dependent antiapoptotic effects of APC on cultivated hippocampal neurons during glutamate excitotoxicity (Gorbacheva et al., 2009, 2010; Savinkova et al., 2014).

It was found that PAR1 activation initiates multidirectional pathways through both G-proteins (Traynelis and Trejo, 2007) and β-arrestins in cultured endotheliocytes (Soh and Trejo, 2011; Roy et al., 2016). The "molecular ensemble" around the receptor and its pattern of phosphorylation by GPCR kinases provide this signal dualism called "biased agonism" (Premont and Gainetdinov, 2007; Reiter et al., 2012). Cytoprotective signaling by APC involves a novel cleavage of PAR1 N-terminal domain at Arg^{46}–Asn^{47} differing from that of thrombin (Arg^{41}–Ser^{42}) and β-arrestin-2-dependent pathway activation (Soh and Trejo, 2011; Roy et al., 2016). β-arrestin recruitment and activation of the Dvl-2 scaffold initiate APC-induced cytoprotection mediated by Rac1. In this case, activated Dvl-2 may provide a platform that recruits effector proteins, such as Rac1-specific guanine nucleotide exchange factors to promote Rac1 activation (Soh and Trejo, 2011). For APC-induced β-arrestin-2-dependent signaling, the colocalization of PAR1 with the endothelial protein C receptor and thrombomodulin in caveolae is required (Griffin et al., 2015; Roy et al., 2016).

The unique mechanism of PAR activation makes it possible to apply peptide analogs of the "tethered ligand" as receptor agonists (Mao et al., 2008; Ramachandran and Hollenberg, 2008; Mosnier et al., 2013). In the present work, we used a nine-amino-acid peptide (AP9, NPNDKYEPF-NH_2), which mimics PAR1 N-terminus beginning at residue Asn^{47} and generated by APC cleavage at Arg^{46}. The protective effects of AP9 via PAR1 activation were confirmed *in vitro* using primary cultures of neurons, mast cells (Savinkova et al., 2014; Babkina et al., 2016), and human keratinocytes (Kiseleva et al., 2014). Moreover, it was previously shown that another PAR1 peptide agonist, TR47, which also formed after PAR1 cleavage at Arg^{46}, demonstrates the general activity profile of APC (Mosnier et al., 2013). Taken together, these data make it possible to hypothesize that AP9 will demonstrate APC-like protective properties, which are expected to be β-arrestin-2-dependent, in ischemic conditions *in vivo*. To test that hypothesis, we used a model of photothrombosis-induced (PT-induced) focal brain ischemia (Lee et al., 2007; Galkov et al., 2020) and different schemes of AP9 intravenous administration.

PT model based on the generation of reactive oxygen species under the action of light induces endothelium damage and triggers thrombogenesis (Lee et al., 2007). PT-induced pathological processes are similar to endogenously formed ones (Kim et al., 2001; Schroeter et al., 2002; Li et al., 2014; Kang et al., 2015; Cotrina et al., 2017). Moreover, PT-induced focal ischemia is characterized by low invasiveness and high reproducibility of the damage volume (Fluri et al., 2015), as well as the precise localization of lesion area in the cerebral cortex (Harrison et al., 2013).

In the present work, we examined the potential effects of PAR1 agonist peptide, AP9, in the mouse model of PT-induced brain ischemia. The role of β-arrestin-2-signaling in intracellular pathways triggered by AP9 was also revealed.

MATERIALS AND METHODS

Animals

Male mice weighing 25–30 g and aged 2.5–3 months were used in the study. Animals were obtained from the nursery for laboratory animals of Shemyakin-Ovchinnikov Institute of Bioorganic Chemistry (Russian Academy of Sciences, Moscow region) and kept under standard conditions (temperature: 22°C, light cycle: 12 h) with unlimited access to water and food. We used BALB/c mice, β-arrestin-2-knockout mice (β-arrestin-2-/- group) kindly provided by Prof. R.R. Gaynetdinov, and animals of genetically related C57BL/6 strain (wild type) (Bohn et al., 1999) with full β-arrestin-2 expression. The total number of animals used was 177 (141 BALB/c mice, 20 C57BL/6 mice, and 16 knockout animals). Six BALB/c mice and one C57BL/6 mouse died during PT induction.

All animals of each strain were randomized into several groups (control groups and groups treated with AP9 at different doses). The randomization scheme was generated using the website Randomization.com[1]. The number of animals in each experimental group (n) is indicated in section "Results" ($n = 4$–10). All experiments were performed according to the

[1]http://www.randomization.com

Directive 2010/63/EU of the European Parliament and the Council of the European Union. Our experimental protocols were approved by the Bioethics Committee of Lomonosov Moscow State University (protocol no. 2018-10-25-93-0-3). All measurements were carried out in a blinded manner. A researcher did not know which group the animals belonged to during the processing of images and video records, as well as during Evans blue dye extraction.

Mouse Genotyping

Modification of the β-*arrestin-2* gene in mice carried out by homologous recombination (Bohn et al., 1999) was confirmed by polymerase chain reaction (PCR). Genomic DNA was isolated from lysates of tail fragments of wild-type and β-arrestin-2-knockout mice by an Extract DNA kit (Eurogen, Russia). PCR was performed using Taq DNA polymerase and standard set of reagents (Thermo Fisher Scientific, United States). During PCR, three primers were used (Eurogen, Russia): primers flanking the insertion site of the genetic construct (forward 5'-GATCAAAGCCCTCGATGATC-3' and reverse 5'-ACAGGGTCCACTTTGTCCA-3'), as well as the primer complementary to donor DNA sequence in the β-*arrestin-2* gene (forward 5'-GCTAAAGCGCATGCTCCAGA-3'). PCR products were separated on a 2% agarose gel with the addition of ethidium bromide. DNA ladder NL002 (Eurogen, Russia) was used as markers; visualization was performed using UV light in a transilluminator. A fragment of 400bp in length indicated the presence of a knockout allele, a 600-bp fragment indicated a wild-type allele. Animals homozygous for the inactivated allele were selected in the experiment.

Western Blotting

β-Arrestin-2 Expression Level

Overanesthetized gene knockout and wild-type animals were transcardially perfused with heparinized saline (40 units/ml). Fragments of the cerebral cortex were isolated on ice and lysed in RIPA buffer and protease inhibitors (Sigma-Aldrich, United States). Samples containing 20 μg of protein were separated by 10% SDS-PAGE, transferred to nitrocellulose membranes, and blocked with 5% skim milk in TBS-Tween 20 (0.05%) for 1 h. The blot was developed by incubation with antibodies against β-arrestin-2 (1:1,000; ab206972, Abcam, United Kingdom) and β-actin (1:1,000; ab8227, Abcam, United Kingdom) overnight at 4°C, followed by incubation with horseradish peroxidase-conjugated anti-rabbit IgG antibodies (1:3,000; sc-2357, Santa Cruz Biotechnology, United States) for 1 h at room temperature. The presence of the target proteins on the blots was recorded using chemiluminescent ECL kit (Thermo Fisher Scientific, United States) and ChemiDoc MP Imaging System (Bio-Rad Laboratories, United States).

GFAP Expression Level

Overanesthetized control and AP9-treated mice were transcardially perfused 96 h after PT. After decapitation, the brain was isolated on ice, the cortex was separated, and the damaged brain tissue in the ipsilateral hemisphere (IH), as well as in the contralateral hemisphere (CH), was isolated by a circular knife 4 mm in diameter. Seventy micrograms of protein was applied into one gel pocket. Western blotting was carried out as described above. Antibodies against GFAP (1:5,000; ab7260, Abcam, United Kingdom), GAPDH (1:5,000; ab181603, Abcam, United Kingdom), and horseradish peroxidase-conjugated anti-rabbit IgG antibodies (1:3,000; sc-2357, Santa Cruz Biotechnology, United States) were used. Quantitative image processing was performed using the Image Lab software (United States). The data were presented as a relative GFAP level taken in CH for 1.

Induction of Ischemic Stroke

Ischemia was induced by photothrombosis (Lee et al., 2007; Galkov et al., 2020). In brief, the mixture of Zoletil 100 (Virbac Sante Animale, France) and Xyla (Interchemie werken "De Adelaar" B.V., Netherlands) at doses of 35 and 3.5 mg/kg (i.p.), respectively, was chosen for anesthesia. Rose Bengal dye (0.15%; Sigma-Aldrich, United States) was injected through a catheter placed into the jugular vein of animals at a dose of 10 mg/kg. An area of 3 mm in diameter localized with the help of a light-tight mask in the sensorimotor area of the cortex of the left hemisphere (2.2 mm lateral to the midline with the epicenter at *bregma*, Franklin and Paxinos, 2001) was illuminated with green laser (λ = 532 nm; Viacho, China) for 5 min. Illuminance on the skull surface was 55–60 lx (Galkov et al., 2020). Mice were sacrificed by an overdose of anesthesia 24 or 96 h after PT.

Previously, we tested the ischemic model and showed that there was no tissue damage in sham-operated mice (administration of saline instead of Rose Bengal dye) according to MRI and 2,3,5-triphenyltetrazolium chloride (TTC) staining data (**Supplementary Figures 1A,B**). We also showed that there was no Evans blue dye leakage in the IH of sham-operated animals (**Supplementary Figure 1C**).

Assessment of Neurological Status

The cylinder and the grid-walk tests were performed before PT induction and for 4 days after it according to the standard protocol (Baskin et al., 2003). The number of cases, when the mouse forelimb contralateral to the damaged hemisphere went through grid holes (stepping errors), and the number of steps performed by that limb were video registered for 5 min. The animals, which performed less than 100 steps, were excluded from the experiment. Sensorimotor deficit in the cylinder test was calculated according to the following formula: asymmetry index = $(t_{after}/t_{before}) \times 100\%$, where t_{after} and t_{before} were the relative contact time of the fore contralateral limb (the contact time of the ipsilateral limb was taken as 100%) after and before PT, respectively. We processed not less than 10 explorations of cylinder walls by each animal in the video records.

Measurement of Ischemic Damage Volume

Lesion volume was assessed using MRI and staining of brain sections with TTC. MRI studies were performed 24 and 96 h after PT on a 7.05-T MR scanner BioSpec 70/30 USR (Bruker, Germany) equipped with fast gradients (105 mT/m/ms

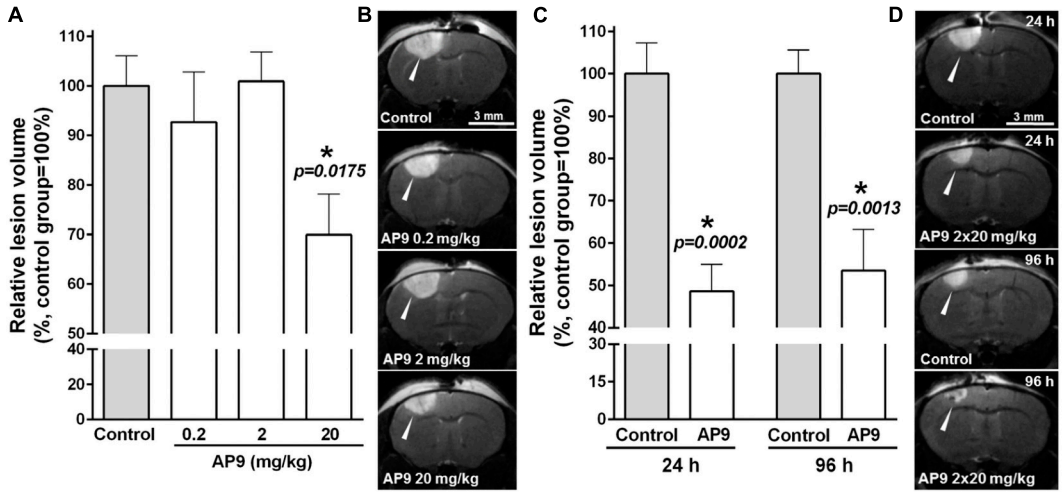

FIGURE 1 | AP9 effects on brain lesion volume after photothrombosis. **(A,B)** A single administration of AP9 at doses of 0.2, 2, and 20 mg/kg: **(A)** relative volume of ischemic damage (one-way ANOVA with Dunnett's correction for multiple comparisons) and **(B)** representative MR images at the level of *bregma* (damaged areas are marked with triangles) 24 h post thrombosis. **(C,D)** A double administration of AP9 at a dose of 20 mg/kg: **(C)** relative volume of ischemic damage (unpaired *t*-test) and **(D)** representative MR images at the level of *bregma* (damaged areas are marked with triangles) 24 and 96 h post thrombosis (*: as compared to the control group).

slew rate). We obtained T_2-weighted MR images using the 2D RARE method with the following scanning parameters: TR/Teeff = 3,000/50 ms; number of slices: 16; slice thickness: 0.4 mm; rare-factor: 4; in-plane resolution: 100 × 100 m; total acquisition time: 9 min 00 s. To measure lesion volume using TTC staining, the animals were decapitated 24 h after thrombosis and the brain was removed. The damage volume was assessed according to the standard protocol as described previously (Galkov et al., 2020).

Digital images were processed in the ImageJ software (NIH, United States). The damage volume was calculated considering an increase in IH size as a result of edema compared with CH (Pialat et al., 2007). Data were presented as relative lesion volume. That parameter in control mice was set as 100%.

Measurement of Blood–Brain Barrier Permeability

Evans blue dye (Sigma-Aldrich, United States) was injected intravenously through a catheter immediately after laser irradiation (80 mg/kg, 2.2% solution). Mice were transcardially perfused with heparinized saline (40 units/ml) 24 h after PT induction. To assess blood–brain barrier (BBB) permeability, dye extraction and determination of its content in both hemispheres were performed as previously described (Kim et al., 2001). The data were expressed as relative Evans blue content in IH. That parameter in CH was taken as 100%.

Tissue Processing and Histological Analysis

Overanesthetized animals were transcardially perfused with 0.1 M phosphate buffer saline (PBS) and 10% formalin 24 or 96 h after PT induction. For immunohistochemistry, the brain was removed, postfixed for 24 h, washed in PBS, and sequentially incubated in 10, 20, and 30% sucrose at room temperature. Then the brain was embedded in an OCT embedding matrix (CellPath, United Kingdom), frozen, and stored at −80°C. For hematoxylin-eosin staining, the brain was removed, fixed in 10% neutral-buffered formalin for 24 h, embedded in paraffin, and cut into 5-μm sections that were stained.

For each animal, cell counting was performed in two sections of the central part of the lesion spaced apart from each other by at least 200 μm. The cells were counted in four non-overlapping fields (300 × 220 μm) of each section both in IH and in CH. The fields of view evenly covered the penumbra region and were located at the outer boundary of the ischemic core in the damaged hemisphere. In CH, we chose mirror areas of the cortex for cell counting (Galkov et al., 2020). Images were processed in the ImageJ software; the obtained data were averaged for one animal.

Hematoxylin-Eosin Staining

The proportion of undamaged neurons was evaluated 24 h after thrombosis. The neurons that were not characterized by nuclear pyknosis, karyorrhexis, karyolysis, hyperchromia, swelling, and alteration of normal cell shape (Hu et al., 2002; Song et al., 2012; Galkov et al., 2020) were considered as undamaged cells. The data were presented as a relative number of undamaged neurons in the penumbra (similar indicator in CH was taken as 100%).

Immunohistochemistry

The number of activated glial cells was evaluated 96 h after thrombosis. Coronal cryosections with 15-μm thickness were immunostained with antibodies against GFAP (1:500; ab10062, Abcam, United Kingdom) and Iba-1 (1:500; 019-19741, Wako, Japan). Secondary antibodies were conjugated with fluorophore Alexa Fluor 594 [anti-mouse IgG (1:1,000; R37121) or anti-rabbit

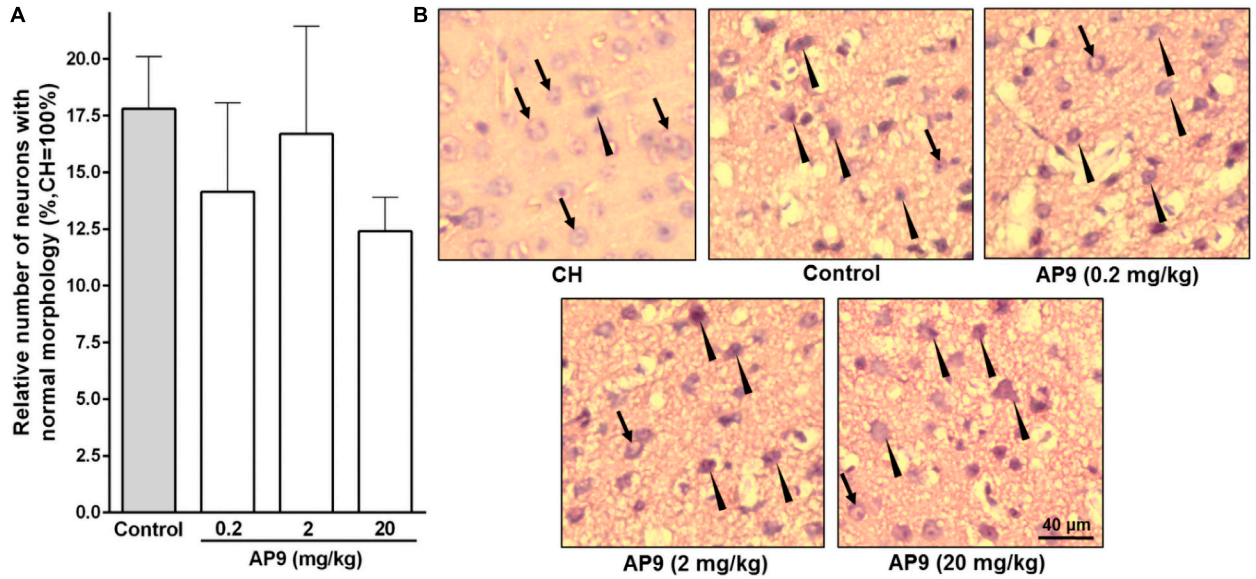

FIGURE 2 | Morphological changes in neurons 24 h post thrombosis in control animals and AP9-treated mice (a single injection, 0.2, 2, and 20 mg/kg). **(A)** Relative number of undamaged neurons in the penumbra (one-way ANOVA). **(B)** Representative micrographs of the penumbral region in IH and a typical micrograph of the mirror region in CH (hematoxylin-eosin staining; arrows indicate cells with normal morphology, triangles indicate cells with signs of damage).

IgG (1:1000; A-11037), Thermo Fisher Scientific, United States]. Cell nuclei were stained with DAPI (Biotium, United States). Images were obtained using confocal laser scanning microscope LSM 710 (Zeiss, Germany). The number of GFAP-positive cells (in two to four layers of cerebral cortex, Cotrina et al., 2017) and Iba-1-positive cells was counted. The data were presented as a relative value taken in CH for 1.

AP9 Structure and Its Administration Scheme

Protease-activated receptor 1 agonist peptide (AP9), consisting of nine amino acids (NPNDKYEPF-NH_2), was synthesized in the Laboratory of Peptide Synthesis of the National Medical Research Center for Cardiology (Moscow) using Fmoc solid-phase synthesis. The homogeneity of the peptide was confirmed by the data of analytical HPLC.

Initially, we used three doses of AP9 (0.2, 2, and 20 mg/kg) dissolved in saline at concentrations of 0.06, 0.6, and 6 mg/ml, respectively. AP9 administration was carried out intravenously 10 min before PT induction (Abdelkarim et al., 2001) through a catheter (as a bolus). In the next experimental series, the injection of AP9 at a dose of 20 mg/kg, which showed maximal efficiency, was performed 10 min before thrombosis and 1 h after PT.

Statistical Analysis

The statistical analysis was performed using the GraphPad Prism 6 software (GraphPad Software Inc., United States). The D'Agostino–Pearson normality test was used to determine correspondence of sample data to normal distribution ($p > 0.1$). The data are expressed as mean ± SEM. The differences between groups were considered as statistically significant at $p < 0.05$. The number of animals (n) and statistical criteria are shown for each experiment. The power analysis performed using the STATISTICA software (StatSoft Inc., United States) showed that the statistical power was more than 0.8 in the case of detecting statistically significant differences between the data groups.

RESULTS

Effect of AP9 on Brain Lesion Volume After Photothrombosis

MRI was used to detect brain damage volume, which directly reflects the severity of ischemia. We found that AP9 effects were dose dependent. AP9 at a dose of 20 mg/kg (a single injection 10 min before PT) caused a statistically significant decrease in lesion volume, which amounted to 69.92 ± 8.21% ($n = 7$) in the AP9-treated group relative to control animals (100.00 ± 6.10%, $n = 7$) 24 h after PT induction. However, we did not observe the effect of AP9 at doses of 0.2 and 2 mg/kg on that parameter, which was 92.70 ± 10.10% ($n = 4$) and 100.90 ± 5.96% ($n = 4$), respectively (**Figures 1A,B**).

The repeated administration of the peptide (i.e., 10 min prior to and 1 h after PT) at a dose of 20 mg/kg enhanced the protective effect of its single injection and led to a statistically significant twofold decrease in lesion volume 24 h after thrombosis. The damage volume was 48.59 ± 6.42% ($n = 7$) in the AP9-treated group and 100.00 ± 7.27% ($n = 7$) in control mice. Moreover, we also evaluated lesion volume 96 h after thrombosis. It was 53.21 ± 9.72% in the AP9-treated group relative to the control value (100.00 ± 5.58%) (**Figures 1C,D**). Thus, MRI results

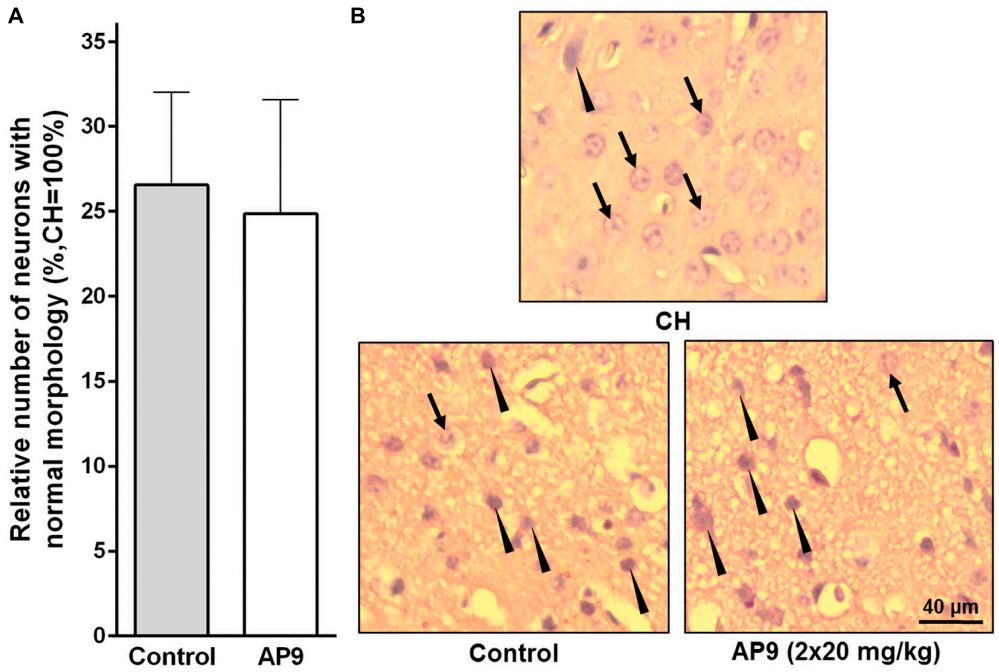

FIGURE 3 | Morphological changes in neurons 24 h post thrombosis in control animals and AP9-treated mice (a double injection, 20 mg/kg). **(A)** Relative number of undamaged neurons in the penumbra (unpaired *t*-test). **(B)** Representative micrographs of the penumbral region in IH and a typical micrograph of the mirror region in CH (hematoxylin-eosin staining; arrows indicate cells with normal morphology, triangles indicate cells with signs of damage).

indicated the preservation of the protective effect of double AP9 administration in the postischemic period.

AP9 Did Not Affect Photothrombosis-Induced Morphological Changes in Neurons

The pathological changes occurring after ischemia induction at the cellular level were assessed by hematoxylin-eosin staining of brain sections. We revealed a significant decrease in the number of neurons without morphological signs of damage in the penumbra compared with the similar areas in CH 24 h after PT (**Figure 2**).

A single injection of the peptide at all three doses used (0.2, 2, and 20 mg/kg) did not affect the proportion of undamaged neurons in IH compared with the control group. These portions were 14.14 ± 3.93% (n = 5), 16.70 ± 4.74% (n = 5), and 12.40 ± 1.50% (n = 7) at doses of 0.2, 2, and 20 mg/kg of AP9, respectively. In the control group of animals, the penumbral region contained 17.80 ± 2.30% (n = 8) neurons with no signs of damage (**Figure 2**).

Two injections (10 min before and 1 h after PT) of AP9 at a dose of 20 mg/kg also did not change the relative number of undamaged neurons in IH. The penumbra was characterized by 26.56 ± 5.47% (n = 5) neurons of normal morphology in the control group of animals and 24.85 ± 6.74% (n = 7) in AP9-treated mice (**Figure 3**).

AP9 Administration Did Not Change Photothrombosis-Induced Glial Cell Activation

According to published data, significant glial cell activation and proliferation are observed in the penumbra 96 h after PT induction. This is supported by enhanced expression of GFAP in activated astrocytes (Li et al., 2014; Cotrina et al., 2017) and Iba-1 in activated microglial cells/macrophages (Li et al., 2014).

In the present study, we also observed a significant increase in the number of activated glial cells in IH compared with CH 96 h after thrombosis induction. However, the effect of AP9 double administration (20 mg/kg, 10 min before and 1 h after thrombosis) on these indices was not found. The relative number of activated astrocytes (GFAP-positive cells) in the penumbra was 8.17 ± 0.51 (n = 5) and 8.55 ± 0.37 (n = 6) in control and AP9-treated animals, respectively (**Figures 4A,B**). For activated microgliocytes/macrophages (Iba-1-positive cells), the values were 6.89 ± 1.04 (control group, n = 5) and 8.52 ± 0.96 (experimental group, n = 6) (**Figures 4C,D**).

Western blotting analysis confirmed that there was no difference between the control group and AP9-treated animals (20 mg/kg, a double administration) in GFAP expression 96 h after photothrombosis. The relative level of GFAP in control animals was 26.74 ± 3.01 in IH and 1.00 ± 0.09 in CH (n = 4). In AP9-treated mice, that parameter was 26.09 ± 2.30 and 1.00 ± 0.10 (n = 4) in IH and CH, respectively (**Supplementary Figure 2**).

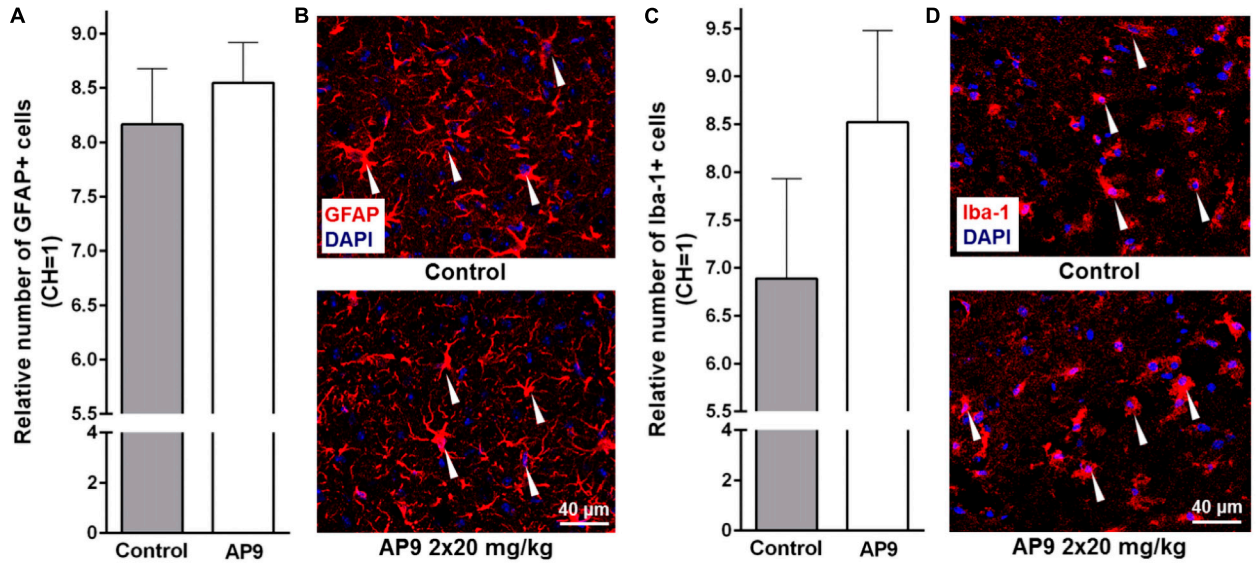

FIGURE 4 | Glial cell activation 96 h post thrombosis in control animals and AP9-treated mice (a double injection, 20 mg/kg). **(A,B)** Immunohistochemistry data on GFAP staining: **(A)** relative number of activated astrocytes (unpaired *t*-test) and **(B)** representative microphotographs of the penumbra. **(C,D)** Immunohistochemistry data on Iba-1 staining: **(C)** relative number of activated microgliocytes/macrophages (unpaired *t*-test) and **(D)** representative microphotographs of the penumbra (GFAP- and Iba-1-positive cells are marked with triangles).

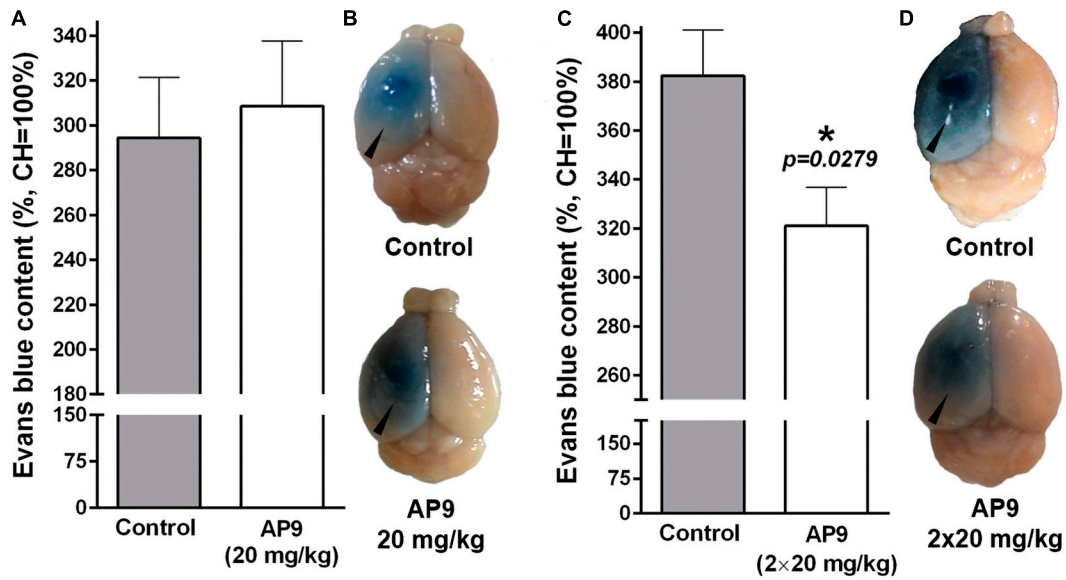

FIGURE 5 | AP9 effects on PT-induced disruption of the BBB 24 h post thrombosis. **(A,B)** A single administration of AP9 (20 mg/kg): **(A)** relative Evans blue dye content in IH (unpaired *t*-test) and **(B)** representative photographs of the whole brains. **(C,D)** A double administration of AP9 (20 mg/kg): **(C)** relative Evans blue dye content in IH (unpaired *t*-test) and **(D)** representative photographs of the whole brains (triangles indicate damaged hemispheres).

Effect of AP9 on BBB Disruption After Thrombosis

Extraction of Evans blue dye is an effective tool to estimate the functional state of the BBB after experimental ischemia (Belayev et al., 1996; Kim et al., 2001). According to published data, the maximal disruption of brain vessel integrity after PT is observed during the first day after its induction (Kang et al., 2015). For this reason, we performed dye extraction from IH and CH 24 h after surgery to assess the potential protective properties of AP9.

A single administration of AP9 at a dose of 20 mg/kg did not affect Evans blue dye content in the damaged hemisphere. That index was 294.40 ± 26.88% (n = 5) and 308.60 ± 28.98% (n = 5) in control and AP9-treated mice, respectively (**Figures 5A,B**). However, a double injection of AP9 (20 mg/kg, 10 min before

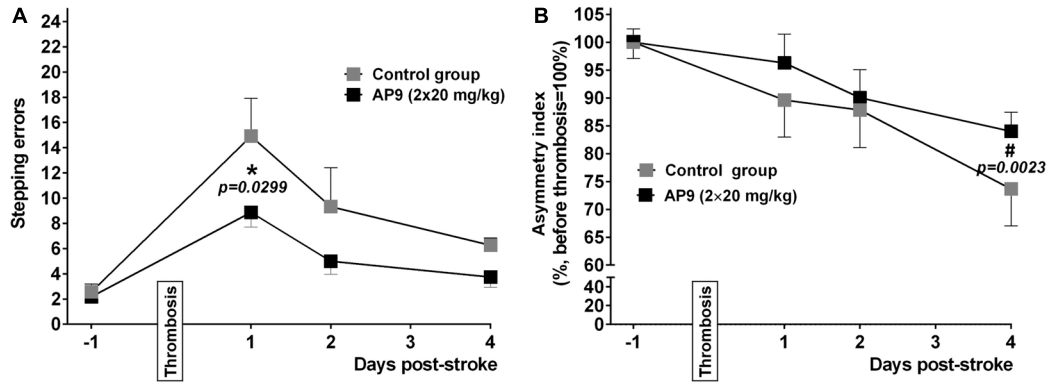

FIGURE 6 | Effects of a double administration of AP9 (20 mg/kg, 10 min before and 1 h after PT) on PT-induced sensorimotor deficit in mice. **(A)** The grid-walk test data. **(B)** The cylinder test data (two-way ANOVA with Šidák correction for multiple comparisons, *: as compared to the corresponding control value, #: as compared to the value before PT).

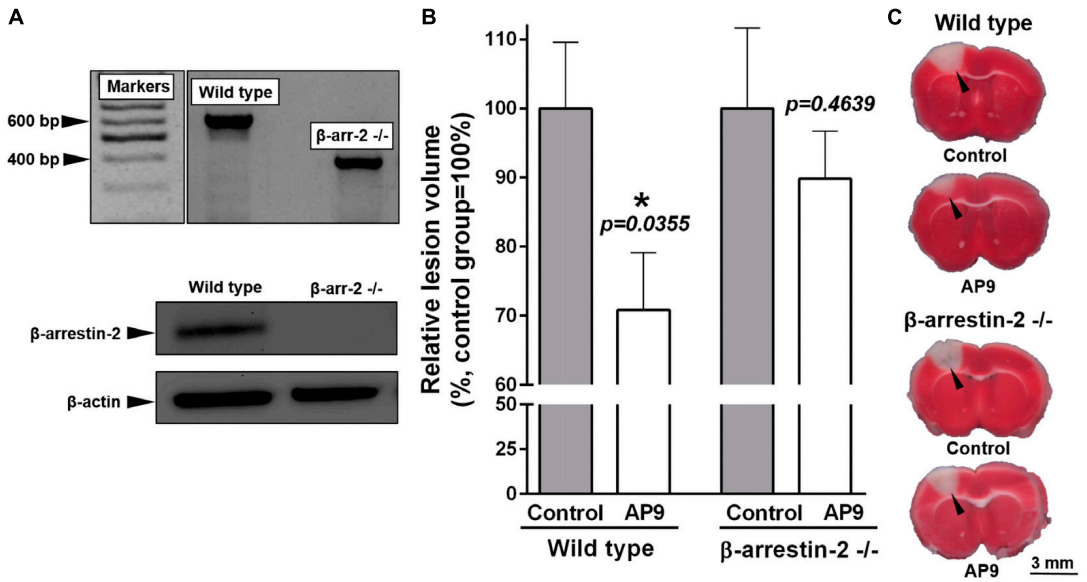

FIGURE 7 | Effect of β-arrestin-2 knockout on AP9 protective action 24 h post thrombosis. **(A)** Confirmation of β-*arrestin-2* gene knockout [results of PCR analysis (above) and western blotting (below)]. **(B)** AP9 (20 mg/kg, a double administration: 10 min before and 1 h after PT) effect on relative lesion volume 24 h after PT in wild-type and gene-knockout mice (unpaired *t*-test for each group of animals). **(C)** Representative images of brain sections at the level of *bregma* (TTC staining; damaged areas are marked with triangles).

and 1 h after thrombosis) demonstrated the protective effect. The relative dye content in IH was 382.40 ± 18.67% (n = 6) in control animals. In mice treated with AP9, this parameter statistically significantly decreased down to 321.10 ± 15.69% (n = 7) (**Figures 5C,D**).

Effect of AP9 on Photothrombosis-Induced Sensorimotor Deficit in Mice

Sensorimotor deficit developing in animals after experimental ischemia is a complex indicator of the severity of this pathology at the level of the whole organism. In the present study, we used the cylinder and the grid-walk tests, which previously showed high efficacy in detecting sensorimotor dysfunction in mice (Baskin et al., 2003; Galkov et al., 2020).

We found that a double injection of AP9 at a dose of 20 mg/kg improved the neurological status of mice in both tests. In the grid-walk test, AP9-treated mice made fewer stepping errors (8.88 ± 1.18 errors/100 steps, n = 9) compared with the control group (14.92 ± 3.00, n = 7, two animals were excluded from the experiment due to the insufficient number of steps performed) 24 h after PT induction (**Figure 6A**). A statistically significant decrease in the asymmetry index measured in the cylinder test developed in the control group by 96 h after PT

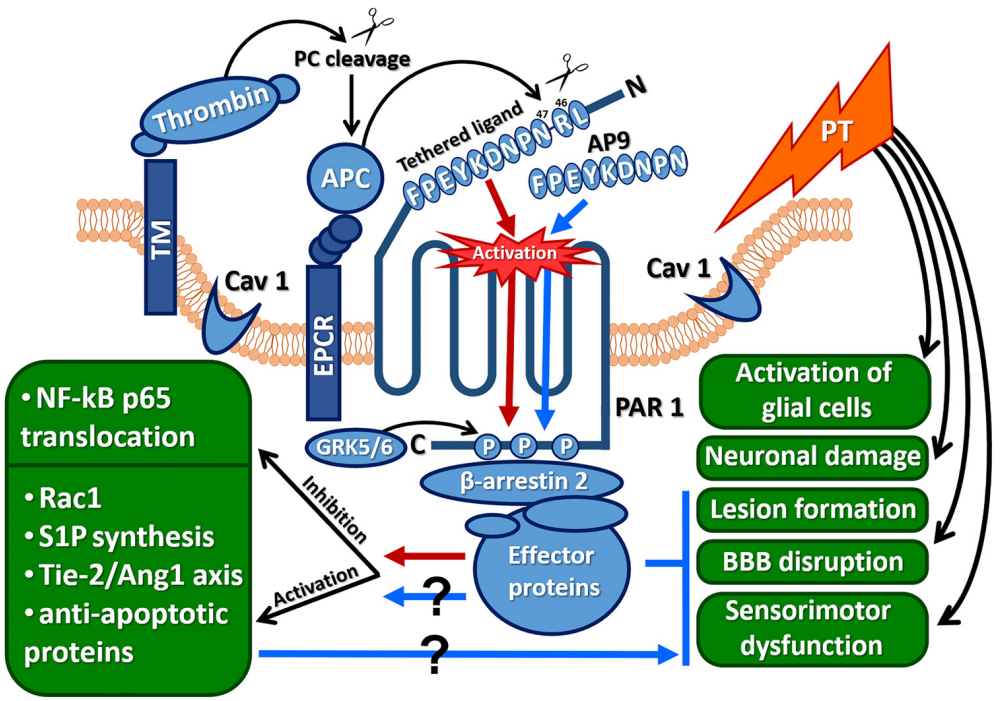

FIGURE 8 | Protective effects of AP9 and possible peptide-triggered cytoprotective pathways similar to those induced by APC (Ang1, angiopoietin 1; AP9, nine-amino-acid peptide analog of PAR1 "tethered ligand"; APC, activated protein C; CAV1, caveolin-1; EPCR, endothelial protein C receptor; GRK 5/6, G-protein-coupled receptor kinases 5 and 6; NF-κBp65, p65 subunit of the nuclear factor κB; PAR1, protease-activated receptor 1; PT, photothrombosis; Rac1, GTPase; S1P, sphingosine-1-phosphate; Tie-2, angiopoietin receptor; red arrows indicate cytoprotective pathways triggered by APC, and blue arrows and lines indicate AP9 effects observed in the present research).

induction (73.64 ± 6.61 and 100.00 ± 2.93% 96 h after PT induction and prior to thrombosis, respectively; n = 7). This decrease was less expressed in the group subjected to AP9 treatment (84.00 ± 3.44 and 100.00 ± 2.39%, respectively; n = 8) (**Figure 6B**).

Impact of β-Arrestin-2 Knockout on AP9 Protective Action in PT

We used mice lacking β-arrestin-2 (Bohn et al., 1999) in order to reveal the contribution of this protein to the protective effects of AP9. According to the data obtained during the genotyping of animals by PCR, all β-arrestin-2-/- mice had knockout of both alleles of the target gene in contrast to wild-type animals. The results of western blotting completely confirmed the absence of β-arrestin-2 expression in knockout animals (**Figure 7A**).

We used TTC staining of brain sections to assess lesion volume. AP9 (20 mg/kg, 10 min before and 1 h after PT) significantly reduced the relative lesion volume in wild-type animals (C57BL/6 strain) 24 h after PT. This parameter was 70.80 ± 8.28% (n = 9) in the treated group and 100.00 ± 9.56% (n = 10) in control mice (**Figures 7B,C**). It was consistent with our MRI data from BALB/c mice. However, we did not find the protective effect of double AP9 injection in β-arrestin-2-/- mice. Lesion volume was 100.00 ± 11.63% (n = 8) in control animals and 89.82 ± 6.91% (n = 8) in AP9-treated mice (**Figures 7B,C**). Thus, β-arrestin-2 expression is required for AP9 protective action in PT-induced brain ischemia.

DISCUSSION

The involvement of hemostatic proteases in the regulation of brain ischemia-induced dysfunctions was demonstrated previously (Xi et al., 2003; Griffin et al., 2004; Suo et al., 2004; Sheehan and Tsirka, 2005). Data on the protective effects of APC and peptide analogs of PAR1 "tethered ligand" generated by APC cleavage at Arg^{46} are of particular interest. The effects of the nine-amino-acid peptide AP9 composed of Asn^{47}–$Phen^{55}$ of PAR1 "tethered ligand" in cultured neurons, mast cells, and keratinocytes were studied in our laboratory. We have shown using selective PAR1 blockers that AP9 increases the survival of neurons after their cocultivation with activated mast cells via PAR1 (Babkina et al., 2016). In addition, the peptide reduced neuronal death under excitotoxic conditions (Savinkova et al., 2014) and accelerated wound healing *in vitro* (Kiseleva et al., 2014). The similarity of PAR1-dependent action of AP9 and APC points to a possibility of AP9 effect implementation through APC-like pathways.

In the present study, we demonstrated for the first time the protective properties of AP9 in the mouse model of ischemic stroke. AP9 injected 10 min before PT at a dose of 20 mg/kg

decreased brain damage volume. The double administration of AP9 (20 mg/kg) 10 min before and 1 h after PT, that is, within the "therapeutic window" (Danton and Dietrich, 2004), reduced not only lesion volume but also BBB disruption and neurological deficit in mice.

It is known that PAR1 is expressed by different components of the neurovascular unit: neurons (Junge et al., 2004; Gorbacheva et al., 2009), astrocytes (Bartha et al., 2000; Wang et al., 2002; Junge et al., 2004), and endothelial cells (Bartha et al., 2000). Accordingly, various types of cells can be considered as a potential target for AP9. Moreover, PT-induced BBB disruption increases the possibility of crossing the BBB by the peptide and leads to expansion of its cell target spectrum.

Nine-amino-acid peptide treatment decreased the lesion volume measured by MRI and Evans blue dye content in the damaged hemisphere after PT. MRI visualizes the brain areas characterized by edema formation (Hoehn et al., 2001), and Evans blue dye extraction allows us to evaluate the functional state of the BBB (Belayev et al., 1996). It indicates that the effects of AP9 are primarily due to the stabilization of the endothelial barrier function after PT-induced ischemia. Our results are in accordance with previous data on the PAR1 peptide agonist TR47, that is, the C-terminal fragment of PAR1 formed after cleavage of the receptor by APC at Arg^{46}. TR47 inhibits endothelial permeability *in vitro* and *in vivo* vascular leakage in mice via APC-like activation of Rac1 (Mosnier et al., 2013).

The observed AP9 effects are similar to those described for APC. In cultured endotheliocytes, APC suppresses NF-κB-modulated genes and inhibits cytokine signaling. Moreover, APC modulates apoptosis pathways, including upregulation of the endothelial Bcl-2 homolog (A1), endothelial NO synthase, and the inhibitor of apoptosis (IAP) (Joyce et al., 2001; Riewald and Ruf, 2005). APC also activates the Ang1/Tie-2 axis (Minhas et al., 2009) and increases S1P synthesis (Feistritzer and Riewald, 2005; Finigan et al., 2005), decreasing disruption of the endothelial barrier. It is possible that all these effects can be triggered in brain endotheliocytes via activation of PAR1 by AP9.

Despite the fact that AP9 beneficial effects were demonstrated on hippocampal neurons under excitotoxic conditions (Savinkova et al., 2014), as well as after their cocultivation with activated mast cells (Babkina et al., 2016), here, AP9 had no neuroprotective action according to histological analysis. It is possible that in addition to glutamate excitotoxicity and immune cell activation, other factors cause neuronal death under ischemic conditions *in vivo* (Durukan and Tatlisumak, 2007). Thus, a direct comparison of the results of *in vivo* and *in vitro* experiments is not applicable. Moreover, the lack of AP9 impact on neurons appears to be related to the method of peptide administration. Endothelial cells are expected to be a direct target of the peptide after its intravenous injection that is confirmed by AP9-mediated BBB stabilization after PT. However, according to the data on the sensorimotor tests, the peptide not only affects endotheliocytes but also indirectly protects other cell types via the regulation of PT-induced edema. Apparently, AP9 prevents cell damage in different components of the neurovascular unit via various cytoprotective pathways similar to APC (**Figure 8**). At the same time, the molecular mechanism of AP9 action needs further detailed study.

The APC-like mechanism of AP9 action is supported by data from β-arrestin-2-knockout animals. The absence of AP9 protective effect in mice lacking β-arrestin-2 indicates that AP9 can trigger β-arrestin-2-dependent pathways. β-Arrestin-2 recruits many effector proteins and provides G-protein-independent signaling via the mechanism of "biased agonism" (**Figure 8**) (Soh and Trejo, 2011; Griffin et al., 2015; Roy et al., 2016). It was previously shown that the localization of PAR1 in caveolae and its association with β-arrestins are necessary for activation of Rac1, which is a key participant in APC-mediated cytoprotective cascades (Soh and Trejo, 2011).

CONCLUSION

In conclusion, the new PAR1 agonist peptide (NPNDKYEPF-NH_2) demonstrates the APC-like protective effects in the mouse model of PT-induced brain ischemia. We suggest that AP9 action is mediated by its effects on the neurovascular unit and brain cells. The molecular mechanism of AP9 action is similar to that of APC. The activation of PAR1 by AP9, as well as APC-mediated PAR1 cleavage induce β-arrestin-2-dependent cytoprotective pathways. Our study shows the potential strategy to the treatment of ischemic brain injury based on a new class of peptide neuroprotectors.

DATA AVAILABILITY STATEMENT

The datasets generated for this study are available on request to the corresponding author.

ETHICS STATEMENT

The animal study was reviewed and approved by the Bioethics Committee of Lomonosov Moscow State University.

AUTHOR CONTRIBUTIONS

MGa performed the research, analyzed the data, and wrote the manuscript. EK performed the histological research. MGu conducted the MRI studies. MS performed the peptide synthesis. LG designed the research and edited the manuscript. All authors contributed to the manuscript revision and read and approved the submitted version.

FUNDING

The work of MGa was supported by the University program "UMNIK" (Lomonosov Moscow State University 2018, project no. 14587Гу/2019) and Russian Foundation for Basic Research (project no. 18-34-00977). The work of EK

was partly conducted in the frame of the IDB RAS state program of Fundamental Scientific Research (project no. 0108-2019-0004).

ACKNOWLEDGMENTS

We are thankful to Alexandra Guseva (Lomonosov Moscow State University) and Ilya Gusev for the help with laser equipment servicing. The team of authors is also thankful to Dmitriy Gorbachev (Shemyakin-Ovchinnikov Institute of Bioorganic Chemistry, Russian Academy of Sciences) and Vladimir Vyushkov (Lomonosov Moscow State University) for the help in mouse genotyping and interpretation of the data obtained.

SUPPLEMENTARY MATERIAL

The Supplementary Material for this article can be found online at: https://www.frontiersin.org/articles/10.3389/fnins.2020.00335/full#supplementary-material

REFERENCES

Abdelkarim, G., Gertz, K., Harms, C., Katchanov, J., Dirnagl, U., Szabo, C., et al. (2001). Protective effects of PJ34, a novel, potent inhibitor of poly (ADP-ribose) polymerase (PARP) in in vitro and in vivo models of stroke. *Int. J. Mol. Med.* 7, 255–260. doi: 10.3892/ijmm.7.3.255

Babkina, I. I., Strukova, S. M., Pinelis, V. G., Reiser, G., and Gorbacheva, L. R. (2016). New synthetic peptide protects neurons from death induced by toxic influence of activated mast cells via protease-activated receptor. *Biochemistry* 10, 126–134. doi: 10.1134/S1990747816010037

Bartha, K., Domotor, E., Lanza, F., Adam-Vizi, V., and Machovich, R. (2000). Identification of thrombin receptors in rat brain capillary endothelial cells. *J. Cereb. Blood Flow Metab.* 20, 175–182. doi: 10.1097/00004647-200001000-00022

Baskin, Y. K., Dietrich, W. D., and Green, E. J. (2003). Two effective behavioral tasks for evaluating sensorimotor dysfunction following traumatic brain injury in mice. *J. Neurosci. Methods* 129, 87–93. doi: 10.1016/S0165-0270(03)00212-7

Belayev, L., Busto, R., Zhao, W., and Ginsberg, M. D. (1996). Quantitative evaluation of blood-brain barrier permeability following middle cerebral artery occlusion in rats. *Brain Res.* 739, 88–96. doi: 10.1016/S0006-8993(96)00815-3

Bohn, L. M., Lefkowitz, R. J., Gainetdinov, R. R., Peppel, K., Caron, M. G., and Lin, F.-T. (1999). Enhanced morphine analgesia in mice lacking β-Arrestin-2. *Science* 286, 2495–2498. doi: 10.1126/science.286.5449.2495

Cotrina, M. L., Lou, N., Tome-Garcia, J., Goldman, J., and Nedergaard, M. (2017). Direct comparison of microglial dynamics and inflammatory profile in photothrombotic and arterial occlusion evoked stroke. *Neuroscience* 343, 483–494. doi: 10.1016/j.neuroscience.2016.12.012

Coughlin, S. R. (2005). Protease-activated receptors in hemostasis, thrombosis and vascular biology. *J. Thromb. Haemost.* 3, 1800–1814. doi: 10.1111/j.1538-7836.2005.01377.x

Danton, G. H., and Dietrich, W. D. (2004). The search for neuroprotective strategies in stroke. *Am. J. Neuroradiol.* 25, 181–194.

Durukan, A., and Tatlisumak, T. (2007). Acute ischemic stroke: overview of major experimental rodent models, pathophysiology, and therapy of focal cerebral ischemia. *Pharmacol. Biochem. Behav.* 87, 179–197. doi: 10.1016/j.pbb.2007.04.015

Feistritzer, C., and Riewald, M. (2005). Endothelial barrier protection by activated protein C through PAR1-dependent sphingosine 1-phosphate receptor-1 crossactivation. *Blood* 105, 3178–3184. doi: 10.1182/blood-2004-10-3985

Finigan, J. H., Dudek, S. M., Singleton, P. A., Chiang, E. T., Jacobson, J. E., Camp, S. M., et al. (2005). Activated protein C mediates novel lung endothelial barrier enhancement: Role of sphingosine 1-phosphate receptor transactivation. *J. Biol. Chem.* 280, 17286–17293. doi: 10.1074/jbc.M412427200

Fluri, F., Schuhmann, M. K., and Kleinschnitz, C. (2015). Animal models of ischemic stroke and their application in clinical research. *Drug Des. Devel. Ther.* 9, 3445–3454. doi: 10.2147/DDDT.S56071

Franklin, K. B. J., and Paxinos, G. (2001). *Mouse Brain in Stereotaxic Coordinates*, 2nd Edn, London: Academic Press.

Galkov, M., Gulyaev, M., Kiseleva, E., Andreev-Andrievskiy, A., and Gorbacheva, L. (2020). Methods for detection of brain injury after photothrombosis-induced ischemia in mice: Characteristics and new aspects of their application. *J. Neurosci. Methods* 329, 1–9. doi: 10.1016/j.jneumeth.2019.108457

Gorbacheva, L., Pinelis, V., Ishiwata, S., Strukova, S., and Reiser, G. (2010). Activated protein C prevents glutamate- and thrombin-induced activation of nuclear factor-κB in cultured hippocampal neurons. *Neuroscience* 165, 1138–1146. doi: 10.1016/j.neuroscience.2009.11.027

Gorbacheva, L. R., Davidova, O., Sokolova, E., Ishiwata, S., Pinelis, V. G., Strukova, S. M., et al. (2009). Endothelial protein C receptor is expressed in rat cortical and hippocampal neurons and is necessary for protective effect of activated protein C at glutamate exitotoxicity. *J. Neurochem.* 111, 967–975. doi: 10.1111/j.1471-4159.2009.06380.x

Gorbacheva, L. R., Storozhevykh, T. P., Pinelis, V. G., Davydova, O. N., Ishiwata, S., and Strukova, S. M. (2008). Activated protein C via PAR1 receptor regulates survival of neurons under conditions of glutamate excitotoxicity. *Biochemistry* 73, 717–724. doi: 10.1134/S0006297908060138

Griffin, J. H., Fernández, J. A., Cheng, T., Guo, H., and Zlokovic, B. V. (2004). Activated protein C and ischemic stroke. *Crit. Care Med.* 32, 247–253. doi: 10.1097/01.CCM.0000126127.87484.2B

Griffin, J. H., Zlokovic, B. V., and Mosnier, L. O. (2015). Activated protein C: biased for translation. *Blood* 125, 2898–2907. doi: 10.1182/blood-2015-02-355974

Harrison, T. C., Silasi, G., Boyd, J. D., and Murphy, T. H. (2013). Displacement of sensory maps and disorganization of motor cortex after targeted stroke in mice. *Stroke* 44, 2300–2306. doi: 10.1161/STROKEAHA.113.001272

Hoehn, M., Nicolay, K., Franke, C., Sanden, Y., and van der, B. (2001). Application of magnetic resonance to animal models of cerebral ischemia. *J. Magn. Reson. Imaging* 14, 491–509. doi: 10.1002/jmri.1213

Hu, X. L., Johansson, I. M., Brännström, T., Olsson, T., and Wester, P. (2002). Long-lasting neuronal apoptotic cell death in regions with severe ischemia after photothrombotic ring stroke in rats. *Acta Neuropathol.* 104, 462–470. doi: 10.1007/s00401-002-0579-8

Joyce, D. E., Gelbert, L., Ciaccia, A., Dehoff, B., and Grinnell, B. W. (2001). Gene expression profile of antithrombotic protein C defines new mechanisms modulating inflammation and apoptosis. *J. Biol. Chem.* 276, 11199–11203. doi: 10.1074/jbc.C100017200

Junge, C. E., Lee, C. J., Hubbard, K. B., Zhang, Z., and Olson, J. J. (2004). Protease-activated receptor-1 in human brain: localization and functional expression in astrocytes. *Exp. Neurol.* 188, 94–103. doi: 10.1016/j.expneurol.2004.02.018

Kang, H., Sohn, I., and Park, C. (2015). Use of indocyanine green for optical analysis of cortical infarcts in photothrombotic ischemic brains. *J. Neurosci. Methods* 248, 46–50. doi: 10.1016/j.jneumeth.2015.03.033

Khoshnam, S. E., Winlow, W., Farzaneh, M., Farbood, Y., and Moghaddam, H. F. (2017). Pathogenic mechanisms following ischemic stroke. *Neurol. Sci.* 38, 1167–1186. doi: 10.1007/s10072-017-2938-1

Kim, G. W., Copin, J.-C., Lewen, A., Watson, B. D., and Chan, P. H. (2001). The cytosolic antioxidant, copper/zinc superoxide dismutase, attenuates blood-brain barrier disruption and oxidative cellular injury after photothrombotic cortical ischemia in mice. *Neuroscience* 105, 1007–1018. doi: 10.1016/S0306-4522(01)00237-8

Kiseleva, E. V., Sidorova, M. V., Gorbacheva, L. R., and Strukova, S. M. (2014). Peptide-agonist of protease activated receptor (PAR1), similar to activated protein C, promotes proliferation in keratinocytes and wound healing of epithelial layer. *Biomed. Khim.* 60, 702–706. doi: 10.18097/pbmc20146006702

Lee, J.-K., Park, M.-S., Kim, Y.-S., Moon, K.-S., Joo, S.-P., and Kim, T.-S. (2007). Photochemically induced cerebral ischemia in a mouse model. *Surg. Neurol.* 67, 620–625. doi: 10.1016/j.surneu.2006.08.077

Li, H., Zhang, N., Lin, H., Yu, Y., Cai, Q., Ma, L., et al. (2014). Histological, cellular and behavioral assessments of stroke outcomes after photothrombosis-induced ischemia in adult mice. *BMC Neurosci.* 15:58. doi: 10.1186/1471-2202-15-58

Mao, Y., Jin, J., and Kunapuli, S. P. (2008). Characterization of a new peptide agonist of the protease-activated receptor-1. *Biochem. Pharmacol.* 75, 438–447. doi: 10.1016/j.bcp.2007.09.002

Minhas, N., Xue, M., Fukudome, K., and Jackson, C. J. (2009). Activated protein C utilizes the angiopoietin/Tie-2 axis to promote endothelial barrier function. *FASEB J.* 24, 873–881. doi: 10.1096/fj.09-134445

Mosnier, L. O., Sinha, R. K., Burnier, L., Bouwens, E. A., and Griffin, J. H. (2013). Biased agonism of protease-activated receptor 1 by activated protein C caused by noncanonical cleavage at Arg46. *Blood* 120, 5237–5246. doi: 10.1182/blood-2012-08-452169

Ossovskaya, V. S., and Bunnett, N. W. (2004). Protease-activated receptors: contribution to physiology and disease. *Physiol. Rev.* 84, 579–621. doi: 10.1152/physrev.00028.2003

Pialat, J.-B., Cho, T.-H., Beuf, O., Joye, E., Moucharaffie, S., Langlois, J.-B., et al. (2007). MRI monitoring of focal cerebral ischemia in peroxisome proliferator-activated receptor (PPAR)-deficient mice. *NMR Biomed.* 6, 335–342. doi: 10.1002/nbm.1157

Premont, R. T., and Gainetdinov, R. R. (2007). Physiological roles of G protein-coupled receptor kinases and arrestins. *Annu. Rev. Physiol.* 69, 511–534. doi: 10.1146/annurev.physiol.69.022405.154731

Ramachandran, R., and Hollenberg, M. (2008). Proteinases and signalling: pathophysiological and therapeutic implications via PARs and more. *Br. J. Pharmacol.* 153, 263–282. doi: 10.1038/sj.bjp.0707507

Reiter, E., Ahn, S., Shukla, A. K., and Lefkowitz, R. J. (2012). Molecular mechanism of β-arrestin-biased agonism at seven-transmembrane receptors. *Annu. Rev. Pharmacol. Toxicol.* 52, 179–199. doi: 10.1146/annurev.pharmtox.010909.105800

Riewald, M., and Ruf, W. (2005). Protease-activated receptor-1 signaling by activated protein C in cytokine-perturbed endothelial cells is distinct from thrombin signaling. *J. Biol. Chem.* 280, 19808–19814. doi: 10.1074/jbc.M500747200

Roy, R. V., Ardeshirylajimi, A., Dinarvand, P., Yang, L., and Rezaie, A. R. (2016). Occupancy of human EPCR by protein C induces β-arrestin-2 biased PAR1 signaling by both APC and thrombin. *Blood* 128, 1884–1893. doi: 10.1182/blood-2016-06-720581

Savinkova, I. G., Gorbacheva, L. R., Bespalova, Z. D., Pinelis, V. G., and Strukova, S. M. (2014). Peptides analogous to tethered ligands liberated by activated protein C exert neuroprotective effects in glutamate induced excitotoxicity. *Biochemistry* 8, 116–120. doi: 10.1134/S1990747813050176

Schroeter, M., Jander, S., and Stoll, G. (2002). Non-invasive induction of focal cerebral ischemia in mice by photothrombosis of cortical microvessels: characterization of inflammatory responses. *J. Neurosci. Methods* 117, 43–49. doi: 10.1016/S0165-0270(02)00072-9

Sheehan, J. J., and Tsirka, S. E. (2005). Fibrin-modifying serine proteases thrombin, tPA, and plasmin in ischemic stroke: a review. *Glia* 50, 340–350. doi: 10.1002/glia.20150

Soh, U. J. K., and Trejo, J. (2011). Activated protein C promotes protease-activated receptor-1 cytoprotective signaling through β-arrestin and dishevelled-2 scaffolds. *PNAS* 108, 1372–1380. doi: 10.1073/pnas.1112482108

Song, M. K., Seon, H. J., Kim, I. G., Han, J. Y., Choi, I. S., and Lee, S. G. (2012). The effect of combined therapy of exercise and nootropic agent on cognitive function in focal cerebral infarction rat model. *Ann. Rehabil. Med.* 36, 303–310. doi: 10.5535/arm.2012.36.3.303

Suo, Z., Citron, B. A., and Festoff, B. W. (2004). Thrombin: a potential proinflammatory mediator in neurotrauma and neurodegenerative disorders. *Curr. Drug Targets Inflamm. Allergy* 3, 105–114. doi: 10.2174/1568010043483953

Traynelis, S. F., and Trejo, J. (2007). Protease-activated receptor signaling: new roles and regulatory mechanisms. *Curr. Opin. Hematol.* 14, 230–235. doi: 10.1097/MOH.0b013e3280dce568

Vu, T.-K. H., Hung, D. T., Wheaton, V. I., and Coughlin, S. R. (1991). Molecular cloning of a functional thrombin receptor reveals a novel proteolytic mechanism of receptor activation. *Cell* 64, 1057–1068. doi: 10.1016/0092-8674(91)90261-V

Wang, H., Ubl, J. J., and Reiser, G. (2002). Four subtypes of protease-activated receptors, co-expressed in rat astrocytes, evoke different physiological signaling. *Glia* 37, 53–63. doi: 10.1002/glia.10012

Xi, G., Reiser, G., and Keep, R. F. (2003). The role of thrombin and thrombin receptors in ischemic, hemorrhagic and traumatic brain injury: deleterious or protective? *J. Neurochem.* 84, 3–9. doi: 10.1046/j.1471-4159.2003.01268.x

Zlokovic, B. V., and Griffin, J. H. (2011). Cytoprotective protein C pathways and implications for stroke and neurological disorders. *Trends Neurosci.* 34, 198–209. doi: 10.1016/j.tins.2011.01.005

Conflict of Interest: The authors declare that the research was conducted in the absence of any commercial or financial relationships that could be construed as a potential conflict of interest.

Copyright © 2020 Galkov, Kiseleva, Gulyaev, Sidorova and Gorbacheva. This is an open-access article distributed under the terms of the Creative Commons Attribution License (CC BY). The use, distribution or reproduction in other forums is permitted, provided the original author(s) and the copyright owner(s) are credited and that the original publication in this journal is cited, in accordance with accepted academic practice. No use, distribution or reproduction is permitted which does not comply with these terms.

frontiers in Neurology

ORIGINAL RESEARCH
published: 08 July 2020
doi: 10.3389/fneur.2020.00551

NEK7 Coordinates Rapid Neuroinflammation After Subarachnoid Hemorrhage in Mice

Gen Li[1,2†], Yushu Dong[1†], Dongdong Liu[1,2], Zheng Zou[1], Guangzhi Hao[1], Xu Gao[1], Pengyu Pan[1] and Guobiao Liang[1*]*

[1] Department of Neurosurgery, General Hospital of Northern Theater Command (General Hospital of Shenyang Military Command), Shenyang, China, [2] Dalian Medical University, Dalian, China

OPEN ACCESS

Edited by:
Emmanuel Pinteaux, University of Manchester, United Kingdom

Reviewed by:
Maria Calvo-Rodriguez, Harvard Medical School, United States
Paul Kasher, University of Manchester, United Kingdom

***Correspondence:**
Pengyu Pan
panpengyu09@sina.com
Guobiao Liang
liangguobiao6708@163.com

[†] *These authors have contributed equally to this work*

Specialty section:
This article was submitted to Stroke, a section of the journal Frontiers in Neurology

Received: *02 June 2019*
Accepted: *15 May 2020*
Published: *08 July 2020*

Citation:
Li G, Dong Y, Liu D, Zou Z, Hao G, Gao X, Pan P and Liang G (2020) NEK7 Coordinates Rapid Neuroinflammation After Subarachnoid Hemorrhage in Mice. Front. Neurol. 11:551. doi: 10.3389/fneur.2020.00551

Background: Subarachnoid hemorrhage (SAH) is a devastating disease which leads to high morbidity and mortality. Recent studies have indicated that, never in mitosis gene A-related expressed kinase 7 (NEK7), is involved in NLRP3 (NLR family, pyrin domain containing 3) associated inflammation, which may result in subsequent cellular and vascular damage. The aim of this study was to investigate whether NEK7 is involved in the pathophysiology of subarachnoid hemorrhage.

Methods: 455 adult male C57B6J mice, weighing 22 to 30 g, were used to investigate the time course of NEK7 expression in the ipsilateral cortex after SAH, and to investigate the intrinsic function and mechanism of NEK7. A vascular puncture model was used to create the mouse SAH model, and intracerebroventricular injection was used to deliver NEK7 recombinant protein, NEK7 small interfering RNA, nigericin, and MCC950. Neurological score, brain water content, Evans blue extravasation, immunofluorescence, and western blot were evaluated for neurological outcome, neuronal apoptosis, blood-brain barrier damage, microglia accumulation, and the mechanism of NEK7 and NLRP3 activation.

Results: Our results exhibited that intrinsic NEK7 was elevated after SAH in the cortex of the left/ipsilateral hemisphere and was colocalized with microglia, endothelial cells, neuron, astrocyte, and oligodendrocyte, and highly expressed in microglia and endothelial cells after SAH. NEK7 recombinant protein aggravated neurological deficits, brain edema, neuronal apoptosis, BBB permeability, microglial accumulation, and activated caspase-1 and IL-1β maturation, while NEK7 small interfering RNA injection reversed those effects. Nigericin administration enhanced ASC oligomerization, caspase-1 and IL-1β maturation without increasing the protein level of NLRP3, and ASC oligomerization and caspase-1 IL-1β maturation reduced when combined with NEK7 knockdown or MCC950 delivery. We found the level of NEK7 expression increased after SAH and could activate the downstream NLRP3 pathway to induce caspase-1, IL-1β expression and then increased the BBB opening, microglia accumulation and neuronal apoptosis after SAH.

Conclusions: This study demonstrated for the first time that NEK7 mediated the harmful effects of neuronal apoptosis and BBB disruption after SAH, which may potentially be mediated by the NEK7/NLRP3 signal. NEK7 served as a co-component for NLRP3 inflammasome activation after SAH. NEK7 may be a promising target on the management of SAH patients.

Keywords: subarachnoid hemorrhage, microglia, NEK7, NLRP3, neuroinflammation, blood-brain barrier

INTRODUCTION

Despite years of efforts, early brain injury—the main contributor to the mortality and poor prognosis of patients after subarachnoid hemorrhage (SAH)—remains a catastrophic complication of a ruptured intracranial aneurysm (1). The pathophysiology of SAH involves an alteration in the brain neural vascular network, involving the arterial, capillary, venous systems, neurons, microglia, surrounding support cells, and the extracellular matrix (2). The precise mechanism of neuronal apoptosis and BBB damage, however, remains elusive.

The NLR family, pyrin domain containing 3 (NLRP3) inflammasome, consists of NLRP3, apoptosis-associated speck-like domain (ASC) and pro-caspase-1. It is a group of innate immune proteins considered to be sensors of pathogen- and damage- associated molecular patterns (3). NLRP3 inflammasome activation promotes the cleavage of pro-caspase 1 and pro- interleukin (IL)-1β into their mature forms, which contributes to the development of type 2 diabetes (4), atherosclerosis (5), gout (6), and Alzheimer's disease (7). Our previous study showed NLRP3 activation increased BBB extravasation, tight junction protein degradation, as well as neuronal apoptosis after CNS injury (8, 9). As a typical inflammation target, the exact mechanism of NLRP3 activation still remains unclear.

Recent studies reported that NEK7, a serine and threonine kinase involved in mitosis, is an essential activator of the NLRP3 inflammasome (10). NEK7-mutant cells showed lower caspase-1 activation and IL-1β production in response to NLRP3-activating stimuli (11). These data suggested that NEK7 acts as a switch between inflammasome activation and cell division (11). We postulated that NEK7 expression was altered after SAH and targeting NEK7 might inactivate NLRP3-inflammasome and downstream IL-1β to preserve neuronal death and BBB permeability. To elucidate the function of NEK7 after SAH, we analyzed the spatial distribution and time course of NEK expression, neurological function, neuronal apoptosis, and BBB permeability after NEK7 interference, and downstream NLRP3 activation.

Abbreviations: ANOVA, analysis of variance; ASC, apoptosis-associated speck-like protein; BBB, blood–brain barrier; BAX, BCL-2-associated X protein; BCL-2, B-cell lymphoma 2; EBI, early brain injury; IL-1β, Interleukin-1 beta; LRR, leucine rich repeat; NBD, nucleotide-binding domain; NEK7, Never in mitosis gene A-related expressed kinase 7; NLRP3, NLR family, pyrin domain containing 3; PBS, phosphate-buffered saline; PYD, pyrin domain; SAH, subarachnoid hemorrhage; TJs, tight junctions; ZO-1, zonula occludens-1.

MATERIALS AND METHODS

Animals

All experimental procedures were approved by the Ethics Committee of the General Hospital of Norther Theater Command (Shenyang Military Command) and was performed in accordance with the guidelines in the National Institutes of Health Guide for the Care and Use of Laboratory Animals, and followed the ARRIVE guidelines. Four-hundred-and-fifty-five (455) adult male C57B6J mice (22 to 30 g), were provided by the Department of Experimental Animals of the General Hospital of Norther Theater Command (Shenyang Military Command, Shenyang, China). Mice were acclimated in a reversed 12 h dark/12 h light cycle environment and provided with free access to water and food.

Experimental Design

The present study contained three experiments, which were designed as follows.

Experiment I

To investigate the time course of NEK7 expression and cell type location of NEK7 after SAH, 44 mice were randomly assigned to seven groups: Sham ($n = 6$), SAH 3 h ($n = 6$), SAH 6 h ($n = 6$), SAH 12 h ($n = 6$), SAH 24 h ($n = 6$), SAH 48 h ($n = 6$) and SAH 72 h ($n = 6$). NEK7 protein expression was detected by Western blot in cortex isolated from the ipsilateral/left hemisphere. Immunohistochemical staining of NEK7, NeuN (neuron marker), GFAP (astrocyte marker), Lectin (endotheliocyte marker), Iba-1 (microglia marker), and NG2 (oligodendrocyte marker) was performed at 24 h post SAH induction to confirm the spatial distribution of NEK7 in the cortex ($n = 6$).

Experiment II

To define the intrinsic function of NEK7 and to screen for effective dosage of NEK7 recombinant protein after SAH, 162 mice were randomly assigned to eight groups: Sham ($n = 24$), SAH ($n = 18$), SAH+NS (normal saline, 2 μL) ($n = 24$), SAH+NEK7 5 ng/μL ($n = 12$), SAH+NEK7 25 ng/μL ($n = 12$), SAH+NEK7 100 ng/μL ($n = 24$), SAH+Scr (scrambled) siRNA ($n = 24$), SAH+NEK7 siRNA ($n = 24$). Beam balance and modified Garcia tests were performed at 24 and 72 h after SAH to assess the neurological deficits in each group ($n = 6$). Furthermore, brain water content was performed at 24 and 72 h post SAH. Evans blue extravasation assessment test at 24 h post SAH induction to evaluate the blood-brain barrier damage. Immunohistochemical staining was also performed to detect

the neuronal apoptosis, endothelial continuity, and microglia accumulation in the cortex of ipsilateral/left hemisphere at 24 h after SAH induction ($n = 6$).

Furthermore, 30 mice were randomly divided into the following groups: Sham ($n = 6$), SAH+NS ($n = 6$), SAH+NEK7 100 ng/μL ($n = 6$), SAH+Scr siRNA ($n = 6$), SAH+NEK7 siRNA ($n = 6$). Western blot was performed to detect the NEK7, NRLP3, ASC, caspase-1, IL-1β, BCL-2, and BAX expression in cortex of the ipsilateral/left hemisphere in each group.

Experiment III

To validate the function of NEK7-denpdent NLRP3 signal activation after SAH induction, 84 mice were assigned to seven groups: Sham ($n = 12$), SAH ($n = 12$), SAH+Vehicle ($n = 12$), SAH+nigericin ($n = 12$), SAH+nigericin+Scr siRNA ($n = 12$), SAH+nigericin+NEK7 siRNA ($n = 12$), and SAH+MCC950 ($n = 12$). Modified Garcia tests and beam balance were performed at 24 h post SAH to evaluate the neurological dysfunction and brain water content, and Evans blue extravasation assessments were carried out to test the blood-brain barrier permeability.

Furhermore, 72 mice were randomly divided into the following groups: Sham ($n = 6$), SAH+NS ($n = 12$), SAH+Ngericin ($n = 12$), SAH+ Ngericin+Scr siRNA ($n = 12$), SAH+Ngericin+NEK7 siRNA ($n = 12$), and SAH+MCC950 ($n = 12$). Immunohistochemical staining was also performed to detect the neuronal apoptosis, endothelial continuity, and microglia accumulation. Western blot was performed to detect the protein expression of NEK7, NLRP3, ASC, caspase-1, IL-1β, BCL-2, and BAX.

SAH Model

SAH model was performed as previously described (12); mice were anesthetized with pentobarbital sodium (40 mg/kg) by intraperitoneal (i.p.) injection, then exposed the bifurcation of the common carotid artery in supine position. The left external carotid artery (ECA) was isolated and distally cut into a 2-mm stump. A 5-0 sharpened monofilament nylon suture was inserted into the left internal carotid artery (ICA) through the ECA, then advanced 3 mm past the bifurcation of the left ICA, until resistance was felt. Sutures were withdrawn and ICA patency confirmed. In the sham group, sutures were not advanced past the internal carotid artery bifurcation, identical to other procedures.

Intracerebroventricular Injection

The operation of intracerebroventricular injection was as previously described (13). A hole, lateral to the bregma 1.0 mm, was drilled on the skull without puncturing the dura. A needle of a 10-μL Hamilton syringe (Microliter 701; Hamilton Company, Reno, NV, USA) was then stereotactically and vertically inserted into the hole, 3.0 mm under the horizontal plane of the bregma, entering the left lateral ventricle. A total 2 μL volume of recombinant NEK7 protein solution (Sino Biological, Beijing, China, 4 μg dissolved in 2 μL sterile saline), nigericin solution (Sigma-Aldrich, Shanghai, China, 4 μg in 2 μL vehicle, vehicle: 2 μL mixture of 9:1 NS and DMSO), or MCC950 solution (Sigma-Aldrich, Shanghai, China, 2 μg in 2 μL vehicle, vehicle: 2 μL mixture of 9:1 NS and DMSO) was infused at a rate of 0.2 μL/min, 1 h after SAH induction, whereas 500 pmol/2 μL of NEK7 siRNA (Santa Cruz Biotechnology, Santa Cruz, CA, USA, 500 pmol in a 2-μL mixture of 1:1 RNase-free water and lipofectamine) or scrambled siRNA was infused at the identical rate 48 h before SAH induction. The syringe was slowly withdrawn at 10 min after infusion.

Neurological Outcome Assessment

Neurological deficits were accessed as previously described, at 24 and 72 h after SAH induction. The modified Garcia scale and beam balance test were used (14). Two blinded observers were employed for grading mean of the neurological score.

SAH Grade

The SAH severity grading score was implemented as previously described (15). The basal cistern was divided into six segments that could be scored from 0 to 3 according to the amount of subarachnoid blood clotting. The total score was calculated by adding the scores from six segments (0–18 points). Animals that received a score <8 were excluded from the study.

Brain Water Content

The brain samples were quickly removed from the skull, separated into the left and right cerebral hemispheres, the cerebellum, and the brain stem. These four parts of the brain were weighed (wet weight), respectively, and the brain samples were then dried at 55°C for 48 h in an oven and weighed again (dry weight). The water content percentage formula was: ([wet weight - dry weight]/wet weight) ×100%.

Evans Blue Extravasation

Evans blue extravasation was performed as previously described (14). Mice were anesthetized by pentobarbital sodium (40 mg/kg) i.p. injection 24 h post-SAH. Evans blue dye (2%, 5 mL/kg; Sigma–Aldrich, St. Louis, MO, USA) was injected into the left femoral vein over 2 min and circulated for 60 min. Mice were euthanized by an intracardial perfusion of phosphate-buffered saline (PBS). The brains were removed and quickly divided into the left and right cerebral hemispheres, weighed, homogenized in saline, and centrifuged at 15,000 g for 30 min. Subsequently, the resultant supernatant was added with equal volume of trichloroacetic acid, incubated overnight at 4°C and centrifuged at 15,000 g for 30 min. Next, the resultant supernatant was collected and spectrophotometrically quantified at 610 nm for Evans blue dye.

Immunofluorescence Staining

Immunofluorescence staining was performed on fixed frozen brain sections as previously described (16, 17). Mice were deeply anesthetized and transcardially perfused with PBS and 4% PFA at 24 h post SAH. Brain samples were isolated and post-fixed in 4% PFA for 24 h, then soaked in 40% sucrose for 1 day. Coronal brain sections (10 μm) were obtained using a cryostat (Leica, Nussloch, Eisfeld, Germany) and permeabilized using 0.3% Triton X-100 in PBS for 30 min. Sections were blocked with 5% donkey serum for 1 and incubated at 4°C overnight with anti–Occludin (1: 100, Abcam, Cambridge, UK), anti-NEK7 (1: 200, Novus, Bio-Techne China, Shanghai,

China), anti-IL-1β, anti–NeuN, anti–GFAP (1: 100), anti–Iba-1, anti–NG2 (1: 50, Abcam, Cambridge, UK) antibody and Lectin (1:200, Vector Laboratories, Burlingame, CA, USA), then incubated with corresponding secondary antibodies for 4 h at room temperature. Images were obtained atbasal cortex with a fluorescence microscope (Olympus, Melville, NY, USA) from slides. Quantification of immunofluorescence intensity was performed with the Measure tool in ImageJ software (National Institutes of Health, Bethesda, MD, USA) and the results of all the groups were normalized to the Sham group. Six image fields per group were analyzed. To evaluate the continuity of tight junctions of ECs, gaps of tight junctions were quantified as the length percentage of whole Occludin staining as per the previous method (18). The length of gaps and whole Occludin staining was measured by the Line tool in ImageJ software (National Institutes of Health, Bethesda, MD, USA) and the percentage was calculated as follows: Gap formation percentage = gap length/whole Occludin length. At least six vessels in each group were analyzed.

TUNEL

TUNEL staining was performed to test neuron apoptosis. Paraffin-embedded left/ ipsilateral hemisphere basal cortex sections (10 mm) were prepared. Apoptotic cells were stained using a Roche *in situ* cell death detection kit (Roche, Basel, Switzerland) according to the manufacturer's instructions. Fluorescent pictures were captured using a fluorescence microscope (Olympus, Melville, NY, USA). The number of TUNEL-positive cells were counted with ImageJ software. To calculate the apoptotic rates, six slides from one group were chosen and the number of TUNEL+ cells were counted in the range of images. The apoptotic rates were calculated by the formula: apoptotic rates = the number of TUNEL+ neurons in the field/ the number of all neurons in the field × 100%.

Western Blot

Western blot was performed as previously described (19, 20). Briefly, a protein sample was extracted from the cortex of the left/ipsilateral hemisphere. Equal amounts of total protein (30 μg) were loaded in the lane of SDS-PAGE gels. After electrophoresis, the protein was transferred onto a PVDF membrane, which was then blocked with blocking buffer for 2 h at room temperature. Subsequently, the membrane was incubated at 4°C overnight with the following antibodies: anti-NEK7 (1:500; Novus, Bio-Techne China, Shanghai, China), anti-NLRP3, anti-ASC (1:500; Abcam, Cambridge, UK), anti-caspase-1, anti–IL-1β (1:500; Santa Cruz Biotechnology, Santa Cruz, CA, USA), anti-BCL-2, and anti-BAX (1:500; Thermo Fisher Scientific, Waltham, MA, USA). β-actin and α-tubulin were used as internal loading controls, anti–β-actin, and anti-α-tubulin primary antibodies (1:2000; Santa Cruz Biotechnology, Santa Cruz, CA, USA). PVDF membranes were incubated with the appropriate secondary antibodies for 2 h at room temperature. Blots were detected by chemiluminescent (ECL Plus; Amersham Bioscience, Arlington Heights, IL, USA). Data were analyzed by densitometry using Quantity One 4.6.2 (Bio-Rad Laboratories, Berkeley, CA, USA).

Statistical Analysis

Data are shown as the mean ± SD. Chi-square tests and one-way ANOVA, followed by Tukey's multiple comparisons test were used to compare the different groups. SPSS 18 software (IBM, Chicago, IL, USA) was utilized to analyze the data, and $P < 0.05$ was considered as statistically significant.

RESULTS

Expression of NEK7 and Cellular Distribution After SAH

To investigate the expression of NEK7 after SAH induction, protein levels of NEK7 was detected by Western blot analysis. A significant increase of NEK7 were found in the ipsilateral/left hemisphere at 24 and 72 h after SAH (**Figures 1A,B**). Furthermore, immunohistochemical staining in the sham group showed that NEK7 expression was colocalized with the NeuN (neuron marker), GFAP (astrocyte marker), Lectin (endotheliocyte marker), Iba-1 (microglia marker), and nerve/glial antigen (NG) 2 (oligodendrocyte marker) in the left/ipsilateral cortex (**Figure 1C**). At 24 h post SAH, NEK7 was obviously elevated in endothelial cells and microglia (**Figures 1D,E**). None of the sham-operated mice died, and eight mice died within 72 h after SAH, due to severe hemorrhagic volume.

Neurological Functions After Recombinant NEK7 Delivery and Interference of NEK7 Expression After SAH

The NEK7 siRNA used in the present study could effectively inhibit the NEK7 expression after SAH. SAH grading score did not display significant differences among the groups at 24 and 72 h after SAH (**Figures 2A,B**). The SAH group showed significant neurological impairment in the modified Garcia test and beam balance, compared with the Sham group at 24 h after SAH induction (**Figures 2C–F**). Mice in the SAH+NEK7 100 ng/μL group had more severe neurological deficits at 24 h post SAH compared with the SAH+NS group, different to that in the SAH+NEK7 5 ng/μL and SAH+NEK7 25 ng group (**Figures 2C–F**). Furthermore, NEK7 siRNA treatment revealed greater improvements in neurological deficits compared with the SAH+Scr siRNA group at 24 h after SAH (**Figures 2C–F**). The Beam balance test exhibited similar trends (**Figures 2C–F**).

Neuronal Apoptosis and BBB Permeability After Recombinant NEK7 Delivery and Interference of NEK7 Expression

Mice from the SAH, SAH+NS, and SAH+Scr siRNA groups showed increased brain water content in both hemispheres at 24 and 72 h after SAH compared with mice in the Sham group (**Figures 3A,B**). The NEK7 100 ng/μL treatment increased the brain water content compared with the SAH+NS group, while the NEK7 siRNA pretreatment significantly reduced the

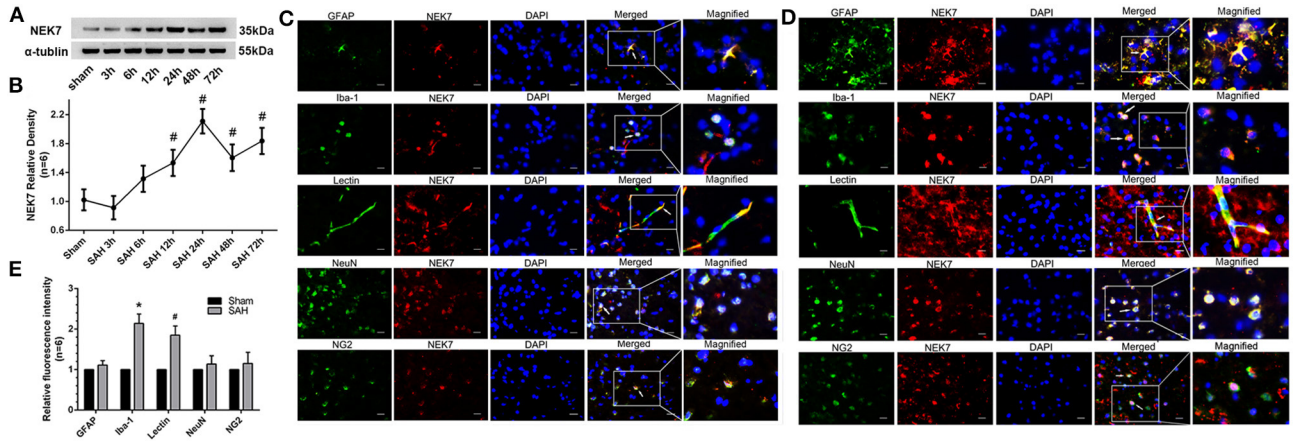

FIGURE 1 | Time course of endogenous NEK7 and cell type location after subarachnoid hemorrhage. **(A,B)** Representative western blot bands and quantitative analysis of NEK7 from the ipsilateral cortex after SAH, $n = 6$. Relative densities of each protein have been normalized against the sham group. #: vs. sham $P < 0.05$. **(C,D)** Representative immunohistochemistry slices of NEK7 (red), GFAP, Iba-1, Lectin, NeuN, NG2, (green) in the sham and SAH group at 24 h after SAH, $n = 1$. Scale Bar = 10 μm. **(E)** Quantitative analysis of NEK7 fluorescent intensity in each type of cell. *: vs. sham (Iba-1) $P < 0.05$, #: vs. sham (Lectin) $P < 0.05$.

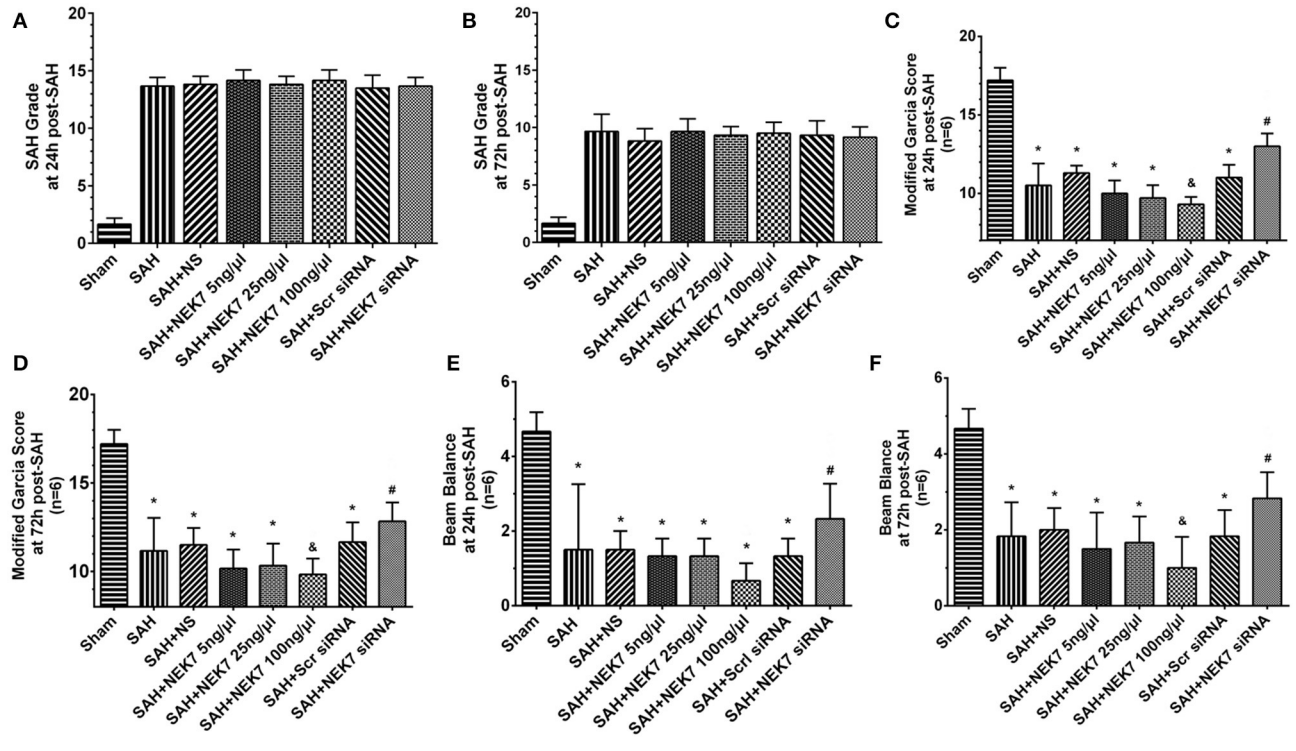

FIGURE 2 | Effects of exogenous NEK7 and NEK7 small interfering RNA treatment on neurological outcomes after subarachnoid hemorrhage. **(A,B)** SAH grading score at 24 and 72 h after SAH **(C-F)** Modified Garcia and Beam balance test at 24 and 72 h after SAH, $n = 6$. *: vs. ham $P < 0.05$, &: vs. SAH+NS $P < 0.05$, and #: vs. SAH+Scr siRNA $P < 0.05$.

brain water content in both hemispheres at 24 and 72 h post SAH (**Figures 3A,B**). Therefore, a dosage of NEK7 100 ng/μL was chosen for further investigation. Apoptosis is a biologically reversible process which is characterized as energy-dependent programmed cell death (21). Neuronal cell apoptosis, a main process of EBI, plays a crucial role in pathophysiology after SAH (22). Mice in the SAH and SAH+NS group showed a significant increase of neuronal apoptosis in the left/ipsilateral cortex. In the SAH+NEK7 100 ng/μL group, mice exhibited a rising number of apoptosis neurons than that in the SAH+NS group, while NEK7 siRNA pretreatment reversed these phenomena (**Figures 3C,D**). Furthermore, the

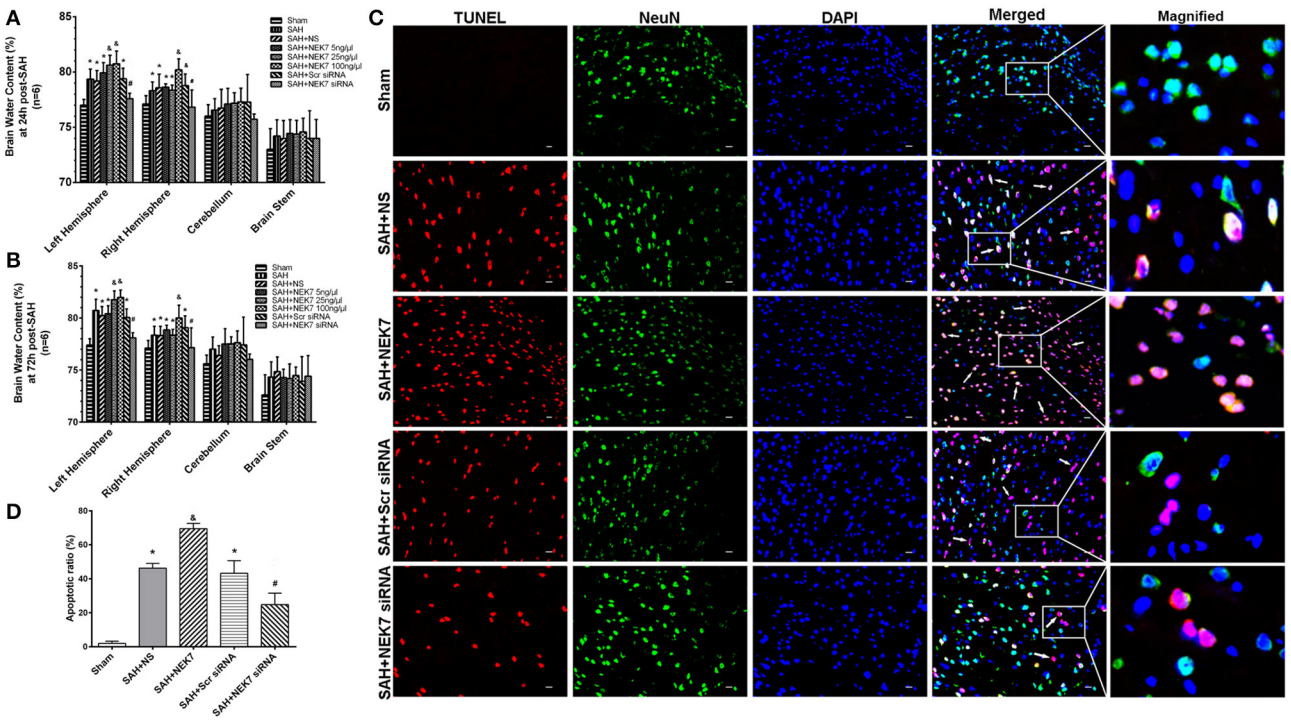

FIGURE 3 | Effects of exogenous NEK7 and NEK7 small interfering RNA treatment on neuronal apoptosis after subarachnoid hemorrhage. **(A,B)** Brain water content assessment at 24 and 72 h after SAH, $n = 6$. **(C)** Representative immunohistochemistry images of TUNEL (red) and NeuN (green) at 24 h after SAH. Scale Bar = 20 μm. **(D)** Apoptotic ratios of each group, $n = 6$. *: vs. sham $P < 0.05$, &: vs. SAH+NS $P < 0.05$, and #: vs. SAH+Scr siRNA $P < 0.05$.

SAH group demonstrated more Evans blue extravasation than the Sham group in the left/ipsilateral hemisphere (**Figure 4A**). The SAH+NEK7 100 ng/μL mice exhibited increased Evans blue leakage compared with the SAH+NS mice, whereas the NEK7 siRNA pretreatment significantly lowered the Evans blue extravasation compared with the SAH+Scr siRNA group (**Figure 4A**). In the immunohistochemical staining images, continuous endothelial cells (Lectin) and Occludin in the sham group were shown. Th Lectin and Occludin continuous structures broke up at 24 h after SAH, and NEK7 treatment significantly aggravated those damages, however, NEK7 siRNA infusion significantly reversed those disruptions at 24 h after SAH (**Figures 4B,C**). There was a significant accumulation of microglia in the SAH+NS group compared to that in the sham group (**Figure 4D**). IL-1β expression in microglia was elevated in the SAH+NS group after SAH and was aggravated by NEK7 infusion, while NEK7 siRNA administration reversed those effects (**Figure 4E**).

NLRP3 Inflammasome Protein and Apoptosis Related Protein Alteration After Recombinant NEK7 Delivery and Specific Inhibition of NEK7 Expression

Expression of NEK7, NLRP3, ASC, caspase-1, and IL-1β was measured *via* western blot at 24 h after SAH. NLRP3 levels in SAH, SAH+NS, SAH+NEK7 100 ng/μL, SAH+Scr siRNA, and SAH+ NEK7 siRNA elevated significantly at 24 h post SAH (**Figures 5A,B**). NEK7 100 ng/μL infusion after SAH increased ASC expression and caspase-1 and IL-1β maturation, however, NEK7 siRNA pretreatment reduced mature caspase-1 and IL-1β expression (**Figures 5A–G**). BCL-2 (B-cell lymphoma 2), is a member of the BCL-2 family of regulator proteins that inhibit apoptosis. It plays an important role in promoting cellular survival and inhibiting the actions of pro-apoptotic proteins (21). BAX (Bcl-2-associated X protein) is a pro-apoptotic protein in the BCL-2 family, which acts on the mitochondrial membrane to promote permeabilization, which is a vital signal in the apoptosis cascade (23). Mice from the SAH and SAH+NS groups showed significantly increased levels of BAX and decreased BCL-2 (**Figures 5H–J**). In the SAH+NEK7 group, expression of BAX rose and BCL-2 reduced, compared to that in the SAH+NS group. While in the SAH+NEK7 siRNA group, expression of BAX was lower, and BCL-2 was more than that in the SAH+Scr siRNA group (**Figures 5H–J**).

Neurological Functions and Neuronal Apoptosis After Nigericin Delivery, Specific Inhibition of NEK7 Expression, and MCC950 Administration

To study whether NLRP3 activation is dependent on NEK7 after SAH, we used nigericin, an activator of NEK7-dependent NLRP3 signal (10), or MCC950, an inhibitor of the NEK7/NLRP3

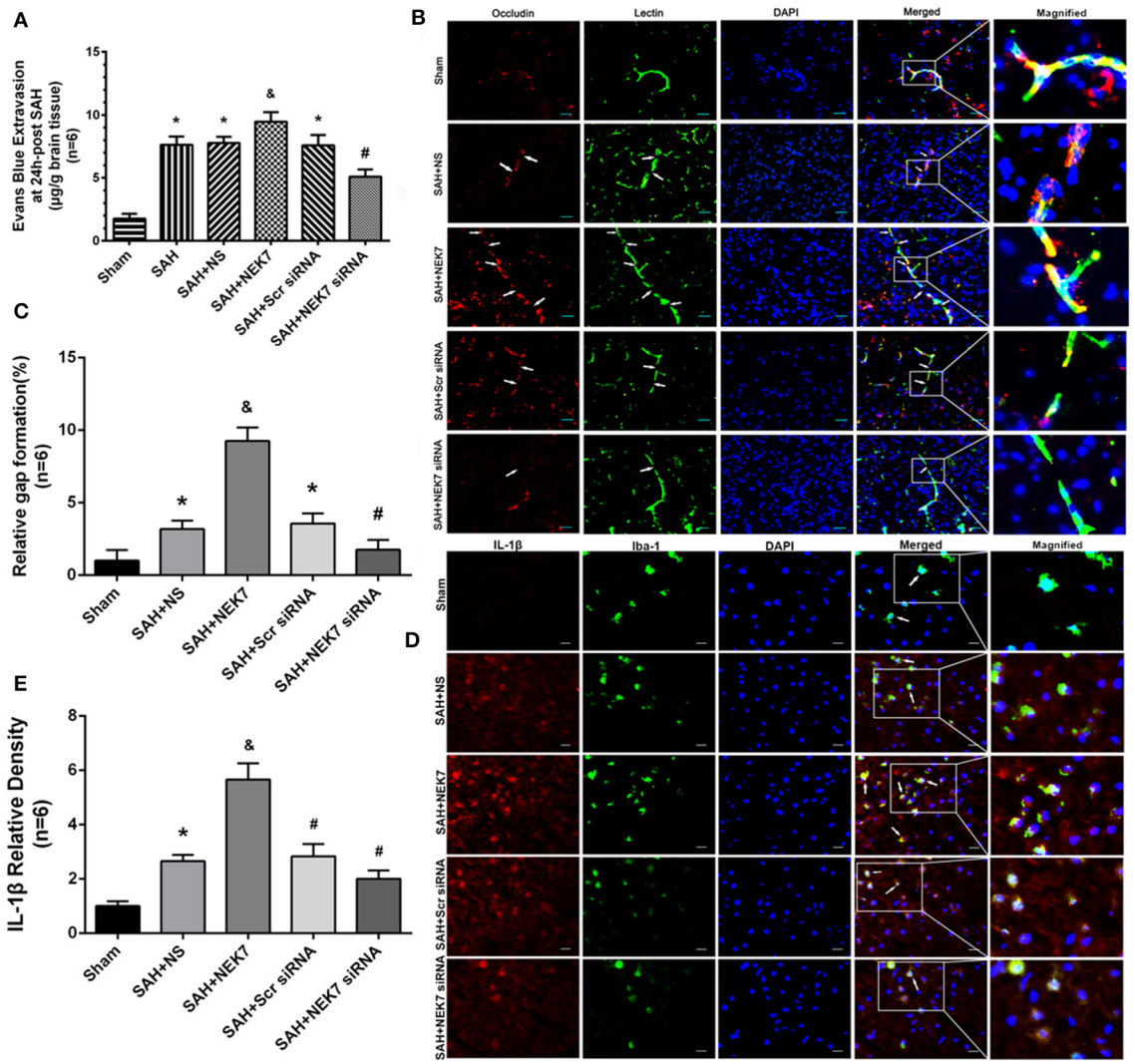

FIGURE 4 | Effects of exogenous NEK7 and NEK7 small interfering RNA treatment on blood–brain barrier and microglia accumulation after subarachnoid hemorrhage. **(A)** Evans blue extravasation evaluation at 24 h after SAH, $n = 6$. **(B)** Representative immunohistochemistry images of Occludin (red) and Lectin (green) at 24 h after SAH. Arrow indicates the breakdown of continuous endothelia cell layer, $n = 6$. Scale Bar = 20 μm. **(C)** Quantitative analysis of endothelial gap in **(B)**. **(D)** Representative immunohistochemistry images of IL-1β (red) and Iba-1 (green) at 24 h after SAH. Arrow indicates the accumulation of microglia and overlap of IL-1β and Iba-1, $n = 6$. Scale Bar = 10 μm. **(E)** Quantitative analysis of IL-1β fluorescent in **(D)**. *: vs. sham $P < 0.05$, &: vs. SAH+NS $P < 0.05$, and #: vs. SAH+Scr siRNA $P < 0.05$.

signal (24), to regulate inflammation post SAH. The SAH grading score did not show significant differences among the groups at 24 h post SAH (**Figure 6A**). The SAH and SAH+Vehcile group showed significant neurological impairment in the modified Garcia score and beam balance test compared with the Sham group (**Figures 6B,C**). Mice in the SAH+negricin group had more severe neurological deficits at 24 h post SAH compared with the SAH+Vehicle group (**Figures 6A–C**). NEK7 siRNA treatment or MCC950 ameliorated neurological deficits, however, were comparable to that of the SAH+Scr siRNA group or SAH+Vehicle group, respectively (**Figures 6A–C**). Compared with the Sham group, the SAH+Vehicle group displayed obvious increasing apoptosis neuron numbers at the left/ipsilateral cortex at 24 h post SAH (**Figures 6D,E**). Nigericin administration increased neuronal apoptosis after SAH, while NEK7 knockdown or MCC950 injection reduced neuronal apoptosis (**Figures 6D,E**).

BBB Permeability After Nigericin or MCC950 Delivery and Specific Inhibition of NEK7 Expression

Mice in the SAH and SAH+Vehicle groups showed increased brain water content in left hemispheres 24 h after SAH, compared with the Sham group (**Figure 7A**). The nigericin treatment increased the brain water content compared with the SAH+

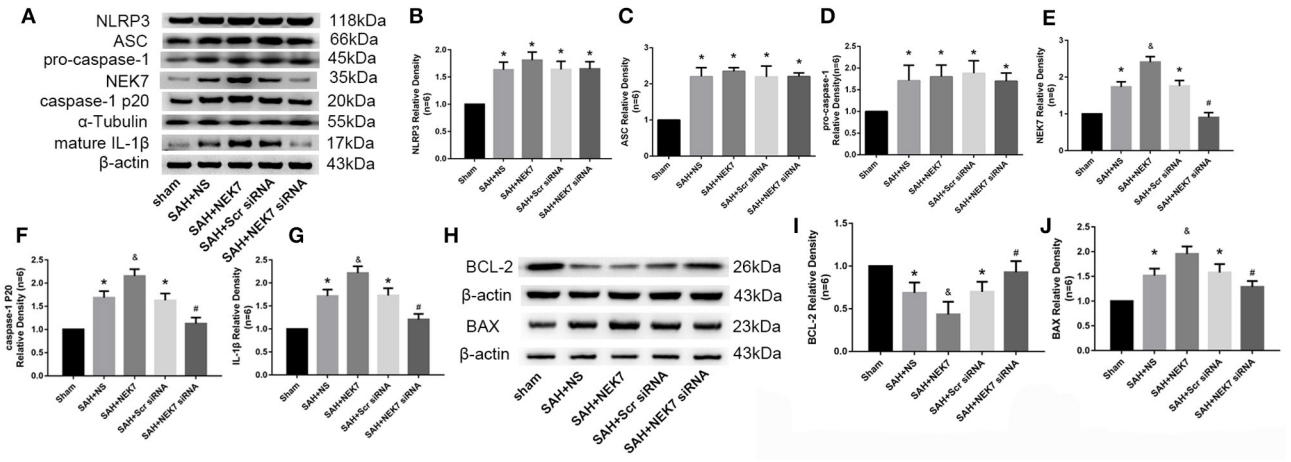

FIGURE 5 | Effects of exogenous NEK7 and NEK7 small interfering RNA pretreatment on NLRP3 activation and apoptosis related protein expression. **(A)** Representative western blot bands of NLRP3, NEK7, caspase-1, ASC, and IL-1β from the ipsilateral cortex after SAH. **(B–G)** Quantitative analysis of NLRP3, ASC, pro-caspase-1, caspase-1 p20, NEK7, and IL-1β, $n = 6$. **(H)** Representative western blot bands of BCL-2 and BAX. **(I,J)** Quantitative analysis of BCL-2 and BAX. Relative densities of each protein have been normalized to the sham group. $n = 6$. *: vs. sham $P < 0.05$, &: vs. SAH+NS $P < 0.05$, and #: vs. SAH+ scrambled siRNA $P < 0.05$.

Vehicle group, however the NEK7 siRNA pretreatment or MCC950 injection significantly reduced the brain water content (**Figure 7A**). Furthermore, the SAH group showed more Evans blue extravasation than the Sham group (**Figure 7B**). The SAH+Nigericin group exhibited increased Evans blue leakage compared with the SAH+Vehicle group, whereas NEK7 siRNA pretreatment or MCC950 delivery significantly lowered the Evans blue extravasation compared with the SAH+Nigericin+Scr siRNA group (**Figure 7B**). Lectin and Occludin continuous structures broke up at 24 h after SAH, and nigericin treatment significantly aggravated those damages, while NEK7 siRNA injection significantly reversed those disruptions (**Figure 7C**). Microglia accumulation was exacerbated and expression of IL-1β in microglia was elevated *via* nigericin administration and was alleviated after NEK7 siRNA pretreatment or MCC950 injection (**Figures 7D,E**).

NEK7 Coordinated NLRP3 Signal Activation After SAH

Expression of NEK7, NLRP3, ASC, pro-caspase-1, caspase-1 and IL-1β was measured *via* western blot at 24 h after SAH. NLRP3 was activated by various stimuli, and we wondered whether NEK7 coordinates NLRP3 activation after SAH. The expression of NEK7, NLRP3, caspase-1, and IL-1β was significantly increased at 24 h after SAH and NEK7 expression peaked at 24 h (**Figures 5A–G**). NEK7 recombinant protein delivery increased ASC oligomerization, caspase-1, and IL-1β maturation without increasing NLRP3 expression, and this was reversed by NEK7 siRNA infusion or MCC950 injection, which indicated that increasing NEK7 and NLRP3 binding activated the downstream signal (**Figures 5A–G**). BCL-2 protein levels in the SAH group were decreased at 24 h after SAH compared to the Sham group, while BAX increased and BCL-2 decreased in the SAH+Vehicle group compared to the sham group (**Figures 5H–J**). NEK7 recombinant protein infusion lowered BCl-2 and elevated BAX, while NEK7 siRNA relieved those effects (**Figures 5H–J**). Nigericin injection increased the expression of caspase-1, IL-1β at 24 h after SAH, which demonstrated that nigericin increased caspase-1 and IL-1β maturation but did not affect NLRP3 and NEK7 expression (**Figures 8A–G,K–Q**). Caspase-1 and IL-1β maturation were decreased at 24 h after SAH in the SAH+nigericin+Scr siRNA group compared to that in the SAH+nigericin+NEK7 siRNA group (**Figures 8A–G,K–Q**). Nigericin treatment could effectively inhibit their BCL-2 expression and enhance BAX expression (**Figures 8H–J**), however NEK7 siRNA treatment (**Figures 8H–J**) or MCC950 administration significantly reversed those trends (**Figures 8R–T**).

DISCUSSION

The present study demonstrated that NEK7 increased after SAH, peaked at 24 h, and was mainly expressed in microglia and endothelial cells. Exogenous NEK7 protein worsened neurological deficits and brain edema, while NEK7 specific inhibition preserved neurological function, neuronal apoptosis, and brain edema. Administration of Nigericin, a NEK7-dependent NLRP3 activator, aggravated neurological deficits, brain edema, microglial accumulation, and BBB disruption, while NEK7 siRNA infusion reversed these phenomena. By further studying the mechanism it was indicated that NEK7 activated the NLRP3 downstream inflammatory pathway, including caspase-1 and IL-1β maturation in endothelial cells which open, leading to increasing BBB extravasation. The microglia were then activated, which subsequently induced neuronal apoptosis by reducing BCL-2 and increasing BAX. NEK7 was recently reported to be critical for the activation of NLRP3 inflammasome and its

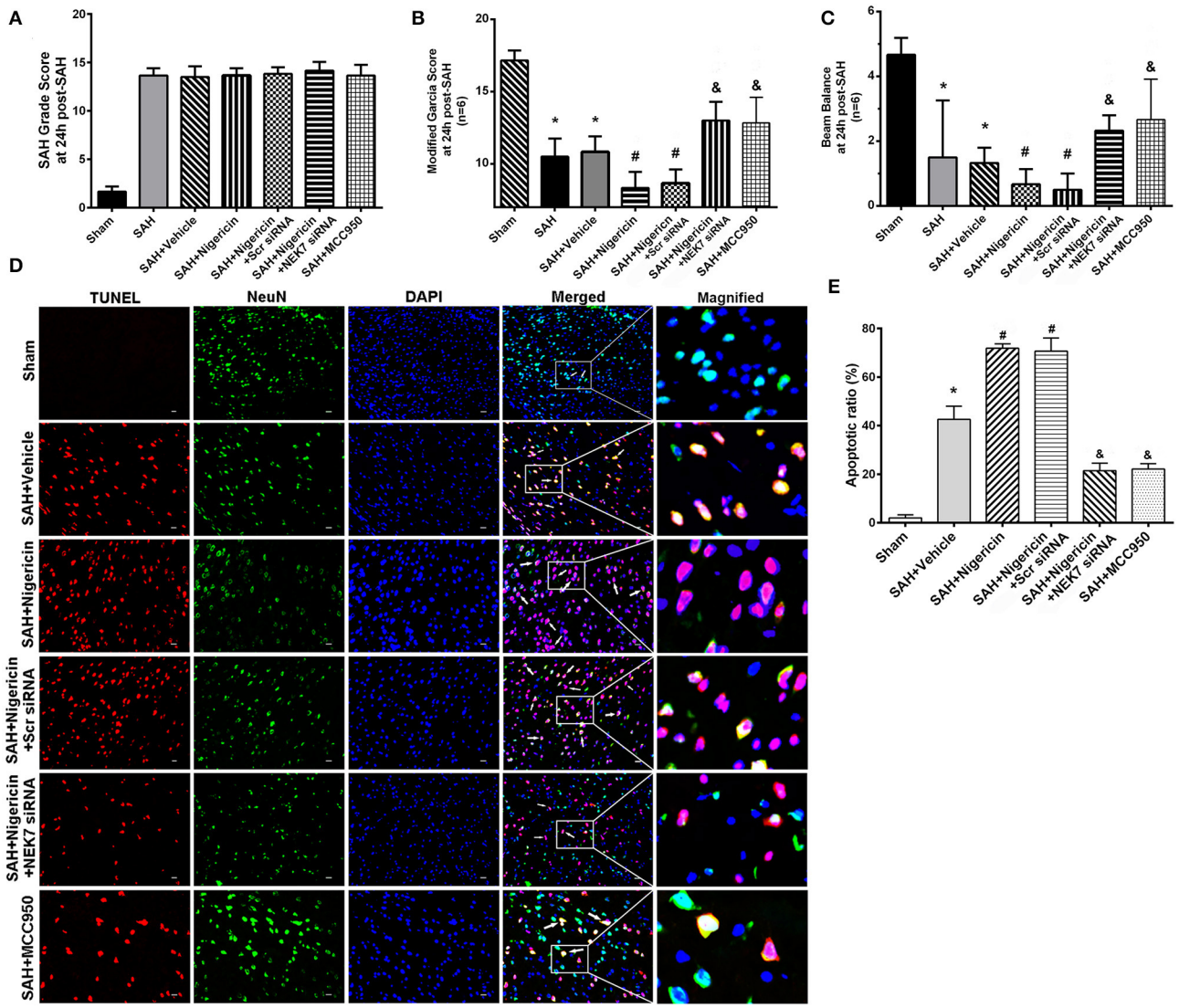

FIGURE 6 | Effects of nigericin, NEK7 small interfering RNA and MCC950 treatment on neurological outcome. **(A)** SAH grading score at 24 and 72 h after SAH **(B,C)** Modified Garcia test and Beam balance test at 24 h after SAH. $n = 6$ for each group. **(D)** Representative immunohistochemistry images of TUNEL (red) and NeuN (green) at 24 h after SAH. Scale Bar=20 μm. **(E)** Apoptotic ratios of each group, $n = 6$. *: vs. sham $P < 0.05$, &: vs. SAH+Vehicle $P < 0.05$, and #: vs. SAH+nigericin+Scr siRNA $P < 0.05$.

downstream inflammatory pathway, to induce caspase-1 and IL-1β maturation (4, 10, 25). NLRP3 inflammasome, which is important for the activation of caspases-1, maturation, and the secretion of proinflammatory cytokines such as IL-1β and IL-18, is a complex with multi-protein components containing three parts: an amino-terminal pyrin domain, a central nucleotide-binding domain, and a C-terminal leucine rich repeat (26). The ASC, and pro-caspase-1 are closely linked with the formation of NLRP3 inflammasome (27). Under the pathological state, NLRP3 is activated, then inflammasome assembly takes place and leads to the IL-1β shearing from pro-IL-1β, then secretion and maturation, which finally causes cell injury and death (7). NLRP3 inflammasome is involved in the initiation and development of several pathophysiological processes of CNS injury including stroke (28), neurodegenerative disease (7), and multiple sclerosis (29).

NEKs (NIMA-related kinase) are a group of evolutionarily conserved protein kinases sharing high amino acid sequence identity with NIMA which controls initiation of cell mitosis during mitotic cell division (30). A decrease in the centrosomal c-tubulin levels and reduction of the microtubule re-growth activity in the NEK7-suppressed cells was observed (31). The NEK7 amino acid sequence contains all of the amino acids conserved in serine/threonine kinases and have no C-terminal extensions (32), is expressed widely in a mouse brain including the Olfactory bulb, cortex, Thalamus, Midbrain, and the Hindbrain

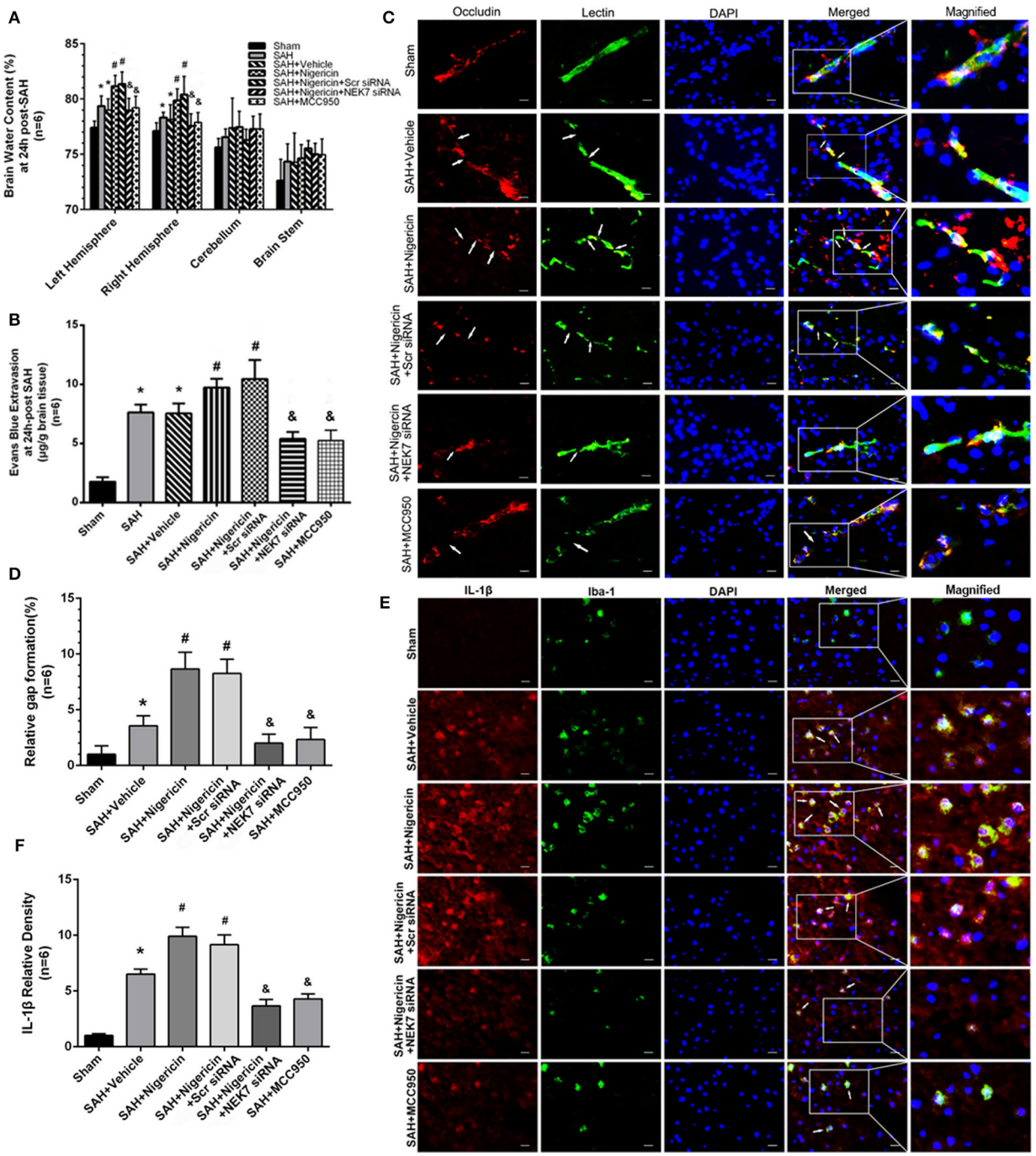

FIGURE 7 | Effects of nigericin, NEK7 small interfering RNA and MCC950 treatment on blood–brain barrier and microglia accumulation after subarachnoid hemorrhage. **(A)** Brain water content assessment at 24 h after SAH, $n = 6$. **(B)** Evans blue extravasation evaluation at 24 h after SAH, $n = 6$. **(C)** Representative immunohistochemistry images of Occludin (red) and Lectin (green) at 24 h after SAH. Arrow indicates the breakdown of continuous endothelia cell layer, $n = 6$. **(D)** Quantitative analysis of endothelial gap in **(C)**. **(E)** Representative immunohistochemistry images of IL-1β (red) and Iba-1 (green) at 24 h after SAH. Arrow indicates the accumulation of microglia and overlap of IL-1β, $n = 6$. Scale Bar = 10 μm. **(F)** Quantitative analysis of IL-1β intensity in **(E)**. *: vs. sham $P < 0.05$, &: vs. SAH+Vehicle $P < 0.05$, and #: vs. SAH+nigericin+Scr siRNA $P < 0.05$.

(33), is considered to be a new inflammasome component, and is also a switch between mitosis and NLRP3 activation (11). A recent study showed that NEK7-mutant mice had a defective IL-1β production response to nigericin (11). NEK7 bound to the leucine-rich repeat domain of NLRP3 in a kinase-independent manner (25) and acted as a coordinator

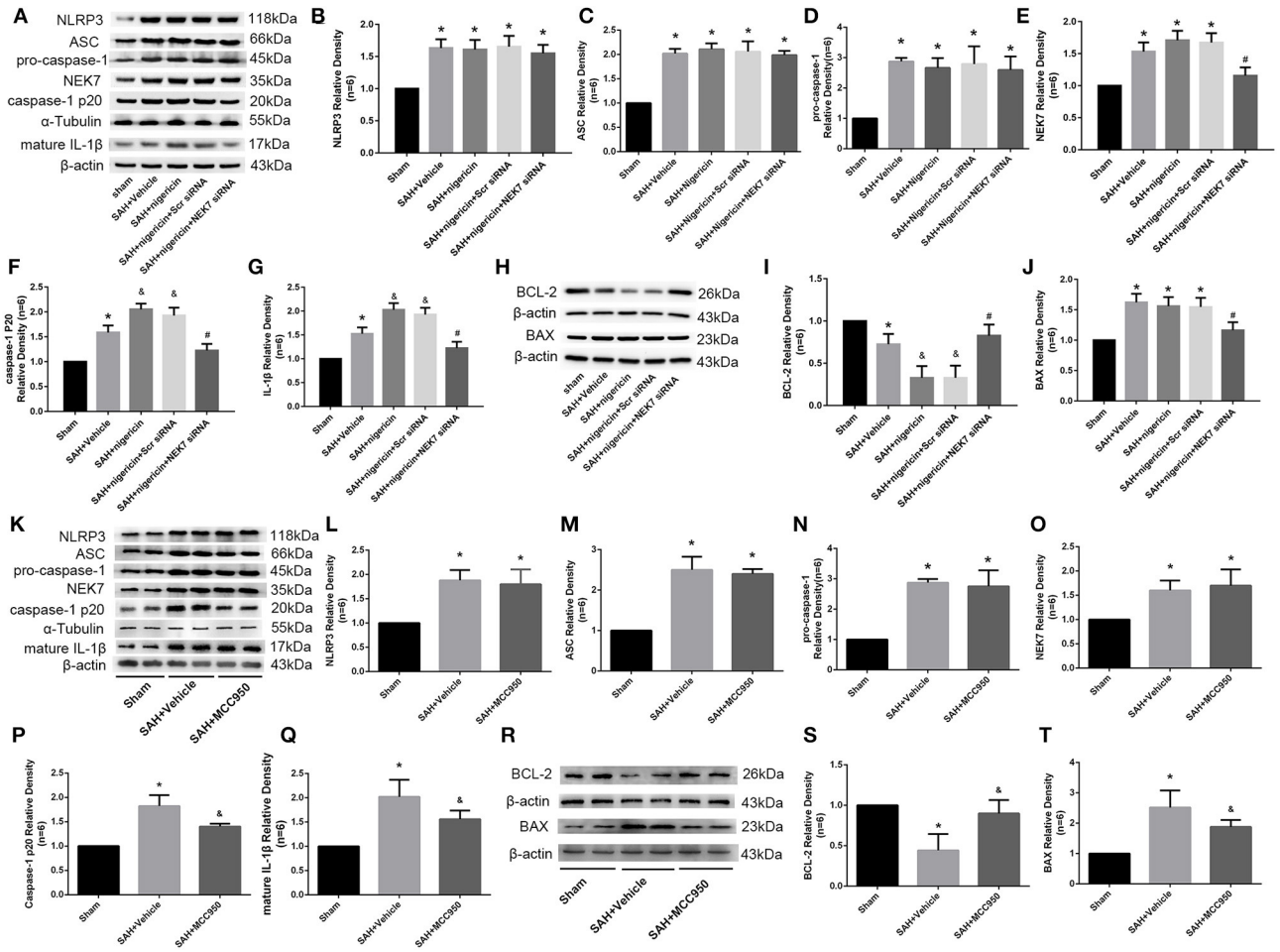

FIGURE 8 | Effects of nigericin, NEK7 small interfering RNA pretreatment, and MCC950 treatment on NLRP3 activation and apoptosis related protein expression. **(A,K)** Representative western blot bands of NLRP3, NEK7, ASC, caspase-1, and IL-1β from the ipsilateral cortex after SAH. **(B–G, L–Q)** Quantitative analysis of NLRP3, ASC, pro-caspase-1, caspase-1 p20, NEK7 and IL-1β, $n = 6$. **(H,R)** Representative western blot bands of BCL-2 and BAX. **(I,J,S,T)** Quantitative analysis of BCL-2 and BAX. Relative densities of each protein have been normalized to the sham group, $n = 6$. *: vs. sham $P < 0.05$, &: vs. SAH+Vehicle $P < 0.05$, and #: vs. SAH+nigericin+Scr siRNA $P < 0.05$.

in NLRP3 inflammasome activation. NLRP3 inflammasome assembly and formation is required for NEK7, which results in the secretion and maturation of IL-1β and IL-18 (11). MCC950 is an orally bioavailable sulfonylurea derived small molecule which selectively interacts with NLRP3 with no effect on NLRC4 and NLRP1 (34), and a number of studies showed its ability to block NLRP3 activation through the NEK7/NLRP3 pathway under pathological conditions (24), however, the precise mechanism is unknown. Some studies have demonstrated that MCC950 could reduce lung ischemia-reperfusion injury and high level of glucose induced retina damage by blocking NEK7-NLRP3 interaction (35, 36). Here we used MCC950 to block NEK7-NLRP3 pathway activation, and found that MCC950 showed similar effects as described in previous publications (37, 38). However, how MCC950 influences the NEK7-NLRP3 pathway still requires further study. Several pathways are pivotal for the NLRP3 inflammasome activation, such as potassium efflux, ROS (reactive oxygen species) signaling, and lysosomal destabilization. 50 mM KCl prevented potassium efflux to inhibit the interaction between NLRP3 and NEK7 induced by ATP, nigericin, or gramicidin in bone-marrow-derived macrophages from C57BL/6J mice carrying mutant NEK7 (25). While LPS-primed $NEK7^{+/+}$or $NEK7^{Cu/Cu}$ macrophages, producing similar amounts of mitochondrial ROS after treatment with nigericin (11). A recent pilot study found that hypokalemia is common in SAH patients (39). Cortical spreading depolarization, a phenomenon which is characterized as serial neuronal exciting *via* K^+ channel open after SAH, was considered as a factor of poor prognosis (40). These studies suggested that K^+ efflux may exist after SAH and could be an activator of NEK7/NLRP3. Recently, NEK7 has been identified as a necessary component of the NLRP3 activation driven by ROS but is independent of K+ efflux (41). The upstream of NEK7/NLRP3 activation after SAH currently remains elusive and requires further investigation.

Microglia are a cluster of specialized macrophages residing in the CNS system and the main source of NLRP3 (42).

Sufficient evidence suggests that they play a critical role in neuroinflammation. Activated microglia produce and secrete pro-inflammatory cytokines, including IL-1β, nitric oxide, and tumor necrosis factor-α, which induce cell death and secondary central nervous system injury. Cultured microglia have recently been shown to produce IL-1β (11), acting as a key mediator of neuronal apoptosis after SAH (43). In addition, Microglia were found to induce neuronal apoptosis *via* reducing BCL-2 and increasing BAX (44). In this study, we showed that NEK7 was expressed in microglia and was elevated after SAH, which in turn elicited neuronal apoptosis by activating NLRP3 and inducing IL-1β releasing. Neuronal apoptosis was alleviated by NEK7 siRNA pretreatment *via* reducing IL-1β and BAX and increasing BCL-2. Microglial accumulation was also found after SAH, providing evidence that targeting NEK7 may reduce neurological deficits by attenuated neuronal apoptosis triggered by microglia activation. Our results displayed that microglial accumulation in the ipsilateral/left cortex was enhanced by exogenous NEK7 administration and nigericin infusion, while it was reversed by NEK7 siRNA pretreatment and MCC950 injection. NEK7 was reported to influence microtubule dynamics, which is also a main factor for cell movement, morphology maintaining, and synaptic outputs of neurons (31, 45, 46). Microtubule activity were also found to be associated with microglia migration (47), however, there are very few studies that mention the exact mechanism of microglia movement after SAH. Based on these results, NEK7 may play a potential role in microglia migration *via* regulating microtubule. Furthermore, Acetylated α-tubulin was recently found to mediate the transport of mitochondria, apposition of ASC to NLRP3 on endoplasmic reticulum, and then activated NLRP3 (48). This indicates that NEK7 might activate NLRP3 *via* activating microtubule acetylation after stroke, which requires further investigation.

The blood-brain barrier can prevent harmful substances from coming into contact with the brain and allows nutrient substances to enter the brain (49). After SAH, the blood-brain barrier opens and leads to blood metabolites coming into direct contact with neurons and surrounding cells, which also leads to vasogenic brain edema (2). Endothelial cells are a main component of the BBB. Endothelial cells maintain the basic function of the BBB though transcellular transport and a tight junction structure. Previous studies indicated that NLRP3 activation induce the BBB open, while NLRP3 deletion preserved BBB permeability by reducing MMP9 and MMP2, which could subsequently degrade the tight junction protein including zonula occludens-1 and TJP2 (50). Expression of NLRP3 rise in endothelial cells after stroke, suggesting that endothelial cells may be a major source of NLRP3 (36, 50). Recent studies reveal that knockdown NEK7 expression could reduce high glucose induced retinal endothelial cell dysfunction (36) and maintain retinal endothelial cell permeability, which suggests that IL-1β itself could increase BBB permeability. In this investigation we demonstrated that brain edema worsened, and Evans blue extravasation increased after SAH, and protein levels of IL-1β rose in endothelial cells. At the same time, knockdown NEK7 ameliorated downstream NLRP3 activation and IL-1β maturation, eventually protecting BBB.

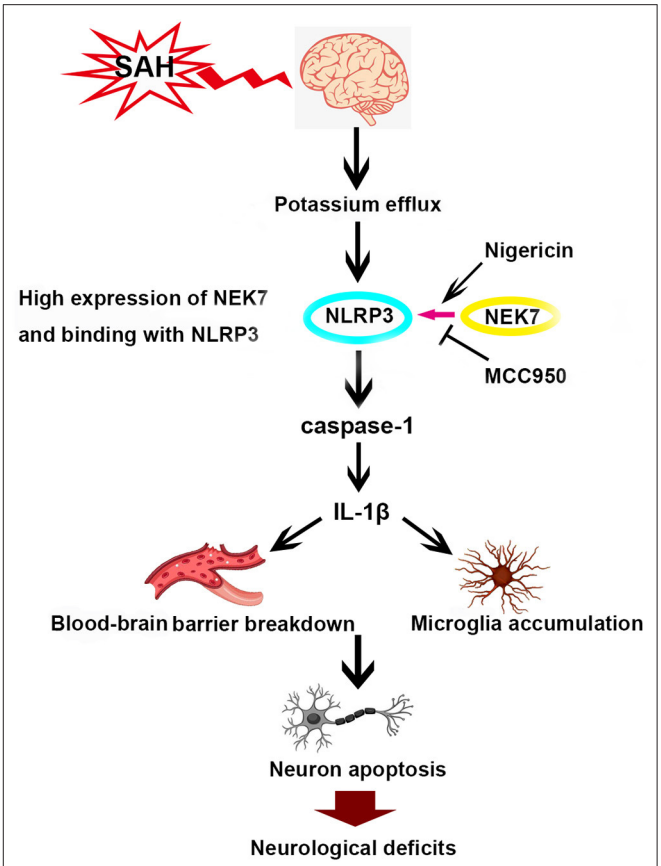

FIGURE 9 | Scheme of NEK7/NLRP3 interaction and downstream signal activation after SAH.

The limitations of this investigation were that data only focused on the NEK7 and NLRP3 inflammasome, while tight junction protein degradation was not studied in detail. After SAH, NF-κB undergoes nuclear translocation, and subsequently, elevated MMP9 transcription and induced basement membrane and tight junction protein degradation, which have all been well-illustrated in other studies. In addition, NEK7 may be located in the extracellular region and could affect surrounding cells. Consistent with previous studies, we found that endothelial cells and microglia highly expressed NEK7, however, whether NEK7-NLRP3 pathway activation in other cells and whether other types of cells secrete NEK7 and have effects on endothelial cells and microglia after SAH, are unknown. Other unknown mechanisms of NEK7 or NLRP3 activation cannot be excluded, therefore, in further studies, more data about the expression of NEK7 in other cell types and the elucidation of mechanisms of other mechanisms are needed.

CONCLUSIONS

This study demonstrated for the first time that NEK7 was elevated in the microglia and endothelial cells of the brain after SAH, and exogenous recombinant NEK7 induced

neuronal apoptosis and blood–brain barrier disruption which subsequently worsens the neurological outcome. This process was potentially mediated by NEK7-NLRP3 activation, which may promote casepase-1 and IL-1β maturation and secretion, and apoptosis related protein alteration in the brain (**Figure 9**). By targeting NEK7, our data and further translational studies may provide benefits for the management of SAH patients.

DATA AVAILABILITY STATEMENT

All datasets generated for this study are included in the article/supplementary material.

ETHICS STATEMENT

The animal study was reviewed and approved by Ethic Committee of General hospital of Northern Theater Command.

AUTHOR CONTRIBUTIONS

YD, GLia, and PP designed the experiment. PP, GLi, DL, ZZ, and GH finished the experiments protocols. GLi and DL carried out data analysis. PP, YD, and GLia prepared and revised the manuscript and gave the final approval of manuscript to be published. All authors contributed to the article and approved the submitted version.

FUNDING

This work was supported by the National Natural Science Foundation of China (Grant Nos. 81671174, 81671313, 81971133), the LIAONING Science and Technology Project (20180550504, 20180550151), the Medical Science Youth Breeding Project of the Chinese People's Liberation Army (17QNP053), and the China Postdoctoral Science Foundation (2016M592951).

REFERENCES

1. Sehba FA, Hou J, Pluta RM, Zhang JH. The importance of early brain injury after subarachnoid hemorrhage. *Progress Neurobiol.* (2012) 97:14–37. doi: 10.1016/j.pneurobio.2012.02.003
2. Zhang JH, Badaut J, Tang J, Obenaus A, Hartman R, Pearce WJ. The vascular neural network–a new paradigm in stroke pathophysiology. *Nat Rev Neurol.* (2012) 8:711–6. doi: 10.1038/nrneurol.2012.210
3. Shao BZ, Cao Q, Liu C. Targeting NLRP3 Inflammasome in the treatment of CNS diseases. *Front Mol Neurosci.* (2018) 11:320. doi: 10.3389/fnmol.2018.00320
4. Jourdan T, Godlewski G, Cinar R, Bertola A, Szanda G, Liu J, et al. Activation of the Nlrp3 inflammasome in infiltrating macrophages by endocannabinoids mediates beta cell loss in type 2 diabetes. *Nat Med.* (2013) 19:1132–40. doi: 10.1038/nm.3265
5. Abdul-Muneer PM, Alikunju S, Mishra V, Schuetz H, Szlachetka AM, Burnham EL, et al. Activation of NLRP3 inflammasome by cholesterol crystals in alcohol consumption induces atherosclerotic lesions. *Brain Behav Immun.* (2017) 62:291–305. doi: 10.1016/j.bbi.2017.02.014
6. Yang G, Yeon SH, Lee HE, Kang HC, Cho YY, Lee HS, et al. Suppression of NLRP3 inflammasome by oral treatment with sulforaphane alleviates acute gouty inflammation. *Rheumatology.* (2018) 57:727–36. doi: 10.1093/rheumatology/kex499
7. Heneka MT, McManus RM, Latz E. Inflammasome signalling in brain function and neurodegenerative disease. *Nat Rev Neurosci.* (2018) 19:610–21. doi: 10.1038/s41583-018-0055-7
8. Dong Y, Fan C, Hu W, Jiang S, Ma Z, Yan X, et al. Melatonin attenuated early brain injury induced by subarachnoid hemorrhage via regulating NLRP3 inflammasome and apoptosis signaling. *J Pineal Res.* (2016) 60:253–62. doi: 10.1111/jpi.12300
9. Zhao H, Pan P, Yang Y, Ge H, Chen W, Qu J, et al. Endogenous hydrogen sulphide attenuates NLRP3 inflammasome-mediated neuroinflammation by suppressing the P2X7 receptor after intracerebral haemorrhage in rats. *J Neuroinflammation.* (2017) 14:163. doi: 10.1186/s12974-017-0940-4
10. Schmid-Burgk JL, Chauhan D, Schmidt T, Ebert TS, Reinhardt J, Endl E, et al. A Genome-wide CRISPR (Clustered Regularly Interspaced Short Palindromic Repeats) Screen Identifies NEK7 as an Essential Component of NLRP3 Inflammasome Activation. *J Biol Chem.* (2016) 291:103–9. doi: 10.1074/jbc.C115.700492
11. Shi H, Wang Y, Li X, Zhan X, Tang M, Fina M, et al. NLRP3 activation and mitosis are mutually exclusive events coordinated by NEK7, a new inflammasome component. *Nat Immunol.* (2016) 17:250–8. doi: 10.1038/ni.3333
12. Li Q, Zhao H, Pan P, Ru X, Zuo S, Qu J, et al. Nexilin regulates oligodendrocyte progenitor cell migration and remyelination and is negatively regulated by protease-activated receptor 1/Ras-Proximate-1 signaling following subarachnoid hemorrhage. *Front Neurol.* (2018) 9:282. doi: 10.3389/fneur.2018.00282
13. Chen Y, Zhang Y, Tang J, Liu F, Hu Q, Luo C, et al. Norrin protected blood-brain barrier via frizzled-4/beta-catenin pathway after subarachnoid hemorrhage in rats. *Stroke.* (2015) 46:529–36. doi: 10.1161/STROKEAHA.114.007265
14. Pan P, Zhang X, Li Q, Zhao H, Qu J, Zhang JH, et al. Cyclosporine A alleviated matrix metalloproteinase 9 associated blood-brain barrier disruption after subarachnoid hemorrhage in mice. *Neurosci Lett.* (2017) 649:7–13. doi: 10.1016/j.neulet.2017.03.050
15. Sugawara T, Ayer R, Jadhav V, Zhang JH. A new grading system evaluating bleeding scale in filament perforation subarachnoid hemorrhage rat model. *J Neurosci Methods.* (2008) 167:327–34. doi: 10.1016/j.jneumeth.2007.08.004
16. Zuo S, Ge H, Li Q, Zhang X, Hu R, Hu S, et al. Artesunate protected blood-brain barrier via sphingosine 1 phosphate receptor 1/phosphatidylinositol 3 kinase pathway after subarachnoid hemorrhage in rats. *Mol Neurobiol.* (2017) 54:1213–28. doi: 10.1007/s12035-016-9732-6
17. Li Q, Chen Y, Li B, Luo C, Zuo S, Liu X, et al. Hemoglobin induced NO/cGMP suppression deteriorate microcirculation via pericyte phenotype transformation after subarachnoid hemorrhage in rats. *Sci Rep.* (2016) 6:22070. doi: 10.1038/srep22070
18. Bauer AT, Burgers HF, Rabie T, Marti HH. Matrix metalloproteinase-9 mediates hypoxia-induced vascular leakage in the brain via tight junction rearrangement. *J Cereb Blood Flow Metab.* (2010) 30:837–48. doi: 10.1038/jcbfm.2009.248
19. Li B, He Y, Xu L, Hu Q, Tang J, Chen Y, et al. Progranulin reduced neuronal cell death by activation of sortilin 1 signaling pathways after subarachnoid hemorrhage in rats. *Crit Care Med.* (2015) 43:e304–11. doi: 10.1097/CCM.0000000000001096
20. Li B, Luo C, Tang W, Chen Z, Li Q, Hu B, et al. Role of HCN channels in neuronal hyperexcitability after subarachnoid hemorrhage in rats. *J Neurosci.* (2012) 32:3164–75. doi: 10.1523/JNEUROSCI.5143-11.2012
21. Taylor RC, Cullen SP, Martin SJ. Apoptosis: controlled demolition at the cellular level. *Nat Rev Mol Cell Biol.* (2008) 9:231–41. doi: 10.1038/nrm2312
22. Chen S, Feng H, Sherchan P, Klebe D, Zhao G, Sun X, et al. Controversies and evolving new mechanisms in subarachnoid hemorrhage. *Prog Neurobiol.* (2014) 115:64–91. doi: 10.1016/j.pneurobio.2013.09.002
23. Czabotar PE, Westphal D, Dewson G, Ma S, Hockings C, Fairlie WD, et al. Bax crystal structures reveal how BH3 domains activate Bax and

nucleate its oligomerization to induce apoptosis. *Cell.* (2013) 152:519–31. doi: 10.1016/j.cell.2012.12.031
24. Coll RC, Robertson AA, Chae JJ, Higgins SC, Munoz-Planillo R, Inserra MC, et al. A small-molecule inhibitor of the NLRP3 inflammasome for the treatment of inflammatory diseases. *Nat Med.* (2015) 21:248–55. doi: 10.1038/nm.3806
25. He Y, Zeng MY, Yang D, Motro B, Nunez G. NEK7 is an essential mediator of NLRP3 activation downstream of potassium efflux. *Nature.* (2016) 530:354–7. doi: 10.1038/nature16959
26. Jha S, Ting JP. Inflammasome-associated nucleotide-binding domain, leucine-rich repeat proteins and inflammatory diseases. *J Immunol.* (2009) 183:7623–9. doi: 10.4049/jimmunol.0902425
27. Bertin J, DiStefano PS. The PYRIN domain: a novel motif found in apoptosis and inflammation proteins. *Cell Death Differ.* (2000) 7:1273–4. doi: 10.1038/sj.cdd.4400774
28. Yang SJ, Shao GF, Chen JL, Gong J. The NLRP3 inflammasome: an important driver of neuroinflammation in hemorrhagic stroke. *Cell Mol Neurobiol.* (2018) 38:595–603. doi: 10.1007/s10571-017-0526-9
29. Malhotra S, Rio J, Urcelay E, Nurtdinov R, Bustamante MF, Fernandez O, et al. NLRP3 inflammasome is associated with the response to IFN-beta in patients with multiple sclerosis. *Brain.* (2015) 138:644–52. doi: 10.1093/brain/awu388
30. de Souza EE, Hehnly H, Perez AM, Meirelles GV, Smetana JH, Doxsey S, et al. Human Nek7-interactor RGS2 is required for mitotic spindle organization. *Cell Cycle.* (2015) 14:656–67. doi: 10.4161/15384101.2014.994988
31. Kim S, Lee K, Rhee K. NEK7 is a centrosomal kinase critical for microtubule nucleation. *Biochem Biophys Res Commun.* (2007) 360:56–62. doi: 10.1016/j.bbrc.2007.05.206
32. Kimura M, Okano Y. Identification and assignment of the human NIMA-related protein kinase 7 gene (NEK7) to human chromosome 1q31.3. *Cytogenet Cell Genet.* (2001) 94:33–8. doi: 10.1159/000048779
33. Feige E, Motro B. The related murine kinases, Nek6 and Nek7, display distinct patterns of expression. *Mech Dev.* (2002) 110:219–23. doi: 10.1016/S0925-4773(01)00573-1
34. Salla M, Butler MS, Pelingon R, Kaeslin G, Croker DE, Reid JC, et al. Synthesis, and biological evaluation of the major human metabolite of NLRP3 inflammasome inhibitor MCC950. *Acs Med Chem Lett.* (2016) 7:1034–8. doi: 10.1021/acsmedchemlett.6b00198
35. Xu KY, Wu CY, Tong S, Xiong P, Wang SH. The selective Nlrp3 inflammasome inhibitor Mcc950 attenuates lung ischemia-reperfusion injury. *Biochem Biophys Res Commun.* (2018) 503:3031–7. doi: 10.1016/j.bbrc.2018.08.089
36. Zhang Y, Lv X, Hu Z, Ye X, Zheng X, Ding Y, et al. Protection of Mcc950 against high-glucose-induced human retinal endothelial cell dysfunction. *Cell Death Dis.* (2017) 8:e2941. doi: 10.1038/cddis.2017.308
37. Luo Y, Lu J, Ruan W, Guo X, Chen S. MCC950 attenuated early brain injury by suppressing NLRP3 inflammasome after experimental SAH in rats. *Brain Res Bull.* (2019) 146:320–6. doi: 10.1016/j.brainresbull.2019.01.027
38. Ren H, Kong Y, Liu Z, Zang D, Yang X, Wood K, et al. Selective NLRP3 (Pyrin Domain-Containing Protein 3) inflammasome inhibitor reduces brain injury after intracerebral hemorrhage. *Stroke.* (2018) 49:184–92. doi: 10.1161/STROKEAHA.117.018904
39. Chen I, Mitchell P. Serum potassium and sodium levels after subarachnoid haemorrhage. *Br J Neurosurg.* (2016) 30:554–9. doi: 10.1080/02688697.2016.1181151
40. Dreier JP, Woitzik J, Fabricius M, Bhatia R, Major S, Drenckhahn C, et al. Delayed ischaemic neurological deficits after subarachnoid haemorrhage are associated with clusters of spreading depolarizations. *Brain.* (2006) 129:3224–37. doi: 10.1093/brain/awl297
41. Gross CJ, Mishra R, Schneider KS, Medard G, Wettmarshausen J, Dittlein DC, et al. K(+) Efflux-independent NLRP3 inflammasome activation by small molecules targeting mitochondria. *Immunity.* (2016) 45:761–773. doi: 10.1016/j.immuni.2016.08.010
42. Xiong XY, Liu L, Yang QW. Functions and mechanisms of microglia/macrophages in neuroinflammation and neurogenesis after stroke. *Prog Neurobiol.* (2016) 142:23–44. doi: 10.1016/j.pneurobio.2016.05.001
43. Schneider UC, Davids AM, Brandenburg S, Muller A, Elke A, Magrini S, et al. Microglia inflict delayed brain injury after subarachnoid hemorrhage. *Acta Neuropathol.* (2015) 130:215–31. doi: 10.1007/s00401-015-1440-1
44. Yan N, Liu Y, Liu S, Cao S, Wang F, Wang Z, et al. Fluoride-induced neuron apoptosis and expressions of inflammatory factors by activating microglia in rat brain. *Mol Neurobiol.* (2016) 53:4449–60. doi: 10.1007/s12035-015-9380-2
45. Hinojosa AJ, Deogracias R, Rico B. The microtubule regulator NEK7 coordinates the wiring of cortical parvalbumin interneurons. *Cell Rep.* (2018) 24:1231–42. doi: 10.1016/j.celrep.2018.06.115
46. Freixo F, Martinez Delgado P, Manso Y, Sanchez-Huertas C, Lacasa C, Soriano E, et al. NEK7 regulates dendrite morphogenesis in neurons via Eg5-dependent microtubule stabilization. *Nat Commun.* (2018) 9:2330. doi: 10.1038/s41467-018-04706-7
47. Valdinocci D, Grant GD, Dickson TC, Pountney DL. Epothilone D inhibits microglia-mediated spread of alpha-synuclein aggregates. *Mol Cell Neurosci.* (2018) 89:80–94. doi: 10.1016/j.mcn.2018.04.006
48. Misawa T, Takahama M, Kozaki T, Lee H, Zou J, Saitoh T, et al. Microtubule-driven spatial arrangement of mitochondria promotes activation of the NLRP3 inflammasome. *Nat Immunol.* (2013) 14:454–60. doi: 10.1038/ni.2550
49. Keaney J, Campbell M. The dynamic blood-brain barrier. *FEBS J.* (2015) 282:4067–79. doi: 10.1111/febs.13412
50. Yang F, Wang Z, Wei X, Han H, Meng X, Zhang Y, et al. NLRP3 deficiency ameliorates neurovascular damage in experimental ischemic stroke. *J Cereb Blood Flow.* (2014) 34:660–7. doi: 10.1038/jcbfm.2013.242

Conflict of Interest: The authors declare that the research was conducted in the absence of any commercial or financial relationships that could be construed as a potential conflict of interest.

Copyright © 2020 Li, Dong, Liu, Zou, Hao, Gao, Pan and Liang. This is an open-access article distributed under the terms of the Creative Commons Attribution License (CC BY). The use, distribution or reproduction in other forums is permitted, provided the original author(s) and the copyright owner(s) are credited and that the original publication in this journal is cited, in accordance with accepted academic practice. No use, distribution or reproduction is permitted which does not comply with these terms.

frontiers in Neuroscience

ORIGINAL RESEARCH
published: 23 September 2020
doi: 10.3389/fnins.2020.576741

A Semiquantitative Non-invasive Measurement of PcomA Patency in C57BL/6 Mice Explains Variance in Ischemic Brain Damage in Filament MCAo

Samuel Knauss[1,2], Carolin Albrecht[1], Ulrich Dirnagl[1,2,3,4,5,6], Susanne Mueller[1,3,7], Christoph Harms[1,2,3,4], Christian Johannes Hoffmann[1,3], Stefan Paul Koch[1,3,7], Matthias Endres[1,2,3,4,5] and Philipp Boehm-Sturm[1,3,7]*

[1] Department of Neurology with Experimental Neurology, Charité-Universitätsmedizin Berlin, Corporate Member of Freie Universität Berlin, Humboldt-Universität zu Berlin, Berlin Institute of Health, Berlin, Germany, [2] German Center for Cardiovascular Research (DZHK), Partner Site Berlin, Berlin, Germany, [3] Center for Stroke Research Berlin, Charité-Universitätsmedizin Berlin, Berlin, Germany, [4] NeuroCure Clinical Research Center, Charité - Universitätsmedizin Berlin, Berlin, Germany, [5] German Center for Neurodegenerative Diseases (DZNE), Bonn, Germany, [6] Quality, Ethics, Open Science, Translation, Center for Transforming Biomedical Research, Berlin Institute of Health, Berlin, Germany, [7] NeuroCure Cluster of Excellence and Charité Core Facility 7T Experimental MRIs, Charité – Universitätsmedizin Berlin, Berlin, Germany

OPEN ACCESS

Edited by:
Yongting Wang,
Shanghai Jiao Tong University, China

Reviewed by:
Peiying Li,
Shanghai Jiao Tong University School of Medicine, China
Xingchun Gou,
Xi'an Medical University, China

***Correspondence:**
Samuel Knauss
samuel.knauss@charite.de

Specialty section:
This article was submitted to Neurodegeneration, a section of the journal Frontiers in Neuroscience

Received: *26 June 2020*
Accepted: *21 August 2020*
Published: *23 September 2020*

Citation:
Knauss S, Albrecht C, Dirnagl U, Mueller S, Harms C, Hoffmann CJ, Koch SP, Endres M and Boehm-Sturm P (2020) A Semiquantitative Non-invasive Measurement of PcomA Patency in C57BL/6 Mice Explains Variance in Ischemic Brain Damage in Filament MCAo. Front. Neurosci. 14:576741. doi: 10.3389/fnins.2020.576741

Numerous studies on experimental ischemic stroke use the filament middle cerebral artery occlusion (fMCAo) model in C57BL/6 mice, but lesion sizes in this strain are highly variable. A known contributor is variation in the posterior communicating artery (PcomA) patency. We therefore aimed to provide a semiquantitative non-invasive *in vivo* method to routinely assess PcomA patency. We included 43 male C57BL/6 mice from four independent studies using a transient 45 min fMCAo model. Edema-corrected lesion sizes were measured by magnetic resonance (MR) imaging 24 h after reperfusion. Time-of-flight MR angiography was performed 7 days before and 24 h after fMCAo. Scores of PcomA size measured 24 h after, but not scores measured 7 days before fMCAo were negatively correlated with lesion size. Variability in PcomA patency explained 30% of the variance in our cohort ($p < 0.0001$, coefficient of determination $r^2 = 0.3$). In a simulation using parameters typical for experimental stroke research, the power to detect a true effect of $d = 1$ between two groups increased by 15% when an according covariate was included in the statistical model. We have demonstrated that *in vivo* measurement of PcomA size is feasible and can lead to increased accuracy in assessing the effect of treatments.

Keywords: stroke, mouse, angiography, MRI, posterior communicating artery, lesion size

INTRODUCTION

Animal models of focal cerebral ischemia are a cornerstone of stroke research, as indicated by over 1.000 experimental treatments for acute stroke that have been evaluated in these models (O'Collins et al., 2006). A prerequisite for a successful translation of preclinical findings into clinical trial is selection of the correct target in preclinical experiments (Dirnagl and Macleod, 2009; Sena et al., 2010). Possibly the greatest risk to reproducibility of results and correct target selection comes from the omnipresence of small sample sizes and correspondingly low statistical power

(Button et al., 2013). Low statistical power can lead to overestimation of effect sizes and low positive predictive value of positive findings but also increases the risk of overlooking the true effects of therapeutics at an early stage (Button et al., 2013; Munafò et al., 2014). Here, we propose a method to increase power and reduce noise in one of the most widely used stroke models and one of the most common animal strains.

The intraluminal filament method of middle cerebral artery occlusion (fMCAo) is among the most commonly used methods to induce focal ischemic stroke in animal studies (Morris et al., 2016). In order to reduce the imbalance of covariates in preclinical stroke models, standard operating procedures and refinements to the methods have been formulated to control known determinants of outcome variables (Connolly et al., 1996; Dirnagl, 2012; Morris et al., 2016). Often, the variance in lesion size, which is one of the main outcome parameters, is as high as 40% of the mean, rendering the generation of robust and reproducible data with prevalently used small sample sizes difficult (Dirnagl, 2006). The extent of this variability greatly depends on the mouse strain used in the experiment (Yang et al., 1997; Kitagawa et al., 1998). One of the most commonly used mouse strains, but at the same time one of the strains with the largest variability in lesion size, is C57BL/6, due to its widespread use for generating genetically modified mice (Kitagawa et al., 1998; Maeda et al., 1998; McColl et al., 2004). One of the factors determining the variability in lesion size is the patency of the circle of Willis in this strain (Kitagawa et al., 1998; Maeda et al., 1998; McColl et al., 2004). Blood supply to the rodent brain is provided through four main arteries: two vertebral arteries posteriorly and two carotid arteries anteriorly. At the base of the brain, these arteries are connected by anastomoses, forming the circle of Willis, with two posterior communicating arteries and one anterior communicating artery. In 1998, Kitagawa showed that the patency of the posterior communicating artery (PcomA) is a crucial determinant of the lesion size in the fMCAo model (Kitagawa et al., 1998). Of note, nomenclature for the communicating arteries in mice is inconsistent in the literature. In this paper, we adhered to the nomenclature used in the work published by Kitagawa et al. (1998) describing the connecting artery between the superior cerebellar artery (SCA) and the posterior cerebral artery (PCA) as PcomA, which corresponds to the P1 segment of the human PCA (Xiong et al., 2017).

In this study, we sought to establish an *in vivo* imaging approach to assess the patency and size of the PcomA as a determinant of lesion size, to be used in adjusting for pre-existing differences in this important covariate. Including this variable in the statistical model to test for treatment effects in preclinical stroke models might increase power and precision to detect true effects and arrive at more precise estimates of effect sizes.

MATERIALS AND METHODS

Animals and Experimental Groups

All experimental procedures were approved by the "Landesamt für Gesundheit und Soziales Berlin" under registration numbers G0005/16, G0065/17 and G0261/17 and were in accordance with national and institutional guidelines for the care and use of laboratory animals and with directive 2010/63/EU of the European Parliament and of the Council of 22 September 2010. The reporting conforms to the ARRIVE guidelines (Kilkenny et al., 2010). A total of 33 C57BL/6J (group 1–3) and 10 C57BL/6N mice (group 4) (10 weeks old, mean weight 25 ± 2 g) were used from control groups of four studies testing different neuroprotective treatments. C57BL/6J and C57BL/6N mice were purchased from Charles River Germany, and the animals were housed in groups of 3–5 per cage with a standard light-dark cycle (12 h:12 h) and *ad libitum* access to food and water. Animals were rested for 7 days upon arrival to the laboratory. Investigating the association between PcomA patency and lesion size was pre-specified as an independent study goal in the study protocols. The animals included in the analysis for the present study were either naïve or treated with a vehicle depending on the respective group (non-reactive mGo53 Antibodies (Wardemann et al., 2003) for group 1 and 3, phosphate buffered saline for group 2 and no treatment for group 4. Group 1 ($n = 10$) was used to establish the method for MRA acquisition and semiquantitative measurement of PcomA size 24 h after fMCAo described below. Five animals in group 1 were used to study PcomA size *ex vivo* by Evans Blue perfusion after MRA acquisition. Group 2 and group 3 (group 2: $n = 13$; group 3: $n = 10$) underwent the same protocol of 45 min fMCAo followed by magnetic resonance imaging (MRI) and magnetic resonance angiography (MRA) 24 h after fMCAo. The sample size for group 2 was calculated assuming an effect size of $r^2 = 0.6$ at an $\alpha = 0.05$ and a power level of 0.8 based on results from group 1.

To test the robustness of the method, we included an additional group from another experimental hardware setup (group 4: $n = 10$). The protocols for 45 min fMCAo were the same in group 4 as in the other groups. The fMCAo surgery and MRI / MRA acquisition were performed by two independent researchers. Groups 2 and 4 underwent additional baseline MRA scans 7 days before fMCAo. **Figure 1** gives an overview of the experiments included in this study.

Randomization, Blinding, and Exclusion Criteria

For randomization, animals were numbered, and operation order was randomly assigned. For all protocols and outcome assessments, the experimenters were blinded. All outcome assessments were performed by observers blinded to previous treatments and outcomes. All animals included in the study ($n = 43$) were included in the analyses.

Model of Middle Cerebral Artery Occlusion in Mice

All experimental procedures were conducted by a trained experimenter following published standard operating procedures (Dirnagl, 2012). A transient fMCAo model was generated as described previously (Engel et al., 2011). Mice were anesthetized using 2.5% (vol/vol) isoflurane for induction and 1.5% (vol/vol) isoflurane for maintenance, mixed in both cases with 30% O_2 and ∼68% N_2O. After permanent occlusion of the ipsilateral external carotid and the common carotid artery, cerebral ischemia was

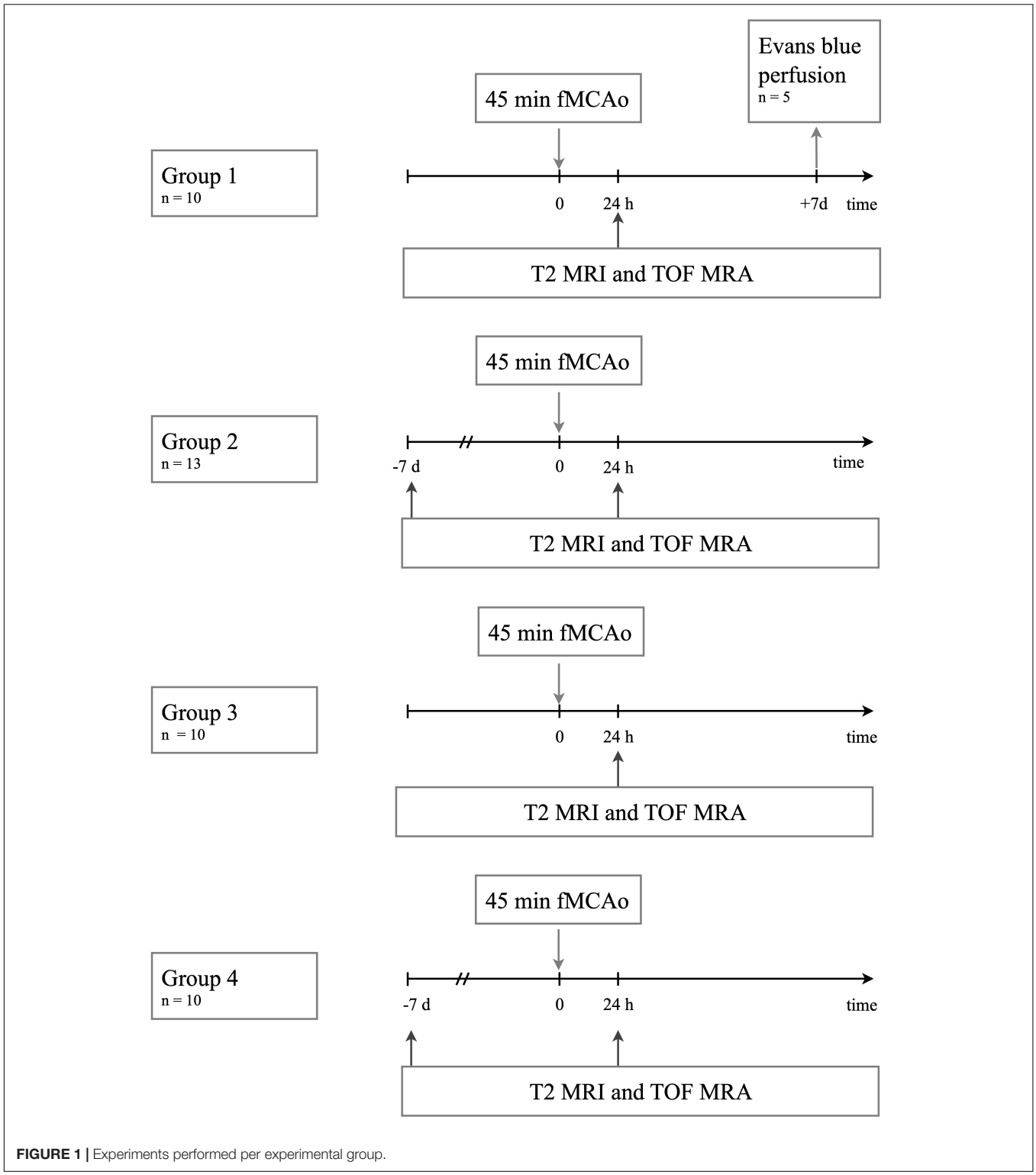

FIGURE 1 | Experiments performed per experimental group.

induced by introducing a 7-0 silicon-rubber-coated fMCAo suture with a coating length of 9–10 mm (monofilament 7019910PK5Re, Doccol Corp., Sharon MA, United States) into the left internal carotid artery and advancing it up to the anterior cerebral artery, thereby occluding the middle cerebral artery. The filament was withdrawn after an occlusion time of 45 min. Rectal temperature was maintained at 37.5 ± 0.5°C throughout the experiment using a feedback-controlled heating pad with a rectal probe (Fine Science Tools GmbH, Heidelberg, Germany). During fMCAo and for at least 2 h after reperfusion, animals

were allowed to recover in a heated cage (Peco Services, Cumbria, United Kingdom). Afterward, they were transferred to the home cage. After fMCAo, animals had access to soft food and were treated with subcutaneous saline injections to ensure adequate hydration after surgery.

Evans Blue Perfusion

For Evans Blue perfusion and vessel fixation, mice were deeply anaesthetized with ketamine and xylazine at the conclusion of the experiment and perfused through the heart with physiological saline followed by 4% paraformaldehyde, Termofisher, W32465, 3% Gelatin (Sigma-Aldrich, G1890), 1% low melting agarose (Sigma Aldrich A4018) and 0.1% Evans Blue (Sigma Aldrich E2129) as described previously (Foddis et al., 2019).

Magnetic Resonance Imaging

Magnetic resonance imaging (MRI) was conducted on a 7-Tesla rodent scanner running Paravision 5.1 software (Pharmascan 70/16, Bruker, Ettlingen, Germany) with a 16 cm horizontal bore magnet and a 9 cm (inner diameter) shielded gradient with a maximum gradient strength of 300 mT/m. Mice were anesthetized under 1.5% isoflurane in a mixture of 30% O_2/68.5% N_2O and scanned under constant respiration monitoring (Small Animal Monitoring & Gating System, SA Instruments, Stony Brook, New York, United States). Animals were placed prone and head fixed on a heated circulating water blanket to ensure a constant body temperature of $37 \pm 0.5°C$.

For groups 1–3, a 72 mm volume resonator (RAPID Biomedical, Rimpar, Germany) was used for transmission, and an actively decoupled mouse head surface coil was used for signal reception. After coil tuning and matching, scout images were acquired. Similar geometry of all scans across animals was assured by using the anterior commissure as a landmark in rostral-caudal direction and the trachea as a landmark in the other directions. T2-weighted images were acquired using a 2D turbo spin-echo sequence (2D RARE) with repetition time (TR) = 4200 ms, echo time (TE) = 36 ms, echo spacing (ΔTE) = 12 ms, RARE factor = 8, 4 averages, 32 contiguous axial slices with a slice thickness of 0.5 mm, field of view (FOV) = 25.6 × 25.6 mm^2, matrix size MTX = 256 × 256, bandwidth BW = 46875 Hz, and total acquisition time TA = 6 min 43 s). Angiography with matching geometry but higher resolution was performed with a non-flow compensated 3D-FLASH time-of-flight (TOF) sequence with TR/TE = 15 ms/2.5 ms, 1 ms sinc-shaped excitation pulse with 22 kHz bandwidth and flip angle FA = 20°, FOV = 25.6 × 25.6 × 16.0 mm^3, MTX = 256 × 223 × 139 zero filled to 256 × 256 × 160, BW = 98684 Hz, TA = 7 min 50 s.

For group 4, a transmit/receive quadrature volume resonator with an inner diameter of 20 mm (RAPID) was used. T2-weighted images were acquired with the same sequence as groups 1–3. Angiography with FOV centered to the FOV of the T2-weighted sequence was acquired with a 3D-FLASH TOF using identical settings as for groups 1–3 but TR/TE = 14 ms/2.3 ms, FOV = 19.2 × 19.2 × 16.0 mm^3, MTX = 192 × 167 × 139 zero filled to 192 × 192 × 160, TA = 5 min 29 s.

Atlas Registration

T2-weighted images were registered to the Allen Brain Atlas[1] as described previously (Koch et al., 2017) using ANTX[2], a custom MATLAB toolbox comprising a segmentation in SPMMouse[3] followed by non-linear warping of tissue probability maps in ELASTIX[4]. The calculated image transformation could then be applied to other images aligned with the T2-weighted scan, including TOF angiograms and lesion masks.

Corrected Lesion Volume

Lesion volume corrected for brain swelling was calculated as described previously (Koch et al., 2017). Briefly, ischemic tissue appearing hyperintense on T2-weighted images 24 h after stroke was manually delineated by an experienced researcher, carefully omitting ventricles, using ANALYZE 5.0 software (AnalyzeDirect, Overland Park, KS, United States), and masks of the same dimensionality as the T2-weighted image were exported in NIFTI format. Using nearest neighbor interpolation, lesion masks were registered to the Allen Brain Atlas. Edema-corrected lesion volume in percent was defined as the volume of the lesion divided by volume of the hemisphere measured in atlas space.

Semiquantitative Assessment of PcomA Patency

ImageJ distribution 1.51m9 (Schneider et al., 2012) was used for post-processing atlas-registered angiograms to obtain scores for PcomA patency and size. Atlas registration allowed us to determine a set of 10 slices that contained the posterior part of the circle of Willis in all animals. To render pixel intensity comparable between individual datasets, we then calculated the signal-to-noise ratio (SNR) of each dataset adjusted as described previously (Gudbjartsson and Patz, 1995; Boehm-Sturm et al., 2011) and set a threshold to 1/10 of the maximum intensity of the dataset, setting all other values to NaN. In the next step, the area between the superior cerebellar artery (SCA) and posterior cerebral artery (PCA) was manually delineated on all selected slices. The maximum SNR in this area depends on background intensity and on the flow signal present, with higher intensities for higher flow. The only larger vessel in this anatomical area is the PcomA (Xiong et al., 2017). We therefore used the maximum SNR measured over the stack of slices as a correlate and semiquantitative score of the flow and thus the patency of the PcomA. Only the side ipsilateral to the ischemic lesion was assessed. ImageJ code is available on www.figshare.com at https://www.doi.org/10.6084/m9.figshare.8950328.

Validation by Manual *in vivo* and *ex vivo* Assessments of PcomA

The semiquantitative assessment of PcomA patency was correlated to an *in vivo* score of PcomA size in the described

[1]http://portal.brain-map.org/

[2]Latest version available under https://github.com/ChariteExpMri/antx2

[3]http://www.spmmouse.org/

[4]http://elastix.isi.uu.nl/

target region assessed and rated from 0 (meaning no vessel) to 3 (large vessel) using the same postprocessing as described above.

To quantitatively validate *in vivo* assessment of PcomA size, a subset of animals was perfused with Evans Blue and *ex vivo* photographs of excised brains were taken. PcomA size was measured in percent of the basilar artery *in vivo* on maximum intensity projections of raw TOF images and *ex vivo* on Evans Blue labeled vasculature.

Simulation

A statistical program was developed in STATA 13.0 (StataCorp, College Station, United States) to simulate a hypothetical two-arm trial testing the effect of a hypothetical treatment. The simulation code was based on work by Egbewale et al. (2014) describing the method to simulate data for clinical trials. Based on assumptions common in preclinical stroke research (Howells et al., 2012), we set the standardized effect size at $d = 1.0$. Setting the α error probability at 0.05 and the power at 0.8, we set the sample size at $n = 14$ per group. A normally distributed covariate with varying degrees of correlation with the outcome variable was introduced. Five different experimental conditions with correlation coefficients between the covariate and the outcome variable of $r^2 = 0$, 0.01, 0.04, 0.09, 0.16, 0.25, 0.29, 0.36, 0.49, and 0.64 were simulated. Outcome analysis was performed by either ANOVA or ANCOVA adjusting for the covariate in each individual experiment. Each hypothetical scenario and outcome analysis combination was repeated 1000 times to obtain reliable estimates of actual power. STATA code is available on www.figshare.com at https://www.doi.org/10.6084/m9.figshare.9752834.

Statistical Evaluation

Data are represented as the Pearson correlation coefficient r or as the coefficient of determination r^2 and calculated probability value (p-value) using the general linear model. For testing of manual ratings measured on an ordinal scale, data are represented as Spearman rank-order correlation coefficient r_S.

Data Availability

Source code for the simulation in STATA and the code for the macro used to postprocess images for semiquantitative measurement in ImageJ are available in the Appendix. All relevant original and Allen Brain Atlas-registered images are publicly available at http://doi.org/10.6084/m9.figshare.9752864.

RESULTS

TOF MRA Can Image PcomA Size After fMCAo

PcomA size was assessed *ex vivo* 7 days after fMCAo in five animals of group 1 (**Figure 2**). *Ex vivo* PcomA vessel size was measured after Evans Blue perfusion in relation to the size of the basilar artery and compared to corresponding measurements obtained *in vivo* 24 h after fMCAo by MR angiography. PcomA size measured by MRA was highly correlated ($n = 5$, $r^2 = 0.81$) with *ex vivo* PcomA size measurements, yet statistical significance was not reached ($p = 0.057$).

Semiquantitative Measurement of PcomA Patency by MRA Is Correlated With Manual PcomA Size Ratings

To validate the semiquantitative measurement of PcomA patency with an independent data analysis method, we compared semiquantitative measurements to independently conducted manual ratings (**Figure 3**). All imaging studies followed the same procedure of atlas registration before being further processed for unbiased semiquantitative measurement. The same atlas-registered datasets were used for evaluation by three trained raters blinded to the total lesion volume. Raters were trained with a standard set from group 1. There was a good correlation of manually rated PcomA size and semiquantitative measurement of PcomA patency (Spearman rank-order correlation coefficient

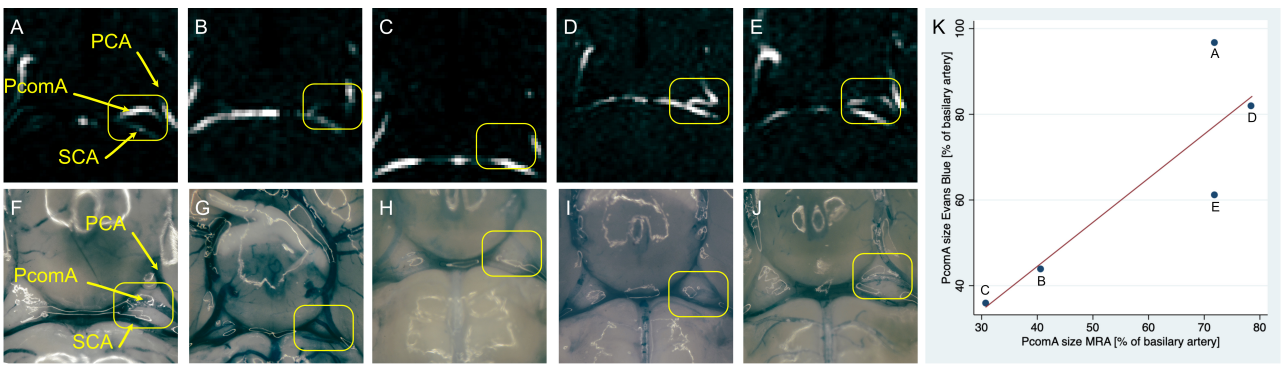

FIGURE 2 | TOF MRA images and corresponding images of vasculature after Evans Blue perfusion. TOF-MR angiography 24 h after fMCAo readily images the circle of Willis and PcomA **(A–E)**. Evans Blue perfusion 7 days after fMCAo clearly depicts the corresponding vasculature **(F–J)**. Yellow boxes highlight the PcomA ipsilateral to the ischemic lesion. Individual data points of images **(A–J)**, respectively, comparing readings of PcomA diameter as percentage of basilar artery diameter from MRA and from images after Evans Blue perfusion **(K)**. PCA – posterior cerebral artery, PcomA – posterior communicating artery, SCA – superior cerebellar artery.

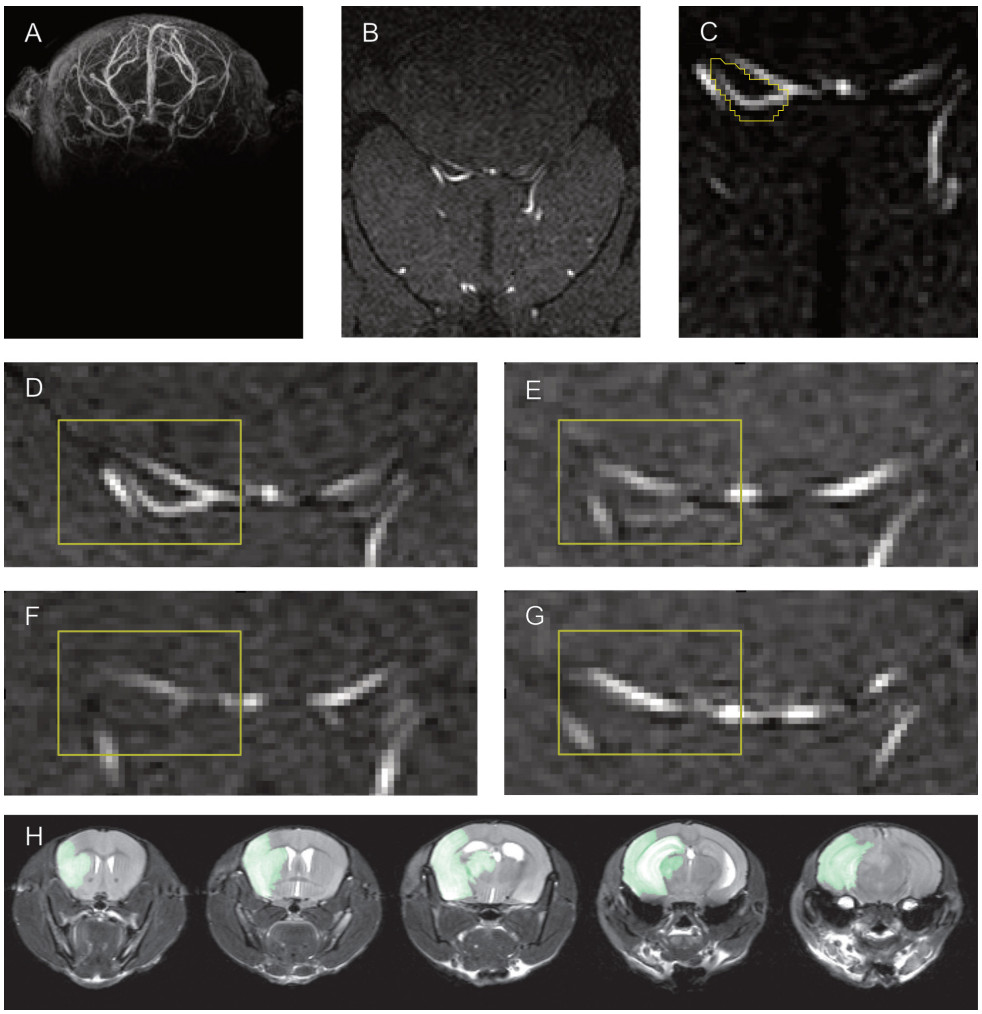

FIGURE 3 | Semiquantitative measurement of PcomA size and manual PcomA assessment. Whole brain TOF MRA recordings **(A)** were normalized to the Allen Brain atlas **(B)** to define a set of slices that contain the location of the PcomA in all animals. Semiquantitative measurements of PcomA patency were taken by assessing the maximum SNR in a manually delineated region of interest between the SCA and the PCA **(C)** in these slices. Examples of Allen atlas-normalized maximum intensity projections with large **(D)**, medium **(E)**, small **(F)** and absent **(G)** PcomA used for the training of raters to manually rate PcomA size. Examples of T2 MRI images used to obtain a mask of the ischemic lesion **(H)**.

$r_S = 0.7$, $p < 0.0001$). Ratings for the size of the PcomA on each side varied between independent raters, but interrater reliability was high (interclass correlation = 0.9, $p < 0.001$).

Semiquantitative Measurement of PcomA Patency Partially Explains Variability in Lesion Size

Unbiased semiquantitative measurement of PcomA patency from TOF angiograms recorded at 24 h after fMCAo significantly negatively correlated with lesion size determined by T2 weighted MRI at 24 h (**Figure 4**) in 4 independent datasets. In the first training set, 62% of intersubject variability of total lesion size was explained by PcomA patency ($r^2 = 0.62$) alone. Applying this algorithm to three independent datasets, 16–49% ($r^2 = 0.16$–0.49) (**Table 1**) of variability in lesion size in these individual groups was explained by differences in semiquantitative PcomA patency measurements. Pooling data from all groups resulted in a highly significant correlation explaining 34% of the variance in the dataset, $r^2 = 0.34$, $p < 0.0001$ (**Figure 5**).

Semiquantitative Measurement of PcomA Patency Prior to fMCAo Cannot Reliably Predict Infarct Size

There was a moderate correlation between mean manual PcomA size ratings before fMCAo and unbiased semiquantitative measurement of PcomA patency 24 h after fMCAo ($r = 0.63$, $r^2 = 0.40$, $p = 0.001$). While there was still a trend for a moderate correlation between mean manual PcomA size ratings before fMCAo and MRI lesion size 24 h after fMCAo (Spearman rank-order correlation coefficient $r = -0.40$, $p = 0.051$), semiquantitative PcomA measurement before fMCAo did not reliably predict lesion size across 2 datasets (group 2 and group

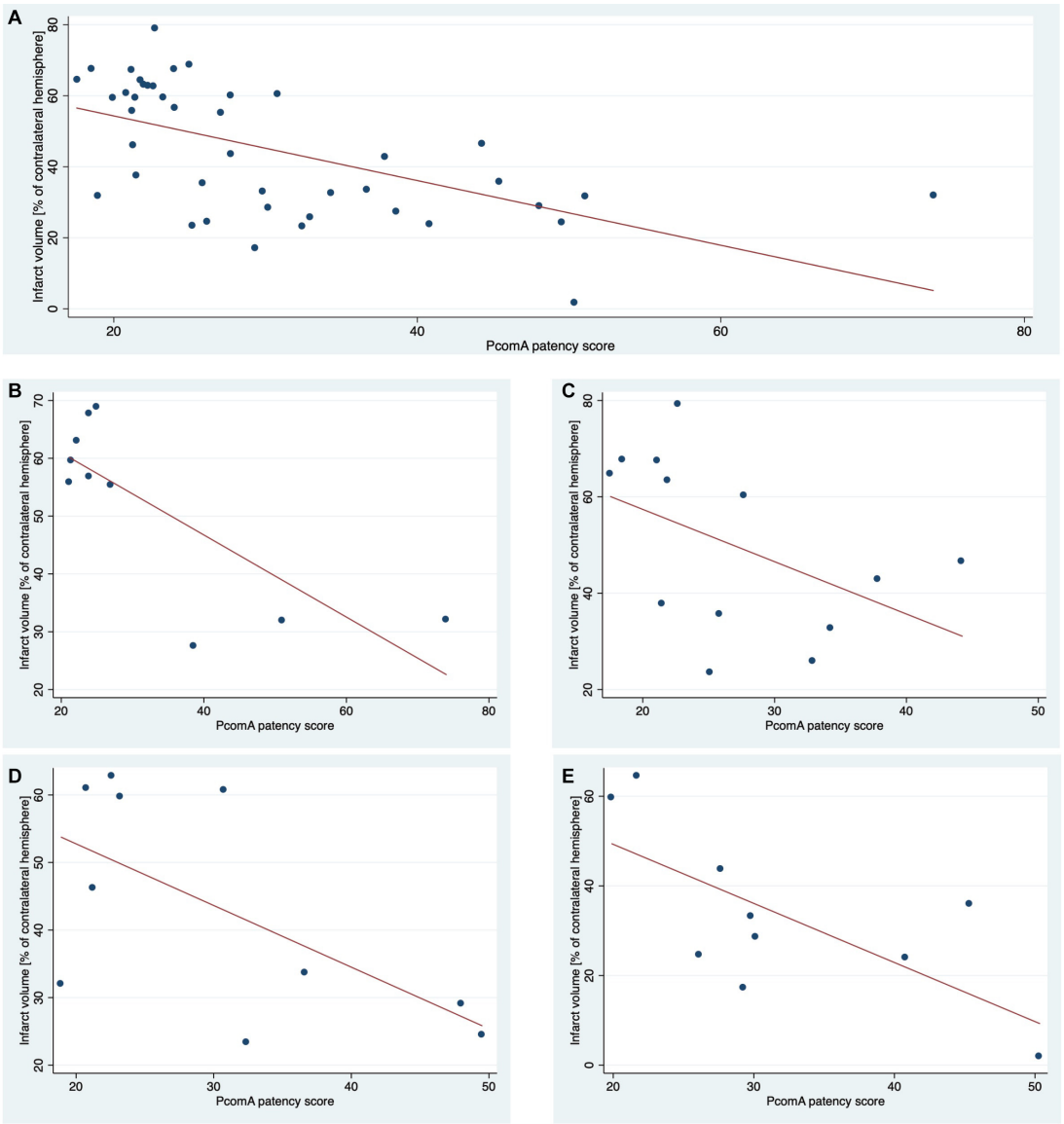

FIGURE 4 | Correlation of PcomA score and lesion size 24 h after fMCAo. Lesion sizes of each animal included in this study and corresponding semiquantitative scores of PcomA patency **(A)**. A method to obtain PcomA scores was developed using group 1 **(B)**. The results were replicated in three additional independent groups 2–4 **(C–E)**.

4; $r = -0.0186$, $r^2 = 0.0003$, $p = 0.933$). For group 1 and group 3, no baseline MRA before fMCAo was recorded.

Including PcomA Size as a Covariate Increases Power in a Simulation Preclinical Stroke Study

We conducted a simulation experiment to test whether the power of the final outcome analysis increases by including a covariate with the magnitude of correlation found for the association between PcomA patency and lesion size in this study. In this simulation, the power to detect an effect with a standardized effect size of $d = 1$ increased by 12% when adjusting for a covariate with a correlation coefficient of $r^2 = 0.25$ and further increased for stronger associations between the covariate and the outcome variable (**Figure 5**).

Distribution of PcomA Phenotypes in C57BL/6 Mice and Correlation With Lesion Size

The vascular anatomy was examined using TOF MRA images recorded 24 h after fMCAo and separate manual ratings of whether the PcomA was patent on each side. In our cohort, we found a complete circle of Willis in 21% (9/43), a patent PcomA on one side in 53% (23/43) and a bilateral lack of patent PcomAs

TABLE 1 | Correlation of semiquantitative scores of PcomA patency and lesion size 24 h after fMCAo.

Group	*n*	Correlation coefficient (*R*)	Coefficient of determination (R^2)	*p*
Group 1	10	−0.76	0.62	<0.01
Group 2	13	−0.4	0.16	0.09
Group 3	10	−0.61	0.38	0.05
Group 4	10	−0.7	0.49	0.023
All Groups	43	−0.58	0.34	<0.0001

in 26% (11/43) of animals. Ischemic lesion size was significantly correlated with PcomA phenotype, with smaller lesion sizes in animals with a complete circle of Willis ($r^2 = 0.32$, $p = 0.0001$).

DISCUSSION

We developed an easy-to-implement semiquantitative method to assess PcomA patency *in vivo* using readily available standard mouse MRI sequences. We demonstrated that the obtained dimensionless score negatively correlates with the lesion size after fMCAo in C57BL/6 mice. In a simulation experiment representative of common study designs in preclinical stroke research, we showed that by including this score as a covariate in the model, the power to detect a true effect increased by almost 20%.

The fMCAo model is widely used to model human focal cerebral ischemia (Kleinschnitz et al., 2015). One of its inherent disadvantages is the high intersubject variability of common outcome parameters. Several variables have been shown to impact lesion volume, one of the most important outcome parameters (Morris et al., 2016); including different parameters of the model itself, such as the occlusion and recovery time (Harada et al., 2005; Liu et al., 2009), the filament and anesthetic used (Michenfelder et al., 1976; Tsuchiya et al., 2003), differences in the surgical technique (Chen et al., 2008) as well as parameters of the animals, such as the species (Carmichael, 2005), strain (Yang et al., 1997; Kitagawa et al., 1998), substrain (Zhao et al., 2019), sex (Alkayed et al., 1998; Zhao et al., 2019), age (Sutherland et al., 1996), and interindividual variation in cerebrovascular anatomy (Barone et al., 1993; Kitagawa et al., 1998; McColl et al., 2004). Species and strain differences in the cerebrovascular architecture and in particular differences in the patency of macroanastomoses formed in the circle of Willis have already been studied previously (Barone et al., 1993; Kitagawa et al., 1998; McColl et al., 2004). In a study in 1998, Kitagawa and colleagues demonstrated species and strain differences of the circle of Willis in mice (Kitagawa et al., 1998; Ankolekar et al., 2012). In the same study, they were able to establish patency of the PcomA as a determinant of parenchymal ATP drop in a model of bilateral carotid artery occlusion and mortality and lesion size in fMCAo. To predict the vascular anatomy, they proposed a method using laser Doppler flow measurement of cerebral microvascular perfusion and a one-minute bilateral common carotid artery (CCA) occlusion. However, this method could neither determine whether the PcomA was patent on one or both sides nor detect the side of a unilaterally patent PcomA. The authors concluded that PcomA

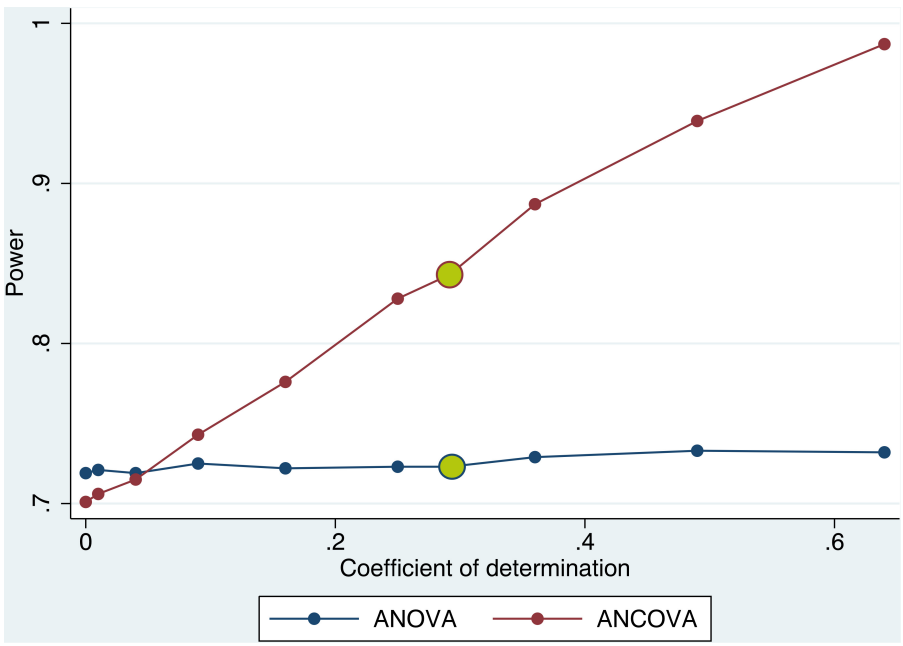

FIGURE 5 | Power to detect an effect of $d = 1$ with and without adjusting for a covariate. Adjusting for a single covariate in the outcome analysis (ANCOVA) increased the power to detect a true effect by up to 25% compared to no adjustment (ANOVA) depending on the magnitude of the correlation coefficient of covariate and outcome variable. Effect size $d = 1$, $n = 14$ per group, 1000 repetitions per condition. Coefficient of determination found in this study for the association of PcomA score and lesion size marked in yellow ($r^2 = 0.34$).

patency should be assessed for every animal in models of cerebral ischemia, but that their own method could be used only to predict forebrain ischemia after bilateral CCA occlusion and not for unilateral MCAo. Additional evidence of the impact of PcomA patency and the variability of PcomA patency in C57BL/6J mice comes from McColl and colleagues: in a small sample of 10 C57BL/6J mice, they found a complete circle of Willis in only 1 animal. In 6 animals, the PcomA was patent only unilaterally, and in another 3 animals, no patent PcomA was found (McColl et al., 2004). In our own cohort of 43 animals, we found a slightly different distribution: we confirmed that a plurality of animals had a single patent PcomA, while almost equal numbers of animals had bilaterally patent PcomAs and complete absence of the posterior part of the circle of Willis. The notion of PcomA patency being one of the main determinants of mortality and lesion size in the fMCAo model is corroborated by a recent exploratory study by Foddis et al. (2019) reporting an almost equal distribution among different PcomA phenotypes (no patent PcomA, unilateral patent PcomA or bilateral patent PcomAs). While the distribution of patent PcomA in C57BL/6 mice in that study differs from the report by McColl and colleagues and our own findings, it still confirms the general conclusion of a high degree of variability in C57BL/6 mice.

Randomization is a cornerstone of all trials of treatment effects. Randomization seeks to prevent bias in the allocation of subjects to treatment groups and is the prerequisite of any statistical testing. To ensure balanced distribution of all known and unknown covariates influencing the dependent variable(s), is the primary goal of randomization. Imbalance in covariates that strongly correlate and determine the outcome variable can lead to an overestimation of the treatment effect or to false negative results, depending on the direction of correlation and the level of imbalance. For clinical trials, methods to adjust for imbalances of known covariates both at the design stage (i.e., stratification) as well as at the stage of data analysis (i.e., by including the covariates in the statistical model) have been commonly adopted (Schneider et al., 2012). The risk of imbalance grows with increasing levels of variability of a given variable in the statistical population and with decreasing sample size. Smaller sample sizes are also associated with an increasing effect of any imbalance in covariates on precision, effect size and power (Button et al., 2013). In preclinical biomedical research, sample sizes are often under 10 animals per group (Button et al., 2013), increasing the impact of imbalance of covariates, especially those (such as PcomA patency) that are strongly correlated with the outcome parameter. We therefore argue that adjustments for imbalances in the distribution of animals with different PcomA statuses could be beneficial for all stroke studies using C57BL/6 mice.

In recent years, high-resolution mouse MRI has become widely available at almost all large stroke research centers. Beckmann and colleagues have demonstrated that high-resolution MRA can be used to non-invasively image cerebrovascular anatomy, including large collaterals in the circle of Willis in mice (Beckmann et al., 1999; Beckmann, 2000). Building on this work, we and others have refined MRA protocols to obtain high-resolution MRA in less than 10 min per animal, rendering the technique applicable for routine use in preclinical stroke research when MRI is included in the study design. Beckman and colleagues proposed using this method for selecting or stratifying animals according to the PcomA status. However, our current data on the inconsistent association of PcomA patency evaluated before fMCAo and the ischemic lesion size, as well as data reported in a recent study by Foddis and colleagues, highlight challenges of this approach (Foddis et al., 2019).

There are several possible explanations for the failure to predict lesion size from pre-fMCAo PcomA evaluation. It is possible that the resolution currently available in TOF MRA sequences is not sufficient to distinguish between smaller PcomA vessel diameters in preischemic conditions. This notion is support by our finding of a moderate, yet statistically not significant ($p = 0.051$), correlation of manual PcomA size ratings before fMCAo and infarct size 24 h after fMCAo, a signal not picked up by our semiquantitative score for PcomA patency. Studies using contrast-enhanced MRA with a cryogenically cooled MR coil and extended recording time demonstrated the technical possibility of imaging vessels with diameters of down to 40 μm (Klohs et al., 2012). Further studies using this technique would be needed to validate this hypothesis. Contrast-enhanced MRA, however, requires long sequences and is inherently invasive, rendering this method less suitable for routine use. In line with the findings reported in this study, Foddis and colleagues found PcomA to be small and not reliably identifiable on MRA in naïve conditions, while under postischemic conditions PcomA is recruited and reaches a vessel size of up to 60% of the basilar artery diameter (Foddis et al., 2019). Despite our finding of a moderate correlation of manual PcomA scores pre-fMCAo and semiquantitative PcomA scores after fMCAo, this might indicate that preischemic PcomA size is only one of several determinants of PcomA perfusion under ischemic conditions. Interindividual differences in collateral recruitment under hypoperfusion might also play a role. In fact, our finding of no reliable prediction of lesion size by preischemic PcomA scores suggests that not the preischemic anatomical size of the PcomA but the postischemic flow after collateral recruitment is what determines ischemic lesion size. Collateral status has recently been shown to be a key predictor of lesion size evolution in the first 24 h in humans (Rao et al., 2020). It can thus be hypothesized that postischemic PcomA flow as measured in this study is only a correlate of a general level of collateral recruitment in the individual animal determining the size of the ischemic lesion. In this scenario, interindividual differences concerning collateral recruitment might be more important for lesion development than the initial PcomA vessel size pre fMCAo. We therefore argue that using a measurement of the postischemic PcomA status by TOF MRA obtained 24 h after fMCAo as a covariate in the outcome analysis is most relevant to adjust for imbalances in interindividual differences of cerebrovascular anatomy and function.

The inaptitude to measure PcomA patency as a determinant of ischemic lesion size in naïve, pre-fMCAo condition is at the same time one to the strongest limitations of the proposed approach. In the case of a treatment paradigm with early treatment within the first 24 h or pre-fMCAo treatment paradigms, the interaction

of the treatment and the PcomA size cannot be excluded. This is particularly problematic for treatments targeting collateral recruitment. In these cases, adjusting for PcomA patency bears the risk of reducing power to detect the treatment effect and cannot be recommended. For experimental paradigms with postischemic treatment randomization later than 24 h after fMCAo, the proposed approach would allow for combining stratified randomization for PcomA status and including PcomA status as a covariate using ANCOVA to control for imbalances of this important covariate. In our study, we focused on variability in acute lesion size as one of the most widely used outcome parameters in experimental ischemic stroke studies and did not include long-term behavioral outcomes. Impact of PcomA patency on long-term behavioral outcomes should be assessed in future studies to test robustness of the proposed approach. To further improve robustness of the described approach and reduce potential bias, we aim to eliminate the currently still required manual input in delineation of the target area and automatise area selection for future studies. A general limitation of the method used, is the indirect measurement of cerebral blood flow (CBF) by morphological TOF MRA imaging. To better assess functional patency and blood flow and relate it to morphological PcomA status, additional measurement of CBF by non-invasive aterial spin labeling (ASL) would be desirable. The scope of the presented work was to use highly standardized widely available sequences easily applicable to routine protocols. We thus did not implement ASL in the current study protocol.

In conclusion, we have shown that including a semiquantitative score of PcomA patency obtained 24 h after fMCAO in the statistical model can explain a large share of previously unexplained intersubject variability in lesion size and thus increase the power to detect treatment effects in preclinical stroke studies. The methods used are easy to implement for study designs with MR imaging. Based on the findings in this study, we therefore suggest to, (i) record an TOF MRA 24 h after fMCAo followed by semiquantitative PcomA measurement in any protocol evaluating experimental stroke therapies in the subacure phase after stroke, (ii) include the semiquantitative score of PcomA patency in the statistical model for outcome assessment. We believe that, mirroring standard procedures in clinical trials for which adjustment for known covariates has become state-of-the-art, similar practices should be adopted for preclinical trials to improve efficiency in therapy selection for clinical translation.

DATA AVAILABILITY STATEMENT

The datasets presented in this study can be found in online repositories. The names of the repository/repositories and accession number(s) can be found below: https://figshare.com/s/117e284677bdbedf08e7; https://figshare.com/s/d1a9072c420c43ed908e; and https://figshare.com/s/e8e03096082a1d5c0f4f.

ETHICS STATEMENT

The animal study was reviewed and approved by the Landesamt für Gesundheit und Soziales Berlin.

AUTHOR CONTRIBUTIONS

SK, CA, UD, SM, CH, CJH, SPK, ME, and PB-S contributed to designing and planning the experiments as well as obtaining official licenses to conduct this study. SK performed the fMCAo surgeries and blinded outcome analyses. CA, SM, and CJH acquired the MRA and MRI datasets. SK, PB-S, and SPK contributed in image normalization and atlas registration. ME, CH, SK, and UD contributed in covariate analysis and simulation design. All authors contributed in drafting and revising the manuscript and approved the manuscript for publication.

FUNDING

Funding was provided by the German Federal Ministry of Education and Research under the ERA-NET NEURON scheme (BMBF 01EW1811), the German Research Foundation (DFG research grant BO 4484/2-1 and EXC NeuroCure) and Fondation Leducq Transatlantic Network of Excellence 15CVD02.

ACKNOWLEDGMENTS

We thank David Schreiber for helping with the logistics of the MRI measurements and Janet Lips for support with animal logistics and handling.

REFERENCES

Alkayed, N. J., Harukuni, I., Kimes, A. S., London, E. D., Traystman, R. J., Hurn, P. D., et al. (1998). Gender-linked brain injury in experimental stroke. *Stroke* 29, 159–166. doi: 10.1161/01.str.29.1.159

Ankolekar, S., Rewell, S., Howells, D. W., and Bath, P. M. W. (2012). The influence of stroke risk factors and comorbidities on assessment of stroke therapies in humans and animals. *Int. J. Stroke* 7, 386–397. doi: 10.1111/j.1747-4949.2012.00802.x

Barone, F. C., Knudsen, D. J., Nelson, A. H., Feuerstein, G. Z., and Willette, R. N. (1993). Mouse strain differences in susceptibility to cerebral ischemia are related to cerebral vascular anatomy. *J. Cereb. Blood Flow Metab.* 13, 683–692. doi: 10.1038/jcbfm.1993.87

Beckmann, N. (2000). High resolution magnetic resonance angiography non-invasively reveals mouse strain differences in the cerebrovascular anatomy in vivo. *Magnet. Reson. Med.* 44, 252–258. doi: 10.1002/1522-2594(200008)44:2<252::aid-mrm12>3.0.co;2-g

Beckmann, N., Stirnimann, R., and Bochelen, D. (1999). High-resolution magnetic resonance angiography of the mouse brain: application to murine focal cerebral ischemia models. *J. Magn. Reson.* 140, 442–450. doi: 10.1006/jmre.1999.1864

Boehm-Sturm, P., Mengler, L., Wecker, S., Hoehn, M., and Kallur, T. (2011). In vivo tracking of human neural stem cells with 19F magnetic resonance imaging. *PLoS One* 6:e29040. doi: 10.1371/journal.pone.0029040

Button, K. S., Ioannidis, J. P. A., Mokrysz, C., Nosek, B. A., Flint, J., Robinson, E. S. J., et al. (2013). Power failure: why small sample size undermines the

reliability of neuroscience. *Nat. Rev. Neurosci.* 14, 365–376. doi: 10.1038/nrn3475

Carmichael, S. T. (2005). Rodent models of focal stroke: size, mechanism, and purpose. *Neurorx* 2, 396–409. doi: 10.1602/neurorx.2.3.396

Chen, Y., Ito, A., Takai, K., and Saito, N. (2008). Blocking pterygopalatine arterial blood flow decreases infarct volume variability in a mouse model of intraluminal suture middle cerebral artery occlusion. *J. Neurosci. Meth.* 174, 18–24. doi: 10.1016/j.jneumeth.2008.06.021

Connolly, E. S. Jr., Winfree, C. J., Stern, D. M., Solomon, R. A., and Pinsky, D. J. (1996). Procedural and strain-related variables significantly affect outcome in a murine model of focal cerebral ischemia. *Neurosurgery* 38, 523–532. doi: 10.1227/00006123-199603000-00021

Dirnagl, U. (2006). Bench to bedside: the quest for quality in experimental stroke research. *J. Cereb. Blood Flow Metab.* 26, 1465–1478. doi: 10.1038/sj.jcbfm.9600298

Dirnagl, U. (2012). Standard operating procedures (SOP) in experimental stroke research: SOP for middle cerebral artery occlusion in the mouse. *Nat. Précéd.* doi: 10.1038/npre.2012.3492.3

Dirnagl, U., and Macleod, M. R. (2009). Stroke research at a road block: the streets from adversity should be paved with meta-analysis and good laboratory practice. *Br. J. Pharmacol.* 157, 1154–1156. doi: 10.1111/j.1476-5381.2009.00211.x

Egbewale, B. E., Lewis, M., and Sim, J. (2014). Bias, precision and statistical power of analysis of covariance in the analysis of randomized trials with baseline imbalance: a simulation study. *BMC Med. Res. Methodol.* 14:49. doi: 10.1186/1471-2288-14-49

Engel, O., Kolodziej, S., Dirnagl, U., and Prinz, V. (2011). Modeling stroke in mice - middle cerebral artery occlusion with the filament model. *J. Vis. Exp. Jove.* 2011:2423. doi: 10.3791/2423

Foddis, M., Winek, K., Bentele, K., Mueller, S., Blumenau, S., Reichhart, N., et al. (2019). An exploratory investigation of brain collateral circulation plasticity after cerebral ischemia in two experimental C57BL/6 mouse models. *J. Cereb. Blood Flow Meta.* 40, 276–287. doi: 10.1177/0271678x19827251

Gudbjartsson, H., and Patz, S. (1995). The rician distribution of noisy mri data. *Magnet. Reson. Med.* 34, 910–914. doi: 10.1002/mrm.1910340618

Harada, H., Wang, Y., Mishima, Y., Uehara, N., Makaya, T., and Kano, T. (2005). A novel method of detecting rCBF with laser-Doppler flowmetry without cranial window through the skull for a MCAO rat model. *Brain Res. Protoc.* 14, 165–170. doi: 10.1016/j.brainresprot.2004.12.007

Howells, D. W., Sena, E. S., O'Collins, V., and Macleod, M. R. (2012). Improving the efficiency of the development of drugs for stroke. *Int. J. Stroke* 7, 371–377. doi: 10.1111/j.1747-4949.2012.00805.x

Kilkenny, C., Browne, W. J., Cuthill, I. C., Emerson, M., and Altman, D. G. (2010). Improving bioscience research reporting: the ARRIVE guidelines for reporting animal research. *PLoS Biol.* 8:e1000412. doi: 10.1371/journal.pbio.1000412

Kitagawa, K., Matsumoto, M., Yang, G., Mabuchi, T., Yagita, Y., Hori, M., et al. (1998). Cerebral ischemia after bilateral carotid artery occlusion and intraluminal suture occlusion in mice: evaluation of the patency of the posterior communicating artery. *J. Cereb. Blood Flow Metab.* 18, 570–579. doi: 10.1097/00004647-199805000-00012

Kleinschnitz, C., Fluri, F., and Schuhmann, M. (2015). Animal models of ischemic stroke and their application in clinical research. *Drug Des. Dev. Ther.* 9, 3445–3454. doi: 10.2147/dddt.s56071

Klohs, J., Baltes, C., Princz-Kranz, F., Ratering, D., Nitsch, R. M., Knuesel, I., et al. (2012). Contrast-enhanced magnetic resonance microangiography reveals remodeling of the cerebral microvasculature in transgenic ArcAβ Mice. *J. Neurosci.* 32, 1705–1713. doi: 10.1523/jneurosci.5626-11.2012

Koch, S., Mueller, S., Foddis, M., Bienert, T., von Elverfeldt, D., Knab, F., et al. (2017). Atlas registration for edema-corrected MRI lesion volume in mouse stroke models. *J. Cereb. Blood Flow Metab.* 39, 313–323. doi: 10.1177/0271678x17726635

Liu, F., Schafer, D. P., and McCullough, L. D. (2009). TTC, Fluoro-Jade B and NeuN staining confirm evolving phases of infarction induced by middle cerebral artery occlusion. *J. Neurosci. Meth.* 179, 1–8. doi: 10.1016/j.jneumeth.2008.12.028

Maeda, K., Hata, R., and Hossmann, K.-A. (1998). Differences in the cerebrovascular anatomy of C57Black/6 and SV129 mice. *Neuroreport* 9:1317. doi: 10.1097/00001756-199805110-00012

McColl, B. W., Carswell, H. V., McCulloch, J., and Horsburgh, K. (2004). Extension of cerebral hypoperfusion and ischaemic pathology beyond MCA territory after intraluminal filament occlusion in C57Bl/6J mice. *Brain Res.* 997, 15–23. doi: 10.1016/j.brainres.2003.10.028

Michenfelder, J. D., Milde, J. H., and Sundt, T. M. (1976). Cerebral protection by barbiturate anesthesia: use after middle cerebral artery occlusion in java monkeys. *Arch. Neurol. Chicago* 33, 345–350. doi: 10.1001/archneur.1976.00500050031006

Morris, G. P., Wright, A. L., Tan, R. P., Gladbach, A., Ittner, L. M., and Vissel, B. (2016). A Comparative study of variables influencing ischemic injury in the longa and koizumi methods of intraluminal filament middle cerebral artery occlusion in mice. *PLoS One* 11:e0148503. doi: 10.1371/journal.pone.0148503

Munafò, M., Noble, S., Browne, W. J., Brunner, D., Button, K., Ferreira, J., et al. (2014). Scientific rigor and the art of motorcycle maintenance. *Nat. Biotechnol.* 32, 871–873. doi: 10.1038/nbt.3004

O'Collins, V. E., Macleod, M. R., Donnan, G. A., Horky, L. L., van der Worp, B. H., and Howells, D. W. (2006). 1,026 experimental treatments in acute stroke. *Ann. Neurol.* 59, 467–477. doi: 10.1002/ana.20741

Rao, V. L., Mlynash, M., Christensen, S., Yennu, A., Kemp, S., Zaharchuk, G., et al. (2020). Collateral status contributes to differences between observed and predicted 24-h infarct volumes in DEFUSE 3. *J. Cereb. Blood Flow Metab.* 40:0271678X2091881. doi: 10.1177/0271678x20918816

Schneider, C. A., Rasband, W. S., and Eliceiri, K. W. (2012). NIH image to imageJ: 25 years of image analysis. *Nat. Methods* 9:671. doi: 10.1038/nmeth.2089

Sena, E. S., van der Worp, H. B., Bath, P. M. W., Howells, D. W., and Macleod, M. R. (2010). Publication bias in reports of animal stroke studies leads to major overstatement of efficacy. *PLoS Biol.* 8:e1000344. doi: 10.1371/journal.pbio.1000344

Sutherland, G. R., Dix, G. A., Auer, R. N., and Koehler, R. C. (1996). Effect of age in rodent models of focal and forebrain ischemia. *Stroke* 27, 1663–1668. doi: 10.1161/01.str.27.9.1663

Tsuchiya, D., Hong, S., Kayama, T., Panter, S. S., and Weinstein, P. R. (2003). Effect of suture size and carotid clip application upon blood flow and infarct volume after permanent and temporary middle cerebral artery occlusion in mice. *Brain Res.* 970, 131–139. doi: 10.1016/s0006-8993(03)02300-x

Wardemann, H., Yurasov, S., Schaefer, A., Young, J. W., Meffre, E., and Nussenzweig, M. C. (2003). Predominant autoantibody production by early human B cell precursors. *Science* 301, 1374–1377. doi: 10.1126/science.1086907

Xiong, B., Li, A., Lou, Y., Chen, S., Long, B., Peng, J., et al. (2017). Precise cerebral vascular atlas in stereotaxic coordinates of whole mouse brain. *Front. Neuroanat.* 11:128. doi: 10.3389/fnana.2017.00128

Yang, G., Kitagawa, K., Matsushita, K., Mabuchi, T., Yagita, Y., Yanagihara, T., et al. (1997). C57BL/6 strain is most susceptible to cerebral ischemia following bilateral common carotid occlusion among seven mouse strains: selective neuronal death in the murine transient forebrain ischemia. *Brain Res.* 752, 209–218. doi: 10.1016/s0006-8993(96)01453-9

Zhao, L., Mulligan, M. K., and Nowak, T. S. (2019). Substrain- and sex-dependent differences in stroke vulnerability in C57BL/6 mice. *J. Cereb. Blood Flow Metab.* 39, 426–438. doi: 10.1177/0271678x17746174

Conflict of Interest: The authors declare that the research was conducted in the absence of any commercial or financial relationships that could be construed as a potential conflict of interest.

Copyright © 2020 Knauss, Albrecht, Dirnagl, Mueller, Harms, Hoffmann, Koch, Endres and Boehm-Sturm. This is an open-access article distributed under the terms of the Creative Commons Attribution License (CC BY). The use, distribution or reproduction in other forums is permitted, provided the original author(s) and the copyright owner(s) are credited and that the original publication in this journal is cited, in accordance with accepted academic practice. No use, distribution or reproduction is permitted which does not comply with these terms.

frontiers in Neuroscience

ORIGINAL RESEARCH
published: 28 October 2020
doi: 10.3389/fnins.2020.591177

Beta-Hydroxybutyrate Enhances BDNF Expression by Increasing H3K4me3 and Decreasing H2AK119ub in Hippocampal Neurons

*Erling Hu, Huan Du, Sen Shang, Yali Zhang and Xiaoyun Lu**

Key Laboratory of Biomedical Information Engineering of Ministry of Education, School of Life Sciences and Technology, Xi'an Jiaotong University, Xi'an, China

Neurological evidence suggests that beta-hydroxybutyrate (BHBA) has positive effects on the central nervous system. Previous studies have explored the molecular mechanisms by which BHBA affects different brain functions, but the effects of BHBA on epigenetic modifications remain elusive. Here, we showed that BHBA enhanced brain-derived neurotrophic factor (BDNF) expression by increasing H3K4me3 and decreasing H2AK119ub occupancy at the *Bdnf* promoters I, II, IV, and VI in hippocampal neurons. Moreover, BHBA treatment induced the upregulation of H3K4me3 and downregulation of H2AK119ub on the global level, both of which were dependent on the L-type calcium channel. Additionally, the BHBA-activated L-type calcium channel subsequently triggered the activation of Ca^{2+}/CaMKII/CREB signaling, and promoted the binding of p-CREB and CBP to *Bdnf* promoters. These results indicate that BHBA regulates cellular signaling and multiple histone modifications to cooperatively modulate BDNF, suggesting a wide range of regulatory effects of BHBA in the central nervous system.

Keywords: beta-hydroxybutyrate, calcium, CaMKII, H3K4 tri-methylation, H2AK119 mono-ubiquitination

OPEN ACCESS

Edited by:
Paulo Henrique Rosado-de-Castro, D'Or Institute for Research and Education (IDOR), Brazil

Reviewed by:
Ming Zhang, Kunming Medical University, China
Yinghua Yu, Xuzhou Medical University, China

****Correspondence:***
Xiaoyun Lu
luxy05@xjtu.edu.cn

Specialty section:
This article was submitted to Neuroenergetics, Nutrition and Brain Health, a section of the journal Frontiers in Neuroscience

Received: *03 August 2020*
Accepted: *12 October 2020*
Published: *28 October 2020*

Citation:
Hu E, Du H, Shang S, Zhang Y and Lu X (2020) Beta-Hydroxybutyrate Enhances BDNF Expression by Increasing H3K4me3 and Decreasing H2AK119ub in Hippocampal Neurons. Front. Neurosci. 14:591177. doi: 10.3389/fnins.2020.591177

INTRODUCTION

Beta-hydroxybutyrate (BHBA) has recently gained increasing attention due to its beneficial effects, such as eliciting advantageous changes in metabolism, reducing inflammation and oxidative stress, as well as improving cognition (Tieu et al., 2003; Reger et al., 2004; Shimazu et al., 2013; Fu et al., 2015). The protective effects of BHBA in the brain have been widely studied. BHBA levels in the body are elevated on a ketogenic diet, during caloric restriction or physical excise and either of these states was found to alleviate some pathological symptoms of neurodegenerative diseases such as Alzheimer's disease, Parkinson's disease, epilepsy, and ischemia (Suzuki et al., 2002; Tieu et al., 2003; Lutas and Yellen, 2013; Yin et al., 2016). Furthermore, BHBA also exerts beneficial effects under normal physiological circumstances, for example by enhancing the learning and memory ability of healthy mice (Zou et al., 2009). Exercise-induced BHBA elevation promotes the expression of brain-derived neurotrophic factor (BDNF) in the hippocampus (Sleiman et al., 2016). However, although many studies explored the underlying mechanisms, they are still not fully understood. In addition to serving as an endogenous energy source that can be used to synthesize ATP in the brain, BHBA is increasingly understood to have broad cellular signaling functions. These include inhibiting class I histone deacetylases (Shimazu et al., 2013), binding to G-protein-coupled

receptors (GPR) (Newman and Verdin, 2017), inhibiting NLRP3 activation (Youm et al., 2015), preventing autophagosome accumulation (Camberos-Luna et al., 2016), repressing H3K27me3 levels (Hu et al., 2018), and acting as a substrate for posttranslational modification of proteins via beta-hydroxybutyrylation at lysine sites (Xie et al., 2016).

Many studies have revealed that BHBA induces BDNF expression when the supply of glucose is insufficient. Our previous study also showed that BHBA was able to promote BDNF expression under normal energy supply (Hu et al., 2018). BDNF is an important trophic factor associated with the improvement of brain function and significant neuroprotective effects. BDNF is a small dimer synthesized and widely distributed in different brain regions, including the hippocampus, amygdala, cortex, forebrain, striatum, and hypothalamus (Aid et al., 2007). In general, the expression of BDNF is controlled by multi-component transcriptional regulation including cAMP response element (CRE)-binding protein (CREB) and epigenetic factors such as histone modifications. The transcriptional activation marks histone H3 lysine 4 trimethylation (H3K4me3) and histone H3 lysine 27 acetylation (H3K27ac), as well as the transcriptional repression mark H3K27 trimethylation (H3K27me3), can directly regulate *Bdnf* transcription in active or repressive ways, leading to changes of promoter occupancy and BDNF expression (Bernstein et al., 2006; Palomer et al., 2016; Hu et al., 2018). The *Bdnf* gene contains nine exons, each of which is regulated by its promoter. Generally, the expression of transcripts from *Bdnf* exons I, II, IV, and VI increases with time, and is important for brain development (Zheng et al., 2012). Interestingly, H3K4me3 and H3K27me3 are consistently distributed in *Bdnf* promoters I to VIII in a strongly bivalent way, so that the gene can be turned on or off rapidly in response to environmental stimuli (Bernstein et al., 2006). In addition, other histone marks, including histone H2A lysine 119 mono-ubiquitination (H2AK119ub) that play a vital role in transcriptional repression, can also co-localize with H3K27me3 in the same chromatin regions to regulate gene transcription (Muller and Verrijzer, 2009). BHBA can increase BDNF expression by elevating the occupancy of H3K27ac at the *Bdnf* promoters and decreasing that of H3K27me3 (Palomer et al., 2016; Hu et al., 2018), suggesting a yet to be investigated potential role of BHBA in regulating histone modifications. However, the locational interaction between the different histone modifications, for example, H3K27me3 and H3K4me3, indicates that the function of BHBA might not just be limited to affecting H3K27me3/ac, but also the other histone marks.

Here, we demonstrated that BHBA enhanced BDNF expression by elevating the transcriptional activation mark H3K4me3 and decreasing the transcriptional repression mark H2AK119ub in hippocampal neurons both *in vivo* and *in vitro*. Furthermore, both the BHBA-triggered increase of H3K4me3 and the decrease of H2AK119ub depend on the L-type calcium channel. These results corroborate the broad functions and diverse mechanisms by which BHBA regulates neuronal genes. The possibility that BHBA modulates the expression of additional neuronal genes to achieve its globally beneficial effects merits further investigation in future studies.

MATERIALS AND METHODS

Animals

The *in vivo* experiments were conducted with 6- to 8-week-old female C57BL/6 mice. The mice were maintained as described previously (Hu et al., 2018). The mice were treated with 60 mg/kg BHBA (dissolved in physiological saline) or only physiological saline twice daily via intragastric gavage for two days in total. The hippocampi were removed and stored at −80°C before further analysis. For *in vitro* experiments, rat hippocampi were isolated from 1-day-old SD rats for culturing primary hippocampal neurons. All experimental procedures involving animals were in strict accordance with institutional, national, and international animal welfare standards, and were approved by the Research Ethics Committee of Xi'an Jiaotong University (Approval No. 201103). All animals were purchased from the Experimental Animal Center of Xi'an Jiaotong University Health Science Center. All mice were fed a normal diet at libitum and were maintained on a 12-h light/dark cycle.

Culture of Primary Hippocampal Neurons

Primary hippocampal neurons from 1-day-old SD rats were extracted and cultivated as described previously (Hu et al., 2018). The hippocampi were isolated in ice-cold Hank's solution and digested with 0.25% trypsin at 37°C for 15 min, followed by centrifugation for 5 min at 300 × *g*. The pellets were re-suspended in Dulbecco's Modified Eagle's Medium (DMEM)/F12 medium (high glucose; hyclone, United States) with 10% fetal bovine serum (FBS, HyClone, GE Healthcare, United States), supplemented with 100 U/ml penicillin (Beyotime, China) and 100 μg/ml streptomycin (Beyotime, China). The cells were counted and then seeded into plates pre-coated with poly-L-lysine (Sigma-Aldrich, United States). After 2 h, the medium was replaced with Neurobasal™ A Medium supplemented with 2% B27 and 2 mM Gln. Half of the medium was changed every 3 days.

Culture of Murine Hippocampal Neuronal Cell Line HT22

The HT22 cell line was purchased from Shanghai Hongshun Biologicals (China) and maintained in high-glucose DMEM supplement with 10% FBS, 100 U/ml penicillin, and 100 μg/ml streptomycin.

Western Blot Analysis

Rat hippocampal neurons were cultured in 6-well plates at an initial concentration of 2×10^6 cells per well. After culturing for 9–10 days, the neurons were treated with 10 μM manidipine, 5 μM KN-62, or 10 μM H89 for 10 min, or left untreated prior to treatment with 2 mM BHBA for another 1 or 12 h. Subsequently, the cells were lysed using 1× lysis buffer (Beyotime, China) containing protease inhibitor cocktail 2 (Roche, Switzerland) directly in the plates to obtain whole-cell lysates. Proteins were separated on SDS/PAGE gels and electroblotted onto PVDF membranes

(GE Healthcare, United States). The membranes were blocked with 5% (w/v) BSA (bovine serum albumin; Sigma-Aldrich, United Kingdom) for 1 h at room temperature, and subsequently incubated with primary antibodies (tri-methyl histone H3 (Lys4) rabbit mAb, ubiquityl-histone H2A (Lys119) rabbit mAb, phospho-CaMKII (Thr286) rabbit mAb, phospho-CREB (SER133) rabbit mAb, WDR5(A-6), anti-BDNF antibody, anti-beta-actin) at 4°C overnight. Then, TBST was used to wash the membranes 3 times, followed by incubation with the horseradish peroxidase (HRP)-conjugated secondary antibody (Abcam, United Kingdom) for 1 h at room temperature. The protein bands were developed using the ImmobilonTM Western Chemiluminescent HRP Substrate (Millipore, United States) and photographed using the FlorChem FC2 System (Alpha Innotech, United States).

Chromatin Immunoprecipitation Followed by Quantitative PCR

Chromatin immunoprecipitation (ChIP) assays were processed using the SimpleChIP Enzymatic Chromatin IP kit (Catalog#9003, Cell signaling Technology) according to the manufacturer's instructions. Briefly, HT22 cells were fixed in 1% formaldehyde for 10 min at room temperature, after which 0.125 M glycine was used to stop the cross-linking for 5 min at room temperature. Then, the samples were washed 2 times with ice-cold PBS supplemented with 1× protease inhibitor cocktail (PIC; Roche, Switzerland). Subsequently, ice-cold 1× Buffer A plus PIC and DTT were added and the cells were incubated on ice for 10 min. The resulting lysates were centrifuged at 2,000 × *g* for 5 min at 4°C to harvest the pellets. Subsequently, 1× Buffer B plus DTT was added to lyse the nuclei, followed by 0.5 μl micrococcal nuclease per IP prep and incubated at 37°C to digest DNA to a length of approximately 150–900 bp. After 20 min, the digestion was stopped by adding 2 μl 0.5 M EDTA. The resulting lysates were centrifuged at 16,000 × *g* and 4°C to harvest the pelleted nuclei. The samples were resuspended in 1× ChIP Buffer with PIC, incubated on ice for 10 min, and then sonicated using a Bandelin ultrasonicator (Sonics, United States) set to 300 W, 50 cycles (1 s each with a duty cycle of 50%). The resulting sonicated mixture was centrifuged at 9,400 × *g* for 10 min at 4°C to remove insoluble material. Supernatants containing DNA-protein complexes were diluted 1:5 with 1× ChIP Buffer. Subsequently, ChIP assays were performed using anti-p-CREB (cell signaling technology), anti-CBP (cell signaling technology), anti-H3K4me3 (cell signaling technology), or anti-H2AK119ub antibodies (Abcam, United Kingdom) and a negative control comprising normal rabbit IgG (Santa Cruz Biotechnology, Inc., United States). Immune complexes were precipitated by adding the magnetic protein G beads and incubating for 2 h at 4°C. The protein G –antibody/chromatin complexes were washed with low salt wash buffer (three times) and a high salt wash buffer (one time). Protein G–antibody/chromatin complexes, as well as the 2% input solution, were eluted with 150 μl 1× ChIP elution buffer two times, and recovered by adding 5 M NaCl and 100 μg/ml protease K and incubating 2 h at 65°C. The beads were separated from the solution using a magnetic separation device and the supernatant was transferred to a fresh tube. Finally, DNA was purified using a DNA purification Kit (DP214; Tiangen, China) according to the manufacturer's protocol, and eluted with 50 μl sterilized deionized water. A 2 μl aliquot of purified DNA was used to perform qRT-PCR, using the primer pairs *Bdnf*-P1, *Bdnf*-P2, *Bdnf*-P3, and *Bdnf*-P4. Quantitative PCR (qPCR) for the measurement of gene expression was performed using the SYBR Green Master Mix on a CFX96TM Real-time system (Bio-Rad, United States).

Calcium Imaging

Rat hippocampal neurons cultured for 8 to 10 days were used for the test. The cells were washed with standard 2 mM Hank's Balanced Salt Solution (HBSS; ThermoFisher Scientific, United States) two times, after which 5 μM Fluo-4AM was used to stain the cells for 15 min, which were then washed again with standard 2 mM extracellular solution. Time-lapse imaging was used at 500 ms/frame for real-time imaging. Neurons were initially given 30 s 2Ca (2 mM Ca^{2+}) to record the basal line followed by 1 min of 2 mM BHBA stimulation, and then rapidly switched back to 2Ca. The intensity of Fluo-4AM fluorescence was analyzed using ImageJ Software.

Enzyme-Linked Immunosorbent Assay

HT22 cells were treated with 2 mM BHBA for 5, 10, or 20 min, or left untreated, and were collected using 0.25% trypsin followed by centrifugation for 5 min at 300 × *g*. The tubes containing the samples were placed into liquid nitrogen for 20 min, and then transferred into a 37°C water bath for 10 min, which was repeated two times. Subsequently, the samples were centrifuged for 5 min at 12,000 *g*, and the supernatants were collected for the detection of PLC activity, using the mouse PLC activity detection kit (Jianglai Biotechnology Company, Shanghai, China) according to the manufacturer's instructions. Samples comprising 50 μl were added into the wells, after which 100 μl of diluted HRP conjugate was added into each well, and the plate was incubated at 37°C for 60 min. The wells were washed with wash buffer five times, after which 50 μl of chromogenic substrate A and 50 μl of chromogenic substrate B were added into each well, and the plate was incubated in the dark at 37°C for 15 min. Finally, 100 μl of stop solution was added into each well and the absorbance at 450 nm was measured.

Statistical Analysis

The data were analyzed using GraphPad Prism V7.0 (GraphPad 264 Software, Inc., San Diego, CA, United States). Two-group comparisons were performed using Student's *t*-test. Multi-group comparisons were performed using a one-way ANOVA followed by *post hoc* Tukey's test. The error bars indicate the SEM. Differences were considered to be statistically significant at $p < 0.05$.

RESULTS

BHBA Treatment Promotes BDNF Expression and Changes Histone H3K4 Trimethylation and Histone H2AK119 Mono-Ubiquitination in *Bdnf* Promoters

Firstly, we verified the increase of BDNF levels in primary hippocampal neurons following treatment with 2 mM BHBA (**Figure 1A**). Actually, we have previously found that BHBA also could increase BDNF expression in murine hippocampal neuronal cell line HT22 cells (Hu et al., 2018). Additionally, mice were gavaged with 60 mg/kg BHBA, twice a day for two days to further assess the *in vivo* effects of BHBA on BDNF. The BDNF levels in the hippocampi of BHBA-treated mice were much higher than in those of control mice (**Figure 1B**). Histone modifications play essential roles in chromatin remodeling and transcriptional regulation. Previous studies indicated that BHBA regulates the lysine 27 tri-methylation of histone H3 (H3K27me3) in *Bdnf* promoters (Palomer et al., 2016). The transcriptional activation mark H3K4me3 is found in a constant balance with the permissive H3K27me3 (Bernstein et al., 2006). Firstly, murine hippocampal neuronal cell line HT22 was treated with 2 mM BHBA for 1 h, followed by ChIP with an antibody against H3K4me3 antibody and measurement of *Bdnf* transcription using real-time qPCR. The occupancy of H3K4me3 in *Bdnf* promoters I, II, III, and IV were significantly increased by BHBA stimulation (**Figure 1C**). It is believed that BHBA broadly regulates epigenetic modification in multiple ways. In addition to H3K4me3, the transcriptional-repression mark histone H2AK119 mono-ubiquitination (H2AK119ub) is also involved in transcriptional regulation, always occurring together with H3K27me3 in the same chromatin regions (Wang et al., 2004). H2AK119ub was found to be directly bound at *Bdnf* promoters I to IV, while BHBA treatment weakened the occupancy of H2AK119ub at these promoters (**Figure 1D**).

BHBA Treatment Causes an Increase of H3K4me3 and a Decrease of H2AK119ub in Hippocampal Neurons *in vitro* and *in vivo*

The effects of BHBA on the global levels of H3K4me3 and H2AK119ub in hippocampal neurons were investigated. After 1 h of treatment, 2 mM BHBA elevated the global H3K4me3 levels in the primary hippocampal neurons (**Figure 2A**). Accordingly, the untreated hippocampal neurons exhibited high levels of H2AK119ub, whereas BHBA treatment significantly reduced the global abundance of H2AK119ub (**Figure 2B**). The *in vivo* results from showed that the total H3K4me3 levels were much higher, and those of H2AK119ub were much lower in the hippocampi of BHBA-treated mice as than those of the control mice, which was consistent with the *in vitro* results (**Figures 2C,D**).

At the same time, WD repeat-containing protein 5 (WDR5), a core subunit of the mixed-lineage leukemia/SET-domain (MLL/SET) complex, which plays a crucial role in regulating global H3K4me3 levels during vertebrate development and hematopoiesis, was detected both *in vitro* and *in vivo* (Wysocka et al., 2005). WDR5 levels were elevated by BHBA both in cultured hippocampal neurons and hippocampi of mice

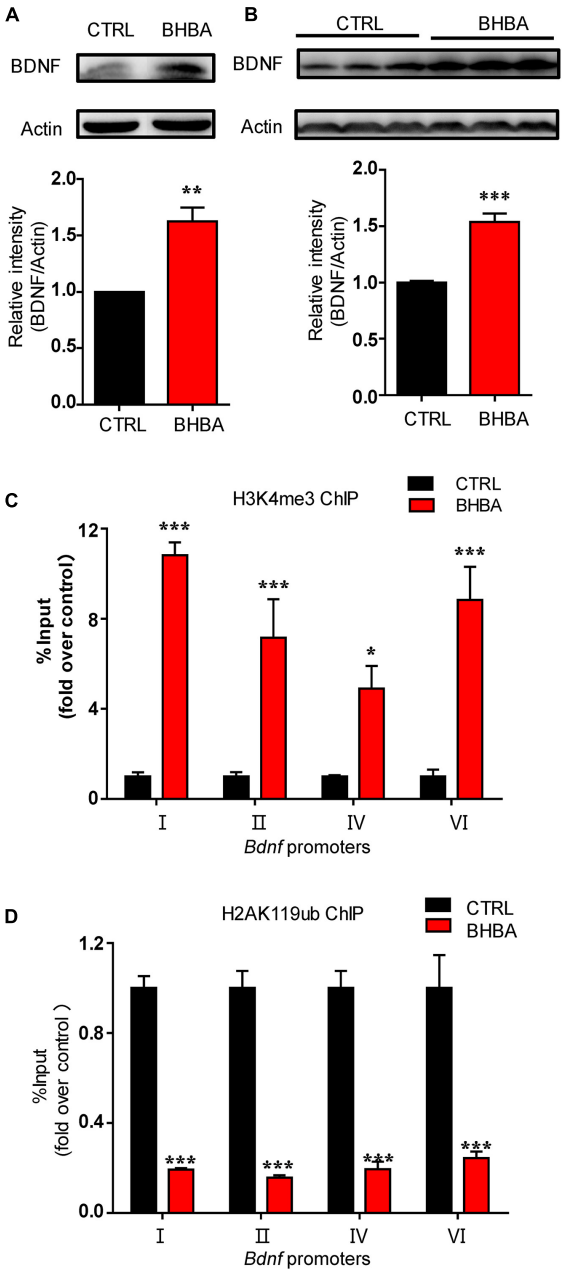

FIGURE 1 | BHBA treatment increased BDNF expression and changed the occupancy of H3K4me3 and H2AK119ub at *Bdnf* promoters in neurons. **(A,B)** Western blot analysis of BDNF levels in hippocampal neurons treated with 2 mM BHBA for 12 h or left untreated ($n = 4$, $F(3, 3) = 27.46$) **(A)**, and in hippocampi of mice treated with 60 mg/kg BHBA, twice 1 day for 2 days and untreated control mice ($n = 8$, $F(3, 28) = 13.19$) **(B)**. **(C,D)** Occupancy of H3K4me3 ($n = 4$, $F(3, 16) = 0.1304$) **(C)** and H2AK119ub ($n = 4$, $F(3, 16) = 3.828$) **(D)** at *Bdnf* promoters from cultured HT22 neurons treated with 2 mM BHBA for 1 h or left untreated. The data represent the mean ± SEM from three independent experiments. $^{*}p < 0.05$, $^{**}p < 0.01$, and $^{***}p < 0.001$.

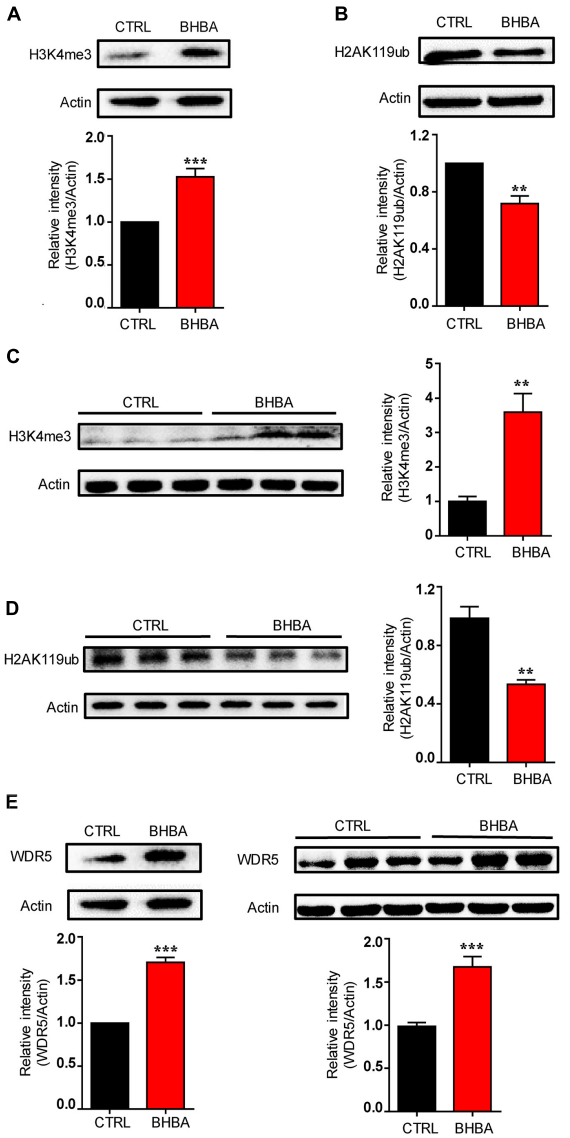

FIGURE 2 | BHBA treatment increased H3K4me3 and decreased H2AK119ub levels in hippocampal neurons both *in vitro* and *in vivo*. **(A,C)** Western blot analysis of H3K4me3 levels in hippocampal neurons treated with 2 mM BHBA for 1 h or left untreated (n = 5, F(4, 4) = infinity) **(A)**, and in hippocampi of mice treated with 60 mg/kg BHBA, twice one day for two days, or untreated control mice (n = 4, F(3, 3) = 23.12) **(C)**. **(B,D)** Western blot analysis of H2AK119ub levels in hippocampal neurons treated with 2 mM BHBA for 1 h or left untreated (n = 4, F(3, 3) = infinity) **(B)**, and in hippocampi of mice treated with 60 mg/kg BHBA, twice 1 day for 2 days, or untreated control mice (n = 4, F(3, 3) = 7.503) **(D)**. **(E,F)** Western blot analysis of WDR5 levels in hippocampal neurons treated with 2 mM BHBA for 1 h or left untreated (n = 3, F(2, 2) = infinity) **(E)**, and from hippocampi of mice treated with 60 mg/kg BHBA, twice 1 day for 2 days, or untreated control mice (n = 4, F(3, 3) = 14.05) **(F)**. The data are presented as mean ± SEM. $^{**}p < 0.01$ and $^{***}p < 0.001$.

(**Figures 2E,F**). These results suggest that BHBA positively regulates H3K4me3, possibly by increasing WDR5 levels in hippocampal neurons. Taken together, these results confirmed the epigenetic regulation of *Bdnf* promoters on H3K4me3 and H2AK119ub in response to BHBA. Therefore, H3K4me3 and H2AK119ub might be involved in regulating BHBA-induced BDNF expression in hippocampal neurons.

BHBA Treatment Activates Calcium Signaling in Neurons

It is believed that changes in epigenetic modifications in cells must be the result of the communication of each cell with the environment, which involves multiple signaling pathways. Calcium signals play crucial roles in these processes. To assess the effects of BHBA on intracellular Ca^{2+} levels, hippocampal neurons were loaded with the calcium-sensitive fluorescence indicator Fluo-4AM, and the changes in fluorescence intensity were measured in all cell bodies of neurons (**Figure 3A**). The hippocampal neurons were kept in PSS (2 mM Ca^{2+}), and PSS was applied for 30 s to obtain the basal Ca^{2+} level. Subsequently, the stimulation was switching from PSS to 2 mM BHBA at the time point of 30 s and maintained for 1 min until the time point of 90 s to switch to PSS again. The intracellular calcium concentration transiently rose after BHBA treatment and was quickly restored to the basal level. Interestingly, another significant rise in intracellular calcium was seen several seconds later (**Figure 3A**). Moreover, phospholipase C (PLC) activity in the hippocampal neurons was also elevated by BHBA (**Figure 3B**). The elevation of cellular Ca^{2+} activates several Ca^{2+}-binding proteins, including calmodulin (CaM) complexes, and promotes the phosphorylation of CaMKII at a threonine residue (T286) in the autoinhibitory domain. In this study, the phosphorylation levels of (CaMKII) in the hippocampal neurons treated with BHBA for 30 min were much higher than in the controls (**Figure 3C**). Significant upregulation of phosphorylated CREB (p-CREB), which is an essential component downstream of p-CaMKII, was also seen in neurons treated with BHBA for 1 h (**Figure 3D**). Similarly, p-CREB levels were much higher in the hippocampi of BHBA-treated mice than in those of control mice (**Figure 3E**). These results demonstrated that BHBA treatment triggered an elevation of intracellular Ca^{2+} and subsequently activated Ca^{2+}/p-CaMKII/p-CREB signaling. Additionally, the binding of p-CREB to *Bdnf* promoters I and II was increased in murine hippocampal cell line HT22 after BHBA treatment for 1 h (**Figure 3F**). Increased binding of nuclear CREB-binding protein (CBP) was also observed in *Bdnf* promoter I. However, no changes were found in *Bdnf* promoter II in both BHBA-treated and untreated neurons (**Figure 3G**). Moreover, CBP levels were also significantly increased in the hippocampi of BHBA-treated mice and hippocampal neurons, repectively (**Figures 3H,I**). Thus, the BHBA-triggered elevation of intracellular calcium levels activated calcium-related signaling, which changed the binding of p-CREB/CBP to the *Bdnf* promoters to facilitate BDNF expression.

Inactivation of Ca^{2+}/CaMKII Inhibits BHBA-Induced BDNF

To assess the role of calcium-related CaM/p-CaMKII signaling in BHBA-induced BDNF, hippocampal neurons were pre-treated

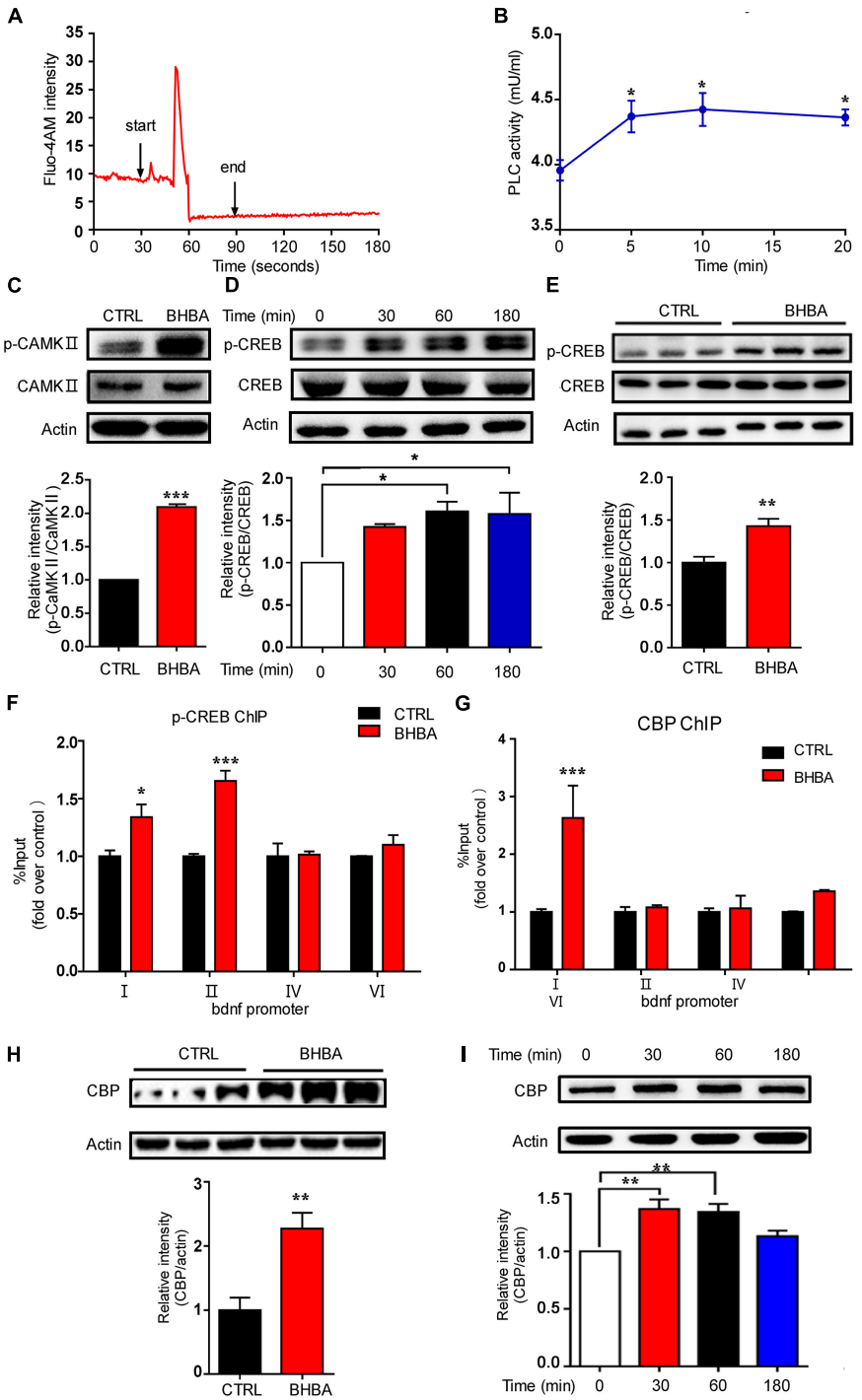

FIGURE 3 | BHBA treatment activated calcium signaling in neurons. **(A)** Representative traces of fluorescence intensity over 3 min of imaging representing intracellular Ca^{2+} concentrations in rat hippocampal neurons stained with Fluo4AM and treated with 2 mM BHBA at the time point of 30 s for another 1 min. **(B)** The activity of phospholipase C (PLC) in rat hippocampal neurons treated with 2 mM BHBA for the indicated time or left untreated (n = 3, $F(3, 8) = 4.589$). **(C)** Western blot analysis of p-CAMKII levels from hippocampal neurons treated with 2 mM BHBA for 1 h or left untreated (n = 3, $F(2, 2)$ = infinity). **(D,E)** Western blot analysis of p-CREB levels in hippocampal neurons treated with 2 mM BHBA for the indicated time or left untreated (n = 3, $F(3, 8) = 3.915$) **(D)**, and from hippocampi of mice treated with 60 mg/kg BHBA, twice one day for two days, or untreated control mice (n = 4, $F(3, 3) = 1.583$) **(E)**. **(F,G)** Occupancy of p-CREB (n = 4, $F(3, 16) = 7.481$) **(F)** and CBP (n = 4, $F(3, 16) = 5.895$) **(G)** at the *Bdnf* promoters of HT22 cells treated with 2 mM BHBA for 1 h or left untreated. **(H)** CBP levels in hippocampi of mice treated with 60 mg/kg BHBA, twice one day for two days, or untreated control mice (n = 4, $F(3, 3) = 1.642$). **(I)** Western blot analysis of CBP levels in hippocampal neurons treated with 2 mM BHBA for the indicated time or left untreated (n = 3 or 4, $F(3, 11) = 8.651$). The data are presented as mean ± SEM. $^*p < 0.05$, $^{**}p < 0.01$, and $^{***}p < 0.001$.

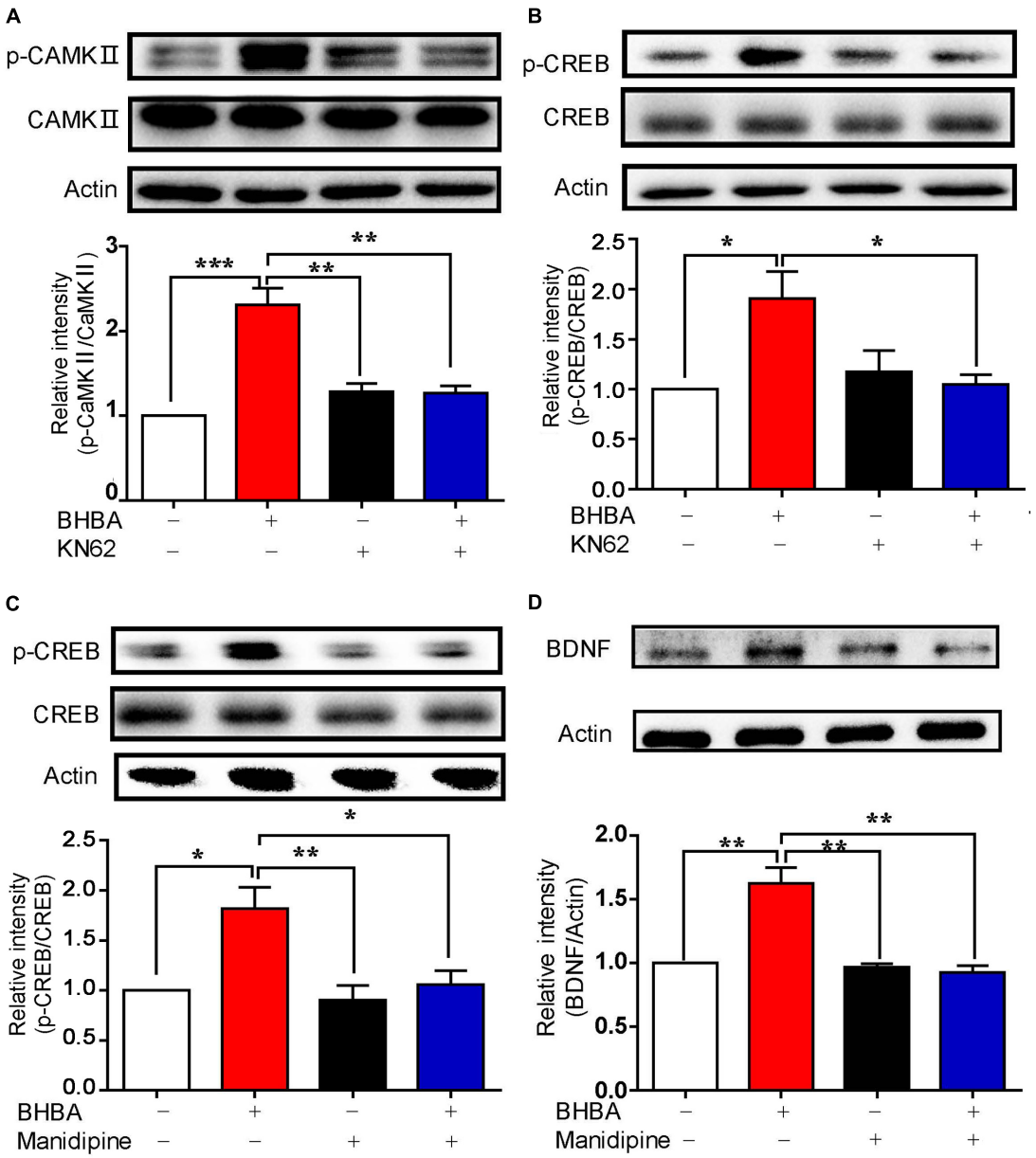

FIGURE 4 | Inhibition of calcium signaling blocked the BHBA-induced increase of BDNF expression. **(A,B)** Western blot analysis of p-CaMKII ($n = 3$, $F(3, 8) = 23.23$) **(A)** and p-CREB ($n = 3$, $F(3, 8) = 5.623$) **(B)** levels in hippocampal neurons treated with 5 μM KN-62 for 10 min prior to treatment with 2 mM-BHBA treatment for another 30 min. **(C)** Western blot analysis of p-CREB levels in hippocampal neurons treated with 10 μM manidipine for 10 min or left untreated prior to treatment with 2 mM BHBA for 1 h ($n = 4$, $F(3, 16) = 8.198$). **(D)** Western blot analysis of BDNF expression in hippocampal neurons treated with 10 μM manidipine for 10 min or left untreated prior to treatment with 2 mM BHBA for 12 h ($n = 4$, $F(3, 12) = 15.43$). The data represent the mean ± SEM from three independent experiments. $^{*}p < 0.05$, $^{**}p < 0.01$, and $^{***}p < 0.001$.

with KN-62, a selective and specific inhibitor of CaM, before BHBA treatment. As expected, the BHBA-induced increase of p-CaMKII was reduced to the basal level by KN-62 (**Figure 4A**). At the same time, the elevation of p-CREB induced by BHBA was also decreased in KN-62-treated neurons, suggesting that the BHBA-induced rise of p-CREB levels depends on the activation of Ca^{2+}/CaM/CaMKII (**Figure 4B**). Since Ca^{2+} influx through L-type VSCCs is one of the main sources of intracellular Ca2 + , hippocampal neurons were pre-treated with manidipine, a blocker of voltage-gated L-type VSCCs, to assess the role of L-type VSCCs in this process. The BHBA-induced increase of p-CREB levels was inhibited by manidipine, suggesting that L-type VSCCs are responsible for the elevation of p-CREB induced by BHBA (**Figure 4C**). A similar trend was observed for BDNF expression in hippocampal neurons pretreated with manidipine (**Figure 4D**). These findings supported the importance of L-type

VSCCs and Ca^{2+}/CaMKII in regulating the induction of BDNF expression by BHBA in hippocampal neurons.

The BHBA-Induced Changes of H2AK119ub and H3K4me3 Depend on Different Ssignals

To further determine the roles of L-type VSCCs and Ca^{2+}/CaM in regulating the BHBA-mediated increase of H3K4me3, hippocampal neurons were pre-treated with either manidipine or KN-62. The increase of H3K4me3 induced by BHBA was partially inhibited by manidipine, while KN-62 did not affect (**Figures 5A,B**), suggesting that the BHBA-induced upregulation of H3K4me3 is, at least in part, dependent on L-type VSCCs but not on CaM/p-CaMKII signaling. We previously found that BHBA also activated the cAMP/PKA signaling pathway in hippocampal neurons (Hu et al., 2018). To assess whether cAMP/PKA signaling plays a role in the BHBA-induced increase of H3K4me3, the hippocampal neurons were pre-treated with the PKA inhibitor H89 prior to BHBA stimulation. Notably, H89 completely blocked the promotion of H3K4me3 by BHBA, suggesting that cAMP/PKA signaling was responsible for the elevation of H3K4me3 levels following BHBA treatment (**Figure 5C**). Moreover, blocking the L-type VSCCs severely weakened the repression of H2AK119ub levels by BHBA, indicating that the BHBA-triggered activation of L-type VSCC-related calcium signaling resulted in the downregulation of H2AK119ub in hippocampal neurons (**Figure 5D**). The inhibition of BHBA on H2AK119ub level was also totally inhibited by KN-62 (**Figure 5E**). However, H89 did not change the inhibitory effect of BHBA on H2AK119ub at all, suggesting that the decrease of H2AK119ub levels was independent of cAMP/PKA signaling (**Figure 5F**). Collectively, these results demonstrated that the changes in H3K4me3 and H2AK119ub levels in hippocampal neurons following BHBA treatment are dependent on different signaling pathways. Overall, the results indicate that the decrease of H2AK119ub depends on L-type VSCCs and CaM/CaMKII signaling, and the increase of H3K4me3 depends on the activation of cAMP/PKA signaling.

DISCUSSION

It is well known that BHBA has a neuroprotective effect in the central nervous system, but the underlying mechanisms are the subject of ongoing research. As a ketone body synthesized primarily in the liver, BHBA can cross the blood–brain barrier to enter the brain and exert beneficial effects through multiple mechanisms (Newman and Verdin, 2017). In the present study, we showed that BHBA promoted the expression of Bdnf by regulating the histone modification on H2AK119 and H3K4. At the mean time, BHBA triggered an elevation of cytosolic Ca^{2+} in cultured hippocampal neurons. Our results are consistent with a previous study (Cheng et al., 2005), which showed that low concentrations of BHBA (0.02 g/l) can rapidly increase the intracellular Ca^{2+} levels in murine L929 fibroblasts, which was blocked by inhibitors of L-type VSCCs and EGTA. It is interesting that a fast slight increase of cytosolic Ca^{2+} was observed after BHBA stimulation, and then a very significant elevation Ca^{2+} level appeared. While whether these two peak were resulted form the intracellular Ca^{2+} release and the consequent extracellular Ca^{2+} influx, or there were corresponding to the HB induced Ca^{2+} signal and a subsequent neuronal firing are still need to be further investigated. Ca^{2+} signaling plays a pivotal role in regulating neuronal activity, and transient increases in cytoplasmic Ca^{2+} activate a variety of important calcium-dependent cellular events, including both the CaMK and PKA pathways (Bok et al., 2003; Hansen et al., 2003). We previously found that BHBA treatment could activate cAMP/PKA signaling, thereby elevating BDNF expression in hippocampal neurons (Hu et al., 2018). Here, we assessed the p-CaMKII level in hippocampal neurons treated with 2 mM BHBA or left untreated and found that BHBA effectively upregulated the p-CaMKII levels in hippocampal neurons. Although we didn't observe the significant increase of p-CaMKII *in vivo* 12 h after BHBA administration (data not show), it might due to the highly dynamic property of CaMKII phosphorylation and dephosphorylation. CaMKII can phosphorylate CREB at serine 133, and once phosphorylated, CREB can recruit transcription coactivators such as CBP and its paralog p300, thereby activating the transcription of target genes. Moreover, the levels of p-CREB and BDNF in both BHBA-treated cultured hippocampal neurons and hippocampi of treated mice were much higher than those of the untreated control groups. At the same time, the binding of p-CREB and CBP to *Bdnf* promoters also increased, implying the activation of *Bdnf* transcription. These results suggested that the BHBA-triggered elevation of intracellular Ca^{2+} levels resulted in the activation of downstream signaling, which was beneficial to the function of the neurons. Transient elevation of intracellular Ca^{2+} can activate several transcription factors that facilitate neuronal function in addition to BDNF. Although we only detected the neuronal expression of BDNF in this study, it is believed that other Ca^{2+}-dependent target genes are also affected by BHBA treatment, which could cooperatively facilitate neuronal activity. However, identifying those factors will require further analysis by RNA-seq or ChIP-seq in further studies. In addition to affecting L-type VSCCs in murine fibroblast L929 cells, BHBA was also reported to modulate *N*-type calcium channels and Cl^- channel in cultured neurons (Juge et al., 2010; Won et al., 2013). Moreover, it was found that BHBA could regulate the activity of sympathetic neurons via FFA3 (Won et al., 2013). Another study showed that ketone bodies, including acetoacetate and BHBA, inhibited glutamate transport by affecting the Cl^--dependence of VGLUT2 (Juge et al., 2010). These studies are in agreement with a pattern of BHBA modulating cellular functions by first affecting surface receptors. It has been reported that BHBA is a main endogenous ligand for two cell-surface receptors, GPR 109A and 41, both of which are Gi/o-protein-coupled receptors. We previously found that GPR109A but not GPR41 was expressed in the mouse hippocampal neuron line HT22. However, blocking Gi-type GPRs with PTX did not change the BHBA-induced increase of p-CREB, suggesting that GPR109A-coupled Gα/i was not responsible for BHBA-induced BDNF expression in

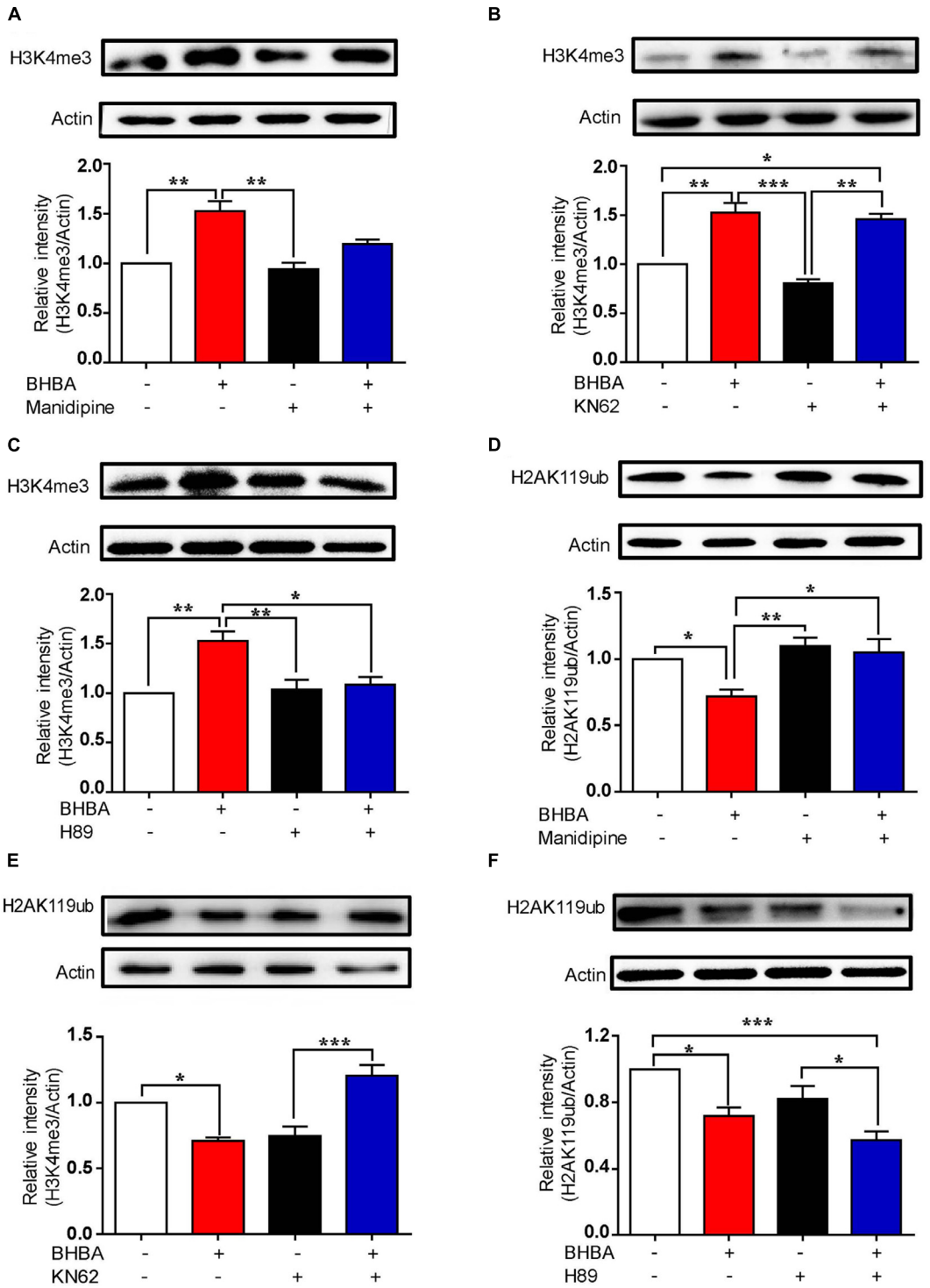

FIGURE 5 | The BHBA-induced changes of H3K4me3 and H2AK119ub depend on different signaling pathways. **(A–C)** Western blot analysis of H3K4me3 levels in hippocampal neurons treated with 10 μM manidipine (n = 3 or 4, $F(3, 10) = 11.27$) **(A)**, 5 μM KN-62 (n = 3 or 4, $F(3, 10) = 18.56$) **(B)**, or 10 μM H89 (n = 3 or 4, $F(3, 11) = 10.84$) **(C)** for 10 min or left untreated prior to treatment with 2 mM BHBA for another 1 h. **(D, E)** Western blot analysis for H2AK119ub levels in hippocampal neurons treated with 10 μM manidipine (n = 3 or 4, $F(3, 10) = 1.898$) **(D)**, 5 μM KN-62 (n = 4, $F(3, 12) = 16.95$) **(E)**, or 10 μM H89 (n = 4, $F(3, 12) = 10.61$) **(F)** for 10 min or left untreated prior to treatment with 2 mM BHBA for another 1 h. The data represent the mean ± SEM from three independent experiments. $^{*}p < 0.05$, $^{**}p < 0.01$, and $^{***}p < 0.001$.

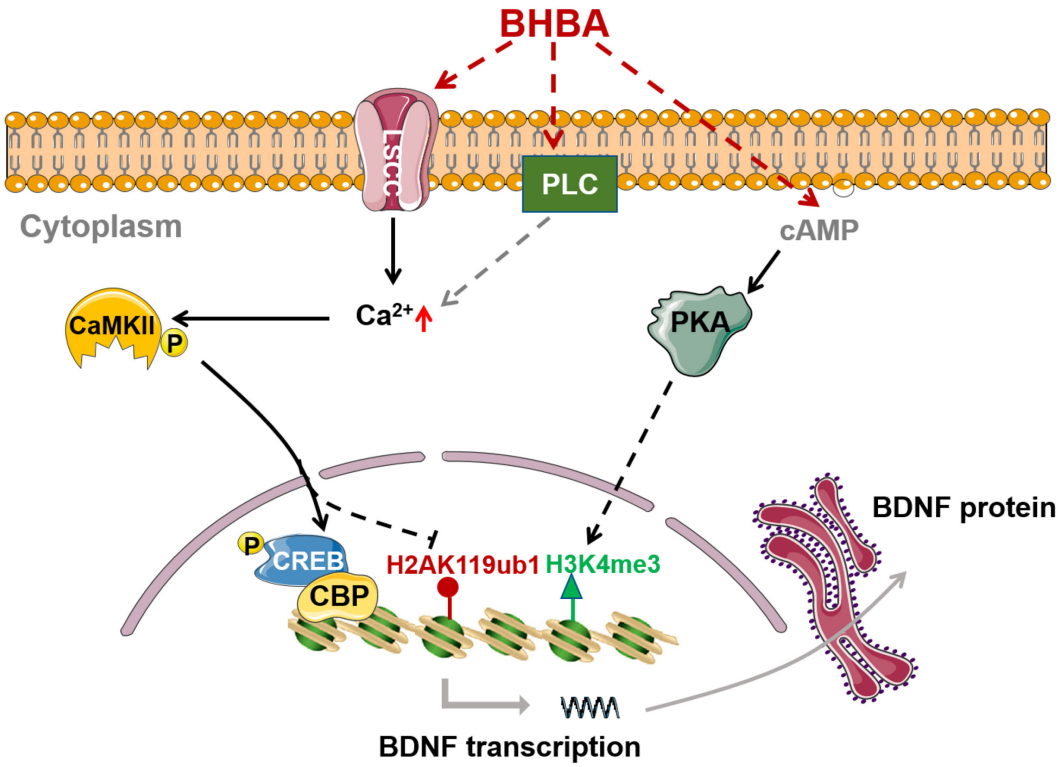

FIGURE 6 | BHBA-induced activation of intracellular signaling and chromatin remodeling in Bdnf promoters in hippocampal neurons. BHBA induces increase of transcriptional mark H3K4me3 as well as decrease of transcriptional mark H2AK119ub occupied in bdnf promoters in hippocampal neurons. Moreover, BHBA-induced changes of H2AK119ub is dependent on the activation of L-type calcium channel and the elevation of intracellular, which subsequently activates Ca^{2+}/CaMKII/p-CREB signaling pathway, and promotes the occupation of p-CREB and CBP in bdnf promoters, thereby enhances BDNF expression. However, BHBA-increased H3K4me3 is dependent on cAMP/PKA activation.

neurons. It has been reported that activation of GPR109A is associated with an increase of intracellular Ca^{2+} levels through the Gβγ subunit/phospholipase Cβ (PLCβ)/inositol-1,4,5-trisphosphate (IP3) pathway in monocyte-derived cells (Offermanns and Schwaninger, 2015).

Our results demonstrated that blocking L-type VSCCs in hippocampal neurons also blocked the effects of BHBA on CaMKII/p-CREB activation, suggesting that the BHBA-induced increase of intracellular Ca^{2+} levels and subsequent activation of CaMKII/p-CREB/BDNF are mediated by L-type VSCCs. However, how BHBA modulates the activation of L-type VSCCs in neurons is still unclear and needs to be further investigated in the future.

It has been reported that BHBA can regulate BDNF transcription by affecting epigenetic modifications, such as increasing the occupancy of the transcriptional activation mark H3K27 acetylation and decreasing that of the transcriptional repression mark H3K27me3 at *Bdnf* promoters (Palomer et al., 2016; Hu et al., 2018). The transcriptional activation mark H3K4me3 was found to act in conjunction with H3K27me3 in a bivalent way in embryonic stem cells, giving them the ability to control gene expression rapidly in response to environmental changes (Bernstein et al., 2006). It has been shown that BHBA treatment decreased the occupancy of H3K27me3 at *Bdnf* promoters II and VI in the hippocampal neuron line HT22 (Hu et al., 2018). In this study, we found that BHBA increased global H3K4me3 levels. Moreover, the H3K4me3 occupancy at *Bdnf* promoters I, II, IV, and VI were also increased after BHBA treatment, indicating that H3K4me3 is involved in the increase of *Bdnf* expression in response to BHBA stimulations, possibly acting cooperatively with H3K27me3. H3K4me3 is a robust epigenetic mark that is involved in regulating synaptic plasticity as well as memory formation and consolidation. Webb et al. (2017) found that a recent contextual fear-conditioned memory elicited memory formation and elevated the global levels of H3K4me3 in the CA1 area. Collins et al. (2019) analyzed H3K4me3 ChIP-seq data from CA1 neurons and found broad H3K4me3 peaks at many learning- and memory-associated genes during memory formation. Moreover, H3K4 is specifically methylated by MLL and SETs, whereby MLL1 is widely expressed throughout the brain and plays crucial roles in synaptic activity and memory (Jakovcevski et al., 2015). The BHBA-induced elevation of WDR5, a core component of the MLL/SET complex, may explain why H3K4me3 levels increased after BHBA treatment since WDR5 is required for the tri-methylation of H3K4 (Wysocka et al., 2005). These results are consistent with

BHBA's neuroprotective role and indicate possible molecular mechanisms of its effects.

The histone site H2AK119 can also be mono-ubiquitinated by polycomb repressive complex 1 (PRC1) and Cullin4B-Ring E3 ligase complex (CRL4B) to repress target genes, and its role in tumorigenesis has been well characterized (Wang et al., 2004; Hu et al., 2012). However, the role of H2AK119ub in the central nervous system is still unclear. We found that the levels of the transcriptional repression mark H2AK119ub were reduced in cultured neurons and the hippocampi of treated mice, indicating that H2AK119ub might be involved in regulating neuronal functions. Other studies have shown that H2AK119ub plays a vital role in transcriptional repression by functionally coordinating with H3K27me3 (Muller and Verrijzer, 2009). In this study, we found that the binding of H2AK119ub to *Bdnf* promoters I, II, IV, and VI was reduced, indicating that H2AK119ub is involved in the BHBA-induced activation of *Bdnf* transcription. H3K27me3 is produced by the histone methyltransferase enhancer of Zeste homolog 2 (EZH2), the catalytic subunit of PRC2, and it is typically added to nucleosomes across upstream promoters and coding regions of PRC2-targeted genes to repress them (Xu et al., 2012). In addition, H3K27me3 was also found to interact with PRC1, while the mono-ubiquitination of H2AK119 by PRC1, in turn, promotes the tri-methylation of H3K27 on H2Aub nucleosomes (Kalb et al., 2014). The fact that H2AK119ub can functionally interact with H3K27me3 also explains the reduction of H2K119ub binding at *Bdnf* promoters after BHBA treatment. Notably, the occupancy of H2AK119ub at *Bdnf* promoters I, II, IV, and VI was decreased, while only the occupancy of H3K27me at *Bdnf* II and VI was found to be reduced by BHBA in our previous study (Hu et al., 2018). CUL4B is a vital component responsible for H2AK119 ubiquitination, acting as a scaffold protein that assembles multiple E3 complexes, including CRL4B via the linker protein DDB1 (Nakagawa and Xiong, 2011a). It has been shown that CUL4B binds to the promoters or enhancer regions of targeted genes, together with EZH2, to silence their transcription by catalyzing H2AK119 mono-ubiquitination and H3K27 tri-methylation (Hu et al., 2012). Although PRC1 and PRC2 usually co-localize at target sites in the chromatin, they rely on different mechanisms. In the "hierarchical" model, the initial event is the binding of PRC2 to chromatin. PRC2 then catalyzes H3K27 tri-methylation, which subsequently recruits PRC1 by interaction with the chromo box (CBX)-containing protein, leading to H2AK119 mono-ubiquitination. In the "alternative" model, PRC1 is recruited to chromatin and then mono-ubiquitinates H2AK119 independently of PRC2 activity (Blackledge et al., 2015). This means that H2AK119ub and H3K27me3 are not always introduced at the same target sites, although most of the time, they work together to inhibit gene transcription. Furthermore, CUL4B can regulate the expression of neuronal genes such as SLC6A12, SYN1, and SNAP2, by targeting the methyltransferase component of H3K4me3, WDR5, for ubiquitination and degradation (Nakagawa and Xiong, 2011b). Together with the discussed literature, our results indicate the possibility that H2AK119ub plays a role in regulating neuronal function by acting cooperatively with H3K4me3 and H3K27me3, allowing neurons to rapidly respond to environmental changes. However, direct evidence for this hypothesis is still lacking. In addition, another study showed that the H2AK119 E3 ubiquitin ligase 2A-HUB can be recruited by N-CoR/HDAC1/3 to form a complex that regulates chromatin remodeling and gene transcription by promoting H2A monoubiquitination (Zhou et al., 2008). Zhu et al. (2007) found that H2A de-ubiquitinase (2A-DUB) interacts with the histone acetyltransferase (HAT) p300/CBP-associated factor (p/CAF) to form an enzymatic complex, which could help HATs provide "optimized" substrates for 2A-DUB to remove the ubiquitin from H2A. As an inhibitor of class-I HADCs, BHBA might affect H2AK119ub levels by changing the interaction of 2A-HUB and N-CoR/HDAC1/3 at the *Bdnf* promoters, or by promoting the formation of p/CAF complexes with 2A-DUB to remove the ubiquitin from H2AK119.

Finally, we found that the BHBA-induced upregulation of H3K4me3 and downregulation of H2AK119ub is dependent on L-type VSCCs by using manidipine to block the impact of BHBA on H3K4me3 and H2AK119ub in neurons. However, we are not aware of reports of any direct evidence demonstrating a relation between H3K4 tri-methylation or H2AK119 ubiquitination with calcium signaling. One study showed that the abundance of the CUL4B-PRC2 complex increases in response to high-glucose stimulus and affects intracellular Ca^{2+} by decreasing Cav1.2 expression (Li et al., 2017). However, in our study, the effect of BHBA on intracellular Ca^{2+} was fast, suggesting that BHBA might directly affect the opening and closing of L-type VSCCs. Moreover, the changes of H3K4me3 and H2AK119ub were found to be downstream of Ca^{2+} signaling. However, it is possible that the BHBA-induced changes of H2AK119ub, in turn, can further influence the Ca^{2+} concentration by affecting the expression of calcium channels such as Cav1.2.

In summary, our study revealed that BHAB stimulation increased histone H3K4me3 and decreased H2AK119ub in hippocampal neurons both *in vitro* and *in vivo*. The occupancy of H3K4me3 and H2AK119ub at *Bdnf* promoters was also correspondingly enhanced and decreased, which contributed to the BHBA-induced expression of BDNF. Moreover, BHBA triggered an increase of intracellular Ca^{2+} via L-type VSCCs, which in turn activated the Ca^{2+}/CaMKII/p-CREB signaling pathway and subsequently induced BDNF expression in primary hippocampal neurons. Furthermore, the BHBA-induced decrease of H2AK119ub was dependent on L-type VSCCs, while the increase of H3K4me3 mainly resulted from BHBA-activated cAMP/PKA signaling (**Figure 6**). Taken together, our findings further enrich the knowledge on the molecular mechanisms by which BHBA induces *Bdnf* expression. We revealed that BHBA also regulates the levels of H2AK119ub and H3K4me3 in addition to the previously reported H3K27me3/ac. These findings broaden the roles of BHBA in modulating the histone code and provides new perspectives for understanding the beneficial effects of BHBA on the CNS.

DATA AVAILABILITY STATEMENT

The raw data supporting the conclusions of this article will be made available by the authors, without undue reservation.

ETHICS STATEMENT

The animal study was reviewed and approved by the Research Ethics Committee of Xi'an Jiaotong University.

AUTHOR CONTRIBUTIONS

XL, YZ, and EH designed the study. EH, HD, and SS carried out the experiments, the data analysis and contributed to preparing the manuscript. All authors discussed the results and contributed to the final manuscript.

FUNDING

This work was supported by grants from the Natural science foundation of Shaanxi province (No. 2018JM7055).

REFERENCES

Aid, T., Kazantseva, A., Piirsoo, M., Palm, K., and Timmusk, T. (2007). Mouse and rat BDNF gene structure and expression revisited. *J. Neurosci. Res.* 85, 525–535. doi: 10.1002/jnr.21139

Bernstein, B. E., Mikkelsen, T. S., Xie, X., Kamal, M., Huebert, D. J., Cuff, J., et al. (2006). A bivalent chromatin structure marks key developmental genes in embryonic stem cells. *Cell* 125, 315–326. doi: 10.1016/j.cell.2006.02.041

Blackledge, N. P., Rose, N. R., and Klose, R. J. (2015). Targeting polycomb systems to regulate gene expression: modifications to a complex story. *Nat. Rev. Mol. Cell Biol.* 16, 643–649. doi: 10.1038/nrm4067

Bok, J., Zha, X. M., Cho, Y. S., and Green, S. H. (2003). An extranuclear locus of cAMP-dependent protein kinase action is necessary and sufficient for promotion of spiral ganglion neuronal survival by cAMP. *J. Neurosci.* 23, 777–787. doi: 10.1152/jn.00779.2002

Camberos-Luna, L., Geronimo-Olvera, C., Montiel, T., Rincon-Heredia, R., and Massieu, L. (2016). The ketone body, beta-hydroxybutyrate stimulates the autophagic flux and prevents neuronal death induced by glucose deprivation in cortical cultured neurons. *Neurochem. Res.* 41, 600–609. doi: 10.1007/s11064-015-1700-4

Cheng, S., Wu, Q., Yang, F., Xu, M., Leski, M., and Chen, G. Q. (2005). Influence of DL-beta-hydroxybutyric acid on cell proliferation and calcium influx. *Biomacromolecules* 6, 593–597. doi: 10.1021/bm049465y

Collins, B. E., Sweatt, J. D., and Greer, C. B. (2019). Broad domains of histone 3 lysine 4 trimethylation are associated with transcriptional activation in CA1 neurons of the hippocampus during memory formation. *Neurobiol. Learn. Mem.* 161, 149–157. doi: 10.1016/j.nlm.2019.04.009

Fu, S. P., Wang, J. F., Xue, W. J., Liu, H. M., Liu, B. R., Zeng, Y. L., et al. (2015). Anti-inflammatory effects of BHBA in both in vivo and in vitro Parkinson's disease models are mediated by GPR109A-dependent mechanisms. *J. Neuroinflamm.* 12:9. doi: 10.1186/s12974-014-0230-3

Hansen, M. R., Bok, J., Devaiah, A. K., Zha, X. M., and Green, S. H. (2003). Ca2+/calmodulin-dependent protein kinases II and IV both promote survival but differ in their effects on axon growth in spiral ganglion neurons. *J. Neurosci. Res.* 72, 169–184. doi: 10.1002/jnr.10551

Hu, E., Du, H., Zhu, X., Wang, L., Shang, S., Wu, X., et al. (2018). Beta-hydroxybutyrate promotes the expression of BDNF in Hippocampal neurons under adequate glucose supply. *Neuroscience* 386, 315–325. doi: 10.1016/j.neuroscience.2018.06.036

Hu, H., Yang, Y., Ji, Q., Zhao, W., Jiang, B., Liu, R., et al. (2012). CRL4B catalyzes H2AK119 monoubiquitination and coordinates with PRC2 to promote tumorigenesis. *Cancer Cell* 22, 781–795. doi: 10.1016/j.ccr.2012.10.024

Jakovcevski, M., Ruan, H., Shen, E. Y., Dincer, A., Javidfar, B., Ma, Q., et al. (2015). Neuronal Kmt2a/Mll1 histone methyltransferase is essential for prefrontal synaptic plasticity and working memory. *J. Neurosci.* 35, 5097–5108. doi: 10.1523/JNEUROSCI.3004-14.2015

Juge, N., Gray, J. A., Omote, H., Miyaji, T., Inoue, T., Hara, C., et al. (2010). Metabolic control of vesicular glutamate transport and release. *Neuron* 68, 99–112. doi: 10.1016/j.neuron.2010.09.002

Kalb, R., Latwiel, S., Baymaz, H. I., Jansen, P. W., Muller, C. W., Vermeulen, M., et al. (2014). Histone H2A monoubiquitination promotes histone H3 methylation in polycomb repression. *Nat. Struct. Mol. Biol.* 21, 569–571. doi: 10.1038/nsmb.2833

Li, Q., Cui, M., Yang, F., Li, N., Jiang, B., Yu, Z., et al. (2017). A cullin 4B-RING E3 ligase complex fine-tunes pancreatic delta cell paracrine interactions. *J. Clin. Invest.* 127, 2631–2646. doi: 10.1172/JCI91348

Lutas, A., and Yellen, G. (2013). The ketogenic diet: metabolic influences on brain excitability and epilepsy. *Trends Neurosci.* 36, 32–40. doi: 10.1016/j.tins.2012.11.005

Muller, J., and Verrijzer, P. (2009). Biochemical mechanisms of gene regulation by polycomb group protein complexes. *Curr. Opin. Genet. Dev.* 19, 150–158. doi: 10.1016/j.gde.2009.03.001

Nakagawa, T., and Xiong, Y. (2011a). Chromatin regulation by CRL4 E3 ubiquitin ligases: CUL4B targets WDR5 ubiquitylation in the nucleus. *Cell Cycle* 10, 4197–4198. doi: 10.4161/cc.10.24.18407

Nakagawa, T., and Xiong, Y. (2011b). X-linked mental retardation gene CUL4B targets ubiquitylation of H3K4 methyltransferase component WDR5 and regulates neuronal gene expression. *Mol. Cell.* 43, 381–391. doi: 10.1016/j.molcel.2011.05.033

Newman, J. C., and Verdin, E. (2017). Beta-hydroxybutyrate: a signaling metabolite. *Annu. Rev. Nutr.* 37, 51–76. doi: 10.1146/annurev-nutr-071816-064916

Offermanns, S., and Schwaninger, M. (2015). Nutritional or pharmacological activation of HCA(2) ameliorates neuroinflammation. *Trends Mol. Med.* 21, 245–255. doi: 10.1016/j.molmed.2015.02.002

Palomer, E., Carretero, J., Benvegnu, S., Dotti, C. G., and Martin, M. G. (2016). Neuronal activity controls Bdnf expression via Polycomb de-repression and CREB/CBP/JMJD3 activation in mature neurons. *Nat. Commun.* 7:11081. doi: 10.1038/ncomms11081

Reger, M. A., Henderson, S. T., Hale, C., Cholerton, B., Baker, L. D., Watson, G. S., et al. (2004). Effects of beta-hydroxybutyrate on cognition in memory-impaired adults. *Neurobiol. Aging* 25, 311–314. doi: 10.1016/S0197-4580(03)00087-3

Shimazu, T., Hirschey, M. D., Newman, J., He, W., Shirakawa, K., Le Moan, N., et al. (2013). Suppression of oxidative stress by beta-hydroxybutyrate, an endogenous histone deacetylase inhibitor. *Science* 339, 211–214. doi: 10.1126/science.1227166

Sleiman, S. F., Henry, J., Al-Haddad, R., El Hayek, L., Abou Haidar, E., Stringer, T., et al. (2016). Exercise promotes the expression of brain derived neurotrophic factor (BDNF) through the action of the ketone body beta-hydroxybutyrate. *eLife* 5:e15092. doi: 10.7554/eLife.15092

Suzuki, M., Suzuki, M., Kitamura, Y., Mori, S., Sato, K., Dohi, S., et al. (2002). Beta-hydroxybutyrate, a cerebral function improving agent, protects rat brain against ischemic damage caused by permanent and transient focal cerebral ischemia. *Jpn. J. Pharmacol.* 89, 36–43. doi: 10.1254/jjp.89.36

Tieu, K., Perier, C., Caspersen, C., Teismann, P., Wu, D. C., Yan, S. D., et al. (2003). D-beta-hydroxybutyrate rescues mitochondrial respiration and mitigates features of Parkinson disease. *J. Clin. Invest.* 112, 892–901. doi: 10.1172/JCI18797

Wang, H., Wang, L., Erdjument-Bromage, H., Vidal, M., Tempst, P., Jones, R. S., et al. (2004). Role of histone H2A ubiquitination in polycomb silencing. *Nature* 431, 873–878. doi: 10.1038/nature02985

Webb, W. M., Sanchez, R. G., Perez, G., Butler, A. A., Hauser, R. M., Rich, M. C., et al. (2017). Dynamic association of epigenetic H3K4me3 and DNA

5hmC marks in the dorsal hippocampus and anterior cingulate cortex following reactivation of a fear memory. *Neurobiol. Learn. Mem.* 142, 66–78. doi: 10.1016/j.nlm.2017.02.010

Won, Y. J., Lu, V. B., Puhl, H. L. III, and dand Ikeda, S. R. (2013). Beta-Hydroxybutyrate modulates N-type calcium channels in rat sympathetic neurons by acting as an agonist for the G-protein-coupled receptor FFA3. *J. Neurosci.* 33, 19314–19325. doi: 10.4161/chan.28956

Wysocka, J., Swigut, T., Milne, T. A., Dou, Y., Zhang, X., Burlingame, A. L., et al. (2005). WDR5 associates with histone H3 methylated at K4 and is essential for H3 K4 methylation and vertebrate development. *Cell* 121, 859–872. doi: 10.1016/j.cell.2005.03.036

Xie, Z., Zhang, D., Chung, D., Tang, Z., Huang, H., Dai, L., et al. (2016). Metabolic regulation of gene expression by histone lysine beta-hydroxybutyrylation. *Mol. Cell.* 62, 194–206. doi: 10.1016/j.molcel.2016.03.036

Xu, K., Wu, Z. J., Groner, A. C., He, H. H., Cai, C., Lis, R. T., et al. (2012). EZH2 oncogenic activity in castration-resistant prostate cancer cells is polycomb-independent. *Science* 338, 1465–1469. doi: 10.1126/science.1227604

Yin, J. X., Maalouf, M., Han, P., Zhao, M., Gao, M., Dharshaun, T., et al. (2016). Ketones block amyloid entry and improve cognition in an Alzheimer's model. *Neurobiol. Aging* 39, 25–37. doi: 10.1016/j.neurobiolaging.2015.11.018

Youm, Y. H., Nguyen, K. Y., Grant, R. W., Goldberg, E. L., Bodogai, M., Kim, D., et al. (2015). The ketone metabolite beta-hydroxybutyrate blocks NLRP3 inflammasome-mediated inflammatory disease. *Nat. Med.* 21, 263–269. doi: 10.1038/nm.3804

Zheng, F., Zhou, X., Moon, C., and Wang, H. (2012). Regulation of brain-derived neurotrophic factor expression in neurons. *Int. J. Physiol. Pathophysiol. Pharmacol.* 4, 188–200.

Zhou, W., Zhu, P., Wang, J., Pascual, G., Ohgi, K. A., Lozach, J., et al. (2008). Histone H2A monoubiquitination represses transcription by inhibiting RNA polymerase II transcriptional elongation. *Mol .Cell.* 29, 69–80. doi: 10.1016/j.molcel.2007.11.002

Zhu, P., Zhou, W., Wang, J., Puc, J., Ohgi, K. A., Erdjument-Bromage, H., et al. (2007). A histone H2A deubiquitinase complex coordinating histone acetylation and H1 dissociation in transcriptional regulation. *Mol. Cell.* 27, 609–621. doi: 10.1016/j.molcel.2007.07.024

Zou, X. H., Li, H. M., Wang, S., Leski, M., Yao, Y. C., Yang, X. D., et al. (2009). The effect of 3-hydroxybutyrate methyl ester on learning and memory in mice. *Biomaterials* 30, 1532–1541. doi: 10.1016/j.biomaterials.2008.12.012

Conflict of Interest: The authors declare that the research was conducted in the absence of any commercial or financial relationships that could be construed as a potential conflict of interest.

Copyright © 2020 Hu, Du, Shang, Zhang and Lu. This is an open-access article distributed under the terms of the Creative Commons Attribution License (CC BY). The use, distribution or reproduction in other forums is permitted, provided the original author(s) and the copyright owner(s) are credited and that the original publication in this journal is cited, in accordance with accepted academic practice. No use, distribution or reproduction is permitted which does not comply with these terms.

frontiers in Aging Neuroscience

ORIGINAL RESEARCH
published: 19 November 2020
doi: 10.3389/fnagi.2020.577899

Disrupted Regional Cerebral Blood Flow and Functional Connectivity in Pontine Infarction: A Longitudinal MRI Study

Ying Wei[1†], Luobing Wu[1†], Yingying Wang[1†], Jingchun Liu[2], Peifang Miao[1], Kaiyu Wang[3], Caihong Wang[1] and Jingliang Cheng[1*]*

[1] First Affiliated Hospital of Zhengzhou University, Zhengzhou, China, [2] Department of Radiology and Tianjin Key Laboratory of Functional Imaging, Tianjin Medical University General Hospital, Tianjin, China, [3] GE Healthcare MR Research, Beijing, China

Abnormal cerebral blood flow (CBF) and resting-state functional connectivity (rs-FC) are sensitive biomarkers of disease progression and prognosis. This study investigated neural underpinnings of motor and cognitive recovery by longitudinally studying the changes of CBF and FC in pontine infarction (PI). Twenty patients underwent three-dimensional pseudo-continuous arterial spin labeling (3D-pcASL), resting-state functional magnetic resonance imaging (rs-fMRI) scans, and behavioral assessments at 1 week, 1, 3, and 6 months after stroke. Twenty normal control (NC) subjects underwent the same examination once. First, we investigated CBF changes in the acute stage, and longitudinal changes from 1 week to 6 months after PI. Brain regions with longitudinal CBF changes were then used as seeds to investigate longitudinal FC alterations during the follow-up period. Compared with NC, patients in the left PI (LPI) and right PI (RPI) groups showed significant CBF alterations in the bilateral cerebellum and some supratentorial brain regions at the baseline stage. Longitudinal analysis revealed that altered CBF values in the right supramarginal (SMG_R) for the LPI group, while the RPI group showed significantly dynamic changes of CBF in the left calcarine sulcus (CAL_L), middle occipital gyrus (MOG_L), and right supplementary motor area (SMA_R). Using the SMG_R as the seed in the LPI group, FC changes were found in the MOG_L, middle temporal gyrus (MTG_L), and prefrontal lobe (IFG_L). Correlation analysis showed that longitudinal CBF changes in the SMG_R and FC values between the SMG_R and MOG_L were associated with motor and memory scores in the LPI group, and longitudinal CBF changes in the CAL_L and SMA_R were related to memory and motor recovery in the RPI group. These longitudinal CBF and accompany FC alterations may provide insights into the neural mechanism underlying functional recovery after PI, including that of motor and cognitive functions.

Keywords: pontine infarction, cerebral blood flow, functional connectivity, motor, cognition

OPEN ACCESS

Edited by:
Piotr Walczak,
Johns Hopkins Medicine,
United States

Reviewed by:
Han Lv,
Beijing Friendship Hospital, Capital Medical University, China
Ying Han,
Xuanwu Hospital, Capital Medical University, China
Yu-Chen Chen,
First Affiliated Hospital, Nanjing Medical University, China

****Correspondence:***
Caihong Wang
fccwangch@zzu.edu.cn
Jingliang Cheng
fccchengjl@zzu.edu.cn

† These authors have contributed equally to this work

Received: *16 July 2020*
Accepted: *12 October 2020*
Published: *19 November 2020*

Citation:
Wei Y, Wu L, Wang Y, Liu J, Miao P, Wang K, Wang C and Cheng J (2020) Disrupted Regional Cerebral Blood Flow and Functional Connectivity in Pontine Infarction: A Longitudinal MRI Study. Front. Aging Neurosci. 12:577899. doi: 10.3389/fnagi.2020.577899

INTRODUCTION

Pontine infarction (PI) accounts for 7% of ischemic strokes and is the most common type of posterior circulation infarction (Wang et al., 2018). Typical clinical manifestations of PI include pure motor hemiplegia, ataxia, dysarthria, dysphagia, and cognitive impairment (Kinjo et al., 2017; Lapa et al., 2017; Li et al., 2020). Long-term follow-up has revealed that some patients with PI

experience a poor prognosis with impaired motor or cognitive function (Mijajlovic et al., 2017; Payabvash et al., 2018). Therefore, understanding the neural mechanisms of behavioral impairment and recovery is crucial in stroke rehabilitation.

In the past few years, neuroimaging studies have been widely used to explore neurobiological mechanisms in the brain under healthy and pathological conditions and have been shown to be useful to predict further behavioral recovery (Haque et al., 2019; Xie et al., 2019; Zhang et al., 2020). Recently, an increasing number of studies have reported that abnormal cerebral hemodynamics represent an important pathophysiological mechanism in the post-stroke brain and that cerebral blood flow (CBF) is disturbed not only in the infarction or peri-infarct areas but also in the remote brain regions that are correlated with injury brain areas (Miao et al., 2018; Wang et al., 2019). Previous studies using single-photon emission computed tomography (SPECT) have also suggested that abnormal perfusion in remote areas, including the cerebellum and supratentorial frontoparietal cortex after PI, and disruption and reorganization of CBF are two of the mechanisms underlying behavioral impairment and improvement (Hoffmann and Watts, 1998; D'Aes and Marien, 2015). However, issues with exposure to ionizing radiation and the use of exogenous tracer agents have limited clinical researches, particularly studies requiring repetitive imaging and longitudinal researches.

Arterial spin labeling (ASL) imaging can quantitatively evaluate regional CBF values using arterial blood as an endogenous diffusion tracer (Deibler et al., 2008). Currently, ASL is a promising alternative technique for investigating the neural basis of various neurological and psychiatric diseases, such as stroke, seizures, Alzheimer's disease, and Parkinson's disease, since the perfusion results detected by ASL are consistent with those detected by conventional techniques. Additionally, ASL detection is non-invasive and non-ionizing (Le Heron et al., 2014; Wiest et al., 2014; Xie et al., 2019; Zhang et al., 2020). Some researchers have investigated CBF patterns of chronic PI by using ASL and have found that patients with PI showed higher CBF values in the contralateral inferior frontal gyrus and lower CBF values in the bilateral cerebellum; moreover, the CBF values in the contralateral cerebellum were closely associated with motor function scores (Wang et al., 2019). However, the processes underlying CBF changes are intrinsic and dynamic during the period of functional damage and subsequent recovery; thus, a longitudinal study is important for gaining comprehensive understanding of the neurobiological underpinnings.

Neurological activity in the brain regions is accompanied by changes of CBF and blood oxygenation, which can be measured by functional magnetic resonance imaging (fMRI) techniques (Detre and Wang, 2002; Fox and Raichle, 2007; Boscolo Galazzo et al., 2014). Resting-state functional connectivity (FC), which is based on detection of the temporal correlations of blood oxygen level-dependent (BOLD) signals between two brain regions, has been used to investigate the cortical reorganization and compensation (Buckner et al., 2013; Guerra-Carrillo et al., 2014). Although early evidence has utilized FC to investigate the neural mechanisms underlying stroke-related behavioral function decline, there is little knowledge about PI, especially longitudinal and within-person changes. In cross-sectional studies, patients with acute PI showed significantly lower FC in the medial prefrontal cortex and precuneus (Jiang et al., 2018), while patients with early chronic PI exhibited decreased FC in the medial prefrontal gyrus, precuneus, right posterior cingulum, and left middle cingulum gyrus (Chen et al., 2019). In a longitudinal-sectional study, some brain regions exhibited special changes during the follow-up period, in which voxel-mirrored homotopic connectivity (VMHC) in the precentral and postcentral gyrus tended to increase gradually, and VMHC in the hippocampus/amygdala was increased throughout the study period, and VMHC in the hippocampus/amygdala and frontal pole in the early stages were associated with the later motor recovery (Shan et al., 2018).

In addition, recent studies have confirmed the association between CBF and FC, and FC might be modulated by regional CBF of the seed (Li et al., 2012; Liu et al., 2013). Network analysis has found that specific network nodes present a higher CBF to main proper network integrity (Liang et al., 2013). According to the neurovascular coupling hypothesis, altered CBF may be coupled with significant changes in the brain FC (Venkat et al., 2016; Zhu et al., 2017). Therefore, some researches have attempted to explore pathophysiological mechanisms and effectiveness of drug therapy in neuropsychiatric disorders using multimodal MRI such as ASL and BOLD fMRI (He et al., 2019; Tan et al., 2020).

Based on the abovementioned knowledge, in order to explore the neural substrates of functional recovery after PI, we first investigated the cross-sectional and longitudinal changes in CBF during the 6 months following PI. After identifying the longitudinal changes in CBF, the progressive FC changes were further explored using these CBF-altered regions as seed. Finally, we also further investigated the relationships among abnormal changes in CBF, FC, and behavioral performance after stroke.

MATERIALS AND METHODS

Participants

Participants were recruited from the First Affiliated Hospital of Zhengzhou University and Tianjin Medial University General Hospital. These subjects provided written informed consent before the study, and the study protocol was approved by the local Research Ethics committee.

The inclusion criteria were as follows: (1) first-onset infarction and within 1 week after onset of symptoms; (2) right-handedness before brain stroke; (2) age from 40 to 80 years; (3) unilateral lesion located in the pontine identified, as identified by MRI examination; and (4) adherence to follow-up tests for 6 months. The exclusion criteria were as follows: (1) secondary hemorrhage and recurrent stroke during follow-up; (2) the score of artery stenosis >2 based on magnetic resonance angiography (Ferguson et al., 1999); (3) severe white matter hyperintensity with a Fazekas scale score >1; (4) history of drug dependence or concomitant neuropsychiatric disorders; (5) severe systemic

TABLE 1 | Demographic and clinical data in the PI and NC groups.

Variable	PI (n = 20)		NC (n = 20)	P-value
	LPI (n = 10)	RPI (n = 10)		
Age, years	60.10 ± 4.40	54.40 ± 7.87	55.67 ± 6.24	P'_{LPI} = 0.06; P'_{RPI} = 0.64
Gender (male/female)	7/3	4/6	12/8	P'_{LPI} = 0.64; P'_{RPI} = 0.28
Years of formal education	10.20 ± 3.52	9.60 ± 1.89	11.11 ± 2.72	P'_{LPI} = 0.45; P'_{RPI} = 0.13
Lesion size at acute phase(ml)	2.75 ± 1.86	1.66 ± 0.75	/	P = 0.11
Stroke to the first follow-up (days)	4.90 ± 1.85	4.60 ± 1.71	/	P = 0.71
Medical history				
Coronary heart disease	1/10	1/10	0/20	P'_{LPI} = 0.39; P'_{RPI} = 0.39
Hypertension	4/10	5/10	4/20	P'_{LPI} = 0.23; P'_{RPI} = 0.09
Hyperlipidemia	4/10	2/10	2/20	P'_{LPI} = 0.05; P'_{RPI} = 0.45
Diabetes	1/10	2/10	1/20	P'_{LPI} = 0.61; P'_{RPI} = 0.19
Smoking	2/10	3/10	2/20	P'_{LPI} = 0.45; P'_{RPI} = 0.17
Drinking	1/10	1/10	1/20	P'_{LPI} = 0.61; P'_{RPI} = 0.61
NIHSS score				
Time 1	3.50 ± 3.92	1.50 ± 2.50		/;/
Time 2	1.70 ± 2.35	1.20 ± 2.09	/	F = 9.57; P_{LPI} = 0.002*
Time 3	1.00 ± 2.21	0.20 ± 0.63		F = 2.65; P_{RPI} = 0.07
Time 4	0.50 ± 1.26	0.10 ± 0.31		
FMT				
Time 1	73.90 ± 33.48	83.20 ± 22.95		/;/
Time 2	85.90 ± 26.52	96.30 ± 7.48	/	F = 7.19; P_{LPI} = 0.001*
Time 3	89.60 ± 25.83	98.40 ± 5.06	/	F = 5.40; P_{RPI} = 0.005*
Time 4	91.20 ± 21.87	99.00 ± 3.16		
RAVLT				
Time 1	34.00 ± 7.11	37.60 ± 11.27	48.11 ± 8.44	P'_{LPI} < 0.001*; P'_{RPI} = 0.01*
Time 2	44.80 ± 7.96	49.50 ± 10.59		F = 18.21; P_{LPI} < 0.001*
Time 3	50.40 ± 12.44	53.00 ± 11.19		F = 13.17; P_{RPI} < 0.001*
Time 4	52.20 ± 7.94	58.88 ± 10.56		
Mean FD				
Time 1	0.116 ± 0.042	0.138 ± 0.047	/	F = 1.158; P_{LPI} = 0.349
Time 2	0.144 ± 0.042	0.146 ± 0.082		F = 0.245; P_{RPI} = 0.864
Time 3	0.139 ± 0.036	0.121 ± 0.073		
Time 4	0.131 ± 0.038	0.134 ± 0.046		

*Data were presented as mean ± SD for continuous data. P_{PI}', P values of demographic data and behavioral test scores between the baseline stage of PI and NC groups; P_{PI}, P value of behavioral scores among PI subgroups at different time-points; P, P value of infarct volume at acute phase between LPI and RPI groups. Time 1, Time 2, Time 3, and Time 4, different time subgroups from 1 week to 6 months after PI. LPI, left pontine infarction; RPI, right pontine infarction; NC, normal control; NIHSS, National Institutes of Health Stroke Scale; FMT, Fugl–Meyer Test; RAVLT, Ray Auditory Verbal Learning Test; Mean FD, mean framewise displacement (FD). *$p < 0.05$.*

comorbidities, including heart failure and cancer; and (6) contraindications for MRI. Finally, 20 patients with unilateral PI were recruited from October 2014 to May 2019, including 10 subjects with lesions on each side. Twenty age-, sex-, and education-matched normal control (NC) subjects were recruited as a control group.

The infarction locations at the acute phase were manually delineated based on the acute diffusion-weighted imaging by using MRIcron software[1]. The lesion masks of all stroke patients were normalized in the Montreal Neurological Institute (MNI) space and then overlaid on a normalized template to generate the lesion distribution probability maps.

[1]www.nitrc.org/projects/mricron

Image Data Acquisition

MRI examinations were performed using a 3.0-Tesla MR imaging system (Discovery MR 750, GE Medical Systems, Waukesha, WI, United States) at 1 week, 1, 3, and 6 months after infarction onset in the PI group, while the NC subjects were examined only once in the same manner. All subjects were instructed to hold still, close their eyes, and think of nothing in particular. Comfortable foam padding and earplugs were used to reduce head motion and scanner noise. Brain perfusion imaging was performed using a three-dimensional pseudo-continuous arterial spin labeling (3D-pcASL) sequence with the following parameters: TR/TE = 5,025 ms/11.1 ms; post label delay = 2,025 ms; spiral in readout of eight arms with 512 sample points; FA = 111°; field-of view (FOV) = 240 × 240 mm;

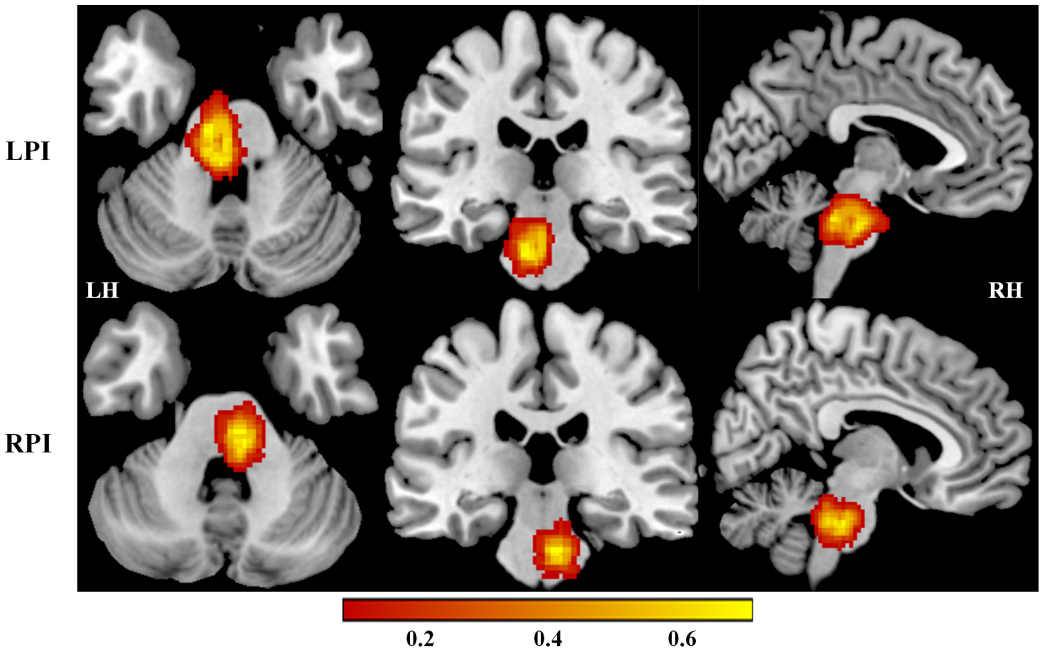

FIGURE 1 | Lesion distribution maps in the LPI and RPI groups. The color bar represents the lesion probability. LH, left hemisphere; RH, right hemisphere; LPI, left pontine infarction; RPI, right pontine infarction.

TABLE 2 | Brain regions with different CBF between the baseline stage of PI and NC group.

Brain regions	Cluster size (voxels)	Peak intensity	MNI coordinates
LPI group			
CBE lobule VIII_L	293	5.550	(−20, −68, −60)
CBE lobule VIIB_R	181	5.691	(44, −64, −54)
CBE Crus I_L	109	3.959	(−52, −48, −38)
IFG_L	140	5.599	(62, −18, −28)
INS_L	77	4.744	(−30, 34, −20)
ITG_R	219	5.268	(−42, −16, 2)
MTG_R	176	5.481	(66, −42, 8)
PCUN_R	343	−4.736	(8, 50, 66)
SPG_L	301	−4.611	(−24, −58, 66)
RPI group			
CBE lobule VIII_L	355	5.773	(−38, −42, −46)
CBE lobule VI_R	440	5.698	(20, −60, −28)
CBE Crus II_R	87	5.009	(16, −88, −32)
SFG_R	79	−4.733	(22, 26, 64)
PreCG_R	87	−4.322	(20, −20, 80)

CBE lobule VIII_L, left cerebellar lobule VIII; CBE Crus I_L, left cerebellar Crus I; CBE lobule VIIB_R, right cerebellar lobule VIIB; IFG_L, left inferior frontal gyrus; INS_L, left insula; ITG_R, right inferior temporal gyrus; MTG_R, right middle temporal gyrus; PCUN_R, right precuneus; SPG_L, left superior parietal gyrus; CBE lobule VI_R, right cerebellar lobule VI; CBE Crus II_R, right cerebellar Crus II; SFG_R, right superior frontal gyrus; PreCG_R, right precentral gyrus; LPI and RPI, left and right pontine infarction.

matrix = 128 × 128; slice thickness = 3.0 mm, no gap, 48 slices, number of excitations = 3, and 1.9 × 1.9 mm in-plane resolution. Spatial-3D T1-weighted images were acquired by using a brain volume sequence with the following imaging parameters: TR/TE = 8.2 ms/3.2 ms; FA = 12°; FOV = 256 × 256 mm; matrix = 256 × 256; slice thickness = 1.0 mm; no gap; 188 slices. Resting-state fMRI data were acquired by using a gradient-echo single-shot echo-planar imaging sequence with the following imaging parameters: TR/TE = 2,000 ms/41 ms; FA = 90°; FOV = 220 × 220 mm; matrix = 64 × 64; slice thickness = 4 mm; 0.5 mm gap; 32 slices; 190 time points. Diffusion-weighted imaging sequences were acquired at the axial plane with TR/TE = 6,000 ms/96 ms; FOV = 256 × 256 mm; slice thickness = 5.0 mm; 1.5 mm gap; 21 slices.

Behavioral Evaluation

Clinical stroke severity was assessed using the National Institutes of Health Stroke Scale (NIHSS), which is a 15-item stroke scale and score ranging from 0 to 42, with a higher score indicating a more serious function impairment (Kasner, 2006). They also underwent more detailed behavioral examination about motor and memory functions. Motor impairment was assessed using the Fugl–Meyer test (FMT) for upper and lower extremities, which is a standardized and reliable motor impairment scale. The score ranges from 0 to 100, with the higher score indicating better performance. The Ray Auditory Verbal Learning Test (RAVLT) was used to explore short-term verbal memory function, and the number of correctly recalled words was recorded as the RAVLT scores.

Image Processing

The CBF images were derived from the pcASL difference images by subtracting the labeled images from the control images.

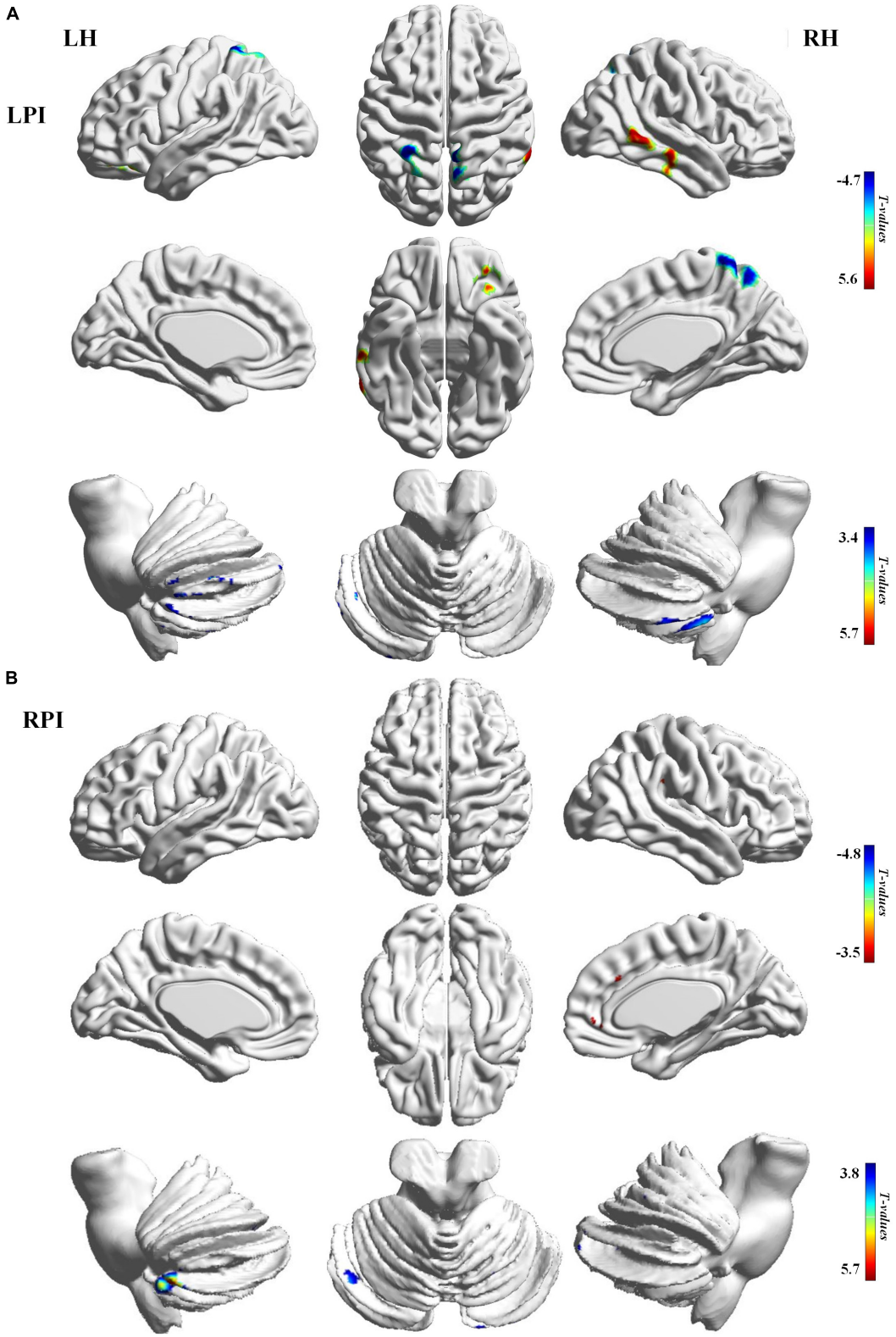

FIGURE 2 | CBF differences between the baseline subgroups of the PI and NC groups. **(A)** Voxel-base analysis showed brain regions with significant CBF alterations in the baseline stage of the LPI group. **(B)** Voxel-base analysis showed brain regions with significant CBF alterations in the baseline stage of the RPI group. The color bar indicated the *t* scores. LH, left hemisphere; RH, right hemisphere; LPI, left pontine infarction; RPI, right pontine infarction.

TABLE 3 | Brain regions with longitudinal CBF changes.

Brain regions	Cluster size (voxels)	Peak intensity	MNI coordinates
LPI group			
SMG_R	58	12.472	(66, −34, 28)
RPI group			
CAL_L	56	9.783	(−10, −102, −12)
MOG_L	127	14.131	(−24, −74, 32)
SMA_R	75	11.436	(8, −10, 68)

SMG_R, right supramarginal; CAL_L, left calcarine sulcus; MOG_L, left middle occipital gyrus; SMA_R, right supplementary motor area; LPI, left pontine infarction; RPI, right pontine infarction.

CBF images were processed using the SPM8 toolbox[2]. First, the individual 3D T1 images were coregistered to the individual ASL images to produce the new individual 3D T1 images. Second, the new individual 3D T1 images were normalized to a standard T1 template in MNI space and segmented into gray matter (GM), white matter, and cerebrospinal fluid maps. Third, the individual CBF images were subsequently written to the spatially normalized 3D T1 GM maps in MNI space and the voxel size for the normalized written images was $2 \times 2 \times 2$ mm^3. Fourth, to reduce individual variance, the spatially normalized CBF maps were transformed into *z* scores by subtracting the mean and dividing by the standard deviation (SD) of the global value within the GM mask. Finally, the images were spatially smoothed using a Gaussian kernel of 6-mm full width at half-maximum (FWHM).

Resting-state functional MRI (rs-fMRI) data were preprocessed using Data Processing and Analysis of Brain Imaging[3] (DPABI) in the SPM 8 software package. The preprocessing included the following steps. First, the first 20 volumes of subjects were removed to allow the signal to reach equilibrium. Second, the remaining 170 volumes were corrected for time delay between slices. For the head motion, we used a threshold of 2 mm translation and 2° rotation, and no subject exceeded this maximum. In this step, the mean framewise displacement (mean FD) was also calculated to characterize the mean head motion (Power et al., 2012). Third, functional images were co-registered to the 3D T1 images, and the remaining dataset was spatially normalized to MNI space and resampled into a voxel size of $3 \times 3 \times 3$ mm^3. Fourth, the images were smoothed by using a Gaussian kernel of 6-mm FWHM, and several covariates were regressed via linear regression. Finally, a temporal band-pass frequency filter (0.01–0.08 Hz) was performed

[2]http://www.Fil.ion.ucl.ac.uk/spm/software/spm

[3]http://rfmri.org/dpabi

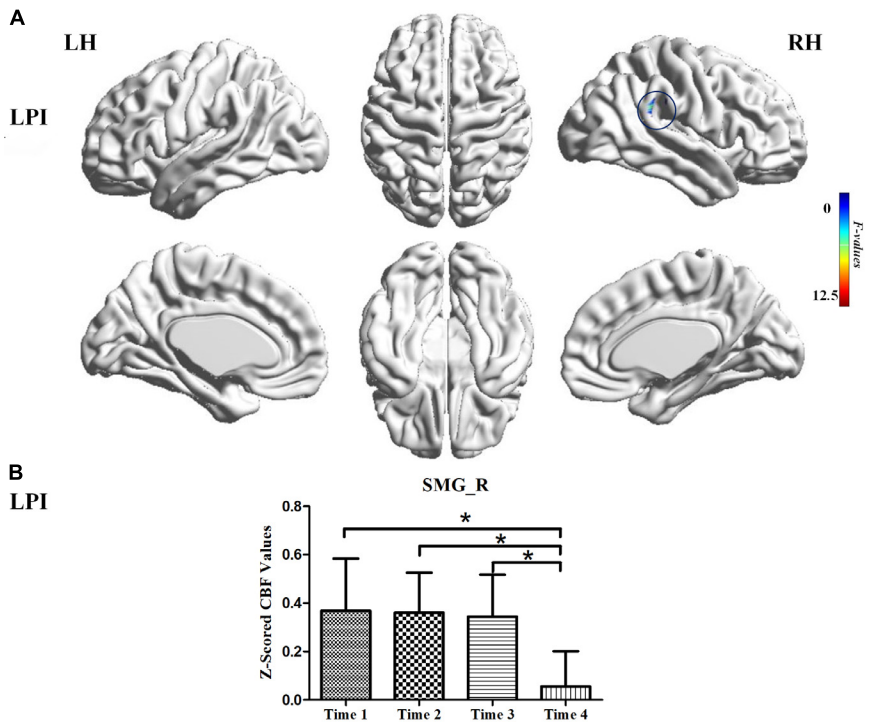

FIGURE 3 | CBF differences among different time-subgroups in the LPI group. **(A)** One-way repeated-measure ANOVA showed brain regions with CBF differences among four follow-up subgroups in the SMG_R. The color bar indicated the *F* scores. **(B)** Bar plots showed the *z*-scored CBF values of the SMG_R at four different time-subgroups and the change trend from the baseline stage to 6 months after infarction. SMG_R, right supramarginal gyrus; Time 1, Time 2, Time 3, and Time 4, different time subgroups from 1 week to 6 months after infarction; LH, left hemisphere; RH, right hemisphere; LPI, left pontine infarction. *$P < 0.05$.

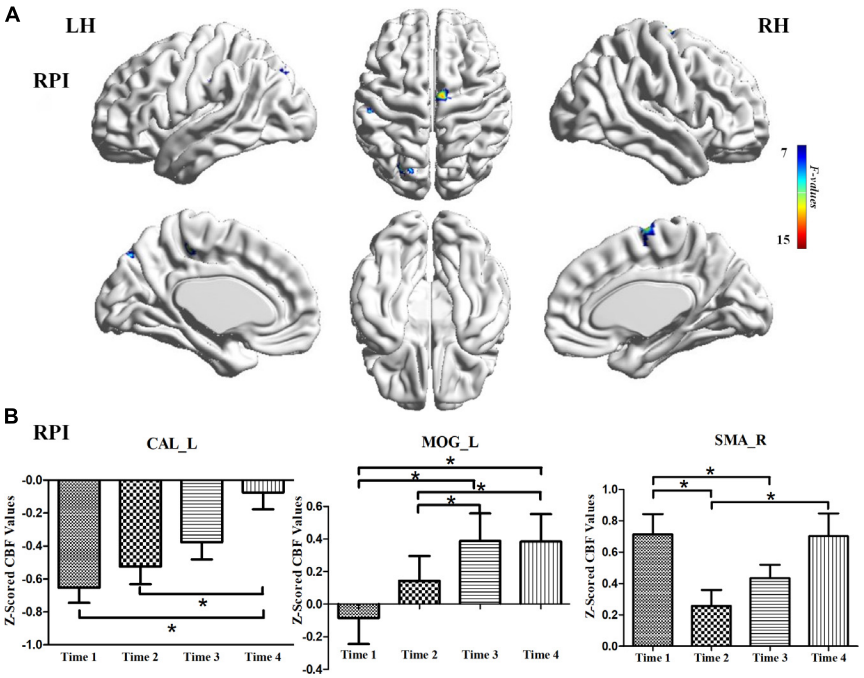

FIGURE 4 | CBF differences among different time-subgroups in the RPI group. **(A)** One-way repeated-measure ANOVA showed brain regions with CBF differences among different time-point subgroups in the CAL_L, MOG_L, and SMA_R. color bar indicated the *F* scores. **(B)** Bar plots showed the *z*-scored CBF values of these significant brain regions at four different time-subgroups and the change trends from the baseline stage to 6 months. CAL_L, the left calcarine sulcus; MOG_L, left middle occipital gyrus; SMA_R, right supplementary motor area; LH, left hemisphere; RH, right hemisphere; RPI, right pontine infarction. *$P < 0.05$.

to reduce low-frequency drift and high-frequency noise. We used the seed-based functional connective method to explore the different FC values over time in PI patients. Brain regions with significant longitudinal CBF changes in the left pontine infarction (LPI) and right pontine infarction (RPI) groups were respectively defined as seed regions of interest (ROIs), and Pearson's correlation coefficients were calculated between the mean time series of each ROI and each voxel in the whole brain GM as the seed-based FC maps. Then, the FC maps were transformed into Fisher's *z* maps for group analysis.

Statistic Analysis

The data at different time points in the same patients were divided into four subgroups, depending on the follow-up time. The demographic differences between the LPI, RPI, and NC groups were analyzed using independent two-sample *t*-tests or chi-square tests in the SPSS 21.0 software (SPSS, Inc., Chicago, IL, United States). The normality of clinical data distribution was tested using the Shapiro–Wilk test. A two-sample *t*-test was used to analyze behavioral differences between baseline subgroups of the PI and NC groups. One-way repeated-measure analysis of variance (ANOVA) and Bonferroni's *post hoc* tests were used to investigate the mean FD and behavioral changes between different LPI and RPI subgroups. All tests were two-tailed, and the significance threshold was set at $P < 0.05$.

For the cross-sectional comparison of CBF at the baseline stage between PI and NC groups, a voxel-wise two-sample *t*-test was performed, with age, sex, and education years as the covariance factors. For longitudinal comparisons, one-way repeated-measure ANOVA and Bonferroni's *post hoc* tests were used to explore the significance of differences in CBF and secondary FC changes among various time-related subgroups in the LPI and RPI groups. In addition, multiple comparisons were corrected using the AlphaSim program (the voxel-wise, $P < 0.001$; the cluster-wise, $P < 0.005$; 5,000 simulations) in the REST toolbox[4] 1.8. Pearson's or Spearman's correlation coefficients were calculated to test the association of normalized *z*-scored CBF values of each brain region with longitudinal CBF changes and behavioral scores over time. The association between the normalized *z*-scored FC values of each brain region showing longitudinal FC

TABLE 4 | Brain regions with longitudinal FC changes.

Seed	Brain regions	Cluster size (voxels)	Peak intensity	MNI coordinates
SMG_R	MTG_L	54	19.297	(−42, −54, 6)
	MOG_L	47	11.281	(−39, −87, 12)
	IFG_L	38	18.582	(−51, 30, 6)

SMG_R, right supramarginal; MTG_L, middle temporal gyrus; MOG_L, middle occipital gyrus; IFG_L, left inferior frontal gyrus.

[4]restfmri.net/forum/

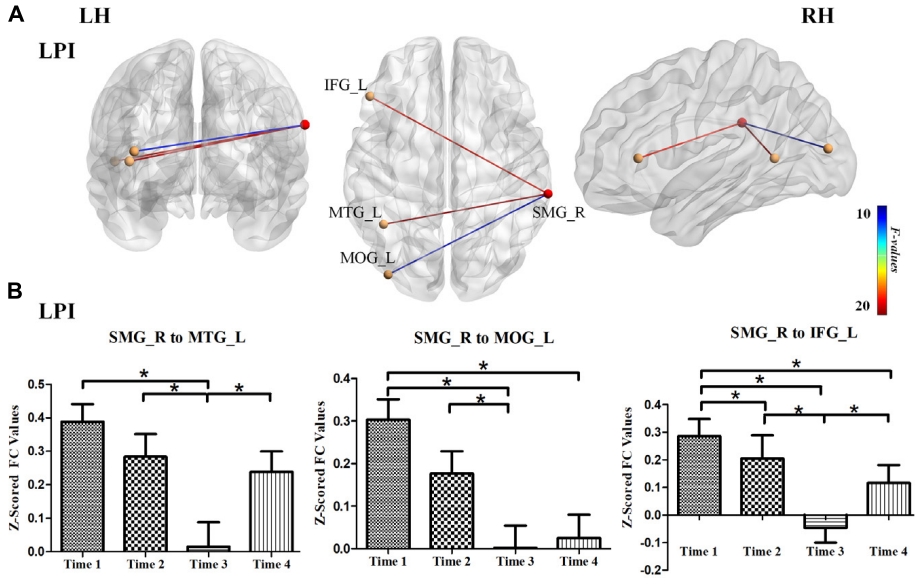

FIGURE 5 | Longitudinal FC changes among different time-subgroups in the LPI group. **(A)** The results for longitudinal analysis of FC using the SMG_R as seed in the LPI group. The red ball represented the seed-ROI, and yellow balls represented brain regions with longitudinal FC changes with seed-ROI. The color of the line indicated *z*-scored FC values. **(B)** Bar plots showed the *z*-scored FC values in significant brain regions with longitudinal FC changes and the change trends over four time points. SMG_R, right supramarginal gyrus; MTG_L, left middle temporal gyrus; MOG_L, left middle occipital gyrus; IFG_L, left inferior frontal gyrus; LH, left hemisphere; RH, right hemisphere; LPI, left pontine infarction. *$P < 0.05$.

changes and motor and memory scores was determined using the same methods.

RESULTS

Demographic and Behavioral Measures

Demographic and clinical characteristics of LPI, RPI, and NC subjects are shown in **Table 1**, **Supplementary Figure S1**, and **Supplementary Table S1** in the **Supplementary Material**. Compared with NC subjects, there were no significant differences in age (P'_{LPI} = 0.06, P'_{RPI} = 0.64), gender (P'_{LPI} = 0.64, P'_{RPI} = 0.28), education years (P'_{LPI} = 0.45, P'_{RPI} = 0.13), and the incidence of other concurrent disease in the LPI and RPI groups. In addition, no significant differences in lesion volume (P = 0.11) and the days from stroke to the first follow-up (P = 0.71) were observed between the LPI and RPI groups in the baseline stage. Compared with the NC group, the LPI and RPI groups in the baseline stage showed significant motor and verbal memory impairment (RAVLT scores, $P'_{LPI} < 0.001$, P'_{RPI} = 0.01). Longitudinal clinical examination in the LPI and RPI patients showed significant improvement over time in FMT (P_{LPI} = 0.001, P_{RPI} = 0.005) and RAVLT scores ($P_{LPI} < 0.0001$, $P_{RPI} < 0.0001$), but only the LPI group showed significant decrease in NHISS scores (P_{LPI} = 0.002, P_{RPI} = 0.07). Furthermore, there was no significant difference among different subgroups in mean FD values (P_{LPI} = 0.349, P_{RPI} = 0.864). The lesion distribution probability maps of the LPI and RPI groups in the acute stage are depicted in **Figure 1**.

Comparison of CBF Between the Baseline Subgroup of the PI and NC Groups

Compared to the NC group, patients with LPI at the baseline stage showed lower *z*-scored CBF values in the bilateral cerebellum, including the left lobule VIII (CBE lobule VIII_L), Crus I (CBE lobule Crus I_L), right lobule VIIB (CBE lobule VIIB_R), the left inferior frontal gyrus (IFG_L), the left insula (INS_L), and right inferior and middle temporal gyrus (ITG_R, MTG_R). In addition, the brain regions with significantly higher *z*-scored CBF values were found in the right precuneus (PCUN_R) and left superior parietal gyrus (SPG_L) (AlphaSim correction, $P < 0.005$, cluster size = 43). Patients with RPI at baseline showed significantly lower *z*-scored CBF values in the bialteral cerebellum including left lobule VIII (CBE lobule VIII_L), right lobule VI (CBE lobule VI_R), and Crus II (CBE Crus II_R) and higher *z*-scored CBF values in the right superior frontal gyrus (SFG_R) and right precentral gyrus (PreCG_R) (AlphaSim correction, $P < 0.005$, cluster size = 43) (**Table 2**, **Figure 2**).

Longitudinal CBF Analysis During the Follow-Up Period After PI

For the LPI group, among the four different time subgroups, patients only exhibited significant CBF changes in the right supramarginal gyrus (SMG_R) after the repeated-measure ANOVA test (AlphaSim correction, $P < 0.005$, cluster size = 54). Moreover, *post hoc* analyses revealed significantly lower *z*-scored CBF values of the SMG_R in the Time 4-subgroup (Bonferroni's

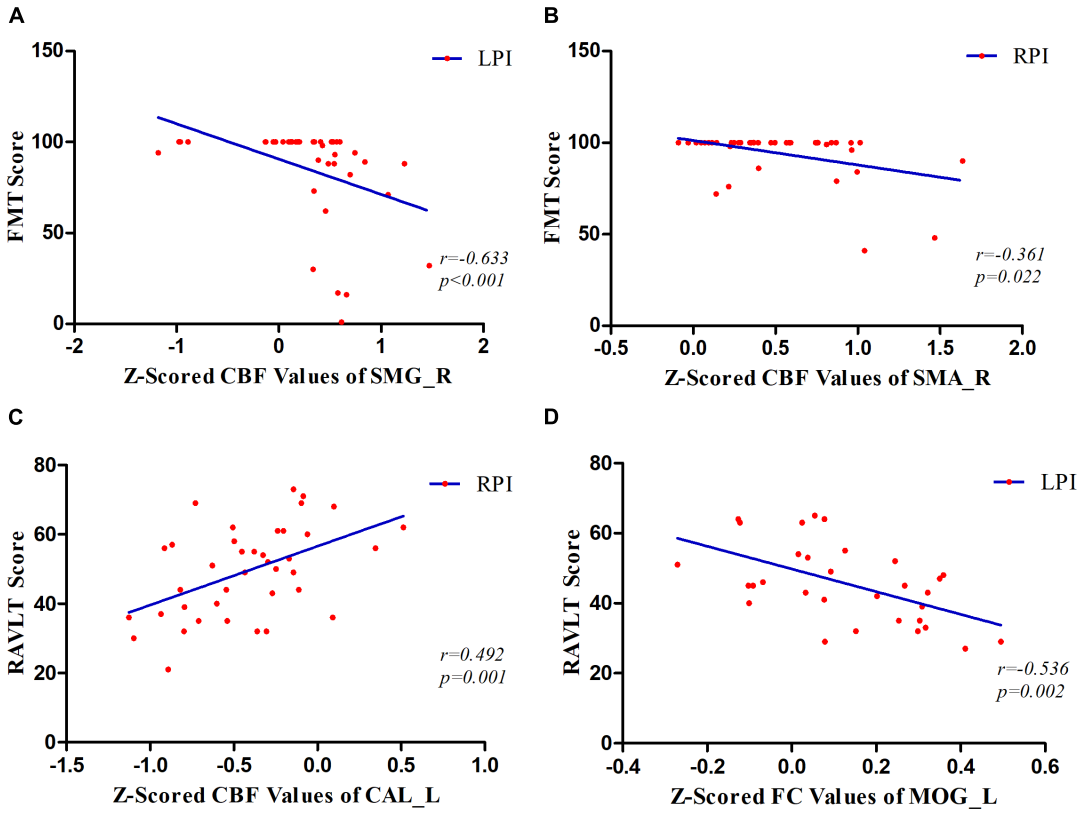

FIGURE 6 | Correlations between *z*-scored CBF values, FC values, and behavioral scores over time. **(A)** The patients in the LPI group showed a significantly negative correlation between dynamic changes of *z*-scored CBF values in the SMG_R and FMT scores over time. **(B)** In the RPI group, the results showed a negative correlation between the longitudinal *z*-scored CBF values of SMA_R and FMT scores. **(C)** In the RPI group, the results showed a positive correlation between longitudinal changes of *z*-scored CBF values in the CAL_L and RAVLT scores. **(D)** In the LPI group, the longitudinal *z*-scored FC values between SMG_R as seed and MOG_L were negatively associated with RAVLT scores. SMG_R, right supramarginal gyrus; SMA_R, right supplementary motor area; CAL_L, left calcarine sulcus; MOG_L, left middle occipital gyrus; FMT, Fugl–Meyer Test; RAVLT, Ray Auditory Verbal Learning Test; LPI and RPI, left and right pontine infarction groups.

post hoc test, $P < 0.001$) (**Table 3**, **Figure 3**). For the RPI group, the patients showed longitudinal changes of CBF in the left calcarine sulcus (CAL_L), left middle occipital gyrus (MOG_L), and right supplementary motor area (SMA_R) (AlphaSim correction, $P < 0.005$, cluster size = 54) (**Table 3**, **Figure 4**). In addition, the *z*-scored CBF values in CAL_L and MOG_L displayed significantly increased trends during the follow-up period. In SMA_R, the *z*-scored CBF values are initially high in the baseline stage, decreasing to a minimum at 1 month, then increasing with time (Bonferroni's *post hoc* test, all $P < 0.001$) (**Figure 4**).

Longitudinal FC Analysis in the LPI and RPI Groups

We further explored longitudinal FC alterations during the follow-up period in the LPI and RPI groups, using brain regions with altered CBF in longitudinal analysis as seed-ROIs. In the LPI group, with the SMG_R as the seed-ROI, patients exhibited significantly altered FC in the left middle temporal gyrus (MTG_L), left middle occipital gyrus (MOG_L), and left inferior frontal gyrus (IFG_L) (AlphaSim correction, $P < 0.005$, cluster size = 16) (**Table 4**, **Figure 5**). Interestingly, *z*-scored FC values in these brain regions showed similar trends of gradual decrease to a minimum at the 3-month time-point, and subsequent increase (Bonferroni's *post hoc* test, all $P < 0.001$) (**Figure 5**), while in the RPI group, there were no brain regions with significant longitudinal differences among the four time-points.

Correlation With Behavioral Function

The correlations between CBF values in brain regions with longitudinal CBF differences and functional improvement are shown in **Figure 6**. We found a significantly negative correlation between dynamic CBF changes in the SMG_R and improvement in motor scores in the LPI group ($r = -0.633$, $P < 0.001$). In the RPI group, the *z*-scored CBF values of the SMA_R showed a significantly negative correlation with motor recovery ($r = -0.361$, $P = 0.022$), and the *z*-scored CBF values of CAL_L showed a significantly positive correlation with verbal memory functional improvement ($r = 0.492$, $P = 0.001$). In addition, correlations between the FC values and behavioral scores over time were also investigated (**Figure 6**). The *z*-scored FC values between the SMG_R and MOG_L were

correlated with verbal memory RAVLT scores (r = 0.536, P = 0.002).

DISCUSSION

In this study, by combining pcASL and rs-fMRI, we investigated the longitudinal changes in CBF and FC during the 6 month follow-up period. These findings suggested that abnormal perfusion first appeared in the acute period and that the LPI and RPI groups at the baseline stage showed significantly lower z-scored CBF values in the bilateral cerebellum and abnormal perfusion in some supratentorial brain regions, as compared with the NC group. The longitudinal study showed the significantly altered CBF in the SMG_R for the LPI group and in the CAL_L, MOG_L, and SMA_R in the RPI group. We further demonstrated that the abnormal perfusion was concomitant with dynamic FC changes during functional recovery. Longitudinal FC changes were found in the MTG_L, MOG_L, and IFG_L when the SMG_R was used as the seed in the LPI group. In addition, these longitudinal changes in the z-scored CBF and FC values were associated with behavioral recovery, including motor and cognitive functions, over time. These results may promote our understanding of the neural pathophysiological underlying recovery from PI.

Cross-Sectional CBF Differences Between PI and NC Subjects

Some cross-sectional studies have investigated abnormal CBF in chronic cortical or subcortical stroke patients (Miao et al., 2018; Obayashi, 2019). A location-dependent study is essential for understanding particular patterns of brain impairment and reorganization after stroke since the location of the lesion plays a vital role in patients' functional outcomes. Our previous studies on CBF changes in chronic PI showed that significantly lower perfusion in the bilateral cerebellum and abnormal perfusion in the ipsilesional cerebellum were associated with motor scores (Wang et al., 2019). In this study, patients with acute LPI showed significantly lower z-scored CBF values in the bialteral cerebellum (left lobule VIII, Crus I, and right lobule VIIB) and ITG_R, MTG_R, IFG_L, and INS_L, and higher z-scored CBF values in the PCUM_R and SPG_L. On the other hand, patients with RPI showed significantly lower z-scored CBF values in the bilateral cerebellum (left lobule VIII, right lobule VI, and Crus II) and higher z-scored CBF values in the SFG_R and PreCG_R at the baseline stage. Coupled with these results, we argued that hypoperfusion of the bilateral cerebellum first appeared at the acute stage and maintained low-level perfusion to the chronic phase. Previous studies have reported that the cerebellum is involved in various motor and cognitive functions, cerebellar anterior lobe lesions may cause the cerebellar motor syndrome, and cerebellar posterior lobe lesions may produce the cerebellar cognitive affective syndrome (Schmahmann, 2004). Therefore, continuous hypoperfusion may be one of the factors in impaired motor and cognitive function after PI. We also found different patterns of CBF changes in some supratentorial brain regions in the LPI and RPI groups. Previous observations have shown that abnormal perfusion of the frontal parietal and temporal areas commonly occurs after unilateral brainstem stroke. Moreover, some studies suggested that factors such as lesion size, number, and location may affect the occurrence of supratentorial hypoperfusion, in which upper PI is more likely to cause ipsilateral supratentorial hypoperfusion, while contralateral supratentorial hypoperfusion is common in the middle pontine to medulla infarctions (Fazekas et al., 1993; Miyazawa et al., 1999; Matsui et al., 2007; D'Aes and Marien, 2015). This may partly explain the inconsistence of supratentorial perfusion patterns in the LPI and RPI groups.

Longitudinal Alterations of CBF in the LPI and RPI Groups

A longitudinal study is an effective way to explore the neurobiological underpinnings of clinical recovery. In our longitudinal investigation, the LPI group showed CBF changes in the SMG_R from baseline to 6 months after infarction and significantly lower z-scored CBF values at the 6 months. The SMG serves as the core region of attentiveness, motor function, and spatial perception (Ciaramelli et al., 2008; Golay et al., 2008). Area-specific cytoarchitecture patterns were investigated in a previous study, which demonstrated that the SMA and pre-SMA were strongly co-activated with the SMG (Ruan et al., 2018). Moreover, a study of chronic stroke patients with upper limb hemiparesis showed better recovery of motor function when the cortical thickness of the SMG was thinner (Ueda et al., 2019). These studies further validated our findings that the CBF changes in the SMG_R correlated with motor recovery after stroke and that the abnormal perfusion of the SMG_R offers a novel approach to explore the neural mechanisms of behavioral recovery. The RPI group showed significant CBF changes in the ipsilateral sensorimotor cortex and contralateral visual cortex, and these brain regions displayed different trends over time. In addition, the dynamic CBF changes in the SMA_R and gradually increased perfusion in the CAL_L were associated with functional recovery in motor and cognitive memory. Some previous studies have demonstrated that memory and attention interact. Rotshtein et al. (2011) suggested that the FC from the thalamus to the visual cortex is associated with working memory performance. Soto and Humphreys (2007) identified increased neural responses in early visual cortices when searching for reappearance of an item from working memory. Thus, the higher z-scored CBF values in the CAL_L may underlie memory recovery over time. Previous studies also have suggested a central role of SMA in the motor network, and early structural and functional changes of SMA are an important predictor of long-term motor outcome (Hannanu et al., 2017; Du et al., 2018). Thus, abnormal perfusion of SMA_R may indicate a neural mechanism of motor recovery after RPI.

At present, the detailed mechanisms underlying CBF changes in local brain regions remain unclear. One possible explanation is the destruction and reorganization of neurovascular coupling.

Numerous studies have demonstrated that neural activity is tightly associated with CBF, and the close temporal and spatial relationship between neural activity and CBF is termed "neurovascular coupling." However, the balance between neural activity and CBF is disrupted after stroke, resulting in hemodynamic abnormalities (Blicher et al., 2012; Bohm et al., 2020). Another possible reason is the disruption of white matter fiber integrity after PI, which may cause progressive anterograde and retrograde degeneration of fiber bundles between original infarction site and the remote regions (Liang et al., 2008). These processes could eventually lead to abnormal CBF patterns in remote regions.

Longitudinal FC Changes in the LPI and RPI Groups

A number of studies have proposed that abnormal perfusion in local brain regions may be a potential cause of local brain structural and functional changes (Yu et al., 2017; Zheng et al., 2019). In this study, we also investigated progressive FC changes during the follow-up period, by taking brain regions with longitudinal CBF changes as seed-ROIs. We found longitudinal FC changes between seeded SMG_R and some regions in the LPI group, including MTG_L, MOG_L, and IFG_L. These FC changes showed a similar trend, gradually decreasing to a minimum at 3 months and then increasing thereafter. Several previous studies have investigated the neural bases of verbal memory and have demonstrated that the left-lateralized frontoparietal network, superior temporal and occipital lobe cortices, and cerebellum are involved in the verbal memory process and that the left SMG is one of the key regions (Emch et al., 2019; Koshy et al., 2019). Impaired verbal memory after disease may lead to functional and structural changes in the homologous brain regions to maintain processing. In our study, the dynamic changes in FC between the SMR_R and MOG_L were associated with RAVLT scores over time in the LPI group. This phenomenon may be a compensatory mechanism aimed at maintaining and promoting the recovery of memory function.

This study had some limitations. First, due to the strict inclusion criteria, the sample size was relatively small, and some studies have suggested that the clinical manifestation and prognosis vary according to the level of PI (Jang, 2012; Huang et al., 2019). In addition, the small sample size also limited the statistical power. Therefore, in further studies, it is necessary to recruit patients with the different level pontine lesions to investigate the mechanisms of behavioral recovery. Second, the recovery of clinical function is a long-term process, and a relatively short follow-up period may be insufficient to observe the exact trends of clinical recovery. We therefore plan to observe these patients in the longer term. Third, in this study, we explored the abnormal perfusion as well as FC in PI during the 6-month follow-up by using ASL and BOLD-fMRI. However, we did not further calculate FC values based on brain regions with abnormal spontaneous BOLD signal oscillation as seeds. Further, we will extend this study through further analysis of BOLD signal changes to comprehensively assess spontaneous brain activity after PI.

In conclusion, we investigated longitudinal alterations of regional CBF and FC in patients with PI. Significantly abnormal perfusion first appeared at the acute stage after infarction. Longitudinal results demonstrated that patients with LPI showed abnormal CBF changes in the SMG_R, while RPI groups showed significant CBF changes in the CAL_L, MOG_L, and SMA_R. Moreover, dynamic CBF changes were accompanied by FC changes during the follow-up period. Correlation analysis demonstrated that longitudinal changes in CBF and FC were significantly correlated with motor or cognitive scores over time. These longitudinal alterations enable us to better understand the neurobiological mechanisms of behavioral recovery after PI.

DATA AVAILABILITY STATEMENT

The raw data supporting the conclusions of this article will be made available by the authors, without undue reservation.

ETHICS STATEMENT

The studies involving human participants were reviewed and approved by the First Affiliated Hospital of Zhengzhou University and Tianjin Medial University General Hospital. The patients/participants provided their written informed consent to participate in this study.

AUTHOR CONTRIBUTIONS

YWe, CW, JL, and JC conceived and designed the experiments. YWe, JL, CW, PM, LW, and YWa performed the MRI scans and behavioral assessment. YWe, KW, and JC wrote the manuscript. All authors contributed to the article and approved the submitted version.

FUNDING

This study was supported by the Natural Science Foundation of China (Nos. 81601467, 81871327, and 81601472).

ACKNOWLEDGMENTS

We are grateful to our patients and their families for their continued support for our study.

SUPPLEMENTARY MATERIAL

The Supplementary Material for this article can be found online at: https://www.frontiersin.org/articles/10.3389/fnagi.2020.577899/full#supplementary-material

REFERENCES

Blicher, J. U., Stagg, C. J., O'Shea, J., Ostergaard, L., MacIntosh, B. J., and Johansen-Berg, H. (2012). Visualization of altered neurovascular coupling in chronic stroke patients using multimodal functional MRI. *J. Cereb. Blood Flow Metab.* 32, 2044–2054. doi: 10.1038/jcbfm.2012.105

Bohm, M., Chung, D. Y., Gomez, C. A., Qin, T., Takizawa, T., and Sadeghian, H. (2020). Neurovascular coupling during optogenetic functional activation: local and remote stimulus-response characteristics, and uncoupling by spreading depression. *J. Cereb. Blood Flow Metab.* 40, 808–822. doi: 10.1177/0271678x19845934

Boscolo Galazzo, I., Storti, S. F., Formaggio, E., Pizzini, F. B., Fiaschi, A., and Beltramello, A. (2014). Investigation of brain hemodynamic changes induced by active and passive movements: a combined arterial spin labeling–BOLD fMRI study. *J. Magn. Reson. Imaging* 40, 937–948. doi: 10.1002/jmri.24432

Buckner, R. L., Krienen, F. M., and Yeo, B. T. (2013). Opportunities and limitations of intrinsic functional connectivity MRNat, I. *Neuroscience* 16, 832–837. doi: 10.1038/nn.3423

Chen, H., Shi, M., Zhang, H., Zhang, Y.-D., Geng, W., and Jiang, L. (2019). Different patterns of functional connectivity alterations within the default-mode network and sensorimotor network in basal ganglia and pontine stroke. *Med. Sci. Monit.* 25, 9585–9593. doi: 10.12659/msm.918185

Ciaramelli, E., Grady, C. L., and Moscovitch, M. (2008). Top-down and bottom-up attention to memory: a hypothesis (AtoM) on the role of the posterior parietal cortex in memory retrieval. *Neuropsychologia* 46, 1828–1851. doi: 10.1016/j.neuropsychologia.2008.03.022

D'Aes, T., and Marien, P. (2015). Cognitive and affective disturbances following focal brainstem lesions: a review and report of three cases. *Cerebellum* 14, 317–340. doi: 10.1007/s12311-014-0626-8

Deibler, A. R., Pollock, J. M., Kraft, R. A., Tan, H., Burdette, J. H., and Maldjian, J. A. (2008). Arterial spin-labeling in routine clinical practice, part 1: technique and artifacts. *Am. J. Neuroradiol.* 29, 1228–1234. doi: 10.3174/ajnr.a1030

Detre, J. A., and Wang, J. (2002). Technical aspects and utility of fMRI using BOLD and ASClinical, L. *Neurophysiology* 113, 621–634. doi: 10.1016/s1388-2457(02)00038-x

Du, J., Yang, F., Zhang, Z., Hu, J., Xu, Q., Hu, J., et al. (2018). Early functional MRI activation predicts motor outcome after ischemic stroke: a longitudinal, multimodal study. *Brain Imaging Behav.* 12, 1804–1813. doi: 10.1007/s11682-018-9851-y

Emch, M., Ripp, I., Wu, Q., Yakushev, I., and Koch, K. (2019). Neural and behavioral effects of an adaptive online verbal working memory training in healthy middle-aged adults. *Front. Aging Neurosci.* 11:300. doi: 10.3389/fnagi.2019.00300

Fazekas, F., Payer, F., Valetitsch, H., Schmidt, R., and Flooh, E. (1993). Brain stem infarction and diaschisis. A SPECT cerebral perfusion study. *Stroke* 24, 1162–1166. doi: 10.1161/01.str.24.8.1162

Ferguson, G. G., Eliasziw, M., Barr, H. W., Clagett, G. P., Barnes, R. W., and Wallace, M. C. (1999). The North American symptomatic carotid endarterectomy trial : surgical results in 1415 patients. *Stroke* 30, 1751–1758. doi: 10.1161/01.str.30.9.1751

Fox, M. D., and Raichle, M. E. (2007). Spontaneous fluctuations in brain activity observed with functional magnetic resonance imaging. *Nat. Rev. Neurosci.* 8, 700–711. doi: 10.1038/nrn2201

Golay, L., Schnider, A., and Ptak, R. (2008). Cortical and subcortical anatomy of chronic spatial neglect following vascular damage. *Behav. Brain Funct.* 4:43. doi: 10.1186/1744-9081-4-43

Guerra-Carrillo, B., Mackey, A. P., and Bunge, S. A. (2014). Resting-State fMRThe, I. *Neuroscientist* 20, 522–533.

Hannanu, F. F., Zeffiro, T. A., Lamalle, L., Heck, O., Renard, F., and Thuriot, A. (2017). Parietal operculum and motor cortex activities predict motor recovery in moderate to severe stroke. *NeuroImage Clin.* 14, 518–529. doi: 10.1016/j.nicl.2017.01.023

Haque, M. E., Gabr, R. E., Hasan, K. M., George, S., Arevalo, O. D., and Zha, A. (2019). Ongoing secondary degeneration of the limbic system in patients with ischemic stroke: a longitudinal MRI study. *Front. Neurol.* 10:154. doi: 10.3389/fneur.2019.00154

He, Z., Sheng, W., Lu, F., Long, Z., Han, S., and Pang, Y. (2019). Altered resting-state cerebral blood flow and functional connectivity of striatum in bipolar disorder and major depressive disorder. *Prog. Neuro Psychopharmacol. Biol. Psychiatry* 90, 177–185. doi: 10.1016/j.pnpbp.2018.11.009

Hoffmann, M., and Watts, A. (1998). Cognitive dysfunction in isolated brainstem stroke: a neuropsychological and SPECT study. *J. Stroke Cerebrovasc. Dis.* 7, 24–31. doi: 10.1016/s1052-3057(98)80018-9

Huang, J., Qiu, Z., Zhou, P., Li, J., Chen, Y., and Huang, R. (2019). Topographic location of unisolated pontine infarction. *BMC Neurol.* 19:186. doi: 10.1186/s12883-019-1411-6

Jang, S. H. (2012). Motor outcome and motor recovery mechanisms in pontine infarct: a review. *NeuroRehabilitation* 30, 147–152. doi: 10.3233/nre-2012-0738

Jiang, L., Geng, W., Chen, H., Zhang, H., Bo, F., and Mao, C.-N. (2018). Decreased functional connectivity within the default-mode network in acute brainstem ischemic stroke. *Eur. J. Radiol.* 105, 221–226. doi: 10.1016/j.ejrad.2018.06.018

Kasner, S. E. (2006). Clinical interpretation and use of stroke scales. *Lancet Neurol.* 5, 603–612. doi: 10.1016/s1474-4422(06)70495-1

Kinjo, Y., Suda, S., Sakamoto, Y., Okubo, S., and Kimura, K. (2017). Ataxic hemiparesis associated with cortical infarct localized in the postcentral gyrus. *Intern. Med.* 56, 2503–2505. doi: 10.2169/internalmedicine.8806-17

Koshy, S. M., Wiesman, A. I., Spooner, R. K., Embury, C., Rezich, M. T., and Heinrichs-Graham, E. (2019). Multielectrode transcranial electrical stimulation of the left and right prefrontal cortices differentially impacts verbal working memory neural circuitry. *Cereb. Cortex* 30, 2389–2400. doi: 10.1093/cercor/bhz246

Lapa, S., Luger, S., Pfeilschifter, W., Henke, C., Wagner, M., and Foerch, C. (2017). Predictors of dysphagia in acute pontine infarction. *Stroke* 48, 1397–1399. doi: 10.1161/strokeaha.116.015045

Le Heron, C. J., Wright, S. L., Melzer, T. R., Myall, D. J., MacAskill, M. R., and Livingston, L. (2014). Comparing cerebral perfusion in Alzheimer's disease and Parkinson's disease dementia: an ASL-MRI study. *J. Cereb. Blood Flow Metab.* 34, 964–970. doi: 10.1038/jcbfm.2014.40

Li, H., Dai, Y., Wu, H., Luo, L., Wei, L., and Zhou, L. (2020). Predictors of early neurologic deterioration in acute pontine infarction. *Stroke* 51, 637–640. doi: 10.1161/strokeaha.119.027239

Li, Z., Zhu, Y., Childress, A. R., Detre, J. A., and Wang, Z. (2012). Relations between BOLD fMRI-derived resting brain activity and cerebral blood flow. *PLoS One* 7:e44556. doi: 10.1371/journal.pone.0044556

Liang, X., Zou, Q., He, Y., and Yang, Y. (2013). Coupling of functional connectivity and regional cerebral blood flow reveals a physiological basis for network hubs of the human brain. *Proc. Natl. Acad. Sci. U.S.A.* 110:1929. doi: 10.1073/pnas.1214900110

Liang, Z., Zeng, J., Zhang, C., Liu, S., Ling, X., and Xu, A. (2008). Longitudinal investigations on the anterograde and retrograde degeneration in the pyramidal tract following pontine infarction with diffusion tensor imaging. *Cerebrovasc. Dis.* 25, 209–216. doi: 10.1159/000113858

Liu, J., Hao, Y., Du, M., Wang, X., Zhang, J., and Manor, B. (2013). Quantitative cerebral blood flow mapping and functional connectivity of postherpetic neuralgia pain: a perfusion fMRI study. *PAIN* 154, 110–118. doi: 10.1016/j.pain.2012.09.016

Matsui, T., Saxena, S., Kawabe, J., Matsunaga, H., Kohagura, K., Higashiyama, S., et al. (2007). Secondary obsessive-compulsive disorder related to diaschisis after pontine infarction, successfully treated with paroxetine. *Psychiatry Clin. Neurosci.* 61, 186–189. doi: 10.1111/j.1440-1819.2007.01635.x

Miao, P., Wang, C., Li, P., Wei, S., Deng, C., Zheng, D., et al. (2018). Altered gray matter volume, cerebral blood flow and functional connectivity in chronic stroke patients. *Neurosci. Lett.* 662, 331–338. doi: 10.1016/j.neulet.2017.05.066

Mijajlovic, M. D., Pavlovic, A., Brainin, M., Heiss, W. D., Quinn, T. J., and Ihle-Hansen, H. B. (2017). Post-stroke dementia - a comprehensive review. *BMC Med.* 15:11. doi: 10.1186/s12916-017-0779-7

Miyazawa, N., Uchida, M., Fukamachi, A., Fukasawa, I., Sasaki, H., and Nukui, H. (1999). Xenon contrast-enhanced CT imaging of supratentorial hypoperfusion in patients with brain stem infarction. *AJNR Am. J. Neuroradiol.* 20, 1858–1862.

Obayashi, S. (2019). Frontal dynamic activity as a predictor of cognitive dysfunction after pontine ischemia. *NeuroRehabilitation* 44, 251–261. doi: 10.3233/nre-182566

Payabvash, S., Benson, J. C., Tyan, A. E., Taleb, S., and McKinney, A. M. (2018). Multivariate prognostic model of acute stroke combining admission infarct location and symptom severity: a proof-of-concept study. *J. Stroke Cerebrovasc. Dis.* 27, 936–944. doi: 10.1016/j.jstrokecerebrovasdis.2017.10.034

Power, J. D., Barnes, K. A., Snyder, A. Z., Schlaggar, B. L., and Petersen, S. E. (2012). Spurious but systematic correlations in functional connectivity MRI networks arise from subject motion. *NeuroImage* 59, 2142–2154. doi: 10.1016/j.neuroimage.2011.10.018

Rotshtein, P., Soto, D., Grecucci, A., Geng, J. J., and Humphreys, G. W. (2011). The role of the pulvinar in resolving competition between memory and visual selection: a functional connectivity study. *Neuropsychologia* 49, 1544–1552. doi: 10.1016/j.neuropsychologia.2010.12.002

Ruan, J., Bludau, S., Palomero-Gallagher, N., Caspers, S., Mohlberg, H., and Eickhoff, S. B. (2018). Cytoarchitecture, probability maps, and functions of the human supplementary and pre-supplementary motor areas. *Brain Struct. Funct.* 223, 4169–4186. doi: 10.1007/s00429-018-1738-6

Schmahmann, J. D. (2004). Disorders of the cerebellum: ataxia, dysmetria of thought, and the cerebellar cognitive affective syndrome. *J. Neuropsychiatry Clin. Neurosci.* 16, 367–378. doi: 10.1176/jnp.16.3.367

Shan, Y., Wang, Y. S., Zhang, M., Rong, D. D., Zhao, Z. L., and Cao, Y. X. (2018). Homotopic connectivity in early pontine infarction predicts late motor recovery. *Front. Neurol.* 9:907. doi: 10.3389/fneur.2018.00907

Soto, D., and Humphreys, G. W. (2007). Automatic guidance of visual attention from verbal working memory. *J. Exp. Psychol. Hum. Percept. Perform.* 33, 730–737. doi: 10.1037/0096-1523.33.3.730

Tan, Y.-W., Liu, L., Wang, Y.-F., Li, H.-M., Pan, M.-R., and Zhao, M.-J. (2020). Alterations of cerebral perfusion and functional brain connectivity in medication-naïve male adults with attention-deficit/hyperactivity disorder. *CNS Neurosci. Ther.* 26, 197–206. doi: 10.1111/cns.13185

Ueda, R., Yamada, N., Abo, M., and Senoo, A. (2019). Correlation analysis of motor function improvement and brain structure for upper limb paralysis. *Neuroreport* 30, 77–81. doi: 10.1097/wnr.0000000000001160

Venkat, P., Chopp, M., and Chen, J. (2016). New insights into coupling and uncoupling of cerebral blood flow and metabolism in the brain. *Croat. Med. J* 57, 223–228. doi: 10.3325/cmj.2016.57.223

Wang, C., Miao, P., Liu, J., Wei, S., Guo, Y., Li, Z., et al. (2019). Cerebral blood flow features in chronic subcortical stroke: lesion location-dependent study. *Brain Res.* 1706, 177–183. doi: 10.1016/j.brainres.2018.11.009

Wang, P., Jia, X., Zhang, M., Cao, Y., Zhao, Z., and Shan, Y. (2018). Correlation of longitudinal gray matter volume changes and motor recovery in patients after pontine infarction. *Front. Neurol.* 9:312. doi: 10.3389/fneur.2018.00312

Wiest, R., Abela, E., Missimer, J., Schroth, G., Hess, C. W., and Sturzenegger, M. (2014). Interhemispheric cerebral blood flow balance during recovery of motor hand function after ischemic stroke–a longitudinal MRI study using arterial spin labeling perfusion. *PLoS One* 9:e106327. doi: 10.1371/journal.pone.0106327

Xie, L., Das, S. R., Pilania, A., Daffner, M., Stockbower, G. E., and Dolui, S. (2019). Task-enhanced arterial spin labeled perfusion MRI predicts longitudinal neurodegeneration in mild cognitive impairment. *Hippocampus* 29, 26–36. doi: 10.1002/hipo.23026

Yu, X., Yang, L., Song, R., Jiaerken, Y., Yang, J., Lou, M., et al. (2017). Changes in structure and perfusion of grey matter tissues during recovery from Ischaemic subcortical stroke: a longitudinal MRI study. *Eur. J. Neurosci.* 46, 2308–2314. doi: 10.1111/ejn.13669

Zhang, N., Qin, J., Yan, J., Zhu, Y., Xu, Y., Zhu, X., et al. (2020). Increased ASL-CBF in the right amygdala predicts the first onset of depression in healthy young first-degree relatives of patients with major depression. *J. Cereb. Blood Flow Metab.* 40, 54–66. doi: 10.1177/0271678x19861909

Zheng, W., Cui, B., Han, Y., Song, H., Li, K., He, Y., et al. (2019). Disrupted regional cerebral blood flow, functional activity and connectivity in Alzheimer's disease: a combined ASL perfusion and resting state fMRI study. *Front. Neurosci.* 13:738. doi: 10.3389/fnins.2019.00738

Zhu, J., Zhuo, C., Xu, L., Liu, F., Qin, W., and Yu, C. (2017). Altered coupling between resting-state cerebral blood flow and functional connectivity in schizophrenia. *Schizophrenia Bull.* 43, 1363–1374. doi: 10.1093/schbul/sbx051

Conflict of Interest: KW was employed by the company GE Healthcare.

The remaining authors declare that the research was conducted in the absence of any commercial or financial relationships that could be construed as a potential conflict of interest.

Copyright © 2020 Wei, Wu, Wang, Liu, Miao, Wang, Wang and Cheng. This is an open-access article distributed under the terms of the Creative Commons Attribution License (CC BY). The use, distribution or reproduction in other forums is permitted, provided the original author(s) and the copyright owner(s) are credited and that the original publication in this journal is cited, in accordance with accepted academic practice. No use, distribution or reproduction is permitted which does not comply with these terms.

frontiers in Aging Neuroscience

ORIGINAL RESEARCH
published: 23 November 2020
doi: 10.3389/fnagi.2020.582455

LongShengZhi Capsule Attenuates Alzheimer-Like Pathology in APP/PS1 Double Transgenic Mice by Reducing Neuronal Oxidative Stress and Inflammation

Zequn Yin[1†], Xuerui Wang[1†], Shihong Zheng[1], Peichang Cao[1], Yuanli Chen[1], Maoyun Yu[2], Chenzhong Liao[1], Zhongyuan Zhang[3], Jihong Han[1,4], Yajun Duan[1], Xiaoxiao Yang[1] and Shuang Zhang[1]**

[1] Key Laboratory of Metabolism and Regulation for Major Diseases of Anhui Higher Education Institutes, College of Food and Biological Engineering, Hefei University of Technology, Hefei, China, [2] School of Biological and Pharmaceutical Engineering, West Anhui University, Lu'an, China, [3] People's Hospital of Zunhua, Tangshan, China, [4] College of Life Sciences, Key Laboratory of Medicinal Chemical Biology, Key Laboratory of Bioactive Materials of Ministry of Education, Nankai University, Tianjin, China

OPEN ACCESS

Edited by:
Marietta Zille, University of Lübeck, Germany

Reviewed by:
Lakshman Kumar Puli, NMIMS University, India
Christina Elizabeth Toomey, University College London, United Kingdom

***Correspondence:**
Xiaoxiao Yang
yangxiaoxiao@hfut.edu.cn
Shuang Zhang
szhang11@163.com

† These authors have contributed equally to this work

Received: *12 July 2020*
Accepted: *16 October 2020*
Published: *23 November 2020*

Citation:
Yin Z, Wang X, Zheng S, Cao P, Chen Y, Yu M, Liao C, Zhang Z, Han J, Duan Y, Yang X and Zhang S (2020) LongShengZhi Capsule Attenuates Alzheimer-Like Pathology in APP/PS1 Double Transgenic Mice by Reducing Neuronal Oxidative Stress and Inflammation. Front. Aging Neurosci. 12:582455. doi: 10.3389/fnagi.2020.582455

Alzheimer's disease (AD) is the most common form of dementia in the elderly. It may be caused by oxidative stress, inflammation, and cerebrovascular dysfunctions in the brain. LongShengZhi Capsule (LSZ), a traditional Chinese medicine, has been approved by the China Food and Drug Administration for treatment of patients with cardiovascular/cerebrovascular disease. LSZ contains several neuroprotective ingredients, including *Hirudo, Astmgali Radix, Carthami Flos (Honghua), Persicae Semen (Taoren), Acori Tatarinowii Rhizoma (Shichangpu),* and *Acanthopanax Senticosus (Ciwujia)*. In this study, we aimed to determine the effect of LSZ on the AD process. Double transgenic mice expressing the amyloid-β precursor protein and mutant human presenilin 1 (APP/PS1) to model AD were treated with LSZ for 7 months starting at 2 months of age. LSZ significantly improved the cognition of the mice without adverse effects, indicating its high degree of safety and efficacy after a long-term treatment. LSZ reduced AD biomarker Aβ plaque accumulation by inhibiting β-secretase and γ-secretase gene expression. LSZ also reduced p-Tau expression, cell death, and inflammation in the brain. Consistently, *in vitro*, LSZ ethanol extract enhanced neuronal viability by reducing L-glutamic acid-induced oxidative stress and inflammation in HT-22 cells. LSZ exerted antioxidative effects by enhancing superoxide dismutase and glutathione peroxidase expression, reduced Aβ accumulation by inhibiting β-secretase and γ-secretase mRNA expression, and decreased p-Tau level by inhibiting NF-κB-mediated inflammation. It also demonstrated neuroprotective effects by regulating the Fas cell surface death receptor/B-cell lymphoma 2/p53 pathway. Taken together, our study demonstrates the antioxidative stress, anti-inflammatory, and neuroprotective effects of LSZ in the AD-like pathological process and suggests it could be a potential medicine for AD treatment.

Keywords: LongShengZhi capsule, Alzheimer's disease, oxidative stress, amyloid-β, Tau, cognition

INTRODUCTION

Alzheimer's disease (AD) is a disease accompanied by behavioral and cognitive impairment, which potently affects the normal social life of the elderly. More than 40 million people worldwide suffer from AD, and many eventually die from serious complications, such as cerebral thrombosis, aspiration pneumonia, and heart failure (Jankowska et al., 2019). Amyloid-β (Aβ) plaques formed by aggregation of Aβ monomer and neurofibrillary tangles (NFTs) formed by hyperphosphorylation of microtubule-associated protein Tau (p-Tau) are considered the two critical biomarkers in AD brains (Congdon and Sigurdsson, 2018). It has been reported that oxidative stress is a conspicuous cause of Aβ aggravation and p-Tau formation for AD development (Jiang et al., 2018).

Aβ is produced from amyloid-β precursor protein (APP) via the amyloidogenic pathway. APP is widely present in various tissues, with its highest expression in the synapses of neurons. APP is synthesized in the endoplasmic reticulum, then transported to the Golgi apparatus, where it is mistakenly cleaved by β-secretase (BACE1) into β-N-terminal and β-C-terminal fragments. The N-terminal transmembrane region of the β-C-terminal fragment is further hydrolyzed by γ-secretase on the cell membrane to release an Aβ peptide (consisting of 39–43 amino acids), and the peptide further aggregates to form Aβ plaques (Hefter et al., 2020). In physiological conditions, the non-amyloidogenic pathway of APP cleavage, which is hydrolyzed by α- and γ-secretase, generates soluble α-APP, p3, and α-C terminal fragments (Dar and Glazner, 2020). In the brains of AD patients, the amyloidogenic pathway appears to be increased.

Presenilin 1 (PSEN1) is one of the subunits of γ-secretase, the mutation of which is highly expressed in most AD patients and considered to be one of the main genetic factors of familial AD (Kabir et al., 2020). PSEN1 mutation may influence the expression of both β-secretase and other subunits of γ-secretase, including PSEN2, nicastrin, presenilin enhancer 2 (PEN2), and anterior pharynx-defective 1 (APH1), thus enhancing the maturation of Aβ (Li et al., 2011; Liu et al., 2019). Oxidative stress in the brain, which may upregulate β-secretase expression and increase the amyloidogenic cleavage of APP, also promotes AD (Sharma et al., 2019). Some natural ingredients, such as folic acid and berberine, have been shown to inhibit the deposition of Aβ by regulating the expression of b- and γ-secretase, which has become a strategy to alleviate the progression of AD (Tian et al., 2016; Cai et al., 2018).

Moreover, extracellular Aβ plaques interfere with the normal growth of neurons and further enhance oxidative stress, represented by overproduction of reactive oxygen species (ROS) (Sultana et al., 2009). Elevated oxidative stress leads to increased DNA, RNA, lipid, and protein oxidation in the brains of AD patients, which causes neuronal cell death (Halliwell, 2006). Antioxidant factors, such as glutathione peroxidase (GSH-PX) and superoxide dismutase (SOD), have been considered therapeutic targets that inhibit AD pathogenesis (Chen et al., 2019). In addition, ROS and Aβ accumulation in the AD brain can potently activate glial cells to release inflammatory cytokines and cause severe brain inflammation (Houtman et al., 2019). The inflammatory cytokines, including interleukin 1β (IL-1β) in the brain, can increase phosphorylation of Tau and make it dissociate from neuronal synapses (Graham et al., 2017). In a physiological state, Tau maintains the stability of neurons and synapses. However, in the AD condition, dissociated p-Tau forms NFTs in neurons, causing synapse damage, which obstructs transmission of neural signals and further aggravates cognitive dysfunction (Hoppe et al., 2010). Therefore, blocking oxidative stress could be an effective strategy to slow the AD process.

Cerebrovascular function is commonly affected in AD patients (Fouda et al., 2019). The clearance of Aβ could be impaired due to cerebrovascular damage in the early stage, which further accelerates AD (Gupta and Iadecola, 2015). In addition, cerebrovascular damage causes insufficient supply of oxygen and glucose in neurons and glial cells, resulting in decreased ATP production and enhanced oxidative stress (Merlini et al., 2011). Long-term chronic hypoxia ultimately causes irreversible structural damage to cells and tissues of the central nervous system (Daulatzai, 2017).

The LongShengZhi capsule (LSZ), a well-known traditional Chinese herbal medicine, has long been prescribed to patients with cardiovascular and cerebrovascular diseases in China. It offers a potent protection against atherosclerotic lesions, ischemic brain damage, and vascular dementia (Ma et al., 2019; Yang et al., 2020). LSZ is made from 12 traditional Chinese medicines, including *Hirudo* (Shuizhi), *Pheretima* (Dilong), *Astmgali Radix* (Huangqi), *Chuanxiong Rhizoma* (Chuanxiong), *Angelicae Sinensis Radix* (Danggui), *Carthami Flos* (Honghua), *Persicae Semen* (Taoren), *Paeoniae Radix Rubra* (Chishao), *Aucklandiae Radix* (Muxiang), *Acori Tatarinowii Rhizoma* (Shichangpu), *Talxilli Herba* (Sangjisheng), and extract of *Acanthopanax Senticosus* (Ciwujia), as shown in **Table 1** (Wei et al., 2019). The 19 main active ingredients in LSZ are listed in **Table 2**. Many of them have clear protective effects on the central nervous system. For example, *Astmgali Radix* can reduce neuroinflammation and cognitive impairment (Huang et al., 2017). *Carthami Flos* seed can attenuate memory impairment induced by scopolamine in mice by ameliorating cholinergic dysfunction and oxidative stress (Kim et al., 2019). *Acanthopanax senticosus* extract also has a neuroprotective effect on nervous system diseases (Li et al., 2014). Moreover, bioactive components contained in LSZ, such as paeoniflorin, isoflavone glucoside, and syringin, have been reported to inhibit oxidative stress to protect neurons (Ding et al., 2013; Zhong et al., 2015).

Our previous studies have shown that LSZ can reduce thrombosis by inhibiting platelet adhesion through reducing oxidative stress and vascular inflammation in the aorta of atherosclerotic mice (Li et al., 2019; Ma et al., 2019). Moreover, we have demonstrated its strong antioxidant role in heart failure (Xu et al., 2020). These findings suggest a potential role of LSZ in AD treatment. Therefore, in this study, we used human APP and mutant presenilin 1 double transgenic (APP/PS1) mice and HT-22 cells to determine the anti-AD-like pathology effect of LSZ.

TABLE 1 | Main ingredients in LSZ.

Ingredients	Local name	Part used	Biological properties
Hirudo	Shuizhi	Dried body	Anti-thrombosis; protection against cerebral ischemia reperfusion injury
Pheretima	Dilong	Dried body	Anti-cerebral thrombosis; anti-inflammation
Astmgali Radix	Huangqi	Root	Neuroprotection; cognition improvement; glucose and lipid metabolism improvement
Chuanxiong Rhizoma	Chuanxiong	Rhizome	Neuroprotection; anti-neuroinflammation; cerebral vascular function improvement
Angelicae Sinensis Radix	Danggui	Root	Blood vessel protection; neuroprotection; anti-neuroinflammation;
Carthami Flos	Honghua	Flower	Cerebral ischemia improvement; anti-neuroinflammation; angiogenesis promotion
Persicae Semen	Taoren	Dried seed	Anticoagulant; neurotrophic
Paeoniae Radix Rubra	Chishao	Root	Microcirculation improvement; Blood vessel dilation; myocardial ischemia prevention; anti-thrombosis
Aucklandiae Radix	Muxiang	Root	Gastrointestinal function improvement; vascular tension regulation
Acori Tatarinowii Rhizoma	Shichangpu	Root	Antidepressant; neuroprotection; inhibiting glial inflammation; cognition improvement
Talxilli Herba	Sangjisheng	Stem	Anti-oxidation; anti-inflammation; anti-cancer
extract of *Acanthopanax Senticosus*	Ciwujia	Stem	Anti-anxiety; neuroprotection; cerebral vascular function protection

MATERIALS AND METHODS

Chemicals and Antibodies

LongShengZhi Capsule (CAT# A14001035472) was provided primarily by the Buchang Pharmaceutical Co. Ltd. (Xi'an, Shaanxi, China). The LSZ ethanol extract solution (LSZ-EES) in PBS was prepared as follows (Li et al., 2019). Bovine serum albumin (BSA), 3-(4,5-dimethylthiazol-2-yl)-2,5-diphenyltetrazolium bromide (MTT), L-glutamic acid (L-Glu), and thioflavin S were purchased from Sigma Aldrich (St. Louis, MO, United States). 2'7'-Dichlorodihydrofluorescein diacetate (DCFH-DA) was purchased from Meilun Biotechnology (Dalian, Liaoning, China). A cocktail of protease inhibitors, PMSF, and enhanced chemiluminescence (ECL) kits were purchased from Millipore (Darmstadt, Germany). Bromphenol blue, eosin Y, heparin, triton X-100, and sodium dodecyl sulfate (SDS) were purchased from the Solarbio (Beijing, China). 4',6-Diamidino-2-phenylindole (DAPI) was purchased from Santa Cruz Biotechnology (Paso Robles, CA, United States). Hematoxylin staining solution, phosphate buffer saline (PBS), BCA protein assay kit, and 4% polyformaldehyde were purchased from Biosharp (Hefei, Anhui, China). Terminal deoxynucleotidyl transferase (TdT)-mediated dUTP nick end labeling (TUNEL) assay kit was purchased from KeyGen Biotech (Nanjing, Jiangsu, China). FAS siRNA kit (CAT# siB13118141431) was purchased from RiboBio Co., Ltd. (Guangzhou, Guangdong, China). Lipofectamine^{TM} RNAiMAX (CAT# 13778030) was purchased from Thermo Scientific (Waltham, MA, United States). Total RNApure reagent (Tri-zol, ZP401-2) was purchased from Zomen Biotechnology Co. Ltd. (Beijing, China). The HiScript II Q Select RT SuperMix for qPCR and AceQ SYBR qPCR Master Mix were purchased from Vazyme (Piscataway, NJ, United States). Annexin V-PE analysis kit, goat anti-rabbit lgG (H + L)-HRP (CAT# LK2001, 1:10000), and goat anti-mouse lgG (H + L)-HRP (CAT# LK2003, 1:10000) were purchased from Sungene Biotech (Tianjin, China). Rabbit anti-PSEN1 (CAT# 20434-1-AP, 1:100), Tau (CAT# 10274-1-AP, 1:1000), Bax (CAT# 50599-2-lg, 1:8000), Bcl-2 (CAT# 12789-1-AP, 1:1000), Bad (CAT# 10435-1-AP, 1:2000), Iba-1 (CAT# 10904-1-AP, 1:300), and FITC-goat anti-mouse IgG (H + L) (CAT# SA00003-1, 1:100), FITC-goat anti-rabbit IgG (H + L) (CAT# SA00003-2, 1:100), and TRITC-goat anti-rabbit IgG (H + L) (CAT# SA00007-2, 1:100) antibodies were purchased from Proteintech Group, Inc. (Chicago, IL, United States). Rabbit anti-APP (CAT# AF6084, 1:300) antibody was purchased from Affinity Biosciences (Changzhou, Jiangsu, China). Rabbit anti-phospho-MAPT-S404 (p-Tau, CAT# AP0170, 1:1000 for WB; 1:100 for IF), IL-1β (CAT# A17361, 1:1000 for WB; 1:100 for IF), NF-κB (CAT# A16271, 1:1000 for WB; 1:100 for IF), β-actin (CAT# AC026, 1:200000), and mouse anti-GAPDH (CAT# AC033, 1:200000) antibodies were purchased from Abclonal (Wuhan, Hubei, China).

TABLE 2 | Main active components in LSZ-EES.

Component	Proportion (~mg·g^{-1})	Component	Proportion (~mg·g^{-1})
Paeoniflorin	3.9	Senkyunolide I	0.05
Calycosin-7-glucoside	0.75	Dehydrocostus lactone	0.03
Amygdalin	0.7	Calycosin	0.03
Hydroxysafflor yellow A	0.49	Ligustilide	0.01
Syringin	0.25	Senkyunolide A	0.01
Ferulic acid	0.15	Oxypaeoniflora	0.01
Eleutheroside E	0.15	Senkyunolide H	<0.01
Isofraxidin	0.13	Ligustrazine	<0.01
Benzoylpaeoniflorin	0.11	3-n-Butylphthalide	<0.01
Astragaloside A	0.1		

Cell Culture

HT-22 cells, a mice hippocampal neuronal cell line (CAT# CP-H042), were purchased from Procell (Wuhan, Hubei, China) and cultured in Dulbecco's Modified Eagle's Medium (DMEM, Biological Industries, Kibbutz Beit Haemek, Israel) containing 10% fetal bovine serum (FBS, AusGeneX, Brisbane, Australia) as

well as 50 μg/mL streptomycin/penicillin (Hyclone, Logan, UT, United States) at 37°C in an atmosphere of 5% CO_2. Cells at ∼90% confluence were treated in serum-free medium.

Cell Viability Assay

Cell viability was detected using MTT assay. In brief, HT-22 cells were plated into 96-well plates (∼10^4 cells/well) and were treated as indicated. After treatment, the culture medium was removed, and cells were added to MTT (0.5 mg/mL) and incubated for 4 h at 37°C. After washing with PBS 3 times and incubating in DMSO (150 μL/well) for 15 min, the optical density at a wavelength of 550 nm was read by a microplate reader (BioTek Instruments, Winooski, VT, United States). The mean of absorbance was expressed as fold changes compared to control samples.

Cell Death Assay

HT-22 cells were seeded in 6-well plates and pre-treated with LSZ-EES for 3 h followed by co-treatment with L-Glu for another 18 h. Then the cells were lifted by trypsin (without EDTA) and washed with cold PBS twice. After incubation with annexin V-PE and 7-aminoactinomycin D (7-AAD) working solution in darkness at room temperature for 20 min, the fluorescence intensity was measured by the fluorescence-activated cell sorting (FACS) assay using a CytoFLEX (Beckman, Brea, CA, United States).

ROS Determination

HT-22 cells were plated in 96-well plates or 6-well plates and pre-treated with LSZ-EES for 3 h, followed by co-treatment with L-Glu for another 18 h. After treatment and removal of the treatment medium, cells were incubated with DCFH-DA (10 μM) working solution for 20 min at 37°C in darkness. After being washed with PBS 3 times, samples in 96-well plates were measured on a microplate reader at 504 nm (excitation) and 529 nm (emission), while the fluorescence images in 6-well plates were captured with a fluorescence microscope (Leica, Wetzlar, Germany).

siRNA Transfection

HT-22 cells in 6-well plates at ∼40% confluence were transfected with FAS siRNA (siFAS, 50 nM/well) or the corresponding negative control siRNA (siCtrl, 50 nM/well) using Lipofectamine^{TM} RNAiMAX in serum-free medium for 24 h, then incubated in complete DMEM medium for another 24 h, followed by the treatment indicated.

Animals

The experiment was conducted with the approval of the Institution Animal Ethics Committee of Hefei University of Technology (HFUT20190116001). All animal experiments were performed in compliance with the guidelines published in the National Institutes of Health (NIH) Guide for the Care and Use of Laboratory Animals. We used male mice in this study, which is widely accepted in AD-related studies, to avoid the hormonal changes, including estrogen, in female mice in AD progress. In addition, all animals were randomized before received treatment. The animals were maintained at a temperature of 24 ± 2°C with a 12-h light/dark cycle and checked daily during the experiment for food intake, water consumption, and bodyweight.

Both male C57BL/6J wild-type mice and APP/PS1 mice (∼2 months old, ∼20 g) without backcrossing were purchased from the Model Animal Research Center of Nanjing University (Nanjing, Jiangsu, China). All the animals were free to access food and drinking water. C57BL/6J wild-type mice fed normal chow were used as the normal control (Group 1, WT, 12 mice/group). APP/PS1 mice were randomly divided into three groups (12 mice/group) and received the following treatment. Group 2 (AC), APP/PS1 mice were fed normal chow. Group 3 (ALN), APP/PS1 mice were fed normal chow containing LSZ at a normal dose (850 mg/100 g food, based on clinical dosage). Group 4 (ALH), APP/PS1 mice were fed normal chow containing LSZ at a high dose (2000 mg/100 g food). The treatment lasted for 7 months as the pathological changes in the brains of APP/PS1 mice at 9 months old are severe enough to be detected.

Morris Water Maze (MWM) Test

The MWM video tracking analysis system (1056001, Beijing ZS Dichuang Technology Development Co., Ltd., Beijing, China) was used to assess spatial learning and reference memory (Vorhees and Williams, 2006). A circular pool was divided into four quadrants and filled with water (22 ± 2°C). A target platform was fixed and immersed at a depth of 2 cm in the middle of the first quadrant. Titanium dioxide was added to the pool to make the platform invisible. A tracking camera was placed above the pool to record the trajectories of the mice. The MWM experiment consisting of a spatial probe test and a hidden platform trial was performed over the next 6 consecutive days as follows (Nunez, 2008). Briefly, in the acquisition training phase, the mouse was placed into the water facing the wall of the pool and swam freely. The length of time it took the mouse to find the underwater platform was recorded. If the mouse did not find the platform within 60 s, we would guide it to the platform and allow it to remain there for 10 s. After training, the animals were removed, dried, and then returned to the cage. Each mouse was trained 4 times a day for 5 consecutive days, entering the water from a different quadrant each time. On the second day after the final acquisition training (day 6), the platform was removed to perform the 60-s probe trial. The mouse was placed in water in the opposite quadrant from where the original platform was located. The trajectories, times of passing through the target quadrant or the original platform, and escape latency that the mice arrived at the hidden platform were recorded.

Y Maze (YM) Test

The YM video tracking analysis system (1056006, Beijing ZS Dichuang Technology Development Co., Ltd., Beijing, China) was used to test the discriminatory working memory and spatial exploration ability of mice (Oboh et al., 2020). Three arms of the YM were randomly defined as the new arm, the starting arm, and the third arm. Mice were placed into the maze at the end of the starting arm and allowed to explore the maze for 3 min. A camera was fixed 1.5 m above the maze to record the trajectory,

distance, and the time and length of time it took the mice to cross the new arm.

Brain Section Preparation

For histological examination, six mice per group were selected randomly and anesthetized with 2% sodium pentobarbital. Mice were then perfused with PBS and 4% paraformaldehyde, followed by collection of whole brain tissue. The brain tissue was quickly frozen with dry ice and then fixed in 4% paraformaldehyde for 24 h at 4°C. Afterward, the brains were dissected and separated into two hemispheres: one for paraffin section preparation and the other for frozen section preparation. Hemispheres for paraffin sections were dehydrated using a HistoPearl automatic dehydrator (Leica, Wetzlar, Germany) and embedded with paraffin. Hemispheres for frozen sections were dehydrated with 15, 20, and 30% sucrose solutions in turn, each for 24 h, and then embedded in optical cutting temperature compound (OCT) and stored at –80°C until sectioning.

For protein and RNA extraction, another six mice per group were euthanatized, and brain tissue was immediately dissected. The cortex and hippocampus were separated and stored at –80°C until processing.

Immunofluorescence Staining and Thioflavin S Staining

The paraffin-embedded brain was cut into 5-μm sections. Expression of p-Tau, PSEN1, NF-κB, IL-1β was detected as follows (Chen et al., 2014). The frozen brain in OCT was cut into 20-μm sections to determine Iba-1 and Aβ plaques. Aβ plaques were detected by co-staining with APP antibody and thioflavin S. Briefly, the sections were blocked with 3% BSA for 1 h at room temperature and then incubated with diluted primary antibody overnight at 4°C. The sections were washed with PBS 3 times, for 10 min each time, and then incubated with FITC-goat anti-rabbit IgG or TRITC-goat anti-rabbit IgG secondary antibodies for 1 h at room temperature. Samples incubated without primary antibody were used as the negative control (NC) to illustrate the specificity of the primary antibody. The sections were washed with PBS for 3 × 10 min and then stained with DAPI solution for nucleus. For Aβ plaque determination, sections were washed with PBS for 3 × 5 min after DAPI staining. The sections were incubated with 0.5% thioflavin S solution for 10 min at room temperature and then washed with 70% alcohol for 15 min and then with PBS for 5 min. The sections were covered with coverslips and kept in the dark until dry. Images were obtained using a ZEISS Scope A1 fluorescence microscope. The ratio of mean of fluorescence intensity (MFI) to cell number or Iba-1-positive cells to cell number were assessed using Photoshop by a technician who was blind to the experiment.

TUNEL Staining

The paraffin-embedded brain was cut into 5-μm sections to detect cell death in brain tissues using a TUNEL assay kit as follows (Ma et al., 2019). Images were observed with a ZEISS Scope A1 fluorescence microscope. The number of TUNEL-positive cells in more than three random fields was counted and quantitated as per mm^2 by a technician who was blind to the experiment and expressed as fold of the WT group.

Quantitative Real Time PCR (qRT-PCR) and Western Blot

After treatment, the total RNA was extracted from HT-22 cells or 30-mg brain tissues using Trizol as follows (Chen et al., 2014). cDNA was synthesized with the same amount of total RNA from each sample with HiScript II Q Select RT SuperMix (+gDNA wiper). qRT-PCR was then performed using the AceQ SYBR qPCR Master Mix reverse transcriptase kit and the primers listed in **Table 3** on LightCycler96 (Roche, Mannheim, Germany). The mRNA expression was normalized by β-actin mRNA in the corresponding samples.

After treatment, HT-22 cells or 30-mg brain tissues were lysed or grated with lysis buffer (Chen et al., 2012). Protein concentration was determined using the BCA protein assay kit. The same amount of protein (50 μg) from each sample was used to determine protein expression of Tau, p-Tau, FAS, Bcl-2, Bad, Bax, NF-κB, IL-1β, p53, GAPDH, or β-actin by Western blot as described (Sun et al., 2017). The signals were detected on Chemiscope 3000 mini (Qinxiang, Shanghai, China) and the band density was quantified using Photoshop.

Statistical Analysis

Based on a survey of data from published research or preliminary studies, we performed *in vitro* studies at least five independent times and decided on the sample size for the *in vivo* studies. All data were analyzed by a technician who was blind to the experiment design and expressed as

TABLE 3 | Sequences of primers for qRT-PCR assay.

Gene	Forward sequences	Reverse sequences
β-actin	ATGGAGGGGAATACAGCCC	TTCTTTGCAGCTCCTTCGTT
IL-1β	GACCTTCCAGGATGAGGACA	AGCTCATATGGGTCCGACAG
IL-10	GCTCTTACTGACTGGCATGAG	CGCAGCTCTAGGAGCATGTG
IL-6	GAGGATACCACTCCCAACAGACC	AAGTGCATCATCGTTGTTCATACA
TNF	CGTCGTAGCAAACCACCAAG	TTGAAGAGAACCTGGGAGTAGACA
SOD1	GCCTTGTGTATTGTCCCCAT	ACCATCCACTTCGAGCAGAA
SOD2	AGACACGGCTGTCAGCTTCT	CTGGACAAACCTGAGCCCTA
GSH-PX	CAATGTAAAATTGGGCTCGAA	GTTTCCCGTGCAATCAGTTC
Bcl-2	CTTTGAGTTCGGTGGGGTCA	GCCCAGACTCATTCAACCAGA
Bad	CCCTTAGAACTGGAGGGAGGA	GTCGCATCTGTGTTGCAGTG
Bax	AGGATGCGTCCACCAAGAAG	CTTGGATCCAGACAAGCAGC
Bcl-xL	CTACCAGGTCGCATGATCCC	CCCGGTTGCTCTGAGACATT
FAS	TGCTTGCTGGCTCACAGTTA	GAATCACTCCAACGGGCTGA
BACE1	GCTGGGAGCTGGATTATGGT	CTATCCGAGCCCGTAGCTTT
APH1a	TATCCACTGCCCATGACTGA	GCAGATTCAAACCCACCAGT
PEN2	TGTTGTGAAGTCGGGAGCAC	AGTACTTCCGGCACAGGTTC

IL-1β/6/10, interleukin 1β, 6 or 10; TNF, tumor necrosis factor; SOD1, superoxide dismutase 1; SOD2, superoxide dismutase 2; GSH-PX, glutathione peroxidase; Bcl-2, B-cell lymphoma 2; Bad, Bcl-2 associated agonist of cell death; Bax, Bcl-2 associated X protein; Bcl-xL, B-cell lymphoma-extra large; FAS, Fas cell surface death receptor; BACE1, beta-site APP-cleaving enzyme 1; APH1a, anterior pharynxdefective 1a; PEN2, presenilin enhancer 2.

mean ± standard deviation (SD). Graph Pad Prism 7.0 was used for statistical analysis. Two-way ANOVA was used to assess significance in ROS and qRT-PCR of the *in vitro* study. One-way ANOVA was used on the other data to assess significance. The Shapiro-Wilk normality test, White test, and Brown-Forsythe test were conducted on the data to evaluate if the values came from a Gaussian distribution (**Supplementary Material**). The differences were considered significant at $p < 0.05$.

RESULTS

LSZ-EES Rescues L-Glu-Induced HT-22 Cell Death and Oxidative Stress

LongShengZhi Capsule has been reported to reduce thrombosis by inhibiting ROS production in human umbilical vein endothelial cells (Li et al., 2019). Thus, we speculated that LSZ may have similar antioxidant effects on neuronal cells. L-Glu is an excitatory neurotransmitter and induces neuronal death by activating oxidative stress (Kritis et al., 2015). A close association between ROS levels and synaptic dysfunctions has been reported (Li et al., 2017). To determine the protective effects of LSZ against neuronal damage, we initially pre-treated HT-22 cells, a neuronal cell line, with LSZ-EES for 3 h. Cells were then treated with L-Glu to induce HT-22 cell death. We found L-Glu exposure increased ROS production to ∼two-fold (two-way ANOVA, $F_{(2,\ 24)} = 21.11$, $p = 0.0002$) of that in the control group (Ctrl). However, the increase was substantially blocked by LSZ-EES co-treatment (two-way ANOVA, 39%, $F_{(2,\ 24)} = 12.61$, $p = 0.0015$ for 10 μg/mL LSZ-EES; 33%, $F_{(2,\ 24)} = 12.61$, $p = 0.0017$ for 20 μg/mL LSZ-EES) (**Figures 1A,B**).

Next, we determined the effect of LSZ on cell viability using the MTT method. As expected, LSZ-EES alone had little effect on cell viability, indicating its high degree of safety to cells ($F_{(4,\ 20)} = 0.756$, $p > 0.05$) (**Figure 1C**). In contrast, L-Glu clearly reduced cell viability by ∼43% ($F_{(3,\ 20)} = 33.39$, $p = 0.0003$), but the reduction was reversed by LSZ-EES treatment ($F_{(3,\ 20)} = 33.39$, $p = 0.0009$ for 10 μg/mL LSZ-EES, $p = 0.0007$ for 20 μg/mL LSZ-EES) (**Figure 1D**). In addition, the results of the flow cytometry experiment show that L-Glu increased the percentage of cell death at early and late stages from ∼4.5% in the control group to ∼18.2%, but the number was significantly reduced to ∼9.5 or ∼8.3% by LSZ-EES treatment at 10 or 20 μg/mL (**Figure 1E**). These results suggest that LSZ-EES can enhance HT-22 cell viability, which is related to the reduction of L-Glu-induced oxidative stress.

Reactive oxygen species is mainly produced by mitochondria, so the neuroprotection of HT-22 cells by LSZ-EES against L-Glu-induced neurotoxicity may be related to its effect on expression of mitochondrial apoptotic genes. The Bcl-2 family is among the essential factors regulating mitochondrial membrane permeability and the mitochondrial apoptosis pathway (Rong and Distelhorst, 2008). Our results show that L-Glu reduced the anti-apoptotic gene Bcl-xL mRNA level (two-way ANOVA, $F_{(1,\ 16)} = 29.14$, $p = 0.0403$) and Bcl-2 protein expression ($F_{(3,\ 16)} = 11.36$, $p = 0.198$), while inducing pro-apoptotic genes, Bax and Bad expression, at protein ($F_{(3,\ 16)} = 6.192$, $p = 0.0152$ for Bax; $F_{(3,\ 16)} = 21.74$, $p = 0.6742$ for Bad) or mRNA levels (two-way ANOVA, $F_{(1,\ 16)} = 4.902$, $p = 0.0003$ for Bax; $F_{(1,\ 16)} = 188.1$, $p < 0.0001$ for Bad). However, the effect of L-Glu on expression of those genes was significantly reversed by LSZ-EES treatment (**Figures 2A-C**), suggesting the anti-mitochondria-associated apoptotic effect of LSZ-EES.

FAS is a pro-apoptotic gene located on the membrane surface and an upstream molecule of the Bcl-2 family (Strasser et al., 2009). Once activated, FAS transmits stimulus signals into the membrane, and its intra-membrane domain leads to programmed cell death (Kaufmann et al., 2012). To determine if LSZ can block the death signal induced by L-Glu from extra-cellular to intra-cellular, we detected expression of FAS and p53. As shown in **Figure 2A**, the FAS mRNA level was significantly activated by L-Glu (two-way ANOVA, $F_{(2,\ 24)} = 186.6$, $p < 0.0001$), but the activation was antagonized by LSZ-EES treatment (two-way ANOVA, $F_{(2,\ 24)} = 186.6$, $p = 0.0009$). Furthermore, LSZ-EES treatment also inhibited L-Glu-induced p53 protein expression, a pro-apoptotic gene responsible for DNA damage ($F_{(3,\ 16)} = 51.29$, $p < 0.001$) (**Figure 2B**). These results suggest LSZ-EES may enhance neuron survival by regulating FAS/Bcl-2/p53 expression.

Therefore, we transfected HT-22 cells with FAS siRNA to indicate the mechanisms of LSZ-EES in regulating neuronal death. As shown in **Supplementary Figure 1**, in cells not transfected with FAS siRNA, LSZ-EES significantly up-regulated protein expression of Bcl-2 (two-way ANOVA, $F_{(3,\ 32)} = 67.63$, $p < 0.0001$) and mRNA expression of Bcl-xL (two-way ANOVA, $F_{(3,\ 32)} = 27.99$, $p < 0.0001$) and down-regulated protein and mRNA expression of Bax (two-way ANOVA, $F_{(3,\ 32)} = 90.43$, $p < 0.0001$ for protein; $F_{(3,\ 32)} = 22.26$, $p < 0.0001$ for mRNA) and mRNA expression of Bad (two-way ANOVA, $F_{(3,\ 32)} = 12.12$, $p < 0.0001$), while in transfected FAS siRNA cells, compared with the L-Glu-exposed group, LSZ-EES pre-treatment failed to regulate Bcl-2 (two-way ANOVA, $F_{(3,\ 32)} = 67.63$, $p > 0.05$), Bcl-xL (two-way ANOVA, $F_{(3,\ 32)} = 27.99$, $p > 0.05$), Bax (two-way ANOVA, protein: $F_{(3,\ 32)} = 90.43$, $p > 0.05$; mRNA: $F_{(3,\ 32)} = 22.26$, $p > 0.05$), and Bad (two-way ANOVA, $F_{(3,\ 32)} = 12.12$, $p > 0.05$) expression, indicating that silencing of FAS eliminated the regulation of apoptotic factors by LSZ-EES. Taken together, these data indicate that LSZ-EES reduces L-Glu-induced ROS production and inhibits neuronal cell death, at least in part, through the FAS/Bcl-2/p53 pathway.

Elevated ROS production is often accompanied by high levels of inflammation in AD patients (Cooney et al., 2014). NF-κB has been shown to play a role in mediating production of inflammatory cytokines in the AD process (Sandireddy et al., 2014). We found that treatment of HT-22 cells with L-Glu increased protein levels of IL-1β ($F_{(3,\ 16)} = 170.3$, $p < 0.0001$) and NF-κB ($F_{(3,\ 16)} = 9.999$, $p = 0.0010$), which were blocked by LSZ-EES treatment ($F_{(3,\ 16)} = 170.3$, $p < 0.0001$ for IL-1β; $F_{(3,\ 16)} = 9.999$, $p = 0.0013$ for NF-κB) (**Figure 2C**). These results show that LSZ-EES may prevent neurons from inflammation by reducing oxidative stress.

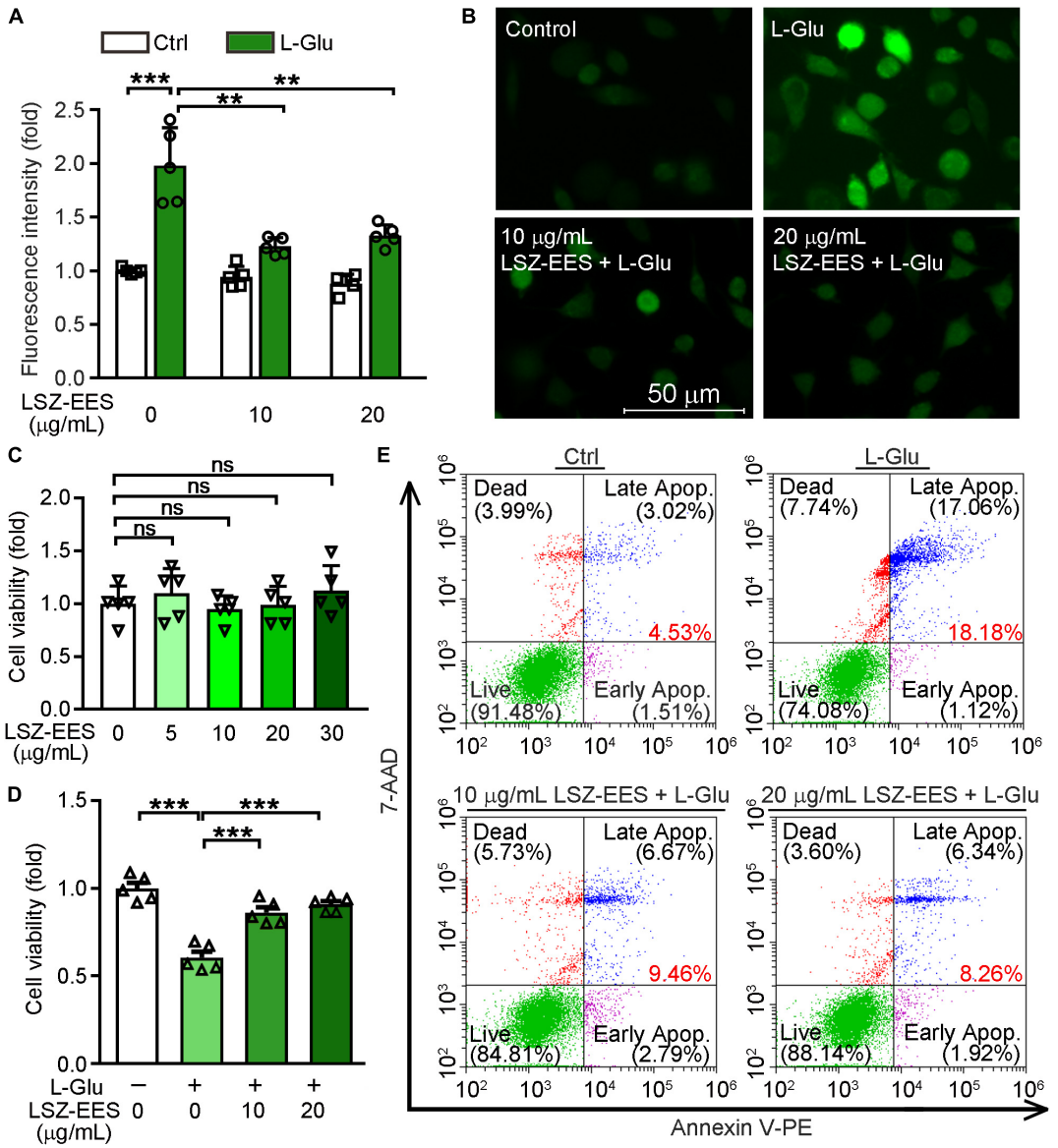

FIGURE 1 | LongShengZhi Capsule Enhances HT-22 Cell Survival by Reducing L-Glu-Induced Oxidative Stress. **(A,B,D,E)** HT-22 cells were pre-treated with LSZ-EES (0, 10, and 20 μg/mL) for 3 h, then co-treated with 20 mM L-Glu for another 18 h; **(C)** HT-22 cells were treated with LSZ-EES at the indicated concentrations for 18 h. ROS levels were detected with DCFH-DA (**A,B**; scale bar: 50 μm). Cell viability was determined by MTT **(C,D)**, and cell death was determined by FACS **(E)**. $^{**}p < 0.01$; $^{***}p < 0.001$; ns, not significant ($n = 5$).

LSZ Improves Cognitive Function in APP/PS1 Mice

Next, we used APP/PS1 mice to determine the cognitive protection of LSZ in the development of AD-like pathology. The 2-month-old APP/PS1 mice were divided into three groups. The animals were fed normal chow, normal chow containing a normal dose (850 mg/100 g food), or a high dose (2000 mg/100 g food) of LSZ, respectively. The age-matched WT mice fed normal chow were used as the normal control. After 7 months of treatment, behavioral experiments, including MWM and YM, were conducted to detect spatial memorizing (**Figure 3A**). In the MWM test, the AC group required significantly more time than the WT group to reach the platform ($F_{(3,\ 20)} = 41.9$, $p < 0.0001$), while LSZ treatment significantly reduced the escape latency ($F_{(3,\ 20)} = 41.9$, $p < 0.0001$) (**Figures 3B,C**). Accordingly, the times for crossing the target platform and quadrant decreased by ∼75% and ∼46%, respectively, in the AC group compared to the WT group ($F_{(3,\ 20)} = 10.29$, $p = 0.0002$ for crossing the target platform, $F_{(3,\ 20)} = 8.663$, $p = 0.0005$ for crossing the target quadrant), while LSZ treatment reversed these parameters by ∼157% for crossing the target platform (AC vs. ALN, $F_{(3,\ 20)} = 10.29$, $p = 0.0068$), and 82% ($F_{(3,\ 20)} = 8.663$, $p = 0.0016$) and ∼64% ($F_{(3,\ 20)} = 8.663$, $p = 0.0129$) for crossing the target quadrant (**Figures 3D,E**).

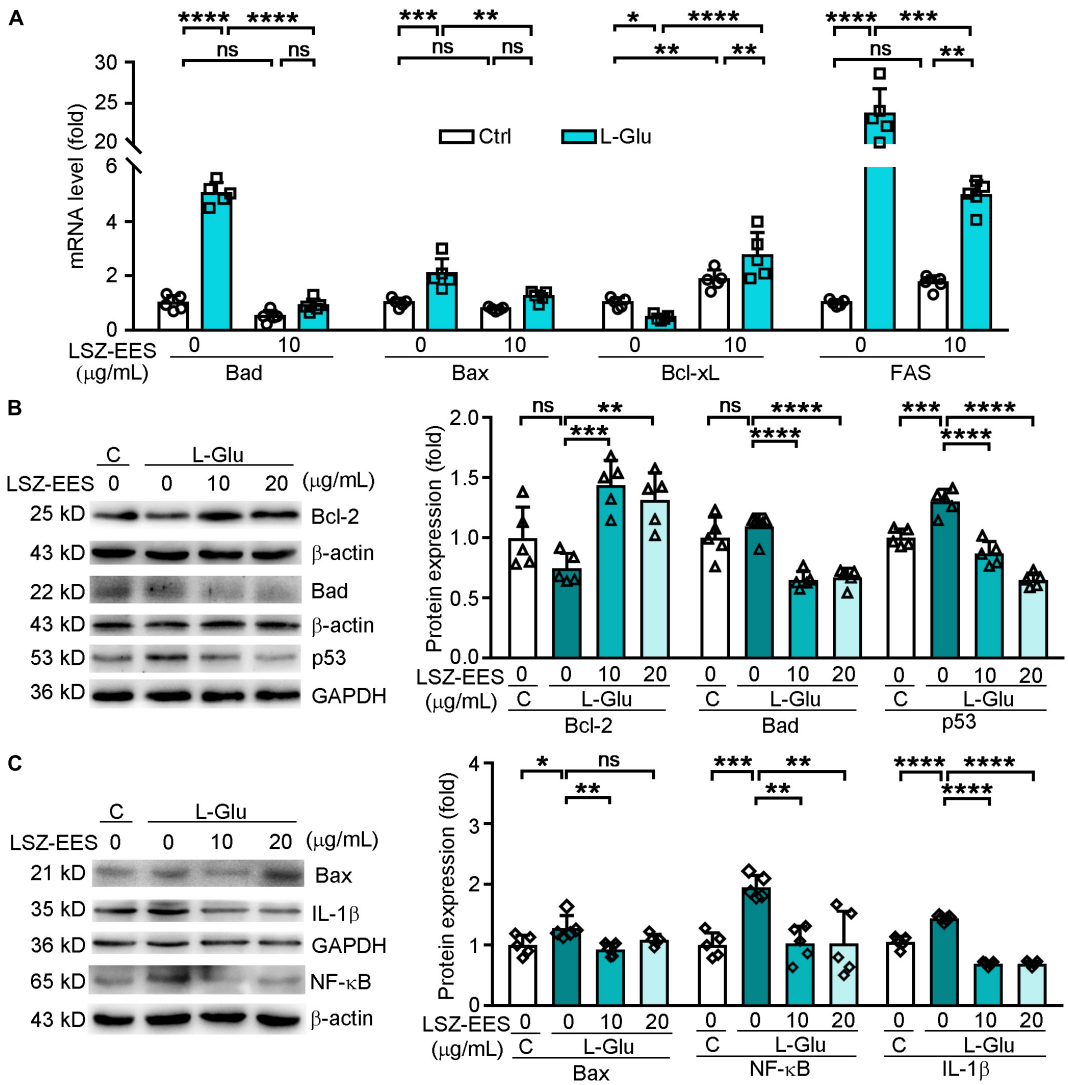

FIGURE 2 | LongShengZhi Capsule Antagonizes L-Glu-induced Expression of Apoptosis-Associated Genes and Inflammatory Cytokines in HT-22 Cells. A: HT-22 cells were pre-treated with LSZ-EES (10 μg/mL) for 3 h, followed by co-treatment with 20 mM L-Glu for another 18 h, or LSZ-EES alone for 21 h; **(B,C)** HT-22 cells were pre-treated with LSZ-EES at the indicated concentrations for 3 h and then co-treated with 20 mM L-Glu for an additional 18 h. Expression of Bad, Bax, Bcl-xL, and FAS mRNA was determined by qRT-PCR **(A)**. Expression of Bcl-2, Bad, p53, Bax, IL-1β, and NF-κB protein was detected by Western blot with quantitative analysis of band density and normalization to β-actin or GAPDH **(B,C)**. $^{*}p < 0.05$; $^{**}p < 0.01$; $^{***}p < 0.001$; $^{****}p < 0.0001$, ns, not significant ($n = 5$).

To eliminate the mutual interference between the two behavioral experiments, the YM test was performed one week later after the MWM test. Our results showed that WT mice had more trajectories in the new arm than the other two arms, showing the normal exploring and learning behavior. In contrast, decreased exploring in the new arm was observed in the AC group but not in the LSZ-treated groups (**Figure 3F**). In addition, compared with the AC group, LSZ treatment increased the relative number (to ∼1.6-fold vs. ∼1.1-fold), distance (to ∼1.6-fold vs. ∼1.5-fold), and time (to ∼1.6-fold vs. ∼1.2-fold) of exploring in the new arm with a greater effect by LSZ at the normal dose ($F_{(3,\ 20)} = 13.13$, $p = 0.0046$ for number; $F_{(3,\ 20)} = 9.215$, $p = 0.0091$ for distance; $F_{(3,\ 20)} = 15.89$, $p = 0.0217$ for time) (**Figures 3G-I**), suggesting that LSZ can enhance the working memory in APP/PS1 mice. Taken together, the results in **Figure 3** indicate that LSZ can repair the cognitive impairment in APP/PS1 mice.

LSZ Attenuates Cell Death and Enhances Antioxidant Enzyme Expression in the APP/PS1 Mouse Brain

Free radical-induced oxidative stress usually occurs in the AD brain (Saito et al., 2019). Excessive oxidative stress promotes neuronal cell apoptosis/death and increases brain damage, which aggravates the AD process (Jiang et al., 2016). In addition, neurons in the CA1 region of hippocampus are more sensitive to age and pathological oxidative stress induced by cerebral

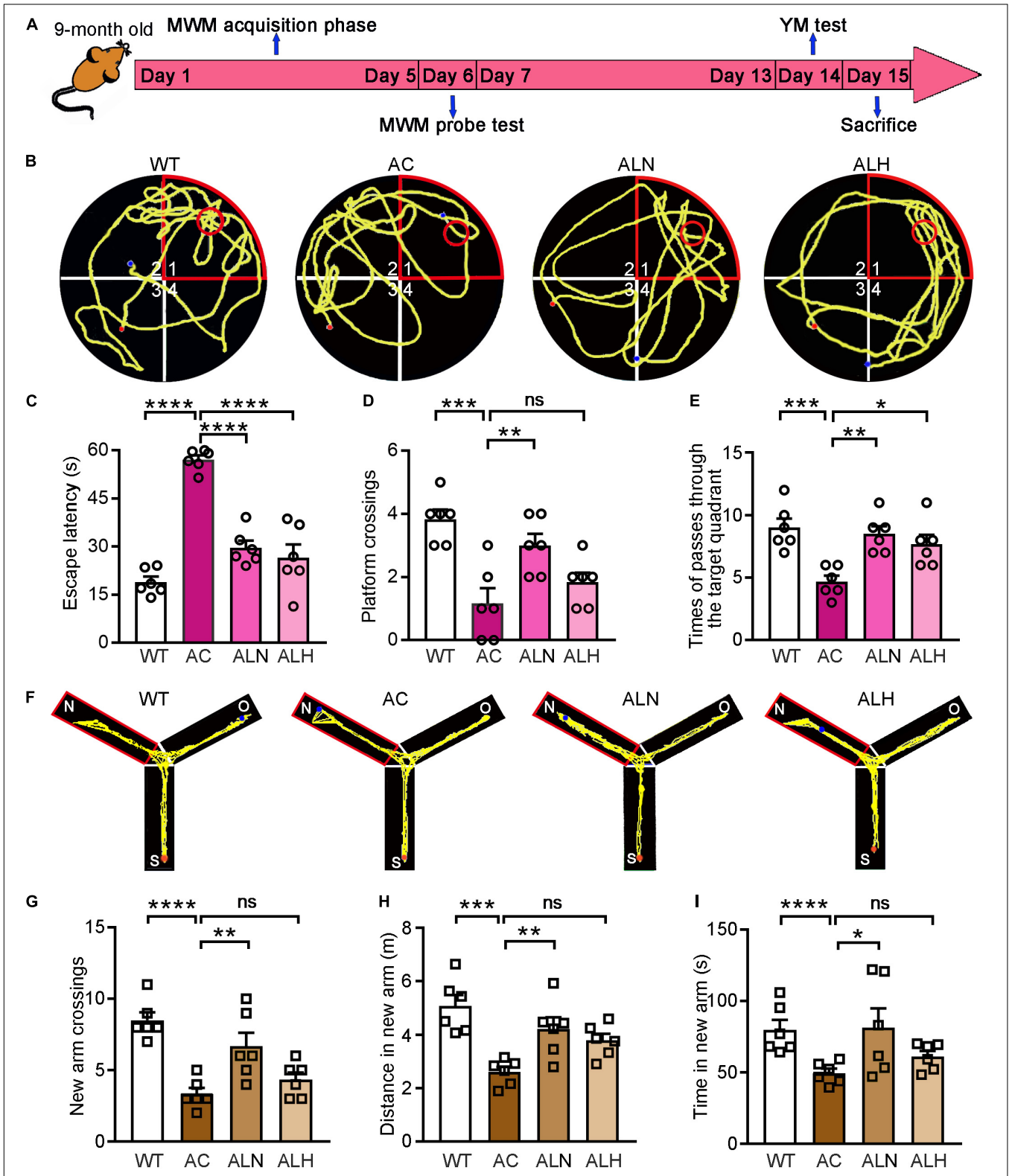

FIGURE 3 | LongShengZhi Capsule Improves Cognitive Functions in APP/PS1 Mice. **(A)** The design of behavioral experiments; **(B–E)** MWM test was conducted on mice. Record of motion trajectory **(B)**, escape latency **(C)**, platform crossings in the target quadrant **(D)**, and times of passing through the target quadrant **(E)** were recorded. The red sector and circle represent the target quadrant and the target platform, respectively, and the yellow curve represents the behavioral track of the mice; **(F–I)** YM test was conducted on mice. Motion behavior track **(F)**, times of crossing new arm **(G)**, distance **(H)**, and time **(I)** in the new arm were recorded. $^{*}p < 0.05$; $^{**}p < 0.01$; $^{***}p < 0.001$; $^{****}p < 0.0001$; ns, not significant ($n = 6$).

ischemia in the AD process (Berkowitz et al., 2017). To determine the neuroprotective effect of LSZ *in vivo*, we performed TUNEL staining on brain tissues. Increased cell death in the CA1 region of the hippocampus ($F_{(3,\ 20)} = 28.97$, $p < 0.0001$) (**Figure 4A**) and cortical areas ($F_{(3,\ 20)} = 13.93$, $p = 0.0003$) (**Figure 4B**) in the AC group was observed, but LSZ treatment significantly reduced cell death in both regions by ∼39% and ∼46% in the hippocampus ($F_{(3,\ 20)} = 28.97$, $p < 0.0001$) and ∼48% in the cortex ($F_{(3,\ 20)} = 13.93$, $p < 0.0001$). Mechanistically, LSZ treatment significantly down-regulated mRNA expression of pro-apoptotic genes, Bax (AC vs. ALN, $F_{(3,\ 20)} = 68.19$, $p = 0.0011$, AC vs. ALH, $F_{(3,\ 20)} = 68.19$, $p = 0.0324$) and Bad (AC vs. ALN, $F_{(3,\ 20)} = 22.73$, $p = 0.0002$; AC vs. ALH, $F_{(3,\ 20)} = 22.73$, $p < 0.0001$), and activated mRNA expression of anti-apoptotic genes, Bcl-xL (AC vs, ALH, $F_{(3,\ 20)} = 65.88$, $p < 0.0001$) and Bcl-2 ($F_{(3,\ 20)} = 135.2$, $p < 0.0001$) in the brains of APP/PS1 mice (**Figure 4C**).

We also examined the mRNA levels of antioxidant genes to determine the association between the neuroprotection effect of LSZ and its antioxidative stress functions in the mouse brain. Compared with the WT group, mRNA levels of GSH-PX, SOD1, and SOD2 in the APP/PS1 mouse brain were slightly affected but potently increased by LSZ treatment (AC vs. ALH, AC vs. ALH, $F_{(3,\ 20)} = 46.99$, $p < 0.0001$ for GSH-PX; AC vs. ALH, $F_{(3,\ 20)} = 24.16$, $p < 0.00015$ for SOD1; AC vs. ALH, $F_{(3,\ 20)} = 19.22$, $p = 0.0194$, AC vs. ALH, $F_{(3,\ 20)} = 19.22$, $p < 0.0001$ for SOD2) (**Figure 4D**). These results show that LSZ can enhance mRNA expression of antioxidant factors and reduce cell death in the brains of APP/PS1 mice.

LSZ Reduces β-Secretase and γ-Secretase Gene Expression and Inhibits Aβ Deposition

Previous studies have shown that the overexpression of mutated PSEN1 in AD brains promotes β-secretase expression and influences γ-secretase activity to enhance Aβ secretion (De Strooper et al., 1998; Al-Atrache et al., 2019). To investigate the effect of LSZ on Aβ secretion and accumulation in APP/PS1 mice, we determined PSEN1 expression by immunofluorescent staining and Aβ accumulation by thioflavin S staining of mouse brain sections. We found in the AC group PSEN1 expression was increased to ∼0-fold of the WT group ($F_{(3,\ 20)} = 188.7$, $p < 0.0001$), while the deposition of Aβ plaques was increased to ∼40-fold of the WT group ($F_{(3,\ 20)} = 192$, $p < 0.0001$) (**Figures 5A-C**). However, PSEN1 expression ($F_{(3,\ 20)} = 188.7$, $p < 0.0001$) and Aβ plaque deposition ($F_{(3,\ 20)} = 192$, $p < 0.0001$) in brain tissues were significantly reduced by LSZ treatment.

Meanwhile, we indicated the specificity of thioflavin S to Aβ plaques by immunofluorescent staining with APP antibody, which can identify the β-C-terminal of APP (**Supplementary Figure 2**). Then we detected that LSZ also reduced the upregulated mRNA levels of BACE1 and γ-secretase subunits, APH1a and PEN2, compared to the AC group ($F_{(3,\ 20)} = 27.62$, $p < 0.0001$ for BACE1; $F_{(3,\ 20)} = 13.08$, $p = 0.001$ for APH1a; $F_{(3,\ 20)} = 46.12$, $p < 0.0001$ for PEN2) (**Figure 5D**). These results indicate that LSZ can reduce Aβ deposition by inhibiting amyloidogenic pathway during the AD-like pathology in APP/PS1 mice.

LSZ Reduces Inflammation and Hyperphosphorylation of Tau in AD Model Mice

Brain inflammation is common in AD patients. It is due to NF-κB-mediated production of inflammatory cytokines by activated microglia, such as IL-1β and TNF (Snow and Albensi, 2016). IL-1β can further promote Tau phosphorylation while TNF increases the β-cleavage of APP, thereby enhancing Aβ production/accumulation and the neuronal cell death (Ghosh et al., 2013). By performing immunofluorescent staining, we found that NF-κB ($F_{(3,\ 20)} = 82.88$, $p < 0.0001$), IL-1β ($F_{(3,\ 20)} = 111.4$, $p < 0.0001$) and Iba-1 (a marker for microglia activation, $F_{(3,\ 20)} = 31.01$, $p < 0.0001$) were increased in the AC group compared with WT mice, but the increases were markedly inhibited by LSZ treatment ($F_{(3,\ 20)} = 82.88$, $p < 0.0001$ for NF-κB; $F_{(3,\ 20)} = 111.4$, $p < 0.0001$ for IL-1β; $F_{(3,\ 20)} = 31.01$, $p < 0.0001$ for Iba-1) (**Figures 6A,B**, **7A**). Similarly, compared with the AC group, LSZ in high dose significantly increased mRNA levels of anti-inflammatory cytokine, IL-10 ($F_{(3,\ 20)} = 12.4$, $p = 0.0009$), and both doses of LSZ treatment decreased mRNA levels of pro-inflammatory cytokines, IL-1β ($F_{(3,\ 20)} = 26.63$, $p < 0.0001$), IL-6 ($F_{(3,\ 20)} = 24.38$, $p < 0.0001$), and TNF (AC vs, ALN, $F_{(3,\ 20)} = 3.799$, $p = 0.0459$; AC vs, ALH, $F_{(3,\ 20)} = 3.799$, $p = 0.0323$) (**Figure 6C**). We further examined Tau expression and its phosphorylation. Compared with the WT group, Tau phosphorylation in the AC group was elevated ($F_{(3,\ 20)} = 106.2$, $p < 0.0001$ for p-Tau MFI/cell number; $F_{(3,\ 20)} = 72.59$, $p < 0.00013$ for p-Tau/total Tau), but the elevation was significantly blocked by LSZ treatment ($F_{(3,\ 20)} = 106.2$, $p < 0.0001$ for p-Tau MFI/cell number; $F_{(3,\ 20)} = 72.59$, $p < 0.0001$ for p-Tau/total Tau), although neither the AD model nor LSZ treatment had an effect on Tau expression (**Figure 7**). Taken together, these results demonstrate that LSZ can reduce NF-κB-mediated brain inflammation and hyperphosphorylation of Tau in APP/PS1 mice.

DISCUSSION

In this study, we used APP/PS1 mice to investigate the therapeutic effect of LSZ on AD-like pathology. We clearly show that LSZ can improve the damaged cognitive functions in APP/PS1 mice (**Figure 3**). LSZ inhibited cell death in the brains of APP/PS1 mice and reduced oxidative stress and consequently regulated Bcl-2 family gene expression (**Figure 4**). LSZ also significantly inhibited glia activation and protein or mRNA expression of inflammatory cytokines (**Figures 6**, **7**). Pathologically, LSZ reduced Aβ accumulation and Tau hyperphosphorylation (**Figures 5**, **7**). Similar to the *in vivo* study, *in vitro* LSZ decreased L-Glu-induced ROS production and enhanced survival of HT-22 cells (**Figure 1**). The neuroprotective effect of LSZ was partly through the FAS/Bcl-2/p53 pathway and NF-κB-mediated inflammation response (**Figure 2** and **Supplementary Figure 1**).

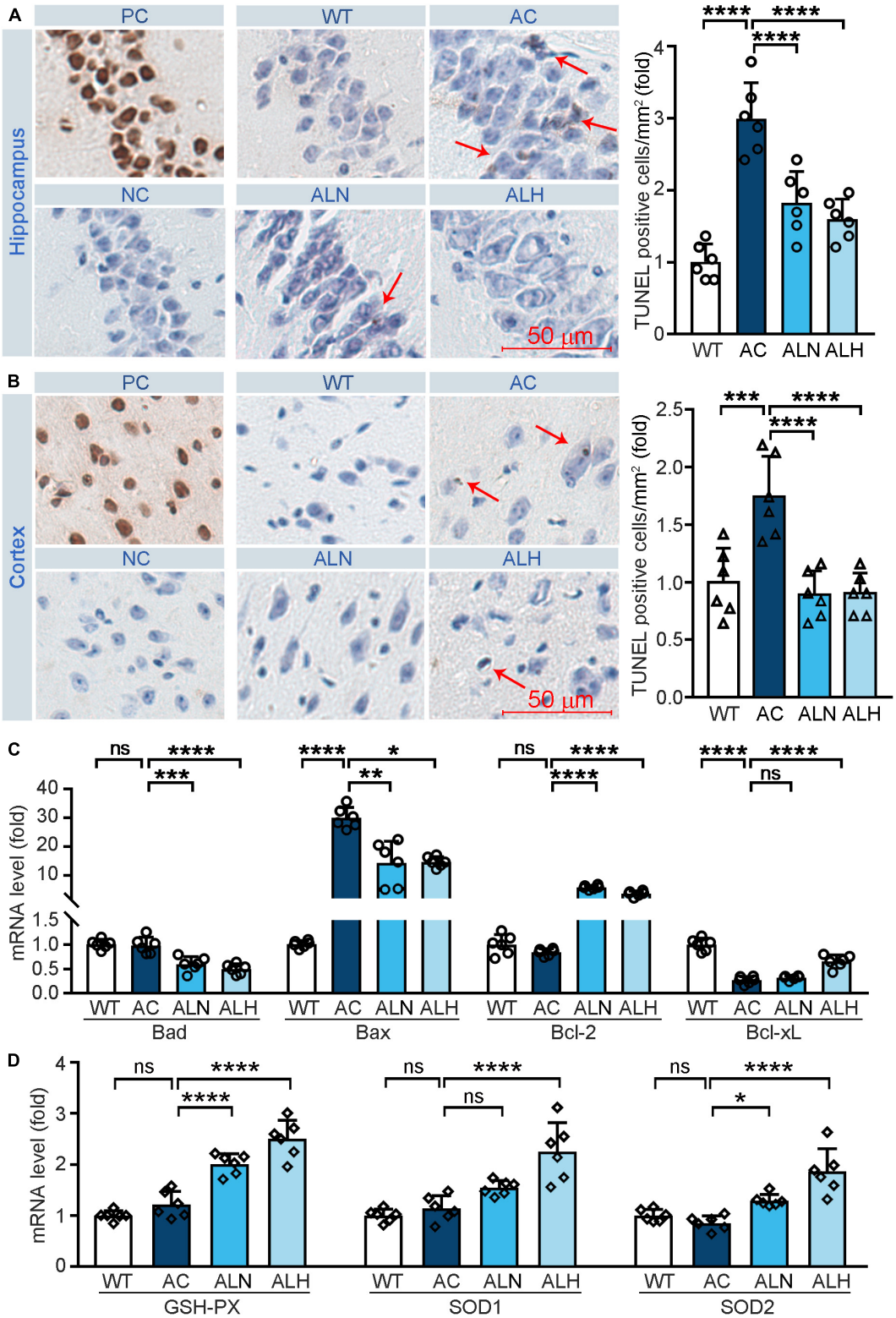

FIGURE 4 | LongShengZhi Capsule Reduces Cell Death and Induces Antioxidant Enzymes in APP/PS1 Mouse Brain. At the end of the experiment as indicated in **Figure 3A**, mouse brain tissues were collected, followed by preparation of cross sections or total RNA. **(A,B)** the sections were used to conduct TUNEL staining to determine cell death (brown, arrow pointed) in THE CA1 region of the hippocampus **(A)** and cortex region **(B)**. PC, Positive control; NC, negative control (scale bar: 50 μm); **(C,D)** mRNA levels of apoptosis-related genes (Bad, Bax, Bcl-2, and Bcl-xL) and antioxidant genes (GSH-PX, SOD1, and SOD2) were detected by qRT-PCR. *$p < 0.05$; **$p < 0.01$; ***$p < 0.001$; ****$p < 0.0001$; ns, not significant ($n = 6$).

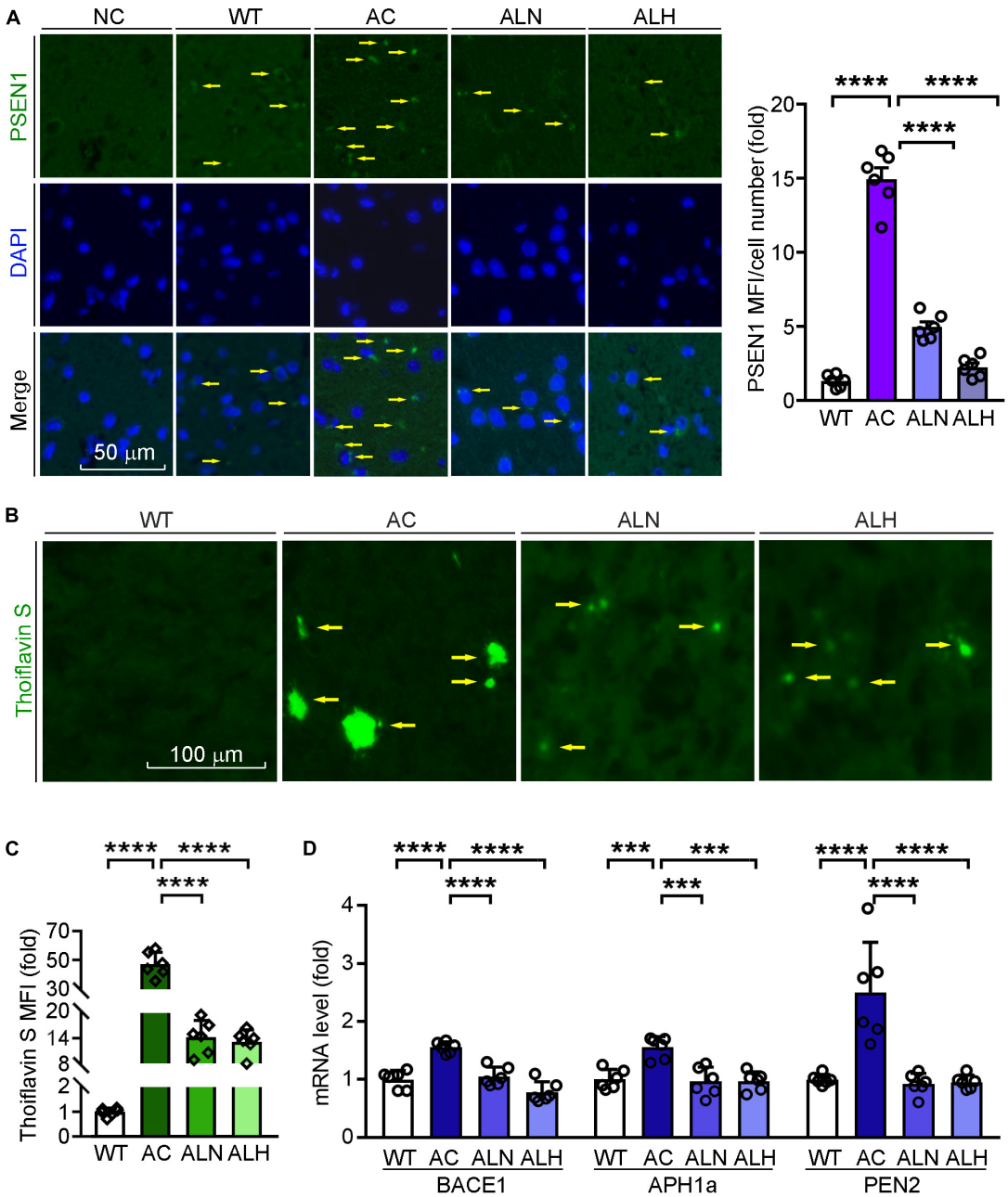

FIGURE 5 | LongShengZhi Capsule Reduces PSEN1 Expression and Aβ Accumulation in APP/PS1 Mouse Brain. **(A)** PSEN1 protein expression (green) in mouse brain sections was determined by immunofluorescent staining with quantitation of MFI/cell number. The nucleus was stained with DAPI (blue). NC: Negative control (scale bar: 50 μm); **(B,C)** brain sections were performed thioflavin S staining with quantitation of Aβ plaques (scale bar: 100 μm); **(D)** mRNA expression of β-secretase and γ-secretase subunit (BACE1, APH1a, PEN2) was detected by qRT-PCR. ***$p < 0.001$, ****$p < 0.0001$ ($n = 6$).

LongShengZhi Capsule as a traditional Chinese medicine for treatment of atherosclerotic cerebral infarction is usually used to treat hemiplegia and stroke caused by atherosclerosis with a high degree of safety. In our previous study, we showed LSZ has few side effects (Li et al., 2019; Ma et al., 2019; Xu et al., 2020). Similarly, in this study, we treated the animal with LSZ for 7 months and found no difference in bodyweight gain, food intake, and the external appearance between control and LSZ-treated groups, which further confirms the high degree of safety of the long-term LSZ treatment.

Oxidative stress and inflammation in the brain are considered important causes of AD. Many factors, such as brain injury, hypoxia, and insufficient cerebral blood flow, can cause excessive production of ROS in the brain. Recent studies have shown a significant decline in cerebral perfusion in the early stages of AD (Fouda et al., 2019). The

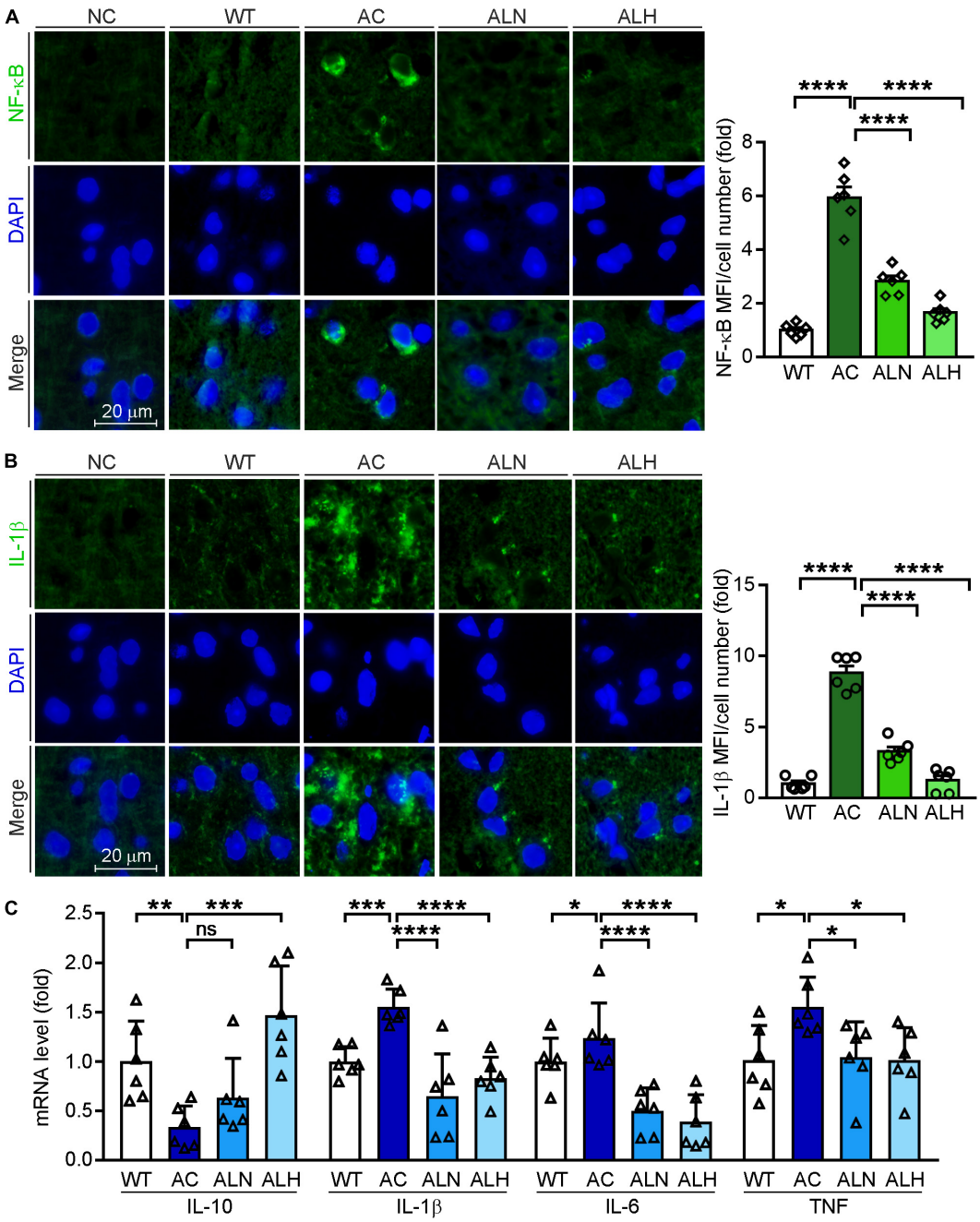

FIGURE 6 | LongShengZhi Capsule Inhibits NF-κB, IL-1β, IL-6, and TNF, but Induces IL-10 Expression. Expression of NF-κB **(A)** and IL-1β **(B)** protein (green) in mouse brain sections was determined by immunofluorescent staining with quantitation of MFI/cell number. The nucleus was stained with DAPI (blue). NC, Negative control (scale bar: 20 μm); **(C)** mRNA levels of IL-10, IL-1β, IL-6, and TNF in the mouse brain was detected by qRT-PCR. $^{*}p < 0.05$, $^{**}p < 0.01$, $^{***}p < 0.001$, $^{****}p < 0.0001$; ns, not significant ($n = 6$).

early defect of cerebral perfusion reduces the removal of Aβ and exacerbates brain oxidative stress (Tarasoff-Conway et al., 2015). Oxidative stress impairs the normal growth of neurons and synapses, as well as the transmission of nerve signals, thereby promoting cognitive damage (Li et al., 2017). Therefore, enhancing cerebral perfusion could be a potential therapeutic for AD. Preclinical experiments have shown that LSZ can also increase cerebral blood flow in experimental animals and reduce cerebral vascular resistance. LSZ improves cerebral blood flow, which suggests an anti-AD potential by targeting Aβ clearing.

In terms of the composition, many components in LSZ have been proven to resist AD. For example, paeoniflorin, the most abundant component in LSZ, reduces the age-onset Aβ

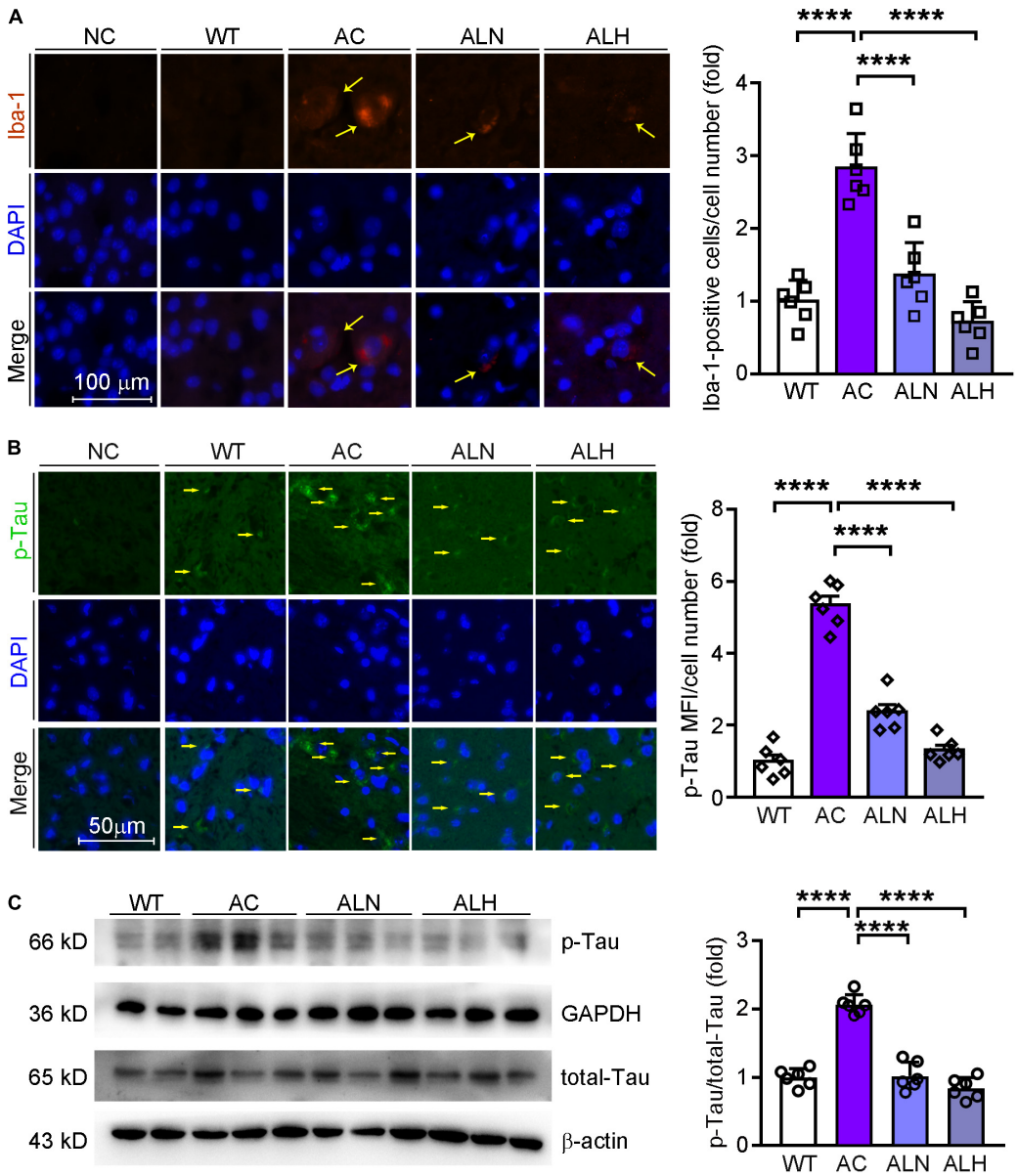

FIGURE 7 | LongShengZhi Capsule Inhibits Microglia Activation and Tau Phosphorylation in APP/PS1 Mouse Brain. Iba-1 (red, **A**) in mouse brain sections was determined by immunofluorescent staining with quantitation of Iba-1-positive cells/cell number, and phosphorylated Tau (p-Tau, green, **B**) in mouse brain sections was determined by immunofluorescent staining with quantitation of MFI/cell number. The nucleus was stained with DAPI (blue); NC indicates the negative control (scale bar: 100 μm for A; 50 μm for B); **(C)** p-Tau and total Tau protein expression were determined by Western blot. Based on the band intensity, the ratio of p-Tau to total Tau was calculated. ****$p < 0.0001$ ($n = 6$).

proteotoxicity by antioxidative stress (Ai et al., 2018). It has strong neuroprotective effects and cognitive preservation effects in intracerebroventricular streptozotocin-induced mice (Wang et al., 2018). Isoflavones, another high-content component in LSZ, have obvious neuroprotective effects (Wang et al., 2018). Isoflavones can attenuate oxidative stress and improve parameters related to AD-like pathology in D-galactose-treated C57BL/6J mice (Hsieh et al., 2009). These studies suggest that LSZ may protect against oxidative stress in AD through these active ingredients. We found LSZ significantly improved the damaged cognitive functions in 9-month-old APP/PS1 mice. Little has been reported thus far about the potential protective effects of LSZ on neurodegenerative diseases and its use as a prescribed medicine for treatment of cerebrovascular disease. However, many bioactive components in LSZ have been demonstrated to improve cognition. For example, paeoniflorin contained in LSZ can significantly improve the performance of aged wild-type rats in passive avoidance tasks (Baltina et al., 2019). Ferulic acid was reported to improve the escape latency of normal mice (Zafeer et al., 2019). These studies

imply that LSZ may protect normal cognition against the damages caused by AD.

Furthermore, we determined that LSZ significantly reduced ROS levels in HT-22 cells and enhanced expression of antioxidant factors, SOD1, SOD2, and GSH-PX, in the APP/PS1 mouse brain. These results suggest that the anti-AD-like pathology effect of LSZ is partly associated with antioxidative stress. The oxidative stress–promoted cell death mainly occurs through mitochondrial pathways, including the Bcl-2 family, FAS, and p53. Aβ can induce expression of apoptosis-related factors by activating the FAS/FASL pathway (Morishima et al., 2001). Aβ can also promote p53 stabilization, which leads to neuronal damage (Lapresa et al., 2019). As expected, in addition to the decline in oxidative stress, cell death was significantly reduced by LSZ treatment both *in vivo* and *in vitro*. We detected that LSZ largely enhanced expression of anti-apoptotic factors Bcl-2 and Bcl-xL while inhibiting expression of pro-apoptotic factors Bax and Bad. We also determined L-Glu-increased expression of FAS and p53 in HT-22 cells was significantly inhibited by LSZ, while the regulation of FAS and the Bcl-2 family by LSZ was blocked by FAS siRNA, indicating LSZ enhances neuron survival partly through the FAS/Bcl-2/p53 pathway. We do not know from the pretreatment mode *in vitro* how long LSZ can be given to continue to exert neuroprotective effects after the onset of neuron toxic. Further exploration is required.

Interestingly, *in vivo*, we noticed higher levels of Bcl-2, SOD, and GSH-PX expression in the brains of APP/PS1 mice treated with LSZ than in wild-type mice. As an anti-apoptotic protein, although the promotion of Bcl-2 has led us to consider an increase in the risk of cancer, its overexpression has been proven to resist Aβ-induced PC12 cell death (Song et al., 2004). Moreover, acting as barriers for cells and body against free radicals, the changes in antioxidant factors SOD and GSH-PX in AD were controversial (Markesbery, 1997). In our study, we observed increased Bcl-2 and antioxidant enzymes levels in LSZ-treated AD mice, even higher than untreated wild type levels. Whether such activation for the long term may cause detrimental effect or not remains unclear and warrants further investigation. However, clinical and basic studies have not reported any adverse events. In the future, the dose titration study should be completed to identify the optimal dose range of LSZ for AD treatment, which can demonstrate its therapeutic effects while keeping antioxidative stress and cell death under control.

Meanwhile, we observed accumulation of Aβ plaques and hyperphosphorylation of Tau were significantly increased in APP/PS1 mouse brains, while LSZ at different doses obviously reduced these two biomarkers. The reduction of Aβ plaques is associated with the inhibition of the amyloidogenic pathway. PSEN1, a subunit of γ-secretase, not only catalyzes the final γ-cleavage of APP but also mediates oxidative stress–induced expression of β-secretase. Thus, activation of PSEN1 results in excessive Aβ production/accumulation in the AD process (Cai et al., 2018). Our results show that PSEN1 expression in AD

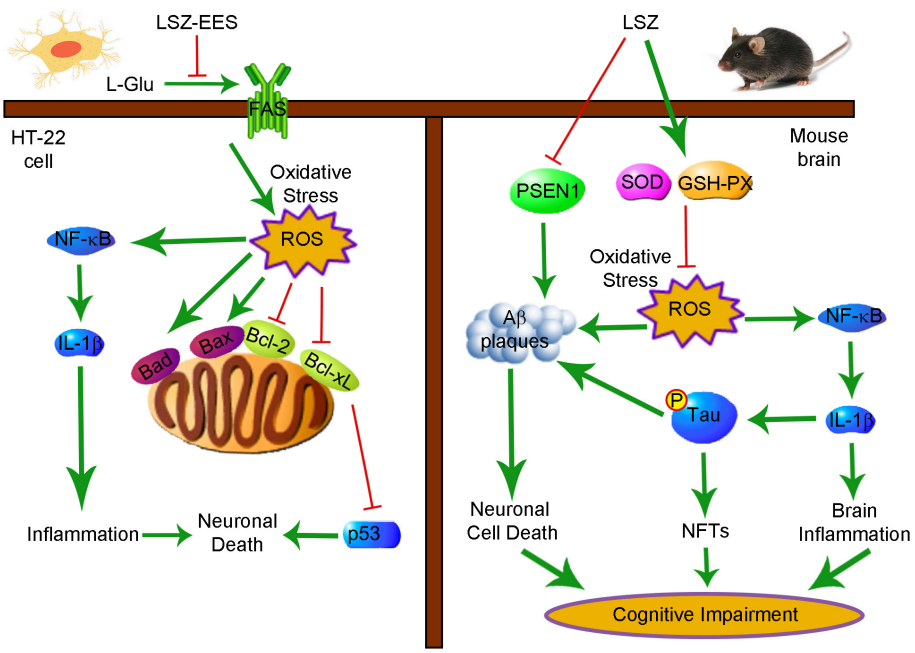

FIGURE 8 | Schematic Showing the Neuroprotection and Anti-AD-Like Pathology Properties of LSZ on HT-22 Cells and APP/PS1 Mice Are Associated with Reducing Oxidative Stress and Inflammation. Bcl-2, B-cell lymphoma 2; Bcl-xL, B-cell lymphoma-extra large; Bad, Bcl-2 associated agonist of cell death; Bax, Bcl-2 associated X protein; FAS, Fas cell surface death receptor; GSH-PX, glutathione peroxidase; IL-1β, interleukin-1β; LSZ, LongShengZhi capsule; LSZ-EES, LSZ ethanol extract solution; L-Glu, L-glutamic acid; NF-κB, nuclear factor kappa-B; NFTs, neurofibrillary tangles; ROS, reactive oxygen species; SOD, superoxide dismutase.

mice was upregulated compared with the WT group, which was reversed by LSZ treatment. In addition, LSZ reduced transcription of BACE1 and another two subunits of γ-secretase, APH1a and PEN2, suggesting that LSZ can inhibit β-secretase and γ-secretase function/expression to decrease Aβ processing. However, we need to determine the exact mechanism by which LSZ affects normal or mutated PSEN1 expression since these transgenic mice express both, which can be recognized by the antibody used in this study.

Expression of p-Tau, another critical biomarker for AD development, can be enhanced by the high level of glia inflammation in the brain, particularly by NF-κB (Barron et al., 2017). In this study, we observed the microglia was significantly activated in the brains of APP/PS1 mice, while LSZ markedly reduced the activation. In addition, increased NF-κB and IL-1β in both APP/PS1 mouse brains and HT-22 cells were substantially reduced by LSZ treatment, suggesting the anti-inflammatory effects of LSZ also play an important role in its functions of anti-AD-like pathology.

In summary, here we report that the protection of LSZ against AD-like pathology may be related to its antioxidant and anti-inflammation functions. Although our study was completed with the APP/PS1 double transgenic mouse model, LSZ inhibits Aβ aggregation and Tau hyperphosphorylation, the basis for AD development. Therefore, we speculate that LSZ may also offer protection against AD in other kinds of AD models with similar rationales, such as 5 × FAD, 3 × Tg mice, and aluminum-induced AD models, all of which have high levels of Aβ plaques, NFTs, and oxidative stress in the brain.

Despite some interesting findings we obtained in this study, there are a few limitations that should be improved in future studies. These limitations include the following: (1) the effect of LSZ on some molecule should be further confirmed by determination of protein expression since mRNA expression does not always mean protein expression; (2) the exact mechanisms of LSZ on AD-like pathology need be further investigated; only its association with oxidative stress/cell death in the brain were reported in this study; (3) the neuroprotective effects of LSZ *in vitro* were only completed in the pretreatment regime; the therapeutic effect of LSZ after AD onset remains to be explored; and (4) we should investigate whether LSZ can also function well with the AD mouse model induced by cholinergic antagonist injection since a different rationale is involved in this kind of model, and such study can further broaden the potential application of LSZ in AD treatment.

CONCLUSION

We demonstrated that LSZ can significantly improve cognitive functions of APP/PS1 mice. LSZ enhances neuron survival in HT-22 cells partly by regulating the FAS/Bcl-2/p53 pathway. LSZ can also decrease oxidative stress and reduce inflammatory cytokine expression *in vitro*. Pathologically, LSZ inhibits AD-induced accumulation of Aβ plaques, hyperphosphorylation of Tau, cell death, and NF-κB-mediated inflammation, and promotes antioxidative gene expression in the brains of APP/PS1 mice (**Figure 8**). Based on the finding that APP/PS1 mice can spontaneously develop AD pathology, our study clearly demonstrates the therapeutic properties of LSZ on AD and suggests its potential clinical application.

DATA AVAILABILITY STATEMENT

The raw data supporting the conclusions of this article will be made available by the authors, without undue reservation.

ETHICS STATEMENT

The animal study was reviewed and approved by the Institution Animal Ethics Committee of Hefei University of Technology.

AUTHOR CONTRIBUTIONS

JH and YD designed the study. ZY, XW, SHZ, PC, and YC performed the experiments. MY, CL, ZZ, and XY modified the file. SHZ and XY prepared the manuscript. All authors reviewed the results and approved the final version of the manuscript.

FUNDING

This work was supported by funding from the International Science & Technology Cooperation Programs of China 2017YFE0110100 to JH, YD, YC, and XY; NSFC grants 81973316 and 81773727 to JH; funding from the Key Research and Development Program of Anhui Province 201904a07020007 to JH; and Fundamental Research Funds for the Central Universities to YD, XY, and YC.

SUPPLEMENTARY MATERIAL

The Supplementary Material for this article can be found online at: https://www.frontiersin.org/articles/10.3389/fnagi.2020.582455/full#supplementary-material

REFERENCES

Ai, L., Yang, F., Song, J., Chen, Y., Xiao, L., Wang, Q., et al. (2018). Inhibition of abeta proteotoxicity by paeoniflorin in *Caenorhabditis elegans* through regulation of oxidative and heat shock stress responses. *Rejuvenation Res.* 21, 304–312. doi: 10.1089/rej.2017.1966

Al-Atrache, Z., Lopez, D. B., Hingley, S. T., and Appelt, D. M. (2019). Astrocytes infected with *Chlamydia pneumoniae* demonstrate altered expression and

activity of secretases involved in the generation of beta-amyloid found in Alzheimer disease. *BMC Neurosci.* 20:6. doi: 10.1186/s12868-019-0489-5

Baltina, L., Sapozhnikova, T., Makara, N., Gabdrakhmanova, S., Baltina, L., and Kondratenko, R. (2019). Paeoniflorin benzoates: synthesis and influence on learning and memory of aged rats in the passive avoidance task. *Nat. Prod. Res.* 10, 1–9. doi: 10.1080/14786419.2019.1662005

Barron, M., Gartlon, J., Dawson, L. A., Atkinson, P. J., and Pardon, M. C. (2017). A state of delirium: deciphering the effect of inflammation on tau pathology in Alzheimer's disease. *Exp. Gerontol.* 94, 103–107. doi: 10.1016/j.exger.2016.12.006

Berkowitz, B. A., Lenning, J., Khetarpal, N., Tran, C., Wu, J. Y., Berri, A. M., et al. (2017). In vivo imaging of prodromal hippocampus CA1 subfield oxidative stress in models of Alzheimer disease and Angelman syndrome. *FASEB J.* 31, 4179–4186. doi: 10.1096/fj.201700229R

Cai, Z., Wang, C., He, W., and Chen, Y. (2018). Berberine alleviates amyloid-beta pathology in the brain of APP/PS1 transgenic mice via inhibiting beta/gamma-secretases activity and enhancing alpha-secretases. *Curr. Alzheimer Res.* 15, 1045–1052. doi: 10.2174/1567205015666180702105740

Chen, Y., Duan, Y., Kang, Y., Yang, X., Jiang, M., Zhang, L., et al. (2012). Activation of liver X receptor induces macrophage interleukin-5 expression. *J. Biol. Chem.* 287, 43340–43350. doi: 10.1074/jbc.M112.403394

Chen, Y., Liu, M., Zhao, T., Zhao, B., Jia, L., Zhu, Y., et al. (2014). Danhong injection inhibits the development of atherosclerosis in both Apoe(-)/(-) and Ldlr(-)/(-) mice. *J. Cardiovasc. Pharmacol.* 63, 441–452. doi: 10.1097/FJC.0000000000000067

Chen, Z., Tao, S., Li, X., Zeng, X., Zhang, M., and Yao, Q. (2019). Anagliptin protects neuronal cells against endogenous amyloid beta (Abeta)-induced cytotoxicity and apoptosis. *Artif. Cells Nanomed. Biotechnol.* 47, 2213–2220. doi: 10.1080/21691401.2019.1609979

Congdon, E. E., and Sigurdsson, E. M. (2018). Tau-targeting therapies for Alzheimer disease. *Nat. Rev. Neurol.* 14, 399–415. doi: 10.1038/s41582-018-0013-z

Cooney, S. J., Zhao, Y., and Byrnes, K. R. (2014). Characterization of the expression and inflammatory activity of NADPH oxidase after spinal cord injury. *Free Radic Res.* 48, 929–939. doi: 10.3109/10715762.2014.927578

Dar, N. J., and Glazner, G. W. (2020). Deciphering the neuroprotective and neurogenic potential of soluble amyloid precursor protein alpha (sAPPalpha). *Cell Mol. Life Sci.* 77, 2315–2330. doi: 10.1007/s00018-019-03404-x

Daulatzai, M. A. (2017). Cerebral hypoperfusion and glucose hypometabolism: key pathophysiological modulators promote neurodegeneration, cognitive impairment, and Alzheimer's disease. *J. Neurosci. Res.* 95, 943–972. doi: 10.1002/jnr.23777

De Strooper, B., Saftig, P., Craessaerts, K., Vanderstichele, H., Guhde, G., Annaert, W., et al. (1998). Deficiency of presenilin-1 inhibits the normal cleavage of amyloid precursor protein. *Nature* 391, 387–390. doi: 10.1038/34910

Ding, J., Yu, H. L., Ma, W. W., Xi, Y. D., Zhao, X., Yuan, L. H., et al. (2013). Soy isoflavone attenuates brain mitochondrial oxidative stress induced by beta-amyloid peptides 1-42 injection in lateral cerebral ventricle. *J. Neurosci. Res.* 91, 562–567. doi: 10.1002/jnr.23163

Fouda, A. Y., Fagan, S. C., and Ergul, A. (2019). Brain vasculature and cognition. *Arterioscler. Thromb. Vasc. Biol.* 39, 593–602. doi: 10.1161/ATVBAHA.118.311906

Ghosh, S., Wu, M. D., Shaftel, S. S., Kyrkanides, S., LaFerla, F. M., Olschowka, J. A., et al. (2013). Sustained interleukin-1beta overexpression exacerbates tau pathology despite reduced amyloid burden in an Alzheimer's mouse model. *J. Neurosci.* 33, 5053–5064. doi: 10.1523/JNEUROSCI.4361-12.2013

Graham, W. V., Bonito-Oliva, A., and Sakmar, T. P. (2017). Update on Alzheimer's disease therapy and prevention strategies. *Annu. Rev. Med.* 68, 413–430. doi: 10.1146/annurev-med-042915-103753

Gupta, A., and Iadecola, C. (2015). Impaired Abeta clearance: a potential link between atherosclerosis and Alzheimer's disease. *Front. Aging Neurosci.* 7:115. doi: 10.3389/fnagi.2015.00115

Halliwell, B. (2006). Oxidative stress and neurodegeneration: where are we now? *J. Neurochem.* 97, 1634–1658. doi: 10.1111/j.1471-4159.2006.03907.x

Hefter, D., Ludewig, S., Draguhn, A., and Korte, M. (2020). Amyloid, APP, and electrical activity of the brain. *Neuroscientist* 26, 231–251. doi: 10.1177/1073858419882619

Hoppe, J. B., Frozza, R. L., Horn, A. P., Comiran, R. A., Bernardi, A., Campos, M. M., et al. (2010). Amyloid-beta neurotoxicity in organotypic culture is attenuated by melatonin: involvement of GSK-3beta, tau and neuroinflammation. *J. Pineal. Res.* 48, 230–238. doi: 10.1111/j.1600-079X.2010.00747.x

Houtman, J., Freitag, K., Gimber, N., Schmoranzer, J., Heppner, F. L., and Jendrach, M. (2019). Beclin1-driven autophagy modulates the inflammatory response of microglia via NLRP3. *EMBO J.* 38:e99430. doi: 10.15252/embj.201899430

Hsieh, H. M., Wu, W. M., and Hu, M. L. (2009). Soy isoflavones attenuate oxidative stress and improve parameters related to aging and Alzheimer's disease in C57BL/6J mice treated with D-galactose. *Food Chem. Toxicol.* 47, 625–632. doi: 10.1016/j.fct.2008.12.026

Huang, Y. C., Tsay, H. J., Lu, M. K., Lin, C. H., Yeh, C. W., Liu, H. K., et al. (2017). Astragalus membranaceus-polysaccharides ameliorates obesity, hepatic steatosis, neuroinflammation and cognition impairment without affecting amyloid deposition in metabolically stressed APPswe/PS1dE9 mice. *Int. J. Mol. Sci.* 18:2746. doi: 10.3390/ijms18122746

Jankowska, A., Wesolowska, A., Pawlowski, M., and Chlon-Rzepa, G. (2019). Diabetic theory in anti-Alzheimer's drug research and development. Part 1: therapeutic potential of antidiabetic agents. *Curr. Med. Chem.* doi: 10.2174/0929867326666191011144818 Online ahead of print

Jiang, L. H., Li, X., Syed Mortadza, S. A., Lovatt, M., and Yang, W. (2018). The TRPM2 channel nexus from oxidative damage to Alzheimer's pathologies: an emerging novel intervention target for age-related dementia. *Ageing Res. Rev.* 47, 67–79. doi: 10.1016/j.arr.2018.07.002

Jiang, T., Sun, Q., and Chen, S. (2016). Oxidative stress: a major pathogenesis and potential therapeutic target of antioxidative agents in Parkinson's disease and Alzheimer's disease. *Prog. Neurobiol.* 147, 1–19. doi: 10.1016/j.pneurobio.2016.07.005

Kabir, M. T., Uddin, M. S., Setu, J. R., Ashraf, G. M., Bin-Jumah, M. N., and Abdel-Daim, M. M. (2020). Exploring the role of PSEN mutations in the pathogenesis of Alzheimer's disease. *Neurotox Res.* 38, 833–849. doi: 10.1007/s12640-020-00232-x

Kaufmann, T., Strasser, A., and Jost, P. J. (2012). Fas death receptor signalling: roles of Bid and XIAP. *Cell Death Differ.* 19, 42–50. doi: 10.1038/cdd.2011.121

Kim, J. H., He, M. T., Kim, M. J., Yang, C. Y., Shin, Y. S., Yokozawa, T., et al. (2019). Safflower (*Carthamus tinctorius* L.) seed attenuates memory impairment induced by scopolamine in mice via regulation of cholinergic dysfunction and oxidative stress. *Food Funct.* 10, 3650–3659. doi: 10.1039/c9fo00615j

Kritis, A. A., Stamoula, E. G., Paniskaki, K. A., and Vavilis, T. D. (2015). Researching glutamate - induced cytotoxicity in different cell lines: a comparative/collective analysis/study. *Front. Cell Neurosci.* 9:91. doi: 10.3389/fncel.2015.00091

Lapresa, R., Agulla, J., Sanchez-Moran, I., Zamarreno, R., Prieto, E., Bolanos, J. P., et al. (2019). Amyloid-ss promotes neurotoxicity by Cdk5-induced p53 stabilization. *Neuropharmacology* 146, 19–27. doi: 10.1016/j.neuropharm.2018.11.019

Li, Q., Chen, Y., Zhao, D., Yang, S., Zhang, S., Wei, Z., et al. (2019). LongShengZhi capsule reduces carrageenan-induced thrombosis by reducing activation of platelets and endothelial cells. *Pharmacol. Res.* 144, 167–180. doi: 10.1016/j.phrs.2019.04.013

Li, T., Li, Y. M., Ahn, K., Price, D. L., Sisodia, S. S., and Wong, P. C. (2011). Increased expression of PS1 is sufficient to elevate the level and activity of gamma-secretase in vivo. *PLoS One* 6:e28179. doi: 10.1371/journal.pone.0028179

Li, X. Z., Zhang, S. N., Wang, K. X., Liu, H. Y., Yang, Z. M., Liu, S. M., et al. (2014). Neuroprotective effects of extract of Acanthopanax senticosus harms on SH-SY5Y cells overexpressing wild-type or A53T mutant alpha-synuclein. *Phytomedicine* 21, 704–711. doi: 10.1016/j.phymed.2013.10.012

Li, Z., Chen, X., Lu, W., Zhang, S., Guan, X., Li, Z., et al. (2017). Anti-oxidative stress activity is essential for amanita caesarea mediated neuroprotection on glutamate-induced apoptotic HT22 Cells and an Alzheimer's disease mouse model. *Int. J. Mol. Sci.* 18:1623. doi: 10.3390/ijms18081623

Liu, L., Ding, L., Rovere, M., Wolfe, M. S., and Selkoe, D. J. (2019). A cellular complex of BACE1 and gamma-secretase sequentially generates Abeta from its full-length precursor. *J. Cell Biol.* 218, 644–663. doi: 10.1083/jcb.201806205

Ma, J., Zhao, D., Wang, X., Ma, C., Feng, K., Zhang, S., et al. (2019). LongShengZhi capsule reduces established atherosclerotic lesions in apoE-deficient mice by ameliorating hepatic lipid metabolism and inhibiting inflammation. *J. Cardiovasc. Pharmacol.* 73, 105–117. doi: 10.1097/FJC.0000000000000642

Markesbery, W. R. (1997). Oxidative stress hypothesis in Alzheimer's disease. *Free Radic Biol. Med.* 23, 134–147. doi: 10.1016/s0891-5849(96)00629-6

Merlini, M., Meyer, E. P., Ulmann-Schuler, A., and Nitsch, R. M. (2011). Vascular beta-amyloid and early astrocyte alterations impair cerebrovascular function and cerebral metabolism in transgenic arcAbeta mice. *Acta Neuropathol.* 122, 293–311. doi: 10.1007/s00401-011-0834-y

Morishima, Y., Gotoh, Y., Zieg, J., Barrett, T., Takano, H., Flavell, R., et al. (2001). Beta-amyloid induces neuronal apoptosis via a mechanism that involves the c-Jun N-terminal kinase pathway and the induction of Fas ligand. *J. Neurosci.* 21, 7551–7560. doi: 10.1523/jneurosci.21-19-07551.2001

Nunez, J. (2008). Morris water maze experiment. *J. Vis. Exp.* 24:897. doi: 10.3791/897

Oboh, G., Adebayo, A. A., Ademosun, A. O., and Olowokere, O. G. (2020). Rutin restores neurobehavioral deficits via alterations in cadmium bioavailability in the brain of rats exposed to cadmium. *Neurotoxicology* 77, 12–19. doi: 10.1016/j.neuro.2019.12.008

Rong, Y., and Distelhorst, C. W. (2008). Bcl-2 protein family members: versatile regulators of calcium signaling in cell survival and apoptosis. *Annu. Rev. Physiol.* 70, 73–91. doi: 10.1146/annurev.physiol.70.021507.105852

Saito, T., Hisahara, S., Iwahara, N., Emoto, M. C., Yokokawa, K., Suzuki, H., et al. (2019). Early administration of galantamine from preplaque phase suppresses oxidative stress and improves cognitive behavior in APPswe/PS1dE9 mouse model of Alzheimer's disease. *Free Radic Biol. Med.* 145, 20–32. doi: 10.1016/j.freeradbiomed.2019.09.014

Sandireddy, R., Yerra, V. G., Areti, A., Komirishetty, P., and Kumar, A. (2014). Neuroinflammation and oxidative stress in diabetic neuropathy: futuristic strategies based on these targets. *Int. J. Endocrinol.* 2014:674987. doi: 10.1155/2014/674987

Sharma, P., Srivastava, P., Seth, A., Tripathi, P. N., Banerjee, A. G., and Shrivastava, S. K. (2019). Comprehensive review of mechanisms of pathogenesis involved in Alzheimer's disease and potential therapeutic strategies. *Prog. Neurobiol.* 174, 53–89. doi: 10.1016/j.pneurobio.2018.12.006

Snow, W. M., and Albensi, B. C. (2016). Neuronal gene targets of NF-kappaB and their dysregulation in Alzheimer's disease. *Front. Mol. Neurosci.* 9:118. doi: 10.3389/fnmol.2016.00118

Song, Y. S., Park, H. J., Kim, S. Y., Lee, S. H., Yoo, H. S., Lee, H. S., et al. (2004). Protective role of Bcl-2 on beta-amyloid-induced cell death of differentiated PC12 cells: reduction of NF-kappaB and p38 MAP kinase activation. *Neurosci. Res.* 49, 69–80. doi: 10.1016/j.neures.2004.01.010

Strasser, A., Jost, P. J., and Nagata, S. (2009). The many roles of FAS receptor signaling in the immune system. *Immunity* 30, 180–192. doi: 10.1016/j.immuni.2009.01.001

Sultana, R., Perluigi, M., and Butterfield, D. A. (2009). Oxidatively modified proteins in Alzheimer's disease (AD), mild cognitive impairment and animal models of AD: role of Abeta in pathogenesis. *Acta Neuropathol.* 118, 131–150. doi: 10.1007/s00401-009-0517-0

Sun, L., Yang, X., Li, Q., Zeng, P., Liu, Y., Liu, L., et al. (2017). Activation of adiponectin receptor regulates proprotein convertase subtilisin/kexin Type 9 expression and inhibits lesions in ApoE-deficient mice. *Arterioscler. Thromb. Vasc. Biol.* 37, 1290–1300. doi: 10.1161/ATVBAHA.117.309630

Tarasoff-Conway, J. M., Carare, R. O., Osorio, R. S., Glodzik, L., Butler, T., Fieremans, E., et al. (2015). Clearance systems in the brain-implications for Alzheimer disease. *Nat. Rev. Neurol.* 11, 457–470. doi: 10.1038/nrneurol.2015.119

Tian, T., Bai, D., Li, W., Huang, G. W., and Liu, H. (2016). Effects of folic acid on secretases involved in abeta deposition in APP/PS1 mice. *Nutrients* 8:556. doi: 10.3390/nu8090556

Vorhees, C. V., and Williams, M. T. (2006). Morris water maze: procedures for assessing spatial and related forms of learning and memory. *Nat. Protoc.* 1, 848–858. doi: 10.1038/nprot.2006.116

Wang, D., Liu, L., Li, S., and Wang, C. (2018). Effects of paeoniflorin on neurobehavior, oxidative stress, brain insulin signaling, and synaptic alterations in intracerebroventricular streptozotocin-induced cognitive impairment in mice. *Physiol. Behav.* 191, 12–20. doi: 10.1016/j.physbeh.2018.03.016

Wei, Z. Y., Xu, W. J., Liu, J., Sun, X. L., Chen, Y. J., Li, Y. T., et al. (2019). [Simultaneous quantification and consistency analysis of 19 representative components in Longshengzhi Capsules by HPLC-QQQ/MS]. *Zhongguo Zhong Yao Za Zhi* 44, 948–953. doi: 10.19540/j.cnki.cjcmm.20181129.008

Xu, S., Wang, Y., Yu, M., Wang, D., Liang, Y., Chen, Y., et al. (2020). LongShengZhi capsule inhibits doxorubicin-induced heart failure by anti-oxidative stress. *Biomed. Pharmacother.* 123:109803. doi: 10.1016/j.biopha.2019.109803

Yang, W., Zhang, L., Chen, S., Yao, Q., Chen, H., Zhou, J., et al. (2020). Longshengzhi capsules improve ischemic stroke outcomes and reperfusion injury via the promotion of anti-inflammatory and neuroprotective effects in MCAO/R rats. *Evid Based Complement Alternat. Med.* 2020:9654175. doi: 10.1155/2020/9654175

Zafeer, M. F., Firdaus, F., Anis, E., and Mobarak Hossain, M. (2019). Prolong treatment with Trans-ferulic acid mitigates bioenergetics loss and restores mitochondrial dynamics in streptozotocin-induced sporadic dementia of Alzheimer's type. *Neurotoxicology* 73, 246–257. doi: 10.1016/j.neuro.2019.04.006

Zhong, M., Song, W. L., Xu, Y. C., Ye, Y., and Feng, L. Y. (2015). Paeoniflorin ameliorates ischemic neuronal damage in vitro via adenosine A1 receptor-mediated transactivation of epidermal growth factor receptor. *Acta Pharmacol. Sin.* 36, 298–310. doi: 10.1038/aps.2014.154

Conflict of Interest: The authors declare that the research was conducted in the absence of any commercial or financial relationships that could be construed as a potential conflict of interest.

Copyright © 2020 Yin, Wang, Zheng, Cao, Chen, Yu, Liao, Zhang, Han, Duan, Yang and Zhang. This is an open-access article distributed under the terms of the Creative Commons Attribution License (CC BY). The use, distribution or reproduction in other forums is permitted, provided the original author(s) and the copyright owner(s) are credited and that the original publication in this journal is cited, in accordance with accepted academic practice. No use, distribution or reproduction is permitted which does not comply with these terms.

frontiers in Neuroscience

ORIGINAL RESEARCH
published: 30 November 2020
doi: 10.3389/fnins.2020.582851

Hydrogen Sulfide Overproduction Is Involved in Acute Ischemic Cerebral Injury Under Hyperhomocysteinemia

Yan Ji, Yusheng Li*, Zichen Zhao, Panxing Li and Yi Xie*

Department of Neurology, The First Affiliated Hospital of Zhengzhou University, Zhengzhou, China

Objectives: This study aimed to identify the involvement of hydrogen sulfide overproduction in acute brain injury under ischemia/reperfusion and hyperhomocysteinemia.

Methods: *In vitro* and *in vivo* experiments were conducted to determine: the effect of sodium hydrosulfide treatment on the human neuroblastoma cell line (SH-SY5Y) under conditions of oxygen and glucose deprivation; the changes of hydrogen sulfide levels, inflammatory factors, energetic metabolism, and mitochondrial function in the brain tissue of rats under either ischemia/reperfusion alone or a combination of ischemia/reperfusion and hyperhomocysteinemia; and the potential mechanism underlying the relationship between homocysteine and these changes through the addition of the related inhibitors. Furthermore, experimental technologies, including western blot, enzyme-linked immunosorbent assay, immunofluorescence, reverse transcription polymerase chain reaction, and flow cytometry, were used.

Results: Our study found that high concentration of sodium hydrosulfide treatment aggravated the decrease in mitochondrial membrane potential, the increase in both mitochondrial permeability transition pore and translocation of cytochrome C, as well as the accumulation of reactive oxygen species in oxygen and glucose deprived SH-SY5Y cells. As a result, neurological deficit appeared in rats with ischemia/reperfusion or ischemia/reperfusion and hyperhomocysteinemia, and a higher water content and larger infarction size of cerebral tissue appeared in rats combined ischemia/reperfusion and hyperhomocysteinemia. Furthermore, alterations in hydrogen sulfide production, inflammatory factors, and mitochondria morphology and function were more evident under the combined ischemia/reperfusion and hyperhomocysteinemia. These changes were, however, alleviated by the addition of inhibitors for CBS, CSE, Hcy, H_2S, and NF-κB, although at different levels. Finally, we observed a negative relationship between the blockage of: (a) the nuclear factor kappa-B pathway and the levels of cystathionine β-synthase and hydrogen sulfide; and (b) the hydrogen sulfide pathway and the levels of inflammatory factors.

Conclusion: Hydrogen sulfide overproduction and reactive inflammatory response are involved in ischemic cerebral injury under hyperhomocysteinemia. Future studies in this direction are warranted to provide a scientific base for targeted medicine development.

Keywords: ischemia, homocysteine, hydrogen sulfide, inflammatory response, mitochondria

OPEN ACCESS

Edited by:
Emmanuel Pinteaux, The University of Manchester, United Kingdom

Reviewed by:
Carla Ines Tasca, Federal University of Santa Catarina, Brazil
Nafisa M. Jadavji, Midwestern University, United States

****Correspondence:***
Yan Ji
jiyannv@126.com
Yusheng Li
yushengli1970@163.com

Specialty section:
This article was submitted to Neuroenergetics, Nutrition and Brain Health, a section of the journal Frontiers in Neuroscience

Received: *13 July 2020*
Accepted: *04 November 2020*
Published: *30 November 2020*

Citation:
Ji Y, Li Y, Zhao Z, Li P and Xie Y (2020) Hydrogen Sulfide Overproduction Is Involved in Acute Ischemic Cerebral Injury Under Hyperhomocysteinemia. Front. Neurosci. 14:582851. doi: 10.3389/fnins.2020.582851

INTRODUCTION

Hydrogen sulfide (H_2S) is an established toxic gas that is characterized by an unpleasant odor of rotten eggs (Wang, 2012). Furthermore, physiological and pathological effects of H_2S as an endogenous signaling molecule have also been described (Fu et al., 2012; Zhang et al., 2015). Indeed, H_2S is identified as the third gaseous transmitter after nitric oxide (NO) and carbon monoxide (CO) (Wang, 2002). Endogenous H_2S is mainly synthesized from both cysteine (Cys) and homocysteine (Hcy), which are catalyzed by the cystathionine β-synthase (CBS) and cystathionine γ-lyase (CSE) enzymes. In fact, Hcy (i.e., an endogenous sulfur-containing amino acid and a metabolite of the essential amino acid methionine), is metabolized by two pathways, namely the methylation and transsulfuration pathways, and the latter is linked to endogenous H_2S formation.

H_2S plays several roles in mammals as a gaseous signal molecule. For example, the activity of the *N*-methyl-D-aspartate (NMDA) receptor, the induction of hippocampal long-term potentiation, the relaxation of vascular smooth muscles and the regulation of blood pressure have been reported to be associated with the physiological concentration of H_2S (Yang et al., 2008; Wang et al., 2015; Tu et al., 2016). Actually, the concentration of H_2S in the mammalian brain is challenging to measure and was reported to vary greatly in previous studies according to the assessment methods utilized (Ishigami et al., 2009; Levitt et al., 2011). In addition, a direct metabolic coupling between H_2S and oxygen (O2) has been described, i.e., while H_2S production is independent from O_2, its metabolism is O_2-dependent. Specifically, although the intracellular H_2S concentration is maintained at low levels through concomitant oxidation, it increases when its oxidation is outbalanced by its production during hypoxia. In fact, permanent occlusion of the middle cerebral artery (MCAO) was shown to increase the endogenous H_2S level in the ipsilateral cortex. This was especially valid for rat that received simultaneous intraperitoneal injection of Cys (Qu et al., 2006). Accumulated evidence also suggests a possible association between the concentration and the effects of H_2S. Specifically, high levels of H_2S are known to cause the generation of both reactive oxygen species (ROS) and reactive nitrogen species (RNS), whereas lower amounts react with hydrogen peroxides (H_2O_2), peroxynitrite ($ONOO^-$), and oxide ion (O^{2-}) (Mikami et al., 2011). In addition, some studies found H_2S to be involved in inflammatory responses (Bhatia, 2012). Specifically, biphasic effects of H_2S on inflammatory signals in murine lipopolysaccharide (LPS)-treated macrophages were reported (Whiteman et al., 2010). Therefore, future studies to better define this relationship are required given the contradictory findings in the literature, i.e., while the administration of sodium hydrosulfide (NaHS, an H_2S donor) significantly increases the infarct volume after MCAO in rats (Ishigami et al., 2009), beneficial effects of H_2S (e.g., decrease in I/R injury and localized inflammatory reaction) can also be observed (Huang et al., 2017). Indeed, the facticity and mechanism associated with the various H_2S effects remain to be defined and future studies should address these questions.

In a previous cohort study, we observed a prominent neurological deficit and poor prognosis in patients with both acute ischemic stroke and elevated levels of plasma Hcy (Ji et al., 2015). Given that these findings urged us to explore the possible pathological mechanism implicated, we performed the present study to observe the effects of different concentration of H_2S on SH-SY5Y cells under oxygen and glucose deprivation (OGD). Furthermore, the changes in H_2S levels, inflammatory factors, energetic metabolism, and cerebral mitochondrial function in rats under I/R alone or a combination of I/R and hyperhomocysteinemia (HHcy) were assessed. Finally, the possible pathologic association between H_2S levels and deteriorated ischemia/reperfusion (I/R) brain injury in patients with HHcy was discussed.

MATERIALS AND METHODS

The study was designed as two approaches: the *in vitro* and *in vivo* studies, and the related experimental process was demonstrated in **Figure 1**.

Antibodies and Reagents

L-methionine, Cys, DL–propargylglycine (PAG), aminooxyacetic acid (AOAA), NaHS, hydroxylamine (HA), *N*-anandamide, and pyrrolidine dithiocarboxylic acid ammonium salt (PDTC) were obtained from Sigma. In contrast, the anti-rabbit horseradish peroxidase (HRP)-conjugated secondary antibodies were purchased from Santa Cruz, whereas the anti-rabbit β-actin antibody and Cytochrome c oxidase IV (COXIV) were developed by Proteintech. In addition, the anti-mouse nuclear factor kappa-B (NF-κB) p65 and glyceraldehyde-3-phosphate dehydrogenase (GAPDH), anti-rabbit histone H3 antibodies were purchased from Abcam, while the anti-rabbit cytochrome C, IkB-alpha (IκBa), P-IκBa and CBS antibodies were obtained from CST. Furthermore, while the primers were procured from Western Biotechnology, the JC-1 mitochondrial membrane potential (MMP), Fluo-3AM (calcium, Ca^{2+}), and ROS assay kits were purchased from BD Biotechnology. The enzyme-linked immunosorbent assay (ELISA) kits for interleukin (IL)-6, -1 and -8 were obtained from Like Beijing, whereas the assay kits for Cys, H_2S, adenosine triphosphate (ATP), and Hcy were acquired from Jiancheng Nanjing. Finally, while the kits for Nuclear and Cytoplasmic Protein Extraction and mitochondria isolation were purchased from Beyotime, those for the mitochondrial permeability transition pore (MPTP) were obtained from GENMED. All drugs were dissolved in saline and administered to rats through intraperitoneal injection.

Animals and Experimental Grouping

Total 135 Male Sprague-Dawley rats (230–260 g) from Chongqing Ensville Biotechnology Co., Ltd. were housed individually with the following conditions: natural light/dark (12/12 h) cycles, temperature of 22–24°C, either normal food or food with 1.7% methionine were provided, and water was available *ad libitum* for 4 weeks. All procedures were reviewed and approved by the Institutional Animal Care and Use

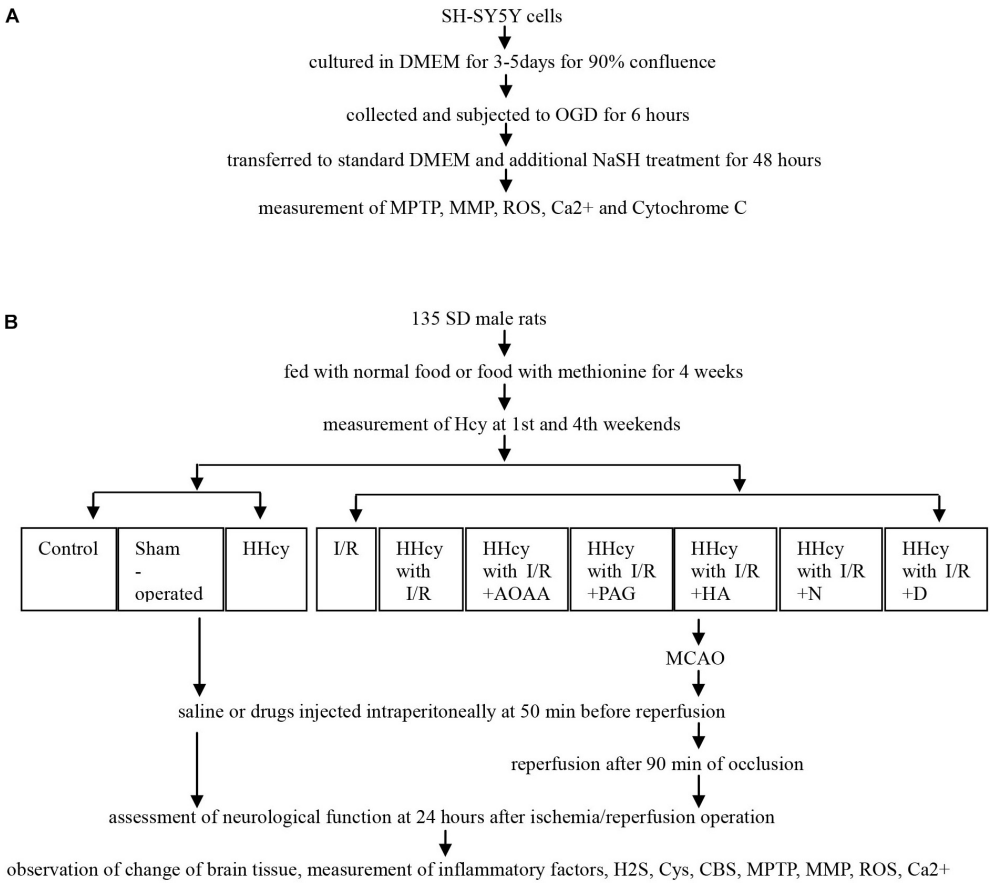

FIGURE 1 | Flowchart of experimental process. **(A)** SY5Y cells were cultured and subjected to OGD and different NaSH treatment, and then collected to measurement of MPTP, MMP, ROS, Ca^{2+} and Cytochorme C. **(B)** SD males fed using normal food or food with methionine were divided into ten groups, and received MCAO or not, saline or inhibitor injected intraperitoneally, and finally assessed for neurological function, morphological change and cytokines levels. *HHcy, hyperhomocysteinemia; I/R, ischemia/reperfusion; AOAA, aminooxyacetic acid; PAG, DL-propargylglycine; HA, hydroxylamine; N, N-anandamide; D, Pyrrolidine dithiocarboxylic acid ammonium salt.

Committee of the University of Zhengzhou, School of Medicine in accord with Animal Care and Use Program Guidelines of the National Institutes of Health. Rats were randomly assigned to the following groups in **Table 1**.

Cells Culture and Treatment

SH-SY5Y neuroblastoma cells were purchased from the Shanghai Cell Bank of the Chinese Academy of Sciences. Successively, they were cultured in high glucose Dulbecco's Modified Eagle Medium (DMEM), supplemented with 10% fetal bovine serum (FBS) and 1% of a penicillin-streptomycin stock, at 37°C in humidified air containing 5% carbon dioxide (CO_2). The serum- and glucose-free DMEM was bubbled with a mixture of 95% nitrogen (N_2) and 5% CO_2 for 30 min and an anaerobic acrylic jar was supplied with the same gas for 6 min. Thereafter, the cells were incubated in the DMEM and then were placed in the jar. The jar was sealed rapidly afterward and placed in an incubator at 37°C. Finally, following 6 h of OGD, the cells were transferred to standard culture conditions and subjected to either a 0, 100, 500, 1,000, or 1,500 μmol/L additional NaSH treatment for 48 h.

I/R Operation and Neurological Function Assessment

Transient brain ischemia was induced through MCAO, as previously described (Zan et al., 2014). In brief, rats were anesthetized with 7% chloral hydrate (0.5 ml/100 g), while their core temperature was maintained at 36.5–37.5°C through a temperature controller pad during the surgery. Following the separation of the right carotid artery from the surrounding tissue, a 3–0 monofilament nylon suture was advanced from the external into the internal carotid artery, until the origin of the middle cerebral artery was blocked. After 90 min of occlusion, the suture was withdrawn to restore blood flow, while either saline or drugs were injected intraperitoneally at 50 min before reperfusion. The wound was then sutured, and rats were allowed to recover from anesthesia before returning to their cages. While sham-operated rats underwent the same procedure, arterial occlusion was not conducted. Animals that died prematurely were excluded from the study. The Zea Longa scale was used for independently evaluating the neurological deficit of rats at 24 h after the operation by two researchers.

TABLE 1 | The detailed data of experiment groups of SDA rats.

Group	*n*	Food	Operation	Treatment
C (control group)	10	Normal	No	Saline (1 ml/kg)
S (sham-operated group)	10	Normal	Sham-operated	Saline (1 ml/kg)
I/R (ischemia/reperfusion group)	15	Normal	I/R operation	Saline (1 ml/kg)
H (HHcy group)	10	Methionine	No	Saline (1 ml/kg)
HI/R (HHcy with I/R)	15	Methionine	I/R operation	Saline (1 ml/kg)
A (HI/R + AOAA group)	15	Methionine	I/R operation	AOAA (1 ml/kg, 10 mg/1 ml)
P (HI/R + PAG group)	15	Methionine	I/R operation	PAG (1 ml/kg, 45 mg/1 ml)
O (HI/R + HA group)	15	Methionine	I/R operation	HA (1 ml/kg, 12.5 mg/1 ml)
N (HI/R + *N*-anandamide group)	15	Methionine	I/R operation	*N*-anandamide (1 ml/kg, 0.2 mg/1 ml)
D (HI/R + PDTC group)	15	Methionine	I/R operation	PDTC (1 ml/kg, 150 mg/1 ml)

HHcy, hyperhomocysteinemia; AOAA, aminooxyacetic acid; PAG, DL*–propargylglycine; HA, hydroxylamine; PDTC, pyrrolidine dithiocarboxylic acid ammonium salt.*

Measurement of Water Content and Infarct Size of Brain Tissue

Rats were decapitated and the whole brain tissue was obtained 24 h after operation. Thereafter, the cerebral tissue was isolated from the olfactory bulb, cerebellum and brainstem, and weighed by an electronic analytical balance (i.e., wet weight). Successively, brain tissues were dried at 65°C for 36–72 h to a constant quality (i.e., the difference between two weighings is less than 1%) in an oven and weighed again (i.e., dry weight). Finally, the brain water content was calculated as the ratio of wet over dry weight.

Similarly, after obtaining the cerebral tissue, coronal sections (2 mm) were prepared. Briefly, they were stored for 5 min in a freezer at −80°C and were then stained with a 1% 2,3,5-triphenyltetrazolium chloride (TTC) solution at 37°C for 15 min. Thereafter, they were fixed using 4% formaldehyde for 24 h and photographed with a digital camera. While the infarct size was traced and quantified with the ImageJ software (National Institutes of Health, Bethesda, MD, United States), it was expressed as a percentage of the bilateral hemisphere.

Transmission Electron Microscope (TEM) Observation for Mitochondrial Morphology

Cerebral tissues were fixed using 2.5% glutaraldehyde for 24 h and then sliced into fragments of 1 mm^3 in size. Subsequently, they were fixed, dehydrated, embedded, cut into 1 μm-thick slices and further dried. Thereafter, they were sliced into ultraslices of 50 nm and finally stained with both uranyl acetate and lead citra to observe the changes in mitochondrial morphology using a transmission electron microscope (TEM) (PHILIPS Tecani-10).

Western Blot for Cytochrome C, IκBa, p-IκBa, NF-κB, and CBS Protein Levels

SH-SY5Y cells were cultured as abovementioned, and then were collected and washed in an ice-cold phosphate buffer saline (PBS). Cell mitochondria were isolated according to the manufacturer's protocol on the mitochondria isolation Kit for measuring cytochrome C protein level in both the mitochondria and cytoplasm separately.

Brain tissues were cut into tiny fragments and put into the homogenate tube, together with 1 ml of RIPA per 100 mg of tissue. The tissues were then homogenized for 20 times and transferred into a centrifuge tube (1.5 ml). Thereafter, the supernatant was collected after a 10 min-long centrifugation (12,000 rpm) at 4°C. To measure the NF-κB protein level, nuclear and cytoplasmic proteins were separately extracted, according to the manufacturer's protocol on the Nuclear and Cytoplasmic Protein Extraction Kit.

Protein concentration was measured using the Bradford assay. Briefly, equal amounts of protein (30 μg) per lane were separated through a 12% sodium dodecyl sulfate–polyacrylamide gel electrophoresis and then transferred onto polyvinylidene difluoride membranes. Thereafter, membranes were incubated with the rabbit anti-cytochrome C (1:2000), rabbit anti-IκBa (1:500), rabbit anti-p-IκBa (1:500), rabbit anti- NF-κB (1:500), rabbit anti-CBS (1:500), goat anti-GAPDH (1:1000), mouse anti-histone H3 (1:1000), rabbit anti-COXIV (1:1000) and rabbit anti-β-actin (1:2000) antibodies at 4°C overnight. This was followed by incubation with secondary antibodies for 2 h at room temperature. Finally, blots were scanned with a light/ultraviolet gel scanning system (Tannon-4200, China) and quantified with an analytic soft system (Labworks^{TM} Analysis Software, United States). Protein levels were normalized to GAPDH, β-actin, COXIV and histone H3.

Measurement of Hcy, IL-1,-6, -8, H_2S, Cys, and ATP Levels in Brain Tissue

Both a plasma sample from the angular vein and a cerebrospinal fluid sample were obtained from rats that received either normal food or food with methionine after 12 h of fasting at the 1st and the 4th weekends. While a capillary tube was rotated into rats' angular vein to obtain the blood samples, cerebrospinal fluid samples were drained from the foramen magnum (exposed through an operation) after rats were anesthetized. The Hcy levels were measured using Hcy assay kits, according to the manufacturer's instructions.

Brain tissue samples were kept in liquid nitrogen, thawed and then added to PBS in a 1:9 ratio. Thereafter, samples were homogenized and centrifuged at 2,000 rpm for 20 min. The

supernatant was then carefully collected and the IL-1, -6, and -8 levels were determined using ELISA analysis kits. Tissues were homogenized as mentioned above. To measure H_2S levels, samples were centrifuged (12,000 rpm) at 4°C for 10 min and the supernatant was collected. Thereafter, levels of H_2S were determined using the H_2S assay kit. In contrast, samples were centrifuged (8,000 rpm) at 4°C for 10 min to assess Cys levels. Subsequently, the supernatant was collected and Cys levels were determined using the Cys Assay Kit. Finally, ATP levels were measured. Samples were boiled in water for 10 min, they were then mixed and extracted for 1 min. This was followed by centrifugation at 3,500 rpm for 10 min and collection of the supernatant. ATP levels were assessed using the ATP Assay Kit (Colorimetric). All procedures followed the manufacturer's instructions on the reagent kits.

Real-Time Polymerase Chain Reaction (RT-PCR) for CBS mRNA

Brain tissues were cut into tiny fragments and mixed with 1 ml of TRIzol reagent (Beyotime) per 100 mg of tissue. They were then homogenized, dissolved and centrifuged (12,000 rpm) at 4°C for 10 min. Thereafter, the supernatant was collected and added to 0.2 ml of chloroform (Shanghai Chemical Reagent Company). Subsequently, the suspension was centrifuged at 10,000 rpm at 4°C for 10 min and the supernatant was then discarded, and the RNA pellet was washed in 75% ethanol and re-suspended in RNAase-free water. The RNA quantity and integrity were verified by agarose gel electrophoresis. In addition, RNA to cDNA reverse transcription was performed on 1 μg of total RNAs using the iScript Reverse Transcription reagent (Western Biotechnology). Successively, quantitative PCR was performed using the Funglyn Biotech Real Time PCR System (Funglyn Biotech, Canada). To determine the cycle threshold (CT) values for CBS and β-actin, SYBR green PCR reagents (Western Biotechnology) were used. Thereafter, a 35× amplification was performed for 4 min, 20 and 30 s at 94, 94, and 72°C, respectively. β-actin was used as an internal control to normalize mRNA abundance. The sequence of oligonucleotides used for RT-PCR was the following: (a) CBS, sense: CCCACCAACGCCAGATTC and antisense: TGCGGTGTCATCGTAGTGC; and (b) β-actin, sense: CCCATCTATGAGGGTTACGC and antisense: TTTAATGTCACGCACGATTTC. During PCR amplification, the amplified products were continuously measured through the determination of their fluorescence emission. All the gene expression data relative to the PCRs were analyzed using the $2^{-\Delta\Delta Ct}$ method and normalized to the β-actin RNA.

Assessment of MPTP, ROS, Ca^{2+} and MMP Levels

SH-SY5Y cells were cultured and treated as mentioned above, washed with cleaning solution, then added 500 μl of dying working solution and incubated for 20 min at 37°C according to the protocol on the MPTP assay kit. Finally, cells were observed using an inverted fluorescence microscope (BM, China).

Rats were decapitated and whole brain tissues were obtained 24 h after I/R operation. Following a PBS wash, a blot of cerebral tissue (100 mg) was cut into tiny fragments and mitochondria were obtained using the Tissue Mitochondria Isolation Kit, according to the manufacturer's protocol. Thereafter, mitochondria were washed with PBS (twice) and centrifuged at 1,500 rpm at 4°C for 5 min. After collecting the supernatant, 200 μl of dying working solution was added and mitochondria were incubated for 30 min at 37°C. Subsequently, they were again washed with PBS (twice) and re-suspended for measuring the mitochondrial permeability transition pore (MPTP) by flow cytometry (CytoFlex, United States).

SH-SY5Y cells and brain tissues were prepared as mentioned above. The cell suspension solution was poured into a centrifuge tube (1.5 ml) and centrifuged (1,500 rpm) at 4°C for 5 min. After collecting the supernatant, the solution was re-suspended in PBS and incubated with a fluorescent probe of DCFH-DA, according to the manufacturer's protocol on the ROS Assay Kit. Finally, the solution was measured using flow cytometry (BD, United States) to determine the ROS levels.

Similarly, the cell suspension solution were incubated with a fluorescent probe, Fluo-3, according to the manufacturer's protocol on the Fluo-3 AM kit, and measured using flow cytometry (BD, United States) to determine the Ca^{2+} levels.

Furthermore, cell suspension was prepared as previously mentioned, then incubated with the JC-1 working solution, washed with the JC-1 staining buffer and resuspended in the JC-1 staining buffer, according to the manufacturer's protocol on the JC-1 MMP Assay Kit. Finally, cells suspension was measured using flow cytometry (BD, United States) to determine the MMP levels.

Statistical Analysis

All experiments were independently performed in triplicates. Data were summarized by means and standard errors (standard error of the mean; SEM). A one-way ANOVA test, followed by Bonferroni *post hoc* testing, was used to compare groups of three or more. Independent *t*-tests were used for two-group comparisons. *P*-values less than 0.05 were considered statistically significant. All statistical analyses were conducted using SPSS 17.0 (SPSS Inc.).

RESULTS

Changes in SH-SY5Y Cells Under the OGD and NaSH Treatment

In vitro part, SH-SY5Y cells simultaneously were subjected to OGD and different concentrations of NaSH treatment. Next, they were collected for assessment of the related protein level, changes in mitochondria and energy metabolism.

Statistical analyses showed significant difference of MMP levels in SH-SY5Y cells among experimental groups [$F(4,10) = 581.68$, $P < 0.000$]. *Post hoc* testing showed obviously decreased MMP levels in cells subjected to OGD and 1,500 μM of NaSH as opposed to cells treated with OGD alone ($P < 0.01$) (**Figure 2A**).

Significant difference of Ca^{2+} levels existed among experimental groups [$F(4,10) = 30.370$, $P < 0.000$]. Compare to

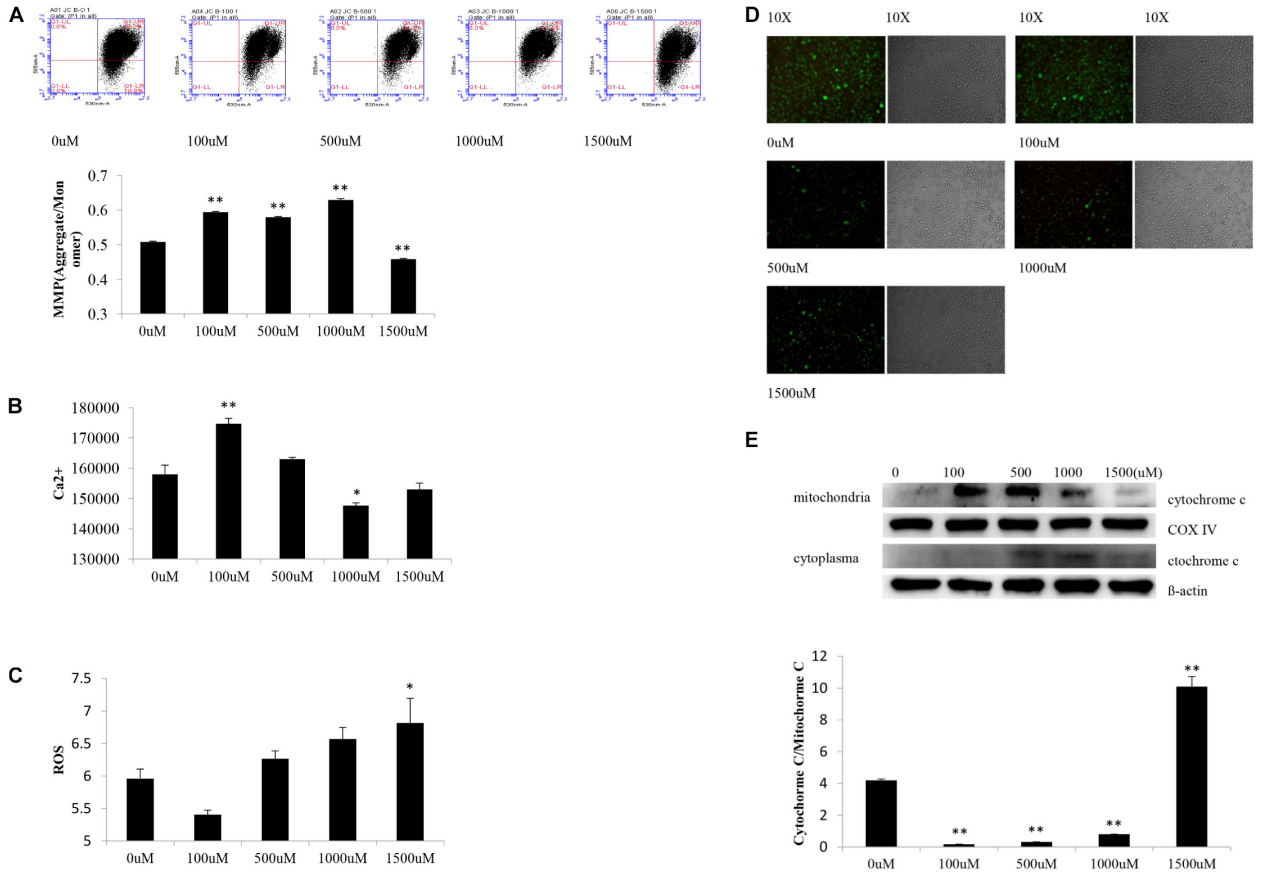

FIGURE 2 | Changes of SY5Y cells subjected to OGD and different concentration NaSH treatment. **(A)** Compared to OGD group, increased MMP levels appeared in cells subjected to OGD and 100, 500, and 1,000 μM NaSH treatment, and decreased MMP levels appeared in cells subjected to 1,500 μM treatment ($n = 3$, $P < 0.01$). **(B)** Compared to OGD group, increased Ca^{2+} levels appeared in OGD and 100 μM of NaSH treatment group ($P < 0.01$) while decreased Ca^{2+} levels appeared in OGD and 1,000 μM of NaSH treated ones ($n = 3$, $P < 0.05$). **(C)** Increased ROS levels appeared in cells subjected to OGD and 1,500 μM treatment compared to OGD group ($n = 3$, $P < 0.05$). **(D)** Compared to OGD group, immunofluorescence showed similar green fluorescence in cells subjected to OGD and 100 μM NaSH treatment, while lower green fluorescence in cells subjected to OGD and 500, 1,000, and 1,500 μM NaSH treatment. **(E)** Compared to OGD group, increased cytochrome C release appeared in cells subjected to OGD and 1,500 μM treatment but decreased in cells subjected to OGD and 100, 500, and 1,000 μM treatment as well ($n = 3$, $P < 0.01$). $^{**}P < 0.01$, $^{*}P < 0.05$, analyzed by one-way ANOVA and Bonferroni *post hoc* test.

cells subjected to OGD alone, increased Ca^{2+} levels appeared in OGD and 100 μM of NaSH treated cells ($P < 0.01$) while decreased Ca^{2+} levels appeared in OGD and 1,000 μM of NaSH treated ones ($P < 0.05$) (**Figure 2B**).

There were significant difference of ROS levels among experimental groups [$F(4,10) = 6.841$, $P < 0.01$]. As opposed to cells subjected to OGD alone, ROS levels increased in cells treated with both OGD and 1,500 μM of NaSH ($P < 0.05$) (**Figure 2C**).

Different appearance of green fluorescence existed among experimental groups. Compared to cells subjected to OGD alone, cells treated with OGD and 500, 1,000, or 1,500 μM of NaSH showed lower green fluorescence (higher MPTP level) while cells treated with OGD and 100 μM of NaSH showed similar green fluorescence (similar MPTP level) (**Figure 2D**).

There were significant difference of cytochrome C release in SH-SY5Y cells among experimental groups [$F(4,10) = 9.238$, $P < 0.01$]. Compared to cells treated with OGD alone, increased translocation of cytochrome C existed in cells subjected to OGD and 1,500 μM of NaSH ($P < 0.01$) but decreased translocation of cytochrome C in OGD and 100, 5,00, and 1,000 μM of NaSH treated cells ($P < 0.01$) (**Figure 2E**).

Neurological Function Change of Experimental Rats

Total 10 groups of rats were included in the *in vivo* part. Specifically, 105 rats were divided into 7 groups and all received I/R operation. Of these, 8 were excluded from our analysis due to a failure of I/R operation. Additional 10 rats were recruited for each of the other 3 groups. Only one group (i.e., 10 rats) received the sham-operation, and all rats survived. As a result, a total of 127 rats were considered for analysis.

The assessment of rats' neurological function according to Zea Longa scores was performed by 2 independent investigators 24 h after I/R operation. Zea Longa scores were identified under 5-scores grades. The detail was as following: zero point

means no neurological impairment, one point means a failure of complete stretch of leg, two points means leg bucking, three points means turning to one side slightly in walking, four points means turning to one side severely in walking, five points means falling to one side in walking. Statistical analyses showed significant difference of Zea Longa scores among experimental groups [$F(9,90) = 46.150$, $P < 0.000$], and *post hoc* testing showed significantly higher scores in both the I/R and HI/R groups compared to all other groups ($P < 0.01$), and decreased by all inhibitors ($P < 0.01$) (**Figure 3A**).

Comparison of Brain Water Content and Infarct Size in Experimental Rats

Significant difference of brain water content existed among experimental groups [$F(9,20) = 20.794$, $P < 0.000$], and *post hoc* testing showed a significantly higher water content in the I/R group and HI/R group compared to the C group, especially in the latter ($P < 0.01$). Furthermore, the water content decreased significantly in the A, P, O, and D groups, as opposed to the HI/R group ($P < 0.05$ or 0.01) (**Figure 3B**). TTC staining showed cerebral infarctions in rats that received I/R operation. Statistical analyses showed significant difference of infarction size among experimental groups [$F(6,14) = 358.431$, $P < 0.000$], and *post hoc* testing showed the first and second largest infarction size of cerebrum tissue in the HI/R and I/R groups, respectively ($P < 0.01$), whereas the A, P, O, N, and D groups was obviously lower ($P < 0.01$) (**Figure 3C**).

Changes in Mitochondrial Morphology of Brain Tissue

Transmission electron microscope were used to observe changes in mitochondrial morphology. As a result, the C and S groups presented a clear myelin sheath and nuclear membrane, as well as abundant round or oval mitochondria with clear crista in the cytoplasm of the cerebral tissue. In contrast, a partly impaired myelin sheath and irregular nuclear membrane were observed in the H group, even though the mitochondria remained unchanged. The morphological change was most evident in the HI/R group, which demonstrated severe edema, vague crista, partial vacuolization, a destroyed myelin sheath, the disappearance of the nuclear membrane and a decrease in organelles. Similar changes, even though to a lesser extent, were also seen in the I/R group. Finally, fewer changes were observed in the A, P, O, N, and D groups (**Figure 4**).

Change of Inflammatory Factors in Experimental Rats

Statistical analyses showed significant difference of IκBα levels among experimental groups [$F(9,20) = 134.199$, $P < 0.000$], and *post hoc* testing demonstrated significantly decreased IκBα levels in all other groups, compared to the C group ($P < 0.05$ or 0.01). Specifically, the first and second lowest IκBα levels were observed in the HI/R and I/R groups, respectively, and increased by all inhibitors ($P < 0.05$ or 0.01) (**Figure 5A**). With regards to the p-IκBα levels, significant difference existed among experimental groups [$F(9,20) = 113.955$, $P < 0.000$], and *post hoc* testing showed the first and second highest levels in the HI/R and I/R groups, respectively ($P < 0.01$). Significant decrease appeared in all inhibitor groups compared to the HI/R group, but only appeared in A, P, O, and D groups as opposed to the I/R group ($P < 0.05$ or 0.01) (**Figure 5B**). The western blot bands of IκBα and p-IκBα are displayed in **Figure 5C**. There were significant

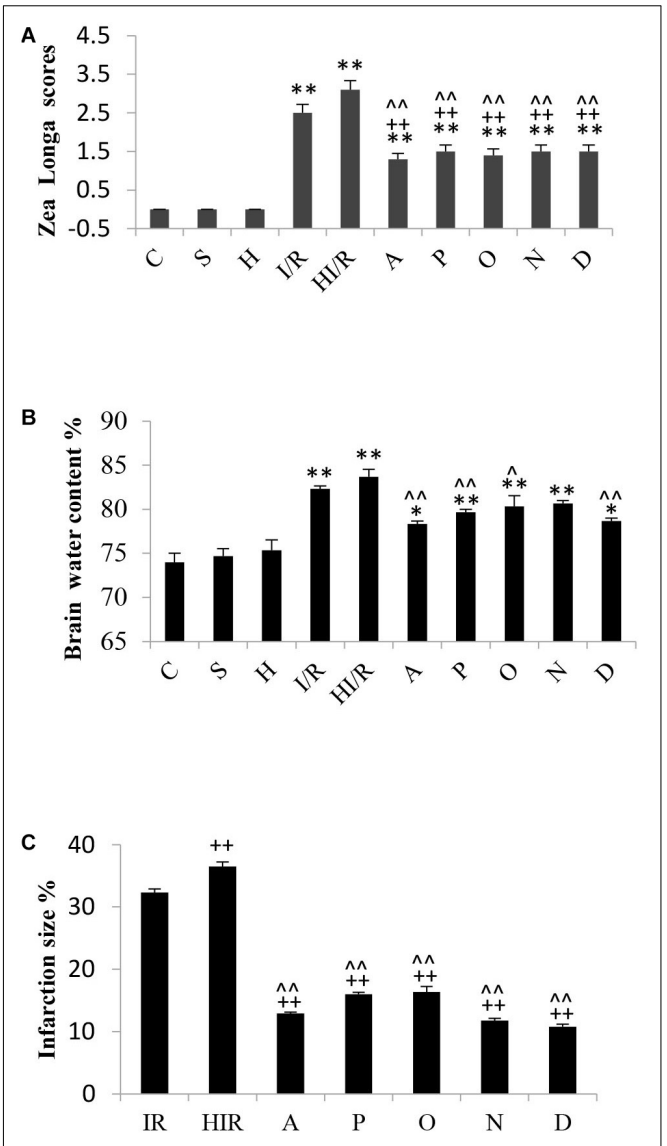

FIGURE 3 | Changes of brain tissue and neurological function in rats 24 h after I/R or not. **(A)** A significant increase of Zea Longa scores appeared in I/R and HI/R groups compared to control groups, especially in the latter, and decreased by all inhibitors ($n = 10$, $P < 0.01$). **(B)** The water content of brain tissue increased evidently in I/R and HI/R groups compared to control groups ($P < 0.01$), and decreased in A, P, O, and D groups when compared to HI/R group ($n = 3$, $P < 0.05$ or 0.01). **(C)** The infarction size of cerebrum tissue in HI/R or I/R group was the first and second largest, separately, and decreased by all inhibitors ($n = 3$, $P < 0.01$). ** or * means $P < 0.01$ or 0.05 versus control, $^{++}$or $^{+}$ means $P < 0.01$ or 0.05 versus I/R group, and ^^ or ^ means $P < 0.01$ or 0.05 versus HI/R group, analyzed by one-way ANOVA and Bonferroni *post hoc* test.

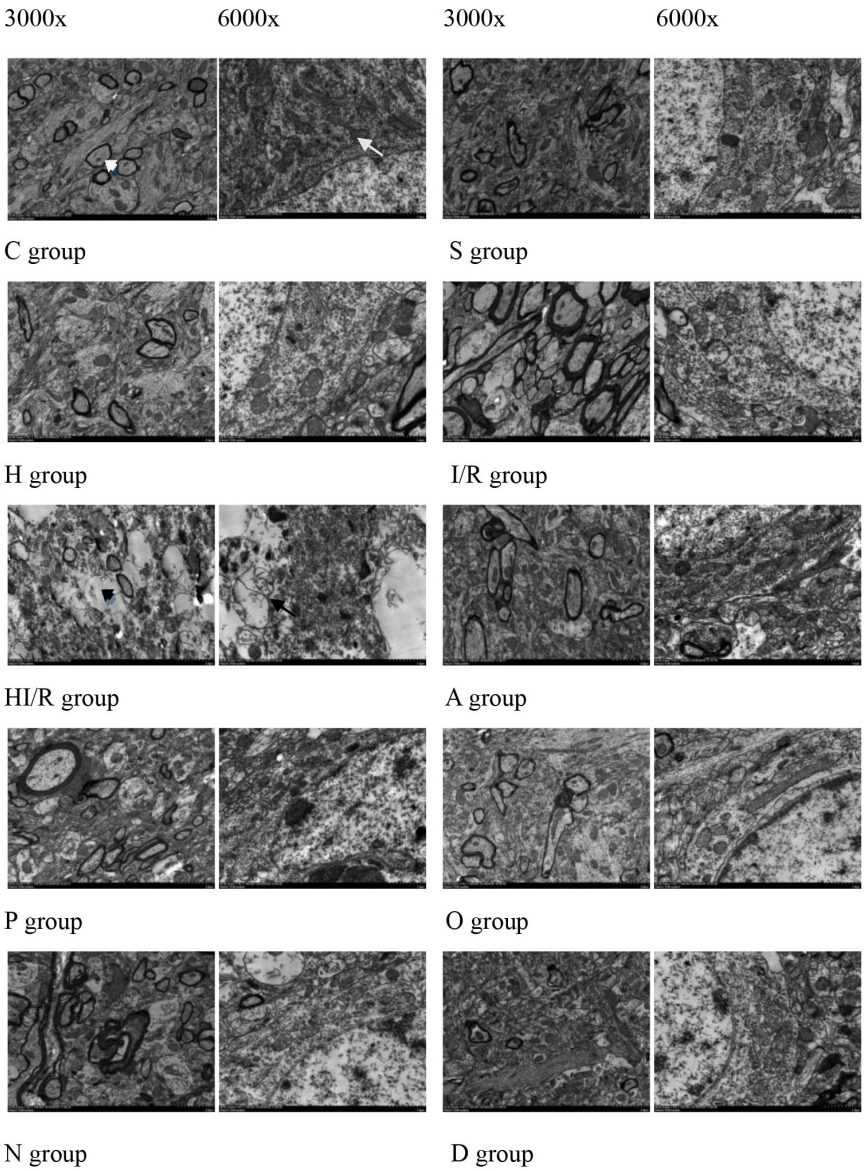

FIGURE 4 | Morphology of cell, myelin sheath, nuclear membrane and mitochondria of brain tissue of the rats 24 h after I/R or not. Abundant round or oval mitochondrial (arrowheads) and clear crista (arrows), myelin sheath and nuclear membrane appeared in the rats of control (C) and sham operated groups (S). Partly impairment of myelin sheath and irregularity of nuclear membrane appeared in H group (H). Myelin sheath destroyed, nuclear membrane disappeared (black arrows), and organelle (black arrowheads) decreased in the rats received I/R, especially I/R combined with HHcy (HI/R). Evident impaired but lesser morphological change in inhibitor groups (A, P, O, N, and D).

difference of NF-κB translocation among experimental groups [$F(9,20) = 1040.637$, $P < 0.000$], and *post hoc* testing showed higher translocation in the I/R and HI/R groups ($P < 0.01$), and decreased by all inhibitors ($P < 0.01$) (**Figure 5D**). The blot bands of NF-κB are demonstrated in **Figure 5D**. Finally, significant difference of the IL-1, IL-6, and IL-8 levels existed among experimental groups [$F(9,20) = 16900.86$, 17695.045, and 336.312, respectively, $P < 0.000$], and *post hoc* testing showed significant increase in the IL-1, IL-6, and IL-8 levels in all groups compared to C group ($P < 0.000$). The highest level was observed in the HI/R group, which was closely followed by the I/R group ($P < 0.000$), and evidently decreased in A, P, O, and D groups ($P < 0.01$) (**Figure 5E**).

Change of Hcy and H_2S Pathway in Experimental Rats

Significant difference of Hcy levels in plasma and cerebrospinal fluid existed among experimental groups [$F(3,16) = 527.566$ and 1563.3, respectively, $P < 0.000$], and *post hoc* testing showed significantly higher Hcy levels in the rats received food with methionine than those fed with normal food ($P < 0.01$)

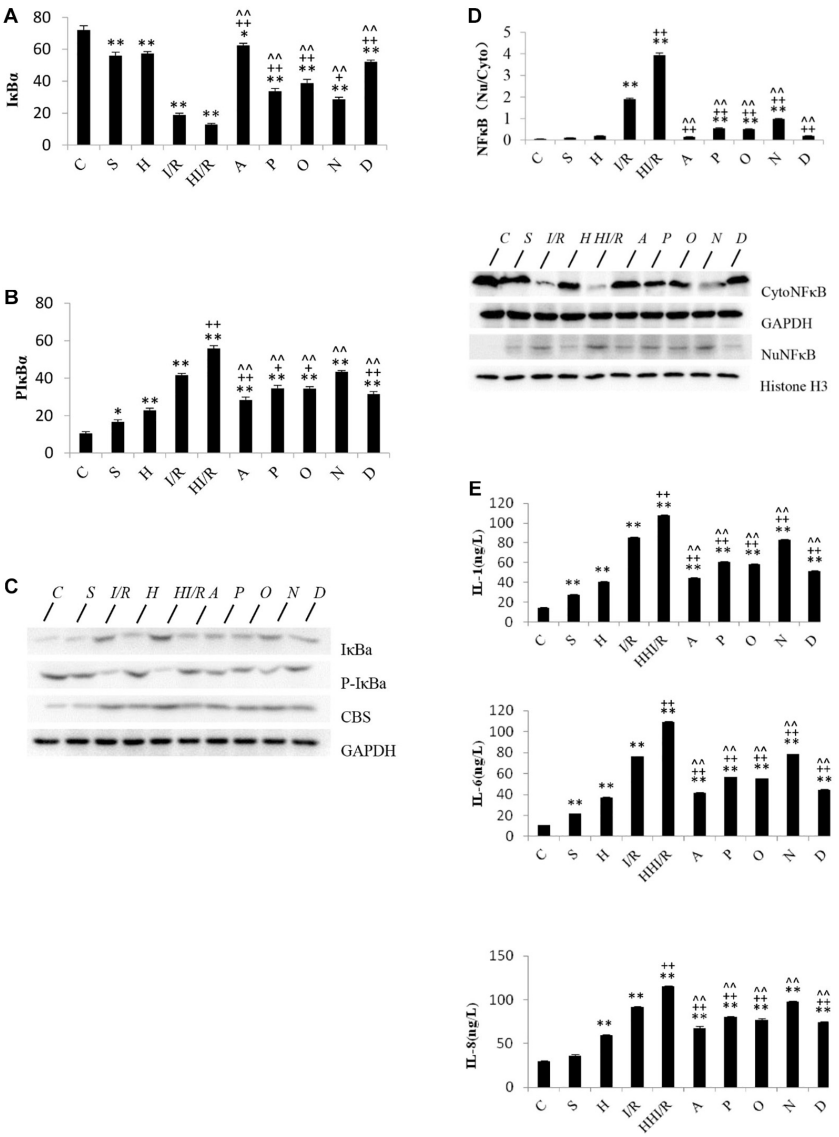

FIGURE 5 | Changes of IκBα, p-IκBα, and NFκB translocation, IL-1, IL-6, and IL-8 levels in cerebrum tissue in rats 24 h after I/R or not. **(A)** IκBα levels decreased significantly in all other groups, compared to the C group ($P < 0.05$ or 0.01). The first and second lowest IκBα levels appeared in the HI/R and I/R groups, respectively ($P < 0.01$), and increased by all inhibitors ($n = 3$, $P < 0.05$ or 0.01). **(B)** The first and second lowest P-IκBα levels appeared in the HI/R and I/R groups, respectively ($P < 0.01$). Significant decrease of p-IκBα levels appeared in all inhibitor groups than in the HI/R group, but appeared in A, P, O, and D groups when compared to the I/R group ($n = 3$, $P < 0.05$ or 0.01). **(C)** The blot band demonstrated changes of IκBα, p-IκBα, and CBS protein levels in each group. GAPDH was used as normalized protein. **(D)** Translocation of NFκB levels into nuclear evidently increased in I/R and HI/R groups compared to control group, and decreased by all inhibitors ($n = 3$, $P < 0.01$). The blot band showed changes of Cyto NFκB and Nu NFκB protein levels in each group. GAPDH and Histone H3 were used as normalized protein, separately. **(E)** The IL-1, IL-6, and IL-8 levels in I/R and HI/R groups significantly increased compared to control groups, especially in the latter, and evidently decreased in A, P, O, and D groups than that in HI/R group and I/R group ($n = 3$, $P < 0.01$). ** or * means $P < 0.01$ or 0.05 versus control, $^{++}$or $^{+}$ means $P < 0.01$ or 0.05 versus I/R group, and ^^ or ^ means $P < 0.01$ or 0.05 versus HI/R group, analyzed by one-way ANOVA and Bonferroni *post hoc* test.

(**Figure 6A**). As far as Cys levels, significant difference existed among experimental groups [$F(9,20) = 1017.961$, $P < 0.000$], and *post hoc* testing showed the lowest concentration in the C group, whereas the HI/R, I/R and H groups had the top three highest levels, respectively ($P < 0.000$). Compared to HI/R group and I/R group, Cys levels evidently decreased in all inhibitor groups ($P < 0.01$) (**Figure 6B**). There were significant difference of CBS levels among experimental groups [$F(9,20) = 183.349$, $P < 0.000$], and *post hoc* testing showed CBS levels in I/R and HI/R groups significantly increased compared to the control group, especially in the latter ($P < 0.01$), and evidently decreased in all inhibitors than in HI/R group but only in A, P, O, and D groups as opposed to I/R group ($P < 0.05$ or 0.01) (**Figure 6C**). Significant difference of CBS mRNA levels existed among experimental groups [$F(9,20) = 32.116$, $P < 0.000$], and *post hoc* testing demonstrated higher CBS mRNA levels appeared in I/R and HI/R

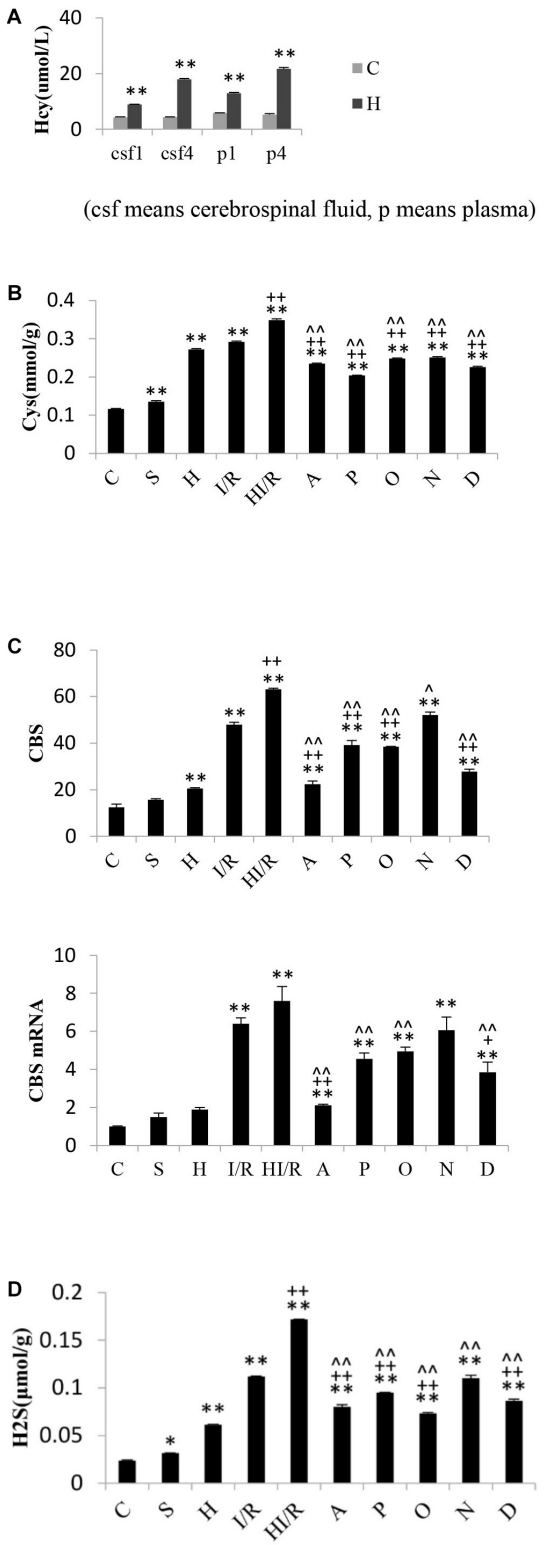

FIGURE 6 | Changes of Hcy levels in rats fed for one and 4 weeks, and Cys, CBS, and H_2S levels in rats 24 h after I/R or not. **(A)** Hcy levels in plasma and cerebrospinal fluid of rats received normal food or food added methionine for 1 week or 4 weeks. A higher Hcy level appeared in H group than that in C group ($n = 5$, $P < 0.01$). **(B)** Cys levels in I/R and HI/R groups significantly increased compared to C group, especially in the latter ($P < 0.01$), and evidently decreased in A, P, O, N, and D groups than that in HI/R group and I/R group ($n = 3$, $P < 0.01$). **(C)** CBS levels in I/R and HI/R groups significantly increased compared to control groups, especially in the latter ($P < 0.01$), and evidently decreased in A, P, O, and D groups than that in HI/R group and I/R group ($n = 3$, $P < 0.01$). CBS mRNA levels in I/R and HI/R groups significantly increased compared to control groups, especially in the latter ($P < 0.01$), and evidently decreased in A and D groups than that in HI/R group and I/R group ($n = 3$, $P < 0.01$). **(D)** H_2S levels in I/R and HI/R groups significantly increased compared to control groups, especially in the latter, and evidently decreased in A, P, O, and D groups than that in HI/R group and I/R group ($n = 3$, $P < 0.01$). ** or * means $P < 0.01$ or 0.05 versus control, $^{++}$or $^{+}$ means $P < 0.01$ or 0.05 versus I/R group, and ^^or ^ means $P < 0.01$ or 0.05 versus HI/R group, analyzed by one-way ANOVA and Bonferroni *post hoc* test.

groups compared to the control group, especially in the latter ($P < 0.01$), and decreased in A, P, O, and D groups compared to HI/R group but only in A and D groups as opposed to I/R group (**Figure 6C**). The blot band of CBS is listed in **Figure 5C**. Similarly, significant difference of H_2S levels existed among experimental groups [$F(9,20) = 919.121$, $P < 0.000$], and *post hoc* testing showed the first and second highest concentrations in the HI/R and I/R groups, and evidently decreased by all inhibitors than in HI/R group but only in A, P, O, and D groups compared to I/R group ($P < 0.01$) (**Figure 6D**).

Change of Mitochondria Function, ROS and Ca^{2+} Levels in Experimental Rats

Through flow cytometry, the decrease in Calcei-AM, the main component of the MPTP assay kit (i.e., a strong fluorescent agent), means the increase in MPTP can be assessed. As a result, significant difference of concentration of Calcei-AM existed among experimental groups [$F(9,20) = 36.066$, $P < 0.000$], and *post hoc* testing showed evidently lower concentration in the I/R and HI/R groups compared to the control group, and increased concentration in A, P, O, and D groups than in I/R group but only in P, O, and D groups compared to HI/R group ($P < 0.05$ or 0.01) (**Figure 7A**). As far as MMP levels, significant difference existed among experimental groups [$F(9,20) = 4488.385$, $P < 0.000$], and *post hoc* testing showed lower levels in I/R and HI/R groups compared to control groups, especially in the latter, and evidently increased in inhibitors groups than in HI/R group but in A, P, O, and D groups as opposed to I/R group ($P < 0.01$) (**Figure 7B**). Similar change of ATP levels existed among experimental groups [$F(9,20) = 123.192$, $P < 0.000$], and *post hoc* testing showed decreased levels in HI/R group and I/R group ($P < 0.01$) (**Figure 7C**). Significant difference of ROS levels existed among experimental groups [$F(9,20) = 13.75$, $P < 0.000$], and *post hoc* testing showed higher levels in the I/R and HI/R groups than in the C group ($P < 0.01$), and decreased in the A group compared to HI/R group ($P = 0.05$) (**Figure 7D**). With regards to the Ca^{2+} level, significant difference existed among experimental groups [$F(9,20) = 164.582$, $P < 0.000$], and *post hoc* testing found highest level in the HI/R group ($P < 0.01$), followed by the I/R group ($P < 0.01$), and evidently decreased in all inhibitor groups compared to HI/R group and I/R group ($P < 0.01$) (**Figure 7E**).

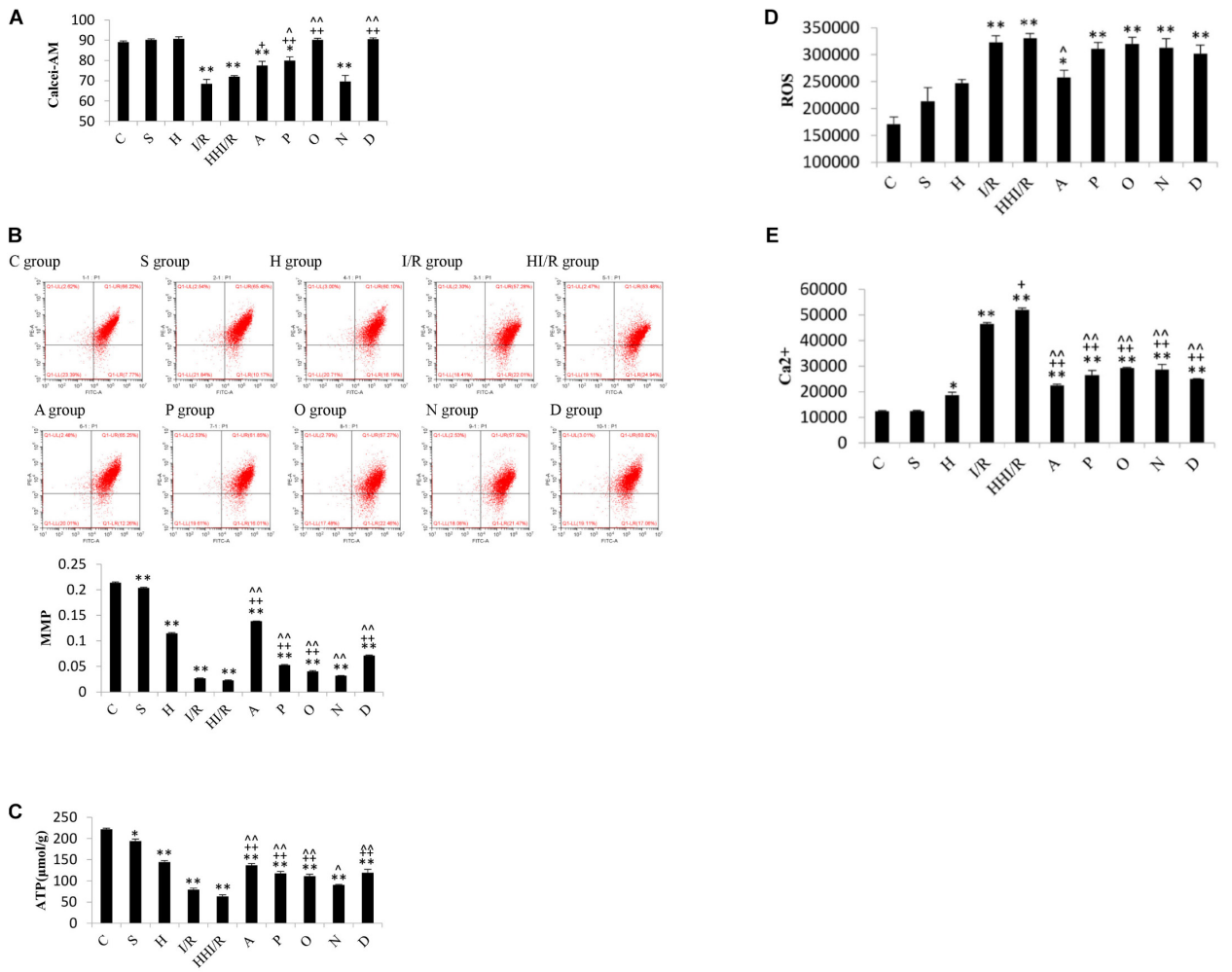

FIGURE 7 | Changes of MPTP, MMP, ATP, ROS, and Ca^{2+} levels in rats 24 h after I/R or not. **(A)** Calcei-AM levels evidently decreased in I/R and HI/R groups compared to control group, and increased significantly by P, O, and D groups (n = 3, $P < 0.05$ or 0.01). **(B)** MMP levels in I/R and HI/R groups significantly decreased compared to control groups, especially in the latter, and evidently increased in A, P, O, and D groups than that in HI/R group and I/R group (n = 3, $P < 0.01$). **(C)** The ATP levels in I/R and HI/R groups significantly decreased compared to control groups, especially in the latter, and evidently increased in A, P, O, and D groups than that in HI/R group and I/R group (n = 3, $P < 0.01$). **(D)** ROS levels increased significantly in I/R or HI/R than that in control groups ($P < 0.01$). **(E)** Ca^{2+} levels in I/R and HI/R groups significantly increased compared to control groups, especially in the latter, and evidently decreased in A, P, O, N, and D groups than that in HI/R group and I/R group (n = 3, $P < 0.01$). ** or * means $P < 0.01$ or 0.05 versus control, $^{++}$or $^{+}$ means $P < 0.01$ or 0.05 versus I/R group, and ^^or ^ means $P < 0.01$ or 0.05 versus HI/R group, analyzed by one-way ANOVA and Bonferroni *post hoc* test.

DISCUSSION

Multiple evidences suggested a definite relationship between elevated plasma Hcy levels and the risk of cardiocerebro-vascular diseases (McCully, 1969; Castro et al., 2006; Maron and Loscalzo, 2009; Ji et al., 2013; Zhao et al., 2017). In a previous study, we observed elevated Hcy levels to be associated with poor prognosis in acute ischemic cerebral infarction patients (Ji et al., 2015). Similarly, various experimental evidences indicated a pathogenic role for Hcy (Kim et al., 1987; Klancnik et al., 1992; Jellinger, 2013; Krishna et al., 2013; Currò et al., 2014; Pushpakumar et al., 2014). A close relationship between HHcy and multiple kinds of neurological diseases has been established. To further explore the effects of HHcy on acute ischemic brain injury and the underlying mechanisms, the present study was performed on OGD plus NaSH-treated SH-SY5Y cells and rat models of I/R and HHcy.

Hcy and Cys are substrates of the CBS and CSE and are thus involved in the endogenous production of H_2S (Griffith, 1987). Although H_2S is the third endogenously produced gasotransmitter and is considered as an important cell signaling molecule, its physiological levels in the body remain to be defined (Goodwin et al., 1989; Warenycia et al., 1989; Savage and Gould, 1990; Han et al., 2006; Ishigami et al., 2009; Levitt et al., 2011). Under the physiologic condition, catabolism of methionine causes an increased Hcy degradation to Cys via the transsulfuration pathway, which spontaneously decomposes and releases H_2S, and then H_2S is rapidly catabolized by the brain tissue (Furne et al., 2008). Therefore, the brain H_2S level

is generally very low at this time. However, the brain H_2S level may increase evidently under pathological condition. In a previous study, Julie et al. observed the anaerobic incubation of brain tissue yielded to higher H_2S release rates than the aerobic incubation at all L-cysteine concentrations (Furne et al., 2008). In the present study, H_2S levels in the brain tissue greatly increased to 110 and 171 nM in the rats under I/R and I/R combined with HHcy, respectively, as opposed to that in control group (24 nM). In concordance, the Cys levels also increased in rats that received either the I/R treatments alone or a combination of I/R and HHcy. To conclude, obvious increases in the H_2S concentration were identified in the brain tissue following an ischemic/reperfusion situation, especially when this was accompanied by an elevated HHcy level.

Several effects associated with H_2S have been reported in the pathophysiological realm. The physiological concentration of H_2S (i.e., low μM) was reported to play cytoprotective effects through the following processes: activation of sarcolemmal KATP channels, activation of the protein kinase C, anti-apoptotic effects and modulation of cellular respiration (Stipanuk et al., 2002). Lower levels of H_2S were identified to stimulate mitochondrial function, whereas higher level were associated with the inhibition of the cytochrome c oxidase, causing the mitochondrial respiration as a state of suspended animation in a dose-dependent manner (Furne et al., 2001; Calvert et al., 2010). Furthermore, supratherapeutic concentrations of H_2S were shown to irreversibly depress mitochondrial respiration, affecting ATP synthesis and further contributing to I/R injury. Previous study found H_2S played both stimulatory and inhibitory effects during the autophagy process (Wang et al., 2017). Its toxic effects are usually observed at relatively high concentrations, i.e., non-physiological levels (high μM to mM), which limits its clinical usefulness for treating patients (Stipanuk et al., 2002). As the dose-response curve of H_2S is bell-shaped, the effects of this compound switch from protective to deleterious based on both the environmental conditions and concentrations (Kumar and Sandhir, 2018). Specifically, while lower concentrations stimulate several physiological processes, including mitochondrial function and antioxidant effects, higher concentrations lead to cell death or other adverse effects.

In the *in vitro* phase of the present study, high concentrations of the NaSH treatment (1,500 μM) were found to cause an increase in the levels of intracellular ROS and MPTP, release of cytochrome C, as well as a decrease in the MMP of SH-SY5Y cells under OGD. In contrast, low concentrations of NaSH treatment (100 μM) appeared beneficial. These reveal high levels of H_2S exacerbate injury to cells under OGD although low levels demonstrate protective effects. *In vivo* phase of the study, the concentrations of H_2S greatly increased in the acute ischemia or when it was combined with HHcy, and the overproduction of H_2S produced a negative impact (Panagaki et al., 2019), such as a worsening in the brain tissue. Specifically, the infarction sizes of the cerebral tissues enlarged, while their water content increased. Furthermore, the energy metabolism of cells was impaired and ATP production decreased. This was followed by Ca^{2+} influx and ROS accumulation. The inflammatory reaction appeared and mitochondrial morphology and function were destroyed. Finally, cytochrome c was released from the mitochondria, which in turn induced cell apoptosis. Such pathological changes were especially obvious in rats that received the combination of I/R and HHcy, suggesting that acute ischemic brain tissue injury deteriorated when it encountered a high Hcy concentration. Higher levels of H_2S probably played a critical role during the pathological process supported by both *in vitro* and *in vivo* works of the study.

To further explore the possible mechanism underlying the involvement of H_2S and HHcy in the acute ischemic injury, we added several inhibitors of CBS, CSE, Hcy, H_2S, and NF-κB to the experimental groups. Specifically, both AOAA and HA were used as antagonists of CBS, whereas PAG was employed as an inhibitor of CSE. In contrast, the *N*-anandamide and PDTC antagonists were aimed for Hcy and NF-κB, respectively. Our results suggested that all inhibitors lessened the neurological function impairment, inflammatory reaction, mitochondria damage and decreased energy metabolism caused by acute ischemia and HHcy. While the AOAA, HA and PAG inhibitors showed obvious effects on the amelioration of the increased CBS, Cys, and H_2S levels in the HHI/R rats, PDTC was more effective on alleviating the release of inflammatory factors. Interestingly, inhibiting CBS, CSE, and Hcy was accompanied by a decrease in inflammatory factors, whereas inhibiting NF-κB was associated with a reduction in the CBS, Cys, and H_2S levels. Therefore, we here propose both the coexistence and interaction of H_2S overproduction and inflammatory factors to be one of the pathological mechanisms underlying the HHI/R process. Furthermore, the AOAA inhibitor was suggested to be extremely useful in modifying both the H_2S overproduction and the inflammatory reaction (Bento et al., 2016). In contrast, the *N*-anandamide inhibitor was less valuable, as it lessened the pathological changes in HHI/R rats only. In addition, mitochondrial function impairment was also involved in the pathological mechanism under HHI/R. In fact, inhibiting NF-κB resulted in a reduction of mitochondrial function impairment in HHI/R rats, whereas blocking either CBS or CSE only partly rectified the impairment. Therefore, it is reasonable to consider that H_2S may indirectly impair mitochondrial function by increasing the inflammatory reaction in the HHI/R condition.

CONCLUSION

To summarize, H_2S overproduction and inflammatory factors are involved in the pathological changes occurring after acute ischemic brain injury and HHcy. Furthermore, mitochondrial dysfunction is also involved in the pathological process. Future studies in this direction are warranted to provide instructive guidance for targeted medicine development.

DATA AVAILABILITY STATEMENT

The original contributions generated for this study are included in the article/supplementary material, further inquiries can be directed to the corresponding authors.

ETHICS STATEMENT

The animal study was reviewed and approved by the Institutional Animal Care and Use Committee of the University of Zhengzhou, School of Medicine.

AUTHOR CONTRIBUTIONS

YJ: conceptualization, methodology, writing – review and editing, project administration, and funding acquisition. YL: supervision, resources, and validation. ZZ: investigation and writing – original draft. PL: formal analysis and investigation. YX: data curation, visualization, and investigation. All authors contributed to the article and approved the submitted version.

FUNDING

This study was funded by Henan Natural Science Foundation, number 162300410297.

REFERENCES

Bento, C. F., Renna, M., Ghislat, G., Puri, C., Ashkenazi, A., Vicinanza, M., et al. (2016). Mammalian autophagy: how does it work? *Annu. Rev. Biochem.* 85, 685–713. doi: 10.1146/annurev-biochem-060815-014556

Bhatia, M. (2012). Role of hydrogen sulfide in the pathology of inflammation. *Scientifica* 2012:159680. doi: 10.6064/2012/159680

Calvert, J. W., Coetzee, W. A., and Lefer, D. J. (2010). Novel insights into hydrogen sulfide–mediated cytoprotection. *Antioxid. Redox Signal.* 12, 1203–1217. doi: 10.1089/ars.2009.2882

Castro, R., Rivera, I., Blom, H. J., Jakobs, C., and Tavares de Almeida, I. (2006). Homocysteine metabolism., hyperhomocysteinaemia and vascular disease: an overview. *J. Inherit. Metab. Dis.* 29, 3–20. doi: 10.1007/s10545-006-0106-5

Currò, M., Gugliandolo, A., Gangemi, C., Risitano, R., Ientile, R., and Caccamo, D. (2014). Toxic effects of mildy elevated homocysteine concnetrations in neuronal-like cells. *Neurochem. Res.* 39, 1485–1495. doi: 10.1007/s11064-014-1338-7

Fu, M., Zhang, W. H., Wu, L. G., Yang, G. D., Li, H. Z., and Wang, R. (2012). Hydrogen sulfide (H2S) metabolism in mitochondria and its regulatory role in energy production. *Proc. Natl. Acad. Sci. U.S.A.* 109, 2943–2948. doi: 10.1073/pnas.1115634109

Furne, J., Saeed, A., and Levitt, M. D. (2008). Whole tissue hydrogen sulfide concentrations are orders of magnitude lower than presently accepted values. *Am. J. Physiol. Regul. Integr. Comp. Physiol.* 295, 1479–1485.

Furne, J., Springfield, J., Koenig, T., DeMaster, E., and Levitt, M. D. (2001). Oxidation of hydrogen sulfide and methanethiol to thiosulfate by rat tissues: a specialized function of the colonic mucosa. *Biochem. Pharmacol.* 62, 255–259. doi: 10.1016/s0006-2952(01)00657-8

Goodwin, L. R., Francom, D., Dieken, F. P., Taylor, J. D., Warenycia, M. W., Reiffenstein, R. J., et al. (1989). Determination of sulfide in brain tissue by gas dialysis/ion chromatography: post-mortem studies and two case reports. *J. Anal. Toxicol.* 13, 105–109. doi: 10.1093/jat/13.2.105

Griffith, O. W. (1987). Mammalian sulfur amino acid metabolism: an overview. *Methods Enzymol.* 143, 366–376. doi: 10.1016/0076-6879(87)43065-6

Han, Y., Qin, J., Chang, X. Z., Yang, Z. X., and Du, J. B. (2006). Hydrogen sulfide and carbon monoxide are in synergy with each other in the pathogenesis of recurrent febrile seizures. *Cell. Mol. Neurobiol.* 26, 101–107. doi: 10.1007/s10571-006-8848-z

Huang, X., Li, Y. B., Li, P., Li, J. P., Bao, H. H., Zhang, Y., et al. (2017). Association between percent decline in serum total homocysteine and risk of first stroke. *Neurology* 89, 2101–2107. doi: 10.1212/WNL.0000000000004648

Ishigami, M., Hiraki, K., Umemura, K., Ogasawara, Y., Ishii, K., and Kimura, H. (2009). A source of hydrogen sulfide and a mechanism of its release in the brain. *Antioxid. Redox Signal.* 11, 205–214. doi: 10.1089/ARS.2008.2132

Jellinger, K. A. (2013). Pathology and pathogenesis of vascular cognitive impairment-a critical update. *Front. Aging Neurosci.* 5:17. doi: 10.3389/fnagi.2013.00017

Ji, Y., Song, B., Xu, Y. M., Fang, H., Wu, J., Sun, S. L., et al. (2015). Prognostic significance of homocysteine levels in acute ischemic stroke: a prospective cohort Study. *Curr. Neurovasc. Res.* 12, 334–340. doi: 10.2174/1567202612666150807112205

Ji, Y., Tan, S., Xu, Y. M., Chandra, A., Shi, C. H., Song, B., et al. (2013). Vitamin B supplementation., homocysteine levels., and the risk of cerebrovascular disease: a meta-analysis. *Neurology* 81, 1298–1307. doi: 10.1212/wnl.0b013e3182a823cc

Kim, J. P., Koh, J. Y., and Choi, D. W. (1987). L-homocysteate is a potent neurotoxin on cultured cortical neurons. *Brain Res.* 437, 103–110. doi: 10.1016/0006-8993(87)91531-9

Klancnik, J. M., Cuénod, M., Gähwiler, B. H., Jiang, Z. P., and Do, K. Q. (1992). Release of endogenous amino acids., including homocysteic acid and cysteine sulphinic acid., from rat hippocampal slices evoked by electrical stimulation of Schaffer collateral-commissural fibres. *Neuroscience* 49, 557–570. doi: 10.1016/0306-4522(92)90226-r

Krishna, S. M., Dear, A., Craig, J. M., Norman, P. E., and Golledge, J. (2013). The potential role of homocysteine mediated DNA methylation and associated epigenetic changes in abdominal aortic aneurysm formation. *Atherosclerosis* 228, 295–305. doi: 10.1016/j.atherosclerosis.2013.02.019

Kumar, M., and Sandhir, R. (2018). Hydrogen sulfide in physiological and pathological mechanisms in brain. *CNS Neurol. Disord. Drug Targets* 179, 654–670. doi: 10.2174/ 1871527317666180605072018

Levitt, M. D., Abdel-Rehim, M. S., and Furne, J. (2011). Free and acid-labile hydrogen sulfide concentrations in mouse tissues: anomalously high free hydrogen sulfide in aortic tissue. *Antioxid. Redox Signal.* 15, 373–378. doi: 10.1089/ars.2010.3525

Maron, B. A., and Loscalzo, J. (2009). The treatment of hyperhomocysteinemia. *Annu. Rev. Med.* 60, 39–54. doi: 10.1146/annurev.med.60.041807.123308

McCully, K. S. (1969). Vascular pathology of homocysteinemia: implications for the pathogenesis of arteriosclerosis. *Am. J. Pathol.* 56, 111–128.

Mikami, Y., Shibuya, N., Kimura, Y., Nagahara, N., Ogasawara, Y., and Kimura, H. (2011). Thioredoxin and dihydrolipoic acid are required for 3-mercaptopyruvate sulfurtransferase to produce hydrogen sulfide. *Biochem. J.* 439, 479–485. doi: 10.1042/BJ20110841

Panagaki, T., Randi, E. B., Augsburger, F., and Szabo, C. (2019). Overproduction of H 2 S., generated by CBS., inhibits mitochondrial Complex IV and suppresses oxidative phosphorylation in Down syndrome. *Proc. Natl. Acad. Sci. U.S.A.* 116, 18769–18771. doi: 10.1073/pnas.1911895116

Pushpakumar, S., Kundu, S., and Sen, U. (2014). Endothelial dysfunction: the link between homocysteine and hydrogen sulfide. *Curr. Med. Chem.* 21, 3662–3672. doi: 10.2174/0929867321666140706142335

Qu, K., Chen, C., Halliwell, B., Moore, P. K., and Wong, P. (2006). Hydrogen sulfide is a mediator of cerebral ischemic damage. *Stroke* 37, 889–893. doi: 10.1161/01.str.0000204184.34946.41

Savage, J. C., and Gould, D. H. (1990). Determination of sulfide in brain tissue and rumen fluid by ion-interaction reversed-phase high-performance liquid chromatography. *J. Chromatogr.* 526, 540–545. doi: 10.1016/s0378-4347(00)82537-2

Stipanuk, M. H., Londono, M., Lee, J. I., Hu, M., and Yu, A. F. (2002). Enzymes and metabolites of cysteine metabolism in nonhepatic tissues of rats show little response to changes in dietary protein or sulfur amino acid levels. *J. Nutr.* 132, 3369–3378. doi: 10.1093/jn/132.11.3369

Tu, P. F., Li, X. J., Li, Q., and Wang, J. (2016). Effects of hydrogen sulfide on cognitive dysfunction and NR2B in rats. *J. Surg. Res.* 205, 426–431. doi: 10.1016/j.jss.2016.06.071

Wang, R. (2002). Two's company., three's a crowd: can H2S be the third endogenous gaseous transmitter? *FASEB J.* 16, 1792–1798. doi: 10.1096/fj.02-0211hyp

Wang, R. (2012). Physiological implications of hydrogen sulfide: a whiff exploration that blossomed. *Physiol. Rev.* 92, 791–896. doi: 10.1152/physrev.00017.2011

Wang, R., Szabo, C., Ichinose, F., Ahmed, A., Whiteman, M., and Papapetropoulos, A. (2015). The role of H2S bioavailability in endothelial dysfunction. *Trends Pharmacol. Sci.* 36, 568–578. doi: 10.1016/j.tips.2015.05.007

Wang, S. S., Chen, Y. H., Chen, N., Wang, L. J., Chen, D. X., Weng, H. L., et al. (2017). Hydrogen sulfide promotes autophagy of hepatocellular carcinoma cells through the PI3K/Akt/mTOR signaling pathway. *Cell Death Dis.* 8:e2688. doi: 10.1038/cddis.2017.18

Warenycia, M. W., Goodwin, L. R., Benishin, C. G., Reiffenstein, R. J., Francom, D. M., Taylor, J. D., et al. (1989). Acute hydrogen sulfide poisoning. Demonstration of selective uptake of sulfide by the brainstem by measurement of brain sulfide levels. *Biochem. Pharmacol.* 38, 973–981. doi: 10.1016/0006-2952(89)90288-8

Whiteman, M., Li, L., Rose, P., Tan, C. H., Parkinson, D. B., and Moore, P. K. (2010). The effect of hydrogen sulfide donors on lipopolysaccharide- induced formation of inflammatory mediators in macrophages. *Antioxid. Redox Signal.* 12, 1147–1154. doi: 10.1089/ars.2009.2899

Yang, G. D., Wu, L. Y., Jiang, B., Yang, W., Qi, J. S., Cao, K., et al. (2008). H2S as a physiologic vasorelaxant: hypertension in mice with deletion of cystathionine gamma-lyase. *Science* 322, 587–590. doi: 10.1126/science.1162667

Zan, L. K., Zhang, X., Xi, Y. F., Wu, H., Song, Y. J., Teng, G. X., et al. (2014). Src regulates angiogenic factors and vascular permeability after focal cerebral ischemia-reperfusion. *Neuroscience* 262, 118–128. doi: 10.1016/j.neuroscience.2013.12.060

Zhang, W. H., Xu, C. Q., Yang, G. D., Wu, L. Y., and Wang, R. (2015). Interaction of H2S with calcium permeable channels and transporters. *Oxidat. Med. Cell. Longev.* 2015:323269. doi: 10.1155/2015/323269

Zhao, M., Wang, X. B., He, M. L., Qin, X. H., Tang, G. F., Huo, Y., et al. (2017). Homocysteine and stroke risk: modifying effect of methylenetetrahydrofolate reductase C677T polymorphism and folic acid intervention. *Stroke* 48, 1183–1190. doi: 10.1161/strokeaha.116.015324

Conflict of Interest: The authors declare that the research was conducted in the absence of any commercial or financial relationships that could be construed as a potential conflict of interest.

Copyright © 2020 Ji, Li, Zhao, Li and Xie. This is an open-access article distributed under the terms of the Creative Commons Attribution License (CC BY). The use, distribution or reproduction in other forums is permitted, provided the original author(s) and the copyright owner(s) are credited and that the original publication in this journal is cited, in accordance with accepted academic practice. No use, distribution or reproduction is permitted which does not comply with these terms.

frontiers in Neuroscience

ORIGINAL RESEARCH
published: 23 December 2020
doi: 10.3389/fnins.2020.609613

MiR-128-3p Alleviates Spinal Cord Ischemia/Reperfusion Injury Associated Neuroinflammation and Cellular Apoptosis via SP1 Suppression in Rat

*Dan Wang, Fengshou Chen, Bo Fang, Zaili Zhang, Yan Dong, Xiangyi Tong and Hong Ma**

Department of Anesthesiology, The First Hospital of China Medical University, Shenyang, China

OPEN ACCESS

Edited by:
Paulo Henrique Rosado-de-Castro, D'Or Institute for Research and Education (IDOR), Brazil

Reviewed by:
Rossella Russo, University of Calabria, Italy
Andreas Wree, University of Rostock, Germany
Jian-Ping Zhang, Guizhou Provincial People's Hospital, China

***Correspondence:**
Hong Ma
mahong5466@yahoo.com

Specialty section:
This article was submitted to Neurodegeneration, a section of the journal Frontiers in Neuroscience

Received: *23 September 2020*
Accepted: *04 December 2020*
Published: *23 December 2020*

Citation:
Wang D, Chen F, Fang B, Zhang Z, Dong Y, Tong X and Ma H (2020) MiR-128-3p Alleviates Spinal Cord Ischemia/Reperfusion Injury Associated Neuroinflammation and Cellular Apoptosis via SP1 Suppression in Rat. Front. Neurosci. 14:609613. doi: 10.3389/fnins.2020.609613

Background: Neuroinflammation and cellular apoptosis caused by spinal cord ischemia/reperfusion (I/R) injury result in neurological dysfunction. MicroRNAs (miRs) have crucial functions in spinal cord I/R injury pathogenesis according to previous evidences. Herein, whether miR-128-3p contributes to spinal cord I/R injury by regulating specificity protein 1 (SP1) was assessed.

Methods: A rat model of spinal cord I/R injury was established by occluding the aortic arch for 14 min. Then, miR-128-3p's interaction with SP1 was detected by dual-luciferase reporter assays. Next, miR-128-3p mimic and inhibitor, as well as adenovirus-delivered shRNA specific for SP1 were injected intrathecally for assessing the effects of miR-128-3p and SP1 on rats with spinal cord I/R injury. SP1, Bax and Bcl-2 expression levels in I/R injured spinal cord tissues were evaluated by Western blotting, while IL-1β, TNF-α, and IL-6 were quantitated by ELISA. Tarlov scores were obtained to detect hind-limb motor function. Evans blue (EB) dye extravasation was utilized to examine blood–spinal cord barrier (BSCB) permeability. Terminal deoxynucleotidyl transferase mediated dUTP nick end labeling (TUNEL) staining was performed for neuronal apoptosis assessment.

Results: MiR-128-3p expression was decreased, while SP1 amounts were increased in rat spinal cord tissue specimens following I/R. SP1 was identified as a miR-128-3p target and downregulated by miR-128-3p. MiR-128-3p overexpression or SP1 silencing alleviated I/R-induced neuroinflammation and cell apoptosis, and improved Tarlov scores, whereas pretreatment with miR-128-3p inhibitor aggravated the above injuries.

Conclusion: Overexpression of miR-128-3p protects neurons from neuroinflammation and apoptosis during spinal cord I/R injury partially by downregulating SP1.

Keywords: spinal cord ischemia/reperfusion injury, miR-128-3p, SP1, neuroinflammation, apoptosis, rat

INTRODUCTION

Spinal cord I/R injury represents the most catastrophic complication generally ensuing multiple events, including thoracoabdominal aortic surgery and spinal cord injury (Wong et al., 2011; Etz et al., 2015). Spinal cord I/R injury may eventually lead to high incidence of paralysis or paraplegia (LeMaire et al., 2012; Coselli et al., 2016). Despite its improvement by clinical operative methods and perioperative approaches, spinal cord I/R injury cannot be prevented completely (Saito et al., 2013; Karatas et al., 2019). Owing to complicated pathogenic factors, such as oxygen free radical-associated lipid peroxidation, excessive calcium accumulation within the cell, leukocyte induction, inflammation, and neuronal apoptosis, which are rapidly induced and evoke serious complications (Li et al., 2014c). Therefore, it is essential to investigate the exact mechanism of spinal cord I/R injury and develop effective therapeutic measures.

SP1 belongs to the specificity protein/Kruppel-like factor family that also comprises SP2, SP3, and SP4 (Wierstra, 2008). Emerging evidences reveal SP1 as an important regulator of multiple cell events such as cell cycle, proliferation, and apoptosis (Nam et al., 2014; Beishline and Azizkhan-Clifford, 2015). Citron et al. suggested that SP1 was expressed in cerebral tissues, with elevated amounts decreasing neuronal survival (Citron et al., 2008). In addition, SP1 was shown to be upregulated in the development of neurological pathologies, including PD (Cai et al., 2020; Wang et al., 2020) and Alzheimer's diseases (Ramanan and Saykin, 2013). Furthermore, Qin et al. (2018) suggested that suppressing SP1 activation effectively inhibited OGD/R-induced inflammatory activation in microglia. Recent evidence indicated that the expression of SP1 under ischemia/hypoxic conditions was increased (Li et al., 2019). Jointly, the aforementioned data revealed the critical influence of SP1 in neurological pathologies.

MicroRNAs (miRNAs) represent a group of small non-coding RNAs with 21–23 nucleotides, which are able to interact with the 3′-UTRs of mRNAs and negatively modulate gene expression via cleavage or translational suppression at the posttranscriptional level (Kim et al., 2009). MiRNAs are highly expressed in the central nervous system, with crucial roles in neuron development, maintenance of neuronal phenotype, and neuroprotection (Saugstad, 2010). In addition, many miRNAs are dysregulated in the spinal cord during the pathogenesis of I/R injury (Song et al., 2016; Balsam, 2017). Meanwhile, synthetic miRNA mimics and anti-miRNA oligonucleotides powerfully mitigate neuroinflammation and neuroapoptosis, and elevate neurological functional recovery in rat models (He et al., 2015; Li et al., 2015; Liu et al., 2017; Li et al., 2018). Recently, miR-128-3p, which is best known as a tumor suppressor (Huang et al., 2015; Zhao et al., 2018), has been found to contribute to central nervous system disorders such as PD (Zhang et al., 2020) and glioma (Huo et al., 2019). Mao et al. (2017) demonstrated miR-128-3p prevented neuron apoptosis by regulating p38α in the initial stage of brain I/R. However, SP1's role in spinal cord I/R-associated injury and the mechanism by which miR-128-3p presents I/R remain unclear. Therefore, the current work aimed to assess the functions of miR-128-3p and SP1 in spinal cord I/R injury. We hypothesized that miR-128-3p relieves neurological damage in spinal cord I/R injury by depleting SP1 to decrease inflammatory reactions and apoptosis. This pathway could emerge as a possible target relieving spinal cord I/R injury -related nerve injury.

Abbreviations: ANOVA, analysis of variance; AV, adenovirus; BCL-2, B cell lymphoma 2; AR, apoptotic rate; BAX, BCL-2 associated X; BCA, bicinchoninic acid; BSCB, blood–spinal cord barrier; DAPI, 4′6-diamidino-2-phenylindole; DMEM, Dulbecco's Modified Eagle Medium; ECL, chemiluminescence; EB, Evans blue; ELISA, Enzyme-linked immunosorbent Assay; IL, interleukin; I/R, ischemia/reperfusion; miRs, microRNAs; HE, hematoxylin and eosin; i.v., intravenous injection; i.p., intraperitoneal injection; MPTP,1-methyl-4-phenyl-1,2,3,6-tetrahydropyridine; MUT, mutant-type; NC, negative control; NS, normal saline; OGD/R, oxygen-glucose deprivation/reperfusion; PD, Parkinson's disease; PVDF, polyvinylidene fluoride; PMSF, phenylmethylsulfonyl fluoride; qRT-PCR, quantitative real-time polymerase chain reaction; RIPA, radio immunoprecipitation; SP1, specificity protein 1; SDS-PAGE, sodium dodecyl sulfate-polyacrylamide gel electrophoresis; TNF, tumor necrosis factor; TMR, tetramethy-rhodamine; TUNEL, terminal deoxynucleotidyl transferase dUTP nick end labeling; UTR, untranslated region; WT, wild-type.

MATERIALS AND METHODS

Animals

In this study, male Sprague-Dawley rats (200–250 g) were provided by the Animal Center of China Medical University, Shenyang (China). All animals ($n = 136$) were housed for at least 1 week before the surgical operation, with freely available rodent chow and water at 22–24°C and 50–60% relative humidity, under a 12 h/12 h light-dark cycle. Animal experiments had approval from the Ethics Review Committee for Animal Experimentation of China Medical University, Shenyang (China) (CMU2020267/2020/03/02), and were carried out in conformity with the National Institutes of Health Guide for the Use and Care of Laboratory Animals (NIH Publications No.80-23, revised 1996).

Rat Model of Spinal Cord I/R Injury

Spinal cord I/R injury was induced in rats via a cross-clamped aortic arch (Li et al., 2014b,c). Briefly, upon anesthesia by intraperitoneally injecting 4% sodium pentobarbital (50 mg/kg; Beyotime Biotechnology, China), endotracheally intubated (24 g trocar sleeve) and lung ventilation was accomplished utilizing a small-animal ventilator (Harvard Apparatus, United States) (tidal 15 mL/kg, breathing frequency 80–100 times/min, breathing ratio 1:1). Body temperatures were kept at 37.5 ± 0.5°C as monitored with a rectal probe. Under aseptic conditions, the left common carotid artery was exposed in the middle of neck. Then, the aortic arch was uncovered through a cervicothoracic incision. Under direct vision, the aortic arch was cross-clamped for 14 min between the left carotid artery and the left subclavian artery to induce ischemia. A catheter (24 g trocar sleeve) was inserted into the femoral artery for blood pressure measurements. After ischemia confirmation [90% reduction of the flow assessed at the femoral artery using a laser Doppler blood flow monitor (Moor Instruments, Axminster, Devon, United Kingdom)], clamp removal was performed, followed by 12-h reperfusion. This procedure was performed in sham animals, except for blockade.

Experimental Protocol

Experimental groups and protocol were shown in **Figure 1**. We used 118 rats and 18 rats for modeling and sham operation, respectively. To measure expression of miR-128-3p and SP1 at various time points (6, 12, 24, 36, and 48 h) after reperfusion, 20 rats were killed at 6, 12, 24, 36, and 48 h after spinal cord I/R, respectively ($n = 4$, at each time point). Subsequently, eight groups were enrolled: (1) Sham group ($n = 14$): same procedure was performed on rats without blockade and 10 μL normal saline was injected inreathecally into each rat prior to sham-operation. (2) I/R group ($n = 14$): cross-clamping for 14 min on rats for ischemia induction. (3) miR-128-3p mimic group ($n = 14$): 10 μL synthetic miR-128-3p mimics were injected intrathecally into each rat prior to ischemia induction once a day for three consecutive days. (4) miR-128-3p negative control (NC) group ($n = 14$): 10 μL synthetic miR-128-3p NC was injected intrathecally into each rat prior to ischemia induction once a day for three consecutive days. (5) miR-128-3p inhibitor group ($n = 14$): 10 μL synthetic miR-128-3p inhibitors were injected intrathecally into each rat prior to ischemia induction once a day for three consecutive days. (6) Adenovirus (AV)-sh-SP1 group ($n = 14$): 20 μL shRNA-SP1 adenovirus at 5×10^{10} PFU/mL was carried out for 2 days before ischemia. (7) AV-sh-NC group ($n = 14$): 20 μL shRNA-NC adenovirus at 5×10^{10} PFU/mL was carried out for 2 days before ischemia. (8) AV-sh-SP1 + miR-128-3p inhibitor group ($n = 14$): 10 μL synthetic miR-128-3p inhibitor were injected intrathecally into each rat prior to ischemia induction once a day for three consecutive days and 2 days before ischemia 20 μL shRNA-SP1 adenovirus at 5×10^{10} PFU/mL was carried out.

Intrathecal Administration

Intrathecal administration of various substances followed a previously reported method (Mestre et al., 1994; Li et al., 2015; He et al., 2016; Li et al., 2018). In brief, upon anesthesia with isoflurane (RWD, Shenzhen, China), rats were placed in the prone position that flexed the rats' back. A 20-μL microsyringe (Gaoge Co., Ltd., Shanghai, China) was positioned in the subarachnoid space at the intervertebral space between L5 and L6 or L4 and L5. The spinal cord of rat terminated between the third and fourth lumbar vertebrae (Padmanabhan and Singh, 1979). This site was chosen so that the injection was restricted to the region where the spinal cord ends and the cauda equine begins in order to minimize the possibility of spinal damage and maximize intervertebral accessibility (Mestre et al., 1994). According to the anatomical structure of the rat, the horizontal position of the connection between the left and right hip joints corresponds to the spinous process space of L5–L6 or the spinous process of L5. When the needle entered the subarachnoid space, a sudden lateral tail-flick was used as a sign of successful puncture. Once correct needle placement was confirmed, the solutions were injected slowly and over the course of 1 min (Judas et al., 2014). Synthetic miR-128-3p mimic, inhibitor and negative control were purchased from Transheep (Shanghai China). A shRNA-SP1 adenovirus (AV-sh-SP1) and NC adenovirus (AV-sh-NC) were provided by IGE Bio. Ltd., (Guangzhou, China). Rats were intrathecally infused with 10 μL of synthetic miR-128-3p mimic, inhibitor and NC, respectively, at a concentration of 500 pmol/10 μL with Entranster^{TM}-*in vivo* transfection regent (Engreen, Beijing, China) to regulate miR-128-3p *in vivo* prior to ischemia induction once a day for three consecutive days. Meanwhile, 2 days before ischemia, intrathecal infusion of 20 μL of shRNA-SP1 or NC adenovirus at 5×10^{10} PFU/mL was carried out, as directed by the manufacturer. Transfection efficacy was assessed by qRT-PCR or Western blotting. Only animals with unaltered motor function after intrathecal injection underwent surgery. The sequences of miR-128-3p mimic, miR-128-3p inhibitor, miR-128-3p NC and AV-sh-SP1 were as follows: miR-128-3p mimic (5′-UCACAGUGAACCGGUCUCUUU-3′), miR-128-3p inhibitor (5′-AGUGUCACUUGGCCAGAGAAA-3′), miR-128-3p NC (5′-CAGUACUUUUGUGUAGUAAA-3′), AV-sh-SP1 (5′-CCGGCCAACTTACAGAACCAGCAAGTTCTCTCGAGAGAACTTGCTGGTTCTGTAAGTTGGTTTTTGAATT-3′).

Neurological Assessment

Hind-limb motor function was examined at 12 h post reperfusion ($n = 8$, at each group) by two investigators blinded to experimental design according to the Tarlov scoring system (Aslan et al., 2009; Li et al., 2014a): 0, Spastic paraplegia and no voluntary movement of lower limbs; 1, Spastic paraplegia and weak hind limb motor function of lower limbs; 2, good antigravity strength with some lower limb movement, but inability to stand; 3, abnormal standing but unable to walk normally; 4, normal motor function.

After neurological evaluation, the rats in all groups were anesthetized with 4% sodium pentobarbital 50mg/kg and perfused transcardially with normal saline. The spinal cords from L4 to L6 were harvested for molecular biology analysis because of their vulnerability to ischemic injury (Li et al., 2014a). There are two methods to identify the L4–L6 segments. On the one hand, in the rat, the sciatic nerve is composed of spinal segments L4, 5, and 6. The roots of these three spinal nerves originate in the spinal cord within the limits of the L1 vertebra, and then must descend distances of 2.7 cm (L4) to 4.5 cm (L6) within the vertebral canal before reaching the periphery (Gelderd and Chopin, 1977). Therefore, L4–L6 spinal segments were identified based on the ascending ends of the posterior fibers of the dorsal root ganglion of L4, 5, and 6. On the other hand, according to the anatomical morphology of the rat spinal cord, the lumbar enlargement of spinal cord in rat is located at the level of vertebrae T12-L1, which corresponds to spinal cord segments L1–L5 (Gilerovich et al., 2008). The L4–L6 segments lie at the upper border, middle and lower border of the L1 vertebra. Therefore, L4–L6 spinal cord segments were identified based on the position of L1 vertebra. At the end of these procedures, all rats were sacrificed under deep anesthesia.

Quantitative Real-Time Polymerase Chain Reaction (qRT-PCR)

After final neurological assessment, total RNA from L4–L6 spinal cord specimens ($n = 4$, at each group) was obtained with TRIzol

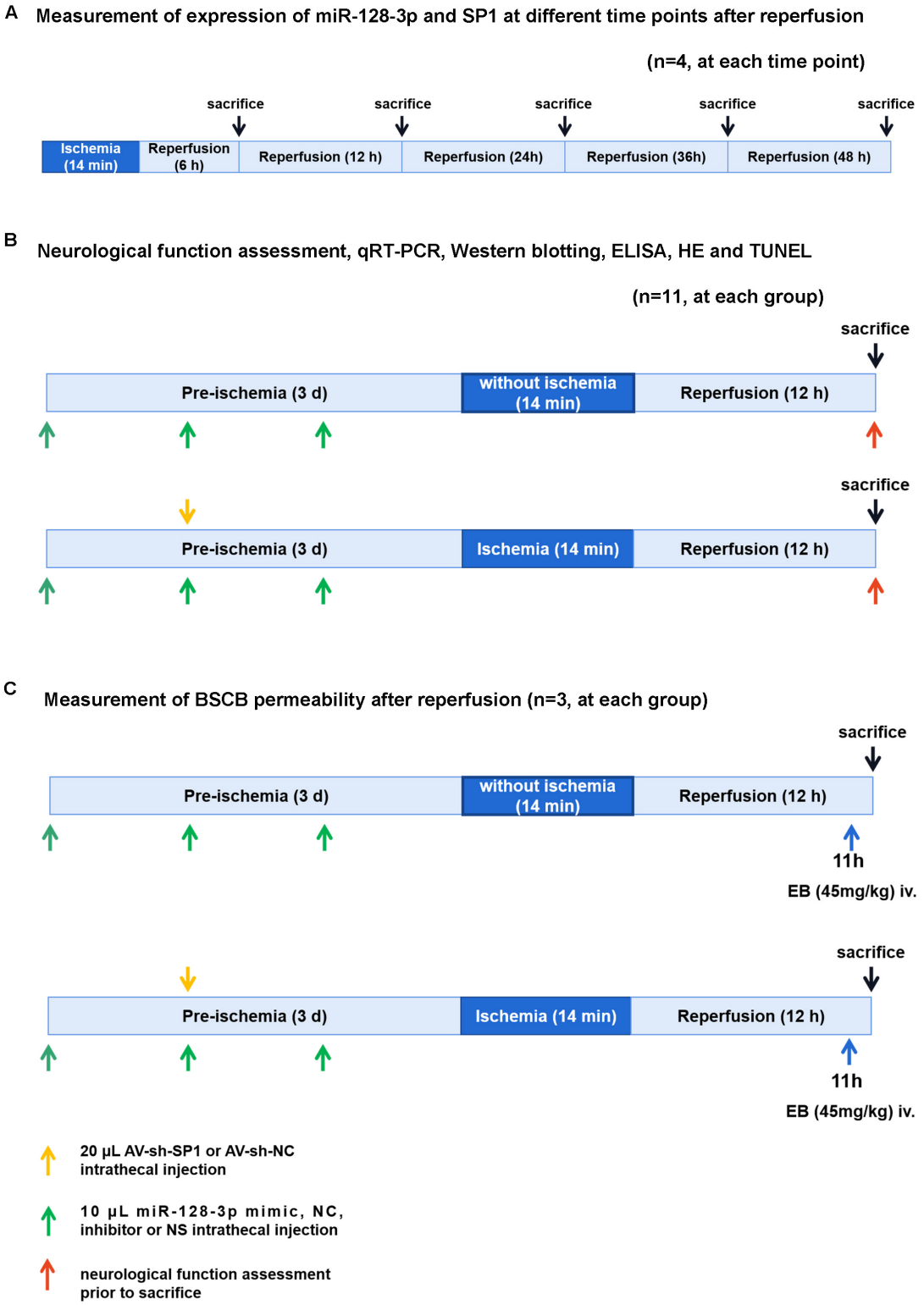

FIGURE 1 | Diagram of the experimental protocols. **(A)** Measurement of expression of miR-128-3p and SP1 at different time points (6, 12, 24, 36, and 48 h) after reperfusion. $n = 4$, at each time point. **(B)** Neurological function assessment ($n = 8$, at each group), qRT-PCR and Western blotting ($n = 4$, at each group), ELISA ($n = 4$, at each group), H&E and TUNEL ($n = 3$, at each group). Rats ($n = 8$, at each group) were euthanized after neurological function assessment. Then 4 rats' spinal cords were used for qRT-PCR and Western blotting and the other 4 rats' spinal cords were used for ELISA. **(C)** Measurement of BSCB permeability after reperfusion ($n = 3$, at each group).

reagent (Takara, Japan) as instructed by the manufacturer. Then, reverse transcription utilized Prime-Script RT reagent Kit with gDNA Eraser (TaKaRa) or MicroRNA Reverse Transcription Kit (Applied Biosystems, United States). Subsequently, qRT-PCR was performed with a SYBR PremixEx TaqII kit (Takara) on an ABI 7500 qRT-PCR instrument (Applied Biosystems) at 95°C (10 min), followed by 40 cycles at 95°C (20 s), 60°C (60 s), 62°C (30 s), and 72°C (30 s). Relative SP1 mRNA and miR-128-3p amounts were assessed by the $2^{-\Delta\Delta Ct}$ method, with GAPDH and U6 as internal references, respectively. The primers (Sangon Biotech, China) employed were as follows: miR-128-3p (forward: 5′-CGTCACAGTGAACCGGTCTCTTT-3′), SP1 (forward: 5′-CTGCAAGGGTCTGATTCTCTA-3′, reverse: 5′-AGCTTGTCCACCTTGAACTA-3′), GAPDH (forward: 5′-GGGGCTCTCTGCTCCTCCCTG-3′, reverse: 5′-AGGCGTCC GATCGGCCAAA-3′), U6 (forward: 5′-CTCGCTTCGGCAGC ACA-3′, reverse: 5′-AACGCTTCACGAATTTGCGT-3′).

Cell Culture

293T cell lines were purchased from cell bank center of Shanghai Institutes for Biological Sciences (SIBS) and were cultured in DMEM (Invitrogen, Thermo Fisher Scientific, Waltham, MA, United States) appended with 10% FBS and 2 Mm glutamine, and 100 μg/ml streotonucin and penicillin (Sangon Technology, Shanghai, China). All of the cells were incubated at 37°C with 5% CO_2 (Yang et al., 2019).

Dual Luciferase Reporter Gene Assay

MiR-128-3p target prediction was performed with TargetScan[1]. For constructing 3′-UTR-luciferase reporters, regions of SP1's 3′-UTR were introduced into pmirGLO (Promega). Then, two wild types named WT1-3′ UTR (binding sites at base pairs [bp] 1437–1443 and 1642–1649) and WT2-3′ UTR (binding site at bp 4373–4379) were constructed by Nanjing TsingKe Co., Ltd. (China). Mutant-type plasmids (MUT1-3′ UTR and MUT2-3′ UTR) were generated with the Directed Mutagenesis system (Invitrogen). Meanwhile, SP1 WT and MT plasmids, respectively, were co-transfected with miR-128-3p mimic or miR-128-3p -NC in 293 T cells with Lipofectamine 2000 (Invitrogen) as directed by the manufacturer. After transfection for 48 h, cell collection and homogenization in passive lysis buffer (Promega G182A) (100 μl) were carried out. Renilla and firefly luciferase activities in triplicate assays were assessed with Luciferase Assay Kit (Beyotime) on a multifunctional microplate reader (PerkinElmer EnSpire, United States).

Hematoxylin and Eosin (H&E) Staining

At 12 h post-modeling, rats (n = 3, at each group) were deeply anesthetized with 4% sodium pentobarbital (50 mg/kg, i.p.). Then, they were perfused transcardially with normal saline, followed by 4% buffered paraformaldehyde (Servicebio G1101, China), and until the right atrium flowed out clear paraformaldehyde and the lungs turned white (Li et al., 2019; Yin et al., 2019). The spinal cords from L4 to L6 were removed rapidly for analysis because of their vulnerability to ischemic injury (Li et al., 2014a). Tissue was fixed with 4% paraformaldehyde for 24 h and embedded in paraffin. Then, paraffin-embedded sections (4 μm) underwent staining with hematoxylin and eosin (H&E) staining kit (Servicebio G1005, China) as directed by the manufacture. Briefly, the 4 μm thick paraffin-embedded sections were firstly deparaffinized and hydrated to water. Second, the sections were stained in hematoxylin solution for 5 min and rinsed in water. Then, the sections were differentiated in 1% hydrochloric acid ethanol solution and restored blue in ammonia solution and washed in slowly running tap water. After then, the sections were dehydrated with 85 and 95% gradient alcohol III, Xylene I, and Xylene II for 5 min, respectively. Stained sections were examined under an optical microscope (Nikon Eclipse E100, Japan) by two blind investigators to judge the morphological appearance of neurons. Normal neurons were defined as viable by the existence of basophilic stippling, whereas necrotic or dead neurons were identified by the existence of diffusely eosinophilic cytoplasm with pyknotic homogenous nuclei (Ding et al., 2009; Li et al., 2014a). Gray matter injury was examined by counting normal motor neurons in its ventral region. Data were calculated as average numbers of intact neurons using ImageJ software (Download from the NIH website[2]) (Li et al., 2014a). Three sections for each rat were assessed in a blinded fashion.

Terminal Deoxynucleotidyl Transferase dUTP Nick End Labeling (TUNEL)

The TUNEL assay was extensively carried out for the detection and quantification of apoptosis in histological tissue sections (Duan et al., 2003). The above tissue sections (n = 3, at each group) underwent staining with TMR (red) TUNEL Cell Apoptosis Detection Kit (Servicebio, G1502, China) as directed by the manufacturer. Following TUNEL labeling, cell nuclei were stained with DAPI (Servicebio G1012, China) for 5 min. Cell apoptosis was assessed by two blinded investigators under a light microscope (Leica, Germany). The nuclei labeled with DAPI appear blue under a fluorescence microscope and the positive apoptotic nuclei were red. The TUNEL-positive cells were recognized as cells double labeled with TUNEL and DAPI and only TUNEL + DAPI were counted. (Li et al., 2018). Finally, the high power fields of spinal cord were randomly selected, and average percentage in three sections/rat of TUNEL-positive cells to total nuclei were calculated by two blind investigators using ImageJ software (Download from the NIH website[2]). The apoptotic rate was calculated as AR = (number of TUNEL-positive cells/total number of nuclei) × 100% (Fu et al., 2020).

Evans Blue (EB) Extravasation

Evans blue (EB) extravasation was carried out to quantitatively and qualitatively assess blood–spinal cord barrier (BSCB) integrity following I/R-associated injury (n = 3, at each group) (Li et al., 2015). After 12 h of reperfusion, Evans blue (EB, 1 mg/ml; Solarbio, China) was administered by intravenous (tail vein) injection (45 mg/kg) 60 min before euthanasia. The rats were anesthetized and perfused transcardially with 500 mL/kg normal

[1]http://www.targetscan.org

[2]https://imagej.nih.gov/ij/

saline, and the L4–L6 segments were removed and underwent fixation with 4% formalin and sectioning at 10 μm (Fang et al., 2013b). EB staining was evaluated under a fluorescence microscope (Olympus, Melville, NY, United States).

Enzyme Linked Immunosorbent Assay (ELISA)

Following 12 h of modeling, L4–L6 segments were obtained ($n = 4$, at each group), homogenized in chilled PBS and submitted to centrifugation (3,000 r/min, 15 min; 4°C). Then, interleukin (IL)-1β, IL-6 and TNF-α amounts were quantified on a microplate reader with ELISA kits (MultiSciences Biotech Co., Ltd., China), as described by the manufacturer. Triplicate experiments were assessed at 450 nm, and results were normalized to protein amounts.

Western Blotting

L4–L6 segments ($n = 4$, at each group) underwent lysis with radioimmunoprecipitation (RIPA) lysis buffer (R0010, Solarbio) supplemented with PMSF (P0100, Solarbio) as previously described (Li et al., 2018). Then, protein concentrations were quantified with a BCA protein assay kit (Beyotime Biotechnology). Equal amounts of protein were resolved by SDS-PAGE (KGP113K, KeyGen Biotech. Co. Ltd., Nanjing, China) and electro-transferred onto PVDF membranes (Millipore, Temecula, CA, United States). Upon blocking with 5% non-fat milk (1 h), the membranes underwent overnight incubation with anti-SP1 (Abcam, ab13370; 1:1000), anti-Bax (Cell Signaling Technology, 2772; 1:1000), anti-Bcl-2 (ProteinTech, 26593-1-AP; 1:1000) and β-actin (ZSGB-BIO, China; 1:5000) primary antibodies at 4°C. Next, the specimens were incubated with HRP-conjugated goat anti-rabbit (ProteinTech, SA00001-2) or anti-mouse (ProteinTech, SA00001-1) antibodies (1 h, 37°C). The membranes were further washed with TBST 3 times. An ECL kit (Bio-Rad, United States) was utilized for visualization, and bands were detected by the Quantity One software (Bio-Rad). ImageJ 1.6.0.24 (National Institutes of Health, United States) was used to quantify the band strength; β-actin served as a reference protein.

Statistical Analysis

SPSS 25.0 (SPSS, United States) was utilized for data analysis. Data are mean ± SD. The Student's *t*-test or Mann–Whitney test was performed for group pair comparisons, while multiple groups were assessed by one-way or two-way ANOVA, with *post hoc* Tukey test. $P < 0.05$ was deemed statistically significant.

RESULTS

Abnormal Expressions of miR-128-3p and SP1 After I/R

MiR-128-3p and SP1 amounts were assessed at 6, 12, 24, 36, and 48 h post-I/R, respectively. As shown in **Figure 2A**, qRT-PCR revealed that miR-128-3p expression was noticeably diminished over time and reached its minimum amounts at 12 h after I/R, in comparison with the sham group ($P < 0.05$). Additionally, qRT-PCR and Western blotting analysis revealed that SP1 mRNA and protein levels were elevated from 6 h post-I/R in comparison with the sham group, and peaked at 12 h (**Figures 2B–D**, $P < 0.05$).

SP1 Is a Direct miR-128-3p Arget

According to results from TargetScan database, a putative miR-128-3p binding site was found in the 3′ UTR of the SP1 gene (**Figure 3A**). This was confirmed by dual-luciferase reporter assays. Luciferase activities of WT1-3′ UTR and WT2-3′ UTR in 293T cells transfected with miR-128-3p mimic exhibited a remarkable decrease, while those of mutant-type (MUT)1-3′ UTR and MUT2-3′ UTR co-transfected with miR-128-3p mimic were unaltered (**Figure 3B**, $P < 0.05$). Furthermore, no disparities were recognized after transfection with NC mimic (**Figure 3B**, $P > 0.05$). The above findings suggested miR-128-3p directly targeted and downregulated SP1.

Intrathecal Administration of miR-128-3p Mimic and Inhibitor Strongly Regulates SP1 Expression *in vivo* After I/R

To investigate miR-128-3p's interaction with SP1 in the spinal cord tissue, miR-128-3p mimic, inhibitor and NC were administered by intrathecal injection for 3 days prior to ischemia. Then, qRT-PCR and Western blotting were carried out to assess miR-128-3p and SP1 mRNA and protein levels in the spinal cord, respectively. Compared with the I/R group, miR-128-3p was upregulated after administration of miR-128-3p mimic (**Figure 4A** $P < 0.05$) but showed no remarkable differences in the miR-128-3p NC group ($P > 0.05$). Significantly, pretreatment with miR-128-3p mimic remarkably reduced I/R-associated SP1 upregulation at the mRNA and protein levels at 12 h post-I/R; conversely, pretreatment with miR-128-3p inhibitor reversed the above effects (**Figures 4B–D**; $P < 0.05$). The above findings jointly suggested that the levels of SP1 were decreased due to overexpressed miR-128-3p and increased after miR-128-3p downregulation.

Intrathecal Pretreatment With miR-128-3p Mimic or AV-sh-SP1 Ameliorates Neurological Function and Histologic Evaluation After I/R

Neurological function in the eight groups according to the Tarlov scores post-I/R was presented in **Figure 5A** Tarlov scores in the I/R group were significantly reduced at 12 h post-I/R compared with the sham group ($P < 0.05$). In comparison with the I/R and miR-128-3p NC groups, the miR-128-3p mimic group showed markedly elevated scores, whereas administration of miR-128-3p inhibitor resulted in lower Tarlov scores ($P < 0.05$). Tarlov scores were comparable in the I/R and miR-128-3p NC groups. Knockdown of SP1 using AV increased Tarlov scores ($P < 0.05$). Meanwhile, Tarlov scores were similar in the I/R and AV-sh-NC groups. Additionally, the miR-128-3p inhibitor + AV-sh-SP1 showed higher Tarlov scores ($P < 0.05$ vs. IR group) indicating AV-sh-SP1 could eliminate the

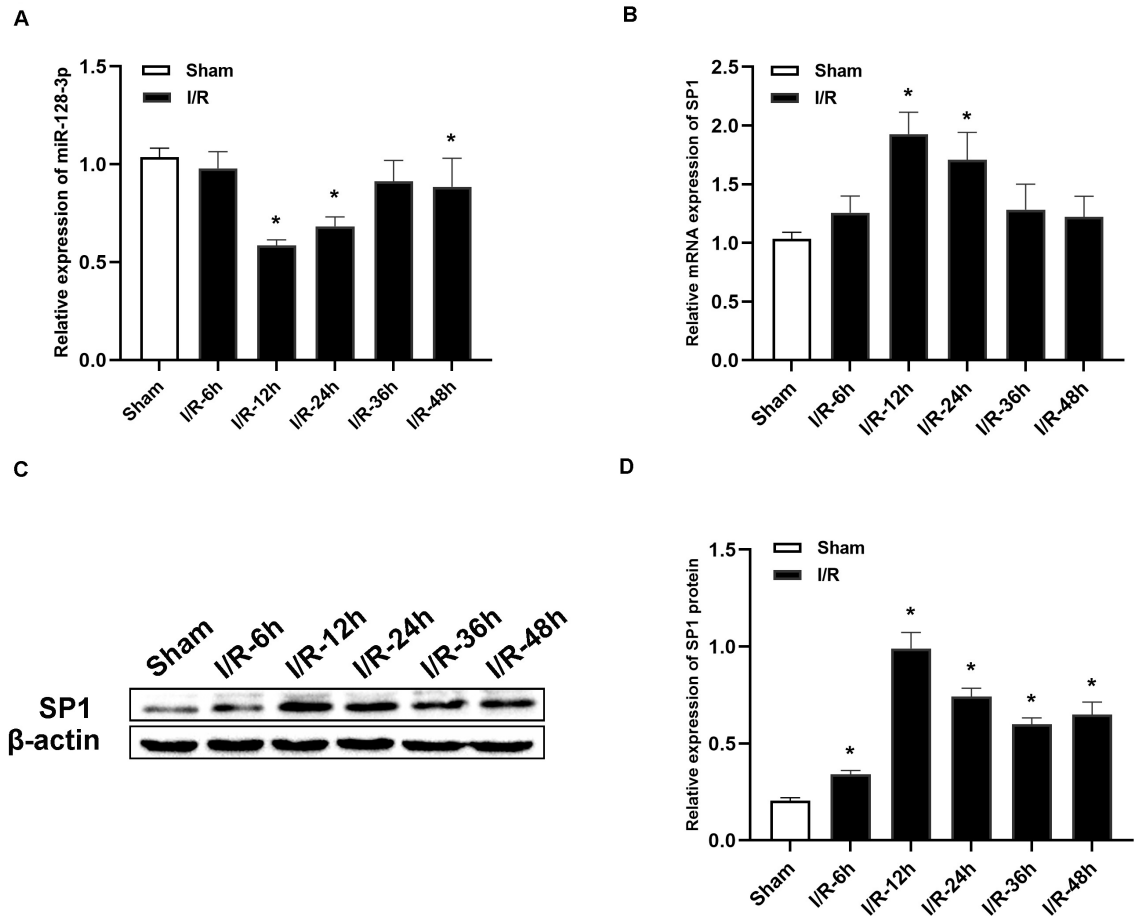

FIGURE 2 | Alterations in miR-128-3p and SP1 expression levels at various time points after spinal cord I/R injury. **(A)** Quantification of miR-128-3p expression in the L4–L6 segments of spinal cord specimens after spinal cord I/R injury. **(B)** Quantification of SP1 mRNA expression in the L4–L6 segments of spinal cord specimens after spinal cord I/R injury. **(C,D)** Western blotting analysis of SP1 protein levels in the L4–L6 segments of spinal cord specimens after spinal cord I/R injury. β-actin was used as a loading control. One-way ANOVA was performed for multiple- group comparisons, followed by the Tukey's test. *$P < 0.05$ vs. sham group.

damage caused by miR-128-3p inhibitor. Consequently, spinal cord I/R injury induced severe neurological deficits of lower limbs; meanwhile, miR-128-3p mimic and AV-sh-SP1 relieved neurological damage, while miR-128-3p inhibitor aggravated neurological deterioration. Likewise, histological findings at 12 h post-I/R revealed that the numbers of intact neurons in the anterior horn were significantly decreased, as shown by the existence of diffusely eosinophilic cytoplasm without cell structure, extensive vacuolation and pkynotic nuclei of neurons. Whereas, more intact neurons with basophilic substance and multipolar structure were seen after treatment with miR-128-3p mimic and AV-sh-SP1; miR-128-3p inhibitor increased necrotic or dead neurons in the anterior horn, while treatment with miR-128-3p inhibitor + AV-sh-SP1 reversed this effect (**Figure 5B**). The numbers of neurons with normal morphology in the anterior horn of spinal cord at 12 h post-I/R was significantly decreased in the I/R group (9 ± 1.000) than in the sham group (25.33 ± 2.082), miR-128-3p mimic group (20.33 ± 2.517), AV-sh-SP1 group (20 ± 1.000) and AV-sh-SP1 + inhibitor group (13.67 ± 2.082) (**Figures 5C**; $P < 0.05$). In the miR-128-3p NC, miR-128-3p inhibitor and AV-sh-NC group the numbers of neurons with normal morphology in the anterior horn were 7.667 ± 2.517, 6.667 ± 1.155, and 8 ± 1.000, respectively and had no marked differences compared with I/R group ($P > 0.05$).

Intrathecal Pretreatment With miR-128-3p Mimic or AV-sh-SP1 Ameliorates BSCB Leakage and Proinflammatory Cytokine Release After I/R

I/R-induced BSCB leakage was evaluated by EB fluorescent dye as described in previous reports (Fang et al., 2013a; Li et al., 2014b,c). As shown in **Figures 6A,B**, I/R notably increased red fluorescence in the gray matter at 12 h after surgery in comparison with sham animals ($P < 0.05$). Intrathecal injection of miR-128-3p mimic or AV-sh-SP1 remarkably reduced fluorescence levels ($P < 0.05$), whereas miR-128-3p inhibitor aggravated BSCB leakage. Moreover, the degree and intensity of fluorescence in the miR-128-3p inhibitor + AV-sh-SP1 group

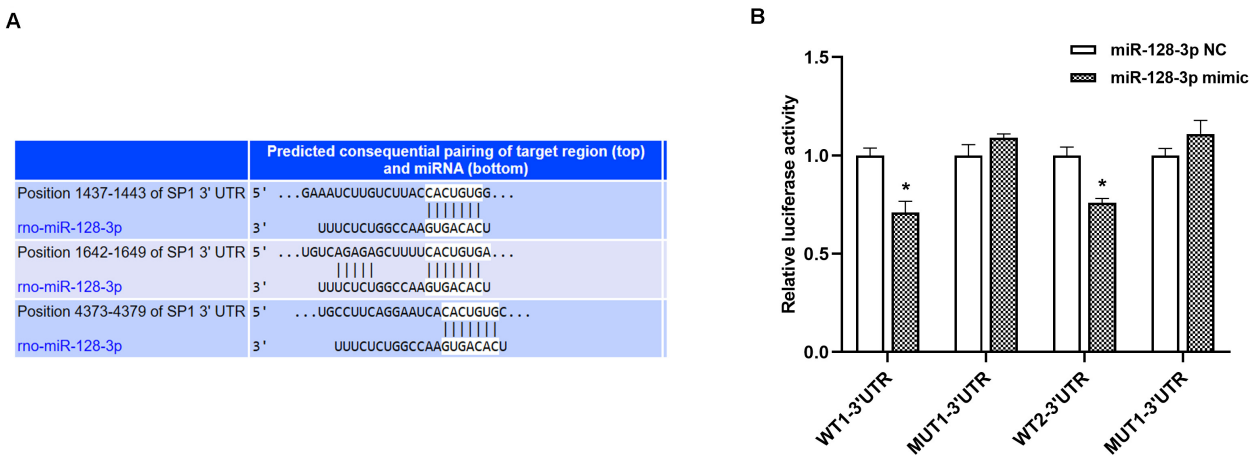

FIGURE 3 | SP1 is a direct miR-128-3p target. **(A)** Prediction of miR-128-3p and SP1 binding sites based on TargetScan. Three predicted conserved miR-128-3p target sites in the 3′UTR of SP1. **(B)** Suppression of SP1 expression by miR-128-3p. Luciferase activity was measured after 48 h of co-transfection of 293T cells with the miR-128-3p mimic and the WT or MUT reporter vector. Compare to the control, miR-128-3p significantly decreased the luciferase activity of the WT vector but not that of the MUT vector. 3′ UTR, 3′untranslated region; WT, wild-type; MUT, mutant-type, SP1, specificity protein 1; NC, negative control. *$P < 0.05$ vs. NC group.

were lower levels ($P < 0.05$). The I/R and NC groups also had no marked differences ($P > 0.05$).

Next, we assessed whether neuronal inflammation is an important response in spinal cord I/R injury development. As shown in **Figures 6C–E**, proinflammatory cytokines, including IL-6, TNF-α, and IL-1β, had remarkably increased amounts at 12 h post-I/R vs. sham group ($P < 0.05$). Interestingly, intrathecal injection of miR-128-3p mimic or AV-sh-SP1 reduced the release of IL-6, TNF-α and IL-1β (vs. I/R group; all $P < 0.05$). In contrast, miR-128-3p inhibitor increased IL-6, TNF-α, and IL-1β amounts (vs. I/R group; all $P < 0.05$), while, IL-6, TNF-α, and IL-1β amounts were reduced in the miR-128-3p inhibitor + AV-sh-SP1 group ($P < 0.05$ vs. inhibitor group), and were comparable in the I/R and miR-128-3P NC groups.

Intrathecal Pretreatment With miR-128-3p Mimic or AV-sh-SP1 Ameliorates Neuronal Apoptosis After I/R

Apoptotic cells in spinal cord samples were represented by TUNEL-positive signals. The results in **Figures 7A,B** showed that the rate of apoptosis was markedly elevated in the I/R group in comparison with sham animals ($P < 0.05$). Apoptosis rate increase was partially restored in the miR-128-p mimic and AV-sh-SP1 group, respectively (both $P < 0.05$), whereas miR-128-3p inhibitor promoted apoptosis. Interestingly, apoptosis rate in the miR-128-3p inhibitor group was restored by AV-sh-SP1 ($P < 0.05$). In addition, the I/R and NC groups showed comparable values ($P > 0.05$). Similarly, to assess the possible mechanism underlying the effects of miR-128-3p and SP1 on apoptosis post-I/R, SP1, Bcl-2 and Bax amounts were assessed by Western blotting upon transfection with miR-128-3p mimic, inhibitor and AV-sh-SP1, respectively. As shown in **Figures 7C–F**, SP1 expression levels were significantly upregulated in the I/R group in comparison with sham group ($P < 0.05$). Meanwhile, miR-128-3p mimic or AV-sh-SP1 remarkably downregulated SP1 ($P < 0.05$). Conversely, miR-128-3p inhibitor upregulated SP1. Interestingly, in the miR-128-3p + AV-sh-SP1 group, the expression of SP1 was inhibited ($P < 0.05$). Bax expression levels changed with the same trends observed for SP1. Bcl-2 was markedly downregulated in the I/R group in comparison with sham animals ($P < 0.05$), and miR-128-3p mimic or AV-sh-SP1 promoted Bcl-2 expression ($P < 0.05$), which was suppressed by miR-128-3p inhibitor. After administration of miR-128-3p inhibitor + AV-sh-SP1, Bcl-2 protein amounts were also elevated ($P > 0.05$). The I/R and NC groups were also comparable. Hence, upregulation of miR-128-3p suppressed apoptosis in rat spinal cord injury after I/R by suppressing SP1 expression.

DISCUSSION

Prominent findings unveiled by this work are that elevated miR-128-3p amounts downregulated the transcription factor SP1, thus ameliorating the impairment of neurons induced by I/R via regulating inflammation and apoptosis.

Cumulative evidences illustrate that miRs are novel molecular targets modulating the pathogenesis of I/R injury (Li et al., 2015, 2017; Liu et al., 2017; Li et al., 2018; Li et al., 2020). The associations of miR-128-3p with central nervous system diseases have been assessed previously. For example, Krichevsky et al. (2006) suggested that miR-128-3p is upregulated in the development of the central nervous system. Additionally, high miR-128-3p amounts in neurons alleviate motor deficits in a mouse model of PD (Tan et al., 2013), and it was recently confirmed that miR-128-3p overexpression in the 1-methyl-4-pheny-1,2,3,6-tetrahydropyridine (MPTP)-injured mouse model of PD reduced hippocampal neuron apoptosis (Zhang

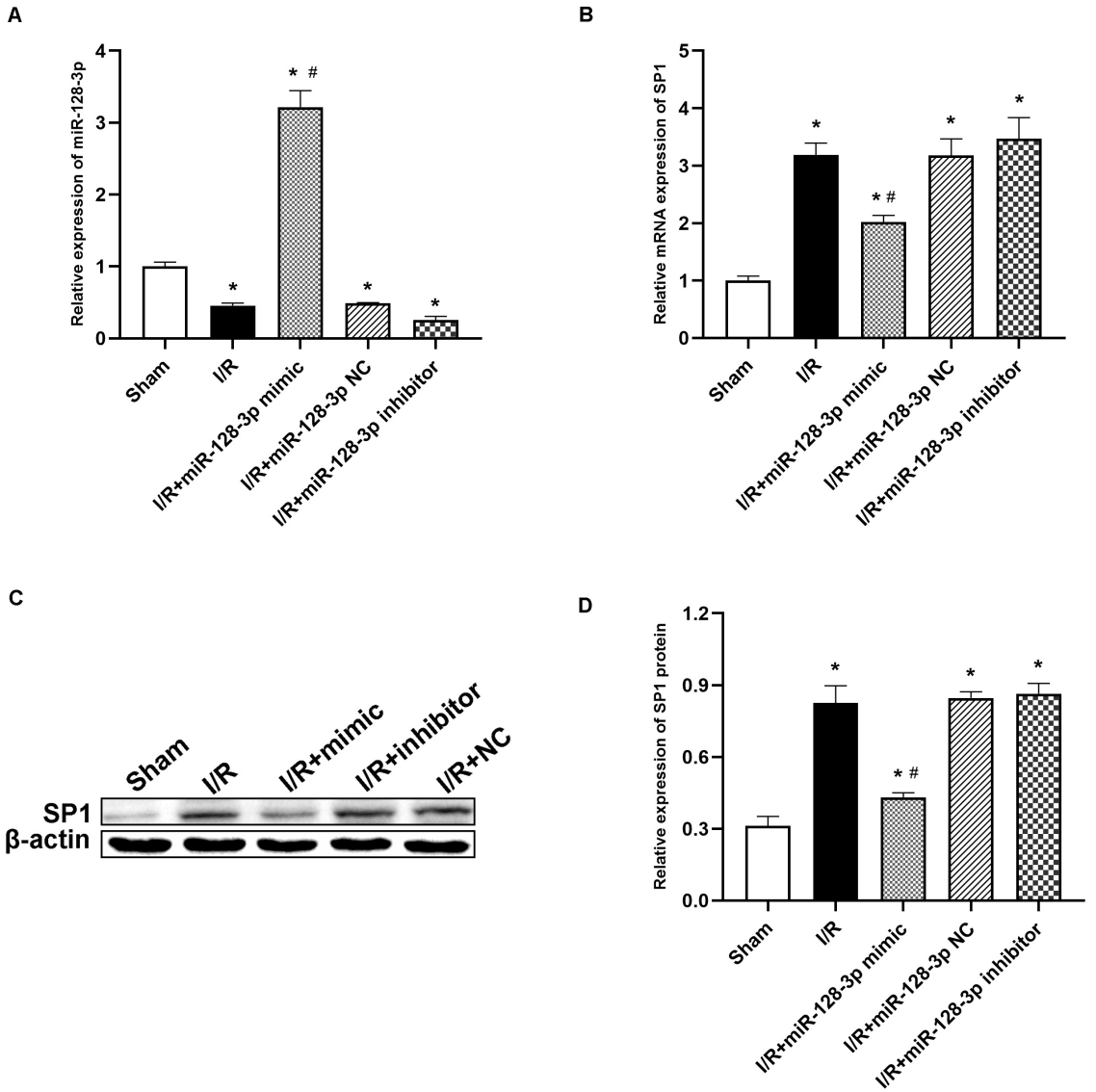

FIGURE 4 | Effects of miR-128-3p mimic and inhibitor on miR-128-3p and SP1 levels in the L4–L6 segments of spinal cord specimens. **(A)** miR-128-3p expression levels in various groups. **(B)** Quantification of SP1 mRNA expression in various groups by qRT-PCR. **(C,D)** Western blot analysis of SP1 protein levels in various groups. β-actin was used as a loading control. One-way ANOVA was performed for the multiple- group followed by the Tukey's test. $^{*}P < 0.05$ vs. sham group, $^{\#}P < 0.05$ vs. I/R and NC group.

et al., 2020). Meanwhile, miR-128-3p protected neurons from apoptosis at the early stage of cerebral ischemia (Mao et al., 2017). The above data suggest miR-128-3p's regulatory role in neuroinflammation and neuroapoptosis post-injury. However, discrepant findings have been reported. While miR-128-3p is considered to enhance neuronal survival in ischemia-induced brain damage (Mao et al., 2017), its inhibition has been shown to induce the protection of cardiomyocytes from I/R injury (Chen et al., 2017). One miR can modulate many target genes, whereas one target gene could be modulated by multiple miRs (Brandenburger et al., 2012; Ksiazek-Winiarek et al., 2013), and functional target genes might depend on pathological conditions, treatments and the effector organ. Thus, it is very possible to encounter discrepancy in expression while examining the same miR in distinct conditions.

Given that neuroinflammation and neuroapoptosis have been shown to be critical phenotypes of spinal cord I/R injury (Li et al., 2015; Bao et al., 2018; Li et al., 2018), we further investigated whether miR-128-3p protected against spinal cord I/R injury by inhibiting inflammation and apoptosis. In this work, miR-128-3p was downregulated in the spinal cord at 6, 12, 24, 36, and 48 h, respectively, post-I/R in comparison with sham animals, and miR-128-3p content reached its lowest point at 12 h after I/R. We, therefore, selected 12 h post-I/R for subsequent assays. Consistently, distinct ameliorations in hind-limb motor function, preservation degrees of BSCB

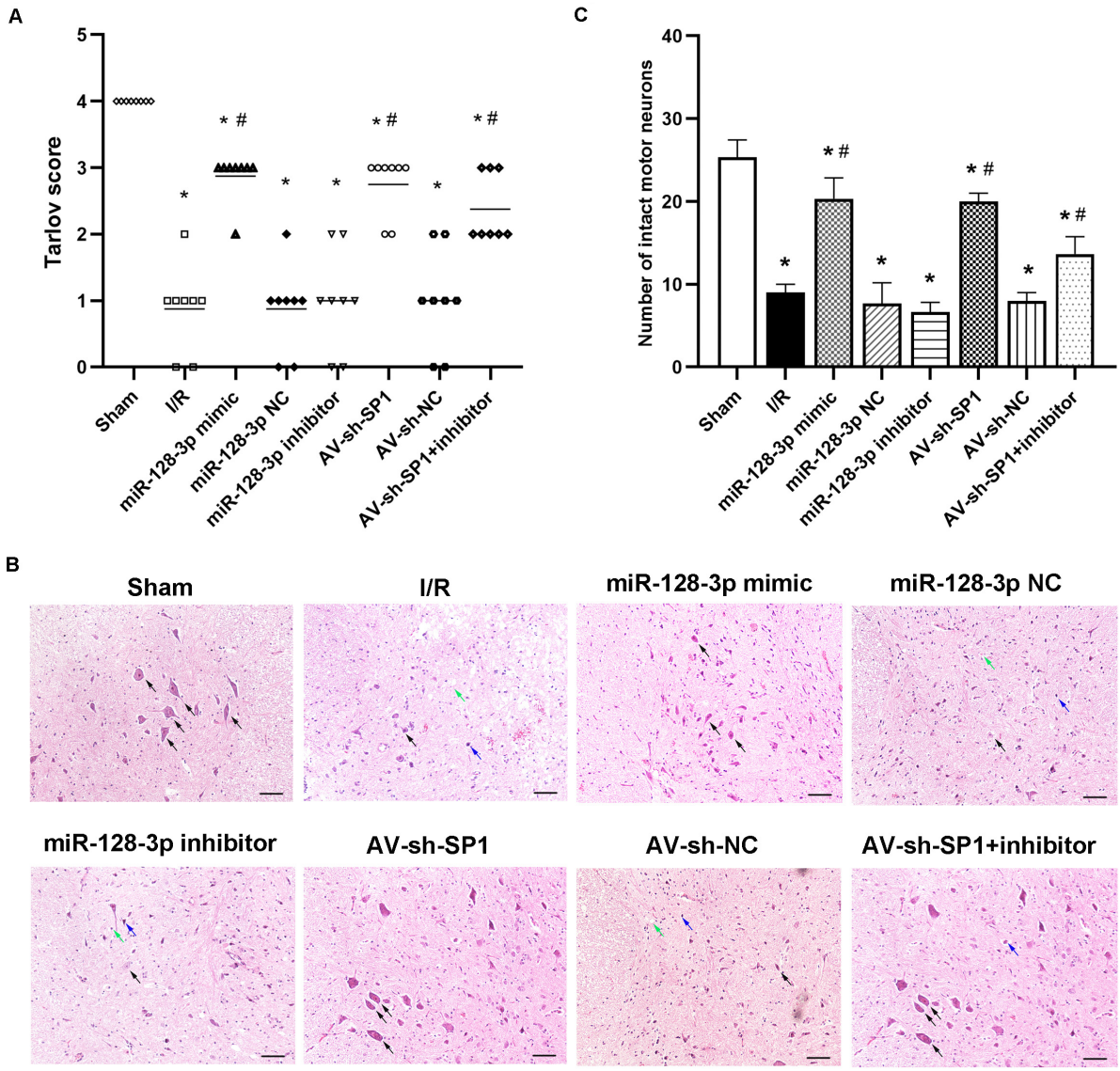

FIGURE 5 | Effects of miR-128-3p mimic and AV-sh-SP1 on neurological function and histologic evaluation after I/R. **(A)** Neurological function scores at 12 h after I/R in eight groups. Tarlov scores ranged from 0 (paraplegia) to 4 (normal). Each symbol represents one rat ($n = 8$). **(B)** Representative sections of L4–L6 spinal cord segments in the central horn of gray matter stained with hematoxylin and eosin 12 h after I/R in eight groups. Scale bar = 100 μm. **(C)** Numbers of intact motor neurons of ventral gray matter in the eight groups. The black arrows indicate normal neurons. The blue arrows indicate dead neurons with a diffuse cytoplasm without cellar structure. The green arrows indicate loosened tissue organization. $^{*}P < 0.05$ vs. sham group. $^{\#}P < 0.05$ vs. IR or NC group.

permeability, reduction in inflammatory factors in ELISA (IL-1β, TNF-α, and IL-6) and numbers of complete neurons were obtained after miR-128-3p mimic administration, as reflected by increased Tarlov scores and reduced EB extravasation. Moreover, we performed TUNEL staining and measured protein levels of Bax and Bcl-2, to investigate the mechanisms by which miR-128-3p might attenuate the neuronal apoptosis after I/R (**Figures 7A,C**). The results showed that TUNEL-positive cells mainly presented a neuronal morphology and were distributed in the anterior horn with increased Bax and decreased Bcl-2 in Western blotting. Following miR-128-3p mimic administration, the TUNEL-positive cells decreased in the anterior horn with decreased Bax and increased Bcl-2. Based on these data, we hypothesized that miR-128-3p might induce neuroprotective effects in spinal cord I/R injury by ameliorating inflammatory cytokine production and apoptotic rate.

To explore the mechanism underlying the neuroprotective effects inducted by miR-128-3p overexpression on spinal cord I/R injury, potential mRNA targeting was examined. MiRs require complementary binding with ≥6 consecutive nucleotides in the 3′ UTR of an mRNA target (Li et al., 2015). Based on TargetScanHuman 7.1 (Li et al., 2018). SP1 mRNA had 8 complementary nucleotides in the 3′ UTR, and the temporal expression patterns of SP1 and miR-128-3p exhibited a negative

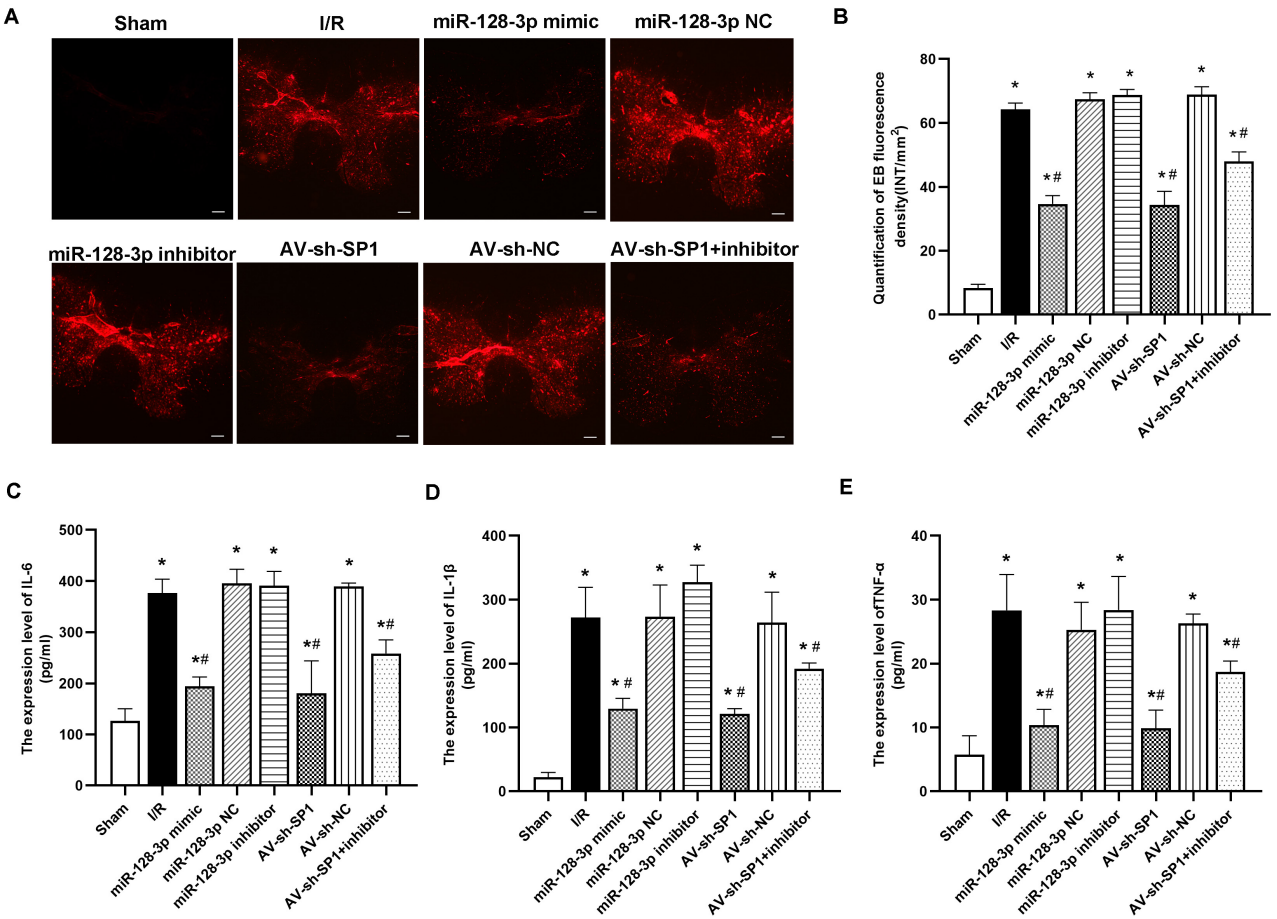

FIGURE 6 | Effects of miR-128-3p mimic and AV-sh-SP1 on blood–spinal cord barrier (BSCB) integrity and IL-6, IL-1β and TNF-α amounts after I/R. **(A)** EB extravasation visualized as red fluorescence by microscopy to evaluate the alterations in BSCB permeability in the eight groups. Scale bar = 200 μm. **(B)** Quantification of EB fluorescence intensity (INT/mm^2). **(C–E)** Measurements of IL-6, IL-1β, and TNF-α expression levels by ELISA in the eight groups. One-way ANOVA was performed for multiple-group comparisons, followed by the Tukey's test. $^*P < 0.05$ vs. sham group. $^{\#}P < 0.05$ vs. IR or NC group.

correlation at 12 h after reperfusion. In accordance with this result, reduced luciferase activity was found after co-transfection with a plasmid harboring the WT 3′ UTR of SP1 and miR-128-3p mimic. To avoid the cellular crosstalk and interactions *in vivo*, these effects were next assessed after pretreatment of rats with miR-128-3p mimic, control and inhibitor, respectively (Li et al., 2017). Administration of miR-128-3p mimic significantly reduced SP1 mRNA and protein amounts, while control and inhibitor miR showed no reductions, receptively (**Figures 4B–D**). Jointly, the above data suggest that miR-128-3p directly suppresses spinal cord SP1 following I/R.

SP1 is a frequently reported DNA-binding protein with a C2H2 zinc finger structure that controls gene transcription in multiple physiological and pathological processes (Chu, 2012). SP1 and related proteins contribute to multiple critical cellular events, including cell growth, differentiation, malignant transformation and apoptosis (Vizcaino et al., 2015). Based on previous literature, SP1 overexpression promotes apoptosis by itself, and malignant cells with SP1 overexpression can avoid SP1-associated apoptosis (Deniaud et al., 2006). In addition, some reports have found that SP1 was upregulated, and SP1 suppression exerted neuroprotection in experimental PD (Yao et al., 2018; Cai et al., 2020). SP1 also favors inflammation in many pathologies (Shin et al., 2015; Yang et al., 2018), and its absence reduces TNF-α, IL-1β, and IL-6 amounts in hypoxia-induced human umbilical vein endothelial cells (HUVECs) (Yang et al., 2018). These findings corroborate Qin et al. (2018), who revealed that suppressing the activation of SP1 effectively inhibits OGD/R-associated inflammation in microglia. Recently, emerging evidences indicate that expression of SP1 under ischemia/hypoxic conditions is increased (Eltzschig et al., 2009; Li et al., 2019). In addition, SP1 expression is upregulated following acute kidney damage associated with I/R (Chen et al., 2017). However, a report described anti-necroptosis effects for human-induced pluripotent stem cell-derived mesenchymal stromal cells-extracellular vesicles (hiPSC-MSCs-EVs) in renal I/R injury by delivering SP1 into target renal cells; meanwhile, SP1 knockout blunted renal protection by hiPSC-MSCs-EVs in rats with I/R injury (Yuan et al., 2017). Such discrepancy may be explained by distinct disease models and study time points for specific

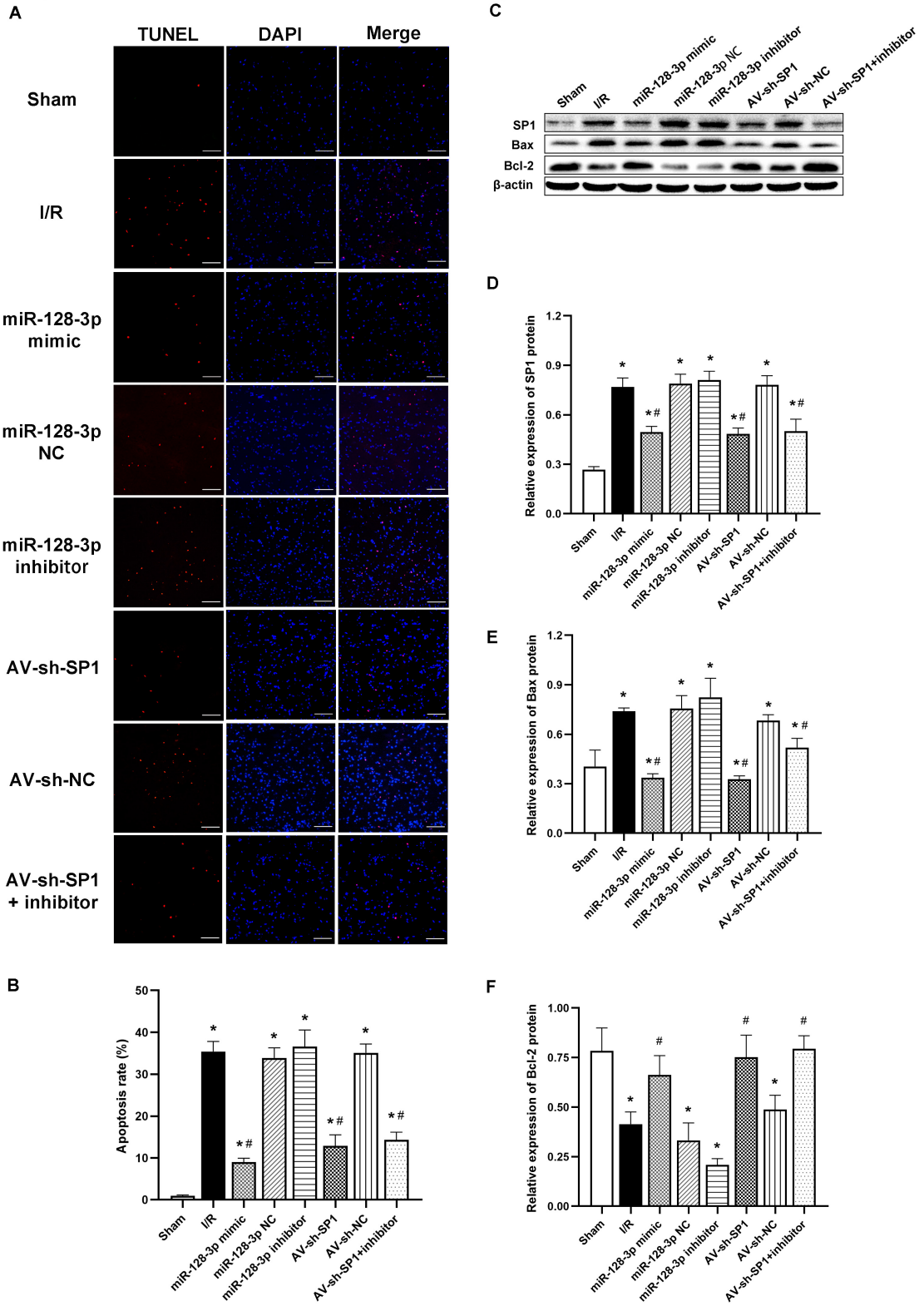

FIGURE 7 | Effects of miR-128-3p mimic and AV-sh-SP1 on neuronal apoptosis and SP1, Bax and Bcl-2 amounts after I/R. **(A)** Cell apoptosis in the ventral gray matter by TUNEL staining (green)and DAPI (blue). Scale bar = 100 μm. **(B)** Quantification of TUNEL-positive neurons in the ventral horn averaged across three independent experiments. **(C–F)** Representative Western blotting and quantitative protein analyses of SP1, Bax and Bcl-2 in the various groups. One-way ANOVA was performed for multiple-group comparisons, followed by the Tukey's test. $^{*}P < 0.05$ vs. sham group. $^{\#}P < 0.05$ vs. IR or NC group.

cell-type activation. A previous study also noted increased SP1 expression in the cortex after brain I/R damage and in primary neurons post-OGD/R (Sun et al., 2015), providing novel insights into the endogenous pathways that prevent ischemia-associated neuronal injury. Moreover, SP1 suppression delays neuronal loss and prolongs survival (Garcia-Morales et al., 2019). Additionally, in the current study, intrathecal injection of AV-sh-SP1 not only induced comparably lower levels of SP1 and resulted in poor production of IL-6, IL-1β, TNF-α, and Bax, but also upregulated Bcl-2, improved neurological function and histological findings, dwindled TUNEL-positive cells in anterior horn, and attenuated EB leakage, in comparison with the I/R group. The current findings suggest that SP1 might represent an inflammation and apoptosis-associated transcription factor, which promotes neuronal survival in spinal cord I/R injury. Moreover, we demonstrated that miR-128-3p targeted SP1, corroborating previous findings that miR-128 plays an essential role in glioma progression via SP1 suppression (Dong et al., 2014). Another report confirmed that high miR-128-3p expression suppresses cell proliferation and differentiation in bovine skeletal muscle satellite cells via SP1 downregulation (Dai et al., 2016).

CONCLUSION

Overall, miR-128-3p suppression provides remarkable protection of the spinal cord I/R injury, involving both anti-inflammatory and anti-apoptotic effects. Prophylactic approaches for spinal cord protection are essential, and this is the first report demonstrating that the miR-128-3p/SP1 axis has critical functions in neuroprotection upon spinal cord ischemia. This report further confirms that miRNAs are neuroprotective molecules affecting spinal cord I/R injury.

DATA AVAILABILITY STATEMENT

The raw data supporting the conclusions of this article will be made available by the authors, without undue reservation, to any qualified researcher.

ETHICS STATEMENT

The animal study was reviewed and approved by Animal Ethics Review Committee for Animal Experimentation of China Medical University.

AUTHOR CONTRIBUTIONS

DW, FC, and HM designed and performed the experiments and obtained the data. DW, BF, ZZ, and YD performed the statistical analysis and wrote the sections of the manuscript. XT wrote the first draft of the manuscript. All authors contributed to manuscript revision, read, and approved the submitted version.

FUNDING

This work was supported by the Natural Science Foundation of China (grant number 81771342).

ACKNOWLEDGMENTS

We would like to acknowledge the reviewers for their helpful comments on this study.

REFERENCES

Aslan, A., Cemek, M., Eser, O., Altunbaş, K., Buyukokuroglu, M. E., Cosar, M., et al. (2009). Does dexmedetomidine reduce secondary damage after spinal cord injury? An experimental study. *Eur. Spine J.* 18, 336–344. doi: 10.1007/s00586-008-0872-x

Balsam, L. B. (2017). Spinal cord ischemia-reperfusion injury: microRNAs and mitophagy at a crossroads. *J. Thorac. Cardiovasc. Surg.* 154, 1509–1510. doi: 10.1016/j.jtcvs.2017.06.010

Bao, N., Fang, B., Lv, H., Jiang, Y., Chen, F., Wang, Z., et al. (2018). Upregulation of miR-199a-5p protects spinal cord against ischemia/reperfusion-induced injury via downregulation of ECE1 in rat. *Cell. Mol. Neurobiol.* 38, 1293–1303. doi: 10.1007/s10571-018-0597-2

Beishline, K., and Azizkhan-Clifford, J. (2015). Sp1 and the 'hallmarks of cancer'. *FEBS J.* 282, 224–258. doi: 10.1111/febs.13148

Brandenburger, T., Castoldi, M., Brendel, M., Grievink, H., Schloesser, L., Werdehausen, R., et al. (2012). Expression of spinal cord microRNAs in a rat model of chronic neuropathic pain. *Neurosci. Lett.* 506, 281–286. doi: 10.1016/j.neulet.2011.11.023

Cai, L.-J., Tu, L., Li, T., Yang, X.-L., Ren, Y.-P., Gu, R., et al. (2020). Up-regulation of microRNA-375 ameliorates the damage of dopaminergic neurons, reduces oxidative stress and inflammation in Parkinson's disease by inhibiting SP1. *Aging* 12, 672–689. doi: 10.18632/aging.102649

Chen, G. H., Xu, C. S., Zhang, J., Li, Q., Cu, H. H., Li, X. D., et al. (2017). Inhibition of miR-128-3p by tongxinluo protects human cardiomyocytes from ischemia/reperfusion injury via upregulation of p70s6k1/p-p70s6k1. *Front. Pharmacol.* 8:17. doi: 10.3389/fphar.2017.00775

Chen, S.-J., Wu, P., Sun, L.-J., Zhou, B., Niu, W., Liu, S., et al. (2017). miR-204 regulates epithelial-mesenchymal transition by targeting SP1 in the tubular epithelial cells after acute kidney injury induced by ischemia-reperfusion. *Oncol. Rep.* 37, 1148–1158. doi: 10.3892/or.2016.5294

Chu, S. (2012). Transcriptional regulation by post-transcriptional modification-role of phosphorylation in Sp1 transcriptional activity. *Gene* 508, 1–8. doi: 10.1016/j.gene.2012.07.022

Citron, B. A., Dennis, J. S., Zeitlin, R. S., and Echeverria, V. (2008). Transcription factor Sp1 dysregulation in Alzheimer's disease. *J. Neurosci. Res.* 86, 2499–2504. doi: 10.1002/jnr.21695

Coselli, J. S., Lemaire, S. A., Preventza, O., De La Cruz, K. I., Cooley, D. A., Price, M. D., et al. (2016). Outcomes of 3309 thoracoabdominal aortic aneurysm repairs. *J. Thorac. Cardiovasc. Surg.* 151, 1323–1337. doi: 10.1016/j.jtcvs.2015.12.050

Dai, Y., Zhang, W. R., Wang, Y. M., Liu, X. F., Li, X., Ding, X. B., et al. (2016). microRNA-128 regulates the proliferation and differentiation of bovine skeletal muscle satellite cells by repressing Sp1. *Mol. Cell. Biochem.* 414, 37–46. doi: 10.1007/s11010-016-2656-7

Deniaud, E., Baguet, J., Mathieu, A. L., Pages, G., Marvel, J., and Leverrier, Y. (2006). Overexpression of Sp1 transcription factor induces apoptosis. *Oncogene* 25, 7096–7105. doi: 10.1038/sj.onc.1209696

Ding, Q., Wang, Q., Deng, J., Gu, Q., Hu, S., Li, Y., et al. (2009). Sevoflurane preconditioning induces rapid ischemic tolerance against spinal cord

ischemia/reperfusion through activation of extracellular signal-regulated kinase in rabbits. *Anesth. Analg.* 109, 1263–1272. doi: 10.1213/ane.0b013e3181b2214c

Dong, Q., Cai, N., Tao, T., Zhang, R., Yan, W., Li, R., et al. (2014). An axis involving SNAI1, microRNA-128 and SP1 modulates glioma progression. *PLoS One* 9:e98651. doi: 10.1371/journal.pone.0098651

Duan, W. R., Garner, D. S., Williams, S. D., Funckes-Shippy, C. L., Spath, I. S., and Blomme, E. A. (2003). Comparison of immunohistochemistry for activated caspase-3 and cleaved cytokeratin 18 with the TUNEL method for quantification of apoptosis in histological sections of PC-3 subcutaneous xenografts. *J. Pathol.* 199, 221–228. doi: 10.1002/path.1289

Eltzschig, H. K., Koehler, D., Eckle, T., Kong, T., Robson, S. C., and Colgan, S. P. (2009). Central role of Sp1-regulated CD39 in hypoxia/ischemia protection. *Blood* 113, 224–232. doi: 10.1182/blood-2008-06-165746

Etz, C. D., Weigang, E., Hartert, M., Lonn, L., Mestres, C. A., Di Bartolomeo, R., et al. (2015). Contemporary spinal cord protection during thoracic and thoracoabdominal aortic surgery and endovascular aortic repair: a position paper of the vascular domain of the European association for cardio-thoracic surgery†. *Eur. J. Cardiothorac. Surg.* 47, 943–957. doi: 10.1093/ejcts/ezv142

Fang, B., Li, X.-M., Sun, X.-J., Bao, N.-R., Ren, X.-Y., Lv, H.-W., et al. (2013a). Ischemic preconditioning protects against spinal cord ischemia-reperfusion injury in rabbits by attenuating blood spinal cord barrier disruption. *Int. J. Mol. Sci.* 14, 10343–10354. doi: 10.3390/ijms140510343

Fang, B., Wang, H., Sun, X. J., Li, X. Q., Ai, C. Y., Tan, W. F., et al. (2013b). Intrathecal transplantation of bone marrow stromal cells attenuates blood-spinal cord barrier disruption induced by spinal cord ischemia-reperfusion injury in rabbits. *J. Vasc. Surg.* 58, 1043–1052. doi: 10.1016/j.jvs.2012.11.087

Fu, J., Sun, H., Wei, H., Dong, M., Zhang, Y., Xu, W., et al. (2020). Astaxanthin alleviates spinal cord ischemia-reperfusion injury via activation of PI3K/Akt/GSK-3β pathway in rats. *J. Orthop. Surg. Res.* 15:275.

Garcia-Morales, V., Rodriguez-Bey, G., Gomez-Perez, L., Dominguez-Vias, G., Gonzalez-Forero, D., Portillo, F., et al. (2019). Sp1-regulated expression of p11 contributes to motor neuron degeneration by membrane insertion of TASK1. *Nat. Commun.* 10:3784.

Gelderd, J. B., and Chopin, S. F. (1977). The vertebral level of origin of spinal nerves in the rat. *Anat. Rec.* 188, 45–47. doi: 10.1002/ar.1091880106

Gilerovich, E. G., Moshonkina, T. R., Fedorova, E. A., Shishko, T. T., Pavlova, N. V., Gerasimenko, Y. P., et al. (2008). Morphofunctional characteristics of the lumbar enlargement of the spinal cord in rats. *Neurosci. Behav. Physiol.* 38, 855–860. doi: 10.1007/s11055-008-9056-8

He, F., Ren, Y., Shi, E., Liu, K., Yan, L., and Jiang, X. (2016). Overexpression of microRNA-21 protects spinal cords against transient ischemia. *J. Thorac. Cardiovasc. Surg.* 152, 1602–1608. doi: 10.1016/j.jtcvs.2016.07.065

He, F., Shi, E., Yan, L., Li, J., and Jiang, X. (2015). Inhibition of micro-ribonucleic acid-320 attenuates neurologic injuries after spinal cord ischemia. *J. Thorac. Cardiovasc. Surg.* 150, 398–406. doi: 10.1016/j.jtcvs.2015.03.066

Huang, C.-Y., Huang, X.-P., Zhu, J.-Y., Chen, Z.-G., Li, X.-J., Zhang, X.-H., et al. (2015). miR-128-3p suppresses hepatocellular carcinoma proliferation by regulating PIK3R1 and is correlated with the prognosis of HCC patients. *Oncol. Rep.* 33, 2889–2898. doi: 10.3892/or.2015.3936

Huo, L., Wang, B., Zheng, M., Zhang, Y., Xu, J., Yang, G., et al. (2019). miR-128-3p inhibits glioma cell proliferation and differentiation by targeting NPTX1 through IRS-1/PI3K/AKT signaling pathway. *Exp. and Ther. Med.* 17, 2921–2930.

Judas, G. I., Ferreira, S. G., Simas, R., Sannomiya, P., Benício, A., Da Silva, L. F., et al. (2014). Intrathecal injection of human umbilical cord blood stem cells attenuates spinal cord ischaemic compromise in rats. *Interact. Cardiovasc. Thorac. Surg.* 18, 757–762. doi: 10.1093/icvts/ivu021

Karatas, Y., Erdi, M. F., Kaya, B., Keskin, F., Cuce, G., Kilinc, I., et al. (2019). Neuroprotective effects of tocilizumab on experimentally-induced spinal cord ischemia-reperfusion injury. *World Neurosurg.* 124, E208–E213.

Kim, V. N., Han, J., and Siomi, M. C. (2009). Biogenesis of small RNAs in animals. *Nat. Rev. Mol. Cell Biol.* 10, 126–139. doi: 10.1038/nrm2632

Krichevsky, A. M., Sonntag, K.-C., Isacson, O., and Kosik, K. S. (2006). Specific microRNAs modulate embryonic stem cell-derived neurogenesis. *Stem Cells* 24, 857–864. doi: 10.1634/stemcells.2005-0441

Ksiazek-Winiarek, D. J., Kacperska, M. J., and Glabinski, A. (2013). MicroRNAs as novel regulators of neuroinflammation. *Mediators Inflamm.* 2013:172351.

LeMaire, S. A., Price, M. D., Green, S. Y., Zarda, S., and Coselli, J. S. (2012). Results of open thoracoabdominal aortic aneurysm repair. *Ann. Cardiothorac. Surg.* 1, 286–292.

Li, Q., Gao, S., Kang, Z., Zhang, M., Zhao, X., Zhai, Y., et al. (2018). Rapamycin enhances mitophagy and attenuates apoptosis after spinal ischemia-reperfusion injury. *Front. Neurosci.* 12:865. doi: 10.3389/fnins.2018.00865

Li, R., Zhao, K. C., Ruan, Q., Meng, C. Y., and Yin, F. (2020). The transcription factor Foxd3 induces spinal cord ischemia-reperfusion injury by potentiating microRNA-214-dependent inhibition of Kcnk2. *Exp. Mol. Med.* 12, 118–129. doi: 10.1038/s12276-019-0370-8

Li, X. G., Du, J. H., Lu, Y., and Lin, X. J. (2019). Neuroprotective effects of rapamycin on spinal cord injury in rats by increasing autophagy and Akt signaling. *Neural Regen. Res.* 14, 721–727. doi: 10.4103/1673-5374.247476

Li, X.-Q., Cao, X.-Z., Wang, J., Fang, B., Tan, W.-F., and Ma, H. (2014a). Sevoflurane preconditioning ameliorates neuronal deficits by inhibiting microglial MMP-9 expression after spinal cord ischemia/reperfusion in rats. *Mol. Brain* 7:69.

Li, X.-Q., Chen, F.-S., Tan, W.-F., Fang, B., Zhang, Z.-L., and Ma, H. (2017). Elevated microRNA-129-5p level ameliorates neuroinflammation and blood-spinal cord barrier damage after ischemia-reperfusion by inhibiting HMGB1 and the TLR3-cytokine pathway. *J. Neuroinflamm.* 14:205.

Li, X.-Q., Lv, H.-W., Tan, W.-F., Fang, B., Wang, H., and Ma, H. (2014b). Role of the TLR4 pathway in blood-spinal cord barrier dysfunction during the bimodal stage after ischemia/reperfusion injury in rats. *J. Neuroinflamm.* 11:62. doi: 10.1186/1742-2094-11-62

Li, X.-Q., Lv, H.-W., Wang, Z.-L., Tan, W.-F., Fang, B., and Ma, H. (2015). MiR-27a ameliorates inflammatory damage to the blood-spinal cord barrier after spinal cord ischemia: reperfusion injury in rats by downregulating TICAM-2 of the TLR4 signaling pathway. *J. Neuroinflamm.* 12:25. doi: 10.1186/s12974-015-0246-3

Li, X.-Q., Wang, J., Fang, B., Tan, W.-F., and Ma, H. (2014c). Intrathecal antagonism of microglial TLR4 reduces inflammatory damage to blood-spinal cord barrier following ischemia/reperfusion injury in rats. *Mol. Brain* 7:28. doi: 10.1186/1756-6606-7-28

Li, X.-Q., Yu, Q., Tan, W.-F., Zhang, Z.-L., and Ma, H. (2018). MicroRNA-125b mimic inhibits ischemia reperfusion-induced neuroinflammation and aberrant p53 apoptotic signalling activation through targeting TP53INP1. *Brain Behav. Immun.* 74, 154–165. doi: 10.1016/j.bbi.2018.09.002

Li, Y., Feng, D., Wang, Z., Zhao, Y., Sun, R., Tian, D., et al. (2019). Ischemia-induced ACSL4 activation contributes to ferroptosis-mediated tissue injury in intestinal ischemia/reperfusion. *Cell Death Differ.* 26, 2284–2299. doi: 10.1038/s41418-019-0299-4

Liu, K., Yan, L., Jiang, X., Yu, Y., Liu, H., Gu, T., et al. (2017). Acquired inhibition of microRNA-124 protects against spinal cord ischemia-reperfusion injury partially through a mitophagy-dependent pathway. *J. Thorac. Cardiovasc. Surg.* 154, 1498–1508. doi: 10.1016/j.jtcvs.2017.05.046

Mao, G., Ren, P., Wang, G., Yan, F., and Zhang, Y. (2017). MicroRNA-128-3p protects mouse against cerebral ischemia through reducing p38 alpha mitogen-activated protein kinase activity. *J. Mol. Neurosci.* 61, 152–158. doi: 10.1007/s12031-016-0871-z

Mestre, C., Pélissier, T., Fialip, J., Wilcox, G., and Eschalier, A. (1994). A method to perform direct transcutaneous intrathecal injection in rats. *J. Pharmacol. Toxicol. Methods* 32, 197–200. doi: 10.1016/1056-8719(94)90087-6

Nam, E.-H., Lee, Y., Zhao, X.-F., Park, Y.-K., Lee, J. W., and Kim, S. (2014). ZEB2Sp1 cooperation induces invasion by upregulating cadherin-11 and integrin 5 expression. *Carcinogenesis* 35, 302–314. doi: 10.1093/carcin/bgt340

Padmanabhan, R., and Singh, S. (1979). Observations on the topographical relations of spinal nerve roots in the rat. *Acta Anat.* 105, 378–380. doi: 10.1159/000145142

Qin, F., Zhao, Y., Shang, W., Zhao, Z.-M., Qian, X., Zhang, B.-B., et al. (2018). Sinomenine relieves oxygen and glucose deprivation-induced microglial activation via inhibition of the SP1/miRNA-183-5p/I kappa B-alpha signaling pathway. *Cell. Mol. Biol.* 64, 140–147. doi: 10.14715/cmb/2018.64.10.23

Ramanan, V. K., and Saykin, A. J. (2013). Pathways to neurodegeneration: mechanistic insights from GWAS in Alzheimer's disease, Parkinson's disease, and related disorders. *Am. J. Neurodegener. Dis.* 2, 145–175.

Saito, T., Saito, S., Yamamoto, H., and Tsuchida, M. (2013). Neuroprotection following mild hypothermia after spinal cord ischemia in rats. *J. Vasc. Surg.* 57, 173–181. doi: 10.1016/j.jvs.2012.05.101

Saugstad, J. A. (2010). MicroRNAs as effectors of brain function with roles in ischemia and injury, neuroprotection, and neurodegeneration. *J. Cereb. Blood Flow Metab.* 30, 1564–1576. doi: 10.1038/jcbfm.2010.101

Shin, I.-S., Shin, N.-R., Park, J.-W., Jeon, C.-M., Hong, J.-M., Kwon, O.-K., et al. (2015). Melatonin attenuates neutrophil inflammation and mucus secretion in cigarette smoke-induced chronic obstructive pulmonary diseases via the suppression of Erk-Sp1 signaling. *J. Pineal Res.* 58, 50–60. doi: 10.1111/jpi.12192

Song, C., Zhang, J., Liu, Y., Pan, H., Qi, H. P., Cao, Y. G., et al. (2016). Construction and analysis of cardiac hypertrophy-associated lncRNA-mRNA network based on competitive endogenous RNA reveal functional lncRNAs in cardiac hypertrophy. *Oncotarget* 7, 10827–10840. doi: 10.18632/oncotarget.7312

Sun, M., Li, M., Huang, Q., Han, F., Gu, J.-H., Xie, J., et al. (2015). Ischemia/reperfusion-induced upregulation of TIGAR in brain is mediated by SP1 and modulated by ROS and hormones involved in glucose metabolism. *Neurochem. Int.* 80, 99–109. doi: 10.1016/j.neuint.2014.09.006

Tan, C. L., Plotkin, J. L., Veno, M. T., Von Schimmelmann, M., Feinberg, P., Mann, S., et al. (2013). MicroRNA-128 governs neuronal excitability and motor behavior in mice. *Science* 342, 1254–1258. doi: 10.1126/science.1244193

Vizcaino, C., Mansilla, S., and Portugal, J. (2015). Sp1 transcription factor: a long-standing target in cancer chemotherapy. *Pharmacol. Ther.* 152, 111–124. doi: 10.1016/j.pharmthera.2015.05.008

Wang, R., Yang, Y., Wang, H., He, Y., and Li, C. (2020). MiR-29c protects against inflammation and apoptosis in Parkinson's disease model in vivo and in vitro by targeting SP1. *Clin. Exp. Pharmacol. Physiol.* 47, 372–382. doi: 10.1111/1440-1681.13212

Wierstra, I. (2008). Sp1: emerging roles – beyond constitutive activation of TATA-less housekeeping genes. *Biochem. Biophys. Res. Commun.* 372, 1–13. doi: 10.1016/j.bbrc.2008.03.074

Wong, D. R., Parenti, J. L., Green, S. Y., Chowdhary, V., Liao, J. M., Zarda, S., et al. (2011). Open repair of thoracoabdominal aortic aneurysm in the modern surgical era: contemporary outcomes in 509 patients. *J. Am. Coll. Surg.* 212, 569–579; discussion 579–581.

Yang, R., Xing, L., Zheng, X., Sun, Y., Wang, X., and Chen, J. (2019). The circRNA circAGFG1 acts as a sponge of miR-195-5p to promote triple-negative breast cancer progression through regulating CCNE1 expression. *Mol. Cancer* 18:4.

Yang, S., Yin, J., and Hou, X. (2018). Inhibition of miR-135b by SP-1 promotes hypoxia-induced vascular endothelial cell injury via HIF-1 alpha. *Exp. Cell Res.* 370, 31–38. doi: 10.1016/j.yexcr.2018.06.001

Yao, L., Dai, X., Sun, Y., Wang, Y., Yang, Q., Chen, X., et al. (2018). Inhibition of transcription factor SP1 produces neuroprotective effects through decreasing MAO B activity in MPTP/MPP+ Parkinson's disease models. *J. Neurosci. Res.* 96, 1663–1676. doi: 10.1002/jnr.24266

Yin, J., Yin, Z., Wang, B., Zhu, C., Sun, C., Liu, X., et al. (2019). Angiopoietin-1 protects spinal cord ischemia and reperfusion injury by inhibiting autophagy in rats. *Neurochem. Res.* 44, 2746–2754. doi: 10.1007/s11064-019-02893-3

Yuan, X., Li, D., Chen, X., Han, C., Xu, L., Huang, T., et al. (2017). Extracellular vesicles from human-induced pluripotent stem cell-derived mesenchymal stromal cells (hiPSC-MSCs) protect against renal ischemia/reperfusion injury via delivering specificity protein (SP1) and transcriptional activating of sphingosine kinase 1 and inhibiting necroptosis. *Cell Death Dis.* 8:3200. doi: 10.1038/s41419-017-0041-4

Zhang, G., Chen, L., Liu, J., Jin, Y., Lin, Z., Du, S., et al. (2020). HIF-1 alpha/microrNA-128-3p axis protects hippocampal neurons from apoptosis via the Axin1-meaiated Wnt/beta-catenin signaling pathway in Parkinson's disease moaeis. *Aging* 12, 4067–4081. doi: 10.18632/aging.102636

Zhao, L., Li, R., Xu, S., Li, Y., Zhao, P., Dong, W., et al. (2018). Tumor suppressor miR-128-3p inhibits metastasis and epithelial-mesenchymal transition by targeting ZEB1 in esophageal squamous-cell cancer. *Acta Biochim. Biophys. Sin.* 50, 171–180. doi: 10.1093/abbs/gmx132

Conflict of Interest: The authors declare that the research was conducted in the absence of any commercial or financial relationships that could be construed as a potential conflict of interest.

Copyright © 2020 Wang, Chen, Fang, Zhang, Dong, Tong and Ma. This is an open-access article distributed under the terms of the Creative Commons Attribution License (CC BY). The use, distribution or reproduction in other forums is permitted, provided the original author(s) and the copyright owner(s) are credited and that the original publication in this journal is cited, in accordance with accepted academic practice. No use, distribution or reproduction is permitted which does not comply with these terms.

frontiers in Neuroscience

ORIGINAL RESEARCH
published: 28 January 2021
doi: 10.3389/fnins.2021.579431

Pathophysiological Changes and the Role of Notch-1 Activation After Decompression in a Compressive Spinal Cord Injury Rat Model

Xing Cheng[1†], Zhengran Yu[1†], Jinghui Xu[1], Daping Quan[2] and Houqing Long[1]*

[1] Guangdong Provincial Key Laboratory of Orthopaedics and Traumatology, Orthopaedic Research Institute/Department of Spine Surgery, The First Affiliated Hospital, Sun Yat-sen University, Guangzhou, China, [2] PCFM Lab, GD HPPC Lab, School of Materials Science and Engineering, Sun Yat-sen University, Guangzhou, China

Surgical decompression is the primary treatment for cervical spondylotic myelopathy (CSM) patients with compressive spinal cord injury (CSCI). However, the prognosis of patients with CSCI varies, and the pathophysiological changes following decompression remain poor. This study aimed to investigate the pathophysiological changes and the role of Notch-1 activation after decompression in a rat CSCI model. Surgical decompression was conducted at 1 week post-injury (wpi). DAPT was intraperitoneally injected to down-regulate Notch-1 expression. Basso, Beattie, and Bresnahan scores and an inclined plane test were used to evaluate the motor function recovery. Hematoxylin and eosin staining was performed to assess pathophysiological changes, while hypoxia-inducible factor 1 alpha, vascular endothelial growth factor (VEGF), von Willebrand factor (vWF), matrix metalloproteinase (MMP)-9, MMP-2, Notch-1, and Hes-1 expression in the spinal cord were examined by immunohistochemical analysis or quantitative PCR. The results show that early decompression can partially promote motor function recovery. Improvements in structural and cellular damage and hypoxic levels were also observed in the decompressed spinal cord. Moreover, decompression resulted in increased VEGF and vWF expression, but decreased MMP-9 and MMP-2 expression at 3 wpi. Expression levels of Notch-1 and its downstream gene Hes-1 were increased after decompression, and the inhibition of Notch-1 significantly reduced the decompression-induced motor function recovery. This exploratory study revealed preliminary pathophysiological changes in the compressed and decompressed rat spinal cord. Furthermore, we confirmed that early surgical decompression partially promotes motor function recovery may via activation of the Notch-1 signaling pathway after CSCI. These results could provide new insights for the development of drug therapy to enhance recovery following surgery.

Keywords: decompression, CSCI, motor function, pathophysiological changes, Notch-1

OPEN ACCESS

Edited by:
Christoph Harms,
Charité – Universitätsmedizin Berlin, Germany

Reviewed by:
Lies De Groef,
KU Leuven, Belgium
Marietta Zille,
University of Lübeck, Germany
Chunyi Wen,
The Hong Kong Polytechnic University, Hong Kong

****Correspondence:***
Houqing Long
longhq@mail.sysu.edu.cn;
houqinglong@163.com

[†]These authors share first authorship

Specialty section:
This article was submitted to Neurodegeneration, a section of the journal Frontiers in Neuroscience

Received: *02 July 2020*
Accepted: *11 January 2021*
Published: *28 January 2021*

Citation:
Cheng X, Yu Z, Xu J, Quan D and Long H (2021) Pathophysiological Changes and the Role of Notch-1 Activation After Decompression in a Compressive Spinal Cord Injury Rat Model. Front. Neurosci. 15:579431. doi: 10.3389/fnins.2021.579431

INTRODUCTION

Cervical spondylotic myelopathy (CSM) is a degenerative condition of the spine that leads to static and dynamic compression of the spinal cord (Karadimas et al., 2013a). CSM in cases of compressive spinal cord injury (CSCI) results in various pathophysiological alterations, such as neuroinflammation, microvasculature changes, ischemic-hypoxic injury,

blood spinal cord barrier (BSCB) destruction, and neuronal cell death (Yu et al., 2011; Hirai et al., 2013; Tetreault et al., 2015; Vidal et al., 2019). Decades ago, it was reported that surgical decompression of the compressed spinal cord can partially recover neurological function in patients and halt CSM progression (Wiberg, 1986; Ishida et al., 1999; Li et al., 2019; Akter et al., 2020). However, our understanding of the physiological and pathological changes following decompression remains poor due to the lack of a reliable animal model of induced CSM. Thus, studies on the pathophysiological changes after decompression may contribute to improved prognoses of patients with CSCI.

In recent years, numerous attempts have been made to establish a CSCI model in different animals, employing methods such as tumor induction (Izumida, 1995), the use of penetrating hydrogels (Yang et al., 2015) or urethane polymers (Kurokawa et al., 2011), the use of spinal hyperostotic mice (twy/twy) (Hirai et al., 2013), and plastic screw implantation (Kanchiku et al., 2001). Among these approaches, hydrogels and polymers are expected be applicable materials that lead to a chronically progressive injury. However, neurological function changes after CSCI have not been reported for the application of polyurethane polymers. Previously, we successfully established a CSCI rat model using a water-absorbable polyurethane polymer sheet (Long et al., 2013), which provided a foundation for exploring pathophysiological changes in the decompressed spinal cord.

Thus far, only four studies have investigated the decompressed state of CSM in animal models (Harkey et al., 1995; Karadimas et al., 2015b; Dhillon et al., 2016; Haddas et al., 2018). Harkey et al. (1995) demonstrated that decompression can improve neurological function and can alter the necrosis and cavitation of spinal cord tissue in a dog model. Karadimas et al. (2015b) reported on an ischemia-reperfusion injury after decompression in a rat model, which could be prevented by treatment with riluzole. Dhillon et al. (2016) suggested that decompression may increase axon growth rates and promote axon sprouting in a rat model. In addition, (Vidal et al., 2017) found that early decompression is important for achieving better neurological outcomes and demonstrated that delayed decompression is associated with increased astrogliosis, microglia activation, and reduced spinal cord blood flow. As few studies have evaluated the decompression state of CSM, further investigations of pathophysiological changes in the decompressed spinal cord are vital to enable the development of comprehensive drug therapy in order to enhance recovery following surgery.

We have found that various changes, including alterations in microvascular density (Long et al., 2014; Cheng et al., 2015), varying degrees of ischemia-hypoxia (Long et al., 2012; Cheng et al., 2019), matrix metalloproteinase (MMP) expression (Cheng et al., 2019), BSCB disruption (Long et al., 2015), and neuron loss (Xu et al., 2017), occured at different time points after chronic CSCI. Structural and cellular changes after decompression, such as the expression of angiogenesis- and BSCB-related factors, have attracted substantial attention in acute and chronic SCI (Ng et al., 2011; Karadimas et al., 2015a; Randi and Laffan, 2017). Nevertheless, the pathophysiological changes occurring in the decompressed spinal cord have not been widely investigated. Increasing evidence suggests that Notch-1 signaling is involved in central nervous system (CNS) diseases and is associated with cell death, angiogenesis, and BSCB function (Fassbender et al., 2011; Cai et al., 2016). By elucidating the physiological and pathological changes and the role of the Notch-1 signaling pathway after decompression in CSCI, new perspectives may be provided for improving the prognosis of CSM patients with decompression. Therefore, based on our previous studies, we further investigated the physiological and pathological changes in the decompressed spinal cord and the effects of Notch-1 pathway inhibition in a rat CSCI model following decompression.

MATERIALS AND METHODS

Animal Studies

The procedures applied in these experiments were approved by the Research Ethics Committee of Sun Yat-sen University and conformed to all relevant regulatory standards (Animal protocol number: 2020458). A total of 73 adult female Sprague–Dawley rats (weighing 250–300 g; aged 28–30 weeks) were included in this study. Ten of these rats were used to evaluate the extent of expansion of the compression material at 1 day post-injury (dpi) ($n = 3$), 1 week post-injury (wpi) ($n = 3$), or 3 wpi ($n = 4$). Thirty-one rats were randomly allocated to the sham ($n = 10$), CSCI ($n = 10$), or CSCI with decompression (CSCI + decompression; $n = 11$) group. Finally, Thirty-two rats were randomly allocated to the CSCI ($n = 10$), CSCI with decompression and control (CSCI + decompression + NC; $n = 11$), or CSCI with decompression and DAPT (CSCI + decompression + DAPT; $n = 11$) group. One rat died in the Sham group and CSCI group respectively, after the initial surgery due to anesthetic accident, One rat in the CSCI group died on the next day after compression surgery. We performed compression surgeries for 76 rats and three of them died. The mortality rate was 3.9%. The rats were housed in groups of 4–5 per cage on a 12/12-h light/dark cycle with free access to food and water.

Intraperitoneal Injection

DAPT solution (1 μg/μL) was prepared by dissolving DAPT powder (MCE, United States) in 0.01 M phosphate-buffered saline (PBS) containing 5% dimethyl sulfoxide. The DAPT solution (1 mg/kg per rat) and a negative control were intraperitoneally injected using a microinjection syringe (Cheng et al., 2020).

Compressive Spinal Cord Injury

Rats in the sham and CSCI groups were anesthetized with a cocktail (3 mg/kg) (Guangzhou FISCLAB Environ. Sci-Tech. Co., Ltd., Guangzhou, China) containing ketamine (31.25 mg/kg), xylazine (1.58 mg/kg), and acepromazine (0.31 mg/kg). Following exposure of the C4–C6 spinal process and laminas from the posterior, C5 laminectomy was conducted to access the epidural space. In the CSCI group, a sheet (1 mm × 3 mm × 1 mm) of water-absorbable polyurethane polymer, (1→4)-3,6-anhydro-a-l-galactopyranosyl-(1→3)-β-D-galactopyranan), was implanted into the C6 epidural space

in the dorsal region of the spinal cord (Hu et al., 2011). A modified polyurethane membrane (synthesized by isocyanates and polyols) was coated on the surface of the polymer sheet to reduce the expansion speed. Spinal cord compression was gradually achieved through slow expansion of the polymer sheet. In contrast, animals in the sham groups received only the C5 laminectomy, without insertion of the polymer. For surgical decompression, the same anesthesia methods were applied, and all animals were reopened. In this step, the polymer was removed in the decompression group. After surgery, the paravertebral muscle was sutured in layers, and the skin incision was stapled. Animals received a subcutaneous injection of lactated Ringer's solution (200 μL) immediately after compression or decompression to prevent dehydration. Penicillin G (80 U/g) was intramuscularly injected to prevent infection during surgery, and carprofen (4–5 mg/kg, Rimadyl, Pfizer) was injected subcutaneously 2 days post-surgery for further pain relief as needed. Both compression and decompression surgeries were performed by the same experienced investigator.

Motor Function Evaluation

To evaluate the motor function recovery after CSCI, the Basso, Beattie, and Bresnahan (BBB) locomotor scale (Basso et al., 1995) and an inclined plane test (IPT) (Rivlin and Tator, 1977) were conducted at 1 dpi and 1, 2, and 3 wpi. BBB scores range between 0 and 21, where a score of 0 reflects complete paralysis and a score of 21 indicates normal locomotion. Lower scores (0–7) denote isolated joint movements with little or no hindlimb movement; intermediate scores (8–13) express intervals of uncoordinated stepping; and higher scores (14–21) express forelimb and hindlimb coordination. For the IPT, rats were placed horizontally on a smooth tilt board. The board was initially placed in a horizontal orientation (0°), and the angle was increased by 5–10° after each attempt. The maximum angle at which the rats remained on the board for 10 s was recorded. Raw BBB score data for the group of CSCI with decompression were used to evaluate the recovery of animals at 3 wpi in comparison with 1 wpi [Recovery BBB score (CSCI): BBB score (3 wpi) – BBB score (1 wpi)]. If the recovery BBB score $\geq$ standard deviation (S.D.) of the recovery BBB score (CSCI), then the case was determined to have significant recovery. If the recovery BBB score $<$ S.D. of the recovery BBB score (CSCI), then the case was determined to have no recovery. This evaluation was conducted by two investigators blinded to the group assignments.

Micro-Computed Tomography

To assess the extent of expansion of the compression material after implantation, the cervical spinal cords of rats in different groups were assessed by micro-computed tomography (micro-CT) (ZKKS-MCT-Sharp-II, Guangzhou Zhongkekaisheng Medical Technology Co., Ltd., Guangzhou, China). Animals were anesthetized with an overdose of 80–120 mg/kg intravenous sodium pentobarbital (Guangzhou Fischer Chemical Co., Ltd.) and transcardially perfused with 0.9% saline followed by 4% paraformaldehyde in 0.1 M phosphate buffer. The whole cervical spinal cord was then carefully harvested and fixed overnight with 4% formaldehyde in phosphate-buffered solution. Prior to micro-CT scanning, the tissues surrounding the spine were carefully removed under a microscope. The compression material of each specimen was presented using 3D-Med 4.3 software (Guangzhou ZhongkeKaisheng Medical Technology Co., Ltd., Guangzhou, China).

Immunohistochemistry

After perfusion, the C5–C7 spinal cord segment was harvested, fixed overnight with 4% formaldehyde in phosphate-buffered solution at 4°C, and then embedded in paraffin. A series of 25-μm-thick spinal cord sections was used for immunohistochemical (IHC) staining. Microwave epitope retrieval was performed before staining. Sections were incubated overnight at 4°C with a mouse monoclonal antibody against hypoxia-inducible factor 1 alpha (HIF-1α) (1:150; ab1, Abcam, Cambridge, United Kingdom), a rabbit polyclonal antibody against Notch-1 (1:200; ab8925, Abcam, Cambridge, United Kingdom), a mouse monoclonal antibody against Hes-1 (1:50; sc-166410, Santa Cruz Biotechnology, Inc., United States), a mouse monoclonal antibody against vascular endothelial growth factor A (VEGFA) (1:200; ab1316, Abcam, Cambridge, United Kingdom), a rabbit polyclonal against von Willebrand factor (vWF) (1:200; ab6994, Abcam, Cambridge, United Kingdom), a rabbit polyclonal against MMP-9 (1:100; ab38898, Abcam, Cambridge, United Kingdom), and a mouse monoclonal antibody against MMP-2 (1:300; ab86607, Abcam, Cambridge, United Kingdom). Subsequently, the sections were sequentially incubated with a ready-to-use DAKO ChemMate EnVision^{TM} kit (K500711; Dako; Agilent Technologies, Inc., Santa Clara, CA, United States) for 30 min at room temperature. Images of each section of the perilesional spinal cord were acquired at 200× or 400× magnification using an XC30 camera mounted on an Olympus microscope (Olympus Corporation, Tokyo, Japan). Three random images at 200× or 400× magnification were also captured for semi-quantitative analysis. The brown area in the sham spinal cord was analyzed, and the background density was excluded to create the standard. Subsequently, the integrated optical density (IOD) was calculated using Image-Pro Plus 6.0 software (Media Cybernetics, Inc., Rockville, MD, United States). Omission of the primary antibody only controls for unspecific staining of the secondary antibodies.

Hematoxylin and Eosin Staining

Briefly, slides were placed in xylene in a 37°C incubator. The slides were hydrated by passing through the following alcohol concentrations (100, 100, 95, 95, 75, 75%). Hematoxylin staining (Guangzhou Fischer Chemical Co., Ltd.) was applied for 2–5 min. The slides were then washed in ddH_2O for 5 min or less, until they turned "blue." The slides were differentiated in 1% acid alcohol (1% HCL in 70% alcohol) for 5 min. After a washing step, the slides were stained in 1% eosin Y (Guangzhou Fischer Chemical Co., Ltd.) for 10 min. Subsequently, the slides were again washed in ddH_2O for 2–5 min. The samples were dehydrated in alcohol solutions of increasing concentration (75, 75, 95, 95, 100, 100%) and were cleared of xylene. Finally, the

slides were mounted with mounting media, and images (20×, 200×, and 400× magnification) were acquired under a light microscope.

Real-Time Quantitative Polymerase Chain Reaction

Total RNA was extracted from the compressed or decompressed spinal cord. The purity of the RNA was determined, and reverse transcription PCR (PrimeScript^{TM} RT reagent kit) and real-time quantitative PCR (RT-qPCR) (SYBR Premix Ex Taq II) were performed following the manufacturer's instructions (Takara Biotechnology Co., Ltd., China). The detailed primer sequences used in RT-qPCR are given in **Supplementary Table S1**. Cycle threshold (CT) values were recorded, and the relative expression of target genes was calculated using the expression $2^{-\Delta\Delta Ct}$ (Hu et al., 2019).

Statistical Analysis

All data are expressed as the mean with 95% confidence intervals (CI) or Medians with interquartile ranges. Statistical tests were performed using GraphPad Prism 7.0 software (San Diego, CA, United States). The motor function recovery results were analyzed by repeated-measures analysis of variance (ANOVA) to reveal overall group differences and significant changes over time. One-way analysis of variance followed by Tukey's *post hoc* test was used for comparisons among multiple groups. Statistical significance was set at $p < 0.05$.

RESULTS

Expansion of Water-Absorbable Compression Material After Implantation

These experiments were designed to evaluate the extent of expansion of polyurethane polymer sheets under the study conditions (**Figure 1A**). As shown in **Figure 1B**, this modified water-absorbable material gradually swelled after implantation and reached a maximal size at 3 wpi. Micro-CT scanning also clearly revealed the extent of expansion at 1 dpi, 1, and 3 wpi (**Figure 1C**).

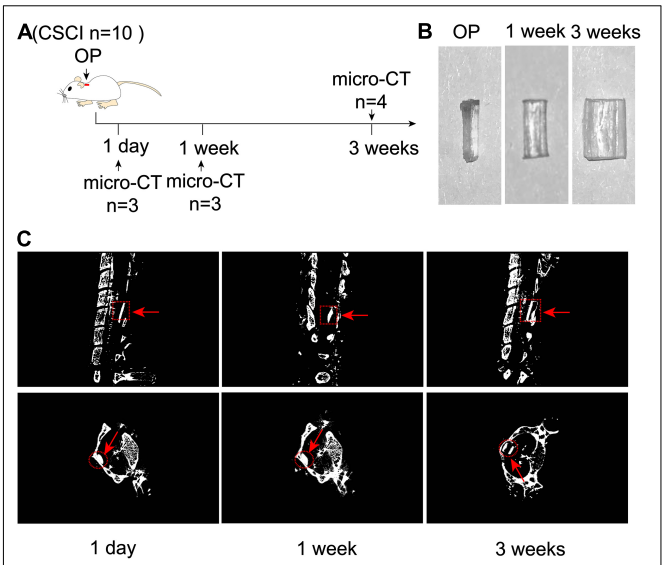

FIGURE 1 | Expansion of compression material after implantation. **(A)** Experimental design. **(B)** Alteration in the water-absorbable polyurethane polymer before and after surgery at 1 and 3 weeks. **(C)** Three-dimensional reconstruction and representative sagittal and transverse micro-CT images of the compressive segment. The red arrow indicates the compression site and material. 1 day post-injury: $n = 3$; 1 week post-injury: $n = 3$; 3 weeks post-injury: $n = 4$.

Early Decompression Partially Promoted Motor Function Recovery After CSCI

Surgical decompression has been regarded as a safe treatment for incomplete CSCI (Bakhsheshian et al., 2017; Sakaura et al., 2019), which results in improved functional status and quality of life for patients with various diseases, including CSM, ossification of the posterior longitudinal ligament (OPLL), and spinal stenosis. Here, we used the BBB score and IPT to evaluate changes in motor function after surgical decompression in a rat model of CSCI (**Figure 2A**). The results showed that the motor function gradually decreased from 1 to 3 wpi after CSCI. However, rats with surgical decompression at 1 wpi exhibited significantly improved motor function compared to rats without decompression (**Figures 2B,C**). Moreover, two of eleven CSCI rats did not recover at 3 wpi in comparison with 1 wpi in terms of BBB score and over 80% of rats exhibited a significant recovery after early decompression in our model (**Figure 2D**).

Structural and Cellular Changes and Hypoxic Level in the Decompressed Spinal Cord

Hematoxylin and eosin (HE) staining revealed histological changes at the injury epicenter under different levels of magnification (**Figure 3A**). The spinal cord was intact in the sham group. In the CSCI without decompression group, the compressed spinal cord exhibited structural damage, including fragmentation of neuronal nuclei, pyknosis, neuropil damage, degradation of the extracellular matrix, interstitial edema, cytoplasmic reduction, and cavity formation. Cellular changes were also observed at 3 wpi following CSCI, including neuron loss and axon degradation. Interestingly, differences were observed in the structural and cellular changes between the groups with and without decompression. After decompression, fragmentation of neuronal nuclei, degradation of the extracellular matrix, pyknosis, neuropil damage, interstitial edema, cytoplasmic reduction, cavity formation, neuron loss, and axon degradation were clearly alleviated.

HIF-1α IHC staining and RT-qPCR were performed to evaluate the hypoxic levels after CSCI (**Figure 3B**). As shown in **Figures 3C,D**, the quantitative analysis results indicate that HIF-1α expression in the spinal cord lesion site was increased after 3 weeks of compression. Preliminary data suggest that surgical compression at 1 wpi may improve the hypoxia environment and

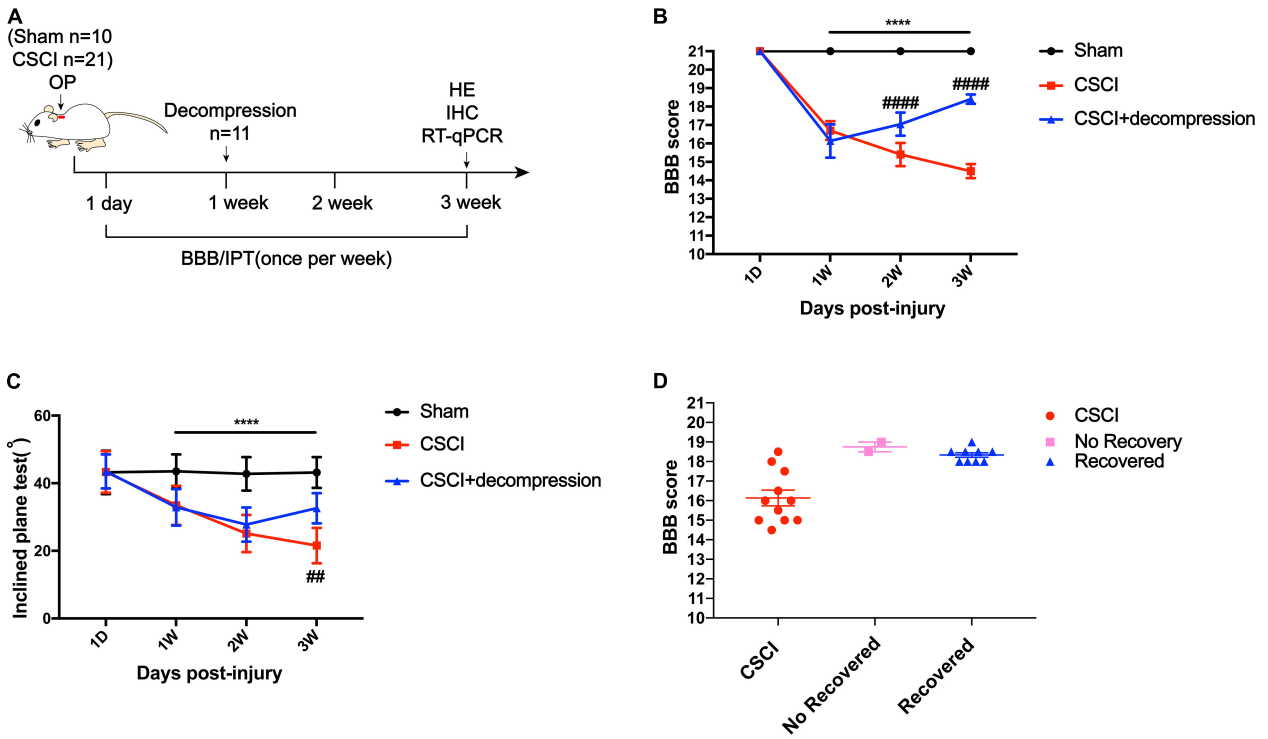

FIGURE 2 | Early decompression promoted motor function recovery after CSCI. **(A)** Experimental design. **(B)** Animals were tested weekly starting from 1 dpi in an open field, and motor function recovery was evaluated according to the BBB score [Two-way ANOVA, $F(1,8) = 66.13$, $p = 0.0043$; $^{****}p < 0.0001$: sham group vs. CSCI group; $^{\#\#\#\#}p < 0.0001$: CSCI group vs. CSCI with decompression group]. **(C)** Animals were tested weekly starting from 1 dpi using the IPT, and the angle (°) was recorded to reveal motor function recovery [Two-way ANOVA, $F(6,112) = 4.861$, $p < 0.001$; $^{****}p < 0.0001$: sham group vs. CSCI group; $^{\#\#}p = 0.0052$: CSCI group vs. CSCI with decompression group]. **(D)** BBB scores for recovered and non-recovery rats after decompression at 3 wpi. The Sham group: $n = 10$; CSCI group: $n = 10$; CSCI with decompression group: $n = 11$. df: the degrees of freedom; Mean ± 95% CI.

decrease HIF-1α expression compared with no decompression. However, further experiments are needed to confirm this notion.

Expression of VEGF, vWF, MMP-9, and MMP-2 in the Decompressed Spinal Cord

Vascular endothelial growth factor (DuBois and Demetri, 2007) and vWF (Randi and Laffan, 2017) have been reported as angiogenesis markers in many diseases, while MMPs such as MMP-9 and MMP-2 are related to inflammation and the BSCB (Na et al., 2015; Yao et al., 2018). Recently, many researchers have suggested that axonal degeneration, vascular dysfunction, and BSCB disruption may be key processes in neurological function recovery following decompression (Badhiwala et al., 2018; Blume et al., 2020). We previously reported on vascular and BSCB alterations as well as a correlation between MMP-9 and motor function recovery after CSCI, which indicated that angiogenesis and MMP may play critical roles in the process of motor function recovery (Long et al., 2014; Cheng et al., 2015, 2019; Xu et al., 2017). Therefore, we further investigated VEGF and vWF expression in spinal cord by using IHC to evaluate the potential effects of surgical decompression on angiogenesis. We also explored the effects of decompression on MMP-9 and MMP-2 (**Figure 4**). The results revealed that VEGF expression level in spinal cord gray matter and vWF expression level in spinal cord white matter were decreased, while MMP-9 and MMP-2 levels were increased in endothelial cells, neurons, and glia of the spinal cord after CSCI. Interestingly, VEGF and vWF levels were dramatically increased after decompression. Moreover, preliminary results suggest that decompression resulted in decreased MMP-9 and MMP-2 expression at 3 wpi (**Figures 4B–E** and **Supplementary Figures S1A,B**). However, further experiments are needed to confirm this notion. These data reveal that decompression may influence angiogenesis and BSCB function in the lesional spinal cord.

Notch-1 Expression Was Up-Regulated and Positively Associated With Motor Function Recovery After Decompression

To investigate whether Notch-1 signaling is activated after decompression, IHC and RT-qPCR were applied to detect the expression of Notch-1 and its downstream gene Hes-1. Preliminary data indicates that decompression lead to an upregulation of Notch-1 and Hes-1 expression levels (**Figure 5** and **Supplementary Figures S1C,D**). However, further studies need to confirm these findings. These preliminary results indicate that the Notch-1 signaling pathway may play a role in motor function recovery after CSCI. Furthermore,

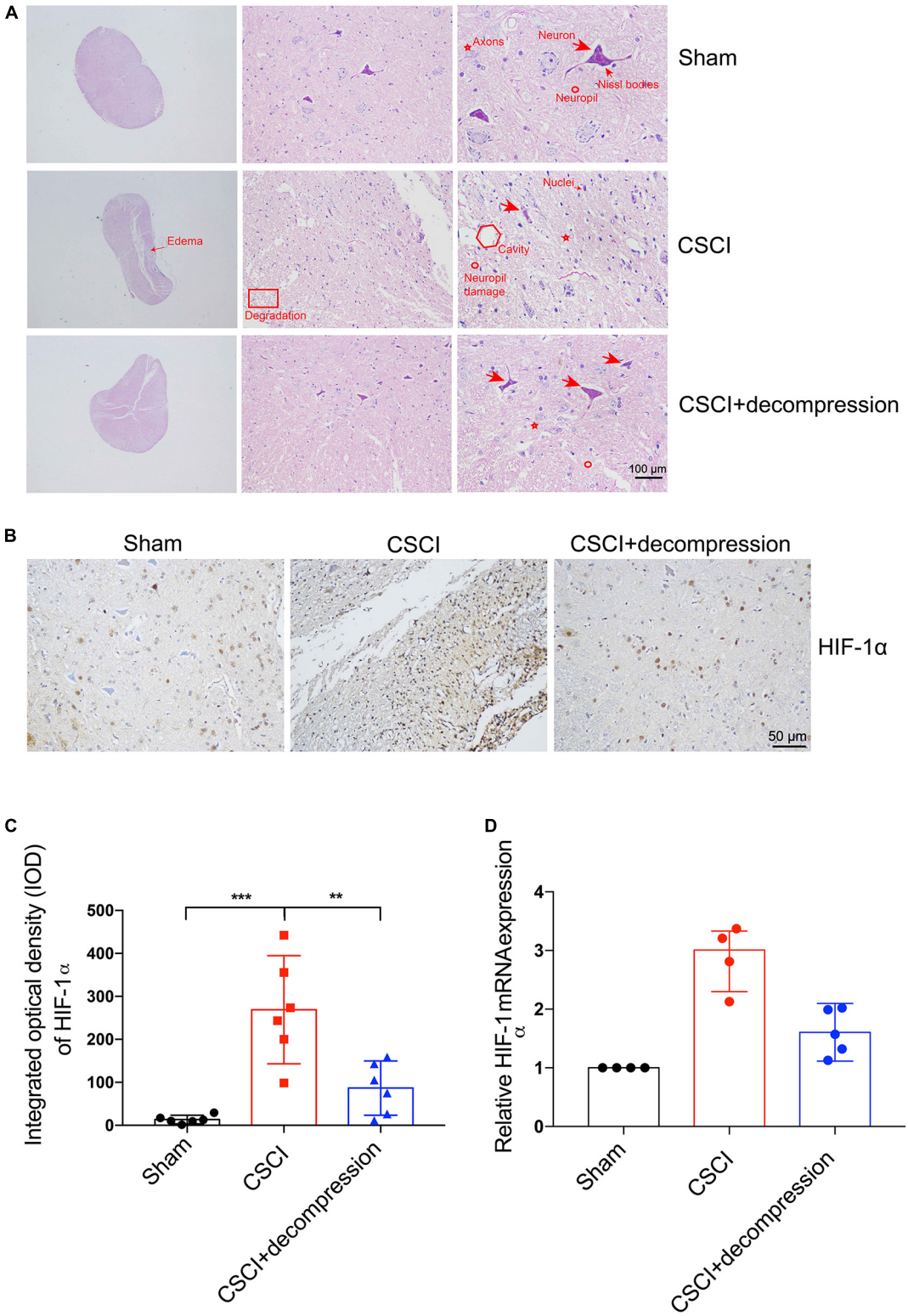

FIGURE 3 | Decompression-protected neurons and improved hypoxia environment after CSCI. **(A)** HE staining of lesion sites from the sham, CSCI, and CSCI with decompression groups (20× , 200× , and 400× magnification; scale bar, 100 μm). **(B)** HIF-1α expression, as assessed by IHC (200× magnification; scale bar, 50 μm). **(C)** HIF-1α IHC staining, as quantitated by the IOD [One-way ANOVA, $F(2,15) = 17.18$, $p < 0.001$; Tukey *post hoc*: ***$p < 0.001$, **$p = 0.003$]. **(D)** Relative HIF-1α expression, as determined by RT-qPCR. HE staining and IHC: $n = 6$ each group; Mean ± 95% CI. RT-qPCR: the Sham group: $n = 4$; CSCI group: $n = 4$; CSCI with decompression group: $n = 5$; Medians ± interquartile ranges, the sample size was too low to perform statistics for these data.

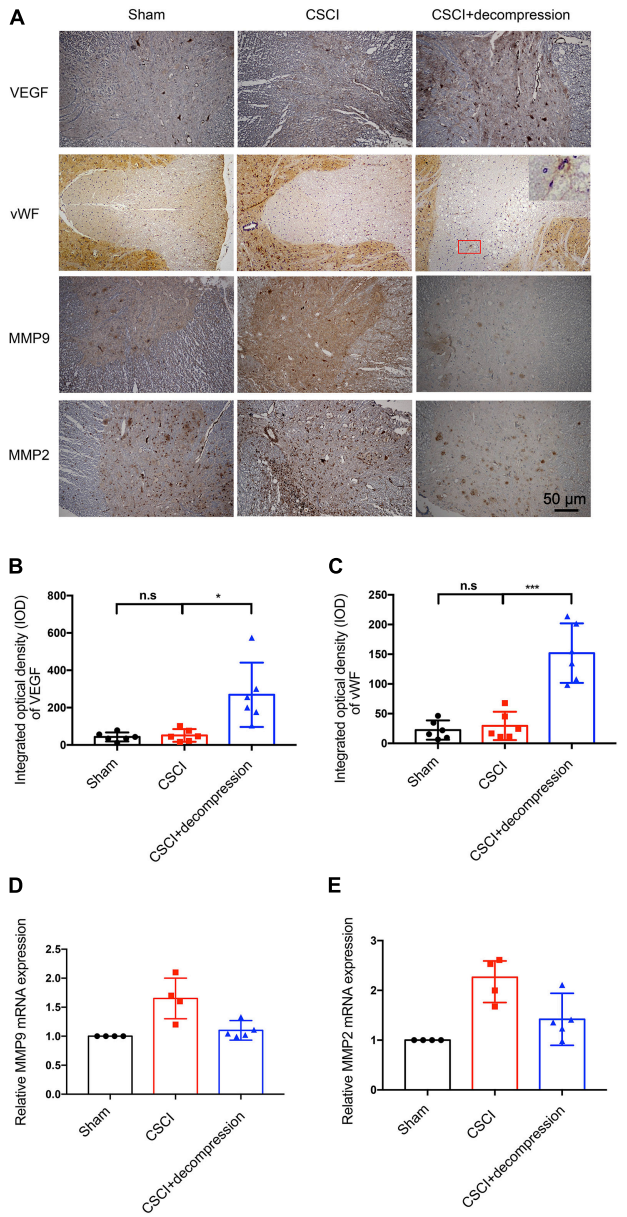

FIGURE 4 | Decompression promoted VEGF and vWF expression and inhibited MMP-9 and MMP-2 expression. **(A)** VEGF, vWF, MMP-9, and MMP-2 expression was assessed by IHC (200× magnification; scale bar, 50 μm). IHC staining of **(B)** VEGF [One-way ANOVA, $F(1.021,5.103) = 10.12$, $p = 0.024$; Tukey *post hoc*: n.s.: not significant; $^{*}p = 0.045$] and **(C)** vWF [One-way ANOVA, $F(1.075,5.376) = 29.33$, $p = 0.002$; Tukey *post hoc*: n.s.: not significant; $^{***}p < 0.001$] as quantitated by analyzing the IOD. Relative expression of **(D)** MMP-9 and **(E)** MMP-2 as assessed by RT-qPCR. IHC: $n = 6$ each group. Mean ± 95% CI; RT-qPCR: the Sham group: $n = 4$; CSCI group: $n = 4$; CSCI with decompression group: $n = 5$; Medians ± interquartile ranges, the sample size was too low to perform statistics for these data.

we down-regulated Notch-1 expression by applying DAPT, a γ-secretase inhibitor, to deactivate the Notch-1/Hes-1 signaling pathway (**Figure 6A**). **Figures 6B,C** clearly show that the motor function recovery was inhibited following down-regulation of Notch-1 after decompression, as the motor function recovery differed from that of the control group at 3 wpi. These results reveal that Notch-1 up-regulation after decompression plays a critical role for motor function recovery in a rat CSCI model.

Effects of Notch-1 Down-Regulation on Pathophysiological Changes in the Decompressed Spinal Cord

As previously described, HE and IHC staining were used to investigate pathological changes in our study. After the down-regulation of Notch-1, the fragmentation of neuronal nuclei, neuropil damage, interstitial edema, cytoplasmic reduction, cavity formation, degradation of the extracellular matrix, neuron loss, and axon degradation were more pronounced than in the group of CSCI without decompression (**Figure 7A**). However, the down-regulation of Notch-1 did not have any effect on the compression-induced hypoxia condition (**Figure 7B** and **Supplementary Figure S2A**). We were not able to detect any difference in our preliminary analysis of HIF-1α expression between the animals with or without DAPT treatment after decompression (**Figure 7C**). Further experiments are needed to confirm this result.

It was previously reported that activation of the Notch-1 signaling pathway can up-regulate VEGF, MMP-2, and MMP-9 by triggering the activation of NF-κB (Li et al., 2016). To further elucidate whether Notch-1 activation is associated with VEGF, vWF, MMP-9, and MMP-2 expression after decompression in the CSCI model, the expression of these factors was detected after Notch-1 down-regulation (**Figure 8**). Interestingly, following the inhibition of Notch-1, VEGF, and vWF expression levels were significantly lower compared with the control group (**Figures 8G,H**). In addition, preliminary data suggest that the down-regulation of Notch-1 increased MMP-9 and MMP-2 expression (**Figures 8I,J** and **Supplementary Figures S2B,C**), however, further experiments are needed to confirm these findings. The correlation among the expression of VEGF, vWF, MMP-9, MMP-2, and Notch-1 is presented in **Figures 8K–N**. The results demonstrate a significant correlation between the expression of Notch-1 and VEGF, vWF, and MMP-9.

Overall, the results indicate that early surgical decompression promoted motor function recovery may through protecting neurons and influencing the expression of angiogenesis-related markers and MMPs. Moreover, activation of the Notch-1 signaling pathway was shown to play an important role in motor function recovery following decompression.

DISCUSSION

Our study clarified the pathophysiological changes that occur in the spinal cord after decompression and demonstrated that early surgical decompression partially promoted motor function recovery in a water-absorbable polyurethane polymer compressive SCI. The motor function improvement achieved by surgical decompression was paralleled by improvements in structural and cellular damage, increased angiogenesis markers

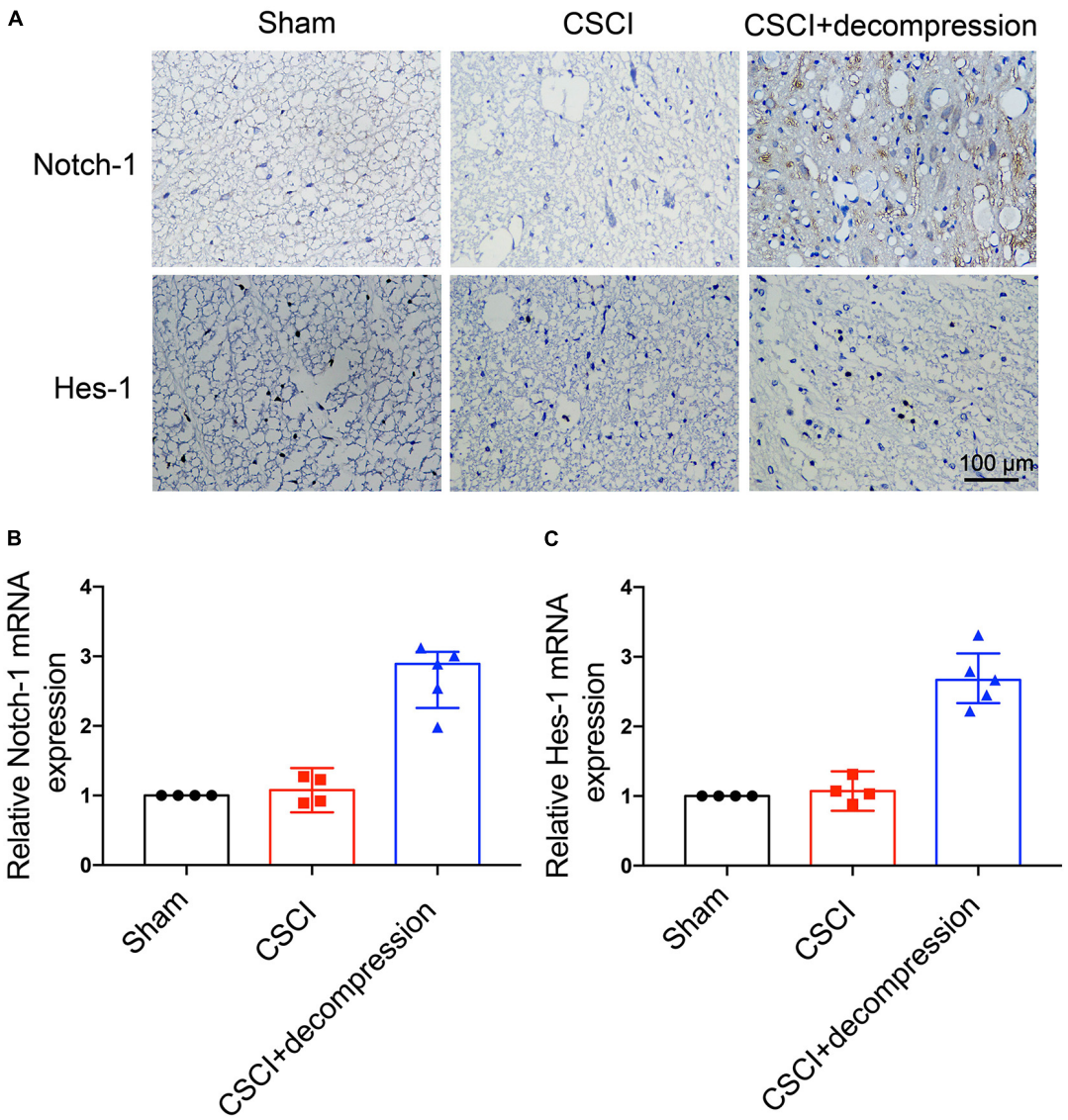

FIGURE 5 | Decompression-induced up-regulated Notch-1 expression. **(A)** Notch-1 and Hes-1 expression was assessed by IHC (400× magnification; scale bar, 100 μm). **(B)** Relative Notch-1 expression and **(C)** relative Hes-1 expression, as assessed by RT-qPCR. IHC: $n = 6$ each group; RT-qPCR: The Sham group: $n = 4$; CSCI group: $n = 4$; CSCI with decompression group: $n = 5$; Medians ± interquartile ranges, the sample size was too low to perform statistics for these data.

(VEGF and vWF), and reduced MMPs (MMP-9 and MMP-2) in the decompressed spinal cord. Moreover, the Notch-1/Hes-1 signal pathway was found to play an important role in the prognosis following decompression.

Due to the lack of a proper spinal cord compression model, pathophysiological changes following decompression are difficult to assess in rodent CSCI models (Akter et al., 2020). A stable, reusable material should also be considered. We therefore characterized rats with a chronic C6 compressive injury by performing IPTs and assessing BBB scores in an open field. The material used in this work gradually expanded after implantation, and therefore, the injured animals developed significant motor dysfunction after 1 wpi. The behavior outcomes in our cervical CSCI model are in line with growing evidence that rats begin to develop motor dysfunction after 1 week post-compression (Wang et al., 2012; Dhillon et al., 2016). Therefore, our study can partially reflect the sub-acute injury process of CSCI. These results indicate that water-absorbable polyurethane polymer may be a suitable material for imitating the occurrence and development of CSM in patients.

In the current study, surgical decompression was able to partially improve the motor function recovery. The pathophysiological mechanisms governing the effects of decompression are complicated. In clinical practice, outcomes are also influenced by the compression degree and symptom duration of each patient. Improvements in structural and cellular changes in the decompressed spinal cord may play a role in the progress of motor function recovery. It has been

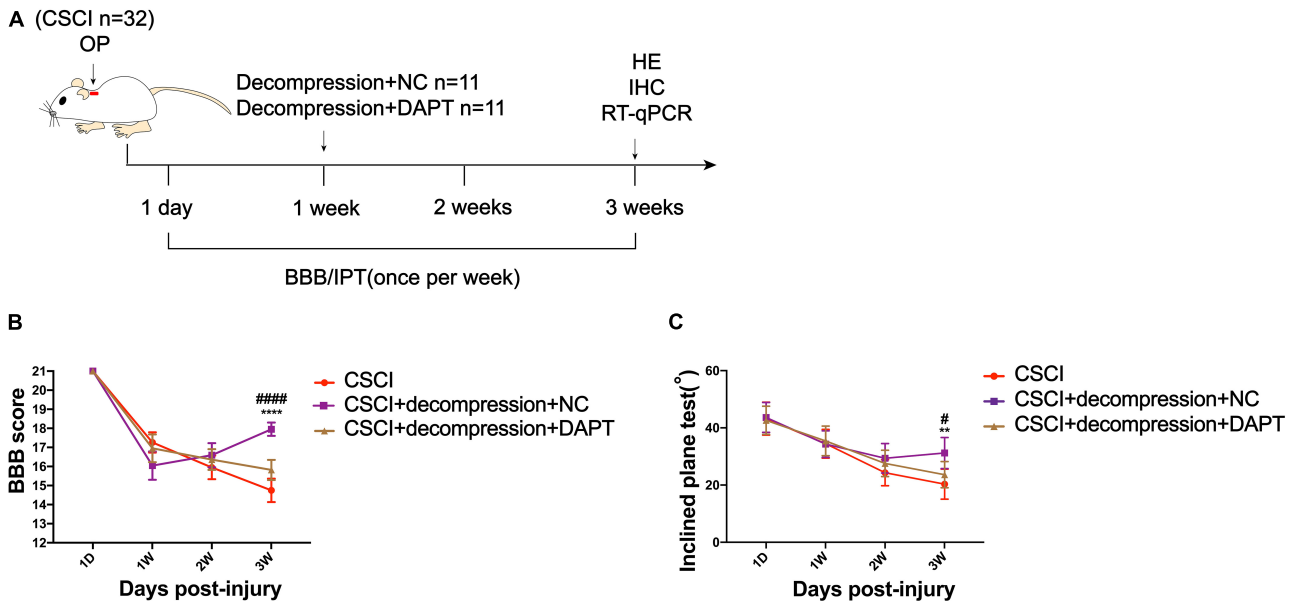

FIGURE 6 | Inhibition of Notch-1 attenuated motor function recovery after decompression. **(A)** Experimental design. **(B)** Animals were tested weekly starting from 1 dpi in an open field, and motor function recovery was evaluated according to the BBB score [Two-way ANOVA, $F(6,116) = 16.85$, $p < 0.0001$; $^{****}p < 0.0001$: CSCI group vs. CSCI with decompression and NC group; $^{\#\#\#\#}p < 0.0001$: CSCI with decompression and NC group vs. CSCI with decompression and DAPT group]. **(C)** Animals were tested weekly starting from 1 dpi using the IPT, and the angle (°) was recorded to reveal the motor function recovery [Two-way ANOVA, $F(6,116) = 3.279$, $p = 0.0412$; $^{**}p = 0.0052$: CSCI group vs. CSCI with decompression and NC group; $^{\#}p = 0.0431$: CSCI with decompression and NC group vs. CSCI with decompression and DAPT group]. The CSCI group: $n = 10$; CSCI with decompression and NC group: $n = 11$; CSCI with decompression and DAPT group: $n = 11$. Mean ± 95% CI.

well-documented that compression-induced neuron loss is paralleled by motor dysfunction (Ogino et al., 1983; Yu et al., 2009). Many factors such as cell death, inflammation, and ischemia can lead to neuron loss (Akter et al., 2020). Tanabe et al. (2011) suggested that HIF-1α may be increased in the twy/twy model and that hypoxic stress may promote neuronal cell death. However, ischemic-hypoxic changes in CSCI have not been widely investigated (Akter et al., 2020). Our data show that hypoxia conditions, which are also associated with motor function recovery, were improved after surgical decompression.

In addition, we observed that angiogenesis markers, i.e., VEGF and vWF, were increased following decompression. It has been reported that vascular dysfunction and angiogenesis may affect myelin damage, glial fibrosis, and necrosis after cervical spinal cord compression (Gooding et al., 1975; Ng and Lee, 2019). Furthermore, reduced blood flow to the spinal cord is associated with vascular dysfunction after compression (Franklin and Ffrench-Constant, 2008; Kurokawa et al., 2011). The molecular mechanisms of angiogenesis in decompression remain unclear. We also found that decompression can significantly decrease MMP-9 and MMP-2 expression. MMPs are associated with BSCB dysfunction (Zhang et al., 2017), and a similar expression pattern in CSM was described by Karadimas et al. (2013b). We previously found that the BSCB is disrupted after long-term spinal cord compression (Xu et al., 2017). Therefore, the high expression levels of MMP-9 and MMP-2 in the lesional spinal cord suggest these factors may play a role in BSCB disruption and that decompression may improve the BSCB by decreasing MMP-9 and MMP-2 expression. However, further research is needed to confirm this interpretation.

Notch signaling in CNS diseases is associated with cell death, angiogenesis, and BSCB function (Fassbender et al., 2011; Cai et al., 2016). Recently, studies have indicated that Notch-1 signaling can modulate VEGF, MMP-9, and MMP-2 expression *in vitro* and *in vivo* (Li et al., 2016). In our study, Notch-1 and its downstream gene Hes-1 were decreased under compression and increased after decompression. More interestingly, the down-regulation of Notch-1 can inhibit angiogenesis marker expression and promote MMP-9 and MMP-2 expression. The role of Notch-1 in angiogenesis is still unclear. Tang et al. (2018) reported that inhibition of the Notch-1/DLL4 pathway promotes angiogenesis in rats, while (Gao et al., 2012) demonstrated that Notch-1/HIF-1α interactions mediate hypoxia-induced angiogenesis in inflammatory arthritis. More investigations are needed to clarify these findings. In our study, HIF-1α expression in the decompressed spinal cord was not influenced by the inhibition of Notch-1. Nevertheless, the improvements in structure and cellular changes were weakened after Notch-1 inhibition. Thus, the underlying mechanisms require further investigation.

The dipeptidic compound DAPT (N-[N- (3,5-difluorophenacetyl) -L-alanyl] -S-phenylglycine t-butyl ester), a γ−secretase inhibitor was tested *in vivo* in Dovey et al. (2001). γ-Secretase displays poor substrate specificity (Panza et al., 2010) and (Takeshita et al., 2007) suggested that γ-secretase can mediate Notch1 cleavage and activation

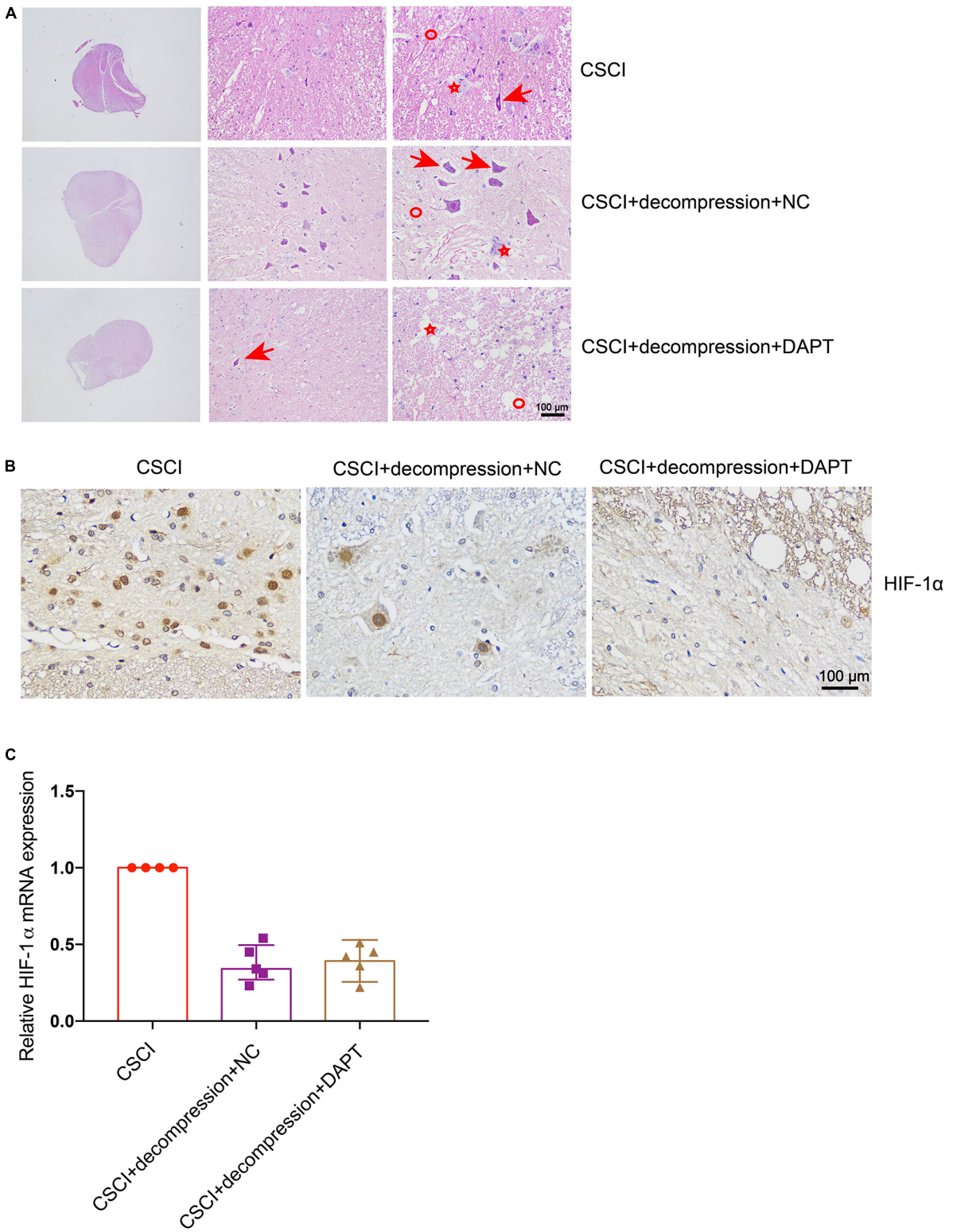

FIGURE 7 | Inhibition of Notch-1 does not have neuron-protective effects on CSCI after decompression. **(A)** HE staining of lesion sites from the CSCI, CSCI with decompression and NC, and CSCI with decompression and DAPT groups (20×, 200×, and 400× magnification; scale bar, 100 μm). **(B)** HIF-1α expression was assessed by IHC (400× magnification; scale bar, 100 μm). **(C)** The relative HIF-1α expression was assessed by RT-qPCR. HE staining and IHC: $n = 6$ each group; RT-qPCR: the CSCI group: $n = 4$; CSCI with decompression and NC group: $n = 5$; CSCI with decompression and DAPT group: $n = 5$; Medians ± interquartile ranges, the sample size was too low to perform statistics for these data.

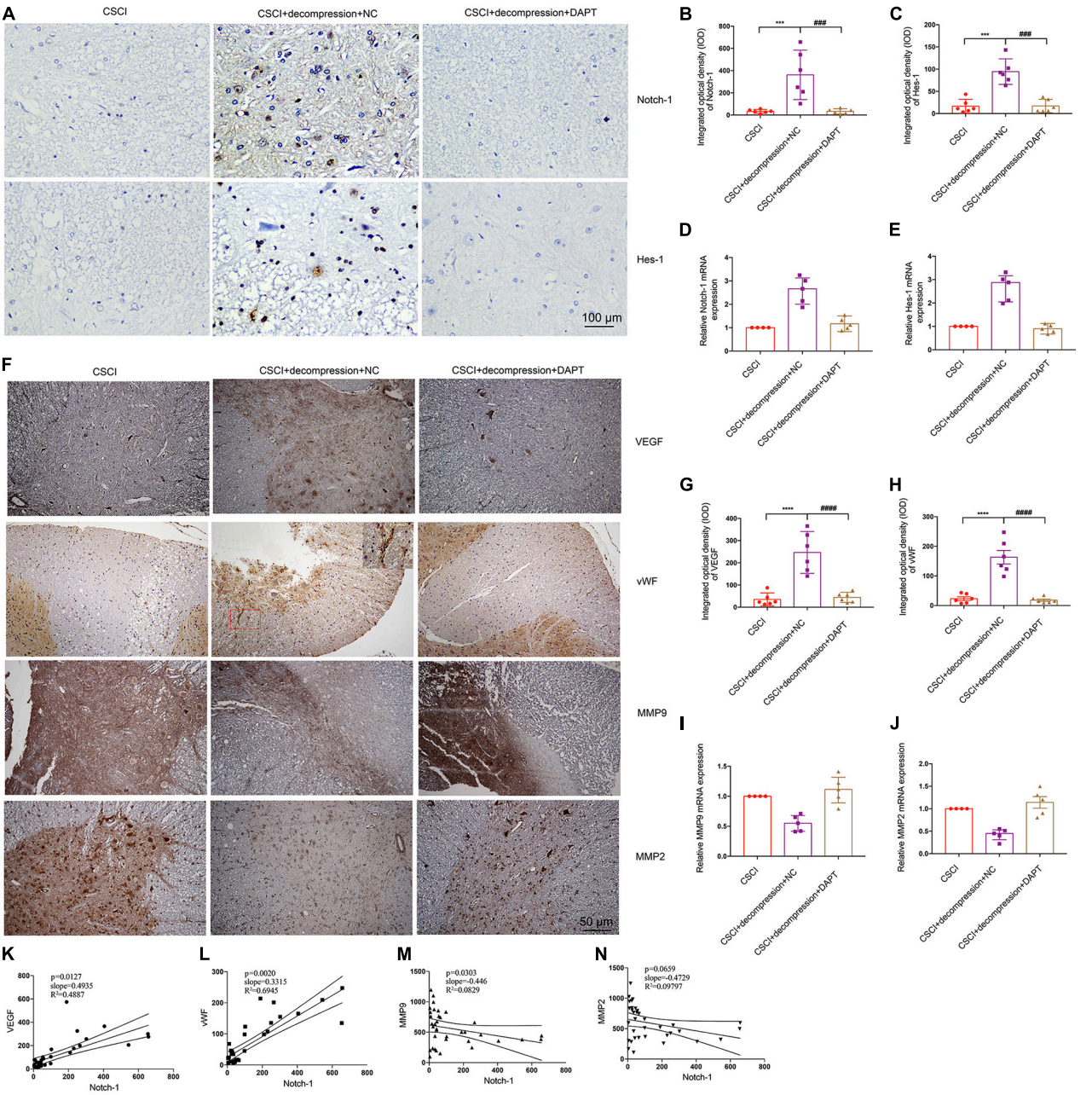

FIGURE 8 | Inhibition of Notch-1 resulted in decreased VEGF, vWF, MMP-9, and MMP-2 expression. **(A)** Notch-1 and Hes-1 expression levels were assessed by IHC (400× magnification; scale bar, 100 μm). IHC staining of **(B)** Notch-1 [One-way ANOVA, $F(2,15) = 14.12$, $p < 0.001$; Tukey *post hoc*: $^{***}p < 0.001$, $^{\#\#\#}p < 0.001$] and **(C)** Hes-1 was quantitated by analyzing the IOD [One-way ANOVA, $F(2,15) = 30.64$, $p < 0.001$; Tukey *post hoc*: $^{***}p < 0.001$, $^{\#\#\#}p < 0.001$]. Relative expression levels of **(D)** Notch-1 and **(E)** Hes-1 were assessed by RT-qPCR. **(F)** VEGF, vWF, MMP-9, and MMP-2 expression levels were assessed by IHC (200× magnification; scale bar, 50 μm). IHC staining of **(G)** VEGF [One-way ANOVA, $F(2,15) = 27.56$, $p < 0.0001$; Tukey *post hoc*: $^{****}p < 0.0001$, $^{\#\#\#\#}p < 0.0001$], and **(H)** vWF [One-way ANOVA, $F(2,15) = 34.93$, $p < 0.0001$; Tukey *post hoc*: $^{****}p < 0.0001$, $^{\#\#\#\#}p < 0.0001$] was quantitated by analyzing the IOD. Relative expression levels of **(I)** MMP-9 and **(J)** MMP-2 were assessed by RT-qPCR. Correlation between Notch-1 expression and **(K)** VEGF, **(L)** vWF, **(M)** MMP-9, and **(N)** MMP-2. IHC: $n = 6$ each group; Mean ± 95% CI. RT-qPCR: the CSCI group: $n = 4$; CSCI with decompression and NC group: $n = 5$; CSCI with decompression and DAPT group: $n = 5$; Medians ± interquartile ranges, the sample size was too low to perform statistics for these data.

by phosphatidylinositol 3-kinase/Akt pathway in postnatal angiogenesis. However, it still needs to be explored whether other signaling molecules/pathways besides Notch-1 may be affected in our CSCI model. In a transgenic mouse model of Alzheimer's Disease, it was demonstrated that DAPT could reverse contextual memory deficit through targeting beta-amyloid (Comery et al., 2005). It has also been reported that DAPT could inhibit all four Notch receptors and is a promising option for cancer

therapy (Shih and Wang, 2007). Moreover, the γ-secretase inhibitor DAPT could decrease angiogenesis and inhibit VEGF-induced endothelial cell proliferation, migration, and survival as well (Takeshita et al., 2007).

To the best of our knowledge, this study is the first to focus on the influence of early surgical decompression on motor function recovery and physiological and pathological changes in CSCI rats. Our findings can serve as a basis for future studies in rodents to explore the molecular and cellular changes underlying motor dysfunction after CSM and decompression-induced improvements.

Nevertheless, our study has several limits. It has been reported that surgical decompression for the treatment of CSM is associated with not only motor function recovery, but also sensory function recovery (Fehlings et al., 2013; Zaveri and Jaiswal, 2019). However, the sensory function was not evaluated in this study. In addition, we found that the inhibition of Notch-1 was associated with the expression of angiogenesis markers and MMPs, but the underlying mechanisms governing these changes were not pursued. Thus, the manner in which Notch-1 modulates the expression of these factors after decompression remains unclear. The NF-κB signaling pathway can be triggered by the activation of Notch-1; therefore, this pathway can be initiated by up-regulated expression of NF-κB target genes, including VEGF, MMP-9, and MMP-2 (Karadimas et al., 2013b). Hence, it would be valuable to explore whether the NF-κB signaling pathway is activated by Notch-1 after decompression in a rat CSCI model. Further research is also needed to demonstrate that activation of Notch-1 is sufficient to induce the protection. Furthermore, although we demonstrated the changes in angiogenesis markers and MMPs in the decompressed spinal cord via histological approaches, the detection of angiogenesis and BSCB disruption via morphological and functional approaches is needed in future work. Given that the sample size in different groups of this exploratory study is not large enough, therefore it is necessary to increase the sample size to further explore the underlying mechanisms of our preliminary findings.

In summary, our study illustrated the preliminary physiological and pathological changes occurring in the compressed and decompressed spinal cord in the sub-acute injury process of CSCI rats. In addition, we confirmed that early surgical decompression can partially improve motor function recovery. Our data indicate that activation of the Notch-1 signaling pathway may play a role in the prognosis of CSCI after decompression, which may provide a new drug approach in order to enhance recovery following surgery.

DATA AVAILABILITY STATEMENT

The raw data supporting the conclusions of this article will be made available by the authors, without undue reservation.

ETHICS STATEMENT

The animal study was reviewed and approved by The first affiliated hospital of Sun Yat-sen University.

AUTHOR CONTRIBUTIONS

XC analyzed the data, wrote the manuscript, and created the figures. ZY performed the experiments and analyzed the data. JX performed the experiments. DQ revised the manuscript and designed the experiments. HL designed the experiments, contributed to manuscript writing, and gave final approval of the manuscript. All authors contributed to the article and approved the submitted version.

FUNDING

This study was supported by the National Natural Science Foundation of China (81450020 to HL).

ACKNOWLEDGMENTS

We thank Prof. Yong Hu (Hong Kong University) for providing the polymer.

SUPPLEMENTARY MATERIAL

The Supplementary Material for this article can be found online at: https://www.frontiersin.org/articles/10.3389/fnins.2021.579431/full#supplementary-material

REFERENCES

Akter, F., Yu, X., Qin, X., Yao, S., Nikrouz, P., Syed, Y., et al. (2020). The pathophysiology of degenerative cervical myelopathy and the physiology of recovery following decompression. *Front. Neurosci.* 14:138. doi: 10.3389/fnins.2020.00138

Badhiwala, J. H., Ahuja, C. S., and Fehlings, M. G. (2018). Time is spine: a review of translational advances in spinal cord injury. *J. Neurosurg. Spine* 30, 1–18. doi: 10.3171/2018.9.SPINE18682

Bakhsheshian, J., Mehta, V. A., and Liu, J. C. (2017). Current diagnosis and management of cervical spondylotic myelopathy. *Global Spine J.* 7, 572–586. doi: 10.1177/2192568217699208

Basso, D. M., Beattie, M. S., and Bresnahan, J. C. (1995). A sensitive and reliable locomotor rating scale for open field testing in rats. *J. Neurotrauma* 12, 1–21. doi: 10.1089/neu.1995.12.1

Blume, C., Geiger, M. F., Brandenburg, L. O., Müller, M., Mainz, V., Kalder, J., et al. (2020). Patients with degenerative cervical myelopathy have signs of blood spinal cord barrier disruption, and its magnitude correlates with myelopathy severity: a prospective comparative cohort study. *Eur. Spine J.* 29, 986–993. doi: 10.1007/s00586-020-06298-7

Cai, Z., Zhao, B., Deng, Y., Shangguan, S., Zhou, F., Zhou, W., et al. (2016). Notch signaling in cerebrovascular diseases (Review). *Mol. Med. Rep.* 14, 2883–2898. doi: 10.3892/mmr.2016.5641

Cheng, X., Long, H., Chen, W., Xu, J., Huang, Y., and Li, F. (2015). Three-dimensional alteration of cervical anterior spinal artery and anterior radicular

artery in rat model of chronic spinal cord compression by micro-CT. *Neurosci. Lett.* 606, 106–112. doi: 10.1016/j.neulet.2015.08.050

Cheng, X., Long, H., Chen, W., Xu, J., Wang, X., and Li, F. (2019). The correlation between hypoxia-inducible factor-1α, matrix metalloproteinase-9 and functional recovery following chronic spinal cord compression. *Brain Res.* 1718, 75–82. doi: 10.1016/j.brainres.2019.04.034

Cheng, X., Xu, J., Yu, Z., Xu, J., and Long, H. (2020). LncRNA Xist contributes to endogenous neurological repair after chronic compressive spinal cord injury by promoting angiogenesis through the miR-32-5p/Notch-1 axis. *Front. Cell Dev. Biol.* 8:744. doi: 10.3389/fcell.2020.00744

Comery, T. A., Martone, R. L., Aschmies, S., Atchison, K. P., Diamantidis, G., Gong, X., et al. (2005). Acute gamma-secretase inhibition improves contextual fear conditioning in the Tg2576 mouse model of Alzheimer's disease. *J. Neurosci.* 25, 8898–8902. doi: 10.1523/JNEUROSCI.2693-05.2005

Dhillon, R. S., Parker, J., Syed, Y. A., Edgley, S., Young, A., Fawcett, J. W., et al. (2016). Axonal plasticity underpins the functional recovery following surgical decompression in a rat model of cervical spondylotic myelopathy. *Acta Neuropathol. Commun.* 4:89. doi: 10.1186/s40478-016-0359-7

Dovey, H. F., John, V., Anderson, J. P., Chen, L. Z., de Saint Andrieu, P., Fang, L. Y., et al. (2001). Functional gamma-secretase inhibitors reduce beta-amyloid peptide levels in brain. *J. Neurochem.* 76, 173–181. doi: 10.1046/j.1471-4159.2001.00012.x

DuBois, S., and Demetri, G. (2007). Markers of angiogenesis and clinical features in patients with sarcoma. *Cancer* 109, 813–819. doi: 10.1002/cncr.22455

Fassbender, J. M., Whittemore, S. R., and Hagg, T. (2011). Targeting microvasculature for neuroprotection after SCI. *Neurotherapeutics* 8, 240–251. doi: 10.1007/s13311-011-0029-1

Fehlings, M. G., Wilson, J. R., Kopjar, B., Yoon, S. T., Arnold, P. M., Massicotte, E. M., et al. (2013). Efficacy and safety of surgical decompression in patients with cervical spondylotic myelopathy: results of the AOSpine North America prospective multi-center study. *J. Bone Joint Surg. Am.* 95, 1651–1658. doi: 10.2106/JBJS.L.00589

Franklin, R. J. M., and Ffrench-Constant, C. (2008). Remyelination in the CNS: from biology to therapy. *Nat. Rev. Neurosci.* 9, 839–855. doi: 10.1038/nrn2480

Gao, W., Sweeney, C., Connolly, M., Kennedy, A., Ng, C. T., McCormick, J., et al. (2012). Notch-1 mediates hypoxia-induced angiogenesis in rheumatoid arthritis. *Arthritis Rheum.* 64, 2104–2113. doi: 10.1002/art.34397

Gooding, M. R., Wilson, C. B., and Hoff, J. T. (1975). Experimental cervical myelopathy. Effects of ischemia and compression of the canine cervical spinal cord. *J. Neurosurg.* 43, 9–17. doi: 10.3171/jns.1975.43.1.0009

Haddas, R., Lieberman, I., Arakal, R., Boah, A., Belanger, T., and Ju, K. (2018). Effect of cervical decompression surgery on gait in adult cervical spondylotic myelopathy patients. *Clin. Spine Surg.* 31, 435–440. doi: 10.1097/BSD.0000000000000719

Harkey, H. L., al-Mefty, O., Marawi, I., Peeler, D. F., Haines, D. E., and Alexander, L. F. (1995). Experimental chronic compressive cervical myelopathy: effects of decompression. *J. Neurosurg.* 83, 336–341. doi: 10.3171/jns.1995.83.2.0336

Hirai, T., Uchida, K., Nakajima, H., Guerrero, A. R., Takeura, N., Watanabe, S., et al. (2013). The prevalence and phenotype of activated microglia/macrophages within the spinal cord of the hyperostotic mouse (twy/twy) changes in response to chronic progressive spinal cord compression: implications for human cervical compressive myelopathy. *PLoS One* 8:e64528. doi: 10.1371/journal.pone.0064528

Hu, C., Bai, X., Liu, C., and Hu, Z. (2019). Long noncoding RNA XIST participates hypoxia-induced angiogenesis in human brain microvascular endothelial cells through regulating miR-485/SOX7 axis. *Am. J. Transl. Res.* 11, 6487–6497.

Hu, Y., Wen, C.-Y., Li, T.-H., Cheung, M. M.-H., Wu, E. X., and Luk, K. D.-K. (2011). Somatosensory-evoked potentials as an indicator for the extent of ultrastructural damage of the spinal cord after chronic compressive injuries in a rat model. *Clin. Neurophysiol.* 122, 1440–1447. doi: 10.1016/j.clinph.2010.12.051

Ishida, Y., Ohmori, K., Suzuki, K., and Inoue, H. (1999). Analysis of dural configuration for evaluation of posterior decompression in cervical myelopathy. *Neurosurgery* 44, 91–95; discussion 95–96. doi: 10.1097/00006123-199901000-00051

Izumida, M. (1995). [A chronic spinal cord compression model in a rat with a 354A tumor]. *Nippon Seikeigeka Gakkai Zasshi* 69, 977–991.

Kanchiku, T., Taguchi, T., Kaneko, K., Yonemura, H., Kawai, S., and Gondo, T. (2001). A new rabbit model for the study on cervical compressive myelopathy. *J. Orthop. Res.* 19, 605–613. doi: 10.1016/S0736-0266(00)00058-9

Karadimas, S. K., Erwin, W. M., Ely, C. G., Dettori, J. R., and Fehlings, M. G. (2013a). Pathophysiology and natural history of cervical spondylotic myelopathy. *Spine* 38, S21–S36. doi: 10.1097/BRS.0b013e3182a7f2c3

Karadimas, S. K., Gatzounis, G., and Fehlings, M. G. (2015a). Pathobiology of cervical spondylotic myelopathy. *Eur. Spine J.* 24(Suppl. 2), 132–138. doi: 10.1007/s00586-014-3264-4

Karadimas, S. K., Klironomos, G., Papachristou, D. J., Papanikolaou, S., Papadaki, E., and Gatzounis, G. (2013b). Immunohistochemical profile of NF-κB/p50, NF-κB/p65, MMP-9, MMP-2, and u-PA in experimental cervical spondylotic myelopathy. *Spine* 38, 4–10. doi: 10.1097/BRS.0b013e318261ea6f

Karadimas, S. K., Laliberte, A. M., Tetreault, L., Chung, Y. S., Arnold, P., Foltz, W. D., et al. (2015b). Riluzole blocks perioperative ischemia-reperfusion injury and enhances postdecompression outcomes in cervical spondylotic myelopathy. *Sci. Transl. Med.* 7:316ra194. doi: 10.1126/scitranslmed.aac6524

Kurokawa, R., Murata, H., Ogino, M., Ueki, K., and Kim, P. (2011). Altered blood flow distribution in the rat spinal cord under chronic compression. *Spine* 36, 1006–1009. doi: 10.1097/BRS.0b013e3181eaf33d

Li, L., Zhang, J., Xiong, N., Li, S., Chen, Y., Yang, H., et al. (2016). Notch-1 signaling activates NF-κB in human breast carcinoma MDA-MB-231 cells via PP2A-dependent AKT pathway. *Med. Oncol.* 33:33. doi: 10.1007/s12032-016-0747-7

Li, P., Zhang, H., Cheng, H., Meng, F., and Li, J. (2019). Recovery process after anterior cervical decompression in patients with cervical spondylotic myelopathy with different natural history. *Clin. Spine Surg.* 32, 337–344. doi: 10.1097/BSD.0000000000000873

Long, H.-Q., Li, G.-S., Cheng, X., Xu, J.-H., and Li, F.-B. (2015). Role of hypoxia-induced VEGF in blood-spinal cord barrier disruption in chronic spinal cord injury. *Chin. J. Traumatol.* 18, 293–295. doi: 10.1016/j.cjtee.2015.08.004

Long, H.-Q., Li, G.-S., Hu, Y., Wen, C.-Y., and Xie, W.-H. (2012). HIF-1α/VEGF signaling pathway may play a dual role in secondary pathogenesis of cervical myelopathy. *Med. Hypotheses* 79, 82–84. doi: 10.1016/j.mehy.2012.04.006

Long, H.-Q., Li, G.-S., Lin, E.-J., Xie, W.-H., Chen, W.-L., Luk, K. D.-K., et al. (2013). Is the speed of chronic compression an important factor for chronic spinal cord injury rat model? *Neurosci. Lett.* 545, 75–80. doi: 10.1016/j.neulet.2013.04.024

Long, H.-Q., Xie, W.-H., Chen, W.-L., Xie, W.-L., Xu, J.-H., and Hu, Y. (2014). Value of micro-CT for monitoring spinal microvascular changes after chronic spinal cord compression. *Int. J. Mol. Sci.* 15, 12061–12073. doi: 10.3390/ijms150712061

Na, W., Lee, J. Y., Kim, W.-S., Yune, T. Y., and Ju, B.-G. (2015). 17β-estradiol ameliorates tight junction disruption via repression of MMP transcription. *Mol. Endocrinol.* 29, 1347–1361. doi: 10.1210/ME.2015-1124

Ng, M. T. L., Stammers, A. T., and Kwon, B. K. (2011). Vascular disruption and the role of angiogenic proteins after spinal cord injury. *Transl. Stroke Res.* 2, 474–491. doi: 10.1007/s12975-011-0109-x

Ng, S. Y., and Lee, A. Y. W. (2019). Traumatic brain injuries: pathophysiology and potential therapeutic targets. *Front. Cell. Neurosci.* 13:528. doi: 10.3389/fncel.2019.00528

Ogino, H., Tada, K., Okada, K., Yonenobu, K., Yamamoto, T., Ono, K., et al. (1983). Canal diameter, anteroposterior compression ratio, and spondylotic myelopathy of the cervical spine. *Spine* 8, 1–15. doi: 10.1097/00007632-198301000-00001

Panza, F., Frisardi, V., Imbimbo, B. P., Capurso, C., Logroscino, G., Sancarlo, D., et al. (2010). REVIEW: γ-Secretase inhibitors for the treatment of Alzheimer's disease: the current state. *CNS Neurosci. Ther.* 16, 272–284. doi: 10.1111/j.1755-5949.2010.00164.x

Randi, A. M., and Laffan, M. A. (2017). Von Willebrand factor and angiogenesis: basic and applied issues. *J. Thromb. Haemost.* 15, 13–20. doi: 10.1111/jth.13551

Rivlin, A. S., and Tator, C. H. (1977). Objective clinical assessment of motor function after experimental spinal cord injury in the rat. *J. Neurosurg.* 47, 577–581. doi: 10.3171/jns.1977.47.4.0577

Sakaura, H., Ohnishi, A., Yamagishi, A., and Ohwada, T. (2019). Differences in postoperative changes of cervical sagittal alignment and balance after laminoplasty between cervical spondylotic myelopathy and cervical ossification

of the posterior longitudinal ligament. *Global Spine J.* 9, 266–271. doi: 10.1177/2192568218784951

Shih, I.-M., and Wang, T.-L. (2007). Notch signaling, gamma-secretase inhibitors, and cancer therapy. *Cancer Res.* 67, 1879–1882. doi: 10.1158/0008-5472.CAN-06-3958

Takeshita, K., Satoh, M., Ii, M., Silver, M., Limbourg, F. P., Mukai, Y., et al. (2007). Critical role of endothelial Notch1 signaling in postnatal angiogenesis. *Circ. Res.* 100, 70–78. doi: 10.1161/01.RES.0000254788.47304.6e

Tanabe, F., Yone, K., Kawabata, N., Sakakima, H., Matsuda, F., Ishidou, Y., et al. (2011). Accumulation of p62 in degenerated spinal cord under chronic mechanical compression: functional analysis of p62 and autophagy in hypoxic neuronal cells. *Autophagy* 7, 1462–1471. doi: 10.4161/auto.7.12.17892

Tang, Q., Jin, H., Tong, M., Zheng, G., Xie, Z., Tang, S., et al. (2018). Inhibition of Dll4/Notch1 pathway promotes angiogenesis of Masquelet's induced membrane in rats. *Exp. Mol. Med.* 50:41. doi: 10.1038/s12276-018-0062-9

Tetreault, L., Goldstein, C. L., Arnold, P., Harrop, J., Hilibrand, A., Nouri, A., et al. (2015). Degenerative cervical myelopathy: a spectrum of related disorders affecting the aging spine. *Neurosurgery* 77(Suppl. 4), S51–S67. doi: 10.1227/NEU.0000000000000951

Vidal, P. M., Karadimas, S. K., Ulndreaj, A., Laliberte, A. M., Tetreault, L., Forner, S., et al. (2017). Delayed decompression exacerbates ischemia-reperfusion injury in cervical compressive myelopathy. *JCI Insight* 2:e92512. doi: 10.1172/jci.insight.92512

Vidal, P. M., Ulndreaj, A., Tetreault, L., Hong, J., and Fehlings, M. G. (2019). The changes in systemic monocytes in humans undergoing surgical decompression for degenerative cervical myelopathy may influence clinical neurological recovery. *J. Neuroimmunol.* 336:577024. doi: 10.1016/j.jneuroim.2019.577024

Wang, J., Rong, W., Hu, X., Liu, X., Jiang, L., Ma, Y., et al. (2012). Hyaluronan tetrasaccharide in the cerebrospinal fluid is associated with self-repair of rats after chronic spinal cord compression. *Neuroscience* 210, 467–480. doi: 10.1016/j.neuroscience.2012.03.016

Wiberg, J. (1986). Effects of surgery on cervical spondylotic myelopathy. *Acta Neurochir. (Wien)* 81, 113–117. doi: 10.1007/BF01401231

Xu, J., Long, H., Chen, W., Cheng, X., Yu, H., Huang, Y., et al. (2017). Ultrastructural features of neurovascular units in a rat model of chronic compressive spinal cord injury. *Front. Neuroanat.* 11:136. doi: 10.3389/fnana.2017.00136

Yang, T., Wu, L., Wang, H., Fang, J., Yao, N., and Xu, Y. (2015). Inflammation level after decompression surgery for a rat model of chronic severe spinal cord compression and effects on ischemia-reperfusion injury. *Neurol. Med. Chir. (Tokyo)* 55, 578–586. doi: 10.2176/nmc.oa.2015-0022

Yao, Y., Xu, J., Yu, T., Chen, Z., Xiao, Z., Wang, J., et al. (2018). Flufenamic acid inhibits secondary hemorrhage and BSCB disruption after spinal cord injury. *Theranostics* 8, 4181–4198. doi: 10.7150/thno.25707

Yu, W. R., Liu, T., Kiehl, T.-R., and Fehlings, M. G. (2011). Human neuropathological and animal model evidence supporting a role for Fas-mediated apoptosis and inflammation in cervical spondylotic myelopathy. *Brain* 134, 1277–1292. doi: 10.1093/brain/awr054

Yu, W.-R., Baptiste, D. C., Liu, T., Odrobina, E., Stanisz, G. J., and Fehlings, M. G. (2009). Molecular mechanisms of spinal cord dysfunction and cell death in the spinal hyperostotic mouse: implications for the pathophysiology of human cervical spondylotic myelopathy. *Neurobiol. Dis.* 33, 149–163. doi: 10.1016/j.nbd.2008.09.024

Zaveri, G. R., and Jaiswal, N. P. (2019). A comparison of clinical and functional outcomes following anterior, posterior, and combined approaches for the management of cervical spondylotic myelopathy. *Indian J. Orthop.* 53, 493–501. doi: 10.4103/ortho.IJOrtho_8_16

Zhang, D., Tang, Q., Zheng, G., Wang, C., Zhou, Y., Wu, Y., et al. (2017). Metformin ameliorates BSCB disruption by inhibiting neutrophil infiltration and MMP-9 expression but not direct TJ proteins expression regulation. *J. Cell. Mol. Med.* 21, 3322–3336. doi: 10.1111/jcmm.13235

Conflict of Interest: The authors declare that the research was conducted in the absence of any commercial or financial relationships that could be construed as a potential conflict of interest.

Copyright © 2021 Cheng, Yu, Xu, Quan and Long. This is an open-access article distributed under the terms of the Creative Commons Attribution License (CC BY). The use, distribution or reproduction in other forums is permitted, provided the original author(s) and the copyright owner(s) are credited and that the original publication in this journal is cited, in accordance with accepted academic practice. No use, distribution or reproduction is permitted which does not comply with these terms.

frontiers in Neurology

ORIGINAL RESEARCH
published: 20 April 2021
doi: 10.3389/fneur.2021.610434

Improved Functional Outcome After Peripheral Nerve Stimulation of the Impaired Forelimb Post-stroke

Shih-Yen Tsai[1], Jennifer A. Schreiber[1,2], Natalie S. Adamczyk[1], Joanna Y. Wu[1], Son T. Ton[1], Ryan C. Hofler[2], James S. Walter[1], Timothy E. O'Brien[3], Gwendolyn L. Kartje[1,4] and Russ P. Nockels[2]*

[1] Edward Hines Jr. Veteran Affairs Hospital, Hines, IL, United States, [2] Department of Neurological Surgery, Loyola University Medical Center, Maywood, IL, United States, [3] Department of Mathematics and Statistics and Institute of Environmental Sustainability, Loyola University Chicago, Chicago, IL, United States, [4] Department of Molecular Pharmacology and Neuroscience, Loyola University Chicago Health Science Division, Chicago, IL, United States

Lack of blood flow to the brain, i.e., ischemic stroke, results in loss of nerve cells and therefore loss of function in the effected brain regions. There is no effective treatment to improve lost function except restoring blood flow within the first several hours. Rehabilitation strategies are widely used with limited success. The purpose of this study was to examine the effect of electrical stimulation on the impaired upper extremity to improve functional recovery after stroke. We developed a rodent model using an electrode cuff implant onto a single peripheral nerve (median nerve) of the paretic forelimb and applied daily electrical stimulation. The skilled forelimb reaching test was used to evaluate functional outcome after stroke and electrical stimulation. Anterograde axonal tracing from layer V pyramidal neurons with biotinylated dextran amine was done to evaluate the formation of new neuronal connections from the contralesional cortex to the deafferented spinal cord. Rats receiving electrical stimulation on the median nerve showed significant improvement in the skilled forelimb reaching test in comparison with stroke only and stroke with sham stimulation. Rats that received electrical stimulation also exhibited significant improvement in the latency to initiate adhesive removal from the impaired forelimb, indicating better sensory recovery. Furthermore, axonal tracing analysis showed a significant higher midline fiber crossing index in the cervical spinal cord of rats receiving electrical stimulation. Our results indicate that direct peripheral nerve stimulation leads to improved sensorimotor recovery in the stroke-impaired forelimb, and may be a useful approach to improve post-stroke deficits in human patients.

Keywords: stroke, recovery, plasticity, middle cerebral artery occlusion, electrical stimulation, implantable device

OPEN ACCESS

Edited by:
Johannes Boltze, University of Warwick, United Kingdom

Reviewed by:
Nathan Makowski, Case Western Reserve University, United States
Masaki Ueno, Niigata University, Japan

****Correspondence:***
Shih-Yen Tsai
shih-yen.tsai@va.gov

Specialty section:
This article was submitted to Stroke, a section of the journal Frontiers in Neurology

Received: *28 September 2020*
Accepted: *15 March 2021*
Published: *20 April 2021*

Citation:
Tsai S-Y, Schreiber JA, Adamczyk NS, Wu JY, Ton ST, Hofler RC, Walter JS, O'Brien TE, Kartje GL and Nockels RP (2021) Improved Functional Outcome After Peripheral Nerve Stimulation of the Impaired Forelimb Post-stroke. Front. Neurol. 12:610434. doi: 10.3389/fneur.2021.610434

INTRODUCTION

Stroke is the fifth leading cause of death in the U.S. and is the most common cause of adult disability. Nearly 4 million stroke survivors live with permanent neurological damage effecting their function and quality of life. Among them, 87% of strokes are ischemic in nature (1). Currently, the only approved treatments for acute ischemic stroke (tissue plasminogen activator and embolectomy) must be administered or performed in the early post-stroke period, which, unfortunately accounts for only 10% of all stroke patients as the rest do not reach a hospital

early enough to receive such interventions (2–4). This leaves roughly 90% of ischemic stroke survivors to rely on rehabilitative therapies which show real but limited success in functional restoration. Among the many complications and sequelae of stroke, more than 75% of patients have upper extremity paresis (5) which includes the inability to properly use the thumb and fingers, as in a grasping motion (6, 7). Thus, improving upper extremity and hand function is of great importance in post-stroke rehabilitation and it is necessary to develop therapeutic approaches for this debilitating aspect of stroke recovery (8).

Neuromuscular electrical stimulation (NMES) has been used to facilitate rehabilitation post-stroke by improving and/or replacing volitional movement to enhance neural motor control, and hence reduce disability (9–11). NMES stimulates nerves to activate paretic muscles, and can be applied as either a supplementary tool combined with other rehabilitation strategies or used alone to improve functional recovery beyond the time of stimulation (12). The actual benefits of NMES are unclear as contradictory results from various clinical studies have emerged (11), and therefore more experimental studies are needed.

NMES can be used via invasive (implanted, percutaneous) or non-invasive (transcutaneous) devices (13, 14). For upper extremity rehabilitation, non-invasive approaches have been applied with conventional therapy in a cyclic pattern, EMG-triggered, or switch-triggered manner to facilitate activation of specific muscles to enhance task performance (15). However, the major issue of transcutaneous devices is that while a specific nerve of interest can be targeted, these devices also activate non-targeted nerves. Moreover, deeper nerves and muscles are more difficult to target using non-invasive techniques. Implanted devices (such as cuff electrodes) target specific nerves and reduce the current required to discharge the nerve while reducing non-targeted nerve activation (10, 16). While some implantable devices have been approved in Europe for use in aiding foot drop in stroke patients, none are currently FDA approved.

Previous studies have suggested that NMES may improve function by inducing neuroplastic changes in the spared motor cortex post-stroke (11, 14, 17). However, this possible cellular mechanism has not been fully investigated. Since changes in cortical efferent circuitry have been reported by our lab and others to play an important role in sensorimotor functional improvement after stroke (18–21), we sought to determine whether post-stroke NMES modulated neuroplasticity and improved function. In this report, we used a rat model of ischemic stroke to produce upper extremity paresis to assess whether peripheral nerve stimulation (*via* nerve cuff electrode) increased functional and volitional recovery in the effected forelimb.

METHODS

Animal Subjects

All animal studies were approved by the Institutional Animal Care and Use Committee of the Edward Hines Jr. Veterans Affairs Hospital. A total of 24 male Long Evans black-hooded rats (2 months of age, HsdBLU:LE, Harlan Laboratories IN, Barrier 217) were used at the beginning of the study. Rats were housed in standard cages (2 rats per cage) with a 12-h light/dark cycle in a fully accredited animal care facility. Rats had access to fresh water and were fed standard laboratory chow (Harlan 2018 Rodent Diet). All rats were number coded by a laboratory member not participating in the study, and investigators conducting behavioral testing and neuroanatomical analyses were blinded to the treatment conditions throughout the experiments.

Experimental Timeline and Overview

The experimental timeline is shown in **Figure 1**.

Behavioral Procedures

When the initial training period began, rats were reduced to 95% of their total body weight by food restriction; water was freely available. Behavioral tests were conducted at approximately the same time of day. Each animal was video recorded separately after the daily tests at baseline, 3 days following stroke, and at the end (8 weeks post-stroke) of the behavioral study. The recorded data was used to calibrate inter-rater variability and reaching error analysis.

Skilled Forelimb Reaching Test

This test was first performed as designed by Whishaw and our laboratory (22, 23) and used as described in our previous work (18, 20, 21, 24). It is well-established that the sensorimotor circuitry controlling motor control and related reaching and grasping of skilled reaching behavior is highly conserved in mammals (25). In brief, animals were placed in a transparent Plexiglas chamber (30 × 36 × 30 cm) with a rectangular opening (1.5 × 3 cm) in one wall. Small round food pellets (45 mg; Bilaney Consultants, Frenchtown, NJ) were placed one after the other onto the shelf at a distance of 1.5 cm from the opening. Rats were placed in the testing chamber daily until they learned to reach through the opening for the pellet, grasp the pellet and bring it to their mouth (a success). Rats were free to use either limb to reach through the opening and limb preference was determined and recorded for each animal. Rats reaching a baseline score with at least 16 successes out of 20 pellets per day for three consecutive days were enrolled in the study for stroke surgery. A maximum time limit of 5 min per session was given. Each rat resumed testing 3 days after stroke, and then daily (Mon-Fri) until the end of the study. The parameters recorded for the skilled forelimb reaching test included (1) the amount of time needed to obtain all 20 pellets, and (2) the success score, i.e., the number of pellets grasped with the preferred limb and placed into the mouth.

Reaching Error Analysis

Each animal was video recorded after the daily tests at baseline, 3 days following stroke, and at the end (8 weeks post-op). Reaching video files were analyzed frame by frame using QuickTime Player. Each reach error was recorded during analysis as described (**Table 1**). Descriptions included (a) the outcome (success or failure) and (b) description of event (short reach, inaccurate aim, bad grasp, etc.). From the described attempts four overarching categories emerged (miss, touch, drop, and success) with two subtypes per category. Categories were assigned a numerical value based on a progression of a reach (1–8). Therefore, rats that

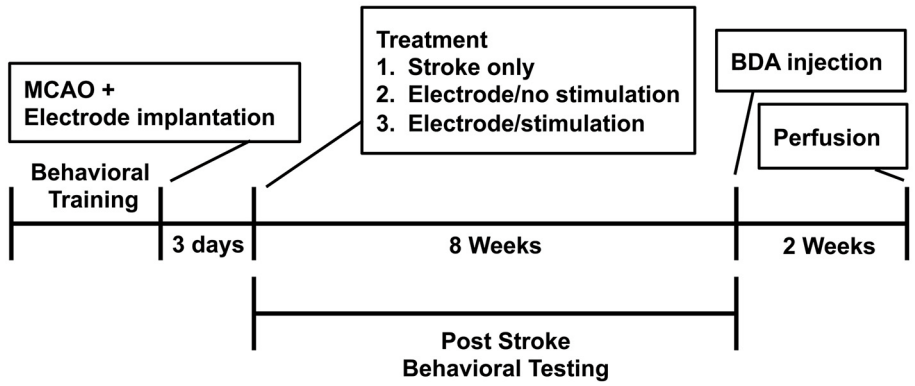

FIGURE 1 | Experimental design and timeline.

were able to grasp received a higher numeric value than rats that could not extend their limb.

Bilateral Tactile Adhesive Removal Task

This task has been shown to be sensitive for the detection of somatosensory deficits following sensorimotor cortex injury (26, 27). Small round adhesive stickers (Creatology adhesive foam sheet, 0.7 mm diameter, Michaels, Irving, TX) were placed onto the plantar surface of both forepaws. The order of contact, contact latency, and removal latency for each paw was recorded independently for each limb. Each rat was given maximal 120 s to complete initiation and removal of the adhesive. One hundred twenty seconds was recorded if the rat did not complete the task in time.

Stroke Surgery

A focal ischemic stroke was induced via middle cerebral artery occlusion (MCAO) modified from Chen et al. (28) and as in our previous work (18, 20, 21, 24). Rats were anesthetized with isoflurane (2–3% in oxygen) and core body temperature was maintained between 36.5 and 37.5°C during the entire procedure. The bilateral common carotid arteries (CCA) were first isolated from a ventral longitudinal cervical incision and the common carotid artery ipsilateral to the hemisphere corresponding to the preferred forelimb was permanently ligated. Rats were then placed in a stereotaxic frame and a vertical incision was made between the eye and ear. The temporalis muscle was retracted, and a burr hole was made to expose the middle cerebral artery (MCA) on the opposite side of the preferred limb, which was subsequently ligated with a 10-0 suture and then transected with microscissors. The contralateral CCA was temporarily occluded for 45 min using an aneurysm clip. After removal of the aneurysm clip, all wounds were closed and rats were either kept warm until awake or were kept anesthetized for nerve electrode cuff implantation. Rats were monitored during the post-op period until fully awake and able to eat and drink.

Nerve Cuff Electrode Placement

Placement of the electrode cuff (MicroProbes for Life Science, Gaithersburg, MD) was performed immediately after completion of MCAO under the same anesthesia (**Figure 2**). The procedure was adapted from Cho et al. (29) as shown in **Figures 2A,B**. Skin incisions were made on the top of the head and at the interscapular region. Additionally, an incision was made along the upper medial aspect of the impaired extremity and extended into the axilla to expose the pectoralis major muscle. The muscle was then retracted to expose the brachial plexus and the median nerve was isolated. A tunnel under the skin was created from the top of the head to the interscapular incision and to the axilla, and the electrode wire was guided into the axilla opening. The median nerve was placed in the electrode cuff and stabilized by sutures (**Figure 2B**). The cuff was custom made with the following specifications: 0.75 mm inner diameter, two 100 μm platinum contacts were situated 1 mm longitudinally apart and 2 mm to the edge of the cuff, an ultra fine lead leaving the cuff at a 45 degree angle with a total silicone encapsulation running for 100 mm, and connected to an *in vivo* 1 MS303-120 right-angled two channel connector (PI Technology, Roanoke, VA). Partial loops of the lead were left in the neck wound to allow for movement and to prevent strain on the electrode/nerve. A small guide hole was placed in the skull frontal bone followed by a stainless steel screw placement. The connector and screw were then covered with a fast-setting dental cement to form a connector cap. The electrical continuity of the electrode leads was tested using an ohmmeter. The head incision was sutured while leaving the top part of the connector cap above the skin and exposed to allow for connection to the stimulator.

Peripheral Neuromuscular Electrical Stimulation

A schematic of the electrical stimulation circuitry is shown in **Figure 2C**. Charge balanced stimulation was used to prevent corrosion of the electrodes and deleterious effects on the nerve.

TABLE 1 | Reaching Error Analysis.

Miss	Touch	Drop	Success
1 – No Extension • Limb contracted • Limb did not extend past window or just past • Curled wrist and digits	*3 – No grasp* • Limb extended past window • Paw and digits are flat or curved toward body • Paw planted flat on pellet – digits do not curl around pellet • Pellet pulled through window or paw lifted up and back	*5 – Early Drop* • Limb extended past window • Paw and digits slightly angled toward pellet • Digits are planted and curled around pellet • Pellet is in paw as limb is retracted • Paw is not brought to mouth but placed on ground near starting position • Pellet falls out of paw while the limb is on the ground or while another reach is attempted	*7 – Partial Success* • Limb extended past window • Paw and digits slightly angled toward pellet • Digits are planted and curled around pellet • Pellet is in paw as limb is retracted • Paw is brought to mouth • Digits are straightened as paw is brought to mouth. Removing pellet from grasp requires multiple licks.
2 – Poor aim • Limb extended past window • Digits curled in grasp motion in air above pellet • Limb/paw ended on either side of pellet and grasps	*4 – Inaccurate grasp* • Limb extended past window • Paw and digits are flat or curved • Digits planted on and curled around pellet • During limb retraction, pellet is either dragged or immediately propelled away from between digits	*6 – Late Drop* • Limb extended past window • Paw and digits slightly angled toward pellet • Digits are planted and curled around pellet • Pellet is in paw as limb is retracted • Paw is brought to mouth • Pellet falls while attempting to remove from grasp	*8 – Complete success* • Limb extended past window • Paw and digits slightly angled toward pellet • Digits are planted and curled around pellet • Pellet is in paw as limb is retracted • Paw is brought to mouth • Digits are straightened as pellet is placed in mouth

The capacitor coupled stimulation balanced the stimulation current during the pulse with an equal and opposite discharge during the inter-pulse period. Rats undergoing stimulation were individually placed into a repurposed forelimb reaching box after their electrode was connected to the stimulator. The leads from the electrode to the stimulator were attached to the roof of the box so the rat could move freely. Using a Grass S11 constant voltage stimulator, stimulation voltage was gradually increased until muscle contraction was felt (deemed threshold level). A 1.5-fold increase over the threshold voltage was applied to induce muscle contraction throughout the 30 min stimulation sessions. Threshold current was determined by measuring the voltage across a 1 K Ohm resistor in series with the stimulating electrode and using Ohm's law to solve for current. Threshold currents were recorded after completion of the electrode cuff implantation. The stimulation parameters were adapted from our previous work on a spinal cord injury model with modifications (30). Other parameters included 1.0 ms in duration of stimulation, delivered every 2 s in 1-s trains of 5 Hz (**Figure 2D**). Daily 30 min stimulation sessions began 3 days after MCAO surgery and continued (Monday–Friday) for a total of 8 weeks. Rats in the Stroke/No E-stim group had the exact same placement of the electrode post-stroke, were placed in the stimulation boxes for the same time period, but did not receive any electrical stimulation. Each stimulation session occurred at least 2 h after the behavioral tests. The staff applying stimulation was different from the staff testing animals.

Biotin Dextran Amine Tracing

When behavioral testing was complete, rats were re-anesthetized with isoflurane (2–3% in oxygen) and secured in a stereotaxic frame. A 2 mm burr hole was made to expose the sensorimotor cortex of the hemisphere opposite to the stroke lesion site. Two 1 μl aliquots of 10% BDA solution in 0.01 M phosphate buffer (pH 7.2) were injected into the caudal forelimb motor cortex (coordinates: 0.5 mm caudal/2.5 mm lateral, 1.0 mm caudal/3.0 mm lateral to bregma, and both at 1.5 mm ventral from the brain surface), as defined electrophysiologically by Neafsey et al. (31).

BDA Histochemistry

BDA histochemistry was performed as previously described by our laboratory (18, 20, 32). Two weeks after BDA injections, rats were euthanized with sodium pentobarbital (100 mg/kg; i.p.) and perfused transcardially with heparinized PBS solution followed by fixative [4% paraformaldehyde (PFA) in 0.1 M phosphate buffer]. The brains and spinal cords were removed, post-fixed, cryoprotected, and frozen sectioned coronally at 40 μm. Sections were collected every 200 μm in one series. Endogenous peroxidases were blocked via incubation with 0.1% hydrogen peroxide solution. Sections were then washed and incubated overnight with an avidin-biotin-peroxidase complex (ABC elite, Vector Labs). The sections were washed again and pre-incubated with 0.4% ammonium nickel sulfate followed by 0.015% 3.3-diaminobenzidine (DAB), and finally reacted with 0.004% hydrogen peroxide. The reaction was stopped by washing with tris buffer and the sections were left to air dry before being lightly counterstained with Nissl stain and coverslipped.

Stroke Size Analysis

Nissl-stained coronal brain sections were quantitatively analyzed every 400 μm between +4.7 to −5.2 mm from bregma according to Paxinos and Watson (33) using a computer-interfaced imaging system (Image J, NIH, Bethesda, MD) as described

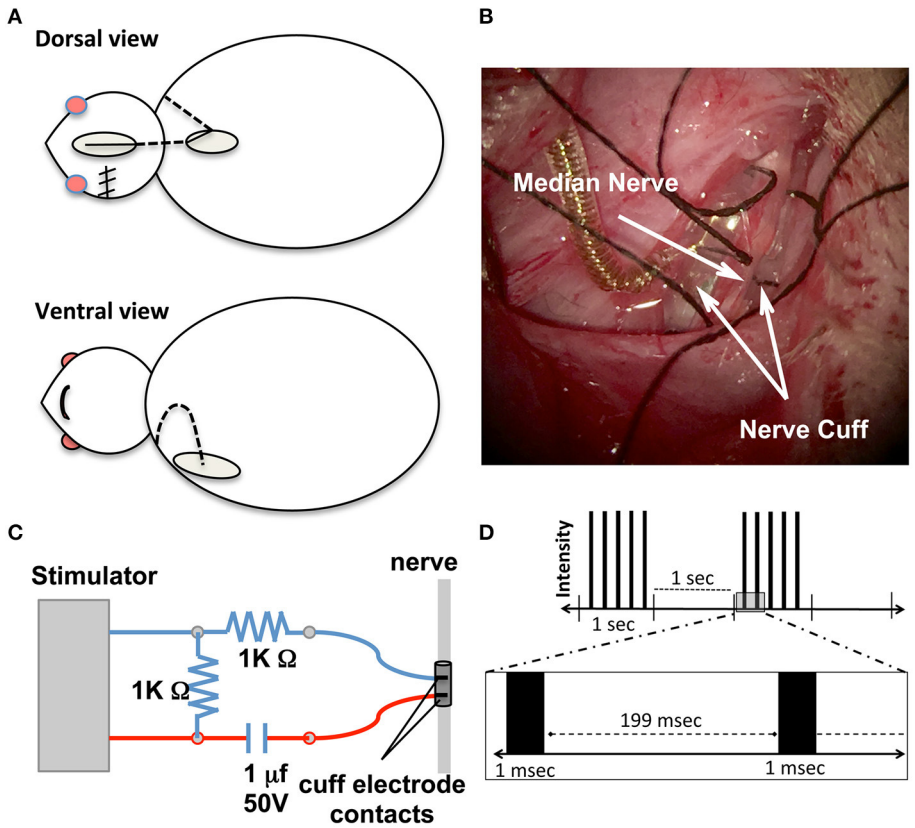

FIGURE 2 | Nerve cuff placement. **(A)** Schematic of surgical procedures for nerve cuff placement. Dotted lines represent the lead wire and ovals represent surgical incision sites. **(B)** Intraoperative photographs of the cuff enclosing the nerve according to the experimental design. Gold colored coil is the lead wire leaving the cuff. Black sutures were tied to keep cuff secure around nerve. **(C)** Schematic diagram of electrical stimulation circuit setups. The stimulator is the power source and **(D)** Schematic demonstration of stimulation parameters. Each black bar represents an individual pulse segment.

previously (18, 20, 21, 34). Stroke size was expressed as a percent of the intact contralateral hemispheric area (total area of the intact contralateral hemisphere minus total area of the ipsilesional hemisphere divided by the total area of the intact contralateral hemisphere).

Neuroanatomical Analysis

The analyses for corticospinal plasticity described in this section were performed as previously reported (18, 35). All analyses were done on coded slides so that the investigator was blinded as to the experimental group. Anatomical structures were identified with the atlas of Paxinos and Watson (33).

Quantification of Corticospinal Tract Labeling Crossing the Midline and in the Dorsal Column

BDA-labeled fibers in the dorsal column were counted using stereological methods (StereoInvestigator, MBF Bioscience, Williston, VT) on the first two C5 sections analyzed for midline fiber crossing. In brief, dorsal column outline tracings were performed under a 2.5X objective. Both the sampling grid size (75 × 75 μm) and the sampling ratio (20%) were optimized to provide adequate sampling of the entire dorsal column. The estimated total BDA-labeled CST fibers of both sections were averaged as an internal reference for BDA injections and staining. This was done in order to standardize the total number of labeled midline crossing fibers in the spinal cord (18).

On sections analyzed, all BDA-positive fibers crossing the midline were counted under a 40X objective. Twenty alternate sections (400 μm apart) at the cervical spinal cord levels C5–C8 were totaled. To correct for inter-animal tracing variability, the total number of crossing fibers was divided by the number of labeled corticospinal fibers in the dorsal column (as determined above) multiplied × 10^4 and expressed as fibers crossing the midline per ten thousand labeled corticospinal axons.

Inclusion/Exclusion Criteria

Skilled Forelimb Reaching Test

Prior to surgery, animals were excluded from the study if they were unable to successfully reach for 16 out of 20 pellets within 5 min after 3 weeks of training on the task. Three days post-stroke, all rats were tested. Animals showing severe deficits were excluded from the study. Severe deficits were defined as the inability of a rat to reach using his impaired forelimb through the open window for at least one out of 20 attempts.

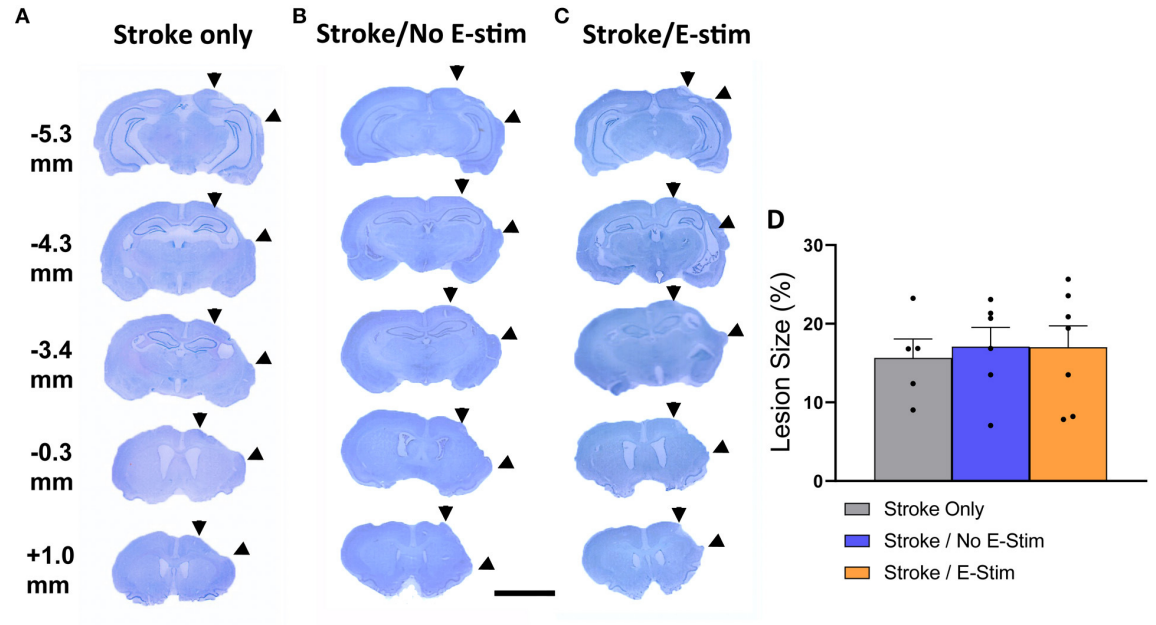

FIGURE 3 | Lesion analysis. Nissl stain sections and their relative distance from bregma showing typical ischemic lesion of all three groups of rats **(A–C)**. Area between two arrowheads on each brain section indicates stroke-induced necrotic regions. The numbers indicate relative distance to bregma. The scale bar indicates 0.5 cm. **(D)** Lesion analysis showed no difference in the lesion size between groups (Stroke only vs. Stroke/No e-stim vs. Stroke/E-stim ANOVA, $p > 0.05$).

Conversely, if a rat showed only a mild deficit 3 days post-stroke, which we defined as reaching successfully for 10 or more pellets out of the 20 attempts, they were excluded from the entire study (21).

Bilateral Tactile Adhesive Removal Task

In order for the handling of the animal to not interfere with the subcutaneous leads and the electrode cuff, animals which struggled excessively during the adhesive removal task at post-op day three were excluded only from this analysis.

Stroke Lesion

Following our previous reports (18, 21), rats were excluded from the study if lesion analysis did not show sensorimotor cortex involvement and/or showed extensive dorsal lateral (DL) striatum involvement.

BDA Labeling

For this analysis, rats demonstrating dorsal column BDA-labeled corticospinal fiber counts of <500 were excluded from crossing fiber analysis due to poor BDA transport or insufficient injection site uptake.

Statistical Analysis

Analyses of all data were performed with SPSS version 13.0 (SPSS Inc., Chicago, IL). A 2-WAY repeated measure ANOVA (time × treatment) was used to analyze differences in the forelimb reaching test between three experimental groups, followed by Tukey *post-hoc* to compare weekly mean values between the three experimental groups. The adhesive removal test was analyzed using Non-parametric Mann-Whitney test. Spinal cord midline crossing index were analyzed using a Student's *T*-test. Forelimb reaching results were correlated with spinal cord midline crossing index. A p value ≤ 0.05 was considered significant. All error bars shown are ±SEM. All bar graphs show individual data points (n value).

RESULTS

At the beginning of the study, 26 animals received skilled forelimb reaching task training. Three animals were removed (n = three) from the study prior to surgery due to failing to reach baseline, i.e., they were not successful at grasping at least 16 out of 20 pellets within 5 min. A total of five animals ($n = 5$) were further excluded from the study 3 days after stroke. Of those, three were removed due to the inability to reach for the pellets (severe deficit), and two were removed because they showed only a mild reaching deficit.

At the completion of electrode cuff implantation, the average threshold currents (mean ± SEM) were 0.11 ± 0.01 mA.

Stroke Lesion in the Sensorimotor Cortex

Stroke lesions in all rats showed ipsilateral sensorimotor cortex necrosis with no or minimal anterior striatum involvement and without other anatomical structure damage (**Figures 3A–C**). There was no statistical difference in stroke size between groups (Stroke only, 15.67% ± 2.4 SEM; Stroke/No E-stim, 17.09%

± 2.45 SEM; Stroke/E-stim, 17.02% ± 2.73 SEM) (one-way ANOVA, $p > 0.05$) (**Figure 3D**).

Functional Improvement After Direct Peripheral Nerve Electrical Stimulation

Skilled Forelimb Reaching

After training on the skilled reaching task, baseline success scores showed no significant difference between the three groups (**Figure 4**). Three days post-MCAO, all rats exhibited a marked deficit in reaching success using their preferred limb with no difference between groups. However, rats receiving electrical stimulation showed significant overall improvement of the skilled forelimb reaching test when compared to stroke only and stroke with sham stimulation (two way repeated-measure ANOVA, main effect time $p < 0.0001$, main effect treatment $p < 0.0001$, interaction $p < 0.001$). Differences in reaching success scores were first apparent 3 weeks post-MCAO between stroke only animals and those receiving electrical stimulation (Tukey, $p < 0.05$). This significant difference between electrical stimulation and stroke only groups continued throughout the remaining weeks ($p < 0.05$ at week 3, 4, and 5, $p < 0.01$ at week 6, $p < 0.001$ at week 7 and week 8). Six weeks after MCAO, those rats receiving stimulation showed significant increases in reaching success compared to those with sham stimulation ($p < 0.01$). This significant increase persisted throughout the remainder of the behavioral testing ($p < 0.001$ at week 7, $p < 0.01$ at week 8). Additionally, the reaching success score of animals receiving electrical stimulation was not significantly different from baseline scores at 8 weeks, with stimulated animals receiving, on average, 83% of the baseline score.

Reaching Error Analysis

Qualitative analysis of the forelimb reaching errors showed a decrease in deficit severity across time that was particularly obvious in rats receiving E-Stim (**Figure 5**). Reaching behaviors were analyzed at pre-stroke baseline, 3 days post-stroke before stimulation, and at the end of 8 weeks just prior to BDA injection. Recordings of three animals in the Stroke only group were dropped from the analysis due to poor recording quality. At 3 days post-stroke, errors were comprised mainly of missed pellets or failure to grasp the pellets. Rats receiving either no stimulation or sham stimulation remained similar in the error types at the end of the study. On the contrary, rats receiving E-stim showed similar errors as the other two control groups at 3 days post-stroke, but improved to less severe categories by the end of the study (**Figures 5A,B**), indicating that not only did electrical stimulation improve overall success in obtaining pellets, but also lessened the impact of the stroke by decreasing the severity of the errors that did persist.

Bilateral Tactile Adhesive Removal Task

In order to examine whether electrical stimulation to the median nerve in the forelimb affected sensory perception, we performed the adhesive removal test on rats that received implantation of an electrode (**Figure 6**). As this test required a longer duration of handling, animals that showed excessive struggle/agitation were excluded from this analysis in order to preserve and not disturb electrode placement. Sensory perception was analyzed using the difference in time it took for the rat to initiate removal of the adhesive sticker from its stroke-affected forepaw compared to its other forepaw. At baseline testing prior to stroke (**Figure 6A**), no difference in latency to initiate removal was observed between the Stroke/no E-stim group ($n = 5$) and the Stroke/E-stim group ($n = 4$). One week post-stroke (**Figure 6B**), the difference in latency to initiate removal between dominant and non-dominant forepaws was increased in both Stroke/no E-stim (mean = 35.7 s) and Stroke/E-stim (mean = 37.8 s) group, indicating a sensory deficit caused by the stroke. However, at 8 weeks post-stroke (**Figure 6C**), rats that received the E-stim therapy showed a significant decrease in latency to initiate between impaired and non-impaired forepaws (mean = 8.1 s) compared to the rats that only received sham stimulation (mean = 30 s) (nonparametric Mann-Whitney test, $p < 0.05$), suggesting that electrical stimulation contributed to improved sensory perception in the stroke-affected limb.

Quantification of Neuronal Plasticity

Compensatory sprouting and neuroanatomical plasticity were analyzed for corticospinal midline crossing fibers originating from the contralesional forelimb cortex using the anterograde neuroanatomical tracer BDA (**Figures 7A,B**). Due to exclusion criteria requiring at least a count of 500 dorsal column BDA-labeled corticospinal fibers, a total of 8 rats (Stroke Only = 3, Stroke/No E-stim = 2, and Stroke/E-stim = 3) were removed from this analysis due to poor BDA transport or insufficient injection site uptake. Since the two control groups showed no statistical difference in crossing fibers, they were pooled as Stroke Control for analysis (**Figure 7C**).

Rats receiving E-stim therapy (**Figure 7D**) exhibited nearly three times the midline crossing index (104.97 ± 19.22 SEM) in the cervical spinal cord as compared to the combined Stroke control group (32.52 ± 5.73 SEM) (**Figure 7E**, $p < 0.05$, Student's t-test). Further analysis (**Figure 7F**) showed that there was a direct correlation between the corticospinal fiber midline crossing index and the final forelimb reaching score for each rat ($r = 0.44$, $p < 0.05$), suggesting a positive relationship between the number of fibers that crossed the midline and functional recovery.

DISCUSSION

Our results show that daily, direct median nerve stimulation to the stroke-impaired forelimb in the adult rat led to significant improvement in the skilled forelimb reaching test, and also reduced the time to initiate adhesive removal on the stroke-impaired limb, indicating significant sensorimotor recovery. Furthermore, this therapy enhanced cortico-efferent plasticity from the contralesional cortex to the deafferented spinal cord, which may be the underlying substrate for the observed improvement in function.

One of the main goals for stroke survivors is improving hand and finger use of the paretic upper extremity, such as flexion/extension and adduction/abduction motion. The median

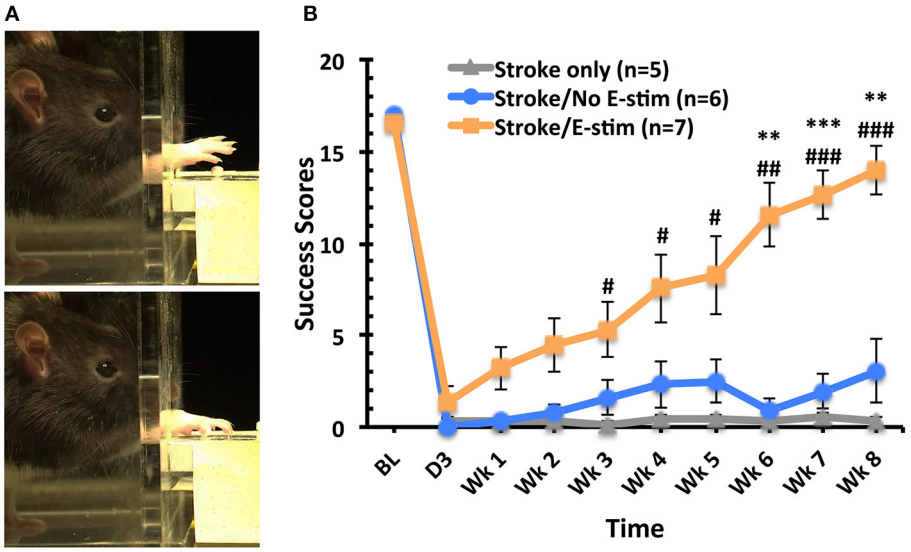

FIGURE 4 | Skilled forelimb reaching task analysis. **(A)** Sequential frames of the skilled forelimb reaching task performed by an adult rat grasping a sugar pellet. **(B)** Success scores for reaching task (out of 20 reaches) across time. No difference between groups at baseline. Marked deficits in successfully obtaining pellets with the stroke-impaired limb were apparent 3 days post-op (before treatment) with no significant difference between groups. Rats receiving electrical stimulation showed significant overall improvement of the skilled forelimb reaching test when compared to stroke only and stroke with sham stimulation (two way repeated-measure ANOVA, main effect time $p < 0.0001$, main effect treatment $p < 0.0001$, interaction $p < 0.001$). Weekly comparison showed that animals receiving electrical stimulation exhibited significant improvement in the success scores than the Stroke only group (#$p < 0.05$ at week 3, 4, and 5, ##$p < 0.01$ at week 6, ###$p < 0.001$ at week 7 and week 8) and Stroke/No e-stim group (**$p < 0.01$ at week 6 and 8, ***$p < 0.001$ at week 7) and the improvement persisted until the end of the study. There was no difference between two control groups at any time point (Tukey's *post hoc* analysis, error bars indicates ±SEM).

nerve was directly targeted in this study as it innervates muscles of the forearm and digits one through four. Furthermore, there are great similarities between humans and rats in performing reaching movements that largely involve the flexion movements that are controlled by the median nerve (37–39). As a mixed nerve, the median nerve also transmits sensory information from the palm and some of the digits (39). Our results showed that direct median nerve stimulation improved performance in a sensorimotor based (skilled reaching task) and a sensory (adhesive removal) task. In the skilled forelimb reaching task, we observed that rats receiving E-stim improved up to 80% or better performance of their baseline values, compared to those who did not receive E-stim. Further analysis of errors leading to non-successful reaches showed that in all three groups rats demonstrated similar types of errors at baseline, which is to be expected since they were essentially "normal" rats. At 3 days post-stroke, and before E-stim was started, the same types of errors were demonstrated across all groups. These errors largely were categorized in the more severe error categories, i.e., inability to aim properly or grasp with their digits. However, there was an exception to this pattern. One rat in the E-stim group did not make as severe of errors. This rat was not excluded from the study as its lesion size and performance on the daily reaching task post-stroke did not differ significantly from the rest of the group.

At the end of the 8 weeks, rats receiving E-stim showed a marked shift in their errors toward categories considered less severe, compared to the stroke/No E-stim group whose errors were predominantly still classified in the more severe categories. This indicated not only an improvement in the total success scores from the reaching task, but a decrease in the overall severity of the stroke impact on forelimb function. Several reports have shown that peripheral electrical stimulation induced neuroplastic changes in the motor cortex (see Chipchase et al. for review) (40), in particular when the stimulation intensity was above the motor threshold (41, 42). Peripheral stimulation of 1.5–2 times the motor threshold (as was used in this study) not only induced a response in the corresponding cortex, but also the contralesional cortex (43–45). This bilateral activation of the cortex may play important roles for cortical reorganization, as the homotopic contralesional cortex is a major site for cortical plasticity leading to functional recovery (20, 46–50).

Our laboratory and others have reported that improved functional outcomes after CNS injury can be induced through a variety of approaches (i.e., neurite inhibitors, pharmacologic interventions, environmental enrichment, stem cells) (18, 51–55). Furthermore, it has been shown that peripheral nerve stimulation induced neuroplastic changes (40), therefore, we sought to determine if E-stim therapy led to new corticospinal connections from the contralesional cortex (47, 56). BDA analysis in the present study revealed that rats which received E-stim had increased spinal cord midline crossings of corticospinal tract axons originating in the contralesional motor cortex and

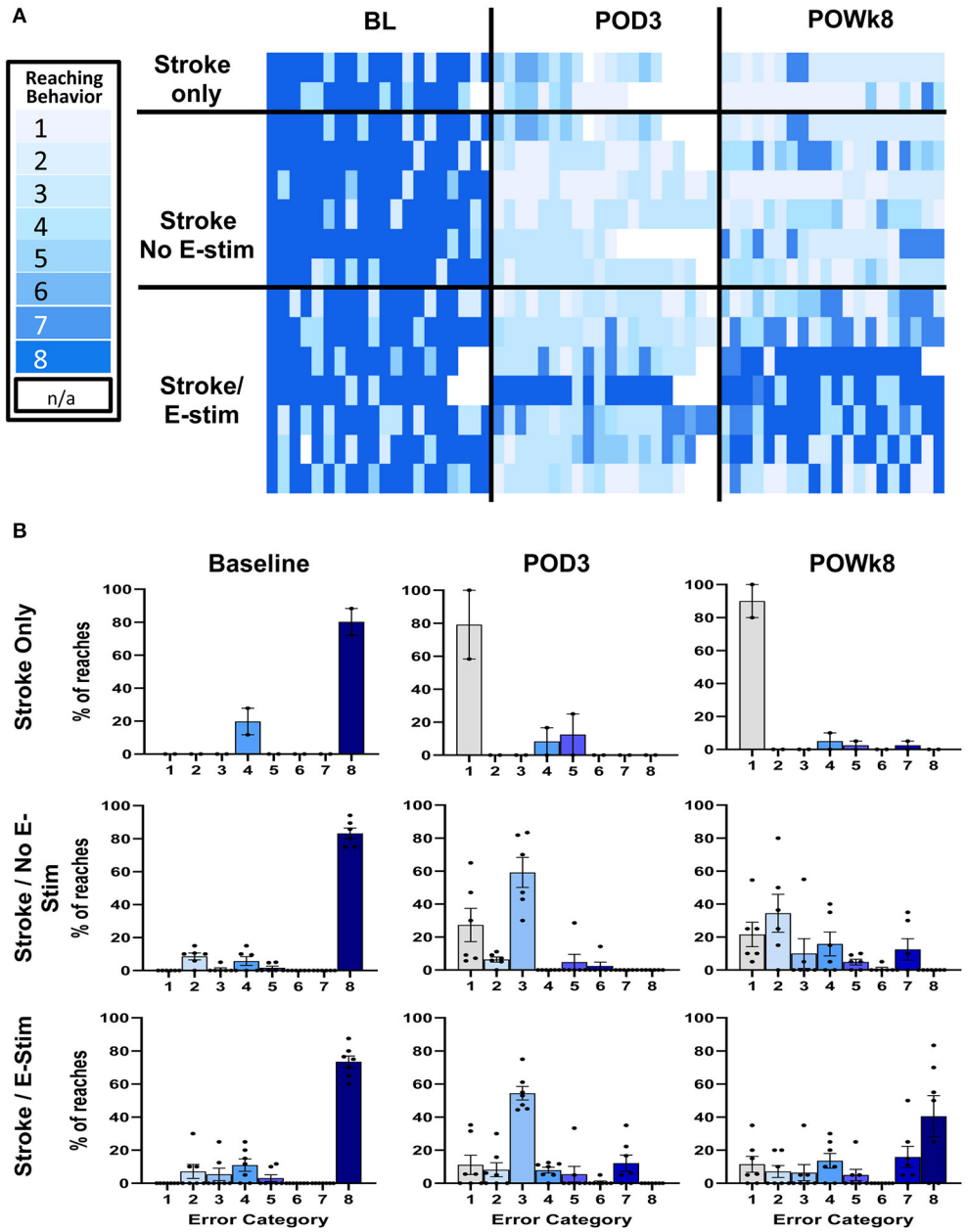

FIGURE 5 | Reaching error analysis. **(A)** Reaching error analysis of individual animals in each experimental group. All animals' reaching behaviors were recorded and analyzed at pre-stroke baseline, 3 days post-op before stimulation, and at the end of 8 weeks before BDA injection. The errors were categorized based on reaching error type. Each trial was composed of 20 different reaches where each reach was categorized independently. Reaching behaviors are categorized as follows and range from the lightest blue to the darkest blue: (1) Miss – no extension, (2) Miss – poor aim, (3) Touch –no grasp, (4) Touch – inaccurate grasp, (5) Grasp – dropped early, (6) Grasp – dropped during eating, (7) Success – arm motions not smooth, and (8) Total Success. White boxes represent missing data points (N/A). **(B)** Bar graph plots of reaching errors. At baseline, most reaches were successes across groups. However, of the unsuccessful reaches, most were in the moderate severity categories. At 3 days post-op (POD3), animals across experimental groups committed errors in the more severe error categories (i.e., 1–3) with less complete success. At the end of behavioral studies (POWk8), animals receiving E-stim not only improved in the number of successful reaches but also committed less errors in the more severe categories. In the non-stimulated groups, animals either showed no improvement (Stroke only) or there was a slightly right shift toward the less severe error categories without increasing success (Stroke/No E-stim).

terminating in deafferented cervical spinal areas. Moreover, by plotting both reaching score and fiber crossing index, two distinct treatment-based populations were evident (**Figure 7F**), which supports the significance of neuroplasticity in functional recovery. This finding is consistent with our previous studies demonstrating that remodeled motor pathways at the spinal cord

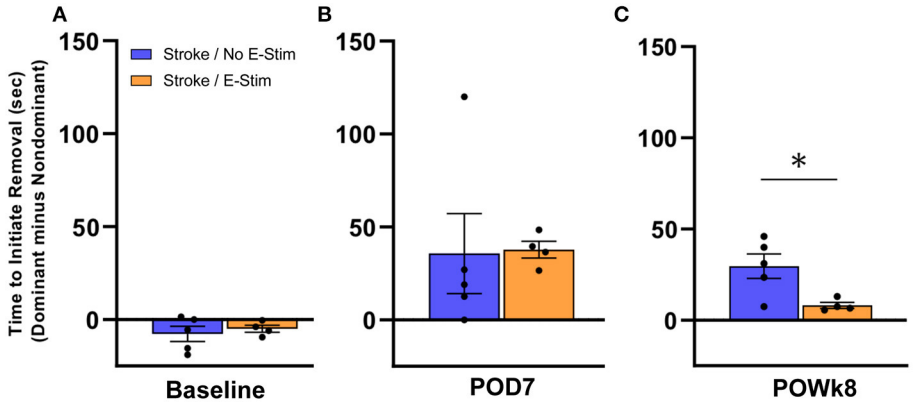

FIGURE 6 | Adhesive removal analysis. Both Stroke/No E-stim and Stroke/E-stim groups showed similar time in the initiation difference between two forelimbs for adhesive removal at pre-stroke baseline **(A)** and such initiation difference increased greatly at 7 days post-stroke **(B)** ($p > 0.05$). **(C)** At the end of behavioral tests, i.e., 8 weeks after stroke, animals receiving direct electrical stimulation on median nerve showed significant less time difference between two limbs to initiate adhesive removal (mean ± SEM, Non-parametric Mann-Whitney test, $^*p < 0.05$).

level correlated with improved function after cortical lesions (18, 35). Although plastic changes in the contralesional cortex may serve as the origin of improved functional outcomes, the role of the perilesional cortex cannot be ignored (57–59). Studies have shown that enhanced synaptic efficacy and either an increase or reorganization of axodendritic synaptic density of the perilesional cortex is also closely associated with spontaneous functional improvement after stroke (60). However, larger stroke size in our model may lessen the availability of intact perilesional cortex in the forelimb area. Further studies will be needed to examine whether anatomical plasticity occurs in response to peripheral electrical stimulation in the perilesional region.

Only young adult animals were examined in the current study (2 months of age at the start of the study). Our previous studies in aged rats showed that improvement in sensorimotor performance (19) and spatial memory (61) can still be achieved post-stroke with the same interventions utilized in young adult rats (18, 24, 32). Therefore, we expect the same approach in this study will lead to similar outcomes in the aged rats. However, we may observe a different recovery pattern, such as delayed recovery (19).

Due to the lack of standard parameters, such as time to start stimulation after stroke and stimulation frequency/intensity, the beneficial effects of NMES on stroke patients cannot be verified easily. The stimulation parameters chosen in the present study were based on our previous report on spinal cord injury in the rat (30). Several clinical studies applying NMES alone suggested sensorimotor function improvement in stroke patients (62, 63) although with stimulation frequencies between 10 and 50 Hz. Further, a report showed that activation at 5 Hz on the cortex did improve stroke patients' motor function (64). Our present study using a lower frequency at 5 Hz is supportive of those clinical studies showing that NMES has great potential to be used alone as an option to promote functional improvement in stroke patients. More importantly, our model can be used to further systemically explore the therapeutic effects of various parameter combinations.

To our knowledge, there is no known research on cellular mechanisms involved in implanted NMES in stroke animals. However, we have considered several possible mechanisms that may contribute to the corticospinal plasticity presented here. (1) Peripheral nerve stimulation could recruit contralesional and surviving ipsilesional cortical neurons to undergo axonal remodeling and motor map reorganization (14, 65–67). (2) Peripheral nerve stimulation could affect all types of neural pathways including sensory, motor, proprioceptive, as well as polysynaptic transmission (44, 45, 63). In this way, future studies should investigate whether median nerve E-stim in this stroke model leads to plastic changes or modulation of structures along the ascending pathway, such as neural modulation in the periaqueductal gray (68). (3) In addition to the plasticity enhancing trophic factors brain-derived neurotrophic factor (BDNF), neurotrophin-3 (NT-3), and cytokines (tumor necrosis factor-alpha, interleukin-6) induced in the spinal cord after stroke (69), plasticity at the spinal cord level may be further enhanced through stimulation-induced changes of the micro-environment such as release of signaling molecules, BDNF (70) and/or insulin-like growth father (IGF) in muscle and spinal cord (71). These trophic factors are known to promote neural growth and enhance neuronal plasticity. Using this model, these trophic factors, and others, should be assayed to determine if changes in their levels could potentially correlate with both function and midline crossing. (4) Peripheral nerve stimulation has recently been shown to lead to subventricular zone (SVZ) neurogenesis (72), which has been implicated as a source of migrating neural progenitors to the lesioned motor cortex (73). Taken together, these possible mechanisms suggest that the neuroplastic effects promoted by peripheral nerve stimulation may not

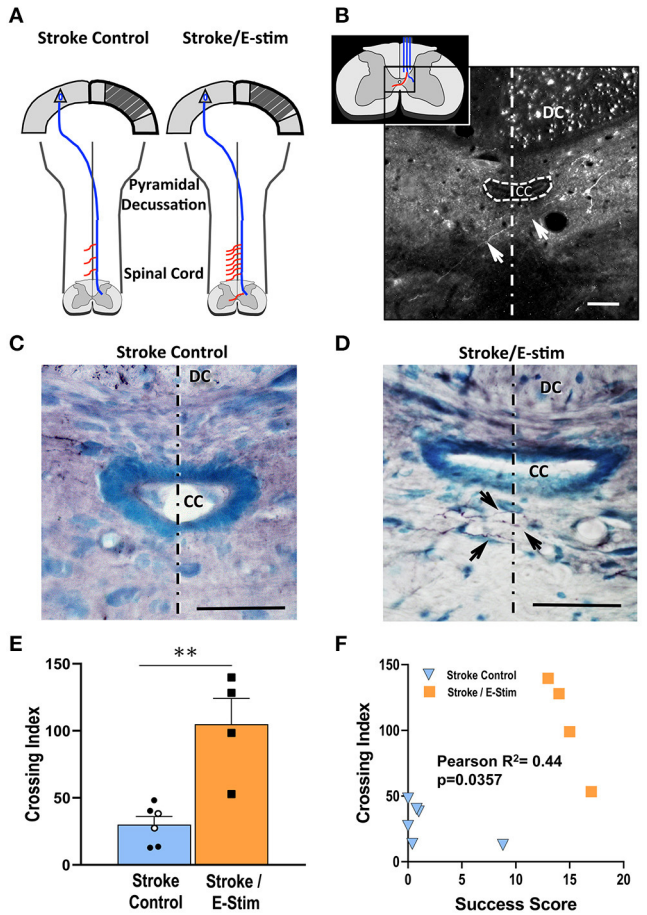

FIGURE 7 | Neuroanatomical analysis. **(A)** Schematic diagram showing corticospinal plasticity presented as more midline crossing fibers (red lines) along the cervical enlargement after stroke and E-stim treatment. Diagram adapted from Wahl et al. (36). **(B)** An enlarged schematic midline fiber crossing diagram (inset) and a representative fluorescent photomicrograph shows an alexa fluor 488 streptavidin-labeled BDA-positive midline-crossing corticospinal fiber (arrows) at C6 level. The fluorescent dots in the right dorsal column are BDA-positive corticospinal fibers. **(C,D)** Photomicrographs of BDA-reacted C6 spinal level sections show differences of corticospinal midline crossing fibers (arrows) between a Stroke Control **(C)** and Stroke/E-stim animals **(D)**. **(E)** Stroke/E-stim treated animals exhibited a significant higher midline crossing corticospinal fiber index in comparison with Stroke control (pooled Stroke Only and Stroke/No E-stim animals) (mean ± SEM, $^{**}p < 0.01$, Student's *t*-test). Black circles represent Stroke/No E-stim and white circles represent Stroke Only animals. **(F)**. Midline crossing corticospinal fibers showed positive correlation with the final forelimb reaching success score across 3 groups of animals ($P < 0.05$). The dotted lines indicate the midline. The scale bar indicates 50 μm. DC, dorsal column; CC, central canal.

only act locally, but also likely involve multiple pathways and cellular mechanisms.

This study provides a reliable animal model to examine the effects of NMES on stroke recovery and to study the underlying mechanisms. There are several points worth mentioning for our model. (1) The nerve cuff electrode reduced animal discomfort during stimulation, allowed for a lower current amplitude (0.11 mA on average) to induce muscle contraction and targeted a specific nerve (median nerve in this study). (2) Utilization of a nerve cuff also allowed for the targeting of a specific nerve (median nerve in this study) and prevented current leakage into the adjacent nerves and tissues, thereby lessening activation of non-targeted nerves (74). (3) Our stimulation paradigm utilized a sub-tetany frequency (5 Hz) compared to other paradigms that utilize higher frequencies that may lead to muscle tetanus (75). Furthermore, a clinical study showed that low frequency stimulation led to activation of bilateral thalami (76) which connect to the sensorimotor cortex and may play an important role in neuroplastic changes. (4) We applied electrical stimulation for only 30 min each day and did not add any additional therapies, yet still yielded improvement in volitional function. Once it is translated for clinical use, the simplicity of this therapy promotes continued patient compliance. (5) Stimulation was delayed until 3 days after stroke, and therefore this intervention may be used in patients that are stabilizing post-stroke and/or missing the time window to receive tPA or thrombectomy. It is believed that most recovery from impairment in humans resulting from enhanced plasticity occurs in the first 1–3 months after stroke (25, 77). The cortical plastic responses to stroke are particularly active within days or weeks after stroke in rodents (78–80). Our reports showed that such plasticity could be enhanced when interventions were given ranging from within a week (18, 19, 32, 52, 53) to months post-stroke in rodents (20, 21). Therefore, the time window to deliver NMES to promote neuronal plasticity and improve functional outcome may be extended beyond the acute stage after stroke in both rodent models and human patients. However, as it is not known for certain, more studies are needed to determine the best time window for clinical use.

In conclusion, median nerve stimulation post-ischemic stroke led to functional recovery on sensorimotor tasks that can potentially be attributed to plastic changes at the cervical spinal cord level. This study has provided an important model for both the cellular mechanisms by which peripheral E-stim promotes functional recovery, and its stimulation paradigm which has high translation potential to the stroke population at large.

DATA AVAILABILITY STATEMENT

The raw data supporting the conclusions of this article will be made available by the authors, without undue reservation.

ETHICS STATEMENT

The animal study was reviewed and approved by Hines VA/Lovell IACUC.

AUTHOR CONTRIBUTIONS

S-YT contributed to the concept and design, acquisition/analysis and interpretation of data, and drafted the major part of the article. JS contributed to acquisition/analysis and interpretation of data, and drafted part of the article.

NA, JWu, and ST contributed to the acquisition/analysis of data. RH contributed to the design and experimental method refinement. JWa contributed to the design and refinement of experimental methods. TO'B contributed to data analysis/interpretation. GK contributed to the concept and design, interpretation of data, and revised the article for important intellectual content. RN originated the concept and design, interpretation of data, revised the article for important intellectual content. All the authors read and approved the final version.

FUNDING

This project was supported by the Paul Kalmanovitz Central Nervous System Repair Research Program, the Department of Veterans Affairs and NIH Grant NS115759.

ACKNOWLEDGMENTS

Special thanks to Dr. Robert Wurster for his helpful discussions and technical support.

REFERENCES

1. Virani SS, Alonso A, Benjamin EJ, Bittencourt MS, Callaway CW, Carson AP, et al. Heart disease and stroke statistics-2020 update: a report from the American Heart Association. *Circulation*. (2020) 141:e139–596. doi: 10.1161/CIR.0000000000000757
2. Ding D. Endovascular mechanical thrombectomy for acute ischemic stroke: a new standard of care. *J Stroke*. (2015) 17:123–6. doi: 10.5853/jos.2015.17.2.123
3. Elgendy IY, Kumbhani DJ, Mahmoud A, Bhatt DL, Bavry AA. Mechanical thrombectomy for acute ischemic stroke: a meta-analysis of randomized trials. *J Am Coll Cardiol*. (2015) 66:2498–505. doi: 10.1016/j.jacc.2015.09.070
4. Lin Y, Schulze V, Brockmeyer M, Parco C, Karathanos A, Heinen Y, et al. Endovascular thrombectomy as a means to improve survival in acute ischemic stroke: a meta-analysis. *JAMA Neurol*. (2019) 76:850–4. doi: 10.1001/jamaneurol.2019.0525
5. Lawrence ES, Coshall C, Dundas R, Stewart J, Rudd AG, Howard R, et al. Estimates of the prevalence of acute stroke impairments and disability in a multiethnic population. *Stroke*. (2001) 32:1279–84. doi: 10.1161/01.STR.32.6.1279
6. Kamper DG, Rymer WZ. Impairment of voluntary control of finger motion following stroke: role of inappropriate muscle coactivation. *Muscle Nerve*. (2001) 24:673–81. doi: 10.1002/mus.1054
7. Lang CE, DeJong SL, Beebe JA. Recovery of thumb and finger extension and its relation to grasp performance after stroke. *J Neurophysiol*. (2009) 102:451–9. doi: 10.1152/jn.91310.2008
8. Takebayashi T, Takahashi K, Moriwaki M, Sakamoto T, Domen K. Improvement of upper extremity deficit after constraint-induced movement therapy combined with and without preconditioning stimulation using dual-hemisphere transcranial direct current stimulation and peripheral neuromuscular stimulation in chronic stroke patients: a pilot randomized controlled trial. *Front Neurol*. (2017) 8:568. doi: 10.3389/fneur.2017.00568
9. Rushton DN. Functional electrical stimulation and rehabilitation–an hypothesis. *Med Eng Phys*. (2003) 25:75–8. doi: 10.1016/S1350-4533(02)00040-1
10. Chae J, Sheffler L, Knutson J. Neuromuscular electrical stimulation for motor restoration in hemiplegia. *Top Stroke Rehabil*. (2008) 15:412–26. doi: 10.1310/tsr1505-412
11. Knutson JS, Fu MJ, Sheffler LR, Chae J. Neuromuscular electrical stimulation for motor restoration in Hemiplegia. *Phys Med Rehabil Clin N Am*. (2015) 26:729–45. doi: 10.1016/j.pmr.2015.06.002
12. Quandt F, Hummel FC. The influence of functional electrical stimulation on hand motor recovery in stroke patients: a review. *Exp Transl Stroke Med*. (2014) 6:9. doi: 10.1186/2040-7378-6-9
13. Takeda K, Tanino G, Miyasaka H. Review of devices used in neuromuscular electrical stimulation for stroke rehabilitation. *Med Devices*. (2017) 10:207–13. doi: 10.2147/MDER.S123464
14. Bao SC, Khan A, Song R, Kai-Yu Tong R. Rewiring the lesioned brain: electrical stimulation for post-stroke motor restoration. *J Stroke*. (2020) 22:47–63. doi: 10.5853/jos.2019.03027
15. Marquez-Chin C, Popovic MR. Functional electrical stimulation therapy for restoration of motor function after spinal cord injury and stroke: a review. *Biomed Eng Online*. (2020) 19:34. doi: 10.1186/s12938-020-00773-4
16. Mortimer J, Bhadra N. Peripheral nerve and muscle stimulation. In: Horch KW, Dhillon GS, editors. *Neuroprosthetics:Theory and Practice* River Edge, NJ: World Scientific Publishing Company (2004). p. 638–82.
17. Smith GV, Alon G, Roys SR, Gullapalli RP. Functional MRI determination of a dose-response relationship to lower extremity neuromuscular electrical stimulation in healthy subjects. *Exp Brain Res*. (2003) 150:33–9. doi: 10.1007/s00221-003-1405-9
18. Papadopoulos CM, Tsai SY, Alsbiei T, O'Brien TE, Schwab ME, Kartje GL. Functional recovery and neuroanatomical plasticity following middle cerebral artery occlusion and IN-1 antibody treatment in the adult rat. *Ann Neurol*. (2002) 51:433–41. doi: 10.1002/ana.10144
19. Markus TM, Tsai SY, Bollnow MR, Farrer RG, O'Brien TE, Kindler-Baumann DR, et al. Recovery and brain reorganization after stroke in adult and aged rats. *Ann Neurol*. (2005) 58:950–3. doi: 10.1002/ana.20676
20. Tsai SY, Papadopoulos CM, Schwab ME, Kartje GL. Delayed anti-nogo-a therapy improves function after chronic stroke in adult rats. *Stroke*. (2011) 42:186–90. doi: 10.1161/STROKEAHA.110.590083
21. Podraza KM, Mehta Y, Husak VA, Lippmann E, O'Brien TE, Kartje GL, et al. Improved functional outcome after chronic stroke with delayed anti-Nogo-A therapy: a clinically relevant intention-to-treat analysis. *J Cereb Blood Flow Metab*. (2018) 38:1327–38. doi: 10.1177/0271678X17730994
22. Castro AJ. The effects of cortical ablations on digital usage in the rat. *Brain Res*. (1972) 37:173–85. doi: 10.1016/0006-8993(72)90665-8
23. Alaverdashvili M, Whishaw IQ. Motor cortex stroke impairs individual digit movement in skilled reaching by the rat. *Eur J Neurosci*. (2008) 28:311–22. doi: 10.1111/j.1460-9568.2008.06315.x
24. Tsai SY, Markus TM, Andrews EM, Cheatwood JL, Emerick AJ, Mir AK, et al. Intrathecal treatment with anti-Nogo-A antibody improves functional recovery in adult rats after stroke. *Exp Brain Res*. (2007) 182:261–6. doi: 10.1007/s00221-007-1067-0
25. Latchoumane CV, Barany DA, Karumbaiah L, Singh T. Neurostimulation and reach-to-grasp function recovery following acquired brain injury: insight from pre-clinical rodent models and human applications. *Front Neurol*. (2020) 11:835. doi: 10.3389/fneur.2020.00835
26. Schallert T, Upchurch M, Lobaugh N, Farrar SB, Spirduso WW, Gilliam P, et al. Tactile extinction: distinguishing between sensorimotor and motor asymmetries in rats with unilateral nigrostriatal damage. *Pharmacol Biochem Behav*. (1982) 16:455–62. doi: 10.1016/0091-3057(82)90452-X
27. Schallert T. Sensorimotor impairment and recovery of function in brain-damaged rats: reappearance of symptoms during old age. *Behav Neurosci*. (1983) 97:159–64. doi: 10.1037/0735-7044.97.1.159
28. Chen ST, Hsu CY, Hogan EL, Maricq H, Balentine JD. A model of focal ischemic stroke in the rat: reproducible extensive cortical infarction. *Stroke*. (1986) 17:738–43. doi: 10.1161/01.STR.17.4.738
29. Cho YR, Pawela CP, Li R, Kao D, Schulte ML, Runquist ML, et al. Refining the sensory and motor ratunculus of the rat upper extremity using fMRI and direct nerve stimulation. *Magn Reson Med*. (2007) 58:901–9. doi: 10.1002/mrm.21408

30. Asgarzadie R, Pan H, Wurster R, Nockels R. Sciatic nerve stimulation enhances motor recovery in spinal cord injured rats. *J Neurotrauma*. (2003) 20:1054. doi: 10.1089/089771503770195894
31. Neafsey EJ, Bold EL, Haas G, Hurley-Gius KM, Quirk G, Sievert CF, et al. The organization of the rat motor cortex: a microstimulation mapping study. *Brain Res*. (1986) 396:77–96. doi: 10.1016/0165-0173(86)90011-1
32. Seymour AB, Andrews EM, Tsai SY, Markus TM, Bollnow MR, Brenneman MM, et al. Delayed treatment with monoclonal antibody IN-1 1 week after stroke results in recovery of function and corticorubral plasticity in adult rats. *J Cereb Blood Flow Metab*. (2005) 25:1366–75. doi: 10.1038/sj.jcbfm.9600134
33. Paxinos G, Watson C. *The Rat Brain in Stereotaxic Coordinates*. 4th ed. New York, NY: Academic Press (1998).
34. Kawamata T, Speliotes EK, Finklestein SP. The role of polypeptide growth factors in recovery from stroke. *Adv Neurol*. (1997) 73:377–82.
35. Emerick AJ, Kartje GL. Behavioral recovery and anatomical plasticity in adult rats after cortical lesion and treatment with monoclonal antibody IN-1. *Behav Brain Res*. (2004) 152:315–25. doi: 10.1016/j.bbr.2003.10.010
36. Wahl AS, Omlor W, Rubio JC, Chen JL, Zheng H, Schroter A, et al. Neuronal repair. Asynchronous therapy restores motor control by rewiring of the rat corticospinal tract after stroke. *Science*. (2014) 344:1250–5. doi: 10.1126/science.1253050
37. Whishaw IQ, Pellis SM, Gorny BP. Skilled reaching in rats and humans: evidence for parallel development or homology. *Behav Brain Res*. (1992) 47:59–70. doi: 10.1016/S0166-4328(05)80252-9
38. Bertelli JA, Taleb M, Saadi A, Mira JC, Pecot-Dechavassine M. The rat brachial plexus and its terminal branches: an experimental model for the study of peripheral nerve regeneration. *Microsurgery*. (1995) 16:77–85. doi: 10.1002/micr.1920160207
39. Rapp FA, Soos MP. *Anatomy, Shoulder and Upper Limb, Hand Cutaneous Innervation*. Treasure Island, FL: StatPearls (2020).
40. Chipchase LS, Schabrun SM, Hodges PW. Peripheral electrical stimulation to induce cortical plasticity: a systematic review of stimulus parameters. *Clin Neurophysiol*. (2011) 122:456–63. doi: 10.1016/j.clinph.2010.07.025
41. McDonnell MN, Ridding MC. Afferent stimulation facilitates performance on a novel motor task. *Exp Brain Res*. (2006) 170:109–15. doi: 10.1007/s00221-005-0192-x
42. Schabrun SM, Ridding MC. The influence of correlated afferent input on motor cortical representations in humans. *Exp Brain Res*. (2007) 183:41–9. doi: 10.1007/s00221-007-1019-8
43. Tsutada T, Tsuyuguchi N, Hattori H, Shimada H, Shimogawara M, Kuramoto T, et al. Determining the appropriate stimulus intensity for studying the dipole moment in somatosensory evoked fields: a preliminary study. *Clin Neurophysiol*. (1999) 110:2127–30. doi: 10.1016/S1388-2457(99)00188-1
44. Torquati K, Pizzella V, Della Penna S, Franciotti R, Babiloni C, Rossini PM, et al. Comparison between SI and SII responses as a function of stimulus intensity. *Neuroreport*. (2002) 13:813–9. doi: 10.1097/00001756-200205070-00016
45. Lin YY, Shih YH, Chen JT, Hsieh JC, Yeh TC, Liao KK, et al. Differential effects of stimulus intensity on peripheral and neuromagnetic cortical responses to median nerve stimulation. *Neuroimage*. (2003) 20:909–17. doi: 10.1016/S1053-8119(03)00387-2
46. Kartje-Tillotson G, Neafsey EJ, Castro AJ. Electrophysiological analysis of motor cortical plasticity after cortical lesions in newborn rats. *Brain Res*. (1985) 332:103–11. doi: 10.1016/0006-8993(85)90393-2
47. Emerick AJ, Neafsey EJ, Schwab ME, Kartje GL. Functional reorganization of the motor cortex in adult rats after cortical lesion and treatment with monoclonal antibody IN-1. *J Neurosci*. (2003) 23:4826–30. doi: 10.1523/JNEUROSCI.23-12-04826.2003
48. Ramic M, Emerick AJ, Bollnow MR, O'Brien TE, Tsai SY, Kartje GL. Axonal plasticity is associated with motor recovery following amphetamine treatment combined with rehabilitation after brain injury in the adult rat. *Brain Res*. (2006) 1111:176–86. doi: 10.1016/j.brainres.2006.06.063
49. Corbett D, Jeffers M, Nguemeni C, Gomez-Smith M, Livingston-Thomas J. Lost in translation: rethinking approaches to stroke recovery. *Pro Brain Res*. (2015) 218:413–34. doi: 10.1016/bs.pbr.2014.12.002
50. Okabe N, Shiromoto T, Himi N, Lu F, Maruyama-Nakamura E, Narita K, et al. Neural network remodeling underlying motor map reorganization induced by rehabilitative training after ischemic stroke. *Neuroscience*. (2016) 339:338–62. doi: 10.1016/j.neuroscience.2016.10.008
51. Z'Graggen WJ, Metz GA, Kartje GL, Thallmair M, Schwab ME. Functional recovery and enhanced corticofugal plasticity after unilateral pyramidal tract lesion and blockade of myelin-associated neurite growth inhibitors in adult rats. *J Neurosci*. (1998) 18:4744–57. doi: 10.1523/JNEUROSCI.18-12-04744.1998
52. Andrews EM, Tsai SY, Johnson SC, Farrer JR, Wagner JP, Kopen GC, et al. Human adult bone marrow-derived somatic cell therapy results in functional recovery and axonal plasticity following stroke in the rat. *Exp Neurol*. (2008) 211:588–92. doi: 10.1016/j.expneurol.2008.02.027
53. Papadopoulos CM, Tsai SY, Guillen V, Ortega J, Kartje GL, Wolf WA. Motor recovery and axonal plasticity with short-term amphetamine after stroke. *Stroke*. (2009) 40:294–302. doi: 10.1161/STROKEAHA.108.519769
54. Beltran EJ, Papadopoulos CM, Tsai SY, Kartje GL, Wolf WA. Long-term motor improvement after stroke is enhanced by short-term treatment with the alpha-2 antagonist, atipamezole. *Brain Res*. (2010) 1346:174–82. doi: 10.1016/j.brainres.2010.05.063
55. Wahl AS, Schwab ME. Finding an optimal rehabilitation paradigm after stroke: enhancing fiber growth and training of the brain at the right moment. *Front. Hum. Neurosci.* (2014) 7:911. doi: 10.3389/fnhum.2013.00911
56. Wahl AS, Buchler U, Brandli A, Brattoli B, Musall S, Kasper H, et al. Optogenetically stimulating intact rat corticospinal tract post-stroke restores motor control through regionalized functional circuit formation. *Nat Commun*. (2017) 8:1187. doi: 10.1038/s41467-01 01090-6
57. Adkins DL, Hsu JE, Jones TA. Motor cortical stimulation promotes synaptic plasticity and behavioral improvements following sensorimotor cortex lesions. *Exp Neurol*. (2008) 212:14–28. doi: 10.1016/j.expneurol.2008.01.031
58. Jones TA, Allred RP, Adkins DL, Hsu JE, O'Bryant A, Maldonado MA. Remodeling the brain with behavioral experience after stroke. *Stroke*. (2009) 40:S136–8. doi: 10.1161/STROKEAHA.108.533653
59. Ruber T, Schlaug G, Lindenberg R. Compensatory role of the cortico-rubro-spinal tract in motor recovery after stroke. *Neurology*. (2012) 79:515–22. doi: 10.1212/WNL.0b013e31826356e8
60. Kim SY, Hsu JE, Husbands LC, Kleim JA, Jones TA. Coordinated plasticity of synapses and astrocytes underlies practice-driven functional vicariation in peri-infarct motor cortex. *J Neurosci*. (2018) 38:93–107. doi: 10.1523/JNEUROSCI.1295-17.2017
61. Gillani RL, Tsai SY, Wallace DG, O'Brien TE, Arhebamen E, Tole M, et al. Cognitive recovery in the aged rat after stroke and anti-Nogo-A immunotherapy. *Behav Brain Res*. (2010) 208:415–24. doi: 10.1016/j.bbr.2009.12.015
62. Peurala SH, Pitkanen K, Sivenius J, Tarkka IM. Cutaneous electrical stimulation may enhance sensorimotor recovery in chronic stroke. *Clin Rehabil*. (2002) 16:709–16. doi: 10.1191/0269215502cr543oa
63. Veldman MP, Maurits NM, Zijdewind I, Maffiuletti NA, van Middelkoop S, Mizelle JC, et al. Somatosensory electrical stimulation improves skill acquisition, consolidation, and transfer by increasing sensorimotor activity and connectivity. *J Neurophysiol*. (2018) 120:281–90. doi: 10.1152/jn.00860.2017
64. Fraser C, Power M, Hamdy S, Rothwell J, Hobday D, Hollander I, et al. Driving plasticity in human adult motor cortex is associated with improved motor function after brain injury. *Neuron*. (2002) 34:831–40. doi: 10.1016/S0896-6273(02)00705-5
65. Okabe N, Himi N, Maruyama-Nakamura E, Hayashi N, Narita K, Miyamoto O. Rehabilitative skilled forelimb training enhances axonal remodeling in the corticospinal pathway but not the brainstem-spinal pathways after photothrombotic stroke in the primary motor cortex. *PLoS ONE*. (2017) 12:e0187413. doi: 10.1371/journal.pone.0187413
66. Okabe N, Narita K, Miyamoto O. Axonal remodeling in the corticospinal tract after stroke: how does rehabilitative training modulate it? *Neural Regen Res*. (2017) 12:185–92. doi: 10.4103/1673-5374.200792
67. Wiersma AM, Fouad K, Winship IR. Enhancing spinal plasticity amplifies the benefits of rehabilitative training and improves recovery from

stroke. *J Neurosci*. (2017) 37:10983–97. doi: 10.1523/JNEUROSCI.0770-17.2017
68. Chen YH, Lee HJ, Lee MT, Wu YT, Lee YH, Hwang LL, et al. Median nerve stimulation induces analgesia via orexin-initiated endocannabinoid disinhibition in the periaqueductal gray. *Proc Natl Acad Sci USA*. (2018) 115:E10720–9. doi: 10.1073/pnas.1807991115
69. Sist B, Fouad K, Winship IR. Plasticity beyond peri-infarct cortex: spinal up regulation of structural plasticity, neurotrophins, and inflammatory cytokines during recovery from cortical stroke. *Exp Neurol*. (2014) 252:47–56. doi: 10.1016/j.expneurol.2013.11.019
70. Hayashi N, Himi N, Nakamura-Maruyama E, Okabe N, Sakamoto I, Hasegawa T, et al. Improvement of motor function induced by skeletal muscle contraction in spinal cord-injured rats. *Spine J*. (2019) 19:1094–105. doi: 10.1016/j.spinee.2018.12.012
71. Polimanti R, Simonelli I, Zappasodi F, Ventriglia M, Pellicciari MC, Benussi L, et al. Biological factors and age-dependence of primary motor cortex experimental plasticity. *Neurol Sci*. (2016) 37:211–8. doi: 10.1007/s10072-015-2388-6
72. Balseanu AT, Grigore M, Pinosanu L-R, Slevin M, Hermann DM, Glavan D, et al. Electric stimulation of neurogenesis improves behavioral recovery after focal ischemia in aged rats. *Front. Neurosci.* (2020) 14:732. doi: 10.3389/fnins.2020.00732
73. Saha B, Peron S, Murray K, Jaber M, Gaillard A. Cortical lesion stimulates adult subventricular zone neural progenitor cell proliferation and migration to the site of injury. *Stem Cell Res*. (2013) 11:965–77. doi: 10.1016/j.scr.2013.06.006
74. Noller CM, Levine YA, Urakov TM, Aronson JP, Nash MS. Vagus nerve stimulation in rodent models: an overview of technical considerations. *Front Neurosci.* (2019) 13:911. doi: 10.3389/fnins.2019.00911
75. Frankel MA, Mathews VJ, Clark GA, Normann RA, Meek SG. Control of dynamic limb motion using fatigue-resistant asynchronous intrafascicular multi-electrode stimulation. *Front Neurosci.* (2016) 10:414. doi: 10.3389/fnins.2016.00414
76. Wegrzyk J, Ranjeva JP, Foure A, Kavounoudias A, Vilmen C, Mattei JP, et al. Specific brain activation patterns associated with two neuromuscular electrical stimulation protocols. *Sci Rep*. (2017) 7:2742. doi: 10.1038/s41598-017-03188-9
77. Zeiler SR, Krakauer JW. The interaction between training and plasticity in the poststroke brain. *Curr Opin Neurol*. (2013) 26:609–16. doi: 10.1097/WCO.0000000000000025
78. Murphy TH, Corbett D. Plasticity during stroke recovery: from synapse to behaviour. *Nat Rev Neurosci*. (2009) 10:861–72. doi: 10.1038/nrn2735
79. Krakauer JW, Carmichael ST, Corbett D, Wittenberg GF. Getting neurorehabilitation right: what can be learned from animal models? *Neurorehabil Neural Repair*. (2012) 26:923–31. doi: 10.1177/1545968312440745
80. Jones TA. Motor compensation and its effects on neural reorganization after stroke. *Nat Rev Neurosci*. (2017) 18:267–80. doi: 10.1038/nrn.2017.26

Conflict of Interest: The authors declare that the research was conducted in the absence of any commercial or financial relationships that could be construed as a potential conflict of interest.

Copyright © 2021 Tsai, Schreiber, Adamczyk, Wu, Ton, Hofler, Walter, O'Brien, Kartje and Nockels. This is an open-access article distributed under the terms of the Creative Commons Attribution License (CC BY). The use, distribution or reproduction in other forums is permitted, provided the original author(s) and the copyright owner(s) are credited and that the original publication in this journal is cited, in accordance with accepted academic practice. No use, distribution or reproduction is permitted which does not comply with these terms.

Advantages of publishing in Frontiers

OPEN ACCESS
Articles are free to read for greatest visibility and readership

FAST PUBLICATION
Around 90 days from submission to decision

HIGH QUALITY PEER-REVIEW
Rigorous, collaborative, and constructive peer-review

TRANSPARENT PEER-REVIEW
Editors and reviewers acknowledged by name on published articles

Frontiers
Avenue du Tribunal-Fédéral 34
1005 Lausanne | Switzerland

Visit us: www.frontiersin.org
Contact us: frontiersin.org/about/contact

REPRODUCIBILITY OF RESEARCH
Support open data and methods to enhance research reproducibility

DIGITAL PUBLISHING
Articles designed for optimal readership across devices

FOLLOW US
@frontiersin

IMPACT METRICS
Advanced article metrics track visibility across digital media

EXTENSIVE PROMOTION
Marketing and promotion of impactful research

LOOP RESEARCH NETWORK
Our network increases your article's readership